GEOTECHNICAL AND GEOENVIRONMENTAL ENGINEERING HANDBOOK

GEOTECHNICAL AND GEOENVIRONMENTAL ENGINEERING HANDBOOK

Edited by

R. Kerry Rowe
QUEEN'S UNIVERSITY,
KINGSTON, ONTARIO, CANADA



Springer Science+Business Media, LLC



Electronic Services <http://www.wkap.nl>

Library of Congress Cataloging-in-Publication Data
Geotechnical and geoenvironmental engineering handbook/edited by
R. Kerry Rowe
p. cm.
Includes bibliographical references.
ISBN 978-1-4613-5699-8 ISBN 978-1-4615-1729-0 (eBook)
DOI 10.1007/978-1-4615-1729-0
1. Engineering geology handbooks, manuals, etc. I. Rowe, R. K.
TA705.G427 2000
624. 1'51—dc21 99-37319
CIP

Copyright © 2001 by Springer Science+Business Media New York
Originally published by Kluwer Academic Publishers in 2001

All rights reserved. No part of this publication may be reproduced, stored in a retrieval system or transmitted in any form or by any means, mechanical, photo-copying, recording, or otherwise, without the prior written permission of the publisher, Springer Science+Business Media, LLC.

Printed on acid-free paper.

Dedicated in memory of

J. R. Booker

E. H. Davis

M. Novak

R. M. Quigley

CONTENTS

List of Figures xxxiii
List of Tables liii
Contributing Authors lix
Preface lxv

I. BASIC BEHAVIOR AND SITE CHARACTERIZATION 1

1. Introduction 3
R. K. Rowe
1.1 Geotechnical and geoenvironmental engineering 3
1.2 Objectives and organization of the book 3
1.3 Limitations 5

2. Basic Soil Mechanics 7
P. V. Lade
2.1 Introduction 7
2.2 Soil types: geologic formation and classification 7
2.2.1 Basic elements, soil forming minerals and types of rock 7
2.2.2 The geologic cycle, soil forming processes and types of soil 8
2.2.3 Soil fabric and structure 9
2.2.3.1 Clay fabric 10
2.2.3.2 Fabric of granular soils 10
2.3 Definitions and relationships between basic soil properties 11
2.4 Seepage through saturated soil 11
2.4.1 Basic head equations 11
2.4.2 Darcy's law and hydraulic conductivity 13
2.5 Basic mechanics 13
2.5.1 Analyses of stress: Mohr's circle 13
2.5.2 Analyses of strain: Mohr's circle 15
2.5.3 Other stress representations and stress paths 16
2.5.3.1 s–t diagram 16
2.5.3.2 p–q diagram 17
2.6 State of stress in the ground 17
2.6.1 Effective stress principle 17
2.6.2 Total vertical (overburden) stress 17
2.6.3 Groundwater table and porewater pressure 18
2.6.4 Effective vertical stress 18
2.6.5 Horizontal stress and K_0 19
2.7 Compressibility and consolidation 19
2.7.1 Elasticity 19
2.7.2 Modulus variation 20
2.7.3 Compression and expansion 21
2.7.4 One-dimensional consolidation 23
2.7.5 Creep 26

2.8 Stress–Strain and strength behavior 28
2.8.1 Drained behavior of sand 28
2.8.2 Undrained behavior of sand 31
2.8.3 Undrained behavior of normally consolidated clay 31
2.8.4 Undrained behavior of overconsolidated clay 31
2.8.5 Drained behavior of clay 33
2.9 Shear strength 34
2.9.1 Effective strength characterization 34
2.9.2 Total strength characterization 35
2.10 Elasto-plasticity, critical state soil mechanics and models for soil stress–strain behavior 36
2.10.1 Critical state soil mechanics 36
2.10.2 Modified Cam Clay model 37
2.10.3 Other models 39
2.11 Dynamic soil behavior 40
2.11.1 Determination of modulus and damping 40
2.11.2 Seismic stability of soil structures 41

3. Engineering Properties of Soils and Typical Correlations 43
P. V. Lade
3.1 Engineering properties and parameters required for characterization 43
3.2 Index tests 43
3.2.1 Grain-size distribution 43
3.2.1.1 Coefficients of uniformity and curvature 43
3.2.2 Particle shape 45
3.2.3 Maximum and minimum void ratios 45
3.2.4 Density index 45
3.2.5 Relative compaction 46
3.2.6 Relative density 46
3.2.7 Atterberg limits 46
3.2.7.1 Liquid limit 46
3.2.7.2 Plastic limit 47
3.2.7.3 Plasticity index 47
3.2.7.4 Liquidity index 48
3.2.7.5 Activity 48
3.2.7.6 Shrinkage limit 48
3.2.8 Expansion index 48
3.2.9 Sensitivity 49
3.2.10 Content of organic material 49
3.2.11 Soil classification 51
3.3 Hydraulic conductivity 51
3.3.1 Laboratory hydraulic conductivity (permeability) tests 51
3.3.2 Typical hydraulic conductivity values and correlations 54
3.4 At rest stress state, K_0 54
3.4.1 Normally consolidated soils 54
3.4.2 Overconsolidated soils 54
3.5 Compressibility and consolidation 55
3.5.1 Elastic properties 55
3.5.1.1 Young's modulus 55
3.5.1.2 Poisson's ratio 55
3.5.2 Compressibility 56
3.5.2.1 Preconsolidation pressure 56
3.5.2.2 Virgin compression 56
3.5.2.3 Swelling and recompression 57
3.5.3 Coefficient of consolidation 57

3.5.4 Creep 58
3.5.5 Remolded or disturbed soils 58
3.6 Swelling and shrinkage 58
3.7 Shear strength 59
3.7.1 Laboratory determination of soil behavior 59
3.7.2 Effective strength parameters 60
3.7.2.1 Granular materials: cohesionless soils 60
3.7.2.2 Clays: cohesive soils 61
3.7.3 Undrained shear strength 62
3.7.3.1 Normally consolidated clays 62
3.7.3.2 Overconsolidated clays 63
3.8 Dynamic properties 64
3.8.1 Shear modulus and damping: low strain level excitation 64
3.8.2 Shear modulus and damping: high strain level excitation 67

4. Site Characterization 69
D. E. Becker
4.1 Introduction 69
4.1.1 The need for site characterization 69
4.1.2 Objectives of site characterization 70
4.2 Site characterization process: an integrated approach 70
4.2.1 Site characterization flowchart 72
4.2.2 Reporting 73
4.3 Planning and design of characterization study 74
4.3.1 Role of codes of practice and guidelines 75
4.3.2 Quality management of site investigation 75
4.3.3 Scope of investigation 75
4.3.4 Selection of field equipment and test methods 78
4.3.5 Cost considerations 79
4.3.6 Offshore investigations 79
4.3.7 Contractual aspects 80
4.4 Investigation components and methods 80
4.4.1 Review of background and existing information 80
4.4.2 Aerial photographs and remote sensing 80
4.4.3 Field reconnaissance and mapping 81
4.4.4 Geophysical surveys 81
4.4.5 Borehole drilling and sampling methods 84
4.4.5.1 Backfilling and sealing of boreholes 86
4.4.6 Field and *in situ* testing 87
4.4.6.1 Standard penetration test (SPT) 89
4.4.6.2 Dynamic cone-penetration test (DCPT) 91
4.4.6.3 Dynamic probing (DP) 91
4.4.6.4 Becker penetration test (BPT) 91
4.4.6.5 Field vane test (FVT) 92
4.4.6.6 Piezo-cone penetration test (CPTU) 92
4.4.6.7 Pressuremeter test (PMT) 93
4.4.6.8 Dilatometer test (DMT) 94
4.4.6.9 Plate-load and screw-plate tests 94
4.4.6.10 Other tests to measure *in situ* horizontal stress 94
4.5 Interpretation of engineering characteristics and properties based on *in situ* tests 96
4.5.1 Use of statistical methods 97
4.6 Observational approach and monitoring 97
4.6.1 Field instrumentation and monitoring 100

4.7 Characterization of groundwater 101
4.7.1 Water levels, piezometric pressures and sampling 102
4.7.2 *In situ* hydraulic conductivity tests 103
4.8 Environmental site characterization 104
4.8.1 Investigation of landfills and contaminated land 104

5. Unsaturated Soil Mechanics and Property Assessment 107
D. G. Fredlund, G. W. Wilson and S. L. Barbour
5.1 Introduction 107
5.1.1 Basic concepts in unsaturated soil mechanics 109
5.2 Soil–water characteristic curve 110
5.2.1 Stages of the soil–water characteristic curve 111
5.2.2 Residual conditions for a soil 113
5.2.3 Mathematical form for the soil–water characteristic curve 114
5.2.4 Laboratory measurement of the soil–water characteristic curve 116
5.2.5 Estimation of the soil–water characteristic curve 117
5.3 Stress state variables of unsaturated soils 120
5.3.1 Measurement of soil suction: matric, osmotic and total suction 121
5.4 Boundary conditions 122
5.4.1 Evaporation, evapotranspiration, and the prediction of the flux boundary condition 124
5.5 Seepage through unsaturated soils 125
5.5.1 Hydraulic conductivity function 126
5.5.2 The water storage function 128
5.5.3 Measurement of the hydraulic conductivity function 128
5.5.4 Estimation of the hydraulic conductivity function and the water storage function from the soil–water characteristic curve 130
5.5.5 Estimation of the water storage function from the soil–water characteristic curve 133
5.5.6 Formulation of the steady state and unsteady state seepage analysis 133
5.6 Shear strength of unsaturated soils 134
5.6.1 Shear strength function with respect to soil suction 134
5.6.2 Measurement of the shear strength function with respect to soil suction 135
5.6.3 Estimation of the shear strength function from the soil–water characteristic curve 136
5.6.4 Formulation for bearing capacity problems 140
5.6.5 Formulation for lateral earth pressure problems 140
5.6.6 Formulations for slope stability problems 140
5.7 Volume change in unsaturated soils 142
5.7.1 Measurement of the volume change function 143
5.7.2 Estimation of the volume change moduli 144
5.7.3 Formulation for the prediction of heave of an expansive soil 144

6. Basic Rock Mechanics and Testing 147
K. Y. Lo and A. M. Hefny
6.1 Introduction 147
6.2 Types of rocks and their classification 147
6.2.1 Rock-forming minerals 147
6.2.2 Rock classification 147
6.2.2.1 Geological classification 148
6.2.2.2 Engineering classification 150
6.3 Laboratory measurements of strength and deformation properties of intact rock 154
6.3.1 Uniaxial compression test 155

6.3.2 Deformation parameters for cross-anisotropic rocks 155
6.3.2.1 Stress–strain relationships in cross-anisotropic rocks 155
6.3.2.2 Evaluation of parameters 157
6.3.2.3 Results of uniaxial compression test 157
6.3.3 Tensile strength tests 157
6.3.3.1 Brazilian test (indirect tension test) 157
6.3.3.2 Direct tension test 159
6.3.4 Triaxial compression test 159
6.3.5 Triaxial extension test 159
6.4 Time-dependent deformation 159
6.4.1 Free swell test 161
6.4.2 Semi-confined swell test 162
6.5 Failure criteria of a brittle material 163
6.5.1 Griffith criterion 164
6.5.2 Hoek–Brown failure criterion 164
6.6 Shear strength of discontinuities 166
6.6.1 Description and measurement of discontinuities 166
6.6.2 Determination of basic friction angle 166
6.6.3 Typical results of tests on rock joints 168
6.7 Measurements of *in situ* horizontal stresses in rock 168
6.7.1 The United States Bureau of Mines (USBM) method 168
6.7.1.1 Example of calculations 170
6.7.2 Hydraulic fracturing method 171

7. Geosynthetics: Characteristics and Testing 173
R. M. Koerner and Y. G. Hsuan
7.1 Introduction 173
7.2 Geotextile properties and test methods 174
7.2.1 Physical properties 174
7.2.2 Mechanical properties 174
7.2.3 Hydraulic properties 176
7.2.4 Endurance properties 177
7.3 Geogrid properties and test methods 179
7.3.1 Physical properties 180
7.3.2 Mechanical properties 180
7.3.3 Endurance properties 180
7.4 Geonet properties and test methods 180
7.4.1 Physical and mechanical properties 181
7.4.2 Hydraulic properties 181
7.4.3 Endurance properties 181
7.5 Geomembrane properties and test methods 181
7.5.1 Physical properties 182
7.5.2 Mechanical properties 183
7.5.3 Endurance properties 185
7.6 Geosynthetic clay liner properties and test methods 185
7.6.1 Physical properties 186
7.6.2 Hydraulic properties 186
7.6.3 Mechanical properties 186
7.6.4 Endurance properties 187
7.7 Geocomposite properties and test methods 187
7.7.1 Separation geocomposites 187
7.7.2 Reinforcement geocomposites 187
7.7.3 Filtration geocomposites 188

7.7.4 Drainage geocomposites 188
7.7.5 Containment (barrier) geocomposites 188
7.8 Degradation mechanisms for polymers 188
7.8.1 Oxidation degradation 188
7.8.1.1 Oxidation degradation mechanisms of polyolefins 189
7.8.1.2 Accelerated tests and lifetime predictions 190
7.8.2 Ultraviolet degradation 190
7.8.3 Biological degradation 191
7.8.4 Hydrolytic degradation 191
7.9 Allowable versus ultimate geotextile and geogrid properties 192
7.9.1 Strength related applications 193
7.9.1.1 Allowable strength approach 193
7.9.1.2 Limit state approach 193
7.9.2 Liquid flow related applications 194
7.10 Summary 194

8. Seepage, Drainage and Dewatering 197
R. W. Loughney
8.1 Introduction 197
8.2 Geology, hydrogeology and hydrology 197
8.2.1 Geology 197
8.2.2 Hydrogeology 197
8.2.3 Hydrology 198
8.2.3.1 Basic flow equations 198
8.2.3.2 Graphical approach 200
8.3 Seepage and drainage 205
8.3.1 Seepage 205
8.3.2 Drainage 205
8.4 Area to be dewatered 206
8.5 Assessment of groundwater conditions 207
8.6 Selection of dewatering systems 208
8.6.1 Dewatering systems 208
8.6.2 Soil stabilization systems 208
8.6.2.1 Vacuum applied to the soil 208
8.6.2.2 Electro-osmosis 213
8.6.3 Cut-off walls: grouting and freezing 214
8.6.4 Open pumping 214
8.6.5 Recharge 214
8.7 Design of the dewatering system 214
8.7.1 Well-screens 215
8.7.2 Filter packs 216
8.7.3 Pump units 217
8.7.4 Piping and fittings 217
8.8 Installation, operation and removal of dewatering systems 218
8.8.1 Installation 218
8.8.2 Operation 218
8.8.3 Removal 218
8.9 Permanent dewatering system 218
8.10 Dewatering specifications 218
8.10.1 Specified end result 219
8.10.2 Specified minimum groundwater control system 219
8.10.3 Specified complete groundwater control system 219
8.10.4 Specialty contractors responsibility 220
8.11 Summary 220

II. FOUNDATIONS AND PAVEMENTS 221

9. Shallow Foundations 223
J. C. Small
9.1 Introduction 223
9.2 Types of Shallow Foundations 223
9.2.1 Strip footings 223
9.2.2 Pad footings 223
9.2.3 Combined footings 224
9.2.4 Raft or mat foundations 224
9.2.5 Inspection 224
9.3 Bearing capacity 224
9.3.1 Uniform soils 225
9.3.1.1 Undrained case 227
9.3.1.2 Drained case 227
9.3.1.3 Accuracy of Terzaghi's factors 228
9.3.1.4 Effect of footing shape 228
9.3.1.5 Net bearing capacity 228
9.3.1.6 General formulae 229
9.3.1.7 Soil layers of finite depth 232
9.3.2 Non-uniform soils 232
9.3.2.1 Strength increasing with depth 234
9.3.2.2 Fissured clays 235
9.3.2.3 Footings on slopes 237
9.3.2.4 Layered soils 238
9.4 Settlement 240
9.4.1 Limits of settlement 240
9.4.2 Settlement computation 240
9.4.3 Theory of elasticity 242
9.4.3.1 One-dimensional conditions 242
9.4.3.2 Three-dimensional problems 242
9.4.4 Rate of settlement 244
9.4.5 Numerical approaches 246
9.4.5.1 Layered soil: finite layer approaches 246
9.4.5.2 Non-linear materials 246
9.4.6 Settlement of footings on sand 247
9.4.6.1 Methods based on the standard penetration test (SPT) 247
9.4.6.2 Method based on static cone penetrometer 249
9.4.7 Methods based on settlement and bearing criteria 250
9.4.8 Estimating the soil parameters 252
9.5 Raft foundations 252
9.5.1 Strip rafts 253
9.5.2 Circular rafts 253
9.5.3 Rectangular rafts 255
9.5.4 Raft foundations of general shape 256
9.6 Reactive soils 257
9.6.1 Rafts on reactive soils 257
9.7 Cold climates 257
9.8 Limit state design 258

10. Pile Foundations 261
H. G. Poulos
10.1 Introduction 261

10.1.1 Design objectives 261
10.1.2 Criteria for design 261
10.1.3 Types of piles and their uses 262
10.2 Pile load capacity 263
10.2.1 Dynamic calculation methods 263
10.2.2 Static calculation methods 264
10.2.2.1 General principles 264
10.2.2.2 Saturated clay soils: α method 264
10.2.2.3 Saturated clay soils: β method 265
10.2.2.4 Non-cohesive soils 266
10.2.2.5 Layered soils 267
10.2.3 Methods using *in situ* test data 268
10.2.3.1 Static cone penetration (CPT) tests 268
10.2.3.2 Standard penetration test (SPT) 268
10.2.4 Uplift capacity 271
10.2.5 Group effects 271
10.2.6 Effects of cyclic loading 271
10.3 Settlement prediction 273
10.3.1 Analysis methods 273
10.3.2 Design charts and equations for single piles 274
10.3.2.1 Non-linear analysis 275
10.3.3 Pile group settlement 275
10.3.3.1 Methods of analysis 275
10.3.3.2 Rapid practical estimation of group settlements 278
10.3.4 Assessment of parameters 280
10.4 Lateral loading 283
10.4.1 Ultimate lateral capacity 283
10.4.1.1 Single piles 283
10.4.1.2 Pile groups 284
10.4.2 Lateral deflection of single piles 285
10.4.2.1 p–y analysis 285
10.4.2.2 Linear elastic solutions 285
10.4.2.3 Non-linear solutions 287
10.4.3 Group effects 287
10.4.4 Assessment of parameters 288
10.4.5 Effects of cyclic loading 290
10.5 General analysis of pile groups 292
10.5.1 Methods of analysis 292
10.5.2 Some elastic-based computer methods 293
10.6 Pile response to externally imposed ground movements 293
10.6.1 Introduction: sources of ground movement 293
10.6.2 Negative friction 294
10.6.3 Expansive soils 296
10.6.4 Piles subjected to lateral ground movements 296
10.6.5 Specific applications 298
10.6.5.1 Piles in unstable slopes 299
10.6.5.2 Piles near an excavation 299
10.6.5.3 Piles in and near embankments 299
10.7 Pile load testing 299
10.7.1 Introduction 299
10.7.2 Static load testing 300
10.7.3 Dynamic pile testing 300
10.7.4 Statnamic testing 301

10.7.5 Interpretation of load test results 302
10.7.5.1 Ultimate load 302
10.7.5.2 Load distribution 302
10.7.5.3 Soil stiffness 303
10.7.6 Integrity testing 303

11. Foundations on Rock 305
K. Y. Lo and A. M. Hefny
11.1 Introduction 305
11.2 Foundations for tall buildings 305
11.2.1 Design considerations 305
11.2.1.1 Bearing capacity 305
11.2.1.2 Allowable bearing pressure 305
11.2.1.3 Differential settlement 309
11.2.1.4 Effect of excavations in rock on adjacent structures 309
11.2.1.5 Base heave 310
11.2.2 Field tests for the measurement of rock mass modulus 310
11.2.3 Socketed piles into rock 313
11.2.3.1 End bearing resistance 314
11.2.3.2 Shaft resistance 314
11.2.3.3 Estimation of average side shear resistance using empirical correlations 314
11.2.3.4 Design of piles socketed into rock 316
11.3 Concrete dams on rock foundations 318
11.3.1 Introduction 318
11.3.2 Methodology 319
11.3.3 Methods of field investigation 319
11.3.4 Strength envelopes of bonded and unbonded contacts 323
11.3.5 Extraction of data from records 326
11.3.6 Methods currently used in stability analysis 327
11.3.7 An example of application of methodology: safety assessment of Barrett Chute Dam 329
11.3.7.1 Design provisions and geological conditions 329
11.3.7.2 Field investigation and condition of contact 330
11.3.7.3 Results of laboratory tests and strength parameters for design analysis 330
11.3.7.4 High uplift pressures measured and remedial measures 331
11.3.7.5 Stability study 332
11.3.8 Experience gained and benefits derived from application of the methodology 332

12. Dynamics of Foundations 337
M. H. El Naggar
12.1 Introduction 337
12.1.1 Design objectives 337
12.1.2 Types of dynamic loads 337
12.1.3 Types of foundations 338
12.2 Shallow foundations 338
12.2.1 Impedance functions of shallow foundations 338
12.2.2 Embedment effects 341
12.2.3 Impedance functions of a layer on halfspace 342
12.3 Deep foundations 344
12.3.1 Impedance functions of piles 344
12.3.2 Pile–soil–pile interaction 346

12.3.3 Impedance functions of pile groups 347
12.3.4 Pile batter 348
12.3.5 Non–linear response of piles 348
12.3.6 Seismic response of pile foundations 348
12.3.7 Experimental studies on response of piles 349
12.3.7.1 Full-scale field tests 349
12.3.7.2 Small prototype field tests 349
12.3.7.3 Small-scale laboratory tests 350
12.3.7.4 Centrifugal modeling 350
12.4 Response of machine foundations 350
12.4.1 Response of rigid foundations in one degree-of-freedom 350
12.4.2 Coupled response of rigid foundations 351
12.4.2.1 Direct solution 351
12.4.2.2 Modal analysis 352
12.4.3 Response of rigid foundations in six degrees-of-freedom 353
12.5 Response of hammer foundations 355
12.5.1 Types of hammers and hammer foundations 355
12.5.2 Design criteria 355
12.5.3 Response of one mass foundation 356
12.5.4 Response of two mass foundation 357

13. Pavement Design 361
R. Haas and B. L. Rodway
13.1 Introduction 361
13.2 Geotechnical and environmental considerations 361
13.2.1 Soils investigation and engineering properties 362
13.2.2 Drainage 363
13.2.3 Compaction 364
13.2.3.1 Basic principles 364
13.2.3.2 Compaction of soils 364
13.2.3.3 Construction equipment for soil compaction 365
13.2.3.4 Compaction of asphalt layers 365
13.2.3.5 Specifications for compaction of asphalt layers 366
13.2.3.6 Asphalt compaction equipment 366
13.2.4 Geosynthetics in pavements 366
13.2.5 Environmental considerations 368
13.3 Framework for pavement design 369
13.3.1 Introduction 369
13.3.2 Design objectives and constraints 369
13.3.3 Components of the design framework 369
13.3.4 Categorization of structural design methods 370
13.4 Design inputs and their characterization 371
13.4.1 Material properties and characterization 371
13.4.1.1 Asphalt concrete 371
13.4.1.2 Portland cement concrete 372
13.4.1.3 Granular bases and subbases 372
13.4.1.4 Reinforcement steel 372
13.4.1.5 Traffic loads 374
13.5 Pavement response models 375
13.5.1 Elastic layer theory 376
13.5.2 The finite element method 376
13.5.3 Simplified (Odemark) elastic layer theory 377
13.6 Structural design of flexible road pavements 377
13.6.1 Review of common design methods 377

13.6.2 Experience-based design 377
13.6.3 Empirically based design: the AASHTO design method 379
13.6.4 Mechanistic-empirical based design: the Asphalt Institute method 380
13.7 Structural design of airfield pavements 382
13.7.1 An overview 382
13.7.2 Airfield pavement types and comparative thicknesses 383
13.7.2.1 Airfield pavement thickness design 384
13.7.3 Airfield pavement failure and safety considerations 386
13.8 Structural design of rigid pavements for roads 386
13.8.1 Types of rigid pavements 386
13.8.2 Basic factors in thickness design 387
13.8.2.1 Flexural strength of concrete 387
13.8.2.2 Subgrade and subbase support 387
13.8.2.3 Design or life-cycle period 387
13.8.3 Thickness design methods 388
13.8.4 AASHTO thickness design procedure (AASHTO 1993) 388
13.8.5 Portland Cement Association thickness design procedure 388
13.8.6 Consideration of joints in design 389
13.8.7 Typical joint configurations 389
13.8.8 Approximate, catalog design approach 389
13.9 Design of overlays 391
13.9.1 Introduction 391
13.9.2 Flexible pavement overlay design methods 391
13.10 Application of reliability to pavement design 392
13.11 Economic evaluation of pavement design alternatives 393
13.11.1 Basic principles and approaches 393
13.11.2 Common methods of economic evaluation 393

III. SLOPE, EMBANKMENT AND WALL STABILITY, AND SOIL IMPROVEMENT 395

14. Slopes and Mass Movements 397
S. Leroueil, J. Locat, G. Sève, L. Picarelli and R. M. Faure
14.1 Introduction 397
14.2 Types of movements 399
14.3 Importance of groundwater conditions in slopes 399
14.3.1 Water flow conditions in soil slopes 399
14.3.2 Particular case of excavations in clays 401
14.3.3 Triggering or aggravating factors related to water 402
14.3.4 Flow nets 402
14.3.5 Particular case of rock slopes 403
14.4 Analysis of slope movements: generalities 404
14.4.1 Pre-failure 405
14.4.2 Failure 406
14.4.3 Post-failure 407
14.4.4 Reactivation 408
14.5 Methods of slope stability analysis 409
14.5.1 General remarks 409
14.5.2 Infinite slope 411
14.5.3 Methods of slices 412
14.5.4 Global method: perturbation method 414
14.5.5 Planar failure 415
14.5.6 Wedge failure 416
14.5.7 Toppling failure 418

14.6 Risk assessment associated to slope movements 420
14.6.1 Total risk 420
14.6.2 Elements at risk and their vulnerability 421
14.6.3 Hazard 421
14.6.4 Tolerable risk 422
14.7 Methods of mitigation 423
14.7.1 Generalities 423
14.7.2 Elimination of the problem or reduction of its consequences 423
14.7.2.1 Relocation 423
14.7.2.2 Complete or partial removal of unstable materials 423
14.7.2.3 Bridging 423
14.7.2.4 Protection of the structures against soil or rock movements 423
14.7.3 Earthworks 424
14.7.4 Earth retaining systems 424
14.7.5 Drainage systems 424
14.7.6 *In situ* reinforcement 426
14.7.7 Anchor systems 427
14.7.8 Vegetation 427
14.7.9 Special techniques 427
14.8 Warning systems 427

15. Soil Improvement 429
R. D. Holtz, J. Q. Shang and D. T. Bergado
15.1 Introduction 429
15.2 Foundation soil improvement techniques 432
15.2.1 Lightweight fill 432
15.2.2 Removal and replacement 433
15.2.3 Consolidation 434
15.2.3.1 Dewatering and groundwater control 434
15.2.3.2 Preloading by surcharge 434
15.2.3.3 Preloading by vacuum 436
15.2.3.4 Consolidation with vertical drains 437
15.2.3.5 Prefabricated vertical drains 441
15.2.4 Chemical, thermal and electrical stabilization 443
15.2.4.1 Stabilization by chemical admixtures 444
15.2.4.2 Lime and lime–cement columns 444
15.2.4.3 Deep soil mixing 445
15.2.4.4 Intrusion and permeation grouting 445
15.2.4.5 Jet grouting 447
15.2.4.6 Thermal treatment 447
15.2.4.7 Artificial ground freezing 448
15.2.4.8 Electro-osmotic and electro-kinetic stabilization 449
15.2.5 Physical stabilization and densification 452
15.2.5.1 Preloading 452
15.2.5.2 Compaction grouting 452
15.2.5.3 Dynamic compaction 453
15.2.5.4 Blast densification 454
15.2.5.5 Vibro-compaction and vibro-replacement 454
15.2.5.6 Inundation (hydromechanical compaction) 456
15.2.5.7 Compaction piles 456
15.2.5.8 Reinforcement of embankments and foundations 457
15.3 Stabilization of slopes 457
15.3.1 Dewatering and groundwater control 458
15.3.2 Ground anchors and tiebacks 458

15.3.3 Soil nailing 458
15.3.4 Micropiles, root piles and pin piles 458
15.3.5 Biotechnical stabilization 459
15.4 Verification and evaluation of soil improvement 460
15.4.1 Inspection during construction 460
15.4.2 Verification of foundation improvement 460
15.4.3 Instrumentation 461
15.4.3.1 Instrumentation and monitoring during construction 461
15.4.3.2 Post-construction monitoring 461

16. Embankments Over Soft Soil and Peat 463
S. Leroueil and R. K. Rowe
16.1 General behavior of clay foundations under embankments 463
16.1.1 Behavior during construction 463
16.1.2 Clay behavior after the end of construction 466
16.1.3 Stage construction 467
16.1.4 Pore pressures 467
16.2 General behavior of reinforced embankments on clay foundations 468
16.3 General behavior of peat deposits under embankments 470
16.3.1 Peat characteristics 470
16.3.2 Pore pressures 471
16.3.3 Behavior during and after construction 472
16.4 Settlements 473
16.4.1 Stress distribution under embankments 473
16.4.2 Construction settlement 474
16.4.3 Long-term settlement 475
16.4.3.1 Primary consolidation settlement 475
16.4.3.2 Contribution of the viscosity of clay to total settlement 475
16.4.4 Effect of embankment reinforcement on settlement 477
16.4.5 Settlement of embankments on peat 478
16.5 Lateral displacements 480
16.6 Consolidation 481
16.6.1 Primary consolidation 481
16.6.2 Consideration of viscous and structuring effects 483
16.7 Stability 484
16.7.1 General remarks 484
16.7.2 Embankments constructed in one stage 484
16.7.2.1 Evaluation of mobilized shear strength, s_u 484
16.7.2.2 Strength of the weathered crust 486
16.7.2.3 Estimation of stability 486
16.7.3 Choice of strength for embankments constructed in several stages 487
16.8 Solutions to problems of stability and settlement 487
16.8.1 General 487
16.8.2 Berms 488
16.8.3 Reinforced embankments on soft clay 488
16.8.3.1 General considerations 488
16.8.3.2 Bearing capacity limits on reinforced embankment height 489
16.8.3.3 Selecting reinforcement properties 492
16.8.4 Reinforced embankments on peat 495
16.8.4.1 Problem definition 495
16.8.4.2 Peat underlain by a firm base 495
16.8.4.3 Peat underlain by a soft clay/marl layer 496
16.9 Practical considerations: construction, instrumentation and observation analysis 497
16.9.1 Design and construction 497

16.9.2 Instrumentation 498
16.9.3 Observation analysis 498

17. Earth Retaining Structures and Reinforced Slopes 501
R. J. Bathurst and C. J. F. P. Jones
17.1 Introduction 501
17.1.1 Types of earth retaining structures 501
17.1.2 Selection of type of retaining wall 504
17.1.3 Reinforced slopes 506
17.1.4 Soil reinforcement concepts 506
17.1.4.1 Reinforcement 506
17.1.4.2 Soil 506
17.1.5 Global factor design approach 507
17.1.6 Limit states design approach 508
17.2 Earth pressure theory 508
17.2.1 Earth pressure at rest 508
17.2.2 Rankine earth pressure theory 508
17.2.3 Compaction stresses 511
17.2.4 Coulomb wedge methods 513
17.2.5 Other 515
17.3 Conventional retaining walls 516
17.3.1 Gravity and cantilever walls 516
17.3.2 Sheet pile walls (cantilever and anchored) 517
17.3.3 Braced excavations 518
17.3.4 Other types of retaining structures (diaphragm walls and cut-offs) 520
17.4 Reinforced soil walls 522
17.4.1 Current design methods 522
17.4.2 Tie-back method 524
17.4.2.1 Limit mode 1: sliding 524
17.4.2.2 Limit mode 2: bearing and tilting 524
17.4.2.3 Limit mode 3: reinforcement layer rupture 525
17.4.2.4 Limit mode 4: pull–out capacity 526
17.4.2.5 Limit mode 5: wedge/slip circle stability 526
17.4.2.6 Limit mode 6: deflections 527
17.4.3 Coherent gravity method 528
17.4.3.1 Limit mode 1: sliding 529
17.4.3.2 Limit mode 2: bearing/tilt 529
17.4.3.3 Limit mode 3: element rupture 529
17.4.3.4 Limit mode 4: element pull–out 529
17.4.3.5 Limit mode 5: wedge/slip circle stability 530
17.4.3.5 Limit mode 6: deflections 530
17.4.4 Soil nailing 530
17.5 Reinforced slopes 531
17.5.1 General 531
17.5.2 Two-part wedge analysis with reinforcement 532
17.5.3 Modified circular slip method 533
17.5.4 Design charts 534
17.6 Reinforcement over voids 535
17.6.1 Analytical methods 535
17.6.1.1 Tension membrane theory 536
17.6.1.2 Arching 536
17.6.1.3 Combined arching and tension membrane theory 536
17.6.1.4 BS 8006 method 537
17.6.2 Reinforcement on embankment piles 537

IV. SPECIAL TOPICS 539

18. Buried Pipes and Culverts 541
I. D. Moore
18.1 Introduction 541
18.1.1 The buried pipe system 541
18.1.2 Pipe types and limit states 541
18.1.3 Analysis of buried pipes 542
18.1.4 Design standards 545
18.2 Loads 545
18.2.1 Static loads: embankments 545
18.2.2 Static loads: trench installation 546
18.2.3 Construction loading 548
18.2.4 Surface live loads 548
18.2.5 Fluid loading 548
18.2.6 Other loading sources 548
18.3 Response 550
18.3.1 Pipe and soil properties 550
18.3.1.1 Pipe modules and wall properties 550
18.3.1.2 Pipe stiffness 550
18.3.1.3 Soil properties 551
18.3.2 Soil–pipe interaction solutions 551
18.3.3 Positive and negative arching 553
18.3.4 Classification for flexible and rigid pipes 553
18.3.5 Thrust and moment 555
18.3.5.1 General expressions 555
18.3.5.2 Limiting values 555
18.3.5.3 Non-circular pipes and culverts 556
18.3.5.4 Empirical limits 556
18.3.6 Deflection 556
18.3.6.1 Deflection limits 556
18.3.6.2 Deflection resulting from static earth pressures: elastic theory 557
18.3.6.3 Deflection resulting from static earth pressures: limiting values 558
18.3.6.4 Deflection resulting from static earth pressures: Spangler's equation 558
18.3.6.5 Pipe stiffness and flexibility 558
18.3.7 Stress and strain 559
18.3.8 Buckling 559
18.4 Backfill selection and pipe installation 560
18.5 Design examples 561
18.5.1 Concrete storm sewer 562
18.5.1.1 Structural design to limit crack width 562
18.5.1.2 Indirect design 563
18.5.1.3 Direct design 563
18.5.1.4 Trench versus embankment loading 564
18.5.2 Large diameter corrugated steel culvert 564
18.5.3 High density polyethylene drainage pipe 566

19. Trenchless Technology 569
G. W. E. Milligan and C. D. F. Rogers
19.1 Introduction 569
19.2 Techniques involving excavation 570
19.2.1 Principles of operation 570
19.2.2 Pipe jacking and microtunneling 570
19.2.3 Auger boring 573

19.2.4 Directional drilling 573
19.2.5 Geotechnical engineering considerations 574
19.2.5.1 Introduction 574
19.2.5.2 Face stability, excavation method and shield thrust force 574
19.2.5.3 Tunnel stability and pipeline friction 576
19.2.5.4 Calculation of ground movements 579
19.2.5.5 Use of lubrication 580
19.2.5.6 Jacking shafts 581
19.2.5.7 Geotechnical considerations for other techniques 581
19.3 Techniques involving ground displacement 582
19.3.1 Principles of operation 582
19.3.2 Moling and guided drilling 582
19.3.3 Pipe bursting 583
19.3.4 Pipe ramming 584
19.3.5 Geotechnical engineering considerations 584
19.3.5.1 Factors influencing void creation 584
19.3.5.2 Void stability and pipeline friction 585
19.3.5.3 Calculation of ground movements 586
19.3.5.4 Influence on the buried infrastructure and adjacent structures and services 588
19.4 Pipeline rehabilitation techniques 588
19.5 Practical application 591

20. Cold Region Engineering 593
J.-M. Konrad
20.1 Introduction 593
20.2 Thermal considerations 593
20.2.1 Heat flow through soils 593
20.2.1.1 Steady state 593
20.2.1.2 Transient state 594
20.2.2 Thermal properties of soils and other materials 595
20.2.2.1 Thermal conductivity 595
20.2.2.2 Heat capacity 595
20.2.2.3 Latent heat 596
20.2.2.4 Thermal resistance 596
20.2.3 Thermal boundary conditions 596
20.2.3.1 Generality 596
20.2.3.2 Freezing and thawing indices at ground surface 598
20.3 Ice formation in freezing soils 600
20.3.1 Unfrozen water content 600
20.3.2 Water migration and ice lens formation 601
20.3.3 Segregation potential of freezing soils for laboratory conditions 602
20.3.4 Segregation potential for field conditions 603
20.3.4.1 SP_{field} from laboratory freezing tests 604
20.3.4.2 SP_{field} from field observations 605
20.3.4.3 SP_{field} from empirical correlations 606
20.3.5 Prediction of frost depth in frost-susceptible soils 606
20.3.6 Frost heave prediction 608
20.3.7 Thaw weakening 609
20.4 Frost susceptibility of soils 609
20.4.1 Limitations of existing frost-susceptibility criteria 609
20.4.2 Rational evaluation of frost susceptibility 610
20.5 Frost action in civil-engineering works 610
20.5.1 Design considerations 610

20.5.2 Foundations 611
20.5.3 Earth retaining structures and excavations 611
20.5.4 Buried structures 611
20.5.5 Highways 612
20.5.5.1 Frost heave 612
20.5.5.2 Thaw-weakening 613
20.5.5.3 Trends in pavement design 613

21. Earthquake Engineering 615
W. D. L. Finn
21.1 Introduction 615
21.2 Seismological aspects 615
21.2.1 Earthquake occurrence 615
21.2.2 Wave type 616
21.2.3 Earthquake magnitude 617
21.2.4 Earthquake statistics 618
21.2.5 Discrete frequency occurrence 618
21.2.6 Earthquake source zones 619
21.2.7 Maximum magnitude, M_x 619
21.2.8 Estimation of maximum magnitude 619
21.2.9 Magnitude from fault break and fault area 620
21.2.10 Probability of occurrence 620
21.3 Wave propagation 620
21.3.1 Elements of wave propagation 620
21.3.2 Strains in the ground 620
21.3.3 Strains in buried pipes 621
21.4 Design ground motions 622
21.4.1 Basic elements 622
21.4.2 Response spectra 622
21.4.3 Simple design spectra 623
21.4.4 Site-specific response spectra 624
21.4.5 Confirmatory dynamic analyses 625
21.4.6 Uniform hazard spectra 625
21.5 Earthquake ground motions 625
21.5.1 Ground motion attenuation relations for crustal earthquakes 625
21.5.2 Ground motion attenuation relations for subduction zone earthquakes 627
21.6 Effects of soil conditions on ground motion 627
21.6.1 Non-linear soil behavior 628
21.6.2 Site classification-based amplification factors 629
21.6.3 NEHRP provisions 630
21.6.4 Effects of topography 631
21.6.5 Motions in sedimentary basins 631
21.6.6 Near-fault effects 632
21.7 Seismic soil–structure interaction 632
21.7.1 Kinematic and inertial soil–structure interaction 632
21.7.2 Tau method for assessing interaction effects 633
21.8 Seismic design of retaining structures 633
21.8.1 Dynamic active and passive earth pressure force 634
21.8.2 Saturated backfill 635
21.8.3 Anchored bulkheads 635
21.8.4 Reinforced soil walls 636
21.8.5 Seismic wall displacements 636
21.8.6 Seismic design for tolerable wall displacement 637
21.8.7 Unyielding walls (rigid) 637

21.8.8 Earth pressures for design of rigid walls 637
21.8.9 Practical considerations 640
21.9 Seismic design of foundations 640
21.9.1 Elements of seismic design of foundations 640
21.9.2 Seismic design requirements for foundations 641
21.9.3 Design pressure based on bearing capacity 641
21.9.4 Design loads 642
21.10 Liquefaction 642
21.10.1 Key factors 642
21.10.2 SPT(N) liquefaction assessment chart 642
21.10.3 Magnitude scaling factor, K_m 644
21.10.4 Overburden pressure scaling factor, K_σ 645
21.10.5 Correction factors for static shear, K_α 645
21.10.6 Core-penetration test (CPT) 645
21.10.7 Shear-wave velocity 646
21.10.8 Becker penetration test (BPT) 647
21.10.9 Seismic settlement 647
21.10.10 Effects of ground improvement 648
21.11 Residual strength and post-liquefaction deformations 649
21.11.1 Factors controlling residual strength 649
21.11.1.1 Effect of sample preparation 649
21.11.1.2 Stress path 650
21.11.1.3 Residual strength as a function of effective confining pressure 651
21.11.2 Post-liquefaction deformations 651
21.12 Embankment dams 652
21.12.1 Equivalent linear analysis 652
21.12.2 Deformations from acceleration data 652
21.12.3 Deformations from stress data 653
21.12.4 Non-linear methods of analysis 653
21.12.4.1 Elastic–plastic methods 653
21.12.4.2 Direct non-linear analysis 653
21.12.5 Recommendations for analysis 654
21.13 Seismic risk in geotechnical earthquake engineering 654
21.13.1 Seismic risk assessment for dams 654
21.13.2 Approaches to risk assessment 654
21.13.3 Some contentious issues 656
21.13.4 Framework for risk assessment 657
21.12.4.1 Example: risk assessment for Keenleyside Dam 657

V. GEOENVIRONMENTAL ENGINEERING 661

22. Geoenvironmental Problem Identification and Risk Management 663
M. Whittaker, J. G. Sprenger and D. D. DuBois
22.1 Introduction 663
22.1.1 Framework for risk-based site management 664
22.1.2 Defining goals 664
22.1.3 Regulatory and societal issues 665
22.2 Site assessment for risk-based site management 667
22.2.1 Scope and objectives 667
22.2.2 Site assessment procedural components 667
22.2.2.1 Stage 1: non-intrusive phase I investigations 667
22.2.2.2 Stage 2: intrusive site assessment 668
22.2.3 Sampling strategies and methods 669
22.2.4 Common difficulties encountered during the site assessment process 670

22.3 Contaminant identification 670
22.3.1 Requirements and objectives 670
22.3.2 Typical contaminants and associated hazards 670
22.3.2.1 Inorganic contamination 670
22.3.2.2 Organic contamination 671
22.3.3 The link between contaminant behavior and risk 671
22.3.3.1 Contaminant partitioning 672
22.3.3.2 Contaminant weathering 672
22.3.4 Selection of analytical parameters 673
22.4 Problem formulation 674
22.4.1 Contaminants 675
22.4.2 Receptors 675
22.4.3 Pathways 675
22.4.4 Conceptual pathway model 679
22.5 Exposure assessment 679
22.5.1 Objectives and link to risk assessment process 679
22.5.2 Basic elements of exposure assessment 680
22.6 Toxicity assessment 681
22.6.1 Objectives and link to risk assessment process 681
22.6.2 Basic elements of toxicity assessment 681
22.6.3 Derivation of exposure limits 682
22.7 Risk characterization 684
22.7.1 Objectives and link to risk assessment process 684
22.7.2 Basic elements of risk characterization 684
22.7.3 Risk description 685
22.7.4 Reporting of uncertainty 685
22.8 Risk communication 686
22.8.1 The need for effective communication 686
22.8.2 External communication 686
22.8.3 Internal communication 686
22.9 Risk management 687
22.9.1 Selection of risk management options 687
22.9.2 Monitoring risk management success 689
22.9.3 Summary 690

23. Physicochemistry of Soils for Geoenvironmental Engineering 691
J. K. Mitchell
23.1 Introduction 691
23.2 Soil mineralogy and composition 691
23.2.1 Mineral compositions and structures 691
23.2.2 Silicate minerals 691
23.2.3 Non-clay minerals in soils 692
23.2.4 Clay mineral structures 692
23.2.5 Clay mineral characteristics 694
23.2.6 Organic matter in soils 694
23.3 Soil water 695
23.3.1 Ice and water structure 695
23.3.2 The influence of dissolved ions 696
23.3.3 Water adsorption by soils 696
23.3.4 Properties of adsorbed water 696
23.4 Clay–water–electrolyte system 697
23.4.1 Ion distributions: the double layer 698
23.4.2 Double layer interactions 699
23.4.3 Factors influencing double layer repulsion 700

23.5 Ion exchange 701
23.6 Soil fabric and its relation to properties 702
23.6.1 Particle associations and fabric scale 703
23.6.2 Single-grain fabrics 703
23.6.3 Multigrain fabrics 703
23.6.4 Fabric–property interrelationships 704
23.7 Physicochemical effects on soil properties and their importance in environmental geotechnics 705
23.7.1 Volume change properties 705
23.7.2 Deformation and strength properties 706
23.7.2.1 Strength 706
23.7.2.2 Stress–strain behavior 707
23.7.2.3 Stress–strain–time behavior 707
23.7.3 Conductivity properties 708
23.7.3.1 Direct flows 708
23.7.3.2 Coupled flows 709
23.7.3.3 Effects of flows on properties 710

24. Contaminant Hydrogeology 711
R. A. Schincariol and R. K. Rowe
24.1 Hydrogeological environments 711
24.1.1 Saturated and unsaturated zones 711
24.1.2 Aquifers and aquitards 711
24.1.3 Hydrogeologic parameters: porosity, hydraulic conductivity and permeability, transmissivity, storativity and specific yield 712
24.1.4 Hydrogeologic variables: hydraulic head, flux and velocity, aquifer recharge and discharge 714
24.1.5 Hydrogeologic controls: lithology, stratigraphy and structure 716
24.1.6 Fractured and karst systems: fracture flow 717
24.2 Contaminants and sources 719
24.2.1 Physical and chemical properties of contaminants 719
24.2.2 Hydraulic characteristics of sources 720
24.2.3 Point and non-point sources 720
24.2.4 Loading history 720
24.3 Principles of contaminant transport 721
24.3.1 Mass transport processes: advection, diffusion and dispersion of solutes 721
24.3.1.1 Advection 721
24.3.1.2 Diffusion 721
24.3.1.3 Dispersion 723
24.3.2 Multiphase flow 724
24.3.3 Attenuation of dissolved solutes: biogeochemical processes 729
24.3.3.1 Acid–base reactions 730
24.3.3.2 Solution, volatilization and precipitation reactions 731
24.3.3.3 Sorption 733
24.3.3.4 Oxidation–reduction reactions 736
24.3.3.5 Hydrolysis 737
24.3.3.6 Complexation reactions 737
24.3.4 Facilitated transport of contaminants: cosolvation and colloidal transport 737

25. Barrier Systems 739
R. K. Rowe
25.1 Applications, mechanisms and scope 739
25.2 Transmissive layers 739
25.2.1 Hydraulic capacity of drainage layers 741

25.2.2 Particulate clogging of drainage layers 742
25.2.3 Biologically induced clogging of leachate collection systems 743
25.2.4 Geotextile "filters" in leachate collection systems 745
25.2.5 Granular drainage material in leachate collection systems 747
25.2.6 Service life of leachate collection drainage material 748
25.2.7 Leachate collection pipes 750
25.3 Low permeability liners 751
25.3.1 Geological barriers 751
25.3.2 Compacted clay liners (CCLs) 752
25.3.2.1 Material selection 752
25.3.2.2 Compaction water content and density 753
25.3.2.3 Estimating the hydraulic conductivity of CCLs 755
25.3.2.4 Construction of CCLs 756
25.3.2.5 Required thickness of CCLs 758
25.3.2.6 Construction quality control and assurance 759
25.3.3 Soil–bentonite liners 761
25.3.4 Geosynthetic clay liners (GCLs) 762
25.3.4.1 Hydration of GCLs and hydraulic conductivity 762
25.3.4.2 Effect of holes in GCLs 765
25.3.4.3 Desiccation and frost action 765
25.3.5 Hydraulic containment 765
25.3.6 Geomembrane liners 768
25.3.7 Single composite liners 768
25.3.8 Double composite liners 769
25.3.9 Vertical cut-off walls 769
25.3.9.1 Slurry trench walls 769
25.3.9.2 Geomembranes 770
25.3.9.3 Sheet pile walls 770
25.4 Liner compatibility with leachate 771
25.4.1 Clay–permeant interaction 771
25.4.2 GCL–permeant interaction 773
25.4.3 Geomembrane–permeant interaction 774
25.5 Diffusion through barriers 776
25.5.1 Dissolved-phase diffusion through porous media 776
25.5.1.1 Diffusion through intact and compacted clays 777
25.5.1.2 Diffusion through GCLs 778
25.5.1.3 Diffusion through unsaturated soil 780
25.5.2 Gaseous-phase diffusion through porous media 781
25.5.3 Diffusion through geomembranes 782
25.5.3.1 Factors affecting diffusion through a geomembrane 783
25.5.3.2 Diffusion of water through HDPE geomembrane 785
25.6 Liner temperature 785
25.7 Contaminant impact assessment and equivalence of liner systems 787
25.7.1 Impact assessment 787
25.7.2 Equivalence of GCL and CCL systems 787
25.8 Liner stability 788

26. Geosynthetics in Liquid-containing Structures 789
J. P. Giroud and R. Bonaparte
26.1 Introduction 789
26.1.1 Types of liquid-containing structures 789
26.1.2 Uses of geosynthetics in liquid-containing structures 789
26.1.3 Geosynthetic liner systems 789
26.1.4 Design considerations 790

26.2 Design of liquid collection layers 790
26.2.1 Introduction to liquid collection 790
26.2.1.1 Liquid collection 790
26.2.1.2 Characteristics of liquid collection layers 791
26.2.1.3 Materials used in liquid collection layers 791
26.2.1.4 Hydraulic head, depth and thickness of liquid 791
26.2.1.5 Design of liquid collection layers 792
26.2.2 Design of primary liquid collection layers 792
26.2.2.1 Analysis of liquid flow in a primary liquid collection layer 792
26.2.2.2 Design of a primary liquid collection layer 794
26.2.2.3 Average head of liquid on top of the primary liner for liquid migration evaluation 794
26.2.3 Design of secondary liquid collection layers 794
26.2.3.1 Analysis of liquid flow in a secondary liquid collection layer 794
26.2.3.2 Design of a secondary liquid collection layer 795
26.2.3.3 Average head of liquid on top of the secondary liner for liquid migration evaluation 796
26.3 Design of filters 796
26.3.1 Introduction of filtration 796
26.3.1.1 Use of filters in liquid-containment structures 796
26.3.1.2 Types of filters 796
26.3.1.3 Functions of filters 796
26.3.1.4 Importance of intimate contact between filter and soil 797
26.3.1.5 Clogging of filters 797
26.3.2 Relevant characteristics of soils and filters 797
26.3.2.1 Characteristics of soils relevant to filter design 797
26.3.2.2 Characteristics of granular filters 798
26.3.2.3 Characteristics of geotextile filters 798
26.3.3 Design of filters 798
26.3.3.1 Filter criteria 798
26.3.3.2 Permeability criterion 799
26.3.3.3 Retention criterion 800
26.3.3.4 Non-clogging criterion 801
26.4 Liquid migration through liners 801
26.4.1 Introduction to liquid migration through liners 801
26.4.1.1 Types of liners 801
26.4.1.2 The low permeability soil component of a composite liner 801
26.4.1.3 Geomembranes 802
26.4.1.4 Liquid migration evaluation 802
26.4.2 Liquid migration through composite liners 803
26.4.2.1 Ideal case: perfect contact 803
26.4.2.2 Description of liquid migration through a composite liner 803
26.4.2.3 Quality of contact between the two components of a composite liner 803
26.4.2.4 Parameters and units used in equations for liquid migration rate evaluation 804
26.4.2.5 General equations for liquid migration rate 805
26.4.2.6 Equations for liquid migration rate for the case of small hydraulic heads 805
26.4.2.7 Limitations of the equations for liquid migration through composite liners 806
26.4.2.8 Leakage through a wrinkle 806
26.4.3 Geomembrane liner 808
26.4.3.1 Geomembrane overlain and underlain by highly permeable media 808

26.4.3.2 Geomembrane overlain by a permeable medium and underlain by a highly permeable medium 808
26.4.3.3 Geomembrane overlain by a permeable medium and underlain by a semi-permeable medium 809
26.5 Stability and deformations of liner systems 810
26.5.1 Introduction 810
26.5.1.1 Types of mechanical actions applied on liner systems 810
26.5.1.2 Instability of soil or waste in contact with linear system 810
26.5.1.3 Deformation of soil in contact with the liner system 811
26.5.1.4 Differential settlement between the soil supporting the liner system and a structure to which the liner system is connected 811
26.5.1.5 Uplift of liner system by fluids 811
26.5.1.6 Concentrated stresses applied on the geosynthetic component of liner system by the materials in contact 811
26.5.2 Geosynthetic strain due to settlement of the supporting medium 812
26.5.2.1 Relationships between geosynthetic deflection and strain 812
26.5.2.2 Relationships between geosynthetic deflection and tension 813
26.5.2.3 Evaluation of the pressure applied on the geosynthetic 814
26.5.2.4 Use of the equations 814
26.5.3 Differential settlement at connection of liner system to rigid structures 815
26.5.3.1 Tension and strain in the geomembrane 815
26.5.3.2 Assumptions 816
26.5.3.3 Presentation of the method 816
26.5.3.4 Practical recommendations 816
26.5.4 Action of wind on geomembranes 817
26.5.4.1 Introduction 817
26.5.4.2 Suction due to wind 817
26.5.4.3 Resistance to wind uplift due to geomembranes self weight 818
26.5.4.4 Prevention of geomembrane uplift 819
26.5.4.5 Analysis of geomembrane uplift 821
26.5.4.6 Anchorage of a geomembrane subjected to wind uplift 824

27. Covers for Waste 825
R. Bonaparte and E. K. Yanful
27.1 Introduction 825
27.2 Types of cover systems 825
27.2.1 Classification of cover systems 825
27.2.2 Examples of cover systems 828
27.2.3 Gas generation and management 828
27.3 Components of hydraulic-barrier cover systems 831
27.3.1 Typical components 831
27.3.2 Surface layer 831
27.3.3 Protection layer 831
27.3.4 Internal drainage layer 832
27.3.5 Hydraulic-barrier layer 833
27.3.6 Gas transmission layer 834
27.3.7 Foundation layer 834
27.4 Capillary-barrier cover systems 834
27.5 Water balance 837
27.5.1 Overview 837
27.5.2 Water balance concept 837
27.5.3 Water balance methods 838
27.5.4 Simplified manual method 838
27.5.4.1 Description of method 838

27.5.4.2 Design of internal drainage layers 841
27.5.4.3 Refinement to simplified manual method 841
27.5.4.4 Design of slope transitions 842
27.5.5 HELP model 843
27.5.6 LEACHM model 845
27.5.7 UNSAT-H 846
27.5.8 Evaluation of models 847
27.5.9 Recommendations 848
27.6 Static slope stability 850
27.6.1 Overview 850
27.6.2 Limit equilibrium analyses 850
27.6.2.1 Overview 850
27.6.2.2 Infinite slope 851
27.6.2.3 Slope of finite length 853
27.6.3 Stress–deformation analyses 856
27.6.4 Shear strength parameters 856
27.6.5 Construction considerations 859
27.6.6 Factors of safety 861
27.7 Seismic slope stability 862
27.7.1 Overview 862
27.7.2 Seismic hazard evaluation 862
27.7.3 Seismic response analysis 864
27.7.3.1 Introduction 864
27.7.3.2 Material property selection 864
27.7.3.3 Simplified response analysis 865
27.7.3.4 Analytical and numerical seismic response analyses 868
27.7.4 Dynamic shear strength 869
27.7.5 Seismic stability and deformation analysis 869
27.7.5.1 Overview 869
27.7.5.2 Pseudo-static factor of safety method 869
27.7.5.3 Modified pseudo-static factor of safety method 870
27.7.5.4 Permanent seismic deformation method 871
27.8 Settlement 872
27.8.1 Mechanisms of settlement 872
27.8.2 Settlement of foundation soils 873
27.8.3 Overall waste compression 873
27.8.4 Settlement due to localized mechanisms 876
27.8.5 Impacts of settlement on cover system 876

28. Monitoring of Contaminants and Consideration of Risk 879
E. McBean, K. Schmidtke, W. Dyck and F. Rovers
28.1 Components of a groundwater monitoring program 879
28.1.1 Determining monitoring well locations and analytical parameters 880
28.1.1.1 Initial site characterization 880
28.1.1.2 Well location 880
28.1.1.3 Analytical parameters 884
28.1.1.4 Refinement of conceptual site model/selection of supplemental well locations 885
28.1.1.5 Corrective action design 885
28.1.1.6 Corrective action monitoring 886
28.1.2 Monitoring well design and construction 887
28.1.2.1 General 887

28.1.2.2 Design considerations 887
28.1.2.3 Well installation documentation 890
28.1.3 Groundwater sampling 890
28.1.3.1 General 890
28.1.3.2 Purging/sampling equipment 890
28.1.3.3 Field quality control/quality assurance (QC/QA) 890
28.1.3.4 Documentation 892
28.1.4 Sampling frequency 892
28.1.5 Monitoring well nests 893
28.2 Statistical analyses of monitoring data 893
28.2.1 Sources of variability of monitoring data 894
28.2.2 Statistical significance testing procedures 895
28.2.2.1 Types of hypotheses 895
28.2.2.2 General steps of hypothesis testing 896
28.2.2.3 Selection of appropriate significance test 897
28.2.2.4 Interpretation of significance tests: acceptance and rejection regions 899
28.2.3 Procedures for single comparisons 900
28.2.3.1 Student's *t*-test 900
28.2.3.2 Cochran's approximation to the Behren's Fisher *t*-test 902
28.2.3.3 Linear regression 903
28.2.4 Procedures for multiple comparisons 904
28.2.4.1 Analysis of variance (ANOVA) 904
28.2.4.2 Multiple regression 906
28.2.5 Non-parametric procedures 906
28.2.5.1 Mann–Whitney (U) test 907
28.2.5.2 Spearman's rank correlation coefficient 908
28.2.5.3 Sign test for paired observations 908
28.2.5.4 Kruskal-Wallis test (or non-parametric ANOVA) 909
28.2.6 Methods for censored data 910
28.2.6.1 Simple substitution methods 910
28.2.6.2 Test of proportions 910
28.2.6.3 Plotting position procedure 911
28.2.6.4 Cohen's test 911
28.2.6.5 Aitchison's method 912
28.2.6.6 Maximum likelihood estimator and alternates 912
28.2.6.7 Poisson model 912
28.2.7 Statistical power 913
28.3 Assessment or risk associated with exceedance of boundary criteria 914
28.3.1 Migration pathways of environmental contaminants 914
28.3.2 Exposure assessment procedures 915
28.3.3 Decisions on risk-based corrective action 916
28.4 The case for innovation: a unique visualization method for demonstrating intrinsic remediation 916

29. *In situ* Containment and Treatment of Contaminated Soil and Groundwater 921
D. J. A. Smyth, R. W. Gillham, D. W. Blowes and J. A. Cherry
29.1 Introduction to contaminated sites 921
29.1.1 Characteristics of contaminated sites 921
29.1.2 Objectives of remediation 922
29.2 Intrinsic remediation 923
29.3 Source-zone restoration 925
29.3.1 Goals and objectives 925

29.3.2 Vadose-zone contamination in the source zone 926
29.3.2.1 Excavation 926
29.3.2.2 Soil vapor extraction and bioventing 927
29.3.2.3 Soil flushing 929
29.3.3 Source-zone restoration in the groundwater zone 929
29.3.3.1 Pumping of immiscible fluids 929
29.3.3.2 *In situ* mass removal from source zones: chemical flushing 930
29.3.3.3 Thermal flushing techniques 932
29.3.3.4 *In situ* mass destruction technologies 932
29.4 Source-zone isolation and containment 933
29.4.1 Source-zone enclosures 933
29.4.2 Covers and bottom barriers 937
29.5 *In situ* plume control and remediation 937
29.5.1 Pump-and-treat remediation 937
29.5.2 Permeable reactive barriers 939
29.5.2.1 General description of barriers 939
29.5.2.2 Hydraulic performance of permeable barrier systems 940
29.5.2.3 *In situ* treatment technologies for contaminated groundwater 942
29.6 Summary 944

30. Management of Contaminated Soil in Engineering Construction 947
P. C. Lucia, G. Ford and H. A. Tuchfeld
30.1 Introduction 947
30.2 Soil management goals 948
30.3 Soil management options 950
30.4 Soil treatment technologies 951
30.5 On-site treatment technologies and containment options 951
30.5.1 Regulatory considerations 953
30.5.1.1 Soil contaminated by petroleum fuel products 955
30.5.1.2 Soil contaminated by hazardous wastes 955
30.5.1.3 Soil contaminated by non-hazardous solid wastes 956
30.5.2 Treatment technologies 956
30.5.2.1 Bioremediation 956
30.5.2.2 Soil vapor extraction 958
30.5.2.3 Stabilization 959
30.5.3 Containment options 959
30.5.3.1 Capping and covers 959
30.5.3.2 Cut-off walls 960
30.5.4 Case study 960
30.6 Off-site treatment technologies and disposal options 962
30.6.1 Regulatory considerations 963
30.6.2 Disposal options 963
30.6.2.1 Non-hazardous waste landfill 963
30.6.2.2 Hazardous waste landfill 964
30.6.2.3 Incineration 964
30.6.2.4 Other off-site management options 964
30.6.3 Treatment technologies 965
30.6.3.1 Aeration 965
30.6.3.2 Bioremediation/landfarming 965
30.6.4 Case study 966

References 967
Index 1063
Conversion Factors US to SI Units 1088

LIST OF FIGURES

FIGURE 2.1 Relationships among soil phases: (a) element of natural soil; and (b) element separated into phases.

FIGURE 2.2 (a) General state of stress in soil element; and (b) Mohr's circle for state of stress.

FIGURE 2.3 (a) Location of pole and stresses on plane at angle α; and (b) principal planes and directions.

FIGURE 2.4 (a) Strained soil element; and (b) Mohr's circle for state of strain, principal strains and their directions (NB: small strain analysis).

FIGURE 2.5 Total and effective stress paths from an undrained triaxial compression test on a remolded, isotropically consolidated kaolinite specimen shown in: (a) s'–t diagram; and (b) p'–q diagram.

FIGURE 2.6 (a) Illustration of plastic yield surface and stress path in p'–q diagram resulting in (b) elastic–plastic (AB and DE) and elastic (BC and CD) stress–strain behavior (modified from Jardine 1992).

FIGURE 2.7 Typical shape of relation between void ratio and effective overburden pressure during compression and expansion of soil.

FIGURE 2.8 One-dimensional consolidation: (a) isochrones of excess pore pressure for an initial uniform pore pressure distribution (modified from Taylor 1948); and (b) degree of consolidation with dimensionless time, T_v, for four initial excess pore pressure distributions (modified from Leroueil & Marques 1996).

FIGURE 2.9 Methods of estimating c_v based on data from a one-dimensional consolidation (odometer) test: (a) Casagrande's log time method; and (b) Taylor's root time method (modified from Cernica 1995).

FIGURE 2.10 Increase in apparent preconsolidation pressure and movement of yield surface (or limit state curve) with secondary compression, where σ'_{vo} is the current effective overburden pressure TS (modified from Tavenas & Leroueil 1977).

FIGURE 2.11 One-dimensional compression of Berthierville clay: (a) preconsolidation pressure as a function of strain rate and temperature; and (b) normalized effective stress–strain curve (modified from Boudali *et al.* 1994 & Kabbaj 1995, reproduced with permission from Leroueil 1997, in Almeida, M. (Ed.), *Recent Developments in Soil and Pavement Mechanics,* Rio de Janeiro, Brazil, A.A. Balkema, Brookfield, Vermont, U.S.A.).

FIGURE 2.12 (a) Stresses applied in triaxial compression test; and (b) stress–strain and volume change behavior of sand in drained tests at three different confining pressures.

FIGURE 2.13 (a) Normalized stress–strain behavior; (b) void ratio variations reaching critical states; and (c) critical state diagram for sand.

FIGURE 2.14 Variation of drained shear strength envelope for sand with: (a) confining pressure; and (b) density.

FIGURE 2.15 Effective stress paths from six undrained triaxial compression tests on water-saturated loose Sacramento River sand (modified from Seed & Lee 1967).

FIGURE 2.16 (a) Normalized stress–strain relations; (b) normalized pore pressure behavior; and (c) normalized effective stress paths for consolidated, undrained tests on normally consolidated clay (p'_c = preconsolidation pressure).

FIGURE 2.17 Normalized data from simple shear tests on K_0 consolidated, undrained tests on Boston Blue clay (modified from Ladd and Foot 1974): (a) normalized stress–strain relations; and (b) normalized ultimate consolidation settlement stress versus OCR.

FIGURE 2.18 Relation of Hvorslev surface for

overconsolidated clay to the void ratio determined from the rebound curve.

FIGURE 2.19 Normalized stress paths for undrained tests on overconsolidated specimens of kaolin clay (modified from Loudon 1967, Atkinson & Bransby 1978).

FIGURE 2.20 Drained triaxial compression test data for Weald clay (a) normalized stress-strain curves; and (b) volume change curves (modified from Henkel 1956, Lambe & Whitman 1979).

FIGURE 2.21 (a) Effective stress failure surface described by Coulomb's failure criterion and by the Mohr–Coulomb failure criterion; and (b) curved failure envelope with straight-line failure criterion fitted for range of stresses in the geotechnical project.

FIGURE 2.22 Determination of shear strength parameters from: (a) s'–t diagram; and (b) p'–q diagram.

FIGURE 2.23 (a) Cambridge p'–q diagram with stress path for drained triaxial compression test reaching failure at the critical state line; (b) e–p' diagram with state path for the drained test; and (c) e–log(p') diagram with parallel virgin compression and critical state lines.

FIGURE 2.24 Modified Cam Clay model with: (a) elliptical yield surface and associated flow; and (b) e–p' relation for determination of volumetric strain used as hardening parameter in the model.

FIGURE 2.25 Illustration of five material parameters required in the modified Cam Clay model.

FIGURE 2.26 Initial yield surfaces (or limit state curves) are biased toward and around the failure line for normally consolidated clayey soils, but less biased for sands, residual soils and soft rocks (modified from Diaz-Rodriquez *et al.* 1992, and reproduced with permission from Leroueil 1997, in Almeida, M. (Ed.), *Recent Developments in Soil and Pavement Mechanics,* Rio de Janeiro, Brazil, A.A. Balkema, Brookfield, Vermont, U.S.A.).

FIGURE 2.27 Determination of equivalent linear parameters, modulus and viscous damping, for soil with non-linear hysteretic characteristics.

FIGURE 3.1 Grain-size distributions for poorly or uniformly graded, gap graded and well-graded soils (MIT grain-size scale): where C_u and C_c are the coefficients of uniformity and curvature, respectively.

FIGURE 3.2 Typical shapes of bulky grains.

FIGURE 3.3 Generalized curves for estimating e_{max} and e_{min} from gradational and particle shape characteristics. Curves are only valid for clean sands with normal to moderately skewed grain-size distributions. Note: The minimum void ratios were obtained from simple shear tests, and they are slightly lower than those determined from ASTM Standard Test Method D 4253 (after Youd 1973, © ASTM, reproduced with permission).

FIGURE 3.4 Plasticity chart with trends of variation in engineering properties.

FIGURE 3.5 Diagram for estimating undrained modulus of clay (modified from Duncan & Buchignani 1976).

FIGURE 3.6 Approximate relation between void ratio and effective overburden pressure for clay sediments, as a function of Atterberg limits (after Lambe & Whitman 1979, *Soil Mechanics SI Version,* © John Wiley & Sons, Inc., New York, reproduced with permission).

FIGURE 3.7 Relationship between compression index, C_c, and initial void ratio (after Leroueil *et al.* 1983, © NRC Press, reproduced with permission).

FIGURE 3.8 Approximate correlations for swelling index of silts and clays (modified from DM-7 1971).

FIGURE 3.9 Correlations between coefficient of consolidation and liquid limit (modified from NAVFAC 1982).

FIGURE 3.10 Predicted relationship between swelling potential and plasticity index for natural soils (modified from Seed *et al.* 1962).

FIGURE 3.11 Correlations between the effective friction angle in triaxial compression and the dry density, density index and gradation for granular soils (modified from NAVFAC 1982).

FIGURE 3.12 Correlations between effective friction angle and plasticity index for fine-grained soils (modified from Kulhawy & Mayne 1990).

FIGURE 3.13 Relation between ultimate friction angle and clay content (after Skempton 1964).

FIGURE 3.14 Relationship between s_u/σ'_p and plasticity index (modified from Tavenas & Leroueil 1987).

FIGURE 3.15 Correction factor versus plasticity index for undrained shear strength determined from vane shear test (VST) (modified from Ladd *et al.* 1977).

FIGURE 3.16 Normalized variation of s_u/σ'_p ratio for overconsolidated clay (modified from Ladd *et al.* 1977).

FIGURE 3.17 General relationship between sensitivity, liquidity index and effective overburden pressure (modified from Houston & Mitchell 1969).

FIGURE 3.18 Variation of normalized shear modulus (a) and damping ratio (b) with single amplitude shear strain and soil plasticity for normally and overconsolidated soils (after Vucetic & Dobry 1991, © ASCE, reproduced with permission).

FIGURE 3.19 Variation of normalized shear modulus with single amplitude shear strain and confining pressure for granular materials (after Ishibashi 1992, © ASCE, reproduced with permission).

FIGURE 3.20 Variation of damping ratio with single amplitude shear strain for granular materials (after Mitchell 1993, *Fundamentals of Soil Behavior*, © John Wiley & Sons, Inc., New York, reproduced with permission).

FIGURE 4.1 Geotechnical circle concept for site characterization.

FIGURE 4.2 Site characterization process flowchart (modified from Taylor & Erikson 1996).

FIGURE 4.3 Influence of the various components of site characterization on quality and satisfying client/project requirements (modified from Site Investigation Steering Group 1993).

FIGURE 4.4 Communications and quality management between groups for site characterization studies (modified from Site Investigation Steering Group 1993).

FIGURE 4.5 Considerations of the interaction between the ground and proposed project when defining site characterization programs (modified from Site Investigation Steering Group 1993).

FIGURE 5.1 Classification of the regions within a saturated–unsaturated soil profile.

FIGURE 5.2 Approaches that can be used in the laboratory to determine the unsaturated soil property functions.

FIGURE 5.3 Example problem illustrating the role of unsaturated soil property functions in performing a combined seepage and slope stability analysis.

FIGURE 5.4 Separation of saturated and unsaturated soil mechanics based on the stress state description.

FIGURE 5.5 A soil–water characteristic curve showing the different stages of desaturation (modified from White *et al.* 1970).

FIGURE 5.6 Definition of variables associated with the soil–water characteristic curve.

FIGURE 5.7 The variation of wetted area of contact area for different stages of desaturation along the soil–water characteristic curve (after Vanapalli 1994, reproduced with permission): (a) boundary effect stage; (b) primary transition stage; (c) secondary transition stage; and (d) residual stage of unsaturation.

FIGURE 5.8 Typical soil–water characteristic curves for four soils from Saskatchewan, Canada.

FIGURE 5.9 Tempe cell, pressure plate apparatus for measuring water content versus matric suction in the low suction range.

FIGURE 5.10 Single specimen, pressure plate cell.

FIGURE 5.11 Approaches that can be used to estimate soil–water characteristic curves for the determination of unsaturated soil property functions when using classification tests and a database.

FIGURE 5.12 (a) Grain-size distribution curve fit for sand; and (b) comparison between experimental and predicted soil–water characteristic curves for sand (after Fredlund *et al.* 1997a, reproduced with permission).

FIGURE 5.13 Suction measurements using thermal conductivity sensors, installed in a test track, Regina, Saskatchewan (modified from Loi *et al.* 1992).

FIGURE 5.14 Illustration of the effect of climate conditions on the porewater pressure profile near the ground surface.

FIGURE 5.15 Measured relationship between soil suction and the ratio of the actual evaporation (AE) to the potential evaporation (PE) for the ground surface.

FIGURE 5.16 Relationship between soil–water

characteristic curve and the hydraulic conductivity for sand and clayey silt.

FIGURE 5.17 Typical hydraulic conductivity functions for sand and clayey silt with the suction plotted on a logarithmic scale.

FIGURE 5.18 Coefficient of water storage, m_2^w, function computed from the soil–water characteristic curve: (a) soil–water characteristic curve; and (b) coefficient of water storage function.

FIGURE 5.19 Flexible walled permeameter developed to control the applied normal stresses and the matric suction (after Huang 1994, reproduced with permission). Not drawn to scale.

FIGURE 5.20 Comparison of measured hydraulic conductivity and hydraulic conductivity functions predicted from the soil–water characteristic curves for silt preconsolidated at 10 (—, ◆), 50 (---, ■) and 200 (·· - ··, ●) kPa, respectively (after Huang 1994, reproduced with permission).

FIGURE 5.21 A typical soil–water characteristic curve for predicting the hydraulic conductivity.

FIGURE 5.22 Extended Mohr–Coulomb failure envelope for unsaturated soils.

FIGURE 5.23 Extended Mohr–Coulomb shear strength envelope showing the strength parameters for a saturated-unsaturated soil: (a) linear strength envelope; and (b) non-linear strength envelope.

FIGURE 5.24 Variation of shear strength with respect to suction for glacial till (modified from Gan *et al.* 1988).

FIGURE 5.25 (a) Soil–water characteristic curves for the compacted till; and (b) comparison of predicted and experimental variation of shear strength with respect to suction (after Vanapalli 1994, reproduced with permission).

FIGURE 5.26 Active, K_a, and passive, K_p, earth pressures for a soil with matric suction.

FIGURE 5.27 Factor of safety versus matric suction for a simple slope.

FIGURE 5.28 Constitutive surfaces for an unsaturated soil expressed using soil mechanics terminology: (a) three-dimensional void ratio and water content constitutive surfaces; and (b) two-dimensional comparison showing volumetric deformation moduli.

FIGURE 5.29 Relationship between curves that define the mass and volume change behavior of an unsaturated soil.

FIGURE 5.30 "Actual" and "analysis" stress paths followed during the wetting of a soil.

FIGURE 5.31 One-dimensional odometer test results showing the effects of sample disturbance.

FIGURE 6.1 Engineering classification for intact igneous rocks (E_t = tangent modulus at 50% ultimate strength); classifies rocks as AM, BH, BL, etc., depending on where E_t and σ_c plot (modified from Deere & Miller 1966).

FIGURE 6.2 Engineering classification for intact sedimentary rocks (E_t = tangent modulus at 50% ultimate strength); classifies rocks as AM, BH, BL, etc. (modified from Deere & Miller 1966).

FIGURE 6.3 Engineering classification for intact metamorphic rocks (E_t = tangent modulus at 50% ultimate strength); classifies rocks as AM, BH, BL, etc. (modified from Deere & Miller 1966).

FIGURE 6.4 Variation of ratio of mass to intact deformation modulus, E_m/E_{int}, with RQD from plate jacking tests, Dworshak Dam (modified from Deere *et al.* 1967).

FIGURE 6.5 Relationship between fracture frequency and ratio of mass to intact deformation modulus.

FIGURE 6.6 Common laboratory tests for obtaining strength and deformation parameters for rocks: (a) uniaxial compression; (b) triaxial compression; (c) triaxial extension; (d) direct tension; and (e) indirect tension (Brazilian).

FIGURE 6.7 Stress–strain relationships and Poisson's ratio for limestone, Gasport Member of Lockport Formation: (a) vertical; (b) 45°; and (c) horizontal samples in test to failure of uniaxial compression tests: □, vertical strain; ○, horizontal strain – Face A; △, horizontal strain – Face B; ×, volumetric strain.

FIGURE 6.8 Scheme of uniaxial compression tests for determining anisotropic elastic parameters. (a) vertical sample; (b) horizontal sample; and (c) inclined sample.

FIGURE 6.9 Comparison of rates of deformation of various tunnels in swelling rocks (modified from PFRA 1951; Einstein *et al.* 1972; Lo *et al.* 1978). (Note: The relative slopes of the lines represent the percentage reduction of tunnel dimensions per log cycle of time.)

FIGURE 6.10 Relationship between swelling potential and calcite content.

FIGURE 6.11 Typical results of a series of semi-confined swell tests on Georgian Bay Shale, where ε_p = swelling potential.

FIGURE 6.12 Effect of applied pressure on horizontal swelling potential of Queenston Shale (1990 investigation, Borehole NF4A; ambient fluid, distilled water).

FIGURE 6.13 Griffith failure criterion in (a) (σ_1, σ_3) space; and (b) (σ_n, τ) space.

FIGURE 6.14 Hoek–Brown failure criterion.

FIGURE 6.15 Illustration of *i*- and β-effects in shear tests.

FIGURE 6.16 Schematic procedure of USBM overcoring measurements.

FIGURE 6.17 Initial stresses in the horizontal plane measured at the Darlington generating station site.

FIGURE 6.18 Typical field data for an overcoring test in dolomite (Goat Island Member, Thorold, Ontario) using the USBM deformation gage, for button sets 1(—), 2 (---) and 3 (- — -).

FIGURE 6.19 Schematic representation of: (a) hydraulic fracturing testing; and (b) impression packer.

FIGURE 6.20 Idealized hydraulic fracturing pressure–time record (reprinted from ISRM 1987a, Kim, K. & Franklin, J.A. Eds. © 1987 with permission of Elsevier Science).

FIGURE 7.1 Typical tensile behavior of different geotextile types using wide-width test specimens (200 mm).

FIGURE 7.2 Direct shear test used to evaluate geosynthetic–geosynthetic or geosynthetic–soil interface strength: (a) direct shear test device; (b) direct shear test data; and (c) Mohr–Coulomb stress space.

FIGURE 7.3 Cross-sections of permittivity and transmissivity test devices, where ΔH = differential height, and ΔL = differential length.

FIGURE 7.4 Typical tensile behavior of different geomembrane types using wide-width test specimens (200 mm) per ASTM D4885.

FIGURE 7.5 Typical axi-symmetrical behavior of different geomembrane types using out-of-plane pressurization per ASTM D5617.

FIGURE 7.6 Water content versus time for GCL samples placed in contact with sand at various water contents (modified from Daniel *et al.* 1993).

FIGURE 7.7 Three stages (A–C) of lifetime of polyolefin geosynthetic materials: Stage A, depletion time of antioxidants; stage B, induction time to onset of polymer degradation; stage C, time to reach 50% degradation of a particular property.

FIGURE 8.1 Minimum depth of borings to avoid boils and/or basal heave.

FIGURE 8.2 Mathematical procedure: (a) unconfined aquifer; and (b) confined aquifer (modified from US Army 1983 and Leonards 1962).

FIGURE 8.3 Mathematical procedure: confined and unconfined aquifer and capacity of a single well (modified from US Army 1983, Leonards 1962, and Jumikis 1971).

FIGURE 8.4 Mathematical procedure: unconfined aquifer (modified from Avery 1951).

FIGURE 8.5 Mathematical procedure: drainage slot–line source of recharge (modified from U.S. Army 1983 and Leonards 1962).

FIGURE 8.6 Graphical and mathematical procedures (modified from Casagrande 1937, and US Army 1983).

FIGURE 8.7 Mathematical procedure for an example situation.

FIGURE 8.8 Graphical procedure for an example situation.

FIGURE 8.9 Use of vertical drains for stratified soils.

FIGURE 8.10 D_{10} grain size and horizontal hydraulic conductivity from pumping tests from the Mississippi and Arkansas river valleys (modified from US Army 1983).

FIGURE 8.11 Detail of eductor well, vacuum well, deep well, suction well and wellpoint.

FIGURE 8.12 Dewatering systems applicable to various soils based on grain size (modified from Moretrench American Corp. 1967).

FIGURE 8.13 Comparison of vacuum applied to deep wells and wellpoints. (P1 = 101kPa, P2 = 101 − 9.8 [0.0136* vacuum (mmHg) − d(m)]

kPa; P3 = 101 − 9.8 [0.0136* vacuum (mmHg)] kPa)

FIGURE 8.14 Comparison of (a) electro-osmotic flow with (b) hydraulic flow (modified from Casagrande 1983).

FIGURE 8.15 Typical electro-osmosis system.

FIGURE 8.16 Selection of filter pack for wells, vacuum wells wellpoints and horizontal drains (modified from US Army 1983).

FIGURE 8.17 Selection of filter pack for wells, vacuum wells, wellpoints and horizontal drains (modified from Driscoll 1986).

FIGURE 9.1 Types of shallow foundation: (a) strip footing; (b) pad footing; (c) combined footing; and (d) waffle slab.

FIGURE 9.2 Smooth strip footing on weightless, cohesionless soil.

FIGURE 9.3 Failure mode for footing at depth D: (a) assumptions made by Terzaghi 1943; and (b) actual failure mode.

FIGURE 9.4 Bearing capacity factors for strip footing (modified from Terzaghi 1943).

FIGURE 9.5 Location of water table, where z_m = the depth to the water-table when beneath the footing.

FIGURE 9.6 Bearing capacity factor, N_γ (modified from Davis & Booker 1971).

FIGURE 9.7 Footing subjected to vertical and horizontal loads plus moments.

FIGURE 9.8 Undrained bearing capacity factor, F_n, for a strip on an infinite layer (a) with undrained shear strength increasing with depth; and (b) with a crust (modified from Davis & Booker 1973).

FIGURE 9.9 Curves of μ_c and N'_c strip on finite layer; undrained shear strength increasing linearly with depth (modified from Matar & Salençon 1977).

FIGURE 9.10 Strip footing on fissured clay.

FIGURE 9.11 Undrained bearing capacity of a strip footing on a fissured clay deposit: (a) containing one or two orthogonal fissure sets; and containing two fissure sets with an included angle of (b) 60°; (c) 45°; and (d) 30° (modified from Lav et al. 1995).

FIGURE 9.12 Definition of terms for a footing on a slope: β = angle of slope with respect to horizontal; D = depth of footing with respect to the level of the horizontal ground; B = footing width; b = horizontal distance leading edge of footing, a, is away from rest of slope, O. $\lambda = b/B$; $\eta = D/B$.

FIGURE 9.13 Suggested design factors for (a) a 2:1 (26.6°) slope; and (b) a 1.5:1 (33.7°) slope (modified from Shields *et al.* 1990). Contours give percent capacity, P.

FIGURE 9.14 Dimensionless limit pressure for strip footing on sand layer overlying clay, case of no surcharge: (a) $\phi = 30°$; (b) $\phi = 35°$; (c) $\phi = 40°$; and (d) $\phi = 45°$ (modified from Michalowski & Shi 1995).

FIGURE 9.15 Bearing capacity for strip footing on sand layer overlying clay layer. $\phi'_{sand} = 40°$ (modified from Burd & Frydman 1997).

FIGURE 9.16 Modified undrained bearing capacity factor, N_m, for square or circular footings on two layer purely cohesive soil (modified from Vesic 1975).

FIGURE 9.17 Chart for evaluating settlement of embedded rectangular footings (modified from Christian & Carrier 1978).

FIGURE 9.18 Chart for evaluating settlement of rigid circular footing on a soil layer of finite thickness.

FIGURE 9.19 Soil profiles considered by Rowe & Booker (1981a,b) in developing elastic solutions.

FIGURE 9.20 Degree of settlement versus time factor for a circular footing on a soil layer drained at the top and bottom (modified from Davis & Poulos 1972).

FIGURE 9.21 Vertical surface displacement beneath circular loading.

FIGURE 9.22 Correlation between blow count and modulus of sand (modified from D'Appolonia *et al.* 1970).

FIGURE 9.23 Observed settlement of footing on sand of various relative densities (modified from Burland *et al.* 1978).

FIGURE 9.24 Strain influence factors for use in Schmertman's method (modified from Schmertman *et al.* 1978): (a) modified strain influence factor distributions; and (b) explanation of pressure terms used in Eq. 9.27.

FIGURE 9.25 Chart for correction of N-values in sand for influence of overburden pressure. Reference value of effective overburden pressure, 107 kPa, i.e. 1 ton/ft (modified from Peck *et al.* 1974).

FIGURE 9.26 Design chart for proportioning shallow footings on sand: (a) $D_f/B = 1$; (b) $D_f/B = 0.5$; and (c) $D_f/B = 0.25$ (modified from Peck *et al.* 1974).

FIGURE 9.27 Strip raft subjected to a point load, P: E_r and E_s = the elastic modulus of the raft and soil, respectively; ν_r and ν_s = the elastic modulus of the raft and soil, respectively.

FIGURE 9.28 (a) Displacement distributions; and (b) moment distributions for strip raft (modified from Brown 1975).

FIGURE 9.29 Circular raft: (a) maximum moments for various stiffnesses; and (b) differential displacements for various stiffnesses ($\nu_r = 0.3$) (modified from Brown 1969).

FIGURE 9.30 Settlement influence factors for rectangular raft on an infinite layer for $L/B = 2$ (modified from Fraser & Wardle 1976).

FIGURE 9.31 Settlement correction factor, S, for $L/B = 2$ (modified from Fraser and Wardle 1976): (a) $\nu_s = 0$; (b) $\nu_s = 0.3$; (c) $\nu_s = 0.5$.

FIGURE 10.1 Adhesion factor u = uplift tests; c = compression tests (modified from Kulhawy & Phoon 1993).

FIGURE 10.2 Variation of bearing capacity factor with friction angle (modified from Berezantzev *et al.* 1961).

FIGURE 10.3 Layered soil profiles: variation of ultimate base capacity with depth: (a) Case A, dense sand below weak layer; (b) Case B, weak soil underlying dense sand; and (c) Case C, dense sand sandwiched between two weak layers. f_{b1}, f_{b2} = limiting base capacity of weak soil; f_{bd} = limiting base capacity of pile in dense sand.

FIGURE 10.4 A typical cyclic stability diagram for a driven pile in clay: $N = 100$ cycles.

FIGURE 10.5 The definition of single pile geometry: (a) bearing stratum Young's modulus = E_b; and (b) distribution of soil Young's modulus, E_s = soil Young's modulus

$$\eta = E_{SO}/E_{SL}.$$

FIGURE 10.6 Settlement of single pile in soil in homogeneous clay.

FIGURE 10.7 Settlement of single pile with linearly increasing modulus.

FIGURE 10.8 Construction of load–settlement curve (modified from Poulos & Davis 1980).

FIGURE 10.9 Settlement of equivalent pier in soil layer

FIGURE 10.10 Proportion of base load for equivalent pier.

FIGURE 10.11 Non-linear correction factors for a flexible fixed-headed pile in stiff clay: (a) deflection correction factor, F_u; and (b) fixing moment correction factor, F_M.

FIGURE 10.12 Non-linear correction factors for a flexible fixed-headed pile in soft clay: (a) deflection correction factor, F_u; and (b) fixing moment correction factor, F_M.

FIGURE 10.13 Group factor exponent, ω_L, for laterally loaded groups: homogeneous soils.

FIGURE 10.14 Some sources of soil movement.

FIGURE 10.15 Simplified approaches to estimating pile head movement: (a) pile movement stabilizes with increasing soil movement ($z_n \geq L_1$); and (b) pile movement continues to increase with increasing soil movement ($z_n < L_1$).

FIGURE 10.16 Elastic solutions for pile movement in expansive soil: uniform pile diameter (modified from Poulos 1989).

FIGURE 10.17 Elastic solutions for unrestrained free-head pile in uniform soil (linear soil movement profile) (reproduced from Chen & Poulos © 1997 with permission of ASCE).

FIGURE 10.18 Elastic solutions for unrestrained free-head pile in "Gibson" soil (linear soil movement profile) (reproduced from Chen & Poulos © 1997 with permission of ASCE).

FIGURE 10.19 Statnamic test: (a) principle of test; and (b) test set-up.

FIGURE 10.20 Elements of a cross-hole sonic logging system (modified from Stain & Williams 1991).

FIGURE 10.21 Typical results of sonic integrity tests on bored piles (modified from Tchepak 1997). Refractogram of (a) a sound pile; and (b) an unsound pile.

FIGURE 11.1 Allowable contact pressure, q_{ba}, for

unweathered jointed rock (modified from Peck *et al.* 1974).

FIGURE 11.2 Bearing pressure coefficient, K_{sp} (modified from CGS 1992).

FIGURE 11.3 Effect of size on rock modulus for plate loading tests (●) 180 kN; (×) 360 kN; (+) 540 kN; (○) 720 kN.

FIGURE 11.4 Notations for pier socketed into rock: L_s = depth of socket, r = radius of socket, B_s = diameter of socket; and Q_t = the total load, Q_b = the load that reaches the base of the socket, Q_s = load carried in side shear.

FIGURE 11.5 Correlations of Horvath *et al.* (1983) and Rowe & Armitage (1984) for estimation of average side shear resistance for conventional rock sockets: (—) Rowe & Armitage (1984) expected values based on log-normal distribution, (––) Horvath *et al.* (1983) lower bound values, (●) Rowe & Armitage (1984) field test results, (■) Carrubba (1997) *in situ* pile test results.

FIGURE 11.6 Load distribution in a rock socket (modified from Pells & Turner 1979).

FIGURE 11.7 Elastic settlement of a complete rock socket (modified from Pells & Turner 1979).

FIGURE 11.8 Embedment reduction factor for shear sockets (modified from Pells & Turner 1979).

FIGURE 11.9 Elastic settlement of shear socket (modified from Pells & Turner 1979).

FIGURE 11.10 Methodology of stability evaluation of concrete dams on rock foundation.

FIGURE 11.11 Strength envelopes of bonded and unbonded contacts.

FIGURE 11.12 Typical "as-built" roughness profile for Barrett Chute Dam. (CH = chainage)

FIGURE 11.13 Diagrams of base pressures (USBR): (a) vertical cross-section; (b) pressure diagram without uplift; (c) uplift pressure diagram; and (d) combined pressure diagram.

FIGURE 11.14 Cross-section of Barrett Chute Dam for stability analysis: A, original design assumption; B, uplift pressure in April 1987 (pretreatment); C, uplift pressure in September (posttreatment); D, bedrock surface; E, grout curtains.

FIGURE 11.15 Measured uplift pressures in the observation wells of Barrett Chute Dam: A, headpond water-level; B, tailrace water-level; C, Phase II investigation; D, installation of relief wells.

FIGURE 12.1 The basic mathematical model used in foundation dynamics: (a) actual system; and (b) basic model of one degree-of-freedom system.

FIGURE 12.2 The co-ordinate system and possible displacements. CG = center of gravity.

FIGURE 12.3 The stiffness and damping parameters for a circular disk on the surface of a half-space: (a) vertical excitation; (b) horizontal excitation; (c) rocking excitation; and (d) torsional excitation. Exact solution by Luco & Westmann 1971, modified from Veletsos & Verbic 1974; Veletsos & Nair 1974. (—) Exact solution, (---) approximate solution, (···) modified cone solution.

FIGURE 12.4 Notations for an embedded foundation: CG = center of gravity.

FIGURE 12.5 Vertical stiffness, f_{v1}, and damping, f_{v2}, parameters for (a) end bearing piles; and (b) floating piles (reproduced from Novak & El Sharnouby © 1983 with permission of ASCE).

FIGURE 12.6 Model for non-linear analysis of piles.

FIGURE 12.7 Notation for coupled motion of embedded foundations.

FIGURE 12.8 Example for the response analysis of machine foundations: Line 1, soil material damping ignored; Line 2, soil material damping considered.

FIGURE 12.9 Types of hammer foundation arrangement.

FIGURE 12.10 Mathematical models for hammer foundations for (a) one degree-of-freedom; and (b) two degrees-of-freedom.

FIGURE 12.11 Example for the response analysis of hammer foundations.

FIGURE 13.1 Schematic of desirable drain installations to control groundwater.

FIGURE 13.2 Schematic illustration of density–moisture curves for standard and modified (AASHTO) compactive efforts.

FIGURE 13.3 Possible locations for geogrid reinforcement in a flexible pavement structure.

FIGURE 13.4 Pavement design framework and major components (modified from TAC 1997).

FIGURE 13.5 Schematic of load transfer mecha-

nism and critical points of stress–strain: (a) stress spreading effect of a flexible pavement structure; and (b) critical stresses and/or strains (← · → tension; → · ← compression).

FIGURE 13.6 Example of thickness design chart from The Asphalt Institute for a conventional flexible pavement with a 150 mm untreated aggregate base (modified from TAI 1991a). MAAT = 7°C.

FIGURE 13.7 US Army Corps of Engineers CBR curve for thickness design of flexible airfield pavement.

FIGURE 13.8 Flexible pavement design curves, B-767 (modified from Federal Aviation Administration 1987).

FIGURE 13.9 Joint designs with load-transfer devices (modified from TAC 1997): (a) dowelled contraction joint; (b) longitudinal sawcut joint; and (c) dowelled expansion joint.

FIGURE 13.10 Asphalt concrete overlay required to reduce measured pavement rebound deflection (RRD) to a design value (modified from TAI 1983).

FIGURE 14.1 Different stages of slope movements.

FIGURE 14.2 Geotechnical characterization of slope movements, and risk assessment, warning devices and mitigation (modified from Leroueil & Locat 1998).

FIGURE 14.3 Main types of slope failures in soil and rock.

FIGURE 14.4 The changes in pore pressure and factor of safety during an excavation of a cut in clay (modified from Bishop & Bjerrum 1960). PWP = porewater pressure, G.W.L. = groundwater level.

FIGURE 14.5 Relationship between the number of landslides and rainfall characteristics in South Korea (modified from Kim *et al.* 1992).

FIGURE 14.6 Flow nets: influence of position of lower aquifer (modified from Lafleur & Lefebvre 1980).

FIGURE 14.7 Groundwater flow model for mountain environment showing the impact of hydraulic conductivity, k, and stratification on flow pattern (modified from Hodge & Freeze 1977). Scales are given as multiples of an arbitrary constant R.

FIGURE 14.8 Variation of yearly rainfall and its relation to the design and failure of slopes in the south of France (modified from Colas *et al.* 1976).

FIGURE 14.9 Boundary conditions for planar failure with pore pressure conditions assumed as a triangular distribution along the sliding plane and the tension crack. ψ_f and ψ_p are the inclination from the horizontal of the slope and failure plane respectively. U and V are hydraulic forces on the failure plane and the face of the crack respectively.

FIGURE 14.10 The three levels of resistance of soils.

FIGURE 14.11 Inclinometer profiles at different times at Selborne (modified from Bromhead *et al.* 1998).

FIGURE 14.12 Relation between slope inclination, slope height and time to failure for London clay cuts (modified from Leonards 1979).

FIGURE 14.13 Factors of safety obtained by total stress analysis of short-term failures versus the plasticity index, I_p (modified from Leroueil *et al.* 1990). I_L = liquidity index.

FIGURE 14.14 Comparison of field and laboratory measurements of residual strength in (a) Upper Lias; and (b) London clay (modified from Chandler 1984).

FIGURE 14.15 Representation of planar features: (a) definition of terms; (b) representation of reference sphere; and (c) equal-area projection (modified from Heok & Bray 1981, and Norrish & Wyllie 1996).

FIGURE 14.16 Various modes of failure of rock masses along discontinuities. The structural data provided in the insert are used in the example.

FIGURE 14.17 Planar failure in infinite slope.

FIGURE 14.18 Bishop's simplified method.

FIGURE 14.19 Stability charts for total stress analyses (modified from Janbu 1954a).

FIGURE 14.20 Stability charts for effective stress analyses (modified from Janbu 1954a).

FIGURE 14.21 Perturbation method: (a) notation; and (b) definition of σ'_0 (modified from Faure 1985).

FIGURE 14.22 Nomogram for estimating a minimum value of the cohesion component of shear strength from the analysis of natural slopes. $\phi' = 30°$.

FIGURE 14.23 Stereoplot of angular data for wedge stability analysis. X, Y, A and B are coefficients used to solve Eq. 14.21. The numbers in brackets refer to the bedding (1) and joint set (3) identified in Fig. 4.16.

FIGURE 14.24 Analysis of toppling failure potential: (a) geometric considerations; and (b) stability conditions (modified from Hoek & Bray 1981).

FIGURE 14.25 Proposed guidelines for assessing risks to life from naturally occurring slope hazards: (a) Cheekeye Fan; (b) British Columbia; and (c) Canada (modified from: (a) Hungr *et al.* 1993; (b) Evans 1997; and (c) Morgan 1997).

FIGURE 14.26 Some design aspects of a buttress.

FIGURE 14.27 Piezometric levels for parallel trench and counterfort drains at drain invert level. (a) Key diagram; (b) h_m/h_0 and $\bar{h}/h_0$ versus $R_s = (k_v/k_h)^{1/2}S/h_0$ for fully penetrating drains ($n = 1.0$) and partially penetrating drains ($n = 4.5$) (modified from Hutchinson 1977).

FIGURE 14.28 Schematic design of an anchor.

FIGURE 15.1 Principle of preloading by surcharge to compensate for primary consolidation settlement (modified from Jamiolkowski *et al.* 1983).

FIGURE 15.2 Excess pore pressure, Δu, after surcharge removal (modified from Jamiolkowski *et al.* 1983).

FIGURE 15.3 Schematic of vacuum preloading system (modified from Shang *et al.* 1998).

FIGURE 15.4 Soil properties before (△) and after (–□–) vacuum preloading consolidation, East Pier Project, Tianjin, China (modified from Shang *et al.* 1998).

FIGURE 15.5 Basic instrumentation of embankment modified with prefabricated vertical drains (PVDs) (modified from Rixner *et al.* 1986a).

FIGURE 15.6 Consolidation using prefabricated vertical drains (PVDs): (a) section of the equivalent cylinder (modified from Holtz *et al.* 1991); (b) PVDs, showing various shapes of cores with nonwoven geotextile filter sleeves (modified from Hausmann 1990); and (c) PVD patterns, showing drain spacing *s* (modified from Holtz *et al.* 1991).

FIGURE 15.7 Schematic of a vertical drain, including disturbed (smear) zone and undisturbed zone (modified from Holtz *et al.* 1991).

FIGURE 15.8 Types of grouting (modified from Hausmann 1990): (a) intrusion grouting; (b) permeation grouting; (c) compaction grouting; and (d) jet grouting.

FIGURE 15.9 Two examples of ground freezing applications (modified from Hausmann 1990): (a) for open excavations; and (b) for tunneling.

FIGURE 15.10 Schematic of electro-osmotic consolidation (modified from Shang 1998).

FIGURE 15.11 Different soil nailing systems and applications (modified from Hausmann 1990): (a) grouted bars; (b) root piles; and (c) anchor plates.

FIGURE 16.1 Trial embankment (section B) at Saint-Alban: (a) location of piezometers; (b) pore pressures measured under the center of the section, as a function of the embankment load (after Leroueil et al. 1978; reproduced with permission, *Canadian Geotechnical Journal*).

FIGURE 16.2 Compilation of observed excess pore pressures in clay foundation in the first place of embankment construction. Isochrone shown is given by Eq. 16.1 for $\bar{B}_m \cong 0.6$. Data from: (●) Tavenas and Leroueil (1980), ○ Ortigao (1980), (△) Kabbaj, M. (1985).

FIGURE 16.3 (a) Effective and total stress paths; and (b) pore pressure under the centerline of an embankment.

FIGURE 16.4 Variation of ratio $\sigma'_{pconv}/\sigma'_{vy}$ with overconsolidation ratio of clay (only sites with OCRs $2 \leq OCR \leq 6$ are presented) (after Leroueil 1996; © reproduced with permission ASCE, Reston, VA, *Journal of Geotechnical Engineering*).

FIGURE 16.5 Behavior of trial embankment at Kalix, Sweden, during construction (modified from Holtz & Holm 1979).

FIGURE 16.6 (a) Effective stress path; and (b) pore pressure under the centerline during stage-construction of an embankment.

FIGURE 16.7 Summary of mechanics in a reinforced embankment on soft soil (modified from Jewell 1996): (a) unreinforced; (b) footing subject to outward shear stress; (c) reduction in bearing capacity, N_c, from outward shear stress; (d) reinforced; (e) rough footing; and (f) increase in bearing capacity, N_c, from inward shear stress.

FIGURE 16.8 Comparison of predicted (—) (Rowe & Soderman 1984) and observed (●) rein-

forcement strains at strain gage location A (modified from Rowe & Soderman 1984).

FIGURE 16.9 Observed excess pore pressure distribution at end of construction for two embankments constructed over peat (modified from Rowe & Soderman 1985b). Data from: ● Raymond (1969), ▲ Rowe *et al.* (1984a). Λ = drainage path, z = depth below peat–fill interface.

FIGURE 16.10 Chart for calculation of vertical stresses caused by embankment (modified from Osterberg 1957).

FIGURE 16.11 Estimation of the end-of-primary *in situ* strain, $\Delta\varepsilon^*$, in excess of that determined from conventional 24-h laboratory odometer test, when strain rate and temperature effects are considered (after Leroueil 1996; © reproduced with permission ASCE, *Journal of Geotechnical Engineering*).

FIGURE 16.12 Net fill height versus fill thickness for various reinforcement tensile stiffness, J, values (modified from Rowe & Soderman 1987): (●) continuous plasticity, (↑) maximum net fill height.

FIGURE 16.13 Effective stresses and lateral displacements at end of construction: (a) Cubzac-les-Ponts; and (b) Saint-Alban B (after Tavenas *et al.* 1979; reproduced with permission *Canadian Geotechnical Journal*).

FIGURE 16.14 Degree of settlement/consolidation curves for two-dimensional flow conditions: (a) permeable top, permeable base; (b) permeable top, impermeable base (modified from Davis & Poulos 1972).

FIGURE 16.15 Strain–time relations in the laboratory and in the field (modified from Ladd *et al.* 1977).

FIGURE 16.16 Strength ratios deduced by different approaches: (●) after Larsson (1980), Jardine and Hight (1987), ■ after Trak et al. (1980).

FIGURE 16.17 Correction to obtain operational strength of a crust beneath an embankment.

FIGURE 16.18 Chart for calculation of factor of safety (modified from Pilot & Moreau 1973).

FIGURE 16.19 Direct sliding failure of the fill or reinforcement.

FIGURE 16.20 Definition of variables used to estimate collapse height for a perfectly reinforced embankment (modified from Rowe & Soderman 1987).

FIGURE 16.21 Bearing capacity factor for non-homogeneous soil (modified from Rowe & Soderman 1987).

FIGURE 16.22 Effect of non-homogeneity on depth of the failure zone beneath a rough rigid footing (modified from Matar & Salençon 1977).

FIGURE 16.23 Rotational failure of embankments on soft soil.

FIGURE 16.24 Design chart for peat underlain by a firm base; see text for assumptions and limitations (modified from Rowe & Soderman 1985b).

FIGURE 16.25 Potential failure mechanism due to lateral thrust and sliding on a deeper low strength layer, e.g. very soft clay beneath a peat layer (modified from Rowe 1997).

FIGURE 16.26 Stages in analysis of settlements using Asaoka's (1978) method: (a) settlement curve for soil layer; and (b) Asaoka's construction.

FIGURE 17.1 Examples of earth retention systems (modified from O'Rourke & Jones 1990 and Bathurst *et al.* 1993): (a) cantilever; (b) crib; (c) braced; (d) tie-back; (e) wrapped face geotextile reinforced soil wall; (f) reinforced soil wall with incremental concrete facing panels; (g) reinforced segmental retaining wall (modular blocks), and (h) soil nailing.

FIGURE 17.2 Example anchored wall systems (after O'Rourke & Jones 1990, © ASCE, reproduced with permission): (a) earth retention with waste tires and geotextiles; (b) wall system with facing plates and rectangular anchors; (c) anchored earth with triangular rebar reinforcement; and (d) wall system with concrete blocks, polymer strips and anchors.

FIGURE 17.3 Geosynthetic reinforced slope.

FIGURE 17.4 Active (a) and passive (b) earth pressure distributions (no groundwater).

FIGURE 17.5 Lateral pressures for the case of a hydrostatic water table behind a wall and cohesionless soils under active earth pressure conditions.

FIGURE 17.6 Active (a) and passive (b) earth pressure distributions due to uniform surcharge (no groundwater).

FIGURE 17.7 Horizontal pressures on a wall due to (a) line, Q_L; and (b) point, Q_P, load surcharges (modified from CGS 1992).

FIGURE 17.8 Calculation of compaction stresses (after Ingold 1979).

FIGURE 17.9 Coulomb wedge theory: (a) active earth force; and (b) passive earth force.

FIGURE 17.10 Log spiral analysis.

FIGURE 17.11 Distribution of pressures and forces for design of gravity (a) and cantilever (b) wall structures (modified from CGS 1992).

FIGURE 17.12 Distribution of pressures and forces for design of cantilever (a) and anchored (b) sheet pile walls.

FIGURE 17.13 Apparent earth pressure distributions for determining forces on supports in braced excavations (modified from CGS 1992): (a) sand; (b) soft–firm clays; and (c) stiff fissured clays.

FIGURE 17.14 Factor of safety with respect to base heave in cohesive soils (modified from Janbu 1954b).

FIGURE 17.15 Settlement adjacent to an open cut (modified from Peck 1969b).

FIGURE 17.16 Concrete diaphragm and cut-off construction (after O'Rourke and Jones 1990, copyright ASCE, reproduced with permission): (a) slurry trench construction; (b) Hydrofraise; (c) soil–cement mixing; (d) Beroto rig; and (e) jet grouting.

FIGURE 17.17 Limit modes of failure for reinforced soil walls: (a) limit mode 1, sliding; (b) limit mode 2; bearing capacity; (c) limit mode 3, reinforcement rupture; (d) limit mode 4, reinforcement pull-out; (e) limit mode 5, wedge/slip circle; and (f) limit mode 6, deformation.

FIGURE 17.18 Limit mode 2: bearing capacity and tilting.

FIGURE 17.19 Limit mode 3: reinforcement layer rupture: (a) contribution of soil self-weight and uniform surcharge; and (b) vertical and horizontal dispersion of load due to surface strip footing.

FIGURE 17.20 Limit mode 4: reinforcement pull-out capacity.

FIGURE 17.21 Limit mode 5: internal wedge stability.

FIGURE 17.22 Empirical curve for estimating maximum lateral wall displacements at end of construction (modified from Mitchell & Christopher 1990). (Based on a 7-m high wall, increase relative displacement 25% for every 20 kPa of uniform surcharge load.)

FIGURE 17.23 Coherent gravity method: (a) position of maximum line of tension in reinforcement layers; and (b) distribution of coefficient of earth pressure for design.

FIGURE 17.24 Pressure distribution along base of reinforced soil mass for coherent gravity method.

FIGURE 17.25 Modified two-part wedge analysis: (a) free-body diagram for unreinforced two-part wedge analysis; and (b) with reinforcement forces.

FIGURE 17.26 Modified circular slip analysis: (a) circular slip geometry; and (b) method of slices.

FIGURE 17.27 Equivalent coefficient of earth pressure, $K = f(\phi, \beta)$ (interslice force oriented at $\lambda = \phi$ to the horizontal).

FIGURE 17.28 Minimum ratio of reinforcement length to slope height, L/H, to contain critical two-part wedge and satisfy sliding and eccentricity criteria (interslice force oriented at $\lambda = \phi$ to the horizontal).

FIGURE 18.1 Definition of terms for the pipe and the surrounding soil: (a) buried pipe and surrounding soil zones; and (b) location of crown, invert, springline, shoulder and haunch.

FIGURE 18.2 Load conditions for circular pipes: (a) vertical and horizontal earth pressures on pipe–soil system; (b) external loads acting directly on the pipe; (c) vertical earth loads at the pipe crown and invert; and (d) approximate vertical and horizontal earth pressure distributions on the pipe (modified from Spangler 1956).

FIGURE 18.3 Pipe burial conditions: (a) conventional trench burial; and (b) pipe under embankment in positive projection condition (pipe crown projects above native ground level).

FIGURE 18.4 Action of the pipe as a ground anchor; limiting forces applied by the ground to the pipe perpendicular to the pipe axis: (a) horizontal force applied by the soil to resist the lateral movement of the pipe; and (b) vertical force applied by soil to the pipe to resist uplift.

FIGURE 18.5 Explanation of arching mechanism: (a) the reference case: a block of elastic soil subjected to earth pressures; (b) positive and negative arching: stiffness less than or greater than the disk.

FIGURE 18.6 Idealized deformation components

around a buried circular pipe: (a) radial pipe deformations under geostatic earth pressures; (b) deformation w_0 for uniform earth pressure component, σ_m; and (c) deformation w_2 for non-uniform earth pressure component, σ_d.

FIGURE 18.7 Example problems: (a) reinforced concrete storm sewer, 0.5-m diameter; (b) corrugated steel culvert, 3-m diameter; and (c) plain HDPE leachate collection pipe, 0.3-m diameter.

FIGURE 19.1 Stability ratios for tunnel in cohesive soil (modified from Atkinson & Mair 1981).

FIGURE 19.2 Dimensionless coefficients F_0–F_3 (from Tunnelling and Underground Space Technology, 11(2), 165–173, Anagnostou & Kovari, "Face stability conditions with earth-pressure-balance shields," 1996, with permission from Elsevier Science Ltd, The Boulevard, Langford Lane, Kidlington OX5 1GB, UK).

FIGURE 19.3 Stability ratios for tunnel in cohesionless soil (modified from Atkinson & Mair 1981): (a) stability number for soil weight; and (b) stability number for surface surcharge.

FIGURE 19.4 Pipes sliding in a stable bore: (a) pipe in soil bore; and (b) pipe in rock bore.

FIGURE 19.5 Ground loading in a cohesionless soil.

FIGURE 19.6 Surface and subsurface settlement curves.

FIGURE 19.7 Application of the modified fluid flow analysis to trenchless techniques involving excavation (similar for expansion, but with "source" and "sink" interchanged): (a) schematic section through pipe jack, with definitions; and (b) analytical framework.

FIGURE 20.1 Temperature–time charts for unsteady heat flow by conduction.

FIGURE 20.2 Thermal conductivity of (a) coarse-grained; and (b) fine-grained soils (modified from Kersten 1949). (—) frozen, (---) unfrozen.

FIGURE 20.3 Thermal energy of water.

FIGURE 20.4 Simplified temperature profile in Stefan's equation.

FIGURE 20.5 Radiation index (modified from Dysli 1990).

FIGURE 20.6 Typical unfrozen water content–temperature relationships for various soils (modified from Nordal & Refsdal 1989).

FIGURE 20.7 Schematic of hydrodynamic and thermal processes in freezing soils (modified from Konrad & Seto 1994).

FIGURE 20.8 Flow chart for obtaining representative values of SP field (w/w_L = ratio of water content, w, to liquid limit, w_L).

FIGURE 20.9 Segregation potential versus overburden pressure for various soils.

FIGURE 20.10 Segregation potential inferred from field data.

FIGURE 20.11 Empirical relationship between segregation potential and soil index properties (modified from Konrad 1998): ▲, $w/w_L > 0.7$; ●, $w/w_L = 0.7$; □, $0.65 < w/w_L < 0.8$ (Rieke et al. 1983).

FIGURE 20.12 Methodology for frost heave prediction.

FIGURE 20.13 Rational approach for frost-susceptibility evaluation.

FIGURE 20.14 Influence of suction in a saturated sandy silt.

FIGURE 21.1 Various types of faulting: (a) right-lateral strike-slip; (b) dip-slip (normal); (c) dip-slip (reverse); and (d) oblique-slip (left-lateral reverse).

FIGURE 21.2 Offsets in strata caused by past earthquakes (modified from Demirtas *et al.* 1996).

FIGURE 21.3 Deformation patterns of the major wave types (modified from Bolt 1976): (a) P-wave; (b) S-wave; (c) Love wave; and (d) Rayleigh wave.

FIGURE 21.4 Earthquake recurrence rates showing G–R line and characteristic earthquakes (modified from Schwartz & Coppersmith 1988).

FIGURE 21.5 Magnitude recurrence relation with a maximum earthquake magnitude.

FIGURE 21.6 Compressional wave propagating at an angle θ to the pipeline.

FIGURE 21.7 Shear wave propagating at an angle θ to the pipe.

FIGURE 21.8 Simple one-degree-of-freedom system: (a) mass–spring damper system; and (b) free-body diagram.

FIGURE 21.9 Logarithmic plot of response spectrum of El Centro corrected accelerogram, 270°, Caltech IIA001.

FIGURE 21.10 Normalized spectral curves suitable for use in building codes (modified from Seed & Idriss 1982).

FIGURE 21.11 Pseudo-acceleration spectrum, Alameda Park, May 11, 1962.

FIGURE 21.12 Amplification of ground motions in soft soils (modified from Idriss 1990).

FIGURE 21.13 Development of design spectra using period-dependent site amplification factors (modified from Martin & Dobry 1994).

FIGURE 21.14 (a) Approximating a ridge formation by a triangular wedge; and (b) infinite wedge excited by plane SH waves (modified from Faccioli 1991).

FIGURE 21.15 Amplitude reduction ratio, τ, as a function of frequency and wave velocity (modified from Clough & Penzien 1993).

FIGURE 21.16 Forces acting on (a) active; and (b) passive failure wedges in Mononobe–Okabe analysis.

FIGURE 21.17 Geometry and notation for partially submerged backfill.

FIGURE 21.18 Static and seismic forces acting on a gravity retaining wall.

FIGURE 21.19 Non-dimensional lateral forces and moments on a rigid wall with unyielding backfill for 1-*g* static horizontal body forces.

FIGURE 21.20 Chart for determining soil–wall system frequency on the basis of shear modulus. ○, parabolic G, $L/H = 5$; △, linear G, $L/H = 5$; □, parabolic G, $L/H = 1.5$. Wall height = 10 m, soil density = 2.

FIGURE 21.21 Peak seismic thrusts for soil profiles with parabolic variation in G ($L/H = 5.0$, $\lambda = 10\%$, $\nu = 0.40$) (modified from Wu & Finn 1999): ––, Wood's (1973) static; —, 84 percentile; ---, upper bound.

FIGURE 21.22 Peak seismic thrusts for soil profiles with parabolic variation in G ($L/H = 1.5$, $\lambda = 10\%$, $\nu = 0.40$) (modified from Wu & Finn 1999): ––, Wood's (1973) static; —, 84 percentile; ---, upper bound.

FIGURE 21.23 Reduction in bearing capacity, R, under seismic loading conditions with (---) and without (—) the inclusion of soil inertia effects as a function of the horizontal seismic coefficient, k_h (modified from Pecker 1996).

FIGURE 21.24 Equivalent footing width for footing subjected to eccentric and inclined loading at failure (modified from CGS 1992).

FIGURE 21.25 Simplified base curve recommended for calculation of CRR from SPT data along with empirical liquefaction data (modified from Seed *et al.* 1985).

FIGURE 21.26 Minimum values for K_σ recommended for clean and silty sands and gravels (modified from NCEER 1997).

FIGURE 21.27 Correction factors to CRR as a function of the initial static shear stress ratio, τ_{st}/σ'_{vo}, and relative density (modified from Harder & Boulanger 1997).

FIGURE 21.28 Curve recommended for calculation of CRR for earthquake magnitude $M = 7.5$ from CPT data along with empirical liquefaction data (modified from NCEER 1997). Liquefaction data: ● Stark & Olson (1995), ▲ Suzuki *et al.* (1995). No liquefaction: ○ Stark & Olson (1995), △ Suzuki *et al.* (1995).

FIGURE 21.29 Curves recommended by workshop for calculation of CRR from corrected shear-wave velocity (modified from NCEER 1997). Boundaries defined by: $\text{CRR} = a\,(V_{sl}/100)^2 + b\,[1/(V_{slc} - V_{sl}) - (1/V_{slc})]$, $a = 0.03$ and $b = 0.9$; $V_{slc} = 220$, 210 and 200 ms^{-1} for sands and gravels with FC ≤ 5, ≈ 5 and $\geq 35\%$, respectively.

FIGURE 21.30 Post-liquefaction volumetric strains as a function of normalized standard penetration resistance and average cyclic stress ratio for $M_w = 7.5$ earthquakes (modified from Tokimatsu & Seed 1987).

FIGURE 21.31 Relationship between volumetric strains in unsaturated sands as a function of cyclic shear strain and penetration resistance for an earthquake magnitude $M_w = 7.5$ (modified from Tokimatsu & Seed 1987).

FIGURE 21.32 Chart for determining the effective shear strain in a soil layer during earthquake shaking (modified from Tokimatsu & Seed 1987).

FIGURE 21.33 Effect of ground improvement techniques on settlement (modified from Yasuda *et al.* 1996). Clear values for: ○, Port Island; ●, Rokko Island. —, range of measured values. Total number of measurements = 25.

FIGURE 21.34 The effect of sample preparation

on undrained simple shear response of Syncrude sand (modified from Vaid *et al.* 1999).

FIGURE 21.35 Effect of stress path on undrained behavior of Toyoura sand (modified from Yoshimine *et al.* 1998). D_r = 39–41%, b = 0.5.

FIGURE 21.36 Correlation of residual strength, S_r, with $(N_1)_{60}$ (modified from Seed & Harder 1990; 100 kPa = 2000 psf). ●, measured SPT data; ○, estimated SPT data; □, construction-induced liquefaction and sliding case histories.

FIGURE 21.37 Elements of deformation analysis.

FIGURE 21.38 Risk management framework proposed by Canadian Standards Association (modified from International Journal on Hydropower and Dams 1998).

FIGURE 21.39 ANCOLD societal risk criteria (based on International Journal on Hydropower and Dams 1998).

FIGURE 21.40 Event tree used for the probability of liquefaction-failure (modified from Lee *et al.* 1998).

FIGURE 22.1 Risk components (modified from Health Canada 1994).

FIGURE 22.2 Top–down approach for risk assessment using step-wise refinement.

FIGURE 22.3 Environmental site management framework.

FIGURE 22.4 Fate and partitioning of common organic contaminants based on contaminant "fugacity" or escape potential (see MacKay *et al.* 1991, 1992, 1993).

FIGURE 22.5 Receptor screening process.

FIGURE 22.6 (a) Pathway process; (b) soil and groundwater screening processes.

FIGURE 22.7 Conceptual exposure pathways model.

FIGURE 22.8 Methods of presenting results of risk calculations.

FIGURE 22.9 Risk management options.

FIGURE 23.1 Soil particle sizes and characteristics.

FIGURE 23.2 Silicon tetrahedron (a) and silica tetrahedra arranged in a hexagonal network (b).

FIGURE 23.3 Octahedral unit (a) and sheet structure of octahedra (b).

FIGURE 23.4 Synthesis pattern for the clay minerals (reproduced from *Fundamentals of Soil Behavior,* J.K. Mitchell © 1993 John Wiley & Sons, Inc. Reprinted with permission of John Wiley & Sons, Inc.).

FIGURE 23.5 Ion–water interaction (as postulated in Frank and Wen (1957)).

FIGURE 23.6 Possible mechanisms of water adsorption by silicate mineral surfaces: (a) hydrogen bonding; (b) ion hydration; (c) attraction by osmosis; and (d) dipole attraction (modified from Mitchell 1993).

FIGURE 23.7 Distribution of ions adjacent to a clay surface according to the concept of the diffuse double layer.

FIGURE 23.8 Energies of repulsion, attraction and net interaction for interacting clay particles minerals (reproduced from *Fundamentals of Soil Behavior,* J.K. Mitchell © 1993 John Wiley & Sons, Inc. Reprinted with permission of John Wiley & Sons, Inc.).

FIGURE 23.9 Structure-determining factors and processes (modified from Mitchell 1993).

FIGURE 23.10 Particle associations in clay suspensions: (a) dispersed and deflocculated; (b) face-to-face aggregated, but deflocculated; (c) edge-to-face-flocculated, but dispersed; (d) edge-to-edge flocculated, but dispersed; (e) edge-to-face flocculated and aggregated; (f) edge-to-edge flocculated and aggregated; (g) edge-to-face and edge-to-edge flocculated and aggregated (modified from van Olphen 1977).

FIGURE 23.11 Soil states in relation to critical or steady state line, and pore pressure and volume changes during deformation where Δu = change in pore pressure (reproduced from *Fundamentals of Soil Behavior,* J.K. Mitchell © 1993 John Wiley & Sons, Inc. Reprinted with permission of John Wiley & Sons, Inc.).

FIGURE 23.12 Composite relationship showing dependence of residual friction angle ϕ_r, on soil composition: A = activity; PI = plasticity index (from *Fundamentals of Soil Behavior,* J.K. Mitchell © 1993 John Wiley & Sons, Inc. Reprinted with permission of John Wiley & Sons, Inc.).

FIGURE 23.13 Volume and pore pressure changes during shear: (a) drained conditions where ΔV = change in volume, and V_o = initial volume; and (b) undrained conditions where Δu =

change in pore pressure (modified from Mitchell 1993).

FIGURE 23.14 Four types of direct flow through a soil mass.

FIGURE 24.1 (a) Potentiometric surface of the Dakota Sandstone, contour interval 100 ft (from Darton 1909, U.S. Geol. Surv. Water Supply Paper 227); (b) Example of a hydrogeologic cross-section describing the pattern of groundwater flow (modified from Domenico & Schwartz 1998, *Physical and Chemical Hydrogeology*). © 1998 John Wiley & Sons, Inc. Reprinted with permission of John Wiley & Sons, Inc.).

FIGURE 24.2 Hydrogeologic cross-sections illustrating the importance of hydraulic conductivity contrasts, continuity of units, and recharge and discharge relations on groundwater flow: (a) sand lenses with little horizontal discharge; (b) sand layers with significant horizontal discharge; and (c) sand layers discharging both bedrock and overburden (modified from Sara 1991, *Practical Handbook of Ground-Water Monitoring,* D.M. Nielsen ed.). © 1991 CRC Press, Inc. Reprinted with permission of CRC Press, Inc.).

FIGURE 24.3 Longitudinal dispersivity versus scale with data classified by reliability (after Gelhar *et al.* 1992, Water Resources Res., v. 28, pp. 1955–1974). © 1992 American Geophysical Union.

FIGURE 24.4 General groundwater contamination scenario with dense, non-aqueous phase liquids (after Kueper & Frind 1991, Water Resources Res., v. 27, pp. 1049–1057). © 1991 American Geophysical Union.

FIGURE 24.5 Interface between air, water and a solid surface (modified from de Marsily 1986, *Quantitative Hydrogeology*). © 1986 Academic Press, Inc. Reprinted with permission of Academic Press, Inc.

FIGURE 24.6 Capillary pressure curves given as a function of the degree of saturation with respect to the wetting and non-wetting phases (modified from Domenico and Schwartz 1998, *Physical and Chemical Hydrogeology*). © 1998 John Wiley & Sons, Inc. Reprinted with permission of John Wiley & Sons, Inc.

FIGURE 24.7 Capillary pressure–water saturation drainage curves for a tetrachloroethene–water system for sands of differing hydraulic conductivity (modified from Kueper & Frind 1991, Water Resources Res., v. 27, pp. 1059–1070). © 1991 American Geophysical Union.

FIGURE 24.8 Typical relative permeability curves (after Demond & Roberts 1987, Water Resources Bulletin, v. 23, pp. 617–628). © 1987 American Water Resources Association. Reproduced by permission of American Water Resources Association.

FIGURE 24.9 The downward percolation of a NAPL in the unsaturated zone is determined by the nature of the spill: (a) a sudden loss results in maximum spreading and a large quantity trapped at residual saturation; and (b) a slow leak causes the product to follow a set of channels and a minimal quantity is trapped at residual saturation (after Domenico & Schwartz 1998, *Physical and Chemical Hydrogeology*). © 1998 John Wiley & Sons, Inc. Reprinted with permission of John Wiley & Sons, Inc.

FIGURE 24.10 Percentages of dissolved carbon dioxide species activities at one atmosphere pressure and at (···) 50, (—) 25 and (––)0°C as a function of pH (after Hem 1995, U.S. Geol. Surv., Water Supply Paper 2254).

FIGURE 24.11 Log *C*–pH diagram for chromium hydroxide complexes (after Domenico & Schwartz 1998, *Physical and Chemical Hydrogeology*). © 1998 John Wiley & Sons, Inc. Reprinted with permission of John Wiley & Sons, Inc.

FIGURE 25.1 Schematic showing (a) base and (b) side slope of barrier system for Kettleman Hills landfill: PLCS = Primary leachate collection system; SLCS = Secondary leachate collection system; GM = Geomembrane (modified from Bryne et al. 1992).

FIGURE 25.2 Schematic showing different collection systems (modified from Rowe 1988).

FIGURE 25.3 Two leachate drainage systems: (a) French drains; and (b) blanket drain (modified from Rowe *et al.* 1995b).

FIGURE 25.4 Schematic showing examples of poor leachate collection system designs: (a) problematic; and (b) even worse. Schematic also shows a leachate mound developed once there is excessive clogging of the geotextile filter and/or the drainage gravel and/or the pipe (modified from Rowe 1992).

FIGURE 25.5 Schematic showing examples of blanket leachate collection system designs includ-

ing a geotextile filter layer (modified from Rowe 1992).

FIGURE 25.6 Distributed clogging model parameters (modified from Rowe & Fleming 1998).

FIGURE 25.7 Method of defining acceptable zone of water content based on compaction, hydraulic conductivity and shear strength considerations (modified from Benson *et al.* 1999).

FIGURE 25.8 Percentage of liners with a compaction water content within a given range having $k \leq 1 \times 10^{-9}$ m s^{-1} (modified from Daniel 1998).

FIGURE 25.9 Percentage of CCLs with $k_{field} \leq 1 \times 10^{-9}$ m s^{-1} versus percentage plotting above the line of optimums (modified from Daniel 1998).

FIGURE 25.10 Hydraulic containment ("hydraulic trap") inward flow but outward diffusion (modified from Rowe 1997).

FIGURE 25.11 Hydraulic trap landfill (Halton) showing potential shadow effect due to landfill construction. Also shown is the subliner contingency layer (modified from Rowe *et al.* 1995b).

FIGURE 25.12 Schematic showing two single composite liner systems: (a) geomembrane (GM) over compacted clay liner (CCL) over an attenuation layer (AL) over an aquifer; and (b) GM over a geosynthetic clay liner (GCL) over an attenuation layer over an aquifer.

FIGURE 25.13 Double layer thickness variations: (a) concentration and valency effects; and (b) dielectric effects (modified from Rowe *et al.* 1995b).

FIGURE 25.14 Hydraulic conductivity versus static confining stress for permeation of synthetic municipal solid waste (MSW) (simulated Keele Valley landfill) leachate (modified from Petrov & Rowe 1997). Distilled water-hydrated, permeant: (■) distilled water, (●) MSW leachate. MSW leachate-hydrated, permeant: ○ MSW leachate.

FIGURE 25.15 Results of regression analysis on diffusion–saturation data (modified from MacKay 1997). (—) $D_\theta/D_a = \exp[-1.03 \exp(0.017\, S_r)^{1.64}]$; where D_θ and D_a = diffusion coefficient of gas through soil pores and air, respectively.

FIGURE 25.16 Variation in temperature at landfill base with leachate head for a number of landfills (modified from Barone *et al.* 1997).

FIGURE 26.1 Five examples of liner systems: (a) single geomembrane liner; (b) single composite liner; (c) double geomembrane liner; (d) double liner with geomembrane primary liner and composite secondary liner; (e) double composite liner.

FIGURE 26.2 Head of liquid on top of the liner in the case of a liner on a slope: (a) hydrostatic conditions; and (b) unconfined flow along the slope (after Giroud 1997, © Geosynthetics International, reproduced with permission).

FIGURE 26.3 Liquid flow in a primary liquid collection layer (modified from Giroud & Houlihan 1995).

FIGURE 26.4 Liquid flow in the primary liquid collection layer, through a defect in the primary liner, and in the secondary liquid collection layer (leakage detection and collection layer), in the case of a double liner: (a) cross-section; and (b) plan view of the secondary liner (modified from Giroud *et al.* 1997a).

FIGURE 26.5 Determination of the linear coefficient of uniformity.

FIGURE 26.6 Graphical solution of Eq. 26.52 for a geomembrane defect having a diameter, d, of 2 mm (after Giroud *et al.* 1997b, © Geosynthetics International, reproduced with permission): q_i = (—) 10^{-7} m s^{-1}, (——) 10^{-8} m s^{-1}, (····) 10^{-9} m s^{-1}.

FIGURE 26.7 Rate of liquid migration through a defect having a diameter, d, of 2 mm in a geomembrane underlain by a medium with a hydraulic conductivity, k_{UM}, and overlain by a medium that is significantly more permeable than the underlying medium, for various values of the head of liquid on top of the geomembrane, h (after Giroud *et al.* 1997c, © Geosynthetics International, reproduced with permission): (—) thickness of the medium of hydraulic conductivity, k_{UM}, underlying the geomembrane is t_{UM} = 0.6 m; (····) thickness of the underlying medium is infinite.

FIGURE 26.8 Geosynthetic deflection: (a) geosynthetic supported by soil; and (b) geosynthetic overlying a void (materials overlying the geomembrane are not shown).

FIGURE 26.9 Geosynthetic deflection under a soil layer.

FIGURE 26.10 Geomembrane connected to a battered wall (after Giroud & Soderman 1995, © Geosynthetics International, reproduced with permission): 1 = position of the geomembrane at

the time of installation; and 2 = position of the geomembrane after settlement.

FIGURE 26.11 Typical configurations of a geomembrane exposed to wind: (a) geomembrane anchored in an anchor trench; (b) geomembrane anchored under a pavement or a layer of soil; (c) geomembrane restrained by a soil layer on a bench; (d) geomembrane restrained by an intermediate anchor trench; (e) geomembrane anchored under a structure at the top and restrained by liquid or solids below a certain level; (f) at bottom of reservoir, geomembrane anchored in anchor trenches; (g) at bottom of reservoir, geomembrane anchored by strips of soil or pavement (after Giroud *et al.* 1995c, © Geosynthetics International, reproduced with permission).

FIGURE 26.12 Geometry of uplifted geomembrane.

FIGURE 26.13 Geomembrane anchorage to resist uplift by wind.

FIGURE 27.1 Hydraulic-barrier cover system.

FIGURE 27.2 Capillary-barrier cover system and partially saturated hydraulic conductivity functions.

FIGURE 27.3 Evapotranspirative cover system, also called monolayer or monocover (modified from Benson & Khire 1995).

FIGURE 27.4 Example of MSW landfill cover: (a) CCL hydraulic barrier; and (b) composite hydraulic barrier. All thicknesses are typical. Note: i = cover slope.

FIGURE 27.5 Example of low-level radioactive waste landfill cover.

FIGURE 27.6 Example of lightweight site remediation cover over soft waste.

FIGURE 27.7 Leachate generation rates at five hazardous waste landfills in units of liters per hectare per day (lphd $\equiv$ l ha^{-1} day^{-1}). Covers incorporate geomembrane hydraulic barriers (modified from Gross *et al.* 1997). Note: symbols and letters identify the five landfills (modified from Gross *et al.* 1997).

FIGURE 27.8 Identification of typical components of hydraulic-barrier cover system and water movement and storage in cover system.

FIGURE 27.9 Capillary-barrier cover system over mine waste at Waite Amulet site, Quebec, Canada (modified from Yanful 1993).

FIGURE 27.10 Water content and air-filled porosity of capillary barrier and mine waste at Waite Amulet site, Quebec, Canada (modified from Woyshner & Yanful 1995).

FIGURE 27.11 Field gaseous oxygen profiles in capillary barrier and mine tailings at Waite Amulet site, Quebec, Canada (modified from Yanful 1993).

FIGURE 27.12 Cover system internal drainage layer: (a) values of (h_{ave}/h_m) or (t_{ave}/t_m) modified from Giroud and Houlihan 1995; and (b) flow continuity at slope bench or transition.

FIGURE 27.13 Conceptualization of HELP water balance model (modified from Schroeder *et al.* 1994a).

FIGURE 27.14 Seepage force and buoyant unit weight for a soil layer overlying a hydraulic barrier on an infinite slope.

FIGURE 27.15 Definition of two-part wedge and flow thickness for the case of a slope of finite height.

FIGURE 27.16 Definition of slope with a tapered soil layer.

FIGURE 27.17 Definition of slope with a partly tapered soil layer.

FIGURE 27.18 Result of direct shear test on a GCL illustrating peak and large-displacement shearing resistances.

FIGURE 27.19 Interpretation of interface or internal shear test on cover system components: (a) test results for peak strength; (b) tangent friction angle, ϕ_{ti}, and apparent adhesion/cohesion, a_i; and (c) secant friction angle, ϕ_{si}. Similar interpretations are applied to large displacement and residual conditions.

FIGURE 27.20 Estimated OII solid waste landfill shear modulus reduction (G/G_{max}) and damping curves. Data from: Idriss *et al.* 1995, Augello 1998, and Matasovic 1998.

FIGURE 27.21 Shear wave velocities, v_s, for southern California solid waste landfills (modified from Kavazanjian *et al.* 1996).

FIGURE 27.22 Results of parametric study comparing calculated peak horizontal acceleration for OII landfill top deck and peak bedrock acceleration (modified from Bray & Rathje 1998). Data from Harder 1991 for earth dams, and Seed *et al.* 1991 for deep cohesionless/stiff cohesive soils.

Shear wave velocity, v_s: (×) medium, (◇) high, (◆) observed at OII.

FIGURE 27.23 Hynes and Franklin (1984) permanent seismic displacement chart (modified from Richardson *et al.* 1995).

FIGURE 27.24 Basic elements of classical Newmark sliding-block analysis with constant yield acceleration, k_y.

FIGURE 27.25 Yield acceleration degradation model: (a) measured shear force–displacement curve; and (b) yield acceleration degradation (modified from Matasovic *et al.* 1997).

FIGURE 27.26 Results of Newmark seismic deformation analysis for constant and degrading yield acceleration at a normal stress = 20.7 kPa (modified from Matasovic *et al.* 1997). (●) peak parameters, (○) residual parameters; and (▲) degradation model.

FIGURE 27.27 Sources of cover settlement.

FIGURE 27.28 Total settlement data for MSW landfills, measured from the time the landfill reaches final grade (data from Edgers *et al.* 1992, König *et al.* 1996, and Spikula 1996).

FIGURE 28.1 Typical overburden well installation (center). Left-hand and right-hand figures, respectively, show optional detail if DNAPL is, or is suspected of being, present, and flush mount installation.

FIGURE 28.2 Typical bedrock well installation: (a) intermediate or deep bedrock well; and (b) shallow bedrock well.

FIGURE 28.3 Protective casing installation. (a) flush-mount; and (b) above-grade.

FIGURE 28.4 Sample stratigraphic and instrumentation logs: (a) for an overburden well; (b) for a bedrock well.

FIGURE 28.5 Typical chain-of-custody record.

FIGURE 28.6 Cumulative probability plots to assess normality of data.

FIGURE 28.7 Example of box plots.

FIGURE 28.8 Example of radial diagram.

FIGURE 28.9 (a,b) SEQUENCE plots for redox parameters and chemical constituents in groundwater at Plattsburg Air Force Base.

FIGURE 29.1 Conceptual models for three cases of point-source contamination: (a) the non-NAPL case; (b) the LNAPL case; and (c) the DNAPL case (reproduced from Cherry *et al.* 1996 with permission).

FIGURE 29.2 Engineered remedial actions for subsurface contamination. Actions may include: (a) source-zone isolation, containment or removal; (b) plume control through the use of pump-and-treat systems; (c) passive to semi-passive plume control through the use of permeable reactive walls; or (d) funnel-and-gate systems case (reproduced from Cherry *et al.* 1996 with permission).

FIGURE 29.3 Elements of a typical soil vapor extraction (SVE)/bioventing system for remediation of VOC contamination in the vadose zone. The key features are the screened well and vacuum pump. Optional features may include passive wells to enhance the flow of air through the zone of contamination, or low permeability ground-surface covers. Upwelling of the water table beneath the vapor extraction wells may inhibit the removal of contaminant mass in these regions.

FIGURE 29.4 The elements of a dual soil vapor extraction (SVE)/air sparging system. Air sparging is used to enhance the removal of VOCs within the capillary fringe and beneath the water table. Johnson *et al.* (1993) suggest that the air-sparge zone is characterized by discrete air flow channels.

FIGURE 29.5 Typical dual pump system for recovery of LNAPLs such as petroleum hydrocarbons in the subsurface. LNAPL liquid and residual will remain in the subsurface following the removal of the recoverable mobile LNAPL.

FIGURE 29.6 Chemical flushing for the enhanced removal of NAPL case (reproduced from Cherry et al. 1996 with permission). The system includes injection wells for the remedial fluids, and withdrawal wells for the recovery of contaminants and remedial fluids. A forced gradient is maintained between the injection and withdrawal wells.

FIGURE 29.7 The conceptual remediation of a source zone and associated plume by pump-and-treat. While remediation of the plume may be achievable over periods of years to decades, the prospects for remediation of the source zone by pump-and-treat are not promising (reproduced from Cherry *et al.* 1996 with permission): (a) plan view; and (b) efficient quality.

FIGURE 29.8 Possible options for the interception and treatment of contaminant plumes by

permeable reactive barriers. Options include: (a) rows of unpumped wells; (b) permeable reactive walls; or (c) funnel-and-gate systems case (reproduced from Cherry *et al.* 1996 with permission).

FIGURE 29.9 Sectional views of groundwater flow through permeable reactive barriers. The barrier systems are installed perpendicular to the horizontal groundwater flow direction, and partially penetrate a surficial granular aquifer. For a permeable reactive wall in (a), the zone of capture for groundwater approaching the barrier is slightly greater than the dimensions of the reactive wall if the hydraulic conductivity of the reactive medium exceeds that of the aquifer. In (b), for a funnel-and-gate system with the same reactive medium, the zone of capture is larger than the dimensions of the treatment gate, but some groundwater flow is diverted around the edges and beneath the low permeability funnel walls.

FIGURE 30.1 Example of potential contamination in an urban area.

LIST OF TABLES

TABLE 2.1 Great rock groups

TABLE 2.2 Definitions and relationships between various soil properties. Refer to Fig. 2.1 and Section 2.3 for notation.

TABLE 3.1 Particle sizes

TABLE 3.2 Roundness criteria and values (after Youd 1973, © ASTM, reproduced with permission)

TABLE 3.3 Maximum and minimum densities for granular soils (modified from Lambe & Whitman 1979)

TABLE 3.4 Relative density, D_r (formerly specific gravity), of various minerals

TABLE 3.5 Atterberg limits of clay minerals (after Lambe and Whitman 1979, *Soil Mechanics SI Version*, © John Wiley & Sons, Inc., New York, reproduced with permission)

TABLE 3.6 Soil classification chart (after ASTM Standard D 2487, © ASTM, reproduced with permission)

TABLE 3.7 Classification of peat structure (after MacFarlane 1969, © University of Toronto Press, reproduced with permission)

TABLE 3.8 Classification of peat based on the modified von Post system (after Landva & Pheeney 1980, © NRC Press, reproduced with permission)

TABLE 3.9 Engineering-use chart for different soil groups (after Wagner 1957). Relative desirability ranges from one (most desirable) to 14 (least desirable). No entry means the soil should not be used for this application

TABLE 3.10 Hydraulic conductivity of soils, k

TABLE 3.11 Approximate values of K^* for sands for initial loading and unloading–reloading

TABLE 3.12 Approximate values of Poisson's ratio for soils

TABLE 3.13 Compressibility of soils (modified from Sowers & Sowers 1970)

TABLE 3.14 Values of $C_{\alpha e}/C_c$ for soils (after Terzaghi *et al.* 1996, *Soil Mechanics in Engineering Practice*, © John Wiley & Sons, Inc., New York, reproduced with permission)

TABLE 3.15 Classification of expansive soils on the basis of shrinkage index and expansion index (based on United States Bureau of Reclamation quoted in Ranganatham & Satyanatayana 1965, and after Anderson & Lade 1981, © ASTM, reproduced with permission)

TABLE 3.16 Values of constant μ used with Equation 3.32 to estimate cyclic shear modulus at low strains (after Hardin & Drnevich 1972)

TABLE 3.17 Values of constant K_2 used with Equation 3.33 to estimate cyclic shear modulus at low strains for sands (after Seed & Idriss 1970)

TABLE 4.1 Summary of geophysical methods: on land

TABLE 4.2 Summary of geophysical methods: offshore

TABLE 4.3 Classification of soil samples

TABLE 4.4 Summary of advantages and disadvantages of *in situ* testing

TABLE 4.5 Summary of applicability of common *in situ* and field tests

TABLE 4.6 Summary of advantages and limitations of some common *in situ* tests

TABLE 4.7 Summary evaluation for determining engineering soil parameters from *in situ* tests

TABLE 4.8 Summary of key reference sources for correlations of engineering properties and design parameters with *in situ* test results

TABLE 4.9 Summary of requirements of groundwater tracers

TABLE 5.1 Summary of some mathematical equations proposed for the soil–water characteristic curve

TABLE 5.2 Salt solutions that provide stable relative humidity environments

TABLE 6.1 Common rock-forming minerals (after Farmer 1968)

TABLE 6.2 Properties of common rock-forming minerals (after Farmer 1968)

TABLE 6.3 Geological classification of igneous rocks (modified from Bowen 1984)

TABLE 6.4 Sedimentary rock classification (after Farmer 1968)

TABLE 6.5 Metamorphic rock classification (after Farmer 1968)

TABLE 6.6 Engineering classification of rock by strength (adapted from ISRM 1978a; CGS 1992)

TABLE 6.7 Classification of rock with regard to RQD value

TABLE 6.8 Summary of method of obtaining the five independent parameters in anisotropic rocks

TABLE 6.9 Typical results of anisotropic elastic parameters for strong and weak rocks

TABLE 6.10 Effect of high horizontal stresses and time-dependent deformation

TABLE 6.11 Swelling potential of various types of rocks from free swell test

TABLE 6.12 Estimation of constants m_b/m_i, s, and a for the generalized Hoek–Brown failure criterion based upon rock-mass structure and discontinuity surface conditions. Note that the values given in this table are for an undisturbed rock mass (adapted from Hoek *et al.* 1995)

TABLE 6.13 Results of simple shear test on rock joints

TABLE 6.14 Calculation of secondary principal stresses from overcoring test data

TABLE 7.1 Primary functions provided by geosynthetics

TABLE 7.2 Typical range of properties for currently available geotextiles

TABLE 7.3 Selected values of geotextile reduction factors against creep deformation

TABLE 7.4 Flow rate ($m^3\ min^{-1}\ m^{-1}$) and reductions from index values, i.e. 10 kPa normal stress, (%)

TABLE 7.5 Recommended test method details for geomembranes and geomembrane seams in shear and in peel

TABLE 7.6 Range of reduction factors for use in Eq. 7.9

TABLE 7.7 Range of partial factors for use in Eq. 7.11

TABLE 7.8 Range of reduction factors for use in Eq. 7.13

TABLE 8.1 Groundwater analysis

TABLE 8.2 Approximate hydraulic conductivity of various soils (from U.S. Army 1983, Driscoll 1986, Cedergren 1989, Powers 1992)

TABLE 8.3 Typical dewatering systems

TABLE 8.4 Installation procedure: wellpoints, vacuum wells, suction wells, eductor wells, deep wells, horizontal drains (wells), vertical drains

TABLE 8.5 Selection of a filter pack

TABLE 9.1 Correction factors (adapted from Vesic 1973, 1975)

TABLE 9.2 Values of factors F_y, F_c, and F_q

TABLE 9.3 Allowable settlements and deflections (adapted from Polshin & Tokar 1957)

TABLE 10.1 Advantages and disadvantages of various pile types (adapted from Tchepak 1997)

TABLE 10.2 Interface friction angle, δ, for piles in sand (adapted from Stas & Kulhawy 1984)

TABLE 10.3 Horizontal stress coefficients (adapted from Stas & Kulhawy 1984)

TABLE 10.4 Limiting values of ultimate shaft and base resistance for piles in sand

TABLE 10.5 Ultimate shaft friction correlation factors for CPT tests (adapted from MELT 1993)

TABLE 10.6 Base capacity factors for CPT (adapted from MELT 1993)

TABLE 10.7 Base factor, K_b (adapted from Decourt 1995)

TABLE 10.8 Recommendations for pile group efficiency estimation

TABLE 10.9 Summary of some correlations for

drained Young's modulus for pile settlement analysis

TABLE 10.10 Homogeneous soil: summary of equations

TABLE 10.11 Elastic lateral response of piles

TABLE 10.12 Approximate solutions for elastic lateral response of long piles (adapted from Pender 1996)

TABLE 10.13 Solutions for elastic lateral response of piles (adapted from Poulos & Hull 1989)

TABLE 10.14 Empirical correlations for Young's modulus in clays (for laterally loaded piles)

TABLE 10.15 Empirical correlations for Young's modulus in sands (for laterally loaded piles)

TABLE 10.16 Summary of some computer programs for pile group analysis

TABLE 11.1 Bearing capacity failure modes in layered and jointed rock mass

TABLE 11.2 Correction factors for N_c and N_γ (adapted from Sowers 1979)

TABLE 11.3 Presumed allowable bearing pressure (adapted from the Canadian Foundation Engineering Manual—CGS 1992)

TABLE 11.4 Summary of field methods for determination of rock mass deformation modulus

TABLE 11.5 Empirical correlations for side shear resistance determination

TABLE 11.6 Stability criteria of concrete dam safety assessment

TABLE 11.7 Classification of concrete–rock contact

TABLE 11.8 Results of tests for basic friction angle, ϕ_b, at a number of Ontario dams

TABLE 11.9 Results of direct tension tests

TABLE 11.10 Results of stability study of Barrett Chute Dam

TABLE 11.11 Strength parameters of "equivalent" contacts (adapted from Lo *et al.* 1991a)

TABLE 12.1 Static stiffnesses of a disk resting on the surface of a homogeneous halfspace

TABLE 12.2 Equivalent radii for a rectangular footing having dimensions a and b

TABLE 12.3 Parameters of cone model footings resting on surface of soil halfspace

TABLE 12.4 Stiffness and damping constants for embedded footings

TABLE 12.5 Stiffness and damping parameters ($\beta = 0$)

TABLE 12.6 Stiffness and damping constants for single piles

TABLE 12.7 Stiffness and damping parameters of horizontal response ($L/R > 25$ for homogeneous soil and $L/R > 30$ for parabolic soil profile) (reproduced from Novak & El Sharnouby © 1983 with permission of ASCE)

TABLE 12.8 Maximum allowable amplitudes for hammer foundations

TABLE 13.1 Physical properties of granular base and subbase materials

TABLE 13.2 Typical gradation requirements for subbase and base (adapted from TAC 1997)

TABLE 13.3 Aircraft versus highway loads

TABLE 13.4 Typical pavement thicknesses (mm) used by Canadian provincial agencies for selected subgrade and traffic loading (traffic loading of 1×10^6 cumulative ESALs) TAC 1997.

TABLE 13.5 Catalog design thicknesses for Portland cement concrete pavements (adapted from MTO 1990)

TABLE 14.1 Suggested semi-quantitative probability scale for landslide hazard magnitude or intensity (adapted from Hungr 1997)

TABLE 14.2 Usual techniques and instruments used in warning systems

TABLE 15.1 Soil improvement methods (adapted from Munfakh 1997a and Holtz 1989)

TABLE 15.2 Lightweight fill materials (adapted from Magnan 1987)

TABLE 15.3 Types of vertical drains, common installation methods and typical geometric characteristics (adapted from Jamiolkowski *et al.* 1983)

TABLE 15.4 Procedures necessary to improve the reliability of predictions of the settlement and consolidation rates of vertical drain installations (adapted from Holtz *et al.* 1991)

TABLE 15.5 Thermal properties of soil (adapted from Mitchell 1993)

TABLE 15.6 Design parameters and common soil properties for electro-osmotic consolidation

TABLE 16.1 Strength properties reported for peats

TABLE 16.2 Approximate required geosynthetic force, T_{req} (kN m^{-1}) ($F^- = 1$) values for embankments on fibrous peat $B_m = 0.34$

TABLE 17.1 Classification scheme for earth retention systems (adapted from O'Rourke & Jones 1990)

TABLE 17.2 Partial factors used in the design of vertical walls and abutments (adapted from Jones 1996)

TABLE 17.3 Partial factors used in the design of reinforced slopes (adapted from Jones 1996)

TABLE 17.4 Comparison of drilled, grouted and driven nails: case histories (adapted from Bruce & Jewell 1987)

TABLE 18.1 Pipe stiffness categories and typical performance limits

TABLE 18.2 Pipe design standards

TABLE 18.3 Soil parameters for trench load analysis

TABLE 18.4 Design values of soil modulus in MPa (adapted from McGrath 1998)

TABLE 18.5 Pipe stiffness classes

TABLE 18.6 C values for a variety of pipes and two backfill moduli

TABLE 18.7 F values for a variety of pipes and two backfill moduli

TABLE 18.8 Design example I: 500-mm diameter reinforced concrete pipe

TABLE 18.9 Bedding factors and equivalent lateral earth pressures for use in direct design

TABLE 18.10 Design example II: 3-m diameter corrugated steel pipe

TABLE 18.11 Design example III: 300-mm diameter HDPE pipe

TABLE 18.12 Arching solutions for HDPE pipe example

TABLE 18.13 HDPE pipe results for bonded, smooth and frictional interface

TABLE 18.14 Flexible pipe design using Iowa deflection equation

TABLE 19.1 Summary of trenchless technology methods

TABLE 19.2 Shield tip resistance pressures, p_s

TABLE 19.3 Pipe–soil interface friction coefficients, tan δ

TABLE 20.1 Thermal properties of various materials

TABLE 20.2 Values of n-factors for different surfaces

TABLE 21.1 Comparison of site classification for attenuation models for shallow crustal events in active regions

TABLE 21.2 Smoothed coefficients used to estimate pseudo-acceleration response spectra (g) for the random horizontal component at 5% damping

TABLE 21.3 Site classification

TABLE 21.4 F_a as a function of site class and earthquake spectral acceleration, S_a, at 0.3 s

TABLE 21.5 F_v as a function of site class and spectral acceleration, S_a at 1 s period

TABLE 21.6 Values of G/G_o and V_s/V_{so}

TABLE 21.7 Summary of energy ratios for SPT procedures (adapted from Seed *et al.* 1985)

TABLE 21.8 Influence of earthquake magnitude on volumetric strain ratio for dry sands (adapted from Tokimatsu & Seed 1987)

TABLE 21.9 Usual minimum criteria for design earthquakes (adapted from CDSA 1995)

TABLE 21.10 Consequence classification of dams (adapted from CDSA 1995)

TABLE 22.1 Types of risk assessment frameworks

TABLE 22.2 Summary of environmental sampling strategies

TABLE 22.3 Examples of industries/activities and their contaminants

TABLE 22.4 Sources of toxicity information

TABLE 23.1 Characteristics and properties of common clay minerals

TABLE 23.2 Practical ranges of flow parameters for fine-grained soils

TABLE 23.3 Direct and coupled flows through soils

TABLE 24.1 Height of capillary rise in sediments (adapted from Fetter 1994)

TABLE 24.2 Range in values of total porosity and effective porosity

TABLE 24.3 Observed effective diffusion coefficients for chloride through a number of soils (adapted from Rowe *et al.* 1995b and Rowe & Weaver 1997)

TABLE 24.4 Effective diffusion coefficients for chloride in porous rock (adapted from Rowe *et al.* 1995b)

TABLE 24.5 Some published Henry's law, log K_{ow}, log K_{oc}, solubility and density values (adapted from Montgomery & Welkom 1989)

TABLE 24.6 Typical f_{oc} values of various sediments

TABLE 25.1 Relationship between average and maximum head on a liner below a drainage layer (adapted from Giroud & Houlihan 1995)

TABLE 25.2 Koerner & Koerner's (1995) recommended minimum values for geotextile filters for use with mild leachate and select waste over the geotextile

TABLE 25.3 Comparison of calculated values of hydraulic conductivity based on Eq. 25.17 and measured values for two Ontario landfills

TABLE 25.4 Recommended minimum testing frequencies: one test for each volume or area noted below (adapted from Daniel & Koerner 1995)

TABLE 25.5 Final bulk GCL void ratios obtained in confined swell tests (adapted from Rowe & Lake 1999)

TABLE 25.6 Basic characteristics of three thermal locked needle-punched GCLs tested

TABLE 25.7 Uptake of water by bentonite (interpreted from Daniel & Shan 1992)

TABLE 25.8 Effect of concentration of permeating NaCl solution and ethanol–water mix on hydraulic conductivity of a particular GCL product at 33–36 kPa

TABLE 25.9 Effect of permeating fluid on hydraulic conductivity of a particular GCL product at 35 kPa (adapted from Ruhl & Daniel 1997)

TABLE 25.10 Summary of results of permeability tests on partially saturated bentonite (adapted from Daniel *et al.* 1993)

TABLE 25.11 Chemical resistance guidelines for some commonly used geomembranes at 38 °C (adapted from Koerner 1998)

TABLE 25.12 Suggested limits of different test values for incubated geomembranes

TABLE 25.13 Range of effective diffusion coefficients for selected contaminants in low activity natural geologic barrier or compacted clay (porosity = 0.31–0.39)

TABLE 25.14 Some effective diffusion coefficients in soil–bentonite liners (22 °C)

TABLE 25.15 Diffusion coefficient in two GCLs as inferred by Lo (1992)

TABLE 25.16 Some published diffusion coefficients in air and water (adapted from Thibodeau 1996; Barone *et al.* 1992)

TABLE 25.17 Typical ranges of partitioning coefficient, S_{gf}, and diffusion coefficient, D_g, and permeability, P_g, for polyethylene geomembranes (see Rowe 1998a for full details and sources of data)

TABLE 25.18 Solubility and diffusion coefficient for water in three types of geomembrane (adapted from Eloy-Giorni *et al.* 1996)

TABLE 25.19 Calculated time for antioxidant depletion based on test data by Hsuan and Koerner (1995) (see Rowe (1998a) for details)

TABLE 25.20 Effect of temperature on diffusion coefficient, D_T, hydraulic conductivity, k_T, in a liner at temperature, T, relative to values at 10 °C (adapted from Rowe 1998a)

TABLE 26.1 Typical hydraulic gradients (critical applications may require designing for higher gradients than those given; adapted from Giroud (1988, 1996) and Luettich *et al.* (1992))

TABLE 26.2 Giroud's retention criterion for geotextile filters (adapted from Giroud 1982, 1988, 1994)

TABLE 26.3 Maximum value, $k_{UM\ max}$ (m s^{-1}), of the hydraulic conductivity of the medium underlying the geomembrane for Eqs 26.37–26.47 to be valid with an acceptable approximation in the case where C_{qo} = 0.21 (good contact) and t_{UM} = 0.6 m (adapted from Giroud *et al.* 1997c)

TABLE 26.4 Minimum value, $k_{UM\ min}$ (m s^{-1}), of the hydraulic conductivity of the medium underlying the geomembrane for Eq. 26.51 (i.e. Bernoulli's

equation for free flow through an orifice) to be valid with an acceptable approximation (adapted from Giroud *et al.* 1997c)

TABLE 26.5 Corresponding values of relative deflection, y/b or y/d, geosynthetic strain, ε, and dimensionless parameter Ω (adapted from Giroud *et al.* 1990)

TABLE 26.6 Typical density, thickness and mass per unit area for geomembranes, and relationship between mass per unit area and threshold wind velocity (adapted from Giroud *et al.* 1995c)

TABLE 26.7 Values of the geomembrane normalized tension, $T/(S_e L)$, as a function of the geomembrane strain, ϵ, the relative uplift, u/L, and the uplift angle, θ (adapted from Giroud *et al.* 1995c)

TABLE 27.1 Comparison of some public-domain water balance models

TABLE 27.2 Run-off coefficients (adapted from Fenn *et al.* 1975) suggested by Koerner & Daniel (1997) for simplified manual water balance calculations

TABLE 27.3 Percolation rates through final cover systems with barriers incorporating geomembranes estimated using the HELP model (adapted from Gross *et al.* 1997)

TABLE 27.4 Interfaces upon which cover system components have undergone sliding

TABLE 27.5 Summary of advantages and disadvantages associated with test devices for measuring interface shear strength (adapted from Gilbert *et al.* 1995)

TABLE 27.6 Engineering measures to increase cover system slope stability factor of safety

TABLE 27.7 Deaggregated peak horizontal bedrock accelerations as a percentage of the aggregated peak probabilistic acceleration of 0.328 *g* for Evansville, Indiana, for a 2% probability of exceedence in 50 years (adapted from USGS Web site)

TABLE 27.8 Earthquake parameters, corresponding peak horizontal bedrock acceleration estimates and peak horizontal accelerations recorded on the top of the Operating Industries Inc. (OII) landfill, California (adapted from Matasovic *et al.* 1998)

TABLE 27.9 Ratio of yield acceleration, k_y, to peak acceleration of cover system as a function of calculated permanent seismic displacement (adapted from Hynes & Franklin (1984) curves, shown in Figure 27.23)

TABLE 27.10 Results of parameter study of calculated post-closure secondary settlements, ($s_{\Delta t}$), as a percentage of initial landfill height, H_1

TABLE 28.1 Purging/sampling equipment usability

TABLE 28.2 Features contributing to the variability in groundwater quality measurements

TABLE 28.3 Examples of sources of error in groundwater monitoring data

TABLE 28.4 Outcomes and errors in statistical testing

TABLE 28.5 Contaminant exposure pathways by medium

TABLE 29.1 Description and characteristics of common low permeability barrier technologies

TABLE 30.1 Advantages and disadvantages of various potential soil clean-up goals

TABLE 30.2 Remedial technology evaluation criteria

TABLE 30.3 Typical contaminant types

TABLE 30.4 Soil treatment technologies generally applicable to compound groups

TABLE 30.5 Types of physical barriers

CONTRIBUTING AUTHORS

Dr S. L. Barbour
Department of Civil Engineering
University of Saskatchewan
57 Campus Drive
Saskatoon
Saskatchewan, Canada S7N 5A9
TEL: 306-966-5369
FAX: 306-966-5427
e-mail: S_L_Barbour@engr.usask.ca

Dr R. J. Bathurst
Department of Civil Engineering
Royal Military College of Canada
Kingston, Ontario, Canada K7K 7B4
TEL: 613-541-6000 x6479
FAX: 613-545-8336
e-mail: bathurst-r@rmc.ca

Dr D. Becker
Golder Associates Ltd
2180 Meadowvale Boulevard
Mississauga, Ontario, Canada L5N 5S3
TEL: 905-567-4444
FAX: 905-567-6561
e-mail: dbecker@golder.com

Dr D. T. Bergado
School of Civil Engineering
Asian Institute of Technology
P.O. Box 4
Klong Luang, Pathumthani, Thailand
TEL: 66-2-516-0110
FAX: 66-2-524-6050
e-mail: bergado@ait.ac.th

Dr D. Blowes
Department of Earth Sciences
University of Waterloo
Waterloo, Ontario, Canada N2L 3G1
TEL: 519-888-4878
FAX: 519-746-3882
e-mail: blowes@sciborg.uwaterloo.ca

Dr R. Bonaparte
GeoSyntec Consultants
1100 Lake Hearn Drive N.E.
Atlanta, Georgia 30342-1523 USA
TEL: 404-705-9500
FAX: 404-705-9400
e-mail: rbonaparte@geosyntec.com

Dr J. A. Cherry
Department of Earth Sciences
University of Waterloo
Waterloo, Ontario, Canada N2L 3G1
TEL: 519-888-4516
FAX: 519-883-0220
e-mail: cherryja@sciborg.uwaterloo.ca

Dr D. DuBois
Golder Associates Ltd
2180 Meadowvale Boulevard
Mississauga, Ontario, Canada L5N 5S3
TEL: 905-567-4444
FAX: 905-567-6561
e-mail: DDuBois@golder.com

Mr W. Dyck
Conestoga-Rovers & Associates Ltd
651 Colby Drive
Waterloo, Ontario, Canada N2V 1C2
TEL: 519-725-3313
FAX: 519-725-1394
e-mail: wdyck@craworld.com

Dr M. H. El Naggar
Department of Civil & Environmental Engineering
University of Western Ontario
London, Ontario, Canada N6A 5B9
TEL: 519-661-4219
FAX: 519-661-3942
e-mail: naggar@uwo.ca

R. M. Faure
Etudes et recherches en Gènie Civil

Centre d'Etude des Tunnels
25 Av. F. Mitterrand
69500 Bron, France
TEL: 33-472-143481
FAX: 33-472-143490
e-mail: rene-michel.faure@cetu.equipement.gouv.fr

Dr W. D. L. Finn
Anabuki Chair of Foundation Geodynamics
Kagawa University
2217-20 Shinmachi
Hayashi-cho
Takamatsu City
761-0396 Japan
TEL: 81-87-864-2170
FAX: 81-87-864-2031
e-mail: finn@eng.kagawa-u.ac.jp

Mr G. Ford
Presidio Trust
P.O. Box 29052
San Francisco, CA 94129-0052 USA
TEL: 415-561-4292
FAX: 415-561-4180
e-mail: gford@presidiotrust.gov

Dr D. G. Fredlund
Department of Civil Engineering
University of Saskatchewan
57 Campus Drive
Saskatoon
Saskatchewan, Canada S7N 5A9
TEL: 306-966-5342
FAX: 306-966-5427
e-mail: Del.Fredlund@skyfox.usask.ca

Dr R. Gillham
Department of Earth Sciences
University of Waterloo
Waterloo, Ontario, Canada N2L 3G1
TEL: 519-888-4658
FAX: 519-746-1829
e-mail: rwgillha@sciborg.uwaterloo.ca

Dr J.-P. Giroud
GeoSyntec Consultants
621 N.W. 53rd St., Suite 650
Boca Raton, FL 33487 USA
TEL: 561-995-0900 x213
FAX: 561-995-0925
e-mail: jpgiroud@geosyntec.com

Dr Ralph Haas
Department of Civil Engineering
University of Waterloo
Waterloo, Ontario, Canada N2L 3G1
TEL: 888-4567 x2176
FAX: 519-888-6197
e-mail: haas@uwaterloo.ca

Dr A. M. Hefny
School of Civil & Structural Engineering
Division of Geotechnics & Surveying
Nanyang Technological University
Nanyang, Singapore 639798
TEL: 65-790-6936
FAX: 65-792-1650
e-mail: camhefny@ntu.edu.sg

Dr R. D. Holtz
Department of Civil & Environmental Engineering
University of Washington
Wilcox Hall 260, Box 352700
Seattle, WA 98195-2700 USA
TEL: 206-543-7614
FAX: 206-685-3836
e-mail: holtz@u.washington.edu

Dr Y. G. Hsuan
Geosynthetics Institute
475 Kedron Avenue
Folsom, PA 19033-1208 USA
TEL: 610-522-8440
FAX: 610-522-8441
e-mail: ghsuan@coe.drexel.edu

Dr C. J. F. P. Jones
Department of Civil Engineering
The University
Newcastle Upon Tyne NE1 7RU UK
TEL: 44-191-222-7117
FAX: 44-191-222-6613
e-mail: c.j.f.p.jones@newcastle.ac.uk

Dr R. M. Koerner
Geosynthetics Institute
475 Kedron Avenue
Folsom, PA 19033-1208 USA
TEL: 610-522-8440
FAX: 610-522-8441
e-mail: Robert.Koerner@cbis.ece.drexel.edu

Dr J.-M. Konrad
Département de génie civil
Fac. des Sciences et de Génie
Université Laval
Sainte-Foy, Quebec, Canada G1K 7P4
TEL: 418-656-2131 x3878
FAX: 418-656-2928
e-mail: Jean-Marie.Konrad@gci.ulaval.ca

Dr P. V. Lade
Department of Civil Engineering
Aalborg University
Sohngaardsholmsvej 57
9000 Aalborg
Denmark
TEL: 45-96-358452
FAX: 45-98-142555
e-mail: Lade@civil.auc.dk

Dr S. Leroueil
Département de Génie civil
Université Laval
Ste-Foy, Qué, Canada G1K 7P4
TEL: 418-656-2601
FAX: 418-656-2928
e-mail: Serge.Leroueil@gci.ulaval.ca

Dr K. Y. Lo
Department of Civil & Environmental Engineering
University of Western Ontario
London, Ontario, Canada N6A 5B9
TEL: 519-661-2125
FAX: 519-661-3942
e-mail: jlemon@eng.uwo.ca

Dr Jacques Locat
Département de Géologie et génie géologique
Université Laval
Ste-Foy, Québec, Canada G1K 7P4
TEL: 418-656-2179
FAX: 418-656-7339
e-mail: Jacques.Locat@ggl.ulaval.ca

Mr R. Loughney
Loughney Associates, Inc.
25 Arrow Point Road
New Preston, CT 06777 USA
TEL: 860-868-9995
FAX: 860-868-1025
e-mail: richard.loughney@snet.net

Dr P. Lucia
GeoSyntec Consultants
1500 Newell Avenue, Suite 800
Walnut Creek, CA 94596 USA
TEL: 925-943-3034
FAX: 925-943-2366

Dr E. McBean
Conestoga-Rovers & Associates Ltd
651 Colby Drive
Waterloo, Ontario, Canada N2V 1C2
TEL: 519-725-3313
FAX: 519-725-1736
e-mail: emcbean@craworld.com

Dr G. Milligan
Geotechnical Consulting Group
9 Lathbury Road
Oxford OX2 7AT UK
FAX: 44-1865-516407
e-mail: g.w.e.milligan@gcg.co.uk

Dr J. K. Mitchell
Via Department of Civil & Environmental Engineering
Virginia Tech
Blacksburg, VA 24061-0105 USA
TEL: 540-231-7351
FAX: 540-231-7532
e-mail: jkm@vt.edu

Dr I. D. Moore
Department of Civil & Environmental Engineering
University of Western Ontario
London, Ontario, Canada N6A 5B9
TEL: 519-661-3997
FAX: 519-661-3942
e-mail: ian@hazzstanl.engga.uwo.ca

Mr Luciano Picarelli
Seconda Università di Napoli
Dipartimento di Ingegneria Civile
Via Roma 21
80125 Aversa, Italy
TEL: 39-81-5010213
FAX: 39-81-5037370
e-mail: picarell@cds.unina.it

Dr H. G. Poulos
Coffey Geosciences Pty. Ltd
142 Wicks Road

North Ryde, NSW 2113 Australia
TEL: 61-2-9888-7444
FAX: 61-2-9888-9977
e-mail: harry_poulos@coffey.com.au

Mr B. L. Rodway
Bruce Rodway and Associates Pty. Ltd
4/15 Mosman Street
Mosman 2088, Australia
TEL: 61-2-9969-6295
FAX: 61-2-9969-6295
e-mail: bruce.rodway@big pond.com

Dr C. D. F. Rogers
School of Civil Engineering
University of Birmingham
Edgbaston
Birmingham B15 2TT UK
TEL: 44-121-414-5066
FAX: 44-121-414-3675
e-mail: c.d.f.rogers@bham.ac.uk

Mr F. Rovers
Conestoga-Rovers & Associates Ltd
651 Colby Drive
Waterloo, Ontario, Canada N2V 1C2
TEL: 519-884-0510
FAX: 519-725-1158

Dr R. K. Rowe
Vice-Principal (Research)
Queen's University
Kingston, Ontario, K7L 3N6
TEL: 613-533-3113
FAX: 613-533-2128
e-mail: kerry@civil.queensu.ca

Dr R. A. Schincariol
Department of Earth Sciences
The University of Western Ontario
London, Ontario, Canada N6A 5B7
TEL: 519-661-3732
FAX: 519-661-3198
e-mail: schincar@julian.uwo.ca

Dr K. Schmidtke
Conestoga-Rovers & Associates Ltd
651 Colby Drive
Waterloo, Ontario, Canada N2V 1C2
TEL: 519-884-0510
FAX: 519-884-0111

Dr Gilles Sève
CETE Mediterraneé
Laboratoire de Nice
56 Bd. Stalingrad
F-06300 Nice
France
TEL: 33-4-92-00-8182
FAX: 33-4-92-00-8199
e-mail: gilles.seve@equipement.gouv.fr

Dr J. Q. Shang
Department of Civil & Environmental Engineering
University of Western Ontario
London, Ontario, Canada N6A 5B9
TEL: 519-661-4218
FAX: 519-661-3942
e-mail: jshang@uwo.ca

Dr J. C. Small
School of Civil Engineering
The University of Sydney
Sydney 2006, NSW Australia
TEL: 61-2-9351-2128
FAX: 61-2-9351-3343
e-mail: j.small@civil.usyd.edu.au

Mr D. Smyth
Department of Earth Sciences
University of Waterloo
Waterloo, Ontario, Canada N2L 3G1
TEL: 519-888-4567 (Ext. 2899)
FAX: 519-746-3882
e-mail: dsmyth@sciborg.uwaterloo.ca

Mr J. Sprenger
GE Canada
2300 Meadowvale Blvd.
Mississauga, Ontario, Canada L5N 5P9
TEL: 905-858-5708
FAX: 905-858-5276
e-mail: james.sprenger@corporate.ge.com

Mr H. A. Tuchfeld
GeoSyntec Consultants
1500 Newell Avenue, Suite 800
Walnut Creek, CA 94596 USA
TEL: 925-943-3034
FAX: 925-943-2366
e-mail: HalT@geosyntec.com

Dr M. Whittaker
Consultant
161 Westminster Avenue
Toronto, Ontario, Canada M6R 1N8
FAX: 905-707-9084
e-mail: mwhittaker@home.com

Dr G. W. Wilson
Department of Mining and Mineral Processing
The University of British Columbia
Forward Building
517-6350 Stores Rd.
Vancouver, BC Canada V6T 1Z4
TEL: 604-822-6781
FAX: 604-822-5599
e-mail: gww@mining.ubc.ca

Dr E. K. Yanful
Department of Civil & Environmental Engineering
University of Western Ontario
London, Ontario, Canada N6A 5B9
TEL: 519-661-4069
FAX: 519-661-3942
e-mail: eyanful@eng.uwo.ca

PREFACE

This handbook aims to discuss, in one volume, a wide array of topics that have entered the mainstream of geopractice (i.e. geotechnical and geoenvironmental engineering) over the past two decades, while at the same time not losing sight of the more conventional aspects of the discipline that remain a core part of the work of geoprofessionals. These topics range from conventional saturated soil mechanics, to unsaturated soil behavior, rock mechanics, hydrogeology and geosynthetics. The book deals with pavements, shallow and deep foundations, embankments, slopes, retaining walls, buried structures, dynamics and earthquakes, risk assessment and management, contaminant transport, groundwater monitoring, and containment, treatment and remediation of contaminated sites.

The 50 contributors to the 30 chapters of the book are all recognized experts in their field—from industry and the academic world. Each chapter was edited and, in order to keep this handbook as one volume, many were reduced to half their original length. Each chapter has been reviewed by at least two experts in the field. Many of these reviewers were contributors to other chapters and are listed in the accompanying list of contributors. In addition, I would like to thank the following individuals who also served as reviewers of one or more chapters: Dr F. S. Barone, Dr S. F. Brown, Dr J. P. Carter, Mr J. M. A. Costa, Dr R. D. Holtz, Dr H. P. Hong, Dr F. Kulhawy, Dr B. Ladanyi, Mr C. Lake, Dr J. Mlynarek, Dr B. Ruth, Dr F. W. Schwartz, Mr G. Skinner, Dr D. Smith, Mr J. Thompson and Dr P. Ullidtz.

Notwithstanding the effort that was made to ensure that each chapter is as correct as practicable, there is little doubt that some errors (typographical or otherwise) will creep into a document of this size, especially in its first printing. Readers are requested to advise the undersigned of any errors (typographical or otherwise) or significant omissions they identify—to the extent possible they will be corrected in subsequent printings.

I am indebted to the numerous contributors to this book who have labored, in their "spare time" to produce a manuscript, respond to editorial and reviewer comments, and helped provide what I hope will be useful contributions to the profession.

Finally, I owe a deep debt of gratitude to my family (Kathy, Katrina, Kieron and Kendall) for their patience and understanding over the past four years as this book has taken shape; to the families of all the authors who will have contributed in a similar fashion to the compilation of each chapter; and to the typists and draftspeople who have assisted in the preparation of the manuscript—especially to Joanne Lemon and Kathy Rowe who have been an invaluable help in getting this book to the publisher.

R. Kerry Rowe
Department of Civil Engineering
Queen's University
Kingston, Ontario, Canada, K7L 3N6
kerry@civil.queensu.ca

I. BASIC BEHAVIOR AND SITE CHARACTERIZATION

1. INTRODUCTION

R. K. Rowe

1.1 Geotechnical and Geoenvironmental Engineering

The work of the geoprofessional has evolved and expanded enormously over the past two decades. The breadth of the discipline is reflected by the number of related international societies (e.g. International Society for Rock Mechanics, International Geosynthetics Society, International Tunnelling Association, International Association for Computer Methods and Advances in Geomechanics, International Association of Hydrogeologists, International Association of Engineering Geology and the Environment to name but a few) and even in the change of name for the International Society for Soil Mechanics and Foundation Engineering to the International Society for Soil Mechanics and Geotechnical Engineering. In particular, geotechnical practice has expanded far beyond the traditional areas of soil mechanics and foundation engineering to include what is now commonly referred to as "geoenvironmental engineering."

While the basic concepts of soil mechanics have not changed significantly in this period (see Chapters 2 and 3), many new concepts have been introduced. There is now a much wider range of field investigation techniques being used in practice (see Chapter 4), and unsaturated soil mechanics (Chapter 5) has been recognized as important to a wide range of both geotechnical and geoenvironmental projects. There have also been advances in the understanding of rock behavior (Chapter 6) and in the use of geosynthetics to aid in the design and construction of a wide range of geotechnical and geoenvironmental engineering projects (Chapter 7).

The past two decades have seen increased interest in the application of limit state design (LSD) consideration in geotechnical engineering and although LSD is far from universally accepted and applied, this trend to increased use of LSD is likely to continue. This handbook includes some discussion of both conventional and limit state approaches as they are presently applied—likely any subsequent edition of this book will see even more emphasis on LSD. Also, there has been a growing interest in risk assessment and risk-based management in geoenvironmental applications and, indeed, across the full spectrum of engineering where the behavior of a "geotechnical structure" may be influenced by extreme events (e.g. as related to natural hazards such as earthquakes, severe rainfall events and floods, hurricanes, tornadoes, ice storms, etc.). This interest already permeates many chapters of the book, but will likely have an even greater influence on later editions.

1.2 Objectives and Organization of the Book

This book is intended as a handbook with two audiences. The first audience will be individuals requiring an introduction to a given topic. These individuals will be seeking an explanation of the basic concepts and method-

R. K. Rowe (ed.), *Geotechnical and Geoenvironmental Engineering Handbook*
© Kluwer Academic Publishers 2001

ologies, and references to more information. The second audience will be practitioners and researchers already knowledgeable in the field but seeking a quick reference to refresh their memory and guidance to other places to look for more information.

Recognizing that very few people will read this book cover to cover, the various chapters of the book have been extensively cross-referenced to assist the reader who opens the book at the section most relevant to their current needs in finding other relevant material in this book. All references are collected together at the end of the book.

This book serves to complement a number of other excellent handbooks available to the geotechnical engineer—especially the *Foundation Engineering Handbook* (Fang 1991) and the *Tunnel Engineering Handbook* (Bickel *et al.* 1996). Although there will be some unavoidable overlap, this handbook seeks to provide a much broader range of coverage than these other handbooks. The desire to cover the field of geotechnical and geoenvironmental engineering in the 30 chapters of one handbook is ambitious. Necessarily, the coverage that can be presented in any chapter is limited—in many cases entire books have been devoted to the subject matter of a given chapter (often authored or co-authored by one or more of the chapter authors). However, it is hoped that each chapter presents the essential information and will direct the reader to other relevant literature.

The material is organized into five groupings of chapters. The first group provides basic information that may be useful in many practical applications in its own right but also provides the reader not knowledgeable in these areas with the background information needed to get the most out of subsequent chapters. These chapters include a basic introduction to soil mechanics (Chapter 2) and typical geotechnical parameters and correlations (Chapter 3). Field investigations for both geotechnical and geoenvironmental applications are covered in Chapter 4. This is followed by an extensive introduction to unsaturated soil mechanics (Chapter 5). Basic rock mechanics is examined in Chapter 6, and Chapter 7 provides an introduction to geosynthetics. Finally, Chapter 8 provides a practical guide to the art of dewatering.

The second group of chapters deals with foundation and pavement issues including shallow and deep foundations in soil (Chapters 9 and 10) and rock (Chapter 11) and the dynamics of foundations (Chapter 12). Chapter 13 examines pavement design for both road and airport pavements.

The third group of chapters addresses the issues of slope, embankment and wall stability and soil improvement. Chapter 14 provides a basic examination of the stability of slopes. Chapter 15 provides insight regarding means of soil improvement that may be required when the existing soil is not adequate to satisfy either serviceability or stability requirements. One of these techniques, soil reinforcement, is examined in more detail in Chapters 16 and 17 as part of a more general examination of embankments on soft soils (Chapter 16) and retaining walls and reinforced slopes (Chapter 17).

The fourth group of chapters deals with "special topics" in geotechnical engineering that may also be relevant to environmental geotechnics. For example, buried pipes and culverts (Chapter 18) have both conventional geotechnical applications (e.g. to transmit water through embankments) and geoenvironmental applications (e.g. in landfill leachate collection pipes). Likewise trenchless technology (Chapter 19), cold region (Chapter 20) and earthquake engineering (Chapter 21) all have applications and implications related to both conventional geotechnical engineering and environmental geotechnics.

The last group of chapters provides the reader with information regarding a number of key aspects of geoenvironmental engi-

neering. Given the important role for risk assessment and risk management, this group of chapters begins with a discussion of these issues (Chapter 22). This is followed by two chapters dealing with fundamental issues of direct relevance to environmental geotechnics and geoenvironmental engineering, namely the physicochemical behavior of soils (Chapter 23) and hydrogeology (Chapter 24). One key aspect of geoenvironmental engineering is the design of containment systems for solid-, hazardous- and mine-waste facilities, liquid-containment facilities and containment as a remediation solution for contaminated sites. This is addressed by three related chapters dealing with barrier systems and covers. Chapter 25 discusses issues such as controlling gradients, leachate collection, low permeability liners and contaminant transport through barrier systems. Chapter 26 looks at geosynthetics in liquid-containment structures (landfills, ponds, lagoons, dams, etc.). This chapter elaborates on some of the issues raised in Chapter 25. Chapter 27 discusses the design of cover systems that will control both fluid (e.g. water) and gas flow (e.g. oxygen into sulphidic mine waste or carbon dioxide and methane out of municipal solid-waste landfills). Chapter 28 provides a statistically based examination of groundwater monitoring that is relevant to monitoring waste containment sites, remediated sites and any other situations where there is concern or potential for groundwater contamination. Finally, Chapters 29 and 30 address the issue of dealing with the management of contaminated groundwater and contaminated soil.

The book seeks to provide essential concepts and details related to many aspects of modern geotechnical and geoenvironmental engineering. However, no book such as this can ever be complete. Major topics such as tunneling, dams, offshore engineering, etc. receive little more than a mention. Even when a topic has a whole chapter devoted to it, this is still only a first step toward providing the reader with access to the wealth of information available in the literature. In selecting references, chapter authors have focused on providing carefully selected key references rather than a vast array of references that can be identified with a library search. It is hoped that this book will serve as a useful tool to both practitioners and students in their engineering projects and research.

1.3 Limitations

This handbook represents a collection of related and edited contributions from across the spectrum of geotechnical and geoenvironmental engineering. However, a handbook is no more than a guide—a starting point. It should not be used as a substitute for the judgment of knowledgeable engineers. Neither the editor, the chapter authors, the reviewers nor the publisher assume any liability for application or misapplication of any statement, figure, table, equation or any other material in this book to a project of any nature, nor do they warrant or guarantee the "correctness" of any statement, figure, table, equation or opinions, or the suitability of any suggested procedures or practice to any specific situation. Geotechnical and geoenvironmental engineering is exciting because every project is different and only a suitably qualified and experienced professional can judge what is the appropriate solution to any problem. The handbook is one of many tools they may use in reaching the solutions but it does not attempt to provide the solution to any specific problems.

2. BASIC SOIL MECHANICS

P. V. Lade

2.1 *Introduction*

The two major technical design considerations in geotechnical engineering are to: (1) avoid catastrophic failure, and (2) avoid excessive deformations (settlements, heave or lateral deformations). In the context of limit state design these are referred to as the ultimate and serviceability limit states, respectively. To perform the design, it is necessary to: (1) calculate the loads from the structure that need transmission into the ground; (2) obtain the behavior characteristics of the soils including, but not limited to, the stress–strain and strength behavior in order to perform the necessary analyses and detailed calculations; and (3) compare the stresses created in the ground by the structure with (a) the available shear strength to evaluate proximity to failure conditions, and with (b) the stress–strain behavior to evaluate deformations. Local building codes may place additional requirements on the design and construction procedures.

These considerations are fundamentally the same for all aspects of design and construction of civil engineering projects. However, soils are different from other engineering materials. Most notably, soils are often non-homogeneous and anisotropic, they cannot sustain tension, and most aspects of their mechanical behavior are non-linear in nature. It is often not possible or economical to obtain all the information desirable for analyses and design, and the analyses performed in geotechnical engineering are simplified relative to the real behavior of the structure in the field. Therefore, engineering judgment as well as local experience are usually required.

This chapter provides a review of basic soil mechanics. As with all other chapters in this handbook, it is intended as a reference and the reader will need to refer to basic textbooks on soil mechanics for detailed explanations, arguments and derivations (e.g. Lambe & Whitman 1979; Holtz & Kovacs 1981; Terzaghi *et al.* 1996; Craig 1997; Powrie 1997).

2.2 *Soil Types: Geologic Formation and Classification*

Two fundamental pieces of information regarding the geology in the field are required for the purpose of design in geotechnical engineering: (1) the geometric arrangement of the soil layers, and (2) the properties of the soils. The geologic origin of natural soil deposits provides important information regarding these two topics, and soils of the same origin have many properties in common. More details may be found in basic textbooks (e.g. Legget 1962; Legget & Hatheway 1988; Costa & Baker 1981; Einsele 1992; Tarbuck & Lutgens 1996).

2.2.1 BASIC ELEMENTS, SOIL FORMING MINERALS AND TYPES OF ROCK

The soil and rock found in the Earth's crust (upper 5–40 km) consist of (by weight): 46.7% oxygen (O), 27.7% silicon (Si), 8.1%

R. K. Rowe (ed.), *Geotechnical and Geoenvironmental Engineering Handbook*
© Kluwer Academic Publishers 2001

TABLE 2.1. Great rock groups

Rock group	Formed by	Examples
Igneous	Cooling and solidification of magma	Granite, basalt
Sedimentary	Weathered rock and soils solidify by cementation, and deposition of dissolved minerals	Conglomerate, sandstone, siltstone, shale, limestone
Metamorphic	Temperature and/or pressure	Quartzite (from sandstone and conglomerate), slate (from shale), marble (from limestone)

aluminum (Al), 16.1% Fe, Ca, Na, K, Mg, and 1.4% others.

The common soil-forming minerals are: quartz (SiO_2) found in silica sands, alumina (Al_2O_3) found in clays, calcite ($CaCO_3$) found in limestone, and cementing agents such as soda (NaO), magnesia (MgO) and others (e.g. FeO).

Soils are formed from weathering of rocks, and the type of soil and its properties depend on the rock from which it originated. Rocks can be divided into three groups as indicated in Table 2.1.

2.2.2 THE GEOLOGIC CYCLE, SOIL FORMING PROCESSES AND TYPES OF SOIL

All types of rock break down to form soils. The geologic processes and their products may be classified by the geologic cycle. Starting with the rock, weathering processes (I) create residual soils (II), which by transportation processes (III) form transported soils (IV), which through rock-formation processes (as reviewed above) form rock again. Each of the two processes (I and III) and two types of soils (II and IV) are useful in reviewing and understanding the most common soil types and formations:

I. Weathering may be either mechanical or chemical. Mechanical weathering forms large particles such as gravel, sand and silt. The types of processes include:

- crystal growth — ice and salt crystals form and grow in joints and fissures in rock
- temperature changes — create stress gradients due to directional and different coefficients of expansion for different minerals
- unloading — causes vertical stress relief, expansion and fracture
- tree roots — grow in cracks in rock
- erosion — due to water, ice and wind

Chemical weathering forms small particles such as clay and dissolves minerals in water. The types of chemical processes include hydration, hydrolysis (feldspar reacts with water to form clay), carbonation, oxidation and solution (dissolution of minerals in groundwater, to be deposited elsewhere). Quartz is a stable mineral that breaks down mainly by mechanical weathering, while feldspar is a relatively unstable mineral that also weathers chemically to form clay particles.

II. Residual soils are weathered, but they have not been transported. The weathering processes form various types of residual soils whose properties depend on: (1) the parent rock (i.e. the type of rock from which they are formed), and (2) the climate in which they are formed (especially the humidity and

temperature). All residual soils have a common characteristic, i.e. their thickness and geometry vary greatly over short distances. This creates many problems in field investigations, determination of the geologic profile (e.g. depth to bedrock) and in construction.

III. Transporting agents include: (1) water, (2) ice and (3) wind. Gravity plays a role in connection with all of these means of transportation, but gravity may also act as a separate transporting agent (e.g. rock slides).

IV. The transported soils are reviewed in relation to the agent that conducted the transportation. Water transportation produces:

- *alluvial deposits* (i.e. stream deposits), which are characterized by mixed, but distinct layers of soil from gravel to clay, created by meandering rivers. Each layer tends to contain uniform grain sizes, and they form lenses with one grain size interspersed in layers of other grain sizes (layers or lenses with coarse grains may be on top of finer grained soil, and vice versa).
- *lacustrine deposits* (i.e. lake deposits), which are characterized by sequential deposition away from the source (e.g. river running into lake) as the slowing water progressively loses its capacity to carry the soil particles. Deposition occurs in the sequence of gravel, sand, silt and clay. In fresh water the clay structure tends to be dispersed (i.e. essentially parallel particle structure). Varved clay may form in quiet water away from the source, with alternating fine layers of clay and silt and fine sand.
- *marine deposits*, which typically involve deposition of fine particles (mainly clay) in salt water. Clay particles are flat and so small that surface forces dominate their behavior. As a river with fresh water and suspended clay particles meets salt water on arrival at the ocean, the clay particles flocculate: As cations, mostly Na^+, but also Ca^{2+} and Mg^{2+}, become attached to the negatively charged surfaces of the clay particles, there is an attraction between the edges and faces of different particles that then form edge-to-face structures. These are characterized by voids full of water. If this structural arrangement is disturbed, it loses much of its strength. This strength loss may be characterized by the sensitivity of the clay.

Glacial (ice) transportation produces:

- glacio-fluvial deposits that are similar to other stream deposits
- glacio-lacustrine deposits that are similar to other lake deposits
- moraine or till, which are created by the action of the glacier. They consist of a variety of particle sizes from clay to boulders created by mechanical (erosion) and chemical weathering and deposited by the glacier. Depending on the location of the till (in front, along the side, or under the glacier), it may be normally consolidated or heavily overconsolidated (due to the overburden pressure of very great magnitudes of glaciers during the ice ages). Because of the large variety of grain sizes and the well-graded grain size curves, till often constitutes a very good construction material for foundations and soil structures.

Wind transportation produces aeolean or wind-blown deposits:

- Sand dunes are characterized by having grain sizes in a very narrow range. Sand dunes move continually, and they move by grains rolling up and spilling over on the back side.
- Loess is composed of silt-size particles that have precipitated in a humid environment, creating rather loose honeycomb grain structures that may collapse upon water inundation. Loess deposits are often characterized by very steep slopes.

2.2.3 SOIL FABRIC AND STRUCTURE

The effects of fabric and structure are as important as the initial void ratio and stress history for understanding the behavior of soils. All types of soils exhibit effects of their initial structure.

2.2.3.1 Clay Fabric

Most naturally occurring deposits of clay are formed in water. In the presence of positively charged cations, as in marine environments, the fabric of the deposit will be flocculated. These edge-to-face structures are characterized by initially random particle orientation and relatively open voids. With consolidation due to further accumulation of overburden soil, the clay particles tend toward more horizontal orientations. In geologic time the cations may be removed from the fabric (e.g. by leaching with fresh water) and it becomes metastable (i.e. even small disturbances may cause the structure to lose strength and collapse, see Bjerrum & Rosenqvist 1956). The degree to which strength (see Section 2.9) is lost may be indicated by the sensitivity, defined as the undrained, intact strength divided by the remolded strength. Examples of extremely metastable clay deposits with sensitivities in the order of 500 are provided by quick clays occurring in Quebec, Norway and Sweden.

Clay deposits formed in the absence of cations, as in rivers and fresh-water lakes, tend to be dispersed (i.e. they have a particle fabric which tends more toward essentially parallel, horizontally oriented particles). The void ratio (see Section 2.3) of a dispersed clay tends to be lower than that of a flocculated clay at the same effective, normal stress (see Section 2.6).

Compaction of clay soils produces an initial fabric that depends on the compaction water content relative to the optimum water content (see Chapter 13, Lambe 1958; Seed *et al.* 1960). For compaction water contents lower than (i.e. on the dry side of) optimum, a flocculated structure is produced. On the other hand, water contents higher than (i.e. on the wet side of) optimum, enable larger shear strains and produce parallel or dispersed particle structures.

After initial deposition, the properties of a clay deposit may change with time (Burland 1990; Leroueil & Vaughan 1990; Schmertmann 1991). This may be due to secondary compression, thixotropy, cementation, cold welding, etc. While secondary compression produces a strength increase related to the decrease in void ratio, the other effects may occur at constant void ratio. These effects result in "structured" soils (Leroueil 1997). Structured soils or soils that have undergone "structuration" exhibit higher preconsolidation pressure, undrained shear strength and initial stiffness than the same soil at the same void ratio, but in unstructured condition.

Disturbance or destructuration may occur due to large deformations that destroy bonds between particles, and this will partially reduce these properties. The large deformations may be caused by compression, shearing and possibly by swelling. Destructuration may be partial or complete and the stiffness-related properties reduce correspondingly. Structure and stiffness-related properties may be recovered to some extent with time.

2.2.3.2 Fabric of Granular Soils

Granular soils also show effects of initial structure (e.g. Oda 1972). The important physical parameter that controls the behavior is the contact normal directions, but other properties such as grain shapes and grain long-axis directions have been used as indicators of the fabric. However, it should be mentioned that deposits made of spherical grains are not isotropic in behavior. With contact normals usually biased toward vertical in most sand deposits, the vertical stiffness and the drained strength are highest in the vertical direction.

Effects of structuration (i.e. aging effects beyond that of secondary compression, such as thixotropy, cementation, cold welding, etc.) similar to those identified in clay soils (see Section 2.2.3.1) have also been recognized in sands (e.g. Mitchell & Solymar 1984; Schmertmann 1991).

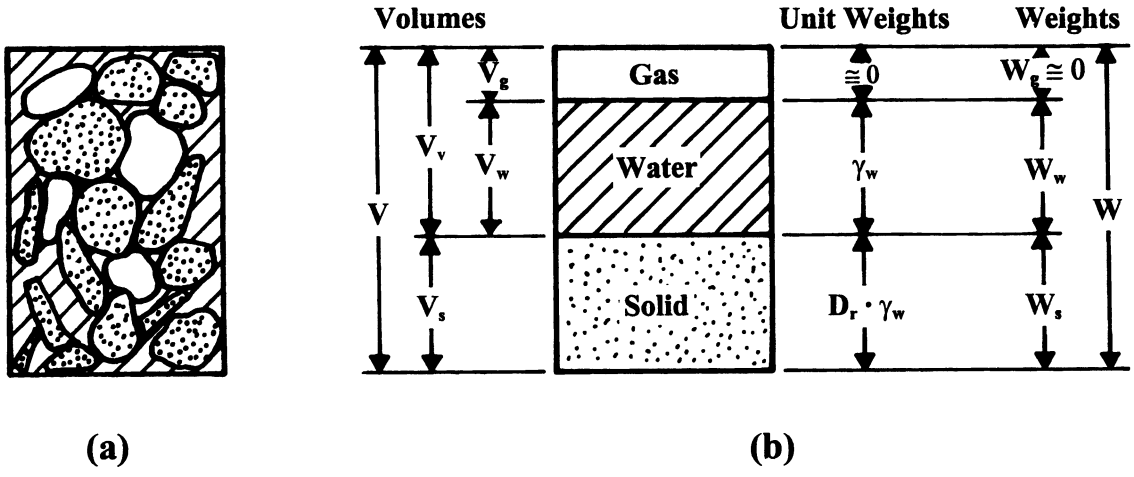


FIGURE 2.1. Relationships among soil phases: (a) element of natural soil, and (b) element separated into phases.

2.3 *Definitions and Relationships between Basic Soil Properties*

All weight–volume relationships are defined in terms of quantities illustrated in Fig. 2.1, in which the idealization of a soil mass, consisting of solids, air and water, is indicated. Table 2.2 gives the definitions and relationships between the most commonly used basic soil properties, where for a given element of soil (see Fig. 2.1) the terms not explicitly defined in Table 2.2 are: V_t = total volume of soil mass, V_v = volume of voids, V_w = volume of water, V_s = volume of solids, W_t = total weight of soil mass, W_w = weight of water, W_s = weight of solids, m_t = total mass of soil, m_w = mass of water, m_s = mass of solids, g = gravitational acceleration (g = 9.81 m s^{-2} on Earth). The relative density (D_r) was formerly known as the specific gravity (G_s), and the density index (I_D) was formerly known as the relative density (D_r), and the maximum and minimum void ratios, e_{max} and e_{min}, are index values obtained by standard procedures. For fully saturated soil, all voids are saturated with water and S_r = 100%. The volumetric water content, θ, is equal to the porosity, n, for a saturated soil. For an unsaturated soil $\theta < n$.

2.4 *Seepage Through Saturated Soil*

2.4.1 BASIC HEAD EQUATIONS

Water flows from a location of higher energy to a location of lower energy, where Bernoulli's energy relation can be used to describe the energy loss occurring between two points on the same flow path in a saturated soil:

$$\frac{v_1^2}{2g} + \frac{u_1}{\gamma_w} + z_1 = \frac{v_2^2}{2g} + \frac{u_2}{\gamma_w} + z_2 + \Delta h \quad (2.1)$$

where $v^2/2g$ = velocity head (m) (v = the groundwater velocity, g = the gravitational acceleration), u/γ_w = pressure head (m) (u = the water pressure at the point of interest and γ_w = the unit weight of water), z = elevation head (m) (the height above some arbitrary but fixed reference point), and Δh = head loss from point 1 to 2 (m).

TABLE 2.2. Definitions and relationships between various soil properties. Refer to Figure 2.1 and Section 2.3 for notation

Soil property	Definition	Remarks
Void ratio	$e = \frac{V_v}{V_s} = \frac{n}{100 - n}$	Decimal form, $e > 0$ Example: 0.63
Porosity	$n = \frac{V_v}{V_t}(\times 100\%) = \frac{100 \times e}{1 + e}$	Percentage, $0 < n < 100\%$ Example: 37%
Degree of saturation	$S_r = \frac{V_w}{V_v}(\times 100\%)$	Percentage, $0 \leq S_r \leq 100\%$ Example: 85%
Density index	$I_D = \frac{e_{max} - e}{e_{max} - e_{min}}(\times 100\%)$	Percentage, $0 \leq I_D \leq 100\%$ Example: 74%
Water content	$w = \frac{W_w}{W_s}(\times 100\%)$	Percentage, $w \geq 0$ Example: 127%
Volumetric water content	$\theta = \frac{V_w}{V_t}(\times 100\%)$	Percentage, $0 \leq \theta \leq 100\%$ Example: 37%
Density	$\rho = \frac{m_t}{V_t}$	SI units: Mg m^{-3}
Dry density	$\rho_d = \frac{m_s}{V_t}$	Typically: 1.6–1.9 Mg m^{-3} Range: 1.0–2.2 Mg m^{-3}
Density of water	$\rho_w = \frac{m_w}{V_w}$	= 1.0 Mg m^{-3} = 10^6 g m^{-3} = 1.0 g cm^{-3}
Density of solids	$\rho_s = \frac{m_s}{V_s}$	Typically: 2.6–2.8 Mg m^{-3}
Relative density of solids	$D_r = \frac{\rho_s}{\rho_w} = \frac{\gamma_s}{\gamma_w}$	Typically: 2.6–2.8
Unit weight	$\gamma = \rho \times g$	SI units: kN m^{-3} English units: lb/ft^3
Dry unit weight of soil mass	$\gamma_d = \frac{W_s}{V_t} = \frac{D_r \times \gamma_w}{1 + e}$	Typically: 15–19 kN m^{-3} Range: 10–22 kN m^{-3}
Unit weight of water	$\gamma_w = \frac{W_w}{V_w}$	= 9.81 kN m^{-3} = 1.0 g cm^{-3} = 62.4 lb/ft^3
Unit weight of solids	$\gamma_s = \frac{W_s}{V_s}$	Typically: 25.5–27.5 kN m^{-3}
Total unit weight	$\gamma_t = \frac{W_t}{V_t} = \frac{D_r + (S_r \times e/100)}{1 + e} \times \gamma_w$	
Total unit weight	$\gamma_t = \left(1 + \frac{w}{100}\right) \times \gamma_d$	
Saturated unit weight	$\gamma_{sat} = \frac{D_r + e}{1 + e} \times \gamma_w$	
Saturated unit weight	$\gamma_{sat} = \left(1 + \frac{w}{100}\right) \times \gamma_d$	
Submerged unit weight	$\gamma' = \gamma_{sat} - \gamma_w$	= buoyant unit weight

The head loss from one point to another on the same flow path is then calculated as the difference between the total heads (and is equal to velocity + pressure + elevation heads) at the two cross-sections. With the possible exception of coarse gravel, flow in soils is laminar and the velocity head is negligible. Thus, the head loss between the two points on the same flow path is given by:

$$\Delta h = \left(\frac{u_1}{\gamma_w} + z_1\right) - \left(\frac{u_2}{\gamma_w} + z_2\right) = h_1 - h_2. \quad (2.2)$$

This equation says that the head loss between points 1 and 2 equals the difference between the total heads:

$$h_i = \left(\frac{u_i}{\gamma_w} + z_i\right) \quad (2.3)$$

where i = 1, 2 at these two points. The hydraulic gradient is defined as the head loss per unit length along the flow path and hence if the distance between points 1 and 2 is Δz, the hydraulic gradient, i, is given by:

$$i = \frac{\Delta h}{\Delta z}. \quad (2.4)$$

2.4.2 DARCY'S LAW AND HYDRAULIC CONDUCTIVITY

The rate of flow of water (or any other fluid or gas) through soil is governed by Darcy's law:

$$q = v_a A = kiA \quad (2.5)$$

where q = flow ($m^3 s^{-1}$), v_a = Darcy flux (also called Darcy velocity and discharge velocity, typical units: $m^3 s^{-1} m^{-2} = m s^{-1}$), k = hydraulic conductivity (formerly called the coefficient of permeability, typical units: $m s^{-1}$), i = hydraulic gradient = head loss per unit length along the flow path (dimensionless), and A = cross-sectional area of flow (m^2). Seepage through soil is discussed in more detail in Chapters 3, 8 and 24.

Typical values of the hydraulic conductivity for different soils are given in Chapter 3. The hydraulic conductivity is often anisotropic (the horizontal hydraulic conductivity frequently being greater than the vertical value) and may vary for a given soil depending on the chemical composition of the permeant and the temperature as discussed in Chapter 25.

The Darcy flux in Darcy's law corresponds to the flow per unit cross-sectional area. The groundwater velocity (also called the average linearized groundwater velocity or the seepage velocity) v, represents the average velocity of the groundwater between two points. The two velocities may be related to each other as follows:

$$v = \frac{v_a}{n}. \quad (2.6)$$

This is the velocity of a tracing agent injected below the groundwater table as it moves from one point to another due to advective transport with the water. This and other contaminant transport mechanisms are discussed in Chapter 24.

2.5 *Basic Mechanics*

2.5.1 ANALYSES OF STRESS: MOHR'S CIRCLE

Figure 2.2a shows a general state of stress acting on a soil element in the ground. The stresses on any plane oriented at an angle α with horizontal may be expressed in terms of the stresses acting on the element:

$$\sigma_a = \frac{\sigma_x + \sigma_y}{2} - \frac{\sigma_x - \sigma_y}{2} \times \cos 2\alpha - \tau_{xy} \sin 2\alpha \quad (2.7)$$

$$\tau_a = \frac{\sigma_x - \sigma_y}{2} \sin 2\alpha - \tau_{xy} \cos 2\alpha. \quad (2.8)$$

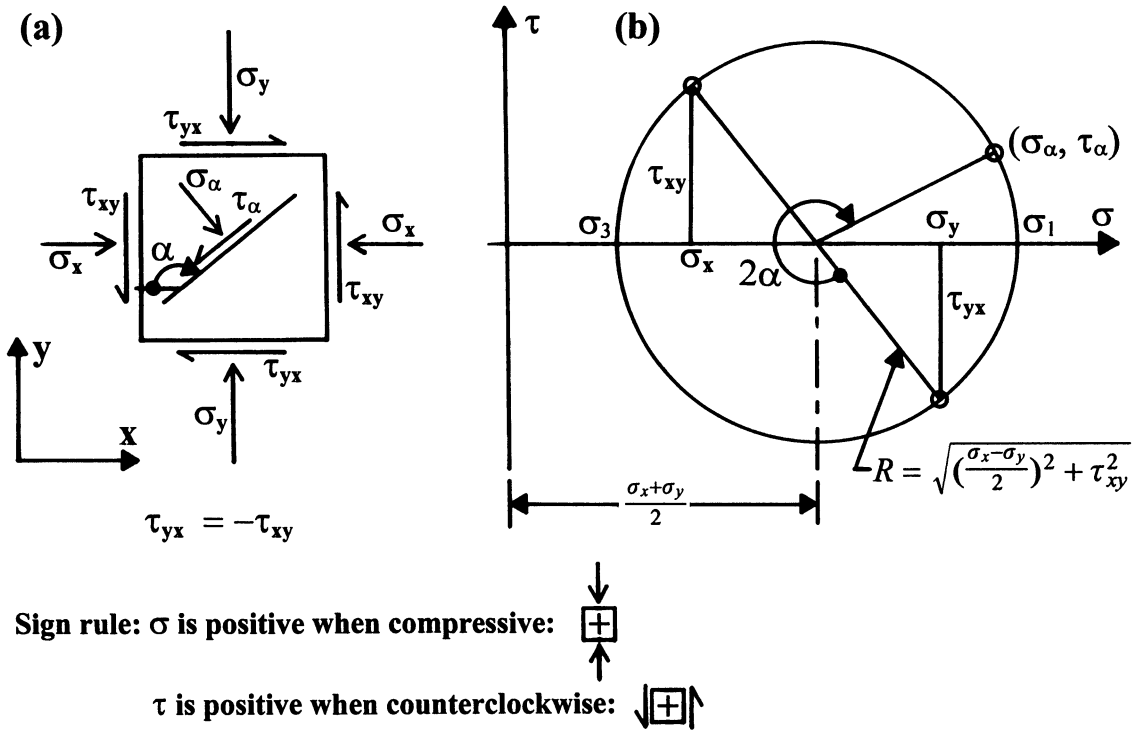


FIGURE 2.2. (a) General state of stress in soil element, and (b) Mohr's circle for state of stress.

These expressions describe a circle, Mohr's circle, in a σ–τ diagram with the same scales on the two axes, as shown in Fig. 2.2b. The principal stresses, σ_1 and σ_3, may be calculated from the following expressions:

$$\sigma_1 = \frac{\sigma_x + \sigma_y}{2} + \left[\left(\frac{\sigma_x - \sigma_y}{2}\right)^2 + \tau_{xy}^2\right]^{1/2} \quad (2.9)$$

$$\sigma_3 = \frac{\sigma_x + \sigma_y}{2} - \left[\left(\frac{\sigma_x - \sigma_y}{2}\right)^2 + \tau_{xy}^2\right]^{1/2}. \quad (2.10)$$

Mohr's circle may also be obtained by construction by setting off the stresses and drawing the circle as implied in Fig. 2.2b. The principal stresses are located at the intersection between the circle and the σ–axis, and their magnitudes may be scaled directly from the diagram.

To find the stresses graphically on any plane through the soil element, the pole method may be used. The pole (origin of planes) is first constructed using the Mohr's circle (see Fig. 2.3a) by drawing a line through one of the stress points (A or B) parallel to the plane on which the stresses act (vertical for point A, horizontal for point B) to intersection with the circle at point P. This is the pole. A line (representing a plane inclined at an angle, β, to the horizontal as shown in Fig. 2.3a) drawn through the pole, P, intersects the circle at the stresses which act on that plane. The values of normal and shear stresses may be read directly on the axes, as indicated on Fig. 2.3a.

Conversely, the plane on which a given set of stresses on Mohr's circle (σ_β, τ_β) acts may be obtained by drawing a line through (σ_β, τ_β) and the pole. In particular, the planes on

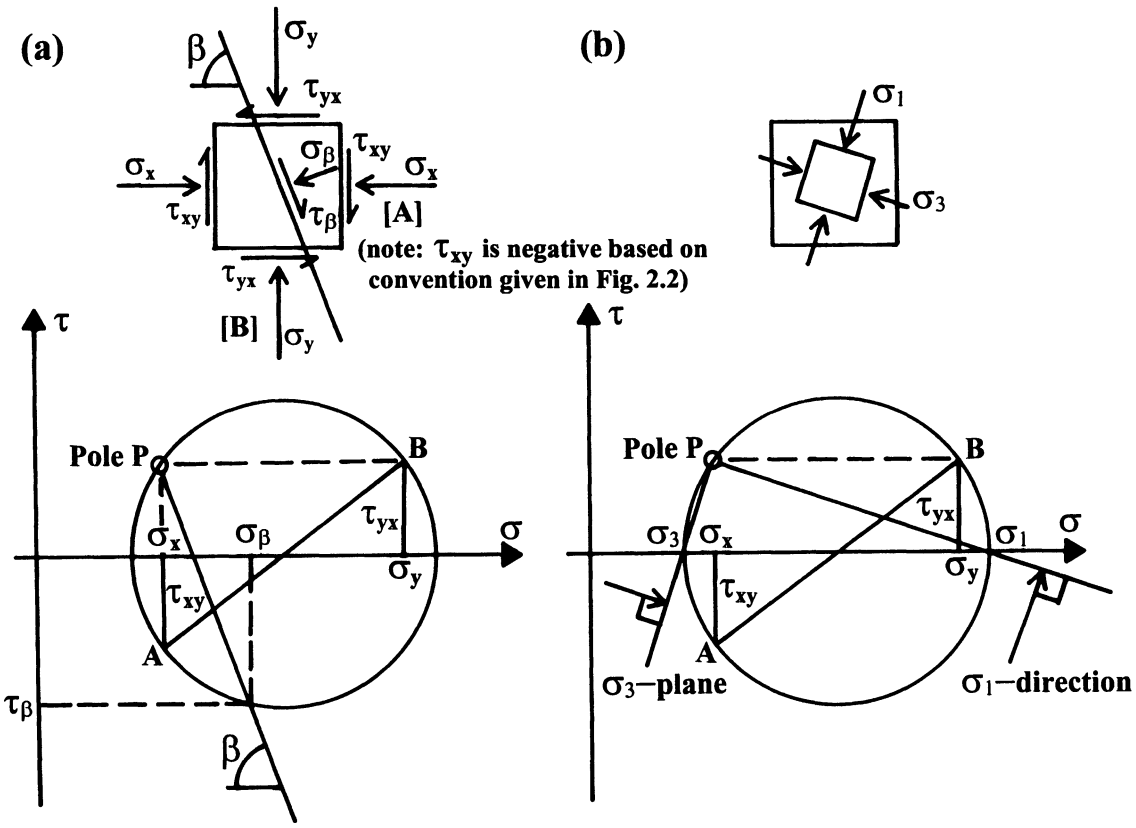


FIGURE 2.3. (a) Location of pole and stresses on plane at angle α, and (b) principal planes and directions.

which the principal stresses act may be determined by drawing lines through the pole and the points where the circle crosses the σ–axis $(\sigma_1, 0)$ and $(\sigma_3, 0)$. These lines represent the principal planes, and the principal stress directions are perpendicular to these planes, as shown in Fig. 2.3b.

2.5.2 ANALYSES OF STRAIN: MOHR'S CIRCLE

Analyses of strains (or strain increments) in two dimensions follow similar expressions as those given above for stresses. The normal stresses, σ, are replaced by normal strains, ε (or the normal strain increment), and the shear stresses, τ, are replaced by half of the engineering shear strains, $\gamma_{xy}/2$ (or half of the engineering shear strain increment).

Similarly, strain analyses may be performed graphically on the Mohr circle for strains (or for strain increments). Figure 2.4a shows a soil element compressed in the vertical direction, expanded in the horizontal direction, and sheared as shown. The sign rule for strains follows that for stresses, as also indicated on the diagram. Figure 2.4b illustrates the Mohr circle for strains. The location of the pole for strains is determined in a similar manner as for stresses, and the planes and directions of principal strains may be determined as indicated.

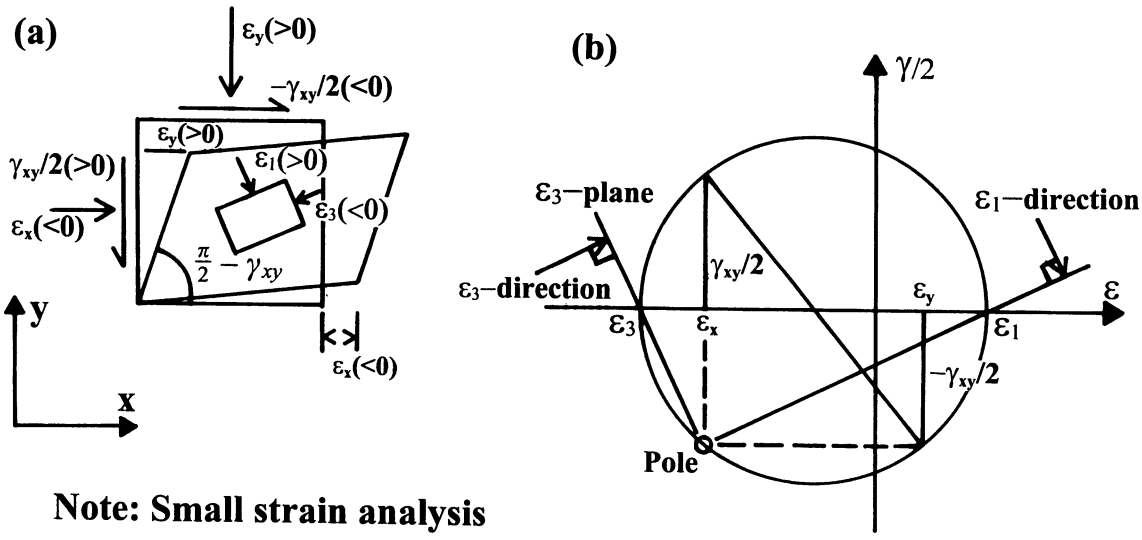


FIGURE 2.4. (a) Strained soil element, and (b) Mohr's circle for state of strain, principal strains and their directions (NB: small strain analysis).

2.5.3 OTHER STRESS REPRESENTATIONS AND STRESS PATHS

Deformations and failure are associated with changes in effective stresses. It is thus important to follow the variations of stresses in soil elements, depicted by the stress paths, to understand and predict their response. Mohr circles are not appropriate to follow stress paths, and other representations have been proposed.

2.5.3.1 *s–t* Diagram

The state of stress in a soil element may be represented uniquely by the top of the Mohr circle given by $(s, t) = [(\sigma_1 + \sigma_3)/2, (\sigma_1 - \sigma_3)/2]$ introduced by Lambe (1964, 1967). The change in stresses is then indicated by the path of this top point (i.e. the stress path). Both total stress paths and effective stress paths (see definition of effective stresses in Section 2.6.1) may be shown on an *s–t* diagram. Figure 2.5a shows the total and effective stress paths in an *s–t* diagram for an undrained triaxial compression test (see Section 2.8).

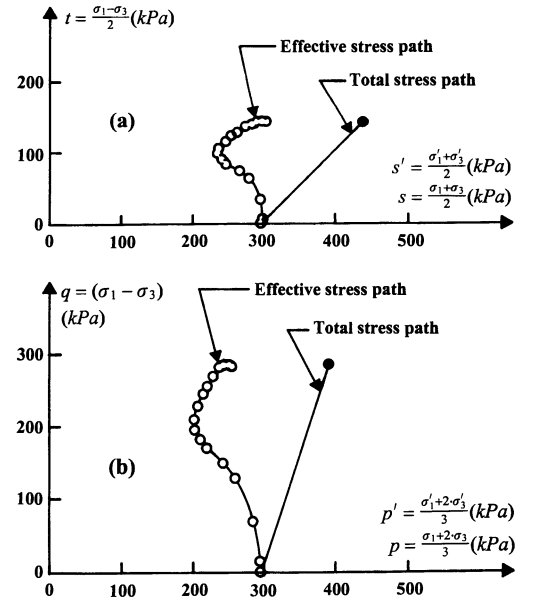


FIGURE 2.5. Total and effective stress paths from an undrained triaxial compression test on a remolded, isotropically consolidated kaolinite specimen shown in: (a) *s'–t* diagram, and (b) *p'–q* diagram.

2.5.3.2 p–q Diagram

The state of stress may also be presented in a diagram of mean normal stress versus maximum deviator stress, $(p, q) = [(\sigma_1 + \sigma_2 + \sigma_3)/3, (\sigma_1 - \sigma_3)]$ as introduced by the Cambridge Soil Mechanics Group (e.g. Schofield & Wroth 1968). Whereas the effect of the intermediate principal stress, σ_2, on the soil behavior may in principle be presented in this diagram (because σ_2 is specifically included in the mean normal stress, p), it is most often used to show results from triaxial tests. The stress path is indicated by the sequence of (p, q)-values through which the stress state passes. As in the s–t diagram, both total stress paths and effective stress paths (see definition of effective stresses in Section 2.6.1) may be shown on a p–q diagram. For triaxial compression tests, $\sigma_2 = \sigma_3$, and Fig. 2.5b presents the total and effective stress paths in a p–q diagram for the same undrained test shown in Figure 2.5a.

The two stress path diagrams have their separate advantages and limitations. The s–t diagram relates directly to the Mohr circle and may therefore be useful in connection with stress analyses in the ground, as indicated above. Since each Mohr circle is represented by a single point, and failure may be indicated by the extreme Mohr circle (see Section 2.9), the s–t diagram provides a clear and uncluttered view of failure conditions, amenable to simple analysis.

The Cambridge p–q diagram provides a larger angle than the s–t diagram in which to indicate the stress paths, as seen in Fig. 2.5, and it provides, in principle, for plotting of results from tests in which σ_2 is different from σ_1 and σ_3. It is also a fundamental diagram employed in critical state soil mechanics (see Section 2.10). Because the s–t diagram does not include any effect of σ_2, it is not possible to relate these two types of stress path diagrams.

Analyses of strengths in the s–t and p–q diagrams are presented in Section 2.9.

2.6 *State of Stress in the Ground*

2.6.1 EFFECTIVE STRESS PRINCIPLE

Deformation and failure of soil occur in response to changes in the forces transmitted through the contact points between the grains that form the soil skeleton. These may be expressed as forces per unit area of a plane through the soil mass (i.e. as stresses). Both normal and shear stresses are transmitted through a given plane in the soil mass, and these stresses influence the deformation and failure of the soil mass. The normal stresses that are effective in producing deformation of the soil mass and in providing shear strength, cannot be calculated directly, but may be determined as the difference between the total normal stress and the pressure in the pores between the soil grains. Thus, the concept of effective stress for a saturated soil, as recognized by Terzaghi in the 1920s (Terzaghi 1923) is expressed as:

$$\sigma' = \sigma - u \tag{2.11}$$

where σ' is the effective normal stress, σ is the total normal stress, and u is the pressure in the fluid in the soil pores (and called the pore pressure). Since the pore fluid cannot take any shear stress and therefore cannot contribute directly to the strength of the soil under normal geotechnical loading conditions, this pore pressure has in the past been referred to as the neutral stress. For the same reason, shear stresses transferred through the soil skeleton are always effective, and they do not require modification due to pore pressures. The concept of effective stress as described by Eq. 2.11 is valid for saturated (or dry) soils. For unsaturated soil, please refer to Chapter 5.

2.6.2 TOTAL VERTICAL (OVERBURDEN) STRESS

The state of stress in the soil under a horizontal ground surface may be calculated from

static considerations. Thus, the total, vertical, normal stress, σ_v, at a given depth in the ground (called the overburden stress) is calculated by summing the weights (per unit area) of the individual soil layers ($\gamma_i h_i$) in a vertical column from the ground surface to the depth of interest:

$$\sigma_v = \sum_{i=1}^{n} \gamma_i h_i \qquad (2.12)$$

where γ_i is the unit weight of the soil mass (i.e. the dry, moist, or saturated unit weight depending on the degree of saturation of the soil), in the ith layer, and h_i is the thickness of that layer and there are n layers above the point at depth $z (z = \sum_{i=1}^{n} h_i)$.

2.6.3 GROUNDWATER TABLE AND POREWATER PRESSURE

The groundwater table is by definition located at the depth where the pressure in the water is atmospheric (i.e. no excess pressure, either positive or negative, exists at the groundwater table). The location of the groundwater table can be established as discussed in Chapter 4.

When there is no vertical flow, the pressure in the pore water, u, is hydrostatic and increases at a constant rate with depth given by:

$$u = h_w \gamma_w \qquad (2.13)$$

where h_w is the depth of the point of interest below the groundwater table. However, in many practical situations there is vertical flow, and in these cases the pore pressure must be either measured (see Chapter 4) or calculated by first establishing the total head, h_T, at the point of interest and then calculating the pore pressure from:

$$u = (h_T - z_i)\, \gamma_w \qquad (2.14)$$

where z_i is the distance from the datum used for calculating the total head, h_T, to the point of interest (z_i is positive if the point of interest is above the datum and negative if below the datum).

In many practical situations the pore pressure will not increase linearly with depth. The importance of pore pressure distributions that do not increase linearly with depth is often underestimated and has been a source of numerous practical problems. The reader is referred to Chapter 5 of Rowe *et al.* (1995b) for more detail on head and pore pressure distributions.

In the capillary zone above the groundwater table (GWT) the pore pressure in the soil is negative. The water is sucked up into this zone by capillary action, or it is hanging and sustained in the pores of the soil skeleton by the surface tension in the miniscus at the water/air interface. The height above the GWT to which the capillary zone reaches depends on the pore sizes and their distribution, the presence of fissures in the ground, and the way in which the water entered this zone (e.g. pulled up from the GWT or from above due to rain storm). Unsaturated soil and soil suction are discussed in Chapter 5.

2.6.4 EFFECTIVE VERTICAL STRESS

The effective vertical stress is obtained by subtracting the pore pressure from the total, vertical stress at each level in the soil column according to the effective stress principle given in Eq. 2.11. Only in the case of dry soil, in which the pore pressure is zero, is the effective stress equal to the total stress.

In the capillary zone, the effect of tension in the water is to increase the effective stress such that it is greater than the total stress. The soil suction above the water table can contribute to the strength of the unsaturated soil (see Chapter 5), but great care is required in making use of this strength in any stability analysis, since it may be lost due to rainfall events and may not contribute at all in fis-

sured materials (see Chapter 14 for a discussion of issues related to slope stability).

2.6.5 HORIZONTAL STRESS AND K_0

The horizontal effective stress in the ground plays an important role in calculation of soil response. The horizontal, effective stress, σ'_h, may be related to the vertical, effective stress, σ'_v, through the value of K_0, as follows:

$$K_0 = \left(\frac{\sigma'_h}{\sigma'_v}\right)_{\varepsilon_h=0} \tag{2.15}$$

where the subscript $\varepsilon_h = 0$ refers to the "at rest" condition of zero horizontal strain. The value of K_0 may be obtained from empirical correlations, as given in Chapter 3, or directly measured, as indicated in Chapter 4.

2.7 *Compressibility and Consolidation*

Deformation of soils, such as settlement and heave, is often assumed to be expressible in terms of relations of the type contained in Hooke's law (i.e. simple proportionality between increments in strains ($\Delta\varepsilon_i$, $\Delta\gamma_{ij}$) and stresses ($\Delta\sigma_i'$, $\Delta\tau_{ij}$)). Even though soil deformation is often irrecoverable, and therefore not elastic, these relations, when appropriately employed, provide approximate and simple means of calculating deformations in soils, e.g. see Chapters 9 and 10.

2.7.1 ELASTICITY

Soils are often assumed to follow the behavior expressed in Hooke's law for isotropic materials:

$$\left.\begin{aligned}
\Delta\varepsilon_x &= \frac{1}{E}[\Delta\sigma'_x - \nu\Delta\sigma'_y - \nu\Delta\sigma'_z] & \Delta\gamma_{yz} &= \frac{1}{G}\Delta\tau_{yz} \\
\Delta\varepsilon_y &= \frac{1}{E}[-\nu\Delta\sigma'_x + \Delta\sigma'_y - \nu\Delta\sigma'_z] \quad \text{and} & \Delta\gamma_{zx} &= \frac{1}{G}\Delta\tau_{zx} \\
\Delta\varepsilon_z &= \frac{1}{E}[-\nu\Delta\sigma'_x - \nu\Delta\sigma'_y + \Delta\sigma'_z] & \Delta\gamma_{xy} &= \frac{1}{G}\Delta\tau_{xy}
\end{aligned}\right\} \tag{2.16}$$

where the ε_is are the normal strains, the γ_{ij}s are the engineering shear strains, E is Young's modulus (dimension of stress), ν is Poisson's ratio (dimensionless), and G is the shear modulus. The shear modulus, G, is related to E and ν as follows:

$$G = \frac{E}{2(1+\nu)}. \tag{2.17}$$

The elastic volumetric strain, $\varepsilon_v = (\varepsilon_x + \varepsilon_y + \varepsilon_z)$, may be expressed in terms of the bulk modulus, K, and the mean normal stress, $\sigma_m = \sigma_{oct} = (\sigma_x + \sigma_y + \sigma_z)/3$, as follows:

$$\varepsilon_v = \frac{\sigma_{oct}}{K} \tag{2.18}$$

where K is also expressible in terms of E and ν:

$$K = \frac{E}{3(1-2\nu)}. \tag{2.19}$$

Inverting the expressions in Eq. 2.16 produces stresses as functions of strains:

$$\left.\begin{aligned}
\Delta\sigma_x &= \lambda\Delta\varepsilon_v + 2G\Delta\varepsilon_x & \Delta\tau_{yz} &= G\Delta\gamma_{yz} \\
\Delta\sigma_y &= \lambda\Delta\varepsilon_v + 2G\Delta\varepsilon_y \quad \text{and} & \Delta\tau_{zx} &= G\Delta\gamma_{zx} \\
\Delta\sigma_z &= \lambda\Delta\varepsilon_v + 2G\Delta\varepsilon_z & \Delta\tau_{xy} &= G\Delta\gamma_{xy}
\end{aligned}\right\} \tag{2.20}$$

where λ is Lamé's constant, which can be expressed as follows:

$$\lambda = \frac{\nu E}{(1+\nu)(1-2\nu)}. \tag{2.21}$$

The constrained modulus, M_c, relates the axial stress increment, $\Delta\sigma_z$, and to the axial strain increment, $\Delta\varepsilon_z$, for one-dimensional compression (i.e. K_0 conditions for which $\varepsilon_x = \varepsilon_y = 0$):

$$\Delta\sigma_z = M_c \Delta\varepsilon_z$$

where (2.22)

$$M_c = \frac{E(1 - \nu)}{(1 + \nu)(1 - 2\nu)}$$

and

$$\Delta\sigma_x = \Delta\sigma_y = \left(\frac{\nu}{1 - \nu}\right)\Delta\sigma_z. \quad (2.23)$$

Note that good judgment is required when choosing values for the elastic moduli and Poisson's ratio for soils, because both vary non-linearly with confining pressure and shear stress.

2.7.2 MODULUS VARIATION

The tangent Young's modulus from triaxial compression tests increases with the confining pressure, σ_3 (Janbu 1963):

$$E = K^* p_a \left(\frac{\sigma_3}{p_a}\right)^n. \quad (2.24)$$

In this equation the modulus number, K^*, and the exponent, n, are dimensionless experimental constants, and p_a is atmospheric pressure in the same units as σ_3 and E. The value of n is typically around 0.5 for sands, while it is 1.0 for normally consolidated clays. Equation 2.24 has been used, separately, for both loading and unloading–reloading conditions.

The strains in soil consist of recoverable (elastic) and irrecoverable (plastic) components. Only elastic strains occur during unloading and reloading, while both elastic and plastic strains are encountered as the soil is loaded the first time (i.e. during primary loading). Figure 2.6b shows the non-linear

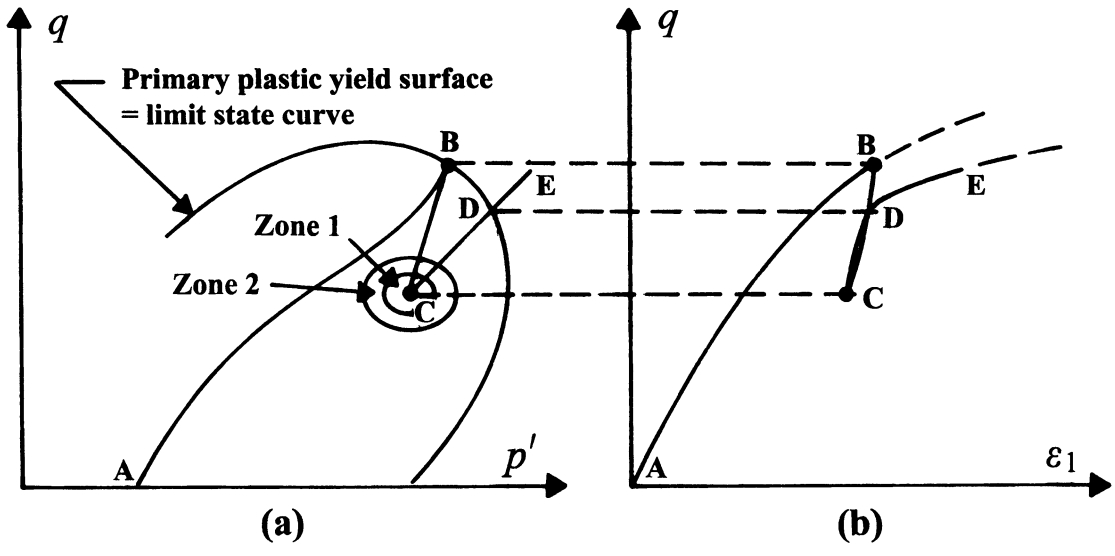


FIGURE 2.6. (a) Illustration of plastic yield surface and stress path in p'–q diagram resulting in (b) elastic–plastic (AB and DE) and elastic (BC and CD) stress–strain behavior (modified from Jardine 1992).

stress–strain curve obtained during primary loading of a soil specimen, while Fig. 2.6a indicates the corresponding stress path from A to B. Plastic yielding results in pushing a plastic yield surface out in the stress diagram, shown in Fig. 2.6a. This yield surface indicates the stress states at which further plastic yielding occurs if the stress path reaches and pushes it further out. If the stress state moves inside the plastic yield surface, say from B to C, unloading results and only elastic strains occur. Reloading (following unloading) from C to D results in elastic straining, and if the yield surface is reached, further loading beyond D produces additional plastic straining, as indicated in Figure 2.6.

Recent carefully performed static experiments (e.g. Jardine 1992; Jamiolkowski *et al.* 1994; Tatsuoka & Kohata 1994) have shown that elastic as well as plastic strains may occur inside the primary plastic yield surface. In the close vicinity of a stress point inside the yield surface (e.g. point C in Fig. 2.6a), and upon stress reversal, the soil response (in Zone 1) is linear and very stiff, reflecting the maximum shear modulus. Stress reversals involving slightly larger stress changes (in Zone 2) experience non-linear elastic soil behavior, and still larger stress reversals (outside Zone 2, but) inside the primary yield surface progressively encounter larger and larger strains, the majority of which are plastic in nature. Thus, the static behavior is similar to that measured in cyclic tests, which produce decreasing shear modulus with increasing strain magnitude, as indicated in Sections 2.11 and 3.8.

2.7.3 COMPRESSION AND EXPANSION

Compression and consolidation are characterized by volume changes due to squeezing air and/or water out from the soil. The compression curve describes the sequence of equilibrium conditions reached after a series of air and water removal increments. The change in volume of a soil is approximately governed by the magnitude and the change in magnitude of the effective major principal stress, which in the field most often is the vertical effective pressure. The typical shape of the relation between void ratio (or water content for fully saturated soil) and effective overburden pressure is shown on the diagram in Fig. 2.7. Here the field virgin compression curve is constructed from the laboratory curve on the basis that all curves, independent of degree of disturbance, go through the point corresponding to $0.4e_0$, in which e_0 is the initial void ratio in the field. The preconsolidation pressure, σ'_p, is the yield stress for the soil, and this is comparable to the maximum past effective pressure to which the soil has been exposed. It separates the part of the compression curve that corresponds to recompression or swelling from the part corresponding to virgin compression. Due to creep and structuration effects occurring with time (see Section 2.2.3), yielding is most often obtained at effective stresses higher than the maximum past effective overburden pressure.

Virgin compression occurs in the range of pressures exceeding the preconsolidation pressure. The semi-logarithmic, straight-line slope of the virgin compression curve is expressed by the compression index, C_c, defined as:

$$C_c = \frac{-\Delta e}{\Delta(\log \sigma')} = \frac{e_2 - e_1}{\log \sigma_1 - \log \sigma_2} \quad (2.25)$$

where points 1 and 2 are located on the virgin compression curve.

If the pressure is reduced, the soil will undergo volumetric expansion, as shown in Fig. 2.7. The semi-logarithmic, straight-line slope of the swelling curve is expressed by the swelling index, C_s, defined by the same equation as that given above, but with points 1 and 2 located on the swelling curve. The swelling index is generally 1/5–1/10 of the compression index.

The slope of the recompression curve is ex-

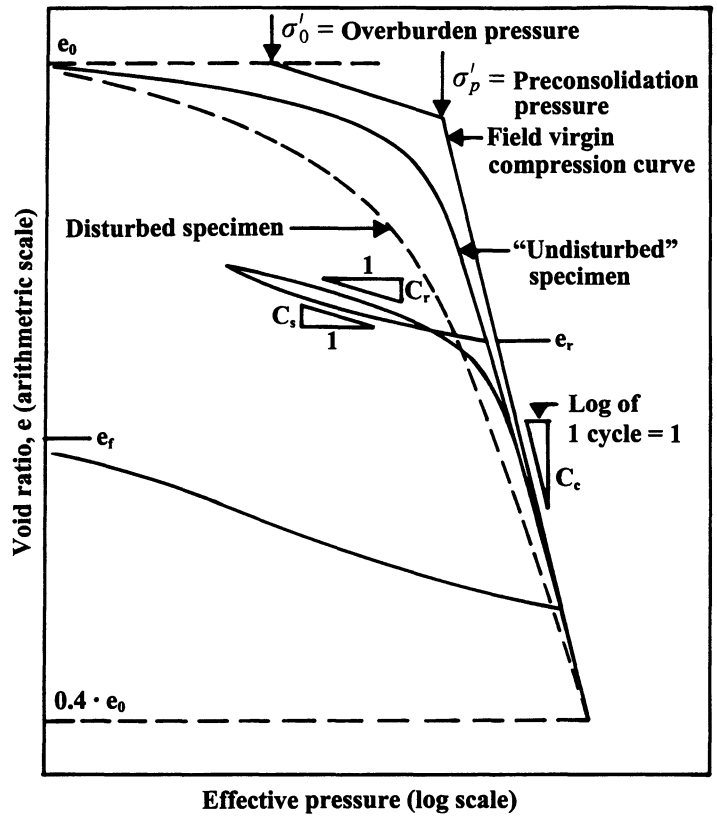


FIGURE 2.7. Typical shape of relation between void ratio and effective overburden pressure during compression and expansion of soil.

pressed by the recompression index, C_r, also defined by the above equation. The value of C_r is approximately equal to the swelling index, C_s. Typical values are given in Chapter 3.

Highly sensitive aged clays in which the preconsolidation pressure has been developed as a result of secondary compression, cementation, or thixotropic mechanisms exhibit low values of C_r/C_c, whereas high values of C_r/C_c are associated with overconsolidated clays containing swelling clay minerals.

The relation between stress and strain may also be shown on straight arithmetic scales, in which case the slope is expressed by the coefficient of volume compressibility, m_v, defined as:

$$m_v = \frac{\Delta\varepsilon_v}{\Delta\sigma'} = \frac{1}{M_c} \tag{2.26}$$

where $\Delta\varepsilon_v$ is the change in volumetric strain and $\Delta\sigma'$ is the corresponding change in effective stress. The dimension of m_v is the reciprocal of stress, and m_v itself is the reciprocal of the constrained modulus in one-dimensional compression, M_c. For a normally consolidated soil, the coefficient of compressibility is related to the compression index as:

$$m_v = \frac{0.435C_c}{(1 + e_0)\Delta\sigma'} \tag{2.27}$$

where e_0 is the initial void ratio.

2.7.4 ONE-DIMENSIONAL CONSOLIDATION

Consolidation refers to the time effect that occurs when water is squeezed out of the soil. Terzaghi (1943) developed the theory of consolidation based on a number of assumptions that are discussed in Section 16.6.1. He developed the equation for one-dimensional consolidation of a layer under constant applied stress:

$$\frac{\partial u_e}{\partial t} = c_v \frac{\partial^2 u_e}{\partial z^2} \tag{2.28}$$

in which u_e is the excess porewater pressure and c_v is the coefficient of consolidation and is given by:

$$c_v = \frac{kM_c}{\gamma_w} = \frac{k}{m_v \gamma_w} = \frac{k(1 + e_0)}{a_v \gamma_w} = \frac{k(1 + e_0)\Delta\sigma'}{0.435 C_c \gamma_w} \tag{2.29}$$

where k = hydraulic conductivity, $a_v = \Delta e / \Delta\sigma'$ and all other terms are as previously defined. Equation 2.28 can be solved subject to the initial condition of constant initial excess pore pressure, u_0, and free drainage at the top and bottom of the layer to obtain the variation in excess pore pressure with time, t, and position, z, as shown Fig. 2.8a, where time is expressed in terms of a dimensionless ratio, T_v, such that:

$$t = T_v \left(\frac{H^2}{c_v}\right) \tag{2.30}$$

where H is the maximum length of drainage (i.e. longest straight-line distance any water molecule has to travel to get out of the consolidating layer).

According to Terzaghi's consolidation theory, the settlement, S_t, can be related to the final, ultimate consolidation settlement, S_u, by the degree of consolidation, U:

$$S_t = US_u = Um_v \Delta\sigma' D \tag{2.31}$$

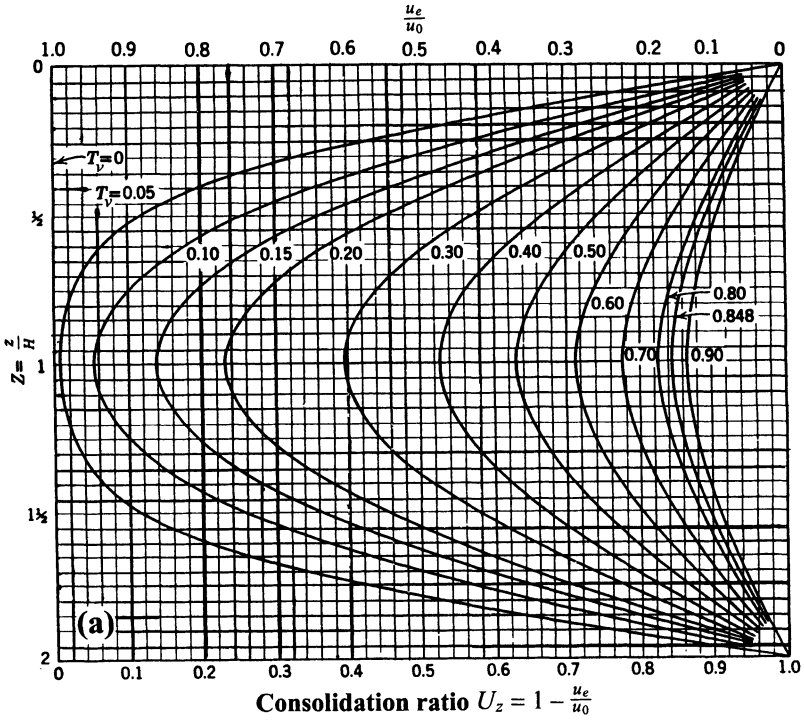
where the degree of consolidation is defined as:

$$U = \frac{1}{D}\int_0^D U_z dz = \frac{1}{D}\int_0^D \left(1 - \frac{u_e}{u_0}\right) dz \tag{2.32}$$

and D is the total thickness of the consolidating layer (which may be different from H in Eq. 2.30). Thus, for example, the degree of consolidation at a given dimensionless time, T_v, (for a constant initial excess pore pressure) can be obtained by taking the ratio of the area to the left of the pore pressure isochrone for that time in Fig. 2.8a and dividing by the total area, and the resulting plot is shown by curve 1 in Fig. 2.8b. A similar approach can be adopted for other initial excess pore pressure distributions to get the degree of consolidation with time plots, as shown by curves 2, 3 and 4 in Fig. 2.8b.

The value of c_v may be calculated from other soil properties as indicated by Eq. 2.29. Alternatively, using the solution to Eq. 2.28, shown by curves in Fig. 2.8b, the value of c_v can be backcalculated from a one-dimensional consolidation (oedometer) test. Two approaches are commonly used: (a) Casagrande's logarithm of time fitting method, and (b) Taylor's square root of time fitting method.

In Casagrande's method, the strain of the soil sample is plotted against the logarithm of time, as shown in Fig. 2.9a. The point corresponding to zero strain is deduced as indicated in Fig. 2.9a by: (a) selecting a point in time, t, in the early stage of consolidation; (b) measuring the difference in strain, Δ, between this point and a point on the curve at time $4t$; (c) marking the strain at a distance



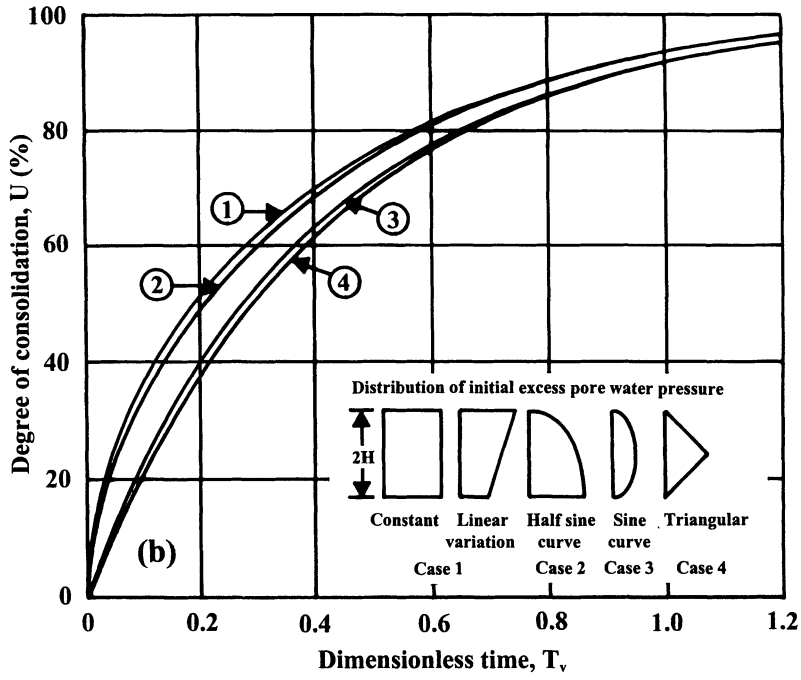
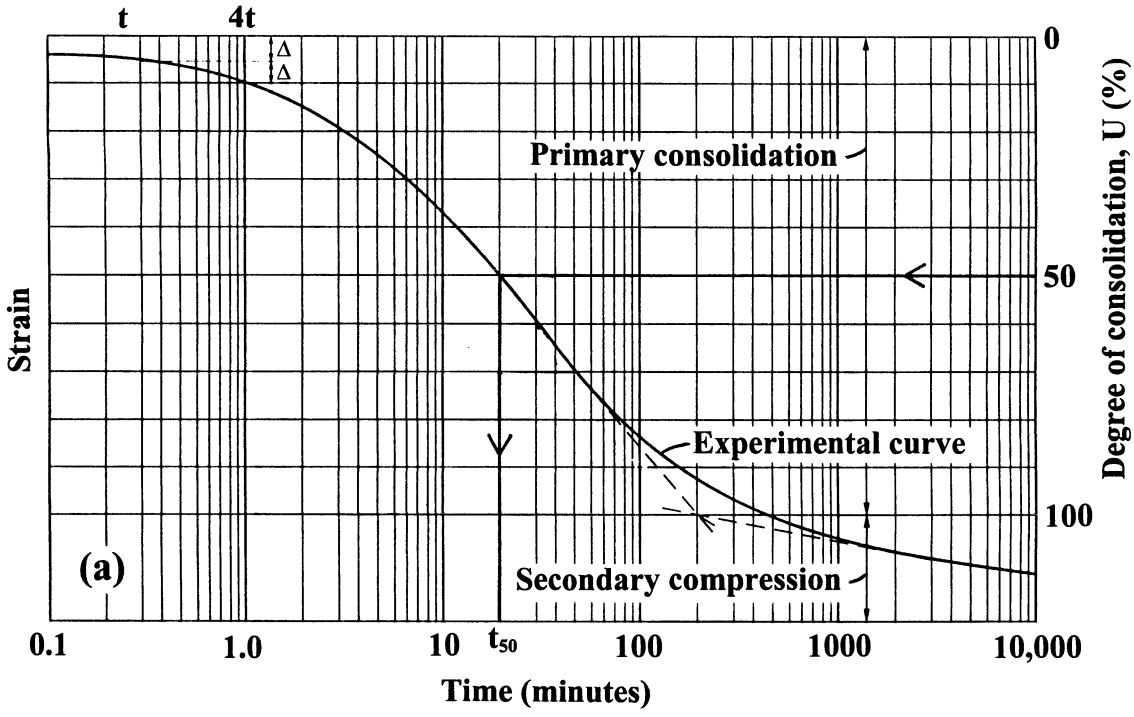


FIGURE 2.8. One-dimensional consolidation: (a) isochrones of excess pore pressure for an initial uniform pore pressure distribution (modified from Taylor 1948), and (b) degree of consolidation with dimensionless time, T_v, for four initial excess pore pressure distributions (modified from Leroueil & Marques 1996).



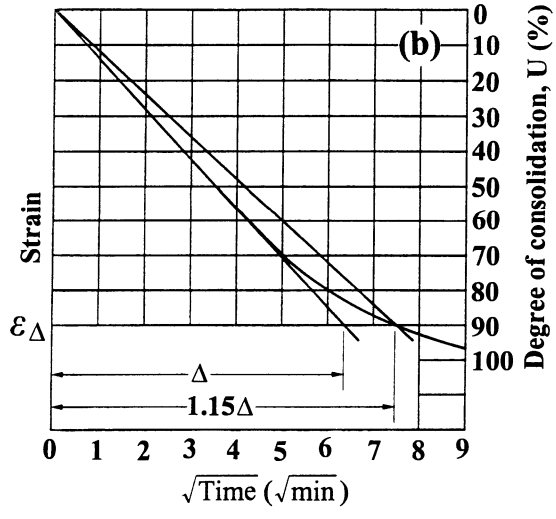


FIGURE 2.9. Methods of estimating c_v based on data from a one-dimensional consolidation (oedometer) test: (a) Casagrande's log time method, and (b) Taylor's root time method (modified from Cernica 1995).

Δ above the point at time, t, as the point of zero theoretical consolidation strain. The strain at 100% consolidation is estimated by finding the intersection of: (a) a line tangent to the straight-line portion of the primary consolidation curve, and (b) a line tangent to the secondary compression part of the curve. The time for 50% consolidation, t_{50}, can then be established as the midpoint between the 0 and 100% consolidation points on the strain axis. The value of $T_v = 0.197$ corresponding to $U = 50\%$ can be determined from Fig. 2.8b, and if H is the drainage path ($H = 0.5D$ if there is two-way drainage as noted earlier) then:

$$c_v = \frac{0.197H^2}{t_{50}}. \tag{2.33}$$

In Taylor's method, the experimental data are plotted against the square root of time, as illustrated in Fig. 2.9b. A tangent is drawn to the straight-line part of the curve and the abscissa, Δ, at some arbitrary strain, ε_Δ, is established, as shown in Fig. 2.9b. A line is then drawn through the origin and a point at the same strain, ε_Δ, with an abscissa of 1.15Δ. The point of intersection of this line with the experimental curve is then taken to indicate the time for 90% consolidation, t_{90}. From Fig. 2.8b, the dimensionless time for $U = 90\%$ is $T_v = 0.848$, and hence for a drainage path, H, the value of c_v can be calculated as:

$$c_v = \frac{0.848H^2}{t_{90}}. \tag{2.34}$$

In general, the values of c_v deduced from Eqs. 2.29, 2.33 and 2.34 will be different. A more detailed discussion of application of consolidation theory to predicting embankment behavior, including the difference between the methods of calculating c_v is provided in Section 16.6.1. It is noted that when c_v is obtained from Eqs. 2.33 and 2.34, then Eq. 2.29 can be used to estimate k from the results of a one-dimensional consolidation test.

2.7.5 CREEP

After completion of primary consolidation under a specific pressure, secondary compression, or creep, continues with time. This time-dependent deformation may be expressed in terms of the secondary compression index, $C_{\alpha e}$, as follows:

$$\Delta e_{\text{creep}} = C_{\alpha e}(\Delta \log t) \tag{2.35}$$

where $C_{\alpha e}$ is determined as the slope of the straight-line portion of the void ratio, e, versus logarithmic time plot after completion of one-dimensional consolidation. The modified secondary compression index (also called the secondary compression ratio) $C_{\alpha\varepsilon}$ is defined as:

$$C_{\alpha\varepsilon} = \frac{C_{\alpha e}}{1 + e_p} \tag{2.36}$$

where e_p is the void ratio at the start of the linear portion of the e versus log t plot, and the creep strain, $\Delta\varepsilon_{\text{creep}}$, is given by:

$$\Delta\varepsilon_{\text{creep}} = C_{\alpha\varepsilon}(\Delta \log t). \tag{2.37}$$

Highly sensitive soils and soils with high compressibility indices will exhibit high rates of secondary compression. For normally consolidated soils, the value of $C_{\alpha\varepsilon}$ for a given soil is approximately proportional to the compression index, C_c (see also Section 3.5.4), whereas overconsolidated soils will have values of $C_{\alpha\varepsilon}$ lower than those corresponding to the same soil under normally consolidated conditions. Secondary compression is particularly important in organic materials and may dominate the time–compression relation, accounting for more than one-half of the total compression.

Aging effects such as secondary compression (as well as structuration effects, see Section 2.2.3) produce preconsolidation pressures under one-dimensional (K_0) conditions that are higher than the maximum past effec-

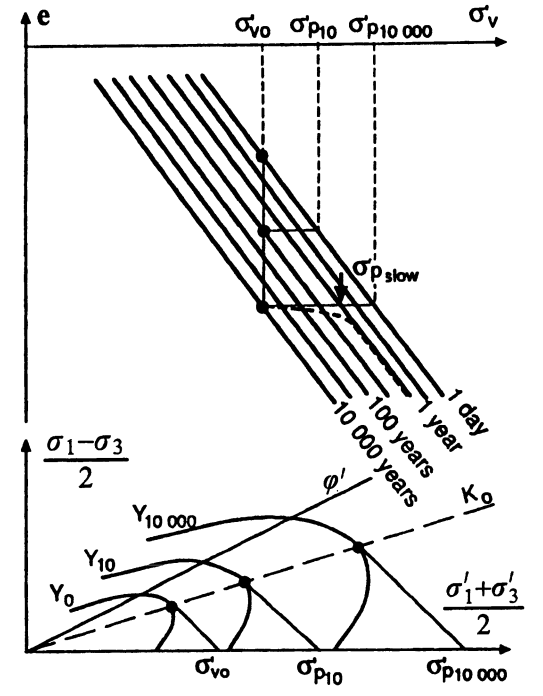


FIGURE 2.10. Increase in apparent preconsolidation pressure and movement of yield surface (or limit state curve) with secondary compression, where σ'_{vo} is the current effective overburden pressure (modified from Tavenas & Leroueil 1977).

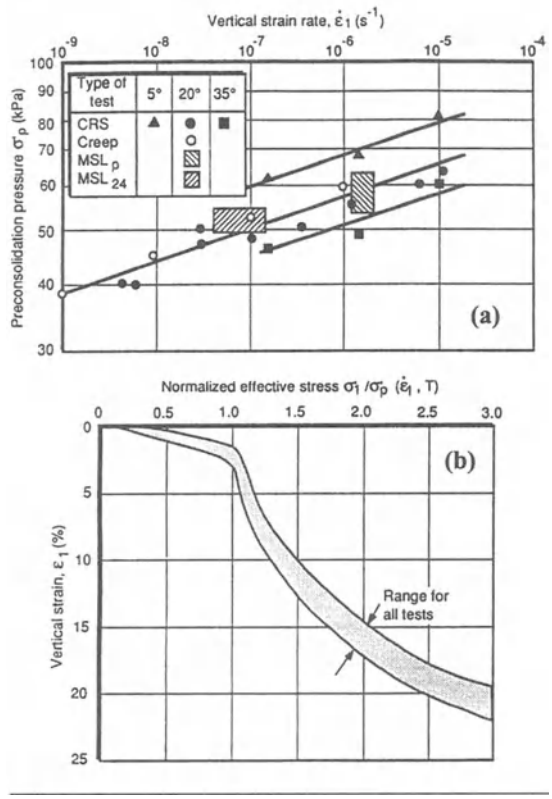


FIGURE 2.11. One-dimensional compression of Berthierville clay: (a) preconsolidation pressure as a function of strain rate and temperature, and (b) normalized effective stress–strain curve (modified from Boudali *et al.* 1994 & Kabbaj 1995, reproduced with permission from Leroueil 1997, in Almeida, M. (Ed.), *Recent Developments in Soil and Pavement Mechanics,* Rio de Janeiro, Brazil, A.A. Balkema, Vermont, U.S.A.).

tive overburden pressure. Figure 2.10 shows a schematic diagram of the increase in apparent preconsolidation pressure, σ'_p, with time following the end of primary consolidation. Thus, the apparent preconsolidation pressure after ten years is indicated as σ'_{p10}. However, the time effect contained in the relations in Fig. 2.10 also implies that the actually obtained preconsolidation pressure depends on the strain rate during reloading. Thus, slow reloading produces an apparent value of σ'_p that is lower than the value indicated by the one-day compression line, as exemplified by the dashed compression curve in Fig. 2.10. Experiments performed by Leroueil *et al.* (1985) show that the entire stress–strain behavior is strain-rate dependent and, in particular, that the preconsolidation pressure increases linearly with log strain-rate, as indicated in Fig. 2.11a. It was also observed that a unique one-dimensional compression curve is obtained when the vertical effective stress is normalized on the preconsolidation pressure for a given strain rate, as shown in Fig. 2.11b.

Figure 2.10 also shows that the yield surfaces tend to be centered around the K_0 compression line, because of stress anisotropy during deposition. This is further discussed in Section 2.10.

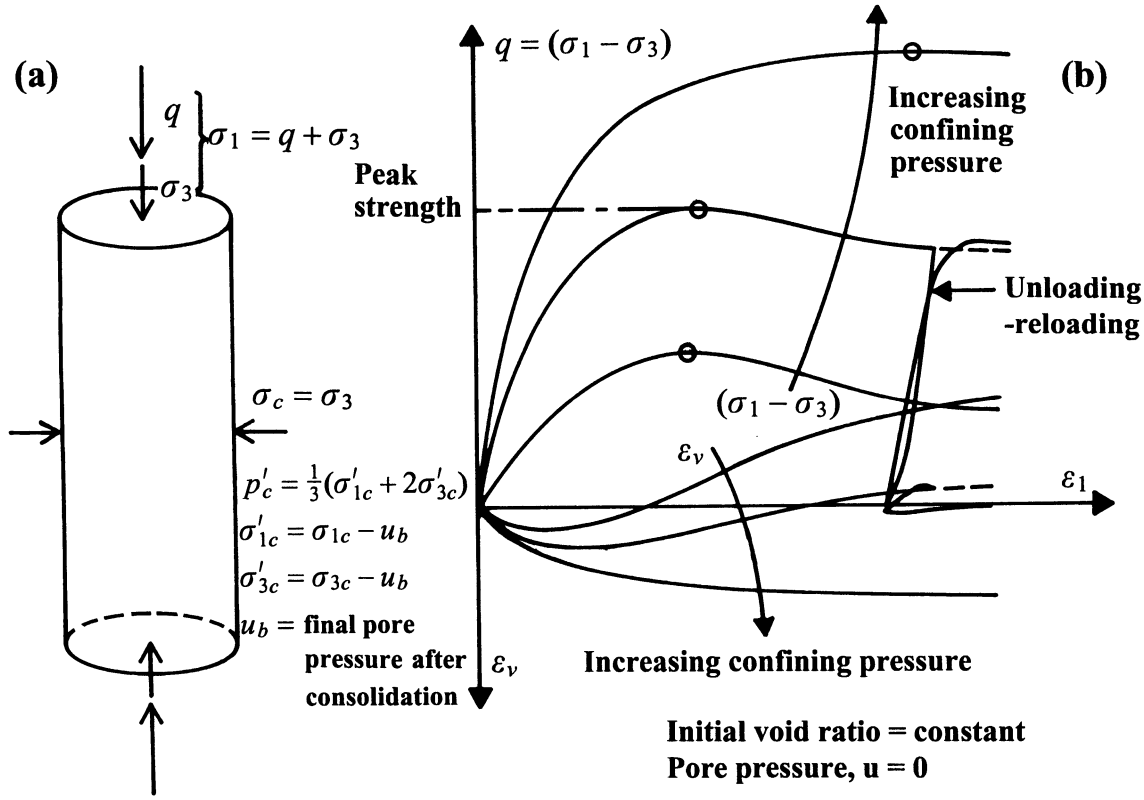


FIGURE 2.12. (a) Stresses applied in triaxial compression test, and (b) stress–strain and volume change behavior of sand in drained tests at three different confining pressures.

2.8 *Stress–Strain and Strength Behavior*

The stress–strain behavior of soils is usually determined from triaxial compression tests and simple shear tests (Bishop & Henkel 1962; Head 1986; Airey & Wood 1987). In the triaxial test the specimen is surrounded by a confining pressure, σ_c, and sheared by applying a deviator stress, $q = (\sigma_1 - \sigma_3)$. Usually the axial strain is determined during compression of the specimen, and the relation between deviator stress, $(\sigma_1 - \sigma_3)$, and axial strain, ε_1, may be plotted (see Fig. 2.12). For drained tests the volumetric strain is determined, while for undrained tests the porewater pressure is measured. Extension tests can also be performed by reducing the vertical stress.

2.8.1 DRAINED BEHAVIOR OF SAND

Typical stress–strain and volumetric strain behavior from drained tests on sand are shown in Fig. 2.12b. The stress–strain behavior is non-linear over the entire range of stresses, and the majority of strains are irrecoverable, as indicated by the unloading–reloading curve for one of the tests. The peak strength increases approximately proportionally with the confining pressure, and the slope of the stress–strain curve (often called the modulus) increases and the strain-to-failure also increases, but less rapidly, with increasing confining pressure. The volumetric strain is initially contractive. This is followed by dilation (expansion) for tests with low confining pressure. The rate of dilation (defined as the slope of the curve of volumetric strain versus

axial strain) is highest at low confining pressure, and it decreases and the behavior eventually becomes only contractive with increasing confining pressure (e.g. see Lee & Seed 1967).

If normalized, the stress–strain relations for sand obtained for different confining pressures are more easily comparable. The principal stress ratio, σ_1'/σ_3', plotted versus axial strain is often used, as shown on the schematic diagram in Fig. 2.13a. A very similar pattern of behavior as that shown in this diagram is obtained for tests performed on specimens with different void ratios, but with the same confining pressure. The dense sand behaves similarly to the specimen with low confining pressure, while the loose sand behavior tends to resemble that of the sand at high confining pressure. The volumetric strain may be presented as variations in void ratio, as shown in Fig. 2.13b. From these two diagrams it may be seen that the sand progresses toward a residual strength and toward the same void ratio at large strains. This critical void ratio depends on the magnitude of the confining pressure. Thus, there is a relation between void ratios and mean effective stress at large strain, the so-called critical states, indicated in Fig. 2.13c, that the sand will tend toward in the process of shearing. If shearing is initiated from a state below the critical state line (point A in Fig. 2.13c), then it will show overall dilation, while the sand will exhibit overall contraction if shearing begins from a state above the critical state line (point B in Fig. 2.13c).

The typical variation of the drained shear strength of sand with confining pressure is illustrated schematically on the p–q diagram in Fig. 2.14a. For a sand with a given initial density the shear strength is composed of two

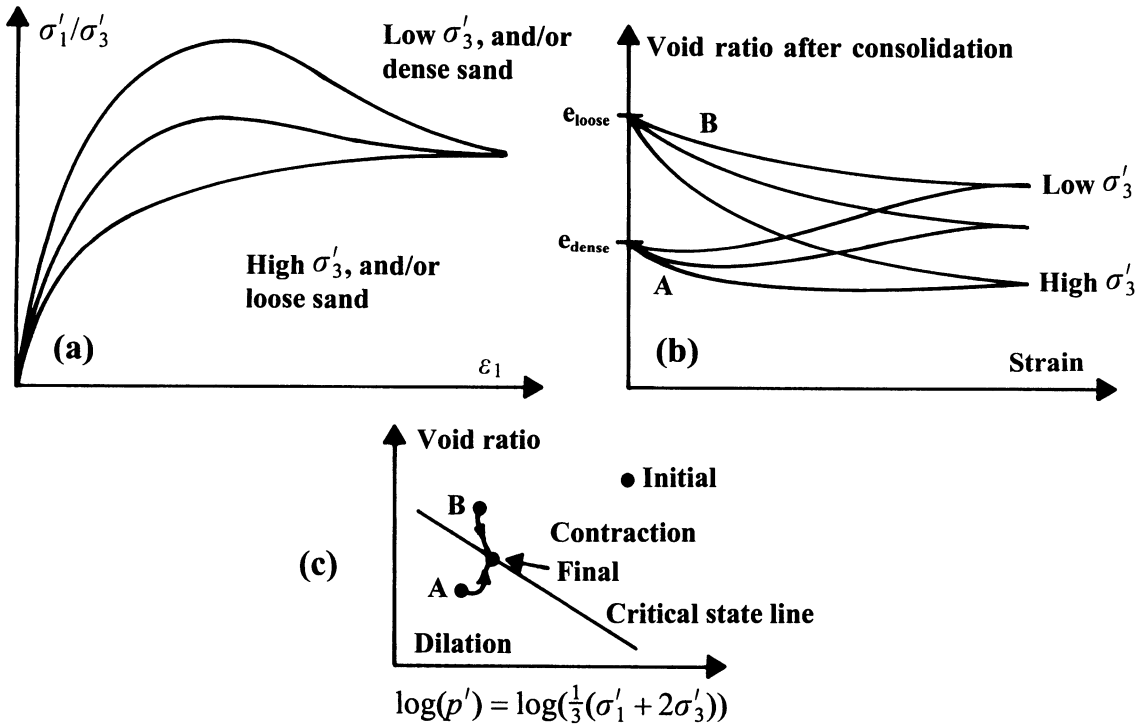


FIGURE 2.13. (a) Normalized stress–strain behavior, (b) void ratio variations reaching critical states, and (c) critical state diagram for sand.

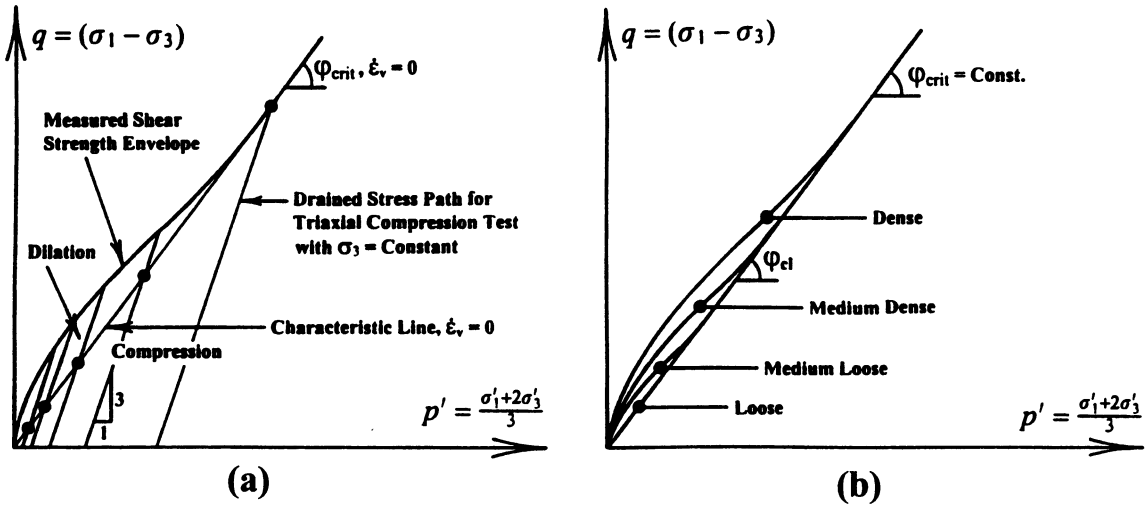


FIGURE 2.14. Variation of drained shear strength envelope for sand with: (a) confining pressure, and (b) density.

contributions. One from the basic friction between sand particles modified by contributions for rearrangement of particles at constant volume. The resulting strength is calculated from the critical friction angle corresponding to the characteristic line in Fig. 2.14a. The second contribution derives from the dilation of the sand during shear. Due to crushing and rearranging the dilation is suppressed at higher pressures and the contribution due to the rate of dilation reduces to zero at very high pressures. Thus, a curved failure surface is observed. Experiments on sands have shown that: (1) the contribution from dilation reduces, and (2) the range of confining pressures in which dilation occurs reduces

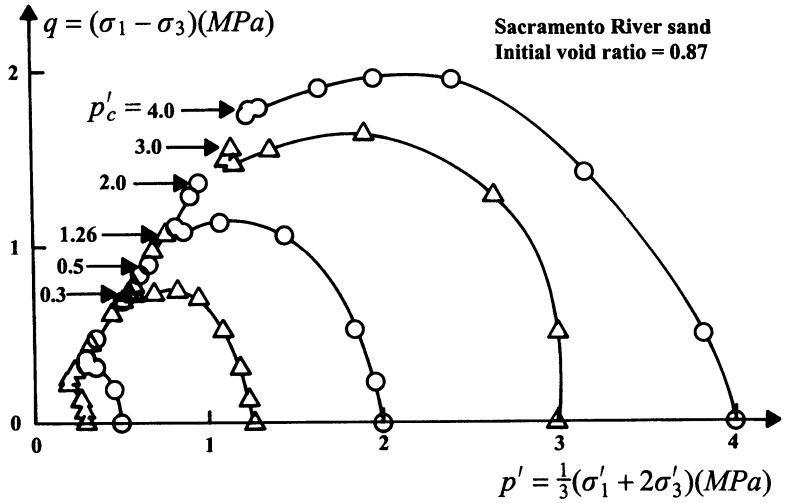


FIGURE 2.15. Effective stress paths from six undrained triaxial compression tests on water-saturated loose Sacramento River sand (modified from Seed & Lee 1967).

with decreasing density, as shown schematically in Fig. 2.14b, and as implied by Fig. 2.13c.

2.8.2 UNDRAINED BEHAVIOR OF SAND

Because of their high permeabilities, sands are rarely loaded sufficiently fast to render them undrained during conventional geotechnical projects. Drained tests therefore best represent the soil behavior for such conditions. Exceptions to this are experienced for rapid loading, as occurs, for example, during earthquakes and pile driving, and for very loose silty sands that may become unstable and produce flow slides, even under static conditions.

The undrained behavior of water-saturated sand is uniquely related to the drained behavior such that pore water pressures increase in the region of volumetric contraction, while they decrease in the region of dilation. The resulting pattern of effective stress paths is exemplified in Fig. 2.15 by six tests on loose Sacramento River sand (Seed & Lee 1967). The undrained strength of dense sand that tends to dilate can become extremely high in the presence of high back pressures (which prevent cavitation), as exist in the ocean bottom (e.g. Lade & Yamamuro 1993).

2.8.3 UNDRAINED BEHAVIOR OF NORMALLY CONSOLIDATED CLAY

For a normally consolidated clay, a unique equilibrium condition exists between void ratio and consolidation pressure. Thus, the initial condition of a normally consolidated clay can only exist along a single compression line on an e–$\log(\sigma'_c)$ diagram, as illustrated in Fig. 2.7. Typical stress–strain and porewater pressure relations are shown in Fig. 2.16a and b for undrained tests on normally consolidated clay. The results are presented in normalized form, obtained by dividing the deviator stress and the pore pressure by the mean consolidation pressure. This tends to produce a single stress–strain relation and a single pore pressure relation (Ladd & Foot 1974). Thus, all variation in stress–strain behavior is accounted for by the implied proportionality of all properties with consolidation pressure, and the consequence of this normalized behavior is that the effective stress paths also normalize, as indicated in Fig. 2.16c.

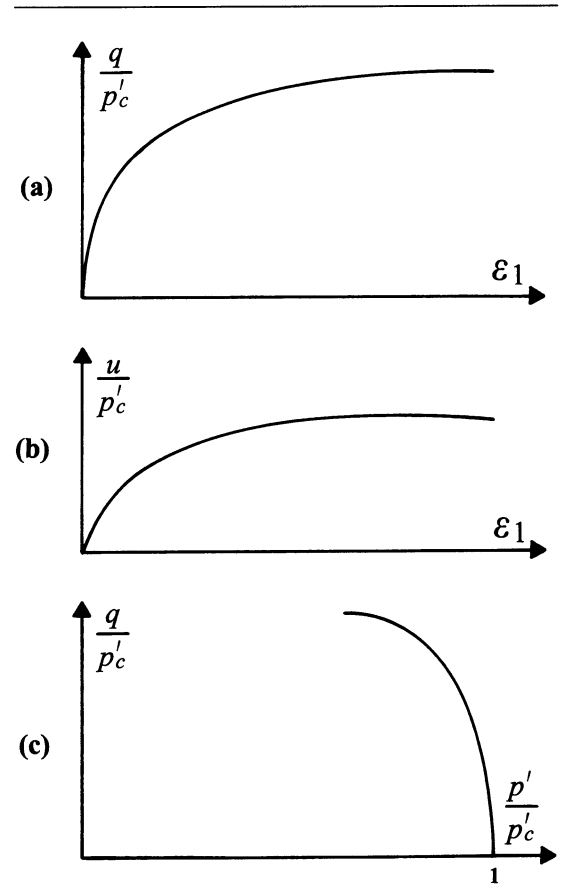


FIGURE 2.16. (a) Normalized stress–strain relations, (b) normalized pore pressure behavior, and (c) normalized effective stress paths for consolidated, undrained tests on normally consolidated clay. [p'_c = consolidation pressure]

2.8.4 UNDRAINED BEHAVIOR OF OVERCONSOLIDATED CLAY

For overconsolidated clay, the normalized stress–strain and pore pressure relations vary with overconsolidation ratio, OCR, defined as:

$$\text{OCR} = \frac{\sigma'_p}{\sigma'_{vo}} \tag{2.38}$$

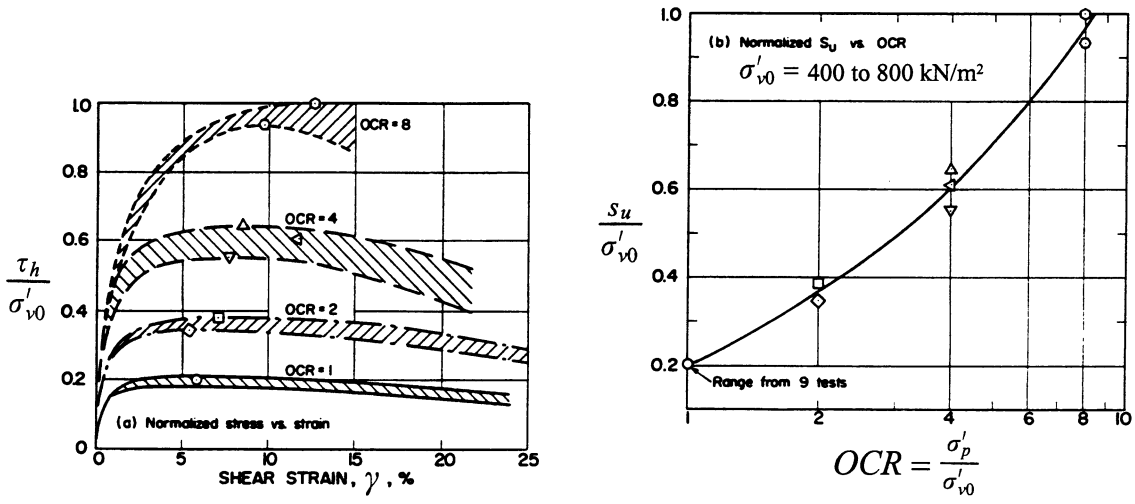


FIGURE 2.17. Normalized data from simple shear tests on K_0 consolidated, undrained tests on Boston Blue clay (modified from Ladd & Foot 1974): (a) normalized stress–strain relations, and (b) normalized ultimate consolidation settlement stress versus OCR.

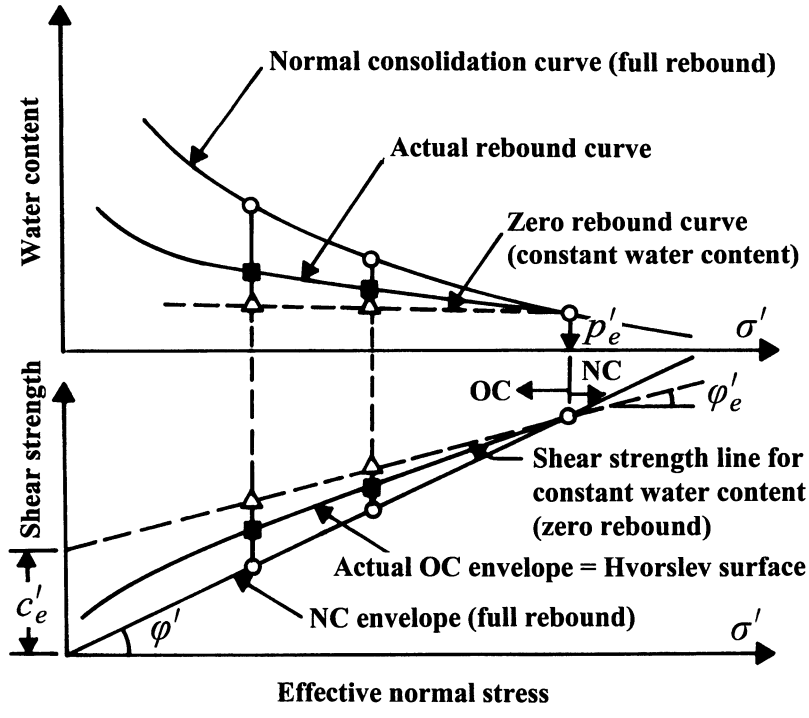


FIGURE 2.18. Relation of Hvorslev surface for overconsolidated clay to the void ratio determined from the rebound curve.

in which σ'_p is the preconsolidation pressure, and σ'_{vo} is the current effective overburden pressure. Similar stress–strain and pore pressure relations are obtained for a given value of OCR, and this implies proportionality of all properties with consolidation pressure for a given value of OCR. However, the normalized stress–strain behavior shows increasing peak strength, increasing modulus, and increasing strain-to-failure with increasing value of OCR, as indicated in Fig. 2.17. The pore pressure is positive for low values of OCR, and it changes to become negative with increasing OCR.

The shear strength of overconsolidated clay follows approximately the concepts proposed by Hvorslev (1937), according to which it is directly related to the void ratio or the water content of a saturated clay, and the shape of the strength envelope reflects the shape and location of the rebound curve, as summarized in Fig. 2.18. In this diagram, the equivalent consolidation pressure, p'_e, is the pressure determined from the virgin compression curve corresponding to the current void ratio. The change in shape of the effective stress paths on a p'–q diagram for a set of undrained triaxial compression tests on specimens with different OCR-values is shown in Fig. 2.19. The stress paths, normalized on the equivalent consolidation pressure, all tend toward the Hvorslev strength envelope.

2.8.5 DRAINED BEHAVIOR OF CLAY

Figure 2.20 illustrates the drained behavior of two clay specimens loaded in triaxial compression at constant confining pressures, and with normalized deviator stresses. The normally consolidated specimen contracts continuously and shows no distinct peak, while the heavily overconsolidated specimen dilates and exhibits a clear peak failure point before reduction in deviator stress toward the residual or critical state.

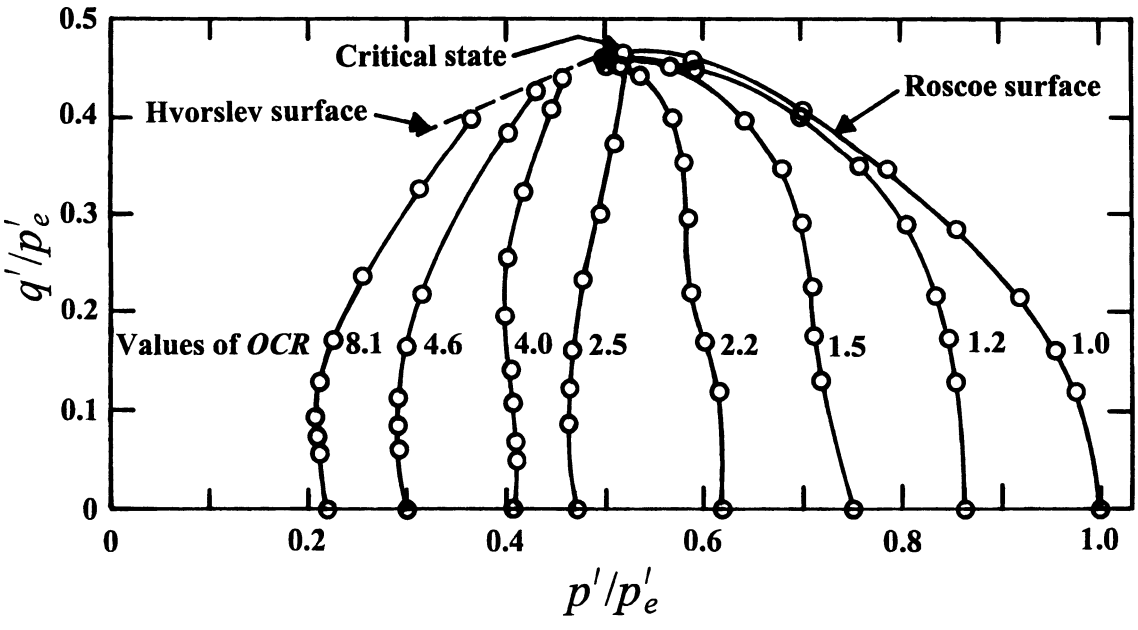


FIGURE 2.19. Normalized stress paths for undrained tests on overconsolidated specimens of kaolin clay (modified from Loudon 1967, Atkinson & Bransby 1978).

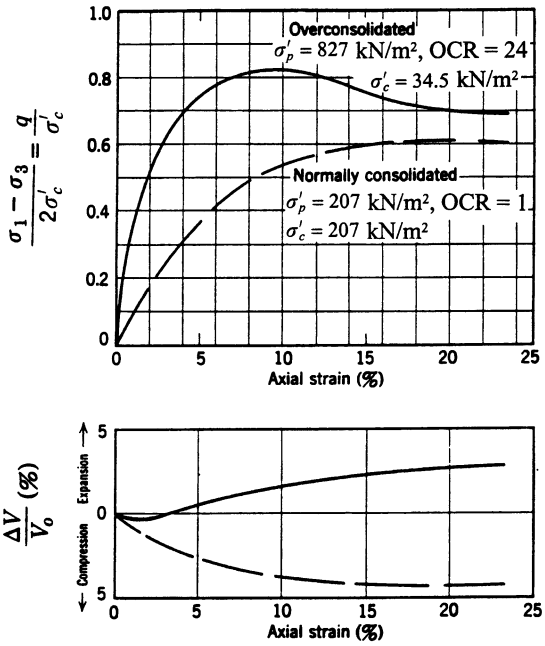


FIGURE 2.20. Drained triaxial compression test data for Weald clay (a) normalized stress–strain curves, and (b) volume change curves (modified from Henkel 1956, Lambe & Whitman 1979).

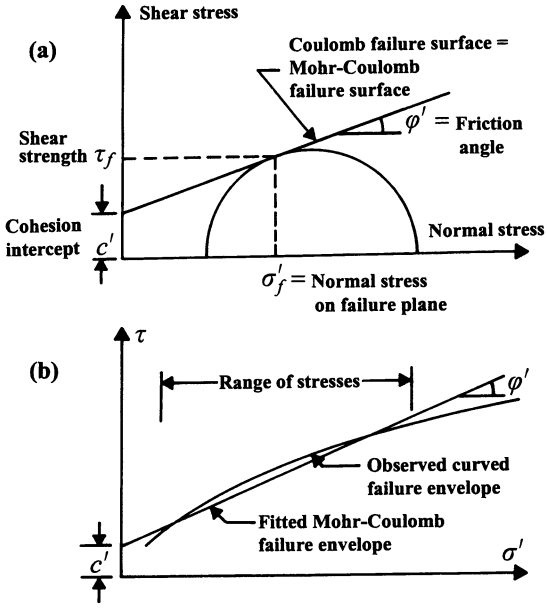


FIGURE 2.21. (a) Effective stress failure surface described by Coulomb's failure criterion and by the Mohr–Coulomb failure criterion, and (b) curved failure envelope with straight-line failure criterion fitted for range of stresses in the geotechnical project.

2.9 *Shear Strength*

Depending on the type of analysis procedure used for calculation of stability (e.g. bearing capacity and slope stability), the shear strength of saturated soil is characterized in terms of either effective stresses or total stresses. Characterization of the behavior of unsaturated soils is described in Chapter 5.

2.9.1 EFFECTIVE STRENGTH CHARACTERIZATION

The effective shear strength of a soil is primarily proportional to the normal stress acting on the soil. This dependency may be described in terms of the stresses acting on the failure plane as expressed by the Coulomb criterion:

$$\tau_f = c' + \sigma'(\tan \phi') \qquad (2.39)$$

where σ' is the normal stress, and τ_f is the shear strength, which is defined as the maximum shear stress that can be sustained on the failure plane. The parameters c' and ϕ' are the effective cohesion intercept and the effective angle of internal friction (often simply called the friction angle) for the soil. The expression describes a straight-line failure surface in a σ–τ diagram, as shown in Fig. 2.21a.

Alternatively, the failure surface may be described in terms of principal stresses, σ_1 and σ_3, as expressed in the Mohr–Coulomb failure criterion:

$$\sigma'_1 = \sigma'_3\left(\frac{1 + \sin \phi'}{1 - \sin \phi'}\right) + 2c'\left(\frac{\cos \sigma'}{1 - \sin \phi'}\right). \qquad (2.40)$$

The two expressions describe the same straight line that forms an envelope to the Mohr circles of stress at failure.

The effective strength parameters c' and ϕ' pertinent to a particular soil may be found

from drained direct shear tests or triaxial compression tests or from consolidated–undrained triaxial compression tests with pore pressure measurements, the latter allowing interpretation of test results in terms of effective stresses.

For saturated sands the effective cohesion is zero, and the (secant) friction angle may be calculated from:

$$\sin \phi' = \left(\frac{\sigma_1' - \sigma_3'}{\sigma_1' + \sigma_3'} \right). \qquad (2.41)$$

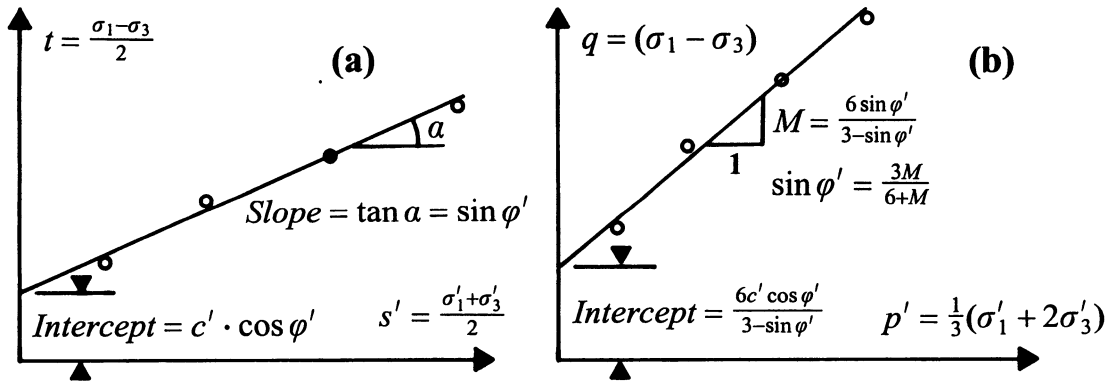
Experiments show that failure envelopes for soils are slightly curved, and that effective cohesion of significant magnitude rarely occurs outside cemented soils. The Mohr–Coulomb description is therefore an approximation to the curved failure envelope, and c' and ϕ' serve as curve-fitting parameters for the particular range of stresses to be found in the tests, as indicated in Fig. 2.21b. The tests should therefore be performed in the range of stresses in the ground to be expected in the geotechnical project.

The strength parameters may also be determined from the s'–t diagram and from the p'–q diagram introduced in Section 2.5.3. Figure 2.22a and b gives the appropriate expressions for determination of c' and ϕ'.

2.9.2 TOTAL STRENGTH CHARACTERIZATION

Total stress analysis procedures require shear strength characterization in terms of undrained shear strength, because the pore pressures developing in the field are unknown. The undrained shear strength embodies the effect of these (unknown) pore pressures. This characterization is usually employed for clays and clayey soils.

For undrained conditions, the shear



Determination of c' and φ' from triaxial compression tests:

1. **Measure α and calculate**
   $\varphi' = \arcsin(\tan \alpha)$
2. **Measure intercept and calculate**
   $c' = Intercept \cdot \frac{1}{\cos \varphi'}$

1. **Measure M and calculate**
   $\varphi' = \arcsin(\frac{3M}{6+M})$
2. **Measure intercept and calculate**
   $c' = Intercept \cdot \frac{3 - \sin \varphi'}{6 \cos \varphi'}$

FIGURE 2.22. Determination of shear strength parameters from: (a) s'–t diagram, and (b) p'–q diagram.

strength of saturated clays can be expressed as:

$$s_u = c_u \quad \text{and} \quad \phi_u = 0 \tag{2.42}$$

where $s_u = (\sigma_1 - \sigma_3)/2$ is often called the undrained shear strength (but this is a misnomer since it is not actually the shear stress on the failure plane at failure) and is independent of total normal stress, c_u is the undrained cohesion intercept of the Mohr–Coulomb failure envelope, and ϕ_u is the undrained friction angle. It should be noted that the undrained shear strength of a soil is not unique and varies depending on the test (method of measurement).

For normally consolidated clay, and indeed for many overconsolidated clays, the undrained shear strength, s_u, is proportional to the preconsolidation pressure, σ'_p, such that for a given soil:

$$s_u/\sigma'_p = \text{constant}. \tag{2.43}$$

For normally consolidated clay this simple normalization implies that in a diagram of void ratio versus log(stress), the compression line (from Fig. 2.7) and the undrained shear strength line are parallel. Similar simple normalization of undrained shear strength is also possible for overconsolidated clay if results with OCR = constant are compared. This is further discussed in Section 3.7.

2.10 *Elasto-Plasticity, Critical State Soil Mechanics and Models for Soil Stress–Strain Behavior*

The deformation of soils may be divided into recoverable and irrecoverable deformations. The recoverable deformation observed during unloading and reloading can be described by elasticity theory, while the irrecoverable behavior may be modeled by hardening plasticity.

Hooke's law for elastic behavior is presented in Section 2.7.1, in which Young's modulus may be taken to vary with confining pressure as indicated in Section 2.7.2, while Poisson's ratio is approximately constant.

The non-linear stress–strain behavior of soils was briefly reviewed in Section 2.8. Both sands and clays exhibit similar behavior patterns. The initial slope of the stress–strain relation increases with confining pressure, as indicated by the modulus variation in Section 2.7.2. The peak strength is essentially proportional with the confining pressure, and it is reached at a strain-to-failure that increases with confining pressure for sands. For normally consolidated, insensitive clay failure occurs with very shallow peaks for which the strain-to-failure is more difficult to distinguish. Overconsolidated clays generally exhibit increasingly pronounced peaks with increasing overconsolidation pressures.

Beyond peak failure the stress–strain relations for all soils approach critical states at which further shearing occurs at constant effective stresses and constant void ratio. For sands, the critical states are located along a line that separates states where the sand dilates from states where it compresses, as illustrated in Fig. 2.13c.

The critical states for a clay are located on a similar line. For normally consolidated clays the virgin compression line and the undrained shear strength line are parallel when plotted on a void ratio–log(stress) diagram. The undrained shear strength for a normally consolidated, insensitive clay occurs at the critical state, because negligible softening is present in such clays.

2.10.1 CRITICAL STATE SOIL MECHANICS

The essence of this behavior of insensitive clays described above is shown in Fig. 2.23, which illustrates some of the essential features of critical state soil mechanics (Roscoe *et al.* 1958). Two lines of critical states are

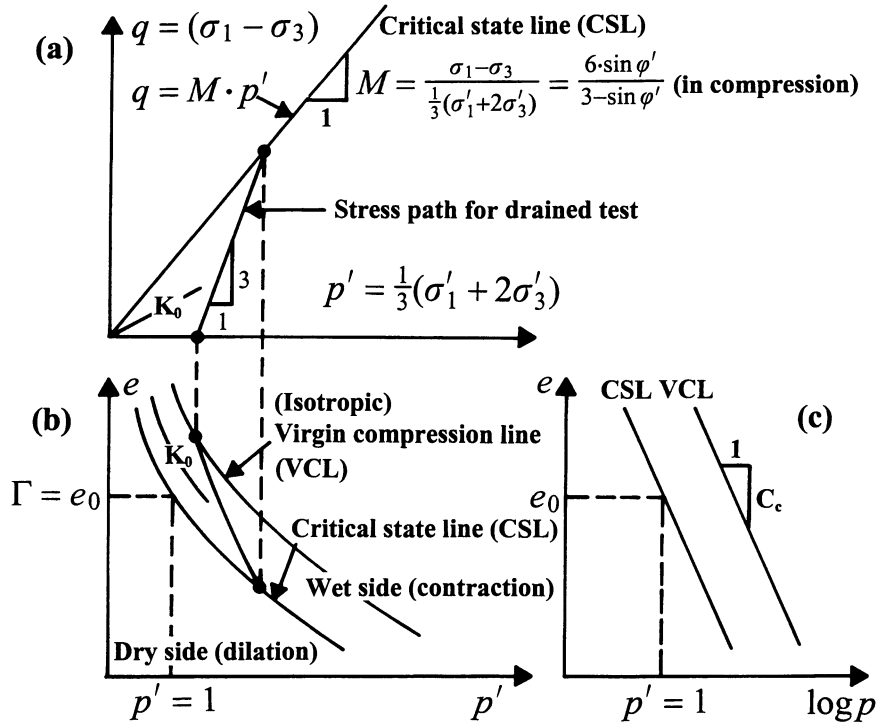


FIGURE 2.23. (a) Cambridge p'–q diagram with stress path for drained triaxial compression test reaching failure at the critical state line, (b) e–p' diagram with state path for the drained test, and (c) e–$\log(p')$ diagram with parallel virgin compression and critical state lines.

shown here: on the Cambridge p'–q diagram in Fig. 2.23a the critical state line is reached at failure, while the e–p' diagram in Fig. 2.23b shows the path of states the specimen follows before reaching the critical state line on this diagram. Above the critical state line on this diagram, the clay is in a so-called "wet" condition, meaning that it will tend to contract and expel water, while below the line the clay is in a "dry" state, indicating that it will dilate and imbibe water when sheared. The states for moderately to heavily overconsolidated clays will be below the critical state line. Figure 2.23c shows the e–p' relations on a semilogarithmic diagram, in which the virgin compression line and the critical state line are parallel for a clay. The consequence is that the volume change pattern is uniquely defined from the location of the current state (in terms of e and p') relative to the critical state line.

2.10.2 MODIFIED CAM CLAY MODEL

This behavior pattern has enabled the development of the hardening plasticity model referred to as the Cam Clay model, in which the volume change is used as the hardening parameter. A similar model for sands has not been successful, because the virgin compression line and the critical state line cross each other, and this consequently negates the unique volume change pattern observed for clays.

The essence of the modified Cam Clay model is illustrated on Fig. 2.24. The yield surface is described by an ellipse located as shown in Fig. 2.24a with one axis along the p'-axis, one end at the stress origin, and with the top point

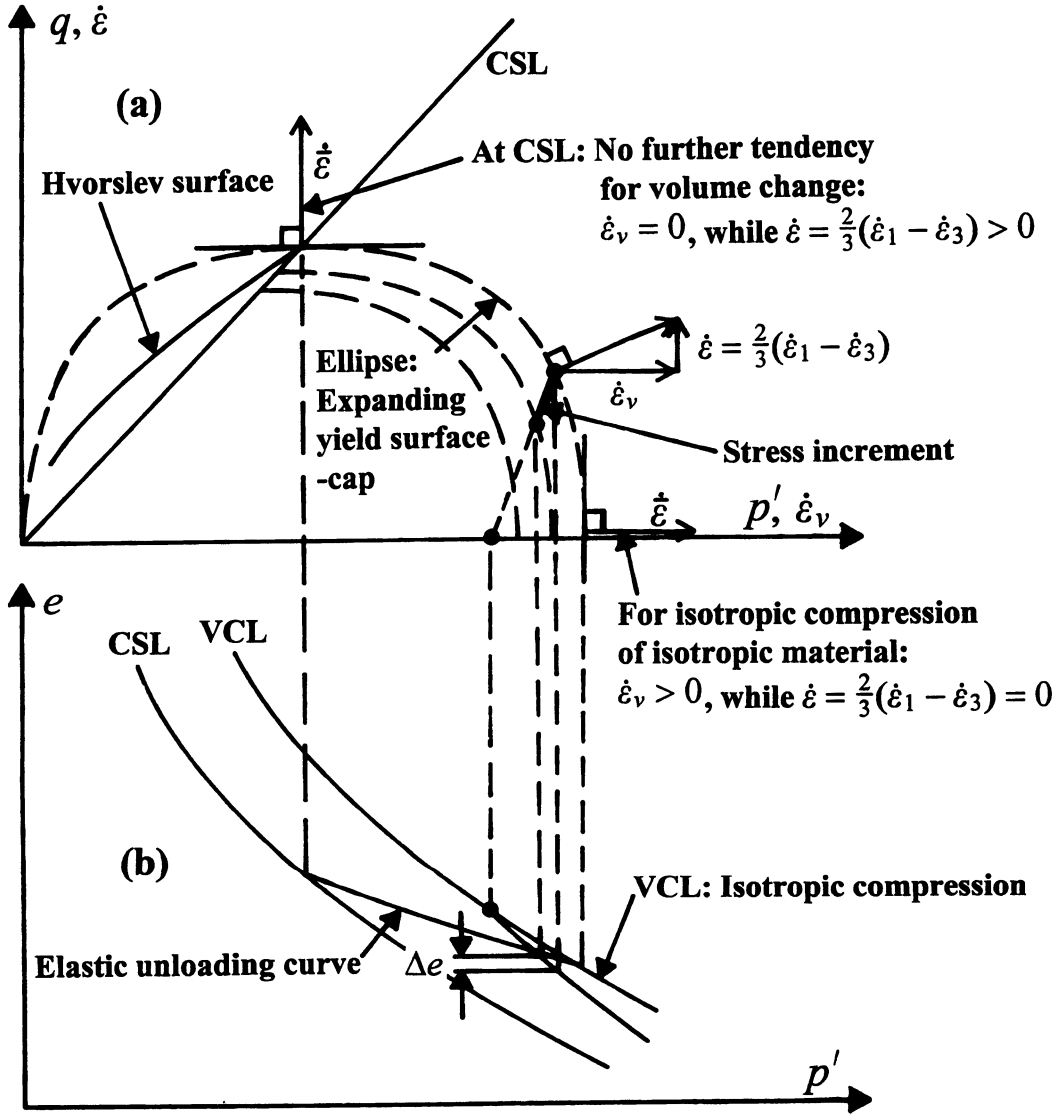


FIGURE 2.24. Modified Cam Clay model with: (a) elliptical yield surface and associated flow, and (b) e–p' relation for determination of volumetric strain used as hardening parameter in the model.

on the critical state line. Superposition of appropriate strain increment vectors on the p'- and q-axes, adoption of associated plastic flow (meaning that the plastic strain increment vectors are perpendicular to the yield surface), and determination of the volumetric strain component of the total plastic strain increment from the e–p' diagram in Fig. 2.24b enables the prediction of non-linear, elasto-plastic stress–strain relations for clay. Both normally consolidated and overconsolidated clays, and drained as well as undrained conditions, can in principle be handled by the model. The five material parameters required for the modified Cam Clay model are indicated on the diagram in Fig. 2.25. Further information and evalua-

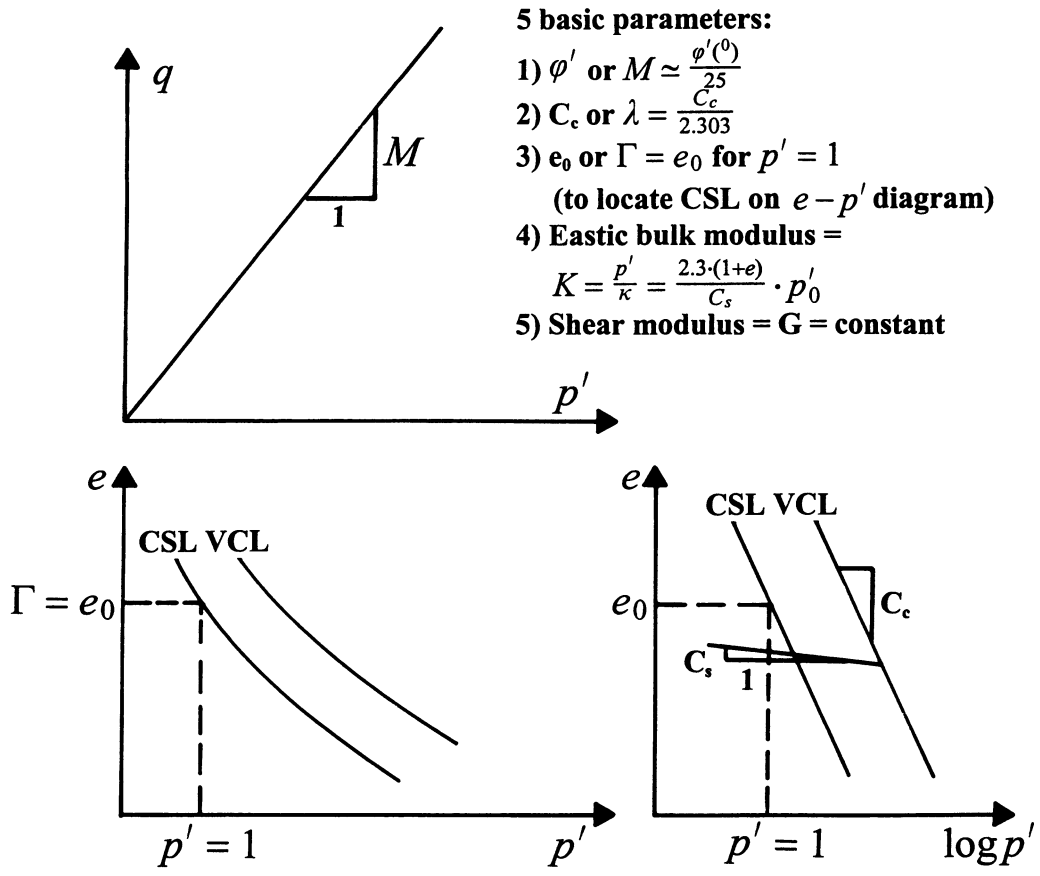


FIGURE 2.25. Illustration of five material parameters required in the modified Cam Clay model.

tion of this model may be found in Roscoe & Burland (1968), Atkinson & Bransby (1978), and Wood (1990).

While the idealized, simple behavior of isotropic clay soils may be represented by the modified Cam Clay model, a number of aspects of real soil behavior are not captured by the concepts behind critical state soil mechanics. Natural clays are most often deposited under K_0 conditions, and the initial fabric, subsequent consolidation due to increasing overburden pressure, and effects of creep and structuration with time (see Section 2.2.3) cause the initial yield surface (or limit state curve) to be biased toward and around the failure line for the normally consolidated soil, as indicated in the s'–t diagram in Fig. 2.26. Thus, the shape and location of the limit state curves for clayey soils are affected by the stress states developing during sedimentation and consolidation. Such bias is less pronounced for sands, residual soils and soft rock.

2.10.3 OTHER MODELS

Non-linear elasto-plastic models have also been developed for sand, but realistic predictions for sand can only be achieved if non-associated flow is employed. This implies that a separate plastic potential function (different from the yield function) has to be defined. Further, volumetric hardening cannot be employed for sand, because both contraction

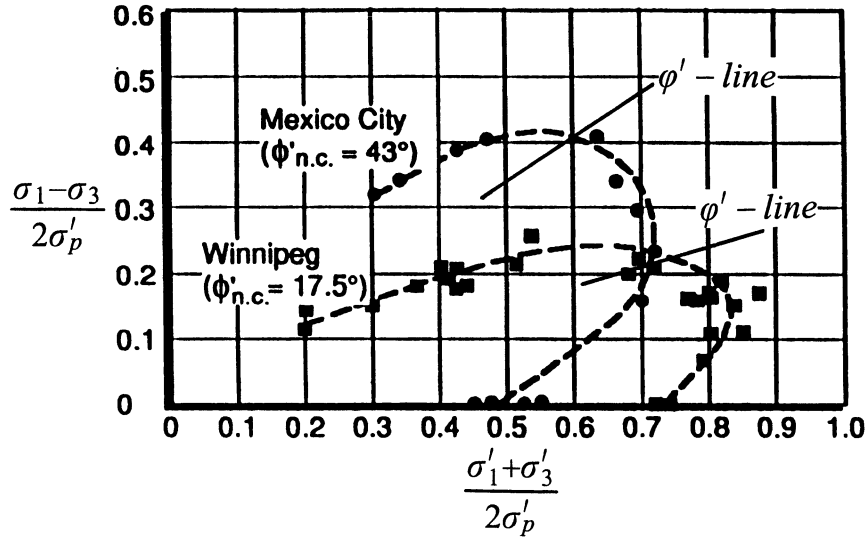


FIGURE 2.26. Initial yield surfaces (or limit state curves) are biased towards and around the failure line for normally consolidated clayey soils, but less biased for sands, residual soils and soft rocks (modified from Diaz-Rodriquez *et al.* 1992, and reproduced with permission from Leroueil 1997, in Almeida, M. (Ed.), *Recent Developments in Soil and Pavement Mechanics,* Rio de Janeiro, Brazil, A.A. Balkema, Brookfield, Vermont, U.S.A.).

and dilation may occur in the hardening regime for sands, resulting in crossing compression and critical state lines, as mentioned above. Other measures of hardening are therefore necessary. Models that are more general and more flexible have been developed and apply to all types of soils including clays. Representative models have been presented by Drucker *et al.* (1957), DiMaggio & Sandler (1971), Lade (1977), Prevost (1978), Dafalias & Herrmann (1980), Mroz *et al.* (1981), Ghaboussi & Momen (1982), Pande & Pietruszczak (1982), Desai & Faruque (1984), Pooroshasb & Pietruszczak (1985), and Lade & Kim (1995).

2.11 *Dynamic Soil Behavior*

Dynamic soil behavior falls into two main categories: (1) problems of foundation design for vibrating equipment, which involve low strain level excitation, and problems of seismic response of the ground to earthquakes, which involve medium–high strain level excitation; and (2) problems of seismic stability analyses of soil foundations, earth dams, or slopes subjected to earthquakes, as well as analyses of foundations for structures subjected to large lateral cyclic forces. The dynamics of foundations is examined in Chapter 12, and geotechnical earthquake engineering is discussed in Chapter 21.

2.11.1 DETERMINATION OF MODULUS AND DAMPING

The soil modulus and damping for machine vibration problems correspond to low strain levels of the order of 1×10^{-6} to 3×10^{-6}. These properties may be determined from field measurements of seismic wave velocity through soil or from special cyclic laboratory tests. The preferred field data come from shear wave velocity measurements obtained by inducing a low level seismic excitation at

one location and measuring directly the time required for the induced shear wave to travel between two known locations. Common tests include up-hole, down-hole and cross-hole wave propagation (see Chapter 4). The shear modulus, G, may be calculated from the shear wave velocity, V_s, according to:

$$G = \rho_t V_s^2 \tag{2.44}$$

where $\rho_t = \gamma_t/g$ = total mass density of the soil.

The modulus, damping and strain level for a particular laboratory cyclic loading test may be calculated directly from the specimen response data. A typical set of results may take the form of a hysteresis loop as shown in Fig. 2.27. The strain level is taken as the single amplitude (half of the peak-to-peak amplitude) cyclic strain. In general, the modulus may be determined as the slope of the hysteresis loop shown in Fig. 2.27:

$$G = \frac{\tau_a}{\gamma_a}. \tag{2.45}$$

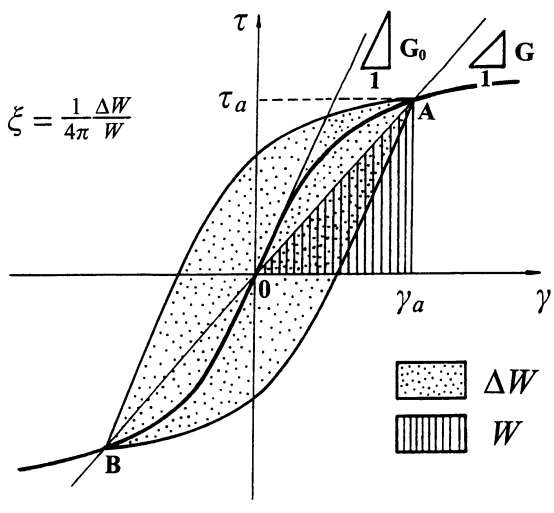


FIGURE 2.27. Determination of equivalent linear parameters, modulus and viscous damping, for soil with non-linear hysteretic characteristics.

The material damping, ξ, may be calculated as a ratio of energies represented by the areas shown in Fig. 2.27:

$$\xi = \frac{1}{4\pi}\left(\frac{\Delta W}{W}\right). \tag{2.46}$$

Note that the equations for modulus and damping assume that the soil behaves as an equivalent elastic, viscous damped material that is linear within the range of strain amplitude specified. Figure 2.27 indicates that the modulus decreases and the damping increases with increasing strain amplitude.

Low strain amplitude shear modulus data may be obtained from laboratory tests and usually involve application of high frequency forced vibration to a cylindrical specimen of soil and measuring the appropriate response (e.g. Drnevich 1976; Novak & Kim 1981). Some test types allow the intensity level of the forced vibration to be varied, thus causing the specimen to be strained different amounts (e.g. Al-Sanad & Aggour 1984; Tawfig *et al.* 1988). High strain level excitation may also be achieved by low frequency cyclic loading tests on laboratory specimens.

Either shear or normal stress cyclic excitation may be used. If simple shear (e.g. Airey & Wood 1987; Kovacs & Leo 1981) or torsion shear (e.g. Ishihara & Li 1972; Dobry *et al.* 1985) specimens are involved such that shear stresses and strains are measured, then the resulting modulus will be the shear modulus, G, as in Eq. 2.45. If the cyclic hysteresis loops are obtained from triaxial test specimens, the resulting modulus will be Young's modulus, E. The shear modulus may be computed from Young's modulus and Poisson's ratio, or vice versa, according to Eq. 2.17. In either case the same damping equation (Eq. 2.46) applies.

2.11.2 SEISMIC STABILITY OF SOIL STRUCTURES

Many methods have been developed for evaluation of stability of soil structures under

static and seismic loading conditions. The cyclic strength of soil is required in order to assess the stability of a soil deposit against liquefaction during an earthquake or to assess the seismic stability of an earth dam. Methods involving laboratory tests (e.g. Pyke *et al.* 1975) and methods involving empirical relations have been developed (e.g. Seed & Idriss 1971). All methods involve comparison of cyclic stress ratio to cyclic strength ratio or some other measure of strength during cyclic loading.

In the laboratory, cyclic stresses are applied to a soil specimen following consolidation to an effective confining pressure equal to the effective overburden pressure on the corresponding soil element in the field. The results of such a cyclic (triaxial or simple shear) test are conveniently expressed as a ratio of the cyclic stress required to cause a certain specified single amplitude cyclic strain or to cause liquefaction in N cycles. The corresponding field strength ratio of cyclic shear stress to effective overburden pressure may be estimated through an empirical correction factor and compared with the anticipated cyclic stress ratio in the field.

Methods have also been worked out in which the cyclic stress ratio anticipated in the field is compared with the results of several types of *in situ* tests and the magnitude of the earthquake. These field methods include standard penetration or equivalent tests, cone penetration tests and flat dilatometer tests. Their description may be found in Ishihara (1996) and Kramer (1996).

3. ENGINEERING PROPERTIES OF SOILS AND TYPICAL CORRELATIONS

P. V. Lade

3.1 Engineering Properties and Parameters Required for Characterization

The purpose of this chapter is to provide simple correlations between engineering properties and index properties for soils. The most important index properties and the tests used for their determination are briefly described. Correlations are provided for: (1) hydraulic conductivity, (2) at rest stress state, (3) compressibility and consolidation, (4) swelling and shrinkage, (5) shear strength and (6) dynamic properties. References are given to the sources of all correlations presented.

Whereas the correlations between engineering properties and index properties presented here may often be helpful, they should not substitute for the testing of intact soil specimens for determination of properties relevant to specific projects. The correlations should rather serve only for estimates of soil parameter values to be used with preliminary analyses. The correlations often represent attempts to unify soil behavior observed on various projects and in research investigations, and not all influential factors may have been recognized or well-defined. Furthermore, variations in testing procedures employed in different laboratories may have influenced the correlations presented. Therefore caution should be exercised when using these correlations.

3.2 Index Tests

Many engineering properties can be correlated with the index properties and the classification of soils. Below is a brief description of the most important index properties and the tests for their determination.

3.2.1 GRAIN-SIZE DISTRIBUTION

The grain-size distribution of a soil can be determined from sieve analyses and/or hydrometer tests according to ASTM Standard Test Method D 422. The grain-size distribution may be conveniently shown on a diagram as in Fig. 3.1. The definitions for boulders, cobbles, gravel, sand, silt and clay are indicated on Fig. 3.1 and in Table 3.1.

3.2.1.1 Coefficients of Uniformity and Curvature

The coefficients of uniformity, C_u, and curvature, C_c, are defined as:

$$C_u = \frac{D_{60}}{D_{10}} \quad \text{(pure number)} \tag{3.1}$$

$$C_c = \frac{(D_{30})^2}{D_{10}D_{60}} \quad \text{(pure number)} \tag{3.2}$$

where D_{60} = particle diameter at which 60% of the soil by weight is finer, D_{30} = particle diameter at which 30% of the soil by weight

R. K. Rowe (ed.), *Geotechnical and Geoenvironmental Engineering Handbook*
© Kluwer Academic Publishers 2001

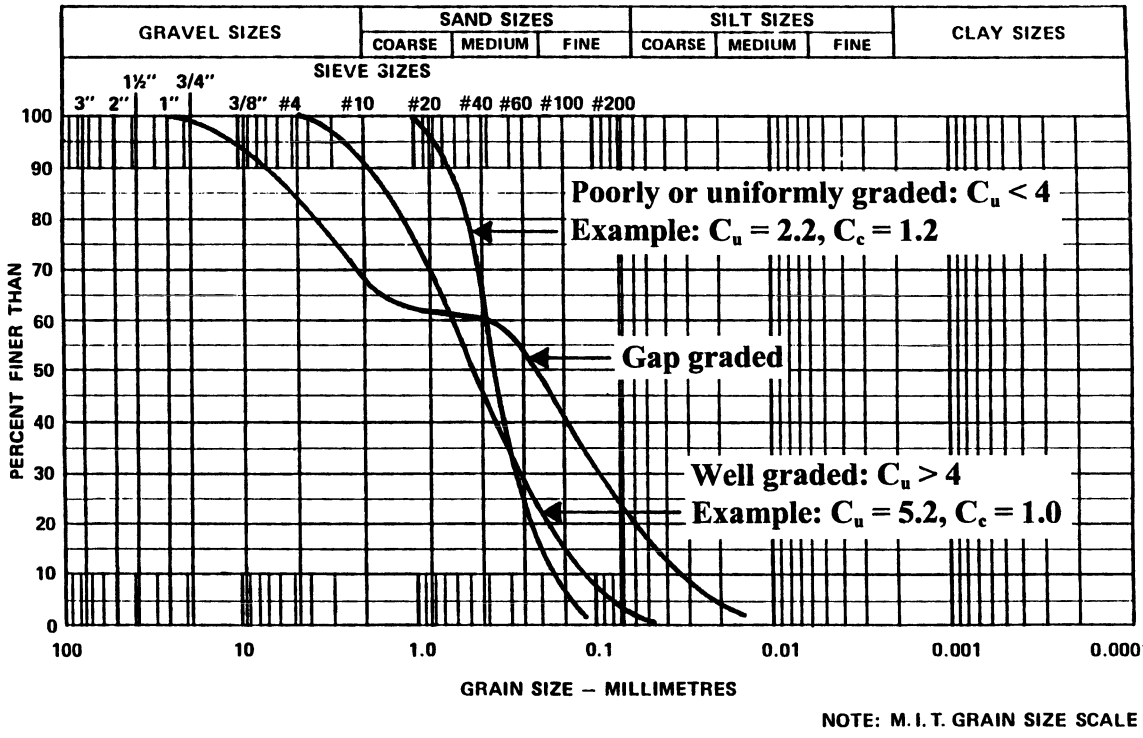


FIGURE 3.1. Grain-size distributions for poorly or uniformly graded, gap graded and well-graded soils (MIT grain-size scale) where C_u and C_c are the coefficients of uniformity and curvature, respectively.

TABLE 3.1. Particle sizes

	Unified classification		
Broad group	ASTM sieve number	mm	BS 1377 (mm)
Coarse-grained			
Boulder	>12″	>305	
Cobble	12″–3″	305–76	>60
Coarse gravel	3″–3/4″	76–19	60–20
Medium gravel			20–6
Fine gravel	3/4″–No. 4	19–4.75	6–2
Coarse sand	No. 4–10	4.75–2.0	2–0.6
Medium sand	No. 10–40	2.0–0.42	0.6–0.2
Fine sand	No. 40–200	0.42–0.075	0.2–0.06
Fine-grained			
Silt and/or clay	<No. 200	<0.075	
Coarse silt			0.06–0.02
Medium silt			0.02–0.006
Fine silt			0.006–0.002
Clay			<0.002

TABLE 3.2. Roundness criteria and values (after Youd 1973, © ASTM, reproduced with permission)

Roundness class	Description	Roundness range (R)*
Very angular	Particles with unworn fractured surfaces and multiple sharp corners and edges	0.12–0.17
Angular	Particles with sharp corners and approximately prismoidal or tetrahedral shapes	0.17–0.25
Subangular	Particles with distinct but blunted or slightly rounded corners and edges	0.25–0.35
Subrounded	Particles with distinct but well-rounded edges and corners	0.35–0.49
Rounded	Irregularly shaped rounded particles with distinct corners and edges	0.49–0.50
Well-rounded	Smooth nearly spherical or ellipsoidal particles	0.70–1.00

* Roundness, R, is the ratio of the average of the radii of the corners of a sand grain image to the radius of the maximum circle that can be inscribed within the grain image.

is finer, and D_{10} = particle diameter at which 10% of the soil by weight is finer.

The value of C_u provides a means of classifying the grain-size distribution as shown in Fig. 3.1. The coefficient of curvature, C_c, is a shape parameter used for classification of granular materials.

3.2.2 PARTICLE SHAPE

The terms for particle shape and roundness and their definitions are given in Table 3.2. Typical shapes of bulky grains are shown in Fig. 3.2.

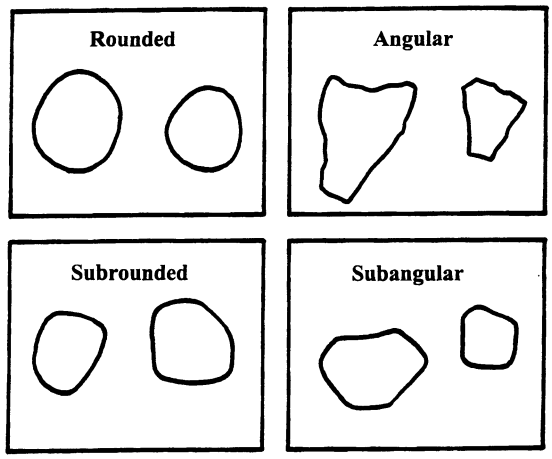


FIGURE 3.2. Typical shapes of bulky grains.

3.2.3 MAXIMUM AND MINIMUM VOID RATIOS

The void ratio for a given granular soil can vary from a maximum to a minimum value, and these values may be different from soil to soil. Procedures for determination of the maximum and minimum void ratios are given by ASTM Standard Test Methods D 4254 and D 4253. A set of curves relating e_{max} and e_{min} to C_u and particle shape for clean sands are shown in Fig. 3.3. Approximate values of the limiting void ratios may be estimated from this figure for normally distributed sands. Table 3.3 gives maximum and minimum void ratios, porosities and dry unit weights for typical granular soils.

3.2.4 DENSITY INDEX

The density index, I_D, indicates the magnitude of the field density relative to the extreme values, and it is defined in terms of void ratios:

$$I_D = \frac{e_{max} - e}{e_{max} - e_{min}} \times 100\% \qquad (3.3)$$

where e_{max} and e_{min} are the maximum and minimum void ratios obtained by standard procedures, as explained above, and e is the void ratio of the soil in the field. The density index was formerly known as the relative density.

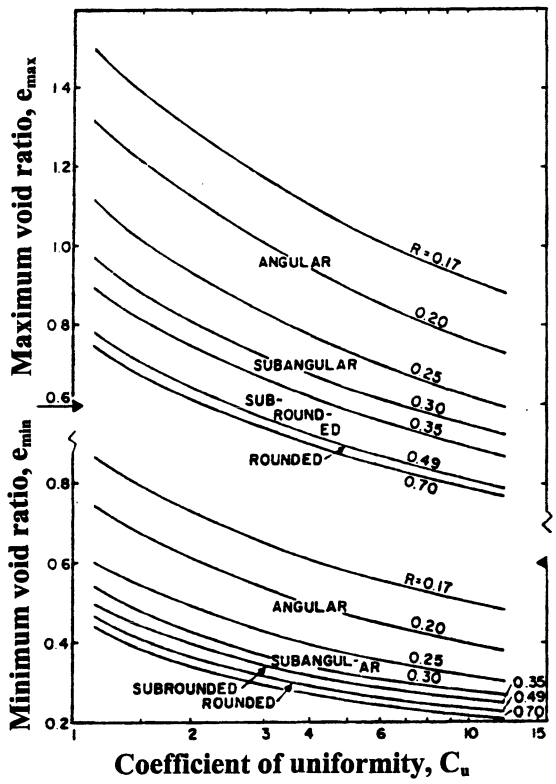


FIGURE 3.3. Generalized curves for estimating e_{max} and e_{min} from gradational and particle shape characteristics. Curves are only valid for clean sands with normal to moderately skewed grain-size distributions. Note: The minimum void ratios were obtained from simple shear tests, and they are slightly lower than those determined from ASTM Standard Test Method D 4253 (after Youd 1973, © ASTM, reproduced with permission).

3.2.5 RELATIVE COMPACTION

The relative compaction of a soil is defined as:

$$RC = \frac{\gamma_{d_{field}}}{\gamma_{d_{max,\ labtest}}} \times 100\% \qquad (3.4)$$

where $\gamma_{d_{field}}$ = dry unit weight in the field, and $\gamma_{d_{max,\ labtest}}$ = maximum dry unit weight obtained by a specified laboratory compaction procedure. For many granular soils a density index (formerly known as the relative density) of 100% may be approximately the same as 100% relative compaction based on the modified Proctor compaction method (ASTM Standard Test Method D 1557). Thus, for many granular soils the relative compaction and the density index are approximately related by the following empirical equation (Lee & Singh 1971):

$$RC = 80 + 0.2I_D \qquad (\text{for } I_D > 40\%). \qquad (3.5)$$

3.2.6 RELATIVE DENSITY

The relative density (formerly known as the specific gravity) of the soil solids is defined as the density of the solids divided by the density of water at 4 °C. It may be determined as specified in ASTM Standard Test Method D 854. The relative densities of various minerals are given in Table 3.4. If the mineral composition of a soil is not known, the best value of relative density is often estimated to be about 2.65 for sands, and about 2.70 for clays. However, it should be noted that the relative density for some soils may vary significantly from these values.

3.2.7 ATTERBERG LIMITS

The Atterberg limits consist of the liquid limit, the plastic limit and the shrinkage limit. Note that the ASTM procedures given below for all three Atterberg limits specify that the tests be performed on only the portion of soil finer than the No. 40 US standard sieve size (0.425 mm).

Most soils are composed of mixtures of different clay minerals and varying amounts of non-clay, non-plastic silt or rock-flour material. Thus, the Atterberg limits of most real soils may vary widely from the values for pure clays given in Table 3.5.

3.2.7.1 Liquid Limit

The liquid limit, w_L, of a fine-grained soil is the arbitrarily defined boundary between the semi-liquid and plastic states. The liquid limit is determined by measuring the water content and the number of blows required to close a specific groove in a standard liquid-limit device. The water content corresponding to 25

TABLE 3.3. Maximum and minimum densities for granular soils (modified from Lambe & Whitman 1979)

	Void ratio		Porosity (%)		Dry unit weight (kN m^{-3})	
	e_{max}	e_{min}	n_{max}	n_{min}	$\gamma_{d_{min}}$	$\gamma_{d_{max}}$
Uniform spheres	0.91	0.35	47.6	26	—	—
Standard Ottawa sand	0.80	0.50	44	33	14.5	17.3
Clean uniform sand	1.0	0.40	50	29	13.0	18.5
Uniform inorganic silt	1.1	0.40	52	29	12.6	18.5
Silty sand	0.90	0.30	47	23	13.7	20.0
Fine–coarse sand	0.95	0.20	49	17	13.4	21.7
Micaceous sand	1.2	0.40	55	29	11.9	18.9
Silty sand and gravel	0.85	0.14	46	12	14.0	22.9

TABLE 3.4. Relative density, D_r (formerly specific gravity), of various minerals

Mineral	Relative density
Anhydrite	3
Attapulgite	2.61
Augite	3.20–3.60
Biotite	2.80–3.20
Calcite	2.70–2.90
Chlorite	2.60–2.90
Dolomite	2.85–2.90
K-feldspars	2.54–2.57
Na–Ca-feldspars	2.62–2.76
Gibbsite	2.30–2.40
Gypsum	2.30–2.34
Halloysite ($2H_2O$)	2.55
Hematite	4.90–5.30
Hornblende	3.00–3.47
Illite	2.60–2.86
Kaolinite	2.50–2.64
Magnetite	5.17–5.18
Montmorillonite	2.75–2.78
Muscovite	2.70–3.10
Olivine	3.27–3.37
Pyrophyllite	2.84
Quartz	2.65
Serpentine	2.20–2.70
Siderite	3.83–3.88
Talc	2.70–2.80

blows is the liquid limit. The test procedure and special apparatus are described in detail in ASTM Standard Test Method D 4318.

3.2.7.2 Plastic Limit

The plastic limit, w_P, of a fine-grained soil is the arbitrarily defined boundary between the plastic and semi-solid states. The plastic limit is determined by measuring the water content of the soil when threads of the soil, 3.2 mm in diameter, begin to crumble. The procedure is described in detail in ASTM Standard Test Method D 4318.

3.2.7.3 Plasticity Index

The plasticity index, I_P, of a fine-grained soil is the range of water contents over which the soil behaves plastically. The plasticity index is defined as:

$$I_P = w_L - w_P. \tag{3.6}$$

Fine-grained soils may conveniently be classified and grouped using the plasticity chart shown in Fig. 3.4. Many engineering properties can be correlated with the liquid limit and plasticity index. Some trends in variations of engineering properties are indicated in Fig. 3.4. Note that there can be exceptions to these trends. More detailed correlations can be found in the following sections.

TABLE 3.5. Atterberg limits of clay minerals (after Lambe and Whitman 1979, *Soil Mechanics SI Version*, © John Wiley & Sons, Inc., New York, reproduced with permission)

Mineral	Exchangeable ion	Liquid limit (%)	Plastic limit (%)	Plasticity index (%)	Shrinkage limit (%)
Montmorillonite	Na	710	54	656	9.9
	K	660	98	562	9.3
	Ca	510	81	429	10.5
	Mg	410	60	350	14.7
	Fe	290	75	215	10.3
	Fe*	140	73	67	—
Illite	Na	120	53	67	15.4
	K	120	60	60	17.5
	Ca	100	45	55	16.8
	Mg	95	46	49	14.7
	Fe	110	49	61	15.3
	Fe*	79	46	33	—
Kaolinite	Na	53	32	21	26.8
	K	49	29	20	—
	Ca	38	27	11	24.5
	Mg	54	31	23	28.7
	Fe	59	37	22	29.2
	Fe*	56	35	21	—
Attapulgite	H	270	150	120	7.6

* After five cycles of wetting and drying.

3.2.7.4. Liquidity Index

The liquidity index, I_L, indicates the nearness of the water content of a natural soil to the liquid limit. The liquidity index is defined as:

$$I_L = \frac{w - w_P}{w_L - w_P} \tag{3.7}$$

where w = natural water content. For most soils $I_L < 1$; however, for some very sensitive (see Equation 3.9) Canadian and Scandinavian clays I_L may exceed unity.

3.2.7.5 Activity

The activity is a measure of the water-holding ability of the clay minerals, and it is defined as:

$$A = \frac{I_P}{\%\text{clay}} \tag{3.8}$$

where %clay = per cent of soil by weight finer than 0.002 mm. The activity of a soil may be used as an indication of the type of clay present in the soil: kaolinite (low activity, 0.4), illite (intermediate activity, 0.9) and montmorillonite (high activity, Ca-montmorillonite, 1.5; Na-montmorillonite 6.0).

3.2.7.6 Shrinkage Limit

The shrinkage limit, w_s, of a fine-grained soil is the water content at which no further shrinkage of a pad of soil occurs upon removal of more water. Details regarding the determination of the shrinkage limit are given in ASTM Standard Test Method D 427. Typical values for clay minerals are given in Table 3.5. The shrinkage limit can be used to evaluate the shrinkage potential and the possibility of development of cracks in earthworks as well as the expansion potential of clayey soils.

3.2.8 EXPANSION INDEX

The expansion index test provides a sensitive measure of potential soil expansion. It is performed by letting a soil specimen swell under a pressure of 6.9 kPa after compaction in a

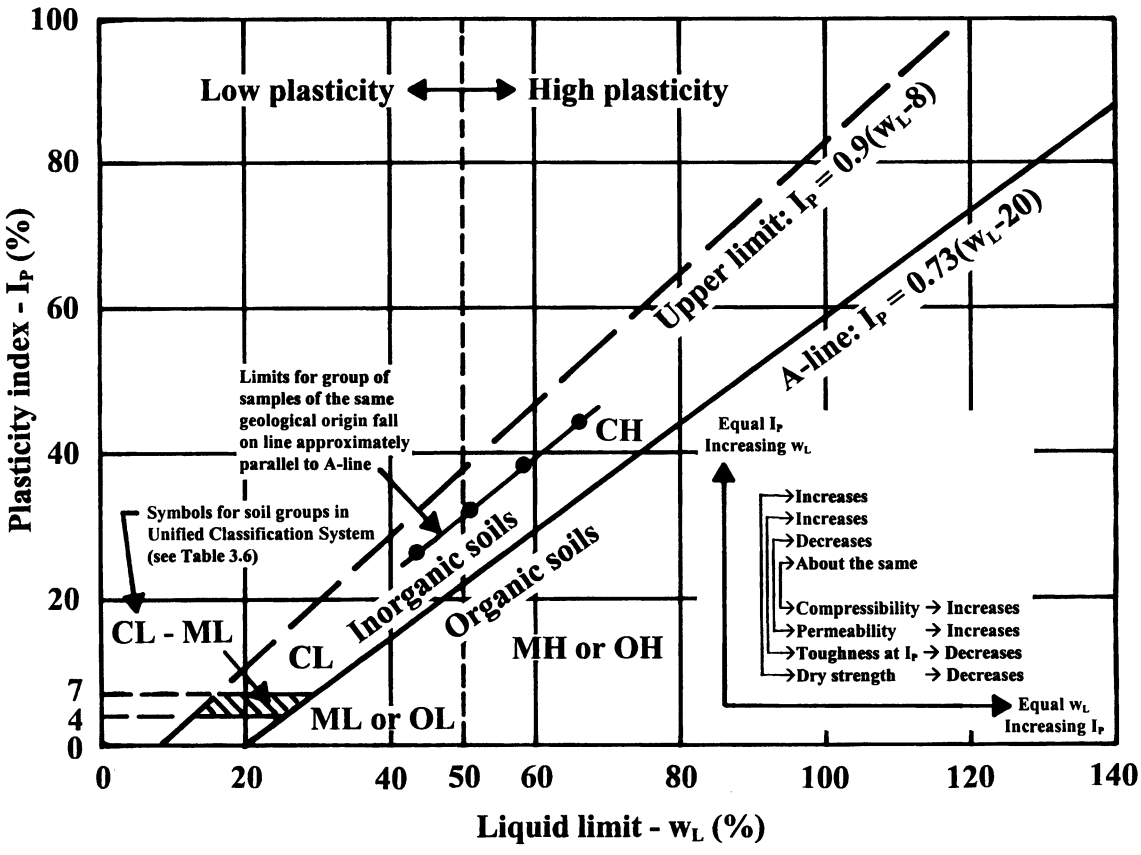


FIGURE 3.4. Plasticity chart with trends of variation in engineering properties.

steel ring at a degree of saturation of 50%. The initial conditions are specified to provide a specimen that will produce a measurable amount of expansion with a fairly wide range and sensitivity in a 24-hour period. The details of the performance of this test are given in ASTM Standard Test Method D 4829.

3.2.9 SENSITIVITY

The sensitivity, S_t, of a soil indicates the effect of remolding on the consistency of a clay soil, and it is calculated as:

$$S_t = \frac{s_u(\text{undisturbed})}{s_u(\text{remolded})} \qquad (3.9)$$

where, s_u (undisturbed) = undrained shear strength of the undisturbed soil, and s_u(remolded) = undrained shear strength of the remolded soil (at the same water content). The sensitivity may be determined from unconfined compression tests or from field or laboratory vane shear tests.

3.2.10 CONTENT OF ORGANIC MATERIAL

The content of organic material of a peat or organic soil sample is determined by igniting the initially oven-dried sample from a water content determination in a furnace at 440 °C. The organic matter is burned away and the amount of organic material is determined as a percentage of the remaining solids:

$$\%\ \text{organic material} = \frac{W_o}{W_s} \times 100\% \qquad (3.10)$$

TABLE 3.6. Soil classification chart (after ASTM Standard D 2487, © ASTM, reproduced with permission)

Criteria for assigning group symbols and group names using laboratory tests[a]				Soil classification	
				Group symbol	Group name[b]
Coarse-grained soils	Gravels	Clean gravels	$C_u \geq 4$ and $1 \leq C_c \leq 3$[e]	GW	Well-graded gravel[f]
More than 50% retained on No. 200 sieve	More than 50% of coarse fraction retained on No. 4 sieve	Less than 5% fines[c]	$C_u < 4$ and/or $1 > C_c > 3$[e]	GP	Poorly graded gravel[f]
		Gravels with fines	Fines classify as ML or MH	GM	Silty gravel[f,g,h]
		More than 12% fines[c]	Fines classify as CL or CH	GC	Clayey gravel[f,g,h]
	Sands	Clean sands	$C_u \geq 6$ and $1 \leq C_c \leq 3$[e]	SW	Well-graded sand
	50% or more of coarse fraction passes No. 4 sieve	Less than 5% fines[d]	$C_u < 6$ and/or $1 > C_c > 3$[e]	SP	Poorly graded sand[i]
		Sands with fines	Fines classify as ML or MH	SM	Silty sand[g,h,j]
		More than 12% fines[d]	Fines classify as CL or CH	SC	Clayey sand[g,h,i]
Fine-grained soils	Silts and clays	Inorganic	$I_P > 7$ and plots on or above "A" line[j]	CL	Lean clay[k,l,m]
50% or more passes the No. 200 sieve	Liquid limit less than 50		$I_P < 4$ or plots below "A" line[j]	ML	Silt[k,l,m]
		Organic	$\frac{\text{Liquid limit, oven dried}}{\text{Liquid limit, not dried}} < 0.75$	OL	Organic clay[k,l,m,n] Organic silt[k,l,m,o]
	Silts and clays	Inorganic	I_P plots on or above "A" line	CH	Fat clay[k,l,m]
	Liquid limit 50 or more		I_P plots below "A" line	MH	Elastic silt[k,l,m]
		Organic	$\frac{\text{Liquid limit, oven dried}}{\text{Liquid limit, not dried}} < 0.75$	OH	Organic clay[k,l,m,p] Organic silt[k,l,m,q]
Highly organic soils	Primarily organic matter, dark in color, and organic odor			PT	Peat

[a] Based on the material passing the 3″ (75 mm) sieve.
[b] If field sample contained cobbles or boulders, or both, add "with cobbles or boulders, or both" to group name.
[c] Gravels with 5–12% fines require dual symbols: GW-GM well-graded gravel with silt; GW-GC well-graded gravel with clay; GP-GM poorly graded gravel with silt; GP-GC poorly graded gravel with clay.
[d] Sands with 5–12% fines require dual symbols: SW-SM well-graded sand with silt; SW-SC well-graded sand with clay; SP-SM poorly graded sand with silt; SP-SC poorly graded sand with clay.
[e] $C_u = D_{60}/D_{10}$; $C_c = (D_{30})^2/(D_{10} \times D_{60})$.
[f] If soil contains ≥15% sand, add "with sand" to group name.
[g] If fines classify as CL-ML, use dual symbol GC-GM, or SC-SM.
[h] If fines are organic, add "with organic fines" to group name.
[i] If soil contains ≥15% gravel, add "with gravel" to group name.
[j] If Atterberg limits plot in hatched area, soil is a CL-ML, silty clay.
[k] If soil contains 15–29% plus No. 200, add "with sand" or "with gravel," whichever is predominant.
[l] If soil contains ≥30% plus No. 200, predominantly sand, add "sandy" to group name.
[m] If soil contains ≥30% plus No. 200, predominantly gravel, add "gravelly" to group name.
[n] $I_P \geq 4$ and plots on or above "A" line.
[o] $I_P < 4$ or plots below "A" line.
[p] I_P plots on or above "A" line.
[q] I_P plots below "A" line.

TABLE 3.7. Classification of peat structure (after MacFarlane 1969, © University of Toronto Press, reproduced with permission)

Predominant characteristic	Category	Name
Amorphous-granular	1	Amorphous-granular peat
	2	Non-woody, fine-fibrous peat
	3	Amorphous-granular peat containing non-woody fine fibers
	4	Amorphous-granular peat containing woody fine fibers
	5	Peat, predominantly amorphous-granular, containing non-woody fine fibers, held in a woody, fine-fibrous framework
	6	Peat, predominantly amorphous-granular containing woody fine fibers, held in a woody, coarse-fibrous framework
	7	Alternate layering of non-woody, fine-fibrous peat and amorphous-granular peat containing non-woody fine fibers
Fine-fibrous	8	Non-woody, fine-fibrous peat containing a mound of coarse fibers
	9	Woody, fine-fibrous peat held in a woody, coarse-fibrous framework
	10	Woody particles held in non-woody, fine-fibrous peat
	11	Woody and non-woody particles held in fine-fibrous peat
Coarse-fibrous	12	Woody, coarse-fibrous peat
	13	Coarse fibers criss-crossing fine-fibrous peat
	14	Non-woody and woody fine-fibrous peat held in a coarse-fibrous framework
	15	Woody mesh of fibers and particles enclosing amorphous-granular peat containing fine fibers
	16	Woody, coarse-fibrous peat containing scattered woody chunks
	17	Mesh of closely applied logs and roots enclosing woody coarse-fibrous peat with woody chunks

where W_o = weight of organic matter (removed upon heating), and W_s = weight of solids in soil mass. Details regarding the determination of the organic material are given in ASTM Standard Test Method D 2974.

3.2.11 SOIL CLASSIFICATION

Soils may be classified according to the unified soil classification system shown in Table 3.6 and described in ASTM Standard D 2487. Such classification is helpful for correlation with engineering properties of soils. Peat may be classified according to the system proposed by MacFarlane, as given in Table 3.7, or by the modified von Post system, as given in Table 3.8.

Table 3.9 gives some significant engineering properties of soils as they relate to the unified soil classification.

3.3 *Hydraulic Conductivity*

3.3.1 LABORATORY HYDRAULIC CONDUCTIVITY (PERMEABILITY) TESTS

Either constant head (e.g. ASTM Standard Test Method D 2434) or falling head permeability tests may be used to obtain the hydraulic conductivity of soils (Lambe & Whitman 1979; Cedergren 1989). Constant head triaxial (flexible wall) hydraulic conductivity tests (ASTM Standard Test Method D 5084) are often used to establish the hydraulic conductivity of compacted clays used in landfill liners, and fixed wall constant flow permeameters are of-

TABLE 3.8. Classification of peat based on the modified von Post system (after Landva & Pheeney 1980, © NRC Press, reproduced with permission)

1. Genera

Bryales (moss) = B; *Carex* (sedge) = C; *Equisetum* (horse tail) = Eq; *Eriophorum* (cotton grass) = Er; *Hypnum* (moss) = H; *Lignidi* (wood) = W; *Nanolignidi* (shrubs) = N; *Phragmites* = Ph; *Scheuchzeria* (aquatic herbs) = Sch; and *Sphagnum* (moss) = S.

2. Designation

With few exceptions natural peats consist of a mixture of two or more genera. The designation adopted in this paper is to list the genera in descending order of content, i.e. the first symbol represents the principal component. For example, a peat classified as ErCS consists mainly of *Eriophorum* remnants, while the content of *Carex* remnants would be lower and that of *Sphagnum* remnants relatively low.

3. Humification (H)

The degree of humification is graded on a scale from one to ten and designated H_1–H_{10}. The various degrees of humification are recognized as shown in the following table:

Degree of humification	Decomposition	Plant structure	Content of amorphous material	Material extruded on squeezing (passing between fingers)	Nature of residue
H_1	None	Easily identified	None	Clear, colorless water	
H_2	Insignificant	Easily identified	None	Yellowish water	
H_3	Very slight	Still identifiable	Slight	Brown, muddy water; no peat	Not pasty
H_4	Slight	Not easily identified	Some	Dark brown, muddy water; no peat	Somewhat pasty
H_5	Moderate	Recognizable, but vague	Considerable	Muddy water and some peat	Strongly pasty
H_6	Moderately strong	Indistinct (more distinct after squeezing)	Considerable	About one-third of peat squeezed out; water dark brown	
H_7	Strong	Faintly recognizable	High	About one-half of peat squeezed out; any water very dark brown	
H_8	Very strong	Very indistinct	High	About two-thirds of peat squeezed out; also some pasty water	Plant tissue capable of resisting decomposition (roots, fibres)
H_9	Nearly complete	Almost not recognizable		Nearly all the peat squeezed out as a fairly uniform paste	
H_{10}	Complete	Not discernible		All the peat passes between the fingers; no free water visible	

4. Water content (B)

In the field the water content of the peat is estimated on a scale from one (dry) to five (very high), designated B_1–B_5. In terms of actual water contents the following ranges are suggested: $B_2 < 500\%$; $B_3 = 500$–1000%; $B_4 = 1000$–2000%; and $B_5 > 2000\%$.

5. Fine fibers (F)

Fine fibers are defined as fibers and stems smaller than 1 mm in diameter or width. They are often of the *Eriophorum* genus, but *Hypnum* and *Sphagnum* stems may also be included if properly specified, e.g. F(H) or F(S). Shrub rootlets may also be included, specified as F(N). No special designation is indicated for plant root hairs, rhizoids or other fibers. The content of fine fibers is graded on a scale from zero to three as follows: F_0, nil; F_1, low content; F_2, moderate content; and F_3, high content.

6. Coarse fibers (R)

Coarse fibers are defined as fibers, stems and rootlets greater than 1 mm in diameter or width. They are often of the *Carex* genus, but *Hypnum* and *Sphagnum* stems may also be included if properly specified, e.g. R(H) or R(S). Shrub (N) rootlets are specified as R(N). The content of coarse fibers is graded on a scale from zero to three as follows. R_0, nil; R_1, low content; R_2, moderate content; and R_3, high content.

7. Wood (W) and shrub (N) remnants

Wood and shrub content is graded on a scale from zero to three as follows: W_0, nil; W_1, low content; W_2, moderate content; and W_3, high content.

TABLE 3.9. Engineering-use chart for different soil groups (after Wagner 1957). Relative desirability ranges from one (most desirable) to 14 (least desirable). No entry means the soil should not be used for this application

Typical names of soil groups	Group symbols	Important properties				Relative desirability for various uses									
						Rolled earth dams			Canal sections		Foundations		Roadways		
													Fills		
		Permeability when compacted	Shearing strength when compacted and saturated	Compressibility when compacted and saturated	Workability as a construction material	Homogeneous embankment	Core	Shell	Erosion resistance	Compacted earth lining	Seepage important	Seepage not important	Frost heave not possible	Frost heave possible	Surfacing
Well-graded gravels, gravel–sand mixtures, little or no fines	GW	Pervious	Excellent	Negligible	Excellent	—	—	1	1	—	—	1	1	1	3
Poorly graded gravels, gravel–sand mixtures, little or no fines	GP	Very pervious	Good	Negligible	Good	—	—	2	2	—	—	3	3	3	—
Silty gravels, poorly graded gravel–sand–silt mixtures	GM	Semi-pervious to impervious	Good	Negligible	Good	2	4	—	4	4	1	4	4	9	5
Clayey gravels, poorly graded gravel–sand–clay mixtures	GC	Impervious	Good to fair	Very low	Good	1	1	—	3	1	2	6	5	5	1
Well-graded sands, gravelly sands, little or no fines	SW	Pervious	Excellent	Negligible	Excellent	—	—	3 if gravelly	6	—	—	2	2	2	4
Poorly graded sands, gravelly sands, little or no fines	SP	Pervious	Good	Very low	Fair	—	—	4 if gravelly	7 if gravelly	—	—	5	6	4	—
Silty sands, poorly graded sand–silt mixtures	SM	Semi-pervious to impervious	Good	Low	Fair	4	5	—	8 if gravelly	5 erosion critical	3	7	8	10	6
Clayey sands, poorly graded sand–clay mixtures	SC	Impervious	Good to fair	Low	Good	3	2	—	5	2	4	8	7	6	2
Inorganic silts and very fine sands, rock flour, silty or clayey fine sands with slight plasticity	ML	Semi-pervious to impervious	Fair	Medium	Fair	6	6	—	—	6 erosion critical	6	9	10	11	—
Inorganic clays of low–medium plasticity, gravelly clays, sandy clays, silty clays, lean clays	CL	Impervious	Fair	Medium	Good to fair	5	3	—	9	3	5	10	9	7	7
Organic silts and organic silt-clays of low plasticity	OL	Semi-pervious to impervious	Poor	Medium	Fair	8	8	—	—	7 erosion critical	7	11	11	12	—
Inorganic silts, micaceous or diatomaceous fine sandy or silty soils, elastic silts	MH	Semi-pervious to impervious	Fair to poor	High	Poor	9	9	—	—	—	8	12	12	13	—
Inorganic clays of high plasticity fat clays	CH	Impervious	Poor	High	Poor	7	7	—	10	8 volume change critical	9	13	13	8	—
Organic clays of medium–high plasticity	OH	Impervious	Poor	High	Poor	10	10	—	—	—	10	14	14	14	—
Peat and other highly organic soils	Pt	—	—	—	—	—	—	—	—	—	—	—	—	—	—

ten used for clay–leacheate compatibility studies (see Chapter 25). The hydraulic conductivity, k, is backcalculated from Darcy's law for the flow of water (or any other fluid) through the soil (see Section 2.4).

For clayey, fine-grained soils the hydraulic conductivity may also be obtained in the laboratory from consolidation tests, either incrementally loaded or performed with constant strain rate. In the field it may be obtained by monitoring the response of the clayey layer to pumping of an adjacent confined aquifer (Rowe et al. 1995; see also Chapter 24).

3.3.2 TYPICAL HYDRAULIC CONDUCTIVITY VALUES AND CORRELATIONS

Soils may be classified according to their hydraulic conductivity. Typical values for different soils are given in Table 3.10.

An empirical correlation between the hydraulic conductivity, k (in m s^{-1}), and the "effective" grain size is given by Hazen's equation (Taylor 1948) for clean uniformly graded materials:

$$k = \frac{(D_{10})^2}{100} \qquad (3.11)$$

where D_{10} = "effective" grain diameter (in mm) at which 10% of the soil weight is finer.

TABLE 3.10. Hydraulic conductivity of soils, k

Soil	k (m s^{-1})	Drainage
Gravel	10^{-3}–1	Good
Coarse sand	10^{-6}–10^{-2}	Good
Medium sand	10^{-6}–10^{-3}	Good
Fine sand	10^{-7}–10^{-4}	Poor–good
Silty sand	10^{-7}–10^{-3}	Poor–good
Silt, loess	10^{-9}–10^{-5}	Poor–fair
Glacial till[a]	10^{-12}–10^{-6}	Very poor[b]–poor
Marine clay[a]	10^{-12}–10^{-9}	Very poor[b]–poor
Clay[a]	10^{-11}–10^{-8}	Very poor[b]–poor

[a] Weathered and fractured clays and tills may have substantially higher hydraulic conductivity than indicated.
[b] Soils with "very poor" drainage make good hydraulic barriers.

Equation 3.11 was obtained from filter sands whose effective sizes (D_{10}) were between 0.1 and 3 mm and for which the coefficient of uniformity, C_u, did not exceed five. Since the hydraulic conductivity can vary substantially from one soil to another, equations such as Equation 3.11 should be used with great caution.

The horizontal hydraulic conductivity is typically between 1.0 and 1.5 times the vertical permeability for homogeneous deposits. For stratified and varved clays the horizontal hydraulic conductivity can be much higher than the vertical hydraulic conductivity.

3.4 At Rest Stress State, K_0

The effective, horizontal stress may be determined from $\sigma'_h = K_0\sigma'_v$ in which the coefficient of earth pressure at rest, K_0, may be estimated from empirical expressions. Additional discussion of K_0 and its measurement in the field is presented in Chapter 4.

3.4.1 NORMALLY CONSOLIDATED SOILS

For normally consolidated soils the values of K_0 may be estimated from (Jaky 1948):

$$K_0 = 1 - \sin \phi' \qquad (3.12)$$

where ϕ' is the effective stress friction angle obtained from a triaxial compression test with a confining pressure of approximately the same magnitude as the horizontal stress to be found in the ground.

3.4.2 OVERCONSOLIDATED SOILS

The coefficient of earth pressure at rest for overconsolidated sands and clays, $(K_0)_{OC}$, may be estimated from (Schmidt 1966):

$$(K_0)_{OC} = (K_0)_{NC} \times (OCR)^{\sin \phi'} \qquad (3.13)$$

where $(K_0)_{NC}$ is the value of K_0 for the soil in the normally consolidated condition, OCR is the overconsolidation ratio, which must be determined from other sources, and ϕ' is the friction angle in triaxial compression. The ap-

proximation formula in Eq. 3.13 has been shown to give reasonable estimates of K_0 for many soils (Mayne & Kulhawy 1982).

3.5 *Compressibility and Consolidation*

3.5.1 ELASTIC PROPERTIES

The elastic modulus and Poisson's ratio are often used in connection with Hooke's law, given in Section 2.7.1, for evaluation of soil deformation. However, the concepts from the theory of elasticity apply to soil only in a very approximate way. Therefore, good judgment is needed when choosing values for the elastic modulus and Poisson's ratio. Typical values given refer to moderate confining pressures and shear stresses corresponding to a factor of safety of two or more.

3.5.1.1 Young's Modulus

The power function given in Eq. 2.24 is often used to express the variation of Young's modulus with confining pressure. The value of K^* varies with density of the soil, and approximate values for the initial modulus are given in Table 3.11. These values are very approximate and serve only to show the order of magnitude. Values of the exponent n typically vary from 0.4 to 0.7 with an average value of about 0.5 for sands, whereas n is about 1.0 for normally consolidated clays.

The unloading–reloading modulus, which more closely represents the elastic behavior of the soil, may also be modeled by Eq. 2.24 using values of K^* in the ranges also listed in Table 3.11. The same values of n apply to both initial loading and unloading–reloading.

TABLE 3.11. Approximate values of K^* for sands for initial loading and unloading–reloading

Density	K_i^* (initial loading)	K_{ur}^* (unloading–reloading)
Dense	1000–2000	2000–3000
Medium	500–1000	1000–2000
Loose	200–500	500–1000

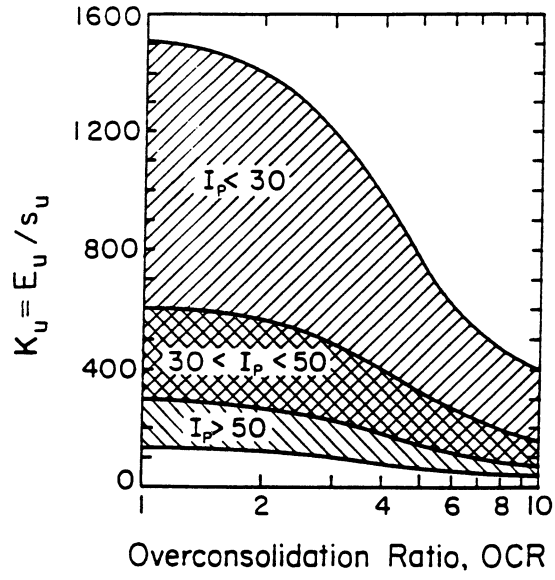


FIGURE 3.5. Diagram for estimating undrained modulus of clay (modified from Duncan & Buchignani 1976).

The undrained modulus for clays may be related to the undrained shear strength, s_u:

$$E_u/s_u = K_u \qquad (3.14)$$

where K_u is given in Fig. 3.5 as a function of plasticity index and overconsolidation ratio.

3.5.1.2 Poisson's Ratio

Table 3.12 gives typical values of Poisson's ratio, ν, for different types of soils.

TABLE 3.12. Approximate values of Poisson's ratio for soils

Soil	Poisson's ratio
Saturated soil, undrained loading	0.5
Clay, drained loading	0.2–0.4
Dense sand, drained loading	0.3–0.4
Loose sand, drained loading	0.1–0.3
Peat, drained loading	0–0.1

3.5.2 COMPRESSIBILITY

One-dimensional compression and expansion of soils was reviewed in Section 2.7.3, and typical quantities are given below.

3.5.2.1 Preconsolidation Pressure

The preconsolidation pressure, σ'_p, is the maximum past effective pressure to which the soil has been exposed. Aging produces a preconsolidation pressure in excess of that from the maximum past pressure. Approximate values of the preconsolidation pressure may be estimated from Fig. 3.6, which relates overburden pressure to void ratio for soils with various values of liquid limit and plasticity index. The preconsolidation pressure, σ'_p, may also be related to the liquidity index, I_L, for soils with sensitivity between one and ten by the relationship (Stas & Kulhawy 1984):

$$\log(\sigma'_p/p_a) = 1.11 - 1.62I_L \qquad (3.15)$$

where p_a is atmospheric pressure. Correlations with field vane strength, s_u(VST), have given (for intact clays, $I_p > 20$, Kulhawy & Mayne 1990):

$$\sigma'_p/s_u(\text{VST}) = 3.54. \qquad (3.16)$$

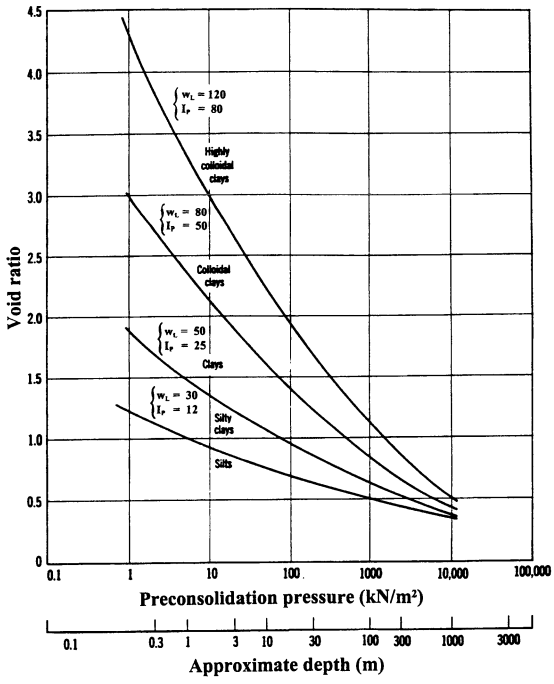


FIGURE 3.6. Approximate relation between void ratio and effective overburden pressure for clay sediments, as a function of Atterberg limits (after Lambe & Whitman 1979, *Soil Mechanics SI Version,* © John Wiley & Sons, Inc., New York, reproduced with permission).

TABLE 3.13. Compressibility of soils (modified from Sowers & Sowers 1970)

Term	Compression index
Slight or low compressibility	0–0.19
Moderate or intermediate	0.20–0.39
High compressibility	0.40 and over

3.5.2.2 Virgin Compression

Terms descriptive of compressibility are given in Table 3.13 together with corresponding values of compression indices. The compression index (Eq. 2.25) of silts and clays has been correlated with the liquid limit (w_L in per cent) (Terzaghi & Peck 1967).

For undisturbed soil:

$$C_c = 0.009(w_L - 10). \qquad (3.17)$$

For remolded soil:

$$C_c = 0.007(w_L - 10). \qquad (3.18)$$

Based on Cam Clay concepts, Wroth & Wood (1978) showed that C_c could be given by:

$$C_c = 0.005D_rI_P \qquad (3.19)$$

while Kulhawy & Mayne (1990) have shown that for a typical relative density of clay (D_r = 2.7) this gives:

$$C_c = I_P/74 \qquad (3.20)$$

which fits reasonably well with the regression through the observed data.

The approximate values of C_c for uniform sands in the pressure range from 100 to 400 kPa may vary from 0.05 to 0.06 for loose sands, and from 0.02 to 0.03 for dense sands.

The semi-logarithmic, straight-line slope of the virgin compression part of the ϵ_v–log σ' relation is expressed by the compression ratio, C_R, defined as:

$$C_R = \frac{\Delta\epsilon_v}{\Delta(\log \sigma')} = \frac{C_c}{1 + e_0} \qquad (3.21)$$

where C_c is the compression index and e_0 is the initial void ratio. Approximate correlations between compression index and void ratio for clays are given in Fig. 3.7.

3.5.2.3 Swelling and Recompression

The swelling index is generally in the order of one-fifth of the compression index. Approximate values may also be obtained from Fig. 3.8.

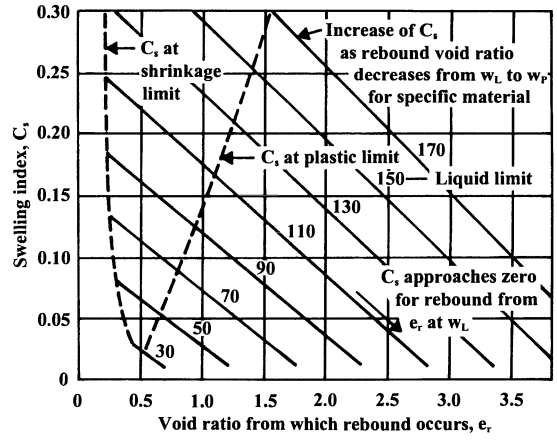


FIGURE 3.8. Approximate correlations for swelling index of silts and clays (modified from DM-7 1971).

3.5.3 COEFFICIENT OF CONSOLIDATION

The soil properties that control the drainage rate of porewater are combined in the coefficient of consolidation, c_v, as defined for vertical consolidation in Equation 2.29. Correlations between the coefficient of consolidation and the liquid limit are shown in Fig. 3.9 for undisturbed and remolded soil.

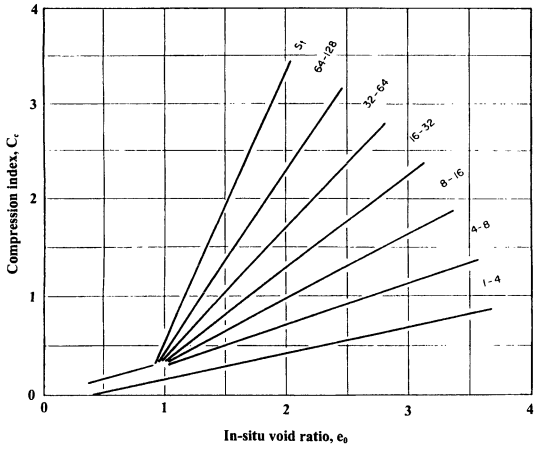


FIGURE 3.7. Relationship between compression index, C_c, and initial void ratio (after Leroueil *et al.* 1983, © NRC Press, reproduced with permission).

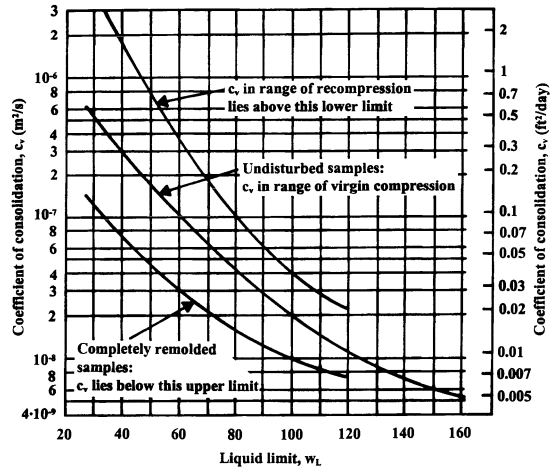


FIGURE 3.9. Correlations between coefficient of consolidation and liquid limit (modified from NAVFAC 1982).

TABLE 3.14. Values of $C_{\alpha e}/C_c$ for soils (after Terzaghi *et al.* 1996, *Soil Mechanics in Engineering Practice,* © John Wiley & Sons, Inc., New York, reproduced with permission)

Material	$C_{\alpha e}/C_c$	$m' = \Delta \log \dot{\varepsilon}_v / \Delta \log \sigma'_p$	$(\Delta\sigma/\sigma)/\Delta \log \dot{\varepsilon}$ (%)
Granular soils including rockfill	0.02 ± 0.01	100–33	2.3–7.2
Shale and mudstone	0.03 ± 0.01	50–25	4.7–9.6
Inorganic clays and silts	0.04 ± 0.01	33–20	7.2–12.2
Organic clays and silts	0.05 ± 0.01	25–17	9.6–14.8
Peat and muskeg	0.06 ± 0.01	20–14	12.2–17.5

3.5.4 CREEP

Table 3.14 gives values of the secondary compression index, $C_{\alpha e}$, in relation to the compression index, C_c, for different soils (Mesri 1987, Mesri *et al.* 1995, Terzaghi *et al.* 1996). Creep or secondary compression is particularly important for organic materials.

3.5.5 REMOLDED OR DISTURBED SOILS

Relative to undisturbed soil, remolding or disturbance lowers the void ratio reached under any applied pressure and eliminates the distinct break in the ε_v–log σ' curve at the preconsolidation pressure. Disturbance also lowers the apparent preconsolidation pressure and the value of the compression index, while increasing the swelling and recompression indices. Disturbance decreases the coefficient of consolidation for both virgin compression and recompression. For an undisturbed soil, the value of c_v usually decreases abruptly at the preconsolidation pressure. This trend is eliminated in severely disturbed soils. Finally, disturbance decreases the coefficient of secondary compression in the range of virgin compression.

3.6 *Swelling and Shrinkage*

To a limited extent the volume change potential may be related to the index properties of a soil. Correlations and classifications of the volume change potential have been based on single index properties or a combination of index properties.

The swelling potential is defined as the percentage swell of a laterally confined soil sample which has soaked under a surcharge of 6.9 kPa after being compacted to the maximum density at optimum water content according to the standard Proctor method (ASTM Standard Test Method D 698). Figure 3.10 shows a correlation between swell-

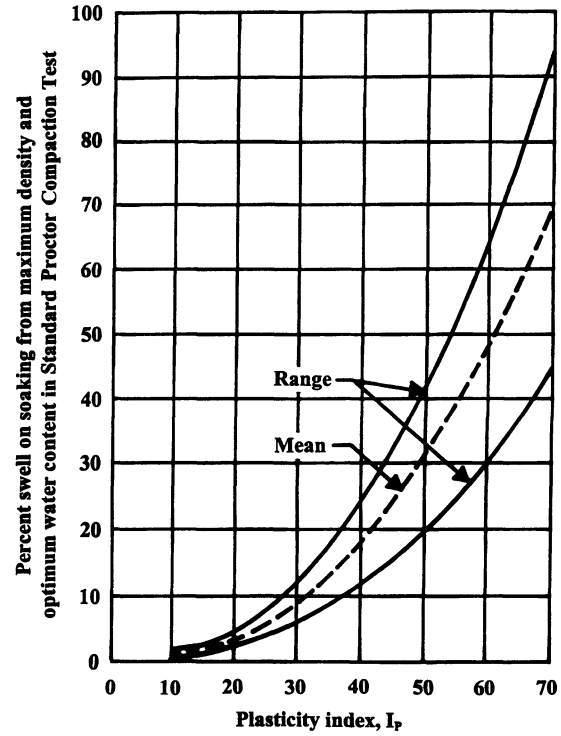


FIGURE 3.10. Predicted relationship between swelling potential and plasticity index for natural soils (modified from Seed *et al.* 1962).

TABLE 3.15. Classification of expansive soils on the basis of shrinkage index and expansion index (modified from US Bureau of Reclamation quoted in Ranganatham & Satyanatayana 1965, and after Anderson & Lade 1981, © ASTM, reproduced with permission)

Swelling potential	Shrinkage index	Expansion index
Very low		0–20
Low	0–20	21–50
Medium	20–30	51–90
High	30–60	91–130
Very high	>60	>130

ing potential and plasticity index for natural soils at the conditions of compaction noted above. This correlation applies to soils with clay contents between 8 and 65%.

An evaluation of the swelling potential, S, may be made on the basis of the shrinkage index, I_S (= liquid limit − shrinkage limit). A classification of expansive soils on the basis of the shrinkage index is given in Table 3.15. Ranganatham & Satyanarayana (1965) indicate the following empirical equation for the swelling potential of natural soils:

$$S(\%) = 41.13 \times 10^{-5} \times (I_S)^{2.67}. \quad (3.22)$$

The swelling potential calculated from this formula is reportedly accurate within ±34%.

The expansion index test, explained in Section 3.2.8, produces a sensitive indication of the expansion potential of soils, and a classification based on the expansion index is also given in Table 3.15.

The amount of swelling and shrinkage depends on the initial water content. If the soil is wetter than the shrinkage limit, then the maximum possible shrinkage will be equivalent to the difference between the actual water content and the shrinkage limit. Similarly, little swelling will occur after the water content has reached some value between the plastic and the liquid limits (Sowers & Sowers 1970).

Estimates of swelling potential, S, and swelling pressure, P_s, may be made from semi-empirical equations which incorporate the plasticity index, the per cent clay in the soil, C, and the initial molding water content, w_i. These equations were derived by Nayak & Christensen (1971) for expansive soils compacted at the optimum water content:

$$S(\%) = 3.5817 \times 10^{-2} \times (I_P)^{1.12}\left(\frac{C}{w_i}\right)^2 + 3.7912 \quad (3.23)$$

$$P_S(\text{kPa}) = 3.32 \times 10^{-3} \times (I_P)^{1.45}\left(\frac{C}{w_i}\right) + 0.925. \quad (3.24)$$

The swelling potential and swelling pressure calculated from these equations correlated well with the values obtained from laboratory tests (coefficients of correlation: S, 0.97; P_s, 0.92).

Direct correlations between volume change potential and index properties can only provide a rough estimate because these index properties do not adequately reflect the effects of soil structure, stress history and mineralogical changes with time. Many factors can influence the actual volume change in the field, and the index properties can only be expected to serve as a guide to the presence and possible behavior of expansive soils in the field.

3.7 *Shear Strength*

3.7.1 LABORATORY DETERMINATION OF SOIL BEHAVIOR

The variation in shear strength of soils with normal stress is most often expressed in terms of the Coulomb failure criterion in Equation 2.39 or the Mohr–Coulomb failure envelope expressed by Equation 2.40 in which the cohesion intercept, c' (or c), and the friction angle, ϕ' (or ϕ), are the soil parameters that characterize individual soils.

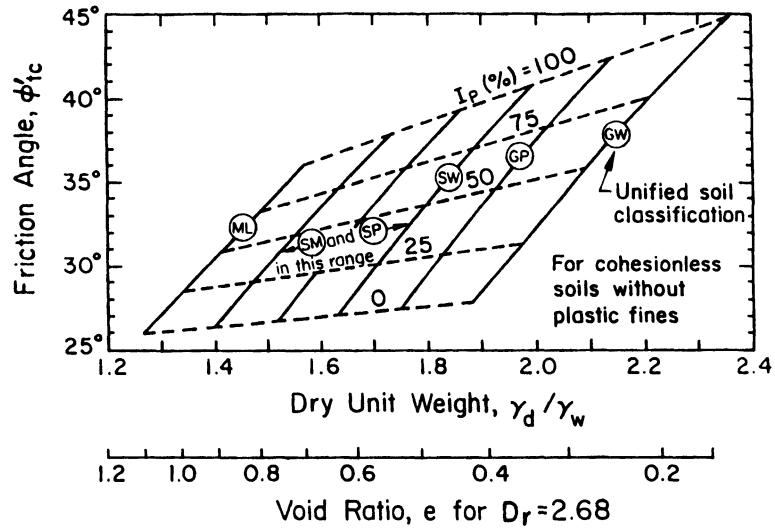


FIGURE 3.11. Correlations between the effective friction angle in triaxial compression and the dry density, density index and gradation for granular soils (modified from NAVFAC 1982).

The values of the cohesion and the friction angle pertinent to a particular soil may be found from direct shear tests, ring shear tests (e.g. Stark & Eid 1993), simple shear tests (e.g. Airey & Wood 1987), or triaxial compression tests (e.g. Bishop & Henkel 1962; Head 1986) performed on intact specimens or specimens prepared to the same conditions as those to be found in the field. The strength parameters may be obtained from consolidated-drained tests (CD-tests), consolidated-undrained tests (CU-tests), or unconsolidated-undrained tests (UU-tests). The strength parameters c and ϕ corresponding to total stresses may be obtained from any of the three types of tests depending on the loading condition in the field. The strength parameters c' and ϕ' corresponding to effective stresses can be obtained from CD-tests or from CU-tests with pore pressure measurements. The choice of test depends on the type of analysis to be made and the intended use of the parameters.

Correlations between shear strength parameters and index properties of soils may be useful for a first estimate and for comparing the results of shear tests on a particular soil with average published data.

3.7.2 EFFECTIVE STRENGTH PARAMETERS

3.7.2.1 Granular Materials: Cohesionless Soils

The shear strength of granular materials (for which the effective cohesion is zero in the absence of true cementation) may be expressed entirely in terms of the effective friction angle, ϕ'.

Figure 3.11 gives correlations between the effective friction angle in triaxial compression and the dry unit weight, γ_d (normalized on the unit weight of water, γ_w = 9.81 kNm^{-3} = 1.0 g cm^{-3} = 62.4 lb/ft^3), density index, I_D (formerly the relative density), grain size and gradation (both indicated by the symbols from the Unified Soil Classification System, see Table 3.6), for granular soils without plastic fines. It should be noted that angular particles may yield friction angles higher than indicated in Fig. 3.11.

An expression for estimating the friction

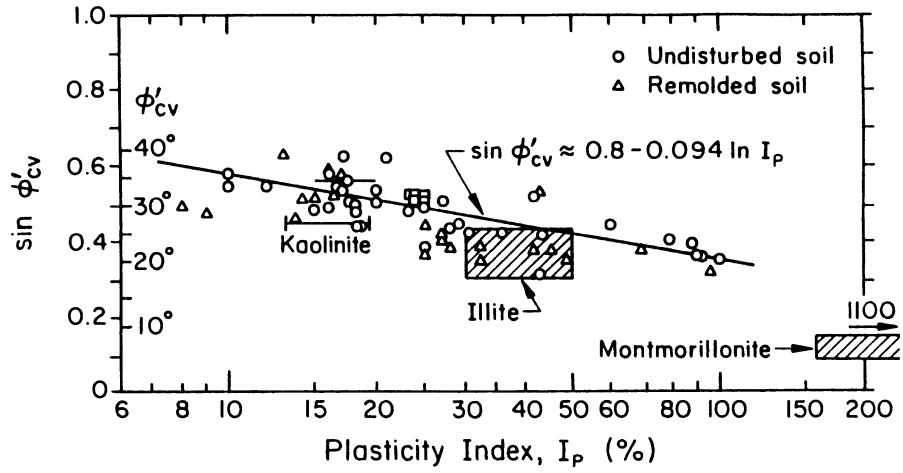


FIGURE 3.12. Correlations between effective friction angle and plasticity index for fine-grained soils (modified from Kulhawy & Mayne 1990).

angle at various void ratios, e, of granular materials is given as follows:

$$\tan \phi' = A/e \tag{3.25}$$

where A is a constant for a given soil, which may be determined from tests. Caquot & Kerisel (1966) suggest A = 0.40 for silts and A = 0.45 to 0.55 for sands.

Bolton (1986) has suggested that the friction angles in triaxial compression, ϕ'_{tc}, and in plane strain, ϕ'_{ps}, may be correlated with the rate of dilation in the following manner:

$$\phi'_{tc} - \phi'_{cv} = 3I_{RD} \tag{3.26}$$

$$\phi'_{ps} - \phi'_{cv} = 5I_{RD} \tag{3.27}$$

where ϕ'_{cv} is the friction angle corresponding to constant volume, and I_{RD} is the relative dilatancy index, defined as:

$$I_{RD} = I_D\left[Q - \ln\left(100\frac{\sigma'_{mf}}{p_a}\right)\right] - R \tag{3.28}$$

where I_D is the density index (formerly known as the relative density), Q is a soil mineralogy and compressibility coefficient (ten for quartz and feldspar, eight for limestone, seven for anthracite, 5.5 for chalk), σ'_{mf} is the effective mean normal stress at failure, and p_a is atmospheric pressure in the same units as σ'_{mf}, and R is a fitting coefficient (and is equal to one for quartz and feldspar sands). The relative dilatancy index, I_{RD}, in Eq. 3.28, should not exceed four.

The value of the friction angle at constant volume, ϕ'_{cv}, is essentially constant and independent of the density index for a given sand, and it is typically 33° for quartz sands and 40° for feldspar sands. Sands containing silt-size particles tend to have lower values of ϕ'_{cv} and Bolton (1986) suggested that most natural sand deposits rarely have values of ϕ'_{cv} greater than 30–33°, and it may be as low as 27° when the silt content is high.

3.7.2.2 Clays: Cohesive Soils

The shear strength of normally consolidated clays in terms of effective stresses can be expressed as in Eqs. 2.39 and 2.40 in terms of the effective friction angle only. The effective friction angle corresponding to maximum obliquity [i.e. $(\sigma'_1/\sigma'_3)_{max}$] may be estimated from Fig. 3.12 in terms of plasticity index for the clay. The friction angle may vary de-

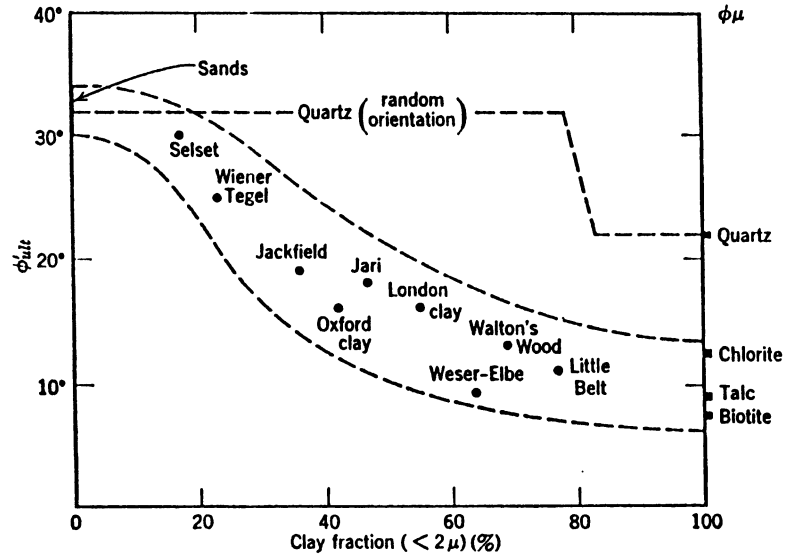


FIGURE 3.13. Relation between ultimate friction angle and clay content (after Skempton 1964).

pending on stress level and mineralogy. Typical ranges of values based on mineralogy (based on Olson 1974) are montmorillonite, 6–15°; illite, 15–28°; kaolinite 24–33°; and quartz, 30–45°. It should be noted that some soils may significantly depart from these values. For example, Mexico City clay has a very high plasticity index ($I_P > 200$), but a friction angle exceeding 40° (Lo 1962). The ultimate or residual effective friction angle of clayey soils may be estimated from Fig. 3.13 in terms of the clay content of the soil. The ultimate friction angle for quartz sand, ϕ_{ult} (shown to the left in Fig. 3.13), is higher than the basic friction angle, ϕ_μ, due to energy required for remolding at constant volume at the ultimate state.

3.7.3 UNDRAINED SHEAR STRENGTH

3.7.3.1 Normally Consolidated Clays

The undrained shear strength, s_u, of normally consolidated clays is proportional to the preconsolidation pressure, σ'_p (which is also the effective overburden pressure, σ'_{vo}), such that s_u/σ'_{vo} = constant for a given soil. Values of s_u/σ'_{vo} may be estimated from Fig. 3.14 as a function of the plasticity index for the soils. Skempton (1957) suggests the following approximation for the dotted line:

$$s_u/\sigma'_{vo} = 0.11 + 0.0037 I_P \qquad (3.29)$$

where I_P is the plasticity index, and s_u is determined from field vane shear tests (VST). The curved line suggested by Bjerrum (1973) fits better with the inorganic clays. The vane shear strengths for organic clays exhibit considerably more scatter than those for inorganic clays.

The undrained shear strength obtained from vane shear tests requires correction for use in design:

$$s_u(\text{field}) = \mu s_u(\text{vane}) \qquad (3.30)$$

where the value of the correction factor, μ, may be obtained from the correlation with the plasticity index in Fig. 3.15. The vane correction (Eq. 3.30 and Fig. 3.15) is most commonly applied to embankment design. Embankment design is discussed in detail in Chapter 16.

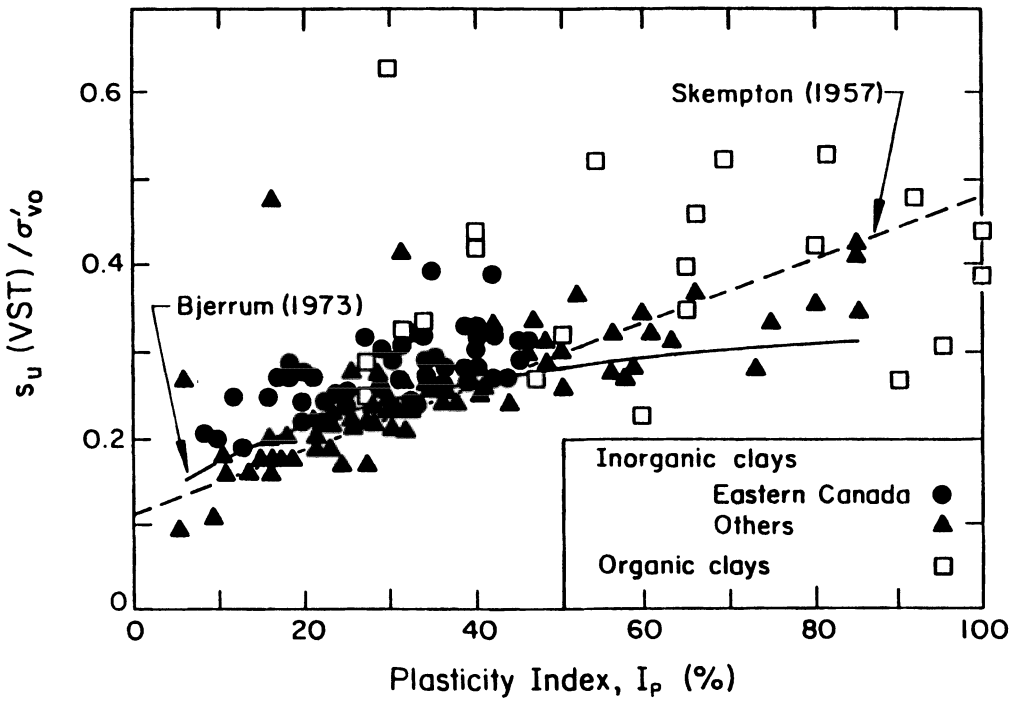


FIGURE 3.14. Relationship between s_u/σ'_p and plasticity index (modified from Tavenas & Leroueil 1987).

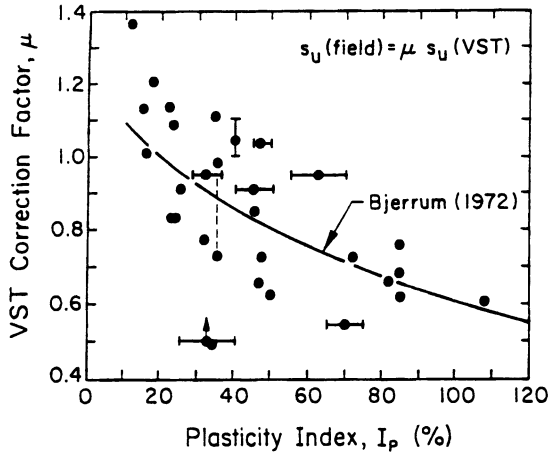


FIGURE 3.15. Correction factor versus plasticity index for undrained shear strength determined from vane shear test (VST) (modified from Ladd *et al.* 1977).

A correlation of the remolded, undrained shear strength of clays with the liquidity index is given by Leroueil et al. (1983):

$$s_u(\text{kPa}) = \frac{1}{(I_L - 0.21)^2}. \qquad (3.31)$$

The s_u/σ'_{vo} ratio for remolded clays is typically 0.3 ± 0.1 (Lambe & Whitman 1979).

3.7.3.2 Overconsolidated Clays

For overconsolidated clays a correlation between the normalized s_u/σ'_{vo} ratio and the overconsolidation ratio is given in Fig. 3.16. The value of σ'_{vo} in $(s_u/\sigma'_{vo})_{OC}$ is the effective present overburden pressure. Values of $(s_u/\sigma'_{vo})_{OC}$ may be estimated from Fig. 3.16 when $(s_u/\sigma'_{vo})_{NC}$ (i.e. the corresponding value for the normally consolidated clay) and the overconsolidation ratio are known.

Generalized relationships between sensitivity, liquidity index and effective overbur-

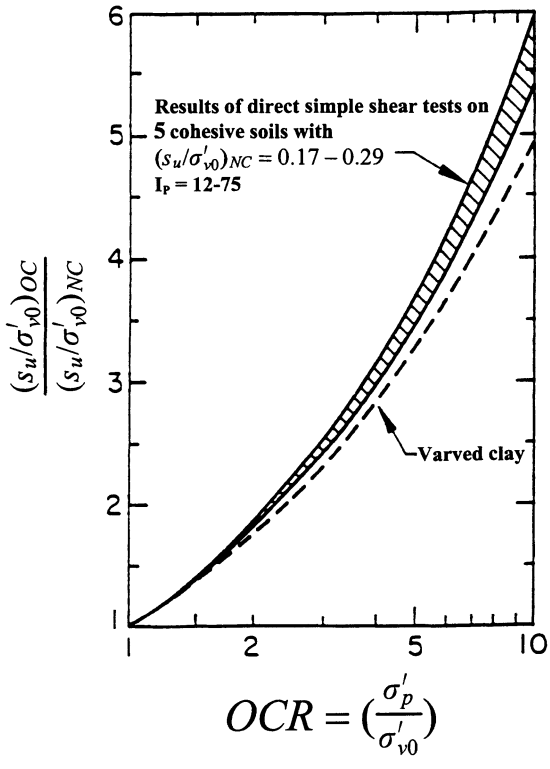


FIGURE 3.16. Normalized variation of s_u/σ_p ratio for overconsolidated clay (modified from Ladd *et al.* 1977).

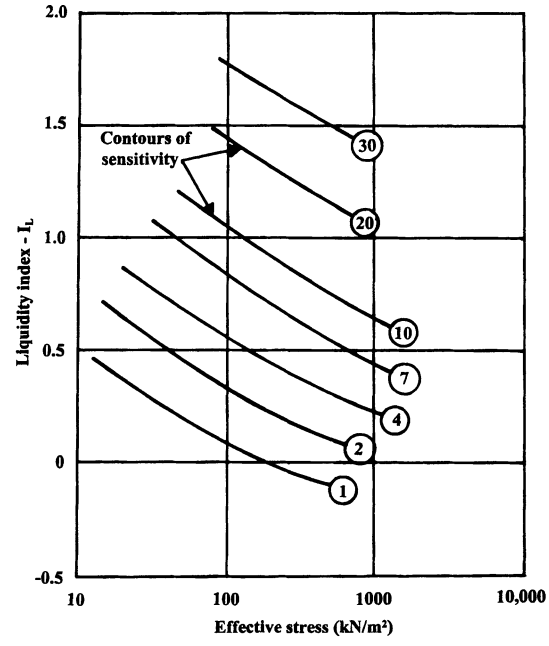


FIGURE 3.17. General relationship between sensitivity, liquidity index and effective overburden pressure (modified from Houston & Mitchell 1969).

den pressure are shown in Fig. 3.17. The preconsolidation pressure rather than the effective overburden pressure should be used for overconsolidated soils when entering Fig. 3.17. Cementation and aging cause higher values of sensitivity than given in Fig. 3.17.

3.8 *Dynamic Properties*

3.8.1 SHEAR MODULUS AND DAMPING: LOW STRAIN LEVEL EXCITATION

Empirical correlations for many sets of data have suggested approximate methods for estimating the shear wave velocity and shear modulus for soils corresponding to low strain excitation. Hardin (1978) has suggested that for many cohesive soils and sands, the maximum shear modulus may be calculated from the following empirical equation:

$$G_{max}/p_a = \frac{625}{0.3 + 0.7e^2}(OCR)^{\mu}(\sigma'_o/p_a)^{0.5} \quad (3.32)$$

where e = void ratio; $\sigma'_o = (\sigma'_1 + \sigma'_2 + \sigma'_3)$ = effective mean normal stress; p_a = atmospheric pressure in the same units as σ'_o; OCR = overconsolidation ratio of the soil; and μ = empirical constant, which depends on the plasticity index (I_p) of the soil, as indicated in Table 3.16. For sands with $I_p = 0$, $\mu = 0$, so that the overconsolidation ratio term reduces to 1.0. For clays, μ increases up to a maximum value of 0.5 at $I_p \geq 100$. For two-dimensional conditions, Yu & Richart (1984) suggest using $\sigma'_m = \frac{1}{2}(\sigma'_a + \sigma'_b)$ rather than σ'_o in Equation 3.32. The value of σ'_m represents the average of the in-plane vertical and horizontal stresses.

TABLE 3.16. Values of constant μ used with Equation 3.32 to estimate cyclic shear modulus at low strains (modified from Hardin & Drnevich 1972)

Plasticity index	μ
0	0
20	0.18
40	0.30
60	0.41
80	0.48
≥100	0.50

TABLE 3.17. Values of constant K_2 used with Equation 3.33 to estimate cyclic shear modulus at low strains for sands (modified from Seed & Idriss 1970)

Void ratio, e	K_2	Density index, I_D (%)	K_2
0.4	70	90	70
0.5	60	75	61
0.6	51	60	52
0.7	45	45	42
0.8	39	40	40
0.9	33	30	33

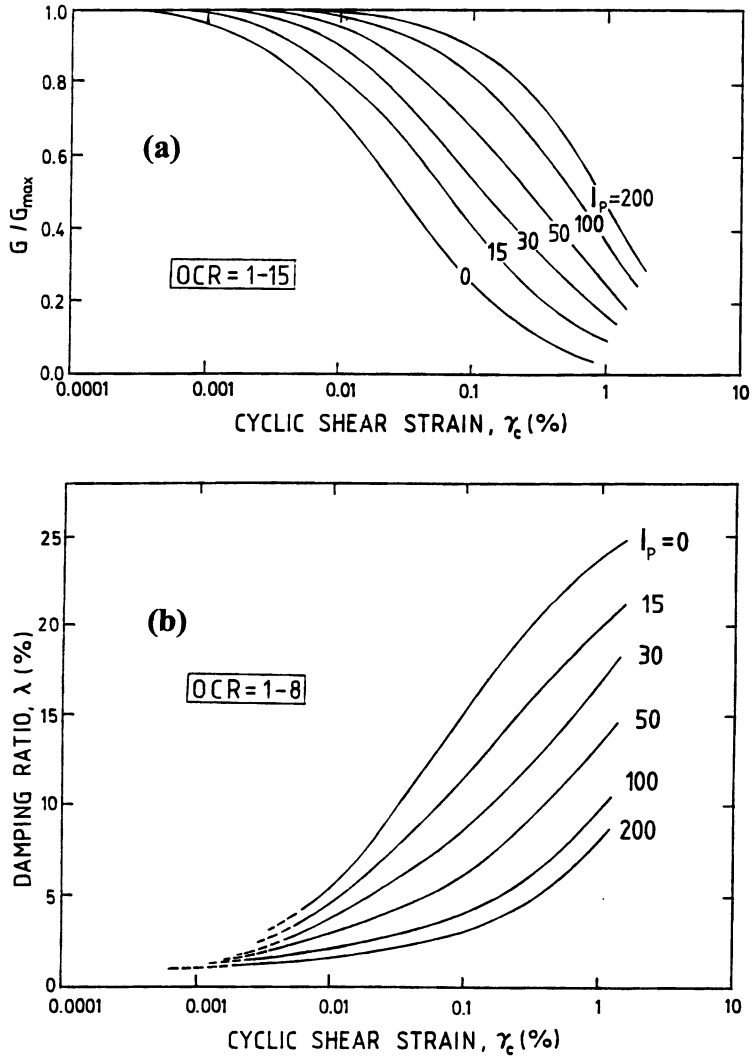


FIGURE 3.18. Variation of normalized shear modulus (a) and damping ratio (b) with single amplitude shear strain and soil plasticity for normally and overconsolidated soils (after Vucetic & Dobry 1991, © ASCE, reproduced with permission).

Seed & Idriss (1970) have shown that for sands and gravels the low strain shear modulus may be calculated from the following equation:

$$G_{max}/p_a = 22K_2(\sigma'_o/p_a)^{0.5} \qquad (3.33)$$

where K_2 is an empirical constant which may be related to the soil type and the void ratio, e, or the density index (formerly relative density), I_D, as shown in Table 3.17. For dense sand, gravel and cobbles with little clay, the value of K_2 is 90–190. For cohesive soils (clays and peat) Seed & Idriss (1970) have found it convenient to relate the low strain cyclic shear modulus to the undrained static shear strength, s_u:

$$G_{max} = K_s s_u \qquad (3.34)$$

where K_s is an empirical dimensionless constant, which depends on soil type. For clays K_s is about 1500–3000. For peats K_s is about 150–160 (very limited database).

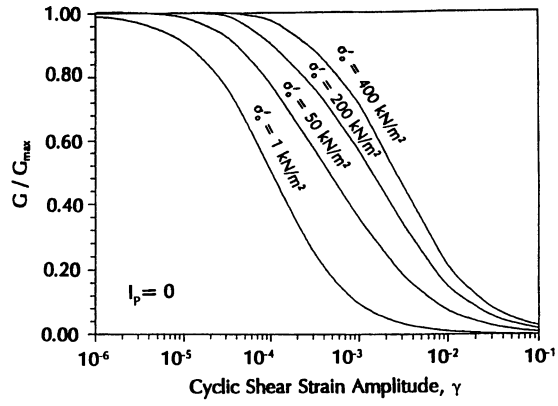


FIGURE 3.19. Variation of normalized shear modulus with single amplitude shear strain and confining pressure for granular materials (after Ishibashi 1992, © ASCE, reproduced with permission).

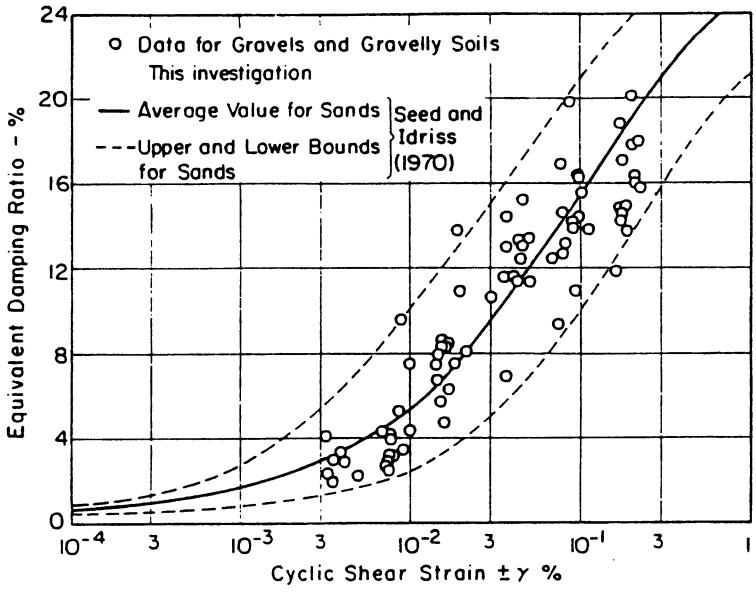


FIGURE 3.20. Variation of damping ratio with single amplitude shear strain for granular materials (after Mitchell 1993, *Fundamentals of Soil Behavior*, © John Wiley & Sons, Inc., New York, reproduced with permission).

Material damping at low strain level excitation is generally less than 5% of critical for most soils (Whitman & Richart 1967). It is important to note that this refers only to material damping, and not to energy loss by radiation away from a vibrating foundation. Radiation damping in machine vibration problems is a function of the geometry of the problem rather than of the physical properties of the soil and is thus beyond the scope of this section.

3.8.2 SHEAR MODULUS AND DAMPING: HIGH STRAIN LEVEL EXCITATION

As indicated in Fig. 2.27, the effect of increasingly higher strain levels is to reduce the modulus and increase the damping of the soil. The curves shown in Fig. 3.18 indicate how the normalized shear modulus and the damping ratio vary with single amplitude shear strain and soil plasticity for normally and overconsolidated soils. Normalized shear modulus for granular soils also varies with confining pressure as indicated in Fig. 3.19, while variation of damping ratios for granular materials is indicated in Fig. 3.20. Shear modulus and damping values at high strains are used mainly in computer programs for analyzing the seismic response of soil under earthquake loading conditions.

The above described empirical relations for modulus and damping pertain to sands and soft normally consolidated clays at low to medium effective confining pressures in the range up to about 30 m overburden. Stiff overconsolidated clays and all soils at high effective confining pressure exhibit lower values of damping and higher values of modulus, especially at high strain levels. In the limit, the modulus and damping values for stiff or strong soils at very high effective confining pressures correspond to values pertaining to crystalline or shale rock.

4. SITE CHARACTERIZATION

D. E. Becker

4.1 Introduction

Site characterization involves the determination of the nature and behavior of all aspects of a site and its environment that could significantly influence, or be influenced by, a project. Geotechnical and environmental aspects should be jointly considered and evaluated. The basic purpose of site characterization is to provide sufficient, reliable information of the site conditions to permit good decisions to be made during assessment, design and construction phases of a project, or as required by regulatory agencies. Site characterization involves determining information on previous and current land use, topography and surface features, hydrogeology, hydrology, meteorology, geology, seismology, geotechnical aspects, environmental aspects, biology, zoology, air quality, water quality, geochemistry and other factors.

This chapter presents an overall perspective of the current state-of-practice. It has been written for a broad variety of readers, ranging from graduate students and young practitioners through to the more experienced practitioner, regulators, and clients and owners. The chapter provides information to assist in the planning and organization of site characterization programs, and to increase the awareness of the variability and uncertainty associated with the ground and the impact of inadequate site characterization on projects. A general awareness and knowledge of site characterization processes and their limitations enhances better communication and understanding amongst the various parties of a project (e.g. owner, client, consultant, regulatory agencies, government and the general public). The key elements of site characterization are identified and briefly discussed. The objectives, philosophy, theoretical considerations and organization of site characterization studies are firstly presented and discussed, followed by identification and discussion of appropriate tools (equipment and test methods) and methods of interpretation. Laboratory testing is part of site characterization; however, it has been discussed in Chapters 2 and 3. This chapter deals mainly with the field component of site characterization studies.

4.1.1 THE NEED FOR SITE CHARACTERIZATION

The largest area of technical and financial risk in civil engineering construction and geoenvironmental projects is associated with the occurrence of ground- (i.e. soil/rock-) related problems (Site Investigation Steering Group 1993). There are hazards and uncertainties in the ground, as a result of natural and man-made processes, that may jeopardize a project and its environment if they are not adequately understood and mitigated. A design or site assessment will not be meaningful or successful if the facts upon which they are based are incorrect. For example, if an inherent weak layer within the ground is not discovered during the investigation, no analysis, no matter how refined and sophisticated, will

R. K. Rowe (ed.), *Geotechnical and Geoenvironmental Engineering Handbook*
© Kluwer Academic Publishers 2001

reliably predict overall performance of the ground. The performance will be controlled by the weak layer. A design solution that has not considered or taken into account the presence of the weak layer may not be appropriate or adequate. Significant effort must, therefore, be made to determine the characteristics of a site by means of appropriate site investigation and testing methods. Each project and site is unique. An investigation should be carried out for every site. In fact, even with site characterization, significant uncertainties and unforeseen events may still occur. An appropriate site characterization will maximize economy by reducing, to an acceptable level, the uncertainties and risk that site conditions pose to a project.

Site characterization also plays an important role in safety assessments and identification of potential environmental effects. The public needs to be reassured that the project is safe during construction, and that it will remain safe thereafter. The project could affect the environment in many ways. For example, construction activities may cause movements and damage to existing structures, lead to changes in the groundwater regime resulting in migration of existing contaminant plumes to areas that previously were not contaminated and, in some circumstances, may release harmful substances into the environment.

4.1.2 OBJECTIVES OF SITE CHARACTERIZATION

The basic objective is to provide sufficient and reliable information and data on the site conditions to a level of detail compatible and consistent with the needs and requirements of the project. The scope of work and requirements of site characterization will vary for each project. From the geotechnical perspective, the investigation should determine: the nature and sequence of soil and rock strata; location of groundwater table and groundwater conditions; engineering properties of the ground such as strength, compressibility and hydraulic conductivity; and other information such as chemical composition of groundwater and sediments that would make them aggressive to normal construction materials.

From the environmental assessment perspective, additional baseline studies also need to be carried out to determine: current air quality, noise and vibration characteristics; current population levels and inventory of flora and fauna species, and to identify the presence of any rare indigenous species that may be threatened by proposed development, both temporarily during construction and in the long term following completion of construction; current surface water quality in terms of potable supply, turbidity, temperature, acidity/alkalinity and habitat for rare indigenous species; current groundwater quality; current hydrogeological flow regimes; private water wells that could be influenced by the proposed development; and any existing zones and concentration of contaminants.

4.2 Site Characterization Process: An Integrated Approach

Site characterization is an integral part of the overall project requirements, and of the site assessment and design process. Figure 4.1 shows the relationships that generally exist for projects. The controlling influence is the specific needs and requirements of the project; assessment and design lie at the kernel of the process. Clearly understanding the needs of the client/owner, from both the technical and financial aspects, for any project is a key fundamental that, perhaps, is too frequently overlooked or ignored in site characterization studies. Prior to the start of any investigation, there must be sufficient effective communication between the client/owner and the consultant undertaking the investigation to ensure that the require-

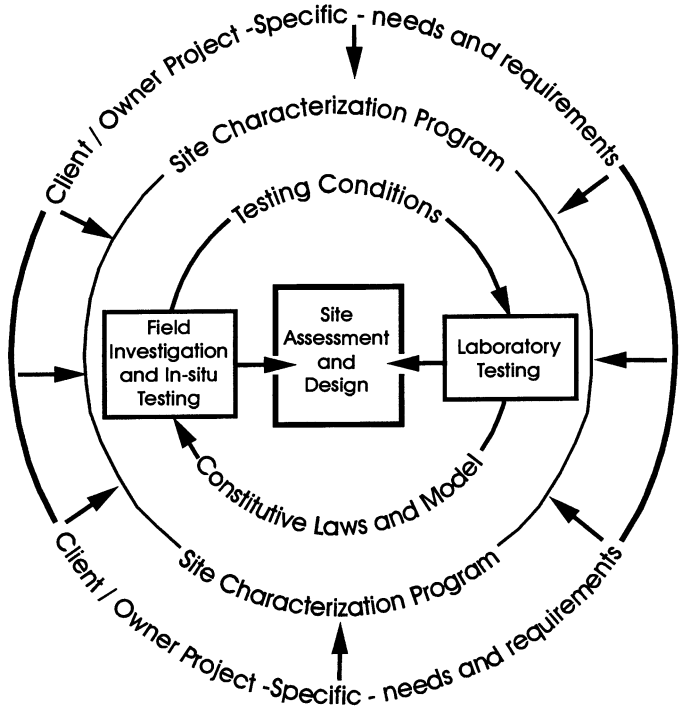


FIGURE 4.1. Geotechnical circle concept for site characterization.

ments of the project are clearly understood, and that the client/owner is made aware of the important relationship that exists between risks and costs. The degree of uncertainty about a site is usually directly related to the cost of site characterization. A degree of uncertainty and risk, however, will always exist for a site, even after large comprehensive investigations have been completed. If the risks and uncertainties have not been reduced to an acceptable level, the investigation has neither been cost-effective nor successful. It is the responsibility of the client/owner to decide what is an acceptable level of risk, after being made aware of the potential consequences and technical limitations associated with various options or level of investigation detail.

The essence of site investigation is the discovery of facts: therefore, an element of research is present in all characterization works. However, the research end should not be the controlling influence in deciding what work is done and it must not compromise the needs of the project nor of the client. Any decision made should always be in the context of: what is best for the project and does the project really need it?

As shown on Fig. 4.1, testing is an inherent part of characterization, assessment and design. Important interrelationships exist between the field and laboratory. Laboratory and *in situ* testing are linked by constitutive relationships of the material being investigated. Field investigation and *in situ* testing results provide not only direct design information and parameters, but also provide data required to define appropriate test conditions in the laboratory. An example of this is the determination of the coefficient of earth pressure at rest, K_0, in the field for subsequent use in the laboratory. Laboratory test

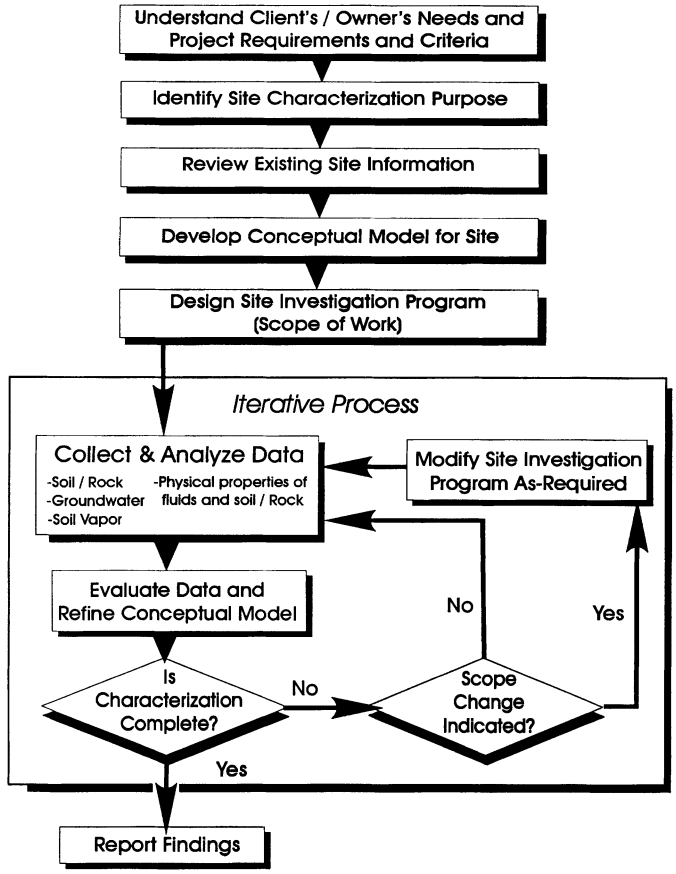


FIGURE 4.2. Site characterization process flowchart (modified from Taylor & Erikson 1996).

results, in turn, provide data to assist in proper evaluation and interpretation of *in situ* testing.

4.2.1 SITE CHARACTERIZATION FLOWCHART

The site characterization process is summarized in Fig. 4.2, which shows that the process is iterative in nature. Ground conditions vary with location across a site and in some cases they can vary significantly over small distances. A large part of the iterative process should take place during the field program. As data are obtained and interpreted, it is often necessary to make changes to the conceptual model and additional data collection is required. During the assessment of data obtained, one should not ignore data simply because they do not fit the general trend or expected behavior. If it is concluded after a thorough evaluation that the test was carried out properly, the test result must be kept. Good test data always tell something or suggest where next to look. Apparent anomalies often provide new insight and provide the stimulus for further work to better characterize and understand a site. The discrepancy may indicate unique behavior. An example of this is described by Jefferies *et al.* (1987).

It is important to build as much flexibility as possible into the characterization program.

Flexibility is enhanced by the following factors: having suitable communications protocol in place with the client/owner and regulators; selecting the right tools (equipment and test methods) and having the ability to change tools should field conditions change; having suitable contingency plans in place that have been discussed with the client/owner; and most importantly, having the "right" people in the field with the appropriate level of authority to make decisions and move the process forward.

A site characterization study should adopt a staged investigation approach consisting of: (1) initial site appraisal through review of available information and reconnaissance; (2) preliminary investigation and assessment; and (3) final, detailed investigation and assessment. Each phase provides input to subsequent phases; they also define areas of the site and/or design aspects that require further investigation in subsequent stages. All three phases will not necessarily be required on all projects.

4.2.2 REPORTING

The site characterization report is very important because different parties will use it to obtain an understanding of the site characteristics for different purposes. The report provides the main vehicle of communications between the parties involved in a project, including regulatory agencies, and it constitutes the primary reference for contractual purposes. For example, geotechnical and hydrogeological baseline, interpretative and design summary reports, in addition to providing the basis for site assessment and design, also define the conditions upon which claims for changed conditions will be assessed from a contractual perspective. The primary purpose of the interpretative geotechnical baseline report (GBR) is to establish a contractual statement of the geotechnical conditions anticipated to be encountered during underground and subsurface construction. These baseline conditions provide the basis for resolution of disputes concerning changed site conditions. The GBR also presents the conditions that formed the basis of design; it should enhance the contractor's understanding of the key project and site constraints, and requirements for excavating and supporting the ground. Previously, this document was commonly referred to as the geotechnical design summary report (GDSR). A discussion of the current status and role of such baseline reports in contracts is provided by Bohlke (1996) and ASCE (1997).

All site information should be formally reported. Reports should: outline the terms of reference, purpose and scope of work; describe the work carried out and summarize the results obtained; provide parameters for design purposes and site assessment; identify the issues and likely problems concerning the site and the project; and provide conclusions and recommendations based on the findings of the characterization work carried out. The discussion and recommendations section of reports should cover all aspects and issues that may affect design, construction and development of a site. A range of design solutions, with guidance on which might be best in terms of cost, schedule, ease of construction, environmental impact, maintenance, longevity and the like, should be provided along with clear statements concerning potential risks that are associated with the various options or alternatives available to the client/owner.

The requirements of reporting may vary considerably from one project to another depending on the nature of the project and the client's/owner's requirements. The scope of reporting or deliverable required should be defined in the early stages of a project. Codes, manuals and guidelines of practice also define minimum requirements and provide recommendations for data presentation and reporting.

4.3 Planning and Design of Characterization Study

A site characterization program should consist of an appropriate combination of field and *in situ* testing, sampled boreholes and laboratory tests carried out on representative samples obtained during the field program. Successful, cost-effective site characterization can only result from thorough and thoughtful planning and implementation. Lack of planning is probably the main factor leading to unsatisfactory results with consequent impact on the project in terms of inadequate design, the wrong solution, undesirable surprises during construction, time delays, additional costs, long-term maintenance, loss of license from regulatory agency and other liabilities. Inadequate characterization can also result from a lack of awareness of the potential problems and hazards (both natural and man-made) that can exist in the ground, inadequate financial resources, insufficient time, inadequate or lack of communications with client/owner, poorly trained or inexperienced field personnel, and lack of technical knowledge, skills and expertise. Reasons for failures of site investigations and a description of case records that illustrate the consequences of inadequate investigations are provided and discussed by Osterberg (1978) and Site Investigation Steering Group (1993).

The controlling influence of the conceptual and planning stages on quality site characterization is shown on Fig. 4.3. The components and people involved are identified in an order reflecting the potential for errors or omissions and consequent impact on the investigation. As the tasks become better defined, the potential for error or omission decreases. The size of the sector box for each component indicates, on a comparative basis, the potential for inadequate performance

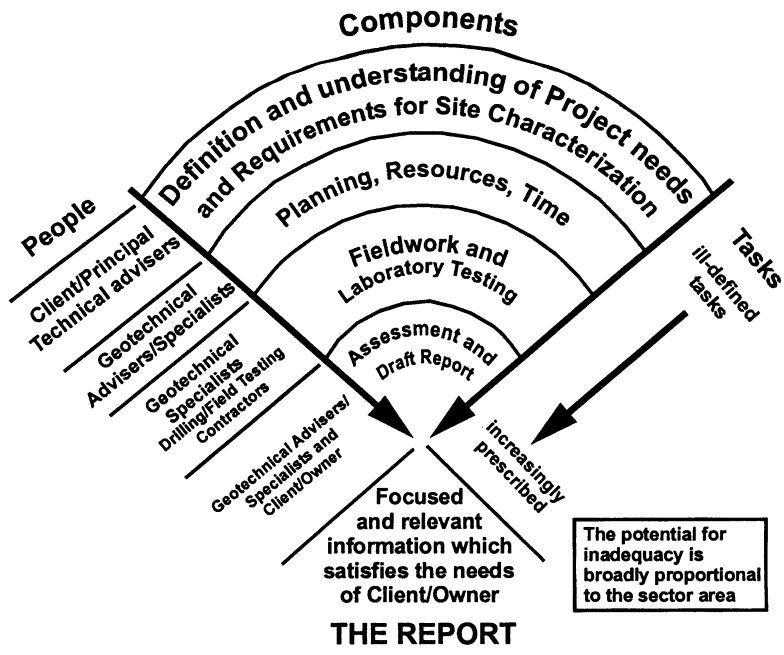


FIGURE 4.3. Influence of the various components of site characterization on quality and satisfying client/project requirements (modified from Site Investigation Steering Group 1993).

(i.e. the larger the area, the greater the potential for error or omission). The early planning stages control performance.

4.3.1 ROLE OF CODES OF PRACTICE AND GUIDELINES

Codes of practice can play a significant role in alleviating some of the problems and shortcomings of the state-of-practice in connection with site characterization studies (Geological Society 1986). Codes are legal documents for quality assurance to obtain or ensure a specific minimum level of technical quality by defining a set of requirements or provisions that must be met. Examples of a code of practice for site investigation include the Danish code (DI 1965), British Standards Institution (BSI) BS 5930 (1981) and Eurocode 7 (CEN 1992). Examples of manuals include the US Navy Design manual (NavFac 1982), the *Canadian Foundation Engineering Manual* (CGS 1992) and *Geoguide 2* (Hong Kong Government 1996). Codes, manuals of practice and guidelines assist engineers in making appropriate decisions to ensure a reasonable level of technical quality and desired level of safety. On the other hand, codes and standards, if not properly and carefully worded, may limit judgment and may decrease flexibility of the designer. Codes should give the designer sufficient freedom to do a good job.

4.3.2 QUALITY MANAGEMENT OF SITE INVESTIGATION

Essential parts of successful site characterization studies are having the "right" people involved and a suitable quality management system in place. The site characterization needs to be carried out under the direction of knowledgeable, experienced and qualified personnel who thoroughly know and understand the key factors that control or significantly affect engineering properties and characteristics, and the limitations of various test methods and equipment used in site characterization work. The drilling contractor also needs to be experienced in drilling, testing and sampling operations for engineering purposes.

Quality begins with the client/owner, who should not select the team solely on the basis of cost. The cost of good advice and quality work is usually insignificant relative to the inevitable cost associated with misjudgment and poor service. The client/owner should: have a clear concept and written scope of the project, which identifies the critical areas of risk as far as practicable and establishes an acceptable level of risk for the project; select the types of professional help needed based on risk areas; and appoint one senior person with authority and responsibility for the project.

The principles of quality management apply to all projects, large or small, and to all tasks, but the more complex the job, the greater the need for a planned approach. Large groups of people of varying disciplines cannot be managed effectively without a formal documented structure defining their roles, responsibilities and accountability. Suitable health and safety plans should also be in place. A formal structured system will prevent oversights and the study will be more efficient. In addition, effective communication is very important to any project. The lines of communication between the various parties need to be clearly defined and followed. Figure 4.4 indicates the usual lines of communications.

4.3.3 SCOPE OF INVESTIGATION

The interaction of the ground and the proposed project needs to be considered when planning the scope or extent of an investigation. One must question how the proposed project will affect the site, and whether the site characteristics will affect the project. Consideration of the zone of ground that is being influenced will assist in defining the type of layout and depth of subsurface exploration. The lateral and vertical extent of investigation should cover all the ground that may be sig-

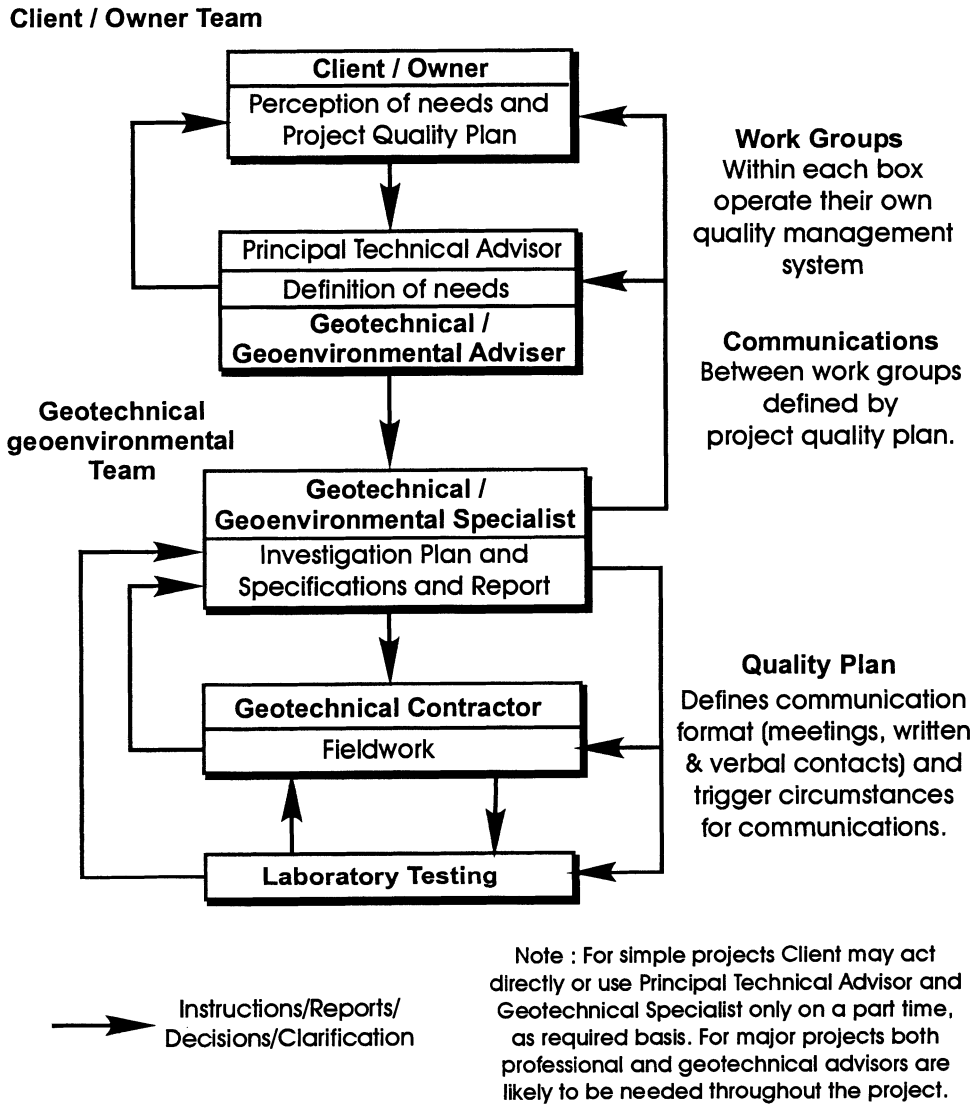


FIGURE 4.4. Communications and quality management between groups for site characterization studies (modified from Site Investigation Steering Group 1993).

nificantly affected by the proposed project. Figure 4.5 illustrates some examples in this regard and identifies some of the technical problems and issues that require consideration.

The extent of ground investigation depends: on the nature of the project; on what is known about the site, including former land use, i.e. was it a gas station or other industrial development that may have introduced contamination or buried structures within the ground?; on the expected variability of site conditions; and on local experience and judgment. A good understanding of both the local and regional geology will assist in planning the number and location of boreholes or other investigation methods. More boreholes and closer spacing would likely be required at sites where previous experience

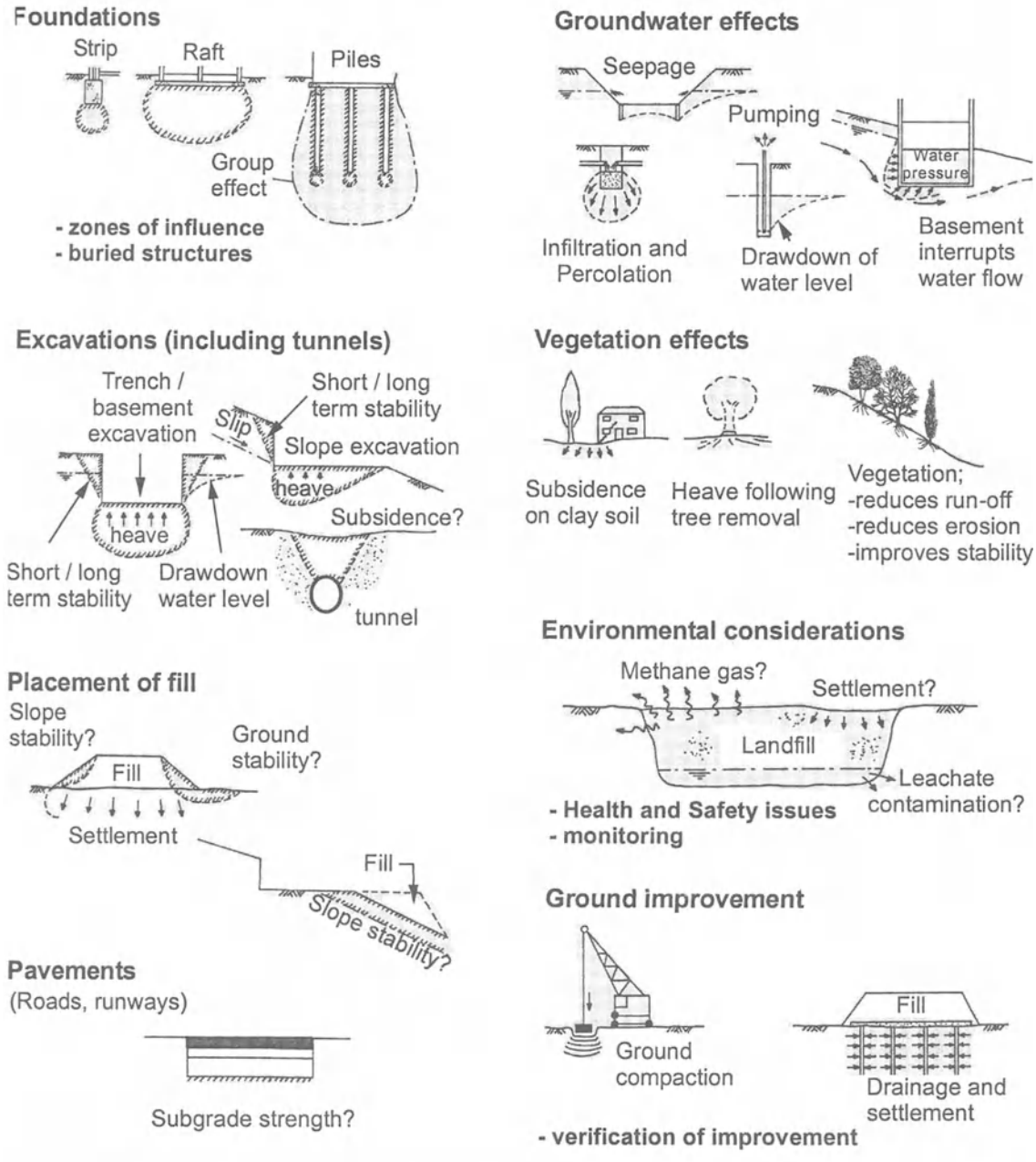


FIGURE 4.5. Considerations of the interaction between the ground and proposed project when defining site characterization programs (modified from Site Investigation Steering Group 1993).

is sparse or non-existent. The boreholes should be located so that a general geological view of the whole site can be obtained with adequate details of the engineering properties of the ground and of groundwater conditions. More detailed information should be obtained at the location of important development, at locations of special engineering difficulty or importance, and where ground conditions are complicated (e.g. suspected buried valleys and old landslide areas). Rigid, preconceived patterns of boreholes should be avoided. Generally, for initial coverage of a site, widely spaced boreholes would be drilled followed by additional investigation in areas that show different conditions, or would likely present problems to the proposed project development.

The use of a single borehole for even a small project is not recommended. Three boreholes are usually considered the minimum. The results from a single borehole can be misleading: for example, drilling into a boulder and thinking that it is bedrock, or in cases where the bedrock surface is highly irregular. Furthermore, in practical terms, once drilling equipment has been mobilized to a site, the cost of an additional one or two boreholes is usually not significant. It is good practice to core about 3 m into rock to prove that bedrock has been encountered. This is especially important in some geological settings such as glaciated regions or where the bedrock may exhibit karst features.

Information and recommendations on the extent of site investigations can be found in various references, codes and manuals such as ASCE (1976), British Standards Institution (1981), NavFac (1982), CGS (1992) and Hong Kong Government (1996).

4.3.4 SELECTION OF FIELD EQUIPMENT AND TEST METHODS

The "correct" choice of test methods and procedures is one of the most important decisions to be made during the planning and progress of a site characterization study. The appropriate choice of equipment and test methods depends on: the location of the site and its accessibility, the nature of the project, the geological setting of the site, the nature of the ground and other site characteristics, whether the site is on land or offshore, and the required accuracy of the prediction of ground behavior. If only classification of soil type and identification of stratigraphy are required, disturbed samples will suffice: such as split-spoon samplers used in conjunction with the standard penetration test (SPT), vibracore samplers and continuous hollow stem auger core samplers. However, if the determination of engineering properties, such as strength and compressibility by laboratory testing, is required, special "undisturbed" samples such as those obtained by thin-walled (Shelby) tubes, piston samplers and/or block sampling will be necessary. *In situ* tests, such as field vane and piezo-cone penetration tests (CPTU), should also be carried out. If empirical correlations will be used to infer the characteristics of the ground, identical equipment and standard procedures should be used and the ground should be similar to that for which the correlations were developed. Marsland (1986) provides a useful discussion on the correct choice of test methods.

Sampling and obtaining quality undisturbed samples of cohesionless materials such as gravels, sands and non-plastic silts below the water table is very difficult. Quality sampling of such soils can only be obtained using expensive soil freezing techniques; which, because of their high costs, are generally only possible in large special projects. Information on soil sampling by freezing is given by Yoshimi *et al.* (1978) and Sego *et al.* (1994). For soils that are significantly disturbed by drilling and sampling operations, it is preferable to use *in situ* testing techniques. The types of *in situ* tests and specific conditions under which each may be used are discussed in Section 4.4.6.

4.3.5 COST CONSIDERATIONS

In general, it is justifiable to spend additional money on investigation, related testing and engineering if doing so is likely to be cost-effective for the project. Expenditure on ground investigation as a percentage of the total project cost is relatively low. Each investigation will bear a price that is consistent with market value for the complexity of the work, the equipment needed and duration of the field work. Although costs can vary significantly depending on project requirements and site conditions, a general rule of thumb is that the cost of an on-land site investigation for design typically ranges from 0.1 to 1.0% of the construction/capital cost of the project. The lower percentage is for large projects and for projects with less critical subsurface conditions; the higher percentage is for small projects and/or projects with difficult subsurface conditions. The level of effort and cost is often about the same for preliminary and final investigations. In general, the combined cost of planning the investigation, supervision, testing and reporting is about the same as the hardware cost of the investigation (i.e. drill rigs, consumable items, samplers and ancillary equipment).

Over the past 25 years, ground investigation prices have been forced down and often are based on minimum cost and maximum speed. This inevitably increases the risk of poor-quality work, unsatisfactory results and client/owner dissatisfaction. Investigations bought cheaply may fail to provide a representative description of site characteristics and the resultant design can be inappropriate for the actual encountered conditions. In such cases, the costs associated with remedial measures, and legal and liability issues are usually well in excess of the cost of the original investigation (Site Investigation Steering Group 1993).

4.3.6 OFFSHORE INVESTIGATIONS

Offshore investigations are generally carried out using the same techniques and equipment as those used for conventional on-land work. The primary differences between on-land and offshore work relate to increased planning, logistics, more sophisticated exploration and survey methods, general support requirements and ancillary equipment such as boats, rafts, barges and drilling platforms. Offshore investigations also use geophysical methods and other specialized surveys much more frequently than on-land work to provide continuous profiles of water depth, soft sediment thickness and depth to hard bottom, and to reduce the number of expensive sampled boreholes. The types of marine geophysics commonly used are summarized in Section 4.4.4. Local coast guard and harbor commissions require sufficient advance notice of proposed offshore work. Approval from these and other agencies is usually required together with navigational permits. Mobilization costs of equipment and personnel vary depending on site location; they can be in the order of tens of thousands of dollars, or more. Because of these factors, offshore geotechnical investigations are relatively expensive and time consuming. They are also more susceptible to delays due to bad weather conditions.

The supply and maintenance of appropriate barges, ships and drilling platforms constitute the major part of the costs for offshore investigations. In order to keep these costs to a minimum, the offshore equipment should be well capable of dealing with the prevailing environmental conditions. In terms of striking an appropriate balance between costs and risk sharing, the client/owner should contract directly the services of drill ships, supply vessels and the like for offshore investigations because these costs are usually much higher than that for engineering. Selecting the appropriate equipment is, therefore, a key component of successful offshore investigations. The size of the offshore equipment required for site investigation work depends primarily on the depth of water, dis-

tance from shore, currents, prevailing winds, wave characteristics and depth of proposed subsurface investigation. Small ships (30–50 m length) are used mainly for seismic surveys and shallow soil sampling operations, which normally do not require fixed anchorage positions. Larger ships may be required for deep water and deep soil sampling and testing.

The operating principles and field deployment for offshore investigation and survey methods are beyond the scope of this chapter. Additional information is provided by Emrich (1971), Noorany (1972), McClelland (1972), Andresen *et al.* (1979) and Carter *et al.* (1986).

4.3.7 CONTRACTUAL ASPECTS

Detailed contract documents with the contractor are important, especially for larger on-land investigations and for offshore work. Many jurisdictions, regulatory agencies and private firms have formulated contract documents based on extensive experience. In general, the formats for these documents are similar. Typical contract documents comprise an invitation to bid, a proposal form, general provisions, technical provisions and drawings describing the program. All aspects of the work, regardless of how trivial they may appear, should be defined in detail. Nothing should be taken for granted or assumed. The proposal form generally consists of a list of all payment items and the estimated quantities for each item. Generally, there is a lump-sum bid item for mobilization and demobilization of equipment and personnel. Other items are usually on a unit price basis, although lump-sum bases are becoming increasingly popular. These items include price per foot of drilling, price per sample, price per standard test and hourly rate for specialized testing and standby. Additional information on contractual aspects is provided in Lowe and Zaccheo (1991) and the Site Investigation Steering Group (1993).

4.4 Investigation Components and Methods

A site investigation consists of many components and may involve many different types of equipment, resources and test methods. The most common components and methods of investigation for both geotechnical and environmental characterization are briefly described in the following sections.

4.4.1 REVIEW OF BACKGROUND AND EXISTING INFORMATION

An initial appraisal of the site based on an examination of existing information will assist in the development of a preliminary understanding of the likely characteristics of the site. The appraisal should be done before planning and carrying out any field work. Valuable information can be obtained from desk studies at low cost. A review of geology, geomorphology, seismicity, former and current land use, water well records, mine records, pedological soil surveys, old and recent aerial photographs, old and recent topographical maps, bathymetric and hydrographic maps, previous reports carried out by government agencies for structures (e.g. roads, bridges, tunnels, canals and the like), university publications, technical papers and climatic data should be included in desk studies. Much of this information is available from all levels of government, research agencies, universities and the military. Sources for such information are identified in BS 5930 (1981), NavFac (1982) and CGS (1992). In addition to the above information, the behavior of existing structures on adjacent or similar sites and/or constructed under similar conditions, and other local experience may also provide useful and valuable information.

4.4.2 AERIAL PHOTOGRAPHS AND REMOTE SENSING

Remote sensing techniques involve looking at the Earth from a distance above its surface. The basis of remote sensing involves mea-

surement or detection of changes in physical properties such as temperature, and visual observations making use of electromagnetic radiation (e.g. infrared, X-rays, ultraviolet, radar, microwave, etc.) and satellite imagery. Such techniques are particularly useful for large-scale characterization and assessing impact on a regional basis, such as siltation from river deltas or hot water discharges by power facilities into bodies of water. Additional information on remote sensing can be found in NavFac (1982), Colwell (1983) and Amos *et al.* (1986).

Comparison of recent and old aerial photographs and topographical maps permits a historical perspective to be gained about the site. They provide valuable information concerning former land use, erosion, possible infilling of ravines, creeks, quarry pits and the like, and provide information on the accessibility and terrain characteristics of the site. Aerial photographs are particularly useful: in areas where little or no work has previously been done; for projects that involve large areas, such as water resources development projects; for projects with long longitudinal or linear features, such as highways and railways; and for site evaluation and selection studies where a number of different alternative sites or routes are being examined. In such studies, it is desirable to gain as much data as possible to compare the various sites and to minimize the use of the much more expensive field drilling and sampling operations. The results of the field exploration program should be used to verify and/or calibrate the aerial photograph interpretation. Additional information is provided by NavFac (1982) and West (1986).

4.4.3 FIELD RECONNAISSANCE AND MAPPING

Subsequent to the desk study review of available information, and prior to drilling, sampling and *in situ* testing, the site should be thoroughly inspected by personnel such as experienced engineering geologists, geotechnical engineers, hydrogeologists and others appropriate to the project. Primary objectives of the field reconnaissance are to confirm desk-top studies and to obtain as much subsurface information as possible without drilling boreholes or excavating test pits. Accessibility of the site, topography, soil profile, slope stability and slope angles, bedrock lithology and structure, surface and subsurface drainage conditions, seeps or springs and other information on groundwater flow are some of the possible information that can be obtained during a field reconnaissance. Maximum use should be made of natural and man-made exposures, such as beach shorelines, river banks, escarpments, quarries, and railway and highway cuts. Important information can also be obtained from the owners of adjacent properties who may have subsurface information and/or a record of the performance of development and structures built on their sites. In addition, local residents can often provide information on groundwater and sources of construction materials. The information obtained during a field reconnaissance, together with that from the review of existing information, is used to assist in defining the scope of subsequent, more detailed investigations.

4.4.4 GEOPHYSICAL SURVEYS

There has been a steady growth in the application of geophysical techniques to geo-civil and geoenvironmental engineering studies. Geophysical methods have proven useful as rapid means of obtaining subsurface information, on a continuous profiling basis, over large areas. They are generally non-destructive in nature and can be carried out from the ground or water surface, and/or from within boreholes. Carrying out the field work is usually quick, typically being done in a day or so. Modern data acquisition systems and computer processing permit the results to be presented very quickly. For some investigations and structures that potentially are sensitive to

having holes drilled in them, the non-destructive nature provides an advantage. Geophysical methods rely on a significant contrast in physical properties (e.g. density, resistivity or electrical conductivity, magnetic susceptibility and velocity of shock waves) being present in the subsurface materials under investigation.

The primary objectives and/or applications in the use of engineering geophysical methods are: to map stratigraphy, determine thickness of strata, depth to bedrock and define major anomalies such as deep buried channels and cavities; to locate aquifers, to determine water quality and map contamination plumes; to locate and define deposits of aggregates and other construction materials; to detect groundwater seepage or leakage paths; to detect voids and buried artifacts such as abandoned shafts, wells, storage drums and old foundations; and to determine engineering properties of strata and their spatial variation. In most of the above applications, geophysical techniques are intended to supplement ground investigation methods; they are not a substitute for drilling, sampling, test pitting and *in situ* testing. The results should be calibrated to borehole data. Geophysical surveys often show variations and anomalies that can be correlated to geological or man-made features. The results from geophysics can be used to interpolate ground conditions between boreholes and to indicate where further boreholes are needed to better investigate the significance of any anomaly identified. By careful planning and proper use of geophysical methods, the number of sampled boreholes required for adequate definition of the subsurface conditions can be reduced and more strategically located.

It is important that the client/owner and personnel in charge of the site investigation be aware of the applicability and limitations of various methods. Some geophysical methods may be useful under one set of subsurface conditions, but offer little to no information or misleading information in others. When used in isolation, geophysical results could be misleading. Poor or unsatisfactory results can be obtained because of one or more of the following reasons: inadequate and/or bad planning, incorrect choice of method and equipment, and inexperienced field personnel (Darracott & McCann 1986). Dissatisfaction with geophysical results can also happen if the expectations from the geophysical work are too high and cannot be practically achieved.

The reliability of the data interpretation is enhanced if more than one geophysical technique and suitably narrow survey grids are used. This enhancement in quality of information obtained is associated with increased effort, equipment and costs. Different geological features will be best studied using different appropriate techniques, depending upon which physical properties of the subsurface materials offer the best chance of being reliably detected. Interference from near-surface and surface infrastructure, common in urban or developed areas, may significantly hinder and limit the usefulness of geophysics in highly developed areas. If there is a doubt about the feasibility or the successful application of geophysical methods, a test survey should be carried out prior to embarking on a detailed program. Some degree of redundancy should be built into the investigation because each method typically responds to different physical properties, and correlations of data from two or more methods usually provide the most meaningful results.

There are many different geophysical techniques, each based on different theoretical principles and which produce different sets of information concerning the properties of subsurface materials. The selection of the most appropriate methods involves consideration of four fundamental but interrelated factors of penetration, resolution, signal-to-noise ratio and contrast in physical properties. Table 4.1 provides a summary of the application of frequently used geophysical

TABLE 4.1. Summary of geophysical methods: on land

Method	Procedure or principal characteristics	Applicability and limitations
Seismic		
Refraction	Time required for seismic waves to travel from source of energy to points of geophone measurement on ground	Preliminary investigation for major stratigraphic units and depth to bedrock
	Refraction of seismic waves at interfaces of different materials gives different sets of arrival times	Limited to 30 m of single layer. Limited by hard layer over soft layer
High resolution reflection	Arrival times of seismic waves reflected from interfaces of adjoining strata	Deep bedrock identification. Useful for locating groundwater. Reflected impulses are weak and easily obscured by other impulses
Vibration	Travel time of transverse or shear waves	Stratigraphy in terms of soil type and thickness and dynamic properties
Uphole, downhole and cross-hole	Measurement of travel times. Geophones on surface and energy source in borehole or geophone downhole with energy source on surface. Energy source in central hole and geophones in surrounding holes	Dynamic ground properties at small strain, rock quality, cavity detection. Unreliable for irregular strata or soft strata with high gravel content
Electrical		
Resistivity	Difference in electrical conductivity or resistivity of various strata measured from surface	Horizontal extent and variation of strata and depths to 30 m. Granular material searches. Fresh/saltwater boundaries. Clay over bedrock. Corrosivity of soils
Drop in potential	Ratio of potential drops between electrodes as a function of current imposed	Similar to resistivity but gives clearer definition on vertical or inclined boundaries
E-logs	Difference in resistivity and conductivity measured in boreholes	Correlation of units between boreholes
Magnetic	Highly sensitive, proton magnetometer measures Earth's magnetic field	Delineation of faults, bedrock, buried utilities and steel drums in ground
Gravity	Differences in density of subsurface materials as indicated by changes in gravitational field	Voids or cavities in bedrock. Tracing steeply inclined and irregular features such as faults, intrusions or domes

techniques for on-land surveys. For offshore or marine geophysical applications, on-land techniques can also be used with suitable instrumentation changes. Of greater use, however, are the techniques summarized in Table 4.2. For proper interpretation and data reduction, it is necessary to apply tidal corrections and to have high quality survey control. Where appropriate, electronic navigational systems such as global positioning systems (GPS) should be used.

Additional information on engineering geophysics and its use for site characterization is provided by ASCE (1974), NavFac (1982), Lowe & Zaccheo (1991) and Charles *et al.* (1996).

TABLE 4.2. Summary of geophysical methods: offshore

Method	Procedure or principal characteristics	Applicability and limitations
Depth recorders (echo-sounding)	Travel time of short pulse of high frequency	Bathymetry up to 100 m. Little sub-bottom penetration. Difficult to assess if reflecting soft bottom sediments or higher density material below seabed
Continuous seismic reflection profilers	Travel time for seismic waves	Cannot differentiate between two dissimilar materials that have similar geophysical properties (i.e. a till and heavily fractured and weathered rock) and of limited use in shallow (i.e. 2 m or so) water because of reflections from seabed
	High frequency (sonar type) 3.5–7 KHz frequency (pinger)	Shallow profiling of bed sediments and near-surface layering within a few meters of bottom. Resolution: 0.1–1.0 m
	Electromechanical transducer acoustic pulse in 400 Hz to 3 KHz region (boomer)	Penetration >100 m in soft sediments; a few tens of meters in gravels and stiff clay. Resolution approximately 1.0 m
	Low frequency, high energy acoustics in 200–800 Hz region (sparker)	Deep seismic profiling of geologic structure of bedrock. Can penetrate more than 1 km in soil or bedrock. Resolution: 2–3 m for high-resolution sparkers, but usually approximately 20 m
Side scan sonar	Sonar image of seabed bottom. Operates at 105 KHz frequency. Reflection of high-frequency pulse of sound from the seabed	High-resolution scanning of bottom surface features. Can differentiate between various materials and locate hazards or obstructions (e.g. bedrock outcrops, sunken vessels, etc.)

4.4.5 BOREHOLE DRILLING AND SAMPLING METHODS

There is a considerable variety of drilling and sampling methods. Some methods are used throughout the world, while others are limited to use on a more regional scale, often dictated by ground conditions and regional state-of-practice. Comprehensive reviews of the standard, conventional borehole drilling and sampling methods are provided in Hvorslev (1948), NavFac (1982), Geological Society (1986), Lowe & Zaccheo (1991) and CGS (1992).

Boreholes are usually vertical, but with some drilling equipment they can be advanced inclined or horizontally. Sampling methods and samplers are designed to minimize disturbance. The quality of samples obtained depends mainly on the drilling methods used to advance the borehole, the sampling equipment used, the experience and care of field staff, and the procedures used in borehole retrieval, transport and storage of samples. Regardless of the method of borehole advancement, the sequence of soil sampling operations is the same, involving lowering of the sampler down to the bottom of the borehole and then hammering or pushing it into the ground for the desired penetration.

The sampling interval used depends on the project requirements. It can range from continuous to as wide an interval as considered appropriate for the project requirements. Normally, sampling intervals range between 0.75 and 1.5 m. Seldom is the interval greater than 3 m. Continuous sampling is necessary if the purpose of the investigation is to accurately define stratigraphy, failure planes and/or possible zones of contamination. The Swedish foil sampler, for example, can be used in soft clays and loose sands to obtain 3-m long samples. Although continuous sampling can be achieved using normal standard samplers, it is a tedious process, especially for deep boreholes. Continuous soil cores can be efficiently obtained using special types of samplers. Examples of these samplers include hollow stem auger coring sleeves and special core barrels designed specifically for coring soil. Vibrocoring techniques can also be used. This type of drilling equipment induces high-frequency vibrations, which in appropriate soils, such as soft to firm clays or sands and silts below the groundwater table, easily penetrate the ground. As the sampling shoe and attached casing are vibrated into the ground, the penetrated soil is recovered as a continuous soil column inside the sampler and casing.

In general, soil samples are classified according to their quality or success in achieving "undisturbed" conditions (Table 4.3). The term undisturbed is somewhat of a misnomer as the drilling and sampling operations, no matter how carefully carried out, impart some disturbance to the soil. The stress relief associated with removal of the sample from the ground can also create disturbance effects on the sample. These disturbance effects can be minimized to some extent if the field stress regime is reasonably duplicated on samples tested in the laboratory.

The two most common types of samplers used in North America and other parts of the world are the split-spoon and Shelby tube. The Dennison and Pitcher samplers are also sometimes used (Lowe & Zaccheo (1991)). The split-spoon sampler obtains disturbed samples as part of the standard penetration test (SPT); it is used for many soil types. The sampler, as the name implies, allows the sampling barrel to be split longitudinally into halves, after the end collars are removed. Additional information on the SPT is provided in Section 4.4.6.

The Shelby tube or thin-walled tube sampler is routinely used to take undisturbed samples of cohesive soils. Tube samplers are steadily pushed into the soil from the bottom of the borehole. In some tube samplers, a piston arrangement prevents caved material at the bottom of the borehole from entering the sampler until the desired depth is reached.

TABLE 4.3. Classification of soil samples (modified from CGS 1992)

Class	Quality	Sampling method	Properties that can be measured[a]
1	"Undisturbed"[b]	Block sample–piston sampler	A–K
2	Slightly disturbed	Open thin-walled tube sampler, such as Shelby tube	A–E, G–K
3	Substantially disturbed	Open thick-walled tube sampler, such as a split-spoon	A–E, G
4	Disturbed	Random samples collected by auger or in pits	A, C–E, G

[a] A, stratigraphy; B, stratification; C, organic content; D, grain-size distribution; E, Atterberg limits; F, density index; G, water content; H, unit weight; I, hydraulic conductivity; J, compressibility; K, shear strength.
[b] Refer to text.

The piston also helps retain the sample by creating a partial vacuum (i.e. suction) above the sample when the sampler is withdrawn. This enhances sample recovery, particularly in soft sediments. It is generally recognized that the best way to enhance soft soil recovery is to use a fixed piston sampler. In other samplers, a removable, thin metal or plastic cylindrical liner encases the soil sample as the sampler penetrates the soil. The liner and encased sample can be removed intact to protect the sample during borehole retrieval and shipment to the laboratory.

Special samplers have been developed to sample lake and seabed sediments. Because of their very soft and at times slurry-like consistency, sample recovery is often limited. Large aluminum samplers ($0.5 \times 0.5 \times 0.5$ m) with hinged cutters at their base are often successfully used. They are dropped (with hinged base open) through water and into the sediments. Using cables, the hinged door is closed to entrap the sample as the sampler is winched up to the surface. Other samplers consist of transparent plexi-glass tubing equipped with a metallic cutting collar. The sampler is dropped, or it can be pushed into the sediments. A peripheral rubber membrane, which is housed inside the cutting collar, is then inflated, using a compressed air source, to effectively create a base retainer that prevents the loss of sample as the sampler is brought to the surface. The clear tubing permits visual inspection of the retained soil column prior to extruding the sample for further detailed examination and testing.

Boreholes for investigation of rock can be advanced by different means, such as: double- or triple-tube core barrels, rotary core drilling with air or water flush, rotary tricone drilling with air or water flush, and percussion or churn drills. The latter two methods only provide cuttings to examine and infer rock types and conditions. They are not generally suitable for more detailed characterization. Cores obtained by means of diamond core drilling are required for laboratory tests. Core barrels vary in size; '*N*' size (50 mm) is most commonly used. Special devices (e.g. core orientator and impression packers) are available to orient the core so that the orientation of fractures and joints in the rock core can be related to field conditions. Closed circuit television (CCTV) cameras are also sometimes used (Institution of Civil Engineers 1996). During coring, special attention should be paid to changes in drilling noise, vibrations, pressure on coring bit, color, and pressure and flow of drilling fluid, because these observations provide important information on rock conditions. For example, a loss or no return of drilling fluid suggests the existence of a highly fractured, pervious zone within the rock mass. A sudden drop in the drill rods suggests the existence of a void or cavity. It is important to carefully note such observations, because the cavities or voids will not be displayed by the recovered core in the core barrel.

4.4.5.1 Backfilling and Sealing of Boreholes

Backfilling of boreholes should be done carefully and thoroughly to minimize subsequent backfill settlement and creation of an open hole, which can be a potential hazard and a liability. Further, the potential for cross-aquifer contamination must be effectively mitigated. This is particularly important if the subsurface conditions involve clay or other low permeability soils that separate two pervious water-bearing strata. The drilling of the borehole provides a connecting pathway between the two aquifers that did not previously exist. Backfilling operations must reinstate, as close as practically possible, the subsurface conditions that existed prior to drilling the borehole. The quality and type of backfill material used depends on location, type of project and if movement of water through the borehole column is to be prevented. In some cases, the soil cuttings resulting from making the borehole and/or a dry granular material will suffice, if properly placed and tamped.

In other cases, the borehole may need to be backfilled completely with a suitable bentonite–cement grout mixture. This method is the most assured means of producing satisfactorily backfilled and sealed holes, and may be required by local jurisdictions and regulatory agencies. Detailed assessment of proper backfilling procedures and recommended procedures for different conditions can be found in Lutenegger *et al.* (1995).

4.4.6 FIELD AND *IN SITU* TESTING

In situ testing is a division of field testing corresponding to the cases where the ground is tested in-place by instruments that are inserted in or penetrate the ground. *In situ* tests are normally associated with tests for which a borehole either is unnecessary or is only an incidental part of the overall test procedure, required only to permit insertion of the testing tool or equipment. The role of specialized *in situ* testing for site characterization and the research and development of *in situ* techniques have received considerable attention over the last 15 years or so. The use of specialized *in situ* testing in geotechnical engineering practice is rapidly gaining increased popularity. In Europe, specialized *in situ* testing has been commonly used for more than 25 years. Improvements in apparatus, instrumentation, technique of deployment, data acquisition and analysis procedure have been significant. The rapid increase in the number, diversity and capability of *in situ* tests has made it difficult for practicing engineers to keep abreast of specialized *in situ* testing and to fully understand their benefits and limitations. Table 4.4 summarizes the primary advantages and disadvantages of *in situ* testing.

The description and applicability of a wide range of geotechnical *in situ* tests for soils has been summarized by numerous researchers in technical symposia and conferences, including ASCE (1974, 1975, 1976, 1978, 1986),

TABLE 4.4. Summary of advantages and disadvantages of *in situ* testing

Advantages	Disadvantages
• Tests are carried out in place in the natural environment without sampling disturbance, which can cause detrimental effects and modifications to stresses, strains, drainage, fabric and particle arrangement	• Samples are not obtained; the soil tested cannot be positively identified. The exception to this is the SPT in which a sample, albeit disturbed, is obtained
• Continuous profiles of stratigraphy and engineering properties/characteristics can be obtained	• The fundamental behavior of soils during testing is not well understood
• Detection of planes of weakness and defects are more likely and practical	• Drainage conditions during testing are not known
• Methods are usually fast, repeatable, produce large amounts of information and are cost effective	• Consistent, rational interpretation is often difficult and uncertain
• Tests can be carried out in soils that are either impossible or difficult to sample without the use of expensive specialized methods	• The stress path imposed during testing may bear no resemblance to the stress path induced by the full-scale engineering structure
• A larger volume of soil may be tested than is normally practicable for laboratory testing. This may be more representative of the soil mass	• Most push-in devices are not suitable for a wide range of ground conditions
	• Some disturbance is imparted to the ground by the insertion or installation of the instrument
	• There is usually no direct measurement of engineering properties. Empirical correlations usually have to be applied to interpret and obtain engineering properties and designs

TABLE 4.5. Summary of applicability of common *in situ* and field tests

Type of test	Soils: Best suited	Soils: Not applicable	Properties that can be obtained	Remarks
Standard penetration test (SPT)	Sand Silt Gravel	Soft–firm clays	Evaluation of compactness and stratification	Most common *in situ* test. Many useful correlations with engineering properties and design
Dynamic cone-penetration test (DCPT)	Sand Gravel Silt	Clay Plastic silt	Qualitative evaluation of variability in compactness	Similar to SPT
Becker penetration test (BPT)	Gravelly and cobbly material	Soft soils	Qualitative evaluation of compactness	Similar to SPT
Piezo-cone-penetration test (CPTU)	Sand Silt Clay	Gravel Till	Continuous evaluation of density and strength of sands. Continuous evaluation of undrained shear strength and overconsolidation ratio (OCR) in clays	Rapidly becoming a common test. Relatively simple to use and reliable. Many useful correlations with engineering properties and design. Continuous stratigraphic profiles
Field vane test (FVT)	Clay Plastic silt	Sand Gravel Till Silt	Undrained shear strength	Test should be used with care, particularly in fissured, varved and highly plastic clays
Pressuremeter test (PMT)	Soft rock Sand, silt Clay Till	Soft sensitive clays	Strength compressibility *in situ* K_0	Self-boring pressuremeter preferable in sands and clays and for K_0 determination
Dilatometer test (DMT)	Sand Silt Clay	Gravel Till	Empirical correlation for soil type, K_0, overconsolidation ratio (OCR), undrained shear strength and modulus	Simple robust tool. Many useful correlations with engineering properties and design
Plate-bearing test and screw-plate test	Sand, silt Clay Till	—	Deformation modulus. Modulus of subgrade reaction	Strictly applicable only if the deposit is uniform; size effects must be considered in other cases
Hydraulic conductivity and pumping tests	Rock Sand Silt Clay Till	—	Evaluation of coefficient of permeability	Variable-head tests in boreholes have limited accuracy. Results reliable to one order-of-magnitude are obtained only from long-term, large-scale pumping tests
Piezometer probe (hydraulic fracturing)	Clay Plastic silt Till	Sand Gravel	*In situ* K_0	Limited to $K_0 < 1$. Also useful for instrumentation and monitoring
Pressure cells	Clay, sand Silt	Till Gravel	*In situ* K_0 Induced stresses from load applications	Useful also for instrumentation and monitoring
Downhole and crosshole seismic (geophysical)	All soils	–	Dynamic modulus of deformation. Shear wave velocity. Shear modulus	Most reliable means of determining dynamic properties of soils

Mitchell (1978 and 1988), Robertson & Campanella (1983), Robertson (1986), Wroth (1984 and 1988), Jamiolkowski *et al.* (1985), ISOPT (1988), Lunne *et al.* (1990), Institution of Civil Engineers (1996) and ISC (1998). The *in situ* tests that are most commonly used in practice are the standard penetration test (SPT), field vane test (FVT), cone-penetration test (CPT) and piezo-cone-penetration test (CPTU), pressuremeter (PMT) and dilatometer (DMT). Other common field tests include plate-bearing tests, pumping tests and other tests to determine hydraulic conductivity, and geophysical surveys. A summary of the applicability of these tests is presented in Table 4.5. Table 4.6 summarizes the advantages and disadvantages of the commonly used *in situ* tests that are discussed in the following subsections.

4.4.6.1 Standard Penetration Test (SPT)

The SPT is the oldest and most widely used *in situ* test. It was first introduced in the USA in the early 1900s and was standardized in the late 1920s or early 1930s. It offers the advantages of low cost, applicability to many soil

TABLE 4.6. Summary of advantages and limitations of some common *in situ* tests

Test	Advantages	Limitations
Standard penetration test (SPT)	• Standardized test that is robust, inexpensive and feasible to carry out in a wide range of materials • Provides a sample • Widely used for many years and has a large database and correlations for most engineering properties • Basis of design for foundations and liquefaction assessment of materials	• Affected by borehole disturbance, such as piping, base heave and stress relief • Affected by equipment to make borehole and by operator • Results are influenced by grain size, soil structure and stress history • Many corrections are required for interpretation and design
Dynamic cone-penetration test and dynamic probing (DCPT and DP)	• Equipment is simple and robust • Large number of tests can be done in a day • Results indicate variability in subsurface condition	• Test is crude and correlations with engineering properties may be unreliable • Test results need to be assessed in conjunction with results from other investigation methods • No sample is obtained
Becker penetration test (BPT)	• Suitable for gravelly, cobbly soils, which present significant problems for other *in situ* tests • Correlatable to SPT • Useful for direct design applications, such as pile driveability	• Not a standardized test and interpretation requires special considerations • Sample obtained not representative because of particle breakage as a result of driving casing
Field vane test (FVT)	• Robust, simple standardized test that is easy to carry out • Direct measurement of shear strength • In some cases, no borehole is needed; but rod friction needs to be eliminated or measured in those applications that require special equipment	• Generally limited to clays with shear strength <150 kPa • Not suitable for most other soils • Results affected by sandy/silty layers and gravel inclusions • Corrections may be required for some soils and results may be misleading in some soils (e.g. silts) • Gives horizontal shear strength • May not give operational strength in fissured soil
Piezo-cone-penetration (CPTU) and seismic cone-penetration tests (CPTS)	• Robust and easy to use standardized test • Continuous profiles are obtained • Test carried out quickly and there is no need for a borehole unless obstructions are encountered • Test results are accurate and repeatable • Different measurements made, which enhance interpretation	• Not suitable for materials with large particles, which obstruct penetration. Best suited for uniform, fine-grained soils • Not easy to penetrate very dense or hard materials • Problems can develop with rod buckling when hard material is suddenly encountered under softer soils

TABLE 4.6. Summary of advantages and limitations of some common *in situ* tests *(continued)*

Test	Advantages	Limitations
	• Many correlations available for most engineering properties and design applications • Avoids disturbance effects associated with boreholes • Large number of tests can be done in a day	• No sample is obtained • Instrument is relatively expensive and some specialized probes still in research and development stage and generally not commercially available • Different methods of interpretation give different results
Pressuremeter test (PMT) and self-boring pressuremeter (SBP)	• Test results give stress–strain relationships for ground tested; not just a single value of an engineering property • Boundary conditions are controlled and well-defined. Testing carried out at both small and large strains • SBP can be inserted in suitable soils with minimal disturbance and avoiding stress relief effects • Useful for determination of *in situ* horizontal stress • Use of loading and unloading cycles can mitigate borehole and other disturbance effects and enhance interpretation • Correlations available for important engineering properties and design applications	• No sample is obtained and test results should be supported by other strength data • Sophisticated, relatively expensive instrument that requires experienced, skilled specialist personnel • Testing is time consuming and on a less continuous basis than CPTU and other tests • Test results affected by procedure, and method of interpretation is important. Different methods of interpretation give different results • Borehole required for Menard type and some soils. Effects of disturbance and stress relief need to be considered and taken into account
Dilatometer test (DMT)	• Robust, simple standardized test that is easy to carry out using same equipment as other tests • Testing is on a near-continuous basis • Results are generally repeatable • Avoids disturbance effects of boreholes • Correlations available for important engineering properties and design applications • Good test for interpretation of *in situ* horizontal stress and deformation at small strain	• Not suited for soils with large particles or that are too dense or hard to permit penetration without use of borehole • No sample is obtained • Different methods of interpretation available which do not give same results • Testing more time consuming and less continuous basis than CPTU • Limited strain imposed during test. Results not well-suited for large strain behavior
Plate-load test (PLT)	• Simple equipment required • Direct assessment of deformation and strength characteristics on a small local scale	• Test is quite specialized, time consuming and expensive • Disturbance effects in boreholes can be important • Scale effects are important, and limit interpretation of results to full-scale, field conditions
Hydraulic fracturing (critical pressure) test	• Uses piezometer that is already installed • Provides direct estimate of pressure to cause cracking in materials such as the core of earth dams	• Only suited to clay soils with $K_0 \leq 1$ • Test method and method of interpretation important, and affect results obtained • Test can damage piezometer installation and subsequent long-term monitoring • Relationship between critical pressure and *in situ* stress is the subject of considerable debate
Pressure cells and stepped-blade	• Potential for direct measurement of *in situ* total stress in soil • Appropriate for instrumentation and monitoring purposes in addition to *in situ* testing	• Affected by borehole and insertion. May need to wait long time before true equilibrium value achieved. Insertion of instrument may permanently affect measurement and not give true indication of actual stresses had no instrument been installed • Interpretation uncertain and subject to debate • Longevity of instruments uncertain for long-term monitoring

types, samples are obtained (albeit disturbed) and a large database from which many useful engineering correlations have been developed. The SPT uses a standard 50-mm outside-diameter split-spoon sampler, which is usually driven into the soil at the bottom of a borehole for 450 mm by means of a 63.5-kg hammer having a free fall of 760 mm. The number of blows required to drive the sampler for each 150 mm of penetration is recorded. The number of blows for the first 150-mm penetration is not used to compute the *N*-value because it may reflect disturbance from the borehole drilling method. The *N*-value is the summation of the number of blows required to drive the sampler the last 300 mm. In dense/hard soils, the sampler may only be driven a few tens of millimeters for blows in excess of 100. For this case, corresponding to practical refusal, the number of blows to advance the sampler is recorded for the actual penetration.

Despite its wide use and simple procedure, the results of the SPT are greatly affected by the drilling and sampling operations; it is also operator dependent (i.e. can vary from one driller to another). A detailed discussion of the possible errors in SPT results has been summarized in NavFac (1982), Decourt (1989) and CGS (1992). Correction or adjustment factors are frequently applied to the measured N-value to account for some of the physical factors affecting the test results. The main corrections are for vertical effective stress (relative to a stress of 100 kPa) and an energy correction corresponding to 60% of the free-fall energy of the SPT (Seed *et al.* 1985 and Skempton 1986). SPT energy transmission has been the subject of recent research work (e.g. ISOPT 1988, Clayton 1990 and 1995, Sy & Campanella 1991a, b and Abou-matar & Goble 1997).

4.4.6.2 Dynamic Cone-Penetration Test (DCPT)

This simple test has similarity to the SPT, except that a solid 60° cone is placed at the end of the drill rods instead of the split-spoon sampler. No sample is obtained. The test can be carried out from ground surface or from the base of a borehole as ground conditions permit. The number of blows required to advance each 300 mm of rod is recorded. The test is usually carried out to practical refusal, typically identified as "bounce" of the hammer on the drive piece or a large number of blows (e.g. 100 or more) for a penetration of only a few millimeters. The main advantages of the DCPT are that it is fast, inexpensive, and it is particularly useful in delineating areas of weak soils overlying stronger strata and in quickly assessing the variability of the soil conditions. It is most suited to granular soils.

4.4.6.3 Dynamic Probing (DP)

This test is more commonly used in European practice and has been described in ISOPT (1988). It also has similarity to the SPT and is carried out from the ground surface without the use of a borehole. The penetration resistance of the soil is measured as a solid 90° cone is driven through the soil by a falling weight hitting an anvil that is attached to rods connected to the cone tip. The number of blows required for each 100 mm of penetration is recorded. Significant friction can develop on the rods; therefore, the rods are rotated at meter intervals and the torque required to rotate the rods is measured. The torque is used to correct the measured blow count for the friction on the rods. The torque reading can be used to calculate the dynamic point resistance (Charles *et al.* 1996).

4.4.6.4 Becker Penetration Test (BPT)

The Becker hammer drill was developed in 1958 in Alberta, Canada, and is now used widely in North America in mining and aggregate resource exploration, particularly in gravelly and bouldery formations. The drilling consists of driving a specially designed double-walled casing into the ground with a double-acting diesel pile hammer, using an air injection, reverse circulation technique to

remove the cuttings from the hole. Details of this hammer drill can be found in Anderson (1968) and Sy & Campanella (1992 a and b). The drilling can be stopped at any depth to carry out sampling, such as SPT or other *in situ* tests, if open-ended casing is used. The casing can also be driven close-ended as a large-scale penetration test, similar to the SPT, to evaluate soil density and pile driveability. The Becker penetration resistance test (BPT) consists of recording the number of blows for each 300 mm of penetration. Because of its large size, the BPT is considered to be more representative in gravelly soils. Correlations have been developed to relate the BPT to the SPT for foundation design and liquefaction assessment. The correlations have attempted to account for variable hammer energy output and shaft resistance acting on the casing (Harder & Seed 1986, Sy & Campanella 1992 a, b and Sy 1996).

4.4.6.5 Field Vane Test (FVT)

The field vane test is one of the most common *in situ* tests for the determination of undrained shear strength of clays. The FVT has been the subject of numerous technical publications and specialty symposia (e.g. Schmertmann 1975, Jamiolkowski *et al.* 1985, Aas *et al.* 1986, ASTM 1988, Becker *et al.* 1988 and Lunne *et al.* 1990). The test is best suited to soft–firm clays; it should not be used in granular soils, non-plastic silts or fibrous peat. The vane consists of four thin rectangular blades welded at right angles to each other on a thin rod. The common height to diameter ratio is about two, with the diameter generally ranging from about 50 to 70 mm. The vane is usually pushed into the soil from the bottom of a borehole and the torque required to rotate the vane is measured, using calibrated springs or a torque wrench. Special vane rods with slip couplings are available to measure rod friction prior to vane shear. With this equipment it may be possible to push the vane into the soil from the ground surface to obtain a continuous profile of vane shear strength. In most cases, however, boreholes are required. The undrained shear strength is computed from the measured torque and dimensions of the vane. In some soils, correction factors may be required to make the vane strength more representative of the field, operational, undrained shear strength (Bjerrum 1972).

4.4.6.6 Piezo-Cone Penetration Test (CPTU)

The piezo-cone penetration test (CPTU) is an example of improved *in situ* techniques that have been developed for site investigations. It is an extension to the standard cone penetration test (CPT). The standard cone penetrometer consists of a 35-mm diameter rod with a 60° conical-shaped tip equipped with electronic sensing elements to measure tip resistance and local side friction on a sleeve. The piezo-cone penetrometer also incorporates a transducer to measure porewater pressure. The penetrometer is pushed at a constant rate of 2 cm s^{-1} into the ground. In general, no pre-boring is required. In addition to the standard three channel piezocone penetrometer, new penetrometers have been developed that include additional sensing elements for the measurement of temperature, inclination, lateral stress and seismic waves. In particular, the seismic cone penetrometer (CPTS), which houses an accelerometer, has proven itself most beneficial in the assessment of liquefaction and determining dynamic soil properties. The CPTU, CPTS and other penetrometers have been the subject of numerous technical publications and speciality symposia and conferences (e.g. Robertson & Campanella 1983, Jamiolkowski *et al.* 1985, ASCE 1986, ISOPT 1988, Lunne *et al.* 1990, Swedish Geotechnical Society 1995, Lunne *et al.* 1997, and ISC 1998).

The CPTU is one of the most commonly used specialized *in situ* tests and is ideal for use in sands, silts, clays and mine-tailings materials. A reliable, continuous stratigraphic

profile, together with important engineering properties, can be interpreted from its results. Further, because the data are collected on a continuous basis, detection of thin, weak layers and/or more pervious layers is possible. This is important because these weaker zones ultimately control the behavior and performance of the soil mass and, in particular, are significant to slope stability and seepage considerations, liquefaction and dynamic stability analysis, and foundation design. These weaker layers often go undetected by conventional borehole drilling and sampling operations. The CPTU also avoids the disturbance effects commonly encountered when drilling boreholes and sampling below the water table. Thus, the CPTU greatly enhances the quality of data gathered in a subsurface investigation. In addition, because of its relative simplicity, ease of operation and high rate of production in terms of depth of soil investigated, the CPTU has proven itself to be very cost-effective.

The interpreted data provide information on: stratigraphy in terms of thickness, gradation and soil type; density (void ratio) and/or state (state parameter) of the more sandy or coarser materials; friction angle (strength) of the more sandy or coarser materials; undrained strength and stress history (OCR) of the more clayey or fine-grained materials; and liquefaction potential evaluation and cyclic resistance. Further, as the cone penetrometer is pushed through the ground, excess porewater pressure is induced, the magnitude of which is controlled by the hydraulic conductivity of the material. If the pushing of the cone is interrupted and the cone is held stationary for a sufficient period of time, the porewater pressure measured by the cone will stabilize to the *in situ* piezometric pressure at the cone tip. Monitoring the rate of porewater pressure change to this stabilized pressure provides data from which the *in situ* hydraulic conductivity can be calculated (Robertson & Campanella 1983, Robertson *et al.* 1992, Lunne *et al.* 1997). From the above operations, the piezometric pressure, gradients and hydraulic conductivity within the ground can also be obtained.

4.4.6.7 Pressuremeter Test (PMT)

A pressuremeter is a cylindrical device with a flexible membrane that imposes a uniform pressure on a borehole wall. The applied pressure and the resulting deformation of the membrane are measured. The outward radial horizontal deformation is only a few millimeters. Pressuremeters are used to measure *in situ* deformation (compressibility), *in situ* horizontal stress and strength of both soil and rock. Several types of pressuremeters are available including the pre-bored, self-boring, push-in and full-displacement pressuremeters (Powell & Uglow 1985). The prebored pressuremeter, which is most commonly of the Menard type, is inserted into a borehole. The test can be used in a wide range of soil and rock conditions. Testing is usually stress-controlled. The instrument consists of three expanding cells, and readings of pressure and volume changes of the membrane (central cell) are recorded as the pressure is increased and decreased. Ground disturbance due to drilling of the borehole can be a significant factor. The self-boring pressuremeter (SBP) is a more sophisticated instrument that incorporates a drilling or cutter head to advance itself without the use of a borehole. There are much less disturbance effects than with the pre-bored type of pressuremeter. SBPs have been used in a variety of soils from sands to very stiff clays to depths as great as 80 m. The full-displacement cone pressuremeter is becoming increasingly available and has promising potential as a valuable investigation tool. The pressuremeter portion of the instrument is located behind the cone portion. The tool is pushed into the ground in the same manner as for the CPTU. Although the method of insertion causes distur-

bance, repeatable results are obtained (Powell & Shields 1995, Whittle 1996). Additional information on pressuremeters and their interpretation is provided in Baguelin *et al.* (1972 and 1978), Mair & Wood (1987), Jefferies (1988), BGS (1990), Lunne *et al.* (1990), CGS (1992), Institution of Civil Engineers (1996), Clarke & Gambin (1998), and ISC (1998).

4.4.6.8 Dilatometer Test (DMT)

The flat plate dilatometer test was developed in Italy in the late 1970s (Marchetti 1980, Marchetti & Crapps 1981). It is generally used to measure soil properties such as *in situ* horizontal stress, stress history (OCR), deformation moduli and undrained shear strength of clays. The Marchetti instrument consists of a 94-mm wide and 14-mm thick flat stainless steel plate. One face of the blade has a 60-mm diameter flexible steel diaphragm, which is used to measure soil contact pressure and the pressure required to move the diaphragm. The Norwegian Geotechnical Institute (NGI) has developed a similar but smaller (77-mm wide and 16-mm thick) plate to fit inside drill pipes for use in offshore investigations. The offshore device is also fitted with a porewater pressure transducer for the measurement of porewater pressure. The dilatometer is connected to rods through which pneumatic tubing and electrical cable are threaded to connect to the dilatometer and the air pressure supply system and readout unit. It is pushed into the ground at the same rate as the CPT–CPTU (2 cms^{-1}) and stopped every 200 mm to carry out testing by increasing air pressure to move the diaphragm. The pressure required to just move the diaphragm and the pressure required to move the diaphragm by 1 mm are measured and recorded. Detailed requirements for equipment, test procedures, accuracy of measurement and presentation of test results are recommended by ASTM Sub-committee D.18.02 (Schmertmann 1986). Additional information and review of the DMT are provided in Jamiolkowski *et al.* (1985), ISOPT (1988), Powell & Uglow (1988), Lunne *et al.* (1990) and Campanella & Robertson (1991).

4.4.6.9 Plate-Load and Screw-Plate Tests

Plate-load tests are generally used to determine stiffness (deformation modulus) and strength properties of ground (soil/rock). The test involves measuring applied loads and penetration (settlement) of a plate into the ground. The test is commonly carried out in shallow trenches or pits and at depth in the bottom of a borehole (Mitchell & Gardner 1975). The applied load is usually achieved by jacking against a reaction provided by kentledge or tension piles. The test is usually carried out either as a stress-controlled test consisting of series of maintained loads of increasing magnitude, or as strain-controlled at a constant rate of penetration. For maintained loads, the ground is allowed to consolidate under each load increment and, thus, drained deformation characteristics are measured. If the rate of penetration in strain-controlled tests is such that no or little drainage occurs, the test results are indicative of undrained behavior. The degree of drainage is governed by the size of the plate, the rate of penetration and applied loading, and soil types. Plate-load test procedures are described in BS 5930 (1981) and ASTM D-1194-72 (1987).

An alternative method to plate-load tests in boreholes is the screw-plate test developed in Europe, which uses a flat-pitch auger device that can be screwed into the soil. The test procedures are similar to plate-load tests and depend on the type of soil being tested and the data required (Janbu & Senneset 1973, Dahlberg 1974).

4.4.6.10 Other Tests to Measure *In Situ* Horizontal Stress

In addition to the pressuremeter and dilatometer tests, *in situ* horizontal stress in soil is

sometimes measured using total stress cells, stepped-blade and hydraulic fracturing. Total stress cells are described in Massarsch (1975 and 1986), Massarsch *et al.* (1975) and Tedd *et al.* (1990). A thin-walled earth pressure cell is pushed into the soil, and readings of pressure are taken normally three to five days after installation. The disturbance and excess porewater pressure effects associated with installation are normally considered to have dissipated in this time. The measured horizontal stress is assumed to correspond to the *in situ* total horizontal stress. To obtain the *in situ* effective horizontal stress, the porewater pressure at the depth of the pressure cell is subtracted from the measured pressure. Watts and Charles (1988) describe a similar technique for the measurement of vertical stress from a borehole.

Hydraulic fracturing or critical pressure testing and its principle for measuring *in situ* horizontal stress in low permeability soils (clays) is described in Bjerrum & Andersen (1972), Bozozuk (1974) and Massarsch *et al.* (1975). A conventional push-in hydraulic piezometer is usually used and installed in the normal manner. After stabilized or equilibrium water levels have been reached, water under pressure is forced through the piezometer into the surrounding soil. The water pressure induces a crack to form in the soil. Theoretically, the crack would form perpendicular to the direction of the minor principal stress in the soil. If the minor principal stress is in the horizontal direction (i.e. $K_0 < 1$), a vertical crack would develop. After initiation of the crack, the source of water pressure is stopped and the decay in water pressure in the piezometer is measured. When the crack just closes, the flow is controlled by the permeability of the soil and a significant change in rate of pressure decrease is observed. The pressure at this change of rate is called the critical pressure (Charles *et al.* 1996) and is assumed to coincide with the *in situ* total horizontal stress. Different techniques have been proposed to evaluate and interpret the measured pressure–time relationship to improve the accuracy of the test results. The hydraulic fracturing test method has limitations because the results can be affected by several factors as discussed in Jamiolkowski *et al.* (1985). Tavenas *et al.* (1975) also discuss the difficulties of determining K_0 *in situ* using hydraulic fracturing, total stress cells and the pressuremeter. Of these three methods they found total stress cells to be the best.

The stepped-blade developed by Handy *et al.* (1982) is similar to total stress cells and dilatometer blade, except that a series of progressively thinner blades comprise the instrument. The stepped-blade is pushed into the soil and stopped at the desired test interval. Readings of pressure on each of the blades are taken. The measured pressure on each blade is plotted against the blade's thickness. The plot is extrapolated to zero blade thickness to estimate the horizontal stress had the blade not been inserted into the soil. This pressure is assumed to be the *in situ* total horizontal stress. The effective stress is then obtained by subtracting the porewater pressure at this location. A piezometer installation would be required.

In situ stress measurement is also important in the characterization of bedrock. Measurements of *in situ* stress in rock have shown that in many locations the horizontal stresses are significantly higher than vertical stresses (Lo 1978 and BS5930). *In situ* stress measurement within the rock mass is described in Chapter 6. This is commonly carried out using overcoring techniques, where strains/deformations of a borehole wall are measured, and by hydraulic fracturing. The deployment and interpretation of *in situ* stress measurements requires specialist expertise and experienced personnel. Additional information on *in situ* stress measurement is provided in Morgan & Panek (1963), Plamer & Lo (1976), Brady & Brown (1993) and Whittlestone & Ljunggren (1996).

4.5 *Interpretation of Engineering Characteristics and Properties Based on* In Situ *Tests*

Currently, most of the interpretation of *in situ* test results is based on a semi-empirical and correlation approach. The correlation and/or interpretation should capture the essence or first-order effects of the ground conditions and behavior during *in situ* testing. Even the most carefully performed tests are of little value if they are not appropriate for the site conditions, and if they fail to take into account the possible differences between test and full-scale behavior. Although existing correlations are useful as a database to which test data can be compared to assess consistency and validity, care must be taken to ensure that appropriate correlations are being used and that they capture the essence of behavior. Multistage or indirect correlations should be avoided wherever possible because they compound errors and often mask critical aspects. The degree to which the volumes of tested ground are representative of the overall ground mass conditions, principal stress rotation considerations, fabric and stress anisotropy, and the effect of disturbance during sampling and insertion of *in situ* tools/probes are important factors and parameters to consider. Additional discussion on these aspects and the choice of test methods and interpretation is provided in Marsland (1986), Houlsby (1998) and ISC (1998).

The influence of the time and duration of loading must also be taken into account. Time and hydraulic conductivity govern development of excess porewater pressure, which in turn governs whether total stress (short term, undrained) or effective stress (long term, drained) parameters are appropriate. The type of test must consider rate of loading effects if it is to represent field behavior. If the soil response is essentially undrained, the test results should be used to infer or interpret undrained characteristics such an undrained shear strength. The results of CPTU tests should, therefore, be used to infer undrained characteristics in clays and drained parameters in sands. Similar consideration should also be given to the degree of deformation or strain induced in the soil during testing. For example, an *in situ* test that imposes very small deformation in the soil is best suited for interpretation of small strain response and *in situ* stresses. In contrast, *in situ* tests that impose large strain/deformation in the soil, such as the CPTU and PMT, should be used to correlate with strength and other large strain behavior.

The results from *in situ* tests are usually correlated and interpreted for the determination and assessment of the following engineering characteristics of soils:

- Soil profiling and classification
- Strength parameters, e.g. undrained shear strength of clays and effective friction angle of sands
- Deformation and stiffness characteristics, e.g. modulus of deformation, shear modulus and maximum shear modulus (static and dynamic)
- Initial states, e.g. density, relative density, state parameter, horizontal stress, stress history (OCR or preconsolidation pressure) and sensitivity
- Hydraulic characteristic parameters, e.g. hydraulic conductivity and coefficient of consolidation
- Direct design applications, e.g. foundation bearing capacity, pile capacities, ground improvement control and verification, liquefaction potential and skirt penetration resistance of offshore gravity-based structures

Numerous correlations between the results of *in situ* tests and engineering properties and designs have been developed and are used in practice. The choice of the most suitable correlations depends on the property or design application being considered, the experience and background of the engineer, and local

state-of-practice. The correlations available have been identified and discussed by several researchers and have been the subject of many national and international conferences and specialty symposia (e.g. Jamiolkowski *et al.* 1985, ASCE 1986, ISOPT 1988, Lunne *et al.* 1990, 1996, 1997, Swedish Geotechnical Society 1995, Institution of Civil Engineers 1996 and ISC 1998). Table 4.7 represents a summary of the applicability and usefulness of the more common *in situ* tests for the assessment of engineering properties and design applications. This table is based on information contained in the technical literature and on the experience of the author. The reader is referred to the above publications and others for the various correlations. Space constraints do not permit the reproduction of the correlations herein. Table 4.8 summarizes the key reference sources for correlations of engineering properties and design parameters with *in situ* test results.

4.5.1 USE OF STATISTICAL METHODS

The use of statistical techniques on the results of the *in situ* tests to enable the determination of realistic mean and standard deviation values of geotechnical parameters is recommended. Reliability analyses are being carried out much more frequently and will eventually become standard practice. *In situ* testing readily lends itself to statistical and probabilistic methods as large quantities of reliable data can be produced by the *in situ* probes and data acquisition systems. The use of geostatistics for geotechnical and environmental applications is discussed in Rouhani *et al.* (1996).

4.6 Observational Approach and Monitoring

There are always uncertainties and unknowns associated with ground conditions at a site, even with careful site characterization. To safely account for these unknowns and to avoid any undesirable surprises and unacceptable performance of structures, an excessive factor of safety or assuming the worst possible conditions could be adopted in design. This can result in very costly and uneconomical design. However, if the project can permit modifications of design during construction, important savings can be realized by continually assessing specific information obtained as construction progresses. The gaps in the information and/or verification of the assumed ground conditions on which design is based are provided by observations, and the design modified as required. This basis of design is called the observational approach. Its use for geotechnical/geological aspects of engineering works has been attributed to Karl Terzaghi (Peck 1969a). It has been frequently used for tunnels, dams and major transportation projects. Because of the added information, it is no longer necessary to design on the basis of most unfavorable conditions; a more economical design may be based on what now appears to be likely conditions.

In order to effectively use the observational approach, two requirements must be satisfied: (1) the presence and general characteristics of possible weak zones must be detected during the site investigation in advance of construction, and (2) special provisions must be made to obtain quantitative information and data on the likely problem zones during construction, before it is too late to modify the design in accordance with the findings. The success of the method depends on the identification of all possible scenarios and the preparation, in advance, of positive courses of action for solving any problems that may be disclosed by the results of observations. The observations can be through general visual surveillance and from appropriate instrumentation and monitoring programs. The data required generally include: measurement of porewater pressures; loads and stresses; horizontal, vertical and angular

TABLE 4.7. Summary evaluation for determining engineering soil parameters from *in situ* tests[a,b]

		Interpreted soil parameters (including use of empirical correlations)													Direct applications					Relative cost of performing test[d]
		Initial states					Strength		Deformation/ compressibility				Hydraulic							
Test[c]	Soil type	γ or D_r	ψ	K_0	σ'_p or OCR	S_t	S_u	ϕ'	E	E'	G_{max}	m_v	k	c_v	Stratigraphy	Shallow foundation	Axial pile capacity	Lateral pile capacity	Liquefaction potential	
SPT	Sand	3	—	—	—	—	—	3	—	4	5	4	—	—	1	1	2	3	1	I
	Clay	—	—	—	—	—	5	—	5	—	—	5	—	—	1	3	4	4	—	
DCPT	Sand	4	—	—	—	—	—	4	—	4	5	4	—	—	5	3	3	—	—	I
	Clay	—	—	—	—	—	—	—	—	—	—	—	—	—	—	—	—	—	—	
FVT	Sand	—	—	—	—	—	—	—	—	—	—	—	—	—	—	—	—	—	—	I
	Clay	—	—	—	3	1	1–2	—	—	—	—	—	—	—	—	2	3	3	—	
CPTU	Sand	2	2	—	—	—	—	2	—	3	4	3	—	—	1	1	2	3	1	II
	Clay	—	—	—	1	—	1–2	—	3	—	4	4	3	3	1	1	3	3	—	
DMT	Sand	3	2	2	—	—	—	3	—	2	4	3	—	—	3	3	4	3	3	II
	Clay	3	—	2	3	—	4	—	2	—	4	4	—	—	3	3	4	3	—	
PMT	Sand	3	—	2	—	—	—	3	—	2	3	3	—	—	5	3	4	2	4	V
	Clay	—	—	2	5	—	3	—	2	—	3	4	—	—	5	3	4	2	—	
PLT	Sand	—	—	—	—	—	—	—	—	1	4	1	—	—	—	1	—	—	—	V
	Clay	—	—	—	—	—	—	—	1	—	4	3	—	—	—	1	—	—	—	
CPTS	Sand	2	2	—	—	—	—	2	—	3	1	3	—	—	1	2	2	3	1	II
	Clay	—	—	—	1	—	1–2	—	3	—	1	4	3	3	1	2	3	3	—	
PIEZ	Sand	—	—	—	—	—	—	—	—	—	—	—	2	3	—	2	—	—	—	II
	Clay	—	—	3	—	—	—	—	—	—	—	—	2	3	—	—	—	—	—	

[a] For definition of symbols, refer to Chapter 2.
[b] Reliability rating scale: 1, high; 2, high–moderate; 3, moderate; 4, moderate–low; 5, low; —, not applicable.
[c] SPT, standard penetration test; DCPT, dynamic cone penetration test; FVT, field vane test; CPTU, piezo-cone penetration test; PIEZ, piezometers and other water sampling probes (including hydraulic fracturing for K_0); DMT, flat plate dilatometer; PMT, pressuremeter test (self-boring); PLT, plate-load test; CPTS, seismic cone penetration test.
[d] Relative cost: I, low; V, high.

TABLE 4.8. Summary of key reference sources for correlations of engineering properties and design parameters with *in situ* test results

In situ test	Soil types	Property or design parameter	References
Standard penetration test (SPT)	Sand Silt Gravel Tailings	Relative density Friction angle Deformation modulus Foundation design Liquefaction evaluation	Decourt (1989), Terzaghi & Peck (1967), Navfac (1982), CGS (1992) Peck *et al.* (1974), Clayton (1995) Seed (1979a), Seed *et al.* (1985), ISC (1998)
Becker penetration test (BPT)	Gravelly and cobbly material	Relative density Foundation design	CGS (1992), Harder & Seed (1986)
Piezo-cone penetration test (CPTU)	Sand Silt Clay Tailings	Stratigraphy Friction angle Relative density State parameter Deformation modulus Constrained modulus Undrained shear strength Stress history (OCR) Coefficient of consolidation and hydraulic conductivity Foundation design Liquefaction evaluation	Robertson (1990), Jefferies & Davies (1991, 1993), ISC (1998) Lunne *et al.* (1997, 1990) Robertson & Campanella (1983) Been *et al.* (1986, 1987) Mayne *et al.* (1998) Robertson *et al.* (1992), Robertson (1986)
Seismic-cone penetration test (CPTS)	Sand Silt Clay Tailings	Shear modulus Seismic velocity	Lunne *et al.* (1997, 1990), Robertson & Campanella (1983)
Dilatometer test (DMT)	Sand Silt Clay Tailings	Deformation modulus At rest Earth pressure (K_0) Stratigraphy Friction angle/relative density Undrained shear strength Foundation design	Lunne *et al.* (1990), Marchetti (1980)
Pressuremeter test (PMT)	Soft rock Sand Silt Clay Till	Deformation modulus At rest Earth pressure (K_0) Stratigraphy Friction angle/relative density Undrained shear strength Foundation design	Lunne *et al.* (1990), Mair & Wood 1987), ISC (1998) Jefferies (1988) Baguelin *et al.* (1978)

displacements; and quantity of seepage or leakage. The methods for making these measurements are discussed below. Some examples of the observational method are given in Terzaghi & Peck (1967), Peck (1969a and 1973) and Charles *et al.* (1996).

4.6.1 FIELD INSTRUMENTATION AND MONITORING

Instrumentation monitoring and visual surveillance are key components of the observational approach. The term monitoring is used to describe the recording of instrument readings and the interpretation of the results. The instruments frequently installed for ongoing monitoring purposes are piezometers for measurement of porewater pressure, monitoring wells for sampling of groundwater, total stress cells for measurement of total earth pressure, settlement plates and cells, extensometers to measure deformation both at the ground surface and within the ground, inclinometers to measure horizontal displacements in the ground, and electro-levels or tilt meters to measure tilt or rotation of the ground and structures. Additional information is provided in Hanna (1985) and Dunnicliff (1988).

Although the proper use of instrumentation and monitoring can be advantageous, the limitations of instruments should be considered to avoid unrealistic expectations of what can be practically achieved. The cost of instrumentation needs to be related to the expected benefit. The cost of the instruments themselves is usually small compared to the total cost of instrumentation including installation, reading, interpretation and assessment of results. It is also unwise to use low-quality instruments and to have them installed by inexperienced but inexpensive field personnel. This combination often produces a false sense of economy.

It is important to recognize that instrumentation, on the assumption that it is installed properly, only monitors behavior or response at its specific location. There is no guarantee that it is representative of the entire ground mass, or that the crucial location has been instrumented. Measurements are usually discontinuous in space and often in time. In addition, in some circumstances the installation of the instrumentation itself may constitute a defect in the ground being monitored (e.g. concentration of seepage effects in a dam). The installation itself may disturb the ground and the presence of the instrument may affect subsequent ground behavior. Some installations also present practical difficulties, which limit the amount or type of instrumentation that can be used. For example, access on natural slopes or embankment slopes can be difficult and costly. Whenever an instrument is installed, the borehole should be backfilled with a material that is similar in compressibility and deformation to the surrounding ground.

It is of little value to read instruments unless the results are recorded, plotted and interpreted without delay. It is good practice for the reader of the instrument to have previous readings available for comparison because this facilitates an immediate check of anomalous readings. To assist with interpretation, results should be presented in a simple form that can be readily understood. The data require careful assessment by experienced personnel taking account of all relevant factors, including climatic conditions. While electronic storage and computer processing can ease the burden of dealing with large quantities of data, this approach has its own pitfalls and does not eliminate the need for a careful assessment of data by experienced personnel.

Deformation of ground in terms of both vertical and horizontal displacements are important indicators of performance. The most common methods for vertical movement are plates installed on the surface of the ground to measure settlement or heave. Vertical and horizontal movements can also be measured

by surveying techniques, such as theodolite, optical level, electro-optic distance (EDM), photogrammetry, and the use of GPS in some applications. The accuracy of measurement should be compatible with the amount of significant or anticipated magnitude of displacement. Reference or benchmark stations must be on stable ground and not subjected to seasonal variations as a function of weather or temperature. Internal vertical displacements of ground are frequently measured using extensometer systems. Magnet extensometers are increasingly being used because they are generally accurate, reliable and easy to use. This extensometer consists of magnets fixed to the sides of a borehole that move relative to a fixed underlying datum point, such as bedrock or hard competent layer. A surficial sensor is lowered down in a central access tube and locates the location of the magnets.

Inclinometers measure and monitor profiles of horizontal movements, distortions and shear zones within the ground. An extensometer can also be incorporated in the same installation. A slope indicator (inclinometer) installation basically consists of specially grooved plastic casing placed within a vertical borehole. The tube has four grooves at right angles to each other. One set of grooves should be in the direction of the anticipated horizontal movement. The inclinometer probe, which is lowered within the casing, following the alignment of the grooves, measures the inclination of the casing from the vertical. Comparison of a series of readings taken at different times provides profiles and magnitudes of ground movements. A satisfactory slope indicator installation requires that the bottom of the casing be anchored into a material that will itself not undergo movement. The fixed base provides the datum from which lateral movements further up the casing can be determined from subsequent readings. If the fixity of the slope indicator casing at the bottom is in doubt, the top of the casing should be surveyed and the results used to correct the readings as required.

The annulus between the borehole walls and the outside of the slope indicator casing should be backfilled with a cement–bentonite grout mixture to ensure an intimate, but not rigid, contact between the casing and the soil. Consideration of the backfill and *in situ* soil compressibility is an important aspect of slope indicator installations. Should the backfill be too stiff, it may be possible for the surrounding softer soil to move around the stiffer backfill column and, if this happens, the actual subsoil movements will not be detected by the slope indicator casing. Further, the flexible bentonite–grout mixture provides an *in situ* seal to prevent the downward migration of possible contaminated material into underlying quality aquifers. Inclinometers are very useful on projects concerning stability such as natural slopes and engineered embankments, anchored bulkheads, sheet pile walls and structures supported on long piles. If properly used, a slope indicator (inclinometer) monitoring program can provide adequate warning of pending instability.

The electro-level is a gravity-sensing electrolytic transducer that provides an output voltage proportional to the tilt angle. It consists of a small sealed plastic case, partially filled with electrolytic fluid and metal electrodes in contact with the electrolyte. Electro-levels can be permanently installed in boreholes or on structures. The system provides a means of measuring tilt to a high degree of accuracy, but their longevity remains a concern (Charles *et al.* 1996).

4.7 Characterization of Groundwater

Groundwater has a significant influence on all projects and project development often impacts groundwater. In some localities groundwater may have elevated concentrations of pollutants or may contain constit-

uents in concentration sufficient to make it aggressive and cause damage to construction materials such as concrete and steel. Characterization of groundwater involves determination of groundwater levels and pressures, hydraulic conductivity and water quality in terms of its chemical composition. Experienced geoenvironmental/geotechnical engineers or hydrogeologists should be consulted and involved during planning stages of the characterization study. Guidelines and reference standards (e.g. BSI 1981, CGS 1992 and ASTM 1997a and b) are also available and they should be consulted during the planning stages for groundwater characterization studies, both from the geotechnical and environmental perspective. A comprehensive review and discussion of groundwater and wells are provided in Driscoll (1986). Issues related to contaminant hydrogeology are discussed in Chapter 25.

4.7.1 WATER LEVELS, PIEZOMETRIC PRESSURES AND SAMPLING

Groundwater conditions and their fluctuations with time are usually investigated by the installation and monitoring of piezometers in boreholes. Groundwater observations made at the time of drilling are not representative in clayey soils and other fine-grained soils, because of their low hydraulic conductivity and the corresponding long periods of time before the water level in the borehole reaches stabilized, equilibrium conditions. Some piezometers, however, can be pushed directly into softer soils without firstly drilling a borehole.

A distinction should be made between standpipes and piezometers. An open well or standpipe installation corresponds to the case of a slotted tube or porous element with no seals, other than at the ground surface. It measures the depth to the groundwater table. A disadvantage of this type of installation is that different layers of soil may be under different pressure conditions; the level measured is not representative of any given layer. This system is only useful for relatively homogenous deposits. A piezometer, on the other hand, is installed with seals and measures the piezometric (porewater pressure) head in the stratum between the seals. A standpipe type of piezometer generally consists of a porous element that is connected to plastic tubing leading to the ground surface. The porewater passes through the porous tip and rises up in the tubing to a distance equal to the porewater pressure in the strata in which the piezometer tip has been installed/sealed. For sands, stabilized conditions are reached quickly; however, in clays several days and perhaps weeks may be required for stable conditions to be reached. The water level within the tube is measured by lowering a small electrical wire down the tube from the ground surface. A buzzer, flashing light or voltmeter indicates when water has been reached.

Consideration of time lag effects is the key factor in the selection of the appropriate type of piezometers for a given project. If the measurement of porewater pressure is to reflect immediate conditions or changes in pressure in real time, the piezometer needs to be a pressure transducer, electrical, vibrating wire or pneumatic type of piezometer for which the measurement does not rely on actual flow or displacement of porewater to occur. These instruments are comparatively expensive and are usually installed in boreholes in the same fashion as for standpipe piezometers. Should only stabilized equilibrium conditions be required, a standpipe type of piezometer would be suitable. Proper installation is critical for satisfactory performance of piezometers. When installed in boreholes, the piezometer tip should be provided with a suitably graded sand pack and bentonite seals placed at a small distance above and below the piezometer tip. A seal should also be placed at ground surface to prevent surface water infiltration. The tip on

hydraulic standpipe piezometers generally consists of a non-metallic or metallic filter with small pore sizes so that the tip can be in direct contact with fine-grained soils if required. A low air-entry tip with a hydraulic conductivity of 3×10^{-4} m s^{-1} is used in saturated soil. If the soil is unsaturated and where negative porewater pressure may develop, a high air-entry tip with hydraulic conductivity of 3×10^{-8} m s^{-1} is used. High air-entry tips may also be used in saturated ground. De-airing or saturating these porous tips is very important for quality installation of hydraulic piezometers.

Special consideration needs to be given to unsaturated soils and sampling of soil, gas and pore fluid from the vadose zone, and measuring matric potential using tensiometers and other methods. Chapter 5 deals with unsaturated soils and provides detailed information.

Samples of the groundwater can be collected from standpipe piezometers and wells for chemical testing purposes. Sampling can be achieved in a variety of ways, including simple bailing techniques, air pressure lifting and pumping. Care should be taken to ensure that the water samples are representative of the water-bearing stratum and that they have not been contaminated or diluted by surface water, or water used to make the boring. Sampling from sealed piezometers or wells is recommended. The water should be flushed several times to ensure that the sampled water is freshly from the water-bearing stratum. Water samples may deteriorate rapidly and should be tested as soon as possible after sampling. The sampling protocol required by the testing agency must be followed. More sophisticated instruments for measuring porewater pressure and collecting groundwater samples are also commercially available. Some of the more common ones are the Waterloo System, BAT sampler and the Westbay Packer System. Details on these systems can be obtained directly from the manufacturers or distributors of geotechnical instrumentation. Additional information is provided in Dunnicliff (1988), Charles *et al.* (1996) and ASTM (1997 a, b). Some specialized piezo-cone penetrometers are also available for sampling groundwater and assessing water quality for contamination studies as the cone is pushed through the soil (Campanella *et al.* 1990, 1994; Robertson *et al.* 1996, 1998; and O'Neil *et al.* 1996).

4.7.2 *IN SITU* HYDRAULIC CONDUCTIVITY TESTS

Determination of the hydraulic conductivity of soil or rock is needed in connection with seepage studies, yield of wells in aquifers and for groundwater control. Milligan (1975) provides a useful summary of the common test methods and difficulties associated with determining *in situ* hydraulic conductivity in soil and rock. The results of *in situ* measurement are more representative of actual field hydraulic conductivity values than the results from laboratory tests on samples. Pumping tests are frequently used to assess aquifer characteristics and hydraulic conductivity. They may also be useful for assessing the hydraulic conductivity of adjacent aquitards. Jezequel & Mieussens (1975) describe a self-boring permeameter. *In situ* hydraulic conductivity tests can also be carried out using properly installed standpipe-type piezometers and wells. Although variable-head (falling or rising) tests in piezometers and wells are most commonly used, constant-head tests are also possible. In the variable-head test, water is either added or removed from the tube, after stabilized conditions have been reached. The change in water level is measured, against time, to obtain time response curves from which the *in situ* hydraulic conductivity can be calculated. The hydraulic conductivity of the piezometer/well filter should be at least one or two orders of magnitude higher than the material to be tested,

otherwise the response measured may be that of the filter instead of the ground. Packer type pressure tests are also used. Summaries of these various tests and methods of interpretation are given in Hvorslev (1951), Mansur & Kaufmann (1962), Gibson (1963), Cedergren (1989), Wilkinson (1967 and 1968), Ahmed *et al.* (1975), NavFac (1982) and Lowe & Zaccheo (1991). The piezo-cone penetration test (CPTU) can also provide estimates of hydraulic conductivity in soils with hydraulic conductivity less than about 10^{-6}–10^{-7} m s^{-1} or lower as discussed in Section 4.4.6.

In addition to the results from piezometers to gain an understanding of the groundwater flow regime, tracer techniques can be used (Siddle *et al.* 1986). Tracer techniques are used in hydrogeological investigations to assess hydraulic connection and the rate of flow of groundwater. The technique involves introducing a measured quantity of an appropriate tracer at a source and detecting the point of emergence by *in situ* monitoring or by combined sampling and laboratory analyses. The success of the approach is subject to many natural unpredictable factors. Care is necessary in the selection of tracers because some tracers can contaminate groundwater and surface water. Table 4.9 summarizes the requirements of tracers. The four main groups of tracers used are colored dyes, particulates, stable chemical compounds and radioactive isotopes. A useful summary of tracer techniques and some case histories of their use are given in Charles *et al.* (1996) and Siddle *et al.* (1986).

4.8 Environmental Site Characterization

Environmental characterization generally includes sampling and monitoring of soil, the vadose zone, lake and river bottom sediments, bedrock, surface water, groundwater and aquifers, waste and contaminants, air and atmospheric constituents, and biological constituents such as flora and fauna, including zooplankton, phytoplankton, benthic communities of macroinvertebrates, and other species. Complete characterization generally requires a multidisciplined team and input from soil scientists, geologists, hydrogeologists, hydrologists, geotechnical and environmental engineers, biologists and other environmental scientists and specialists. The appropriate characterization works for a site depend on the specific requirements for each project. As such, they will generally vary from one project to another.

The process of site characterization and many of the investigative methods and tools used in environmental characterization and assessment of contaminated sites are essentially the same as those used for geotechnical characterization. However, for environmental characterization, special care and attention must be paid to drilling and sampling protocols, potential cross-aquifer contamination vertically in a borehole, baseline studies, and health and safety plans and procedures. Guidelines for investigation of landfills and contaminated land are presented and discussed in the Site Investigation Steering Group—Part 4 (1993). Standards relevant to environmental site characterization are provided in ASTM (1997a, b). Additional information and discussion of aspects of environmental characterization are presented in Chapter 23.

4.8.1 INVESTIGATION OF LANDFILLS AND CONTAMINATED LAND

Investigation of landfills and contaminated land requires special consideration and attention. A written health and safety plan, which incorporates safety and emergency response procedures, needs to be prepared prior to the start of any field work. All site personnel must be given appropriate training and provided with protective clothing, as appropriate. Recommended field operations in

TABLE 4.9. Summary of requirements of groundwater tracers

Properties	
Singularity:	the tracer should not occur naturally in the groundwater under investigation
Stability:	the tracer should be chemically and biologically stable; it should be unaffected by sunlight or pH of the groundwater, and should be resistant to adsorption by clay minerals, peat and fine-grained materials
Non-toxicity:	the tracer should be free from contaminants and should not be harmful to vegetation, man or animals
Inoffensive:	the use of tracer should not cause a nuisance to other water users downstream of the project area
Cost:	the technique should preferably be relatively inexpensive
Performance	
Travel:	the tracer should travel at, or as close as possible to, the same velocity as the water it is tracing
Accurate dosing:	the injection procedure should permit controlled introduction of tracer into a specific aquifer
Sampling reliability:	samples should accurately represent the concentrations occurring in the field
Accurate detection:	the tracer should be detectable at low concentrations
Analysis	
Qualitative assessment:	tests should indicate positive hydraulic connections
Quantitative analysis:	quantitative analysis results should provide information on flow rates

terms of drilling, sampling, handling of samples, monitoring, site security, and procedures for personnel leaving a contaminated site need to be described in the safety plan. All personnel involved in the investigation of landfills and contaminated land should carry appropriate insurances; provision of Certification of Insurance should be a contractual requirement.

Special care is required to ensure that cross-contamination does not occur either between boreholes or as a borehole is advanced. Drilling and sampling equipment must be cleaned between samples and special drilling procedures, such as the use of a series of sealed casings, need to be used to avoid carrying contamination down into an underlying aquifer. Special consideration needs to be given to the sealing of boreholes as discussed in Section 4.4.5.

Site specific protocols are required for taking of samples, and arrangements need to be made for the disposal of borehole cuttings. Frequently this includes disposal of the material in registered landfills and other waste management facilities. Testing as specified by regulations and local jurisdictions is required before taking contaminated material off-site.

Samples obtained need to be clearly labelled and clearly identified, e.g. using colorcodes to indicate the nature and category of the material placed in the sample container. Precautions need to be taken while transporting the samples to testing laboratories to ensure that no leakage or spillage takes place. Signed chain of custody papers for samples should be implemented so that accurate tracking of a sample can be achieved. All samples not sent for testing should, whenever possible, be stored on site in appropriately marked and secured areas.

5. UNSATURATED SOIL MECHANICS AND PROPERTY ASSESSMENT

D. G. Fredlund
G. W. Wilson
S. L. Barbour

5.1 *Introduction*

Early theoretical soil mechanics dealt mainly with saturated soil from below the groundwater table, i.e. positive porewater pressures (see Chapter 2). The soil above the groundwater table has negative porewater pressures and is known as the vadose zone. Recent theories for unsaturated soil behavior have taken on the form of extensions of classical (saturated) soil mechanics theories. While parallels and similarities between saturated and unsaturated soil mechanics are present, variations exist that make the practice of unsaturated soil mechanics somewhat different in character from saturated soil mechanics. Differences lie primarily in the assessment of appropriate soil properties and soil property functions, and in the flux boundary condition between the soil and the atmosphere. This chapter presents the fundamental theories of unsaturated soil mechanics, and emphasizes those elements of unsaturated soil mechanics that differ from saturated soil mechanics. Unsaturated soil mechanics can be categorized into three classical areas of study: seepage, shear strength and volume change. Paradigm shifts in analysis associated with the assessment of soil properties become an important factor when moving from theory to practice of unsaturated soil mechanics.

The term *unsaturated soil mechanics* is used in the sense that the theories and formulations apply to all soils with negative porewater pressures; namely, soils commonly found in the vadose zone. Figure 5.1 illustrates that soils may have a continuous air phase, an occluded air phase, or even be saturated. There is a smooth transition from the unsaturated soil mechanics to saturated soil mechanics. Saturated soils are a special case of the more general unsaturated soils. Unsaturated soil mechanics is relevant to many practical problems such as:

- Damage induced to structures on unsaturated, expansive soils
- Contaminant migration in the vadose zone
- Design of covers for waste disposal facilities and mining rehabilitation schemes
- Slope failures after periods of high precipitation
- Stability of loosely compacted fills
- Stability of cuts or trenches in the vadose zone
- Cohesive backfills in earth-retaining structures
- Bearing capacity of foundations in the vadose zone
- Roads, railway and airfield performance

R. K. Rowe (ed.), *Geotechnical and Geoenvironmental Engineering Handbook*
© Kluwer Academic Publishers 2001

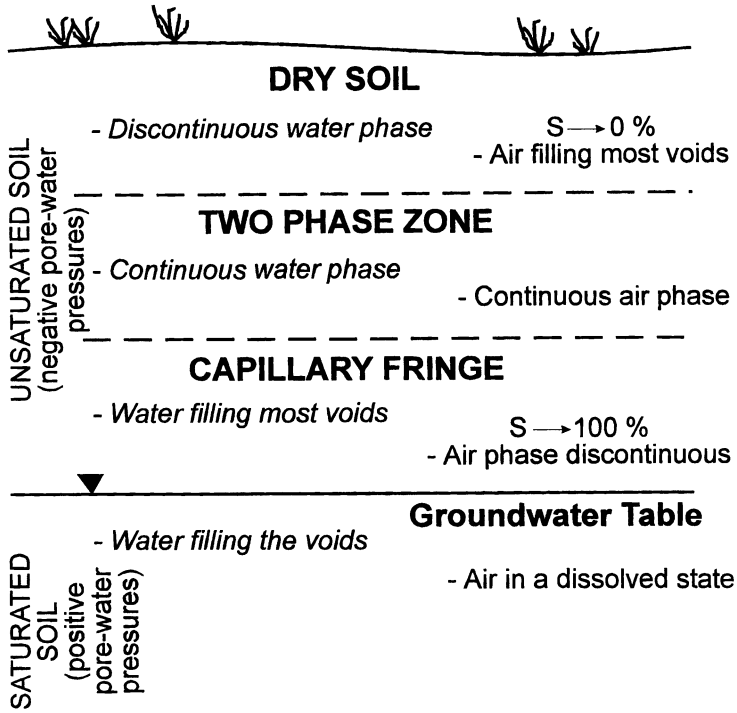


FIGURE 5.1. Classification of the regions within a saturated–unsaturated soil profile.

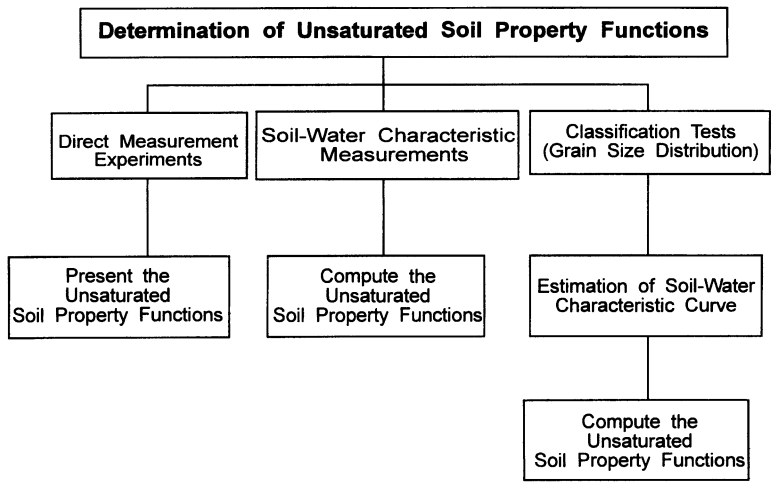


FIGURE 5.2. Approaches that can be used in the laboratory to determine the unsaturated soil property functions.

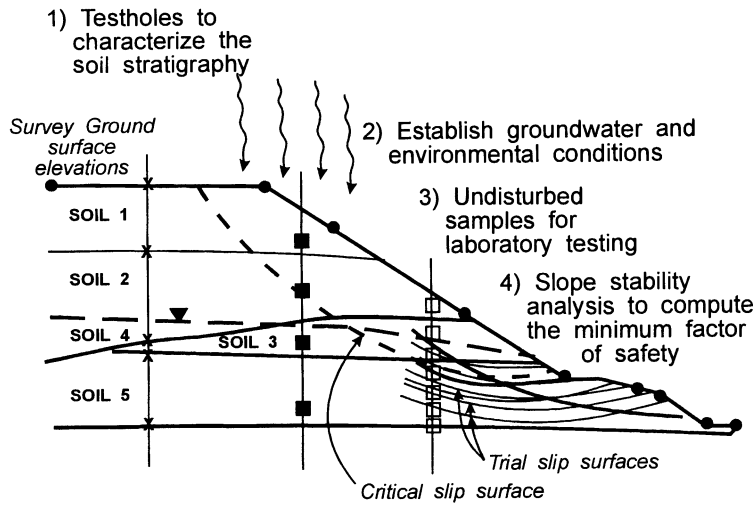


FIGURE 5.3. Example problem illustrating the role of the unsaturated soil property functions in performing a combined seepage and slope stability analysis.

The major focus of a typical geotechnical engineering project involves the assessment of the soil properties. All theoretical, predictive engineering tools have constitutive relationships that contain soil properties embedded within their mathematical models. For unsaturated soil, the soil properties tend to be highly non-linear and are generally represented in terms of the unsaturated soil property functions. These functions must either be measured, indirectly computed or estimated in a cost-effective manner (Fredlund 1995). Figure 5.2 illustrates the types of approaches that can be used in the assessment of unsaturated soil property functions. Each of the suggested procedures is further developed in this chapter.

Appropriate boundary conditions, particularly at the ground surface, are also an important component in the analysis of unsaturated soils. Varying the soil properties and the boundary conditions allows the engineer to address a range of questions related to: what will happen under variable conditions that may occur at sometime in the future?

Consider the example of a slope stability study in order to focus on the role of soil property functions and boundary conditions. Figure 5.3 shows a typical slope along with an outline of the information required in order to perform an analytical study. A relevant question might be: under what rainfall conditions, i.e. intensity and duration, is the slope likely to fail? The problem can be reduced to a saturated–unsaturated seepage study and a soil–atmosphere interactive study, which provide information for a limit equilibrium slope stability study.

5.1.1 BASIC CONCEPTS IN UNSATURATED SOIL MECHANICS

The description of the stress state for an unsaturated soil becomes a fundamental building block for unsaturated soil mechanics. In the early 1960s, researchers began to recognize the need for two independent stress state variables for unsaturated soil (Bishop & Blight 1963). In the early 1970s, a theoretical basis and justification for the use of two independent stress state variables was provided (Fredlund & Morgenstern 1977). The justification for two independent stress state variables was based on the superposition of equilibrium stress fields for each phase of a

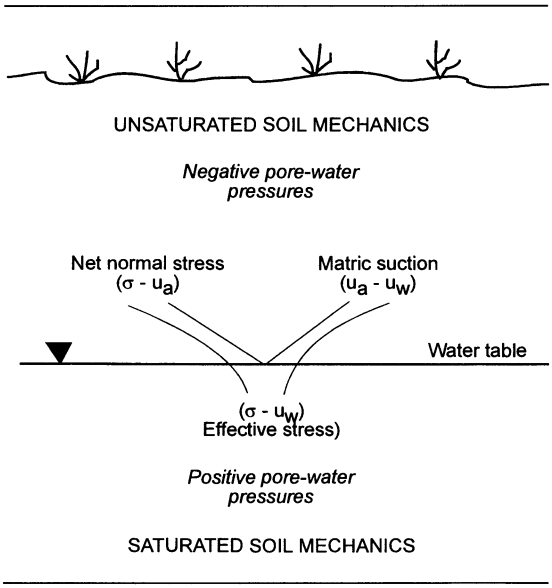


FIGURE 5.4. Separation of saturated and unsaturated soil mechanics based on the stress state description.

multiphase system. Figure 5.4 illustrates the stress state variables for saturated and unsaturated soils.

Three possible combinations of independent stress state variables can be justified from theoretical continuum mechanics. The three combinations are net normal stress ($\sigma - u_a$), matric suction ($u_a - u_w$), and effective stress ($\sigma - u_w$); where σ = total normal stress, u_w = porewater pressure, and u_a = pore-air pressure. Net normal stress ($\sigma - u_a$), embraces the activities of man, which are dominated by applying and removing total stress, i.e., fills, applied loads and excavations. Matric suction ($u_a - u_w$), embraces the impact of the climatic environment above the ground surface.

Total suction ψ, is comprised of matric suction ($u_a - u_w$), and osmotic suction, π:

$$\psi = (u_a - u_w) + \pi. \qquad (5.1)$$

Matric suction is closely related to the surrounding environment and is known to vary with time due to environmental changes. Osmotic suction is related to the salt content in the porewater present in the soil. Changes in osmotic suction may effect the mechanical behavior, overall volume change and shear strength of a soil. Many of the engineering problems involving unsaturated soils are a result of changes in the surrounding environment. For example, a slope may become unstable due to the reduction of matric suction caused by an increase in porewater pressure from water infiltrating into the soil.

The change in osmotic suction is generally less significant than the change in matric suction. Laboratory data have shown that a change in total suction is essentially equivalent to a change in matric suction during changes in water content (Krahn & Fredlund 1972). However, the effect of osmotic suction may be significant in cases where chemical contamination of the soil alters the salt content of the porewater, or construction occurs in saline soils or marine conditions. The change in osmotic suction must be taken into account in theses types of problem analysis. In the remainder of this chapter, it is assumed that the effects of osmotic suction are negligible and total suction and matric suction are equivalent, i.e. $\pi = 0$.

5.2 *Soil–Water Characteristic Curve*

The soil–water characteristic curve, also referred to as the water retention curve, has played a dominant role in understanding the behavior of unsaturated soils in disciplines such as soil science, soil physics, agronomy and agriculture. As a consequence of the long history associated with the use of the soil–water characteristic curve, large amounts of information and experimental data are available from these disciplines. The soil–water characteristic curve is now recognized as one part of the water phase constitutive relationship in geotechnical engineering. The soil–water characteristic curve is of greatest value in predicting unsaturated soil property func-

tions. As a result, it is essential that the nature and theory behind the soil–water characteristic curve be well understood when implementing unsaturated soil mechanics.

The soil–water characteristic curve is a relationship between the amount of water in the soil and the soil suction, or stress, on the soil. The water content of the soil is plotted as a function of matric suction. Suction is usually plotted on a logarithmic scale to accommodate the large range of suctions, approximately six orders of magnitude. Negative values cannot be plotted on a logarithmic scale, and as a result, suction is plotted as a positive value. Remember that suction represents a negative porewater pressure in the soil. The amount of water in the soil, plotted arithmetically, is generally quantified in terms of volumetric water content, θ; but can also be expressed as gravimetric water content, w, or degree of saturation, S (see Chapter 2 for definitions of θ, w and S). Figure 5.5 defines the typical features of a soil–water characteristic curve.

Volumetric water content, θ, is defined as the ratio of the volume of water to the total volume of soil. Relationships can be written between the various volume–mass designations for water content. The relationship between volumetric water content, θ, and other variables is:

$$\theta = \frac{Se}{1 + e} = Sn \tag{5.2}$$

where e = void ratio, S = degree of saturation, and n = porosity. The relationship between volumetric water content, θ, and gravimetric water content, w, can be written as:

$$\theta = w\rho_d/\rho_w \tag{5.3}$$

where ρ_d = dry density of the soil, ρ_w = density of water, and w = gravimetric water content.

5.2.1 STAGES OF THE SOIL–WATER CHARACTERISTIC CURVE

An initially saturated soil specimen desaturates when it is subjected to an increase in soil suction. Different saturation stages can be identified as desaturation takes place. Figure 5.5 shows the desaturation stages along the desorption, or drying, branch of a soil–water characteristic curve. Similar stages apply to the adsorption, or wetting, branch of the soil–water characteristic curve. Figure 5.6 illustrates both the desorption and adsorption curves and the definitions associated with the soil–water characteristic curve. The follow-

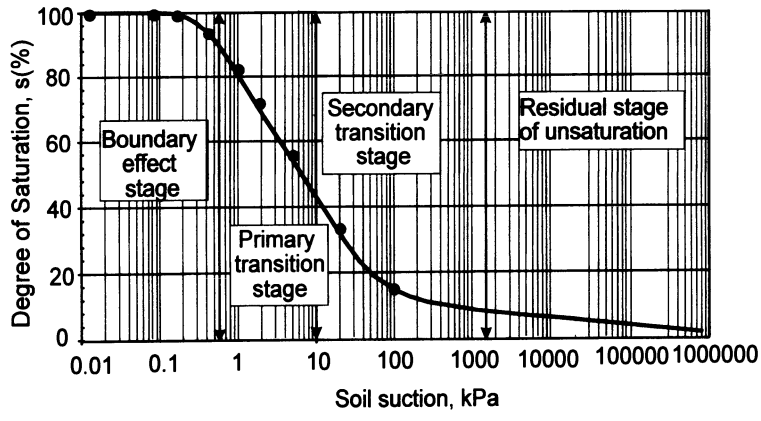


FIGURE 5.5. A soil–water characteristic curve showing the different stages of desaturation (modified from White *et al.* 1970).

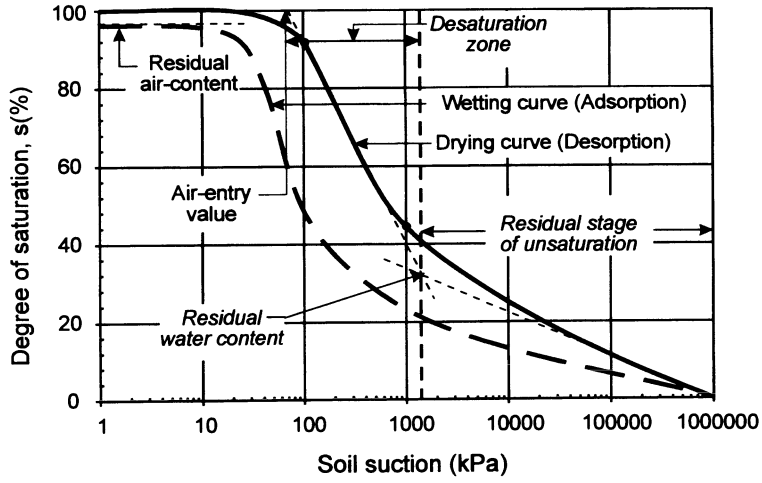


FIGURE 5.6. Definition of variables associated with the soil-water characteristic curve.

ing definitions and descriptions of the soil–water characteristic curve are made using the desorption, or drying, curve. There are three identifiable stages of desaturation: the boundary effect stage, transition stage and residual stage of saturation (Fig. 5.5).

Figure 5.7 illustrates the variation of wetted area of contact for different stages of the soil–water characteristic curve (Vanapalli 1994). The boundary effect stage ranges from full saturation of the soil to the air entry value (Fig. 5.5). The soil is essentially saturated in this stage. The air entry value of the soil $(u_a - u_w)_b$, is a soil suction value at which the largest pores in the soil begin to drain and air enters the pores in the soil. The air entry value is sometimes referred to as the "bubbling pressure." The air entry value is seen on the graph by the change in slope on the curve. The slope of the curve in the boundary effect stage is not horizontal (zero slope), as there is a slight change of water content from zero suction to the air entry value as a result of compression of the soil. If the curve is extended back into the negative suction range, i.e. positive porewater pressures, the slope of the curve would represent the coefficient of volume change, m_v, for a saturated soil.

In the boundary effect stage, flow takes place through the voids in a manner similar to that for a saturated soil. The unsaturated hydraulic conductivity, $k_{(u_a-u_w)}$, is equal to the saturated hydraulic conductivity, k_s, up to the air entry value of the soil. The shear strength contribution due to soil suction is primarily

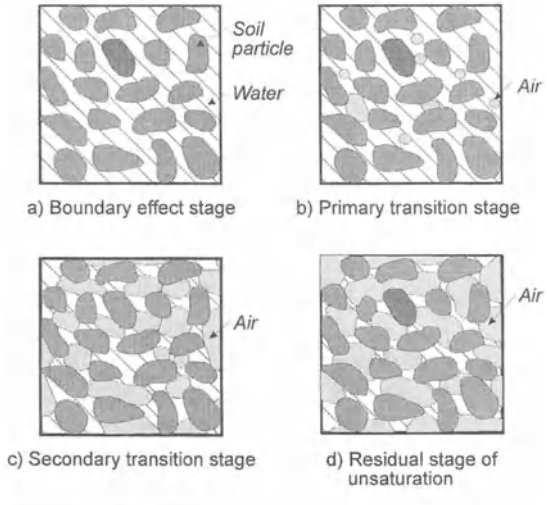


FIGURE 5.7. The variation of wetted area of contact area for different stages of desaturation along the soil–water characteristic curve (after Vanapalli 1994, reproduced with permission): (a) boundary effect stage; (b) primary transition stage; (c) secondary transition stage; and (d) residual stage of unsaturation.

through the wetted interaggregate contact area points. As there is little change in the water content of the soil at suctions below the air entry value, the shear strength contribution due to suction, represented by ϕ^b, is equal to the effective angle of internal friction, ϕ', up to the air entry value of the soil.

The soil desaturates in the transition stage. The flow of water in the pores of the soil remains in the liquid phase as the applied suction increases. The water content in the soil declines significantly with increasing suction. When the soil desaturates in this stage, the soil properties are no longer constant, as for the boundary effect stage. The soil properties are a function of the suction, or stress, in the soil, and are called the unsaturated soil property functions. Flow occurs through progressively smaller size pores as the soil suction increases. The connectivity of the pores, or voids, continues to reduce with increasing values of suction, as the pathways for flow are reduced. Thus, the unsaturated hydraulic conductivity, $k_{(u_a-u_w)}$, drops as the soil suction increases. The wetted area of contact at the interaggregate contacts reduces as desaturation continues (Fig. 5.7). The contribution of shear strength due to the suction decreases with the desaturation of the soil in this stage. As a result, there is a non-linear variation in the shear strength of the soil with respect to soil suction beyond the air entry value of the soil.

Eventually, large increases in suction lead to relatively small changes in water content. This stage is referred to as the "residual stage of saturation." There is a fraction of relatively immobile water in the pores of the soil at this stage, which has little or no contribution to the flow in the pores (Huang 1994). Water movement in this stage is primarily through vapor transport. The water content of the soil at the beginning of the residual stage is called the "residual water content." The wetted area of contact is significantly reduced, compared to the saturated state, and soil suction is not significantly effective in contributing towards the shear strength of the soil. The various stages along the soil–water characteristic curve provide a physical model for understanding the unsaturated soil property functions. There is a close relationship between both the hydraulic conductivity and the soil–water characteristic curve to the shear strength behavior of an unsaturated soil.

5.2.2 RESIDUAL CONDITIONS FOR A SOIL

The "residual water content", and its corresponding soil suction, have been defined in a number of ways in the literature. However, consistent use of these terms is lacking. Some researchers suggest that a water content corresponding to a suction of approximately 1500 kPa may be used to define the residual water content (van Genuchten 1980). This value of suction corresponds to the wilting point of many plants.

Residual conditions for a soil will be defined as the point where water movement in the liquid phase ceases, or the point where vapor phase transport becomes the primary mechanism for moisture movement in the soil. Desaturation beyond residual conditions appears to occur primarily as a result of vapor movement up to the point where the soil water content is in equilibrium with the vapor pressure in the surrounding environment. The arbitrary value of 1500 kPa may, or may not, correspond to the residual conditions for a given soil. Residual conditions for a soil will depend on the soil type and the pore size distribution within the soil. Graphically, the residual state can be seen on the soil–water characteristic curve at the second break in curvature at high suction values (Fig. 5.6).

The following graphical construction is suggested for defining the residual state of a soil (Fig. 5.6, dashed lines). First, in the transition stage of the soil–water characteristic curve, draw a line tangent through the inflection point on the straight-line portion of the curve. Second, in the residual stage of the soil–water characteristic curve, extend a

straight line back from the portion of the curve passing through 1 000 000 kPa. The residual state of the soil, soil suction and corresponding water content, is defined as the point where the line extended from 1 000 000 kPa intersects the previous tangent line.

The residual state, or residual stress state, for gravel, sand, silt and their mixtures is well-defined and generally occurs at relatively low values of suction, i.e. between zero and 500 kPa suction range. For clays with low plasticity, the residual stress will generally be in the range 500–1500 kPa. However, for intermediate to highly plastic soil the residual state can be greater than 1500 kPa. In some cases, such as highly plastic, intact clays, it is difficult to define the residual break in the curve.

There is a common value of total suction, i.e. the sum of matric suction and osmotic suction, where all types of soil approach a zero water content. The total suction value corresponds to approximately 1 000 000 kPa. Experimental results of Croney *et al.* (1958), Russam (1958), Fredlund (1964), and Vanapalli (1994) on various soils support this value. This experimentally observed behavior is also supported using thermodynamic principles (Richards 1965). Engineers are generally interested in the performance of geotechnical structures in the relatively low suction range of 0–500 kPa. Suction values approaching 1 000 000 kPa, and the corresponding low water contents, are useful when defining flux boundary conditions for use in coupled soil–atmosphere modeling. Therefore, it is of value to mathematically define the soil–water characteristic curve over the entire range of suctions.

Typical desorption branches of soil–water characteristic curves for different soils are shown in Fig. 5.8. A coarse-grained soil, such as gravel or sand, has large interconnected pores and shows a tendency to desaturate rapidly with increasing values of suction. The rate of desaturation decreases with an increase of fines in a soil. The water holding capacity, or storage capacity, of a soil corresponding to a particular value of suction is higher for a soil with a higher percentage of fines. The air entry value $(u_a - u_w)_b$, and the residual suction value, ψ_r, can be expected to be higher for soils that have more fines.

5.2.3 MATHEMATICAL FORM FOR THE SOIL–WATER CHARACTERISTIC CURVE

Analysis of geotechnical problems involving unsaturated soils is complex and is carried out using computers. Defining the soil–water characteristic curve mathematically is required, since the soil–water characteristic curve is used to predict the unsaturated soil

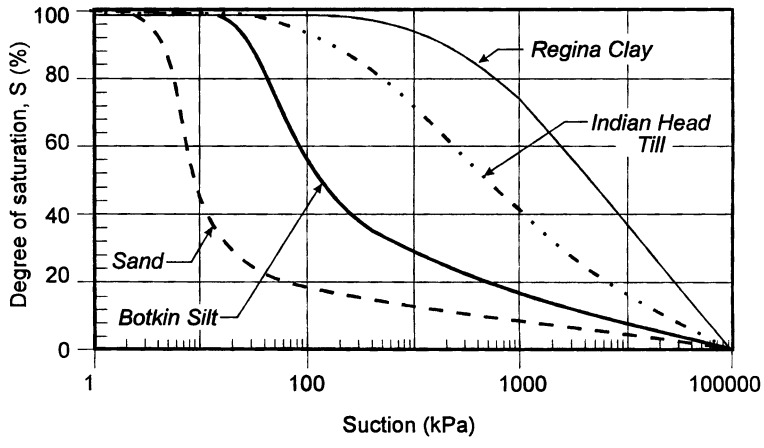


FIGURE 5.8. Typical soil–water characteristic curves for four soils from Saskatchewan, Canada.

property functions. Several equations have been proposed for the soil–water characteristic curve and are summarized in Table 5.1.

Many of the equations in Table 5.1 do not properly model the entire suction range. Most of the equations are asymptotic to horizontal lines in both the low and high suction ranges, in the boundary effect stage and residual stage, respectively. In the boundary effect stage, the equations produce a curve that is horizontal at the maximum water content from zero suction to the air entry value. If this line is extended back into the negative suction range (positive porewater pressures), it would yield a zero value for coefficient of volume change, m_v. In the residual stage, the equations produce a curve that does not pass through zero water content at a suction of 1 000 000 kPa.

The equation proposed by Fredlund & Xing (1994) provides a mathematically based function defining the soil–water characteristic curve over the entire range of suctions form zero to 1 000 000 kPa. The relationship is empirical, but is derived using the assumption that the soil consists of a set of interconnected pores that are randomly distributed. The equation, written in terms of volumetric water content, θ, is:

$$\theta = C(\psi)\left[\frac{\theta_s}{\{\ln[e + (\psi/a)^n]\}^m}\right] \qquad (5.4)$$

where θ = volumetric water content; θ_s = saturated volumetric water content, a = a suction value corresponding to the inflection point on the curve, which has physical meaning in its relationship to the air entry value of the soil; n = soil parameter related to the slope of the soil–water characteristic curve in the transition stage, ψ = soil suction, i.e. matric suction at low suctions and total suction at high suctions; m = parameter related to the residual water content; θ_r = volumetric water content at residual conditions; e = natural number, 2.71828 . . .; and $C(\psi)$ = correction function that forces the soil–water characteristic curve through a suction of 1 000 000 kPa at zero water content.

The correction factor is defined as:

$$C(\psi) = \left\{1 - \frac{\ln[1 + (\psi/\psi_r)}{\ln[1 + (1\,000\,000/\psi_r)}\right\} \qquad (5.5)$$

where ψ_r = suction value corresponding to residual water content, θ_r.

Equation 5.4 can be written in a dimensionless form by dividing both sides of the equation by the saturated volumetric water content so that for an incompressible soil:

$$\Theta = S = C(\psi)\left\{\frac{1}{\ln[e + (\psi/a)^n]}\right\}^m. \qquad (5.6)$$

Equation 5.5 can be used to best fit the desorption or adsorption branches of soil–water characteristic curve data over the entire range of suctions. The fitting parameters, i.e. a, n, and m values, can be determined using

TABLE 5.1. Summary of some mathematical equations proposed for the soil–water characteristic curve

Soil parameter[a]	Equation	Reference
a_g, n_g	$\theta_w = \theta_s/[1 + (\psi/a_g)^{n_g}]$	Gardner (1958)
a_{vg}, n_{vg}, m_{vg}	$\theta_w = \theta_s/[1 + (\psi/a_{vg})^{n_{vg}}]^{m_{vg}}$	van Genutchen (1980)
a_m, n_m, m_m where $m_m = 1 - (1/n_m)$	$\theta_w = \theta_s/[1 + (\psi/a_m)^{n_m}]^{m_m}$	Mualem (1976)
a_b, n_b, m_b where $m_b = 1 - (2/n_m)$	$\theta_w = \theta_s/[1 + (\psi/a_b)^{n_b}]^{m_b}$	Burdine (1953)
a_f, n_f, m_f and ψ_r	$\theta_w = C(\psi)\theta_s/\{\ln[e + (\psi/a_f)^{n_f}]\}^{m_f}$	Fredlund & Xing (1994)

[a] See section 5.2.3 for definition of term.

a non-linear regression procedure such as the one proposed by Fredlund & Xing (1994).

The soil parameters (a, m, and n) associated with each equation in Table 5.1 have a similar meaning to the soil parameters described for the Fredlund & Xing equation. The a parameter bears a relationship to the air entry value, while the n parameter is the slope of the straight-line portion of the soil–water characteristic curve.

5.2.4 LABORATORY MEASUREMENT OF THE SOIL–WATER CHARACTERISTIC CURVE

The soil–water characteristic curve is relatively easy to measure in the laboratory. However, the required test equipment has not found its way into all soil laboratories. The cost of performing the soil–water characteristic curve test is generally less than performing a one-dimensional oedometer test.

The experimental determination of the soil–water characteristic curve is divided into two parts. In the low suction range, where suctions are less than 1500 kPa, a pressure plate apparatus (Fig. 5.9) is used. Suctions greater than 1500 kPa are established using an osmotic desiccator. The Tempe cell is an acrylic pressure plate device with a 100 kPa (1 bar) ceramic high air entry disk. The soil specimen is placed inside the acrylic chamber in contact with the ceramic disk. In geotechnical engineering, the soil specimens are initially in an undisturbed state and water is added to saturate the specimen at the start of the test. Air pressure is applied to the chamber and water is forced out through the high air entry disk. Time is allowed for the soil to reach an equilibrium. Once an equilibrium is reached, the air supply is disconnected and the Tempe cell with the soil specimen is weighed. The air supply is reconnected to the Tempe cell and an increased pressure is applied. This process is repeated until 100 kPa (1 atm) of suction is reached. At this point, the soil specimen is removed from the Tempe cell and the volume and water content of the soil are measured.

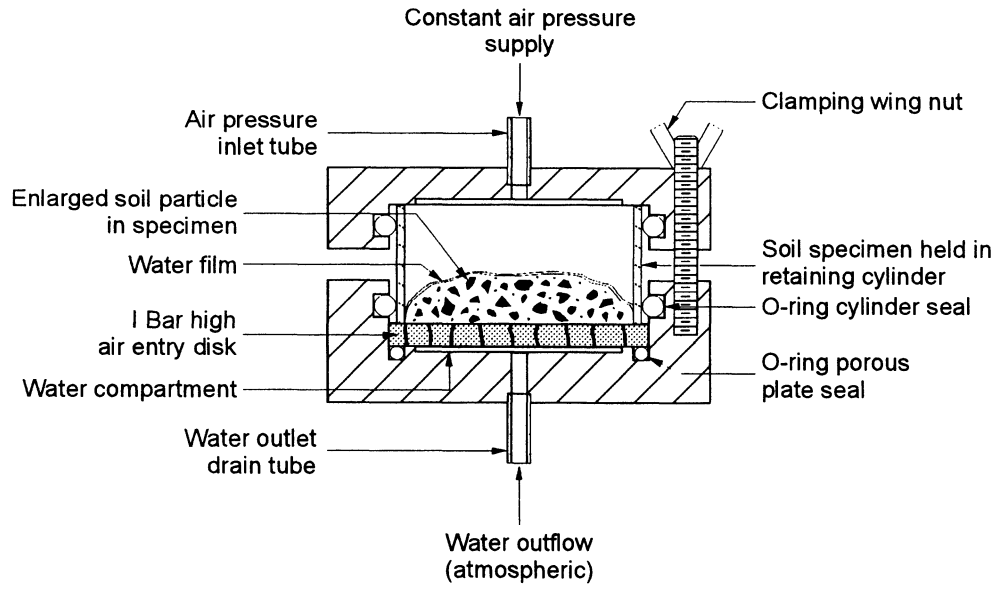


FIGURE 5.9. Tempe cell, pressure plate apparatus for measuring water content versus matric suction in the low suction range.

Other commercially available pressure plate devices allow tests to be performed up to 1500 kPa. These devices were designed for use in areas other than geotechnical engineering, and each device has certain limitations. Several attempts have been made to develop an apparatus more suitable for geotechnical engineering. A single specimen, pressure plate device that allows a nominal surcharge pressure to be applied to a soil specimen and permits a more realistic total stress situation to be examined is shown in Fig. 5.10. The pressure range is limited to 500 kPa, and it is not possible to measure changes in the volume of the specimen. Other equipment for measuring the soil–water characteristic curve is at the experimental stages (Leong & Rahardjo 1997a, 1997b) of development.

At suction values greater than 1500 kPa, an osmotic dessicator is used to determine the water contents. A salt solution, selected to provide a fixed relative humidity environment, is placed in the bottom of the osmotic dessicator. Examples of salt solutions are given in Table 5.2. The soil specimen can be prepared such that the soil either dries to equilibrium or wets to the equilibrium condition. A slight hysteresis will be observed depending on the stress path. The soil samples are approximately 1 g in size.

5.2.5 ESTIMATION OF THE SOIL–WATER CHARACTERISTIC CURVE

There are several approaches that can be used to estimate an approximate soil–water characteristic curve (Figs 5.2 and 5.11). Some

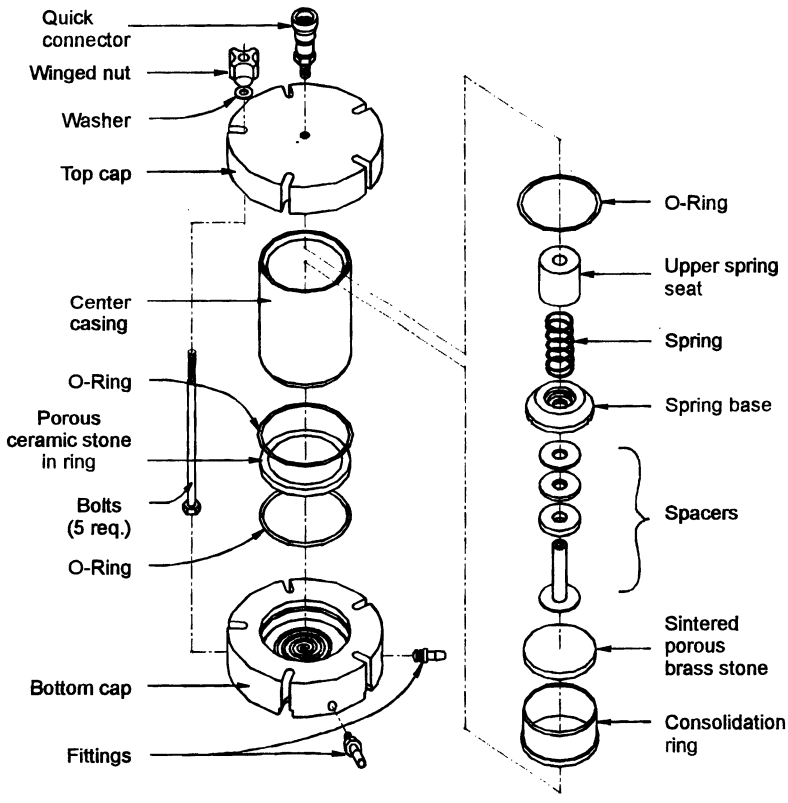


FIGURE 5.10. Single specimen, pressure plate cell.

TABLE 5.2. Salt solutions that provide stable relative humidity environments

Total suction (kPa)	RH	g NaCl-1000 ml^{-1} H_2O	g KCl-1000 ml^{-1} H_2O[a]
98.0	0.999 27	1.3	1.2
310.0	0.997 74	3.8	5.3
980.0	0.992 78	13.1	17.0
3100.0	0.977 64	39.0	52.7
9800.0	0.930 08	122.5	165.0

[a] At 20 °C.

attempts have been made to correlate fitting parameters for a soil–water characteristic curve with the plasticity and grain size distribution classification properties of a soil (Ahuja *et al.* 1985, Pessaran 1995). Presently, these correlations are approximate and based on limited data. Further studies may prove these relationships to be applicable to engineering practice.

The use of operations research techniques on a large database holds promise due to the large volumes of data on soil–water characteristic curves available from other disciplines. The database can be used in conjunction with a knowledge-based system to determine the most reasonable soil–water characteristic curve, or the grain-size curves can be matched in order to estimate soil–

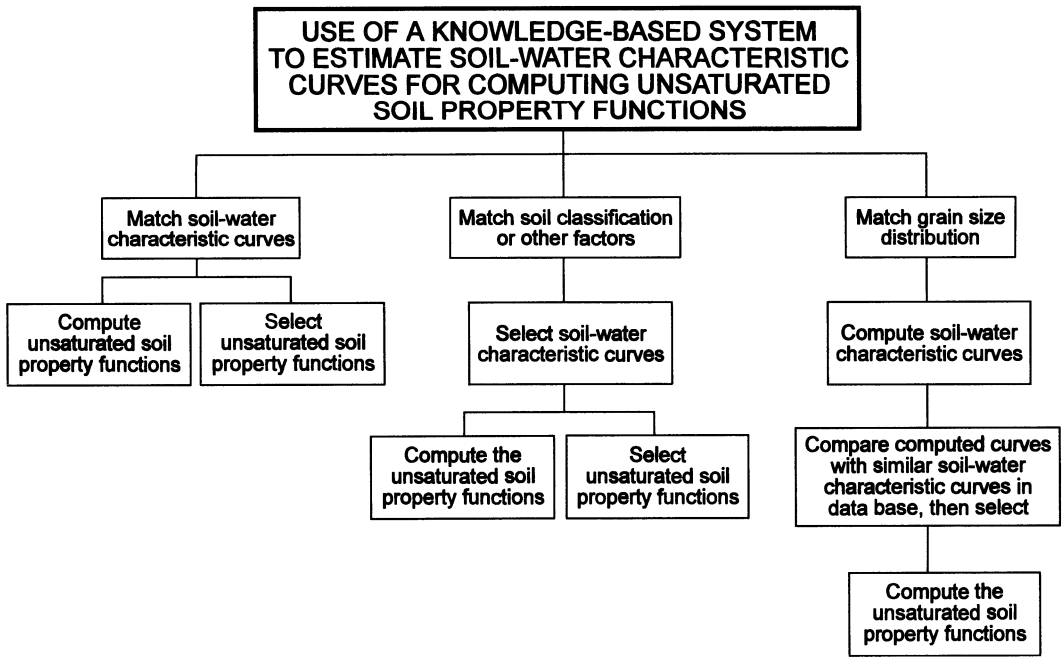


FIGURE 5.11. Approaches that can be used to estimate soil–water characteristic curves for the determination of unsaturated soil property functions when using classification tests and a database.

water characteristic curves (Fredlund *et al.* 1997a). Three different approaches could be adopted, as shown in Fig. 5.11. Engineering judgment is involved to determine if the soil–water characteristic curves and unsaturated soil property functions are reasonable.

The first approach involves matching measured soil–water characteristic curves with soil–water characteristic curves already in a database. The measured soil–water characteristic curves can be used either to compute the unsaturated soil property functions or to select unsaturated soil property functions already in the database.

The second approach involves matching measured classification properties, such as grain-size curves, with classification properties in the database. Once one or more similar soils have been found in the database, corresponding soil–water characteristic curves can be retrieved. As in the first approach, the soil–water characteristic curve data can then be used either to compute the unsaturated soil property functions or to select unsaturated soil property functions already in the database.

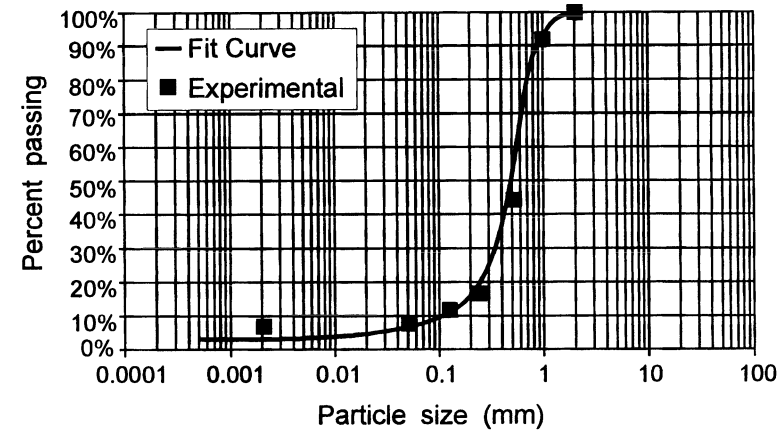
The third approach uses the measured grain-size distribution curve to directly compute the soil–water characteristic curve. The mathematical equation that is used to describe the soil–water characteristic curve can also be used for fitting the grain-size distribution curve. The Fredlund & Xing (1994) form of the equation, given below, is suggested for the grain-size distribution curve since the equation can independently characterize the two extremes of the function:

$$P = C(d_r)\frac{100}{\{\ln[e + (d/a_s)^{n_s}]\}^{m_s}} \qquad (5.7)$$

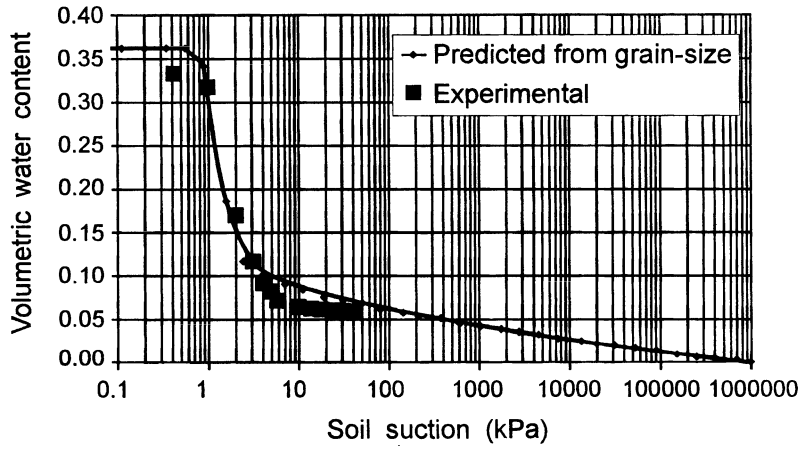
where P = grain-size per cent passing; 100 = 100% passing; e = 2.718 . . . ; d = diameter of the particles in mm; a_s = parameter corresponding to the inflection point on the grain-size curve, related to the largest particles in the distribution; n_s = parameter related to the uniformity of the particle size distribution and having a character similar to the uniformity coefficient, C_u; m_s = parameter related to residual particle sizes; and $C(d_r)$ = correction factor to ensure that the function goes through a lower limit particle diameter, e.g. 0.000 01 mm.

The grain-size distribution curve parameters, i.e. a_s, n_s and m_s, are obtained by performing a best-fit regression analysis on particle size data from an existing database. The grain-size curve parameters allow the grain-size distribution curve of a soil to be represented as a continuous mathematical function that can be further analyzed. The grain-size distribution curve forms the basis for a theory to estimate the pore-size distribution in the soil. This is true only to a degree, and the volume–mass properties must also be taken into consideration in the form of a "packing factor" (Fredlund *et al.* 1997a). Several attempts have been made to characterize the pore-size distribution from the grain-size distribution (Gupta & Larson 1979; Ghosh 1980; Arya & Paris 1981; Ahuja *et al.* 1985; Haverkamp & Parlange 1986). Information from the pore-size distribution can be used for the estimation of the soil–water characteristic curve.

Fredlund *et al.* (1997a,b) showed that it is possible to estimate the soil–water characteristic curve from a grain-size distribution curve provided the procedure is "trained" with the assistance of a knowledge base. Figure 5.12a shows a best-fit of the grain-size curve for a sand sample. The soil–water characteristic curve predicted from the grain-size distribution curve is compared with experimental data in Fig. 5.12b. The results are encouraging for sands and silts, but further research is required when using this procedure for clayey soils.



(a)



(b)

FIGURE 5.12. (a) Grain-size distribution curve fit for sand, and (b) comparison between experimental and predicted soil–water characteristic curves for sand (after Fredlund *et al.* 1997a, reproduced with permission).

5.3 *Stress State Variables of Unsaturated Soils*

Three sets of possible stress states exist for an unsaturated soil, net normal stress ($\sigma - u_a$), matric suction ($u_a - u_w$), and effective stress ($\sigma - u_w$), where σ = total normal stress, u_w = porewater pressure, and u_a = pore-air pressure (see Section 5.1.1). Although three sets of stress state variables exist, only two sets are independent. Fredlund and Morgenstern (1977) found that the stress state for an unsaturated soil could be defined by the two independent stress state sets. The stress tensors associated with the stress state variables are given below.

Stress state set No. 1:

$$\begin{bmatrix} (\sigma_x - u_a) & \tau_{yx} & \tau_{zx} \\ \tau_{xy} & (\sigma_y - u_a) & \tau_{zy} \\ \tau_{xz} & \tau_{yz} & (\sigma_z - u_a) \end{bmatrix} \quad (5.8a)$$

Stress state set No. 2:

$$\begin{bmatrix} (\sigma_x - u_w) & \tau_{yx} & \tau_{zx} \\ \tau_{xy} & (\sigma_y - u_w) & \tau_{zy} \\ \tau_{xz} & \tau_{yz} & (\sigma_z - u_w) \end{bmatrix} \quad (5.8b)$$

Stress state set No. 3:

$$\begin{bmatrix} (u_a - u_w) & 0 & 0 \\ 0 & (u_a - u_w) & 0 \\ 0 & 0 & (u_a - u_w) \end{bmatrix} \quad (5.8c)$$

In the special case of a saturated soil, the air pressure, u_a, is equal to the water pressure, u_w, and the three stress tensors reduce to one single stress tensor. The stress state variables most often used in the formulations of unsaturated soils problems are sets 1 and 3.

Research has found that it is convenient to combine the stress state variables in the form of stress points. A system of stress point designations has emerged within critical state soil mechanics (see Chapter 2) for an unsaturated soil (Wheeler & Sivakumar 1992). Stress point designation can be written in terms of net mean normal stress, p, a deviator stress, q, and matric suction, r, for an unsaturated soil:

$$p = \left(\frac{\sigma_1 + \sigma_2 + \sigma_3}{3}\right) - u_a \quad (5.9a)$$

$$q = \{1/2[(\sigma_2 - \sigma_3)^2 + (\sigma_3 - \sigma_1)^2 + (\sigma_1 - \sigma_2)^2]\} \quad (5.9b)$$

$$r = (u_a - u_w). \quad (5.9c)$$

5.3.1 MEASUREMENT OF SOIL SUCTION: MATRIC, OSMOTIC AND TOTAL SUCTION

The measurement of soil suction is key to the practical implementation of unsaturated soil mechanics theory. The direct measurement of matric suction values, *in situ* and in the laboratory, from zero to several atmospheres of pressure has proven to be a great challenge. The pressure plate apparatus and axis-translation technique was the earliest procedure used in the laboratory to measure matric suction. The increase in air pressure in the chamber surrounding the specimen kept the porewater pressure positive and prevented cavitation in the chamber above the pressure transducer. The first *in situ* direct measurements of matric suction were made with the use of tensiometers. The "Quick Draw" tensiometer (manufactured by Soilmoisture Inc.) has proven satisfactory for some geotechnical engineering applications.

Conventional tensiometers have two major drawbacks; the inability to measure suctions greater than 1 atm, and the need for daily servicing in the field. Recent developments on tensiometers that can go beyond the limit of 1-atm suction limit provide hope that direct measurement of matric suction may become part of engineering practice (Ridley 1993; Ridley & Burland 1993; Guan & Fredlund 1997). The key to being able to take direct measurements in the high suction range appears to lie with the care in the manufacturing of the sensor and the conditioning of the water used in the sensor.

Indirect measurement can also be made using a thermal conductivity sensor to obtain the matric suction in a soil. The thermal conductivity sensor is placed in contact with the soil, and the water content in the porous ceramic tip is allowed to come to equilibrium with the water content of the soil. To measure the matric suction in the soil, the sensor is heated and the rate of cooling is measured and used to determine the water content of the ceramic sensor tip.

The indirect measurement of matric suction using thermal conductivity sensors has several advantages. Measurements in the high suction (low water content) range are possible. The sensors do not need daily servicing, and are almost maintenance free once

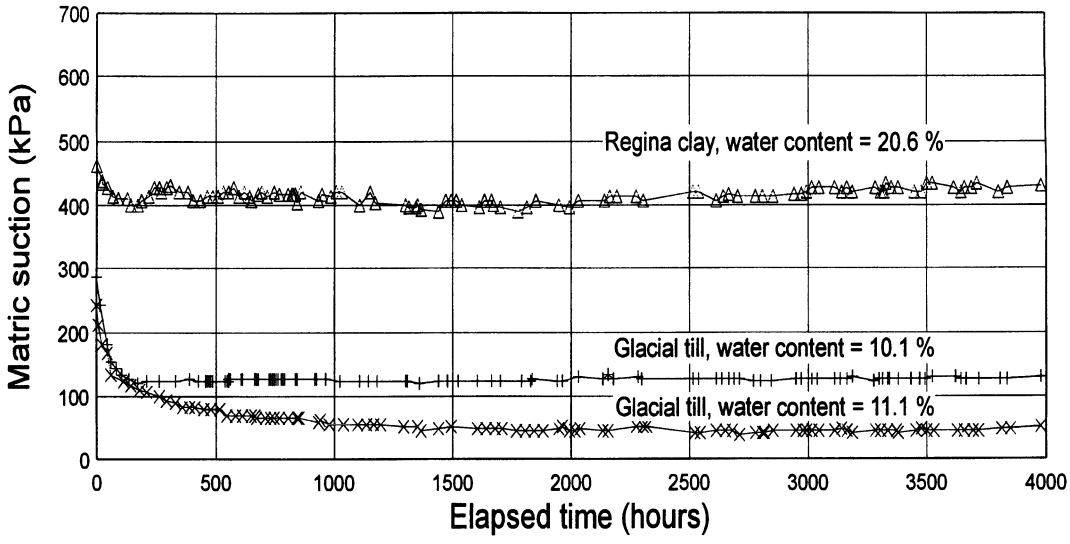


FIGURE 5.13. Suction measurements using thermal conductivity sensors, installed in a test track, Regina, Saskatchewan (modified from Loi *et al.* 1992).

in place. Measurements can be made using digital technology and the data can be downloaded from a data acquisition system at regular intervals. The use of thermal conductivity sensors has shown encouraging results (Fredlund 1992). Figure 5.13 shows the results of long-term measurements on the subgrade soil of a test track in Regina, Canada. The test track was housed in a controlled environment and measurements showed essentially constant values of matric suction for more than one year, with suctions as low as 60 kPa being measured.

Measurement of total suction holds potential in cases where the suction values are relatively large. Thermocouple psychrometers, thermistor psychrometers, and the filter-paper technique have been used with similar degrees of success. Each technique is dependent on the relative humidity of the air immediately adjacent to the soil mass. The techniques, though simple to employ, produce considerable scatter in the data. More research is required particularly with the filter-paper technique where the calibration curve is the soil–water characteristic curve for the filter paper.

Osmotic suction can be measured indirectly using the squeezing technique (Krahn & Fredlund 1972). The electrical conductivity of the porewater is measured and correlated to the total concentration of dissolved salts in the soil, which is then related to the osmotic suction. The electrical conductivity is directly related to the osmotic pressure regardless of the type of salts present in the soil (Fredlund & Rahardjo 1993).

5.4 *Boundary Conditions*

Boundary value numerical modeling requires that a boundary condition be defined at all boundaries. When performing seepage analysis, the surfaces forming the extremities of the soil continuum under consideration are designated as either a flux or water pressure head. The ground surface–atmosphere flux boundary condition is based on the climate (Fig 5.14), and this surface condition is the most difficult boundary condition to quantify.

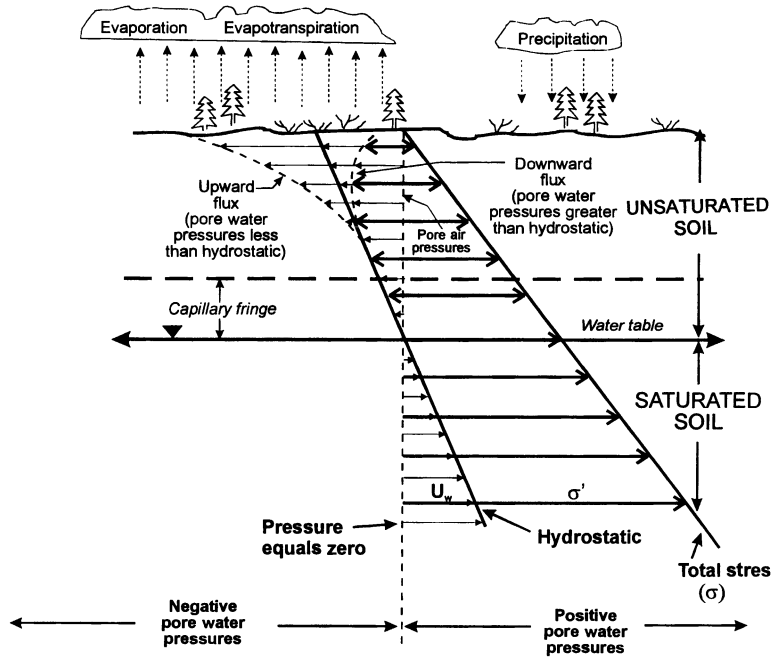


FIGURE 5.14. Illustration of the effect of climate conditions on the pore water pressure profile near the ground surface.

The components that make up the flux boundary condition are precipitation, evaporation, transpiration, infiltration and runoff. Precipitation conditions at a site are often known from past meteorological records and are available for design purposes. The evaporative flux must be computed using one of several models (MEND 1993). Only recently, engineers have begun to include the role of soil suction in computing the rate of evaporation from the ground surface. Infiltration and runoff are a function of the condition of the soil and the soil suction.

There are many complexities associated with the vadose zone region of unsaturated soil, because of the fissured and fractured nature of this region. There is a tendency in geotechnical engineering to avoid analysis of this zone due to the complexity of the analysis required. However, in many cases it is an understanding of the vadose zone that holds the key to the performance of subgrades, slopes and the foundations of most engineered structures.

One of the characteristics of the upper portion of the vadose zone is its ability to release water vapor to the atmosphere at a rate that is dependent on the hydraulic conductivity of the intact portions of the soil. Downward flow of water can occur through the fissures under a gradient of unity ($dh/dl = 1$). There appears to be little impedance to inflow of water into the soil until the soil swells and the mass becomes intact, or until the fissures and cracks are filled with water.

A common misconception is that water can always enter the soil at the ground surface. If the soil is intact, the maximum flux of water at the ground surface is controlled by the saturated hydraulic conductivity of the soil together with the water content and suction values at the soil surface. The maximum flux into the soil may be a very low value. On a sloping ground surface, the surface layer may

become saturated and have a higher hydraulic conductivity than the underlying soil. This results in anisotropy in the hydraulic conductivity and water runs down the top layers of soil on the slope, but may not enter the underlying soil.

5.4.1 EVAPORATION, EVAPOTRANSPIRATION, AND THE PREDICTION OF THE FLUX BOUNDARY CONDITION

The prediction of the moisture flux boundary condition at the soil surface depends on a knowledge of the rate of infiltration during precipitation events and the rate of evaporation during subsequent dry periods. Evaporation is an energy driven process that depends on climatic factors such as solar radiation, relative humidity, temperature and wind speed. Potential evaporation from a water surface is computed from the mass transfer equation, first proposed by Dalton in 1802, as a function of the difference between the vapor pressure between the water surface and the overlying air:

$$PE = f(u)(e_s - e_a) \tag{5.10}$$

where PE = the rate of potential evaporation (mm day^{-1}), e_s = saturation vapor pressure at the water surface temperature (kPa), e_a = vapor pressure of the air in the atmosphere above the water (kPa), and $f(u)$ = an empirical transmission function depending on the mixing characteristics of the air above the evaporating surface (Gray 1970).

The actual evaporation from an unsaturated soil surface can be computed using the modified Penman formulation developed by Wilson (1990):

$$AE = \frac{\Gamma Q + \eta E}{\Gamma + \eta A} \tag{5.11}$$

where AE = actual evaporative flux; Γ = slope of saturation versus temperature curve at the temperature of the air; Q = net radiation; η = psychrometric constant; $E = f(u)e_a(B - A)$, where $f(u)$ is a function of wind speed, surface roughness and eddy diffusion; e_a = vapor pressure in the air above the soil surface; B = inverse of the relative humidity of the air; and A = inverse of the relative humidity of the soil surface.

The relative humidity in the soil at the ground surface is related to the suction in the soil (Edlefsen & Anderson 1943):

$$h_r = e^{(\psi W_v g/RT)} \tag{5.12}$$

where h_r = relative humidity in the unsaturated soil voids, ψ = total suction in the liquid water phase, W_v = molecular weight of water (0.018 kg mol^{-1}), g = acceleration due to gravity, R = universal gas constant (8.314 J K^{-1} mol^{-1}), and T = absolute temperature (K).

In an alternative approach, the ratio of the actual evaporative flux (AE) to the potential evaporative flux (PE), AE/PE, can be obtained by combining Dalton's equation (Eq. 5.10) with the relationship between relative humidity and soil suction (Eq. 5.12), where the empirical transmission function, $f(u)$, is assumed to be the same for both the soil surface and the water surface. This gives:

$$\frac{AE}{PE} = \frac{(e_0 - e_a)}{(e_s - e_a)} \tag{5.13}$$

where e_0 = actual vapor pressure of the air. To express Eq. 5.13 in terms of relative humidity, the numerator and denominator are divided by the saturated vapor pressure:

$$\frac{AE}{PE} = \frac{(h_r - h_a)}{(1 - h_a)} \tag{5.14}$$

where h_a = the relative humidity of the air above the evaporating soil and water surfaces.

The relative humidity in the soil at the ground surface is computed on the basis of a heat and mass equation (Wilson *et al.* 1994). Substituting Eq. 5.12 into Eq. 5.14 gives:

$$\frac{AE}{PE} = \frac{[e^{(\psi W_v g/RT)} - h_a]}{(1 - h_a)}. \tag{5.15}$$

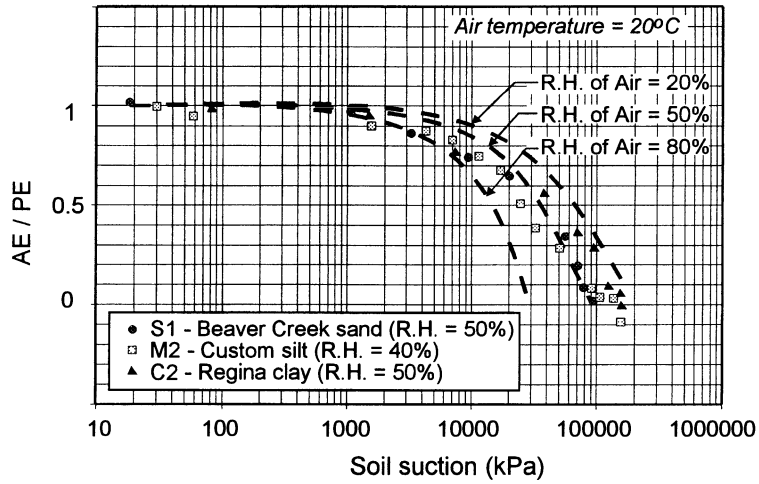


FIGURE 5.15. Measured relationship between soil suction and the ratio of the actual evaporation (AE) to the potential evaporation (PE) for the ground surface.

The actual and potential rates of evaporation are only equal when water is freely available. Experimental data (Wilson *et al.* 1997) show that the rate of actual evaporation relative to the potential evaporation (AE/PE) is a function of the suction in the soil (Fig. 5.15). The AE/PE ratio was found to be the same for three soils ranging from sand to highly plastic clay. The actual rate of evaporation decreases as the soil suction increases, or the soil dries out. The use of potential evaporation during prolonged dry periods, when suctions in the soil increase, may give inaccurate estimates of the actual rate of evaporation.

The AE/PE ratio is also dependent on the relative humidity of the air above the soil. Contour lines of the AE/PE ratio are shown in Fig. 5.15 along with the experimental data of the three soils.

5.5 *Seepage through Unsaturated Soils*

For an unsaturated soil, Darcy's law applies in the sense that the Darcy flux, v, is proportional to the hydraulic head gradient, dh/dl. The hydraulic conductivity of the soil is no longer constant, as in a saturated soil, since the volume of water in the soil depends on the suction in the soil. Darcy's law for an unsaturated soil can be written in terms of the hydraulic conductivity as a function of the soil suction (or negative porewater pressures) (Childs & Collis-George 1950). For example, in the x-direction:

$$v_x = -k_x(u_w)\frac{dh}{dx} \tag{5.16}$$

where v_x = Darcy flux (velocity) in the x-direction; dh/dx = hydraulic gradient in the x-direction; $k_x(u_w)$ = hydraulic conductivity in the x-direction as a function of negative porewater pressure. Similar definitions apply to the other two cartesian directions.

The cross-sectional area of the soil available for water flow is related to the water content. The water content of an unsaturated soil decreases as the soil desaturates. The dependence of the hydraulic conductivity on the water content is based on the assumption that Darcy's law holds and water can only flow through the wetted portion of the soil. This is a useful assumption for many applications in unsaturated soil mechanics, but may not be applicable to all situations, especially where Darcy's law does not apply.

5.5.1 HYDRAULIC CONDUCTIVITY FUNCTION

Gardner (1958) proposed a form for the hydraulic conductivity function for an unsaturated soil. The equation required two soil properties for its definition, one related to the air entry value and the other related to the rate at which the soil desaturates. Other hydraulic conductivity functions have been suggested that allow greater flexibility in defining the hydraulic conductivity function of an unsaturated soil over a wide range of soil suction (Fredlund *et al.* 1994).

The nature of the hydraulic conductivity function can be visualized by comparing the shape of the hydraulic conductivity curve with the shape of the soil–water characteristic curve. Figure 5.16 compares the soil–water characteristic curves and hydraulic conductivity functions for sand and clayey silt. The hydraulic conductivity for both soils remains relatively constant from zero suction up to the air entry value of the soil. The change in the hydraulic conductivity of a soil occurs at approximately the air entry value of the soil. Beyond the air entry value, the hy-

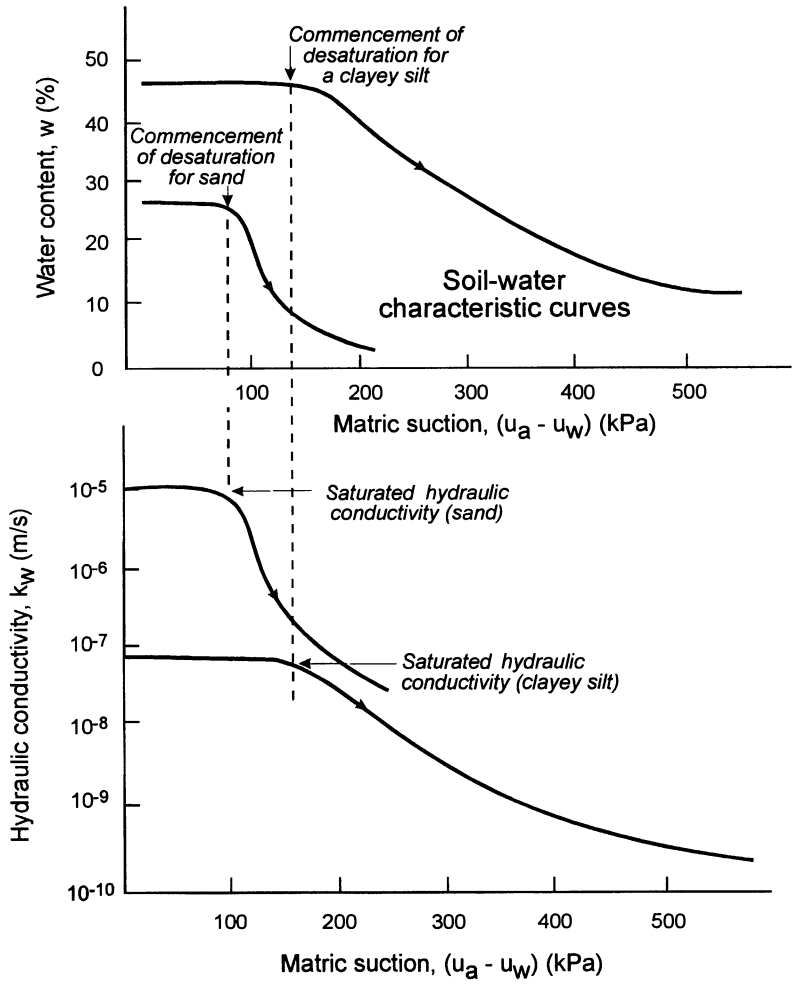


FIGURE 5.16. Relationship between soil–water characteristic curve and the hydraulic conductivity for sand and clayey silt.

draulic conductivity decreases rapidly with increasing suction for both soils. The decrease in the hydraulic conductivity is due to the reduction in the cross-sectional area of flow. The initial hydraulic conductivity, or saturated hydraulic conductivity, k_s, of the sand is shown to be about two orders of magnitude greater than that of the clayey silt. As the suction increases, it is possible that the hydraulic conductivity of the sand will decrease by more than two orders of magnitude. Under certain conditions, it is possible for the clayey silt to be more permeable than the sand.

Figure 5.16 shows a curved relationship between matric suction and the logarithm of hydraulic conductivity. The function can be linearized by plotting matric suction on a logarithmic scale (Fig. 5.17). The function should remain essentially linear until the residual suction of the soil is reached.

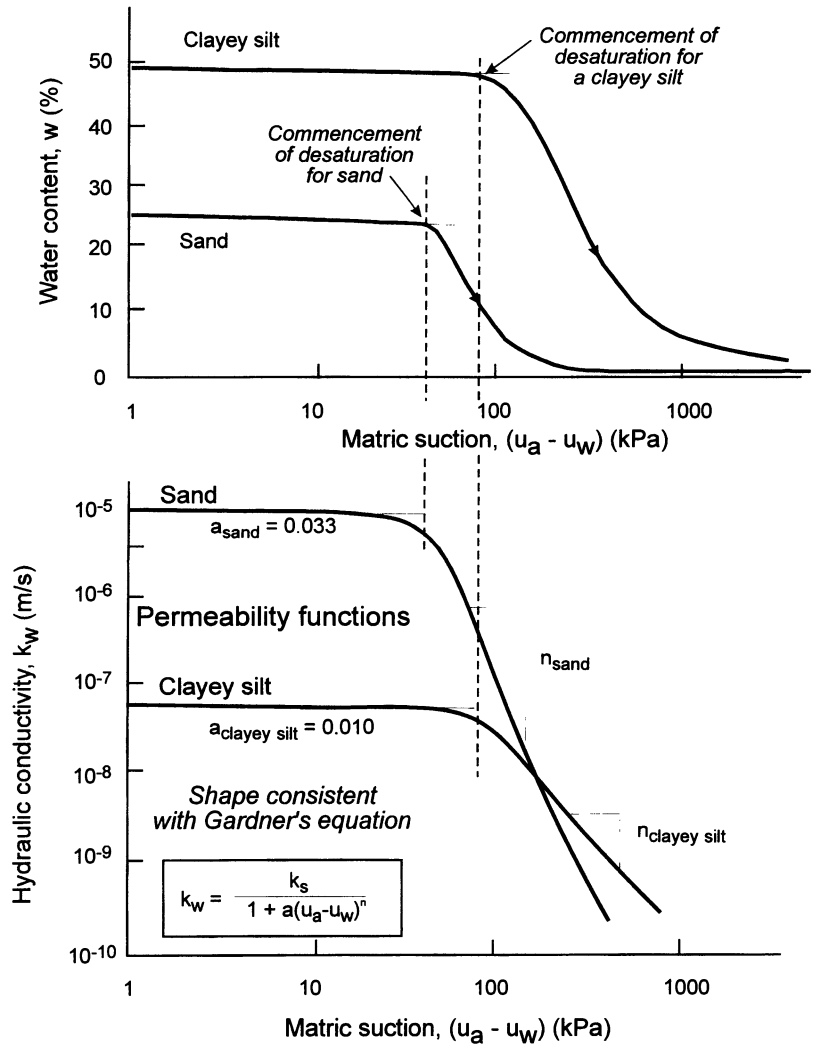


FIGURE 5.17. Typical hydraulic conductivity (permeability) functions for sand and clayey silt with the suction plotted on a logarithmic scale.

5.5.2 THE WATER STORAGE FUNCTION

The water storage function can be defined as the slope of the soil–water characteristic curve. Differentiation of the soil–water characteristic curve yields the water storage function for an unsaturated soil. Figure 5.18 shows a soil–water characteristic curve and the plot of the corresponding water storage function. The water storage function becomes highly non-linear as the soil desaturates. The water storage function is required in conjunction with the hydraulic conductivity function when performing a transient flow analysis on an unsaturated soil.

5.5.3 MEASUREMENT OF THE HYDRAULIC CONDUCTIVITY FUNCTION

Unsaturated soil hydraulic conductivity is a non-linear soil property function that requires considerable testing for its definition. It is important to be able to measure the unsaturated soil properties. Due to cost, the laboratory testing of unsaturated soils may never enjoy the level of routine as has been the case for saturated soils. Possibilities have emerged for the indirect estimation or prediction of unsaturated soil property functions.

Steady state and unsteady state testing procedures have been successfully used to mea-

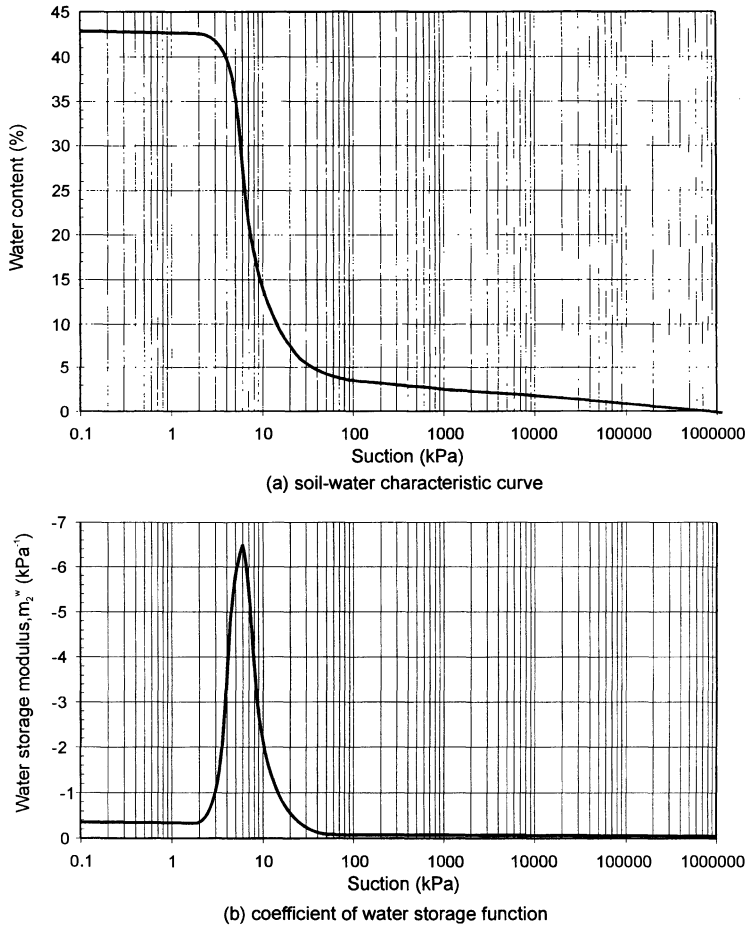


FIGURE 5.18. Coefficient of water storage, m_2^w, function computed from the soil–water characteristic curve: (a) soil–water characteristic curve, and (b) coefficient of water storage function.

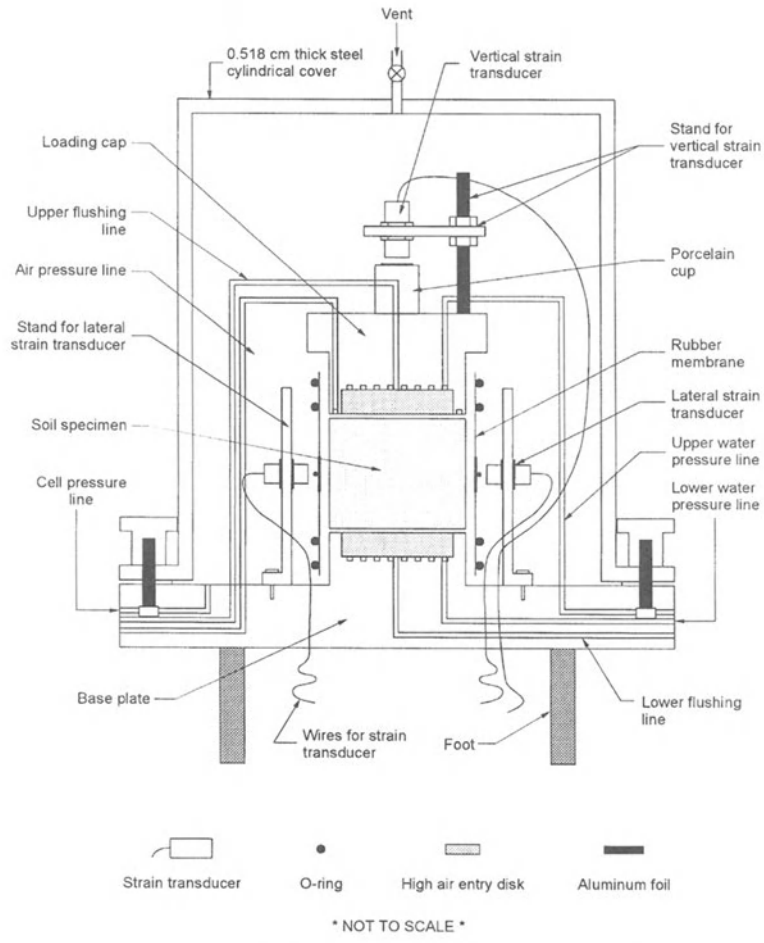


FIGURE 5.19. Flexible walled permeameter developed to control the applied normal stresses and the matric suction (after Huang 1994, reproduced with permission). Not drawn to scale.

sure the hydraulic conductivity of a soil under varying applied soil suction (and varying degrees of saturation) (Fredlund & Rahardjo 1993). Unsteady state testing procedures require the application of transient flow analysis in the interpretation of the data.

The steady state testing procedure is relatively easy to perform, provided the applied suctions do not exceed 100 kPa. Each specimen may require one or more weeks when testing at different applied suctions. The hydraulic conductivity that can be measured using the typical apparatus shown in Fig. 5.19 is limited to soils where the saturated hydraulic conductivity, k_s, is less than that of the high air entry value ceramic disk. The smallest value for hydraulic conductivity that can be measured is approximately 1×10^{-13} ms^{-1}. Extending the apparatus beyond 100 kPa of suction requires the use of the axis-translation technique.

A typical set of flow data is presented for an initially slurried, consolidated silt subjected to various net normal stresses and matric suctions in a flexible wall permeability testing apparatus (Huang 1994). The soil–water characteristic curves were measured for the consolidated specimens using a pres-

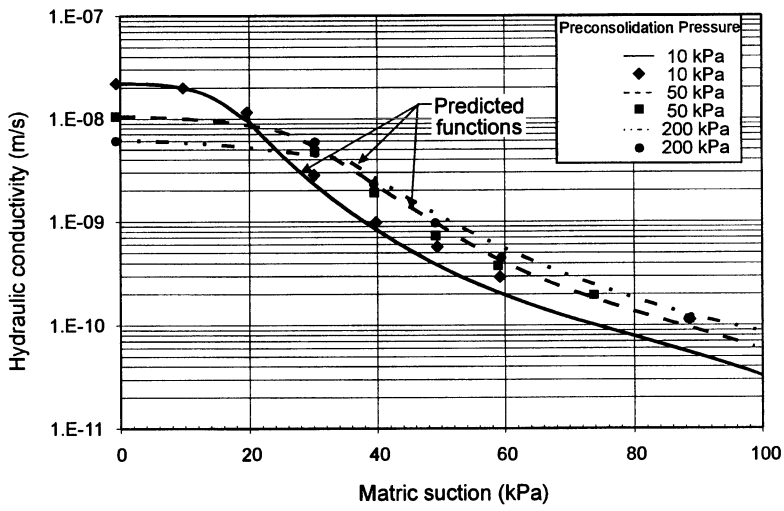


FIGURE 5.20. Comparison of measured hydraulic conductivity and hydraulic conductivity functions predicted from the soil–water characteristic curves for silt preconsolidated at 10 (—, ◆) 50 (—, ■) and 200 (—,●) kPa, respectively (after Huang 1994, reproduced with permission).

sure plate cell, for the suction range from zero to 300 kPa. Dessicator tests were conducted for the suction range beyond 1500 kPa. Figure 5.20 show the predicted hydraulic conductivity function, using the equation developed in the next section, and the measured hydraulic conductivity function. There is reasonably close agreement between the measured and predicted values.

5.5.4 ESTIMATION OF THE HYDRAULIC CONDUCTIVITY FUNCTION AND THE WATER STORAGE FUNCTION FROM THE SOIL–WATER CHARACTERISTIC CURVE

The hydraulic conductivity function of an unsaturated soil can be predicted with sufficient accuracy for many engineering applications with a knowledge of the saturated hydraulic conductivity and the soil–water characteristic curve. Several investigators have proposed empirical functions for predicting the hydraulic conductivity function (Huang *et al.* 1994). The soil–water characteristic curve equation developed by Fredlund *et al.* (1994) defines the water content–suction relationship over the entire suction range. This curve can be used to compute the hydraulic conductivity function, the relationship between hydraulic conductivity and soil suction.

Childs and Collis-George (1950) proposed a statistical model to predict the hydraulic conductivity based on the random variation of pore sizes in a soil. This model was first modified by Marshall (1958), and further modified by Kunze *et al.* (1968). The calculations are performed by dividing the volumetric water content versus suction relationship into several water content increments (Fig. 5.21). This is equivalent to integration along the volumetric water content axis.

The following numerical integration procedure can be used along the soil–water characteristic curve to compute data points that can be best-fit to form the hydraulic conductivity function. The integration is carried out between the saturated volumetric water content and the volumetric water content under residual conditions:

$$k(\theta_i) = k_s K_{SC} \frac{\theta^{Ps}}{n^2} \sum_{j=1}^{m} [(2j + 1 - 2i)\psi_j^{-2}] \quad (5.17)$$

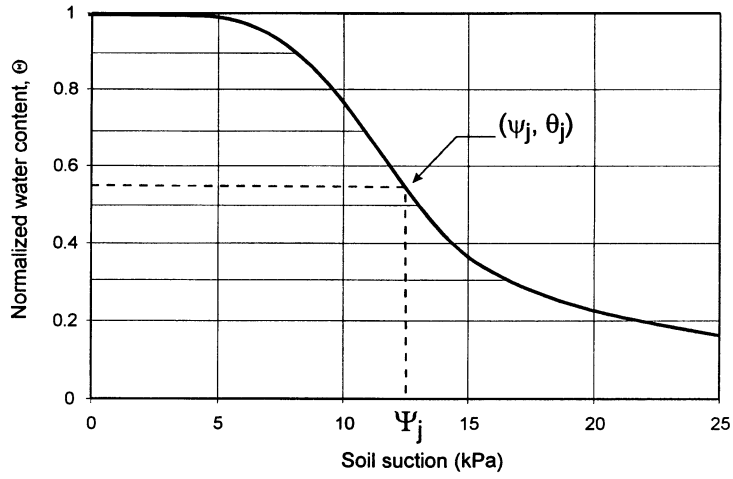


FIGURE 5.21. A typical soil–water characteristic curve for predicting the hydraulic conductivity.

where: $k(\theta_i)$ = calculated hydraulic conductivity for a specified volumetric water content; θ_i, corresponding to the ith interval; i = interval number that increases with decreasing water content (for example, i equals 1 identifies the first interval that closely corresponds to the saturated water content, θ_S, and $i = m$ identifies the last interval corresponding to the lowest water content, θ_l, on the experimental soil–water characteristic curve); j = counter from i to m; K_{SC} = a curve fitting, "matching factor" (discussed below); p_S = a constant that accounts for the interaction of pores of various sizes; m = total number of intervals between the saturated volumetric water content, θ_S, and the lowest volumetric water content, θ_l, on the experimental soil–water characteristic curve; and n = total number of intervals computed between the saturated volumetric water content, θ_S, and zero volumetric water content, i.e. $\theta_W = 0$, (note that $n = m\,[\theta_S/(\theta_S - \theta_l)]$; $m \leq n$; and $m = n$ when $\theta_l = 0$); and ψ_j, is the suction (kPa) corresponding to the midpoint of jth interval.

The calculation of the hydraulic conductivity, $k(\theta_i)$, at a specific volumetric water content, θ_i, involves the summation of soil suction values that correspond to the water contents at and below a particular volumetric water content, θ_i. The matching factor, K_{SC}, is necessary in order to provide a fit between the computed unsaturated hydraulic conductivity and the measured saturated hydraulic conductivity. The shape of the hydraulic conductivity function is determined by the terms inside the summation-sign portion of the equation. These terms are obtained from the soil–water characteristic curve. Equation 5.16 can be expressed in the form of a "relative" hydraulic conductivity function, $k_r(\theta)$, by dividing by $(k_S K_{SC})$.

$$k_r(\theta_i) = \sum_{j=1}^{m} \frac{2(j-i)+1}{\psi_j^2} \Bigg/ \sum_{j=1}^{m} \frac{2j-1}{\psi_j^2}. \quad (5.18)$$

Equation 5.18 can be written in an integral form for volumetric water contents ranging from the saturated volumetric water content to residual conditions:

$$k_r(\theta) = \int_{\theta_r}^{\theta} \frac{\theta - x}{\psi^2(x)} dx \Bigg/ \int_{\theta_r}^{\theta_s} \frac{\theta_s - x}{\psi^2(x)} dx \quad (5.19)$$

where x = a variable of integration representing water content.

Most proposed models require a knowledge of the residual water content in order

to predict the relative hydraulic conductivity function, $k_r(\theta)$. Brooks & Corey (1964), Mualem (1976a, 1976b) and van Genuchten (1980) suggest different methods for the extrapolation of the measured soil–water characteristic curve data and the determination of the residual water content. The conventional procedure consists of two steps. First, the residual water content of the soil under consideration is estimated from the experimental data. Then, the measured soil–water characteristic curve data are fitted using a mathematical equation over the volumetric water content range from saturation, θ_S, to residual water content, θ_r. Integration is then carried out using the best-fit soil–water characteristic curve.

Fredlund *et al.* (1994) proposed a mathematical relationship and theoretical basis for the hydraulic conductivity function. The accuracy of the prediction of the hydraulic conductivity function was shown to significantly improve when the complete soil–water characteristic curve is used and following conditions are prescribed:

$$\theta = \theta_r; \qquad k_{res} = \text{constant} \qquad (5.20)$$

where θ_r = volumetric water content at residual conditions; and k_{res} = hydraulic conductivity at residual conditions.

The function is based on the entire soil–water characteristic curve, from saturation, where the soil suction is zero, to a water content of zero, or 1 000 000 kPa. It is assumed that the ease of water flow is related to the amount of water in the soil matrix. Although the hydraulic conductivity function can be computed down to zero water content, it should be noted that the function may be more indicative of vapor flow in the region beyond the residual stress state. As a result, it may be more reasonable to leave the hydraulic conductivity as a constant, k_{res}, beyond the residual state. To calculate the hydraulic conductivity using Eqs. 5.19 and 5.6, it is convenient to perform the integration along the soil suction axis. Therefore, Eq. 5.19 can be transformed into:

$$k_r(\psi) = \int_{\psi}^{\psi_r} \frac{\theta(y) - \theta(\psi)}{y^2}\theta'(y)dy \Bigg/ \int_{\psi_{aev}}^{\psi_r} \frac{\theta(y) - \theta_s}{y^2}\theta'(y)dy \qquad (5.21)$$

where ψ_{aev} = air entry value of the soil under consideration; ψ_r = suction corresponding to the residual water content, θ_r; ψ = a variable of integration representing suction; y = a variable of integration representing suction; and θ' = the derivative of the soil–water characteristic curve, i.e. Eq. 5.6.

Equation 5.6 fits the experimental data over the entire soil suction range, and the integrations of Eq. 5.21 can be performed for suction values from the air entry value to 1 000 000 kPa for all types of soils. This simplifies the prediction procedure for the hydraulic conductivity, since the residual water content and residual soil suction values (θ_r or ψ_r) do not need to be known when computing the hydraulic conductivity function.

To avoid the numerical difficulties associated with performing the integration over the soil suction range from the air entry value, ψ_{aev}, to a suction of 1 000 000 kPa, it is more convenient to perform the integration on a logarithm scale. Therefore, the following variation of Eq. 5.21 is preferred:

$$k_r(\psi) = \int_{\ln(\psi)}^{b} \frac{\theta(e^y) - \theta(\psi)}{e^y}\theta'(e^y)dy \Bigg/ \int_{\ln(\psi_{aev})}^{b} \frac{\theta(e^y) - \theta_s}{e^y}\theta'(e^y)dy \qquad (5.22)$$

where b = ln(1 000 000) and e = 2.718 28. . .

The accuracy of the prediction of the hydraulic conductivity function depends not only on the closeness of the best-fit curve to the experimental soil–water characteristic curve data, but also on the prediction model adopted. Mualem (1986) concluded that

there was no single model that fitted every soil type. The proposed models have been found to be most satisfactory for sandy soils, whereas agreement with experimental data may prove to be unsatisfactory for finer-grained soils. The flexibility of Eq. 5.21 can be increased by multiplying the results by the dimensionless water content raised to a power, i.e. Θ^q. The variable Θ^q uses a correction factor, q, to take into account the tortuosity of the soil pores (Mualem 1986) as shown in the following equation. Therefore, more accurate predictions can be obtained by using the following modifications of Eq. 5.21:

$$k_r(\psi) = \Theta^q(\psi) \int_{\ln(\psi)}^{b} \frac{\theta(e^y) - \theta(\psi)}{e^y} \theta'(e^y) dy \Bigg/ \int_{\ln(\psi_{aev})}^{b} \frac{\theta(e^y) - \theta_s}{e^y} \theta'(e^y) dy. \quad (5.23)$$

Based on research work by Kunze *et al.* (1968), the value of the power, q, can be assumed to be one unless there is reason to assume otherwise.

The hydraulic conductivity function can be computed for an unsaturated soil using the following procedure. The four parameters of the soil–water characteristic curve, i.e. a, n, m and ψ_r, are first determined through the use of a non-linear least square procedure applied to Eq. 5.6. The numerical integration of Eq. 5.22 can be performed using the numerical integration procedure described by Fredlund *et al.* (1994). Neither of the residual values, residual water content, θ_r, nor suction at residual water content, ψ_r, are explicitly required during the calculation of the hydraulic conductivity function.

5.5.5 ESTIMATION OF THE WATER STORAGE FUNCTION FROM THE SOIL–WATER CHARACTERISTIC CURVE

The water storage function, defining the amount of water in the soil, is required when performing a transient seepage analysis on an unsaturated soil. For a saturated soil, the water storage property is referred to as the coefficient of volume change, m_v, i.e. the relationship between effective stress and volume change; see Chapter 2. When suction is applied to the soil and the air entry value is exceeded, there is a change in the volumetric water content due to either a change in volume or to the desaturation of the soil. The slope of the soil–water characteristic curve defines the amount of water stored in the soil, and this value is required for unsteady state seepage analyses involving unsaturated soils.

The relationship between soil suction and the water storage coefficient (Fig. 5.18) of an unsaturated soil, m_w^2, can be predicted with sufficient accuracy for most engineering problems through a knowledge of the saturated coefficient of volume change and the soil–water characteristic curve. The water storage coefficient, m_w^2, is obtained by differentiating the equation representing the soil–water characteristic curve, written in terms of volumetric water content, with respect to soil suction.

5.5.6 FORMULATION OF THE STEADY STATE AND UNSTEADY STATE SEEPAGE ANALYSIS

The steady state, partial differential flow equation for an unsaturated soil is formulated by satisfying conservation of mass for a representative elemental volume. The partial differential equation is non-linear because hydraulic conductivity in the flow law is a function of the porewater pressure, which, in turn, is part of the hydraulic head. An unsaturated soil is similar to a heterogeneous soil with a spatially variant hydraulic conductivity:

$$k_x(u_w)\frac{\partial^2 h}{\partial x^2} + k_y(u_w)\frac{\partial^2 h}{\partial y^2} + \frac{\partial k_x(u_w)}{\partial x}\frac{\partial h}{\partial x} + \frac{\partial k_y(u_w)}{\partial y}\frac{\partial h}{\partial y} = 0. \quad (5.24)$$

Numerical methods, such as the finite element technique, have become necessary tools for solving saturated-unsaturated modeling in engineering practice. Today, there are a number of software packages available that provide great flexibility in solving saturated/unsaturated seepage problems.

For unsteady state conditions, the storage of water within the soil must be taken into account. Equation 5.24 can be expanded to accommodate unsteady (or transient) conditions:

$$k_x(u_w)\frac{\partial^2 h}{\partial x^2} + k_y(u_w)\frac{\partial^2 h}{\partial y^2} + \frac{\partial k_x(u_w)}{\partial x}\frac{\partial h}{\partial x} + \frac{\partial k_y(u_w)}{\partial y}\frac{\partial h}{\partial y} = \frac{m_w^2}{\gamma_w}\frac{\partial h}{\partial t} \quad (5.25)$$

where m_w^2 = water storage coefficient, γ_w = unit weight of water, and t = time.

5.6 *Shear Strength of Unsaturated Soils*

The shear strength equation for an unsaturated soil can be approximated as a linear combination of the effect of two independent stress state variables, i.e. $(\sigma_n - u_a)$ and $(u_a - u_w)$:

$$\tau = c'(\sigma_n - u_a)\tan\phi' + (u_a - u_w)\tan\phi^b. \quad (5.26)$$

A three-dimensional representation of Equation 5.26 is presented in Fig. 5.22. The change in shear strength with respect to soil suction is often linear (Fredlund *et al.* 1978) over a limited stress range. The change in shear strength with respect to soil suction can also be non-linear (Gan *et al.* 1988) which will give rise to the type of failure surface shown in Fig. 5.23. It is possible to mathematically represent a non-linear form for the unsaturated shear strength envelope over a limited range of suctions. The non-linear form can be estimated through the use of the soil–water characteristic curve and the saturated shear strength parameters of the soil.

5.6.1 SHEAR STRENGTH FUNCTION WITH RESPECT TO SOIL SUCTION

The relationship between soil suction and the shear strength of an unsaturated soil is re-

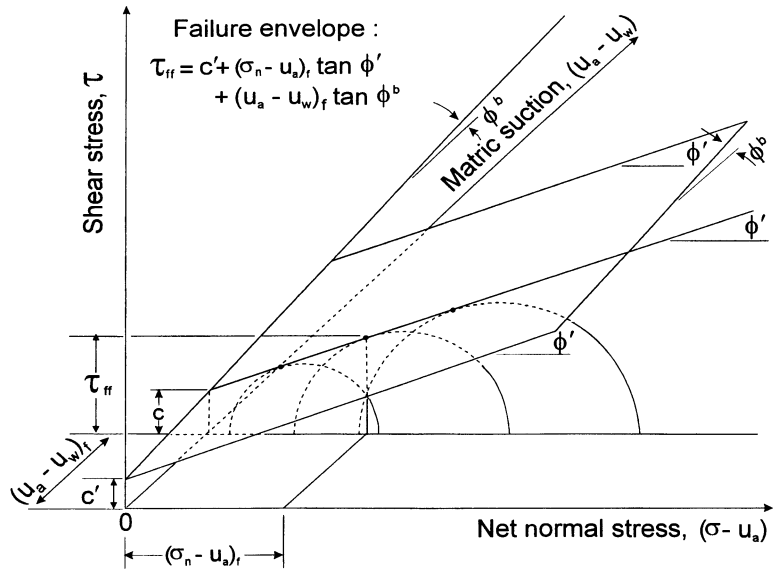
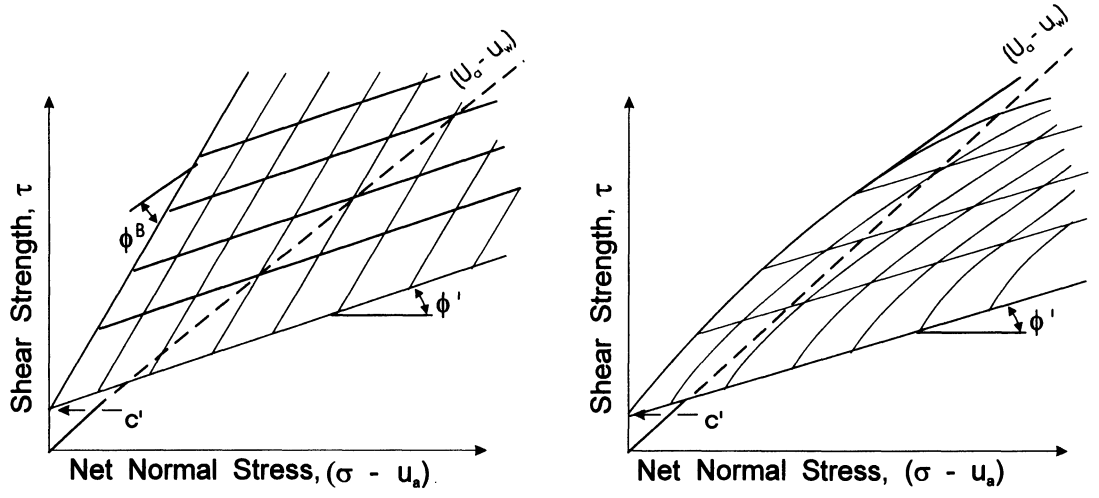


FIGURE 5.22. Extended Mohr–Coulomb failure envelope for unsaturated soils.



(a) Linear strength envelope *(b) Non-linear strength envelope*

FIGURE 5.23. Extended Mohr–Coulomb shear strength envelope showing the strength parameters for a saturated-unsaturated soil: (a) linear strength envelope; and (b) non-linear strength envelope.

ferred to as the shear strength function. This relationship can be satisfactorily predicted for many engineering problems through the use of the saturated shear strength parameters and the soil–water characteristic curve.

The slope of the plot of shear strength versus soil suction, ϕ^b, bears a similarity in shape to the soil–water characteristic curve (Gan *et al.* 1988). Figure 5.23 shows that the angle defining the relationship between shear strength and soil suction, ϕ^b, begins to deviate from the effective angle of internal friction, ϕ', as the soil desaturates at suctions greater than the air entry value. As the soil suction reaches a value corresponding to the residual water content, the ϕ^b angle appears to approach an angle near to zero degrees, or it may even go negative.

The shear strength function can be obtained by integrating along the soil–water characteristic curve. The following shear strength expression as a function of soil suction and the effective shear strength parameters were obtained by Fredlund *et al.* (1996b).

$$\tau(u_a - u_w) = c' + \Theta^p(\sigma - u_a)\tan\phi' + \Theta^p(u_a - u_w)\tan\phi' \quad (5.27)$$

where $\Theta = \theta(u_a - u_w)/\theta_s$; and $\theta(u_a - u_w)$ = the volumetric water content at any soil suction, which can be represented by the equation for the soil–water of characteristic curve; p = a fitting parameter to account for any non-linearity between the area and volume representation of the amount of water contributing to the shear strength.

5.6.2 MEASUREMENT OF THE SHEAR STRENGTH FUNCTION WITH RESPECT TO SOIL SUCTION

The laboratory measurement of shear strength with respect to soil suction can be made using either a triaxial apparatus or a direct shear apparatus. In either case, the apparatus must be modified to allow for the independent measurement, or control, of the pore-air pressures and the porewater pressures (Fredlund & Rahardjo 1993). The pore-air pressure can be applied through a coarse, or extremely low air entry ceramic

disk. The porewater pressures can be measured with a high air entry disk, which is sealed with epoxy to the lower base plate.

A modified direct shear apparatus (Gan *et al.* 1988) has proven to be superior to a triaxial apparatus when testing unsaturated soils, because it has a reduced length of the drainage path for pore-pressure equalization. Even with the modifications to reduce the drainage path, testing in the direct shear apparatus will often require two days for equalization under the applied stress, and then one day to apply the shear stress to failure. Since the shear strength relationship is non-linear, several specimens must be tested or else multistage testing is required. Testing using the triaxial apparatus can require considerably more time. Unsaturated soil shear strength testing is time consuming and great care must be exercised with respect to the testing procedures.

Figure 5.24 illustrates a typical series of consolidated drained multistage direct shear tests on a compacted glacial till. All specimens were prepared in a similar manner using static compaction and then subjected to suctions as high as 500 kPa. The ϕ^b angle between shear strength and matric suction deviates from the ϕ' value of 25.5° once the air entry value of the soil, approximately 150 kPa, is exceeded.

A series of test results are presented for the same glacial till tested at dry of optimum condition (Fig. 5.25a, b). The tests were conducted at different levels of net normal stress and matric suction. The soil–water characteristic curves were developed using a pressure plate apparatus for the suction range of 0–1500 kPa, and osmotic dessicator for the suction of 2500–300 000 kPa (Fig. 5.25a). The measured shear strength parameters were $c' = 0$, and $\phi' = 23.5°$. Figure 5.25b shows good agreement between the experimental results and the predicted variation of shear strength with suction.

5.6.3 ESTIMATION OF THE SHEAR STRENGTH FUNCTION FROM THE SOIL–WATER CHARACTERISTIC CURVE

The shear strength function is the relationship between soil suction and the shear strength for an unsaturated soil. This relationship can be predicted for many engineering problems with the saturated shear

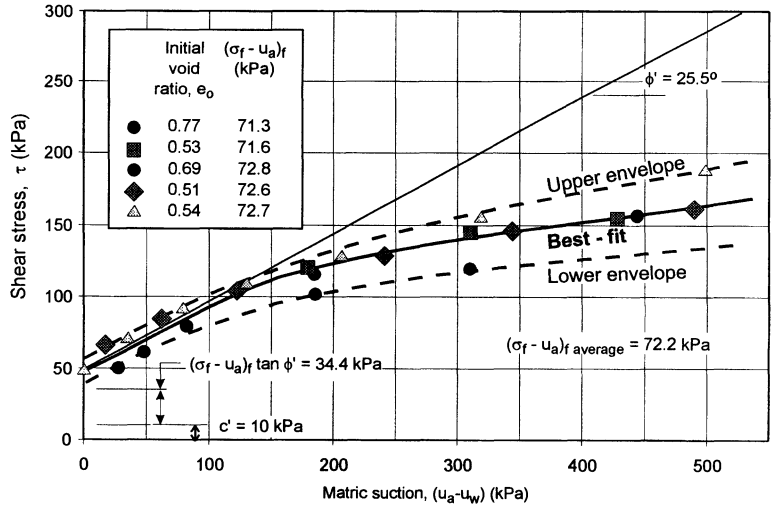
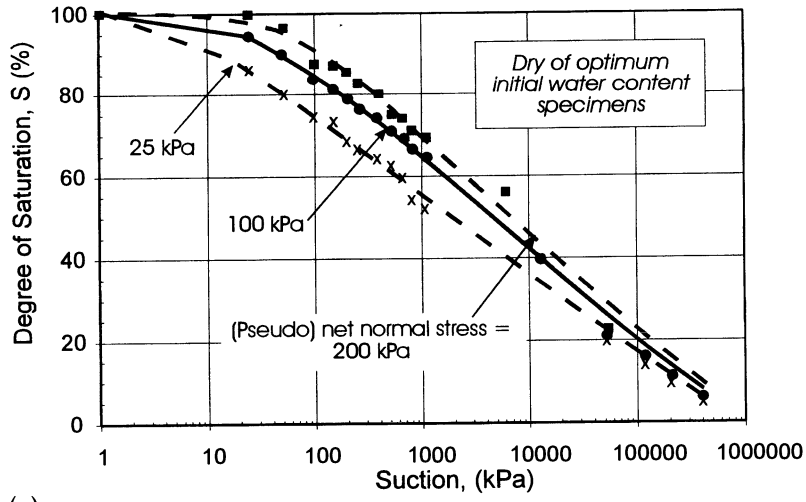
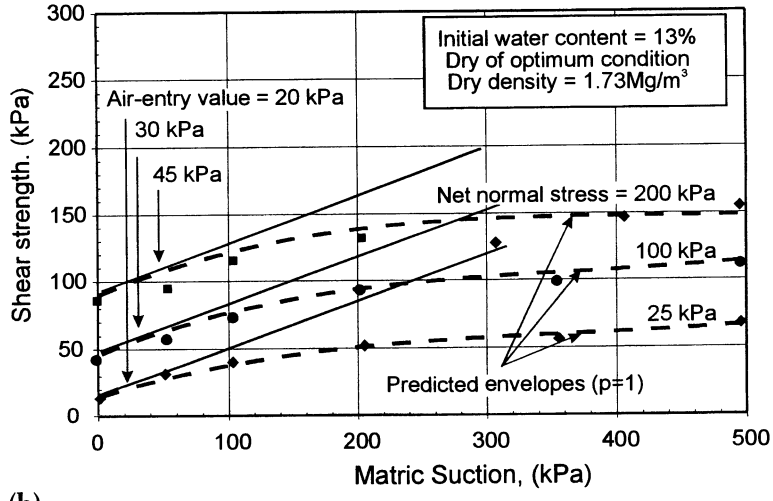


FIGURE 5.24. Variation of shear strength with respect to suction for glacial till (modified from Gan *et al.* 1988).



(a)



(b)

FIGURE 5.25. (a) Soil–water characteristic curves for the compacted till; and (b) comparison for predicted and experimental variation of shear strength with respect to suction (after Vanapalli 1994, reproduced with permission).

strength parameters and the soil–water characteristic curve (Fredlund *et al.* 1996b, Vanapalli *et al.* 1996).

At low suctions, the soil remains essentially saturated and a change in porewater pressure produces the same change in shear strength as the change in total stress (under drained conditions). The ϕ^b angle, corresponding to suctions below the air entry value of the soil, will be equal to the effective angle of internal friction, ϕ'. As the soil desaturates, the ϕ^b angle decreases because water no longer covers the entire void space in the failure plane. The decrease in shear strength is related to the volumetric water content of the soil. However, the relationship need not be directly proportional to the volumetric water content.

The shear strength relationship becomes

non-linear when tests are performed over a wide range of suctions (Gan *et al.* 1988). At lower values of soil suction, i.e. at high degrees of saturation, the porewater pressure acts directly to increase the stress contributing to shear strength. This condition applies until the soil begins to desaturate, after which the increase in shear strength can be related to the effective wetted area of contact, A_w. The effective wetted area of contact can be assumed to be proportional to the water volume in the soil in accordance with Green's theorem (Fung 1977). The effective wetted area of contact, A_w, is defined as:

$$A_w = \frac{A_{tw} - A_{dw}}{A_{tw}} \tag{5.28}$$

where A_{tw} = total wetted area of contact in the saturated state, and A_{dw} = wetted area of contact at any volumetric water content or degree of saturation.

The effective wetted area of contact, A_w, is approximately 1.0 in the "boundary effect stage" since the soil is essentially saturated, i.e. $A_{dw} = 0$. The ϕ^b angle is equal to the effective angle of internal friction, ϕ', up to the air entry value. The first significant desaturation commences in the transition stage, i.e. past the air entry value $(u_a - u_w)_b$, and the wetted area of contact, A_w, decreases. In this stage, the shear strength increase due to an increase in matric suction results in an angle, ϕ^b, which is lower than ϕ'. In the residual stage of unsaturation, the wetted area of contact decreases considerably. The value of ϕ^b in this stage can decrease, increase, or remain relatively constant as suction increases.

The normalized volumetric water content, Θ_e, can be defined with respect to the residual water content of the soil:

$$\Theta_e = \frac{\theta - \theta_r}{\theta_s - \theta_r}. \tag{5.29}$$

The normalized volumetric water content can also be taken as being equal to the dimensionless volumetric water content θ/θ_s when the entire soil–water characteristic curve is used and θ_r is assumed to be zero. The following relationship can be written between the effective wetted area of contact, A_w, and the normalized volumetric water content, Θ_e:

$$A_w = \Theta_e^p \tag{5.30}$$

where p = fitting parameter.

The shear strength contribution from soil suction, τ_{us}, written in terms of the effective wetted area of contact, A_w, can be expressed as:

$$\tau_{us} = \psi(A_w \tan \phi'). \tag{5.31}$$

Substituting Eq. 5.30 into Eq. 5.31 gives:

$$\tau_{us} = (u_a - u_w)[\Theta_e^p(\tan \phi')]. \tag{5.32}$$

The incremental change in shear strength due to a change in suction, $d\tau$, can be shown by differentiating Eq. 5.32 with respect to soil suction $(u_a - u_w)$. The value of $(\tan \phi^b)$ at any value of suction can then be written as:

$$\begin{aligned} \tan \phi^b &= \frac{d\tau_{us}}{d(u_a - u_w)} \\ &= \left[(\Theta_e^p) + (u_a - u_w)\frac{d(\Theta_e^p)}{d(u_a - u_w)} \right] \tan \phi'. \end{aligned} \tag{5.33}$$

Up to the air entry value of the soil, Θ_e is equal to unity and there is little change in the effective wetted area of contact, A_w. The rate of change of the normalized volumetric water content, Θ_e, i.e. $d(\Theta_e^p)/d(u_a - u_w)$, is equal to zero up to the air entry value of soil. Therefore, $\tan \phi^b$ is equal to $\tan \phi'$ up to the air entry value of the soil, i.e. in the boundary effect stage. The rate of change of Θ_e is negative for increments of suction beyond the air entry value, i.e. in the transition stage. However, the overall shear strength contribution due to suction, $d\tau$, in Eq. 5.33 is positive. This occurs because a reduction in the effective wetted area of contact, A_w, due to an incremental increase in suction, produces a net contribution due to suction that is positive

and hence there is an increase in the shear strength. At high values of soil suction, i.e. in the residual stage of unsaturation, Θ_e is small and the overall change in shear strength can be negative. The net summation of $\{(\Theta_e^p) + (u_a - u_w)\,[d(\Theta_e^p)/d(u_a - u_w)]\}\,(\tan \phi')$ in Eq. 5.33 may approach negative values, i.e. the incremental increase in suction results in a greater loss in the effective wetted area than the contribution to the shear strength from the increment of suction. As a result, the overall contribution of an increase in soil suction in the residual stage of unsaturation may result in a reduction in the shear strength.

There is experimental evidence to illustrate that the shear strength can decrease with an increase in suction (Donald 1956, and Escario & Juca 1989). A decrease in shear strength is most likely to occur for sands and gravels that desaturate quickly. Donald (1956) shows a drop in shear strength after a suction value of 10–15 kPa for four sands tested. For soils that have a high percentage of fines, a shear strength drop is possible only at large values of suction. Escario and Juca (1989) have observed increases in shear strength up to suction values of 1000 kPa for clayey sand. However, for suction values from 1000 to 4000 kPa, a drop in shear strength was observed.

For soils such as highly plastic clays, there is no clearly defined residual state of unsaturation. Such soils show an increase in shear strength even at relatively high values of suction. Escario and Juca (1989) report increases in shear strength for Guadalix red clay at suction values as high as 10 000 kPa.

The effective angle of internal friction, ϕ', appears to be essentially independent of the suction in the soil. Vanapalli (1994) showed that ϕ' was independent of soil suction for glacial till specimens prepared at various densities and initial water contents for a range of suction from zero to 500 kPa. Karube (1988) reported similar results for kaolinitic clay. Drumright (1989) reported that ϕ' appeared to increase slightly with suction. However, Escario and Juca (1989) have found that ϕ' was independent of soil suction for Madrid clayey sand, but not for Guadalix red clay, when tested over a wide range of suction values (0–10 000 kPa). For all practical purposes, ϕ' can be assumed to be constant for suction ranges from zero to 500 kPa, which is generally the range of practical interest in engineering.

The shear strength of an unsaturated soil at any given value of suction can be written as:

$$\tau = [c' + (\sigma_n - u_a)\tan \phi'] + (u_a - u_w)[(\Theta_e^p)(\tan \phi')]. \quad (5.34)$$

When the pore-air pressure equals the pore-water pressure, the first part of the right-hand side of Eq. 5.34 represents the saturated shear strength of the soil. The first part of Eq. 5.34 is a function of normal stress as the shear strength parameter, c', is constant for a given saturated soil. The second part of Eq. 5.34 represents the shear strength contribution due to suction and can be predicted using the soil–water characteristic curve. The soil–water characteristic curve, along with the saturated shear strength parameters, yields the shear strength contribution due to suction. The prediction of the unsaturated shear strength depends on the definition of the residual state and the fitting parameter, p. A value of $p = 1$ can be used for inactive soils such as sand, silt and some fine soils, for suctions ranging from zero to 500 kPa. A value of p equal to one means that the effective wetted area of contact is equal to the effective volumetric water content. The fitting parameter, p, is used to obtain better correlations between the predicted and experimental shear strength data.

The following summarizes a procedure for predicting the shear strength of an unsaturated soil.

1. A mathematical relationship is found for the soil–water characteristic curve for the suction range 0–1 000 000 kPa. A non-linear minimization technique can be used to find the equation for the soil–water characteristic curve. The three curve fitting parameters, i.e. a and n, should be selected so that the predicted curve matches the measured values for the soil–water characteristic curve.
2. A graphical construction technique for the soil–water characteristic curve is used to determine the residual state of the soil (residual water content and corresponding suction).
3. The shear strength function can be predicted using Eq. 5.34, and assuming that p is equal to one for relatively low values of suction, i.e. 0–500 kPa range. The shear strength parameters, c' and ϕ', are required as input parameters.
4. The shear strength function can also be predicted by using the normalized water content, Θ_e, in Eq. 5.34 along with a p value greater than 1, e.g. 2 to 4.

5.6.4 FORMULATION FOR BEARING CAPACITY PROBLEMS

Several engineering applications, such as bearing capacity, lateral earth pressures and slope stability, involve the shear strength of a soil. The bearing capacity of a soil, and other similar plasticity problems, can be viewed as an extension of saturated soil mechanics. The limiting, or failure, condition for a saturated soil is given by:

$$\tau = c' + (\sigma_n - u_a)\tan \phi'. \qquad (5.35)$$

Equation 5.35 can be extended to an unsaturated soil by including the effect to shear strength due to matric suction as given below:

$$\tau = c' + (\sigma_n - u_a)\tan \phi' + (u_a - u_w)\tan\phi^b. \qquad (5.36)$$

In an unsaturated soil, cohesion can be visualized as two components: the effective cohesion, c', and a component due to matric suction, $(u_a - u_w)\tan \phi^b$. The total cohesion, c, can be written as:

$$c = c' + (u_a - u_w)\tan \phi^b. \qquad (5.37)$$

Equation 5.35 can be written in a form similar to that for saturated soils by substituting Eq. 5.37 into Eq. 5.36:

$$\tau = c + (\sigma_n - u_a)\tan \phi'. \qquad (5.38)$$

Conventional bearing capacity theory, given in Chapter 9, can be applied to unsaturated soils where cohesion is the total cohesion, c as given in Eq. 5.37, and ϕ' is the friction angle of the soil.

5.6.5 FORMULATION FOR LATERAL EARTH PRESSURE PROBLEMS

Unsaturated conditions in a soil, soil suctions greater than zero, have the net effect of increasing the cohesion in the soil. As detailed in the previous section (Section 5.6.4), the soil has a total cohesion with two components. The active pressure in an unsaturated soil decreases from the active pressure in a saturated soil (see Fig. 5.26). Conversely, the passive pressure in an unsaturated soil increases from the passive pressure in a saturated soil (see Fig. 5.26). When the linear form of the unsaturated shear strength equation is used, the mathematical equations for the active and passive earth pressures of an unsaturated soil take the same form as for a saturated soil, see Chapter 17.

5.6.6 FORMULATIONS FOR SLOPE STABILITY PROBLEMS

The general limit equilibrium (GLE) method provides a general force and moment equilibrium equation for the calculation of the factor of safety of a slope (see Chapter 14 for a detailed discussion). When going from a saturated to an unsaturated soil, only the shear forced mobilized along the base of the trial slip surface changes. Since the matric suction component of shear strength is considered as part of the cohesion of the soil, the conventional factor of safety equations do not need to be re-derived, and one can use the com-

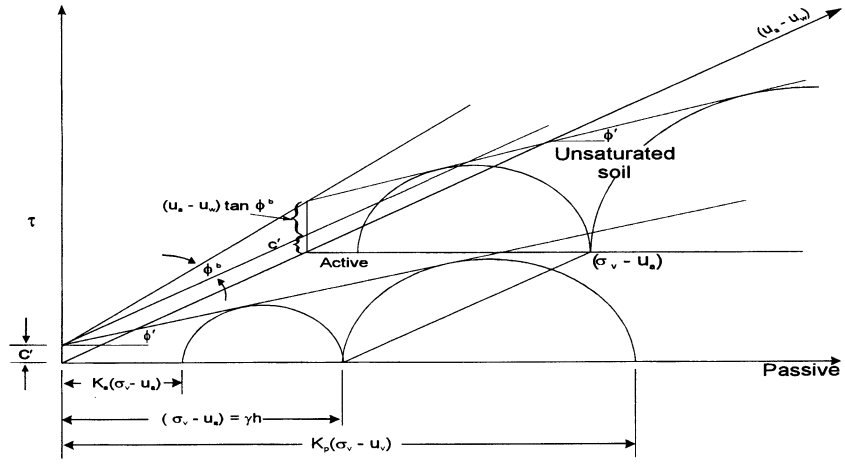


FIGURE 5.26. Active, K_a, and passive, K_p, earth pressures for a soil with matric suction.

puter programs written for saturated soils to solve unsaturated soil problems. The soils in the negative porewater pressure region must be subdivided into several discrete layers, each layer having a constant value of cohesion, and the porewater pressures set to zero. The two main disadvantages of this approach are that cohesion is not a continuous function, and the appropriate cohesion values for each soil layer must be computed manually.

Two independent equations for factor of safety can be derived: one with respect to moment equilibrium, and the other with respect to horizontal force equilibrium. Moment equilibrium can be satisfied with an arbitrary point above the central portion of the slip surface. The center of rotation is an obvious point for moment equilibrium for a circular slip surface. The center of moments is determined when both force and moment equilibria are satisfied.

Figure 5.27 illustrates the effect of soil suction on the computed factor of safety. Relatively small increase in soil suction, e.g. less than 100 kPa, can increase the computed factor of safety by more than 50%. The influence of negative porewater pressures can be very substantial, particularly for shallow slip surfaces.

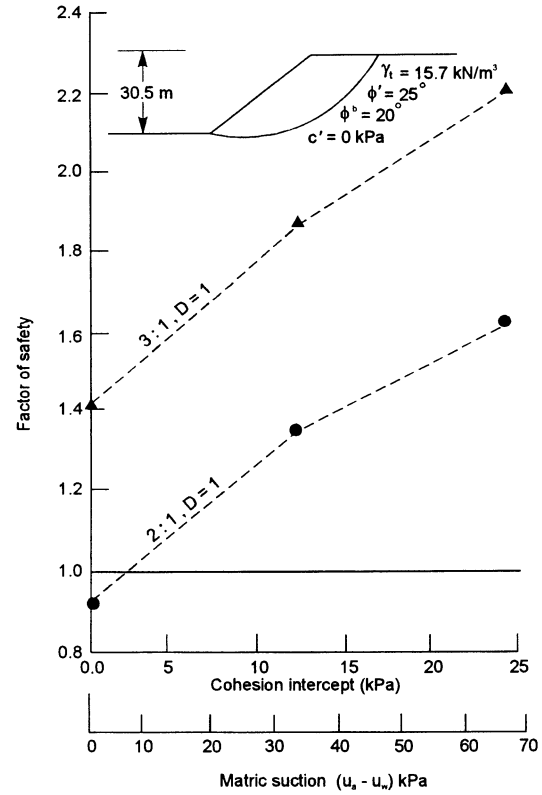


FIGURE 5.27. Factor of safety versus matric suction for a simple slope.

5.7 *Volume Change in Unsaturated Soils*

The volume change constitutive behavior of an unsaturated soil can be written in several possible forms (Fredlund 1979, Fredlund & Morgenstern 1977), such as the elasticity form, the compressibility form, and the soil mechanics terminology form. The classical soil mechanics form for the one-dimensional, K_0, loading of a saturated soil involved the relationship between void ratio and effective stress with the slope of the relationship defined as the coefficient of compressibility, a_v. However, two independent constitutive relationships are required to define the volume–mass properties of an unsaturated soil in terms of the stress state variables. The need for two independent constitutive relations for an unsaturated soil can be demonstrated using chain rule differentiation of the basic volume–mass relationship, i.e. $Se = wD_r$ (see Chapter 2). The incremental form of the mass–volume relationship can then be integrated from initial to final conditions:

$$\int_{e_0}^{e_f} S\mathrm{d}e + \int_{S_0}^{S_f} e\mathrm{d}S = D_r \int_{w_0}^{w_f} \mathrm{d}w. \quad (5.39)$$

Using soil mechanics terminology, the change in void ratio, de, of an unsaturated soil under general, three-dimensional, isotropic loading can be written as:

$$\mathrm{d}e = a_t \mathrm{d}\,(\sigma_{mean} - u_a) + a_m \mathrm{d}(u_a - u_w) \quad (5.40)$$

where a_t = coefficient of compressibility with respect to a change in net normal stress, $\mathrm{d}(\sigma_{mean} - u_a)$; a_m = coefficient of compressibility with respect to a change in soil suction, $\mathrm{d}(u_a - u_w)$.

A second constitutive relationship, namely, the water phase constitutive equation can be expressed as a change in water content. For three-dimensional loading, the water phase constitutive relation can be written as:

$$\mathrm{d}w = b_t \mathrm{d}\,(\sigma_{mean} - u_a) + b_m \mathrm{d}(u_a - u_w) \quad (5.41)$$

where b_t = coefficient of water content change with respect to a change in net normal stress, $\mathrm{d}(\sigma_{mean} - u_a)$; b_m = coefficient of water content change with respect to a change in soil suction, $\mathrm{d}(u_a - u_w)$.

The above constitutive equations can be visualized as constitutive surfaces on a three-dimensional plot, with each abscissa representing one of the stress state variables, and the ordinate representing the soil volume–mass property (Fig. 5.28a). The a_t, a_m, b_t and b_m coefficients can be visualized as volumetric deformation coefficients. The constitutive surfaces (shown in Fig. 5.28a) can be reduced to a two-dimensional plot that shows the relationship between the various volumetric deformation coefficients (Fig. 5.28b).

The constitutive relationships can also be written for other loading conditions, i.e. stress paths. When the net confining stress on the soil is equal to zero, the resulting equation is a relationship between gravimetric water content and soil suction, which gives one form of the soil–water characteristic curve:

$$\mathrm{d}w = b_m \mathrm{d}(u_a - u_w). \quad (5.42)$$

The soil–water characteristic curve is more often written in terms of volumetric water content, θ:

$$\mathrm{d}\theta = m_2^w \mathrm{d}(u_a - u_w). \quad (5.43)$$

The constitutive relations can be formulated within the critical state framework, proposed by Wheeler (1991), which uses three stress state parameters, p, q, r, and two volume–mass parameters, water content, w, and void ratio, e, to indicate the phase relations. Specific volume, v, and void ratio, e, are related as follows:

$$v = 1 + e \quad (5.44)$$

The void ratio and the gravimetric water content constitutive surfaces can be combined on one plot by multiplying the water content by the relative density of the soil, i.e. wD_r. A generalized plot of the loading branches

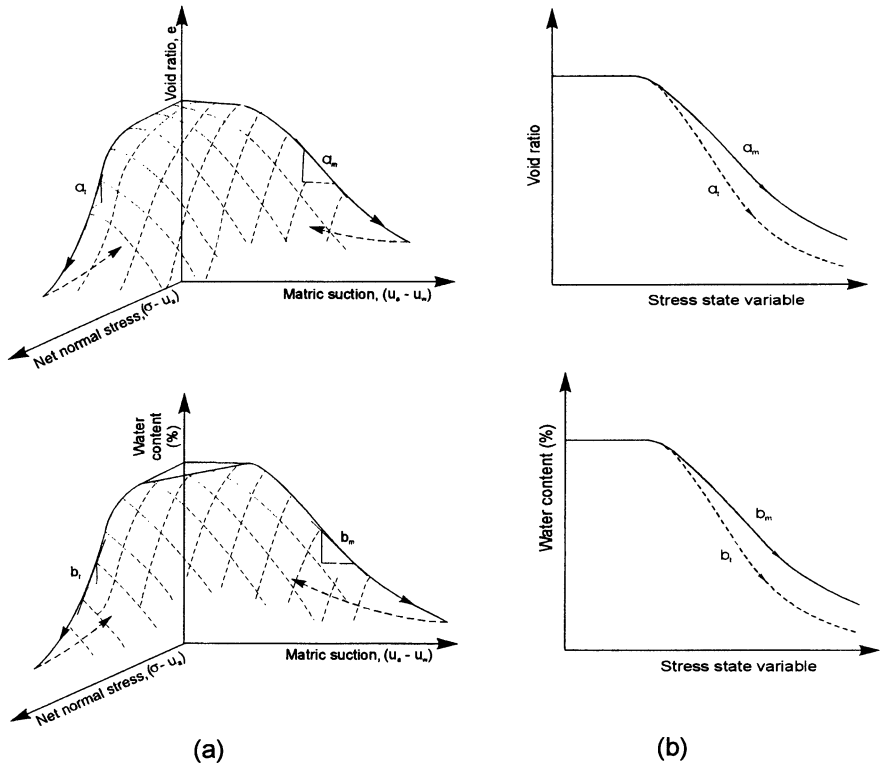


FIGURE 5.28. Constitutive surfaces for an unsaturated soil expressed using soil mechanics terminology: (a) three-dimensional void ratio and water content constitutive surfaces, and (b) two-dimensional comparison showing volumetric deformation moduli.

associated with the limiting conditions on all constitutive surfaces is shown in Fig. 5.29. For the condition of zero suction, the water content and void ratio constitutive relations overlap.

5.7.1 MEASUREMENT OF THE VOLUME CHANGE FUNCTION

Several stress paths exist along which an element can be loaded or unloaded. The most general loading stress path is the three-dimensional loading path. The three-dimensional loading path is also the most difficult to follow, and it is often desirable to use a more specialized loading path. Common stress paths for loading are: isotropic loading, uniaxial loading, biaxial loading, plane strain and K_0 loading. Isotropic loading (the changes in suction are always isotropic in nature), has become the reference loading condition in critical state soil mechanics.

The definition of the extreme limits on the overall volume change and water content constitutive relationships is made using three independent laboratory tests. The three relationships to be defined are: void ratio, e, and net total stress $(\sigma - u_a)$; water content, gravimetric or volumetric, and matric suction $(u_a - u_w)$; and the ratio of the slope of the void ratio change to the water content change in response to a change in suction.

A conventional one-dimensional oedometer test, or a triaxial isotropic loading test, is used to define the relationship between void ratio and net total stress. The results of this test are referred to as the compression

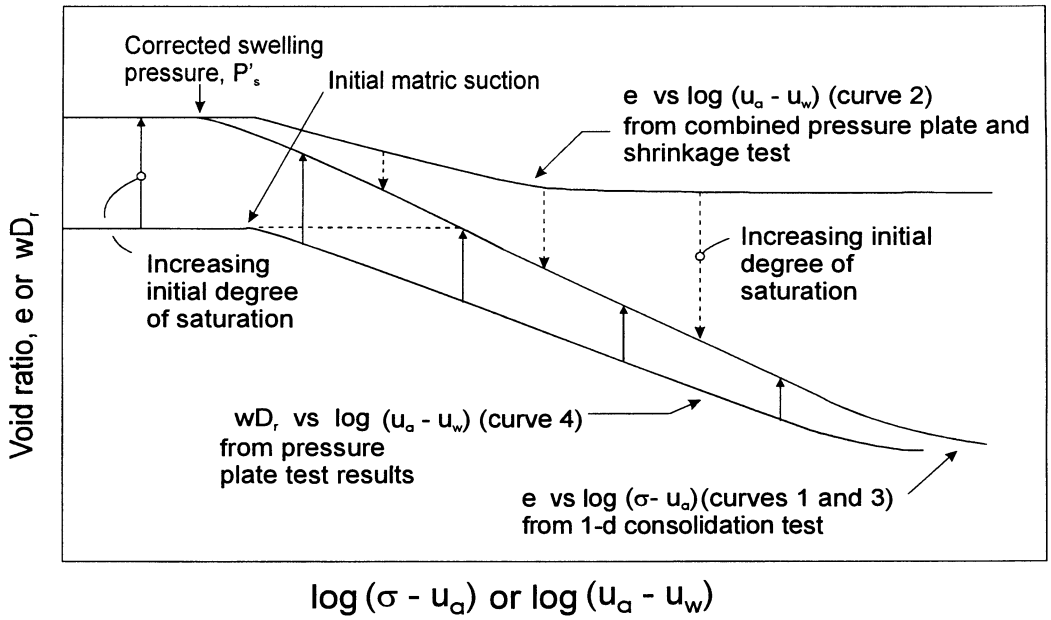


FIGURE 5.29. Relationship between curves that define the mass and volume change behavior of an unsaturated soil.

curve for the soil, and the relationship is equivalent to the void ratio versus effective stress for a saturated soil. A pressure plate apparatus is used to define the relationship between gravimetric, or volumetric, water content and matric suction. The test can be performed under various applied total stresses, but is often performed with the net total stress equal to zero. The test results are referred to as the soil–water characteristic curve for the soil. The shrinkage test is used to define the ratio of the slope of the void ratio versus water content in response to a change in suction. Data from the above three tests are used to define the extremes of the void ratio and water content constitutive surfaces. Typical data for silt and glacial till, compacted dry of optimum are given by Ho *et al.* (1992).

5.7.2 ESTIMATION OF THE VOLUME CHANGE MODULI

The volume change function is the relationship between the soil suction and the volume change of an unsaturated soil. While further research is needed in order to be able to estimate the relationships between the loading constitutive surfaces, it is possible to determine other means of relating moduli on the void ratio constitutive surface by assuming that the unloading constitutive surface is unique for monitoring conditions (Fig. 5.29). This procedure can be used to predict the heave in expansive soils. Then, the *in situ* stress state (overburden pressure and matric suction) in the field can be transferred on to the total stress plane to give the swelling pressure of the soil. The unloading moduli on the total stress plane is taken to correspond to the wetting of an expansive soil and used in the prediction of total heave.

5.7.3 FORMULATION FOR THE PREDICTION OF HEAVE OF AN EXPANSIVE SOIL

To predict heave, the initial and future stress states must be established and the stress path between the initial and final stress states

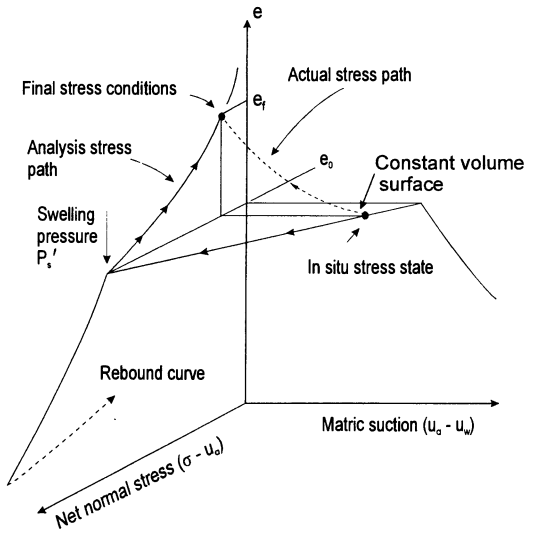


FIGURE 5.30. "Actual" and "analysis" stress paths followed during the wetting of a soil.

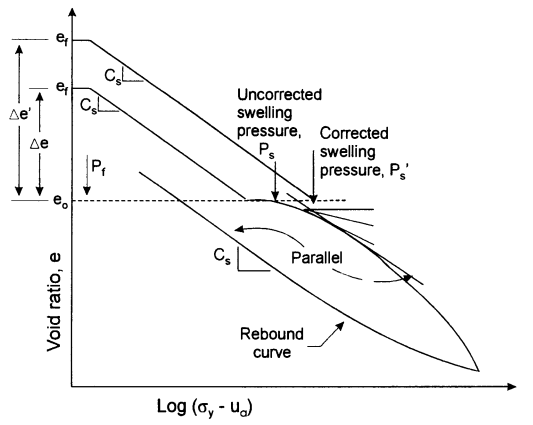


FIGURE 5.31. One-dimensional oedometer test results showing the effects of sample disturbance.

must be understood. Figure 5.30 shows a comparison between the actual and analysis stress paths for an element of expanding soil. The initial stress state is defined in terms of "corrected" swelling pressure. The word "corrected" is used to indicate that the effect that sampling disturbance must be taken into account in establishing the swelling pressure of the soil (Yoshida *et al.* 1983). Figure 5.31 shows the procedure for correcting for sampling disturbance.

The calculation for predicting total heave is similar to the procedure used for settlement calculations. The amount of total heave is computed from the swelling index and the changes in void ratio corresponding to the initial and final stress states. The following formulation is based on the assumption that the stress paths have been projected on to the net normal stress plane. The total heave stress path follows the rebound curve, i.e. C_s, from the initial to the final stress state. The equation of the rebound portion of the oedometer test data is:

$$\Delta e = C_s \log\left(\frac{P_f}{P_0}\right) \qquad (5.45)$$

where Δe = change in void ratio between the initial and final stress states, i.e. $e_f - e_0$; e_0 = initial void ratio; e_f = final void ratio; C_s = swelling index; P_0 = initial stress state, which is equivalent to the corrected swelling pressure, P_s', P_f = final stress state.

The initial stress state, P_0, is the sum of the overburden pressure and the matric suction equivalent (Fig. 5.29):

$$P_0 = (\sigma_v - u_a) + (u_a - u_w)_e \qquad (5.46)$$

where σ_v = total overburden pressure; $(\sigma_v - u_a)$ = net overburden pressure; u_a = pore-air pressure; u_w = porewater pressure; and $(u_a - u_w)_e$ = matric suction equivalent.

Equation 5.46 defines the initial stress state, P_0, which is measured as the corrected swelling pressure in the oedometer test. The final stress state, P_f, accounts for the changes in total stress and the estimate of the final porewater pressures. The final stress state can be written as:

$$P_f = \sigma_v + \Delta\sigma_v - u_{wf} \qquad (5.47)$$

where $\Delta\sigma_v$ = change in total stress, due to fill or excavation, and can be a positive or negative change, respectively; and u_{wf} =

predicted or estimated final porewater pressure.

The total heave, ΔH, from several soil layers can be written as the sum of the heave from each individual layer, Δh:

$$\Delta H = \Sigma \Delta h_i = \Sigma \frac{C_s}{1 + e_0} h_i \log \frac{P_{fi}}{P_{0i}} \quad (5.48)$$

where h_i = thickness of the layer under consideration, e_{oi} = initial void ratio of the soil layer, and e_{fi} = final void ratio of the soil layer.

Prediction of the final porewater pressures is required to predict total heave. The prediction of porewater pressures must take into consideration the surface flux moisture boundary conditions, an unsaturated soils analysis, and the fluctuation of the groundwater table. Surface flux boundary conditions are dependent on the climatic conditions. On a smaller scale, man-made causes, such as irrigation or leaky pipes, can effect the final porewater pressures.

There are three possibilities for the prediction of the final porewater pressure conditions. First, it can be assumed that the water table will rise to the ground surface creating a hydrostatic condition. The greatest amount of total heave will be predicted using this assumption. Second, it can be assumed that the porewater pressure approaches a zero value throughout its depth. This may appear to be a realistic assumption; however, it is not an equilibrium condition. In many situations, this assumption may provide a suitable estimate for the final porewater pressures. Third, it can assumed that for long-term equilibrium conditions the porewater pressure will remain slightly negative. This assumption predicts the smallest amount of total heave. It is also possible to have variations of the above assumptions within the soil profile. There may also be a limit placed on the depth to which wetting will occur. Most of the heave that occurs is in the uppermost soil layer, as this is the layer where the greatest changes in matric suction generally occur.

There is still much research required in the area of overall volume change in unsaturated soils. The theoretical context for volume change has been established. It is only a matter of time before suctions can be measured *in situ* and new procedures are forthcoming (Thompson 1997).

6. BASIC ROCK MECHANICS AND TESTING

K. Y. Lo
A. M. Hefny

6.1 Introduction

The application of rock mechanics to solve engineering problems requires some knowledge of engineering geology and an appreciation of the difference between parameters measured in the laboratory and the design parameters used in field problems. This concept is particularly important in the practice of rock engineering because laboratory tests described in subsequent sections are performed on small specimens of intact rock. In contrast, the rock mass in the field is often dissected by various discontinuities such as joints. Therefore, quantities of engineering importance measured in the laboratory, such as the elastic modulus and strength, can seldom be directly used in the field. However, the results of laboratory measurements do form an intrinsic component of the knowledge required for design. The parameters measured in the laboratory may serve as: (1) an index to correlate experience between different rock formations, (2) an index to represent the variation of material behavior over a proposed site, (3) upper bound values such as elastic modulus and strength, and (4) a component to which a "correction factor" may be applied to obtain the design value.

6.2 Types of Rocks and their Classification

6.2.1 ROCK-FORMING MINERALS

Rocks are composed of minerals, which are formed by the combination of naturally occurring elements. The most common elements, comprising approximately 98% of the Earth's crust, are: oxygen (O), silicon (Si), aluminum (Al), iron (Fe), calcium (Ca), sodium (Na), potassium (K) and magnesium (Mg). Although there are hundreds of recognized minerals, only a few are common. Tables 6.1 and 6.2 summarize the common rock-forming minerals and their properties.

Mohs' scale, used in Table 6.2, is a standard of ten minerals by which the hardness of a mineral may be rated. Hardness is defined as the ability of a mineral to scratch another. The scale is unity for the softest mineral (talc) and is ten for the hardest (diamond).

6.2.2 ROCK CLASSIFICATION

Rocks may be classified according to their geological characteristics or their engineering properties. The geological classification of rocks refers to the mineralogy, fabric, chemistry, crystallography and the texture of rocks. Engineering classifications are based on

R. K. Rowe (ed.), *Geotechnical and Geoenvironmental Engineering Handbook*
© Kluwer Academic Publishers 2001

TABLE 6.1. Common rock-forming minerals (after Farmer 1968)

Feldspar	
Orthoclase	$KAlSi_3O_8$
Plagioclase	$\left\{\begin{matrix} NaAlSi_3O_8 \\ CaAl_2Si_2O_8 \\ \text{variable} \end{matrix}\right\}$
Quartz	SiO_2
Mica	
Muscovite	$KAl_2(Si_3Al)O_{10}(OH)_2$
Biotite	$K_2(MgFe)_6(SiAl)_8O_{20}(OH)_4$
Amphibole	
Hornblende	Na, Ca, Mg, Fe, Al silicate
Pyroxene	
Augite	Ca, Mg, Fe, Al silicate
Olivine	$(MgFe)_2SiO_4$
Calcite	$CaCO_3$
Dolomite	$CaMg(CO_3)_2$
Kaolinite	$Al_2Si_2O_5(OH)_4$
Iron oxide	Fe_2O_3, $2Fe_2O_3 \cdot 3H_2O$

strength, deformation and fracturing characteristics of rocks.

6.2.2.1 Geological Classification

The three main classes of rocks are igneous, sedimentary and metamorphic. Igneous rocks are formed by crystallization of molten magma. The mode of crystallization of the magma, at depth in the Earth's crust or by extrusion, and the rate of cooling affect the rock texture or crystal size. The igneous rocks are subdivided into plutonic, hypabyssal and volcanic, according to their texture. They are further subdivided into acid, intermediate and basic, according to the silica content, as shown in Table 6.3. Sedimentary rocks are formed from the consolidation of sediments. Table 6.4 shows the classification of the sedimentary rocks. Metamorphic rocks are derived from pre-existing rocks by temperature, pressure and/or chemical changes. Table 6.5

TABLE 6.2. Properties of common rock-forming minerals (after Farmer 1968)

Mineral	Hardness (Mohs' scale, 1–10)	Relative density	Fracture	Structure
Orthoclase feldspar	6	2.6	Good cleavage at right angles	Monoclinic. Commonly occurs as crystals
Plagioclase feldspar	6	2.7	Cleavage nearly at right angles–very marked	Triclinic. Showing distinct cleavage lamellae
Quartz	7	2.65	No cleavage. Choncoidal fracture	Hexagonal
Muscovite	2.5	2.8	Perfect single cleavage into thin easily separated plates	Monoclinic. Exhibiting strong cleavage lamellae
Biotite	3	3		
Hornblende	5–6	3.05	Good cleavage at 120°	Hexagonal–normally in elongated prisms
Augite	5–6	3.05	Cleavage nearly at right angles	Monoclinic
Olivine	6–7	3.5	No cleavage	No distinctive structure
Calcite	3	2.7	Three perfect cleavages. Rhomboids formed	Hexagonal
Dolomite	4	2.8	Three perfect cleavages	Hexagonal
Kaolinite	1	2.6	No cleavage	No distinctive structure (altered feldspar)
Hematite	6	5	No cleavage	Hexagonal

TABLE 6.3. Geological classification of igneous rocks (modified from Bowen 1984)

	Type			
Grain size	Acid >65% silica	Intermediate 55–65% silica	Basic 45–55% silica	Ultrabasic <45% silica
Plutonic (coarse)	Granite Granodiorite	Diorite	Gabbro	Picrite Peridotite Serpentinite Dunite
Hypabyssal	Quartz Orthoclase porphyries	Plagioclase porphyries	Dolerite	Basic dolerites
Extrusive (fine)	Rhyolite Dacite	Pichstone Andesite	Basalt	Basic olivine basalts
Major mineral constituents	Quartz, orthoclase, sodium-plagioclase, muscovite, biotite, hornblende	Quartz, orthoclase, plagioclase, biotite, hornblende, augite	Calcium-plagioclase, augite, olivine, hornblende	Calcium-plagioclase, olivine, augite

TABLE 6.4. Sedimentary rock classification (after Farmer 1968)

Method of formation	Classification	Rock	Description	Major mineral constituents
Mechanical	Rudaceous	Breccia Conglomerate	Large grains in clay matrix	Various
	Arenaceous	Sandstone	Medium, round grains in calcite matrix	Quartz, calcite (sometimes feldspar, mica)
		Quartzite	Medium, round grains in silica matrix	Quartz
		Gritstone	Medium, angular grains in matrix	Quartz, calcite, various
		Breccia	Coarse, angular grains in matrix	
	Argillaceous	Clay	Micro-fine-grained plastic texture	Kaolinite, quartz, mica
		Shale Mudstone	Harder-laminated compacted clay	
Organic	Calcareous	Limestone	Fossiliferous, coarse or fine grained	Calcite
	Carbonaceous (siliceous, ferruginous, phosphatic)	Coal		
Chemical	Ferruginous	Ironstone	Impregnated limestone or clay (or precipitated)	Calcite, iron oxide
	Calcareous (siliceous, saline)	Dolomitic limestone	Precipitated or replaced limestone, fine grained	Dolomite, calcite

TABLE 6.5. Metamorphic rock classification (after Farmer 1968)

Classification	Rock	Description	Major mineral constituents
Massive	Hornfels	Micro-fine grained	Quartz
	Quartzite	Fine grained	Quartz
	Marble	Fine–coarse grained	Calcite or dolomite
Foliated	Slate	Micro-fine grained, laminated	Kaolinite, mica
	Phyllite	Soft, laminated	Mica, kaolinite
	Schist	Altered hypabyssal rocks, coarse grained	Feldspar, quartz, mica
	Gneiss	Altered granite	Hornblende

TABLE 6.6. Engineering classification of rock by strength (adapted from ISRM 1978a; CGS 1992)

Strength			Range of uniaxial compressive strength (MPa)
Grade	Classification	Field identification method	
R0	Extremely weak	Indented by thumbnail	<1
R1	Very weak	Crumbles under firm blows of geological hammer; can be peeled with a pocket knife	1–5
R2	Weak	Can be peeled by a pocket knife with difficulty; shallow indentations made by a firm blow with point of geological hammer	5–25
R3	Medium strong	Cannot be scraped or peeled with a pocket knife; specimen can be fractured with a single firm blow of geological hammer	25–50
R4	Strong	Specimen requires more than one blow of geological hammer to fracture	50–100
R5	Very strong	Specimen requires many blows of geological hammer to fracture	100–250
R6	Extremely strong	Specimen can only be chipped by the geological hammer	>250

shows a classification of the metamorphic rocks according to their physical structure, i.e. massive or foliated.

6.2.2.2 Engineering Classification

1. Intact rocks. The engineering classifications of intact rocks (rocks free of planes of weakness) are based on the strength and deformation properties of the rock. Among the systems that use only one parameter (strength) for classification are those of Attewell & Farmer (1976) and the International Society of Rock Mechanics (ISRM 1978a). The ISRM classification was also recommended in the *Canadian Foundation Engineering Manual* (CGS 1992). In this classification, the rock may range from extremely weak to extremely strong depending on the uniaxial compressive strength or the approximate field identification method, as shown in Table 6.6.

Based on the laboratory measurements of strength and deformation of rocks, Deere and Miller (1966) established a two parameter classification system. The two parameters are the ultimate strength (uniaxial strength) and the tangent modulus of elasticity at 50% of the ultimate strength. Figures 6.1, 6.2 and 6.3 summarize the engineering classification

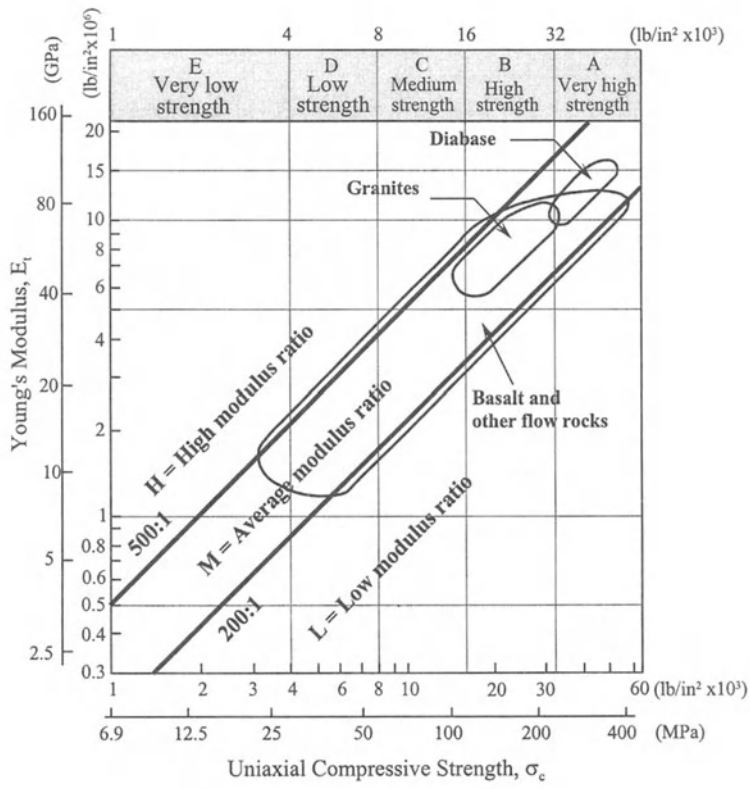


FIGURE 6.1. Engineering classification for intact igneous rocks (E_t = tangent modulus at 50% ultimate strength); classifies rocks as AM, BH, BL, etc., depending on where E_t and σ_c plot (modified from Deere & Miller 1966).

for igneous, sedimentary and metamorphic rocks, respectively, as given in Deere & Miller (1966). The modulus ratio appearing in the figures is the ratio of elastic modulus to the uniaxial compressive strength.

2. Fractured rocks. Recognizing the important effects of geological discontinuities on the strength and deformability of rock masses, the classification system should include information about spacing, aperture, roughness, filling, weathering and orientation of these discontinuities, in addition to the strength of the rock material. The ISRM (1978a) has recommended a classification system based on these properties. Some important indices of the rock-mass quality are the fracture frequency, velocity ratio and rock quality designation (RQD).

1. Fracture frequency. The fracture frequency is the number of fractures per meter of the rock core drilled. A low fracture frequency is indicative of good quality in a rock mass. As the fracture frequency increases, the quality of the rock mass becomes poorer and the *in situ* modulus of deformation decreases. The use of fracture frequency in estimation of the ratio of mass to intact deformation moduli will be discussed in a later section.
2. Velocity ratio. The velocity ratio, the ratio of the field seismic velocity to the laboratory sonic velocity, was first proposed as a quality index of rock mass by Onodera (1963). The field seismic velocity can be determined from a refraction seismic survey by up-hole

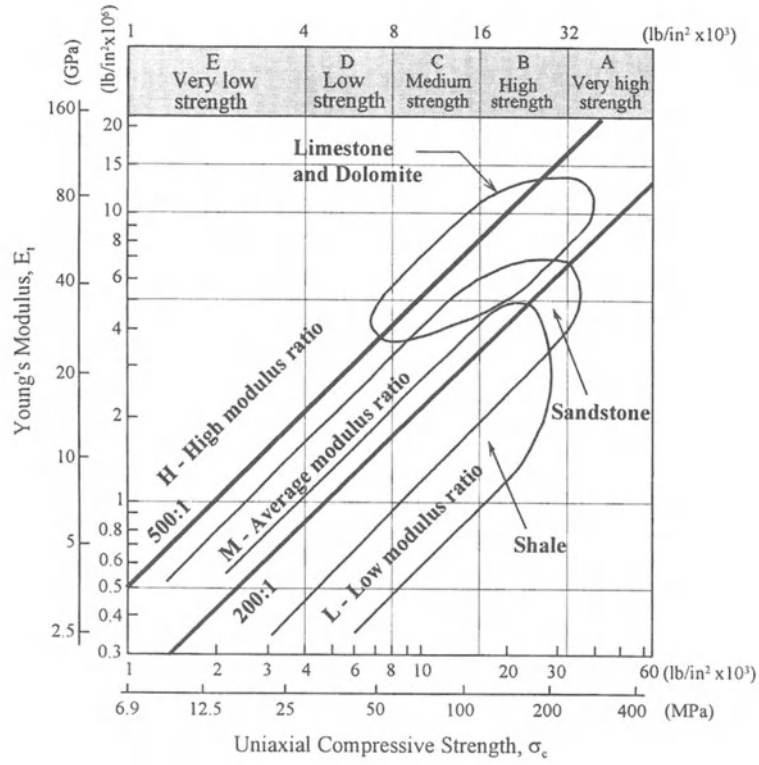


FIGURE 6.2. Engineering classification for intact sedimentary rocks (E_t = tangent modulus at 50% ultimate strength); classifies rocks as AM, BH, BL, etc. (modified from Deere & Miller 1966).

shooting, by continuous three-dimensional sonic logging in a drill hole, or from cross-hole seismic velocities. The velocity determined in the laboratory is a function of the properties of the intact rock, whilst the field velocity is influenced additionally by the number, orientation and type of discontinuities in the path of the pulse. The velocity ratio is thus a measure of the rock mass quality. A velocity ratio approaching unity is a representative of a high quality massive rock with only a few tight joints. Conversely, if open discontinuities exist, the quality of the rock becomes poorer and the velocity ratio is reduced.

3. Rock quality designation (RQD). A commonly used index of rock mass quality, which is based on a modified core-recovery procedure, was proposed by Deere (1964). The RQD is determined by summing the total length of core recovered, considering only intact pieces of 100 mm or more in length. The RQD is the percentage ratio of the summed core length to the total core drilled. The relationship between RQD and rock quality is given in Table 6.7.

An important application of the indices described in the previous sections is to estimate the deformation modulus of rock mass, which often forms the controlling design criterion in most engineering projects. Figure 6.4 shows the variation of the ratio of mass to intact deformation modulus, E_m/E_{int}, with RQD given by Deere *et al.* (1967). The "mass" moduli were

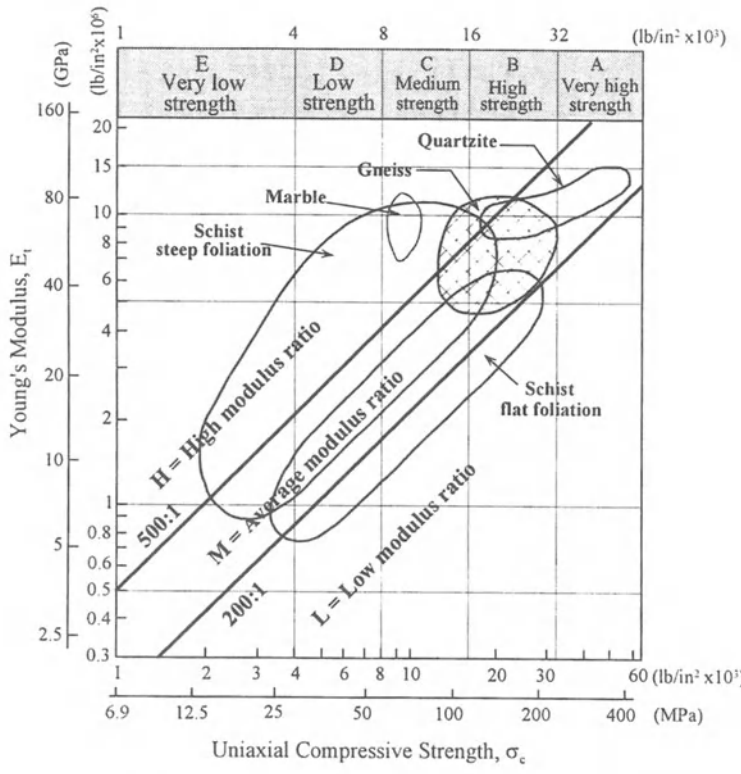


FIGURE 6.3. Engineering classification for intact metamorphic rocks (E_t = tangent modulus at 50% ultimate strength); classifies rocks as AM, BH, BL, etc. (modified from Deere & Miller 1966).

obtained from plate jacking tests of 0.86-m diameter performed in unlined adits at Dworshak Dam site. Although there are scatter in data, there is a trend that E_m/E_{int} decreases sharply with a decrease in RQD from 100 to about 60%. Below an RQD value of 60%, it is unlikely that a definite correlation between RQD and E_m/E_{int} exists. Similar observations were reported in Coon & Merritt (1970) and Bieniawski (1978).

Figure 6.5 shows a correlation between the fracture frequency and the ratio of mass to intact deformation modulus, E_m/E_{int}. The mass moduli shown in the figure were computed from field measurements of deformation in tunneling projects in different rock formations with measured *in situ* stresses. In the same figure, a theoretical curve (Walsh 1965) is also shown. The relationship between E_m/E_{int} and fracture frequency provides a satisfactory representation of the effects of fracturing on deformation of rock mass.

A case record of assessing the mass

TABLE 6.7. Classification of rock with regard to RQD value

Classification	Very poor	Poor	Fair	Good	Excellent
RQD (%)	<25	25–50	50–75	75–90	90–100

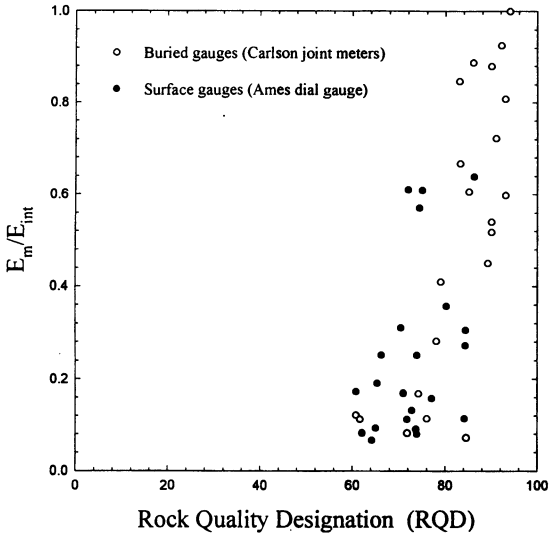


FIGURE 6.4. Variation of ratio of mass to intact deformation modulus, E_m/E_{int}, with RQD from plate jacking tests, Dworshak Dam (modified from Deere *et al.* 1967).

modulus for the design of Darlington nuclear generating station is presented in Lo *et al.* (1987b).

4. Other classification systems. Detailed classification systems developed for the design of temporary supports of tunnels in fractured rocks have been developed, including the rockmass rating (RMR) system developed at the South African Council for Scientific and Industrial Research (CSIR) by Bieniawski (1974, 1976, 1984, 1989) and the Q system developed at the Norwegian Geotechnical Institute (NGI) by Barton *et al.* (1974).

6.3 *Laboratory Measurements of Strength and Deformation Properties of Intact Rock*

In the design of structures in rocks, the strength and deformation parameters of the rock units must be known. It has been well-recognized that these parameters when determined from rock cores represent the property of intact rocks and therefore usually overesti-

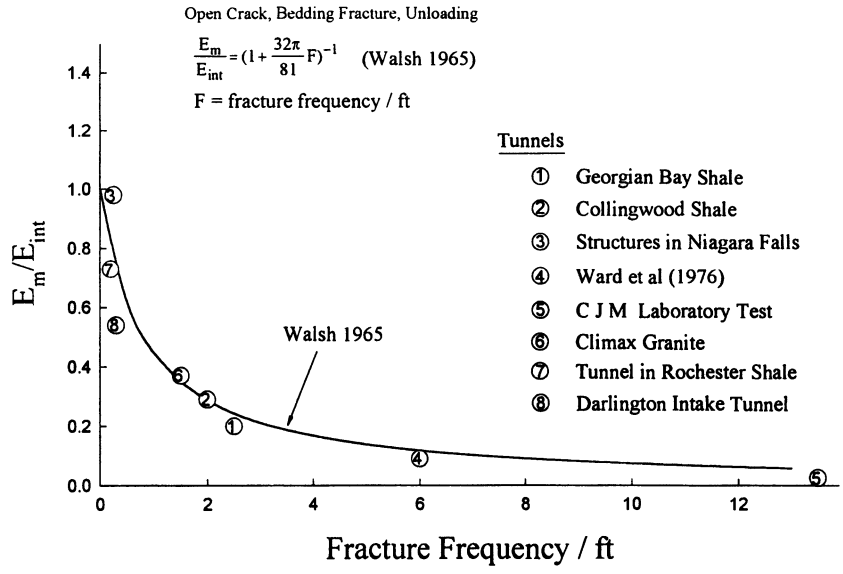


FIGURE 6.5. Relationship between fracture frequency and ratio of mass to intact deformation modulus.

mate the mass strength and modulus due to the existence of geological discontinuities. However, several important uses may be made of these parameters in the design process, such as:

- When the rock is relatively intact, as for example when the rock quality designation (RQD) approaches 100%, the mass modulus and strength approach those of the intact rock.
- As illustrated in Section 6.2.2.2, the modulus determined from rock cores together with a classification system may be used as a basis for correlation with the mass modulus, serving as a parameter for defining zones of different compressibility at a proposed site for a major structure, or summarizing experience in different geological conditions.
- In some problems involving high stress concentration, the induced stresses in the field do indeed exceed the strength of intact rocks.
- The strength of intact rock is an important parameter for the selection of excavation method, including the selection for tunnel boring machine.

This section summarizes some of the important laboratory tests conducted on intact rock for the determination of the deformation and strength parameters. Figure 6.6 shows the different type of tests required to obtain the complete failure envelope of intact rock.

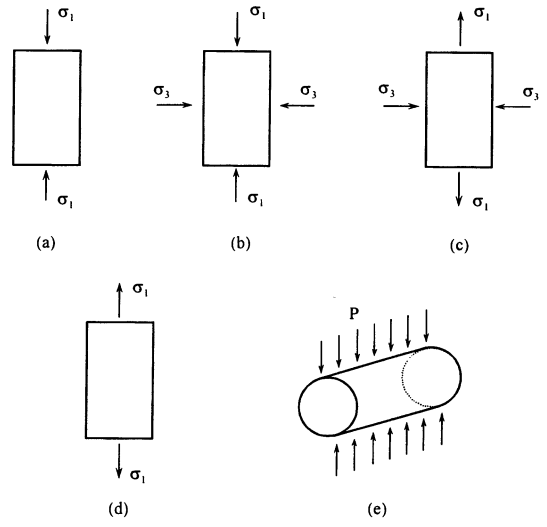


FIGURE 6.6. Common laboratory tests for obtaining strength and deformation parameters for rocks: (a) uniaxial compression; (b) triaxial compression; (c) triaxial extension; (d) direct tension; and (e) indirect tension (Brazilian).

6.3.1 UNIAXIAL COMPRESSION TEST

In the uniaxial compression test, a cylindrical specimen of rock is loaded axially to failure at a constant rate (Fig. 6.6a). The axial and lateral strains are monitored by strain gages. The results of the test provide the values of uniaxial strength, elastic modulus and Poisson's ratio. An example of test results is shown in Fig. 6.7a. Detail test procedure is given by ISRM (1979d) and ASTM (D2938-86) for isotropic rocks. For sedimentary rocks, the method described in Lo & Hori (1979) may be used for obtaining the anisotropic deformation parameters as described in the following section.

6.3.2 DEFORMATION PARAMETERS FOR CROSS-ANISOTROPIC ROCKS

6.3.2.1 Stress–Strain Relationships In Cross-Anisotropic Rocks

Rock of sedimentary origin may often exhibit cross-anisotropic behavior, with the mechanical behavior being isotropic along bedding planes but anisotropic in orthogonal planes. The stress–strain relationships of a cross-anisotropic rock unit can be described by the following equations (Hearmon 1961), taking the z-axis as the vertical direction (normal to bedding) and the x- and y-axes in horizontal directions:

$$\varepsilon_z = \frac{\sigma_z}{E_v} - \nu_{hv}\frac{\sigma_x}{E_h} - \nu_{hv}\frac{\sigma_y}{E_h} \qquad (6.1)$$

$$\varepsilon_x = \frac{\sigma_x}{E_h} - \nu_h\frac{\sigma_y}{E_h} - \nu_{vh}\frac{\sigma_z}{E_v} \qquad (6.2)$$

$$\varepsilon_y = \frac{\sigma_y}{E_h} - \nu_{hv}\frac{\sigma_z}{E_v} - \nu_h\frac{\sigma_x}{E_h} \qquad (6.3)$$

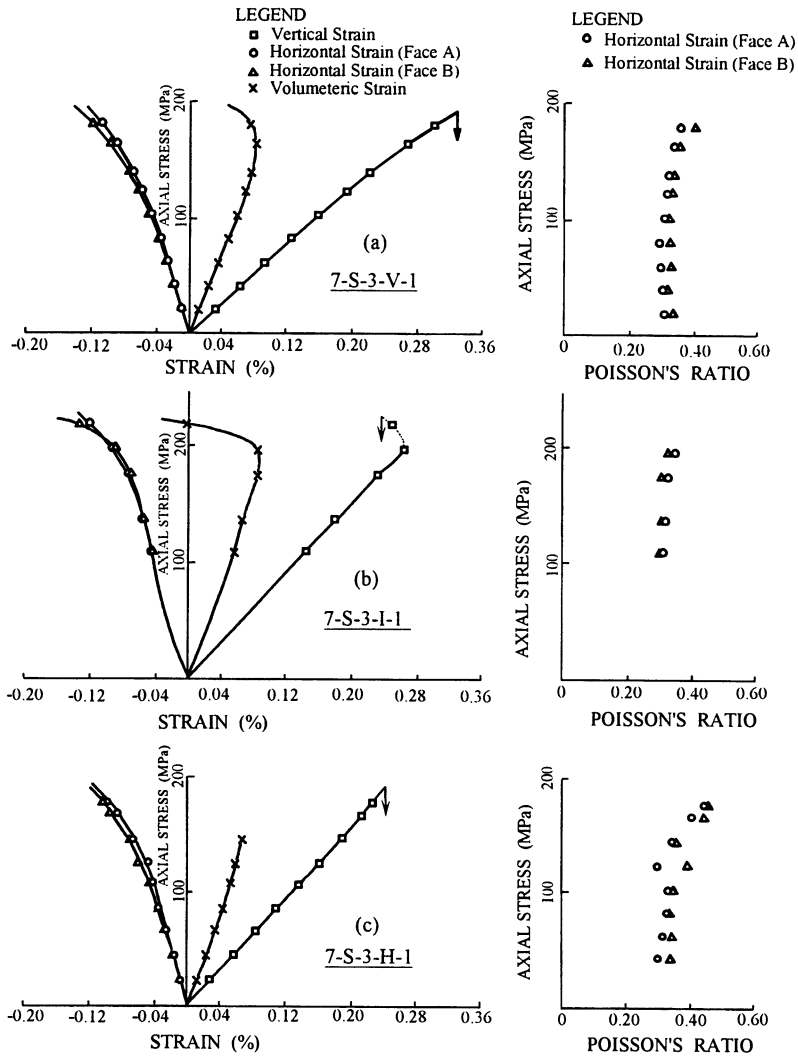


FIGURE 6.7. Stress–strain relationships and Poisson's ratio for limestone, Gasport Member of Lockport Formation: (a) vertical; (b) 45°; and (c) horizontal samples in test to failure of uniaxial compression tests. □, vertical strain; ○, horizontal strain–face A; △, horizontal strain–Face B; ×, volumetric strain.

$$\gamma_{zx} = \tau_{zx}/G_{vh} \tag{6.4}$$

$$\gamma_{yz} = \tau_{yz}/G_{vh} \tag{6.5}$$

$$\gamma_{xy} = \frac{\tau_{xy}}{G_h} = \frac{2(1 + \nu_h)}{E_h}\tau_{xy} \tag{6.6}$$

where E_v = elastic modulus in vertical direction, E_h = elastic modulus in horizontal direction, ν_{vh} = Poisson's ratio for effect of vertical stress on horizontal strain, ν_{hv} = Poisson's ratio for effect of horizontal stress on vertical strain, ν_h = Poisson's ratio for effect of horizontal stress on horizontal strain, and G_{vh} = independent shear modulus. From strain energy consideration, it may be shown that:

$$\nu_{hv}/E_h = \nu_{vh}/E_v. \tag{6.7}$$

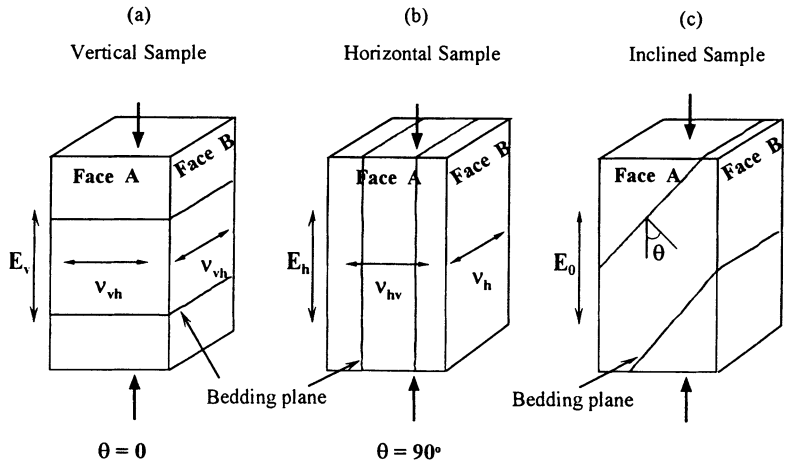


FIGURE 6.8. Scheme of uniaxial compression tests for determining anisotropic elastic parameters. (a) vertical sample; (b) horizontal sample; and (c) inclined sample.

The cross-anisotropic system is therefore completely described by five independent elastic parameters: E_v, E_h, ν_{vh}, ν_h and G_{vh}.

6.3.2.2 Evaluation Of Parameters

The five independent parameters can be obtained by performing uniaxial compression tests on oriented samples (at least three orientations, $\theta = 0$, 45 and 90°, where θ denotes the angle between the direction of the axial stress and the normal to the bedding plane, Fig. 6.8). Table 6.8 summarizes the equations required to calculate the parameters from the measured quantities in each test.

It should be noted that the redundancy of the five equations in Table 6.8 for four independent parameters E_v, E_h, ν_{hv} and ν_h enables the validity of Eq. 6.7 to be checked. For rocks to be isotropic, the necessary and sufficient conditions to be met are $E_v = E_h$ and $1/G_{vh} = 2(1 + \nu_h)/E_h$.

6.3.2.3 Results Of Uniaxial Compression Test

Based on the study carried out by Lo & Hori (1979) on sedimentary rocks from Southern Ontario, typical anisotropic elastic parameters obtained for strong rocks of the Lockport Formation and Trenton Formation and for weak rocks (Collingwood Shale and Georgian Bay Shale) are shown in Table 6.9. Typical results of a uniaxial compression test on a specimen of limestone (Lockport Formation) are given in Fig. 6.7.

It can be seen from Table 6.9 that the shaly limestone of the Lockport Formation exhibits distinct anisotropy. The ratio of E_h/E_v is 1.7. The limestone of the Trenton Formation appears to be isotropic.

For the Collingwood Shale, both individual layers of black and gray shales are significantly anisotropic. The ratio of E_h/E_v is 1.8 for the black shale layers and 2.4 for the grey shale layers. The shear modulus, G_{vh}, is substantially lower than G_h, the shear modulus co-planar with the bedding plane of the black shale. The Georgian Bay Shale is markedly anisotropic; the ratio of E_h/E_v is 2.2 and the value of the shear modulus, G_{vh}, is very low.

6.3.3 TENSILE STRENGTH TESTS

6.3.3.1 Brazilian Test (Indirect Tension Test)

The test procedure is given in Mellor & Hawkes (1971) and ISRM (1978b). This test is intended to measure indirectly the tensile

TABLE 6.8. Summary of method of obtaining the five independent parameters in anisotropic rocks

Orientation of sample	Parameter obtained	Measured quantity in test	Equation to obtain parameters from measured quantities
Vertical, $\theta = 0$	E_v	σ_z, ε_x, ε_y, ε_z	$E_v = \sigma_z/\varepsilon_z$
	ν_{vh}		$\varepsilon_x = \varepsilon_y = -\nu_{vh}\sigma_z/E_v$
Horizontal, $\theta = 90°$	E_h	σ_x, ε_x, ε_y, ε_z	$E_h = \sigma_x/\varepsilon_x$
	ν_{hv}		$\varepsilon_z = -\nu_{hv}\sigma_x/E_h$
	ν_h		$\varepsilon_y = -\nu_h\sigma_x/E_h$
θ	G_{vh}	σ_θ, ε_θ	$\frac{1}{E_\theta} = \frac{\varepsilon_\theta}{\sigma_\theta} = \frac{1}{E_v}\cos^4\theta + \frac{1}{E_h}\sin^4\theta + \left[\frac{1}{G_{vh}} - \left(\frac{\nu_{hv}}{E_h} + \frac{\nu_{vh}}{E_v}\right)\right]\sin^2\theta\cos^2\theta$[a]

[a] From Jaeger and Cook (1969).

TABLE 6.9. Typical results of anisotropic elastic parameters for strong and weak rocks

Rock material	E_v (10^7 kPa)	E_h (10^7 kPa)	ν_{vh}	ν_{hv}	ν_h	G_h (10^7 kPa)	G_{vh} (10^7 kPa)	E_h/E_v
Lockport Formation								
Shaly limestone	2.67	4.50	0.16	0.25	0.23	1.83	1.48	1.7
Trenton Formation								
Limestone	5.5	5.5	0.35	0.40	0.24	2.0	1.6	1.0
Collingwood Shale								
Black shale	2.04	3.73	0.18	0.33[a]	0.12	1.7	0.6	1.8
Gray shale	0.98	2.32	0.20	0.47[a]	0.12	1.0	—	2.4
Georgian Bay Shale								
Shale	0.55	1.21	0.13	0.29[a]	0.25	0.48	0.07	2.2

[a] Calculated from energy equation.

strength of rock specimens. In this test (Fig. 6.6e), a cylindrical specimen of rock is loaded diametrically between platens in a compression machine. At failure, the sample will split along the loaded diameter and parallel to its axis. The tensile strength of the specimen, σ_t, is calculated using the following formula:

$$\sigma_t = \frac{2P}{\pi Dl} \tag{6.8}$$

where P = the load at failure, D = the diameter, and l = the length of the test specimen.

By performing this test on re-cored specimens with different orientations, the tensile strength anisotropy may be investigated.

6.3.3.2 Direct Tension Test

The test procedure is given by ISRM (1978c), the ASTM (D2936-84), and Lo *et al.* (1991b). In this test (Fig. 6.6d), a specimen of rock is subjected to a direct uniaxial tensile stress until failure. The tensile strength of rock is the maximum tensile stress carried by the specimen.

While the Brazilian test is simple to perform, it is realized that the failure occurs in a biaxial state of stress where one principal stress is highly compressive. The measured "indirect tensile strength" is usually significantly higher than the strength measured by the direct tension test. Therefore, it is recommended for field cases where the mode of failure is likely to be purely tensile that the direct tensile strength be measured and used in design (Lo *et al.* 1991b).

6.3.4 TRIAXIAL COMPRESSION TEST

The recommended test procedure is described by the ISRM (1978d), the ASTM (D2664-86), and Lo *et al.* (1991b). In this test (Fig. 6.6b), the cylindrical specimen is subjected to a confining pressure, σ_3, then the axial stress is increased until failure. The state of stress at failure represents a point on the strength envelope. By performing a series of tests under different confining pressures appropriate to the field stress range, the strength envelope may be established.

6.3.5 TRIAXIAL EXTENSION TEST

This test (Fig. 6.6c), together with the direct tension test, is used to obtain the envelope in the tensile stress region. In this test, the cylindrical specimen is subjected to a lateral stress and then a tensile axial stress is applied until failure. The test procedure is given in Lo *et al.* (1991b).

The use of tests described in the preceding sections is illustrated for a number of design problems in Chapter 11.

6.4 Time-Dependent Deformation

Swelling rocks cause major problems in the design and construction of underground struc-

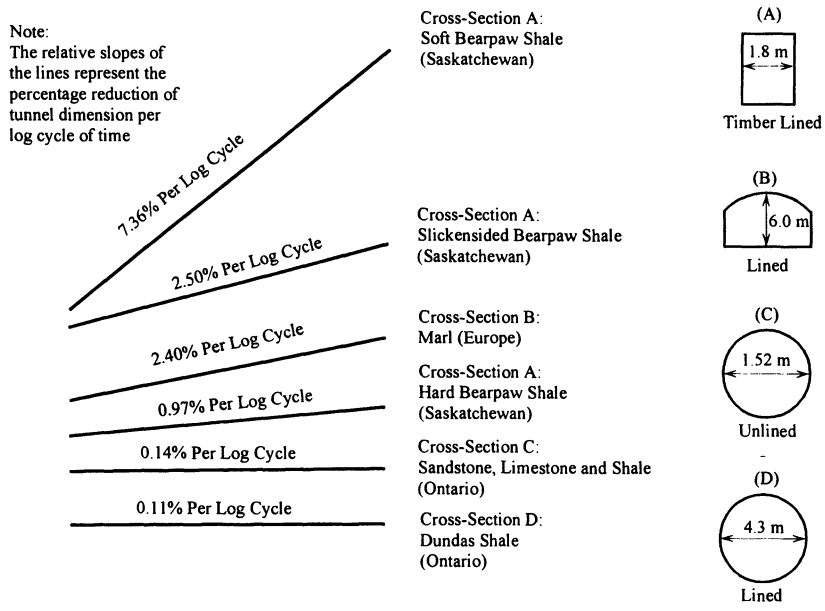


FIGURE 6.9. Comparison of rates of deformation of various tunnels in swelling rocks (modified from PFRA 1951; Einstein *et al.* 1972; Lo *et al.* 1978). (Note: The relative slopes of the lines represent the percentage reduction of tunnel dimension per log cycle of time.)

tures. Time-dependent deformations, in the form of invert heave and lateral inward deflection, have been observed in tunnels in different parts of the world resulting, in many cases, in costly remedial and maintenance work. The results of field observation of several tunnels are summarized and illustrated in Fig. 6.9 and the type of short- and long-term problems involved are summarized in Table 6.10.

The swelling behavior of rocks is highly dependent on boundary conditions, loading conditions, and stress history. Therefore, tests that do not provide a precise definition of these conditions are not amenable to interpretation and hence not suitable for obtaining design parameters. Two simple tests for determining the time-dependent deformation behavior of rocks, where boundary and constraint conditions are well defined, are described below.

TABLE 6.10. Effect of high horizontal stresses and time-dependent deformation

Type of structure	Short term (during construction)	Long term
Open excavation	Heave and buckling of floor Movement along bedding planes	Heave and buckling of floor Long-term deformation in unsupported excavation Stress increases in support system leading to distress
Tunnels	Movement along bedding planes at or near springline Local "failure" at crown and invert in soft rock Invert heave	Displacements (inward) increase with time in unlined tunnels Stress increases in lining leading to distress

6.4.1 FREE SWELL TEST

In a free swell test (Lo *et al.* 1978) a cylindrical specimen is cut from the rock core. Three pairs of gages are mounted onto the specimen in the vertical (normal to bedding) and two orthogonal (parallel to bedding) directions. The specimen is stored in a temperature-controlled room with 100% humidity or immersed in the ambient fluid expected in the field. The unrestrained deformations in the three directions are monitored with time. Typically, the relationship between swelling strain and logarithm of time between ten and 100 days is approximately linear both in the vertical and horizontal directions. The slope in this interval for each direction is defined as the swelling potential. The swelling potential of some shales and shaly limestones measured in different tunneling projects are summarized in Table 6.11. It should also be noted that swelling behavior in the horizontal direction, i.e. along the bedding planes of shales, is isotropic for all the rocks tested. The vertical and horizontal swelling potentials serve as a useful index to assess the degree of severity of swelling and to delineate regions of high swelling along the length of a tunnel.

The calcite content of the specimen in free swell tests on shales is often determined. The test can be performed in a Chittick apparatus (Dreimanis 1962) by measuring the volume of CO_2 resulting from the reaction between carbonates in the sample and 6*N* hydrochloric acid. The relationship between vertical

TABLE 6.11. Swelling potential of various types of rocks from free swell test

Rock type			Rate of deformation (% strain per log cycle of time) Horizontal	Vertical
Silurian	Lockport	Gasport Dolomitic Limestone	0.02 (8)	0.01 (2)
		Gasport Shaly Limestone	0.08 (3)	0.08 (3)
	Rochester Shale (Niagara)		0.07 (4)	0.16 (2)
	Cabot Head Shale (Hamilton–Wennorth)		0.30 (6)	1.10 (3)
Ordovician	Queenston Shale (Oakville)		0.04 (9)	0.14 (3)
		(Niagara)	0.25 (42)	0.37 (32)
	Georgian Bay	Shaly limestone (West of Toronto) Etobicoke Creek	0.05 (6)	0.22 (3)
		Shale with 7% calcite (Downtown Toronto) CN Tower	0.03 (10)	0.20 (5)
		Shale with 1% calcite (Downtown Toronto) CN Tower	0.14 (2)	—
		Skydome & Scotia Plaza	0.15–0.20	0.25–0.30
	Collingwood	Gray mudstone–Duffin Creek	0.15 (10)	0.45 (5)
		Black shale–Duffin Creek	0.00 (3)	0.00 (2)
	Trenton–Black River	Shaly limestone–Wesleyville	0.06 (8)	0.09 (4)
		Limestone–Wesleyville	0.00 (2)	0.00 (1)

and horizontal swelling potential and calcite content is illustrated in Fig. 6.10. The lines drawn are envelopes of the available data. It may be seen that as the calcite content increases the swelling potential generally decreases. The reason for this phenomenon is that the calcite acts as a cementing agent to reduce swelling. This index test may be used as a first indication of the problem of swelling.

6.4.2 SEMI-CONFINED SWELL TEST

The semi-confined swell test was developed (Lo *et al.* 1978; modified by Lo & Lee 1990) to study the stress dependency of the time-dependent deformation of swelling rocks. In this test, a vertical load is applied on a specimen submerged in a representative ambient fluid in a temperature-controlled room. The load is applied perpendicular and parallel to the bedding planes to investigate the swelling under load in different directions. The swelling strain in the loading direction is monitored by a dial gage, and the lateral strains in two orthogonal horizontal directions are monitored by strain gages mounted on cantilever beams.

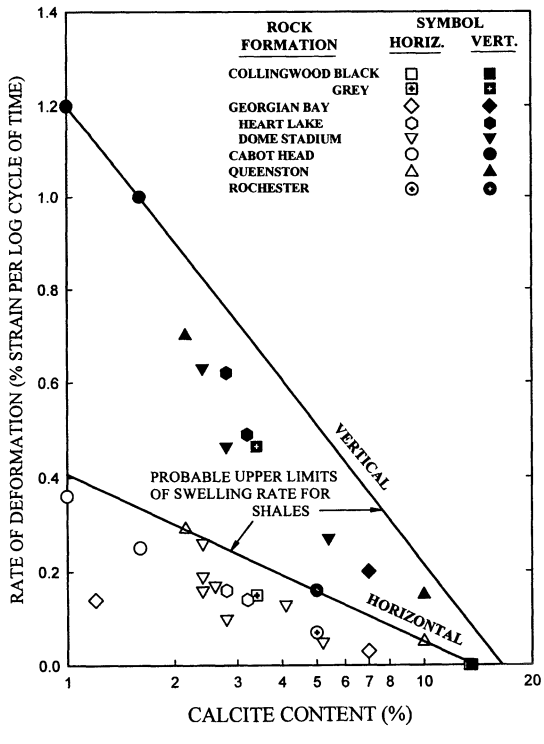


FIGURE 6.10. Relationship between swelling potential and calcite content.

The results of a series of semi-confined swell tests on Georgian Bay Shale shown in Fig. 6.11 were used for the design of tunnels and shafts beneath and in the vicinity of the Sky Dome in Toronto (Lo *et al.* 1987a). It may be seen that as the stress increases, the swelling potential decreases. Results of free swell and semi-confined tests have been employed for the design of underground structures since the early 1980s, including tunnels in shaly limestones for cold water intake and discharge for the Darlington nuclear station (Lo & Lukajic 1984).

Experience gained from testing on several rock formations showed that, in general, the stress–swelling rate relationship is non-linear. The relationship is linear in semi-log scale for Queenston Shale (Fig. 6.12). The intersection of the stress–swelling potential line with the horizontal axis gives the critical "suppression" pressure, under which no time-dependent deformation occurs. Further discussion of the stress–strain–time relationship may be found in Hefny *et al.* (1996) and Lo & Hefny (1996).

Other complementary methods for complete description of swelling behavior of rocks and concrete expansion under alkali–aggregate reaction are described elsewhere (Lo *et al.* 1997).

Based on the results of the swell tests described, analytical solutions for the stresses and displacements in the lining of tunnels driven in rocks possessing time-dependent deformation behavior have been developed by Lo & Yuen (1981). The solutions were given as explicit functions of time and took into account: (a) the complete state of initial

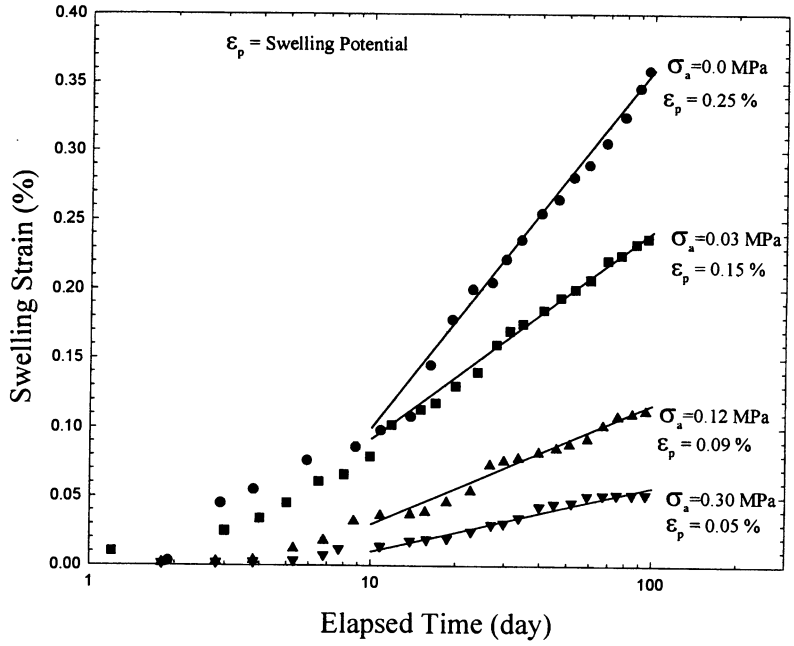


FIGURE 6.11. Typical results of a series of semi-confined swell tests on Georgian Bay Shale where ε_p = swelling potential.

stress; (b) the time-dependent deformation parameters of the lining as well as the rock, obtained from results of free and semi-confined swell tests; and (c) the time lapsed between excavation and lining installation. This method of design has been successfully used for the design of underground structures cited in the preceding paragraph.

For shales that exhibit long-term swelling behavior, a more detailed model to account for the non-linear relationship between stress and swelling strain rate was developed (Hefny *et al.* 1996). Explicit solutions for stresses and displacements in the lining and rock using this model were presented in Lo & Hefny (1996).

ISRM (1989) described several other methods for testing of swelling rocks.

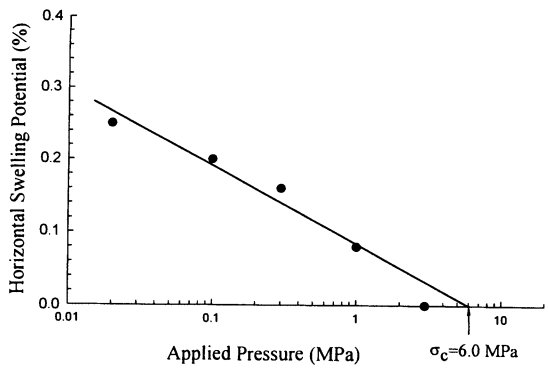


FIGURE 6.12. Effect of applied pressure on horizontal swelling potential of Queenston Shale (1990 investigation, Borehole NF4A, ambient fluid, distilled water).

6.5 *Failure Criteria of a Brittle Material*

A failure criterion of a brittle material defines the state of stress at which rupture of a specimen occurs. Two commonly used criteria, the Griffith criterion and the Hoek–Brown criterion, are described below.

6.5.1 GRIFFITH CRITERION

The Griffith theory of fracture (1924) was originally developed to explain why the mechanical tensile strength measured in tests on a brittle material such as glass is much less than the theoretical molecular bond strength of the material. Griffith postulated the existence of microcracks (or flaws) randomly distributed within a material that may appear to be intact. Using the Inglis solution (1913) for stress distribution around an elliptical crack, Griffith showed that, under uniaxial tension, the criterion of crack propagation is:

$$\sigma_1 = \sqrt{\frac{\Omega E}{\pi c}} \tag{6.9}$$

where Ω = the energy released per unit crack surface area, E = the modulus of elasticity, and c = half the crack length.

Under compressive stresses, the Griffith criterion in principal stress (σ_1, σ_3) space is

$$(\sigma_1 - \sigma_3)^2 - 8\sigma_t(\sigma_1 + \sigma_3) = 0 \quad \text{if } \sigma_1 + 3\sigma_3 \geq 0 \tag{6.10}$$

$$\sigma_t = -\sigma_3 \quad \text{if } \sigma_1 + 3\sigma_3 < 0 \tag{6.11}$$

where σ_t is the tensile strength. The criterion in shear and normal stress (τ, σ_n) space is

$$\tau^2 + 4\sigma_t\sigma_n = 4\sigma_t^2. \tag{6.12}$$

The theoretical requirements of Griffith criterion in (σ_1, σ_3) and (τ, σ_n) spaces are illustrated in Fig. 6.13a and b, respectively. For $\sigma_3 = 0$, the ratio of the uniaxial compressive strength ($\sigma_1 = \sigma_c$) to the tensile strength is eight. In practice, this ratio is not constant and may vary from six to 12 for some rocks. It can be shown that for $\sigma_n = 0$, the ratio of cohesion (c) to tensile strength is two. The ratio of cohesion to tensile strength for clays ranges between two to three (Lo & Morin 1972) and for concrete–rock contact in concrete dams is approximately two (Lo *et al.* 1991b).

Although it is often referred to as a failure criterion, the Griffith criterion is, in effect, a criterion for the state of stress required for crack propagation in brittle materials and not related to the failure (rupture) condition. Since the points of crack propagation and rupture for the uniaxial tensile field are very close, it is expected that this theory is applicable to field problems in which the stress range is tensile or involves only low compressive stresses.

6.5.2 HOEK–BROWN FAILURE CRITERION

The Hoek–Brown failure criterion (1980) is an empirical criterion originally developed for applications in underground excavation

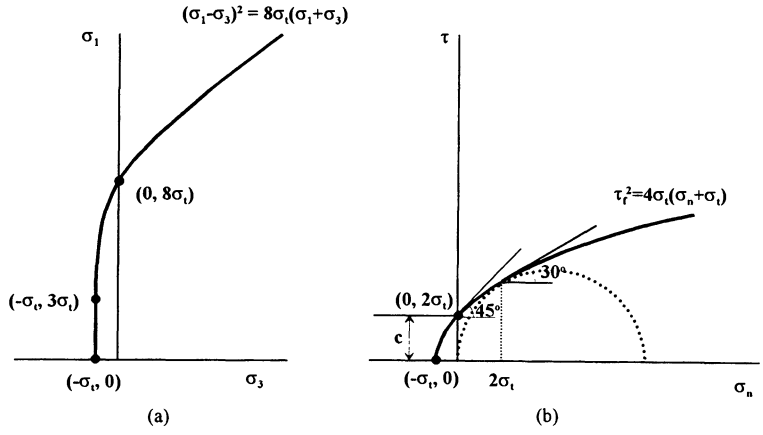


FIGURE 6.13. Griffith failure criterion in (a) (σ_1, σ_3) space, and (b) (σ_n, τ) space.

design. This criterion was updated in 1988 (Hoek & Brown 1988) and modified in 1992 (Hoek *et al.* 1992). The following form incorporates both the original and modified versions of the criterion (Hoek *et al.* 1995).

$$\sigma_1 = \sigma_3 + \sigma_c\left(m_b\frac{\sigma_3}{\sigma_c} + s\right)^a \qquad (6.13)$$

where m_b, s and a = parameters that depend upon the characteristics of the rock mass; σ_c = the uniaxial compressive strength of the intact rock material; and σ_1 and σ_3 = the "axial" and "confining" principal stresses, respectively.

For most rocks of good to reasonable quality in which the rock mass strength is controlled by tightly interlocking angular rock pieces, the value of the parameter a is equal to 0.5 and Eq. 6.19 takes the form of the original criterion:

TABLE 6.12. Estimation of constants m_b/m_i, s, and a for the generalized Hoek–Brown failure criterion based upon rock mass structure and discontinuity surface conditions. Note that the values given in this table are for an undisturbed rock mass (adapted from Hoek *et al.* 1995)

Generalized Hoek–Brown criterion

$$\sigma_1 = \sigma_3 + \sigma_c\left(m_b\frac{\sigma_3}{\sigma_c} + s\right)^a$$

σ_1 = major principal effective stress at failure
σ_3 = minor principal effective stress at failure
σ_c = uniaxial compressive strength of intact pieces of rock
m_b, s and a are constants that depend on the composition, structure and surface conditions of the rock mass[a]

Structure		Surface condition	Very good: very rough, unweathered surfaces	Good: rough, slightly weathered, iron-stained surfaces	Fair: smooth, moderately weathered or altered	Poor: Slickensided, highly weathered surfaces with compact coatings or fillings containing angular rock fragments	Very poor: slickensided, highly weathered surfaces with soft clay coatings or fillings
	Blocky: very well interlocked undisturbed rock mass consisting of cubical blocks formed by three orthogonal discontinuity sets	m_b/m_i	0.6	0.4	0.26	0.16	0.08
		s	0.190	0.062	0.015	0.003	0.0004
		a	0.5	0.5	0.5	0.5	0.5
	Very blocky: interlocked, partially disturbed rock mass with multifaceted angular blocks formed by four or more discontinuity sets	m_b/m_i	0.4	0.29	0.16	0.11	0.07
		s	0.062	0.021	0.003	0.001	0
		a	0.5	0.5	0.5	0.5	0.53
	Blocky/seamy: folded and faulted with many intersecting discontinuities forming angular blocks	m_b/m_i	0.24	0.17	0.12	0.08	0.06
		s	0.012	0.004	0.001	0	0
		a	0.5	0.5	0.5	0.5	0.55
	Crushed: poorly interlocked, heavily broken rock mass with a mixture of angular and rounded blocks	m_b/m_i	0.17	0.12	0.08	0.06	0.04
		s	0.004	0.001	0	0	0
		a	0.5	0.5	0.5	0.55	0.6

[a] m_i is the parameter m_b for intact rock.

$$\sigma_1 = \sigma_3 + (m_b \sigma_c \sigma_3 + s\sigma_c^2)^{1/2}. \quad (6.14)$$

For intact rock, the parameter s is equal to unity and it decreases rapidly to very small values for fractured rock masses. For poor quality rock masses, $s = 0$ and Eq. 6.13 becomes:

$$\sigma_1 = \sigma_3 + \sigma_c \left(m_b \frac{\sigma_3}{\sigma_c} \right)^a. \quad (6.15)$$

Typical values of m_b, s and a, which appear in Eqs 6.13–6.15, are shown in Table 6.12. Hoek *et al.* (1995) introduced relationships between these material parameters and an index called the geological strength index (GSI). Methods for estimating the value of GSI for a given rock mass are given in Hoek *et al.* (1995).

Figure 6.14 shows a schematic representation of the Hoek–Brown failure criterion.

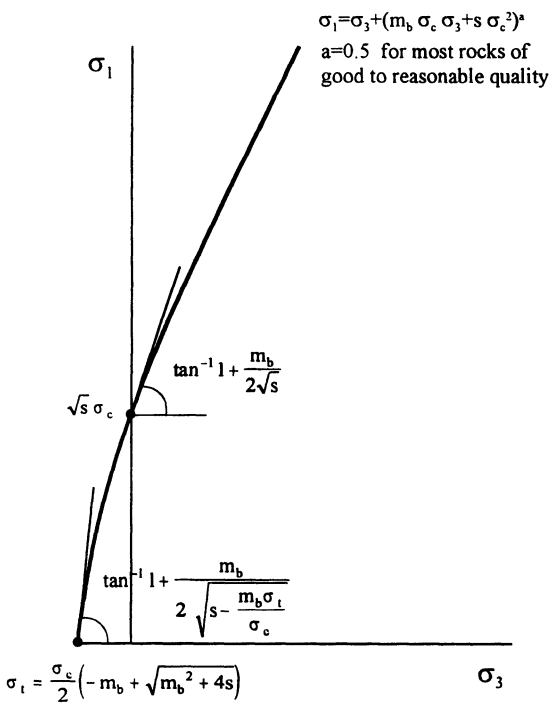


FIGURE 6.14. Hoek–Brown failure criterion.

6.6 *Shear Strength of Discontinuities*

Discontinuities are planes of weakness that dissect the rock medium causing the rock mass to be weaker, more deformable, and more permeable than intact rock. It is a collective term, including joints, bedding planes, schistocity planes, faults and other features of weakness.

Determination of shear strength parameters of rock joints and contact surface between concrete and rock foundations are of crucial importance for stability analysis of rock slopes and underground excavations as well as concrete dams on rock foundations.

6.6.1 DESCRIPTION AND MEASUREMENT OF DISCONTINUITIES

The parameters that should be measured to describe discontinuities such as rock joints are:

- number of joint sets
- orientation of joint sets–strike and dip
- spacing of joints
- continuity of joint
- roughness of joint
- degree of joint surface weathering
- properties of filling (gouge) material.

6.6.2 DETERMINATION OF BASIC FRICTION ANGLE

The shear strength of rock joints, whether in the field or in the laboratory, consists of two components. The major component is the basic friction angle, ϕ_b, which corresponds to the sliding on a smooth horizontal plane between two blocks in contact. The second component (i-effect) is the interlocking effect of the asperities, the importance of this component being dependent on the geometry and strength of the asperities and the normal stress applied. If the plane of shear is not coplanar with the joint or contact plane, an additional component (β-effect) will also

play a role in the shearing resistance (Fig. 6.15).

The objective in the laboratory test program is to obtain the basic friction angle by accounting for the i-effect and β-effect of each test. With ϕ_b deduced, the i-effect operative in the field may be incorporated to obtain the shear strength in the field. This procedure is necessary since the shear behavior in the laboratory-scale tests is influenced by asperities measured in millimeters, while in the field the shear behavior is affected by roughness angle, i, which may be measured in the order of meters.

The measured quantities in simple shear tests are (Fig. 6.15): N = constant force in the vertical direction; T = horizontal force in the direction of applied shear; δ_h = relative horizontal displacement between the upper and lower half of the specimen; and δ_v = relative vertical displacement, positive for dilatancy. The expression for the basic friction angle, ϕ_b, taking into account the i-effect and β-effect is (Lo *et al.* 1991b):

$$\phi_b = \phi_{obs} - i_{obs} \tag{6.16}$$

where ϕ_{obs} = the angle without correction, which is simply calculated from the observed normal ($\sigma_n = N/A$) and shear stresses ($\tau = T/A$), where A is the cross-sectional area of the specimen:

$$\phi_{obs} = \tan^{-1}(\tau/\sigma_n). \tag{6.17}$$

i_{obs} = the angle calculated from the measurement of the displacements in the shear test by using the relation:

$$i_{obs} = \tan^{-1}(\delta_v/\delta_h). \tag{6.18}$$

Equation 6.16 suggests that the angle β does not appear explicitly and that the basic friction angle can be calculated directly from the measurements of the shear test no matter how the joint inclines from the direction of shearing.

In Fig. 6.15b and c, two possible cases are considered concerning the observed vertical movement. When the roughness angle, i, is greater than the average angle of inclination of the joint β, i_{obs} is positive; i.e. an upward movement would be observed in the shear test (apparent positive dilatancy). On the contrary, when the angle i is smaller than β, then i_{obs} is negative and a downward movement would therefore be observed (apparent negative dilatancy).

Lo *et al.* (1991b) showed that $i_{obs} = i - \beta$, and therefore an independent check for i_{obs} and $(i - \beta)$ is possible from the horizontal–vertical displacement curve obtained by the shear test and from the direct measurement of roughness of the joint.

Details of measuring the roughness of the joint surface and of using the simple shear test for measuring the basic friction angle are described in Lo *et al.* (1991b).

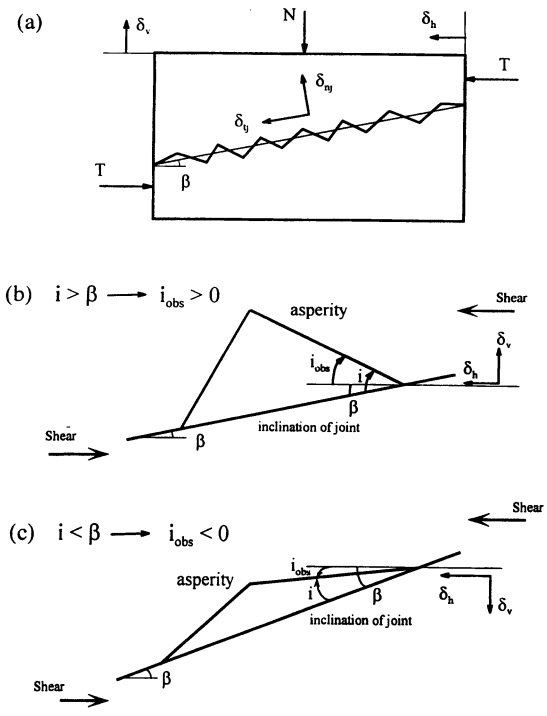


FIGURE 6.15. Illustration of i- and β-effects in shear tests.

6.6.3 TYPICAL RESULTS OF TESTS ON ROCK JOINTS

To illustrate the magnitude of the joint roughness parameters, Table 6.13 summarizes the calculation of the basic friction angle of the rock from the results of simple shear tests on a relatively smooth joint and a rough joint of calcareous shale in the Lindsay Formation at the Darlington nuclear generating station site. A method of checking the internal consistency of test results is given in Lo *et al.* (1991b). More details for the application of the results to field problems are given in Chapter 11.

A different approach for determining the shear strength of rock joints was given in Barton (1973 and 1976), Barton & Choubey (1977), and Barton & Bandis (1990).

6.7 *Measurements of* In Situ *Horizontal Stresses in Rock*

For the design of underground structures in rocks for various purposes, the magnitudes and directions of initial stresses in the rock mass must be known. Two methods of stress measurements that are often used in North America are the overcoring method using the United States Bureau of Mines (USBM) deformation gage and the hydraulic fracturing method. Other methods of stress measurements such as the Leeman technique (Leeman 1968), the solid inclusion stress gage (Rocha & Silverio 1969) and the hollow inclusion triaxial stress gage (Worotnicki & Walton 1976) are also available. This section describes briefly the USBM overcoring method and the hydraulic fracturing method as well as the procedure of stress calculation.

6.7.1 THE UNITED STATES BUREAU OF MINES (USBM) METHOD

The design of the USBM gage permits the calculation of the stresses in a plane perpendicular to the axis of the test borehole. Details of the instrument and the techniques of measurement have been described by Hooker & Bickel (1974). A modification of the technique of measurement has been developed for vertical downhole measurements (Palmer & Lo 1976; Lo *et al.* 1979a, b). A schematic procedure of measurements is shown in Fig. 6.16. After drilling the test borehole (150 or 94 mm in diameter) to the desired depth, a 38-mm pilot hole is drilled at the bottom of and concentric with the test hole. After the gage is firmly installed in the pilot hole, the overcoring process is started. Continuous readings for the change in deformation across three diameters at 60° apart are monitored during the overcoring process. The deformation modulus of rock at the test depth is measured by performing a biaxial test on the recovered overcore using the same USBM gage used in the field. The modulus can be calculated using the thick-wall cylinder formula.

TABLE 6.13. Results of simple shear test on rock joints

	J-2 (smooth)[a]			J-6 (rough)[b]		
Joint material	Fossiliferous calcareous shale			Calcareous shale		
σ_n, kN m^{-2}	345	690	1380	345	690	1380
τ_{max}, kN m^{-2}	172	338	622	301	510	889
δ_{hf}, mm	0.25	1.3	1.3	1.0	0.6	1.04
ϕ_{obs}, deg	26.5	26.1	25.6	41.1	36.5	32.8
i_{obs}, deg	−1.7	−2.4	−3.0	9.9	2.6	0
ϕ_b, deg	28.2	28.5	28.6	31.2	33.9	32.8
Average ϕ_b		28			33	

[a] For joint J-2: $\beta = 3.1°$; $i = 2.4°$ before test; $i = 0.2°$ after test.
[b] For joint J-6: $\beta = 4°$; $i = 9.1°$ before test; $i = 6.3°$ after test.

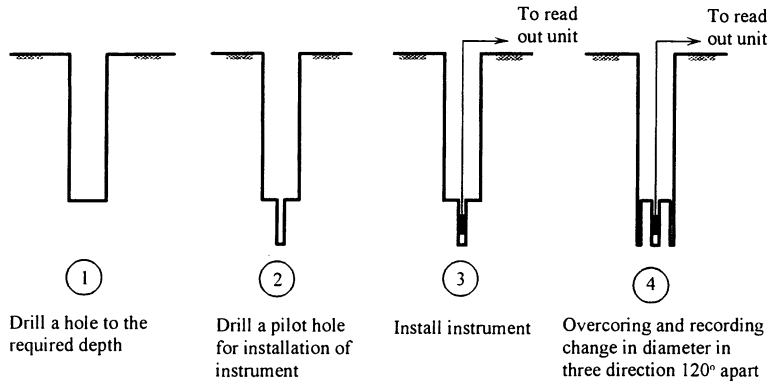


FIGURE 6.16. Schematic procedure of USBM overcoring measurements.

Since the stresses are determined in only one plane, measurements in three orthogonal boreholes are required to determine the complete state of stresses in three dimensions. In rocks of sedimentary origin where the planes of beddings are nearly horizontal, the horizontal plane is likely to be one of the principal planes and the overburden stress is one of the principal stresses. Under such conditions, the complete state of stress in the rock may be determined in a single vertical borehole. Examples of such stratigraphy may be found in Southern Ontario and the results of measurements have been reported by Palmer and Lo (1976) and Lo *et al.* (1979a, b) and applied to design of underground structures (Lo & Lukajic 1984; Lo *et al.* 1984; Lo 1986; and Trow & Lo 1989). For convenience the procedure of initial stress calculations is outlined in Table 6.14.

TABLE 6.14. Calculation of secondary principal stresses from overcoring test data[a]

Major principal stress (P)	$P = \frac{E}{6d(1-\nu^2)}\left\{U_1 + U_2 + U_3 + \frac{1}{2^{1/2}}[(U_1-U_2)^2 + (U_2-U_3)^2 + (U_3-U_1)^2]^{1/2}\right\}$
Minor principal stress (Q)	$Q = \frac{E}{6d(1-\nu^2)}\left\{U_1 + U_2 + U_3 - \frac{1}{2^{1/2}}[(U_1-U_2)^2 + (U_2-U_3)^2 + (U_3-U_1)^2]^{1/2}\right\}$
Angle from diameter U_1 to P, i.e. θ (counterclockwise)	$\theta = \frac{1}{2}\tan^{-1}\left[\frac{3^{1/2}(U_2-U_3)}{2U_1-U_2-U_3}\right]$
Quadrant of θ	if $U_2 > U_3$ and $U_2 + U_3 < 2U_1$ then θ is between 0 and 45° if $U_2 > U_3$ and $U_2 + U_3 > 2U_1$ then θ is between 45 and 90° if $U_2 < U_3$ and $U_2 + U_3 > 2U_1$ then θ is between 90 and 135° if $U_2 < U_3$ and $U_2 + U_3 < 2U_1$ then θ is between 135 and 180°

[a] E = average deformation modulus; ν = Poisson's ratio; d = diameter of the pilot hole; U_1, U_2, U_3 = measured changes in borehole diameter across three diameters at 60° rotation; and U is positive for an increasing diameter.

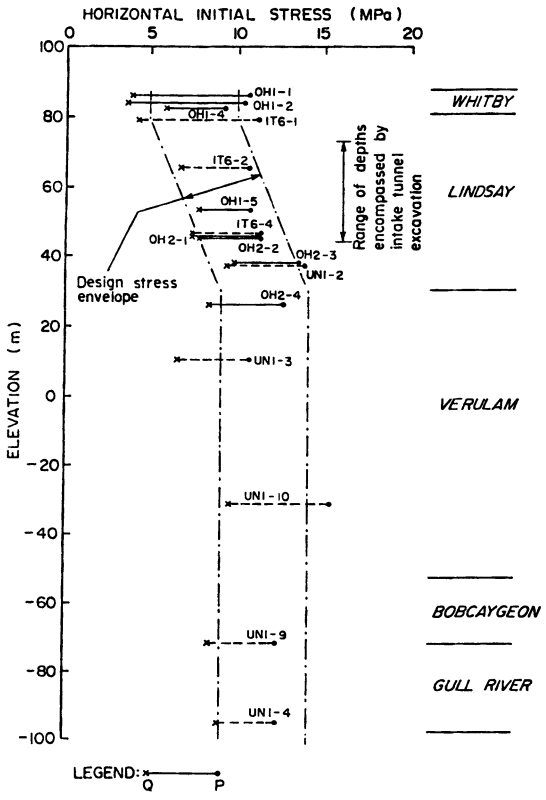


FIGURE 6.17. Initial stresses in the horizontal plane measured at the Darlington generating station site.

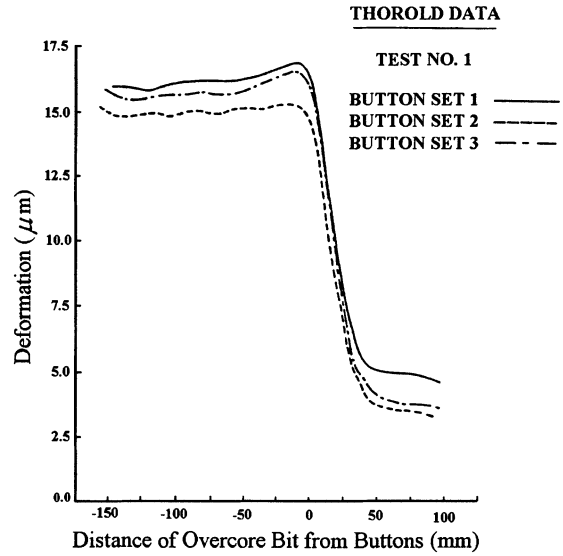


FIGURE 6.18. Typical field data for an overcoring test in dolomite (Goat Island Member, Thorold, Ontario) using the USBM deformation gage, for button sets 1 (——), 2 (– – –) and 3 (– ——–).

Figure 6.17 shows typical results of initial stress measured using the USBM deformation gage (data marked as OH and IT) for the design of the facilities for the Darlington generating station. The design envelopes for the major (P) and minor (Q) principal horizontal stresses as given by Lo & Lukajic (1984) are shown in the figure.

6.7.1.1 Example Of Calculations

Figure 6.18 shows typical field data for an overcoring test in dolomite (Goat Island Member, Thorold, Ontario) using the USBM deformation gage. The change in diameter of the pilot hole is plotted against the distance of overcore bit from buttons (measuring plane) in three directions (button set 1, button set 2 and button set 3). The gage was installed such that the reference direction (button set 1) was east. The change in diameter as interpreted from Fig. 6.18 is $U_1 = 11.7\ \mu m$, $U_2 = 11.9\ \mu m$, and $U_3 = 13.1\ \mu m$. The values of deformation modulus, E, and Poisson's ratio, ν, were determined, respectively, as 71 GPa and 0.30.

Substituting for the values of U_1, U_2, U_3, E, ν and d (38 mm or 1.5 in) in the first two equations in Table 6.14, the values of the major (P) and minor (Q) principal horizontal stresses are calculated as 13 and 12.1 MPa, respectively. Substituting for the values of U_1, U_2 and U_3 in the third equation in Table 6.14, the angle of P measured counterclockwise from the U_1 direction, θ, is calculated as 27°. Since $U_2 < U_3$ and $U_2 + U_3 > 2U_1$, then θ lies between 90 and 135°, according to the relations given in Table 6.14. Therefore, the direction of P is N 27° W.

6.7.2 HYDRAULIC FRACTURING METHOD

Although there are several methods available for *in situ* measurements of stresses, the only practical technique for determination of stresses at great depths is the hydraulic fracturing method.

The test procedure is described in the published works of Haimson who has made important progress in the development of the hydraulic fracturing technique (see e.g. Haimson & Fairhurst 1969 and Haimson 1978a). The procedure is also described in ISRM (1987a).

The test is performed by pumping water at a constant flow rate in a sealed section of the borehole (Fig. 6.19a). The pressure is increased until a critical value P_{c1}, the breakdown pressure (fracture initiation pressure, Fig. 6.20), is reached and a fracture is induced. After maintaining pumping for a short time to extend the fracture beyond the zone of influence of the borehole (about three times the borehole diameter), the injection is stopped and the hydraulic system is "shut-in", yielding the shut-in pressure, P_s. The pressurization cycle is repeated several times to obtain the fracture reopening pressure, P_{c2}, and additional measurements of the shut-in pressure. After the test is performed, the inclination and the direction of the induced hydrofractures at the borehole wall are determined using an impression packer and a magnetic orienting instrument, Fig. 6.19b.

In case of formation of a vertical fracture, the conventional method for initial stress calculation is applicable (Haimson & Fairhurst 1969). The vertical *in situ* stress is considered as one of the principal stresses in the ground, and the fracture is assumed to develop perpendicular to the minimum horizontal principal stress. This minimum *in situ* horizontal stress, σ_h, is taken to be equal to the recorded shut-in pressure, P_s:

$$\sigma_h = P_s. \tag{6.19}$$

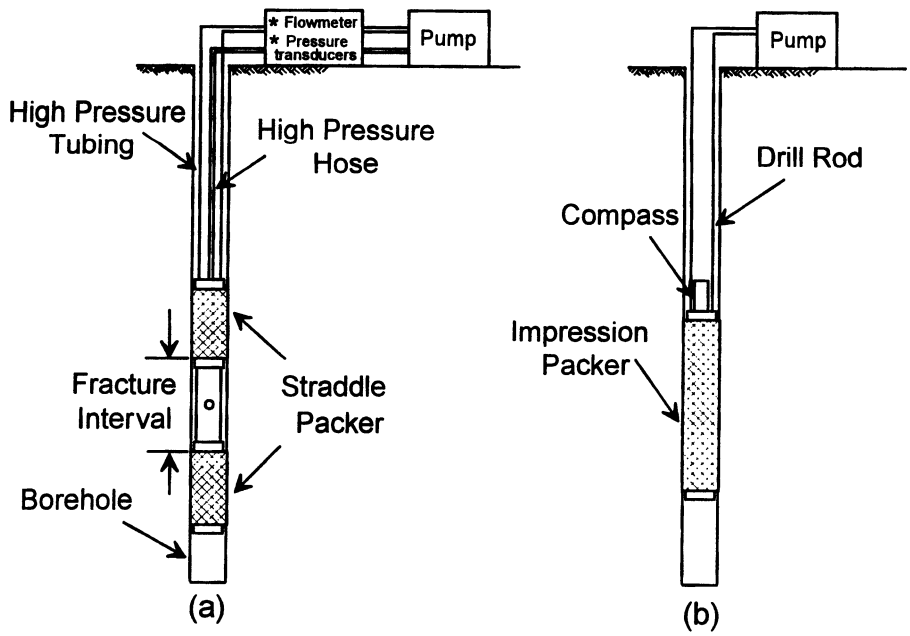


FIGURE 6.19. Schematic representation of: (a) hydraulic fracturing testing, and (b) impression packer.

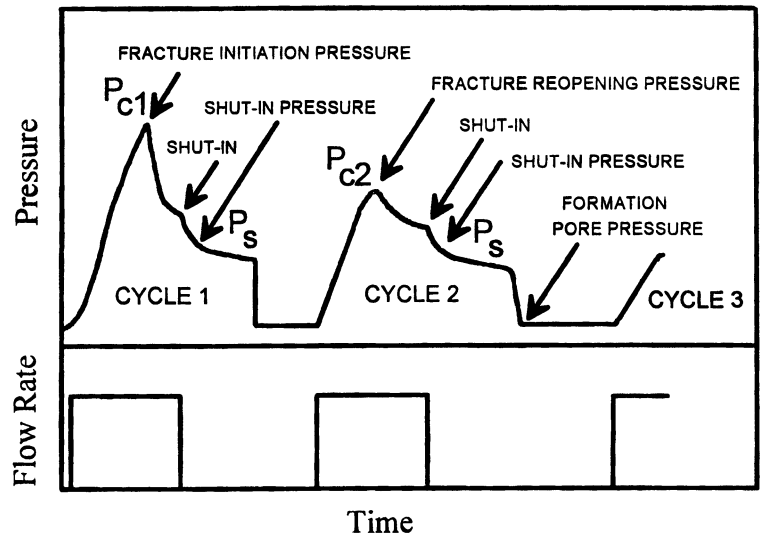


FIGURE 6.20. Idealized hydraulic fracturing pressure–time record (reprinted from ISRM 1987a, Kim, K. & Franklin, J.A. Eds. © 1987 with permission of Elsevier Science).

The maximum horizontal stress, σ_H, is calculated using the following relationship:

$$\sigma_H = 3P_s - P_{cl} + T \qquad (6.20)$$

where T = tensile strength of rock. Equations 6.19 and 6.20 are commonly used to calculate the minimum and the maximum horizontal stresses, respectively. To account for the initial porewater pressure, P_0, at the test depth, Haimson (1978a, 1978b, 1985), Haimson & Lee (1980), and Haimson *et al.* (1989) the following equation was used (assuming the rock is porous and at the same time impermeable to the wellbore fracturing fluid):

$$\sigma_H = 3P_s - P_{cl} - P_0 + T. \qquad (6.21)$$

Results of hydraulic fracturing tests at Darlington are shown in Fig. 6.17 (data marked as UN1–4, etc.). The stresses at shallow depths were measured by USBM gage and at greater depths by the hydraulic fracturing method. It may be seen that at El 40 m elevation, where both methods were used, the results of stress determined were similar.

In hydraulic fracture tests in which horizontal fractures are induced, the conventional method cannot be used for the interpretation of results. For cases where both horizontal and vertical fractures are obtained in impression packer tests, it is necessary to determine which fracture has occurred first.

Closed form solutions for horizontal and mixed-mode fractures including strength anisotropy have been given by Hefny & Lo (1992, 1995) and Lo & Hefny (1993) by following the stress paths from start of test to hydraulic fracture. Several case histories were analyzed using this method for calculating the initial stresses at several sites in Canada where horizontal and mixed-mode fractures were induced by the hydraulic fracturing test. The results of stress determination using this stress path method have been found to be consistent with performance of underground structures.

7. GEOSYNTHETICS: CHARACTERISTICS AND TESTING

R. M. Koerner
Y. G. Hsuan

7.1 Introduction

Geosynthetics are polymeric materials that are used in below-grade construction in a broad and ever-increasing range of applications. The majority of the applications generally fall into the areas of geotechnical, environmental, transportation and hydraulic engineering. A number of specific applications using geosynthetics will be described in Chapters 13–19, 25–27 and 29, 30. Before dealing with applications, however, it is necessary to present the salient characteristics of the various geosynthetics and the most relevant test methods and properties. This chapter is focused on providing that type of background material. While the literature is abundant with references on geosynthetic properties and test methods, this review is quite brief. It follows the general description in Koerner (1998), which is more detailed.

In so far as a categorization of geosynthetics is concerned (and the sections to be followed in this chapter), the following applies:

- Geotextiles (GT): woven or non-woven fabrics used primarily for separation, reinforcement, filtration and drainage.
- Geogrids (GG): grid-like sets of interconnected ribs with large apertures primarily used for soil reinforcement.
- Geonets (GN): net-like sets of integrally joined overlapping ribs used for in-plane drainage.
- Geomembranes (GM): polymeric sheets used as barriers for the containment of liquids, gases or solids.
- Geosynthetic clay liners (GCLs): thin layers of bentonite generally contained between two geotextiles used as barriers for containment of liquids, gases or solids.
- Geocomposites (GC): a broad range of materials consisting of two, or more, geosynthetics (sometimes with biodegradable materials or with soil) used for separation, reinforcement, filtration, drainage or contaminant.

In describing the many test methods to be presented (International Standards Organization, ISO, test methods will be referenced whenever available), it is instructive to keep in mind the primary function that the geosynthetic is called upon to serve. In so doing, the major test method(s) can usually be identified. Geosynthetics *vis-à-vis* the primary functions that they serve are given in Table 7.1.

After the discussion of properties and test methods of the various types of geosynthetics, the last section will be on a general discussion of the usual design approach so as to serve as an introduction for forthcoming chapters on specific applications of each type of geosynthetics. A brief summary as to the significance of laboratory testing concludes the section.

R. K. Rowe (ed.), *Geotechnical and Geoenvironmental Engineering Handbook*
© Kluwer Academic Publishers 2001

TABLE 7.1. Primary functions provided by geosynthetics

Type	Separation	Reinforcement	Filtration	Drainage	Containment
Geotextiles	Yes	Yes	Yes	Yes	–
Geogrids	–	Yes	–	–	–
Geonets	–	–	–	Yes	–
Geomembranes	–	–	–	–	Yes
Geosynthetic Clay Liners	–	–	–	–	Yes
Geocomposites	Varies	Varies	Varies	Varies	Varies

7.2 *Geotextile Properties and Test Methods*

Geotextiles are typically woven or non-woven fabrics made from polypropylene (PP) or polyester (PET) fibers, filaments or yarns using conventional textile manufacturing facilities. There is considerable variety in the final product, with commercial geotextiles typically ranging in mass per unit area from 135 to 1000 g m^{-2}, and in strength from 9 to 180 kN m^{-1} for filtration or separation applications. Geotextiles with a higher mass per unit area and strength are also available for severe installation conditions and reinforcement applications. Other polymers, such as high density polyethylene (HDPE), polyamide (PA) and polyvinyl alcohol (PVA) are also used, but to a lesser extent than PP and PET. Due to the inherent variability of different geotextiles, product-specific properties are always needed. Fortunately, much of the testing is reasonably standardized in both international (ISO) and regional organizations (American Society for Testing and Materials, ASTM; European Committee for Standardization, CEN; etc.).

7.2.1 PHYSICAL PROPERTIES

The primary physical properties of geotextiles are specific gravity, mass per unit area, thickness and stiffness. All are straightforward index properties to measure. Table 7.2 shows typical ranges for these properties.

7.2.2 MECHANICAL PROPERTIES

The major mechanical properties of geotextiles are listed in Table 7.2 along with typical values. The list contains both index and performance properties. In the latter group is the wide-width tensile strength and the friction behavior of geotextiles. Both properties warrant special commentary since they apply to all geosynthetics.

The wide-width tensile strength of geotextiles (and other geosynthetics) is evaluated so as to replicate plane strain conditions in the field. While somewhat subjective, the width of the test specimen is set at 200 mm in ISO 10319 and many regional standards as well. The general response for different types of geotextiles is shown in Fig. 7.1. The stress–strain response varies with the type of geotextile being evaluated due to resin type and fabric structure variation.

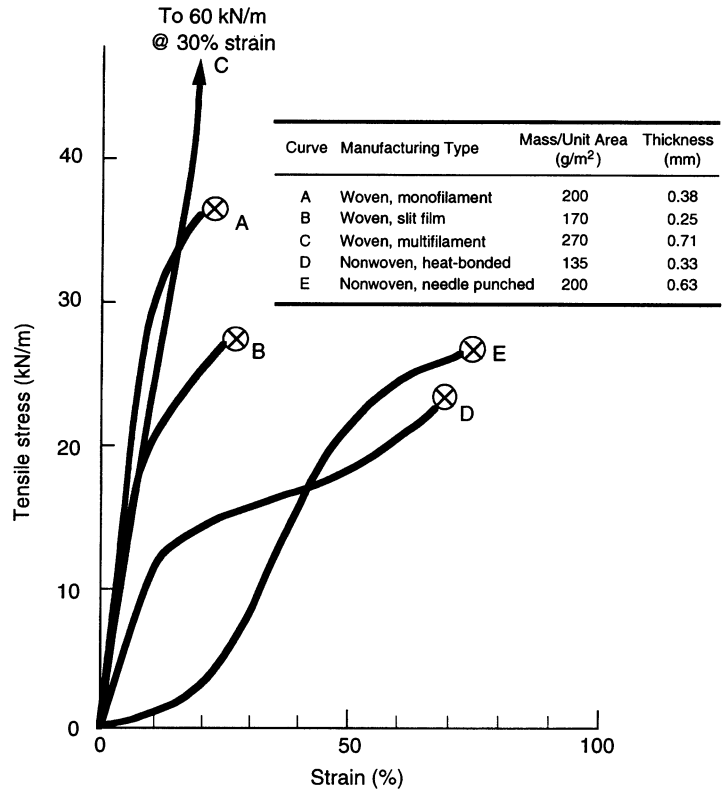
The friction behavior for geotextiles (and other geosynthetics) is a particularly important property for the design engineer. This property is evaluated using a direct shear adaptation of the conventional soil testing procedure. The test is considered to be a performance test rather than an index test, since the condition of soil, such as soil type, moisture content and compaction density, influences

TABLE 7.2. Typical range of properties for currently available geotextiles

Physical properties	
Specific gravity	0.9–1.7
Mass per unit area, g m^{-2}	135–1000
Thickness, mm	0.25–7.5
Stiffness, mg cm^{-1}	0–25,000
Mechanical properties	
Compressibility	Nil to high
Tensile strength (grab), kN	0.45–4.5
Tensile strength (wide width), kN m^{-1}	9–180
Confined tensile strength, kN m^{-1}	18–180
Seam strength, % tensile	50–100
Cyclic fatigue strength, % tensile	50–100
Burst strength, kPa	350–5200
Tear strength, N	90–1300
Impact strength, J	14–200
Puncture strength, N	45–450
Friction behavior, % soil friction	60–100
Pullout behavior, % geotextile strength	50–100
Hydraulic properties	
Porosity (non-wovens), %	50–95
Open size (sieve size), mm (No. 10–200)	2.0–0.075
Open area (wovens), %	0–36
Permittivity, s^{-1}	0.02–2.2
Permittivity under load, s^{-1}	0.01–3.0
Transmissivity, m^2 min^{-1}	0.01×10^{-3} to 2.0×10^{-3}
Soil retention:	
Turbidity curtains	M.b.e.[a]
Silt fences	M.b.e.[a]
Endurance properties	
Installation damage, % of fabric strength	0–70
Creep response	G.n.p. if <40% strength is being used[b]
Confined creep response	G.n.p. if <50% strength is being used[b]
Stress relaxation	G.n.p. if <40% strength is being used[b]
Abrasion, % of geotextile strength	50–100
Long-term clogging	M.b.e. for critical conditions[a]
Gradient ratio clogging	M.b.e. for critical conditions[a]
Hydraulic conductivity ratio	0.4–0.8 appear to be acceptable

[a] M.b.e.–must be evaluated.
[b] G.n.p.–generally no problem.

the result. The property is both a product- and project-specific test in that similitude to the actual situation must be as close as possible. Each detail must be replicated if realistic shear strength parameters are to be generated. Important considerations in this regard are test configuration (size and shape), type of hydrating liquid (undrained or drained conditions), normal stress (magnitude and duration), strain rate and strain displacement. The latter is particularly important if the interface being investigated suggests lower residual strength than peak strength. The sketches of Fig. 7.2 illustrate the typical test set-up, typical response for a sequence of normal stress tests (showing strain softening behavior), and the method of obtaining peak and residual shear strength parameters.



Curve	Manufacturing Type	Mass/Unit Area (g/m^2)	Thickness (mm)
A	Woven, monofilament	200	0.38
B	Woven, slit film	170	0.25
C	Woven, multifilament	270	0.71
D	Nonwoven, heat-bonded	135	0.33
E	Nonwoven, needle punched	200	0.63

FIGURE 7.1. Typical tensile behavior of different geotextile types using wide-width test specimens (200 mm).

7.2.3 HYDRAULIC PROPERTIES

When geotextiles are used in filtration and drainage functions, the hydraulic properties of geotextiles are important. Table 7.2 lists the common tests and typical range of values. Within this group porosity, open area, permittivity and transmissivity will be mentioned.

1. *Porosity*. The amount of open space in the fiber network of non-woven geotextiles. It is related to the ability of liquid to flow through or within the geotextile, but is rarely measured directly. Instead, it is calculated from other properties of the geotextile, as shown in Eq. 7.1:

$$n = 1 - \frac{M_A}{\rho_f t_{GT}} \qquad (7.1)$$

where n = porosity (dimensionless); M_A = mass per unit area, i.e. weight (g m^{-2}); ρ_f = density (g m^{-3}); and t_{GT} = thickness of the geotextile (m). Eq. 7.1 indicates that for a given geotextile's mass and density, the porosity is proportional to the thickness. Thickness, in turn, is related to the applied normal stress.

2. *Percent open area* (POA). A geotextile property that has applicability for woven geotextiles. POA is a comparison of the total open area (the void space between adjacent yarns) to the total specimen area. *Apparent opening size* (AOS) is used for all geotextiles. The AOS, equivalent opening size (EOS), or O_{95} all refer to the same specific pore size, the difference being that AOS and EOS are sieve numbers defined by an appropriate standard, while O_{95} is the corresponding

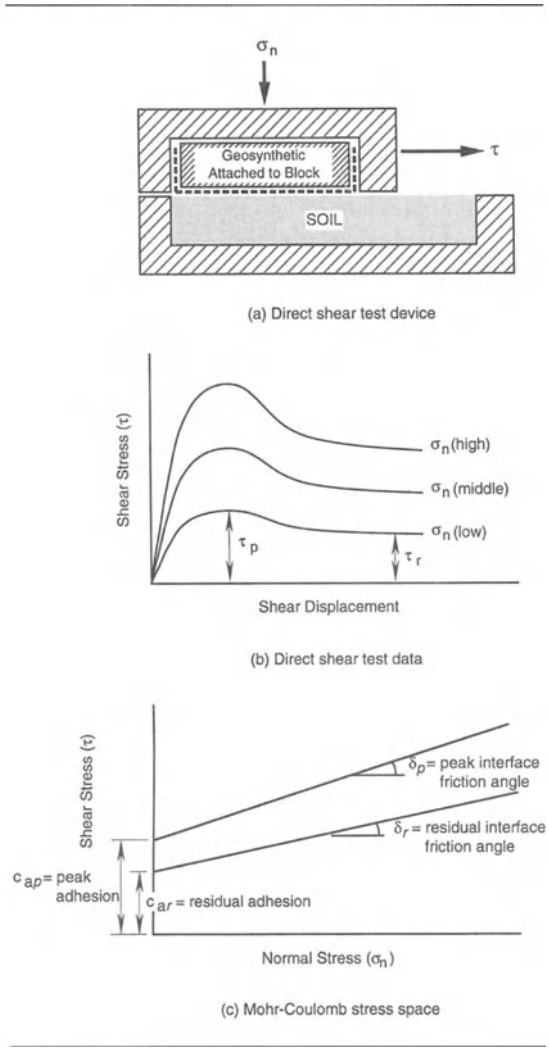


FIGURE 7.2. Direct shear test used to evaluate geosynthetic–geosynthetic or geosynthetic–soil interface strength: (a) direct shear lest device, (b) direct shear test data, and (c) Mohr-Coulomb shear space.

sieve-opening size in millimeters. The value is obtained according to ASTM D 4751 by sieving of known-diameter glass beads through the geotextile in a prescribed manner. As alternatives to the dry-sieving test, there are a number of wet-sieving methods using well-graded standard soil (ISO/DIS 12956).

3. *Permeability*. Permeability of a geotextile is measured via an adapted soil testing procedure using a constant-head or falling-head permeameter (ISO/DIS 11058). Due to the compressible nature of fabrics, however, a geotextile-related parameter called *permittivity* is used. This parameter incorporates the fabric's thickness, i.e.:

$$\psi = \frac{k_n}{t_{GT}} \tag{7.2}$$

where ψ = permittivity (s^{-1}), k_n = permeability (properly called *hydraulic conductivity*) normal to the geotextile (m s^{-1}), and t_{GT} = thickness of the geotextile (m). A schematic of a permittivity test device is shown in Fig. 7.3a.

In a somewhat similar manner *transmissivity* is defined as:

$$\theta = k_p t_{GT} \tag{7.3}$$

where θ = transmissivity of the geotextile ($m^2\ s^{-1}$ or $m^3\ s^{-1}\ m^{-1}$), k_p = permeability (hydraulic conductivity in the plane of the geotextile (m s^{-1}), and t_{GT} = thickness of the geotextile (m). A number of test devices are configured to model the above formulation, where liquid (usually water) flows in the plane of the geotextile in a parallel flow trajectory (Fig. 7.3b). Koerner & Bove (1983) provide a review of such devices including ISO/DIS 12958.

7.2.4 ENDURANCE PROPERTIES

As indicated in Table 7.2, there are a number of potentially significant endurance properties, of which creep and clogging tests are particularly important.

Creep is the term commonly applied to the elongation of a material under constant load. Since polymers are generally considered creep-sensitive materials, it is an important property to evaluate for geosynthetics used in the reinforcement function. The test specimens should be of the wide-width variety (≃200 mm) and are usually stressed by means of stationary hanging weights. Since

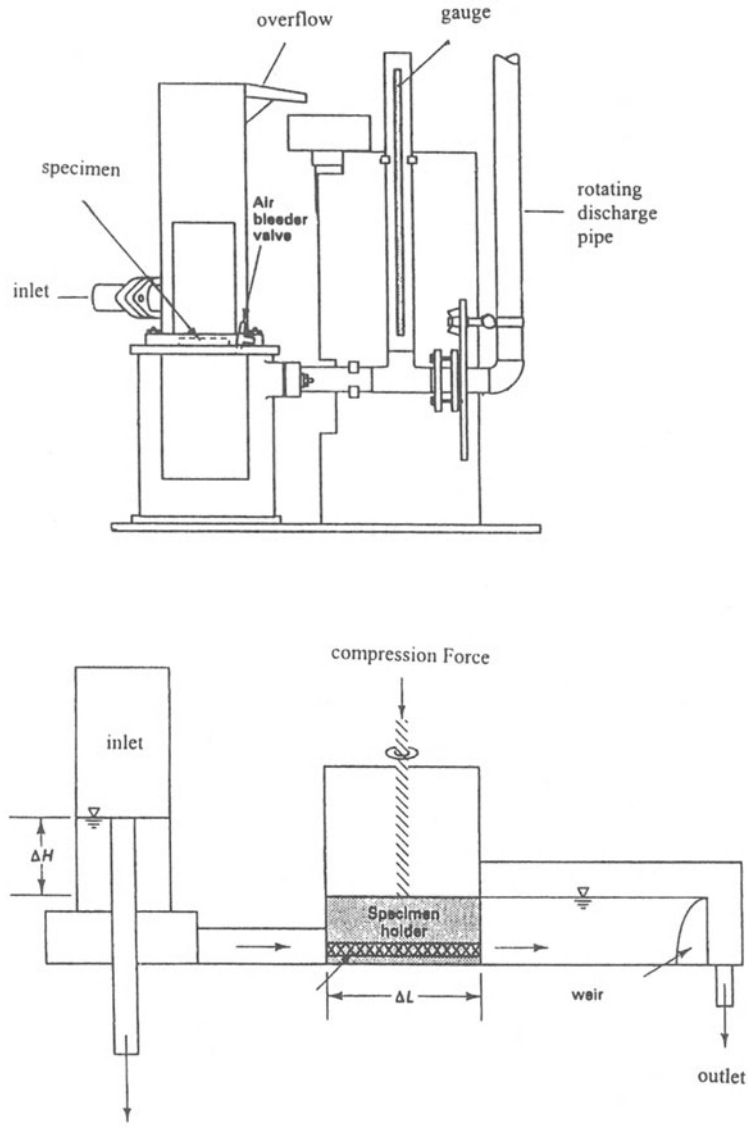


FIGURE 7.3. Cross-sections of permittivity and transmissivity test devices, where ΔH = differential height, and ΔL = differential length.

the test duration is generally long (up to 10,000 h), a number of tests are often conducted simultaneously by cascading the test specimens and their respective loads. The set-up can also be horizontal with a number of specimens connected to one another. Selected creep reduction values to be used in reinforcement applications from the literature are given in Table 7.3. The design aspect of the creep property will be explained in Section 7.9.

Other than long-term degradation, which will be discussed for all geosynthetic polymers in Section 7.8, the issue of excessive clogging is often of concern. There are three laboratory methods available for its assess-

TABLE 7.3. Selected values of geotextile reduction factors against creep deformation[a]

	den Hoedt [1986]	Lawson [1986]	Task force no. 27 [1991]	Koerner [1998]
Geotextile fiber/yarn type				
Polypropylene[b]	4.0	2.5–5.0	5.0	3.0–4.0
Polyethylene[b]	4.0	2.5–5.0	5.0	3.0–4.0
Polyamide	2.5	1.5–2.5	2.9	2.0–2.5
Polyester	2.0	1.5–2.5	2.5	2.0–2.5

[a] These values are for use in avoiding creep deformation completely, i.e. the zero-creep condition.
[b] Refers to polyolefin geotextile yarns, not to oriented homogeneous geogrids, which are less sensitive to creep.

ment: long-term flow, gradient ratio and hydraulic conductivity ratio tests. All three tests are performance tests. They must be performed using the candidate geotextile and soil with the intended, or simulated, permeant. In the long-term flow test, the flow rate is monitored throughout the duration of the test, which normally runs for 1000 h (Wayne & Koerner 1993). The gradient ratio test is performed according to ASTM D5101. In this test, the hydraulic head at various locations in a soil–geotextile column is measured. Head differences are then converted to hydraulic gradients, and the GR value is calculated according to Eq. 7.4. The Army Corps of Engineers suggests that GR values greater than 3.0 indicate non-acceptable geotextiles for the type of soil under test:

$$GR = \frac{\Delta h_{GT+25S}/t_{GT+25}}{\Delta h_{50S}/t_{50}} \qquad (7.4)$$

where Δh_{GT+25S} = head change (mm) from the bottom of the geotextile to 25 mm of soil above the geotextile, t_{GT+25} = geotextile thickness (mm) plus 25 mm of soil, Δh_{50S} = head change (mm) between 50 mm of soil above the geotextile, and t_{50} = 50 mm of soil.

Alternatively, one could conduct the hydraulic conductivity ratio test, which is performed according to ASTM D5084. The HCR value is determined as:

$$HCR = \frac{k_{sg}}{k_g} \qquad (7.5)$$

where HCR = hydraulic conductivity ratio, i.e. permeability ratio; k_{sg} = permeability of soil–geotextile system; and k_s = permeability of the soil. See Williams & Abouzakhm (1989) for details of the test, and Luettich & Williams (1989) for an interpretation of the resulting values. Typically, HCR values of 0.4–0.8 signify equilibrium flow conditions. Values higher than 0.8 suggest soil piping may be of concern, and values less than 0.4 may indicate excessive clogging.

7.3 *Geogrid Properties and Test Methods*

Geogrids are of two different categories. One category is made from polyolefin sheets with openings that are drawn in a machine and/or cross-machine direction to form a unitized and relatively stiff grid structure. Unidirectional types are made from HDPE and biaxial types are made from PP. The second category of geogrids is made from high tenacity PET yarns (each yarn consisting of many individual filaments), which are fabricated on weaving or knitting looms into a relatively flexible grid structure. Fiberglass has also been used to make geogrids in this category. These flexible types of geogrids are subsequently coated with PVC, bitumen or latex to provide dimensional stability during handling and installation. Geogrids of both categories provide reinforcement as their primary function.

7.3.1 PHYSICAL PROPERTIES

Many of the physical properties of geogrids can be measured directly and are relatively straightforward. These include the type of structure, junction type, aperture size and thickness. Other properties that are of interest are density (ASTM D1505), which is associated with the type of polymer; mass per unit area (ASTM D5261), which varies over a tremendous range from 200 to 1000 g m^{-2}; and per cent open area, which varies from 40 to 95%.

7.3.2 MECHANICAL PROPERTIES

Single rib strength and junction strength of geogrids are both index tests and are performed in an unconfined state (GRI GG-1, GRI GG-2). The performance test for geogrid strength, however, should be measured in a wide-width manner (recall Fig. 7.1). ISO 10319 requires geogrid test specimens to consist of at least three sets of longitudinal ribs. Ultimate strengths of commercially available products range from 13 to 370 kN m^{-1}.

Shear strength of geogrids with respect to adjacent materials, e.g. soils, geomembranes, etc., is performed in a direct shear box as described in Section 7.2.2. All of the issues that were presented in that section are also to be considered with geogrids, in particular the size of the shear box. Geogrids with apertures as large as 50 mm will require a large shear box, e.g. at least 300 mm^2.

Two additional strength tests associated with geogrids are its anchorage strength from soil pull-out, and anchorage strength within wall connections. These tests, arguably the largest of all geosynthetic tests, are meant to simulate the actual conditions as closely as possible (Bathurst & Simac 1994).

7.3.3 ENDURANCE PROPERTIES

There are at least two important endurance considerations with respect to the long-term performance of geogrids: creep and chemical resistance. Creep is a function of polymer type, its orientation state, applied stress level, type of local application, service temperature, service environmental factors and anticipated service lifetime. The test was described in Section 7.2.4 and Table 7.3 presents some data from the literature. With the number of variables, however, product specific tests are always recommended. ISO/DIS 13431 presents a testing procedure. It is, however, silent on the method of data interpretation.

Chemical resistance is a concern particularly when geogrids are being used in an aggressive environment. Clearly, applications in landfills where the geogrid is exposed to leachate are such situations. The incubation is done at an elevated temperature, typically 50°C, and the removed samples are tested for possible changes in their index strength properties. Degradation of geosynthetics will be discussed in more detail in Section 7.8.

7.4 Geonet Properties and Test Methods

Geonets (biaxial-type) are made from HDPE in a slotted counter-rotating die, which results in two parallel sets of ribs integrally joined at their cross-over locations. The resulting apertures are diamond-shaped and approximately 10–15 mm in size. When a biaxial geonet is measured in a transmissivity test, the flow rate is approximately equal in all directions. A newer geonet (triaxial type) consists of a central parallel set of ribs covered by smaller sets of ribs on the top and bottom. The main direction of flow is in the machine direction, and these geonets are generally targeted toward side-slope drainage where the flow direction is known.

Whatever the type, geonets always serve as planar drainage materials. As such, their upper and lower surfaces must always be covered. Typically, a geotextile is on at least one

surface (if not both) so as to allow flow to enter into the geonet.

7.4.1 PHYSICAL AND MECHANICAL PROPERTIES

The density (ASTM D1505), thickness (ASTM D5199), and mass per unit area (ASTM D5261) of geonets are measured via established tests. Other physical properties, such as rib dimensions, planar angles made by the intersecting ribs, cross-planar angles made at junction locations, aperture size and shape, etc., can be measured directly and are relatively straightforward to obtain.

7.4.2 HYDRAULIC PROPERTIES

The in-plane hydraulic test to determine planar flow rate, or transmissivity, of geonets should be performed according to ISO/DIS 12958. Some important considerations are:

- The specimen size must be 150 × 150 mm, or larger. Kolbasuk *et al.* (1992) have shown that sample size and aspect ratio, i.e. length–width ratio, can have a significant effect on the resulting measured flow rates.
- As an index test, the geonet test specimen is sandwiched between rigid plates.
- Normal stresses are typically applied for a 15-min duration, and flow rates are measured at different hydraulic gradients during a subsequent 15-min duration.
- Compressive stress is then increased to the next level and the process is repeated.
- As a performance test, the geonet test specimen is sandwiched between the replicated cross-section proposed in the field. Compressive stress, type of permeant, temperature and test duration are all important considerations and at the discretion of the parties involved.
- De-aired water at 6 p.p.m., or lower, of dissolved oxygen is not explicitly specified, although for critical situations it might be necessary.

The geotextile covering the surface(s) of a geonet is an important consideration, in that it must serve as a filter and as a separator. As a filter its permeability and opening size are important, while as a separator its tensile strength (and related strength properties) is important.

A flow test that evaluates both the permeant passing the geotextile (permittivity) and the flow within the geonet (transmissivity) is also available according to GRI GC-1.

7.4.3 ENDURANCE PROPERTIES

If *compressive creep* of a geonet occurs, the transmissivity will decrease in linear proportion to its reduction in thickness. The resin density and fabricated structure of the geonet are both relevant in this regard. The test should be performed long enough to give insight into the possibility, e.g. 1000-h tests, at a minimum, are common.

Intrusion refers to the deformation of the covering materials, primarily geotextiles, occupying some of the space of the geonet's apertures. The geonet's transmissivity is reduced accordingly. Table 7.4 shows the reduction in flow rates for two different configurations under various normal stress. Hwu *et al.* (1990) and Eith & Koerner (1992) have studied and reported on this phenomenon. The situation must be modeled in the laboratory test so as to obtain a realistic design value.

Extrusion refers to fine soil particles passing through geotextile voids into the apertures of the geonet. This situation is unacceptable under any condition. Particular concern is when fine-grained soils, e.g. GCL or CCL, are placed adjacent to the geotextile covering of the geonet.

7.5 Geomembrane Properties and Test Methods

The majority of geomembranes are relatively thin sheets of flexible thermoplastic materi-

TABLE 7.4. Flow rate ($m^3\ min^{-1}\ m^{-1}$) and reductions from index values, i.e. 10 kPa normal stress, (%)

Normal stress (kPa)	Cross-section	Hydraulic gradient (i)					
		0.03	0.06	0.12	0.25	0.50	1.00
50	HDPE (both sides)	0.005	0.011	0.019	0.032	0.055	0.095
	GT/clay (one side)	0.004	0.008	0.013	0.022	0.038	0.059
	Difference	0.001	0.003	0.006	0.010	0.017	0.036
	Reduction[a]	20	27	31	31	31	38
250	HDPE (both sides)	0.005	0.011	0.017	0.028	0.048	0.077
	GT/clay (one side)	0.004	0.008	0.012	0.019	0.032	0.052
	Difference	0.001	0.003	0.005	0.009	0.016	0.025
	Reduction[a]	20	27	29	32	33	32
500	HDPE (both sides)	0.005	0.010	0.017	0.027	0.047	0.072
	GT/clay (one side)	0.004	0.007	0.012	0.018	0.028	0.043
	Difference	0.001	0.003	0.005	0.009	0.019	0.029
	Reduction[a]	20	30	29	30	40	40

[a] Per cent reduction.

als. There are many different types of polymers that are used in making of geomembranes. The most widely used polymers are high density polyethylene (HDPE), very flexible polyethylene (VFPE), including both very low density polyethylene (VLDPE) and linear low density polyethylene (LLDPE), and polyvinyl chloride (PVC). Polymers, such as flexible polypropylene (fPP), chlorosulfonated polyethylene (CSPE), ethylene interpolymer alloy (EIA) and ethylene propylene diene monomer (EPDM), are somewhat less widely used. It should be recognized that other materials are continuously merging into this category of geosynthetics.

Geomembranes can be divided into three groups based on their physical appearance: smooth, textured and reinforced geomembranes. The smooth sheet is the basic manufactured product for HDPE, VFPE, PVC and fPP geomembranes. Textured geomembranes are specially formed to enhance surface roughness in order to improve interface friction with adjacent materials; they are available in HDPE, VFPE and PVC geomembranes. The techniques for making the texturing in HDPE and VFPE geomembranes are described in detail by Donaldson (1994). Reinforced geomembranes are manufactured by incorporating a layer of polyester scrim between two layers (called "plys") of membrane. The membrane generally is an elastomeric material, exhibiting a low tensile strength. The scrim provides the strength for the geomembrane. CSPE, EIA and EPDM geomembranes are manufactured in this style.

There are a tremendous number of possible tests for geomembranes, many of which are material-specific and site-specific. Only the most common will be discussed.

7.5.1 PHYSICAL PROPERTIES

Within the physical property category there are many possible tests: thickness (smooth sheet (ASTM D5199), textured sheet (ASTM D5994), asperity height (GRI GM-12)), density (both resin and formulation) (ASTM D1505), melt index (melt flow and flow rate ratio) (ASTM D1238), and vapor transmission (water and solvent) (ASTM E96). The vapor transmission test is quite contentious in its methodology and significance.

Vapor transmission is conducted with a liquid (water, solvent or other liquid) in a cup having the candidate geomembrane making the closure. When placed in a constant humidity chamber, the changing weight can be monitored over time. Procedures allowing for

the calculation of the vapor transmission rate in units of g m^{-2} per day, and many other aspects of diffusion testing, are available in Rowe (1998a).

7.5.2 MECHANICAL PROPERTIES

In the category of mechanical properties of geomembranes, there are many important properties, including tensile strength (index, wide-width, axi-symmetric), seam strength (shear and peel), various resistance strengths (tear, impact and puncture), interface shear and anchorage (to a wide range of soils). In addition, the test method varies with the style of geomembrane and the type of polymer, as shown in Table 7.5. The variation of stress–

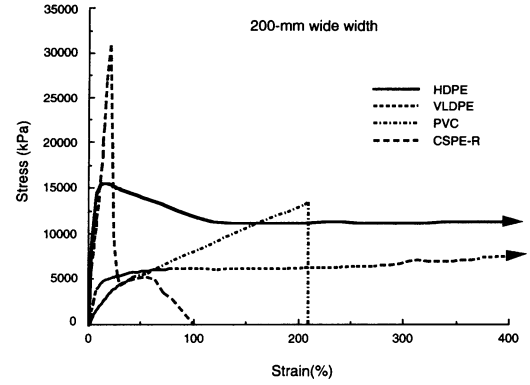


FIGURE 7.4. Typical tensile behavior of different geomembrane types using wide-width test specimens (200 mm) per ASTM D4885.

TABLE 7.5. Recommended test method details for geomembranes and geomembrane seams in shear and in peel

Type of test	HDPE	VFPE & PP	PVC	Reinforced[a]
Tensile test on sheet				
ASTM test method	D638 [426]	D638 [426]	D882 [427]	D751 [428]
Specimen shape	Dumb-bell	Dumb-bell	Strip	Grab
Specimen width, mm	6.3	6.3	25	100 (25 grab)
Specimen length, mm	115	115	150	150
Gage length, mm	33	33	50	75
Strain rate, mm min^{-1}	50	500	500	300
Strength[c]	Force/($w \times t$)	Force/($w \times t$)	Force/($w \times t$)	Force
Strain, mm mm^{-1}	Elong/33	Elong/33	Elong/50	Elong/75
Modulus	From graph	From graph	From graph	n/a[b]
Shear test on seams				
ASTM test method	D4437 [429]	D4437 [429]	D3083 [430]	D751 [428]
Specimen shape	Strip	Strip	Strip	Grab
Specimen width, mm	25	25	25	100 (25 grab)
Specimen length, mm	150 + seam	150 + seam	150 + seam	225 + seam
Gage length, mm	100 + seam	100 + seam	100 + seam	150 + seam
Strain rate, mm min	50	500	500	300
Strength[c]	Force/($w \times t$)	Force/($w \times t$)	Force/($w \times t$)	Force
Peel test on seams				
ASTM test method	D4437 [429]	D4437 [429]	D413 [431]	D413 [431]
Specimen shape	Strip	Strip	Strip	Strip
Specimen width, mm	25	25	25	25
Specimen length, mm	100	100	100	100
Gage length, mm	n/a[b]	n/a[b]	n/a[b]	n/a[b]
Strain rate, mm min^{-1}	50	500	50	50
Strength[c]	Force/w	Force/w	Force/w	Force/w

[a] This category of scrim-reinforced geomembranes includes CSPE-R, fPP-R, EIA-R and EPDM-R.
[b] n/a = not applicable.
[c] Force = maximum force attained at specimen failure (ultimate or break); w = specimen width (mm); t = specimen thickness (mm).

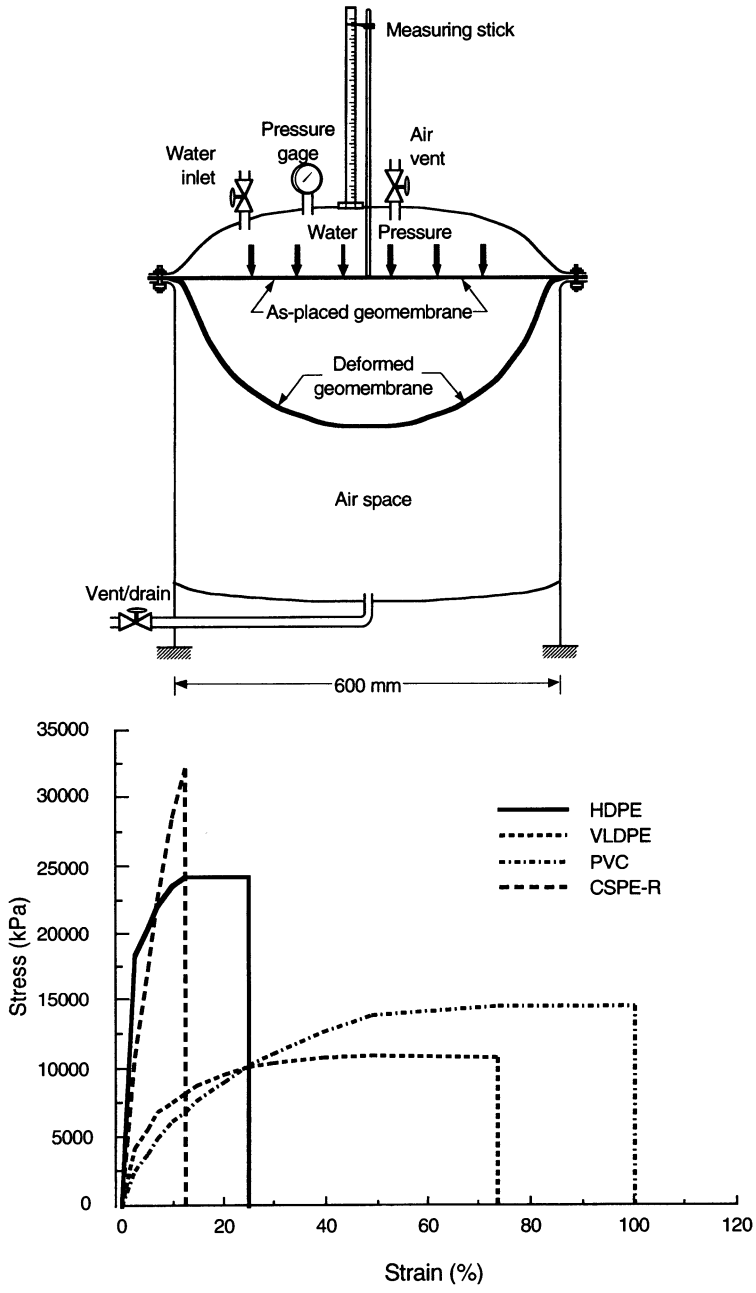


FIGURE 7.5. Typical axi-symmetrical behavior of different geomembrane types using out-of-plane pressurization per ASTM D5617.

strain behavior of different types of geomembrane is illustrated using the wide-width tensile test, as shown in Fig. 7.4. Particularly controversial in the above list of tests, however, are the axi-symmetric and seam tests.

The axi-symmetric test is generally meant to model geomembranes placed over yielding subgrades, such as the covers over landfills. The concern regarding the geomembrane is differential settlement of solid waste materials, e.g. the covers of landfills. While ASTM D5617 describes the procedure, the test is usually conducted at a pressurization rate of 7 kPa min^{-1}, which results in data of the type shown in Fig. 7.5. However, this pressurization rate is so fast that stress relaxation cannot occur and can result in biased information due to poor similitude to the generally slow development of the actual strain as arising from subsidence in the field.

Geomembrane seam tests are also contentious, particularly the peel test. In conducting the test one rarely monitors peel elongation and the issue of partial peel separation is difficult to quantify. Neither of these issues (peel elongation and peel separation) are in agreement among the various segments of the geomembrane industry.

7.5.3 ENDURANCE PROPERTIES

The detailed discussion of endurance properties for each type of polymer used in geosynthetics will be presented in Section 7.8. However, there are two properties that are specifically important to geomembranes that should be mentioned here: chemical resistance and stress crack resistance.

Chemical resistance of geomembranes is determined via an immersion protocol (ASTM D5322 for laboratory immersion or ASTM D5496 for field immersion), followed by a suite of physical and mechanical tests according to ASTM D5747. The data from the incubated samples are compared to the as-received material and assessed over a 120-day period. The data assessment, *per se*, is made by agreement of the parties involved. It should be noted that chemical mixtures involving organic solvents are the most aggressive in degrading the properties of geomembranes (and other geosynthetics as well). Degradation rates, however, vary widely attesting to the necessity of properly simulated testing.

Stress cracking of polymeric materials can be caused by two mechanisms: slow crack growth and rapid crack propagation. Failure induced by rapid crack propagation is usually associated with cold temperature, preexisting flaws and impact loading. Thus, this type of failure is less common than that induced by slow crack growth.

Stress cracking via slow crack growth can take place in many different types of polymers (Williams 1984). In geosynthetics, HDPE products are more susceptible to stress cracking than others due to their high crystallinity (Aspe 1988). Geosynthetics made from HDPE should be properly evaluated to ensure their stress crack resistance. The standard test method for evaluating HDPE geomembranes is ASTM D5397. An acceptable HDPE geomembrane should have a failure time greater than 200 h at 30% yield stress (Hsuan & Koerner 1995a).

7.6 Geosynthetic Clay Liner Properties and Test Methods

Owing to their basic manufacturing, geosynthetic clay liners (GCLs) are composite materials. All types except one consist of a thin layer of bentonite ($\simeq$10-mm thick) placed between two geotextiles. The GCL structure is maintained in its composite form by adhesives, needle punching or stitch bonding. The atypical GCL is adhesively bonded bentonite to a geomembrane.

As far as test methods and properties of GCLs are concerned, the bentonite, its composite structure and the nature of the geotex-

tile (or geomembrane) carrier materials are all relevant.

7.6.1 PHYSICAL PROPERTIES

The major GCL physical properties are moisture content (ASTM D4643), adhesive type (if present), thickness (bentonite and composite), and mass per unit area (bentonite and composite) (ASTM D5993). All can be measured, including identification of the clay type, which is accomplished by either X-ray diffraction or by use of a methylene-blue procedure (Heerten *et al.* 1993).

7.6.2 HYDRAULIC PROPERTIES

In the category of GCL hydraulic properties are the hydration liquid, swell index (ASTM D5890), moisture absorption, fluid loss, permeability and flux. Permeability and flux are, by far, the most important.

The flow rate (or *flux*) through a GCL is measured in a flexible wall permeameter per ASTM D5887. A major issue in conducting the test is the value of effective normal stress on the test specimen during liquid permeation. High values of effective stress give low values of flux and vice versa. The type of permeating liquid is obviously critical with site-specific liquids being ultimately the logical selection. The test procedure readily produces a value of flux in units of 1 m^{-2} per day. To obtain *permeability*, a thickness value is needed. The thickness of the hydrated test GCL specimen after conclusion of the test is somewhat ambiguous. Test specimens often have a gradually curved surface and the stitch bonded products actually exhibit a pillowed pattern. Using average values of thickness, typical ranges of permeability of GCLs with respect to water are from 1×10^{-11} to 5×10^{-11} m s^{-1} (Daniel *et al.* 1997).

7.6.3 MECHANICAL PROPERTIES

Within the mechanical property category are tension tests (wide-width tensile test (ASTM D4595)), confined wide-width tensile test (Wilson-Fahmy *et al.* 1993), axi-symmetric (Koerner *et al.* 1996), puncture resistance, interface shear and lateral squeezing.

With respect to *interface shear* strength there are three interfaces of concern: the upper GCL surface to its overlying material, the lower GCL surface to its subgrade material, and the internal strength of the GCL. The first two items are obviously site-specific, the last item is product-specific. Testing of all interfaces is usually performed in the hydrated state. This is due to the high suction capacity of bentonite, which will invariably cause the GCL to hydrate. Figure 7.6 illustrates that even on sand of 1.0% water content, the bentonite hydrates to 50% within a few weeks (Daniel *et al.* 1993). The hydrated bentonite is itself low in shear strength and can easily become fugitive. Large-scale test plots have shown that hydrated bentonite extruded through woven geotextiles lubricating the interface with a geomembrane creating slides of overlying cover systems (Koerner *et al.* 1997 and Daniel *et al.* 1998). Also, with the low shear

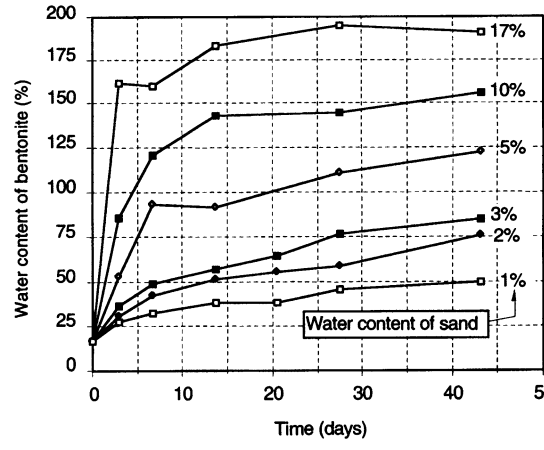


FIGURE 7.6. Water content versus time for GCL samples placed in contact with sand at various water contents (modified from Daniel *et al.* 1993).

strength of the hydrated bentonite it is necessary that the needle punching or stitch bonding be strong enough to withstand the site-specific stresses on the internal strength of the composite material. Typically, such conditions exist on steep side-slopes. Clearly, carefully configured laboratory tests are necessary to assess each of these three interface conditions.

The hydrated bentonite brings about another issue and that is product thinning due to *lateral squeezing* of the bentonite when the GCL is placed under non-uniform stress. This can come about from equipment loads, stones/rocks in the subgrade soil or in the cover soil. The situation is, in essence, a bearing capacity problem wherein sufficient fill thickness is necessary before vehicle trafficking, and quality control/quality assurance must be exercised throughout the construction phase of the project.

7.6.4 ENDURANCE PROPERTIES

The primary endurance properties of GCLs are freeze–thaw behavior, shrink–swell behavior, adsorptive capacity, water and solute breakout time.

Of the group, freeze–thaw and shrink–swell have been evaluated and found to be much less sensitive to these actions when compared to CCLs (Boardman & Daniel 1996; Daniel *et al.* 1997; and Kraus *et al.* 1997). The bentonite (when protected by the covering geotextiles) has a remarkable capability of self-healing.

Chemical adsorptive capacity is clearly a limiting factor of GCL with respect to CCLs. Even though bentonite has a tremendous adsorptive capability, there is simply too little mass to compare favorably to CCLs. The current strategy to mute this criticism of GCLs is to consider a two-part soil liner consisting of a GCL placed in association with a CCL. However, the CCL now utilizes locally available clays in which the permeability is higher than the regulated value. In composite form, such liners are three-component materials, i.e. GM–GCL–CCL. This obviously is a site-specific design situation, see (Koerner & Daniel 1995).

7.7 Geocomposite Properties and Test Methods

Since geocomposites can consist of any type of geosynthetic in combination with another geosynthetic (or with soil materials), this section will be function-specific with respect to the geocomposite under consideration (recall Table 7.1).

7.7.1 SEPARATION GEOCOMPOSITES

The major geosynthetic type within the separation geocomposite category is erosion control materials. When geosynthetic-based (rather than hard-armor-based), these products are flexible and can be tested by any one of a number of tests.

Within the index test category are tension (various types), open area (for infill and growth) and flexibility (for intimate contact with the soil subgrade). All of these tests are reasonably well-positioned in so far as standard tests are concerned.

The performance test category is in the early stages of development. At the minimum, resistance-to-erosion tests are necessary, but are not standardized. Large-scale laboratory or outdoor facilities are currently being used. The objective is generally to collect the run-off along with the soil sediment. One then compares different erosion control products to one another for a relative assessment.

7.7.2 REINFORCEMENT GEOCOMPOSITES

With fiberglass and steel strands woven into a polymer fiber matrix, one has reinforcement geocomposites with tensile strengths up to 2000 kN m^{-1}. The definitive test is obviously a tension test, but the width of the test

specimen in light of the testing machine capacity and proper gripping is a major consideration.

7.7.3 FILTRATION GEOCOMPOSITES

In a manner paralleling graded soil filters, filtration geocomposites can be made by needle punching together geotextiles of different porometry. The resulting geocomposite product is tested as with any other filter material in that permeability (or permittivity), opening size and long-term behavior are the most significant. Regarding long-term behavior the hydraulic conductivity ratio test described in Section 7.2.3 should be considered.

7.7.4 DRAINAGE GEOCOMPOSITES

In the category of drainage geocomposites there are wick drains, sheet drains and edge drains. All consist of a drainage core surrounded by a geotextile. The functions of the geotextile are as a filter (to allow liquid to pass into the drainage core) and as a separator (to prevent soil from entering and clogging the drainage core). Details on geotextile filtration products have been provided in Section 7.2.

The drainage core must be evaluated for its planar flow, i.e. its transmissivity, as with any other geosynthetic drainage core. ISO/DIS 12958, modified for the particular product's specific dimensions, is generally used for determination of the planar flow rate (see Section 7.4.2. It is important to use the project-specific cross-section so as to assess the amount of flow reduction due to intrusion and to conduct the test long enough to assess the possibility of creep of the drainage core, or of the covering geotextile.

7.7.5 CONTAINMENT (BARRIER) GEOCOMPOSITES

Geocomposites containing a geomembrane, e.g. with a geotextile or geonet, obviously take the barrier properties of the geomembrane. Thus the tests presented in Section 7.5 apply. As far as the other component(s) is concerned, its primary function must be assessed and tests conducted in accordance with the materials involved. The appropriate section in Chapter 7 should be consulted.

7.8 Degradation Mechanisms for Polymers

It is important to understand various degradation mechanisms in order to evaluate and ensure the durability of the geosynthetics. As indicated in the previous chapters, there are several types of polymers being used in manufacturing geosynthetics, e.g. PE, PP, PVC, PET, etc. As such, individual treatment of each polymer's degradation is not possible. Instead only the major chemical degradation mechanisms that involve geosynthetic polymers are discussed. They are oxidation (all types), ultraviolet (all types), biological (with respect to PVC) and hydrolytic (with respect to PET) degradations.

7.8.1 OXIDATION DEGRADATION

Polymers of different chemical structure vary markedly in their susceptibility to oxidation degradation. For polymers that are commonly used in geosynthetics, the rate of oxidation decreases in the following order (Grassie & Scott 1985):

$$PP > PE > PET > PVC$$

Since polyolefins, such as PP and PE, are the most susceptible materials (polyolefins refer to polymers containing only hydrogen and carbon atoms), the focus of this section is on the oxidation degradation of polyolefins. The degradation mechanisms of polyolefins will be described, followed by accelerated degradation tests and the methodology of lifetime

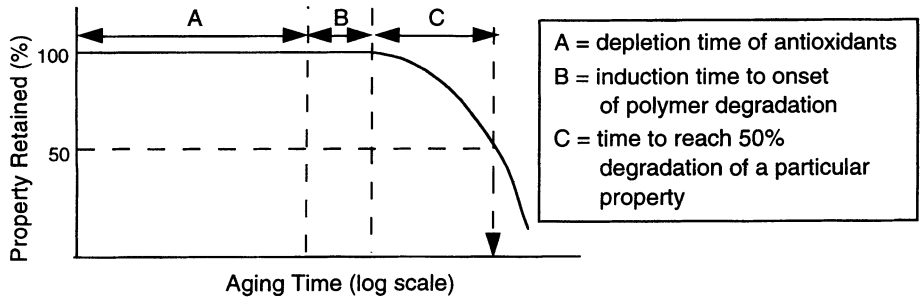


FIGURE 7.7. Three stages (A–C) of lifetime of polyolefin geosynthetic materials: Stage A, depletion time of antioxidants; stage B, induction time to onset of polymer degradation; stage C, time to reach 50% degradation of a particular property.

prediction when oxidation is the primary mechanism.

7.8.1.1 Oxidation Degradation Mechanisms of Polyolefins

In order to prolong the service life of polyolefins, antioxidants are always added into the polymer formulation to retard the onset of the oxidation. Figure 7.7 illustrates the influence of antioxidants on the overall lifetime of the material. A large portion of the material's lifetime is contributed by the antioxidants. Thus, it is essential to understand the function of antioxidants and their interaction in oxidation processes.

There are four groups of antioxidants being used in polyolefin geosynthetics. Each group of antioxidants has a unique function as explained by Grassie & Scott (1985). Furthermore, the operational temperature is different for each group of antioxidants (Fay & King 1994). Other than being depleted by chemical reactions, antioxidants can also be depleted by physical loss via either volatilization or dissolution (Luster 1986).

There are many different methods to evaluate the depletion of antioxidants. The most precise method is to extract the antioxidants from the polymer and analyze for their quantity using high-performance liquid chromatography. However, this is a very complex procedure due to the small quantity of antioxidants present in the formulations. Alternatively, the oxidative induction time (OIT) test indirectly measures the amount of antioxidants in the geosynthetic. There are two different OIT tests: standard OIT (ASTM D3895) and high-pressure OIT (ASTM 5885). A detailed description of these two tests regarding their advantages and disadvantages was presented by Hsuan & Koerner (1998). However, it should be noted that although these two OIT methods can effectively assess the amount of antioxidants in HDPE geomembranes, there is still ongoing research necessary to evaluate antioxidants in PP geosynthetics, particularly PP geotextiles.

After the antioxidants are completely consumed, the lifetime of the material enters into stages B and C as shown in Fig. 7.7. Now the polymer is no longer protected and oxidation degradation begins to occur in the polymer chains. The oxidation degradation of polyolefins involves a series of free radical reactions. These reactions can be divided into three stages: initiation, propagation and acceleration (Hsuan & Koerner 1998).

As oxidation proceeds, degradation occurs in the polymer via either cross-linking under oxygen deficiency, or chain scission under abundant oxygen (Grassie & Scott 1985).

This results in a decrease in molecular weight. Eventually, and after a relatively short induction period, i.e. stage B, the mechanical properties of the polymer change according to the extent of the degradation. This is labeled stage C in Fig. 7.7. An indirect qualitative method to assess changes in molecular weight of the polymer is the melt index (MI) test ASTM D1238. The test evaluates the melt flow behavior of the polymer. A high melt index value indicates a low molecular weight, and vice versa. As for the mechanical properties, tensile break stress and break strain are more sensitive to molecular weight changes than are yield stress and yield strain (Hsuan & Guan 1997).

Both the material itself and the service environment can affect the rate of oxidation reactions. Regarding the material, the amount of tertiary carbon atoms, crystallinity and transition metals are important factors (Hsuan *et al.* 1993). Also, the degrees of orientation of the manufactured product can also impede the diffusion of oxygen (Rapoport *et al.* 1977). Environmental factors include oxygen concentration, moisture and temperature (Salman *et al.* 1998).

7.8.1.2 Accelerated Tests and Lifetime Predictions

As illustrated in the previous two subsections, the lifetime of polyolefin geosynthetics is finite and is strongly dependent on the type and amount of antioxidants being added to the product. Acceleration methods are commonly used in the laboratory to predict the lifetime of the material. The most commonly used acceleration method to increase the degradation rate is by the use of elevated temperatures. Thomas & Ancelet (1993) and Yim & Godin (1993) used elevated temperatures to accelerate the depletion of antioxidants in HDPE geomembranes. Salman *et al.* (1997) also utilized a similar acceleration technique on polyolefin geotextiles and geogrids. Hsuan & Koerner (1998) indicate that the lifetime of antioxidants in HDPE geomembranes can be predicted using Arrhenius modeling. The predicted lifetime of antioxidants in a commercially available HDPE geomembrane sample varied from 50 to 200 years at a service temperature of 20 °C depending on the test environment and conditions. This signifies that the incubation condition must be carefully designed to simulate field conditions as closely as possible.

In the currently practiced manufacturing quality control specification of HDPE geomembranes (GRI-GM13), the OIT test is required. The minimum value is either 100/min for standard OIT (Std-OIT) or 400 min for high-pressure OIT (HP-OIT). Furthermore, the depletion rate of the antioxidant package is evaluated using a forced-air oven at 85 °C for 90 days. The incubated specimen must retain at least 55% of its initial OIT value for Std-OIT, or 80% for HP-OIT.

7.8.2 ULTRAVIOLET DEGRADATION

Ultraviolet (UV) light refers to the wavelength region less than 400 nm in the solar spectrum. Since energy is inversely proportional to the wavelength, photons in the UV region have energy levels that are compatible with the bond energy of polymers, which are unique for each chemical bond (Hirt & Searle 1964). Photodegradation occurs when the photon energy exceeds the bond energy. This phenomena is almost exclusively contributed by UV light. All polymers are degradable by UV light, but to varying degrees. For polyolefins, photodegradation is always associated with oxidation. Combination of the two reactions is referred to as photo-oxidation. Once free radicals are created by energy provided from photons, they rapidly react with the available oxygen. The basic polymer degradation reactions involved in the photo-oxidation are similar to the oxida-

tion process described in the previous section. As with oxidation, the types of antioxidants are very important for the longevity of geosynthetics that are exposed to sunlight (Vink 1986). In addition to antioxidants, carbon black is used as a UV stabilizer. Carbon black functions as a light absorber. The typical carbon black content in polyolefin geomembranes is 2–3%, beyond this amount the mechanical properties begin to diminish.

Since PVC geomembranes contain up to 35% plasticizers, both the polymer and plasticizer must be able to resist UV degradation. The major chain degradation process of PVC is zip-elimination of HCl and the simultaneous formation of conjugated double-bonds, which can induce the formation of free radicals (Ivan 1993). Similar to polyolefins, transition metals, such as iron, also have a significant effect on the photo-oxidation of PVC (Joffe & Ranby 1976).

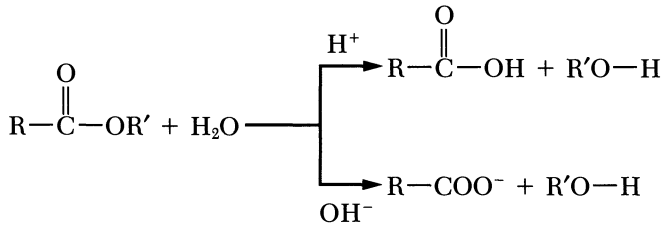
At the present time, simulation of outdoor UV degradation by laboratory weatherometers is still a controversial issue. Furthermore, fluctuation of ambient conditions makes the simulation very challenging. Currently, there are two types of weatherometers that are commonly used: xenon arc and UV fluorescent. The xenon weatherometer can generate an artificial light spectrum that is similar to sunlight. For geosynthetics, the operation procedure is according to ASTM D4355. In contrast, the UV weatherometer can select different fluorescent lights in either the UV-A or UV-B region of the spectrum. There is no visible light generated. The operational procedure for HDPE geomembranes is according to GRI-GM10. For other geosynthetics, ASTM D5208 can be used. Researchers are constantly attempting to correlate data between weatherometers and outdoor exposure. Baker & Marienfeld (1995) presented data for PP geotextiles in both field and xenon arc weatherometer, and Comer *et al.* (1998) studied the UV resistance of PP geomembranes in both the field and UV weatherometer. Recognize that results of such correlations are only valid at those particular field locations. An accurate prediction of the UV resistance of exposed geosynthetics remains a difficult challenge.

7.8.3 BIOLOGICAL DEGRADATION

Biological degradation refers to two chemical activities: (1) assimilatory processes, in which constituents of plastics serve as sources of nutrients for organisms; (2) dissimilarity processes, in which the plastic is chemically damaged by corrosive substances produced and secreted by an organism (Kuster 1976). Most geosynthetic polymers are considered to be resistant to microbial attack due to their high molecular weight. However, additives that are contained in the polymer are more susceptible to biological degradation than the basic polymers due to their low molecular weight. Their biodegradability depends on the physical and chemical properties of the specific additives used in the formulation. For geosynthetics that contain a high percentage of additives, such as plasticized PVC geomembrane, a simulated test should be performed to verify the material's resistance to microbials. Bright (1993) has summarized current test methods and reviewed their advantages and limitations.

7.8.4 HYDROLYTIC DEGRADATION

Hydrolysis is a chemical reaction that involves decomposition of a substance by water. Only PET geosynthetics (geotextiles and geogrids) are susceptible to this reaction. The ester group in the PET reacts with water leading to chain scission in the polymer. The reaction is accelerated in the presence of acid or alkaline environments as indicated in Eqs 7.6 and 7.7 (Morrison & Boyd 1992). This is particularly the case in alkaline environments.



$$R-\overset{\overset{O}{\|}}{C}-OR' + H_2O \xrightarrow{H^+} R-\overset{\overset{O}{\|}}{C}-OH + R'O-H \quad (7.6)$$

$$R-\overset{\overset{O}{\|}}{C}-OR' + H_2O \xrightarrow{OH^-} R-COO^- + R'O-H \quad (7.7)$$

Two different phenomenon can occur in the hydrolysis of PET depending on the pH level. In neutral and acidic conditions, i.e. pH $\leq$ 7 hydrolysis is an "internal" reaction and is mainly governed by the diffusion of water and H^+ ions into the amorphous phase. In contrast, "external" hydrolysis occurs under high alkaline conditions, pH > 10. Furthermore, it has been found (Halse *et al.* 1987a,b and Sprague 1990) that calcium cations induce a greater acceleration than sodium cations under the same pH level.

The hydrolytic resistance of PET products depends on two intrinsic material properties. They are the molecular weight and carboxyl end group (CEG) (Schmidt *et al.* 1994). The current AASHTO specification for PET geosynthetic reinforcing materials requires PET yarns to have a number-average molecular weight greater than 25,000 and a CEG value less than 30 mmol g^{-1}.

The lifetime prediction of the PET yarns under acidic and alkaline environments has been studied by Salman *et al.* (1997). Their results showed that at a pH = 7 condition, the half-lifetime of the PET yarns being evaluated was approximately 100 years. However, at a highly alkaline condition of pH = 12, the half-lifetime decreased to 10 years.

7.9 *Allowable versus Ultimate Geotextile and Geogrid Properties*

It is important to recognize that many of the preceding test properties represent idealized (or in-isolation) conditions and, therefore, result in the maximum possible numeric property values if used directly in design; i.e. they result in upper-bound values. Yet, when practicing the design-by-function process, the laboratory value should be as close as possible to the perceived field situation; i.e. the values should be performance-related. The equation is usually expressed as:

$$\text{Factor of safety (FS)} = \frac{\text{Allowable (test) property}}{\text{Required (design) property}} \quad (7.8)$$

In this context most laboratory test values generally cannot be used directly; they must be suitably modified for *in situ* conditions. This could be done directly in the test procedure, for example, by conducting a completely simulated performance test; but in most cases this is simply not possible. Simulating installation damage, performing long-term creep testing, using site-specific liquids, reproducing *in situ* porewater stress, providing complete stress state modeling, and so on, are generally not feasible. To account for such differences between the laboratory measured test value and the desired allowable value, two approaches can be taken:

- For strength and flow related applications, the laboratory obtained value can be modified by reduction factors to better simulate site specific conditions.
- For strength related applications, the laboratory obtained value can be adjusted by using partial factors on the rupture or limiting strain value at the anticipated end of the site specific design life.

7.9.1 STRENGTH RELATED APPLICATIONS

For applications dealing with geotextiles (such as separation and reinforcement problems) and with geogrids (such as reinforcement problems), either of the following approaches can be used.

7.9.1.1 Allowable strength approach

The allowable strength approach uses a laboratory generated, short-term, in-isolation strength value, T_{ult}, and reduces it to an allowable strength value, T_{allow}, by site-specific reduction factors:

$$T_{allow} = T_{ult}\left(\frac{1}{RF_{ID} \times RF_{CR} \times RF_{CD} \times RF_{BD}}\right) \quad (7.9)$$

$$T_{allow} = T_{ult}\left(\frac{1}{\Pi RF}\right) \quad (7.10)$$

where T_{allow} = allowable tensile strength for use in design; T_{ult} = ultimate tensile strength from the laboratory test, usually wide-width tensile test, but occasionally other related strength tests; RF_{ID} = reduction factor for installation damage; RF_{CR} = reduction factor for creep; RF_{CD} = reduction factor for chemical degradation; RF_{BD} = reduction factor for biological degradation; and ΠRF = cumulative value of all reduction factors. Table 7.6 gives recommended values for the above reduction factors depending on the type of application. It is important to note that if additional site-specific factors are involved, e.g. seams or intentionally made holes, they can be included in the formulation accordingly. Conversely, if any of the listed factors have been included in the laboratory test it would appear in the above formulation as a value of 1.0.

7.9.1.2 Limit state approach

A related, but somewhat different, approach is called limit (or ultimate) state design and is based on an initial value of creep rupture, or a limiting strain to reach a desired lifetime. This approach is embodied in the British Standard BS 8006, and uses creep rupture in the laboratory test thereby avoiding a creep reduction term, *per se*. The formulation is given in Eqs 7.11 and 7.12:

$$T_{des} = T_B\left(\frac{1}{f_m \times f_d \times f_{env}}\right) \quad (7.11)$$

$$T_{des} = T_B\left(\frac{1}{\Pi f}\right) \quad (7.12)$$

where T_{des} = design tensile strength; T_B = laboratory generated tensile strength leading to creep rupture or to a limiting strain at the

TABLE 7.6. Range of reduction factors for use in Eq. 7.9

Function or application	Installation damage (RF_{ID})		Creep[a] (RF_{CR})		Chemical degradation (RF_{CD})		Biological degradation (RF_{BD})	
	GT[a]	GG[d]	GT[c]	GG[d]	GT[c]	GG[d]	GT[c]	GG[d]
Separation	1.1–2.5	n/a[b]	1.5–2.5	n/a	1.0–1.5	n/a	1.0–1.2	n/a
Embankments	1.1–2.0	1.1–1.4	2.0–3.5	2.0–3.0	1.0–1.5	1.1–1.4	1.0–1.3	1.0–1.2
Slopes	1.1–1.5	1.1–1.4	2.0–3.0	2.0–3.0	1.0–1.5	1.1–1.4	1.0–1.3	1.0–1.2
Walls	1.1–2.0	1.1–1.4	2.0–4.0	2.0–3.0	1.0–1.5	1.1–1.4	1.0–1.3	1.0–1.2

[a] Low end of the range refers to applications that have relatively short service lifetimes and/or situation where creep deformation is not critical to system performance.
[b] n/a, not available.
[c] GT = geotextile.
[d] GG = geogrid.

TABLE 7.7. Range of partial factors for use in Eq. 7.11

Function or application	Material (f_m)		Damage (f_d)		Environment (f_{env})	
	GT	GG	GT	GG	GT	GG
Separation	1.2–1.4	n/a	1.1–2.5	n/a	1.0–1.5	n/a
Embankments	1.3–1.7	1.2–1.5	1.1–2.0	1.1–1.4	1.0–1.7	1.1–1.5
Slopes	1.3–1.7	1.2–1.5	1.1–1.5	1.1–1.4	1.0–1.7	1.1–1.5
Walls	1.5–2.0	1.3–1.7	1.1–2.0	1.1–1.4	1.0–1.7	1.1–1.5

end of the anticipate design life, e.g. extrapolated creep rupture curve or isochronous curves of extrapolated strain data; f_m = partial factor related to uncertainty of the intrinsic properties of the material; f_d = partial factor for short- or long-term damage; and f_{env} = partial factor for environmental effects. Table 7.7 gives recommended values for the above partial factors depending on the type of application.

7.9.2 LIQUID FLOW RELATED APPLICATIONS

For hydraulic applications dealing with geotextiles (either flow through them as in filtration, or flow within them as in drainage) and for drainage composites (like geotextile–geonet or geotextile–drainage core materials), the formulation for allowable flow parallels the approach of Section 7.9.1.1. Note that drainage cores take many possible shapes: including columns, nubs, cuspations, webbing, mats, ribs, etc. In all cases a geotextile is bonded to the drainage core as the product is manufactured. The reduction factors are completely different and now refer to liquids flowing through or within the respective geosynthetic product. The allowable flow rate approach uses a laboratory generated, short-term, in-isolation, flow value using water as the permeant. The reduction factors are obviously completely different and now refer to liquids flowing through, q_{ult}, and reduces it to an allowable flow rate, q_{allow}, by site-specific reduction factors:

$$q_{allow} = q_{ult}\left(\frac{1}{RF_{SCB} \times RF_{CR} \times RF_{IN} \times RF_{CC} \times RF_{BC}}\right) \quad (7.13)$$

$$q_{allow} = q_{ult}\left(\frac{1}{\Pi RF}\right) \quad (7.14)$$

where q_{allow} = allowable flow rate for use in design; q_{ult} = ultimate flow rate from the appropriate laboratory test, usually the permittivity or transmissivity test; RF_{SCB} = reduction factor for soil clogging and blinding; RF_{CR} = reduction factor for creep reduction of void space; RF_{CC} = reduction factor for chemical clogging; RF_{BC} = reduction factor for biological clogging; and ΠRF = cumulative value of all reduction factors. Table 7.8 gives recommended values for the above reduction factors depending on the type of application. It is important to note that if additional site-specific factors are involved, e.g. blocking of a geotextile's surface by riprap or concrete blocks, they can be included in the formulation accordingly. Conversely, if any of the listed factors have been included in the laboratory test it would appear in the formulation as a value of 1.0.

7.10 Summary

In closing this section on laboratory testing of geosynthetics it is important to emphasize that the entire design process falls apart without representative testing values. Recall Eq.

TABLE 7.8. Range of reduction factors for use in Eq. 7.13

Function or application	Soil clogging and blinding (RF_{SCB})		Creep reduction of voids (RF_{CR})		Intrusion into voids (RF_{IN})		Chemical clogging (RF_{CC})		Biological clogging (RF_{BC})	
	GT[a]	GC[b]	GT[a]	GC[b]	GT[a]	GC[b]	GT[a]	GC[b]	GT[a]	GC[b]
Embankments	2–4	3–5	1.5–2.0	2–3	1.0–1.2	1.1–1.5	1.0–1.2	1.1–1.3	1.0–1.3	1.1–1.5
Slopes	2–4	3–5	1.5–2.0	2–3	1.0–1.2	1.1–1.5	1.0–1.2	1.1–1.3	1.0–1.3	1.1–1.5
Walls	2–4	3–5	1.5–2.0	2–3	1.0–1.2	1.1–1.5	1.0–1.2	1.1–1.3	1.0–1.3	1.1–1.5
Underdrains	5–10	5–10	1.0–1.5	1.0–1.5	1.0–1.2	1.1–1.5	1.2–1.5	1.5–2.0	2–4	2–5
Erosion control	2–10	2–10	1.0–1.5	1.0–1.5	1.0–1.2	1.1–1.5	1.0–1.2	1.1–1.3	2–4	2–5
Landfill leachate	5–10	5–10	1.5–2.0	2–3	1.0–1.2	1.1–1.5	1.2–1.5	1.5–2.0	5–10	5–10

[a] GT = geotextile used as a filter.
[b] GC = drainage composite including geotextile(s) as a filter/separator.

7.8, from which it is inferred that no amount of design accuracy is useful beyond the accuracy of the allowable (test) property value. In this regard, the laboratory test must be crafted so as to be both product-specific and site-specific. The use of literature values for permanent and/or critical applications is completely inappropriate. Also to be noted is that only the design engineer knows (or should know) the site-specific conditions. Thus it is encumbent on the design engineer (*not* on the geosynthetics manufacturer) to provide the requisite value for the envisioned site-specific conditions.

In this regard, it is recognized that many design engineers do not have a geosynthetics laboratory, *per se*. Furthermore, to mobilize and equip such a laboratory is quite expensive. Fortunately, there are a number of such laboratories that are available. These are either independent laboratories, or are within research institutes or universities. The concern to the writers of this section is to be sure that such new and emerging laboratories are indeed capable of performing the tests in the manner prescribed in the appropriate test standards. All of these laboratories (independent, institute and university) should be accredited for the tests that they advertise as being capable of performing. Such laboratory accreditation programs are available on a world-wide basis.

8. SEEPAGE, DRAINAGE AND DEWATERING

R. W. Loughney

8.1 Introduction

Each year thousands of projects require some type of groundwater control. Whether it is minor seepage or a complex groundwater flow, a proper assessment of the conditions at the site and the selection of an appropriate groundwater control system is essential to the successful completion of the project. This chapter will describe procedures that can be of assistance in the assessment, selection, design, installation, operation and removal of groundwater control systems.

8.2 Geology, Hydrogeology and Hydrology

8.2.1 GEOLOGY

The geology of the site should be reviewed and the soils identified as to whether they are river channel, flood-plain, delta, glacial, shore, wind-blown, or still-water deposits or residual soils. Generally for flood-plain, lake and wind deposits, the soils are more consistent and are less likely to have significant differences within the site that is to be dewatered. River channel, delta and glacial soil deposits and residual soils can vary considerably within the site that is to be dewatered. Where rock is encountered, the type and quality of the rock should be established. For limestone, coral, basalt and sandstone rock formations the history of the general area should be reviewed in detail.

8.2.2 HYDROGEOLOGY

Although there may be considerable existing information about the hydrogeology of the general area of interest, very seldom is this data sufficient for a particular construction site. As discussed in more detail in Chapter 4, the site investigation should include sufficient borings that extend below the final subgrade to the depth required to intercept all pervious strata that could cause boils in and/or the heave of the subgrade due to water pressures in the pervious strata as shown in Fig. 8.1. To avoid boils or basal heave, it is necessary that there be an adequate factor of safety, F, where:

$$F = D\gamma'/h\gamma_w > 1 \qquad (8.1)$$

where D = the minimum depth below the excavation that the borings should extend (see Fig. 8.1); h = the height to which water rises in a monitor (at depth D) above the base of the excavation; and γ_{sat} and γ' = the average saturated unit weight and submerged unit weight of the soil between the base of the excavation and depth D, respectively; γ_w = average unit weight of water; and $\gamma' = \gamma_{sat} - \gamma_w$.

The borings should define the hydrogeology of the site and provide detailed descriptions of: the soil, rock and water encountered; the depth at which water was encountered; the loss or gain of water during drilling; any soil heave; voids encountered within the bore hole; collapse of the bore hole and any other difficulties encountered. Piezometers (ob-

R. K. Rowe (ed.), *Geotechnical and Geoenvironmental Engineering Handbook*
© Kluwer Academic Publishers 2001

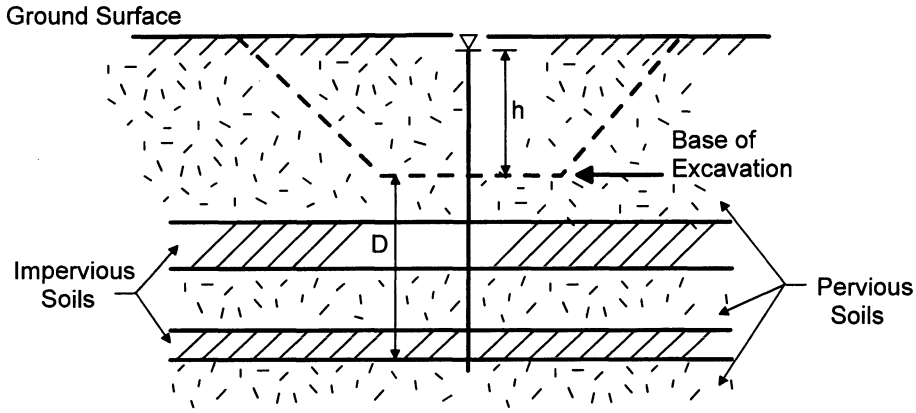


FIGURE 8.1. Minimum depth of borings to avoid boils and/or basal heave.

servation wells) should be installed in the various pervious strata and other sensitive strata. Whenever possible, the water-level data should be collected over at least a year so that the seasonal effect on the water-levels can be established. Groundwater samples should be taken and analyzed, as a minimum, for the constituents shown in Table 8.1. The investigation should identify any evidence of contamination in the soil or water. Rock samples should be classified with particular care as to the degree of weathering and presence of fissures, cracks and voids in the rock. For most rocks, pressure testing of the bore hole will provide a good indication of the hydraulic conductivity (see Section 4.7). Coral, limestone, dolomite, basalt and sandstone rocks have a history of being very pervious and should be considered so until proven otherwise. For large projects that could be significantly impacted by the groundwater, often a pumping test is performed to confirm the hydraulic conductivity inferred from the geotechnical data.

TABLE 8.1. Groundwater analysis

	Units
ph	—
Color	—
Turbidity	—
Conductivity	$\mu\Omega\ cm^{-1}$
Total dissolved solids	$mg\ l^{-1}$
Total alkalinity, $CaCO_3$	$mg\ l^{-1}$
Carbonate alkalinity, $CaCO_3$	$mg\ l^{-1}$
Bicarbonate alkalinity, $CaCO_3$	$mg\ l^{-1}$
Hydroxide alkalinity, $CaCO_3$	$mg\ l^{-1}$
Chloride, as Cl	$mg\ l^{-1}$
Nitrate, as N	$mg\ l^{-1}$
Temperature	°C
Iron, as Fe	$mg\ l^{-1}$
Floride, as F	$mg\ l^{-1}$
Phosphate, as PO_4	$mg\ l^{-1}$
Total hardness, $CaCO_3$	$mg\ l^{-1}$
Calcium hardness, $CaCO_3$	$mg\ l^{-1}$
Magnesium hardness, $CaCO_3$	$mg\ l^{-1}$
Manganese, as Mn	$mg\ l^{-1}$
Copper, as Cu	$mg\ l^{-1}$
Sulfate, as SO_4	$mg\ l^{-1}$
Silica, as SiO_2	$mg\ l^{-1}$

8.2.3 HYDROLOGY

8.2.3.1 Basic Flow Equations

As discussed in Section 2.4, the flow of water through porous media is described by Darcy's law:

$$v = ki \tag{8.2a}$$

$$Q = vA \tag{8.2b}$$

where v = Darcy velocity (flux), k = hydraulic conductivity, i = hydraulic gradient, Q = volume of water, and A = the cross-sectional area. Under three-dimensional steady state flow conditions, the continuity equation can be written as:

$$\frac{\partial v_x}{\partial x} + \frac{\partial v_y}{\partial y} + \frac{\partial v_z}{\partial z} = 0 \tag{8.2c}$$

where v_x, v_y, v_z = the Darcy velocities in the three Cartesian directions. Combining Eq. 8.2a and 8.2c gives Laplace's equation, which has been solved for a wide range of boundary conditions relevant to dewatering. The most commonly used solutions are based on the following assumptions (Driscoll 1986):

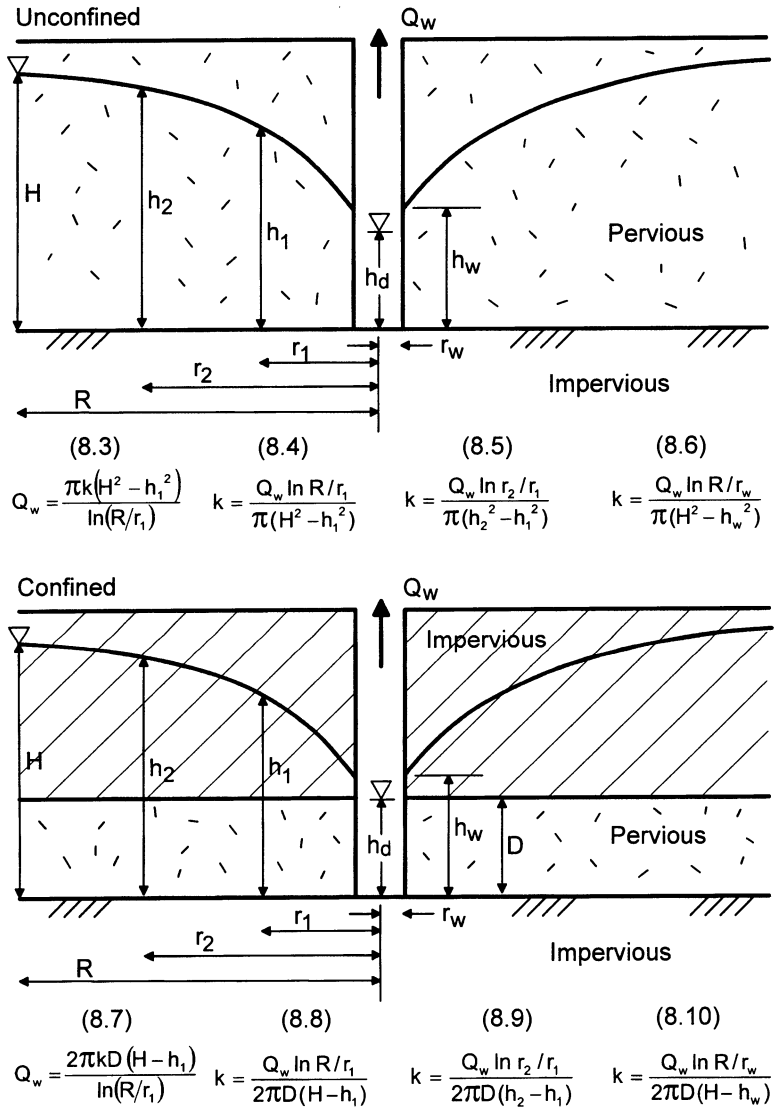


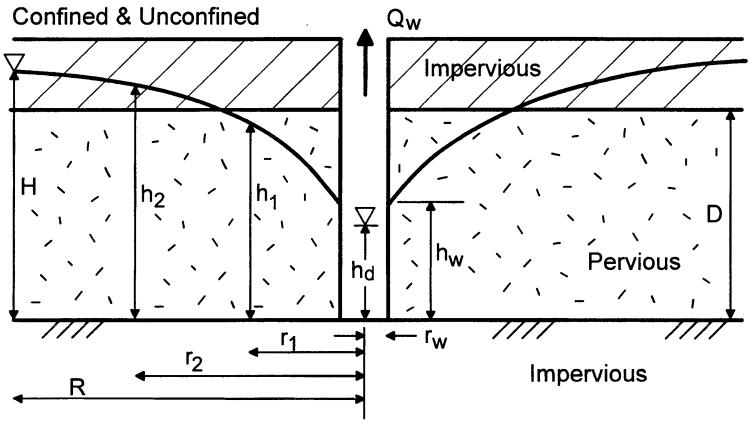
FIGURE 8.2. Mathematical procedure: (a) unconfined aquifer, and (b) confined aquifer (modified from US Army 1983 and Leonards 1962).

- the water bearing soils have a uniform hydraulic conductivity, are not stratified and have a constant saturated thickness;
- the well is 100% efficient;
- the well-screen penetrates the entire aquifer;
- the flow through the aquifer is laminar;
- the initial water table is flat;
- equilibrium has been reached and the drawdown and radius of influence no longer change with continued pumping at the same rate.

Though many of these assumptions may not occur in practice the solutions can be used to calculate the approximate volumes of water that can be expected for most conditions encountered in construction. A number of the mathematical and graphical solutions commonly used are given by Eqs 8.3–8.26 in Figs 8.2–8.6.

8.2.3.2 Graphical Approach

For most projects that require dewatering a pumping test is not provided as part of the



(8.11)

$$Q_w = \frac{\pi k(2DH - D^2 - h_1^2)}{\ln(R/r_1)}$$

(8.12)

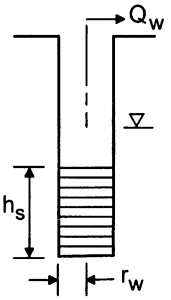
$$k = \frac{Q_w \ln R/r_1}{\pi(2DH - D^2 - h_1^2)}$$

(8.13)

$$k = \frac{Q_w \ln r_2/r_1}{\pi(2Dh_2 - D^2 - h_1^2)}$$

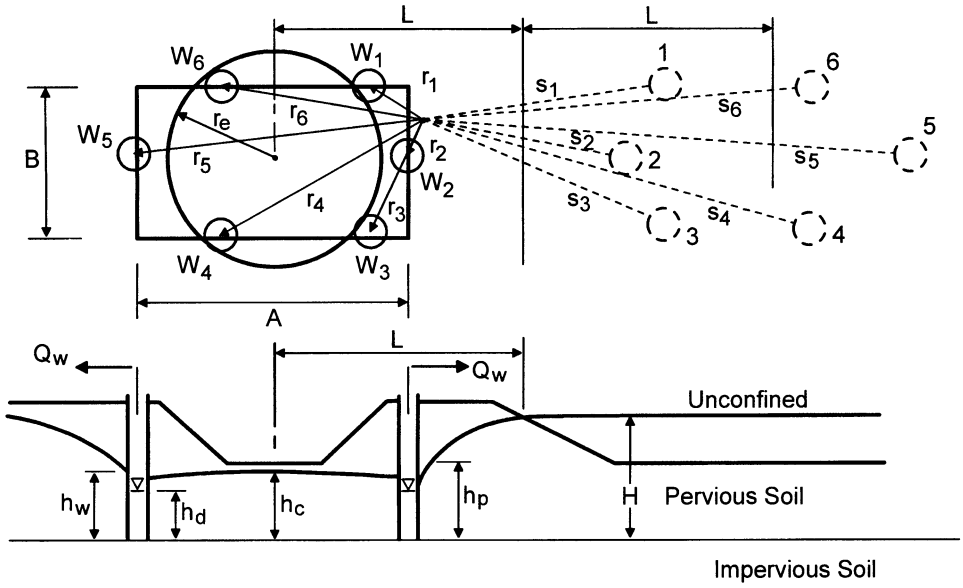
(8.14)

$$k = \frac{Q_w \ln R/r_w}{\pi(2DH - D^2 - h_w^2)}$$



$$Q_w = 2\pi r_w h_s \frac{\sqrt{k}}{15} \quad m^3/s \quad (8.15)$$

FIGURE 8.3. Mathematical procedure: confined and unconfined aquifer and capacity of a single well (modified from US Army 1983, Leonards 1962, and Jumikis 1971).



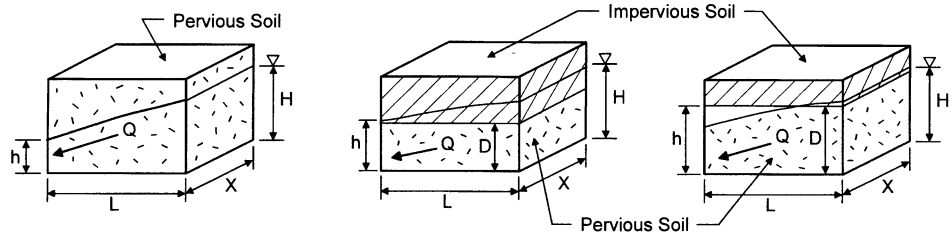
$$r_e = 1.15\sqrt{\frac{AB}{\pi}} \qquad (8.16)$$

$$Q_T = \frac{\pi k(H^2 - h_c^2)}{\ln(2L/r_e)} \qquad (8.17)$$

$$h_p^2 = H^2 - \frac{1}{\pi k}\left(Q_{w1}\ln\frac{s_1}{r_1} + \text{------} + Q_{w6}\ln\frac{s_6}{r_6}\right) \qquad (8.18)$$

Q_T / Q_w = No. of Wells

FIGURE 8.4. Mathematical procedure: unconfined aquifer (modified from Avery 1951).



UNCONFINED **CONFINED** **CONFINED AND UNCONFINED**

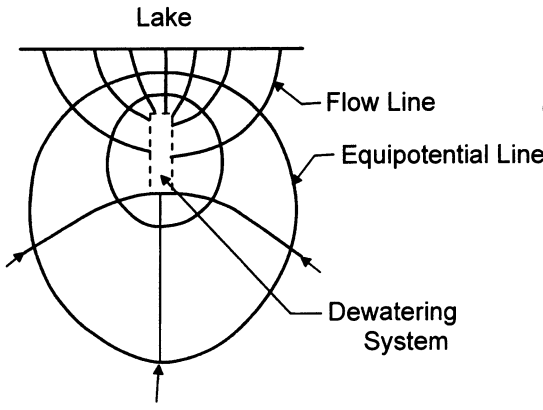
$$Q = \frac{kX(H^2 - h^2)}{2L} \qquad (8.19)$$

$$Q = \frac{kDX(H - h)}{L} \qquad (8.20)$$

$$Q = \frac{kX(D^2 - h^2)(2DH - D^2 - h^2)^*}{2L(D^2 - h^2)} \qquad (8.21)$$

Use for closely spaced wells, wellpoints, horizontal drains.
For a moving excavation maintain 30 m (100 ft) of system acting in advance and behind the area being dewatered by the system.

FIGURE 8.5. Mathematical procedure: drainage slot–line source of recharge (modified from US Army 1983 and Leonards 1962).



Unconfined

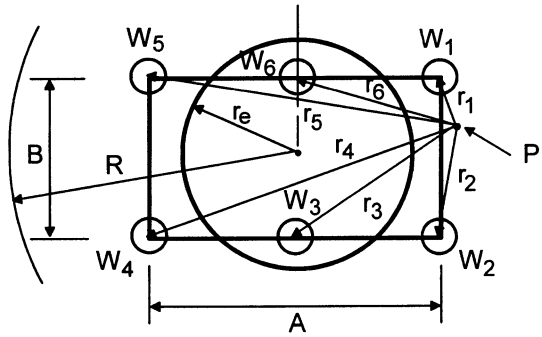
$$Q = \frac{k(H^2 - h_c^2)N_f / N_e}{2} \quad (8.22)$$

Confined

$$Q = kD(H - h_c)\, N_f / N_e \quad (8.23)$$

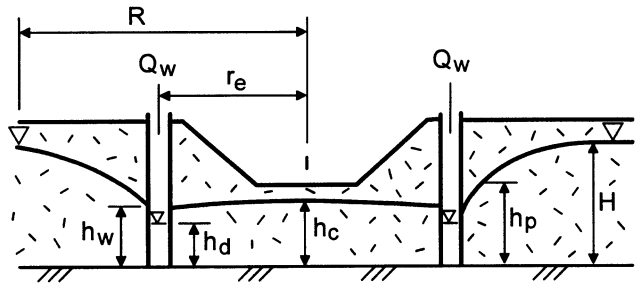
N_f = number of flow tubes

N_e = number of potential drops



$$r_e = 1.15\sqrt{\frac{AB}{\pi}} \quad (8.24)$$

$$Q_T = \frac{\pi k(H^2 - h_c^2)}{\ln R/r_e} \quad (8.25)$$



$$h_p^2 = H^2 - \frac{1}{\pi k}(Q_{w1} \ln R/r_1 + Q_{w2} \ln R/r_2 + ----+ Q_{w6} \ln R/r_6) \quad (8.26)$$

FIGURE 8.6. Graphical and mathematical procedures (modified from Casagrande 1937, and US Army 1983).

pretender data. A procedure that can be used to select dewatering systems for these projects is as follows. Estimate the hydraulic conductivity, k, from the available geotechnical data and other data such as local water supply wells. Referring to an applicable equation in Figures 8.2–8.6, select as appropriate the H, D, h, h_c, r, r_e, x and L from the geometry of the project. Where L is not applicable, an approximate R can be ascertained from:

$$R = C(H - h_w)k^{0.5} \quad (8.27)$$

where k is in m s^{-1}; C = 3000 for wells and 1500–2000 for a single line of closely spaced wells or wellpoints; and R, H and h_w are in meters.

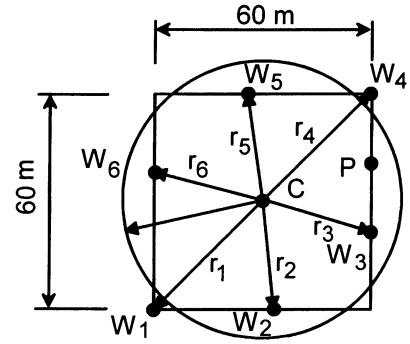
Figures 8.7 and 8.8 illustrate how these equations can be used to calculate the estimated volume of water, Q_T, that will be needed to be pumped to dewater an excavation. Assuming $k = 2 \times 10^{-4}$ m s^{-1} and for values of H = 18 m and h_c = 10.7 m (see Fig. 8.7), one can calculate R from Eq. 8.27 and hence deduce $Q = Q_T$, r_e and Q_w (for a

$R = 3000(H - h_c)\sqrt{k}$ [assume 75% of $(H - h_c)$] From Eq. 8.27

$\therefore R = 3000\,(0.75)\,(18 - 10.7)\,\sqrt{(0.0002\ m/s)} = 232m$

$r_e = 1.15\sqrt{\frac{60^2}{\pi}} = 39m$ From Eq. 8.16

$Q_T = \frac{\pi k(H^2 - h_c^2)}{\ln(R/r_e)} = \frac{3.14\,(0.0002)\,(18^2 - 10.7^2)}{\ln(232/39)} = 0.074\ m^3/s$ From Eq. 8.25

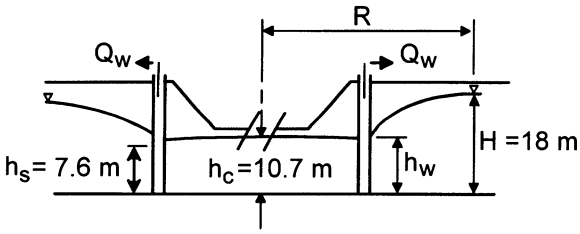


$Q_w = 2\pi r_w \frac{\sqrt{k}}{15} h_s$ From Eq. 8.15a

$= 6.28\,(0.3)\frac{\sqrt{0.0002}}{15}\,(7.6)$

$= 0.0135 m^3/s$

$Q_T / Q_w = 0.074/0.0135 = 5.5$ say 6 wells



From Fig. 8.8 obtain drawdowns at various distances

Distance From Well to Point C (m)	Drawdown at Point C (m)	Distance From Well to Point P (m)	Drawdown at Point P (m)
W_1 (r_1) 43	1.2	72	0.8
W_2 (r_2) 31	1.3	48	1.0
W_3 (r_3) 32	1.3	20	1.7
W_4 (r_4) 43	1.2	20	1.7
W_5 (r_5) 30	1.3	40	1.2
W_6 (r_6) 30	1.3	60	0.9
Total Drawdown	7.6		7.3

FIGURE 8.7. Mathematical procedure for an example situation.

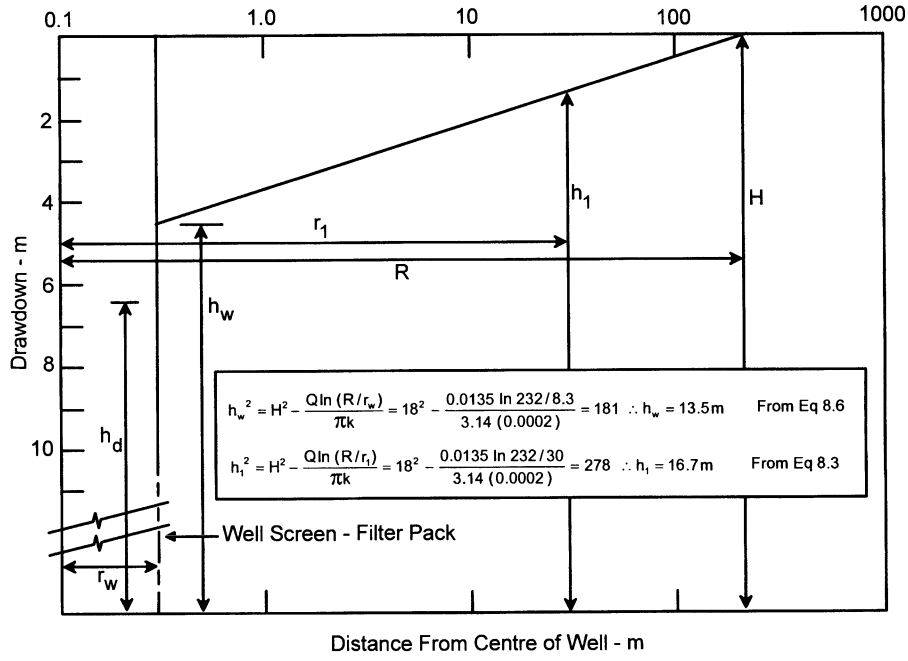


FIGURE 8.8. Graphical procedure for an example situation.

single well of radius r_w = 0.3 m and well-screen h_s = 7.6 m) from Eqs 8.25, 8.16 and 8.15, respectively. One can then divide the estimated volume of water required to dewater the excavation, Q_T, by the estimated flow for a single well, Q_w, and obtain the initial number of dewatering wells required for the project. Using the flow of water for a single well, Q_w, the radius of the well or filter pack, r_w, and the appropriate H, R or L, the drawdown, h_w, at the perimeter of the well-screen or filter pack, r_w, and the drawdown, h_1, at distance r_1, 30 m away from the well can be calculated using appropriate equations from Figs 8.2 or 8.3 as shown in Fig. 8.8. With this data, plot a distance drawdown graph as shown in Fig. 8.8. At selected site locations, e.g. points C and P on Fig. 8.7, which should include an operating dewatering well, measure the distance from each dewatering well, e.g. W_1, W_2, . . . , W_6 in Fig. 8.7) to each selected site location. From the distance drawdown curve (Fig. 8.8), obtain the cumulative drawdown caused by all of the wells at each location as shown on Fig. 8.7.

With all the wells operating, assume that the wells will have an efficiency of 70% (the depth of the drawdown at the perimeter of the well-screen or filter pack over the depth of the drawdown inside of the well). One then modifies the arrangement and number of wells to accommodate the desired drawdowns at specific locations. Often, smaller capacity wells have to be used to adjust for the efficiency of the wells. The efficiency of a well can vary from 10 to 90% depending on the well-screen, filter pack and the installation procedure used. In addition to the drawdown in the wells due to the inefficiency of the wells, additional drawdown occurs in the wells where the thickness of the aquifer is reduced more than 20%; a condition that often occurs for unconfined aquifers. The distance drawdown graph for the initial well capacity

can be adjusted in direct proportion to the change in the new yield of the well. Also, the expected yield from each dewatering well has to be adjusted for the interference from the other dewatering wells. The closer the dewatering wells are spaced the greater is the interference and the larger is the reduction in the yield from each dewatering well. Lowering the level of the water within the dewatering wells to near the bottom of the well-screens, and/or applying a vacuum to the well-screens, where conditions permit, will help to offset some of the reduction in the yield of the dewatering wells, provided the formation is similar along the length of the wetted well-screens. Generally, the pumps used are capable of lowering the water close to the bottom of the well so as to maximize the yield from the dewatering wells.

8.3 *Seepage and Drainage*

8.3.1 SEEPAGE

In general, excavation below the groundwater level will cause seepage through the sides and up through the bottom of the excavation and this seepage can cause problems during construction. The movement of the water exerts seepage pressures on the soils that can reduce stability and cause failures. The groundwater pressures should be reduced to the extent that excessive flow and movement and/or loosening of the soils will not occur.

8.3.2 DRAINAGE

The control of seepage can be accomplished by draining the soils concurrent with and/or in advance of the excavation below the groundwater level. Sometimes ungraded coarse gravel is used along the perimeter of the excavation to drain the soils. Problems may arise if the soils being drained flow through the coarse gravel and are removed by pumping, resulting in the loss of ground and a change in the density of the soils. Occasionally, the ungraded coarse gravel is placed over the soil beneath the subgrade of the structure to drain the excavation. In these cases, if the groundwater is allowed to rise above the subgrade of the structure and then the groundwater is lowered rapidly within the coarse gravel, the head in the soils beneath the coarse gravel may not dissipate quickly and the soils may become unstable and settlement will occur. These problems can be eliminated by using a better form of predrainage as described below.

For many projects, pervious strata overlay less pervious strata or pervious strata are sandwiched between less pervious strata (see Fig. 8.9). The less pervious strata restrict

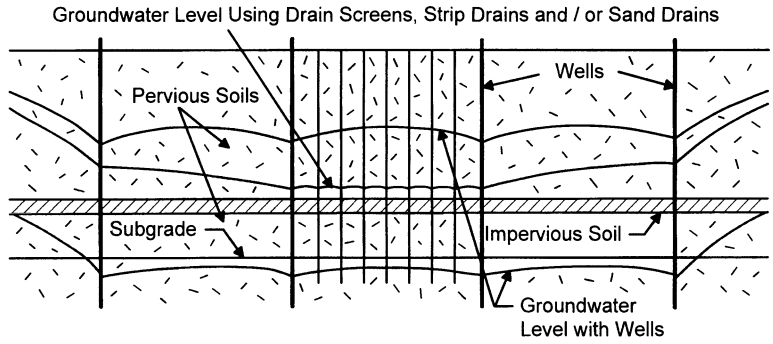


FIGURE 8.9. Use of vertical drains for stratified soils.

the levels to which the groundwater can be lowered by various types of dewatering systems. For example, wells spaced at 15 m can leave 1.5–4.5 m of water in a pervious strata overlaying a less pervious strata. Where the groundwater can be lowered to the required depths in deeper pervious strata by wells, the height of the groundwater remaining perched in the pervious strata above a less pervious strata, can be lowered to acceptable heights (0.6 m), using vertical drains or angle drains that extend into the lower pervious strata. To control the last 0.3–0.6 m of water remaining above an impervious layer, ditches or a sand-bag wall can be used. For this procedure to function the deeper pervious strata should be at least as permeable as the upper pervious strata.

The vertical drain screens or angle drain screens should extend from the full height of the initial groundwater in the upper pervious strata to the depth in the lower pervious strata that is needed to accept the volume of water transmitted by the drain screens as illustrated in Fig. 8.9. For most soil conditions the drain screen should be encased in the type of filter pack described in Section 8.7.2. The design and installation procedures for the vertical and angle drains are the same as would be used for wells, wellpoints and vacuum wells. Sand drains or prefabricated vertical drains (strip drains, wick drains) can be used to provide the vertical drainage where a low volume of water is to be drained (see also Section 15.2.3). The strip drains should have an interior vertical space that provides free vertical movement of the water. The strip drains can be installed using conventional strip drain rigs where the soil is suitable for this type of installation. Sand drains can be installed by jetting or jet and drive casing procedures, as would be used for the installation of wells and wellpoints. The sand suitable for the sand drains is described in Section 8.7.2 with less than 10% passing the 0.295 mm (No. 50) sieve.

8.4 Area to be Dewatered

For most construction sites control of surface water is essential. More dewatering projects have been inundated by surface water rather than by groundwater. Ditches and/or berms should be provided around the top of the site to divert surface water away from the excavation. Ditches, sumps and pumps should be provided at the toe of the slope to collect and discharge surface water outside of the excavation. For deep excavations, ditches, sumps and pumps should be provided at intervals along the slope of the excavation to collect and dispose of the surface water and hence prevent serious erosion of the slope by surface water. For example, to excavate 26 m below the level of Lake Michigan, 580 eductor wells pumping 265 l s^{-1} were required to dewater the 975-m perimeter excavation. Surface water control was an essential part of the groundwater control system. During heavy storms spray from the lake came across the top of the cofferdam at the rate of 1260 l s^{-1}. An extensive berm and slope protection and sumping system were required to control this surface water.

Any changes in the natural conditions can have a significant effect on the dewatering. New structures, existing and discarded utilities, old piles, bore holes, cuts and fills, etc., may alter the flow of groundwater and surface water, change the levels of the groundwater, develop perched water conditions, provide short or longer flow paths from open bodies of water, which may significantly influence the dewatering plans for a site. Lowering of the groundwater may expose existing timber piles and cause their deterioration. Furthermore, dewatering may cause settlement of compressible soils and thus can damage existing structures and utilities. Also the lowering of the groundwater can cause the

migration of contaminants within the adjacent lands towards the dewatered site. Storage and/or spills of contaminated substances at/or near the site may require special groundwater control measures that will contain and/or remove the contaminants. The presence of a former coal storage pile can result in a concentration of iron in the groundwater that can be 100 times higher than the iron content in the groundwater in adjacent areas. Often this can require a dewatering system that is entirely different from the dewatering system used for the adjacent areas. The effect that dewatering could have on a potable water system should be evaluated.

8.5 *Assessment of Groundwater Conditions*

Any assessment of the groundwater conditions should involve a review of the site geology and an identification of the type of soil deposits. The area that will need dewatering should be defined. Seasonal changes in lake, river and groundwater levels, and rainfall should be ascertained. The possibility of high river levels many miles upstream of the site, which may cause water pressures in the soils beneath the site to rise considerably higher than the river levels at the site, should be explored. A rise in lake or river levels can significantly affect the volume of water that must be pumped. Under certain conditions the increase in volume is directly related to the percentage increase in the rise of the lake or river level.

The normal sources of groundwater recharge at the site should be defined. New sources of groundwater and water from lakes or rivers should be investigated and assessed. These sources include: open channels; sheet piling that is not properly interlocked or does not have a tight connection to an existing structure; sheet piling and other cut-off walls that do not extend into an impervious soil; porous backfill; gaps beneath an existing pile-supported structure, gravel or stone placed under existing structures; pipe lines; unlined ponds and lakes, bore holes that are not grouted; drainage systems and previous dewatering systems. The soil borings should be studied and the stratigraphy of the soils and rocks plotted. The grain-size distribution curves for the soils should be reviewed. The soil samples should be examined. Soils that are dense, well-graded and/or contain more than 10% of fines will have considerably lower hydraulic conductivity. Soils that are loose, poorly graded, clean and/or have rounded grains will have considerably higher conductivity. Hazen's formula for the hydraulic conductivity of clean, loose sand is:

$$k = C(D_{10})^2 \tag{8.28}$$

where k = the hydraulic conductivity in m s^{-1}, C varies from 0.4–1.5, and D_{10} = the effective grain size in centimeters. However, a slight amount of silt or clay can significantly reduce the hydraulic conductivity implied by this equation. The formula should be used with considerable care until it can be correlated with local experience as shown in Fig. 8.10. Tables 3.10 and 8.2 illustrate typical hydraulic conductivity values of various sands. Equations for calculating k from a pumping test are given in Figs 8.2 and 8.3. If the value of k estimated from the bore hole log descriptions and the grading curves, is different to that based on a pumping test, normally the k from the pumping test would be used. If the value of k from the falling head and/or the rising head tests is different to that estimated from the bore hole log descriptions and gradations curves, the higher k value would normally be used. If the estimated k from the rock descriptions is different to that from the pressure test in the rock, usually the higher k would be used. The groundwater samples should be analyzed for minerals, chemicals, pH, dissolved solids, conductivity and con-

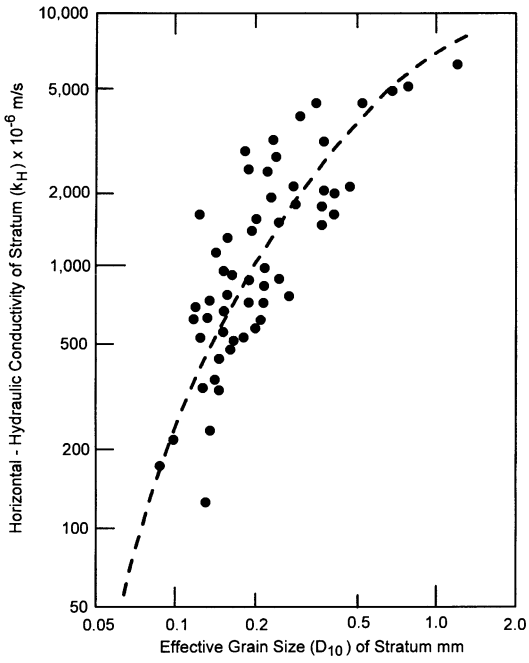


FIGURE 8.10. D_{10} grain size and horizontal hydraulic conductivity from pumping tests from the Mississippi and Arkansas river valleys (modified from US Army 1983).

taminants, which could cause deterioration, clogging and/or malfunctioning of the dewatering systems, or that may require treatment of the groundwater, and/or could result in environmental damage.

TABLE 8.2 Approximate hydraulic conductivity of various soils (from US Army 1983, Driscoll 1986, Cedergren 1989, Powers 1992)

Type of sand (Unified Soil Classification System)	k[a]
Sandy silt[b]	5–20
Silty sand	20–50
Very fine sand	50–200
Fine sand	200–500
Fine–medium sand	500–1000
Medium sand	1000–1500
Medium–coarse	1500–2000
Coarse sand and gravel	2000–5000

[a] Hydraulic conductivity, $k = \kappa \times 10^{-6}$ (m s^{-1}).
[b] E.g., for sandy silt: 5×10^{-6} m $s^{-1} \leq k \leq 20 \times 10^{-6}$ m s^{-1}).

8.6 *Selection of Dewatering Systems*

8.6.1 DEWATERING SYSTEMS

After reviewing the geology, hydrogeology, hydrology, site conditions, groundwater conditions, construction procedures, specified groundwater control requirements and the local labor requirements, a groundwater control system(s) is selected. Table 8.3 lists the most conventional dewatering systems used, and Table 8.4 lists the normal installation procedures and their advantages and disadvantages. Figure 8.11 illustrates the various systems, and Fig. 8.12 shows the applicable dewatering systems for the various types of soils.

For the vast majority of groundwater control projects the installation procedures and the types of groundwater control systems selected will be controlled by the geology, hydrogeology, hydraulics, site conditions, and the experience of the person(s) responsible for the dewatering. As the dewatering system is being installed the individual wells, wellpoints, eductor wells, vacuum wells, electroosmosis cathodes and anodes are tested, and the dewatering design and installation procedures are modified as required for the site conditions encountered. Very seldom does the final dewatering system exactly correspond to the initial dewatering concept.

8.6.2 SOIL STABILIZATION SYSTEMS

8.6.2.1 Vacuum Applied to the Soil

Vacuum applied to the filter pack of a wellpoint, deep well or a horizontal drain can be used to stabilize unstable sand and silt, sandy silt and medium–coarse silt. Also, a vacuum applied to the bottom of a soft soil layer can be used to surcharge and strengthen the soft soil (Halton *et al.* 1965). The pressure within the filter pack is lowered below atmospheric pressure. This action causes porewater to flow to the filter pack, where it is removed,

TABLE 8.3. Typical dewatering systems

Conditions	Wellpoint system	Vacuum well	Suction well	Eductor well	Deep well	Horizontal drain (well)
Sandy silt, sand & silt, silt, clay[a]	ok[c]	ok[c]	—	ok[c]	ok[c]	ok[c]
Silty sand, silty gravel	ok[c]	ok[c]	—	ok[c]	ok[c]	ok[c]
Fine sand	ok[c]	ok[c]	—	ok[c]	ok[c]	ok[c]
Medium sand	ok	ok	ok	Fair	ok	ok
Coarse sand	ok	ok	ok	Fair	ok	ok
Sandy gravel, gravels[b]	ok	ok	ok	Poor	ok	ok
Pervious soil overlaying less pervious soil or rock at/or above subgrade	ok	ok[d]	—	ok	ok[e]	ok[f]
Less pervious soil between pervious soils	ok[g]	ok[g]	Poor	ok[g]	ok[g]	ok[c]
Pervious rock	ok	ok	ok	ok	ok	—
Subgrade less than 6.7 m (22′) below water level	ok	ok	ok	ok	ok	ok
Subgrade more than 6.7 m (22′) below water level	Multistage	Multistage	Multistage	ok	ok	Multistage
System within excavation	Yes	Yes	Yes	Optional	Optional	Yes
Adaptability to changes	Good	Better	Good	Fair	Fair	Poor
Groundwater with high p.p.m. iron, manganese, etc.	Fair	Fair	Fair	No	Difficult	No
Capacity per unit, l min^{-1}	0.4–95	0.4–151	0.19–1.9[h]	0.4–189	0.0004–19[h]	1.1–1140
Spacing of units, m	1–4.6	1–6	>6 m	1.8–12	>3	m^{-1}
Energy efficiency	Good	Good	Good	Poor	Fair	Good
Cost efficiency per unit	Good	Good	Good	Fair	Fair	Good

[a] Vacuum is applied to filter pack, electro-osmosis may be needed.
[b] For large volumes sump and/or cut-off wall.
[c] Requires filter pack.
[d] Requires penetration into rock or less pervious soil or large air-handling capacity.
[e] Requires close spacing or combination deep well and wellpoint system, or deep well system with cut-off wall.
[f] Need to penetrate into less pervious soil or rock.
[g] May require filter packs.
[h] For suction wells and deep wells the capacity per unit is measured in $m^3\ min^{-1}$.

TABLE 8.4. Installation procedure: wellpoints, vacuum wells, suction wells, eductor wells, deep wells, horizontal drains (wells), vertical drains

Method	Depth (m)	Diameter (mm)	Advantages	Disadvantages
Reverse rotary[a]	>60	460–1220	Less development; more productive well	Higher mobilization cost; boulders a problem; drill rig needs to set 3 m above water level and to set over the hole; high cost; slow
Cable tool[b,c]	>60	150–1500	Low mobilization cost; penetrates most formations; cased hole; works in limited head room	Slow; often requires telescoping casings; drill rig set over hole; medium unit cost; seldom used
Hollow stem auger[b,c]	<30	100–200	Low mobilization cost; fast cased hole; low unit cost; readily available	Difficult to install filter pack; tends to smear pervious strata in stratified formations; unable to penetrate tills, boulders, rock; drill sets over the hole
Down-the-hole hammer & drill[a]	>60	100–610	Fast, cased and uncased hole, cuttings removed by air; penetrates soil and rock	Difficult to add and remove casing; uncased hole in soils tends to collapse; drill rig sets over the hole; high unit cost
Water jetted-wellpoint, wells, holepuncher, holepuncher and casing[b,c]	<70	38–610	Provides the best well; fast, mobile, requires little or no development; does not need to set over hole; lowest unit cost; readily available; cased hole where needed; cuttings removed by water	Mobilization cost can be significant for depths greater than 30 m; not suited for dense tills, boulders and most rock formations; may need pre-drilling by auger; for tills, hard clay, requires a minimum no. of holes to be competitive
Bucket auger[a]	<40	460–1220	Low mobilization cost; fast, suitable for most soils; low unit price; readily available	Clay, bentonite, slurry used to keep hole open; drills larger diameter hole than needed; may require extensive development; not efficient for fine sands and layered soils; difficult time with boulders, rock and hard till; filter pack required; drill rig sets over hole
Double-wall driven casing[b,c]	>60	100–610	Average mobilization cost; air used to remove cuttings; little or little or no development required; readily penetrates cobbles and boulders; cased hole; works in limited head room	Not suitable for clay tills; drill rig sets over hole; high unit cost; limited no. of drills available

TABLE 8.4. *(Continued)*

Method	Depth (m)	Diameter (mm)	Advantages	Disadvantages
Rotary drill[a]	>60	100–610	Average mobilization cost; suitable for most soils and rock; medium unit cost	Slurry is recirculated to keep hole open; extensive development may be required; filter pack required; drill rig sets over hole; slow in cobbles, boulders and rock
Dual rotary casing and down-the-hole hammer[b,c]	>60	100–610	Average mobilization cost, fast; penetrates cobbles, boulders and rock; air removes cuttings; little or no development; cased hole; works in limited head room	High unit cost; drill rig sets over the hole; limited number of drill rigs available
Vibratory casing[b,c]	<40	100–610	Fast; installation rig does not set over hole; penetrates most soils; little or no development; low unit price; cased hole with bottom plug	Mobilization costs can be significant; not suited for rock and clay tills; tends to smear varved sand, silts and clays; equipment not readily available; requires a minimum no. of holes to be competitive; bottom plug left in hole
Earth augers[a,b]	>60	100–610	Good for pre-drilling holes in clay and till; low unit price; fast; low mobilization cost	Generally another procedure must be used for the completion of the well; drill needs to set over the hole; uncased hole
Trencher[a,b]	<6.7	300–610	Cased hole; no drilling fluid used; very fast; very low unit cost; no development required	High mobilization cost; large quantities of filter material required; trencher needs to be 0.6 m above water level; needs to set over hole; not suited for boulders, large rock fragments, developed areas; limited no. of machines available

[a] Artesian pressures above the drill level are a problem.
[b] Filter pack not required for coarse sand, sand and gravel and gravels: smaller diameter hole can be used.
[c] Holes can be at an angle.

and increases the effective stress in the soil over a small area. The differential pressure within the filter pack decreases with depth and becomes zero when all the available vacuum is used to raise the water collected in the filter pack to the pump. As illustrated in Fig. 8.13, if an eductor or a deep well pumping unit is used to remove the water collected in the filter pack, all of the applied vacuum can be used to create a significantly larger differential pressure within the filter pack, which increases the effective stress in the soil over a larger area. The practical vacuum limit is 0.71 m Hg^{-1} (9.5 m). Vacuum well stabilization requires person-

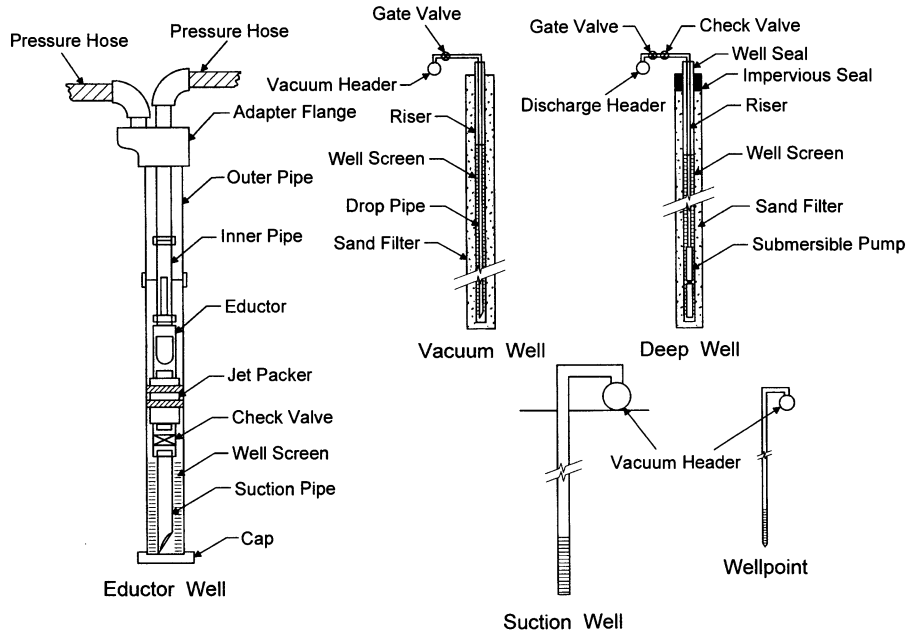


FIGURE 8.11. Detail of eductor well, vacuum well, deep well, suction well and wellpoint.

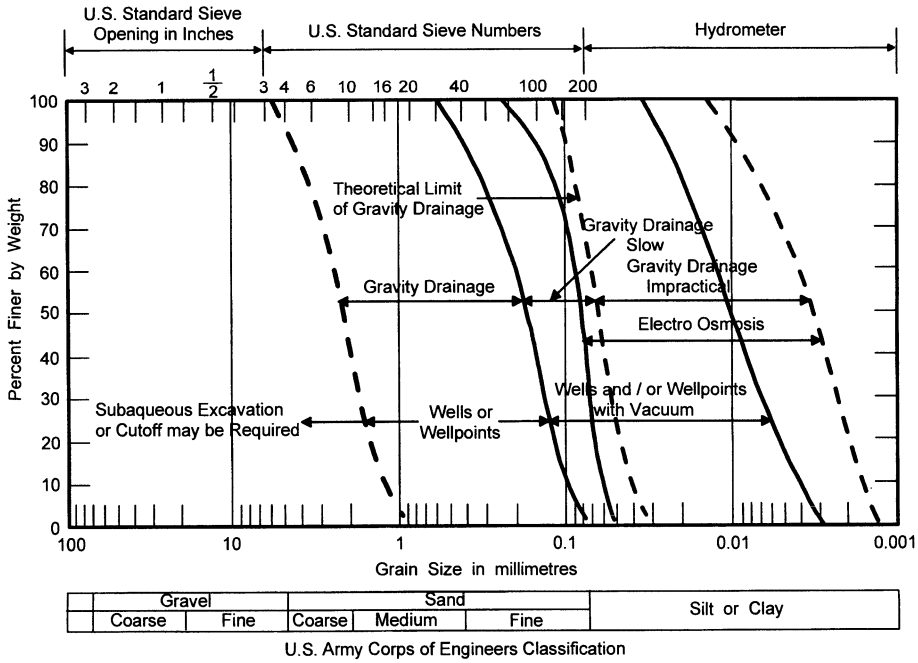


FIGURE 8.12. Dewatering systems applicable to various soils based on grain size (modified from Moretrench American Corp. 1967).

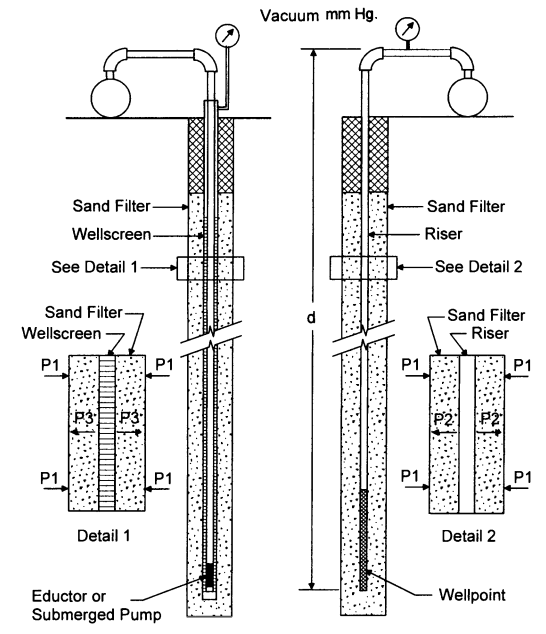


FIGURE 8.13. Comparison of vacuum applied to deep wells and wellpoints. P1 = 101kPa; P2 = 101 − 9.8[0.0136 * vacuum (mm Hg) − d(m)] kPa; P3 = 101 − 9.8[0.0136 * vacuum (mm Hg)] kPa.

nel that are experienced in the design, installation and operation of the system.

8.6.2.2 Electro-osmosis

Electro-osmosis can be used to stabilize unstable sand and silt, coarse–fine silt and clays (see also Section 15.2.4.8). As illustrated on Fig. 8.14, the application of a direct current (D.C.) potential across an anode and a cathode causes the porewater and part of the boundary film of water that is attached to the soil particles to move to the cathode. This action directs the seepage pressures from the anode to the cathode, increases the effective stress in the soil, reduces the water content of the soil and causes a chemical exchange that strengthens the soil. Most soils have an electro-osmotic hydraulic conductivity of 0.5 $\times 10^{-6}$ m s^{-1} V cm^{-1}. When this potential gradient is applied to soils with a hydraulic conductivity of less than 0.5 $\times 10^{-6}$ m s^{-1} the rate of flow through the soil will increase in direct proportion to the ratio of electric osmosis conductivity to the hydraulic conductivity of the soil. This significantly greater equivalent hydraulic gradient developed by electro-osmosis in silts and clays as compared to the hydraulic gradient developed by a vacuum permits greater spacing of the anodes and cathodes, allows a much larger area to be treated, reduces the treatment time, causes a larger reduction in the water content of the soils, develops higher effective stress in the soils and provides considerably more stable soils. Electro-osmosis stabilization requires personnel that are experienced in the design, installation and operation of the system. A schematic of a typical system is shown in Fig. 8.15. Examples of its application are given in

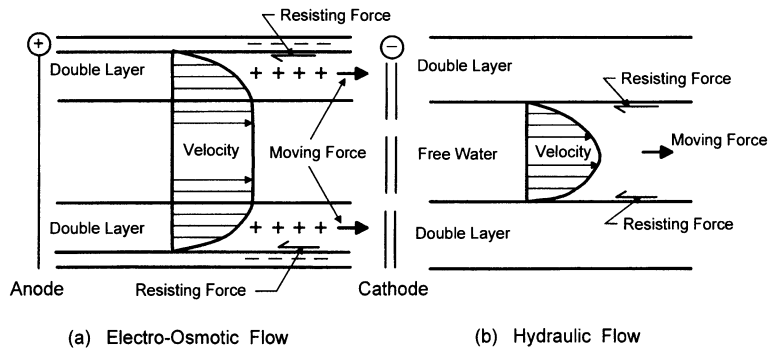


FIGURE 8.14. Comparison of (a) electro-osmotic flow with (b) hydraulic flow (modified from Casagrande 1983).

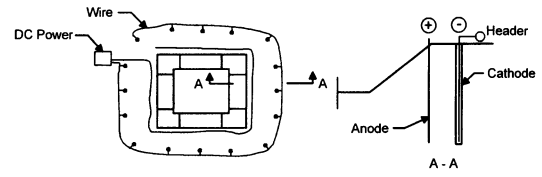


FIGURE 8.15. Typical electro-osmosis system.

(Casagrande (1952, 1983), Richardson (1953), Loughney (1954), Casagrande *et al.* (1961, 1981), Soderman & Milligan (1961) and Fetzer (1967).

8.6.3 CUT-OFF WALLS: GROUTING AND FREEZING

Steel sheet piling, slurry trenches, slurry diaphragm walls, secant piles, grouting, soil mix walls, jet grouting, tremie seals, freeze walls, chemical injection, compressed air, and earth pressure shields can be used to partially or fully control the groundwater (see Chapter 15). Where partial control of the groundwater is performed a dewatering system such as wellpoints, wells, eductor wells and horizontal drains can be used to supplement the cut-off wall. The cut-off wall methods require personnel that are experienced in design and construction of the procedure selected. Proper instrumentation is required to ascertain that the desired results are being obtained.

8.6.4 OPEN PUMPING

Where the soil is coarse gravel, cobbles, boulders, broken rock, fissured rock or weathered rock, the groundwater often can be controlled by sump pumping, from sumps and ditches located at the perimeter of the excavation. However, care should be taken that the open pumping does not remove soil and cause damage to the area and/or cause the volume of water being removed to increase rapidly. Where the volume of water being removed is excessive, the flow may need to be reduced by cut-off wall procedures.

8.6.5 RECHARGE

Conditions at the site may require that the groundwater be maintained at a desired level outside of the excavation. This can be achieved by using cut-off walls and/or recharging the groundwater. Where site conditions permit dyked or excavated areas can be used as reservoirs to recharge the groundwater. This method has the advantage that it more readily allows the groundwater removed to be used as the source of water for recharging. Also, vertical drains can be used in the recharge area to pass water into lower layers where necessary. Where recharge wells are used, the geochemistry of the groundwater being removed may be such that it is necessary to use an outside source of recharge water.

8.7 Design of the Dewatering System

For most dewatering projects, the equation that is most appropriate for the dewatering system(s) is selected from Eqs 8.3–8.26 (Figs 8.2–8.6), and then the hydraulic conductivity is used to calculate the volume of water that should be expected from each pervious strata for the given site conditions. Alternatively, commercial software packages can be used. The number, spacing, capacity, location, and depth of the units (wellpoint, vacuum well, deep well, eductor well, horizontal drain) that will be required to pump the volume of water and lower the groundwater to the desired levels are estimated. The capacity of each unit to produce the estimated volume and the corresponding lowering of the groundwater is checked using the appropriate equations. As needed, the system is modified until the required yield and drawdown are obtained. Due allowance should be made for the inefficiencies of the units. Very seldom does a unit produce the theoretical capacity. The efficiency of the well is the drawdown at the perimeter of the well-screen

or well filter divided by the drawdown inside of the well. Depending on the installation procedure used, the filter pack and the well-screen, the efficiency of a well can range from less than 10 to 90%. As the efficiency of a well decreases, the number of wells required to provide the desired drawdown increases. Seldom does a unit operating as part of a group produce the efficiency of a single unit operating alone. Project records have shown that when the excavation is enclosed by a dewatering system consisting of wells that extend the full depth of the aquifer and are spaced 12–30 m around the site, the flow to each operating well may be only one-quarter to one-half of the flow to one well operating alone that has the same length of wetted well-screen (filter) with the same drawdown within the well. As the spacing of the wells decreases, the yield of the wells will also decrease. If the length of wetted screen or filter is reduced, the yield of the well will usually be reduced almost proportionately. Generally, a greater capacity is required initially to remove the water in storage and maintain the construction schedule.

8.7.1 WELL-SCREENS

For most construction projects, slotted plastic, wire wrapped galvanized steel or mild steel louvered screens are used for wells. Where the groundwater conditions are corrosive, stainless steel or fiberglass screens may be needed. Wire mesh screens or plastic screens are normally used for wellpoints, vacuum wells and suction wells. The well-screen openings are obtained by using wire wrapped, mesh wrapped, slotted, punched, drilled and sliced methods. Wire wrapped and mesh wrapped are the most efficient screens. The size of the openings in well-screens are selected to be compatible with the soils being dewatered or with the filter pack when a filter pack is used. Often, soil formations such as coarse sand, coarse sand and gravel, graveley sand, sandy gravel and gravel do not require filter packs. For these soils if the installation procedure used does not require a filter pack, a well-screen opening that will retain 50% of the finer soil is usually suitable. When a filter pack is required because of the soil formation and/or the installation procedure used, a well-screen opening that retains 90% of the filter pack is usually suitable. Often, well-screens are reused for construction projects, the screen opening size is set and a filter pack suitable for the screen opening is used. The filter pack selected may not be suitable for the soil formation. This practice can result in inefficient wells or wells that pump sand. The maximum flow that should be initially considered for a chosen length of wetted well-screen can be estimated from Eq. 8.15 (Fig. 8.3). Where the soil formation is suitable, a longer length of well-screen should be used to offset the inefficiency of the well. The additional screen length provides a larger drainage area and a greater depth that the water inside the well can be lowered, which increases the yield of the well. Quite often the length of the well-screen is governed by construction procedures and the soil formation. All pervious strata above the structures subgrade should be intercepted by the well-screen. All pervious strata below the structures subgrade should be intercepted by the well-screen, to the depth needed, to prevent boils in and/or a heave of the bottom of the excavation because of the existence of water pressures in pervious soil strata below subgrade (Eq. 8.1 and Fig. 8.1). When the well-screen is completely submerged a vacuum can be applied to the well-screen to increase the yield of the well.

The diameter of wellpoints, vacuum well and suction well screens range from 32 to 203 mm in diameter. The standard jetting wellpoint is 38–51 mm in diameter. Deep well well-screens range from 102 to 1524 mm in diameter. Mostly 102–610 mm diameter well-screens are used. Wellpoint and vacuum

well-screen should have a diameter that will keep the head losses at the entrance of the water into the well-screen and the head loss from the friction of the water flowing up the riser pipe to the vacuum header, excluding vacuum lift loss, to less than 1 m. Deep well well-screen diameter should be large enough to provide adequate clearance between the inside of the well-screen and the outside of the pumping unit. For volumes greater than 12.5 l s^{-1}, a minimum of 50 cm should be provided between the inside of the well-screen and the outside diameter of the pump bowl. The outside diameter of the well-screen and the slot area should be large enough that the volume of water entering the well-screen does not develop an entrance velocity greater than 0.3 m s^{-1} (Walton 1962). Assume that 50% of the open area is blocked by grains of soil.

8.7.2 FILTER PACKS

Where filter packs are required because of the soil formation and/or the installation procedure, the well-screen should retain 70–90% of the filter pack, depending on the procedure selected. Several procedures for the selection of filter packs are shown in Figs. 8.16 and 8.17 and Table 8.5. For fine sands, very fine sands and silts, the Corps of Engineers criteria (Fig. 8.16) provide the more suitable procedure to follow in selecting a filter pack. For soil formations with various strata of silt, fine sand, medium sand, coarse sands and gravel, usually a clean washed concrete sand with 90% passing the 2.0 mm (US No. 10) sieve and less than 10% passing the 0.3 mm (US No. 50) sieve is a more appropriate filter. For soil formations consisting of fine–medium sand, medium sand, coarse sand and gravel, the criteria in Fig. 8.17 are usually used to select a filter pack.

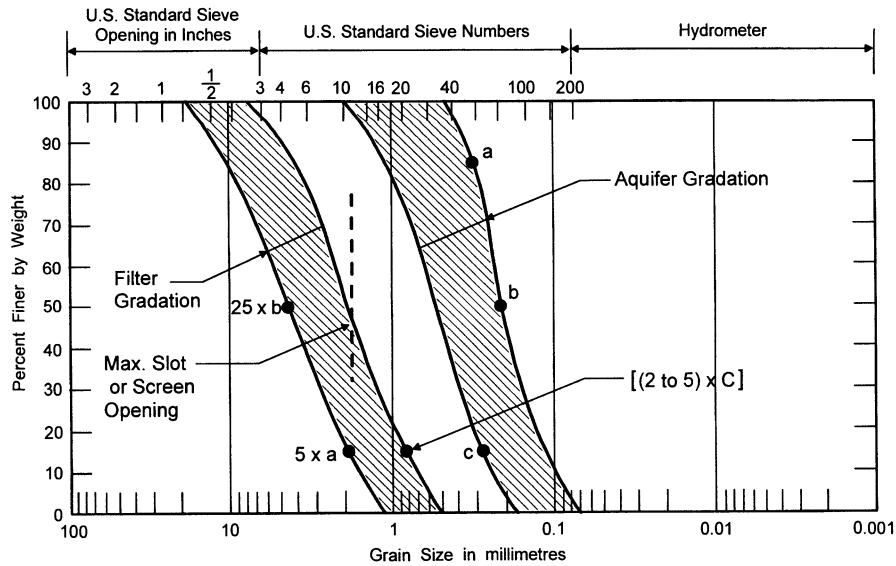


FIGURE 8.16. Selection of filter pack for wells, vacuum wells, wellpoints and horizontal drains (modified from US Army 1983).

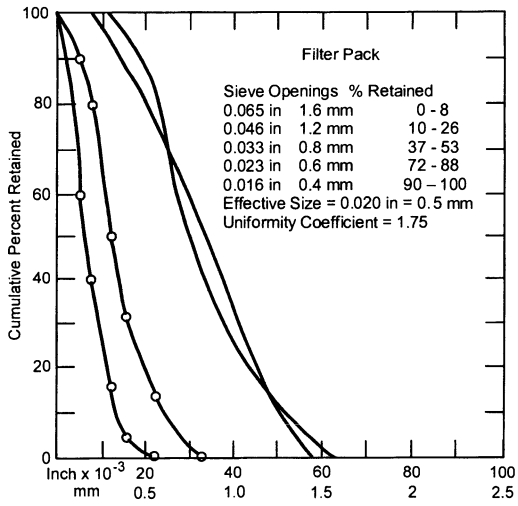


FIGURE 8.17. Selection of filter pack for wells, vacuum wells, wellpoints and horizontal drains (modified from Driscoll 1986).

8.7.3 PUMP UNITS

The pump selected should have a capacity, a total discharge head (TH), and a net positive suction head (NPSH) that is 15% greater than needed. The depth that the pump is placed below the pumping water-level in the well should meet the NPSH requirements. For most construction projects the deep well pumping units are located close to the bottom of the wells to permit lowering the water within the well-screen as deep as possible so as to maximize the flow from the wells. Where submersible pump motors are used, the required cooling water flow over the motor should be provided by sleeves where necessary. The components of the pump unit should be compatible with the groundwater. The height that the wellpoint pump is above the lowered groundwater, plus the head loss from the flow of water through the piping to the pump, should be within the NPSH of the pump. The horizontal or vertical wellpoint pump should have an auxiliary vacuum pump to provide the air-handling capacity required for the site and system conditions.

8.7.4 PIPING AND FITTINGS

The piping and fittings used should be of sufficient size to keep the head losses, from the friction of the water flowing through the piping and fittings, to the amounts that are within the available total suction lift and total pumping head of the units. The piping and fittings should consist of materials that are compatible with the quality of water being pumped. For most construction projects plastic, aluminum or steel piping and fittings are used. Each pumping unit should be

TABLE 8.5. Selection of a filter pack[a]

- Selected grain-size curve for the finest material
- For a uniform formation with a 40% retained size that is 0.25 mm or less, use a 4–6 multiplier
- When the formation sediment has a highly non-uniform gradation and includes silt and clay stringers use a 6–10 multiplier
- Place this multiplier of the 70% retained size on the graph as the 70% size of the filter
- Through this initial point in the filter pack draw a smooth curve representing material with a uniformity coefficient of 2.5 or less. Draw the curve so that the filter pack is as uniform as practical. The uniformity coefficient is the 40% size retained divided by the 90% size retained
- Select five sieve sizes that cover the range of the curve
- Allow eight percentage points above and below the fraction to be retained at any point on the curve
- Use this band width as the range of material that can be used when selecting the filter pack
- Select a screen slot size that will retain 90% of the filter pack material

[a] See also Fig. 8.17.

equipped with a valve that can be used to regulate the flow. Each deep well pumping unit should have a check valve at the top of the well discharge piping, before the regulating valve.

8.8 *Installation, Operation and Removal of Dewatering Systems*

8.8.1 INSTALLATION

The improper installation of wellpoints, vacuum wells, suction wells, eductor wells, deep wells, horizontal wells and their component parts is a major problem that occurs with dewatering systems. Either the wrong installation procedure is used and/or the installer does not know how to install the dewatering system. It is essential that the designer and the installer be skilled in the procedure selected. Very few persons are skilled in all the dewatering procedures. The installation methods most commonly used and their advantages and disadvantages are shown in Table 8.4.

8.8.2 OPERATION

Observation wells (piezometers) should be installed along the perimeter and within the excavation to monitor the groundwater levels in all pervious strata encountered from the water-level to the depth below subgrade, so that the upward pressure of the water above subgrade in each pervious stratum does not exceed the submerged weights of the soils. The groundwater levels should be monitored daily along with the volume of water being pumped and the number of pumping units operating. If the dewatering system is a submersible pump deep well system or a horizontal drain system a 100% standby source of electric power should be provided, connected, and ready to operate. If a turbine pump deep well system is used, dual electric and diesel engine powered units or diesel powered units can be used. If the dewatering system is a wellpoint, vacuum well, suction well, and/or an eductor well system a 100% standby pumping capacity should be provided, connected, and ready to operate. At least 15% redundant parts should be available at the job site. The standby source of power or pumping unit should be operated a minimum of 4 h per week. The dewatering system should be operated the necessary hours per day, and days per week, that will maintain the water-levels at the desired levels and that will provide sufficient time to activate the standby units and the standby source of power before the water-levels rise above the allowable levels.

8.8.3 REMOVAL

The wells, wellpoints, eductor wells, vacuum wells, horizontal drains, vertical drains and angle drains should be sealed and/or removed in accordance with the local procedures required at each site upon completion of dewatering.

8.9 *Permanent Dewatering System*

The same procedures that are used to select and design the temporary groundwater control system are used for a permanent groundwater control system. Materials are used that will last the expected lifetime of the permanent system. Greater emphasis is placed on the efficiency of the system, the maintenance required, the power consumed, and the location and access to the permanent system.

8.10 *Dewatering Specifications*

The groundwater control specifications should clearly state the intent of the specifications and the responsibilities of the owner and the contractor. Projects where there is

not a clearly defined dewatering specification or where the dewatering specifications are not enforced can result in changes, delays, disputes and damage to the project that result in additional costs, which can be as much as 100 times greater than the cost of the initial dewatering system. The three types of specifications presently used are discussed below.

8.10.1 SPECIFIED END RESULT

The owner furnishes a specification that defines the responsibilities of the owner and the contractor and in detail clearly states the end results desired, the means that will be used to monitor compliance with the specifications and the action(s) that will be taken when the specifications are not satisfied. The design, installation, operation and removal of the groundwater control system are the contractor's responsibility. The contractor's procedures are subject to the review and approval of the owner's engineers, as a starting procedure, which will be modified by the contractor, if required, to meet the specifications at no additional expense to the owner. The owner's engineers monitor and require compliance with the specifications. This form of specifications is suitable for most projects and is the most commonly used specification. Its advantages are: as more information becomes available during installation and operation, the system can be modified promptly; the cost is known; the owner's engineers, who seldom have the technical knowledge and the field experience, are not required to design a groundwater control system, oversee the installation and operation, or recognize changes that need to be made as additional information becomes available during the installation, operation and maintenance of the system. This form of specifications has the following disadvantages: the groundwater control system selected may be best for the contractor's work but not the best system for the total project or the contractor may be inexperienced and changes, delays and disputes develop.

8.10.2 SPECIFIED MINIMUM GROUNDWATER CONTROL SYSTEM

The owner's engineers design and specify the minimum groundwater control system that can be installed and anything required beyond the minimum system is the responsibility of the contractor. This form of specification has the advantages that: a minimum groundwater control system will be installed initially and that the contractor will endeavor to maximize its use; generally there is a more thorough review of the available data; the initial groundwater control system is the best system for the overall project; and the costs are set. The disadvantages are: changes that should be made during the installation and operation seldom can be implemented promptly; and the owner's engineers need to have the technical knowledge and field experience to design the groundwater control system and oversee the installation and operation of the system.

8.10.3 SPECIFIED COMPLETE GROUNDWATER CONTROL SYSTEM

The owner's engineers design the groundwater control system and anything required beyond that design is the owner's responsibility. The advantages of this form of specification are: a more thorough review of the available data is made when designing the system; the initial dewatering system is a system that would be best for the overall project; changes can be made without dispute; there is less risk for the contractor. The disadvantages of this form of specifications are: the owner's engineers seldom have the technical and field experience to design and oversee the installation and operation of the dewatering system; the costs are not set; additional information obtained during the installation and operation is not readily entered into the system.

8.10.4 SPECIALTY CONTRACTOR'S RESPONSIBILITY

For any of the above specifications the owner can stipulate that a qualified specialty dewatering contractor, whose principal business is 75% dewatering and who is capable and has experience in the design, installation and operation of the types of systems that would be used, will perform the design, installation and operation of the dewatering system. The specialty dewatering contractor would be a subcontractor to the contractor. Also, the dewatering work could be let out directly by the owner to a qualified specialty dewatering contractor.

8.11 Summary

Groundwater control commences early in the project and when it is not properly performed, damages, delays and consequential damages occur, which may result in additional costs that may greatly exceed the initial groundwater control cost. Water that may not be a concern at one site may be a major problem at another site if not properly controlled. If sufficient geotechnical information is provided, a correct assessment is made of the site conditions and the appropriate specifications are defined and enforced, the desired groundwater control should be obtained.

II. FOUNDATIONS AND PAVEMENTS

9. SHALLOW FOUNDATIONS

J. C. Small

9.1 *Introduction*

Shallow foundations can be classified as those that are constructed on the ground surface or at shallow depth beneath the ground surface. A foundation is usually termed "shallow" if it is at a depth that is less than its breadth.

The purpose of a shallow foundation is to apply the structural loads to the ground by spreading the load over a larger area. The size of the footing can be selected so that the contact pressure between the footing and the soil is small enough to reduce settlement to acceptable levels and provide a target factor of safety against the possibility of a bearing failure.

Shallow foundations may be of several different types, and the selection of the appropriate type will depend on the structural loads and the foundation conditions. Some commonly used shallow foundation types are discussed in the next section.

9.2 *Types of Shallow Foundations*

9.2.1 STRIP FOOTINGS

A strip footing is one that is long compared to its width. Such foundations (see Fig. 9.1a) are typically used to support continuous masonry walls.

Strip footings are constructed by excavating a trench with a backhoe (or by hand), placing a reinforcing cage and pouring concrete into the trench. If permitted by the local building code, and the trench is able to stand open without collapsing (e.g. clayey soils) then formwork may not be needed except to form that part of the foundation that is above ground level. For sandy soils, the trench has to be excavated and fully formed before concrete can be poured, as the trench will not stay open.

9.2.2 PAD FOOTINGS

For support of isolated loads, such as column loads, or support of raised slabs or flooring, pad footings may be used (Fig. 9.1b). The process of construction is similar to that for strip footings.

It is also generally recommended that in

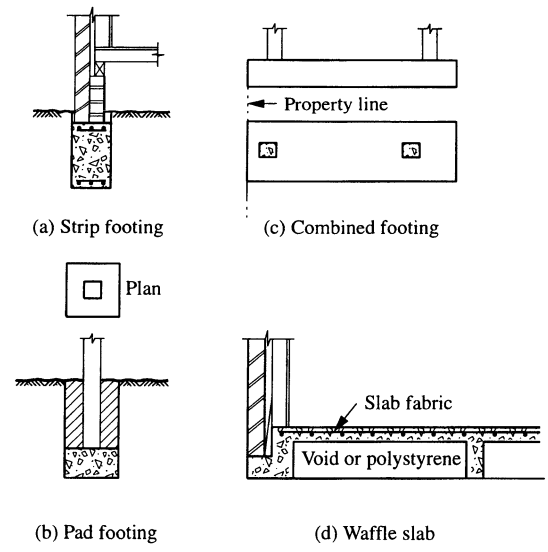


FIGURE 9.1. Types of shallow foundation: (a) strip footing, (b) pad footing, (c) combined footing, and (d) waffle slab.

R. K. Rowe (ed.), *Geotechnical and Geoenvironmental Engineering Handbook*
© Kluwer Academic Publishers 2001

sandy areas or on sites that may be subjected to wind or water erosion, footings should be constructed at least 300 mm below the surface to prevent any undermining. In cold climates, footings should be founded below the depth of frost penetration so that they are not affected by frost heave. It is also prudent to backfill against the sides of such foundations with non-frost susceptible soil. This is discussed more fully in Chapter 20.

9.2.3 COMBINED FOOTINGS

A combined footing may be necessary when a column load is close to a property boundary, and the foundation cannot be made large enough to support the load without encroaching onto the neighboring property (Fig. 9.1c). In this case the footing is combined or tied to a nearby footing, which provides additional support.

9.2.4 RAFT OR MAT FOUNDATIONS

For special conditions, i.e. in areas of swelling soils, or where pad footings would need to be large to support loads, a raft or mat foundation may be used. Rafts are often reinforced concrete slabs, which for tall buildings can be several meters thick.

For smaller scale construction, rafts can be stiffened under walls and columns by making the raft thicker at the point of loading. In areas where reactive soils exist, it is common to construct a "waffle" slab, so called because it consists of stiffened ribs running perpendicular to each other under the slab (Fig. 9.1d). The upper flat portion of waffle slabs can be cast on polystyrene blocks so that swelling of the soil does not affect the slab or raft but merely compresses the polystyrene.

9.2.5 INSPECTION

The requirements for inspection of holes or the soil surface prior to placing concrete are usually provided in codes of practice or local building regulations (e.g. AS 28702, 1990). Most codes or regulations require that the hole should be inspected (for any type of footing) to make sure that it does not contain any water or soil that has fallen in from the sides.

For mat or slab-on-ground foundations, often vapor barriers are used (under the slab), which consist of an impermeable membrane such as a PVC sheet. In this case the sheet needs to cover the entire base of the slab, and pass under edge and internal beams to restrict moisture from entering the slab. Lapped joints should be inspected for at least 200-mm overlap, and penetrations for pipes should be taped, although this again depends on local regulations.

9.3 *Bearing Capacity*

Theoretical solutions for the bearing capacity of shallow foundations are generally based on the theory of plasticity, where the soil is assumed to behave as a rigid plastic material that fails according to the Mohr–Coulomb failure criterion. Shallow foundations may be defined as those that are founded at a depth, D, which is less than the full width, B, of the foundation (B may be taken as the width of a strip, the diameter of a circle or the smaller dimension of a rectangular footing). Solutions are obtained by establishing the stress-characteristic fields beneath a foundation. The stress characteristics are lines that show the orientation of the planes on which the stresses in the soil have reached the critical combination, τ_f and σ_f, as shown in Fig. 9.2. The method is described by Hill (1983) and Wu (1976).

Many solutions to bearing capacity problems have been obtained using classical plasticity theory; however, for more complex problems, i.e. layered soils and eccentric loadings, approximate methods may have to be used to obtain solutions. Such methods include those based on the bound theories of plasticity, whereby upper and lower bounds to the collapse load may be found (Sloan and

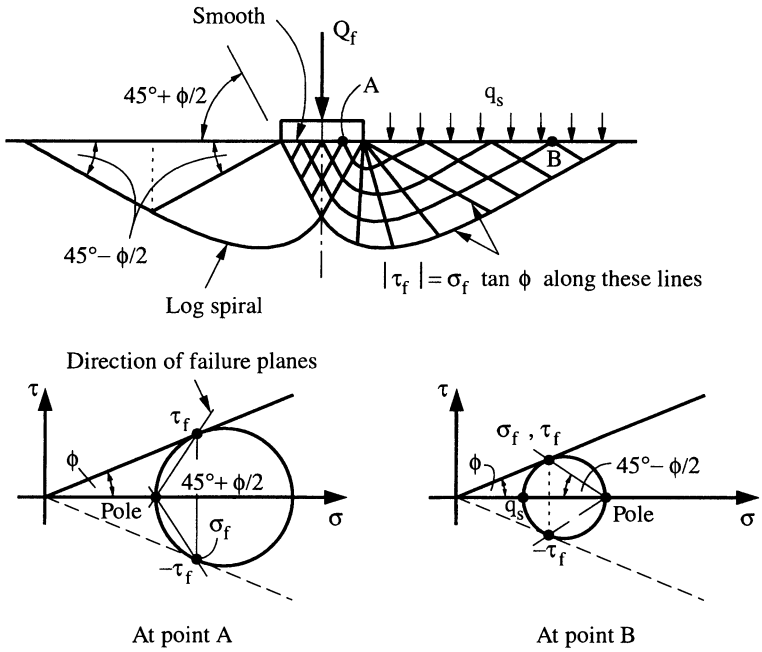


FIGURE 9.2. Smooth strip footing on weightless, cohesionless soil.

Yu 1996). The true collapse load, therefore, lies between the bounds that have been established.

Other methods include finite element techniques (see Zienkiewicz 1979) or finite difference methods, as used in the commercially available computer program FLAC (ITASCA 1996). Obviously, a great deal more effort is involved in setting up finite element meshes or finite difference grids and computing ultimate loads than in using the results of a theoretical solution, and so such numerical techniques are limited to problems involving complex geometry, loading or material properties. If collapse loads are required from finite element models, a plot of the load applied to a foundation versus the deflection of the foundation can be made, and the collapse load determined by locating the point at which large deflections occur for a small increase in load. However, care must be taken with the type of elements used, the proximity of boundaries and the way that the load is incrementally applied to the foundation if accurate collapse loads are to be predicted. This has been discussed by Sloan & Randolph (1982).

9.3.1 UNIFORM SOILS

For soil layers that can be considered to be of infinite depth and having uniform strength with depth, i.e. the cohesion, c, and angle of shearing resistance, ϕ, are constant, the well-known Terzaghi (Terzaghi 1943) equation may be used (Eq. 9.1). This equation applies to strip footings of width B subjected to vertical loading as shown in Fig. 9.3a:

$$q_u = cN_c + 0.5\gamma BN_\gamma + q_s N_q \qquad (9.1)$$

where q_u = the ultimate pressure that can be carried by the foundation; q_s = the surcharge acting on the surface of the soil; B = the full width of the strip; γ = the unit weight of the soil below the foundation level; c = the cohesive strength of the soil; and N_c, N_γ, N_q are

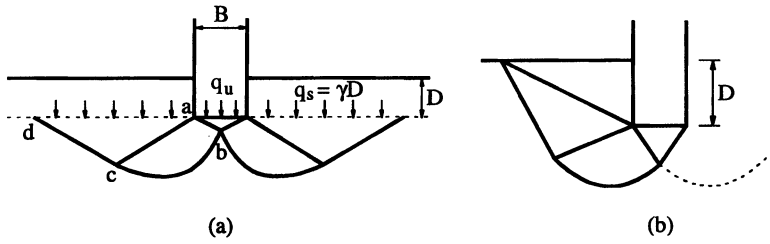


FIGURE 9.3. Failure mode for footing at depth D: (a) assumptions made by Terzaghi (1943); and (b) actual failure mode.

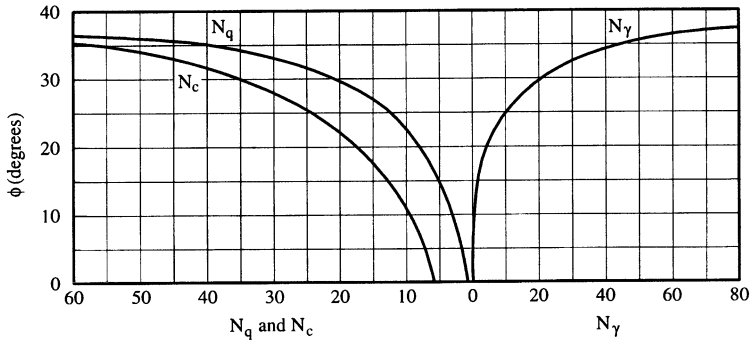


FIGURE 9.4. Bearing capacity factors for strip footing (modified from Terzaghi 1943).

bearing capacity factors that depend on the angle of shearing resistance of the soil, ϕ. Values presented by Terzaghi (1943) are shown in Fig. 9.4.

The formula of Eq. 9.1 consists of three terms, the first arising from the cohesive strength of the material, the second from the self-weight of the soil beneath the foundation, and the third from the surcharge considered to be applied at foundation level (see Fig. 9.3a). For foundations that are not on the surface of the soil, the surcharge is considered to be equal to the pressure exerted by the soil above foundation level. Plastic failure is, therefore, not considered in the soil above foundation level and so some error exists because of this assumption, however, for most practical purposes the error is small. Figure 9.3b shows the characteristics for the case where the soil above footing level is considered. Shearing would have to take place through the surcharge in this case, as can be seen from the figure.

The ultimate bearing capacity of a foundation depends upon on the rate of loading and will be different depending on whether it is loaded rapidly, so that the soil does not drain, or whether it is loaded slowly, so that all pore pressures have dissipated. Typically, the rate of loading of low permeability soils, e.g. clays, is such that "undrained" conditions (no pore pressure dissipation) are assumed. For permeable soils, e.g. sands, the excess pore pressures are usually negligible and "drained" conditions prevail. The drained case can also be used to assess the long-term bearing capacity of low permeability soils, e.g. clays.

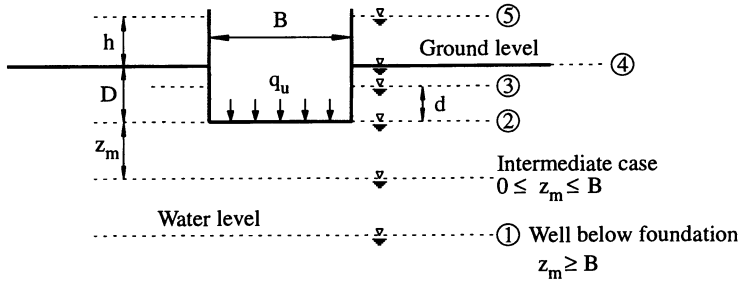


FIGURE 9.5. Location of water table, where z_m = the depth to the water table when beneath the footing.

9.3.1.1 Undrained Case

Although it is well-known that effective stresses govern the behavior of a soil under undrained conditions, it has been found adequate to perform bearing capacity calculation using the undrained shear strength, s_u (see Chapter 2), and the bearing capacity equation becomes:

$$q_u = 5.14 s_u + \gamma_{bulk} D \qquad (9.2)$$

where D = the depth of the foundation, and γ_{bulk} = the bulk unit weight of the soil above foundation level. It should be noted that Eq. 9.2 can be obtained from Eq. 9.1 by taking $c = s_u$ and $\phi = 0$.

9.3.1.2 Drained Case

For the drained loading case, the effective strength parameters are used with Eq. 9.1, i.e. $c = c'$, $\phi = \phi'$; however, the drained case is a little more complex than the undrained case if the water table is in the vicinity of the foundation. Figure 9.5 shows several different cases for the level of the water and for each case, the method of calculating the total ultimate pressure that can be applied at foundation level is given in Eq. 9.3:

$$\left.\begin{aligned}
&\text{Case (1)} \quad q_u = c'N_c + 0.5\gamma_{bulk} B N_\gamma + \gamma_{bulk} D N_q \\
&\text{Case (2)} \quad q_u = c'N_c + 0.5\gamma_{sub} B N_\gamma + \gamma_{bulk} D N_q \\
&\text{Case (3)} \quad q_u = c'N_c + 0.5\gamma_{sub} B N_\gamma + \{[\gamma_{bulk}(D - d)] + \gamma_{sub} d\} N_q + \gamma_w d \\
&\text{Case (4)} \quad q_u = c'N_c + 0.5\gamma_{sub} B N_\gamma + \gamma_{sub} D N_q + \gamma_w D \\
&\text{Case (5)} \quad q_u = c'N_c + 0.5\gamma_{sub} B N_\gamma + \gamma_{sub} D N_q + \gamma_w (D + h)
\end{aligned}\right\} \qquad (9.3)$$

where γ_{sub} = the submerged unit weight of the soil; γ_w = the unit weight of water; γ_{bulk} = the bulk unit weight of the soil; and D, d, h = the distances shown on Fig. 9.5

It may be noted that q_u is the total stress that can be applied at foundation level and therefore in Eq. 9.3, the effective ultimate bearing pressure has been calculated and the water pressure added if the water is above foundation level.

If the water-level is at a depth of less than one foundation width, B, beneath the footing, i.e. intermediate of Cases 1 and 2, simple empirical corrections are sometimes made to allow for the changed unit weight of the soil beneath the footing. This assumes that the water-level only begins to affect the unit weight of the soil being pushed aside by the foundation when it reaches a distance of B beneath it, and that as the water table rises further, the overall unit weight of the soil can be computed from a simple linear interpolation:

$$\gamma = \gamma_{sub} + \frac{z_m}{B}(\gamma_{bulk} - \gamma_{sub}) \qquad (9.4)$$

where γ_{bulk} = the unit weight of soil corresponding to the minimum water content above the

water table, and z_m = the depth to the water table when beneath the footing (see Fig. 9.5).

The unit weight calculated from Eq. 9.4 is used in the self-weight term (N_γ term) of the bearing capacity equation.

9.3.1.3 Accuracy of Terzaghi's Factors

The bearing capacity factors that were computed by Terzaghi were obtained approximately by considering the contributions of cohesion, self-weight of the soil and the surcharge separately and then adding (or superimposing) the results. The effect of this approximation has been examined by Davis & Booker (1971), who obtained a rigorous plasticity theory solution to the problem. They considered all effects contributing to the bearing capacity to be acting together in obtaining their solution.

The results of this analysis are shown for the coefficient N_γ in Fig. 9.6, where it may be seen that the Terzaghi coefficient is not greatly in error for a rough footing base. For a smooth footing, the values of N_γ can be seen to be overestimated by the Terzaghi theory; however, for most practical purposes, the Terzaghi factors are accurate enough.

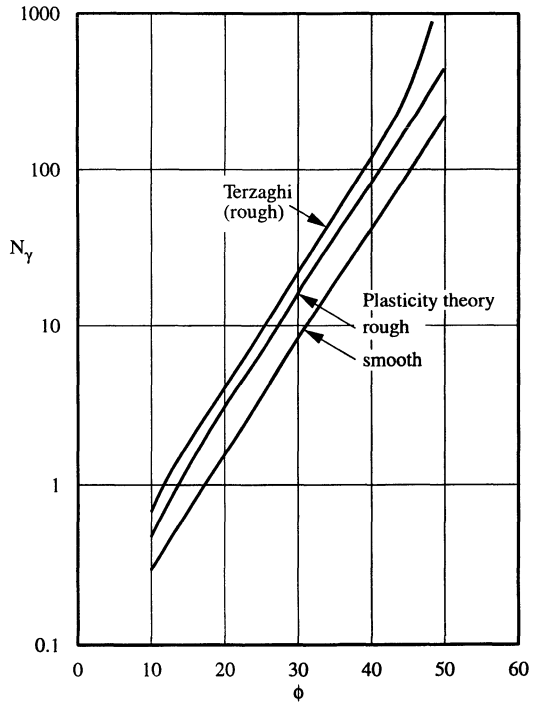


FIGURE 9.6. Bearing capacity factor, N_γ (modified from Davis & Booker 1971).

9.3.1.4 Effect of Footing Shape

The Terzaghi bearing capacity factors were computed for strip foundations, i.e. the length of the foundation is large compared to its width, and therefore do not apply to footings of other shapes. For footings that are square or circular in plan, the following formulae have been proposed (Terzaghi & Peck 1967):

$$\begin{aligned} q_u &= 1.2cN_c + 0.6\gamma RN_\gamma + q_sN_q \quad \text{Circular} \\ q_u &= 1.2cN_c + 0.4\gamma BN_\gamma + q_sN_q \quad \text{Square} \end{aligned} \tag{9.5a}$$

where R = the radius of a circular footing, and B = the full width of a square footing. For undrained conditions, the bearing capacity is given by:

$$q_u = 6.2s_u + \gamma_{bulk}D. \tag{9.5b}$$

The effect of footing shape is discussed more fully in Section 9.3.1.6.

9.3.1.5 Net Bearing Capacity

The value of bearing capacity, q_u, as computed from equations such as Eqs 9.1 or 9.3 gives the ultimate total pressure that can be applied at foundation level. If a hole is excavated for a foundation, the stress at foundation level is reduced by an amount equal to the overburden pressure. Therefore we should be able to apply a total stress at foundation level equal to the overburden pressure to return to initial conditions. It is only stresses above overburden pressure that will contribute to bearing failure.

This observation leads to the concept of *net bearing pressure*, which is useful in computing the allowable loads that can be applied to a foundation. The net bearing capacity is defined as:

$$q_{netu} = q_u - q_{ob} \tag{9.6}$$

where q_{netu} = the ultimate net load, q_u = the bearing capacity, and q_{ob} = the total overburden stress at foundation level.

The allowable load, q_{all}, that can be applied (at foundation level) can be computed from:

$$q_{all} = \frac{q_{netu}}{F} + q_{ob} \tag{9.7}$$

where F = the factor of safety.

Equation 9.7 shows that if the factor of safety were infinitely large, then the allowable load is equal to the overburden pressure. This implies that if a load equal to that of the excavated soil were applied, there is no possibility of failure, i.e. F is infinite since the initial conditions have been reinstated. This is the basis for the design of what are called "floating foundations" or "fully compensated foundations."

9.3.1.6 General Formulae

Loads on foundations may not always be vertical or applied at the central point of the foundation, or the foundation may not be on level ground. In order to take into account many other factors that may affect the bearing capacity, the following general bearing capacity equation (Eq. 9.8) has been proposed by Vesic (1973, 1975).

$$q_u = cN_c\zeta_c + 0.5\gamma BN_\gamma\zeta_\gamma + q_sN_q\zeta_q. \tag{9.8}$$

The correction multipliers, ζ, are obtained from Table 9.1 by multiplying together individual correction factors if they are applicable. For example:

$$\begin{aligned}\zeta_c &= \zeta_{cs}\zeta_{ci}\zeta_{cd}\zeta_{c\beta}\zeta_{c\delta}\\ \zeta_\gamma &= \zeta_{\gamma s}\zeta_{\gamma i}\zeta_{\gamma d}\zeta_{\gamma\beta}\zeta_{\gamma\delta}\\ \zeta_q &= \zeta_{qs}\zeta_{qi}\zeta_{qd}\zeta_{q\beta}\zeta_{q\delta}\end{aligned} \tag{9.9}$$

and the additional subscripts s, i, d, β, δ indicate that the correction factors apply for foundation shape, inclination, depth, slope of soil surface and slope of foundation base, respectively (see Fig. 9.7).

The bearing capacity factors, N_c, N_q, N_γ may be obtained from Fig. 9.4 or from Vesic (1973, 1975). For eccentric loads, it is assumed that the load acts at the center of a foundation of reduced size. For example, if the eccentric load, V, shown in Fig. 9.7, were acting at the point X at eccentricities, e_B, e_L, then the footing would be treated as one having a reduced area of B' by L', where the reduced dimensions are given by:

$$\begin{aligned}B' &= B - 2e_B\\ L' &= L - 2e_L.\end{aligned} \tag{9.10}$$

If the footing is subjected to a moment, M_L, in the L direction and a moment, M_B, in the B direction and has an applied vertical load, V, an equivalent loading system can be obtained by placing the vertical load at eccentricities e_L and e_B (see Fig. 9.7) where:

$$\begin{aligned}e_L &= M_L/V\\ e_B &= M_B/V.\end{aligned} \tag{9.11}$$

The correction multipliers in the general bearing capacity equation, Eq. 9.8, can also be computed from values given by Meyerhof (Meyerhof 1953, 1963) or by Hansen (1970). Hansen's correction factors include the effects of the slope of the soil surface and the slope of the base of the foundation. The correction multipliers may be computed by multiplying the correction factors together as for the Vesic case, Eq. 9.9.

Worked Example

A square footing 1.5 × 1.5 m in plan, is founded at a depth of 1m in a deep layer of clay. The footing is loaded by an inclined load and moment loadings, such that the load can be considered to act eccentrically at a point 0.3 m away from each of the center lines of the footing.

The water table is at foundation level and the

TABLE 9.1. Correction factors (adapted from Vesic 1973, 1975)[a]

Factor	Cohesion, c	Self-weight, γ	Surcharge, q
Foundation shapes, s	ζ_{cs}	$\zeta_{\gamma s}$	ζ_{qs}
	$= 1 + \frac{B'}{L'}\frac{N_q}{N_c}$	$= 1 - 0.4\frac{B'}{L'}$	$= 1 + \frac{B'}{L'}\tan\phi$
Inclined loading, i	ζ_{ci}	$\zeta_{\gamma i}$	ζ_{qi}
	$= 1 - \frac{mH}{B'L'cN_c}$ $(\phi = 0)$	$= \left[1 - \frac{H}{V + B'L'c\cot\phi}\right]^{m+1}$	$= \left[1 - \frac{H}{V + B'L'c\cot\phi}\right]^{m}$
	$= \zeta_{qi} - \frac{1 - \zeta_{qi}}{N_c\tan\phi}$ $(\phi > 0)$		
Foundation depth, d	ζ_{cd}	$\zeta_{\gamma d}$	ζ_{qd}
	$= 1 + 0.4\xi$ $(\phi = 0)$	$= 1.0$	$= 1 + 2\tan\phi(1 - \sin\phi)^2\xi$
	$= \zeta_{qd} - \frac{(1 - \zeta_{qd})}{N_c\tan\phi}$ $(\phi > 0)$		
Surface slope, β[b]	$\zeta_{c\beta}$	$\zeta_{\gamma\beta}$	$\zeta_{q\beta}$
	$= 1 - [2\beta/(\pi + 2)]$ $(\phi = 0)$	$= (1 - \tan\beta)^2$	$= (1 - \tan\beta)^2$
	$= \zeta_{q\beta} - \frac{1 - \zeta_{q\beta}}{N_c\tan\phi}$ $(\phi > 0)$	Note: $N_\gamma = -2\sin\beta$ $(\phi = 0)$[c]	
Base tilt, δ[c]	$\zeta_{c\delta}$	$\zeta_{\gamma\delta}$	$\zeta_{q\delta}$
	$= 1 - [2\delta/(\pi + 2)]$ $(\phi = 0)$	$= (1 - \delta\tan\phi)^2$	$= (1 - \delta\tan\phi)^2$
	$= \zeta_{q\delta} - \frac{1 - \zeta_{q\delta}}{N_c\tan\phi}$ $(\phi > 0)$		

[a] V, vertical load; H, horizontal load; B, foundation width; L, foundation length ($L > B$); e_B, eccentricity parallel to B; e_L, eccentricity parallel to L; $B' = B - 2e_B$; $L' = L - 2e_L$; $m = (2 + x)/(1 + x)$; $x = B/L$ if H parallel to B; $x = L/B$ if H parallel to L; $\xi = D/B$ if $D/B \leq 1$; $\zeta = \tan^{-1}(D/B)$ if $D/B > 1$.

[b] $\beta < \pi/4$, where β is in radians.

[c] $\delta < \pi/4$, where δ is in radians.

[d] $q_u = cN_c\zeta_{c\beta} + 1/2\gamma BN_\gamma + q_sN_q\cos\beta$ $(\phi = 0^0)$ if only applying surface slope correction.

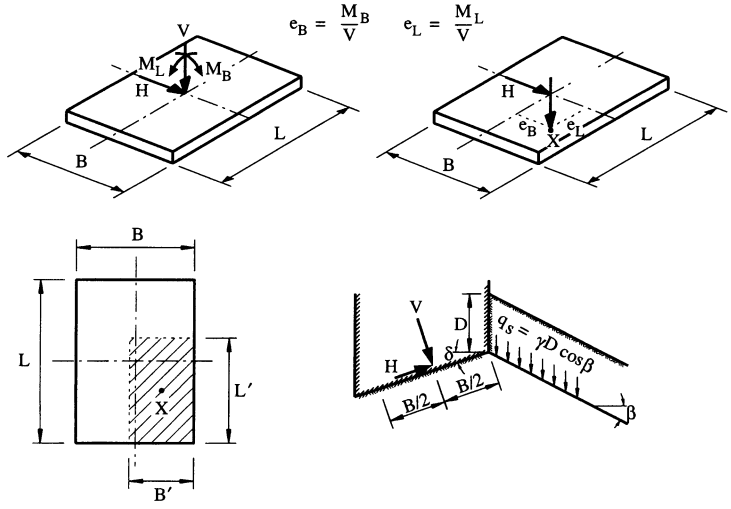


FIGURE 9.7. Footing subjected to vertical and horizontal loads plus moments.

saturated unit weight of the clay may be taken as γ_{sat} = 17 kN m^{-3} (as can the bulk unit weight of the clay above water-level). The horizontal component of the inclined load acts along a diagonal of the footing, i.e. at 45° to each center-line. If the magnitude of the inclined load is 100 kN and it is inclined at 60° to the horizontal, compute the bearing capacity of the footing (a) when it is loaded rapidly so that the soil is in an undrained condition; and (b) long term (after excess pore pressure dissipation).

The strength properties of the clay are s_u = 60 kPa; $\phi_u = 0$; $c' = 0$; $\phi' = 28°$.

Solution: Because the load is eccentric we must calculate the reduced length and breadth of the footing.

$$L' = L - 2e_L = 1.5 - 2 \times 0.3 = 0.9 \text{ m}$$

$$B' = B - 2e_B = 0.9 \text{ m}.$$

The components of the load are $H = 100 \cos 60°$ = 50 kN, and $V = 100 \sin 60°$ = 86.6 kN.

1. Undrained loading. The undrained bearing capacity factors are obtained from Fig. 9.4 (setting $\phi = 0$) as $N_c = 5.14$, $N_q = 1$, $N_\gamma = 0$.

In this case we have to compute the factor m, which depends upon whether the horizontal load is parallel to side B or L. Because the loading is at an angle to both sides for this problem, it is necessary to compute $m = m_B \sin^2\theta + m_L \cos^2\theta$ (as suggested by Vesic 1975), where θ is the angle of the inclined load to the long side, L, of the foundation. As the footing is square, $m_B = m_L$ = (2 + 1)/(1 + 1) = 1.5 and the angle is 45°, so that m = 1.5.

Using Table 9.1, the Vesic correction factors are given by:

$$\zeta_c = \zeta_{cs}\zeta_{cd}\zeta_{ci}$$

$$= \left(1 + \frac{B'N_q}{L'N_c}\right)(1 + 0.4\xi)\left(1 - \frac{mH}{B'L'cN_c}\right)$$

$$= (1 + 0.194)(1 + 0.266)(1 - 0.30)$$

$$= 1.058$$

$$\zeta_q = \zeta_{qs}\zeta_{qd}\zeta_{qi}$$

$$= \left(1 + \frac{B'}{L'}\tan\phi\right)$$

$$\times [1 + 2\tan\phi(1 - \sin\phi)^2\xi]$$

$$\times \left(1 - \frac{H}{V + B'L'c\cot\phi}\right)^m$$

$$= 1 \times 1 \times 1 = 1$$

and so the ultimate bearing capacity, q_u, is given by:

$$q_u = s_u N_c \zeta_c + \gamma D N_q \zeta_q$$
$$= (60 \times 5.14 \times 1.058) + (17 \times 1 \times 1 \times 1.0)$$
$$= 343 \text{ kPa.}$$

2. Drained loading. For $\phi = 28°$, the bearing capacity factors from Fig. 9.4 are $N_q = 17$, $N_\gamma = 16$. We now may compute the correction factors from Table 9.1 (with $m = 1.5$)

$$\zeta_q = \zeta_{qs}\zeta_{qd}\zeta_{qi}$$
$$= (1 + 0.532)(1 + 0.199)(1 - 0.438) = 1.031$$
$$\zeta_\gamma = \zeta_{\gamma s}\zeta_{\gamma d}\zeta_{\gamma i}$$
$$= (1 - 0.4)(1.0)(1 - 0.253) = 0.448$$

and so the bearing capacity for drained conditions is:

$$q_u = 0.5\gamma_{sub} B' N_\gamma \zeta_\gamma + \gamma D N_q \zeta_q$$
$$= [0.5 \times (17 - 9.81) \times 0.9 \times 16 \times 0.448]$$
$$+ (17 \times 1 \times 17 \times 1.031)$$
$$= 23.2 + 297.9$$
$$= 321 \text{ kPa.}$$

Therefore, for this particular problem, the drained bearing capacity is the lowest.

For eccentric loading such as in this example, the reduced footing size would be used to compute the ultimate vertical load, Q_u, that the footing could carry, i.e. $Q_u = q_u L'B'$. In all of the above calculations, the reduced footing size B' has been used, except where calculating m and ξ (see Table 9.1) as suggested by Das (1990).

9.3.1.7 Soil Layers of Finite Depth

The solutions for the bearing capacities of foundations mentioned so far have been for soils that are of infinite depth. It is of interest to examine the effect of a very strong layer at a finite depth beneath the surface of the soil layer. Solutions to this problem have been found by Mandel & Salençon (1972), who considered a strip footing on a uniform layer of soil, i.e. strength parameters are constant, underlain by a rough rigid base. The conditions assumed for the interface between the rigid base and the layer of soil are important because they influence the collapse load; other base conditions have also been considered in this paper. The rough based solution is more applicable to soils where it would be expected that there would be some shearing resistance between the soil and the underlying rock, and so only results for the rough base are considered here.

The bearing capacity of strip footings having a full width B may be computed from:

$$q_u = (cN_cF_c) + (0.5\gamma BN_\gamma F_\gamma) + (q_s N_q F_q) \quad (9.12)$$

where the bearing capacity coefficients are the same as for the Terzaghi equation, but are modified by the factors F_c, F_γ, and F_q, which depend upon the depth, h, of the soil layer.

Table 9.2 gives values of the factors F_γ, F_c and F_q. The values in the tables may be seen to depend on the angle of shearing resistance and the ratio of the footing width to the layer depth, B/h. It may be noted that the correction factors were computed for a smooth footing base and by considering the effects of cohesion, self-weight of the soil and surcharge separately.

9.3.2 NON-UNIFORM SOILS

Inhomogeneity can be due to the soil strength increasing with depth, or perhaps being stronger at the surface due to overconsolidation. The soil beneath a foundation may also consist of different layers of material or the soil strength may simply be different at different places on a site. In the latter case, the footing should be designed for the soil strength at the location of the footing, or if this is not known, a conservative approach is to design footings for the lowest strength.

Solutions have been found for the case where the soil strength varies uniformly with depth or where the soil is layered, and these solutions are presented in the following sections.

TABLE 9.2. Values of factors F_γ, F_c, and F_q

$\phi\downarrow$	$B/h\rightarrow$	1	2	3	4	5	6	8	10	15	20	30	40
Factor F_γ													
30°	$B/h \leq 1.3:1.0$		1.20	2.07	4.23	9.90	24.8	178	1450	3.81×10^5	1.3×10^8	1.95×10^{13}	
20°	$B/h \leq 2.14:1.0$			1.07	1.28	1.63	2.20	4.41	9.82	97	340	2.6×10^5	7×10^5
10°	$B/h \leq 4.07:1.0$					1.01	1.04	1.12	1.36	2.28	4.33	20	113
0°	$F_\gamma = 1$ for all B/h												
Factor F_c													
30°	$B/h \leq 0.63:1.0$	1.13	2.50	6.36	17.4	50.2	150	1444	1.48×10^4	5.81×10^6			
20°	$B/h \leq 0.63:1.0$	1.01	1.39	2.12	3.29	5.17	8.29	22.0	61.5	905	1.50×10^4		
10°	$B/h \leq 1.12:1.0$		1.11	1.35	1.62	1.95	2.33	3.34	4.77	11.7	29.4		
0°	$B/h \leq 1.414:1.0$		1.02	1.11	1.21	1.30	1.40	1.59	1.78	2.27	2.75	3.72	
Factor F_q													
30°	$B/h \leq 0.63:1.0$	1.12	2.42	6.07	16.5	47.5	142	1370	1.40×10^4	5.50×10^6			
20°	$B/h \leq 0.86:1.0$	1.01	1.33	1.95	2.93	4.52	7.14	18.7	51.9	763	1.26×10^4		
10°	$B/h \leq 1.12:1.0$		1.07	1.21	1.37	1.56	1.79	2.39	3.25	7.37	17.9	92.3	
0°													

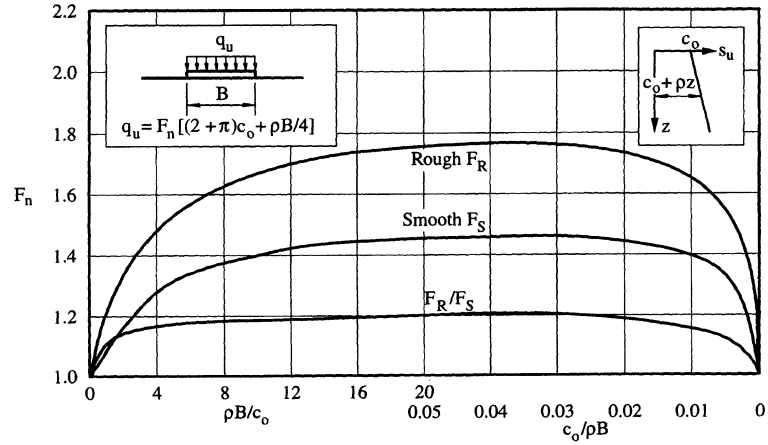
9.3.2.1 Strength Increasing with Depth

Strip Loading on Infinitely Deep Soil Layer. Solutions to the problem where the undrained shear strength of the soil increases linearly with depth have been produced by Davis & Booker (1973) for the case of a strip footing. The ultimate bearing capacity of the foundation for vertical load is:

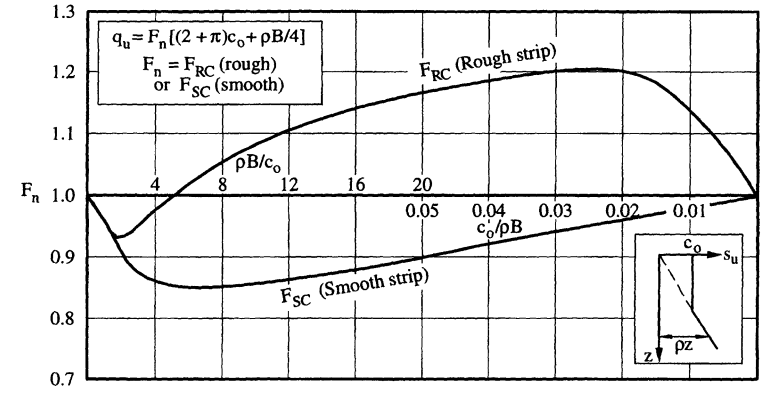
$$q_u = F_n[(2 + \pi)c_0 + \rho B/4] \qquad (9.13)$$

where c_0 = the cohesive strength at the surface of the soil, ρ = the rate of increase of cohesive strength with depth, B = the full width of the footing, and F_n = a factor that is presented in Fig. 9.8a. In the figure, the factor F_n is presented for both rough, F_R, and smooth, F_S, foundations.

Factors were also presented by Davis & Booker for a soil having a crust. The crust is assumed to have a cohesion, c_0, to a depth where it intersects the line $c = \rho z$ (see inset to Fig. 9.8b). The factor F_n is presented in Fig. 9.8b for both rough and smooth footings, where the factor is again used with Eq. 9.13.



(a)



(b)

FIGURE 9.8. Undrained bearing capacity factor, F_n, for a strip on an infinite layer (a) with undrained shear strength increasing with depth, and (b) with a crust (modified from Davis & Booker 1973).

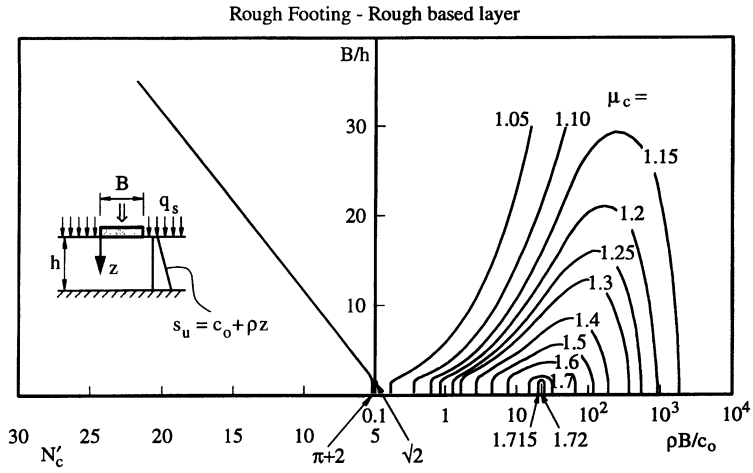


FIGURE 9.9. Curves of μ_c and N'_c. Strip on finite layer; undrained shear strength increasing linearly with depth (modified from Matar & Salençon 1977).

Soil Layers of Finite Depth. The case of an undrained clay with a cohesion that varies with depth has been examined by Matar & Salençon (1977) for the case of a strip footing on a soil layer of finite depth (overlying a rough, rigid base).

The bearing capacity of the strip is:

$$q_u = q_s + \mu_c c_0 \left(N'_c + \frac{\rho B}{4c_0} \right) \qquad (9.14)$$

where q_s = the surcharge, N'_c = the bearing capacity factor given by Fig. 9.9, μ_c = the correction factor given in Fig. 9.9, c_0 = the cohesion at the surface, and ρ = the rate of increase in cohesion with depth.

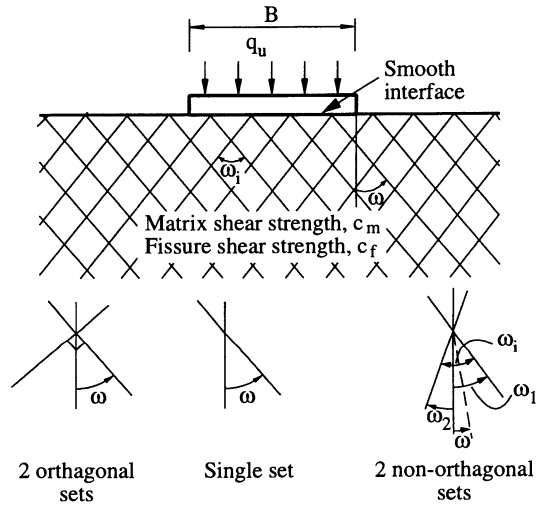


FIGURE 9.10. Strip footing on fissured clay.

9.3.2.2 Fissured Clays

Some clay deposits, especially overconsolidated clays, can contain fissures that have a lower strength than the matrix due to shearing and weathering. Some solutions have been obtained to this problem (Davis 1980 & Booker 1991) for the case of a strip footing.

Solutions to the problem have also been presented by Lav *et al.* (1995) for the case of a smooth strip footing resting on a weightless, purely cohesive material that has a regular set of fissures. The problem considered is shown in Fig. 9.10. The angle between the sets of fissures is ω_i, while the fissures lie at an angle, ω, to the vertical.

If the cohesive strength of the fissures is c_f and the strength of the intact soil between the fissures is c_m, then the undrained bearing

capacity of the strip footing can be expressed in terms of c_m. Results are presented in Fig. 9.11a–d, which shows the effects of the fissures on the bearing capacity for joint sets with an included angle, ω_i, of 90, 60, 45 and 30°. Where there is a set of orthogonal fissures or a single set, i.e. Fig. 9.11a, the inclination, ω, of one set is used. Where the fissures are not orthogonal, (Fig. 9.11b–d) the mean inclination of the two sets of fissures is used, $(\omega_1 + \omega_2)/2$, to indicate the inclination of the fissure sets where ω_1, ω_2 are as shown in Fig. 9.10. Solutions have been evaluated for several values of the ratio of the fissure strength to the strength of the solid material, c_f/c_m.

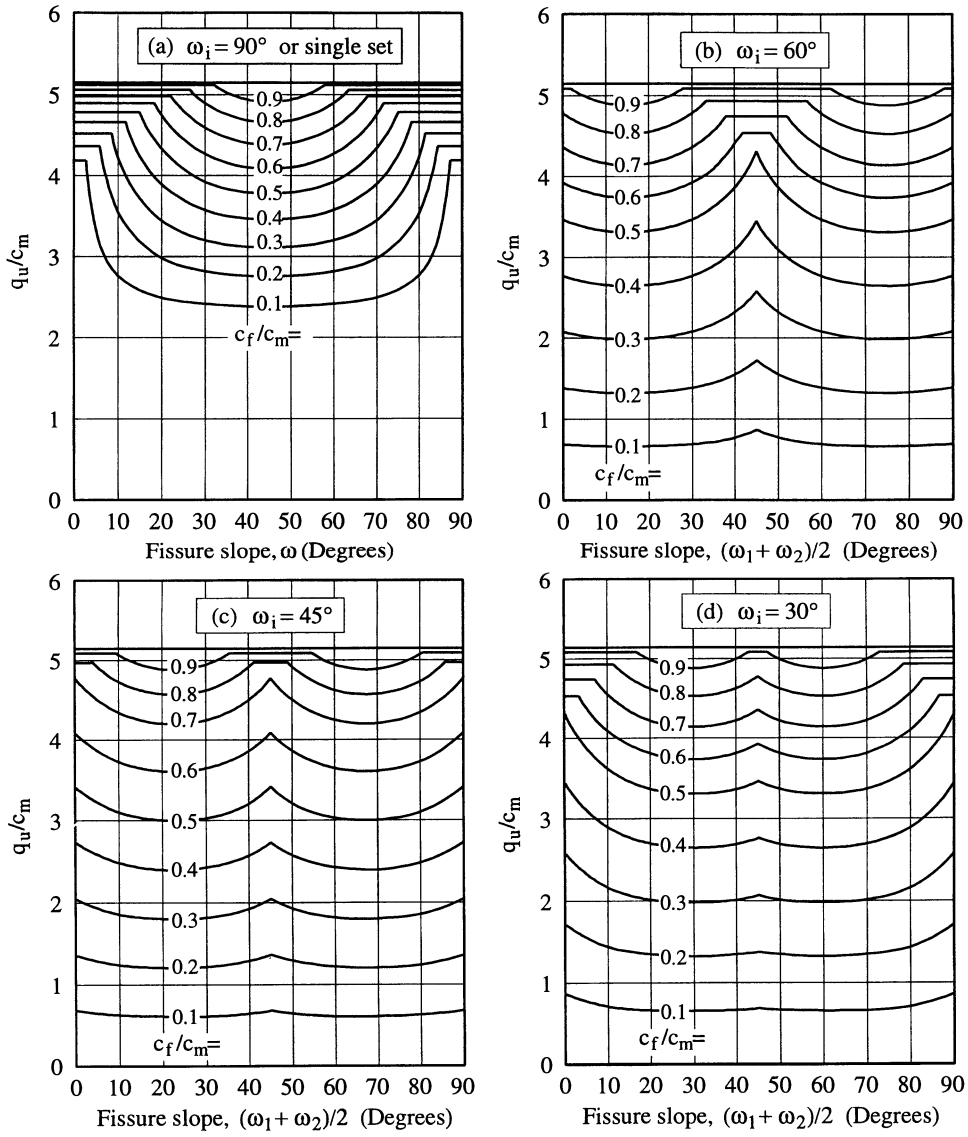
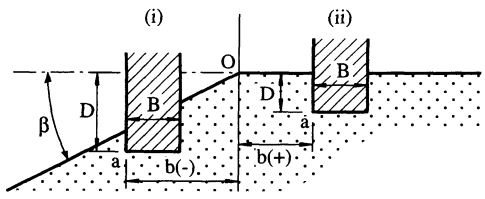


FIGURE 9.11. Undrained bearing capacity of a strip footing on a fissured clay deposit: (a) containing one or two orthogonal fissure sets; and containing two fissure sets with an included angle of (b) 60°, (c) 45°, and (d) 30° (modified from Lav *et al.* 1995).



Legend:

Note:
$\lambda = b/B$
$\eta = D/B$

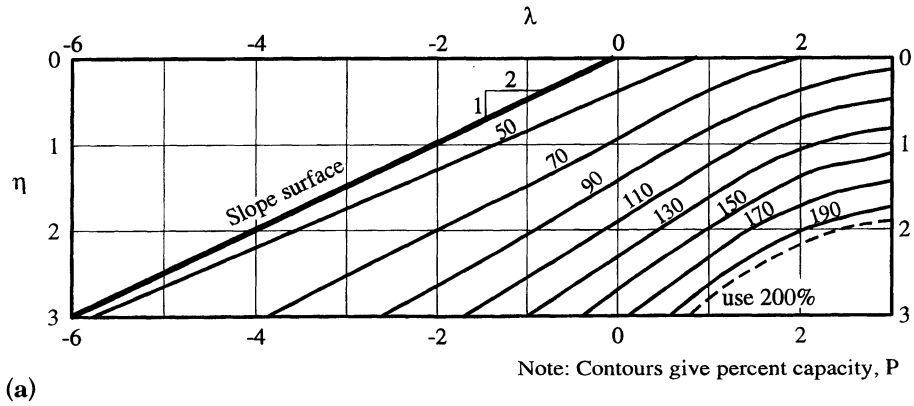
β = angle of slope with respect to horizontal
D = depth of footing with respect to the level of the horizontal ground
B = footing width
b = horizontal distance leading edge of footing is away from crest of slope

FIGURE 9.12. Definition of terms for a footing on a slope.

9.3.2.3 Footings on Slopes

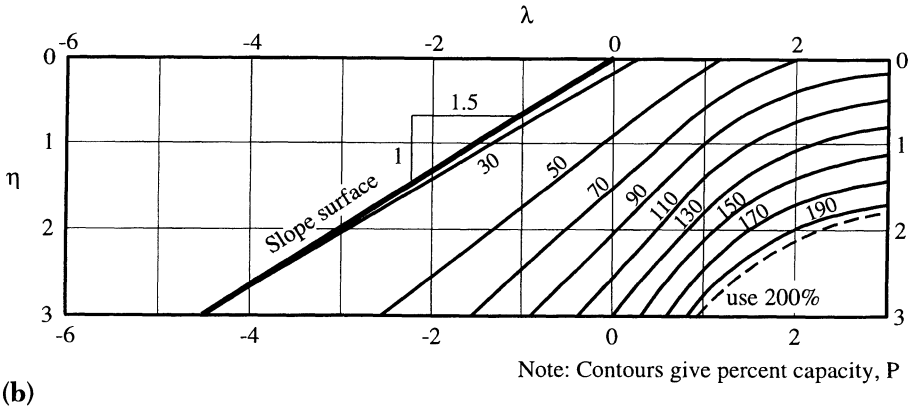
The bearing capacity of footings on slopes (rather than on level ground) is of interest to engineers as abutments to bridges are often founded on valley walls or are at the top of a slope. Shields *et al.* (1990) have produced design charts that are based on the centrifuge tests of Gemperline (1988) and other model tests.

Figure 9.12 shows the locations of footings with respect to the slope, and definitions of the non-dimensional terms λ and η, which give the location of the strip footing with respect to the slope. Design charts for two slopes ($2H:1V$) and ($1.5\,H:1V$) on cohesionless soil are shown in Fig. 9.13a, b. The charts show contours of the percentage capacity, *P*,



Note: Contours give percent capacity, P

(a)



Note: Contours give percent capacity, P

(b)

FIGURE 9.13. Suggested design factors for (a) a 2:1 (26.6°) slope, and (b) a 1.5:1 (33.7°) slope (modified from Shields *et al.* 1990). Contours give per cent capacity, *P*.

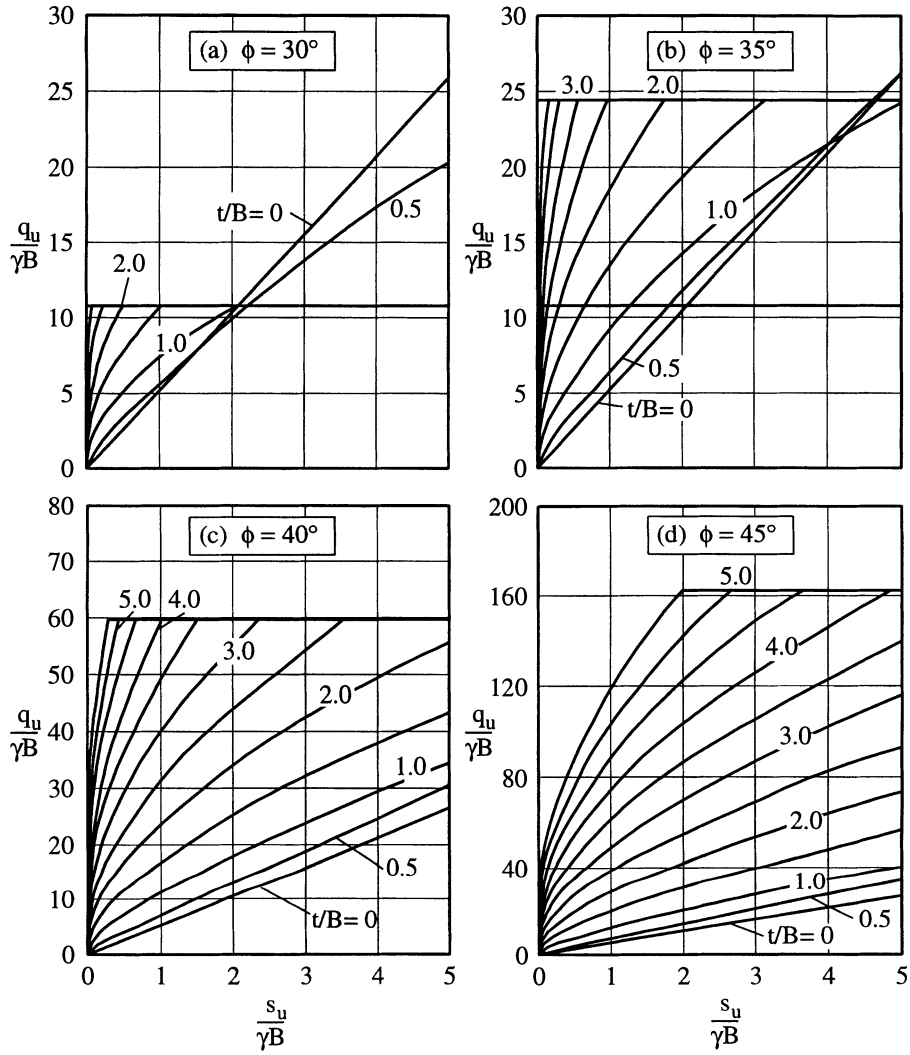


FIGURE 9.14. Dimensionless limit pressure for strip footing on sand layer overlying clay. Case of no surcharge: (a) $\phi = 30°$, (b) $\phi = 35°$, (c) $\phi = 40°$, and (d) $\phi = 45°$, (modified from Michalowski & Shi 1995).

of a footing on level ground that the footing in a slope can carry.

The bearing capacity of a footing in a slope is, therefore, for a cohesionless soil, given by:

$$q_u = 0.5\gamma B N_{\gamma q} \tag{9.15}$$

where $N_{\gamma q}$ may be found from $N_{\gamma q} = PN_{\gamma qR}$ and

$$N_{\gamma qR} = [10^{(0.1159\phi - 2.386)}][10^{(0.34\ -0.2\log_{10}B^*)}] \tag{9.16}$$

and the value of ϕ is in degrees. The value of $B^* = B$ if the footing width is in inches or $B^* = 39.4B$ if the footing width, B, is in meters in the above formula.

9.3.2.4 Layered Soils

The bearing capacity of footings on layered soils presents a more difficult problem than that of a footing on a uniform soil, and so solutions are less plentiful and often approxi-

mate in nature. Problems may be divided into two categories: those involving sand and clay layers, and those involving clay layers of different strengths.

Sand and Clay Layers. If a loading is applied to a foundation that is constructed on a sand layer overlying a clay layer, then the footing can punch through the sand into the clay layer beneath, especially if the clay layer is soft. This type of failure has been examined by Meyerhof (1974), Hanna & Meyerhof (1980), Michalowski & Shi (1995) and Burd & Frydman (1997).

The solutions of Michalowski and Shi (1995) were obtained through the use of a kinematic approach, which will yield an upper bound to the bearing capacity of a footing, and so one would expect their collapse loads to be somewhat higher than the true solution. These solutions are presented in Fig. 9.14a–d. The numerical results of Burd & Frydman (1997) were obtained from finite element and finite difference-based computer codes, and so may still contain some error. These results (for an angle of friction of the sand of 40°) are presented in Fig. 9.15.

In these figures, the full width of the foundation is B, the thickness of the sand layer is t, the undrained shear strength of the clay is s_u, the angle of friction of the sand is ϕ' and the unit weight of the sand is γ. The ultimate bearing capacity of the footing is q_u.

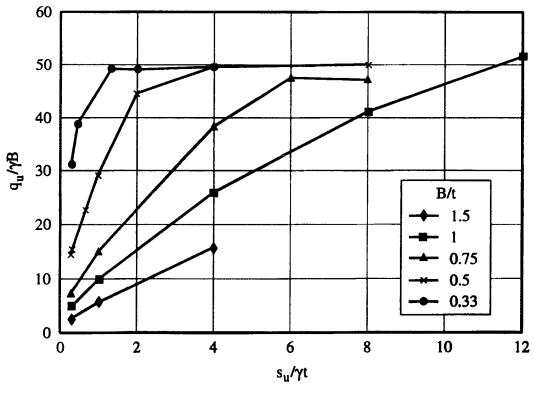


FIGURE 9.15. Bearing capacity for strip footing on sand layer overlying clay layer. $\phi'_{sand} = 40°$ (modified from Burd & Frydman 1997).

Solutions to this problem should be bounded by the solution for a footing on clay when the sand layer becomes thin and by the solution for a footing on sand when the sand layer becomes thick (as the failure would occur through the surface sand layer). Thus the accuracy of the results can roughly be assessed by looking at the limiting cases as illustrated below. For deeper sand layers, the value of $q_u/\gamma B$ should approach $\frac{1}{2}N_\gamma$ because the failure would occur through the sand alone. The rigorous plasticity solutions of Davis & Booker (1971) show that this value should be about 45 for a rough strip footing on a sand layer having an angle of friction of 40° (Fig. 9.6). The charts of Michalowski and Shi show a value of 60 for this case, while Burd & Frydman's solution shows a value of about 50.

For thin sand layers, the results should be that for a clay layer alone, so that a plot of $q_u/\gamma B$ versus $s_u/\gamma B$ should be a straight line with a gradient of 5.14 as in this case $q_u = N_c s_u$ and N_c is equal to the classical value of $(2 + \pi)$. This is certainly true for the Michalowski and Shi results; however, it is not so easy to see on the plot of Burd & Frydman because their plot is of $q_u/\gamma B$ versus $s_u/\gamma t$.

It can therefore be concluded that the results of both methods of analysis are overestimating bearing capacities for deeper sand layers with high angles of friction (>40°), although if appropriate factors of safety are used, then the charts should be a reasonable guide for foundation design.

Clay Layers of Different Strengths. For clay layers of different stiffnesses some solutions are available for the undrained case where the angle of shearing resistance can be taken as $\phi = 0$ (Vesic 1975). For the case where a soft clay layer (having an undrained shear strength, s_{u1}) overlies a deep stiffer clay layer

(having an undrained shear strength, s_{u2}), the bearing capacity is given by Vesic (1975) as:

$$q_u = s_{u1}N_m + q_s \qquad (9.17)$$

where the coefficient N_m can be found from Fig. 9.16 for square or circular footings.

For the case where a stiff clay layer (having undrained strength s_{u1}) overlies a deep soft clay layer (s_{u2}), then the bearing capacity can be estimated from:

$$N_m = \frac{1}{\beta} + \kappa\zeta_c N_c \ (\leq \zeta_c N_c) \qquad (9.18)$$

where $\kappa = s_{u2}/s_{u1}$, $\beta = BL/[2(B + L)H]$ and ζ_c is the bearing capacity shape factor for the footing (see Eq. 9.9). (Figure 9.16 shows the dimensions B, H, L = footing length.)

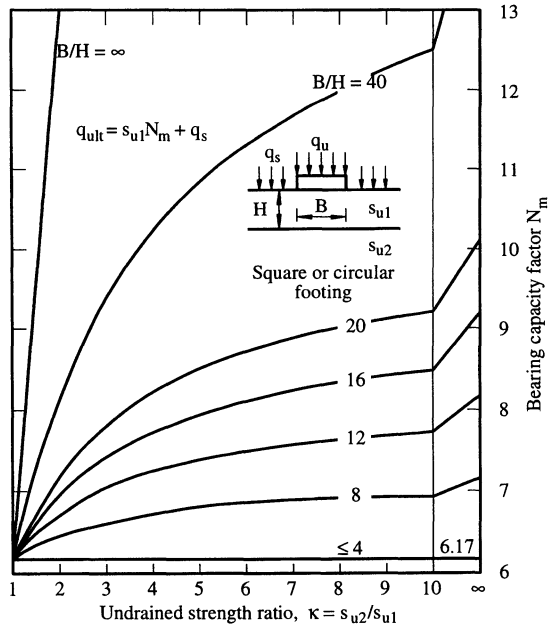


FIGURE 9.16. Modified undrained bearing capacity factor, N_m, for square or circular footings on two layer purely cohesive soil (modified from Vesic 1975).

9.4 *Settlement*

If a structure settles substantially with very small differential settlements (settlements are almost uniform everywhere) then the structure is unlikely to sustain any damage, although if settlement is too large, the structure will be subject to serviceability problems, i.e. water, gas, and sewer pipes, and other services, may be damaged.) It is the differential settlements that cause cracking and damage to structures, i.e. movement of one part of a structure relative to another. Tilt may also be a problem for crane rails or machinery that has to remain level.

It is therefore necessary to try to limit the differential settlements as well as the overall vertical movements of a structure. The magnitude of allowable settlements depends on the type of structure or the purposes for which the foundation is to be used. Here only static loadings are considered. Chapter 12 examines the dynamic response of foundations.

9.4.1 LIMITS OF SETTLEMENT

Allowable deflections (or angular distortions) of different structures have been proposed by Skempton and MacDonald (1956), Bjerrum (1963a) and Grant *et al.* (1974). More recently, Boone (1995) has proposed a method for determining damage to structures that relies on many factors such as the ground movement profile, the geometry of the structure and the critical strains in the building materials.

Allowable angular distortions for different types of structures and construction materials have also been presented by Polshin & Tokar (1957) and these are shown in Table 9.3. It may be seen from this table that, in general, stiffer structures such as those constructed from masonry, are more likely to be damaged than flexible structures such as those having steel frames with sheet cladding.

9.4.2 SETTLEMENT COMPUTATION

When a load is applied to a footing on a non-cohesive, free-draining soil like a sand or a

TABLE 9.3. Allowable settlements and deflections (adapted from Polshin & Tokar 1957)

Item no.	Description of standard value	Subsoil: Sand and clay in hard condition	Subsoil: Clay in plastic condition
1	Slope of crane-way, as well as tracks for bridge-crane truck	0.003	0.003
2	Difference in settlement of civil and industrial building column foundations:		
	• For steel and reinforced concrete frame structures	$0.002l$	$0.002l$
	• For end rows of columns with brick cladding	$0.007l$	$0.001l$
	• For structures where auxiliary strain does not arise during non-uniform settlement of foundations (l = distance between foundation centers)	$0.005l$	$0.005l$
3	Relative deflection of plain brick walls:		
	• for multi-storey dwellings and civil buildings		
	At $l/H < 3$	0.0003	0.0004
	At $l/H \gg 5$	0.0005	0.0007
	(l = length of deflected part of wall, H = height of wall from foundation footing)		
	• for one-storey mills	0.0010	0.0010
4	Pitch of solid or ring-shaped foundations of high rigid structures (smoke stacks, water towers, silos, etc.) at the most unfavorable combination of loads	0.004	0.004

Kind of building and type of foundation	Average settlement (cm)
Buildings with plain brick walls on continuous and separate foundations with the wall length, l, to the wall height, H (H counted from the foundation footing):	
$l/H > 2.5$	8
$l/H < 1.5$	10
Buildings with brick walls, reinforced with reinforced concrete or reinforced brick belts (not depending on the ratio of l/H)	15
Framed buildings	10
Solid reinforced concrete foundations of blast furnaces, smoke stacks, silos, water towers, etc.	30

gravel, the soil will deform immediately and will reach its final settlement (provided there is no creep settlement). However, as discussed in Chapter 2, when a load is applied to a saturated clay, the load is partly supported by the soil skeleton and partly by the porewater. There is therefore an increase in the porewater pressure beneath the foundation and water will begin to flow from areas of high water pressure to areas of low water pressure, and as it does, the soil beneath the footing undergoes a volume reduction. The footing will therefore settle with time until all excess pore pressures have dissipated, at which time the footing will have reached its final settlement (again if creep is not considered).

When the load is first applied, the footing

will undergo an initial settlement, with the soil deforming at constant volume (since the water does not have time to flow through the soil). This can only occur if the load is not one-dimensional so that shear deformation can take place.

Generally, it is the final settlement of a foundation that is of interest, as this is the largest settlement that will occur and therefore this leads to the largest differential settlements. However, the time–deflection behavior may be of importance in some cases.

9.4.3 THEORY OF ELASTICITY

Working loads applied to foundations are usually selected so that they are well below the ultimate bearing capacity of the building. It is therefore possible to treat the soil as an elastic material, provided that the elastic modulus used in any computations is appropriate for the stress range that occurs in the ground beneath the footing.

9.4.3.1 One-dimensional Conditions

For one-dimensional loadings, i.e. where the load is large in extent compared to the thickness of the soil layer, such as a surcharge, the elastic theory of Terzaghi (1923) may be used (see also Chapter 2). One-dimensional theory is based on the assumption that the strain will be entirely vertical and that there will be no lateral strains. The soil layer is divided into horizontal layers each of thickness h_i, and the stress increases are computed at the center of each layer. The coefficient of compressibility, m_v, is found from an oedometer test (see Sections 2.7 and 3.5) and is calculated from the strain in the specimen divided by the stress change. As the value of m_v is dependent on the stress level, the appropriate value should be used for each layer. A value corresponding to the mean stress, i.e. intermediate of the initial stress and the stress after application of the load, is appropriate. Vertical settlement, S, is then given by:

$$S = \sum_{i=1}^{N} m_{vi} \Delta\sigma'_{vi} h_i \qquad (9.19)$$

where m_{vi} = the coefficient of compressibility of layer i of the soil; $\Delta\sigma'_{vi}$ = the increase in vertical effective stress in layer i of the soil; h_i = the thickness of the ith layer of soil; and N = the number of layers into which the soil is divided.

For strictly one-dimensional problems the stress increase $\Delta\sigma'_{vi}$ should be the same for all layers and equal to the applied uniform load; however, vertical stress increases are often calculated for rectangular or circular loading shapes using three-dimensional solutions for the stress increases. This is in effect carrying out a pseudo three-dimensional analysis as stresses are calculated from three-dimensional solutions, and then the one-dimensional equation (Eq. 9.19) is used to compute settlements.

9.4.3.2 Three-Dimensional Problems

For problems that are three-dimensional in nature, elastic solutions for the settlement of foundations of various shapes and stiffnesses and subjected to various types of loadings, are available and may be found in books such as the one by Poulos & Davis (1974). Provided that the appropriate solution can be found, the settlement of the foundation can be calculated.

For obtaining the initial settlement, S_i, of the footing, the undrained elastic modulus, E_u, and Poisson's ratio, ν_u, of the soil are needed. As the soil is assumed to undergo zero volume change the value of ν_u is taken to be 0.5, as this can be shown to be the requirement for zero volume change in an isotropic material. For computing the final settlement, S_f, the drained elastic modulus, E' and Poisson's ratio, ν', are used (see Section 3.5). For free-draining sands and gravels, only the drained parameters will apply.

The settlement of flexible footings, which are rectangular in plan (of length, L, by breadth, B) and founded at depth, D, in uni-

form soil layers of finite depth, may be computed from the charts of Christian & Carrier (1978). These charts are reproduced in Fig. 9.17 and apply only to the undrained case ($\nu_u = 0.5$). Elastic solutions are normally presented in non-dimensional form, so that they apply to a wide range of problems. In addition, solutions for strip- or rectangular-shaped loadings, are often presented for the edge (strip) or corner (rectangle) because the solutions may then be superimposed. For example, the deflection at the center of a rectangle may be obtained by dividing the rectangular loaded area into four equal rectangular areas and summing the deflections under the corners of each.

Figure 9.18 shows solutions for a rigid circular foundation constructed on a layer of soil of finite thickness. This plot may be used to calculate both initial and final settlements, as the solutions have been evaluated for a range of Poisson's ratios. The solutions apply only to foundations on the surface of the clay layer, and may also be used for square footings since the settlement of a square footing may be approximated as the settlement of a circular footing having the same area in plan, with very little error.

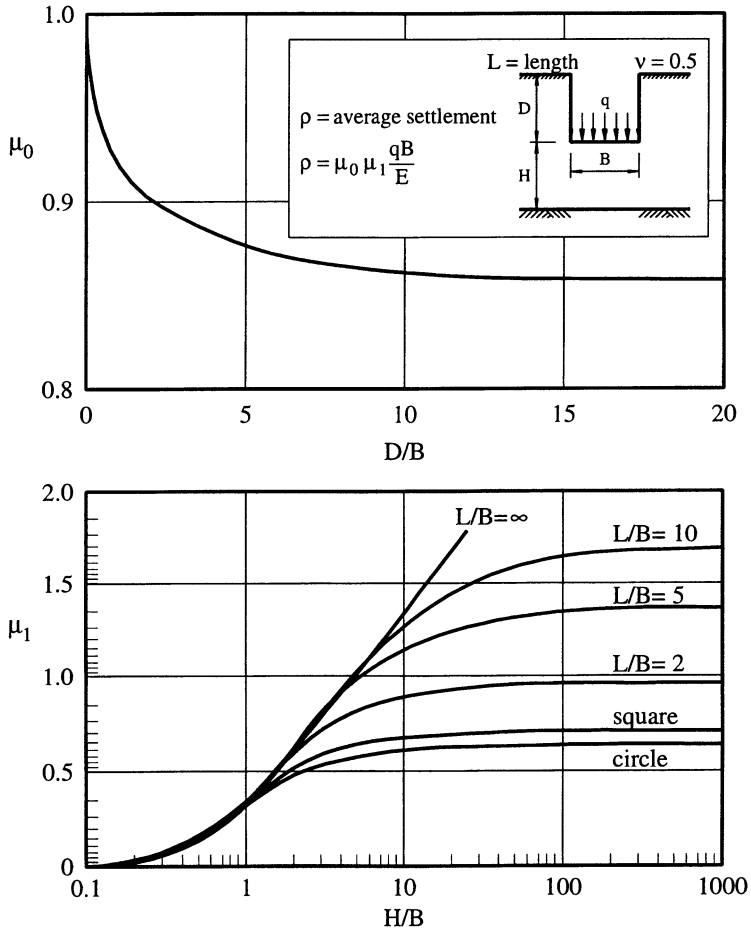


FIGURE 9.17. Chart for evaluating settlement of embedded rectangular footings (modified from Christian & Carrier 1978).

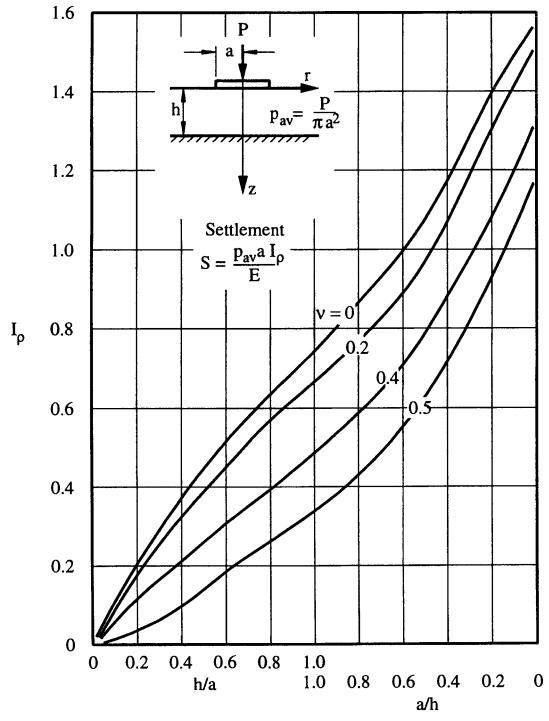


FIGURE 9.18. Chart for evaluating settlement of rigid circular footing on a soil layer of finite thickness.

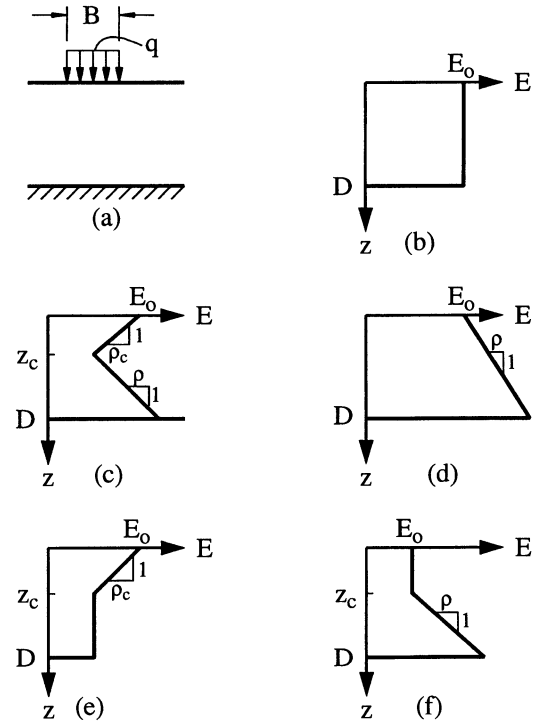


FIGURE 9.19. Soil profiles considered by Rowe & Booker (1981a,b) in developing elastic solutions.

Often the stiffness and hence Young's modulus, E, of the soil is not uniform with depth as assumed for Figs 9.17 and 9.18. Rowe and Booker (1981a,b) obtained elastic solutions for non-homogeneous soil with variations in Young's modulus with depth as shown in Fig. 9.19. These charts readily allow the calculation of settlement for a range of Young's modulus profiles, values of Poisson's ratio, ν, and footing rigidities (flexible and rigid) for both strip (Rowe & Booker 1981a) and circular (Rowe & Booker 1981b) footings. In Fig. 9.19, E_o = modulus of soil at the surface, D = layer depth, ρ_c = rate of decrease in soil modulus of crust, ρ = rate of increase of soil modulus below crust, and z_c = thickness of the soil crust.

9.4.4 RATE OF SETTLEMENT

The rate at which footings settle may be estimated by carrying out a consolidation analysis. It is generally assumed that the soil is totally saturated, and that as water flows from the soil, the soil skeleton slowly deforms. The volume change in the soil skeleton is assumed to be equal to the volume of water that flows from the soil.

If the problem is one-dimensional, there can be no initial settlement, i.e. upon application of a load, as the porewater is incompressible; but for three-dimensional problems, shear deformation of the soil can take place and so the soil can undergo an initial undrained deformation at constant volume.

Plots have been produced to allow estimates to be made of the rate of consolidation of footings, and an example of such a plot is shown in Fig. 9.20 (Davis & Poulos 1972). This plot is for a circular footing of radius a resting on the surface of a clay layer of thickness h, which may

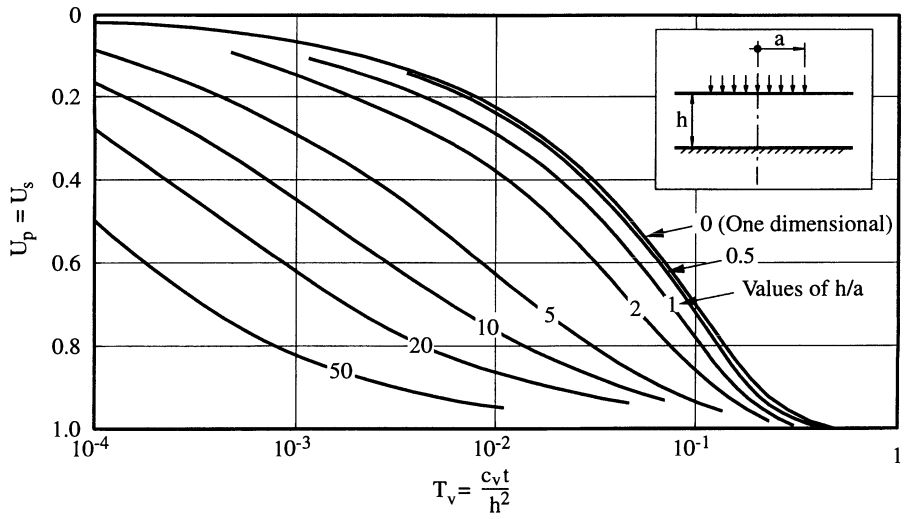


FIGURE 9.20. Degree of settlement versus time factor for a circular footing on a soil layer drained at the top and bottom (modified from Davis & Poulos 1972).

drain across its upper surface and through its lower surface. It is assumed that the load is applied to the footing at time $t = 0$ and then held constant. In the plots, the degree of consolidation, U, is plotted versus the dimensionless time factor, T_v, where:

$$T_v = \frac{c_v t}{h^2}. \tag{9.20}$$

If the extent of the load is large enough, it can be seen that the consolidation curve reaches the one-dimensional curve ($h/a = 0$). The coefficient of consolidation, c_v, under one-dimensional conditions may be found from an odometer test as is described in Section 2.7.

The degree of consolidation, U, is defined as:

$$U = \frac{S_t - S_i}{S_f - S_i} \tag{9.21}$$

where S_t = the settlement at any time, S_f = the final settlement, and S_i = the initial settlement. Initial and final settlements can be calculated using the appropriate elastic moduli and Poisson's ratios as described above (Section 9.4.3.2).

Settlement at any time, t, can therefore be computed (from Eq. 9.21) once the degree of consolidation is known and the initial and final settlements have been found.

Worked Example

A square footing having a side of 2 m is constructed on a layer of soft clay that is 4-m thick and has the following properties: $E' = 8$ MPa; $\nu' = 0.3$; $c_v = 0.8$ m^2 a^{-1}; $E_u = 12$ MPa; $\nu_u = 0.5$.

The footing is constructed on a granular base layer of permeable material, so that the surface of the clay layer may be considered drained. The base of the clay layer is underlain by sand, and so drainage can take place at the base of the clay layer also.

If a vertical load of 400 kN is applied to the footing, what would be the expected settlement of the footing after one year?

Solution: The pressure applied to the footing would be $p_{av} = 400$ kN/(2m $\times$ 2m) = 100 kPa. The square footing may be treated as a circular footing of area equal to the square, therefore, $\pi a^2 = 2 \times 2$, giving $a = 1.128$ m. The thickness of the soil layer to the radius of the footing would be: $h/a = 4/1.128 = 3.55$, or $a/h = 0.28$.

1. Drained case. Figure 9.18 gives (for Poisson's ratio, $\nu' = 0.3$) an influence factor, $I_\rho = 1.1$. Therefore the final settlement, S_f, is given by:

$$S_f = \frac{p_{av} a I_\rho}{E'} = \frac{100 \times 1.128 \times 1.1}{8} = 15.5 \text{ mm}.$$

2. Undrained case (or initial settlement). Figure 9.18 gives an influence factor of $I_\rho = 0.84$ (for $\nu_u = 0.5$). The initial settlement, S_i, is therefore given by:

$$S_i = \frac{p_{av} a I_\rho}{E_u} = \frac{100 \times 1.128 \times 0.84}{12} = 7.9 \text{ mm}.$$

3. At one year, the time factor can be computed as:

$$T_v = \frac{c_v t}{h^2} = \frac{0.8 \times 1}{16} = 0.05$$

and so from Fig. 9.20, the degree of consolidation, U, can be found to be 0.81. We can therefore write:

$$U = \frac{S_t - S_i}{S_f - S_i} = \frac{S_t - 7.9}{15.5 - 7.9} = 0.81.$$

And solving for S_t, gives the settlement at one year, $S_t = 7.9 + 0.81\ (15.5 - 7.9) \approx 14$ mm.

9.4.5 *Numerical Approaches*

Finding the appropriate analytic solution based on the theory of elasticity may be difficult, especially if the soil is anisotropic or consists of layers that have different stiffnesses. In such cases, numerical solutions are often necessary and some of these methods are discussed in the following sections.

9.4.5.1 LAYERED SOIL: FINITE LAYER APPROACHES

Computer programs can be useful in the situation where the soil is layered. Finite layer programs have been developed (Small & Booker 1986, 1996) that allow elastic anisotropic layered soils subjected to multiple surface loadings to be analyzed. The surface loadings may be strip, circular or rectangular in shape, and the programs may be used to find elastic deflections only, or the time–settlement behavior of a loading. One advantage of the formulation is that solutions may be found for a Poisson's ratio of 0.5, i.e. the undrained solution.

The finite layer method is particularly easy to use, as the only information required is the thickness of each layer and the material properties of each layer (Small & Booker 1986). The only restriction is that the material properties of each material layer do not vary laterally (but can vary from layer to layer).

Shown in Fig. 9.21 is a plot of the surface deflection computed beneath a single circular loading applied to the surface of a soil layer consisting of two isotropic sublayers where the modulus of the uppermost layer is greater than that of the bottom layer. All the parameters used in the computation and the geometry of the problem are shown on this plot.

9.4.5.2 NON-LINEAR MATERIALS

For soft clays or soils loaded close to failure, the use of simple elastic models will not be applicable, and a more sophisticated means of analysis is needed. The most common methods used are finite element techniques or finite difference-based methods. Many commercially available computer codes can perform non-linear analyses for problems that are two- or three-dimensional in nature. The computer code FLAC (fast Lagrangian analysis of continua) is a popular means of analysing geotechnical problems (ITASCA 1996). Various soil models may be implemented, one of the most popular being the Cam clay model, which was developed for clays (Britto & Gunn 1987) and implemented in the finite element code CRISP.

One advantage of these numerical models is that complex geometries, loadings and material distributions can be included in the analysis.

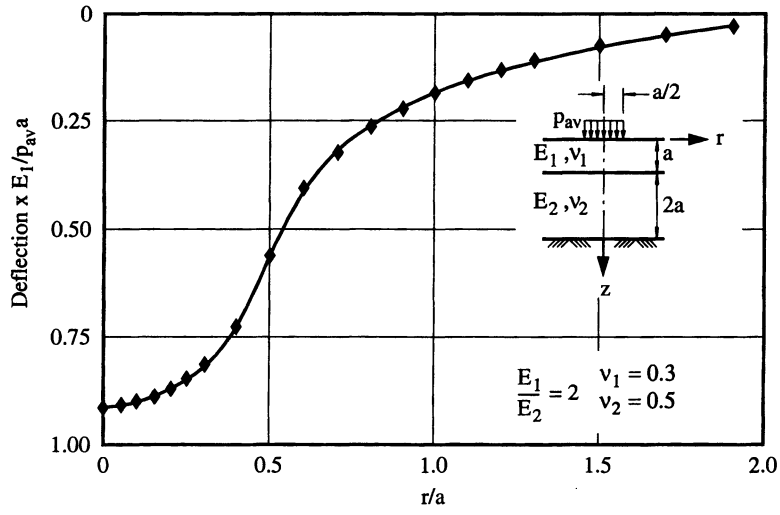


FIGURE 9.21. Vertical surface displacement beneath circular loading.

9.4.6 SETTLEMENT OF FOOTINGS ON SAND

Often, footing design for sand foundations is based on field test results (such as the standard penetration test or cone penetrometer results) because of the difficulty of sampling and testing sand samples in the laboratory, i.e. testing samples at the correct density. The design must again be based on both settlement criteria and bearing criteria.

Generally, a small or narrow footing subjected to an increasing pressure will have an unacceptably small margin of safety against a bearing capacity failure before it settles too much, whereas a larger or wider foundation will reach a given settlement criterion before the margin of safety against a bearing capacity failure is exceeded. Therefore, for smaller foundations, bearing capacity influences design, but for larger foundations, settlement is of greater importance.

Vibration can cause footings on loose sand to settle unduly as the sand will tend to densify (or even liquefy if it is saturated); however, this aspect is not considered in the following. Footings to be constructed on loose sands, which are often the result of hydraulically placed fills, should be considered in the light of potential vibration or earthquake hazard and densification of the sand deposit may be necessary by means such as vibroflotting.

9.4.6.1 Methods Based on the Standard Penetration Test (SPT)

D'Appolonia *et al.* (1970) presented a method based on obtaining the elastic modulus of the sand from the average SPT blow count taken over one footing width, B, beneath the foundation. The settlement of a footing can be found once the modulus is obtained, by use of the theory of elasticity (see Section 9.4.3). The relationship between elastic modulus, E', and the blow count is shown in Fig. 9.22 (ν' is the Poisson's ratio of the sand).

Burland *et al.* (1977) presented a compilation of observed data, which can be used to estimate the settlement of footings on sands of different densities. The deflection of a foundation per unit applied pressure is presented for different footing widths B, as shown in Fig. 9.23. Suggested upper limits

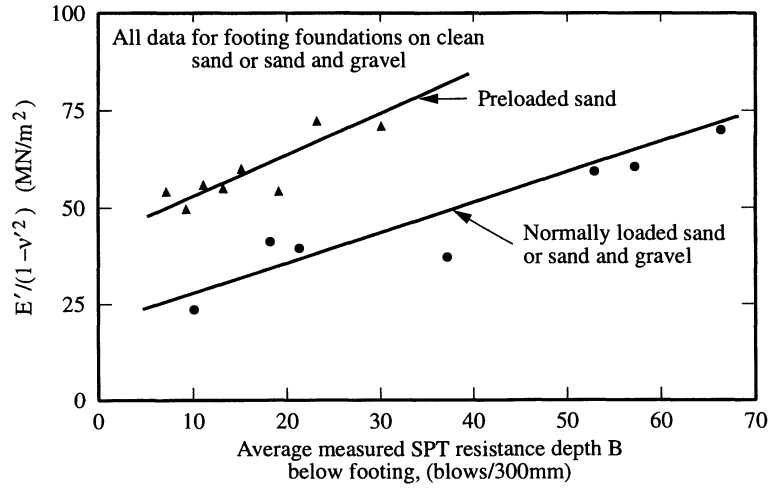


FIGURE 9.22. Correlation between blow count and modulus of sand (modified from D'Appolonia *et al.* 1970).

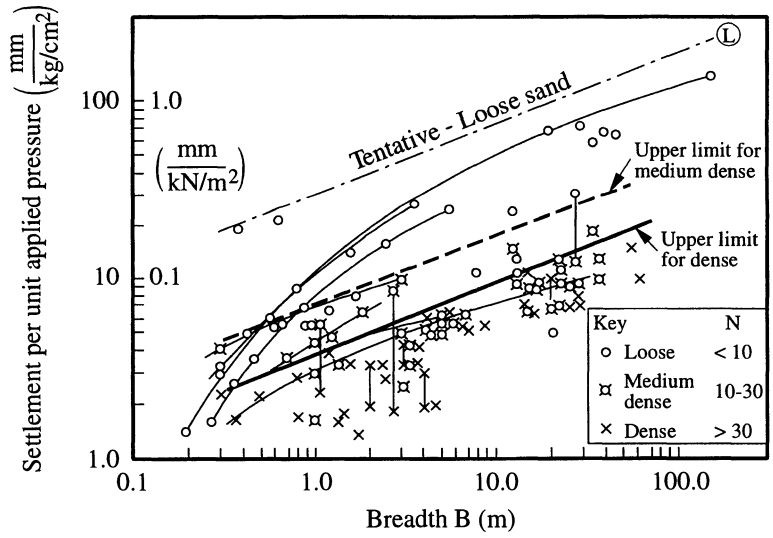


FIGURE 9.23. Observed settlement of footings on sand of various relative densities (modified from Burland *et al.* 1978).

for the deflection are shown (as lines) on the plot for dense, medium dense and loose sands. The density of the sand can be determined from the SPT blow count as shown in the inset to Fig. 9.23.

Parry (1977) presented a method based on SPT results in which the likely settlement of strip or rectangular footings of width B may be computed. The SPT blow count at a representative depth of $3/4B$ beneath the base of the footing is used in the design, and this is not corrected for depth or for the effects

of the water table. If N_m is the SPT blow count at the representative depth, then the settlement of a footing may be estimated from:

$$\rho = 300 \frac{p_{av} B}{N_m} \tag{9.22}$$

where p_{av} is in MPa, B is in meters, and ρ = the settlement of the footing in mm.

To be able to use any of these methods for settlement calculation, the load applied to the footing must be well below the collapse load, and so a bearing capacity check is required to verify that there is an adequate factor of safety against collapse at the design load.

9.4.6.2 Method Based on Static Cone Penetrometer

The approach of Schmertman (1970) and Schmertman *et al.* (1978) is based on cone penetrometer results. The soil is divided up into N depth increments or layers and the expected settlement, ρ_i, is then computed from the formula:

$$\rho_i = C_1 C_2 \Delta p \sum_{i=1}^{N} \frac{\Delta z_i}{E_{s_i}} I_{z_i} \tag{9.23}$$

where C_1 = a correction to allow for strain relief from embedment; C_2 = a correction for time dependent increase in settlement; Δp = the net applied footing pressure, $\Delta p = p - p_0$ (see below); Δz_i = the depth increment; I_{z_i} = the influence factor for soil layer i (see Fig. 9.24); and E_{s_i} = the elastic modulus of soil layer i.

Factor C_1 allows for strain relief due to embedment of a footing and is computed from the ratio of the overburden pressure at foundation level, p_0, to the net pressure increase at foundation level $\Delta p = p - p_0$ (p = the applied pressure).

$$C_1 = 1 - 0.5 \frac{p_0}{\Delta p}. \tag{9.24}$$

Note that C_1 must be greater than or equal to 0.5.

Factor C_2 is used to allow for creep of the foundation and is given by:

$$C_2 = 1 + 0.2 \log \left(\frac{t}{0.1} \right) \tag{9.25}$$

where t = the time in years.

The soil is divided into a number of horizontal layers and the elastic modulus of the soil is estimated from the cone penetrometer tip resistance, q_c. The elastic modulus may be found from the following correlations:

$$\left.\begin{array}{ll} \text{Long or strip footings } L/B \geq 10 & E_{s_i} = 3.5 q_c \\ \text{Axisymmetric footings or } L/B = 1 & E_{s_i} = 2.5 q_c \end{array}\right\} \tag{9.26}$$

L = length and B = breadth of a rectangular footing.

The strain distributions beneath footings are different depending on the footing shape and vary between the two extremes of the distributions for a strip or for a square footing. Therefore, different influence factor diagrams are used for square (or circular) and strip footings (see Fig. 9.24). For intermediate cases, i.e. rectangular footings of length L and breadth B (L/B from 1 to 10), interpolation between the two diagrams may be used. I_z may be assumed to vary linearly between 0.1 and 0.2 on the I_z-axis and relative depth to vary from $2B$ to $4B$ on the depth axis.

It may be noted that the peak value on the influence factor plots varies and is given by:

$$I_{zp} = 0.5 + 0.1 \left(\frac{\Delta p}{\sigma'_{vp}} \right)^{1/2}. \tag{9.27}$$

The effective stress used in computing the peak value of the influence factor σ'_{vp} is calculated at the depth shown in the inset to Fig. 9.24.

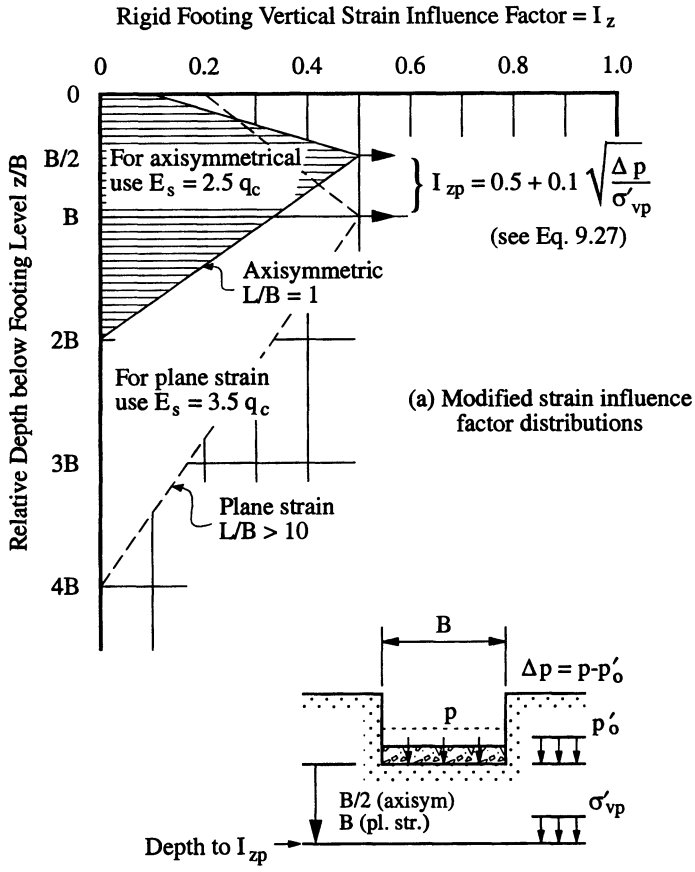


FIGURE 9.24. Strain influence factors for use in Schmertman's method (modified from Schmertman *et al.* 1978): (a) modified strain influence factor distributions, and (b) explanation of pressure terms used in Eq. 9.27.

9.4.7 METHODS BASED ON SETTLEMENT AND BEARING CRITERIA

Some methods of footing design (for sands) are based on both settlement and bearing criteria. An example of this is the approach of Peck *et al.* (1974). This method is based on SPT results, and allows for a factor of safety of two against a bearing capacity failure or an allowable settlement of 25 mm.

To design footings using this approach, the field SPT results must be corrected to allow for the effect of depth. The correction factor, C_N, is shown plotted against vertical effective stress in Fig. 9.25, so that at any depth the corrected blow count, N_{cor}, can be obtained by multiplying the field value, N_{field}, by the correction factor:

$$N_{cor} = N_{field} \times C_N. \tag{9.28}$$

The average corrected blow count over a depth of one footing width beneath the foundation is then used to design the foundation using the charts shown in Fig. 9.26. This is straightforward if the size of the footing is known and an allowable pressure is being ob-

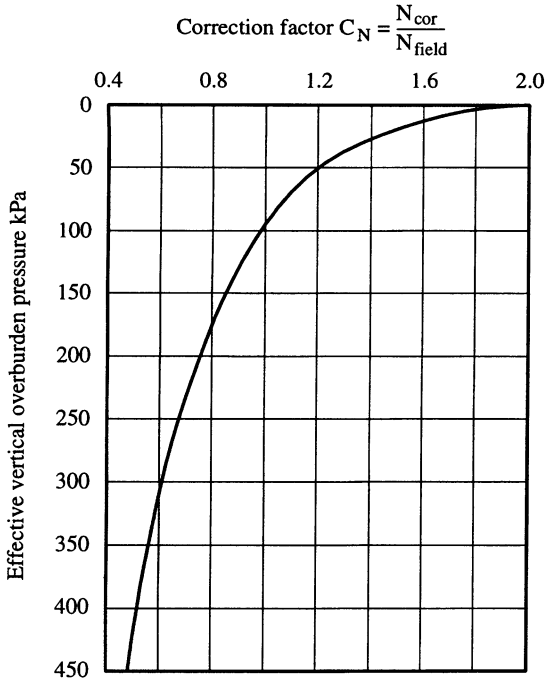


FIGURE 9.25. Chart for correction of N-values in sand for influence of overburden pressure. Reference value of effective overburden pressure, 107 kPa, i.e. 1 ton/ft, (modified from Peck *et al.* 1974).

tained, but if the applied pressure is known and the footing size is to be determined, some trial and error is required as the average blow count over one footing depth may change with the size of the footing selected. Full details of the method are given in the book by Peck *et al.* (1974).

A correction is also made for the effect of the water table by multiplying the allowable pressure (from Fig. 9.26) by the correction factor C_w where:

$$\left.\begin{aligned} C_w &= 0.5 + 0.5D_w/(D+B) \quad D_w \leq D+B \\ C_w &= 1.0 \qquad\qquad\qquad\quad D_w > D+B \end{aligned}\right\}. \tag{9.29}$$

In the above equation, B = the footing width, D = the footing depth, and D_w = the depth of water below the surface. It may be seen that the correction is 0.5 when the water table is at the surface and 1.0 when greater or equal to one footing width below the base of the foundation: anywhere between these two extremes, the formula (Eq. 9.30) provides a linear interpolation. The reasoning is that the unit weight of the cohesionless material will be approximately halved when submerged

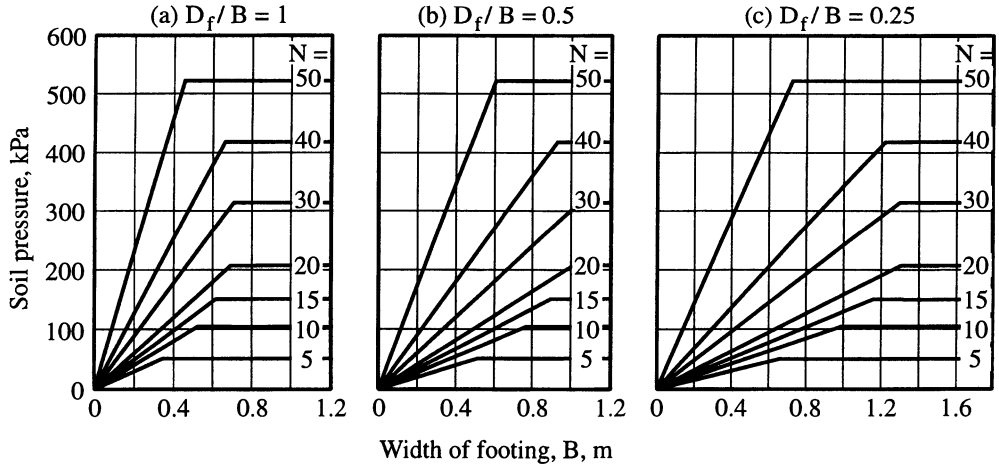


FIGURE 9.26. Design chart for proportioning shallow footings on sand: (a) $D_f/B = 1$, (b) $D_f/B = 0.5$, and (c) $D_f/B = 0.25$ (modified from Peck *et al.* 1974).

and so the bearing capacity will be similarly reduced.

9.4.8 ESTIMATING THE SOIL PARAMETERS

In order to use the analytical methods described previously it is necessary to estimate the soil parameters. For many of the more complex non-linear soil models, this may require special laboratory testing, although for models like the Cam clay model, the parameters can all be estimated from standard laboratory triaxial and odometer tests.

Here attention will be restricted to estimating elastic soil properties, as these form the basis of many of the hand-based methods of calculation mentioned previously. The soil parameters needed, E_u, E' and ν', are generally obtained either from laboratory tests or from *in situ* tests. Commonly used field tests are the standard penetration tests (SPT), plate loading tests, pressuremeter tests, dialatometer tests, static cone penetration tests and screw plate tests. See Chapter 7 for more detail on field testing and properties of soils.

These field tests often rely upon empirical correlations between the test result and a particular parameter, e.g. correlations between elastic modulus and the SPT or elastic modulus and the cone penetrometer resistance, q_c, as was seen in Section 9.4.6 on the settlement of footings on sand. As was stated before, laboratory testing is rarely used for sands, as it is difficult to keep sand samples in an undisturbed state (at the same density) as in the field. Correlations between shear modulus of sands and field test results from pressuremeters, dialatometers, SPT tests and cone penetration tests have been presented by Décourt (1994) for use in the computation of settlement of footings.

For clays, the elastic moduli can be found from triaxial testing or from field tests. Triaxial testing normally involves consolidating undisturbed soil samples back to the *in situ* stress state before loading them in an undrained condition (to obtain the undrained parameters) or in a drained condition (to obtain the drained parameters). Methods of testing have been described in Davis & Poulos (1968) and in Ladd & Foott (1974). For clays also, a common procedure is to relate the undrained modulus, E_u, to the undrained shear strength of the clay, s_u. This and other methods have been discussed in Sections 2.7 and 3.5 of this book.

9.5 *Raft Foundations*

While settlements of pad footings may be calculated by treating the foundation as being perfectly flexible or perfectly rigid, it is generally necessary to take into account the actual stiffness of a raft or mat foundation. This is because differential settlements or moments and shears in the raft usually need to be calculated, and so the structural rigidity of the foundation has to be considered.

Often solutions are found by treating the soil beneath the raft as consisting of a series of springs (a Winkler foundation) as this makes the analysis simpler; however, such methods are to be used with caution as they cannot represent true soil behavior. For example, a flexible raft carrying a uniform vertical loading (over the whole raft) would be predicted to settle uniformly with no differential settlement apparent if on a spring foundation, and this is obviously contrary to observed behavior. A rigid raft would also make all the springs compress equally, and hence the load in each spring would be equal. Measurement of contact stress below rigid rafts shows that the contact stress is generally larger at the edges (for a uniform loading on the raft), and so the load distribution in the springs would again not be modeling the correct behavior.

It is therefore desirable to treat the foundation as an elastic continuum, as the observed behavior of rafts can be more closely

simulated. Full finite element analyses may be necessary if the soil has highly non-linear properties, but generally the theory of elasticity is sufficient as rafts are not designed to carry loads that are going to cause yielding of the soil. A soil modulus representative of the stress levels in the soil can be used in such cases.

Solutions have been found to some problems involving rafts constructed on an elastic continuum, but the solutions are limited because it is difficult to present results for all raft shapes and for different soil conditions, such as layering or modulus increasing with depth. Selvadurai (1979) contains analytic solutions to problems involving rafts on elastic continua; however, most solutions have been based on numerical procedures. Some of the available solutions are presented in the following sections.

9.5.1 STRIP RAFTS

A strip raft may be classified as a raft that has a length, L, that is much greater than its width, B. Solutions to such a problem have been presented by Brown (1975) for a strip raft, having a length to width ratio L/B of ten, resting on an infinitely deep elastic soil. The raft is considered to be loaded by a point load, which is located at a distance, sL, from one end, as is shown in Fig. 9.27. The results are presented for a single point load as the solutions may be superimposed if more than one point load is acting on the raft.

Shown in Fig. 9.28a are the solutions for the deflections in the strip raft, while Fig. 9.28b shows the moments in the raft. These particular solutions are for the case where the relative stiffness of the raft to the soil, K, has a value of 0.01. The relative stiffness is defined as:

$$K = \frac{16E_r I(1 - \nu_s)}{\pi E_s L^4} \tag{9.30}$$

where E_r = the elastic modulus of the raft; I = the second moment of area of the raft ($I = Bt^3/12$ for a strip raft of thickness, t); E_s = the modulus of the soil and ν_s = the Poisson's ratio of the soil.

Solutions for the moment or displacement in the raft are presented in non-dimensional form at various positions, x, along the strip raft, for a point load of magnitude, P. If several point loads are applied along the raft, the appropriate values of P (corresponding to each load) should be used when computing the moments or deflections before superimposing, i.e. adding, them.

9.5.2 CIRCULAR RAFTS

Brown (1969) has also obtained solutions for circular rafts subjected to uniform vertical

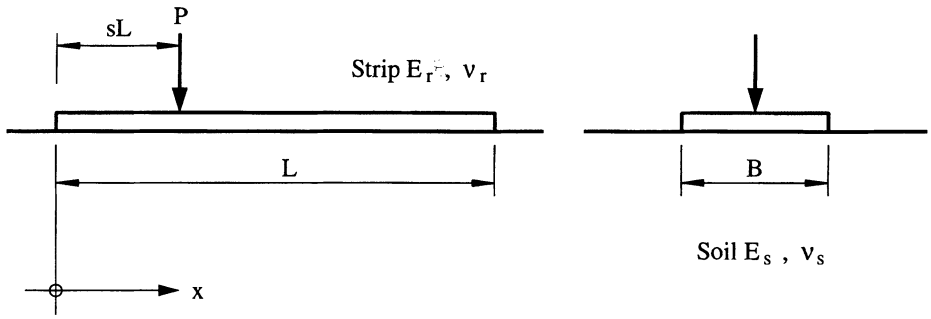
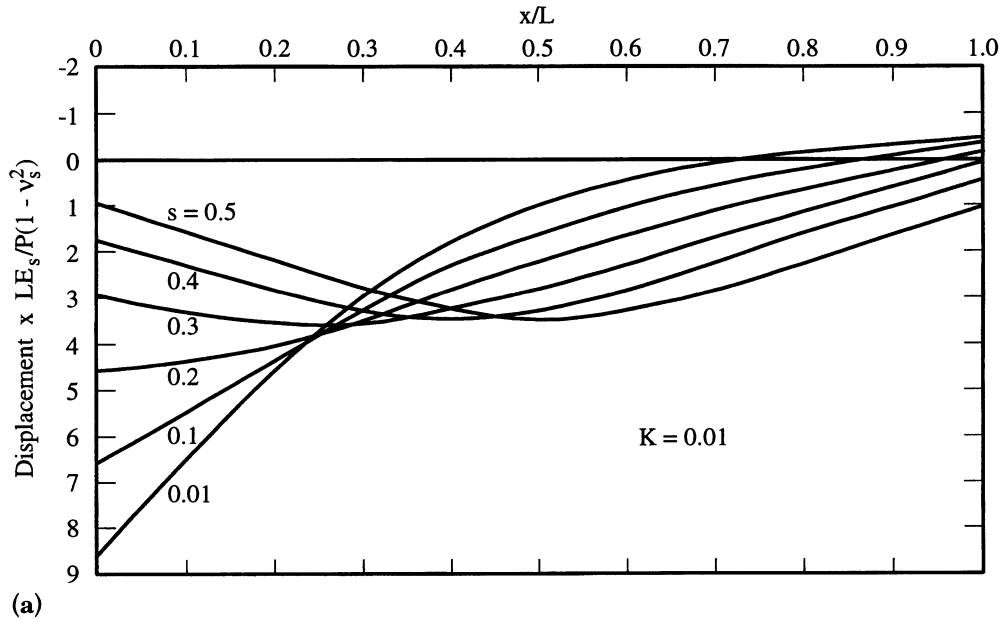


FIGURE 9.27. Strip raft subjected to a point load, P: E_r and E_s = the elastic modulus of the raft and soil, respectively; ν_r and ν_s = the elastic modulus of the raft and soil, respectively.



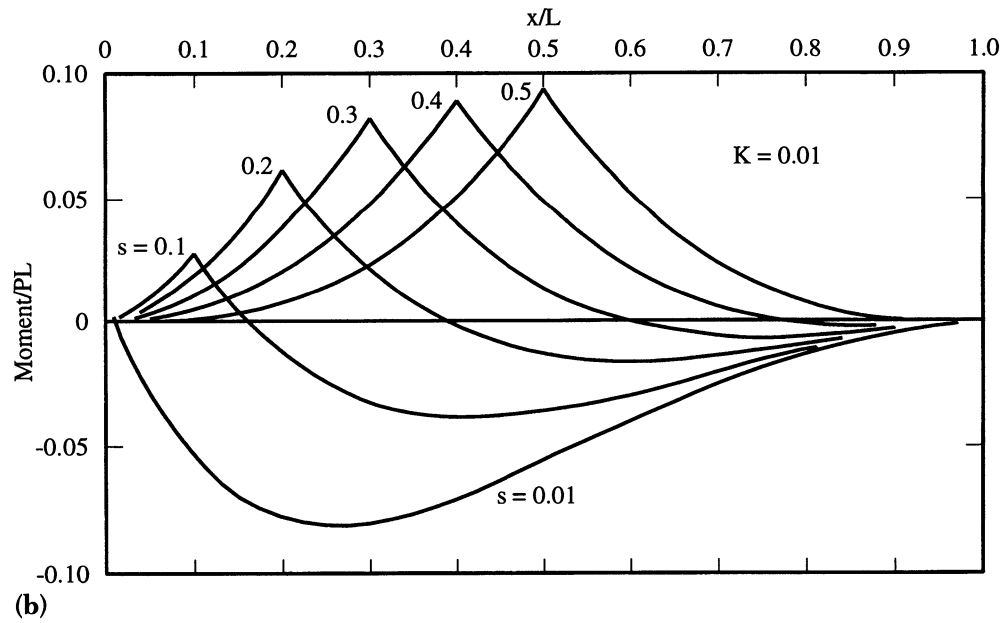


FIGURE 9.28. (a) Displacement distributions, and (b) moment distributions for strip raft (modified from Brown 1975).

loading, q, over their entire upper surface. The raft is assumed to be of thickness t and radius a, and to rest on a layer of soil of depth h. In this case, the relative stiffness of the raft, K, is defined as:

$$K = \frac{E_r(1 - \nu_s^2)}{E_s}\left(\frac{t}{a}\right)^3. \qquad (9.31)$$

Maximum moment in the raft occurs at its central point, and this moment is shown plotted in non-dimensional form against raft stiffness, K, in Fig. 9.29a. Solutions are presented for different depth to radius ratios, h/a, and for two extremes of Poisson's ratio, $\nu = 0$ and 0.5. In this case, the moments presented in the plot are actually moments per unit length, i.e. would have units such as kNm m^{-1} run. Differential deflections in the raft are shown in Fig. 9.29b for various soil layer depths and Poisson's ratios. For a circular raft, the differential deflection is defined as the difference in displacement between the center and the edge of the raft.

Booker & Small (1983) have extended the charts of Brown to include the effects of the walls as well as the base raft of a tank. The restraining effect of the walls at the outer circumference of the base, means that there is a moment generated there that is opposite in sign to the moment at the center of the base and may be large if the walls are stiff enough to resist the rotation at the base–wall junction.

9.5.3 RECTANGULAR RAFTS

Rafts of rectangular shape (in plan) that carry a uniformly distributed load, q, have been analyzed by Fraser & Wardle (1976). The

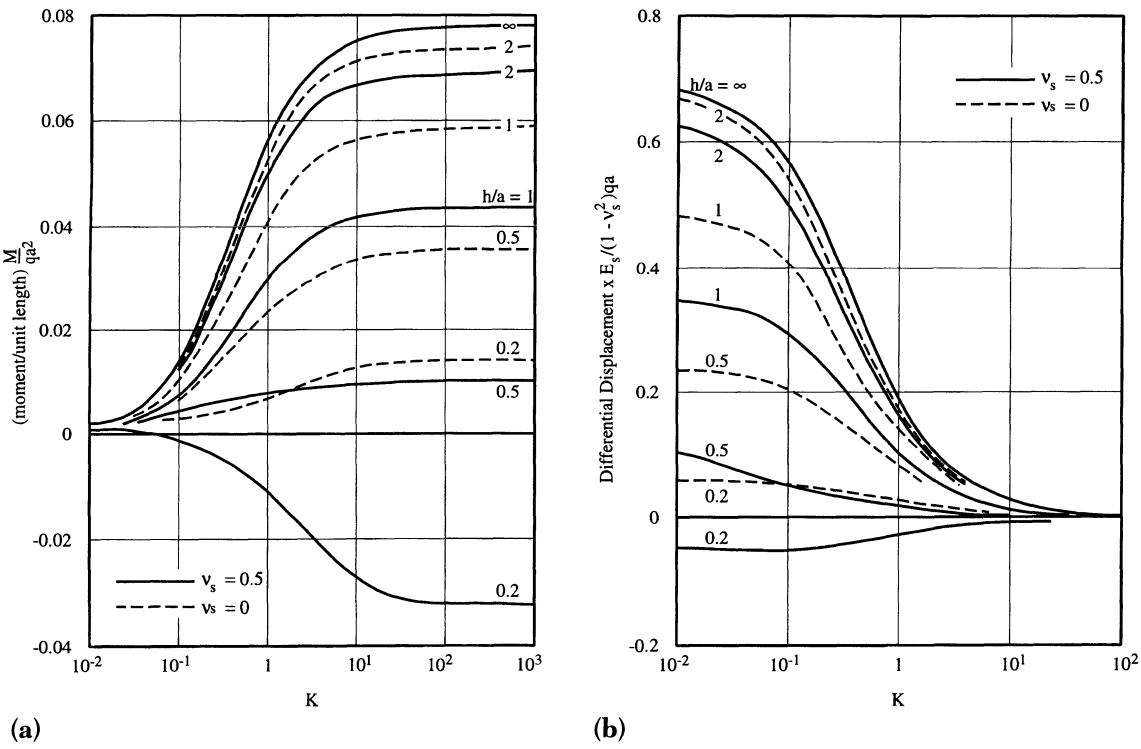


FIGURE 9.29. Circular raft: (a) maximum moments for various stiffnesses and (b) differential displacements for various stiffnesses ($\nu_r = 0.3$) (modified from Brown 1969).

rafts are assumed to be constructed on a layered soil profile, and methods are given in the paper to enable an equivalent elastic modulus and Poisson's ratio to be determined for the layered system so that it may be treated as a uniform material.

The raft of length L and width B is shown as the inset to Fig. 9.30. The relative stiffness, K, of the raft as defined by Fraser & Wardle as:

$$K = \frac{4E_r(1 - \nu_s^2)t^3}{3E_s(1 - \nu_r^2)B^3} \qquad (9.32)$$

where the terms have the same meanings as for the strip raft (see Section 9.5.1), and ν_r = the Poisson's ratio of the raft. In Fig. 9.30, points α, β, γ, δ are identified on the raft. The deflections at these points, and the differential deflections between these points can be calculated by use of the influence factors shown on the figure. For instance, the curve labeled I_α would be used to compute the settlement at point α, whereas $I_{\alpha\beta}$ would be used to compute the differential settlement between points α and β.

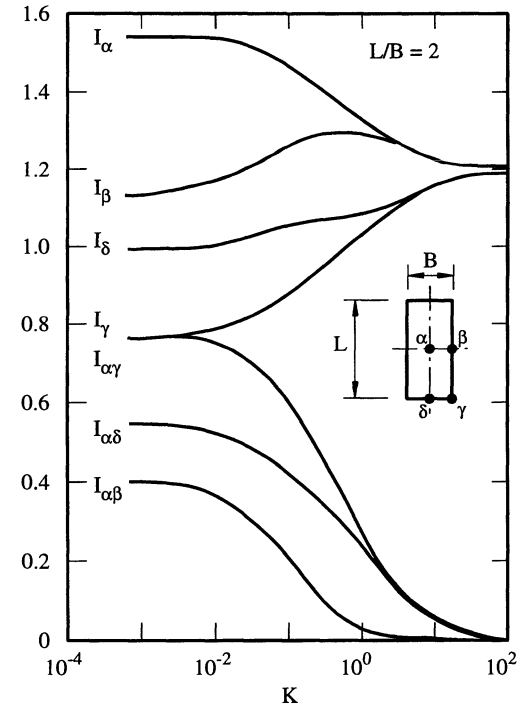


FIGURE 9.30. Settlement influence factors for rectangular raft on an infinite layer for $L/B = 2$ (modified from Fraser & Wardle 1976).

To compute the deflection or differential deflection ρ^{si} for an infinitely deep soil layer the following equation is used:

$$\rho^{si} = \frac{p_{av}B(1 - \nu_s^2)}{E_s} I \qquad (9.33)$$

where I = the appropriate influence factor as determined from Fig. 9.30, and p_{av} = the pressure applied to the raft. To compute the settlement or differential settlement for a soil layer that is not semi-infinite, corrections need to be applied to ρ^{si}. The actual displacement, ρ, is computed from the following expression:

$$\rho = S\rho^{si} \qquad (9.34)$$

where S = a correction factor, which is found from charts like those shown in Fig. 9.31 (for a raft with a length to breadth ratio, L/B, of 2).

Similar charts have been provided by Fraser and Wardle to enable moments to be computed in the raft. This involves calculating moments for the case where the soil is infinitely deep, and then applying a correction for soil layers of finite depth, as was done for displacements.

9.5.4 RAFT FOUNDATIONS OF GENERAL SHAPE

When the raft is of general shape and is subjected to general loading (which may include point loads, moments or uniform loads), it becomes difficult to provide solutions in the form of charts. For more complicated cases, it is necessary to use computer programs, and these may analyze raft behavior by using finite difference methods or by use of finite element methods (e.g. Zhang & Small 1994).

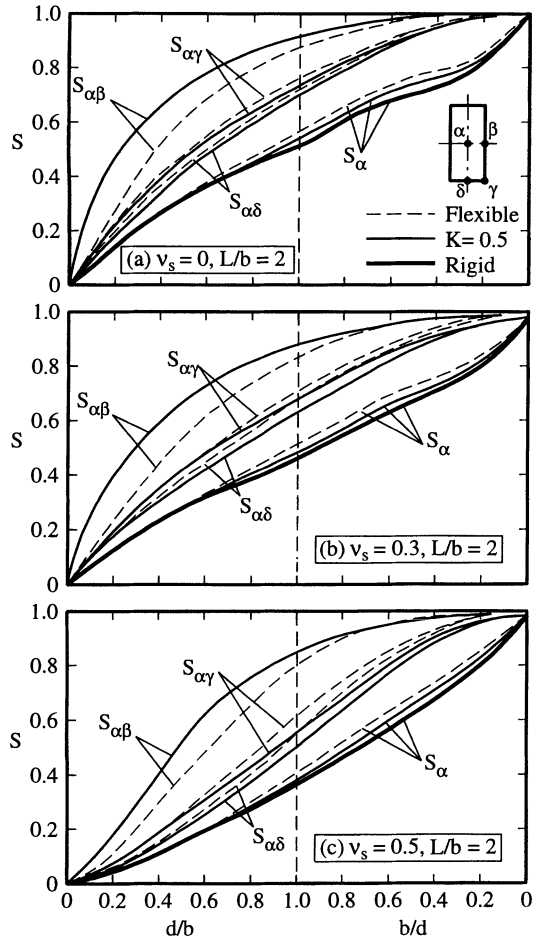


FIGURE 9.31. Settlement correction factor, S, for $L/B = 2$ (modified from Fraser & Wardle 1976): (a) $\nu_s = 0$; (b) $\nu_s = 0.3$; (c) $\nu_s = 0.5$.

9.6 *Reactive Soils*

Soils such as plastic clays, which contain clay minerals like montmorillonites or smectites, tend to shrink when their moisture content decreases or to swell as their moisture content increases. Soil suctions exist in the uppermost partially saturated "active zone" in the soil, and it is changes in these suctions (due to moisture content variations) that cause shrink–swell behavior, as discussed in Chapter 5.

Swelling can cause damage to structures especially if differential movements occur in the structure. For example, moisture changes may be small beneath the center of a raft or mat foundation, and so little swelling or shrinking will occur. At the edges of the foundation, moisture changes are larger, and so swell–shrink movements are large. This creates differential movements in the foundation which are seasonal, and this can cause damage if the raft is not stiff enough to resist the movements. A technique for predicting the heave of expansive soils is given in Section 5.7.3 of this book.

9.6.1 RAFTS ON REACTIVE SOILS

The swelling and shrinking of reactive soils can produce differential movements in raft foundations, and this is usually due to soil movements at the edges of the raft where moisture changes are most likely to occur. Rafts constructed in areas where soils are reactive are generally stiffened with ribs, i.e. waffle slabs, as shown in Fig. 9.1d.

If swelling and shrinkage movements take place around the edges of a raft foundation, the raft will undergo uplift at the edges (swelling) or will be supported on a mound of soil if the soil shrinks away at the edges. Analysis of this type of behavior has been examined by Sinha & Poulos (1996) using finite element analysis of the raft, and finite element methods have been used by Li *et al.* (1996) to analyze moisture flow and soil–structure interaction for a stiffened raft foundation.

9.7 *Cold Climates*

In cold climates, when the ground begins to freeze, water can be drawn upward towards the surface by capillary action (from the water table below) and can form ice lenses. The lenses usually grow perpendicular to the direction of heat flow, which for most soils is parallel to the ground surface. The increase in volume of the ice will cause the surface of

the soil to heave, and these upward movements can be very large, i.e. 300 mm or more, causing structural damage.

Frost-susceptible soils are those that have pores small enough to produce ice lenses at the freezing front, i.e. the surface separating frozen and non-frozen soil. Silty materials, fine silty sands with more than 15% of particles finer than 0.02 mm and lean clays having a plasticity index <12, varved clays and chalks are most susceptible to frost heave, while gravels and clean sands are not because of their high permeability. Clays are less susceptible to heave because their low permeability prevents the flow of water (and hence the formation of ice lenses).

For a soil to exhibit frost heave, there must be sufficiently low temperatures, water available in the soil and the soil must be of a type (as mentioned above) that is frost susceptible. Freezing tests may be carried out on soil samples to determine frost heave potential.

Freezing of a foundation may be due to sub-zero climatic conditions, or it may be due to man-made causes, e.g. freezer rooms or ice rinks (see Chapuis 1988). In the former case, resistance to frost heave may be engineered by draining the soil, founding footings below the depth of frost penetration or replacing frost-susceptible soils by non-susceptible materials such as gravels or sands. For man-made sources of low temperature, these methods may also be used, or good insulation provided, between the soil and the structure.

Prediction of frost heave is not generally a simple matter, as any analysis involves computation of the heat flow in the soil, the thermal properties of the soil, the cooling rate and suction at the frost front as discussed in Chapter 20. Such analyses have been reported by Konrad & Morgenstern (1982a) & Nixon (1991). Field measurements and numerical predictions of the measured heaves are also reported in Hayhoe & Balchin (1990).

9.8 *Limit State Design*

The design approaches presented in the forgoing sections of this chapter, are based on satisfying settlement criteria at working loads and checking if the working load has a prescribed factor of safety, F, against a bearing capacity failure. This is what is termed "working stress design" (WSD), as one global factor of safety is used to relate the allowable and applied load.

More recently, the concept of limit state design (LSD) has been applied to problems involving soil and rock mechanics, and this approach is becoming more popular in codes of practice around the world. The advantage of the LSD approach is that the uncertainty in individual loads or soil strengths may be factored differently, depending on the amount of uncertainty involved in estimating them. It is not therefore necessary to rely on one factor of safety as is generally done with WSD. There are many issues involved in LSD and the reader is referred to two papers by Becker (1996a,b) for a more complete discussion.

There are two main methods of applying LSD currently in use:

1. Soil strengths are factored down so that a reduced soil resistance, R_d, is computed, and the applied loads are factored up to estimate S_d. In calculating S_d, different factors may be applied to different types of loadings (e.g. dead load or live load); and in determining R_d, different factors are applied to soil strengths (e.g. cohesion, c, or tan ϕ). The requirement for design is then that $R_d \geq S_d$. This is the design approach commonly used in Europe.
2. Soil resistance is factored down. A single reduction factor, Φ, is applied to the soil resistance, and this factor takes account of all uncertainties involved. Partial factors of safety are applied to the loads, and these can be different according to the uncertainty as was discussed in (1) above. This approach can be written:

$$\Phi R_n \geq \Sigma \alpha_i S_{ni} \quad (9.35)$$

where Φ = the resistance factor; R_n = the resistance that may be calculated using unfactored soil strength parameters, or could be the resistance measured from a field loading test; α_i = the load factors; and S_{ni} = the load components, i.e. dead load, live load, wind load. This is the approach favored in North America.

The factored strength approach (point 1 above) has the advantage that different factors can be applied to different soil strength parameters (such as c and $\tan\phi$); while the factored resistance approach (point 2) has the advantage that it can be applied to both calculated resistances and measured resistances, i.e. field tests.

In the writer's opinion, the factored resistance approach is the most suitable for a wide range of soil mechanics problems because of the fact that reducing soil strengths can lead to different failure mechanisms and lead to erroneous results. For example, in designing a retaining wall with a concentrated load on the surface of the retained soil (at some distance back from the face of the wall), the failure surface may not include the surface load if full strength soil parameters are used, but may pass behind the load if factored strengths are used. This problem is also pointed out by Becker (1996a), who gives the example of a vertically loaded footing. The shape of the plastic zone beneath the footing will change with the angle of shearing resistance, ϕ, and so the resistance based on factored strength is not the same as factored resistance.

An important factor in all design methods, whether WSD or LSD, is how the characteristic strengths are obtained for the soil strength parameters. There is always a scatter in measured data (say s_u values) for soils, and therefore some characteristic value has to be chosen for design. Often this is a mean value, although this is not always so. The way in which the characteristic value is calculated will determine how the resistance factors should be selected in LSD, and this is often addressed in codes of practice.

10. PILE FOUNDATIONS

H. G. Poulos

10.1 Introduction

10.1.1 DESIGN OBJECTIVES

A major function of piles is to transmit foundation loads through relatively weak or loose strata to stiffer underlying soil or rock strata. Piles may also be used to carry uplift loads, to carry loads below scour level in marine situations, to resist lateral loadings, and to reduce the settlement of shallow pad or raft foundations. Resistance of piles to vertical loads is supplied by a combination of pile shaft friction and end bearing, and even with nominally end bearing piles, significant resistance can be derived from shaft friction. Piles subjected to lateral loads rely mainly on the resistance developed near the ground surface. The soil in this region is often disturbed or else subjected to seasonal moisture changes that may affect the soil strength and stiffness significantly. Thus, prediction of the lateral behavior of piles may be even more difficult than vertical behavior.

The design of pile foundations involves a number of stages, including:

1. Selection of the type of pile and installation method.
2. Estimation of the size of the piles and the number of piles to obtain a sufficient margin of safety against failure of the supporting soil and the pile material.
3. Estimation of the settlement of the foundation, and the differential settlement between adjacent foundations, and adjustment of the design (if necessary) to satisfy the settlement and differential settlement criteria.
4. Consideration of the effects of any lateral loads that may be transferred from the structure to the foundation, and in particular, the estimation of the lateral deflection of the foundation due to such loads.
5. Consideration of the effects of ground movements that may occur due to external causes (e.g. shrinking and swelling) and the assessment of the consequent pile forces and deflections.
6. Evaluation of pile performance from appropriate pile loading tests, and interpretation of these tests to evaluate parameters that may be used to predict the performance of the actual foundation.

In this chapter, the above issues are addressed, and practical approaches to the evaluation of various geotechnical aspects of pile performance are presented. Some discussion of the main characteristics of pile behavior under static loading are also given. The response of pile foundations to dynamic and seismic loads is considered in Chapters 12 and 21, respectively. Attention is concentrated on piles in soil deposits, since piles socketed into rock are dealt with in Chapter 11.

10.1.2 CRITERIA FOR DESIGN

The design of the piles must satisfy criteria related to the strength, deformation and durability of the piles. In relation to strength, criteria are applied to both the geotechnical strength, i.e. the load carrying capacity of the soil, and the structural strength of the pile it-

R. K. Rowe (ed.), *Geotechnical and Geoenvironmental Engineering Handbook*
© Kluwer Academic Publishers 2001

self. The geotechnical and structural strength criteria depend on the basis of the design method. Traditional methods have relied on an overall safety factor against ultimate failure, so that the design criteria can be expressed as:

$$Q = Q_u/F \qquad (10.1)$$

where Q = design load, Q_u = ultimate load, F = overall factor of safety.

Equation 10.1 applies to both axial and lateral loadings. Typical factors of safety for the geotechnical strength of pile foundations range between about two and three, depending on the method of calculation of the capacity, the extent of the designer's experience and knowledge of the site and the geotechnical conditions, and the likely consequences of failure. In cases where there is extensive experience of the site and pile load tests have been carried out, values of safety factor as low as 1.5 may be appropriate. On the other hand, where knowledge of the site is limited, and the consequences of failure may be extreme, safety factors of three or more may be appropriate.

In recent years, there has been an increasing tendency for limit state design methods to be used (Becker 1996a,b). These incorporate the use of partial safety factors applied to the pile resistances, and load factors applied to the loadings. The design criterion for ultimate limit state design is then:

$$\Phi_u Q_u > Q_d \qquad (10.2)$$

where Φ_u = reduction factor for pile resistance, Q_u = ultimate pile resistance, Q_d = factored design load, including appropriate load combinations.

Equation 10.2 applies to both axial and lateral loadings, and to structural and geotechnical strengths. The load factors, and the reduction factors for geotechnical and strength resistance of piles, are generally specified in standards or codes of practice. Typical values for the geotechnical resistance reduction factors range from about 0.4 to 0.8, depending on factors similar to those considered in assessing the overall factor of safety.

For the serviceability limit state the design criteria for deformations may be stated generally as:

Estimated deformation

$$< \text{allowable deformation} \qquad (10.3)$$

Estimated differential deformation

$$< \text{allowable differential deformation.} \qquad (10.4)$$

Equations 10.3 and 10.4 apply to both vertical and lateral deformations (including tilts). The allowable deformations and differential deformations depend primarily on the nature of the structure; typical values are quoted by Bjerrum (1963b) and Grant *et al.* (1974).

For durability, the usual design criterion is that the piles shall have a design life that exceeds the design life of the structure to be supported; this is usually 50 years or more for permanent structures.

10.1.3 TYPES OF PILES AND THEIR USES

Piles are generally classified according to the pile material (timber, steel, concrete), the method of installation (driven, driven and cast-*in situ*, bored or drilled shafts, screwed, and composite), or the effect of the installation procedure on the surrounding soil. The last is probably the most useful means of classification, and three main types can be identified: displacement piles, low-displacement piles and non-displacement piles. Displacement piles include driven timber, precast concrete and closed-ended steel piles, and cause relatively large horizontal and ground movements during installation. Low-displacement piles include driven steel H-piles, open-ended steel tube piles and some forms of screwed piles (e.g. the 'Atlas' piles); their installation causes considerably less lateral and vertical ground movements than a displacement pile. Non-displacement piles include various types

of bored and auger piles, and generally induce only small ground movements (ideally zero, but in practice, some movements are almost inevitable). The method of installation of a pile can have a significant effect on its load capacity and load–settlement behavior. Details of the various types of piles and their installation methods are given by Tomlinson (1977) and Fleming *et al.* (1992). Table 10.1 summarizes some of the advantages and disadvantages of some typical pile types.

The choice of pile type is governed by a number of factors, but Tomlinson (1995) identifies three main factors: location and type of structure, ground conditions, and durability. These considerations usually narrow the choice of pile type to one or two basic types, and then the final choice is often made on the basis of cost.

10.2 Pile Load Capacity

10.2.1 DYNAMIC CALCULATION METHODS

The total load capacity of driven piles has been estimated for many years by means of driving or dynamic pile formulae. Such formulae (of which there are several hundred)

TABLE 10.1. Advantages and disadvantages of various pile types (adapted from Tchepak 1997)

Pile type	Advantages	Disadvantages
Precast (reinforced concrete)	Displacement pile performance Confidence in founding conditions Relatively low unit costs	Potential problems with noise and vibrations Long lengths require mechanical splice joints Pile caps required Relatively weak in bending and tension
Bored (drilled shafts)	Do not necessarily require pile caps Free from noise and vibrations High bending moment resistance for larger diameters	Spoil removal required (particularly expensive in sites suspected of being contaminated) Bentonite/drilling fluids messy; can result in uncertain pile performance Can be expensive
Enlarged base driven cast-*in-situ* piles	Displacement pile performance Confidence in founding conditions Basing energy varied to suit large range of soil conditions Low cost (high founding levels)	Potential vibration problems Pile caps usually required
Continuous flight auger (CFA) piles	Free from noise and vibration Usually relatively fast installation	Relatively high cost No "feel" for founding conditions other than on hard rock Spoil removal required Non-displacement pile performance Comprehensive site investigation essential
Screw piles	Displacement pile performance Found at high levels with confidence in performance No spoil removal No problems with nose or vibrations	Pile caps generally required Relatively low bending moment capacity

relate ultimate load capacity to pile set (the permanent vertical movement of the pile per hammer blow) and assume implicitly that the resistance of the pile under static load is the same as under dynamic load or driving conditions. Despite the widespread use of driving formulae, there are fundamental objections to their use, since the pile is not stressed simultaneously at all points by the hammer blow, as is assumed in the Newtonian theory that usually underpins driving formulae. More satisfactory simulation of the pile-driving process can be achieved by using a one-dimensional wave equation analysis, such as that pioneered by Smith (1960). Further developments of this analysis have been made by Randolph & Simons (1986) and Lee *et al.* (1988), using dynamic pile response theory to obtain the stiffness and damping characteristics of the pile–soil system.

Even with the improved theories, the main functions of pile-driving analyses are to estimate the driveability of the pile with the available equipment, and to assess the stresses developed in the pile during driving. Dynamic analyses have limitations when applied to the prediction of pile load capacity, and in particular, the effects of "set-up" of clay soils surrounding the pile are likely to cause the static load capacity to differ from the resistance developed during driving. More reliable estimates of pile capacity can be obtained when the pile is re-struck after allowing some time for dissipation of excess pore pressures (set-up) to occur.

Dynamic pile testing makes use of the wave equation theory, and when properly applied, is capable of giving reasonable estimates of pile capacity, not only for driven piles, but also for cast-*in-situ* piles. This type of testing is discussed further in Section 10.7.3.

10.2.2 STATIC CALCULATION METHODS

10.2.2.1 General Principles

A very widely used approach for estimating the ultimate load capacity is to use a static analysis, which utilizes conventional soil mechanics techniques in conjunction with measured soil strength properties. In this approach, the ultimate load capacity, P_u, is calculated as the sum of the ultimate shaft capacity, P_{su}, and the ultimate base capacity, P_{bu}, less the weight of the pile, W_p. In turn, P_{su} and P_{bu} are related to the unit ultimate shaft and base resistances, so that:

$$P_u = \int f_s C \, dz + f_b A_b - W_p \qquad (10.5)$$

where f_s = ultimate shaft friction, C = pile perimeter, f_b = ultimate base resistance, A_b = area of pile base, W_p = pile weight. The value of f_s is usually obtained by use of Coulomb's equation; while the ultimate base resistance, f_b, is usually derived from bearing capacity theory. The usual principles of soil mechanics (see Chapter 2) can be applied, i.e. undrained analyses use total stresses and undrained values of f_s and f_b, while long-term or drained analyses use effective stresses and drained values of f_s and f_b.

10.2.2.2 Saturated Clay Soils: α Method

For the estimation of undrained pile capacity in saturated clay soils, f_s is usually related to the undrained shear strength via an adhesion factor α, and hence the total stress method of pile capacity calculation is usually termed the "alpha" method. Thus:

$$f_s = \alpha s_u F_1 \qquad (10.6)$$

where α = adhesion factor, s_u = undrained shear strength, F_1 = reduction factor for pile slenderness. The value of α is a function of s_u, and has been empirically derived by a number of investigators. Figure 10.1 shows the correlation developed for bored piles by Stas & Kulhawy (1984). Alternative correlations have been developed by Kulhawy & Phoon (1993) for ground conditions ranging from soft clay to strong rock. In this correlation, s_u represents the undrained shear strength. The considerable scatter in this correlation should be noted. For

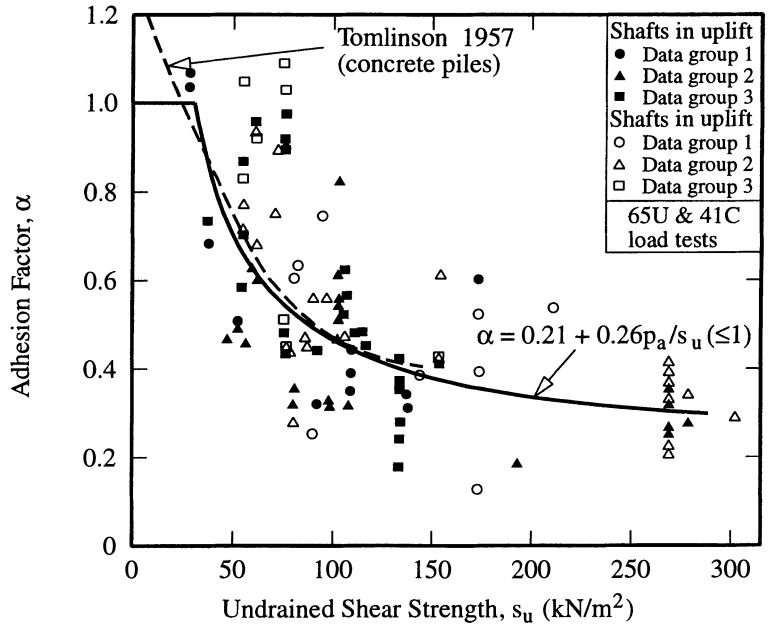


FIGURE 10.1. Adhesion factor (modified from Kulhawy & Phoon 1993). u = uplift tests; c = compression tests.

driven piles an alternative approach was developed by Fleming *et al.* (1985), who related α to the normalized undrained shear strength:

$$\alpha = 0.5/(s_u/\sigma'_v)^{1/2} \qquad \text{For } s_u/\sigma'_v < 1 \qquad (10.7a)$$

$$\alpha = 0.5/(s_u/\sigma'_v)^{1/4} \qquad \text{For } s_u/\sigma'_v > 1 \qquad (10.7b)$$

where σ'_v = vertical effective stress at the point in question along the pile shaft.

The reduction factor for pile slenderness, F_1, has been suggested by Semple & Rigden (1984) to be related to the pile length-to-diameter ratio, L/d:

$$F_1 = 1 \text{ for } L/d < 50 \qquad (10.8a)$$

$$F_1 = 0.7 \text{ for } L/d > 120. \qquad (10.8b)$$

F_1 is interpolated linearly between 1.0 and 0.7 for $120 > L/d > 50$.

F_b is obtained from undrained bearing theory:

$$f_b = N_c s_{ub} + \sigma_{vb} \qquad (10.9)$$

where N_c = bearing capacity factor, s_{ub} = average undrained shear strength within a depth of two base diameters below the pile base, σ_{vb} = total overburden stress at level of pile base. N_c is related to the relative depth of the pile base, and can be approximated as:

$$N_c = 6 + L/d_b \leq 9 \qquad (10.10)$$

where L = pile length, d_b = pile base diameter.

10.2.2.3 Saturated Clay Soils: β Method

There has been a tendency in recent years towards the use of an effective stress approach, rather than a total stress approach, to the calculation of pile shaft capacity. It is argued that the high pore pressure gradient set up near the pile shaft by loading the pile dissipates rapidly, and thus drained conditions prevail at the shaft–soil interface. The ultimate shaft friction is then given as:

$$f_s = K_s \sigma'_v \tan \delta \qquad (10.11a)$$

$$= \beta \sigma'_v \qquad (10.11b)$$

where K_s = lateral stress coefficient, σ'_v = effective vertical stress at the point in question, δ = effective interface friction angle between soil and shaft, β = shaft friction coefficient = $K_s \tan \delta$. Burland (1973) demonstrated that a lower limit of β for driven piles in normally consolidated clay is β_{nc}, where:

$$\beta_{nc} = (1 - \sin \phi')\tan \phi' \qquad (10.12)$$

and Φ' = effective angle of internal friction of the clay.

For typical values of Φ' in the range 20–30°, β_{nc} varies only between 0.24 and 0.29. Such values are in accordance with measurements of both positive and negative friction on driven piles in soft clay. For overconsolidated clays, β is greater than β_{nc}. If the overconsolidation ratio (OCR) is known, Meyerhof (1976) suggests that β can be estimated as:

$$\beta = \beta_{nc} (\text{OCR})^{0.5}. \qquad (10.13)$$

For bored piles, provided that the pile is formed promptly after excavation of the shaft, little change in the *in situ* effective stress state in the soil should occur, and Eq. 10.11 may be used with $K_s = K_0$, the coefficient of earth pressure at rest. In heavily overconsolidated clay, some allowance for stress relaxation is recommended by Fleming *et al.* (1985), who suggest two alternatives: a reduction of the value of K_s by 20%, i.e. to 0.8 K_0; or using the mean stress between the *in situ* horizontal stress and that due to the wet concrete in the pile shaft, i.e. $K_s = (1 + K_0)/2$.

Despite the use of effective stresses to compute the shaft capacity, the ultimate base capacity, f_b, is usually still calculated from the total stress approach in Eq. 10.9.

10.2.2.4 Non-Cohesive Soils

For piles in sand or gravel, or piles in saturated clays under long-term drained conditions, effective stress analysis of ultimate load capacity is appropriate. If the cohesive component of drained strength is ignored, the ultimate shaft friction, f_s, and ultimate base resistance can be expressed as:

$$f_s = K_s \sigma'_v \tan \delta \qquad (10.14)$$

$$f_b = N_q \sigma'_{vb} \qquad (10.15)$$

where N_q = bearing capacity factor, σ'_{vb} = effective vertical overburden stress at level of pile base.

Equation 10.14 is the same equation as that in the β method for clays (Eq. 10.11). Conventional methods of calculation for piles in sand and gravel (e.g. Broms 1966; Nordlund 1963) assume that both f_s and f_b increase, more or less linearly, with depth. However, initial interpretations of the research by Vesic (1969) and others suggested that the average shaft friction and base resistance did not increase linearly with depth, but that they reached limiting values at depths of between 5 and 20 diameters, depending on the relative density of the soils. This phenomenon was attributed by some to a form of arching, together with the effects of soil compressibility and the reduction of friction angle with increasing stress level. While there is some controversy over this hypothesis (Kulhawy 1984), there is now a prevailing view that f_s and f_b may continue to increase with increasing depth, but at a decreasing rate. For practical design purposes, it is not uncommon to adopt limiting values of both f_s and f_b for piles in sands and gravels.

Figure 10.2 shows a commonly used solution for the bearing capacity factor, N_q, as a function of the angle of internal friction, Φ. In using this chart, the value of Φ for driven piles should be $(\Phi_0 + 40)/2$ degrees; while for bored piles, a value of $\Phi_0 - 3$ degrees should be adopted, where Φ_0 is the initial angle of friction of the soil in the vicinity of the pile base prior to pile installation. More comprehensive solutions for N_q, incorporating the effects of the relative compressibility of the soil and relative embedment depth, are presented by Kulhawy (1984) and Fleming *et al.* (1992).

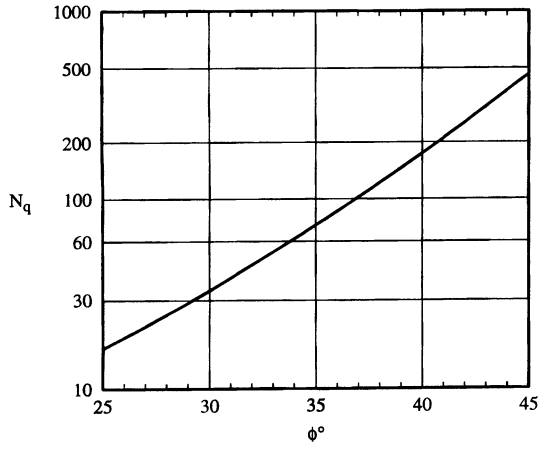


FIGURE 10.2. Variation of bearing capacity factor with friction angle (modified from Berezantzev *et al.* 1961).

of six diameters has been recommended by Meyerhof & Sastry (1978).

For Case B, where a weak layer underlies a dense sand layer, the presence of the weak layer affects the base capacity if the base is less than six times the base diameter, d_b, above the weak layer. The base capacity can be assumed to decrease linearly from the value for the dense sand layer to the value for the weak layer for distance, z_d, less than $6d_b$. More recent research by Matsui (1993), suggests that a depth of influence of three base diameters, rather than six diameters, is more realistic.

Where a dense sand layer is sandwiched between two weak layers, then the effects of the two weak layers must be considered together (Case C in Fig. 10.3).

TABLE 10.2. Interface friction angle, δ, for piles in sand (adapted from Stas & Kulhawy 1984)

Interface materials	Ratio of interface friction angle to soil friction angle, δ/ϕ	Typical field analogy
Sand/rough concrete	1.0	Cast-*in-situ*
Sand/smooth concrete	0.8–1.0	Precast
Sand/rough steel	0.7–0.9	Corrugated
Sand/smooth steel	0.5–0.7	Coated
Sand/timber	0.8–0.9	Pressure-treated

Tables 10.2–10.4 give some correlations for the parameters δ, K_s and the limiting values of shaft friction, f_{sl}, and end bearing, f_{bl}, for piles in sands.

10.2.2.5 Layered Soils

Proper consideration of layered soil profiles is important when estimating the ultimate base capacity of piles. Three important cases of layered soil profiles have been considered by Meyerhof (1976) and Meyerhof & Sastry (1978). These cases are illustrated in Fig. 10.3. In Case A, where a dense sand layer underlies a weak layer, the full base capacity is not developed until the pile penetration is some diameters into the dense sand. Meyerhof (1976) suggests ten diameters, but this may be excessively conservative; and a value

TABLE 10.3. Horizontal stress coefficients (adapted from Stas & Kulhawy 1984)[a]

Foundation type and method of installation	Ratio of horizontal stress coefficient to *in situ* value, K/K_0
Jetted pile	0.5–0.67
Drilled shaft, case-*in-situ*	0.67–1.0
Driven pile, small displacement	0.75–1.25
Driven pile, large displacement	1–2

[a] Typical values of K_0 are given in Chapter 3.

TABLE 10.4 Limiting values of ultimate shaft and base resistance for piles in sand

Soil type and condition	Limiting shaft friction, f_{sl} (kPa)	Limiting base resistance, f_{bl} (MPa)	Source
Very loose sand, Loose sand/silt	48	1.9	API (1984)
Medium dense silt, Loose sand, Medium dense sand/silt	67	2.9	API (1984)
Dense silt, Medium dense sand, Dense sand/silt	80	4.8	API (1984)
Dense sand, Very dense sand/silt	96	9.6	API (1984)
Dense gravel, Very dense sand	115	12.0	API (1984)
Calcareous sand (uncemented)			
Driven piles	10–20	1–4[a]	Nauroy *et al.* (1986)
Bored piles	60–100[a]	0.5–3[a]	Poulos (1988b, 1989)

[a] Depends on soil compressibility: smaller values for more compressible soils.

10.2.3 METHODS USING *IN SITU* TEST DATA

10.2.3.1 Static Cone Penetration (CPT) Tests

Two broad approaches have been adopted for utilizing static cone penetration test (CPT, see Chapter 4) data to predict pile capacity:

- Correlations between cone resistance values and both ultimate shaft friction and ultimate base capacity (e.g. De Ruiter & Beringen 1979; Bustamante & Gianeselli 1982; Poulos 1989).
- Correlations between sleeve friction and ultimate pile shaft friction (Schmertmann 1975, 1978). This approach is often considered to be less reliable than the above method because of the difficulties in accurately measuring sleeve friction.

A useful adaptation of the method of Bustamante and Gianeselli (1982) is summarized by Frank & Magnan (1975). The ultimate shaft friction, f_s, and base capacity, f_b, are given by:

$$f_s = (q_c/b) \leq f_{sl} \tag{10.16}$$

$$f_b = k_c q_c \tag{10.17}$$

where q_c = measured cone tip resistance, b = shaft factor, f_{sl} = limiting ultimate shaft friction, k_c = base factor.

Table 10.5 gives recommended values of b and f_{sl}, which depend on soil type and pile type. Values of k_c are given in Table 10.6. Here, the value of q_c used in Eq. 10.17 should be the average value within a distance of 1.5 base diameters above and below the base. Excessively large and low values are excluded from the average (Bustamante and Gianeselli 1982).

10.2.3.2 Standard Penetration Test (SPT)

Meyerhof (1956) introduced correlations between ultimate shaft resistance, f_s, ultimate base resistance, f_b, and SPT data, which are still widely used in practice (see Chapter 4 for a discussion of the SPT test). Further correlations are summarized by Meyerhof

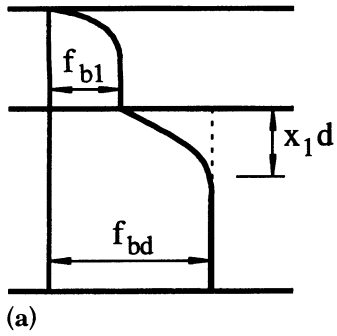


FIGURE 10.3. Layered soil profiles: variation of ultimate base capacity with depth: (a) Case A, dense sand below weak layer; (b) Case B, weak soil underlying dense sand; and (c) Case C, dense sand sandwiched between two weak layers. f_{b1}, f_{b2} = limiting base capacity of weak soil; f_{bd} = limiting base capacity of pile in dense sand. Typically x_1 and x_2 are between 3 and 6.

TABLE 10.5. Ultimate shaft friction correlation factors for CPT tests (adapted from MELT 1993)

	Clay and silt					Sand and gravel			Chalk	
Pile type	Soft	Stiff		Hard		Loose	Medium	Dense	Soft	Weathered
Drilled										
b	—	—	75[a]	—	—	200	200	200	125	80
f_{sl}, kPa	15	40	80[a]	40	80[a]	—	—	120	40	120
Drilled removed casing										
b	—	100	100[b]	—	100[b]	250	250	300	125	100
f_{sl}, kPa	15	40	60[b]	40	80[b]	—	40	120	40	80
Steel driven closed-ended										
b	—	120		150		300	300	300		
f_{sl}, kPa	15	40		80		—	—	120	[c]	
Driven concrete										
b	—	75		—		150	150	150		
f_{sl}, kPa	15	80		80		—	—	120	[c]	

[a] Trimmed and grooved at the end of drilling.
[b] Dry excavation, no rotation of casing.
[c] In chalk, f_s can be very low for some types of piles; a specific study is needed.

TABLE 10.6. Base capacity factors for CPT (adapted from MELT 1993)

	Soil type		q_c (MPa)	k_c	
				Non-displacement pile	Displacement pile
Clay silt	A	Soft	<3		
	B	Stiff	3–6	0.40	0.55
	C	Hard(clay)	>6		
Sand gravel	A	Loose	<5		
	B	Medium	8–15	0.15	0.50
	C	Dense	>20		
Chalk	A	Soft	<5	0.20	0.30
	B	Weathered	>5	0.30	0.45

(1976) and Poulos (1989). More comprehensive correlations have been developed by Decourt (1982, 1995). In the latter work, the following expressions are suggested:

$$f_s = \alpha(2.8N_{60} + 10)\text{kN m}^{-2} \quad (10.18)$$

$$f_b = K_b(\bar{N}_{60})_b \text{ kN m}^{-2} \quad (10.19)$$

where N_{60} = SPT value (normalized to 60% energy efficiency) along pile shaft; $\alpha = 1$ for displacement piles in all soil types and non-displacement piles in clays, and 0.5–0.6 for non-displacement piles in granular soils; $(\bar{N}_{60})_b$ = average of N_{60} values in vicinity of pile tip; K_b = base factor, as set out in Table 10.7.

There are alternative recommendations for the use of SPT data, e.g. Robert (1997), whose correlations are generally more conservative for driven piles, but less conservative for bored piles. Robert has also found

TABLE 10.7. Base factor, K_b (adapted from Decourt 1995)

Soil type	Displacement piles	Non-displacement piles
Sand	325	165
Sandy silt	205	115
Clayey silt	165	100
Clay	100	80

that timber piles, because of their taper, mobilize a higher ultimate skin friction than driven piles with uniform cross-sections, typically by a factor of 1.8 for both sand and clay.

10.2.4 UPLIFT CAPACITY

For piles without an enlarged base, the ultimate uplift capacity, Q_{ut}, can be estimated:

$$Q_{ut} = (\bar{f}_{st} A_s) + W \qquad (10.20)$$

where f_{st} = average uplift shaft resistance; A_s = shaft surface area; W = weight of pile, allowing for buoyancy where applicable.

In cohesive soils, f_{st} can be taken to be the same as for downward loading. In sands, De Nicola & Randolph (1993) have demonstrated that the ratio of the shaft resistance in tension, f_{st}, and compression, f_s, is related to the relative compressibility of the pile:

$$\frac{f_{st}}{f_s} = \{1 - 0.2 \log_{10}[100/(L/d)]\} \times (1 - 8\eta + 25\eta^2) \qquad (10.21a)$$

$$\eta = \nu_p \left(\frac{L}{d}\right)\left(\frac{G_{av}}{E_p}\right) \tan \delta \qquad (10.21b)$$

where L = pile length, d = pile diameter, η = dimensionless pile compressibility factor, ν_p = Poisson's ratio of pile material, δ = pile–soil interface friction angle, G_{av} = average value of soil shear modulus along shaft, E_p = Young's modulus of pile material.

For piles with an enlarged base, Q_{ut} can be taken as the lesser of:

1. the sum of the weight of the pile and the ultimate uplift resistance of the entire base area (similar to an anchor pull-out);
2. the sum of the weight of the pile, the frictional force along the shaft, and the ultimate uplift resistance of the net base area.

In saturated clays and silts, the long-term uplift capacity may be considerably less than the short-term capacity because of the dissipation of negative porewater pressures (Meyerhof & Adams 1968). For calculation of the ultimate uplift resistance of the base, the solutions of Rowe & Davis (1982a) for anchor plates may be used.

10.2.5 GROUP EFFECTS

It is convenient to define a pile group efficiency, Y, for ultimate capacity:

$$Y = \frac{\text{ultimate capacity of pile group}}{\text{sum of ultimate capacities of individual piles}}. \qquad (10.22)$$

Early methods of estimating Y were often based purely on geometry, e.g. the Converse Labarre formulae and Feld's rule (Poulos & Davis 1980), but it is now recognized that such approaches are deficient in not considering the soil and pile characteristics. Table 10.8 summarizes recommendations for the estimation of Y for various situations. It should be emphasized that these approaches are approximate only.

10.2.6 EFFECTS OF CYCLIC LOADING

Cyclic or repeated axial loading can arise from the action of wave or wind forces and can be an important factor in the design of piles for offshore structures, transmission towers and some tall buildings. The application of cyclic loading to piles can have at least two detrimental effects:

1. a possible reduction or "degradation" of pile resistance, especially shaft resistance;
2. accumulation of permanent displacements.

If the loading is applied rapidly, there may be a counterbalancing effect of loading rate, which tends to increase pile resistance.

The degradation of shaft resistance has been found to be a function of the cyclic displacement and the number of cycles (Mat-

TABLE 10.8. Recommendations for pile group efficiency estimation

Case	Group efficiency, Y	Remarks
Driven piles in loose–medium dense sand	1.0	Y may be considerably >1: adopt-1 for design
End-bearing piles on rock, dense sand, or gravel	1.0	Base resistance is not much affected by group action, even at small spacings
Bored friction piles in sand	0.67	For "customary spacings": i.e. 3 ± 1 diameters
Friction piles in clay: cap above surface	Lesser of $P_B/\Sigma P_u$, or 1.0[a]	Make allowance for any soft layers below base
	$\{1/[1 + (\Sigma P_u/P_B)^2]\}^{0.5}$	Make allowance for any soft layers below base

[a] P_B = ultimate load capacity of block containing piles and soil; ΣP_u = sum of ultimate capacities of individual piles.

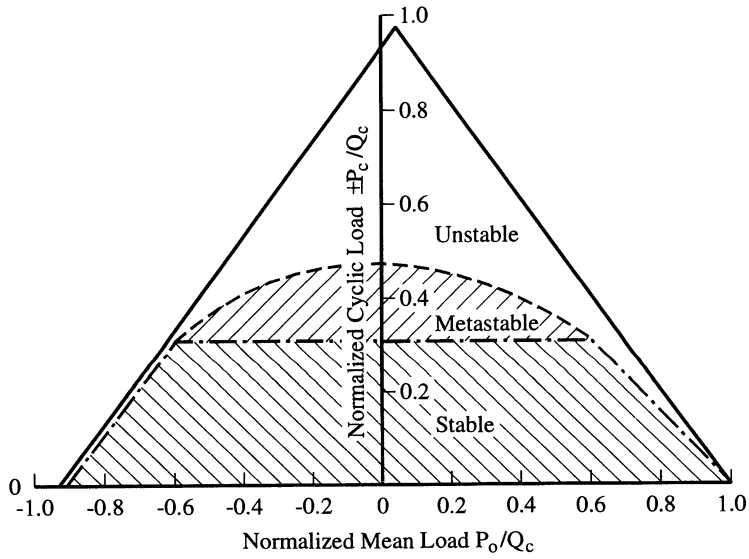


FIGURE 10.4. A typical cyclic stability diagram for a driven pile in clay: N = 100 cycles.

lock & Foo 1979; Poulos 1988a, b). Using a simplified characterization of shaft resistance degradation, it is possible to analyze the axial response of a pile subjected to various combinations of mean and cyclic loading. The results of such an analysis can be represented in the form of a cyclic stability diagram, which is a normalized plot of mean load, P_0, versus cyclic load, P_c, each normalized with respect to the ultimate compressive load capacity, Q_c (Poulos 1988a). A typical cyclic stability diagram is shown in Fig. 10.4 for a driven offshore pile in clay. Three main regions can be identified:

1. A cyclically stable region, in which cyclic loading has no influence on the axial pile capacity.
2. A cyclically metastable region, in which cyclic loading causes some reduction of axial capacity, but the pile does not fail within the specified number of cycles.
3. A cyclically unstable zone, in which cyclic

loading causes sufficient reduction of axial capacity for the pile to fail within the specified number of cycles of load.

A useful estimate of the cyclic load representing the boundary between the stable and metastable zones of the cyclic stability diagram may be obtained from the following expression developed by Randolph (1983):

$$P_{\dot{Y}}/P_{su} \leq 1/(\Pi_1)^{1/2} \qquad (10.23)$$

where $P_{\dot{Y}}$ = the cyclic load, which just avoids slip between the pile and soil; P_{su} = the ultimate shaft load capacity, and:

$$\Pi_1 = \frac{8}{\lambda\zeta}(L/d)^{\theta} \qquad (10.24)$$

in which λ and ζ are defined in Eq. 10.26 below, and L and d = the pile length and diameter, respectively.

10.3 Settlement Prediction

10.3.1 ANALYSIS METHODS

There are four main means of modeling pile–soil interaction:

1. Via load-transfer (t–z) curves, which relate local shear stress to local displacement along the pile; these are, in effect, non-linear independent spring support characteristics describing the soil–pile response at a particular location on the pile (e.g. Coyle & Reese 1966; Kraft *et al.* 1981; Randolph 1994a,b).
2. Via elastic theory, which idealizes the soil as an elastic continuum, and allows consideration of interaction between different portions of the pile through the soil (e.g. Butterfield & Banerjee 1971; Banerjee & Davies 1977; Poulos & Davis 1980).
3. Via simplified analysis methods, which consider localized shear around the pile and can lead to convenient closed-form solutions (e.g. Randolph & Wroth 1978; Fleming *et al.* 1992).
4. Via numerical analyses, which utilize advanced constitutive models of soil behavior (e.g. Jardine *et al.* 1986; Trochanis *et al.* 1991).

The load transfer, or t–z, method is widely used in practice for estimating the load–settlement behavior of a single pile, especially for offshore pile design, and for cases where non-linear soil–pile behavior has to be considered or the soil is stratified. The method involves modeling the pile as a structural member supported by discrete springs that represent the resistance of the soil along the shaft and at the base of the pile. The relationships between local load transfer, t, and local displacement, z, are generally referred to as t–z curves. These curves were originally obtained empirically, but may now be obtained more satisfactorily via theoretical relationships with the stiffness of the surrounding soil (e.g. Kraft *et al.* 1981; Randolph 1994b). Such curves may be relatively complex, and incorporate such factors as non-linearity, strain softening and cyclic loading effects.

Once the pile and soil characteristics have been defined, the relationship between applied load and pile head settlement can be obtained from what is now a reasonably routine structural analysis.

Different methods that utilize the theory of elasticity in general give very similar solutions for the pile settlement. For example, for a typical pile in a soil whose modulus increases linearly with depth, four independent linear analyses (Banerjee & Davies 1977; Randolph & Wroth 1978; Poulos 1979a, 1989) give solutions for settlement that agree to within ±7%, which is adequate for practical purposes.

Jardine *et al.* (1986) have employed a finite element analysis using approach (d) above to analyze a pile in a homogeneous clay layer. This problem has been analyzed by various alternative methods in categories (1) and (2) above by Poulos (1989), and for a realistic pile stiffness, the resulting load–settlement curves have been found to agree well with

the finite element solutions of Jardine *et al.* (1986). There is therefore a strong indication from these comparisons that the method of analysis is not a critical factor in single pile settlement prediction, provided that the method is soundly based.

Despite the wide use of load–transfer analyses in practice, attention will be focused here on the methods in (2) and (3) above, as they lend themselves to the development of parametric solutions and design charts.

10.3.2 DESIGN CHARTS AND EQUATIONS FOR SINGLE PILES

For routine design applications, it is convenient to use parametric solutions derived for a pile in an elastic soil whose modulus increases linearly with depth. Figure 10.5 defines the geometry and parameters of the problem. The pile head settlement, S, can be expressed as:

$$S = \frac{P}{E_{SL}d} I_\rho \qquad (10.25)$$

where P = applied load, d = pile diameter, E_{SL} = Young's modulus at the level of the pile tip, and I_ρ = the settlement influence factor.

Values of I_ρ have been given by Poulos (1979a) and Poulos & Davis (1980), and are shown to be dependent on a number of dimensionless parameters, including L/d, $K_b = E_pR_A/E_{SL}$ (pile stiffness factor); E_{SO}/E_{SL} and E_b/E_{SL}, where E_p = pile Young's modulus, R_A = area ratio (ratio of area of pile section to the gross cross-sectional area of the pile), E_{SO} = soil Young's modulus at surface, E_b = Young's modulus of bearing stratum on which the tip rests.

From the closed-form solutions obtained by Randolph (Fleming *et al.* 1992), the following explicit expression can be derived for I_ρ:

$$I_\rho = 4(1+\nu_s)\left[1 + \frac{1}{\pi\lambda}\frac{8}{(1-\nu_s)}\frac{\eta_1}{\xi}\frac{\tanh(\mu L)}{\mu L}\frac{L}{d}\right] \Bigg/ \left[\frac{4}{(1-\nu_s)}\frac{\eta}{\xi} + \frac{4\pi\rho}{\zeta}\frac{\tanh(\mu L)}{\mu L}\frac{L}{d}\right] \qquad (10.26)$$

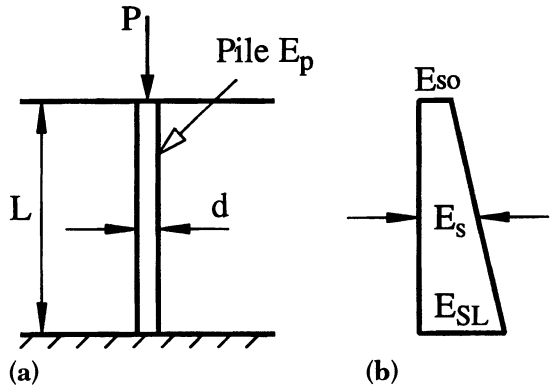


FIGURE 10.5. The definition of single pile geometry: (a) bearing stratum Young's modulus = E_b; and (b) distribution of soil Young's modulus, $\eta = E_{SO}/E_{SL}$. E_s = soil Young's modulus.

where, referring to Fig. 10.6, $\eta = d_b/d$; d_b = the diameter of the pile tip, $\xi = E_{SL}/E_b$, $\rho = \bar{E}_s/E_{SL}$ ($\bar{E}_s$ = average value of soil Young's modulus along shaft):

$$\left.\begin{aligned} \lambda &= 2(1+\nu_s)E_p/E_{SL} \\ \zeta &= \ln[\{0.25 + [2.5\rho(1-\nu_s) - 0.25]\xi\}2L/d] \\ \mu L &= 2\left(\frac{2}{\zeta\lambda}\right)^{0.5}\frac{L}{d} \end{aligned}\right\}. \qquad (10.27)$$

The settlement of the pile, S_z, at any depth, z, can be approximated as:

$$S_z = S_L \cosh[\mu(L-z)] \qquad (10.28)$$

where S_L = the settlement at the tip. Thus, the ratio of the top: tip settlements is cosh (μL). In applying the above elastic solutions, the immediate or undrained settlement (for piles in clay) is calculated with E_{SO} and E_{SL} put equal to the undrained Young's modulus values, and I_ρ being the value relevant to the undrained value of ν_s (0.5 for a saturated

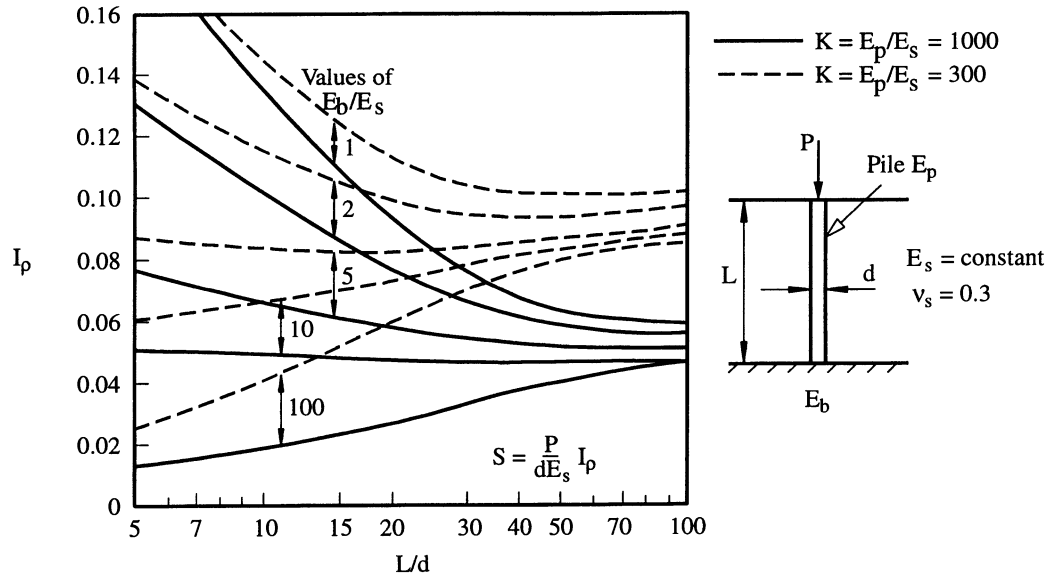


FIGURE 10.6. Settlement of single pile in homogeneous clay.

clay). For total final settlement calculation in sand or clay, E_{SO} and E_{SL} = the drained Young's modulus values, and I_ρ = the influence factor for the drained value of ν_s.

For typical values of pile stiffness factor K_b, values of I_ρ are shown in Fig. 10.6 for a homogeneous clay deposit and in Fig. 10.7 for a soil whose modulus increases linearly with depth. These solutions have been derived via spreadsheet solution of Eq. 10.26.

For layered soil profiles, it is adequate for most practical purposes to replace the layered soil along the pile shaft by an equivalent homogeneous soil, with the pile base resting on a soil whose modulus represents the soil stiffness in the region influenced by the base. Poulos (1994a) provides a simple means of estimating this modulus.

10.3.2.1 Non-Linear Analysis

The above solutions are derived from linear elastic theory and are generally adequate for piles in clay and piles that derive most of their resistance from shaft friction. However, for large-diameter piles, or piles that derive a substantial proportion of their resistance from the base, the load–settlement behavior may become markedly non-linear at normal working loads. In such cases, an approximate simple procedure has been developed by Poulos & Davis (1980). This method involves the construction of a tri-linear load–settlement curve, as illustrated in Fig. 10.8. In addition to the settlement influence factor, it is necessary to estimate the ultimate shaft and base resistances (see Section 10.2), and the proportion of load carried by the base, β_b. Solutions for β_b are given by Poulos & Davis (1980), and may also be derived from the solutions of Randolph (Fleming *et al.* 1992).

10.3.3 PILE GROUP SETTLEMENT

10.3.3.1 Methods of Analysis

At least seven broad categories of analysis procedures have been employed for group settlement calculation:

1. Simplified procedures that reduce the group to an equivalent raft (e.g. Terzaghi & Peck 1967; Tomlinson 1986).

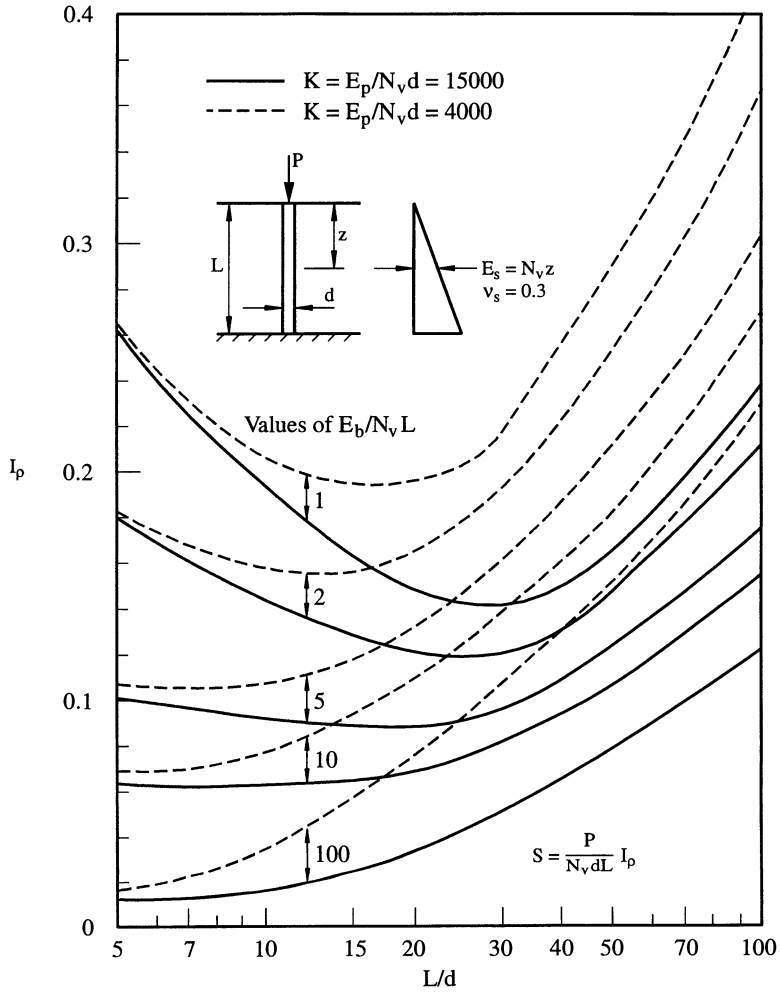


FIGURE 10.7. Settlement of single pile in soil with linearly increasing modulus.

2. Simplified methods that reduce the group to an equivalent pier (e.g. Poulos & Davis 1980; Poulos 1993; van Impe 1991).
3. The settlement ratio method, in which the settlement of a single pile (at the average load level) is multiplied by a settlement ratio, which is usually derived from one of the methods outlined below (e.g. Poulos 1979b; Fleming *et al.* 1985).
4. Methods that compute the response of a single pile via elastic theory, and which consider pile–soil–pile interaction via interaction factors that are also computed from some form of elastic theory (e.g. Poulos 1968; Randolph & Wroth 1979; Hirayama 1991; Polo & Clement 1988).
5. Hybrid methods that compute the single pile response from a load-transfer analysis, while pile–soil–pile interaction is allowed for via the use of elastic theory (e.g. O'Neill *et al.* 1977; Chow 1986; Lee 1993).
6. Complete boundary element methods, in which each pile is divided into discrete elements and pile–soil–pile interaction is considered between each of these elements via the use of elastic theory (e.g. Butterfield & Douglas 1981; Poulos & Hewitt 1986).

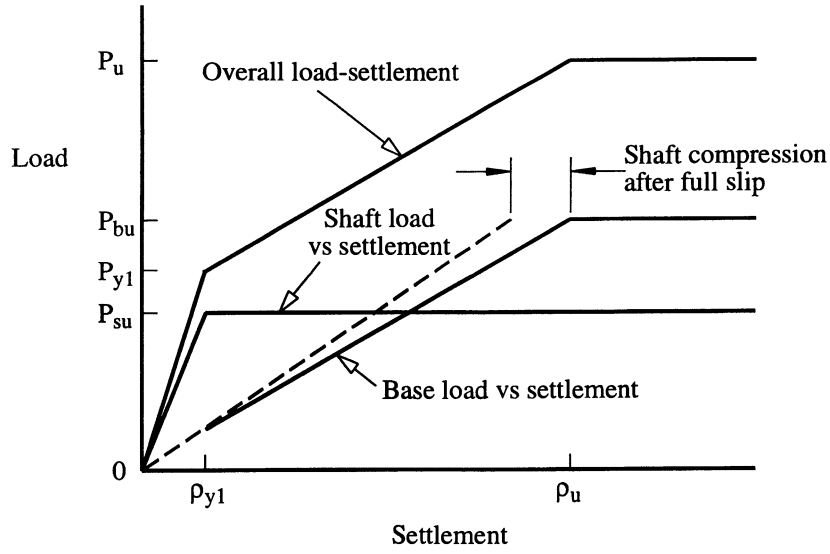


FIGURE 10.8. Construction of load–settlement curve (modified from Poulos & Davis 1980).

7. Finite element methods, which often simplify the group to an equivalent plane-strain or axisymmetric system (e.g. Ottavini 1975; Pressley & Poulos 1986).

A number of comparisons have been published between various methods, and it has been found that a similar settlement is predicted by the various methods based on elastic theory, e.g. Poulos & Randolph (1983), Chow (1986), and Lee (1993). Poulos (1993) has found that, for end-bearing groups, the equivalent raft method tends to overestimate the settlement of groups containing a small number of piles, although it gives reasonable values for groups containing 16 or more piles. The equivalent raft method is found to be better suited to analyzing a group of friction piles, and can give adequate solutions for groups as small as four piles. O'Neill & Ha (1982) have found that hybrid and elastic methods can give similar results, provided that the input soil parameters are chosen appropriately, while Pressley & Poulos (1986) have demonstrated that the load–settlement response of a pile group, using a linear finite element analysis, is similar to that predicted via an interaction factor analysis.

Poulos (1994a) has examined the relative importance of various factors that may influence the load–settlement behavior of a group. Among the factors that are very important are the soil modulus around and beneath piles, and the soil moduli between the piles and well below the pile tips. The effects of installation on the soil characteristics within the pile group can be very important, particularly for piles in sand. It is now well-understood that the effects of driving a group of piles in sand is to densify, stiffen and strengthen the soil around the interior piles in the group. Thus, the load–settlement behavior of a pile within a group may be quite different to that of a single isolated pile, and the group settlement ratio may be less than unity in some cases. O'Neill (1983) summarizes published data that demonstrates that the group settlement ratio decreases as the average group breadth decreases, and may be as low as 0.2 for closely spaced piles driven into loose sand. It is therefore clear that injudicious application of theoretical analyses, without a clear understanding of the significance of some of the key factors, may lead to highly inaccurate estimates of group settle-

ment, particularly in sands (e.g. Poulos 1968; Leonards 1972). Fortunately, such inaccuracies tend to be on the conservative side, i.e. the predicted settlements are larger than the true settlement.

10.3.3.2 Rapid Practical Estimation of Group Settlements

For rapid practical estimation of group settlements without recourse to a computer, there are at least three convenient methods that may be employed: the settlement ratio method, the equivalent raft method, and the equivalent pier method.

In the settlement ratio method, the group settlement, S_G, is related to the single-pile settlement as follows:

$$S_G = R_s S_{iav} \qquad (10.29)$$

where S_{iav} = settlement of single pile at the average load of a pile in the group, and R_s = settlement ratio. S_{iav} can be estimated either by calculation (Eq. 10.25) or from the results of a pile load test on a prototype pile.

Theoretical values of R_s for various pile groups in homogeneous and non-homogeneous soil profiles have been presented by Poulos (1977, 1979b) and Butterfield & Douglas (1981). A particularly useful approximation for the settlement ratio has been derived by Randolph (Fleming *et al.* 1992):

$$R_s \simeq n^w \qquad (10.30)$$

where n = number of piles in the group; w = exponent depending on pile spacing, pile proportions, relative pile stiffness, and the variation of soil modulus with depth. For typical pile proportions and pile spacings, Poulos (1989) has suggested the following approximate "rules of thumb": $w \simeq 0.5$ for piles in clay, and $w \simeq 0.33$ for piles in sand.

The equivalent raft method suggested by Tomlinson 1986) involves the representation of the pile group by a raft located at an appropriate depth below the surface. Poulos (1993) found that this approach gives generally satisfactory results. The equivalent pier method (Poulos & Davis 1980), involves the replacement of the pile group by an equivalent pier consisting of the piles and the soil between them. For estimating the settlement of driven pile groups, the equivalent pier method has the following advantages:

- it does not require detailed consideration of the response of single piles within the group, which may have been influenced by installation effects;
- it reflects the increasing proportion of the load that is carried by the pile tips because of pile–soil–pile interaction effects;
- it can be extended to include non-linear load–settlement response;
- it allows an assessment to be made of the rate of settlement of pile groups in clay.

Figure 10.9 presents dimensionless solutions for a pier in a homogeneous soil, bearing on a stratum of equal or greater stiffness. The compressibility of the pier has been chosen to be representative of the average value of a pile and soil block with piles at a spacing of about three diameters. For short piers, the relative compressibility is unimportant unless the pier is very compressible, or unless it is founded on a very stiff stratum. Figure 10.9 may be used with sufficient accuracy for a pier in a non-homogeneous soil, by using an average soil modulus along the shaft of the pier. Solutions for the proportion of base load are given in Fig. 10.10, and are useful if the approximate approach illustrated in Fig. 10.8 is used to estimate the load–settlement curve to failure.

In utilizing the equivalent pier approach, the following points should be noted:

1. The diameter, d_e, of the equivalent pier should be such that it has an equal total surface area (shaft and base) to the enclosed "block" of piles and soil. For a block of square plan area $B \times B$, d_e will

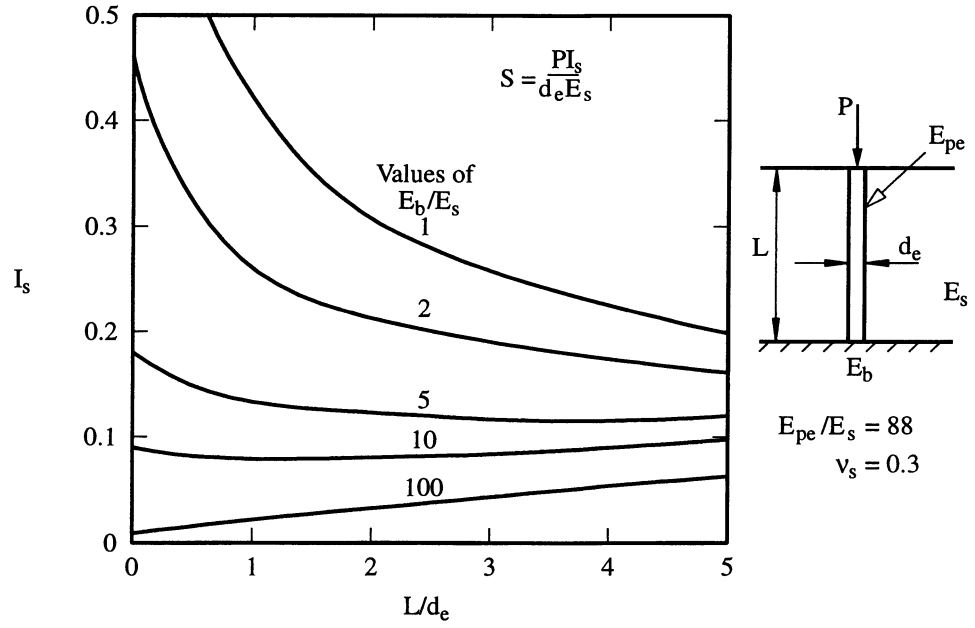


FIGURE 10.9. Settlement of equivalent pier in soil layer.

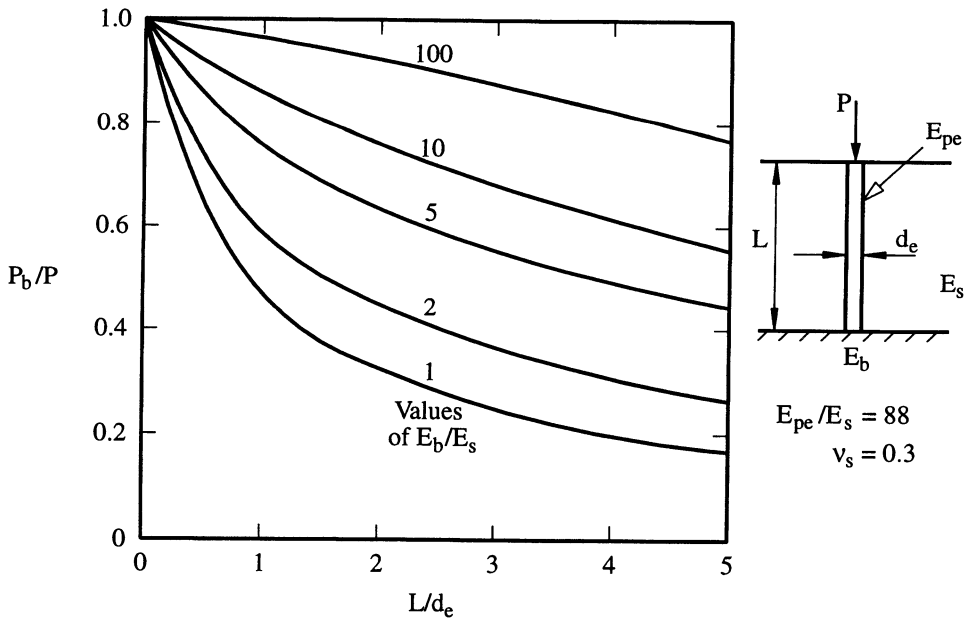


FIGURE 10.10. Proportion of base load for equivalent pier.

lie between 1.13b and 1.27B, depending on the length of the block.
2. The Young's modulus of the pier is taken as the area-weighted average value for the pile–soil block.
3. In selecting the Young's modulus, E_b, of the bearing stratum, consideration needs to be given to the effects of installation. An average value (weighted with respect to the relative depth below the base of the pier) should be used as discussed by Poulos (1994a).
4. For a non-linear analysis, the ultimate shaft and base resistances of the group (which are not necessarily the same as those for the equivalent pier) are computed. If a computer analysis is to be performed, the equivalent average ultimate skin friction and end-bearing values can be obtained by dividing the computed shaft and base resistances by the shaft and base areas of the pier, respectively.

10.3.4 ASSESSMENT OF PARAMETERS

For predictions of pile settlement, the key geotechnical parameter required is the stiffness of the soil. If an analysis based on elastic continuum theory is used, then the soil stiffness can be expressed in terms of a Young's modulus, E_s, or shear modulus, G_s. Both the magnitude and distribution of these moduli are important. It cannot be emphasized too strongly that E_s (or G_s) are not constants, but depend on many factors, including soil type, initial stress state, stress history, the method of installation of the pile, the stress system and stress level imposed by the pile or pile group, and whether short- or long-term conditions are being considered. The most satisfactory procedure for assessing the soil modulus is to carry out pile load tests on prototype piles and backfigure the modulus from the observed load–settlement response, using the same theory that will be used for the actual settlement prediction. Because this is not always possible, especially in the preliminary stages of design, it is usual practice to correlate the soil modulus with the results of simple *in situ* tests, such as the standard penetration test (SPT) and cone penetration test (CPT), or with the results of field or laboratory strength tests.

Four different values of Young's modulus can be distinguished for pile settlement analysis:

1. The value E_s for the soil in the vicinity of the pile shaft. It will tend to influence strongly the settlement of a single pile and pile groups.
2. The value E_{sb} immediately below the pile tip; this will also tend to influence the settlement of single pile and pile groups.
3. The initial tangent value E_i for the soil between the piles; this will reflect the small strains in this region and will affect the settlement interaction between the piles.
4. The value of E_{sl} for the soil well-below the tips. This value will influence the settlement of a group increasingly as the group size increases.

E_s and E_{sb} will both be influenced by the installation process, and would be expected to be different for bored piles and for driven piles. On the other hand, E_{si} and E_{sl} are unlikely to be influenced by the installation process, but rather by the initial stress state and stress history of the soil. An interesting corollary is that the method of installation is likely to have a much more significant effect on the settlement of a single pile, which depends largely on E_s or E_{sb}, than on the settlement of a pile group, which may depend to a large extend on E_{sl} and E_{si}.

Table 10.9 summarizes some suggested correlations for E_s, E_{si} and E_{sl}. In all cases, the correlations relate to the drained Young's modulus, and therefore to the calculation of final settlements. There appears to be little information available on the modulus E_{sb} below the tip of a driven pile. It is suggested that, for clays, the same correlation be used for E_{sb} as for E_s; while for sands, E_{sb} should be three–five times that given by the correlation for E_s.

TABLE 10.9. Summary of some correlations for drained Young's modulus for pile settlement analysis[a–e]

	Near-shaft modulus, E_s (MPa)		Small strain modulus, E_{si} (MPa)		Modulus well-below pile tips, E_s (MPa)	
Clays						
	$(2.5 \pm 0.5)N$	(Decourt *et al.* 1989)	$14N$	(Hirayama 1991)	$(0.5 \pm 0.2)N$	(Stroud 1974)
Driven piles						
	$(15 \pm 5)s_u$	(Poulos 1989)	$49.4q_c^{0.695} \cdot e_0^{-1.13}$	(Mayne & Rix, 1993)	$(7.5 \pm 2.5)q_c$	
	$(500 \pm 5)q_c$	(Callanan & Kulhawy 1985)				
			$1500s_u$	(Hirayama 1991)		
Bored piles						
	$(150–400)s_u$	(Poulos & Davis 1980)			$(150 \pm 50)s_u$	
	$10q_c$	(Christoulas & Frank 1991)			$(0.5–0.7)M$	
Silica sands						
	$(2.5 \pm 0.5)N$	(Decourt *et al.* 1989)	$16.9N^{0.9}$	(Ohsaki & Kawasaki 1973)	$7N^{0.5}$	(Denver 1982)
Driven piles	$(7.5 \pm 2.5)q_c$	(Poulos 1989)	$53q_c^{0.61}$	(Imai & Tonouchi 1982)	$(7 \pm 4)q_c$	(Jamiolkowski *et al.* 1988)
Bored piles	$(3 \pm 0.5)q_c$	(Poulos 1993)				

[a] Values of E_s and E_{si} for sands are for single isolated pile. In a group, the values may be increased, depending on pile spacing and initial density.
[b] Below pile tip, E_{sb} can be taken as equal to E_s for clays and bored piles in sands; and three–five times E_s for driven piles in sands.
[c] Above values of E_s and E_{sb} are for use in an elastic analysis. Higher values are appropriate for non-linear analyses (e.g. the initial tangent values for a hyperbolic model should be 1.4–1.6 times the values in this table).
[d] N is the SPT value (blows per 300 mm, MPa), and should be corrected to a rod energy of 60%.
[e] q_c = cone penetrometer resistance in MPa; s_u = undrained shear strength in MPa; e_0 = initial void ratio; M = constrained modulus.

The values of E_s and E_{sb} in Table 10.9 are meant to be used in elastic or elastic–plastic analyses of settlement, and represent a secant modulus at typical working load levels of one-third to one-half of ultimate load. However, if a non-linear analysis is employed, the initial tangent values of E_s and E_{sb} should be greater than the values in Table 10.9.

If the simple theoretical solutions such as those in Figs 10.6 and 10.10 are used, it is necessary to estimate average values of Young's modulus along the shaft and below the pile tip. Unless the piles are very slender or compressible, it is usually adequate to adopt an average modulus along the shaft of the pile (or the equivalent pier). Below the pile tip, a weighted average modulus, $E_{sb(e)}$, can be estimated as described by Poulos (1994a).

Worked Example

A group of 16 piles in a square (four × four) configuration is to be driven through a 15 m thick clay layer to a medium dense sand layer. Each of the piles is a 0.5 m outside-diameter steel tube, with

a 20 mm wall thickness, with the tip resting just on the sand layer. The piles are driven closed-ended and attached to a rigid cap and are spaced 1.5 m center-to-center. The weight of the pile is 36 kN.

The clay layer has an average undrained shear strength of 60 kPa and a bulk unit weight of 18 kN m^{-3}. The sand layer has an average SPT value of 20. Compute: (1) the ultimate capacity of the group; (2) the group settlement under a 12 MN serviceability load, using (a) the settlement ratio method; (b) the equivalent pier method, and (c) the equivalent raft method.

Solution:

1. The ultimate capacity of a single pile will be calculated first, and then consideration will be given to group effects. For the estimation of ultimate shaft friction, the total stress, α, method will be used; while for the ultimate end bearing resistance, correlations with SPT will be used.

Using the correlations from Figure 10.1, the value of α for $s_u = 60$ kPa is 0.64. The length-to-diameter ratio, L/d, of each pile is $15/0.5 = 30$, and from Equation 10.8a, the factor $F_1 = 1.0$. Therefore, from Equation 10.6, the average shaft friction is $f_s = 0.64 \times 60 \times 1.0 = 38$ kPa.

From the correlations of Decourt (1995) in Table 10.7, for driven piles, the ultimate end bearing capacity is $f_b = 325N$ kPa = 6.5 MPa. This value exceeds the limiting value of f_b in Table 10.4 of 4.8 MPa for piles in medium–dense sand; hence, a f_b value of 4.8 MPa (4800 kPa) will be adopted.

From Equation 10.5, ignoring the shaft resistance in the top 1 m of the clay:

$$P_u = [(38 \times \pi \times 0.5 \times 14) + (4800 \times \pi \times 0.25^2) - 36] = 1.74 \text{ MN}$$

Thus, for the single pile failure mode, the ultimate axial capacity of 16 piles is $16 \times 1742 \simeq 27.9$ MN.

Group effects will now be checked, and the capacity of the group as a block will be computed. The overall width of each side of the block is $3 \times 1.5 + 0.5 = 5.0$ m. Allowing for soil–soil failure around the block, the ultimate shaft resistance is $4 \times 5 \times 14 \times 60 = 16\,800$ kN. The end bearing capacity of the block base is $5 \times 5 \times 4800 = 120\,000$ kN. The weight of the piles and soil in the block is (approximately) $(16 \times 36) + (5 \times 5 \times 15 \times 18) = 7326$ kN. The ultimate capacity of the block is then $P_B = 16\,800 + 120\,000 - 7326 = 129\,474$ kN $\simeq 129.5$ MN. This is substantially greater than the value of 27.9 MN for the single pile failure mode.

Using the Terzaghi & Peck approach, the ultimate group capacity is ~27.9 MN. If the approach of Poulos & Davis (1980) is adopted, the efficiency factor (from Table 10.8) is found to be $\{1/[1 + (27872/129474)^2]\}^{0.5} = 0.98$, and therefore the ultimate group capacity is $0.98 \times 27\,872 = 27\,315$ kN $\simeq 27.3$ MN.

The overall factor of safety, for the serviceability load of 12 MN is 2.28 (Poulos & Davis 1980) or 2.32 (Terzaghi & Peck 1967).

2. Settlement calculation.

(a) Settlement ratio method. In this method, the settlement of a single pile at the average load is calculated first. Using the elastic analysis described in Section 10.3.2, it is necessary to calculate first the pile stiffness factor $K = E_P R_A / E_{SL}$. For the steel tube pile, $R_A = \pi \times 0.48 \times (0.20/\pi) \times 0.25^2 = 0.152$. It will be assumed that the pile Young's modulus, E_P, is 200 000 MPa, and that the soil Young's modulus in the clay is constant and equal to $400s_u$ (Table 10.9), i.e. $E_{SL} = 400 \times 60 = 24\,000$ kPa = 24 MPa. Thus, $K = 200\,000 \times (0.153/24) = 1275$. For the underlying sand, Young's modulus will be assumed to be $E_{sb} = 2.5N$ MPa (Table 10.9) = 50 MPa.

Figure 10.6 will be used to estimate the single pile settlement, and the relevant dimensionless parameters are as follows: $L/d = 30$, $E_b/E_s = 50/24 \simeq 2.1$, $K = 1275$. Interpolating from this figure, $I_\rho = 0.067$. The average load per pile is $12/16 = 0.750$ MN, and therefore the single pile settlement is $0.750 \times [0.067/(0.5 \times 24)] = 0.0042$ m (4.2 mm).

From Eq. 10.28, the settlement ratio can be estimated as $R_s = n^w$, and in this case, it will be assumed that w = 0.5, so that $R_s = 16^{0.5} = 4.0$. The group settlement is then $4.2 \times 4.0 = 16.8$ mm.

(b) Equivalent pier method. The equivalent diameter, d_e, of the pier is taken as $1.2 \times 5.0 = 6.0$ m, and therefore $L/d_e = 15/6.0 = 2.5$. The ratio

$E_b/E_s = 2.1$ as before. From Fig. 10.9, the settlement factor, I_s, is 0.20. The settlement of the equivalent pier is then $12.0 \times [0.20/(6.0 \times 24)] = 0.0167 = 16.7$ mm.

(c) Equivalent raft method. It will be assumed that the equivalent raft is located at a depth of two-thirds of the pile length, i.e. 10 m below the surface. Assuming a 1 : 4 spread of the load to this depth (as recommended by Tomlinson 1986) the width of each side of the equivalent raft is $5.0 + (2 \times 10 \times 0.25) = 10.0$ m. The area of the raft is therefore 100 m^2, and the average applied pressure is $12/100 = 0.12$ MPa. Therefore the problem is reduced to a square raft on a two layer system, consisting of a 5 m layer with a modulus of 24 MPa, underlying a deep layer with a modulus of 50 MPa. An elastic analysis of this problem (assuming a Poisson's ratio of 0.3 for each layer), gives an average settlement of 26.9 mm. This value should be corrected for the depth of embedment of the raft, and using the results quoted by Poulos (1993), this factor is found to be 0.72. The estimated settlement of the equivalent raft is therefore $0.72 \times 26.9 = 19.4$ mm.

It will be observed that in this case, all three approximate methods give similar computed settlements. As a matter of interest, a computer analysis using the interaction factor approach via the computer program DEFPIG (see Section 10.6) gives a settlement of 19.7 mm, which is also in general agreement with the above hand-calculation methods.

10.4 Lateral Loading

10.4.1 ULTIMATE LATERAL CAPACITY

The ultimate lateral resistance of a laterally loaded pile or group is unlikely to be the controlling factor for design unless large deflections can be tolerated, e.g. anchor piles for offshore structures. Methods for calculating ultimate lateral resistance generally consider the static equilibrium of the pile or group at the point of failure.

10.4.1.1 Single Piles

Two modes of failure need to be considered for a single pile:

1. Failure due to yielding of the soil along the length of the pile (termed "short-pile failure" by Broms 1964a).
2. Failure due to yielding of the pile itself at the point of maximum moment (termed "long-pile failure" by Broms 1964a).

Solutions for the ultimate lateral resistance of a pile under both the above modes can be obtained by assuming a distribution of ultimate lateral pile–soil pressure, p_y, and considering the statics of the problem. The best-known and most widely quoted results are those of Broms (1964a,b), who considered two soil types:

- a uniform purely cohesive soil, e.g. an overconsolidated clay under undrained conditions);
- a cohesionless soil, e.g. sand.

For the pile in uniform clay, Broms took the ultimate lateral pile–soil pressure, p_y, at any point along the pile as:

$$p_y = 9s_u \tag{10.31}$$

where s_u = undrained shear strength. However, he allowed for a "dead" zone of zero reaction from the surface to a depth of 1.5 diameters.

For the pile in cohesionless soil, Broms adopted (rather conservatively):

$$p_y = 3K_p\sigma'_v \tag{10.32}$$

where K_p = Rankine passive pressure coefficient = $\tan^2(45 + \Phi'/2)$, Φ' = effective friction angle of soil, σ'_v = effective vertical stress at the point in question.

Both a free-headed (or unrestrained) pile and a fixed-headed (or restrained) pile were analyzed.

Broms derived dimensionless charts for the ultimate lateral resistance of a pile subjected to an eccentrically applied lateral load for "short-pile" and "long-pile" failure of piles in sand and in clay. These charts have been reproduced widely (e.g. Poulos & Davis

TABLE 10.10. Homogeneous soil: summary of equations[a]

Head condition	Failure mode	a	b	c
Free-head	Shortpile	0.25	$\gamma + 0.5(\gamma + 1)$	$-0.25(\gamma - 1)^2$
	Longpile	0.5	$\epsilon + \gamma$	$-\bar{M}\gamma$
Fixed-head	Shortpile	0	1	$\gamma - 1$
	Longpile	0.5	γ	$-2\bar{M}\gamma$
	Intermediate	0.25	0.5	$-0.25(\gamma - 1)^2 - \bar{M}\gamma$

[a] $\bar{M}_y = M_y/p_y dL^2$, where M_y = yield moment of pile section, p_y = ultimate lateral pile–soil pressure, d = the diameter of a pile, and L = length; $\gamma = \zeta/L$, where ζ = depth of "dead zone", i.e. no soil resistance, below surface; $\epsilon = e/L$, where e = M/H = eccentricity of applied loading above soil surface.

1980). In using the charts, the values of H_u (the ultimate lateral food) for both short-pile failure and long-pile failure are computed, and the lesser value is taken.

Poulos (1985) has developed a general solution for piles in a two-layer cohesive soil. This solution involves the solution of a quadratic equation of the form:

$$aH^{*2} + bH^* + c = 0 \qquad (10.33)$$

where $H^* = H/p_y dL$, p_y = ultimate lateral pile–soil pressure. For the special case of a single homogeneous layer, the coefficients a, b and c in Eq. (10.32) are given in Table 10.10, together with a definition of the various parameters involved.

Meyerhof (1995) has provided a summary of an alternative approach to the estimation of ultimate lateral capacity, which incorporates the effects of load eccentricity and inclination.

10.4.1.2 Pile Groups

For pile groups, the ultimate lateral load should be taken as the lesser of:

- the sum of the ultimate lateral loads of the piles in the group,
- the ultimate lateral load of an equivalent block representing the group.

In the latter case, only the "short-pile" capacity of the equivalent block should be considered. For clays, the use of Broms' solution is not appropriate for the equivalent block calculation because of the assumed "dead" zone of zero soil resistance extending from the surface to a depth of 1.5 diameters; while this may be reasonable for a normal single pile, it is unrealistic for a relatively short block. It is therefore suggested that the ultimate lateral capacity of the block be calculated from consideration of statics, using a zone of zero reaction of $1.5d$, where d is the diameter of a single pile in the group.

For the case of a free-head equivalent block of length L and diameter or width D, it may readily be shown that the ultimate lateral load, H_u, is:

$$H_u = p_y DL\{[(1 + 2e/L)^2 + 1]^{0.5} - (1 + 2e/L)\} \qquad (10.34)$$

where e = eccentricity of load above groundline, p_y = ultimate lateral pile–soil pressure.

For the fixed-head case:

$$H_u = p_y DL \qquad (10.35)$$

If the concept of a zone of zero soil resistance is adopted, the length of the equivalent block is the actual length minus $1.5d$, the eccentricity of loading is $e = 1.5d$, and the width is the projected width of the group in the direction of loading.

The provision of raking piles increases the ultimate lateral resistance of a pile group, and an estimate of the effect of raking piles can be obtained by considering static equilibrium of the group. The raking of the outer piles of the group generally has the major influence on group behavior.

10.4.2 LATERAL DEFLECTION OF SINGLE PILES

Methods of predicting the lateral deflection and rotation of a laterally loaded pile usually rely either on the theory of subgrade reaction (Broms 1964a, b) or on the theory of elasticity using some form of boundary element analysis (Poulos 1971a; Budhu & Davies 1987, 1988), or finite element analysis (Randolph 1981). It has been found that solutions from these various approaches are in relatively close agreement (Poulos 1982a).

The load–deflection and load–rotation relationships for a laterally loaded pile are highly non-linear and the application of a linear theory, whether based on a subgrade reaction approach or an elastic approach, can be expected to give only an approximate prediction of deflection and rotation. A more logical approach is to use a theory in which non-linearity of the soil is introduced into the analysis (Kubo 1985; Poulos 1973). Non-linear response can be incorporated into the elastic continuum approach, by specifying a limit to the lateral pressures that can be developed between the pile and the soil. The well-known and widely used "p–y" analysis developed by Reese, Matlock and their coworkers (see Reese *et al.* 1974) is an example of a non-linear analysis based on subgrade reaction theory and is described briefly below.

10.4.2.1 p–y Analysis

The p–y analysis is the lateral analog of the t–z analysis for load–settlement prediction and involves the idealization of the soil resistance as a series of relationships between local lateral pressure, p, and local lateral deflection, y, at various depths along the pile shaft. The pile itself is modeled as an elastic beam supported by the non-linear springs whose characteristics are represented by the p–y curves. The bending of the pile under lateral and moment loading can be carried out by a finite difference or finite element analysis, and the relationship between lateral loading and deflection can then be obtained.

The most widely used p–y curves are those derived empirically from lateral pile load tests, and typical forms have been presented by Reese *et al.* (1974) for piles in sand, and by Matlock (1970) and Sullivan *et al.* (1979) for piles in clay. Baguelin & Frank (1979) discuss the use of pressuremeter tests to derive p–y curves, while alternative approaches have been reviewed by Murchison & O'Neill (1984) for cohesionless soils, and Gazioglu & O'Neill (1984) for cohesive soils.

10.4.2.2 Linear Elastic Solutions

Where approximate deflection and rotation predictions are sufficient, linear theories may be adequate provided that appropriate secant values of the soil modulus, relevant to the level of load to be applied to the pile, are input into the theory. On the basis of elastic continuum solutions from a simplified form of boundary element analysis for a soil whose modulus increased linearly with depth, the groundline deflection and rotation of a fully embedded single free-head vertical pile, and the pile bending moments, may be expressed in the form shown in Table 10.11. The pile

TABLE 10.11. Elastic lateral response of piles[a]

Quantity	Free-head	Fixed-head
Groundline deflection, ρ	$Hf_{\rho H} + Mf_{\rho M}$	$Hf_{\rho F}$
Groundline rotation, θ	$Hf_{\theta H} + Mf_{\theta M}$	0
Max. positive moment, M_{max}	HdI_{MH}	—
Fixing moment at pile head, M_f	—	$-Hd\,I_{MF}$

[a] See Tables 10.12 and 10.13 and text for the various factors.

TABLE 10.12. Approximate solutions for elastic lateral response of long piles (adapted from Pender 1996)[a]

Factor	Case 1: constant E_s	Case 2: linearly increasing, E_s	Case 3: parabolic E_s
E_s	E_s = constant	$E_s = mz$	$E_s = E_{SD}\sqrt{z}/d$
K	E_p/E_s	E_p/md	E_p/E_{SD}
L_c/d	$0.50K^{0.36}$	$1.3K^{0.222}$	Between cases 1 and 2
$f_{\rho H}$	$1.3K^{-0.18}/E_{sd}$	$3.2K^{-0.333}/md^2$	$2.14K^{-0.29}/E_{SD}d^2$
$f_{\rho M} = f_{\theta H}$	$2.2K^{-0.45}/E_sd^2$	$5.0K^{-0.556}/md^3$	$3.43K^{-0.53}/E_{SD}d^2$
$f_{\theta M}$	$9.2K^{-0.73}/E_sd^3$	$13.6K^{-0.778}/md^4$	$12.16K^{-0.77}/E_{SD}d^3$
$f_{\rho F}$	$f_{\rho H} - (f_{\theta H}^2/f_{\theta M})$	$1.33K^{-0.333}/md^2$	$f_{\rho H} - (f_{\theta H}^2/f_{\theta M})$
I_{MH}	αK^b	$\alpha K^b(\not> 8)$	—
α	$0.12 + 0.24f + 0.1f^2$	$0.6f$	—
b	$\exp(-1.3 - 0.34f)$	$0.17f^{0.3}$	—
f	M/dH	M/dH	—
L_{Mmax}	$0.40L_c$	$0.41L_c$	—
I_{MF}	$0.24K^{0.27}$	$0.37K^{0.222}$	—

[a] See text for definition of terms.

TABLE 10.13. Solutions for elastic lateral response of piles (adapted from Poulos & Hull 1989)[a]

Factor	Case 1: constant E_s	Case 2: linearly increasing, E_s
E_s	E_s = constant	$E_s = mz$
K	E_p/E_s	E_p/md
L_c/d	$2.09K^{0.25}$	$1.81K^{0.20}$
L_e	L_c if $L \geq L_c$	L_c if $L \geq L_c$
	L if $L < L_c/3$	L if $L < L_c/3$
x	$\log_{10}(L_e/d)$	$\log_{10}(L_e/d)$
$L \geq L_c$		
$f_{\rho H}$	$(1.65 + 3.40x)/E_sL_c$	$(13.10 + 11.09x)/mL_c^2$
$f_{\rho M} = F_{\theta H}$	$(5.52 + 9.08x)/E_sL_c^2$	$(34.63 + 11.09x)/mL_c^3$
$f_{\theta M}$	$(64.98 + 37.95x)/E_sL_c^3$	$(156.1 + 37.14x)/mL_c^4$
$f_{\rho F}$	$(1.336 + 1.64x)/E_sL_c$	$(5.669 + 4.14\log_{10}x)/mL_c^2$
I_{MF}	$(L_c/d)\ (0.098 + 0.042x)$	$(L_c/d)\ (0.23 + 0.44\log_{10}x)$
$L < L_c/3$		
$f_{\rho H}$	$(0.976 + 2.196x)/E_sL$	$(3.18 + 9.70x)/mL^2$
$f_{\rho M} = f_{\theta H}$	$(0.70 + 3.23x)/E_sL^2$	$(2.41 + 12.71x)/mL^3$
$f_{\theta M}$	$(1.09 + 6.29x)/E_sL^3$	$(1.84 + 18.65x)/mL^3$
$f_{\rho F}$	$(0.54 + 0.55x)/E_sL$	$(0.77 + 1.081x)/mL^2$
I_{MF}	$(L/d)\ (0.55 - 0.014x)$	$(L/d)\ (0.76 - 0.35x)$

[a] See text for definition of terms; note: for $L_c/3 < L < L_c$, linearly interpolate between solutions for $L < L_c/3$ and $L \geq L_c$.

is of embedded length L, diameter or width d, and Young's modulus E_p, and is subjected to a horizontal load, H, and a moment, M, at the groundline. Solutions for the various flexibility and moment coefficients are shown in Tables 10.12 and 10.13. Pender (1996) has collected solutions from Budhu & Davies (1987, 1988) and Gazetas (1991), which are shown in Table 10.12. This table gives solutions for a flexible pile, i.e. a pile whose

length is greater than the critical length, L_c; and applies for three idealized distributions of the Young's modulus of soil with depth. Table 10.13 gives alternative, and somewhat more accurate, solutions, developed by Poulos and Hull (1989), for the cases of a uniform modulus and a linearly increasing modulus with depth. Solutions are given for both a "flexible" pile and a rigid pile, whose length is less than one-third of the critical length, L_c. Other approximate solutions are available for flexible piles (e.g. Randolph 1981). The solutions in Tables 10.12 and 10.13 can be evaluated readily via spreadsheet or mathematical programs such as MATHCAD.

10.4.2.3 Non-Linear Solutions

Because of the marked non-linearity of pile response to lateral loads, proper estimation of the lateral load–deflection behavior of piles requires an approach that takes account of local yielding of the soil, especially near the soil surface. A convenient non-linear approach has been described by Poulos & Davis (1980) and Budhu & Davies (1987, 1988), in which the elastic solutions for pile deflection, rotation and moment are modified by yield factors. These factors depend primarily on applied load level, relative pile flexibility and the distribution of soil stiffness.

For piles subjected to a lateral load, the groundline deflection, ρ, and rotation, θ, may be expressed as:

$$\rho = \rho_{el}/F_u \qquad (10.36)$$

$$\theta = \theta_{el}/F_\theta \qquad (10.37)$$

where ρ_{el} = deflection from elastic theory, θ = rotation from elastic theory, and F_u and F_θ = yield deflection and rotation factors. Values of F_u and F_θ are presented by Poulos & Davis (1980) for soils with both a uniform soil modulus and a linearity increasing modulus with depth. Budhu & Davies (1987, 1988) also give simplified expressions for these factors, although they appear to contain some inconsistencies.

Alternative solutions have been presented by Poulos & Hull (1989) for fixed-head piles in typical stiff clay and soft clay profiles. The pile head deflection is given by Eq. 10.36, while the pile head fixing moment, M_F, is expressed as:

$$M_F = M_{FE}/F_M \qquad (10.38)$$

where M_{FE} = pile head moment from linear elastic theory and F_M = yield moment factor. Figures 10.11 and 10.12 show the solutions for flexible piles in a stiff clay and in a soft clay. The effect of relative pile flexibility is incorporated via the critical length, L_c (see Tables 10.12 and 10.13). The application of these results is illustrated via an example in Section 10.4.6.

10.4.3 GROUP EFFECTS

A method of calculating the deflection and rotation of a pile group has been described by Poulos & Davis (1980). The method involves the superposition of lateral interaction factors, and parallels the approach for calculating the settlement and load distribution in axially loaded groups. Randolph (1981) presents very useful approximations for the various interaction factors involved. From this analysis, it is possible to derive a group deflection ratio, R_ρ, that relates the group and single pile deflections. For groups with either a pinned or fixed (non-rotating) connection to the pile cap, the lateral and axial responses can be de-coupled. The lateral deflection of the pile cap, ρ_g, can then be expressed as:

$$\rho_g = \rho_{lav} R_\rho \qquad (10.39)$$

where ρ_{lav} = horizontal deflection of a single pile at the average load level of a pile in the group, and R_ρ = group deflection ratio. As a practical approximation, R_ρ can be expressed as:

$$R_p = n^{\omega_L} \qquad (10.40)$$

where n = number of piles in group, and ω_L = exponent depending on pile and soil characteristics. For piles in a homogeneous soil layer, Fig. 10.13 plots ω_L as a function of critical length and pile spacing. Similar values of ω_L also apply for a fixed-head group in which the pile heads do not rotate.

For more accurate and general analyses of pile group response, a more general analysis is required, such as that outlined in Section 10.5.

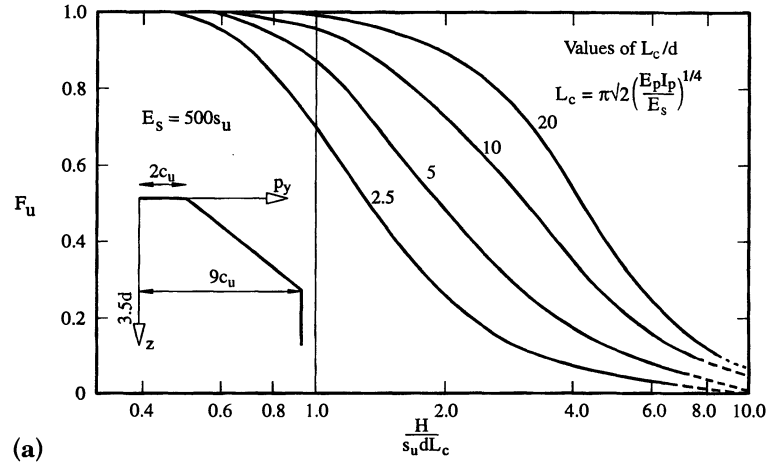
10.4.4 ASSESSMENT OF PARAMETERS

In predicting the lateral load–deflection behavior of piles using a non-linear analysis based on elastic theory, the following parameters are required:

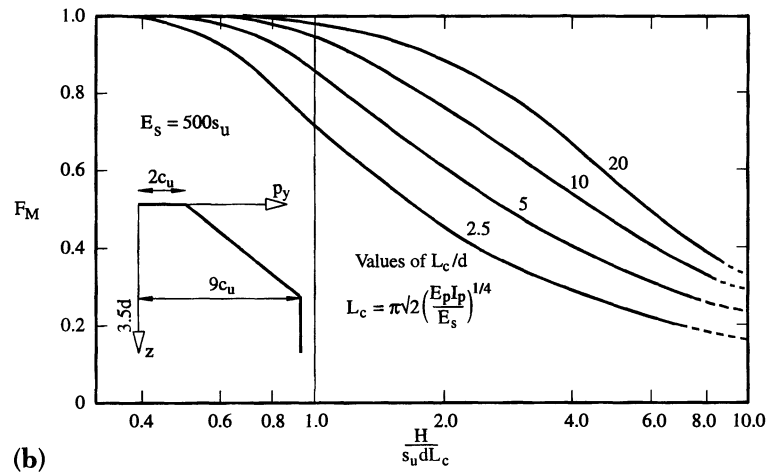
- the magnitude and distribution of Young's modulus, E_s, for static loading;
- the magnitude and distribution of pile–soil yield pressure, p_y, for static loading.

The assessment of p_y has been discussed in Section 10.4.1, and hence attention is concentrated on Young's modulus, E_s.

Some success in predicting static pile re-

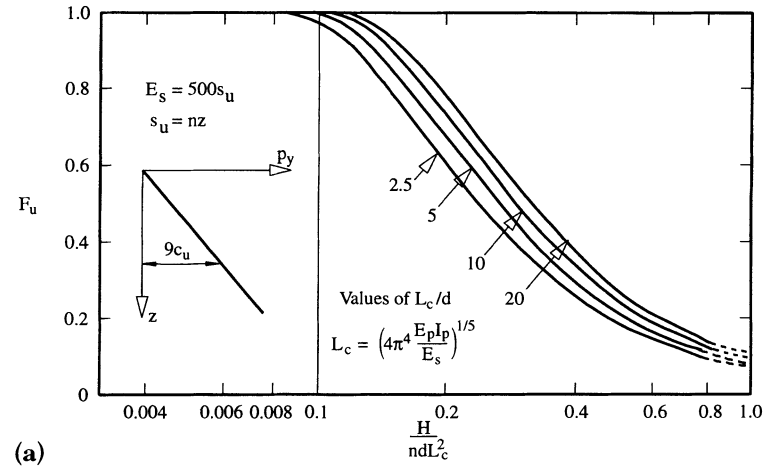


(a)



(b)

FIGURE 10.11. Non-linear correction factors for a flexible fixed-headed pile in stiff clay: (a) deflection correction factor, F_u; and (b) fixing moment correction factor, F_M.



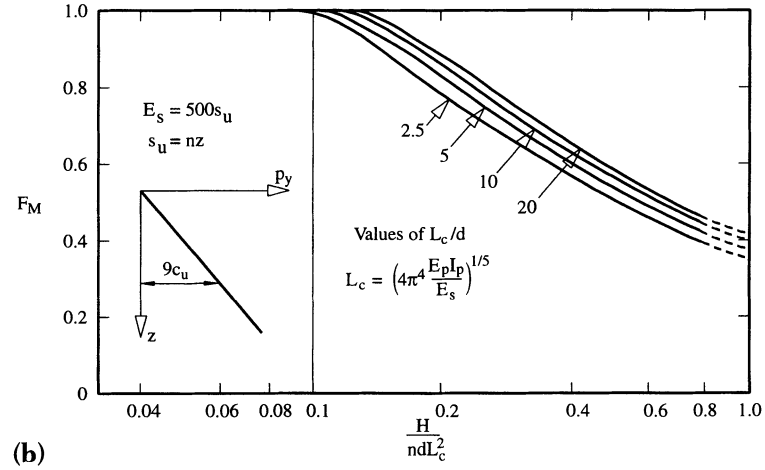


FIGURE 10.12. Non-linear correction factors for a flexible fixed-headed pile in soft clay: (a) deflection correction factor, F_u; and (b) fixing moment correction factor, F_M.

sponse has been achieved by using the results of *in situ* plate load tests carried out at various depths to determine E_s, but such tests are rarely carried out in routine investigations. The most satisfactory means of determining E_s is to carry out a lateral pile load test and to backcalculate the modulus by fitting the observations to the theory. This procedure has been described by Poulos & Davis (1980) and has the following advantages.

1. The actual soil profile is tested by a pile installed in the same manner as the prototype pile.
2. The modulus is determined in relation to the theory to be used for the prototype pile.

In the absence of *in situ* test information of lateral pile load test data, it is necessary to estimate E_s on the basis of previous experience via empirical correlations. Caution must, however, be exercised in employing such correlations, to ensure that the value of E_s is used with the theory from which it was derived, or else has been modified to allow for differences between the various theories. Tables 10.14 and 10.15 summarize some of the available corre-

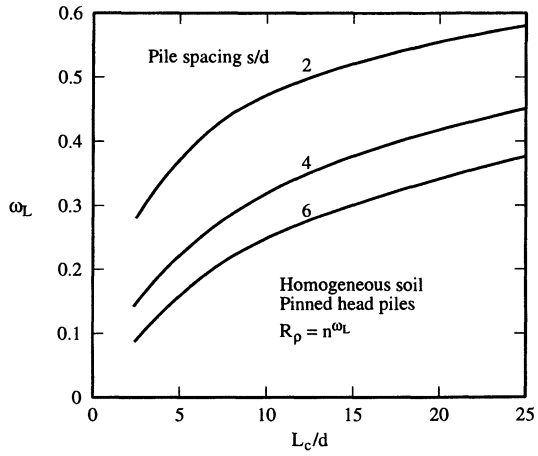


FIGURE 10.13. Group factor exponent, ω_L, for laterally loaded groups: homogeneous soils.

lations for clays and sands. These have been expressed in terms of Young's modulus, E_s, and where the original correlation has been for the modulus of subgrade reaction, k, it has been assumed that $E_s = kd$, where d = pile diameter or width. For the case of a linearly increasing modulus with depth, the rates of increase of Young's modulus and of subgrade reaction modulus have been taken to be equal.

For clays under short-term loading conditions, Poisson's ratio, ν_s, may be taken as 0.5 for saturated clays, and about 0.4 for unsaturated clays; while for long-term loading ν_s is the drained value, which typically ranges between 0.3 and 0.45, the higher values being relevant to softer clays. For sands, ν_s usually lies in the range 0.3–0.4.

10.4.5 EFFECTS OF CYCLIC LOADING

Cyclic or repeated loading on a pile generally has a deleterious effect on the lateral response of a pile. At least four phenomena may arise:

- a reduction in ultimate lateral pressure due to a reduction of soil strength,
- a reduction in soil stiffness near the pile,
- formation of a "gap" near the soil surface due to breakaway between the pile and the soil,
- accumulation of permanent displacement if the load cycles about a non-zero mean value.

A number of approaches have been developed to consider the effects of cyclic lateral loading, and these include: non-linear p–y analyses using modified p–y envelopes for cy-

TABLE 10.14. Empirical correlations for Young's modulus in clays (for laterally loaded piles)

Relationship	Theory	Reference	Remarks
E_{si}/s_u			
300–600	Non-linear subgrade reaction	Jamiolkowski & Garassino (1977)	Initial tangent modulus for driven piles in soft clays
180–450	Non-linear boundary element	Poulos (1973)	Tangent modulus from model tests on jacked piles
280–400	Non-linear subgrade reaction	Kishida and Nakai (1977)	Tangent modulus
100–180	Linear boundary element	Banerjee (1978)	Secant value
N_{hi} MPa m^{-1} s_u, kPa	Non-linear subgrade reaction	Sullivan *et al.* (1979)	Tangent values of rate of modulus increase $E_{si} = N_{hi}z$
0.8 12–25			
2.7 25–50			
8 50–100			
27 100–200			
80 200–400			

TABLE 10.15. Empirical correlations for Young's modulus in sands (for laterally loaded piles)

Relationship	Theory	Reference	Remarks
$N_{hi} = 0.19I_D^{1.16}$, MPa m^{-1} where I_D = density index (%)	Non-linear subgrade reaction	Jamiolkowski and Garassino (1977)	Tangent value for driven piles in saturated sands
Condition N_{hi}, MPa m^{-1} Loose 5.4 Medium 15.3 Dense 34.0	Non-linear subgrade reaction	Reese *et al.* (1974)	Tangent value for driven piles in submerged sands
N_h = 8–19 MPa m^{-1} (av. 10.9)	Linear boundary element	Banerjee (1978)	Secant value I_s
$E_{si} = 1.6N$ MPa where N = SPT value	Non-linear subgrade reaction	Kishida and Nakai (1977)	Tangent value

clic loading (e.g. Matlock 1970); incorporation of a degradation model into the lateral response analysis, with the degradation of lateral resistance being dependent on plastic stress reversal (e.g. Matlock *et al.* 1978; Swane and Poulos 1984); incorporation into the analysis the degradation of lateral resistance and modulus as a function of cyclic strain and number of cycles (e.g. Poulos 1982b).

Poulos (1982b) has presented a series of correction factors for cyclic loadings that may be applied to the lateral behavior computed from a static analysis. These analyses indicate that cyclic loading effects are likely to be more severe for stiff clays than for soft clays. They also suggest that failure in stiff clays can be quite abrupt for relatively small increases in cyclic load level.

Worked Example

A group of four steel tube piles is to be driven into a deposit of stiff clay. The piles are 500-mm outside diameter, with a 20-mm wall thickness, and are embedded 12 m into the clay. The piles are in a square configuration, with a center-to-center spacing of 2 m, and are to be subjected to a lateral load of 3.0 MN. It will be assumed that the piles are rigidly attached to a substantial pile cap, so that the pile heads can be considered as fixed against rotation. The clay has an average undrained shear strength, s_u, of 120 kPa.

Estimate the lateral deflection of the group, and the fixing moment at the pile heads.

Solution: From Table 10.14, a tangent Young's modulus of $300s_u$ (= 36 MPa) will be adopted. The moment of inertia of the tube pile is:

$$I_p = \pi(0.500^4 - 0.460^4)/64 = 0.000\,87 \text{ m}^4.$$

For a solid pile:

$$I_p = \pi \times 0.500^4/64 = 0.003\,07 \text{ m}^4.$$

Assuming a Young's modulus of 200 000 MPa for the steel tube, the equivalent modulus for a solid pile would be:

$$E_p = 2\,000\,000 \times 0.000\,87/0.003\,07$$
$$= 56\,680 \text{ MPa}.$$

Using the solution of Poulos & Hull (1989):

$$K = E_p/E_s = 56\,680/86 = 1574$$

and the critical length, L_c, from Table 10.13, is:

$$L_c = 2.09 \times K^{0.25} \times d = 6.58 \text{ m}.$$

Since the pile length of 12 m is greater than L_c, the pile can be considered to be flexible, with $L_e = L_c = 6.58$ m.

For a single fixed-head pile, the linear elastic value of groundline deflection is (from Table 10.11), $\rho = H.f_{\rho F}$, where H = applied load. From Table 10.13, $f_{\rho F} = (1.336 + 1.64x)/(E_sL_c)$, and $x = \log_{10}(L_e/d) = 1.119$. Thus:

$$f_{\rho F} = (1.336 + 1.64 \times 1.119)/(36 \cdot 6.58)$$
$$= 0.013\,36 \text{ m MN}^{-1}.$$

The average load per pile is $H = 3.0/4 = 0.75$ MN. Therefore the linear elastic deflection is:

$$\rho_{ee} = 0.75 \times 0.013\,36 = 0.010 \text{ m}.$$

Carrying out similar calculations for the pile head fixing moment:

$$I_{MF} = (6.58/0.5)$$
$$\times (0.098 + 0.042 \times 1.119) = 1.908.$$

The fixing moment at the pile head is therefore:

$$M_{fe} = -HdI_{MF} = -0.75 \times 0.5 \times 1.908$$
$$= -0.716 \text{ MNm}.$$

The effects of non-linearity are considered now. For the stiff clay profile, the yield factors in Fig. 10.11 will be used. $H/(s_u d L_c) = 0.75/(0.12 \cdot 0.5 \cdot 6.58) = 1.90$, and $L_c/d = 6.58/0.5 = 13.2$. Thus, $F_u = 0.82$ and $F_M = 0.81$. The single pile deflection is then $0.010/0.82 = 0.0122$ m, and the pile head fixing moment $= 0.716/0.81 = 0.884$ MNm.

Finally, consideration is given to group effects. From Eq. 10.39, the group deflection is $\rho_g = \rho_{1av} R_\rho$, and from the approximation in Eq. 10.40, $R_\rho = n^{\omega_L}$. For $s/d = 2.0/0.5 = 4$, and $L_c/d = 13.2$, $\omega_L = 0.36$, assuming that these values of ω_L also apply to fixed-head piles. The group deflection is then $\rho_g = 0.0122 \times 4^{0.36} = 0.020$ m. It should be noted that no allowance has been made for group effects on the pile head moment, but such group effects are generally modest and considerably less than the effects on deflection.

10.5 General Analysis of Pile Groups

10.5.1 METHODS OF ANALYSIS

For pile groups subjected to simultaneous axial and lateral loading, a number of methods of analysis have been developed. Most of these methods can be classified into one of the following categories:

1. Simple statical methods: these consider the group as a simple statically determinate system, and ignore the effect of the soil. They inherently assume the piles to be pinned to the pile cap, and can only provide approximate estimates of the axial and lateral forces in the piles.
2. Equivalent bent methods: these reduce the pile group to a structural frame and then use a structural analysis to estimate group movements and individual pile head forces and moments (e.g. Saul 1968; Reese *et al.* 1970). Such methods can be modified to take some account of pile–soil–pile interaction, i.e. interaction through the soil among the piles (Poulos and Davis 1980).
3. Methods based on elastic theory: elastic analyses are used to compute single pile responses to the various components of load, and then interaction factors are used to take account of pile–soil–pile interaction. Some methods in this category are discussed further in Section 10.5.2.
4. Hybrid methods: these employ load transfer, t–z, analyses to estimate axial response of single piles and p–y analyses to estimate lateral response. Interaction factors, or some alternative form of elastic analysis, are then used to allow for the effects of pile–soil–pile interaction (e.g. Focht & Koch 1973; O'Neill *et al.* 1977).
5. Finite element methods: these may take several forms, including simplified plane strain analyses (e.g. Desai 1974)), simplified axially symmetrical analyses (e.g. Hooper 1973; Naylor & Hooper 1974) or full three-dimensional analyses (e.g. Ottaviani 1975; Adachi *et al.* 1994).

Comparisons of a number of these methods have been presented by Poulos & Davis (1980), Poulos & Randolph (1983), O'Neill & Ha (1982), Pressley & Poulos (1986), and Poulos (1989).

TABLE 10.16. Summary of some computer programs for pile group analysis

Program	Analytical approach	Capabilities	Remarks
PGROUP	Elastic boundary element analysis	Linear variation of soil modulus with depth Horizontal loading in one direction Piles raked in plane of vertical and horizontal loading Pile–cap contact modeled	Rigorous analysis, but accuracy limited by level of discretization of piles, particularly when considering lateral response. Requires considerable computer resources and relatively slow and labor-intensive to run
DEFPIG	Boundary element analysis of single piles with interaction factors for pile groups	Any variation of soil modulus Yielding and slip allowed for by limiting stress Horizontal loading in one direction Piles raked in plane of vertical and horizontal loading Pile–cap contact modeled	Versatile program, with main limitation being the approximate treatment of variations in modulus with depth. Microcomputer version available, but relatively slow and non-interactive
PIGLET	Elastic closed form solutions (single piles), interaction factors for groups	Linear variation of soil modulus with depth Separate modulus for axial and lateral loading Horizontal loading in any direction, torsional loading Piles raked in any direction	Fast and simple program but limited to linear response, extensively checked against more rigorous analysis. Microcomputer-based, with fully interactive data input/editing. Can analyze groups of up to 300 piles

10.5.2 SOME ELASTIC-BASED COMPUTER METHODS

A number of computer programs have been developed for the analysis of pile groups under general loading conditions. Probably the three most widely used programs for pile group analysis are PGROUP, DEFPIG and PIGLET. The programs have been compared by Poulos & Randolph (1983) and found to give reasonably similar results. All three of these programs are based on elastic continuum analysis. A brief survey of the capabilities and limitations of the three programs has been given by Randolph (1992) and is reproduced in Table 10.16.

10.6 Pile Response to Externally Imposed Ground Movements

10.6.1 INTRODUCTION: SOURCES OF GROUND MOVEMENT

There are many circumstances in which pile foundations may be subjected to loadings arising from vertical and/or lateral movements of the surrounding ground. Figure 10.14 illustrates a number of these circumstances. In such cases, at least two important aspects of pile foundation design must be considered:

- the movements of the piles caused by the ground movements;

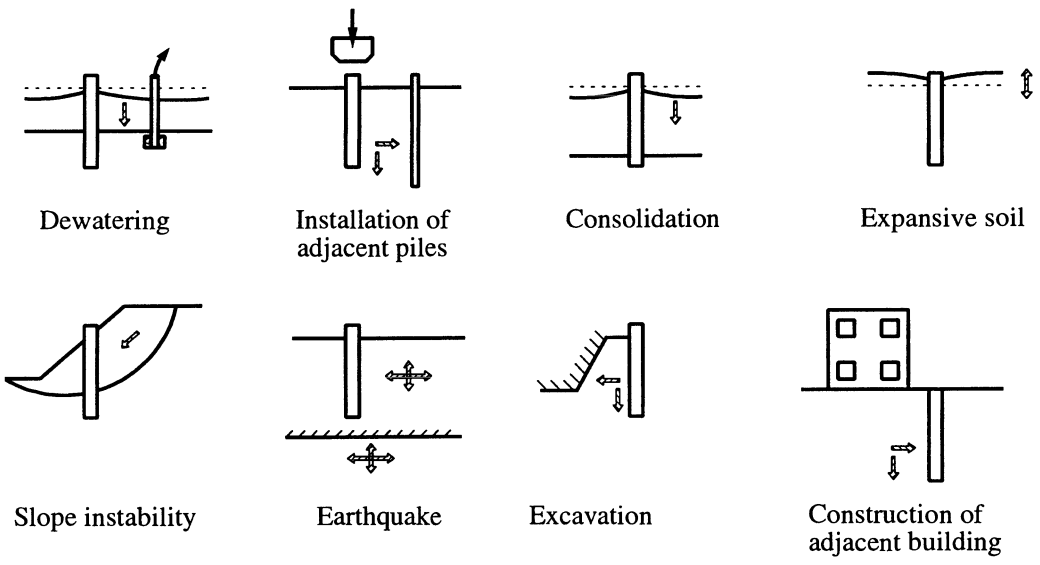


FIGURE 10.14. Some sources of soil movement.

- the additional forces and/or bending moments induced in the piles by the ground movements, and their effect on the structural integrity of the piles.

These two aspects will be considered below for some selected cases of ground movement. It should be emphasized that, in general, the geotechnical axial and lateral load capacity of a pile is unlikely to be seriously affected by ground movements.

10.6.2 NEGATIVE FRICTION

It has long been recognized that pile foundations located within a settling soil layer will be subjected to negative friction stresses caused by the downward movement of the soil relative to the pile. As a consequence, an additional "downdrag" force will be developed within the pile and the pile head will experience additional settlement.

There is a widespread misconception that negative friction leads to a reduction in ultimate axial load capacity of piles, and some methods of design attempt to compute a reduced axial load capacity in which the downdrag load caused by negative friction is subtracted from the original load capacity. The allowable axial load is then assessed on the basis of this reduced load capacity. Such a concept is not valid, since a pile can only fail geotechnically if the pile moves past the soil, whereas negative friction requires the soil to move past the pile.

Computer analyses of the effects of negative friction can be carried out by incorporating the "free field" ground movements into an analysis of pile–soil interaction (e.g. Poulos & Davis 1980). However, for simpler practical applications, approximate methods of calculation can be used (e.g. Fellenius 1989; Poulos 1997b). Figure 10.15 illustrates the approach adopted in the latter reference. A pile of length L is located in a soil profile consisting of a consolidating layer, of thickness L_1, which is underlain by a stable nonconsolidating layer, L_2. It is assumed that the settlement of the consolidating layer decreases linearly with depth, from S_0 at the surface to zero at depth L_1. The neutral plane

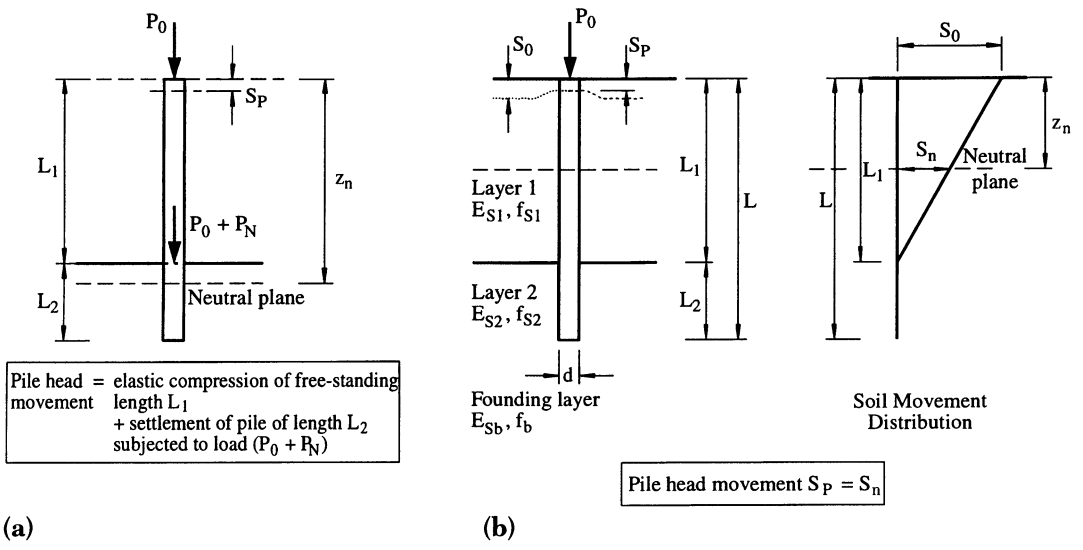


FIGURE 10.15. Simplified approaches to estimating pile head movement: (a) pile movement stabilizes with increasing soil movement ($z_n \geq L_1$), and (b) pile movement continues to increase with increasing soil movement ($z_n < L_1$).

is the location along the pile where the pile friction changes from negative to positive, and is located at a depth z_n.

To compute the maximum force in the pile and the pile head movement, the following procedure may be followed:

1. The maximum force, P_{max}, in the pile is the force at the location of the neutral plane, and is the sum of the applied load and the maximum downdrag force.
2. The pile head movement is the larger of the following two values:
   - the elastic compression of the pile above the neutral plane, plus the settlement of that portion of the pile below the neutral plane; the latter component may be estimated from pile settlement theory, assuming a pile length $(L - Z_n)$ subjected to the computed maximum axial force, P_{max};
   - the "free-field" vertical movement of the soil at the level of the neutral plane.

These two "options" are illustrated in Fig. 10.15a and b, respectively.

In summary, the hand calculation procedure is:

1. Compute the maximum possible value of $z_n(z_{nmax})$.
2. Compute the maximum axial force in the pile as follows:

$$P_{nmax} = P_0 + f_a c z' \quad (10.41)$$

where P_0 = applied load at pile head, f_a = average negative skin friction above neutral plane, c = pile shaft diameter, and where:

$$z' = L_1 \text{ if } z_{nmax} > L_1;$$

and

$$z' = z_{nmax} \text{ if } z_{nmax} < L_1.$$

3. Compute the pile head settlement, using the "options" shown in Fig. 10.15a, b, and adopt the larger value.

The above approach assumes, implicitly, that full mobilization of the negative skin friction above the neutral plane occurs. While this may be reasonable for piles in soft clays, it is not necessarily accurate for piles in stiffer clays, where the ground movements may be small. It may also not be valid for pile groups, as the effects of pile–soil–pile interaction may inhibit the development of pile–soil slip along inner piles of the inner group. In such cases, analyses considering pile–soil interaction are preferable (e.g. Chow *et al.* 1990; Kuwabara & Poulos 1989).

The detrimental effects of negative friction can be reduced by the application of suitable coatings along the pile in the settling portion of the soil profile. Bitumen is the most commonly used coating material.

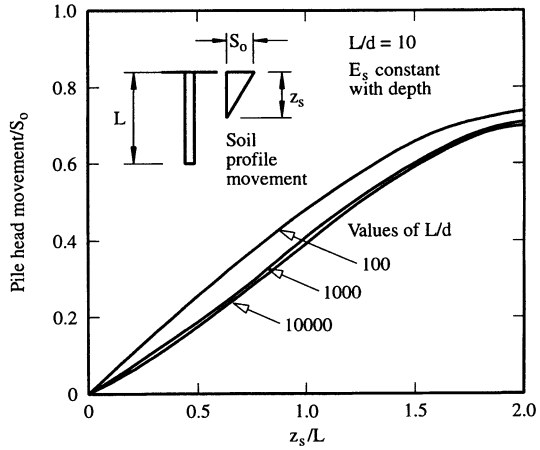


FIGURE 10.16. Elastic solutions for pile movement in expansive soil: uniform pile diameter (modified from Poulos 1989).

10.6.3 EXPANSIVE SOILS

Piles in expansive soils may be subjected to alternating heave and settlement of the ground in response to environmentally induced moisture changes in the soil. The design of piles in expansive soils again involves two main issues: the maximum axial force induced in the piles by the ground movements, and the amount of pile head movement. In principle, the same approach may be adopted for pile design as with negative friction.

However, there are at least three practical difficulties that may arise:

1. The soil may be stiff and the ground movements may not be sufficient to cause full mobilization of the ultimate shaft resistance.
2. Assessment of the ultimate shaft resistance of piles in expansive soils is generally more difficult than in soft clays, because the expansive soils are often only partly saturated.
3. Tensile forces are induced in the pile by swelling movements and these forces may cause concrete piles to crack if not properly reinforced.

As an aid to the assessment of pile head movement in relation to ground surface movement, Fig. 10.16 shows theoretical solutions developed by Poulos (1989). These have been found to give useful indications of the movement of model piles in laboratory tests (Challa & Poulos, 1991). Charts for the estimation of pile forces are given by Nelson & Miller (1992).

10.6.4 PILES SUBJECTED TO LATERAL GROUND MOVEMENTS

The response of piles subjected to lateral ground movements may be analyzed by an extension of the techniques employed to analyze the behavior of piles subjected to lateral loads (e.g. Poulos & Davis 1980; Maugeri & Motta 1991). A key aspect of such analyses is the estimation of the "free-field" ground movements, since these movements play a major role in determining the pile behavior.

If the distribution with depth of free-field movements can be simplified, it is possible to develop useful design charts to enable approximate assessment of the pile head de-

flection and the maximum bending moment in the pile. Chen & Poulos (1997) have presented two series of such charts, one for a pile in a soil subjected to a uniform movement with depth (to a depth z_s below the surface); and the other for a soil in which the horizontal movement decreases linearly with depth, from a maximum at the surface to zero at a depth z_s. The first movement profile may be relevant to piles in unstable soil slopes, while the linear profile may be relevant for piles adjacent to embankment construction.

For the linear soil movement profile, Figs 10.17 and 10.18 present charts for pile head movement and maximum moment, for a homogeneous (uniform) soil, and a "Gibson" soil whose modulus increases linearly with depth. The pile head is unrestrained.

As discussed by Chen & Poulos (1997), these solutions assume that the soil remains elastic, and they therefore generally give an upper bound estimate of the pile moment and deflection. The extent of the possible overestimation increases with increasing lateral soil movements, due to the progressive departure from elastic conditions that results from the development of plastic flow of the soil past the pile.

As an example of the application of both a theoretical computer analysis and the design charts, the case reported by Kalteziotis *et al.* (1993) is considered. Two rows of piles were used to stabilize a sliding slope on which a semi-bridge structure had been built. The soil conditions consisted mainly of lacustrine deposits, with a thickness of more than 100 m, overlying bedrock of Triassic marl. Among the piles were three steel pipe piles instrumented with strain gages, aiming to study the lateral reaction mechanism in a landslide;

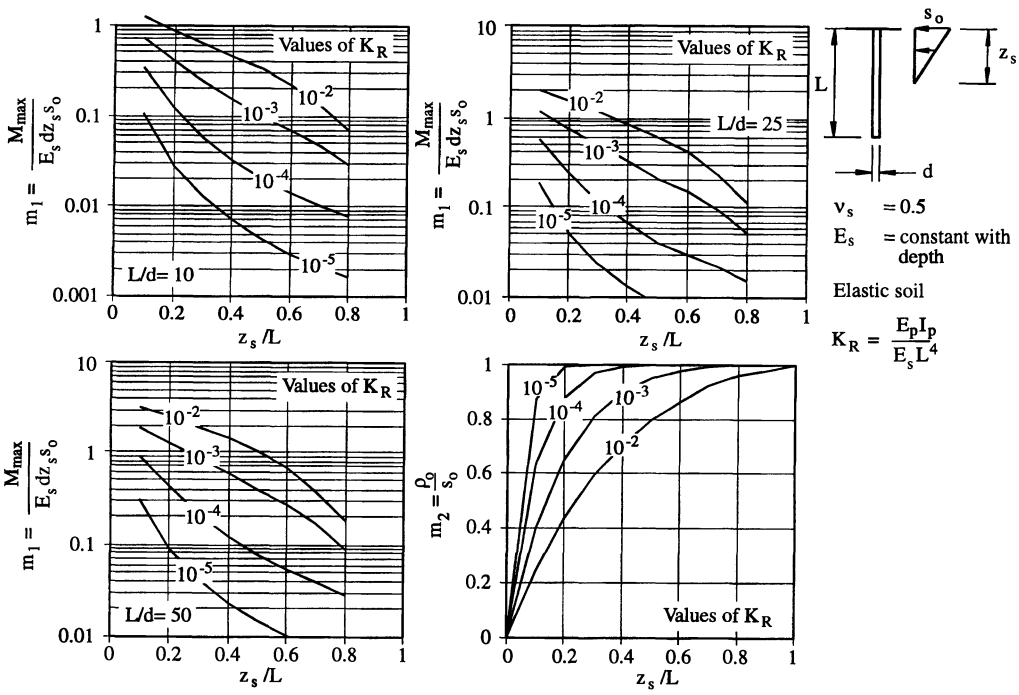


FIGURE 10.17. Elastic solutions for unrestrained free-head pile in uniform soil (linear soil movement profile) (reproduced from Chen & Poulos © 1997 with permission of ASCE).

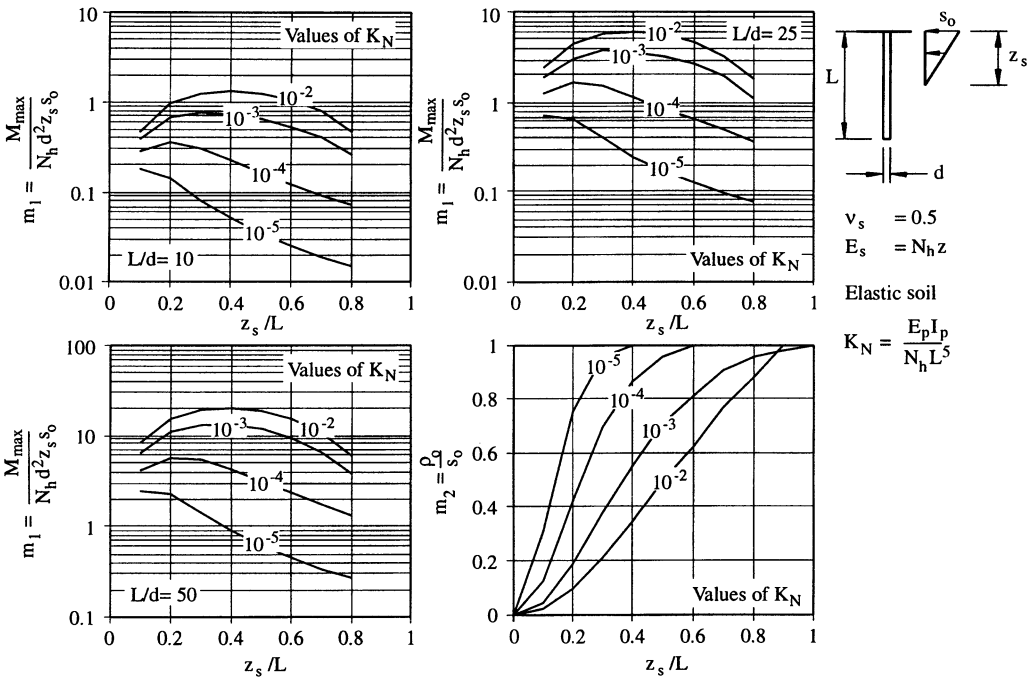


FIGURE 10.18. Elastic solutions for unrestrained free-head pile in "Gibson" soil (linear soil movement profile) (reproduced from Chen & Poulos © 1997 with permission of ASCE).

results were presented only for one of these. All the piles had a length of 12 m and the steel piles had an external diameter of 1.03 m, a wall thickness of 18 mm and a flexural stiffness, E_pI_p, of 1540 MN m^{-2}. The center-to-center spacing of the piles was 2.5 m.

In the theoretical analysis reported by Chen & Poulos (1997), a triangular soil profile, with a maximum movement of 3.5 mm at the soil surface and zero at a depth of 6 m below the surface, was adopted on the basis of the reported inclinometer data. Based on the results of the pressuremeter tests reported by the authors, the limiting soil pressure was taken to be 0.9 and 3.2 MPa for the moving soil layer and the stable soil layer, respectively; while the corresponding soil Young's modulus values were taken to be 15 and 70 MPa.

The predicted results agreed reasonably well with those measured, with reasonable agreement being observed between the predicted and the measured distributions of bending moment and deflection. The maximum bending moment was developed at about 6.2 m below the soil surface, which is very close to the assumed sliding surface. The design charts may also be used to estimate the maximum moment and deflection. In this case, L/d = 12/1.03 = 12, z_s/L = 6/12 = 0.5, K_R = 1540/(43 · 12^4) = 1.7 × 10^{-3} (the average E_s was taken as 43 MPa), and from Fig. 10.17 m_1 = 0.17, so that M_{max} = 0.17 · 43 · 1.03 · 6 · 0.0035 = 0.16 MN m, which compares with the measured value of 0.15 MN m. Also, m_2 = 0.92, and so ρ_0 = 0.92 · 3.5 = 3.2 mm, which is in good agreement with the measured 2.7 mm.

10.6.5 SPECIFIC APPLICATIONS

There are a number of important specific applications of the analysis of piles subjected to

lateral soil movements. Three of these are listed below.

10.6.5.1 Piles in Unstable Slopes

There are two important aspects of piles in unstable slopes: first, the effect on the piles of the ground movements, i.e. the induced bending moments and deflections; and second, the effect, on the slope, of the shear resistance provided by the piles, i.e. the reinforcing effect of the piles.

Lee *et al.* (1991) discuss how the effect of the slope on the piles can be assessed and describe the various possible modes of behavior. In addition, the design charts presented by Chen & Poulos (1997) provide a simple approach for preliminary assessment. Viggiani (1981) and Poulos (1994b) discuss means by which an assessment can be made of the stabilizing effect of the piles on the slope.

10.6.5.2 Piles Near An Excavation

The ground movements caused by excavation may induce substantial bending moments in nearby piles, as well as axial downdrag forces. Failure of existing piles may result (e.g. Poulos 1997a). Simplified design charts to enable approximate estimate of pile deflection and bending moment have been presented by Poulos & Chen (1996) for unsupported excavations, and Poulos & Chen (1997) for supported excavations. In the latter reference, factors are presented to take account of distance from the excavation, the excavation depth, the pile stiffness, the soil strength, and the stiffness and spacing of the struts supporting the excavation.

10.6.5.3 Piles In and Near Embankments

The construction of road embankments and fills causes lateral and vertical soil movement, which can have an adverse effect on the adjacent piles supporting structures, bridges or utilities. A number of instrumented case studies have been reported (e.g. Heyman 1965; Leussink & Wenz 1969), and centrifuge studies have also been undertaken in recent years (e.g. Stewart *et al.* 1994).

A number of methods of design have been employed, several of which are based on assumed pressure distributions and which are unreliable, as discussed by Poulos (1996). Stewart *et al.* (1994) have developed a useful empirical approach, based on the results of centrifuge tests, while some design charts have been developed by Poulos (1994b), based on theoretical boundary element analyses. More recently, Goh *et al.* (1997) have undertaken analyses via an approach similar in principle to that described by Poulos (1994b). They have derived the following useful approximations for the maximum bending moment, M_{max}, induced in a pile by embankment loading:

$$M_{max} = \lambda \exp[\beta(q/s_u)] \cdot s_u d h_s^2 \qquad (10.42)$$

$$\lambda = 1.88(K_R)^{0.5} \qquad (10.43)$$

$$\beta = 0.18(K_R)^{-0.1} \qquad (10.44)$$

$$K_R = E_p I_p / E_s h_s^4 \qquad (10.45)$$

where s_u = undrained shear strength of clay, d = pile diameter, h_s = depth of clay layer, q = the applied embankment loading. Comparisons between the bending moments computed from the above equations and the design charts produced by Poulos (1994b) suggest that these equations tend to give conservative estimates of the bending moments for relatively flexible piles.

10.7 Pile Load Testing

10.7.1 INTRODUCTION

Pile testing is usually carried out for one of the following reasons:

- to serve as a proof test to ensure that failure does not occur before a selected proof

load (greater than the working load) is reached;
- to assess the ultimate load capacity as a check on the value calculated from a static or dynamic calculation, or to obtain back-calculated soil data enabling other piles to be designed;
- to obtain the load–settlement behavior of a pile (especially in the region of the anticipated working load), which can be used to predict the settlement of pile groups or other types of piles; or
- to indicate the structural soundness of a pile.

It should be emphasized that in many cases, the results of a test on a single pile cannot be extrapolated directly to predict the behavior of pile groups or other piles. The area of influence of a single pile is much less than that of a large group, so that the influence of deep-seated compressible layers may not be apparent in a pile load test although such layers may critically affect the behavior of a pile group. Pile load tests should therefore be accompanied by detailed site investigation to accurately define the entire soil profile (see Chapter 4).

In this section, a number of pile test procedures are described briefly, including static load tests, dynamic testing, Statnamic testing and integrity testing.

10.7.2 STATIC LOAD TESTING

Static load testing is generally regarded as providing the definitive or "benchmark" test results for piles. It involves the application of a series of static loads to a pile, these loads being left on either for a specific period of time or until a specified rate of pile movement is achieved. Tests can be performed for compression, tension and lateral loadings. The load is most commonly applied via a jack acting against a reaction beam that is restrained by an anchorage system (usually comprising either reaction piles or cable anchors), or by jacking against a mass (kentledge). The load on the pile is usually measured via a load cell, while pile movements are usually measured by displacement transducers or dial gages acting off simply supported reference beams. Most static loading tests are limited to about 5000–10 000 kN, and although tests to much higher loads have been performed, these are not common because of the substantial costs involved.

Errors in the interpretation of the test results can arise because of interaction effects between the pile and the anchoring system, or between the measuring system and the kentledge. A number of these error sources are discussed by Poulos & Davis (1980), who demonstrated that the use of cable anchors generally results in less interaction effects than if reaction piles are used.

One alternative approach to static load testing of bored piles involves the use of an Osterberg cell (Osterberg 1989), which is cast in or near the pile base and pressure is applied to the cell. The base is thus jacked downward, while the shaft provides reaction and is jacked upward. The test can continue until the element with the smaller capacity reaches its ultimate resistance. Using the Osterberg cell, load tests of up to 150 MN have been carried out. However, it must be borne in mind that, like all load tests, this approach has limitations. It is confined to bored piles in which the cell is installed. Also, great care must be taken in interpreting the results, as interaction between the base and the shaft will cause the measured deflection of each to be less than the real deflection would be. Thus, the apparent base and shaft stiffnesses from the measured load–displacement curves will be too large unless appropriate allowance is made for base–shaft interaction.

10.7.3 DYNAMIC PILE TESTING

Dynamic pile testing involves impact applied to the pile head and the measurement of strain and acceleration developed at the pile head as a function of time.

The equipment used for carrying out dynamic pile loading tests comprises:

- two sets of strain gages and accelerometers (bolted at diametrically opposite faces of the pile); and
- a portable field computer to condition and collect the data, and to store the signals.

The impact for the test is usually provided by a piling hammer. This causes a stress wave to be propagated down the pile, to reflect off the toe. The downward traveling wave may be partially or completely reflected by irregularities or discontinuities in the pile shaft, and by interaction with the surrounding soil to produce "upward traveling waves". The field computer receives the measured signals of strains and accelerations, and these are integrated to produce force and velocity results. A number of relationships are used to model the passage of upward and downward traveling waves and it is from these relationships that a prediction of pile performance is made. The predictions are made initially by pile driving analysis/analyser (PDA) methods and should be confirmed by signal matching methods (Rausche *et al.* 1985).

Signal matching provides the most reliable means of predicting the performance of a pile tested by dynamic methods. The pile and the soil data are modeled according to the best estimates made by the operator performing the analysis, and a calculation is made using wave equation methods. The calculated signals are displayed on the computer screen along with the measured signals. The operator then performs a number of iterations, varying the input data until a satisfactory match between the measured and calculated signals is obtained. Once a satisfactory match is obtained, a plausible model of the pile–soil system is deemed to be established, and from this, the mobilized static loading can be predicted. A further advantage of signal matching methods is that the distribution of the resistance of the pile down the pile shaft and the pile toe is predicted. The signal matching process permits a prediction of the static load–movement to be made. In addition, defects in the pile can be identified via premature separation of the force and velocity traces.

Studies of the accuracy of dynamic testing suggest that it can usually predict the static test result within an accuracy of ±25%, and frequently better. The accuracy increases for tests performed on driven piles in comparison to cast-*in-situ* piles, but good results have also been reported for large diameter bored piles. For driven piles, especially in fine-grained soils, the most reliable results are achieved when the piles are restruck some time after initial driving. Such a procedure permits dissipation of the excess pore pressures developed during driving and more closely reflects the conditions that prevail for static loading tests.

10.7.4 STATNAMIC TESTING

Statnamic testing is a relatively recent innovation, having been developed jointly in Canada and the Netherlands in the early 1990s (Bermingham & Janes 1989; Middendorp *et al.* 1992). The principle of the test is illustrated in Fig. 10.19. The downward force on the pile is obtained by burning fast-expanding solid fuel in a combustion chamber, resulting in a large pressure acting upward on a reaction mass. The mass is accelerated to 20 g, in turn producing an equal and opposite force acting downward on the pile. The load is applied in a linearly increasing manner, followed by a gradual unloading, which is achieved by controlled venting of the pressure. The reaction mass, usually rings of concrete or steel, provide the resistance, and needs to be only 5% of the total load to be applied to the pile. During the test, a state-of-the-art load cell and laser sensor, built into the Statnamic device, act in concert with a high speed lap-top computer to measure load and pile movement directly, taking up to 4000 readings per second. Comparative tests on piles subjected to Statnamic testing and conventional static loading tests have provided very good agreement in load–settle-

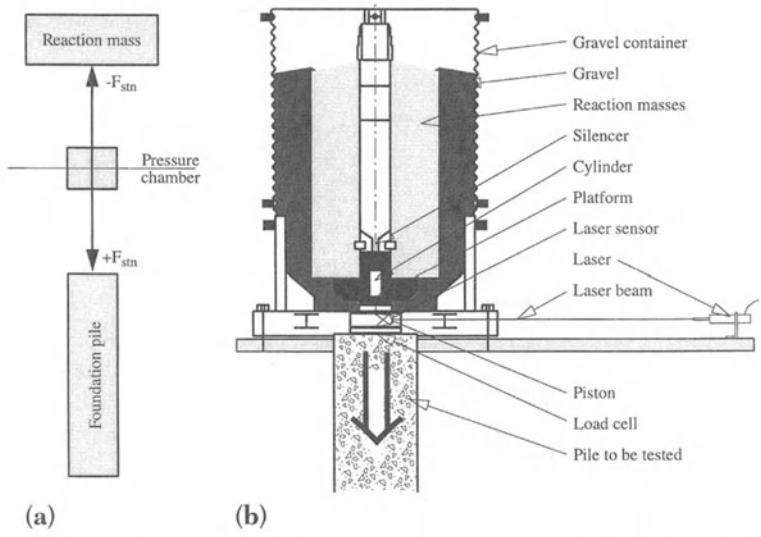


FIGURE 10.19. Statnamic test: (a) principle of test, and (b) test set-up.

ment performance. Statnamic devices are available for routine testing of piles to loads in excess of 30 000 KN.

Statnamic testing appears to offer a number of advantages over other types of testing, including:

- the test is quick and easily mobilized;
- pile performance is measured cost-effectively;
- high loading capacity is available;
- the system is flexible and adaptable, e.g. single piles or pile groups can be tested for compression loading and also lateral loading characteristics; and
- the test is quasi-static, and does not produce harmful compression and tension stresses, which have the potential of damaging a pile.

10.7.5 INTERPRETATION OF LOAD TEST RESULTS

10.7.5.1 Ultimate Load

The interpretation of the ultimate load capacity from pile load tests is open to considerable debate. Several procedures have been developed and are passionately defended by their proponents. However, the simplest and most consistent approach appears to be to define the ultimate axial load capacity as that load that causes a pile head settlement of 10% of the pile diameter.

10.7.5.2 Load Distribution

To obtain some indication of the load distribution between shaft and base from uninstrumented piles, testing procedures have been proposed by van Weele (1957) and Woodward *et al.* (1972). However, a simpler procedure has been suggested by Poulos (1987), in which the linear post-slip portion of the load–settlement curve is extended back to zero settlement. Such a procedure is, at best, approximate.

The provision of instrumentation along a pile enables the distribution of displacement, strain or load to be deduced at various depths. Such instrumentation may consist of "tell-tale" strain rods, strain gages, or load cells, and is most easily installed in bored piles prior to their installation; however, it is possible to mount suitable strain gages on driven piles prior to driving. From the re-

sulting measurements, it is possible to estimate the distribution of shaft resistance versus depth, and hence the contributions of the shaft and base to the pile resistance. They may also enable a check on structural integrity of the pile to be made. For driven piles, measurements of the strain distribution in piles after installation have revealed the existence of very significant residual stresses. If these are not allowed for, the measurement of additional stresses due to the applied loading will not reflect the true shaft and base resistances (e.g. Holloway *et al.* 1975).

10.7.5.3 Soil Stiffness

The load–settlement relationship may be used to estimate the distribution of soil Young's modulus, E_s, along the pile. It is first necessary to assume a reasonable distribution of modulus along the pile, e.g. based on *in situ* SPT or CPT data. Often, a simple linear distribution of modulus with depth may be adequate. From the theoretical solutions for settlement, the relationship between pile head flexibility (settlement per unit load) may be plotted as a function of a reference modulus value. The required reference value will be that which gives the value measured in the load test at the working (or serviceability) load.

If details are available of the strain distribution along the pile shaft, then it is possible to obtain a better estimate of both the distribution and magnitude of the soil modulus by matching the observed and theoretical strain distributions. A computer analysis will generally be required for this procedure.

10.7.6 INTEGRITY TESTING

Integrity testing is a low-strain non-destructive form of testing in which the main objective is to detect the presence of any defects in a pile, e.g. cracks, waists, voids or soil inclusions. A comprehensive review of integrity tests is given by Turner (1997). Such tests fall into two classes:

1. Those that require pre-construction planning and that require the insertion of equipment into the pile during construction, to enable a test to be carried out on completion.
2. Tests that may be applied to an existing pile, and that therefore do not require pre-planning.

One of the most effective methods in the first category is the cross-hole sonic logging method (Levy 1970; Stain & Williams 1991). The test involves the lowering of two piezo-electric probes, one a sonic emitter and the other a receiver, down two parallel access tubes embedded within the pile. Figure 10.20 illustrates a typical test set-up. The method is restricted to bored piles, and tests the continuity of the concrete between the tubes by measuring its effect on the propagation of the sonic wave between the emitter

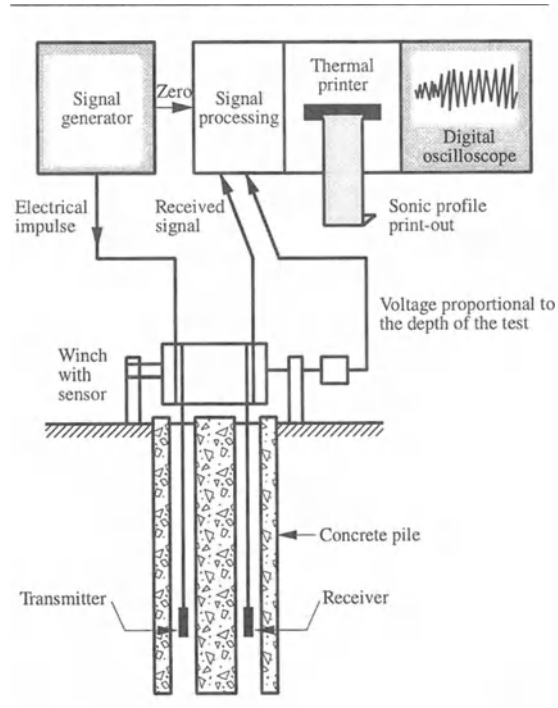


FIGURE 10.20. Elements of a cross-hole sonic logging system (modified from Stain & Williams 1991).

and the receiver. Sound concrete shows good transmission characteristics; but the presence of soil, voids or other foreign material can affect the transmission signal. In general, two pairs of tubes are installed within the pile.

The most common form of test that does not necessarily require pre-planning is the sonic integrity test. The test involves the application of a blow to the pile head (usually with a plastic mallet) and the measurement of the time of arrival of reflected waves, via a transducer at the surface. If the pile is sound, the reflected wave will return at a time which is dependent on the wave velocity of the pile material and the length of the pile. If the pile contains defects, premature reflections of the stress waves will occur. Typical records of sound and unsound piles are shown in Fig. 10.21 (Tchepak 1997). Interpretation of the wave traces (or "reflectograms") requires both experience and caution, as reflections can occur not only because of defects, but also because of changes in soil stratigraphy and changes in pile geometry.

Sonic integrity testing has a number of attractive features: the tests can be performed quickly and economically, an immediate indication of pile integrity can be obtained, and no special treatment (other than a sound pile head surface for the hammer blow) is required prior to the test. Analytical studies to evaluate the capabilities of sonic integrity tests in detecting details of defects have been reported by Liao & Roesset (1997). However, it must also be borne in mind that the test has several limitations, in that it cannot detect gradual changes in cross-section, curved forms, small defects or inclusions, and local loss of concrete cover. In addition, it is generally limited to piles having a length of no more than about 20–25 m.

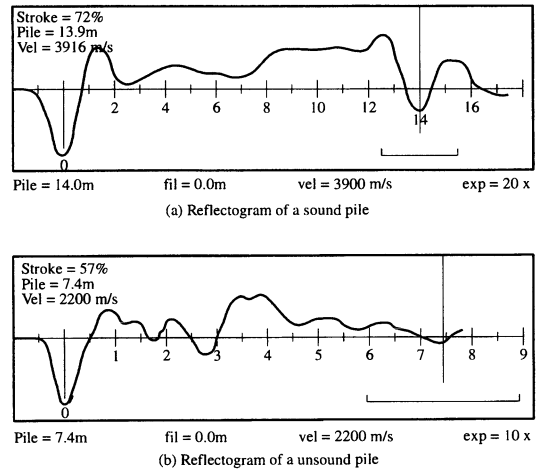


FIGURE 10.21. Typical results of sonic integrity tests on bored piles (modified from Tchepak 1997). Refractogram of (a) a sound pile, and (b) an unsound pile.

11. FOUNDATIONS ON ROCK

K. Y. Lo
A. M. Hefny

11.1 Introduction

This chapter covers two main topics. The first deals with the design principles for foundations on rock specially those for tall buildings (Section 11.2): both shallow footings and piles socketed in rocks are addressed. The second topic deals with the safety assessment of concrete dams on rock foundations (Section 11.3).

11.2 Foundations for Tall Buildings

11.2.1 DESIGN CONSIDERATIONS

11.2.1.1 Bearing Capacity

The loads associated with tall buildings are large and may result in high contact pressures being applied to the rock mass. Although settlement criteria often control the design of foundations supported by rock, the bearing capacity of the rock mass must be calculated to assess the stability.

The appropriate method for assessing the bearing capacity of foundation at a site depends entirely on the geological condition. For sound intact rock mass, the strength of the rock is so high that bearing capacity is rarely an issue. It should be noted that for strong sound rock, the stresses in the structural section of the foundation may control the design. There are several potential modes of failure (Jurgenson 1934; Sowers 1979) for a layered and jointed rock mass, as shown in Table 11.1. Equations for calculating the ultimate bearing capacity for each mode are also provided in Table 11.1 in conjunction with Table 11.2.

11.2.1.2 Allowable Bearing Pressure

The allowable bearing pressure may be defined as the maximum bearing stress to be applied to the rock mass to provide an adequate factor of safety against bearing capacity failure and to ensure that settlement is within tolerable limits. The allowable bearing pressure for foundations supported on rocks can be obtained from: 1. codes, 2. semi-empirical methods, 3. bearing capacity theories, and 4. *in situ* tests.

1. Codes. For preliminary design purposes, it is sometimes useful to estimate the allowable bearing pressure, which will depend on the type and condition of rock, based on presumed values given in city and national building codes. While the city codes are derived from local experience and geology, the national codes are often more general. These presumed values are usually conservative; however, the engineer should ensure that they are applicable to the particular conditions relevant to the site under consideration.

Table 11.3 shows presumed allowable bearing pressure for different rock types and conditions as given by the CGS (1992).

R. K. Rowe (ed.), *Geotechnical and Geoenvironmental Engineering Handbook*
© Kluwer Academic Publishers 2001

TABLE 11.1. Bearing capacity failure modes in layered and jointed rock mass

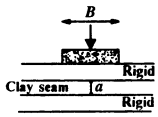
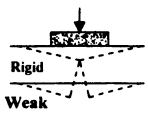
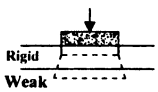
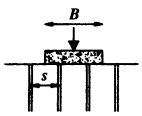
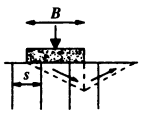
Bearing capacity failure mode			
Illustration	Description	Mode	Ultimate bearing capacity (q_{ult})
	Clay seam sandwiched between two rigid layers	Squeezing out of weak clay seam	Use the Jurgenson solution (1934) $q_{ult} = \frac{s_u B}{2a}$ where s_u = the undrained shear strength for the clay, B = the foundation width, and a = the thickness of the clay seam
	Thick rigid layer overlying weak compressible layer	Flexure failure	Minimum $q_{ult} \approx$ twice the tensile strength of the upper rock layer
	Thin rigid layer overlying weak compressible layer	Punching failure	Mininum $q_{ult} \approx$ tensile strength of the upper rock layer
	Open joints with $s < B$	Uniaxial compression of the "rock columns"	q_{ult} = uniaxial compressive strength of the upper rock layer
	Closed joints with $s < B$	General wedge shear failure	Use the Bell solution (e.g. Kulhawy & Goodman 1987) $q_{ult} = cN_c + \frac{B\gamma}{2} N_\gamma + \gamma D_f N_q$ where B = base width; D_f = foundation depth below rock surface; γ = unit weight of rock; $N_c = 2N_\phi^{1/2}(N_\theta + 1)$; $N_\gamma = N_\phi^{1/2}(N_\phi^2 + 1)$; $N_q = N_\phi^2$; $N_\phi = \tan^2[45° + (\phi/2)]$; c and ϕ = shear strength parameters of rock mass at operative stress level. For circular, square or rectangular footing use correction factors for N_c and N_γ given in Table 11.2

TABLE 11.2. Correction factors for N_c and N_γ (modified from Sowers 1979)

Foundation shape[a]	Correction factor for N_c	Correction factor for N_γ
Circular	1.20	0.70
Square	1.25	0.85
Rectangular		
$L/B = 2$	1.12	0.90
$L/B = 5$	1.05	0.95

[a] L = foundation length; B = foundation width.

TABLE 11.3. Presumed allowable bearing pressure (modified from the Canadian Foundation Engineering Manual–CGS 1992)[a]

Types and conditions of rocks	Strength of rock material	Presumed allowable bearing pressure (MPa)
Massive igneous and metamorphic rocks (granite, diorite, basalt, gneiss) in sound condition[b]	High–very high	10
Foliated metamorphic rocks (slate, schist) in sound condition[b,c]	Medium–high	3
Sedimentary rocks	Medium–high	1–4
Cemented shale, siltstone, sandstone, limestone without cavities, thoroughly cemented conglomerates, all in sound condition[b,c]		
Compaction shale and other argillaceous rocks in sound condition[b,d]	Low–medium	0.5–1
Broken rocks of any kind with moderately close spacing of discontinuities (0.3 m or greater), except argillaceous rocks (shale)		1
Limestone, sandstone, shale with closely spaced bedding		[e]
Heavily shattered or weathered rocks		[e]

[a] The tabulated values of the allowable bearing pressure are estimates and may need to be adjusted upwards or downwards in a specific case. No consideration has been made for the depth of embedment of the foundation.
[b] Sound rock conditions allow minor cracks at spacing not closer than 1 m.
[c] The above values for sedimentary or foliated rocks apply where the strata or the foliation are level or nearly so, and, then, only if the area has ample lateral support. Tilted strata and their relation to nearby slopes or excavations should be assessed by a person knowledgeable in this field of work.
[d] These rocks are apt to swell on release of stress; and on exposure to water they are apt to soften and swell.
[e] To be assessed by examination *in situ*, including test loading if necessary.

2. Semi-empirical methods.

1. RQD. Figure 11.1 shows a correlation between the allowable bearing pressure and rock quality designation (RQD) as suggested by Peck *et al.* (1974) (see Section 6.2.2.2 for definition of RQD). This correlation is intended only for unweathered jointed rock where the joints are generally tight. If the value of allowable pressure exceeds the uniaxial compressive strength of intact rock, the allowable pressure is taken as the uniaxial compressive strength. This correlation should be considered only as a first crude step in design (Peck 1976).
2. Strength of rock cores. A method for the assessment of the allowable bearing pressure is proposed by the *Canadian Foundation Engineering Manual* (CGS 1992). The allowable bearing pressure, q_{ba}, is given by:

$$q_{ba} = \sigma_c K_{sp} \qquad (11.1)$$

where σ_c = the average uniaxial compressive strength determined from rock cores, K_{sp} = an empirical factor given by Fig. 11.2. The coefficient K_{sp} takes into account the width of foundation, the spacing and aperture of discontinuities in the rock mass, and contains a nominal factor of safety of three against lower bound bearing capacity of foundation (Ladanyi *et al.* 1974).

3. Bearing capacity theories. The ultimate bearing capacity of the rock mass is determined by the potential mode of failure, which in turn is dependent on the geological fea-

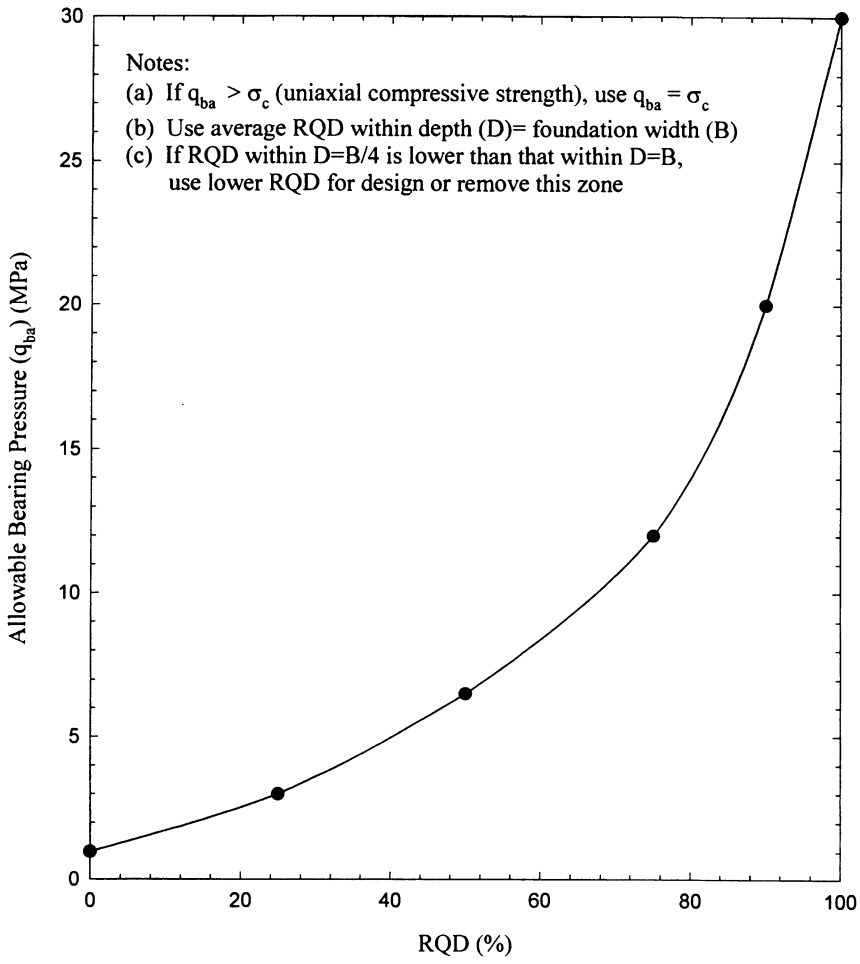
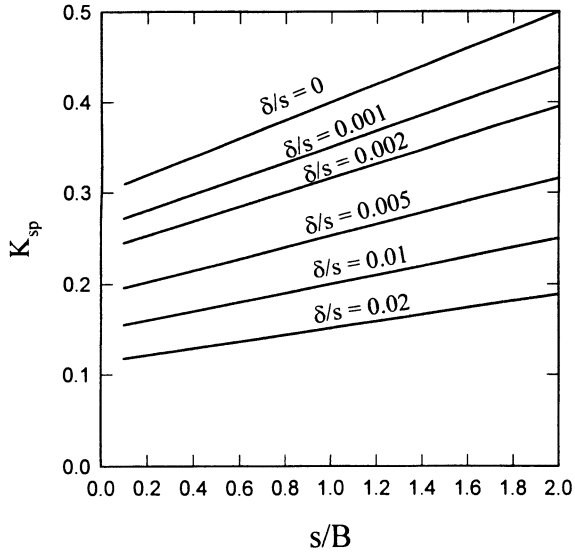


FIGURE 11.1. Allowable contact pressure, q_{ba}, for unweathered jointed rock (modified from Peck *et al.* 1974).

tures of the rock mass. Approximate bearing capacity equations may be developed by employing plastic solutions for a particular geological condition. Some of these modes of failure have been discussed by Jurgenson (1934) and Sowers (1979). The mechanics of failure corresponding to these cases of rock layering and these cases of jointing are summarized in Table 11.1. The strength that governs the failure mode and approximate expressions for bearing capacities are also included in the table.

The allowable bearing pressure, q_{ba}, may be calculated from the ultimate bearing capacity (as obtained from Table 11.1) divided by a factor of safety. For most structural foundations, the minimum acceptable factor of safety is three, with a structural load comprised of the full dead load plus the full live load (ASCE 1995).

Using the "characteristics method" (Sokolovskii 1960, 1965), Serrano & Olalla (1994, 1996) presented a method for calculat-



$$K_{sp} = \frac{3 + s/B}{10\sqrt{1 + 300\,\delta/s}}$$

where:

s = spacing of discontinuities
δ = aperture of discontinuities
B = footing width

VALID FOR:

$0.05 < s/B < 2.0$
$0 < \delta/s < 0.02$
$s > 300$ mm
$\delta < 5$ mm
(or $\delta < 25$ mm if filled with debris)

FIGURE 11.2. Bearing pressure coefficient, K_{sp} (modified from CGS 1992).

ing the ultimate bearing capacity of rock mass based on the Hoek–Brown empirical failure criterion. They proposed the range of safety factors to be used with their method to calculate the allowable bearing pressure considering the variability of the rock parameters. For details, refer to the references.

4. *In situ* tests. Field tests such as plate load tests may be used to evaluate the ultimate capacity and the load–deformation characteristics of the rock mass from which the allowable pressure can be calculated. Refer to Section 11.2.2 for more details.

11.2.1.3 Differential Settlement

Differential settlement between columns is usually the controlling design factor for foundations of tall buildings constructed on or in rocks. Differential settlement between columns exerts additional stresses in the structural members of the building and may lead to distress. Usually the structural members are designed to withstand certain allowable differential settlement between columns. An analysis should be performed to make sure that the resulting differential settlements in the rock mass under the applied pressures never exceed the allowable values. Otherwise, change in foundation design or special rock treatment should be considered. To calculate the deformations in rocks, the rock mass modulus should be obtained at representative locations of the site. Several field test methods are available for evaluating the rock mass modulus, as discussed in Section 11.2.2. For methods of calculating settlement for foundations on rock, refer to Wyllie (1992) and Kulhawy & Carter (1992a).

11.2.1.4 Effect of Excavations in Rock on Adjacent Structures

For construction of tall buildings, excavations into rock for foundations and substructures are often carried out. As a result of the relief of the *in situ* stresses, significant horizontal displacements occur during excavation, in cases of high initial horizontal stresses in rock

such as in southern Ontario (Lo 1986). Significant time-dependent deformation may also follow in rock formations of shales and shaly limestones. The displacements, both elastic and time-dependent, may pose a problem to the adjacent structures, because most buildings are not specifically designed for static horizontal movements at the foundation level. Horizontal movements, particularly horizontal differential displacement, may induce tensile stress and thus cracking in the structures surrounding the excavation.

In these design cases, the magnitude and distribution of elastic and time-dependent deformation in adjacent rocks should be evaluated. The initial stresses may be determined by the methods described in Chapter 6, and the mass modulus may be evaluated by the methods described in Section 11.2.2. Methods for the computation of elastic and time-dependent displacements were described in a case record of the design and construction of the Scotia Plaza, a 69-story-high complex in downtown Toronto (Trow & Lo 1989).

11.2.1.5 Base Heave

When the horizontal initial stresses in rock are high and the rock is horizontally thinly layered or bedded, the excavation may result in the loss of the vertical confinement required for stability. In this case, the floor of the excavation may fail by buckling upwards. This may decrease the stiffness of the rock mass below the foundations resulting in additional settlement upon loading.

11.2.2 FIELD TESTS FOR THE MEASUREMENT OF ROCK MASS MODULUS

For the design of structures supported on and in rocks, the deformation modulus of the rock mass should be obtained. In Chapter 6, laboratory methods for obtaining the deformation modulus for intact rock were given. In the field, rocks often contain joints and fractures, rubble zones, clay seams, and other zones of weakness that cause the mass deformation modulus to be much smaller than the deformation modulus for intact rock. Therefore for large projects and for structures sensitive to settlement, it is important to carry out field tests to determine the rock mass deformation modulus under the range of working stresses and at appropriate scales. Table 11.4 summarizes methods for determination of rock mass modulus in the field. The main advantages and disadvantages for each test are also listed.

The plate load test is the most commonly used *in situ* test for rock mass modulus determination. However, depending on the geological conditions, the results are sometimes dependent on the size of the plate used in the test. For example, as part of the foundation investigation for the Skydome Stadium in Toronto (Lo *et al.* 1987a; Lo & Cooke 1989), two series of plate load tests were conducted on shale with stronger layers of limy shale or limestone interbeds. Fractures were usually horizontal, although some near-vertical and sloping fractures were observed. The average fracturing spacing ranged from 240 to 700 mm with the fracture aperture ranging from 6 to 12 mm. Most fractures were observed to be filled with clay.

Each series of tests consisted of loading three different size plates (diameters of 229, 457 and 762 mm) to a load of 720 kN in four cycles of equal load increments. The modulus at each peak load at test site no. 1 is plotted against size, r^3, in Fig. 11.3, where r is the radius of the plate. It may be seen that the modulus decreases with increasing size of the plate from a value of 1750 to 310 MPa at a peak load of 720 kN. The reason for the decrease in modulus with increasing plate size is the increase in the zone of influence under loading. At this test site, both the thickness and frequency of weak zones are high.

TABLE 11.4. Summary of field methods for determination of rock mass deformation modulus

Test	Test principle	Main advantage	Main disadvantage
Plate load (bearing) test	It is the most common *in situ* test used in rock mechanics. A load is applied to a prepared flat surface of the rock mass through a rigid or flexible plate and the resulting normal deformation is measured. Using the relationship between the normal displacement of the surface of a semi-infinite elastic solid and the applied pressure, the deformation modulus can be obtained. The test can be performed in shallow pits or trenches, at the bottom of boreholes, or in excavated underground test galleries. When two opposite rock surfaces are loaded and monitored for deformation in a test gallery, the test is usually referred to as a "uniaxial jacking test." Test procedures and interpretation of test data can be found in ISRM (1979a,b) and ASTM (D4394-84 and D4395-84)	Simple	Site preparation and excavation of test galleries are expensive Small volume of rock mass is often influenced by the test (refer to Section 11.2.2 for the size effect) A disturbed zone around the excavated test tunnel usually leads to conservative results
Large flat jack test	Large hydraulic flat jacks are placed into a narrow slot cut into an exposed rock surface, e.g. walls of test adit when testing underground. Pressure is applied to the flat jacks and the resulting normal rock deformation is measured. The rock mass deformation modulus is evaluated from relationships between the applied pressure and the resulting deformation. Test procedures and calculations can be found in ISRM (1986)	Simple Large volume of rock mass is influenced by the test Performed in a relatively non-disturbed zone of rock mass	Needs skilled drilling personnel Flat jacks are generally non-recoverable Weak theoretical background Seating problem
Pressure tunnel (chamber) test	A section of a circular tunnel is lined with a waterproof material and sealed-off by means of bulkheads. Water pressure is applied in the prepared section and the resulting rock deformation is measured. The rock mass modulus is calculated using the elastic solution of a thick cylinder under internal pressure with its external diameter being infinity. Test method and calculations can be found in Stagg (1968)	Large volume of rock mass is influenced by the test	Expensive
Radial jacking test	It is a variation of the pressure tunnel test, where the uniformly distributed radial pressure on the surface of the circular tunnel is applied by means of flat jacks positioned on a reaction frame. Test procedures and method of calculating the rock mass deformation modulus can be found in ISRM (1979c) and ASTM (D4506-90)	Large volume of rock mass is influenced by the test	Expensive

TABLE 11.4. *(Continued)*

Test	Test principle	Main advantage	Main disadvantage
Dilatometer test	There are two types of dilatometers: flexible and stiff. In the flexible type, e.g., Colorado School of Mines cell, a uniformly distributed pressure is applied to a borehole wall by hydraulically expanding a flexible membrane. The resulting hole expansion (dilation) is determined by measuring the volume of the injected fluid or directly by displacement transducers in the probe. The deformation modulus at the test section is calculated from relationships between the applied pressure and the resulting dilation. Testing method is described in ISRM (1987). In the stiff type, e.g., Goodman jack, instead of applying a uniform pressure to the full cross-section of the borehole, unidirectional pressure is applied to the wall of the borehole by means of two opposed curved steel platens each covering a 90° sector. The testing procedures and interpretation of data are described in ISRM (1996) and ASTM (D4971-89)	Easily performed Inexpensive By performing the test at different depths and locations, the variation of deformability with depth and across the site can be obtained	Small volume of mass is influenced by test. Therefore, the modulus obtained is comparable to the laboratory modulus but not to the rock mass modulus
Tunnel relaxation test	A tunnel is excavated and the deformations of the rock walls are measured during tunnel excavation. The mass modulus is backcalculated using numerical analysis or relationships between the observed deformations and initial stresses (Lo & Lukajic 1984)	Modulus backcalculated is representative of field value	Expensive due to tunnel excavation
Dynamic tests	Compressional and shear wave velocities are determined from a surface or downhole seismic method. The dynamic Young's modulus and the dynamic shear modulus of the rock mass are calculated from relationships between the moduli and both the mass density of the rock and the compressional and shear wave velocities (Oliveira & Graca 1987)	Fast Inexpensive Can be performed at any depth	Parameters determined are usually higher than the static parameters Parameters correspond to low stress and strain levels, which are not representative for most static design cases
Stress relief test	A vertical circular hole is drilled into the rock mass and the resulting diametric displacement due to the relief of *in situ* stresses is measured. The modulus is calculated from the displacements measured and *in situ* stress conditions separately measured. Test method and calculations can be found in Lo *et al.* (1987b)	Relatively simple Inexpensive	Ease of installation is limited to relatively shallow depth

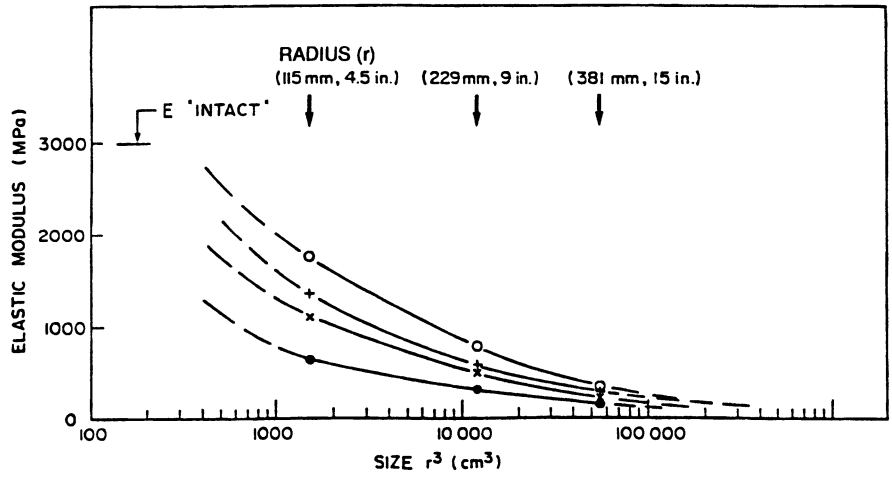


FIGURE 11.3. Effect of size on rock modulus for plate loading tests: (●) 180 kN; (×) 360 kN; (+) 540 kN; (O) 720 kN.

At a larger plate diameter, the zone of influence is larger so that more weak zones are included within the zone of influence under applied stress. In addition, the stress intensity for a given peak load is higher for a smaller plate. Laboratory tests have shown that the modulus of the weak zones increases due to consolidation. Hence, the modulus of the weak zones increases during the plate loading tests by a greater amount under the plate of smaller size. These two factors contribute to the decrease of the deformation modulus with increasing plate size at constant peak loads as shown in Fig. 11.3. The application of the results to design with guides for foundation construction is illustrated in Lo & Cooke (1989).

11.2.3 SOCKETED PILES INTO ROCK

When the quality of the rock mass at the surface is poor, shallow footings may be impractical or uneconomical. In this case, the foundation can be socketed into rock as shown in Fig. 11.4. Typically, the ratio of socket depth to diameter is 3 to 1 (CGS 1992). The capacity of piles socketed into rock is derived from two components: socket base capacity and

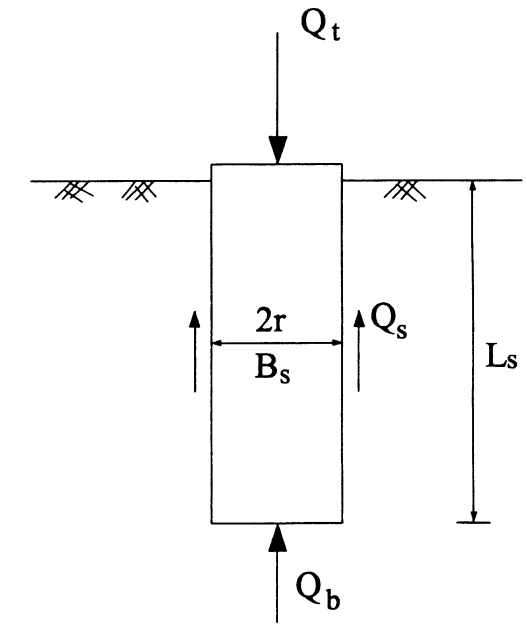


FIGURE 11.4. Notations for pier socketed into rock: L_s = depth of socket, r = radius of socket, B_s = diameter of socket; Q_s = load carried in side shear; and Q_t and Q_b = the total load and the load that reaches the base of the socket.

shaft capacity. The design assumptions of socketed piles vary from region to region. Typically one of three different design assumptions is used wherein the capacity is assumed to be derived from: (a) base resistance only, (b) shaft resistance only, or (c) a combination of the base and shaft resistance.

In the following sections, the behavior of socketed piers in rocks under axial load will be discussed. For the behavior under lateral load, refer to Poulos & Davis (1980), Kulhawy & Carter (1992b), Carter & Kulhawy (1992), and Wyllie (1992).

11.2.3.1 End Bearing Resistance

When the design is based on the base capacity partially or totally, the bottom of the socket should be cleaned from any debris remaining due to socket excavation. The existence of such material may produce large deformation before the bearing capacity is mobilized.

For stability, the portion of load carried by the base should not exceed the end bearing resistance. The end bearing resistance is defined as the allowable pressure multiplied by the area of the base. Alternatively, the contact pressure under working load, q_b, should be less than the allowable bearing pressure, q_{ba}. The allowable bearing pressure can be calculated by the methods presented in Section 11.2.1.2. The CGS (1992) suggested to multiply the value obtained from Eq. 11.1 by a depth factor, d, to include the effect of embedment (according to Ladanyi & Roy, 1971). Therefore, Eq. 11.1 becomes:

$$q_{ba} = \sigma_c K_{sp} d \qquad (11.2)$$

where σ_c = average uniaxial compressive strength of rock core; K_{sp} = empirical factor given by Fig. 11.2, d = depth factor = $1 + [0.4\ (L_s/B_s)] \leq 3$, L_s = depth of the socket; and B_s = diameter of the socket.

11.2.3.2 Shaft Resistance

The ultimate socket shear load, Q_{sf}, is conventionally calculated as the average side shear resistance, q_{sf}, multiplied by the surface area of the walls of the socket:

$$Q_{sf} = \pi B_s L_s q_{sf} \qquad (11.3)$$

where B_s = the socket diameter, and L_s = the socket length as shown in Fig. 11.4.

The value of shear resistance mobilized at the concrete–rock interface is affected by many factors (e.g. see Rowe & Armitage 1987a). These factors include the socket roughness, strength of concrete and the rock material, the interface strength properties, geometry of the socket, deformation properties of the concrete and the rock mass, Poisson's ratios, creep properties of the concrete and rock, initial stress in the ground and swelling characteristics of the rock. The effect of roughness of the socket walls is emphasized by most investigators. It is therefore considered that the reliable method to determine q_{sf} is to perform a full-scale field test using the same wall roughness that is expected in the actual sockets.

11.2.3.3 Estimation of Average Side Shear Resistance Using Empirical Correlations

Several empirical correlations exist in the literature for the determination of the average side shear resistance, q_{sf}, at the socket interface (e.g. Rosenberg & Journeaux 1976; Williams & Pells 1981; Horvath *et al.* 1983; Rowe & Armitage 1984; Kulhawy & Phoon 1993). A common approach in these correlations is to relate q_{sf} to the uniaxial compressive strength of the weaker of the pier concrete or the rock core. Some of these correlations are summarized in Table 11.5 for two cases: conventional piers (relatively smooth piers) and grooved piers (rough piers).

Horvath *et al.* (1983) and Rowe & Armitage (1984) proposed the same form of correlation for conventional piles, namely: $q_{sf}/p_a = \lambda(\sigma_c/p_a)^{1/2}$, but the values of λ differ (refer to

TABLE 11.5. Empirical correlations for side shear resistance determination[a]

Case	Correlation	Remarks
Conventional piers (relatively smooth walls)	$\frac{q_{sf}}{p_a} = \lambda\sqrt{\frac{\sigma_c}{p_a}}$	λ = 1.41 (Rowe & Armitage 1984) λ = 0.63–0.94 (Horvath *et al.* 1983) Carter & Kulhawy (1988) indicated that λ = 0.63 is a conservative value suitable for design purposes.
	$q_{sf} = \alpha\beta\sigma_c$	Williams and Pells (1981) α = reduction factor for strength. It includes roughness effect in some implicit manner β = reduction factor due to the presence of discontinuities For determination of α and β, refer to graphs provided by Williams & Pells (1981)
	Log q_{sf} − Log σ_c linear relationship	Rosenberg & Journeaux (1976) Determine q_{sf} from the graph given by Rosenberg & Journeaux (1976)
Grooved piers	$\frac{q_{sf}}{p_a} = \lambda\sqrt{\frac{\sigma_c}{p_a}}$	λ = 1.89 (Rowe & Armitage 1984) Correlation is for sockets with grooves of depth and width greater than 10 mm, at spacing between 50 and 200 mm
	$q_{sf} = 0.8\sigma_c\sqrt{RF}$ $RF = \frac{\Delta r L_t}{r L_s}$	Horvath *et al.* (1983) RF = roughness factor, Δr = average height of grooves in socket, L_t = total travel length along the socket wall profile, r = nominal radius of the socket, and L_s = nominal length of the socket

[a] q_{sf} = average side shear resistance, σ_c = uniaxial compressive strength of the weaker of rock or concrete, p_a = atmospheric pressure = 101.3 kN m^{-2}.

Table 11.5). Using the database of load tests developed by Rowe & Armitage (1984) supplemented by additional load tests in Florida limestone presented by Bloomquist & Townsend (1991) and McVay *et al.* (1992), Kulhawy & Phoon (1993) re-analyzed the data by using site average. The same form of correlation as that given by Horvath *et al.* (1983) and Rowe & Armitage (1984) was obtained.

The correlation of Williams & Pells (1981) considers an additional reduction factor, which reflects the effect of the deformability of the rock mass as described by the presence of discontinuities. Their correlation covered a wide range of roughness and no distinction was made between smooth and rough walls.

It should be noted that the data used to derive these correlations are highly scattered. In addition, the values of the average side shear resistance estimated from these correlations are widely different. For example, the λ factor for conventional piles in the Rowe and Armitage correlation is about twice that in the Horvath *et al.* correlation. For illustration, these two correlations are plotted in Fig. 11.5, along with the data used by Rowe and Armitage to derive their correlation. However, it should be noted that there was a fundamental difference in design approach adopted in conjunction with the selection of these values. Horvath *et al.* (1983) and Carter & Kulhawy (1988) sought conservative (lower bound) values of q_{sf} for use in a conventional working stress design approach. While Rowe & Armitage sought the expected (average) value and combined the use of this with a limit states design approach and the site partial factor, PF, applied to q_{sf}, which

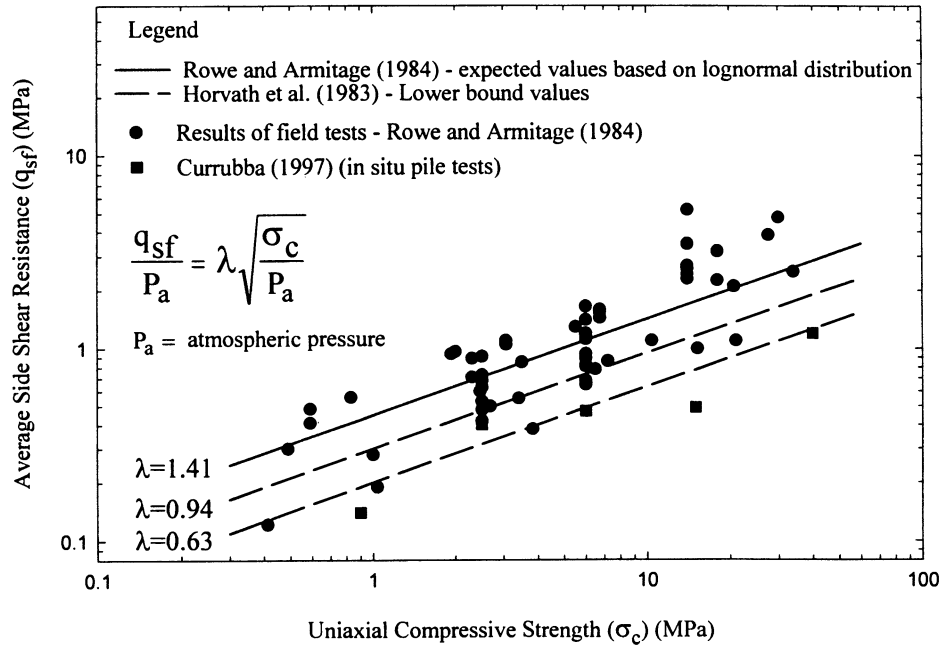


FIGURE 11.5. Correlations of Horvath *et al.* (1983) and Rowe & Armitage (1984) for estimation of average side shear resistance for conventional rock sockets: (——) Rowe & Armitage (1984) expected values based on log-normal distribution, (— —) (Horvath *et al.* 1983) lower bound values.

accounted for the scatter of data and allowed the selection of a design value $q_{sfd} = q_{sf}/PF$ that would provide a specific level of confidence in performance. This limit states approach allows the use of consistent characteristic parameters when assuming the serviceability and ultimate limit states.

Recent results of *in situ* pile tests show that while a group of data may compare favorably to one correlation, another group may compare favorably with another correlation. For example, Lam *et al.* (1991) and Carrubba (1997) report results that are consistent with the Horvath *et al.* correlation, while Radhakrishnan & Leung (1989) report results that are consistent with the Rowe & Armitage correlation.

The widely different results of field tests presented by various investigators show that care is needed in the selection of design parameters. Correlations such as those given in Table 11.5 should be used with an appropriate factor of safety or partial factors (e.g. see Rowe & Armitage 1987a, b) that allow for the variability. Like all correlations, these correlations are intended for use in preliminary design and when side shear resistance is critical to the success or cost of a project, site specific field tests should be performed to establish side shear resistance for that site and method of shaft construction. In particular, it is noted that auger smear or a bentonite film along the socket can significantly reduce side shear resistance.

11.2.3.4 Design of Piles Socketed into Rock

1. Elastic analysis. A simple method for the design of socketed piles in rocks is to consider that the rock-socket system behaves elastically. This requires that both the concrete

and the rock materials behave elastically and the bond at the interface between the pier concrete and the rock remain unbroken (no slip).

Elastic solutions for a single compressible pile in an elastic half space were presented by Poulos & Mattes (1969) and Osterberg & Gill (1973). Pells & Turner (1979) extended their solutions to cover a wide range of geometries and stiffnesses that may be encountered with rock sockets. From the solutions presented by Pells & Turner, both the distribution of load between end bearing and side shear in a rock socket and the settlement of pile head can be determined.

Suppose that it is required to determine the dimensions (diameter B_s and length L_s) of a pile socketed into rock, where both the base and shaft resistance are to be considered. The pile will support a load Q_t, at its head. Young's modulus of concrete is E_c, and the deformation modulus of rock mass is E_r. The allowable bearing pressure is q_{ba}, the allowable average side shear resistance is q_{sa}, and the allowable settlement at the pile head is u_{ca}. Using the elastic solutions of Pells & Turner (1979) and the iterative technique of Ladanyi (1977), the pile can be designed as follows:

1. Choose a suitable socket diameter, B_s.
2. Assuming that the load is carried by side resistance only (i.e. ignore the base resistance), calculate the maximum length, L_{max}, of the socket from:

$$Q_t = \pi B_s L_s q_{sa}. \tag{11.4}$$

3. Choose a socket length L_s less than L_{max}. Using the ratio L_s/B_s and E_c/E_r and Fig. 11.6, find the ratio of the load that reaches the base, Q_b, to the total load, Q_t, ($n = Q_b/Q_t$).
4. Calculate the average side shear:

$$q_s = \frac{(1-n)Q_t}{\pi B_s L_s}. \tag{11.5}$$

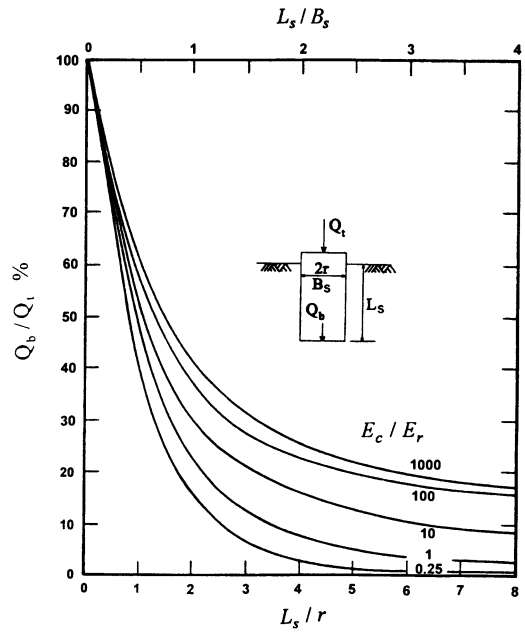


FIGURE 11.6. Load distribution in a rock socket (modified from Pells & Turner 1979).

5. Repeat steps 3 and 4 until $q_s = q_{sa}$. The corresponding L_s is the required socket length.
6. Check that the bearing pressure at the socket base is less than the allowable bearing pressure:

$$q_b = \frac{nQ_t}{(\pi B_s^2/4)} \leq q_{ba}. \tag{11.6}$$

7. Check that the settlement of the pile head, u_c, is less than the allowable settlement, u_{ca}:

$$u_c = \frac{Q_t}{rE_r} I_s \leq u_{ca} \tag{11.7}$$

where the influence factor, I_s, is obtained from Fig. 11.7.

If the load is supported by shaft resistance only, calculate the socket length directly from Eq. 11.4. Equation 11.7 still can be used to calculate the settlement at the pile head. Use

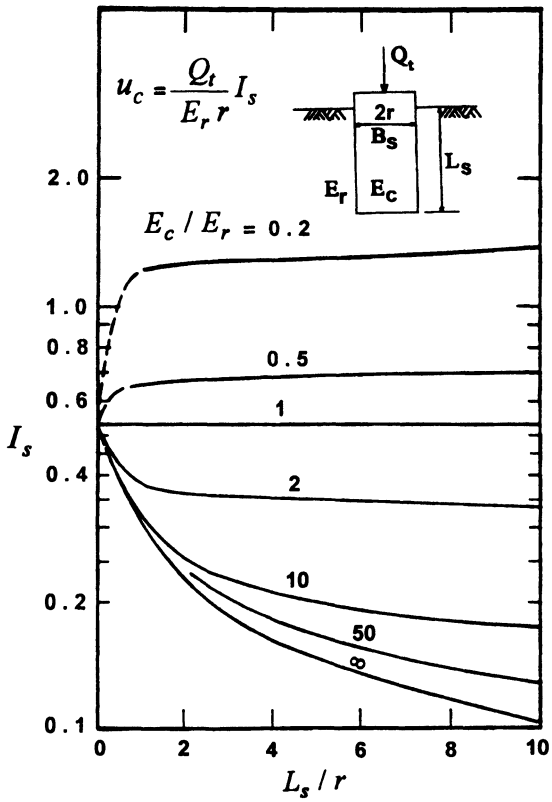


FIGURE 11.7. Elastic settlement of a complete rock socket (modified from Pells & Turner 1979).

Figs 11.8 and 11.9 instead of Fig. 11.7 to obtain I_s.

It should be noted that the use of the elastic solution requires that the value of the allowable average side shear resistance used in design be in the linear elastic range. Therefore, the value of the ultimate shaft resistance should be reduced by 50% to arrive at q_{sa} (CGS 1985).

Results of monitoring of three drilled pier foundations socketed into weak shale for two years for the Hamilton General Hospital were reported by Horvath (1989). Horvath concluded that the elastic theory may be used to estimate the displacement behavior of drilled pier foundations socketed into rock even when the rock is considered to be relatively weak.

2. Other design methods. In the elastic solution presented in the previous section, it is assumed that the bond between concrete and rock remains unbroken (no slip). Rowe and Armitage (1987a, b) presented a design method that allows for possible slip at the pier–rock interface. Their design method is based on satisfying a settlement limitation and ensuring that there is an adequate factor of safety against collapse. Design examples are given in Rowe and Armitage (1987b, c).

Some other design approaches reported in the literature include Kulhawy & Goodman (1980), Kulhawy & Carter (1992b), and Hassan *et al.* (1997).

11.3 Concrete Dams on Rock Foundations

11.3.1 INTRODUCTION

Several issues should be considered in the design and safety assessment of concrete dams on rock foundations. The strength and stiffness of the foundation rock mass are of paramount importance. They play a major role in the overall stability of the dam and the resulting settlement. The shear strength parameters of the concrete–rock interface control the sliding stability of the dam. Other design issues include controlling seepage under the dam, and erosion, leaching or solution effects in the foundation.

The following sections deal with the stability assessment at the dam foundation interface. The methodology developed by Lo *et al.* (1991a, b) for the safety assessment of concrete dams on rock foundations is summarized. The methodology was developed during the early stage of a long-term program for the safety assessment of existing dams that was initiated by Ontario Hydro in 1985. The

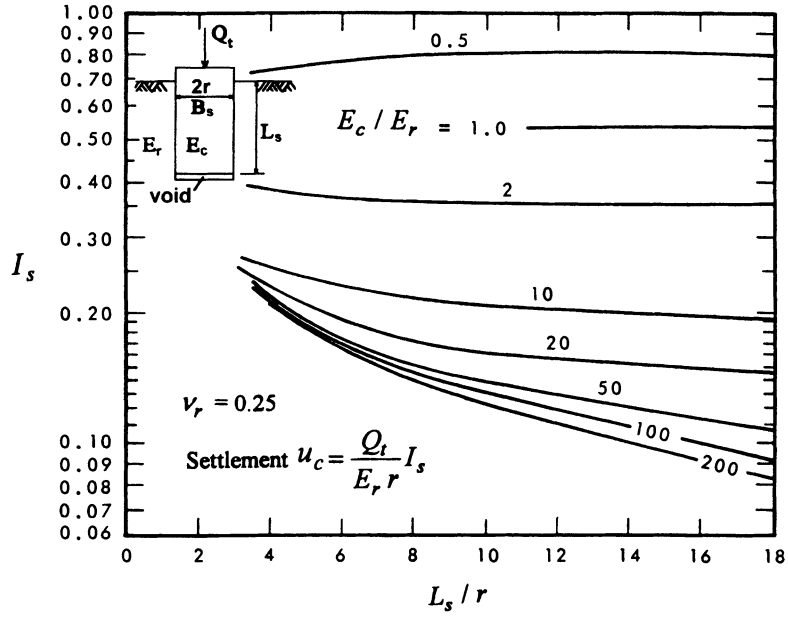


FIGURE 11.8. Embedment reduction factor for shear sockets (modified from Pells & Turner 1979).

assessment is performed on a common, rational basis without the introduction of unnecessary conservatism, which may lead to unnecessary expensive remedial measures. Experience of using this methodology was reported by Lo *et al.* (1991a, b) and Lo & Grass (1994). Lo & Hefny (1998) updated the experience of using this approach to 38 dams.

Methods for stability analysis used in several organizations are reviewed. A case record is also analyzed to illustrate the application of the methodology.

11.3.2 METHODOLOGY

A summary of the methodology is shown in Fig. 11.10. The assessment begins with a Phase I study with conservatively assumed strength parameters for the dam–foundation interface. If the results of the design review meet the engineering standards, the stability condition is considered to be satisfactory and no further work is required. The stability criteria adopted here are shown in Table 11.6. It may be noted that the difference in the requirement of factors of safety between Case A (assumed strength parameters) and Case B (measured strength parameters) is significant and reflects the increased level of confidence in the foundation conditions and shear strength parameters resulting from the measurements.

If a dam does not meet the standards after Phase I study, a more detailed investigation is performed during Phase II for dams with high hazard ratings. The investigation consists of three main components: field investigation, laboratory tests and further study of factors affecting stability as illustrated in Fig. 11.10.

11.3.3 METHODS OF FIELD INVESTIGATION

Based on considerations of geology, records of construction, and performance and accessibility, a field program of investigation is planned for an existing dam. The main objectives of the field work are:

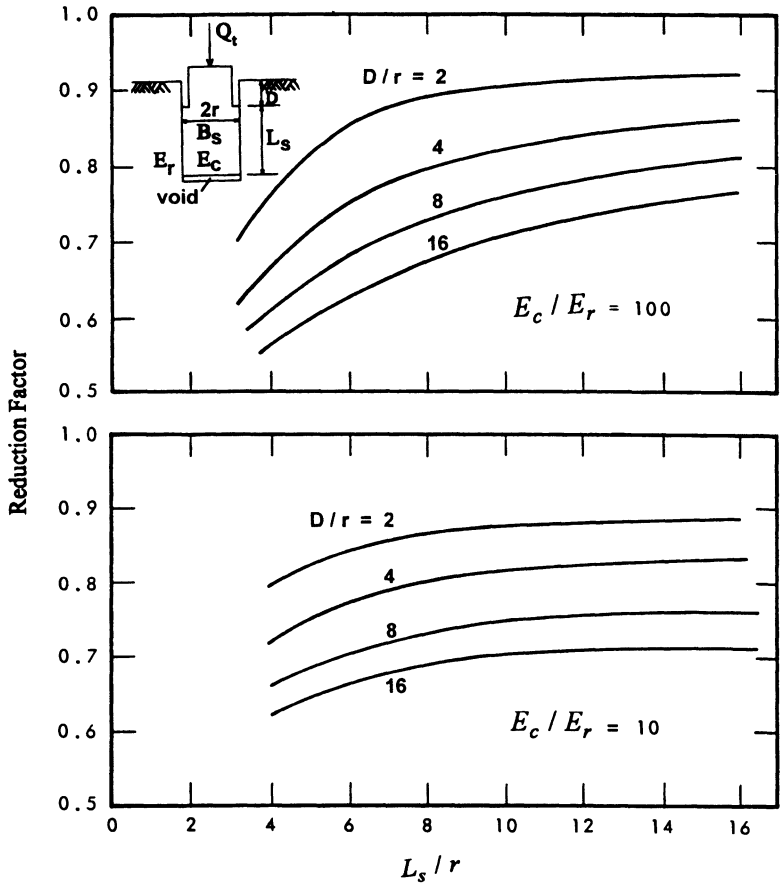


FIGURE 11.9. Elastic settlement of shear socket (modified from Pells & Turner 1979).

- to recover samples at the concrete–rock contact and rock foundation for laboratory tests,
- to investigate the contact condition, and
- to furnish critical geological information where required.

The drilled holes are usually used later for installation of piezometers for the measurement of uplift pressures, and for pressure testing to detect continuity of flow channels at or below the dam–foundation interface.

From the condition of core recovered at the interface, the concrete–rock contact is classified into three categories: bonded, weakly bonded and unbonded, as shown in Table 11.7.

From the point of view of strength of the contact surface, bonded contacts can sustain significant tension and possess cohesion. Only friction is available for strength of unbonded contacts. For weakly bonded contacts, it is most likely that breakage is mainly a result of drilling, but the contact would have been intact *in situ*. However, the tensile strength and cohesion would be smaller than of bonded contacts recovered by the same drilling crew and technique. For this case, the minimum tensile strength measured in the laboratory is ascribed to the contact (≈0.18 MPa).

The scope of the drilling program is governed by previous information available, the complexity of the geological condition, and

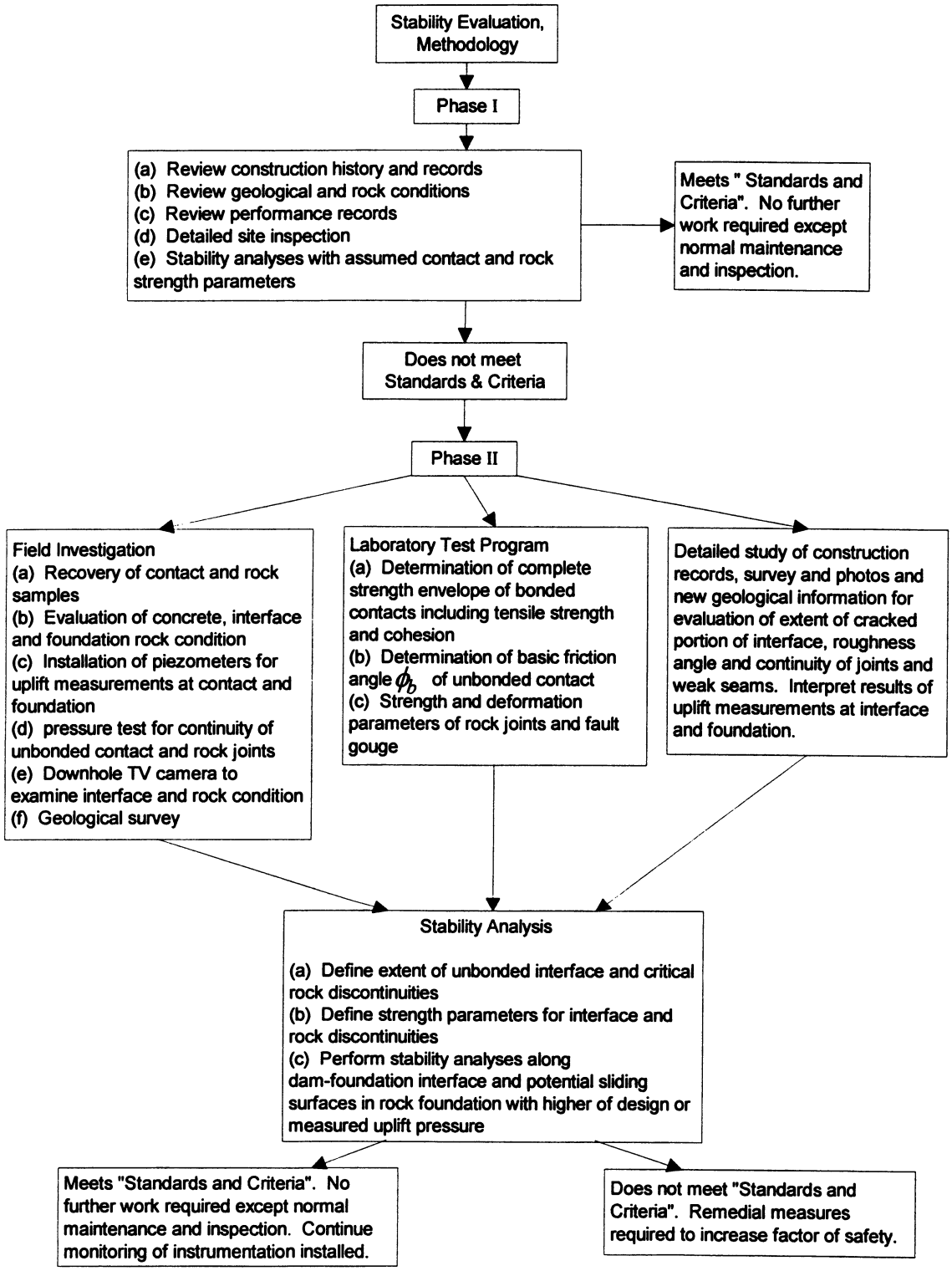


FIGURE 11.10. Methodology of stability evaluation of concrete dams on rock foundation.

TABLE 11.6. Stability criteria of concrete dam safety assessment

Loading condition	Definition of loading condition	Factor of safety	
		Case A: assumed strength parameters	Case B: strength parameters determined by tests on contact and rock samples
Normal	Maximum operating reservoir load with and without ice load	3	2
Unusual	Inflow design flood condition	2	1.5
Extreme	Maximum operating reservoir with and without ice load + seismic load	1	1

TABLE 11.7. Classification of concrete–rock contact

Contact classification	Condition of contact	Notes on strength of contact
Bonded contact	The core of the concrete–rock contact is intact when received, or partial or inclined breakage has occurred at the contact due to rock fracture during drilling	The contact can sustain significant tension and possess cohesion. Appropriate test to be performed on specimen
Weakly bonded contact	Contact is broken when received, but fracture surface is fresh and matching good. Sometimes small concrete fragments adhere to the rock surface or vice versa. Or, although the contact is intact when received, it breaks during specimen preparation for testing	It is most likely that breakage is mainly a result of drilling, but the contact would have been intact *in situ*. The tensile strength and cohesion would be smaller than those of bonded contacts. The minimum tensile strength measured in laboratory is ascribed to the contact ($\approx$0.18 MPa)
Unbonded contact	Contact is broken when received, often in pieces. No fresh fracture surface is identified. The rock surface is weathered and often coated with calcite deposits. Matching of rock and concrete portions is either impossible or very poor	Only friction is available for strength

the size and importance of the dam. A reasonable guideline for spacing of boreholes is approximately 30 m, or alternate dam monoliths, which ever is less. Additional boreholes should be drilled if information from this first series of boreholes suggests the possible existence of a "critical" section.

A main objective of the field program is to define the condition of the concrete–rock contact and the extent of the unbonded dam–foundation interface. For this purpose, several methods are employed: (a) direct examination of drilled-cores, as described previously; (b) down-hole TV camera to examine the contact condition *in situ*; and (c) water pressure tests in packed off sections at the contact.

11.3.4 STRENGTH ENVELOPES OF BONDED AND UNBONDED CONTACTS

It may be seen from Fig. 11.10 that the key element of the methodology is the determination of strength parameters of the interface between the dam and the rock foundation. This process involves two steps: (a) the measurement of the strength of bonded and unbonded specimens using specialized laboratory tests; and (b) interpretation of laboratory results in (a), together with results of water pressure and other field tests, to arrive at a set of strength parameters appropriate for stability analysis.

It is particularly important to assess the values of tensile strength and cohesion because of their impact on results of stability analysis as will be seen in a subsequent section.

1. Bonded contact. The problem of determination of the strength of the interface is illustrated in Fig. 11.11. If a dam is constructed in the best possible manner, it is theoretically possible that the interface is completely and uniformly bonded. Under such an ideal condition, a sample taken at a particular location and tested by an appropriate method will yield results representative not only at that location, but also representative of the entire interface. A series of direct tension, triaxial extension and compression tests, as described in Chapter 6, will yield the strength envelope as shown by Curve I. Curve I is characterized by the tensile strength, σ_t, and the cohesion, c_i, of intact contact and a variable friction angle, ϕ_i, because the envelope is non-linear. Experience with 38 dams investigated in Ontario (Lo & Grass 1994; Lo & Hefny 1998) has shown that only one dam (Saunders Dam in the St Lawrence River System) closely approaches this

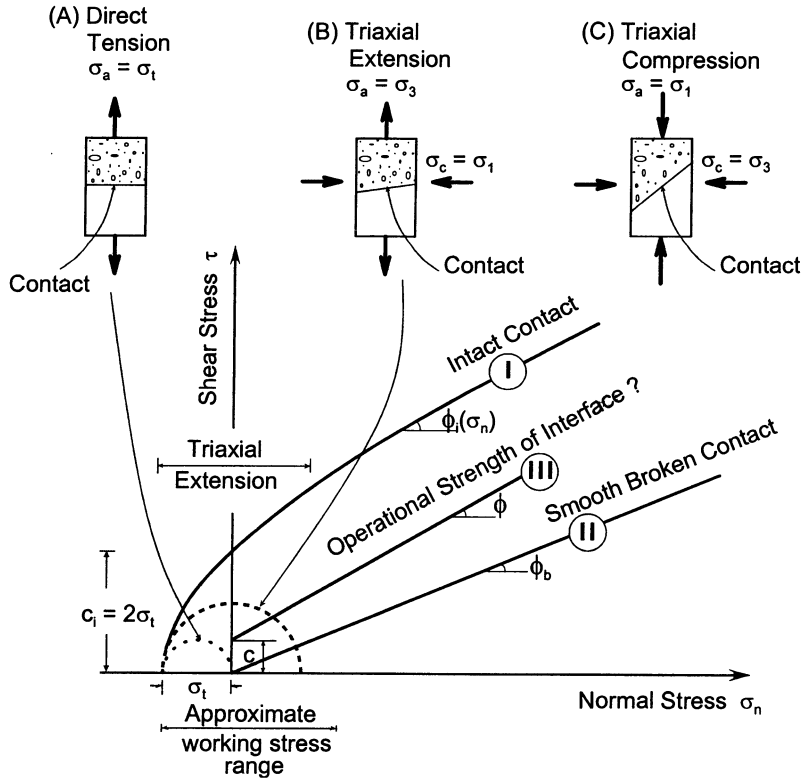


FIGURE 11.11. Strength envelopes of bonded and unbonded contacts.

ideal condition. In general, Curve I defines the upper bound of the strength of interface.

2. Unbonded contact. In contrast, if an existing dam was built with poor construction control exacerbated by deterioration due to aging, it is conceivable that the entire interface is unbonded. A specimen taken at the interface will show a broken contact between concrete and rock. A series of simple shear tests, corrected for the effects of inclination of contact surface and roughness angle (Chapter 6), will yield the strength of a smooth broken contact as illustrated by Curve II, which defines the lower bound of strength.

It should be noted that the friction angle defined by Curve II is the basic friction angle, ϕ_b, to which the field roughness angle may be added to obtain the overall friction angle.

The results of measurements of ϕ_b by the method described in Section 6.6.2 are summarized in Table 11.8. For the purpose of comparison, the basic friction angles for concrete on concrete and rock joints are also included. From Table 11.8, it may be observed that:

- the basic friction angle of the contact is not very sensitive to rock type, ranging from 30 to 39°;
- the values of ϕ_b for contact samples are comparable to those of rock

TABLE 11.8. Results of tests for basic friction angle, ϕ_b, at a number of Ontario dams

Type of contact	No. of tests	Range (°)	Average ϕ_b (°)	Dam
Concrete–gneiss	25	27–47	35	Barrett Chute, Coniston, McVittie, Cameron Falls, Chat Falls, Trethewey Falls, Hanna Chute, South Falls, Otto Holden, Otter Rapids, Dog Lake 2, Fredrick House
Concrete–granite	7	32–34	33	Cameron Falls, Nipissing, Bingham Chute, Elliott Chute, McConnel
Concrete–crystalline limestone	4	34–42	38	Barrett Chute, Mountain Chute, Stewartville
Concrete–shaly limestone	10	30–39	35	Rannyey Falls, Lakefield, Hagues Reach
Concrete–dolostone	5	30–35	32	Saunders, PGS
Concrete–greywacke	6	32–37	36	Red Rock Falls, Matabitchuan
Concrete–quartzite	5	37–40	38	Red Rock Falls, Stinson, Wanapitei
Concrete–diabase	5	37–41	39	Rayner, Wanapitei
Concrete–porphyry	2	37–38	37	Sandy Falls
Concrete–pegmatite	1	35	35	McVittie
Concrete–concrete	5	29–36	32	
Joint in gneiss	11	29–42	34	Barrett Chute, Coniston, Otter Rapids
Joint in crystalline limestone	5	28–37	32	Barrett Chute, Stewartville, Chanaux
Joint in shaly limestone	8	28–36	32	Saunders, Lakefield
Joint in dolostone	4	27–36	33	Saunders
Joint in greywacke	3	29–34	32	Red Rock Falls
Joint in quartzite	7	31–36	33	Red Rock Falls, Stinson
Joint in diabase (horizontal)	7	27–37	33	Rayner, Wanapitei
Joint in diabase (vertical)	6	25–36	30	Rayner
Joint in red schist	2	30–34	33	Rayner

joints, the average ϕ_b for joints ranging from 30 to 34°; and
- the basic friction angle of concrete to concrete sliding lies in the lower range of ϕ_b of contact samples.

3. Operational strength on interface

For most existing dams, the field conditions lie anywhere between the upper and lower bounds of strength. The problem is therefore to establish the strength envelop representative of the interface, operational under working stress range and suitable for use in stability analysis. While it is, in principle, possible to establish the upper and lower bounds of the strength envelope in Fig. 11.11 and perform a sufficient amount of field investigation to obtain the operational strength envelope (Curve II), experience gained from past investigations showed that the most practical equation to be used is:

$$\tau = c + \sigma_n \tan \phi \qquad (11.8)$$

with $c = (1 - \eta)c_i$, $c_i = 2\,\sigma_t$, and $\phi = \phi_b + i$; where τ = the operational shear strength of the interface; c and ϕ = the operational shear strength parameters that may be used directly in stability analysis; η = the unbonded area ratio of the interface; c_i = the cohesion of intact contact; σ_n = the normal stress; ϕ_b = the basic friction angle of contact; i = the roughness angle measured in the field; and σ_t = the tensile strength.

The tensile strength should be determined by direct tension tests with appropriate interpretation regarding the modes of rupture. The cohesion, c_i, is obtained from the relationship $c_i = 2\sigma_t$, based on the classical Griffith theory (1921) of fracture of brittle materials and experimental evidence (Lo *et al.* 1990). The friction angle, ϕ, is the sum of the basic friction angle, ϕ_b, and the roughness angle, i, measured in the field. The value of ϕ will be somewhat lower than ϕ_i, the friction angle of intact contact, and this simplification is therefore conservative. The unbonded area of the interface, η, is assessed by field investigation and construction records. A factor of safety may be applied to the measured direct tensile strength depending on the amount and variability of results available.

Results of direct tension tests from 38 dams are shown in Table 11.9. Of the 111 tests, 58 specimens (52%) failed along the contact. The value of σ_t varied from 0.18 to 2.62 MPa, with an average of 0.88 MPa. The tensile strengths for rupture in rock and mixed mode failure (defined as having 25% of the failure surface outside the contact surface) are comparable to that for failure along the contact. The tensile strengths for failure in concrete are higher. The values measured for failure in glue represent the tensile strengths of poorly developed glues.

The minimum tensile strength of 0.18 MPa, which had been measured from samples taken at several different sites, reflects the minimum tensile strength that is required for the core recovery. It is interesting to note that the bonded contact of some fairly old

TABLE 11.9. Results of direct tension tests

Mode of failure	Number of samples	$\sigma_{t\,min}$ (MPa)	$\sigma_{t\,max}$ (MPa)	$\sigma_{t\,ave}$ (MPa)
Along contact	58	0.18	2.62	0.88
In concrete[a]	17	0.31	3.25	1.69
In rock	6	0.18	1.97	0.72
In glue	8	0.56	2.15	1.58
Mixed[b]	22	0.19	2.06	0.93

[a] Includes samples failed along boundary of large aggregates.
[b] Defined as having more than 25% of failure surface outside contact area.

dams (constructed in or before 1925) still possess tensile strengths comparable in magnitude to newer dams constructed after 1946.

It should be emphasized that the tensile strength of contact at any particular location depends on the following:

- preparation of the foundation rock surface;
- quality and type of cement;
- type of bedrock;
- concrete age and condition;
- blast damage fracturing, and
- slow solutioning at contact.

Therefore, a significant variation of the contact condition and tensile strength may be expected between different dam sites and even within the same dam site.

11.3.5 EXTRACTION OF DATA FROM RECORDS

Along with the field and laboratory programs, records of construction and performance of the dam, which had been studied in Phase I, are reviewed. The objectives of this review are:

1. to synthesize all historical and current geological information, to assess the rock condition in general and the continuity of joints and weak seams or layers in the foundation in particular;
2. to review construction practice and procedure and any variation thereof in a particular dam site, which may have an effect on the contact condition, and to compare these with the contact conditions revealed in the Phase II investigation; and
3. to review and interpret construction records and surveys of foundation rock surface so as to assess the roughness angle, i, that is operative under field conditions.

At the Barrett Chute Main Dam, which was founded on hornblende biotite gneiss and crystalline limestone, the roughness angles were formed by blasting along joint surfaces. The foundation rock surface profiles were surveyed at every 0.6-m section of the dam before concrete for the gravity dam was poured. The profiles at three sections of the dam are illustrated in Fig. 11.12. It may be seen that the roughness angles in the gneiss

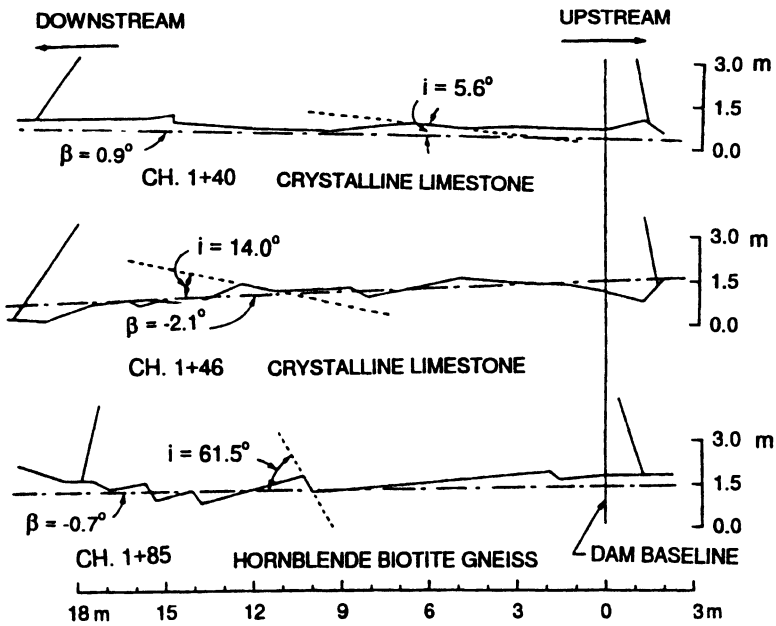


FIGURE 11.12. Typical "as-built" roughness profile for Barrett Chute Dam. (CH = Chainage).

rock are generally much higher than those in crystalline limestone rock. It must be noted, however, that the integrity of the rock asperity has to be established before the full value roughness angle, i, can be used (in conjunction with ϕ_b) for stability analysis.

The application of the methodology discussed in the preceding sections will be illustrated by a case history.

11.3.6 METHODS CURRENTLY USED IN STABILITY ANALYSIS

In this section, methods for sliding stability analysis used in several organizations are reviewed and compared.

1. Method used in China. According to the instructions for design of hydraulic structures, the following two equations have been suggested in China for stability analysis:

$$FS = \frac{(\Sigma V - \Sigma U)\tan \phi_s}{\Sigma H} \qquad (11.9)$$

$$FS = \frac{(\Sigma V - \Sigma U)\tan \phi + cA}{\Sigma H} \qquad (11.10)$$

where FS = factor of safety; ΣV = the summation of vertical forces; ΣU = the summation of uplift; ΣH = summation of horizontal forces; $\tan \phi_s$ = the sliding friction coefficient of unbonded contact ($c = 0$); $\tan \phi$ = shear friction coefficient; c = shear cohesion; A = area of foundation base per unit length of the dam.

Either one of these two equations can be selected for use by the designer of the project according to their experience. The main reason for accepting the two equations is that the dams in China were designed using either Eq. 11.9 or 11.10, and all these dams have operated safely for a long time. Therefore, the dam safety could be ensured if the factor of safety satisfied either one of the two safety criteria.

For the case of Eq. 11.9, the minimum factor of safety is defined to be equal to 1.05–1.10 for the usual loading combination, 1.0–1.05 for an unusual loading combination, and 1.0 for an extreme loading combination. When using Eq. 11.10, the factor of safety should be greater than 3.0 for usual loading and greater than 2.5 for unusual loading.

The parameters of $\tan \phi_s$, $\tan \phi$ and c should be obtained based on laboratory and/or *in situ* tests. For large dams, the results obtained from *in situ* tests are necessary. An average value from the lower values of test results is recommended for use.

2. Method used by US Bureau of Reclamation (USBR). In the method used by the USBR, Eq. 11.10 is accepted, in principle, for computation of the factor of safety. It emphasizes that the values $\tan \phi$ and c should be obtained from actual tests, but does not suggest a methodology for the determination of strength parameters.

For gravity dams, the required minimum factor of safety, FS, should be greater than 3.0 for a usual loading condition, 2.0 for an unusual loading condition, and 1.0 for an extreme loading condition. It is also required to check the stability condition for cracking at the heel of the dam.

The USBR method of analysis is illustrated in Fig. 11.13. In the initial steps of computation, the normal stress on the base at the upstream face, σ_A, in Fig. 11.13b is computed without consideration of uplift pressure. Then σ_A is compared with the minimum allowable compressive stress, σ_{zu}.

The criterion of cracking is governed by the minimum allowable compressive stress without internal hydrostatic pressure, using the equation:

$$\sigma_{zu} = p\gamma_w h - \frac{\sigma_t}{FS_t} \qquad (11.11)$$

where σ_{zu} = the minimum allowable compressive stress at the upstream face; p = a reduction factor to account for drains ($p = 1$

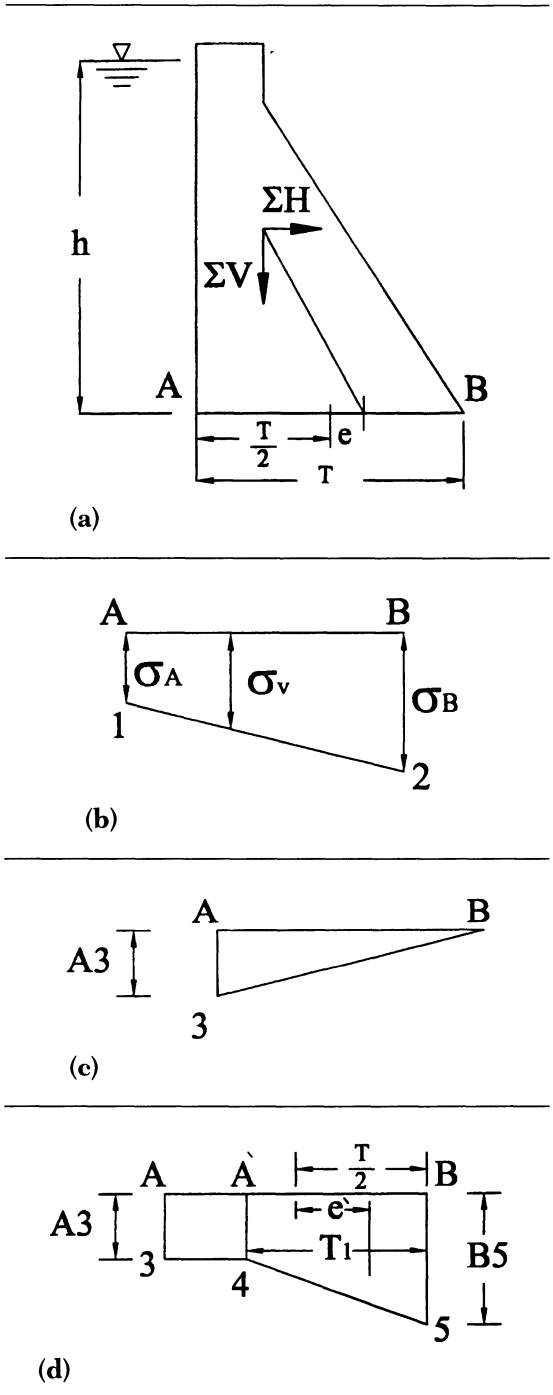


FIGURE 11.13. Diagrams of base pressures (USBR): (a) vertical cross-section, (b) pressure diagram without uplift, (c) uplift pressure diagram, and (d) combined pressure diagram.

when drains are not present, $p = 0.4$ when drains are used); γ_w = the unit weight of water; h = the depth below reservoir surface; σ_t = the tensile strength of contact; and FS_t = the factor of safety for tensile strength (FS_t = 3.0, 2.0 and 1.0 for usual, unusual and extreme loading conditions, respectively). The allowable value of σ_{zu} for a usual loading condition should never be less than zero. It is therefore clear that tensile strength may be used in both new and existing dams.

In assessing the extent of cracking, however, it is assumed that a horizontal crack extends from the upstream face to a point where the vertical stress (σ_V in Fig. 11.13b) is equal to the uplift pressure, *A*3, at the upstream face (Fig. 11.13d). The uplift pressure along the crack is assumed uniform and equal to the uplift at the upstream face.

It is significant to note that the tensile strength of the contact is neglected in this step of computation for the extent of cracking, in contrast to establishing the allowable minimum compressive stress.

The section analyzed is considered satisfactory, if the calculated stress at the downstream face does not exceed the allowable stress, and the calculated factor of safety is greater than or equal to the required factor of safety.

The USBR analysis is a limit equilibrium method satisfying force and moment equilibrium. An inconsistency arises, however, in permitting the use of tensile strength for the determination of initiation of cracking while tensile strength is neglected for the calculation of extent of cracking. To remove this inconsistency, the USBR method has been extended to allow for tensile strength by Lo *et al.* (1990). This modified method results in a smaller calculated length of the hypothetical crack and therefore leads to a higher computed factor of safety.

3. Method used by the US Federal Energy Regulatory Commission. The Federal Energy Regulatory Commission, Office of Hydropower Licensing, provided *"Guidelines for the Evaluation of Hydropower Projects"*. The design philosophy generally follows those of USBR and the method of crack analysis along the contact is also similar. The factors of safety adopted for high hazards dams are identical to those of USBR.

The guidelines do not permit the use of tensile strength along the contact, based on the premise that weak seams and fractures in bedrock may exist immediately below the dam foundation interface. While there are many cases where such a rock condition exists, there are also many other cases where the rock is free of any important weak zones or discontinuities near the contact, where foundation treatment has been properly performed during construction. This stipulation in the guidelines is unnecessarily restrictive.

11.3.7 AN EXAMPLE OF APPLICATION OF METHODOLOGY: SAFETY ASSESSMENT OF BARRETT CHUTE DAM

11.3.7.1 Design Provisions and Geological Conditions

The main dam of the Barrett Chute hydroelectric generating station (capacity 178 MW) was constructed between 1938 and 1942. It is a concrete gravity structure 27-m high, 21-m wide at the base and 360-m long.

The grout curtain consists of two parallel lines of grout holes, spaced at 1.5 m, installed to a depth of 9 m into rock. The foundation drainage system comprises a box drain at the concrete–rock contact. The locations of these provisions are shown in Fig. 11.14. No pressure relief wells were installed during construction.

The bedrock consists of six different interlayered rock types, most of which contain several weak zones. The rock structure is characterized by major bedding planes (N 50°

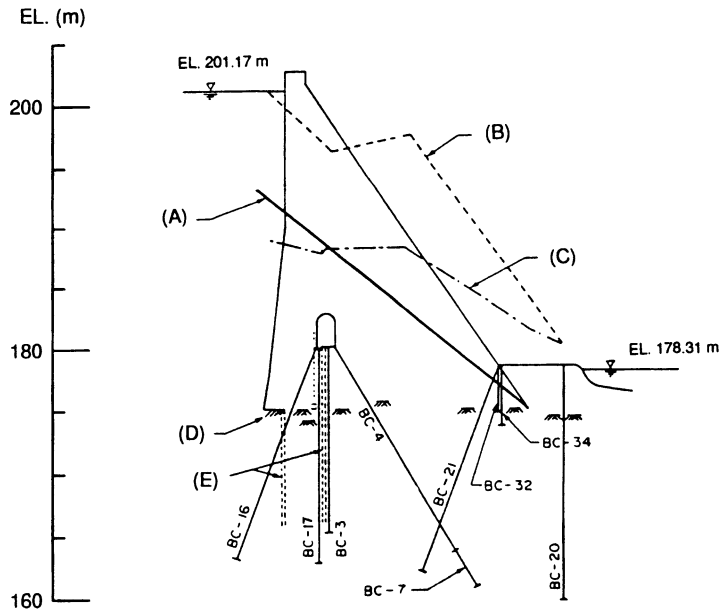


FIGURE 11.14. Cross-section of Barrett Chute Dam for stability analysis: A, original design assumption; B, uplift pressure in April 1987 (pretreatment); C, uplift pressure in September (post-treatment); D, bedrock surface; E, grout curtains.

W/25–30° NE). Five sets of shear joints with spacing of about 1–3 m were also founded in the main dam area.

As a result of these geological conditions, the excavated rock surface during construction has a "saw tooth" feature, and the contact between the dam foundation and rock is not a plane surface. This complex geometry makes it impossible to predict what inclination of the contact would be obtained during drilling for sample recovery. Thus, the test program had to be continuously modified to optimize sample usage because of these practical difficulties. Fortunately, the apparatus was designed to accommodate a wide variety of sample sizes and inclination of contact so that "less than ideal" samples recovered may be tested (see Chapter 6).

11.3.7.2 Field Investigation and Condition of Contact

Subsequent to the Phase I study, the field program consisting of 29 boreholes for Phase II was carried out in 1987. In addition to recovery of contact and rock samples for laboratory testing, pressure tests and dye tests were performed in selected boreholes to detect any interconnection of flow channel through the contact or rock discontinuities. In one region (CH. 0 + 91 to 1 + 83), it was found that pressure response in holes adjacent to the test hole was almost instantaneous, indicating strong hydraulic connectivity. An additional 17 boreholes were drilled in 1988.

A study of the contact conditions of the cores recovered indicated that there was no evidence of concentration of unbonded contact at any particular area and the unbonded contacts were roughly evenly distributed. Based on these results, together with information from pressure tests, it was deduced that for overall condition of the entire dam approximately 40% of the interface was unbonded. At the critical sections between CH. 1 + 22 and 1 + 55, the unbonded portion reached 50%. This value will be used to arrive at the strength parameters for stability analysis.

11.3.7.3 Results of Laboratory Tests and Strength Parameters for Design Analysis

1. Bonded contacts. A series of direct tension, triaxial extension and triaxial compression tests (see Chapter 6, Section 6.3) was performed on bonded contacts between concrete and the two main foundation rock types, hornblende biotite gneiss and crystalline limestone. The results showed that the strength parameters of bonded contact may be represented by tensile strength $\sigma_t = 482$ kPa, cohesion $c = 964$ kPa, and friction angle $\phi = 62°$ (Lo *et al.* 1991a).

2. Unbonded contacts. The strengths along the unbonded contact were obtained using the method described in Chapter 6 (Section 6.6.2). The results of tests on unbonded contacts show that the basic friction angle, ϕ_b, for concrete–limestone contacts is approximately 40°. The value of ϕ_b for concrete–gneiss contacts varies from 35 to 43°, averaging 39°. A value of ϕ_b of 40° is therefore adopted.

The geometric components of shear strength, as occurring in the field, must be added to the basic friction. The roughness profiles of selected chainages are shown in Fig. 11.12. It may be seen that the base of the dam is essentially horizontal overall, so that the β-effect may be neglected. The roughness angle, i, is taken to be 5°. The operative friction angle of the unbonded portion of the dam in the field is therefore $\phi = \phi_b + i = 45°$.

3. Overall strength parameters for stability analysis. The percentage of unbonded area has been deduced to be 0.5 previously. Applying this reduction factor to the tensile strength and cohesion of bonded contacts, the complete set of strength parameters for

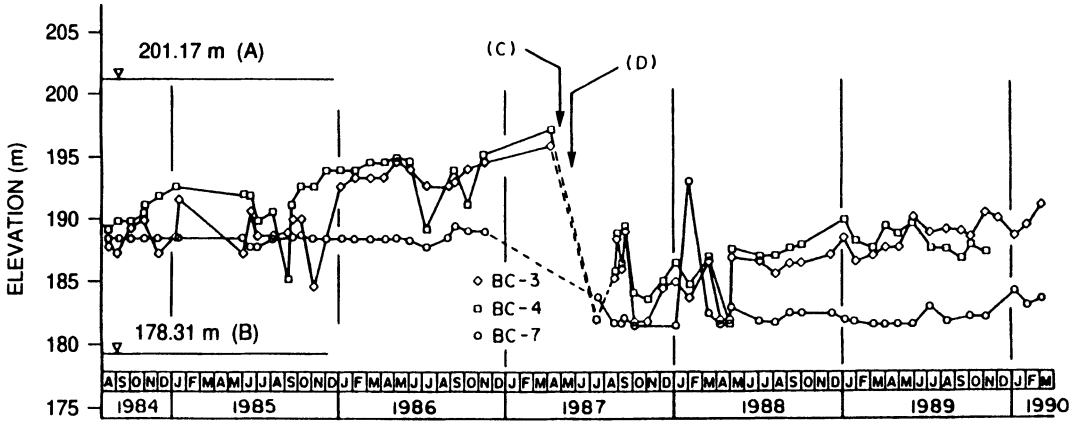


FIGURE 11.15. Measured uplift pressures in the observation wells of Barrett Chute Dam: A, headpond water-level; B, tailrace water-level; C, Phase II investigation; D, installation of relief wells.

stability analysis are: σ_t = 241 kPa, c = 482 kPa, and ϕ = 45°.

For the major joint sets in limestone, the strength parameters used are: c = 0, ϕ = 32°, and for joints in hornblende biotite gneiss, c = 0, ϕ = 35°.

11.3.7.4 High Uplift Pressures Measured and Remedial Measures

As part of the Phase II investigation, the results of uplift pressure measurement were reviewed in detail in 1987. Typical results are shown in Fig. 11.15 for variation of uplift pressures with time and in Fig. 11.14 for comparison with "design uplift" used for design of the dam in 1938. From these results, the following observations were made:

- Zones of high uplift pressure persisted. At some locations, the uplift pressures were about twice the design value.
- At zones of high uplift pressure, the uplift pressures were increasing with time at constant upstream water-level, e.g. see observation holes BC-3 and BC-4.

It is clear that the grout curtain and drainage provision were ineffective with respect to design requirements. The bedrock at zones of high uplift pressure is interlayered crystalline limestone, altered limestone, pegmatite and quartzitic gneiss, each of which contains several weak seams with apparent downstream dips. By coincidence, the sections from CH. 1 + 16 to 1 + 83 were not keyed into rock. It is therefore evident that such an unfavorable condition could not be allowed to persist. Corrective measures, in the form of relief wells, were immediately undertaken to reduce the high uplift pressure. For this purpose, the pressure relief wells were drilled to depths ranging generally from 12 to 23 m, according to the geological condition, to intersect water-bearing discontinuities in the rock. The effectiveness of the corrective measure may be seen in Figs 11.14 and 11.15. The uplift pressure was reduced considerably to values closer to the design value. Results of measurement subsequent to 1987 indicated that there was a slight tendency for the uplift pressures to increase with time. Continuous surveillance has been undertaken and the performance of the dam will be further assessed in the future. Stability analyses using the input data obtained are discussed in the following section.

TABLE 11.10. Results of stability study of Barrett Chute Dam

Method	ΣV kN	ΣH kN	ΣU kN	ΣM kN · m	e (or e')	Case 1[a] T_c[c] m	Case 1[a] FS	Case 2[b] T_c[c] m	Case 2[b] FS_1	Remarks
Before treatment										
A	6917	3283	3969	7464	1.08	1.28	0.90	0	3.90	USAC
B	6917	3283	3969	7464	4.30	2.68	0.90	0	3.90	USBR
C	6917	3283	3969	7464		3.5	0.84	0	3.51	Ontario Hydro
D	6917	3283	3969	7464	4.30	2.68	0.90	0	3.90	Modified USBR
After treatment										
A	6917	3283	1300	7464	1.08	0	1.70	0	4.70	USAC
B	6917	3283	1300	7464	1.43	0	1.70	0	4.70	USBR
C	6917	3283	1300	7464		0	1.66	0	4.58	Ontario Hydro
D	6917	3283	1300	7464	1.43	0	1.70	0	4.70	Modified USBR

[a] Case 1: FS = factor of safety; $\phi = 45°$; $c = \sigma_t = 0$.
[b] Case 2: FS_1 = factor of safety; $\phi = 45°$, $c = 482$ kPa; $\sigma_t = 241$ kPa.
[c] T_c = crack length.

11.3.7.5 Stability Study

Of special interest to the present study is the high uplift pressure measured during investigation in 1987. This high pressure has subsequently been drawn by drilling relief wells. It is evident, therefore, that this dam has been subjected to and withstood a "critical test" recently.

The section analyzed is shown in Fig. 11.14, representing the highest sections of the dam. In these sections, the base of the dam was not keyed in. The measured pretreatment and post-treatment uplift pressures used in the analyses are shown.

Four methods of analysis were used:

- the US Army Corps of Engineers (USAC) method,
- the US Bureau of Reclamation (USBR) method,
- Ontario Hydro method, and
- the modified USBR method, (this takes tensile strength into consideration, and the derivation of this method is described in Lo *et al. (1990).*

The results of computation are shown in Table 11.10. The factor of safety, FS, is that obtained for $c = 0$; while FS_1 denotes the factor of safety with $c = 482$ kPa.

From Table 11.10, three important observations may be made:

1. If cohesion is neglected, FS is below unity in all cases considered during the period of high uplift pressure that the dam had experienced. Within this framework of limit equilibrium analysis, it is evident that neglecting cohesion is too conservative since the dam was in normal operation.
2. If cohesion is considered, the factor of safety FS_1 is clearly adequate in all cases, consistent with the performance of the dam.
3. After pressure relief, the factors of safety FS and FS_1 increase substantially. Irrespective of the methods of computation, therefore, the beneficial effect of drainage holes as remedial treatments is decisive.

11.3.8 EXPERIENCE GAINED AND BENEFITS DERIVED FROM APPLICATION OF THE METHODOLOGY

Since the start of the dam safety program of Ontario Hydro, 38 concrete dams on rock foundations have undergone Phase II study (Lo & Hefny 1998). These dams were built between 1907 and 1968, with heights ranging from 6 to 72 m. The operational or "equiva-

12. DYNAMICS OF FOUNDATIONS

M. H. El Naggar

12.1 Introduction

Geotechnical engineers encounter problems related to the dynamic loading of foundations when designing foundations for machinery and vibrating equipment or designing foundations for structures subjected to seismic loading. This chapter will focus on the former case and the latter will be treated in Chapter 21.

12.1.1 DESIGN OBJECTIVES

The design of foundations for vibrating equipment is always governed by displacement considerations. The displacement of foundations subjected to dynamic loads depends on the type and geometry of the foundation, the flexibility of the supporting ground and the type of dynamic loading. The main objective of the design is to limit the response amplitudes of the foundation in all vibration modes to the specified tolerance. Usually the tolerance is set by the machine manufacturer to ensure a satisfactory performance of the machine and minimum disturbance for people working in its immediate vicinity. Another objective that could be extremely important in some cases is to limit vibration propagating from the footing into the surroundings.

To achieve these objectives, the design of a machine foundation involves a trial-and-error procedure (Gazetas, 1991). This procedure includes the following steps:

1. Estimating the dynamic loads. This step is described in Section 12.1.2.
2. Establishing the soil profile and evaluating the soil properties required for the dynamic analysis (shear modulus, mass density, Poisson's ratio and material damping ratio).
3. Based on experience, selecting the type and trial dimensions of the foundation (discussed in Section 12.1.3) and with the clients input, establishing the performance criteria.
4. Computing the dynamic response of the trial foundation (step 3) supported by the given soil profile (step 2) due to the estimated load (step 1) and comparing the response with the performance criteria. If the response is not satisfactory, modifying the dimensions of the foundation (step 3) and repeating the analysis until satisfactory design is achieved.

12.1.2 TYPES OF DYNAMIC LOADS

The type of response of a system depends on the nature of the loads applied. The loads and responses resulting from them can be periodic, transient or random. Rotating machines produce centrifugal periodic forces due to unbalanced rotors. An unbalanced mass, m_e, rotating with an eccentricity, e, and circular velocity, ω, produces a centrifugal force, $P = m_e e\omega^2$. Its horizontal (vertical) component is $P = m_e e\omega^2 \cos\omega t(\sin \omega t)$ where t is time. Reciprocating machines produce biharmonic inertia forces and centrifugal forces associated with the motion of the piston, the fly wheel and the crank mechanism. Arya *et al.* (1979) provide tables for typical values of eccentricity for rotating ma-

R. K. Rowe (ed.), *Geotechnical and Geoenvironmental Engineering Handbook*
© Kluwer Academic Publishers 2001

chines, and unbalanced forces and couples for different crank arrangements. Das (1995) describes the mathematical derivation of these forces. In design situations, the excitation forces should be provided by the manufacturer of the machine. Transient loading is characterized by a non-periodic time history of limited duration. The load time history could be smooth, as the one produced by hammer blows, or more irregular, similar to that generated by crushers and shredders. This type of loading is represented either by an analytical expression or by a set of digital data. Random loading is an irregular process, which cannot be predicted mathematically with accuracy because it never repeats itself exactly. Fluctuating forces produced by mills, pumps and crushers are typical of this category. A random force and its effect is most meaningfully treated in statistical terms, and its energy distribution with regard to frequency is described by a power spectral density (power spectrum). Detailed information on dynamic loading may be found in Barkan (1962), Richart (1975), Arya *et al.* (1979) and Prakash & Puri (1988).

12.1.3 TYPES OF FOUNDATIONS

Machine foundations are designed as block foundations, wall foundations, mat foundations or frame foundations. Block foundations are solid blocks of concrete with sizable thickness, wall foundations are block foundations with cavities, and mat foundations are foundations with a limited thickness compared to their surface dimensions. Block foundations, the most common type, and wall foundations behave as rigid bodies. Mat foundations of small depth may behave as elastic slabs. Sometimes the foundation features a joint slab supporting a few rigid blocks for individual machines. The foundations can rest directly on soil (shallow foundations) or on piles (deep foundations). The foundation type results in considerable differences in response.

12.2 Shallow Foundations

The dynamic response of foundations depends on stiffness and damping characteristics. This section presents a general introduction to this subject and a summary of approaches and formulae that can be used to evaluate the stiffness and damping of shallow foundations.

12.2.1 IMPEDANCE FUNCTIONS OF SHALLOW FOUNDATIONS

The basic mathematical model used in the dynamic analysis is a lumped mass with a spring and dashpot, shown in Fig. 12.1. If the mass, m, is free to move in only one direction, e.g. vertical, it is said to have one degree-of-freedom. The foundation block has six degrees-of-freedom, three translational and three rotational. These are the displacements along the axes x, y and z, and rotation about the same axes (Fig. 12.2).

The response of the mass depends on the nature of the soil reaction, which is modeled by both the spring and the dashpot. The spring represents the elasticity of the soil and is characterized by the stiffness constant, k, which is defined as the force that produces a unit compression (or extension), v, of the spring in the positive direction of the displacement of the mass. The dashpot represents damping caused by energy dissipation. Damping stems from two sources, energy dissipated through waves spreading away from the foundation (radiation damping) and energy dissipated due to the imperfect elasticity of the soil (hysteretic or material damp-

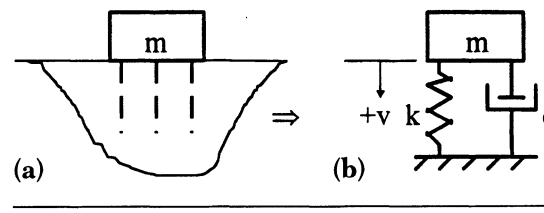


FIGURE 12.1. The basic mathematical model used in foundation dynamics: (a) actual system, and (b) basic model of one degree-of-freedom system.

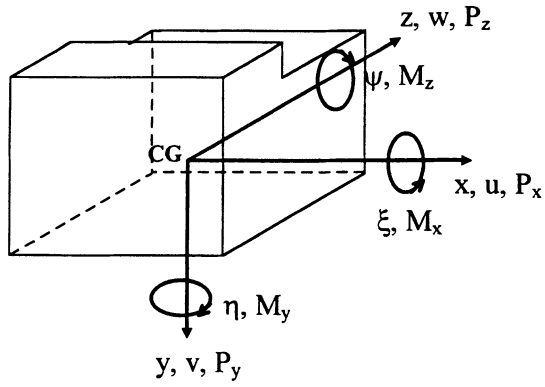


FIGURE 12.2. The co-ordinate system and possible displacements. CG = centre of gravity.

ing). A characteristic feature of damping forces is that they lag the displacement and are out of phase with the motion.

Shallow foundations are often idealized by a massless circular disk. The stiffness and damping constants of a massless circular disk resting on the surface of a linear viscoelastic halfspace were obtained using a three-dimensional or two-dimensional continuum approach. The analytical solutions were initiated by Reissner (1936) and followed by the contribution of many researchers, e.g. Bycroft (1965), Luco & Westman (1971), Veletsos & Verbic (1973), Veletsos & Nair (1974), Kobori *et al.* (1971) to name a few. The finite element and boundary element solutions were introduced by Lysmer and Kuhlemyer (1969), Kausel *et al.* (1975), Veletsos & Wei (1971) and Luco & Hadjian (1974). For circular bases the complex stiffness, K_i (also called the dynamic impedance function), associated with direction, i, is obtained by the determination of the relationship between a harmonic force acting on a massless disk resting on the surface of the halfspace and the resulting displacement of the disk. This complex stiffness can be expressed in terms of the true stiffness constant, k_i, and damping constant, c_i, as:

$$K_i = \bar{k}_i[k_i'(a_0) + ia_0c_i'(a_0)] \tag{12.1}$$

in which $\bar{k}_i$ = static stiffness; $a_0 = (\omega R/V_s)$ = dimensionless frequency; R = the disc radius; $V_s = (G/\rho)^{1/2}$ = shear wave velocity of the soil, G and ρ are the soil shear modulus and mass density, respectively; and k_i' and c_i' = stiffness and damping constants normalized as follows: $k_i' = k_i/\bar{k}_i$, $c_i' = (V_s/\bar{k}_iR)c_i$. In the case of an isotropic homogeneous halfspace, the approximate static stiffness constants for the vertical translation, v, horizontal translation (sliding), u, rocking, ψ, and torsion, η, are shown in Table 12.1, in which ν = Poisson's ratio and G = the soil shear modulus. Figure 12.3 shows the variation of k_i' and c_i' with frequency.

For shapes which differ from circular, the real non-circular base is replaced by an equivalent circular base with a suitable radius. The radius of the equivalent circular foundation is usually determined by equating the areas of the actual base, A_0, and equivalent base for vertical and horizontal translations, the moments of inertia, I_0, for rotation in the vertical plane (rocking) and the polar moments of inertia, J_0, for torsion about the vertical axis. For rectangular bases having dimensions a and b, the equivalent radii are given in Table 12.2.

Meek & Veletsos (1974), Meek & Wolf (1992a, b, 1994) and Wolf (1995) used cone idealization to model foundations on a homogeneous soil halfspace. In this idealization, the dynamic impedance functions

TABLE 12.1. Static stiffnesses of a disk resting on the surface of a homogeneous halfspace

Vertical	Horizontal	Rocking	Torsion
$\bar{k}_v = \frac{4GR}{1-\nu}$	$\bar{k}_u = \frac{8GR}{2-\nu}$	$\bar{k}_\psi = \frac{8GR^3}{3(1-\nu)}$	$\bar{k}_\eta = \frac{16GR^3}{3}$

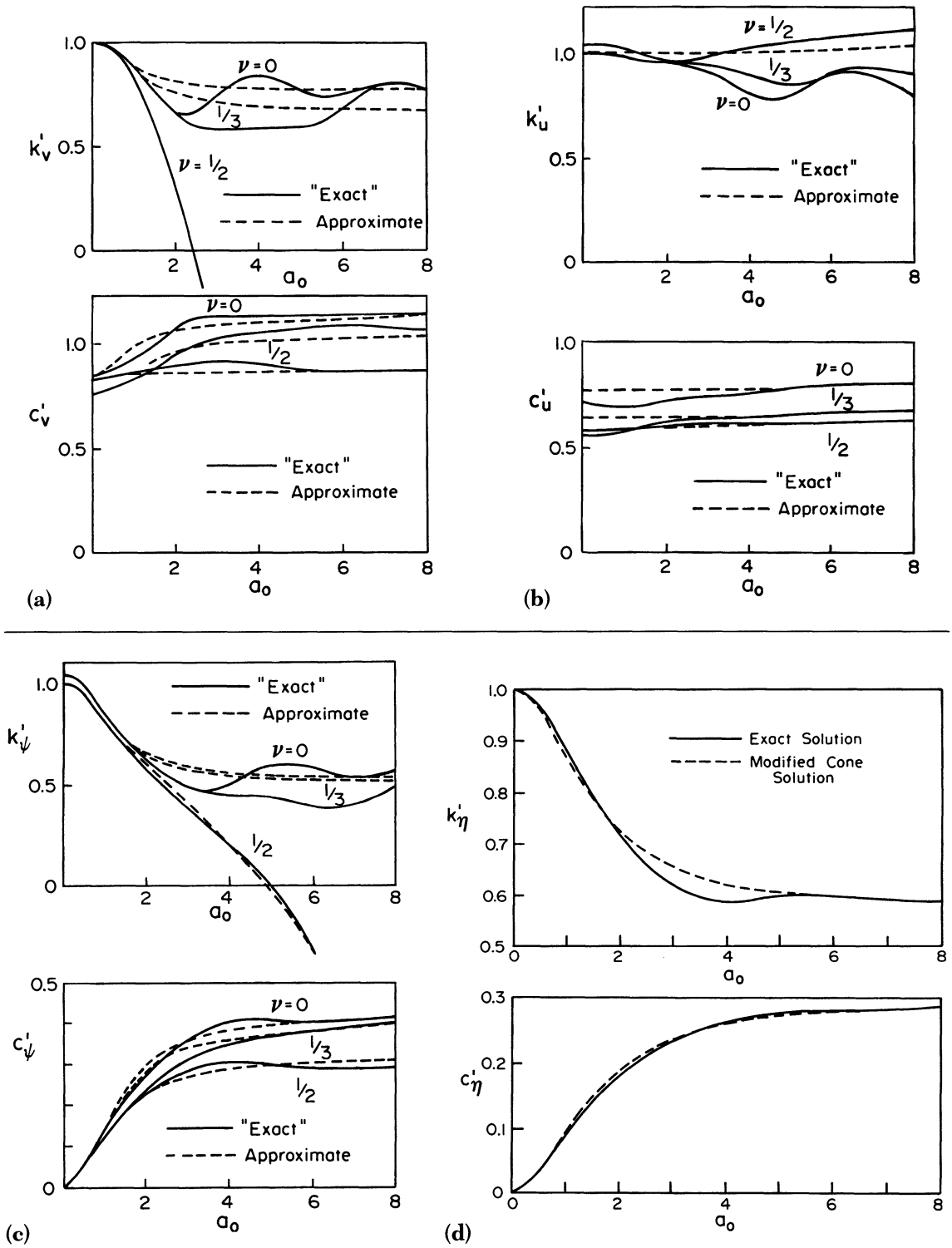


FIGURE 12.3. The stiffness and damping parameters for a circular disk on the surface of a halfspace: (a) vertical excitation, (b) horizontal excitation, (c) rocking excitation, and (d) torsional excitation. (Exact solution by Luco & Westmann 1971, modified from Veletsos & Verbic 1974; Veletsos & Nair 1974). (—) Exact solution, (---) approximate solution, (...) modified cone solution.

TABLE 12.2. Equivalent radii for a rectangular footing having dimensions a and b

Vertical	Horizontal	Rocking	Torsion
$R = \sqrt{\frac{ab}{\pi}}$	$R = \sqrt{\frac{ab}{\pi}}$	$R = \sqrt[4]{\frac{a^3b}{3\pi}}$	$R = \sqrt[4]{\frac{ab(a^2 + b^2)}{6\pi}}$

TABLE 12.3. Parameters of cone model footings resting on surface of soil halfspace

	Vertical	Horizontal	Rocking	Torsion
R	$(A_0/\pi)^{1/2}$	$(A_0/\pi)^{1/2}$	$(4I_0/\pi)^{1/4}$	$(2J_0/\pi)^{1/4}$
V	V_P $\nu \le 1/3$ $2V_s$ $\nu \ge 1/3$	V_s	V_P $\nu \le 1/3$ $2V_s$ $\nu \ge 1/3$	V_s
Z_0/R	$\frac{\pi}{4}(1 - \nu)\left(\frac{V}{V_s}\right)^2$	$(\pi/8)(2 - \nu)$	$\frac{9\pi}{32}(1 - \nu)\left(\frac{V}{V_s}\right)^2$	$\frac{9\pi}{32}$
μ	0 $\nu \le 1/3$ $2.4\left(\nu - \frac{1}{3}\right)\rho A_0 R$ $\nu \ge 1/3$	0	0 $\nu \le 1/3$ $1.2\left(\nu - \frac{1}{3}\right)\rho I_0 R$ $\nu \ge 1/3$	0

are expressed by Eq. 12.1, where $\bar{k}_i$ is given in Table 12.1, the model parameters are given in Table 12.3 and k_i' and c_i' are given by:

$$k_i'(a_0) = 1 - \frac{\mu}{\pi}\frac{z_0}{R}\frac{V_s^2}{V}a_0^2 \qquad (12.2)$$

and

$$c_i'(a_0) = 1 - \frac{z_0}{R}\frac{V_s}{V} \qquad (12.3)$$

where V = the pertinent wave velocity as given in Table 12.3, in which V_p = the dilational wave velocity = $\{2(G/\rho)[(1 - 2)/(1 - 2\nu)]\}^{1/2}$.

To account for the material (hysteretic) damping in these models, the correspondence principle is used. The damped stiffness and damping constants including the soil hysteretic damping, β, are then:

$$k_{i\beta}'(a_0) = 1 - \frac{\mu}{\pi}\frac{z_0}{R}\frac{V_s^2}{V}a_0^2 - \beta\frac{z_0}{R}\frac{V_s}{V}a_0 \qquad (12.4)$$

and

$$c_{i\beta}'(a_0) = \frac{z_0}{R}\frac{V_s}{V} + \frac{2\beta}{a_0}k_i'. \qquad (12.5)$$

12.2.2 EMBEDMENT EFFECTS

Embedment is known to increase both stiffness and damping, but the increase in damping is more significant. The finite element approach has been used to calculate the stiffness and damping of embedded foundations by a number of investigators, e.g. Urlich & Kuhlemeyer (1973) and Kausel & Ushijima (1979). Boundary element solutions were formulated by Kobayashi & Nishimura (1983), Wolf & Darbre (1984) and Karabalis & Beskos (1985). Alternatively, the response of embedded footings can be approximated by assuming that soil reactions acting on the base are equal to those of a surface footing, and the reactions acting on the footing sides are equal to those of an independent layer overlying the halfspace (Fig. 12.4). Novak and associates (Novak & Beredugo 1972, Beredugo & Novak 1972 and Novak & Sachs 1973) found that this approximate approach

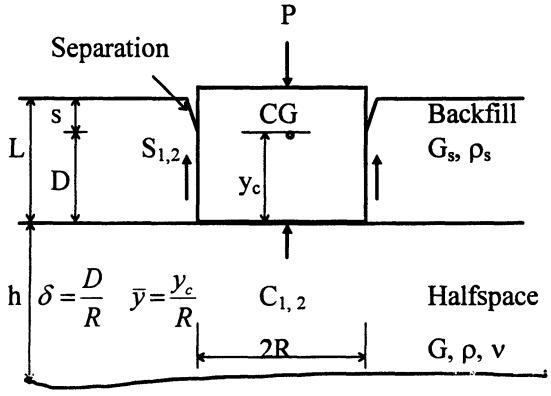


FIGURE 12.4. Notations for an embedded foundation: CG = centre of gravity.

works quite well, especially for higher frequencies. Using plane strain solutions for side reactions and half-space solution for base reactions, and the notations in Fig. 12.4, the stiffness and damping constants are given in Table 12.4.

The parameters C, in Table 12.4, relate to the reactions acting on the base (Veletsos & Verbic, 1973 and Veletsos & Nair, 1974) and parameters S relate to side reactions (Novak *et al.* 1978). Parameters C and S are frequency dependent. However, given all the approximations involved in modeling dynamic soil behavior it is often sufficient to select suitable constant values to represent the parameters over a limited frequency range. Such constant values are suggested in Table 12.5. The lack of confining pressure at the surface often leads to separation of the soil from the foundation, which reduces the effectiveness of embedment. This effect can be corrected approximately by considering an effective embedment depth, D, smaller than the true one. An extensive set of tables and charts for stiffness and damping constants of embedded footings of arbitrary shapes is given in Gazetas (1991).

12.2.3 IMPEDANCE FUNCTIONS OF A LAYER ON HALFSPACE

The impedance functions of a shallow layer are different from that of the halfspace. In

TABLE 12.4. Stiffness and damping constants for embedded footings

Motion	Stiffness constant, k	Damping constant, c
Vertical	$GR[C_{v1} + (G_s/G)\delta S_{v1}]$	$R^2(\rho G)^{1/2}\left[C_{v2} + S_{v2}\delta\left(\frac{\rho_s}{\rho}\frac{G_s}{G}\right)^{1/2}\right]$
Torsional	$GR^3[C_{\eta 1} + (G_s/G)\delta S_{\eta 1}]$	$R^4(\rho G)^{1/2}\left[C_{\eta 2} + S_{\eta 2}\delta\left(\frac{\rho_s}{\rho}\frac{G_s}{G}\right)^{1/2}\right]$
Horizontal	$GR[C_{u1} + (G_s/G)\delta S_{u1}]$	$R^2(\rho G)^{1/2}\left[C_{u2} + \delta\left(\frac{\rho_s}{\rho}\frac{G_s}{G}\right)^{1/2} S_{u2}\right]$
Rocking	$GR^3\left[\bar{y}^2 C_{u1} + \frac{G_s}{G}\delta\left(\frac{\delta^2}{3} + \bar{y}^2 - \delta\bar{y}\right)S_{u1}\right]$	$R^4(\rho G)^{1/2}\left[\bar{y}^2 C_{u2} + \delta\left(\frac{\rho_s}{\rho}\frac{G_s}{G}\right)^{1/2}\left(\frac{\delta^2}{3} + \bar{y}^2 - \delta\bar{y}\right)S_{u2}\right]$
	$+ GR_\psi^3\left(C_{\psi 1} + \frac{G_s}{G}\delta_\psi S_{\psi 1}\right)$	$+ R_\psi^4(\rho G)^{1/2}\left[C_{\psi 2} + \delta_\psi\left(\frac{\rho_2}{\rho}\frac{G_s}{G}\right)^{1/2} S_{\psi 2}\right]$
Coupling	$-GR\left[y_c C_{u1} + \frac{G_s}{G}\delta\left(y_c - \frac{D}{2}\right)S_{u1}\right]$	$-R^2(\rho G)^{1/2}\left\{y_c C_{u2} + \delta\left(\frac{\rho_s}{\rho}\frac{G_s}{G}\right)^{1/2}[y_c - (D/2)]S_{u2}\right\}$

TABLE 12.5. Stiffness and damping parameters ($\beta = 0$)

Motion	Soil	Side layer		Halfspace	
Vertical	Cohesive	$S_{v1} = 2.7$	$S_{v2} = 6.7$	$C_{v1} = 7.5$	$C_{v2} = 6.8$
	Granular	$S_{v1} = 2.7$	$S_{v2} = 6.7$	$C_{v1} = 5.2$	$C_{v2} = 5.0$
Horizontal	Cohesive	$S_{u1} = 4.1$	$S_{u2} = 10.6$	$C_{u1} = 5.1$	$C_{u2} = 3.2$
	Granular	$S_{u1} = 4.0$	$S_{u2} = 9.1$	$C_{u1} = 4.7$	$C_{u2} = 2.8$
Rocking	Cohesive	$S_{\psi 1} = 2.5$	$S_{\psi 2} = 1.8$	$C_{\psi 1} = 4.3$	$C_{\psi 2} = 0.7$
	Granular	$S_{\psi 1} = 2.5$	$S_{\psi 2} = 1.8$	$C_{\psi 1} = 3.3$	$C_{\psi 2} = 0.5$
Torsion	Cohesive and granular	$S_{\eta 1} = 10.2$	$S_{\eta 2} = 5.4$	$C_{\eta 1} = 4.3$	$C_{\eta 2} = 0.7$

the case of a shallow layer, the stiffness increases and geometric damping decreases or even vanishes. Studies of the behavior of strata suggest that geometric damping may completely vanish if the excitation frequency is lower than the first natural frequency of the soil layer (Kobori *et al.* 1971 and Nogami & Novak 1976). For a homogeneous soil layer, the first vertical and horizontal natural frequencies, ω_v and ω_u, respectively, are:

$$\omega_v = \frac{\pi V_s}{2H}\left(\frac{2(2-\nu)}{1-2\nu}\right)^{1/2} \tag{12.6}$$

and

$$\omega_u = \frac{\pi V_s}{2H}. \tag{12.7}$$

At frequencies lower than ω_v and ω_u, the only source of damping is the material damping. In this case, the damping parameters may be:

$$S_{u2} = 2\beta\frac{S_{u1}}{a_0} \tag{12.8}$$

and

$$S_{v2} = 2\beta\frac{S_{v1}}{a_0}. \tag{12.9}$$

The static stiffness of a footing embedded in a layer of limited thickness in the horizontal and rocking modes was derived by Elsabee & Morray (1977) and in the vertical and torsional modes by Kausel & Ushijima (1979). The impedance functions are defined similar to Eq. 12.1. In this case $\bar{k}$ are the static stiffnesses of circular foundations embedded in a soil layer of total depth, H, and are given by:

$$\bar{k}_v = \frac{4GR}{1-\nu}\left(1+1.28\frac{R}{H}\right)(1+0.47\delta) \times\left[1+2(0.85-0.28\delta)\frac{(D/H)}{1-(D/H)}\right] \tag{12.10a}$$

$$\bar{k}_u = \frac{8GR}{2-\nu}\left(1+\frac{1}{2}\frac{R}{H}\right)\left(1+\frac{2}{3}\delta\right)\left(1+\frac{5}{4}\frac{D}{H}\right) \tag{12.10b}$$

$$\bar{k}_\phi = \frac{8GR^3}{3(1-\nu)}\left(1+\frac{1}{6}\frac{R}{H}\right)(1+2\delta)\left(1+0.7\frac{D}{H}\right) \tag{12.10c}$$

$$\bar{k}_{u\phi} = (0.4\delta - 0.03)R\bar{k}_u \tag{12.10d}$$

$$\bar{k}_\eta = \frac{16GR^3}{3}(1+2.67\delta). \tag{12.10e}$$

These empirical expressions for the stiffness suggested by these authors are referred to the center of the base and are valid for $\delta = D/R \leq 1.5$, $D/H \leq 0.75$ and $R/H \leq 0.5$. Kausel & Ushijima (1979) recommend taking k' and c' equal to the halfspace functions (Eq. 12.1 and Fig. 12.3), except for c' in the low frequency range. For frequencies below the first layer natural frequencies, it would be safe to ignore geometric damping completely, and the damping can be established as a fraction of stiffness giving c as:

$$c = \bar{k}k'\frac{2\beta}{\omega}. \tag{12.11}$$

Similar formulae for foundations on shallow layer can be found in Gazetas (1991). The solutions for impedance functions of shallow

foundations on different soil profiles are incorporated in an efficient computer program, Dyna5 (Novak *et al.* 1999).

12.3 Deep Foundations

Stiffness and damping of piles are affected by interaction of the piles with the surrounding soil. To account for this interaction, a few approaches are employed: the continuum approach (Tajimi 1969, Kobori *et al.* 1977 and Novak & Nogami, 1977); the lumped mass model (Penzian *et al.* 1964, Matlock *et al.* 1978); the finite element method (Kuhlemeyer, 1979, Blaney *et al.*, 1976, Wolf & von Arx, 1978); boundary element solutions (Kaynia & Kausel, 1982 and Davies *et al.*, 1985); and simplified approach (Gazetas & Dobry, 1984, Dobry & Gazetas, 1985 and Dobry & Gazetas, 1988). In groups of closely spaced piles, the character of dynamic stiffness and damping is further complicated by interaction between individual piles. It is useful therefore to discuss single piles first.

12.3.1 IMPEDANCE FUNCTIONS OF PILES

Dynamic behavior of piles depends on frequency and the properties of both the pile and soil. The pile is described by its length, bending and axial stiffness, tip and head conditions, mass and batter. Soil behavior depends on soil properties and their variation with depth and layering. The impedance functions of piles can be described as:

$$K_i = k_i(a_0) + i\omega c_i(a_0). \qquad (12.12)$$

Dynamic stiffness is generated by calculating the forces needed to produce vibration of the pile head, having a unit amplitude in the prescribed direction. Novak (1974) described the stiffness constants, k_i, and the constants of equivalent viscous damping, c_i, for individual motions of the pile head as shown in Table 12.6, where E_p = the Young's modulus of the pile; A, I and G_pJ = its cross-sectional area, moment of inertia and torsional stiffness, respectively. R = the radius of circular piles and equivalent radius for non-circular piles.

The symbol $f_{1,2}$ in Table 12.6 represents dimensionless stiffness and damping functions, whose subscript 1 indicates stiffness and 2 indicates damping. These functions depend on the following parameters: the relative stiffness of the pile and soil, E_p/G; dimensionless frequency, a_0; the slenderness ratio, L/R, in which L = pile length; material damping of both the soil and pile; the variation of soil and pile properties with depth; and the tip and head conditions. To account accurately for all these factors, the use of a computer is necessary. A method suitable for such calculations and accounting for an arbitrary soil profile has been presented by Novak & Aboul-Ella (1978) and extended to include pile separation by Novak & Sheta (1980). These solutions are based on plane strain soil reactions and their use is facilitated by an efficient computer program, Dyna5 (Novak *et al.* 1999). However, not all factors affecting function, f, are of equal importance in all situations. The most important factors are: E_p/G, the soil profile and, for the vertical direction, the tip condition. The stiffness and damping parameters, $f_{1,2}$, are given for a few basic cases in Table 12.7, for horizontal re-

TABLE 12.6. Stiffness and damping constants for single piles

Vertical	Horizontal	Rocking	Coupling	Torsion
$k_v = \frac{E_pA}{R}f_{v1}$	$k_u = \frac{E_pI}{R^3}f_{u1}$	$k_\psi = \frac{E_pI}{R}f_{\psi 1}$	$k_c = \frac{E_pI}{R^2}f_{c1}$	$c_\eta = \frac{G_pJ}{V_s}f_{\eta 2}$
$c_v = \frac{E_pA}{V_s}f_{v2}$	$c_u = \frac{E_pI}{R^2V_s}f_{u1}$	$c_\psi = \frac{E_pI}{V_s}f_{\psi 2}$	$c_c = \frac{E_pI}{RV_s}f_{c2}$	$c_\eta = \frac{G_pJ}{V_s}f_{\eta 2}$

TABLE 12.7. Stiffness and damping parameters of horizontal response ($L/R > 25$ for homogeneous soil and $L/R > 30$ for parabolic soil profile) (reproduced from Novak & El Sharnouby © 1983 with permission of ASCE)

Soil profile	ν	E_p/G	$f_{\psi 1}$	f_{c1}	f_{u1}	f^p_{u1}	$f_{\psi 2}$	f_{c2}	f_{u2}	f^p_{u2}
	0.25	10 000	0.2135	−0.0217	0.0042	0.0021	0.1577	−0.0333	0.0107	0.0054
		2500	0.2998	−0.0429	0.0119	0.0061	0.2152	−0.0646	0.0297	0.0154
		1000	0.3741	−0.0668	0.0236	0.0123	0.2598	−0.0985	0.0579	0.0306
		500	0.4411	−0.0929	0.0395	0.0210	0.2953	−0.1337	0.0953	0.0514
		250	0.5186	−0.1281	0.0659	0.0358	0.3299	−0.1786	0.1556	0.0864
G_{soil}	0.4	10 000	0.2207	−0.0232	0.0047	0.0024	0.1634	−0.0358	0.0119	0.0060
		2500	0.3097	−0.0459	0.0132	0.0068	0.2224	−0.0692	0.0329	0.0171
Homogeneous		1000	0.3860	−0.0714	0.0261	0.0136	0.2677	−0.1052	0.0641	0.0339
		500	0.4547	−0.0991	0.0436	0.0231	0.3034	−0.1425	0.1054	0.0570
		250	0.5336	−0.1365	0.0726	0.0394	0.3377	−0.1896	0.1717	0.0957
	0.25	10 000	0.1800	−0.0144	0.0019	0.0008	0.1450	−0.0252	0.0060	0.0028
		2500	0.2452	−0.0267	0.0047	0.0020	0.2025	−0.0484	0.0159	0.0076
		1000	0.3000	−0.0400	0.0086	0.0037	0.2499	−0.0737	0.0303	0.0147
		500	0.3489	−0.0543	0.0136	0.0059	0.2910	−0.1008	0.0491	0.0241
		250	0.4049	−0.0734	0.0215	0.0094	0.3361	−0.1370	0.0793	0.0398
G_{soil}	0.4	10 000	0.1857	−0.0153	0.0020	0.0009	0.1508	−0.0271	0.0067	0.0031
		2500	0.2529	−0.0284	0.0051	0.0022	0.2101	−0.0519	0.0177	0.0084
Parabolic		1000	0.3094	−0.0426	0.0094	0.0041	0.2589	−0.0790	0.0336	0.0163
		500	0.3596	−0.0577	0.0149	0.0065	0.3009	−0.1079	0.0544	0.0269
		250	0.4170	−0.0780	0.0236	0.0103	0.3468	−0.1461	0.0880	0.0443

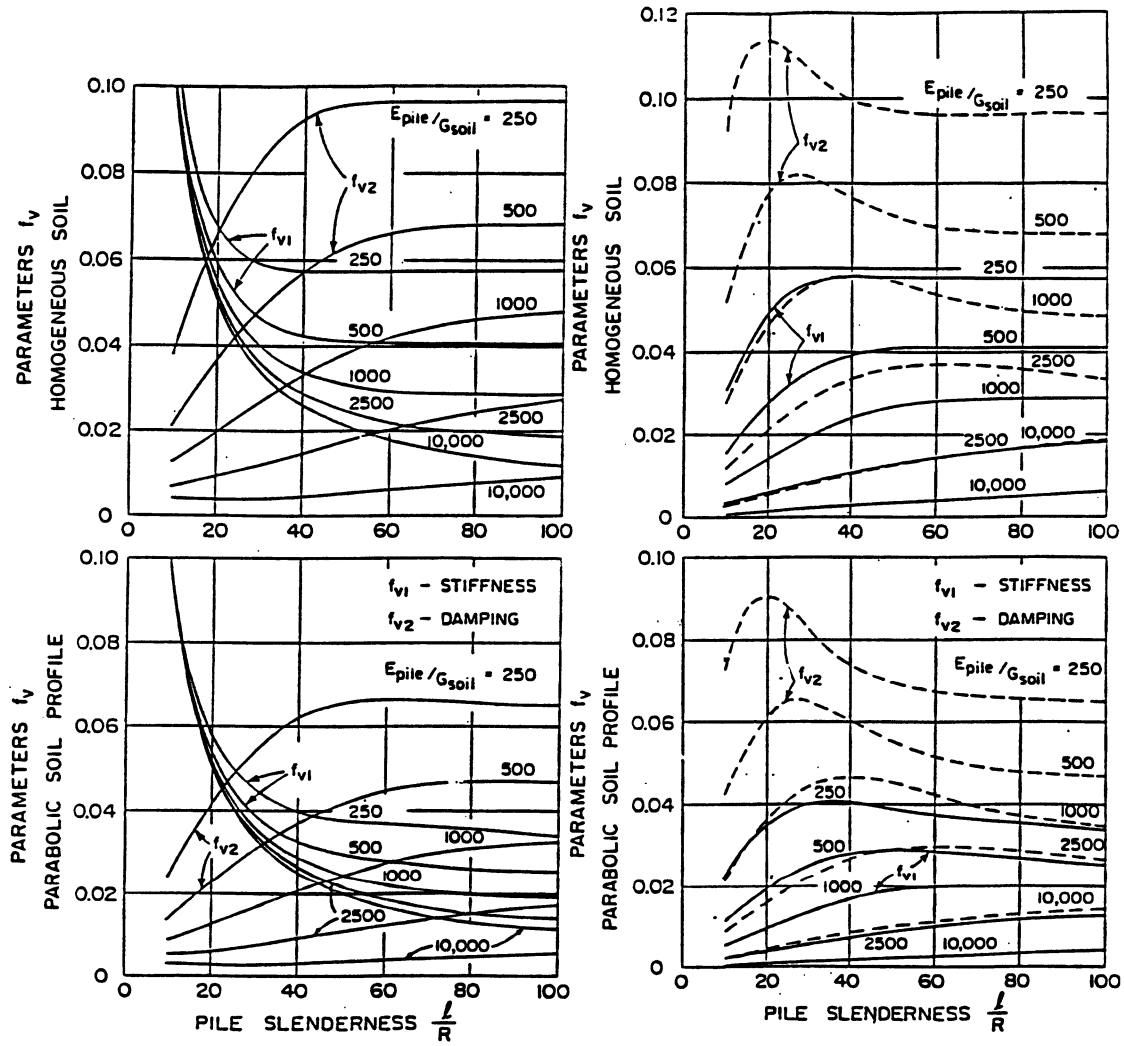


FIGURE 12.5. Vertical stiffness, f_{v1}, and damping, f_{v2}, parameters for (a) end bearing piles, and (b) floating piles (reproduced from Novak & El Sharnouby © 1983 with permission of ASCE).

sponse, and Fig. 12.5, for vertical response, for a dimensionless frequency, $a_0 = 0.3$. For other cases, see Novak & El Sharnouby (1983), which provides extensive coverage of a wide range of parameters, and the effect of limited stratum depth is also described.

Gazetas (1991) presented simple algebraic expressions to describe stiffness and damping constants of piles. These expressions are curve fits to rigorous numerical results and are reasonably accurate. Wolf (1995) generalized the cone model and produced expressions that can be used to develop the stiffness and damping parameters of piles.

12.3.2 PILE–SOIL–PILE INTERACTION

When piles in a group are closely spaced, they interact with each other because the displacement of one pile contributes to the displacement of others. For static loads, Poulos (1968, 1971b, 1979b) studied interaction between piles extensively (see also Chapter 10).

The studies of dynamic pile–soil–pile interaction are relatively recent and few in number. Wolf & von Arx (1978) and Wolf *et al.* (1981) used the finite element method, Waas and Hartmann (1981) developed a semi-analytical solution, Aubery & Chapel (1981) employed a boundary element approach, and Nogami (1980) and Sheta & Novak (1982) developed approximate solutions. These studies indicate that: dynamic group effects are profound and differ considerably from static group effects; dynamic stiffness and damping of piles groups vary with frequency, and these variations are greater than for single piles; group stiffness and damping can be either reduced or increased by pile–soil–pile interaction. Dynamic group effects are quite complex and there is no simple way of alleviating these complexities. The only simplifications available are the interaction factors approach and the approximate approach due to Dobry & Gazetas (1988) and Gazetas & Makris (1991) in which the interaction problem is reduced to the consideration of cylindrical wave propagation.

12.3.3 IMPEDANCE FUNCTIONS OF PILE GROUPS

To obtain an accurate analysis of dynamic behavior of pile groups it is necessary to use a suitable computer program. However, a simplified approximate analysis, can be formulated on the basis of interaction factors, α, introduced by Poulos (1971b) for static analysis and extended to the dynamic case by Kaynia & Kausel (1982), who presented charts for dynamic interaction. The interaction factors derive from the deformation of two equally loaded piles and give the increase in deformation of a pile due to deformation of an equally loaded neighboring pile. For a homogeneous halfspace, the interaction factors between two piles may be given by (Dobry & Gazetas 1988; Gazetas & Makris 1991).

$$\alpha_v \approx \frac{1}{(2)^{1/2}}\left(\frac{S}{d}\right)^{-0.5} \exp^{[-\beta\omega(S/V_s)]} \exp^{[-i\omega(S/V_s)]} \quad (12.12a)$$

and

$$\alpha_u(\theta^0) \approx \alpha_u(0^0)\cos^2\theta + \alpha_u(90^0)\sin^2\theta$$

where

$$\alpha_u(0^0) \approx \frac{1}{2}\left(\frac{S}{d}\right)^{-0.5} \exp^{[-\beta\omega(S/V_{La})]} \exp^{[-i\omega(S/V_{La})]}$$

and (12.12b)

$$\alpha_u(90^0) \approx 0.75\alpha_v$$

where α_v and α_u = vertical and horizontal interaction factors, respectively; S/d = pile spacing to diameter ratio; θ = the angle between the direction of load action and the plane in which piles lie; and V_{La} = the so-called Lysmer's analog velocity = $[3.4V_s/\pi(1-\nu)]$.

To analyze a pile group using the interaction factors approach, the impedance functions of single piles and the interaction factors are calculated first, then the group impedance functions are computed. The stiffness and damping constants of individual piles are calculated using expressions given in Table 12.6 or formulae due to Gazetas (1991). The interaction factors are calculated using Eq. 12.12 or charts due to Kaynia & Kausel (1982). The impedance functions of a pile group of n piles are then given by:

$$K_v^G = \bar{k}_v \sum_{i=1}^{n}\sum_{j=1}^{n} \varepsilon_{ij}^v \quad (12.13a)$$

$$K_h^G = \bar{k}_h \sum_{i=1}^{n}\sum_{j=1}^{n} \varepsilon_{2i-1,2j-1}^h \quad (12.13b)$$

$$K_r^G = \bar{k}_h \sum_{i=1}^{n}\sum_{j=1}^{n} \varepsilon_{2i,2j}^h \quad (12.13c)$$

$$K_c^G = \bar{k}_h \sum_{i=1}^{n}\sum_{j=1}^{n} \varepsilon_{2i-2j}^h \quad (12.13d)$$

where K_v^G, K_h^G, K_r^G and K_c^G = the vertical, horizontal, rocking and coupling group stiffnesses, respectively. In Eq. 12.13, $\bar{k}_v$ = the static vertical stiffness of the single pile, $[\varepsilon^v] = [\alpha]_v^{-1}$, where α_{ij}^v = complex interaction factors between piles i and j, $\alpha_{ii}^v = \bar{k}_v/K_v$, and K_v = the complex vertical impedance function of the single pile. Similarly, $\bar{k}_h$ = the static horizontal stiffness of the pile $[\varepsilon^h] = [\alpha]_h^{-1}$, where α_{ij}^h =

complex interaction coefficients for the horizontal translations and rotations. The formulation of the $[\alpha]_h$ can be found in Novak & Mitwally (1987) and El Naggar & Novak (1995a).

12.3.4 PILE BATTER

Pile batter can be accounted for approximately by calculating first the pile stiffnesses for a vertical pile, assembling them as a stiffness matrix in element co-ordinates and transforming this matrix into horizontal and vertical global co-ordinates (Novak 1979).

12.3.5 NON-LINEAR RESPONSE OF PILES

For large displacements, piles behave in a non-linear fashion. The finite element method can handle non-linearity, but the solution is very costly and can be inaccurate (Trochanis *et al.* 1988). The most practical model for non-linear analysis is the lumped mass model in which the soil stiffness and damping are discretized and represented by isolated springs and dashpots. Such models are popular in offshore technology where large displacements are expected. El Naggar & Novak (1995b, 1996) developed a non-linear lumped mass analysis (Fig. 12.6) and used it to model the piled foundations of offshore towers.

12.3.6 SEISMIC RESPONSE OF PILE FOUNDATIONS

One of the primary considerations for design of bridge foundations in seismically active regions is the response of the foundation sys-

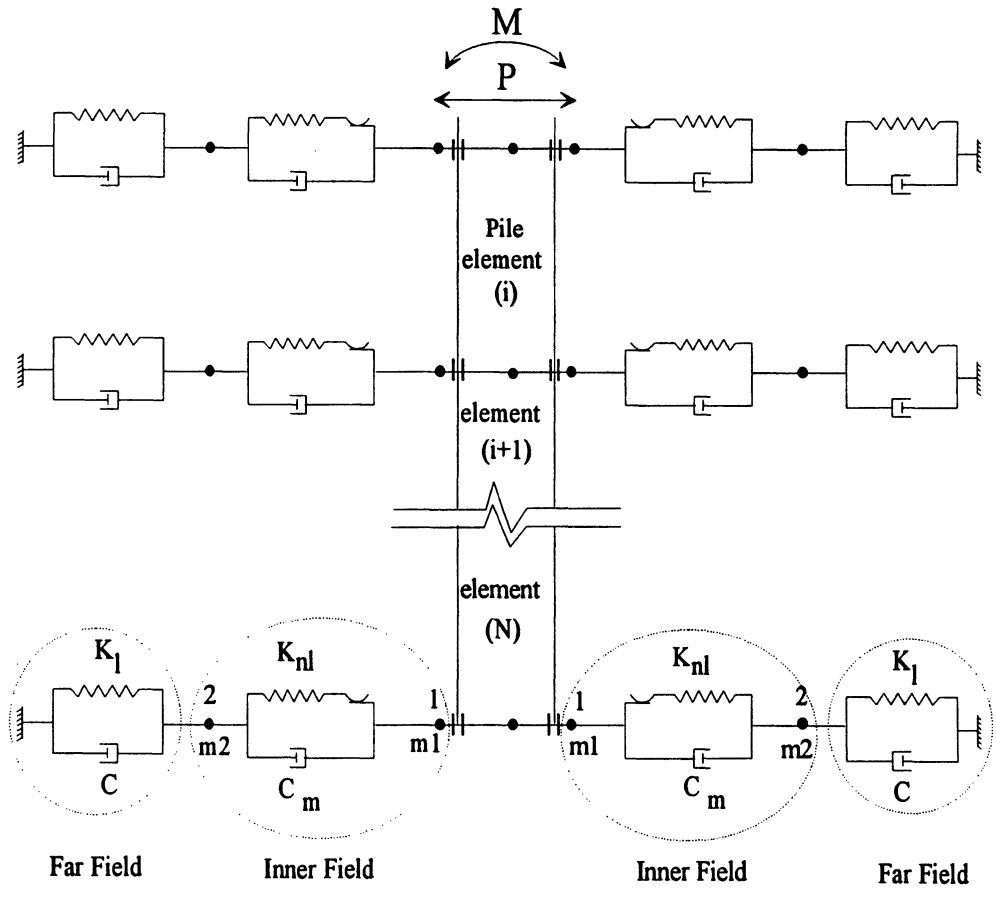


FIGURE 12.6. Model for non-linear analysis of piles.

tem to seismic loads, which are viewed currently as being primarily horizontal. The common foundation system in these situations involves a group of piles. In the analysis of these foundations, consideration should be given to three main aspects: the pile–soil–pile interaction effects on the group capacity and its response to the seismic (dynamic) loading; the effects of the soil non-linearity, and probably the pile non-linearity for concrete and wood piles, on the group impedance functions; and the kinematic (ground-motion-induced) loading. Thus, the problem is rather complicated and several approximations are called for to simplify the problem.

Gazetas and co-workers (Dobry & Gazetas, 1988; Makris & Gazetas, 1992; Gazetas *et al.*, 1993) developed a simple beam-on-dynamic-Winkler-foundation (BDWF) and used it to determine the impedance functions of single piles and pile groups. The soil is modeled as a Winkler foundation resisting the pile motion by continuously distributed frequency dependent linear springs and dashpots along the pile length. The coefficients of these springs and dashpots are frequency dependent and determined using algebraic expressions, developed by matching the dynamic pile–head displacements from Winkler and finite element analyses. The form of the damping coefficients is first determined from the cone model by Wolf *et al.* (1992) and the numerical values are then calibrated by curve-fitting finite element results. The spring constants are derived solely through curve fitting. The group effect is accounted for through the superposition approach using dynamic interaction factors. Mylonakis *et al.* (1997) further extended this approach to account for kinematic interaction and solved the seismic response of the bridge-foundation system.

Wolf and Darbre (1986) developed a time domain analysis that can be used to calculate the seismic response of bridge foundations. This analysis involves the indirect boundary element method to account for non-linearity stemming from soil separation and can handle both kinematic loading and inertial loading, non-linearity due to slippage and separation; however, it requires enormous computational effort.

An approximate procedure may be used to account for the soil non-linearity due to seismic excitation. In this procedure, a ground response analysis is performed first to obtain the free-field site response using any available code (e.g. SHAKE91; Idriss and Sun 1992). This analysis yields a shear strain profile that can be used to determine strain-compatible soil properties. These properties are then used to compute the dynamic stiffnesses of the pile group using one of the approaches discussed in Section 12.3.3. These stiffnesses are used to model the foundation system in the superstructure analysis.

12.3.7 EXPERIMENTAL STUDIES ON RESPONSE OF PILES

Various types of dynamic tests of piles are conducted to validate and calibrate the available methods of analysis. They differ according to the size of the piles and the test medium and technique employed. The main types are described below.

12.3.7.1 Full-Scale Field Tests

In these tests, full-scale piles are installed in the natural deposit. The main advantages of this technique are that natural soil response is examined and unobstructed wave propagation is allowed. However, the cost of carrying out this type of test is substantial. Experimental studies that fall in this category include Tuzuki *et al.* (1992), Mizuno & Iibat (1992), Hakulinen (1991), Kobayashi *et al.* (1991), Musser (1996), Masuda *et al.* (1986), Kobori *et al.* (1991), Crouse & Cheang (1987) and El-Marsafawi *et al.* (1992).

12.3.7.2 Small Prototype Field Tests

Field experiments with small prototype pile are easier and less expensive to conduct while still allowing for unobstructed wave propagation. The work described by Novak & Grigg

(1976), Novak & El-Sharnouby (1984), El-Marsafawi *et al.* (1992) and Burr *et al.* (1997) falls into this category.

12.3.7.3 Small-scale Laboratory Tests

These tests are conducted with very small model piles in test bins or tanks. The small-scale laboratory tests are popular because they are inexpensive, easy to organize and independent of the weather. The deficiencies are the difficulty in modeling an undisturbed natural deposit, achieving meaningful confining pressure and providing a medium for unobstructed wave propagation. Different solutions were proposed and implemented to alleviate these difficulties, however, they cannot be eliminated. Experiments reported by Kana *et al.* (1986) fall into this category.

12.3.7.4 Centrifugal Modeling

In this technique, a small-scale model of the pile or pile group is installed in a small bin filled with sand or remolded clay. This bin is suspended in a centrifuge. At the operating speed, the model is exposed to centrifugal forces far in excess of the gravity force, making it possible to reproduce prototype gravity-induced stresses in soil in the small-scale model. Thus confining stress is identical in both the prototype and model soils, and consequently the stress–strain relation is the same in both the prototype and the model. Experimental studies using this technique are described in Scott *et al.* (1977, 1982), Prevost & Scanlan (1983) and Ting & Scott (1984).

12.4 Response of Machine Foundations

The foundation depicted in Fig. 12.2 can vibrate in any or all six possible modes due to excitation loading from the vibrating machine it supports. For ease of analysis, some of these modes can be considered separately (e.g. vertical or torsional) and design is carried out by considering the displacement due to these modes separately.

12.4.1 RESPONSE OF RIGID FOUNDATIONS IN ONE DEGREE-OF-FREEDOM

The governing equation of motion is obtained by considering the dynamic equilibrium of the foundation. As an example, the governing equation of the vertical vibration is derived and solved. For mathematical convenience, the excitation force is represented in a complex number notation. The governing equation for motion, $v(t)$ is:

$$m\ddot{v} + c\dot{v} + kv = Pe^{i\omega t}. \qquad (12.14)$$

Because the excitation force is complex, the response is also complex and is given by:

$$v(t) = v_c\, e^{i\omega t} \qquad (12.15)$$

where v_c is a complex amplitude. Substituting for $v(t)$ in Eq. 12.14 yields:

$$v_c = \frac{1}{k - m\omega^2 + i\omega c} P \qquad (12.16)$$

With mathematical manipulation of v_c and substituting into Eq. 12.15, $v(t)$ is given as:

$$v(t) = \frac{P}{[(k - m\omega^2)^2 + \omega^2 c^2]^{1/2}} e^{i(\omega t + \phi)} \qquad (12.17)$$

where $\phi = \tan^{-1}(-\omega c/k - m\omega^2)$ and the real response is given by the real part of Eq. 12.17, i.e:

$$v(t) = \frac{P}{[(k - m\omega^2)^2 + \omega^2 c^2]^{1/2}} \cos(\omega t + \phi). \qquad (12.18)$$

The stiffness and damping constants k and c are established as described in Sections 12.2 and 12.3 and are frequency dependent, hence the response has to be calculated using Eq. 12.18. However, if they can be considered frequency independent in the frequency range of interest, Eq. 12.18 can be rearranged and the real amplitude can be written as:

$$v = \frac{P}{k_v} \frac{1}{\left\{\left[1 - \left(\frac{\omega}{\omega_0}\right)^2\right]^2 + 4D^2\left(\frac{\omega}{\omega_0}\right)^2\right\}^{1/2}} = v_{st}\varepsilon \quad (12.19)$$

in which the natural frequency, $\omega_0 = (k_v/m)$, the damping ratio, $D = c_v/2\,(k_v m)^{1/2}$ $v_{st} = P/k_v$ = the static displacement and ϵ = dynamic amplification factor given by:

$$\varepsilon = \frac{1}{\left\{\left[1 - \left(\frac{\omega}{\omega_0}\right)^2\right]^2 + 4D^2\left(\frac{\omega}{\omega_0}\right)^2\right\}^{1/2}}. \quad (12.20)$$

For a harmonic excitation, the maximum displacement is given by:

$$v_{max} = \frac{P}{k} \frac{1}{2D(1 - D^2)^{1/2}}. \quad (12.21)$$

This maximum appears at frequencies, $\omega_m = \omega_0\,(1 - 2D^2)^{1/2}$ and $\omega'_m = \omega_0\,1/(1 - 2D^2)^{1/2}$ for constant amplitude (P = constant) and quadratic excitations ($P = m_e\,e\,\omega^2$), respectively.

12.4.2 COUPLED RESPONSE OF RIGID FOUNDATIONS

The coupled motion in the vertical plane represents an important case because it results from excitation by moments and horizontal forces acting in the vertical plane. The center of gravity of the footing and the machine considered together, CG, is taken as the reference point (origin of co-ordinates). The horizontal sliding, $u(t)$, and rocking, $\psi(t)$, describe the coupled motion as indicated in Fig. 12.7. For a simple rectangular footing as shown in Fig. 12.7, the mass moment of inertia of the system is:

$$I = \frac{m_1}{12}(a^2 + b^2) + m_1\left(y_c - \frac{b}{2}\right)^2 + m_2 y_m^2 \quad (12.22)$$

where m_1 = the mass of the footing and m_2 = the mass of the machine. The stiffness constants, k_{uu}, $k_{u\psi}$ and $k_{\psi\psi}$ are described as the stiffness constants for translation and rotation at the base of the footing, transformed to the reference point, CG. If the stiffness constants referred to the center of the base are k_u and k_ψ (calculated as described in Sections 12.2 or 12.3), the stiffness constants referred to CG are:

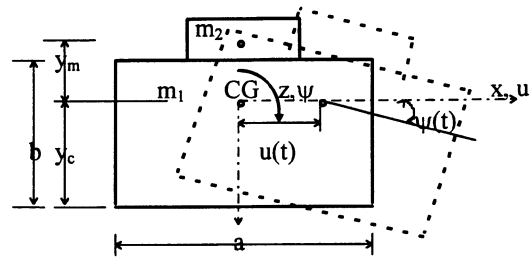


FIGURE 12.7. Notation for coupled motion of embedded foundations.

$$k_{uu} = k_u,\ k_{\psi\psi} = k_\psi + k_u y_c^2 \quad \text{and} \quad k_{u\psi} = k_{\psi u} = -k_u y_c. \quad (12.23)$$

The excitation loading is composed of horizontal force, $P(t)$, and a moment, $M(t)$. With mass, stiffness and loading established, the governing equations of the coupled motion can be written by expressing the condition of equilibrium in translation and rotation as:

$$m\ddot{u} + k_{uu}u + k_{u\psi}\psi + c_{uu}\dot{u} + c_{u\psi}\dot{\psi} = P(t) \quad (12.24a)$$

$$I\ddot{u} + k_{\psi u}u + k_{\psi\psi}\psi + c_{\psi u}\dot{u} + c_{\psi\psi}\dot{\psi} = M(t) \quad (12.24)$$

in which, for the sake of brevity, $u(t) = u$ and $\psi(t) = \psi$.

Two approaches can be used to solve Eq. 12.24: the direct solution and modal analysis.

12.4.2.1 Direct Solution

It is mathematically accurate. The harmonic excitation is described as a set of complex

functions, i.e. $P(t) = Pe^{i\omega t}$ and $M(t) = (Py_e)e^{i\omega t} = Me^{i\omega t}$, where y_e = vertical distance between the horizontal force and CG, and hence the particular solutions to Eq. 12.25 are also complex, i.e. $u(t) = u_c e^{i\omega t}$ and $\psi(t) = \psi_c e^{i\omega t}$. Upon substituting these particular solutions into Eq. 12.24 and solving the resulting equation using Kramer's rule, the real motion of the centre of gravity is obtained as:

$$u(t) = u\cos(\omega t + \phi_u) \quad \text{and} \quad \psi(t) = \psi\cos(\omega t + \phi_u) \tag{12.25}$$

where the true vibration amplitudes u and ψ are given (Novak & Beredugo 1972) by:

$$u = P\left(\frac{\alpha_1^2 + \alpha_2^2}{\varepsilon_1^2 + \varepsilon_2^2}\right)^{1/2} \quad \text{and} \quad \psi = M\left(\frac{\beta_1^2 + \beta_2^2}{\varepsilon_1^2 + \varepsilon_2^2}\right)^{1/2}. \tag{12.26}$$

The auxiliary constants, α, β and ε are given as:

$$\left.\begin{aligned} \alpha_1 &= k_{\psi\psi} - I\omega^2 - (M/P)k_{u\psi} \quad \alpha_2 = [c_{\psi\psi} - (M/P)c_{u\psi}]\omega \\ \beta_1 &= k_{uu} - m\omega^2 - (P/M)k_{u\psi} \quad \beta_2 = [c_{uu} - (P/M)c_{u\psi}]\omega \\ \varepsilon_1 &= mI\omega^4 - (mk_{\psi\psi} + Ik_{uu} + c_{uu}c_{\psi\psi} - c_{u\psi}^2)\omega^2 + k_{uu}k_{\psi\psi} - k_{u\psi}^2 \\ \varepsilon_2 &= -(mc_{\psi\psi} + Ic_{uu})\omega^3 + (c_{uu}k_{\psi\psi} + c_{\psi\psi}k_{uu} - 2c_{u\psi}k_{u\psi})\omega \end{aligned}\right\} \tag{12.27}$$

The phase shifts between the excitation forces and the response, ϕ_u and ϕ_ψ, are given by:

$$\phi_u = -\tan^{-1}\left(\frac{\alpha_1\varepsilon_2 - \alpha_2\varepsilon_1}{\alpha_1\varepsilon_1 + \alpha_2\varepsilon_2}\right) \quad \text{and} \quad \phi_\psi = -\tan^{-1}\left(\frac{\beta_1\varepsilon_2 - \beta_2\varepsilon_1}{\beta_1\varepsilon_1 + \beta_2\varepsilon_2}\right). \tag{12.28}$$

12.4.2.2 Modal Analysis

The principal advantages of this approximate approach are that it yields natural frequencies and damping ratios in addition to amplitudes and that it involves simple algebra. First, the natural frequencies and modes of free vibration are calculated, through the solution of the eigenvalue problem by putting the damping coefficients and excitation forces to zero and substituting the particular solutions into Eq. 12.24, and are given by:

$$\omega_{1,2}^2 = \frac{1}{2}\left(\frac{k_{uu}}{m} + \frac{k_{\psi\psi}}{I}\right) \mp \left[\frac{1}{4}\left(\frac{k_{uu}}{m} - \frac{k_{\psi\psi}}{I}\right)^2 + \frac{k_{u\psi}^2}{mI}\right]^{1/2}. \tag{12.29}$$

With these two natural frequencies, ω_j (j = 1, 2), the two vibration modes are:

$$a_j = \frac{u_j}{\psi_j} = \frac{-k_{u\psi}}{k_{uu} - m\omega_j^2} = \frac{k_{\psi\psi} - I\omega_j^2}{-k_{u\psi}}. \tag{12.30}$$

The generalized force amplitudes are:

$$P_j = Pu_j + M\psi_j \text{ and } M_j = mu_j^2 + I\psi_j^2. \tag{12.31}$$

The modal co-ordinates u_j and ψ_j can be chosen to an arbitrary scale; e.g. $\psi_j = 1$ and $u_j = a_j$. The two modal damping ratios pertinent to the vibration modes are:

$$D_j = \frac{1}{2\omega_j M_j}(c_{uu}u_j^2 + c_{\psi\psi}\psi_j^2 + 2c_{u\psi}u_j\psi_j). \tag{12.32}$$

Then, the footing translation and rocking are:

$$u(t) = \sum_{j=1}^{2} q_j u_j \sin(\omega t + \phi_j) \quad \text{and} \quad \psi(t) = \sum_{j=1}^{2} q_j\psi_j \sin(\omega t + \phi_j) \tag{12.33}$$

in which q_j and ϕ_j are:

$$q_j = \frac{P_j}{M_j[(\omega_j^2 - \omega^2)^2 + 4(D_j\omega_j\omega)^2]^{1/2}} \quad \text{and} \quad \phi_j = -\tan^{-1}\left(\frac{2D_j\omega_j\omega}{\omega_j^2 - \omega^2}\right). \tag{12.34}$$

If the damping in the system is small, the results from modal analysis are very close to the results obtained from the direct approach.

impedance functions K_{ij}. Then, considering the dynamic equilibrium of forces and moments in the directions X and ψ, the governing equations in the two directions are:

$$\left.\begin{aligned} m\ddot{u} + K_{uu}u + K_{uv}v + K_{uw}w + K_{u\xi}\xi + K_{u\psi}\psi + K_{u\zeta}\zeta &= P_X(t) \\ I_\psi\ddot{\psi} - D_{YX}\ddot{\xi} - D_{YZ}\ddot{\zeta} + K_{\psi u}u + K_{\psi v}v + K_{\psi w}w + K_{\psi\xi}\xi + K_{\psi\psi}\psi + K_{\psi\zeta}\zeta &= M_X(t) \end{aligned}\right\} \quad (12.35)$$

where I_i = mass moment of inertia in direction i and D_{ij} = products of inertia.

Similar equations can be written in the other four directions. This is a system of linear algebraic equations for the complex amplitudes, which can be readily solved using the same direct approach used for the planar case.

12.4.3 RESPONSE OF RIGID FOUNDATIONS IN SIX DEGREES-OF-FREEDOM

When the rigid foundation is of general shape, the response is in six degrees-of-freedom (Fig. 12.2), all of them, possibly, coupled. Similar to the analysis in the vertical plane case, the stiffness constants are described at the base of the footing, then transformed to the reference point, CG. The stiffness and damping are described in terms of

Worked Example

Evaluate the response of the machine foundation shown in Fig. 12.8a. The machine weighs 89 kN and

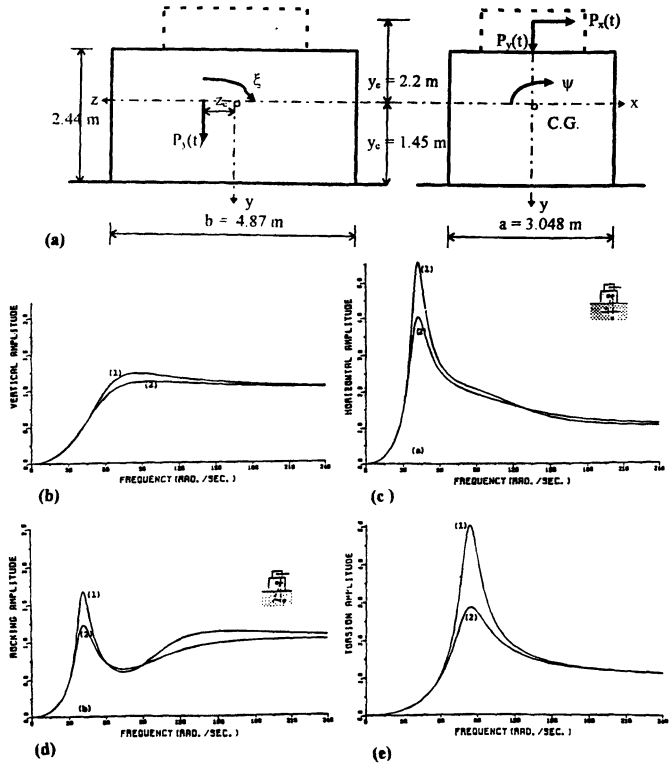


FIGURE 12.8. Example for the response analysis of machine foundations: Line 1, soil material damping ignored; line 2, soil material damping considered.

rests on the surface of a homogeneous halfspace whose properties are as follows: shear wave velocity, $V_s = 150\ \text{ms}^{-1}$; mass density, $\rho = 1602\ \text{kgm}^{-3}$; Poisson's ratio, $\nu = 0.25$; and material damping (viscous damping ratio), $\beta = 0.05$; the total mass of the system, $m = 9.6 \times 10^4$ kg; and mass moment of inertia about the z-axis, $I_z = 1.6 \times 10^5\ \text{kgm}^{-2}$.

Solution: Equivalent radii (Table 12.2) $R = R_u = R_v = (ab/\pi)^{1/2} = 2.174$ m, $R_\psi = (ba^3/3\pi)^{1/2} = 1.96$ m $G = \rho V_s^2 = 3.6 \times 10^7\ \text{N m}^{-1}$.

Stiffness and damping constants (Tables 12.4 and 12.5 with no embedment, i.e. $S_{ij} = 0$):

$$k_{vv} = GRC_{v1} = 3.6 \times 10^7 \times 2.174 \times 5.2$$
$$= 4.074 \times 10^8\ \text{N m}^{-1}$$
$$c_{vv} = R^2(\rho G)^{1/2}C_{v2} = (2.174)^2 \times (1602 \times 3.6 \times 10^7)^{1/2} \times 5 = 5.68 \times 10^6\ \text{N m}^{-1}\ \text{s}^{-1}$$
$$k_{uu} = GRC_{u1} = 3.6 \times 10^7 \times 2.174 \times 4.7$$
$$= 3.683 \times 10^8\ \text{N m}^{-1}$$
$$c_{uu} = R^2(\rho G)^{1/2}C_{u2} = (2.174)^2 \times (1602 \times 3.6 \times 10^7)^{1/2} \times 2.8$$
$$= 3.18 \times 10^6\ \text{N m}^{-1}\ \text{s}^{-1}$$
$$k_{\psi\psi} = G(R^3\bar{y}^2C_{u1} + R_\varphi^3 C_{\varphi 1}) = 3.6 \times 10^7\left[2.174^3 \times \left(\frac{1.448}{2.174}\right)^2 \times 4.7 + 1.96^3 \times 3.3\right]$$
$$= 1.668 \times 10^9\ \text{N m rad}^{-1}$$
$$c_{\psi\psi} = (\rho G)^{1/2}(R_\psi^4 C_{\psi 2} + R^4\bar{y}^2C_{u2}) = 2.4 \times 10^5\left[1.96^4 \times 0.5 + 2.174^4 \times \left(\frac{1.448}{2.174}\right)^2 \times 2.8\right]$$
$$= 1.15 \times 10^7\ \text{N m rad}^{-1}\ \text{s}^{-1}$$
$$k_{u\psi} = GRy_cC_{u1} = -3.6 \times 10^7 \times 2.174 \times 1.448 \times 4.7$$
$$= -5.34 \times 10^8\ \text{N rad}^{-1}$$
$$c_{u\psi} = -R^2(\rho G)^{1/2}y_cC_{u2}$$
$$= -2.174^2 \times 2.403 \times 10^5 \times 1.448 \times 2.8$$
$$= -4.611 \times 10^6\ \text{N rad}^{-1}\ \text{s}^{-1}.$$

Natural frequencies and damping ratios:

Vertical

$$\omega_0 = (k/m)^{1/2}$$
$$= (4.074 \times 10^8/9.603 \times 10^4)^{1/2}$$
$$= 65.14\ \text{rad s}^{-1}\ D = c/2(km)^{1/2}$$
$$= 5.68 \times 10^6/2(4.074 \times 10^8 \times 9.603 \times 10^4)^{1/2}$$
$$= 0.454.$$

Coupled (horizontal and rocking) vibration:

$$\omega_{1,2}^2 = \frac{1}{2}\left(\frac{k_{uu}}{m} + \frac{k_{\psi\psi}}{I}\right) \pm \left[\frac{1}{4}\left(\frac{k_{uu}}{m} - \frac{k_{\psi\psi}}{I}\right)^2 + \frac{k_{u\psi}^2}{mI}\right]$$

$$\therefore\ \omega_1 = 41.3\ \text{rad s}^{-1} \qquad \omega_2 = 112.3\ \text{rad s}^{-1}.$$

The material damping is accounted for through the correspondence principle, i.e.:

$$k'_{vv} = k_{vv} - 2\beta c_{vv}\omega_0 = 4.074 \times 10^8 - 0.1 \times 5.68 \times 10^6 \times 65.14 = 3.708 \times 10^8\ \text{N m}^{-1}$$
$$c'_{vv} = c_{vv} + 2\beta k_{vv}/\omega_0 = 5.68 \times 10^6 + 0.1 \times 4.074 \times 10^8/65.14 = 6.306 \times 10^6\ \text{N m}^{-1}\ \text{s}^{-1}.$$

Similarly

$$k'_{uu} = 3.551 \times 10^8\ \text{N m}^{-1} \qquad c'_{uu} = 4.071 \times 10^6\ \text{N m}^{-1}\ \text{s}^{-1}$$
$$k'_{\psi\psi} = 1.62 \times 10^9\ \text{N m}^{-1}\ \text{rad}^{-1} \qquad c'_{\psi\psi} = 1.554 \times 10^7\ \text{N m}^{-1}\ \text{rad}^{-1}\ \text{s}^{-1}$$
$$k'_{u\psi} = -5.149 \times 10^8\ \text{N rad}^{-1} \qquad c'_{u\psi} = -5.904 \times 10^6\ \text{N rad}^{-1}\ \text{s}^{-1}$$

Natural frequencies, damping ratios and response with material damping included:

Vertical

$$\omega_0 = (k'/m)^{1/2} = 62.14\ \text{rad s}^{-1}$$
$$D = c/2(k'm)^{1/2} = 0.528.$$

Coupled horizontal and rocking vibration:

$$\omega_1 = 40.75\ \text{rad s}^{-1} \qquad \omega_2 = 110.34\ \text{rad s}^{-1}$$
$$D_1 = 0.188 \qquad D_2 = 0.563.$$

The vertical response: with $P = m_e e \omega^2$ and $k = m\omega_0^2$, the amplitude is (Eq. 12.19):

$$v = \frac{m_e e\omega^2}{m\omega_0^2}\varepsilon = \frac{m_e e}{m}(\omega/\omega_2)^2\varepsilon$$

(Fig. 12.8b in dimensionless form: $A_v = vm/m_e e$).

Coupled motion: using the direct analysis (Eqs 12.25 through 12.27), the horizontal and rocking amplitudes are shown in Fig. 12.8c and d in dimensionless form:

$$A_u = u\frac{m}{m_e e} \quad \text{and} \quad A_\psi = \frac{I}{m_e e y_e}.$$

12.5 Response of Hammer Foundations

Shock producing machines generate dynamic effects, which differ from those of rotating machines, and the design of their foundations, therefore, requires special consideration.

12.5.1 TYPES OF HAMMERS AND HAMMER FOUNDATIONS

There are many types of hammers. They can be divided according to their function into forging hammers and die stamping hammers, or according to their mode of operation, into drop, steam and pneumatic hammers. More details can be found in Major (1962).

Different foundation arrangements are used for hammers. In small hammers, the anvil is mounted directly on the foundation (Fig. 12.9a). Viscoelastic suspension of the anvil is usually provided (Fig. 12.9b). The foundation block is most often cast directly on soil (Fig. 12.9a, b). When the transmission of vibration in the vicinity and adjoining facilities is of concern, the block may be supported on a pad (Fig. 12.9c) or vibration isolating elements (Fig. 12.9d).

12.5.2 DESIGN CRITERIA

The design of a hammer foundation must ensure satisfactory performance of the hammer and minimum disturbance to the environment. These objectives are met by limiting the vibration amplitudes, settlement, physiological effects and stresses to the given tolerances.

1. Vibration amplitudes. The limits on the vibration amplitudes should be specified by

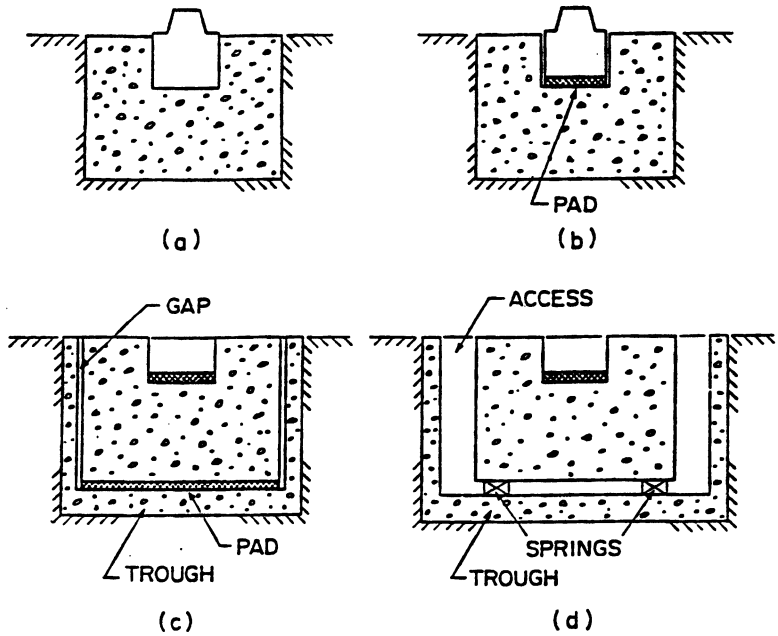


FIGURE 12.9. Types of hammer foundation arrangement.

TABLE 12.8. Maximum allowable amplitudes for hammer foundations

Head weight (kN)	Max. anvil amplitude (mm)	Max. foundation amplitude (mm)
<100	1	1.2
200	2	1.2
>300	4	1.2

the manufacturer. In the absence of such specifications, a few values of maximum allowable amplitudes are suggested in Table 12.8, or an estimate is made based on experience.

2. Physiological effects. They are related to vibration velocity and acceleration rather than displacement. The vibration velocity can be calculated approximately as $\dot{v}_m = v_m\omega_0$ where v_m = the maximum displacement and ω_0 = the natural frequency of the foundation. For data on human perceptibility have been collected see Richart *et al.* (1970).

3. Stresses. Stresses in all parts of the foundation have to remain within allowable limits. Dynamic stress is repetitive and fatigue effects have to be accounted for. To account for the fatigue in stresses in the machine components, a factor of safety greater than three should be considered in the design.

4. Mass of the foundation block. The adequacy of the foundation mass is best proven by detailed analysis of stresses and amplitudes. Some guidelines have been suggested for the preliminary choice of the weight of the foundation block. Assuming the anvil weight = $20G_0$, where G_0 is the weight of the head, the weight of the block, G_b, can be estimated by:

$$G_b = 75G_0\left(\frac{C_0}{C_r}\right)^2 \qquad (12.36)$$

where C_0 = the maximum velocity of the head and C_r = 5.6 ms^{-1} (Rausch 1950).

5. Vibration effects on environment. Vibration propagates from the footing into the surroundings in the form of ground motion. The vertical amplitude of the ground motion, v_r, at a distance, r, from the foundation vertical axis can be evaluated approximately as:

$$v_r = v_0\left(\frac{r_0}{r}\right)^{1/2} e^{-\alpha(r-r_0)} \qquad (12.37)$$

where v_0 = footing amplitude, r_0 = the distance of the footing edge from its vertical axis and α = empirical coefficient ranges from 0 to 0.05 m^{-1}. Equation 12.37 was derived assuming a surface wave whose vertical axis was greater than its horizontal axis. However, the physical properties of the soil medium differ considerably from the ideal properties assumed in theory. Consequently, the motion actually observed differs from the theoretical pattern. Hence, for practical calculations the horizontal amplitude may be considered equal to the vertical one. The response of a structure located near the hammer foundation can be predicted using the methods of structural dynamics.

12.5.3 RESPONSE OF ONE MASS FOUNDATION

When the anvil is rigidly mounted (Fig. 12.9a) and the hammer blow does not act eccentrically, the foundation response can be analyzed using a one degree-of-freedom model (Fig. 12.10a). With the notation of Fig. 12.10a, the governing equation of the response is:

$$m\ddot{v} + c\dot{v} + kv = 0 \qquad (12.38)$$

in which m = the mass of foundation with the anvil and frame. The solution to Eq. 12.38 corresponding to initial velocity of the system, $\hat{c}$, can be written as:

$$v(t) = \frac{\hat{c}}{\omega_0'}e^{-D\omega_0 t}\sin\omega_0' t \qquad (12.39)$$

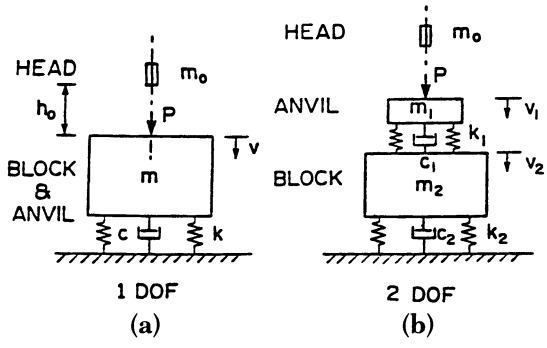


FIGURE 12.10. Mathematical models for hammer foundations for (a) one degree-of-freedom, and (b) two degrees-of-freedom.

where $\omega_0' = \omega_0(1 - D^2)^{1/2}$, $D = c/2(km)^{1/2}$. The initial velocity of the system, $\hat{c}$, can be obtained from the consideration of the collision between the head whose mass is m_0 and the foundation having mass m. Assuming a collision of two free bodies yields:

$$\hat{c} = (1 + k_r)c_0 \frac{m_0}{m + m_0} \qquad (12.40)$$

where k_r = coefficient of restitution and ranges from 0 to 1, with 0.5 adequate for design purposes. The peak displacement occurs at the time, $t_m = (1/\omega_0')\tan^{-1}(1 - D^2/D)^{1/2}$ and the peak displacement, $\hat{v}$, follows from Eq. 12.39. The peak force transmitted into the ground is $F = \hat{v}[k^2 + (c\omega_0)^2]^{1/2}$ and the peak stress is $\sigma = F/A_b$, where A_b = the base area.

12.5.4 RESPONSE OF TWO MASS FOUNDATION

When the anvil rests on an elastic pad (Figs. 12.9b or c), a hammer foundation should be considered as a two mass system (Fig. 12.10b). In this model, m_1 = the mass of the anvil and m_2 = the mass of the footing; k_1 and c_1 = the stiffness and damping constants of the pad, and k_2 and c_2 = the stiffness and damping of the soil or piles supporting the footing. Stiffness and damping of foundations can be evaluated using the approaches described in Sections 12.2 and 12.3. The stiffness and damping constants of a pad can be given by:

$$k_p = \frac{E_p A_p}{d} \quad \text{and} \quad c_p = 2\beta_p \frac{k_p}{\omega_0} \qquad (12.41)$$

where E_p, A_p, d and β_p = Young's modulus, area, thickness and material damping of the pad, respectively; and ω_0 = natural frequency of the block calculated with k_p.

The duration of the collision between the hammer head and the anvil is short relative to the system natural periods, hence free vibration of both masses, $v_1(t)$ and $v_2(t)$ is assumed. First, the damping is neglected and the equations of motion follow as:

$$\begin{aligned} m_1\ddot{v}_1 + k_1v_1 - k_1v_2 &= 0 \\ m_2\ddot{v}_2 - k_1v_1 + (k_1 + k_2)v_2 &= 0. \end{aligned} \qquad (12.42)$$

Solving the eigenvalue problem stemming from Eq. 12.38, the natural frequencies are:

$$\omega_{1,2}^2 = \frac{1}{2}\left(\frac{k_1}{m_1} + \frac{k_1 + k_2}{m_2}\right) \mp \left[\frac{1}{4}\left(\frac{k_1}{m_1} - \frac{k_1 + k_2}{m_2}\right)^2 + \frac{k_1^2}{m_1 m_2}\right]^{1/2}. \qquad (12.43)$$

The damped response is evaluated approximately using the modal analysis and assuming that the damping mode is approximately the same as the undamped mode, the damping ratio and generalized mass of mode j (j = 1, 2) are given by:

$$\begin{aligned} D_j &= \frac{1}{2\omega_j M_j}[c_1(v_{1j} - v_{2j})^2 + c_2 v_{2j}^2] \\ M_j &= m_1 v_{1j}^2 + m_2 v_{2j}^2. \end{aligned} \qquad (12.44)$$

The amplitudes v_{ij} are determined from the initial conditions and are given by:

$$v_{11} = \frac{\hat{c}}{\omega_1}\frac{\omega_2^2 - \omega_a^2}{\omega_2^2 - \omega_1^2}$$

$$\text{and } v_{12} = \frac{\hat{c}}{\omega_2}\frac{\omega_\alpha^2 - \omega_1^2}{\omega_2^2 - \omega_1^2} \quad (12.45a)$$

$$v_{21} = v_{11}\left(1 - \frac{\omega_1^2}{\omega_a^2}\right) \text{ and } v_{22} = -v_{21}\frac{\omega_1}{\omega_2} \quad (12.45b)$$

where $\omega_a = (k_1/m_1)^{1/2}$. The damped vibration of the anvil and the footing is then given by

$$v_1(t) = v_{11}e^{-D_1\omega_1 t}\sin\omega_1' t + v_{12}e^{-D_2\omega_2 t}\sin\omega_2' t$$
$$v_2(t) = v_{21}e^{-D_1\omega_1 t}\sin\omega_1' t + v_{22}e^{-D_2\omega_2 t}\sin\omega_2' t. \quad (12.46)$$

The peak displacements occur at time, $t_m = (1/\omega_1')\tan^{-1}[(-D^2{}_1)^{1/2}/D_1]$, where $\omega_1' = \omega_1(1 - D_1^2)^{1/2}$. Finally, the peak force transmitted to the ground is $F = \Sigma_j \hat{v}_{2j}[k_2^2 + (c_2\,\omega_j')^2]^{1/2}$.

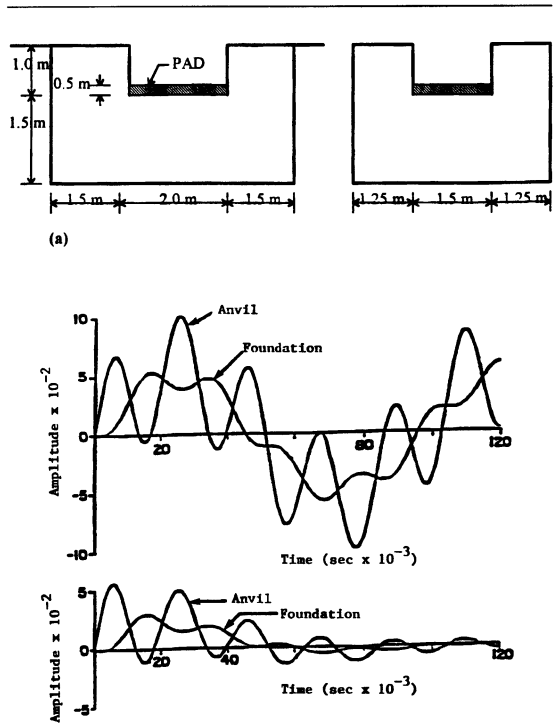


FIGURE 12.11. Example for the response analysis of hammer foundations.

Worked Example

Evaluate the response of the hammer foundation shown in Fig. 12.11a and characterized by the following data. Hammer: G_0 = 13.35 kN, G_1 = 266.7 kN, weight of frame, G_F = 222.5 kN, C_0 = 6.5 ms^{-1}, frequency of blows 40–90 blow min^{-1} and k_r = 0.5. Soil: V_s = 152.4 ms^{-1}, ρ = 1922 kg m^{-3}, ν = 0.25, β = 0.05, depth to bedrock = 30.48 m and allowable stress = 0.287 MPa. Backfill: G_s = 0.5G, ρ_s = 0.75ρ and ν_s = 0.25. Pad anvil (hard felt): d = 0.1524 m, E_p = 103.43 MPa, A_p = 3.0 m (2 × 1.5), β_p = 0.05 and allowable stress = 3.45 MPa. Foundation block: ρ = 2400 kg m^{-3}, base dimensions = 5 × 4 m^2, total depth = 2.5 m.

Solution:

$$G_b = 2400 \times 9.81(5 \times 4 \times 2.5 - 1 \times 2 \times 1.5)$$
$$= 1106.6 \text{ kN} \cong 75$$
$$\times 13.35(6.5/5.6)^2 \text{ kN, therefore OK}$$
$$m_0 = G_0/g = 13.35 \times 10^3/9.81 = 1361 \text{ kg}$$
$$m_1 = G_1/g = 266.7 \times 10^3/9.81 = 27216 \text{ kg}$$
$$m_2 = m_b + m_F = (1106.6 + 222.5) \times 10^3/9.81$$
$$= 1.355 \times 10^5 \text{ kg}$$
$$k_1 = k_p = E_p/A_p/d = 103.43 \times 10^6 \times 3/0.1524$$
$$= 2.036 \times 10^9 \text{ N m}^{-1}.$$

Stiffness of the embedded footing:

$$R = (ab/\pi)^{1/2} = (5 \times 4/\pi)^{1/2} = 2.524 \text{ m}$$
$$G = \rho V_s^2 = 1922 \times (152.4)^2 = 4.464 \times 10^7 \text{ Pa}.$$

Assume effective embedment D = 2.5 − 0.9 = 1.6 m, therefore δ = 1.6/2.524 = 0.63.

$$k_2 = GR(C_1 + G_s/G\delta S_1)$$
$$= 4.464 \times 10^7 \times 2.524(5.2 + 0.5 \times 0.63 \times 2.7)$$
$$= 6.82 \times 10^8 \text{ N m}^{-1}.$$

Damping of footing: $C_2 = 5.0/2$ (theoretical damping is overestimated)

$$c_2 = R^2(\rho G)^{1/2}\left[C_2 + S_2\delta\left(\frac{\rho}{\rho}\frac{G_s}{G}\right)^{1/2}\right]$$

$$= 2.524^2(1922 \times 4.464 \times 10^7)^{1/2} \times [2.5 + 6.7 \times 0.63(0.75 \times 0.5)^{1/2}]$$

$$c_2 = 9.488 \times 10^6 \text{ N m}^{-1} \text{ s}^{-1}\hat{c} = (1 + k_r)c_m \frac{m_0}{m + m_0}$$

$$= (1 + 0.5) \times 6.5 \times \frac{1361}{1361 + 27216} = 0.463 \text{ m s}^{-1}$$

$$\omega_{1,2}^2 = \frac{1}{2}\left(\frac{k_1}{m_1} + \frac{k_1 + k_2}{m_2}\right) \mp \left[\frac{1}{4}\left(\frac{k_1}{m_1} - \frac{k_1 + k_2}{m_2}\right)^2 + \frac{k_1^2}{m_1 m_2}\right]^{1/2}$$

$$\omega_1^2 = 0.4149 \times 10^4(\text{s}^{-1})^2 \quad \omega_1 = 64.41 \text{ s}^{-1}$$

$$\omega_2^2 = 9.0781 \times 10^4(\text{s}^{-1})^2 \quad \omega_2 = 301.2 \text{ s}^{-1}$$

$$\omega_a = \left(\frac{k_1}{m_1}\right)^{1/2} = \left(\frac{2.036 \times 10^9}{27216}\right) = 273.6 \text{ s}^{-1}$$

$$\omega_a^2 = 7.4865 \times 104(\text{s}^{-1})^2$$

$$v_{11} = \frac{0.463 \times 10^3}{64.41}\frac{9.0781 - 7.4865}{9.0781 - 0.4149} = 1.321 \text{ mm}$$

$$v_{12} = \frac{0.463 \times 10^3}{301.3}\frac{7.4865 - 0.4149}{9.0781 - 0.4149} = 1.255 \text{ mm}$$

$$v_{21} = 1.321\left(1 - \frac{0.4149}{7.4865}\right) = 1.247 \text{ mm}$$

$$v_{22} = -1.247\frac{64.41}{301.3} = -0.267 \text{ mm}.$$

The peak undamped displacement (Eq. 12.46 with $D = 0$):

$$\hat{v}_1(\text{anvil}) = v_{11} + v_{12} = 1.321 + 1.255 = 2.576 \text{ mm}$$

$$\hat{v}_2(\text{footing}) = v_{21} + |v_{22}| = 1.247 + 0.267 = 1.515 \text{ mm}$$

$$c_{ij} = 2\beta k_1/\omega_j (j = 1, 2)$$

$$c_{11} = 0.1 \times 2.036 \times 10^9/64.41 = 3.161 \times 10^6 \text{ N m}^{-1} \text{ s}^{-1}$$

$$c_{12} = 0.1 \times 2.036 \times 10^9/301.2 = 0.676 \times 10^6 \text{ N m}^{-1} \text{ s}^{-1}$$

$$M_1(\text{Eq. 12.44}) = 27216(1.321)^2 + 1.355 \times 10^5 \times (1.255)^2 = 260\,909 \text{ kg m}^{-2}$$

$$M_2 = 52\,525.5 \text{ kg m}^{-2}$$

$$D_1(\text{Eq. 12.44}) = \frac{1}{2 \times 64.41 \times 260\,909} \times [3.161 \times 10^6(1.321 - 1.247)^2 + 9.488 \times 10^6 \times 1.247^2] = 0.44$$

$$D_2 = \frac{1}{2 \times 301.3 \times 52\,525.5} \times [0.676 \times 10^6(1.255 + 0.267)^2 + 9.488 \times 10^6 \times 0.267^2] = 0.07$$

$$\omega_1' = \omega_1(1 - D_1^2)^{1/2} = 64.41(1 - 0.44^2)^{1/2} = 57.84 \text{ s}^{-1}$$

$$t_m = \frac{1}{\omega_1'}\tan^{-1}\frac{(1 - D_1^2)^{1/2}}{D_1} = 0.019 \text{ s}.$$

The total response is calculated from Eq. 12.46 and plotted in Fig. 12.11b.

13. PAVEMENT DESIGN

R. Haas
B. L. Rodway

13.1 Introduction

Pavement design encompasses three major interrelated components: (a) geotechnical investigation and considerations; (b) structural analysis of alternative designs, including performance prediction; and (c) economic evaluation of the alternative designs. In a broader sense, pavement design is a major part of pavement management, which itself is a part of infrastructure or asset management (Haas *et al.* 1994; Hudson *et al.* 1997).

The basic types of pavement structures include:

1. Flexible: normally consisting of (a) hot mix asphalt concrete on untreated granular base and subbase, or (b) bituminous surface treatment on a granular base. Variations include asphalt treated granular base, and full-depth asphalt layers directly on the subgrade. Another variation is concrete block pavements on a sand base, which, for design purposes, can be treated as flexible pavements.
2. Rigid: normally consisting of plain, jointed (with dowels) Portland cement concrete slabs on a granular subbase. Variations include non-dowelled joints (for low volume facilities), asphalt or cement treated rather than granular subbase, and continuously reinforced concrete.
3. Composite: consisting of hot mix asphalt concrete on Portland cement concrete.

The expected performance of a pavement design for any given situation depends directly on several key factors, including the quality and consistency of the materials used, the subgrade support conditions, traffic repetitions and loads, environmental conditions, drainage and on the quality of construction. With the exception of traffic, all of these factors incorporate geotechnical considerations to some degree. Compaction of the subgrade and overlying pavement layers is also an inherent critical factor.

The intent of the chapter is to address the geotechnical considerations in pavement design, to provide sufficient basic information regarding pavement structural design and to provide design examples. While the primary emphasis is on flexible pavements, structural design of rigid pavements is also a very important topic and receives attention, as does application of the reliability concept to design.

Economic evaluation is also part of a complete design project. The major elements involved are summarized at the conclusion of the chapter.

13.2 Geotechnical and Environmental Considerations

Much material exists on the subject of geotechnical considerations in pavement design. One of the best references available, which consolidates a wide range of knowledge, has been provided in a 1996 Rankine lecture (Brown 1996), and by Papagiannakis & Schwartz (1998).

R. K. Rowe (ed.), *Geotechnical and Geoenvironmental Engineering Handbook*
© Kluwer Academic Publishers 2001

13.2.1 SOILS INVESTIGATION AND ENGINEERING PROPERTIES

The purpose of a soils investigation is to identify those site conditions and engineering properties of the soils involved that will influence the design and construction of the pavement. Since Chapter 4 covers geotechnical site characterization in detail, this section concentrates on those aspects which are relevant to pavement design and construction.

More specifically, the purpose of a pavement-related soils investigation includes:

1. Identifying the subgrade soil type(s) and engineering properties.
2. Establishing the depth to bedrock (if this is a possible factor in the particular design and construction situation).
3. Establishing the existing pavement layer thicknesses and material properties if a rehabilitation design (rather than a new pavement design) is involved.
4. Identifying the groundwater and/or drainage conditions.

Field equipment and test methods have been described in Chapter 4. For pavement design, the key subgrade soil properties obtained from field sampling commonly include: particle size analysis, moisture content and Atterberg limits, as well as the moisture–density relationship for compacted samples. This latter aspect is discussed further in Section 13.2.3. As well, many pavement design methods use a strength or bearing capacity (the latter term is common in Europe) characterization in terms of modulus of resilience, M_R.

M_R is the ratio of deviator stress to recoverable or resilient strain in a dynamic triaxial test (for both cohesionless materials, such as silts, sands and gravels, as well as cohesive soils). Since dynamic triaxial tests are seldom carried out, except in special cases, for complexity, cost, time and other reasons, an approximate empirical relationship has been established between M_R and a simpler California Bearing Ratio (CBR) test:

$$M_R(\text{MPa}) = 10.3\ \text{CBR (or } 1500\ \text{CBR if } M_R \text{ is in psi).} \quad (13.1)$$

The CBR test is described in ASTM D1883. It is an index test, which compares the resistance to penetration of a 50-mm diameter piston into a compacted subgrade, subbase or base material to that of a standard crushed granular material. CBR is defined as the percentage ratio of the force required to penetrate 12.7 mm into the compacted material as compared to the standard material. Weak clays will often range as low as CBR 2–6, while compacted granular materials may be well above CBR 50.

For bound materials, such as cement stabilized base aggregate, asphalt concrete, etc., M_R is usually established through indirect, dynamic diametral tension tests on cores or compacted cylindrical specimens. The specimens are edge loaded so that the center is in tension (diametral tensile stress is calculated from the load and geometry of the specimens), and recovered diametral displacement is measured by extensometers or proximeters. M_R is then the ratio of calculated diametral stress to recoverable strain. Procedures for carrying out resilient modulus testing are described in ASTM D4123.

Both the CBR and M_R tests are applicable to materials being evaluated for a new pavement design and for a rehabilitation design for an existing pavement (such as an overlay). In the latter case, coring is usually carried out to establish existing layer thicknesses, and/or to obtain samples for testing.

A typical "soils report" for pavement design would include information on the following (MTO 1990): (a) reference data on project location, length, etc.; (b) general data on existing conditions such as pavement width and shoulders, surface type, year of construction, etc.; (c) design criteria such as alignment and grade, geometrics (cross-sections, slopes), etc.; (d) specific data on the existing pavement, if a rehabilitation design is in-

volved, such as surface distresses, roughness, drainage conditions, culverts, etc.; (e) physiographic and subsurface soils data (physiographic region, geological history, frost penetration, freezing index, bedrock type, etc.); (f) soil investigation details; (g) alternative designs considered and evaluated, final selection, including drainage design; and (h) recommendations for construction.

13.2.2 DRAINAGE

Water in pavement structures comes mainly from surface infiltration, including shoulders and groundwater. The latter is usually due to a high water table, or capillary rise where silty or fine sandy soils are involved.

Subsurface soil investigations should identify the position of the groundwater table. As well, at the design stage, potential effects caused by the construction should be assessed. For example, cut slopes or fills on slopes may either intercept the groundwater table or block the natural drainage path, thereby creating the potential for erosion or raising of the groundwater table.

Rural roads normally use ditches to collect excess surface water. In urban areas, however, edge drainage is controlled with curbs, gutters and catchbasins.

For groundwater control, proper slope drainage, interceptor drains and collector subdrains should be used, as schematically illustrated in Fig. 13.1.

Water in pavement structures can affect structural and functional performance, where the former relates to load carrying capacity and the latter to accelerated deterioration and thus loss of serviceability to users. These effects can involve:

1. Frost action, in terms of frost heaving, and subsequently "frost boils" upon thawing. Particularly susceptible are fine-grained silty and fine sandy materials.
2. Loss of strength in both the granular layers and the subgrade. This occurs under saturated or near-saturated conditions when moving wheel loads cause excess pore water pressures.
3. "Pumping" of fine materials at rigid pavement joints under moving wheel loads. The net result can be significant stepping or faulting at the joint.
4. Loss of durability in asphalt concrete due to "stripping" (bond failure between the aggregate particles and the asphalt), and in Portland cement concrete due to deicing salts in solution.

Effective drainage of the pavement structure is critical in minimizing the loss of structural and functional performance. Collector subdrains (see Fig. 13.1) and highly permeable open-graded drainage layers in the pavement structure (below the asphalt concrete surface layers and on the granular base, normally 100 mm in thickness and stabilized with 1.5–2.0% asphalt cement for constructability reasons) can achieve this objective. A detailed

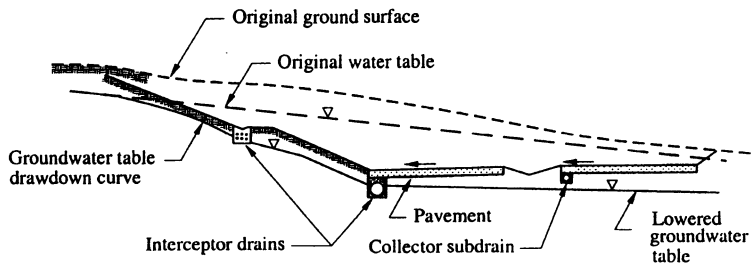


FIGURE 13.1. Schematic of desirable drain installations to control groundwater.

description is given in (MTO 1990). It is important that these open-graded layers not only have adequate permeability but also filtering capacity to prevent the migration of fines from adjacent soils. Thus, the design criteria in this reference are:

1. to ensure adequate permeability:

$$\frac{D_{15}(\text{open graded})}{D_{15}(\text{subsoil})} > 5 \qquad (13.2a)$$

2. to prevent migration of soil fines:

$$\frac{D_{15}(\text{open graded})}{D_{85}(\text{subsoil})} < 5. \qquad (13.2b)$$

where 15% and 85% of the soil is smaller than D_{15} and D_{85}, respectively.

13.2.3 COMPACTION

13.2.3.1 Basic Principles

Compaction is the process by which a mass of material, e.g. soil, aggregate, asphalt mix, etc., is reduced in volume by the momentary application of loading, e.g. rolling, tamping or vibration. It involves the expulsion of air and consequent decrease in voids without significantly changing the gradation of the material. For asphalt mixtures, compaction is the single most important factor influencing the long-term performance of the pavement as it affects stability, durability, fatigue resistance, skid resistance, moisture ingress as well as fracture strength (Hughes 1989).

In soils and unbound granular materials, compaction is influenced by the soil type, moisture content, gradation, particle shape (particularly for granular materials) and the subsequent environment of the compacted product. On the other hand, compaction of an asphalt mixture is affected by such factors as asphalt grade and content, mix design, temperature, type and configuration of the compaction equipment, etc.

13.2.3.2 Compaction of Soils

The key engineering properties of soils, including granular materials, are shear strength, compressibility and hydraulic conductivity. The primary function of compaction is therefore to increase shear strength, decrease compressibility and decrease permeability.

Compaction of cohesive and cohesionless soils should be considered separately (Hilf 1991). Cohesive soils contain a significant proportion of fines (silt and clay). They include Unified Soil Classification (USC) system groups CH, CL, MH, ML, SC, SM, GC, GM and borderline cases (see Section 3.2.11 for more details). Cohesive soils can compact to a low hydraulic conductivity, as discussed in Chapter 25. Cohesionless soils, on the other hand, include relatively clean sands and gravels that remain pervious even when well compacted. They are defined under USC groups SW, SP, GW, GP and the borderline cases.

Generally speaking, the strength or shearing resistance of soils increases with increasing density (TAI 1987a). Two factors that control the dry density of the compacted mass are the moisture content and the compactive effort. Thus, moisture–density curves are used to specify field compaction, as shown schematically in Fig. 13.2. The compacted dry density exhibits a maximum at an "optimum" moisture content for a given compactive effort. At a higher compactive effort, represented in Fig. 13.2 by the modified AASHTO curve, a higher dry density is achieved at a lower optimum moisture content. Details of the standard AASHTO (often referred to as the Standard Proctor) and the modified AASHTO tests are covered in ASTM designations D698 and D1557 and AASHTO designations T99 and T180, respectively.

It should be noted that the shape of the curves in Fig. 13.2 varies significantly with the type of soil. For example, clays often have a curve such as in Fig. 13.2, while silts and sands typically have a less well-defined relationship.

There are significant differences in the shear strength behavior of compacted cohesive and cohesionless soils (Hilf 1991). Cohe-

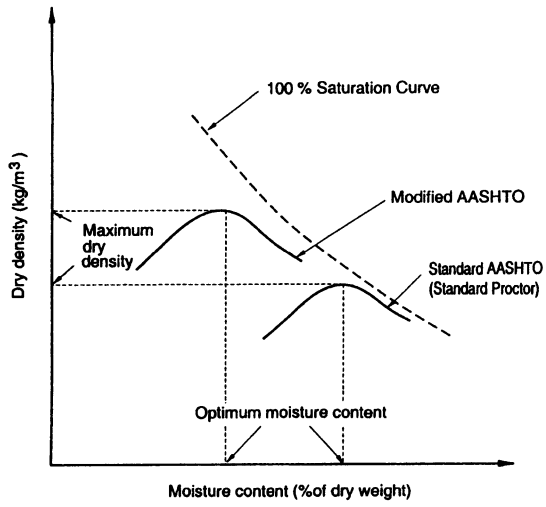


FIGURE 13.2. Schematic illustration of density–moisture curves for standard and modified (AASHTO) compactive efforts.

sionless soils, particularly sands and gravels, are relatively pervious and are often quite sensitive to water content during the compaction process; i.e. their dry densities can decrease rapidly with moisture contents higher than the optimum. A detailed discussion of the factors to be considered in specifying compaction quality control and evaluating shear strength for cohesionless soils is provided in Hilf (1991).

13.2.3.3 Construction Equipment for Soil Compaction

Compaction equipment is available in a large variety of types, sizes and configurations. It is important to carefully select or recommend the most appropriate type based on the type of soil, moisture conditions and the specifications for the finished, compacted product. Experience has shown that no single type of compaction device is completely suitable for all soils and situations. Rather, it is useful to discuss the range of applicability of a particular type of equipment with respect to type of soil, density desired and cost.

Common types of equipment include: sheepsfoot (tamping) rollers, rubber tire rollers, smooth steel wheel rollers (static or vibratory mode), vibrating baseplate compactors, and power tampers or rammers. Desirable specifications appropriate for different applications are given, for example, in Hilf (1991).

Sheepsfoot rollers are applicable to cohesive soils, while steel wheel rollers are applicable to cohesionless soils (usually in the vibratory mode). Baseplate and power tampers are primarily used in small or difficult to access areas, on both cohesive and cohesionless soils, and hot mix asphalt concrete. For regular asphalt compaction, however, steel wheel compaction (usually in a vibratory mode, but depending on thickness of layer and type of aggregate) is first applied, followed by rubber tire rollers and finished with static steel wheel compaction.

Most specifications for compaction of subgrade materials are based on stating the target dry density of the compacted product as a percentage of the laboratory maximum dry density, i.e. 95%, 98%, etc. In some cases, limits are also stated for the allowable range of moisture content.

Generally, standard AASHTO compaction (ASTM D-698 or AASHTO T-99) is used for embankments and backfills specifications, while modified AASHTO T-180 or ASTM D-1557 is used for specifying compaction of granular base layers for pavements.

13.2.3.4 Compaction of Asphalt Layers

Proper compaction of hot mix asphalt concrete is essential because reducing air voids to an acceptable level improves the strength, resistance to deformation, resistance to moisture damage and impermeability of the mix. It is also known that compaction improves fatigue resistance, skid resistance and fracture strength.

The final compaction of an asphalt pavement is affected by two categories of factors:

material properties and initial density. Material-related factors include asphalt (temperature susceptibility and rheology), aggregate properties (texture, shape, gradation, maximum size and absorption), and mix design. The initial density is influenced by factors such as subgrade support, lift thickness, environment (temperature), equipment, rolling sequence and procedure. Detailed treatment of these factors is found in Hughes (1989) and in TAI (1988).

13.2.3.5 Specifications for Compaction of Asphalt Layers

The subject of specifications is well documented in the paving literature, such as in Hughes (1989). There are three types of specifications: method, end result and long-term performance. Method specifications are the oldest type in practice, and are based on detailing for the contractor step-by-step procedures, equipment, etc. End-result specifications are based on limits for as-placed properties, such as voids, density, binder content, etc. Long-term performance based specifications, a relatively more recent approach, involve limits on damage or distress, such as fatigue cracking, rutting, thermal cracking and surface roughness at various pavement ages.

A typical example of method specification may read, "a minimum of three passes of a 10–12 t steel roller, followed by three passes with a pneumatic tire roller, with a minimum load of 1000 kg per wheel, and finally sufficient passes of an 8–10 t roller to iron out roller marks for finishing". A typical end-result specification sets mean target values and acceptable tolerance limits for the field density relative to results obtained in thelaboratory mix design, e.g. field density shall be no less than 95% of the laboratory density. A typical example of a long-term performance based specification might be to specify surface rut depths no greater than 5, 10 and 15 mm at 5, 10 and 15 years of age, respectively.

The most common laboratory mix design method used for many years in North America and in many other countries worldwide has been the Marshall method. It involves compaction of various design formulations of hot mix asphalt concrete, normally in a 100 mm diameter steel mold, with a number of blows of a flat plate steel hammer appropriate to the design situation requirements. The method is described in detail in various references, including (Roberts *et al.* 1996). A strong possibility exists, however, that the Marshall method will eventually be superseded by the "Superpave" mix design method, a result of the Strategic Highway Research Program (SHRP 1994). This is a volumetric-based method, which uses a gyratory shear type of compaction device.

13.2.3.6 Asphalt Compaction Equipment

In modern construction practice, initial compaction of the asphalt concrete is provided by the paver screed. Factors influencing the effectiveness of modern vibratory screed pavers are: (a) speed of the paver, (b) uniformity of the asphalt concrete mix, and (c) thickness of mat being placed, relative to the maximum size aggregate used in the mix.

Rollers are used to compact the asphalt mat immediately behind the paver. There are two basic types in use: (a) static or vibratory steel wheel rollers, and (b) pneumatic or rubber tire rollers, as previously noted in Section 13.2.3.3. The effectiveness of such types of rollers is treated in more detail in Geller (1982).

13.2.4 GEOSYNTHETICS IN PAVEMENTS

The use of geosynthetics in road and airfield applications has increased markedly over the past two or three decades. Several reasons exist: (a) the range of geosynthetic types and associated economy has increased; (b) technological advancements in design and construction have occurred; and (c) there has been increasing recognition of the value and

usefulness of geosynthetics in various design situations.

The various classes of geosynthetics, test methods and properties have been covered in Chapter 7. Within these classes, there are many variations of types, and various manufacturers or suppliers. Consequently, it is important that the "engineering" of a geosynthetic into a pavement or any other application carefully recognizes the types available, their properties and the design situation requirements if the application is to be successful.

Design requirements for pavements can generally be classified according to one or more of the following functions: (a) filtration; (b) drainage; (c) separation; and (d) reinforcement.

A primary use for geotextile filters in pavement structures is for collector subdrains (see Fig. 13.1). These subdrains consist of narrow trenches located about 300 mm from the edge of the pavement surface (or immediately below the end of the open-graded drainage layer, if used, as noted in Section 13.2.2), with a flexible perforated or slotted plastic pipe commonly 100 or 150 mm in diameter wrapped with a geotextile and surrounded by crushed stone. Alternatively, the subdrain may consist of crushed stone wrapped in a geotextile. These configurations are described and illustrated in detail in (Koerner 1998).

Geocomposites represent an alternate to the type of collector subdrain described above. These consist of egg-carton or fingerboard shaped cores wrapped with a geotextile, which can also be used to serve both the filtration and drainage function when installed in a narrow trench at the edge of the pavement. Again, a more detailed description is provided in (Koerner 1998), who also provides a list of manufacturers.

Geosynthetic separators, e.g. non-woven geotextiles, have had a significant impact on pavement engineering, particularly for pavement structures on weak subgrades. Without a suitable separating layer, in these cases the soft (silty, clay–silt or fine sand) subgrade material can "pump" up into the granular subbase or base under repeated traffic loads, and/or it can contaminate the granular material through frost action. The end result is a weakened, more frost-susceptible subbase and base. Geotextiles may also be used for reinforcement purposes, particularly where deformations are expected to be sufficiently large to mobilize the tensile strength. However, geogrids, as subsequently discussed, may be more effective for reinforcement applications involving pavement structures. While many good references exist in this area, *Geosynthetics Case Histories* (Raymond & Giroud 1993) has a number of well-described applications.

Another separation application for geotextiles in pavements is for waterproofing between an existing pavement and an overlay. In this case, an emulsified asphalt is first sprayed on the existing surface, as an adhesive, and the geotextile is rolled on, followed by the overlay. While many kilometers of construction have occurred with this application, there are serious reservations among a number of pavement engineers about the effectiveness of the application. Primarily, it is felt that because water can and does enter the pavement structure through the shoulders and slopes, the so-called waterproofing function is not effective. Moreover, because of the relatively impermeable barrier, water can in fact become trapped between the overlay and the existing surface, with the net result being stripping of asphalt at the underside of the overlay.

Reinforcement of a pavement structure can be a very effective application for geosynthetics, particularly in the case of weak subgrade conditions and using high tensile strength geogrids. Another reinforcement function is the use of high strength geogrids to reduce or minimize the "reflection" of cracks in an existing pavement through an

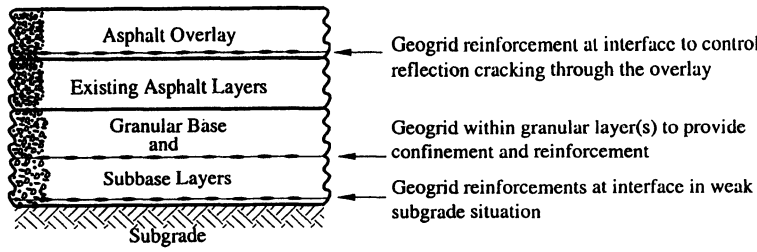


FIGURE 13.3. Possible locations for geogrid reinforcement in a flexible pavement structure.

overlay. Figure 13.3 illustrates the potential locations for reinforcement in a pavement structure.

The overlay reinforcement application in Fig. 13.3 is accomplished by "tacking" the geogrid to the existing pavement surface and then placing the overlay. While a number of products have been used, Glas Grid™ has seen the most widespread application to date.

Constructability plays a key role in this type of application and that is largely why installation of geogrids within asphalt layers has been very limited. The technical and cost effectiveness of geogrids to prevent reflection cracking through overlays has not yet been well established for two basic reasons: (a) lack of long-term field performance data, and (b) lack of comparative life cycle economic analysis.

Geogrid reinforcement within granular layers can be very effective, provided that location is properly selected on an engineering analysis basis. There is considerable design literature available, much of which has been summarized in Koerner (1998). As well, geogrid reinforcement at the interface between a weak subgrade (where the CBR is less than about 6–8, or the modulus of resilience, M_R, is less than about 60–80 MPa) and the granular layers can be quite effective. Again, this is well summarized in Koerner (1998). There should, however, be a note of caution. It is possible that in the longer term, where clay, silt or fine, sandy subgrades are involved, some intrusion of fines into the granular layers may occur because of the openings in the geogrid.

13.2.5 ENVIRONMENTAL CONSIDERATIONS

At the design stage, the environmental factors of concern are precipitation or moisture, temperature and solar radiation. Each has a major influence on the performance of materials and the pavement structure.

Moisture ingress into the pavement structure has a number of possible effects: reduction in bearing capacity of the subgrade, subbase and base; moisture damage of the asphalt concrete; corrosion of reinforcing steel in Portland cement concrete, etc.

Minimizing the reduction of bearing capacity through proper drainage has been discussed in Section 13.2.2. Asphalt concrete moisture damage can occur in the form of "stripping", which is separation of the asphalt binder from the aggregate particles. It is a complex phenomenon, largely related to chemical and physical interaction between the aggregate mineral type and the asphalt binder. Several treatment alternatives with additives or modifiers exist for asphalt–aggregate combinations prone to stripping. Most common is the use of about 1–1.5% hydrated lime added at the mix plant. Corrosion of reinforcing steel can be mitigated by the use of stainless steel and epoxy coating, where warranted (see Section 13.4.1.4).

Temperature changes have adverse effects on performance. Extreme high temperatures are associated with effects such as curling and warping stresses in rigid pavements and bleeding (flushing of the asphalt to the surface) and rutting problems in asphalt pavements. At the other extreme, low temperatures can cause widening of joints and cracking in rigid pavements and thermal contraction cracking in asphalt pavements. The latter is a major problem over much of North America and parts of Europe and Asia. It is primarily related to the type of asphalt binder and low temperature conditions. A great deal of research in the area has been carried out, and binder specifications and test methods, as well as low temperature mix test methods, have been developed in SHRP (1994).

Another serious effect of low temperature changes in cold regions is the spring thaw process. The freeze–thaw cycle is associated with a lag in temperature changes at different depths of the pavement. Trapped moisture in the underlying layers, resulting from the pavement thawing from the top down, weakens the structure and results in excessive damage by traffic during the spring. Chapter 20 provides a more detailed treatment of this topic. Again, proper drainage, as discussed in Section 13.2.2, can be an important mitigating factor.

Solar radiation has the primary effect of hardening the asphalt concrete layer through increased oxidation or volatilization of the lighter molecules in the binder. The possible effects include block cracking, particularly in more temperate climates.

13.3 Framework for Pavement Design

13.3.1 INTRODUCTION

Pavement design has evolved to a multiplicity of procedures ranging from very simple to fairly complex. Notwithstanding the large number of methods, there seems to be a common framework that underlines all methods (Haas *et al.* 1994). This section outlines the generic framework underlying pavement design and its major components.

13.3.2 DESIGN OBJECTIVES AND CONSTRAINTS

The primary objectives in pavement design would ideally include all of the following: maximum economy to the road or airfield authority as well as the user; adequate safety, serviceability and structural integrity over the design life; resistance to environmental degradation; minimal noise, air pollution and land-use impact concerns; and good aesthetics.

Some of these objectives are contradictory and consequently the final design is normally a trade-off between competing objectives. More specific design objectives arise from the nature of the project, and the design process itself. Such specific objectives are, for example, maximizing use of local materials, minimizing the overall project cost, maximizing the accuracy of performance predictions, etc. (Haas *et al.* 1994).

Major constraints facing the design process are either economic or technical in nature and can include the following: time and funds available for the design and construction; allowable limits on serviceability, layer thicknesses, etc.; available materials; testing, construction and maintenance resources available; capabilities of the structural and economic models; and quality and quantity of data.

13.3.3 COMPONENTS OF THE DESIGN FRAMEWORK

A framework for pavement design is shown in Fig. 13.4. Any individual design method might incorporate some of the components in the framework, only implicitly or intuitively, such as design objectives and constraints, reliability level and climatic factors. Three of the major inputs, i.e. soil and materials prop-

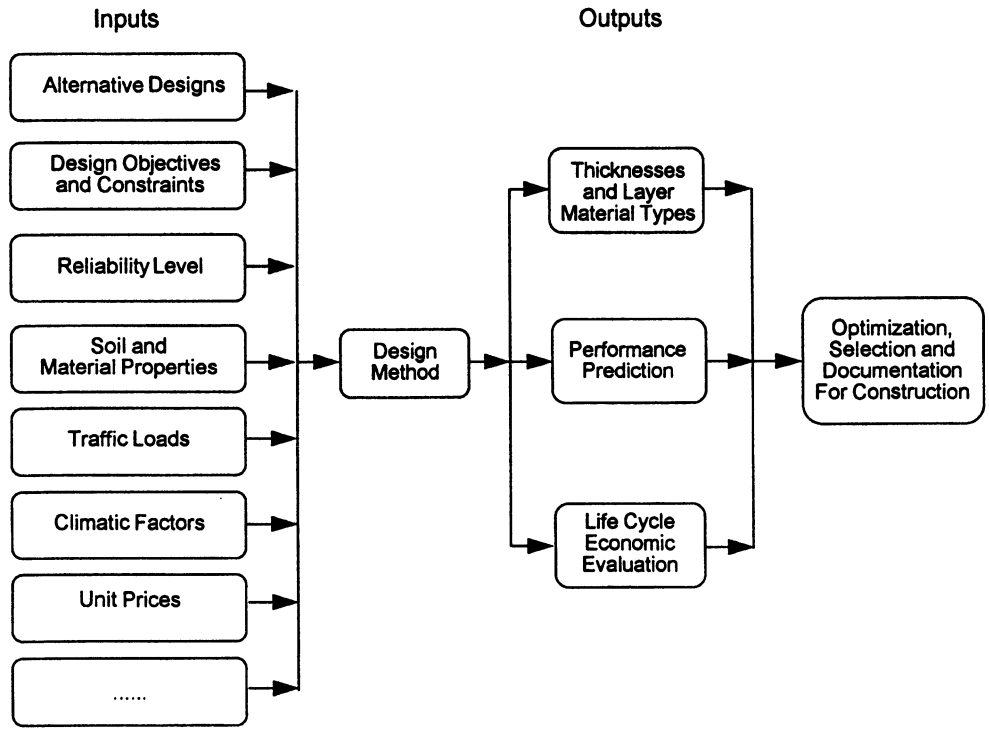


FIGURE 13.4. Pavement design framework and major components (modified from TAC 1997).

erties, traffic loads, and environmental factors, are further discussed in the next section.

13.3.4 CATEGORIZATION OF STRUCTURAL DESIGN METHODS

All methods of pavement structural design fall into one of the following three basic categories:

1. Experience-based (prescriptive) methods using standard layer thicknesses for various conditions of traffic, types of subgrade soil, class of highway, drainage, etc. With this approach, a major limitation is that experience cannot be easily extrapolated to new materials, different types of traffic loads and environmental conditions, and different construction and maintenance practices.
2. Empirical methods in which relationships between some measured pavement response, usually deflection, and field observations of performance are utilized to arrive at thickness designs for various levels of traffic loads. Most of the limitations of the experience-based (prescriptive) methods also apply to this approach.
3. Theory-based methods, often called mechanistic-empirical methods. These relate calculated values of stress, strain or deflection at some point(s) in the pavement structure to observed performance under various axle load repetitions. This approach has the advantage of considerable flexibility because of: (a) its theoretical basis, (b) the capability of using past experience for "calibration" purposes, and (c) the potential for transfer from one environment to another. However, all theory-based design methods still have some empirical components and require additional work to make them consistent, reliable and routine.

These design methods are further described in various textbooks, major reports and man-

uals. Example textbooks include Ullidtz (1987, 1998) and Haas *et al.* (1994). Other key references from Europe include Powell *et al.* (1984), Brown *et al.* (1985) for flexible pavements, Mayhew & Harding (1986) for rigid pavements, and Nunn & Merrill (1997) for flexible and composite pavements. As well, there is a very comprehensive publication from Delft University in Holland on the theory and practice of pavement design (Molenaar 1983).

There are many other similar excellent references in the Middle East, Africa, Asia, Australia, South America and elsewhere. Readers might contact asphalt or Portland cement associations in these regions for further information or advice. Most, if not all, would likely have web sites. For example, the International Society for Asphalt Pavements can be accessed at www.asphalt.org.

13.4 Design Inputs and Their Characterization

There are three principal inputs to the design process: soil and material properties, traffic loads, and environmental factors.

13.4.1 MATERIAL PROPERTIES AND CHARACTERIZATION

Traditionally, many pavement design methods use empirical tests to characterize the subgrade soil, granular materials and the asphalt or Portland cement concrete layer materials. Examples of empirical tests include the California Bearing Ratio (CBR) for subgrade soils and granular materials, as noted in Section 13.2.1. There is a trend, however, to more fundamentally based mechanistic characterization procedures involving triaxial, shear, torsional and other types of testing. These testing methods try to establish the response properties (elastic, viscoelastic, etc.) of the materials under load. In practice, the model used to characterize a material is often, of necessity, a practical simplification of the true state of nature. Consequently, a trade-off is sought between the complexity of the testing and analytical procedures and the ability of engineers to perform the tests and the calculations in a cost-effective manner. The subsequent paragraphs review the key materials used in pavements.

13.4.1.1 Asphalt Concrete

Asphalt concrete represents the major pavement surfacing material. It consists of a combination of coarse and fine aggregate and asphalt binder, mixed in a heated condition, and placed and compacted mechanically. A comprehensive description of binder and aggregate properties, and specifications and mix design procedures is provided in (SHRP 1994; Roberts *et al.* 1996; TAC 1997).

Key properties that impact on the long-term performance of asphalt concrete pavements include: mixture stiffness, strength (resistance to permanent deformation), durability, low temperature cracking resistance, fatigue resistance and permeability.

The traditional mix design approach (e.g. the Marshall method, Section 13.2.3.5) is based on criteria that prescribe minimum levels of strength (stability), and allowable ranges of flow and voids content. A relatively new, performance-based mix design approach within the "Superpave" system, developed as part of the Strategic Highway Research Program (SHRP 1994), is being adopted by some road and airport authorities. It provides a comprehensive approach to mix design that considers site specific requirements, traffic, climate and the other structural factors. However, there are reservations about its capabilities in several parts of the world. It appears that the most valued part of Superpave, currently, is the comprehensive and fundamental characterization of the asphalt binder and the selection of binder grades to suit the extremes of temperature under which the mix is required to perform.

Asphalt is also used in cold mixes, which

are made with emulsified or cutback asphalt and aggregate at low or ambient temperatures. Emulsified asphalt and cold mixes have become popular in rehabilitation and maintenance work, primarily in low-volume road situations.

13.4.1.2 Portland Cement Concrete

Portland cement concrete is produced by mixing cement, aggregates and water. The cement reacts with water to produce the binding structure, which determines the properties of the hardened concrete. Structurally, concrete has high compressive strength, but relatively low tensile strength. Since pavement slabs under traffic loading act principally as flexural members, flexural strength testing is used for the design of concrete pavements. The third-point loading beam test is commonly used for establishing the design flexural strength (ASTM C78).

Aside from load-related deterioration, concrete pavements are also subject to environmental degradation (aging) and chemical attack. For this reason, different types of cements have been developed for particular applications. Example specifications for cements and concrete are available from such organizations as the American Society for Testing and Materials (ASTM, USA), International Union of Testing and Research Laboratories (RILEM, Europe) and the American Concrete Pavement Association (USA), as well as in the manuals and specifications of many larger road and airfield authorities.

13.4.1.3 Granular Bases and Subbases

Base and subbase layers in a pavement structure distribute traffic-induced stresses to tolerable levels for subgrades under flexible pavements. For rigid pavements the subbase layer provides a construction platform and uniformity of support for the slab. These layers normally consist of crushed naturally occurring mineral aggregate, e.g. sands and gravels, and/or crushed rock, and there are three main categories: dense graded, treated (with Portland cement or asphalt) and open-graded drainage layers.

In general, properties of granular materials are dependent on gradation, moisture content, density, stress state (particularly for unbound granular materials), and the aggregate shape and texture. The required physical properties will vary with type of application. Table 13.1 provides typical limiting values for these physical properties. The stress dependency of granular materials can be a major issue in structural design and will be further addressed in Section 13.5.1 on elastic layer theory.

Table 13.2 summarizes typical gradation requirements for granular subbase, base and open-graded base as well as asphalt treated base (TAC 1997). More detailed treatment of testing and limiting requirements for aggregates are available in various ASTM and RILEM standards, in (Roberts *et al.* 1996), from the Strategic Highway Research Program (SHRP 1994) and from organizations such as the National Stone Association in Washington DC. A summary description of the various tests is also available in (TAC 1997).

13.4.1.4 Reinforcement Steel

The principal use of steel in jointed rigid pavements is for load-transfer devices (dowels) at transverse joints and tie bars for longitudinal joints; in continuously reinforced concrete pavements, steel reinforcement grids are used. Details of steel reinforcement design in pavements are provided in such sources as (AASHTO 1993).

The limitation in the long-term performance of steel is corrosion. Special treatments may be necessary in some situations to ensure prevention of premature rusting and loss of functionality. Epoxy coatings and the use of stainless steel are example treatment alternatives for load transfer devices in pavements, but they are not yet being widely used.

TABLE 13.1. Physical properties of granular base and subbase materials

Physical test	ASTM designation	Typical limiting values		
		Granular subbase	Granular base	Asphalt stabilized base
Magnesium sulphate soundness loss	C88 [875]			
Coarse aggregate				
Fine aggregate		25	20	
Los Angeles Abrasion Loss, % max.		20	25	
Sand equivalent, % min.	C131 [876]	50	45	60
Liquid limit	D2419 [877]	30	40	
Plasticity index	D4318 [84]	25 max.	25 max.	
% with at least one crushed face +4.75-mm fraction, min.	D4318 [84]	6 max.	6 max.	
Lightweight particles, % max.	—	—	60	50
Flat and elongated particles, % max.	C123 [878]	5	5	
California Bearing Ratio (CBR)	D4791 [879]	15	15	
@ 100% of ASTM D698 [858], min.	D1883 [852]	40	80 (PCC)[a]	
			100 (ACP)[b]	

[a] If used in a Portland cement concrete pavement application.
[b] If used in an asphalt concrete pavement application.

TABLE 13.2. Typical gradation requirements for subbase and base (adapted from TAC 1997)

Sieve size[a] (mm)	Subbase	Well-graded base[b]		Open-graded base[b]	Asphalt stabilized base[b]
		25 mm	19 mm		
75	100				
37.5				100	
25	55–100	100			100
19			100	50–100	85–100
16		70–90			
12.5				25–70	
9.5		50–75	50–80	15–50	50–75
4.75	25–100	35–60	40–70	5–15	35–65
2.36	15–80				
1.18	15–45	15–40	15–40	0–8	15–40
0.600	10–35				
0.315		8–20	8–25		5–25
0.150	5–15	5–15	5–18		
0.075	0–8	2–8[c]	2–8[c]	0–5	2–8

[a] Data from [880].
[b] Figures are a measure of the percent passing.
[c] The upper limit on this size is reduced to 5% by some agencies in order to improve layer permeability properties.

13.4.1.5 Traffic Loads

1. Flexible pavements (roads). Specific axle group loads for trucks can be converted to an equivalent standard axle using a load equivalency factor (LEF):

$$\text{LEF} = \left[\frac{\text{specific axle group load}}{\text{standard axle group load}}\right]^4. \quad (13.3)$$

Equation 13.3 is often referred to as the "fourth-power law". In actual fact, the exponent varies with axle group type, pavement type, thickness and other factors. However, an exponent of four can be used as an approximation.

LEFs are transformed into equivalent single axle loads (ESALs), where the standard for an ESAL is 80 kN or 18 kips. Thus, for an actual single axle load of 80 kN (the numerator in Eq. 13.3), where the standard axle load is also 80 kN, the LEF = $(80/80)^4 = 1$. For a 100 kN actual single axle load, the LEF = $(100/80)^4 = 2.5$. This means that one 100 kN load would impose 2.5 times the damage of one 80 kN load, and would be considered as 2.5 ESALs. In other words, the LEF is calculated for each specific or individual axle load group in the traffic stream, and multiplied by the number of passes of that group to estimate the ESALs. Thus, 10^6 passes of 100 kN single axle loads would represent 2.5×10^6 ESALs.

Because of the difficulty in obtaining individual axle group load data, approximate estimation methods are often used for design purposes. One of these was developed in the SHRP program for estimating (outside) design lane annual flexible pavement ESALs based on average annual daily traffic (AADT), truck percentage (TP) and truck factor (TF), which is the number of ESALs per truck:

For one lane:

$$\text{ESAL} = 182.5 * \text{AADT} * \text{TP} * \text{TF} \quad (13.4a)$$

For two lanes:

$$\text{ESAL} = 182.5 * \text{AADT} * \text{TP} * \text{TF} * [1.57 - 0.083 * \log_e(\text{AADT}/2)] \quad (13.4b)$$

For more than two lanes:

$$\text{ESAL} = 182.5 * \text{AADT} * \text{TP} * \text{TF} * [1.44 - 0.083 * \log_e(\text{AADT}/2)] \quad (13.4c)$$

where: "lanes" = the number of lanes for a given direction, TP = the fraction of heavy vehicles, and TF = 0.76 for flexible pavements and TF = 1.15 for rigid pavements.

It must be strongly emphasized that the truck factor (TF) varies with region, and calibration to local conditions should be carried out if at all possible. As well, calibration of the constants in the above equations to local conditions is desirable.

2. Rigid pavements (roads). Estimation of traffic loading for the design of concrete or rigid pavements is similar in concept to that for flexible pavements. Studies have shown that LEF for rigid pavements are generally influenced by: (a) the failure criterion used, e.g. fatigue cracking, joint failure, terminal serviceability, etc.; (b) pavement strength, thickness D of the slab; (c) pavement stiffness (particularly the concrete to subgrade moduli ratio E_c/E_s); and (d) the inter-axle spacing in tandem and tridem axles. Flexible pavement ESALs will therefore differ from rigid ESALs estimated from the same traffic data. Generally the rigid pavement ESALs are larger than the corresponding flexible pavement ESALs. Procedures for estimating both rigid and flexible pavement ESALs can be found in (AASHTO 1993).

3. Airfields. Table 13.3 lists the loading characteristics of a number of aircraft, new and old, for comparison with the highway loading given at the bottom of the table. The aircraft wheel loads are approximately ten times the legal highway maximum and the tire pressures are almost double. Some military aircraft have small tires with pressures as high as 3.1 MPa (1450 psi), but because the wheel loads are small, they do not usually result in significant pavement damage.

TABLE 13.3. Aircraft versus highway loads

Aircraft	Maximum mass (t)	Tire pressure (MPa)	Wheel load (t)
Antonov 225	600	1.15[a]	20[a]
B-747	397	1.40	23
B-777	310	1.48	24
B-707	150	1.24	18
Concorde	185	1.26	22
C5A Galaxy	350	0.80	14
DC-10	270	1.24	26
B-727	95	1.15	22

[a] Typically highway traffic consists of tire pressures less than 0.70 MPa and axle loads are typically limited to 9.1, 17.0 and 24 t for dual-tired single, tandem and tridem axles, respectively. Single-tired steering axles are typically limited to 5.5 t.

As shown in the table, the mass of the aircraft is not reflected in the wheel loads. For many years aircraft have, to a large extent, been designed not to overstress existing pavements. This has been accomplished by providing larger aircraft with more wheels and increasing the wheel spacings. In addition to higher tire pressures and loads, modern jet aircraft subject pavements to large horizontal braking and cornering forces. These can produce slippage failures, resulting from surface layers of asphalt sliding over the underlying layer.

The airfield situation also differs from highways in that wheel loads are much more evenly distributed across the pavement width. This is due to the large variety of aircraft wheel configurations and the low degree of channelization relative to the road situation. Field observations of aircraft movements have shown that successive passes of aircraft along a pavement are normally distributed about the pavement centerline. Statistically, the degree of "wander" can be reasonably characterized by a standard deviation and is found to be significantly different for runways, taxiways and aircraft docking bays. This spreading of aircraft wheel loads across the pavement width to different degrees affects the pavement thickness required for different parts of the airport.

Impact loads during landing do not constitute a significant problem for pavements except that rubber buildup occurs, which diminishes runway texture. Having used up much of its fuel during flight, the aircraft is considerably lighter at landing than at takeoff. A Boeing 747, for example, uses approximately 140 t of fuel flying from Los Angeles to Sydney, thereby reducing its 400 t takeoff weight to 260 t at landing. Furthermore, much of its remaining load is "taken on the wings" until a later stage of the landing. Also, asphalt has a stronger/stiffer response to high-speed loading. As with the road situation, most asphalt pavement problems develop on airfields in areas that are subjected to slow moving or stationary loads. Wheel loads up to 20% greater than the static value have been measured during aircraft rotation, immediately before leaving the runway at takeoff. But again, because this is a high-speed event, pavements are not unduly affected.

Because heavy aircraft loadings are ten times greater than those of road vehicles, the cost of generating much-needed empirical design data by accelerated load testing of full-scale pavements is often prohibitive, and very little has been done in this respect. This contrasts with the highway situation where many accelerated loading facilities exist throughout the world to produce data for road pavement designers. However, a full-scale test loading facility for aircraft, at the time of writing this handbook, is under construction at Atlantic City in the USA.

13.5 *Pavement Response Models*

Mechanistic design of pavements relies upon the engineer being able to estimate the stress–strain behavior of the pavement structure under simulated field-load conditions. Structural models for calculating these responses range from simple to complex. This section reviews,

in broad terms, the key features of the common pavement response models.

13.5.1 ELASTIC LAYER THEORY

The general concept of the elastic layer theory is reviewed in various textbooks, such as Ullidtz (1998), Huang (1993), Croney & Croney (1997) and Haas *et al.* (1994). The pavement is commonly represented by a model based on the following assumptions: (a) each layer consists of a homogeneous linear-elastic material and is of finite thickness, (b) the layer materials are isotropic, (c) full friction exists between layers and there is no shear stress at the surface. Wheel loads are assumed to be static and are represented by vertical stress uniformly distributed over circular areas.

Some computer programs, such as CIRCLY4 (Wardle & Rodway 1998a) accommodate material anisotrophy, slip between layers and non-uniform loading including shear. Models based on dynamic loadings have also been developed; however, their complexity has limited any widespread adoption.

The actual load response of many pavement materials is elasto-plastic and stress-dependent. The layered elastic method can account for stress dependence to a limited degree by dividing granular layers into sublayers and assigning moduli to each sublayer. This allows the modulus to change with depth, but not with horizontal distance. Elastic layer theory cannot take account of plasticity. Despite these limitations it is used by pavement engineers as the best currently practical method of estimating stresses in a layered system.

Pavement design methods, which are mechanistic-empirical (see Section 13.6.4), relate the estimated elastic strains to pavement performance. Typically, the vertical compressive strain at subgrade level is related to repetitions to cause surface rutting failure, and the tensile strain at the underside of the asphalt or other bound layers is related to repetitions to cause cracking. The performance relationships are established by a process of calibration against the observed rutting and cracking performance of in-service roads or test pavements. It is important that the pavement model used in the calibration process is also used when designing new pavements: the use of a pavement model from one design method with a performance relationship from another will produce an invalid design.

Several computer codes exist for solving the elastic layer equations. One commonly used in North America is ELSYM5 (McTRANS™). Other widely used elastic layer programs include CIRCLY (Wardle 1996), and its most current version CIRCLY4 (Wardle & Rodway 1998a), Shell's BISAR, which is described in the *Shell Pavement Design Manual*, personal computer version, SPDM-PC (Preston 1996) and JULEA (FAA 1995a), which was developed at the US Army Corps of Engineers.

CIRCLY4, LEDFAA (Layered Elastic Design, Federal Aviation Administration (FAA 1995a)) and SPDM-PC are pavement design programs that use layered elastic programs (CIRCLY, JULEA and BISAR, respectively) to calculate strains, then use the strains to perform the required design calculations. The aircraft pavement design programs, APSDS (Airport Pavement Structural Design System) and LEDFAA (see Section 13.7.2.1) differ from road design programs in that they cater for vehicle wander, which must be taken into account in aircraft pavement design.

All three programs run under Windows, and incorporate databases for material properties, vehicle loadings and empirical failure criteria, thus eliminating the need to re-key data. They are also all highly automated.

13.5.2 THE FINITE ELEMENT METHOD

The finite element method (FEM) involves dividing a pavement structure into a large number of small elements. Each element can be assigned deformation properties that are different from those of the other elements. It therefore potentially allows a more realistic

representation of pavements than using the layered elastic method of analysis. As well, it is considered by some to be the tool most likely to overcome the limitations of the elastic layer theory. In fact, the "First National Symposium on 3D Finite Element Modeling For Pavement Analysis and Design" was held November 8–10, 1998 in Charleston, West Virginia, sponsored by the US Federal Highway Administration, West Virginia University and the West Virginia Department of Transportation (Shoukry 1998).

Although FEM has been in existence for more than two decades, it has not yet been adopted in the pavement field, partly because of the large computer time required to handle realistic pavement problems, and because of the extreme difficulty in obtaining the required input material properties. Nevertheless, it is seriously being considered in a project currently underway, known as "AASHTO 2002", which is intended to produce a successor to AASHTO's empirical method of pavement design (AASHTO 1993).

13.5.3 SIMPLIFIED (ODEMARK) ELASTIC LAYER THEORY

A simplified elastic layer theory was originally formulated by Odemark in Sweden and is described in detail in Jung and Phang (1974). In its simplest form, the pavement structure becomes a two-layer system consisting of the subgrade and an equivalent single flexible pavement layer on the subgrade. This equivalent layer is determined through transforming the individual layers into equivalent granular material. An example of the practical application of the theory is described in a new Ontario design method called OPAC 2000 (He *et al.* 1996).

13.6 Structural Design of Flexible Road Pavements

Structural design of asphalt pavements for roads and airports has evolved to a multitude of methods. Almost every provincial or state road authority has customized its own design approach. It is not feasible or logical to provide a detailed coverage of all available methods in this subsection. Instead, a very condensed overview of several common methods will be given.

13.6.1 REVIEW OF COMMON DESIGN METHODS

Two current reviews of flexible pavement design methods are provided in TAC (1997) and in Nunn & Merrill (1997). The theoretical basics are given elsewhere (Molenaar 1983, Ullidtz 1987, Haas *et al.* 1994 and Ullidtz 1998).

13.6.2 EXPERIENCE-BASED DESIGN

As noted in Section 13.3.4, a common yet practical approach for pavement design is the use of standard sections or a catalog of experience-based designs. The standard sections are very useful as indicators of the probable range of design alternatives for the observed range of conditions.

A comprehensive example of catalog designs is provided by the National Cooperative Highway Research Program (NCHRP) Project 1-32, titled "Catalog of Current State Pavement Design Features" (ERES 1998). It covers both flexible and rigid pavements, and a wide range of climatic conditions. An example for rigid pavements is subsequently provided in Section 13.8.8. Because of the magnitude of information, the project results are only available in CD format (from NCHRP in Washington, DC, which is part of the Transportation Research Board).

Another illustration of such catalog designs is given in the *Pavement Design and Management Guide* (TAC 1997). Table 13.4 presents designs for the Canadian provinces, one territory (Yukon) and one federal agency (Public Works and Government Services Canada), for a design traffic loading of one million ESALs.

A typical standard section prescribes classes of subgrade strength, traffic loadings, and environmental conditions to which it ap-

TABLE 13.4. Typical pavement thicknesses (mm) used by Canadian provincial agencies for selected subgrade and traffic loading (traffic loading of 1×10^6 cumulative ESALs) (TAC 1997)

Subgrade type	Conventional pavement structure course	BC	AB	SK	MB	ON	QC	NB	NS	NF	YT[d]	PW & GSC
Weak[a]	Asphalt concrete	100	100	100	100	130	105	140	150	120	100	100
	Asphalt stabilized granular		50									
	Granular base	300	300	150	175	150	200	150	150	150	150	200
	Granular subbase			360	350	450–600	525–675	450	300	300	150	450
	Select granular	300								500	450	
	Total	700	450	610	625	730–880	830–980	740	600	1070	850	750
Medium[b]	Asphalt concrete	100	90	80	100	130	105	140	150	120	100	100
	Asphalt stabilized granular		50									
	Granular base	300	230	150	150	150	200	150	150	150	150	200
	Granular subbase			260	225	450	525–675	450	250	300	150	300
	Select granular	300								500	300	
	Total	700	370	490	475	730	830–980	740	550	1070	700	600
Strong[c]	Asphalt concrete	100	80	60	100	130	105	140	125	120	100	100
	Asphalt stabilized granular		50									
	Granular base	300	200	180	100	150	200	150	150	150	150	150
	Granular subbase				100	150	300–450	450	200	300	150	150
	Select granular	0–300								500	150	
	Total	400–700	330	240	300	430	605–755	740	475	1070	550	400

[a] Lacustrine clay: CBR ≡ 3.0; Group Index, ~20; Unified Soil Classification, CH.
[b] Glacial till: CBR ≡ 5.0; Group Index, ~10–12; Unified Soil Classification, CL.
[c] Clayey gravel: CBR ≡ 20; Group Index, ~2; Unified Soil Classification, GC.
[d] Yukon has alternative designs of bituminous surface treatment (BST) on 300 mm of granular base on 450, 300 and 150 mm of select granular, respectively, for the three subgrade types.
[e] BC = British Columbia, AB = Alberta, SK = Saskatchewan, MB = Manitoba, ON = Ontario, NB = New Brunswick, NS = Nova Scotia, PEI = Prince Edward Island, NF = Newfoundland, YT = Yukon, PW & GSC = Public Works and Government Services Canada.

plies. Most of these standard sections were developed from the experience gained in using the existing design methods.

Whatever the source of a catalog design, it is important to emphasize that engineering judgement should be used to recommend the final design alternative. An example of an experience-based design illustrates how it may be used as an initial step in a more complete design, or as a final design if the scale of the project does not warrant further investigation. Suppose a two lane access road is proposed on a weak subgrade (CBR ~ 3) in Ontario and is expected to carry average annual daily traffic (AADT) of 600 during a design period of 20 years. Assume commercial vehicles amount only to 10% with an average truck factor of 2.1, an annual growth rate of 3%, and 300 days per year with truck traffic. Granular base equivalencies for Ontario are 1 mm granular base = 2.25 mm asphalt concrete = 1.50 mm asphalt stabilized base = 0.67 mm granular subbase. It may be noted that many agencies use such equivalencies, as an approximation, but caution should be exercised as they can vary considerably and are in effect calibrated to local conditions.

The cumulative design ESALs is found as AADT $\times$ 300 $\times$ 0.10 $\times$ 2.1 $\times$ $[(1 + 0.03)^{20} - 1]/0.03$, giving an approximate value of 1.02×10^6 ESALs. Table 13.4 indicates the following conventional flexible pavement structure might be initially considered:

Layer	*Thickness* (mm)	*Granular base equivalent* GBE (mm)
Asphalt concrete	130	130 $\times$ 2.25 = 293
Granular base	150	150 $\times$ 1.00 = 150
Granular subbase	525	525 $\times$ 0.67 = 350
		Total GBE ~ 790

It should be emphasized that selecting a thickness design, as in the example, is only a preliminary step. For a larger project, more detailed consideration is usually warranted in order to evaluate alternative possible designs or make an enhancement to the initial, preliminary design.

13.6.3 EMPIRICALLY BASED DESIGN: THE AASHTO DESIGN METHOD

The AASHTO design method is one of the most widely used empirical methods both in the USA and in many other countries. It has undergone several updates since the original procedure based on the AASHO Road Test in the early 1960s. The major modifications (AASHTO 1993) can be summarized as follows: (a) introduction of resilient modulus to characterize the layer materials, (b) improved quantification of environmental effects, and (c) incorporation of the reliability concept in the design process.

The basic design equation for flexible pavements estimates the number of ESALs a pavement section can carry as a function of the structural number (SN), the terminal serviceability index level and the resilient modulus of the subgrade:

$$\log_{10}(W_{18}) = Z_R + S_o * \log(SN + 1) + \frac{\log_{10}\left[\frac{\Delta PSI}{(4.2 - 1.5)}\right]}{0.40 + [1094/(SN + 1)^{5.19}]} + 2.32 * \log_{10}(M_R) - \Omega \quad (13.5)$$

where SL = 8.27 if M_R is in psi and SL = 3.25 if M_R is in mP_a; M_R is the resilient modulus of the subgrade (psi) (see Section 13.2.1); W_{18} = the term used in the AASHTO equation for the number of equivalent single axle load (ESAL) applications; Z_R = the standard normal deviate; S_o = the combined standard error of the traffic prediction and performance prediction, e.g. the overall standard deviation of the design inputs; ΔPSI is the difference between initial serviceability index, P_o, and the terminal serviceability index, P_t (note that P_o usually ranges between 4.2 and 4.5, and P_t be-

tween 2.0 and 2.5; also, the constant 4.2 in Eq. 13.5 can actually be varied to reflect a higher or lower expected P_0 for local conditions).

SN is indicative of the pavement total thickness required and is given as a linear combination of the individual layer thicknesses and their drainage coefficients:

$$SN = \sum_{i=1}^{n} a_i D_i m_i \qquad (13.6)$$

where n is the total number of layers; a_i is the ith layer structural coefficient; D_i is the ith layer thickness (cm); and m_i is the ith layer drainage coefficient.

The structural coefficients, a_i, vary with resilient modulus; but typical values often used are 0.42 for asphalt concrete, 0.14 for granular base and 0.11 for granular subbase.

The drainage layer coefficients are functions of the quality of drainage; estimates are given in (AASHTO 1993) for a range of excellent to very poor drainage and a range of times the pavement structure is exposed to near-saturation conditions. Values of m_i vary from 1.40 (excellent with less than 1% exposure time) to 0.40 (very poor with greater than 25% exposure time).

The standard normal deviate, Z_R, corresponds to the reliability level, R, chosen by the designer and is the tail area of the normal distribution. For example, if R is chosen as 90%, the corresponding Z_R, e.g. the 10% tail area, which can be found in standard normal curve area tables, is -1.28. AASHTO suggests R levels between 80 and 99.9% for rural freeways or expressways, 75–95% for rural arterial and collector roads, and 50–80% for local rural roads. As an example, standard tables would show for an R of 50% the corresponding $Z_R = 0.000$, an R of 75% would give $Z_R = -0.674$ and an R of 99.9% would give $Z_R = -3.090$. The range of suggested R values and tables for Z_R are provided in AASHTO (1993).

AASHTO recommends that the standard deviation of the design inputs, S_0, should be selected as representative of local conditions. However, few if any authorities have collected sufficient as-built data to estimate S_0 for design purposes. Thus, representative values of $S_0 = 0.45$ (which was derived from AASHO Road Test data) for flexible pavements and $S_0 = 0.35$ for rigid pavements are commonly used.

Present serviceability index (PSI), is a measure of the level of service provided to road users and varies between zero and five. A perfect pavement would be at PSI = 5, and PSI = 0 would represent an impassable pavement. PSI is primarily related to road roughness and is described in AASHTO (1993). The initial or as-build PSI, noted as P_0 in Eq. 13.5, was 4.2 for flexible pavements at the AASHO Road Test; but modern construction methods now usually result in a P_0 of 4.5 or higher. Consequently, the constant of 4.2 is provided in the middle part of Eq. 13.5 (rather than simply using a denominator of $4.2 - 1.5 = 2.7$), so that adjustments can be made for local conditions. The terminal level of PSI, noted as P_T, usually ranges from about 2.5 to 2.0, where the higher value would be applicable to expressways and the lower value to local roads.

The design procedure is rather complex to carry out manually but there is a computer program termed DARWin, which is available for purchase (AASHTO 1998). The key inputs are: (a) estimate of traffic loading in design period (ESALs); (b) loss of serviceability over the design period (ΔPSI); (c) resilient modulus of the subgrade, M_R, (d) the overall standard deviation, S_0, of the design inputs; and (e) design reliability or target confidence level, as reflected in Z_R.

13.6.4 MECHANISTIC-EMPIRICAL BASED DESIGN: THE ASPHALT INSTITUTE METHOD

The Asphalt Institute developed a widely used mechanistic-empirical based design method based on elastic layer theory, which

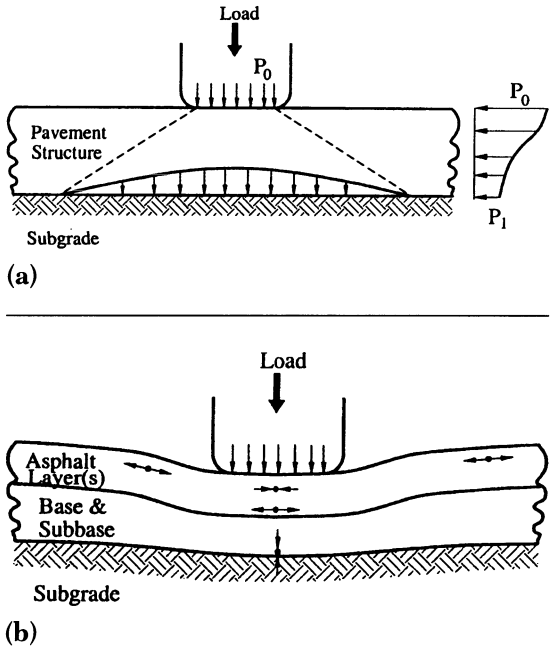


FIGURE 13.5. Schematic of load transfer mechanism and critical points of stress–strain: (a) stress spreading effect of a flexible pavement structure, and (b) critical stresses and/or strains (←•→ tension; →•← compression).

incorporates both mechanistic and empirical state-of-the-art information (TAI 1991a). A computer program for the procedure is available (TAI 1991b).

The design philosophy is based on the structural function of the pavement being to transfer the traffic loads to the subgrade without exceeding either the strength of the subgrade or the internal strength of the pavement itself. Figure 13.5 illustrates this concept. In Fig. 13.5a, the wheel load is transmitted to the pavement through the tire at an approximately uniform pressure, P_0. The pavement distributes the wheel load over a larger area so that the maximum pressure on the subgrade is only P_1. The design process involves selecting the pavement materials and thicknesses such that P_1 is within the subgrade capacity. Figure 13.5b shows the critical stresses and strains; for example, fatigue failure can result due to excessive tensile stress–strain cycles at the bottom of the asphalt layer.

The Asphalt Institute procedure can be summarized as follows: (a) obtain input data on subgrade resilient modulus, expected traffic loading, surface and base material types, and climatic (temperature and drainage) conditions; (b) calculate initial design thicknesses/alternatives; (c) conduct economic analysis of various alternatives; and (d) select the final design cross-section. This procedure is applicable for all traffic types (highways or airfields). Steps (a) and (b) are outlined in the following discussion.

In the Asphalt Institute method, the subgrade strength is characterized by the resilient modulus, M_R (see Section 13.2.1). The design M_R is derived from a set of repeated tests (normally ten) as either the 60th, the 75th or the 87.5th percentile value (using a cumulative frequency plot of percent equal to or greater on the vertical axis versus M_R on the horizontal axis) depending on traffic loading in ESALs. The 60th percentile value of M_R is for $\leq 10^4$ ESALs, 75th for 10^4–10^6 ESALs, and 87.5th for $>10^6$ ESALs. Since the plot is in ascending order, the 87.5th percentile is the lower value of M_R and represents a higher degree of conservatism (because of the higher traffic level).

Estimation of the design traffic (ESALs) is based on applying truck factors and appropriate traffic growth rates to the estimated traffic composition in the base year of analysis (see Section 13.4.1.5).

The required pavement thickness can be obtained according to the previously noted computer program, CP4 (TAI 1991b); alternatively it has been simplified into several design charts covering three flexible pavement types: (a) conventional, consisting of asphalt concrete on untreated aggregate base, (b) emulsified asphalt mixes on untreated aggregate base; and (c) full depth asphalt concrete on subgrade.

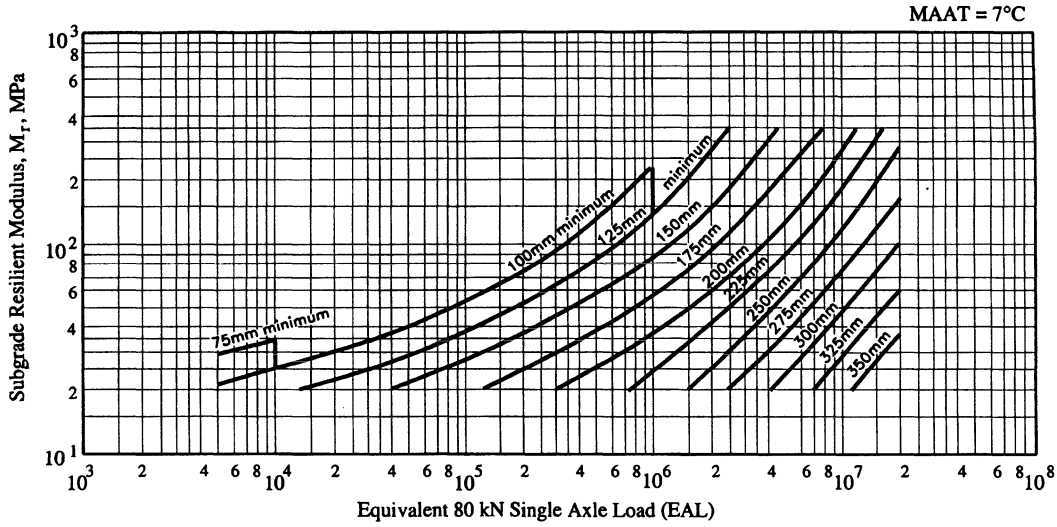


FIGURE 13.6. Example of thickness design chart from The Asphalt Institute for a conventional flexible pavement with a 150 mm untreated aggregate base (modified from TAI 1991a). MAAT = 7°C.

These charts allow the selection of the necessary design thicknesses as a function of the subgrade modulus, M_R and the design ESALs for an average climatic condition in terms of mean average annual temperature (MAAT). All design charts include a minimum thickness of asphalt concrete surface. Figure 13.6 shows a typical design chart for a conventional flexible pavement with 150 mm untreated aggregate base and in an area where the MAAT is 7°C.

As an example, suppose that the estimated design traffic is 3×10^6 ESALs (note TAI uses the designation EAL for ESALs) and the design subgrade M_R is 40 MPa. From Fig. 13.6, this design traffic requires a minimum asphalt thickness of 150 mm. However, the combination of 3×10^6 ESALs traffic and 40 MPa subgrade would require a total asphalt thickness of about 240 mm (by interpolation). If, for economic reasons, it was desired to use the minimum, then the difference (240 − 150 = 90 mm of asphalt) could be converted into extra granular base. If the equivalency were 1 mm of asphalt = 2 mm granular base (which is an approximate equivalency used by many agencies), the 90 mm of asphalt would convert to $90 \times 2 = 180$ mm of granular base. Thus, the final design would be 150 mm of asphalt concrete on 150 (thickness of untreated aggregate base represented in Fig. 13.6) + 180 (converted thickness) = 330 mm of granular base.

13.7 Structural Design of Airfield Pavements

13.7.1 AN OVERVIEW

While the techniques of design, construction and maintenance of airfield pavements are generally similar to those appropriate for roads, there are important differences which must be taken into account in order to provide pavements that are satisfactory for aircraft.

Aeroplanes are designed for flying but are much less stable and controllable than cars when traveling at high speed along the ground. Landing speeds of modern aircraft are typically 260–280 km h^{-1} in all conditions. Unlike car drivers, pilots cannot in-

crease their safety margin by slowing down to take into account wet and uneven pavements, high crosswinds and poor visibility. Aircraft land on multi-tired undercarriages that are located close to the center of gravity, not at each corner like road vehicles, and so are inherently less stable.

Aquaplaning is a serious hazard, which is easily avoided on the road by slowing down. Surface water on airfield pavements, however, either present as sheet flow or in the form of localized puddles, is a major concern on runways. Drainage of water is more difficult than from roads due to the smaller allowable crossfalls (1.5%) and larger pavement widths (typically 60 m). Thus, it is essential to provide an adequately textured surface (for good, wet-weather braking) to tight initial level tolerances. It is also essential to have very high degrees of compaction of all layers if surface trueness is not to be lost by subsequent compaction under the very heavy aircraft wheel loads.

Loose stones on a road surface lead to chipped paintwork and perhaps to broken windscreens, but the ingestion of stones or pavement fragments by jet engines can have catastrophic consequences. Therefore it is vital that airfield pavements be maintained in a condition where the surface will not produce loose material.

Because of the larger pavement widths compared to roads, moisture conditions beneath sealed airfield pavements are generally more uniform and stable. Within about 1–3 years after construction, moisture contents reach equilibrium values that are independent of the compaction moisture content.

13.7.2 AIRFIELD PAVEMENT TYPES AND COMPARATIVE THICKNESSES

In areas not subject to frost, major flexible airfield pavements often consist of unbound layers of heavily compacted, graded crushed stone with a relatively thin (30–60 mm) asphalt concrete surfacing layer. Thicker (125 mm or more) asphalt concrete surface layers and base courses bound by either cement or asphalt are also used, particularly in regions where frost effects must be taken into account. To accommodate the largest aircraft, pavement thicknesses range from 500 to 2000 mm depending upon subgrade strength.

Hot-sprayed bituminous seals are used on many airfield pavements, particularly those designed for lighter aircraft and non-jet aircraft. The main distinction between sealing of airfield pavements and road sealing practice is that there is much more concern about loose stones in the case of pavements trafficked by jet aircraft. Higher binder spray rates are used to firmly secure the stones, and also to extend the pavement life. Airfield pavements receive less load repetitions by comparison with roads, so the binder is likely to fail by aging and embrittlement rather than by load-induced fatigue.

Rigid airfield pavements usually consist of unreinforced jointed concrete slabs. Slab sizes of up to 7.6 m have often been used, but smaller sizes of 5–6 m are now commonly favored. Load sharing between slabs is provided by dowels at longitudinal and transverse construction joints and by aggregate interlock, with or without dowels at transverse contraction joints. Concrete mixtures sometimes contain larger (37 mm) size aggregates to improve load transfer directly by improved interlock and indirectly by reducing concrete drying shrinkage. Base courses consist of lean mix concrete or 200 mm of graded crushed stone such that it is not susceptible to pumping. Pumping is less of a problem for airfield pavements, however, than it is on roads due to the much lower frequency of loading. Cement or asphalt bound graded crushed stone base courses are also used, and can have an open-graded structure to function as a drainage layer. Joints are now usually sawn rather than wet-formed. The practice with respect to joint sealants is location specific. In Australia, for example, where extremes of tempera-

ture and frost do not occur, joint sealing is now undertaken only when justified by specific circumstances. This permits the use of much narrower (3–5 mm) joints, which cannot then harbor large loose stones. By comparison, in freezing zones it is common practice to use wider, sealed joints (up to 12 mm or more in width) for extended pavement life and reduced maintenance.

Slab thicknesses range up to 525 mm, but 350–400 mm is more typical to cater for modern large aircraft. These thicknesses compare with 230 mm typically used for major highway pavements. The thicker airfield pavements undergo smaller thermal movements. This has beneficial implications for load transfer across joints and also for sealant policy as compared to roads.

In recent years, some interlocking concrete block pavements have been utilized, chiefly on aprons, as for example in the new Hong Kong airport; at Dallas-Fort Worth; Luton, near London; and Cairns, in Australia. The use of blocks, however, in areas where aircraft use near-full jet thrust is of serious concern because of the risk of failure occurrences under these conditions.

13.7.2.1 Airfield Pavement Thickness Design

Thickness design methods, as for roads, can be classified into: (a) experience-based methods; (b) empirical methods; and (c) mechanistic-empirical methods. For various reasons, including the advent of new, heavier aircraft, such as the Boeing 777, there is a trend toward the more fundamental mechanistic-empirical methods.

The experience-based and empirical design procedures for flexible airfield pavements are adapted largely from the original US Corps of Engineers CBR method originally developed in 1942. Extrapolations were subsequently made, using Boussinesq's single layer elastic theory as aircraft wheel loads increased. Validation was carried out by full-scale trafficking tests, the last of which was completed in 1971. Since then, pavement engineers have relied almost exclusively on the Corps' tests to calibrate their models and to provide empirical "anchors" to their theoretical analyses. The development of the Corps' CBR design method is described in Pereira (1977). A summary of the Corps' work in flexible and rigid pavements is given in Ahlvin (1991).

To accommodate multiwheeled landing gears, the Corps used the concept of equivalent single wheel load (ESWL). It is intended to be the single wheel load that causes pavement damage equal to that caused by a multiwheel gear at its actual load. In practice it is defined as the load on a single wheel that will produce the same maximum deflection at subgrade level as the multiwheel gear. Thus the S-77-1 method (Pereira 1977) adopts elastic vertical deflection at subgrade level as the indicator of the rate at which deformation develops at the pavement surface. The Corps' empirical relationship between aircraft loads, CBR, and required flexible pavement thickness is shown in Fig. 13.7.

The later Corps of Engineers full-scale testing (Ahlvin *et al.* 1971) confirmed that their early deflection-based design curves overstated the pavement damage caused by

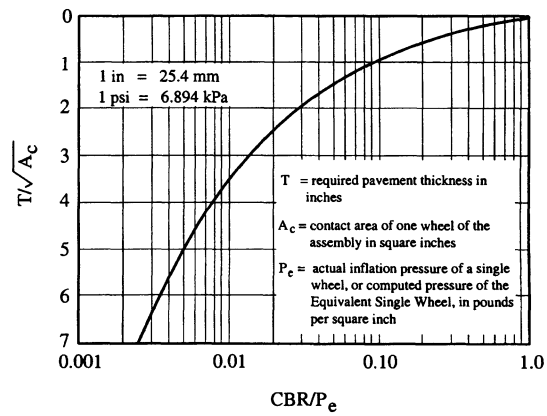


FIGURE 13.7. US Army Corps of Engineers CBR curve for thickness design of flexible airfield pavement.

multiwheeled gears. This led to the introduction of empirical pavement thickness reduction factors (alpha factors), which result in increasing thickness reduction with increasing wheel numbers and load repetitions. The design thickness of the pavement is obtained by multiplying the "standard" thickness, T, from Fig. 13.7 by alpha. As an example, for 10 000 coverages, the alpha factors are 0.995, 0.90, 0.825 and 0.788 for single wheels, duals, four-wheel (e.g. B-747) and six-wheel gears, respectively. A plot of alpha factor versus coverage is provided in S-77-1 (Pereira 1997) for different number of wheels.

The S-77-1 method (Pereira 1997) is the basis of many of the world's airfield pavement design methods, including that used by the US Federal Aviation Administration (FAA). It is also the basis of the International Civil Aviation Organization's (ICAO's) system for load rating of aircraft and for publishing aerodrome flexible pavement strength data (ICAO 1983). A typical FAA design chart, reproduced from FAA Advisory Circular, Airport Pavement Design and Evaluation (FAA 1995b) is shown in Fig. 13.8.

The layered elastic method was introduced into regular airfield design practice in the mid-1990s with the release of the computer program LEDFAA (Layered Elastic Design, Federal Aviation Administration) (FAA 1995a) and also the Australian-developed APSDS (Airport Pavement Structural Design System) (Rickards 1994; Wardle and Rodway 1995 and 1998b).

LEDFAA and APSDS use layered elastic programs, JULEA and CIRCLY, respectively, to compute load-induced vertical strains at the subgrade level, which must then be related to observed test track pavement performance. This step in the design process is purely empirical. The new methods are empirical to the same degree as the conventional S-77-1 empirical CBR method and are calibrated against the same full-scale tests. Consequently, they predict pavement thickness requirements that are similar to the conventional method. Confident prediction of the thicknesses required by new significantly different aircraft wheel arrangements requires empirical data that are relevant to the new aircraft. The FAA's national airport pavement test machine under construction at Atlantic City, at the time of preparation of this handbook, is designed to provide such data.

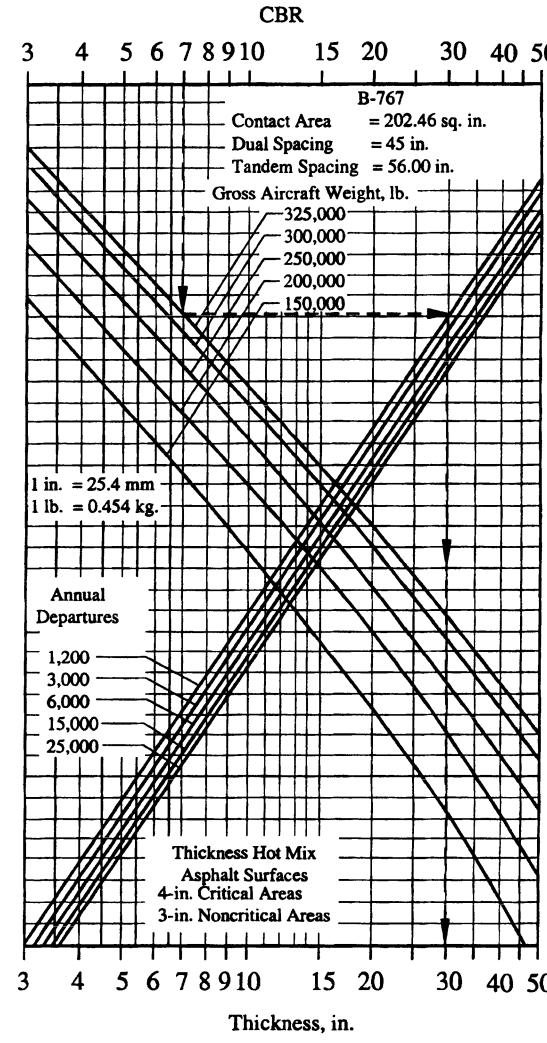


FIGURE 13.8. Flexible pavement design curves, B-767 (modified from Federal Aviation Administration 1987).

This does not mean that the introduction

of "mechanistic" methods based on layered elastic analysis are not a significant advance in pavement design. The computational power eliminates the need for earlier simplifications such as the single layer theory, the equivalent single wheel load concept and the pass-to-coverage ratio, which were necessary to make computations manageable. They also make possible a more rigorous process of calibration against available or future pavement performance data. As well, they facilitate the introduction of new materials, both bound and unbound, and greatly simplify the calculation of the combined effects of mixes of aircraft types and weights. In summary, for aircraft that were represented by the full-scale tests, they provide the designer with a fast tool to design layered pavement structures to cater to complex aircraft traffic mixes.

It may be noted that The Asphalt Institute also publishes a flexible airport pavement design manual, *Asphalt Pavements for Air Carrier Airports* (TAI 1987b). It is based on mechanistic empirical principles, with strain criteria based on elastic layer calculations. Design charts for different types of aircraft and varying subgrade strains are provided; also, a computer program available from The Asphalt Institute can be used as an alternative.

13.7.3 AIRFIELD PAVEMENT FAILURE AND SAFETY CONSIDERATIONS

Airfield pavements must be maintained in a condition that allows for the safe operation of the aircraft that use them. From this point of view, a pavement is considered to have failed if: (a) the surface has spalled or has a tendency to produce loose stones or pavement fragments that could be ingested by a jet engine; (b) water ponds on the surface, which could lead to loss of braking capability in wet weather; (c) loss of surface texture occurs due to rubber buildup in touchdown zones, or to flushing of bitumen to the surface; or (d) excessive roughness exists, making control of the aircraft difficult.

Cracking of the surface does not itself constitute failure in these terms but, unless attended to, can lead to the foregoing failure conditions. This is particularly so if the ingress of water causes a loss of pavement strength or debonding at pavement layer interfaces.

13.8 Structural Design of Rigid Pavements for Roads

Portland cement concrete pavements distribute loads to the subgrade over a much larger area than flexible pavements. The concrete slab acts as a rigid structural member, transmitting the loading mainly through bending; hence the alternate name, rigid pavements. The design process must consider both traffic and environmental stresses. Design of joints and/or reinforcement is extremely important in rigid pavements to control cracking and movement. Consequently, rigid pavements are commonly classified according to the type of joints and/or reinforcement.

13.8.1 TYPES OF RIGID PAVEMENTS

There are four common types of rigid pavements: (a) jointed plain concrete pavements (JPCP) with dowelled or undowelled joints; (b) jointed reinforced concrete pavements (JRCP), typically with dowelled joints; (c) continuously reinforced concrete pavements (CRCP); (d) prestressed or post-tensioned concrete pavements.

The JPCP is the most common type in most countries. As the name implies, the pavement is constructed using plain concrete (without reinforcement) with tranverse joints, typically at a maximum spacing of 4.5 m. Jointed reinforced concrete pavements (JRCP) are constructed with reinforcing steel and dowel bars for load transfer at the construction joints. Joint spacings in this case are larger, typically up to 12 m.

Continuously reinforced pavements (CRCP) are built without contraction joints

and are commonly used in warmer climates such as the southern states of Texas and Arizona. Unlike the JRCP, CRCP pavements are relatively heavily reinforced and transverse cracks develop at closer intervals. The reinforcement holds the cracks together tightly to maintain a high degree of load transfer.

Prestressed or post-tensioned pavements have only been used in specialized locations, where the more effective reinforcement is applied to reduce the required concrete thickness. The cost implications associated with the method of construction have resulted in literally no applications of prestressed/post-tensioned pavements to roads.

13.8.2 BASIC FACTORS IN THICKNESS DESIGN

The structural design of rigid pavements seeks to establish the optimal thickness of the concrete slab that will result in the lowest total life-cycle cost. The key factors are: (a) flexural strength of the concrete, (b) strength of subgrade and the subbase, (c) traffic loading, and (d) design period.

Other factors requiring consideration in design include the drainage, erosion (of base) and reliability factor. Estimation of traffic loading was treated in section 13.4.1.5. The other primary design factors are subsequently highlighted.

13.8.2.1 Flexural Strength of Concrete

In most design methods the key criterion is fatigue cracking under repeated loadings. Flexural strength (usually termed the modulus of rupture in rigid pavement design) is important in design because it determines the bending stress cycles and amplitude which translate to fatigue cracking under repeated loading.

It is usually established from laboratory testing of 28-day aged beams by third point loading, as described in ASTM C78. For airport pavements, 90-day testing of beams is normally used. The 7- and 14-day tests are used for construction quality control and for opening to traffic decisions.

13.8.2.2 Subgrade and Subbase Support

Although stresses transmitted to the subgrade are relatively low for rigid pavements compared to flexible pavements, the underlying layer is still an important part of the load carrying system. It is thus necessary to estimate the level of subgrade/subbase support before designing the slab thickness.

This support is defined in terms of the Westergaard modulus of subgrade reaction, k. It is equal to the load intensity (force per area) divided by the deflection resulting from that load. The k-values may be estimated from plate-loading tests (k depends on the size of plate used; 750 mm is normal for airfields and 450 mm for roads). However, the California Bearing Ratio (CBR) value (see Section 13.2.1) has been found to correlate well with k-value. Since the CBR test is simpler than the plate loading test, k-value is usually estimated from CBR test results. In addition, AASHTO (1993) provides a nomograph for estimating k-values from subgrade soil resilient modulus, M_R, and from other parameters. The Portland Cement Association tabulates estimated increases in k-values arising from using untreated and treated subbases (PCA 1984).

13.8.2.3 Design or Life-Cycle Period

The terms life-cycle and design or analysis period each find common use, and may vary from less than 20 to 40 years or more. Since traffic forecasting becomes less reliable for longer periods, a design period of 20 years is often used (PCA 1984). There are examples, however, where shorter or longer design periods have been justified, such as special project roads where the usage of the facility is only a few years, or a high volume facility where user delays or service interruptions due to future maintenance are economically unacceptable if they occur before 20 years.

The design period selected has a direct impact on the thickness design (due to traffic loading) and hence upon the initial cost of pavement construction. Final selection is ultimately an engineering judgment based on economic analysis of pavement costs and upon the service level to road users.

13.8.3 THICKNESS DESIGN METHODS

Thickness design, along with joint and base design, are important elements in the overall design process. The approaches to designing the appropriate thickness, range from the simple one of using previous experience, i.e. the catalog approach, to the empirical approach to a mechanistic-empirical approach.

An example of a widely used approach in North America and various other countries around the world is that of the AASHTO design procedure (AASHTO 1993), which is empirical. The PCA design procedure (CPCA 1984) is an example of the mechanistic-empirical approach. The basic features of each are briefly described in the following subsections. Unfortunately, neither method lends itself to being described in a few pages and/or illustrated conveniently with numerical examples (readily available computer programs, as subsequently referred to, provide a convenient means for use of these methods). Consequently, an approximate "catalog" approach example is subsequently provided, similar to that previously used for flexible pavements.

13.8.4 AASHTO THICKNESS DESIGN PROCEDURE (AASHTO 1993)

The design procedure recommended by AASHTO (1993) is based on empirical equations developed from the results of the AASHO road test conducted in Ottawa, Illinois, in the late 1950s and early 1960s.

The basic design equation for rigid pavements is similar in form to that for flexible pavements (see Eq. 13.5). It has undergone some modifications to include variables not considered at the road test. Principal additions or modifications to the original design equations include a provision for variable load transfer at joints, and a drainage coefficient for concrete pavements. Both the flexible and rigid design procedures now also incorporate the concept of reliability.

The following are the major design variables used in the AASHTO procedure: (a) The present serviceability index (PSI), in terms of as built PSI (p_o), and terminal PSI (p_t) when rehabilitation is required; adjustments can be made where expansive or frost-susceptible soils occur; (b) traffic, in terms of ESALs; (c) concrete properties in terms of:

- 28-day flexural strength, S'_c (the average value is used since the AASHTO method incorporates a reliability concept);
- modulus of elasticity, E_c;
- load-transfer coefficient (J-factor);
- drainage coefficient, C_d.

Detailed descriptions of the variables and design examples can be found in AASHTO (1993). As well, the previously noted computer program DARWin™ is available (AASHTO 1998).

13.8.5 PORTLAND CEMENT ASSOCIATION THICKNESS DESIGN PROCEDURE

The thickness design procedure developed by the Portland Cement Association (PCA) is mechanistically based. Conventional design factors of concrete properties, foundation support and loadings are used in the procedure; however, additional factors such as joint load-transfer and concrete shoulders are incorporated into the design. It has been verified extensively by correlation to performance of pavements at the AASHO road test and other road tests and to studies of the performance of many in-service pavements. More information on the development and basis of the PCA design procedure is given in (CPCA 1984).

The procedure optimizes pavement thickness using two failure mechanisms. The first is fatigue, which requires pavement stresses

due to repeated loads to be kept within safe limits to prevent fatigue cracking. The second mechanism is erosion of foundation and shoulder material, which must be limited to minimize the effects of pavement deflections at slab edges, joints and corners. The criterion for erosion is needed to assess distresses such as faulting, pumping and shoulder distress, which are unrelated to fatigue. For full details concerning this procedure see CPCA (1984). A simplified method for concrete pavement street design is also available from the American Concrete Pavement Association (ACPA 1992), and in the Portland Cement Association's information series 184 (PCA 92).

13.8.6 CONSIDERATION OF JOINTS IN DESIGN

Joints in concrete pavements are used to accommodate the volume changes of the material due to temperature. However, all joints represent a discontinuity in the pavement. As a result, several major distress types in concrete pavements, such as faults and breakouts at joints, are associated with the behavior of the joints. Thus, the design of transverse and longitudinal joints is critical to the performance of rigid jointed pavements. The components of joint design that must be considered include FHWA (1987): (a) load transfer at the transverse joints and spacing; (b) spacing between longitudinal joints; (c) joint sealant reservoir; and (d) ties between longitudinal joints. It should be noted that these considerations apply to rigid pavements for roads. In the airfield situation, because of thicker slabs, temperature movements are relatively small and thus expansion joints are not normally needed. Also, many designers do not tie longitudinal joints as this can result in longitudinal mid-slab cracks.

13.8.7 TYPICAL JOINT CONFIGURATIONS

Various joint designs are described in the literature, and summarized in (TAC 1997). The major ones involving load-transfer devices are:

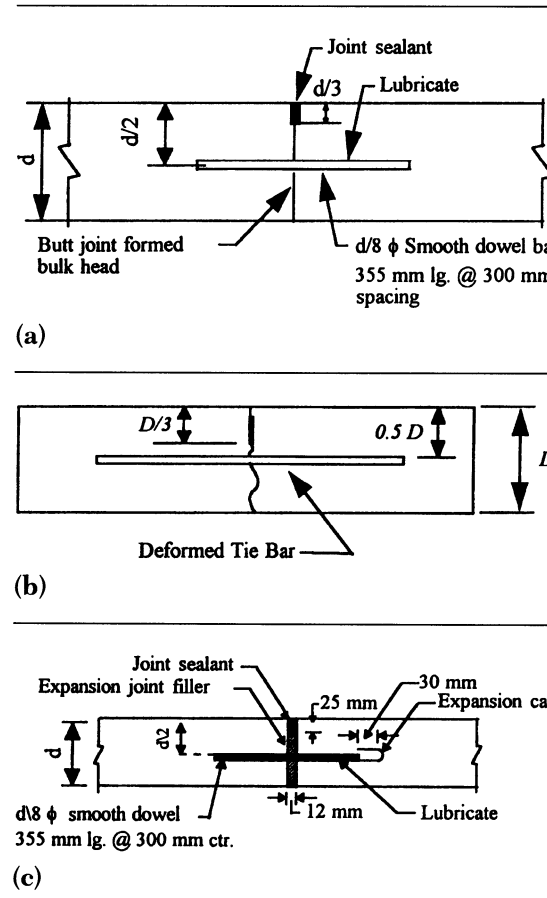


FIGURE 13.9. Joint designs with load-transfer devices (modified from TAC 1997): (a) dowelled contraction joint; (b) longitudinal sawcut joint; and (c) dowelled expansion joint.

(a) dowelled contraction joints, (b) longitudinal sawcut joints with tie bars, and (c) dowelled expansion joints. Details, as recommended in TAC (1997), are shown in Fig. 13.9.

13.8.8 APPROXIMATE, CATALOG DESIGN APPROACH

Catalog designs can be used as an approximation, particularly where a short or small project is involved and/or as a forerunner for a more complex design by the AASHTO or PCA methods. However, few catalog tables have been available, one exception being that published by the Ministry of Transportation of Ontario and shown in Table 13.5 (MTO 1990).

TABLE 13.5. Catalogue design thicknesses for Portland cement concrete pavements (adapted from MTO, 1990)[a,h,i,j,k,l,m]

	Erodable subgrade[a] (clays, silts and fine-grained sands)						Non-erodable subgrade[a] (tills and granulars)					
	Undowelled[b,c]			Dowelled[c,d,e]			Undowelled[b,c]			Dowelled[c,d,e]		
Traffic classification	Treated base[f]	OGDL[g]	Direct on subgrade	Treated base[f]	OGDL[g]	Direct on subgrade	Treated base[f]	OGDL[g]	Direct on subgrade	Treated base[f]	OGDL[g]	Direct on subgrade
Two-lane, rural or urban												
AADT < 1000		150	150					150	150			
1000 < AADT < 2000	150	175	200					150	150			
2000–3500	175	200	240	150	175	200	150	175	200			
AADT > 3500				200	225	300				175	215	250
Rural multi-lane				200	240	300				200	225	250
Urban multi-lane				225	250	300				225	250	275

[a] The minimum concrete slab thickness is measured in millimeters.
[b] Undowelled; i.e. plain concrete slabs with no dowels in transverse joints.
[c] For plain slabs random joint spacings of 4, 5.75, 5.5, and 3.6 m are recommended.
[d] Dowelled, i.e. either plain concrete slabs with dowels in transverse joints or reinforced slabs with dowels in transverse joints.
[e] For reinforced slabs joint spacings of 12–13.75 m are recommended.
[f] Minimum thickness of treated base to be 125 mm of plant mix asphalt, cement-treated material, or lean concrete base.
[g] Open-graded drainage layer (OGDL) minimum thickness = 100 mm. Construction may require 100–150 mm of granular soil below OGDL.
[h] Skewing of transverse joints 0.6 m in 3.6 m is recommended for all transverse joints (OPSD 509 and 510 series).
[i] All designs to have tie bars or hook bolt dowels at longitudinal joints.
[j] Where paved shoulders are warranted, tied concrete paved shoulders are recommended. Tied concrete shoulders extend the fatigue life of the pavement equivalent to an additional 25-mm Portland cement concrete (PCC) pavement thickness.
[k] Designs assume not more than 15% truck traffic.
[l] For development of detailed structural designs for particular projects the method in [904] is recommended.
[m] Continuously reinforced pavements are not included in these guidelines.

It should be emphasized that the values in Table 13.5 are minimums and that a number of factors have to be taken into account in arriving at a final design.

As an example of the use of Table 13.5, consider a design situation with an average annual daily traffic (AADT) of 10 000 averaged over a pavement life of 20 years on a multi-lane rural highway with an erodible subgrade. From the table, only a design with dowelled joints is applicable, and the following minimum thickness options exist: (a) 200-mm Portland cement concrete (PCC) slab on treated base, or (b) 240 mm PCC on a minimum 100-mm open-graded drainage layer (OGDL), or (c) 300 mm PCC directly on the subgrade.

A comprehensive study in the USA under the National Cooperative Highway Research Program (NCHRP) Project 1-32 provides a *Catalog of Current State Pavement Design Features* (ERES 1998). The format is very similar to that of Table 13.5, but extends into higher traffic volumes, involves all the rigid pavement types previously identified, and covers a wide range of climatic conditions. Because of the volume of data, the results are only available on CD-ROM, from the Transportation Research Board (TRB 1998).

13.9 Design of Overlays

13.9.1 INTRODUCTION

The traditional and most widely used method for protecting a deteriorating pavement, reducing roughness, restoring surface friction, and strengthening the pavement structure is with an overlay of hot mix asphalt (HMA). Overlays generally include a leveling course, to correct the contour of the old pavement, followed by one or more HMA courses to provide needed thickness.

13.9.2 FLEXIBLE PAVEMENT OVERLAY DESIGN METHODS

Two major methods in common use are those described in guides or manuals of The American Association of State Highway and Transportation Officials (AASHTO 1993) and The Asphalt Institute (TAI 1983).

The Asphalt Institute's overlay design method in their manual series MS-17, *Asphalt Overlays for Highways and Streets* (TAI 1983), can be used as an example. It involves a deflection survey with a Benkelman beam. This is a static deflection method where the rebound or recoverable deflection under a 40-kN dual tire load is measured after the vehicle slowly moves forward. It has been used as a standard in many countries around the world for decades, but is being superseded by such dynamic deflection devices as the falling weight deflectometer (FWD). Correlations between FWD and Benkelman beam measurements are available but require caution in their use (Haas *et al.* 1994).

The results of the Benkelman beam deflection survey are adjusted to a reference temperature of 21°C, and a representative rebound deflection (RRD) is calculated as the mean of the measurements plus two standard deviations. This means that only about 5% of the Benkelman beam measurements would exceed the RRD value. Depending on the time of year the survey is done, i.e. fall, a critical period, i.e. spring, adjustment factor may also be used for those areas where spring weakening (due to thaw) of the pavement is the governing consideration.

Using the design ESALs (termed EAL_d in The Asphalt Institute method) and the RRD value, the thickness of overlay needed to strengthen an inadequate pavement may be calculated, or the length of time before an overlay is needed may be estimated.

The thickness of overlay can be calculated as follows: (a) establish the representative rebound deflection (RRD); (b) estimate the design ESALs (EAL_d) that the pavement will be required to carry in the future, using conventional traffic projection methods; (c) enter the overlay thickness chart, Fig. 13.10, at the RRD and move up or down, depending upon

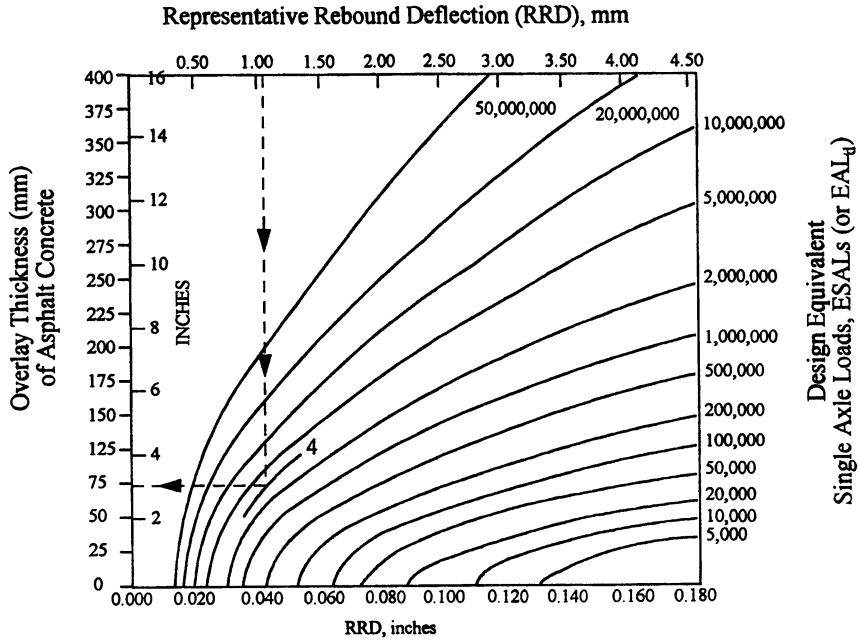


FIGURE 13.10. Asphalt concrete overlay required to reduce measured pavement rebound deflection (RRD) to a design value (modified from TAI 1983).

which units are used, to the curve representing the design ESALs (EAL_d). Then move horizontally and read the thickness of overlay required.

For example, using a design ESALs (EAL_d) = 4×10^6, and RRD = 1050 μm (1.05 mm), the required overlay thickness from Fig. 13.10 is 75 mm.

Although this chart is relatively simple to use, The Asphalt Institute pavement design computer program, HWY, CP-4 (TAI 1991b) is expedient. Data can be entered in either SI or Imperial units. The program enables the designer to perform the traffic analysis in a systematic manner and to make appropriate estimates with structural parameter inputs, including pavement temperature and different asphalt concrete overlay modulus values. It is also possible to use not only deflection measurements obtained with the standard Benkelman beam, but those obtained with other devices such as the falling weight deflectometer (FWD).

13.10 Application of Reliability to Pavement Design

Variability is a fact of daily life. For the pavement engineer, many factors contribute to our inability to accurately predict pavement performance. Sources of variability include normal measurement (random) errors that affect all the measured material parameters, model errors (all models are approximations of reality), and the inherent variability of material properties from one pavement section to the next. Another source of errors, and probably the most important, is the approximate nature with which the amount and composition of future traffic on the facility are predicted.

While it has been common practice to design pavements on a deterministic basis, there is growing recognition of the need to incorporate variability in the design process. A number of studies and initiatives have explicitly addressed the issue the application of reliability concepts to pavement design (Haas

et al. 1994, Ullidtz 1998). These are reflected, for example, in the *AASHTO Guide for Design of Pavement Structures* (AASHTO 1993), and in the new OPAC 2000 design method (He *et al.* 1996).

13.11 Economic Evaluation of Pavement Design Alternatives

13.11.1 BASIC PRINCIPLES AND APPROACHES

One of the most significant benefits of a pavement management system is the potential of achieving the best possible value for the available public resources (Haas *et al.* 1994). This is accomplished by comparing investment alternatives at both the network and project levels. The economic comparison of the feasible design alternatives should consider the following key categories of costs over the life cycle of the facility: (a) capital cost of constructing the pavement; (b) agency costs of maintaining the pavement throughout the life cycle; (c) vehicle operating costs; (d) environmental (direct/indirect) cost implications; and (e) other user-related costs due to future maintenance/rehabilitation or reconstruction, e.g. delays, accidents, etc.

The analysis should also consider several direct and indirect benefits associated with design alternatives. The key benefit components are: (a) savings in vehicle operating costs due to an improved facility; (b) savings in user delay costs, accident costs, etc.; (c) increased property value/comfort, etc.

Economic evaluation requires good cost data. Although agency costs can easily be established from construction and maintenance data from previous projects, it is not so straightforward to determine user costs or benefits. Common practice is to consider user benefits in terms of cost savings arising from an improved pavement. Several pavement parameters affect different components of user costs including surface roughness, surface friction, etc. Among the major studies in recent years on causal relationships between pavement characteristics and their effects on user costs is the highway design and maintenance (HDM) study undertaken by a World Bank international effort (Paterson 1987).

13.11.2 COMMON METHODS OF ECONOMIC EVALUATION

The available methods of economic analysis for evaluating alternative pavement designs, together with examples, have been summarized in (Haas *et al.* 1994, TAC 1997). Most commonly used is the present worth method on costs alone, benefits alone or net benefits, i.e. costs minus benefits. This method provides the ability to consider a stream of costs and/or benefits occurring at different times over the specified design/analysis or life-cycle period and thereby facilitates comparison over a common platform. The effect of time on money is achieved by applying an acceptable rate of discount.

The present worth method involves multiplying all costs (and benefits if included) during the life cycle by a present worth factor:

$$\text{PWF} = 1/(1 + i)^n \qquad (13.7)$$

where i is the discount rate and n is the year in which the cost (or benefit) occurs.

PWFs can be found in tables published in various books, or easily calculated using Eq. 13.7. The critical issue is the selection of i, since it can have a major effect on PWF and in turn the estimation of present worth of costs and/or benefits. Some agencies specify i as a policy decision, while others relate i to the real value of money, e.g. interest rate minus inflation rate.

Since the economic evaluation of pavement design alternatives is essential to identifying the one which is most cost-effective in any given design situation, it is further essential that the evaluation is rigorous and thorough with all assumptions, data sources, etc. clearly identified.

III. SLOPE, EMBANKMENT AND WALL STABILITY, AND SOIL IMPROVEMENT

14. SLOPES AND MASS MOVEMENTS

S. Leroueil
J. Locat
G. Sève
L. Picarelli
R. M. Faure

14.1 Introduction

The study of slope movements is complicated because they can take very different configurations and mechanisms ranging from rock topple to mudflow, can involve a variety of materials ranging from hard rock to sensitive clay and loess, and can result from a variety of phenomena ranging from rapid snow melt or heavy rainfall to earthquake. Leroueil *et al.* (1996b) defined four different stages of slope movement (Fig. 14.1): (a) the pre-failure stage, including deformations associated with changes in stresses, viscous deformations, and strains and displacements associated with progressive failure; (b) the onset of failure characterized by the formation of a continuous shear surface through the entire soil or rock mass or by the separation of an unstable rock mass from the slope (rock fall or toppling); (c) the post-failure stage, which includes movement of the soil or rock mass involved in the landslide, from just after the onset of failure until it essentially stops; and (d) the reactivation stage, when the soil or rock mass slides along one or several pre-existing shear surfaces. This reactivation is generally occasional. Continuous movements with seasonal variations of the rate of movement (active landslides), which are the rule in some countries and geological environments, represent a peculiar situation that might be associated with reactivation since these movements occur along well-defined shear surfaces.

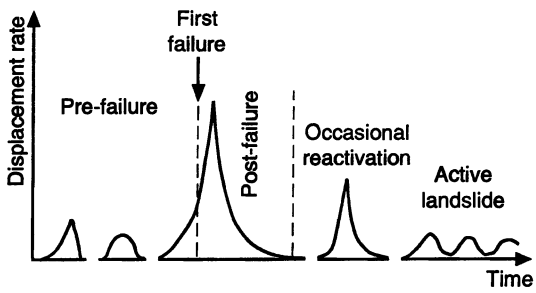


FIGURE 14.1. Different stages of slope movements.

Leroueil *et al.* (1996b) proposed a method for characterizing slope movements. For given type and stage of movement, the geotechnical characterization includes con-

R. K. Rowe (ed.), *Geotechnical and Geoenvironmental Engineering Handbook*
© Kluwer Academic Publishers 2001

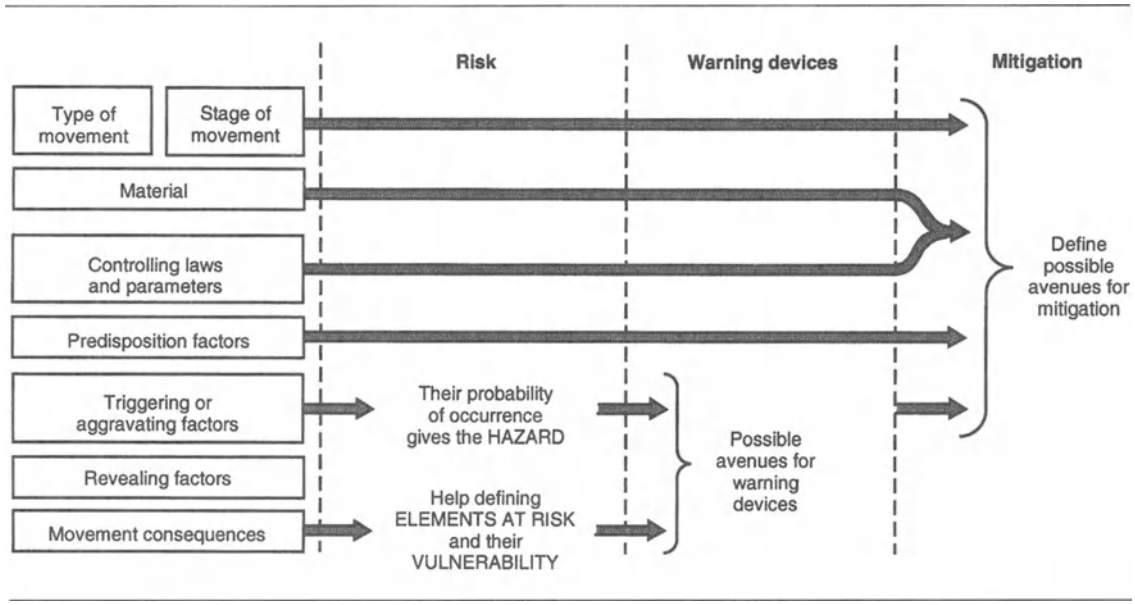


FIGURE 14.2. Geotechnical characterization of slope movements, and risk assessment, warning devices and mitigation (modified from Leroueil & Locat 1998).

sideration of a number of factors associated with slope stability and/or slope movements, as indicated on the left-hand side of Fig. 14.2: (a) the laws and parameters controlling the phenomenon, e.g. Mohr–Coulomb criterion, and c' and ϕ' at the failure stage; (b) the predisposition factors, which give information about the present situation and determine the slope response following the occurrence of a triggering factor, e.g. the presence of a weak layer; (c) the triggering factors, which lead to failure, or aggravating factors, which produce a significant modification of stability conditions or of the rate of movement (the most common are rainfall, earthquakes and erosion); (d) the revealing factors, which provide evidence of slope movement but generally do not participate to the process (presence of cracks for example); and (e) the possible consequences of the movement, e.g. destruction of houses. The triggering or aggravating factors can be temporary, e.g. heavy rainfall, or progressive, e.g. erosion.

The main types of movement that can be observed *in situ* are described in Section 14.2. A detailed description of the different stages of movements is given in Section 14.4. The analysis of different slope movements may require completely different mechanical approaches, constitutive laws and parameters. The mechanical behavior of the materials that can be involved in slope movements are described in Chapter 2 for saturated soils, in Chapter 5 for unsaturated soils and in Chapter 6 for rocks.

Slopes are usually formed in an environment that is largely controlled by geology. Knowledge of the local geology and geomorphology, and a good quality geotechnical investigation are thus essential for a good understanding of the behavior of a slope. Also, instrumentation and monitoring are often important for understanding the mechanisms of rupture and/or movements, identifying the kinematics of the slope, evaluating slope stability, designing mitigation systems or establishing warning systems, and finally for evaluating the efficiency of the stabilizing

technique used. The case of submarine mass movements is different as it involves very different approaches for either describing landslide features or carrying geotechnical investigations. For more in depth analysis of submarine slides, the reader is referred to Hampton *et al.* (1996).

14.2 Types of Movements

Bromhead (1992) subdivided slope movements into three major families: slides, flows and falls. Slides involve material that remains largely in contact with the parent or underlying materials during the movement that takes place along a discrete shear surface. A flow involves movement of material without the concentration of displacement at a single shear surface. Finally, a fall usually takes place on steep faces in soil and rock, and involves immediate separation of the falling material from the parent rock or soil mass. Slope movements, however, require a more detailed description, and more precise classifications have been proposed in Varnes (1978), Hutchinson (1988) and Cruden and Varnes (1996). The main classes are rotational and translational slides, toppling failures, falls, spreads and flows.

Slides can be rotational or translational, as illustrated in Fig. 14.3a–f, but can also have more complex geometries. Figure 14.3h illustrates a fall, whereas Fig. 14.3g shows a topple, a type of failure obtained when there is rotation of a mass of material around an axis at its bottom. Spreads of rocks or soils (Fig. 14.3i and j) may be associated with the softening of an underlying layer due to high pore pressures, unfavorable dip, seismic loading, etc.

Some flows initiate from landslides and are associated with what has been previously called post-failure movements. They depend mostly on the physical characteristics of the material involved (unit weight, relative density, water content, liquidity index, etc.) and on the geometry of the slope, especially its angle to the horizontal. Flows may include slow earthflows in plastic clays and weathered clay shales; landslides in sensitive clays; debris flows initiated by heavy rainfalls; flows following the "impact collapse" of weak rocks; loess flows; rock avalanches; etc.

14.3 Importance of Groundwater Conditions in Slopes

As the behavior of soil is controlled by effective stresses (or by porewater pressure and total stress in unsaturated soils in slopes) and since in many cases, the total stresses do not vary significantly in natural slopes, knowledge of the porewater pressures is essential to any analysis. In rocks, the water pressure acts along discontinuities and may also have an important influence on stability.

14.3.1 WATER FLOW CONDITIONS IN SOIL SLOPES

The porewater regime in slopes is rarely steady due to continuous changes of boundary conditions depending on rainfall, snowmelt, . . . , and more generally on both infiltration and evapotranspiration.

The infiltration of water into an unsaturated soil is a complex process and depends on the general stratigraphy, the presence of cracks and fissures at shallow depths, the saturated hydraulic conductivity, the degree of saturation, and the variation of the hydraulic conductivity of the soil with the degree of saturation (see Section 5.5). It follows that the antecedent water content generally has an important influence on the pore pressure response of the soil to rainfall (Johnson & Sitar 1990; Gullà & Sorbino 1996; Collins & Znidarcic 1998). In addition to this more or less "vertical infiltration," pore pressure buildup can also come from coarser underlying soil layers or the substratum (Johnson & Sitar 1990). The slope response has to be examined on the basis of local experience.

Even in saturated materials, changes in

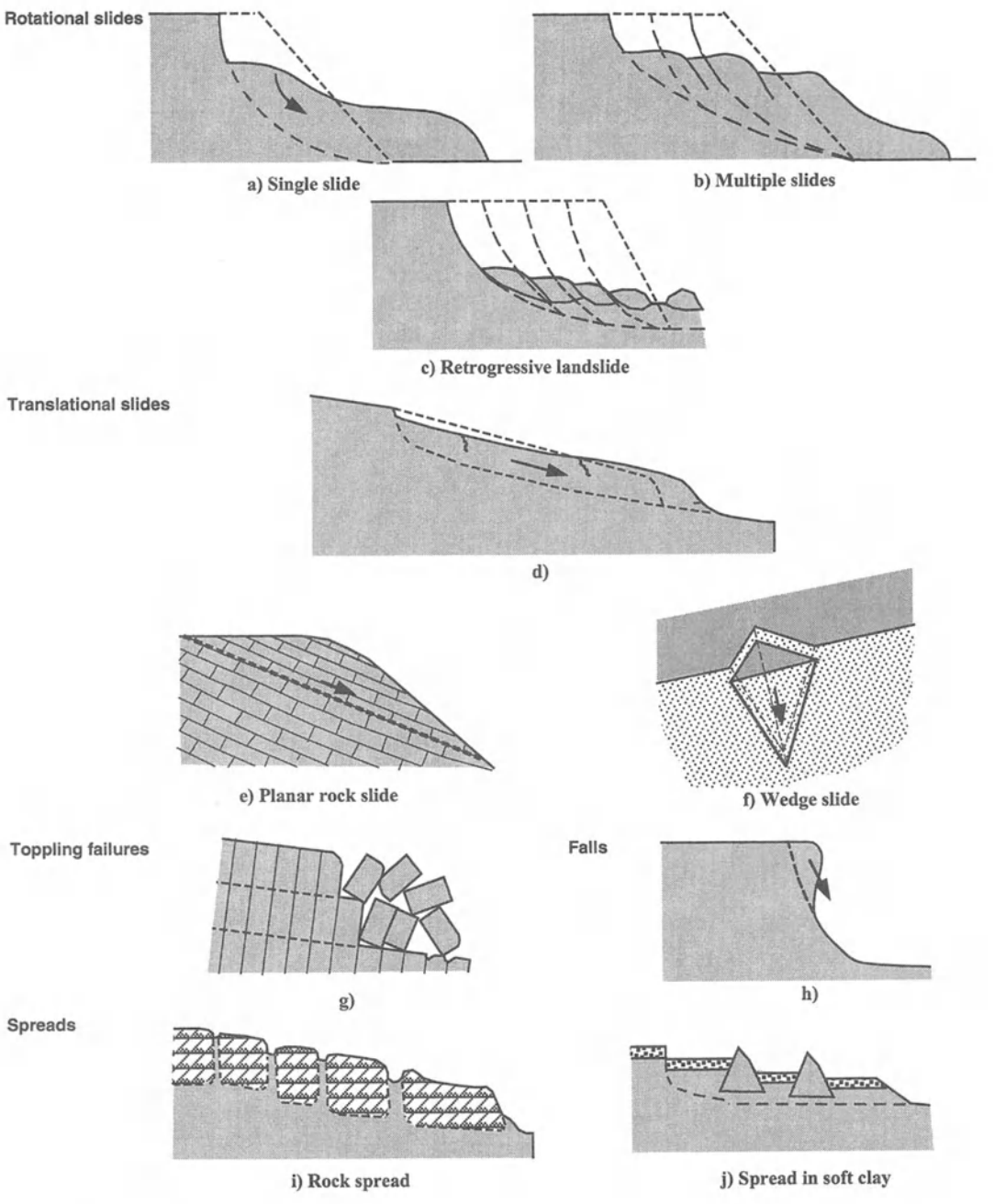


FIGURE 14.3. Main types of slope failures in soil and rock.

boundary conditions generally take time to propagate through the soil mass. One consequence is that pore pressures in a slope are continuously changing; another consequence is that the annual changes in porewater pressure in a clay deposit generally decrease with distance away from the boundaries (e.g. see Kenney & Lau 1984; Leroueil 2000). Water flows in slopes are thus often complex and, when possible, pore pressures should be measured with piezometers.

14.3.2 PARTICULAR CASE OF EXCAVATIONS IN CLAYS

Bishop & Bjerrum (1960) discussed the problem of excavation in (saturated) clays and illustrated the process of change in pore pressure and factor of safety with time in Fig. 14.4. Associated with the reduction in total stress, there is a decrease in porewater pressure, Δu. Assuming the soil is saturated and perfectly elastic (isotropic and linear), Δu would be equal to the change in mean principal stress, Δp. With time, the clay swells and pore pressures come to an equilibrium corresponding to long-term conditions (Fig. 14.4b). The time necessary for pore pressure to equilibrate is highly variable from site to site, depending on the geometry of the problem, the hydraulic conductivity, the boundary conditions, the stratigraphy and the swelling characteristics of the soil: it is about one month in the Mexico City clay for excavation depths of 4.5–8 m (Alberro 1979); 5–6 months at Saint-Hilaire, Québec, for a depth of 8 m (Lafleur *et al.* 1988); and about 50 years for a 10 m deep excavation in London clay (Skempton 1977; Chandler 1984). Below a valley that started eroding about 300 000 years ago, Fenelli & Picarelli (1990) observed pore pressures much smaller than those corresponding to steady state conditions, and even negative at some depths.

Eigenbrod (1975) indicated that full equilibration of pore pressures is obtained when the dimensionless time factor T:

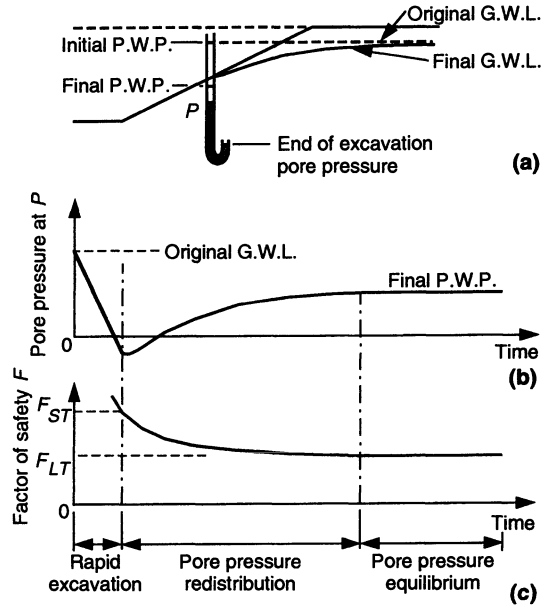


FIGURE 14.4. The changes in pore pressure and factor of safety during an excavation of a cut in clay (modified from Bishop & Bjerrum 1960). PWP = porewater pressure, G.W.L. = groundwater level.

$$T = c_{vs}t/H^2 \qquad (14.1)$$

is equal to 0.33 (where t = the time, H = the depth of the excavation and c_{vs} = the coefficient of consolidation evaluated for swelling conditions, see Section 2.7). This was, however, for a theoretical case in which the clay was excavated up to an impervious substratum. For cases in which the bottom of the excavation remains in the clay deposit, the time factor T can take larger values (Laflamme & Leroueil 1999).

The main difficulty in predicting the time necessary to reach equilibrium comes from the uncertainty regarding the coefficient of consolidation under swelling conditions for the overconsolidated soil. Experience with eastern Canada clays indicates that representative c_{vs} values can be obtained on the basis of the small strain shear modulus G_{max} (see Section 2.11) and a representative hydraulic conductivity (Laflamme & Leroueil 1999).

14.3.3 TRIGGERING OR AGGRAVATING FACTORS RELATED TO WATER

The main triggering or aggravating factors related to water are:

1. Intense rainfall. Intense rainfall often triggers shallow landslides and debris flows in steep slopes. This can result from erosion, but also from infiltration in unsaturated soils and strength reduction (see Section 5.6.1). Even if the relationship between rainfall characteristics and landslide activity is indirect, such relationships have been empirically defined in several countries, for local geological and climatic conditions. Figure 14.5 shows an example, presented by Kim *et al.* (1992) for landslides in South Korea, in which two parameters are used to define rainfall, the two-day antecedent rainfall and the maximum hourly rainfall, and in which landslide activity is divided into three categories.

2. Snowmelt. In mountainous areas and in cold climate countries such as Scandinavia and Canada, snowmelt provides a continuous supply of water over several weeks, generates an increase in pore pressures in the soil, and is often an important triggering factor. This is clearly the case in Quebec where 54% of the landslides occur in April and May (Lebuis *et al.* 1983). The phenomenon is increased when snowmelt is rapid. Jorstad (1968) reports the case of an intensive snowmelt causing 36 landslides in a small area in Norway; Wieczorek *et al.* (1989) report that in Utah about 150 debris flows and other types of landslides were triggered by the melting of snow during an unusually warm period.

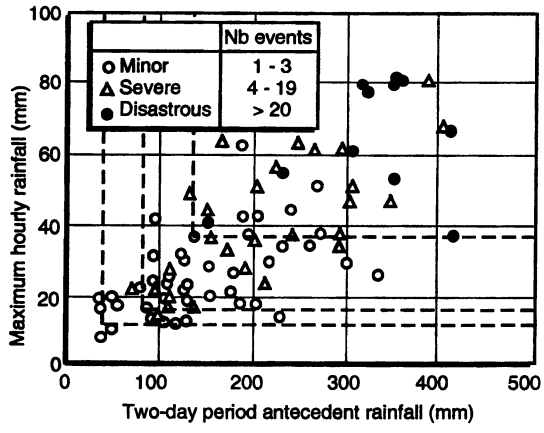


FIGURE 14.5. Relationship between the number of landslides and rainfall characteristics in South Korea (modified from Kim *et al.* 1992).

3. Rapid drawdown. When the water-level of a reservoir adjacent to a slope is rapidly lowered, the stabilizing effect of the water pressure on the slope is decreased in a manner similar to an excavation.

4. Dynamic loading. Dynamic loading such as those induced by earthquakes (e.g. see Seed & Wilson 1966, Fenelli *et al.* 1992, and Chapter 21), vibrating machines (see Chapter 12), pile driving (see Chapter 10), etc., can induce an increase in porewater pressure and reduce the strength of the soil. This is particularly true in loose silty and sandy soils.

14.3.4 FLOW NETS

As explained in Section 14.3.1, the porewater regime in slopes is often hydrodynamic. However, in many cases, the analysis of the porewater regime in slopes is simplified by supposing a steady flow governed by constant hydraulic conditions. The flow net corresponding to steady state conditions depends on the geometry of the problem, the heterogeneity of the hydraulic conductivity due to stratigraphy as well as hydraulic conductivity anisotropy. Figure 14.6 shows flow nets that indicate the direction of groundwater flow and the total head distribution (the equipotentials are lines of constant total head, see Section 2.4) in three different slope conditions. They indicate that, as often observed in practice, the geometry of the problem tends to induce a downward flow under the crest of the slope and an upward flow under the toe of the slope. More complex flow conditions are shown in Fig. 14.7.

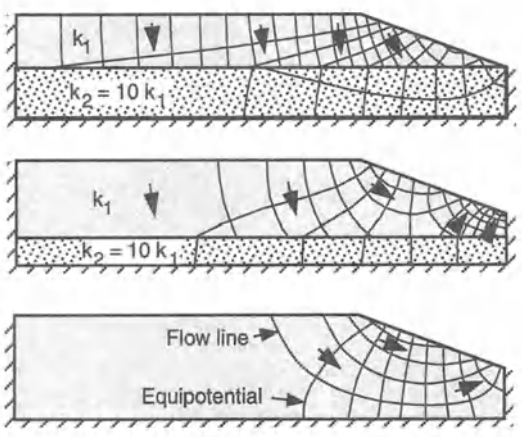


FIGURE 14.6. Flow nets: influence of position of lower aquifer (modified from Lafleur & Lefebvre 1980).

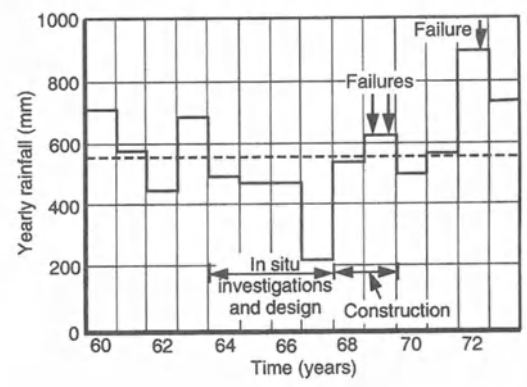


FIGURE 14.8. Variation of yearly rainfall and its relation to the design and failure of slopes in the south of France (modified from Colas *et al.* 1976).

In the analysis, the boundary conditions governing the flow net should correspond to the worst conditions. In fact, the pore pressures observed during a limited period of observation are probably not the most critical that the slope will experience in the future. A good illustration of this difficulty is presented by Colas *et al.* (1976); they reported a case where the stability of slopes along a highway was investigated during a dry period, leading the designers to adopt relatively steep grades for cut slopes in Tertiary overconsolidated deposits; failures were later experienced when the yearly rainfall exceeded the conditions prevailing during the site investigation (Fig. 14.8).

14.3.5 PARTICULAR CASE OF ROCK SLOPES

In rock slopes, the role of pore pressure is similar to that in soils up to when movement

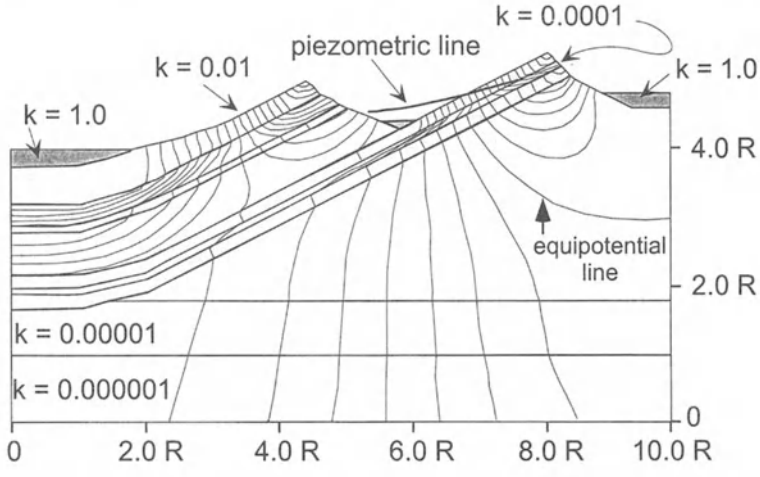


FIGURE 14.7. Groundwater flow model for mountain environment showing the impact of hydraulic conductivity, k, and stratification on flow pattern (modified from Hodge & Freeze 1977). Scales are given as multiples of an arbitrary constant R.

starts. Water pressure is manifest along the various discontinuities that are interconnected. Once movement is initiated, the pore pressures generally drop rapidly. Another important consideration is that rock masses generally have high anisotropic hydraulic conductivity since this is largely influenced by joint opening and spacing. The hydraulic conductivity in fractured or jointed materials is often represented by a simple parallel plate model (e.g. see Louis 1969):

$$k = \frac{ge^3}{12\eta b} \tag{14.2}$$

where g = the gravitational acceleration, η = the dynamic viscosity of water, e = the joint opening and b = the joint spacing. Thus, the hydraulic conductivity increases as a function of the cube of the opening, and hence the anisotropy of the hydraulic conductivity is greatly influenced by the orientation of joints.

For slope stability issues in hard rocks, the pore pressure distribution is often simplified with triangular distributions (see Fig. 14.9) with pore pressure at the atmospheric pressure at the top and at the base of the slope.

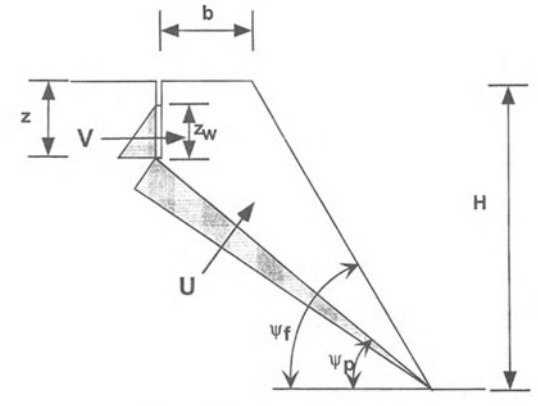


FIGURE 14.9. Boundary conditions for planar failure with pore pressure conditions assumed as a triangular distribution along the sliding plane and the tension crack. ψ_f and ψ_p are the inclination from the horizontal of the slope and failure plane, respectively. U and V are hydraulic forces on the failure plane and the face of the crack respectively.

There are few data on groundwater systems in large rock masses such as mountains, although an interesting study at this scale has been reported by Hodge and Freeze (1977). As indicated by the flow system shown in Fig. 14.7, they studied some hypothetical cases of groundwater flow in mountains including considerations of the effect of anisotropy due to stratigraphic changes (alternating limestone and shale). In these large-scale cases, the pore pressure distribution is similar to that in soils.

14.4 Analysis of Slope Movements: Generalities

In a stable slope, soils are generally in an "overconsolidated" state and essentially behave elastically. Small changes in effective stresses, such as those associated with normal seasonal changes in groundwater conditions, are then generally associated with small deformations or displacements. However, when failure is considered, it is important to keep in mind that soils are, in general, characterized by three levels of strength (Fig. 14.10): (a) the peak strength envelope of the "overconsolidated" material is generally characterized by an effective friction angle and some effective cohesion; (b) at large strains, in the normally consolidated range and even in the "overconsolidated" range when deformations are ho-

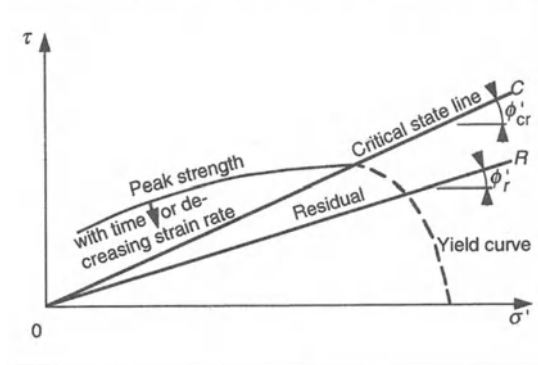


FIGURE 14.10. The three levels of resistance of soils.

mogeneous and not localized, the soil is on the critical state line and the strength is characterized by a friction angle ϕ'_{cr} (or ϕ'_{nc}) and no cohesion (see Section 2.10); and (c) when there is a shear surface on which particles are oriented along the direction of movement, the strength is characterized by the residual strength envelope and a friction angle ϕ'_r. The residual friction angle ϕ'_r is smaller than the critical state friction angle ϕ'_{cr} in soils made up of platy particles, but the two are very close in soils made up of non-platy particles (Lupini *et al.* 1981). It is also worth noting that the peak strength envelope is influenced by strain rate and time, but that these factors have no significant effect on the critical state and residual friction angles (Lo & Morin 1972; Leroueil & Marques 1996).

For most cases of rock slope stability, the shear strength resisting the action of gravity is mobilized along discontinuities, including roughness (Patton 1966) and interlocking (Ladanyi & Archambault 1970). Many models have been proposed to analyze the shear strength of rock masses along discontinuities. Hoek & Bray (1981) provide a good database to help evaluate the friction angle; see also Section 6.6. As will be indicated in Section 14.4.2, the combined effects of roughness and interlocking can be taken into account either as an apparent increase in friction angle or as an increase in an apparent cohesion. The apparent cohesion and friction angle are both greatly influenced by normal stresses and are difficult to estimate. A simplified approach for the estimation of the apparent cohesion will, however, be presented later for the case of planar failures.

14.4.1 PRE-FAILURE

In a stable slope, the soil is generally "overconsolidated" and average effective stresses along any potential failure surface are below the peak strength envelope. When the state of stress is relatively close to the peak strength envelope, creep develops at a rate increasing with the stress level. This explains why observed creep rates in clay slopes are larger when pore pressures are high (Mitchell & Eden 1972; Tavenas & Leroueil 1981). When the state of stress locally reaches the peak strength envelope there is local failure, and the stresses progressively move toward the critical state strength and possibly the residual shear strength envelope. This local reduction of shear stress is associated with the development of progressive failure. A good example of development of progressive failure has been observed in the Selborne experimental cut in an overconsolidated clay (Cooper *et al.* 1998; Leroueil 2000). The stability of the cut was progressively reduced by increasing pore pressures in a recharge zone within the clay mass. Figure 14.11 shows horizontal displacement profiles observed at different times in an inclinometer, (I-06), situated in the central part of the slope. At time B (day −171) and time C (day 88), the deformations are continuous; on the

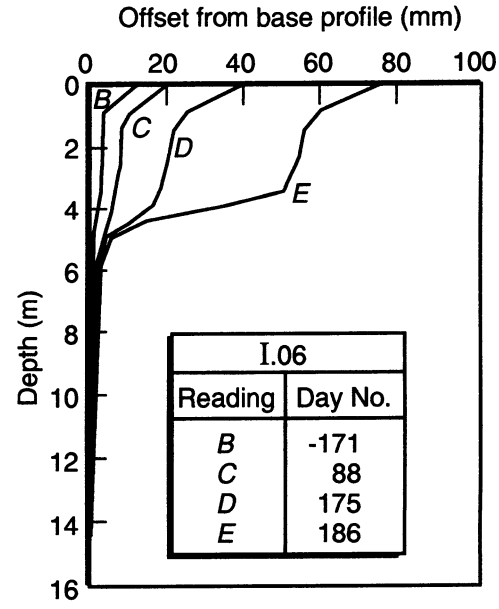


FIGURE 14.11. Inclinometer profiles at different times at Selborne (modified from Bromhead *et al.* 1998).

other hand, at time D (day 175) and time E (day 186, ten days before collapse), there is localization of movements at a depth of about 4.7 m.

An important feature of pre-failure movements is that they involve the entire soil mass and have thus to be analyzed by volumetric methods using, for example, finite element techniques. The application of such models to slopes has been described in Wood *et al.* (1995), Adachi *et al.* (1996, 1998) and Potts *et al.* (1997). The reader is also referred to Duncan (1992).

14.4.2 FAILURE

When the process of progressive failure extends along a shear zone through the entire soil mass, there is general failure. The processes leading to first-time failure are complex and can be even more complicated by the presence of fissures, joints, etc. It follows that the average strength parameters mobilized at failure are generally difficult to assess, and it is only with ductile materials that the strength parameters defined in laboratory can be directly used for field conditions. For other cases, local experience gained from past failures and back-analyses are very useful for the definition of representative strength parameters. For example, the following strength parameters corresponding to a first-time failure have been reported in the literature: $c' = 4$–6 kPa and $\phi' = 26$–$29°$ for Norwegian clays (Janbu 1977); $c' = 7$–12 kPa, $\phi' = 28$–$33°$ for eastern Canada clays (Tavenas & Leroueil 1981); and $c' = 1$ kPa, $\phi' = 20°$ in brown London clay (Skempton 1977; Chandler 1984). Lo & Lee (1974) and Lefebvre (1981) also found that the mobilized strength in eastern Canada clays is close to the large strain strength of the "overconsolidated" material, as obtained in laboratory tests.

In natural slopes where the porewater pressures can be established, stability analyses are usually performed in terms of effective stresses. However, when there are changes in total stress or in boundary pore pressures that are very rapid compared to the time necessary for the soil mass to reach a new equilibrium, stability analyses are usually performed in terms of total stresses.

As discussed in Section 14.3.2, for excavations in clays, the pore pressures are at their minimum value and the factor of safety is at its maximum at the end of excavation (see Fig. 14.4). This factor of safety is defined as F_{ST}, ST being used for short-term. With time, the pore pressures come to equilibrium corresponding to the new boundary conditions and the factor of safety progressively decreases to reach the long-term factor of safety, F_{LT}. Leroueil (2000) illustrates this aspect with the case of the 27° slope at Saint-Hilaire, Québec (Lafleur *et al.* 1988) which had a factor of safety that decreased from about 1.46 at the end of excavation to a value very close to 1.00 in the long term. This can also be illustrated with a relation between slope height, slope inclination and time to failure, as empirically established for cuts in brown London clay (Fig. 14.12). The long-term factor of safety, F_{LT}, is usually estimated on the basis of an effective stress analysis.

Assuming that the excavation time is small compared to the time necessary to reach pore pressure equilibrium, F_{ST} is generally estimated on the basis of the undrained shear

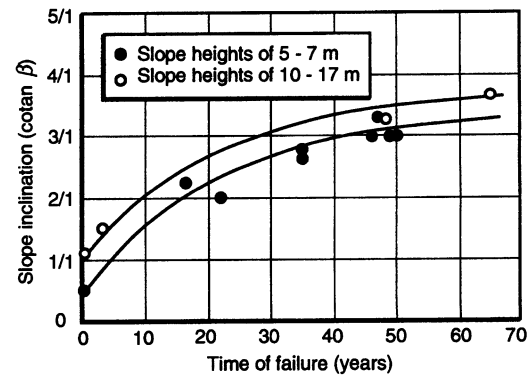


FIGURE 14.12. Relation between slope inclination, slope height and time to failure for London clay cuts (modified from Leonards 1979).

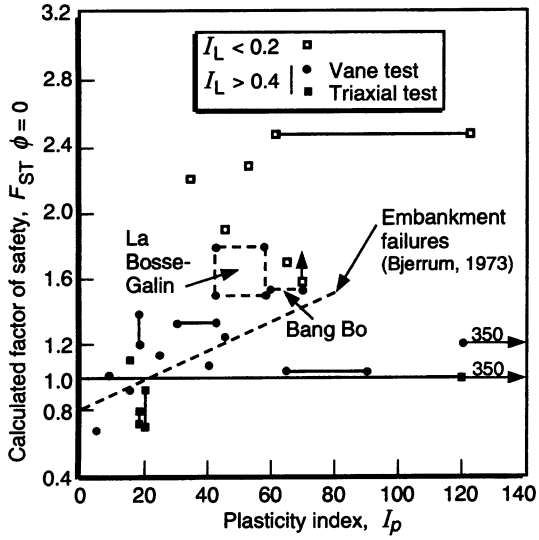


FIGURE 14.13. Factors of safety obtained by total stress analysis of short-term failures versus the plasticity index, I_p (modified from Leroueil *et al.* 1990). I_L = liquidity index.

strength of the clay (total stress analysis). Chandler (1984), Leroueil *et al.* (1990) and Leroueil (2000) reviewed case histories of cuts failing during excavation or shortly after. On the basis of this information, summarized in Fig. 14.13, it was observed that:

- In clays with a liquidity index, I_L (see Section 3.2.7) larger than 0.4, failure occurs at a factor of safety, estimated from undrained stability analysis generally based on the uncorrected vane shear strength, close to 1.0 and, in all cases except La Bosse Galin and Bang Bo, smaller than 1.35.
- The case of La Bosse Galin (Blondeau & Queyroi 1976) is meaningful. It took three weeks to reach the depth of 4 m at which point failures occurred at a factor of safety calculated on the basis of the uncorrected vane shear strength varying between 1.45 and 1.85. However, piezometric data indicated that pore pressures were equilibrating during excavation. The failure was therefore a long-term failure and it is thus not surprising that failure occurred with a calculated short-term factor of safety in the order of 1.65. The situation was apparently similar at Bang Bo (Leroueil 2000).
- In stiff clays (clays having a liquidity index smaller than 0.2 and often fissured), the undrained shear strength of the clay, as measured in undrained compression triaxial tests, overestimates the shear strength back-analyzed from failures by a factor that is typically equal to two, but could be greater.

In the case of rock masses, the stress history during mountain building or tectonic activity often generates shearing along bedding or structural joints. The strength along these discontinuities is influenced by normal stresses and has a tendency to decrease with increasing relative displacements. For closely jointed rock masses, other factors such as interlocking contribute to the shearing resistance (Ladanyi & Archambault 1970) and, with increasing joint density, the behavior becomes similar to the one of granular soils.

14.4.3 POST-FAILURE

What happens just after failure depends on the redistribution of the potential energy that becomes available at failure. This energy can be dissipated: (a) in friction at the contact between the moving soil mass and the underlying layers and/or within the moving soil mass; (b) by disaggregating or remolding the materials involved in the landslide; and (c) in kinetic energy (movement). In the case of a landslide in ductile materials, most of the energy is dissipated in friction and, consequently, the rate of movement is slow. On the other hand, when the material displays strain-softening behavior or brittleness the kinetic energy and thus the rate of movement and the run-out distance may become important.

When the large-strain strength of the material is small, flow slides may develop. The processes involved are complex and the reader should refer to specialized documents (e.g. Takahashi 1991). With these flow slides,

the normalized travel distance (L/H, where L = the travel distance and H = the change in elevation of the material involved in the flow) depends on the characteristics of the material (grain-size distribution, water content) and on the geometry and boundary conditions of the run-out path. It also increases with the volume of the failed mass.

Following failure of rock masses, there is fragmentation and the physical and mechanical characteristics of the resulting material have little similarity to those in the initial state. Thus, the post-failure behavior of these masses is sometimes better described by principles of fluid mechanics than soil or rock mechanics. The case of the La Valette slide, in the French Alps, is a good example of a mass movement for which the post-failure behavior evolved from rock mechanics, to soil mechanics and finally to fluid mechanics (Colas and Locat 1993).

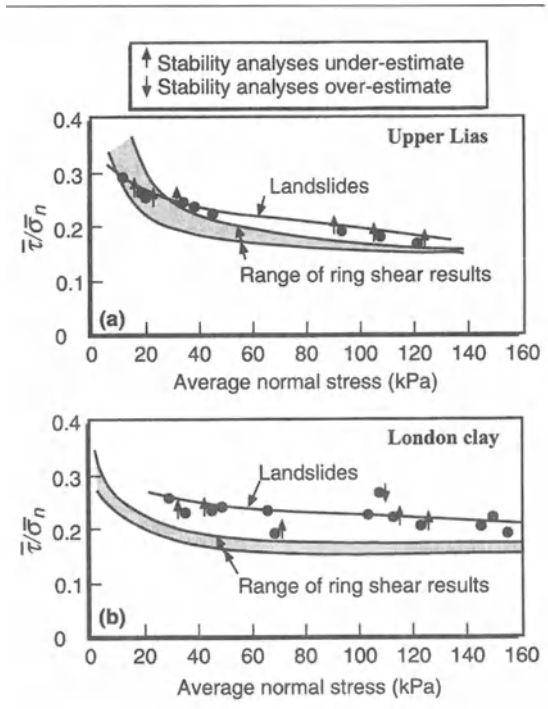


FIGURE 14.14. Comparison of field and laboratory measurements of residual strength in: (a) Upper Lias; and (b) London clay (modified from Chandler 1984).

14.4.4 REACTIVATION

Reactivation may occur along a pre-existing failure surface on which there has been, in most cases, a reorientation of plate-shaped clay particles. The movements are then localized with the sliding of a soil mass over an essentially rigid base. For these cases, limit equilibrium analyses are fully justified (Section 14.5). The strength parameters to take into account are generally characterized by a residual friction angle, ϕ'_r, and an effective cohesion equal to zero. General correlations between residual friction angle and physical characteristics of clayey materials are presented in Chapters 3 and 23 (Sections 3.7.2 and 23.7.2). It is worth noting, however, that, due to an irregular shear surface, an incomplete orientation of the particles and to the possible presence of coarse elements along the shear surface, the residual friction angle mobilized *in situ* may be slightly larger than the one obtained in the laboratory. For Upper Lias and London clay, Chandler (1984) and Skempton (1985) found that the field strength is slightly higher than the residual shear strength measured in ring shear tests by an equivalent of 1–3° on the residual friction angle (Fig. 14.14).

Reactivation may involve what are usually called active landslides and reactivated landslides. In active landslides, the rate of displacement varies with the seasonal changes of the groundwater level. This is particularly true for translational landslides in which the driving forces do not change significantly with time. The rates of displacement are generally small, varying between some centimeters to some meters per year (Urciuoli 1990).

In contrast to active landslides, reactivated landslides may be associated to sudden and fairly rapid displacements (Hutchinson 1987; D'Elia *et al.* 1998). Hutchinson (1987) listed a number of mechanisms that can produce such movements, including: (a) a rapid increase in pore pressure due to filling of cracks or breaking of a pipe; (b) a rapid change in

load distribution along the shear surface; (c) an increase in strength along the shear surface due to cementation or chemical changes, which could give some brittleness to the material involved; and (d) seismic effects. In this last case, the main movements may be delayed relatively to the earthquake (D'Elia *et al.* 1985), probably due to pore pressure redistribution in the soil mass.

14.5 Methods of Slope Stability Analysis

14.5.1 GENERAL REMARKS

Stability is usually characterized by a factor of safety, F, defined as the ratio between the available shear strength and the mobilized shear stress necessary to maintain equilibrium. The shear stresses mobilized along a potential shear surface in a slope result from the geometry of the problem and gravity forces as well as from stress history and the coefficient of earth pressure at rest, K_0. For saturated soils, the shear strength is a function of the effective stress normal to the plane of rupture being considered and thus depends on pore pressure:

$$\tau_f = c' + \sigma'_n \tan \phi' = c' + (\sigma_n - u) \tan \phi'. \quad (14.3)$$

The shear strength of unsaturated soils is discussed in Chapter 5 (Section 5.6.1) and formulations for slope stability problems are given in Section 5.6.6. When there is a rapid loading or unloading in clayey materials, or an extremely rapid change in total stresses in silty or sandy materials so that the changes in pore pressures have no time to equilibrate, the undrained shear strength is usually considered.

The shear strength of rock masses can be described by various failure criteria (see Chapter 6, especially Sections 6.5 and 6.6). However, the most commonly used failure criterion for slope stability problems is Mohr–Coulomb.

Stability analyses are generally performed with limit equilibrium methods assuming a rigid–plastic soil (or rock) behavior and the validity of the Mohr–Coulomb criterion. Most methods of analysis have been formulated in two dimensions and most experience is related to these methods. It is worth noting, however, that landslides are often three-dimensional and that the factor of safety calculated for the central section with a two-dimensional model is smaller than the three-dimensional factor of safety. The reader is referred to Gens *et al.* (1988), Hungr *et al.* (1989), Morgenstern (1992) and Faure *et al.* (1996) for more details concerning three-dimensional analyses. However, according to Sève (1998), three-dimensional analyses are justified only when the ratio of the length of the slide over its width is larger than ten. Except for wedge failures, all the analyses presented in this chapter are two-dimensional.

The minimum factor of safety value required for a slope varies from country to country and can depend on local conditions like population density, physical settings and economic considerations. It could also vary depending on the estimated and accepted risks associated with the potential slope movement, and on the degree of sophistication of the investigation or, more generally, the uncertainty regarding the input parameters (see in particular Lacasse & Nadim 1994; Sällfors *et al.* 1996). When the actual factor of safety is close to 1.0, or equal to 1.0 as evidenced by a failure, and that mitigation measures are planned, an increase of the factor of safety by 20–30% is usually considered acceptable.

In soils, where the moving mass is generally considered as a continuum, stability is usually calculated by the so-called "methods of slices" or by the global so-called "perturbation method." Methods exist for circular failure surfaces and for failure surface of any shape. The methods of slices are described in Section 14.5.3 and the perturbation method is presented in Section 14.5.4. The particular case of a plane failure surface parallel to the surface (infinite slope) is considered in Section 14.5.2.

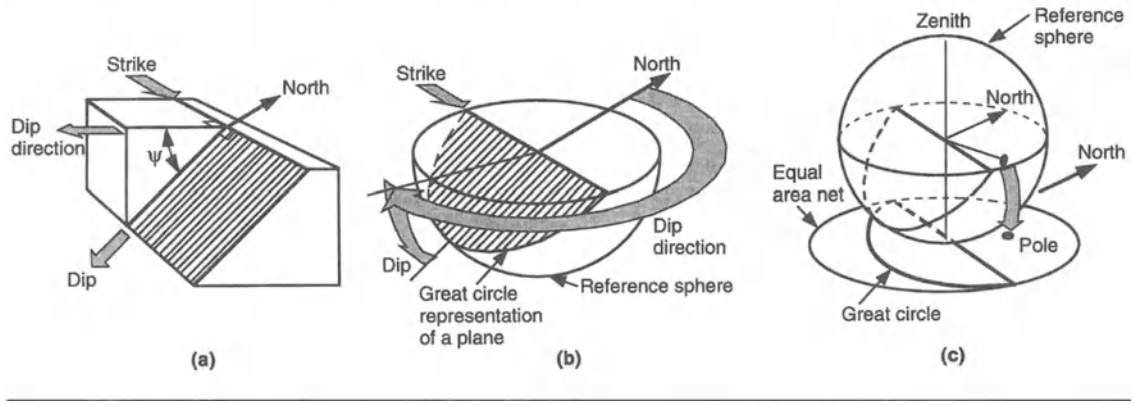


FIGURE 14.15. Representation of planar features: (a) definition of terms; (b) representation of reference sphere; and (c) equal-area projection (modified from Hoek & Bray 1981 and Norrish & Wyllie 1996).

In rocks, where stability is often controlled by discontinuities, the identification of the potential failure type can be assessed by stereographic projections. Stereographic projections allow for the representation of structural features, such as discontinuities, as a function of their dip and dip direction (or the strike of the plane). Referring to Fig. 14.15a, the dip is the inclination of the plane below the horizontal and the dip direction is the azimuth of the maximum dip of the plane.

This information can be represented in three dimensions on a reference sphere (Fig. 14.15b). The intersection of the plane passing through the center of the sphere and the sphere is the great circle (Fig. 14.15b). The intersection of the radial line normal to the plane and the sphere is the pole of the plane (Fig. 14.15c). A two-dimensional representation of the great circle and the pole of the plane is obtained by equal-area projection (stereonet), as indicated in Fig. 14.15c.

Because of the necessity to describe the joint system, some variables are represented by symbols that differ from those commonly used for soils (see Fig. 14.9).

The four main types of failure that occur in rock masses are: (a) planar; (b) wedge; (c) rock fall; and (d) toppling. In the cases of planar and wedge failures, respectively discussed in Sections 14.5.5 and 14.5.6, the major differences in the equations are due to differences in geometry. For toppling (Section 14.5.7), the formulation is mostly based on the geometry of the problem, especially when cohesion is not considered. These modes of failure are illustrated in Fig. 14.16 for a friction angle of 30° and zero cohesion (circular dashed line in the figure). This figure represents four sets (or families) of discontinuities. Each family is represented by a great circle of the plane and its pole (numbers 1–4). The slope surface is also represented by a great circle and is shown as a dashed line. Since friction angle is assumed constant, its value is the same in all directions. Therefore, the friction cone can be represented by a circle corresponding to a dip equal to the friction angle. The shaded area represents the intersection of the friction cone and the great circle of the slope surface.

From kinematics, discontinuities (e.g. number 1 in Fig. 14.16) for which the great circle passes through the shaded area would indicate a potential instability (planar failure) since the slope of the plane would be less than the slope angle but more than the friction angle. Similarly, planes intersecting in the shaded area (e.g. wedge: 1, 3 or wedge: 1, 2 in Fig. 14.16) would also be considered

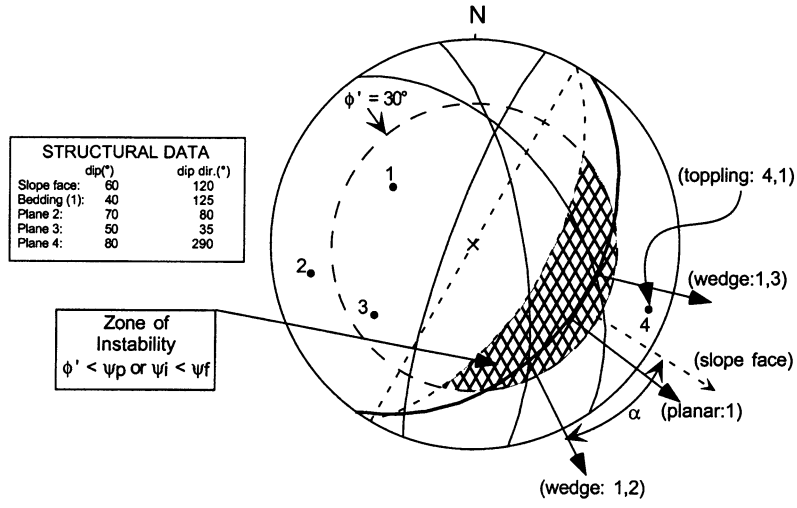


FIGURE 14.16. Various modes of failure of rock masses along discontinuities. The structural data provided in the insert are used in the example.

potentially unstable (wedge failure) since the inclination of the line of intersection of the two planes forming the wedge would be less than the slope face but more than the friction angle. The azimuths of the lines of intersection of these two wedges are indicated by the two arrows noted (wedge 1,3) and (wedge 1,2) in Fig. 14.16. The case of simple toppling failures is discussed in Section 14.5.7.

Rock slope stability analyses have been described in detail by several authors, in particular Hoek & Bray (1981) and Norrish & Wyllie (1996).

14.5.2 INFINITE SLOPE

The term "infinite slope" is used to designate a uniform slope in which a slide would involve a plane failure surface parallel to the slope surface at a depth much smaller than the width and the length of the involved mass of material. In these conditions, the potential landslide body can be represented by a single slice delimited by the ground surface, the potential sliding surface and two parallel vertical sections.

For steady seepage parallel to the slope and the groundwater level, h_w, above the slip surface, the factor of safety, F, is defined for the parameters indicated in Fig. 14.17:

$$F = \frac{c' + (\gamma z \cos^2 \beta - u) \tan \phi'}{\gamma z \sin \beta \cos \beta}. \quad (14.4)$$

When the effective cohesion, c', is equal to zero, the groundwater level is at the surface and the flow parallel to the slope surface, the factor of safety, F, becomes:

$$F = \frac{(\gamma - \gamma_w) \tan \phi'}{\gamma \tan \beta}. \quad (14.5)$$

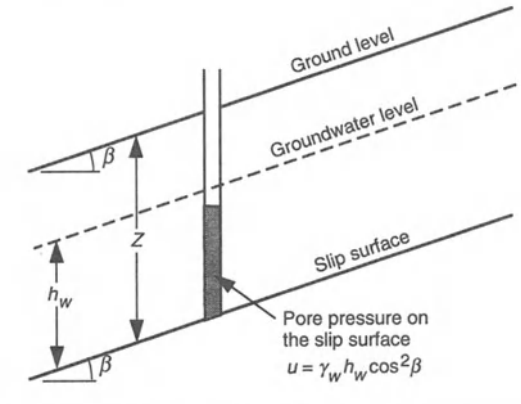
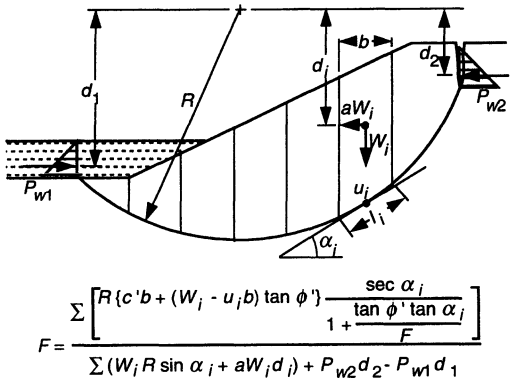


FIGURE 14.17. Planar failure in infinite slope.



$$F = \frac{\Sigma\left[R\{c'b + (W_i - u_i b)\tan\phi'\}\dfrac{\sec\alpha_i}{1 + \dfrac{\tan\phi'\tan\alpha_i}{F}}\right]}{\Sigma(W_i R\sin\alpha_i + aW_i d_i) + P_{w2}d_2 - P_{w1}d_1}$$

FIGURE 14.18. Bishop's simplified method.

14.5.3 METHODS OF SLICES

In these methods, the potential sliding mass is subdivided into n slices, as shown in Fig. 14.18. Each slice is in equilibrium under the forces acting on it: its own weight, W_i; interslice forces; and a total reaction at the base, which can be subdivided into an effective force ($\sigma'_i l_i$) and a porewater force ($u_i l_i$). Other aspects that may have to be considered include:

- Seismic forces: possible earthquake effects are generally considered by introducing in the stability analysis a horizontal force applied in the center of gravity of each slice (pseudostatic method) corresponding to an acceleration, "$a \times g$," applied to the mass of material (see Chapter 21 and Section 27.7.5).
- Submerged slopes and rapid drawdown: submergence of the toe of a slope can be taken into account by considering a horizontal force, P_{w1}, as indicated in Fig. 14.18. When the water-level rapidly decreases (rapid drawdown), there is a change in stability conditions since the external pressure applied by water disappears. The strength to take into account for such situation depends on the rate of decrease of the water-level, the coefficient of consolidation of the soil, and the geometry of the problem. If the soil has time to drain, an effective stress analysis must be applied to stabilized conditions; if the soil has no time to drain, undrained strength must be used.
- Open fissures: no strength can be mobilized in open fissures or cracks. However, if there is water in the cracks, the force due to this water (P_{w2} in Fig. 14.18) must be taken into account in the analysis.

The methods of analysis should ensure the conditions of equilibrium for each slice and for the entire mass. Some methods satisfy all these conditions (Morgenstern & Price 1965; Spencer 1967; Sarma 1973); some do not. This is the case for the ordinary method of slices (Fellenius 1927), which does not take into account the interslice forces, and Bishop's simplified method (Bishop 1955), which neglects the vertical component of the interslice forces.

The expression for the factor of safety calculated with the Bishop's simplified method is given in Fig. 14.18. Experience has shown that the ordinary method of slices (Fellenius 1927) gives factors of safety lower than all other methods. On the other hand, the methods satisfying all the conditions of equilibrium provide, for circular slip surfaces, factors of safety that are very close to the one obtained with Bishop's simplified method (Fredlund & Krahn 1977). As a consequence, this last method is often used for circular slip surfaces. When the slip surface is not circular, one of the methods proposed in Morgenstern & Price (1965), Spencer (1967), Janbu (1968), or Sarma (1973) can be used. Duncan & Wright (1980) and Sève (1998) compared the factors of safety computed using the methods quoted above for several cases. They conclude that the factors of safety deduced using these different methods are usually in a range of 10% and always in a range smaller than 20%.

Many commercial stability analysis programs are available. However, for very simple cases, and in order to get an approximate value of the factor of safety, stability charts can be used. Figures 14.19 and 14.20 give those developed for circular failure surfaces by Janbu

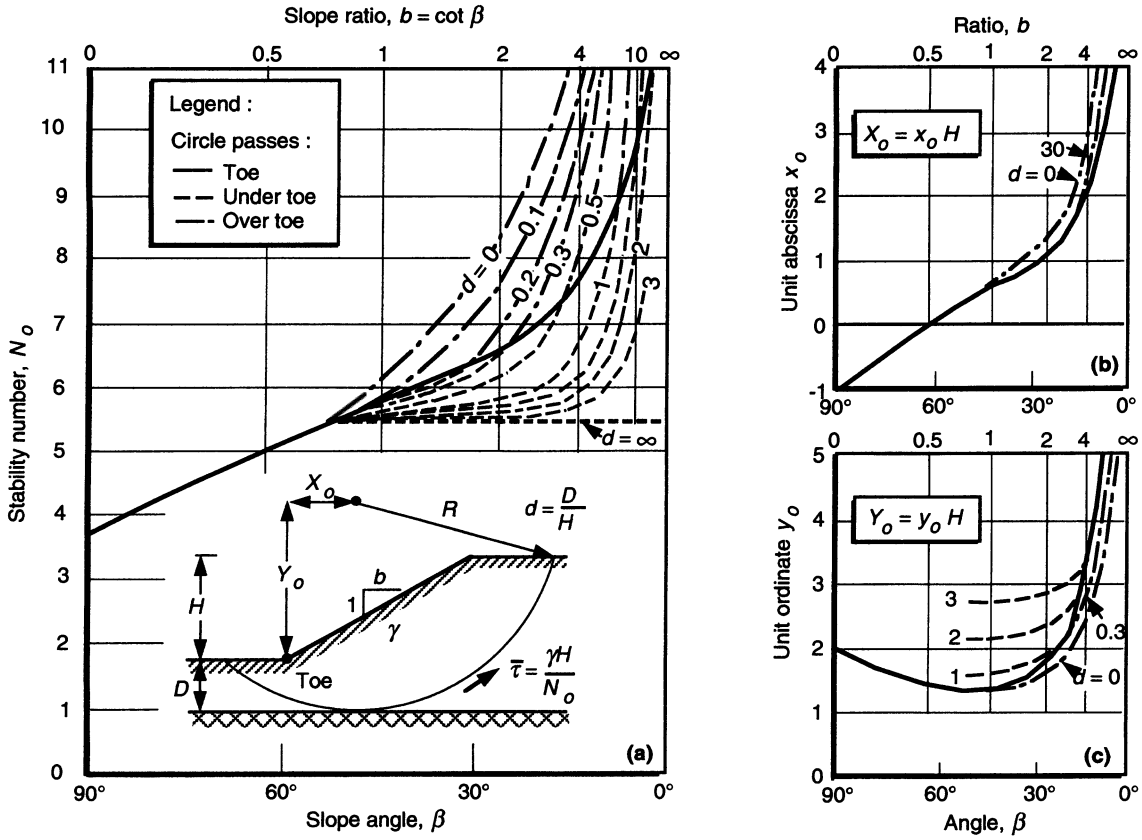


FIGURE 14.19. Stability charts for total stress analyses (modified from Janbu 1954a).

(1954a; see also Janbu 1996) for total stress and effective stress analyses, respectively.

Figure 14.19 shows the stability chart for total stress analysis. The minimum factor of safety is defined by:

$$F_{\min} = N_0 \frac{s_u}{\gamma H} \qquad (14.6)$$

where s_u = the undrained shear strength (constant or average) and N_0 is a stability number (minimum value).

The co-ordinates of the center of the critical circle are given by:

$$X_0 = x_0 H, \qquad Y_0 = y_0 H. \qquad (14.7)$$

The dimensionless numbers N_0, x_0 and y_0 are plotted as a function of the slope ratio b = cot β and the location of the rock, or hard layers, $d = D/H$, in Fig. 14.19.

As mentioned by Janbu (1996), Eq. 14.6 and Fig. 14.19 can be used to find the maximum average shear stress $\bar{\tau} = s_u/F_{\min}$ required for equilibrium, independently of the strength of the soil:

$$\bar{\tau}_{\max} = \frac{\gamma H}{N_0}. \qquad (14.8)$$

Figure 14.20 presents the stability chart for effective stress analysis. The minimum factor of safety is defined by:

$$F_{\min} = N_{cf} \frac{c'}{p_d}. \qquad (14.9)$$

For simple slopes:

$$p_d = \gamma H \qquad (14.10a)$$

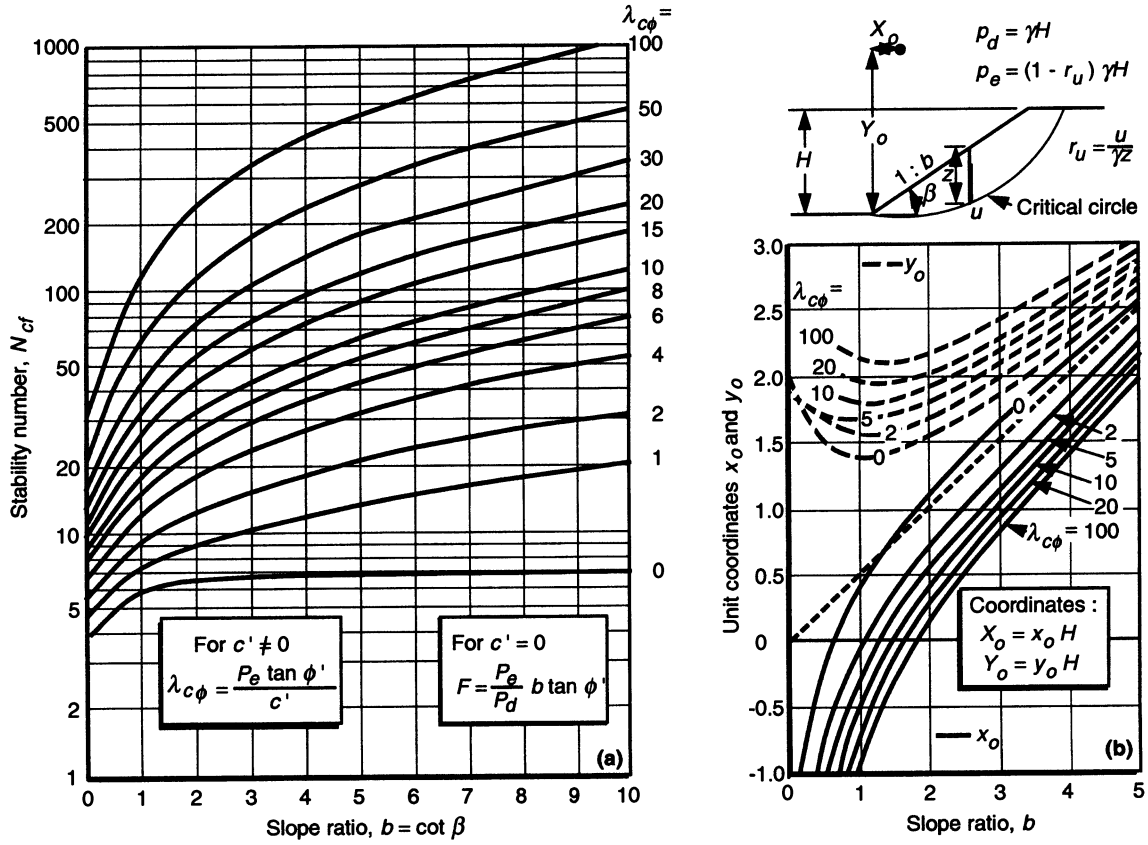


FIGURE 14.20. Stability charts for effective stress analyses (modified from Janbu 1954a).

or

$$p_d = (\gamma H - \gamma_w H_w). \qquad (14.10b)$$

N_{cf} can be obtained from Fig. 14.20a as a function of the slope ratio b and the parameter

$$\lambda_{c\phi} = \frac{p_e \tan \phi'}{c'} \qquad (14.11)$$

where $p_e = (1 - r_u)\, p_d$ and $r_u = u/\gamma z$ (see Fig. 14.20).

Most often, toe circles were found to be critical. The center co-ordinates (X_0, Y_0) of the critical toe circle can be deduced from Eq. 14.7, using the x_0 and y_0 values given in Fig. 14.20b.

14.5.4 GLOBAL METHOD: PERTURBATION METHOD

The perturbation method is a global method proposed by Raulin *et al.* (1972) and Faure (1985). Considering a slip surface, this approach assumes that the total normal stress, σ_n, at a point such as M (Fig. 14.21a) can be written as $\sigma_0\,(\lambda + \mu \tan \alpha)$. σ_0 is the initial total stress, which can be chosen as the Fellenius' stress $\gamma H \cos^2 \alpha$ (see Fig. 14.21a for the meaning of the symbols). σ_0 can also be defined so that σ'_0 can be compatible with the effective vertical stress $(\gamma H - u)$ at point M on the Mohr circle, as indicated in Fig. 14.21b (see Faure 1985 and Faure *et al.* 1996 for details). λ and μ are parameters that are numerically obtained to satisfy the equations

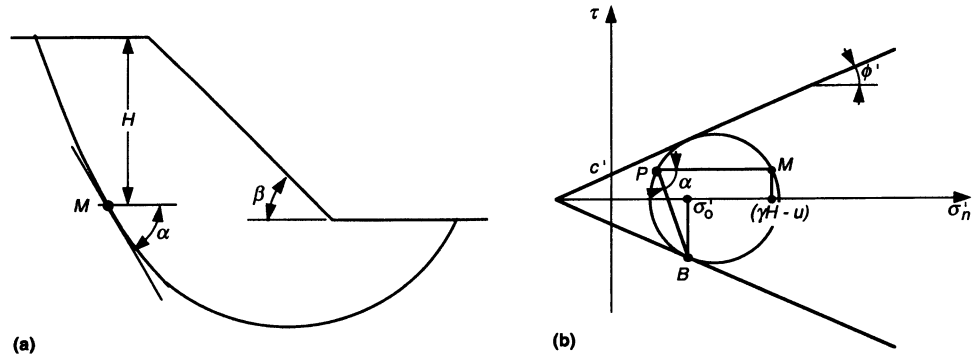


FIGURE 14.21. Perturbation method: (a) notation, and (b) definition of σ'_0 (modified from Faure 1985).

of equilibrium; their values are generally found close to 1.0 and 0.0, respectively. This method, applicable to any shape of slip surface is found to give F values similar to those obtained with methods of slices and has been widely used in France for more than 20 years.

14.5.5 PLANAR FAILURE

A planar failure is defined as a sliding of a rock (or soil) mass that takes place along a single plane (see Fig. 14.3e). From a kinematics point of view, a simple planar failure along a given plane must meet, as a minimum, the following conditions (see Fig. 14.9 for the symbols used):

1. the sliding plane, ψ_p, must have (for rock) a dip direction within 20° of that of the slope angle, ψ_f;
2. the failure plane must daylight in the slope face, i.e. $\psi_p < \psi_f$;
3. the dip of the sliding plane must be greater than the friction angle, i.e. for dry slopes, $\psi_p > \phi'$; and
4. there must be lateral joints on either side of the block to ensure that there is no significant side friction.

The general equation used for planar analysis (Hoek & Bray 1981) is:

$$F = \frac{c'A + [W(\cos\psi_p - a\sin\psi_p) - U - V\sin\psi_p + T\cos\theta]\tan\phi'}{W(\sin\psi_p + a\cos\psi_p) + V\cos\psi_p - T\sin\theta} \quad (14.12)$$

where c' = the cohesion; ϕ' = the friction angle; ψ_p = the angle of the failure plane; A = the area of the failure plane; W = the weight of the block; U and V = the forces exerted by pore pressures along the failure plane and the tension crack, respectively (Fig. 14.9); T = the force applied to the rock by reinforcement members (if any) at an angle θ with the normal to the failure surface, and a = the horizontal acceleration applied to the soil or rock mass in case of an earthquake as a proportion of gravitational acceleration g (see Chapter 21).

From the geometry of Fig. 14.9, the geometric variables can be derived as:

$$A = (H - z)\ \text{cosec}\ \psi_p \quad (14.13)$$

$$U = \frac{1}{2}\gamma_w z_w (H - z)\ \text{cosec}\ \psi_p \quad (14.14)$$

$$V = \frac{1}{2}\gamma_w z_w^2. \quad (14.15)$$

For the case where the tension crack is at the back of the crest of the slope we have:

$$W = \frac{1}{2}\gamma H^2 \left\{\left[1 - \left(\frac{z}{H}\right)^2\right]\cot\psi_p - \cot\psi_f\right\} \quad (14.16)$$

and for a tension crack located in the slope:

$$W = \frac{1}{2}\gamma H^2 \times \left[\left(1 - \frac{z}{H}\right)^2 \cot \psi_p(\cot \psi_p \tan \psi_f - 1)\right]. \quad (14.17)$$

The position of the tension crack and its depth are difficult to determine. Hoek and Bray (1981) proposed relationships that can be used as a first estimate: the critical depth of the tension crack ($z = z_c$) and its distance ($b = b_c$) from the crest of the slope (see Fig. 14.9) could be defined as follows (see Hoek & Bray 1981 for explanations):

$$z_c = H[1 - (\cot \psi_f \tan \psi_p)^{1/2}] \quad (14.18)$$

and

$$b_c = H[(\cot \psi_f \cot \psi_p)^{1/2} - \cot \psi_f]. \quad (14.19)$$

evaluate a minimum value for the cohesion mobilized in a slope, considering that the factor of safety of the slope is larger than 1.0. It is based on two assumptions: (a) the slope is at an angle close to equilibrium, i.e. $F \sim 1$; and (b) the friction angle measured in the direct shear box represents the reference friction angle of the rock so that any other component of the mobilized shear strength can be assumed as included in the cohesion parameter c'. Using these assumptions, it is possible to carry out a computation of cohesion of fictitious slopes where the tension crack is at the critical location ($b = b_c$) and at the critical depth ($z = z_c$) given by Eqs 14.18 and 14.19 (see Fig. 14.9). In such a case, the calculated value of c' is directly proportional to the height of the slope, H. Therefore, knowing the friction angle, ϕ', and assuming that $F = 1$ and that there is no reinforcement, Eq. 14.12 can be modified so that:

$$\frac{c'}{H} = \frac{(W \sin \psi_p + V \cos \psi_p) - (W \cos \psi_p - U - V \sin \psi_p) \tan \phi'}{AH}. \quad (14.20)$$

In most instances, the friction angle is obtained by direct shear tests on pre-cut surfaces in order to minimize the roughness. In such a case, and depending on the degree of polishing, the measured friction angle may be influenced by the presence of a film of water (wet surface). If the degree of roughness of the cut surface is very small, friction angle values can approach those of pure minerals. In this case, the presence of water could either decrease or increase the friction angle (Mitchell 1993). These test results thus give a reference friction angle for the rock surface but do not provide any cohesion component of the shear strength that is related, for example, to roughness or interlocking along the potential failure surface or to the rock mass itself.

A simple approach is proposed hereafter to

This relationship is illustrated in a c'/H versus ψ_p diagram (Fig. 14.22) for $\phi' = 30°$, a unit weight of 25 kN m^{-3}, and three water pressure conditions (see Fig. 14.9): (a) dry slope ($z_w = 0$); (b) tension crack half-filled ($z_w/z_c = 0.5$); and (c) tension crack full of water ($z_w/z_c = 1.0$).

For example, for a slope in shale ($\phi' = 30°$) with a height $H = 30$ m, a slope angle $\psi_f = 60°$, and a failure plane angle $\psi_p = 40°$, the minimum cohesion required to maintain the stability would be 36 kPa (30 × 1.20), 50 kPa (30 × 1.65) and 75 kPa (30 × 2.5) for the three water pressure conditions.

14.5.6 WEDGE FAILURE

Examples of two potential wedge failures (wedges 1, 2 and 1, 3) have been shown in Fig. 14.16. In this case, the bedding plane (1)

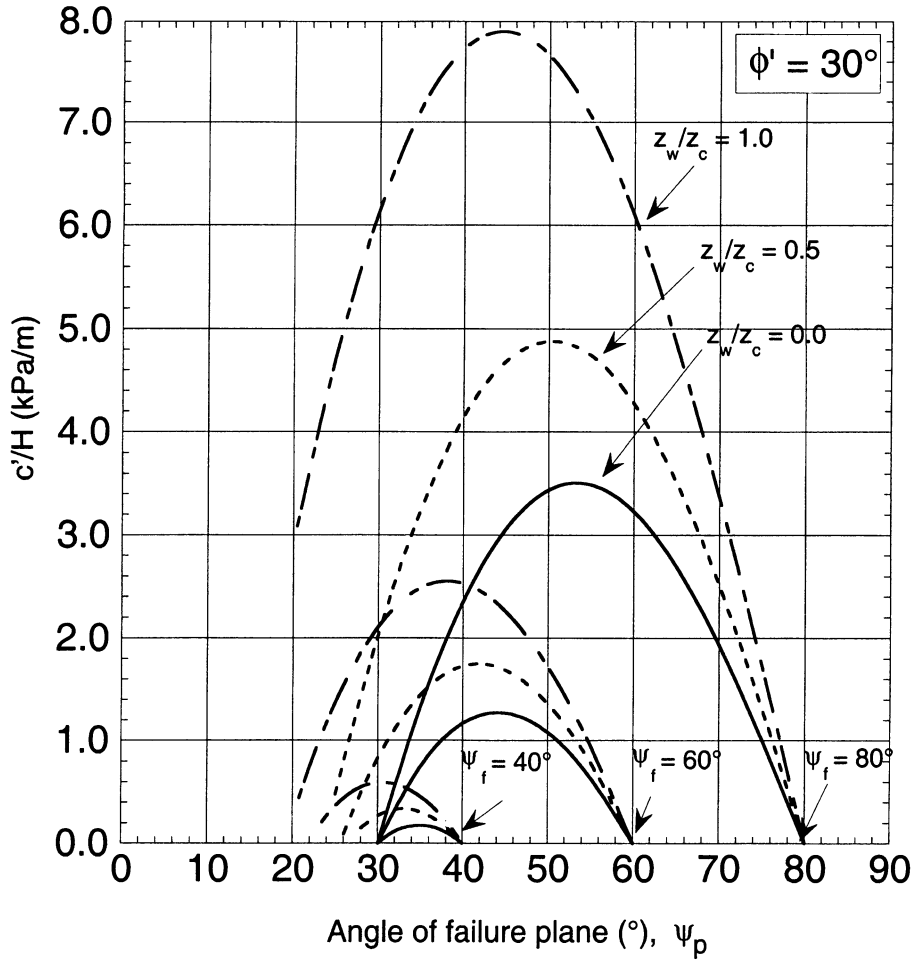
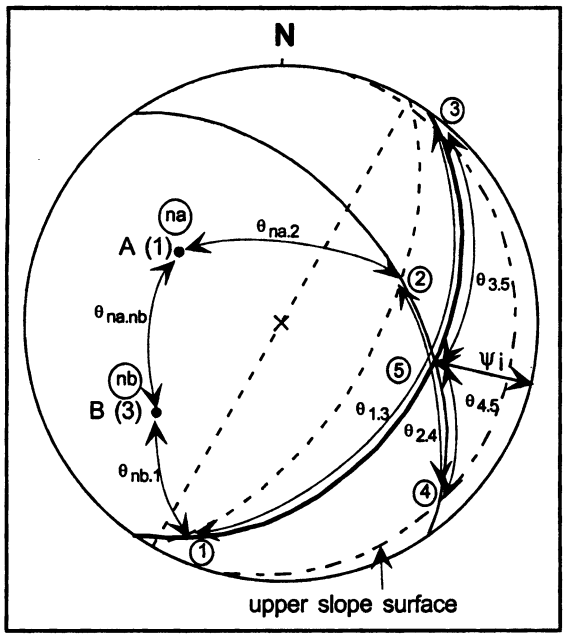


FIGURE 14.22. Nomogram for estimating a minimum value of the cohesion component of shear strength from the analysis of natural slopes. $\phi' = 30°$.

intersects two other planes (2 and 3) in the shaded area, thus leading to two potential wedge failures, as described in Section 14.5.1. For the stability analysis, Hoek & Bray (1981) propose the following relationships to compute the factor of safety, F:

$$F = \frac{3}{\gamma H}(c'_A X + c'_B Y) + \left(A - \frac{\gamma_w}{2\gamma} X\right) \tan \phi'_A + \left(B - \frac{\gamma_w}{2\gamma} Y\right) \tan \phi'_B \quad (14.21)$$

where c'_A and ϕ'_A, and c'_B and ϕ'_B = the cohesion and friction angle for planes A and B, respectively; γ and γ_w = the unit weights of the rock and water, respectively; H = the height of the wedge, defined as the difference in the elevations of the upper and lower ends of the line of intersection of the two planes. X, Y, A and B are non-dimensional factors reflecting the geometry of the wedge, which are described in Fig. 14.23. The plane identified by A (bedding: 1) is the one having the smallest dip, while plane B corresponds to joint set



$$X = \frac{\sin\theta_{24}}{\sin\theta_{45}\cos\theta_{2.na}}$$

$$Y = \frac{\sin\theta_{13}}{\sin\theta_{35}\cos\theta_{1.nb}}$$

$$A = \frac{\cos\psi_a - \cos\psi_b\cos\theta_{na.nb}}{\sin\psi_5 \sin^2\theta_{na.nb}}$$

$$B = \frac{\cos\psi_b - \cos\psi_a\cos\theta_{na.nb}}{\sin\psi_5 \sin^2\theta_{na.nb}}$$

STRUCTURAL DATA FOR WEDGE ANALYSIS

	dip(°)	dip dir.(°)
Slope face:	60	120
Upper slope surface:	10	115
Bedding (1):	40 (A)	125
Plane 3:	50 (B)	35

Angular intersection convention

1: plane A and slope face
2: plane B and slope face
3: plane A and upper slope
4: plane B and upper slope
5: A and B (A < B)
θ: angle between two planes

FIGURE 14.23. Stereoplot of angular data for wedge stability analysis. X, Y, A and B are coefficients used to solve Eq. 14.21. The numbers in brackets refer to the bedding (1) and joint set (3) identified in Fig. 14.16.

3 in Fig. 14.16. The procedure for evaluating the various geometrical combinations is described in Hoek & Bray (1981). This procedure always assumes that sliding will take place along the line of intersection between the two planes. In order to use Fig. 14.23, the numbering sequence must be respected. A numerical program for solving Eq. 14.21 is provided in Abramson (1985).

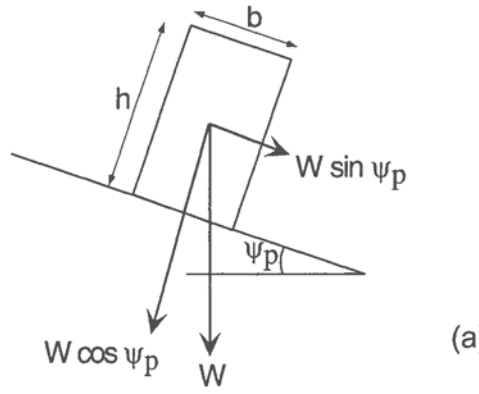
The analysis of wedge failure can be simplified if no cohesion and pore pressure are considered. In such a case, Eq. 14.21 can be simplified to take into account only friction and reduces to:

$$F = A \tan \phi'_A + B \tan \phi'_B. \quad (14.22)$$

Hoek & Bray (1981) propose a series of charts that make Eq. 14.22 very useful for a rapid evaluation of joint conditions which can lead to stability problems.

14.5.7 TOPPLING FAILURE

When the possibility of toppling is considered, stability is defined in terms of the relative position of the center of gravity and the angle of the sliding plane (Fig. 14.24a). In the case of drained slopes and neglecting cohesion, it is possible to identify simple condi-



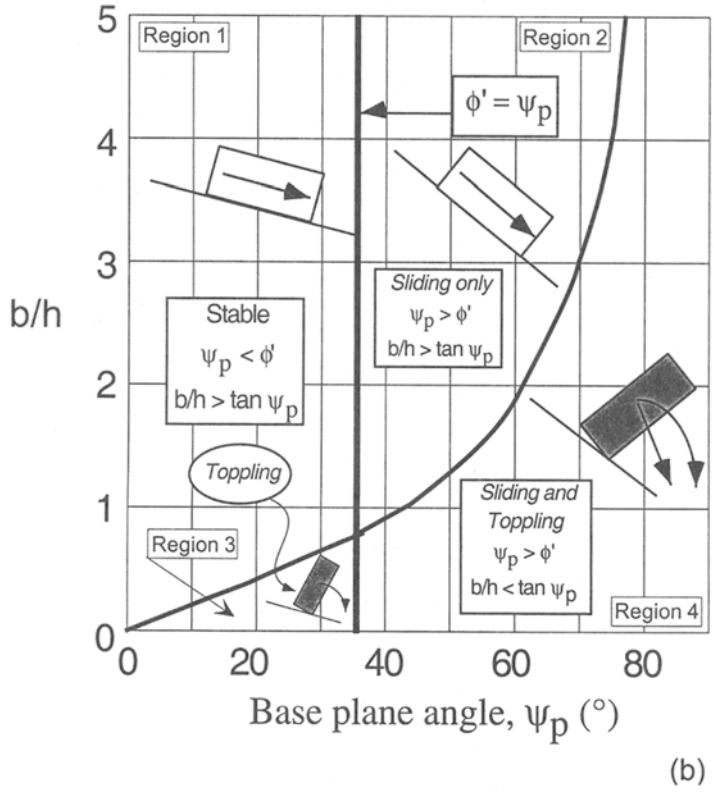


FIGURE 14.24. Analysis of toppling failure potential: (a) geometric considerations, and (b) stability conditions (modified from Hoek & Bray 1981).

tions of stability. Figure 14.24b shows, assuming a purely frictional contact between the block and its base, four regions identified as:

- Region 1: where $\psi_p < \phi'$ and $b/h > \tan \psi_p$, the block is stable.
- Region 2: where $\psi_p > \phi'$ and $b/h > \tan \psi_p$, the block will slide without toppling.
- Region 3: where $\psi_p < \phi'$ and $b/h < \tan \psi_p$, the block will topple without sliding.
- Region 4: where $\psi_p > \phi'$ and $b/h < \tan \psi_p$, the block can both rotate and slide.

Choquet & Tanon (1985) proposed that the kinematic condition to have toppling be defined as:

$$(90° - \psi_p) \leq (\psi_f - \phi' + k) \quad (14.23)$$

where $k = 0$ for $\psi_p < 20°$ and $k = 0.67\ (\psi_p - 20°)$ for $\psi_p > 20°$.

Figure 14.24 shows the stability conditions for a single block. In most cases, however, the stability analysis for toppling must take into account the interaction between various blocks (Goodman & Bray 1976). The interaction of the various blocks makes the analysis of toppling more complex and requires the use of numerical methods (Hittinger 1978). Pritchard & Savigny (1990) presented a detailed analysis of the numerical modeling of toppling, suggesting that discrete element methods are well suited for this type of analysis as they can more easily model large displacements.

A simplified approach has been proposed by Choquet & Tanon (1985) who presented various charts to estimate the stability conditions based on computations carried out by Hittinger (1978). In these computations, it was assumed that: (a) the columns of the model have a constant width, Δx; (b) the basal plane over which the rotation takes place is at an angle of 15°; and (c) there are no pore pressures within the slope. Choquet & Tanon (1985) give the factor of safety, F, against toppling, based on the width of the limiting columns, Δxe, to be:

$$F = \frac{\Delta x}{\Delta xe} \quad (14.24)$$

where Δxe = the column width that would induce a toppling failure, everything else being constant. So, if the value of Δx is smaller than the limiting value, Δxe, there would be failure. It is therefore not surprising that from Eq. 14.24, the mitigation against toppling failure can be performed by changing the aspect ratio of the column, e.g. reducing column height or by tying columns together using reinforcement.

14.6 Risk Assessment Associated to Slope Movements

Slope movements are responsible for considerable socioeconomic losses (Brabb & Harrod 1989; Schuster 1996). In India, Italy, Japan and the USA alone, the costs associated to landslides are somewhere between one and five billion US dollars per year for each country (Schuster 1996). Casualties are also important. This situation explains the growing interest for hazard and risk assessment associated with slope movements in general, rapid landslides such as debris flows and rock avalanches in particular.

When associated to slopes, risk has often been considered in terms of failure. This indeed constitutes an important proportion of the problems encountered, particularly when risk is examined in terms of loss of life. However, this does not satisfy all the geotechnical engineering needs. In particular, for linear structures or infrastructure, such as bridges, roads, railway tracks, pipelines, etc., to be built in zones of precarious stability, there are also questions related to movements and rates of movement.

For the risk assessment of slope movements, the first step consists of defining all possible dangers, i.e. all possible slope movements that can affect a given area. Then, each danger has to be characterized. To do so, the characterization of slope movements proposed by Leroueil *et al.* (1996b), and schematically shown in Fig. 14.2 can be used for risk assessment, because it forces the engineer to answer a series of questions essential to the understanding of the situation (Leroueil & Locat 1998).

14.6.1 TOTAL RISK

Varnes *et al.* (1984) defined the total risk, R_T, as the set of damages resulting from the occurrence of a phenomenon. It can be described by:

$$R_T = \Sigma H R_i V_i \quad (14.25)$$

where H = the hazard or the phenomenon-occurrence probability within a given area and a given time period; R_i (for $i = 1–n$) = the elements at risk, potentially damaged by the phenomenon; and V_i = the vulnerability of each element represented by a damage degree comprised between 0 (no loss) and 1 (total loss). These factors are described in the following sections.

14.6.2 ELEMENTS AT RISK AND THEIR VULNERABILITY

The elements at risk, R_i, can be classified into four categories: (a) individuals, (b) properties and goods, (c) activities, and (d) social functions. They can suffer consequences directly from the phenomenon or from induced phenomena. For example, the destruction of a house by a landslide is a direct consequence of the event, whereas flooding of a town due to the damming of a river by a landslide is an indirect consequence. All these elements have to be considered in a risk analysis.

The elements at risk as well as their vulnerability should be deduced from the "movement consequences," in the geotechnical characterization of slope movements (Fig. 14.2, second column from the left). In particular, the rate of movement is of major importance when the element "loss of life" is considered; when movements are relatively slow, people have time to escape.

14.6.3 HAZARD

Hazard is the probability that the considered phenomenon occurs. In the context of slopes, this phenomenon may be, for example, a first-time failure or an active landslide that would reach a rate of displacement in excess of a given value. This can also be examined on the basis of the geotechnical characterization of slope movements (Fig. 14.2) since the probability of a failure or an excessive rate of movement is the probability that the triggering or aggravating factor reaches a given value leading to failure or to this excessive rate of movement.

When considering a landslide, two stages of the geotechnical characterization previously mentioned are involved: the failure stage, followed by the post-failure stage. As a consequence, the hazard, H, has to be subdivided into two parts, as indicated in Eq. 14.26: the hazard H_f, associated to the possibility that a failure occurs; and the hazard $H_{post\text{-}f}$, associated to the possibility that the post-failure stage has specific characteristics:

$$H = H_f \times H_{post\text{-}f}. \tag{14.26}$$

For example, the probability that a landslide reaches a house at a distance, L, from the toe of a slope is the hazard associated with a first failure multiplied by the hazard associated with the possibility that the run-out distance will be larger than L. When elements, such as vehicles, are moving or are temporarily in the area at risk, the probability analysis has to be modified accordingly (see the example presented in Bunce *et al.* 1997).

The estimated hazard depends on uncertainty, which may come from three different sources: parameter uncertainty, model uncertainty and human uncertainty (Morgenstern 1995). The parameter uncertainty can be subdivided into two parts: (a) the uncertainty that depends on the spatial variation of the parameters characterizing the material and the predisposition factors; and (b) the uncertainty due to the temporal variation of the triggering or aggravating factors. It is because of these latter variations that there can be a failure or a change in the rate of movement.

To estimate the hazard associated with parameter uncertainty, a probabilistic model can be applied to a deterministic solution. In the case of failure, the model can be based on limit equilibrium (see Section 14.5), and failure is supposed to occur at a calculated factor of safety of 1.0. The probability of failure then becomes the probability that F be-

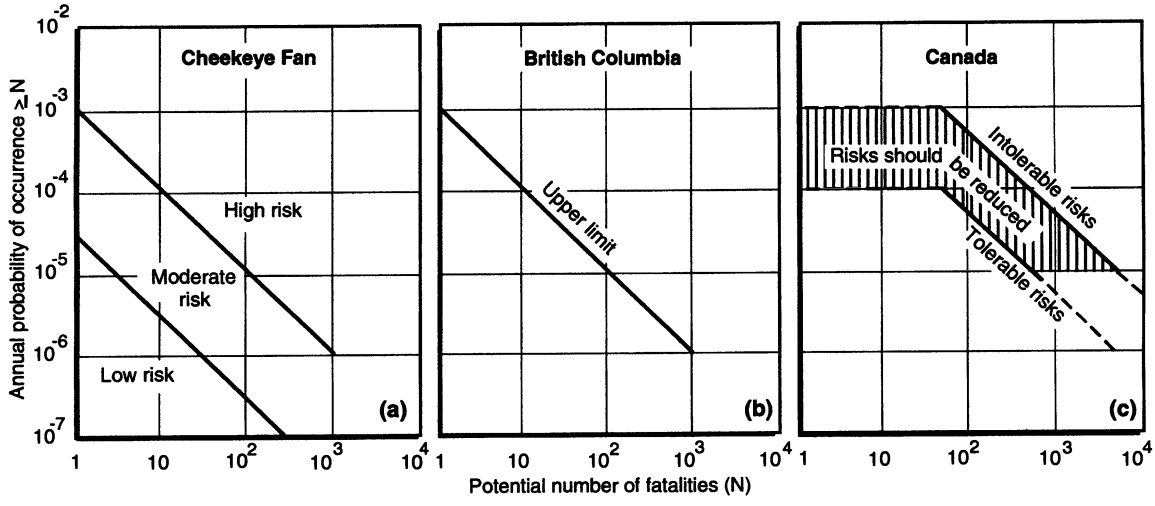


FIGURE 14.25. Proposed guidelines for assessing risks to life from naturally occurring slope hazards (a) Cheekeye Fan, (b) British Columbia, and (c) Canada: (modified from: (a) Hungr *et al.* 1993; (b) Evans 1997; and (c) Morgan 1997).

comes smaller than 1.0. The advantage of considering this approach is well illustrated in Lacasse and Nadim (1994).

In general, the probability of occurrence of slope movements is very difficult to predict and engineers need to use all available sources of information that can help in defining hazard, semi-quantatively or qualitatively. These sources (see Locat & Leroueil 1997, 1998) can be: (a) geotechnical information, e.g. as explained by Tavernas *et al.* (1983a), to have large retrogressions of landslides in clay, liquidity indices larger than 1.0 are required; (b) historical information (past is often a good indication of the future in terms of landslide activity); (c) geomorphological information; and (d) climatic-landslide activity (many relationships have been locally established to relate rainfall and landslide activity; an example is shown in Fig. 14.5).

14.6.4 TOLERABLE RISK

Tolerable risk is generally defined by a domain in a diagram showing the annual probability of occurrence of a specific event as a function of the risk. Figure 14.25 shows examples that have been defined in Canadian contexts and where the risk considered was in terms of loss of life. However, as it is often difficult to define the hazard quantitatively, semi-quantitative and qualitative scales have been proposed. Table 14.1 shows the one proposed by Hungr (1997).

Because the definition of what is tolerable may have social (Fell 1994; Finlay & Fell 1997), economic, environmental, political and legal (Bunce *et al.* 1997) implications, it cannot be defined by engineers alone. For the same reasons, it also varies from one country to another.

TABLE 14.1. Suggested semi-quantitative probability scale for landslide hazard magnitude or intensity (adapted from Hungr 1997)

Term	Range of frequency (1 year^{-1})
Very high probability	>1/20
High	1/100–1/20
Medium	1/500–1/100
Low	1/2500–1/500
Very low	<1/2500

14.7 Methods of Mitigation

14.7.1 GENERALITIES

When dealing with a slope of precarious stability and/or presenting a risk that is considered too high, there are three main options: (a) do nothing to the slope and try to reduce the possible consequences of movements; (b) do nothing to the slope, but put a warning system in place to reduce the risk of movement affecting the safety of people; or (c) improve the safety of the slope in order to reduce the hazard and risk associated with its potential movements to an acceptable level. The first option is discussed in Section 14.7.2, warning systems are briefly presented in Section 14.8, the most usual mitigation methods are described in Sections 14.7.3–14.7.9 and 15.3. Schuster (1995), Holtz & Schuster (1996), Wyllie & Norrish (1996a), and Sève and Pouget (1998) can be examined for more details on stabilization techniques. In all cases, a clear understanding of the processes involved is required.

For the solutions considered to improve a given situation, reductions in hazard and risk have to be examined as a function of the cost in order to select the most appropriate solution based on the cost/benefit ratio. As indicated by Morgenstern (1995), even if the absolute risk and hazard are not well known, the hazard and risk improvements are more precise since a number of the uncertainties are the same for all the solutions considered.

14.7.2 ELIMINATION OF THE PROBLEM OR REDUCTION OF ITS CONSEQUENCES

14.7.2.1 Relocation

When the size of the moving or potentially moving mass is too important, or when the cost associated with mitigation is considered too high, the possibility of relocation of structures (roads for example) must be examined. Obviously, it is preferable to consider such a possibility during the planning phase.

14.7.2.2 Complete or Partial Removal of Unstable Materials

This solution can be considered when the volume of unstable materials is not too important. The stability of the new slope has to be verified.

This approach is, in particular, adapted to the case of unstable rock blocks, which can be removed by pushing them downslope or destroyed by explosive or expansive injections.

14.7.2.3 Bridging

This possibility can be considered when the unstable zone is relatively narrow and can be spanned by a structure founded on the stable sides of the main slide.

14.7.2.4 Protection of the Structures Against Soil or Rock Movements

There are several situations that can justify specially designed foundations (Sève & Pouget 1998). For example, when the slide is shallow, it may be possible to design foundations for resisting the forces applied by the moving material. If the rate of movement is small, deep foundations can be inserted into shafts of larger dimensions so that the moving soil mass is not in contact with the foundations. Finally, when the rate of movement is very small, some structures and foundations can be designed in such a way that they can be readjusted from time to time.

An alternative approach is to provide protection systems against falling or sliding materials. These may be nets or walls that can stop the moving material. They may also be systems that divert the moving material, e.g. a debris flow, from the elements at risk, e.g. houses. Or they may be in the form of sheds or tunnels.

Finally, dykes can be used for containing mudflows, debris flows, etc. The main difficulty is to make sure that the capacity of the reservoir is large enough to avoid an overtopping of the dykes.

14.7.3 EARTHWORKS

Earthworks are the most common method of slope mitigation. Several approaches can be considered: reduction of slope height; flattening the slope; reduction of gravity forces in the upper part of the slope by removing materials or replacing some by lightweight fill; addition of buttresses, counterweights or berms at the toe of the slope; and partial or complete substitution of weak materials for better ones, generally granular (larger friction angle; better drainage characteristics), to a depth larger than the failure surface. Slope height reduction or flattening are generally more efficient for shallow movements. Toe counterweights and buttresses are generally more efficient for deep-seated landslides (Bromhead 1992), and not suited for long translational landslides.

Due to irregular initial slope profiles, complex or badly defined failure surface(s), etc., it is often difficult to define an "optimized new profile". In this case, the "neutral point" method proposed by Hutchinson (1977) can help. The moving mass is subdivided into vertical slices and the effect of a small load applied locally at the surface is considered. Such a small load applied to one of the slices has two effects: it changes the effective stress applied on the failure surface and modifies the distribution of overturning moments. This latter effect is positive at the toe and negative at the crest. On the other hand, the load always increases the effective stress. The neutral point is defined where the two effects neutralize each other (the load does not modify the factor of safety) and forms a boundary between the area of the soil mass on which a fill (or a cut) would improve its stability and the area for which the reverse would hold.

When designing buttresses, several aspects have to be considered: (a) the stability of the slope in general, (b) the stability of the buttress (overturning and sliding on its base), and (c) the possibility that the buttress could be overtopped by soils moving down from the upper part of the slope or could trigger another landslide downstream (Fig. 14.26).

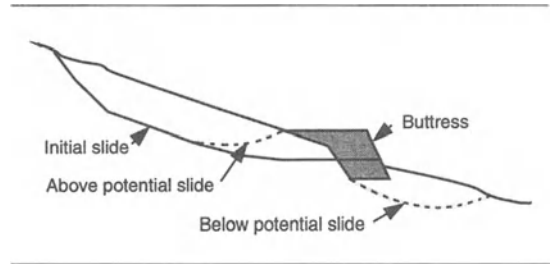


FIGURE 14.26. Some design aspects of a buttress.

14.7.4 EARTH RETAINING SYSTEMS

The earth retaining systems are generally used when there is not enough space to get satisfactory stability conditions with the type of earthworks described in the previous section. They thus have a steep slope or are vertical. These systems can be subdivided in two main classes: rigid systems and flexible systems, as discussed in Chapter 17. For their design, the following general aspects have to be examined: (a) the overall stability of the slope; (b) the stability of the retention system; and (c) the possibility that the material from the upper part of the slope could overtop the stabilizing system (see Chapter 17 for details).

14.7.5 DRAINAGE SYSTEMS

Because of the importance of porewater pressure in slope stability (see Section 14.3), drainage is often used for slope stabilization. The efficiency of drainage systems depends on factors such as:

- the geometry of the problem and of the soil units,
- the nature of the soils (including the hydraulic conductivity and anisotropy),
- the presence of cracks or fissures,
- water flow within the slope.

Thus, the uncertainty associated with the efficiency of a drainage system is usually larger than that associated with other mitigation techniques. The choice for the best location

of drains, trenches, wells or other drainage systems is based on hydrogeologic information, but can be facilitated by surface measurement of the variation of the electric potential induced by the water flow in the soil (Gress & Faure 1996). The design of drainage systems is often based on a minimum increase of 30% of the factor of safety, and their efficiency on site should be verified with piezometers.

Most systems use gravity flow, but other techniques such as pumps or siphons (Gress 1992) are sometimes used. Consideration should be given to the long-term efficiency of drainage systems and periodic maintenance is generally required. Several approaches that can be considered for drainage are briefly described below (also see Chapter 8 and Cedergren 1989):

1. Earthworks. Buttresses, counterweight fills, total or partial replacements and earth retaining structures can facilitate drainage if they are made up of coarse materials or if they incorporate drains.

2. Control of surface waters. Surface waters should be diverted away from the slope. This can be done with surface protection against infiltration or by diversion ditches.

3. Counterforts and trench drains. Counterforts are drains that penetrate into solid ground beneath a slip surface and therefore also provide some mechanical buttressing (Bromhead 1992). Trench drains may or may not penetrate beneath the slip surface. In this latter case, they contribute to stability only through a decrease in pore pressure. As indicated by Hutchinson (1977), due to intermittent recharge from infiltration, a variable inflow of groundwater from upslope, and nonhomogeneous and non-isotropic hydraulic conductivity, the piezometric levels in between parallel trench drains are variable with time, and thus difficult to define. Figure 14.27 shows an approach for the design of counterforts and trench drains (Hutchinson 1977). Figure 14.27a defines the different parameters. In particular, S = the distance between drains, h_d = the piezometric head on the drainage inverts before drainage, $\bar{h}$ = the average piezometric head between the drains on plane FG. If A = the drain spacing (= S + drain width), the average piezometric head on the whole plane EH is defined as:

$$h_{av} = \bar{h}S/A. \qquad (14.27)$$

Figure 14.27b presents the normalized average piezometric head, $\bar{h}/h_0$, versus $R_s = (k_v/k_h)^{1/2}S/h_0$, which becomes equal to S/h_0 when the hydraulic conductivity is isotropic. At levels other than the drain invert, Bromhead (1992) suggests linear interpolation between the head values on the drain invert level and those at the surface or at the base of the stratum.

4. Drainage trenches. Drainage trenches are usually made of coarse material, often with geotextile as filter, but can also incorporate geosynthetic drains (see Chapter 7). Their depth may be up to 6 m. However, Deniau *et al.* (1981) describe two cases in which a trench was constructed to a depth of 12–15 m, as a slurry trench, but with a biodegradable mud in order to give the material constituting the trench a high hydraulic conductivity. Drainage trenches can be very efficient when they go deeper than the slip surface. If not, there is doubt as to the extent that the lowering of the water table will decrease the pore pressures on the slip surface.

5. Drainage wells. When connected to other wells, drainage wells can behave in a manner similar to trenches (see Chapter 8).

6. Drainage tunnels and galleries. These are methods applicable to large slopes, in deep open pit mines in particular.

7. Subhorizontal drains. Subhorizontal drains are generally constructed from polyvinylchloride (PVC), since it is less susceptible to corrosion than steel. They are generally in-

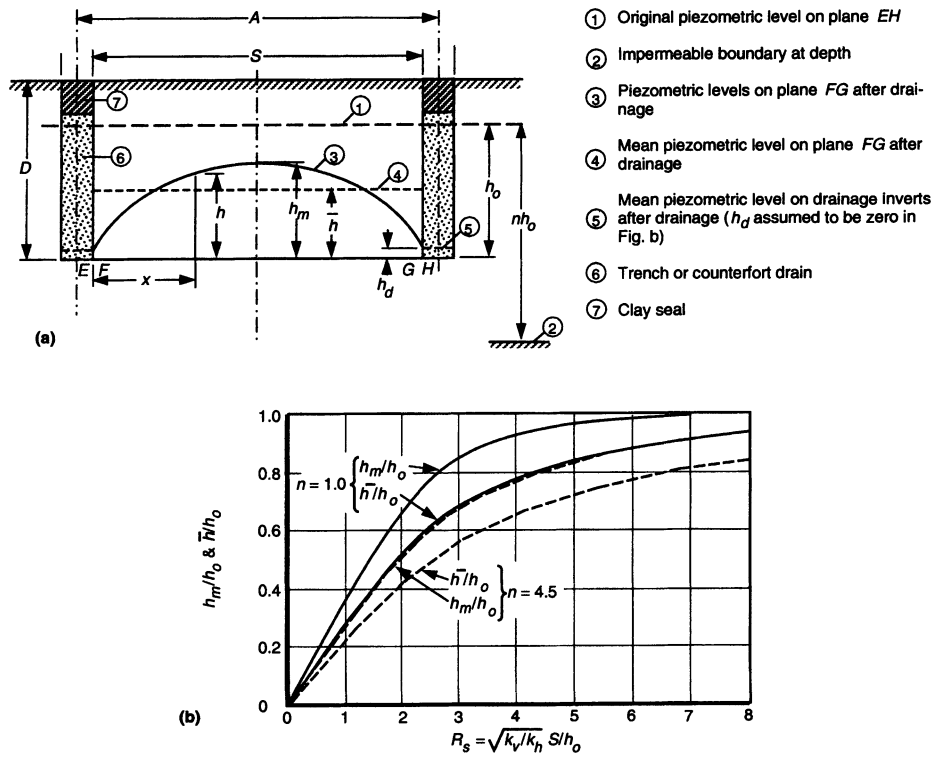


FIGURE 14.27. Piezometric levels for parallel trench and counterfort drains at drain invert level. (a) Key diagram; (b) $\bar{h}_m/h_0$ and $\bar{h}/h_0$ versus $R_s = (k_v/k_h)^{1/2}S/h_0$ for fully penetrating drains ($n = 1.0$) and partially penetrating drains ($n = 4.5$) (modified from Hutchinson 1977).

stalled from the lower part of the slope, or from galleries or large wells, at an inclination often between 2 and 6° with the horizontal. Their efficiency is generally difficult to predict and their spacing is often defined on site, depending on the performance of the first drains installed.

14.7.6 *IN SITU* REINFORCEMENT

In situ reinforcement is the inclusion of resistant elements in the moving soil mass in order to improve its shearing resistance. Soil reinforcement systems include small diameter flexible structural elements such as "nails" (see Section 15.3.3) or micropiles (see Section 15.3.4), and stiffer elements such as concrete piles, sheet piles and large diameter steel pipes (see Section 10.6). The stabilization of a landslide is achieved when resisting forces are mobilized in the nails, micropiles or piles. Since this requires soil displacements along the failure surface, full efficiency of soil nailing and piling is thus usually delayed. The beneficial effects are thus progressive and residual movements may occur during months after installation of the reinforcement system (Sève & Leca 1995; Sève & Pouget 1998). In the design process, it is important to take into account the compatibility of deformation at failure of the different elements (soil, nail or pile, and soil–nail (soil–pile) interface).

Failure or malfunctioning of a reinforced system may come from different sources: (a) insufficient strength of the inclusion (tensile and shear strengths), (b) lack of adhesion between the soil and the inclusion, (c) plastic failure of either the inclusion or the soil around it, and (d) overall instability of the system.

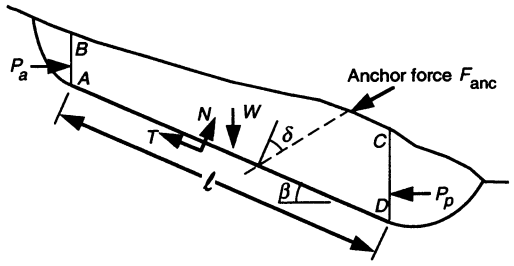


FIGURE 14.28. Schematic design of an anchor.

Techniques for the design of these systems have been proposed by Schlosser (1982), Blondeau *et al.* (1984), and Elias & Juran (1991). Details on the "multicriteria" approach proposed by Schlosser (1982) are also given in Clouterre (1991).

14.7.7 ANCHOR SYSTEMS

Anchors increase the normal effective stresses, and hence the shear strength, along a potential or actual failure surface. For the case presented in Fig. 14.28 and considering the soil to be dry and homogeneous, and that the forces P_a and P_p result from active and passive failures, respectively, the initial factor of safety, F_0 (without anchors), is given by:

$$F_0 = \frac{c'l + (W\cos\beta + P_p \sin\beta - P_a \sin\beta)\tan\phi'}{W\sin\beta + P_a\cos\beta - P_p\cos\beta}. \tag{14.28}$$

For a failure to occur along the surface AD, the parameters c' and ϕ' must be such that $F_0 = 1.0$.

When anchor forces, F_{anc}, are applied with an inclination δ to the direction normal to AD, then the factor of safety becomes:

$$F_0 + \Delta F = \frac{c'l + [W\cos\beta + (P_p - P_a)\sin\beta]\tan\phi' + F_{anc}\cos\delta\tan\phi'}{W\sin\beta + (P_a - P_p)\cos\beta - F_{anc}\sin\delta}. \tag{14.29}$$

It is found that F_{anc} takes a minimum value when the inclination δ is equal to:

$$\delta = \tan^{-1}\left(\frac{F + \Delta F}{\tan\phi'}\right). \tag{14.30}$$

Due to possible movements of the soil with time, the tension in the anchors can also vary with time. To deal with this, it may be worth installing tension gages in order to monitor and possibly readjust the tension in the anchor.

14.7.8 VEGETATION

The most important effect of vegetation is to reduce erosion. Vegetation also contributes to improved stability through the roots, which reinforce the soil, and evapotranspiration, which increases the suction, and thus the strength of the soil. Vegetation can be considered alone or, more generally, in combination with other stabilizing techniques (see Section 15.3.5 and Gray & Sotir 1992 for additional references).

14.7.9 SPECIAL TECHNIQUES

There are many other techniques such as jet grouting, injection of cementing agents like lime or cement, and heating or freezing that have occasionally been used for slope stabilization (see Chapter 15).

14.8 Warning Systems

Warning systems do not modify the hazard (probability of occurrence of the event), but contribute to reducing the consequences of the movement and thus the risk, in particular the risk associated to the loss of life. Many systems have been proposed and the selection of an appropriate system can take advantage of the geotechnical characterization shown in Fig. 14.2, as discussed below.

At a pre-failure stage, the warning system can be applied either to revealing factors or

to aggravating factors. The revealing factors can be the opening of fissures or the movement of given points in the slope. In these cases, the warning criterion can be a magnitude or a rate of movement. When associated with the triggering or aggravating factors, there is a need to first define the relation between the magnitude of the controlling factors and the stability or the rate of movement of the slope. The warning criterion can be a given pore pressure, a given stage of erosion, a minimum suction in a soil (e.g. loess) deposit, etc.

At the failure stage, the warning system can only be linked to revealing factors, generally a sudden acceleration of movements or the disappearance of a target.

At the post-failure stage, the warning system must be associated with the expected consequences of the movement. Its choice will, in particular, depend on the rate of movement and run-out distance.

For active or reactivated slides, the warning system can be applied to the triggering or aggravating factors, the revealing factors, or some of the possible consequences of the movement.

The alarm can come from the monitoring and the analysis of the evolution of significant parameters, or when one or more parameters reach a critical level (see Sève & Durville 1995 for more details). The actions triggered by the alarm can be automatic or can necessitate human intervention. These actions can be:

- forbid access to a predefined zone, a road, etc.;
- evacuate a predefined zone;
- increase the protection of structures or buildings by reinforcing the slope, using pumps, etc.;
- limit the use of structures (reduce the speed on a road, limit the weight of vehicles, etc.); or
- inform the public or the users of facilities about the dangers.

The most common techniques and instruments used in warning systems are listed in Table 14.2.

TABLE 14.2. Usual techniques and instruments used in warning systems

Kinematic
Surface
Usual survey methods
Electro-optic distance measuring devices
Photogrammetry
Extensometer
Clinometers
Settlement gages
Inverted pendulum
Movement or contact detectors
Electrical wires and fences
Subsurface
Inclinometers
Failure detectors
Hydrology
Piezometers
Flow meters
Others
Rain gage
Geophones

15. SOIL IMPROVEMENT

R. D. Holtz
J. Q. Shang
D. T. Bergado

15.1 Introduction

If during the design of a foundation, the geotechnical engineer finds, for example, that the bearing capacity of the soils at the site are inadequate or if estimates of the total and differential foundation settlements are intolerable, then alternate approaches to the design must be considered (Holtz 1991; Munfakh 1997a). The project may be abandoned as being infeasible or too expensive, or it may be possible to relocate the facility to a more suitable site. For buildings and some bridges, an alternate shallow foundation type such as a mat or raft may be appropriate, or in some cases, a compensated foundation is a feasible alternative (see Chapter 9). Probably the most common alternate foundation to be considered for structures is a deep foundation of one type or another. Pile foundations and drilled shafts are discussed in Chapter 10 and in Kulhawy (1991). The design and construction of embankments on soft soils and peat pose special problems, and these are discussed in Chapter 16.

Inadequate slope stability is another class of problems facing the geotechnical engineer. Abandonment or relocation of the facility, mentioned above for foundations, are also possibilities for slopes, but a number of other techniques for mitigating slope instability are more commonly employed (see Chapters 14 and 17; Holtz & Schuster 1996; Wyllie & Norrish 1996b).

When faced with slope instability or poor foundation conditions, another approach that the geotechnical engineer should always consider is techniques to improve the properties of the soils at the site. The terms soil improvement, ground modification and ground improvement are used interchangeably. A number of foundation and slope treatment alternatives are possible, and the choice of the most appropriate method or methods depends on the soil types involved, whether predominately granular or cohesive, and the type, function and performance requirements of the facility.

In recent years, the interest in soil improvement techniques for foundations and slopes has greatly increased, primarily due to the world-wide increase in the cost of land together with an increase in environmental awareness (Munfakh 1997a). The increased cost of conventional construction, especially deep foundations, undoubtedly has contributed to this interest also.

Munfakh (1997a) gives five major functions of soil improvement applied to foundations and slopes:

- increasing bearing capacity;
- controling deformations and accelerating consolidation;
- providing lateral stability for slopes and excavations;
- seepage cut-off and other types of environmental control; and
- increasing resistance to liquefaction of loose, saturated granular deposits.

R. K. Rowe (ed.), *Geotechnical and Geoenvironmental Engineering Handbook*
© Kluwer Academic Publishers 2001

Other purposes for soil improvement include treatment of soils subject to collapse, swelling and frost action. If carried out at or near the ground surface, soil improvement is an inexpensive and relatively simple process. On the other hand, if it is carried out at some depth, a more rigorous geotechnical investigation and analysis are required along with the use of specialized equipment and construction procedures (Munfakh 1997a).

Problem slopes and foundation soils can be improved by:

1. reducing the load and therefore the stress on the foundation or in the slope;
2. removing the problem soils and replacing them by more competent materials;
3. increasing the shear strength and reducing the compressibility of the problem materials; and
4. reinforcing embankments on soft foundations or unstable slopes.

Under category 3, the shear strength can be increased and compressibility reduced by: (a) consolidation of soft foundation materials; (b) chemical stabilization; and (c) physical stabilization, including densification by various methods.

These methods and their variations are listed in Table 15.1. All have been used singly

TABLE 15.1. Soil improvement methods (modified from Munfakh 1997a and Holtz 1989)

Improvement method or technique	Treatment classification	Applicable soils	Primary applications	Variations and remarks
Reduced stress	Reduced stress	All	Embankments, slopes	Lightweight fill materials
Removal and replacement	Removal and replacement	Soft cohesive, organic soils, peat	Embankments, small structures	Full depth (complete) or partial displacement by weight and controlled excavation or blasting
Dewatering	Consolidation	Clays, silts, possibly peat	Foundations, excavations	Active pumping
Surcharging, preloading	Consolidation	Clays, silts, possibly peat	Embankments, foundations	With or without vertical drains Vacuum preloading
Vertical drains	Consolidation	Clays, silts	Embankments, foundations	Sand drains Prefabricated geocomposite drains
Stabilization by admixtures	Chemical	Silts, clays, especially swelling	Subgrades for highway and airport pavements, erosion control	Near-surface treatment with lime, Portland cement, other chemicals and fly ash
Lime and lime-cement columns	Chemical	Silts, clays	Embankments, foundations, excavations	
Deep soil mixing	Chemical	All soils	Deep excavations, seepage and environmental cut-off	Cement and cement-bentonite admixtures
Intrusion and permeation grouting	Chemical	Fissured rock; all granular soils, including coarse silts	Foundations, seepage cutoffs, liquefaction mitigation, environmental remediation	Portland and microfine cements Chemicals (bitumen, silicates, acrylates, etc.)

TABLE 15.1. *(Continued)*

Improvement method or technique	Treatment classification	Applicable soils	Primary applications	Variations and remarks
Jet grouting	Chemical	All soils	Foundations, tunnels and other excavations	
Heat and freezing	Thermal	Loose sands and silts	Foundations, deep excavations, subgrades	Vitrification (heat) used for environmental remediation
Electro-osmosis and electrokinetic stabilization	Electrical	Silts and clays	Slopes, foundations	
Preloading (prestraining)	Densification	Granular soils	Foundations	
Compaction grouting	Densification	Granular soils	Foundations, tunnels	
Dynamic compaction	Densification	Granular soils and fills, waste materials	Foundations, embankments	
Blast densification	Densification	Granular soils	Foundations, embankments	
Vibrocompaction and vibroreplacement	Densification	Granular soils	Foundations, embankments	Stone and sand columns Vibroconcrete columns
Inundation	Densification	Loose and collapsing sands and silts	Foundations	
Compaction piles	Densification	Loose granular deposits	Foundations	Useful for stratified deposits where vibromethods are inappropriate
Geosynthetic reinforcement	Reinforcement	All soils	Foundations, embankments, retaining walls	
Drainage	Reinforcement	All types	Slopes, excavations	Interception Pore pressure Control Dewatering
Ground anchors, tiebacks	Reinforcement	All types	Slopes, excavations	Post-tensioned Prestressed
Soil nailing	Reinforcement	All types	Slopes, excavations	New Austrian Tunneling Method applied to slopes and excavations
Micro-piles, root piles, pin piles	Reinforcement	All types	Slopes, excavations, foundations	Suitable for retrofit
Biotechnical	Reinforcement	All types	Slopes, erosion control	

or in combination, although some methods are much more popular than others are, and some have only been used on an experimental basis.

Soil improvement is a rapidly developing field, and because of the many soil improvement techniques available today and their many benefits, selection of the best method for a specific site and project is not easy. To help assess which technique(s) may be the most appropriate; the following nine factors should be considered (Mitchell 1981; Munfakh 1997b):

1. The operational criteria for the facility, e.g. stability requirements, allowable total settlement and rate of settlement, seepage criteria, durability and maintenance requirements, etc. This will establish the level of improvement required in terms of properties such as strength, modulus, compressibility, hydraulic conductivity, etc. (see Chapter 2 for the definition of the terms and Chapter 3 for typical values).
2. The area, depth and total volume of soil to be treated.
3. Soil type and its initial properties; depth to groundwater table.
4. Availability of materials, e.g. sand, gravel, water, admixtures, etc.
5. Availability of equipment and required skills.
6. Construction; environmental factors, such as site accessibility and constraints, waste disposal, erosion, water pollution; and effects on adjacent facilities and structures.
7. Local experience and preference; politics and tradition.
8. Time available.
9. Cost.

Several examples of how these factors are considered in method selection and cost analyses are given in Mitchell (1981), Holtz (1989) and Munfakh (1997b). Depending on the size of the project, the choice of an appropriate construction procedure requires a detailed comparative cost analysis of several alternative designs, and for reasons discussed by Holtz (1989), field test sections are often desirable to establish the behavior of alternates to conventional solutions.

Good general references on the methods in Table 15.1 include Mitchell (1981), Eggestad (1983), Brandl (1983), Broms and Anttikoski (1983), Welsh (1987), Holtz (1989), Van Impe (1989), Hausmann (1990), Moseley (1993), Moseley & Priebe (1993), Bergado *et al.* (1996), Schaefer (1997), and Munfakh (1997a). Holtz & Schuster (1996) and Wyllie & Norrish (1996b) deal with stabilization techniques, particularly those applicable to soil and rock slopes. Case histories are reported in the following conference proceedings edited by Welsh *et al.* (1987), Esrig & Bachus (1991), Kramer & Holtz (1991), Borden *et al.* (1992), Rollins (1994), Hryciw (1995), and Schaefer (1997).

15.2 Foundation Soil Improvement Techniques

15.2.1 LIGHTWEIGHT FILL

Because both stability and settlement of foundations depend on the load applied to the foundation soils, problem foundation soils can often be improved by simply reducing the load and, therefore, the stress on the foundation. For buildings, bridges and tanks, such an approach is rarely feasible because it entails a complete redesign of the structure. On the other hand, for embankments on soft foundations, reduced stress is a viable design alternative, especially if it involves lightweight fill materials.

Various types of lightweight materials that have been used in embankments include wood bark and sawdust; bailed peat; fuel ash, slag, etc.; cellular concrete; expanded clay or shale; oyster and clam shells; shredded waste tires; and expanded polystyrene (Holtz 1989). Table 15.2 summarizes the commonly used lightweight fill materials. Because their compacted densities are significantly less than those of soils ordinarily used in embankment construction, the effective weight of the embankment can be reduced significantly by the use of these

TABLE 15.2. Lightweight fill materials (modified from Magnan 1987)

Material	γ(kN m^{-3})
Residues from wood industry (bark and sawdust)	8–10
Dried or pulverized peat	3–5
Compressed bales of peat	8–10
Rice hull ash	8
Clam shells	10–14
Fly ash	10–14
Used tires, with or without other fill materials	6–8
Light cellular concrete	6–10
Expanded clay	5–10
Expanded polystyrene	<1
Extruded polypropylene	<1
Compressed plastic waste blocks	4–5

materials. In addition to their low unit weights, many of these materials have a reasonable compressive modulus and a high angle of shearing resistance due to their interlock capabilities, especially after compaction.

Lightweight fill materials are often expensive, especially if they are manufactured (expanded shales and clays, expanded polystyrene, lightweight concrete, etc.), and costs can range up to US$100 m^{-3}. Even if they are a waste material, e.g. sawdust, bark, shells, cinders, shredded waste tires, slag, fly ash, bottom ash, etc., and free at the source, they must be transported to the site. In many instances, transportation costs alone have made the use of a lightweight material uneconomical, but each case should be examined on its merits.

In addition to cost, lightweight materials have other problems of which designers should be aware; see Holtz (1989) for details. For example, the crushing strength of some lightweight materials is relatively low, and care must be taken during construction to avoid damaging the material, especially if conventional compaction equipment is used. Also sawdust and bark may biologically degrade and create both engineering and environmental problems if subjected to cycles of wetting and drying.

Expanded polystyrene (EPS) or "geofoam" (a term coined by Horvath (1995)) deserves special mention. It is extremely lightweight (average density about 20 kg m^{-3}), is molded into large blocks (typically about 600 × 1200 × 2400 mm and weighing about 350 N), and can be made sufficiently strong to be able to support construction workers and ordinary highway pavement and traffic loads with tolerable settlements. Although experience with EPS in North America is somewhat limited, it has been successfully used on hundreds of projects (embankments on peat and other soft soils and behind bridge abutments) in Scandinavia for the past 25 years. Horvath (1995) and the special issue of the *Journal of Geotextiles and Geomembranes* (Vol. 15, Nos. 1–3, 1997) provide the most complete information on geofoam, including its manufacture, properties, and analysis and design for a number of applications including lightweight fill.

Design with lightweight fill is straightforward. A reduced unit weight is used in conventional stability and settlement analyses, and alternative materials are selected depending on cost, including transportation and availability. Construction, performance and environmental problems discussed above should also be kept in mind.

15.2.2 REMOVAL AND REPLACEMENT

A simple way to improve a soft or problem soil site is to remove the problem soils and replace them with higher quality materials. This treatment is most common for organic deposits and very soft clays, but it has also been used for loose deposits of granular materials, collapsing soils, as well as for landfills, dumps, mine wastes, etc. (in short, any place where there are stability problems or excessive settlements predicted). This method is suitable for highways and other types of embankments, as well as for foundations of many structures. In the case of buildings and other structure foundations, the replacement fill is often called a "structural" fill.

Holtz (1989) summarizes excavation and replacement techniques for highway embankments. Depending on the specific geotechnical conditions at the site and operational considerations, complete removal, partial excavation, and removal by displacement and partial excavation, or displacement by blasting may be most appropriate. These techniques may also be appropriate for structural fills. However, it should be noted that replacement can cause environmental problems, e.g. when crossing wetlands, and in some cases there may be problems on disposal of the material removed if it is contaminated.

15.2.3 CONSOLIDATION

When a saturated soil is loaded, pore pressures in excess of the existing static groundwater pressure are created. As this excess porewater pressure dissipates, the volume of the soil decreases and surface settlements occur. This process is called consolidation, and the rate of settlement depends on the hydraulic conductivity of the soil (see Sections 2.7, 3.5, 9.4 and 16.6). Because fine-grained soils have a lower hydraulic conductivity, they may take a long time to compress, but as they do, they become denser and stronger, and the rate at which they settle gradually decreases. This basically is the principle of stabilization by consolidation; foundation soils can be improved by allowing them to consolidate, gain strength and increase in stability.

In practice, consolidation can be accomplished by dewatering and subsurface drainage, and more commonly by surcharging and preloading, either with or without the use of vertical drains, such as sand or geocomposite drains.

15.2.3.1 Dewatering and Groundwater Control

Although dewatering is often thought of as a part of the construction of temporary excavation support systems, permanent dewatering systems are also very common (see Chapter 8). It is in this latter area that dewatering and groundwater control become part of foundation soil improvement. Good general references on the subject are Powers (1991, 1992) and CGS (1992). Traditional dewatering methods applied to soil improvement and several case histories of dewatering for soil stabilization are given in Hausmann (1990), Kramer & Holtz (1991), and Abramson (1997).

At some sites, soft soils are underlain by sands that can provide drainage under a foundation; or some deposits are strongly stratified with continuous silt and sand layers capable of serving as drainage layers. However, for the case of very wide embankment fills, water entering these drainage layers must flow laterally long distances. Large head losses and high excess porewater pressures can develop in the intermediate drainage layers, which decrease their efficiency as drains and increases instability. Where this occurs, trench drains, sand drains or even well points can be installed near the toe of an embankment to decrease the porewater pressure in the intermediate drainage layers (Holtz 1989; Hausmann 1990).

15.2.3.2 Preloading by Surcharge

By preloading soft foundation soils, the settlement that would occur under the final structural load can be achieved before construction, and hence post-construction settlements are significantly reduced or eliminated. Preloading refers to the process of compressing foundation soils prior to placement of the final permanent construction load. If the temporary applied load exceeds the final loading, the excess is referred to as surcharge load. Because primary consolidation settlement predominates at many soft clay sites, it is the only factor considered in the design of many projects. On the other hand, secondary compression can be important in some soil deposits, and procedures have been developed for designing surcharges to greatly reduce secondary settlements.

Terzaghi's one-dimensional consolidation theory is the usual way to estimate the time for surcharge removal. The final consolidation settlement of a clay under the design surcharge load, $\Delta\sigma = p_f + p_s$, as discussed in detail in Section 16.4, is given by the following equation for a normally consolidated clay:

$$S_{f+S} = \frac{H}{1 + e_0} C_c \log\left(\frac{\sigma'_{v0} + p_f + p_s}{\sigma'_{v0}}\right) \qquad (15.1)$$

where H = the thickness of the soft clay stratum with an initial void ratio e_0 and compression index C_c, and initial vertical effective stress σ'_{v0}. For overconsolidated soils, significant compression would only occur at stress greater than the preconsolidation pressure, σ'_p (see Section 16.4).

The principle of preloading by surcharge to compensate for primary consolidation settlement is shown in Fig. 15.1. The settlement–time relationship for the design load p_f applied to a soil is shown by curve p_f, and S_f is the final consolidation settlement that would occur if the design load alone were applied without any surcharge. When a surcharge p_s is additionally applied, the settlement–time relationship is the lower curve, and the settlement under $\Delta\sigma = p_f + p_s$ is S_{f+S}. When the settlement under surcharge reaches S_f at time t_{SR}, the surcharge can then be removed.

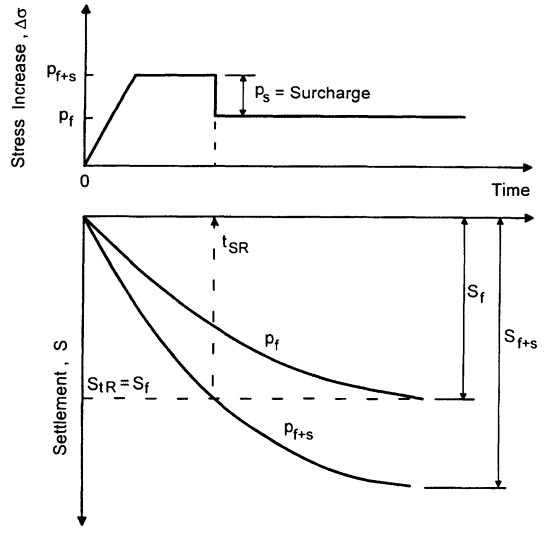


FIGURE 15.1. Principle of preloading by surcharge to compensate for primary consolidation settlement (modified from Jamiolkowski *et al.* 1983).

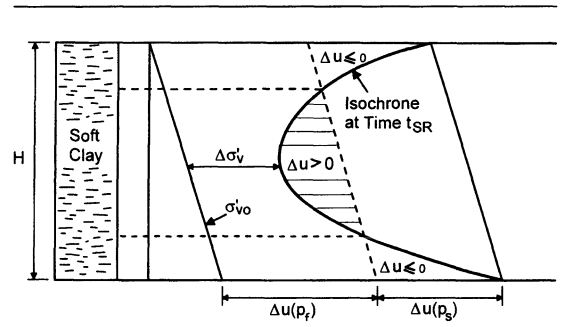


FIGURE 15.2. Excess pore pressure Δu after surcharge removal (modified from Jamiolkowski *et al.* 1983).

Designs to reduce the length of time for primary settlement to occur are quite straightforward (Fig. 15.1). From the settlement curves for the two loads p_f and $p_f + p_s$ the time for surcharge removal, t_{SR}, can be calculated. Without vertical drainage, this time can be quite long; otherwise the middle portion of the clay layer will still be consolidating, as shown in Fig. 15.2. At this time, the average degree of consolidation (see Section 2.7.4) is:

$$U_{f+S} \geq U_{SR} = S_f/S_{f+S} \qquad (15.2)$$

where S_{f+S} is calculated from Eq. 15.1 and the average degree of consolidation can be calculated (Johnson 1970a) from:

$$U_{f+s} = \frac{\log[1 + (p_f/\sigma'_{v0})]}{\log\{[1 + (p_f/\sigma'_{v0})][1 + (p_s/p_f)]\}}. \qquad (15.3)$$

To further minimize consolidation settlements under the load p_f, it is necessary to remove the surcharge p_s at the time t_{SR}, at which time the consolidation ratio is not less than:

$$U_z = p_f/p_{f+S}. \qquad (15.4)$$

If all these conditions are satisfied, then upon removal of the surcharge, p_s, all the succeeding settlement will be secondary. Most surcharge fill designs eliminate the primary consolidation.

Reduction of secondary compression is important especially with peat and other organic soils that consolidate rapidly and have a large secondary compression, but it may also be important when vertical drains are used, because the primary consolidation can take place quite rapidly. Secondary compression settlements can be reduced to tolerable amounts with appropriate design procedures (e.g. Johnson 1970a; Jamiolkowski *et al.* 1983; Mesri & Feng 1991). See also CGS (1992) and Section 16.8 for additional information on preloading.

15.2.3.3 Preloading by Vacuum

The principles of using vacuum for preloading of soft clayey soils were first introduced in the early 1950s (Kjellman 1952). When a vacuum is applied to a soil mass, it generates a negative porewater pressure. If the total stress remains unchanged, the negative pore pressure increases the effective stress in the soil and this leads to consolidation. A schematic of the vacuum preloading method is shown in Fig. 15.3. The working platform consists of a sand layer through which vertical drains are placed in the soil. The vertical drains must be above any sand layer to sustain the vacuum pressure. A flexible geomembrane (polyethylene) liner covers the area and keys into an anchor trench, which provides a watertight seal. A perforated pipe system is placed beneath the liner to collect water. Specially prepared vacuum pumps capable of pumping water as well as air are connected to the collection system. It is essential that the area to be consolidated is totally sealed and isolated from any surrounding permeable soils in order to avoid the loss of vacuum. Leaks must also be avoided. Since pinholes or cracks in the sealing membrane are difficult to locate and repair, the membrane should be covered with water, which will also minimize potential damage from foot traffic and wildlife. When the required preloading pressure is higher than the capacity of the vacuum pumps, a surcharge fill may be used in conjunction with the vacuum method, as shown in Fig. 15.3. The fill must be free from stones or sharp objects. If a fill is placed on the membrane liner during the vacuum period, it may be necessary to add a leak detection system under the liner to help locate leaks.

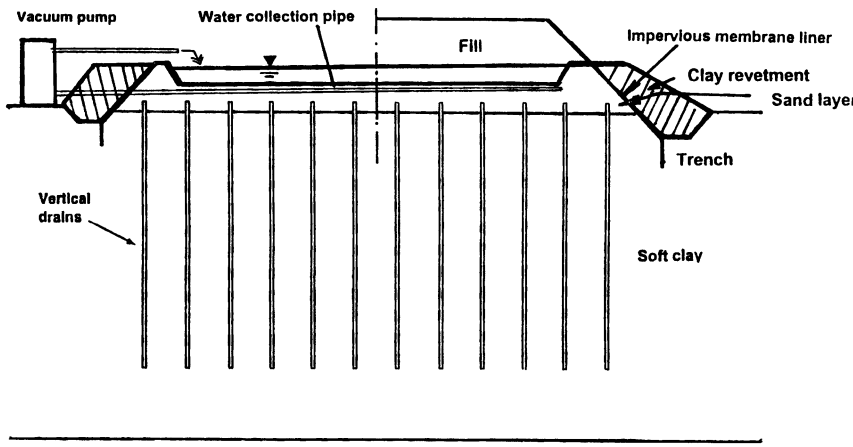


FIGURE 15.3. Schematic of vacuum preloading system (modified from Shang *et al.* 1998).

The vacuum method has the following characteristics (Shang *et al.* 1998):

- A vacuum pressure of more than 80 kPa (600 mm Hg) can be achieved in practice using available vacuum equipment, which is equivalent to a fill of 4–4.5 m in height.
- The lateral deformation of soil is inward due to the suction generated by the vacuum (instead of soil "squeeze-out" encountered in a surcharge preloading process, tensile cracks may develop adjacent to the treated area).
- There is no need to control the rate of vacuum application to prevent a bearing capacity failure because applying a vacuum pressure leads to an immediate increase of the effective stress and hence strengthening of the soil.

Despite a relatively good understanding of the principles of the vacuum method (Holtz & Wager 1975), the technique was not used widely in geotechnical engineering practice until the early 1980s, due mainly to high cost. The technology gained the attention of the Asian geotechnical community in the late 1980s (Qian *et al.* 1992) due to advances in geosynthetics and the shortage of land along shorelines. Prefabricated vertical (wick) drains, which are effective, cost efficient and easy to install compared to sand drains, have made the cost of the vacuum method acceptable.

A number of projects have been undertaken in the Netherlands, France, Malaysia, Sweden and China. One of the largest projects was the East Pier Project in Xingang Port, Tianjin, China (Shang *et al.* 1998). The soil improvement project was conducted on 480 000 m^2 of reclaimed land using the vacuum preloading method. After 29 months, including a preloading period of 135–247 days, the average consolidation settlement reached 2.0 m, corresponding to increases in undrained shear strength of two- to four-fold, as shown in Fig. 15.4. The study showed that the vacuum method was an effective tool for

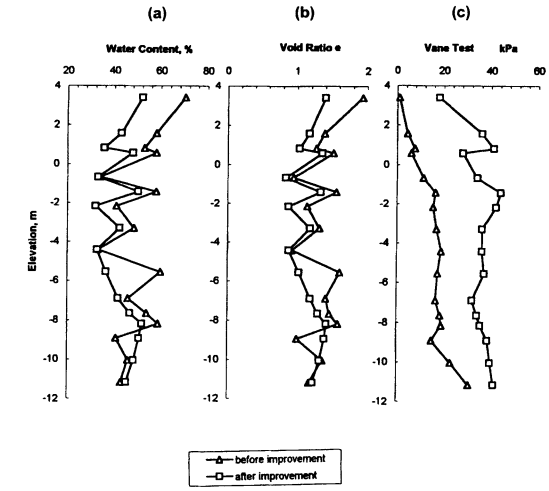


FIGURE 15.4. Soil properties before (△) and after (–□–) vacuum preloading consolidation, East Pier Project, Tianjin, China (modified from Shang *et al.* 1998).

the consolidation of very soft, highly compressible clayey soils over a large area. The technique is especially feasible in cases where there is a paucity of suitable materials for use as a surcharge and extremely low shear strength. Access to a power supply for the vacuum pumps is necessary.

Additional information on vacuum preloading can be found in Thevanayagam *et al.* (1994), Thevanayagam & Nesarajah (1996).

15.2.3.4 Consolidation with Vertical Drains

In thick deposits of soft clay, the time required for consolidation under a surcharge may be unacceptably long and/or foundation instability may be a serious concern. In such cases, it is often economically advantageous to install some type of vertical drain in the foundation soil to decrease the length of drainage path and thereby speed up the consolidation. Figure 15.5 shows a typical vertical drain installation and instrumentation. Because the rate of consolidation is inversely proportional to the square of the length of drainage path, the benefits of reducing the flow distance are to reduce (a) the

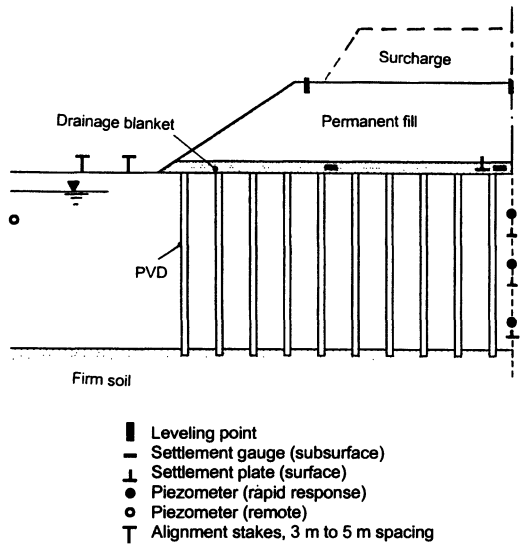


FIGURE 15.5. Basic instrumentation of embankment modified with prefabricated vertical drains (PVDs) (modified from Rixner *et al.* 1986a).

time required for surcharge loading, (b) the thickness of surcharge fill, and (c) the size of berms, if any (see Section 16.8.2). These benefits are partially offset by the cost of the drains and the drainage blanket that is required to conduct water outside the loaded area (Fig. 15.5). Furthermore, collector drains in the drainage blanket, which further increase cost, may also be required beneath very wide fills.

Various types of vertical drains, their common installation methods and pertinent geometric characteristics are given in Table 15.3. Sand drains were widely used after their invention in 1926 until the development of the modern prefabricated vertical drains in 1972. Since then, a large number of prefabricated geocomposite vertical drains (see Section 15.2.3.5), probably more than 50 different types, have appeared on the market. Competition has appreciably decreased their cost, and installation procedures have been improved to permit rapid, simple installations to depths approaching 60 m and at rates up to 1 m s^{-1}. Today it is fair to say that prefabricated vertical drains have made all types of sand drains virtually obsolete; see Johnson (1970b), Holtz *et al.* (1991), and Hansbo (1981, 1993).

Vertical drains will be most efficient in those soil deposits in which primary consolidation settlement is important. Because vertical drains are neither useful for nor intended to reduce secondary settlements, they are ordinarily ineffective in organic materials, particularly high permeability peat. However, peat is frequently underlain by soft soils that

TABLE 15.3 Types of vertical drains, common installation methods and typical geometric characteristics (modified from Jamiolkowski *et al.* 1983)

Drain type	Common installation methods	Drain diameter (m)	Typical spacing (m)	Maximum length (m)
Sand drain	Driven or vibratory closed-end mandrel (displacement type)	0.15–0.6	1–5	≤30
Sand drain	Hollow stem continuous-flight auger (low displacement)	0.3–0.5	2–5	≤35
Sand drain	Jetted (non-displacement)	0.2–0.3	2–5	≤30
Prefabricated sand drains "sandwicks"	Driven or vibratory closed-end mandrel; flight auger; rotary wash boring (displacement or low displacement)	0.06–0.15	1.2–4	≤30
Prefabricated vertical drains	Driven or vibratory closed-end mandrel (low displacement)	0.05–0.1[a]	1.2–3.5	≤60

[a] Equivalent diameter.

may be effectively treated with vertical drains. When properly designed, vertical drains may be especially beneficial in soils with a highly developed macrofabric, because the vertical drains permit intermediate previous layers to function as horizontal drains. However, as noted by Holtz *et al.* (1991), to achieve an economical drain design at such sites requires a very high quality subsurface investigation and laboratory testing program.

Soil and Drain Parameters Required. The parameters required for the design of vertical drains on soft cohesive deposits are:

- coefficients of consolidation for horizontal, c_h, and vertical flow, c_v;
- stress history of the deposit, σ'_p, OCR;
- extent of the disturbed or "smeared" zone, d_s, and hydraulic conductivity of the remolded clay within the smeared zone, k_r;
- discharge capacity of the drains, q_w, and its variation with total lateral stress, σ_h, and time, t (this factor is important for very long drains).

Site Investigation and Laboratory Testing Program. To provide sufficient information for a detailed design of the vertical drainage system, a comprehensive program of *in situ* testing as well as high-quality soil sampling and laboratory testing will be necessary. The particular program will depend on the size of the project and a preliminary assessment of whether the clay deposit is likely to possess a strong macrofabric. The program should obtain the following information for the deposit: (a) macrofabric, geometry of the drainage paths, and the drainage boundaries; (b) consolidation and permeability characteristics in both vertical and horizontal directions; (c) stress–strain and strength characteristics; and (d) stress history. The first two items are important for the prediction of the magnitude and rate of settlement. The stress–strain and strength properties may be necessary for a stability analysis of the preloading fill. Depending on the strength of the foundation, stage construction may be required to avoid failure during construction; therefore, an evaluation of the partially consolidated strength may also be necessary (Ladd 1991).

Designers have often neglected the importance of stress history and its impact on design. Whether there is a real need for preloading and vertical drainage depends on the relationship between stress history and the magnitude of total stress imposed on the deposit. As with the vertical coefficient of consolidation, c_v, the horizontal coefficient c_h is also strongly dependent on the stress history of the deposit. Furthermore, it is important to select c_h at an effective stress level corresponding to that *in situ*; otherwise erroneous results will be obtained. These points are discussed in some detail in Jamiolkowski *et al.* (1983) and Holtz *et al.* (1991).

To obtain more reliable predictions of settlement and consolidation rates, the recommendations in Table 15.4 have been developed. They represent a compromise between *in situ* and laboratory techniques.

TABLE 15.4. Procedures necessary to improve the reliability of predictions of the settlement and consolidation rates of vertical drain installations (adapted from Holtz *et al.* 1991)

Uniform clay[a]	Clay with macrofabric[a]
Small projects	
Laboratory c_h	Field k_h plus laboratory m_v[b]
Piezocone dissipation tests	Piezocone dissipation tests
Large projects	
Field k_h plus laboratory m_v[b]	Trial embankment
Piezocone dissipation tests	Field k_h plus laboratory m_v[b]
Trial embankment (maybe)	Piezocone dissipation tests

[a] For all projects investigate the macrofabric and drainage paths of the deposit by means of borings (preferably with continuous undisturbed sampling) and piezocone testing.
[b] m_v = coefficient of volume compressibility.

When dealing with vertical drains, Johnson (1970b) is worth consulting because much of it is also applicable to prefabricated drains. Other good sources of information about drain types, design, selection and installation include Hansbo (1979), Mitchell (1981), Jamiolkowski *et al. (1983), Choa (1985), TRB (1986), Rixner et al.* (1986a, b), Holtz *et al.* (1991), CFEM (1992), Hansbo (1993), and Bergado *et al.* (1996).

Theory of Consolidation with Vertical Drainage. Barron (1948) presented the first exhaustive treatment of the consolidation of a soil cylinder containing a central drain well. The assumptions and the solutions for different boundary conditions are given in Holtz *et al.* (1991), Hansbo (1993), and Bergado *et al.* (1996), and only the results will be given here.

For the case of radial drainage only, the average degree of consolidation under ideal conditions (no smear and no well resistance) is:

$$U_h = 1 - \exp\left(\frac{-8T_h}{F}\right) \qquad (15.5)$$

where $F = F_1(n)$ and the function

$$F_1(n) = \frac{n^2}{n^2 - 1}\log_e(n) - \frac{3n^2 - 1}{4n^2} \qquad (15.6)$$

The time factor $T_h = c_h t / d_e^2$, c_h = coefficient of horizontal consolidation, d_e = diameter of the equivalent soil cylinder (Fig. 15.6a), d_w = equivalent diameter of the drain (Fig. 15.6a), and $n = d_e/d_w$ is called the drain spacing ratio.

If the drain is band-shaped (Fig. 15.6b), then as suggested by Hansbo (1979), the equivalent diameter, d_w, should be that of a cylinder having the same circumference as the drain; or $d_w = [2(a + b)]/\pi$, where a and b are the width and thickness of the drain, respectively.

Diameter of the equivalent soil cylinder, d_e, depends on how the drains are installed in the field. Two patterns, triangular and square, are commonly assumed for analysis, as shown in

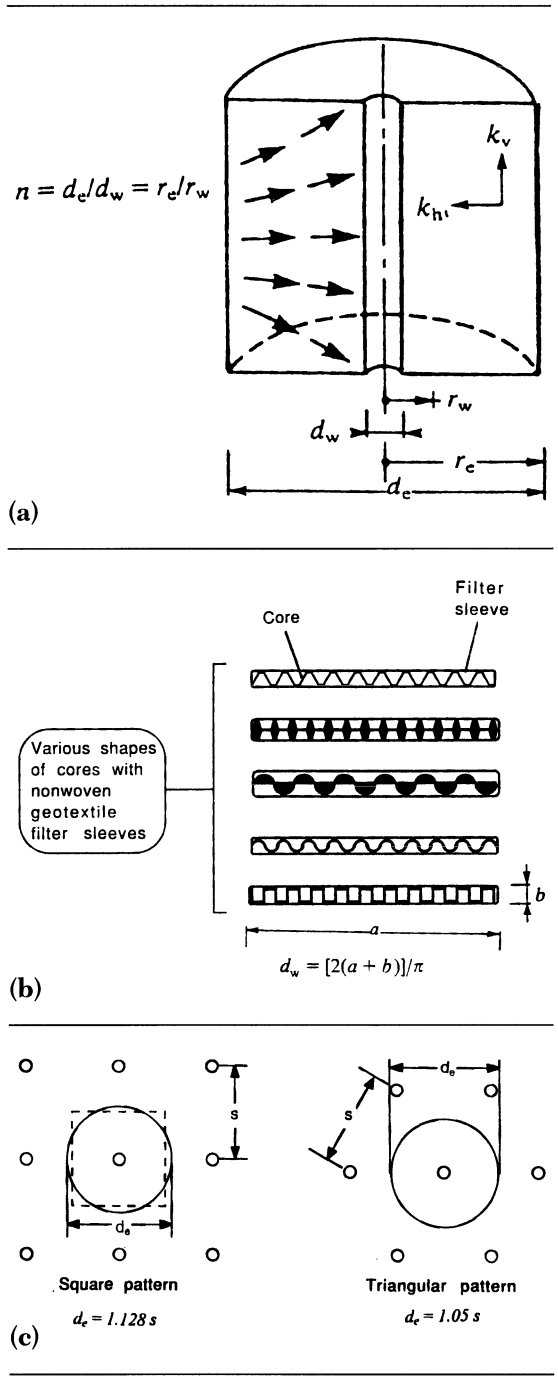


FIGURE 15.6. Consolidation using prefabricated vertical drains (PVDs): (a) section of the equivalent cylinder (modified from Holtz *et al.* 1991); (b) PVDs, showing various shapes of cores with nonwoven, geotextile filter sleeves (modified from Hausmann 1990); and (c) PVD patterns, showing drain spacing s (modified from Holtz *et al.* 1991).

Fig. 15.6c. Barron (1948) showed that the triangular pattern was slightly more economical, although the difference from a practical point of view is small. The square pattern is easier to layout and control in the field.

Equation 15.5 assumes that the drains can be installed without any changes in the properties of the surrounding clay, which is impossible in practice. The degree of disturbance caused by drain installation depends on the soil sensitivity and macrofabric. Another factor influencing drain performance is its discharge capacity, q_w. Both these factors have been studied by Barron (1948) and Hansbo (1979; 1981), and Eq. 15.5 for the average degree of consolidation can be modified by adapting a value of F, which is the sum of the drain-spacing factor $F_1(n)$, the smear factor $F_S(n)$, and the well resistance factor $F_w(n)$, or:

$$F = F_1(n) + F_S(n) + F_w(n) \qquad (15.7)$$

To account for the effects of soil disturbance during installation, a zone of disturbance with a reduced hydraulic conductivity is assumed around the vicinity of the drain, as shown in Fig. 15.7. The smear effect factor is:

$$F_S(n) + \log_e\left(\frac{n}{N_S}\right) - 0.75 + \left(\frac{k_h}{k_r}\right)\log_e(N_S) \qquad (15.8)$$

where $N_S = d_S/d_w$; d_S = the diameter of the disturbed or smeared zone around the drain. The disturbed or remolded soil has a lower hydraulic conductivity, k_r, than the undisturbed clay, k_h.

If during consolidation, the discharge capacity of the drain is reached, the overall consolidation process is retarded. Assuming that Darcy's law can be applied for flow along the vertical axis of the drain, the factor $F_w(n)$ is (see Fig. 15.7):

$$F_w(n) + \log_e(n) - 0.75 + \pi z\left[(2l - z)\left(\frac{k_h}{q_w}\right)\right] \qquad (15.9)$$

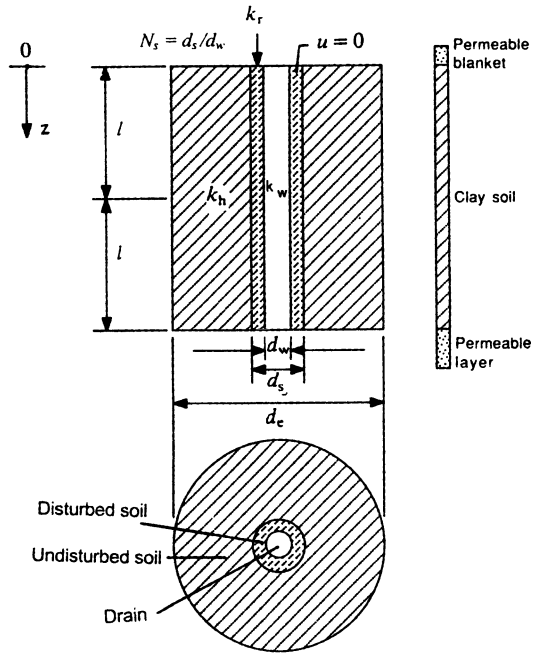


FIGURE 15.7. Schematic of a vertical drain, including disturbed (smear) zone and undisturbed zone (modified from Holtz *et al.* 1991).

where l = characteristic length of the drain, which is the half the length of the drain for fully penetrating drains and equal to the length for partially penetrating drains; q_w = the well discharge capacity = $A_w k_h$ = cross-sectional area of the drains times the horizontal hydraulic conductivity of the undisturbed clay; and z = depth measured from the ground surface.

Holtz *et al.* (1991) also discuss combined radial and vertical drainage, time-dependent loading, and the limitations of the Terzaghi–Barron theory.

15.2.3.5 Prefabricated Vertical Drains

Modern prefabricated vertical drains (PVDs) appear to be modeled after the original Kjellman "wick"; they have a rectangular cross-section, typically about 100 × 4 or 5 mm, and are manufactured in long, thin strips or bands. Most PVDs are a geocomposite and consist of a plastic core with grooves, studs or

channels that is surrounded by a filter, most commonly made of a non-woven geotextile, but in a few cases, a heavy paper filter is used (see Fig. 15.6b). The core carries the excess water to the ground surface, and the filter keeps soil particles from entering the core. The core also supports the filter during installation and helps to resist *in situ* soil pressures.

Good general references on PVDs include TRB (1986), Rixner *et al.* (1986a, b), Holtz *et al.* (1991), CFEM (1992), Hansbo (1993), Bergado *et al.* (1996), and Schaefer (1997). For case histories of PVD installations see Hansbo (1993), Bergado *et al.* (1996) and Schaefer (1997).

Design of Prefabricated Vertical Drains (PVDs). The area requiring drainage can be established from the site plan. The soil profile established during the subsurface investigation program together with the anticipated applied loads would usually dictate the lengths of the drains required. The input required to the design equations includes: (a) the soil properties; (b) the boundary and drainage conditions; (c) the desired degree of consolidation; (d) the drain installation pattern assumed (square or triangular); and (e) the equivalent diameter of the prefabricated drains. The Barron–Kjellman design equations (Eqs. 15.5–15.9) can be solved to give the drain spacing, s, using a spreadsheet program on a personal computer. In addition, Hansbo (1979) and Bergado *et al.* (1996) have charts that are helpful for preliminary designs. The drain spacing may be varied to optimize the design. Closer drain spacing decreases consolidation time but increases installation costs. In the design process, it may also be necessary to consider such factors as the smear zone and drain characteristics such as well resistance; how these factors theoretically influence the average degree of consolidation was discussed in the previous section.

The smear zone surrounding the drains is generated by the soil disturbance from the installation of the PVD. The degree of disturbance depends on the size and shape of the mandrel used to install the drains, soil macrofabric and the installation procedure (whether driven, pushed or vibrated). The mandrel cross-section should be minimized, while at the same time, it must have adequate stiffness. Based on work by Holtz & Holm (1973) and Akagi (1979), Hansbo (1987) recommended that the diameter of the smear zone be assumed as $d_s = 2d_w$ (Fig. 15.7). This relationship has been experimentally verified in the laboratory and in the field in soft Bangkok clay (Bergado *et al.* 1996).

Finally, the material characteristic of the prefabricated drains must be appropriately considered. The information required includes: (a) the discharge capacity of the drain considering lateral stress, possible drain folding or kinking; (b) transverse permeability of the filter sleeve; (c) mechanical properties; and (d) durability of the proposed drains. Information on these factors is presented in Rixner *et al.* (1986a) and Holtz *et al.* (1991).

The discharge capacity, q_w, of PVDs varies considerably depending on how the drain is made, its installed length, and whether the drain is folded because of large settlements. The length is important because q_w decreases with increasing lateral pressure, which causes the filter sleeve to squeeze into the drain core channels and reduce the cross-sectional area of the channels. Folding of the drain also reduces the area available for flow in the core. Both Holtz *et al.* (1991) and Bergado *et al.* (1996) present laboratory data showing the discharge capacity of several commonly available drains. Analytical and experimental studies summarized in Holtz *et al.* (1991) indicate that well resistance has little or no influence on consolidation rates of PVD installations, even for long drains, as long as q_w is at least 100–150 $m^3\ a^{-1}$.

The transverse hydraulic conductivity of the PVD depends on the characteristics of the geotextile filter surrounding the drain. Durability depends on the particular poly-

mers used to make the drain and their resistance to the chemical and biological environment at the site. Geotextile filtration design is discussed in Section 26.2.4, while durability considerations are given in Section 7.8. Mechanical properties of PV drains are discussed in Holtz *et al.* (1991). Evaluation of new drains is discussed in Holtz *et al.* (1991, 1997) and Bergado *et al.* (1996). Sample drain specifications are given in Rixner *et al.* (1986a) and Holtz & Christopher (1987).

In 1998, the installed costs of prefabricated drains were as low as US$1.60 m^{-1} and up to more than US$3.00 m^{-1}. These costs do not consider the cost of a drainage blanket, working mat, mobilization, pre-drilling, etc. For comparison, sand drains cost around US$13–16 m^{-1}.

Hansbo (1983) gives an example comparing the cost of preloading with vertical drains versus piles for a small building on soft clay. The optimum solution depends on the cost of surcharge fill versus cost of piles, and how much time is available for the preloading.

Installation, Inspection and Evaluation of Results. The most common installation procedure is by a closed-end mandrel driven by an attachment to a crane or end loader (Rixner *et al.* 1986a, b). Depending on the site conditions and construction sequence, pre-drilling through the embankment or upper dense layers may be required. Although prefabricated drains are much smaller in cross-section than the old sand drains, the installation patterns are similar to those for sand drains (square or triangular) with typical spacing ranging between 1.2 and 3.6 m (or greater).

Details of most foundation treatment construction operations are usually left to the contractor, but in the case of vertical drainage projects, there are some construction and installation details that the designer should consider. These include the type and shape of the mandrel, the end shoe, method of installation of the mandrel, and the sequence of the installation operations. Other construction considerations include site preparation, a working platform, fill placement rates and/or stages, removal of the surcharge, and alternate surcharges (water, vacuum). As with most geotechnical construction, well-trained and conscientious field personnel are very important to the success of the project. Visual inspection by the design engineer or his/her representative of all aspects of the construction (site preparation, drain installation, fill placement, surcharge removal, if any, etc.) is essential.

In many preloading and vertical drainage designs, it is necessary to be able to control the rate of fill placement, and this is best done by a program of field instrumentation and measurements. Common instrumentation includes piezometers, settlement plates, inclinometers, and plan and elevation surveys (see Section 15.4.3). For major projects, instrumentation programs are essential, and they may also be required for small projects in which fill failure would be disastrous. Site monitoring should be carried out not only during construction, but also as long as practical afterwards. The objective of the long-term measurements is to verify settlement predictions made during the design phase. Section 15.4 further discusses issues of verification and evaluation of soil improvement.

If the Drains do not Perform as Expected. Sometimes the soil conditions at a site are actually worse than originally anticipated, and the drains may not perform as expected. In this case, possible solutions include: (a) install additional drains at decreased spacing, (b) increase the surcharge level, (c) increase the time for consolidation, and (d) reduce the acceptance criteria. An investigation aimed at establishing "what went wrong and why" is advisable because this information will be useful in deciding what course of action to take and in the redesign.

15.2.4 CHEMICAL, THERMAL AND ELECTRICAL STABILIZATION

The use of various chemical additives as well as the application of thermal and electrical

energy in various forms are among the oldest foundation soil improvement techniques. Chemical stabilization can involve mixing and compaction of near-surface soils, if necessary. The chemicals can be mixed at some depth with special equipment or alternatively injected under pressure (various "grouting" techniques). Thermal treatments include both heating and artificial ground freezing (AGF); stabilization with electrical energy includes electro-osmotic consolidation and electro-kinetic stabilization.

15.2.4.1 Stabilization by Chemical Admixtures

For many years, highway and airport engineers have used various chemical admixtures to chemically stabilize problem subgrade soils. Chemical substances such as lime (both slaked and unslaked or quicklime), Portland cement, asphalt, tar, fly ash and calcium chloride have been used, either alone or in some combination, to mitigate the problems associated with construction on soft subgrades, swelling and shrinking clays, and soils subject to frost action. Chemical stabilization is especially applicable for light structures such as pavements, one-story buildings, and small tanks. Construction techniques are well-developed, relatively simple and inexpensive. The chemistry of lime–cement and other materials used for soil stabilization is discussed in Van Impe (1989), Hausmann (1990), Winterkorn & Pamukcu (1991), Bergado *et al.* (1996), and Abramson (1997). Hausmann (1990) describes how admixtures are used in pavement design and to stabilize industrial waste materials.

15.2.4.2 Lime and Lime–cement Columns

Traditionally, chemical stabilization was only applicable to near-surface compacted soils. However, during the past 20 year or so, equipment and procedures have been developed that can apply and mix lime and cement *in situ* to make stabilized columns to significant depths. Lime and lime–cement columns were developed in Sweden in the 1970s. Deep mixing methods were developed in Japan also in the 1970s; both lime and cement are quite commonly used. Other additives such as Portland cement, gypsum, and fly ash together with quicklime extend the range of soils that can be effectively stabilized to inorganic and organic silts and clays with significant organic contents. In some cases, besides the desirable engineering properties of the subsoil, the relative cost of lime versus Portland cement determines the types of additives used.

The most common applications of lime and lime–cement columns are for improving the stability of natural and excavated slopes and for reducing the settlements of shallow foundations, especially for highway embankments and small structures. For deposits of soft clays less than 15–20 m in thickness, the entire depth can be stabilized; for deeper deposits, the stabilized zone acts like a deep "dry crust" layer that serves to spread the load and significantly reduce settlements. Thus the method is very appropriate for structures such as highway embankments, small, flexible buildings, and tanks that can tolerate some settlement.

Detailed information on lime and lime–cement columns can be found in Holtz (1989), Van Impe (1989), Broms (1991b and 1993), Bergado *et al.* (1996), Schaefer (1997), Broms & Boman (1978) and Munfakh (1997a). Columns are commonly 0.5–0.6 m in diameter with a maximum length of 15 m, although machines capable of making columns 1 m in diameter and 20 m deep are available. Depending on the soil type, desired rate of strength gain, initial soil water content, ambient temperature, and other factors, the amount of quicklime utilized is 6–8% by dry weight of soil. If Portland cement is used, as high as 25% cement content may be required to achieve the desired results. Because of more uniform mixing, constant temperature, and better control, both the amount and rate of strength gain is greater in laboratory tests than is usually achieved in the field.

Design for the bearing capacity of lime column foundations, individual columns and column groups is detailed in Broms (1991b, 1993), who recommends procedures analogous to common design procedures for single piles and pile groups in soft clays, and using an analysis in terms of total stresses (see Chapter 10). For settlement analyses, both total and differential settlements must be estimated, and these calculations become especially important when the stabilized depth is less than the thickness of the compressible material.

15.2.4.3 Deep Soil Mixing

Although somewhat similar in concept to lime–cement columns, deep soil mixing (DSM) utilizes multiple arrays of long hollow stem augers with discontinuous flights or paddles to mix soils *in situ* with a cement grout. The augers, usually crane-supported, are introduced into the ground, and at the same time, the grout is pumped out at low pressure through holes located at multiple intervals on the hollow stem. Treatment depths can range up to 50 m or more, while typical auger diameters range from 0.55 to 1.0 m or greater. Sometimes, steel H-sections or sheet piles sections are inserted into the columns for additional strength and bending resistance. Although most of the grout consists of cement, bentonite (about 5% by weight of cement) may be added to decrease the hydraulic conductivity for cut-off applications. Sometimes other stabilizing agents such as lime and fly ash are used.

Although the majority of DSM in applications involve a grout or slurry, i.e. the so-called "wet method", the "dry jet method" (DJM) is also sometimes used. In the DJM, lime or cement powder is forced into the soil through holes in the mixing paddle using compressed air (Tòth 1993; Bergado *et al.* 1996). Probably the two most common forms of DSM in use are the cement deep mixing (CDM) method (sometimes called the DCM) and the soil mix wall (SMW) method. DSM methods are applicable to both cohesive and granular soils, although the augers cannot penetrate large particles, a serious limitation when DSM is used for cut-offs and groundwater control in deposits with boulders and cobbles.

Both the CDM and SMW methods stabilize the entire soil column, which can be expensive if only certain weak layers at depth require treatment. A variation of DSM technology that has particular advantage in such cases is the so-called spreadable wing (SWING) method and its variations, as described in Yang *et al.* (1998).

DSM has been used on many projects for cut-offs for dams and levees as well as for environmental containment, foundation stabilization, permanent and temporary excavation support, and liquefaction mitigation. Several case histories illustrating these applications are presented in Yang (1994), Yang & Takeshima (1994) and Schaefer (1997).

Design methods for DSM are not as well-developed as for lime–cement columns. Depending on the application, design mainly consists of estimating the desired engineering properties of the *in situ* soil, e.g. strength, compressibility, hydraulic conductivity, and then conducting laboratory tests with different percentages of cement plus other additives to obtain the needed properties. The remainder of the design is conventional geotechnical design.

15.2.4.4 Intrusion and Permeation Grouting

Grouting is defined (Hausmann 1990; Winterkorn & Pamukcu 1991) as the injection of a fluid material, generally under pressure through drilled holes, into voids or fissures in rock or soil, or between those materials and a structural material or component. Its purpose is of course to improve the physical characteristics of the soil deposit or rock formation, e.g. increased strength, decreased compressibility, or decreased hydraulic conductivity. To achieve these objectives, many different grouting materials have

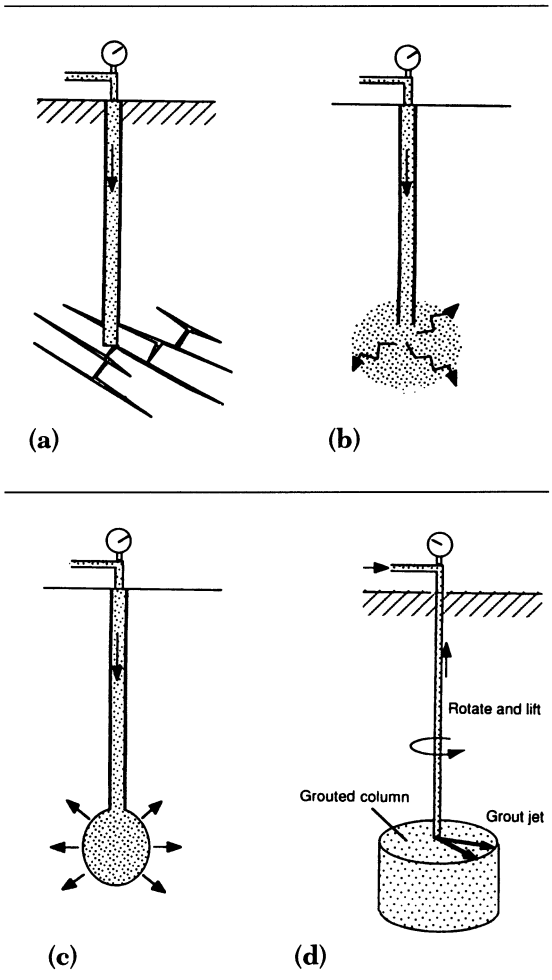


FIGURE 15.8. Types of grouting (modified from Hausmann 1990): (a) intrusion grouting, (b) permeation grouting, (c) compaction grouting, and (d) jet grouting.

been used and numerous techniques have been developed.

In any discussion of grouting, it is important to distinguish between displacement or densification grouting (called compaction grouting, see Section 15.2.5.2), and non-densification grouting. These latter grouting processes are intrusion grouting, permeation grouting and jet grouting (discussed separately in Section 15.2.4.5). These techniques are illustrated in Fig. 15.8.

Intrusion, fracture or slurry grouting (Fig. 15.8a) is a technique in which fluid grout is injected under pressure causing controlled fracturing of the ground. Theoretically, the first fractures are perpendicular to the minor principal stress direction, but observations have shown that they usually follow the weaker bedding planes and joints. Repeated injections tend to cause fractures along different planes. The hydraulic conductivity of the soil decreases, and some densification probably occurs, although it is secondary to the strength increase resulting from hardened grout lenses.

In permeation grouting, the voids of a soil or rock are filled with grout, but little change in the physical structure of the soil or rock occurs (Fig. 15.8b). Materials injected include: (a) particulate grouts, including Portland and micro-fine cement, fly ash, clay (bentonite) or mixtures of these components; and (b) chemical grouts, such as lime, sodium silicates, acrylates, phenols, etc., in solution. Chemical grouts can permeate smaller pore sizes, as they are liquids with a low viscosity and no solid particles to clog the soil pores. As with cement grouts, they offer the added benefit of cementing soil particles together. However, they are more costly than particulate grouts.

According to Hausmann (1990), grouting with clay, lime and cement has been used for the repair of masonry walls, to fill cracks in load-bearing structures, and to stop unwanted seepage in rock fissures for a few hundred years. Grouting for seepage cut-offs in dam foundations began before 1890, and became quite common and highly developed by the 1930s (Weaver 1991). Applications to tunnels and foundations developed concurrently. Chemical grouting started in the mid-1920s with silicate-based grouts. Acrylamide grouts (e.g. AM-9) were developed in 1951 (Karol 1982), and they were almost an ideal grout in terms of their penetration, viscosity, gel time and strength imparted to the grouted soil mass. However, they are toxic and thus no longer available. Today sodium-silicate-based grouts

are the most widely used, although other organic monomers and resins are available.

Grouting is most likely to be feasible for stabilization of locally important deposits of loose sands, fractured fissured rock, collapsible soils, waste landfills and dumps, loosely backfilled strip-mined areas, and karstic and cavernous limestone areas. The strength and stiffness of the grouted soil can be predicted rather well in advance. However, for seepage cut-offs and reduction in hydraulic conductivity, as well as for mitigation of soil liquefaction, verification of the effectiveness of grouting is more problematic. In all cases, high quality geotechnical investigations are required, and the advice of specialty grouting contractors is very valuable.

Detailed descriptions of grouting are given in Van Impe (1989), Hausmann (1990), Winterkorn & Pamukcu (1991), Gallavresi (1992), and Littlejohn (1993), while up-to-date overviews are provided in Bruce (1994b), Abramson (1997) and Munfakh (1997a). See Weaver (1991) for information about grouting dam foundations. Karol (1982) gives a complete description of chemical grouts, while Baker (1982) and Raabe & Esters (1993) present details about structural chemical grouting. Most of these references have case histories on grouting, as do Kramer & Holtz (1991) and Borden *et al.* (1992).

15.2.4.5 Jet Grouting

Jet grouting is a relatively new technology. According to Kauschinger *et al.* (1992), it started in Japan about 1965, and the technology developed rapidly and quickly spread to Italy, Germany and Brazil. As illustrated in Fig. 15.8d, in jet grouting, high-pressure (up to 50 MPa) air or water jets, either singly or in multiples mounted on a central drill stem, are rotated in the soil to cut and mix it with an injected grout material such as Portland cement. Jet grouting is able to construct relatively uniform columns of improved soil, 1–2 m in diameter, in a wide variety of soil conditions. The columns can form continuous walls or panels of solidified soil, or they can be connected to form cells.

In recent years, jet grouting has gained wider international acceptance as a viable soil stabilization technique, probably because of three factors: (1) it is applicable to sand, silt and clay deposits; (2) it has been actively promoted by specialty contractors; and (3) jet grouting has been frequently discussed in recent books, papers and conferences, including a number of well-documented successful case histories. It has been increasingly widely used for soft ground tunneling and to stabilize deep excavations in urban areas (e.g. see Bruce 1994b).

Detailed information on the properties, construction processes and design of jet grouting is given in Van Impe (1989), Winterkorn and Pamukcu (1991), Gallavresi (1992), Kauschinger *et al.* (1992), Bell (1993), Munfakh (1997a), and Schaefer (1997). In addition to these references, Kramer & Holtz (1991) and Borden *et al.* (1992) give case histories on jet grouting.

15.2.4.6 Thermal Treatment

If the temperature of a soil is increased above 100 °C, drying, consolidation and an increase in strength will occur. Higher temperatures, e.g. 600–1000 °C, can produce even more-stable soils, and very high temperatures can actually fuse the mineral grains, as occurs in pottery and brick making. In the context of soil improvement, thermal treatment refers to heating clayey soils at temperatures of 600 °C and above. The process results in irreversible changes in the engineering properties of soils. The reported field tests included the thermal treatment of unsaturated loess and weak clays in east Europe and Russia (Terzaghi *et al.* 1996). A major drawback of thermal treatment is that it consumes a lot of energy. Examples in the literature indicate that 50–100 l of fuel oil may be needed to stabilize 1 m^3 of soil (Hausmann 1990).

Recently, plasma technology has come under investigation as an approach for thermal ground modification. Plasma is a highly ionized gas that exists at temperatures between 4000 and 12 000 °C. It can be used to melt soil into magma, which later cools to form igneous rock (Circeo & Mayne 1994). At present, only laboratory-scale tests of the process have been conducted and the applicability of the technique in the field remains to be studied.

Most published applications of deep thermal stabilization have been in Russia and eastern Europe, where, apparently, energy is relatively cheap. For additional information, see Broms (1979), Mitchell (1981), Broms and Anttikoski (1983), Van Impe (1989), Hausmann (1990), and Munfakh (1997a).

15.2.4.7 Artificial Ground Freezing

Artificial ground freezing (AGF) has been used in the mining and civil construction fields for over a century to solve difficult foundation problems, such as the ingress of groundwater during construction, and to provide temporary structural support for excavation and subsurface construction. Frozen soils are quite strong and relatively incompressible in comparison to their thawed state, so artificially freezing the ground is a potential stabilization method. Probably because of cost, it has primarily been used for temporary support of excavations and tunnels. It is suitable for a wide range of soil or rock types. Typical applications include retaining structures for open excavations and ground support and seepage control during tunneling in granular soils, as shown in Fig. 15.9.

To complete an AGF cut-off wall, freeze pipes are installed at the required locations. A refrigerant (typically $CaCl_2$ brine) is circulated through each pipe to cool the ground and freeze the soil porewater around each freeze pipe. Cylinders of frozen soil around adjacent pipes expand until overlapping occurs and forms a continuous barrier.

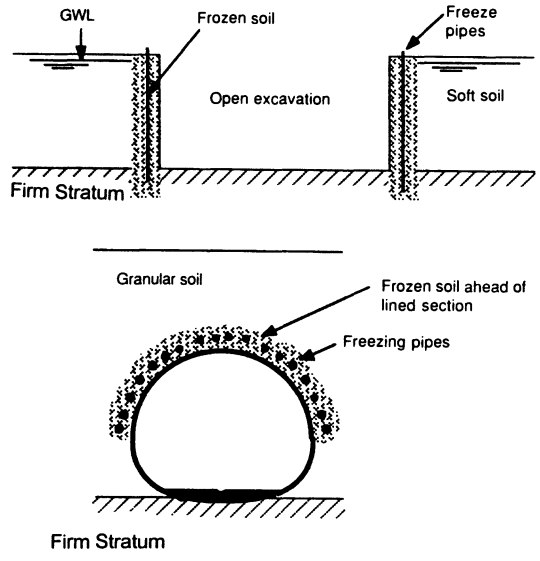


FIGURE 15.9. Two examples of ground freezing applications (modified from Hausmann 1990): (a) for open excavations; and (b) for tunneling.

Since heat flow through soil is almost entirely by conduction (Mitchell 1993), a two-dimensional (x, y) heat flow in soil can be expressed through a diffusion equation (Carslaw & Jaeger 1959):

$$\frac{\partial}{\partial x}\left(k_{Tx}\frac{\partial T}{\partial x}\right)+\frac{\partial}{\partial y}\left(k_{Ty}\frac{\partial T}{\partial y}\right)+Q=\left(C+L_F\theta\frac{\partial \theta_u}{\partial T}\right)\frac{\partial T}{\partial t} \quad (15.10)$$

where T = temperature (°C); t = time, k_{Tx} and k_{Ty} are the thermal conductivities in the x and y directions, respectively (W m^{-1} °C^{-1}); Q = applied boundary heat flux (W m^{-2}); C = volumetric heat capacity (kJ m^{-3} °C^{-1}), which consists of two components, i.e. that of unfrozen soil and frozen soil, respectively, which have to be accounted for separately in computations; L_f = latent heat of fusion of water = 334 kJ kg^{-1}; θ = volumetric water content of soil; and θ_u = unfrozen volumetric water content. The soil temperature variation as a function of time and location can be ob-

TABLE 15.5. Thermal properties of soil (modified from Mitchell 1993)

Material	Value
Thermal conductivity, k_T (W m^{-1} $°C^{-1}$)	
Air	0.024
Water	0.60
Ice	2.25
Shale	1.56
Granite	2.76
Copper	389
Soil	0.25–2.5 (~1.7)
Heat capacity (kJ kg^{-1} $°C^{-1}$)	
Water	4.186
Ice	2.093
Minerals	0.710
Volumetric heat capacity (kJ m^{-3} $°C^{-1}$)	
Unfrozen soil	$\gamma_d(72.4 + 427w)^{a,b}$
Frozen soil	$\gamma_d(72.4 + 213w)^{a,b}$

[a] γ_d = dry unit weight, kN-m^{-3}.
[b] w = gravimetric water content = mass of water/mass of dry soil.

tained by solving Eq. 15.10 using commercially available computer software with known parameters and boundary conditions. Table 15.5 lists the thermal properties of soil, air, water, ice and minerals (Mitchell 1993).

Ground freezing engineering has been summarized in Hausmann (1990). In general, the procedure is expensive and justifiable economically only if more conventional methods are impractical on account of specific site conditions (Terzaghi *et al.* 1996). One of the most complete references on ground freezing is Jessberger (1979). For additional information, see Broms (1979), Mitchell (1981), and Broms & Anttikoski (1983), Van Impe (1989), Hausmann (1990), CGS (1992), Munfakh (1997a), and Abramson (1997).

15.2.4.8 Electro-osmotic and Electro-kinetic Stabilization

Electro-osmosis is a technique used for the consolidation and strengthening of soft, saturated clayey soils. As shown in Fig. 15.10, when a direct current (d.c.) voltage is applied to soil via electrode poles, the soil porewater will be attracted towards the direction of the negative terminal (cathode) due to the interaction of the electric field, the ions in the porewater and the soil particles. If drainage is provided at the cathode and prohibited at the anode, consolidation will be induced by electro-osmosis, resulting in the lower soil

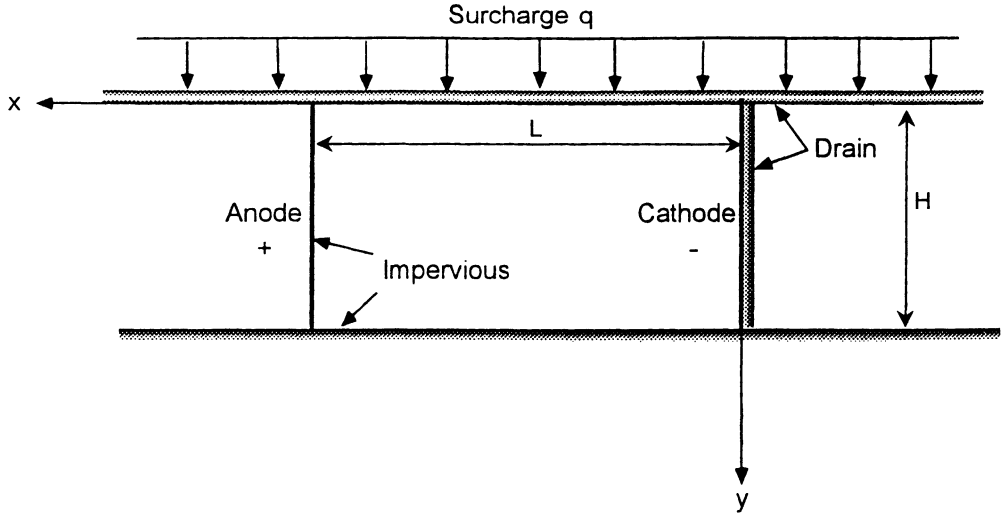


FIGURE 15.10. Schematic of electro-osmotic consolidation (modified from Shang 1998).

water content, higher shear strength and lower compressibility. In addition, electrochemical reactions associated with an electro-osmotic process alter the physical and chemical properties of the soil and lead to a further increase in shear strength (Mitchell 1993).

Casagrande (1959) first applied the technique of electro-osmosis to strengthen and stabilize soft silty clays in the middle 1930s. Since then, successful field tests have been reported that used electro-osmosis to strengthen silty clays and soft sensitive clays; to stabilize earth slopes and to reinforce steel piles installed in clayey soils (Bjerrum *et al.* 1967; Casagrande 1983; Lo *et al.* 1991c). Electro-osmotic consolidation has been considered for projects requiring a rapid improvement in the properties of soft clayey soils.

When an open cathode and sealed anode condition is present, a negative porewater pressure is generated upon the application of a d.c. electrical field. In one dimension, the pore pressure generated by electro-osmosis, $u_{eo}(x, t \rightarrow \infty)$ (kPa), at a distance, x(m), to the cathode is given (Esrig 1968) by:

$$u_{eo}(x) = -\frac{k_e}{k_h}\gamma_w U(x) \qquad (15.11)$$

where k_e(m^2 sV^{-1}) = electro-osmotic permeability, k_h(m s^{-1}) = hydraulic conductivity, γ_w = 9.81 kN m^{-3} = unit weight of water, and $U(x)$ (V) = electrical potential at distance x to the cathode.

Equation 15.11 states the pore pressure induced by electro-osmosis is negative and proportional to the electrical potential, i.e. it has a maximum magnitude at the anode and zero at the cathode. The negative pore pressure results in an increase in the effective stress in the soil, leading to consolidation, as described in the conventional consolidation theory. Knowing the pore pressure generated by electro-osmosis, the time rate of electro-osmotic consolidation can be estimated by conventional consolidation theory.

The electro-osmotic permeability, k_e, governs the water flow in a soil mass under an electrical gradient in the similar way as the hydraulic conductivity governs the flow in soil under a hydraulic gradient. When both the anode and cathode are open to drainage and the hydraulic gradient is set to zero, k_e can be obtained by measuring the flow velocity across a soil plug using an empirical relation (Mitchell 1993):

$$q_e = k_e E \qquad (15.12)$$

where q_e = water flow vector due to an electrical gradient (m s^{-1}), and E = electric field intensity vector (V m^{-1}), defined as:

$$E = -\bar{\nabla} U \qquad (15.13)$$

The power consumption per cubic meter of soil mass per hour is calculated from:

$$p = \kappa E^2 \qquad (15.14)$$

where p = unit power consumption (kW m^{-3}) and κ = electrical conductivity of the soil (S m^{-1}).

Equation 15.14 indicates that the power consumption of electro-osmotic treatment increases with the soil electrical conductivity and applied electric field. Table 15.6 summarizes the typical ranges of soil and electrical properties that are suitable and have been used for electro-osmotic consolidation.

A two-dimensional electro-osmotic consolidation model was recently developed (Shang 1998) that can take the effects of both preloading and electro-osmotic consolidation into account.

The most predominant electrochemical effects during an electro-osmotic process include the development of a pH gradient, the generation of gases and heating. The pH of soil water will increase rapidly to as high as 11 or 12 at the cathode and decrease to almost two at the anode. Consequently, metallic anodes will corrode. Oxygen gas is gener-

TABLE 15.6. Design parameters and common soil properties for electro-osmotic consolidation

Parameter	Unit	Typical range
Hydraulic conductivity, k_h	m s^{-1}	10^{-10}–10^{-8}
Electro-osmotic permeability, k_e	m^2 s V^{-1}	$\sim 10^{-9}$
Electrical conductivity of soil, κ	siemens m^{-1}	0.01–0.5
Electric field intensity, E	V m^{-1}	20–100
Coefficient of consolidation, c_v	m^2 s^{-1}	10^{-8}–10^{-7}
Hourly power consumption, p	kWh m^{-3} h^{-1}	0.01–1

ated at the anode and hydrogen gas at the cathode due to hydrolytic reactions. The electrical current also generates heating. The seriousness of these effects is directly related to the applied voltage and current. It is usually desirable to minimize heating effects to reduce power consumption. It has been found that applying polarity reversal and intermittent (pulse) current can reduce pH gradient and corrosion and increase the electro-osmotic permeability of the soil, thus improving the efficiency of electro-osmotic treatment (Shang *et al.* 1996).

The evaluation of electro-osmotic consolidation on a specific soil can be conducted according to the following procedure:

1. Determination of parameters. In addition to conventional soil properties such as the grain size; preconsolidation pressure; shear strength; water content; hydraulic conductivity, k_v; and coefficient of consolidation, c_v; the parameters required for a treatability analysis include the electro-osmotic permeability, k_e; electrical conductivity, κ; intensity of electric field, E; and power consumption, p. All these parameters can be obtained from laboratory tests prior to field application. Table 15.6 lists the typical ranges of the major parameters for soils that are suitable for electro-osmotic treatment.

2. Electrical operation system in field applications. The electrical operation system can be designed based on the parameters obtained from laboratory tests and from the geotechnical investigation of the site. Typically, the electrode poles consist of metallic rods or pipes installed vertically into the ground with prefabricated vertical drains (see Section 15.2.3.5) installed at the cathode, as shown in Fig. 15.10. The depth of the electrode insertion should be equal to the thickness of the soil layer to be treated. The upper portion of the electrodes in contact with the ground surface crust or top drainage layer should be electrically insulated using a dielectric coating to avoid short-circuiting due to the presence of surface water (Lo *et al.* 1991c).

The material, layout and spacing of electrodes and the applied voltage are of utmost importance to a successful field application. Among the most commonly used conducting metallic materials, the best results were reported using electrodes made of iron and copper rather than aluminum (Sprute & Kelsh 1980). Electrodes made of carbon-coated steel rods and graphite have been used in laboratory studies to prevent electrode corrosion.

The typical spacing between anodes and cathodes reported in the literature ranged from 1 to 3 m (Casagrande 1983; Lo *et al.* 1991c). In general, an approximately uniform electric field gives the best results (Casagrande 1983). To achieve an approximately uniform electric field, the spacing between electrode rods of the same polarity should be much less than the spacing of the opposite polarity.

Power supply capacity can be estimated based on the soil's electrical conductivity and

electrode layout. It has been found that a more dramatic voltage drop takes place at the soil–electrode contacts at a higher applied voltage, which made the treatment less efficient (Casagrande 1983; Shang *et al.* 1996). Therefore, a lower voltage applied across a smaller anode–cathode spacing is desirable to generate the required electric field. However, the cost of electrodes and installation should also be considered. The final design will be based on a balance of the cost of electrodes and electrode installation as well as the treatment efficiency. For additional information, see Arman (1978), Broms (1979), Mitchell (1981, 1993), U.S. Navy (1983), Van Impe (1989) and Hausmann (1990).

Electro-kinetic stabilization is a hybrid between electro-osmosis and chemical grouting. The infusion of certain stabilization chemicals into silty and clayey soils is made more efficient by the application of an electrical potential difference to the soil mass. The procedure seems to be more effective in silty soils, which are otherwise difficult to grout ordinarily. Information on this technique can be found in Broms (1979) and Mitchell (1981).

15.2.5 PHYSICAL STABILIZATION AND DENSIFICATION

Although granular soils generally make good foundation materials, sometimes settlement can be a problem, especially with loose deposits, even if the magnitude of the settlement is relatively small in comparison with the behavior of similar foundations on cohesive soils. The explanation for this is twofold. First, because of their high hydraulic conductivity, granular soils settle rapidly, often during construction, and most structures are much more sensitive to rapid settlements, especially differential and distortion settlements, than to slow settlements. Second, granular soil deposits tend to be much more heterogeneous and variable than cohesive soil deposits, and this variability is a major challenge in foundation design.

Most of the techniques described in this section are applicable to loose granular materials, collapsible soils, and some waste fills and dumps. In addition, some vibro-replacement methods, including stone columns, can also be used in cohesive soils. The possibility of liquefaction due to earthquakes or other vibrations may also lead designers to consider foundation soil improvement at sites with loose granular materials and a high groundwater table. In such cases, in addition to the specific treatment methods described in this section, reference to Kramer & Holtz (1991), Hryciw (1995), and Mitchell *et al.* (1995) is recommended.

15.2.5.1 Preloading

Preloading greatly increases the soil modulus, significantly decreases the settlements of granular deposits, and therefore is a possible treatment method for granular soils (Broms 1991a). The physical reasons why preloading, or more precisely prestraining, works is discussed by Holtz (1991) in connection with its consequences for settlement predictions. If the prestraining has occurred naturally, e.g. by sand dunes or glaciation, then conventional site investigation techniques may seriously overestimate the compressibility of these deposits; geologic evidence thus becomes an important component of the site investigation in granular deposits. If a deposit is unloaded by erosion, glaciation or human excavation, then that deposit has been prestrained and is therefore less compressible. All these possibilities should be carefully considered prior to embarking on a program of foundation soil improvement.

15.2.5.2 Compaction Grouting

Compaction grouting involves the injection of low slump mortar or grout under relatively high pressures (2–4 MPa) in order to displace and compact *in situ* soils. The grout usually consists of silty sand (10–30% fines), Portland cement, and sometimes other additives such as fly ash, fluidizers, and accelerators. Additional details are given in Munfakh

(1997a) and Schaefer (1997). According to Broms (1991a), after compaction grouting of loose sands, the SPT *N*-values are increased by of a factor of 3–5, while the CPT penetration resistance can be increased by about 100% (see Section 4.4.6 for details regarding SPT and CPT tests).

Compaction grouting has been used most often to arrest or eliminate foundation settlements, to lift and level concrete slabs, and for the stabilization of foundation slabs on grade. It has also been used successfully to control surface settlements occurring during soft ground tunneling (Baker *et al.* 1983; Welsh *et al.* 1987), to rectify sinkhole problems (Schmertmann *et al.* 1986), and to density liquefiable soils under both new and existing structures (Graf 1992b; Kramer & Holtz 1991). Additional case histories are reported in Borden *et al.* (1992) and Schaefer (1997).

Warner (1982) provides a historical description of the development of compaction grouting, while Graf (1992a), Warner *et al.* (1992), and Schaefer (1997) provide overviews of current practice and recent developments.

For the design of compaction grouting, the most complete treatment is by Rubright and Welsh (1993), who discuss in detail design methods and parameters, construction procedures and equipment, and quality assurance–quality control requirements and methods.

15.2.5.3 Dynamic Compaction

Densification of a deposit by repeatedly dropping a heavy weight onto its surface is called dynamic compaction. Typical weights are between 5 and 30 t (Mg) and drop heights, H, range between about 10 and 25 m, although much greater weights and drop heights have been utilized in special cases. Spacing between the drop points depends on the soil type, thickness of the deposit, and the location of the groundwater table, but typically ranges between 2 and 15 m. An aerial view of the grid pattern produced by dynamic compaction would look like a series of approximately equally spaced craters. Conventional crawler cranes can be used for weights up to about 18 t (Mg) and drop heights up to 30 m. Beyond that, conventional equipment must be modified with special cables, swivels and drum brakes, or other special equipment used.

Dynamic compaction is very effective for densifying loose partially saturated sands, municipal solid wastes, strip-mined areas, building rubble, loosely dumped fill including rock fill, and the like. With saturated sands, liquefaction occurs upon impact, and as the excess pore pressures dissipate, densification occurs. Densification of finer-grained and less permeable materials is somewhat questionable, especially if they are saturated, because of the time required for the excess pore pressures to dissipate. It is possible that the use of prefabricated vertical drains (see Section 15.2.3.5) together with dynamic compaction could be used at such sites. Dynamic compaction of highly organic and peat deposits is not recommended.

The depth of densification depends on factors other than just the energy of compaction (mass of the falling weight and height of drop), but this depth, D (in m), can be estimated rather well by:

$$D = n(WH)^{0.5} \tag{15.15}$$

where W = mass of weight in tonnes (Mg); H = height of fall in meters; and n = an empirical coefficient, with an average value about 0.5, and with a range between 0.3 and 0.8. The lower value of n applies to landfills and other highly variable deposits, while the higher values have been achieved in clean, uniform sand deposits.

The degree of densification and improvement that can be expected in some deposits is large, and depends largely on the total applied energy. Some soil properties will be improved at least 100% and in some cases, up to 400% increases have been observed, although there does appear to be an upper limit of improvement (Leonards *et al.* 1980). The depth to the groundwater table and the

presence of intermediate silty and clayey layers, calcium carbonate seams, coral layers, etc., will also significantly influence the degree of improvement.

Lukas (1986; updated in 1995) provides an extensive discussion of dynamic compaction. It describes the deposits where dynamic compaction is suitable and the degree of improvement attainable, gives suggestions for project monitoring, and discusses off-site effects such as vibrations and lateral displacements. Other useful information is included on equipment required, contracting, costs and specifications. See Welsh *et al.* (1987), Van Impe (1989), Broms (1991a), CGS (1992), Slocombe (1993), Bergado *et al.* (1996), Munfakh (1997a), and Schaefer (1997) for additional useful information on dynamic compaction. This latter reference and Rollins (1994) also report on a number of successful case histories. Time dependent increases in sand strength and densities have been observed after blast densification, but with the exception of Lukas (1997), dynamic compaction has not commonly produced a similar response.

Dynamic compaction may be an appropriate treatment method for collapsible soils, as discussed in Holtz (1989) and Rollins & Kim (1994). Its use is also described in Lukas (1986), Holtz (1989) and Schaefer (1997) for the densification of uncontrolled fills, and industrial, mining and municipal solid wastes.

15.2.5.4 Blast Densification

Detonation of buried explosives can very effectively densify deposits of clean saturated uncemented sands. The process is similar to that of dynamic compaction, in that vibrations and liquefaction of the deposit results in subsequent densification. With greater depths, because the effective stresses are greater, larger charges are required to achieve the same results. Nevertheless, treatments have been attempted down to 40 m.

Mitchell (1981) reports that equivalent relative densities of 75–80% are possible, but that the results are likely to be somewhat erratic, depending on the homogeneity of the deposit. Dense layers and lenses are likely to be loosened somewhat, but the overall improvement will probably be satisfactory. Van Impe (1989) states that if the initial relative density is less than 50%, then increases of 15–30% are possible; however, the improvement is significantly less if the initial relative density is 60% or greater.

An almost immediate surface settlement of between 2 and 10% of the layer thickness will occur after blasting. There may be some problems with evaluating the effectiveness of the blasting by means of penetration tests, i.e. SPT, CPT (see Section 4.4.6) because these tests often show little improvement immediately after blasting; however, after several weeks, they do indicate that the density has in fact increased (Mitchell & Solymar 1984). The phenomenon of time effects in sands has been discussed in Mitchell (1986a) and Schmertmann (1991). Solymar (1984), Solymar *et al.* (1984), and Solymar & Mitchell (1986) describe a project where a very deep loose sand deposit was densified by blasting and different vibro-compaction techniques. Another case history was the use of blasting to densify very loose lehar and debris flow deposits that resulted from the 1980 eruption of Mt St Helens (Hachey *et al.* 1994).

Besides Mitchell (1981), useful information on the design of blast densification, e.g. depth, spacing and weight of charges, use of delays, etc. can be found in Van Impe (1989), Hausmann (1990), Broms (1991a), CFEM (1992), Narin Van Court & Mitchell (1995), Munfakh (1997a), and Schaefer (1997).

15.2.5.5 Vibro-Compaction and Vibro-Replacement

Vibro-Compaction Methods: Granular Soils. Another way to densify loose deposits of clean granular materials is to insert some type of vibrating probe, tube, rod or section into the

deposit at different locations across the site. Sometimes water jets or air pressure are used to aid in the insertion, and usually the probe, supported by a crane, is repeatedly inserted and withdrawn at the same location. In the vibro-flotation and sand-compaction pile systems, water and additional sand are added during withdrawal of the probe so that a column of denser granular material remains after the process is completed. Other vibratory compaction systems include the Foster Terra-Probe, a rod with several blades attached ("vibrowing"), the Franki Y-Probe, and the Mueller "flexiprobe" and resonant compaction (MRC) systems.

Useful references for design and construction quality control of these methods include Welsh *et al.* (1987), Van Impe (1989), Broms (1991a), CGS (1992), Moseley & Priebe (1993), Bergado *et al.* (1996), Schaefer (1997), and Munfakh (1997a). In addition to these references, useful case histories are given in Esrig & Bachus (1991).

Vibro-Replacement Methods: Cohesive Soils. For cohesive soils, vibration alone will not densify or improve the soil, so some other material such as sand (sand compaction piles, SCP or "Vibrocompozer" piles), sand and gravel (sand–gravel piles), gravel (stone columns) or even concrete (vibro-concrete columns, VCC) is introduced into the soil and densified by vibration. Sometimes, sand and stone columns are grouted after installation. Interestingly, hand-dug stone columns were used to support the Taj Mahal in India (Handa 1984).

Sand and stone columns are constructed in a manner very similar to the vibro-compaction methods described above. A crane-supported vibro-probe 300–450 mm in diameter is inserted, often assisted by water jets, into the soft soil. Then clean gravel or crushed stone is dumped in 0.3–1.2-m lifts into the annulus created around the probe. The probe repeatedly vibrates the stone to densify and force it into the surrounding soil. This method is called the "wet" method or sometimes the "top feed" method. If the soils are too soft for the hole to stand open, the probe is left in the hole momentarily with water jets flowing; the water and fines are used to stabilize the hole as stone is dumped into the annulus between the hole and probe. Some probes are available with a skip at the top of a long feeder tube, which deposits the stone at the bottom of the hole while the probe is in place; this is called the "dry" or "bottom feed" method. Muhfakh (1997a) refers to the wet methods as "vibro-replacement" and the dry top feed method as "vibro-displacement." In both methods, the diameter of the completed columns is somewhat larger than the probe diameter; a typical range is between 0.6 and 1.2 m or larger.

Usually between 15 and 35% of the volume of the soft soils is replaced by stone. The columns are installed in a triangular or rectangular grid pattern at typical center-to-center spacings of 1.5–3.5 m. Common lengths are between 6 and 12 m, although some columns greater than 30 m have been installed (Moseley & Priebe 1993).

Vibro-replacement methods are appropriate for a rather wide range of soils including silty sands down to clays. Stratified sands or sands with some clay, which cannot be effectively treated by vibro-compaction methods, are good candidates for stone columns. They are not recommended for soft, highly sensitive clays or for peat or other organic soils. The method works best in soils with shear strengths between 30 and 60 kPa, although they have been used in clays with strengths as low as 15 kPa.

In addition to the reports by DiMaggio (1978) and Barksdale & Bachus (1983), useful information on the design and construction of sand and stone columns can be found in Aboshi & Suematsu (1985), Barksdale (1987), Munfakh *et al.* (1987), Van Impe (1989), Broms (1991a), Moseley & Priebe (1993), Bergado *et al.* (1996), Schaefer

(1997), and Munfakh (1997a). Successful case histories are reported by Munfakh *et al.* (1987), Esrig & Bacchus (1991), Hryciw (1995), Bergado *et al.* (1996), and Schaefer (1997); a failure reported by Mathis and Munson (1987) is summarized by Holtz (1989).

Settlement analyses for foundations stabilized with stone columns are either: (1) simple, approximate methods; or (2) rather sophisticated methods using the theories of elasticity and/or plasticity. When theoretical settlement predictions are compared to field measurements, the results are not very encouraging, but these analyses have shown that significant reductions in settlement occur if the columns are closely spaced and penetrate the clay layer completely. Although theoretical settlement predictions of partially penetrating stone columns can be made, there is little field evidence to verify the results. However, charts developed using elastic theory and finite element analyses by Balaam *et al.* (1977) are simple to use and satisfactory for preliminary design purposes. See also Moseley & Priebe (1993) and Bergado *et al.* (1996).

Stone columns act as drains, so the time rate of consolidation for a foundation with stone columns is significantly increased. This characteristic also makes them suitable for liquefaction mitigation, as discussed in Baez (1995) and Schaefer (1997).

Vibro-Concrete Columns. Vibro-concrete columns (VCC) are constructed using the same equipment as bottom-feed ("dry") stone columns, and the final product is in fact rather similar in concept to cast-in-place concrete piles. Schaefer (1997) presents a complete discussion of VCC design practice, construction, quality control–quality assurance concepts, and case histories of several successful VCC installations for the foundations of tanks, highway and railway embankments, and buildings.

15.2.5.6 Inundation (Hydromechanical Compaction)

Collapsing and subsiding soils are rather common in some localities, and they can pose serious problems for the foundation engineer. Examples include loess soils as well as the remains of mudflows, slope wash, alluvial fans, etc., in arid regions. These soils have in common a loose, open, "honeycomb" structure that collapses when wetted (thus the term "hydrocompactable"), loaded, or even vibrated. Holtz (1989) discusses the treatment of these soil deposits in some detail.

According to Bara (1978), the most economical treatment method for collapsible soils is inundation. This can be done in two ways (US Navy 1983): (1) by pumping from wellpoints, so that seepage forces are directed downwards applying a consolidating force; and (2) by prewetting, flooding or ponding with water over the area to be densified. Depending on the nature of the cementation or bonding between soil grains, inundation will result in a compression of up to 8–10% of the thickness of the collapsible soil layer. This increases the density of the layer and thereby reduces its compressibility under surface loads such as embankments.

Hausmann (1990) briefly describes the compaction of dry fills by inundation, as well as the compaction of rock fill with water jets.

15.2.5.7 Compaction Piles

Although not commonly considered a method of foundation soil improvement, compaction piles may be a low-cost and effective alternate for the densification of loose granular soils. As mentioned by Broms (1991a), such deposits, especially if they are silty or stratified, are not easily improved by techniques such as dynamic compaction, vibro-compaction or vibro-replacement. Because compaction piles improve by both vibration and displacement, they are related in concept to both vibro-compaction and vibro-

replacement. Thus timber piles because of their shape and low cost, e.g. telephone and power pole rejects, are often the preferred compaction pile type.

Most of the time, the piles are left in place, but if for some reason they are withdrawn, then the hole must be backfilled during withdrawal; a procedure carried out more easily with a pipe pile closed with a hinged driving shoe (Solymar & Reed 1986).

15.2.5.8 Reinforcement of Embankments and Foundations

Soil reinforcement is another form of physical stabilization. Because soils generally have poor to no tensile strength, the inclusion of tensile elements arranged in a special way can greatly increase the stability of, for example, embankments and foundations on soft or weak soils. Embankment instability results in part from the weight of the overlying fill and in part from a tendency of the fill to spread laterally due to internal earth pressures in the embankment. Both factors impose shear stresses on the foundation soils, and if these stresses are greater than the shear strength of the soil, failure will occur. Thus to be effective, reinforcement placed at the interface between the embankment and the foundation must reduce the transfer of these shear stresses from the embankment to the foundation: this is the basic principle of embankment reinforcement. Materials used at one time or another to reinforce embankments include fascines, corduroy, short sheet piles and tie rods (Wager & Holtz 1976); steel nets and meshes, landing mats, used automobile tire casings (Forsyth & Egan 1976); and geosynthetics, particularly geotextiles and geogrids (see Sections 7.2 and 7.3). Design of geosynthetic reinforced embankments on soft foundations is discussed in detail in Chapter 16 and in Bonaparte *et al.* (1987), Holtz (1989), Holtz (1990), and Holtz *et al.* (1997), among others.

Analytical research and numerous laboratory model tests have shown that the bearing capacity is increased and especially the differential settlement is decreased when shallow foundations on sand are reinforced in some manner. However, very few full-scale case histories are available illustrating an economical and successful use of the technique, probably for the reason that it is more economical to utilize other *in situ* foundation soil improvement techniques discussed in Section 15.2.5, or simply to excavate and replace the loose soils with a structural fill (Section 15.2.2). Because of the magnitude of the loads, reinforcement of structure foundations on soft clays is probably rarely feasible. See also Hausmann (1990) for additional discussion on foundation reinforcement.

15.3 Stabilization of Slopes

Many of the soil improvement techniques described above for foundations are also effective for improving the stability of slopes. Because mitigation of slope instability is covered in Section 14.7, only a few additional comments and references will be given here.

One of the more complete recent references on landslides is the *Transportation Research Board Special Report 247* (Turner & Schuster 1996). Included are two chapters on stabilization of slopes: one on soil slopes (Holtz & Schuster 1996) and one on rock slopes (Wyllie & Norrish 1996b). These chapters provide information and case histories on various stabilization techniques that are appropriate for slope instability problems: unloading of slopes, lightweight fills, surface and subsurface drainage, buttresses and various types of *in situ* reinforcement and stabilization techniques. Pertinent to this chapter are ground anchors and tiebacks, soil nailing, micropiles, root- and pin-piles, and biotechnical stabilization.

15.3.1 DEWATERING AND GROUNDWATER CONTROL

As mentioned in Section 15.2.3.1, dewatering is often thought of in connection with the construction of temporary excavation support systems, but permanent dewatering systems are also very common for slope stabilization (see Section 14.7.5). Traditional as well as special dewatering methods, including several case histories, applied to slope stabilization are discussed in Hausmann (1990), Kramer and Holtz (1991), and Holtz & Schuster (1996).

15.3.2 GROUND ANCHORS AND TIEBACKS

The use of ground anchors and tiebacks to stabilize both temporary and permanent slopes is well-developed (see Section 14.7.7). Besides Holtz & Schuster (1996) and Wyllie & Norrish (1996b), good references on tiebacks include Hanna (1982), Schnabel (1982), Weatherby (1982), Cheney (1984), Munfakh *et al.* (1987), Hausmann (1990), Juran & Elias (1991), and CGS (1992). Schaefer (1997) provides information on ground anchors.

15.3.3 SOIL NAILING

Soil nailing is a composite *in situ* slope reinforcement system that consists of "nails" (steel bars, rods, cables or tubes) driven into the slope or grouted into predrilled boreholes, welded wire mesh attached to the nails with anchor plates, and a 75–150-mm layer of shotcrete. These three components, plus the soil in the slope, form a coherent reinforced-soil structure capable of stabilizing natural slopes and temporary excavations. Soil nailing differs from tieback anchor support systems in that the nails are passive elements and are not post-tensioned; also the nails are usually spaced more closely than tiebacks. Typical spacings are between 1 and 6 m, depending on the strength of the soils and the height of the slope. Figure 15.11 illustrates different soil nailing systems and applications.

Soil nailing is further discussed in Section 17.4.4. Holtz & Schuster (1996) and Munfakh (1997a,b) provide overviews of soil nailing, while Juran & Elias (1991) presents design details. Schaefer (1997) has a valuable critique of the common design methods and information on the performance of soil-nailed walls in recent earthquakes.

A system similar to soil nailing has been developed by Koerner (1984) for stabilizing slopes with shallow layers of loose soils. Instead of shotcrete, a geotextile (Section 7.2) or geonet (Section 7.4) is attached to the nails with anchor plates, and as the nails are installed, they pull the surface netting or geotextile into the soil. This action puts tension into the net or geotextile, and at the same time the near-surface soils in the slope are constrained. Koerner & Robbins (1986) and Schaefer (1997) show how anchored geosynthetics may be analyzed for stability, while the use of these systems for erosion protection is discussed in Ghiassian *et al.* (1997).

15.3.4 MICROPILES, ROOT PILES AND PIN PILES

As noted in Holtz & Schuster (1996) and Munfakh (1997a,b), another approach to the *in situ* reinforcement of slopes in soils and soft rocks is the use of small diameter (75–300 mm) bored and cast- or grouted-in-place reinforced concrete piles. These piles are called micropiles, root piles or pin piles by various authors and agencies. In the smaller-diameter range, reinforcing is by a central steel rod or pipe, while the large diameter versions may be provided with a reinforcing-bar cage bound with spiral reinforcement. In slope stabilization applications, a sufficient number of micropiles is installed in the slope to form a monolithic block of reinforced soil or rock that extends below the critical sliding surface (Fig. 15.11). The reinforcement provided by micropiles is strongly influenced by their three-dimensional root-like geometric arrangement. In fact, the original developer

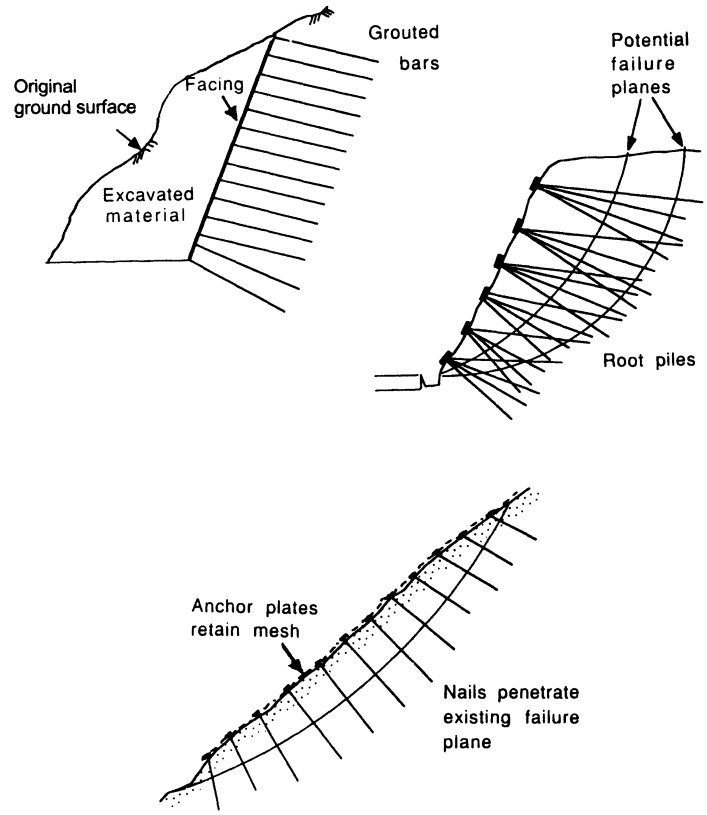


FIGURE 15.11. Different soil nailing systems and applications (modified from Hausmann 1990): (a) grouted bars; (b) root piles; and (c) anchor plates.

of micropiles, Fernando Lizzi, termed the system "reticulated root piles" when he patented the system in 1952. Root piles have been extensively used for underpinning of structural foundations. In the past 20 years or so, however, root piles have been increasingly used for slope stabilization.

Details about the classification, design, construction, quality assurance–quality control, and testing; summaries of these systems and recent developments in micropile technology and research are included in Bruce (1992, 1994a) and Schaefer (1997).

15.3.5 BIOTECHNICAL STABILIZATION

As noted in Holtz and Schuster (1996) and Munfakh (1997a), vegetative and biotechnical stabilization (vegetation used together with structural slope stabilization techniques) is a rapidly developing slope stabilization technology. Although the basic concepts are not particularly new, recent research and development permits a more effective use of vegetation for slope stabilization than in the past. Vegetation contributes to slope stability through: (1) root reinforcement, and (2) pore pressure reduction by rainfall interception and evapotranspiration. Systems that combine vegetation with manufactured structural elements, termed biotechnical stabilization, have a number of advantages over vegetation alone or conventional structural elements in many applications. They are a more effective stabilization agent than vegetation alone, and

they are often less expensive and more environmentally friendly than structural systems alone. Examples of each are given in Gray & Leiser (1982), Gray & Sotir (1995), and Schaefer (1997).

15.4 Verification and Evaluation of Soil Improvement

The geotechnical design process does not end when the plans and specifications have been signed, sealed and delivered. The design is not finished until the construction has been completed and the foundation or slope is performing satisfactorily. This is especially true where some type of soil improvement has been carried out. To ensure satisfactory construction and performance of the completed system, careful, competent inspection during construction is essential. Visual observations and physical testing are obviously important components of construction inspection and, although perhaps less obvious, geotechnical instrumentation for measurements during construction is also an important component of construction monitoring. With some types of soil improvement, e.g. consolidation with vertical drainage, reinforcement, and chemical stabilization, it may be desirable for instrumentation and monitoring to continue for many years after construction is complete, especially if the particular treatment technology is considered experimental or if the stability of the site is marginal.

The following sections are adapted from Holtz (1989) with additional input from Van Impe (1989), Kramer & Holtz (1991), and Broms (1991a).

15.4.1 INSPECTION DURING CONSTRUCTION

The importance of well-trained, competent, and conscientious field and inspection personnel cannot be over emphasized. This is the only way to ensure that the essential features of the design are actually carried out on site. Good inspection is a requirement for almost all foundation work, since it is easy in such work for mistakes to get buried! With most if not all soil improvement techniques, so much is dependent on the success of the treatment, that inspection and instrumentation is not the place to cut cost.

In selecting soil improvement alternatives, the designer should keep in mind the level of inspection required by the method and the competency of the field personnel likely to be available on site. To insure success, the on-site project engineer must have an intimate knowledge of the design assumptions to be able to make correct decisions about problems that will inevitably arise during construction. Uninformed construction decisions often result in cost overruns, contractor claims, or even failures. Ideally, the designer should have direct contractual control over the field personnel on the project to insure that construction procedures are properly carried out. In lieu of this, the designer should become involved in training project engineers and field inspectors prior to construction, so that they will be aware of the important design concepts and key construction details in the treatment method. This is especially important if construction inspection and field control are by outside contract.

15.4.2 VERIFICATION OF FOUNDATION IMPROVEMENT

In many cases, the verification for the soil improvement method was simply a matter that no obvious failures occurred and that the project was apparently successfully completed. Such informal verification may be sufficient for some sites and treatment methods. However, additional measures are required to be sure the degree of improvement was sufficient and that it covered the intended area and depth. Of particular interest in this regard are problem soils and deposits such as swelling, collapsible, and subsiding soils;

loose saturated sands in earthquake prone regions; dredged materials; wastes of all types, including Municipal Solid Waste (MSW) dumps and landfills, mine tailings, strip mines areas, slurry ponds, and the like. In many of these deposits, changes in the strength and compressibility may take place gradually with time. In other cases, it would be desirable to be able to verify that the treatment has in fact been effective before, for example, an earthquake occurs or a final pavement is placed.

Depending on the soils at the site, site conditions, method of treatment employed and time since soil improvement, the required verification can be obtained by *in situ* testing (e.g. Mitchall 1986b; Welsh 1986), geophysical techniques and laboratory tests on undisturbed samples of the treated soil. The validity of these comparative analyses will depend of course on how much reliable "before treatment" information of a similar nature is available.

15.4.3 INSTRUMENTATION

In addition to visual observations by field personnel, measurements of movements and pore pressures are often necessary to verify the success of a particular soil improvement method. In almost all the treatment methods described in this chapter, information from construction monitoring is an essential part of the geotechnical design. In selecting the soil improvement alternate, the designer should consider whether instrumentation and field measurements are possible. If there is doubt that the required instrumentation can be procured or that such measurements can be competently made, then an alternative requiring less instrumentation, even though it might mean more expensive construction, should be selected.

Valuable sources of information about geotechnical instrumentation are Hanna (1985) and Dunnicliff (1988), while Mikkelsen (1996) is applicable particularly to slopes.

15.4.3.1 Instrumentation and Monitoring During Construction

Little or no instrumentation is required, for example, where soft soils are completely excavated and replaced by suitable fill materials. On the other hand, considerable instrumentation and construction monitoring are needed for a surcharge fill and stage loading with or without vertical drains, for many of the chemical and physical stabilization methods, and for reinforced embankments.

The amount and extent of instrumentation installed on a project depends on its size and particular circumstances. If a project is large and the required construction time will be long, it is desirable to install a lot of instrumentation in the early phases of the project, because the measurements may permit design changes that could substantially reduce construction costs.

Some soil improvement methods may require special instrumentation to see that the treatment is progressing satisfactorily or that it is being applied uniformly. In other cases, it may be used to control the process, e.g. dynamic compaction or grouting, or the rate of construction of the embankment. In reinforcement stabilization projects, it may be desirable to have strain gages, for example, attached to the geotextile or geogrid to get an idea of the reinforcement efficiency as construction proceeds.

Surprisingly, field data are often collected but not analyzed during construction. Field measurements are primarily intended to obtain information that relates to the progress of the work; hence, the collected data have value only if promptly analyzed and reported. This requires a deliberate organizational effort to designate responsible personnel for this purpose, and Dunnicliff (1988) gives some recommendations on this point.

15.4.3.2 Post-Construction Monitoring

Often it is difficult to provide for long-term post-construction monitoring of projects in

which some type of soil improvement was attempted. If the project is apparently successfully completed with no failures or excessive deformations, the temptation is to forget it and get on with the next job. Especially if the soil improvement technology is new to the designer, it is worth considering setting up a program to obtain surveys of deformations and settlements of the structure or slope and, if appropriate, obtain maintenance records for the facility. If instrumentation was installed, and it is still functioning, periodic readings and plotting of the results is also very valuable. In the case of a new treatment technology, or unusual soil or site conditions, a good case could be made for obtaining public research funds for a formal follow-up and report to benefit not only the particular project designer, but also the geotechnical profession at large. There is no question that the great progress made in soil and site improvement during the past several years has largely come about through the willingness of geotechnical engineers and designers to report to others their successes and their failures. This process advances the art and practice of geotechnical engineering to the benefit of society.

16. EMBANKMENTS OVER SOFT SOIL AND PEAT

S. Leroueil
R. K. Rowe

16.1 General Behavior of Clay Foundations Under Embankments

In the analysis of the behavior of embankments on clay foundations it has commonly been assumed that the behavior is perfectly undrained during construction and that drainage and consolidation start only after the end of construction. This approach has been widely used and has generally performed well for conventional design situations. However, observations during construction have shown that while this approach may often provide reasonable designs, the actual behavior may be more complicated and that conventional undrained analyses may overpredict pore pressures and lateral displacements. Thus, if one wishes to predict the actual behavior of an embankment on clay, it is essential to have a good knowledge of the mechanical behavior of natural clays, as described in Chapter 2, and to understand what may happen under an embankment during construction as described in Section 16.1.1.

16.1.1 BEHAVIOR DURING CONSTRUCTION

As in most geotechnical problems, it becomes possible to understand soil response only when the corresponding stress path is known. Under embankments, the effective stress paths can be deduced from pore pressure observations. Figure 16.1 shows the excess pore pressures, Δu, observed beneath the centerline during the construction of embankment B at Saint-Alban (Leroueil *et al.* 1978a). At a depth of 2.5 m, the pore pressure increase is small up to a γH value of about 25 kPa and then rises roughly at the same rate as the total applied vertical stress. The behavior is essentially the same at a depth of 5 m, but with a change at γH = 48 kPa. At greater depths, the pore pressure increase remains small in comparison with the applied stress. In general, two phases of behavior can be identified: the first during which the pore pressure increase is low; the second during which the increase in pore pressure is approximately equal to the increase in total vertical stress.

Significant partial consolidation during construction has been reported by a number of investigators (e.g. Law & Bozozuk 1979; Tavenas & Leroueil 1980; Ortigao 1980; Kabbaj 1985; Rowe *et al.* 1995d). The pore pressure increase observed during the first phase of loading under more than 30 embankments (characterized by $\bar{B}_1 = \Delta u/\Delta\sigma_v$) is plotted in Fig. 16.2 as a function of the normalized depth, z/D, with D being the thickness of the clay layer. Two observations were made by Leroueil *et al.* (1978b): first, $\bar{B}_1$ is smaller than predicted when perfectly undrained behavior is assumed; and second, the $\bar{B}_1$ versus z/D relationship has the shape of a consolida-

R. K. Rowe (ed.), *Geotechnical and Geoenvironmental Engineering Handbook*
© Kluwer Academic Publishers 2001

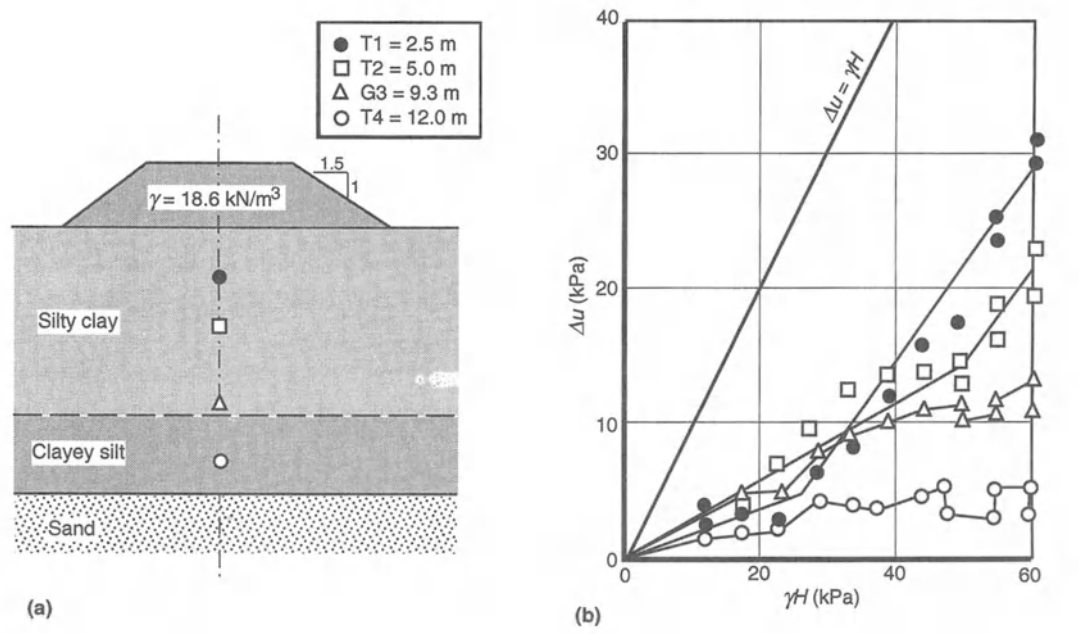


FIGURE 16.1. Trial embankment (section B) at Saint-Alban: (a) location of piezometers; (b) pore pressures measured under the centre of the section, as a function of the embankment load (after Leroueil *et al.* 1978a; reproduced with permission, *Canadian Geotechnical Journal*).

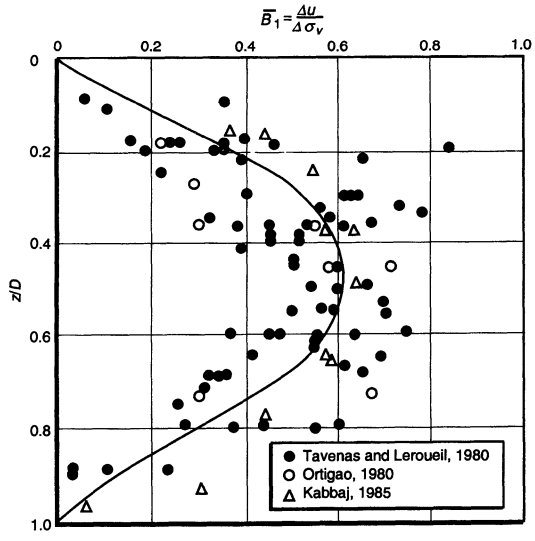


FIGURE 16.2. Compilation of observed excess pore pressures in clay foundation in the first phase of embankment construction. Isochrone shown is given by Eq.16.1 for $\bar{B}_m \equiv 0.6$. Data from (●) Tavenas & Leroueil (1980), ○ Ortigao (1980), (△) Kabbaj (1985).

tion isochrone, indicating that in these cases there is significant consolidation during the early stages of construction when the soil is overconsolidated. The amount of consolidation that occurs during the early stages of construction will vary with the consolidation characteristics of the clay, the thickness of the clay deposit, the drainage conditions and the rate of loading of the embankment and this can explain the scatter of data evident in Fig. 16.2. This said, however, there does appear to be a general tendency that can be approximated by an isochrone of the form:

$$\bar{B}_1 = \bar{B}_m \left[1 - \left(\frac{z}{\Lambda} - 1 \right)^2 \right] \qquad (16.1)$$

where z = the distance from the upper drainage boundary, Λ = the drainage path ($\Lambda = 0.5D$ in Fig. 16.2), and $\bar{B}_m$ = the maximum pore pressure ratio. The value of $\bar{B}_m$ can be expected to vary from case to case as can be

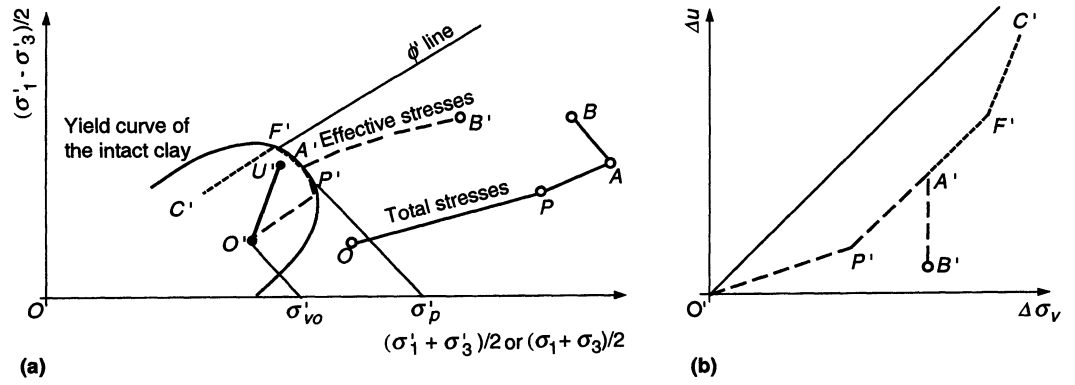


FIGURE 16.3. (a) Effective and total stress paths, and (b) pore pressure under the centerline of an embankment.

seen from the data in Fig. 16.2. This figure shows an isochrone for $\bar{B}_m \cong 0.6$.

If the behavior of the clay foundation under an embankment were perfectly undrained, the effective stress path for a point at or near the centerline would be as O′–U′ in Fig. 16.3a. However, as a consequence of the rapid consolidation during early stages of construction, the effective stress path may be O′–P′, reaching the limit state curve at P′, at a vertical effective stress, σ'_v, close to the preconsolidation pressure, σ'_p, of the clay. As the clay becomes normally consolidated, its coefficient of consolidation is reduced by a significant amount and the behavior becomes essentially undrained. Due to the shape of the limit state curve of natural clays (see Section 2.10), further loading is associated with a stress path such as P′–A′, under an essentially constant vertical effective stress equal to σ'_p. Such a stress path corresponds to an increase in pore pressure equal to the increase in total stress ($\bar{B}_2 = \Delta u/\Delta\sigma_v = 1.0$), as shown in Fig. 16.1 during the second phase of loading.

The change in pore pressure generation during construction is thus associated with the yielding of the soil when the effective stress path reaches the limit state curve. This *in situ* vertical yield stress, (σ'_{vy}), has been compared with the preconsolidation pressure measured in conventional 24-h oedometer tests, (σ'_{pconv}) (Morin *et al.* 1983; Leroueil 1996). The results can be summarized as follows: for overconsolidation ratios (OCRs, estimated on the basis of laboratory tests) between 1.2 and 2, there is a good agreement between the two parameters; at lower OCRs, laboratory tests generally slightly underestimate *in situ* values, typically by 10%; for OCRs larger than 2, laboratory tests generally overestimate *in situ* values, as indicated in Fig. 16.4. Based on data for clays with $2 \leq \text{OCR} \leq 6$ (Fig. 16.4), Leroueil (1996) proposed:

$$\sigma'_{vy} = \frac{\sigma'_{pconv}}{0.64 + 0.26\ \text{OCR}}. \qquad (16.2)$$

The overestimation of σ'_{vy} by laboratory tests in overconsolidated clays with OCR > 2 can be explained by the shape of the limit state curve of natural clays and the fact that coefficient of earth pressure at rest, K_0, is high in these materials (Leroueil *et al.* 1978b). If the embankment is built to a height in excess of that corresponding to point A in Fig. 16.3, the effective stress path will continue up to F′, on the strength envelope of the normally consolidated clay, where there is local failure

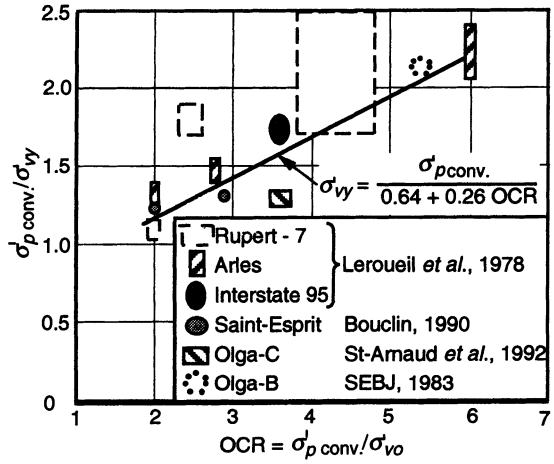


FIGURE 16.4. Variation of ratio $\sigma'_{pconv}/\sigma'_{vy}$ with overconsolidation ratio of clay (only sites with OCRs $2 \leq OCR \leq 6$ are presented) (after Leroueil 1996; reproduced with permission ASCE, *Journal of Geotechnical Engineering*).

and then possibly to the critical state C′. Between F′ and C′, the increase in excess pore pressure is larger than the increase in total stress ($\bar{B}_3 = \Delta u/\Delta\sigma_v > 1.0$) as shown in Fig. 16.3b. It should be noted that $\bar{B}_1$, $\bar{B}_2$ and $\bar{B}_3$ discussed above are incremental values during different stages of loading and do not correspond directly to the conventional $\bar{B} = (\Delta u/\Delta\sigma)$ under the entire loading (where $\Delta\sigma = \gamma H$). Hence a high value of $\bar{B}_3$ does not necessarily mean that the embankment is unstable. As discussed later, pore pressure may develop even after construction is completed, i.e. when there is no increase in total stress, but $\bar{B}$ may still be less than unity.

The pore pressure generated during the construction of an embankment and the corresponding stress path have a direct influence on settlements and lateral displacements. The observations of the Kalix test embankment (Holtz & Holm 1979) shown in Fig. 16.5 (with P′ and F′ conditions corresponding to those in Fig. 16.3a) illustrate this fact.

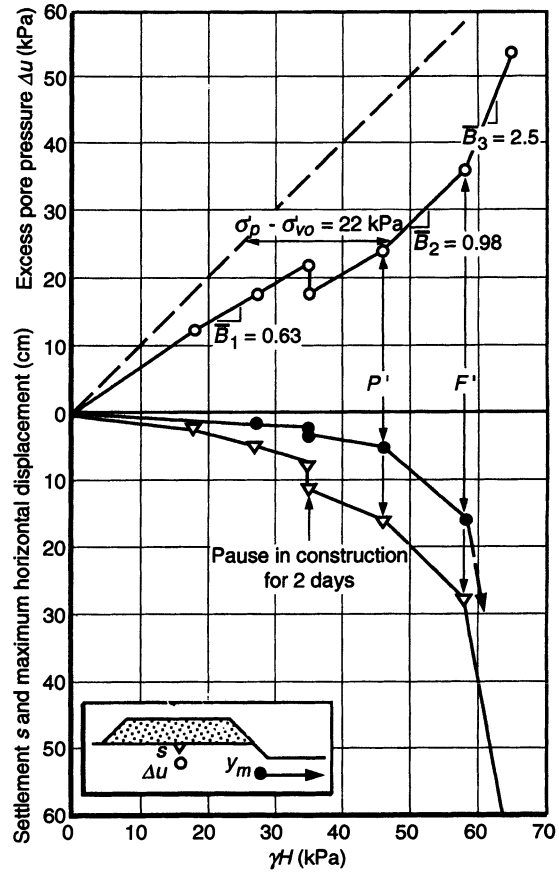


FIGURE 16.5. Behavior of trial embankment at Kalix, Sweden, during construction (modified from Holtz & Holm 1979).

16.1.2 CLAY BEHAVIOR AFTER THE END OF CONSTRUCTION

During construction the effective stress path is such as O′–P′–A′ (Fig. 16.3a). The total stress state at the end of construction is at A and the pore pressure is defined as the horizontal distance between A and A′. During the consolidation stage, after the end of construction, the effective stress condition moves along A′–B′, whereas the total stress state moves from A to B under an essentially constant vertical total stress (allowing here for some stress redistribution and hence some change in $\sigma_1 - \sigma_3$).

16.1.3 STAGE CONSTRUCTION

As the vertical effective stress increases beyond σ'_p, there is a decrease in void ratio and an increase in undrained shear strength. Consequently, if the initial undrained shear strength is too small to ensure the stability of the embankment under its final height, the strength can be progressively increased by constructing the embankment in stages, with sufficiently long periods of consolidation between the stages to allow pore pressure to decrease and strength to increase. In some cases, there may be little or no measurable strength gain in a reasonable time and conventional stage construction may not be useful (e.g. see Lo & Stermac 1965; Stermac *et al.* 1967). In some cases, relatively large strains (thus consolidation) are necessary before observing a measurable strength increase. The consolidation process can be accelerated by appropriate use of vertical drains (see Section 15.2.3).

Figure 16.6a presents a typical stress path at or near the embankment centerline during stage construction. During the second and following stages, loading is associated with stress paths such as B′–D′ and E′–G′ on the new limit state curves. If loading is continued beyond the point G′, then this soil element can reach local failure at F'_E, and will then move towards the critical state of the soil, C'_E, corresponding to the new void ratio of the soil. The corresponding pore pressures are as illustrated in Fig. 16.6b, with pore pressure increases during the reloading stages approximately equal to the increase in total vertical stress near the embankment centerline.

16.1.4 PORE PRESSURES

Pore pressures generated during the construction of an embankment are generally as illustrated in Fig. 16.3b, with $\bar{B}_1$ during the early stages of loading as described by Fig. 16.2 and Eq. 16.1. At the end of construction, the vertical effective stress is generally close to the preconsolidation pressure of the clay and in this case the excess pore pressure that will dissipate after construction is given by:

$$\Delta u = \Delta\sigma_v - (\sigma'_p - \sigma'_{vo}). \qquad (16.3)$$

When the embankment is loaded to such a height that local failure is reached at point F′ (Fig. 16.3a), there may be softening of the clay associated with an increase in pore pressure larger than the increase in total vertical

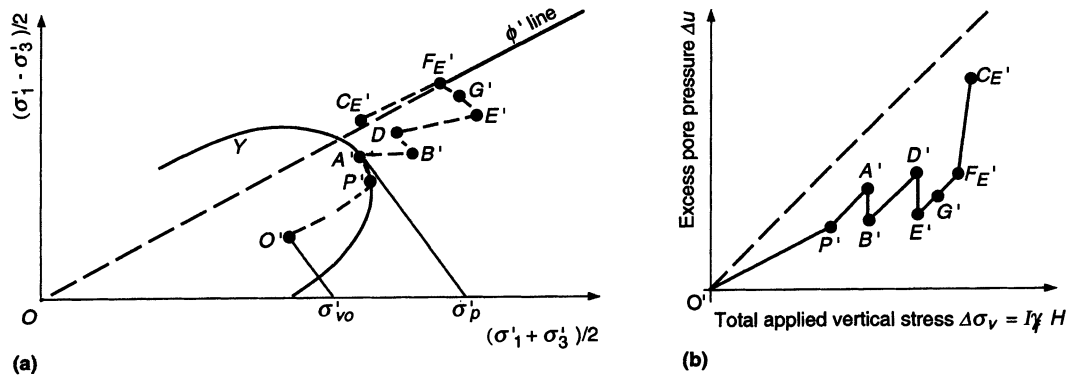


FIGURE 16.6. (a) Effective stress path, and (b) pore pressure under the centerline during stage-construction of an embankment.

stress (Fig. 16.3b) and the stress path may be along F′–C′. As indicated by Folkes and Crooks (1985) and Leroueil and Tavenas (1986), there are some field cases where the behavior is essentially undrained, many cases like those discussed here where there is some yielding after partial dissipation of pore pressure, and some cases in which yielding was not reached during construction. In this latter situation, the pore pressures rapidly decrease after the end of construction.

16.2 General Behavior of Reinforced Embankments on Clay Foundations

The earth pressure that develops within the fill placed over a soft clay foundation causes outward shear stresses on the clay, which serve to reduce the bearing capacity of the underlying foundation and hence reduce the stability of the embankment (Fig. 16.7a–c). Thus the stability can be increased by the in-

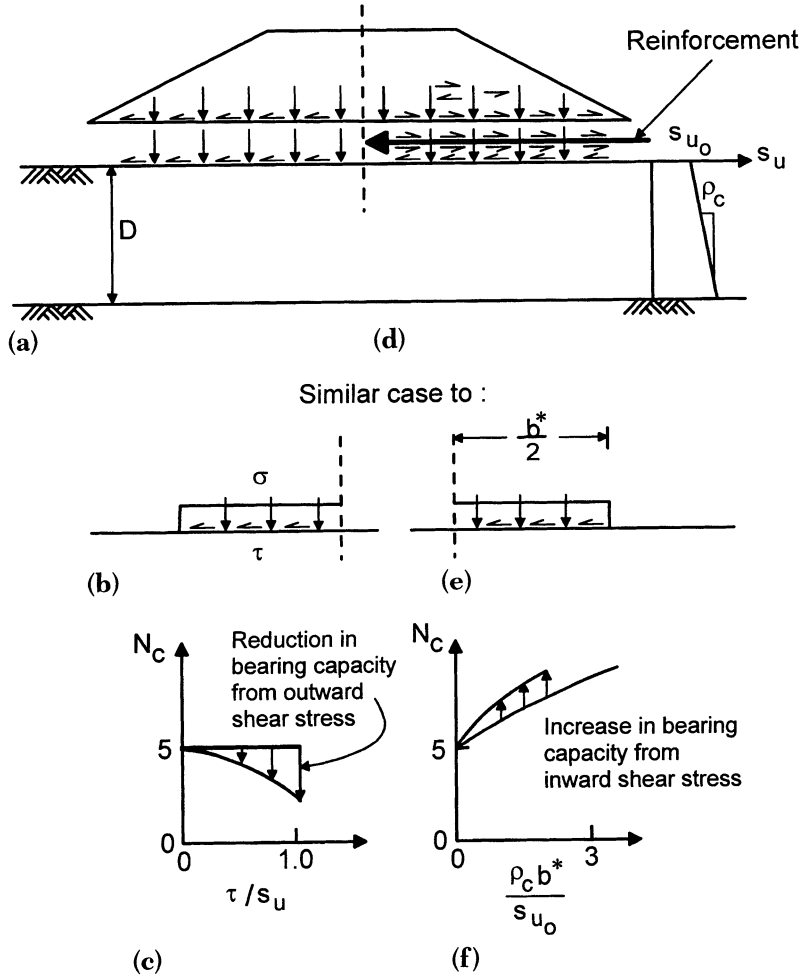


FIGURE 16.7. Summary of mechanics in a reinforced embankment on soft soil (modified from Jewell 1996): (a) unreinforced; (b) footing subject to outward shear stress; (c) reduction in bearing capacity, N_c, from outward shear stress; (d) reinforced; (e) rough footing; and (f) increase in bearing capacity, N_c, from inward shear stress.

clusion of one or more layers of reinforcement in the fill at (or close to) the fill–clay interface. The reinforcement serves two primary functions. First, it resists some or all of the earth pressure that develops within the embankment, thereby reducing the disturbing forces. The extent to which it attracts the horizontal thrust depends on the stiffness of the reinforcement relative to the underlying soil and the shear strength, s_u, of the foundation. The movement of the reinforcement and adjacent soil will be the same until slip occurs at the interface. Thus, in response to the development of earth pressure as the embankment is constructed, there will be some lateral movement away from the centerline and a sharing of the horizontal thrust between the reinforcement and the underlying foundation. The degree of load sharing will be controlled by considerations such as strain compatibility and the relative stiffness of the reinforcement and foundation.

The second primary function of the reinforcement is to resist the lateral deformations of the foundation that would otherwise occur in response to the applied vertical load. If the soil below the reinforcement is trying to move more than the movement of the reinforcement, then the reinforcement will induce an inward shear stress on the foundation (see Fig. 16.7d–f). The magnitude of this shear stress depends on the axial stiffness of the reinforcement, the strength and stiffness of the foundation and, in particular, the shear strength at or near the fill–foundation interface. This shear stress serves to increase the embankment stability if the thickness of the soft soil layer, D, is less than 0.7 times the width of the reinforced embankment, b^* (details of how to calculate b^* will be given in Section 16.8.3.2) or if the undrained shear strength increases with depth.

The effectiveness of reinforcing embankments on soft foundations depends on the relative stiffness of the reinforcement and underlying foundation soil. Given the stiffness of most readily available reinforcement (typically woven geotextiles or geogrids; see Chapter 7 for a discussion of these materials; but steel strips or grids may also be used), reinforcement tends to have the greatest effect on soft foundations ($s_u < 30$ kPa).

The behavior of reinforced embankments can best be explained in the context of the analysis of observed field behavior. Rowe & Soderman (1984) examined the behavior of an unreinforced and a reinforced embankment constructed on a relatively thin (3.3 m) layer of organic clay ($s_u \cong 8$ kPa) underlain by dense sand. The unreinforced embankment failed quickly when the fill height reached about 1.8 m. In contrast to the rapid failure of the unreinforced embankment, the reinforced embankment experienced relatively ductile failure at a height of 2.75 m. Both the observed and calculated reinforcement strains exhibited the same general trends as shown in Fig. 16.8. The analysis indicated that for fill heights less than 1 m, the mobilized shear stress was less than the shear strength of the soil and the strains in the reinforcement were small. As the fill increased from 1 to 2 m, there was an increase in the strain in the reinforcement as a region of plastic failure developed within the clay. Once the soil had reached its shear strength along a potential failure surface (at a fill height of about 2 m here), the embankment was completely dependent upon the geosynthetic reinforcement for the support of additional fill and, as a consequence, the strains increased rapidly as more fill was added. In this case, the geosynthetic–soil interface strength was reached over a significant length of the geosynthetic at a height of about 2.7 m and, since the geosynthetic could not sustain any additional load, this corresponded to the limiting strain shown in Fig. 16.8 and failure of the embankment.

In the case examined above, even with this very soft clay ($s_u \cong 8$ kPa) and relatively stiff geotextile reinforcement (strength $T_f = 200$

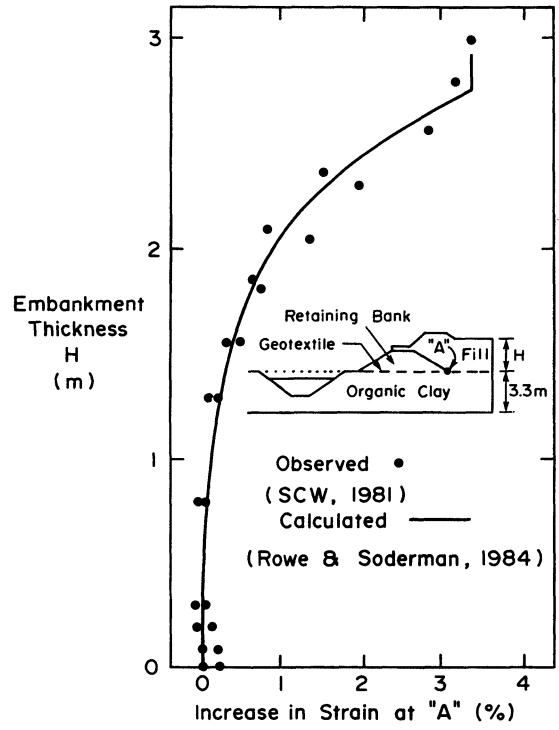


FIGURE 16.8. Comparison of predicted — (SCW 1981) and observed (●) reinforcement strains at strain gage location A (modified from Rowe & Soderman 1984).

kN m^{-1} and tensile stiffness J = 2000 kN m^{-1}), the reinforcement was only significantly mobilized after extensive shear failure had developed within the foundation soil. Taking the collapse height to be 2.75 m and applying a factor of safety of 1.3, the working height for a reinforced embankment with this reinforcement and soil profile would have been about 2.1 m. At this height, the strain in the reinforcement would only have been about 1%, even though this height is a little above the height at which the unreinforced embankment collapsed. Thus the reinforcement usually does not play a significant role in providing a stabilizing force until the soil has reached its shear strength along a potential failure surface. For this reason, one must be careful in assessing the shear strength of the soil and particular care is required on brittle soils that experience significant strain softening (see Mylleville & Rowe 1991).

As noted in Section 16.1.1, for most embankment cases the soil will be initially overconsolidated and there will be relatively rapid dissipation of pore pressures and small lateral displacements until the soil becomes normally consolidated. This has been examined theoretically by Rowe and Li (1999) and shown to have significant implications with respect to increasing stability. However, it is generally (and conservatively) not considered in the design of reinforced embankments, and undrained conditions are normally assumed from the commencement of construction. Partly as a consequence of this, the observed strains in reinforcement are often less than those expected based on the design assumption of undrained conditions.

Soil reinforcement may be used in conjunction with vertical drains (see Sections 15.2.3.4 and 15.2.3.5) and stage construction (Section 16.1.3) to accelerate the rate at which an embankment can be constructed to a desired grade. The reinforcement allows construction of thicker lifts in each stage and hence fewer stages are needed (see Li & Rowe 1999).

16.3 General Behavior of Peat Deposits Under Embankments

16.3.1 PEAT CHARACTERISTICS

There are many different classification systems with different definitions of what constitutes "peat" (e.g. see Landva *et al.* 1983; Hartlén & Wolski 1996). Unfortunately, these systems are not very consistent and the inorganic component (ash content) of peat may range from less than 20 up to 80%. Thus the term "peat" is often used to include organic soils that may range from jelly-like organic silts and very soft organic clay "muds", to extremely coarse-fibrous meshes of woody remains and fibers.

The wide range of classification for "peat" has led to much confusion, since a "peat" with 80% ash content and a significant clay

component will respond to embankment loads in a manner similar to a clay (as discussed in Section 16.1) whereas a fibrous peat with less than 20% ash content may behave more like a frictional material than a cohesive material. For the purposes of this book, the term "peat" is reserved for soils with less than 20% ash content. Even with this restriction, there can be a variety of peats ranging from amorphous granular peats to coarse fibrous peats (see Section 3.2.11 and Table 3.7).

Peats typically have a high natural water content (50–2000%), high void ratio (usually 5–15, but may be up to 25) and high compressibility. The hydraulic conductivity of peat is typically high at high void ratios, but reduces significantly as the peat compresses (Lefebvre *et al.* 1984). Due to the high void ratio and compressibility, it is usually not practical to obtain realistic strength parameters from conventional triaxial tests (these yield "friction angles" of 45–55° based on envelopes drawn when the tests were terminated due to excessive deformation rather than shear failure (see Adams 1961; Edil & Dhowian 1981; Rowe *et al.* 1984b). Also, due to the fibrosity of many peats, it may be difficult obtaining reliable strength parameters from direct shear tests for these peats. Landva (1980) has had success using ring shear apparatus and Rowe (Rowe *et al.* 1984b; Rowe & Mylleville 1996; and various unpublished reports) has obtained clearly defined failure envelopes using the Norwegian simple shear apparatus. Table 16.1 summarizes the strength properties obtained for some Canadian peats. Good predictions of embankment behavior have been obtained using these strength parameters evaluated in this manner (see Rowe *et al.* 1984b; Rowe & Mylleville 1996).

16.3.2 PORE PRESSURES

Because of the high initial hydraulic conductivity of peat, some pore pressure dissipation will occur during construction; however, excess pore pressures will be developed and they normally reach a maximum value at the end of construction. In a similar manner to that already described in Section 16.1 for the early stages of loading on clay, the observed increase in pore pressure in peat due to embankment loading can be characterized in terms of the pore pressure parameter $\bar{B} = \Delta u/\Delta\sigma_v$ and Eq. 16.1, as shown in Fig. 16.9.

The range of $\bar{B}_m$ values that can be deduced from published field cases is typically 0.1–0.35, although values as high as 0.8–0.9 have been reported (Lupien *et al.* 1983; Adams 1965).

It may be expected that the magnitude of the maximum excess pore pressures and, hence the likelihood of failure, will depend on the rate of loading. Weber (1969) reported that in his experience with peat deposits in the San Francisco Bay area, fills in excess of 1.5 m above original ground level were subject to collapse. The exact height at which instability occurred depended upon the foun-

TABLE 16.1. Strength properties reported for peats

Description and classification category (see Table 3.7)	Natural water content (%)	c'(kPa)	ϕ'(°)	Reference
Fine fibrous peat				
C11	527	1	26	Rowe *et al.* (1984b)
C9	656	1.2	26	Personal Files
Coarse fibrous peat				
C13	680	2.5	28	Rowe & Mylleville (1996)
C12	1450	0.5	29	Personal Files
Sphagnum peat	1200–1500	2.5	27	Landva (1980)
	1200–1500	3.5	33	Landva (1980)

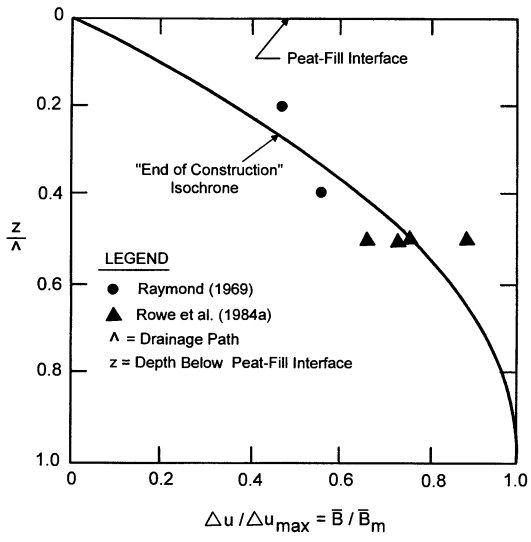


FIGURE 16.9. Observed excess pore pressure distribution at end of construction for two embankments constructed over peat (modified from Rowe & Soderman 1985b). Data from: ● (Raymond 1969), ▲ (Rowe *et al.* 1984). Λ = drainage path, z = depth below peat–fill interface.

dation condition and rate of loading. At a construction rate of 0.9 m of fill per week, he reported a collapse of a fill at a height of 2.4 m. At an even slower construction rate (0.15–0.3 m per week), fills to a height of about 3 m could be constructed without failure.

16.3.3 BEHAVIOR DURING AND AFTER CONSTRUCTION

The peats examined in the investigations summarized in Table 16.1 all exhibited an essentially frictional behavior, with a friction angle typically between 26 and 29°. The initial effective stresses both within the peat and any very soft clay or silt layer below the peat are initially very low. If loaded too quickly, i.e. without significant pore pressure dissipation during loading, the only shear strength available to carry the load is a small apparent cohesion (only a few kPa for the peats examined in Table 16.1 and this is due to the tensile strength of the fibers in the peat) and the tensile strength of any root mat, which acts like reinforcement. Thus when loaded quickly, peats are likely to fail. For example, Flaate and Rygg (1964), Ripley and Leonoff (1961) and Lupien *et al.* (1983) report "shear failures" that, on the basis of the published data, appear to involve failure in the peat and not in the soil underlying peat. These failures do not usually involve the formation of a definite sliding surface. Rather, the collapse involves rapid and excessive shear deformations that give rise to large embankment settlement, lateral movement and "mud" waves. In this context, collapse will be distinguished by the fact that additional fill will not increase the height of the embankment unless steps are taken to stabilize the embankment, i.e. allowing pore pressure dissipation during construction, use of berms, etc.

The behavior of a number of unreinforced embankments constructed on peat underlain by a weak layer has been reported in the literature (MacFarlane & Rutka 1959; Lea & Brawner 1963; Weber 1969; Raymond 1969; Rowe & Mylleville 1996). Collapse in these cases usually involves formation of a crack in the embankment and a block-like slide moving on or just below the boundary between the peat and the underlying soft soil.

Field observations have established that embankments constructed on peat settle rapidly during construction (loading) and then continue to settle at a reduced rate after loading (e.g. Hanrahan 1964; Adams 1965; Weber 1969; Rowe *et al.* 1984a,b). An examination of the time–settlement curves indicates that "primary" consolidation occurs relatively quickly (typically 5–200 days after construction) for typical thicknesses of peat (2–10 m), after which the settlement continues to increase with time due to secondary compression. However, significant excess pore pressures have also been observed at times long after the time–settlement curve indicates that "primary" consolidation is complete. These excess pore pressures appear to re-

main at a relatively constant value for considerable periods of time (e.g. Adams 1965; Rowe *et al.* 1984a). The reasons for this behavior have not generally been agreed upon (e.g. see Adams 1965; Landva & La Rochelle 1983). It could be that these excess pore pressures are "creep induced pore pressures" resulting from time-dependent compression of both the peat fibers and of the organic structure itself, they could also be due to a rise of the water table within the embankment. Clearly, the possibility of the presence of these excess pore pressures for long periods of time may have important consequences when considering stage loading of a peat deposit and, in such cases, it would be advisable to provide instrumentation to measure the pore pressure and to use this information to monitor the construction.

From the available data, it may be concluded that where drainage of the peat is provided and a slow rate of construction is used, there will be little difficulty in constructing low (2 m or less) embankments on peat, although settlements may be large. However, when an impervious fill is used or where the peat is underlain by soft marl or clay, it may not be possible to construct even low embankments on the peat unless special measures are taken to ensure stability, e.g. provide drainage, berms, geotextiles, use of lightweight fill, etc.

16.4 Settlements

16.4.1 STRESS DISTRIBUTION UNDER EMBANKMENTS

The vertical stress increase due to an embankment is generally calculated assuming isotropy and elasticity of the soil, and by:

$$\Delta\sigma_v = I\gamma_f H \qquad (16.4)$$

in which I = the influence factor, γ_f = the unit weight of the fill material, and H = the thickness of embankment fill.

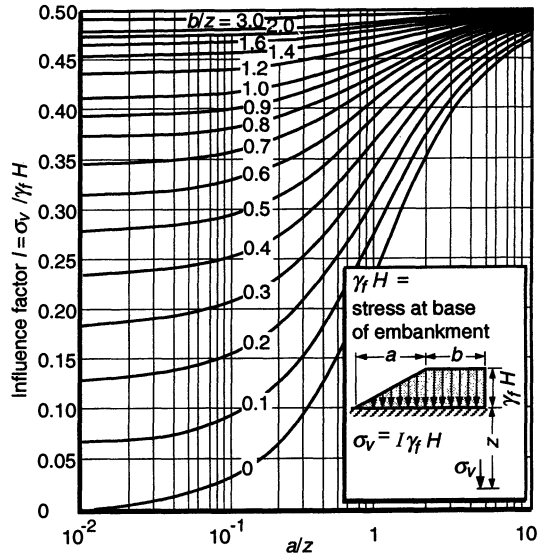


FIGURE 16.10. Chart for calculation of vertical stresses caused by embankment (modified from Osterberg 1957).

For long and trapezoidal embankments, the solution proposed by Osterberg (1957), Fig. 16.10, is generally adequate. This solution gives the change in stress at depth z due to the trapezoidal applied stress shown in the insert. To obtain the stress at any point, one must use the principle of superposition. Thus at the centerline one would multiply the value deduced by two, i.e. an equal contribution from each side. For a point away from the centerline, one would need to use Fig. 16.10 twice (once for the geometry on the left of the point of interest, and once for the geometry on the right). Similarly, berms could also be approximately considered by extending the use of superposition to include the contribution of the berm to the change in stress at the point of interest. Poulos & Davis (1974) give a compendium of elastic solutions that may be used for more complex cases. Alternatively, numerous computer programs are available for calculating stresses in elastic media.

It is important to note that stress distribu-

tion changes during consolidation and this can affect the final settlement. Considering a point a on the surface of the compressible deposit, a point b of interest within the deposit and a point e at the bottom of the deposit, different aspects to be considered include:

- The total vertical stress applied at a given point, b, in the foundation decreases with the expulsion of water associated with the settlement (change in soil thickness) that has occurred above this point (S_{ab}):

$$\Delta q = -\gamma_w S_{ab}. \tag{16.5}$$

- On the other hand, the total vertical stress increases due to the fact that the upper part of the natural soil deposit, and possibly the lower part of the embankment, has moved below the water table. If $\Delta\gamma$ is the increase in unit weight of the soil when it becomes submerged and if h_w is the rise of water table above its initial level, and S_{ae} is the surface settlement, then:

$$\Delta q = \Delta\gamma(S_{ae} + h_w). \tag{16.6}$$

- The reference pore pressure changes due to the settling of the point, b, and a possible change of the water table. If the entire deposit is influenced by this latter change, then:

$$\Delta u = \gamma_w(S_{be} + h_w) \tag{16.7}$$

in which S_{be} = settlement of point b. Recognizing that $S_{ab} = S_{ae} - S_{be}$ and combining Eqs 16.4–16.7, the change in effective stress due to embankment construction is given by:

$$\Delta\sigma'_v = (\Delta\gamma - \gamma_w)(S_{ae} + h_w) + I\gamma_f H. \tag{16.8}$$

When the change in water table affects only the upper boundary of the consolidating layer and not the water pressure at the bottom, the change in stress applied by the embankment varies with depth, but is close to:

$$\Delta\sigma'_v = \Delta\gamma(S_{ae} + h_w) - \gamma_w(S_{ae} + 0.5h_w) + I\gamma_f H. \tag{16.9}$$

Although the changes in effective stress arising from Eqs 16.5–16.9 have often been neglected, they do need to be considered because the change in effective stress, $\Delta\sigma'_v$, can be quite significant and the use of these equations is quite straightforward.

16.4.2 CONSTRUCTION SETTLEMENT

The settlement S_c at the end of construction results from the sum of the recompression settlement, S_r (O′ towards P' in Fig. 16.3), and a settlement, S_u, resulting from undrained shearing (P′–A′ in Fig. 16.3):

$$S_c = S_r + S_u. \tag{16.10}$$

Consider a layer, i, of thickness D_i. If a representative point in the layer with an initial effective stress, σ'_{voi}, and void ratio, e_{oi}, experiences an increase in stress, $\Delta\sigma_v$, due to the embankment, then the recompression settlement, S_{ri}, of this layer can be calculated as:

If $(\sigma'_{voi} + \Delta\sigma_v)$ is less than the preconsolidation pressure, σ'_p, then:

$$S_{ri} = \frac{D_i}{1 + e_{oi}} C_{si} \log\left(\frac{\sigma'_{voi} + \Delta\sigma}{\sigma'_{voi}}\right). \tag{16.11a}$$

Otherwise, if $\sigma'_{vo} + \Delta\sigma_v \geq \sigma'_p$

$$S_{ri} = \frac{D_i}{1 + e_{oi}} C_{si} \log\left(\frac{\sigma'_p}{\sigma'_{voi}}\right) \tag{16.11b}$$

where C_{si} is the swelling index for the layer (see Sections 2.7.3 and 3.5.2 and Fig. 2.7). Now the total recompression settlement, S_r, can be obtained by summing the values for each layer, giving:

$$S_r = \sum_{i=1}^{n} S_{ri}. \tag{16.12}$$

The undrained shearing settlement, S_u, associated to the stress path P′–A′ in Fig. 16.3 results from plastic flow of the normally consolidated clay. This could be evaluated using a suitable finite element program and representative soil parameters. Alternatively, the following relation established by Tavenas and Leroueil (1980) on the observations of 12 embankments on clay from different countries could be used as an approximation:

$$S_u = (0.07 \pm 0.03)(H - H_{nc}) \quad (16.13)$$

where H_{nc} = the height of the embankment when the foundation clay becomes normally consolidated (point P′ in Fig. 16.3). H_{nc} can be estimated from the concepts described in Section 16.1.1.

16.4.3 LONG-TERM SETTLEMENT

16.4.3.1 Primary Consolidation Settlement

At the end of construction, the effective stress conditions below the centerline of an embankment often correspond to a vertical effective stress close to the preconsolidation pressure of the clay. The long-term settlement is thus associated with an effective stress increase from σ'_p to $(\sigma'_{vo} + \Delta\sigma)$ and can be calculated as follows for a homogeneous layer of thickness D_i:

$$S_{di} = \frac{D_i}{1 + e_{oi}} C_{ci} \log\left(\frac{\sigma'_{voi} + \Delta\sigma}{\sigma'_{pi}}\right). \quad (16.14)$$

At the end of primary consolidation, when the excess pore pressures have dissipated, the settlement of embankments can usually be calculated on the basis of parameters from the conventional 24-hour oedometer test (see also Section 16.4.3.2). Due to the fact that the normally consolidated branch of the compression curve is not always linear, C_c has to be taken as a secant compression index between the preconsolidation pressure and the final vertical effective stress. Typical correlations for C_c are given in Section 3.5.2.

The total post-construction settlement, S_d, is the sum of the settlements, S_{di}, of the different soil layers:

$$S_d = \sum_{i=1}^{n} S_{di} \quad (16.15)$$

Thus the total settlement, S, is given by adding Eqs 16.10 and 16.15, namely:

$$S = S_r + S_u + S_d \quad (16.16)$$

16.4.3.2 Contribution of the Viscosity of Clay to Total Settlement

It has been shown (Leroueil *et al.* 1985a; Imai & Tang 1992) that, during one-dimensional compression and in laboratory conditions, the behavior of clays is controlled by a unique effective stress–strain–strain rate $(\sigma'_v, \varepsilon_v, \dot{\varepsilon}_v)$ [or $(\sigma'_v, e, \dot{e}_v)$] relationship. At a given stress, the lower the strain rate, the higher the strain. This applies during both primary and secondary consolidation. In particular and as a first approximation, it can be considered that the logarithm of the preconsolidation pressure varies linearly with the logarithm of the strain rate. It can also be shown that the slope $m' = \Delta \log \dot{\varepsilon}_v / \Delta \log \sigma'_p$ is in fact equal to the ratio $C_c/C_{\alpha e}$, where $C_{\alpha e}$ is the secondary compression index as defined in Section 2.7.5. Table 3.14 gives typical values of $C_{\alpha e}/C_c$ and m' for different types of soils. For inorganic clays, $C_{\alpha e}/C_c$ is typically about 0.04 (Mesri & Godlewski 1977).

Temperature also influences the behavior of clay. At a given strain rate and at a given effective stress, the higher the temperature, the higher the strain (Leroueil & Marques 1996). Since the temperature beneath an embankment may be different from that of the laboratory and the field strain rate is generally smaller than that in the laboratory by a few orders of magnitude, the settlements *in situ* could be different from those expected for

the same stress increase in laboratory conditions.

Using the viscous model described above, Leroueil (1988, 1996) evaluated the strain component, $\Delta\varepsilon_s^*$, that should be added to the strain, estimated on the basis of the conventional 24-h oedometer test, to evaluate the strain at the end of the *in situ* primary consolidation in the field. Considering the end-of-primary consolidation (EOP) to correspond to a degree of consolidation of 95% according to one-dimensional consolidation theory (Section 2.7.4), the strain rate at this time can be described by (Leroueil 1988, 1996):

$$\dot{\varepsilon}_{EOP} = 0.16ku_o'/(\gamma_w\Lambda^2) \qquad (16.17)$$

where k = hydraulic conductivity of the clay, u_o' = initial excess pore pressure, and Λ = maximum drainage length. Assuming that the temperature *in situ* is about 12 °C below that in the laboratory, the viscous strain, $\Delta\varepsilon_s^*$, and settlement S_{vi} can be deduced from the strain rate model to be given by:

$$S_{vi} = D_i\Delta\varepsilon_s^* = \frac{D_iC_c}{(1+e_o)m'} \times \left[\log(6\times10^{-9}) - \log\left(\frac{0.16u_o'k}{\gamma_w\Lambda^2}\right)\right] \qquad (16.18)$$

where D_i = the layer thickness, C_c = compression index under the final effective stress, e_0 = initial void ratio, m' = $\Delta \log \dot{\varepsilon}_v/\Delta \log \sigma_p'$ = $C_c/C_{\alpha e}$ = a strain rate factor having typical values as given in Table 3.14. Figure 16.11 shows $\Delta\varepsilon_s^*$ as a function of $C_c/(1+e_0)$ and $\dot{\varepsilon}_{EOP}$ for an m' value of 32.

In the previously described "viscous approach", the settlement of layer i at the end of primary consolidation would be the sum of the settlement, S_{di}, calculated from Eq. 16.14, using the compression parameters obtained in 24-h oedometer tests, and the viscous settlement S_{vi} defined as Eq. 16.18. This gives an upper limit of settlements since it

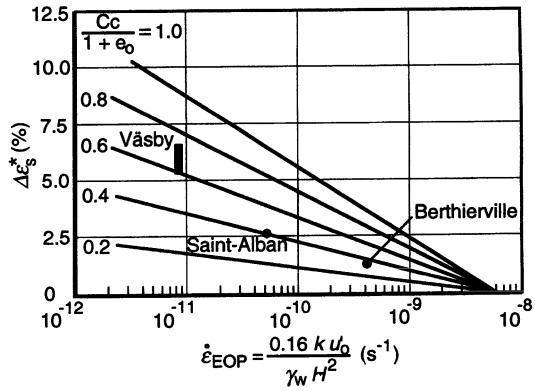


FIGURE 16.11. Estimation of the end-of-primary *in situ* strain, $\Delta\varepsilon^*$, in excess of that determined from conventional 24-h laboratory oedometer test, when strain rate and temperature effects are considered (after Leroueil 1996; reproduced with permission ASCE, *Journal of Geotechnical Engineering*).

neglects the effects of possible disturbance of the specimens tested in laboratory, and the fact that during consolidation *in situ* structure may develop when there is a combination of low strain rate and significant elapsed time and this would reduce the effect of the strain rate (Leroueil *et al.* 1996a).

Mesri & Choi (1985) suggest that the settlement at the end of primary consolidation be calculated from Eq. 16.14, with compression parameters deduced from incremental loading oedometer tests with reloading at the end of primary consolidation (when the excess pore pressure becomes negligible). This approach leads to predicted settlements smaller than those estimated from conventional 24-h oedometer tests since these latter incorporate some secondary compression. It is thus thought that the Mesri & Choi (1985) approach (also called EOP approach) provides a lower limit of settlements.

Mesri & Choi (1985) and Mesri *et al.* (1994) found that settlement predicted using the EOP approach gives results representative of observed field settlements. On the

other hand, detailed studies performed by Kabbaj *et al.* (1988) on four different sites from Canada and Sweden show that the EOP approach significantly underestimates *in situ* settlements. Leroueil (1988) and Leroueil (1996) indicates that the observed settlements are in rather good agreement with the viscous model described above. Other detailed studies and experience gained in Sweden (Larsson 1986), France (Magnan 1992) and elsewhere (Leroueil 1988) confirm the importance of rate effects during primary consolidation.

The apparently contradictory observations noted above are thought to be due to the effects of: (a) sample disturbance, which increases laboratory strains; and (b) structuring effects, which can decrease *in situ* strains. Unfortunately, there is no validated method for evaluating the ability of a soil to develop structure in *in situ* conditions. On the basis of all these remarks and observations, Leroueil (1996) recommended the following approach:

- For typical projects in clays of low compressibility [$C_c/(1 + e_0)$ values less than 0.25], $\Delta\varepsilon_s^*$ is smaller than 2.5% and is often compensated by some disturbance of the clay and some rise in the water table (see Section 16.4.1), which is often neglected in analyses for these soils. In these cases conventional 24-hour oedometer test results, which already include some secondary compression, can be used, as indicated in Section 16.4.3.1, without any additional viscous correction (described in this section).
- When vertical drains are used to accelerate the consolidation process (see Sections 15.2.3.4 and 15.2.3.5) or when the clay deposit is thin or stratified, the *in situ* strain rate at the end of primary consolidation is larger than 3×10^{-10} s^{-1} in most cases. Consequently, $\Delta\varepsilon_s^*$ remains relatively small and, for the same reasons as those indicated above, the conventional 24-hour oedometer test results can be used as indicated in Section 16.4.3.1 without the correction for viscous effects described in this section.
- In highly compressible clays [$C_c/(1 + e_0)$ values larger than 0.25] or for embankments of special importance (test embankments, embankments for which the magnitude of the settlements may have important consequences), viscous effects could be significant and should be considered as described above.

After the end of primary consolidation, the settlement continues with time due to secondary consolidation. The secondary settlements can be estimated as:

$$S_s = DC_{\alpha\varepsilon} \log\left(\frac{t}{t_p}\right) = \frac{DC_{\alpha e}}{1 + e_p} \log\left(\frac{t}{t_p}\right) \qquad (16.19)$$

in which $C_{\alpha\varepsilon}$ and $C_{\alpha e}$ are measured in oedometer tests (see Section 2.7.5) or estimated from C_c (see Table 3.14); D = the thickness of the clay layer; t_p = the time at the end-of-primary consolidation, which can be practically estimated as the time necessary to obtain a degree of consolidation of 95% (as discussed in Section 16.6); t = the time of interest; and e_p = the void ratio at time t_p.

16.4.4 EFFECT OF EMBANKMENT REINFORCEMENT ON SETTLEMENT

The inclusion of suitable reinforcement at or near the base of the embankment may reduce undrained shear deformations relative to what would have occurred at the same fill height without reinforcement. However, in most practical cases one will not be comparing settlement at the same fill height. The fact that reinforcement is being used usually means that the embankment will be constructed to a greater height than an unreinforced embankment for the same soil profile. This will mean a larger zone of shear failure in the soil for the same factor of safety and, consequently, potentially larger undrained shear deformations than would have been ex-

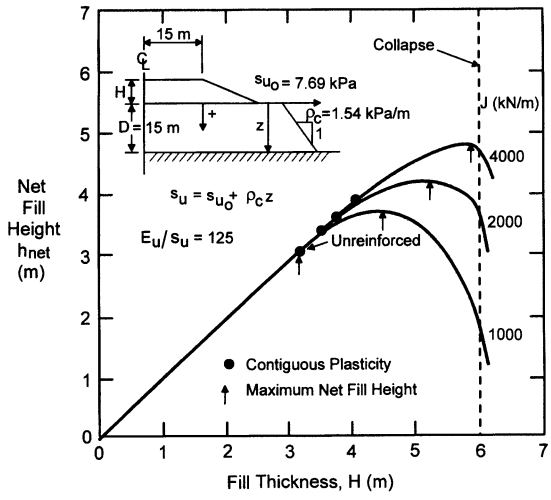


FIGURE 16.12. Net fill height versus fill thickness for various reinforcement tensile stiffness, J, values (modified from Rowe & Soderman 1987): (●) continuous plasticity, (↑) maximum net fill height.

pected for an unreinforced embankment at the same factor of safety against collapse. The magnitude of the undrained deformations will depend significantly on the stiffness of reinforcement used near the base of the embankment.

To illustrate the point made above, consider an embankment and soil profile as shown in the insert to Fig. 16.12. For this soil profile an unreinforced embankment will collapse at a fill thickness $H = 3$ m. Provided there is sufficient reinforcement to maintain equilibrium, the embankment can be constructed to a maximum fill thickness of 6 m. This limit is imposed by bearing capacity considerations (to be discussed in Section 16.8.3) and no amount of reinforcement allows a higher embankment under these foundation conditions unless other methods of soil improvement (see Chapter 15 and Section 16.8) are also introduced. Figure 16.12 shows a plot of the calculated net fill height, h_{net}, beneath the shoulder versus the fill thickness, H, (where $h_{net} = H - S_u$ and it is assumed $S_r \cong 0$) for a reinforcement with tensile stiffness, J, of 1000, 2000 and 4000 kN m^{-1}. In all cases, the calculated collapse fill thickness is essentially the same (6 m), however with $J =$ 1000 kN m^{-1} the embankment could only be constructed to about 3.6 m above original grade before the undrained shear deformation became excessive. In contrast, for $J =$ 4000 kN m^{-1}, the maximum net fill height was about 4.7 m. Thus when dealing with reinforced embankments one could achieve a practical failure height that is less than the collapse height predicted from limit equilibrium or bearing capacity considerations. This necessitates limiting the allowable strain in the reinforcement as discussed in Section 16.8.3.

The inclusion of reinforcement in an embankment has very little effect on long-term settlements, S_d, that would be calculated for an unreinforced embankment with the same fill height as described in Section 16.4.3. However, reinforcement may provide the additional stability required to allow the placing of a surcharge (see Section 16.8.3).

16.4.5 SETTLEMENT OF EMBANKMENTS ON PEAT

Peat deposits typically experience significant settlement by the end of construction, additional consolidation settlement and secondary compression. Due to the low initial stresses, equations such as Eqs 16.11 and 16.14 generally cannot be used to establish the construction settlement, S_{ri}, and consolidation settlement, S_{di}, of a layer. Rather, total settlement, S, of a peat deposit of thickness, D must either be established based on data from consolidation tests (oedometer) giving Δe versus $\Delta\sigma'_v$:

$$S = \int_0^D \frac{\Delta e(z)}{1 + e_o} dz = \int_0^D \varepsilon_v(z) dz \quad (16.20)$$

where $\Delta e(z)$ and $\varepsilon_v(z)$ will depend on $\Delta\sigma'_v(z)$, which may vary with depth, z. Alternatively, one can estimate the settlement, S:

$$S = \varepsilon_v D \tag{16.21}$$

where ε_v = a function of the change in vertical effective stress, $\Delta\sigma'_v$. In the simplest case, assuming a linear relationship between strain and effective stress increase, ε_v is given by:

$$\varepsilon_v = \Omega\left(\frac{\Delta\sigma'_v}{p_a}\right) \tag{16.22}$$

where p_a = atmospheric pressure and, based on data from a large number of field cases (see Rowe 1984), $\Omega = 0.24$ represents a minimum settlement, $\Omega = 0.66$ represents a typical situation (recognizing wide scatter of data), $\Omega = 1.6$ (for $\Delta\sigma'_v \leq 40$ kPa) represents an upper bound to most field data.

When considering embankments on peat the change in effective stress will usually depend on the settlement and will, as a first approximation, be given by:

$$\Delta\sigma'_v(z) = \gamma_f H - \gamma_w S - \Delta u(z) \tag{16.23}$$

where H = the fill thickness and S = the settlement (assuming here that the water table is at or very close to the original ground level, as is often the case) and that the unit weight of the fill does not increase significantly, and $\Delta u(z)$ is the change in pore pressure at depth z (e.g., due to a rise in water table into the embankment). It also assumes that the embankment is wide compared to the peat deposit thickness.

To estimate the end of construction settlement, S_r, one can use the end of construction pore pressure isochrone given by Eq. 16.1 to calculate the end of construction change in stress, $\Delta\sigma'_v(z)$, and then combining Eqs 16.20, 16.22 and 16.23, integrating and solving for S_r gives:

$$S_r = \Omega\gamma_f HD(1 - \bar{B}_m D/\Lambda + \bar{B}_m D^2/3\Lambda^2)/$$
$$[p_a + \Omega\gamma_w D(1 - \bar{B}_m D/\Lambda + \bar{B}_m D^2/3\Lambda^2)] \tag{16.24}$$

and $\Lambda = 0.5D$ for two-way drainage and $\Lambda = D$ for one-way drainage. End of construction values of $\bar{B}_m$ for peat typically range between 0.1 and 0.35 (see Section 16.3.2). This equation can be evaluated using a hand calculator. For typical combinations of parameters ($B_m \leq 0.35$), the settlement at the end of construction, S_r, ranges between 80 and 100% of the "final" consolidation settlement, i.e. $S_r \cong 0.9S \pm 0.1S$. The "final" settlement corresponds to $\bar{B}_m = 0$ and Eq. 16.24 reduces to:

$$S = \frac{\Omega\gamma_f HD}{(p_a + \Omega\gamma_w D)} \tag{16.25}$$

Equation 16.22 suffers from the presumption that the strain is linearly proportional to effective stress where, in fact, the peat becomes stiffer with increasing applied stress. A generally conservative, i.e. tending to overpredict settlement, bi-linear approximation is given by:

$$\Omega = 1.33 \text{ for } \left(\frac{\Delta\sigma'_v}{p_a}\right) \leq 0.4 \tag{16.26}$$

$$\Omega = 0.33 + 0.4\, p_a/\Delta\sigma'_v \text{ for } \left(\frac{\Delta\sigma'_v}{p_a}\right) > 0.4. \tag{16.27}$$

For values of $\Delta\sigma'_v/p_a \leq 0.4$, Eqs 16.24 and 16.25 can be used directly to get an upper bound on end of construction, S_r, and final settlement, S (including some secondary compression). For $\Delta\sigma'_v/p_a \geq 0.4$, an iterative solution can be obtained by estimating S_r and S, calculating Ω from Eq. 16.27, calculating an improved estimate of S_r and S from Eqs 16.24 and 16.25 and repeating the procedure until convergence is attained.

Settlements due to secondary compression can be particularly significant for embankments on peat, especially if the embankment was not surcharged. There is evidence that this settlement can be calculated using Eq. 16.19 and values of $C_{\alpha e}/C_c$ for peat given in Table 3.14 ($C_{\alpha e}/C_c = 0.06 \pm 0.01$). There has been some questioning of the $C_{\alpha e}/C_c$ concept for peat (Fox *et al.* 1992), however more recent research on the same peat (Mesri *et al.*

1997; Fox *et al.* 1999) provides additional support for the concept and suggests that departures from the concept in the laboratory test may be due to biodegradation of the peat in the laboratory.

When dealing with embankments where the surface settlement and especially differential settlement of the embankment with time can be problematic, e.g. road embankments, surcharging of the embankment, has been successfully used as a means of reducing or delaying the onset of secondary compression after removal of the surcharge (e.g. see Mesri *et al.* 1997). As noted by Rowe *et al.* (1984a), the surcharge should be applied to the embankment over the entire peat deposit and not just over the thicker portions of the deposit.

16.5 Lateral Displacements

Field observations of embankments on clay show that the lateral displacements during and at the end of construction can generally be described as a function of the settlement under the centerline of the embankment. In the overconsolidated region (from O′ to P′, Fig. 16.3), the maximum lateral displacement under the toe of the embankment is linearly related to the surface settlement under the center of the embankment. Tavenas *et al.* (1979) found:

$$y_{mr} = (0.18 \pm 0.09)S_r. \qquad (16.28a)$$

During the following phase, when the soil is normally consolidated (P′A′F′ in Fig. 16.3), the increase in maximum horizontal displacement is very close to the increase in settlement and Tavenas *et al.* (1979) found that on average:

$$y_{mu} = (0.91 \pm 0.2)S_u. \qquad (16.28b)$$

The distribution of lateral displacements with depth at the end of construction is directly dependent on the effective stress condition in the foundation, as shown in Fig. 16.13. If the clay has become normally consolidated over the full depth of the deposit (Fig. 16.13a), the displacement curve, $y = f(z)$, reflects this homogeneous condition and roughly corresponds to the classical theoretical solution (Poulos 1972). If only a part of the foundation has become normally consolidated as for the Saint-Alban B test fill (Fig. 16.13b), the $y = f(z)$ curve reflects the resulting non-uniform condition with small deformations developing in the lower, still overconsolidated clay, and large deformations occurring in the upper normally consolidated clay.

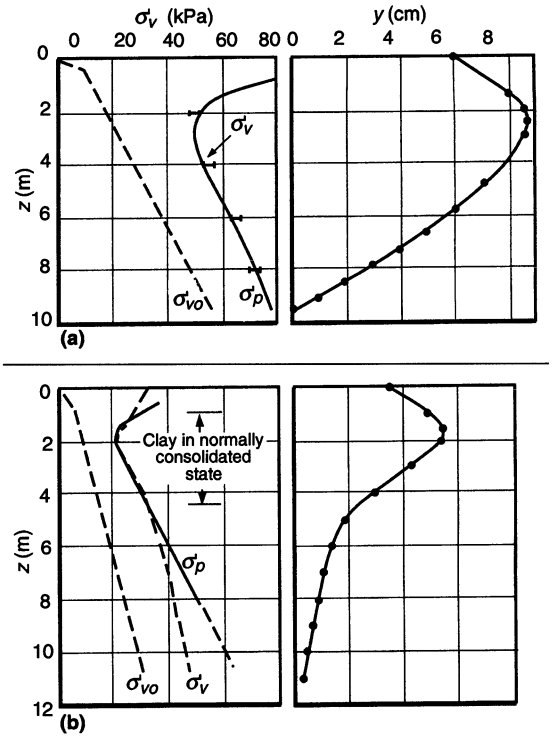


FIGURE 16.13. Effective stresses and lateral displacements at end of construction: (a) Cubzac-les-Ponts, and (b) Saint-Alban B (after Tavenas *et al.* 1979; reproduced with permission, *Canadian Geotechnical Journal*).

Tavenas *et al.* (1979) noted two points concerning the long-term lateral displacements: first, the distribution of lateral displacement with depth does not significantly change fur-

ther after the end of construction; second, the increase in lateral displacement varies linearly with the increase in settlement. For embankments with a factor of safety, F, a full width b and crest width B on a clay layer of thickness D, where $0.9 \leq b/D \leq 2.3$, $0.35 \leq (b - D)/D \leq 0.9$, $1.25 \leq F \leq 1.5$ and side slopes of 1.5 : 1, the relationship between the increase in maximum horizontal displacement, Δy_{md}, and the increase in settlement, ΔS_d, was given by:

$$\Delta y_{md} = (0.16 \pm 0.02)\Delta S_d. \quad (16.28c)$$

Thus the total horizontal displacement is given by summing Eq. 16.28a–c to give:

$$y_m = y_{mr} + y_{mu} + \Delta y_{md}. \quad (16.29)$$

For different geometries, the ratio y_m/S varies, having a tendency to decrease when the factor of safety rises and/or at lower embankment side slopes.

16.6 Consolidation

16.6.1 PRIMARY CONSOLIDATION

The settlements that occur following construction (see Section 16.4.3) develop with time due to consolidation of the soil as the excess pore pressures dissipate. Traditionally, consolidation has been predicted based on Terzaghi's (1925) theory for one-dimensional consolidation as discussed in Section 2.7.4 and Fig. 2.8. This theory is based on several hypotheses, some of which may not be fully realized in practice. Specifically, the hypotheses are:

1. The strains in the clay layer are one-dimensional and small.
2. The flow of water is one-dimensional and is controlled by Darcy's law.
3. The clay layer is homogeneous.
4. The soil particles and the pore liquid are incompressible.
5. The soil is saturated.
6. The hydraulic conductivity is constant.
7. There is a linear relation between the vertical effective stress and the void ratio.
8. The soil is not viscous, thus not influenced by time or strain rate.

In practice, the strain will not be purely one-dimensional and the flow of water is generally two-dimensional. To take this into account, Biot (1941, 1955) proposed a general theory for predicting pore pressure dissipation and consolidation settlement, which is implemented in many modern finite element codes. Also, Davis & Poulos (1972) provided general solutions to the two- and three-dimensional consolidation equations in a graphical form that can be readily used in practice, as shown in Fig. 16.14 (note: Davis & Poulos also give solutions for additional cases).

Variances from hypotheses 2–5 and 7 are likely to result in excess pore pressures that are smaller than the theoretical values and the settlements at a given time, which are larger than the theoretical values.

Contrary to hypothesis 6, the hydraulic conductivity k is not constant, but decreases with the void ratio, e. As a first approximation, it follows the law:

$$k = k_r \exp[2.3(e - e_r)/C_k] \quad (16.30)$$

where k_r = the hydraulic conductivity at the reference void ratio, e_r, and C_k is close to $0.5e_0$ (Tavenas *et al.* 1983b).

Finally, as indicated in Sections 16.4.3.2 and 16.6.2, clays are viscous and this influences pore pressure generation and the consolidation process. Thus, the coefficient of consolidation is not a basic property of a soil. As a consequence, it depends on the way it is estimated (see Section 2.7.4). Experience shows that:

$$c_v(\text{Casagrande; Eq. 2.33}) < c_v$$

$$(\text{Taylor; Eq. 2.34}) < c_v = \frac{kM_c}{\gamma_w} (\text{Eq. 2.29}). \quad (16.31)$$

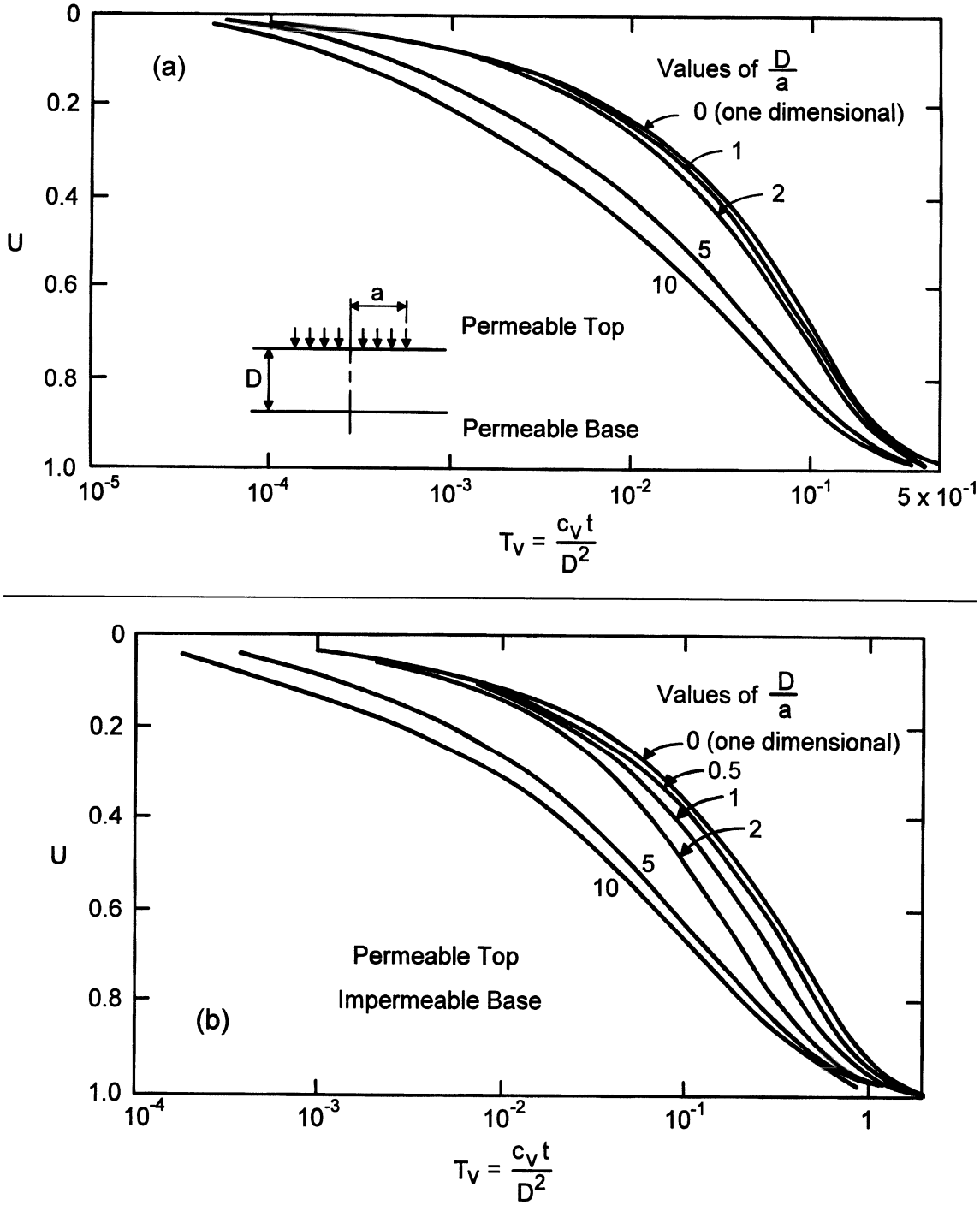


FIGURE 16.14. Degree of settlement/consolidation curves for two-dimensional flow conditions: (a) permeable top, permeable base; (b) permeable top, impermeable base (modified from Davis & Poulos 1972).

Furthermore, experience also shows that the coefficient of consolidation in the field is larger than that calculated from laboratory data using the method of Casagrande. Compiling data from 16 embankments, Leroueil (1988) found an average ratio of 20 between these two parameters. Thus, when possible, it is desirable to use a numerical model to take into account the variation in consolidation characteristics with depth using representative laws for the compression curve and the permeability–void ratio relation.

As a consequence of hypothesis 7, Terzaghi's theory also considers the degree of consolidation U, defined in terms of pore pressure, to be equal to that defined in terms of settlement. This is often not the case, especially for soils that are initially overconsolidated and become normally consolidated during loading. In such a case, separate consideration can be given to the settlement and pore pressure dissipation in the overconsolidated and normally consolidated stages, e.g. see discussion in Section 16.1.1 recognizing that the rate of settlement in the normally consolidated state will depend on the excess pore pressures remaining when the soil becomes normally consolidated. The excess pore pressures at the end of construction are best established by field measurement. Alternatively, they can be calculated either from current numerical models or, based on the discussion in Section 16.1.2, approximated as the difference between the final expected effective stress and the preconsolidation pressure.

The settlement at time t after the end of construction can then be expressed as:

$$S(t) = S_r + S_u + U_{nc} S_d \qquad (16.32)$$

where S_d is given by Eqs 16.14 and 16.15, and U_{nc} the degree of consolidation in the normally consolidated range. U_{nc} is given approximately by Fig. 2.8b for a dimensionless time, $T_v = c_{v_{nc}} t/\Lambda^2$ (where Λ is the drainage path) or by Fig. 16.14 for $T_v = c_{v_{nc}} t/D^2$ (where D = layer thickness irrespective of drainage path). Figure 16.14a is for a layer with a permeable top and bottom, and Fig. 16.14b is for a layer with a permeable top and impermeable bottom.

16.6.2 CONSIDERATION OF VISCOUS AND STRUCTURING EFFECTS

As indicated in Sections 2.7.5 and 16.4.3.2, clays (and also peats) are viscous and this influences the settlement during primary consolidation. As schematically shown in Fig. 16.15, there are two extreme possibilities (Jamiolkowski *et al.* 1985): curve A assumes that creep occurs only after the end-of-primary consolidation, and consequently, the strain at the end-of-primary consolidation would be the same *in situ* (ε_{vA} on field curve A in Fig. 16.15) and in the laboratory. Curve B assumes that viscous strains develop during primary consolidation and, consequently, the strain at the end-of-primary consolidation is larger *in situ* (ε_{vB} on field curve B in Fig. 16.15) than in the laboratory. The viscous model described in Section 16.4.3.2 corresponds to curve B. However, if structure develops under small strain rates for *in situ* conditions, the *in situ* strain at the end-of-primary consolidation could be smaller than ε_{vB} (see Section 16.4.3.2).

A consequence of the viscous behavior of

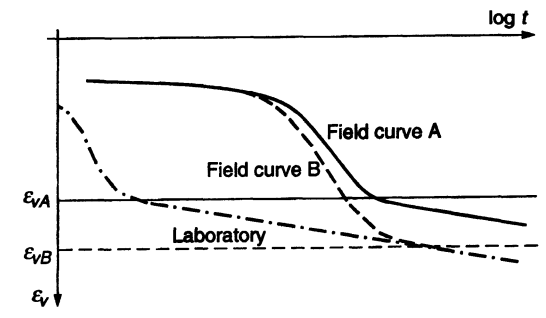


FIGURE 16.15. Strain–time relations in the laboratory and in the field (modified from Ladd *et al.* 1977).

clays is that, in some cases involving high compressibility clays and a long drainage path, the pore pressures continue to increase after the end of construction (Crooks *et al.* 1984; Kabbaj *et al.* 1988; Leroueil 1996; Hinchberger & Rowe 1998).

16.7 Stability

16.7.1 GENERAL REMARKS

Ladd (1991) defined three types of stability analysis: (a) a total stress analysis (TSA); (b) an undrained strength analysis (USA), and (c) an effective stress analysis (ESA). A total stress analysis is often used in single-stage construction analysis and is usually based on the undrained strength profile prior to construction. In undrained strength analysis, the *in situ* undrained shear strength is computed as a function of the pre-shear effective stress. This type of analysis is often used in evaluating the stability of stage-constructed embankments.

Several authors have examined effective stress analyses (Tavenas *et al.* 1980; Ladd 1991) and noted several inherent difficulties: (a) the evaluation of pore pressures and thus of the effective stress normal to the failure surface; (b) the assumption that, at any time, the overall factor of safety is equal to the local factor of safety at different points along the potential failure surface; (c) the choice of representative effective stress strength parameters; and (d) the definition of the factor of safety.

Numerical methods that can be used for stability analyses are described in Section 14.5.

16.7.2 EMBANKMENTS CONSTRUCTED IN ONE STAGE

16.7.2.1 Evaluation of Mobilized Shear Strength, s_u

As indicated in Section 16.1, clay foundations generally do not behave in an undrained manner during the early stages of construction. Also, for other reasons such as sample disturbance, different stress paths, strain rate effects, influence of the intermediate principal stress, etc., the undrained shear strengths, s_u, measured in undrained laboratory or *in situ* tests may not be directly applicable under an embankment and are used on an empirical or semi-empirical basis. Several approaches have been proposed and will be described below. To gain confidence with the results of stability analyses, it is recommended that at least two of these approaches be considered in practical applications. Since vane shear strength and preconsolidation pressure profiles are available in most projects, the corresponding approaches can be used, but other approaches may also be used, based on the regional experience.

1. Field vane test approach. Back-analyses of numerous failures have shown that the vane shear strength often overestimates the average strength mobilized under embankments. Bjerrum (1972) suggested that a correction factor, μ, which decreases from 1.0 to 0.6 when the plasticity index increases from 20 to 100 (Fig. 3.15), be used to adjust vane shear strength for design purposes. Similarly, correction factors as a function of the liquid limit were proposed by Pilot (1972) and Helenelund (1977).

2. Preconsolidation pressure approach. Mesri (1975) suggested that the ratio, s_u/σ'_p, between the strength available at failure and the preconsolidation pressure of the clay is essentially constant and equal to 0.22. Larsson (1980) and Jardine & Hight (1987) computed ratios between the strength mobilized at failure and the preconsolidation pressure, generally obtained in conventional 24-hour oedometer tests. It was generally found that the ratio s_u/σ'_p slightly increases from about 0.19 at a plasticity index of ten to about 0.28 at a plasticity index of 80 (see Fig.

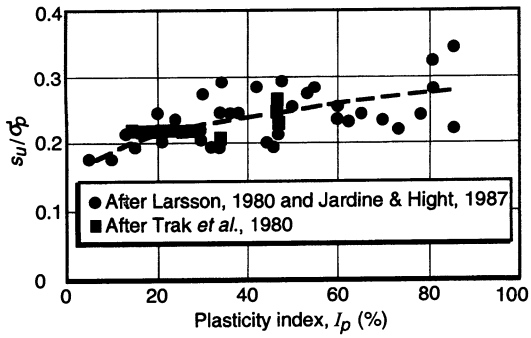


FIGURE 16.16. Strength ratios deduced by different approaches: (●) after Larsson 1980; Jardine & Hight 1987; ■ after Trak *et al.* 1980.

16.16). As noted by Leroueil *et al.* (1985b) and Ladd (1991), the upper values often correspond to organic clays.

3. Recompression and SHANSEP approaches. Ladd (1969) proposed a methodology in which the undrained shear strength is obtained from a laboratory program of CK_0U shear tests on samples consolidated under K_0 conditions (see Sections 2.6.5 and 3.4) and sheared under undrained conditions (called CK_0U tests) in different modes of failure: compression under the central part of the embankment, direct simple shear where failure is close to horizontal, and extension near the toe. The Norwegian Geotechnical Institute (Bjerrum 1973) uses the "recompression technique" in which the specimens are reconsolidated to *in situ* stresses prior to shearing. Ladd & Foott (1974) proposed the SHANSEP technique in which the specimens are first consolidated well beyond their preconsolidation pressure, and maintained in these conditions or rebounded to various OCRs before being subjected to undrained shear tests. Ladd *et al.* (1977) showed that the results can generally be written as:

$$\left(\frac{s_u}{\sigma'_{vc}}\right)_{oc} = \left(\frac{s_u}{\sigma'_{vc}}\right)_{nc} \mathrm{OCR}^m \qquad (16.33)$$

in which m is a parameter approximately equal to 0.8. By consolidating the specimens beyond their preconsolidation pressure, the SHANSEP approach neglects the influence of structure on the strength of clays. For this reason, Ladd (1991) specifies that "SHANSEP is strictly applicable only to mechanically overconsolidated and truly normally consolidated soils exhibiting normalized behavior." According to Leroueil & Jamiolkowski (1991), this approach could be conservative.

4. Direct simple shear (DSS) test approach. "For preliminary design and for final design of less important projects involving 'ordinary' soils with low to moderate anisotropy," Ladd (1991) recommends the use of CK_0U direct simple shear test results for stability analyses. He observed average strength ratios, s_u/σ'_{vc} of 0.225 for 16 non-varved normally consolidated clays (i.e. very close to 0.22 reported by Mesri 1975) and of 0.26 for nine normally consolidated silts and organic soils.

5. Unconfined (UC) and unconsolidated undrained (UUC) compression test approach. Due to swelling of the specimens following sampling and the influence of small defects in the specimens, the test results are often smaller and more scattered than those obtained from tests where the sample has been reconsolidated. As a consequence, this approach is likely to underestimate stability (other things being equal) and is generally not recommended when there are significant economic consequences to underestimating the stability. However, this approach has been successfully and extensively used in some countries (especially Japan, see Nagase 1967).

6. USALS approach. Trak *et al.* (1980) indicated that the large strain strength measured in triaxial compression tests, called USALS, may be representative of the strength mobilized at failure under embankments for some clays from eastern Canada.

As shown in Fig. 16.16, the USALS values reported by the authors are close to the field values reported by Larsson (1980) and Jardine & Hight (1987).

7. CPT tip resistance approach. The cone penetration tip resistance, q_c (or the value corrected for pore pressure behind the tip, q_T), is related to the undrained shear strength of the clay (see Section 4.4.6), and has been used to evaluate design strength (Lunne *et al.* 1976; Hanzawa 1989). The advantage of this test is that it provides a continuous strength profile, which may allow detection of weak layers that might be missed with other approaches. Because it has not been calibrated yet against failure, the CPT tip resistance is invariably used together with other measurements when establishing the design strength.

8. Effective stress analysis approach. Back-analyses performed in effective stress, on the basis of pore pressures measured at failure indicate that the mobilized strength parameters are close to those of the normally consolidated clay (Parry 1968; Rivard & Lu 1978; Hanzawa *et al.* 1982; Pilot *et al.* 1982). However, due to the difficulty of predicting pore pressures in the entire foundation of the embankment, the effective stress analysis is not commonly used in simple limit equilibrium analyses.

16.7.2.2 Strength of the Weathered Crust

Because it is generally weathered and fissured, the mobilized strength of the surface crust of clay deposits is smaller than that measured in vane shear tests (Lo 1970). Corrections have thus been proposed by a number of investigators. For example, Tavenas and Leroueil (1980) and Lefebvre *et al.* (1987) suggested that the operational strength in the crust is given as shown in Fig. 16.17.

16.7.2.3 Estimation of Stability

The geometry of an embankment is chosen on a case-by-case basis. The desired calculated factor of safety at the end of construction is often between 1.3 and 1.5, with the actual target value depending on the project and the consequences of a failure.

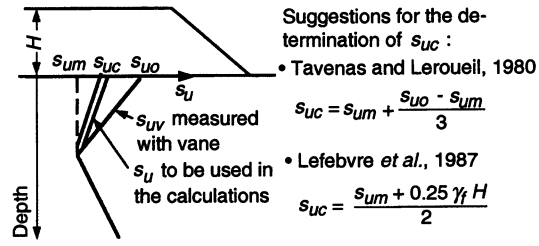


FIGURE 16.17. Correction to obtain operational strength of a crust beneath an embankment.

The stability is generally evaluated using limit equilibrium analysis incorporated into computer programs (see Section 14.5). However, charts corresponding to simplified conditions (e.g. full-fill strength, no tension cracks) can be used for preliminary design. Figure 16.18 presents charts for the case of

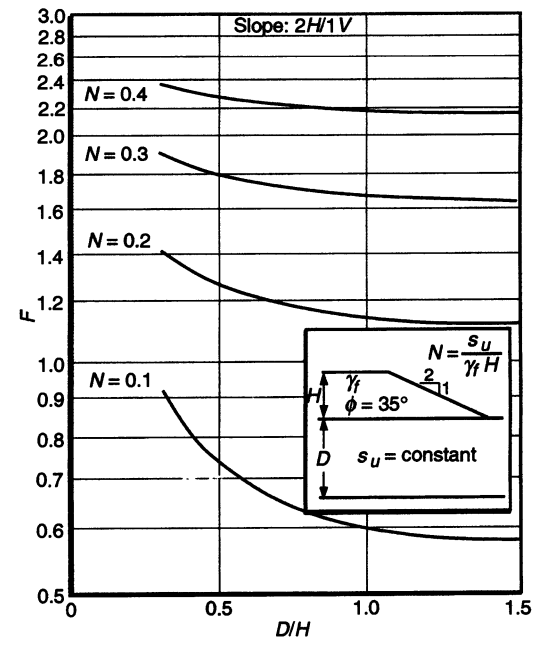


FIGURE 16.18. Chart for calculation of factor of safety (modified from Pilot & Moreau 1973).

an embankment on a clay deposit of constant undrained shear strength.

16.7.3 CHOICE OF STRENGTH FOR EMBANKMENTS CONSTRUCTED IN SEVERAL STAGES

Although there are many reported failures of single-stage embankments, which have allowed the calibration of the stability methods mentioned in Section 16.7.2, there is a paucity of well-documented failures of stage-constructed embankments. Nevertheless, several approaches have been proposed that are based on the observation that, for stresses exceeding the preconsolidation pressure, the undrained shear strength increases with decreasing void ratio and increasing effective stress.

1. Field vane test approach. The vane shear strength measured under embankments has often been used to evaluate the stability of stage-constructed embankments. However, observing ratios s_{uv}/σ'_{vc} under embankments between 0.18 and 0.25, and smaller than the ratio s_{uv}/σ'_p of the intact clay, Tavenas *et al.* (1978) suggested that the Bjerrum's correction considered in single-stage construction (Section 16.7.2.1) should not be applied to the vane shear strength measured under embankments for stability analyses of stage-constructed embankments. Law (1985) came to the same conclusion. They explained the decrease in s_{uv}/σ'_p by a loss of clay structure when it becomes normally consolidated.

2. CPT tip resistance approach. There is evidence (e.g. Leroueil *et al.* 1995) that the cone penetration test can be used for the evaluation of the strength increase under stage-constructed embankments in terms of the change in $q_T - \sigma_v$. Research is in progress to establish the validity of this approach for more general application.

3. Vertical effective stress approach. Using an analogy with the s_{uv}/σ'_p ratio suggested in Mesri (1975) for single-stage construction, Leroueil *et al.* (1985b) proposed an estimation of the shear strength on the basis of the vertical effective stress, using a strength ratio $s_{uv}/\sigma'_{vc} = 0.25$. Such a value would take into account the fact that the largest strength increase develops in compression, under the center of the embankment.

4. SHANSEP approach. In staged construction, where the soil has become normally consolidated along most of the failure surface, the recompression and SHANSEP techniques are similar. They also seem more appropriate since the main criticisms formulated for single-stage constructions (the fact that the effects of structure and partial drainage are not considered) are not relevant to the second and subsequent stages.

16.8 Solutions to Problems of Stability and Settlement

16.8.1 GENERAL

Whenever possible, embankments are constructed with conventional fill materials, in one single stage, on the natural soil deposit. However, to obtain satisfactory factor of safety, to have acceptable post-construction settlements, and to satisfy construction constraints such as limited site area or maximum duration of construction, special solutions may be required. Table 15.1 summarizes the solutions most commonly considered and Chapter 15 discusses many of these solutions. These solutions can be classified into five different groups:

1. Eliminate the problem by replacing the soils of unfavorable characteristics or by using lightweight fill materials (see Section 15.2.1 and Rowe & Soderman 1986).
2. Improve the stability of the embankment by using lateral berms (Section 16.8.2) or reinforcement (Section 16.8.3 and 16.8.4), and/or by building the embankment in several stages (Section 16.7.3).

3. Reduce the post-construction settlements by using a temporary surcharge (Section 15.2.3.2).
4. Accelerate consolidation with vertical drains or drainage trenches (Sections 15.2.3.4 and 15.2.3.5).
5. Improve the soft soil foundation with lime columns, electro-osmosis (Section 15.2.4), preloading or compaction (Section 15.2.5), etc.

In some cases it may be necessary or desirable to combine solutions from a number of groups. The following will focus on the common solutions not discussed in detail in Chapter 15.

16.8.2 BERMS

The stability of embankments can be improved by either flattening the side slopes (in some cases to as much as 10 *H*: 1*V*; see Rowe 1982) or by the use of berms. The dimensions of the berms are usually established based on stability considerations (see Section 16.7), but the height of a berm is typically 40–50% of the height of the embankment. Due to common limitations on the space available for embankment construction (either for economic or environmental reasons) berms are not as widely used these days as in the past, since the same effect often can be achieved by the use of alternative techniques (e.g. basal reinforcement). For example, Rowe and Soderman (1985b) illustrate that either the use of basal reinforcement or lightweight fill can have a similar effect to berms in terms of improving the performance of embankments on peat.

16.8.3 REINFORCED EMBANKMENTS ON SOFT CLAY

16.8.3.1 General Considerations

As discussed in Section 16.2, under appropriate conditions, the provision of basal reinforcement, i.e. reinforcement located at or near the fill–clay interface, can substantially increase embankment stability and hence allow the construction of a higher embankment than would be possible under single-stage loading for the same soil profile without the use of reinforcement. When one cannot achieve the desired grade with an adequate factor of safety by single-stage loading without reinforcement, the following steps should be followed.

- Step 1. Establish whether it is possible to construct a reinforced embankment to the desired fill thickness. This involves the application of bearing capacity theory as described in Section 16.8.3.2. If the desired thickness can be achieved, proceed to Step 2 below. If it cannot be achieved using reinforcement alone then an alternative method of addressing stability is required, e.g. use of stage construction in conjunction with provision of vertical drains, or the use of lightweight fill. The stability calculation already performed in Step 1 indicates the maximum fill thickness that can be placed in the first stage of construction. Alternatively, this stability calculation may be used to assess the thickness/density of lightweight fill that would be required.
- Step 2. Establish the reinforcement force required to achieve the desired fill thickness at the desired factor of safety using limit equilibrium methods as discussed in Section 16.8.3.3.
- Step 3. Check the potential for sliding of the embankment on top of the upper layer of reinforcement (embankment splitting) due to the earth pressure that will develop in the fill. Referring to Fig. 16.19, this can be achieved by considering horizontal equilibrium and checking the factor of safety from:

$$F = 0.5n\gamma_f H^2 \tan \phi'_{ds} / [K_a(0.5\gamma_f H^2 + qH)] \quad (16.34)$$

where K_a = the Rankine active earth pressure coefficient corresponding to the friction angle of the fill (see Section 17.2.2), ϕ'_{ds} = the soil–reinforcement friction angle in direct shear (see Sections 7.2.2 and 7.3.2), q = the surcharge (if any) acting on the embankment, and all other terms are as

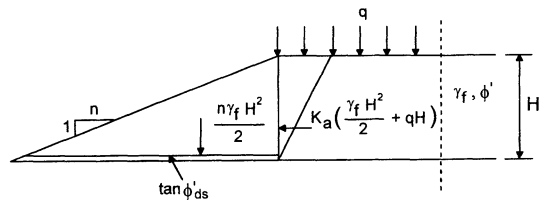


FIGURE 16.19. Direct sliding failure of the fill or reinforcement.

defined in Fig. 16.19 or previously defined. While this mechanism should be checked, for typical values of embankment side slope, n, with $n \geq 1.5$ (see Fig. 16.19), it rarely controls the design.

In addition to the foregoing, consideration should also be given to long-term settlement and rate of consolidation in the same manner to that discussed in Sections 16.4.3 and 16.6, respectively.

In the preceding and following discussions it is assumed that the fill is a free-draining frictional material. Lower quality fills, e.g. cohesive fills, have been used and the analysis presented herein can be readily extended to deal with a cohesive fill, however, these fills introduce a number of additional problems such as tension cracking in the fill, significant pore pressure changes due to rainfall events, potentially low soil–reinforcement interface strength for some types of reinforcement, creep of the fill, etc., which are beyond the scope of this handbook.

16.8.3.2 Bearing Capacity Limits on Reinforced Embankment Height

Historically, bearing capacity calculations have been based on the Prandtl (1920) solution ($q_u = 5.14s_u$), which was developed for strip loading on a deep homogeneous layer. However, it has been found in numerous cases that reinforced embankments on very soft to soft clays may be stable at heights up to 2 m above the theoretical collapse height based on Prandtl's theory (Humphrey & Rowe 1991; Rowe 1997a). The reasons for this include: (a) most soils would have been slightly overconsolidated before loading (see Section 16.1); (b) there is usually a significant increase in undrained strength with depth in these deposits and the effect is not correctly considered by using an "average strength"; and (c) often the very soft layer is underlain by a firm stratum at relatively shallow depth, i.e. depths less than 0.7 times the width of the embankment, and the presence of this firm stratum can significantly increase the bearing capacity. This has been recognized by a number of investigators (Humphrey & Holtz 1986; Rowe & Soderman 1987; Houlsby & Jewell 1988). Rowe and Soderman (1987) synthesized the bearing capacity factors of Davis & Booker (1973) and Matar & Salençon (1977) and proposed a design methodology, involving only hand calculations, that can be used to allow for the effects of both strength increase with depth and the presence of a stiff layer at a depth of less than 0.7 times the embankment width.

Since an embankment will generally be trapezoidal in shape and the plasticity solutions are for a rigid footing, an approximation must be made to obtain the equivalent width of the embankment b^*. Since the vertical pressure at the edge of a rigid footing at the point of collapse is $(2 + \pi)s_{uo}$ (where s_{uo} is the undrained shear strength directly beneath the footing), the equivalent width of a rigidly reinforced embankment, b^*, can be taken to be the distance between the points on either side of the embankment when the applied pressure, $\gamma_f h^*$, is equal to $(2 + \pi)s_{uo}$ as shown in Fig. 16.20. Thus:

$$\begin{aligned} b^* &= B + 2n(H - h^*) \\ &= B + 2n[H - (2 + \pi)s_{uo}/\gamma_f] \end{aligned} \tag{16.35}$$

The bearing capacity, q_u, of the equivalent rigid footing of width b^* is given by:

$$q_u = N_c s_{uo} + q_s \tag{16.36}$$

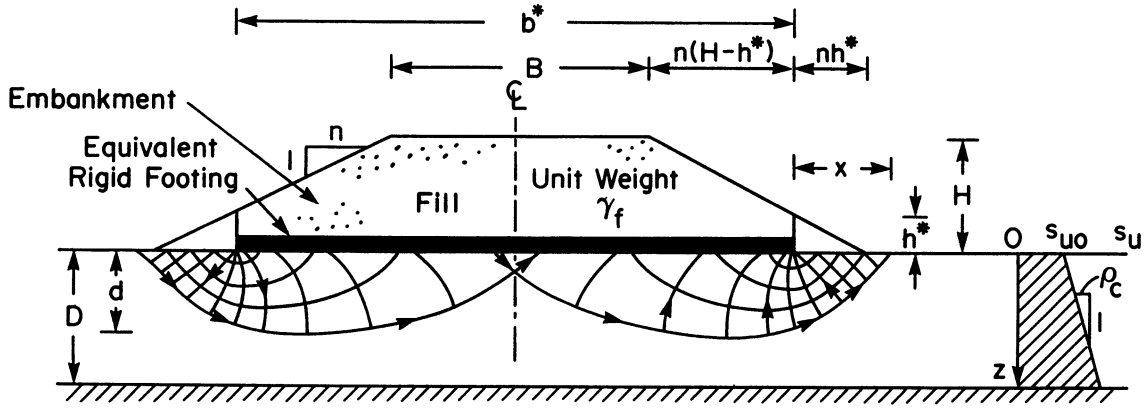


FIGURE 16.20. Definition of variables used to estimate collapse height for a perfectly reinforced embankment (modified from Rowe & Soderman 1987).

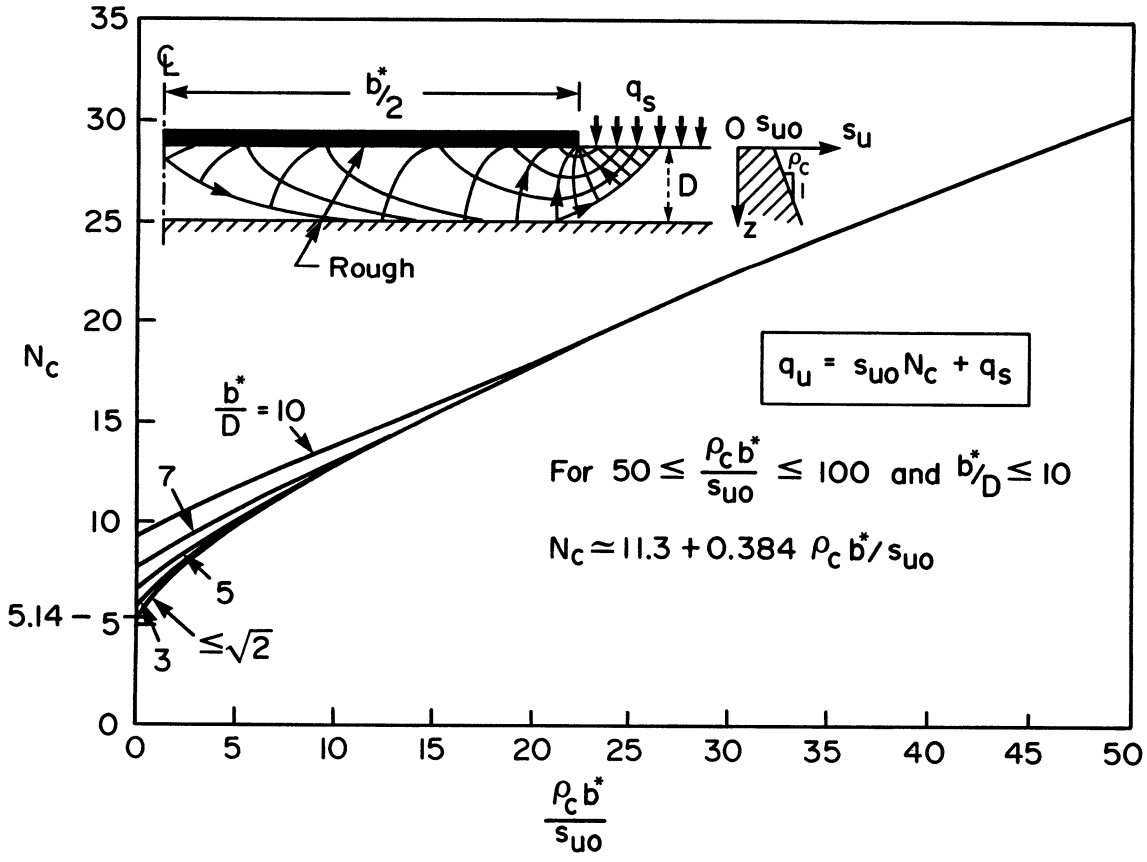


FIGURE 16.21. Bearing capacity factor for non-homogeneous soil (modified from Rowe & Soderman 1987).

where q_s is a uniform surcharge pressure applied to the foundation soil surface outside of the footing width. The bearing capacity factor N_c is obtained from Fig. 16.21. Inspection of Fig. 16.20 shows that the triangular edge of the embankment (beyond the equivalent rigid footing) provides a surcharge that would increase stability, and hence an estimate of q_s in terms of the pressure applied by this triangular distribution is required. Figure 16.22 shows the depth, d, to which the failure mechanism is expected to extend. The lateral extent of the plastic region involved in the collapse of a rigid footing extends a distance x from the footing, where x is approximately equal to the minimum of: d as obtained from Fig. 16.22 and the actual thickness of the deposit, D.

Thus, distributing the applied pressure due to the triangular distribution over a distance x gives:

$$q_s = 0.5n\gamma_f(h^*)^2/x \quad \text{for } x > nh^* \qquad (16.37a)$$

and

$$q_s = 0.5(2\,nh^* - x)\gamma_f h^*/(nh^*) \quad \text{for } x \leq nh^*. \qquad (16.37b)$$

The bearing capacity of an equivalent rigid footing can then be calculated from Eqs 16.36–16.37, and this may be compared with the average applied pressure, q_a, due to the embankment over the width b^*:

$$q_a = \gamma_f[BH + n[H^2 - (h^*)^2]]/b^*. \qquad (16.38)$$

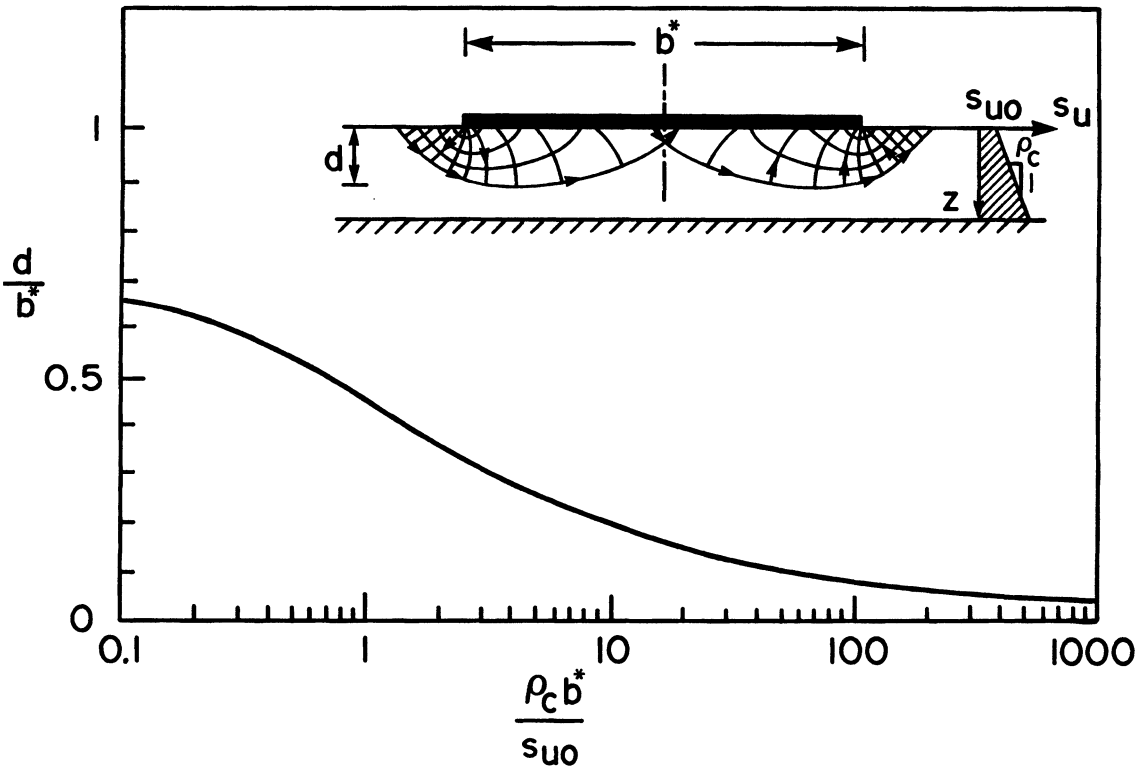


FIGURE 16.22. Effect of non-homogeneity on depth of the failure zone beneath a rough rigid footing (modified from Matar & Salençon 1977).

For the purposes of estimating the maximum possible factor of safety (defined here as $F = q_u/q_a$) that could be achieved for a given embankment geometry and soil profile, q_u and q_a can be calculated directly from Eqs 16.35–16.38.

The maximum possible factor of safety, F, calculated above was obtained without considering the amount or properties of the reinforcement and implicitly assumes that the reinforcement has sufficient strength and stiffness to develop the required reinforcement forces without breaking or excessive deformation. Having established that it is possible to build the embankment to the desired factor of safety, the next step (to be discussed in Section 16.8.3.3) is to select reinforcement that has sufficient strength and stiffness to achieve the desired factor of safety.

16.8.3.3 Selecting Reinforcement Properties

The reinforcement needs to be selected such that it develops the force required to maintain equilibrium with the desired factor of safety at a strain that will not permit excessive undrained shear deformation (see Section 16.2). There are a number of different approaches, but they are generally based on some form of limit equilibrium analysis (see Section 14.5).

Most commonly, this involves some form of slip circle analysis, wherein for any trial slip circle an additional restoring moment is included in the calculation of moment equilibrium and this restoring moment is equal to the force in the reinforcement, T, multiplied by a lever arm between the center of the trial circle and the point of action of the tensile force in the reinforcement. There has been considerable debate regarding the appropriate selection of the lever arm, with estimates ranging from the radius of the circle, R (see Fig. 16.23, this assumes the reinforcement deforms to a tangent to the slip circle at the point of interaction), as a maximum, to the vertical distance from the center of the circle to a horizontal line drawn through the reinforcement, Y_T, (see Fig. 16.23, this assumes that the tensile force in the reinforcement acts in the horizontal direction). Using limit analysis, Michalowski (1998) has theoretically established that the reinforcement should be considered to be horizontal. Furthermore, back-analysis of a number of cases by Palmeira *et al.* (1998) indicates that this approach also gives a good prediction of the

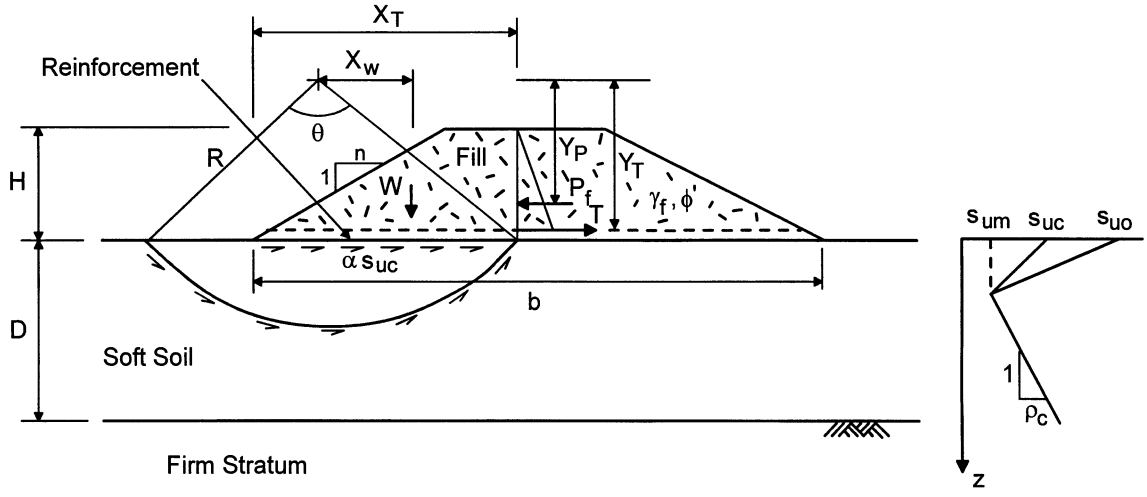


FIGURE 16.23. Rotational failure of embankments on soft soil.

factor of safety for embankments that have failed.

There are two approaches to establishing the required reinforcement force, T, to maintain stability at a given factor of safety. The first uses the expected strength profile in the soil (see Section 16.7.2) and the expected fill properties, assumes trial value of T_t, and performs a series of limit equilibrium analyses to establish the minimum factor of safety, F, associated with that value of T_t. By trial and error, one can adjust the value of T_t until the minimum value of F corresponds to the desired factor of safety, F_d, (typically 1.3–1.5) thereby yielding the required force, T_{req}. However, T_{req} must not exceed the maximum force, T_l, that can be developed in the reinforcement and which is given by the sum of the horizontal thrust in the fill, P_f, and the resisting shear force that can be transferred to the soil, P_s, e.g. see Fig. 16.23, thus:

$$T_l = P_f + P_s \tag{16.39}$$

where

$$P_f = 0.5K_a\gamma_f H^2 \tag{16.40}$$

and the earth pressure coefficient, K_a, is based on the factored mobilized fill friction angle, $\phi'_f = \tan^{-1}[(\tan \phi')/F_d]$, and

$$P_s = \alpha s_{uc} X_T / F_d \tag{16.41}$$

where s_{uc} = the operational shear strength at the soil interface, α = a reduction factor to reflect any reduction in shear strength that may occur at the reinforcement–foundation interface, and X_T = the distance from the toe of the embankment to the point where the circle intersects the reinforcement (see Fig. 16.23).

Referring to Fig. 16.23, an alternative approach, and the one recommended here is to:

1. Obtain design shear strength parameters for the foundation, s_u^*, by dividing by the desired factor of safety, F_d, ($s_u^* = s_u/F_d$).
2. Take the fill unit weight as the maximum expected and adopt a friction angle for the fill equal to the critical state value, ϕ'_{cv} (in recognition that it is difficult to gain good compaction of fill on very soft foundations that require basal reinforcement, especially near the bottom of the embankment).
3. Assume a trial slip circle as shown in Fig. 16.23, such that a vertical line from the point of intersection of the circle and the reinforcement passes through the crest of the embankment (note the slip circle is not carried through the fill; rather, the fill is modeled as described in 4. below).
4. Separate the consideration of the overturning moments of the fill from that of the foundation (as recommended by Jewell 1996) by replacing the fill by a horizontal thrust, P_f, given by Eq. 16.40, with K_a evaluated for $\phi' = \phi'_{cv}$ acting at the centroid of the horizontal pressure (lever arm Y_p) and a vertical force equal to the weight of the fill to the left (in Fig. 16.23) of the point of intersection between a given trial slip circle and the reinforcement, acting at the centroid of this block of fill (lever arm X_w).
5. Consider a trial slip circle with a restoring moment, m_s, due to the shear strength along the surface in the clay given by:

$$m_s = R^2 \int_0^\theta s_u^* d\theta. \tag{16.42}$$

6. For a given trial slip circle, evaluate the force required to maintain equilibrium from:

$$T = (WX_w + P_f Y_p - m_s)/Y_T. \tag{16.43}$$

7. Check that the force calculated in step 6 can be mobilized, namely $T \leq T_l$, with T_l given in Eq. 16.39. (Note: If $T > T_l$ then the desired factor of safety cannot be achieved irrespective of how much reinforcement is provided and additional means of soil improvement will be required, see Section 16.8.1).
8. Repeat steps 3–7 to find the maximum value of T and this becomes the required force, T_{req}.

Once the desired design force, T_{req}, has been established (by either method described above) it remains to select the reinforcement with the required strength and stiffness. With respect to the strength, the reinforcement is required to have an allowable strength, T_a, or design strength, T_D, larger than T_{req}.

Rowe & Mylleville (1993) discuss the use of steel strip reinforcement and the selection of T_D for steel. If geosynthetic reinforcement is used, then T_D is selected to support the required load fully until consolidation is 90% complete (see Section 16.6). Two approaches are commonly adopted for establishing the allowable and design strength, T_a or T_D. The simplest and most commonly used method in North America is to calculate the allowable strength, T_a, by reducing the short-term ultimate strength by a number of reduction factors as discussed in Section 7.9.1.1. The alternative limit state approach (mostly used in Europe) is to establish the load leading to rupture or limiting strain (based on the geosynthetic properties) at the end of the design life and then use these partial factors as discussed in Section 7.9.1.2 to obtain the design strength, T_D. Both approaches have proven successful in the past.

The failure height and required reinforcement calculated as described above using limit equilibrium, e.g. based on a slip circle failure mechanism, relate to the ultimate limit state (collapse) and provide no indication regarding the serviceability limit state (deformations prior to or at failure). In some instances, the embankment may have failed due to excessive displacements (serviceability limit state) prior to reaching the collapse height (ultimate limit state). In some instances, excessively large displacements may be required to cause failure of reinforced embankments. This has been recognized by Jewell (1982), Rowe & Soderman (1985a), Bonaparte & Christopher (1987), Mylleville & Rowe (1988, 1991) and Rowe & Mylleville (1989, 1990), who have each made recommendations regarding what maximum strain in reinforcement should be allowed for a range of different soil conditions.

It has also been found that for soft plastic cohesive soils where there is a significant increase in strength with depth, i.e. a rate of increase in undrained strength with depth $\rho_c \geq 1$ kPa m^{-1}, a maximum allowable strain of 5% will often provide a conservative estimate of the failure height of the embankment. However, it should be emphasized that special care is required in designing embankments on soils that are susceptible to strain softening at the anticipated rate of straining associated with the proposed construction schedule and that the allowable strain in these cases may be substantially less than 5%. The reader is referred to Mylleville & Rowe (1988, 1991) and Rowe & Mylleville (1989, 1990) for a more detailed discussion of the relationship between strain in the reinforcement and that in the underlying soil.

Having established a reasonable allowable strain, ε_a, (e.g. if it is 5%, $\varepsilon_a = 0.05$) then required tensile stiffness of the reinforcement is given by:

$$J_{req} = \frac{T_{req}}{\varepsilon_a} \tag{16.44}$$

where T_{req} and ε_a are obtained as described above.

The foregoing has dealt with a single layer of reinforcement. The single layer may be replaced by a few layers provided that they are all located relatively close to the bottom of the embankment with a layer of granular soil between each layer. Thus if there are m layers (provided that $m \leq 3$ in these applications) each with allowable strength, T_a, or design strength, T_D, one requires that:

$$(T_a \text{ or } T_D) \geq T_{req}/m \tag{16.45}$$

and

$$J_{req} = \frac{T_{req}}{m\varepsilon_a}. \tag{16.46}$$

16.8.4 REINFORCED EMBANKMENTS ON PEAT

16.8.4.1 Problem Definition

Due to the pore pressure dissipation that occurs during construction (see Section 16.3), there is no simple limit equilibrium method that can be used to assess the stability of embankments constructed on peat (see Section 16.3.1 for qualifications regarding what is meant by the term "peat").

Rowe & Soderman (1985b, 1986) have reported the results of a series of finite element analyses that examine the effect of geosynthetic reinforcement on the stability and deformation of embankments on peat. The method of analysis has been validated against case histories (e.g. Rowe *et al.* 1984b; Rowe & Mylleville 1996).

The peat parameters ($c' = 1.8$ kPa, $\phi' = 27°$, $\nu' = 0.15$, $K_0 = 0.18$, $e_0 = 9$) were selected based on a review of the literature. It would be considered unusual for a fibrous peat to have a combination of parameters significantly worse than those used, although this possibility cannot be excluded. The cases examined involved low granular embankments with heights above original ground surface of 2.5 m or less, a crest width of 13.4 m and 2:1 side slopes resting on peat deposits with depths of 3, 5 and 8 m. The granular fill was assumed to have $c' = 0$, $\phi' = 32°$, $\gamma = 20$ kN m^{-3}. The end of construction pore pressure distribution was assumed to be as shown in Fig. 16.9 for a maximum pore pressure $\bar{B}_m = 0.34$. The solution presented in the following takes into account the fact that some settlement, S_r, does occur during construction and is represented in terms of the end of construction fill height, h, above the original ground level (i.e. where $h = H\text{-}S_r$, and H = the fill thickness; see Section 16.4.5).

16.8.4.2 Peat Underlain by a Firm Base

The shear deformations and stability of embankments on peat can be improved by including a layer of suitable reinforcement at or near the interface between the peat and the fill. Figure 16.24 gives design curves relating the design height, h (above original ground level; $h = H - S_r$, as noted above) to the reinforcement tensile stiffness, J, for embankments on peat deposits 3, 5, and 8 m thick underlain by a firm base; interpolation can be used for intermediate thicknesses.

Referring to Fig. 16.24, for the conditions examined a desired end of construction height of 1.5 m above original ground level and $\gamma_f = 20$ kN m^{-3}, no reinforcement would be required if the peat deposit was 3 m deep, but reinforcement with a tensile stiffness $J >$ 800 kN m^{-1} would be required for a peat deposit 8 m deep. A major reason for the difference is the fact that, other things being equal, for an 8 m thick deposit the settlement during construction will be between two–three times that for a 3 m deposit and the reinforcement is required to carry the load due to the additional fill below the ground surface that would be present for the 8 m deposit. Settlement can be estimated as described in Section 16.4.5.

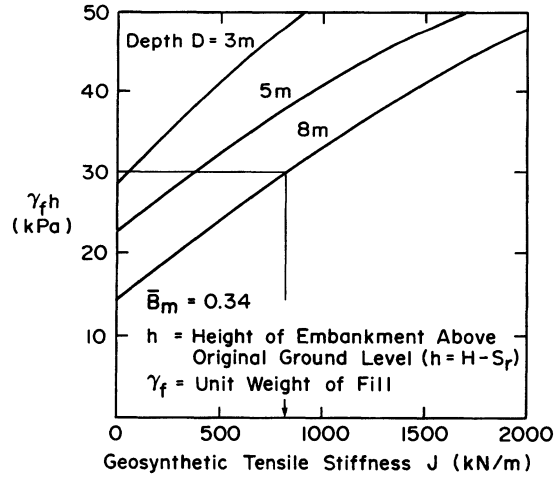


FIGURE 16.24. Design chart for peat underlain by a firm base; see text for assumptions and limitations (modified from Rowe & Soderman 1985b).

16.8.4.3 Peat Underlain by a Soft Clay/Marl Layer

Peat deposits are often encountered in regions that have been subjected to "recent" glaciation. Frequently, the depositional history of these deposits involves the sedimentation of clay, silts or lake marl followed by the formation of a peat deposit that will usually be covered by some form of living vegetation. Because the peat has low unit weight, the clay, silt or marl in a recent normally consolidated deposit will be very weak just below the peat, although the increase in effective stress with increasing depth will generally result in a significant increase in strength with depth below the peat. For the cases reported in the literature, the vane shear strength in a very soft stratum below the peat is typically in the range 5–15 kPa, although shear strengths as low as 2 kPa have been reported.

It has generally been observed (e.g. MacFarlane & Rutka 1959; Lea & Brawner 1963; Weber 1969; Raymond 1969) that construction and maintenance problems and shear failure are far more likely to occur when the peat is underlain by a weak soil than when it rests on a firm stratum. Collapse in these cases usually involves formation of a crack in the embankment and a block-like slide moving on or just below the boundary between the peat and the soft soil.

Figure 16.25 shows an embankment on a peat layer underlain by very soft clay. The active earth pressure in the fill creates a lateral thrust. The applied pressure due to the embankment resting on the peat also induces a lateral thrust in the peat. This lateral thrust must be resisted by the passive resistance that can be developed in the peat, the tensile force in the reinforcement and the shear strength that can be mobilized at (or near) the peat/very soft clay interface. Generally, due to the low effective stress in the peat outside the embankment, the passive resistance is negligible (unless berms are used; see Section 16.8.2). Thus the reinforcement and the shear strength at the peat–very soft clay interface must resist the lateral force. Initially, the contribution of the very soft clay is small and hence even with very high strength reinforcement there is a severe limit to the embankment height that can be achieved in single-stage construction. However, the reinforcement (either geosynthetic or natural root mat or both) does allow some fill to be placed (while maintaining stability) and with

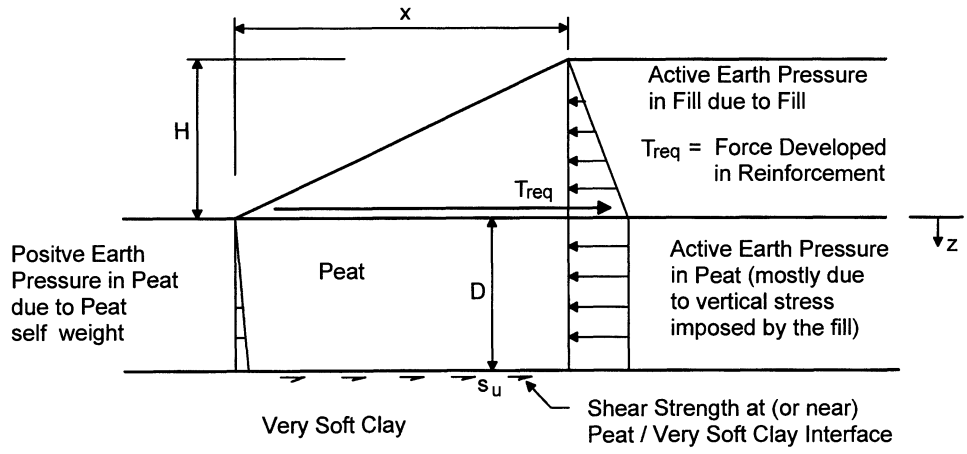


FIGURE 16.25. Potential failure mechanism due to lateral thrust and sliding on a deeper low strength layer, e.g. very soft clay beneath a peat layer (modified from Rowe 1997).

time the consequent increase in effective stress in the very soft soil will give rise to an increase in strength and hence more fill can be placed in a second stage of construction.

To assess stability, one can perform slip circle calculations to identify the critical slip circle through the peat and/or through the peat and clay, but to do so one must make some assumptions about the distribution of excess pore pressure both vertically, e.g. based on Eq. 16.1 and horizontally. This approach may not always capture the worst case and consideration should also be given to non-circular failure mechanisms such as that shown in Fig. 16.25. In this case, the fill is modeled as earth pressures (as discussed in Section 16.8.3.3) and the objective is to deduce the reinforcement force required to achieve the desired factor of safety (as discussed in Section 16.8.3.3). The required reinforcement force, T_{req}, can be calculated by assuming that at the end of construction: (a) there will be a settlement, S_r, of the fill into the peat so the total thickness of fill material will be $H = h + S_r$ and peat thickness will be $D' = D - S_r$; (b) the water table remains constant; (c) the excess pore pressures are as given by Eq. 16.1; (d) the submerged unit weight of the peat is negligible; and (e) the apparent cohesion of the peat can be conservatively neglected. One can write an approximate equation for horizontal equilibrium:

$$T_{req} = 0.5\gamma_f h^2 K_{af} + K_{af}\gamma_f h S_r + 0.5K_{af}\gamma'_f S_r^2 + (\gamma_f h + \gamma'_f S_r) \times \left[K_{ap} + \frac{2}{3} B_m D'(1 - K_{ap})\right] - s_{ur} x/F \quad (16.47)$$

where in addition to the terms defined in Fig. 16.25 and above:

$$K_a = \tan^2(45 - \phi'/2) \quad (16.48)$$

and K_{af} and K_{ap} = the values of the active earth pressure coefficient, K_a, evaluated for friction angle $\phi' \cong \phi'_{cv}$ for the fill and $\phi' \cong \tan^{-1}[(\tan \phi'_{peat})/F]$, respectively; ϕ'_{peat} = the friction angle of the peat; and $\gamma'_f = \gamma_f - \gamma_w$.

In order to evaluate the required force, T_{req} (Eq. 16.47), it is necessary to estimate the settlement, S_r, that will occur by the end of construction. This may be evaluated as discussed in Section 16.4.5. Once the T_{req} has been established, the required strength and tensile stiffness can be established using Eqs 16.44–16.46 as discussed in Section 16.8.3.3 with a typical allowable strain for peat, ε_a, of 5–8% (provided that these strains do not exceed the allowable strain in reinforcement).

Equation 16.47 represents a simple limit equilibrium approach that can be adopted in assessing reinforcement requirements. A more sophisticated alternative approach is to perform finite element analyses. For example, using the parameters discussed in Section 16.8.4.1, Rowe & Soderman (1986) analyzed a number of cases where peat was underlain by soft clay. Based on these analyses and those already discussed for peat underlain by a firm base they deduced approximate values of the reinforcement force, T_{req}, required to maintain stability with a factor of safety of unity as indicated in Table 16.2. The values can be approximately used by finding a result in the table corresponding to the factored strength $s^*_{uo} = s_{uo}/F$, where s_{uo} = the expected undrained shear strength of the clay near the peat–clay interface. Intermediate values of peat thickness and clay strength can be estimated by interpolation.

16.9 Practical Considerations: Construction, Instrumentation and Observation Analysis

16.9.1 DESIGN AND CONSTRUCTION

The upper part of soft clay and peat deposits (crust and root mat, respectively) is generally stronger than the underlying soil and should be left in place to allow the passage of vehi-

TABLE 16.2. Approximate required geosynthetic force, T_{req} (kN m^{-1}) (F = 1) values for embankments on fibrous peat $\bar{B}_m$ = 0.34

Peat thickness (m)	Underlying strata	Strength of underlying strata, s^*_{uo} (kPa)	Maximum height of fill above original ground level (m)[b,c]			
			1.0	1.5	2.0	2.5
3	Firm	—	NRR	NRR	25	60
	Clay	15	NRR	NRR	25	60
		10	NRR	NRR	30	65
		7.5	NRR	15	40	70
		5	NRR	40	80	PF
		2.5–5	15	110	PF	PF
5	Firm	—	NRR	30	50	75
	Clay	15	NRR	30	50	75
		10	10	60	110	PF
		7.5	25	100	PF	PF
8	Firm	—	65	75	95	120

[a] See Rowe and Soderman 1985b, 1986 for limitations.
[b] NRR, no reinforcing required.
[c] PF, potential failure for the assumed conditions: do not construct.

cles and protect the underlying soil from disturbance. This crust is often covered by a permeable fill layer that, in addition to improving the bearing capacity of the upper layer, facilitates the consolidation of the clay or peat layer. In cases where the crust is non-existent, or rather soft or thin, a geosynthetic can be placed over the natural soil as a separator and/or reinforcement layer (see Chapter 7). In order to avoid disturbance of the clay deposit, the lower part of the embankment should not be heavily compacted. When clayey soils are used as fill material, the compaction conditions must be selected to avoid their collapse when wetted and to limit long-term creep movements. The use of an appropriate construction procedure is crucial to the success of the project (see Holtz *et al.* 1997).

16.9.2 INSTRUMENTATION

In order to evaluate the degree of consolidation and the strength of the clay, it is desirable to instrument the clay foundation with piezometers and settlement gages. This is particularly important in stage construction to estimate when the following stage could be constructed and to what level. When there are services, structures or piles close to the embankment, it can be important to monitor the lateral displacements using inclinometers.

16.9.3 OBSERVATION ANALYSIS

The monitoring data obtained during and after construction should be used to verify how the observed behavior compares with the parameters used in design, and where appropriate the calculations can be upgraded.

As indicated in Fig. 16.1 and Section 16.1.1, the observation of pore pressures generated during construction under the centerline of an embankment can generally be used to calculate the vertical yield stress of the clay at the level of the piezometer. It can also give an indication of local shear failure when the ratio $\Delta u/\Delta\sigma$ becomes larger than 1.0.

The strain between two deep settlement gages can be used in conjunction with pore pressure measurements to define an *in situ* effective stress–strain curve, that can then be

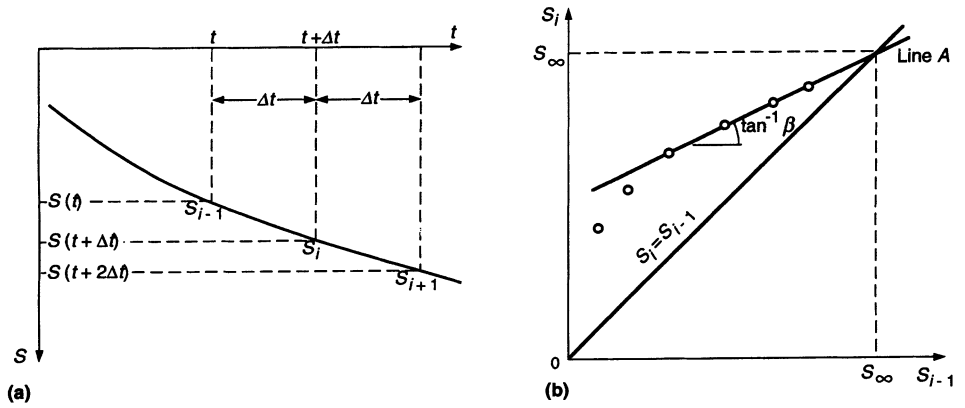


FIGURE 16.26. Stages in analysis of settlements using Asaoka's (1978) method: (a) settlement curve for soil layer, and (b) Asaoka's construction.

compared with the compression curve assumed for the sublayer considered.

When the clay deposit and the consolidation conditions are relatively simple, Asaoka's (1978) method can be used during the consolidation process to evaluate the magnitude of the final settlement as well as a representative coefficient of consolidation. This method involves the following procedure: (a) plot the settlement, $S(t)$, of the compressible layer with time (Fig. 16.26a); (b) choose a time interval, Δt, and read from the curve the settlement, S_i, at times $(t_0 + i\Delta t)$ for $i = 0, 1, 2 \ldots$. (Fig. 16.26a); (c) plot S_{i-1} versus S_i on a special diagram and draw the line A (Fig. 16.26b); and (d) the point at which $S_{i-1} = S_i$ corresponds to the final settlement, S_f. The slope of the line A can be used to calculate the average coefficient of consolidation of the clay, using one of the following equations:

1. For the case of a vertically drained compressible layer (Asaoka 1978):

$$c_v = -\frac{5\Lambda^2}{12\Delta t} ln\beta \qquad (16.49)$$

in which Λ = the drainage path ($\Lambda = D$, the thickness of the layer for one-way drainage and $\Lambda = 0.5D$ for two-way drainage).

2. For the case where vertical drains are used (Magnan & Deroy 1980):

$$c_v = -\frac{d_e^2 F(n)}{8\Delta t} ln\beta \qquad (16.50)$$

in which d_e and n =, respectively, the diameter of the zone of influence of each drain, and the drain spacing ratio ($n = d_e/d_w$, where d_w = the equivalent diameter of the drains); and $F(n)$ is defined as discussed in Section 15.2.3.4.

The Asaoka method can be used for embankments constructed in one stage or in several stages separated by periods of consolidation at constant load.

17. EARTH RETAINING STRUCTURES AND REINFORCED SLOPES

R. J. Bathurst
C. J. F. P. Jones

17.1 Introduction

For many years engineering practice for earth retaining structures emphasized earth pressures and their application in choosing an appropriate design and support system. In the last 25 years there has been a dramatic growth in new construction technologies and products for retaining soil. In particular there has been increasing use of reinforcing elements, either by incremental burial to create reinforced soils or by systematic *in situ* installation to produce soil nailing. Rapid developments in polymer manufacturing have led to a wide range of polymeric products (geosynthetics) (see Chapter 7). These materials are now routinely used to reinforce the soil in retaining wall and slope applications, and to control soil drainage. Reinforced soils and soil nailing have changed the ways built-up and *in situ* walls are constructed by providing economically attractive alternatives to conventional methods. The use of these products in reinforced soil applications has led to many different earth retention systems.

17.1.1 TYPES OF EARTH RETAINING STRUCTURES

Table 17.1 summarizes current earth retention methods for both externally and internally stabilized systems. An externally stabilized system uses an external structural wall to resist earth forces. An internally stabilized system involves reinforcements installed within the soil and extending beyond the potential failure mass. Here the use of shear transfer to mobilize the tensile capacity of closely spaced reinforcing elements has freed retaining structures of the need for a structural wall by substituting a composite system of reinforcing elements and soil. A facing may be required on an internally stabilized system to prevent local raveling and deterioration.

Figure 17.1 shows that traditional walls may be regarded as externally stabilized systems. Gravity walls, in the form of a cantilever structure (Fig. 17.1a) or gravity elements, e.g. cribs (Fig. 17.1b), support the soil through weight and stiffness to resist sliding, overturning, and excessive shear and moments. Bracing, in the form of internal struts or rakers (Fig. 17.1c), provides temporary support for *in situ* walls. Tie-backs (Fig. 17.1d) provide support through the pull-out capacity of anchors established in stable soil outside of the zone of potential failure.

Internally stabilized walls are represented in Fig. 17.1 by reinforced soils with horizontally layered elements, such as metallic strips, polymeric geogrids or geotextiles (Fig. 17.1e–g), and soil nailing (Fig. 17.1h). Soil

R. K. Rowe (ed.), *Geotechnical and Geoenvironmental Engineering Handbook*
© Kluwer Academic Publishers 2001

TABLE 17.1. Classification scheme for earth retention systems (adapted from O'Rourke & Jones 1990)

Externally stabilized systems	Internally stabilized systems
In situ walls	*In situ* reinforcement
Timber	Soil nailing
Precast concrete	Reticulated micropiles
Sheet piles	Soil doweling
Soldier piles	Reinforced soils
Cast-*in-situ*	Metallic, glass-fiber
Slurry wall	Polymeric reinforcement strips, geogrids and geotextiles
Secant pile	Geocells
Tangent pile	Anchored earth
Bored-in-place (piles not contiguous)	
Soil-cement	
Braced: Internal struts, Rakers	Tied-back: Augered, Pressure injected, Driven
Gravity walls	Hybrid systems
Concrete	Gabion/reinforced soil
Segmental retaining walls (masonry concrete)	Reinforced segmental (masonry concrete) retaining walls
Cantilever	Special materials
Counterfort	Polymer fiber, filament and mesh impregnated soil
Gabion	Low density fills
Crib	Expanded low density concrete and cement
Bin	Geofoam
Cellular cofferdam	

nailing uses metallic bars or dowels, which are installed during *in situ* construction. A key aspect of an internally stabilized system is its incremental form of construction. In effect, the soil mass is partitioned so that each partition receives support from a locally inserted reinforcing element. This process is just the opposite of what occurs in a conventional back-filled wall where earth pressures are integrated to produce an overall force resisted by the structure. The overall earth pressure in reinforced soil, for example, is actually differentiated by the multiple layers of reinforcement. In soil nailing, multiple levels of bars or dowels interconnect the soil mass so that each potential failure surface is crossed by enough elements to maintain stability.

Hybrid systems combine elements of both internally and externally supported soils. Geosynthetic reinforced segmental retaining walls (see Fig. 17.1g) fall within this class and use a hard facing comprising a column of dry-stacked modular concrete units (Bathurst and Simac 1994). The modular concrete facing units are produced using machine molded (masonry) or wet-casting methods and are available in a wide range of shapes, sizes and finishes. The dry- stacked (mortarless) concrete blocks are discrete units that transmit shear through interface friction, concrete keys, mechanical connectors or a combina-

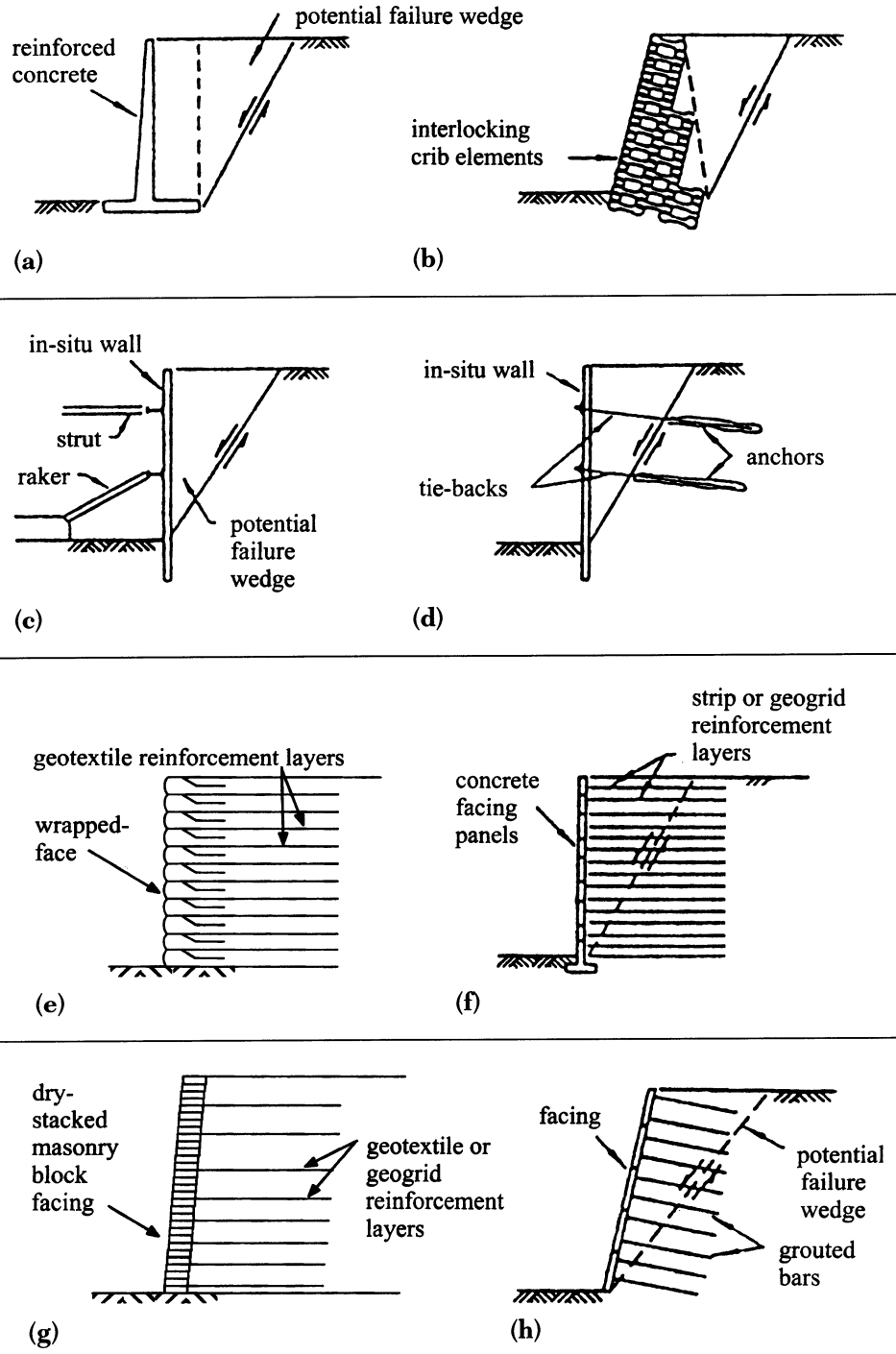


FIGURE 17.1. Examples of earth retention systems (modified from O'Rourke & Jones 1990 and Bathurst *et al.* 1993): (a) cantilever; (b) crib; (c) braced; (d) tie-back; (e) wrapped face geotextile reinforced soil wall; (f) reinforced soil wall with incremental concrete facing panels; (g) reinforced segmental retaining wall (modular blocks); and (h) soil nailing.

tion of these methods. In addition to providing structural stability to the composite facing–geosynthetic–soil structure, they also act as a temporary form work during placement and compaction of backfill soils. Most proprietary units are 80–600 mm in height, 150–800 mm in width (toe to heel), and 150–800 mm in length. The modular units typically vary from 14 to 48-kg each. The modular concrete units may be solid, hollow, or hollow and infilled with a free-draining granular soil. Segmental retaining walls are usually constructed with a stepped face, which results in a facing batter that ranges from 3 to 15° from the vertical.

However, modular facing systems are not restricted to concrete materials. Timber facings, expanded polymeric geocells (Bathurst & Crowe 1992) and wire mesh gabion units (Simac *et al.* 1997a,b) have also been employed to construct hybrid systems. In some cases, geogrids have been substituted for the metallic wire in stone-filled baskets used in gabion structures (O'Rourke 1987).

There is a wide variety of reinforcing components and the possibilities of combining elements of externally and internally stabilized systems are extensive. Anchored earth systems have been developed that involve aspects of reinforced soil and soil anchoring. Figure 17.2 illustrates applications originating from Austrian, Japanese and British practitioners. All these applications utilize multiple layers of closely spaced reinforcement and thus are similar in construction to the methods employed for reinforced soils. The Austrian application involves polymeric strips connecting concrete wall blocks and semicircular anchors (Fig. 17.2d), while the Japanese application exploits the local passive resistance of small rectangular anchor plates (Fig. 17.2b). The British method (Jones *et al.* 1996, Murray & Irwin 1981) employs reinforcing steel bent into triangular anchors (Fig. 17.2c). Pullout resistance is mobilized by friction along the straight portion of the steel and by passive pressure mobilized at the triangular anchor. Anchored earth concepts have been extended even to waste automobile tires, as illustrated in Fig. 17.2a (Jones 1996). The tires may be tied together with metal bars or polymer strips.

A common objective for soil reinforced systems has been to transform soil into an engineered medium, which is less soil-like because of enhanced mechanical properties. An innovation that directly modifies the mechanical properties of retaining wall soils includes polymer impregnation of soils by mixing soil with continuous polymer filaments. The reinforcing element described by Leflaivre *et al.* (1983) is a polyester filament of 0.1-mm diameter and a tensile strength of 10 N. The placement requires the simultaneous projection of sand, water and filament. Approximately 0.1–0.2% of the composite material is filament, producing a total length of reinforcement of 200 m per m^3. Cohesive strengths of 100–200 kPa have been reported for the material. Similar mechanical behavior has been developed by the inclusion of small 60 × 40 mm polymeric mesh elements into sand. The inclusion of 0.2% by weight of mesh elements can increase the shear strength of sandy soil by 25–60% (Mercer *et al.* 1984).

In some cases, particularly when very soft compressible soils underlie highway walls and abutments, it may be advantageous to replace the soil entirely by a lightweight material including geofoam (expanded polystyrene). Low density cements and soil–cement products have been used for similar applications. The use of geofoam has also been proposed to reduce active earth pressures against rigid basement walls and abutments (Horvath 1995, Karpurapu & Bathurst 1992) and as seismic buffers (Bathurst & Alfaro 1996).

17.1.2 SELECTION OF TYPE OF RETAINING WALL

The selection of the appropriate form of retaining wall for a particular application depends upon a number of factors including:

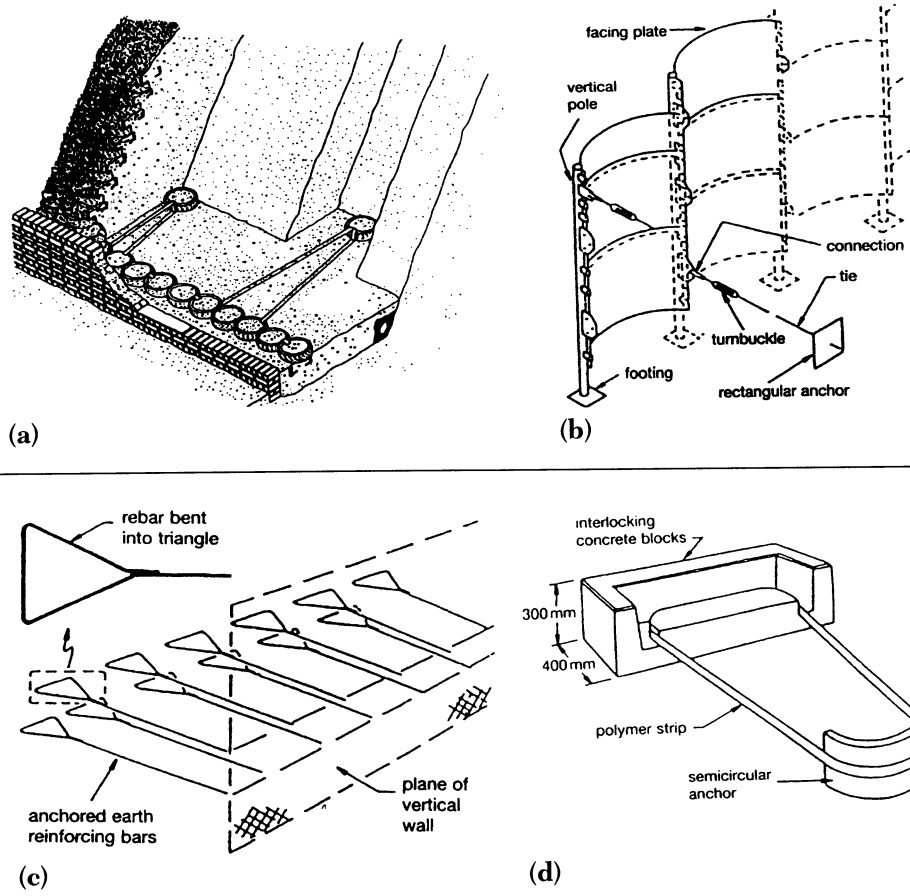


FIGURE 17.2. Example anchored wall systems (after O'Rourke & Jones 1990, © ASCE, reproduced with permission): (a) earth retention with waste tires and geotextiles; (b) wall system with facing plates and rectangular anchors; (c) anchored earth with triangular rebar reinforcement; and (d) wall system with concrete block, polymer strips and anchors.

- Location of the proposed retaining wall, its position relative to other structures and the amount of space available, including the necessity or otherwise to confine the support system within the site boundaries.
- Height of the proposed retaining wall and the topography of the ground to be formed.
- Subsurface stratigraphy and groundwater conditions.
- Extent of ground movement acceptable during construction and in service, and the effect of movement of the retaining wall on nearby structures and services.
- Availability of materials.
- Time available for construction.
- Appearance.
- Design life and maintenance.
- Experience and familiarity of the construction technique by the contractor.
- Environmental considerations.

The use of any particular system may also be influenced by historical and cultural considerations and importantly by the availability or absence of recognized codes of practice. This is particularly the case with new retention systems such as reinforced soil, which in some countries has only recently gained acceptance with the introduction of codes of practice by regulatory authorities.

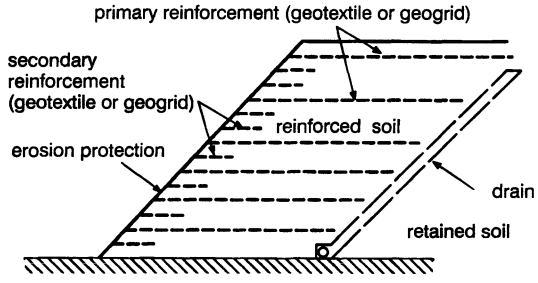


FIGURE 17.3. Geosynthetic reinforced slope.

17.1.3 REINFORCED SLOPES

The necessity for a structural facing system is obviated if the facing slope is shallow enough that mass movement of the steepened soil is not likely. The introduction of geosynthetics, including geotextiles and geogrids, has led to the construction of reinforced soil slopes with slope angles that are steeper than what can be safely achieved with unreinforced slope systems (see Chapter 14). An example of a reinforced soil slope is illustrated in Fig. 17.3. The primary reinforcement layers perform the reinforcement function, while lower strength layers of reinforcement are often used to help stabilize the near-slope soils during construction. In some cases it is good construction practice to include a chimney drain to intercept groundwater. These drains may include geotextile-wrapped free-draining granular stone. Facing treatments, including vegetative cover or geosynthetic erosion control products, are required to protect against surficial erosion of the slope face. In some cases the reinforcement is extended along the slope face to give a wrapped-face construction (Fig. 17.1e).

17.1.4 SOIL REINFORCEMENT CONCEPTS

17.1.4.1 Reinforcement

The effect of placing reinforcement in soil in the direction of tensile strain is to restrict deformation and to generate a force that is proportional to the resultant strain developed in the reinforcement. An equilibrium condition is reached dependent upon the longitudinal stiffness of the reinforcement and the load–displacement characteristics of the soil. Longitudinal stiffness of the reinforcement governs the deformation (or strains) that occurs in the reinforced soil. The longitudinal stiffness of a reinforcement layer, J, is equal to the product of elastic modulus, E, and the effective cross-sectional area, A, of the reinforcement. Soil strength is improved until a limiting value of strain is achieved; with further shear displacement the improvement in soil strength remains constant.

17.1.4.2 Soil

The properties of the fill material and the stress state of the material have a marked influence on its behavior when reinforced. The ideal reinforced soil is a well-drained, well-graded granular material, providing long-term durability, stability during construction, and having good physiochemical properties. In the normal stress range associated with reinforced soil structures, post-construction movements do not normally occur when well-graded granular soils are used.

Fine-grained soils are normally poorly drained, and efficient stress transfer between the reinforcement and soil may not be immediate. Fine-grained soils often exhibit visco-plastic behavior, thereby increasing the chance of unacceptable post-construction movements.

The density of a soil has an effect on the stress–strain relationship in soils; accordingly, relative density will influence some aspects of reinforced soil performance. Dense soil in the drained condition dilates during shear, whereas loose soil has a lower deviator stress, no peak value and exhibits volumetric reduction.

The effect of a dilating soil on the normal stress of a reinforcing element can be significant, leading to enhanced frictional shear stress transfer between the soil and the reinforcement. However, the increase in stress

may reduce rapidly with increasing shear strain. Some reinforcing materials such as "high adherence strips" rely upon the restrained dilatancy effect to develop the apparent interface friction used in design (parameter μ^* in Section 17.4.3.4).

The mobilized shear strength of a soil subject to compressive loads increases with increasing axial and lateral strain, until a peak shear strength, ϕ'_p, is mobilized. In elastic–plastic soils, shear strength continues to be mobilized at peak values when strains are required to produce the peak shear strength. In the case of strain softening soils, the mobilized shear strength decreases as strains exceed those required to mobilize peak strength. At large strains the mobilized shear strength achieves a constant minimum value, ϕ'_{cv}. According to Cornforth (1964) and Bolton (1986), the peak angle of friction, ϕ'_p, of granular soils occurs at lateral tensile strains in the range 3–6% and the constant volume angle of friction, ϕ'_{cv}, occurs at tensile strains in the range 6–12%. Typical ϕ'_{cv} values for granular soils range from 33 to 40°.

A number of analytical methods use the peak angle of friction, ϕ'_p, in design of walls and slopes. Bolton (1986) has proposed the following relationship to calculate the peak friction angle of a granular soil under plane strain conditions, i.e. the condition most often assumed to apply to retaining wall and slope structures:

$$\phi'_p = \phi'_{cv} + 0.8\psi_{max} \qquad (17.1)$$

where ψ_{max} is the peak dilatancy angle of the soil during shear. For well-compacted granular fills the peak plane strain dilatancy angle, ψ_{max}, used in Eq. 17.1 can be estimated as $\psi_{max} = 6.25I_R$ (degrees), where I_R = the relative dilatancy index of the soil (Bolton 1986). For well-compacted granular soils used in walls and slopes not exceeding 10 m in height, the relative dilatancy index of the soil can be estimated by $I_R = 5I_D - 1$, where I_D = relative density ($I_D = e_{max} - e/e_{max} - e_{min}$). The peak friction angle, ϕ'_p, under radial symmetric loading, i.e. triaxial test conditions, is typically less than that measured under true plane strain conditions. The peak friction angle, ϕ'_p, under triaxial conditions can be estimated from Eq. 17.1 using $\psi_{max} = 3.75I_R$.

The selection of a value of the friction angle for design, ϕ'_{des}, depends upon the quality of the fill used in design. Selection of $\phi'_{des} = \phi'_p$ is appropriate for walls, abutments and reinforced slopes constructed with good frictional fill. In the case of slopes and embankments over weak foundations, $\phi'_{des} = \phi'_{cv}$ is appropriate. The large strain constant volume angle, ϕ'_{cv}, has been used for ultimate limit state analysis in limit states design since large strains are typically associated with collapse conditions. As the constant volume shear strength is the lowest value achievable, no partial factor is required (see Sections 17.1.6, 17.4.1 and 17.5.1). In North America, the global factor design approach is common and the peak friction angle, ϕ'_p, is typically used in retaining wall and slope design to avoid undue conservatism. The selection of the appropriate value of friction angle for design should always be based on applicable codes of practice and local experience.

17.1.5 GLOBAL FACTOR DESIGN APPROACH

Geotechnical engineers have traditionally designed earth structures based on a global factor of safety approach. For each failure mechanism, a single global factor of safety, F, is calculated based on the ratio of the resistance of the structure, R, to the load effects, S, hence:

$$F = \frac{R}{S} \qquad (17.2)$$

A state of failure is assumed to exist if $F \leq 1$. A fundamental shortcoming of this method is that no attempt is made to distinguish between uncertainty in material

strength (resistance, R), and structure loading effects, S. Nevertheless, the large amount of experience that has been gained by geotechnical engineers using a global factor design approach has led to safe design. Indeed, limit states design methods described below have been calibrated against the database of experience from traditional global factor of safety methods.

17.1.6 LIMIT STATES DESIGN APPROACH

Limit states design (LSD) has been used by structural engineers in North America and Europe for many years. LSD methods are at various stages of acceptance and development for geotechnical structures. Limit states are defined as conditions under which a structure or a component no longer performs its intended function. Limit states typically include collapse (ultimate limit states) and deformation (serviceability limit states) criteria (see Section 17.4.1 for example LSD methods for reinforced soil walls). Nevertheless, different LSD approaches are used in Europe and North America. In Europe, a "factored strength" approach is used, while in North America a "factored overall resistance" approach is used (Becker 1996a). Regardless of the approach, the basic design criterion is that the resistance capacity, R, of the earth structure must be greater than load demand, S, for an acceptable level of safety, hence:

$$R > S. \tag{17.3}$$

In both the European and North American approaches the specified or characteristic loads are multiplied by partial factors to arrive at design loads. The difference in philosophy is related to the treatment of the resistance side of Eq. 17.3. In the European factored strength approach, partial factors are applied directly to each strength parameter contributing to the applicable limit state. In the North American factored overall resistance approach, the total resistance is first calculated using unfactored strength parameters and then the total resistance is multiplied by a single resistance factor to obtain the factored resistance for design.

Values of partial factors which have been used in the UK for the design of vertical walls, bridge abutments and reinforced slopes are shown in Tables 17.2 and 17.3.

17.2 Earth Pressure Theory

17.2.1 EARTH PRESSURE AT REST

The ratio of horizontal to vertical effective stress for an element of soil can be estimated as discussed in Sections 2.6.5 and 3.4. Often the "coefficient of earth pressure at rest," K_0, is approximated by:

$$K_0 = \frac{\sigma'_h}{\sigma'_v} = 1 - \sin \phi' \tag{17.4}$$

where σ'_v = vertical effective stress, e.g. $\sigma'_v = \gamma z - \gamma_w(z - z_w)$, where γ = the bulk unit weight of the soil, z = depth below the soil surface, γ_w = the unit weight of water, and z_w = the depth of the horizontal static water table below the soil surface (if applicable).

17.2.2 RANKINE EARTH PRESSURE THEORY

Rankine earth pressure theory can be used to calculate the magnitude and distribution of active and passive earth pressures behind vertical earth retaining structures. Retained soils are assumed to have a cohesion, $c' \geq 0$, and friction angle, $\phi' \geq 0$. For cases in which a retaining wall will translate outward horizontally or rotate outward about the toe, the magnitude of horizontal active earth pressure can be calculated by:

$$\sigma'_a = K_a\sigma'_v - 2c'(K_a)^{1/2} \tag{17.5}$$

where K_a = the "coefficient of active earth pressure" expressed by:

$$K_a = \frac{1 - \sin \phi'}{1 + \sin \phi'} \tag{17.6}$$

TABLE 17.2. Partial factors used in the design of vertical walls and abutments (adapted from Jones 1996)

	Partial factor	Ultimate limit state	Serviceability limit state
Loads	Soil unit weight (within and at top of structure), f_{es}	1.5[a]	1.0[a]
		1.0[b]	1.0[b]
		1.0[c]	1.0[c]
	External dead loads (e.g. line or point loads), f_{ff}	1.2[a]	1.2[a]
		1.0[b]	1.0[b]
		1.0[c]	1.0[c]
	External live loads		
	Traffic loading, f_q	1.5[a]	1.5[a]
		1.5[b]	1.5[b]
	Bridge loading, f_{eq}	1.5(HA)[a]	1.5(HA)[a]
		1.3(HA+HB)[a]	1.3(HA+HB)[a]
		1.5(HA)[a]	1.5(HA)[a]
		1.3(HA+HB)[b]	1.1(HA+HB)[b]
	Temperature effects, f_{eq}	1.3	1.3
	Earth pressure behind structure, f_{es}	1.5[a]	1.0[a]
		1.5[b]	1.0[b]
		1.0[c]	1.0[c]
	Horizontal loads due to shrinkage and creep, f_{ef}	1.2[a]	1.2[a]
		1.2[b]	1.2[b]
		1.0[c]	1.0[c]
Materials	Soil materials, f_{ms}		
	Applied to tan ϕ'_{des}	1.0	1.0
	Applied to c'	1.6	1.0
	Applied to s_u	1.0	1.0
	Reinforcement, f_m	Varies with type (e.g. metallic or polymeric)	Varies with type (e.g. metallic or polymeric)
Soil/reinforcement interaction	Sliding on surface, f_s	1.3	1.0
	Reinforcement pull-out, f_p	1.35	1.0
Bearing capacity	Foundation, f_{bc}	1.35	1.0
Sliding	Base of structure, f_{ss}	1.2	1.0
	Soil–soil interface, f_{ss}	1.2	1.0
Economic ramifications of failure	Structure of strategic importance (highway bridge or dam), f_n	1.1	1.0
	Other structures, f_n	1.0	1.0

[a] When checking maximum reinforcement tension and foundation pressure.
[b] When checking maximum overturning loads, pull-out resistance and sliding on base.
[c] When considering dead loads only, foundation settlement and the reinforcement tension at the serviceability limit state. HA and HB are uniformly distributed and non-uniformly distributed highway loadings defined in the UK bridge code BS 5400 (1995).

For the passive loading condition in which a retaining wall translates horizontally into the retained soil or rotates inward about the toe, the horizontal passive earth pressure can be calculated by:

$$\sigma'_p = K_p\sigma'_v + 2c'(K_p)^{1/2} \quad (17.7)$$

where K_p = the "coefficient of passive earth pressure" and can be calculated using $K_p = 1/K_a$. Coefficients of earth pressure intro-

TABLE 17.3. Partial factors used in the design of reinforced slopes (adapted from Jones 1996)

	Partial factor	Ultimate limit state	Serviceability limit state
Loads	Soil unit weight, f_{es}	1.5	1.0
	External dead loads, f_{ff}	1.2	1.0
	External live loads, f_q	1.3	1.0
Materials	Soil materials, f_{ms}		
	Applied to tan ϕ'_{des}	1.0	1.0
	Applied to c'	1.6	1.0
	Reinforcement, f_m	Varies	Varies
Soil–reinforcement interaction	Sliding on surface, f_s	1.3	1.0
	Reinforcement pull-out, f_p	1.3	1.0
Sliding	Base of structure, f_{ss}	1.2	1.0
	Soil/soil interface, f_{ss}	1.2	1.0

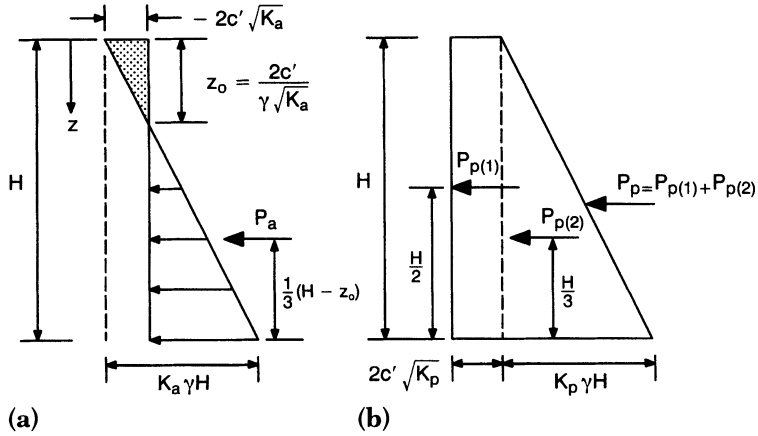


FIGURE 17.4. Active (a) and passive (b) earth pressure distributions (no groundwater).

duced thus far show that for a frictional soil, $K_a < K_0 < K_p$.

Distributions for active and passive earth pressures due to soil self-weight are illustrated in Fig. 17.4 for a dry soil. Since retained soils cannot exert a tensile stress at the back of a structure, the negative active earth pressure zone at the top of the wall predicted for soils with $c' > 0$ is usually ignored for gravity structures (Fig. 17.4a).

The total active earth force, $\boldsymbol{P}_a$, or total passive earth force, $\boldsymbol{P}_p$, acting against a vertical wall can be calculated by integrating the earth pressure distributions over the height of the wall, H. For $c' = 0$, the earth pressure distributions become triangular and the active earth force for the case of dry soil becomes:

$$\boldsymbol{P}_a = \frac{1}{2} K_a \gamma H^2 \tag{17.8}$$

and the passive earth force:

$$\boldsymbol{P}_p = \frac{1}{2} K_p \gamma H^2. \tag{17.9}$$

If a horizontal static water table condition exists behind a retaining wall, Eqs 17.5 and 17.7 must be used with effective unit soil weights ($\gamma' = \gamma - \gamma_w$) for the soil as applicable, and a triangular hydrostatic water pressure distri-

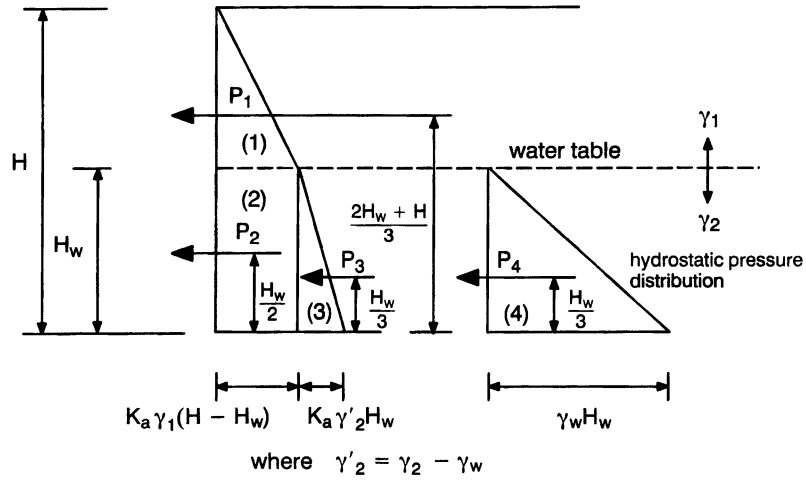


FIGURE 17.5. Lateral pressures for the case of a hydrostatic water table behind a wall and cohesionless soils under active earth pressure conditions.

bution added to lateral earth pressures acting against the wall. An example is illustrated in Fig. 17.5. It should be noted that the soil located behind the wall will have a higher bulk unit weight below the water table (where it is fully saturated) than above the water table where the soil is only partially saturated, i.e. $\gamma_2 > \gamma_1$ in Fig. 17.5. Good engineering practice is to avoid the accumulation of water behind the wall by directing surface water away from the structure or installing drains in the back-fill.

Additional horizontal pressures may be developed against a wall due to vertical loads applied at the surface of the retained soil. Horizontal pressures and loads due to a uniformly distributed surcharge pressure, q, can be calculated as illustrated in Fig. 17.6. Horizontal pressures and loads due to point or line load surcharges can be calculated using Fig. 17.7. Horizontal pressures and loads generated by surcharge effects (e.g. see Fig. 17.6) are added to the distributions illustrated in Figs 17.4 and 17.5.

17.2.3 COMPACTION STRESSES

Compaction of cohesionless soils behind retaining walls can lead to additional horizontal stresses. Compaction-induced stresses can be estimated using the method by Ingold (1979) illustrated in Fig. 17.8. Compaction stresses in excess of active earth pressures are assumed to be developed over a depth, d_c, where:

$$d_c = \frac{1}{K_a}\left(\frac{2Q/w}{\pi\gamma}\right)^{1/2} \qquad (17.10)$$

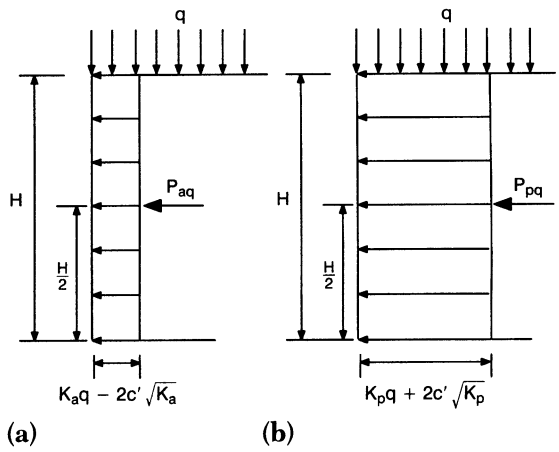
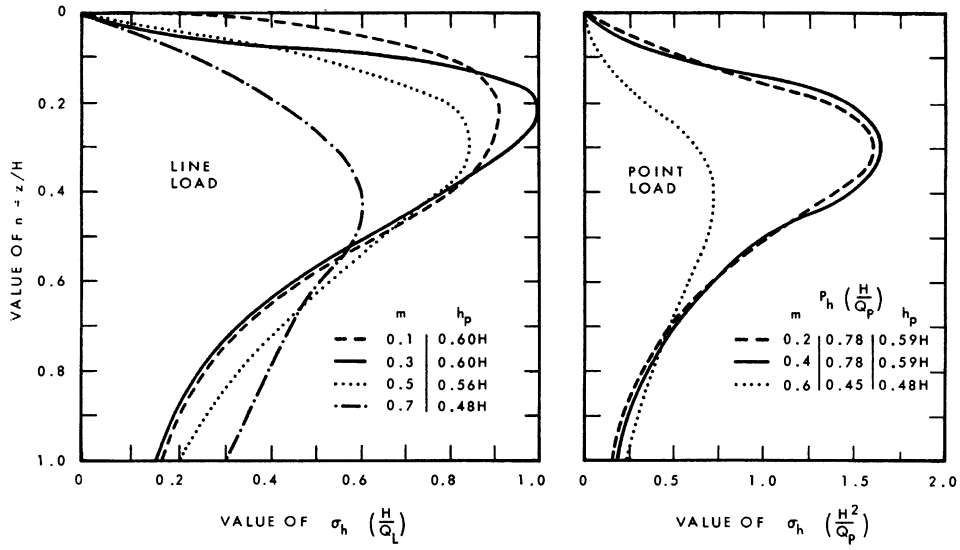
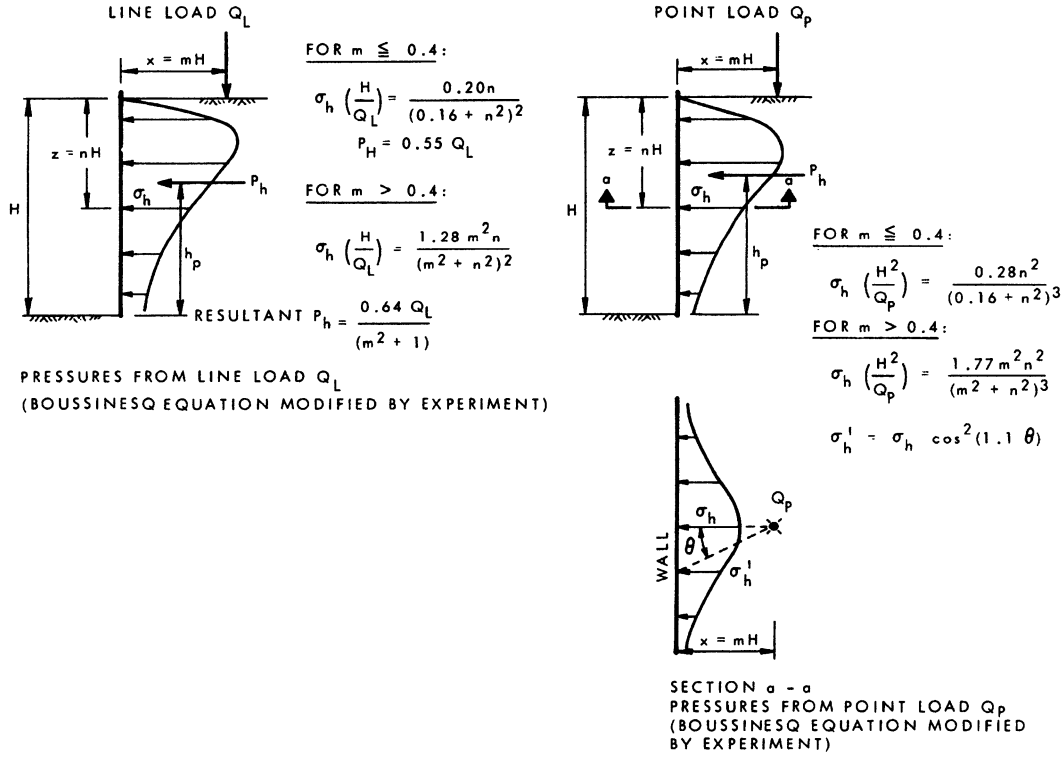


FIGURE 17.6. Active (a) and passive (b) earth pressure distributions due to uniform surcharge (no groundwater).



(a)



(b)

FIGURE 17.7. Horizontal pressures on a wall due to (a) line, Q_L, and (b) point, Q_P, load surcharges (modified from CGS 1992).

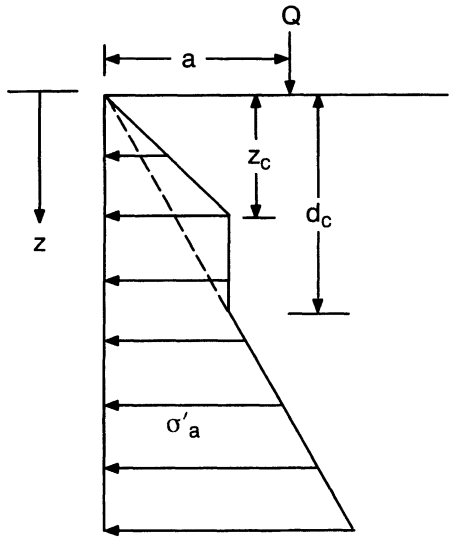


FIGURE 17.8. Calculation of compaction stresses (after Ingold 1979).

where Q = the roller load (dead load plus dynamic load) and w = the roller length perpendicular to the wall length. Compaction stresses are assumed to increase linearly with depth to:

$$z_c = K_a \left(\frac{2Q}{\pi\gamma}\right)^{1/2}. \qquad (17.11)$$

Over the depth $z_c \leq z \leq d_c$ the active earth pressure is constant and equal to:

$$\sigma'_a = \left[\left(\frac{2Q\gamma/w}{\pi}\right)\right]^{1/2}\left(\frac{w}{a+w}\right) \qquad (17.12)$$

where a = the distance of the roller edge from the back of the wall. Below depth d_c compaction stresses are assumed to be less than active earth pressure values, and hence horizontal stresses can be calculated using Rankine active earth pressure theory. The value of d_c has been found to be about 6 m when conventional compaction plant and specifications are employed. This is reflected in a number of codes of practice relating to reinforced soil, including the UK, French and Australian codes (1992, 1995, 1996), respectively. Duncan *et al.* (1991a, b) have produced a series of design charts to calculate earth pressures due to compaction effects based on a hysteretic theory by Duncan and Seed (1986).

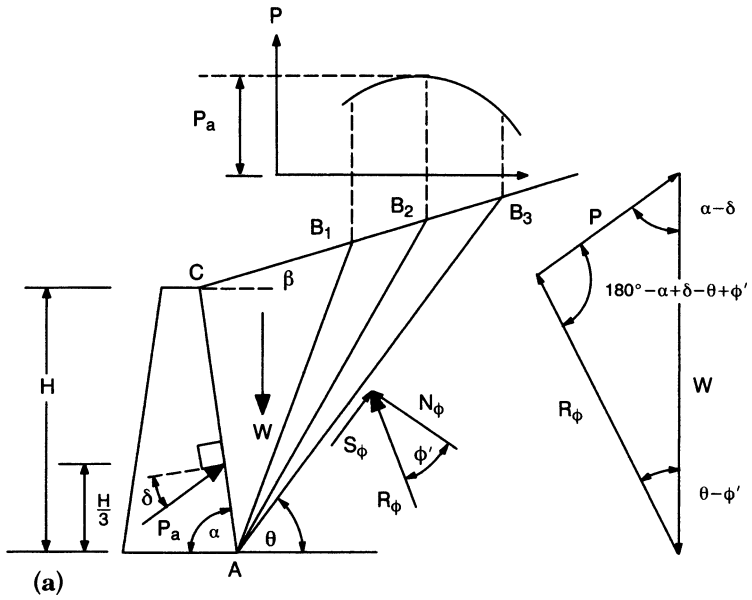
17.2.4 COULOMB WEDGE METHODS

A general approach to find the active earth force at the back of an earth retaining structure is the Coulomb wedge method. This method involves finding the free body soil volume (wedges ABC) in Fig. 17.9a, which gives a maximum value of the vector $\boldsymbol{P}$. This value is the active earth force, $\boldsymbol{P}_a$, and can be calculated using a force polygon as illustrated in the figure. In a graphical solution to the force polygon, the magnitude of vector $\boldsymbol{P}$ can be obtained by projecting lines from the top and bottom of the weight vector, $\boldsymbol{W}$, at the orientations shown in the vector diagram.

The Coulomb wedge method is very general and allows walls with irregular back slope geometries to be analyzed. In addition, the Coulomb wedge solution can be used to solve problems in which the wall–soil face is not vertical, interface shear between the wall and soil is mobilized, and additional surface distributed loads are present behind the wall. Surcharge loads falling within trial wedges (ABC) are treated as additional vertical loads in the force polygon solution. For cohesionless ($c' = 0$) dry soils and the simple geometry shown in Fig. 17.9a, the active earth pressure coefficient, K_a, can be calculated using the following closed-form solution:

$$K_a = \sin^2(\phi' + \alpha)\Big/\left[\sin^2(\alpha)\sin(\alpha - \delta)\right.$$
$$\left.\times\left\{1 + \left[\frac{\sin(\phi' + \delta)\sin(\phi' - \beta)}{\sin(\alpha - \delta)\sin(\alpha + \beta)}\right]^{1/2}\right\}^2\right] \qquad (17.13)$$

Here, α = the slope of the wall back face, δ = the interface friction angle between the wall and retained soil and β = the back slope angle (Fig. 17.9a). The active earth force $\boldsymbol{P}_a$



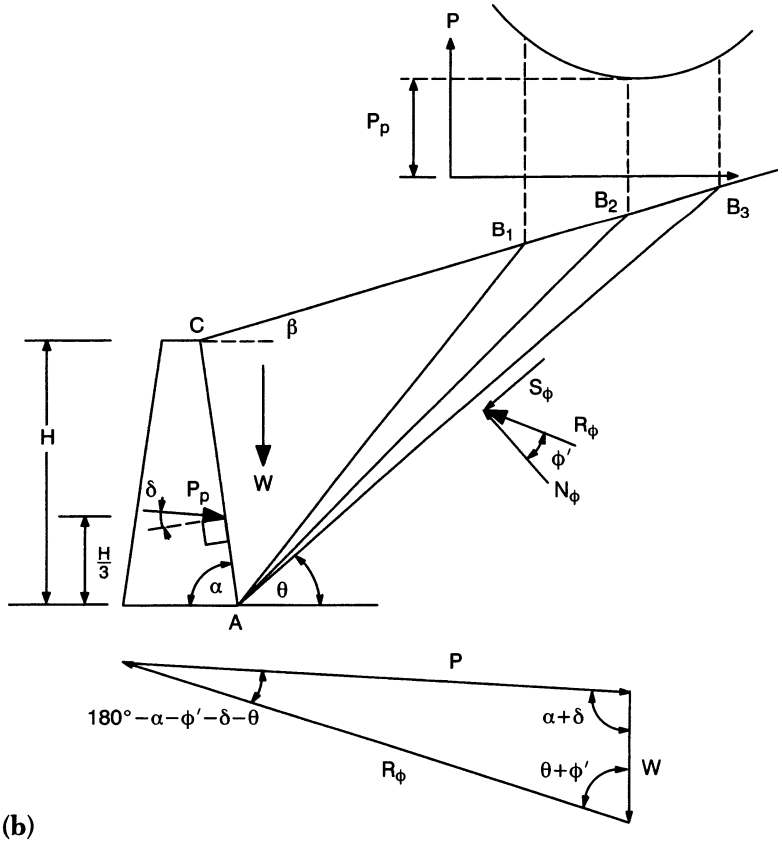


FIGURE 17.9. Coulomb wedge theory: (a) active earth force; and (b) passive earth force.

is calculated using Eq. 17.8. A reasonable estimate for interface friction angle between soil and concrete is $\delta = 2\phi'/3$.

The passive earth force can be calculated for the same conditions described above, but assuming that the wall moves inward and/or rotates inward about the toe as described in Section 17.2.2. The trial soil wedge in Fig. 17.9b, which gives a minimum value for vector $\boldsymbol{P}$ in a force polygon construction, is the passive earth force, $\boldsymbol{P}_p$, acting against surface AC. For the simple case illustrated in Fig. 17.9b, the closed form solution for the coefficient of passive earth pressure is:

$$K_p = \sin^2(\alpha - \phi') \Big/ \left[\sin^2(\alpha)\sin(\alpha + \delta) \times \left\{1 - \left[\frac{\sin(\phi' + \delta)\sin(\phi' + \beta)}{\sin(\alpha + \delta)\sin(\alpha + \beta)}\right]^{1/2}\right\}^2\right] \quad (17.14)$$

In the limit of $\alpha = 90°$ and $\delta = \beta = 0$ the equations for K_a and K_p are identical to the Rankine earth pressure solutions described in Section 17.2.2 for cohesionless soil.

The Coulomb wedge approach is based on force equilibrium, and the point of application of the earth forces $\boldsymbol{P}_a$ and $\boldsymbol{P}_p$ must be assumed. For the simple geometry shown in Fig. 17.9, the earth forces are assumed to act at $H/3$ above the heel of the wall. Similarly, the distribution of earth pressures must be assumed. Conventional practice for the simple geometry in Fig. 17.9 is to assume a triangular distribution of earth pressure acting parallel to the vector $\boldsymbol{P}_a$ or $\boldsymbol{P}_p$ as appropriate.

17.2.5 OTHER

Log spiral failure mechanisms (Fig. 17.10) have been used to calculate the out-of-balance force to be carried by horizontal reinforcement layers in slopes and walls (Leshchinsky *et al.* 1995). An advantage of this method is that moment equilibrium is also satisfied, i.e. the problem is statically determinate. The trace of a log spiral surface is given by:

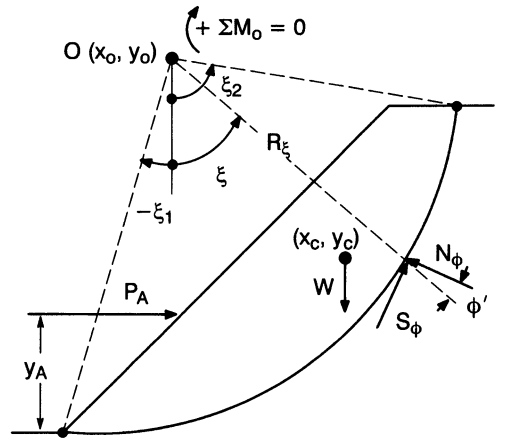


FIGURE 17.10. Log spiral analysis.

$$R_\xi = A \exp(-\xi \tan \phi') \quad (17.15)$$

where the orientation of the radius, R_ξ, of the log spiral is measured by angle ξ. For an assumed surface (i.e. a trial log spiral failure mechanism defined by any three independent parameters x_O, y_O and A), the moment equilibrium equation about the pole, O, can be explicitly written as:

$$\Sigma M_O = W(x_c - x_O) - \boldsymbol{P}_A(y_O - y_A) = 0 \quad (17.16)$$

where $\boldsymbol{W}$ is the weight of the assumed failure mass acting at the centre of gravity of the mass (x_c, y_c). Note that the moment about the log spiral pole is independent of the distribution of normal and shear stresses over the log spiral because its resultant must pass through the pole. The critical mechanism corresponds to the trace that yields the maximum value of $\boldsymbol{P}_A$ required to satisfy Eq. 17.16. Clearly the point of application, y_A, of the equivalent out-of-balance horizontal force, $\boldsymbol{P}_A$, will influence the magnitude of $\boldsymbol{P}_A$. Here it is assumed *a priori* that $y_A = H/3$.

Two-part wedge analyses have also been

employed to calculate earth forces acting on retaining wall structures. This approach adapted for the case of reinforced soil slopes is discussed in Section 17.5.2.

17.3 Conventional Retaining Walls

Conventional retaining walls are typically rigid structures that depend on self-weight and the weight of the backfill to support the retained soil. Rigid retaining walls include concrete gravity, cantilever and counterfort retaining walls as well as crib walls. Some examples are illustrated in Fig. 17.1a, b.

17.3.1 GRAVITY AND CANTILEVER WALLS

The distribution of pressures and forces to calculate load and resistance quantities for design are illustrated in Fig. 17.11. The forces acting on the wall are typically calculated using Rankine or Coulomb earth pressure theories. Potential failure mechanisms are base sliding, foundation collapse due to bearing capacity failure of the foundation soils, and/or excessive settlement of the structure. Structure settlement due to elastic compression and/or consolidation of the foundation soils can be carried out using the principles described in Chapter 9. Base sliding resistance, $\boldsymbol{S}_L$, is calculated as:

$$\boldsymbol{S}_L = \boldsymbol{R}_v \tan \delta = (W_v + \boldsymbol{P}_{av})\tan \delta \quad (17.17)$$

where W_v = the weight of the concrete plus the soil above the base heel in the case of a cantilever wall and $\boldsymbol{P}_{av}$ = the vertical component of active earth force acting on the wall. Quantity δ = the interface friction angle between the base of the wall and the foundation. Cantilever walls are typically more economical than gravity retaining walls because they use the mass of soil above the heel slab to provide additional stability. Passive earth forces are often neglected in stability analyses

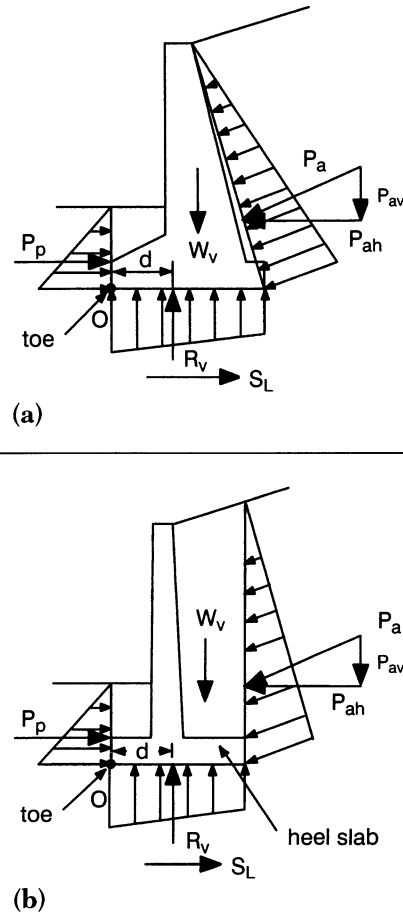


FIGURE 17.11. Distribution of pressures and forces for design of gravity (a) and cantilever (b) wall structures (modified from CGS 1992).

of gravity and cantilever walls because they may not be present for the life of the structure. The destabilizing or load side in base sliding calculations is due to the horizontal active earth component, $\boldsymbol{P}_{ah}$, in Fig. 17.11. In conventional global factor of safety design approaches, the factor of safety against base sliding ($F = \boldsymbol{S}_L/\boldsymbol{P}_{ah}$) is typically specified to be not less than 1.5–2.0.

For limit states design the base sliding mode of failure may be expressed as:

$$f_{ss}\boldsymbol{P}_{ah} \leq \frac{\boldsymbol{R}_v \tan \delta_{des}}{f_{ms}} \quad (17.18)$$

where δ_{des} = the design value of footing–soil interface friction (e.g. $\delta_{des} = 2\phi'_{des}/3$), and f_{ss} and f_{ms} are partial factors (Table 17.2).

The calculation of the applied pressure and foundation capacity at the base of a gravity or cantilever wall is based on conventional bearing capacity theory described in Chapter 9. The location (distance, d) of the net foundation load, $\boldsymbol{R}_v$, acting at the base of the wall can be calculated by considering the sum of moments about the toe of the structure (point O in Fig. 17.11) as follows:

$$d = \frac{\Sigma M_O}{\boldsymbol{R}_v} = \frac{\Sigma M_O}{(\boldsymbol{W}_v + \boldsymbol{P}_{av})}. \qquad (17.19)$$

Typical minimum specified global factors of safety against bearing capacity failure are in the range 1.5–2.0.

17.3.2 SHEET PILE WALLS (CANTILEVER AND ANCHORED)

Sheet pile wall earth retaining wall structures are flexible structures constructed by driving a row of interlocking steel sheet piles into soil. They may be used for permanent or temporary works and are common in permanent shoreline applications or for excavation support. Cantilever sheet pile walls (Fig. 17.12a) are typically restricted to an exposed height, $H \leq 5$ m. In order to increase the height of a sheet pile wall, reduce stresses in the sheet pile sections and reduce displacements, a sheet pile wall may be constructed with one or more anchors (Fig. 17.12b). Regardless of the construction type, the distributions of earth pressures that develop behind and in front of the wall are influenced by wall flexibility and have been shown to differ from those developed against rigid earth retaining wall structures. Nevertheless, Rankine or Coulomb earth pressure theory is used to simplify design and analysis.

The resistance to active earth pressures behind a cantilever sheet pile wall (Fig. 17.12a) is provided by the passive earth force, $\boldsymbol{P}_p$, developed over depth, d, to the assumed point of rotation O. The sum of active and passive earth pressures developed below point O is replaced by an equivalent reaction force, $\boldsymbol{R}_O$, which is assumed to act at point O. The designer must first determine the value of dimension d that satisfies moment equilibrium about point O. In the global factor of safety approach for design, a factor of safety, F, may be applied to the resisting moment by using $\boldsymbol{P}_p/F$ in the calculation of passive earth force. To ensure that the theoretical point of rotation O can develop, the driving depth is typically increased by 20%, i.e. $D = 1.2d$. The distribution of internal moment in the sheet pile wall is calculated using the unfactored earth pressure distribution between the top of the sheet pile wall and point O. The maximum moment and flexural strength of the pile material are used to select a suitable sheet pile section. Finally, the depth, d, must be great enough that the value of $\boldsymbol{R}_0$ required to satisfy horizontal equilibrium is not less than the net earth force acting below point O.

The earth pressure distributions and forces used to design an anchored sheet pile wall according to the "free earth support method" are illustrated in Fig. 17.12b. In this approach the sheet pile wall is assumed to rotate about a point O at the pile tip. The magnitudes and distributions of active and passive earth pressure are calculated in the same manner as for cantilever walls (including the application of a factor of safety to the passive earth force if a global factor of safety design approach is adopted, i.e. $\boldsymbol{P}_p/F$). Depth, d, is calculated to be the value for which the sum of moments about the anchor point, A, are zero. The anchor load, $\boldsymbol{T}_A$, is then calculated based on horizontal force equilibrium. The resulting internal bending moments are also illustrated in the figure and can be calculated from the design net earth pressure distribution. As the flexibility of the wall increases the maximum moment calculated using the free earth support method becomes progressively larger.

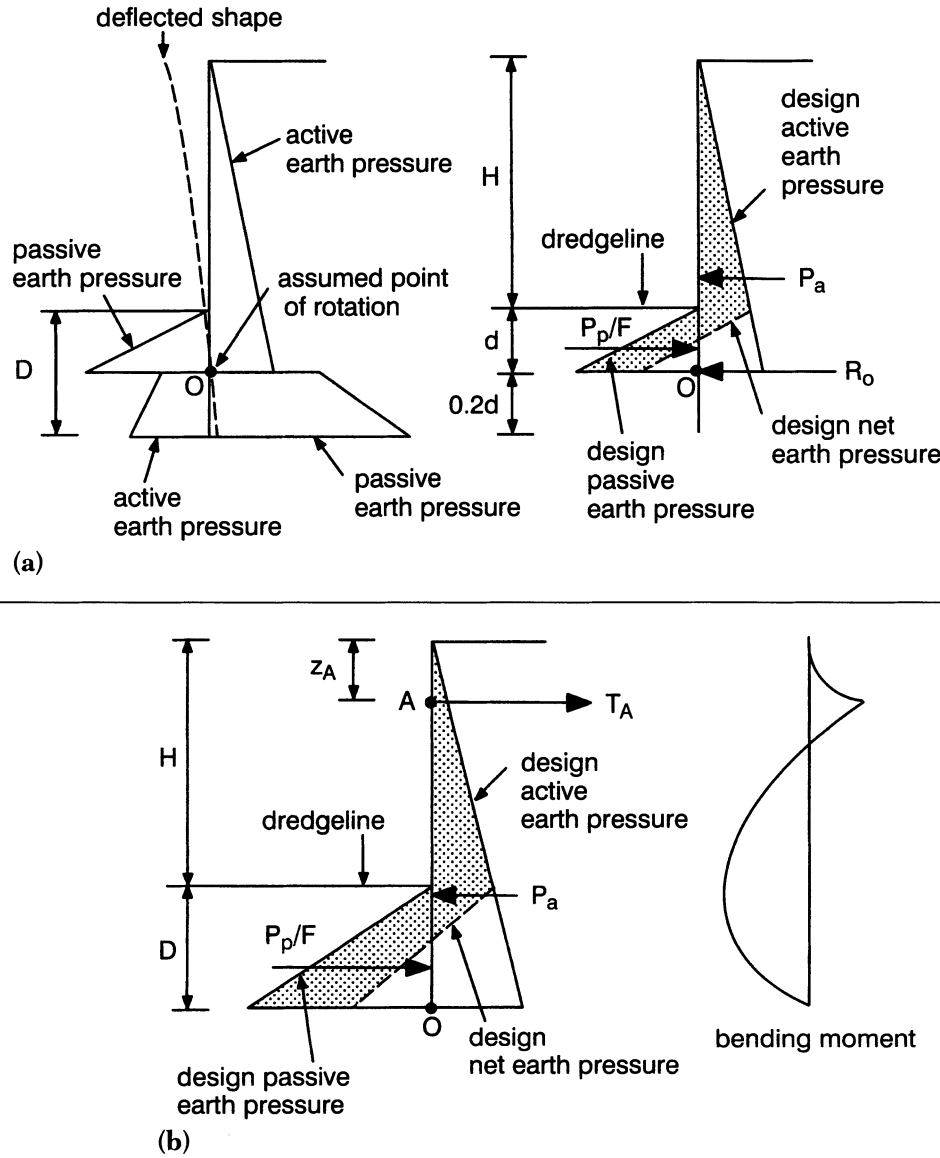


FIGURE 17.12. Distribution of pressures and forces for design of cantilever (a) and anchored (b) sheet pile walls.

Similarly, wall flexibility leading to soil pressure redistribution will influence the magnitude of tie force T_A. Rowe (1952, 1957) proposed a moment reduction method to adjust results of the free earth support method so as to reduce conservativeness in the selection of an acceptable pile section modulus, see also Bowles (1996) for details of Rowe's moment reduction method.

17.3.3 BRACED EXCAVATIONS

The magnitude and distribution of earth pressures required to select structural components of braced excavations cannot be pre-

dicted accurately using conventional earth pressure theory. Rather, empirically derived "apparent" earth pressure distributions are used to partition earth pressures to horizontal struts in braced excavations (Terzaghi *et al.* 1996). For sand soils the distribution shown in Fig. 17.13a is recommended, where H = the height of the excavation and γ = the bulk unit weight of the soil. The distribution illustrated in Fig. 17.13b is recommended for soft–firm clays based on total stresses. Where a great depth of soft clays exists below the excavation, the value of the apparent pressure should be calculated using $m = 0.4$ and s_u equal to the undrained shear strength of the soil. For a firm clay or lateral support at the base of the excavation, a value of $m = 1.0$ may be used. In no case should the maximum lateral pressure be less than $0.3\gamma H$ in Fig. 17.13b. For stiff–hard fissured clays the apparent earth pressure distribution in Fig. 17.13c is recommended. The magnitude of maximum apparent earth pressure depends on the type of clay, the amount of fissuring and amount of reduction in clay shear strength with time. The distribution illustrated in Fig. 17.13c is expressed in terms of total stresses, but the method is not based on total stresses. Hence, if fissures in the clay are anticipated to be filled with water, a hydrostatic water pressure distribution should be added to the distribution shown.

Deep excavations in soft–firm clays must be checked against possible base heave failure. The factor of safety against base heave, F_{sb}, for cohesive soils can be calculated as:

$$F_{sb} = \frac{N_b s_u}{(\gamma H + q)} \tag{17.20}$$

where S_u = the undrained shear strength of the soil below the excavation and q = the magnitude of adjacent uniformly distributed surcharge loads. The dimensionless bearing capacity factor, N_b, can be estimated from Fig. 17.14. For braced excavations in cohesionless soils, base heave may occur due to piping or heave associated with groundwater flow.

The placement of side support (e.g. lagging boards) and horizontal bracing as excavation progresses results in movement of the surrounding soils towards the excavation and

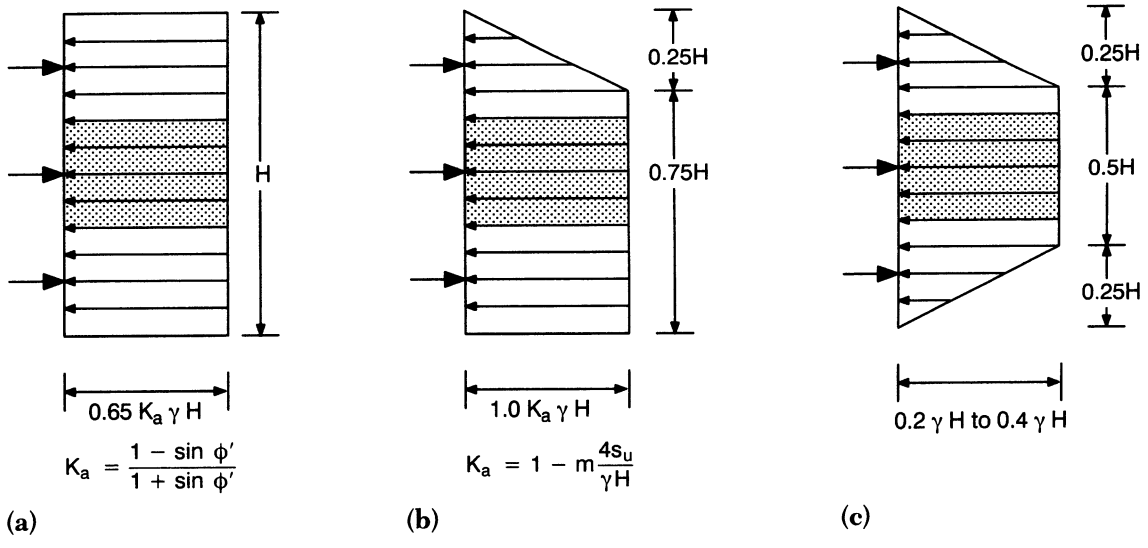


FIGURE 17.13. Apparent earth pressure distributions for determining forces on supports in braced excavations (modified from CGS 1992): (a) sand, (b) soft–firm clays, and (c) stiff fissured clays.

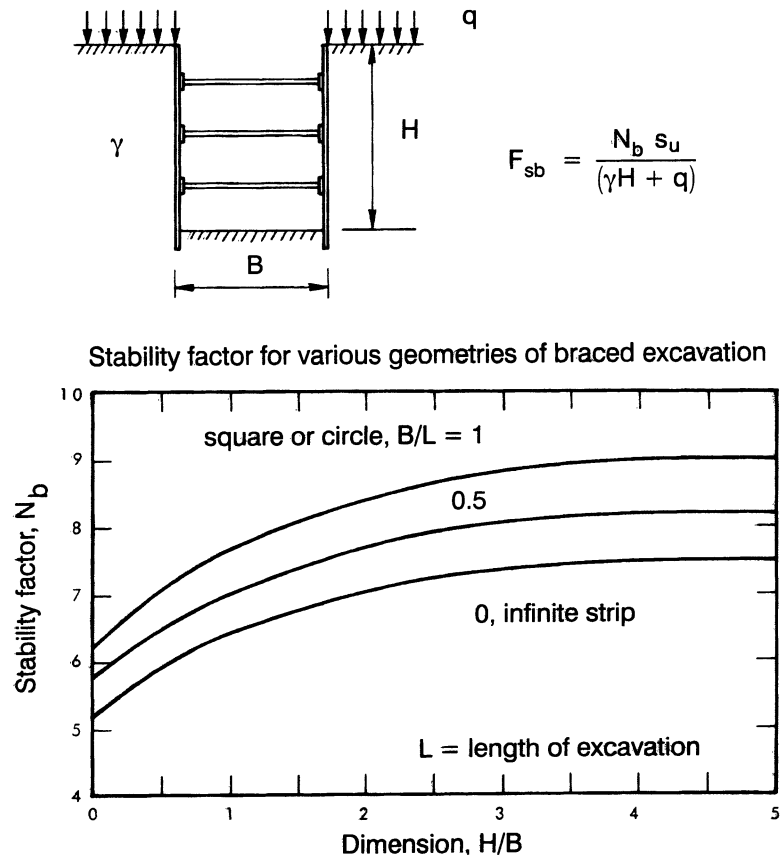
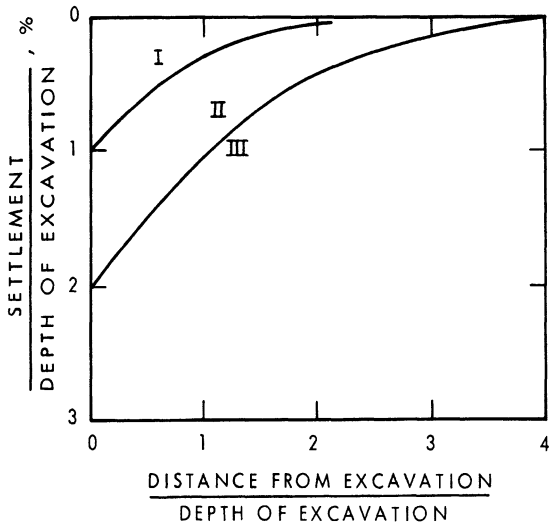


FIGURE 17.14. Factor of safety with respect to base heave in cohesive soils (modified from Janbu 1954b).

corresponding surface settlement. Figure 17.15 has been developed from field measurements and can be used to estimate the magnitude and distribution of surface settlements adjacent to a braced excavation.

17.3.4 OTHER TYPES OF RETAINING STRUCTURES (DIAPHRAGM WALLS AND CUT-OFFS)

It is often necessary to have excavation and support systems that provide unrestricted access for construction and that also limit ground movements associated with adjacent structures. The success of many recent deep excavations in urban environments is due to developments in construction equipment. Figure 17.16 illustrates five different methods for installing cast *in-situ* diaphragm walls and cut-offs. Figure 17.16a illustrates a clamshell rig for concrete slurry wall construction. The Hydrofraise method (Fig. 17.16b) was developed for the excavation of *in situ* panels through soil and rock. This advanced system consists of a heavy metal frame at the base of which are two counter-rotating drums with tungsten-carbide teeth. A pump, mounted centrally within the unit, removes spoil and cuttings suspended in a bentonite slurry. The device is capable of excavating rock with compressive strengths of 100 MPa and can advance panels to 130-m depths with tight vertical tolerances in the range of 1%. Tolerance of less than 0.5% can be achieved using computer-controlled equipment. Wall thick-



Zone I = sand and soft to hard clay
Zone II = very soft to soft clay when the depth of clay below excavation is limited or when $F_{sb} > 1.3$
Zone III = very soft to soft clay when $F_{sb} < 1.3$
F_{sb} = factor of safety against base failure

FIGURE 17.15. Settlement adjacent to an open cut (modified from Peck 1969b).

nesses between 600 and 2800 mm are possible. Potential disadvantages of the use of the Hydrofraise system include: high cost, short life of the supporting slurry because of adjacent soil contamination, and disruption due to the presence of cobbles and boulders.

In situ wall construction can also be produced by soil–cement mixing, Fig. 17.16c (see also Section 15.2.4). This method uses three- or two-axes hollow stem augers,which churn and mix the soil as water and cement are introduced through the base of the augers. Soil–cement mixtures can be adjusted to obtain different compressive strengths in the range 5–10 MPa. Structural walls can be built using H-piles in the soil–cement columns to provide flexural strength. These are installed before hardening of the soil–cement mixture.

The Benoto rig (Fig. 17.16d) was developed to install secant pile walls and drilled shafts. The rig rotates a casing and special end-tube, equipped with cutting teeth, into the ground as soil is removed from inside by a mechanical grab. Reinforcing steel is then placed and concrete placed in the pile as the casing and tube are withdrawn.

Jet grouting involves drilling a vertical hole and then grouting by means of high pressure water jets to cut, replace and mix *in situ* soil with a cementing agent, Fig. 17.16e (see also Section 15.2.4.5). Jet grouting can be performed by single, double and triple fluid systems. Soil–cement columns formed by jet grouting are also used as groundwater cut-off systems, stabilizing units at the base of excavations and underpinning elements to protect adjacent structures from excavation-induced ground movements.

The inherent bending stiffness of diaphragm walls is a valuable asset in controlling adjacent ground movements. In San Francisco, for example, the use of concrete diaphragm walls for deep basement and rapid transit excavation resulted in a 50–75% reduction in lateral wall movements compared with sheet pile walls braced similarly in approximately the same soil conditions (Clough *et al.* 1989). Post-tensioned (Gysi *et al.* 1975) and precast concrete diaphragm walls have also been used to increase bending capacity and reduce wall deflections.

Slurry walls are excavated using bentonite or polymeric slurries. Polymeric slurry behaves quite differently compared to bentonite, acting as a pseudoplastic fluid without forming a filter cake. Bentonite relies on thixotropic gel viscosity to provide trench support. Polymeric slurries are approximately ten times more expensive than bentonite, but disposal costs of used bentonite can be high due to lack of suitable disposal sites. The polymer is reusable and only a small quantity of polymer is usually required for a project. Disposal of the spent polymer can be carried out by the addition of an agglomerator followed by discharge directly into a sewer.

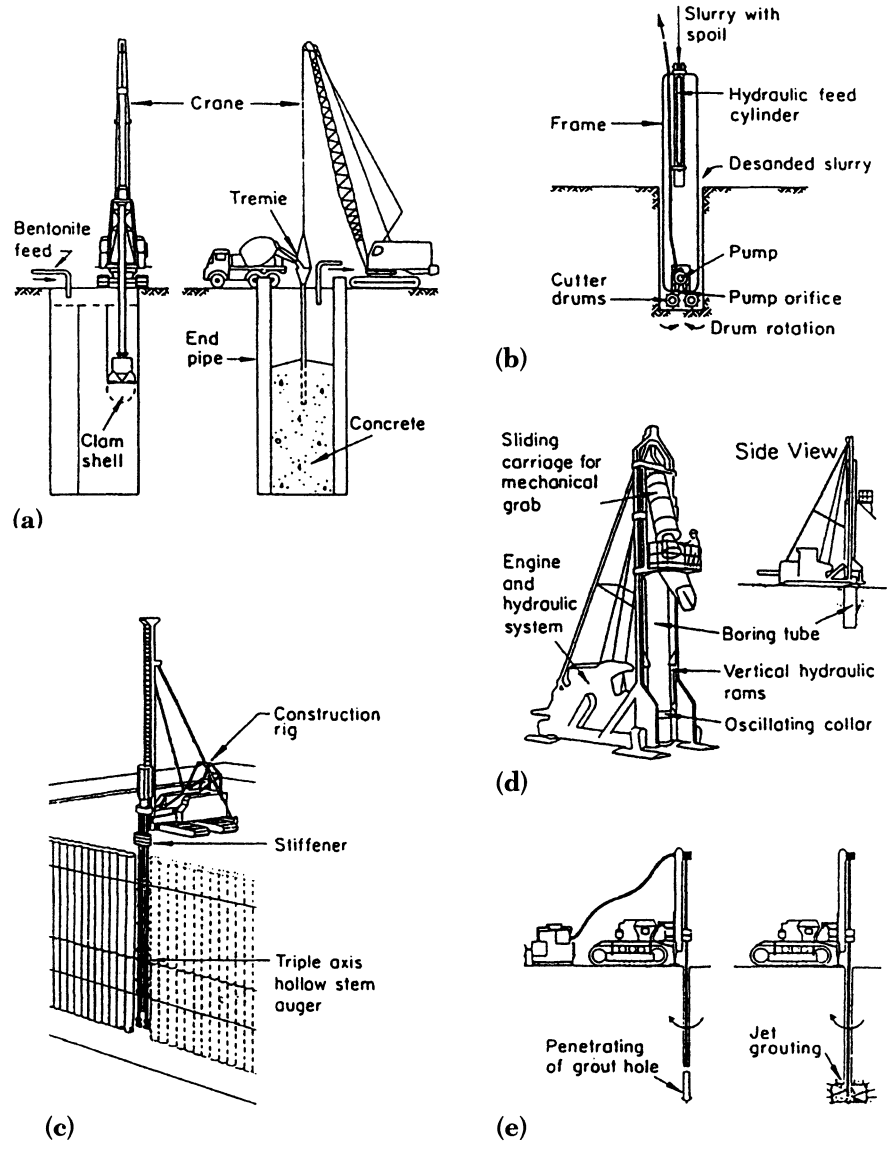


FIGURE 17.16. Concrete diaphragm and cut-off construction (after O'Rourke & Jones 1990, © ASCE, reproduced with permission): (a) slurry trench construction; (b) Hydrofraise; (c) soil–cement mixing; (d) Benoto rig; and (e) jet grouting.

17.4 Reinforced Soil Walls

17.4.1 CURRENT DESIGN METHODS

Current design methods for reinforced soil walls can be classified as either coherent gravity or tie-back methods. The coherent gravity method (Mitchell & Villet 1987, Ministeres des Transports 1979) was developed initially for structures reinforced with steel strip (inextensible) reinforcements. The tie-back method is based upon limit equilibrium methods. It is independent of the reinforcement material and is used with both inextensible and extensible reinforcements and with anchors.

In the context of reinforced soil wall design, two limit states (see Section 17.1.6) are considered:

1. Ultimate limit state, at which collapse mechanisms form in the ground or the retaining structure or when movement of a retaining structure leads to severe structural damage in other parts of the structure or in nearby structures or services.
2. Serviceability limit state, at which movements of the retaining structure affect the appearance or efficient use of the structure or nearby structures or services which rely upon it.

The limit states may be defined in terms of limit modes. Design evaluation involves ensuring the stability of the structure against failure by the limit modes appropriate for the circumstances. In the case of vertical walls and abutments, six limit modes are considered, Fig. 17.17. Limit mode 1 involves sliding failure of the structure: (a) on the interface between the reinforced fill and the subsoil, or (b) within the reinforced fill on a soil–soil interface or soil–reinforcement interface. Limit mode 2 involves bearing failure of the structure. Limit mode 3 involves tensile failure of the reinforcement. Limit mode 4 involves pull-out failure of reinforcing elements. Limit mode 5 involves wedge/slip circle stability failure. Limit mode 6 involves deformation.

Limit modes 1–5 relate to the ultimate limit state. Limit mode 6 is a serviceability state. Other limit modes may be appropriate in certain circumstances and must be

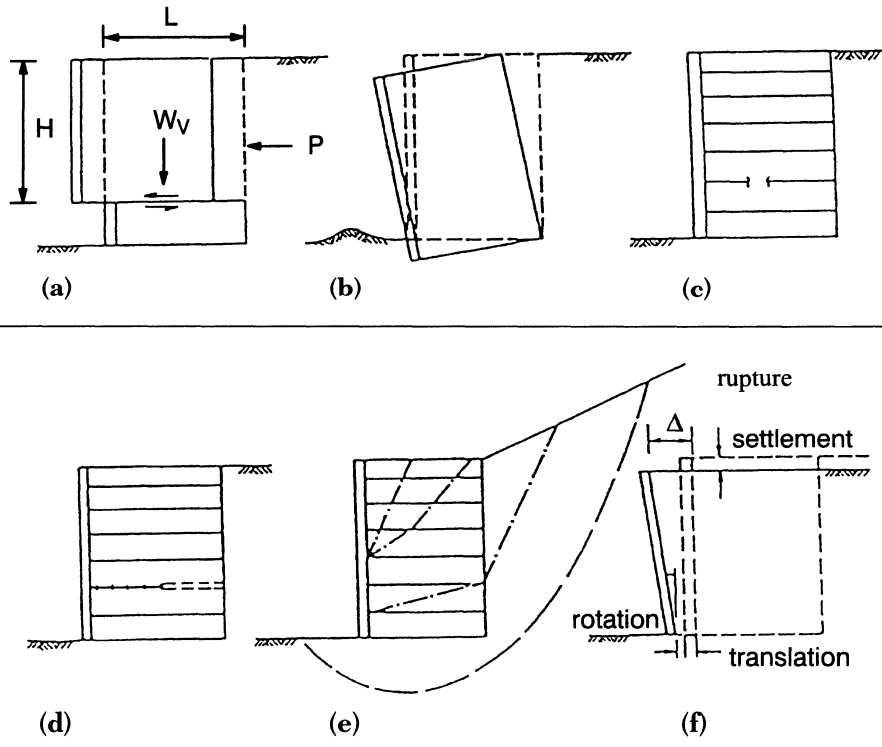


FIGURE 17.17. Limit modes of failure for reinforced soil walls: (a) limit mode 1, sliding; (b) limit mode 2, bearing capacity; (c) limit mode 3, reinforcement rupture; (d) limit mode 4, reinforcement pull-out; (e) limit mode 5, wedge/slip circle; and (f) limit mode 6, deformation.

checked accordingly. For example: (a) where three-dimensional effects could influence the structure, (b) where the structure could be subject to seismic loading (see Chapter 21), (c) where the structure could be subject to cyclic loading, and (d) where the structure could be subject to accidental flooding.

At the ultimate limit state, calculations are needed to evaluate stability. At the serviceability limit state, calculations may not be necessary and requirements may be satisfied by reference to similar structures and details.

In the limit mode method of analysis, limit mode 6, covering deformation, has to be considered. This mode is used to check the serviceability of any structure and is also used to calculate the stress state applicable in the analysis. The analytical model used is sensitive to the type of reinforcement used, e.g. an extensible reinforcement may lead to greater structural deflection during and post construction than if inextensible (stiff) reinforcement is specified. The use of stiff reinforcement can result in additional stress being attracted to the reinforcement, a point implicitly acknowledged in the coherent gravity method where the K_0 stress state is used in the analysis.

17.4.2 TIE-BACK METHOD

17.4.2.1 Limit Mode 1: Sliding

The stability of the structure against forward sliding is checked at the base of the structure or at any level within the structure including each soil–reinforcement interface (Fig. 17.17a) as follows:

1. Long-term stability on a soil–soil interface.

$$f_{ss}\boldsymbol{P} \leq \frac{\boldsymbol{W}_v \tan \phi'_{des}}{f_{ms}} + \frac{c'}{f_{ms}}L. \quad (17.21)$$

2. Long-term stability on a soil–reinforcement interface:

$$f_s\boldsymbol{P} \leq \alpha' \frac{\boldsymbol{W}_v \tan \phi'_{des}}{f_{ms}} + \alpha'_{sr}\frac{c'}{f_{ms}}L. \quad (17.22)$$

3. Short-term stability on a soil–soil interface:

$$f_{ss}\boldsymbol{P} \leq \frac{s_u}{f_{ms}}L. \quad (17.23)$$

4. Short-term stability on a soil–reinforcement interface:

$$f_s\boldsymbol{P} \leq \frac{\alpha'_{sr}s_u}{f_{mc}}L \quad (17.24)$$

where $\boldsymbol{P}$ = the destabilizing horizontal factored force = $\frac{1}{2}K_{des}f_{es}\gamma H^2$ for the simple case of backfill pressure only; H and L = the height and length of the sliding mass, respectively; $\boldsymbol{W}_v$ = the vertical factored resistance force = $f_{es}\gamma HL$ for the simple case of no surcharge loading and horizontal fill; ϕ'_{des} = the design angle of shearing resistance under effective stress conditions (Section 17.1.4.2); c' = the cohesion of the soil under effective stress conditions; s_u = undrained shear strength of the soil; α' = the coefficient of interaction relating soil–reinforcement bond angle to tan ϕ'_{des}; α'_{sr} = the cohesive coefficient of interaction relating soil cohesion to soil–reinforcement bond. Partial factors are defined in Table 17.2 for vertical walls and abutments.

17.4.2.2 Limit Mode 2: Bearing and Tilting

This limit mode should be checked for the following conditions: (a) horizontal forces are at a maximum and vertical forces are at a minimum, and (b) both horizontal and vertical forces are at a maximum.

1. Bearing. For structures situated on good subsoils a trapezoidal pressure distribution beneath the structure may be assumed

(Fig. 17.18). The maximum factored bearing pressure, $q_a(\max)$, acting under the toe should satisfy:

$$q_a(\max) = \frac{1}{L}\left(\boldsymbol{W}_v + \frac{6\boldsymbol{P}e}{L}\right)$$

$$= f_{es}\gamma H\left[1 + K_a\left(\frac{H}{L}\right)^2\right] \quad (17.25)$$

$$\leq \frac{q_{ult}}{f_{bc}} + \gamma D_m.$$

Here e = the eccentricity of the disturbing force $\boldsymbol{P}$, which acts at a height $H/3$ in the simple case; D_m = the embedment depth; f_{bc} = the partial factor for bearing capacity of the foundation; q_{ult} = the ultimate bearing capacity of the foundation soil (Chapter 9); and γ = soil unit weight.

2. Tilting. The overturning movement with respect to the toe must be less than the restoring movement, hence:

$$\frac{\boldsymbol{W}_v L}{2} > \boldsymbol{P}e. \quad (17.26)$$

If the limit mode 2 condition is not satisfied, the stability of the structure can be increased by widening the base width of the structure.

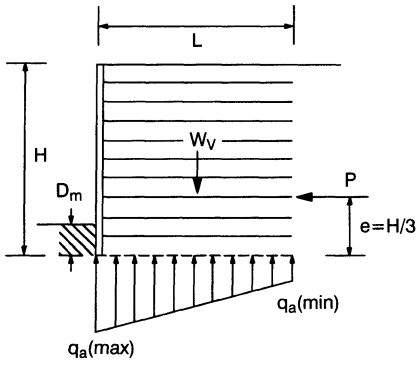


FIGURE 17.18. Limit mode 2: bearing capacity and tilting.

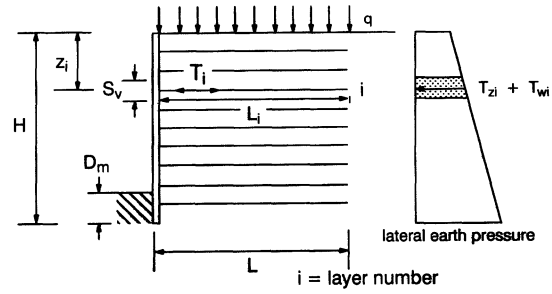
17.4.2.3 Limit Mode 3: Reinforcement Layer Rupture

Consider layer i of reinforcing members in Fig. 17.19. The maximum ultimate limit state tensile force, $\boldsymbol{T}_i$, at a depth z_i below the top of the structure is given by:

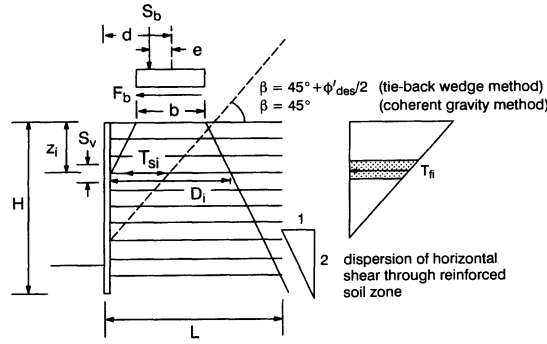
$$\boldsymbol{T}_i = \boldsymbol{T}_{z_i} + \boldsymbol{T}_{w_i} + \boldsymbol{T}_{f_i} + \boldsymbol{T}_{m_i} + \boldsymbol{T}_{s_i}. \quad (17.27)$$

$\boldsymbol{T}_{z_i}$ = the design tensile force due to the self-weight of the reinforced fill above reinforcement layer i (Fig. 17.19a):

$$\boldsymbol{T}_{z_i} = \left[K_{des} f_{es}\gamma z_i - 2\frac{c'}{f_{ms}}(K_{des})^{1/2}\right]S_v. \quad (17.28)$$



(a)



(b)

FIGURE 17.19. Limit mode 3: reinforcement layer rupture: (a) contribution of soil self-weight and uniform surchage; and (b) vertical and horizontal dispersion of load due to surface strip footing.

Here, S_v = the reinforcement spacing.

T_{w_i} = the force due to the uniform surcharge pressure, q, on top of the structure:

$$T_{w_i} = K_{des} f_{ff} q S_v. \quad (17.29)$$

For the combined effect of height and fill and a uniform surcharge only (Fig. 17.19a):

$$T_{z_i} + T_{w_i} \geq 5 S_v \left(z_i + \frac{f_{ff} q}{f_{es} \gamma} \right). \quad (17.30)$$

T_{s_i} = the force due to the vertical loading, S_b, applied to a strip contact area of width, b, on top of the structure (Fig. 17.19b):

$$T_{s_i} = K_{des} S_v f_{eq} \frac{S_b}{D_i} \left(1 + \frac{6e}{b} \right) \quad (17.31)$$

where $D_i = z_i + b$ if $z_i \leq 2d - b$; and $D_i = d + (z_i + b)/2$ if $z_i > 2d - b$. If $z_i > 2b$ then:

$$T_{s_i} = K_{des} S_v f_{eq} \frac{S_b}{D_i}. \quad (17.32)$$

T_{f_i} = the force due to the horizontal shear applied to a strip contact area of width b on top of the structure (Fig. 17.19b) and is calculated as:

$$T_{f_i} = 2 S_v f_{eq} F_b \Theta (1 - z_i \Theta) \quad (17.33)$$

where $\Theta = \tan (45° - \phi'_{des}/2)/(d + b/2)$.

T_{m_i} = the force due to the bending moment, M_i, caused by external loading acting at the back of the reinforced soil zone over the height, z_i and is calculated as:

$$T_{m_i} = 6 \frac{K_{des} S_v M_i}{L_i^2}. \quad (17.34)$$

The tensile strength of the reinforcement layer i required to satisfy load and stability is:

$$\frac{T_D}{f_n} \geq T_i \quad (17.35)$$

where T_D = the design strength of the reinforcement and f_n = the partial factor to account for economic ramifications of failure.

17.4.2.4 Limit Mode 4: Pull-Out Capacity

The perimeter, P_i, of reinforcement layer i required to satisfy local stability requirements (Fig. 17.20) is:

$$P_i = T_i \left\{ \mu L_{e_i} \left[\frac{(f_{es} \gamma z_i + f_{ff} q)}{f_n f_p} \right] + \frac{\alpha_{sr} c' L_{e_i}}{f_{ms} f_n f_p} \right\} \quad (17.36)$$

where T_i = the maximum value of the design tensile force calculated for limit mode 3 (above); P_i = the total horizontal width of the top and bottom faces of the reinforcing element i per unit length of wall; μ = the coefficient of friction between the fill and the reinforcing elements = α' tan ϕ'_{des}/f_{ms}; and L_{e_i} = the length of reinforcement in the resistant zone. Note that P_c is the perimeter length of a reinforcing strips per unit length of wall. For reinforcement sheets $P_i = 2$. P_i is dimensionless (e.g. m/m).

17.4.2.5 Limit Mode 5: Wedge/Slip Circle Stability

Wedges are assumed to behave as rigid bodies and may be any size and shape. Stability of any wedge is maintained when frictional forces acting on the potential failure plane in connection with the tensile resistance/bond

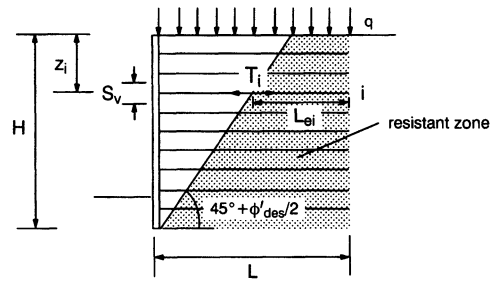


FIGURE 17.20. Limit mode 4: reinforcement pull-out capacity.

of the group of reinforcing elements embedded in the fill beyond the plane are able to resist the applied loads tending to cause movement (Fig. 17.21). The following loads and forces are considered in the analysis: (a) self-weight of the fill in the wedge; (b) any uniformly distributed surcharge load, q; (c) external vertical loading, S_b; (d) horizontal shear from any external loading, F_b; (e) frictional and cohesive forces acting along the potential failure plane, S_k; (f) the normal reaction on the potential failure plane, N_k. It is often assumed that no potential failure plane intersects the soil surface in front of a footing (e.g. BS 8006 1995). The wedge stability check ensures that the calculated frictional resistance does not exceed the tensile capacity, and vice versa, of any layer of elements.

Various potential failure planes are considered (Fig. 17.21), and a graphical search made for the maximum value of $\boldsymbol{P}_{ak}$, as described in Section 17.2.4. For a simple structure with a horizontal backfill and only a uniform surcharge load, the orientation of the potential failure plane can be estimated to be $\beta = (45° - \phi'/2)$. The resistance provided by any layer of reinforcing elements is taken as the smaller value of: (a) the adherence or frictional resistance of the elements embedded in the resistant zone, (b) the tensile resistance of the reinforcement elements. The total resistance of the layers of elements anchoring the wedge is obtained from:

$$\sum_{j=1}^{n}\left[\frac{\boldsymbol{T}_{D_j}}{f_n} \text{ or } \frac{P_i L_{ip}}{f_p f_n}\left(\mu f_{es}\gamma z_i + \mu f_{ff} q + \frac{\alpha'_{sr} c'}{f_{ms}}\right)\right] > \boldsymbol{P}_{ak} \tag{17.37}$$

where $\boldsymbol{T}_{D_j}$ is the sum of the design strengths of the reinforcement layers above layer i and L_{ip} is the length of each reinforcement layer in the resistant zone for the critical internal wedge, i.e. most critical wedge in Fig. 17.21.

When the facing consists of a structural element formed in one piece, potential failure planes passing through the facing may be neglected. However, for segmental retaining wall structures or other systems with discrete facing column materials, e.g. reinforced gabion walls, the interface between facing units must be considered as a potential failure surface. For these systems, the shearing resistance available at each interface must be considered explicitly in facing and internal stability modes of failure (Simac *et al.* 1993, Bathurst & Simac 1994).

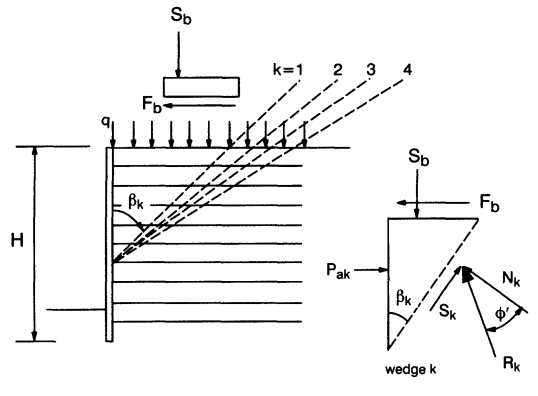


FIGURE 17.21. Limit mode 5: internal wedge stability.

17.4.2.6 Limit Mode 6: Deflections

Deformation, Δ, (Fig. 17.17f) should be checked at the following stages:

1. After considering limit modes 1–4 assess whether the correct design stress, K_{des}, has been used. If $\Delta \geq 0.001H$ the use of $K_{des} = K_a$ is justified. If $\Delta \leq 0.001H$, $K_{des} = K_0$ and the use of the coherent gravity method described below is justified.
2. At the end of construction.
3. At the end of the specified design life of the structure.

BS 8006 (1995) recommends that post-construction internal strains should not exceed 0.5% for bridge abutments and 1% for other

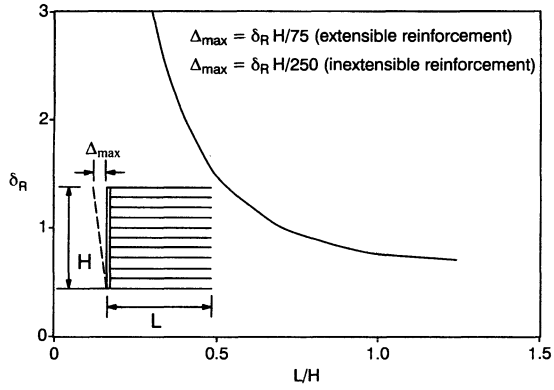


FIGURE 17.22. Empirical curve for estimating maximum lateral wall displacements at end of construction (modified from Mitchell & Christopher 1990). (Based on a 7-m high wall, increase relative displacement 25% for every 20 kPa of uniform surcharge load.)

walls to meet serviceability limits. An empirical method to estimate post-construction deformation of vertical walls is shown in Fig. 17.22.

17.4.3 COHERENT GRAVITY METHOD

The coherent gravity method of analysis was developed for metallic strip reinforcement, but is equally applicable to other relatively inextensible reinforcement products such as steel mesh. The coherent gravity analysis for the internal stability of reinforced soil structures assumes:

1. The reinforced mass is divided into an active zone and a resisting zone, divided by the line of maximum tension in the reinforcement, Fig. 17.23a.
2. The state of stress within the reinforced mass varies.
3. An apparent coefficient of adherence between the reinforcing elements and the fill based upon pull-out tests is assumed in the resistant zone.
4. A Meyerhof pressure distribution is assumed to exist beneath and within the reinforced fill.

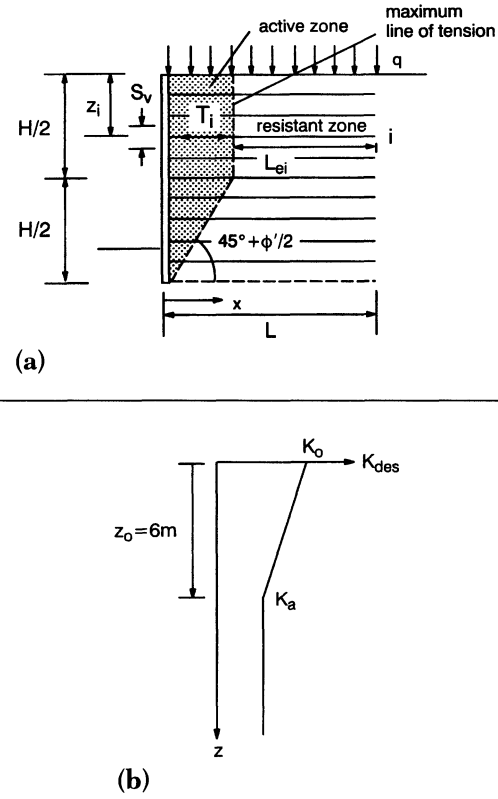


FIGURE 17.23. Coherent gravity method: (a) position of maximum line of tension in reinforcement layers; and (b) distribution of coefficient of earth pressure for design.

5. Cohesionless fills are used in the reinforced soil zone.

An empirical coefficient, K_{des} is used to calculate lateral earth pressures and is assumed to vary with depth as illustrated in Fig. 17.23b:

$$K_{des} = K_0\left(1 - \frac{z}{z_0}\right) + K_a\frac{z}{z_0} \quad \text{when } z \le (z_0 = 6 \text{ m}) \tag{17.38}$$

$$K_{des} = K_a \quad \text{when } z > (z_0 = 6 \text{ m}). \tag{17.39}$$

Here K_0 and K_a are calculated using Eqs 7.4 and 7.6, respectively.

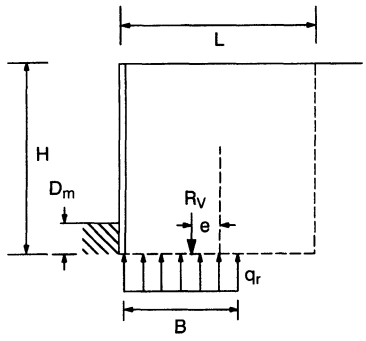


FIGURE 17.24. Pressure distribution along base of reinforced soil mass for coherent gravity method.

17.4.3.1 Limit Mode 1: Sliding

This check is similar to the general case using the tie-back method of analysis (see Section 17.4.2.1).

17.4.3.2 Limit Mode 2: Bearing/Tilt

The bearing pressure assumed with the coherent gravity analysis is shown in Fig. 17.24.

$$q_r = \frac{R_v}{B} = \frac{R_v}{L - 2e} \qquad (17.40)$$

where L = the reinforcement length at the base of the reinforced soil mass; e = the eccentricity of the resultant factored vertical load, R_v, about the centerline of the base; B = the equivalent base width; and q_r = the factored bearing pressure acting at the base of the reinforced soil mass. The imposed bearing pressure, q_r, should be less than the ultimate bearing capacity, q_{ult}, of the foundation soil where:

$$q_r \leq \frac{q_{ult}}{f_{bc}} + \gamma D_m. \qquad (17.41)$$

Here D_m = the embedment depth of the wall and q_{ult} = the ultimate bearing capacity of the foundation (Chapter 9).

17.4.3.3 Limit Mode 3: Element Rupture

The maximum tensile force, $\boldsymbol{T}_i$, to be resisted by the reinforcement layer i at depth z_i is given by:

$$\boldsymbol{T}_i = \boldsymbol{T}_{p_i} + \boldsymbol{T}_{s_i} + \boldsymbol{T}_{f_i}. \qquad (17.42)$$

1. $\boldsymbol{T}_{p_i}$ = the contribution to reinforcement load from vertical load due to soil self-weight, uniform surcharge loading, and bending moment resulting from external applied surface loads:

$$\boldsymbol{T}_{p_i} = K_{des}\sigma_{v_i}S_v = K_{des}\left(\frac{R_{v_i}}{L_i - 2e_i}\right)S_V \qquad (17.43)$$

where σ_{v_i} = the average stress acting at the reinforcement elevation; R_{v_i} = the resultant factored load (excluding surface strip loads) acting on the reinforcement layer; and e_i = the eccentricity of load R_{v_i}, from the mid-length of the reinforcement layer.

2. $\boldsymbol{T}_{s_i}$ = the contribution to reinforcement load from a surface vertical strip loading and can be calculated using the method described for the tie-back method (Fig. 17.19b) or a similar approach described in BS 8006 (1995).
3. $\boldsymbol{T}_{f_i}$ = the reinforcement load due to the horizontal shear force, F_b, applied to a strip contact area of width b, (see Fig. 17.19b) and is calculated as:

$$\boldsymbol{T}_{f_i} = \frac{2f_{ff}F_bS_v}{d + \frac{b}{2}}\left[1 - z_i\Big/\left(d + \frac{b}{2}\right)\right]. \qquad (17.44)$$

In this approach, angle β in Fig. 17.19b is set to 45°.

The rupture capacity of reinforcement layer i should exceed the value calculated using Eq. 17.33.

17.4.3.4 Limit Mode 4: Element Pull-Out

Experimental observations with metallic strip reinforcements have shown that the coefficient of friction of the reinforcement varies under different conditions. The coherent

gravity method of analysis uses an apparent friction coefficient, μ^*, which is assumed to vary with depth. For $z \leq 6$ m:

$$\mu^* = \mu_0\left(1 - \frac{z}{z_0}\right) + \frac{z}{z_0}\tan\phi' \quad (17.45)$$

where $\mu_0 = 1.2 + \log C_u$ for high adherence reinforcement, C_u = the uniformity coefficient for the particle size distribution of the fill, and $\mu_0 = 0.4$ for smooth strip reinforcement. For $z > 6$ m:

$$\mu^* = \tan\phi' \quad (17.46)$$

for high adherence reinforcement and grids, and $\mu_0 = 0.4$ for smooth strip reinforcement. For the simple case of a horizontal backfill surface as illustrated in Fig. 17.23, $z_0 = 6$ m.

The maximum tensile capacity, $\boldsymbol{T}_i$, of layer i based on adherence capacity is calculated by:

$$\boldsymbol{T}_i \leq \frac{2B_i\mu}{f_p f_n}\int_{L_i - L_{ei}}^{L_i} f_{es}\sigma_v(x)dx \quad (17.47)$$

where f_p = the partial factor for pull-out resistance; B_i = the width of the reinforcement; L_{ei} = the length of reinforcement beyond the line of maximum tension, Fig. 17.23a; μ = the value of the coefficient of friction or μ^*; and $\sigma_v(x)$ is the vertical stress along length x of the reinforcement.

17.4.3.5 Limit Mode 5: Wedge/Slip Circle Stability

The coherent gravity method of analysis does not normally consider this limit mode of failure. However, failures of retaining walls in 1986 designed using the coherent gravity method suggest that this limit condition should be checked (Lee *et al.* 1995).

17.4.3.6 Limit Mode 6: Deflections

This check is the same as the general case using the tie-back method of analysis (see Section 17.4.2.6).

17.4.4 SOIL NAILING

Soil nailing (Fig. 17.1h) is a process in which excavation walls and slopes are stabilized *in situ* by installing relatively short, fully bonded steel bars or other reinforcing materials according to a regular and relatively closely spaced pattern (see also Section 15.3.3). At every stage during the top down construction, excavation beneath the toe of the stabilized soil is required. This is only possible if the soil is able to provide self-supporting stability during the excavation.

A number of standards/recommendations exist for the analysis of soil nailing, including the Japanese Design Code (JHPC 1987), (FHWA 1993a,b), and the British Standard (BS 8006 1995). In European practice for near-vertical walls with horizontal nails, the tensile component of reinforcement strength is assumed to be the primary load carrying component and the contribution of shear/bending is secondary.

The design of soil nailing is based upon equilibrium methods. Most design is carried out using computer programs. Bruce and Jewell (1987) have developed expressions which can be used for preliminary design based on four dimensionless parameters (Table 17.4). The analysis of soil nailing by kinematical methods has been developed by Gudehus (1972), Stocker *et al.* (1979), and Gässler & Gudehus (1983).

The construction method for soil nailing includes the following steps:

1. Excavate soil layer of 1.0–1.5-m depth.
2. Protect exposed face of soil, normally using spray concrete reinforced with wire mesh.
3. Drive in nail or nails at a predetermined angle of inclination and spacing, using

TABLE 17.4. Comparison of drilled, grouted and driven nails: case histories (adapted from Bruce & Jewell 1987)

Parameter	Definition	Drilled and grouted	Driven
Length ratio	$\frac{\text{Maximum nail length}}{\text{Excavation height}}$	0.5–0.8	0.5–0.6
Bond ratio	$\frac{\text{Hole diameter} \times \text{length}}{\text{Nail spacing}}$	0.3–0.6	0.6–1.1
Strength ratio	$\left(\frac{\text{Nail diameter}^2}{\text{Nail spacing}}\right) \times 10^{-3}$	0.4–0.8	1.3–1.9
Performance ratio	$\frac{\text{Outward movement (top of structure)}}{\text{Excavation height}}$	0.001–0.003	No data

percussion, rotary drilling, flushing, vibration or pneumatic methods.
4. Grout area between the nails and the soil to ensure bond between the soil and the nail.
5. Cover the exposed ends of the nail with spray concrete.
6. Repeat steps 1–5.

Most nails are installed either by track-mounted drill rigs or by percussion methods. A relatively novel development is to install the nail by ballistic penetration. The key to this new approach is the acceleration of the nail from the front, thereby putting the nail in tension during the period of time it is penetrating the soil (Myles 1993).

17.5 Reinforced Slopes

17.5.1. GENERAL

The concept of reinforced slopes using geosynthetics was introduced in Section 17.1.3 (Fig. 17.3). Stability analysis methods are typically based on refinements to conventional limit equilibrium methods for unreinforced soil slopes (Chapter 14). These methods have been adapted to include the additional resisting forces that may be mobilized by geosynthetic reinforcement layers that intersect potential failure surfaces.

Modified two-part wedge and circular slip methods are described below. It should be noted that for brevity in this chapter, these methods are formulated using a global factor of safety approach and assuming unsaturated cohesionless soils described by a peak friction angle. However, the limit state philosophy can be used in a similar manner to that described for reinforced soil wall structures in Section 17.4. For limit state design of reinforced slopes, soil weight and external forces used on the load side of equilibrium equations are increased by partial load factors. The soil properties and reinforcement strengths on the resistance side of equilibrium equations are reduced by applying appropriate partial factors. The resulting limit equilibrium equations for each limit state must satisfy Eq. 17.3. Partial factors for reinforced slope design are summarized in Table 7.3.

The analytical expressions for reinforced slope stability analysis presented below are easily modified to include the influence of horizontal and vertical components of ground acceleration during earthquake loading (see Chapter 21). A comprehensive review of these "pseudostatic" limit equilibrium methods of analysis for reinforced slopes and walls can be found in the paper by Bathurst & Alfaro (1996).

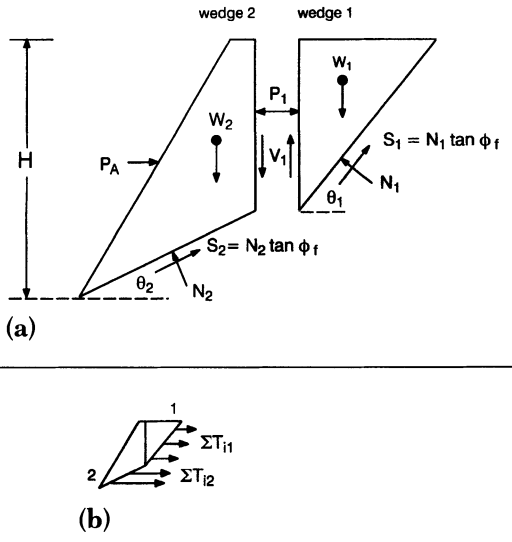


FIGURE 17.25. Modified two-part wedge analysis: (a) free-body diagram for unreinforced two-part wedge analysis; and (b) with reinforcement forces.

17.5.2 TWO-PART WEDGE ANALYSIS WITH REINFORCEMENT

The general solution for a trial two-part wedge failure mechanism under static loading is illustrated in Fig. 17.25. The horizontal and vertical forces $\boldsymbol{P}_1$ and $\boldsymbol{V}_1$, acting on wedge 2 from wedge 1 are, respectively:

$$\boldsymbol{P}_1 = \frac{\boldsymbol{W}_1}{\lambda \tan \phi_f + B_1 A_1} \tag{17.48}$$

$$\boldsymbol{V}_1 = \lambda \boldsymbol{P}_1 \tan \phi_f \tag{17.49}$$

where:

$$A_1 = \frac{1}{\sin \theta_1 - \tan \phi_f \cos \theta_1} \tag{17.50}$$

$$B_1 = \tan \phi_f \sin \theta_1 + \cos \theta_1. \tag{17.51}$$

The quantity λ = the inter-wedge shear mobilization ratio and varies over the range $0 \leq \lambda \leq 1$. Parameter ϕ_f = the factored soil friction angle expressed as:

$$\phi_f = \tan^{-1}(\tan \phi / F). \tag{17.52}$$

Where ϕ = friction angle of the soil (i.e. typically $\phi = \phi'_p$). The horizontal out-of-balance force, $\boldsymbol{P}_A$, is calculated as:

$$\boldsymbol{P}_A = \boldsymbol{P}_1 - B_2 A_2 (\boldsymbol{W}_2 + \boldsymbol{V}_1) \tag{17.53}$$

where:

$$A_2 = \frac{1}{\tan \phi_f \sin \theta_2 + \cos \theta_2} \tag{17.54}$$

$$B_2 = \tan \phi_f \cos \theta_2 - \sin \theta_2. \tag{17.55}$$

By setting $F = 1$ (i.e. $\phi_f = \phi$) an equivalent total active earth pressure coefficient for the slope can be calculated as:

$$K_a = 2\boldsymbol{P}_A / \gamma H^2 \tag{17.56}$$

for the most critical trial geometry (i.e. trial search that yields a maximum value for $\boldsymbol{P}_A$). The total required design strength of the horizontal layers of reinforcement is taken as $\Sigma \boldsymbol{T}_i = \boldsymbol{P}_A$.

The two-part wedge analysis degenerates to a single wedge analysis by restricting trial searches to $\theta_1 = \theta_2$ and setting $\lambda = 0$. An alternative strategy, which uses the approach by Woods and Jewell (1990), is to rewrite Eq. 17.53 as:

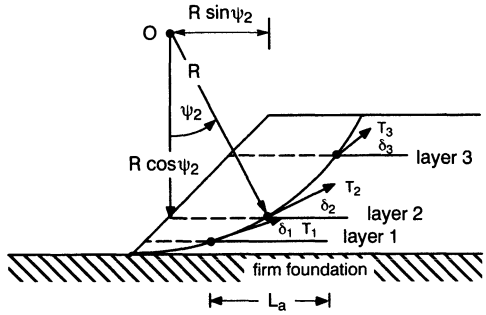
$$\boldsymbol{P}_A = \boldsymbol{P}_1 - \frac{B_1 A_1 \Sigma \boldsymbol{T}_{i1}}{\lambda \tan \phi_f + B_1 A_1} - \Sigma \boldsymbol{T}_{i2} - B_2 A_2 (\boldsymbol{W}_2 + \boldsymbol{V}_1). \tag{17.57}$$

The factor of safety for a given two-part wedge geometry corresponds to the value of F that yields $\boldsymbol{P}_A = 0$. The factor of safety for a slope corresponds to the minimum value of F from a search of all potential failure geometries. It should also be noted that in this approach the same global F is applied to the reference design tensile strength of the reinforcement and pullout capacity. Equation 17.57 illustrates that the value of F against collapse is independent of the location of the reinforcement layers for $\lambda = 0$.

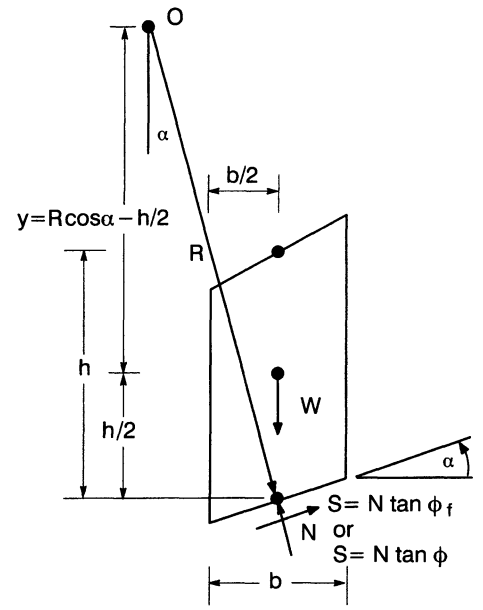
17.5.3 MODIFIED CIRCULAR SLIP METHOD

Conventional methods of slices can be modified to account for the additional restoring moment due to reinforcement layers. The general case can be referred to Fig. 17.26. Moment equilibrium leads to the following equation to calculate the factor of safety, F, against collapse:

$$F = \frac{M_R + \Delta M_R}{M_D} \tag{17.58}$$



(a)



(b)

FIGURE 17.26. Modified circular slip analysis: (a) circular slip geometry; and (b) method of slices.

where M_R = moment resistance due to soil shear strength, ΔM_R = increase in moment resistance due to the reinforcement, and M_D = driving moment.

Using the Bishop's simplified method:

$$M_D = R\Sigma \boldsymbol{W} \sin \alpha. \tag{17.59}$$

The moment resistance due to cohesionless soil shear strength is:

$$M_R = R\Sigma \left(\frac{\boldsymbol{W} \tan \phi \sec \alpha}{1 + \tan \alpha \tan \phi_f} \right). \tag{17.60}$$

The additional resisting moment due to the tensile capacity of the reinforcement is calculated as:

$$\Delta M_R = R\Sigma \boldsymbol{T}_i \cos(\psi_i - \delta_i). \tag{17.61}$$

The summation term in Eq. 17.61 considers the available reinforcement tensile force in each layer (lesser of tensile reinforcement strength based on over-stressing or pull-out) and the orientation, δ_i, of the force with respect to the horizontal. Since geosynthetic reinforcement products are flexible, the restoring force, $\boldsymbol{T}_i$, can be argued to act tangent to the slip surface at incipient collapse of the slope. This assumption leads to the summation term in Eq. 17.61 becoming $\Sigma \boldsymbol{T}_i R$. This approach is used in Federal Highway Administration (1996) guidelines. It is important to note that in the above formulation the influence of reinforcement capacity, $\boldsymbol{T}_i$, on base sliding resistance is not considered.

An alternative strategy is to modify the "ordinary method" (e.g. Fredlund & Krahn 1977). In this approach, equations for vertical and horizontal equilibrium of slices include forces due to mobilized reinforcement tensile capacity. Hence, these parameters directly affect base sliding resistance. The resisting moment term in Eq. 17.58 becomes:

$$M_R = R \tan \phi \, \Sigma \boldsymbol{W} \cos \alpha \tag{17.62}$$

and the incremental resisting moment due to reinforcement layers is:

$$\Delta M_R = R\Sigma \boldsymbol{T}_i[\cos(\psi_i - \delta_i) + \sin(\psi_i - \delta_i)\tan\phi] \quad (17.63)$$

where the summation term in Eq. 17.63 is with respect to reinforcement layers. An advantage of the modified "ordinary method" is that Eq. 17.58 is a linear function of F. This approach is used by the Public Works Research Institute (1992) in Japan with $\delta_i = 0$ for retaining walls and $\delta_i = \psi_i$ for slopes. In the Japanese approach, the distribution of total reinforcement load is assumed to be uniform with depth for slopes less than 45° from horizontal. For steeper slopes, including walls, the static portion of the required reinforcement load is assumed to increase linearly with depth.

17.5.4 DESIGN CHARTS

This section presents a series of design charts that can be used to provide preliminary designs for slopes constructed over stable foundations and comprising cohesionless soils. The charts have been generated using a conventional two-part wedge limit equilibrium method of analysis and cover the case of simple geometry with a range of slope angles from 90 (vertical) to 30°, and a range of soils with friction angles from 20 to 50°. The assumptions used to generate the charts are:

1. The foundation soils below the toe of the slope are stable and any potential instability is restricted to the soil volume above the elevation of the toe.
2. The groundwater table is below the toe of the slope.
3. The properties of the soil are uniquely described by a uniform bulk unit weight, γ, and design friction angle, ϕ (degrees).
4. The intersection of failure surfaces with the slope boundaries occurs at the toe of the slope and at points beyond the crest.

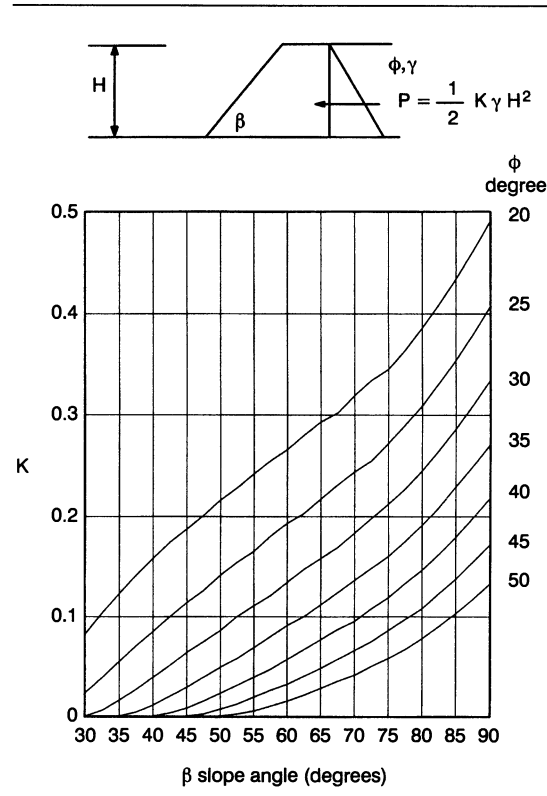


FIGURE 17.27. Equivalent coefficient of earth pressure, $K = f(\phi, \beta)$ (interslice force oriented at $\lambda = \phi$ to the horizontal).

5. The interslice forces act at an angle of $\lambda = \phi$ to the horizontal.

Figure 17.27 gives the maximum equivalent coefficient of active earth pressure based on a search of all potential two-part wedges for given β and ϕ values and assuming that the interslice friction angle $\lambda = \phi$. After taking the appropriate K from the chart, the minimum number of reinforcement layers, N_{min}, can be calculated:

$$N_{min} \geq \frac{1}{2}(K\gamma H^2)/T_a. \quad (17.64)$$

Here the term T_a denotes the design tensile strength of the geosynthetic reinforcement.

The calculation of the minimum length of reinforcement is based on:

1. All reinforcement lengths are equal, i.e. truncation is parallel to the slope face.
2. The reinforced zone must contain the critical unreinforced two-part wedge.
3. The reinforced zone must have sufficient width that the slope does not slide outwards.
4. The reinforced zone must have sufficient width that tensile vertical stresses are not developed along the surface of the foundation soils, i.e. base eccentricity must fall within the middle third of the base width.

The results of analyses are presented in normalized form L/H in Fig. 17.28 for the condition $\lambda = \phi$. Here L = the length of reinforcement and H = the height of the slope.

The calculation of maximum reinforcement spacing, S_v, at any depth z below the crest of the slope can be carried out using the following relationship:

$$S_v \geq \frac{T_a}{K\gamma z}. \tag{17.65}$$

The maximum spacing of primary reinforcement layers should not exceed 1 m. Secondary reinforcement layers (Fig. 7.3) should be placed at a vertical spacing not exceeding 0.6 m and should extend 2 m into the slope.

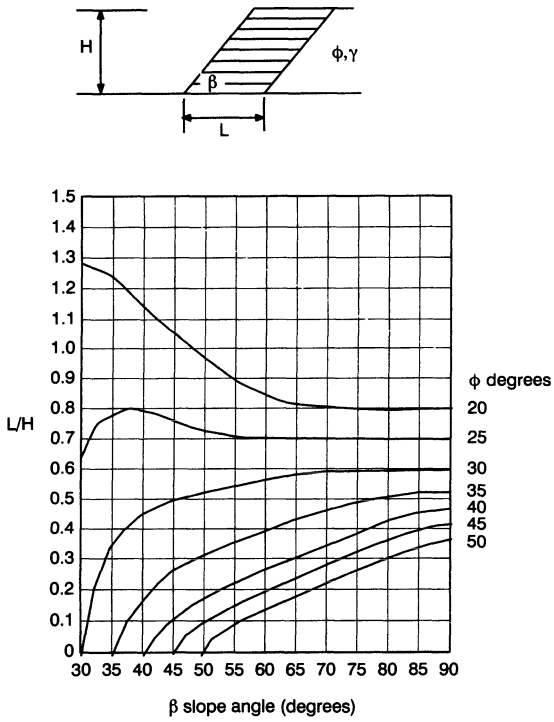


FIGURE 17.28. Minimum ratio of reinforcement length to slope height, L/H, to contain critical two-part wedge and satisfy sliding and eccentricity criteria (interslice force oriented at $\lambda = \phi$ to the horizontal).

17.6 *Reinforcement Over Voids*

Voids can occur under embankments or other earthworks due to a variety of causes, including cavities resulting from solution activity, the collapse of underground mine workings, differential foundation settlements, or thawing of subsurface ice lenses. Tensile reinforcing elements may be used to support highway embankments and other soil structures over voids. Bonaparte & Berg (1987) have subdivided these applications into two categories: (a) design to resist complete collapse into the void, while accepting loss of serviceability (i.e. provide temporary support); (b) design the reinforced soil structure to behave as a beam or slab with sufficient bending stiffness to limit deformations to an acceptable level (i.e. provide long-term support).

17.6.1 ANALYTICAL METHODS

Current methods of design of tension membranes adopt a conservative approach, due to the uncertainties involved and the simplicity of the analytical techniques employed. The soil and reinforcement are assumed to be resting initially on a firm foundation. With the development of a void under the reinforcement the overlying soil deflects into the void. The deflection of the soil layer generates arching within the soil above the reinforcement, and the load in the reinforcement

over the void is less than the theoretical weight of the soil above the void.

17.6.1.1 Tension membrane theory

The length of reinforcement required for embedment beyond the edges of the voids is controlled by the soil–reinforcement interface shear behavior. The pull-out capacity of membrane reinforcement may be calculated using:

$$P_u = \sigma_v L \alpha' \tan \phi' \qquad (17.66)$$

where σ_v = the vertical pressure acting on the anchorage length; L = the embedded length of reinforcement, and α' = the soil–reinforcement interaction coefficient.

Assuming that the reinforcement spanning a void transmits tensile stresses but not shear stresses and that the soil–reinforcement interface above the void is frictionless, the applied stress to the membrane is normal. For plane strain conditions, it is convenient to assume that the shape of the membrane is described by an arc of a circle. The tensile resistance, T_{max}, in a layer of reinforcement spanning an infinitely long void of width b has been given by Giroud (1981) as:

$$T_{max} = J_{sec}\left[\frac{2f(\varepsilon)}{180/\pi}\sin^{-1}\left(\frac{1}{2f(\varepsilon)}\right) - 1\right] \qquad (17.67)$$

where:

$$f(\varepsilon) = \frac{1}{4}\left(\frac{2y}{b} + \frac{b}{2y}\right). \qquad (17.68)$$

Here, J_{sec} = the secant tensile stiffness of the reinforcement (e.g. kN m^{-1}) and y = the maximum vertical reinforcement deflection (m). Strain in the reinforcement, ε, is obtained by dividing the reinforcement tensile resistance by the secant tensile stiffness.

17.6.1.2 Arching

Arching above the void may cause a reduction in vertical stress. In the case of a void under an embankment, arching reduces the stress and the tension in the reinforcement spanning the void by transferring part of the stress to adjacent stable portions of the embankment. Terzaghi (1943) has presented an approximate method for calculating the vertical stress on a horizontal plane at the base of a soil mass due to yielding of part of the base. It is assumed that yielding produces vertical shear surfaces from the edge of the void to the surface. An expression for the vertical stress under plane strain yielding conditions is given by:

$$\sigma_v = \frac{by}{2K\tan\phi}\{1 - \exp[-(K\tan\phi 2h/b)]\} \qquad (17.69)$$

where K = the ratio of horizontal to vertical earth pressure along vertical shear surfaces, and h = the height of soil. Similarly, Kezdi (1975) has developed an equivalent expression for vertical stress developed over a circular yielding surface of diameter D:

$$\sigma_v = \frac{Dy}{4K\tan\phi}\{1 - \exp[-(K\tan\phi 4h/b)]\} \qquad (17.70)$$

where:

$$K = 1.06(\cos^2\theta + K_a \sin^2\theta) \qquad (17.71)$$

and $\theta = \pi/4 + \phi/2$.

17.6.1.3 Combined Arching and Tension Membrane Theory

Giroud *et al.* (1988) developed an analytical method for the design of reinforcement spanning a void, which combines both arching and tension membrane theory. The solution involves uncoupling the soil response due to arching from the reinforcement response associated with the tension membrane theory using a two-step approach. First, the behavior of the soil fill is analyzed using classical arch theory: this provides pressure at the base of

the soil layer on that portion of the reinforcement located above the void. Second, tension membrane theory is used to establish a relationship between the pressure on the reinforcement, the tensile stress and strain in the reinforcement, and the deflection. An inherent assumption in this uncoupled two-step approach is that the deformation required to generate a soil arch is compatible with the tensile strain required to mobilize the reinforcement tension.

17.6.1.4 BS 8006 Method

The tension membrane theory assumes that the deflected shape of the reinforcement is circular; in reality, the weight of the fill acting on the reinforcement over the unsupported void causes the membrane to deform into a catenary shape. However, to simplify the analysis BS 8006 (1995) assumes that the load is actually distributed along the horizontal span of the reinforcement rather than along the actual deflected length. In this case, the shape of the deflected reinforcement is parabolic. The equation governing the extension of an unsupported membrane, which assumes the shape of a parabola, cannot be solved directly as it has two unknowns. However, by utilizing the geometry of the subsided soil mass and assuming a constant volume of soil in the subsided soil mass, a relationship can be derived for the maximum allowable extension, ε_{max}, in the unsupported reinforcement given a maximum acceptable differential deformation, d_s/D_s:

$$\varepsilon_{max} = 8\frac{(d_s/D_s)^2(D + 2H/\tan\theta_d)^6}{3D^6} \qquad (17.72)$$

where d_s/D_s = the differential deformation criterion for the surface of the embankment, D = the cavity diameter, H = the height of the fill of the embankment, and θ_d = the angle of draw of the embankment. The angle of draw, θ_d, is usually equated to the peak angle of friction of the fill, ϕ'_p. If the value of d_s/D_s is set at the maximum acceptable limit required to maintain serviceability at the surface of the embankment or highway (e.g. 1% for high speed roads and 2% for lower class roads), the resulting value of ε_{max} derived from Eq. 17.72 will be the maximum allowable extension in the reinforcement over the period of time which the material is required to act.

In the development of the value of ε_{max} in Eq. 17.72, it is frequently assumed that no soil arching occurs in the embankment material above the unsupported reinforcement. This is because vibrations caused by traffic can result in the breakdown of the arching action. In this situation the reinforcement is required to support the full weight of the fill material together with any surcharge for the life of the structure.

17.6.2 REINFORCEMENT ON EMBANKMENT PILES

The use of embankment piles to support fills, lightweight structures and bridge abutments is growing. Loads generated by the fill or structures are carried by friction along the sides of the piles or through pile caps at the top of the piles. The piles and pile caps are normally designed to carry the total load of the embankment (Swedish Road Board, 1974).

A development described by Broms & Wong (1985) and Reid & Buchanan (1984) is to provide a polymeric reinforcing membrane spanning in catenary between the pile caps. The tension membrane reduces the horizontal loads on the piles caused by the placement and compaction of fill: this reduces the possibility of tilting the pile caps and the punching through of the fill between the piles. Importantly, the provision of the tension membrane permits the spacing of the piles to be increased and the size of the pile caps to be reduced. The design of tension membranes over piles is given comprehensive treatment in BS 8006 (1995) and is described by Jones *et al.* (1996) and Kempton *et al.* (1998).

IV. SPECIAL TOPICS

18. BURIED PIPES AND CULVERTS

I. D. Moore

18.1 Introduction

18.1.1 THE BURIED PIPE SYSTEM

A variety of buried pipe infrastructure is needed to service the needs of our communities and resource industries for electrical, water, gas and oil supply, power development, storm-water and sanitary sewer systems, and highway and railway culverts. The conduit surrounded by soil is both loaded and supported by the earth and porewater: and geotechnical engineers are frequently called upon to provide advice regarding various design and construction issues. This chapter describes issues associated with pipe loading and load capacity, and the construction of buried pipeline infrastructure. Other chapters contain related material associated with trenchless pipe-laying technologies (Chapter 19), slope stability (Chapter 14) and frost and thermal effects (Chapter 20).

Figure 18.1a shows a gravity flow pipe or culvert buried under an earth embankment. Generally, the zone of "structural" backfill soil placed directly adjacent to the pipe is specially selected to provide a stable supporting environment, and often consists of granular soil. The "bedding" soil placed beneath the pipe is also specially prepared. Beyond these materials lie lower quality soils: undisturbed native material and lower quality (generally native) soil backfill.

Design and selection of the soil materials is important, since the pipe does not act as an isolated structural element subjected to clearly defined loads, but as one component in the complete pipe–soil system. The pipe carries part of the earth pressures, and part is carried around the pipe through the backfill. The stiffness and uniformity of the backfill soil influences both the proportion of loads reaching the pipe, and the pipe's load carrying ability.

Figure 18.1b defines key locations around the pipe circumference. The crown, springlines and invert are generally those positions where the pipe reaches critical limit states, though shoulders and haunches can also be critical as a result of non-uniform surface loading or narrow bedding at the invert.

18.1.2 PIPE TYPES AND LIMIT STATES

Table 18.1 contains a summary of six different pipe categories, together with a classification as rigid or flexible, and details of key performance limits. The wide variety of materials used in pipe manufacture (ceramics, metals and polymers) have stiffness, strength, ductility and durability characteristics that can vary by orders of magnitude. There are also substantial variations in pipe wall geometry (plain, corrugated or profiled, uniform or composite systems) that lend further complexity. However, in all cases, the stiffness and configuration of the soil around the pipe can affect pipe performance. Performance limits significantly influenced by the surrounding soil are marked in the table. This table also includes the categories of pipe stiffness relative to the surrounding ground. Relative stiffness is influenced by two different

R. K. Rowe (ed.), *Geotechnical and Geoenvironmental Engineering Handbook*
© Kluwer Academic Publishers 2001

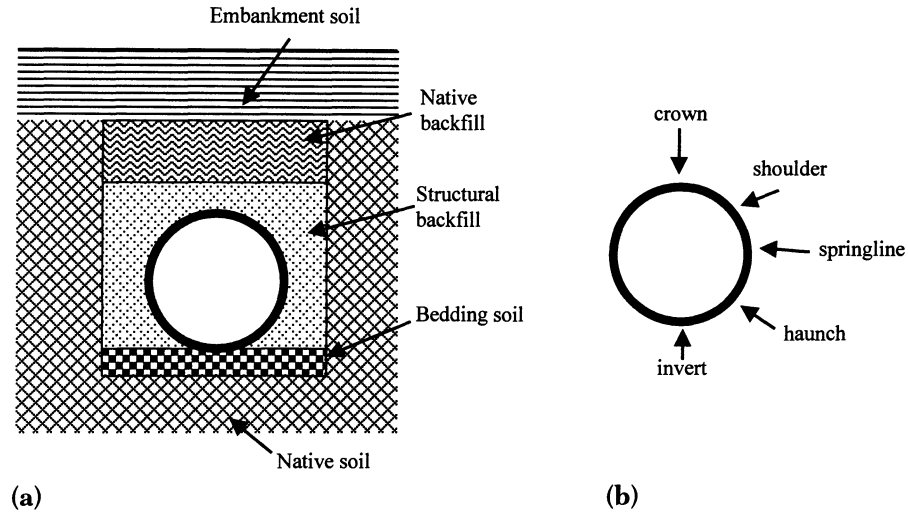


FIGURE 18.1. Definition of terms for the pipe and the surrounding soil: (a) buried pipe and surrounding soil zones; and (b) location of crown, invert, springline, shoulder and haunch.

types of pipe and soil deformation: bending (associated with non-uniform external pressures leading to deformations from circular to oval or other non-circular shape); and hoop compression (uniform and non-uniform pressures reducing pipe circumference). Pipe stiffness categories are:

- Rigid: where the pipe stiffness in bending and ring compression is very large relative to the soil.
- Semi-flexible: where the pipe stiffness in bending is of similar magnitude to the soil, but where stiffness in ring compression is very large.
- Flexible: where the pipe is flexible in bending relative to the soil, but where stiffness in ring compression is very large.
- Compressible: where the pipe is flexible in bending relative to the soil, and stiffness in ring compression is similar to that of the soil.

These stiffness categories will be defined more precisely in Section 18.3.4, as will the manner in which the stiffness influences load sharing between the soil and pipe, and the resistance to deformation.

18.1.3 ANALYSIS OF BURIED PIPES

There are many different pipe types, and many different empirical and semi-empirical procedures have been developed for pipe analysis and design. Product development history and geography have led to design practice that varies considerably from region to region. A major breakthrough occurred with the development of closed-form solutions by Burns & Richard (1964) and Hoeg (1968), examining the pipe response based on elastic response of a thin circular shell and the solid material surrounding it. This permits rational predictions of behavior for many different pipes, based on the elastic properties and the geometry of each particular product. A unified method of analysis that can predict the different responses of rigid, flexible and compressible pipes is then possible, independent of the empirical and semi-empirical procedures.

Another key development has been the formulation of computer analyses based on the finite element method. These developments are summarized in the following paragraphs.

Two-dimensional procedures can model

TABLE 18.1. Pipe stiffness categories and typical performance limits

Pipe materials	Stiffness[a]	Material failure	Deflection	Buckling	Durability
Clay	Rigid	Cracking[a]	No	No	Abrasion
Reinforced concrete	Rigid	Cracking[a], steel yield[a]	No	No	Abrasion, corrosion[a]
Cast iron	Rigid	Cracking	No	No	Corrosion[a]
Ductile iron (DI), corrugated steel (CS) aluminum (Al)	Semi-flexible, flexible	Yield or crushing	Ovaling[a]	Global[a]	Abrasion corrosion[a]
Thermoplastics (PVC, HDPE, PP)	Flexible, compressible	Short-term yield[a], long-term cracking[a]	Ovaling[a] and hoop compression[a]	Global[a] and local[a]	UV degradation, solvents
Glass-reinforced plastic (GRP)	Flexible	Cracking[a]	Ovaling[a]	Global[a]	Solvents

[a] Performance limit influenced by backfill soil.

TABLE 18.2. Pipe design standards[a]

Pipe materials	ASTM	AS/NZS	BS and EN	CSA	ISO
Concrete (C)	C14 (ASTM)	3725 (AS/NZ)	BS 8010	A5 (CSA)	
Corrugated steel (CS)	A796 (ASTM)	2566 (AS/NZ)	EN 1295-1	C140 (CSA)	
Ductile iron (DI)					
Culvert	A716 (ASTM)		BS 8010		TR 7186 (ISO/TR)
Sewer	A746 (ASTM)				
Glass-reinforced plastic (GRP)	D3262 (ASTM)	2566 (AS/NZ)	EN 1295-1		TR 7370 (ISO)
High density polyethylene (HDPE)					
Smooth wall	F810 (ASTM)	2566 (AS/NZ)	EN 1295-1		TR 7074 (ISO/TR)
Corrugated	F892 (ASTM)				
Profile wall	F894 (ASTM)		EN 12666-1		TR 8772 (ISO/TR)
Polyvinylchloride (PVC)					
Sewers	D3034 (ASTM)	2566 (AS/NZ)	EN 1295-1	B182.1 (CSA)	TR 7074 (ISO/TR)
Large diameter	F679 (ASTM)				
Corrugated	F949 (ASTM)		EN 1401-1	B182.4 (CSA)	DIS 4435 (ISO/DIS)
Reinforced concrete (RC)	C76 (ASTM)	3725 (AS/NZ)	EN 1295-1	A257.2 (CSA)	
Vitrified clay pipe (VC)	C301 (ASTM)	4060 (AS/NZ)	EN 1295-1	A60.1 (CSA)	

[a] ASTM, American Society for Testing and Materials; AS/NZS, Australian and New Zealand Standard; BS, British Standard; EN, European Standard; CSA, Canadian Standards Association; ISO, International Standards Organization (TR, technical report).

the specific geometry and material response of the pipe structure, and the zones of soil below, beside and above the pipe (e.g. Katona 1978; Duncan 1979). The influence of soil placement, which can be significant for flexible and long-span structures, can also be modeled. The response to live load can be estimated, provided vehicles can be represented as line loads extending along the culvert axis. Ultimate limit states can be assessed once suitable procedures are available to deal with plastic mechanisms and buckling response (e.g. Moore 1987; Seed & Raines 1988).

Three-dimensional procedures can more accurately capture the influence of live load effects, including three-dimensional load distribution through the fill covering the structure (e.g. Moore & Brachman 1994; Fernando & Carter 1998).

New constitutive models have been incorporated into finite element procedures, allowing consideration of more complex material response on the pipe–soil interaction, e.g. the reinforced concrete pipe wall model of Katona 1978, and the visco-plastic models for HDPE pipe of Zhang & Moore 1998.

This chapter presents a unified approach to analysis of buried pipes and culvert structures based on the elastic continuum analysis of Hoeg (1968). Key empirical equations used for flexible and rigid pipe design are also described and explained.

18.1.4 DESIGN STANDARDS

Table 18.2 shows some of the relevant standards used in pipe design and specification. Design examples are included in this chapter to illustrate use of a unified design approach, as well as traditional empirical design methods.

18.2 Loads

Loads on buried pipes arise in a number of ways, and the following subsections describe the influence of the geostatic stresses (loads associated with earth weight), surface live loads, fluid loads, loads induced by ground movements and dynamic events, and other load sources. Some can be characterized effectively using simple equations. Others are more difficult to quantify, as a result of the complexity of the mechanical response of the system or because of the vagaries of the load source.

Loading must be distinguished as either acting on the pipe–soil system, Fig. 18.2a, or directly on the pipe itself, Fig. 18.2b. The former will generally be used here, since it permits unified assessment of pipes of different material, wall type and stiffness categories. Empirical design procedures generally focus on the vertical load acting across the pipe at the level of the pipe crown, W_v, Fig. 18.2c, rather than the more complete loading pattern. This may be augmented by approximate lateral loading conditions for some of the empirical design methods, Fig. 18.2d.

Buried pipe analysis is generally conducted based on considerations of the total soil stresses acting on the system. In some circumstances, the loads are best subdivided into components associated with the soil skeleton (the effective stresses) and the external water pressures (the pore pressures). Most of the discussion in this chapter is based on the use of total stresses, though fluid pressure loading is explicitly described in Section 18.2.5.

18.2.1 STATIC LOADS: EMBANKMENTS

Vertical, σ_v, and horizontal, σ_h, earth pressures applied to the pipe–soil system, Fig. 18.2a, can be calculated in the conventional way where geostatic conditions apply:

$$\sigma_v = \gamma H \tag{18.1}$$

$$\sigma_h = K\sigma_v \tag{18.2}$$

for soil unit weight γ, depth to the crown, H, and coefficient of lateral earth pressure, K. The quantity $W_p = \sigma_v D$ is often referred to as the "prism load", meaning the weight of

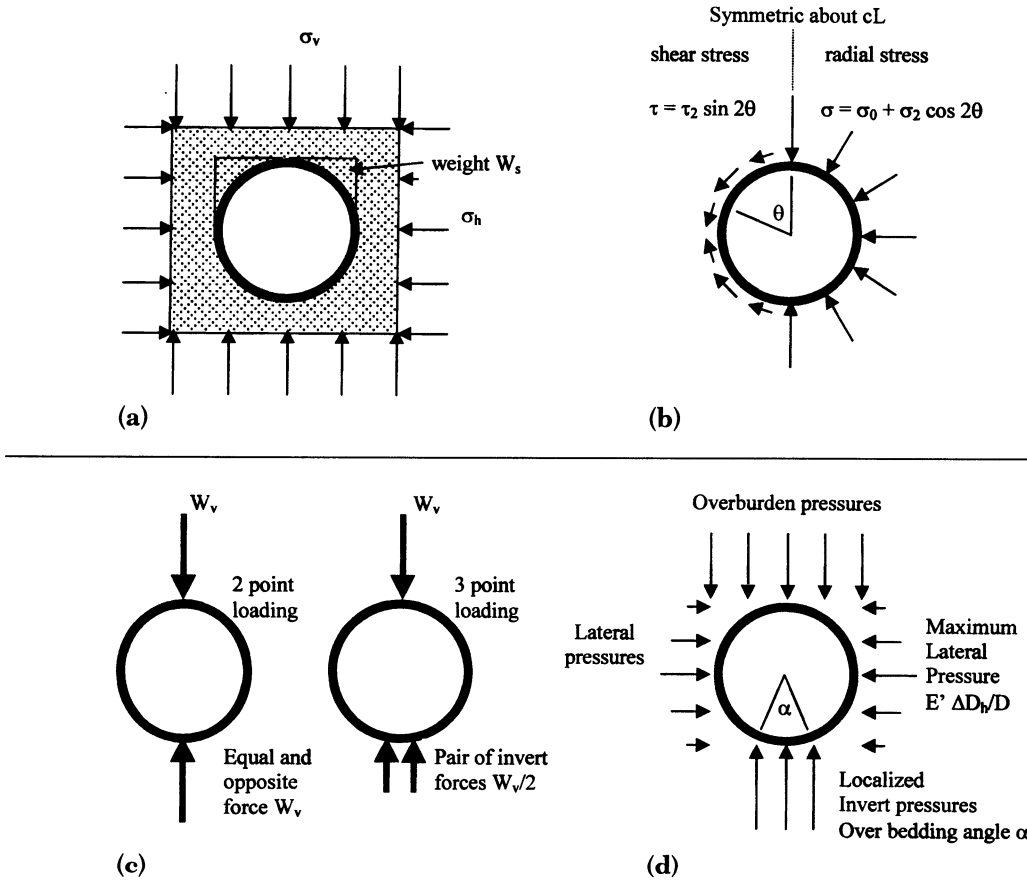


FIGURE 18.2. Load conditions for circular pipes: (a) vertical and horizontal earth pressures on pipe–soil system, (b) external loads acting directly on the pipe, (c) vertical earth loads at the pipe crown and invert, and (d) approximate vertical and horizontal earth pressure distributions on the pipe (modified from Spangler 1956).

the column of soil extending across the pipe diameter, D (from springline to springline), and up to the ground surface.

These equations ignore the weight:

$$W_s = 0.25\gamma D^2(1 - \pi/4) = \gamma 0.054 D^2 \quad (18.3)$$

of backfill soil in each of the two zones of soil directly over the shoulders, Fig. 18.2a. This weight can be important for long span (large diameter) culverts at shallow burial depth. The equations are also based on the assumption that the influence of groundwater can be neglected (the water table is below the pipe) or can be implicitly included in the soil parameters (for example, the unit weight, γ, and lateral earth pressure coefficient, K).

18.2.2 STATIC LOADS: TRENCH INSTALLATION

Is has long been recognized that backfill soil placed into a trench moves downward relative to the native soil at the sides, and that frictional shear stresses develop between the backfill and the trench walls. The shear stresses reduce the vertical force, W_t, transmitted through the trench backfill to the pipe crown at depth, H. Marston & Anderson

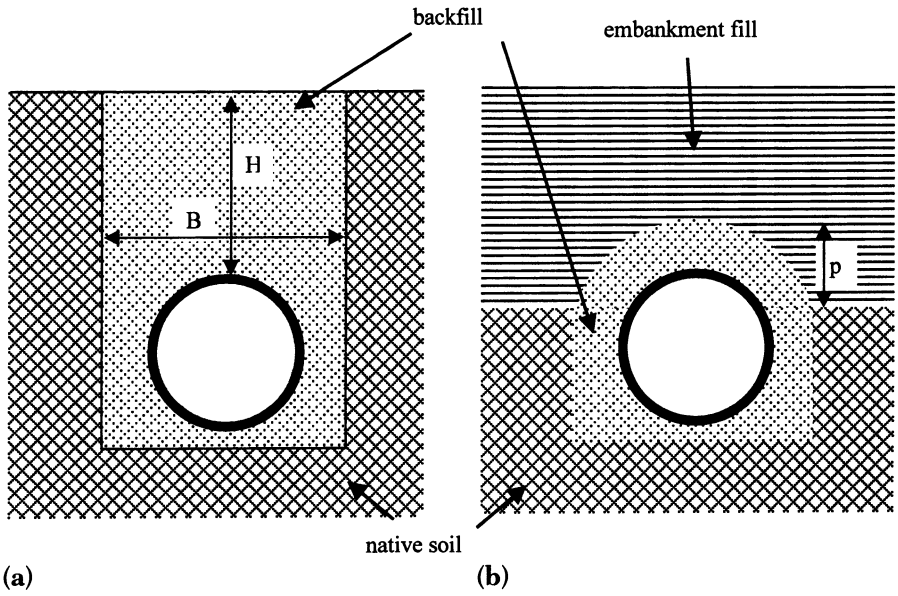


FIGURE 18.3. Pipe burial conditions: (a) conventional trench burial; and (b)pipe under embankment in positive projection condition (pipe crown projects above native ground level).

(1913) adapted the silo arching theory of Janssen (1895) to express vertical load, W_t, as a function of soil unit weight, γ, trench width, B, lateral earth pressure coefficient, K, and friction coefficient, μ, between backfill and native soil at the sides of the trench, Fig. 18.3a. Re-expressing the trench arching solution in terms of average vertical stress in the backfill, σ_v:

$$\sigma_v = W_t/B = C_t \gamma B \qquad (18.4)$$

$$C_t = (1 - e^{-2K\mu H/B})/(2K\mu). \qquad (18.5)$$

For very shallow or very wide trenches where H/B is small, differentiation of C_t reveals that C_t approaches H/B, so that σ_v is given by γH and the geostatic stress solution, Eq. 18.1, is recovered.

As trench depth becomes large, the exponential term in Eq. 18.5 becomes small and C_t approaches $1/(2K\mu)$. The vertical stress, σ_v, then approaches the limit $\gamma B/(2K\mu)$. This occurs because the shear stresses at the sides of the trench are then large enough to balance the extra weight of each additional layer of backfill. Table 18.3 contains a standard set of $K\mu$ values often used in pipe design. "Arching" coefficient C_t is sometimes presented in graphical form in codes of practice and design guides.

Many other burial configurations have been defined in terms of the trench arching theory, where the distance the pipe crown protrudes above the native ground surface (the pipe "projection", p) is varied, Fig. 18.3b. These empirical procedures have been extended to include discussions of pipe under

TABLE 18.3. Soil parameters for trench load analysis

Soil type	$K\mu$
Granular, no cohesion	0.19
Maximum for sand and gravel	0.165
Maximum for saturated top soil	0.150
Maximum for most soils	0.130
Maximum for saturated clay	0.110

embankment loading, with the intention of explaining measurements of pipe load in the field that exceed overburden pressures (the phenomenon referred to as "negative arching"). These procedures all rely on empirical "settlement" coefficients to capture the effects of geometry and the movement of the prism of soil over the pipe relative to the surrounding soil. Negative arching will be discussed further in Section 18.3.3, where techniques are introduced that permit load calculation without the need for empirical "trench arching" theory. Spangler & Handy (1973) provide details of the empirical load calculation procedures.

18.2.3 CONSTRUCTION LOADING

One important source of applied loading relates to temporary construction loads during placement of soil at the sides and over the top of a buried pipe. These are associated with transient loads from construction vehicles, compaction equipment and the influence of unbalanced earth loads (when backfill is placed unevenly on each side of the pipe). While earth loads generally dominate the design and performance of deeply buried pipelines, construction loads can be critical for shallow buried structures. Recent studies by Webb *et al.* (1995) provide guidelines for soil placement and compaction around metal, concrete and polymer pipes.

18.2.4 SURFACE LIVE LOADS

The effect of live loads acting at the ground surface on underlying buried pipes has often been considered in terms of the corresponding vertical stress, σ_v, at the crown of the pipe. It is common to simply add this to the static vertical earth pressures prior to calculations of thrust and moment, though such procedures ignore the effect of pipe–soil interaction.

One commonly used procedure estimates σ_v using the Boussinesq solution, examining the stress that develops at a depth H and lateral distance x from the surface point load P:

$$\sigma_v = 3P/(2\pi H^2)(1 + x^2/H^2)^{-5/2}. \quad (18.6)$$

Another alternative is to use simple prism models to estimate load attenuation with depth:

$$\sigma_v = P/A_H \quad (18.7)$$

where the vertical surface load, P, is spread over horizontal area, A_H, at depth H. If the surface load is applied over a surface rectangle of length l_0 and width b_0, the area at depth H is:

$$A_H = (l_0 + mH)(b_0 + mH). \quad (18.8)$$

Parameter m = the extent to which the area increases with depth (it defines the sideslopes of the prism). Recommended values of m include values of 1 or 1.15 from AASHTO (1994) and 1.45 from AS/NZS 2566.

18.2.5 FLUID LOADING

Pressure from gas or water within the pipe, σ_i, leads to tensile hoop stresses in the walls of the pipe and a wall force, N, per unit length:

$$N = -\sigma_i r. \quad (18.9)$$

Submarine structures can experience large external fluid pressures, σ_e, producing a compressive wall force per unit length of:

$$N = \sigma_e r. \quad (18.10)$$

18.2.6 OTHER LOADING SOURCES

Ground movements in the vicinity of a pipeline due to seismic ground motion, landslides and frost action may all affect the pipeline within it, Selvadurai (1985). Both lateral and axial ground movements can cause structural distress. Offshore pipeline structures are particularly susceptible to seabed instability or

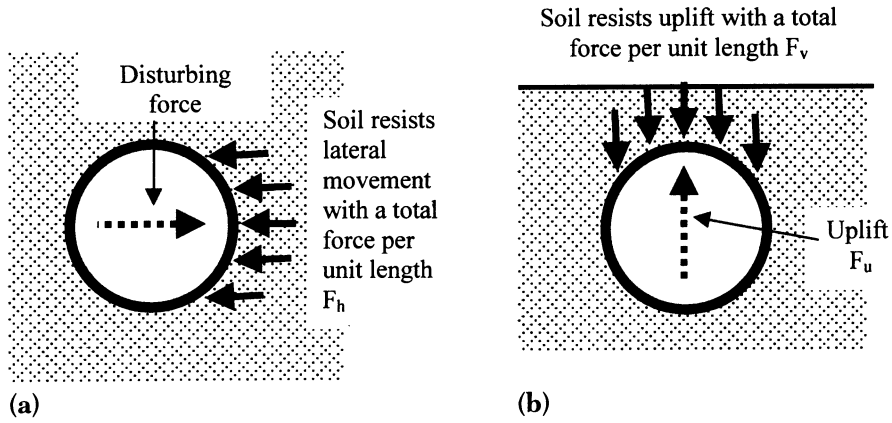


FIGURE 18.4. Action of the pipe as a ground anchor, limiting forces applied by the ground to the pipe perpendicular to the pipe axis: (a) horizontal force applied by the soil to resist the lateral movement of the pipe, and (b) vertical force applied by soil to the pipe to resist uplift.

creep over longer periods of time. Pipeline location should be chosen to avoid or minimize the risk of such ground movements.

Lateral earth movements past a pipeline will generate a lateral force per unit length, F_h, which must be resisted by the pipeline (see Fig. 18.4a). Analysis of the pipeline performance will require an estimate of the lateral force, F_h.

Trautmann & O'Rourke (1985) have investigated the lateral response of pipelines in sand, using soil box tests and reviewing available solutions. They conclude that the anchor force coefficient, $N_{hs}(\phi, H/D)$, of Rowe & Davis (1982b) provides reasonable estimates of peak lateral force per unit length, F_h, accounting for friction angle of the sand, ϕ', unit weight, γ' (bulk unit weight if above the water table, submerged unit weight if below), and normalized burial depth, H/D:

$$F_h = N_{hs}\gamma' HD. \tag{18.11}$$

Trautmann & O'Rourke also provide guidelines on methods of calculating force–displacement relationships, to obtain lateral force, F_h, as a function of lateral soil movement (where F_h has not fully mobilized soil strength and reached a peak value).

Pipe response in clay has been investigated by Paulin *et al.* (1998), who confirm that the anchor force coefficient, $N_{hc}(H/D)$, of Rowe & Davis (1982a) also provides reasonable, though somewhat large solutions for clays of undrained shear strength, s_u:

$$F_h = N_{hc}s_u D. \tag{18.12}$$

Buoyancy force, F_u, per unit length:

$$F_u = \gamma_w \pi D^2/4 \tag{18.13}$$

can be significant when pipelines are placed underwater at shallow covers, and burial needs to be sufficient to generate a resisting force, F_v (see Fig. 18.4b) greater than F_u in the circumstances where the pipeline can be filled (or partially filled) with air.

Trautmann *et al.* (1985) have examined resistance to uplift for pipelines in sands, and have concluded that the anchor force coefficient, $N_{vs}(\phi', H/D)$ of Rowe & Davis (1982b) provides reasonable solutions for force per unit length resisting uplift, F_v, provided by:

$$F_v = N_{vs}\gamma' HD \tag{18.14}$$

though forces are overestimated at depths greater than 4*D*.

Thermally induced loads can be substantial when the pipe is restrained axially and large temperature changes develop. This is particularly true when the pipe is manufactured from a material like HDPE, which has a high coefficient of thermal expansion. Careful design of thrust end restraints is then required, or provision made to accommodate the large axial movements that develop when the ends are not restrained. Assessment of the influence of the compressive or tensile axial forces may also be needed during design.

Seismic analysis of long span metal culverts by Byrne *et al.* (1996) suggests that the effect of vertical acceleration exceeds that of horizontal acceleration. They suggest that seismically induced thrust can be estimated from static thrust using F_v, the ratio of vertical acceleration to acceleration due to gravity, g, CHBDC (1998). Earthquake loading of pipes is discussed further in Section 21.3.3.

Finally, significant forces can arise in curved pipes filled with fluid moving at high velocity. Thrust blocks and other forms of additional restraint are needed where forces are large and ground support is inadequate to resist those forces.

18.3 Response

18.3.1 PIPE AND SOIL PROPERTIES

18.3.1.1 Pipe modulus and wall properties

Pipe structural properties in the circumferential direction generally control the structural design of pipelines and culverts. These include the modulus, E_P, the cross-sectional area per unit length, A_P, and the second moment of area per unit length, I_P.

For a long plain pipe of wall thickness t:

$$A_P = t \tag{18.15}$$

$$I_P = t^3/12. \tag{18.16}$$

Pipe modulus should be reduced by the factor $(1 - \nu_P^2)$ when the plain pipe is very long (and axial restraint is sufficient to result in plane strain conditions).

For profiled wall structures the section properties A_P and I_P are a function of the wall geometry. Modulus should not be reduced by $(1 - \nu_P^2)$ for such structures, since the axial restraint is typically low.

Modulus E_P represents the effective elastic modulus of the pipe wall. This requires averaging in the case of composite structures (e.g. reinforced concrete, glass-reinforced plastic) and a "secant" modulus parameter where stress–strain response is either non-linear or time dependent.

18.3.1.2 Pipe Stiffness

Historically, the results of laboratory pipe load tests have been used to classify pipe, and develop empirical and semi-empirical design methods. For example, "pipe stiffness" (PS) is measured for thermoplastic pipes by compressing the pipe between two rigid steel plates and measuring the deflection as a function of the vertical load (e.g. ASTM D2412):

$$\text{PS} = \text{vertical load per unit length/vertical deflection.} \tag{18.17}$$

PS for thermoplastic pipes varies with the magnitude of the vertical deflection, and a deflection corresponding to 5% decrease in vertical diameter is generally used for evaluations of standard pipe stiffness.

PS for a short pipe segment can be expressed as a function of flexural stiffness, $E_P I_P$, and radius, r:

$$\text{PS} = E_P I_P/[r^3(\pi/4 - 2/\pi)]. \tag{18.18}$$

Ring stiffness constant is another index measure of pipe wall rigidity obtained using the parallel plate load test:

$$\text{RSC} = \text{vertical load per unit length}/0.03 \tag{18.19}$$

$$\text{RSC} = 6.44 E_P I_P/D^2. \tag{18.20}$$

In this case, the pipe is deflected to 3% vertical diameter decrease.

In practice, the parallel plate loading test produces a complex three-dimensional pipe response so the theoretical relationships given by Eqs 18.18 and 18.20 can substantially overestimate stiffness. Furthermore, the time dependent response of polymer materials is such that measurements made at different rates of deformation and at different deflection levels will have different effective pipe moduli, E_P. Three-dimensional analysis capable of capturing the rate dependent stiffness of the material is needed to establish true relationships between PS, RSC, A_P and I_P, Moore (1994).

18.3.1.3 Soil Properties

Backfill properties have a great influence on pipe performance. While it is unusual to have precise information regarding the constitutive behavior of the backfill and native soils, Selig (1990) tested a series of backfill materials and developed non-linear soil parameters for three materials: well-graded granular soil (SW), silt (ML) and lean clay (CL). McGrath (1998) used these parameters to develop design values of soil modulus, which were successfully used to interpret a field testing program for reinforced concrete, corrugated steel and profiled polyethylene pipe. McGrath's modulus values are for three different densities relative to peak values obtained using the Standard Proctor test (85, 90 and 95%). They are presented in Table 18.4 for six different levels of effective vertical earth pressure (7, 35, 70, 140, 275 and 410 kPa).

18.3.2 SOIL–PIPE INTERACTION SOLUTIONS

Various workers have published theoretical solutions to estimate the response of a pipe of radius r, modulus E_P and section properties I_P and A_P when it is buried in a soil of modulus E_s and Poisson's ratio ν_s. Solutions have been developed for two idealized interface conditions: (a) perfect adhesion of the soil to the structure (the perfectly rough, no-slip or bonded interface condition), and (b) zero adhesion (the full-slip or smooth interface condition). Intermediate response can be evaluated using numerical solutions that account for the finite shear strength of the pipe–soil interface (e.g. Katona 1978).

Elastic solutions for pipe–soil interaction include those of:

- Burns & Richard (1964), who examined the response of a pipe installed with no ap-

TABLE 18.4. Design values of soil modulus in MPa (adapted from McGrath 1998)

Soil type[a]	RD[b]	Vertical stress level[c]/(kPa)					
		7	35	70	140	275	410
Granular materials (SW, SP, GW, GP)	85	3.2	3.6	3.9	4.5	5.7	6.9
	90	8.8	10.3	11.2	12.4	14.5	17.2
	95	13.8	17.9	20.7	23.8	29.3	34.5
Silty backfill (ML)	85	2.5	2.7	2.8	3.0	3.5	4.1
	90	4.6	5.1	5.2	5.4	6.2	7.1
	95	9.8	11.5	12.2	13.0	14.4	15.9
Clay soils (CL)	85	0.9	1.2	1.4	1.6	2.0	2.4
	90	1.8	2.2	2.4	2.7	3.2	3.6
	95	3.7	4.3	4.8	5.1	5.6	6.2

[a] Unified Classification System.
[b] Density relative to maximum from Standard Proctor Test, e.g. ASTM D-698.
[c] Level of vertical effective stress at end of burial.

plied stress and then subjected to vertical overburden pressure, σ_v, and horizontal pressure, $\sigma_h = [\nu_s/(1 - \nu_s)]\,\sigma_v$; and Hoeg (1968), who examined the more general case where $\sigma_h = K\sigma_v$ (for arbitrary K). These solutions approximate loading conditions such as pipe burial where ground stresses develop after the pipe is in place.

- Einstein & Schwartz (1979), who considered the response of a thin elastic pipe inserted in prestressed elastic ground, $\sigma_h = K\sigma_v$; this solution is useful for examining problems such as tunneling and pipe jacking where the ground stresses are active before the pipe is installed.
- Moore (1988), who examined the behavior of thin elliptical pipes for both the initially unstressed and prestressed ground cases.
- Moore (1990), who developed three-dimensional solutions for thin or thick elastic pipes in non-uniform elastic ground.

The solution of Hoeg (1968) is adapted here for use in buried circular pipe or culvert analysis. Use will be made of the techniques developed by Gumbel (1981) and Moore (1988) to relate solutions for the initially unstressed ground case to those for prestressed ground (allowing both pipe burial and tunneling/jacking problems to be examined using the same solution).

The following equations can be used to calculate the distribution of radial stress, σ, and shear stress, τ, on the external boundary of the pipe at angle θ from the crown, Fig. 18.2b:

$$\sigma = \sigma_0 + \sigma_2 \cos 2\theta \qquad (18.21)$$

$$\tau = \tau_2 \sin 2\theta. \qquad (18.22)$$

Once these are established, the stress resultants and deformations of the pipe can be calculated (expressions are provided in later sections). For elastic soil responding under onedimensional conditions, coefficient of lateral pressure at rest, K_0, is related to Poisson's ratio of the soil:

$$K_0 = [\nu_s/(1 - \nu_s)]. \qquad (18.23)$$

More realistic ground response features higher lateral earth pressures as given in Section 3.4, which provides values for normally and overconsolidated soils.

For pipes buried then loaded through placement of backfill, mean σ_m and deviatoric σ_d stress components are defined:

$$\sigma_m = (\sigma_v + \sigma_h)/2 \qquad (18.24)$$

$$\sigma_d = (\sigma_v - \sigma_h)/2 \qquad (18.25)$$

For pipes inserted within prestressed ground:

$$\sigma_m = 0.25(\sigma_v + \sigma_h)/(1 - \nu_s) \qquad (18.26)$$

$$\sigma_d = 0.125(\sigma_v - \sigma_h)/[(1 - \nu_s)/(3 - 4\nu_s)]. \qquad (18.27)$$

Factors A_m, $A_{d\sigma}$ and $A_{d\tau}$ are defined to give stresses on the pipe in terms of the mean and deviatoric field stresses. The uniform component of radial stress is given by:

$$\sigma_0 = A_m\sigma_m \qquad (18.28)$$

$$A_m = 2(1 - \nu_s)/[1 + C(1 - 2\nu_s)]. \qquad (18.29)$$

The non-uniform component of radial stress is given by:

$$\sigma_2 = A_{d\sigma}\sigma_d \qquad (18.30)$$

$$A_{d\sigma} = 4(1 - \nu_s)[4 + 3C(1 - 2\nu_s) - 2F]/\Delta \quad \text{for a bonded interface} \qquad (18.31)$$

$$A_{d\sigma} = 12(1 - \nu_s)/(2F + 5 - 6\nu_s) \quad \text{for a smooth interface.} \qquad (18.32)$$

The non-uniform component of shear stress is given by:

$$\tau_2 = A_{d\tau}\sigma_d \qquad (18.33)$$

$$A_{d\tau} = 16(1 - \nu_s)(F + 1)/\Delta \quad \text{for a bonded interface} \qquad (18.34)$$

$$A_{d\tau} = 0 \quad \text{for a smooth interface.} \qquad (18.35)$$

The denominator in Eqs 18.31 and 18.34 is given by:

$$\Delta = C(1 - 2\nu_s)(5 - 6\nu_s + 2F) + 2F(3 - 2\nu_s) + 4(3 - 4\nu_s) \quad (18.36)$$

where the two stiffness parameters C and F are defined by Hoeg (1968) as:

$$C = E_s D/[2(1 + \nu_s)(1 - 2\nu_s)E_p A_p] \quad (18.37)$$

$$F = E_s D^3/[48(1 + \nu_s)E_p I_p]. \quad (18.38)$$

18.3.3 POSITIVE AND NEGATIVE ARCHING

"Arching" is the term generally used to express load transfer from low stiffness to high stiffness components of a multicomponent load-support system. Factors A_m, $A_{d\sigma}$ and $A_{d\tau}$ are used to define the extent of arching between the backfill and the pipe.

Figure 18.5a shows a block of soil subjected to earth pressures. Radial and shear stresses around the disk of soil are given by: $\sigma_0 = \sigma_m$, $\sigma_2 = \sigma_d$, $\tau_2 = \sigma_d$. If a pipe is inserted into the ground at this location prior to application of the earth pressures, then if the pipe stiffness:

- is equal to the disk of soil it "displaces" (Fig. 18.5a), then a "neutral" condition arises, where the pipe carries the "soil prism" directly over it and:

$$A_m = 1 \quad (18.39)$$

- is less than the disk of soil it displaces, then "positive arching" develops, where the arching factor A_m is less than one (Fig. 18.5b);
- is greater than the disk of soil it displaces, then "negative arching" occurs, where arching factor A_m is greater than one (Fig. 18.5b).

For pipe inserted into prestressed ground, the "neutral condition" occurs if the pipe is rigid and permits no displacements at its external boundary and soil stresses are maintained equal to the geostatic stress values, Eqs 18.24 and 18.25. Pipes of any lower stiffness permit deformations that reduce the stresses acting on the pipe below the preexisting ground stresses.

18.3.4 CLASSIFICATION FOR FLEXIBLE AND RIGID PIPES

Pipe rigidity or flexibility can be defined using Hoeg's relative stiffness parameters C

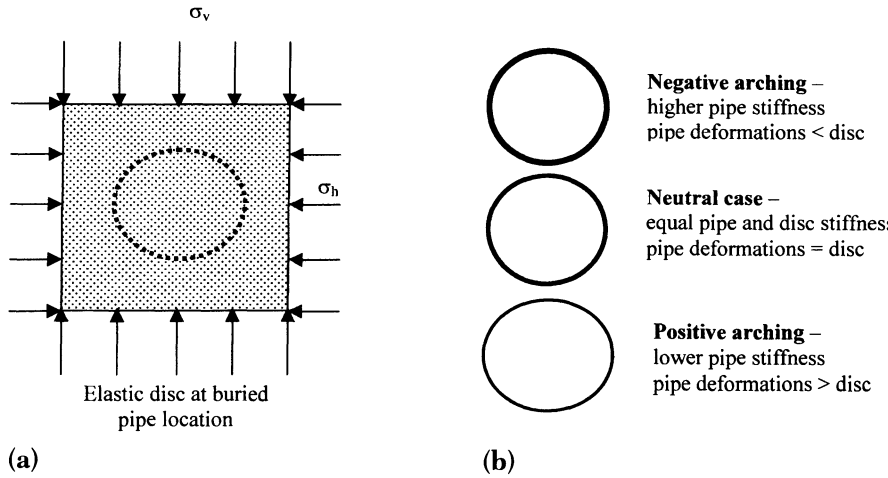


FIGURE 18.5. Explanation of arching mechanism: (a) the reference case: a block of elastic soil subjected to earth pressures; (b) positive and negative arching stiffness less than or greater than the disk.

and F (Eqs 18.37 and 18.38). Structures with low C or F experience negative arching, while those with large values of C or F experience positive arching. Elastic predictions of pipe response can be inspected to classify the soil–pipe system using C and F, as shown in Table 18.5. Also shown are typical examples of these pipe classes.

Tables 18.6 and 18.7 give examples of C and F for six specific reinforced concrete, corrugated metal and high density polyethylene pipes. Also shown are values of arching factors A_m and $A_{d\sigma}$ calculated using Eqs 18.29 and 18.32. Results are given for two different soil moduli, E_s, to reveal how soil modulus influences the soil structure interaction.

An inspection of Tables 18.6 and 18.7 indicates that:

- Rigid pipes have arching factors that are largely independent of soil modulus: the role of the soil around rigid pipes is to spread the earth pressures around the circumference rather than change the magnitude of those earth pressures (this is discussed further in Section 18.5.1).
- Flexible pipes are stiff in hoop compression and attract a uniform component of earth pressure from the soil ($A_m > 1$ indicating negative arching); the non-uniform components of earth pressure are reduced by the backfill soil (positive arching); soil modulus has a significant effect on the magnitude of $A_{d\sigma}$ (i.e. the deflections and bending moments).
- Compressible structures like profiled HDPE pipes have negligible value of $A_{d\sigma}$; and positive arching means that $0 < A_m < 1$, which is controlled by soil modulus.

TABLE 18.5. Pipe stiffness classes

Pipe class	C values	F values	Examples
Rigid pipe	$0.1 > C$	$0.1 > F$	Cast iron, reinforced concrete and clay
Semi-rigid pipe	$0.1 > C$	$10 > F > 0.1$	Long span reinforced concrete, ductile iron, rib stiffened corrugated steel
Flexible pipe	$0.1 > C$	$F > 10$	Corrugated steel and aluminum, PVC, glass reinforced plastic, polypropylene, plain polyethylene
Compressible pipe	$100 > C > 0.1$	$F > 10$	Profiled polyethylene
Empty cavity	$C > 100$	$F > 10$	

TABLE 18.6. C values for a variety of pipes and two backfill moduli shown

Product	Diameter (mm)	Modulus (GPa)	A_p (mm^2 mm^{-1})	E_s = 40 MPa		E_s = 10 MPa	
				C	A_m[c]	C	A_m[c]
Reinforced concrete pipe[a,b]	450	30	90	0.006	1.39	0.002	1.40
	2100	30	220	0.012	1.39	0.003	1.40
Corrugated steel pipe	450	200	1.3	0.066	1.33	0.017	1.38
	2100	200	5.8	0.070	1.33	0.017	1.38
HDPE							
Plain[b]	200	0.6	18	0.71	0.92	0.18	1.24
Profiled	450	0.6	6.4	4.51	0.32	1.13	0.76

[a] Reinforced concrete pipe properties adjusted to include area of steel with modulus of concrete.
[b] Moduli of plain polyethylene and reinforced concrete pipes adjusted by $(1 - \nu_p^2)^{-1}$ to characterize long pipes.
[c] Arching factor.

TABLE 18.7. F values for a variety of pipes and two backfill moduli

Product	Diameter (mm)	Modulus (GPa)	I_p (mm^4 mm^{-1})	E_s = 40 MPa		E_s = 10 MPa	
				F	$A_{d\sigma}$[c]	F	$A_{d\sigma}$[c]
Reinforced concrete pipe[a,b]	450	30	60 000	0.03	2.57	0.01	2.61
	2100	30	887 333	0.22	2.30	0.06	2.54
Corrugated steel pipe	450	200	25	12	0.31	3	0.92
	2100	200	1770	17	0.23	4	0.73
HDPE							
Plain[b]	200	0.6	501	17	0.23	4	0.72
Profiled	450	0.6	127	767	0.01	192	0.02

[a] Reinforced concrete pipe properties adjusted to include area of steel with modulus of concrete.
[b] Moduli of plain polyethylene and reinforced concrete pipes adjusted by $(1 - \nu_p^2)^{-1}$ to characterize long pipes.
[c] Arching factor. Calculations are based on a smooth pipe–soil interaction.

18.3.5 THRUST AND MOMENT

Three approaches can be used to evaluate stress resultants thrust N and bending moment M: (a) general expressions in terms of interface stresses σ_0, σ_2 and τ_2; (b) expressions derived from elastic continuum solutions for rigid or flexible conditions; and (c) empirical procedures developed for specific pipe classes. The first of these is used below for the general design procedure; the latter two are used to provide limiting values for rigid and flexible pipes.

18.3.5.1 General Expressions

Thrust and moment can be estimated once interface pressure components σ_0, σ_2 and τ_2 have been evaluated (Eqs 18.28, 18.30 and 18.33). For harmonic interface stresses defined by Eqs 18.21 and 18.22, thrusts at the crown, N_{cr}, and springline, N_{sp}, are given by:

$$N_{cr} = \sigma_0 r - (\sigma_2/3 + 2\tau_2/3)r \quad (18.40)$$

$$N_{sp} = \sigma_0 r + (\sigma_2/3 + 2\tau_2/3)r \quad (18.41)$$

while bending moments at the crown, M_{cr}, and the springline, M_{sp}, are given by:

$$M_{cr} = (\sigma_2/3 + \tau_2/6)r^2 \quad (18.42)$$

$$M_{sp} = -(\sigma_2/3 + \tau_2/6)r^2. \quad (18.43)$$

18.3.5.2 Limiting Values

For buried flexible pipes, moments are assumed negligible and thrust limits can be calculated assuming C is small, and F is large:

$$N_{sp} = \sigma_v r[(1 - \nu_s)/(3 - 2\nu_s)][5 - 2\nu_s + K(1 - \nu_s)]$$

bonded interface (18.44)

$$N_{sp} = \sigma_v r(1 - \nu_s)(1 + K)$$

smooth interface. (18.45)

For buried rigid pipes, C and F are small, yielding:

$$N_{sp} = \sigma_v r(1 - \nu_s)[1 + K + 2(1 - K)/(3 - 4\nu_s)]$$

bonded interface (18.46)

$$N_{sp} = \sigma_v r(1 - \nu_s)[1 + K + 2(1 - K)/(5 - 6\nu_s)]$$

smooth interface (18.47)

$$M_{sp} = -\sigma_v r^2(1 - K)(1 - \nu_s)/(3 - 4\nu_s)$$

bonded interface (18.48)

$$M_{sp} = -\sigma_v r^2 (1 - K)(1 - \nu_s)2/(5 - 6\nu_s)$$

smooth interface. (18.49)

Analogous expressions exist for pipes inserted within prestressed ground.

Each of these expressions is dependent on Poisson's ratio, ν_s, but is independent of other elastic soil or pipe properties. This occurs because soil and pipe moduli affect the interaction stresses only for semi-rigid pipes ($10 > F > 0.1$) and compressible pipes ($100 > C > 0.1$).

18.3.5.3 Non-Circular Pipes and Culverts

Parametric studies examining the behavior of non-circular pipes and culverts indicate that springline thrust is a function of the ratio of rise R (crown to invert distance) to span S (springline to springline distance), (e.g. see Moore 1988, CHBDC 1998). Circular culvert solutions Eqs 18.21–18.38 ($S/R = 1$) will overpredict thrust (i.e. are conservative) for $S/R > 1$, but may underpredict thrust (i.e. may be unconservative) for $S/R < 1$. Moments are also influenced by pipe shape; this is particularly important for rigid pipes.

18.3.5.4 Empirical Limits

Marston & Anderson (1913) developed empirical guidelines for rigid pipes buried in trenches. They assumed such pipes carry all of the vertical force acting in the column of backfill soil (Fig. 18.2a):

$$W_t = 2N_{sp} = B\sigma_v = C_t\gamma B^2. \quad (18.50)$$

Empirical limits were also developed for the loads, W_e, that develop on rigid pipes buried under embankments. These had:

$$W_e = 2N_{sp} = (1.2 \text{ to } 1.8)D\sigma_v \quad (18.51)$$

depending on the backfill soil and the location of the pipe relative to the original ground surface. A review of Eqs 18.46 and 18.47 indicates that for $K = 0.5$ and $\nu_s = 0.1$ to 0.4, $W_e = 2.N_{sp} = (1.1 \text{ to } 1.7)D\sigma_v$, agrees well with the empirical earth load calculations like those presented by Spangler & Handy (1973).

For "flexible" pipes like corrugated metal culverts, White & Layer (1960) suggested that the "prism load", W_p (the weight of the column of soil directly above the pipe), generates thrusts at the pipe sides:

$$N_{sp} = r\sigma_v. \quad (18.52)$$

This equation forms the basis of some design procedures (e.g. AISI, 1990).

Evaluation of Eq. 18.44 gives $N_{sp} = 1.2$ to $1.7r\sigma_v$ for bonded interface and $\nu_s = 0.1$ to 0.4. These higher values match field measurements, (e.g. Webb *et al.* 1999) where conventional "ring compression theory" based on the soil prism load has been found to be unconservative. Negative arching is considered in some flexible metal culvert design standards, (e.g. CHBDC, 1998).

18.3.6 DEFLECTION

18.3.6.1 Deflection Limits

Pipe deflection results from both permanent and transient loads. While negligible for rigid pipes that are correctly designed and installed, deflections for non-rigid pipes can be significant and are an important design consideration. The deflection of these flexible and compressible pipes is largely controlled by the stiffness of the backfill supporting the buried structure.

While pipe response to static earth pressures can be estimated using rational procedures, response to construction loads is difficult or impossible to predict, since it is subject to the particular installation practices, soil placement, compaction procedure and loading history. Deflection of very flexible and compressible structures must be carefully controlled during construction. Contractors are obliged to maintain deflection within limits specified by a code or the pipe designer.

Typical deflection limits are:

- 5% for corrugated metal structures, e.g. AS/NZS 2566.1.
- 5–6% for GRP pipes; e.g. ASTM D3262-96, AS/NZS 2566.1.
- 7.5% for profile wall HDPE pipe; e.g. ASTM F894-95, AS/NZS 2566.1.
- 3.3–11% for plain HDPE pipe; e.g. ASTM F714-97, AS/NZS 2566.1.
- 6–7.5% for PVC pipes; e.g. ASTM F679-95, 949-96, D3034-97, AS/NZS 2566.1, CSA B182.1-87.

18.3.6.2 Deflection Resulting From Static Earth Pressures: Elastic Theory

Pipe deflections occur as a result of the uniform stress, σ_0, acting on the pipe, as well as non-uniform stresses, $\sigma_2 \cos 2\theta$ and $\tau_2 \sin 2\theta$ (see Fig. 18.2b). Using the estimate of uniform component of radial stress, σ_0, and the non-uniform components, σ_2 and τ_2, from Eqs. 18.28, 18.30 and 18.33 the radial deflection of the pipe, w, is given by:

$$w = w_0 + w_2 \cos 2\theta \tag{18.53}$$

$$w_0 = \sigma_0 r^2 / E_p A_p \tag{18.54}$$

$$w_2 = (2\sigma_0 + \tau_2) r^4 / (18 E_p I_p). \tag{18.55}$$

The deflections vary around the pipe circumference as a function of θ in a manner similar to the applied stresses (Fig. 18.6a). Dependence of displacement components w_0 and

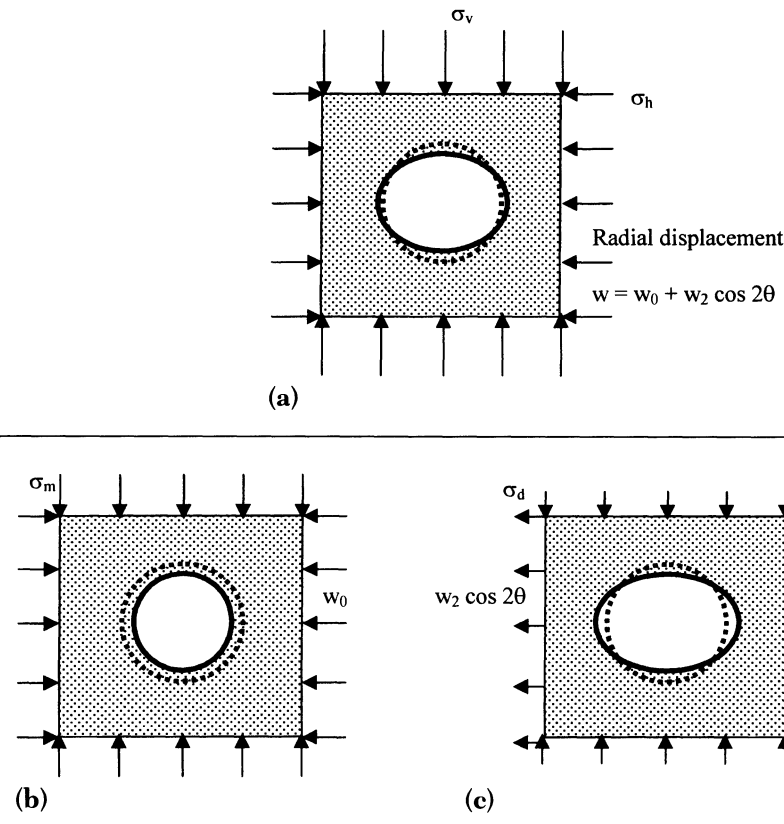


FIGURE 18.6. Idealized deformation components around a buried circular pipe: (a) radial pipe deformations under geostatic earth pressures; (b) deformation w_0 for uniform earth pressure component, σ_m; and (c) deformation w_2 for non-uniform earth pressure component, σ_d.

w_2 on σ_m and σ_d, respectively, is illustrated in Fig. 18.6b and c.

The changes in the vertical and horizontal pipe diameters, ΔD_v and ΔD_h, can be found from w:

$$\Delta D_v = -2(w_0 + w_2) \quad (18.56)$$

$$\Delta D_h = -2(w_0 - w_2). \quad (18.57)$$

18.3.6.3 Deflection Resulting from Static Earth Pressures: Limiting Values

The decrease in vertical pipe diameter can be evaluated for limits of soil to pipe stiffness parameters C and F. For an empty cavity (F and C very large):

$$\Delta D_v = -2\sigma_v r(3 - K)(1 - \nu_s)(1 + \nu_s)/E_s. \quad (18.58)$$

For a flexible pipe that is stiff in hoop compression (F large, C negligible):

$$\Delta D_v = -8\sigma_v r(1 - K)(1 - \nu_s)(1 + \nu_s)/[(3 - 2\nu_s)E_s]. \quad (18.59)$$

For a rigid pipe (F and C negligible):

$$\Delta D_v = 2\sigma_v r(1 - K)r^4(1 - \nu_s)/[3E_pI_p(3 - 4\nu_s)] - 2\sigma_v r^2(1 + K)(1 - \nu_s)/(E_pA_p). \quad (18.60)$$

18.3.6.4 Deflection Resulting from Static Earth Pressures: Spangler's Equation

Spangler (1956) developed a procedure for predicting the changes in horizontal diameter of flexible metal pipes. The modified Iowa deflection equation, as the revised form of Spangler's semi-empirical equation is known, provides an estimate of horizontal pipe diameter increase:

$$\Delta D_h = D_L K_b(2\sigma_v r)/(E_pI_p/r^3 + 0.061E'). \quad (18.61)$$

Spangler employed an earth pressure distribution like that shown in Fig. 18.2d, assuming: (a) a finite width bedding support at the invert characterized using K_b, which is chosen based on the angle of bedding support at the invert α, Fig. 18.2d (e.g. $K_b = 0.105$ for $\alpha = 45°$); (b) a time-dependent response quantified using an empirical "deflection lag factor" D_L (typically between one and 1.5); (c) a parabolic distribution of side pressures with maximum magnitude occurring at the springline and equal to the product of soil stiffness parameter, E', and normalized lateral pipe deflection equal to $\Delta D_h/D$:

$$\sigma_h = E'\Delta D_h/D. \quad (18.62)$$

It is also generally assumed that the change in horizontal pipe diameter is equal and opposite to the change in the vertical diameter. While this is not unreasonable for corrugated metal pipes where the uniform component of radial deflection is negligible, it is not valid for compressible pipes. Furthermore, the soil parameter E' is an empirical model-dependent quantity that depends on pipe size and pipe material, as well as soil type. Finally, the procedure Eq. 18.62 for calculating lateral earth pressures implies zero pressure at zero lateral deflection. Instead, non-zero lateral earth pressures such as $\sigma_h = K\sigma_v$ should be recovered.

Despite these shortcomings, studies have been conducted to provide guidance on selection of E', Howard (1977), and various design procedures employ this procedure (e.g. glass-reinforced plastic pipe design, AWWA C905-88).

18.3.6.5 Pipe Stiffness and Flexibility

Pipe deflection is controlled for some products by specifying limits for pipe stiffness (PS), ring stiffness constant (RSC), or flexibility factor (FF) defined by:

$$FF = S^2/E_pI_p \quad (18.63)$$

where S is the culvert span (springline to springline). These limits effectively control

the flexural rigidity of the pipe, $E_P I_P$, the objective being to limit the bending deformations that occur, particularly during construction (when soil resistance to pipe bending is low). Control of FF is used in design of long span metal culverts (e.g. ASTM A796-98).

18.3.7 STRESS AND STRAIN

Once thrust and moment have been estimated, the maximum compressive circumferential wall stress, σ_c (compression positive), can be calculated from:

$$\sigma_c = N/A_P + |M|y_c/I_P \qquad (18.64)$$

and the maximum tensile circumferential pipe wall stress, σ_t, from:

$$\sigma_t = N/A_P - |M|y_t/I_P. \qquad (18.65)$$

Estimates are best made at the crown and springline using the thrust and moment given in Eqs 18.40–18.49. The y_c and y_t values used here are the distance from the neutral axis of the pipe section to the extreme fibers, respectively, in compression and tension. Stability against material failure can be determined after comparing σ_c and σ_t with the stress limits in compression and tension.

Circumferential (tension positive) strain, ε_θ, can be estimated from circumferential wall stress, σ:

$$\varepsilon_\theta = -\sigma/E_p$$

for uniaxial stress (e.g. profiled pipe) (18.66)

$$\varepsilon_\theta = -\sigma(1 - \nu_p^2)/E_p$$

for plane strain (e.g. plain pipe). (18.67)

One alternative for calculating strain is to express maximum circumferential strain as a function of pipe deflection, ΔD, distance to the extreme fibre, y, pipe diameter, D, and an empirical "strain factor" D_f (sometimes referred to as a shape factor):

$$\varepsilon_{max} = D_f(t/D)(\Delta D_v/D) \qquad (18.68)$$

where t may be replaced by $2y$ for profiled or corrugated pipes. Empirical values of D_f ranging 4.5–8 are employed, depending on pipe stiffness (e.g. ASTM D3262-96). This semi-empirical approach seeks to account for strain amplification in the haunches due to localized bedding support at the invert, Fig. 18.2d. The effect of construction-induced deformations on strain is sometimes estimated by setting $\Delta D_v/D$ in Eq. 18.68 to the levels of pipe deflection allowed during installation (see Section 18.3.6).

18.3.8 BUCKLING

Since the earth and groundwater pressures induce compressive hoop thrusts in the buried pipe, the potential exists for flexible pipe systems to buckle circumferentially. Two methods have generally been used to estimate the compressive thrusts that induce buckling, N_b.

Early workers characterized the backfill soil as a series of elastic springs. The soil stiffness for this "Winkler" or "subgrade reaction" model is given by E'. The critical thrust can then be represented as:

$$N_b = 2(E_P I_P E'/r)^{1/2} \qquad (18.69)$$

where E' = an empirical value of soil stiffness. It is not necessarily the same as the value of E' used in the modified Iowa deflection equation. Both should be back-calculated from field data; one for deflection, the other for pipe buckling. This approach has been used in many codes of practice, with empirical correction factors added to account for the effect of shallow burial and groundwater pressure (e.g. AWWA C905).

Alternatively, the soil can be represented as an elastic solid (e.g. AS2566.1 and the ASTM standard for polyethylene manhole design). In that case, critical hoop thrust is given by

$$N_b = 1.2p_f(E_P I_P)^{1/3}\{E_s/(1 - 2\nu_s)\}^{2/3}R_h \qquad (18.70)$$

where p_f = a performance factor; E_s and v_s = the modulus and Poisson's ratio for the soil,

respectively; and R_h = a factor that accounts for the influence of burial depth and extent of backfill soil (as discussed below).

Comparisons of Eqs 18.69 and 18.70 with measurements of maximum thrust at buckling indicate that the performance of Eq. 18.70 is superior (Moore 1989). Performance factor p_f was estimated by Moore (1989) as 0.55 for granular backfill soils.

The elastic continuum model also permits rational assessment of backfill geometry through correction factor R_h (Moore *et al.* 1994). R_h is a function of H/D, normalized bending stiffness, F, minimum width of backfill soil, W, adjacent to the pipe and the ratio of moduli for native and backfill soils, E_0/E_s. Lower bounds for R_h are given by:

$$R_h = 11.4/(11 + D/H) \leq 1 \quad \text{for } W/D \text{ large} \quad (18.71)$$

$$R_h = 20/(56 + D/H) \quad \text{for } W/D = 0.1 \text{ and } E_0/E_S = 0.1. \quad (18.72)$$

More detailed values of R_h are provided in Moore *et al.* (1994).

Some pipe products also have the potential for local buckling. Corrugated and profile walled structures composed of thin structural elements can develop local short wavelength buckles within individual components of the wall. Soil support is important in these circumstances since it controls the level of bending and hoop strain that develops in the pipe, and also acts to provide local lateral resistance to buckling deformations (Moore & Laidlaw, 1997).

18.4 Backfill Selection and Pipe Installation

Guidelines on pipe installation practice are available (e.g. ASTM A798-97 and D2321-89, AS/NZS 2566.2, BS 8010, ISO/TR 7073: 1998 and 10465-1:1993). Issues to be considered include:

- Care is needed when the native foundation soil beneath the pipe is expansive, soft or unstable; special treatment may be required in such conditions to stabilize the material and prevent excessive deformations.
- Over-excavation under the pipeline must be controlled since longitudinal bending will likely occur where variable bedding settlements develop along the pipeline.
- Restrictions are placed on the types of backfill materials, with preference to granular materials; clay backfills are generally avoided around flexible structures; fines in granular backfills are usually limited to a maximum of 5%; pipe design should include consideration of stone impingement where large size particles are employed for drainage applications.
- Minimum trench widths are specified to permit effective placement and compaction of backfill materials at the sides of the pipe; the placement and compaction of that backfill is far more important than efforts to minimize loads by keeping trench width narrow (see the discussion in the following paragraph); a space of width 500 mm between the pipe and the trench wall is generally needed (even larger for pipe diameters greater than 1 m); the space should be wider than the compaction equipment in use.
- Maximum trench widths are specified, since construction of trench width greater than that used in design, leads to increases in earth loads expected to reach the crown of the pipe.
- Uniform bedding soil is placed in the bottom of the trench below the pipe; compaction of the bedding directly under the pipe can lead to line loading at the invert and possibly distress at invert and haunches; bending moments are reduced if the bedding is not compacted directly under the pipe, though the outer bedding should still be compacted.
- Placement of soil under the haunches and compaction of that material reduces local bending in the pipe; material can be sliced in this area with shovels, or tampers may be used.

- Rammers generally provide the best method of soil compaction in the vicinity of the pipe and are considerably more effective than vibratory plates (McGrath, 1998).
- Granular bedding is permeable, and may serve as a path for groundwater; trench plugs or lateral drains may be needed to control groundwater flow.
- Minimum spacing between parallel pipelines of one diameter or 600 mm (whichever is larger), is needed to permit placement of sidefill.
- Restrictions should be placed on the use of large size compaction equipment in the vicinity of the pipe (the mass of static compaction equipment, and the energy of dynamic equipment).
- Backfill soils placed more than 300 mm or one pipe diameter above the pipe may be native materials, but care is needed to keep large particles away from the pipe, and to compact the backfill beneath roads, water crossings and other pipelines; native soil should also be compacted in populated areas and under cultivated land.
- Native and backfill soils must have compatible gradations to prevent fines migration; alternatively, suitable geotextiles should be used to separate the different soil zones; care is needed in selecting a suitable geotextile and ensuring adequate construction controls (Rowe & Seychuk 1995).
- Care is needed when removing trench boxes or other temporary trench-side support (such as sheet piling); the objective is to prevent loss of side support to the pipe; trench walls must have adequate strength, particularly when flexible pipe is being installed.
- Care is needed with jointing, to prevent inflow of groundwater into the pipe and subsequent loss of backfill.
- Adequate supervision of pipe laying work is required unless large variations in pipe placement, trench excavation and backfill selection, placement and compaction can be tolerated (this is not generally the case).

18.5 *Design Examples*

Three example problems are included to demonstrate pipe design using the procedures outlined in this chapter: (a) rigid pipe: a reinforced concrete storm sewer (Fig. 18.7a) (b) flexible pipe: a corrugated steel culvert (Fig. 18.7b) (c) compressible pipe: a plain high density polyethylene landfill drainage pipe (Fig. 18.7c).

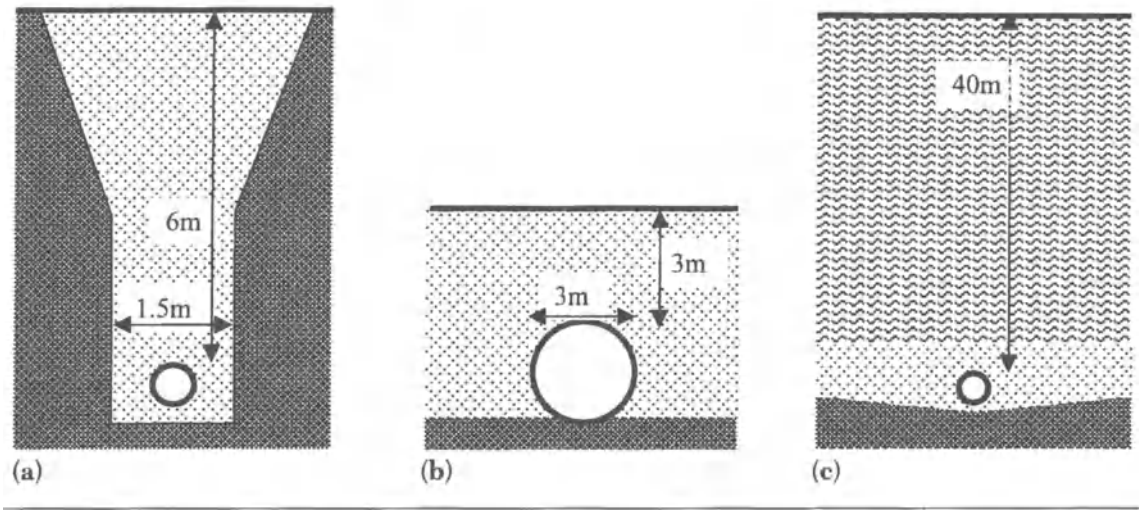


FIGURE 18.7 Example problems: (a) reinforced concrete storm sewer, 0.5-m diameter; (b) corrugated steel culvert, 3-m diameter; and (c) plain HDPE leachate collection pipe, 0.3-m diameter.

18.5.1 CONCRETE STORM SEWER

A reinforced concrete pipe with external diameter of 500 mm is examined at a burial depth of 6 m within a trench of 1.5 m width. Table 18.8 contains all dimensions, material properties and estimates of pipe response. Pipe response is assumed to be unrestrained in the axial direction, due to the flexible joints that would be used in this application. Comparison of values calculated for C and F with Table 18.5 verifies that the pipe is effectively rigid compared with the soil surrounding it.

18.5.1.1 Structural Design to Limit Crack Width

Structural capacity of reinforced concrete pipe is quantified by measuring crack development in the laboratory under diametrically opposed line loads. A limit to crack width is generally specified in the pipe design standard being used (e.g. 0.25 mm, ASTM C655M-95). This serves as a serviceability limit, designed to limit the ingress of moisture and prevent damage to the reinforcing steel. A two- or three-point load test is used to measure W_{cr}/SF, Fig. 18.2c, the factored

TABLE 18.8. Design example I: 500-mm diameter reinforced concrete pipe

Description	Value	Source
Cover, H (m)	6	
Backfill classification Well-graded sand (% of max. Proctor)	SW90	
Trench width, B (m)	1.5	
Trench friction coefficients, $K\mu$	0.165	Table 18.3
Bedding factor, BF	2	Table 18.9
Soil modulus, E_s (MPa)	12	Table 18.4
Poisson's ratio, ν_s	0.3	
Unit weight, γ (kNm^{-3})	20	
Coefficient of lateral pressure, K	0.4	Table 18.9
Radius, r (mm)	250	
Thickness, t (mm)	40	
Modulus, E_p (MPa)	33 000	
Area, A_P (mm^2 mm^{-1})	40	Eq. 18.15
Second moment of area, I_P (mm^4 mm^{-1})	5333	Eq. 18.16
Relative hoop stiffness, C	0.0044	Eq. 18.37[b]
Relative bending stiffness, F	0.137	Eq. 18.38[c]
Trench arching, C_t	2.22	Eq. 18.5
Trench load, $W_v = C_t\gamma B^2$ (kNm^{-1})	100	Eq. 18.50
Embankment load, $W_v = 2N_{sp}$ (kNm^{-1})	87[a]	Eq. 18.51
Cracking load, W_{cr} (kNm^{-1})	43	Eq. 18.75
Vertical stress		
$\sigma_v = \gamma H$ (kPa)	120[a]	Eq. 18.1
$\sigma_v = C_t\gamma B^2/D$(kPa)	200	Eq. 18.4
Cracking moment, M_{sp} (kN m m^{-1})	−1.75	Assume rigid Eq. 18.48
Cracking load, W_{cr} (kN m^{-1})	39	Eq. 18.76

[a] Embankment case governs.
[b] Stiff in hoop compression.
[c] Stiff in circumferential bending.

vertical load per unit length that generates cracks of this size. The safety factor (SF) is used to adjust "ultimate" to "design" load, e.g. values of 1.25–1.5 are specified in ASTM C655M-95 depending on pipe class. The three-point load test has a pair of closely spaced supports at the invert, and produces bending moments and their associated cracks, which are virtually identical to those resulting from two-point loading.

Pipe performance in the field is then evaluated, using either "direct" or "indirect" design procedures to relate W_{cr} to the vertical earth load, W_v, supported by the pipe. This earth load is calculated based on the embankment or trench burial condition:

$$W_v = W_e \quad \text{for embankment burial} \qquad (18.73)$$

$$W_v = W_t \quad \text{for trench burial.} \qquad (18.74)$$

18.5.1.2 Indirect Design

In indirect design, the vertical earth load, W_v, is related to the factored vertical cracking load, W_{cr}/SF, using the empirical bedding factor (BF):

$$W_{cr}/SF = W_v/BF. \qquad (18.75)$$

The bedding factor relates earth load, W_v, to the vertical force that produces the same peak bending moment (and therefore cracking) under parallel plate loading, W_{cr}/SF (Fig. 18.2c). The bedding factor depends on the extent to which backfill distributes earth loads around the pipe. Table 18.9 specifies BF values for different types of burial condition in a manner which is typical of codified design practice. Increases in backfill stiffness and uniformity, i.e. backfill quality, lead to increases in BF.

18.5.1.3 Direct Design

An alternative procedure is to work directly using bending moment (so-called "direct design"). Springline moment associated with the limiting cracks can be estimated from the vertical cracking load, W_{cr}, assuming the pipe sample responds as an elastic ring (e.g. Young & Trott, 1984):

$$M_{sp} = W_{cr}r(\pi^{-1} - 0.5)/SF \qquad (18.76)$$

This is then equated to the springline bending moment, M_{sp}, calculated to occur in the field. Soil–structure interaction analysis is used to estimate M_{sp} based on burial condition (in particular, the lateral earth pressure ratio, K, since this controls bending moment and is influenced by the quality of backfill soil and its placement).

Rational "direct" design methods using soil– structure interaction analysis can be developed for any standard bedding conditions provided standard definitions of K(BF) are established. Table 18.9 gives approximate values of K(BF) for the four bedding conditions. More comprehensive earth pressure distributions and their associated values of K(BF) have also been proposed and implemented for reinforced concrete pipe design, McGrath & Kurdziel (1991).

TABLE 18.9. Bedding factors and equivalent lateral earth pressures for use in direct design

Class	Bedding & haunch[a]	Cover	BF		K
			Trench	Embankment	
A	15-MPa concrete	Dense backfill	3–5	3–5	0.6–0.75
B	SW90	Compacted granular	1.9	2–3	0.4–0.6
C	SW80 or ML85	Lightly compacted	1.5	1.8–2.5	0.2–0.5
D	Loose	Loose	1.1	1.3	0–0.1

[a] Compaction to percentage of maximum modified Proctor density.

18.5.1.4 Trench versus Embankment Loading

This particular design example demonstrates that the trench burial condition may not lead to effective decreases in vertical earth loads. In this case, the trench is too wide to induce effective arching. Both embankment, W_e, and trench, W_t, loads are estimated in Table 18.8. The embankment load is found to be less than the trench load. Conventional design assumes the whole weight of the trench backfill rests on the rigid pipe, rather than just the column of soil over the pipe, and the weight of this wide column exceeds that predicted for embankment loading. Clearly, shear stresses at the sides of the trench can reduce, not increase, earth loads on the pipe; so the use of all the weight of the backfill in this wide trench leads to overconservative estimates of pipe load.

18.5.2 LARGE DIAMETER CORRUGATED STEEL CULVERT

A 3-m diameter corrugated metal culvert is examined in the second design example. Table 18.10 contains details of all calculations and results. The culvert is buried 3-m within a road embankment. Corrugated steel plate of 152-mm wavelength and depth 52-mm is used, where thickness is 2-mm. Section properties I_p and A_p are values obtained from a product handbook, AISI (1990).

Design calculations using flexible pipe lim-

TABLE 18.10. Design example II: 3-m diameter corrugated steel pipe

Description	Value	Source
Cover, H(m)		
Backfill classification Well-graded sand	SW85	
Soil modulus, E_s (MPa)	10	Table 18.4
Poisson's ratio, soil, ν_s	0.3	
Unit weight, γ (kN m^{-3})	20	
Coefficient of lateral pressure, K	0.35	
Radius, r (mm)	1500	
Thickness, t (mm)	2	
Area, A_p (mm^2 mm^{-1})	2	Tabulated data for 152 × 52 plate
Second moment of area, I_p (mm^4 mm^{-1})	12500	Tabulated data for 152 × 52 plate
Pipe modulus, E_p (MPa)	200000	
Poisson's ratio, pipe, ν_p	0	Assume zero for corrugated material
Yield stress, σ_y (MPa)	250	
Relative hoop stiffness, C	0.072	Eq. 18.37
Relative bending stiffness, F	1.7	Eq. 18.38
Vertical stress, σ_v (kPa)	60	Eq. 18.1
Springline thrust, N_{sp} (kN m^{-1})	119.2	Assume flexible Eq. 18.44
Factor of safety against crushing, SF_y	4	Eq. 18.77
Correction factor, for extent of backfill, R_h	1	Assume deeply buried in wide zone of backfill
Critical thrust (for buckling), N_b(kN m^{-1})	2199	Eq. 18.70
Factor of safety against buckling SF_b	18	Eq. 18.81
Deflection Earth load only, ΔD_v (mm)	−17.7	Assume perfectly flexible Eq. 18.59
Per cent deflection $\%\Delta D_v$	−0.6	

its for thrust and deflection are illustrated. The relative flexibility, F, for this structure is calculated to be 1.7, which would be assessed as being in the "semi-rigid" category in Table 18.5. This results from use of the large size corrugation pattern for a structure of relatively small diameter (3 m). Consideration of bending effects is therefore included, by calculating the bending stresses that result at springlines (the location of maximum wall thrust).

The performance limits are now discussed in turn:

- Wall crushing at the springline. This results from springline thrust; a factor of safety (SF_y) is introduced to ensure that wall stress at working loads is less than the yield stress:

$$SF_y = \sigma_y A_P / N_{sp}. \quad (18.77)$$

  The strength of bolted wall seams should also be designed for $SF_y N_{sp}$.

- Deflection (decrease in vertical diameter) as obtained from Eq. 18.59 must be less than the deflection limit (the conventional value is 5%); a value of 0.6% is calculated (very low due to the high bending stiffness of the structure).
- Bending stresses at the springlines associated with pipe ovaling leading to change in diameter, ΔD_v, and no change in pipe circumference, $\Delta D_h = -\Delta D_v$, are given by:

$$\sigma_t = 6E_P (y_t/D)(\Delta D_v/D) \quad (18.78)$$

$$\sigma_c = -6E_P (y_c/D)(\Delta D_v/D). \quad (18.79)$$

For the deflection associated with static earth load (0.6%), the bending stress is 60 MPa, leaving a factor of safety against first yield of:

$$F_y = \sigma_y/[(N_{sp}/A_P) + 6E(y_c/D)(-\Delta D_v/D)] \quad (18.80)$$

TABLE 18.11. Design example III: 300-mm diameter HDPE pipe

Description	Value	Source
Cover, H(m)	40	
Backfill classification, uniform stone	SW95	
Soil modulus, E_s (MPa)	29	Table 18.4 for 275-kPa stress
Poisson's ratio, soil, ν_s	0.25	
Unit weight of waste, γ (kN m^{-3})	12.5	
Coefficient of lateral pressure, K	0.35	
Radius, r (mm)	160	
Dimension ratio, DR	23	
Thickness, t (mm)	13.9	
Area, A_p (mm^2 mm^{-1} = t)	13.9	
Second moment of area, I_p (mm^4 mm^{-1} = $t^3/12$)	224	
Pipe modulus, E_p (MPa)	200	50 year modulus for HDPE
Poisson's ratio, pipe, ν_p	0	Assume zero axial restraint
Yield stress, σ_y (MPa)	9	
Relative hoop stiffness, C	2.67	Eq. 18.37
Relative bending stiffness, F	353	Eq. 18.38
Vertical stress, σ_v (kPa)	500	Eq. 18.1
Correction factor, R_h	1	Deeply buried, wide backfill
Critical thrust, N_b (kN m^{-1})	120	Eq. 18.70

TABLE 18.12. Arching solutions for HDPE pipe example

	Bonded interface condition		Smooth interface condition	
	Value	Source	Value	Source
Arching factor				
A_m	0.64	Eq. 18.29	0.64	Eq. 18.29
$A_{d\sigma}$	0.77	Eq. 18.31	0.01	Eq. 18.32
A_{dt}	1.56	Eq. 18.34	0.00	Eq. 18.35
Springline thrust, N_{sp} (kN m^{-1})	55.1	Eq. 18.41	34.8	Eq. 18.41
Crown thrust, N_{cr} (kN m^{-1})	13.3	Eq. 18.40	34.6	Eq. 18.40
Springline moment, M_{sp}, (kN mm^{-1})	0.015	Eq. 18.43	0.018	Eq. 18.43
Maximum hoop stress, σ_{max} (MPa)	4.4	Eq. 18.64	3.0	Eq. 18.64
Factor of safety				
Yield, SF_y	2.0		3.0	
Buckling, SF_b	2.0	Eq. 18.81	3.5	Eq. 18.81
Uniform displacement, w_0 (mm)	2.0	Eq. 18.54	2.0	Eq. 18.54
Non-uniform displacement, w_2 (mm)	2.9	Eq. 18.55	3.3	Eq. 18.55
Diameter change, ΔD_v (mm)	−9.8	Eq. 18.56	−10.7	Eq. 18.56

equal to 2.1. Construction induced deformation will also produce local bending stresses. The conventional deflection limit associated with flexible metal pipe (5%), gives an elastic bending stress of 500 MPa. This structure, therefore, should be limited to, say, 1% during construction to limit local bending stresses to 100 MPa (giving a final factor of safety of 1.4 against first yield). This should not be difficult, since the structure is very stiff.

- Springline thrust leading to elastic buckling with factor of safety (SF_b) of 18 being obtained from:

$$SF_b = N_b/N_{sp}. \quad (18.81)$$

18.5.3 HIGH DENSITY POLYETHYLENE DRAINAGE PIPE

The last example problem features a HDPE drainage pipe, Table 18.11. The ends of this structure have been assessed where there is zero axial constraint. Relative stiffness values calculated are $C = 0.8$ and $F = 353$, placing the pipe in the compressible pipe range (Table 18.5). Soil–structure interaction has therefore been evaluated using arching factors A_m, $A_{d\sigma}$ and A_{dt} (Table 18.12). The calculated value of $A_m = 0.64$ indicates that there will be positive arching and soil stresses around the pipe, which are reduced below those in the free field. Therefore, soil modulus in the vicinity of the pipe is chosen from

TABLE 18.13. HDPE pipe results for bonded, smooth and frictional interface

Quantity	Bonded	$\mu_i = 0.18$	Smooth
N_{sp}, kN m^{-1}	55.1	39.9	34.8
N_{cr}, kN m^{-1}	14.3	29.9	34.6
M_{sp}, kN m m^{-1}	0.015	0.016	0.018
σ_{max}, MPa	4.9	4.3	3.0
$\Delta D_v/D$, %	−3.0	−3.3	−3.3

TABLE 18.14. Flexible pipe design using Iowa deflection equation

Coefficient of soil reaction, E' (MPa)	20	
Bedding factor, K_b	0.105	Assumes bedding angle $\alpha = 45°$
Deflection, ΔD_v (mm)	−9	Eq. 18.61
Percent deflection, $\%\Delta D_v$	−4.7	

Table 18.4 for the 275-kPa stress level, rather than the total vertical stress 500 kPa.

The interface condition between soil and pipe must be chosen, and the example calculation shows values estimated for both "smooth" and "bonded" interface cases. More advanced analysis using a frictional interface ($\tan \delta = 0.18$) is presented in Table 18.13. These results show that the bonded interface approximation produces conservative pipe wall stresses. The smooth interface solution produces a conservative prediction of pipe deformation.

Pipe design considers factor of safety against yield:

$$SF_y = \sigma_y/\sigma_c \tag{18.82}$$

as well as buckling and pipe deflection. Pipe design should also consider the influence of stress concentrations resulting from stone contact forces and perforations (Brachman 1999). Since the pipe wall stresses in this particular example are already at maximum working limits, this pipe design is inadequate if it is to be perforated and placed within large-sized gravel.

Also shown is a calculation for pipe deflection made using the Iowa deflection equation (Table 18.14). This produces a higher estimate of vertical pipe deflection.

19. TRENCHLESS TECHNOLOGY

G. W. E. Milligan
C. D. F. Rogers

19.1 Introduction

Trenchless technologies cover a wide range of methods of installing new cables, pipes, ducts and small-diameter tunnels in the ground without open excavation between the start point and end point. For the smaller sizes, the installed structure is of circular cross-section, but for larger sizes in suitable ground conditions non-circular sections may be possible. The larger-size installations at substantial cover depth provide an alternative to conventional tunneling methods, while at shallow depths trenchless technologies usually compete with installation in open trench. For small-diameter pipes, techniques such as microtunneling and directional drilling provide the only economic methods of installation at depth. Trenchless technologies also include various methods of on-line replacement and renovation of existing pipes and ducts. A useful summary of the methods available is provided in *Trenchless Technology Guidelines*, produced by the International Society for Trenchless Technology (ISTT).

Once in the ground, pipes and ducts installed by trenchless methods are subject to similar load regimes to those installed in trenches; design for these conditions is covered in Chapter 18. However, the installation procedures often impose more onerous loading on the pipes than do the long-term in-service conditions. This chapter is therefore mainly concerned with the geotechnical aspects of the installation procedures and their influence on the success of the work and the design of the pipes or culverts. One by-product of this is that the installed structures may need to be of a higher quality than would normally be the case for similar structures installed in open trench.

Trenchless technologies are summarized in Table 19.1. However, the boundaries between different techniques are not always distinct, for instance between auger boring and some methods of microtunneling using auger systems. Variations in terminology may also occur between different countries. In Europe, "microtunneling" is used to describe installation of pipes smaller than man-entry size (less than 900 or 1000 mm internal diameter, ID) by pipe jacking methods, while "pipe jacking" refers to installation of pipes up to about 3000 mm ID; in the USA "microtunneling" covers installation of pipes of all diameters up to about 3000 mm ID using a remotely controlled tunneling machine.

Trenchless technologies are mainly used for the installation of new service pipes and ducts, but there are also important techniques for replacement of existing services at either the same or larger diameter. Techniques may be divided generally into those involving excavation of the ground, covered in Section 19.2, and those involving displacement of the ground, covered in Section 19.3. Techniques for rehabilitation of existing pipelines are introduced briefly in Section 19.4, while some of the many uses of trenchless technologies are discussed in Section 19.5.

R. K. Rowe (ed.), *Geotechnical and Geoenvironmental Engineering Handbook*
© Kluwer Academic Publishers 2001

TABLE 19.1. Summary of trenchless technology methods

Method	Pipe internal diameter (mm)	Drive length (m)	Ground conditions	Directional control
Pipe jacking	900–3000+	Typically 100–500	All soils	Yes; accuracy ± 50–100 mm
Microtunneling	250–1000	Up to about 120	All soils; problems with obstructions, e.g. boulders	Yes; accuracy ± 25–50 mm
Auger boring	150–900	Up to about 120	All except hard rock; problems in unstable soils, below water table, also with obstructions, e.g. boulders	Some control; accuracy ≈50 mm
Horizontal directional drilling	500–1500	Up to about 2000	All soils; problems with obstructions, e.g. boulders	Steerable both horizontally and vertically; accuracy ≈1% of length
Guided drilling	50–600	Up to about 600	All soils; problems with obstructions, e.g. boulders	Steerable both horizontally and vertically; accuracy ≈150 mm
Moling	50–200	Typically 10–20; up to 75 possible	Not hard rock or very soft soils; beware obstructions	Only if steerable moles are used; accuracy ±50–100 mm
Pipe bursting	100–500	Up to about 120	Most soils	Follows line of existing pipe
Pipe ramming	50–1200	Up to about 75	Not through rock	None

19.2 Techniques Involving Excavation

19.2.1 PRINCIPLES OF OPERATION

The techniques involving excavation all depend on the same basic principle, of excavating the ground to the external dimensions of the pipe to be inserted, or a slightly larger diameter, and pushing or pulling a lining pipe into the excavated hole. With pipe jacking, microtunneling and auger boring, the pipe is of relatively large diameter in relation to the drive length, and the lining pipe is pushed forward from the rear end. Directional and guided drilling usually involves pipes with much greater length/diameter ratio; in this case a pilot hole is drilled, then the hole enlarged if necessary by pulling back a reaming tool. One or two stages of reaming may be required to reach the required diameter, and the lining pipe is then pulled behind the final reamer to complete the installation.

Some details of the different methods are covered in the next three sections, and the geotechnical engineering considerations relevant to them in Section 19.2.5.

19.2.2 PIPE JACKING AND MICROTUNNELING

These techniques usually involve pushing a "string" of pipes through the ground, excavating at the front end using a suitable steer-

able tunneling shield, and adding additional pipes at the rear end as the drive advances. Work starts from a jacking pit or shaft in which the hydraulic jacks to push the pipeline are located, reacting against a thrust wall at the back of the pit or a previously installed length of pipeline. Spoil from the tunnel excavation is removed at the jacking shaft, and new pipes inserted.

The method of excavation in stable ground conditions may vary from hand excavation using pneumatic tools from within a simple shield, to mechanical excavation using backacters, cutter booms or tunnel-boring machines with rotating cutting heads. For all except the last, excavated sections of noncircular cross-section are possible. In unstable ground, various traditional methods such as breasting boards may allow hand excavation, but fully enclosed systems using slurry or earth-pressure-balance types of tunneling machine are becoming increasingly popular. In very soft clays, simple shields in which the soil is allowed to extrude through controlled ports in the closed face of the shield can be very effective. Shields are usually driven forward by the pipeline, but some incorporate their own jacks so that the cutting head may be driven forward independently, reacting against the leading pipe, and the pipes then closed up behind by the main rams. All shields are steerable, using two or more short-stroke jacks. A drive normally ends at a reception pit, from which the shield may be recovered or relaunched for the next drive. However, "blind" drives, in which the pipe terminates underground, are possible, although the shield may have to be sacrificed unless it is specially designed to be recovered through the installed pipeline.

To help reduce frictional forces between the pipeline and the ground, the ground is often excavated (whether by hand or machine) to slightly larger dimensions than the extrados of the pipes. The presence of a small open annulus around the pipes allows the introduction of a lubricating fluid, such as bentonite slurry, the effects of which are discussed further below.

Excavated spoil is usually removed in wheeled skips through the pipeline, though other methods such as conveyors or clay pumps may be used. In slurry systems the spoil is transported by the slurry, which is pumped back to the surface, where separation facilities are needed to remove the soil from the slurry.

Pipes for pipe jacking are made in a wide variety of materials: clay, glass-reinforced plastic, steel, ductile iron and, most commonly, plain or reinforced concrete. The pipes have to be strong enough to resist the high longitudinal forces imposed on them during jacking, and in particular the stress concentrations caused at pipe joints due to small angular misalignments between one pipe and the next. To maintain a smooth outer surface profile along the pipeline, joints must be formed within the thickness of the pipe wall. The effects of stress concentrations are usually reduced by the incorporation of a compressible packing material in the joint. Research has shown that chipboard and medium density fiberboard are more effective packing materials than plywood or solid timber of similar thickness (Milligan & Ripley 1989; Boot & Husein 1991). Joints are normally made watertight by the incorporation of a rubber sealing ring, often supplemented by internal caulking of the joint gap. Details of pipe dimensions, joint details, allowable loads, etc. should be obtained from the manufacturers.

The main jacking system typically involves two, three or four hydraulic jacks mounted in a frame in the jacking pit. The forces applied to the rearmost pipe are distributed using a thrust ring between the jacks and the pipe. The jacking system may involve long-stroke jacks, or short-stroke jacks and a set of spacer units; the system must be tailored to the arrangements for removing spoil and inserting

pipes, and to the expected rate of progress. A thrust wall to provide reaction for the jacks is usually built into the rear wall of the jacking pit, or, if space is limited, into a short "backshunt" tunnel. The jacking forces are ultimately transmitted into the ground by passive pressures against the thrust wall. Alternatively, reaction may be provided by a length of pipeline installed in a previous drive, through the frictional resistance between the pipes and the soil. Pipe jacks at shallow depth or through embankments may require piles or ground anchors to provide the necessary jacking reaction.

In long drives, the jacking force may increase to the extent that it exceeds the capacity of the jacks, thrust wall or pipes. In these cases, before failure occurs, an interjack station may be inserted. This consists of a telescopic combination of steel sleeve and special pipe incorporating subsidiary jacks. The interjack station allows the pipes ahead of it to be advanced using these jacks, then the pipes behind it to be brought up, closing the interjack again, using the main rams. In principle, any number of interjack stations may be incorporated. The maximum length of drive may then be greatly extended, especially in combination with lubrication; the practical limit is usually controlled by other requirements such as access, safety for workers, or the economics of spoil removal over increasing lengths.

Most pipe jacks are designed to be straight, though it is possible to jack around curves of reasonably large radius; special techniques are being developed to allow jacking around tighter curves. Straight drives are usually controlled by a laser, mounted in the thrust pit and illuminating a target in the shield. Checks are made by conventional surveying methods. Curved pipelines are more difficult and may require sophisticated laser systems or gyrocompass controls. Tolerances for line and level are usually specified, typically in the range $\pm$25–100 mm depending on end-use and pipe diameter. Level control is generally more important, particularly for gravity sewers. However, it should be realized that tight line and level tolerances may not be needed, and are not in themselves sufficient to ensure that angular misalignments between successive pipes are kept small enough. Steering corrections within these limits must be kept gradual, and it may be preferable to allow line tolerances to be exceeded rather than correct a deviation too rapidly. Allowable jacking loads on pipes reduce rapidly with joint misalignment angle, due to stress concentrations in the joints. There is a strong case for specifications to include an allowable jacking load limitation based on joint angles. Well-controlled pipe jacks should be able to keep joint angles in the range 0–0.3°, or 0.5° in difficult ground conditions (such as ground of rapidly varying density, containing boulders or other obstructions, or very soft soils that cannot provide the reaction necessary to facilitate steering).

Microtunneling is required for smaller diameter pipelines. This is identical in principle to pipe jacking, but since man-entry is not possible, the excavation and removal of spoil must be done by remote control. Two main systems have been developed: the first uses an auger along the pipeline to remove the spoil, with a cutting head to suit the ground conditions, driven from the thrust pit; the second is a miniaturized version of a slurry-tunneling machine, with a full-face cutting head and slurry spoil-transport system. Microtunneling drives are usually relatively short, less than 100 m in length between shafts; interjacks are not feasible, provision of lubrication is more difficult, and the load capacity of the small-diameter pipes is limited. While machines are available to cope with all soil types from soft clay to hard rock, mixed or unstable ground conditions may cause problems. For instance, an obstruction such as a large boulder will halt the machine and retrieval may be very expensive and disruptive, involving excavation from the surface or a rescue tunnel from the far end. Some systems

allow the machine to be retrieved through the pipeline in the event of it becoming stuck.

Various specialist systems have been developed: one, for instance, allows the installation of a flexible plastic pipe by driving a steel pipe containing the plastic pipe, and then withdrawing the steel pipe for re-use; in another, an existing pipeline is "eaten" by the tunneling machine and a new pipeline of larger diameter jacked in to replace it.

For further general information on pipe jacking and microtunneling see Thomson (1993). Much practical information and advice is contained in the publications of the UK Pipe Jacking Association, in particular the *Guide to Best Practice* (1995).

19.2.3 AUGER BORING

Auger boring predates microtunneling and is a simple method commonly used for driving a steel pipe through an existing embankment, to provide a casing through which a service pipe, duct or cable is subsequently installed. Precise directional tolerance is therefore less important. Most systems have very limited ability to steer the pipe, which usually consists of lengths of steel pipe welded together and pushed through the embankment while soil is excavated and removed from its front end. The cutting head is powered by flight augers, which are located in the steel casing and transport the muck back to the launch pit. Auger microtunneling differs mainly in that the pipe is made up of short discrete units so that it can be undertaken at depth from a shaft of limited diameter. The cutting head may be independently driven and the augers are located in temporary steel casings inside the permanent pipe. A space is deliberately left to allow a laser beam to focus on a target at the head, and an adjustable shield allows close tolerance steering.

Auger boring construction takes place at ground level or between shallow launch and reception pits. The boring equipment is driven by hydraulic jacks along a track in the drive pit.

19.2.4 DIRECTIONAL DRILLING

Directional drilling includes two different techniques, horizontal directional drilling (HDD) and guided drilling or boring (see Table 19.1). They are both normally operated by surface-mounted machines and both install a pilot bore, which is reamed out for larger sizes. In the past there have been major differences in technology and application between the two, but there is now an increasing overlap in methods and capabilities.

HDD uses large, powerful and expensive equipment for installing relatively long lengths of pipe for crossings under major waterways or similar obstructions. The pilot drill string is not rotated, but a mud motor turns the cutting head, creating the bore. The drill is usually mounted on a wheeled or tracked vehicle, with pickets or ground anchors used to provide additional reaction when necessary. Various drill bits are available for different ground conditions. The drilling fluid is also used to transport the drill returns and may be plain water in fine-grained soils, but is often a sophisticated drilling mud designed to transport material, lubricate and provide hole stability. Curvatures in both horizontal and vertical directions are possible, steering being by means of a "bent sub" in the drill string behind the cutting head, which is turned to produce a change in orientation.

Guided drills are small, relatively low-cost machines much used in urban and suburban situations for the installation at shallow depth of pressure pipes and cable ducts. The majority of the work is for pipes up to 200 mm in diameter, but recently more powerful "midi" machines capable of installing pipes up to 600-mm diameter have been introduced and find a use for mid-length crossings. Guided drilling machines use a rotating drill rod, with wedge-shaped "chisel" heads to allow steering. When continually rotated, the drill follows a straight line through the ground, but when advanced without rotation the wedge causes it to deviate in the direction required. The location and orientation of the head is

often detected by signals from a sonde housed in the drill head. Small-diameter pipes are installed by drilling a hole of slightly greater diameter than the pipe, then pulling the pipe through the excavated hole as the drill is retracted. For larger-diameter pipes, a small-diameter pilot hole is drilled, then enlarged using a reaming tool, which is pulled back with the service pipe attached behind it. There are now several thousand guided drilling machines in operation and in terms of lengths of installation, this is the most important of the trenchless technology methods. In the past, HDD and guided drilling have mainly been used for pressure pipes, cable ducts, etc., for which precise control of gradient was not essential, while pipe jacking and microtunneling were necessary for gravity sewer pipes. However, improved control of alignment is likely to make these techniques increasingly viable for gravity pipelines.

19.2.5 GEOTECHNICAL ENGINEERING CONSIDERATIONS

19.2.5.1 Introduction

There are four main elements of any trenchless technique involving excavation: (a) a method of excavation; (b) a means of removing the spoil; (c) a lining pipe; and (d) a system for pushing or pulling the pipe. Many systems have been developed. However, similar geotechnical considerations apply in most cases. These relate to:

- the stability of the excavated face;
- the choice of excavation method and resulting shield thrust force;
- stability of the excavated hole, and "frictional" forces between pipe and ground;
- closure of ground onto the pipe and resulting ground movements; and
- design of the thrust wall or other reaction system.

Geotechnical aspects are considered here mainly in relation to pipe jacking and microtunneling, which have been the subject of detailed studies. These aspects, covered briefly in the following sections, are discussed in greater detail in Thomson (1993). Some of the theoretical concepts apply equally to other techniques, but in general their success owes mainly to practical experience in the development and use of equipment and procedures; particular problems associated with these are discussed briefly in Section 19.2.5.7

19.2.5.2 Face Stability, Excavation Method and Shield Thrust Force

The method of excavation adopted is dependent on the stability of the excavated face. Hand excavation is only safe if the face is stable and serious soil collapse or water inflow will not occur. On the other hand, for cohesionless soils below the water table, a tunneling machine (probably slurry-type) that can control soil and water pressures will be essential. Stability of tunnel faces in cohesive soils has been studied theoretically and by model tests, and the results summarized by Atkinson & Mair (1981). The pressure, σ_T, required to maintain stability of the tunnel face is given by:

$$\sigma_T \geq \gamma(H + D/2) - T_c s_u \qquad (19.1)$$

where γ = unit weight of soil, H = depth of cover, D = diameter of tunnel, s_u = undrained strength of the soil, and T_c = the stability number.

The value of T_c may be obtained from Fig. 19.1, in which P is an unsupported length of tunnel behind the face. In pipe jacking, microtunneling and auger boring, P is usually small or zero.

Obviously, if σ_T is zero or negative, no pressure is needed and the face is stable unsupported; this is commonly the case in trenchless technologies, unless the drive is very deep or the soil very soft. At the other extreme, an excessively pressurized tunnel face will yield outwards, causing heave of the ground. To prevent this occurring:

$$\sigma_T \leq \gamma(H + D/2) + T_c s_u \qquad (19.2)$$

Within these limits for collapse or "blow-out", a factor of safety of 1.5–2.0 on s_u is

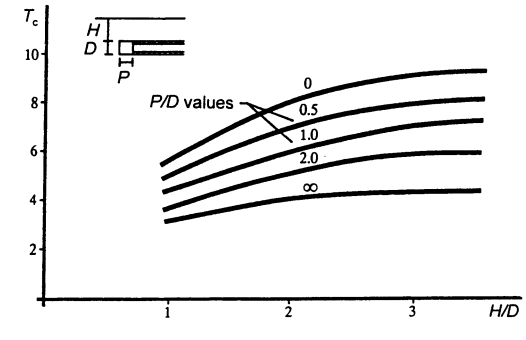


FIGURE 19.1. Stability ratios for tunnel in cohesive soil (modified from Atkinson & Mair 1981).

needed to prevent excessive ground settlement or heave (Mair 1987).

More generally, Anagnostou & Kovari (1996) have presented an expression for the effective support pressure, σ'_T, for soil with both cohesion and friction:

$$\sigma'_T = F_0\gamma' D - F_1 c' + F_2\gamma'\Delta h - F_3 c' \frac{\Delta h}{D} \qquad (19.3)$$

where γ' = submerged unit weight of soil; D = tunnel diameter; c' = soil cohesion; $\Delta h = h_0 - h$, where h_0 = external water head and h = water head at face; and F_0–F_3 are dimensionless coefficients obtained from the plots in Fig. 19.2. To obtain the total support

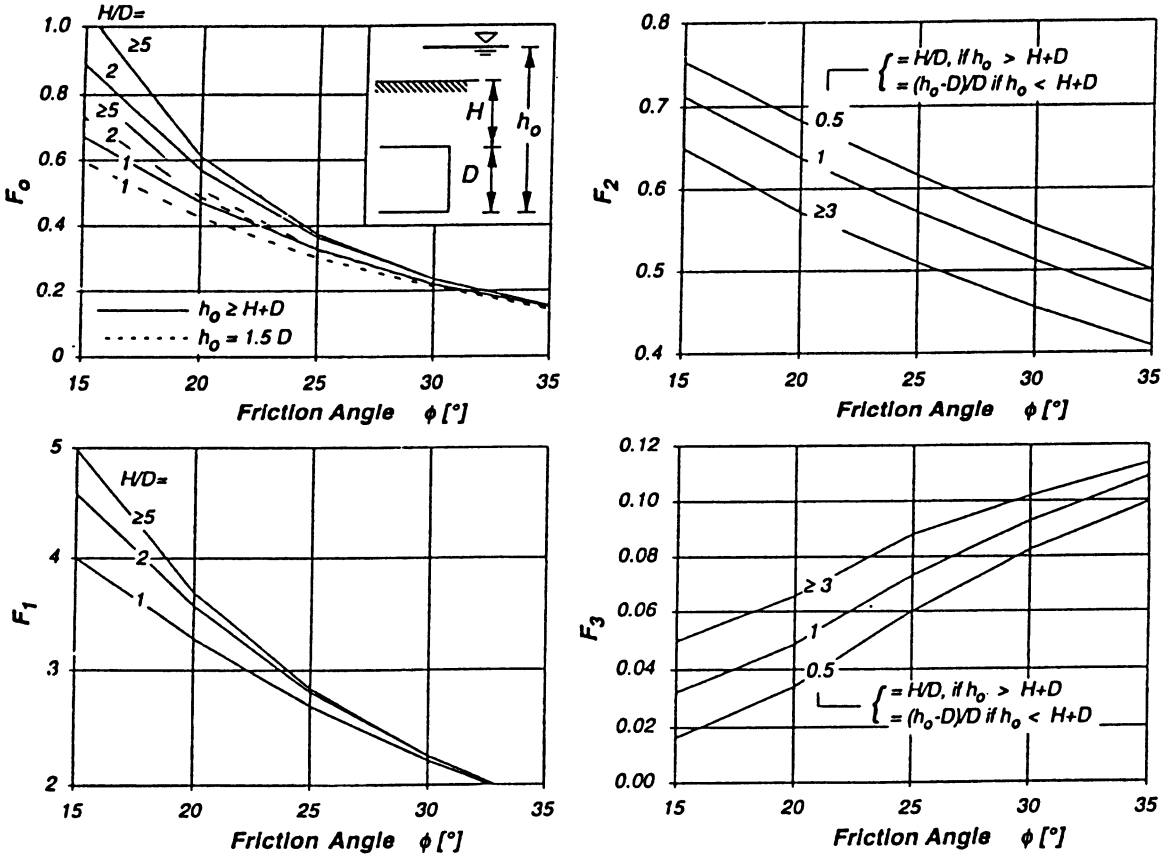


FIGURE 19.2. Dimensionless coefficients F_0–F_3 (reprinted from Tunnelling and Underground Space Technology, 11(2), 165-173, Anagnostou & Kovari, "Face stability conditions with earth-pressure-balance shields," 1996, with permission from Elsevier Science Ltd, The Boulevard, Langford Lane, Kidlington OX5 1GB, UK).

pressure the water pressure at the face must be added to the effective support pressure.

The total face resistance transmitted to the pipeline is the sum of the force due to the support pressure over the face area and the cutting force, P_s, from the edge of the shield being driven into the soil. The latter is given by:

$$P_s = \pi D_s t_s p_s \qquad (19.4)$$

where D_s = external diameter of shield, t_s = thickness of cutting edge of shield, p_s = tip resistance pressure. Typical values of p_s, after Herzog (1985), are given in Table 19.2. However, the actual value of tip resistance is very sensitive to the details of face excavation. In rock and very stiff cohesive soils it is usual to excavate, whether by machine, pneumatic tools or drill-and-blast, to a diameter slightly greater than the external diameter of the shield, in which case the tip resistance may be reduced to zero. Damp, fine sands and silts above the water table will usually also provide a stable face in the short term due to capillary tensions, allowing similar overexcavation.

The final component of resistance to the forward movement of the shield is the friction between the sides of the shield and the ground. This may be assessed using similar methods to those for estimating pipe–soil friction discussed in the next section.

19.2.5.3 Tunnel Stability and Pipeline Friction

The resistance to forward sliding of the pipeline behind the shield depends very much on the stability of the excavated tunnel bore. Stability in cohesive ground may be assessed using Eq. 19.1 and Fig. 19.1, with the value of T_c for an infinite length P. Again, for most trenchless bores the hole will be stable except in very soft clays, at large depth, or for large-diameter pipe jacks. The internal pressure, σ_T, to maintain stability of tunnel bores in cohesionless soil, may be assessed from the following equation, after Atkinson & Mair (1981):

$$\sigma_T = \sigma_S T_S + \gamma D T_\gamma \qquad (19.5)$$

where σ_s = surface surcharge loading, T_s = stability number for surface surcharge, γ = unit weight of soil, D = diameter of tunnel bore, and T_γ = stability number for soil weight. The values of the stability numbers are given in Fig. 19.3. For a tunnel below the

TABLE 19.2. Shield tip resistance pressures, p_s

Soil type	p_s (kPa)
Soft rock, cemented soil	12000
Gravel	7000
Dense sand	6000
Medium-dense sand	4000
Loose sand	2000
Stiff–hard clay	3000
Soft–firm clay	1000
Silt, alluvium	400

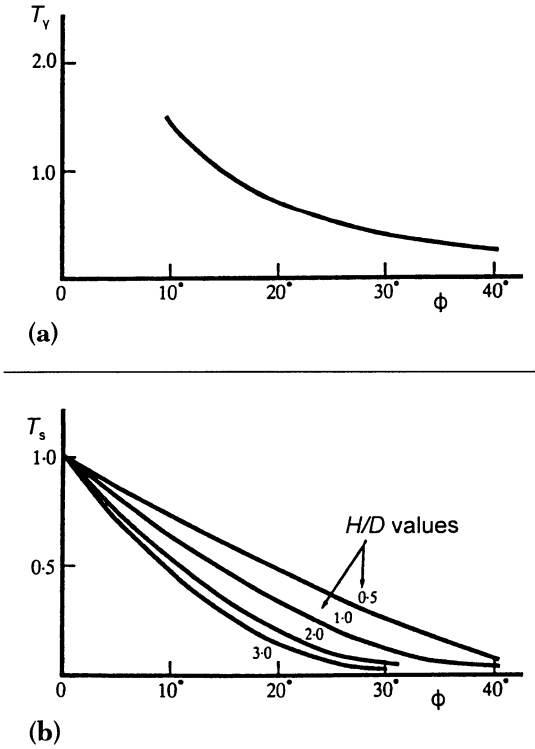


FIGURE 19.3. Stability ratios for tunnel in cohesionless soil (modified from Atkinson & Mair 1981): (a) stability number for soil weight; and (b) stability number for surface surcharge.

water table, a buoyant unit weight, γ', must be used instead of γ in Eq. 19.5, and the water pressure added to obtain the total pressure.

Traditionally, the resistance to sliding of the pipeline has been estimated on the basis of empirical data such as tabulated in Craig (1983) and Stein *et al.* (1989). These are given as apparent frictional forces per unit external area of the pipe; however, they show a very wide scatter of possible values even in a single soil type, and better estimates may be obtained by considering the basic mechanics of pipe–soil interaction under different conditions.

In most cases, the shield used for pipe jacking or microtunneling is of slightly larger diameter than the pipes; this "overcut", combined with any overexcavation at the face, ensures that in stable ground the pipes are sliding along the base of an open bore. The overcut is generally kept to the minimum required to ensure that the ground does not close on to the pipes, as a large overcut may lead to unacceptable ground settlements above the tunnel. Estimation of likely ground closure and settlement is discussed further below. At the end of a drive, any overcut remaining open may be grouted up to minimize further settlements in the long term.

Two simple theoretical models are appropriate for assessing sliding resistance of pipes in an open bore. In rock, stiff clays, silts and sands, the interaction between pipe and ground is frictional, and the resistance, F, per unit length of pipe is given theoretically by $F = W_p \tan \delta$, where W_p = the weight of unit length of pipe and δ = the interface friction angle between soil and pipe (see Fig. 19.4). Values of δ may be obtained from interface tests in a shear box, or from published values. Some values quoted in Herzog (1985) and Norris & Milligan (1992) are given in Table 19.3.

Norris & Milligan (1992) also found from field measurements that the theoretical resistance should typically be increased by about 25% to allow for the effects of misalignments in nominally straight drives. O'Reilly & Rogers (1987) have suggested that for drives through rock, an additional factor to account for non-vertical reactions between pipe and

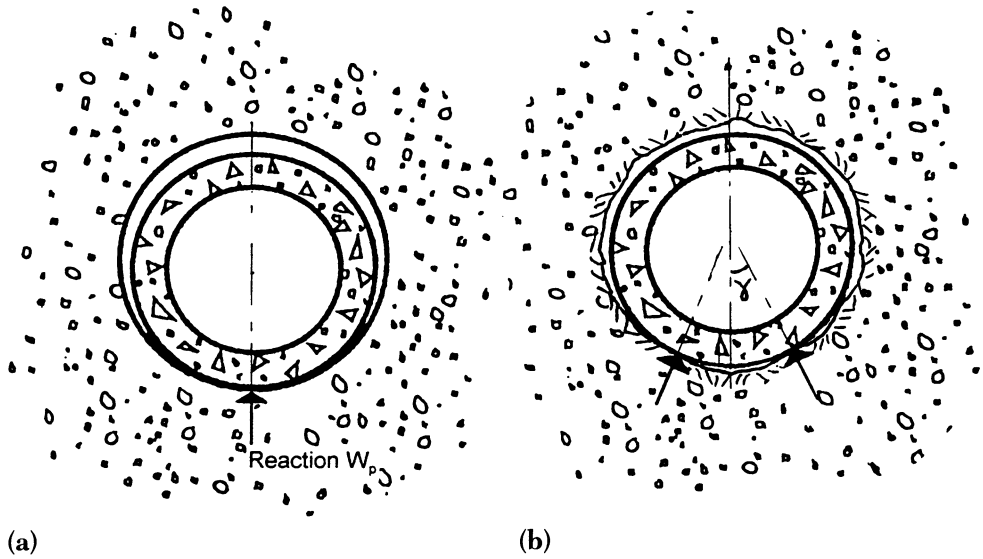


FIGURE 19.4. Pipes sliding in a stable bore: (a) pipe in soil bore; and (b) pipe in rock bore.

TABLE 19.3. Pipe–soil interface friction coefficients, tan δ

For steel and concrete pipes (Herzog 1985)			For concrete pipes (Norris & Milligan 1992)		
Soil type	Steel	Concrete	Soil type	δ(°)	tan δ
Gravel	0.55	0.88	Dense silty sand	38	0.78
Sand	0.45	0.65	Loose sand and gravel	32	0.62
Loam, marl	0.35	0.40	Glacial till (clay)	19	0.34
Low-grade clay	0.30	0.35	Weathered mudstone	17	0.31
Clay	0.20	0.25	London Clay	13	0.23

rock should be included, so that $F = W_p \tan \delta/\cos \gamma$ (see Fig. 19.4b). In softer cohesive soils, the interaction between pipe and ground may be adhesive in nature, and the resistance to forward sliding per unit length, F, is then given by $F = \alpha s_u b$, where α = an adhesion factor as used in pile design (see Chapter 10), s_u = the undrained soil strength, and b = the width of contact between pipe and ground. Haslem (1986) has suggested that b may be calculated using elastic theory for contact between two curved surfaces, but a common-sense estimate is probably sufficient given the other uncertainties involved.

If the ground is not stable, it will collapse onto the pipes, making contact with the full periphery of the pipes. In soft clay, the resistance to forward sliding will then be given by the undrained "adhesion", probably equal to the remolded shear strength of the soil, acting over the full surface area of the pipes. For cohesionless soils, a number of models of the soil–pipe interaction have been proposed, mostly based on or similar to Terzaghi's (1943) "trap door" analysis. This is shown in Fig. 19.5. The frictional resistance, F, to forward sliding due to the earth pressures on the pipes is then given by:

$$F = \frac{\pi D_e}{2}(\sigma'_v + \sigma'_h)\tan \delta \qquad (19.6)$$

where

$$\sigma'_h = K(\sigma'_v + 0.5\gamma' D_e) \qquad (19.7)$$

$$\sigma'_v = \sigma'_{v_1} \exp\left[\frac{-K \tan \phi'(H - H_1)}{B}\right] + \frac{\gamma' B}{K \tan \phi'}\left\{1 - \exp\left[\frac{-K \tan \phi'(H - H_1)}{B}\right]\right\} \qquad (19.8)$$

$$\sigma'_{v_1} = \frac{\gamma B}{K \tan \phi'}\left[1 - \exp\left(\frac{-K \tan \phi' H_1}{B}\right)\right] \qquad (19.9)$$

and

$$B = \frac{D_e \tan(45° - \phi'/2)}{2} + \frac{D_e}{2 \sin(45° + \phi'/2)}. \qquad (19.10)$$

Here γ = the bulk unit weight above the water table, γ' = the submerged unit weight below the water table, H_1 = the depth to the

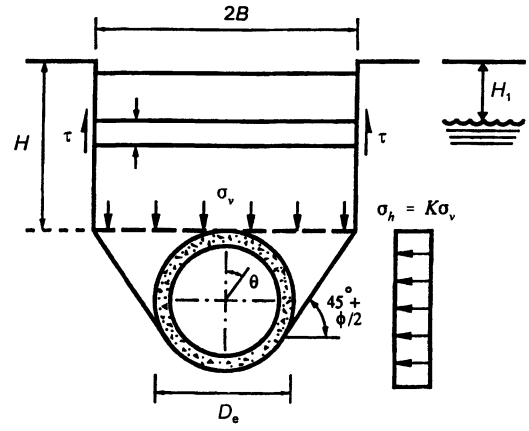


FIGURE 19.5. Ground loading in a cohesionless soil.

water table, and D_e = the external diameter of the pipes. Prior to tunneling, hydrostatic conditions are assumed in the groundwater. The parameter K is the earth pressure coefficient relating horizontal and vertical effective stresses; it must have a value between the active and passive coefficients, and may reasonably be taken as the coefficient at rest, K_0, and equal to $(1 - \sin \phi')$ in sands and gravels (see Chapter 3). The frictional resistance due to the self-weight of the pipes must then be added to give the total sliding resistance; the end result is a resistance very much greater than for pipes sliding in an open tunnel bore.

Even when the tunnel bore is stable, some ground closure will occur due to the unloading of the ground around the opening; if the overcut is insufficient the ground may make contact with the pipes and increase the sliding resistance over that for the simple "open-bore" model. By treating the ground as being elastic, standard solutions from elasticity theory may be applied (Poulos & Davis 1974). For initial total stresses in the ground at depth z of $\sigma_v (= \gamma z)$ and σ_h, the reduction in horizontal and vertical radius, δ_h and δ_v, respectively, are:

$$\delta_h = \frac{(1 - \nu)}{4G} D(3\sigma_h - \sigma_v), \qquad \delta_v = \frac{(1 - \nu)}{4G} D(3\sigma_v - \sigma_h). \tag{19.11}$$

While, if internal supporting pressure, p, is applied, the radius in all directions is increased by:

$$\delta_p = \frac{pD}{4G} \tag{19.12}$$

where G and ν = respectively, the elastic shear modulus and Poisson's ratio for the soil; and D = the diameter of the tunnel bore.

Stress concentrations will also occur around the tunnel, and the maximum circumferential stress, σ_c, at the surface of the tunnel will be given by $(3\sigma_h - \sigma_v)$ or $(3\sigma_v - \sigma_h)$, whichever is the greater (the relative values of σ_v and σ_h will depend on the degree of overconsolidation of a clay deposit, as discussed in Chapter 3). Plastic yielding of clay will occur, and tunnel deformations start to increase more rapidly, when $(\sigma_c - 2p)$ exceeds $2s_u$. There is then no simple general solution for ground deformations, but for axisymmetric conditions with σ_h and σ_v both equal to σ_0:

$$\frac{\delta}{a} = \frac{s_u}{2G}\left(\frac{a}{r}\right) \exp(N^* - 1) \tag{19.13}$$

where δ = radical inward movement at radius, r; a = radius of tunnel bore $\approx D/2$; $N^* = \sigma_0/s_u$ and is called the stability ratio.

Initial undrained deformations will set up changes in porewater pressure, which will dissipate with time, allowing further movements to occur. The complete analysis of the time-dependent closure of ground onto pipes or tunnels, and the resulting ground–pipe interaction pressure, is complex and would have to be solved by finite element analysis. Such sophistication is unlikely to be justified for most applications, and the simple equations given above are sufficient to assess whether problems are likely to occur and make a reasonable decision about the overcut needed.

Even for pipes sliding in an open bore, time effects can be important in clays of high plasticity. The low value of interface friction angle for London Clay given in Table 19.2 is applicable while the pipeline is moving. Once the pipe has stopped, jacking resistance to restart movement increases in only a few minutes, and may increase by 50% or more after a few hours. Increases in low plasticity glacial clay have been found to be smaller, with a maximum of about 35% over a three-day break.

19.2.5.4 Calculation of Ground Movements

Here again, methods developed for tunnels may be applied to trenchless techniques. For

small pipe diameters, movements are likely to be very small provided ground collapse and loss of soil into the excavated bore is prevented. However, for pipe jacking and larger microtunneling work, movements may be sufficient to affect surface structures, or services or foundations beneath the surface.

The most commonly used method for predicting a surface settlement profile is an empirical one, based on a Gaussian distribution curve. The surface settlement, S_0, is described by:

$$S_0 = S_{max} \exp^{(-x^2/2i^2)} \quad (19.14)$$

$$S_{max} = \frac{V_s}{i(2\pi)^{1/2}} \quad (19.15)$$

where S_{max} = the settlement above the centerline of the tunnel, x= the horizontal distance from the centerline, i= the value of x at the point of inflexion of the curve (see Fig. 19.6), and V_s = the total volume of the settlement trough. Provided the tunnel face is kept stable, settlements due to movements there are very small; the total settlement volume may then be obtained as the volume loss along the pipeline, which is equal to the volume of the overcut around the pipe. O'Reilly & New (1982) published the following expressions:

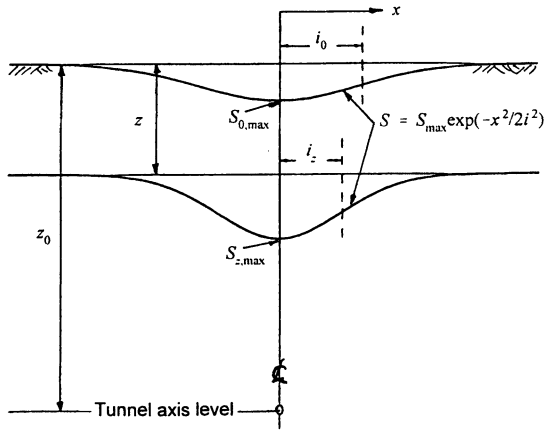


FIGURE 19.6. Surface and subsurface settlement curves.

$$i = 0.28z_0 - 0.12 \quad \text{in granular soils} \quad (19.16)$$

$$i = 0.43z_0 + 1.1 \quad \text{in cohesive soils} \quad (19.17)$$

with z_0 = the depth to tunnel axis and dimensions of meters.

A method of estimating subsurface settlement in cohesive soil has been presented by Mair *et al.* (1993). The volume of the settlement trough is taken to be the same at all depths, with the width at depth z varying in accordance with:

$$\frac{i}{z_0} = 0.175 + 0.325\left(1 - \frac{z}{z_0}\right). \quad (19.18)$$

When $z = 0$, this expression gives a close approximation to the O'Reilly & New expression for normal values of z_0.

An alternative method of calculating ground movements is to use the flow method of Sagaseta (1987), discussed below in Section 19.3.5.3 in relation to pipe bursting.

Large settlements (or heaves) may occur if inadequate or excessive pressures are applied at the tunnel face in soft ground (see Section 19.2.5.2). These pressures may be applied by the slurry in the head of a slurry-tunneling machine, or by the soil in the pressure chamber of an earth-pressure-balance machine (EPBM). The latter results from the balance between the rate of excavation at the cutter head and the rate of extraction of spoil by the screw conveyor from the pressure chamber. A skilled operator is needed to maintain the pressure within the required limits, though increasingly assistance is provided by pressure sensors at various point within the head of the machine.

In addition to these short-term ground movements, long-term settlements may occur due to consolidation of clay soils, particularly when seepage towards the tunnel causes increased effective stresses in the ground around it.

19.2.5.5 Use of Lubrication

The resistance to forward movement of the pipes may be reduced by the use of a lubricat-

ing layer between the pipes and the soil. Although simply coating the pipes with some lubricating material may have some effect, full lubrication requires that the tunnel bore is stable and the overcut remains open and is completely filled with lubricating fluid. In unstable ground, the primary action of the fluid is to provide an internal support pressure to prevent collapse of the tunnel bore. A bentonite slurry is usually used, designed to form a filter cake in cohesionless ground and allow sufficient pressure to be applied to counteract groundwater pressure and support the soil (Eq. 19.5). Various polymer materials are also available as an alternative to bentonite slurries.

Provided the overcut is kept open, the pipes are able to become partially or completely buoyant in the fluid, depending on their diameter and weight. The effective weight causing friction forces with the soil will then be reduced; for fully buoyant pipes (larger diameter pipe-jacked pipes), the pipes will in fact press against the roof of the tunnel as the effective weight becomes negative. Since the shear strength of the slurry itself is minimal, the jacking resistance can be reduced to very low values, allowing drive lengths of several hundred meters with moderate jacking forces. As an example, a 1.2-m external diameter pipe was jacked through fine sands below the water table. With fully effective lubrication, the jacking resistance was only 2.6 kN m^{-1} (equivalent to about 0.7 kPa averaged over the external surface area of the pipe), and this matched quite well the calculated frictional resistance for a buoyant pipe in a stable bore. At this rate, a drive of over 1.5-km length would be possible with a jacking force of 4000 kN. In contrast, the jacking resistance in this job increased to 41.6 kN m^{-1} when the lubrication system was not operational.

19.2.5.6 Jacking Shafts

Drive and reception shafts may be formed in a variety of ways, such as sheet piling with timber framing, concrete segments, or caissons. The thrust wall may be constructed as part of the shaft, or as a separate structure to distribute jacking forces onto the shaft wall. Resistance will usually be provided by the earth pressure at the back of the wall. In calculating this resistance, it must be recognized that intimate contact between wall and ground be achieved, probably by grouting, and that some movement is needed to mobilize passive pressures in the ground. In difficult ground conditions the design and construction of the shafts for pipe jacking or microtunneling may constitute a major part of the work, but cannot be covered in detail in this chapter.

19.2.5.7 Geotechnical Considerations for Other Techniques

Geotechnical problems with auger boring generally relate to the lack of precise control over the stability of the face. It should not be used in cohesionless soils below the water table, as the inflow of soil cannot readily be prevented. Similarly, there is a danger that voids may be created in any loose soil. Steering is fairly primitive, so that if an obstruction such as a boulder is encountered, which cannot be removed or forced out of the way, the bore will have to be abandoned.

With guided boring, directional control is good, so that if an obstruction is encountered it is possible to withdraw the drill a suitable distance and then continue again along a different line. The relatively shallow depth of most bores allows the drill head to be tracked quite accurately from the surface. Drills can operate in most ground conditions, and it is possible to retract the drill if necessary to change bits to cope with a change in ground conditions. However, it may not be possible to penetrate coarse gravel and cobbles. The water or "mud" used to assist drilling also helps to stabilize the drill hole and to lubricate the pipe as it is pulled through the ground.

Horizontal directional drilling often suffers

from the lack of good information on ground conditions, due to its use under major obstructions such as a river or airport runways, where boreholes are very expensive or even impossible. Likely ground conditions should be assessed carefully in the light of the geological history of the site; for instance, the sediments beneath a river crossing may be related to the past regimes of the river. Relatively high mud pressures in the drill hole are required to return the excavated material over the full length of the drill, and zones of high permeability, including fractures and fissures in rock, may lead to unacceptable losses, while unexpectedly low soil strength with insufficient overburden may lead to blow-out failures. Correct design of the drilling mud for the ground conditions is essential, as it must be able to perform its functions of lubrication, spoil transport and powering of the mud motors at the drill head, without excessive loss into the ground.

19.3 Techniques Involving Ground Displacement

19.3.1 PRINCIPLES OF OPERATION

The techniques involving ground displacement all work on the same fundamental principle of soil displacement to create a void into which a pipe is pulled or pushed. In the case of moling, the displacement tool creates an opening in an undisturbed soil mass, which is marginally larger in diameter than the external diameter of the pipe or cable that is pulled into place. Where an existing pipeline needs replacing, the replacement pipeline can be installed along the same route by pipe bursting or pipe removal. Pipe bursting involves a tool which is generally pulled through the existing pipe to burst or split it and expand the void to a diameter that is larger than the new pipe. The replacement pipe can have a similar or larger internal diameter than the original and can either be pulled or jacked into position, depending upon its type. Pipe removal refers to the process of pulling the existing pipe into a shaft, where it is shattered, prior to insertion of the new pipeline. Pipe ramming involves the installation of a relatively thick-walled steel pipeline, with an annular cutting shoe fixed to its leading edge, by hydraulic or pneumatic impacts. The soil that enters the pipe during this process is subsequently removed and the pipe(s) or cable(s) are fed through the permanent casing.

These techniques are described in more detail in the next three sections. Sufficient detail is provided to allow the geotechnical engineer to understand the important features of the operations, although for more information on the construction aspects, reference should be made to Kramer *et al.* (1992). The important geotechnical engineering considerations for practical application are discussed in Section 19.3.5.

19.3.2 MOLING AND GUIDED DRILLING

There are several techniques that work on the principle of void creation in an undisturbed soil mass, including rod pushing (sometimes termed thrust boring), impact moling, steerable moling and jet drilling. As with the excavation techniques, there can be confusion caused by different usage of terminology and similarity of methods. All techniques require an adequate site investigation to ensure that nothing lies in the path or within the zone of influence of the operation.

In rod pushing, a string of solid steel rods is pushed into the soil by hydraulic rams, with the rams being retracted and a new rod added to the string once it is sufficiently advanced. The leading rod is usually fitted with a tapered head having a greater base diameter than the rods. Since there is no facility for steering, a pit usually needs to be excavated and the jacking frame needs to be installed, anchored to enable both pushing and pulling operations, and accurately set to line and level. Once the leading rod has reached its target, often an exca-

vated reception pit, either the pipe can be pulled in directly (if sufficiently small) or an expander can be drawn through in progressive stages prior to pipe installation. This technique is usually restricted to pipes of up to 150-mm diameter and lengths of 30 m.

Impact moles were introduced to improve both drive length and efficiency relative to rod pushing. These consist of a pneumatically or hydraulically powered hammer contained within a torpedo, or mole, of typically 1–2-m length. The mole has a tapered leading edge and is advanced progressively by the hammer action of the drive mechanism. Once the hole has been formed, the pipe is attached to the head of the mole and pulled into position as the tool is drawn back to the starting point. There is no facility for steering a standard impact mole. To minimize the potential for the mole to rise to the surface, the technique is normally restricted to a depth of at least ten times the diameter of the mole. The mole also can deviate from its desired route by encountering the interface between strata of different consistencies or by meeting obstacles (cobbles, rubble, roots, etc.). Thus it is necessary to track the mole as it progresses. This can be done by fitting a sonde, or signal generator, to the head of the mole and monitoring the strength of the signal transmitted to the ground surface to allow the operator to detect any significant changes in direction. Since there is no facility to steer an impact mole, however, the only recourse available to the operator is to withdraw the mole and try again at a different location.

Steerable moles, which have a head that is angled as though sliced obliquely through a cylinder, and a facility for mole rotation, have been developed but are not in widespread use. Jet drilling operates according to the same principle as steerable moling except that a water jet is forced from the leading edge of the mole. Impact and steerable moling are generally used for smaller-diameter pipelines (typically up to 200 mm) and, although the length of drives is increasing, the practical limit on length concerns not only the robustness of the pipe being drawn in, but also the power losses down the hoses that feed the hammer.

19.3.3 PIPE BURSTING

Pipe bursting or splitting is used where an existing pipe needs to be replaced due to structural or operational inadequacy. The bursting unit is usually pulled along the existing pipe and aims to cause outward displacement by multiple fragmentation of a rigid pipe or longitudinal splitting of a flexible pipe. In its simplest form, the burster consists of a tapered mandrel that is steadily pulled through the pipe. Where a steel, lead or ductile plastic pipe needs replacement, the burster will have a single, prominent, sharpened fin that splits the pipe prior to enlargement by increasing the diameter, i.e. the gap at the point of splitting is increased accordingly. The pulling forces required to break out the existing pipe can prove to be very large, however, and thus either static hydraulic expansion or dynamic thrusting is usually employed. In the case of hydraulic expansion, the cone of the burster is made up of segments. The burster is advanced with the segments in the closed position, stopped when further advancement is resisted and the segments are expanded outwards from the axis of the burster to create a void that is greater in diameter than the body of the burster (which is in turn greater in diameter than the following replacement pipes). The segments are then closed and the burster is advanced once more. In the case of dynamic pipe bursting, an impact hammer is built into the burster such that it operates in a similar manner to a guided impact mole. Repeated dynamic thrusts advance the burster in small increments. This generally fragments the pipe more thoroughly than hydraulic expansion.

The choice of burster for any particular site depends upon the type of existing pipe, the

surrounding soil and the likely zone of influence of the burster. The primary problem faced by a bursting unit occurs in cases where the joints in the existing pipe are very strong (e.g. bolted collar joints around cast iron pipes), where the existing pipe is surrounded by concrete (perhaps only at isolated points along its length), where lengths of existing pipe are reinforced or where the existing pipe passes close by or through an existing structure. In such cases, local excavation may prove necessary to effect the break-out of the existing pipe.

The replacement pipe is either pulled (continuous flexible pipe) or jacked (pipe in discrete lengths) into position. Damage to the external surface of the replacement pipe can occur due to scoring by fragments of the burst pipe. In addition, some countries do not allow shards of broken pipe to remain in the ground. One means of avoiding these problems is to use the pipe removal technique.

19.3.4 PIPE RAMMING

Pipe ramming is generally used for relatively short crossings where good access is available. The technique essentially involves a strong, relatively thick-walled steel pipe being driven into the ground by repeated blows of a pneumatic or hydraulic hammer. The leading edge of the steel pipe is generally fitted with a cutting shoe, which has a marginally greater external diameter than the pipe. The process is thus not dissimilar to that of driving a tube for soil sampling. The pipe is advanced into the ground, the hammer is withdrawn, a new length of steel pipe is welded on and the pipe is advanced once again. The resistance to penetration, which together with the structural capacity of the pipe determines the length that can be driven, derives from a combination of face resistance on the cutter, and frictional resistance on the external and internal surfaces of the pipe. However, in some soil conditions a plug may form in the end of the pipe and the resistance to driving will rise to that for a closed-ended tube (*cf.* a cylindrical driven pile). The ground displacements in this case would increase considerably (Rogers & Chapman 1995a).

19.3.5 GEOTECHNICAL ENGINEERING CONSIDERATIONS

The geotechnical engineer must consider the means of and factors controlling void creation, the stability of the displaced soil around the void and the effects of outward soil displacement away from the void. These factors not only influence the choice of equipment and the way in which it should be used, but also whether damage to the adjacent buried infrastructure or overlying structures could occur.

19.3.5.1 Factors Influencing Void Creation

The two primary influences on void creation are the means by which the soil is displaced and the geotechnical properties of the soil. The means of void creation described above can be categorized as dynamic displacement, or static displacement either with or without forward displacement. The dynamic displacement techniques cause associated vibrations in the surrounding soil, which are dependent upon the frequency of the dynamic action used to displace the soil. Slow hammer action and high frequency vibrations will thus affect the soil in different ways, depending upon the soil type and state. Consideration of the type of construction operation will consequently be addressed for each category of soil type in turn. In addition, the effects of the operation will be influenced by the stress state (essentially the effective confinement, p') in the surrounding soil.

In an unsaturated, essentially cohesionless soil, there is the facility for immediate shearing and compression to take place. In a very loose soil, such as a sand dune, compression is likely to occur readily (i.e. with relatively little effort) in the immediate vicinity of the

operation. However, disturbance of the soil structure is likely also to induce collapse settlements in the soil overlying the operation, since volume reduction associated with shearing results in no arching in the overlying soil. This can increase the resistance to outward expansion considerably above that expected for a compressible soil. Such collapse is more likely to occur if dynamic techniques are used, high frequency vibrations being highly effective at causing collapse in such soils. If the soil is relatively dense, however, the soil will not readily compress and there will be larger magnitudes of outward displacement that extend over a greater distance from the operation. The process of outward displacement necessarily causes shearing within the soil and in dense soils this is associated with dilation, or volume increase. The difficulty in achieving outward displacement is consequently wholly dependent upon the mean normal effective stress. Vibration induced by dynamic techniques in this case is likely to restrict the extent of displacements and ease the passage of the void creation tool.

In a saturated, relatively impermeable soil, neither compression nor dilation can occur immediately and thus void creation is associated with undrained shearing. If the soil is heavily overconsolidated, undrained shearing will be associated with negative porewater pressure generation (the soil wishes to dilate) and the mean normal effective stress will increase. This will make void creation harder. Conversely, if the soil is normally consolidated or lightly overconsolidated, undrained shearing will be associated with positive porewater pressure generation and void creation will be easier since the mean effective stress will decrease. This in turn has implications for directional control of, for example, steerable moling, which relies upon the resistance along the length of the mole to effect directional change.

The second influence on porewater pressures concerns the dynamic nature of the operation. Vibration, which is in effect repeated small shearing, will result in a progressive increase in porewater pressures, which will reduce the resistance to void creation. Vibration will also facilitate local densification of soil and, if applied at an appropriate frequency, can fluidize the soil.

If the soil does not fall into one of the above categories, then engineering judgment has to be applied to predict the resistance to void creation as the tool attempts to shear/compress the soil. In cases of cemented soil, weak rock and intact rock, the resistance to soil displacement increases greatly, and can result in the expansive technique becoming impractical or impossible. In such a case, some form of "down-the-hole" hammer drilling is necessary, a technique that needs to be employed with care. Where boulders, cobbles, buried timber, objects in fill or tree roots lie in the path or close to the operation, these will similarly increase the resistance to void expansion and in some cases cause progress to be halted. As mentioned earlier, local enhancement of the pipeline structure (e.g. bolted collars, concrete surrounds) or adjacent structures can similarly inhibit progress of a pipe bursting operation and must be dealt with carefully. If progress is greatly impeded or halted for whatever reason, then either the tool must be retracted or local excavation will be required. In order to avoid these undesirable actions in all but the most exceptional of circumstances, it is important that the expansion equipment is (considerably) more than sufficient for the length and anticipated ground conditions, accounting also for any power loss to the head that may occur when working at the farthest end of the drive.

19.3.5.2 Void Stability and Pipeline Friction

When assessing void stability, similar considerations to those presented for excavation techniques (Section 19.2.5.2) are relevant. However, the techniques involving expansion often occur at much shallower depths than those involving excavation and the sur-

rounding ground has been altered due to shearing/compression. A void can remain stable due to either negative porewater pressure (sometimes termed suction, or cohesion), and/or the creation of a stable surrounding structure in which arching can develop. The former is a time-dependent effect, void instability being more likely if delays occur in the operation.

The pipeline friction depends on the coefficient of friction between the pipe material and the surrounding soil/fragment(s) of original pipe and the mean effective stress acting normal to the pipe wall. The ease of pipe insertion is thus greatly dependent on whether the void collapses or remains stable and at what point(s) along the length of the pipeline this occurs. In addition, a single continuous length of pipe with a smooth external surface will be easier to install than a pipe made up of discrete lengths that is jacked into place. This is because there is the facility for soil or shards to be trapped in the joints (depending on their configuration), thereby increasing the resistance to forward movement.

The process of insertion of the pipeline can also have a considerable influence on the pipe itself. The pipe will tend to undergo scoring when advanced against sharp soil particles and (particularly) shards of existing pipe, the degree of scoring being dependent upon the hardness of the pipe. This can be allowed for by thickening the wall of the pipe (i.e. including a sacrificial thickness), by coating the pipe with a harder material (such as a thin steel coating), installing a liner and subsequently inserting the service pipe, and/or providing protective sleeves over (any) pipe joints. It should be noted that severe scoring could weaken the pipe structure, especially if it is subsequently subjected to cyclic loading, and in very severe cases could lead to isolated puncturing of the pipe wall. A further important influence concerns pipes that are pulled into the line, particularly if the pipe material is relatively extensible. The tensile forces involved in insertion will result in residual stresses and/or elongation that can alter the structural performance of the installed pipe as the material undergoes relaxation. It should be noted that the tensile stress application will be differential along the length of the pipeline and there will be highly concentrated stresses around the connection with the void creation tool. Jacked pipes, which are installed under compression, are less likely to suffer from residual stresses, but must be capable of withstanding the likely maximum jacking loads without structural distress (both to the pipe barrel and, where concentrated stresses occur, to the area around the joints).

19.3.5.3 Calculation of Ground Movements

The trenchless pipelaying techniques described in Section 19.3 all result in either forward soil displacement as the void creation tool approaches any point under consideration, (differential) radial outward displacement, possibly some degree of backward displacement as the tool passes and possibly some further forward displacement as the pipeline is inserted. In addition, long-term heave (upward) or settlement (downward) displacements can occur as a result of excess porewater pressure dissipation. The degree of forward displacement is likely to be most pronounced in the case of pipe ramming, but significant forward displacements will also occur with moling and dynamic pipe bursting. This is of concern where buried services cross the line of the drive within the zone of influence of the construction technique, since the service will undergo additional distress due to radial displacement. Prediction of the forward movements is not straightforward, but can be attempted on the basis of published research papers, e.g. Rogers & Chapman (1995a,c). The radial displacements are usually greater and thus more important to predict.

The prediction of radial displacements usually involves calculating the short-term displacements caused by static outward

expansion, adjusting the pattern in the case of dynamic expansion and then anticipating the long-term displacements on the basis of the excess negative or positive porewater pressures generated. The radial displacements can be predicted using finite element analyses, via charts based upon empirical measurements (Leach & Reed, 1985) or by theoretical equations. Chart analyses usually rely only upon surface observations and thus give no clear or accurate indication of the likely subsurface displacement pattern, which is often of most importance. Simple theoretical analysis calibrated using site measurements or laboratory test data (e.g. Rogers & Chapman 1995b) thus provides an attractive option in cases where the subsurface pattern is predicted from the operation outwards (rather than from the surface downwards). As with all such predictions, the findings must be tempered by carefully applied engineering judgment.

Sagaseta (1987) proposed an analytical technique based on a fluid flow model that could be applied to tunnel displacements. According to this model, the ground is simulated by a fluid. The ground displacement pattern generated by a volume loss at a point (a sink) at a specified depth, z, can be estimated by assuming that undrained, constant volume soil displacements occur as the result of an equal and opposite source located vertically above it at a distance z above the ground surface (Fig. 19.7). An adjustment to the dis-

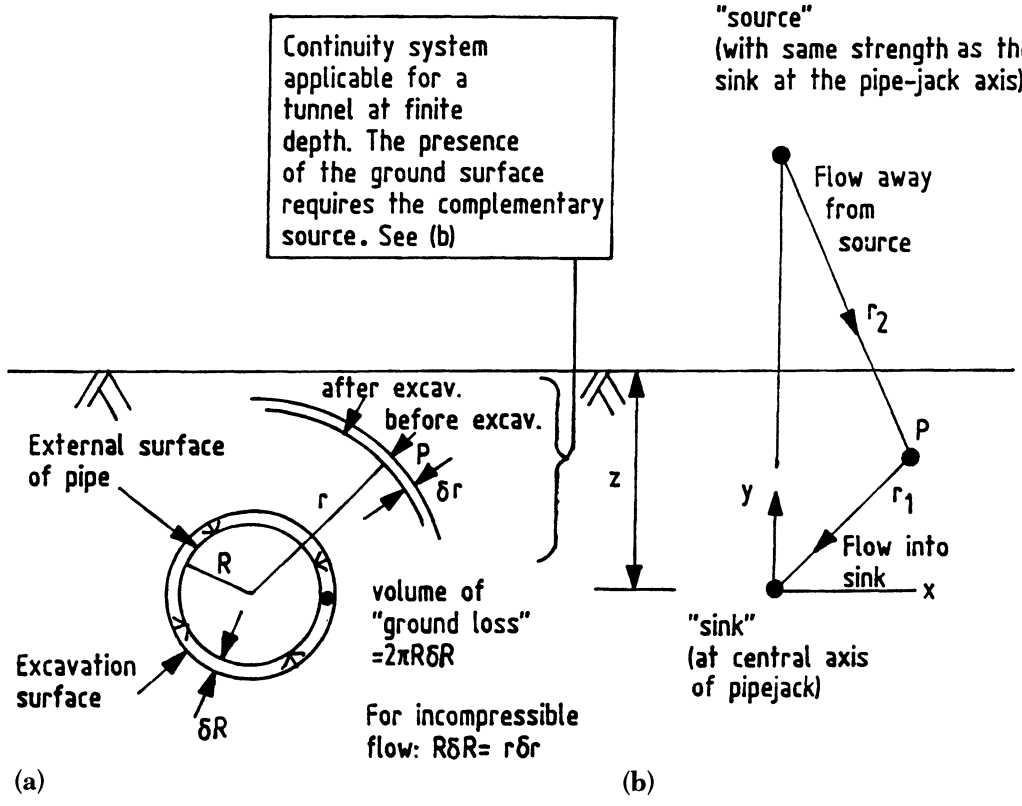


FIGURE 19.7. Application of the modified fluid flow analysis to trenchless techniques involving excavation (similar for expansion, but with "source" and "sink" interchanged): (a) schematic section through pipe jack, with definitions; and (b) analytical framework.

placement pattern close to the ground surface is made to account for the surface shear stresses generated as a result of the assumptions made. This technique can therefore be used to predict the immediate displacement pattern in saturated, fine-grained soils. The long-term displacements that result from equilibration of porewater pressures can subsequently be estimated on the basis of the initial state of the soil.

This technique has been reversed in order to predict the displacements resulting from an expansive operation such as pipe bursting (Rogers & Chapman 1998). In addition, the technique has been adjusted to allow for contraction and dilation of the soil in order that a truer picture of the displacements in a wide variety of soils can be determined directly. The principle is similar to that shown in Fig. 19.7, but with the "sink" and "sources" reversed. Where dynamic pipe bursting is used, the residual displacements are likely to be limited to a smaller zone of influence due to more effective local densification of the soil (Chapman *et al.* 1996).

19.3.5.4 Influence on the Buried Infrastructure and Adjacent Structures and Services

The patterns of ground displacement must first be predicted, as discussed in Section 19.3. The response of adjacent buried and/or overlying services or structures to the displacement pattern then needs to be assessed based on the relative stiffnesses and the form of the service/structure. This is done by tracing it onto the displacement pattern and hence estimating the maximum displacement that it would undergo (i.e. if its stiffness were less than or equal to the soil). The relative displacement of the service/structure can then be calculated on the basis that no movement will occur outside the zone of influence of the operation. If the stiffness of the service/structure is significantly greater than the soil and it can either move relative to the soil or is strong enough to restrain the soil and hence limit the soil displacements, then the relative displacement (e.g. maximum curvature) can be reduced.

Important in this analysis is a consideration of the strength and continuity of the service/structure concerned. For example, if the expansive operation were to take place close below the surface of a continuous road pavement structure that is strong enough to resist cracking, the surface displacements will be lower than those of a free ground surface. The displacement pattern in such a case will be more radial in nature and there will be a greater degree of compression within the soil. If the surface consists of a thin, weak pavement structure, then a single crack is likely to occur directly above the line of the operation. If, however, the surface were to consist of small, discrete blocks then a more extensive pattern of smaller cracks might be expected over the full width of the surface zone of influence.

19.4 Pipeline Rehabilitation Techniques

If an existing pipeline becomes, or is likely soon to become, structurally or operationally inadequate, then there are five fundamental options available:

1. The pipeline can be abandoned and a new pipeline can be constructed in parallel.
2. The pipeline can be replaced on-line using a "pipe eating" type of microtunneling, drilling or auger boring equipment.
3. The pipeline can be replaced following pipe removal or bursting/splitting and diametrical expansion.
4. The pipeline can be replaced using trench excavation.
5. The existing pipeline can be rehabilitated.

Methods by which the first three options can be effected have been discussed earlier in this chapter, with all three being suitable for some degree of up-sizing and size-for-size re-

placement. The fourth, traditional option is always to be considered, although it will result in considerable surface disruption that might be or might not prove acceptable depending upon where it is located. However, it should be noted that where the pipeline has lateral connections, some means of remotely remaking the connections will be needed if surface disruption is to be avoided totally using trenchless techniques. If local excavations are required to make lateral connections, however, then the benefits over trenching can become significantly reduced, although small local excavations will nevertheless be much less disruptive to pavement structures and surface operations than full trench excavation. The fifth option, discussed below, is only viable where some size reduction of the pipeline is acceptable.

The choice of rehabilitation over other techniques depends partially upon the reason for renovation/replacement. If the existing pipeline has become operationally inadequate due to poor hydraulic performance or leakage (either egress of fluid, in which case beware of local surrounding soil erosion, or ingress of water), but otherwise remains structurally sound, the case for simple restoration of the hydraulic condition or watertightness is strong. If the existing pipeline has deteriorated in a structural sense also, the rehabilitation technique will (usually) need to provide structural enhancement, with the new liner/lining acting in combination with the existing pipe structure. It is thus important to determine the condition of the existing pipeline and this is usually done using a closed-circuit television camera survey.

The geotechnical considerations of the structural performance of a new pipeline constructed using trenchless techniques (i.e. covering the first three options listed above) have been considered earlier in this chapter and will not be discussed further here. When compared with pipelines installed by trenching, the advantages of rehabilitation are that the surrounding soil remains undisturbed and will usually therefore be relatively stiff. When installing a pipe in a trench, it is usually impossible to reinstate the natural soil to provide the same degree of support as when it is in its undisturbed state. For this reason, a high quality fill is commonly introduced to surround the pipes and backfill the trench (depending upon its location), creating additional cost and environmental damage. Thus it is the pipe–soil system, rather than the pipe in isolation, that needs to be considered in determining the structural performance of rehabilitated pipes and pipes installed by trenching.

One further important consideration here is the intimacy of the association between an existing pipe and a new liner or coating. Many rehabilitation processes will produce a lining that has insufficient structural capacity alone to resist applied loading. Such processes are prohibited in general in current design unless there is full bonding and hence interaction between the existing pipe and the liner. The lining needs to act in combination with the existing pipe to counteract soil loading and any dynamic or static imposed loading. This type of structural calculation has been discussed in Chapter 18. However, if the existing pipeline is no longer watertight, or if it might lose its watertightness as a result of the rehabilitation process (for example, during intensive cleaning operations prior to treatment), then the hydrostatic effects of water pressure acting on the lining alone must be considered. If the pipeline is deeply buried beneath the groundwater table, the hydrostatic pressure can become considerable and the liner, which is often thin, can be susceptible to buckling, if flexible, or cracking, if rigid. In such a case the liner must be designed to be sufficiently strong to resist buckling/cracking, or some means of grouting behind the liner should be used to prevent the hydrostatic pressure acting directly on it.

The traditional means of providing a full

lining is to use sliplining techniques. The pipeline to be treated is taken out of service, cleaned and a new (generally thin-walled) liner is pulled and/or pushed into place. Any lateral connections then need to be made, either by hand in local surface excavations or remotely using robotic techniques, prior to testing the system for water/airtightness and recommissioning. High density polyethylene liners, for example, are often installed in this manner since they can often be bent sufficiently to be passed into the pipeline in one continuous length without additional excavation (e.g. via a manhole). An alternative system is to use welded lengths of a less deformable material, such as thin-wall stainless steel.

In order to make this process more efficient, techniques of reducing the diameter of the liner during insertion, and then expanding the diameter once it is in place, have been developed. This greatly eases the insertion process and reduces the risk of scoring of the external pipe surface, as well as ensuring a tight fit to the existing pipe structure and minimizing the loss of cross-sectional area of the pipeline. Such techniques are applied to continuous lengths of medium- or high-density polyethylene pipe. One technique is known as *rolldown*, in which the liner is diametrically compressed by passing it through a series of rollers such that it is elastically, but not plastically, deformed (i.e. the yield point of the plastic is not reached). The liner is then fed, in one continuous operation, into the host pipeline, the ends of the liner thereafter being sealed and the original diameter being restored by pumping in water under pressure. It should be noted that rerounding would occur automatically within weeks, although pressure is usually applied as an expediency.

A second technique is known as *die drawing* or *swage lining*. In this case, the liner is pulled by a winch through a die. For smaller diameters, the process is carried out at ambient temperatures, whereas for larger pipes, the die and even the liner may be heated prior to diametrical reduction. The liner is thereafter expanded when in place and any lateral connections remade, as before.

A further variation of this idea consists of the insertion of collapsed, or folded, sections of thermoplastic pipe, which are subsequently rerounded using hot air, hot water or steam. The liner in this case is folded into a C or U shape using a thermomechanical process, delivered to site in its deformed shape and then heated to make it flexible prior to insertion. One advantage of the heating process used to reround the liner is that it will deform readily around bends and into any surface irregularities in the pipe wall, thus ensuring a close fit. In addition, indentations in the liner will occur where lateral connections occur in the host pipe, making it easier to determine their location for making remote controlled connections.

Cured-in-place resin-impregnated soft liners can be installed to produce a similar end result, although via a different process. A flexible, permeable tube made from a geotextile is fully impregnated with a polyester or epoxy resin and a catalyst, and is cut to the required length. This tube is then either drawn into place and filled with cold water to force the liner against the host pipe wall or installed by inversion. For installation by inversion, the tube is fixed to a ring at the insertion point (for example, a manhole for sewer renovation) and is progressively installed using cold water under pressure such that the tube is turned inside out as it passes through the ring and the host pipe. Once it has reached the reception point (often a second manhole), the cold water is replaced by recirculated hot water for a period of a few hours to cure (heat cured) or an ultraviolet light is passed down the inflated tube (light cured). Whichever technique is used, and several companies offer such a service, the resins and/or geotextile thickness can be de-

signed for the particular job being undertaken. In general, epoxy resins produce superior adhesion with the host pipe, whereas polyester resins have a superior chemical resistance. Liner design is commonly offered by the contracting companies.

A further form of liner that can be installed in small spaces, such as from the base of a manhole, is a spirally wound liner. This type of liner is formed from a continuous strip of plastic, which is ribbed on one side and smooth on the other, and has interlocking edges. The strip is fed into a winding device at the base of the manhole, which produces a pipe by interlocking the edges. The pipe, which is typically 25-mm smaller in diameter than the host pipe (assuming that a reasonably true, intact bore exists), is progressively fed into the host pipe and the annular gap is subsequently grouted using a cementitious grout or polyurethane foam. The winding process produces a ribbed external surface, which adds to the liner strength, and a smooth internal surface. An alternative process was developed that allowed a spirally wound pipe to be formed and inserted as above, but then the liner was wound in reverse allowing the diameter to increase, as the spiral joints slip, with the aid of an expander tool. This allows the liner to come into contact with the host pipe wall and obviates the need for grouting, although grout can be added during the winding process to aid sealing, bonding with the host pipe and resistance to hydrostatic pressure.

The final technique involves a continuous sprayed liner. This can be formed from cementitious mortar or resin. For non-man-entry pipelines a polymer mix can be applied as a thin coating to improve the hydraulic properties of the host pipe, using robotic devices to spray the material. However, this technique is still undergoing commercial development. This type of liner rarely provides significant structural strength. In the case of man-entry pipes, reinforcement can be placed prior to spraying shotcrete or Ferrocement. The reinforced lining in this case is designed for full internal and external load.

19.5 *Practical Application*

In some cases, the range of trenchless techniques now available will prove highly attractive since access cannot be readily gained to the surface. In the majority of cases, however, the engineer is faced with a choice between surface excavation or trenchless construction. In these cases, the engineer must make an appropriate engineering decision based upon both hydraulic and structural considerations and on cost. The hydraulic considerations focus on both the size of the new/replacement pipe and its hydraulic performance in relation to pipes laid by trenching and, where relevant, to an existing pipeline that is being replaced. The structural considerations of the two broad alternatives have been isolated in this chapter and Chapter 18 with respect to the pipeline itself and its immediate surround. In addition the influence of trenchless technology operations on adjacent services and buried structures has been highlighted, as would be the case for traditional tunneling. Similar considerations are necessary for trenching operations, however, although the effects of trenching are often overlooked. For example, trenching or utility cut patching can cause a significant reduction in the life of road pavement structures (Shahin & Crovetti 1987).

The principal considerations for geotechnical engineering in connection with trenchless methods have been introduced in the sections above. It is important to emphasize the need for appropriate site investigation if these techniques are to be used successfully. Problems arise mainly where ground conditions vary significantly along a drive, where "mixed-face" conditions can occur, from unexpected groundwater pressures, and from

the presence of obstructions, whether natural or man-made, or other services already present. The relative importance of these will depend on the type of project and the ground conditions. For example, obstructions may be dealt with relatively easily in a stable face in a pipe-jacked tunnel, but may prevent completion of a microtunneling, moling or ramming operation. However, the same pipe jack encountering a lens of water-bearing sand will suffer face collapse, which may endanger miners and lead to large surface settlements. Thus although trenchless techniques can provide considerable advantages, serious problems such as obstruction or deviation of a drive, or large settlements, can require expensive remedial measures.

Trenchless techniques are often used for crossings beneath rivers and canals, major roads and railways. Conventional ground investigation in such cases may be very expensiveor unacceptable, but the consequences of problems due to unexpected ground conditions may be very serious. Use of directional drilling as a ground exploration technique along the line of a proposed pipe jack might be considered in these circumstances. In other cases, consideration should be given to the use of geophysical methods to interpolate information between boreholes, for instance, on the depth to a sand–clay or soil–rock interface. In urban areas, the ground will often be highly congested with buried services. Underground mapping techniques, such as ground-probing radar and infrared thermography, should be added to the ground investigation program, and the desk study should be as extensive as possible. The site investigation process needs especially careful design since techniques that, for example, recognize cables may not react to plastic water-filled pipelines. In addition, the observational approach involving careful site monitoring should be adopted while construction takes place so that any changes in conditions or unexpected events can be perceived and appropriate action taken at the earliest opportunity.

Trenchless technology is a relatively new subject that is increasingly being introduced into general engineering practice. New trenchless techniques are being developed, the currently available techniques are being refined and confidence in the use of equipment is increasing. The direct costs of trenchless technology are consequently falling and the risk associated with the use of the techniques is reducing. The instinctive decision to dig a trench for even a small-scale construction operation must be reconsidered. The pipeline engineer must therefore weigh carefully the disadvantages and advantages of both trenching and trenchless techniques.

20. COLD REGION ENGINEERING

J.-M. Konrad

20.1 Introduction

Permafrost underlies about one-quarter of the world's land surface and most of the engineering aspect has been well-covered in Andersland & Anderson (1978), Johnston (1981) and Andersland & Ladanyi (1994). This chapter considers more specifically the problems associated with seasonal freezing and thawing of soils in which there is no perennially frozen ground. Frost action may cause extensive damage to buildings, infrastructure such as roads and utility lines and other civil-engineering structures. All such facilities should be designed and constructed to avoid serious functional problems, costly maintenance and unduly short service life. The behavior of soils is strongly influenced by temperature and, therefore, an appreciation of heat transfer in soils is of utmost importance to cold region engineering.

Ground temperatures can be predicted, in principle, if the boundary conditions and the thermal properties of each soil layer are known, especially with available finite element models. It is beyond the scope of this chapter to give details of numerical methods since it is intended to provide basic information about heat transfer in soils and guidance for simplified predictions of frost depth, frost heave and freezing-induced water content increase, and some design mitigations against frost action. Frost heave mechanics is covered extensively to provide the necessary background for the design engineer.

20.2 Thermal Considerations

20.2.1 HEAT FLOW THROUGH SOILS

20.2.1.1 Steady State

Steady state (i.e. time independent) heat flow through homogeneous soils by conduction is given by the Fourier equation:

$$Q_x = -\lambda \frac{dT}{dx} A$$

$$\text{or} \quad q_x = \frac{Q_x}{A} = -\lambda \frac{dT}{dx} = -\lambda T_G \quad (20.1)$$

where Q_x = heat flow in the x-direction per unit time (W), q_x = heat flux (W m^{-2}), λ = thermal conductivity (W m^{-1} K^{-1}), T = temperature (K); x = distance (m), A = area (m^2).

Heat flux is thus proportional to the temperature gradient, T_G, and the proportionality constant is referred to as the thermal conductivity. The negative sign in Eq. 20.1 indicates that heat flow is in the direction of decreasing temperature, i.e., warm to cold.

In homogeneous materials not undergoing phase change, the distribution of temperature at steady state is linear for planar one-dimensional conduction. In layered soils, each with its own constant thermal conductivity, the heat flux normal to the bedding can be computed from:

$$q_x = T_1 - T_2 \Big/ \sum_{i=1}^{n} \frac{d_i}{\lambda_i} \quad (20.2)$$

R. K. Rowe (ed.), *Geotechnical and Geoenvironmental Engineering Handbook*
© Kluwer Academic Publishers 2001

or from

$$q_x = \bar{\lambda}\frac{T_1 - T_2}{D}$$

where $\bar{\lambda} = D/\sum_{i=1}^{n} d_i/\lambda_i$ = the equivalent thermal conductivity. D = the total thickness of the layered system, d_i is the thickness of layer i, T_1 and T_2 = imposed temperature boundary conditions. The temperature distribution is piecewise linear and obeys the following relationship at each interface:

$$\lambda_{i+1} T_{G_{i+1}} = \lambda_i T_{G_i} . \qquad (20.3)$$

The heat flux per unit length for one-dimensional radial heat flow in homogeneous material without phase change is:

$$q_r = 2\pi\lambda(T_0 - T_1)/\ln\frac{r_1}{r_0} \qquad (20.4)$$

where r_0 is the inner radius maintained at a fixed temperature, T_0; and r_1 is the outer radius at a temperature T_1.

The temperature distribution given by Eq. 20.5 is non-linear as heat flows through elements with increasing areas if $T_0 > T_1$ or with decreasing areas if $T_0 < T_1$:

$$T(r) = T_0 - (T_0 - T_1)\ln\frac{r}{r_0}\Big/\ln\frac{r_1}{r_0}. \qquad (20.5)$$

20.2.1.2 Transient State

Transient conduction processes, in which the temperature at a given point varies with time, are commonly encountered in engineering design. They generally fall into two classes: the process that ultimately reaches steady state conditions, and the process in which the thermal boundary conditions change with time.

For a homogeneous material, without phase change, the governing equation of one-dimensional heat transfer is:

$$\frac{\partial T}{\partial t} = \alpha\frac{\partial^2 T}{\partial x^2} \qquad (20.6)$$

where t = time; α = thermal diffusivity = λ/C ($m^2\ s^{-1}$), where C = volumetric heat capacity ($J\ m^{-3}\ K^{-1}$).

Equation 20.6 is analogous to the well-known consolidation equation in which temperature is replaced by pore pressure and thermal diffusivity by the coefficient of consolidation. As for the consolidation problem, solutions for unsteady state heat transfer can be presented in terms of temperature–time charts (Fig. 20.1) using dimensionless

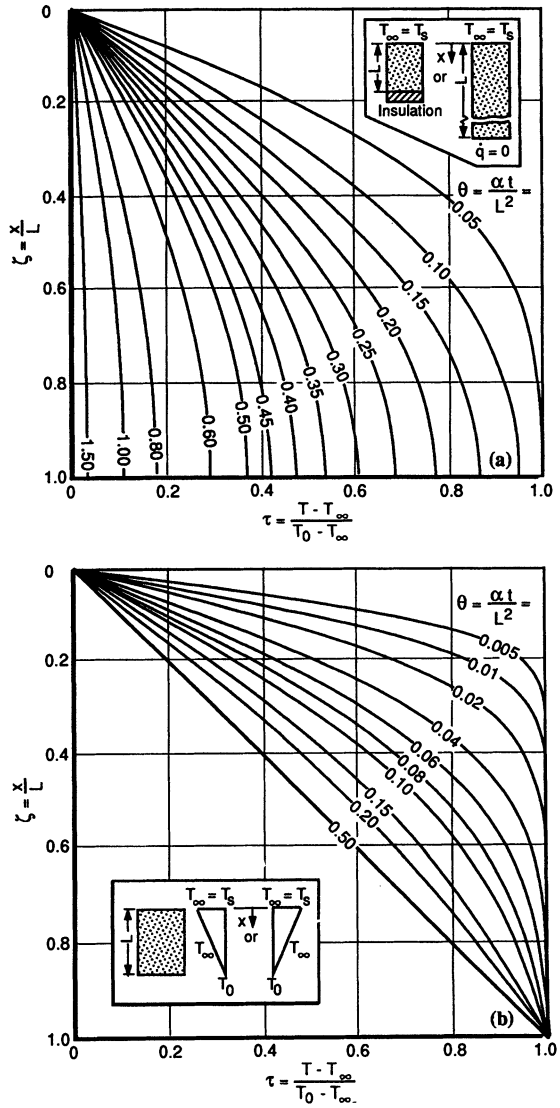


FIGURE 20.1. Temperature–time charts for unsteady heat flow by conduction.

ratios θ, relative time = $\alpha t/L^2$; ζ, relative position = x/L; and τ, relative temperature = $(T - T_\infty)/(T - T_0 - T_\infty)$, where T_∞ represents the temperature at steady state. These charts may be used to evaluate temperature profiles for cases involving conductive heat flow if the following conditions apply: (a) constant thermal diffusivity and no internal heat source; (b) the conducting medium has a uniform initial temperature, T_0; and (c) the temperature at the boundary is changed to a new value, T_∞, for $t > 0$.

In many time-dependent conduction processes actual initial and/or boundary conditions may be more complex than those corresponding to the analytical solutions, geometry may be irregular, thermal properties may be temperature dependent and phase change may be present. Numerical techniques may be used to compute temperature–time distributions using the many available computing codes. This aspect will not be discussed further in this chapter.

20.2.2 THERMAL PROPERTIES OF SOILS AND OTHER MATERIALS

The thermal properties needed for the analysis of thermal problems in soils are the thermal conductivity, the volumetric heat capacity and the latent heat of fusion associated with phase change of interstitial water. In this section, sufficient information on the thermal properties of different materials is provided to enable the reader to apply various analytical methods for calculation of temperature–time distributions.

20.2.2.1 Thermal Conductivity

The thermal conductivity, λ, of soil depends on its density, water content, mineralogy, grain size and temperature. Kersten (1949) has measured the thermal conductivity for a wide range of both frozen and unfrozen soils at different water contents and dry densities, as shown in Fig. 20.2.

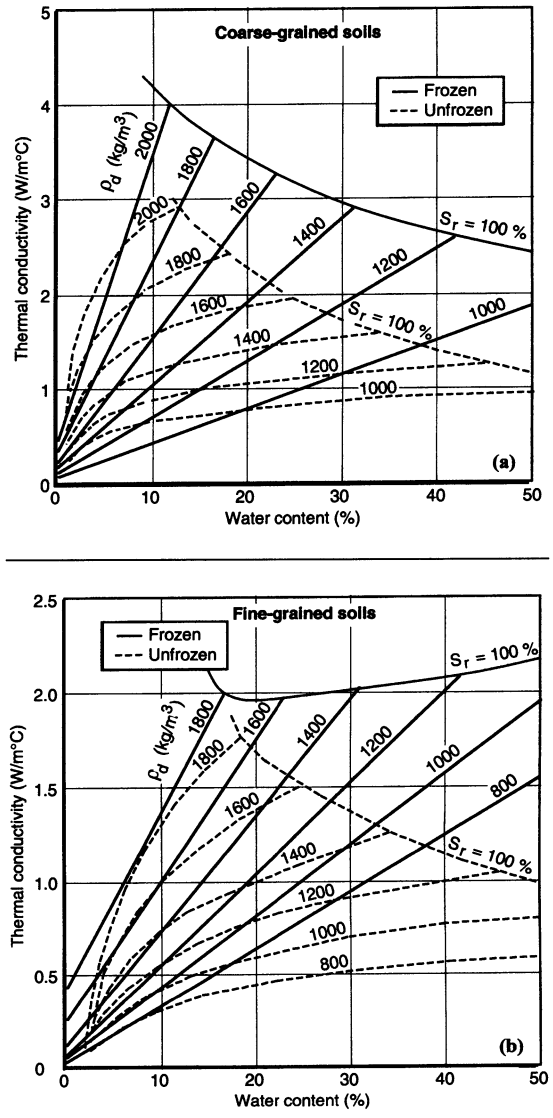


FIGURE 20.2. Thermal conductivity of (a) coarse-grained, and (b) fine-grained soils (modified from Kersten 1949). — frozen, (---) unfrozen.

20.2.2.2 Heat Capacity

The specific heat is defined as the quantity of heat required to raise the temperature of a given material by 1 °C. When expressed on a per unit mass basis, this quantity of heat is referred to as the specific heat capacity, c, and when expressed on a per unit volume basis, it is known as the volumetric heat capacity, C.

For unfrozen soils, the volumetric heat capacity can be estimated from:

$$C_u = c_s\rho_d + \frac{w}{100}c_w\rho_d \qquad (20.7)$$

where c_s = specific heat capacity of soil grains = 800 J kg^{-1} K^{-1} (average value), c_w = specific heat capacity of water = 4200 J kg^{-1} K^{-1}, w = water content (% dry weight), ρ_d = dry density (kg m^{-3}).

For frozen soils, the volumetric heat capacity is estimated from:

$$C_f = c_s\rho_d + \frac{w_u}{100}c_w\rho_d + \frac{w - w_u}{100}c_i\rho_d \qquad (20.8)$$

where c_i = specific heat capacity of ice = 2050 J kg^{-1} K^{-1}, w_u = unfrozen water content (see section below).

The thermal diffusivity, α, which is defined as the ratio of thermal conductivity to volumetric heat capacity, is readily calculated ($\alpha = \lambda/C$). It represents the rate at which a material will undergo a temperature change in response to boundary condition changes.

20.2.2.3 Latent Heat

As depicted on Fig. 20.3, the latent heat of pure water, L, is associated with phase change from solid to liquid. When ice is progressively heated, thermal energy is absorbed by the ice–water system under constant phase change temperature until all ice is melted. Conversely, when water is progressively cooled, thermal energy is released by the ice–water system under constant phase change temperature until all water is frozen. In both cases, the latent heat for water, L, is 334 kJ kg^{-1} or 334 MJ m^{-3}.

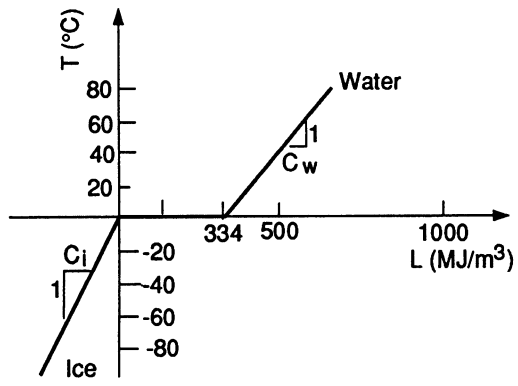


FIGURE 20.3. Thermal energy of water.

For a soil (saturated or unsaturated), the latent heat of freezing or thawing is related to water content as:

$$L_s = \frac{w}{100}\frac{\rho_d}{\rho_w}L. \qquad (20.9)$$

20.2.2.4 Thermal Resistance

The concept of thermal resistance is widely used for characterizing the thermal properties of construction materials such as walls, polystyrene insulation and bricks. The thermal resistance, R, per unit area is defined as the difference in temperature between two surfaces divided by the heat flux between them. It can be viewed as another form of Eq. 20.1 since:

$$R = \frac{\Delta T}{q} = \frac{\Delta x}{\lambda}. \qquad (20.10)$$

R is thus expressed as m^2 KW^{-1} and manufacturers usually also specify Δx.

For instance, extruded polystyrene has a thermal resistance of 0.92 m^2 K^{-1} W for a 25.4-mm thick panel, which yields a thermal conductivity of 0.0254/0.92 = 0.028 W m^{-1} K^{-1}. Table 20.1 presents a summary compiled from various sources (Dysli 1990; Johnston 1981) of thermal properties for materials used by the geopractitioner.

20.2.3 THERMAL BOUNDARY CONDITIONS

20.2.3.1 Generality

Several thermal boundary conditions can be used with the heat conduction equation:

TABLE 20.1. Thermal properties of various materials[a]

Material	λ(W m^{-1} K^{-1})	c(kJ kg^{-1} K^{-1})	C(kJ m^{-3} K^{-1})
Air (20 °C)	0.026	1.00	1.2
Water			
10 °C	0.55	4.22	4217
20 °C	0.60	4.18	4174
Ice			
0 °C	2.24	2.11	1935
−10 °C	2.32	2.03	1865
−20 °C	2.43	1.96	1800
Snow			
ρ = 100 kg m^{-3}	0.06	0.21	210
ρ = 500 kg m^{-3}	0.59	1.05	1050
Minerals			
Quartz	4.8–7.7	~0.75	~2000
Feldspar	1.9		
Biotite	2.0		
Rocks			
Granite	2.9–4.1	~0.80	~2100
Gneiss	2.7–4.6	~0.85	~2200
Quartzite	5.4–8.1	~0.85	~2100
Limestone	1.5–3.3	0.85–2.20	2000–5200
Sandstone	2.3–6.5	0.90–2.00	2200–5000
Mudstone	1.5–3.5	1.00–2.20	2100–4600
Soils (unfrozen, saturated)			
Clays	0.9–1.8	1.4–2.1	2600–3400
Silts	1.2–2.4	1.2–1.8	2500–3100
Gravelly sands	1.2–3.0	1.1–1.8	2400–3000
Peat	~0.6	~3.0	~4000
Common materials			
Steel	70	0.48	3800
Aluminum	220	0.95	2600
Copper	400	0.39	3500
Glass	0.8	0.9	2400
Concrete	1.8	1.10	2600
PVC	0.22	1.50	2000
Bituminous concrete	~1.5	1.0	2300
Insulation			
Polystyrene			
Extruded	0.03–0.04	1.40	40
Expanded	0.05–0.06		
Saw dust			
Dry	0.16		
Unfrozen, saturated	0.30–0.35		
Frozen, saturated	0.60–0.70		
Wood chips			
Unfrozen	0.70–0.85		
in situ, dry	0.18		
Wood bark	0.5		
Straw fibers	0.04–0.05		
Recycled plastic chips			
Laboratory	0.3–0.4		
In situ	0.5		
Tire chips (dry)	0.40		

[a] Moisture pick-up in the field must be considered.

1. Prescribed temperature: this temperature may be constant, or a function of time, or position, or both.
2. No flux across the boundary: according to Eq. 20.1, this condition means that $dT/dx = 0$, or that the temperature profile is normal to the boundary.
3. Prescribed flux across the surface: $dT/dx \neq 0$ and is equal to q/λ.
4. Linear heat transfer at the surface: if the flux across the surface is proportional to the temperature difference between the surface and the surrounding medium: $\kappa(T - T_M)$, where T_M = the temperature of the medium and κ is a constant.
5. Other boundary conditions: such as forced convection, natural convection, non-linear heat transfer and radiation may be used, but will not be discussed herein. Further details may be found in Carslaw & Jaeger (1959).

20.2.3.2 Freezing and Thawing Indices at Ground Surface

The actual thermal boundary condition at the ground surface is best described in terms of a prescribed net heat flux that varies with time both seasonally and daily. In practice, however, the time-dependent net heat flux is difficult to estimate since it results from solar radiation (dependent upon surface reflectivity and orientation, clouds, latitude, season and day), long-wave radiation (dependent upon temperature of surface and surrounding medium, clouds, temperature and humidity gradients in the atmosphere), and air flow over the surface (dependent upon temperature, wind speed, surface roughness and flow regime, evaporation, condensation, evapotranspiration).

Historically, the depth of frost penetration was first estimated by Stefan (1891) for a large water body with the assumptions that the latent heat is the only heat to be removed during freezing and that thermal energy stored as volumetric heat in the frozen zone, i.e. the ice sheet, is neglected. The initial temperature in the water is assumed to be 0°C and constant with depth. Adapting Stefan's solution to a saturated soil at given water content and dry density subjected to a step-freezing temperature, T_s, the equation of continuity at the frozen–unfrozen interface is (Fig. 20.4):

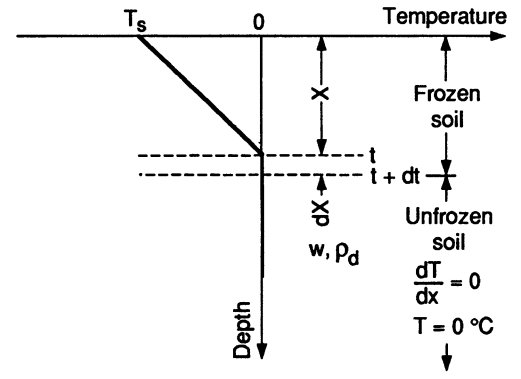


FIGURE 20.4. Simplified temperature profile in Stefan's equation.

$$L_s \frac{dX}{dt} = \lambda_f \frac{T_s}{X} \qquad (20.11)$$

which, after integration, yields the relationship between frost depth and duration of freezing:

$$X = \left(\frac{2\lambda_f T_s t}{L_s}\right)^{1/2} \text{ with } L_s = \frac{w}{100}\frac{\rho_d}{\rho_w} L \qquad (20.12)$$

where X = the depth of frost penetration and t = the duration of freezing.

If the surface temperature varies with time, integration of Eq. 20.11 gives:

$$X = \left[\frac{2\lambda_f \int_0^t T_s(t)dt}{L_s}\right]^{1/2} = \left(\frac{2\lambda_f I_{sf}}{L_s}\right)^{1/2} \qquad (20.13)$$

where I_{sf} = the integral of the surface temperature with time. It is a measure of freezing intensity, referred to as the ground surface freezing index, and is usually expressed in °C-days.

Stefan's simplified approach can also be

used to estimate the thaw depth in permafrost as:

$$X = \left[\frac{2\lambda_t \int_0^t T_s(t)dt}{L_s}\right]^{1/2} = \left(\frac{2\lambda_t I_{st}}{L_s}\right)^{1/2} \qquad (20.14)$$

where I_{st} = the integral of the surface temperature with time and is a measure of thawing intensity, referred to as the ground surface thawing index. It is also expressed in degrees C days. λ_t is the thermal conductivity of the thawed soil. L_s corresponds to the latent heat of the frozen soil and accounts for the actual ice content, which can be significant if segregated ice is present. In areas of seasonal freezing, Eq. 20.14 can be used to estimate the length of the thawing period, given a maximum frost depth computed from Eq. 20.13 as discussed below.

Since air-temperature data are readily available from meteorological stations and ground surface temperatures are not, engineers have established correlations between these two parameters. Furthermore, in practice, the actual surface temperature variations are replaced by the surface freezing and thawing indices. Thus, thermal boundary conditions are usually related to the air-freezing, I_{af}, and air-thawing, I_{st}, indices:

$$I_{sf} = n_f I_{af} \quad \text{and} \quad I_{st} = n_t I_{at} \qquad (20.15)$$

where n_f and n_t = empirical coefficients called the "n-factor" for freezing and thawing, respectively. The magnitude of the n-factors depends on the same factors as those affecting the net heat flux at ground surface. Table 20.2 compiles available data from (US Army 1966; Smith 1986; Dysli 1990).

The extreme range of n-factor values may reflect the range of geographical location, but also of climatic characteristics such as atmospheric relative humidity, solar radiation, precipitation, wind speed, etc. For these reasons, Dysli (1990) proposed to use the following relationship to estimate surface-freezing index from air-freezing index:

TABLE 20.2. Values of n-factors for different surfaces

Surface type	n_f	n_t
Snow	1.0	—
Sand and gravel (probable range for northern conditions)	0.6–1.0	1.3–2.0
Asphalt pavement (free of snow or ice)	0.4–1.0	1.4–2.3
Concrete pavement (free of snow or ice)	0.25–0.95	1.3–2.1

$$I_{sf} = I_{af} - \text{RI} \qquad (20.16)$$

where RI = the radiation index, which can be related to the net global radiation over the freezing period measured by a pyranometer. RI can also be estimated directly from the average length of exposure to sun over the whole freezing period or more crudely from an estimate of exposure to sun (nil, low, medium, high). The relationship presented in Fig. 20.5 is valid for Switzerland and is useful for the design of highways.

Applying the Swiss relationship to North American conditions, say to Quebec City characterized by an average air-freezing in-

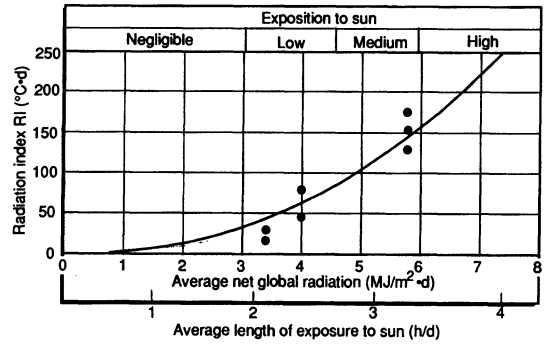


FIGURE 20.5. Radiation index (modified from Dysli 1990).

dex of 1000 °C-days and by about 3 *h* per day of sun exposure from November to April yields a radiation index of 120 °C-days and a surface-freezing index of 880 °C-days. It is usual to consider that n_f = 0.8–0.9 for an asphalt pavement, i.e. I_{sf} is 800–900 °C-days. Both approaches suggest similar values of I_{sf}, but more data on radiation are needed for North America.

20.3 *Ice Formation in Freezing Soils*

When a saturated coarse-grained soil freezes with unimpeded drainage of the excess porewater away from the freezing front, porewater will be changed into pore ice without change in the soil's porosity. However, if the same soil freezes in a closed system, the pore space expands by 9% as water changes into ice. Usually, these soils are referred to as non frost-susceptible.

When a fine-grained-soil freezes, water from the unfrozen soil is attracted to the freezing front where it forms an ice lens causing frost heave well in excess of the 9% original unfrozen pore space increase. These soils are referred to as frost-susceptible.

20.3.1 UNFROZEN WATER CONTENT

When a fine-grained soil is frozen not all the water within the soil pores freezes at 0 °C (Bouyoucos 1916; Lovell 1957). In air-free and solute-free soils, water coexisting with ice is presumed to exist as thin films of adsorbed water and as capillary water that lies outside the range of adsorption forces but fails to freeze because it occupies spaces too narrow to be penetrated by a curved ice–water interface. Several factors govern the phase composition of a frozen soil: specific surface area, temperature, applied pressure, osmotic pressure of the soil solution, pore-size distribution, particle packing geometry, and exchangeable adsorbed ions (Anderson & Tice 1972; Nersesova & Tsytovitch 1963; Anderson & Morgenstern 1973). For a given soil, most of these factors are fixed and the unfrozen water content, w_u, is the amount of liquid water in a soil at a given sub-zero temperature, usually expressed as a percentage of the dry weight of the soil.

Typical unfrozen water content curves are shown in Fig. 20.6 for various soils. In general, significant amounts of unfrozen water exist in clays at temperatures lower than 10 °C, while most of the porewater freezes within a few tenths degree Celsius of zero in silty soils. As for unsaturated soils in which air–water menisci in the pores produce negative porewater pressures (or suctions), the ice–unfrozen water menisci in partially frozen soils also cause negative pressures in the water films.

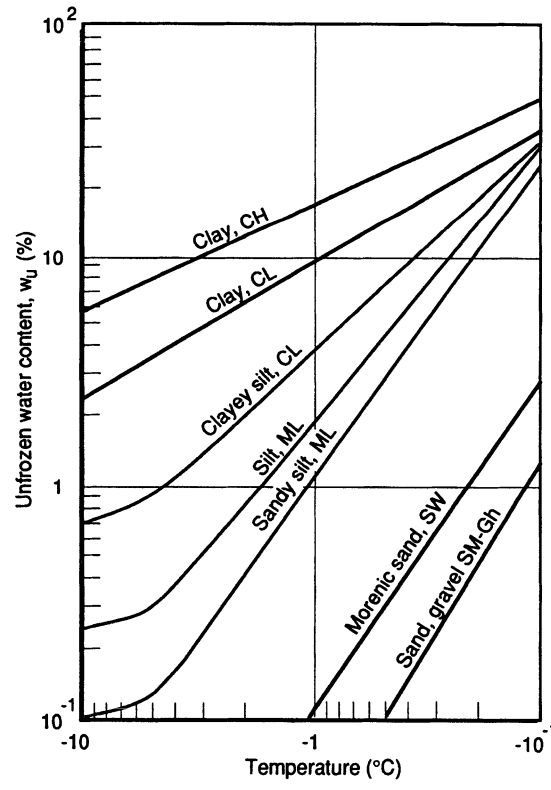


FIGURE 20.6. Typical unfrozen water content–temperature relationships for various soils (modified from Nordal & Refsdal 1994).

20.3.2 WATER MIGRATION AND ICE LENS FORMATION

The fact that not all the water in a fine-grained soil freezes at a unique temperature, but rather over a given range and that it exists in a state of suction, has a significant impact on water migration when a saturated porous medium is frozen under a temperature gradient. Once nucleated, the ice crystals propagate into pore space through the maximum pore-size openings. The highest temperature at which ice can grow in the soil pores is termed the pore freezing temperature, T_p. It is mainly a function of soil type, pressure and solute concentration. In general, the more finer grained a soil, the lower the pore freezing temperature. The pore freezing front is defined herein as the T_p isotherm.

Experimental observations on specimens frozen under a temperature gradient suggest that even though much of the porewater is frozen, water transport still occurs in the frozen soil past the pore freezing front in response to temperature-induced unfrozen water content gradients and suction gradients. The migratory water freezes at the segregation freezing temperature, T_s, which is lower than T_p (Freden 1965; Hoekstra 1969; Penner & Goodrich 1980; Konrad & Morgenstern 1982b). The zone between the pore freezing front, T_p, and the segregation freezing front, T_s, has been referred to as the frozen fringe (Miller 1972).

The hydraulic conductivity in the frozen fringe is related to the amount of unfrozen water and decreases continuously from the pore freezing front to the segregation freezing front. Furthermore, because water flows through the frozen fringe, unfrozen water content is a function of both temperature and suction as outlined in Konrad & Duquennoi (1993). This has serious impacts on the hydraulic conductivity of the frozen fringe, which cannot be considered as a simple soil property.

Figure 20.7 illustrates schematically the hydrodynamic and thermal conditions for a

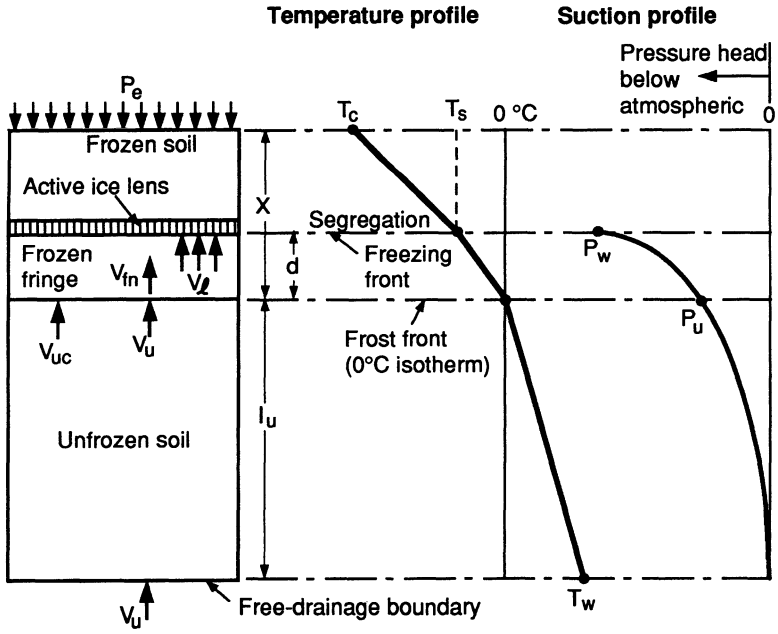


FIGURE 20.7. Schematic of hydrodynamic and thermal processes in freezing soils (modified from Konrad & Seto 1994).

soil freezing under open-system conditions, i.e. with free access to water. Water flowing to the active ice lens may be drawn from three distinct sources:

1. water generated within the frozen fringe, where freezing occurs at invariant porosity and accumulates at the segregation freezing front at a rate v_{fn};
2. water leaving the unfrozen soil as a result of suction-induced consolidation and entering the frozen fringe at a rate v_{uc}; and
3. water from an external supply entering at a rate v_u.

The overall rate of water migration to the active ice lens, v_l is thus the sum of these three distinct fluxes:

$$v_l = v_{fn} + v_{uc} + v_u. \quad (20.17)$$

At the segregation freezing front, the migrating water freezes and the rate of ice lens growth, dh/dt, is readily obtained considering an increase in volume of 9%.

$$dh/dt = 1.09v_l. \quad (20.18)$$

Pore freezing in the frozen fringe without changing the pore volume requires that a given quantity of porewater must be removed as ice forms and is flowing to the ice lens where it freezes. The flux v_{fn} is associated with transient freezing and can be approximated by:

$$v_{fn} = 0.09\varepsilon n dX/dt \quad (20.19)$$

where n = the porosity, ε = a factor taking into account the amount of unfrozen water remaining in the frozen fringe, dX/dt = the rate of frost penetration. The rate of ice lens growth corresponding to this mechanism is:

$$(dh/dt)_{fn} = 1.09v_{fn} = (0.1)\varepsilon n dX/dt. \quad (20.20)$$

This has been known as the heave rate associated with the freezing of porewater of the unfrozen soil solely.

20.3.3 SEGREGATION POTENTIAL OF FREEZING SOILS FOR LABORATORY CONDITIONS

From a phenomenological point of view, frost heave mechanics can be regarded as a problem of impeded drainage in a layered medium to an ice–water interface that exists in the frozen soil at the segregation freezing front. The soil freezing characteristics should therefore be related to the characteristics of the frozen fringe, i.e. the relationship between hydraulic conductivity and unfrozen water content. In view of the complexity of one-dimensional frost heave modeling (Konrad 1994), it appears that precise point measurements of hydraulic conductivity, temperature and suction within the frozen fringe would not ultimately be of direct value in a predictive frost heave model. Instead, representative overall frozen fringe characteristics should be deducible from controlled laboratory freezing tests or from field observations and should constitute adequate input parameters to a general formulation of simultaneous heat and mass transfer in freezing soils.

If the suction-induced effective stresses in the unfrozen soil do not exceed the preconsolidation pressure, it is justified to set v_{uc} to zero in Eq. 20.17 in overconsolidated soils. Furthermore, if freezing is studied near thermal steady state, i.e. at the formation of the final ice lens in laboratory step-freezing tests, v_{fn} is equal to zero and Eq. 20.17 reduces to:

$$v_l = v_u. \quad (20.21)$$

Konrad & Morgenstern (1980) demonstrated that overall frozen fringe characteristics in incompressible soils (high OCR value) can be obtained in the laboratory without detailed measurements at the scale of the frozen fringe. A simple analysis of seepage in the frozen fringe at the onset of formation of the final ice lens in step-freezing tests, i.e. at a rate of cooling close to zero, showed that the porewater velocity entering into the unfrozen soil, v_u, is proportional to temperature gradi-

ent in the frozen fringe provided that the suction at the pore-freezing front is constant:

$$v_u = \frac{P_w - P_u}{d}\bar{k}_f = \left(\frac{P_w - P_u}{T_s}\bar{k}_f\right)T_G = SP(T_G) \quad (20.22)$$

where P_w = suction head at the ice lens (m); P_u = suction head at the frost front (m); $\bar{k}_f$ = overall hydraulic conductivity of the frozen fringe (m s^{-1}).

The constant of proportionality, i.e. the slope of the linear relationship between v_u and the temperature gradient in the frozen fringe, is defined as the segregation potential parameter, SP. Since SP is a parameter that partly reflects the overall hydraulic conductivity of the frozen fringe, which, in turn, is dependent upon the overall unfrozen water content, it is expected that factors affecting w_u will also affect SP.

The segregation potential extended to transient freezing is at least dependent upon the following variables (Konrad 1989a):

$$SP = f(\text{soil type, porosity, OCR, pore fluid, } dT_f/dt, P_u, P_e, N, \ldots). \quad (20.23)$$

The first four factors relate basically to the porous medium subjected to freezing. Soil type includes all the physical properties such as gradation, mineralogy of the fine fraction, specific surface and surface charge density. The porosity, n, reflects the degree of packing of the soil. The overconsolidation ratio, OCR, controls freezing-induced consolidation of the unfrozen soil. Finally, the pore fluid relates to porewater chemistry.

The other factors given in Eq. 20.23 relate to the freezing conditions. The rate of cooling of the frozen fringe, dT_f/dt, is defined herein as the change of temperature per unit time at the frost front and can be calculated (Konrad 1987) as:

$$\frac{dT_f}{dt} = \frac{dT_f}{dX}\frac{dX}{dt} \quad (20.24)$$

where dX/dt = the rate of frost front advance and dT_f/dX = the temperature gradient in the frozen fringe. P_u = the suction head at the frost and P_e = the overburden pressure at the segregation freezing front. Finally, the segregation potential is also affected by the number of freeze–thaw cycles, N (Konrad 1989b).

20.3.4 SEGREGATION POTENTIAL FOR FIELD CONDITIONS

To successfully predict water migration rates in the field using Eq. 20.23, SP must be obtained from laboratory freezing tests on representative samples using representative values of dT_f/dt, P_u and P_e. In the field, small frost penetration rates combined with small temperature gradients in the frozen soil near the frost front result in extremely small rates of cooling of the frozen fringe. The suctions at the frost front are generally very small owing to small water migration rates consistent with relatively small temperature gradients in the field. The overburden pressure at the freezing front can be estimated as a function of frost depth, X, as:

$$P_e = \gamma_f X \quad (20.25)$$

where γ_f = the unit weight of the frozen soil.

These field conditions can be satisfactorily approximated by step-freezing tests on representative samples, i.e. undisturbed, subjected to the range of field overburden pressures. Conditions with small rates of cooling are obtained at the formation of the final ice lens, i.e. when the rate of frost penetration approaches zero. Low values of P_u would be achieved by choosing a warm plate temperature close to 0 °C (about 0.5–1 °C) in order to force the final ice lens to form close to the external water source, hence a relatively small flow path.

It is emphasized that in the field where frost penetration rates may be different from zero during most of the freezing period, water for ice lens growth comes first from the excess water in the pores, $(v_{fn})_{field}$, and if required from the surrounding medium, $(v_u)_{field}$, such that:

$$(v_{fn} + v_u)_{field} = SP_{field}(T_{G_{field}}) \quad (20.26)$$

with $SP_{field} = (v_u/T_G)_{lab}$.

20.3.4.1 SP_{field} from Laboratory Freezing Tests

It is recommended to use undisturbed samples wherever possible so that the factors characterizing the *in situ* conditions (soil structure, void ratio, degree of saturation and pore fluid chemistry) are preserved. If, for economic reasons, it is not possible to justify tests on undisturbed samples, reconstituted soil specimens, preferably overconsolidated, reproducing as close as possible soil structure, water content and porewater chemistry can be used. Figure 20.8 is a simplified flow chart that specifies the type of testing that may be used by the designer to estimate the frost heave parameter operative in the field depending on the stress and thermal history of a natural soil deposit.

Frost heave data are shown on Fig. 20.9 for conditions representative of field freezing. Most of the data were obtained from step-freezing tests. The segregation potential is sensitive to overburden pressure and can be expressed for many soils ranging from sandy silts to clays as:

$$SP_{field} = SP_0 \exp(-aP_e) \quad (20.27)$$

where SP_0 = the segregation potential at zero overburden and a is a soil constant. Since the segregation potential considers the actual temperature boundary conditions, it is not too critical to define a standard test, provided

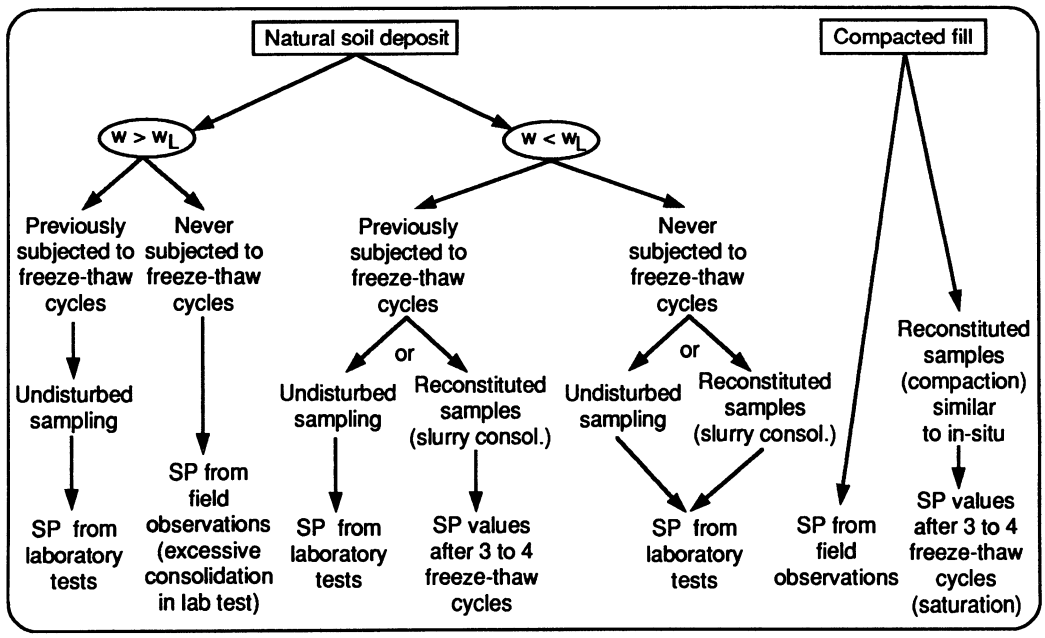


FIGURE 20.8. Flow chart for obtaining representative values of SP field (w/w_L = ratio of water content, w, to liquid limit, w_L).

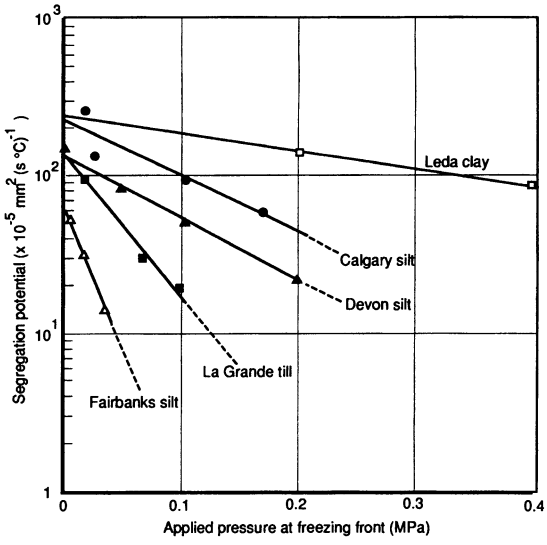


FIGURE 20.9. Segregation potential versus overburden pressure for various soils.

that the test results consider the factors discussed above.

20.3.4.2 SP_{field} from Field Observations

The segregation potential can also be obtained directly from field observations where surface heave and temperature data are available from:

$$SP_{field} = \frac{dh/dt}{1.09T_{G_{field}}}. \qquad (20.28)$$

Figure 20.10 illustrates the procedure for determining SP of a subgrade soil. Frost penetrates through the base material without significant surface heave and enters subgrade soil in early December. During freezing of the subgrade, until reaching a depth of 1.3 m, frost heave rate is relatively constant (0.68 mm per day) and the average temperature gradient in the frozen soil near 0°C is 9.2 °C

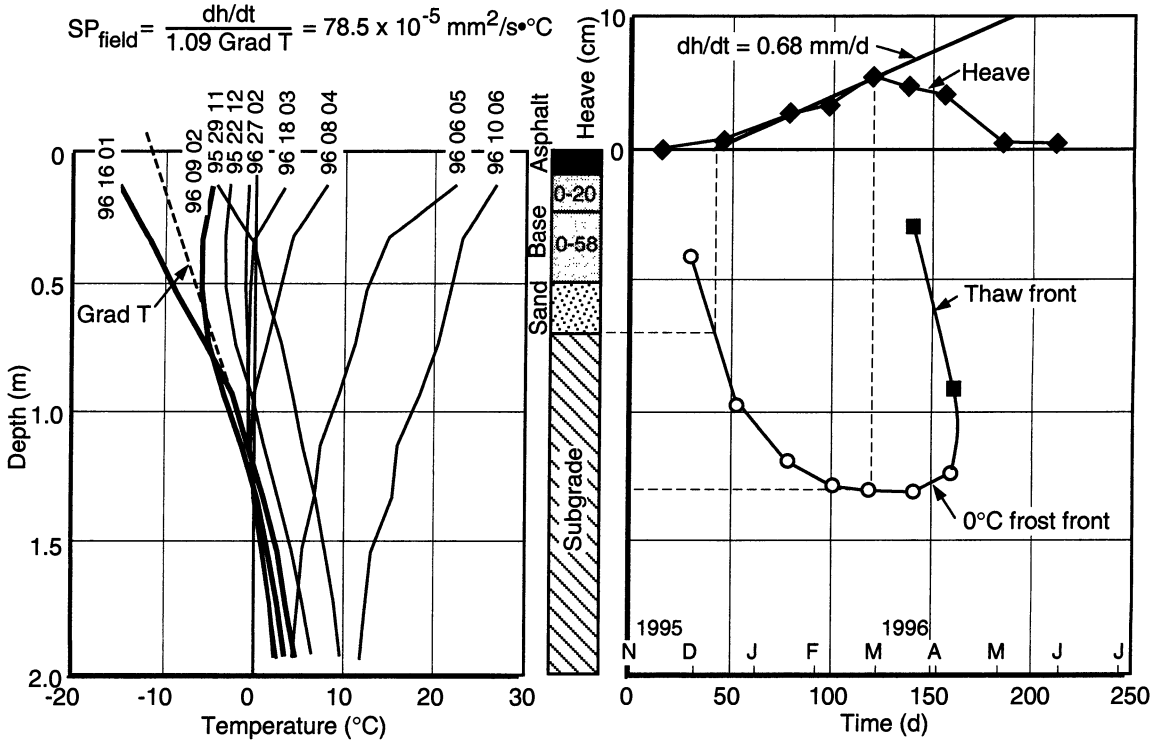


FIGURE 20.10. Segregation potential inferred from field data.

m^{-1}. SP_{field} is thus 0.68/(1.09)(0.0092) = 68 $mm^2\ °C^{-1}$ per day = $79.10^{-5}\ mm^2\ °C^{-1}\ s^{-1}$. This approach is especially recommended in compressible soils such as lightly overconsolidated soft clays and when undisturbed samples are difficult or too expensive to obtain.

20.3.4.3 SP_{field} From Empirical Correlations

An estimate of the SP value for a given soil can also be obtained from empirical correlations. Rieke *et al.* (1983) showed that the frost heave susceptibility increased with increasing percentage of fines, decreasing activity of the fine fraction, and for a specific fine fraction mineralogy, increasing liquid limit of the fine fraction. Recently, Konrad (1998) has shown that SP is best related to d_{50} of the fines fraction (<74 μm), w/w_L (ratio of water content to liquid limit) and mineralogy.

The segregation potential for zero applied pressure can be estimated using the empirical relationship presented in Fig. 20.11. For a ratio w/w_L equal to 0.7, the empirical relationship is best fit by:

$$SP_0(S_S) = [116 - 75 \log d_{50}(FF)] \times 10^3\ mm^4\ °C^{-1}\ s^{-1}\ g^{-1}. \quad (20.29)$$

where $d_{50}(FF)$ is expressed in μm.

Knowing the value of the specific surface area of the fines fraction (FF) SP_0 readily follows. If the soil is at a different water content, it is suggested to apply a correction to SP_0 using the following relationship:

$$SP_0(w) = SP_0 + 9 \times 10^{-3} \log(w/0.7w_L)\ mm^2\ °C^{-1}\ s^{-1}. \quad (20.30)$$

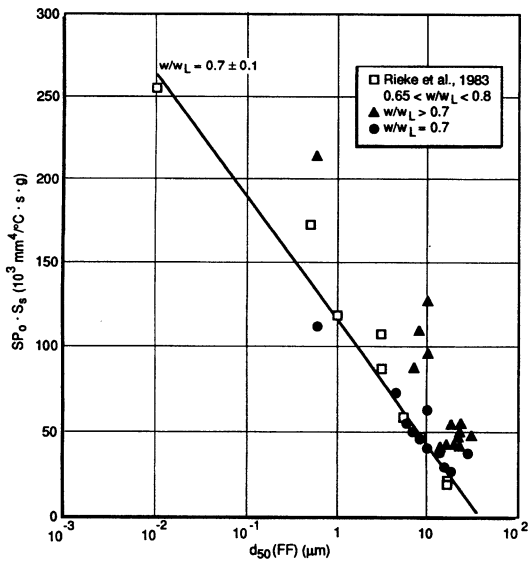


FIGURE 20.11. Empirical relationship between segregation potential and soil index properties (modified from Konrad 1998): ▲, $w/w_L > 0.7$; ●, $w/w_L = 0.7$; □, $0.65 < w/w_L < 0.8$ (Rieke *et al.* 1983).

20.3.5 PREDICTION OF FROST DEPTH IN FROST-SUSCEPTIBLE SOILS

While frost depth in non-frost-susceptible soils is readily estimated with Eq. 20.13, the calculation of frost depth in frost-susceptible soils must account for the release of latent heat associated with the formation of ice lenses. An extension to Stefan's approach yields enough accuracy for practical considerations. Using the segregation potential to quantify the rate of ice formation with Stefan's assumptions gives the modified Stefan equation:

$$X = \left[\frac{2(\lambda_f - SP\ L)I_{sf}}{L_s}\right]^{1/2} \quad (20.31)$$

where SP = the value of the segregation potential in $m^2\ s^{-1}\ °C^{-1}$; L = the latent heat of water, i.e. 334 MJ m^{-3}; λ_f = the thermal conductivity of the frozen soil from Kersten's relationship given in Fig. 20.2, L_s is given by Eq. 20.12 and I_{sf} is obtained as discussed in Section 20.2.3.2.

Worked Example

Calculate the frost depth for a saturated clayey silt characterized with an SP value of $250 \times 10^{-5}\ mm^2\ s^{-1}\ °C^{-1}$ and a water content of 25% in an area where the freezing index at the ground surface I_{sf}, is 1000 °C-days. (NB: For a non-frost-susceptible soil SP = 0.)

Solution: Figure 20.2 gives $\lambda_f = 1.9$ W m^{-1} °C^{-1} = 1.9 J(s m °C)$^{-1}$.

$$\text{SP}\,L = (250 \times 10^{-11})(334 \times 10^6) = 0.835 \text{ J/(s m °C)}$$

$$L_s = (0.25)(1600/1000)(334 \times 10^6)$$

$$= 134 \times 10^6 \text{ J m}^{-3} \text{ (from Eq. 20.12)}$$

$$I_{sf} = 1000 \times 24 \times 3600 = 86.4 \times 10^6 \text{ °C s}$$

and hence from Eq. 20.31:

$$X = \left[\frac{2(1.9 - 0.835)86.4 \times 10^6}{134 \times 10^6}\right]^{1/2} = 1.17 \text{ m.}$$

It is noted here that X represents in fact the thickness of the frozen soil rather than the frost depth because it includes the surface heave due to ice lensing.

Neglecting the latent heat from ice lensing, i.e. using Eq. 20.13, would result in a prediction of frost depth of 1.56 m, i.e. an overprediction of about 30%.

Equation 20.31 always overpredicts the depth of freezing because the volumetric heat component from both the frozen and unfrozen soil is neglected. Furthermore, the heat flow from the unfrozen soil is also neglected. One might consider a dimensionless correction factor, λ^*, dependent on the thermal ratio β and the fusion parameter μ to improve the accuracy of the prediction (Aldrich 1956):

$$X_{corr} = \lambda^* X \tag{20.32}$$

For soils with high water content, λ^* is close to one and Eq. 20.31 is reasonable, especially because it considers ice lensing. For northern climates with high air-freezing indices, β is relatively small and λ^* is larger than 0.9. Equation 20.31 is then also satisfactory. The correction becomes more important, however, in more temperate climates and in relatively dry or well-drained soils. Values of λ^* are given in the *Canadian Foundation Engineering Manual* (CGS 1992).

This simplified approach can also be used efficiently in layered soils, such as highways.

Worked Example

Calculate the frost depth in layered system consisting of a 1-m thick silty sand at a water content of 8% underlain by a deposit of a saturated clayey silt characterized with an SP value of 250 × 10^{-5} mm^2 s^{-1} °C and a water content of 25% in an area where the freezing index at the ground surface, I_{sf}, is 1000 °C-days with a freezing period, t_f, of 130 days. The surface layer is unsaturated and does not result in ice lensing.

Solution: Figure 20.2 gives $\lambda_f = 1.0$ W(m °C)$^{-1}$ = 1.0 J(s m °C)$^{-1}$.

$$L_s = (0.08)(1800/1000)(334 \times 10^6)$$

$$= 48 \times 10^6 \text{ J m}^{-3}.$$

Equation 20.13 can be used to calculate the time required to completely freeze the upper layer:

$$I_{s1} = \frac{D^2 L_s}{2\lambda_f}$$

where I_{s1} is the freezing index for a frost penetration of depth D.

$$I_{s1} = \frac{(1)^2(48 \times 10^6)}{(2)(1)} = 24\,106 \text{ °C s} = 277 \text{ C days.}$$

To transform I_{s1} into a period, it is assumed that the temperature variation is sinusoidal, i.e.:

$$t_1 = \frac{\cos^{-1}(I_{sf} - 2I_{s1})/I_{sf}}{\pi} t_f$$

$$= \frac{\cos^{-1}[1000 - (2 \times 277)/1000]\ 130}{\pi} \tag{20.33}$$

$$= 41 \text{ days.}$$

To calculate the maximum frost depth, use Eq. 20.2 to calculate the equivalent thermal conductivity of the system as:

$$\bar{\lambda} = \frac{X}{(D_1/\lambda_{f_1}) + \{(X - D_1)/[\lambda_{f_2} - \text{SP}(L)]\}} \tag{20.34}$$

and the weighted value of the latent heat of the system as:

$$\bar{L}_s = \frac{L_{s1}D_1 + L_{s2}(X - D_1)}{X}. \tag{20.35}$$

The maximum frost depth is then obtained from Eq. 20.13 with the weighted parameters:

$$X = \left(\frac{2\bar{\lambda} I_{sf}}{\bar{L}_s}\right)^{1/2}. \tag{20.36}$$

Since X is the unknown, it must be obtained iteratively from Eqs 20.34–20.36. The example gives the following results:

$$X = \left(\frac{2\bar{\lambda}I_{sf}}{\bar{L}_s}\right)^{1/2}$$

$$= \left[\frac{2(1.02)1000 \times (86.4)10^3}{7710^6}\right]^{1/2} = 1.51 \text{ m}.$$

The same approach can also be used to estimate the required thickness of a given insulation to prevent undue frost penetration into a frost-susceptible horizon.

Worked Example

Given the previous example, calculate the styrofoam thickness to be placed above the frost-susceptible layer in order to have a frost depth of only 1.15 m. The thermal conductivity of the styrofoam is 0.03 W m^{-1} $°C^{-1}$:

$$\bar{\lambda} = X/(D_1/\lambda_{f_1}) + \{(X - D_1)/[\lambda_{f_2} - \text{SP}(L)]\} + \frac{e}{\lambda_i}$$

and

$$\bar{L}_s = \frac{L_{s1}D_1 + L_{s2}(X - e - D_1)}{X}$$

where X is known.

Solving iteratively gives $e = 0.075$ m.

20.3.6 FROST HEAVE PREDICTION

To predict frost heave in the field, the engineer must first obtain a representative value of the segregation potential at the active ice lens, SP_{field}, as discussed in Section 20.3.4. The frost heave, h, is then calculated from:

$$h = 1.09\int \text{SP}_{\text{field}} T_{G_{\text{field}}} dt \qquad (20.37)$$

where $T_{G_{\text{field}}}$ = the temperature gradient in the frozen zone near the frost front and is obtained by solving the coupled heat- and mass-transfer equations for the specific field problem. Figure 20.12 outlines the procedure for the prediction of one-dimensional frost heave versus time for given thermal conditions. The temperature distribution in the field is obtained either from a numerical approach, from a closed-form solution, from a simplified method as discussed above, or directly from observations at an instrumented site. The temperature gradient in the frozen soil adjacent to the frost front (it approximates the temperature gradient in the frozen fringe) is calculated as a function of time. Knowing the relationship between SP and overburden pressure (laboratory freezing tests, field data or empirical correlations), the rate of water migration to the freezing front is readily computed from Eq. 20.26. Integration over time provides total heave. Often, a simpler calculation by assuming a constant value of $T_{G_{\text{field}}}$ during the freezing yields a good approximation of frost heave. It is noted that heave from expansion of *in situ* porewater is already included in SP_{field} as discussed earlier.

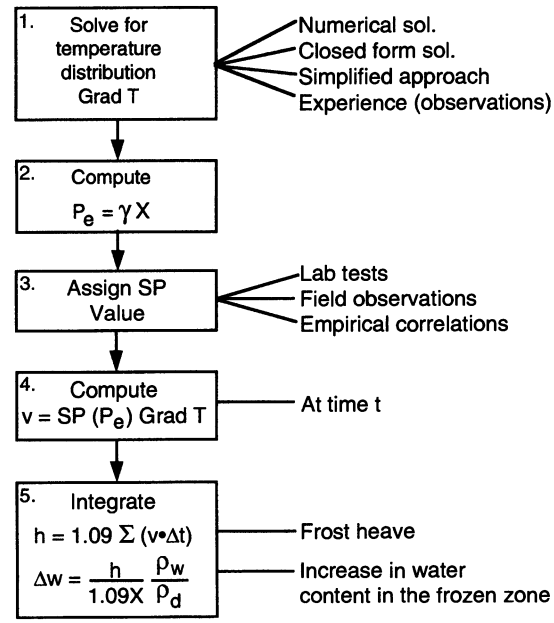


FIGURE 20.12. Methodology for frost heave prediction.

Worked Example

Calculate the amount of frost heave for the layered system examined in the second worked example.

Solution: The average surface temperature is 1000/130 = −7.7 °C, and the average temperature gradient in the frost-susceptible layer is −7.7/(1 + 0.25) = −6.15 °C m^{-1} since the frost depth is about 1.5 m. Surface heave is thus computed using Eq. 20.37 as:

$$h = 1.09 SP_{field} T_{G_{field}} (t_f - t_1)$$
$$= (1.09)(250 \times 10^{-11})(6.15)(89 \times 24 \times 3600)$$
$$= 0.13 \text{ m}.$$

The increase in water content in the frost-susceptible layer can also be calculated as:

$$\Delta w = \frac{1}{1.09} \frac{h}{(X - D_1)} \frac{\rho_w}{\rho_d}$$
$$= \frac{(0.13)(1000)}{(1.09)(1.5 - 1.0)(1600)} \quad (20.38)$$
$$= 0.16 = 16\%.$$

For non-frost-susceptible soils, i.e. no water migration towards the freezing front, frost heave depends on whether excess porewater can be expelled during freezing as would be the case for a thick layer of clean sand or gravel or when excess porewater cannot freely escape as ice enters into the soil pores because of the presence of a clay layer below the sand layer. In the first case, frost heave is negligible, while in the latter frost heave in saturated soils during closed-system is obtained from:

$$h = 0.09(\rho_d/\rho_w) w X \quad (20.39)$$

where X = the thickness of frozen non-frost-susceptible soil.

20.3.7 THAW WEAKENING

With thawing the moisture accumulated during the freezing process is released and generally causes a decrease in suction (porewater pressures may even become positive). As a result, the resilient modulus is reduced and considerable deformation or failure may occur. In highway engineering, considerable work has been done by the US Army Corps of Engineers and the reader may find key references in Cole *et al.* (1986), Johnson *et al.* (1978) and Chamberlain (1973). While the significance of moisture tension in modeling resilient response of soils is well recognized (Bergen & Monismith 1973; Fredlund *et al.* 1975; Brown & Pappin 1981), more attention needs to be devoted to the prediction of moisture content with time under the actual environmental conditions.

Thawing of frozen soil is also associated with volume change leading to thaw settlement and thaw consolidation. Considerable work was done on these aspects by Morgenstern & Nixon (1971) and the reader is referred to the textbooks edited by Johnston (1981) and Andersland & Anderson (1978). A special mention is made for sensitive clays that are highly frost susceptible when subjected to freezing for the first time (excavation, cuts, etc.) since they display significant strength loss during thaw. The undrained shear strength, the thaw consolidation volume change and the strength after consolidation may be related to the initial liquidity index (Leroueil *et al.* 1991).

20.4 Frost Susceptibility of Soils

20.4.1 LIMITATIONS OF EXISTING FROST-SUSCEPTIBILITY CRITERIA

From a survey of more than 100 frost-susceptibility test methods (Chamberlain 1981), it is possible to identify, in general, three levels of sophistication in estimating the frost susceptibility of soils. The first level, type I, methods, are primarily based on the per cent of soil finer than a specified particle size, commonly 0.074 or 0.02 mm. Since frost susceptibility is directly related to unfrozen water content and applied stress and other factors discussed in Section 20.3.3, type I methods cannot successfully yield adequate and reliable decisions.

The second level, type II, methods, are generally based on soil type or classification of particle-size curves, additional soil properties such as Atterberg limits, pore-size distri-

bution, hydraulic conductivity of unfrozen soil, capillary rise, etc. Type II methods, although more time-consuming and costly than type I methods, have limitations as well, since most of the parameters are only partially related to the characteristics of the frozen fringe.

The third level, type III, methods require a laboratory freezing test and/or observations of frost heave and/or thaw weakening and eventually some predictions. Freezing test procedures differ widely and generally provide heave rate values specific to each procedure. Substantial differences in temperature gradient (not always reported in the literature) in the various tests result then, according to Sections 20.3.2 and 20.3.3, to significant variations in heave rate and consequently in apparent degree of frost susceptibility.

20.4.2 RATIONAL EVALUATION OF FROST SUSCEPTIBILITY

The frost-susceptibility criteria described above lead only to the acceptance or rejection of soils without specifying the degree of damage resulting from frost action. Konrad & Morgenstern (1983) have proposed a more rational approach for assessing the relative frost susceptibility of saturated soils. The method is illustrated in Fig. 20.13 and essentially uses the concept of the segregation potential to predict frost heave and/or water (ice) content after freezing for given thermal and geological conditions, but also includes project requirements and acceptable risk. Non-frost-susceptible backfill is thus defined according to the acceptable response during freezing. It should not be specified solely based upon grain-size characteristics, as discussed in Section 20.3.4.3. Water availability is essential for severe frost action. For instance, compaction on the dry side of optimum in backfill material reduces frost heave.

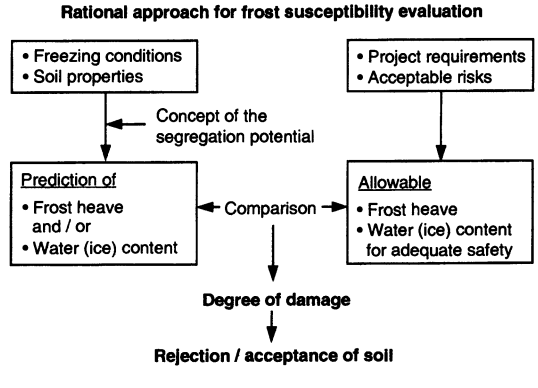


FIGURE 20.13. Rational approach for frost-susceptibility evaluation.

20.5 Frost Action in Civil-Engineering Works

20.5.1 DESIGN CONSIDERATIONS

In cold regions, the design engineer evaluates the following:

1. The thermal boundary conditions, usually associated with the temperature variation in the air, at the structure–air or soil–air interface, as discussed in Section 20.2.3. For design purposes, as recommended by the *Canadian Foundation Engineering Manual* (CGS 1992), it is common practice to use a design air-freezing index, I_{ad}, defined with respect to the mean air-freezing index, I_{am}, as:

$$I_{ad} = 100 + 1.29I_{am}. \qquad (20.40)$$

When historical climatic data are available, the design air-freezing index can also be taken as that of the coldest winter over the last ten year period.

The actual design freezing index at the air–structure or air–soil interface is obtained through the empirical "*n*"-factors outlined in Section 20.2.3.2. The presence of snow must also be considered, using a layered system approach with thermal properties given in Table 20.1.

In artificial freezing, the thermal boundary conditions are usually tempera-

ture conditions imposed by the freezing system and must specify the duration of freezing. In some cases, artificial thaw may also be considered.
2. The geological conditions used to assess the type of soils, the position of the groundwater table and the proximity to other water sources, the drainage paths, stress history, water content and degree of saturation of each soil unit.
3. The geotechnical soil properties, including both physical and thermal properties.
4. The project requirements in terms of allowable deformations (heave and thaw), allowable strength and allowable freezing-induced expansion pressures.
5. The effect of frost action in terms of adfreezing, differential responses under unheated or partially heated appurtenances to a primary structure, temporary excavations in winter subjected to fairly rapid thaw and the formation of frost-induced shrinkage cracks.

20.5.2 FOUNDATIONS

The conventional approach for protection of building foundations against frost action is to locate shallow foundations at a depth greater than the design depth of frost penetration (Eqs 20.13, 20.31 and 20.40). In some cases, thin soil cover may be supplemented with insulating material. A design methodology for insulated foundations has been presented by Robinsky and Bespfug (1973) and given in the *Canadian Foundation Engineering Manual* (CGS 1992).

Moist soil in contact with shallow foundations or piles can freeze to their sides, developing a substantial adfreeze bond. Backfill that is frost susceptible can heave and transmit uplift forces to the foundation. Average adfreeze strengths typically range from 65 kPa for fine-grained soils frozen to wood or concrete to 100 kPa for steel structures (Penner 1974). According to the *Canadian Foundation Engineering Manual* (CGS 1992), it is good practice to backfill against foundations with non-frost-susceptible soil (see Section 20.4). Furthermore, provision should be made for drainage around the foundation perimeter, below the maximum frost depth.

20.5.3 EARTH RETAINING STRUCTURES AND EXCAVATIONS

Earth retaining structures are subjected to many pressure distributions depending on the direction of relative wall movement, drainage and frost action. Horizontally and vertically acting frost heave forces can greatly exceed any earth pressure and may cause cracking and tilting. Experimental data is scarce! Sui *et al.* (1988) have measured horizontal frost heave forces on full-scale retaining walls backfilled with relatively frost-susceptible soils. For a wall height of 1.6 m, the horizontal pressure distribution was trapezoidal with a maximum value of 0.15–0.2 MPa at a depth of about two-thirds of the wall height. Further details are given in Konrad & Shen (1994).

Traditionally, frost protection has been accomplished by using non-frost-susceptible backfill and by placing the foundation below the frost depth. Nordal & Refsdal (1994) have proposed alternative solutions using thermal insulating materials.

Morgenstern & Sego (1981) found a strong correlation between tie-back loads and average air temperature, which can be accounted for by the alternate freezing and thawing of the ground adjacent to the sheet pile wall. Freezing of fine-grained soils around a sheeted excavation may result in an increase in water content in a zone close to the excavation due to ice lensing and frost heave forces. In unsupported excavations subjected to unplanned freezing (late winter–early spring), stability problems may be encountered during thaw, especially in highly frost-susceptible clays.

20.5.4 BURIED STRUCTURES

Utility systems (water, sewage) in cold regions must be operative at all time despite

severe climatic conditions. The reader is referred to the *Cold Climate Utilities Manual* (1986) for details and design methods.

20.5.5 HIGHWAYS

Frost action in highways and urban roads is responsible on the one hand for differential surface movements both in the longitudinal direction and in cross-sections owing to the formation of ice lenses in frost-susceptible soils and on the other hand for the seasonal variations in bearing capacity due to ice melting during thaw, which causes a variation in moisture content with time in the different soil layers. The rational understanding of these frost-induced phenomena requires the prediction of: (a) the amount and spatial distribution of frost heave with time, which is also related to the amount of excess ice in each soil layer; and (b) water content distribution with time as thaw progresses.

The thermal regime of cold regions with freezing indices ranging from 800 to 2000 °C-days generally produces the following features:

1. A frost penetration period of about 3–4 months, in which the frost advance rate is higher in the granular base materials and slower in the frost-susceptible subgrade.
2. Frost depths larger than 1.2 m (depending essentially on moisture content of materials and on frost susceptibility of subgrade soil).
3. A relatively rapid thaw with duration of about 2–3 weeks.
4. Thaw fronts progressing from pavement surface downward and from the base of the frozen subgrade upwards.
5. Occurrence of one or several thaw cycles during the freezing period resulting in shallow thaw beneath the pavement.

20.5.5.1 Frost Heave

The key of a successful frost heave prediction is the use of relevant soil properties. Assuming that both base and subbase granular material are non-frost-susceptible, it can be argued that surface heave depends mainly on the freezing characteristics of subgrade soil. Close examination of the conditions in the subgrade reveals that three distinct zones may be found in the subgrade:

- Zone 1, which is an unsaturated zone if the water table is fairly low.
- Zone 2, which is saturated by capillary action and subjected to negative pore pressures.
- Zone 3, which is a saturated subgrade with hydrostatic pore pressures.

In zone 3, laboratory freezing tests have shown that SP varies with overburden pressure. In zone 2, SP decreases with increasing suction (Konrad & Seto 1994). Field tests confirm the dependence of SP on suction, as shown by Fig. 20.14 for a sandy silt obtained at two sections of the same road with Shelby tubes. At Section A, frost heave rate was 0.3 mm per day with a water table at a depth of 4.0–5.0 m, and at Section B it was 0.48 mm per day with a water table at a depth of 3.0 m. In both cases, water content measurements confirmed that the subgrade was saturated by capillary action. In zone 1, SP varies with degree of saturation. In general, it is acceptable to assume a value of SP close to 0.

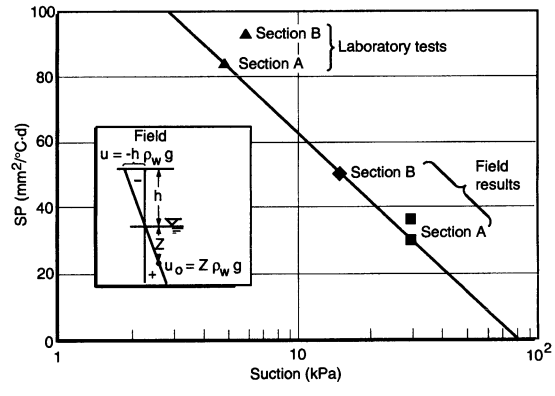


FIGURE 20.14. Influence of suction in a saturated sandy silt.

20.5.5.2 Thaw-Weakening

The existence, in many cases, of two thaw fronts renders the problem more complex than that treated by Morgenstern & Nixon in the early 1970s (1991) for one-dimensional consolidation of thawing permafrost. During and after the thaw period, the pavement design engineer must assess the rate of pore pressure dissipation in the frost-susceptible subgrade and the variation of water content in the subbase and base material with time.

The latter is of utmost importance as the deformation and strength properties are strongly related to the degree of saturation of the granular pavement foundation materials. Soil–water characteristic curves of these materials are required to assess the evolution of stress state and deformation properties with time. Needless to say that pore pressure development during traffic loading depends upon the drainage capacity of these pavement foundation layers; which, in turn, is directly related to the hydraulic conductivity and thus to gradation and type of material as well.

As the lower thaw front retreats upwards and water from the ice lenses is liberated and cannot readily escape owing to the presence of an impervious frozen subgrade barrier, it will carry some of the overburden pressure. Under this pressure gradient, water redistribution occurs into subgrade soil that stayed unfrozen during the whole winter. This water redistribution mechanism leads to an increase in water content of the subgrade that never froze and geotechnical engineers referred to it as swelling. Once, the subgrade is completely thawed, water then migrates in an upward direction and may contribute to further water content increase in the foundation materials before it can drain laterally.

20.5.5.3 Trends in Pavement Design

Pavement design in cold regions is a complex task. Clearly, it is the water content in each layer, including natural subgrade soils, that controls structural deterioration and ultimately failure of a flexible pavement. Since the water content varies with time, pavement design must take into account these variations. In frost-free areas, it is acceptable that pavements are designed as discussed in Chapter 13. However, this may not be sufficient in regions with significant variations in layer properties throughout the year.

A mechanistic pavement design procedure developed by the US Army Corps of Engineers considers critical strains and pavement damage that are calculated daily and assume that damage results are additive over the life of a pavement. To calculate strains at different locations in the pavement structure, it is, however, necessary to consider the actual layers with their respective thickness, water content and properties.

While this pavement design procedure appears quite complex, not necessarily in principles but because many soil properties may be required as input, it is clear that pavement damage will be a function of climate, type of subgrade and its ability to create excess ice in forms of ice lenses, rate of thaw and the ability of foundation material to evacuate excess water liberated at the thaw front and finally of the swelling characteristics of the subgrade. For all these reasons, it is unlikely that standard pavement design may be an optimal solution; rather it is suggested that more geotechnical investigations and engineering be done on each site. Adequate design may be more expensive that standardized design, but it will lead to economy from a long-term perspective since the actual life of the pavement structure is increased.

21. EARTHQUAKE ENGINEERING

W. D. L. Finn

21.1 Introduction

This chapter presents the concepts and procedures used by geotechnical earthquake engineers to design safe structures in a seismic environment. Geotechnical engineers tackle a wide range of problems; establishing design ground motions, the seismic design of foundations, analysis of soil–structure interaction, estimating seismic pressures against retaining and basement walls, evaluation of liquefaction potential, seismic response analysis of earth structures, post-liquefaction behavior of soil structures, evaluating the design of remediation measures and seismic risk analysis for critical facilities such as embankment dams with seismic liquefaction hazard potential.

It is impossible to deal in detail with most of these topics within the confines of a single chapter. In some areas, such as evaluating liquefaction potential and estimating seismic pressures, the key concepts and procedures can be presented compactly. In others, such as evaluating the seismic response of embankments, this is not possible. In these cases, the concepts are explained but for the most part the reader is directed to references for details of the procedures.

There is a limited review of seismological concepts. Seismological reports are the basis for seismic design of any critical project. It is imperative that the geotechnical engineer who will participate in the development of seismic design criteria should be able to understand the basis for the recommendations of a seismological report and be able to appreciate the uncertainties associated with them.

21.2 Seismological Aspects

21.2.1 EARTHQUAKE OCCURRENCE

Earthquakes are generated by the interaction between tectonic plates. These plates move with velocities that are considered constant over geological time. There are two main classes of earthquakes: interplate earthquakes, which occur mainly at the boundaries of the tectonic plates; and intraplate earthquakes, which occur in the interior of the plates far from the boundaries.

Interaction at the plate boundaries determines the characteristics of the interplate earthquake sources. If the plates slide past each other, strike-slip earthquakes occur at fairly shallow depths less than 70 km. An example is the San Andreas strike-slip fault in California, which is the boundary between the North American plate and the Pacific plate. If one plate overrides the other and forces it to bend down into the asthenosphere, a subduction zone develops, which can give rise to earthquakes at a variety of depths. Some of these earthquakes occur in the subducting plate, others in the overriding slab. Large earthquakes are associated with slip between the locked segments of the subducting and overriding plates. On the west coast of Chile, subduction earthquakes have occurred at depths up to 650 km. Finally,

R. K. Rowe (ed.), *Geotechnical and Geoenvironmental Engineering Handbook*
© Kluwer Academic Publishers 2001

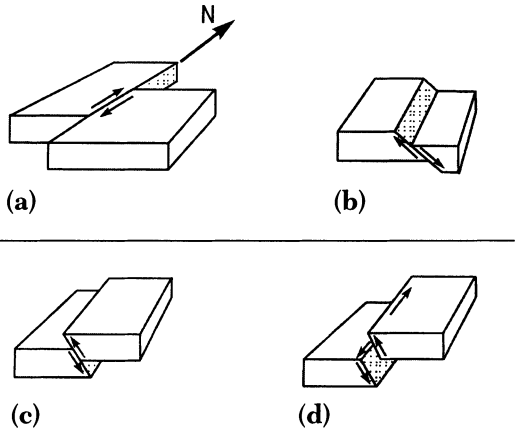


FIGURE 21.1. Various types of faulting: (a) right-lateral strike-slip; (b) dip-slip (normal); (c) dip-slip (reverse); and (d) oblique-slip (left-lateral reverse).

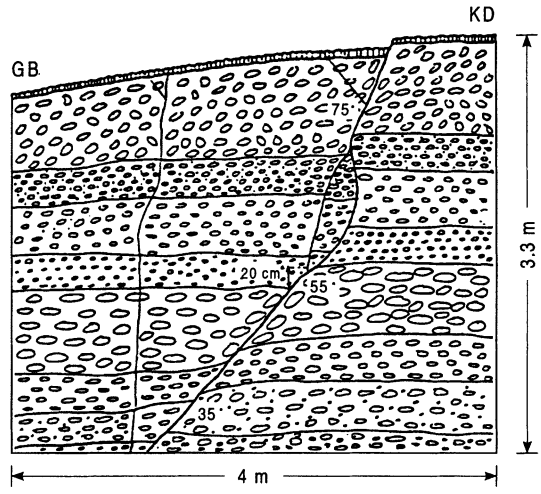


FIGURE 21.2. Offsets in strata caused by past earthquakes (modified from Demirtas *et al.* 1996).

when plates collide head on, very large mountains are created and the potential for very large earthquakes exists. The collision between the Indo-Australian plate and the Eurasian plate created the Himalayas. In this region, design earthquakes with magnitudes up to $M = 8.5$ have been proposed.

Earthquakes are associated with faults (Fig. 21.1), and are described with reference to movement of the fault: strike-slip, normal, reverse and oblique. Each of these types of slip generates its own specific radiation pattern of seismic ground motions (Reiter 1990).

In addition to natural seismicity, earthquakes are also induced by the impoundment of large reservoirs behind dams. Loading the ground surface in this way appears to activate local faults and can generate earthquakes of substantial magnitude. In some instances, earthquakes have also been generated by the pumping of fluids under high pressures back into the geological structures. This type of seismicity is classified as induced seismicity.

There are three sources of seismicity data: instrumental, historical and geological. Because of the limited time frame of instrumental data (about 100 years), historical and geological data play a major part in extending the earthquake record. Historical data are derived from diverse sources, such as inscriptions on stone columns (e.g. in the eastern Mediterranean) and from chronicles and letters (Ambraseys 1988). The use of geological data (called paleoseismic data) is increasing and is becoming routine for major projects involving critical structures. The data on past events are derived from digging trenches across faults and inferring both the magnitude and the date of the events from dislocations and offsets in the sedimentary sequences (Sieh & Jahns 1984). A typical example is shown in Fig. 21.2.

21.2.2 WAVE TYPE

Four principal wave types generated by an earthquake are important in engineering applications. The deformation pattern of the ground during passage of these waves is illustrated in Fig. 21.3 (Bolt 1976). The compression waves, also called P-waves, travel fastest, at about 5.5 km s^{-1} in hard rock. The particle displacements occur along the direction of propagation and create zones of compression and extension as shown in Fig. 21.3a. The shear or S-waves travel at about 3.0 km s^{-1}.

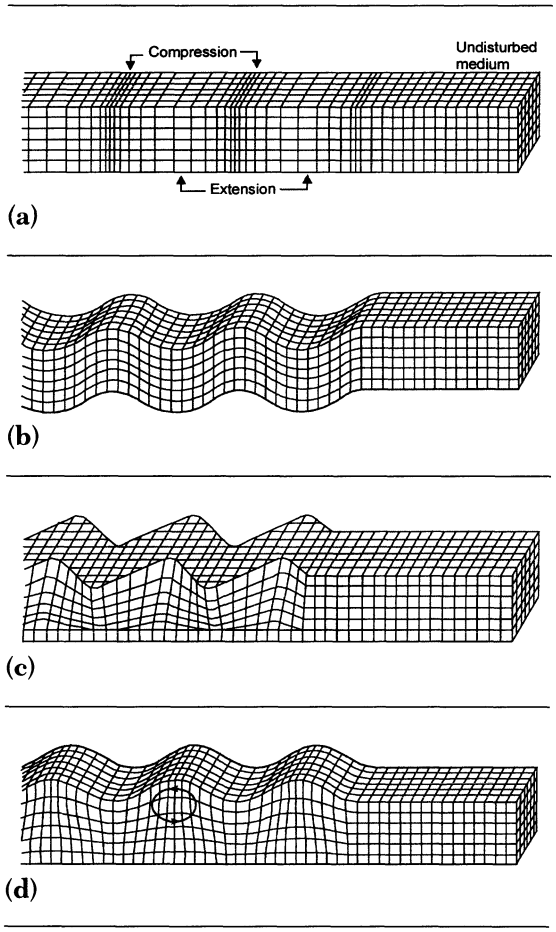


FIGURE 21.3. Deformation patterns of the major wave types (modified from Bolt 1976): (a) P-wave, (b) S-wave; (c) Love wave; and (d) Rayleigh wave.

The particles move normal to the direction of wave propagation, as shown in Fig. 21.3b. The Rayleigh waves travel at about 92% of the speed of the S-waves. The particles describe the retrograde motion shown in Fig. 21.3d. The Love waves (Fig. 21.3c) are surface shear waves with no vertical component, and are slower than Rayleigh waves. The shear waves (S), cause most damage in earthquakes, followed by Rayleigh waves, which tend to have the longest periods and therefore affect long period structures the most.

21.2.3 EARTHQUAKE MAGNITUDE

The magnitude frequently quoted in newspaper accounts of earthquakes is the Richter or local magnitude, M_L. It is defined as "the logarithm to the base 10 of the maximum seismic wave amplitude in thousands of a millimeter recorded on the (standard) Wood–Anderson seismograph at a distance of 100 km from the epicenter," (Richter 1958).

The most commonly used magnitude scales are the surface wave magnitude, M_s, the body wave magnitude, m_b, and the moment magnitude, M_w. M_s is based on the amplitude of (Rayleigh) waves with a period of about 20 s. It is limited to relatively shallow earthquakes <70-km deep and is usually measured at distances of >1000 km from events $M_s \geq 5$. During earthquakes at great depths, Rayleigh waves are not generated well. The body wave magnitude, m_b, is a world-wide scale based on the maximum amplitude in the first few cycles of P-wave motion observed on vertical seismograms. The waves have a period of about 1 s. These waves are best observed at distances greater than 1000 km. The body wave magnitude does not adequately describe the strength of large earthquakes that generate very large fault ruptures because it is based on a relatively short period motion. In eastern North America, a magnitude, m_{Lg}, is used. This scale uses Love waves with a period of about 1 s. In Japan, a different local magnitude, M_{JMA}, is used by the Japanese Meteorological Agency. This is a long period measurement. Since Japanese earthquakes are often used in Western databases, it is important to keep the differences in the definitions of magnitude in mind.

Moment magnitude was developed to achieve a single unified magnitude scale applicable to earthquakes of all sizes, depths and locations. This scale is based on seismic moment, M_0, defined by:

$$M_0 = GAD \tag{21.1}$$

where G = the shear modulus, A = the area of the fault rupture, and D = the average slip between opposite sides of the fault.

The moment magnitude, M_w, is defined as:

$$M_w = (\log M_0 - 16.05)/1.5. \quad (21.2)$$

This magnitude is consistent with other magnitudes over a wide range of magnitudes. It does not saturate as the other magnitudes do that are period dependent. For example, magnitudes based on a 1-s period can reflect properly only the energy release or deformation from faults whose dimensions are of the order of tens of kilometers or less, because their wavelength is about 10 km. M_s, which is based on a period of 20 s and a wavelength of 80 km, cannot fully represent the energy release or deformations from faults whose rupture length is many hundreds of kilometers.

21.2.4 EARTHQUAKE STATISTICS

Gutenberg & Richter (1944), on the basis of world-wide seismicity, developed the linear relationship (G–R line) between frequency of occurrence and magnitude:

$$\log_{10} N(M) = a - bM \quad (21.3)$$

where $N(M)$ = number of earthquakes per year with magnitude greater than or equal to M, and a and b = constants for a given seismic zone. The number N is associated with a given area and time. Alternatively, $N(M)$ can be given by:

$$N(\geq M) = \exp^{\alpha-\beta M} = N_0 \exp^{-\beta M}. \quad (21.4)$$

There is a threshold magnitude, M, below which the occurrence of earthquakes are not recorded completely for a given seismographic layout, population distribution, etc. Fitting the Gutenberg–Richter (G–R) equation to incomplete data (at low end) will flatten the slope of the line and indicate higher occurrence rates for larger earthquakes. Therefore, it is imperative to ensure that any data used to establish the rates of occurrence of earthquakes are complete for the time period under consideration.

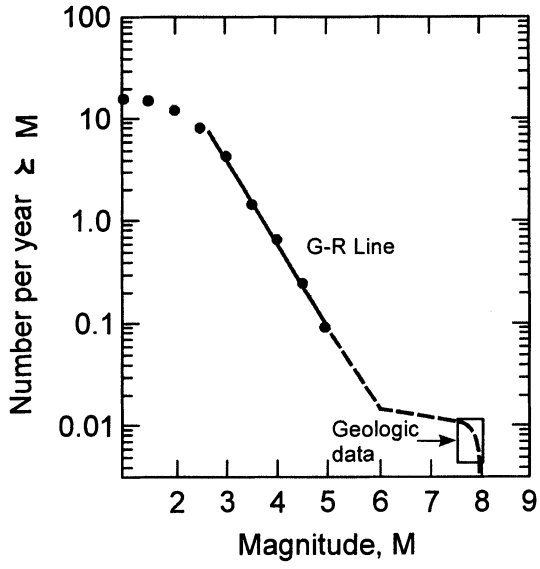


FIGURE 21.4. Earthquake recurrence rates showing G–R line and characteristic earthquakes (modified from Schwartz & Coppersmith 1984).

The G–R equation does not always hold. Some fault segments tend to have many occurrences of an earthquake of a particular size or of earthquakes in a narrow range of magnitudes. These earthquakes are often called characteristic earthquakes, and tend not to lie on the G–R line based on smaller earthquakes. An example is shown in Fig. 21.4.

21.2.5 DISCRETE FREQUENCY OCCURRENCE

It is necessary to know how often an earthquake of a particular magnitude may occur so that its contribution to seismic hazard or seismic risk, such as liquefaction, can be independently assessed. However, it is not possible to deal directly with discrete magnitudes, so the earthquakes are put into bins with magnitude labels, M, but including earthquakes with $M \pm dM$ where dM is arbitrary. The frequency occurrence of the bin magnitudes is given by a discrete frequency relation.

The number of earthquakes in each bin can be calculated as follows. Assuming that the range in magnitude is $dM = \pm 1/4$, the number of earthquakes in magnitude bin M, $n(M)$, is given by:

$$n(M) = N_0\{\exp^{[-\beta(M-1/4)]} - \exp^{[-\beta(M+1/4)]}\} = N_0[\exp^{(\beta/4)} - \exp^{(-\beta/4)}] \exp^{-\beta M} \quad (21.5)$$

yielding the discrete frequency relation:

$$n(M) = N_{0d} \times \exp^{(-\beta M)}. \quad (21.6)$$

21.2.6 EARTHQUAKE SOURCE ZONES

Seismicity of a region is defined by finite source zones each with uniform seismicity, (i.e. with a specified rate of occurrence defined by values of the parameters a and b or α and β in the G–R equation and a specified maximum magnitude). The source zones may be areal sources, line (vertical fault) or inclined plane (dipping fault) sources. Probabilistic seismic hazard analysis is based on these homogeneous source zones.

21.2.7 MAXIMUM MAGNITUDE, M_x

There is an upper limit to the maximum magnitude expected in a given source zone based on historical, geological or tectonic reasons. This entails a curved portion in the frequency of occurrence curves so that the equation can have the form:

$$N(\geq M) = N_0 \exp(-\beta M)\{1 - \exp[-\beta(M_x - M)]\}. \quad (21.7)$$

The factor $\{1 - \exp[-\beta(M_x - M)]\}$ produces a curve giving a smooth approach to zero rate of occurrence at $M = M_x$ in the plotted cumulative distribution (Fig. 21.5).

21.2.8 ESTIMATION OF MAXIMUM MAGNITUDE

The following procedures are among those used to estimate the maximum magnitude:

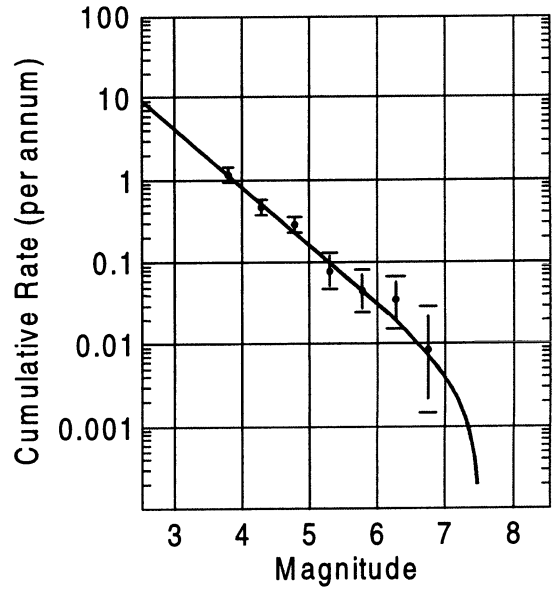


FIGURE 21.5. Magnitude recurrence relation with a maximum earthquake magnitude.

1. Use the largest previous earthquake if the observation period is significantly longer than the return period of the maximum earthquake.
2. Use correlations between maximum fault break and magnitude (Bonilla *et al.* 1984).
3. Estimate maximum magnitudes from plate tectonic models, slip rates, etc.
4. Base magnitude on geological studies, such as trenching to detect past events and strata displacements, or height of fault scarps, etc.
5. In some cases, arbitrary estimates are used: 0.5-magnitude greater than largest known historical event. This approach is typically used when the type of information required for accurate estimates is not available or the cost of acquiring the information, if retrievable, is not justified.

For zones of high seismicity, such as California, the contribution to significant risk at moderate probabilities comes from earthquakes near the estimated maximum magnitude. For zones of low seismicity, such as

eastern North America, the probability of occurrence of earthquakes near the maximum can be much less than the probability being considered in the risk estimate. In these cases, the choice of maximum magnitude may be less important for projects with a time horizon that is short relative to the return period of the maximum earthquake.

21.2.9 MAGNITUDE FROM FAULT BREAK AND FAULT AREA

Various attempts have been made to relate the magnitude of an earthquake to the characteristics of the fault break, such as rupture length and rupture area. Bonilla *et al.* (1984) gave an expression for the surface magnitude:

$$M_s = 6.04 + 0.708 \log L \qquad (21.8)$$

with a standard error, $s = 0.306$. The length of rupture, L, is in kilometers. This equation is based on all fault types. Some authors, such as Slemmons *et al.* (1989), give equations for each fault type.

Other researchers have correlated magnitude with fault rupture area, e.g. Wyss (1979):

$$M_s = 4.15 + \log A \qquad (21.9)$$

where A = the area of the fault rupture surface in square kilometers.

21.2.10 PROBABILITY OF OCCURRENCE

The following basic assumptions are made in estimating the probability of occurrence:

- Earthquake occurrence is independent of space and time.
- The probability density function is given by the Poisson distribution:

$$p(n) = \frac{(Nt)^n \exp(-Nt)}{n!} \quad n = 0, 1, 2, \text{etc.} \qquad (21.10)$$

where N = the rate of occurrence per year for the source, t = the time period under consideration, and $p(n)$ = the probability of n earthquakes occurring in time t. The probability of at least one earthquake occurring is p_e:

$$p_e = 1 - \exp(-Nt). \qquad (21.11)$$

Thus, for example, the probability that an earthquake with a return period of 100 years will occur during 100 years is obtained from Eq. 21.11 using $t = 100$ years and $N = 0.01$, giving $p_e = 63\%$. More generally, the probability of an earthquake occurring within its return period is 63%.

21.3 *Wave Propagation*

21.3.1 ELEMENTS OF WAVE PROPAGATION

Assume the largest wave amplitude, a_m, is associated with a harmonic wave of circular frequency, ω (wave period, $T = 2\pi/\omega$). Since the wave is propagating in space and time, both types of variables must be present in the wave form:

$$a = a_m \sin(\kappa x - \omega t). \qquad (21.12)$$

For a constant wave amplitude, $\sin(\kappa x - \omega t)$ must remain constant, thus:

$$\kappa x - \omega t = C_1$$

$$\kappa \frac{dx}{dt} - \omega = 0 \qquad (21.13)$$

$$\frac{dx}{dt} = V_w = \frac{\omega}{\kappa}$$

where V_w = wave speed and x = displacement in direction of propagation. A similar analysis for spatial period shows that the wave number, $\kappa = 2\pi/L$, where L = wavelength.

21.3.2 STRAINS IN THE GROUND

The strains in the ground caused by the propagating wave may be readily calculated for any wave type using the following procedure. Assume that for a compressive harmonic wave, the particle displacement, y_p, is in the direction of propagation, x, and is given by:

$$y_p = A \sin(\omega t - \kappa x). \quad (21.14)$$

The particle velocity, v_p, is:

$$v_p = \frac{\partial y_p}{\partial t} = \omega A \cos(\omega t - \kappa x) \quad (21.15)$$

therefore:

$$\therefore A \cos(\omega t - \kappa x) = v_p/\omega. \quad (21.16)$$

The strain in the ground, ε_x, is given by:

$$\varepsilon_x = \frac{\partial y_p}{\partial x} = -\kappa A \cos(\omega t - \kappa x). \quad (21.17)$$

Therefore, combining Eqs 21.16 and 21.17 gives:

$$\varepsilon_x = \left(-\frac{\kappa}{\omega}\right) v_p = -\frac{v_p}{V_p} \quad (21.18)$$

where V_p = the compression wave velocity.

The result may be expressed as:

$$\text{Strain} = \frac{\text{particle velocity}}{\text{wave velocity}} \quad (21.19)$$

where particle and wave velocities are in the same direction.

21.3.3 STRAINS IN BURIED PIPES

Strains in buried pipes caused by earthquake shaking are readily calculated if it is conservatively assumed that there is no slip between the pipe and the ground. Thus, for compressional waves along the pipe:

$$\varepsilon_{\text{pipe}} = \varepsilon_{\text{ground}} = \frac{v_p}{V_p}. \quad (21.20)$$

When the wave is propagating at an angle, θ, to a pipeline, the same formula for strain can be employed provided the particle velocity is resolved parallel to the pipe and the apparent wave velocity along the pipe is substituted for the wave propagation velocity. The procedure is explained by means of an example.

Consider compressional wave fronts 1-s apart as shown in Fig. 21.6. From Fig. 21.6, the apparent propagation velocity along the pipe is:

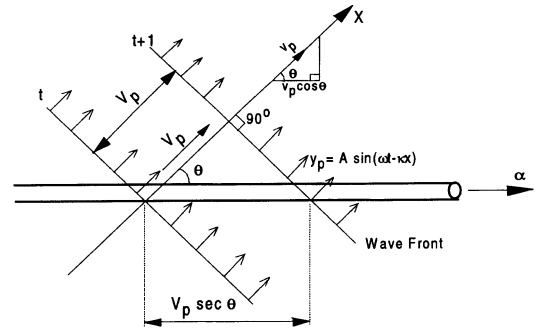


FIGURE 21.6. Compressional wave propagating at an angle θ to the pipeline.

$$V_\alpha = V_p (\sec \theta) \quad (21.21)$$

Particle velocity in the direction of the pipe is:

$$v_\alpha = v_p \cos \theta. \quad (21.22)$$

Therefore, the maximum strain in the pipe is:

$$\varepsilon_\alpha = \frac{\text{particle velocity}}{\text{apparent wave velocity}} = \frac{v_p \cos^2 \theta}{V_p}. \quad (21.23)$$

The axial strain is a maximum at $\theta = 0°$.

When the propagating wave is a shear wave (Fig. 21.7), then the particle velocity is nor-

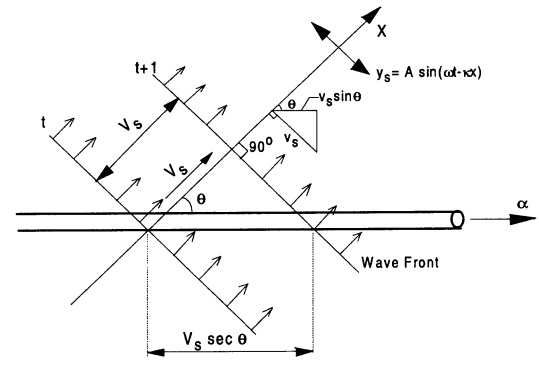


FIGURE 21.7. Shear wave propagating at an angle θ to the pipe.

mal to the direction of propagation and the strain in the pipe, ε_α, is given by:

$$\varepsilon_\alpha = \frac{\text{particle velocity along pipe}}{\text{apparent wave velocity along pipe}} = \frac{v_s}{V_s} \sin\theta \cos\theta. \quad (21.24)$$

The axial strain is a maximum at $\theta = 45°$.

21.4 Design Ground Motions

21.4.1 BASIC ELEMENTS

The simple one-degree-of-freedom system in Fig. 21.8a contains most of the significant elements controlling dynamic response; mass = m, spring stiffness = k, viscous damping coefficient = c, and excitation by ground acceleration = $\ddot{u}_g(t) = d^2u/dt^2$.

The force system for dynamic equilibrium is shown in Fig. 21.8b, where F_D = damping force = $c\dot{u}$, F_S = spring force = ku, F_I = inertia force = $m\ddot{u}(t)$.

Note that the stiffness and damping depend on the relative movement between the structure and the ground. The total displacement of the structural mass $u_t(t)$ = the sum of the ground displacement, $u_g(t)$, and the displacement of the structural mass relative to the ground, $u(t)$:

$$u_t(t) = u_g(t) + u(t). \quad (21.25)$$

The equilibrium equation for the structure is:

$$F_I + F_D + F_S = 0 \quad (21.26)$$

$$m(\ddot{u}_g + \ddot{u}) + c\dot{u} + ku = 0 \quad (21.27)$$

$$\ddot{u} + (c/m)\dot{u} + (k/m)u = -\ddot{u}_g(t) \quad (21.28)$$

$$\ddot{u} + 2\lambda\omega\dot{u} + \omega^2 u = -\ddot{u}_g(t) \quad (21.29)$$

where $\ddot{u}_g(t)$ and $\ddot{u}(t)$ = the accelerations of the ground and of the mass relative to the ground, respectively; $\dot{u}(t)$ = velocity of the mass relative to the ground; $\omega = (k/m)^{1/2}$ natural (circular) frequency; and $\lambda = 0.5c/(km)^{1/2}$ fraction of critical damping or damping ratio. The critical damping above which no free vibration occurs is:

$$c_{cr} = 2(km)^{1/2} \quad \text{or} \quad 2m\omega. \quad (21.30)$$

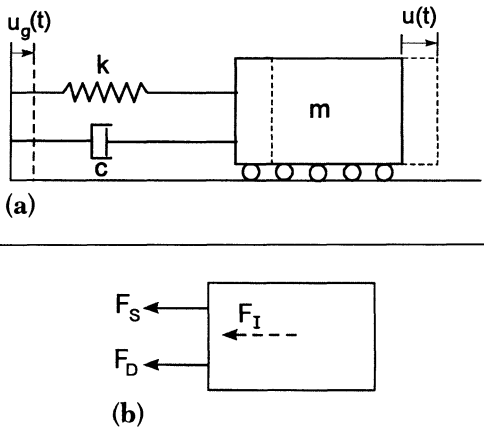


FIGURE 21.8. Simple one-degree-of-freedom system: (a) mass–spring damper system; and (b) free-body diagram.

21.4.2 RESPONSE SPECTRA

The response spectrum of a ground motion parameter such as acceleration, velocity or displacement for a specified level of damping is a plot of the maximum value of that quantity as a function of the frequency or period of a one-dimensional structure under a specific seismic excitation. A good introduction to response spectra is given by Chopra (1981).

Spectra can be computed for peak displacement, peak velocity and peak acceleration. However, peak velocity and peak acceleration spectra are not usually used in design. In practice, spectra are drawn for pseudo-relative velocity (S_v or PSV) and pseudo-acceleration, S_a or PSA. S_v and S_a are defined in terms of S_d, the ordinates of the peak displacement spectrum:

$$S_d = U_{max} \quad (21.31)$$

where U_{max} = the maximum displacement at each period for a constant level of damping:

$$S_v = \omega S_d \tag{21.32}$$

$$S_a = \omega^2 S_d. \tag{21.33}$$

Since S_d, S_v and S_a are all related, they may be plotted on the same chart as a function of frequency or period. Such a plot, for the El Centro earthquake of 1940, known as a tripartite logarithmic plot, is shown in Fig. 21.9. The motivation for defining S_v and S_a, as described above, is as follows. During an earthquake, the maximum elastic energy, E_{max}, is stored in a structure of weight W at peak displacement U_{max} and can be shown to be related to the pseudo-velocity, S_v, not the peak velocity, by $E = (1/2)(W/g)S_v^2$. The elastic base shear in the structure, V_{max} is related to S_a by $V_{max} = (W/g)S_a$.

Different parts of the response spectrum control the seismic behavior of different kinds of structures. Stiff structures with low period (high natural frequency) will be affected most by the acceleration parts of the spectrum. Structures of intermediate frequency will be controlled by the pseudo-velocity part of the spectrum and long period structures will be controlled by the displacement region of the spectrum.

21.4.3 SIMPLE DESIGN SPECTRA

Design is generally carried out using smooth spectral shapes. The peaks and valleys in spectra from real records (Fig. 21.9) cannot be used effectively in design because of the major uncertainties associated with the frequency content of any future motions at the site and the uncertainties associated with the dynamic periods of the structure itself.

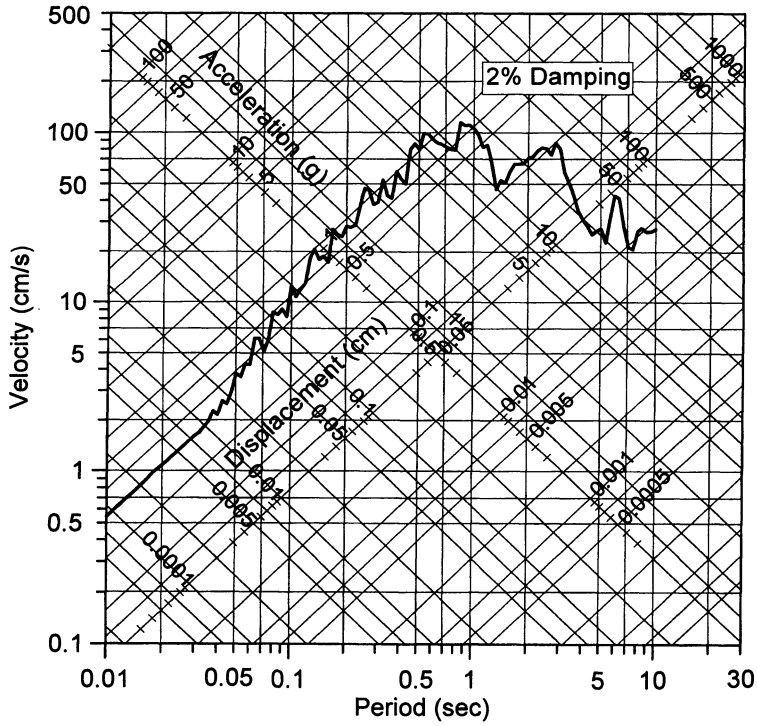


FIGURE 21.9. Logarithmic plot of response spectrum of El Centro corrected accelerogram, 270°, Caltech IIA001.

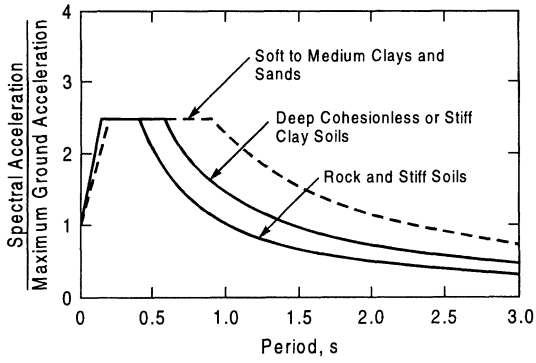


FIGURE 21.10. Normalized spectral curves suitable for use in building codes (modified from Seed & Idriss 1982).

Spectral shapes for use in design are found in the *National Building Code of Canada* (NRCCa,b 1995), and in the US *Uniform Building Code* (ICBO 1997). Some industry organizations such as the American Petroleum Institute have recommended design spectra for use by their members (API 1993).

As an example of design spectra, the spectra proposed by Seed and Idriss (1982) for use in building codes, which are normalized to the maximum ground acceleration, are shown in Fig. 21.10. Spectral shapes can be anchored to acceleration levels established by probabilistic analysis to provide spectra for design of particular projects. These idealized Seed and Idriss spectra are derived from the spectra of ground motions recorded on different soil types.

21.4.4 SITE-SPECIFIC RESPONSE SPECTRA

For important and critical structures, it is usual to develop site-specific design spectra, following procedures described below. Spectra are usually developed for two different levels of motions: operating level events (OLE) and design level events (DLE). The names of these levels of design motions vary with area of application.

Operating level events are usually moderate earthquakes with a high probability of occurring at least once in the life of the structure. The structure is designed to resist these events without any significant damage so that the structure or facility can continue to operate. Design level events are rare large earthquakes. Because of the low probability of occurrence, significant damage is acceptable, but collapse and loss of life must be avoided.

The ground motions for these events can be characterized by response spectra and/or time histories of motion. For critical structures, design is often done on the basis of response spectra and confirmatory dynamic analyses are conducted using ground motions that cover the frequency range of the design spectra adequately.

The development of site-specific spectra involves:

1. Seismotectonic characterization, i.e. seismic source evaluation, source to site attenuation (see Section 21.5) and site evaluation.
2. Seismic exposure assessment: for OLE events probabilistic analysis may be used to help rank the significance of the earthquake sources and to select events that are likely to contribute most to ground motions at a site for a range of spectral periods. In the most general case, near-field, mid-field and far-field events are considered. The selection of DLE events involves a more deterministic approach. Events are often classified as maximum credible events.
3. Ground motion characterization: select and suitably scale ground motion records from earthquakes similar to the design events in magnitude, epicentral distance, types of faulting, site conditions, etc. Estimate the site specific motions by site response analysis using rock input motions if possible. Non-linear analysis is recommended (Schnabel *et al.* 1972; Lee & Finn 1978). The result of these steps is a set of tuned ground motion records for the site and associated response spectra.

4. Design ground motion specification: specify smooth response spectra and associated sets of representative records for dynamic analysis. The smoothed spectra are usually based on the mean or 84% levels obtained from a statistical analysis of the representative ground motion spectra.

Design spectra should not be based solely on a statistical analysis of the response spectra from representative records, though such analyses play a major part. Consideration should be given to the following items before selecting a design spectrum: (a) acceptable level of damage; (b) consequences of failure; (c) method of analysis and associated level of conservatism; (d) uncertainties in material properties; (e) brittleness or ductility of structure; (f) level of damping; and (g) extent and quality of seismic data base, also how well is local seismicity understood and associated with known geologic features.

21.4.5 CONFIRMATORY DYNAMIC ANALYSES

Select a sufficient number of ground motion records representing the range of design ground motions associated with OLE and DLE events to cover the desired frequency range. Most records have significant energy over a fairly narrow band. Thus, no single record in the original group from which the design response spectra were developed contains sufficient energy to be representative over the broad frequency band represented by the design spectrum. For this reason, confirmatory analysis should be conducted using records from the near-, mid- and far-field to match the frequency content of the design spectra.

21.4.6 UNIFORM HAZARD SPECTRA

The design spectra described earlier were derived from earthquake records scaled to peak ground accelerations only. The peak ground acceleration may be selected at a specified probability of exceedance based on a probabilistic seismic hazard analysis.

The probability of exceedance for periods other than that of the peak ground acceleration is unknown. To ensure that the probability of exceedance at any period is the same, a uniform hazard spectrum is used to define the design spectrum. This is developed by conducting a seismic hazard analysis for a specified probability of exceedance of the spectral acceleration (or velocity) over the full range of periods relevant to the design. Recorded earthquake motions are then scaled to match the design spectrum at all periods. This scaling is conducted using computer software such as RASCAL (Silva & Lee 1987). A very lucid explanation of the process of developing spectrum-compatible motions may be found in Clough & Penzien (1993).

The uniform hazard response spectrum leads to a consistent treatment of hazard in the design of structures of different periods. However, no natural earthquake motions would have the spectral amplitude characteristics of the spectrum-compatible motion over the entire spectrum. Using spectrum-compatible motions for predicting non-linear analysis can lead to inflated estimates of seismic displacements (Naeim & Lew 1995).

21.5 Earthquake Ground Motions

21.5.1 GROUND MOTION ATTENUATION RELATIONS FOR CRUSTAL EARTHQUAKES

The basic input to seismic hazard calculations is an estimate of the expected ground motion at a site at a given distance from an earthquake of a given magnitude, usually expressed as moment magnitude. This motion may be characterized by peak ground motion parameters such as acceleration, velocity and displacement, or ground motion spectra. Ground motion attenuation relationships, which define how ground motion parameters decay with distance from the source, are used

TABLE 21.1. Comparison of site classification for attenuation models for shallow crustal events in active regions

Boore *et al.* (1993)	Abrahamson & Silva (1997); Sadigh *et al.* (1997)	Campbell (1997)	Idriss (1990)
Average V_s = 620 m s^{-1}	Rock, shallow soil	Hard rock, soft rock	Rock and stiff soil
Average V_s = 310 m s^{-1}	Deep soil	Firm soil	Deep soil
V_s < 180 m s^{-1}	Soft soil	Soft soil, shallow soil	Soft soil

to provide ground motion estimates for a site. There are many such relationships and as more data become available, existing attenuation relationships are updated. A state-of-the-art assessment of the main attenuation relations in use in North America may be found in a special issue of *Seismological Research Letters* (SSA 1997).

Attenuation relations tend to be regionally specific. For example, in North America, very different attenuation relations are used in the west and the east because of radically different geological and tectonic structures. Relations also tend to be specific with respect to the type of faulting (see Section 21.2.1 for definition of types of faults). Attenuation from subduction sources is different than from strike-slip sources. There are also differences between attenuation from strike-slip sources and reverse or thrust faults.

Attenuation relations may be site-specific in the sense that the relation may be established for a particular soil condition such as rock, soft soil, deep stiff soil, shallow stiff soil, etc. Some attenuation relations define these conditions by means of descriptive adjectives. Boore *et al.* (1993) characterized the site conditions by means of the time averaged shear wave velocity in the top 30 m of the site. Site classifications used in five different attenuation models are shown in Table 21.1.

The characteristics of attenuation relations will be illustrated using the attenuation relation for crustal sources by Boore *et al.* (1997):

$$\ln Y = b_1 + b_2(M - 6) + b_3(M - 6)^2 + b_5 \ln r + b_v \ln \frac{V_S}{V_A} \tag{21.34a}$$

where

$$r = (r_{jb}^2 + h^2)^{1/2} \tag{21.34b}$$

$$b_1 = \begin{cases} b_{1SS} & \text{for strike-slip earthquakes} \\ b_{1RS} & \text{for reverse-slip earthquakes} \\ b_{1ALL} & \text{if mechanism is not specified.} \end{cases} \tag{21.34c}$$

and examples of other parameters are given in Table 21.2.

In this equation, Y = the ground-motion parameter (peak horizontal acceleration or pseudo-acceleration response, g); the predictor variables are moment magnitude, M, distance, r_{jb}(km), and average shear-wave velocity to 30 m, V_s (m^{-1} s). Note that h = a regression parameter.

TABLE 21.2. Smoothed coefficients used to estimate pseudo-acceleration response spectra (g) for the random horizontal component at 5% damping

Period	b_{1SS}	b_{1RS}	b_{1ALL}	b_2	b_3	b_5	b_V	V_A	h	σ_{lnY}
0.000	−0.313	−0.117	−0.242	0.527	0.000	−0.778	−0.371	1396	5.57	0.520
0.200	0.999	1.170	1.089	0.711	−0.207	−0.924	−0.292	2118	7.02	0.502
1.000	−1.133	−1.009	−1.080	1.036	−0.032	−0.798	−0.698	1406	2.90	0.613

The many different definitions of distance, r, from the earthquake source used in attenuation relations are illustrated in Abrahamson & Shedlock (1997). The Boore *et al.* (1997) distance, r_{jb}, is the closest horizontal distance to the vertical projection of the rupture surface. In the case of a vertical fault, this is the same as the distance to the fault break. For dipping faults, the distance can be as low as zero when the source is within the vertical projection of the rupture surface.

The attenuation relation (Eq. 21.34) is valid for earthquake magnitudes ranging from $M = 5.5$ to 7.5 and for distances $D \leq 80$ km. Values of the coefficients in Eq. 21.34 are given for the attenuation of spectral accelerations at periods from 0 to 2 s. The complete table of coefficients is given in Boore *et al.* (1997). A few lines from the table of parameters are given in Table 21.2 to illustrate the structure of such tables. The entries for zero period are the coefficients for peak horizontal acceleration. In Table 21.2, $\sigma_{\ln Y}$ is the square root of the overall variances of the regression, so that the mean plus one σ value of the natural logarithm of the ground motion parameter Y in Eq. 21.34 is $\ln Y + \sigma_{\ln Y}$.

Abrahamson & Silva (1997) have developed attenuation relations valid for periods up to 5 s. These may be particularly useful in developing spectra for tall buildings.

21.5.2 GROUND MOTION ATTENUATION RELATIONS FOR SUBDUCTION ZONE EARTHQUAKES

Youngs *et al.* (1997) provide attenuation relations for horizontal response spectral acceleration (5% damping) for subduction earthquakes applicable to rock and soil sites. These attenuation relationships are considered appropriate for earthquakes with $M = 5$ and greater, and for distances to the rupture surface from 10 to 500 km.

Most attenuation models for subduction zone events are based on recordings from Japan and South America. Most of these events were recorded at large distances. However, recordings were made during the 1985 Michoacan earthquake at distances as small as 13 km, although recordings within 30 km were sparse. Youngs *et al.* (1997) show that peak ground motions from subduction zone earthquakes attenuate more slowly than those from shallow crustal earthquakes and that intraslab earthquakes produce larger peak ground accelerations than interface earthquakes for the same magnitude and distance. However, the database contains a very limited number of intraslab recordings.

21.6 *Effects of Soil Conditions on Ground Motion*

A number of factors contribute to the amplification of incoming rock motions at soil sites. The first important factor is the relative stiffness between the soil and the rock. This is usually characterized by the impedance ratio, ζ. The impedance of a soil layer is the mass density multiplied by the shear-wave velocity of the material. Therefore, the impedance ratio $\zeta = \rho_s V_{ss}/\rho_r V_{sr}$, where ρ = the mass density, V_s = the shear-wave velocity, and S and R refer to the surface layer and underlying rock, respectively.

For example, consider a uniform elastic undamped surface layer. If the incoming wave motion in the bedrock from the source is a harmonic wave and has the same period as that of the elastic surface layer, then the amplification of the motion in the surface of the soil layer according to Okamoto (1973) is:

$$A = 2/\zeta. \tag{21.35}$$

This amplification includes the effect of impedance, resonance and the doubling of the motion at the free surface. If there is no surface layer of soil, then the amplification of the incoming motion at the surface of the layer is $A = 2$.

In the above example, the incoming mo-

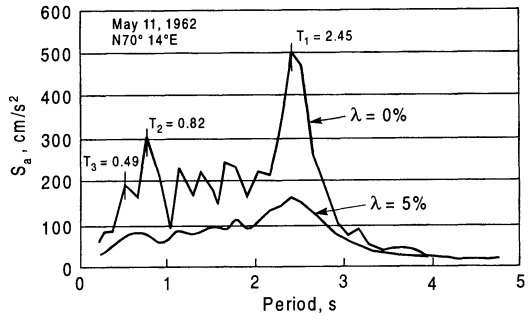


FIGURE 21.11. Pseudo-acceleration spectrum, Alameda Park, May 11, 1962.

tions were assumed to have the same period as the surface layer of soil. Now consider how the periods of the surface layer are manifested in recorded ground motions. The natural periods, T_n, of a uniform elastic layer of thickness H and a shear-wave velocity of V_s are:

$$T_n = (4H/V_s)/(2n - 1) \quad n = 1, 2, \text{etc.} \qquad (21.36)$$

The ratios between the individual periods of the layer are:

$$T_1 = (4H/V_s),\ T_2 = (1/3)T_1,\ T_3 = (1/5)T_1, \text{ etc.} \qquad (21.37)$$

This relationship may be seen clearly in the ground response at Alameda Park in Mexico City during an earthquake in 1962. The ground motions are characterized in Fig. 21.11 by the response spectrum for pseudo-acceleration. The zero damping spectrum is used to clearly define the peaks. Significant peaks in the spectrum are associated with the natural periods of the ground. Note the location of T_1, T_2, T_3, etc., and that they have the relation to each other close to that described above.

In Fig. 21.11, the response spectra are shown for different damping ratios. Even a modest 5% damping, which would not be untypical of structures undergoing reasonable strong motion without damage, reduces very significantly the response of the structure. Therefore, there are three important factors controlling the effects of surface layers on ground motion: (a) the impedance ratio, ζ; (b) the relationship between the high energy periods of the bedrock motions and the periods of the surface layer; and (c) the amount of damping in the soil layer.

21.6.1 NON-LINEAR SOIL BEHAVIOR

The amplification of the softer sites during the Loma Prieta earthquake was studied by Idriss (1990), and he provided the amplification chart shown in Fig. 21.12, which gives the amplification of the ground motions at the surface with respect to rock or firm ground. The greatest amplifications occur at the lower accelerations. At accelerations higher than 0.4g, the motions are attenuated at the site. This is due to the fact that the stiffness and damping of the soft soils are strain-dependent. Under very strong shaking, the stiffness is reduced substantially and the damping is increased. The net effect for strong shaking is to reduce the amplitude of the high–medium frequency ground motions. The strengths of the weak soils, of course, impose a definite limit on the maximum acceleration that can be transmitted to the surface. Accelerations cannot generate

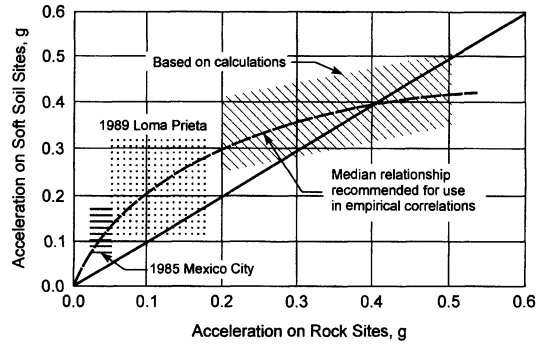


FIGURE 21.12. Amplification of ground motions in soft soils (modified from Idriss 1990).

shearing stresses in excess of the strength of the soil under dynamic loading conditions.

21.6.2 SITE CLASSIFICATION-BASED AMPLIFICATION FACTORS

For any given uniform site, the impedance ratio is fixed and the level of response will depend heavily on the correspondence between the site periods and the periods of the incoming motion. The fundamental site period is given by $T = 4H/V_s$. Therefore, the period, and hence, the response to a given input motion, depends on the thickness of the layer and the shear-wave velocity. For layers of equal thickness, the shear-wave velocity accurately reflects the period. Furthermore, if the differences in mass densities between rock and surface layer are neglected, the shear-wave velocity is also an index of relative impedance.

These ideas have led to a new way of characterizing sites for estimating the potential amplification of earthquake motions. The time-averaged shear-wave velocity in a constant thickness layer comprised of the materials in the top 30 m of a site is taken as an index of potential site amplification. This procedure has been adopted by the US National Hazards Reduction Program (NEHRP) for characterizing sites for code purposes.

The classification of sites based on V_s is shown in Table 21.3 (FEMA 1997). Because the shear-wave velocity may not be known in a given area, or may not be measured at a particular site, alternative indices of amplification that correspond to the shear-wave velocity criteria are also used. These are the average standard penetration resistance, $\bar{N}$, for cohesionless soils, and the average undrained shear strength, $\bar{s}_u$, for clays in the top 30 m of the geological profile at the site (see Section 4.4.6 for a discussion of how N and s_u are obtained in the field).

TABLE 21.3. Site classification[a]

Site class	Site-class name/generic description	Site-class definition
A	Hard rock	$\bar{V}_s > 1500$ m s^{-1}
B	Rock	$760 < \bar{V}_s \leq 1500$ m s^{-1}
C	Very dense soil and soft rock	$360 < \bar{V}_s \leq 760$ m s^{-1}, or with either $\bar{N} > 50$; or $\bar{s}_u \geq 100$ kPa
D	Stiff soil	$180 < \bar{V}_s \leq 360$ m s^{-1}, or with either $15 \leq \bar{N} \leq 50$; $50 \leq \bar{s}_u \leq 100$ kPa
E	A soil profile with	$\bar{V}_s < 180$ m s^{-1}, or with either $\bar{N} < 15$; or $\bar{s}_u < 50$ kPa
	Or	
	Any soil profile with	More than 3 m of soft clay defined as soil with PI > 20, $w \geq 40\%$, and $s_u < 25$ kPa
F	F_1: soils vulnerable to potential failure or collapse under seismic loading such as liquefiable soils, quick and highly sensitive clays, collapsible weakly cemented soils	
	F_2: peats and/or highly organic clays ($H > 3$ m of peat and/or highly organic clay where H = thickness of soil)	
	F_3: very high plasticity clays ($H > 8$ m with PI > 75)	
	F_4: very thick "soft/medium stiff clays" ($H > 36$ m)	

[a] Exception: when the soil properties are not known in sufficient detail to determine the site class, class D shall be used. Site classes E or F need not be assumed unless the authority having jurisdiction determines that site classes E or F could be present at the site or in the event that site classes E or F are established by geotechnical data.

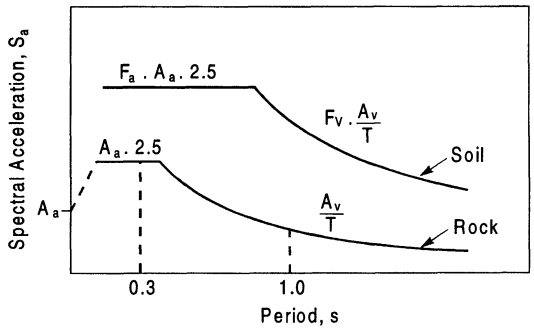


FIGURE 21.13. Development of design spectra using period-dependent site amplification factors (modified from Martin & Dobry 1994).

21.6.3 NEHRP PROVISIONS

NEHRP adopted the spectral shape for site class B (Table 21.3), shown in Fig. 21.13 as the basis for design. The spectrum is constructed using spectral values at periods of $T = 0.3$ and 1.0 s. At $T = 0.3$ s, the spectral value is $2.5A$, where A is the effective site acceleration at the appropriate probability of exceedance. Similarly, the spectral value at the period $T = 1.0$ s is the value with the appropriate probability of exceedance. The curved part of the spectrum varies as $1/T$.

NEHRP adopted two site coefficients for constructing free-field acceleration response spectra for soil sites from the given rock spectrum as shown in Fig. 21.13. The coefficient F_a is used for the short period motion and the coefficient F_v for the longer period motion. Together the factors are intended to cover the period range 0.2–3.0 s.

These site coefficients are a function of site class and intensity of shaking, specified by spectral acceleration. The five different general site classes, A–F, are given in Table 21.3. Site specific geotechnical investigations and dynamic site response analyses are recommended for soils falling into class F.

The values of the site coefficients, F_a and F_v, appropriate for the different site classes and the different levels of shaking were drawn from the results of hundreds of site response analyses using both equivalent linear and non-linear methods. The analyses were all calibrated first on data from the 1989 Loma Prieta earthquake. Variations in the values of the site coefficients, F_a and F_v, reflect the non-linear response of soil to strong shaking. Hence, they become smaller as the acceleration increases. Values of F_a are given in Table 21.4, and of F_v in Table 21.5, for different levels of peak ground accelerations. The values for F_a are mean values. The values of F_v were highly variable depending on site conditions and input motions. Therefore, F_v values are given at the mean plus one standard deviation level. For more detailed discussion of foundation factors see Finn (1995).

TABLE 21.4. F_a as a function of site class and earthquake spectral acceleration, S_a, at 0.3 s

	Spectral response acceleration at 0.3 s[a]				
Site class	$S_s \leq 0.25$	$S_s = 0.5$	$S_s = 0.75$	$S_s = 1.00$	$S_s \leq 1.25$
A	0.8	0.8	0.8	0.8	0.8
B	1.0	1.0	1.0	1.0	1.0
C	1.2	1.2	1.1	1.0	1.0
D	1.6	1.4	1.2	1.1	1.0
E	2.5	1.7	1.2	0.9	[b]
F	[b]	[b]	[b]	[b]	[b]

[a] Use straight-line interpolation for intermediate values of S_s.
[b] Site-specific geotechnical investigation and dynamic site response analyses are recommended.

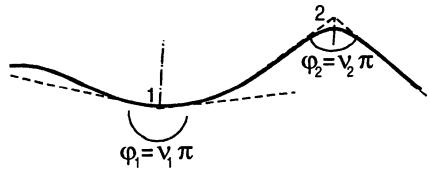
TABLE 21.5. F_v as a function of site class and spectral acceleration, S_a, at 1 s period

	Spectral response acceleration at 1 s period[a]				
Site class	$S_s \leq 0.25$	$S_s = 0.5$	$S_s = 0.75$	$S_s = 1.00$	$S_s \leq 1.25$
A	0.8	0.8	0.8	0.8	0.8
B	1.0	1.0	1.0	1.0	1.0
C	1.7	1.6	1.5	1.4	1.3
D	2.4	2.0	1.8	1.6	1.5
E	3.5	3.2	2.8	2.4	[b]
F	[b]	[b]	[b]	[b]	[b]

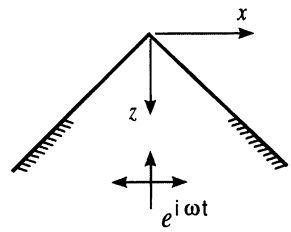
[a] Use straight-line interpolation for intermediate values of S_s.
[b] Site-specific geotechnical investigation and dynamic site response analyses are recommended.

21.6.4 EFFECTS OF TOPOGRAPHY

Aki (1988) used the simple structure of a triangular wedge (Fig. 21.14a) to illustrate the effects of topography. This structure may be used to model approximately ridge–valley topography as shown in Fig. 21.14b by Faccioli (1991). An exact solution exists for the wedge for SH waves propagating normal to the ridge and polarized parallel to the ridge axis. Displacement amplification at the vertex is $2/\nu$ where the ridge angle is $\nu\pi$ ($0 < \nu < 2$). In Fig. 21.14a, the amplification of the crest relative to the base is ν_1/ν_2. Thus the simple solution provides a rough estimate of the relative amplification at the crest of the ridge or de-amplification in a valley.



(a)



(b)

FIGURE 21.14. (a) Approximating a ridge formation by a triangular wedge, and (b) infinite wedge excited by plane SH waves (modified from Faccioli 1991).

Amplification of motions at the crest of a ridge relative to the base is also supported by damage patterns during the 1980 Fruili earthquakes in Italy (Brambati *et al.* 1980), the Chilean earthquake of 1985 (Celebi 1987, 1991), the 1985 Loma Prieta earthquake and the 1994 Northridge earthquake.

21.6.5 MOTIONS IN SEDIMENTARY BASINS

Surface waves have been recorded by strong-motion instruments at sites in deep sedimentary basins. These waves arrive later than the shear body waves and have periods in the general range of 3–10 s. At some sites the largest amplitudes at long periods may be due to surface waves.

Sediment filled basins are usually the locations of greatest residential and industrial development. Ground motions on these sites generated by shear waves propagating vertically are usually estimated by one-dimensional shear beam models, using either equivalent linear methods (Schnabel *et al.* 1972) or nonlinear models (Finn 1988; Lee & Finn 1978). Body waves trapped in the basin may amplify the motion and increase the duration over that

predicted by one-dimensional analysis. These effects were very pronounced in the 1985 Mexico City and 1994 Northridge earthquakes.

Ground motion estimations near the edges of sediment-filled valleys require two- and three-dimensional analysis in order to ensure that the surface waves appear in the computed responses (e.g. Graves *et al.* 1998).

The effects of surface topography and sediment-filled valleys on site response have been summarized by Silva (1988).

21.6.6 NEAR-FAULT EFFECTS

Large velocity pulses have been noted in ground motion recordings near faults where the motions have propagated towards the recording station. The conditions that give rise to this directivity effect have been reviewed by Somerville & Graves (1996).

Somerville (1998) suggested that the directivity effects in the near-fault region of strike-slip faults may not be adequately represented in empirical ground motion attenuation relations. This is especially true of relations that use an average of the two horizontal ground motion components, since the fault normal motions may be up to 1.5 times the average motion. Data from the Kobe earthquake (Finn *et al.* 1996) confirm that potential directivity effects should be taken into consideration in estimating design loads in the near field.

21.7 Seismic Soil–Structure Interaction

Seismic soil structure interaction has the following beneficial effects: (a) the period and damping of the vibrating structure are increased; (b) energy can flow from the vibrating building back into the soil; (c) uplift of foundation slab reduces forces transmitted to building; (d) large foundation slabs can reduce the high frequency motions and hence reduce the input motions to the structure; but (e) rocking increases the relative displacements and hence can increase overturning moments (called the P–δ effect).

The NEHRP *Recommended Provisions for Seismic Regulations for New Buildings and Other Structures* proposed in March 1997 (FEMA 1997) give approximate methods for calculating the damping and period of a building on a flexible foundation soil. Based on these parameters, a reduction in the seismic base shears for the rigid base structure is allowed. The procedures are somewhat complicated and cannot be conveniently summarized here.

21.7.1 KINEMATIC AND INERTIAL SOIL–STRUCTURE INTERACTION

Soil–structure interaction may be classified into two types: kinematic and inertial interaction. Kinematic interaction describes the modification of the ground motions by the structure due to its stiffness only. The additional modifications of ground motions introduced by the accelerating mass of the structure is attributed to inertial interaction.

The effects of kinematic interaction are produced by the scattering and reflection of incident waves from the foundation. These secondary motions modify the free-field ground motions to produce resultant ground motions at foundation levels that may be significantly different from the free-field motions. The significance of kinematic interaction depends on the characteristics of the incident waves and the size, embedment and flexibility of the foundation. Kinematic interaction is generally most pronounced for the high frequency components of the motion because the associated wavelengths are comparable to the dimensions of large foundations such as rafts or slabs.

Inertial interaction describes the secondary motions generated in the foundation soils by the inertia forces generated in the structure and foundation. The inertial forces are usually more significant at the fundamental period of the structure, so inertial interaction is more pronounced in a narrow period range around the fundamental period.

Therefore, kinematic and inertial interaction modify different parts of the spectrum. Kinematic effects are pronounced at the higher frequencies and inertial interaction at the fundamental frequency with little effect on the higher frequency responses.

21.7.2 TAU METHOD FOR ASSESSING INTERACTION EFFECTS

Clough & Penzien (1993) proposed a method for estimating the effect of kinematic interaction on the input motions to the rigid basemat. The ratio of the amplitude of a harmonic component of the basemat in translation to the same harmonic of the free-field motion is given by τ, where:

$$\tau = \frac{1}{\alpha}[2(1 - \cos \alpha)]^{1/2} \qquad (21.38a)$$

where

$$\alpha = \frac{\omega D}{V_a} = \frac{2\pi D}{L} \qquad (21.38b)$$

and ω = the circular frequency of the harmonic under consideration, D = the dimension of the structure in the direction of wave propagation, V_a = the apparent wave speed in the ground, and L = the wavelength corresponding to ω. The ratio τ is plotted in Fig. 21.15.

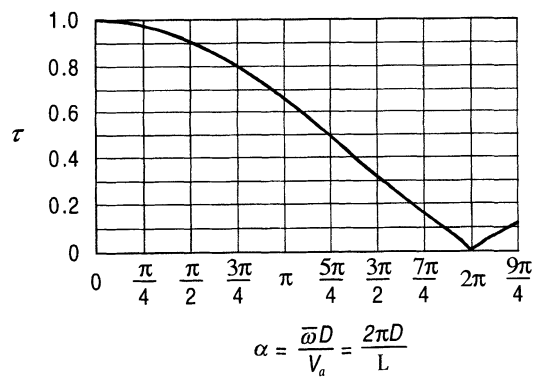


FIGURE 21.15. Amplitude reduction ratio, τ, as a function of frequency and wave velocity (modified from Clough & Penzien 1993).

21.8 Seismic Design of Retaining Structures

The static design of retaining structures was discussed in Chapter 17 and reference should be made to that chapter for the basic concept of wall design. Seismic design may be based on two different approaches. The walls can be designed to resist the inertial earthquake forces or to limit displacements of the structure to tolerable levels. A basic element in both approaches is the calculation of the active or passive seismic pressures against the retaining structure during seismic excitation. These pressures are usually calculated using the Mononobe–Okabe method (Okabe 1926; Mononobe & Matsuo 1929).

In this method, the effects of earthquake shaking are simulated by applying vertical and horizontal inertia forces, $k_h W$ and $k_v W$, to the active and passive failure wedges of weight, W, behind the wall as shown in Fig. 21.16. The parameters k_h and k_v are called the seismic coefficients and are defined by $a_h = k_h g$ and $a_v = k_v g$, where a_h and a_v are horizontal and vertical accelerations. The values of k_h and k_v may be defined by codes or selected on the basis of experience. When not defined by codes, k_h is usually selected between 0.5 and 0.8 times the peak ground acceleration, a_p; k_v is often taken as 0.5–0.7 k_h. Studies of the failure of quay walls in Japan during earthquakes suggest that $k_h = 0.33 (a_p/g)^{1/3}$.

The Mononobe–Okabe method assumes that the wall movements are sufficient to fully mobilize the shearing resistance along the base of the failure wedge, as is the case for Coulomb's active and passive earth pressure theories (see Section 17.2). Dynamic tests on model retaining walls indicate that the movements required to develop the dynamic active earth pressure force are on the order of those movements required to develop the static active earth pressure force (Sherif *et al.* 1982).

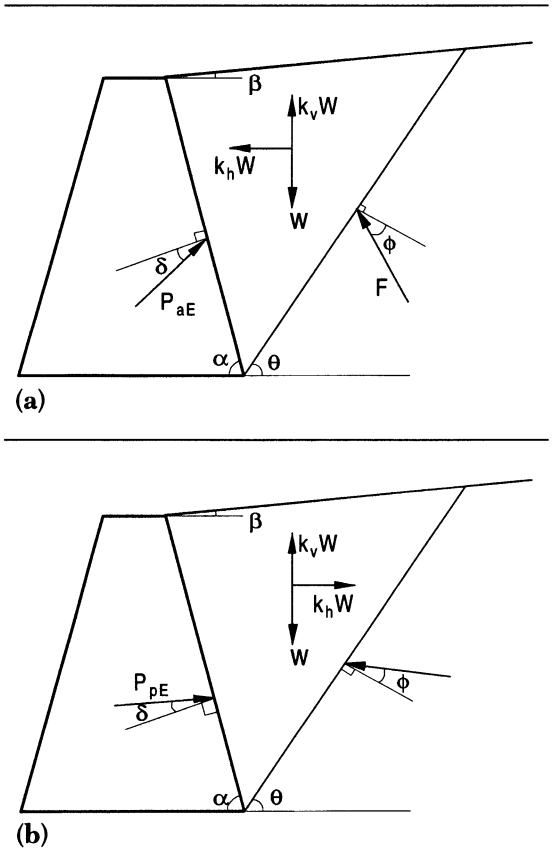


FIGURE 21.16. Forces acting on (a) active, and (b) passive failure wedges in Mononobe–Okabe analysis.

21.8.1 DYNAMIC ACTIVE AND PASSIVE EARTH PRESSURE FORCE

The Mononobe–Okabe relationship for P_{AE} for dry backfills with unit weight γ is given by:

$$P_{AE} = \frac{1}{2}\gamma H^2[K_{aE}(1 - k_v)] \qquad (21.39)$$

and acts at the angle of wall friction, to the normal to the back of the wall of height H (Whitman & Christian 1990).

The dynamic active earth pressure coefficient, K_{aE}, is equal to:

$$K_{aE} = \sin^2(\phi + \alpha - \psi)/\cos\psi \sin^2\alpha \sin(\alpha - \delta - \psi) \times \left\{1 + \left[\frac{\sin(\phi + \delta)\sin(\phi - \psi - \beta)}{\sin(\alpha - \delta - \psi)\sin(\alpha + \beta)}\right]^{1/2}\right\}^2. \qquad (21.40)$$

The seismic inertia angle, ψ, represents the angle that the resultant of the gravity force and the inertial forces make with the vertical direction and is given by:

$$\psi = \tan^{-1}\left[\frac{k_h}{(1 - k_v)}\right]. \qquad (21.41)$$

If the wall and soil wedge are rotated through the angle ψ, the resulting force vector representing the vectorial sums of W, k_hW and k_vW becomes vertical and the dynamic problem becomes equivalent to the static Coulomb earth pressure problem. Existing tables of lateral pressure coefficients for static loading can then be used to determine the dynamic lateral pressures. Then the active lateral dynamic force is given by:

$$P_{aE} = [K_a(\beta^*, \alpha^*) \cdot F_{aE}] \cdot \frac{1}{2}[\gamma(1 - k_v)]H^2 \qquad (21.42)$$

where H = actual height of the wall, $\beta^* = \beta + \psi$, $\alpha^* = \alpha - \psi$, and ψ is computed using Eq. 21.41 and:

$$F_{aE} = \frac{\sin^2(\alpha - \psi)}{\cos\psi \sin^2\alpha}. \qquad (21.43)$$

The dynamic passive earth pressure coefficient, K_{pE}, is equal to:

$$K_{pE} = \sin^2(\alpha - \phi + \psi)/\cos\psi \sin^2\alpha \sin(\alpha + \delta + \psi) \times \left\{1 - \left[\frac{\sin(\phi + \delta)\sin(\phi - \psi + \beta)}{\sin(\alpha + \delta + \psi)\sin(\alpha + \beta)}\right]^{1/2}\right\}^2 \qquad (21.44)$$

where $\psi = \tan^{-1}[k_h/(1 - k_v)]$.

The radical in the equation for K_{aE} and K_{pE} must remain positive for real solutions. Therefore, for active conditions $k_h \leq (1 - k_v)\tan(\phi + \beta)$, and for passive conditions $k_h \leq (1 - k_v)\tan(\phi + \beta)$. The vertical seismic coefficient does not have a significant effect on the seismic lateral forces for the usual ratios of k_v/k_h ranging from 0.3 to 0.7 for values of k_h up to 0.4. The error in neglecting k_v is gen-

erally less than 10%, except when $k_h > 0.5$ and $k_v/k_h > 0.5$.

21.8.2 SATURATED BACKFILL

The presence of water in the backfill behind a retaining wall has three effects: (1) it increases the total unit weight and hence the inertial forces within the backfill, (2) seismic porewater pressures may be generated by the earthquake shaking, and (3) hydrodynamic pressures may develop independently against the wall.

The inertial forces in saturated soils depend on the relative movement between the backfill soil particles and the porewater that surrounds them. If the permeability of the soil is small enough, the porewater moves with the soil during earthquake shaking. For this restrained water condition, the inertial forces will be proportional to the total unit weight of the soil. In the case of clean gravels, where the permeability is very high, however, the porewater may act independently while the soil skeleton moves back and forth. Under this free-water condition, inertial forces from the saturated soil will be proportional to the buoyant unit weight of the soil.

In the free-water condition, hydrodynamic pressures can develop against the wall. The resultant hydrodynamic force is calculated using the equation (Westergaard 1931):

$$P_w = (7/12) \cdot k_h \gamma_w h^2 \qquad (21.45)$$

where γ_w = the unit weight of water and h = the depth of water. The force is assumed to act at a height $0.4h$. The static water force must be added to the hydrodynamic thrust to give the total water force against the wall.

The Mononobe–Okabe method can be modified for the restrained water conditions to account for the presence of porewater within the backfill (Matsuzawa *et al.* 1985). If no significant porewater pressures are developed, the soil thrust from partially submerged backfills may be computed using an average unit weight based on the relative volumes of soil within the active wedge that are above and below the phreatic surface:

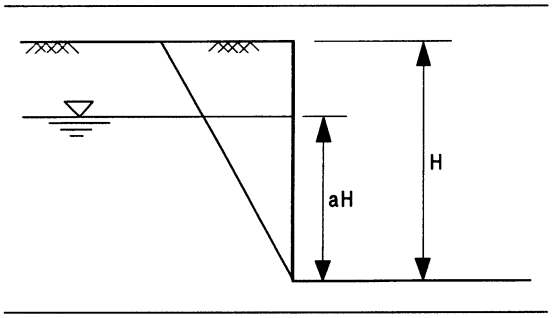


FIGURE 21.17. Geometry and notation for partially submerged backfill.

$$\bar{\gamma} = a^2\gamma_{sat} + (1 - a^2)\gamma_m \qquad (21.46)$$

where γ_m = the unit weight of moist soil, γ_{sat} = the saturated unit weight, and a is defined in Fig. 21.17. The static water pressure must be added to the total soil thrust.

If seismic porewater pressures develop during shaking, represented on the average by the ratio, r_u, of the porewater pressure, u, to the effective overburden pressure, σ', the active soil thrust acting on a yielding wall can be computed using Eq. 21.39 with:

$$\gamma = \gamma_b(1 - r_u) \qquad (21.47)$$

where γ_b = buoyant unit weight. The seismic inertia angle, ψ, is now given by:

$$\psi = \tan^{-1}\left[\frac{\gamma_{sat}k_h}{\gamma_b(1 - r_u)(1 - k_v)}\right]. \qquad (21.48)$$

An equivalent hydrostatic thrust based on a fluid of unit weight $\gamma_{eq} = \gamma_w + r_u\gamma_b$ must be added to the soil thrust (Ebeling & Morrison 1992).

21.8.3 ANCHORED BULKHEADS

Ebeling & Morrison (1992) have proposed a seismic design procedure for anchored bulkheads based on the free earth support method and Rowe's moment reduction procedure.

The bulkhead is first designed for static

loading conditions. The active seismic force on the back of the wall and the seismic passive force in front of the wall are calculated using the Mononobe–Okabe method for the different drainage conditions described in the previous section. The required depth of wall penetration is obtained by summing moments about the tie–rod connection to the wall. The tie–rod resistance is obtained by summing all horizontal forces acting on the wall. The distribution of bending moments are then calculated and the design bending moments determined using Rowe's moment reduction factors, based on wall flexibility.

The design tie-rod force is conventionally set at a level 30% greater than the anchor resistance computed above. The anchor block is located a sufficient distance from the wall so that the active wedge developing behind the wall does not intersect the passive wedge in front of the anchor block. The active failure plane is assumed to originate at the point of rotation of the wall. The size of the block is based on horizontal force equilibrium.

Kitajima & Uwabe (1979) summarized the performance of 110 quay walls during earthquakes in Japan since 1960. Most of the walls were anchored bulkheads. They categorized the damage to anchor bulkheads as a function of the permanent horizontal displacement at the top of the sheet pile. Their study shows that the level of damage increased in proportion to the displacements greater than 10 cm. Details of this study are given by Kramer (1996).

21.8.4 REINFORCED SOIL WALLS

Seismic design and analysis of reinforced soil walls are, in many aspects, very similar to that for gravity-type retaining walls. The primary difference is that an internal seismic stability analysis should also be performed as part of the design for these walls. The internal stability analysis incorporates the effects of the inertial force generated by the reinforced soil volume on individual reinforcing elements during an earthquake as a pseudo-static horizontal load. The FHWA has recently published design guidelines for seismic design and analysis for reinforced soil walls (Elias & Christopher 1996).

21.8.5 SEISMIC WALL DISPLACEMENTS

Richards & Elms (1979) proposed a method for the seismic design of gravity walls based on displacement criteria. The displacements are estimated using the Newmark (1965) sliding-block procedure. The forces on the wall are shown in Fig. 21.18.

The wall will begin to slide when the sum of the horizontal forces, $k_h W_w$ and $(P_{AE})_h$ exceeds the shearing resistance, T. If the coefficient of sliding friction is ϕ_s, then the resistance to sliding horizontally is given by the equation:

$$T = [W_w + P_{aE} \cos(\alpha - \delta)]\tan \phi_s. \quad (21.49)$$

The horizontal driving forces are $k_h W_w$ and $P_{aE} \sin(\alpha - \delta)$. Equating driving and resisting forces gives:

$$k_h = \times \left[\tan \phi_s - \frac{P_{aE} \sin(\alpha - \delta) - P_{aE} \cos(\alpha - \delta) \tan \phi_s}{W_w} \right] \quad (21.50)$$

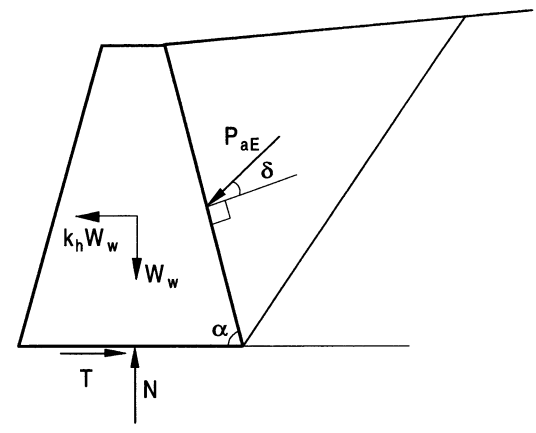


FIGURE 21.18. Static and seismic forces acting on a gravity retaining wall.

This seismic coefficient, k_h, is just sufficient to initiate sliding of the wall. The associated acceleration $a_y = k_h g$ is called the yield acceleration. Richards & Elms (1979) proposed the following equation for evaluating the permanent displacement of the wall during an earthquake with peak ground velocity v_p and peak ground acceleration a_p. The permanent displacement is given by:

$$d_{perm} = 0.087 \frac{v_p^2 a_p^3}{a_y^4}. \quad (21.51)$$

The Newmark (1965) and Richards & Elms (1979) equations tend to provide an upper bound for the wide range of displacements computed by Franklin & Chang (1977). Kramer (1996) gives an excellent description of displacement analysis.

21.8.6 SEISMIC DESIGN FOR TOLERABLE WALL DISPLACEMENT

The first step is to calculate the yield acceleration, a_y, that will allow the tolerable deformation, d_t, to occur under ground motions with a peak velocity v_p and a peak acceleration a_p using Eq. 21.51. This gives:

$$a_y = \left(0.087 \frac{v_p^2 a_p^3}{d_t}\right)^{1/4}. \quad (21.52)$$

The weight of wall, W_w, required to limit the permanent displacement to the tolerable value, from Eq. 21.50 is:

$$W_w = \frac{P_{aE} \sin(\alpha - \delta) - P_{aE} \cos(\alpha - \delta) \tan \phi_s}{\tan \phi_s - k_h}. \quad (21.53)$$

The dynamic force P_{aE} in Eq. 21.53 is computed using Eq. 21.40 with $k_h = a_y/g$. Whitman & Liao (1985) have shown that a factor of safety of 1.1–1.2 reduces the probability of exceeding the allowable tolerable displacement to less than 5%.

21.8.7 UNYIELDING WALLS (RIGID)

The Mononobe–Okabe method is not applicable to rigid immovable walls because a failure plane does not develop behind the wall. Several researchers have used elastic wave theory to derive expressions for seismic pressures against rigid walls (Matsuo & Ohara 1960; Wood 1973; Veletsos & Younan 1994). Others have used a modified shear beam model, which incorporates horizontal normal stresses (Arias *et al.* 1981; Finn *et al.* 1994; Veletsos *et al.* 1995; Wu & Finn 1996, 1999). For many years, Wood's solution has been the one used most in practice.

Wood provided non-dimensional static elastic solutions for lateral forces, F_{sr}, and overturning moments, M_{sr} for different L/H ratios and Poisson ratios, ν, for 1g horizontal acceleration (Fig. 21.19) (where L = the distance between the wall and another boundary that is rigid relative to the backfill, and H = the wall height). The point of application of F_{sr} above the base of the wall, Y_{sr}, is given by:

$$Y_{sr} = \frac{M_{sr}}{F_{sr}}. \quad (21.54)$$

Forces and moments caused by a harmonic excitation with peak acceleration, $k_h g$, are obtained by multiplying the non-dimensional values by $\rho H^2 k_h g$ or $\gamma H^2 k_h$.

In the cases of a wide backfill and a peak horizontal acceleration, $A_{max} = k_h g$, the lateral seismic force against the wall, when $\Omega < 0.5$ is given approximately for $\nu = 0.4$ by:

$$F_{sr} = \gamma H^2 (\cdot k_h) = \rho H^2 (\cdot A_{max}) \quad (21.55)$$

acting at a height of about $0.63H$ above the back of the wall. This is called Wood's static force (Fig. 21.21).

21.8.8 EARTH PRESSURES FOR DESIGN OF RIGID WALLS

Wu & Finn (1996) proposed an alternative analysis based on the modified shear beam model, which gives pressures within 5% of the exact modal solution proposed by Wood

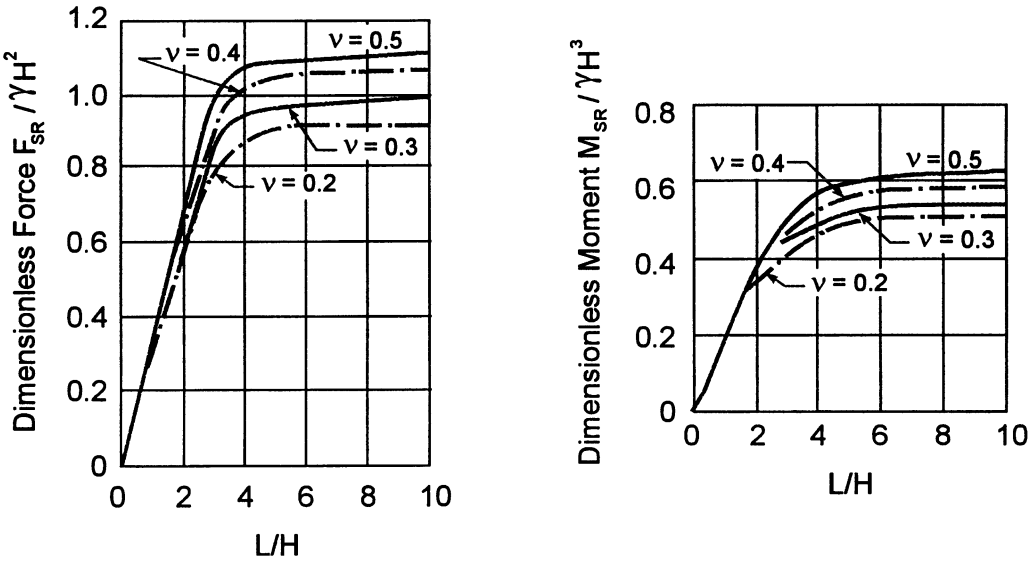


FIGURE 21.19. Non-dimensional lateral forces and moments on a rigid wall with unyielding backfill for 1-*g* static horizontal body forces.

(1973) for a wide range of all controlling parameters and which converges very rapidly.

Wu & Finn (1999) developed design charts for estimating the dynamic pressures against rigid walls for three types of soil profile, namely; uniform, linear and parabolic variations of shear modulus with depth. For the latter two cases, the shear moduli, G, are assumed to vary from zero at the ground surface to G_{soil} at the bottom of the soil profile. For most analyses, a Poisson's ratio of $\nu = 0.4$ and a damping ratio $\lambda = 10\%$ were used. The analyses were conducted assuming viscoelastic response. Simple corrections for nonlinear response are given later.

Peak dynamic thrusts are presented as functions of the ratio of the predominant frequency of the earthquake motions, ω, to the fundamental frequency of the wall–soil system, ω_{11}, which is established in the course of analysis and may initially be estimated from the maximum shear modulus in the backfill (Fig. 21.20).

In the presentation of the results, the computed seismic lateral forces, Q_{max}, are normalized by dividing by $\rho H^2 A_{max}$, where ρ = the mass density, H = the height of the wall, and A_{max} = the peak-ground acceleration. Envelopes of lateral forces corresponding to upper bound and 84% levels for a parabolic variation in G are shown in Fig. 21.21 for $L/H = 5.0$ and Fig. 21.22 for $L/H = 1.5$. These charts cover the cases of relatively long backfill and short backfill, respectively. These charts give design forces at the upper bound and 84 percentile levels for the common case where the modulus varies parabolically with depth. Wu & Finn (1999) should be consulted for additional results, including the effects of variations in ν and damping ratio.

The principal findings are:

- Under seismic loads, the upper bound peak seismic thrusts, Q_{max}, against walls with semi-infinite backfills could be as high as $1.7\rho H^2 A_{max}$ for a uniform soil profile, $1.35\rho H^2 A_{max}$ for a parabolic soil profile, and $1.15\rho H^2 A_{max}$ for a linear soil profile.
- The more uniform the backfill is, the larger the seismic thrust against the wall.

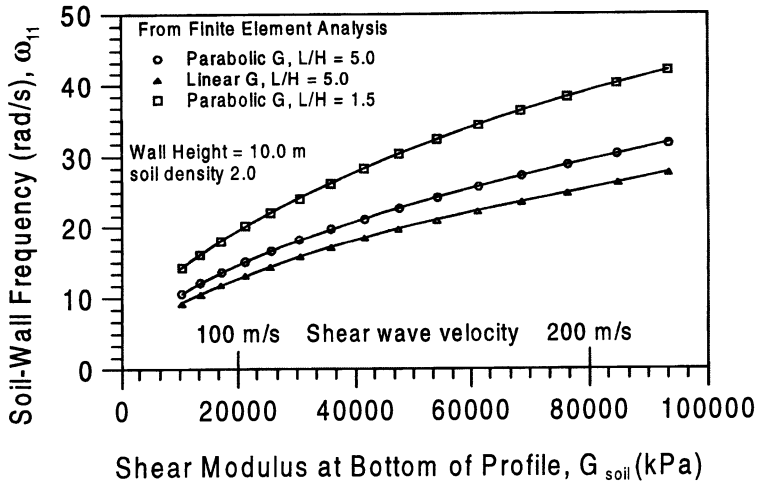


FIGURE 21.20. Chart for determining soil–wall system frequency on the basis of shear modulus: ○, parabolic G, $L/H = 5$; △, linear G, $L/H = 5$; □, parabolic G, $L/H = 1.5$. Wall height = 10 m, soil density = 2 (Mg m^{-3}).

- Amplification of seismic thrusts at resonance are much larger for backfills with $L/H = 1.5$ than for backfills with $L/H = 5.0$. The peak seismic thrust against walls with $L/H = 1.5$ reaches $1.7\rho H^2 A_{max}$ because of this amplification.
- The height of the resultant seismic thrust above the base of the wall varies from $0.64H$ for the uniform G profile to approximately $0.5H$ for the linear and parabolic G profiles.
- The static lateral pressures, typically at rest pressures, must be added to the dynamic pressures for design.

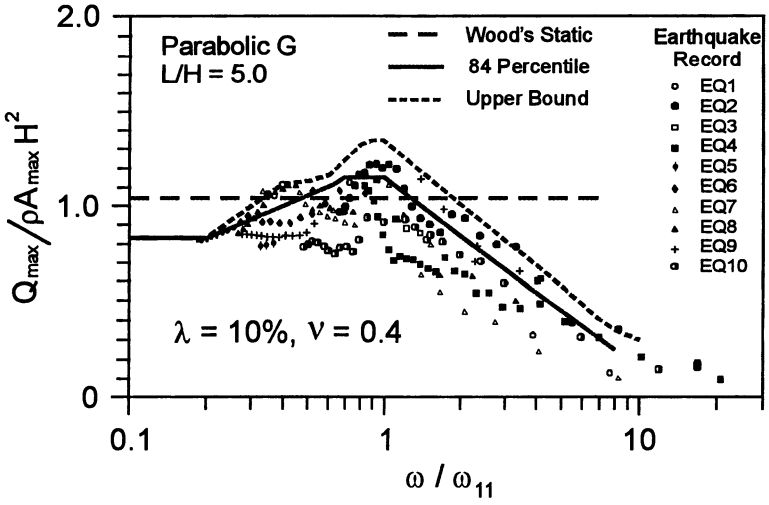


FIGURE 21.21. Peak seismic thrusts for soil profiles with parabolic variation in G ($L/H = 5.0$, $\lambda = 10\%$, $\nu = 0.40$) (modified from Wu & Finn 1999): – –, Wood's (1973) static; —, 84 percentile; ---, upper bound.

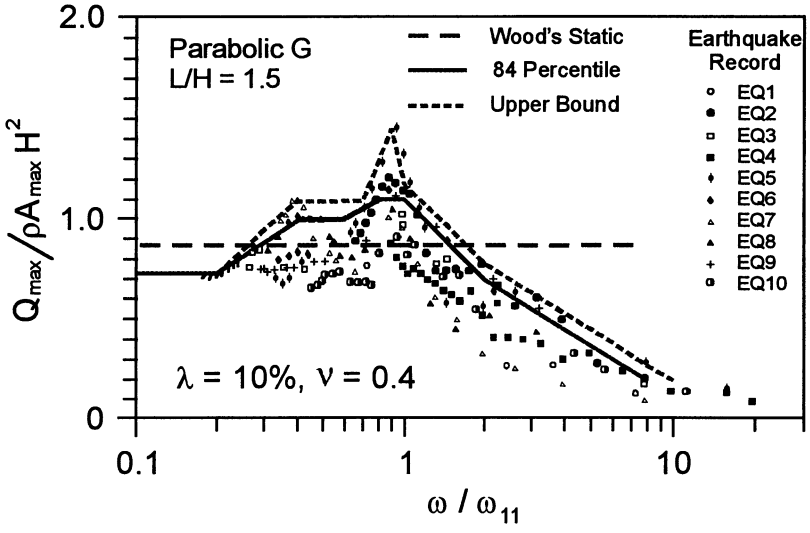


FIGURE 21.22. Peak seismic thrusts for soil profiles with parabolic variation in G (L/H = 1.5, λ = 10%, ν = 0.40) (modified from Wu & Finn 1999): – –, Wood's (1973) static; —, 84 percentile; ---, upper bound.

21.8.9 Practical Considerations

The shear modulus can be estimated from shear-wave velocity measurements made by seismic cone-penetration tests or from correlations with cone-bearing values, q_c, or standard penetration blow counts, N (see Chapter 4). During strong shaking, the modulus will be reduced because the modulus of soil is strain-dependent. The reduction in modulus for strong shaking can be estimated approximately on the basis of judgment or by a one-dimensional response analysis of the backfill using the program SHAKE (Schnabel *et al.* 1972). The modulus reduction table in NEHRP (FEMA 1997) is also useful (Table 21.6). In cases where the distribution of shear moduli with depth does not follow one of the profiles above, it is suggested that an average shear modulus weighted with respect to depth be used. In many cases involving basement walls, the elastic analysis is likely to be accurate enough except for very strong shaking. The advice of the geotechnical engineer in establishing the frequency of the soil–wall system is recommended.

TABLE 21.6. Values of G/G_o and V_s/V_{so}

	Ground acceleration coefficient, A_v			
	≤0.10	≤0.15	≤0.20	≥0.30
G/G_o	0.81	0.64	0.49	0.42
V_s/V_{so}	0.90	0.80	0.70	0.65

21.9 Seismic Design of Foundations

21.9.1 ELEMENTS OF SEISMIC DESIGN OF FOUNDATIONS

Very few foundation failures have occurred during earthquakes except in cases where liquefaction occurred or sensitive clays lost their strength and stiffness under cyclic loading. The foundation failures in Mexico City during the 1985 Michoacàn–Guerrero earthquake provide some of the few examples of failure under earthquake loading that could not be attributed to liquefaction. In this earthquake, foundations with low static safety factors or significant load eccentricities behaved poorly. However, even in these cases,

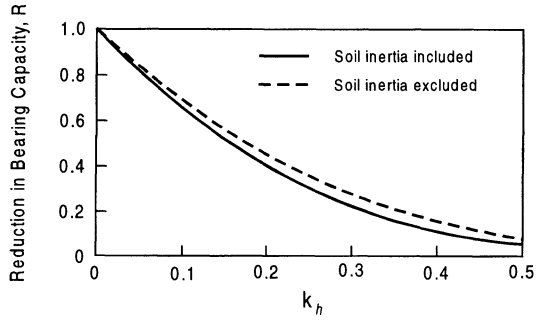


FIGURE 21.23. Reduction in bearing capacity, R, under seismic loading conditions with (---) and without (—) the inclusion of soil inertia effects as a function of the horizontal seismic coefficient, k_h (modified from Pecker 1996).

there is a possibility that the soil strength was also degraded (Girault 1986).

Eurocode 8, Part V (CEN 1994) deals explicitly with the effects of these seismic forces and states that in calculating the bearing capacity of a shallow foundation under earthquake loading, one should "include the load inclination and eccentricity arising from the inertial forces of the structure as well as the possible effects of the inertia in the soil".

Bearing capacity formulae are developed by analyzing the stability of a mass of soil moving under the footing load along slip surfaces. If the inertia forces acting on this soil mass are included, the effect is to generate additional shear stresses, which reduce the bearing capacity. Recent studies (Paolucci & Pecker 1997; Shi & Richards 1995) show that the reduction in bearing capacity due to soil inertia is not more than 15–20% for $k_h \leq 0.3$ (Fig. 21.23). The major reduction in bearing capacity comes from load inclination and the eccentricity of the resultant load on the foundation.

21.9.2 SEISMIC DESIGN REQUIREMENTS FOR FOUNDATIONS

A basic assumption of seismic design of foundations is that the foundation soils do not liquefy during the earthquake or undergo significant degradation of strength and stiffness. If these conditions are likely to occur, then a decision must be made to either: (a) improve the soil conditions; or (b) develop a design that can cope with these conditions.

There are two distinct requirements for the seismic design of foundations on stable soils. First, the overturning moment taken about the toe of the footing should be balanced by the dead load of the building with an adequate factor of safety. Second, one must ensure that the stresses generated in the foundation soils by the seismic moments do not exceed the specified design stresses based on the overall stability of the foundation nor the specified stresses to ensure that the settlements remain within tolerable limits.

21.9.3 DESIGN PRESSURE BASED ON BEARING CAPACITY

The bearing capacity of a footing loaded eccentrically by an inclined resultant force is considered to be the same as the bearing capacity of the reduced effective footing shown in Fig. 21.24, when loaded centrally by the same inclined force. The dimensions of the reduced area, B' and L', in terms of the plan dimensions of the actual footing (B and L) and the eccentricity, e, are width $B' = B - 2e$, and length $L' = L - 2e$. The bearing capacity of the effective footing may be calculated using a bearing capacity formula for

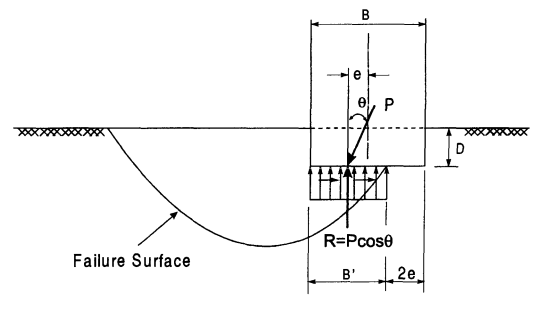


FIGURE 21.24. Equivalent footing width for footing subjected to eccentric and inclined loading at failure (modified from CGS 1992).

concentric inclined loading (see Section 9.3; CGS 1992; Meyerhof 1963; Bowles 1996). Because of the short-term application of the seismic loads, a smaller factor of safety can be adopted for seismic design of foundations.

21.9.4 DESIGN LOADS

The seismic design of structures according to the provisions in building codes are now based on capacity design in many jurisdictions, particularly North America, the EU and New Zealand. The design loads may be less than the loads that initiate yielding in the constructed structure for the following reasons. The yield moment used in design is taken as a fraction of the yield moment of the material. For steel, the fraction is typically 0.85–0.90. The yield stress is a specified stress, but the yield stress of the steel supplied by the manufacturer is usually greater than this to avoid problems of meeting the specifications with prescribed reliability. The yield stress supplied may be on the average 10% higher than the specified yield stress. Finally, the practical requirements of design and construction may require somewhat larger members and somewhat greater reinforcement than calculated for design. These effects result in a structure that yields at loads that may be in the range of 1.5–2.8 times the design loads, depending on the code used in design.

It is very important to take the overstrength factor into account when specifying the design loads for the foundation (CEN 1994; NRCC 1995a,b; ICBO 1997). Not only because the loads are greater, but because under seismic loading a significant increase is allowed in the bearing capacity of the footing, which reduces the factor of safety.

21.10 Liquefaction

21.10.1 KEY FACTORS

The primary factors controlling the liquefaction of saturated cohesionless soils are the intensity and duration of earthquake shaking, and the density of the soil. In engineering practice, the potential for liquefaction is assessed usually by using liquefaction assessment charts where the *in situ* compactness of the soil is characterized by the standard penetration resistance (SPT), N, cone penetration resistance (CPT), q_c, the Becker penetration resistance or *in situ* shear-wave velocity, V_s (see Chapter 4 for details regarding these tests). The standard charts are based on a magnitude 7.5 earthquake. The intensity of earthquake shaking is usually represented by the effective average cyclic stress ratio (CSR).

Seed & Idriss (1971) formulated the following equation for calculation of CSR:

$$\begin{aligned} \text{CSR} &= (\tau_{av}/\sigma'_{v0}) \\ &= 0.65(a_{max}/g)(\sigma_{v0}/\sigma'_{v0})r_d \end{aligned} \tag{21.56}$$

where a_{max} = the peak horizontal acceleration at ground surface generated by the earthquake; g = the acceleration of gravity; σ_{v0} and σ'_{v0} = total and effective vertical overburden stresses, respectively; and r_d = a stress reduction coefficient (see NCEER 1997 for the latest values for r_d). The latter coefficient provides an approximate correction for flexibility of the soil profile. An approximate expression for r_d used in Japan is:

$$r_d = 1.0 - 0.015H \tag{21.57}$$

where H = the depth below the surface in meters of the location where the stress is being evaluated.

21.10.2 SPT(N) LIQUEFACTION ASSESSMENT CHART

Seed and his colleagues (Seed 1979a; Seed *et al.* 1985) developed correlations between the SPT(N)-value and the cyclic stress ratio to cause liquefaction (CSR_{crit}) during earthquakes of magnitude M = 7.5. The correlations, which are presented in Fig. 21.25, were based on the observed response of sites during earthquake loading. Sites were consid-

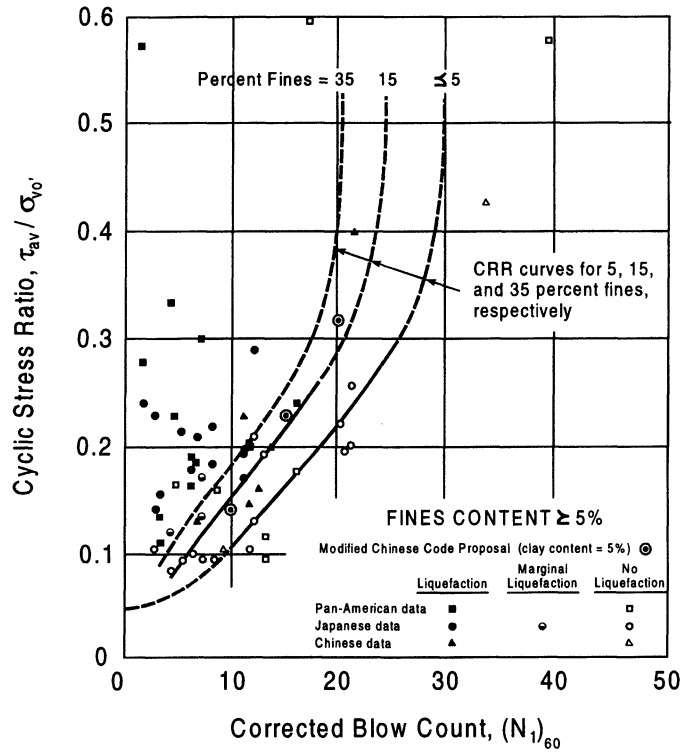


FIGURE 21.25. Simplified base curve recommended for calculation of CRR from SPT data, along with empirical liquefaction data (modified from Seed *et al.* 1985).

ered to have liquefied based on observed surface features, such as sand boils. Lower bound curves, separating liquefied from non-liquefied sites, are shown in Fig. 21.25, corresponding to various fine contents of the sand.

To compare the ground conditions at one site with those of another, it is necessary to standardize the measured penetration values to a standard driving energy and effective overburden pressure. Seed normalized the SPT to an energy level of 60% of the free-fall potential energy of the hammer and an effective overburden pressure of 100 kPa. Hence, the correlations presented in Fig. 21.25 show the normalized SPT(N) value, i.e. $(N_1)_{60}$.

The correction for energy level may be made using the data in Table 21.7 or by direct measurement of the energy imparted to the rods by the falling hammer.

A commonly used correction factor, C_N, for overburden pressure is that proposed by Liao and Whitman (1986):

$$C_N = (P_a/\sigma'_{v0})^{0.5} \tag{21.58}$$

where σ'_{v0} is expressed in the same units as standard atmospheric pressure, P_a. $(N)_{60}$ at σ'_{v0} is corrected to $(N_1)_{60}$, i.e. to $(N)_{60}$ at 100 kPa nominal pressure by:

$$(N_1)_{60} = C_N(N)_{60}. \tag{21.59}$$

Judgment is required in limiting the maximum value of the correction factor. Generally, the upper limit is taken in the range 1.5–2.0.

The chart in Fig. 21.25 is based on a magnitude $M = 7.5$, an effective overburden pressure of 100 kPa and level ground conditions. The last condition means that there are

TABLE 21.7. Summary of energy ratios for SPT procedures (adapted from Seed *et al.* 1985)

Country	Hammer type	Hammer release	Estimated rod energy (%)	Correction factor for 60% rod energy
Japan[a]	Donut	Free-fall	78	78/60 = 1.30
	Donut	Rope and pulley with special throw release	67	67/60 = 1.12
USA	Safety	Rope and pulley	60	60/60 = 1.00
	Donut[b]	Rope and pulley	45	45/60 = 0.75
Argentina	Donut	Rope and pulley	45	45/60 = 0.75
China	Donut	Free-fall[c]	60	60/60 = 1.00
	Donut	Rope and pulley	50	50/60 = 0.83

[a] Japanese SPT results have additional corrections for borehole diameter and frequency effects.
[b] Prevalent method in the USA today.
[c] Pilcon-type hammers develop an energy ratio of about 60%.

no static shear stresses on potential failure planes. The popularity of the Seed & Idriss (1982) method for assessing liquefaction resulted in it being applied outside the conditions on which the chart in Fig. 21.25 was based. Especially, it began to be applied to embankment dams and their foundations. In these situations, overburden pressures are much higher and large static shear stresses exist on potential failure planes. These applications challenged engineers and researchers to adapt the basic liquefaction resistance curve to these changed conditions and to other earthquake magnitudes. This adaptation resulted in corrections being applied to the critical cyclic resistance ratio (CCRR) read from the chart at a specified $(N_1)_{60}$ by means of correction factors K_m for magnitude, K_σ for pressure effects, and K_α for static shear effects. The corrected critical cyclic resistance ratio, CCRR (τ_{av}/σ'_0), corresponding to $(N_1)_{60}$, is then given by:

$$\text{CCRR}_{\text{CORR}} = \text{CCRR} \times K_m \times K_\sigma \times K_\alpha. \quad (21.60)$$

The development of these factors is reviewed here and values recommended by NCEER (1997) for use in practice, are given.

The state-of-the-art for evaluating liquefaction was first reviewed in 1985 by a committee of the US National Research Council (NRC 1985). It was reviewed again by a committee set up by the National Center for Earthquake Engineering Research (NCEER) in 1997 (NCEER 1997). The procedures described here reflect the current state of the document, although some further revisions may occur in 1999. This document defines the current state of knowledge and is likely to be the reference document for practice.

For some time, there has been concern about the fact that the liquefaction resistance curve is aligned through the origin. After reviewing the available data, the NCEER committee proposed a modification to the basic Seed curve in Fig. 21.25. The modification, shown by the dotted curve, is tangent to the old curve at $N = 10$ and cuts the vertical axis at a stress ratio of $\tau/\sigma'_0 = 0.05$.

21.10.3 MAGNITUDE SCALING FACTOR, K_m

A range of magnitude scaling factors are presented. These differ from the factors suggested by Seed & Idriss (1982), which are widely used in practice, in assigning higher scaling factors to magnitudes less than 7.5 to reflect the observed field data on liquefaction occurrence at the lower magnitudes. NCEER (1997) recommends the scaling factor K_m: developed by Idriss (NCEER 1997)

$$K_m = 10^{2.24}/M^{2.56}. \quad (21.61)$$

21.10.4 OVERBURDEN PRESSURE SCALING FACTOR, K_σ

A correction for overburden pressure must be made to the critical cyclic resistance ratio associated with the corrected $(N_1)_{60}$ value by the correction factor K_σ. K_σ is defined here as the cyclic resistance ratio of a soil at $\sigma'_{v0}(\sigma'_{v0} > 100$ kPa) divided by the ratio at $\sigma'_{v0} = 100$ kPa. The cyclic resistance is defined at 100% porewater pressure or 5% axial strain in cyclic triaxial tests. Values for K_σ used widely in practice are taken from the average curve proposed by Seed & Harder (1990). The data represent K_σ values from a wide variety of sand types and geological environments. Therefore, there is a wide scatter in the data about the average curve.

Since 1990, a lot of new data have become available on K_σ, up to confining pressures as high as 2500 kPa. Important sources of new data are given in Arango (1996), Vaid & Thomas (1994), and Pillai & Byrne (1994). After reviewing all these data, NCEER (1997) recommended the curve shown in Fig. 21.26 for taking into account the effects of effective overburden pressure on liquefaction potential. The committee are currently considering providing three correction curves, with the curve in Fig. 21.26 being applicable to medium-dense sand. A higher curve would be recommended for loose sand, a lower curve for dense sand.

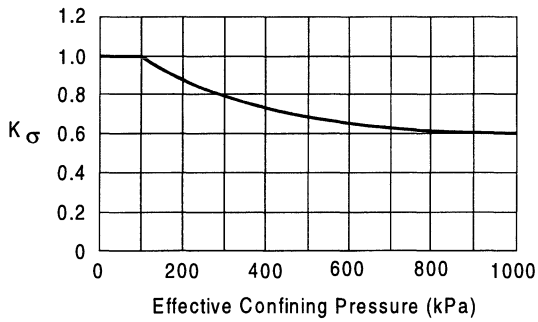


FIGURE 21.26. Minimum values for K_σ recommended for clean and silty sands and gravels (modified from NCEER 1997).

21.10.5 CORRECTION FACTORS FOR STATIC SHEAR, K_α

The Seed *et al.* (1985) liquefaction assessment chart is based on data from level or nearly level ground. There are no initial static shear stresses on potential failure planes. When the chart is used to evaluate the liquefaction potential of earth dams or their foundations, potential failure planes may carry large initial static shear stresses. Correction factors, K_α, have been developed to correct the critical cyclic resistance ratio for the effects of static shear. The K_α factors currently used in practice are those recommended by Seed & Harder (1990).

Harder & Boulanger (1997) have suggested a revised version of the Seed & Harder (1990) chart, which has a much narrower range of K_α values. For this chart, a triggering criterion of 3% shear strain was adopted (Harder & Boulanger 1997). Harder & Boulanger were influenced in selecting this criterion by the results of their tests involving static shear, both parallel and perpendicular, to the direction of shaking. They found that the influence of the direction of static shear was not very significant if a 3% triggering criterion was adopted. The correction factor recommended by Harder & Boulanger (1997) is shown in Fig. 21.27. The correction factor applies for effective overburden pressures less than 300 kPa.

The NCEER committee are still tentative about recommending values of K_α for use in practice. It would be better to incorporate the effect of static shear by conducting tests directly on high quality samples to obtain a combined factor $K_{\sigma\alpha}$, which will reflect the coupled effects of confining pressure and static shear on cyclic resistance.

21.10.6 CORE-PENETRATION TEST (CPT)

The liquefaction assessment chart based on the normalized CPT tip resistance, q_{c1}, recommended in NCEER (1997), is shown in Fig. 21.28. The chart is valid for an earth-

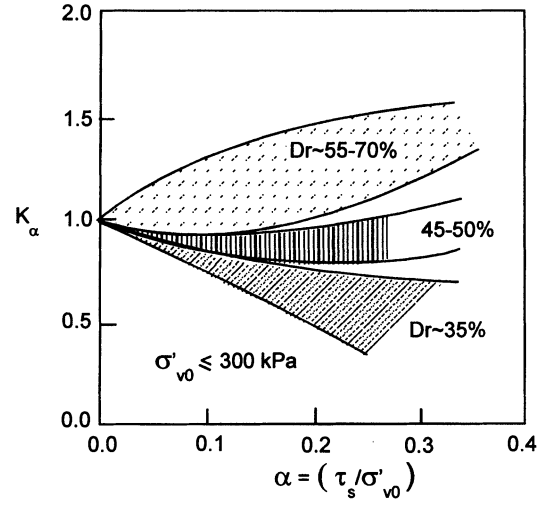


FIGURE 21.27. Correction factors to CRR as a function of the initial static shear stress ratio, τ_{st}/σ'_{v0}, and relative density (modified from Harder & Boulanger 1997).

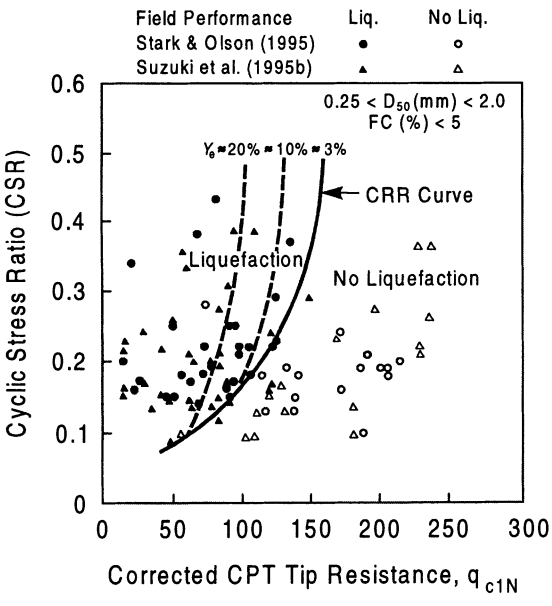


FIGURE 21.28. Curve recommended for calculation of CRR for earthquake magnitude $M = 7.5$ from CPT data along with empirical liquefaction data (modified from NCEER 1997). Liquefaction data: ● (Stark & Olson 1995), ▲ (Suzuki *et al.* 1995). No liquefaction: ○ (Stark & Olson 1995), △ (Suzuki *et al.* 1995).

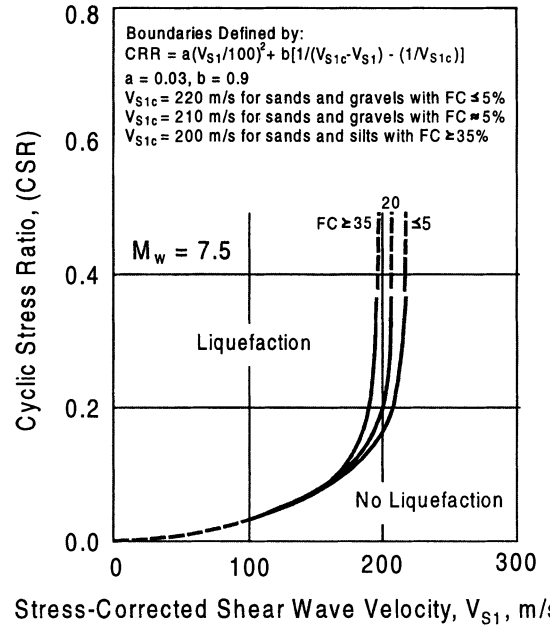


FIGURE 21.29. Curves recommended by workshop for calculation of CRR from corrected shear-wave velocity (modified from NCEER 1997). Boundaries defined by: CRR = $a\,(V_{sl}/100)^2 + b\,[1/(V_{slc} - V_{sl}) - (1/V_{slc})]$, $a = 0.03$ and $b = 0.9$; $V_{slc} = 220$, 210 and 200 ms^{-1} for sands and gravels with FC $\leq$5, $\approx$5 and $\geq$35%, respectively.

quake with a magnitude $M = 7.5$. The correction factors used on the SPT data are also used on the CPT data.

21.10.7 SHEAR-WAVE VELOCITY

The liquefaction assessment chart, based on average shear-wave velocity normalized to a vertical confining pressure of 100 kPa, is shown in Fig. 21.29 (NCEER 1997). The chart is valid for uncemented Holocene age soils and an earthquake magnitude, $M = 7.5$. The modified shear-wave velocity, V_{s1}, is defined as:

$$V_{s1} = V_s(P_a/\sigma'_{v0})^{0.25}. \qquad (21.62)$$

The other correction factors used with the SPT chart are also applied here.

21.10.8 BECKER PENETRATION TEST (BPT)

In the BPT, a double-walled casing is driven into the ground with a diesel pile hammer (Section 4.4.6.4). The test is standardized by reducing the blow counts to constant standard combustion conditions, following procedures established by Harder & Seed (1986). The standardized Becker blowcounts are then converted to SPT blowcounts, N. This is done on the basis of correlations developed by Harder & Seed (1986) on the basis of BPT and SPT tests run side by side to depths of less than 10 m. The Becker test has been used in evaluating gravelly soils in dam foundations where the penetration depths are far deeper than those for which correlations are available.

There is hardly any direct data linking the Becker blowcount directly to field liquefaction. Even if friction is accounted for properly (Sy & Campanella 1994), there is still concern whether correlations established in sand can be applied to the Becker casing when it is driven through coarse gravel. There is as yet no fully accepted solution to the friction problem associated with deep penetrations or driving through dense material after remediation.

21.10.9 SEISMIC SETTLEMENT

Both saturated and unsaturated sands tend to settle during earthquake shaking. Settlements in unsaturated sands are unlikely to be very significant unless the sand is loose. Large settlements are typical in loose saturated sands because of the development of high porewater pressures and even full liquefaction. Settlements in saturated sands may be estimated using the chart developed by Tokimatsu & Seed (1987) shown in Fig. 21.30. This figure gives the volumetric strains for an earthquake with reference magnitude M_w = 7.5 as a function of the normalized standard penetration resistance $(N_1)_{60}$ and cyclic stress ratio. The cyclic stress ratio is computed using Eq. 21.56. The volumetric strains corresponding to other earthquake magnitudes

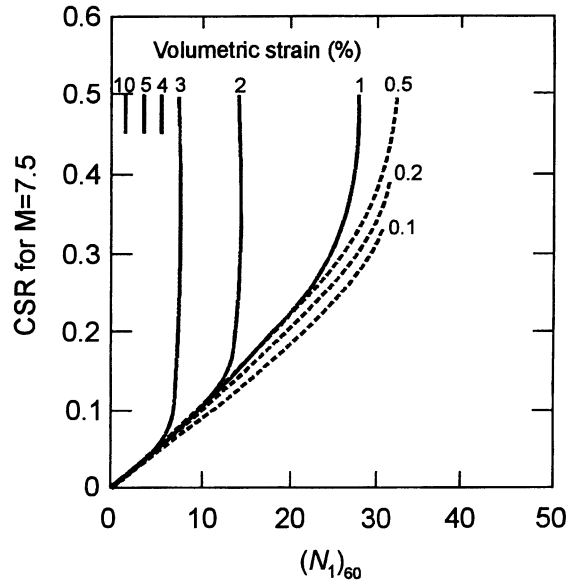


FIGURE 21.30. Post-liquefaction volumetric strains as a function of normalized standard penetration resistance and average cyclic stress ratio for M_w = 7.5 earthquakes (modified from Tokimatsu & Seed 1987).

may be calculated using the magnitude scaling factors for volumetric strain, given in Table 21.8. In order to calculate the seismic settlements, the site is divided into layers of roughly constant $(N_1)_{60}$ values. The seismic settlement of each layer is obtained by multiplying the layer thickness by the estimated volumetric strain for that layer. The layer set-

TABLE 21.8. Influence of earthquake magnitude on volumetric strain ratio for dry sands (adapted from Tokimatsu & Seed 1987)

Earthquake magnitude	Number of representative cycles at $0.65\tau_{max}$	Volumetric strain ratio, $\varepsilon_{C,N}/\varepsilon_{C,N=15}$
8.5	26	1.25
7.5	15	1.0
6.75	10	0.85
6	5	0.6
5.25	2–3	0.4

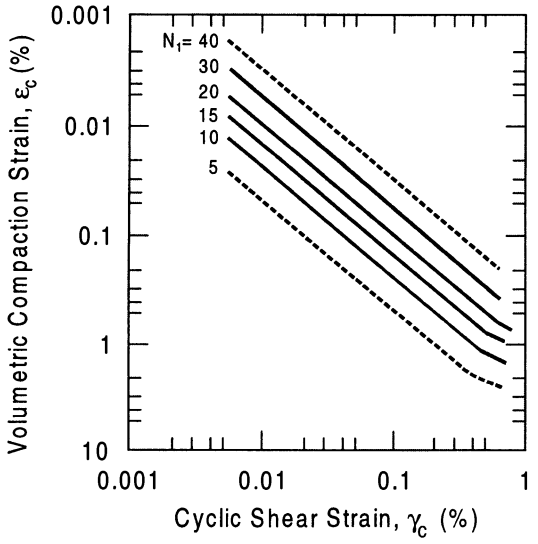


FIGURE 21.31. Relationship between volumetric strains in unsaturated sands as a function of cyclic shear strain and penetration resistance for an earthquake magnitude M_w = 7.5 (modified from Tokimatsu & Seed 1987).

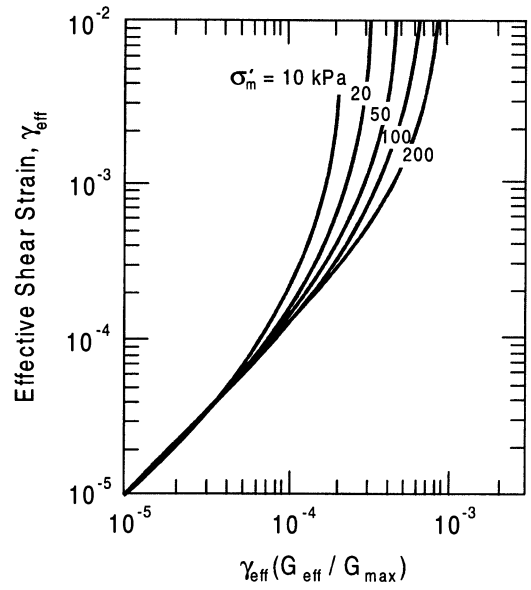


FIGURE 21.32. Chart for determining the effective shear strain in a soil layer during earthquake shaking (modified from Tokimatsu & Seed 1987).

tlements are summed to obtain the total seismic settlement for the site.

The settlements in unsaturated sands are estimated using the chart by Tokimatsu & Seed (1987) shown in Fig. 21.31. In this chart (developed for M = 7.5), the volumetric strain is given as a function of the normalized standard penetration resistance, N_1, and the cyclic shear strain γ_c (%). The cyclic shear strain, γ_c, is taken to be the average effective shear strain during shaking, γ_{eff}. The effective strain, γ_{eff}, is obtained from Fig. 21.32. The parameter $\gamma_{eff}(G_{eff}/G_{max})$ in Fig. 21.32 is given by Eq. 21.63, which is a variation of Eq. 21.56:

$$\gamma_{eff}(G_{eff}/G_{max}) = (0.65a_{max}\sigma_v r_d)/(gG_{max}) \quad (21.63)$$

where G_{max} = the shear modulus of the soil at small strain. The term $\gamma_{eff}(G_{eff}/G_{max})$ = the effective average cyclic shear stress in Eq. 21.56 divided by G_{max}. G_{max} (in kPa) can be estimated from the correlation given by Seed & Idriss (1970).

$$G_{max} = 4400[(N_1)_{60}]^{1/3}(\sigma'_m)^{1/2} \quad (21.64)$$

where σ'_m = mean normal effective stress in kPa.

The volumetric strains at an earthquake magnitude other than M_w = 7.5 may be found using the strain ratio factors in Table 21.8.

The procedure described above takes only one horizontal component of motion into account. Multiply the volumetric strain due to compaction for each layer by two to correct for multidirectional shaking effects, as recommended by Tokimatsu & Seed (1987), to get the representative volumetric strain for each layer.

21.10.10 EFFECTS OF GROUND IMPROVEMENT

Yasuda *et al.* (1996) conducted post-earthquake settlement measurements on Port and

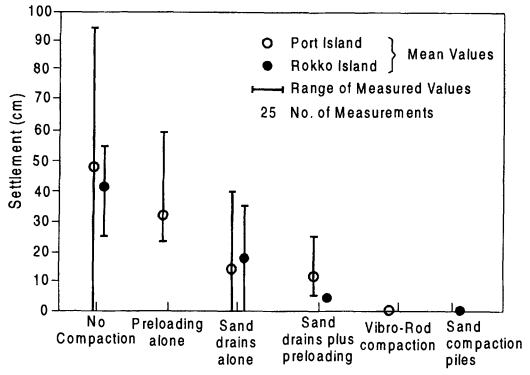


FIGURE 21.33. Effect of ground improvement techniques on settlement (modified from Yasuda *et al.* 1996). Clear values for: ○, Port Island: ●, Rokko Island. —, range of measured values. Total number of measurements = 25.

Rokko Islands to establish the effectiveness of the different remediation methods for improving the seismic performance of the site during the Kobe earthquake in 1995. The results of their survey are summarized in Fig. 21.33, which shows the variation in settlement for the different remediation techniques.

Sand drains were widely used in conjunction with preloading to accelerate the settlement of the alluvium clay stratum before construction on Port and Rokko Islands. The sand drains were installed by first driving closed pipes through the fill into the clay deposit. This produced some densification of the fill. The densification increased the resistance to liquefaction. At a number of sites, the fill was densified using a vibro-rod or sand compaction piles (see Section 15.2 for a description of foundation soil improvement techniques).

21.11 Residual Strength and Post-Liquefaction Deformations

The post-liquefaction behavior of earth structures such as dams or slopes should be assessed using both limiting equilibrium analysis and deformation analysis. Limiting equilibrium is a useful screening tool for potential instability problems, but the extent and location of remediation should be assessed primarily on the basis of deformation criteria. For many dams, especially those with substantial freeboard, criteria based on factor of safety alone can result in unnecessary remediation costs.

Large displacement post-liquefaction analysis has been used in the evaluation of the consequences of liquefaction and the design of remediation measures since 1988. It has been the subject of several reviews (Finn 1993, 1999; Ledbetter & Finn 1993), which may be consulted for background theory and case histories. The post-liquefaction behavior of liquefied soils is controlled by the residual strength and the strain level required to reach it.

21.11.1 FACTORS CONTROLLING RESIDUAL STRENGTH

Recent research (to be summarized below) suggests that the residual strength measured within the strain capacity of laboratory equipment is a function of: (a) sample preparation technique, (b) stress path followed during loading, and (c) effective confining pressure.

21.11.1.1 Effect of Sample Preparation

Many laboratory studies of liquefaction use samples prepared by moist tamping, air pluviation or pluviation under water. Moist tamped samples can be formed at void ratios unrepresentative of field conditions and are less uniform than pluviated samples (Vaid & Negussey 1988). Vaid *et al.* (1999) have demonstrated that the residual strengths measured on samples prepared in different ways are quite different (Fig. 21.34). Vaid *et al.* (1999) have also shown that by using pluviation in water it was possible to reconstitute samples which gave residual strengths very

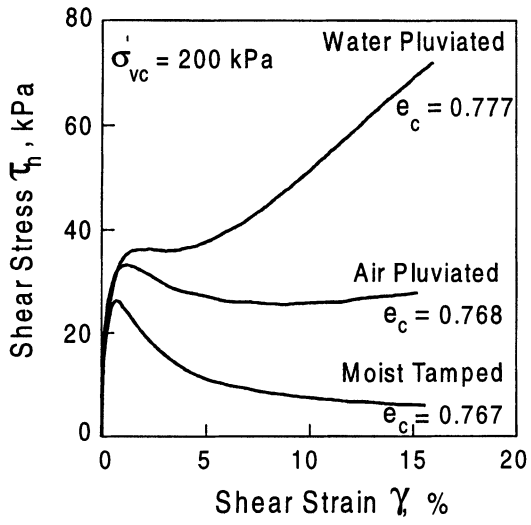


FIGURE 21.34. The effect of sample preparation on undrained simple shear response of Syncrude sand (modified from Vaid *et al.* 1999).

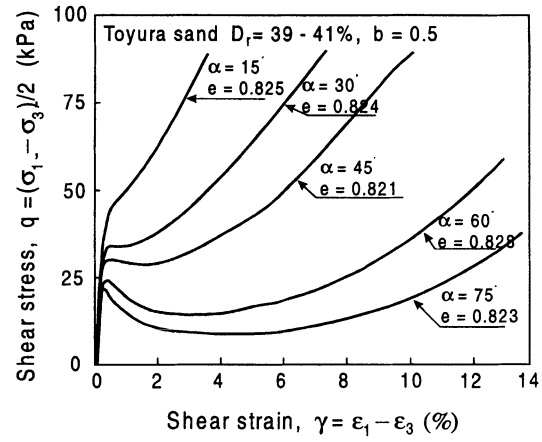


FIGURE 21.35. Effect of stress path on undrained behavior of Toyoura sand (modified from Yoshimine *et al.* 1998). D_r = 39–41%, b = 0.5.

similar to those obtained from the original undisturbed samples of recent sands.

These results provide a strong argument for using pluviation under water to form representative samples of soils that were originally deposited under water or were placed by hydraulic fill construction. The moist tamping method would seem to be more appropriate for unsaturated compacted soils.

21.11.1.2 Stress Path

Vaid & Chern (1985) were among the first to draw attention to the fact that the residual strength measured in extension was much smaller than the strength in compression and that sands in a given state were much more contractive in extension than in compression. These samples showed remarkable uniformity before and after testing and the test results should not be dismissed as being due to non-uniformity of the test specimens in extension tests and the development of necking at large strains.

Uthayakumar & Vaid (1998) and Yoshimine *et al.* (1998) have explored the effects of stress path on residual strength over a wide range of stress paths defined by α, the inclination of the principal stress to the vertical axes of the sample, and the parameter $b = (\sigma_2 - \sigma_3)/(\sigma_1 - \sigma_3)$, which is a measure of the intermediate principal stress. The samples were tested using the hollow cylinder torsional shear device. Typical examples of this kind of data (Yoshimine *et al.* 1998) are shown in Fig. 21.35. These results suggest that different residual strengths should be assigned to different parts of the liquefied region depending on the predominant stress conditions. This selective use of shear strength for design is not new. Bearing capacity under offshore structures in the North Sea is evaluated using compression, simple shear and extension strength data to suit stress conditions at different locations along potential sliding surfaces.

At some loose densities, sands may not show contractive behavior in triaxial compression tests. This is especially true for angular sands. Therefore, design decisions based only on compressive undrained tests on loose sands may be potentially unconservative. Tests conducted by Vaid *et al.* (1998) suggest that these sands may not become compres-

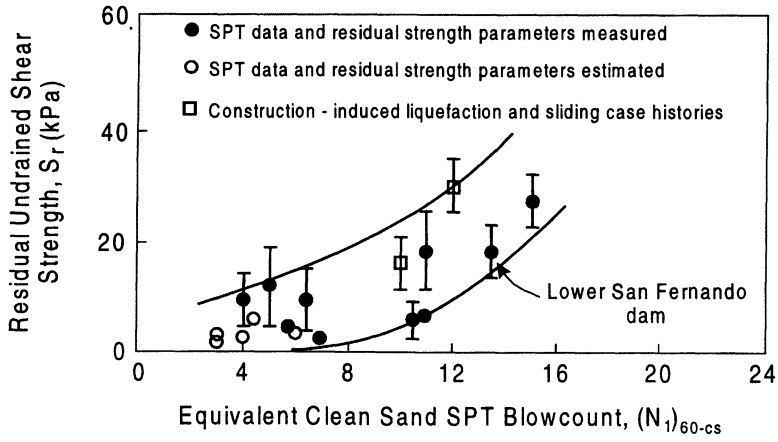


FIGURE 21.36. Correlation of residual strength, S_r, with $(N_1)_{60}$ (modified from Seed & Harder 1990; 100 kPa = 2000 psf). ●, measured SPT data; ○, estimated SPT data; □, construction-induced liquefaction and sliding case histories.

sive until very high confining pressures are used, approaching 1000 kPa.

21.11.1.3 Residual Strength as a Function of Effective Confining Pressure

The concept of expressing the residual strength as a fraction of the effective confining pressure has been used in engineering practice on several water-retaining and tailings dams, including the Sardis Dam in 1989 (Finn *et al.* 1991). For the most part, the ratio selected has been between 0.06 and 0.1. Similar results have been reported by Baziar & Dobry (1995) and by Ishihara (1993). A value of $S_r/p' = 0.23$ was used in the analysis of Duncan Dam, based on extensive testing of frozen samples (Byrne *et al.* 1994). Laboratory justification of this concept has been provided by Vaid & Sivathayalan (1996) and Vaid & Thomas (1994). The triaxial extension tests conducted by Vaid & Thomas (1994) show an almost linear dependence of the normalized residual strength on the void ratio, with the normalized residual strength varying from 0.05 to 0.20 as the void ratio changes from 0.95 to 0.82. This covers the range of normalized strengths found by other investigators.

Seed (1987) developed a correlation between $(N_1)_{60}$ and the undrained residual strength, S_r, from the back analysis of past flow slides. An updated version of this correlation was proposed by Seed & Harder (1990), which is shown in Fig. 21.36. Lower bound strengths from this correlation are very often used in practice, although occasionally values approaching the 33rd percentile have been used. In either case, these values are small at low $(N_1)_{60}$ values and frequently result in the prediction of instability and the need for substantial remediation.

21.11.2 POST-LIQUEFACTION DEFORMATIONS

Large deformation analysis to evaluate post-liquefaction deformations was first used in 1989 on the Sardis Dam (Finn 1990; Finn *et al.* 1991). The analysis, incorporated in the finite element computer program TARA-3FL (Finn & Yogendrakumar 1989) is based on the undrained stress–strain relations of the liquefied materials. The analysis considers the change in shear strength due to liquefaction and models the progressive deformation until equilibrium is reached.

Since the deformations may become large,

it is necessary to update progressively the finite element mesh. Each calculation of incremental deformation is based on the current shape of the dam, not the initial shape as in conventional finite element analysis. An independent assessment of the equilibrium of the final position should be conducted using a conventional static stability analysis. The factor of safety calculated in this way should be unity or greater, depending on whether the deformations occurred relatively slowly after the earthquake or during it when inertia forces were acting.

21.12 Embankment Dams

21.12.1 EQUIVALENT LINEAR ANALYSIS

The dynamic response of an earth dam is usually computed in engineering practice using an equivalent linear (EQL) method of two-dimensional analysis, such as that incorporated in the computer programs QUAD-4 (Idriss *et al.* 1973) or FLUSH (Lysmer *et al.* 1975). The results may be corrected approximately for three-dimensional effects (Mejia & Seed 1983). These corrections were used in the back analyses of Oroville Dam to the 1975 earthquake (Vrymoed 1975). The corrections are based on altering the shear modulus in the two-dimensional analysis so that the fundamental two-dimensional period matches the equivalent three-dimensional elastic period. Dakoulas & Gazetas (1986) have studied this problem further. Despite matching the fundamental period, the contributions of higher harmonics may be substantially underestimated. Therefore, assessing the seismic response of embankment dams in narrow valleys requires the exercise of engineering judgment, since the higher harmonics are likely to have their greatest effect at the crest of the dam.

The EQL analyses are conducted in terms of total stresses and so the effects of seismically induced porewater pressures are not reflected in the computed stresses and accelerations. Also, since the analyses are elastic, they cannot predict the permanent deformations directly. Therefore, equivalent linear methods are used only to get the distribution of accelerations and shear stresses in the dam. Semi-empirical methods are used to estimate the permanent deformations and pore-water pressures using the acceleration and stress data from the equivalent linear analyses (Seed *et al.* 1975). Finn (1993) has presented a detailed review of these methods.

21.12.2 DEFORMATIONS FROM ACCELERATION DATA

Various potential sliding surfaces in the embankment are analyzed statically to find the inertia force $F_I = (W/g)a_y$ required to cause failure (Fig. 21.37). The average yield acceleration, a_y, is then deduced from this force. The average acceleration time-history of the sliding block is obtained usually from a QUAD-4 analysis. The yield acceleration is deducted from the average acceleration time-history and the net acceleration (the shaded area in Fig. 21.37), is available to generate permanent displacements (Newmark 1965). The analysis is conducted on the equivalent model of a horizontal sliding block on a plane with only one-way motions allowed (Fig. 21.37).

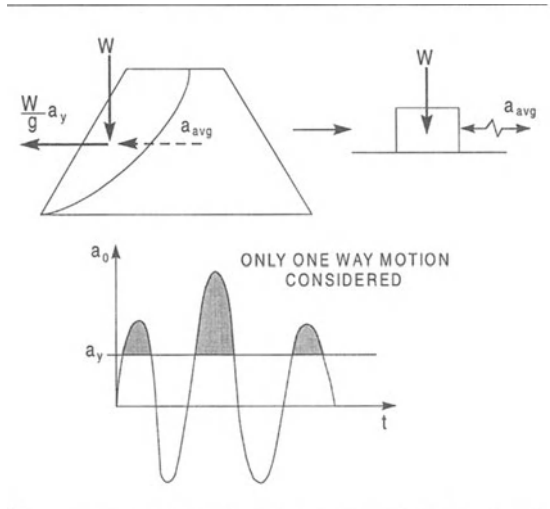


FIGURE 21.37. Elements of deformation analysis.

21.12.3 DEFORMATIONS FROM STRESS DATA

A more detailed picture of potential strains and deformations is obtained using Seed's semi-empirical method (Seed 1979b). The computed dynamic stresses in soil elements in the dam are converted to equivalent uniform stress cycles and are applied to laboratory specimens in consolidated states similar to corresponding elements in the dam. The resulting strains in the laboratory specimens are assigned to the corresponding elements in the dam. This procedure gives an incompatible set of strains which, however, are an indication of the potential for straining at selected locations within the dam.

A major motivation for the development of more general constitutive relations has been the need to model non-linear behavior in terms of effective stresses and to provide reliable estimates of porewater pressures and permanent deformations under seismic loading.

21.12.4 NON-LINEAR METHODS OF ANALYSIS

A hierarchy of constitutive models is available for the non-linear dynamic response of embankment dams to earthquake loading. The models range from the relatively simple hysteretic non-linear models to complex elastic–kinematic hardening plasticity models. Detailed critical assessments of these models may be found in Finn (1988) and Marcuson *et al.* (1992). This review presents the main true non-linear procedures used in current practice and outlines their advantages and limitations.

21.12.4.1 Elastic–Plastic Methods

The more comprehensive elastic–plastic models of soil behavior under cyclic loading are based on either a kinematic hardening theory of plasticity using multi-yield surfaces, or a bounding surface theory with a hardening law that defines the evolution of the plastic modulus. These constitutive models are complex and incorporate some parameters not usually measured in field or laboratory testing. Soil is treated as a two-phase material using coupled equations for the soil and water phases. The coupled equations and the more complex constitutive models make heavy demands on computing time (Finn 1988).

Validation studies of the elastic–plastic models suggest that, despite their theoretical generality, the quality of response predictions is strongly path dependent (Saada and Bianchini 1987; Finn 1988). When loading paths are similar to the stress paths used in calibrating the models, the predictions are good. As the loading path deviates from the calibration path, the prediction becomes less reliable.

Typical elastic–plastic methods used in practice to evaluate the seismic response of embankment dams are DYNAFLOW (Prevost 1981), DIANA (Kawai 1985), DSAGE (Roth 1985), DYNARD (Moriwaki *et al.* 1988), and FLAC (Itasca 1996).

21.12.4.2 Direct Non-Linear Analysis

The direct non-linear approach is presented as incorporated in the program TARA-3 (Finn *et al.* 1986) because there is extensive experience in using this method in practice. In addition, the program has been validated in an extensive series of centrifuge tests conducted on behalf of the US Nuclear Regulatory Commission (Finn 1988).

In this model, the behavior of soil in shear is assumed to be non-linear and hysteretic. The response of the soil to uniform all-round pressure is assumed to be non-linearly elastic and dependent on the mean normal effective stress.

The objective during analysis is to follow the stress–strain curve of the soil in shear, during both loading and unloading. Checks are built into the program to establish whether or not a calculated stress–strain point is on the stress–strain curve and correction forces are applied to bring the point back on the curve if necessary. To simplify the computations, the stress–strain curve is assumed to be hyperbolic. This curve is defined

by two parameters, which are fundamental soil properties, i.e. the strength, τ_{max}, and the *in situ* small strain shear modulus, G_{max}.

The response of the soil to an increment in load, either static or dynamic, is controlled by the tangent shear and tangent bulk moduli appropriate to the current state of the soil. The moduli are functions of the level of effective stress and therefore excess porewater pressures must be continually updated during analysis, and their effects on the moduli taken progressively into account.

During seismic shaking, two kinds of porewater pressures are generated in saturated soils: transient and residual. The residual porewater pressures are due to plastic deformations in the sand skeleton. These persist until dissipated by drainage or diffusion and therefore they exert a major influence on the strength and stiffness of the soil skeleton. These pressures are modeled in TARA-3 using the Martin *et al.* (1975) porewater pressure model.

21.12.5 RECOMMENDATIONS FOR ANALYSIS

The dynamic response analyses of embankment dams is still largely based on technology developed in the 1970s and which represents the very first attempts to carry out non-linear analysis by equivalent linear procedures. The stresses and accelerations calculated in this way are input into other procedures for assessing the performance of the dam. These procedures appear to work quite well provided the behavior of the dam is not strongly non-linear and significant pore pressures do not develop. Seed *et al.* (1989) note that this method can occasionally predict large displacements that do not occur when there is strong non-linearity or high porewater pressures. The Newmark (1965) procedure, based on sliding-block analysis, is particularly inappropriate when a large zone has liquefied in the embankment or foundation. The more comprehensive non-linear methods described above are especially appropriate for evaluating the permanent displacements resulting from strong shaking with or without the presence of liquefaction.

21.13 Seismic Risk in Geotechnical Earthquake Engineering

21.13.1 SEISMIC RISK ASSESSMENT FOR DAMS

Seismic risk analysis provides a rational basis for the evaluation of dam safety during an earthquake. It is a process by which the consequences of exposure to a range of probabilistic seismic hazards are determined. The consequences are most often expressed in terms of both loss of life and economic loss at various probabilities of exceedance.

Risk analysis in the field of embankment dams is relatively new in engineering practice and most engineers do not have the knowledge or experience for making decisions on the basis of risk assessment. Risk assessment was adopted by the US Bureau of Reclamation (USBR) in 1995 and the US Army Corps of Engineers in 1997. The objective of USBR was "to ensure that structures do not create unacceptable risks to public safety and welfare, property, the environment and cultural resources". The Canadian Standards Association has developed the general framework for risk management shown in Fig. 21.38. There are two main structures in the framework, risk assessment and risk control, both of which form the basis for decisions on risk management.

21.13.2 APPROACHES TO RISK ASSESSMENT

The simplest approach to introducing probabilistic methods into the evaluation of dam safety is to formulate safety guidelines in which the hazard to the dam is defined probabilistically as a function of the potential consequences of failure expressed in general terms. The probability of the failure is not evaluated. The dam safety guidelines formu-

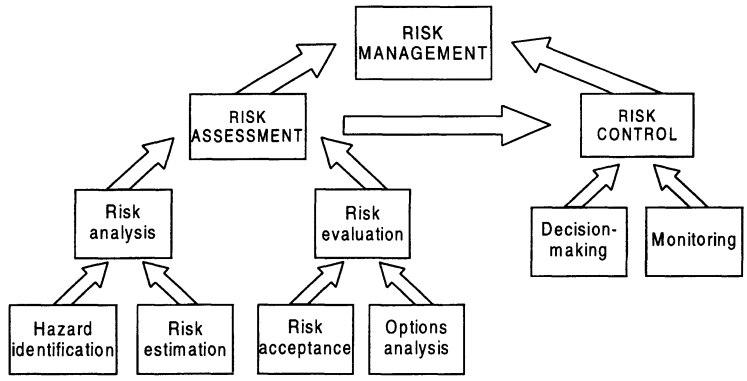


FIGURE 21.38. Risk management framework proposed by Canadian Standards Association (modified from International Journal on Hydropower and Dams 1998).

lated by the Canadian Dam Safety Association (CDSA) (1995), are a good example of this approach. These guidelines have been adopted nationally. The CDSA recommendations on hazards specifications are outlined in Table 21.9 as a function of three categories of consequences of failure. The categories are defined in Table 21.10. The procedure for safety analysis of dams, once the seismic hazard is selected, follow conventional deterministic procedures such as stability calculations based on limit equilibrium and finite element methods. However, for "high consequence dams" in moderate to high seismic zones, seismic response and displacement analyses should be considered. Formal risk analysis is commonly used in many areas of engineering practice, but it is by no means widely embraced as yet for the seismic safety evaluation of embankment dams.

TABLE 21.9. Usual minimum criteria for design earthquakes (adapted from CDSA 1995)

	Minimum design earthquake (MDE)[a]	
Consequence category	Deterministically derived	Probabilistically derived (Annual exceedance probability)
Very high	MCE[b]	10^{-4}
High[c]	50–100% MCE[b]	10^{-3}–10^{-4}
Low	—	10^{-2}–10^{-3}

[a] MDE (minimum design earthquake) firm ground accelerations and velocities can be taken as 50–100% of MCE[b] values. For design purposes, the magnitude should remain the same as the MCE.

[b] For a dam site, MCE (maximum credible earthquake) ground motions are the most severe ground motions capable of being produced at the site under the presently known or interpreted tectonic framework.

[c] In the "high" consequence category, the MDE is based on the consequences of failure. For example, if one incremental fatality would result from failure, an annual exceedance probability (AEP) of 10^{-3} could be acceptable, but for consequences approaching those of a "very high" consequence dam, design earthquakes approaching the MCE would be required.

The Australian National Committee on Large Dams (ANCOLD) has been in the forefront in promoting formal risk assessment. In 1994, ANCOLD released its guidelines on risk assessment (McDonald 1997). Key elements of their guidelines, which are representative of emerging practice, are given below:

- For new dams, and the upgrading of existing dams, ensure that the average risk of death of particular members of the public from dam failure does not exceed 10^{-6} per exposed person per annum. Do not subject any person, being a member of the public, to a risk greater than 10^{-5} per annum.
- For existing dams, individual risks up to ten times those for new dams could be tolerable, subject to application of the ALARP

TABLE 21.10. Consequence classification of dams (adapted from CDSA 1995)

	Potential incremental consequences of failure[a]	
Consequence	Loss of life	Economic, social, environmental
Very high	Large increase expected[b]	Excessive increase in social, economic and/or environmental losses
High	Some increase expected[b]	Substantial increase in social, economic and/or environmental losses
Low	No increase expected	Low social, economic and/or environmental losses
Very low	No increase	Small dams with minimal social, economic and/or environmental losses. Losses generally limited to the owner's property; damages to other property are acceptable to society

[a] Incremental to the impacts that would occur during an earthquake, but without failure of the dam. The type of consequence, e.g. loss of life or economic losses, with the highest rating, determines which category is assigned to the structure.
[b] The loss-of-life criteria, which separate the "high" and "very high" categories, may be based on risks that are acceptable or tolerable to society, taken to be 0.001 lives per year for each dam. Consistent with this tolerable societal risk, the minimum criteria for a "very high" consequence dam (MCE) should result in an annual probability of failure less than 1 : 100 000.

principle, i.e. keep the risk "as low as reasonably possible".

- Ensure that new dams, and dams being upgraded, satisfy the societal risk criterion given by the objective curves in Fig. 21.39.
- Ensure that existing dams satisfy the societal risk criterion given by the lower curve of Fig. 21.39, but carefully consider the ALARP principle.

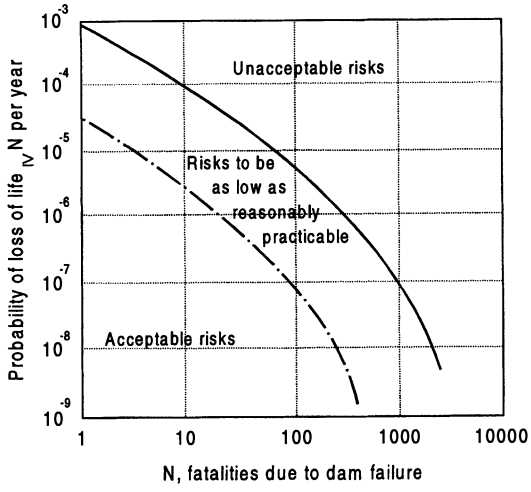


FIGURE 21.39. ANCOLD societal risk criteria (based on International Journal on Hydropower and Dams 1998).

- Ensure that a dam complies with both individual risk and societal risk criteria. In assessing compliance with individual and societal risk criteria, use a recognized methodology, such as the procedures set out by the US Bureau of Reclamation to estimate expected loss of life.

Note the crucial difference between formal risk assessment and the standards approach. The probabilities are now specified for the consequences, whereas in the standard approach, the emphasis is on the probability of the hazard.

21.13.3 SOME CONTENTIOUS ISSUES

Estimating the risk of loss of life is a contentious issue. In particular, there is debate about whether it should be expressed as expected losses per annum or losses associated with an actual event. Losses per event are more likely to arouse social and political opposition than expected values. In some cases, even economic losses probably should be considered on an event basis. Coping with losses from catastrophic events like earthquakes is not like dealing with losses from car accidents or on life insurance policies. Insur-

ance companies when considering earthquake losses do not usually consider the expected losses. They are more concerned with the conditional probabilities of loss. Even the conditional probabilities are often ignored by moving the largest earthquake closest to the insured portfolio. The companies are very sensitive to the threat that, if and when the earthquake occurs, they may go broke because of having to meet all the losses at once. These features of potentially catastrophic events do not seem to be well-represented in conventional seismic risk procedures.

21.13.4 FRAMEWORK FOR RISK ASSESSMENT

The framework for formal risk assessment defines how to go from probabilistic specification of seismic hazard to the determination of the probabilities associated with different levels of consequences. The form of the framework depends on the potential failure modes of the dam. An example is presented from a paper by Lee *et al.* (1998). The paper describes how the probability of different levels of post-liquefaction damage and consequences were assessed for Keenleyside Dam in British Columbia by Hydro and Power Authority. BC Hydro has been actively promoting risk assessment for its projects (Hartford 1997). The emphasis here is on describing the framework of the risk assessment process.

21.13.4.1 Example: Risk Assessment for Keenleyside Dam

The framework used by Lee *et al.* (1998) is given in Fig. 21.40. There is a long sequence of complex steps between the specification of the seismic hazards and the calculation of the probabilities of different levels of damage and associated consequences. The sequence of steps is called an event tree. The development of an appropriate event tree is a complex task requiring a wide range of skills and considerable judgment. The event tree by itself, even without the probability assessments, leads to a much better understanding of the risk to the dam. It can be useful in planning remedial measures or risk management.

The first step is to specify the seismic hazard in level 1 (Fig. 21.40). A range of shaking intensities is specified by peak ground accelerations. Each level of acceleration has its probability of exceedance. The potential for liquefaction, all other things being equal, depends on the duration of strong shaking. Duration is represented by the earthquake magnitude in the techniques used in engineering practice for assessing liquefaction potential (Seed *et al.* 1985). Therefore, the magnitudes contributing most to the specified levels of shaking are obtained from a conventional seismic hazard assessment using a program such as EZ-FRISK, 4.0 (Risk Engineeering 1997), which allows de-aggregation of the magnitudes contributing most to each level of seismic risk. On this basis, the magnitudes in level 2 can be obtained. Level 3 in the event tree is the designation of the liquefaction model to be used in the analysis. The conventional models such as Seed *et al.* (1985) and Robertson & Campanella (1985), based on the standard penetration tests (SPT) and the cone penetration tests (CPT), respectively, are used deterministically. Liao *et al.* (1988) and Youd & Noble (1998), using the database for the deterministic models, have developed charts that allow the estimation of the probability of liquefaction for a given level of shaking and a given level of liquefaction resistance to cyclic loading (CRR) specified by data from standard penetration or cone penetration tests. In the Keenleyside study, only the Liao *et al.* (1988) probability model was actually used. If both models had been used, then weighting factors would have been assigned to each. Cyclic resistance ratios, CRR, with probabilities of liquefaction of 0.85, 0.50 and 0.15 are used to assess the potential damage to the dam in

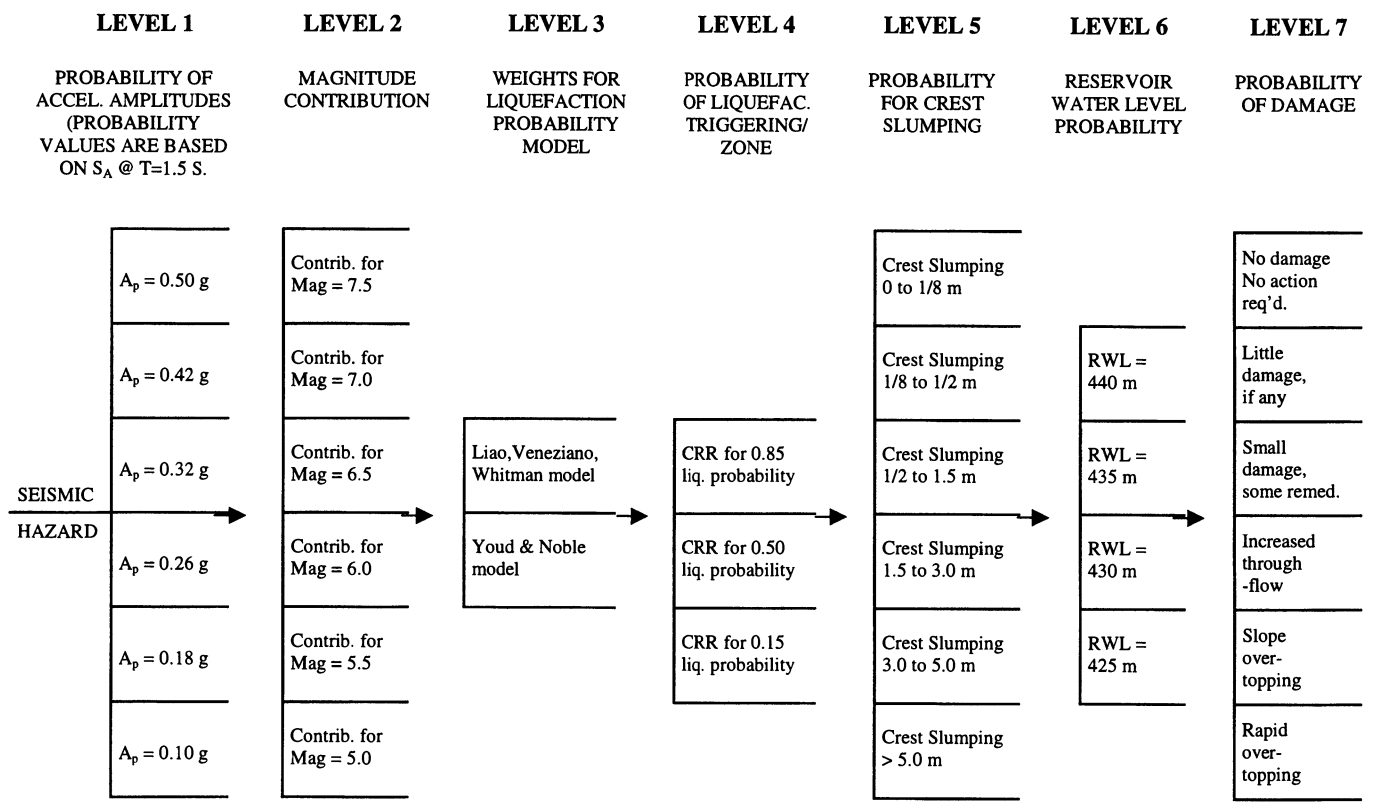


FIGURE 21.40. Event tree used for the probability of liquefaction-failure (modified from Lee *et al.* 1998).

terms of displacements such as loss of freeboard (crest slumping). These analyses are carried out by finite element analyses using post-liquefaction stress–strain–strength properties in the liquefied soils.

Six different levels of crest slumping are used to characterize the potential performance of the dam. At this stage, the conditional probabilities of these different levels may be introduced, based on computed response data and taking into account potential variations in properties of the materials, uncertainties in the analysis procedure itself and the exercise of judgment. The definition of performance is a very critical part of the entire process. A simple criterion based on safety of factor against slope failure has been found to be unsatisfactory (Lee *et al.* 1998; Whitman 1984). The probabilities based on such a narrow criterion appear to be overly sensitive to some details of the analyses.

The next step is evaluating the consequences. The consequences of the loss of freeboard associated with crest slumping obviously depend on the level of the reservoir. The probability of the reservoir being at specific levels can be calculated from the long-term records of reservoir operation, and consequently, probabilities can be assigned to the reservoir level being at a number of representative stages, as shown in Fig. 21.40. Judgments must now be made of the damage potential for the different combinations of crest settlement and reservoir level. This is the difficult part and requires expert judgment to assign subjective probabilities.

Placing the range in reservoir levels, in level 6 of the event tree, after the displacement analyses in level 5, emphasizes the role that the reservoir level plays in assessing the consequences of failure. However, the level of the reservoir also affects the stresses in the dam before failure and hence, needs to be incorporated into the finite element analyses so that strictly speaking the node for reservoir level should also be placed before the node for displacement analysis.

Whatever reservations one may have about the probability of the various consequences derived from a risk assessment analysis, it is clear that constructing the event tree forces one to think in a very detailed way about the process by which failure develops in the dam, and therefore, it contributes to a deep understanding of how the dam is likely to behave. This is a very positive benefit of any well-conducted risk assessment study.

If one now considers how the consequences might be mitigated, other events may need to be taken into account. The consequences may be dealt with in some situations by relying on evacuation of those who might be affected downstream. For such an evacuation to be effective, the consequences of the earthquake in the downstream area on transportation routes, on the communities at risk and on communications need to be taken into account. This would require an extension of the event tree to cope with these other events, which impact the mitigation of the consequences. If mitigation depends on lowering the reservoir level, then the impact of the earthquake on procedures for doing this needs to be taken into account. Clearly, the full range of risk assessment involves a very comprehensive investigation on all consequences of the earthquake, both directly on the dam itself, on the operating environment of the dam and on the region surrounding dam and reservoir. Full risk assessment is a very expensive process and requires a range of high-level skills that is not yet widely available.

V. GEOENVIRONMENTAL ENGINEERING

22. GEOENVIRONMENTAL PROBLEM IDENTIFICATION AND RISK MANAGEMENT

M. Whittaker
J. G. Sprenger
D. D. DuBois

22.1 Introduction

The issue of contaminated land carries with it significant environmental and economic implications. A key question is how best to fulfill the interests of all those with a stake in contaminated land (owners, potential vendors/purchasers, consultants, the public, the regulators and so on) while ensuring that the land is returned to a condition that is protective of the users and does not present a long-term environmental liability.

Increasingly, contaminated sites are being managed through consideration of the risks they pose to human and environmental health. The process of identifying and evaluating the significance of risks is known as risk assessment; the process through which identified risks are controlled or mitigated is known as risk management.

The objective of this chapter is to provide the reader with an overview of how geoenvironmental issues relating to the contaminated subsurface may be addressed by considering the risks to human and environmental health. In essence, risk assessment can be viewed as a framework for evaluating the likelihood of adverse effects on humans and the wider ecological environment resulting from exposure to a contaminant. Use of risk assessment at contaminated sites provides a customized, clearer, more comprehensive means of discriminating between, and identifying appropriate solutions for the potential issues of concern associated with a contaminated site than by direct comparison with generic non-health-based standards.

Typically, the risk-based approach has proven to be most valuable in situations where financial or technical constraints rule out a more conventional solution, e.g. where portions of the site underlie existing building structures or services, where landfill disposal is prohibitively expensive, or where the contaminated material is deep lying and cannot be removed. However, its application is by no means confined to such situations, and risk-based site management is now frequently being applied in a wider sense as a recognized clean-up framework in many jurisdictions across Canada, the USA and Europe.

This chapter is specifically intended to provide an overview of and commentary on the risk assessment/risk management framework as it applies to the management of contami-

R. K. Rowe (ed.), *Geotechnical and Geoenvironmental Engineering Handbook*
© Kluwer Academic Publishers 2001

nated sites. It is intended primarily as a commentary for risk assessment practitioners and not as a prescriptive manual or work sheet. The key technical elements of the risk assessment process are considered, with emphasis placed upon the underlying principles essential to understanding the issues and applying them in practice. Where appropriate, relevant non-technical issues such as risk communication and legal matters are also discussed.

22.1.1 FRAMEWORK FOR RISK-BASED SITE MANAGEMENT

Environmental risk assessment at contaminated sites entails characterization of the source of an environmental hazard, identification of exposure routes through which a contaminant may come into contact with a receptor, assessment of the relationship between the contaminants and the adverse effects produced (if any) and, finally, estimation of the effect (CCME 1996). The primary role of a risk assessment is a technical framework in which potentially contaminated land can be examined, target remediation levels derived, and the environmental issues caused by the presence of contamination managed to protect human and environmental health.

During risk assessment, a major requirement is to identify the key contaminants, pathways and receptors associated with a site, and, at the same time, rule out possible risk scenarios found to be of little or no significance. The three risk components are shown in Fig. 22.1. To achieve this, most site assessments are progressed to the appropriate level of investigation by means of an iterative process of refinement, which seeks to draw an accurate picture of the site through the gradual accumulation of information obtained using increasingly intrusive examination techniques. For risk-based site assessments, the information gathering should be done in an interactive (with all project stakeholders, including the public) and progressive, or "top–down refinement," manner. The top–down approach is illustrated in Fig. 22.2.

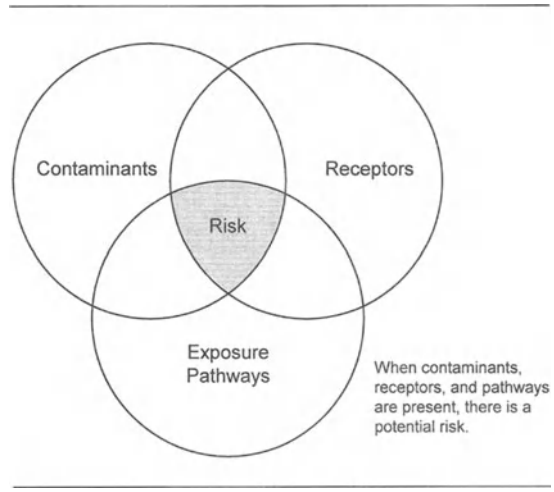


FIGURE 22.1. Risk components (modified from Health Canada 1994).

Beginning at the top level, with the most simplified approach, Table 22.1 summarizes the characteristics of the four main types of risk assessment frameworks in use at the present time. If conservative models based on gross assumptions indicate that no significant environmental problems are present, then more sophisticated examination is not warranted. The most widely used frameworks are the types III and IV, and these approaches will be examined in more detail throughout this chapter.

22.1.2 DEFINING GOALS

The principal goal of contaminated site remediation is to provide acceptable protection to the site users in the context of a specified land use. With the key word "acceptable" being somewhat subjective, the intensity and extent of restoration activities can vary significantly with differing interpretations of what is, or is not, acceptable. Regulators often strive to provide guidance on this issue by issuing generic soil and groundwater remediation criteria, and these are utilized in traditional ap-

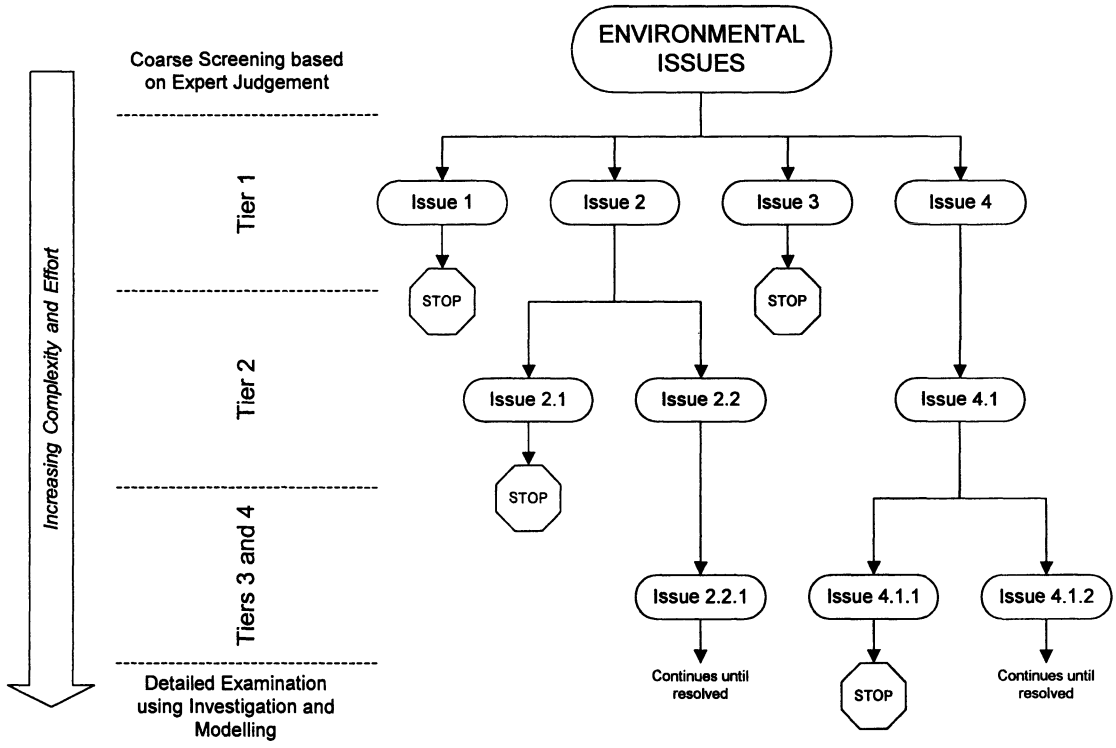


FIGURE 22.2. Top–down approach for risk assessment using step-wise refinement.

proaches to dealing with the definition of adverse effects of contamination by providing general "trigger" levels and remediation goals for the project team (e.g. MoE 1997). These generic criteria are often health-based risk management principles, but necessarily incorporate assumptions that are conservative, in order that they can be applied widely to many situations.

Assessment and management of contaminated land within a site-specific risk-based framework, as opposed to using generic criteria, addresses the issue of acceptability by allowing the environmental issues arising from the presence of contaminating substances to be prioritized according to their significance and in a way that considers site-specific factors such as land use, proximity to environmentally sensitive areas, and the actual geologic and hydrogeologic conditions encountered at the site. In this way, insignificant or trivial environmental effects can be identified and quickly removed from the site management plan, allowing site management resources to be focused on the significant environmental issues; furthermore, the conservative assumptions (on, for example, soil porosity, the rate of contaminant degradation or the groundwater flow regime) used in the generic criteria can be identified and modified accordingly.

22.1.3 REGULATORY AND SOCIETAL ISSUES

The application of risk assessment in the management of contaminated land in North

TABLE 22.1. Types of risk assessment frameworks

Type I: non-analytical method
- Simplest method (advantage)
- Based on the comparison of observed environmental concentrations to tabulated criteria determined according to conservative, exposure assumptions
- Lack of site-specific realism
- Lack of quantitative confidence in results due to generalized nature of generic criteria

Type II: best professional judgment methods
- Risk assessment performed according to the best professional judgment of the environmental consultant/risk assessment team
- Very little procedural guidance
- Outcome highly dependent on the expertise of the assessor
- Can be highly site specific (advantage)
- Can be flexible (advantage)
- Results may not be independently reproducible (disadvantage)

Type III: RAGS-type method
- Consistent with framework developed in the US Environmental Protection Agency's method entitled "Risk Assessment Guidance for Superfund" (RAGS)
- High degree of procedural guidance available, which produces independently reproducible results (advantage)
- Widely accepted method
- Framework consists of four stages: problem formulation, toxicity assessment, exposure assessment and risk characterization
- Lack of site specificity, since RAGS method advocates the use of default factors (and conservatism) in various model parameters (can be disadvantage)

Type IV: enhanced RAGS-type method
- Method based on RAGS but with a significant evolutionary advancement because of the incorporation of scientifically based procedures (advantage)
- More realistic and able to quantify risk estimates and degree of uncertainty in estimates (advantage)
- Disadvantage to regulatory and regulated communities since unfamiliarity with such issues as probabilistic and statistical concepts
- Increased effort, time and cost associated with increased degree of site-specific realism (can be disadvantage)

America has gained widespread recognition by regulatory agencies in recent years (USEPA 1997; CCME 1996). In fact, the majority of Western industrialized countries have developed or are in the process of developing risk-based soil and groundwater quality criteria (CARACAS 1998). These are often based on the "Risk Assessment Guidance for Superfund" (RAGS)-type approach, but do differ in some aspects, and so the risk assessment team should become familiar with applicable regulations in the appropriate jurisdiction at the outset of the risk assessment.

A single universal approach has not yet been defined, although the 1996 American Society for Testing and Materials (ASTM) document (ASTM 1996) for risk-based corrective action (RBCA, pronounced "Rebecca") is the most widely practiced. The ASTM RBCA standard was developed to provide an overall process to assess risks associated with total petroleum hydrocarbon (TPH) sites. It incorporates methods developed under the USEPA superfund program for hazardous waste sites. In essence, it integrates site assessment, remedial action selec-

tion, and monitoring through the use of USEPA risk assessment methodologies.

22.2 *Site Assessment for Risk-Based Site Management*

22.2.1 SCOPE AND OBJECTIVES

Site assessment is considered to be the most critical stage of problem identification and risk management at contaminated sites. Information obtained during this phase of the site management program invariably provides the basis upon which the entire site management plan is founded and may be used to determine the nature and magnitude of any risks the site may pose, and the type and extent of risk management alternatives that might be required. The situation is often further complicated by a variety of social, financial and legal issues that must be factored into the assessment process. The primary objective of any site assessment is to provide accurate, reliable data on the environmental condition of the site.

Key site assessment goals may include any or all of the following items: identifying sources of contamination both on and off site; determining the extent, location and nature of contamination both on site and off site; assessing the geological and hydrogeological characteristics of the subsurface; identifying the type and locations of any underground structures, including service utilities, that may be present on site; obtaining information pertinent to geotechnical matters, e.g. soil stability, foundation design; identifying site users, both human and ecological. An account of conventional site characterization components and methods is provided in Chapter 4.

22.2.2 SITE ASSESSMENT PROCEDURAL COMPONENTS

An environmental site assessment (ESA) is usually carried out in two stages in a top–down manner:

22.2.2.1 Stage 1: Non-Intrusive Phase I Investigations

The first stage of site assessment is usually a conventional non-intrusive investigation and is intended to identify the potential for a site to have been impacted. Available information is assembled on the existing condition of the site, its past and present uses and any issues of potential environmental concern. At this stage, the focus is not only on the most immediate or obvious risk scenarios that could potentially arise at the site, but also those areas where a more detailed investigation could be required.

As described in Chapter 4, phase I assessments typically comprise one or more site visits and a background/historical survey. A limited, non-intrusive field monitoring program may also be undertaken. Knowledge of the site is maximized through the use of site photographs, personal interviews with individuals familiar with the historic site, site records, maps, aerial photographs, local and regional authority records and library sources. Information collected at this stage may relate to any or all of the components of the contaminant–exposure–receptor paradigm, including actual or potential site users (human and ecological), groundwater migration pathways, the presence of neighboring receptors (human and ecological) or sensitive water bodies, land usage at the site and the immediate vicinity.

In proceeding this way, an inventory is compiled of potential hazards associated with the site, the likely exposure routes and the potential human and/or ecological receptors. If, upon completion of the initial investigation, it appears that potential sources of contamination exist at or adjacent to the site, or that there is potential for off-site migration of contaminants, then an intrusive phase II investigation is usually warranted.

For an in-depth account of standard procedures in phase I environmental site assessments (ESA), the reader is directed toward the numerous technical manuals and stan-

dard practice documents that are currently available (e.g. CSA 1994; ASTM E1527).

22.2.2.2 Stage 2: Intrusive Site Assessment

Progression to the second stage of site assessment involves the accumulation of more detailed information on the subsurface environmental condition of the site. The objective of the phase II environmental assessment is to better characterize the nature, extent and distribution of contaminants identified during the initial stage as being of actual or potential concern, such that the actual risks posed by the site can be more accurately evaluated. This is accomplished by a combination of intrusive environmental sampling and subsequent chemical analysis.

Ideally, phase II ESAs should themselves comprise several stages: an initial planning stage, a site investigation and sample analysis stage, and a data evaluation stage. Allowance should be made to continually move information between these stages, since this often results in a more focused and insightful final product. It is not uncommon, for example, for the preliminary results of an analytical program to be used to direct further sampling and analysis.

The initial planning stage of the investigation will draw heavily upon the findings of the phase I ESA to determine the number, location and type of samples to be taken. At this stage, consideration is given to the nature of the contaminants under investigation, as different contaminants exhibit varying subsurface distribution characteristics. This point is elaborated upon in the following section. Sampling is usually accomplished through the groundwater or vapor use of boreholes/monitoring wells and/or test pits, which permit sampling of subsurface soil/groundwater and/or vapors at various depth intervals (see Chapter 4 for details). Figure 22.3 illustrates the phased approach to environmental site assessment (leading to remediation) and the interaction of ESA with the risk assessment process.

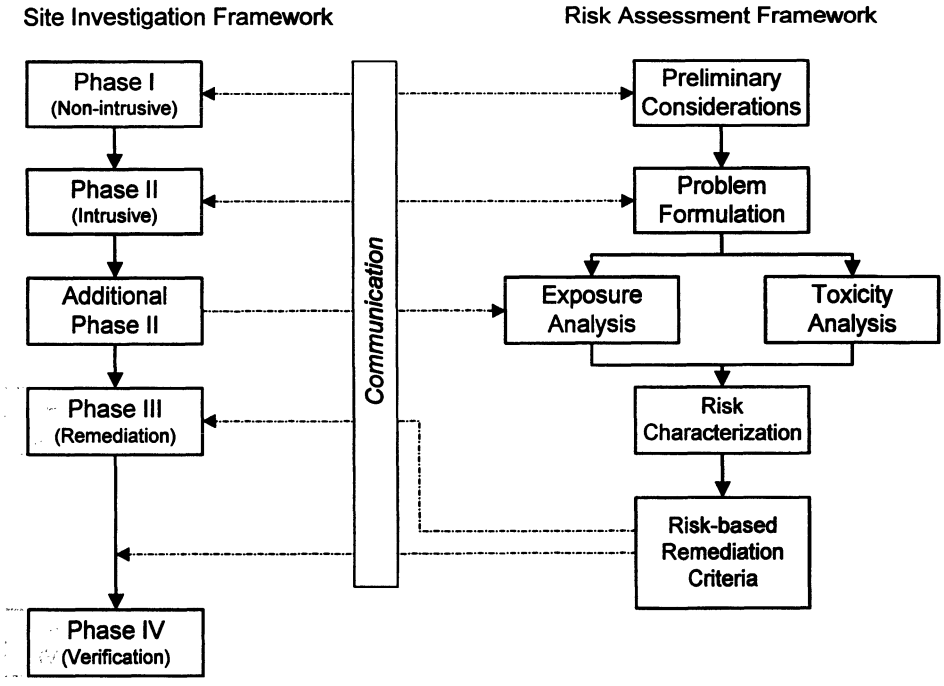


FIGURE 22.3. Environmental site management framework.

22.2.3 SAMPLING STRATEGIES AND METHODS

When designing a site sampling strategy, it is important to be mindful of the spatial and temporal variations in contaminant concentrations that may occur across a site, as well as the heterogeneity of the site subsurface.

There are two main approaches to sampling at contaminated sites: probabilistic (random) sampling; and deterministic sampling, in which decisions are made on where to sample based on some previous knowledge of the site and/or the investigation. Random sampling is favorable for any statistical treatment of data collected, which is often the case where quantitative risk assessment is applied or when the site is evenly or randomly contaminated.

Sampling should be carried out according to the recognized USEPA, ASTM (both US standards) or CCME (Canadian) protocols to ensure the necessary level of quality assurance (e.g. USEPA 1997; ASTM E1527;

TABLE 22.2. Summary of environmental sampling strategies[a]

Type of sampling design	Conditions when the sampling design is useful
Haphazard sampling	A very homogeneous population over time and space is essential if unbiased estimates of population parameters are needed. This method of selection is *not* recommended due to difficulty in verifying this assumption
Judgment sampling	The target population should be clearly defined, homogeneous, and completely assessable so that sample selection basis is not a problem. Specific environmental samples are selected for their unique value and interest rather than for making inferences to a wider population
Probability sampling, simple random sampling	The simplest random sampling design. Other designs below will frequently give more accurate estimates of means if the population contains trends or patterns of contamination
Stratified random sampling	Useful when a heterogeneous population can be broken down into parts that are internally homogeneous
Multistage sampling	Needed when measurements are made on subsamples or aliquots of the field sample
Cluster sampling	Useful when population units cluster together areas of specific historic use, and every unit in each randomly selected cluster can be measured
Systematic sampling	Usually the method of choice when estimating trends or patterns of contamination over space. Also useful for estimating the mean when trends and patterns in concentrations are not present or they are known *a priori* or when strictly random methods are impractical
Double sampling	Useful when there is a strong linear relationship between the variable of interest and a less expensive or more easily measured variable
Search sampling	Useful when historical information, site knowledge, or prior samples indicate where the object of the search may be found

[a] Modified from Gilbert (1987).

CCME 1996; MoEE 1996a). Gilbert (1987) provides an insightful discussion of different sampling strategies (see Table 22.2).

22.2.4 COMMON DIFFICULTIES ENCOUNTERED DURING THE SITE ASSESSMENT PROCESS

As stated in the opening paragraph of this section, information obtained during site assessment often underpins the entire problem identification and risk management process. It is crucial, therefore, to ensure that data of sufficient quality and volume are collected throughout the site assessment phase. The number and location of data points should reflect not just the size of the contaminated site, but also the number of environmental compartments into which the contaminant(s) may have partitioned and the type of sampling regime selected (deterministic versus random). Where a number of subsurface phases are suspected of having been impacted by a particular contaminant, then this should be reflected in the variety of samples taken. Petroleum products, for example, can potentially give rise to soil vapors, dissolved phase contamination, a residual phase adsorbed to soil natural organic matter and free-phase contaminant. It may be necessary to sample each of these subsurface phases in order to gain an accurate picture of the extent of contamination. It follows that composite samples, taken from more than one location are only used for contaminant screening but are of little use as input data for risk assessments.

22.3 Contaminant Identification

22.3.1 REQUIREMENTS AND OBJECTIVES

Contaminant identification within geoenvironmental problem identification and risk management is concerned principally with establishing the source, abundance, distribution and direction, and speed of movement of contaminants in the subsurface media. Invariably, a combination of complex contaminants together with their degradation products, heterogeneous soil subsurfaces and confounding site-specific factors, e.g. site location, topography, give rise to a variety of technical challenges that must be addressed to fully characterize the contaminants present at a site.

22.3.2 TYPICAL CONTAMINANTS AND ASSOCIATED HAZARDS

The inherent diversity in materials and processes used in industrial activities has given rise to a multitude of potentially contaminating substances. Certain classes of contaminant are routinely associated with certain industries, and this assists the risk assessor in selecting which contaminants could be of concern at a particular site. In general, contaminants are classified according to their chemical characteristics. There are two main families of chemical contaminant: inorganic and organic. Examples of each, together with typical sources are provided in Table 22.3.

22.3.2.1 Inorganic Contamination

This is usually associated with the presence of metals, but also includes cyanides and other anions such as chlorides, sulphates and nitrates. Metal contamination is common at former industrial sites, and can be associated with activities such as mining, smelting, steel production, landfarming, scrap metal yards, vehicle maintenance, manufacturing, sewage treatment and the like. In particular, arsenic, cadmium and lead are known to be acutely toxic to both plants and humans, whereas zinc, copper and nickel are primarily phytotoxic (harmful to plants).

Cyanides are commonly associated with mining, manufactured gas plants and waste disposal facilities, whereas sulphates are produced by numerous industrial processes. Both represent a hazard to human and ecological receptors, in addition to acting as corrosive agents on building foundations.

TABLE 22.3. Examples of industries/activities and their contaminants

Inorganic contaminants	Organic contaminants
Examples	Examples
Iron (Fe), manganese (Mn)—usually of concern for aesthetic reasons in water supplies	Polynuclear aromatic hydrocarbons (PAHs)
Heavy metals—silver (Ag), mercury (Hg), cadmium (Cd), zinc (Zn), copper (Cu), lead (Pb), chromium (Cr), arsenic (As)	Phenols
Acids and bases	Pesticides
Cyanide	Non-chlorinated solvents
	Chlorinated solvents
	Polychlorinated biphenyls (PCBs)
	Petroleum hydrocarbons
Typical sources	Typical sources
Mining and smelting operations	Fuel dispensing
Mine tailings and tailings ponds	Degreasing operations
Landfills	Electrical conductors
Sewage	Bulk storage depots
Metal plating operations (Ag, Cr)	Sewage
Paint, painting operations (Pb, Cd)	Metal plating operations
Pulp mills (Hg)	Paint, painting operations
Wood treatment (Cu, Cr, As)	Wood treatment
Auto wrecking yards	Auto industry
Industrial and municipal landfills	Home heating
Thermal power stations	Industrial and municipal landfills
Imported fill soils (when imported to a site from one of the primary source areas)	Power stations

22.3.2.2 Organic Contamination

Organic contaminants include petroleum products (from gasolines to heavy fuel oils to bitumen), coal tar, solvents (including chlorinated compounds), phenols, dioxins and expanded polychlorinated biphenyls (PCBs). These contaminants differ widely in their chemical composition and inherent toxicity. In considering the risks associated with these contaminants, it is important to recognize that organic contaminants are usually mixtures of many individual chemical compounds (gasoline, for example, comprises several thousands of compounds), each exhibiting different chemical, physical, biological and toxicological properties, and that this can result in multiphase environmental partitioning following a spill event. Many organic contaminants, most notably benzene and polynuclear aromatic hydrocarbons (PAHs), are considered to be carcinogenic to humans.

Common vapor phase contaminants include methane, carbon dioxide, carbon monoxide, hydrogen sulphide and sulphur dioxide, as well as low molecular weight volatile organic compounds (VOCs), which exist either in vapor or liquid phases. These substances present a variety of risks, including combustion, asphyxiation, corrosion and health impacts following inhalation.

22.3.3 THE LINK BETWEEN CONTAMINANT BEHAVIOR AND RISK

In considering the various types of contaminant that may be faced by the risk assessor, and how these contaminants should be characterized in order to begin the problem identification process, it is important to understand what happens to a contaminant following its release into the natural environment. In particular, because the toxicity and exposure characteristics (and, therefore, the risks) associated with a particular contaminant are influenced by the chemical form of

the contaminant and its distribution in the environment, attention should be given to elucidating how contaminants partition in the environment, and how their composition or chemical form could change following a release (Sims 1990). This is also important in establishing the routes by which exposure could occur. In broad terms, the characteristics that govern contaminant environmental fate and partitioning can be considered as inherent properties of the released material and the properties acquired as a result of contaminant weathering and subsurface attenuation. These are physical, chemical and biological processes that alter the chemical form and, therefore, the subsurface behavior of chemical contaminants. Both inherent and acquired characteristics must be considered in order to obtain a complete picture of the exposure scenarios presented by a particular contaminant.

22.3.3.1 Contaminant Partitioning

The partitioning of contaminants between the available air, water, soil, natural organic matter (NOM), mineral and free-product phases during their passage through the subsurface is governed by the fundamental physical, chemical and biological properties of the contaminants and the geology and hydrogeology of the subsurface.

Different contaminants will partition throughout the subsurface in a variety of ways. For metals, it is important to consider the conditions of the subsurface, especially parameters such as pH and redox potential. These parameters affect the chemical form of metals, which in turn influences the extent to which the contaminants are bound in the soil phase or mobilized in groundwater. Arsenic, for example, can exist in over 30 different forms, each exhibiting its own particular toxicity (Hrudey & Pollard 1993).

Organic contaminants can be complex mixtures of individual compounds and often partition into several phases. For organic non-aqueous-phase liquids (NAPL), for example, it is generally possible to identify six phases into which the mixture may partition (Hrudey and Pollard 1993):

- immobilized pockets of residual contamination in the unsaturated soil;
- individual contaminant constituents adsorbed to soil natural organic matter (NOM) or mineral matter;
- the vapor phase, through evaporation;
- the aqueous phase, dissolved in groundwater in the saturated or interstitial zone;
- mobile component, termed non-aqueous-phase liquid (NAPL), which is either less dense (LNAPL) or more dense (DNAPL) than water; and
- a contaminated water emulsion.

Figure 22.4 illustrates simplified partitioning behavior of four common environmental contaminants.

Knowledge of the subsurface partitioning allows appropriate risk management technologies to be selected and targeted accordingly. The application of groundwater pump and treatment technologies that focus only on removing contaminants from groundwater, for example, fail to target the residual contamination in the vadose zone and can result in an unnecessarily prolonged, expensive and ultimately ineffective site clean-up operation. Sources of fate and partitioning information for organic contaminants are provided by MacKay *et al.* (1992–1997); Howard (1989, 1991).

22.3.3.2 Contaminant Weathering

A variety of interactions take place between the contaminant and the soil–groundwater matrix that affect the chemical composition of the contaminants and their partitioning throughout the subsurface. These processes are collectively referred to as weathering. Specifically, weathering can be divided into four main processes: (i) volatilization, (ii) dissolution, (iii) chemical alteration, and (iv) biotransformation (Brady *et al.* 1998). Since these processes affect the chemical form of the con-

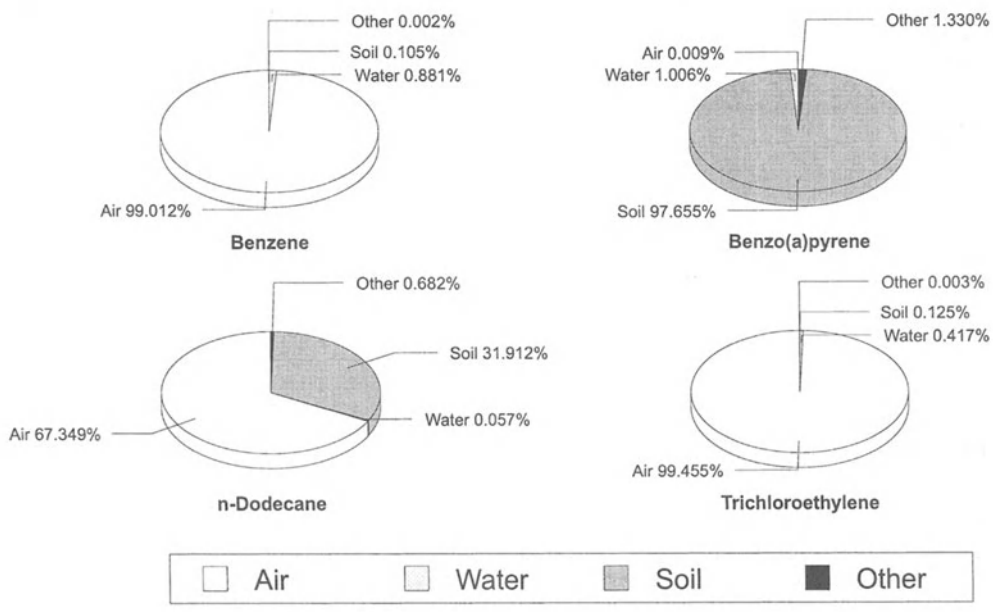


FIGURE 22.4. Fate and partitioning of common organic contaminants based on contaminant "fugacity" or escape potential (see MacKay *et al.* 1991, 1992, 1993).

taminant, they have significant bearing upon how a particular contaminant may be sampled and analyzed, the hazard that it represents, the routes via which exposure can occur and the manner in which it should be treated. For example, trichloroethylene, though itself a fairly mobile, noncarcinogenic hazard, can be degraded into vinyl chloride, a more mobile and reportedly more potent carcinogen.

22.3.4 SELECTION OF ANALYTICAL PARAMETERS

The selection of analytical parameters directed by the nature of the contaminants are identified as being of greatest concern during the phase I site assessment/contaminant identification process. Often, however, risks at contaminated sites can be estimated by considering the presence of one or more individual compounds (usually those of greatest toxicological significance), known as surrogate compounds. The analysis of surrogates may require interrogation of the contaminant matrix beyond conventional "prescriptive" analytical parameters, i.e. standard sets of analytical parameters. Thus, it is advisable to arrange for analyses to be completed by one of the many professionally certified analytical laboratories to ensure that the analytical procedures and techniques used during analyses will be in compliance with standard procedure.

The range of analytical techniques available varies considerably depending upon the type of contamination being examined. Analysis is most effectively accomplished by a phased analytical approach, in which non-specific screening techniques, such as are used to obtain information on the total concentrations of organics, and more sophisticated techniques are then applied to target individual contaminants of greatest toxicological concern.

Screening techniques usually involve measurement of total oil and grease, total petroleum hydrocarbons, total metal loading and total extractable hydrocarbons by gas chromatography (GC) and solvent extraction

methods. These techniques allow the amounts of broad collective "groups" of contaminants to be estimated. While this is useful for elucidating the extent of contamination, for the purposes of the risk-based site management it is essential that an assessment of the contaminant extends beyond the measurement of bulk containment concentrations to provide information on specific contaminants and weathering. Individual chemicals are usually detected by gas chromatography–mass spectrometry (GC–MS) or inductively coupled plasma–mass spectrometry (ICP–MS) methods. Target compounds should be those of toxicological significance: benzene, toluene, ethylbenzene and xylene (BTEX); polynuclear aromatic hydrocarbons (PAHs); surrogate compounds; and, special categories such as phenols, volatile aromatic compounds, ketones and so on. Depending on how these latter techniques are employed, it is also possible to shed light on the movement, age and source of a particular contaminant, although this requires the input of a specialist analytical chemist.

It is crucial that appropriate analytical parameters be selected if the results of the ESA are to match the expectations of the risk characterization. In particular, because the chemical form of a contaminant often has considerable bearing upon the severity of the hazard it represents and its mobility in the environment, analytical techniques should be selected according to their ability to impart information on the specific chemical form of greatest concern. The use of generic analytical criteria, such as total extractable hydrocarbons or total metal analyses, does not discriminate between the chemical form or the toxic potential of the chemical under analysis, and thus provide only marginal insight into the true nature of the risk to human and ecological health (Whittaker *et al.* 1995). Similarly, the reporting of chemicals as "non-detects" should be treated with caution by the risk assessor, as analytical methodologies are sometimes unable to resolve highly complex mixtures of contaminants (absence of proof is not proof of absence). Importantly, method detection limits for analytical techniques employed should be below the maximum acceptable contaminant concentration. This point is elaborated upon in Section 22.3.4.

22.4 Problem Formulation

Problem formulation, as the initial stage of the risk assessment process, provides the foundation for the subsequent stages of the risk assessment. This is sometimes referred to as a screening level risk assessment. The aim is to devise a conceptual model that correctly simulates the anticipated usage of the site. This model can be used to understand and discriminate between significant and insignificant environmental risks by considering the three risk components: the contaminants present at the site of interest, the humans and ecological receptors that use the site, and the exposure pathways of contact that are possible between the contaminants and the receptors. These contaminants, receptors and exposure pathways are examined in some detail to identify the combinations that are possible and contribute the most potential risk. Where no contaminant-exposure route-receptor link can be reasonably established, the risk to the receptor in question is deemed insignificant. These insignificant risks can then be eliminated from further consideration or "screened" out. The significant risks that remain are, therefore, derived from any potential link between the three risk components: contaminant, exposure, receptor. These risks can then be examined and quantified in more detail through an in-depth exposure, toxicology and risk characterization (the subsequent stages of the risk assessment), after which they too may prove to be insignificant, or at least "tolerable." At the qualitative screening level, distinguishing between significant and insignificant risks relies heavily on the experience of the risk assessor: in some cases, comparing

site soil and groundwater quality to generic criteria provides a useful indication of where risks may be significant or not.

22.4.1 CONTAMINANTS

The presence, type, amount and distribution of contaminants across the site must be estimated as described in Section 22.3, and this is usually achieved through a site investigation as detailed in Section 22.2. Correct identification of the type and amount of contaminants present at a site is clearly pivotal to establishing the hazard (and, therefore, the risk) associated with a contaminated site. Also important are the details of the fate and partitioning of contaminants. The linkages between contaminant type, fate and partitioning, and the associated human health and environmental risks are described in Section 22.3.

22.4.2 RECEPTORS

Receptor screening involves determining the identity, sensitivity and behavioral characteristics of all site users that could potentially be exposed to the contaminants of concern. This may include humans, plants, animals, fish, soil invertebrates and other valued ecosystem components. For the purposes of risk assessment, the term "site users" should include all areas potentially affected by the contamination (both on and off site) and taking into account the current or intended usage of the site.

The goal of this task is to develop a list of potential receptors, their toxicological sensitivities and site use characteristics, which can be used as a basis for more detailed receptor analysis in subsequent stages of the risk assessment. Sensitive receptors, such as endangered species, would also have to be identified and included within the assessment. Figure 22.5 illustrates a conceptual framework for receptor screening.

22.4.3 PATHWAYS

Screening of pathways requires consideration of the potential exposure routes by which receptors identified in the previous task could be exposed to risk. There are three funda-

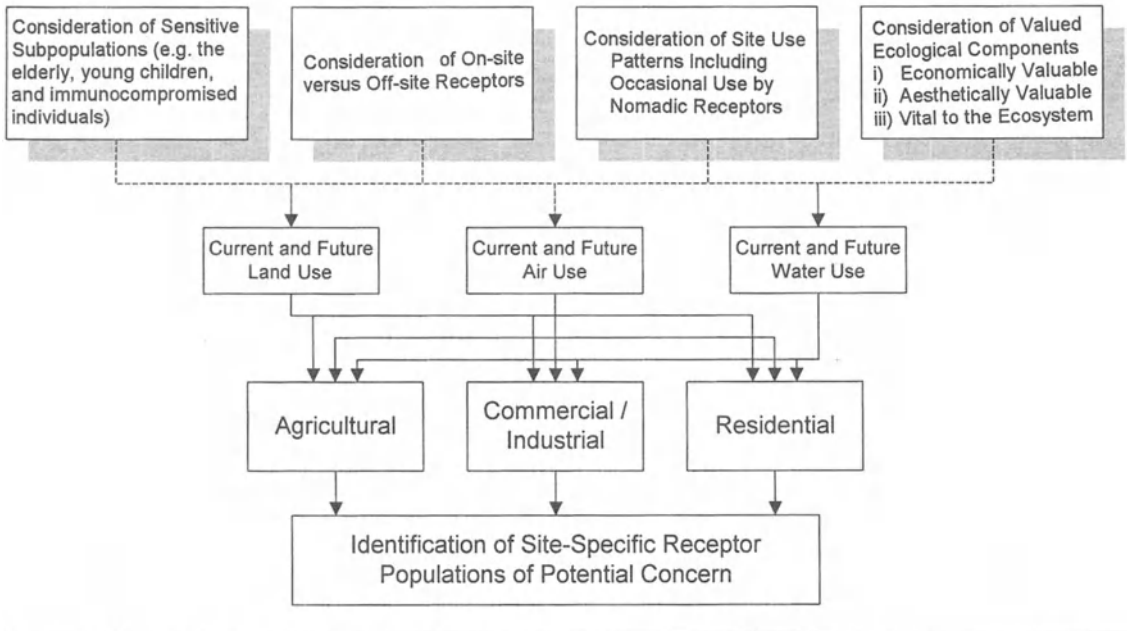


FIGURE 22.5. Receptor screening process.

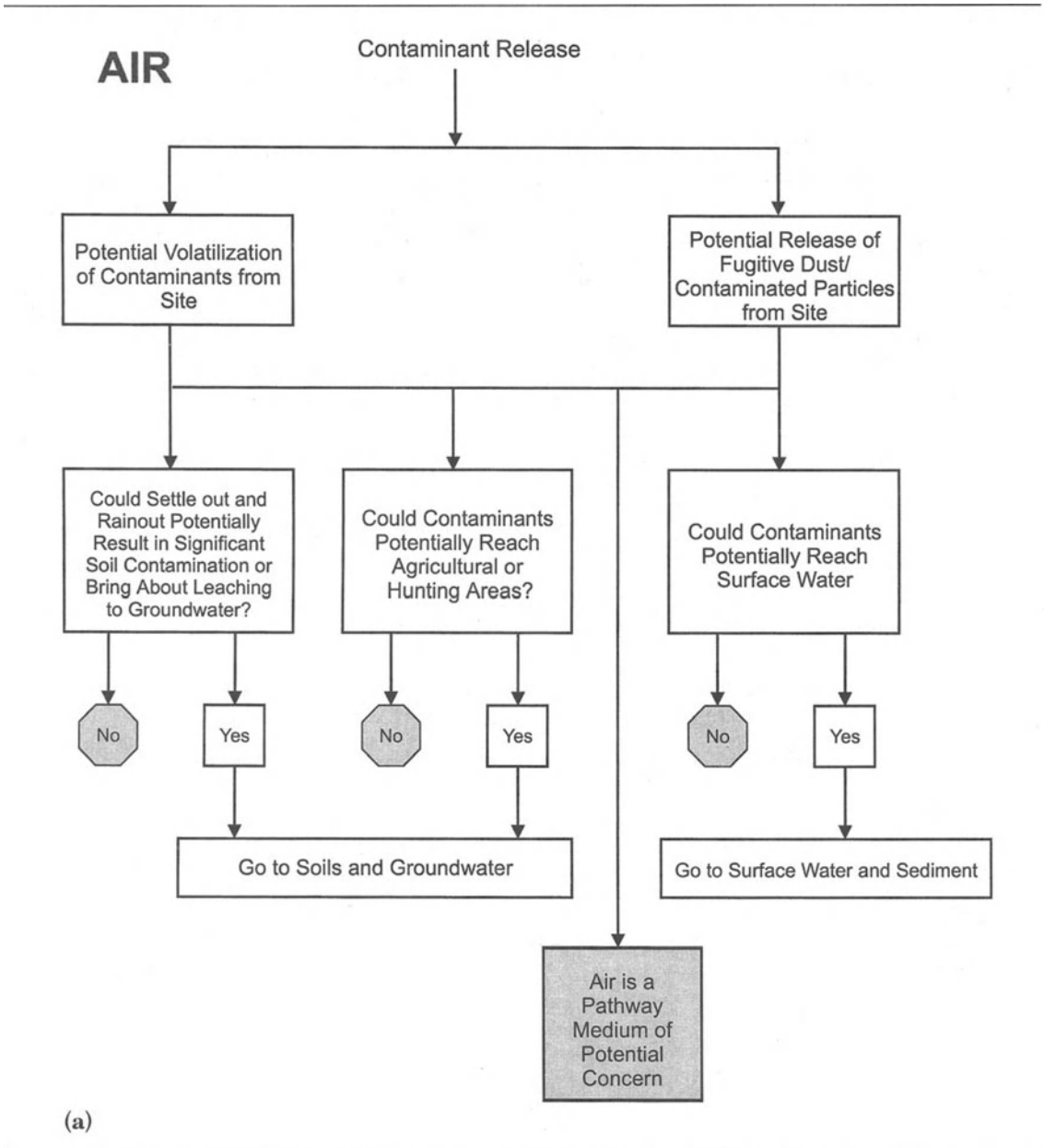


FIGURE 22.6. (a) Pathway process.

mental exposure routes to be examined: ingestion of contaminants (either directly, or through consumption of contaminated materials, including garden produce); inhalation of volatile contaminants, or contaminants carried on dust particles; and dermal contact, where the receptor is exposed by direct contact with contaminants. Receptor exposure to contaminants is usually based on some combination of these pathways. At this stage, the detailed features of the exposure need not be considered or quantified: the goal is to compile a descriptive list of all potential exposure routes (see Fig. 22.6a, b).

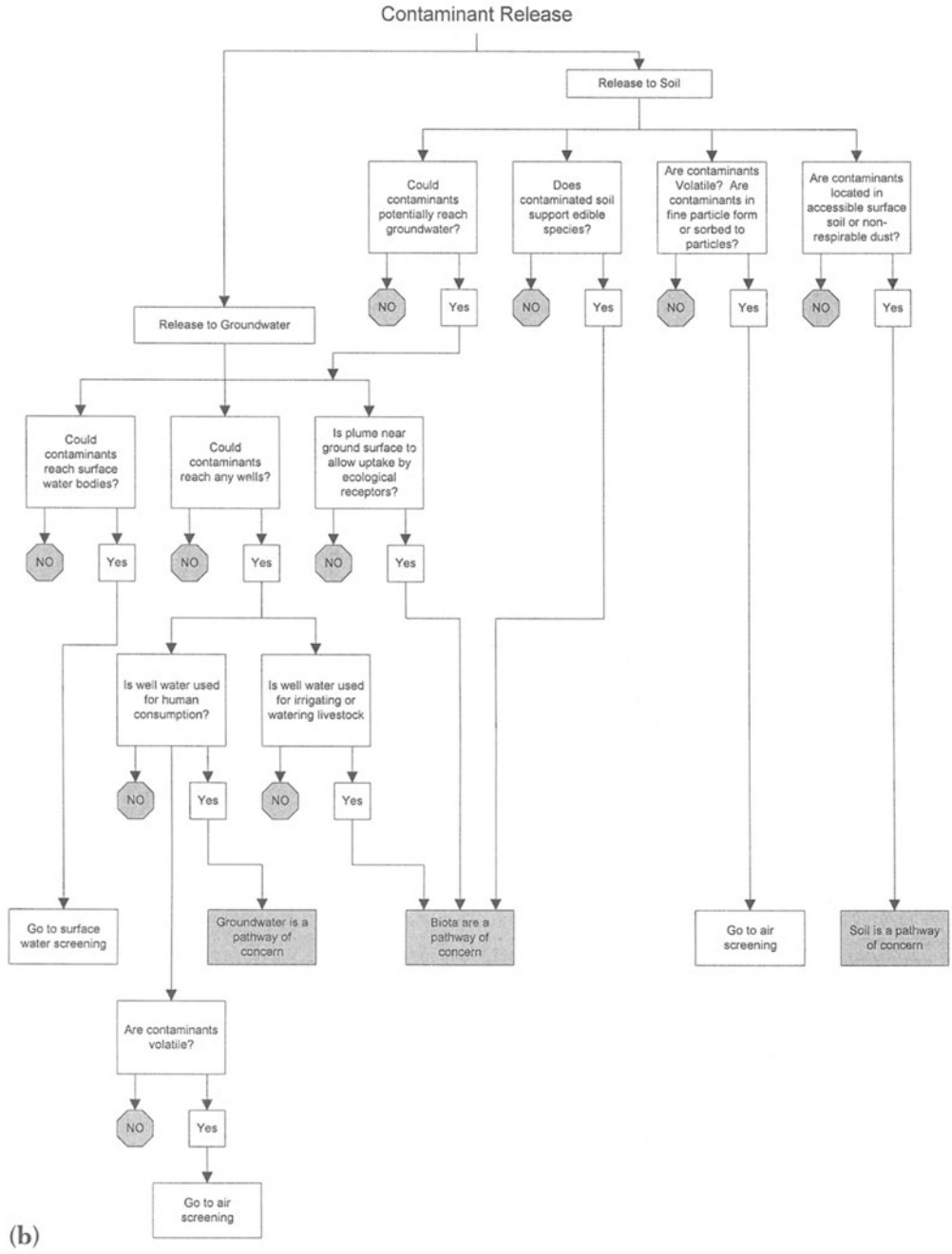


FIGURE 22.6 (Continued). (b) Soil and groundwater screening process (modified from USEPA 1989).

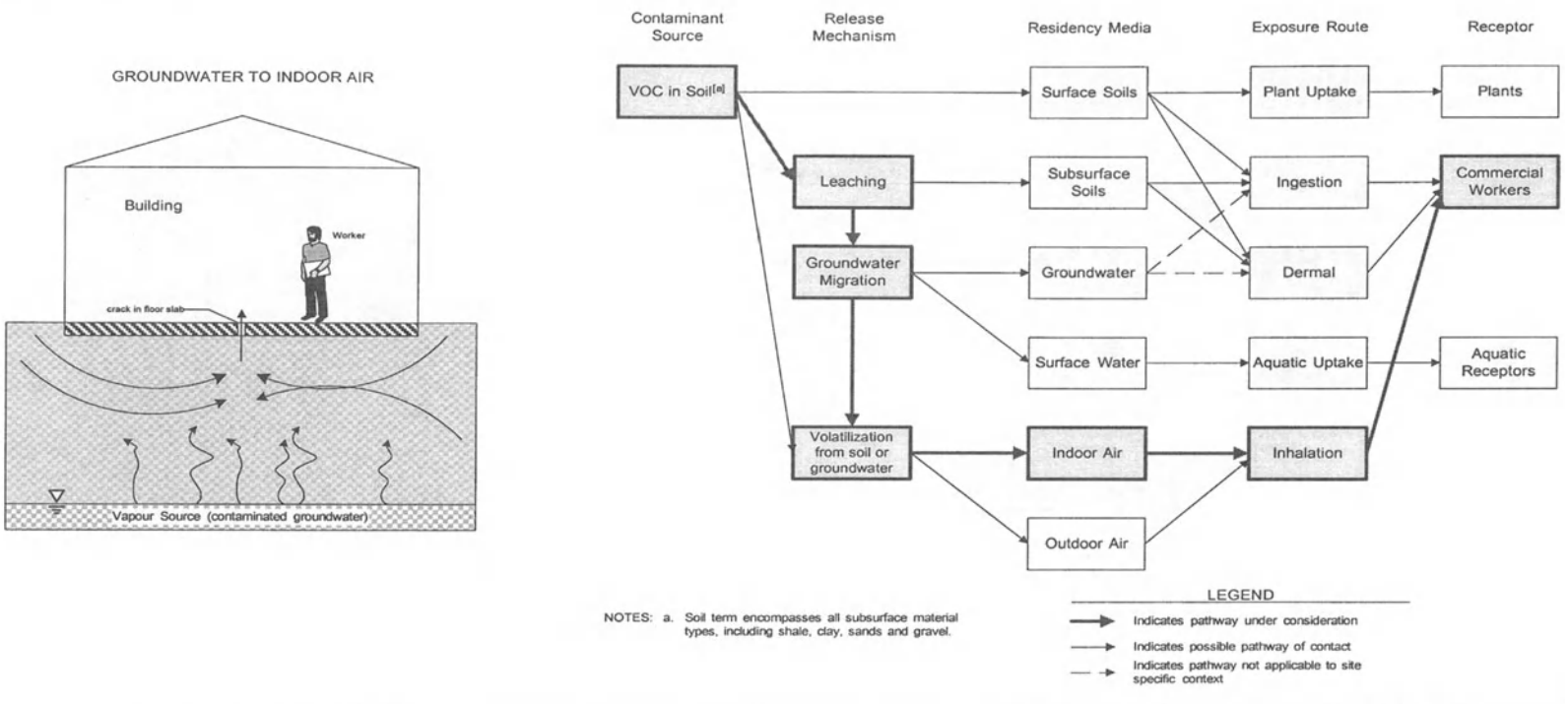


FIGURE 22.7. Conceptual exposure pathways model.

22.4.4 CONCEPTUAL PATHWAY MODEL

The combination of contaminant–pathway–receptor connections (termed environmental components) that emerge from the screening process form the basis of the conceptual model, which simulates the site condition and potential areas of environmental concern. The conceptual model not only provides a qualitative examination of the potential risk scenarios but guides the subsequent quantitative risk assessment, if required. It should also be used to guide additional refinements of the site assessment. Figure 22.7 provides an example of a conceptual pathway model.

In developing the conceptual model, the risk assessor is always seeking to summarize the relationship between contaminants, exposure pathways and receptors taking into account the technical requirements of the project.

Questions answered by the conceptual model include:

- Is it possible for the contaminants to come into contact with the site users?
- What substances are on the site? Where are they in the environment? How much is there?
- What/who are the site users (current or future)? How do/will they use the site?

If by examination of the potential risks there is no route by which the contaminants can come in contact with the receptors, then the contamination does not present a risk (no exposure, no risk) and the risk is deemed insignificant. In such cases, an acceptable environmental risk scenario is considered to prevail, i.e. the risks identified were not considered significant, and the risk assessment should terminate at this stage with recommendations for environmental management controls that maintain the conditions under which the "acceptable risk" situation is prevalent. However, if risks to users are considered to be potentially significant, i.e. there is a possibility that exposure could occur now or sometime in the future, then the remaining quantitative stages of the risk assessment should be completed. These are described in the following sections.

22.5 *Exposure Assessment*

22.5.1 OBJECTIVES AND LINK TO RISK ASSESSMENT PROCESS

Exposure assessment is the first stage in the assessment following problem formulation, and is carried out for all contaminating substances, receptors and pathways of exposure considered to be of potential significance during the initial problem formulation/risk screening stage.

In the exposure assessment stage, the magnitude of the potential exposures for the combinations of substances, site users and pathways identified in the conceptual model are evaluated using specified technical procedures, equations and models. Contact rates between contaminants and receptors are quantified by estimating the amount of substances at the site, the physical and chemical properties of the substances of concern and the biological characteristics of the site users, and the estimated duration of exposure for given land use scenarios; this is usually expressed as an amount of chemical intake by the receptor over a specified period of time. Estimated exposures may then be compared to documented exposure limits (or potency factors) to reveal whether acceptable limits have been exceeded and action is required.

Questions answered by the exposure analysis include:

- How much contact between the substance and the site users can occur?
- Which pathway is contributing the most contact?
- What is the acceptable level of exposure of the contaminant?

The exposure assessment is usually carried out in tandem with the toxicity assessment stage of risk assessment described in Section 22.6, since information from these components form the basis of the risk evaluation of exposure and tolerance. For example, the toxicity data of a chemical may be specific to a certain route of exposure intake; likewise, toxicity data may indicate that a certain receptor is particularly sensitive to a contaminant, requiring specific exposure assessment for this receptor.

22.5.2 BASIC ELEMENTS OF EXPOSURE ASSESSMENT

Exposure assessment is achieved by the application of mathematical exposure models and equations that have been developed to simulate exposure route. Thus, models exist for quantifying migration of contaminants through soil to indoor air and subsequent inhalation by humans; or ingestion of contaminated soil by children or small animals, etc. These models are continually being upgraded by researchers and risk assessors to improve their accuracy in predicting the exposure conditions. Selection of appropriate exposure models and choice of input parameters and assumptions require judgment on behalf of the risk assessor as well as communication with other stakeholders, e.g. regulators, the public. Simulation of exposure routes should only be carried out by suitably qualified and experienced practitioners.

The input for the exposure assessment may be obtained from: studies of the concentrations of various contaminants through affected environmental media (air, soil, groundwater and surface water), which may be accomplished through modeling of contaminant fate and distribution (see Chapter 25); an assessment of contaminant bioavailability (ability to participate in biological interactions); an analysis of receptor characteristics (to determine when and how often exposure can occur); and an assessment of the potential media through which exposure may occur, e.g. soil characteristics, groundwater flow, air flux patterns. The last analysis for human receptors requires gaining an understanding of receptor physiological characteristics, lifestyle and habits in context of the contaminated site.

In conducting the exposure assessment, exposures for each potential receptor are estimated for each individual pathway (see Fig. 22.7), as well as for the background (non-contaminated) scenario. Thus, for a human receptor, contaminant exposure may be estimated by any or all of the three principal routes of ingestion, inhalation or direct contact, and in some cases may be summed to produce a total exposure value. It should be noted that a distinction is sometimes made between the contact exposure to a particular chemical, termed the potential dose, and the internal dose, which is the amount of chemical absorbed into the body. Most exposure models use the potential dose to describe exposure, i.e. a bioavailability of 100%, as the most conservative scenario. A distinction is also sometimes made between chemicals that act systematically, i.e. they must be adsorbed into the body to cause adverse effects, and those that act locally, i.e. do not require adsorption. For the former, which encompasses the majority of common contaminants, the exposure can be expressed as potential or critical dose rate, e.g. milligrams of chemical per kilogram of body weight per day. For locally acting contaminants, exposure rate is expressed as the duration or frequency of contact. This approach is most appropriate for gases, acid/alkalis and so on. In most cases, the exposure scenarios of greatest significance will become evident, and can then be appropriately simulated.

Many jurisdictions across Canada and the USA have specified exposure models for conducting risk assessments. These approaches may require emphasis to be placed on certain

exposure scenarios, or on particular transport media of concern, e.g. sensitive potable water supplies, depending on their unique circumstances. Most are based upon USEPA guidelines (e.g. EPA 1997) and the reader is directed toward these documents as a source of additional information.

Equation 22.1 describes a typical calculation for ingestion exposure.

$$\text{LADD} = \frac{C_{soil} \times IR_{soil} \times RAF_{ing} \times EF \times ED}{BW \times AT} \quad (22.1)$$

where LADD = lifetime average daily dose (mg kg^{-1} per day^{-1}), C_{soil} = concentration of chemical in soil (mg kg^{-1}), IR_{soil} = ingestion rate of soil (mg day^{-1}), RAF_{ing} = relative absorption factor (fraction, usually 1.0), EF = exposure frequency (days y^{-1}), ED = exposure duration (y), BW = receptor body weight (kg), and AT = averaging time (days). Equation 22.1 describes a typical calculation for ingestion exposure.

22.6 *Toxicity Assessment*

22.6.1 OBJECTIVES AND LINK TO RISK ASSESSMENT PROCESS

Toxicity assessment is conducted for all chemicals of concern identified during the problem formulation, and involves identifying the toxicity associated with the different exposure scenarios. The aims of the toxicity assessment are to identify potential toxicological effects associated with contaminants of concern, and provide an estimate of the amount of chemical exposure that could be considered acceptable without any adverse health effects (for noncarcinogenic chemicals) or within acceptable degrees of risk (for carcinogenic chemicals). In assessing the toxicity of a contaminant, it is important to classify the substances of concern as being either carcinogenic or noncarcinogenic, depending on their mode of toxic action.

22.6.2 BASIC ELEMENTS OF TOXICITY ASSESSMENT

To achieve the objectives of the toxicity assessment as described previously, information is needed on such factors as:

- The mode of toxicological action of the contaminant, i.e. is the contaminant a threshold noncarcinogenic chemical, where adverse effects are noted only above a certain "threshold" dose, or is it a non-threshold (carcinogenic) chemical, where adverse effects are assumed across the entire dose range.
- The exposure limit for contaminants of concern. This is expressed as either a reference dose (RFD), an allowable daily intake (ADI) or tolerable daily intake (TDI) for threshold chemicals, and as a potency factor, or risk-specific dose (RSD), which expresses the dose rate associated with a specific lifetime cancer risk, for non-threshold chemicals. The dose associated with an increase in lifetime cancer risk of one in one million is typically used as the limit of acceptable risk in the USA and Canada, though one in 100 000 and one in 10 000 risks may be employed by certain other jurisdictions.
- Consideration of other factors relating to toxicity, such as the sensitivity of various receptors, the chemical form of the contaminant (e.g. metal speciation or organic isomer presence), the presence of multiple exposure/toxicity components associated with chemical mixtures and simultaneous exposures.

Toxicology information is available from a variety of sources including literature sources, databases, e.g. Integrated Risk Information System (IRIS 1997), USEPA Health Effects Assessment Summary Table (HEAST 1997) and through suitably designed toxicity studies. In all cases, it is recommended that the acquisition/selection of toxicity information be only carried out by an experienced and qualified toxicologist.

Further considerations on contaminant toxicity include the chemical form of the contaminant, the importance of which is described in Section 22.3, the contaminant bioavailability, i.e. its ability to participate in biological activities, and the synergistic effects on toxicity caused by mixtures of contaminants. It is again recommended that interpretations in regard to the above only be carried out by experienced and appropriately trained personnel.

Questions answered by the toxicity analysis include:

- What types of adverse health effects may substances cause after exposure?
- What is the relationship between the magnitude of exposure and the probability or frequency of occurrence of the adverse health effects?
- What level of exposure can be tolerated without adverse effects?

22.6.3 DERIVATION OF EXPOSURE LIMITS

For chemicals with threshold-type, i.e. highly non-linear, dose–response relationships, the safety factor approach is used to estimate the threshold dose that would not produce measurable adverse effects in humans. The procedure used involves the division of the no-observed-adverse-effect-level (NOAEL) of exposure, usually determined from laboratory studies on animals, by appropriate uncertainty factors to derive an exposure limit (USEPA 1989f; Klaassen & Eaton 1991; Health Canada 1993). Typically, uncertainty factors of 100-fold are applied to the NOAEL:

- ten-fold extrapolation between laboratory species and humans; and
- ten-fold for interindividual differences in the human population, i.e. to account for sensitive subpopulations.

If the toxic effect upon which the exposure limit is based is judged to be severe, then additional uncertainty factors of five- or ten-fold, or larger, may be applied to the NOAEL (Health Canada 1993). If the available data are less than ideal, e.g. no information is available following chronic or long-term exposure, further uncertainty factors of two to ten-fold may be applied, depending on a scientific judgment of the weight-of-evidence available (Klaassen & Eaton 1991). The exposure limits developed by such procedures have been called "acceptable daily intakes" (ADIs) by agencies such as Health Canada and the World Health Organization, and "reference doses" by the USEPA (Barnes & Dourson 1988; Klaassen & Eaton 1991). The adoption of exposure limits based on the above procedures assumes that there is a rate of exposure to the chemical, below which no adverse effects would be observed, i.e. where the risk or probability of adverse effects is zero, for practical purposes.

For non-threshold chemicals, i.e. genotoxic carcinogens, the exposure limit is based on cancer potency factors (CPF), which are derived from extrapolating high exposure rates (from experimental studies) where effects can be measured to low exposure rates considered to pose acceptable risks to human health. The mathematical models used to extrapolate the exposure rates are conservative. A commonly used model is the linearized multistage model (Armitage & Doll 1961). A value for negligible risk is selected to calculate a risk-specific dose as the exposure limit. A common value for acceptable negligible risk is one in one million (1×10^{-6}) and corresponds to a risk that is insignificant. The exposure limit can be calculated by:

$$EL = \frac{ILCR}{CPF} \tag{22.2}$$

where ILCR = incremental lifetime cancer risk, i.e. 1×10^{-6}; CPF = cancer potency factory; EL = exposure limit. Detailed discussion of applying uncertainty factors for risk assessment can be found in Faustman and Omenn (1996).

Table 22.4 summarizes a list of sources

TABLE 22.4. Sources of toxicity information

Source	Agency/government	Comment
Existing Data and Information		
Integrated Risk Information System (IRIS)	US Environmental Protection Agency	Website: www.epa.gov/iris
Health Effects Assessment Summary Tables (HEAST)	US Environmental Protection Agency	Published annually
Canadian Environmental Protection Act (CEPA)	Environmental Canada, Health Canada	Publications available through Canadian Federal Government
Canadian Council of Ministers of the Environment (CCME)	Environment Canada, Health Canada	Publications available through Canadian Federal Government
National Institute of Health (NIH) National Toxicology Program (NTP)	NIH/NTP	Website: ntp-db.niehs.nih.gov
Canadian Centre of Occupational Health and Safety (CCOHS)	CCOHS	Website: www.ccohs.ca
Agency for Toxic Substances and Disease Registry (ATSDR)	ATSDR	Hardcopy and CD-ROM published periodically. Website: atsdr1.atsdr.cdc.gov:8080/
American Conference of Governmental Industrial Hygienists (ACGIH)	ACGIH	Published guidelines and rationale to the development of guidelines
National Institute for Occupational Safety and Health (NIOSH)	NIOSH (Centers for Disease Control, US Department of Health and Human Services)	Published guidelines available. Website: www.cdc.gov/niosh
Occupational Safety and Health Association (OSHA)	US Department of Labor	Website: www.osha-slc.gov
Toxicology Excellence for Risk Assessment (TERA)	TERA	Website: www.tera.org
Ontario Ministry of Environment (OMOE)	Ontario Provincial Government	Publications available through Provincial Government
Ontario Ministry of Labour (OMOL)	Ontario Provincial Government	Publications available through Provincial Government
British Columbia Ministry of the Environment, Lands and Parks (BCE)	BC Provincial Government	Website: www.env.gov.bc.ca
Massachusetts Department of Environmental Protection (MDEP)	Massachusetts State Government	Website: www.magnet.state.ma.us/dep/
California Environmental Protection Agency (Cal EPA)	California State Government	Website: www.calepa.cahwnet.gov
World Health Organization (WHO)	WHO	Published monographs on wide-ranging issues, health information may be hard to retrieve. Website: www.who.org
US Air Force Total Petroleum Hydrocarbon Criteria Working Group (TPHCWG)	US Government	Website: voyager.wpafb.af.mil
Region 3 and Region 9 USEPA	Regional USEPA	EPA website (above) has links to Regional Information
***De novo* synthesis of toxicity information**		
Specialist toxicology and risk assessment consultants		
Specialist toxicity testing laboratories		

and/or agencies that provide peer-reviewed toxicity data through published literature or on-line databases (including World Wide Web addresses).

22.7 *Risk Characterization*

22.7.1 OBJECTIVES AND LINK TO RISK ASSESSMENT PROCESS

The final stage of the risk assessment process is risk characterization. This stage integrates the information from the toxicity analysis and exposure analysis stages to estimate the magnitude and nature of the risk (a probability), if any, to which the site users may be subjected.

Risk characterization involves two steps: (i) estimating risks by comparing estimated exposure (as described in Section 22.5) with the acceptable exposure limit (as described in Section 22.6), followed by (ii) a description of the estimated risks in the context of the site-specific factors, background conditions, future land use, uncertainties, and other economic and societal factors. The results of the risk characterization form the basis for subsequent risk management decisions.

22.7.2 BASIC ELEMENTS OF RISK CHARACTERIZATION

Risk estimation may be achieved by either correlating exposure and toxicity assessments to establish whether the site specific exposure is acceptable, or by "back-calculating" maximum allowable soil and groundwater concentrations starting from acceptable exposure limits for each exposure scenario. In this latter methodology, the lowest soil and groundwater concentration across all exposure scenarios is considered to be most protective of human and ecological health, and may therefore be used as acceptable criteria for the site.

Correlation of exposure and toxicity assessments may be expressed as either a hazard quotient (HQ, for threshold chemicals), a numerical cancer risk (NCR) estimate (for non-threshold chemicals) or an exposure ratio (ER) value (which can be applied to both chemical types). The choice of methodology is usually determined by the regulatory agency, in consideration of risk communication requirements. For the HQ approach, the risk is estimated by comparing predicted exposure and exposure limit according to:

$$\mathrm{HQ} = \frac{\text{Dose rate}}{\text{Exposure limit (threshold)}}. \quad (22.3)$$

An HQ value exceeding one, or in some cases 0.1 (reference value depends on regulatory requirements), implies an unacceptable exposure condition.

An NCR estimate is calculated according to:

$$\text{NCR estimate} = \text{dose rate} \times \text{cancer potency factor}. \quad (22.4)$$

The NCR estimate produces a value for the incremental increased risk of acquiring cancer expressed as a probability, e.g. one chance per one million. The USEPA maximum acceptable incremental risk has been set at one in 1 000 000 and this is the most widely adopted value.

The ER value is determined by:

$$\mathrm{ER} = \frac{\text{Dose rate}}{\text{Exposure limit (threshold or non-threshold)}}. \quad (22.5)$$

It is generally considered that the ER approach is preferable for communicating risks to the public because threshold and non-threshold are placed on a similar basis, and because the negative connotations associated with the terms "hazard" or "cancer risk" are reduced, although this latter consideration has no technical substance.

22.7.3 RISK DESCRIPTION

Evaluated risks are most effectively described by making a comparison between risks associated with different scenarios, e.g. site-specific versus background conditions, one exposure route versus another, or exposure-specific risks versus estimated "safe" exposure-risk scenarios, which invariably include one or more conservative uncertainty factors.

Concerns over the description of risks range from the overestimation of risks due to the incorporation of overly conservative factors into exposure limits, to the underestimation of risks due to insufficient accounting for information uncertainties, synergistic effects of multiple exposures, and the toxicity of chemical mixtures.

22.7.4 REPORTING OF UNCERTAINTY

It should be noted that the results of risk assessments should not be provided in absolute terms, without a description of the inherent assumptions, judgments and potential variations that unavoidably arise during the risk assessment process. For example, data obtained from a single sample taken from a single borehole at a site suspected of being contaminated provides information on the identity and concentration of contamination at the point of sampling only. The variation of contaminant identity and concentration with time, areal and vertical extent, and subsurface media can only be assumed, based upon experience and with knowledge of site geology, hydrogeology and so on.

The quantitative results of a risk assessment can usually be presented in one of three ways: point estimates, as a range, or as a probability distribution (see Fig. 22.8).

Where an analysis has been carried out with input parameters or a range of input values, specifically chosen to simulate the exposure conditions, the results of analysis are respectively provided as a single point or range estimated. Discussions relating to uncertainty focus on the reasons why specific values were chosen.

When the analysis is required to more realistically reflect actual conditions, distributions that better describe the variable, e.g. the distribution of body weight for the study population, can be used in the analysis. The analysis is completed with random selection

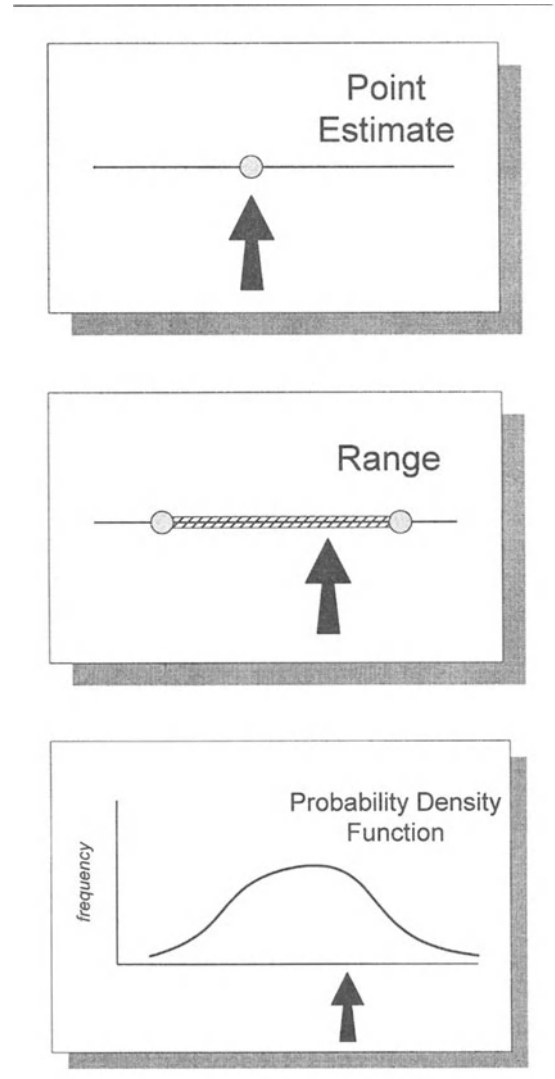


FIGURE 22.8. Methods of presenting results of risk calculations.

of input parameter combination and the results can be presented as a distribution.

Assessments that do not acknowledge such uncertainties risk being laid open to misinterpretation. Presentation of this type of information, or the description of uncertainty, should not be seen as admissions of ineptitude on behalf of the proponent; rather, full reporting of uncertainty provides a mechanism by which the realities of the site's environmental condition can be more fully understood and communicated to all project stakeholders.

22.8 *Risk Communication*

22.8.1 THE NEED FOR EFFECTIVE COMMUNICATION

Risk assessment/risk management projects differ from more conventional environmental management projects in that they invariably involve a broad number of stakeholders, including regulators (from a variety of jurisdictional levels), site owners, developers, lawyers, financial institutions, environmental consultants and the public. These stakeholders have varied interests in the project, and are likely to have differing views, perspectives and understandings of what risk assessment is, what is acceptable and what it can achieve. It is important that there is a clear and mutual understanding between the project team, the stakeholders and the regulatory body(ies) with regards to the scope of the risk assessment and the required level of protection for human and ecological site users. This can only be achieved through communication. Identifying and agreeing upon risk-based restoration, scope and ultimate restoration goals early in the process not only speeds up the remediation process (to everybody's benefit), but also builds and sharpens confidence that the risk assessment has taken into account a broader range of issues to ensure adequate protection for human and ecological site users. In summary, effective communication helps to ensure that all project stakeholders move in unison toward the optimal goal of site restoration. Effective communication resulting in stakeholder commitment is, therefore, critical to the successful application of a risk-based approach to contaminated land management. Two "forms" of communication should be formally accounted for: external communication and internal communication.

22.8.2 EXTERNAL COMMUNICATION

External communication encompasses the necessary public communications program associated with most projects where environmental issues are required to be addressed. This form of communication is often characterized by an atmosphere of scepticism and potential confrontation. Communication regarding environmental issues can become emotionally charged and should be co-ordinated/facilitated by a communication specialist. The primary initial goal of external communication should be to develop a working platform that is founded on a credible, confident and common understanding with the public. The underlying role of risk assessment as a framework for identifying, prioritizing and managing human and ecological health risks. When communicating risks to the general public, it is particularly crucial that the risk assessment option is explained as a legitimate means of providing protection to human health and the environment, and not as a "high tech" means of "risking away" the real issues. It is often forgotten that a risk-based approach was used to develop many generic soil and groundwater criteria, which the remediation industry and the community have accepted.

22.8.3 INTERNAL COMMUNICATION

Internal communication requirements stem from a growing recognition that the manage-

ment of contaminated land within a risk-based context requires effective communication not just between project stakeholders, but also between the various scientific and technical disciplines that may be represented in the project team (Whittaker *et al.* 1998). Key disciplines are engineering (for risk management and remediation activities), chemistry (for understanding the fate and partitioning of contaminants), geology and hydrogeology (for site assessment, including soil types, and groundwater flow patterns), environmental microbiology (for understanding the effects on spilled oily wastes on soil microbial consortia) and toxicology (for defining the ecological and human health risks presented by contaminants). In problem identification for risk assessment, it is imperative that dialogue is initiated between the toxicologist, chemist and the field engineer during the planning and design stages of the field investigation program, rather than after the field work has been completed. This communication will ensure that the field sampling is directed not just by contaminant abundance and/or availability, but also by toxicology, pathways and exposure concerns.

22.9 Risk Management

As discussed above, completion of the problem formulation and risk assessment will quantify the environmental risk associated with a site and provide the proponent with an understanding of how and what level of significance environmental risks may be presented at a site. Clearly, if the risks are evaluated to be at unacceptable levels for any valued receptor, then the proponent must carry out work to mitigate these exposures. On this basis, the objective of an environmental risk management strategy is to provide suitable protection to the human and ecological site uses from the potential environmental exposure.

The implemented risk-based measures should specifically address the dominant components of the environmental risk and reduce the exposure to acceptable levels.

22.9.1 SELECTION OF RISK MANAGEMENT OPTIONS

Typically, a range of mitigative risk management measures are required to address issues identified in the risk assessment. At a conceptual level, risk management measures are directed to either removing or reducing contaminant levels, blocking exposure pathways or changing the habits or presence of the receptor (Fig. 22.9). Such measures include, but are not limited to, extraction (contaminant removal), encapsulation (barrier installation), avoidance (by modifying land use to restrict receptor exposure), treatment (by physical, chemical or biological remedial methods) or a combination of these alternatives. It is generally recognized that a single remedial method is often insufficient to satisfactorily remediate more complex sites that have required the use of risk-based approach. Effective risk management should, therefore, endeavor to apply a combination of mitigative measures or in sequence (as sometimes termed the "treatment train") (Sims 1990).

Evaluation of the preferred restoration alternatives (e.g. see Chapters 30 and 31) should involve all stakeholders and should take into account evaluation/selection criteria that encompass all aspects of the restoration. The relative significance of the evaluating criteria usually becomes apparent following interactive discussion between all project stakeholders, and should be weighted to reflect the relative site-specific importance of the criteria. Key factors for selection of the preferred risk management options can include:

1. Technical effectiveness: considers the suitability of the proposed risk management strategy within the context of the site management goals.

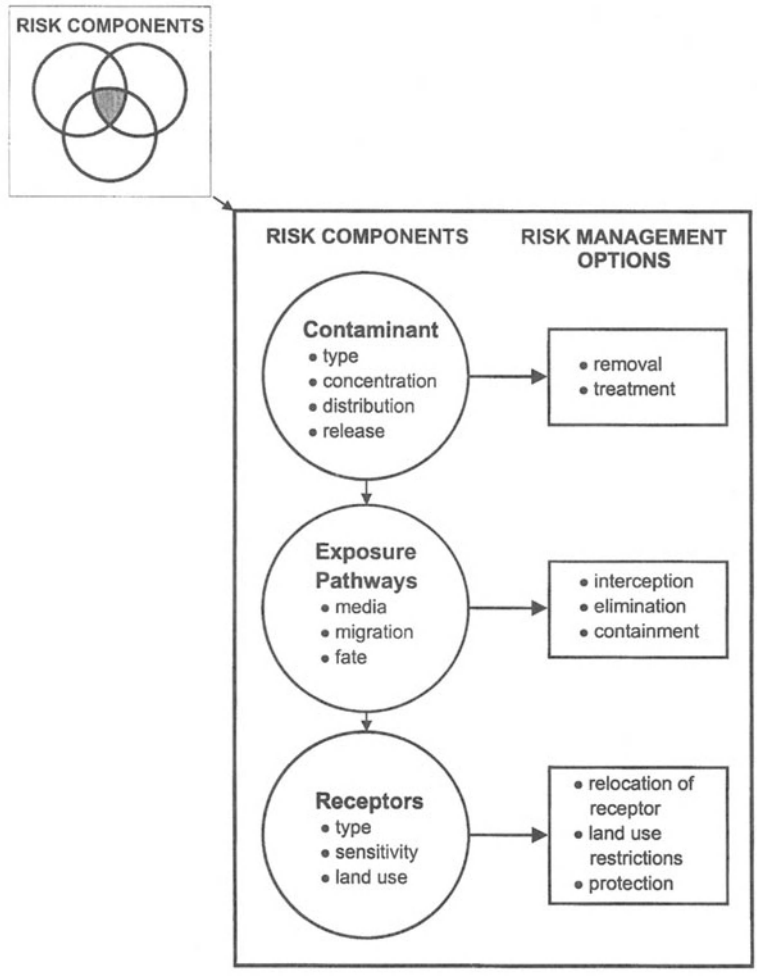


FIGURE 22.9 Risk management options.

2. Long-term performance: considers the longevity of the proposed risk management approach.
3. Degree of protection: examines the degree of protection that the strategy provides, assuming that the strategy has been effectively implemented.
4. Regulatory approvals: examines the approval requirements for the strategy to be implemented.
5. Environmental assessment requirements: considers the need for public environmental assessment of the proposed strategy.
6. Construction constraints: examines the difficulties associated with installation and maintenance of the proposed risk management measures.
7. Community acceptance: considers factors relating to community acceptance of risk management options, including both the installation and construction period, and the long-term operation.
8. Implementation time: may be important if rapid risk management controls are required.
9. Operational maintenance: considers the

need for operational maintenance of proposed risk management controls.
10. Capital costs: examines the total cost of installing or setting up of risk control measures.
11. Long-term operation and maintenance costs: considers the on-going cost of the strategy to continuously provide the required protection.
12. Potential costs associated with residual liabilities (e.g. costs associated with incomplete clean-up, legal fees).

22.9.2 MONITORING RISK MANAGEMENT SUCCESS

When the remedial strategy has been chosen it is important to evaluate the proposed measures in the context of the initial risk assessment to ensure that suitable protection has been or will be achieved. When contaminant removal or extraction has been selected, for example, this evaluation is a straightforward verification of post-extraction conditions. In other situations where the contamination has been encapsulated by a soil or synthetic barrier (e.g. see Chapters 26–28), for example, the verifying risk assessment would have to confirm the integrity of the environmental control barrier as well as confirm its effectiveness in containing the contaminants of concern (e.g. see Chapters 25 and 29). Where contaminant remediation has been carried out, evaluation could entail monitoring compliance with the risk based clean-up criteria through additional confirmatory sampling and analysis.

Finally, in situations where risks have been managed through engineered environmental control measures that allow the contaminants to remain in place, e.g. encapsulation, it is necessary to have in place some mechanism for ensuring that current and future land owners are informed of the site-specific conditions that environmental measures impose on future site operation. Specifically, these limitations relate to any on-going monitoring that may be required to ensure compliance, the constraints placed on land use and, as a consequence of these constraints, the depreciation in value of the land due to the continued presence of contaminants thereon. In most cases this notification can be achieved by a description of the limitations on some component of the title of the property. Though this type of notice of restriction can create a stigma for the site in question, it should be remembered that good science has been used to establish the specific conditions under which the environmental protection is provided and that the total cost of implementing the risk-based strategy can be significantly lower than the cost of full extraction of contamination. The whole simulation process is based on real, probable land use scenarios and even though various levels of conservatism may be included in the assessment, the results and consequential measures are specific only to the site and the land use scenarios under assessment. In the event of the land use changes, the revised land uses are to be examined in the context of the initial risk assessment to ensure that adequate protection continues to be provided.

The "parking lot" example is best used to illustrate land use dependency and the need for notification to future land owners/users. Consider a contaminated site where the on-site impact is such that exposure is caused by inhalation of frequent dust and/or direct contact with the soil. Combined use of the site can be provided by the installation of a barrier in the form of a parking lot pavement, paved walkways, swimming pool, tennis courts, layer of soil for ornamental gardens, etc. These remedial measures, though sufficient for the intended land use are not sufficient for any land use such as residential, where the exposure would occur. Consequently, notification of constraints must remain accessible for future land owners for all situations where risk management measures

have been installed to control/manage the risk due to environmental impact.

22.9.3 SUMMARY

The risk assessment/risk management process should be viewed as a versatile, powerful analytical process that can be used to examine simulated aspects of an environmental issue for specific-site conditions. The range of complexity of a risk assessment can vary from a simple screening comparison with existing criteria to a full quantitative risk assessment. In all cases, the complexity of the assessment should be appropriate for the problem and "common sense" should prevail in order to develop an acceptable solution for all stakeholders.

23. PHYSICOCHEMISTRY OF SOILS FOR GEOENVIRONMENTAL ENGINEERING

J. K. Mitchell

23.1 Introduction

The goals of geoenvironmental engineering include: (1) safe containment of wastes, (2) clean-up of contaminated ground and groundwater, (3) prevention of contamination and pollution, and (4) enhancement of the natural and man-made environment. Attainment of these goals inevitably involves activities on, in, or with the earth. Therefore, soils and their properties and behavior over a range of conditions are of major importance in geoenvironmental engineering. The purpose of this chapter is to identify and summarize aspects of soils that are important in dealing with geoenvironmental problems, such as those considered in subsequent chapters of this handbook. They include contaminant hydrogeology and contaminant migration (Chapter 24), clay liners (Chapter 25), geosynthetics in waste containment systems (Chapter 26), landfill covers (Chapter 27), *in situ* containment and treatment of contaminated soil and groundwater (Chapter 29), and contaminated soil management (Chapter 30). Much of the information in this chapter is covered in more detail in Mitchell (1993).

23.2 Soil Mineralogy and Composition

A soil is typically composed of several types of solid particles, water, dissolved materials and gases. The solid particles include tremendous range of sizes (Fig. 23.1). Although attention is focused on the solid phase in most geotechnical studies, properties of water and the influences of system chemistry must also be taken into account in geoenvironmental engineering.

23.2.1 MINERAL COMPOSITIONS AND STRUCTURES

Gravel, sand and silt-size particles in a soil are usually silicate minerals of the same type as the rock from which they are derived. The most abundant elements in these minerals are oxygen (91.8 vol % and almost 50 wt % in igneous rocks), silicon (about 25 wt % and 0.8 vol %), and aluminum. Magnesium, iron, calcium, potassium and many other elements may be present in small amounts. Clay-size particles are usually hydrous aluminum silicate minerals of various types.

23.2.2 SILICATE MINERALS

Silicate minerals, the dominant minerals in rocks, are composed of silica tetrahedra $(SiO_4)^{4-}$ held together and arranged in various ways. A silicon tetrahedron and silicon tetrahedra arranged in a hexagonal sheet pattern are shown in Fig. 23.2. Many arrangements are possible owing to the small size and high charge of the silicon atom. This accounts

R. K. Rowe (ed.), *Geotechnical and Geoenvironmental Engineering Handbook*
© Kluwer Academic Publishers 2001

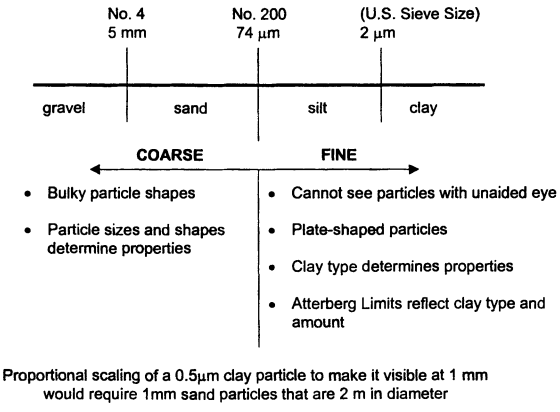


FIGURE 23.1. Soil particle sizes and characteristics.

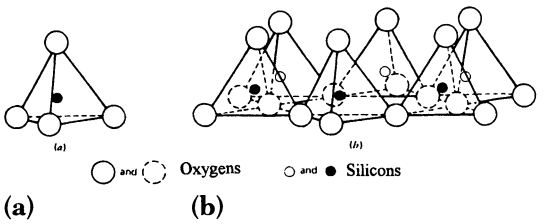


FIGURE 23.2. Silicon tetrahedron (a) and silica tetrahedra arranged in a hexagonal network (b).

for the many different silicate mineral types in nature. Tetrahedra may be independent or associate in pairs, in rings, in chains, in bands, in sheets and in three-dimensional frameworks. The greater and more complex the association, the more stable and resistant to breakdown is the structure.

23.2.3 NON-CLAY MINERALS IN SOILS

Because soil particles are products of rock weathering and because different silicate minerals have different resistances to weathering, the relative proportions of specific minerals in soils differ greatly from those in the source rocks. Quartz, which accounts for only 12% of igneous rocks, is the most abundant mineral in soils because of its resistant framework structure. On the other hand, feldspar, which accounts for 59% of igneous rocks, is usually present only in small amounts in soils. Micas, although present in igneous rock in only relatively small amounts, are quite resistant to weathering; thus they are often found in both the coarse and fine fractions of a soil.

Carbonates (such as calcite), sulfates (such as gypsum) and oxides, (especially iron oxides), may also be present in a soil, and these materials require special attention in geoenvironmental engineering. Carbonates and sulfates are sufficiently soluble that they may react with wastes, thus influencing such things as waste containment barrier effectiveness and *in situ* treatment technologies. Iron oxides, usually identifiable by the yellow–red colors imparted to a soil, are left behind from weathering processes. They are found most commonly in wet, warm–tropical climates, and they can act as cementing agents within the soil.

23.2.4 CLAY MINERAL STRUCTURES

Clay minerals are characterized by: (1) small particle size, generally <2 μm; (2) platy morphology (except for halloysite, which has tubular particles, and attapulgite, which has lath-like particles); (3) plasticity when mixed with water; (4) high resistance to weathering, which reflects high structural stability; and (5) net negative particle charge. The net negative charge results from isomorphous substitution during mineral formation, wherein a replacing cation has a valence lower than the replaced cation. The magnitude of the electro-negativity is measured in terms of the cation exchange capacity (equivalents kg^{-1}).

Different clay mineral structures are formed from different associations of silica tetrahedra and aluminum or magnesium octahedra. An octahedron unit and a sheet structure formed by octahedra are shown in Fig. 23.3. A synthesis pattern for the major clay mineral groups is shown in Fig. 23.4. Silicon tetrahedral sheets and octahedral sheets are stacked in regular ways to form the unit

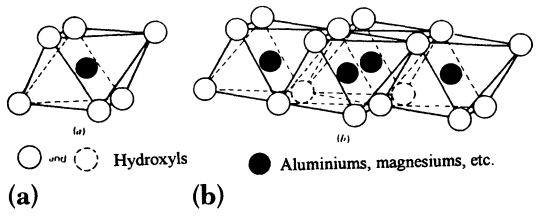


FIGURE 23.3. Octahedral unit (a) and sheet structure of octahedra (b).

cell layers shown in the figure. The actual mineral particles, with the exception of halloysite, consist of stacks of many hundreds or thousands of layers. Pyrophyllite is a 2:1 mineral structure without isomorphous substitution. It is not a clay mineral because it is not found in the very small particle sizes typical of clay, it is electrically neutral, and it is not plastic when mixed with water. Some salient features of the clay minerals likely to be encountered on geoenvironmental projects are:

- *Kaolinite* consists of 1:1 unit layers held together by hydrogen bonds. It occurs in relatively large particles, has low plasticity and does not swell.
- *Halloysite* in its hydrated state consists of two 1: 1 unit cell layers separated by a single layer of water molecules. Particles are hollow tubes. The water layer is irreversibly removed by drying, and possibly also as a result of pressure, with collapse to a structure similar to kaolinite.
- *Smectite minerals* consist of stacked 2:1 unit layers and differ in the isomorphous substitution in both the tetrahedral and octahedral sheets. In montmorillonite, the most common mineral in the group, one of every six aluminum atoms in the octahedral layer is replaced by magnesium. Because the unit layers are not strongly bonded, water and cations can enter between them,

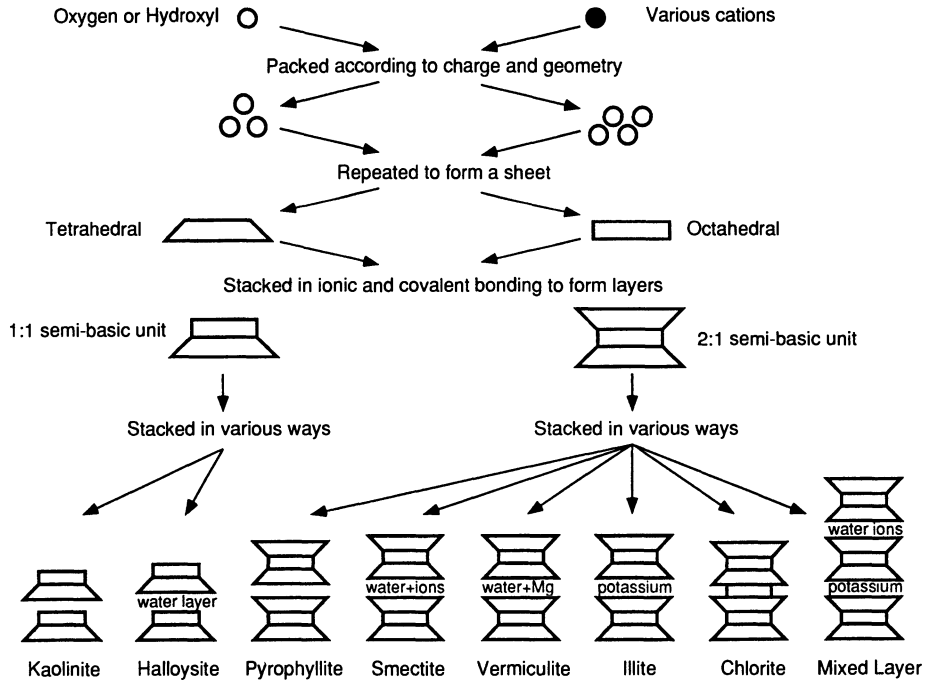


FIGURE 23.4. Synthesis pattern for the clay minerals (reproduced from *Fundamentals of Soil Behavior*, J.K. Mitchell © 1993 John Wiley & Sons, Inc. Reprinted by permission of John Wiley & Sons, Inc.).

accounting for the highly expansive character of the smectite minerals. Bentonite, which is widely used in drilling mud, contaminant containment barriers, landfill liners (see Chapter 25), and covers (see Chapter 27), is a montmorillonite of volcanic origin.

- *Vermiculite*, which is less common than smectite, has a more organized interlayer structure, with Mg^{2+} or Ca^{2+} and water between the layers. It is not as expansive as smectite.
- *Illite* or *hydrous mica* contains interlayer K^+, which fits well into the holes in the silica sheets. The potassium ions bond the unit layers together strongly enough that illite is non-expansive. Illite is the most frequently encountered clay mineral in sedimentary soils in temperate climates.
- *Chlorite* has an octahedral-type layer holding the 2 : 1 layers together. It is neither expansive nor very abundant in soils.
- *Mixed-layer clays* are composed of regularly or randomly stacked layers of different unit cell types, e.g. montmorillonite–illite. Mixed-layer clays are common in soils.
- *Attapulgite* has a double silica chain structure, and occurs as lath or thread-like particles. It is useful for drilling-mud in chemical and saline environments because of its high stability in suspensions in comparison to bentonite.
- *Allophane* is clay-like material without definable crystal structure, i.e. a material that is amorphous to X-rays. It is often found in areas of intense weathering, such as wet, tropical climates.

23.2.5 CLAY MINERAL CHARACTERISTICS

The special, and often unusual, properties of clays are a direct consequence of: (1) their very small particle size and, therefore, very large specific surface; (2) unbalanced surface forces; (3) net negative electrical charge; and (4) platy, tubular and lath-like particle shapes. The possible ranges in each physical, chemical and mechanical property of a given soil are determined by the type and amount of each mineral, the particle sizes and shapes, the types of cations adsorbed to balance the electro-negativity, and the composition of the porewater. Data on these characteristics can be obtained from representative, but disturbed samples. However, the actual values of a property in any case depend on the water content and unit weight, the state of stress, the temperature and the availability of water. Undisturbed samples or appropriate *in situ* tests are needed to determine these properties.

Table 23.1 provides information on some characteristics and properties of common clay mineral types. The properties of smectite vary over the widest range. Because of its very high specific surface, corresponding to its very small particle size, its properties are very susceptible to changes in the composition of the pore fluid, e.g. salt concentration, cation type, dielectric constant and pH.

Real soils are seldom composed solely of one mineral type. The specific values of different properties of a soil cannot be assumed to be in proportion to the amounts of the different minerals that are present because of physical and chemical interactions. Nonetheless, a little clay goes a long way in influencing soil properties, because the specific surface of the clay phase contributes the greatest proportion of the total surface area of the soil, and water is adsorbed approximately in proportion to the specific surface. As a consequence, a relatively small amount of clay in a wet soil is sufficient to coat larger particles, fill the voids between the larger particles, and produce physical properties that are more characteristic of the clay than of the silt and sand that may be present. Thus, identification of the clay minerals present is of great value in understanding and predicting probable behavior.

23.2.6 ORGANIC MATTER IN SOILS

Organic matter occurs in soils in a variety of forms, ranging from large, visible items such as roots, twigs and leaves, to finely divided

TABLE 23.1. Characteristics and properties of common clay minerals

	Kaolinite	Halloysite	Smectite	Illite	Mixed layer
Structure	1:1	1:1	2:1	2:1	2:1
Basal spacing, nm	0.72	1.0	1.0↑	1.0	1.0–1.7
Cation exchange capacity, eq. kg^{-1}	0.03–0.15	0.05–0.40	0.8–1.5	0.1–0.4	Variable
Specific surface, $m^2\ g^{-1}$	10–20	35–70	Up to 800	65–100	Variable
Particle shape	Plates	Tubes	Plates/films	Plates	Plates
Usual location	Warm, humid	Wet, volcanic	Warm, dry	Temperate	Anywhere
Relative particle size	Large	Small	Very small	Medium	Variable
Liquid limit, %	30–75	35–70	100–900	60–120	50–150(?)
Plastic limit, %	25–40	30–60	50–100	35–60	30–60(?)
Activity	< 0.5	0.1–0.5	1–7	0.5–1	0.5–1.5(?)
Shrink/swell	Negligible	No swell, collapse on drying	Very high	Low	Moderate
Hydraulic conductivity, $m\ s^{-1}$	10^{-7}–10^{-9}	10^{-7}–10^{-9}	10^{-9}–10^{-11}	10^{-8}–10^{-9}	10^{-8}–10^{-11}
Compression index	0.2–0.3	—	1.0–2.6	0.5–1.1	—
Shear strength, ϕ', deg	24–30	—	5–17	17–26	—

material and colloidal-size particles of carbohydrates, proteins, fats, resins, waxes and hydrocarbons, which are products of biological decay. Decomposing organic material usually imparts a dark color to a soil, often an odor, and results in increased soil plasticity and compressibility. Soils with significant organic matter content will usually exhibit irreversible decreases in plasticity and compressibility if dried.

Organic compounds that are disposed or spilled into the ground react with the organic matter in the soil. Hydrocarbon wastes that are adsorbed onto soil organic matter are difficult to remove. The organic phase plays an important role in *in situ* biodegradation processes, and is the source of carbon dioxide and methane from aerobic and anaerobic decomposition processes.

23.3 *Soil Water*

The water phase of a soil may comprise a substantial proportion of the total soil volume. For example, in a saturated soil at a water content of 50%, the volume of water will be about 1.35 times the volume of solid material. Accordingly, the properties of soil water and the interactions of the water and solid phases of a soil are important to the overall physical and chemical behavior of the material.

23.3.1 ICE AND WATER STRUCTURE

The eight outer shell electrons in a water molecule are associated in pairs located in a tetrahedral arrangement. This results in separations between the centers of positive and negative atomic charges, making each molecule a strong dipole that can be oriented in an electrical field. Individual water molecules are attracted to each other by hydrogen bonds. In ice a sufficient number of hydrogen bonds is formed to produce a solid structure. Ice breaks down to water when about 15% of the possible hydrogen bonds are ruptured. At room temperature about half the possible hydrogen bonds are broken. Without hydrogen bonding and the open structure that results, the density of water would be about 1.84 g cm^{-3}, rather than 1.0 g cm^{-3}.

23.3.2 THE INFLUENCE OF DISSOLVED IONS

As a result of their uneven charge distribution and dipolar character, water molecules are attracted to ions in solution, resulting in ion hydration. Water molecules move from their normal structure into positions in the hydration shell of an ion, provided their energy state is less as water of hydration than as normal water. Ions disrupt normal water structure. A schematic model for ion–water interaction is shown in Fig. 23.5.

23.3.3 WATER ADSORPTION BY SOILS

Given that water consists of oxygen ions held together by hydrogen, and silicate mineral surfaces are composed of oxygen ions held together by silicon, water is attracted to and strongly adsorbed on soil particle surfaces. All details of the mechanisms of attraction are not known. Some proposed mechanisms are shown in Fig. 23.6. Of these, it seems most likely that hydrogen bonding is important in wet soils, and surface attraction of hydrated ions is significant for drier soils.

Water is strongly attracted to a distance of about 1.0 nm, i.e. three molecular layers, from a silicate layer surface (Sposito 1984) and has a structure different from that of normal water. Surface forces influence water structure out to 10 nm from particle surfaces. To put this in perspective, consider a low plasticity clay soil having a specific surface area of 20 $m^2\ g^{-1}$, and a high plasticity clay with a specific surface area of 200 $m^2\ g^{-1}$. Each has a water content corresponding to an average water layer thickness on the particle surfaces of 5 nm. The water content of the low plasticity clay, e.g. a kaolinite, would be 10%; whereas, the water content of the high plasticity clay would be 100%. These water contents are in the ranges characteristic of compacted clays (10–20%) and saturated, natural clays (50–100%). Thus, most compacted fine-grained soils contain water that is strongly influenced by the surface properties of the particles, and water properties in more plastic materials can be influenced by surface adsorption forces to relatively high water contents.

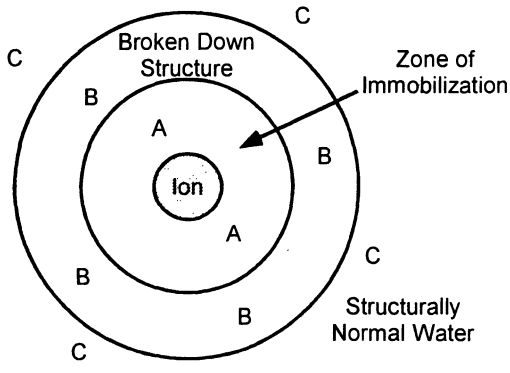


FIGURE 23.5. Ion–water interaction (as postulated in Frank and Wen 1957).

23.3.4 PROPERTIES OF ADSORBED WATER

Some characteristics and properties of adsorbed and free water in soil pores that are important in geoenvironmental engineering are:

- Available data suggest that adsorbed water has a hydrogen bonded structure that includes random networks and five-coordinated molecular rings.
- Energy is released during the adsorption of water on soil surfaces.
- The structure of the water adsorbed on soil particle surfaces differs from that of ice and normal water.
- Adsorbed water exhibits both freezing point depression and supercooling.
- There is no evidence for abnormal water viscosity or failure of Darcy's law in soils of the type usually encountered. For practical purposes, the viscosity and diffusion properties of soil water are the same as for pure water.

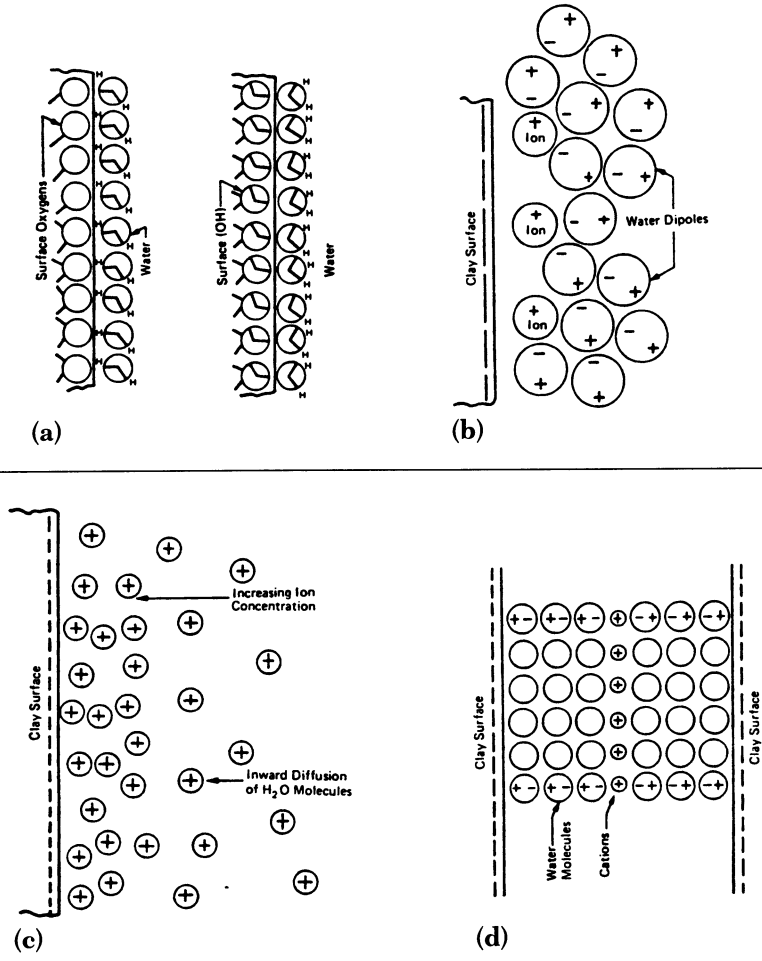


FIGURE 23.6. Possible mechanisms of water adsorption by silicate mineral surfaces: (a) hydrogen bonding, (b) ion hydration, (c) attraction by osmosis, and (d) dipole attraction (modified from Mitchell 1993).

- The dielectric constant of strongly adsorbed water may be less than that of free water.

23.4 *Clay–Water–Electrolyte System*

The clay particles in a soil behave as lyophobic colloids. In liquid suspensions they are small, solid particles that: (1) are two-phase systems with a large interfacial surface area, (2) exhibit behavior that is dominated by surface forces, and (3) can flocculate in the presence of small amounts of salt. Electrical double layer theory provides a basis for understanding many aspects of the behavior of such colloidal systems. This understanding can be used for explanation of many aspects of soil properties, soil–waste interactions and their effects on engineering properties, ion exchange phenomena, and adsorption processes. It is also useful for development and evaluation of different methods for remediation of contaminated ground.

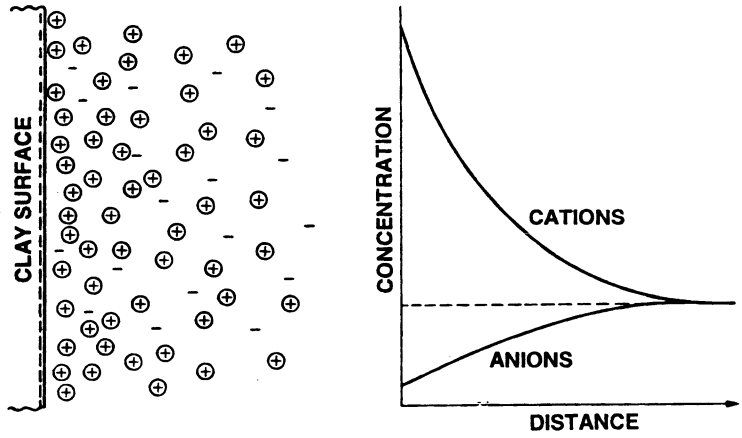


FIGURE 23.7. Distribution of ions adjacent to a clay surface according to the concept of the diffuse double layer.

23.4.1 ION DISTRIBUTIONS: THE DOUBLE LAYER

A representative distribution of cations and ions in solution near the surface of a clay particle is shown in Fig. 23.7. Cation and anion distributions depend on the combined effects of two forces: (1) the electrostatic attraction (cations) or repulsion (anions) of the negatively charged particle surface, and (2) the escaping tendency of the cations and the inward diffusion tendency of the anions owing to the spatial variations in concentration. The charged surface and the distributed charge in the adjacent phase are together termed the diffuse double layer.

The differential equation used to compute ion concentration and electrical potential versus distance in the double layer is obtained by combining: (1) the Boltzmann equation for ion concentration as a function of potential; and (2) the Poisson equation for relating potential, charge and distance.

The Boltzmann equation is:

$$n_i = n_{i0} \exp(- v_i e\psi/kT) \qquad (23.1)$$

where n_i = the concentration of an ion species, i, at a point within the double layer (ions m^{-3}); n_{i0} = reference ion concentration at a point where ions are no longer influenced by the particle surface forces; v_i = valence of ion species; e = electronic charge (1.602×10^{-19} coulomb); ψ = electrical potential (V) at the point (defined as the work to bring a positive unit charge from an infinite distance to the specified point in the electric field); k = Boltzmann constant (1.38×10^{-23} JK^{-1} per molecule), where k = the gas constant (R) per molecule, ($k = R/N$, where N is Avogadro's number); and T = temperature (K).

The Poisson equation relating potential, charge, and distance is:

$$\frac{d^2\psi}{dx^2} = -\frac{\rho}{\varepsilon} \qquad (23.2)$$

where x = distance from the surface in meters, ρ = charge density at point (ρ = charge per unit volume = $e\sum v_i n_i$ in C m^{-3}), ε = electrical permittivity of the medium (C^2 J^{-1} m^{-1}).

The electrical permittivity measures the ease with which molecules can be polarized and oriented in an electric field. Permittivity can be expressed in terms of dielectric constant, D, and permittivity of vacuum, ε_0, as $\varepsilon = \varepsilon_0 \times D$. The dielectric constant is equal

to the ratio of the electrostatic capacity of condenser plates separated by a given material to that of the same condenser with vacuum between the plates. The dielectric constant of water at 20 °C is about 80 and the dielectric constant of vacuum is 1.0. Dielectric constants for non-polar hydrocarbons are generally less than ten. The permittivity of vacuum, ε_0, is 8.8542×10^{-12} C^2 J^{-1} m^{-1}.

Substitution for n_i from Eq. 23.1 into $\rho = e\sum v_i n_i$ gives:

$$\rho = e\sum v_i n_{i0} \exp(- v_i e\psi/kT) \qquad (23.3)$$

which, when substituted into Eq. 23.2 gives:

$$\frac{d^2\psi}{dx^2} = -\frac{e}{\varepsilon}\sum v_i n_{i0} \exp(- v_i e\psi/kT). \qquad (23.4)$$

This is the differential equation that is solved to determine the electrical potential and ionic distributions in the diffuse part of the double layer. ψ is negative because of the negative particle surface charge. ψ_0, the value of ψ at a particle surface, can be up to a few tens of millivolts. Van Olphen (1977) and Mitchell (1993) give examples of solutions.

23.4.2 DOUBLE LAYER INTERACTIONS

The practical importance of the ionic distributions in the diffuse layer is that when the elevated cation concentration extends a large distance from particle surfaces, i.e. a thick diffuse layer condition, interparticle repulsive forces are high. This condition is associated with deflocculation of suspensions and swelling of expansive clays. If the cations balancing the negatively charged clay particles are compressed against the particle surfaces, i.e. a thin diffuse layer condition, suspensions flocculate and expanded clays may shrink.

Figure 23.8 shows curves of repulsion and attraction versus distance from a particle surface. Repulsion is caused by double layer interactions, i.e. cations from overlapping double layers repel each other. Attraction is caused by van der Waals' forces, which are universal forces of attraction caused by fluc-

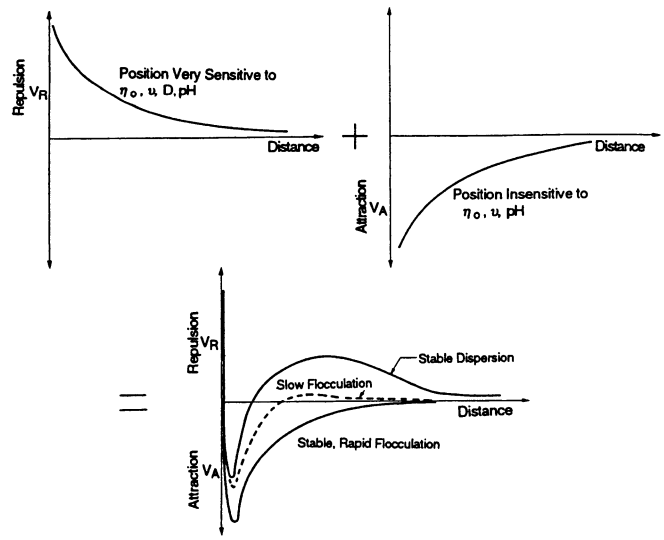


FIGURE 23.8. Energies of repulsion, attraction and net interaction for interacting clay particle minerals (reproduced from *Fundamentals of Soil Behavior*, J.K. Mitchell © 1993 John Wiley & Sons, Inc. Reprinted by permission of John Wiley & Sons, Inc.).

tuating dipoles. Not shown on the repulsion figure is the short range repulsion (Born repulsion), which resists interpenetration of matter.

Combining the two curves gives a net curve of interaction. Net curves of interaction change as the double layer changes. The van der Waals' attraction is rather insensitive to system variables. The character of the interaction curve has a major influence on flocculation–deflocculation and particle arrangements and their stability in sedimented, consolidated or compacted deposits of clay. High repulsion barriers in suspensions prevent particles from getting close to each other and thus cause or maintain dispersion. When the repulsion barrier is small or does not exist, the attractive force causes or maintains flocculation.

23.4.3 FACTORS INFLUENCING DOUBLE LAYER REPULSION

A useful measure of the "thickness" of the double layer is the distance to the center of gravity of the diffuse layer charge distribution, i.e. the distance where there is equal balancing charge both toward and away from the particle surface. Designating this distance by $1/K$:

$$1/K = \left(\frac{\varepsilon_0 DkT}{2n_0 e^2 v^2}\right)^{1/2}. \qquad (23.5)$$

Equation 23.5 provides a basis to examine the effects of changing some of the system variables, because an increase in $1/K$ means an increase in interparticle repulsion. Flocculation–deflocculation behavior is considered in non-active (low PI) clays such as kaolinite, while shrink–swell behavior is considered for active (high PI) clays such as bentonite. Recall that water and ions are mostly free in non-active clays such as kaolinite (low plasticity soils), whereas they are mostly under the influence of particle surface forces in active clays such as smectite (high plasticity soils). In inactive clays, increasing $1/K$ causes an increased tendency for deflocculation and dispersion. In active clays, increasing $1/K$ causes swell. The influences of changes in pore solution chemistry, as given by Eq. 23.5 are:

- As the reference ion concentration, n_0, increases, $1/K$ decreases, interparticle repulsion decreases and the tendency for flocculation increases.
- As cation valence, v, increases, $1/K$ decreases and the flocculation tendency increases.
- As dielectric constant, D increases, $1/K$ increases, causing deflocculation or swelling.
- According to Eq. 23.5, an increase in temperature increases $1/K$. However, an increase in temperature also causes a decrease in dielectric constant, and the net effect of temperature change on $1/K$ is small.

Although not directly accounted for in Eq. 23.5, changes in pH may have a large influence on the colloidal behavior of clays. This is because changing the pH will cause changes in the particle surface charge density.

Clay particles have either O^{2-} or $(OH)^-$ exposed on their surfaces and alumina, $Al(OH)_3$, exposed on the edges of the octahedral layers. Two characteristics of these surfaces influence flocculation–deflocculation and swelling behavior. First, the $(OH)^-$ on the surfaces and edges can dissociate, with some H^+ ions moving into solution. More dissociation will occur at high pH because of the smaller concentration of H^+ already in solution. The net negative charge of the particle surface or edge increases as the H^+ leaves the particle. The increased negative surface charge attracts more cations, increasing the thickness of the double layer. Second, alumina is amphoteric; it ionizes positively at low pH and negatively at high pH. As a consequence, positive diffuse layers can develop at the edges of some clay particles, especially the 1:1 minerals, at low pH.

As a result, low pH promotes a positive edge–negative surface interaction, often leading to flocculation. High pH promotes stable suspensions or dispersions. Minerals like kaolinite and halloysite (1:1 minerals) are more sensitive to pH changes than the 2:1 minerals, because more surface (OH) are exposed. In addition, the thickness–diameter ratio of the 1:1 minerals is larger, thus exposing more alumina and (OH) on their edges. The behavior of the 2:1 minerals is not nearly as influenced by pH changes.

23.5 *Ion Exchange*

Double layer cations and anions are exchangeable. Changes in the type of adsorbed cation, in particular, may produce changes in physical properties, e.g. a smectite with calcium as the adsorbed cation balancing the particle electro-negativity, is much less plastic and expansive than the same clay with sodium as the exchangeable cation. Bentonite with sodium may have a liquid limit around 600%, whereas with calcium it may only be around 100%.

Ion exchange reactions are stoichiometric. Particle structure is not affected by ion exchange. The most commonly found cations in surficial soils are usually in the following decreasing order of abundance: Ca^{2+}, Mg^{2+}, Na^{+} and K^{+}. The most common anions, in order of decreasing abundance are SO_4^{2+}, Cl^{-}, PO_4^{3+} and NO_3^{-}. In marine clays and many sediments, however, Na^{+} and Cl^{-} are the most common cations and anions.

Isomorphous substitution is the most important source of ion exchange capacity, with broken bonds at particle edges and replacement of the hydrogen of an exposed hydroxyl by another type of cation contributing to the total exchange capacity in some cases.

Ion exchange usually occurs in an aqueous environment, and it is almost instantaneous for low plasticity clays like kaolinite, but may take hours for clays like illite, and a day or more for high plasticity clays like smectite. In general, as the valence increases and the size of the ion decreases, the replacing power of an ion increases.

A general cation replacement series, in order of increasing replacement power is:

$$Na^{+} < Li^{+} < K^{+} < Rb^{+} < Cs^{+} < Mg^{2+} < Ca^{2+} < Ba^{2+} < Cu^{2+} < Al^{3+} < Fe^{3+} < Th^{4+}.$$

Replacement can occur in the other direction, against the general trend shown above, by the law of mass action if the replacing ion is at high concentration.

The development of generally applicable quantitative theories for ion exchange has been difficult because of the great complexity of the system and the large number of variables involved. Fortunately, for many engineering applications, knowledge of general trends is adequate.

Anions can be adsorbed onto particle edges and can possibly replace some surface $(OH)^{-}$ ions. Some anion types can be preferentially adsorbed, including phosphate, silicate, arsenate and molybdate. Phosphate, PO^{3-}, and silicate, SiO^{4-}, have tetrahedral structures and are similar in size and geometry. If a phosphate attaches to a clay particle, then the electro-negativity of the clay increases and dispersion increases. This is an important reason why phosphates are effective dispersing agents for soils.

Organophillic clays can adsorb organic contaminants. Organic compounds interact with clays by:

- Adsorption of organic compounds on clay surfaces in aqueous systems. The amount depends on the available surface and the ability of the organic molecules to displace water molecules.
- Cationic organic compounds exchange for inorganic adsorbed cations.

- Intercalation, which involves the entry of organic molecules between silicate layers and may be particularly important in the kaolin minerals.
- Attraction of large organic molecules to clay surfaces by van der Waals' forces.

Organophillic clays are manufactured by attaching an organic compound (such as $(NH_4)^+$–organic) to the clay by an ion exchange reaction. The modified clay can act as an adsorbent for other organic compounds.

23.6 *Soil Fabric and Its Relation to Properties*

Mineralogy and pore solution chemistry by themselves are insufficient to define the properties of a soil that are needed to properly address projects and problems in geoenvironmental engineering. Volume change properties control compression and swelling; stress-deformation and strength properties determine displacements and stability of geoenvironmental structures such as waste landfills; and conductivity properties control the effectiveness of waste containment barriers and contaminant transport.

Soil–water–electrolyte systems are particulate systems, with the solid particles distributed, arranged and bonded in different ways. The arrangement of particles, particle groups and pore spaces is termed the fabric. The fabric and its resistance and response to changes in ambient conditions define the structure. The structure reflects all facets of soil composition, history, present state and environment. Structure-determining factors and processes are summarized in Fig. 23.9. Extensive description, illustration and discussion of soil fabric and structure, and their relationships to the properties of coarse- and fine-grained soils are given in Chapters 8 and 11 of Mitchell (1993).

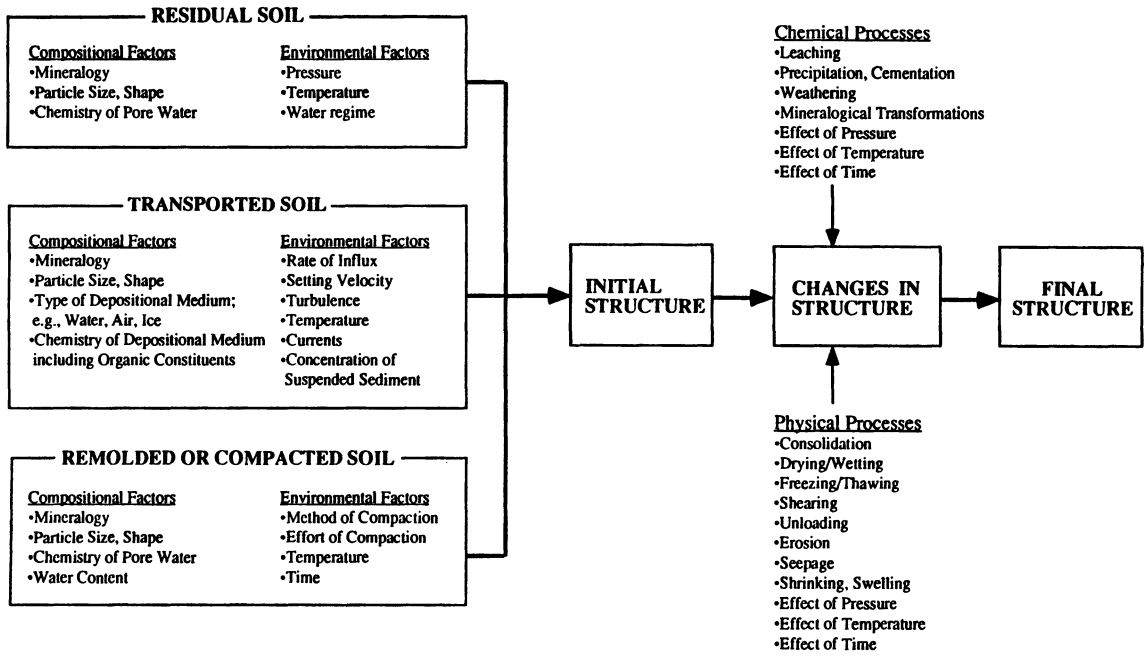


FIGURE 23.9. Structure-determining factors and processes (modified from Mitchell 1993).

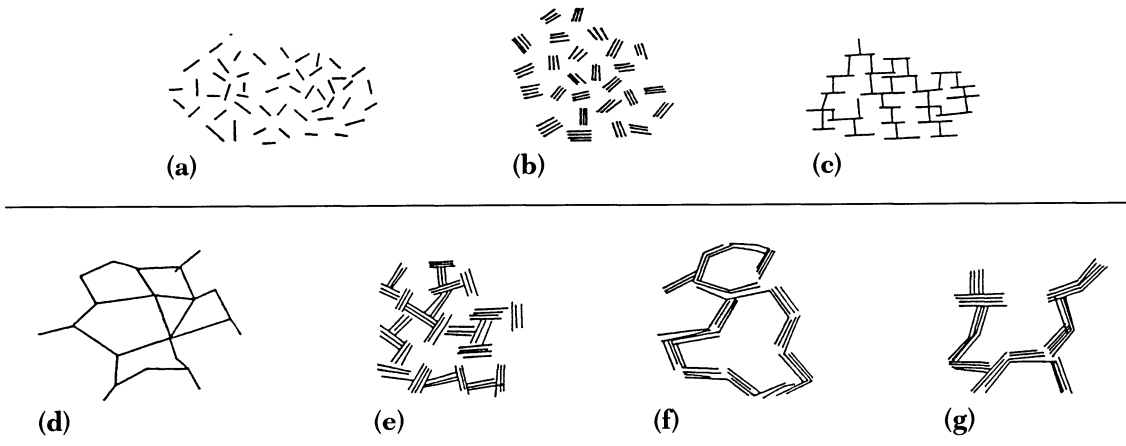


FIGURE 23.10. Particle associations in clay suspensions: (a) dispersed and deflocculated; (b) face-to-face aggregated, but deflocculated; (c) edge-to-face flocculated, but dispersed; (d) edge-to-edge flocculated, but dispersed; (e) edge-to-face flocculated and aggregated; (f) edge-to-edge flocculated and aggregated; (g) edge-to-face and edge-to-edge flocculated and aggregated (modified from van Olphen 1977).

23.6.1 PARTICLE ASSOCIATIONS AND FABRIC SCALE

Soil fabric should be considered relative to three levels of scale:

- *Microfabric*. Regular aggregations of particles and the very small pores between them. Microfabric units are up to a few tens of micrometers across. Types of units in clay suspensions, such as bentonite slurries, used for slurry trenches and cut-off walls are shown schematically in Fig. 23.10.
- *Minifabric*. Aggregations of the microfabric units and the larger pores between them. Minifabric units are up to a few hundred micrometers in size. Particle arrangements in the clay matrix phase of a compacted soil containment barrier can be similar to those shown in Fig. 23.10; however, the individual units will be much closer together, and the inter-unit void spaces will be much smaller.
- *Macrofabric*. A larger volume that may contain cracks, fissures, root holes, laminations, etc. Macrofabric features can have a dominating influence on the gross fluid flow and strength properties of a soil formation. A goal in the engineering of soil-based cut-off walls, liners and covers for waste containment is to assure that macrofabric features that could act as flow paths do not form during construction or in the future (see Chapter 25).

23.6.2 SINGLE-GRAIN FABRICS

Coarse silt, sand and gravel particles are so large that, in the absence of interparticle cementation, they behave as independent units. Non-clay minerals in soils are in this size range and, with the exception of mica, they are bulky in shape. Clean, cohesionless materials have void ratios typically in the range 0.4–1.0 (porosity in the range 25–50%). As most particles are at least slightly elongated, different fabrics are possible for the same material at the same void ratio. Although the consequences of this are minor as regards hydraulic conductivity, different fabrics are known to be responsible for differences in shear-induced compression–dilation behavior and liquefaction resistance.

23.6.3 MULTIGRAIN FABRICS

Single-grain fabric is rare in soils containing fine silt and clay, because the interparticle at-

traction and repulsion forces acting on each small particle are of a magnitude comparable to gravitational forces. Accordingly, multigrain arrangements of the types shown schematically Fig. 23.10 are formed. The stability of aggregates and the ease with which particles can be moved within the material are dependent on both physical and chemical factors. Hence, the variations in properties at a given soil density can be large, with the greatest ranges likely in materials that have a high liquidity index (ratio of the water content less the plastic limit to the plasticity index, i.e. (WC-PL)/PI).

23.6.4 FABRIC–PROPERTY INTERRELATIONSHIPS

Several principles relate the fabric and structure of a soil to its mechanical properties, thus providing a basis for understanding and predicting behavior over a range of existing and future conditions.

1. Under a given effective consolidation pressure, a soil with a flocculated fabric will be less dense than a soil with a deflocculated fabric.
2. At the same void ratio, a flocculated soil with randomly oriented particles and particle groups is more rigid than a deflocculated soil.
3. At stresses greater than the preconsolidation pressure, further stress increase causes a greater change in fabric of a flocculated soil structure than in a deflocculated structure.
4. The average pore diameter and range in pore sizes are smaller in deflocculated soil fabrics than in flocculated fabrics.
5. Shear displacements usually orient platy particles and particle groups with their long axes in the plane of shear.
6. Anisotropic consolidation stresses align platy particles and particle groups with their long axes in the major principal plane.
7. Stresses are unlikely to be distributed

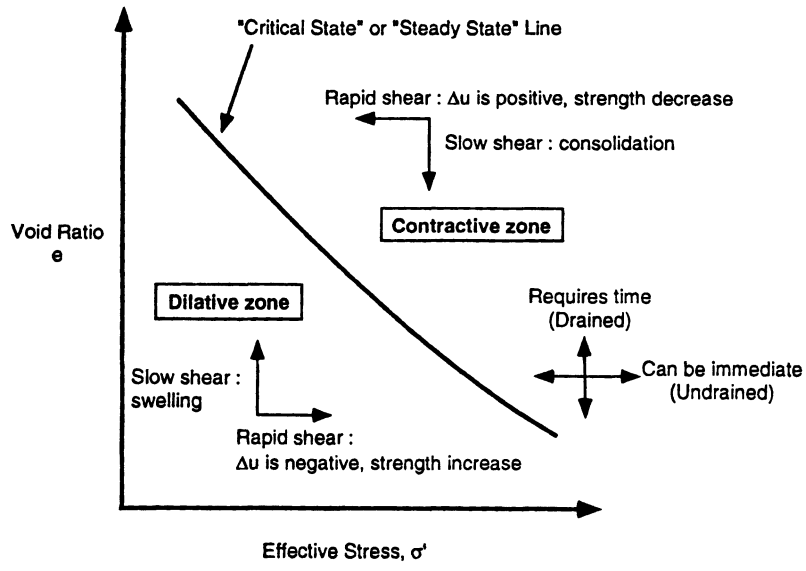


FIGURE 23.11. Soil states in relation to critical or steady state line, and pore pressure and volume changes during deformation where Δu = change in pore water pressure (reproduced from *Fundamentals of Soil Behavior*, J.K. Mitchell © 1993 John Wiley & Sons, Inc. Reprinted by permission of John Wiley & Sons, Inc.).

uniformly among all particles and particle groups.
8. Different stress–deformation histories can produce different structures at the same void ratio.
9. Volume change tendencies determine pore pressure development during undrained deformation.
10. Changes in structure of a saturated soil at constant volume are accompanied by immediate changes in effective stress.
11. Changes in structure of a saturated soil at constant effective stress are accompanied by changes in void ratio. The change in void ratio is time-dependent, owing to the time required for water to enter or drain from the soil.
12. In partially saturated soils, changes in structure can be accompanied by immediate changes in both void ratio and effective stress.

Points 9, 10 and 11 are illustrated and summarized by Fig. 23.11. In general, normally consolidated to slightly overconsolidated clays and saturated loose sands are contractive; whereas, heavily overconsolidated clays and dense sands are dilative.

23.7 Physicochemical Effects on Soil Properties and Their Importance in Environmental Geotechnics

23.7.1 VOLUME CHANGE PROPERTIES

Several compositional and environmental factors control the compression and swelling properties of a soil. Meaningful quantitative predictions are usually only possible if undisturbed samples or *in situ* tests are used to measure the response to a change in stress, chemical and biological environment, or temperature.

1. *Physical interactions*. Bending, sliding, rolling and crushing of soil particles accompany compression. These processes are most important in soils at low void ratios.
2. *Physicochemical interactions*. These interactions originate in the particle surface forces that are responsible for double layer repulsion, surface and ion hydration, and interparticle attractive forces. They are most important in the formational stages of most fine-grained soil deposits when they are under low pressure and at high water content and void ratio. This concept is embodied in the principle of chemical irreversibility of clay fabric (Bennett & Hurlbut 1986), which states that the chemical environment is critical during the initial stages of fabric formation in sediments in water. After the initial flocculation and deposition of particles, the fabric is much less important, with mechanical energy rather than chemical energy being the dominant factor affecting behavior.
3. *Chemical and organic environment*. Chemical precipitates cement particles together. Organic matter influences surface forces and water and organic chemical adsorption properties.
4. *Mineralogical detail*. Small differences in structural details of the expansive clay minerals, such as lattice charge deficiency (Brindley & MacEwan 1953) and *b*-dimension of the crystal lattice (Davidtz & Low 1970) have major effects on soil swelling. The formation of hydroxy-cation interlayers of Fe-OH, Al-OH and Mg-OH reduces the cation exchange capacity and restricts swelling.
5. *Fabric and structure*. Compacted expansive soils with flocculent structures swell more than compacted expansive soils with dispersed structures.
6. *Stress history*. An overconsolidated soil is less compressible, but more expansive, than the same material normally consolidated to the same void ratio. Anisotropic consolidation usually results in anisotropic compression and swelling behavior.
7. *Temperature*. An increase in temperature will usually cause a decrease in volume under drained conditions. If drainage is prevented, a temperature increase causes an increase in porewater pressure and a de-

crease in effective stress. Quantitative analysis in terms of the compressibility and thermal expansion properties of soil solids and water is given in Mitchell (1993).

8. *Porewater chemistry*. Any change in the pore solution chemistry that decreases double layer thickness reduces swell and swell pressure in soils containing expansive clay minerals. For soils containing only non-expansive clay minerals, the porewater chemistry has relatively little effect on the compression behavior once the initial fabric has formed and the structure has stabilized under a moderate level of effective stress.
9. *Stress path*. The magnitude of compression and swelling associated with a given change in stress is usually path-dependent. Loading or unloading in stages can give very different volume change behavior than obtained if the stress change is made in one step, as shown, for example, by Seed *et al.* (1962a).

Expansive clays such as bentonite and attapulgite are widely used for geoenvironmental applications including cut-off walls, liners and covers. Thus, the swelling properties of these materials in suspension, in soil–bentonite and cement–bentonite mixes, and in geosynthetic clay liners are important. Both an osmotic pressure theory of swelling, which is based on double layer theory (Bolt 1956; Mitchell 1993), and a water adsorption (hydration) theory, in which swelling is attributed to surface hydration (Low 1987, 1992), have been proposed to explain swelling quantitatively. Each accounts well for some aspects of swelling phenomena; however, neither accounts for all observations. The effective specific surface area, i.e. the relative proportions of fully expandable and partially expandable layers, controls swelling. When the clay content is high and particle dissociation into unit layers is extensive, the effective specific surface area is large, and swelling is large and very sensitive to the magnitude of double layer repulsive forces. As shown earlier, these forces are very dependent on the pore fluid composition.

23.7.2 DEFORMATION AND STRENGTH PROPERTIES

The stress–deformation and stress–deformation–time behavior of soils must be considered when ground movements and stability are of interest. In geoenvironmental engineering, the deformations and integrity of waste containment barrier components, landfills and tailings dams are important during and following construction.

23.7.2.1 Strength

In the absence of chemical cementation, the strength of sand and normally consolidated clay is given by:

$$\tau_{ff} = \sigma'_{ff} \tan \phi' \qquad (23.6)$$

in which τ_{ff} = the shear stress on the failure plane at failure, σ'_{ff} = the normal effective stress on the failure plane, and ϕ' = the effective stress friction angle. The magnitude of the effective stress friction angle depends on several factors, including: (1) sliding friction between particle surfaces in contact, (2) dilation during shear, (3) particle rearrangements during shear, and (4) grain crushing. Each of these depends on soil mineralogy, gradation, porosity, structure and confining pressure. In reality, ϕ' for most soils is not constant but decreases slightly with increasing effective confining pressures, thus producing curved strength failure envelopes. Mitchell (1993) gives further discussion of the frictional characteristics of soil minerals.

True cohesion is strength in excess of that given by Eq. 23.6. True cohesion is caused by: (1) chemical cementation between particles by carbonates, silica, alumina, iron oxides, and organic compounds; (2) interparticle electro-static and electro-magnetic attractions; and (3) primary valence bonding

and adhesion generated as a result of prior compression and unloading (overconsolidation). According to Ingles (1962) chemical cementation in consolidated sediments may account for tensile strengths up to about 500 kPa; whereas, electro-static and electromagnetic attractions (van der Waals' forces) may contribute only a few tens of kilopascals of tensile resistance, even in a very fine-grained soil.

Apparent cohesion exists in partially saturated soils owing to positive interparticle effective stresses generated by capillary pressures (see Chapter 5). The magnitude of this apparent cohesion increases with decreasing particle size, and may range from a few kilopascals in sands to several hundred kilopascals in clays.

For many soils, the maximum or peak strength is greater than the residual strength, which is measured after shear displacements of a few to several tens of millimeters. The difference between the two for a given soil is a function of structural stability, porosity and confining pressure. A composite relationship, derived from Kenney (1967), Lupini *et al.* (1981), Skempton (1985) and others, showing residual friction angle as a function of amount of clay in a soil is given in Fig. 23.12. Knowledge of the residual strength of a soil is important in such geoenvironmental applications as the stability of landfills.

As a change in temperature causes a change in void ratio, a change in effective stress, or a change in both, temperature changes cause changes in strength. For a saturated soil under undrained conditions, temperature increase causes a decrease in effective stress, so strength decreases. Under drained conditions, temperature increase causes consolidation. The effect on strength depends on the relative influences of this consolidation and any subsequent changes in temperature on effective stress (Mitchell 1993). The undrained strength of clays is strain rate dependent, with an increase of about 10% for each order of magnitude increase in strain rate.

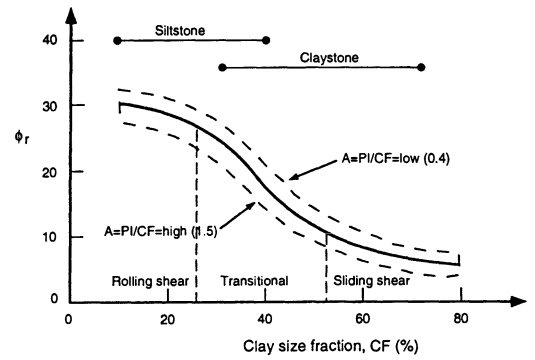


FIGURE 23.12. Composite relationship showing dependence of residual friction angle, ϕr, on soil composition: A = activity; PI = plasticity index (from *Fundamentals of Soil Behavior*, J.K. Mitchell © 1993 John Wiley & Sons, Inc. Reprinted by permission of John Wiley & Sons, Inc.).

23.7.2.2 Stress–Strain Behavior

Stress–strain behavior ranges from very brittle for some quick clays, cemented soils, heavily overconsolidated clays and dense sands, to ductile for insensitive and remolded clays and loose sands. The stiffness is both structure and effective stress dependent. Shear deformation of structured saturated soil is accompanied by volume change if drainage is allowed, or change in porewater pressure and effective stress if drainage is prevented, as shown in Fig. 23.13. Under constant total confining stress the magnitude of generated pore pressure is strain dependent. Temperature increase causes a decrease in modulus, i.e. a softening of the soil.

23.7.2.3 Stress–Strain–Time Behavior

Soils undergo both creep (continuing deformation under constant stress) and stress relaxation (continuing reduction in shear stress carried by the soil at constant deformation). The form of behavior is the same for all soil types; however, the magnitude of the effects

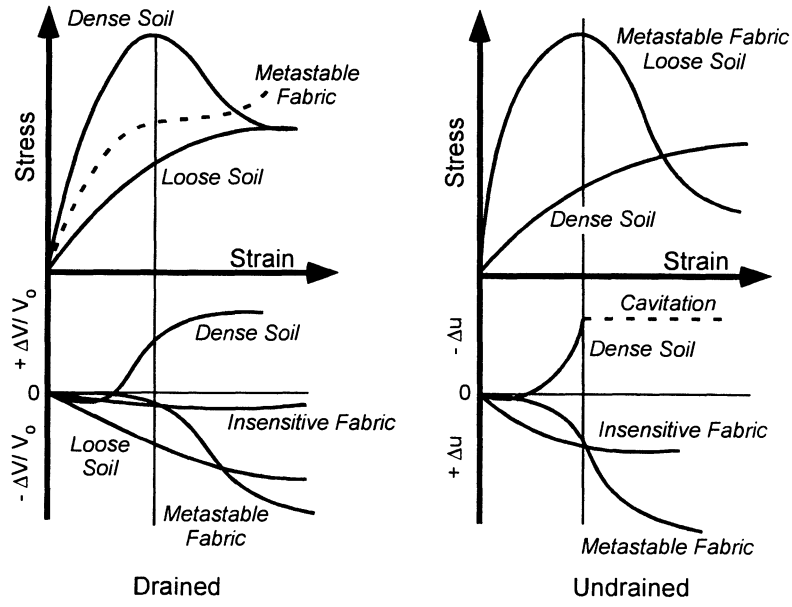


FIGURE 23.13. Volume and pore pressure changes during shear: (a) drained conditions where ΔV = change in volume and V_0 = initial volume; and (b) undrained conditions where Δu = change in pore pressure (modified from Mitchell 1993).

increases with plasticity, activity and water content of the soil, and with increases in deviatoric stress. Deformation under sustained stress usually leads to increased stiffness under the action of subsequent increase in the deviatoric stress. Some soils, however, fail under sustained deviatoric stress significantly less (as much as 50%) than the peak stress measured in a normal strength test. This creep rupture is particularly important in overconsolidated soils under drained conditions and sensitive normally consolidated soils under undrained conditions.

23.7.3 CONDUCTIVITY PROPERTIES

Evaluation of fluid and chemical flows is an essential part of geoenvironmental projects involving contaminant transport and waste containment. Heat and electrical flows must be considered in many methods for site remediation. Accordingly, flow processes and conductivity properties of soils must be known. Both direct flows, in which a gradient of one type causes flow of the same type, and coupled flows, in which a gradient of one type causes a flow of another type, must be considered.

23.7.3.1 Direct Flows

Four types of direct flows through soils are shown in Fig. 23.14. Each is described by a well-known steady state equation, which is valid provided the flow process does not change the state of the soil. The equations shown are for flow in one dimension. The cross-sectional area normal to the flow is designated by A, H is hydraulic head, V is voltage, T is temperature, and C is chemical concentration. The coefficient k_h is the hydraulic conductivity, σ_e is the electrical conductivity, k_t is the thermal conductivity, and D is the diffusion coefficient. Practical ranges of values for these coefficients are given in Table 23.2. Mitchell (1991, 1993) provides detailed analyses of these flow types and coefficients.

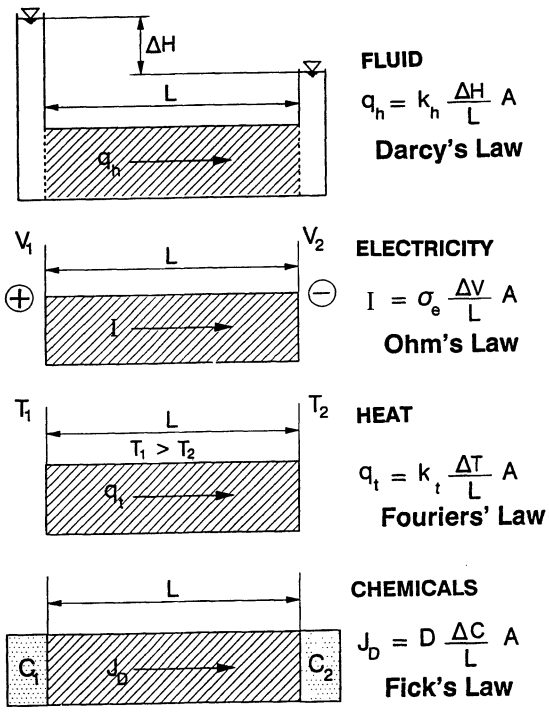


FIGURE 23.14. Four types of direct flow through a soil mass.

Diffusive chemical transport is important in soils having a hydraulic conductivity less than about 1×10^{-9}–1×10^{-10} m s^{-1}. Whereas the hydraulic conductivity, k_h, decreases rapidly with decreasing soil particle size, the effective diffusion coefficient, D, is relatively insensitive to particle size. Detailed analysis of diffusion in soils is given in Sections 24.3 and 25.5 of this handbook, and in Quigley *et al.* (1987), Shackelford & Daniel (1991a), and Rowe *et al.* (1995b).

23.7.3.2 Coupled Flows

Owing to the internal non-homogeneity of ion distributions, restrictions to ionic movement resulting from electrostatic attraction and repulsion, and the dependence of these interactions on temperature and chemical concentrations, several microscopic and macroscopic effects develop when a wet soil is subjected to flow gradients of different types. Among them are that a flow gradient X, of one type can cause a flow J, of another type, according to:

$$J_i = L_{ij}X_j. \tag{23.7}$$

The L_{ij} are coupling coefficients. The different types of coupled flows involving hydraulic, thermal, electrical and chemical gradients are indicated in Table 23.3.

Advection, the hydraulic transport of dissolved and suspended materials, is the dominant mode of chemical transport in most groundwater flow situations and is a major contributor, along with molecular diffusion, to the contaminant transport across waste containment barriers (see Section 25.5). Of the other coupled flows listed in Table 23.3, those of most importance in fine-grained soils are: (1) thermo-osmosis, the movement of water under a temperature gradient; (2) electro-osmosis, the movement of water under an electrical gradient; (3) chemical osmosis, the flow of water across a clay layer induced by a chemical gradient; (4) isothermal heat transfer, the flow of heat with moving groundwater; and (5) electrophoresis, the movement of charged particles in an electrical field.

TABLE 23.2. Practical ranges of flow parameters for fine-grained soils[a]

Parameter	Minimum	Maximum
Porosity, n	0.1	0.7
Hydraulic conductivity, k_h (m s^{-1})	1×10^{-11}	1×10^{-6}
Thermal conductivity, k_t (W m^{-1} K^{-1})	0.25	2.5
Electrical conductivity, σ_e (S m^{-1})	0.01	1.0
Electro-osmotic conductivity, k_e (m^2 s^{-1} V^{-1})	1×10^{-9}	1×10^{-8}
Diffusion coefficient, D (m^2 s^{-1})	2×10^{-11}	2×10^{-9}

[a] The above values are for saturated soil. They will be less in partly saturated soil.

TABLE 23.3. Direct and coupled flows through soils

	Gradient, X			
Flow, J	Hydraulic head	Temperature	Electrical potential	Chemical concentration
Fluid	Hydraulic conduction (Darcy's law)	Thermo-osmosis	Electro-osmosis	Chemical osmosis
Heat	Isothermal heat transfer	Thermal conduction (Fourier's law)	Peltier effect	Dufour effect
Current	Streaming current	Thermoelectricity (Seebeck effect)	Electrical conduction (Ohm's law)	Diffusion and membrane potentials
Ion	Advection	Thermal diffusion of electrolyte (Soret effect)	Electrophoresis	Diffusion (Fick's law)

Quantification of coupled flows requires determination of coupling coefficients applicable to the system, and is formulated using irrevesible thermodynamics (Katchalsky & Curran 1967). Yeung & Mitchell (1992) give a general solution for combined hydraulic, electrical and chemical flows through a clay barrier system.

23.7.3.3 Effects of Flows on Properties

Prolonged application of potential fields and flow of material and energy through a soil may change the state and properties of the material. The changes may be beneficial, as for clay consolidation by electro-osmosis, or detrimental, as for shrinkage cracking of a clay containment barrier as a result of exposure to non-polar organic liquids. Among the effects that may develop are: (1) hydro-consolidation by seepage forces; (2) electro-osmotic consolidation; (3) electrochemical reactions, including gas generation, electrode decomposition, ion exchange and pH changes; (4) thermal drying; (5) swelling and shrinking caused by chemical concentration differences and/or changes in pore fluid composition.

The magnitude of these effects depends on the type and size of potential gradients, soil and pore fluid composition, and initial state and structure of the soil. The finer grained the soil, the more active the clay minerals, and the lower the void ratio, the more important are chemically and electrically induced fluid flows through the soil relative to hydraulic flow. The higher the water content and void ratio, and the greater the compressibility, the larger are the changes in soil state caused by application of the different potential fields.

24. CONTAMINANT HYDROGEOLOGY

R. A. Schincariol
R. K. Rowe

24.1 Hydrogeological Environments

While advances into understanding the complexities of contaminant migration through porous media and fractured rock are continually being made, nothing is more important to understanding contaminant migration, and designing remedial systems, then a complete model of the hydrogeological environment. One must understand the hydrostratigraphy and other factors that control fluid flow at a site before one can hope to understand or control contaminant migration.

24.1.1 SATURATED AND UNSATURATED ZONES

In the subsurface, the region above the water table is referred to as the vadose or unsaturated zone (see Chapter 5), whereas the region below the water table is referred to as the phreatic or saturated zone. However, the terms saturated and unsaturated zones require some clarification because the distinction between the two zones is actually based on fluid pressure and not degree of saturation. Typically, the water table is defined by the water level in a shallow well or piezometer screened across the vadose–phreatic boundary. The water pressure is less than atmospheric in the vadose zone, and greater than atmospheric in the phreatic zone. The capillary fringe is a zone above the water table where fluid saturations are high, close to 100%, but fluid pressures are less than atmospheric pressure owing to tension of the sediment–surface–water contact (see Chapter 5). The capillary fringe is thicker in fine-grained sediments than coarse-grained sediments because of the greater tension created by the smaller pore openings (Table 24.1). Due to heterogeneity in pore sizes the capillary fringe forms an irregular zone above the water table.

24.1.2 AQUIFERS AND AQUITARDS

An aquifer is a saturated permeable geologic unit that can transmit significant quantities of water to wells under ordinary hydraulic gradients. Unconsolidated sands and gravels, sandstones, limestones and fractured rock are common aquifers. In contrast, an aquitard is a saturated low permeability geologic unit that transmits significantly less water than adjacent aquifers. Clays, shales and unfractured crystalline rock are common aquitards. These definitions are subjective and came into use to suit the needs of water-supply hydrogeology. However, in contaminant hydrogeology, aquifers and aquitards are usually defined within a particular hydrogeologic setting or hydrostratigraphic framework. Gorelick *et al.* (1993) emphasize this by stating that "an aquifer has a clear meaning only when ac-

R. K. Rowe (ed.), *Geotechnical and Geoenvironmental Engineering Handbook*
© Kluwer Academic Publishers 2001

TABLE 24.1. Height of capillary rise in sediments (adapted from Fetter 1994)

Sediment	Grain diameter (mm)	Pore radius (mm)	Capillary rise (m)
Fine silt	0.008	0.002	7.5
Coarse silt	0.025	0.005	3
Very fine sand	0.075	0.015	1
Fine sand	0.15	0.03	0.5
Medium sand	0.3	0.06	0.25
Coarse sand	0.5	0.1	0.15
Very coarse sand	2	0.4	0.04
Fine gravel	5	1	0.015

companied by a description of the hydrogeologic setting, the nature of the contamination problem, and the attendant regulatory and public concerns". Therefore the two terms, aquifer and aquitard, must be viewed as relative; a silt layer might be considered an aquifer in a silt–clay system and an aquitard in a silt–sand system (Gorelick *et al.* 1993). Typically aquitards define the boundaries or act as confining layers of aquifers. If an aquifer is bounded above by an aquitard it is called a confined aquifer. If a water table forms the upper boundary it is an unconfined aquifer.

24.1.3 HYDROGEOLOGIC PARAMETERS: POROSITY, HYDRAULIC CONDUCTIVITY AND PERMEABILITY, TRANSMISSIVITY, STORATIVITY AND SPECIFIC YIELD

Porosity, or more accurately, total porosity, n_t, is defined as the ratio of the volume of voids, V_v, in sediment or rock to the total volume, V_t, of the sample. However, for purposes of quantifying the relative volume of porous media through which groundwater actually flows, the parameter effective porosity, n_e, is more appropriate. Effective porosity, n_e, is defined as the ratio of the volume of interconnected pore space to the total volume of the sample. Thus isolated or dead-end channels that do not contribute to groundwater flow are excluded. Effective porosity implies some connectivity through the sediment or rock and is more closely related to permeability than total porosity. The total and effective porosity for unconsolidated sediments are usually similar. However, they may not be similar in lithified sediment or rocks (see Table 24.2). It is the effective porosity that determines the advective velocity of groundwater.

Hydraulic conductivity and permeability are the two basic properties that describe the ability of a porous medium to transmit fluid. Hydraulic conductivity was defined in Sections 2.4.2 and 3.3 as a basic soil property. From a hydrogeologic perspective, hydraulic conductivity, k, which has dimensions of length/time (e.g. m s^{-1}), depends on properties of porous medium and properties of fluid. In the geotechnical literature, the term, "coefficient of permeability," is sometimes used to mean the same as hydraulic conductivity. However, this term is being dropped because of potential confusion with the intrinsic permeability, k_i. Intrinsic permeability describes the capacity for flow of any fluid through a porous medium and has units of squared length (e.g. m^2). Unlike hydraulic conductivity, the intrinsic permeability is only a function of porous media properties. The relationship between hydraulic conductivity, k, and permeability, k_i, is:

$$k = \frac{k_i \rho_f g}{\mu_f} \tag{24.1}$$

TABLE 24.2. Range in values of total porosity and effective porosity

	Total porosity	Effective porosity
Anhydrite[a]	$5 \times 10^{-3} - 5 \times 10^{-2}$	$5 \times 10^{-4} - 5 \times 10^{-3}$
Chalk[a]	$5 \times 10^{-2} - 4 \times 10^{-1}$	$5 \times 10^{-4} - 2 \times 10^{-2}$
Limestone, dolomite[a]	$0–4 \times 10^{-1}$	$1.0 \times 10^{-3} - 5 \times 10^{-2}$
Sandstone[a]	$5 \times 10^{-2} - 1.5 \times 10^{-1}$	$5 \times 10^{-3} - 1 \times 10^{-1}$
Shale[a]	$1 \times 10^{-2} - 1 \times 10^{-1}$	$5 \times 10^{-3} - 5 \times 10^{-2}$
Salt[a]	5×10^{-3}	1×10^{-3}
Granite[b]	1×10^{-3}	5×10^{-6}
Fractured crystalline rock[b]	—	$5 \times 10^{-7} - 1 \times 10^{-4}$

[a] Data from Croff *et al.* (1985).
[b] Data from Norton and Knapp (1977).

where ρ_f and μ_f = the density and dynamic viscosity of the fluid, respectively; and g = the gravitational acceleration constant. Given that ρ_f and μ_f vary with the composition and temperature of the fluid, hydraulic conductivity will also vary.

Chapter 3 (Table 3.10) and hydrogeology textbooks (e.g. Domenico & Schwartz 1998; Freeze & Cherry 1979), present tables of hydraulic conductivity for various geologic materials. Most tabulated values assume pure water and a temperature of 15.6°C, i.e. ρ_f = 1000 kg m^{-3}. These tabulated values provide only approximate values and should be used only when site-specific data are not available. When dealing with deep basinal brines, highly contaminated waters, non-aqueous phase liquids, vapors, or any fluid whose viscosity or density varies significantly from pure water (15.6°C) permeability becomes the dominant term of usage.

Hydraulic conductivity and permeability can be measured in the laboratory. These techniques are discussed in Section 3.3.1. While laboratory values are commonly used, care must be exercised in extrapolating laboratory data to the field scale. Large-scale heterogeneities in geologic materials can cause large deviations from local values. If site-wide or field-scale values are required, aquifer pumping tests, which effectively "average" aquifer properties over the area of influence, give much more representative values. Several hydrogeology texts give an introduction to aquifer tests and hydraulic testing (e.g. Domenico & Schwartz 1998; Fetter 1994). Kruseman & de Ridder (1990) present the most definitive text for the analysis and evaluation of aquifer pumping test data. Permeability values can also be calculated from empirical equations based on porous media characteristics, such as grain and pore size (Bear 1972). These relationships are often imprecise and are usually only applicable to well-sorted, unconsolidated porous media.

Transmissivity and storativity are field-scale properties that define the transmissive and storage properties of geologic units of some specified thickness. Transmissivity, or coefficient of transmissibility, is the product of the average hydraulic conductivity and the saturated thickness of the aquifer, H:

$$T = kH. \tag{24.2}$$

The storativity, or coefficient of storage, is the volume of water released from storage of a saturated confined aquifer of thickness H per unit surface area per unit decline in the hydraulic head. Mathematically, storativity is defined as:

$$S = S_s' H \tag{24.3}$$

where S_s' = the specific storage or the volume of water that a unit volume of aquifer (confined) releases from storage under a unit decline in hydraulic head. The release of water from storage under a decreasing head stems from the reduction in porosity due to increasing effective stress and the expansion of water. The specific storage is defined mathematically as:

$$S_s' = \rho_w g(\alpha_v + n\beta) \qquad (24.4)$$

where α_v = the vertical aquifer compressibility, β = the compressibility of water, and other symbols are as defined earlier. Specific storage has the dimensions of L^{-1} and the storativity is dimensionless, as it is the ratio of the volume of water released per volume of aquifer. Values of storativity for confined aquifers range from 5×10^{-5} to 5×10^{-3} (Kruseman & de Ridder 1990).

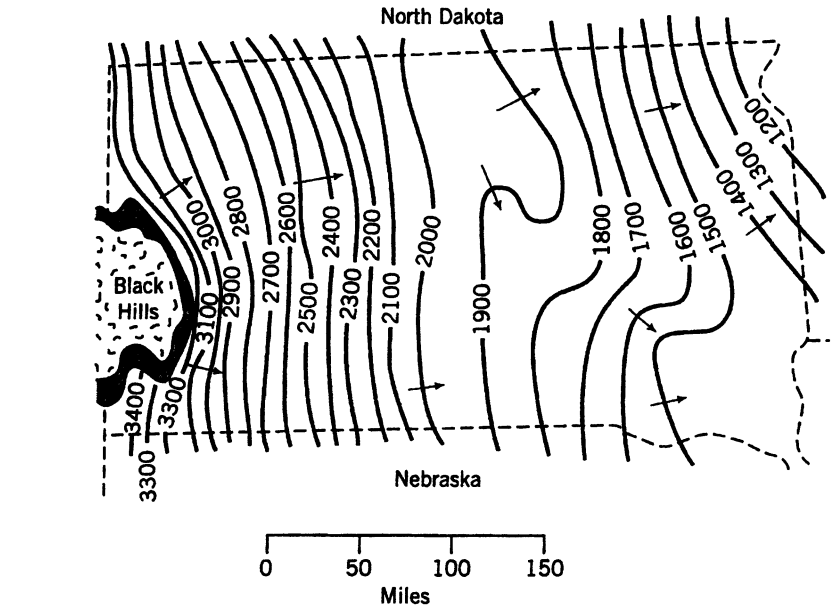
Specific yield is the storage property of an unconfined aquifer. It is equal to the volume of water that an unconfined aquifer releases from storage, via gravity drainage, per unit surface area of aquifer per unit decline of the water table. Johnson (1967) has summarized typical values of specific yield for various sediments and rock types. These values range from 0.03 (clay) and 0.08 (silt) to 0.38 (dune sand) and 0.44 (peat).

24.1.4 HYDROGEOLOGIC VARIABLES: HYDRAULIC HEAD, FLUX AND VELOCITY, AQUIFER RECHARGE AND DISCHARGE

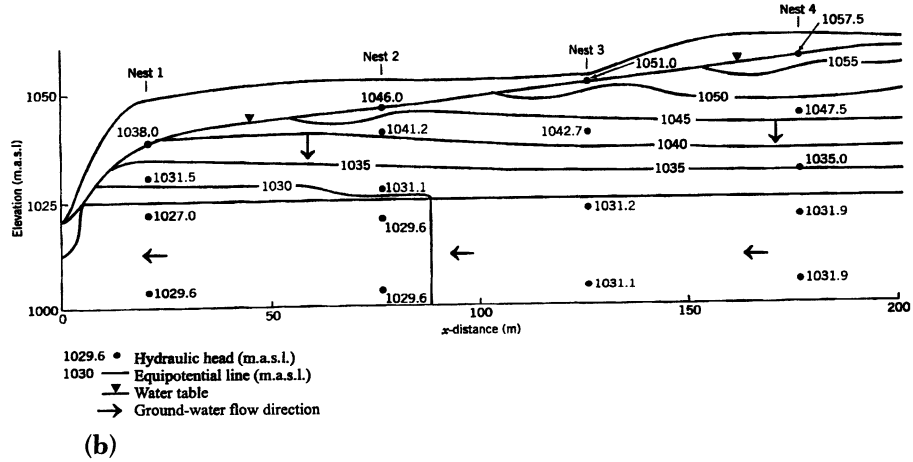
Hydraulic or total head, h, pressure head, $h_p = u_w/\gamma_w$, and fluid or porewater pressure, u_w, were defined earlier in Section 2.4. The water table represents the surface where the fluid pressure is atmospheric (gage pressure equals zero) and thus h = water table elevation measured with respect to some datum. Values of hydraulic head, including water table elevation, are required to calculate the directions of groundwater flow. While numerous methods exist to measure hydraulic head in boreholes, wells and piezometers (see Section 4.7 and Nielsen 1991; Fetter 1994; Rowe *et al.* 1995b), some important considerations regarding the use of hydraulic head data should be recalled:

- The length and position of the screened interval in a well or piezometer can influence the water-level observed in the well. The measured water-level is an integrated average of the hydraulic heads over the screened interval. Thus, large screen lengths for deep monitors could mask important differences in hydraulic head. Furthermore, water table elevations should be taken from wells screened over the vadose–phreatic zone interface. As water-levels rise above the top of the screen, the water-level becomes unrepresentative of true water table elevation.
- Hydraulic heads are often measured across a site to understand spatial and temporal gradients. Measurements of hydraulic head within a single aquifer provide the data to construct a potentiometric map (Fig. 24.1a). One must be careful to ensure that the potentiometric map is related to a single aquifer. It is assumed that flow in the aquifer is horizontal, and vertical gradients are absent. Thus, one cannot make potentiometric maps of low-permeability units as flow typically has a large vertical component. Vertical gradients are typically assessed in hydrogeological cross-sections (Fig. 24.1b). Here a vertical section is aligned parallel to the direction of mean groundwater flow. Domenico & Schwartz (1998) present an excellent discussion of mapping flow in geological systems.
- If significant differences in groundwater density exist hydraulic head measurements should be corrected to a common density before comparing data or calculating gradients (Jorgensen *et al.* 1982). Methods for correcting data to equivalent freshwater heads are provided in Pickens *et al.* (1987).

From Darcy's law (Section 2.4.2), the Darcy velocity, v_a, also called the specific discharge, discharge velocity or Darcy flux, may be calculated:



(a)



(b)

FIGURE 24.1. (a) Potentiometric surface of the Dakota Sandstone, contour interval 100 ft (from Darton 1909, U.S. Geol. Surv. Water Supply Paper 227). (b) Example of a hydrogeologic cross-section describing the pattern of groundwater flow (modified from Domenico & Schwartz, 1998, *Physical and Chemical Hydrogeology*, © 1998 John Wiley & Sons, Inc. Reprinted by permission of John Wiley & Sons, Inc.).

$$v_a = -k\frac{\Delta h}{\Delta l} \qquad (24.5)$$

where Δl = the flow distance between points of h measurement. However, as noted in Section 2.4.2, although v_a can have the dimensions of velocity, it corresponds to flow per unit cross-sectional area and it is not the velocity of groundwater. It is best referred to as the Darcy flux.

The average groundwater velocity, which gives an indication of the velocity at which

contaminants are advected by the bulk flow of groundwater, is called the average linear groundwater velocity, v, or the seepage velocity. It is defined as the Darcy flux divided by the effective porosity, n_e:

$$v = \frac{v_a}{n_e} = -\frac{k}{n_e}\frac{\Delta h}{\Delta l}. \qquad (24.6)$$

Thus, the average linear groundwater velocity can be calculated indirectly from measurements of hydraulic conductivity, effective porosity, and hydraulic gradient. Alternately, it can be measured directly with tracer tests. Domenico & Schwartz (1998) outline some basic aspects of tracer tests.

Recharge of groundwater depends on infiltration of precipitation through the vadose zone and across the water table, or leakage from surface water bodies. Discharge from unconfined aquifers takes place as evapotranspiration, springs or seeps, and base-flow to effluent streams. Recharge and discharge to deeper confined aquifers occurs via leakage across confining units. Discharge to both unconfined and confined aquifers occurs through the pumping of wells.

Quantifying aquifer recharge and discharge relations is extremely important to many groundwater supply, dewatering, or contaminant transport and remedial action programs. Recharge and discharge rates are controlled by the precipitation, evapotranspiration, and the topography and geology of the basin or watershed. Recharge and discharge rates are very difficult and expensive to measure directly in the field. Furthermore, they are often highly variable both temporally and spatially. Most often, they are obtained by quantifying various components of the water balance for a drainage basin and/or estimating values from the calibration of steady state or transient groundwater models for the basin. Dingman (1994) provides a general review of the water balance and various techniques to quantify components. For a more detailed and applied approach, the *Handbook of Hydrology* (Maidment 1993) has separate chapters that focus on quantifying each component of the hydrologic cycle. Stephens (1996) provides a detailed review of field techniques for estimating recharge, and Anderson and Woessner (1992) discuss the application and use of numerical models for groundwater problems.

24.1.5 HYDROGEOLOGIC CONTROLS: LITHOLOGY, STRATIGRAPHY AND STRUCTURE

The permeability, porosity and geometry of the aquitard–aquifer systems at a site depend directly or indirectly on the lithology, stratigraphy and structure of the regional and local geologic setting. The geologic setting is usually heterogeneous and complex at all scales and geological training is a prerequisite to understanding the distribution and geometry of aquifers and aquitards.

The lithology of a geologic deposit describes the type of rock or sediment. Rocks and sediments are described in terms of their mineralogy, grain size and orientation, and packing at the local, hand-specimen or outcrop scale. It is the lithology that determines if a geologic deposit is a consolidated, unconsolidated or lithified sediment; a fractured or unfractured rock; and weathered or unweathered. All of these factors and many more control the local porosity and permeability of the geologic deposit.

The stratigraphy of the aquifer–aquitard system is concerned with the arrangement, orientation and chronological order of the lithologic units. Hydrogeologists often group or subdivide traditional stratigraphic units into units that possess similar permeability, called hydrostratigraphic units. Sedimentary systems can range from the dominantly horizontal layered units of lacustrine or marine depositional environments, to the highly heterogeneous and lenticular material found in alluvial or

glaciofluvial sediments. Structural disruptions due to folding, faulting, uplift and fracturing can alter the geometry, continuity and hydraulic conductivity of geologic units.

The pattern of groundwater flow depends on the geometry and permeability distribution of the aquifers and aquitards. Typically, if the permeability contrast between aquifer–aquitard systems is two orders of magnitude or greater, flow lines tend to become almost horizontal in the aquifers and almost vertical in the aquitards (Freeze & Cherry 1979). However, actual flow directions depend on the location of recharge and discharge areas in relation to the continuity of the hydrostratigraphic units. Sara (1991) presents a series of figures, shown here as Fig. 24.2a–c, which illustrate this concept. The figures display a landfill over a sedimentary deposit with higher permeability sand lenses within a lower permeability material. Underlying this sedimentary deposit is the regional bedrock aquifer. Figure 24.2a illustrates that even with two orders of magnitude difference between the sand lenses and surrounding sediment, lack of connectivity among the lenses and the influence of the underlying regional aquifer, result in vertical flow in the sand lenses. When the lens continuity is increased, and connection to surface discharge is allowed, flow has a much more pronounced horizontal component in the sand layers (Fig. 24.2b). Only when the permeability of the regional aquifer is reduced does flow become dominantly vertical in the low permeability sediments and horizontal in the sand layers (Fig. 24.2c).

The lithology, stratigraphy and structure of aquitard–aquifer systems are usually established during a site investigation. A site investigation usually involves an examination of air photographs, topographic and geologic maps, and a review of existing geotechnical borings and water well records for the area (see Chapter 4). Following this early phase of the study, the site is usually visited and test borings, detailed mapping of hydrostratigraphic units and fracture traces, and geophysical surveys are carried out. Finally, wells and piezometers may be installed for a complete assessment of on-site aquifer–aquitard relations, permeabilities, gradients and water quality. Chapter 4 discusses the geotechnical and environmental site characterization. Additional references include hydrogeology texts by Domenico and Schwartz (1998) and Fetter (1994), monitoring handbooks by Nielsen (1991), and various regulatory guidelines (e.g. MoEE 1996b; CCME 1994; US EPA 1992a).

24.1.6 FRACTURED AND KARST SYSTEMS: FRACTURE FLOW

In fractured rocks, the interconnected fractures are considered to be the main pathways for fluid flow, while the matrix or solid rock blocks are considered to be much less permeable. Karst systems behave much the same way.

To organize studies of fractured media two approaches are typically followed: equivalent porous medium or discrete fracture. The equivalent porous medium approach assumes that the fractured mass of rock is hydraulically equivalent to a porous medium. In effect, this assumes that a set of porous medium parameters can be defined to characterize the hydraulic and transport behavior. With the equivalent porous medium approach a geologic unit is considered to have a sufficiently high fracture density that the structure of the fracture network need not be described in detail. This simple approach is complicated by the difficulty in justifying that the network of interconnected fractures is of sufficient density to provide an equivalent porous medium. Furthermore, the inherent heterogeneity and evolving scales of fracture networks makes defining a representative elementary volume difficult. Readers interested in learning more about these problems and flow and transport in fractured rock can refer to Domenico & Schwartz (1998), Bear *et al.* (1993) and NRC (1996).

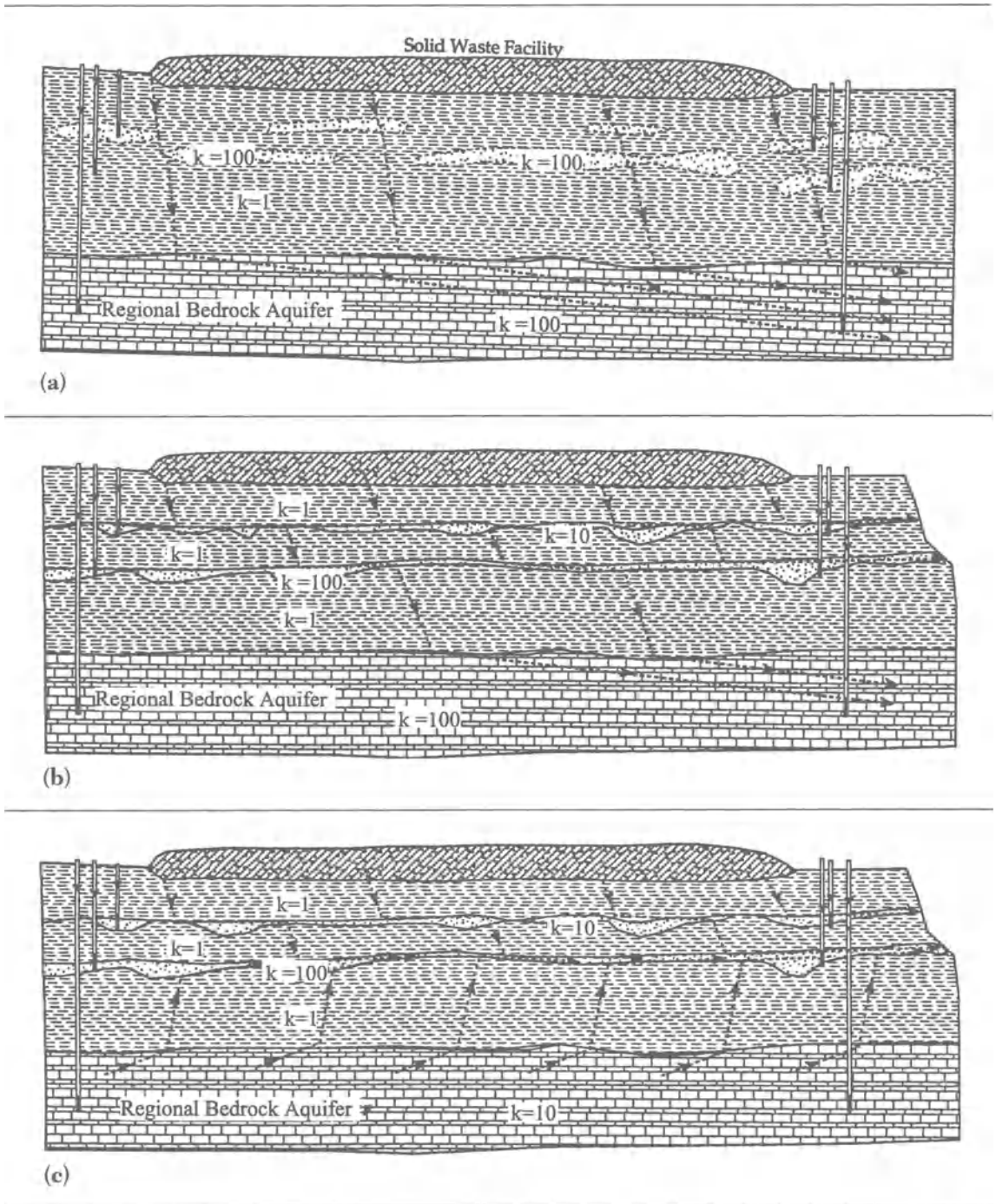


FIGURE 24.2. Hydrogeologic cross-sections illustrating the importance of hydraulic conductivity contrasts, continuity of units, and recharge and discharge relations on groundwater flow: (a) sand lenses with little horizontal discharge; (b) sand layers with significant horizontal discharge; and (c) sand layers discharging both bedrock and overburden (modified from Sara 1991, *Practical Handbook of Ground-Water Monitoring*, D.M. Nielsen ed., © 1991 CRC Press, Inc. Reprinted by permission of CRC Press, Inc.).

In the discrete-fracture approach, the fracture network is described in terms of individual fractures. This approach also presents several difficulties. First, extensive field testing is required even to begin to characterize the fracture properties, e.g. length, width, aperture, orientation, fracture density, wall smoothness. Second, the fracture apertures, and thus hydraulic conductivity, depend upon the three-dimensional stress field. This coupling has implications both in field testing, where boreholes are pumped or stressed, and in natural changes to the stress field. Finally, in larger apertures, flow could be turbulent, which invalidates Darcy's law.

24.2 *Contaminants and Sources*

24.2.1 PHYSICAL AND CHEMICAL PROPERTIES OF CONTAMINANTS

A contaminant is generally defined as a miscible (aqueous) or immiscible (non-aqueous) phase liquid, or soluble or insoluble solid phase, which is added to water as a consequence of human activities. The dominant physical properties of a contaminant that would control contaminant transport include density, viscosity and volatility. A key chemical property influencing the abundance of a contaminant in water is the contaminant solubility. Abundance also is controlled by a variety of chemical interactions that may occur among native groundwaters, aquifer materials, and other contaminants once a given contaminant has entered the groundwater flow system. These chemical and geochemical reactions are beyond the scope of this book, but are well-covered in texts such as Stumm & Morgan (1996); Morel (1983); Hounslow (1995). Physical and chemical properties of typical contaminants are found in the chemical literature (Montgomery & Welkon 1990) or from manufacturers' safety data sheets (MSDS).

The solubility defines the maximum quantity of mass that will go into solution per unit volume of solution under specified conditions. However, contaminants are seldom found in groundwater at their theoretical solubilities. This behavior is explained by several factors, such as the heterogeneous nature of flow fields at pore and aquifer scales, the complex kinetics of dissolution, and mixing of waters containing other solutes or contaminants. Fortunately, for many contaminants, their theoretical solubilities are low. For example, non-polar compounds like polychlorinated biphenyls (PCBs), commonly exhibit low solubility due to the polar structure of water.

Another important way contaminants occur are as non-aqueous phase liquids (NAPLs). An NAPL encompasses contaminants present as a distinctly separate liquid phase, like gasoline. NAPLs can migrate as a separate liquid phase, a dissolved phase and a vapor phase.

The two physical properties that largely control how NAPLs migrate are their density and volatility. Dense non-aqueous phase liquids (DNAPLs) are denser than water and, thus, sink through water. Light non-aqueous phase liquids (LNAPLs) are less dense than water and float on water. In unsaturated systems, these chemical compounds can migrate in the vapor phase. The extent of partitioning into the vapor phase, the compound's volatility, is determined by its vapor pressure. The vapor pressure of the compound is a measure of its solubility in a gas phase. The greater the vapor pressure of an organic or NAPL the greater the tendency for volatilization and spreading as a vapor phase in the unsaturated zone. NAPL migration is discussed more fully in Section 24.3.2.

The viscosity of a NAPL is mainly used to assess its relative mobility. As shown by Eq. 24.1, the hydraulic conductivity of a particular fluid–porous media combination is inversely proportional to the viscosity. While viscosity is most important in assessing the relative mobilities of NAPLs it can also be important with miscible contaminants. At

high concentrations, as typically found near the source, the contaminant plume viscosity and density may significantly control plume migration (Kimmel & Braids 1980; Van de Molen & Van Ommen 1988; LeBlanc & Celia 1991; Schincariol *et al.* 1994, 1997; Zhang *et al.* 1998).

24.2.2 HYDRAULIC CHARACTERISTICS OF SOURCES

The hydraulic characteristics of the source can significantly influence dissolved contaminant transport in the unsaturated and saturated zones. For example, increased recharge at landfills, disposal pits, holding ponds and lagoons, or recharge wells and infiltration galleries often causes a mounding of the water table at these sources. This mounding creates a zone of elevated hydraulic head that perturbs the regional groundwater flow field and results in a local radial spread of contamination. Furthermore, the increased local gradients, and water saturation of some wastes, increases contaminant loadings to the subsurface.

24.2.3 POINT AND NON-POINT SOURCES

The terms point and non-point describe the degree of localization of the source. A point source is characterized by an identifiable, relatively small and fairly well-defined source. Point sources include leaking storage tanks, disposal ponds, landfills, injection wells or leaking pipelines. Usually, these sources produce a reasonably well-defined plume. A non-point source refers to a more spatially distributed source, such as the large-scale loading that results from the atmospheric fallout of airborne contaminants. Alternatively, it could be a large grouping of distributed sources, such as herbicide, pesticide, and nitrate contaminants that result from farming practices, or nutrient loadings from septic beds or leaking sewer systems. In these cases, there are typically no well-defined plumes, but a large enclave of contamination with extremely variable concentrations.

There are also significant differences between point and non-point sources from a remedial perspective. Contaminant plumes from point sources are often candidates for direct remedial action or plume control and remediation (see Chapters 29 and 30). However, non-point plumes are typically candidates for passive remedial action. This includes preventative source control (reduction in fertilizer use, repair of sewer systems) and natural attenuation. The most common approach to groundwater remediation for non-point source contamination has been to treat the groundwater at the well as it is removed for use (Gorelick *et al.* 1993).

24.2.4 LOADING HISTORY

The loading history describes how the concentration of a contaminant, or its flux, varies as a function of time at the source. A spill or one-time release of contaminants from a storage lagoon or tank is an example of a pulse loading. Here, the source produces contaminants at a fixed concentration for a short period of time. Long-term leakage from a landfill, storage lagoon or tank is termed continuous source loading. In some cases, the continuous source loading could be at a constant concentration. This loading might occur with NAPL contamination, where the NAPL source can dissolve at a slow rate over many years. However, most often the source loadings at industrial sites or operational landfills have a non-constant loading function. In this case, the concentration of chemicals added to a storage lagoon may vary depending on manufacturing needs, techniques, or plant owner. The waste type added to sanitary landfills will also vary with geographic area and clients served. Seasonal factors, such as precipitation and evaporation, will also influence both the concentration and flux of contaminants in waste ponds or landfills. Closed ponds or landfills may exhibit a decaying concentration function, as contaminants are leached from the solid wastes or the

waste stream biodegrades (see Rowe *et al.* 1995b).

The source loading function, along with the physical and chemical mass transport processes discussed in Section 24.3, will control the contaminant distributions in plumes. Increasing complexity in the loading function will translate directly into increasingly variable concentration distributions.

24.3 Principles of Contaminant Transport

24.3.1 MASS TRANSPORT PROCESSES: ADVECTION, DIFFUSION AND DISPERSION OF SOLUTES

Mass occurring in groundwater as ions, molecules or solid particles is transported by three processes: advection, mechanical dispersion and diffusion. All three processes operate simultaneously in flowing groundwater.

24.3.1.1 Advection

Advection is mass transport, or the movement of dissolved solute, due simply to the flowing groundwater. The direction and rate of transport coincide with the groundwater. The velocity of transport is equal to the average linear groundwater velocity. In aquifers, advection is the dominant process. Therefore, if one understands the flow system or hydrogeological environment, one understands advective transport. Similarly, factors that influence groundwater flow patterns, such as water table configuration, pattern of geologic layering and hydraulic conductivity of geologic units, recharge and discharge relations, control the direction and rate of advective mass transport. If advection is the only process operating, mass added to a streamtube, defined by bounding flowlines, will remain in the streamtube.

24.3.1.2 Diffusion

Whenever contaminants exist in groundwater, there will be zones of low and high concentration. Molecular or ionic diffusion is the process where dissolved mass moves from areas of high concentration to areas of low concentration. Mixing is caused by random molecular motion due to the thermal kinetic energy of the solute. For a simple aqueous non-porous system, at fairly low concentration, Fick's law describes how the chemical mass flux is proportional to the concentration gradient:

$$J = -D_0 \text{grad}(C) \tag{24.7}$$

where J = the chemical mass flux (negative sign indicating that transport is in the direction of decreasing concentration), D_0 = a proportionality constant called the diffusion coefficient in free solution, and C = the concentration. Diffusion coefficients are temperature dependent. Values for most major ions can be found in Robinson and Stokes (1970).

In a porous medium, the diffusion coefficient must be smaller than that in a fluid environment due to the hindering effect of collisions with solids, and the tortuous fluid pathways. To account for these effects, a porous media diffusion coefficient, D_p, is introduced so Fick's law for diffusion in porous media becomes:

$$J = -D_p \text{grad}(C). \tag{24.8}$$

There are several relationships for calculating D_p. Greenkorn and Kessler (1972) express D_p as a function of porosity and tortuosity:

$$D_p = \frac{nD_0}{(L_e/L)} \tag{24.9a}$$

where the tortuosity is defined as the ratio of the length of a flow channel for a fluid particle, L_e, to the length of a porous medium sample, L. Thus the value (L_e/L) is always greater than one in porous media. However, since one is dividing by tortuosity (L_e/L), it has the same effect as more conventional definitions. Bear (1972) also defines D_p as a

function of porosity and tortuosity, T^*, but where tortuosity has a different definition:

$$D_p = nT^*D_0 \qquad (24.9b)$$

and T^* is reported to range from 0.56 to 0.8. According to Rowe *et al.* (1995b), the porous media diffusion coefficient is related to D_0 by the relationship:

$$D_p = D_0 W_T \qquad (24.9c)$$

where W_T = a complex tortuosity factor that depends on the porosity of the soil, geometric tortuosity, a fluidity factor related to adsorbed double layer water and electrostatic interaction. These latter factors may be particularly important for diffusion through clayey soils. It is often convenient to replace D_p in Eq. 24.8 by:

$$D_p = nD_e \qquad (24.9d)$$

yielding:

$$J = -nD_e \text{grad}(C) \qquad (24.10)$$

where D_e is defined here as the effective diffusion coefficient.

Unfortunately, the terminology relating to diffusion is somewhat confused with similar words being used to mean different things. For example, Domenico & Schwartz (1998) refer to D_p as the "effective diffusion" coefficient; however, in the geotechnical literature (e.g. Shackelford & Daniel 1991a,b; Rowe *et al.* 1995b) the "effective diffusion" coefficient does not include porosity and is as defined by Eq. 24.10. Thus the reader needs to be very careful in clarifying the definition in a given context prior to using a diffusion coefficient in numerical calculation.

When dealing with contaminant migration through soils, it is important to recognize that diffusive transport is also influenced by electro-osmotic flow and that the effective diffusion coefficient deduced in the laboratory or back-figured from field profiles is really a bulk mass transfer coefficient. It can incorporate the effects of a number of related processes including true diffusion, osmotic flow and, due to the need to maintain an ion balance, electrically induced flow (Rowe *et al.* 1995b). For a given soil, the diffusion of a particular contaminant is temperature dependent. In addition, the diffusion coefficient of even a "conservative" contaminant such as chloride can be influenced as much by the chemical composition of the leachate (due to the effect on both the availability of cations to migrate with chloride and osmotic flow) as by temperature over typical temperature ranges. This is illustrated by the range of observed (deduced) effective diffusion coefficients summarized in Table 24.3.

The nature of the porous media (and its effect on geometric tortuosity) does have

TABLE 24.3. Observed effective diffusion coefficients for chloride through a number of soils (adapted from Rowe *et al.* 1995b and Rowe & Weaver 1997)

Soil type	Method of evaluation	Effective diffusion coefficient, D_e ($m^2\ a^{-1}$)
Uniform sand or gravel	Laboratory, at 23°C	0.03
Silt and silty sand	Laboratory, at 23°C	0.022–0.028
Low activity clayey soils	Laboratory, at 22°C	0.017–0.021
	Laboratory, at 10°C	0.01–0.025
In situ silty clay below waste	Field	0.006–0.02
Leda clay	Field	0.006
Water-laid clay till	Field	0.01
Freshwater glaciolacustrine clay	Field	0.012–0.018

TABLE 24.4. Effective diffusion coefficients for chloride in porous rock (adapted from Rowe *et al.* 1995b)

Rock	Effective porosity (%)	Effective diffusion coefficient, D_e (m^2 a^{-1})
Sandstone	3.4	0.002–0.003
Mudstone	9.2	0.002–0.003
Shale	10.8	0.005
Mudstone	23.8	0.006

some effect on the effective diffusion coefficient. For example, the diffusion through uniform sand and gravel is greater than through silt, which, in turn, is greater than through clays and clayey tills. Diffusion can also occur through porous rock such as chalk, sandstone and shale. Observed (deduced) effective diffusion coefficients for a number of porous rocks are given in Table 24.4.

Diffusion operates independently of groundwater flow. In aquifers, or primarily high velocity hydrogeological environments, it is secondary in importance to advection and dispersion. However, in aquitards, in which advection or groundwater flow velocities are very small, diffusion can become the dominant transport mechanism (see Rowe *et al.* 1995b).

Matrix diffusion into or out of low permeability clay lenses in aquifers or porous blocks of fractured media plays an important role in contaminant migration. Here, contaminants being transported through the more permeable zone, e.g. aquifer adjacent to a clay lens or a fracture in a clay or porous rock, diffuse into the adjacent low permeability unit, thereby reducing contaminant concentrations in the permeable zone. If not anticipated, this process may lead to misinterpretation of groundwater monitoring data. Matrix diffusion both reduces the magnitude and delays the arrival time of the contaminant peak at a point (Rowe *et al.* 1995b). Field evidence indicates that this effect can be significant (Rowe & Booker 1989). Matrix diffusion can also substantially reduce the effectiveness of conventional "pump and treat" clean-up strategies. This is caused by the slow but persistent release of contaminants back into the permeable zone by diffusion once the concentration in the permeable zone drops below that in the adjacent low permeability material.

Diffusion can also be of importance in unsaturated soils below landfills. The diffusion of dissolved species is reduced with reducing degrees of saturation (volumetric water content), as discussed in Section 25.5.1. Conversely, however, the diffusion of vapor (e.g. volatile organic compounds or oxygen) can be enhanced as the degree of saturation is reduced, see Section 25.5.2.

24.3.1.3 Dispersion

Dispersion, or more formally hydrodynamic dispersion, spreads mass beyond the area it normally would occupy due to advection alone. Stated another way hydrodynamic dispersion will move mass out of flow or stream tubes. Hydrodynamic dispersion occurs as a consequence of two processes, diffusion as discussed above, and mechanical dispersion. These two contributions to hydrodynamic dispersion are represented mathematically as:

$$D = D_{md} + D_e \qquad (24.11)$$

where D = the coefficient of hydrodynamic dispersion and D_{md} = the coefficient of mechanical dispersion. The use of the effective diffusion coefficient, D_e (rather than the porous media diffusion coefficient, D_p) in Eq. 24.11 is important because the coefficient of hydrodynamic dispersion that appears in most formulations of the groundwater transport equation already has the porosity factored out.

Mechanical dispersion is mixing caused by the convoluted pathways that water and contaminants (solutes, molecules, particles) follow while flowing through porous or fractured

media. Essentially, mechanical dispersion is caused by local variations in velocity around some mean velocity of flow (average linear groundwater velocity). Thus, mechanical dispersion is purely an advective process related to the statistical variability in the grain-size distribution in the aquifer and is not driven by a chemical potential like diffusion. The more heterogeneous the aquifer is, the greater the irregularity of the flow paths and the deviation about the mean velocity will be, and the greater the mechanical dispersion. This relationship with average linear groundwater velocity is reflected in the equations for the coefficients of mechanical dispersion:

$$D_{md-L} = \alpha_L v \text{ and } D_{md-T} = \alpha_T v \quad (24.12)$$

where α_L and α_T = the longitudinal and transverse dispersivities of the porous medium (units of length), and D_{md-L} and D_{md-T} = the longitudinal and transverse dispersion coefficients. D_{md-L} quantifies mechanical dispersion in the direction of flow, while D_{md-T} quantifies transverse spreading. In actuality, there are two transverse components of spreading, one in the horizontal plane and one in the vertical plane.

Although Eq. 24.12 is the commonly accepted relation for the coefficient of mechanical dispersion, the order of dependence on velocity is only approximate, i.e. $D_{md-L} \propto v$. Greenkorn (1983) has explained the reasons for this uncertainty. Furthermore, while it is agreed the dispersivity is a medium property, quantifying dispersivity is difficult. Numerous studies on dispersivity from the column to field scale have been undertaken. Gelhar *et al.* (1992) undertook a critical review of field experiments from 59 sites around the world (Fig. 24.3). Of approximately 106 values for longitudinal dispersivity only 14 values were highly reliable. The reliable values ranged from 10^{-2} to 10^{-1} m for column experiments to 10^{-1} to 2 m for relatively small-scale field studies (over a maximum distance of approximately 100 m). Many published dispersivity values are unrealistically large. They suffer from errors related to the collection and interpretation of field data, which force dispersivity values to be larger than actual values (Domenico & Schwartz 1998). Furthermore, many published estimates of dispersivity are no more than numerical model calibration or curve-fitting values (Anderson 1984), and can be subject to a variety of other errors. While it is known that dispersivity is scale dependent, no larger, properly conducted, field experiments have been carried out to quantify scale dependence.

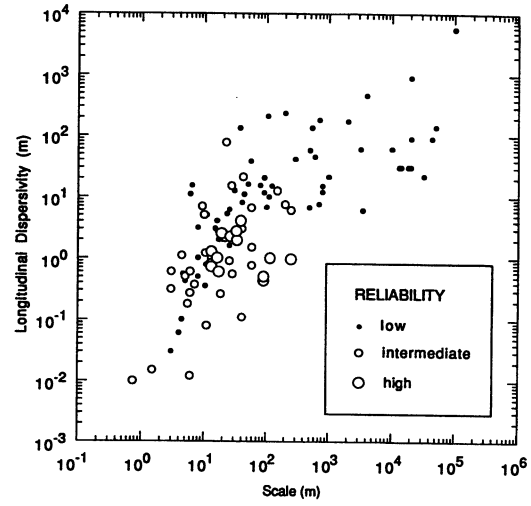


FIGURE 24.3. Longitudinal dispersivity versus scale with data classified by reliability (after Gelhar *et al.* 1992, *Water Res.*, v. 28, p. 1955–1974. © 1992 American Geophysical Union).

24.3.2 MULTIPHASE FLOW

Many contamination problems involve more than one fluid phase (e.g. aqueous phase, non-aqueous phase, and vapor phase). Figure 24.4 illustrates a conceptual DNAPL spill, where the non-aqueous phase contaminants occur as residual fluid within the pores and ponded on a low permeability layer. Complexity is added because the DNAPL dissolves into groundwater to form a large aque-

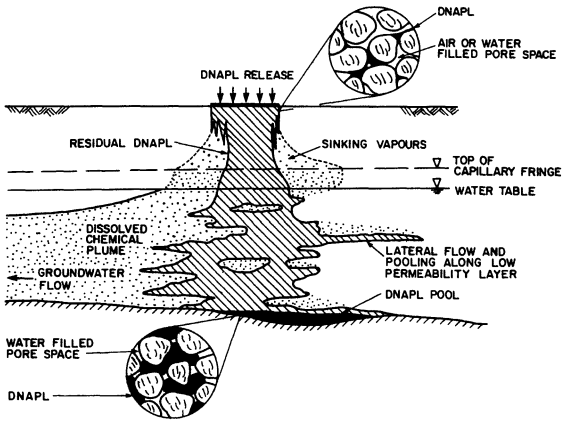


FIGURE 24.4. General groundwater contamination scenario with dense, non-aqueous phase liquids (after Kueper & Frind 1991, *Water Resources Res.*, v. 27, p. 1049–1057. © 1991 American Geophysical Union).

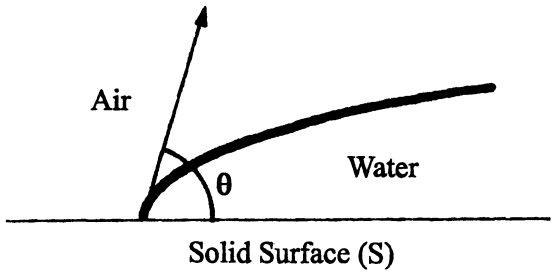


FIGURE 24.5. Interface between air, water and a solid surface (modified from de Marsily, 1986, *Quantitative Hydrogeology*. © 1986 Academic Press, Inc. Reprinted by permission of Academic Press, Inc.).

ous phase plume, and volatilizes into the unsaturated zone to create a vapor plume. Problems involving NAPLs or multiphase flow are much more complex than dissolved plumes.

When several fluids occupy a porous medium, their flow characteristics will be governed by the proportion of each fluid in the medium. Their relative abundance is described by the volumetric saturation, S_i, of the fluids:

$$S_i = V_i/V_v \qquad (24.13)$$

where V_i = the volume of the ith fluid, and V_v = the volume of voids.

When two fluids are in contact with each other, or a fluid is in contact with a solid, there is a free interfacial energy between them created by the difference between the forces that attract the molecules toward the interior of each phase and those that attract the molecules through the contact surface. The interfacial energy is characterized by the interfacial or surface tension, σ_{ij}. Interfacial tension is defined as the work required to separate a unit area of one substance (i) from that of another (j), and is expressed as a force per unit length. When two or more fluids are present, there is a preference for one fluid to be attracted to a surface over the others. The term wettability describes the preference of fluids to wet a surface. According to Demond and Roberts (1987), the only direct measure of wettability is the contact angle. The contact angle, as in Fig. 24.5, is given by Young's equation (de Marsily 1986):

$$\cos\theta = \frac{\sigma_{sa} - \sigma_{sw}}{\sigma_{aw}} \qquad (24.14)$$

where θ is measured from 0 to 180° in the denser fluid (in Fig. 24.5, the water). If $\theta < 90°$, the fluid (here water) is said to be wetting with respect to the solid. If $\theta > 90°$, the fluid is said to be non-wetting. This is the case of the air in Fig. 24.5. Wettability is unique for given types of solids and fluids. However, it is generally found that: water is always the wetting fluid with respect to oil or air on rock-forming minerals; oil is a wetting fluid when combined with air, but a non-wetting fluid when combined with water; and oil is the wetting fluid on organic matter, such as peat or humus, in relation to either water or air (Albertsen *et al.* 1986).

In the fluid domain (Fig. 24.5), on either side of the interface, the pressure is not the same. The pressure discontinuity across any

curved interface separating immiscible fluids is called the capillary pressure, P_c, and is given by:

$$P_c = P_{nw} - P_w \qquad (24.15)$$

where P_{nw} = the pressure of the non-wetting fluid, and P_w = the pressure of the wetting fluid. Capillary pressure is a function of the radius of curvature, r, of the interface between the two fluids and of the surface tension, σ_{ij}, existing between them:

$$P_c = \frac{2\sigma_{ij}}{r}. \qquad (24.16)$$

In a fluid sense, capillary pressure is a measure of the tendency of a porous medium to imbibe the wetting phase or to repel the non-wetting phase (Bear 1972). Domenico & Schwartz (1998) explain that capillary pressure can be thought of as the pressure required to move a particle of non-wetting fluid into a pore filled with wetting fluid. Thus, because small pores provide resistance to entry due to capillarity, non-wetting fluids will tend to move through the coarser, more permeable zones in a heterogeneous medium. This behavior traps globules of water. A more detailed understanding of how immiscible fluids displace one another can be obtained by studying capillary pressure curves (Fig. 24.6). Capillary pressure curves illustrate the pressure–saturation relationship as the fluid initially saturating the medium is slowly displaced by the other fluid.

The radius of curvature of the menisci separating the fluids in the porous medium is a function of saturation. Accordingly, capillary pressure depends on the saturations of non-wetting and wetting fluids (Fig. 24.6). Drainage is the displacement of the wetting fluid by the non-wetting fluid and imbibition is the displacement of the non-wetting fluid by the wetting fluid. The curves show the value of capillary pressure that must be exceeded for displacement to take place at each relative

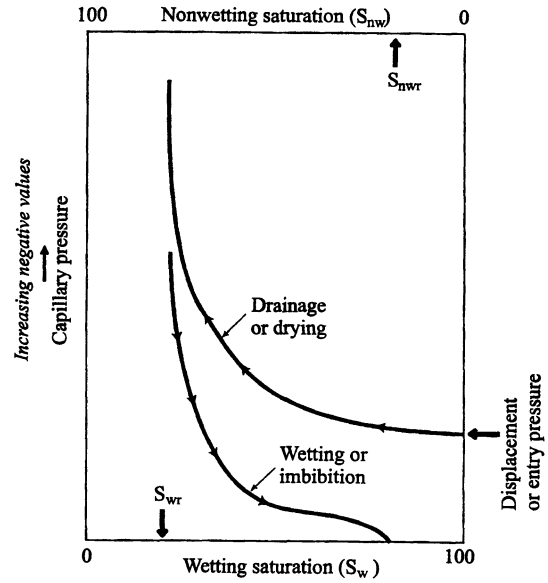


FIGURE 24.6. Capillary pressure curves given as a function of the degree of saturation with respect to the wetting and non-wetting phases (modified from Domenico & Schwartz, 1998, *Physical and Chemical Hydrogeology.* © 1998 John Wiley & Sons, Inc. Reprinted by permission of John Wiley & Sons, Inc.).

saturation. The drainage curve starts off at 100% wetting fluid saturation and some finite value of capillary pressure. For the non-wetting fluid to displace the wetting fluid, this value of capillary pressure, termed the entry pressure, must be exceeded. The curve is essentially a succession of equilibrium states for increasing values of saturation in non-wetting fluids that are very close to each other. As the wetting saturation decreases, the capillary pressure becomes more negative. As the suction increases, the displacement process eventually stops when the capillary pressure tends to infinity. The saturation value at which it stops is known as the residual wetting saturation (designated S_{wr} in Fig. 24.6). At the residual saturation there is no longer a continuum of the wetting fluid and pressures can no longer be transmitted across the pore network. The wetting or imbibition

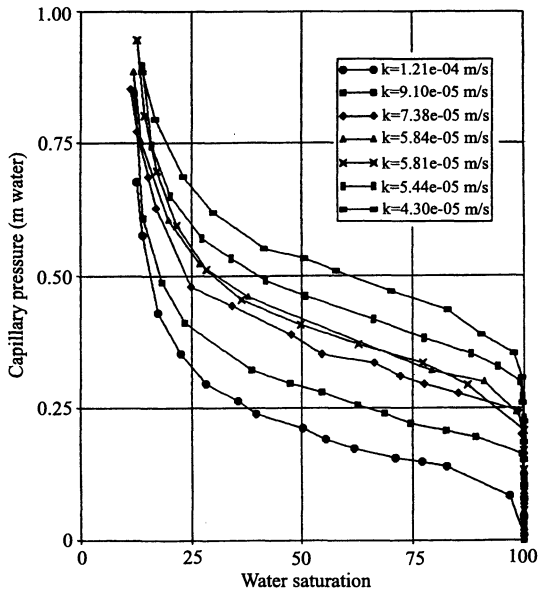


FIGURE 24.7. Capillary pressure–water saturation drainage curves for a tetrachloroethene–water system for sands of differing hydraulic conductivity (modified from Kueper & Frind, 1991, *Water Resources Res.*, v. 27, p. 1059–1070. © 1991 American Geophysical Union.).

curve shows the opposite process. However, it does not follow the same pathway as the drying curve since the non-wetting fluid occupies a different pore network during imbibition than during drainage. Note also that for a zero capillary pressure some saturation remains in a non-wetting fluid. This is the residual non-wetting saturation (designated S_{nwr} in Fig. 24.6).

Kueper & Frind (1991) present capillary pressure curves for a tetrachloroethylene–water system for sands of differing hydraulic conductivity (Fig. 24.7). These curves show that the entry pressure decreases with increasing hydraulic conductivity. Curves like this can be used at contaminated sites to assess the potential for DNAPL to enter underlying fine-grain material that may serve initially as migration barriers. The reader is referred to Kueper & McWhorter (1991) for details.

The capillary pressure curves illustrate how immiscible fluids tend to interfere with one another as they flow. In essence, because some of the pore networks are occupied with an immiscible fluid these networks are unavailable for the "other" fluid. This concept is readily illustrated by looking at Darcy's law for one-dimensional multiphase flow in a homogeneous medium, as given by Demond & Roberts (1987).

$$q_i = -\frac{k_i k_{ri}}{\mu_i}(\nabla P_i - \rho_i g \nabla h) \qquad (24.17)$$

where q_i = the flow of the ith fluid per unit area of the medium, k_i = the intrinsic permeability; k_{ri} = the relative permeability to the ith fluid, h = the elevation, and μ_i, P_i, ρ_i are the viscosity, pressure and density of the ith fluid, respectively. The relative permeability to the ith fluid is defined as:

$$k_{ri} = \frac{k_{eff}}{k_i} \qquad (24.18)$$

where k_{eff} = the effective permeability of the medium to the ith fluid. Effective permeabilities are generally obtained by measurement in the laboratory or from published experimental results. A detailed discussion of effective and relative permeabilities can be found in Corey (1986).

How k_{ri} varies between zero and one depends on many elements including: fluid densities, viscosities, and interfacial tension; wetting angle; relative saturation, media pore-size distribution; and whether the system is undergoing imbibition or drainage. Figure 24.8 illustrates many features common to most relative permeability curves:

- The simultaneous flow of both immiscible fluids is only possible if the residual wetting and non-wetting saturation are exceeded (in Fig. 24.8 $S_w > 0.2$; $S_{nw} > 0.1$).
- When both fluids are present the relative permeabilities rarely sum to one.

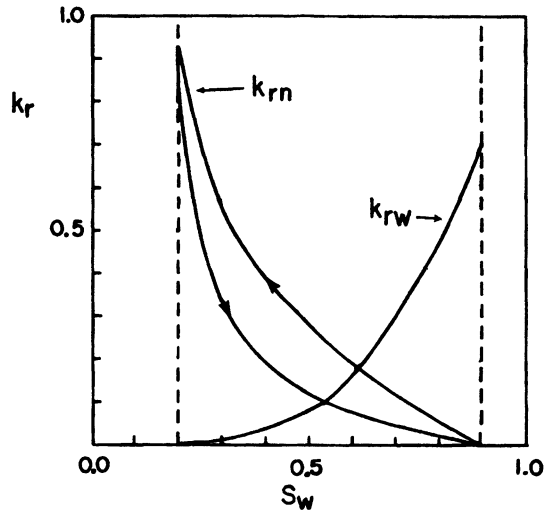


FIGURE 24.8. Typical relative permeability curves (after Demond & Roberts, 1987, *Water Resources Bulletin*, v. 23, p. 617–628. © 1987 American Water Resources Association. Reproduced by permission of American Water Resources Association.).

- When at residual wetting saturation, the relative permeability of the non-wetting fluid is close to one. At residual non-wetting saturation, the relative permeability of the wetting fluid is much less than one. Thus, the presence of a wetting fluid at residual saturation has little influence on the flow of a non-wetting fluid, while the presence of a non-wetting fluid at residual saturation interferes considerably with the flow of a wetting fluid.
- For comparable saturations $k_{rn} > k_{rw}$ (Fig. 24.8). One reason for this is that the wetting fluid occupies the smaller pores that contribute least to flow, while the non-wetting fluid occupies the larger pores that contribute most to flow.

Readers can refer to Demond & Roberts (1987) and texts by Dullien (1979) and Marle (1981) for a more detailed review of capillary pressure or relative permeability curves.

The level of residual saturations has important implications regarding the mobility of NAPLs and DNAPLs. At residual wetting saturation, the wetting fluid is held by capillary forces in the narrowest parts of the pore space. At residual non-wetting saturation, the non-wetting fluid, in a water-wet aquifer, occurs as an isolated blob in the center of pores. In the unsaturated zone, it is common to find water, air and a NAPL such as oil. Here, water is the wetting fluid, air is the non-wetting fluid, and oil has intermediate wetting properties (non-wetting with respect to water but wetting with respect to air, as discussed by Wilson & Conrad (1984)). Because immiscible fluids behave differently in the saturated zone and unsaturated zone, the residual saturations differ. Residual saturations in the unsaturated zone generally range between 0.1 and 0.2 (Cohen & Mercer 1993). In the saturated zone, where the NAPL is usually the non-wetting fluid, residual saturation values range from approximately 0.1 to 0.5.

Domenico & Schwartz (1998) present many examples of DNAPL and NAPL migration and have an excellent discussion of conceptual models for multiphase migration. In addition, Schwille (1988) presents detailed experimental studies on DNAPL migration in heterogeneous porous and fractured media.

One important key to understanding the migration of NAPLs at a site is understanding the hydrogeological setting or environment (Section 24.1); most importantly a detailed characterization of aquifer and aquitard permeability heterogeneities (hydrostratigraphy). While detailed field characterization is costly, an added problem at a NAPL-contaminated site is that drilling can perforate low permeability zones and enhance downward NAPL migration.

When an LNAPL or DNAPL is released on the ground surface, the free product percolates down toward the water table under gravity driven flow. As the NAPL locally displaces porewater and soil gas, it moves from pore to pore, once saturations exceed residual saturation. Therefore, the rate and area

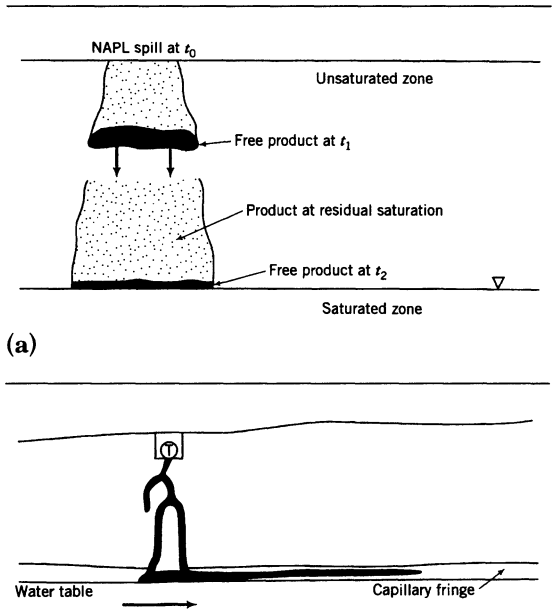


FIGURE 24.9. The downward percolation of a NAPL in the unsaturated zone is determined by the nature of the spill: (a) a sudden loss results in maximum spreading and a large quantity trapped at residual saturation; and (b) a slow leak causes the product to follow a set of channels and a minimal quantity is trapped at residual saturation (after Domenico & Schwartz 1998, *Physical and Chemical Hydrogeology*. © 1998 John Wiley & Sons, Inc. Reprinted by permission of John Wiley & Sons, Inc.).

of NAPL spill influences migration patterns. A large volume release over a short time period will trap a relatively large volume of NAPL at residual saturation (Fig. 24.9a). In comparison, slow leakage over a long time, will greatly increase the volume NAPL reaching the water table (Fig. 24.9b). Thus, if the volume of the spill is relatively small, and includes a sufficiently large area, the NAPL could be trapped in the unsaturated zone at residual saturation. Domenico & Schwartz (1998) discuss quantitative methods to calculate the depth of the residual saturation and other relevant parameters necessary to access NAPL migration in the field.

As the NAPL moves downward, it also tends to spread horizontally due to capillary forces (Fig. 24.9a). However lateral migration is most influenced by media heterogeneities and low permeability zones (Fig. 24.4). As LNAPL encounters the capillary fringe, the water saturations increase and relative permeability decreases. At this point, buoyancy forces become important; LNAPL accumulates and once some critical thickness is achieved, would flow down-gradient. Recent studies (Farr *et al.* 1990; Lenhard & Parker 1990; Huntley *et al.* 1992) show that instead of occurring as a discrete layer at the top of the capillary fringe (the classical model), LNAPL will be distributed throughout and above the capillary fringe. According to Huntley *et al.* (1992), this more realistic model for LNAPL saturation would provide for much less mobility than is suggested for high LNAPL saturation within a single layer. Furthermore, water table fluctuations can redistribute LNAPL across a larger zone. Lehnard *et al.* (1993) show how rapidly rising water tables can trap LNAPL below the water table.

Because DNAPLs are more dense than water, they will continue to move downward, displacing water in the saturated zone. Spreading will continue until the DNAPL is at residual saturation. As with all NAPLs, flow will be very sensitive to permeability variations. DNAPL will accumulate on low permeability units, moving "downhill" with the topography of the boundary (Fig. 24.4). Because most hydrogeological environments are highly heterogeneous on a local scale, DNAPL distributions are often highly complex with numerous isolated pools of DNAPL. DNAPL at residual saturation and in pools also serves as important sources for vapor phase or aqueous (dissolved) phase contamination (Fig. 24.4).

24.3.3 ATTENUATION OF DISSOLVED SOLUTES: BIOGEOCHEMICAL PROCESSES

The concentration of dissolved solutes often is reduced because of chemical reactions.

Such reactions can take place entirely in the aqueous phase, or involve the solid matrix of the porous or fractured medium. Mass transfer reactions that commonly alter contaminant concentrations in groundwater are:

1. acid–base reactions;
2. solution, volatilization and precipitation reactions;
3. surface reactions;
4. oxidation–reduction reactions;
5. hydrolysis; and
6. complexation reactions.

All of these processes probably will not be important at any given site. However, depending on site geology and contaminant type, one or several of these reactions could exhibit significant control on contaminant transport.

24.3.3.1 Acid–base reactions

Acid–base reactions are important in groundwater because they influence the pH and control ion concentrations. One of the most important natural weak acid–base systems is the CO_2–water system. This involves a set of reactions initiated when CO_2 is dissolved in water:

$$\left.\begin{aligned} CO_2(g) + H_2O &= H_2CO_3(aq) \\ H_2CO_3(aq) &= H^+ + HCO_3^- \\ HCO_3^- &= H^+ + CO_3^{2-} \end{aligned}\right\}. \quad (24.19)$$

Carbonate species are the most important participants in reactions that control the pH of natural waters (Hounslow 1995). How the relative concentration of the carbonate species changes with pH is shown in Fig. 24.10. In natural waters, the dissolved CO_2 species, bicarbonate (HCO_3^-) and carbonate (CO_3^{2-}), produce most of the alkalinity. Alkalinity is defined as the capacity of a solution to react with, or neutralize, a strong acid. It is determined by titrating a specified volume of water, with a strong acid such as HCl, to a specific end-point (typically pH 4.5). Standard test methods for alkalinity determination can be found in American Society for Testing and Materials (ASTM) designation D 1067. Natural groundwaters are usually alkaline because of the abundance of dissolved CO_2 species, bicarbonate and carbonate. Other non-carbonate contributors to alkalinity, such as hydroxide, silicate, borate and the organic ligands, especially acetate and propo-

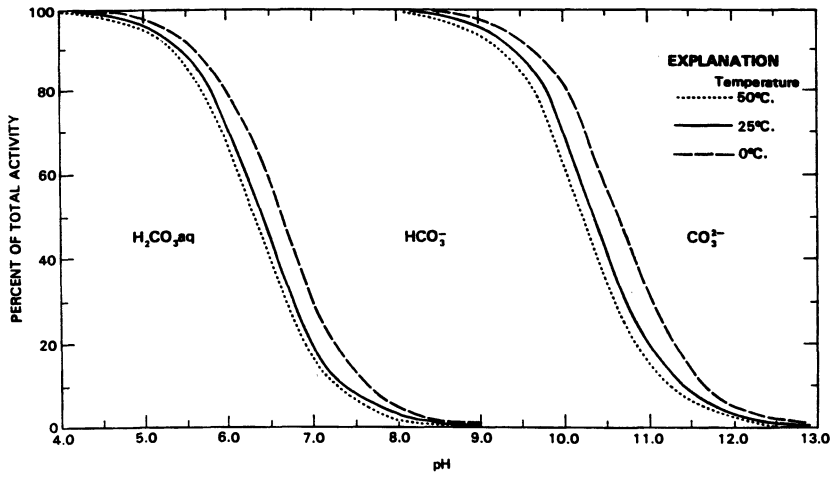


FIGURE 24.10. Percentages of dissolved carbon dioxide species activities at one atmosphere pressure and at (···) 50, (—) 25 and (––)0°C as a function of pH (after Hem 1995, *U.S. Geol. Surv.*, Water Supply Paper 2254).

nate, are only important if present in significant amounts (Hounslow 1995). However, this situation may change as a result of contamination, e.g. oxidation of sulfide minerals from metal mines. Typically, alkalinity is reported in terms of milliequivalents per liter (meq L^{-1}) $CaCO_3$. Example alkalinity calculations, and a much more detailed description of acid–base reactions, carbonate equilibria and alkalinity can be found in Drever (1982).

Carbonate reactions and their control on water chemistry and pH also influence how one samples groundwaters. Exposure of groundwater to atmospheric partial pressures of CO_2 often results in the removal of CO_2 from the solution. This raises the pH of the solution and can result in various metals being precipitated. In addition, the cation equilibria with solid phases can also change. Thus, the common practice of filtering and adding acid or acidifying groundwater samples for metals analysis.

24.3.3.2 Solution, Volatilization and Precipitation Reactions

Gas solution and exsolution are commonly modeled using equilibrium concepts based on Henry's law. The Henry's law equation for CO_2 is:

$$K_H = \frac{P_{CO_2}}{CO_2(aq)} \tag{24.20}$$

where K_H = Henry's law constant, with units like atm m^3 mol^{-1} or bar m^3 mol^{-1}, P_{CO_2} = partial pressure of CO_2 (atm) in the gas phase, and $CO_2(aq)$ = the molar concentration of CO_2 gas in solution (mol m^{-3}). In applications, the concentration of $CO_2(aq)$ = H_2CO_3 (aq).

The Henry's law expression for gases (Eq. 24.21) is the same expression for the volatilization of dissolved organic solutes from water:

$$P_{org} = K_H C_{org} \tag{24.21a}$$

where P_{org} = the partial pressure of the organic compound in the vapor phase (atm), and C_{org} = the concentration in the aqueous phase (mol m^{-3}). Henry's law can also be expressed as

$$P_{org} = K'_H C_{org} \tag{24.21b}$$

where P_{org} = the solute concentration in air (mol L^{-1}), C_{org} = the aqueous solute concentration (mol L^{-1}) and K'_H = the dimensionless Henry coefficient:

$$K'_H = \frac{K_H}{RK} \tag{24.22}$$

where R = the ideal gas constant (8.205×10^{-5} atm m^3 mol^{-1} $°K^{-1}$ = 8.314×10^{-5} bar m^3 mol^{-1} $°K^{-1}$) and K = the temperature of the water (degrees kelvin). The volatilization of pure organic solvents is typically described by Raoult's law:

$$P_{org} = x_{org} P^{\circ}_{org} \tag{24.23}$$

where x_{org} = the mole fraction of the organic solvent, and P°_{org} = the vapor pressure of the pure organic solvent. The Henry's law constants and vapor pressures of all US EPA priority pollutants can be found in Montgomery & Welkom (1990) along with other physicochemical data such as water solubility, vapor density, octanol-water (K_{ow}) and organic-carbon water (K_{oc}) partition coefficients. A number of these parameters are summarized in Table 24.5. The relative volatility of a substance can be related to the Henry's law coefficient K_H and if $K_H < 10^{-7}$ atm m^3 mol^{-1}, the substance is considered to have low volatility (Lyman *et al.* 1982). A value of $10^{-7} \leq K_H \leq 10^{-5}$ atm m^3 mol^{-1} is considered to correspond to slow volatilization. Volatilization is usually important for $10^{-5} < K_H < 10^{-3}$ atm m^3 mol^{-1} and the process will occur quickly for $K_H > 10^{-3}$ atm m^3 mol^{-1}. Volatilization is important for problems of NAPL (organic) contamination within the unsaturated and capillary zone (Fig. 24.4). Volatilization is also important for issues related to sample collection and analysis. Volatilization can reduce

TABLE 24.5. Some published Henry's law, log K_{ow}, log K_{oc}, solubility and density values (adapted from Montgomery & Welkom 1990)

Compound	Henry's law constant (atm m^3 mol^{-1})	$\log_{10} K_{oc}$ (−)	$\log_{10} K_{ow}$ (−)	Solubility in water at 25°C (mg L^{-1})	Density at 20°C (g mL^{-1})
Acetone	3.97×10^{-5}	−0.43	−0.24	∞	0.79
Benzene	5.38×10^{-3}–5.48×10^{-3}	1.69–2.00	1.56–2.15	1780–1800	0.876
bis-(2 ethylhexyl)phthalate	1.1×10^{-5}	5.0	4.2–5.11	0.05–0.4	0.985
2-Butanone (MEK)	4.66×10^{-5}	0.09	0.26–0.29	2.5×10^5	0.805
Chlorobenzene	3.6×10^{-3}–4.45×10^{-3}	1.68–2.52	2.71–2.98	295–503	1.1
Chloroethane	8.5×10^{-3}–1.46×10^{-2}	0.51	1.43	4700	0.897
Chloroform	2.9×10^{-3}–5.3×10^{-3}	1.64	1.9–1.97	7200–9600	1.48
p-Cresol	7.9×10^{-7}	1.69	1.67–1.94	18000–23000	1.01–1.03
Di-n-butyl phthalate	6.3×10^{-5}	3.14	4.31–4.79	9–4500	1.046
1,2 Dichlorobenzene	1.2×10^{-3}–2.4×10^{-3}	2.26–3.23	3.38–3.55	93–156	1.3
1,4 Dichlorobenzene	2.7×10^{-3}–4.4×10^{-3}	2.2	3.37–3.62	65–90	1.25
1,1 Dichloroethane	4.3×10^{-3}–5.9×10^{-3}	1.48	1.78	5.060	1.17
1,2 Dichloroethane	9.1×10^{-4}–1.3×10^{-3}	1.15–1.28	1.45–1.48	7890–8650	1.23–1.25
1,1 Dichloroethene	1.5×10^{-2}–2.1×10^{-2}	1.81	1.48–2.13	273–6400	1.21
trans-1,2 Dichloroethene	6.7×10^{-3}–3.8×10^{-1}	1.77	2.09	6300	1.26
Dichloromethane	2.0×10^{-3}–3.2×10^{-3}	0.94	1.25–1.30	13000–19400	1.33
Ethylbenzene	6.4×10^{-3}–8.7×10^{-3}	1.98–2.41	3.05–3.15	77–208	0.867
Naphthalene	3.6×10^{-4}–1.2×10^{-3}	2.74–3.52	3.01–4.70	20–40	1.14–1.16
Pentachloro-phenol	2.8×10^{-7}–3.4×10^{-6}	2.95–2.96	2.75–2.86	20–25	1.98
Phenol	1.7×10^{-7}–4.0×10^{-7}	1.24–1.43	1.46–1.48	67000–93000	1.058
1,1,2,2-Tetrachloroethane	3.8×10^{-4}–4.6×10^{-4}	1.66–2.07	2.39–2.56	2870–2970	1.59
Tetrachloroethene (PCE)	2.9×10^{-3}–1.5×10^{-2}	2.32–2.56	2.10–2.60	150–485	1.62
Toluene	6.7×10^{-3}	2.06–2.18	2.11–2.80	220–627	0.867
1,1,1-Trichloroethane	1.3×10^{-2}–1.8×10^{-2}	2.0–2.18	2.17–2.49	300–1334	1.31–1.34
Trichloroethene (TCE)	9.1×10^{-3}–1.2×10^{-2}	1.81–2.10	2.29–3.30	1100–1470	1.46
Vinyl chloride	5.6×10^{-2}–2.78	0.39	0.60	915–8800	0.91

the concentration of organic contaminants in water samples if exposed to the atmosphere.

The dissolution and precipitation of solids are two of the most important factors controlling the chemistry of groundwater. In natural waters, a recharging groundwater obtains almost all its solute load from the dissolution of minerals along the flow path. If geochemical conditions change along the flow path, mineral precipitation can occur removing some of the dissolved mass. Low pH, metal-rich, contaminant plumes can precipitate minerals as the plume disperses and the pH gradually increases. Because other ions are typically present in groundwaters these mineral dissolution–precipitation reactions are best quantitatively analyzed using geochemical speciation models. For the details of chemical equilibria and rates in natural waters readers are referred to aquatic chemistry texts such as Stumm & Morgan (1996), Morel (1983), and Drever (1982).

24.3.3.3 Sorption

The reaction between solutes and solids plays an extremely important role in controlling the chemistry of groundwater. Sorption reactions can be subdivided into two main types: hydrophobic sorption of organic compounds and ion exchange reactions. For example, non-polar organic molecules partition onto solid organic matter on or within the mineral grains of a soil. Ion exchange typically involves the exchange of cations in solution with other cations on the surface of clay minerals in the soil. In the case of a contaminant sorption, this results in a reduction in concentration in the aqueous phase. This sorption is manifest by a reduction in contaminant velocity relative to the groundwater flow. The term retardation is used to describe this velocity reduction.

The case of ion exchange is somewhat different. The decrease in the concentration of the ion of interest in solution, e.g. K^+, Na^+, Pb^{2+}, Cd^{2+}, Fe^{2+}, Cu^{2+}, is accompanied by an increase in pore fluid concentration of the desorbed ion, e.g. Ca^{2+}, Mg^{2+} as discussed by Rowe *et al.* (1995b).

Sorption is commonly represented by a simple one-parameter model or K_d approach. The sorption isotherm, describing the equilibrium between solute and sediment, is represented as a simple linear isotherm (isopleth):

$$S = K_d C \tag{24.24}$$

where S = the mass sorbed per unit mass of dry soil (mg g^{-1}), K_d = the distribution coefficient (cm^3 g^{-1}), and C = the equilibrium solution concentration (mg L^{-1}). In reality, sorption isotherms can take on a complex functional form. However, the linear isotherm is easy to incorporate into mass-transport models and works fairly well for modeling sorption of organic contaminants at relatively low concentrations.

Values of K_d are typically obtained in the laboratory from sorption batch experiments, column tests, diffusion tests (see Rowe *et al.* (1995b), or estimated from empirical correlations (e.g. Karickhoff *et al.* 1979; Schwarzenback & Westall 1981):

$$K_d = K_{oc} f_{oc} \tag{24.25}$$

where K_{oc} = the partition coefficient of a compound between organic carbon and water (cm^3 g^{-1}) and f_{oc} = the weight fraction of organic carbon in the soil ($g_{organic\ carbon}$ g_{solids}^{-1}). Values of f_{oc} can be measured in the laboratory. A synthesis of some f_{oc} data at particular sites illustrates how variable the parameter can be (Table 24.6). While K_{oc} values are available for many contaminants (see Table 24.5 and Montgomery & Welkom 1990), a good correlation exists between log K_{oc} and a more often referenced parameter, the octanol-water partition coefficient, K_{ow}. Various regression equations between log K_{oc} and log K_{ow} can be found in Domenico & Schwartz (1998) and Lyman *et al.* (1982).

The simple linear isotherm (Eq. 24.24) has

TABLE 24.6. Typical f_{oc} values of various sediments

Field site	Type of deposit	Sediment texture	f_{oc}	Reference
Borden, Ontario	Glaciofluvial	Fine–medium sand	0.0002	Jackson *et al.* (1985)
Gloucester, Ontario	Glaciofluvial	Regressional sands and gravels	0.0001–0.0035	Mackay *et al.* (1986)
		Stratified clayey silt and silt	0.0029–0.0059	
		Subaqueous outwash gravels, sands and silts	0.0131–0.0015	
Palo Alto, Baylands	Unknown	Silty sand	0.01	Mackay & Vogel (1985)
River Glatt, Switzerland	Glaciofluvial	Sand and gravel	<0.0001–0.01	Schwartzenbach & Giger (1985)
Oconee River, Georgia	River sediment	Sand	0.0057	Karickhoff (1981)
		Coarse silt	0.029	
		Medium silt	0.02	
		Fine silt	0.0226	
Sarnia, Ontario	Glaciolacustrine	Clay	0.0058	Rowe *et al.* (1995b)
Milton, Ontario	Till	Clayey till	0.0029–0.0045	Rowe *et al.* (1993)

limitations and can break down under a number of conditions as follows:

- For hydrophilic organic compounds: Karickhoff (1984) recommends that a hydrophobic sorption model (K_d approach) should only be used for organic compounds with solubilities less than 10^{-3} M.
- For low f_{oc} values: sorption of organic compounds on inorganic surfaces, which is normally considered negligible, can be significant. McCarty *et al.* (1981) have developed an empirical equation to estimate the critical organic fraction, f_{oc}^{*}, where sorption due to organic and inorganic solids equals:

$$f_{oc}^{*} = \frac{S_a}{200(K_{ow})^{0.84}} \qquad (24.26)$$

  where S_a = the surface area of the soil ($m^2\ g^{-1}$) and K_{ow} = the octanol-water partition coefficient. The surface area depends on the clay content and mineralogy (typical values reported (Yong 1985) range from 15 $m^2\ g^{-1}$ for kaolinite to 80 $m^2\ g^{-1}$ for illites and chlorites, to 800 $m^2\ g^{-1}$ for montmorillonites). Values of K_{ow} can be found in Montgomery & Welkom (1990) and some values are given in Table 24.5 (in terms of $\log_{10} K_{ow}$).
- For relatively large organic concentrations: a linear isotherm does not limit the amount of solute that can be sorbed onto the solid. Non-linear isotherms, however, often fit the experimental data better. Two of the most common relationships are the Freundlich and Langmuir isotherm:

$$\text{Freundlich} \qquad S = K_f C^m \qquad (24.27)$$

$$\text{Langmuir} \qquad S = \frac{S_m K_l C}{1 + K_l C} \qquad (24.28)$$

  where K_f and K_l = empirical coefficients related to the extent of sorption, m = an empirical constant (often ranging from 0.7 to 1.2), and S_m = the maximum sorptive capacity for the soil.
- If the organic compound carries a charge. Some organic acids and bases ionize to some extent depending on the pH of the groundwater.

Batch tests and empirical correlations are useful in quantitatively describing sorption. However, they do not fully represent *in situ* conditions and could be subject to error from a number of sources. Particular care is needed in the application of laboratory parameters because they may either underestimate or overestimate the amount of sorption that can occur in the field (e.g. see Rowe *et al.* 1995b).

The K_d approach has been used to describe metal sorption on mineral surfaces. However, one must be cautious in applying such a simple one-parameter model to what with metals is a much more complex process. Even cation-exchange reactions provide a more sophisticated approach. In these reactions, an exchange of ions takes place between ions in solution and ions sorbed on clay minerals or other oxide surfaces. However, the extent of the exchange depends both on the mineralogy of the clay (or nature of the oxide surface) and the chemical composition of the groundwater. For example, Rowe *et al.* (1995b) show that the sorption of a cation on a given clay is highly dependent on the presence of competing cations. Thus, either the sorption characteristics must be empirically evaluated under conditions as close as possible to that expected in the field, or rigorously evaluated in terms of multiparameter equilibrium models. These models apply the law of mass action, which accounts for properties of the solution and the solid surfaces.

It is possible to model sorption using more realistic multiparameter equilibrium models. Such models are now being incorporated into state-of-the-art contaminant transport models; however, they are complex and require considerable data. Stollenwerk (1991) uses such an approach to study the sorption of molybdate (MoO_4^{2-}) on ferrihydrite, which coats quartz grains of an outwash aquifer.

Stumm & Morgan (1996) provided a more detailed review of ion exchange and sorption isotherms.

When estimating sorption parameters, e.g. K_d, it is important to recognize that both empirical equations, e.g. Eq. 24.26, and laboratory batch tests or column studies have numerous limitations. For example, in order for a laboratory batch or column test to adequately represent the exchange process, actual field samples of ambient groundwater or leachate (or water with similar major ion concentrations), and porous media are used along with actual contaminant(s) of interest. However, several major difficulties arise with this approach. First, it is very difficult not to alter the geochemical characteristics of the geologic materials as they are sampled and sent to the laboratory. Most basic are the invasion of O_2 and the degassing of CO_2, which can alter the redox condition and pH of the samples. In some cases this can cause the precipitation of iron and manganese hydroxides, which have a strong affinity for the sorption of cationic and anionic trace contaminants. Second, a batch test does not represent the field conditions where the advancing zone of contamination continuously supplies ions to the exchange sites. In the field this can result in some contaminants being less retarded in certain zones due to a change in exchange properties, and other geochemical changes such as a change in the redox state and the precipitation of minerals. Finally, one must be careful not to extrapolate isotherm data. At low concentrations many contaminants exhibit a linear trend, which would appear to support a linear or K_d approach. However, at higher concentrations the type of surface reactions may change substantially shifting the functional form of the isotherm.

24.3.3.4 Oxidation–Reduction Reactions

Oxidation–reduction reactions or redox reactions are very important in contaminant hydrogeology because they can control the mobility of metal ions in solution, and biodegradation or biotransformation reactions. While biotransformation reactions can attenuate organic contaminants, daughter products are not necessarily less toxic. For example, the biotransformation of trichloroethylene can result in the formation of vinyl chloride, which is more toxic than its parent. Micro-organisms act as catalysts speeding up the very sluggish redox reactions. Micro-organisms occur ubiquitously in the subsurface and are most often found as colonies attached as films on porous media or fracture surfaces. Some micro-organisms thrive under aerobic conditions; others prefer anaerobic conditions. The need for biological mediation of most redox processes encountered in natural waters means that approaches to equilibrium depend strongly on biota activities (Stumm & Morgan 1996). While equilibrium calculations and approaches greatly aid attempts at understanding redox patterns in natural waters they only provide boundary conditions and rates of approach toward which the system must be proceeding.

Field electrode measurements of redox potentials present additional difficulties and often these measurements are meaningless. Stumm & Morgan (1996) comment on this:

> Values obtained depend on the nature and rates of the reactions at the electrode surface and are seldom meaningfully interpretable. Even when suitable conditions for measurement are obtained, the results are significant only for those components whose behavior is electrochemically reversible at the electrode surface.

The assessment of biodegradation and redox processes in groundwater systems is very difficult because it requires considerable knowledge about both groundwater geochemistry and applied microbiology. Chapelle (1993) nicely bridges this gap and provides a comprehensive text that focuses on the impact of microbial processes on pristine and contaminated groundwater systems. Domenico & Schwartz (1998) present an excellent up-to-

date synthesis of how redox processes and microbial systems influence groundwater geochemistry and remediation.

24.3.3.5 Hydrolysis

Hydrolysis is another transformation reaction that can operate on organic compounds; however, unlike biodegradation, it is not catalyzed by micro-organisms. Hydrolysis reactions involve the substitution of a water molecule, or an OH^- ion, for another atom or group of atoms in an organic molecule. Hydrolysis reactions are very prevalent in the aquatic environment, and often the products are less ecologically and toxicologically harmful than the unhydrolyzed reactants (Stumm & Morgan 1996). In addition, the introduction of a hydroxyl group into the parent molecule makes the product more soluble in groundwater, and more susceptible to biodegradation (Neeley 1985).

24.3.3.6 Complexation Reactions

Complexation reactions involve the combination of simpler cations, anions and sometimes organic molecules, to form a "complex". An example is one of the possible hydrolysis reactions of a metal (Cr^{3+}) with a ligand (OH^-) to form a complex $Cr(OH)^{2+}$:

$$Cr^{3+} + OH^- = Cr(OH)^{2+}. \quad (24.29)$$

Sometimes complexes can react themselves with ligands:

$$Cr(OH)^{2+} + OH^- = Cr(OH)_2{}^+. \quad (24.30)$$

Most inorganic complexation reactions are kinetically fast, with respect to groundwater flow, so they can be examined quantitatively using equilibrium concepts. Calculation of the distribution of a given total metal concentration among various complexes involves the solution of a series of mass law equations. Figure 24.11 illustrates the outcome of such a process for assessing the speciation of Cr as controlled by solution pH.

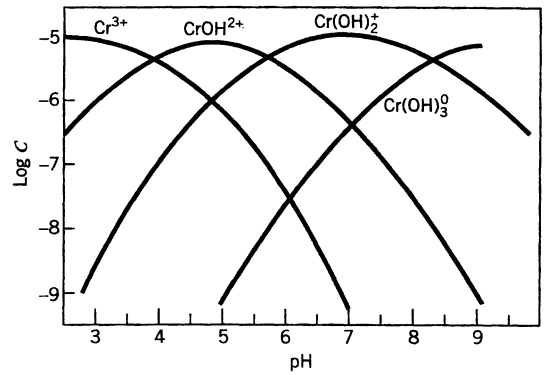


FIGURE 24.11. Log C–pH diagram for chromium hydroxide complexes (after Domenico & Schwartz 1998, Physical and Chemical Hydrogeology. © 1998 John Wiley & Sons, Inc. Reprinted by permission of John Wiley & Sons, Inc.).

Complexation facilitates the transport of toxic metals such as cadmium, chromium, lead and uranium. In general, metals in groundwater are most soluble at low pHs, where most of the metal mass exists as a charged ion. Ignoring the effects of sorption, this mobility declines once the pH increases to a point when equilibrium is reached with a solid phase, such as a metal hydroxide, sulfide or carbonate. Since most natural groundwaters are neutral or alkaline, equilibrium with the solid phase determines that aqueous metal concentrations will be small. It is under these circumstances that complexes can enhance the solubility and mobility of metals.

24.3.4 FACILITATED TRANSPORT OF CONTAMINANTS: COSOLVATION AND COLLOIDAL TRANSPORT

Facilitated transport occurs when the mobility of a contaminant increases as a result of physical, chemical or biological changes in the aquifer or aquitard. Cosolvation and colloidal transport are two major examples of facilitated transport that will be discussed here.

Cosolvation is the process by which the mobility of a contaminant is enhanced by the

presence of a solvent (Gorelick *et al.* 1993). Through cosolvation hydrophobic contaminants, such as PCBs, which are practically immobile in the aqueous phase, can become much more soluble when chlorinated solvents are present. Typically, cosolvation is most significant near the source, where solvent concentrations are likely to be high (Gorelick *et al.* 1993).

Colloidal transport occurs when small organic or inorganic particles, generally less than about 1 μm in diameter, move through porous, fractured and karst media. Colloids can be contaminants themselves, such as viruses and bacteria present in waste waters, and organic macromolecules generated in landfill leachates (Gournaris *et al.* 1993). Alternately, harmless colloids, such as clay and humic substances, can become contaminant collectors and facilitators when low mobility contaminants, such as trace metals, radionuclides or organic compounds, sorb onto their large surface areas. As long as colloids do not aggregate, or undergo physico-chemical collection on solid surfaces (McCarthy & Zachara 1989), they can move through the pore networks of gravels, sands and silts. Penrose *et al.* (1990) and Champ *et al.* (1984) have found significant colloid-facilitated radionuclide transport. Additional field studies include the work of Gschwend & Reynolds (1987), who examined colloid formation and transport in relation to a large sewage plume.

If surfactants are present in groundwaters they can also greatly increase the solubility of immiscible organic compounds. The surfactants form a microemulsion in water, trapping immiscible organic compounds, and allow them to stay dissolved and move through an aquifer. These emulsion-trapped organic compounds have similar fate and transport characteristics to that of metals bound up on colloids (USEPA 1992a).

One additional important concept with colloids involves the filtration of groundwater samples. The standard environmental filter has a pore size (0.45 μm) which is the middle of the colloidal size range. The problem arises that this filter does not provide a clean cut-off, between dissolved and colloidal species that are mobile, and colloids and larger particles that are not. Large concentration differences between filtered and unfiltered samples have been observed for metals (Puls & Barcelona 1989; Puls & Powel 1992; Puls *et al.* 1992; Pohlman *et al.* 1994). Therefore, many states, and some programs of the US Environmental Protection Agency, now prohibit filtration for metals analyses. This is due to potential sampling artifacts, created during the purging process, that lead to the production of turbid samples, or artifacts generated during the filtration process itself (Puls & Paul 1995; USEPA 1992a). If field filtration exposes a water sample to the atmosphere, the sample can oxidize dissolved ferrous iron to form a ferric hydroxide precipitate ($Fe(OH)_3$). In turn, other metals in solution may sorb onto the ferric hydroxide colloids, and both the colloid and sorbed metals will be removed from the sample by field filtration (USEPA 1992a). In most instances, proper well construction, and low-flow purging and sampling of monitoring wells, can eliminate the need to field-filter groundwater samples (Puls & Paul 1995).

25. BARRIER SYSTEMS

R. K. Rowe

25.1 *Applications, Mechanisms and Scope*

Barrier systems are intended to minimize the movement of liquids and/or gases from one location to another. Typical example applications include the use of liners for canals, ponds, dams, waste disposal facilities and spill protection around tanks. The liquids to be "contained" may range from water (e.g. in canals, ponds and dams) to contaminated water (e.g. in landfills; sewage lagoons; brine ponds; or contaminated groundwater) to relatively pure chemicals (e.g. hydrocarbons) stored in tank farms. In these applications the primary objective is to limit the physical escape of the liquid to either surface water or groundwater. In situations where the liner is in contact with contaminated water over long periods of time (e.g. lagoons, landfill liners, etc.), a secondary objective may also be to limit chemical migration by the process of diffusion (Section 24.3.1) whereby contaminants migrate from a point of high concentration (e.g. in the retained fluid) to points of lower concentration (e.g. in groundwater).

Other barriers include covers for solid and mining waste that serve to control the influx of a fluid (e.g. water in landfill covers) or a gas (e.g. oxygen in covers for acidic mine waste). They may also be intended to minimize the outward flux of liquids (e.g. perched leachate in a landfill) or gases (e.g. methane generated in a municipal solid waste landfill).

Barrier systems typically control the flow of liquids by virtue of having a liner component with a low hydraulic conductivity (Section 24.1.3) and, often, by having a transmissive layer adjacent to the liner (e.g. see Fig. 25.1).

This chapter provides basic information concerning obtaining and maintaining (as long as possible):

- high transmissivity of granular layers used to control hydraulic head or gas pressure (Section 25.2),
- low hydraulic conductivity of clay liners and minimizing leakage through composite liner systems (Section 25.3),
- liner compatibility with leachate (Section 25.4),
- minimizing diffusive transport of dissolved contaminants and gases (Section 25.5),
- the effect of temperature on liner performance (Section 25.6),
- assessing equivalency of liner systems (Section 25.7), and
- stability of liner systems (Section 25.8).

Other design considerations related to liners in liquid-containing structures are provided in Chapter 26, while Chapter 27 discusses covers for waste and Chapters 29 and 30 include a discussion of the use of barriers for containment of both contaminated groundwater and soil.

25.2 *Transmissive Layers*

High transmissivity layers may be used above liners to minimize the hydraulic head act-

R. K. Rowe (ed.), *Geotechnical and Geoenvironmental Engineering Handbook*
© Kluwer Academic Publishers 2001

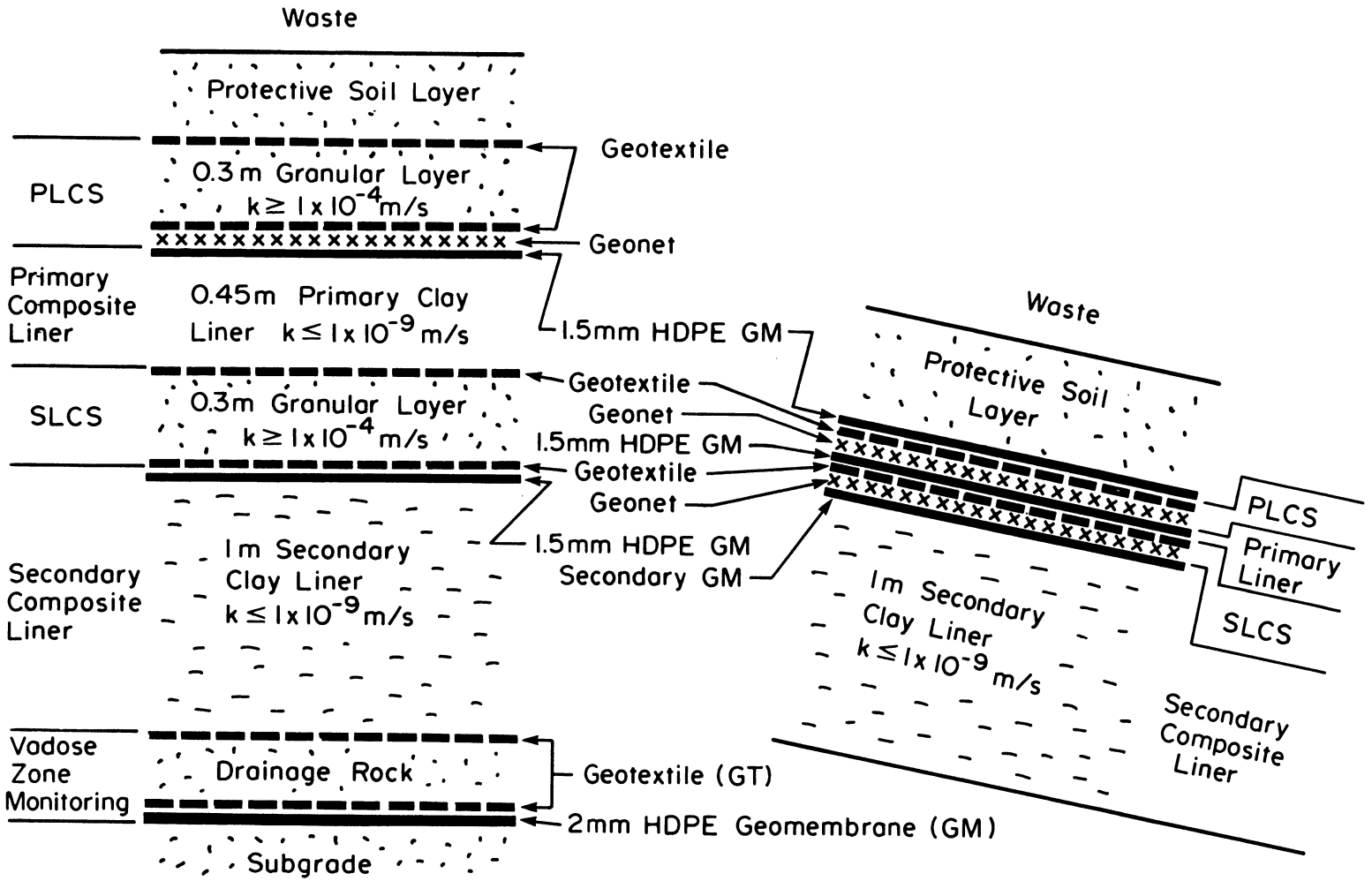


FIGURE 25.1. Schematic showing (a) base and (b) side slope of barrier system for Kettleman Hills landfill: PLCS = Primary leachate collection system; SLCS = Secondary leachate collection system; GM = Geomembrane (modified from Byrne *et al.* 1992).

ing on the liner (and hence minimize flow through the liner) or below liners in covers to allow recovery of gas and control gas pressures that could otherwise cause instability of a low permeability cover. These transmissive layers may be constructed from granular materials or geosynthetics or a combination of both, e.g. see Fig. 25.1. In either case, the primary design objective is to provide a layer with sufficient hydraulic capacity to allow transmission of the fluid to the collection point without allowing a build-up of head (pressure) that exceeds the design value.

25.2.1 HYDRAULIC CAPACITY OF DRAINAGE LAYERS

In the simplest terms, ensuring adequate hydraulic capacity of drainage layers involves consideration of the transmissivity of the layer, T (where $T = kB$ and k is the hydraulic conductivity and B is the thickness of the layer), the hydraulic gradient, i, and the required flow to be accommodated, q_{des}. Thus for a desired factor of safety, F, the required transmissivity of the layer is given by:

$$T_{req} \geq \frac{Fq_{des}}{iw} \qquad (25.1)$$

where w = the width of drainage layer through which the flow q_{des} must pass.

Equation 25.1 is most appropriate when designing a transmissive layer intended to conduct flow q_{des} from one point in the layer to another without significant additional fluid input. However, in many practical situations, the drainage layer is intended to collect percolation that is relatively uniformly distributed (e.g. q_o in Fig. 25.2) and conduct it to drainage pipes (see Fig. 25.2). Typically, a design objective in these cases is to maintain a maximum head, h_{max}, less than the thickness of the transmissive layer, B.

For steady state conditions and the simplest case of a flat base (shown in Fig. 25.2a)

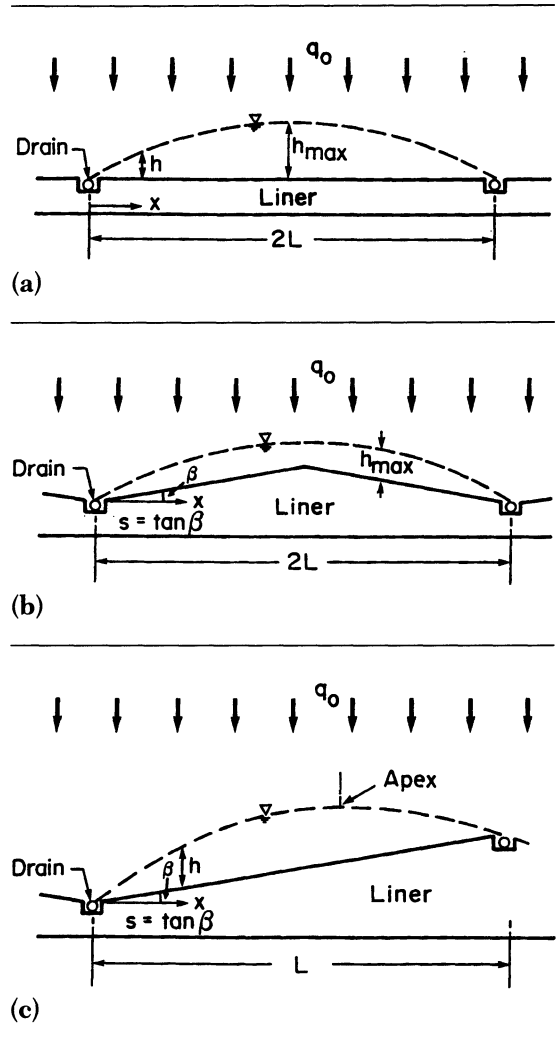


FIGURE 25.2. Schematic showing different collection systems (modified from Rowe 1988).

the maximum head, h_{max}, on the liner is given by:

$$h_{max} = L\left(\frac{q_o}{k}\right)^{1/2} \qquad (25.2)$$

and where L = the half-horizontal distance between drains as shown in Fig. 25.2a and k = the hydraulic conductivity of the material through which the water is flowing laterally to the drains. The average head $h_{avg} = 0.785h_{max}$.

For the situation shown in Fig. 25.2b, the

maximum leachate head is often calculated using Moore's (1983) equation, however, as indicated by Giroud & Houlihan (1995), Moore's equation may result in a significant underestimate of h_{max} (by a factor of two, or more) for slopes of more than a few percent and/or values of $q_o/k < 0.01$ and hence should not be used. They proposed an alternative, more accurate equation for the maximum head, h_{max}:

$$h_{max} = 0.5Lj[(\tan^2\beta + 4q_o/k)^{1/2} - \tan\beta] \quad (25.3a)$$

where

$$j = 1 - 0.12\exp\{-[\log_{10}(1.6\lambda)^{0.625}]^2\} \quad (25.3b)$$

and

$$\lambda = \frac{q_o}{k\tan^2\beta}. \quad (25.4)$$

Equation 25.3 is valid for all the situations shown in Fig. 25.2, reduces to Eq. 25.2 for $\beta = 0$, and is easy to use (it can be further simplified by taking $j = 1$ for an error of 12% or less).

The average head, h_{avg}, acting on the liner varies and is given by:

$$h_{avg} = \Lambda h_{max} \quad (25.5)$$

where typical values of Λ are given in Table 25.1. Other representations and a more detailed discussion are given in Section 26.2.2.

TABLE 25.1. Relationship between average and maximum head on a liner below a drainage layer (adapted from Giroud & Houlihan 1995)

λ	Λ	λ	Λ
0	0.5	1.0	0.80
0.05	0.56	1.2	0.83
0.1	0.6	1.5	0.85
0.15	0.63	3.0	0.87
0.2	0.67	10	0.85
0.35	0.7	30	0.82
0.6	0.75	50	0.81
0.8	0.79	1000	0.79
		∞	0.785

One can readily show that for a value of $k \geq 10^{-5}$ m s^{-1}, $q_o \leq 0.2$ m a^{-1}($\leq 6 \times 10^{-9}$ m s^{-1}) and drains at a spacing of 20 m, the maximum steady state head is likely less than a typical drainage layer thickness of 0.3 m. For a 1% slope, the spacing between drains as shown in Fig. 25.2b could be 30 m and still maintain a maximum head of less than 0.3 m. As a consequence, these drainage layers are often specified to have a hydraulic conductivity greater than 10^{-5} m s^{-1}. Unfortunately, while this may provide the required drainage immediately after construction, a reduction in hydraulic conductivity due to biological, chemical or particulate clogging may quickly result in an excessive leachate mound as discussed in the next subsection. When there is potential for clogging, special care is required to ensure adequate long-term drainage capacity.

In this chapter the discussion of drainage layers is restricted to granular layers such as the primary (PLCS) and secondary (SLCS) granular collection layers shown in Fig. 25.1a. However, similar considerations also apply to geosynthetic drainage layers as discussed in Section 26.2.

25.2.2 PARTICULATE CLOGGING OF DRAINAGE LAYERS

A number of failures have occurred due to drainage layers having inadequate hydraulic conductivities and the consequent development of excessive seepage forces (e.g. see Rowe 1998a). In a number of cases these failures have occurred due to the accumulation of fines in material that initially had an adequate hydraulic conductivity. In order to avoid particulate clogging it is necessary to: (a) ensure that there is a suitable filter between the drainage layer and adjacent soil or waste, e.g. the geotextile and "protective soil layer" shown in Fig. 25.1a; and (b) develop an appropriate design and construction plan that will minimize the accumulation of fines.

The design of filters is discussed in Section 26.3. However, it is noted here that even a

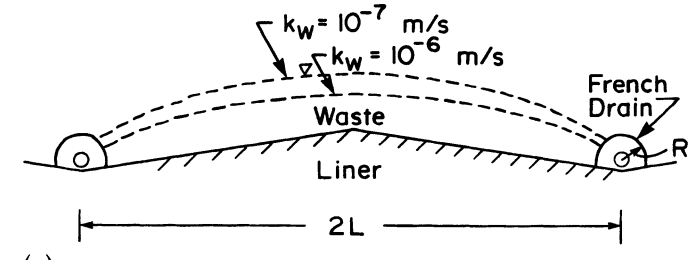
relatively small proportion of fines (0.5–1%) in a sand protective layer separated from an underlying geonet drainage layer (see Section 7.4) by a geotextile filter (see Section 7.2) has the potential to cause significant particulate clogging of the underlying geonet (e.g. see Giroud *et al.* 1998a). The same amount of fines would have a negligible effect on the performance of a 0.3-m thick coarse gravel drainage layer.

25.2.3 BIOLOGICALLY INDUCED CLOGGING OF LEACHATE COLLECTION SYSTEMS

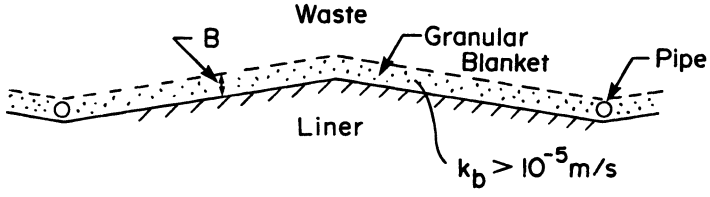
One of the most critical drainage applications is the collection of leachate in landfills. These collection systems typically take the form of toe drains (common in old landfills) around the edge of the waste and/or underdrain systems below the waste. Underdrain systems may take the form of French drains (typically perforated pipes embedded in granular material (e.g. see Figs 25.3a and 25.4) at some spacing, granular drainage blankets with perforated pipes at some specified spacing (see Fig. 25.3b), and geosynthetic (geonet) drainage layers (e.g. see Fig. 25.1b). Geotextiles are often used as filters between the waste and the drainage layer, especially when either coarse drainage material, e.g. gravel, or geonets are used to provide a drainage blanket. Key issues in the design of these systems are the need to provide adequate drainage, prevent structural failure, e.g. crushing, or other pipe failure, and to minimize clogging.

There is a growing body of evidence that the performance of these systems (especially those shown in Fig. 25.3a) can be greatly impaired by clogging and a number of failures have been reported in the literature (see Rowe 1998a,b for a review of clogging of geotextiles and granular material, respectively).

The clogging problem arises because municipal solid waste leachate contains nutrients that will encourage bacterial growth in geotextile filters, in granular drainage layers, around the perforations in the leachate collection pipes and within the pipes. Clogging of the leachate collection system involves the filling of the void space between solid parti-



(a)



(b)

FIGURE 25.3. Two leachate drainage systems: (a) French drains; and (b) blanket drain (modified from Rowe *et al.* 1995b).

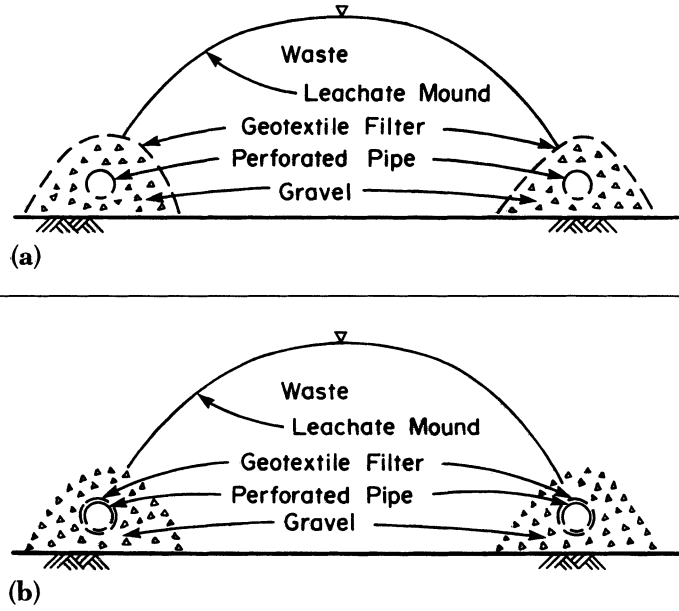


FIGURE 25.4. Schematic showing examples of poor leachate collection system designs: (a) problematic; and (b) even worse. Schematic also shows a leachate mound developed once there is excessive clogging of the geotextile filter and/or the drainage gravel and/or the pipe (modified from Rowe 1992).

cles as a result of a combination of biological, chemical and physical events. Particulate clogging can be a problem in some cases (Section 25.2.2), however, a major component of the clogging is microbiologically related.

Microbiological and chemical studies (Brune *et al.* 1994; Rowe *et al.* 1995c, 1997c,d and Rittmann *et al.* 1996) suggest that the clogging of drainage systems is the result of a mobilization of inorganic constituents of waste, e.g. metals such as calcium, iron, etc., by a process involving fermentative bacteria together with iron- and manganese-reducing bacteria, followed by precipitation processes involving primarily methanogenic- and sulfate-reducing bacteria. The clog typically has a soft (organic) and hard (predominantly $CaCO_3$) component. The rate of clogging is related to the flow through the critical component of the system, the void size, the temperature in the collection system (generally higher temperature implies faster clogging) and the leachate chemistry. The reduction in void space caused by biofilm growth and chemical precipitation (Brune *et al.* 1994; Vandevivere & Baveye 1992; McBean *et al.* 1993; Rowe *et al.* 1995c, 1997d; Fleming *et al.* 1999) results in a concurrent reduction in the hydraulic conductivity of these drainage systems and hence a reduction in their capacity to laterally transmit leachate. Fleming *et al.* (1999) report a field case where after four years a coarse, uniformly graded gravel (50-mm nominal size) experienced at least a three-order-of-magnitude drop in hydraulic conductivity due to the build-up of clog material. Rowe (1998a) gives experimental data showing a decrease in six–seven orders-of-magnitude in a uniform (6-mm nominal) gravel size material. A decrease in hydraulic conductivity, k, to or around 10^{-7}–10^{-8} m s^{-1} is sufficient to inhibit lateral drainage and cause the build-up of a leachate mound. However, this decrease in k is not sufficient to significantly inhibit vertical movement of contaminants since it is still several orders-

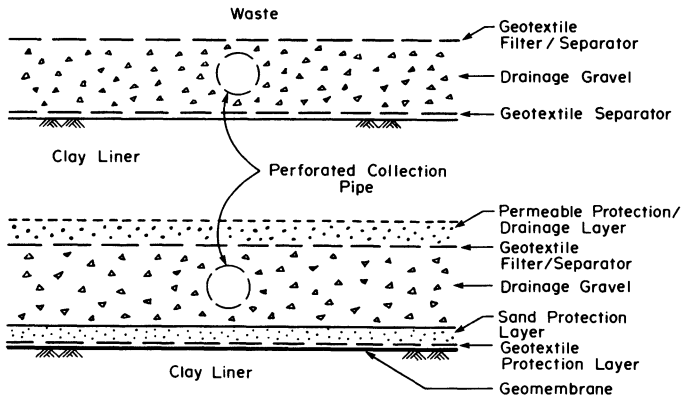


FIGURE 25.5. Schematic showing examples of blanket leachate collection system designs including a geotextile filter layer (modified from Rowe 1992).

of-magnitude higher than the hydraulic conductivity of the underlying liner that will control vertical flow.

Both laboratory experiments and field evidence show that clogging is directly related to leachate mass loading (Koerner & Koerner 1994; Fleming *et al.* 1999; Rowe *et al.* 2000a; Rowe 1998a). The leachate mass loading is a function of: (a) the concentration of volatile fatty acids (represented in terms of chemical oxygen demand, i.e. COD) and metals (especially calcium) in the leachate; (b) the flow rate per unit area; and (c) elapsed time. Thus when leachate that is generated over a large area of the landfill is directed through a filter surrounding isolated drainage gravel (French drains, see Fig. 25.4a) or, even worse, a filter wrapped around the pipe itself (Fig. 25.4b), there is a confluence of flow across the filter and the confluence factor is approximately equal to the area of the landfill over which the leachate going to this pipe is generated, divided by the area of the filter material through which the leachate must flow. Since clogging depends on flow rate per unit area, this confluence of flow increases the mass loading per unit time and hence increases the rate of clogging of the geotextile and the drainage gravel (it is assumed here that clogging of pipes is mitigated by regular cleaning). However, even more important is the effect that clogging has when it does occur. When the resistance to flow into the drainage pipe is increased, a leachate mound will develop in the waste between the drains (see Fig. 25.4). This mound will maintain some flow to the pipe, but will also increase flow out through the underlying liner. Based on this, Rowe (1992) cautioned against designs such as those shown in Figs 25.3a and 25.4. The field investigations discussed by Rowe (1998a,b) confirm the soundness of this recommendation. Geotextiles used to wrap drains or pipes have been found to experience a drop in hydraulic conductivity of between two and five orders-of-magnitude (to as low as 4×10^{-8} m s^{-1}; Rowe 1998a).

25.2.4 GEOTEXTILE "FILTERS" IN LEACHATE COLLECTION SYSTEMS

Many regulatory authorities now recommend or require the use of a blanket drainage layer (see Fig. 25.3b), although details regarding exactly what is required vary substantially. Rowe (1992) recommended the use of a suitably selected geotextile as a blanket filter as part of a blanket underdrain layer (see Fig. 25.5) to reduce clogging of the drainage layer.

TABLE 25.2. Koerner & Koerner's (1995) recommended minimum values for geotextile filters for use with mild leachate[a] and select waste over the geotextile[b]

Property	Woven monofilament	Nonwoven needle-punched
Mass per unit area, g m^{-2}	200	270
POA, %[c]	10	—
O_{95}, mm[d]	—	0.21
Grab strength, N	1400	900
Trapezoidal tear, N	350	350
Puncture strength, N	350	350
Burst strength, kPa	1300	1700

[a] Total suspended solid (TSS) and biochemical oxygen demand (BOD_5) ≤ 2500 mg L^{-1}.
[b] No hard or coarse material; for coarse or hard material over geotextile, the strength requirements may need to be increased.
[c] POA, relative open area.
[d] O_{95}, filtration opening size.

The findings of Rowe *et al.* (1995c), Fleming *et al.* (1999) and Koerner & Koerner (1995) provide some evidence that a suitable blanket geotextile will function adequately. These investigations demonstrated that the geotextile provided good protection to the granular drainage material, which experienced relatively little clogging compared to that observed when there was no geotextile filter between the waste and stone drainage medium. Koerner & Koerner (1995) recommended that for mild leachate, a geotextile in contact with the waste should have the properties given in Table 25.2.

Giroud (1996a) has discussed the issue of geotextile clogging as part of a broad review of filter design. He tentatively recommends that sand and nonwoven geotextile filters should not be used even if the waste has been stabilized to produce low strength leachate by pretreatment. Rather, he recommends the use of monofilament woven geotextiles with a minimum filtration opening size (O_{95}) of 0.5 mm and a minimum relative open area (POA) of 15%, with a preference for a POA greater than 30%. The rationale for these recommendations arises from the observations that:

1. the specific surface area for monofilament woven geotextile is much smaller than for nonwoven geotextiles and this decreases the surface area for biofilm growth;
2. the woven filter allows more effective and rapid movement of fine material, i.e. material not intended to be retained, and leachate through the filter; and
3. due to their compressibility, the filtration characteristics of a nonwoven geotextile vary with applied pressure and the critical filtration characteristics should be assessed under design pressures which could be up to 500 kPa.

There is some evidence to suggest that geotextiles selected in accordance with Giroud's (1996a) recommendations are likely to experience less clogging and reduction in hydraulic conductivity with time than geotextiles that simply meet the requirements of Koerner & Koerner (1995 and Table 25.2).

It is important to recognize that Giroud's (1996a) recommendations are based on the premise that one wishes to minimize clogging of the filter. This may indeed be the case for some design situations, e.g. if one insists on using a design such as is shown in Fig. 25.3a even though the use of French drains is generally not recommended. However, while excessive clogging is undesirable, the processes that cause clogging also provide leachate treatment and, in so doing: (a) decrease the potential for clogging at more critical zones, e.g. near collection pipes; and (b) reduce the level of leachate treatment required after re-

moval of leachate from the landfill. Although the subject of ongoing research, it appears desirable to design the leachate collection system to maximize leachate treatment while maintaining its design function (Fleming *et al.* 1999). Under these circumstances, and using a design such as the one shown in Fig. 25.5, a granular or nonwoven geotextile filter may actually be desirable provided that the hydraulic conductivity did not drop to such a point as to cause sufficient perching of leachate to have negative effects such as side seeps.

Based on published data, it appears unlikely that the hydraulic conductivity of the geotextile selected in accordance with either Giroud's (1996a) or Koerner & Koerner's (1995) recommendations (Table 25.2) would be below 4×10^{-8} m s^{-1} (1.3 m a^{-1}) for normal conditions and more likely it would be of the order of 1×10^{-7} m s^{-1} or higher. If the geotextile was used in a blanket drain, e.g. see Fig. 25.5, one can quickly establish that there would be negligible perched leachate on the geotextile for typical rates of leachate generation (less than 3×10^{-8} m s^{-1} or 1 m^3 a^{-1} m^{-2}). Thus, while recognizing that geotextiles will clog, based on the available data it appears that an appropriately designed and selected geotextile used to protect gravel in a blanket drain may improve the performance and the service life of the drainage gravel and, based on available evidence, they do not appear to cause excessive perched leachate mounding.

25.2.5 GRANULAR DRAINAGE MATERIAL IN LEACHATE COLLECTION SYSTEMS

Since the clogging of granular material may be the result of a combination of particulate clogging, clogging due to chemical precipitation and biofilm growth, the rate of clogging can be minimized by:

- maximizing the flow velocity in the drain;
- maximizing the void size; and
- minimizing the surface area available for biofilm growth.

By maximizing the flow velocity, one reduces the residence time for leachate in the collection system, thereby reducing the amount of sedimentation of particulates and chemical precipitation that can occur. The available evidence would suggest that clogging is greater under saturated conditions than for unsaturated conditions (clogging may, in fact, be greatest near the boundary between the saturated and unsaturated zone). Thus, it is desirable to keep drainage systems pumped.

Maximizing the void size within the granular material tends to increase the initial hydraulic conductivity and reduces the likelihood of voids becoming blocked. Since void size is about 20% of the characteristic particle size, it follows that a larger characteristic particle size will result in larger voids (in fact, $O_f \cong 0.2d_{15}$; see Section 26.3.2.2).

Biofilm growth is related to the surface area available on the particles forming the drainage layer. Since the specific surface, i.e. the surface area per unit volume, is inversely proportional to the characteristic particle size of the granular material (Cooke & Rowe 1999), the surface area (and rate of clogging) may be reduced by increasing the characteristic size of the granular material used.

It has been found (in the field and laboratory) that sands with an initial hydraulic conductivity of 10^{-4} to 10^{-5} m s^{-1} clog quickly. While suitably selected sands may serve a purpose as a protection layer or granular filter (see Figs 25.1 and 25.5b) they are not recommended for use in the granular drainage layer.

German investigators (Lechner 1994; Brune *et al.* 1994) recommend that granular drainage material should have a grain-size distribution between 16 and 32 mm. Canadian authorities (MoE 1998) recommend that granular drainage material have $D_{85} \geq 37$ mm; $D_{10} \geq 19$ mm; a uniformity coefficient $C_u = D_{60}/D_{10} < 2$ and no more than 1% finer than 0.075 mm (i.e. passing the US No. 200 sieve) and require that a suitable geotextile or graded granular filter/separator be installed between the drainage

layer and both the waste and any underlying liner. Current research would indicate that the 16–32-mm gravel recommended by the German investigators represents a minimum requirement for good, long performance of leachate collection systems. A minimum thickness of 0.3 m of granular drainage material is usually recommended for the drainage blanket (TA Siedlungsabfall 1993; MoE 1998) with a minimum of 0.5 m at the location of perforated leachate collection pipes (MoE 1998). Current research suggests that the service life can be maximized by the use of systems such as that shown in Fig. 25.5b where the granular drainage blanket below the geotextile meets the recommendations in MoE (1998) cited above and the "permeable protection drainage layer" above the geotextile meets the German (Lechner 1994; Brune *et al.* 1994) recommendations of a grain-size distribution between 16 and 32 mm.

The drainage gravel may be either rounded or angular (e.g. crushed stone), however particular care is needed to provide adequate protection to underlying geomembrane liners. Recent research (Tognon *et al.* 1999) indicates that geotextiles alone may not provide adequate long-term protection of geomembranes when there is a combination of a coarse gravel drainage layer and high pressure, i.e. large waste thickness.

25.2.6 SERVICE LIFE OF LEACHATE COLLECTION DRAINAGE MATERIAL

Based on the observations from field and laboratory studies (Sections 25.2.3 and 25.2.5), Rowe & Fleming (1998) developed an approximate method for estimating the service life of drainage gravel used either as part of a French drain system (Fig. 25.3a) or in a blanket drain (Fig. 25.3b). The approach is based on the observation that while clogging is induced by biological processes, the clog material is predominantly composed of inorganic precipitates with calcium representing a proportion, f_{Ca}, of the clog (encrustation) material (see Brune *et al.* 1994; Fleming *et al.* 1999). Thus the rate of clogging can be related to the change in the concentration of calcium in leachate, $c_L(t)$ between the time the leachate enters the collection system and the time it is collected. The yield of clog material, i.e. the volume of clog material deposited per unit volume of leachate flow, $Y(t)$, at time t is given by:

$$Y(t) = c_L(t)/(\rho_c f_{Ca}) \tag{25.6}$$

where ρ_c = the density of the clog material. Assuming that the flow, Q, per unit length of pipe into one-half of a collection pipe is given by:

$$Q = q_o L \tag{25.7}$$

where q_o = the leachate flux through the waste and L = the drainage path length (see Fig. 25.2), the volume of pore space, $V(t)$, that would be occupied by clog material at some time, T, is given by:

$$V(t) = \int_0^T \frac{c_L(t) q_o L}{\rho_c f_{Ca}} \, dt. \tag{25.8}$$

If the Ca concentration is c_{L1} for $T < T_1$ and then linearly decreases to c_{L2} at $T = T_2$, after which it remains constant at c_{L2}; then the total clog volume for $t > T_2$ is given by:

$$V(t) = 0.5\omega(c_{L1} - c_{L2})(T_1 + T_2) + \omega c_{L2} t \tag{25.9}$$

where $\omega = q_o L/(\rho_c f_{Ca})$. Thus the time $t = T$ required to obtain a uniform clog through a French drain, such as those shown in Fig. 25.3a, is given by:

$$T = \frac{\pi R^2 \nu_f}{4\omega c_{L2}} - \frac{(c_{L1} - c_{L2})(T_1 + T_2)}{2c_{L2}} \tag{25.10}$$

for a French drain of radius R, and where ν_f = the reduction in pore space required to cause "clogging." Experimental studies (see Rowe 1998a; Rowe *et al.* 2000a,b) suggest that gravel-size material experiences a significant decrease in hydraulic conductivity (by about six orders-of-magnitude) when $\nu_f \cong 0.9 n_o$ (n_o is the initial porosity and typically $n_o \cong 0.4$–0.5 for relatively uniformly graded gravel).

Based on field observations at the Keele Valley landfill (Fleming *et al.* 1999), it is considered likely that the clogging of blanket

drains (see Fig. 25.6) will not be uniform and that in fact there may be a concentration of clogging toward the collection pipes. Thus it is assumed that the clog filled porosity reduction, v_f', and the portion of the overall drainage blanket thickness subject to clogging, B', both vary linearly from essentially zero at the up-gradient edge of the drainage path ($x = 0$, $Q = 0$) to a maximum value $v_f' = v_f$ and $B' = B$ within a zone defined by $(L - a) \leq x \leq L$ near the collection pipe (see Fig. 25.6). Thus the volume of mineral clog corresponding to a reduction in porosity, v_f', is given by:

$$V_{tot} = \int_0^L v_f'(x)B'(x)dx \qquad (25.11)$$

where

$$\begin{aligned} v_f'(x) &= v_f x/(L - a) && \text{for } x < L - a \\ &= v_f && L - a < x < L \\ B'(x) &= Bx/(L - a) && \text{for } x < L - a \\ &= B && L - a < x < L \end{aligned}$$

and hence

$$V_{tot} = \frac{v_f BL(1 + 2a/L)}{3}. \qquad (25.12)$$

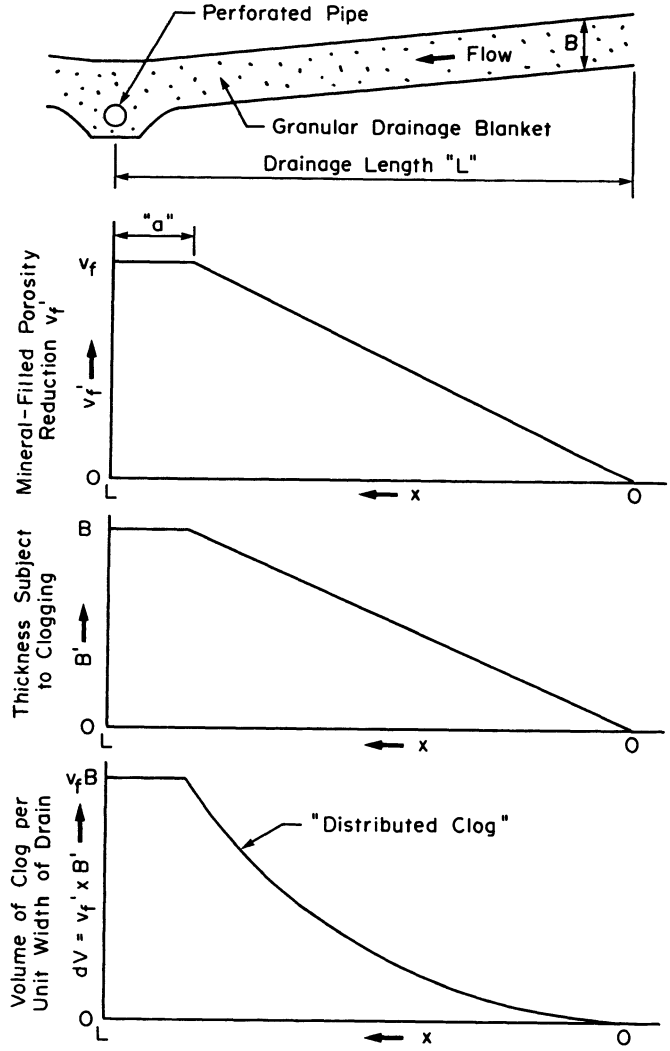


FIGURE 25.6. Distributed clogging model parameters (modified from Rowe & Fleming 1998).

The time to reach the degree of clogging represented by V_{tot} is calculated by solving for the rate of mineral volume growth given by Eq. 25.8 in general terms and Eq. 25.9 for a decreasing concentration of Ca with time. Combining Eqs 25.9 and 25.12 gives the time required for clogging as:

$$T = \frac{(1 + 2a/L)B\rho_c f_{Ca} v_f}{3q_o c_{L2}} - \frac{(c_{L1} - c_{L2})(T_1 + T_2)}{2c_{L2}} \quad (25.13)$$

for a blanket drain of thickness B.

Fleming *et al.* (1999) found that $f_{Ca} \cong 0.26$, while Brune *et al.* (1994) found $f_{Ca} \cong 0.21$. The Fleming *et al.* (1999) study also found $\rho_c \cong 1.5$ g cm^{-3}. The decrease in leachate concentration, $c_L(t)$, with time is more difficult to estimate. Data suggest that the calcium concentration in leachate decreases with time as the landfill moves from the acetogenic phase to the methanogenic phase and the average leachate pH increases to greater than seven. Initial concentrations in Canada are typically around 1650 mg L^{-1} (Rowe 1994), while Ehrig & Scheelhaase (1993) report an average of 1200 mg L^{-1} in Europe. Based on European data (Robinson & Gronow 1993; Ehrig & Scheelhaase 1993), the Ca concentration in leachate is expected to decrease to approximately 150 mg L^{-1} or less during the stable methane phase. After about 20 years, two Canadian landfills (each having an average pH > 7) had a Ca concentration of about 360 and 320 mg L^{-1}, respectively (Rowe 1994). It should be recognized that the leachate characteristics and the calcium concentration will vary between the time it leaves the waste, i.e. enters the collection system, and when it is collected. Strictly speaking, the calcium concentrations c_{L1}, c_{L2} should represent the decrease in concentration in the leachate between the time it enters the collection system and when it is collected. However, there is a paucity of data showing this drop and hence generally the estimated calcium concentration in the leachate is used. If this is based on data from within the landfill itself, i.e. before it enters the collection system, then this is a conservative assumption, i.e. will overpredict the rate of clogging. However, if the concentrations are based on data at the "end of pipe," i.e. after the leachate has been through the system, it is not clear whether or not the predicted clogging rate will be conservative and caution is required.

Rowe & Fleming (1998) applied this approach to estimate the time for clogging of a Canadian landfill with a French drain drainage system and obtained predictions that were consistent with the observed period when substantial leachate mounding was observed.

The foregoing represents a simple engineering approach to estimating the time to clogging that can be used in hand calculations. In this context, the service life of the leachate collection system is defined as the period of time that the leachate collection system controls the head to below the design value, e.g. 0.3 m in many cases. Once the head on the liner exceeds the design value, the collection system has "failed" to meet its design objective even though it will still collect some leachate. This is the approach that was used to estimate the service lives of drainage layers given in a Canadian landfill standard (MoE 1998). The approach does not explicitly consider biological processes or factors such as the particle size (it is assumed that the material is gravel). Currently, a more sophisticated computer model is being developed (Rowe *et al.* 1997b) that may be used to model the biological processes and the progressive development of clogging.

25.2.7 LEACHATE COLLECTION PIPES

Leachate collection pipes need to have: (a) sufficient hydraulic capacity to transmit leachate without the build-up of a leachate

mound exceeding regulatory requirements (often 0.3 m); (b) an internal diameter that will allow TV inspection and cleaning; (c) perforations that will allow leachate to move into the pipe, minimize the potential for clogging, facilitate cleaning and minimize impact on the structural performance of the pipe; and (d) deformations and stresses that will not impair its performance.

The hydraulic design of collection pipes is usually governed by the need to provide adequate drainage during a rainfall event when the cell is in the early stages of development and will be governed by the intensity of rainfall events, the area to be drained by a given pipe, and the slope of the pipe. The pipe diameter can then be selected based on the Manning formula:

$$Q = 1.49AR_H^{0.66}s^{0.5}/N \qquad (25.14a)$$

where Q = the flow in the pipe (in $m^3\ s^{-1}$), A = wetted area (m^2), R_H = the hydraulic radius (m) and is equal to the wetted area divided by the wetted perimeter, s = the pipe slope (−) and N is the coefficient of roughness. Koerner (1998) suggests that for plastic pipe with a smooth interior $0.009 \leq N \leq 0.01$ and for plastic pipe with a profiled or corrugated interior $0.018 \leq N \leq 0.025$. For a circular pipe flowing almost full:

$$Q \cong 0.47D^{2.66}s^{0.5}/N \qquad (25.14b)$$

where D = the internal diameter of the pipe (m). To meet the requirement of being able to readily inspect and clean the pipe, a minimum internal diameter of 0.15 m is often specified (e.g. MoE 1998) with clean-out points at regular intervals (usually not exceeding 300 m).

The selection of perforations is a somewhat contentious issue. Some regulatory environments prefer slots, although these can both weaken the pipe and may not be optimal for cleaning. Circular holes (perforations) need to be large enough to minimize clogging and facilitate cleaning by jetting. A minimum perforation diameter of 12 mm (MoE 1998) may be adequate, but preferably the perforations will be larger and of similar magnitude to the wall thickness of the pipe, subject to the restriction that the holes should not allow movement of the drainage gravel into the pipe. It is essential that leachate collection pipes be regularly inspected and cleaned while the clog material is still "soft." Once the clog material hardens it becomes very difficult to remove.

The deformations and stresses developed in the pipe will depend on the type of pipe, the applied vertical stress and the bedding conditions. This is discussed in more detail in Chapter 18.

25.3 *Low Permeability Liners*

25.3.1 GEOLOGICAL BARRIERS

When present, a suitable geological barrier represents one of the cheapest and best long-term liners for a wide range of applications (canals, lagoons, landfills, etc.). Typically, the geological barrier consists of a low hydraulic conductivity clayey layer. Near the ground surface, these layers are often weathered and fractured, and it is usually necessary to excavate to some depth below the weathered crust to reach material that will have sufficiently low bulk hydraulic conductivity. As noted by Rowe *et al.* (1995b), fractures may extend to depths well below the weathered zones and they report cases where fractures have extended to 10–15 m even though the weathered crust only extended to 4–6-m depth.

The suitability of a natural geological unit as a liner can normally only be assessed after a detailed hydrogeologic investigation aimed at identifying the extent and continuity of the unit and its bulk hydraulic conductivity, i.e. large-scale hydraulic conductivity that takes

account of local features such as fractures, see Chapter 24. Typical ranges of hydraulic conductivity are given in Table 3.10. Consideration also needs to be given to the thickness of the unit, the potential for future desiccation cracking, and/or chemical interaction with the fluid being retained and geotechnical issues such as the stability of any cut in this unit (see Chapter 14).

The remaining thickness of a natural geologic unit after excavation for construction of the fluid-retaining structure (e.g. lagoon, landfill, etc.) may vary considerably depending on: (a) local geologic conditions; (b) grade and materials balance considerations; (c) the potential for basal heave, e.g. due to the potentiometric head in any underlying aquifer, and other stability considerations; and (d) the thickness required to provide adequate contaminant attenuation (see Section 25.5). The level of attenuation required will depend on the nature of the contaminants, and the nature and reasonable use (either present or future) of the groundwater (e.g. see MoE 1998; Bouchard *et al.* 1992; Rowe *et al.* 1995b). Typically, this thickness is 3 m or more and may be tens of meters. However, with adequate investigation, thicknesses smaller than 3 m may be justified.

25.3.2 COMPACTED CLAY LINERS (CCLs)

Compacted clay liners (CCLs) represent an alternative means of obtaining a low hydraulic conductivity clayey liner when a suitable, natural geologic deposit is not available. This may be necessary because of the absence of suitable clay on site or because the existing clay has a bulk hydraulic conductivity that is too high due to macrostructures (e.g. fractures) but has sufficient plasticity that it can be reworked as a clay liner.

The quality of a CCL will depend on: (a) the characteristics of the clayey soil used; (b) the method of compaction and, in particular, the compaction water content; and (c) the protection against desiccation after construction. CCLs may range in thickness from 0.3 to 3 m or more, although typical thicknesses range between 0.6 and 1.2 m. The selection of the required thickness may be based on: (a) the need to provide adequate hydraulic resistance, since the hydraulic gradient, and hence the Darcy flux (Section 24.1), across the liner decreases with increasing liner thickness (all other things being equal); (b) the need to provide adequate contaminant attenuation (Section 24.3); (c) the need to minimize the effects of construction or post-construction related defects (e.g. local zones of higher hydraulic conductivity, desiccation, etc.); and (d) the presence of other liner components (e.g. a geomembrane in a composite liner, see Section 25.3.7) or a double liner (Section 25.3.8). Like most engineered liners, CCLs require protection from the elements, e.g. sun and frost, and consideration must be given to the potential long-term effects of differential settlements.

25.3.2.1 Material Selection

CCLs are most commonly constructed from soils that are classified as CL, CH or SC in the unified classification system (see Section 3.2.11 and Table 3.6). The source of the material may include glacial tills, lacustrine, deltaic or aeolian deposits, residual soils or, by crushing, weathered mudstones and shales (e.g. see Lopes *et al.* 1992). Typically, CCLs are expected to have a hydraulic conductivity of 1×10^{-9} m s^{-1} (or less).

With adequate compaction (see Section 13.2.3 for a discussion of compaction tests, compaction curves and definition of terms such as optimum water content), this usually can be achieved for a soil containing a minimum of 15–20% of the particles with a size smaller than 2 μm, a plasticity index, I_p, greater than 7% ($I_p > 7\%$), an activity of 0.3 or greater, and less than 50% gravel, i.e. $D_{50} < 4.75$ mm.

The suitability of a given soil should be assessed by an appropriate laboratory testing

program to: (1) establish the variability and potential suitability of the proposed material with respect to grain size and plasticity; and (2) assess the hydraulic conductivity as a function of compaction conditions to establish the acceptable compaction zone with respect to hydraulic conductivity. At a minimum, this may involve:

- standard Proctor compaction tests (ASTM D698) at different water contents to establish standard Proctor optimum water content (and maximum dry density); and
- hydraulic conductivity tests (e.g. ASTM D5084) on these samples to establish the range of water contents and dry densities over which a satisfactory hydraulic conductivity, k, is achieved.

However, caution is required in interpreting the results of these laboratory hydraulic conductivity test results. A laboratory hydraulic conductivity value that exceeds the specified value is usually a good indication of potential problems in the field; however, an acceptable laboratory value does not necessarily imply good field behavior (see discussion in Section 25.3.2.3).

Daniel (1998) recommends a more extensive laboratory program than that described above involving:

- compaction of the soil over a range of compactive energy (this allows one to establish the line of optimums shown in Fig. 25.7);
- performing hydraulic conductivity tests on these compacted samples;
- defining a water content range over which acceptable hydraulic conductivity is achieved;
- limit acceptable dry density–water content relationship to ensure adequate shear strength (and possibly to limit susceptibility to desiccation cracking).

This would result in an "acceptable zone" as indicated schematically in Fig. 25.7. Whether this level of effort is required is still subject to debate.

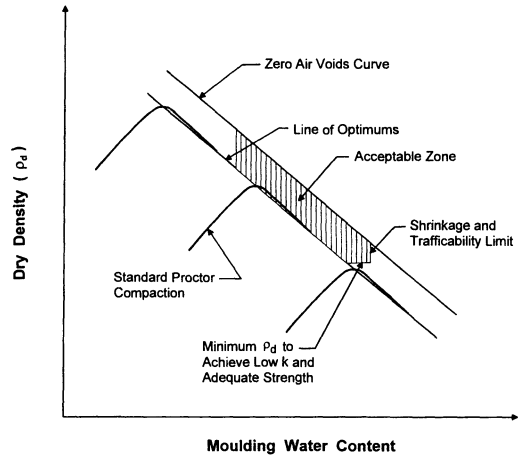


FIGURE 25.7. Method of defining acceptable zone of water content based on compaction, hydraulic conductivity and shear strength considerations (modified from Benson *et al.* 1999).

Special care is needed with soils of low plasticity ($7 < I_p < 15\%$) to ensure that the desired hydraulic conductivity can be achieved. Care is also required with high plasticity clay ($I_p > 30\%$) since these can form hard clods that may be difficult to break up when constructing the liner and because they are particularly susceptible to shrinkage and cracking if allowed to dry after compaction.

In cases where the *in situ* soil has inadequate clay minerals to achieve the desired hydraulic conductivity, bentonite (a commercially processed soil consisting predominantly of the clay mineral smectite; see Chapter 23) may be mixed with a silty sand or sandy silt soil (as discussed in Section 25.3.3) to reduce the hydraulic conductivity of the amended soil.

25.3.2.2 Compaction Water Content and Density

In order to achieve a low hydraulic conductivity, a CCL should be compacted at a water content that is near or higher than the standard Proctor optimum water content and

with a degree of saturation, S_r, greater than that corresponding to the degree of saturation at standard Proctor optimum, $S_{r_{opt}}$, i.e. $S_r \geq S_{r_{opt}}$, which means that the combination of (ω, ρ_d) should plot in the crosshatched zone shown in Fig. 25.7. (See Section 13.2.3 for a discussion of compaction and Mitchell *et al.* (1965) for a discussion of the effect of water content on hydraulic conductivity.)

Liners with a significant percentage of water contents below the standard Proctor optimum water content will typically have a macrostructure that gives rise to a high hydraulic conductivity (see Fig. 25.8). This can be explained by the observation that in order to provide sufficient plasticity to break up clods and develop a suitable clay fabric in the liner, the soil should be compacted at a water content near, or above, the plastic limit. Since, in North America, the plastic limit is often close to or slightly above the standard Proctor optimum water content, ω_{opt} (Leroueil *et al.* 1992a,b), standard Proctor optimum is generally a lower limit for the water content in order to obtain a good liner. Increasing water content, ω, above standard Proctor optimum, ω_{opt}, has been found to substantially increase the probability of achieving a hydraulic conductivity of 1×10^{-9} m s^{-1} (Fig. 25.8). An examination of the cases reported by Benson *et al.* (1994) indicates that the average compacted water content of 11 CCLs with $1 \times 10^{-11} \leq k \leq 1 \times 10^{-10}$ m s^{-1} was PL + 2% while the average for 13 liners with $1 \times 10^{-10} \leq k \leq 1 \times 10^{-9}$ m s^{-1} was PL + 1%, where PL is the plastic limit. In contrast, the average for four liners with $k > 1 \times 10^{-9}$ m s^{-1} was PL − 7.5%.

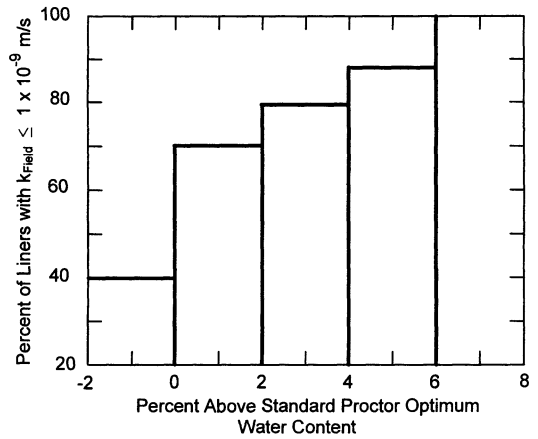


FIGURE 25.8. Percentage of liners with a compaction water content within a given range having $k \leq 1 \times 10^{-9}$ m s^{-1} (modified from Daniel 1998).

It is noted that the relationship between optimum water content, ω_{opt}, and PL varies from soil to soil and care is required in the use of any empirical relationship. For example, Morin & Todor (1977) report that for red tropical soils in South America:

$$\omega_{opt} = 0.61\ PL - 0.84\ (\text{std. dev.} = 3.4\%) \quad (25.15a)$$

and for red tropical soils in Africa:

$$\omega_{opt} = 0.58\ PL - 4.5\ (\text{std. dev.} = 4.2\%). \quad (25.15b)$$

Well-compacted clay liners will typically have an initial degree of saturation, S_r, exceeding 90%; although some low hydraulic conductivity liners ($k < 1 \times 10^{-9}$ m s^{-1}) have been constructed with initial degrees of saturation as low as 83% (e.g. see Benson *et al.* 1994; Trast & Benson 1995). Liners with $S_r < 83\%$ typically have $k > 1 \times 10^{-9}$ m s^{-1}. This is consistent with the observation by Benson and Boutwell (1992) that there was a strong correlation between achieving $k < 1 \times 10^{-9}$ m s^{-1} and a combination of dry density and water content that plot on or above the line of optimums, see Figs 25.7 and 25.9. Daniel (1998) has suggested a minimum of 70–80% of (ω, ρ_d) points plotting above the line of optimums, i.e. $P_o > 70$–80%, be specified for CCL, while also cautioning the need to ensure adequate internal shear strength of the CCL and interface strength with adjacent

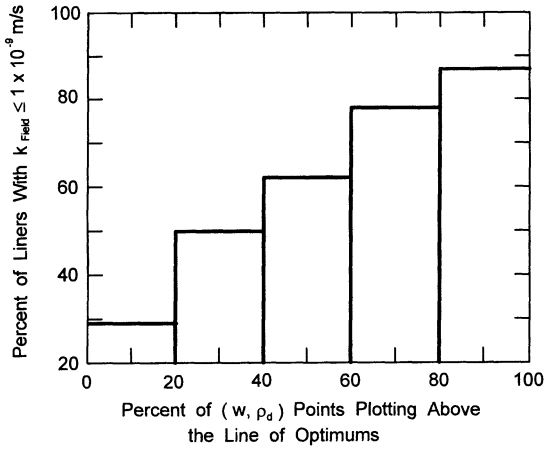


FIGURE 25.9. Percentage of CCLs with $k_{field} \leq 1 \times 10^{-9}$ m s^{-1} versus percentage plotting above the line of optimums (modified from Daniel 1998).

materials, e.g. geomembrane liners—see Sections 25.8 and 27.6.

Although the compacted dry density, ρ_d, may be important in terms of where the liner lies relative to the line of optimums (the degree of saturation) as discussed above, there is no significant correlation between the field hydraulic conductivity and the percent compaction. Thus, specifying ρ_d to be 95% of that obtained by standard Proctor compaction (or other arbitrary percentage) does not provide any assurance of a low hydraulic conductivity liner.

Although it is generally agreed that clay should be compacted such that the water content and dry density points (ω, ρ_d) generally plot above the line of optimums, there is not complete freedom in the choice of water content. If the water content is too high there may be problems with trafficability and obtaining adequate compaction with heavy equipment (Daniel 1998). Furthermore, difficulty may be experienced in obtaining both a sufficiently smooth surface on the liner or the shear strength may not be adequate to ensure stability. Leroueil *et al.* (1992a) proposed an empirical relationship for estimating the undrained shear strength, s_u, of clays that plot above the A-line (see Fig. 3.4) and have a value of $(\omega - \omega_{opt})/I_p \geq -0.06$, namely:

$$s_u(\text{kPa}) = 140 \exp[-5.8(\omega - \omega_{opt})/I_p]. \quad (25.16)$$

This equation can be used to make a preliminary estimate of shear strength for both stability and trafficability considerations. Like all empirical relations, it should be used with caution and appropriate laboratory tests should be conducted to ascertain the actual shear strength on important projects or where there are significant cost or safety implications if the shear strength is not correctly evaluated. This may be especially critical when constructing composite liners (see Sections 25.3.7, 25.3.8 and 25.8). Ensuring adequate shear strength should be considered when specifying the allowable water content–density relationship for a CCL.

25.3.2.3 Estimating the Hydraulic Conductivity of CCLs

Benson *et al.* (1994) have examined the hydraulic conductivity achieved for soils from 67 landfills in North America where natural clay liners, i.e. excluding soil bentonite mixtures, etc., were used and developed an empirical relationship between the hydraulic conductivity and a number of soil and compaction variables. This equation can be rewritten as:

$$k_F = \exp\left[-22.96 + \left(\frac{894}{w}\right) - 0.08I_p - 0.029S + 0.32(G)^{1/2} + 0.02C\right] \quad (25.17a)$$

where k_F = the estimated field hydraulic conductivity in m s^{-1}, w = the weight of the compactor in kN, I_p = the plasticity index in percent, S = the initial degree of saturation in percent, G = the percent gravel, and C =

the percent clay. Like all empirical equations, this equation should not be used without independent verification for a particular project (see Section 25.3.2.4).

Equation 25.17a may be useful for estimating hydraulic conductivity under low stress conditions, e.g. as might be obtained using a sealed double-ring infiltrometer (SDRI). In many practical (e.g. landfill) applications the liners will be consolidated under the weight of the overlayer material (e.g. waste) and this has been shown (e.g. see King *et al.* 1993) to cause a reduction in hydraulic conductivity. By comparing hydraulic conductivity values, k_σ, obtained from tests on samples consolidated to different effective stress levels, σ', with the field value, k_F, obtained under low stress conditions using a SDRI, Trast and Benson (1995) obtained the following empirical relationships.

For soils with $k_F > 1 \times 10^{-9}$ m s^{-1} (σ' in kPa):

$$k_\sigma/k_F = 1 - 0.018(\sigma' - 10) \quad \text{for } 10 \leq \sigma' < 44 \text{ kPa} \quad (25.17b)$$

$$k_\sigma/k_F = 0.4 - 0.0027(\sigma' - 44) \quad \text{for } 44 \leq \sigma' \leq 147 \text{ kPa} \quad (25.17c)$$

For soils with $k_F < 1 \times 10^{-9}$ m s^{-1}:

$$k_\sigma/k_F = 1 - 0.0059(\sigma' - 10) \quad \text{for } 10 \leq \sigma' < 44 \text{ kPa} \quad (25.17d)$$

$$k_\sigma/k_F = 0.8 - 0.0017(\sigma' - 44) \quad \text{for } 44 \leq \sigma' \leq 147 \text{ kPa.} \quad (25.17e)$$

Equation 25.17 cannot always be applicable since hydraulic conductivity will also depend on compaction conditions not considered in Eq. 25.17, the compressibility of the clay, the void ratio–hydraulic conductivity relationship, etc. Thus, the equation should only be used as an initial guide to estimate the hydraulic conductivities that might be achieved for a given soil, weight of the compactor and effective stress level. The hydraulic conductivity that can be achieved in the field can only be properly evaluated by constructing a test pad where the soil is compacted in the field using the proposed construction specifications and then performing tests to confirm that the desired hydraulic conductivity was achieved (see Sections 25.3.2.4–25.3.2.6).

Table 25.3 provides a comparison between measured hydraulic conductivity under a number of stress conditions for two Canadian landfill liners with values predicted using Eq. 25.17. It can be seen that in these cases the predicted values exceed the observed values. In most cases, but not all (e.g. see Section 25.3.5), overpredicting the hydraulic conductivity would be conservative.

25.3.2.4 Construction of CCLs

Successful construction of a low hydraulic conductivity CCL using soil that meets the requirements outlined in Section 25.3.2.1 is highly dependent on: (a) water content control; (b) breakup of clods of soil and homogenization of non-uniform soils; (c) lift thickness; and (d) method of compaction and equipment used.

The soil used to construct a CCL needs to be broken up to minimize clod size and especially for dry, hard, clay-rich soil it is essential that these clods be wetted to the point that they can be readily remolded by the compaction equipment as discussed in Section 25.3.2.2. Daniel & Koerner (1995) recommend a maximum particle size of between 25 and 50 mm stones generally cannot be broken up. Low hydraulic conductivity liners have been sucessfully constructed with stones up to 100 mm in size provided that the liner is of a thickness exceeding 0.9 m. Large stones could be a problem with thin liners (<0.6 m) due to the fact that these stones can have voids adjacent to them due to movement during compaction (see Rowe *et al.*

TABLE 25.3. Comparison of calculated values of hydraulic conductivity based on Eq. 25.17 and measured values for two Ontario landfills

		Hydraulic conductivity ($m\ s^{-1}$)					
Soil[a]	Compactor weight (kN)	Predicted k_F	Predicted at	Observed at	Predicted at	Observed at	Reference
Halton landfill			$\sigma' = 25$ kPa	$\sigma' = 25$ kPa[b]	$\sigma' \cong 100$ kPa	$\sigma' = 100$ kPa[b]	Rowe *et al.* (1993)
WHT	180	2×10^{-9}	1.5×10^{-9}	1.4×10^{-10}	5×10^{-10}	0.8×10^{-10}	
WHT	300	3×10^{-10}	2.7×10^{-10}	1.1×10^{-10}	2×10^{-10}	0.8×10^{-10}	
UHT	300	3×10^{-10}	2.7×10^{-10}	1.4×10^{-10}	2×10^{-10}	0.8×10^{-10}	
Keele Valley landfill				Field[c]	$\sigma' \cong 145$	$\sigma' = 145$	
WHT	300	3×10^{-10}		0.7×10^{-10}	1.9×10^{-10}	0.8×10^{-10}	King *et al.* (1993)

[a] WHT, weathered Halton till; UHT, unweathered Halton till.
[b] Based on flexible wall permeameter test consolidated to σ'.
[c] Based on field lysimeter below liner.

1993). Oversize particles need to be removed using a mechanized stone picker or by hand.

Prior to placing a lift, the surface of the compacted lift should be rough and may need to be scarified using an industrial disk before constructing the new lift. The loose thickness of lifts used to construct CCLs should generally not exceed 230 mm and the compacted thickness should not exceed about 150 mm. The sheepsfoot/padfoot compactor used should have long feet (>150 mm), which can fully penetrate the lift being compacted into the underlying lift to break up interfaces between the lifts (see Rowe *et al.* 1993). The compactor should have a weight of 180 kN or greater, and typically five (or more) passes are required to achieve the desired compaction.

When placing the first lift over an underlying engineered system it may be necessary to compact a sacrificial layer using a lightweight smooth drum roller to avoid causing damage to the underlying material (e.g. secondary leachate collection/leak detection layer). The sacrificial layer compacted with the smooth drum roller is unlikely to meet the hydraulic conductivity requirement and should not be considered as contributing to the effective thickness of the CCL (see Rowe *et al.* 1993). Also, a smooth drum roller will usually be required to smooth the surface of the final lift after it has been compacted with the sheepsfoot/padfoot compactor.

CCLs may experience an increase in hydraulic conductivity with time of several orders-of-magnitude if not adequately protected against desiccation cracking or frost damage (e.g. Othman & Benson 1993; Bouchard *et al.* 1992). Potentially, this is particularly problematic for covers where it is difficult to provide adequate long-term protection. However, care is also required with the protection of any liner that may be exposed to drying or freezing conditions. For base liners in landfills, protection against desiccation may involve frequent watering using a water truck or covering the liner with a damp geotextile or, most effectively, 150–300 mm of soil and keeping the geotextile–soil damp. The CCL can also be covered with a geomembrane; however, particular care is needed in this case to avoid desiccation of the CCL below the geomembrane due to thermal gradients established in the liner. The most effective means of protecting landfill liners against frost is to schedule liner construction such that an adequate thickness of waste can be placed over the liner before the onset of freezing conditions (see Chapter 20 for a discussion of frost penetration).

25.3.2.5 Required Thickness of CCLs

The required thickness of a CCL varies from one regulatory environment to another and the rational basis for the choice is often hard to find. Thickness may be important in terms of: (a) providing adequate contaminant attenuation potential; or (b) ensuring that the liner has adequate hydraulic conductivity. An assessment of attenuation capacity requires consideration of advective–diffusive contaminant transport as well as appropriate retardation mechanisms (see Sections 24.3 and 25.7) and the thickness required may include part CCL and part lower quality compacted soil or an existing (natural) attenuation layer. The issue of thickness versus ensuring adequate hydraulic conductivity has been the subject of some debate as discussed below.

Benson & Daniel (1994) have performed statistical studies considering the potential for advective transport through CCLs constructed using different numbers of lifts. Based on this they recommend a minimum thickness of 0.6–0.9 m for a CCL constructed in four–six lifts of 0.15-m compacted thickness. This conclusion has been questioned (see Fuleihan & Wissa 1995 and closure by Benson & Daniel 1995) from the perspective that if a liner is well-compacted then there is

no trend of increasing hydraulic conductivity with decreasing liner thickness.

As noted in Section 25.3.2.2, one of the most important factors related to construction of a good quality CCL from material meeting the requirements of Section 25.3.2.1 is the water content control and use of appropriate compaction equipment that will bring (ρ_d, ω) above the line of optimums. Liners compacted at water content dry of optimum, i.e. at a water content below standard Proctor optimum, generally give a hydraulic conductivity greater than 1×10^{-9} m s^{-1} (e.g. see Fuleihan & Wissa 1995 or Benson & Daniel 1995). Liners reported to have been constructed wet of optimum using heavy (weight $\geq$ 180 kN) sheepsfoot/padfoot rollers with long penetration feet (>150 mm) generally, but not necessarily, had hydraulic conductivities less than 1×10^{-9} m s^{-1} (*loc. cit.*). The reasons for values exceeding 1×10^{-9} m s^{-1} are unclear, but are likely related to quality control that was not as good as might have been expected; in the writer's experience this is usually associated with lack of attention to water content control.

With appropriate material compacted at the correct water content using the right equipment and with appropriate quality control and assurance it should be possible to construct a low hydraulic conductivity liner that is relatively thin. However, recognizing that field conditions and people involved with the project are not always perfect, there is no question that increasing the number of lifts reduces the probability of a local defect significantly impacting on the liner performance. Two lifts are much better than one. The extent to which more than two lifts are required to achieve the desired hydraulic conductivity will, as shown by Benson & Daniel (1994) depend on variability that is likely to occur in a given layer. Thus there is an economic trade-off between the level of attention that must be paid to construction, the number of lifts required and the acceptable risk of the liner not meeting the design hydraulic conductivity specifications, which can only properly be evaluated on a site-specific basis. Increasing thickness provides some level of increased assurance of meeting the specified hydraulic conductivity, within limits, but is no substitute for ensuring the soil is properly homogenized, brought to the correct water content and the clay clods are kneaded into a low hydraulic conductivity liner using appropriate compaction equipment. As noted by Fuleihan & Wissa (1995):

> Surprisingly, many practitioners were still not aware that construction quality and molding conditions have a much greater effect than thickness on the quality of a clay liner, even though Lambe (1958) showed as early as 1958 the several order-of-magnitude influence that molding conditions can have on the hydraulic conductivity of a compacted clay liner.

Once the specified hydraulic conductivity of the liner has been achieved, the required thickness will depend on factors like the potential for contaminant transport (see Section 25.7). In all cases, attention must be paid to preventing desiccation cracks and frost damage.

25.3.2.6 Construction Quality Control and Assurance

Construction specifications typically indicate the water content and compacted clay density to be achieved; here, the critical issue is that the combination of water content, ω, and dry density, ρ_d, measured for a liner should plot above the line of optimums for a well-constructed liner, see Section 25.3.2.2 and Fig. 25.7.

A well-trained engineer/technician can usually identify whether the water content is correct by eye and feel (as noted earlier, the desired water content is often close to the plastic limit). A soil that appears and feels dry will usually give poor performance if compacted into the liner. Tests to establish the

TABLE 25.4. Recommended minimum testing frequencies: one test for each per volume or area noted below (adapted from Daniel & Koerner 1995)

Parameter	Method ASTM	Soil source[a] (m^3)	In loose lift (m^3)	After compaction (m^2 per lift)
Water content (field)	D-3017[b]	—	—	750
	D-2216	2000	800	750
Density (field)	D-2922[b]	—	—	750
	D-1556/2167	—	—	15 000
Atterberg limits	D-4318	5000	800	750
Per cent clay	D-422	5000	800	750
Per cent gravel	D-422	5000	800	750
Compaction curve	D-698	5000	4000	—
Hydraulic conductivity	D-5084	10 000	—	2000[c]
Construction oversight			Continuous	Continuous

[a] Or each change in material type.
[b] Values are field measurements.
[c] Value is m^2 of finished liner.

water content and density achieved should be used to document the liner construction; however, there is no substitute for having a well-trained engineer/technician overseeing the liner construction on a full-time basis and ensuring that adjustments are made to water content as needed.

Quality control procedure involves checking the soil meets the specifications in terms of Atterberg limits, percentage of clay and gravel and that the CCL meets the specifications in terms of water content, dry density and hydraulic conductivity. Table 25.4 gives recommended testing methods and minimum testing frequency (partially based on Daniel & Koerner (1995) and partially based on the writer's experience).

In the USA, SDRIs are often used to establish the field hydraulic conductivity. However, provided that adequate water content control is achieved and the liner is compacted to a degree of saturation of 87% or higher (e.g. see Trast & Benson 1995), and provided there is no visible evidence of macrostructure, e.g. desiccation cracks, flexible wall hydraulic conductivity tests performed on Shelby tube samples provide a good indication of the hydraulic conductivity of the liner.

If Shelby tube samples are taken, then this area of the liner must be stripped to below the depth of the Shelby tube penetration over a width exceeding the width of the compactor and the liner must be reconstructed according to the original procedure.

Liner construction procedures are best verified by construction of a test pad prior to construction of the actual liner. This provides a means of acquainting the contractor with potential problems and calibrating the quality control and assurance procedures. Test pads will typically be 10–15-m wide and 15–30-m long.

Due to the inherent variability of soil it may be anticipated that at times parameters evaluated in accordance with Table 25.4 may not meet the specifications. Daniel & Koerner (1995) recommend allowing up to 3% of water content and dry density results falling outside the specified range in any one lift or area provided that no water content is less than 2% below or more than 3% above the specified values and no dry density is less

than 80 kg m^{-3} below the required value. Other specifications may also require that no water content may be below standard Proctor optimum. If the liner is found to be out of specifications, additional tests will likely be required to establish the extent of the problem area requiring repair.

If the water content is within range, but the dry density is too low, the problem may be rectified by more passes of the compactor.

25.3.3 SOIL–BENTONITE LINERS

In situations where suitable natural soils are not available for use in a compacted clay liner, bentonite may be added to a non-cohesive soil, e.g. silty sand, to achieve a liner with the required hydraulic conductivity. Key considerations in the selection of bentonite and design of these mixed-soil liners is the grain-size distribution of the base soil, the amount of bentonite and the mineralogy of the bentonite. Typically, the bentonite used is a sodium bentonite, calcium bentonite, or sodium activated calcium bentonite (see Chapter 23 for a discussion of clay mineralogy), although a wide range of modified bentonites, e.g. organobentonites, are also available. Both powdered and granular bentonites have been used, although Goldman *et al.* (1990) recommend that only powdered bentonite be used since it is said to mix more uniformly throughout the soil.

The proportion of bentonite in the soil mixture typically ranges between 4 and 10%, and this may give hydraulic conductivities of 10^{-9}–10^{-11} m s^{-1}. However, it is important to establish the optimum proportions of bentonite and water content on a site-specific basis. This is usually achieved by compacting different soil mixes with different amounts of bentonite at different water contents and then performing laboratory hydraulic conductivity tests on the compacted samples. Chapuis (1990) describes a simple approximation technique for estimating hydraulic conductivity and provides suggestions regarding the associated laboratory study. Care is needed to examine the hydraulic conductivities under the maximum gradient that could occur (e.g. with the development of a leachate mound) to ensure that there will not be an increase in hydraulic conductivity due to internal erosion of the bentonite, i.e. transport of the bentonite out of the liner by water flow.

Successful construction of low hydraulic conductivity soil–bentonite liners is highly dependent on: (a) obtaining and maintaining a homogeneous mixture of the base soil and bentonite, and avoiding segregation prior to and during placement; (b) compaction and water content control; and (c) lift thickness. If the soil–bentonite liner is to be used as a landfill liner, it is recommended that the liner be at least 200-mm thick and either special effort be devoted to ensuring uniform mixing of bentonite and negligible segregation prior to placement or, like other CCLs, the soil–bentonite liner be compacted in a number of layers. Good success has been achieved constructing soil–bentonite liners using padfoot compactors with a weight of 180 kN (or greater). Smooth drum rollers have also been used with success. In all cases, it is desirable to establish the required construction procedure based on the construction and evaluation of a test pad prior to liner construction.

A key consideration in the selection and design of soil–bentonite liners is the potential for chemical interaction between the clay and the fluid to be retained (see Section 25.4). Although sand–bentonite specimens have been shown to be more resistant to freeze-thaw cycles than clay or till specimens in laboratory tests (Wong & Haug 1991), as with normal CCLs, it is still prudent to protect the sand–bentonite liners against desiccation and frost. Testing for construction quality control may follow that given in Table 25.4.

25.3.4 GEOSYNTHETIC CLAY LINERS (GCLs)

GCLs (see Section 7.6) provide a convenient and potentially economical low permeability alternative to CCLs both in covers and base liners in many situations. Due to the fact that it is a manufactured product, typically produced using either powdered or granular sodium bentonite, a high level of quality control can be achieved. Since they are relatively thin ($\simeq$10 mm), there is also the potential for either minimizing the excavation required prior to placing the GCL or alternatively the use of a thin GCL may allow more air space, e.g. for waste disposal. However, the fact that they come in thin sheets that are seamed by overlapping does mean that considerable care is required during construction to avoid tearing the GCL sheets or opening the seams, especially when cover soil is being placed over the GCL. GCLs will usually need to be placed on a prepared foundation layer. Careful consideration must be given to the stability of liner systems involving GCLs and other geosynthetics (see Sections 25.8, 26.5 and 27.6).

25.3.4.1 Hydration of GCLs and Hydraulic Conductivity

As will be shown in subsequent sections, both the hydraulic conductivity, k, and diffusion coefficient, D, of a GCL are highly dependent on the bulk GCL void ratio, e_B (defined by Petrov & Rowe (1997) to be the ratio volume of void to the volume of solids in the GCL including both the geotextiles and bentonite). This may depend on: (a) the method of GCL manufacture; and (b) the confining stress at which hydration of the GCL occurs. Petrov *et al.* (1997b) showed that the final bulk GCL void ratio of a needle-punched GCL and an otherwise similar GCL without needle punching, i.e. fiber-free, varied substantially with the values for the needle-punched geotextile being much lower (better) under otherwise similar conditions (compare columns 2 and 3 of Table 25.5). Thermal locking of the needle-punched fibers can also have a beneficial influence on the bulk GCL void ratio as noted below.

TABLE 25.5. Final bulk GCL void ratios obtained in confined swell tests (adapted from Rowe & Lake 1999)

	Final bulk void ratio, e_B		
		With needle punching[b]	
Confining stress (kPa)	No needle punching[a]	No thermal locking[a]	Thermal locking[b]
6	7.58	5.12	3.98
25	4.04	3.23	2.97
100	2.58	2.26	2.25
200	1.96	1.68	1.69

[a] Based on data from Petrov *et al.* (1997b).
[b] Data from Lake & Rowe (2000a).

Thermal locked GCLs are needle-punched GCLs where the bottom geotextile has been heated after needle punching. This bonds the needle-punched fibers to the carrier geotextile (i.e. the bottom geotextile during the manufacturing process), minimizing pull-out of the fibers from the geotextile. Columns 3 and 4 of Table 25.5 compare the final bulk GCL void ratio for two otherwise similar needle-punched GCLs, except that in one case there is no thermal locking (column 3) and in the other there is thermal locking of the fibers (column 4). As can be seen, at lower confining stresses needle punching and thermal locking give a lower value of e_B and hence may be expected to improve the performance of a GCL (other things being equal) in terms of both hydraulic conductivity and diffusion.

The results presented in Table 25.5 are for confined, constant stress swell (CSS) tests, where the stress is applied prior to hydration. The effect of thermal locking is even more evident in post-hydration confinement where the sample is allowed to hydrate at a low confining stress (6 kPa) and then, after hydration, the stress is applied. This might correspond to the case where a GCL used as part of a composite liner is left to hydrate (e.g. from the under-

lying soil) with only the leachate collection system in place and with little or no waste being placed until after hydration had occurred. As shown by Lake & Rowe (2000a), in this case the beneficial effect of thermal locking is manifest throughout the stress history.

The relationship between the effective confining stress, σ'_v, and the bulk GCL void ratio, e_B, under confined swell conditions depends on the type of GCL manufacturing process. Recognizing that for a given method of manufacturing there will be variability between similar samples of the same GCL at the same confining stress, it is still useful to have some idea of how the bulk void ratio varies with confining stress. These relationships need to be developed for each type of GCL, and for a given GCL will vary with hydrating conditions (e.g. the fluid used to hydrate the GCL and whether the stress was applied before or after hydration). To illustrate the effect of the type of manufacturing process, Rowe & Lake (1999) fitted regression curves to the data obtained for the three types of GCLs indicated in Table 25.6, yielding the following relationships for confined swell condition and hydration with distilled water:

$$\log_{10} \sigma'_v \cong 3.25 - 0.57e_B \quad \text{for the NWNWT GCL} \quad (25.18a)$$

$$\log_{10} \sigma'_v \cong 3.5 - 0.69e_B \quad \text{for the WNWT GCL} \quad (25.18b)$$

$$\log_{10} \sigma'_v \cong 2.9 - 0.32e_B \quad \text{for the WNWBT GCL.} \quad (25.18c)$$

Variability in a given manufactured product may result in some deviation from these relationships and hence they only serve to illustrate general trends and should not be used for detailed design without independent verification.

Extensive research has been conducted into the hydraulic conductivity of GCLs as a function of confining stress and permeant type and concentration as summarized by Rowe (1998a). In particular, it has been shown by Petrov & Rowe (1997) that for a given permeant, there is a log-linear relationship between the hydraulic conductivity, k (in m s^{-1}), and the bulk GCL void ratio, e_B. For example, for the needle-punched NWNWT GCL and conditions they examined, the hydraulic conductivity with respect to distilled water was given by:

$$\log_{10} k(\text{m s}^{-1}) \cong -11.8 + 0.29e_B. \quad (25.19)$$

The coefficients in this relationship can be expected to vary from GCL to GCL; however, the important point here is that the hydraulic conductivity decreases with decreasing bulk GCL void ratio (which is, in turn, related to stress as implied by Eq. 25.18).

More generally, it can be concluded that when hydrated and permeated with water, GCLs have a low hydraulic conductivity, e.g. 7×10^{-12}–7×10^{-11} m s^{-1} depending on hydrating and applied stress conditions during permeation. However, since this arises from the presence of bentonite, careful consideration must be given to the potential for an increase in hydraulic conductivity due to clay

TABLE 25.6. Basic characteristics of three thermal locked needle-punched GCLs tested

Generic symbol used in paper	Bentonite	Carrier geotextile	Cover geotextile	GCL mass (g m^{-2})[a]
NWNWT	Granular	PP nonwoven	PP nonwoven	5270
WNWT	Granular	PP woven	PP nonwoven	5380
WNWBT[b]	Powdered	PP woven	PP nonwoven	4990

[a] Minimum values.
[b] Cover geotextile filled with a minimum of 600 g m^{-2} of powder bentonite.

leachate interaction as discussed in more detail in Section 25.4. However, it is noted here that the relationship implied by Eq. 25.19 may change when the GCL is permeated with leachate. For example, for the same NWNWT GCL used to obtain the results summarized in Eq. 25.19, the hydraulic conductivity was bounded by:

$$-11.4 + 0.42e_B < \log_{10} k \text{ (m s}^{-1}) < -11.2 + 0.42e_B \quad (25.20)$$

when hydrated with water and subsequently permeated using a synthetic leachate based on the typical leachate chemistry at the Keele Valley landfill (see Petrov & Rowe 1997).

For typical values of e_B, the difference between the hydraulic conductivity with respect to water (Eq. 25.19) and synthetic leachate (Eq. 25.20) is about one order-of-magnitude. This means that when considering the use of GCLs in landfill liner systems, one should use a hydraulic conductivity for the anticipated leachate when performing contaminant impact calculations to assess equivalency (see Section 25.7).

The results used to obtain Eq. 25.20 were for a GCL hydrated with water and then permeated with synthetic leachate. Petrov & Rowe (1997) showed that a sample hydrated with leachate and then permeated with leachate had twice the hydraulic conductivity of an otherwise similar sample initially hydrated with water. Thus, careful consideration needs to be given to the hydrating conditions when evaluating the hydraulic conductivity.

Since the hydration of GCLs with water prior to permeation with leachate generally results in a lower hydraulic conductivity as discussed above and in Section 25.4, the level of hydration that can be achieved prior to contact with leachate is an important question. Daniel & Shan (1992) indicated that in contact with soil at the wilting point, sodium bentonite can be expected to have a water content rise to about 50%. They performed a number of tests where the bentonite from a GCL was in contact with sand at different water contents. Table 25.7 summarizes the bentonite-water content after 40–45 days for bentonite placed in contact with (0.1–0.2 mm) sand at different water contents (at 14 kPa pressure). It can be seen that under these circumstances, the bentonite is very efficient in its uptake of water from the underlying soil.

TABLE 25.7. Uptake of water by bentonite (interpreted from Daniel & Shan 1992)

Sand initial water content (%)	Bentonite water content at 40–45 days (%)
1	50
2	75
3	88
5	128
10	156
17	193

Bonaparte *et al.* (1996) performed hydration tests on three different GCL products in contact with a compacted clay (PL = 22%, I_p = 19%, ω_{opt} = 20%) placed at three different water contents (ω_{opt} − 4%, ω_{opt}, ω_{opt} + 4%). Even for the driest soil ($\omega \sim 16\%$) the GCL moisture content increased from initial values of 15–20% up to about 40% within 20 days. At the higher water content there was greater hydration. For compacted soil at ω = 24%, after 75 days the GCL water content had increased to 70–90% depending on the product. Their test suggested that the uptake of moisture over a period of 25 days was not significantly affected by the applied pressure over the stress range of 5–390 kPa. Eberle & von Maubeuge (1997) also report an example where a GCL installed "dry" ($\omega \sim 9\%$) over a sand with a moisture content of 8–10% was hydrated to a moisture content over 100% in less than 24 h and increased to 140% after 60 days.

25.3.4.2 Effect of Holes in GCLs

Shan & Daniel (1991) examined the effect of puncturing a GCL by cutting holes in 152-mm diameter GCL specimens. The samples were allowed to hydrate under a confining stress of 14 kPa. Under these test conditions the bentonite swelled to completely fill the 12-mm and 25-mm diameter holes and the hydraulic conductivity only increased from 2×10^{-11} m s^{-1} with no punching to 5×10^{-11} m s^{-1} with the 25-mm puncture. However, two out of the three 75-mm holes were reported to have not sealed and left an opening of 12-mm diameter giving a very high hydraulic conductivity (the upper limit measurable with the equipment used). These tests suggest that in this test the GCL had the capacity to effectively self-heal small holes but not large holes or tears. However, it should be recognized that this type of test does not simulate many practical situations. If a stone punched a hole in the GCL, the stone will likely stay in the hole. Also, the potential for puncturing will depend on the robustness of the cover geotextile. The GCL should be carefully installed in a manner that will avoid holes in the GCL.

25.3.4.3 Desiccation and Frost Action

GLCs are subject to potential changes in hydraulic conductivity due to desiccation; however, preliminary work by Boardman & Daniel (1996) indicates that while the bentonite in GCLs did form open cracks upon drying, these cracks closed due to swelling upon rewetting. Thus although the initial hydraulic conductivity was high ($\sim 10^{-7}$ m s^{-1}), after a few days it had reduced to a value similar to the original value ($\sim 7 \times 10^{-11}$ m s^{-1}). Eith *et al.* (1991) reported laboratory tests where the hydraulic conductivity was found to decrease from an initial value of 4×10^{-12} to 1.5×10^{-12} m s^{-1} after ten freeze–thaw cycles. While these results are encouraging, they were performed under a limited range of conditions and more field data as required to verify these findings.

GCLs subjected to limited freeze–thaw conditions (Hewitt & Daniel 1997; Kraus *et al.* 1997) were found to perform well with no evidence of cracking, and no significant increase in hydraulic conductivity was observed related to the freeze–thaw of the GCL sheets. Again, there is a need for more field data to verify these encouraging findings. These findings are in contrast to those of Othman & Benson (1993) who observed a significant (one–two or more orders-of-magnitude) increase in the hydraulic conductivity of a conventional CCL subjected to freeze–thaw cycles. Thus the, albeit limited, available evidence would suggest that GCLs may be preferable to CCLs where the liner cannot be protected from desiccation and freeze–thaw, e.g. in covers.

25.3.5 HYDRAULIC CONTAINMENT

In most liner applications the hydraulic head acting on top of the liner exceeds that below the liner and hence there is a gradient tending to cause fluid flow from inside to outside the liner. The magnitude of the outward flow is given by Darcy's law (Sections 2.4 and 24.1) and is controlled in part by the low hydraulic conductivity of the liner. However, in some cases one can take advantage of the presence of a high water table or artesian conditions to induce an inward flow. Thus, if the head in the leachate collection layer surrounding the waste is less than that in the surrounding hydrogeologic environment then the consequent inward flow can be used to resist outward diffusion of contaminants (see Fig. 25.10). This is called hydraulic containment or, sometimes, a natural "hydraulic trap." Joseph & Mather (1993) have advocated a form of hydraulic containment in the UK. The Gallatin National Balefill in Illinois, USA, was approved in 1987 on the basis of its operation as a hydraulic trap (Burke & Haubert 1991). In Ontario, Canada, there was considerable debate in 1987–1988 concerning the proposal to operate the Halton

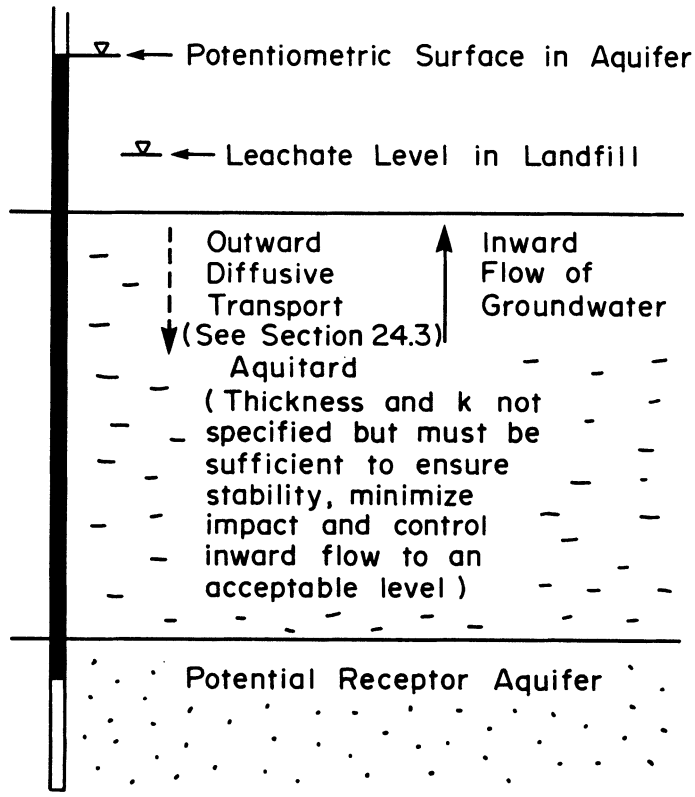


FIGURE 25.10. Hydraulic containment ("hydraulic trap") inward flow but outward diffusion (modified from Rowe 1997b).

landfill as a hydraulic trap. Approval was granted in 1989 and the landfill has been operating as a hydraulic containment site since 1992 (Rowe *et al.* 1993, 1996a, 1998b, 2000c). This approval was a landmark decision, which was followed by the approval, construction and operation (since 1995) of a number of hydraulic containment landfills. The Halton landfill has a CCL over a granular "subliner contingency layer" (see Fig. 25.11) overlying a relatively low hydraulic conductivity till layer. Under normal operations the subliner contingency layer is saturated and operated in a passive mode, i.e. no human intervention. In the event of an unexpected drop in water levels in the underlying aquifer or an unexpected increase in leachate head acting on the compacted liner, this layer can be operated to control impact on the very sensitive underlying aquifer. The Grimsby landfill, which has been in operation since 1995, also has a hydraulic containment design. It has a reworked till liner (CCL) directly on a fractured till layer, which is underlain by a fractured limestone aquifer.

Subsequent to the approval of the Halton and Grimsby landfills, the Essex–Windsor and North Simcoe landfills have also been approved for operation as hydraulic containment sites using an intact natural clayey barrier (Section 25.3.1); and the "Adams Mine," a worked-out open-pit quarry, has been conditionally approved as a hydraulic containment facility, located in fractured hard rock, without any liner as such.

Like all approaches, hydraulic contain-

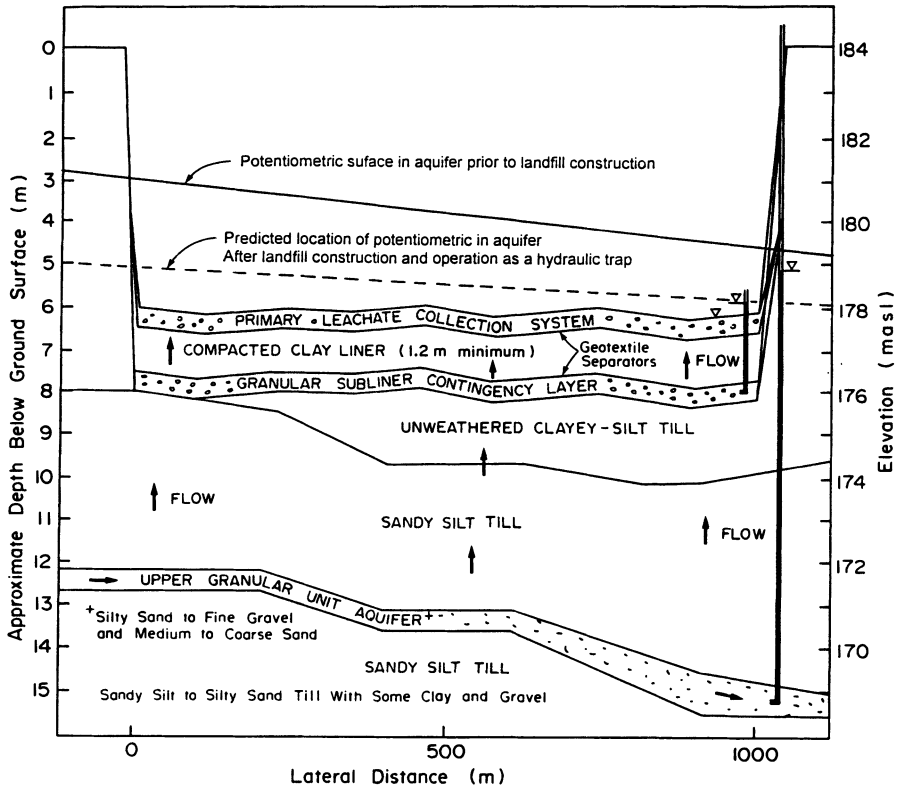


FIGURE 25.11. Hydraulic trap landfill (Halton) showing potential shadow effect due to landfill construction. Also shown is the subliner contingency layer (modified from Rowe *et al.* 1995b).

ment has both advantages and disadvantages as summarized by Rowe (1992, 1995a, 1997b; Rowe *et al.* 1995b). The primary advantages are: (a) the relative ease of construction, development and operation; (b) relatively low construction costs; and (c) inward flow provides some resistance to outward diffusion. For hydraulic containment to work it is essential to control the leachate head on the base of the landfill to a level that will induce inward flow. This is not as easy as it may first appear. Thus the primary disadvantages of this approach are: (a) the design is sensitive to the effects of clogging of leachate collection systems, see Section 25.2.3; (b) careful consideration must be given to the potential for the landfill construction causing a change in the natural water levels (i.e. the "shadow effect"; see Rowe 1992; Rowe *et al.* 1995b, 1998b); and (c) the success of the design may be sensitive to future natural changes in water levels. There are ways of addressing all of these issues (e.g. see Rowe 1995a; Rowe *et al.* 1995b, 1998b); however, they do increase the complexity and cost of the design.

Irrespective of whether one is using physical containment involving a geomembrane over clay or hydraulic containment, it is necessary to control the leachate mound in the landfill and collect and treat the leachate that is generated. For landfills with a soil cover, the increased amount of leachate requiring collection and treatment due to groundwater coming into the landfill (typically of the order of 0.001 $m^3\ a^{-1}\ m^{-2}$ for landfills in southern Ontario) is small and hence there is little im-

pact on the operating cost relative to a landfill with a composite liner system and no contribution of groundwater to the volume of leachate generated and collected. For landfills with a low infiltration cover, the groundwater flow may represent in the order of 25% of the leachate generated; however, this is for relatively small volumes of leachate being generated.

Although hydraulic containment is not always an option, in the right hydrogeologic environment it represents a viable alternative to more conventional barrier designs and should not be eliminated as an option by regulations.

25.3.6 GEOMEMBRANE LINERS

Geomembranes are planar, relatively impermeable polymeric sheets used in contact with soil or rock (Section 7.5). Due to their low permeability, they make excellent liners for fluid-retaining structures. This application is discussed in detail in Chapter 26. When used over a permeable layer, there is considerable potential for leakage through holes in the geomembrane (Section 26.4.3). Geomembranes are often combined with an underlying low permeability soil layer to form a composite liner as discussed in Sections 25.3.7 and 26.4.2. When the geomembrane is used to contain fluids other than water, careful consideration should be given to potential interaction of the geomembrane with the fluid (Section 25.4.3) and the potential for contaminant escape due to diffusion (Section 25.5.3). The service life of a geomembrane liner will be highly dependent on the exposure condition and temperature of the liner (Section 25.6).

25.3.7 SINGLE COMPOSITE LINERS

Single composite liners consist of a geomembrane (Section 25.3.6) over a low hydraulic conductivity soil liner/aquitard (Section 24.1.1 and 25.3.1–25.3.4). In landfill applications this typically involves an HDPE geomembrane over a CCL or GCL. Usually, but not always, there will be an attenuation layer of natural soil below the CCL or GCL before reaching a saturated aquifer (see Section 24.1.1 for definition of an aquifer) as shown in Fig. 25.12.

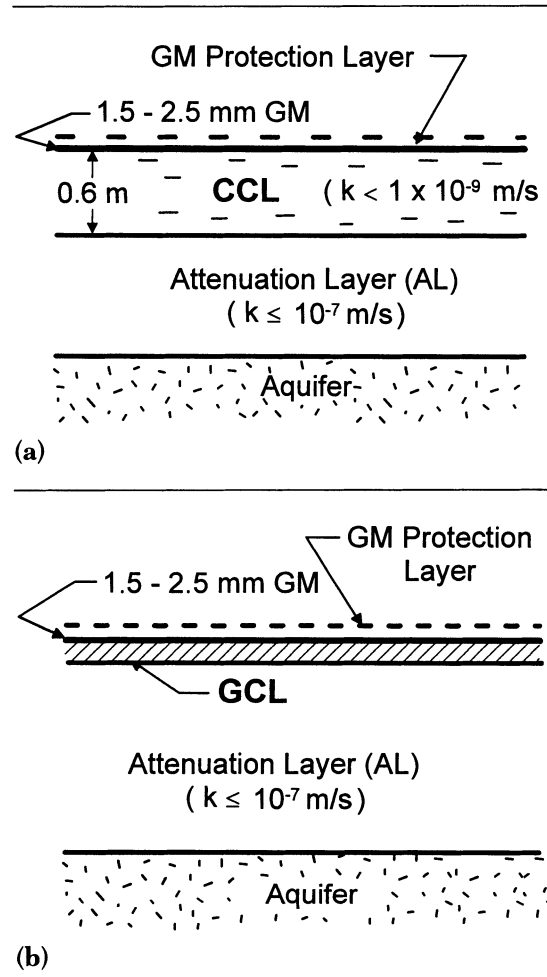


FIGURE 25.12. Schematic showing two single composite liner systems: (a) geomembrane (GM) over compacted clay liner (CCL) over an attenuation layer (AL) over an aquifer; and (b) geomembrane (GM) over a geosynthetic clay liner (GCL) over an attenuation layer (AL) over an aquifer.

The geomembrane provides the primary barrier to the movement of fluid; however, the presence of the low permeability layer in contact with the geomembrane serves to substantially reduce the leakage through defects/holes in the geomembrane. Leakage through composite liners has been reviewed by Rowe

(1998a), and simple equations for calculating leakage through holes in geomembranes are given in Section 26.4. The low permeability liner and underlying attenuation layer also play an important role as a diffusion barrier and zone for attenuation of certain organic contaminants, which can readily diffuse through geomembranes (Section 25.5). Other key considerations, e.g. stability and deformations, are discussed in Chapter 26 and 27.

25.3.8 DOUBLE COMPOSITE LINERS

Double composite liners, e.g. see Fig. 25.1, consist of two single composite liners separated by a drainage layer. Both geonets (Section 7.4) and granular layers (Section 25.2) may be used provided that the geomembranes are adequately protected. The issues related to each composite liner are similar to those discussed in Section 25.3.7. The primary objective of the drainage layer between the liners is to control the head acting on the second liner and hydraulically isolate the flows in the second composite liner from any leachate mounding above the primary geomembrane and any flow through the primary composite liner. Thus, it is essential that the secondary liquid collection layer (sometimes called the "leak detection system," since under some circumstances it can be used to detect flow or leakage through the primary liner) be designed to have sufficient long-term transmissivity to control the head on the secondary geomembrane for as long as required (Section 26.2.3).

25.3.9 VERTICAL CUT-OFF WALLS

There is a growing movement toward "containment" as a primary "remediation" strategy for many contaminated sites where alternative approaches have proven ineffective or are too expensive (see Chapters 22, 28, 29 and 30 for a discussion of issues related to contaminated groundwater and soil). This "containment" will frequently involve the construction of a vertical cut-off wall around part or all of the contaminated site and possibly (but rarely) a retrofitted "base liner" below the site (see O'Donnell *et al.* 1995). Vertical cut-off walls may consist of slurry trench walls, geomembrane walls or sheet pile walls. A detailed discussion of the state-of-practice with respect to these walls is provided in O'Donnell *et al.* (1995). Daniel & Koerner (1995) provide a discussion of construction quality assurance and construction quality control (CQA/CQC) for these walls. The key concerns with all of these walls is: (a) ensuring sufficient uniformity and quality of construction that leakage is controlled to an acceptably low level; (b) the difficulty of detecting small leaks; (c) long-term durability, e.g. the potential effects of interaction with contaminants. The significance of these concerns can be reduced, but not eliminated, by combining the use of a vertical cut-off wall with hydraulic containment where the head in the contained zone is maintained below that outside the walled area to induce an inward flow (Section 25.3.5). The disadvantage of this is that it requires active control (pumping and treatment of contaminated groundwater). When combined with hydraulic containment, the primary functions of the cut-off wall are: (a) to reduce the volume of groundwater that needs to be pumped to maintain the inward gradient; (b) to limit density driven contaminant migration, e.g. movement of dense nonaqueous phase liquids, (DNAPLs) that might not be otherwise controlled by an inward gradient; (c) to provide a diffusion barrier (see Rowe 1996).

25.3.9.1 Slurry Trench Walls

Slurry trench walls are usually constructed by excavating existing soil using a backhoe or clamshell. To provide stability during construction, the trench is filled with a slurry, which is maintained with a slurry level above the groundwater level.

The slurry is typically a clay–water mixture (usually bentonite and water) or a cement–

bentonite–water mixture. Slurry trenches are then backfilled with either: (a) a mixture of bentonite, soil and water with a consistency of high slump concrete; or (b) a plastic concrete. Cement–bentonite–water slurry walls are left in place and the mix hardens to form the cut-off wall.

These walls may be used to contain, capture and redirect flow of contaminated water, gases or free-phase liquids. There are practical limits to the depths that can be achieved and the type of ground conditions in which they can be constructed. The short- and long-term hydraulic conductivity that can be achieved requires careful consideration. In particular, construction quality control and its effect on initial hydraulic conductivity, the effect of changes in groundwater condition and freeze–thaw, i.e. desiccation and cracking, the effect of interaction with the contaminants to be retained and the long-term hydraulic conductivity all need to be considered. In addition, it must be recognized that even if there is no outward flow there is still potential for contaminants to diffuse across the barrier (see Rowe 1996).

25.3.9.2 Geomembranes

Due to the very low permeability of geomembranes (Sections 7.5 and 25.3.6) they provide an excellent barrier to water and some contaminated waters. The geomembrane may either be used alone or with soil–bentonite and cement–bentonite backfills to create a composite liner. Typically, HDPE geomembranes are used and, as in the case of landfill liners, the greatest challenge is placing the geomembrane with a minimum of holes and providing good interlock between the sheets of geomembrane such that leakage is minimized (see O'Donnell *et al.* 1995). As in the case of landfill liners, consideration must be given to potential interaction between the "leachate" to be contained and the geomembrane (Section 25.4) as well as the potential for diffusion through the geomembrane (Section 25.5).

25.3.9.3 Sheet Pile Walls

Although there is extensive experience in the use of steel sheet pile walls in conventional geotechnical engineering applications, the use of this technique in geoenvironmental applications has been limited. This is primarily due to concerns regarding: (a) providing an interlock that will adequately control movement of contaminated fluids through the wall; and (b) the service life of the wall, i.e. the potential for corrosion in chemically aggressive environmental applications. As discussed in O'Donnell *et al.* (1995), sealable interlocks have been developed that use a sealant that is chemically compatible with the applicable environmental conditions. Resistance to corrosion can be provided by using: (a) thicker steel sections; or (b) sections with an organic coating, e.g. pitch that has been made more damage resistant than normal pitch by combining with vinyl or epoxy resins.

Field data on leakage across sheet pile walls are limited. Based on limited data, O'Donnell *et al.* (1995) suggest a permittivity, Ψ, similar to that of a 0.6-m thick soil–bentonite wall (for $k \sim 10^{-9}$ m s^{-1}; $\Psi \sim 1.7 \times 10^{-9}$ s^{-1}) with values in the range 6×10^{-9}–1×10^{-9} s^{-1} being reported for walls sealed with an organic polymer sealant. Due to the paucity of field experience, there is a need for long-term, large-scale field monitoring to provide better data regarding the long-term effectiveness of sheet piles as a contaminant barrier. Ideal applications for sheet pile walls may include: (a) reducing leakage from reservoirs; (b) reducing volumes of fluid that need to be pumped in hydraulic containment applications, especially when the sheet piles can be driven to a low hydraulic conductivity unit below the more permeable unit to be isolated; (c) allowing construction of reactive walls (see Section 29.5); and (d) temporary support during the excavation of contaminated soils.

25.4 *Liner Compatibility with Leachate*

There is potential for interaction between contaminated water or other liquids, e.g. hydrocarbons, when they come into contact with and migrate through all types of liners. The effects, if any, will depend on factors such as the chemical characteristics of the fluid, the characteristics of the liner, period of exposure, applied stress and temperature.

25.4.1 CLAY–PERMEANT INTERACTION

Clay minerals are the primary contributor to the low hydraulic conductivity of natural geologic barriers (Section 25.3.1), CCLs (Section 25.3.2), soil–bentonite liners (Section 25.3.3), GCLs (Section 25.3.4), soil–bentonite vertical cut-off walls (Section 25.3.9) and they contribute significantly to the performance of composite liner systems (Sections 25.3.7 and 25.3.8). Clay mineralogy is discussed in Chapter 23. The potential for interaction needs to be understood in terms of the potential for: (a) a change in crystal lattice volume, e.g. K^+ or NH_4^+ fixation by vermiculates can cause a significant decrease in crystal lattice volume and cation exchange capacity (see Rowe *et al.* 1995b); and (b) double layer expansion or contraction. As indicated in Fig. 25.13, typically interaction with a clay double layer is due to the effect of ions in the permeant fluid (see Fig. 25.13a; Section 23.4 and 23.5) and due to the effect of organic contaminant on the dielectric constant, ε, of the pore fluid (see Fig. 25.13b, Section 23.4 and Rowe *et al.* 1995b).

Rowe *et al.* (1995b) indicate that most inactive soils whose minerals consist of illites and chlorites are relatively insensitive to typical municipal solid waste leachate. They may in fact experience a decrease in hydraulic conductivity (Griffin *et al.* 1976) due to Na^+ adsorption (accompanied by desorption of Ca^{2+} and Mg^{2+}) and the consequent double layer expansion (see Fig. 25.13a) coupled with possible bacterial clogging. In contrast, soils containing significant amounts of swelling minerals (e.g. vermiculite, montmorillonite, interlayered illite–smectite; see Rowe *et al.* 1995b) may experience *c*-axis contraction or expansion with consequent increases or decreases in hydraulic conductivity, respectively. For example, K^+ fixation by vermiculite may cause a 28% decrease in crystal volume as well as a contraction in double layer

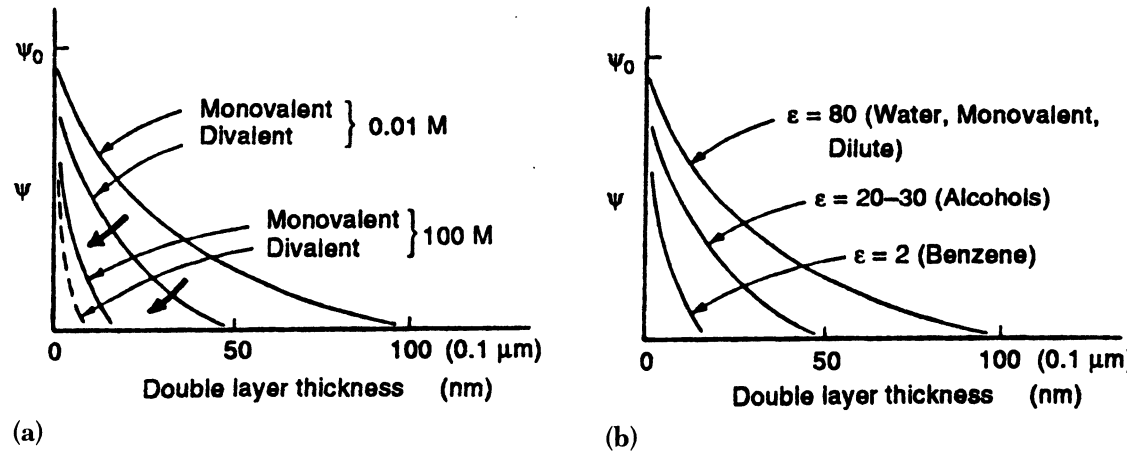


FIGURE 25.13. Double layer thickness variations: (a) concentration and valency effects; and (b) dielectric effects (modified from Rowe *et al.* 1995b).

thickness (Rowe *et al.* 1995b). Sodium bentonite (composed primarily of sodium montmorillonite) may experience a considerable increase in hydraulic conductivity when permeated with a solution containing Ca^{2+} or Mg^{2+} or even a solution with a high concentration of Na^{+} due to the effect of valence and concentration on double layer thickness.

Organic compounds with a low dielectric constant have been shown (e.g. Fernandez & Quigley 1985; Madsen & Mitchell 1988) to cause double layer contraction and higher hydraulic conductivity through macropores in the flocculated clay. When dealing with organic contaminants, an additional complicating factor is the effect of the organic compound on the viscosity of the permeating fluid, which may cause a decrease in hydraulic conductivity at some concentrations even though the intrinsic permeability remains the same (see Section 24.1.3 for definitions of these terms and see Rowe *et al.* 1995b for an extensive discussion of this effect). At higher concentrations of the organic compound, both the hydraulic conductivity and intrinsic permeability may increase.

The effects of clay–permeant interaction can be reduced by the presence of an applied effective stress, especially if the stress was applied prior to permeation (e.g. see Foreman & Daniel 1986; Fernandez & Quigley 1988; Rowe *et al.* 1995b; Petrov *et al.* 1997a,b; Petrov & Rowe 1997). This reduced effect is due to consolidation, which decreases the void ratio and the size of the macropores.

All clays have some potential for a change in hydraulic conductivity when permeated. While some clays, e.g. those rich in smectite, vermiculite or interlayered illite–smectite, have greater potential for interaction than others, e.g. illite, the only way to assess whether there is a potential problem is to examine the effect of the particular contaminant of interest on the proposed liner material.

Techniques for assessing potential clay–permeant interaction may include both direct and inferential (index) tests as described by Rowe *et al.* (1995b). Direct methods involve permeating a sample of the proposed liner material with the permeant of interest and monitoring the change in hydraulic conductivity. Both flexible wall (fixed gradient) and rigid wall (fixed flow) permeameters may be used and each has advantages and disadvantages (e.g. see Daniel *et al.* 1985). To properly assess the potential for interaction, the permeant should be passed through the clay until chemical equilibrium is reached (or nearly reached). However, this may require many pore volumes of permeation and for a low hydraulic conductivity soil the tests may take an excessively long time using flexible wall permeameters where limitations of the applied gradient result in a relatively small Darcy flux. Small-scale fixed-ring permeameters operated with a constant flow (e.g. Fernandez & Quigley 1985) allow higher gradients for low permeability soils and hence shorter testing times. However, concern might be raised regarding the potential for side wall leakage and the effect of seepage induced stresses when testing samples at low applied stresses, which are applicable to some liner applications (e.g. ponds, lagoons, etc.). Petrov *et al.* (1997a) compared both techniques when examining clay–leachate interaction for GCLs and found that similar results could be obtained by both approaches.

Indirect approaches of assessing potential clay–leachate compatibility problems may involve an examination of the effects of the liquid of interest or the Atterberg limits of the clay (e.g. Acar & Seals 1984; Daniel *et al.* 1985). Another approach is to examine the effect of mixing the fluid and clay on the mineralogy of the clay (see Rowe *et al.* 1995b). However, while these techniques may be a useful screening tool, they should still be coupled with an appropriate hydraulic conductivity testing program (with appropriate controls) if there is any concern about possible interaction.

25.4.2 GCL–PERMEANT INTERACTION

Rowe (1998a) provided a detailed review of GCL hydraulic conductivity testing. It has been found that the hydraulic conductivity of a GCL is highly dependent on the hydrating conditions and the applied effective stress during permeation. These factors combined with the type of GCL manufacturing process used, water content prior to hydration and mass of bentonite all significantly influence the GCL thickness and while there is some correlation between hydraulic conductivity, k, and thickness, H, there is a great deal of scatter. Petrov *et al.* (1997b) showed that by plotting the bulk void ratio, e_B, rather than thickness, H, against hydraulic conductivity, k, one obtains a much better correlation and much less scatter of the data for a given permeant. This is consistent with the conventional geotechnical engineering concept of a strong correlation between the void ratio and hydraulic conductivity.

The hydraulic conductivity to water of a number of commercially available GCLs ranges between about 5×10^{-11} m s^{-1} at "low" (3–4 kPa) confining stress to 1×10^{-11} m s^{-1} at "intermediate" (34–38 kPa) confining stress, and 7×10^{-12} m s^{-1} at "high" (109–117 kPa) confining stress. It is of interest to note that at a confining stress of about 35 kPa, the six products tested (see Rowe 1998a) had a very similar hydraulic conductivity to water (7×10^{-12}–1×10^{-11} m s^{-1}).

TABLE 25.9. Effect of permeating fluid on hydraulic conductivity of a particular GCL product at 35 kPa (adapted from Ruhl & Daniel 1997)

Permeating fluid	Hydraulic conductivity (m s^{-1})
Tap water	7×10^{-12}
Real leachate	$<1 \times 10^{-12}$
Synthetic leachate	1×10^{-11}
High strength synthetic leachate	2×10^{-8}

Table 25.8 shows the change in hydraulic conductivity of a GCL with the concentration of NaCl and ethanol (note that the decrease in hydraulic conductivity for a 25 and 50% ethanol–water mix is due to decreased viscosity; see Petrov *et al.* 1997b). Table 25.9 summarizes changes in hydraulic conductivity of a GCL permeated with different real and simulated leachates. The hydraulic conductivity with respect to real leachate obtained by Ruhl & Daniel (1997) (Table 25.9) was lower than that obtained with tap water. Grant *et al.* (1997) also reported low GCL hydraulic conductivity values for tests with a real municipal solid waste leachate. It can be seen that in general the changes in hydraulic conductivity for modest strength leachates (Table 25.9), salt solutions (<0.6 N; Table 25.8) or ethanol–water mix (<25% ethanol; Table 25.8) are all modest

TABLE 25.8. Effect of concentration of permeating NaCl solution and ethanol–water mix on hydraulic conductivity of a particular GCL product at 33–36 kPa

Concentration NaCl (N)	Hydraulic conductivity (m s^{-1})[a]	Proportion ethanol % (by mass)[b]	Hydraulic conductivity (m s^{-1})[b]
0	1.3×10^{-11}	0	1.6×10^{-11}
0.1	2.0×10^{-11}	25	7.3×10^{-12}
≅0.13[c]	7.3×10^{-11}	50	6.0×10^{-12}
0.6	9.3×10^{-11}	75	4.1×10^{-11}
2	4.7×10^{-10}	100	2.0×10^{-9}

[a] Data from Petrov & Rowe (1997).
[b] Data from Petrov *et al.* (1997b).
[c] Synthetic (simulated Keele Valley landfill) leachate without bacteria.

and the hydraulic conductivity is still low ($<10^{-10}$ m s^{-1}). However, a high concentration permeant can result in very significant changes in hydraulic conductivity.

The confining stress at the time of hydration and the hydrating fluid can also have an effect on the final hydraulic conductivity. For example, Fig. 25.14 shows an increase in the hydraulic conductivity of a GCL when permeated with synthetic leachate. At a low confining stress (3–4 kPa) the increase is by almost an order-of-magnitude. At an intermediate confining stress (30–35 kPa) the increase is by a factor of six. The increases in hydraulic conductivity evident in Fig. 25.14 need not be a problem if the liner system has been designed based on the higher values, which reflect interaction with leachate.

Daniel *et al.* (1993) examined the effect of partial hydration on the hydraulic conductivity of a GCL. They found that when the partially saturated GCL was permeated with concentrated hydrocarbons, the hydraulic conductivity was high (see Table 25.10) for a low initial water content (17 and 50%). It was close to that of water (except for trichloroethylene) at a water content of 100%, and less than that due to water at higher water contents. Thus it was not necessary for the GCL to be fully saturated to have a low hydraulic conductivity.

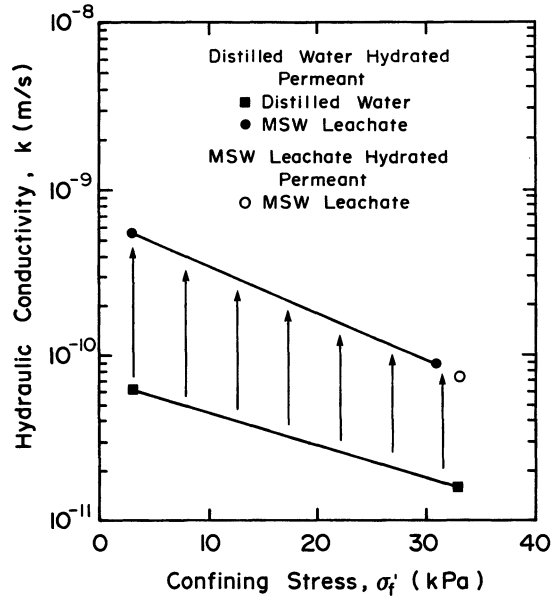


FIGURE 25.14. Hydraulic conductivity versus static confining stress for permeation of synthetic municipal solid waste (MSW) (simulated Keele Valley landfill) leachate (modified from Petrov & Rowe 1997). Distilled water-hydrated, permeant: (■) distilled water; (●) MSW leachate. MSW leachate-hydrated, permeant: ○ MSW leachate.

25.4.3 GEOMEMBRANE–PERMEANT INTERACTION

Geomembranes are used to "contain" fluids because of their very high resistance to fluid flow. However, it is essential that the geomembrane have sufficient compatibility with the fluid to maintain this resistance for the service life of the facility.

Based on extensive testing, general chemical resistance guidelines have been developed for a number of geomembranes, e.g.

TABLE 25.10. Summary of results of hydraulic conductivity tests on partially saturated bentonite (adapted from Daniel *et al.* 1993)

Permeating liquid, w_0	Hydraulic conductivity (m s^{-1})			
	17%	50%	100%	125%
Benzene	3×10^{-7}	2×10^{-7}	5×10^{-11}	No flow
Gasoline	4×10^{-7}	4×10^{-7}	4×10^{-11}	No flow
Methanol	3×10^{-7}	3×10^{-7}	3×10^{-11}	No flow
Trichloroethylene	4×10^{-5}	4×10^{-7}	3×10^{-10}	No flow
Water	$1–2 \times 10^{-11}$	—	—	—

TABLE 25.11. Chemical resistance guidelines for some commonly used geomembranes at 38 °C (adapted from Koerner 1998)

Chemical	Geomembrane type[a,b]		
	HDPE	PVC	CSPE
General			
Aliphatic hydrocarbons	✓		
Aromatic hydrocarbons	✓		
Chlorinated solvents	✓		
Oxygenated solvents	✓		
Crude petroleum solvents	✓		
Alcohols	✓	✓	
Acids			
Organic	✓	✓	✓
Inorganic	✓	✓	✓
Heavy metals	✓	✓	✓
Salts	✓	✓	✓

[a] HDPE = high density polyethylene, PVC = polyvinyl chloride, CSPE = ethylene interpolymer alloy.
[b] ✓ = generally good resistance.

see Table 25.11. However, for materials not listed (e.g. very flexible polyethylene, polypropylene, etc.) or for chemical solutions and mixtures not listed or for all critical projects where geomembrane–chemical interaction could have significant consequences, it is necessary to perform chemical resistance tests on the geomembrane of interest using the fluid of interest. Typically (e.g. see Koerner 1998), this involves immersing samples ("coupons") of the geomembrane in the fluid (using an appropriate sealed container and temperature) and removing coupons for testing at 30, 60, 90 and 120 days according to ASTM D5322 and D5496. The coupons are then tested to identify changes in physical, mechanical and possibly diffusion characteristics. Procedures such as in ASTM D5747 specify the test methods to be used.

At present, there are no well-established rules for assessing what is an acceptable variation from other original geomembrane properties after immersion in the chemical of interest. Koerner (1998) has suggested that a geomembrane is "resistant" to chemical interaction if the properties listed in the first column of Table 25.12 vary from the original

TABLE 25.12. Suggested limits of different test values for incubated geomembranes

Thermoset and thermoplastic polymers, e.g. PVC, CSPE (after Little 1985)[a]	
Permeation rate, g m^{-2} h^{-1}	<0.9
Change in	
Weight, %	<10
Volume, %	<10
Tensile strength, %	<20
Elongation at break, %	<30
100 or 200% modulus, %	<30
Hardness, points	<10
Semicrystalline polymers, e.g. HDPE (after Koerner 1998)	
Permeation rate, g m^{-2} h^{-1}	<0.9
Change in	
Weight, %	<2
Volume, %	<1
Yield strength, %	<20
Yield elongation, %	<30
Modulus, %	<30
Tear strength, %	<20
Puncture strength, %	<30

[a] For low crystallinity polymers (e.g. very flexible polyethylene, flexible polypropylene) Koerner (1998) recommends that the properties should be the same as those for thermoset and thermoplastic polymers and the values for resistance should be slightly more restrictive. PVC = polyvinyl chloride, CSPE = ethylene interpolymer alloy, HDPE = high density polyethylene.

values by less than the values given in the second column of Table 25.12.

25.5 *Diffusion through Barriers*

As discussed in Section 24.3.1.2, diffusion is a process whereby mass moves from areas of high concentration (potential) to areas of low concentration. This is often modeled using Fick's first law:

$$J = -D_p \frac{dC}{dz} \qquad (25.21)$$

where J = the mass flux at a point (mass per unit area per unit time), D_p = a bulk diffusion coefficient (also called the porous media diffusion coefficient for porous media as discussed in Section 24.3.1.2), and dC/dz = the concentration gradient at that point. Diffusion may occur in gas, liquids and solid phases, and all three are of potential interest to the geoenvironmental engineer.

In general terms, the diffusion coefficient in a gaseous phase is many orders-of-magnitude higher than in water; which, in turn, is orders-of-magnitude higher than in a solid. For example, the bulk diffusion coefficient, D_p, for the volatile organic compound dichloromethane is of the order of 10^{-5} m^2 s^{-1} in air, 10^{-10} m^2 s^{-1} in the porewater of a CCL, and 10^{-12} m^2 s^{-1} in an HDPE geomembrane. Thus in the liner system shown in Fig. 25.1 contaminant migration through an intact composite liner will involve:

- diffusion through the geomembrane (controlled by a low diffusion coefficient but also a potentially high concentration gradient due to the small 1.5–2.5-mm thickness of typical geomembrane liners);
- diffusion through the pore structure of an essentially saturated CCL (controlled by a higher diffusion coefficient but also by a smaller gradient than for the geomembrane such that the resistance of the two components of the system to the diffusion of dichloromethane (DCM) is of a similar order-of-magnitude); and
- diffusion predominantly through the gas-filled pores of the granular secondary leachate collection (SLCS) drainage layer (controlled by diffusion coefficient in air and the volumetric gas content, θ_a, for a drainage layer that is kept pumped and at a low degree of saturation).

The process is then repeated through the secondary liner.

25.5.1 DISSOLVED-PHASE DIFFUSION THROUGH POROUS MEDIA

Diffusion of dissolved contaminants through a porous medium will occur through the water-filled pores of the medium and so it is convenient to separate out the effect of porosity (or volumetric water content) from the effective diffusion coefficient such that for a saturated soil Eq. 25.21 becomes:

$$J = -n_e D_e \frac{dC}{dz} \qquad (25.22a)$$

or more generally for an unsaturated soil (see Section 25.5.1.3 for more discussion):

$$J = -\theta_e D_{e\theta} \frac{dC}{dz} \qquad (25.22b)$$

where n_e = the effective porosity of a saturated soil; D_e = the effective diffusion coefficient; θ_e = the effective volumetric water content ($\theta_e = n_e$ for $S = 100\%$); $D_{e\theta}$ = the effective diffusion coefficient for an unsaturated soil at a volumetric water content, θ ($D_{e\theta} = D_e$ for $S = 100\%$).

Several mechanisms influence the "diffusive" movement of ions or molecules through a soil. These include diffusion itself, electrical flow (e.g. where the rate of movement of a cation is influenced by rate of movement of an anion in order to maintain electrical neutrality and vice versa), and osmotic flow (where there is water flow from the area of low contaminant concentration to the area of high contaminant concentration). Thus when an effective diffusion coefficient is measured

by typical laboratory means (e.g. see Rowe *et al.* 1988; 1995b), it is in fact a bulk mass transfer coefficient that includes all of these effects. Fortunately, experience has shown that parameters evaluated in this way do provide a good prediction of observed field behavior (Rowe *et al.* 1995b; 1998b).

Various texts (e.g. Bear 1979) attempt to relate the diffusion coefficient in soil to the diffusion coefficient in free solution, D_o (Section 24.3.1.2) by a geometric "tortuosity" factor to account for the more tortuous path the contaminant must take in soil. This may have some justification in sands, but fails to account for a number of other important factors such as the decreased fluidity of adsorbed double layer water, electrostatic interaction, etc. which influence the effective diffusion coefficient through clayey soils. Since these effects may vary from soil to soil and contaminant to contaminant, the ratio (D_e/D_o) of the effective diffusion coefficient to free solution coefficient will vary from soil to soil and even from one contaminant to another in the same soil depending on the contaminant being considered, the soil mineralogy and porewater chemistry, and the leachate composition (see Rowe *et al.* 1995b).

In addition to being influenced by soil mineralogy, porewater chemistry, soil fabric and leachate chemistry, the effective diffusion coefficient will also depend on temperature. Although corrections can be made to try to adjust for these factors they fail to account for interaction effects. Hence, if a diffusion coefficient is important for a particular project, it is best to obtain an experimental value using the proposed soil, a leachate composition as close as practical to that expected and at a temperature as close as practical to the expected field temperature. Fortunately, despite all the complicating factors involved, the diffusion coefficient varies over a relatively narrow range (relative to other parameters such as hydraulic conductivity) and provided a reasonable attempt is made to pick appropriate parameters, quite good predictions of field behavior can be achieved (see Rowe *et al.* 1995b).

For many soils and contaminants, the effective porosity, n_e, will be very close to the total porosity, n, (e.g. Rowe *et al.* 1988; 1995b). However, there are circumstances where the effective porosity may be less than the total porosity (e.g. due to anion exclusion in some soils). The effective porosity may vary from one contaminant to another (e.g. the effective porosity for chloride may not be the same as for dichloromethane) and may not be the same as the effective porosity used to calculate average linearized groundwater velocity when considering advective contaminant transport (Section 24.1.4 and Eq. 24.6). While this is an unfortunate complication, in practical terms generally either advection dominates (in which case n_e can be taken to be the effective porosity with respect to advection) or diffusion dominates (in which case n_e can be taken to be the effective porosity with respect to diffusion).

When dealing with systems where diffusive transport is significant (typical of liners that are performing their design function of controlling advective transport to an advective flux of 0.03 m a^{-1} or less; see Rowe *et al.* 1995b), both the effective porosity and diffusion coefficient can be established from appropriate laboratory tests. In situations where one is considering diffusive transport through liner systems it will also, generally, be necessary to consider the effect of biodegradation and geochemical processes, which will also influence the dissolved concentrations, e.g. see Section 24.3.3.

25.5.1.1 Diffusion through Intact and Compacted Clays

There is now a body of field evidence showing the importance of diffusion in low permeability materials that range over a geological time-scale, i.e. over 10 000–15 000 years since the last Ice Age, and over a period of

TABLE 25.13. Range of effective diffusion coefficients for selected contaminants in low activity natural geologic barrier or compacted clay (porosity = 0.31–0.39)

	Effective diffusion coefficient, D_e[a]	
	($m^2\ s^{-1}$)	($m^2\ a^{-1}$)
Chloride[b,c]	$2–8 \times 10^{-10}$	0.006–0.25
Potassium[b]	$5–7.5 \times 10^{-10}$	0.016–0.024
Sodium[b,c]	$2–4.8 \times 10^{-10}$	0.006–0.015
Zinc[c]	$3.7–7 \times 10^{-10}$	0.012–0.022
Acetone[c]	5.6×10^{-10}	0.018
Aniline[c]	6.8×10^{-10}	0.021
Benzene[c]	$2.5–3.6 \times 10^{-10}$	0.008–0.011
Chloroform[c]	7×10^{-10}	0.022
Dichloromethane[c]	$2.5–8.5 \times 10^{-10}$	0.008–0.027
1,4 Dioxane[c]	4×10^{-10}	0.013
Toluene[c]	$0.6–3 \times 10^{-10}$	0.002–0.01
Trichloroethene[c]	$2.5–3.5 \times 10^{-10}$	0.008–0.011

[a] Data from Barone *et al.* 1989; Barone 1990; Rowe *et al.* 1988; Myrand *et al.* 1987; Karickhoff *et al.* 1979; Rowe & Barone 1991; McKay & Trudell 1989) and unpublished reports.
[b] Some values obtained over the temperature range 7–10 °C.
[c] Some values obtained over the temperature range 20–23 °C.

about 25 years since contaminant migration has been monitored beneath landfills with a low permeability liner (see Rowe *et al.* 1995b). Typical field and laboratory diffusion coefficients for chloride are given in Table 24.3 and vary from about 2×10^{-10} to 8×10^{-10} $m^2\ s^{-1}$ depending on soil, leachate and temperature. Table 25.13 gives the reported effective diffusion coefficients for a number of selected contaminant diffusions through low activity clays. Values were obtained over the two temperature ranges as noted. While the diffusion coefficient increases with increasing temperature (all other things being equal), other factors such as leachate chemistry often have had a greater effect than temperature. For example, the values reported for sodium include two of 2×10^{-10} $m^2\ s^{-1}$ at 10 °C. Based on the influence of temperature on the free solution diffusion coefficient (see Rowe *et al.* 1995b), a value of 2×10^{-10} $m^2\ s^{-1}$ at 10 °C should increase to 2.7×10^{-10} $m^2\ s^{-1}$ at 22 °C. However, other experimental data include one diffusion coefficient of 3.7×10^{-10} $m^2\ s^{-1}$ at 7 °C for industrial waste leachate, one at 4.6×10^{-10} $m^2\ s^{-1}$ at 10 °C for municipal solid waste leachate and one at 4.8×10^{-10} $m^2\ s^{-1}$ at 22 °C for a simple NaCl solution (see Rowe *et al.* 1995b for details). Thus, it is best to establish parameters for the appropriate leachate and temperature if reliable parameters are needed.

Table 25.14 gives a number of published diffusion coefficients for soil–bentonite liners.

25.5.1.2 Diffusion through GCLs

Similar to the hydraulic conductivity of GCLs, the diffusion coefficient of GCLs depends in large part on the bulk void ratio of the GCL; which, in turn, depends on the applied stress conditions. The diffusion coefficient can be estimated from relatively simple tests (see Rowe *et al.* 1997a, 1998a) by monitoring the mass transfer across the GCL. This mass transfer is primarily controlled by the porous media diffusion coefficient, D_p, i.e. $D_p = n_e D_e$.

Lake & Rowe (2000b) examined the diffusion of inorganic contaminants through a GCL and found a linear relationship between the porous media diffusion coefficient, D_p,

TABLE 25.14. Some effective diffusion coefficients in soil–bentonite liners (22 °C)

Bentonite (%)	Porosity, $n(-)$	Contaminant	Diffusion coefficient ($m^2\ s^{-1}$)	Diffusion coefficient ($m^2\ a^{-1}$)
0	0.3–0.33	Bromide[a]	$10–11 \times 10^{-10}$	0.033–0.035
		Trichloroethene[a]	$6.6–7.3 \times 10^{-10}$	0.021–0.023
4	0.37	Bromide[a]	6×10^{-10}	0.02
		Trichloroethene[a]	4.4×10^{-10}	0.014
5	0.4	Chloride	7.9×10^{-10}	0.025

[a] Data from Gullick (1998).

and the bulk GCL void ratio, e_B. For a simple 3–5 g L^{-1} NaCl solution, the relationship between D_p and e_B for chloride ($1 \leq e_B \leq 3.5$) was given by:

$$D_p \cong (1.02e_B - 0.89) \times 10^{-10} (m^2\ s^{-1}). \quad (25.23)$$

It should be noted that the diffusion coefficient, e.g. as given by Eq. 25.23, is dependent on the chemical species, the void ratio and the other chemical constituents in the leachate, and the background chemistry of the soil below the GCL. Thus, Lake & Rowe (2000b) showed that the chloride porous media diffusion coefficient obtained at a given void ratio increased from $D_p \cong 1 \times 10^{-10}\ m^2\ s^{-1}$ for a 4.6 g L^{-1} NaCl solution to $D_p \cong 3 \times 10^{-10}\ m^2\ s^{-1}$ for a 114 g L^{-1} brine solution. For a given permeant, the relationship between bulk GCL void ratio and diffusion coefficient was relatively independent of the test type (constant volume or constant stress) or hydrating conditions (i.e. pre- or post-confinement), or method of GCL manufacture (at least for the three GCLs examined, see Table 25.6). However, the relationship between applied stress and bulk GCL void ratio did depend on the type of manufacturing process and hydrating conditions (see Section 25.3.4).

The relationship between applied stress and diffusion coefficient will vary depending on the GCL manufacturing process, fluid used to hydrate the GCL, and the leachate characteristics. That said, a preliminary estimate of the diffusion coefficient for chloride through the three GCLs listed in Table 25.6 can be obtained using Eq. 25.18 (depending on the GCL) and Eq. 25.23 (chloride), recognizing that these results were obtained for GCLs hydrated with distilled water under confined conditions and using a 3–5 gl^{-1} NaCl solution as the source "leachate." Equations such as these may be useful in preliminary design calculations; however, if these calculations indicate that the diffusion coefficient is a key parameter, then the diffusion coefficient should be measured directly from a constant stress diffusion test using the proposed GCL, hydrating conditions and leachate (see Rowe *et al.* 1998a).

Tests have also been conducted to examine sorption and diffusion of organic contaminants through GCLs and it has been found (Rowe & Lake 1999) that:

1. The sorption of organic compounds, e.g. volatile organic compounds (VOCs), in conventional GCLs is low. However, this sorption can be substantially increased by combining activated carbon with the bentonite.
2. The diffusion coefficients for organic contaminants through GCLs are of a similar order-of-magnitude to that for inorganic contaminants at a given bulk GCL void ratio.
3. Diffusion tests for volatile organic compounds are much more difficult than those for inorganic contaminants.

Diffusion can be an important consideration with respect to contaminant impact of well-

TABLE 25.15. Diffusion coefficient in two GCLs as inferred by Lo (1992)

	Effective diffusion coefficient, D_e ($m^2\ s^{-1}$)		
Liner material	Chloride	Lead	1,2 dichlorobenzene
Normal GCL	2.4×10^{-10}	5.9×10^{-10}	9.8×10^{-11}
Organo-clay	4.9×10^{-10}	9.0×10^{-10}	1.5×10^{-10}

designed and operated landfill facilities (see Rowe *et al.* 1995b). It can also impact on laboratory hydraulic conductivity tests where diffusion of chloride ahead of the advective contaminant front may be misinterpreted as indicating a macrostructure and preferential flow paths.

The observation that there will be an "early" diffusive movement of contaminant ahead of the advective front in hydraulic conductivity tests can be used to obtain an estimate of diffusion characteristics. For example, Lo (1992) used an early version of the program POLLUTE (Rowe & Booker 1997a) to fit the concentration profile in the effluent for tests performed using the GCL "CL" and obtained diffusion coefficients as summarized in Table 25.15. It was inferred that the diffusion coefficient for lead was greater than that for chloride, while the diffusion coefficient for 1,2 dichlorobenzene was reported to be less than for chloride. Diffusion coefficients for the modified organo-clay were reported to be up to 50% greater than for conventional bentonite.

Compared to conventional bentonite, the organo-clay tested by Lo (1992) provided much less "sorption capacity" for lead but much more sorption for 1,2 dichlorobenzene.

25.5.1.3 Diffusion through Unsaturated Soil

Suitable natural clay liners will usually be saturated. Good CCLs may have a degree of saturation between 87 and 100% and often between 95 and 100% (see Section 25.3.2). If the liner is loaded, e.g. due to placement of waste over the liner, then it may be expected that due to consolidation the degree of saturation will increase. For these soils, the effective diffusion coefficient is essentially the same as the saturated diffusion coefficient discussed in Section 25.5.1.1. However, if necessary, the diffusion through these liners may be modeled using Eq. 25.22b and a value of $D_{e\theta}$ as discussed below.

Compacted clay and composite liners are often underlain by an unsaturated zone, which may include natural unsaturated silts, sands or gravels or an engineered secondary leachate collection system, e.g. see Fig. 25.1. For these soils the volumetric water content, θ, is less than the porosity. In addition, the effective diffusion may be substantially smaller than for saturated soil (Klute & Letey 1958; Porter *et al.* 1960). Rowe and Badv (1996a,b) examined dissolved phase diffusion through unsaturated silt, sand and fine gravel and found that the diffusion coefficient, $D_{e\theta}$, for the unsaturated soils they examined was given by:

$$D_{e\theta} = \left(\frac{\theta - \theta_{min}}{n - \theta_{min}}\right) D_e \qquad (25.24a)$$

where $D_{e\theta}$ = the effective diffusion coefficient in the unsaturated soil at a volumetric water content, θ; n, D_e = the volumetric water content (total porosity) and effective diffusion coefficient in the same soil under saturated conditions; and θ_{min} = the water content at which there is no interconnected water through which diffusion can occur. For their tests, Rowe & Badv (1996a,b) found that $\theta_{min} \cong 0$ and Eq. 25.24a reduces to:

$$D_{e\theta} = \left(\frac{\theta}{n}\right) D_n \qquad (25.24b)$$

(where $D_e \cong 0.028–0.033$ m^2 a^{-1} in their test on silt, sand and gravel with $n = 0.34–0.38$).

Rowe & Badv (1996a,b; Badv & Rowe 1996) demonstrated that advective–diffusive transport through a CCL underlain by unsaturated silt, sand or gravel could be well-predicted using finite layer theory (Rowe & Booker 1997a). It was also shown that mechanical dispersion (Section 24.3.1.3) was very small for clay, silts, sands and fine gravels at volumetric water contents greater than 0.04 and a Darcy flux less than 6×10^{-10} m s^{-1}, i.e. 0.02 m a^{-1}. However, for a coarse gravel drainage layer (20–45-mm particle size) with a volumetric water content of 0.027–0.035, advective transport and mechanical dispersion was dominant over diffusion through the unsaturated coarse gravel at Darcy fluxes of between 6×10^{-10} and 8×10^{-8} m s^{-1} (0.02–2.5 m a^{-1}). For this case, they found that the coefficient of hydrodynamic dispersion (Section 24.3.1.3), D (m^2 s^{-1}), could be given by:

$$D = D_{e\theta} + \alpha v \ (\text{m}^2\ \text{s}^{-1}) \qquad (25.25a)$$

where $D_{e\theta}$ (m^2 s^{-1}) is given by Eq. 25.24, α (m) = the dispersivity given by:

$$\alpha = 35200v + 0.013 \ (\text{m}) \qquad (25.25b)$$

the average linearized groundwater velocity, v (m s^{-1}), is given by:

$$v = v_a/\theta \ (\text{m s}^{-1}) \qquad (25.25c)$$

where v_a (m s^{-1}) = the Darcy flux through the liner and θ (−) is the volumetric water content of the coarse gravel. Equation 25.25b must be used with the units defined above.

The unsaturated diffusion coefficient as defined above will be important with respect to the transport of non-volatile contaminants. It may also control transport of volatile contaminants when the degree of saturation is sufficiently high that there is no significant interconnected gas-filled void. However, for low degrees of saturation, the migration of volatile organic compounds will be dominated by diffusion in a gaseous phase as discussed in Section 25.5.2.

25.5.2 GASEOUS-PHASE DIFFUSION THROUGH POROUS MEDIA

Unsaturated soils may have continuous gas-filled pore space and under these circumstances the movement of volatile contaminants and other gases of potential environmental concern (e.g. the diffusion of oxygen through a cover and into sulphidic mine tailings as discussed in Chapter 27, and the migration of methane generated by municipal solid waste) will be predominantly through the continuous gas-fill pores. In these cases, the diffusive flux is given (again by Fick's law) as:

$$J = -\theta_a D_\theta \frac{dC}{dz} \qquad (25.26)$$

but where θ_a = the effective air porosity; D_θ = the diffusion coefficient of the gas of interest through a porous medium with a volumetric water content, θ (or degree of saturation, S_r); and C = the concentration in the gaseous phase. There will be a relationship between the gaseous phase concentration and the dissolved phase concentration, which is given by Henry's law (see Section 24.3.3.2, Eq. 24.22 and Table 24.5).

The gaseous diffusion coefficient through porous media, D_θ, is often related to the diffusion of gas through air, D_a. van Bavel (1952) found that for dry soil and sand mixtures with porosities between 0.1 and 0.6, $D_\theta/D_a = 0.58$. Many studies have been conducted to examine the variation in the ratio D_θ/D_a with the degree of saturation, and these results are summarized in Fig. 25.15. The results cover a range of materials (sands, silts, sand–bentonite, loams, till and clay) with no particular pattern being noticed due to the material itself. Figure 25.15 shows that at low degrees of saturation the data are fairly consistent and approach van Bavel's ratio of

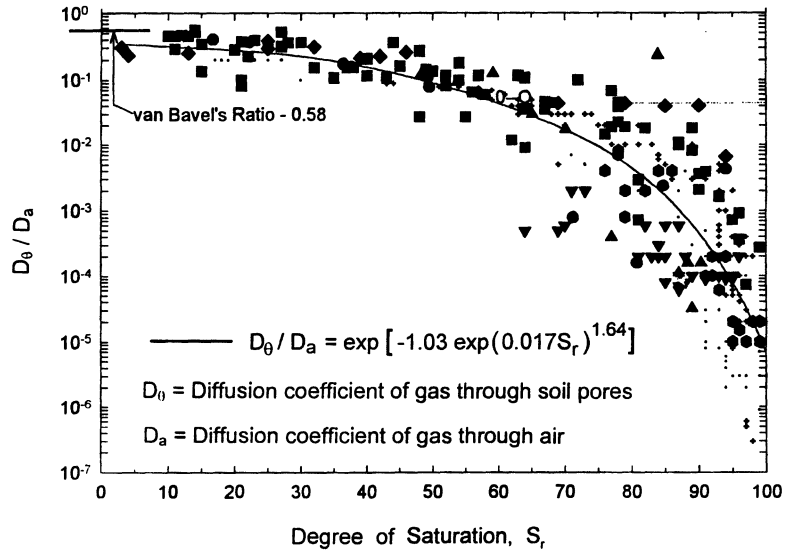


FIGURE 25.15. Results of regression analysis on diffusion–saturation data (modified from MacKay 1997): (—) $D_\theta/D_a = \exp[-1.03 \exp(0.017\ S_r)^{1.64}]$; where D_θ and D_a = diffusion coefficient of gas through soil pores and air, respectively.

0.58. As the degree of saturation increases, the value of D_θ/D_a decreases significantly and the scatter increases. The high scatter at high degrees of saturation is likely due to variability in the effective porosity where in two samples with the same degree of saturation and total porosity but different grain distribution may have different amounts of connected gaseous pore space. If one sample has many continuous gaseous pores the value of D_θ will be much larger than for the second sample with the same number of gaseous pores but where the paths between pockets of gaseous pores are blocked by water-filled pores.

Based on the data presented in Fig. 25.15, the "best-fit" relationship between D_θ/D_a and the degree of saturation, S_r, is given by:

$$D_\theta/D_a = \exp[-1.03 \exp(0.017S_r)^{1.64}]. \quad (25.27)$$

S_r is expressed in percent. It can be seen from Table 25.16 that the diffusion coefficient in air, D_a, and water, D_o, typically differs by about four orders-of-magnitude. As was the case for diffusion in the dissolved phase, the diffusion coefficient in air increases with increasing temperature. In both cases, the variation is approximately linear with temperature.

The foregoing has focused on the migration of gases through the primary pore structure of the soil. This is likely to be valid where there is no significant secondary porosity, e.g. fractures. However, soil covers may desiccate and crack due to both heating and frost action (Section 25.3). If cracks occur there may be much greater gas migration through the secondary pores (cracks) than through the primary gas-filled pores (intact soil).

25.5.3 DIFFUSION THROUGH GEOMEMBRANES

Water and contaminants dissolved in water or in other solvent can diffuse through a geomembrane. Considering diffusion within the geomembrane itself, Fick's law can be written as shown in Eq. 25.21 where $C = C_g$ is the mass of the penetrant per unit volume of geomem-

TABLE 25.16. Some published diffusion coefficients in air and water (adapted from Thibodeau 1996; Barone *et al.* 1992)

	In air @ $D_a \times 10^5$ ($m^2\ s^{-1}$)	T Temperature, (°C)	In water $D_o \times 10^9$ ($m^2\ s^{-1}$)	T Temperature, (°C)
Acetic acid	1.33	25	0.88	20
Acetone	1.09	0	1.15	22
Ammonia	2.8	25	1.76	20
Aniline	0.72	25	0.98	22
Benzene	0.88	25	1.15	25[a]
Butyric acid	0.76	25[a]	0.92	25[a]
Carbon dioxide	1.64	25	1.77	20
Chlorine	0.93	0	1.45	25
Chloroform	0.91	0	1.06	22
p-cresol	0.77	25	0.87	25
1,2 dichloroethane	0.90	25[a]	1.07	25[a]
1,4 dichlorobenzene	0.68	25[a]	0.81	25[a]
Dichloromethane	1.04	25[a]	1.26	25[a]
Ethylbenzene	0.75	25[a]	0.91	25[a]
Hydrogen	4.1	25	5.85	25
Methyl ethyl ketone	0.85	25[a]	0.99	25[a]
Nitrogen	1.3	0	2.0	20
Propionic acid	0.95	25[a]	1.01	25[a]
Oxygen	2.06	25	2.35	25
Toluene	0.85	25[a]	0.96	25[a]
Water	2.56	25		
m-xylene	1.23	25[a]	0.79	25[a]

[a] Calculated as per Yaws (1995).

brane. This may be related to the concentration in fluid by a Henry's law relationship:

$$C_g = S_{gf} C_f \tag{25.28}$$

where S_{gf} = the solubility or partitioning coefficient, or Henry's coefficient; C_f = the equilibrium concentration in the fluid. Thus with the same fluid on either side of the geomembrane (e.g. air or water) Fick's law for mass flux across the geomembrane can be written as:

$$J = -D_g \frac{dC_g}{dz} = -S_{gf} D_g \frac{dC_f}{dz} = -P_g \frac{dC_f}{dz} \tag{25.29}$$

where P_g = the permeability of the geomembrane (not to be confused with hydraulic conductivity or intrinsic permeability discussed in Section 24.1.3). Diffusive transport across the geomembrane is described by:

$$\frac{\partial C_f}{\partial t} = D_g \frac{\partial^2 C_f}{\partial z^2}. \tag{25.30}$$

The diffusion coefficient, D_g, and solubility coefficient, S_{gf}, will depend on the nature of the source fluid and the geomembrane and may be obtained using techniques described in Rowe (1998a). Table 25.17 summarizes published values of S_{gf}, D_g and P_g for a range of contaminants through polyethylene geomembranes.

25.5.3.1 Factors Affecting Diffusion through a Geomembrane

Diffusion coefficient D_g and solubility S_{gf} of a contaminant for a given geomembrane in-

TABLE 25.17. Typical ranges of partitioning coefficient, S_{gf}, and diffusion coefficient, D_g, and permeability, P_g, for polyethylene geomembrane (see Rowe 1998a for full details and sources of data)

Chemical	Solution	S_{gf} (−)	$D_g \times 10^{12}$ ($m^2\ s^{-1}$)	$P_g \times 10^{15}$ ($m^2\ s^{-1}$)
Acetic Acid	Aqueous	0.015	0.11–0.29	1.65–4.35
	Pure	0.0086	0.52–0.58	4.47–5.0
Acetone	Aqueous	0.013–0.2	<0.0001	<0.02–0.27
	Pure	0.01–0.012	0.51–0.91	6.1–10.9
Benzene	Aqueous	54.3–57.2	0.037	2010–2120
	Pure	0.08	2.0–4.2	160–340
Carbon tetrachloride	Aqueous			48–57
	Pure	0.18–0.2	0.66–2.4	432
Chlorobenzene	Pure	0.083–0.11	2.2–3.6	200–350
Chloroform	Aqueous			17–25
	Pure	0.134–0.153	1.8–5.9	790
Chloride	Aqueous	0.0008	0.1–0.3	0.08–5
Cyclohexane	Aqueous	2378	0.012	2.8×10^4
	Pure		0.61	
Dichloromethane	Aqueous	1.8–5.6	0.58–2.28	1000–6600
	Pure	0.06	2–10	294
1,1 Dichloroethane	Aqueous			1000–2500
1,2 Dichloroethane	Aqueous	7.2	3.6–6.8	3000–6000
Ethylbenzene	Pure	0.1	2.8	280
Heptane	Pure	0.065–0.066	1.52–1.74	100–115
n-Hexane	Pure	?	2.08–3.6	
Methyl ethyl ketone	Aqueous	>0.025		300–800
	Pure	0.018–0.019	0.75–0.86	13–16
n-Octane	Pure	0.08	1.9	150
Propanoic acid	Pure	0.021	0.3–0.32	6.3–6.7
Tetrachloroethane	Aqueous			7800–8700
Tetrachloroethene	Pure	0.19–0.22	3.8	720
Toluene	Aqueous	63.5–192	0.2–0.56	22 000–98 000
	Pure	0.08–0.09	0.18–4.4	230–490
Trichloroethene	Aqueous	94–189	0.2–0.76	38 000–70 000
	Pure	0.11–0.2	7.7–85	1320–1810
m-xylene	Aqueous	193–370	0.31–0.36	60 000–112 000
	Pure	0.093	1.5–3.7	340
o-xylene	Aqueous	422		
	Pure		0.94	
p-xylene	Aqueous	387		
	Pure		1.6	
Xylene	Aqueous	499–556	0.2–1.8	110 000–500 000
	Pure	0.083–0.095	4.7	390
Water		<0.0003–0.001	0.29–9.0	0.1–0.9

crease with temperature. The product of these two parameters, the permeability ($P_g = S_{gf}D_g$) is highly dependent on the similarity of the penetrant and polymer. Based on research by August & Tatzky (1984) and Rowe *et al.* (1995a, 1996b), the permeability through HDPE geomembranes has the following order:

ions (Cl^-, Na^+, Zn^{2+}, Ni^{2+}, Mn^{2+}, Cu^{2+}, Cd^{2+}, Pb^{2+})
and alcohols < acids < nitroderivatives
< aldehydes < ketones
< esters < ethers
< hydrocarbons.

Chlorinated hydrocarbons (e.g. dichloromethane; 1,1 dichloroethane; 1,2 dichloroethane) can diffuse through an HDPE geomembrane and be detected in the porewater on the other side in a matter of days (Rowe *et al.* 1995a, 1996b), whereas the diffusion of salts (Na^+, Cl^-, and heavy metal salts) was negligible in tests conducted over five years at room temperature.

The "permeability" P_g also depends on the type of geomembrane and decreases with increasing crystalinity. For example, Park *et al.* (1995) reported that the permeability ($P_g = S_{gf}D_g$) of xylene in very low density polyethylene (VLDPE) was almost twice that through HDPE.

25.5.3.2 Diffusion of Water through HDPE Geomembrane

Eloy-Giorni *et al.* (1996) performed a detailed study of water movement through intact geomembranes and concluded that the concept of hydraulic conductivity (as defined by Darcy's law) is not appropriate for describing water transport (and by inference the advective transport of contaminants) through hydrophobic geomembranes. In particular, they demonstrated that a difference in pressure head across a geomembrane of up to 200 m had no significant effect on the movement of water molecules across a 1.7-mm thick HDPE geomembrane ($\rho_g = 940\,kg\,m^{-3}$). Likewise, a head difference of up to 400 m had no significant effect on water movement across a 1- and 1.6-mm thick, t_{GM}, PVC geomembrane (ρ_g = 1260 kg m^{-3}). As discussed by Rowe (1998a), one can expect negligible diffusion of water through intact geomembranes used as fluid-retaining structures. This is in part due to the very low "permeability" $P_g = S_{gf}D_g$ as evident from the parameters given in Table 25.18 and in part due to the fact that in most cases the relative humidity is very high on both sides of the geomembrane.

25.6 *Liner Temperature*

The temperature of the liner can have a profound effect on: (a) the service life of the liner; (b) hydraulic conductivity; and (c) diffusion through the liner. In landfill applications, the temperature of the liner may be related to the level of leachate mounding above the liner (see Fig. 25.16) as discussed by Rowe (1998a).

The service life of geomembrane liners will depend, in part, on the rate of antioxidant depletion (see Hsuan & Koerner 1995b;

TABLE 25.18. Solubility and diffusion coefficient for water in three types of geomembrane (adapted from Eloy-Giorni *et al.* 1996)

	S_{gf} (−)	D_g ($m^2\,s^{-1}$)	ρ_g ($kg\,m^{-3}$)	t_{GM} (mm)
HDPE	8×10^{-4}	2.9×10^{-13}	940	1.7
PVC	7×10^{-2}	4.4×10^{-13}	1260	1.0, 1.6
Bituminous	9×10^{-3}	8×10^{-13}	1150	5

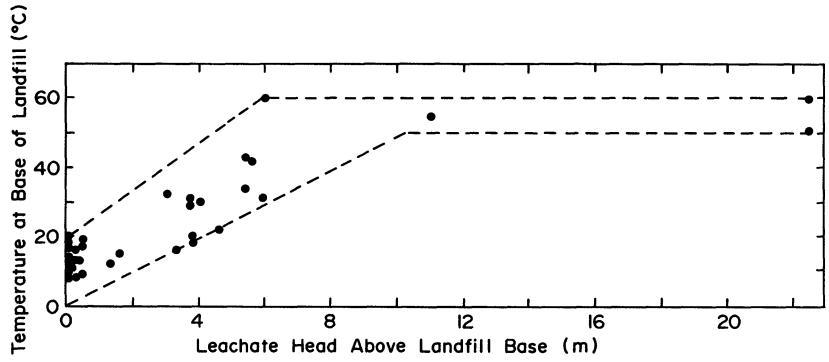


FIGURE 25.16. Variation in temperature at landfill base with leachate head for a number of landfills (modified from Barone *et al.* 1997).

TABLE 25.19. Calculated time for antioxidant depletion based on test data by Hsuan and Koerner (1995b) (see Rowe 1998a for details)

Temperature (°C)	Series I[a] (years)	Series III[b] (years)
10	111	453
15	98	299
20	59	200
25	44	135
30	33	93
35	25	65
40	19	45
45	14	32
50	11	23
55	9	17
60	7	12

[a] Series I: Moving water on both surfaces of geomembrane.
[b] Series III: Stationary water on only one surface.

TABLE 25.20. Effect of temperature on diffusion coefficient, D_T, hydraulic conductivity, k_T, in a liner at temperature, T, relative to values at 10 °C (adapted from Rowe 1998a)

Temperature (°C)	D_T/D_{10}	k_T/k_{10}
10	1.0	1.0
20	1.4	1.3
25	1.6	1.5
35	2.0	1.8
50	2.7	2.4
65	3.5	2.9

Rowe 1998a), and Table 25.19 illustrates how the projected time for antioxidant depletion changes with temperature and the potential for water moving past the surface to increase the leaching of antioxidants. Temperature also has the potential to decrease the service life of clay liners if it is sufficient to cause desiccation of the liner (see Rowe 1998a).

Temperature can influence the hydraulic conductivity and diffusion coefficients, as shown in Table 25.20, which gives the ratio of the values at temperature, T, to that at 10 °C. Domenico and Schwartz (1998) indicate that the groundwater temperature at a depth of 10–20 m is typically 1–2 °C higher than local mean temperature and hence a temperature of 5–10 °C would be typical groundwater temperature in the northern USA and southern Canada. From Table 25.20, it can be seen that diffusive and advective transport are 40 and 30%, respectively, higher at 20 °C than at 10 °C, and 100 and 80%, respectively, higher at 35 °C. If the liner temperature is to remain relatively constant, then constant diffusion and hydraulic conductivity parameters relevant to that temperature may be used. However, if the temperature of the liner changes with time, e.g. due to leachate

mounding (see Fig. 25.16), then some consideration may need to be given to the effect of the change in these parameters with temperature on the impact calculations. The approach proposed by Rowe & Booker (1997b) readily models change in D and the effect of a change in k with time as appropriate.

25.7 *Contaminant Impact Assessment and Equivalence of Liner Systems*

25.7.1 IMPACT ASSESSMENT

The assessment of the suitability of a liner system should, in principle, be related to the potential impact on water quality (especially groundwater) due to the proposed landfill and liner system. This assessment typically involves the solution of the advection–dispersion equation subject to appropriate boundary conditions (e.g. see Rowe *et al.* 1995b for a detailed discussion). Factors that influence the potential impact include: (a) the landfill source concentration and its decay characteristics; (b) the advective flux (leakage) across the barrier system; (c) the thickness of any "attenuation" layer between the base of the low permeability liner(s) and the receptor aquifer (or distance to the water table if the liner is constructed in the unsaturated portion of the aquifer); (d) diffusion (especially for VOCs) across the barrier system; (e) sorption/retardation in the liner and underlying soil; (f) biodegradation; (g) dilution in the aquifer; (h) the service life of the engineered components of the landfill (e.g. covers/caps, leachate collection systems, liners); (i) the mode of operation of the landfill; (j) landfill size and geometry; and (k) consolidation of the liner and any underlying compressible soils.

Consolidation (item k) is usually not considered on the grounds that it is transient and provides water for "dilution" of contaminants; however, it should be noted that consolidation may be significant if one is calculating travel times and, in particular, first arrival times. It may be hypothesized that the "premature" arrival of contaminant in leakage detection systems is, in part, attributable to failure to consider consolidation effects in assessing the expected travel times. More research is required into this aspect.

Items (a)–(j) can be readily modeled using existing contaminant transport theory and codes (e.g. Rowe & Booker 1997a,b). However, the factors considered in modeling impact tend to be regulatory driven and vary from one country to another, and hence the assessment of what represents an "adequate" barrier system will vary from regulatory environment to regulatory environment. Thus one cannot generalize about "equivalency" of liner systems since what is "equivalent" depends on what is being compared and how it is being compared.

25.7.2 EQUIVALENCE OF GCL AND CCL SYSTEMS

Rowe (1998a) illustrates the evaluation of the equivalence of a liner system involving a GCL with one involving a CCL. When comparing liner systems, consideration should be given to factors such as:

1. The hydraulic resistance over the contaminating lifespan of the landfill, including the effects of leachate mounding and clay–leachate interaction for both compacted clays and GCLs. Consideration should also be given to the potential for internal erosion when there may be high gradients.
2. The contact conditions between the geomembrane and "clay." The geotextile component of the GCL may control transmissivity at the interface between the GCL and geomembrane and any assessment of leakage should be based on experimental data for the proposed geomembrane and GCL under anticipated stress conditions.
3. The presence of wrinkles may be a problem with respect to the long-term perfor-

mance of composite liner systems in landfills.
4. The quality of a CCL is highly dependent on the construction control, e.g. compaction equipment, water content, etc. These CCLs are also prone to desiccation cracking. GCLs are easier to place and their long-term performance is less sensitive to desiccation effects; however, care is required to ensure that overlapped seams do not move and open up when overlying layers are placed.
5. The stability of the liner system and the potential for shear failure either at the interface between materials or within a layer itself both during construction and during placement of the waste.
6. The potential for diffusion, sorption and biodegradation. Since CCLs are often not specified to have a minimum organic carbon content, sorption cannot be relied on without independent tests. If sorption is required to control impact to a regulatory driven level, it is possible to specify a minimum organic carbon content and/or use modified clays in the GCL to achieve the desired level of sorption. For both CCL and GCL systems, some consideration should be given to the migration of metals, organic compounds and organo-metallic complexes that may be encountered in leachate.

25.8 *Liner Stability*

A detailed discussion of liner stability is beyond the scope of this chapter. Stability issues are dealt with in Chapter 14 and Chapters 26 (Section 26.5) and 27 (Sections 27.6 and 27.7) deal with specific issues related to stability of liner systems and cover systems, respectively. However, it is worth noting here that there have been a number of failures associated with liner construction (see Rowe 1998a). These cases illustrate the need to give careful consideration to the potential for sliding: (a) during barrier construction; (b) during expansion of existing landfills; and (c) during landfilling over the barrier system. The likelihood of failure occurring can be minimized by:

1. appropriate design and materials selection (including appropriate laboratory tests, selection of reasonable parameters, and appropriate stability analyses);
2. good CQC/CQA to ensure that the barrier system is installed as designed;
3. development plans for expanded landfills that limit toe excavation and overfilling and define allowable conditions for construction of the expansion area and a means of monitoring adherence to the development plans;
4. operations plans that include consideration of stability as the waste is placed and means of monitoring adherence to the operations plans;
5. contingency plans in the event of changed conditions occurring during construction (e.g. excessive rain, unexpected foundations conditions, etc.); and
6. disposal alternatives so that waste can be diverted if expansion schedules are not met.

26. GEOSYNTHETICS IN LIQUID-CONTAINING STRUCTURES

J. P. Giroud
R. Bonaparte

26.1 Introduction

26.1.1 TYPES OF LIQUID-CONTAINING STRUCTURES

The liquid-containing structures considered herein are those constructed with soil; thus, concrete dams, concrete reservoirs, cavities excavated in rock and steel tanks are not considered. The liquid-containing structures considered include: structures used for liquid storage (e.g. embankment dams, liquid impoundments excavated in soil or surrounded with dikes), structures used for liquid conveyance (canals) and structures used to prevent liquid from migrating into the ground (lined landfills). This chapter addresses analysis and design methods for liquid-containing structures. Required geosynthetic material properties and engineering parameters are addressed. The geosynthetic materials themselves are not discussed, however, and the reader is referred to Chapter 7 for information on this subject.

26.1.2 USES OF GEOSYNTHETICS IN LIQUID-CONTAINING STRUCTURES

Geosynthetics are extensively used in liquid-containing structures. These include: geomembrane liners, geosynthetic clay liners, geonet drainage layers, geotextile filters and geogrid reinforcement in liner systems; geotextile filters in embankment dams and bank protection systems; geonets and geocomposites in the internal drainage system of embankment dams; geotextile and geogrid reinforcement used to construct embankments with steep slopes for dams, levees, landfills, etc.; and geomats, geocells and other specialized geosynthetics used for erosion control.

26.1.3 GEOSYNTHETIC LINER SYSTEMS

Many liquid-containing structures include one or several low permeability layers, referred to as liners (see Section 25.3). These low permeability layers are generally incorporated into liner systems where low permeability materials are associated with high permeability materials. These two categories of materials are associated to perform complementary functions: the function of the liners, i.e. the low permeability materials, is to prevent or minimize the migration of liquid; and the function of liquid collection layers, i.e. the high permeability materials, is to collect and remove liquid. The removal of liquid is important because it reduces the head of liquid on top of the underlying liner, which reduces the rate of liquid migration through that liner (see Section 26.2.1.4 for more details on head).

In Chapter 26, the terminology "liner system" is used to designate liner systems where at least one component is a geosynthetic.

R. K. Rowe (ed.), *Geotechnical and Geoenvironmental Engineering Handbook*
© Kluwer Academic Publishers 2001

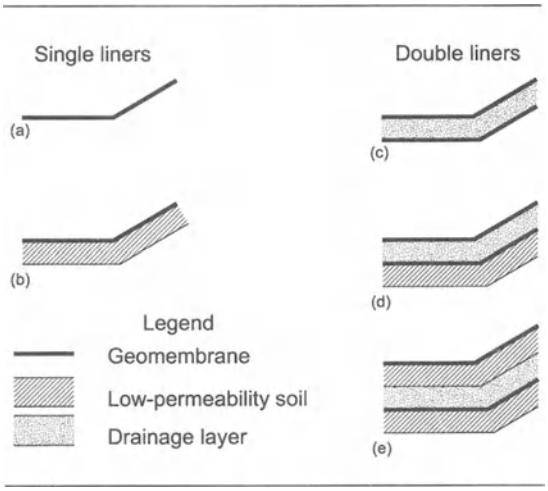


FIGURE 26.1. Five examples of liner systems: (a) single geomembrane liner, (b) single composite liner, (c) double geomembrane liner, (d) double liner with geomembrane primary liner and composite secondary liner, (e) double composite liner.

Chapter 26 complements Chapter 25, which provides information regarding the natural soil components of liner systems, by providing additional information regarding the geosynthetic components of liner systems.

Examples of liner systems are given in Fig. 26.1. A composite liner is a liner composed of two or more components, typically a geomembrane on a layer of compacted clay (or clayey soil), or a geomembrane on a geosynthetic clay liner. A double liner is a liner system that includes two liners (the primary liner on top, and the secondary liner underneath) separated by a drainage layer called the "leakage detection and collection layer" or "secondary liquid collection layer". The function of the secondary liquid collection layer is to detect liquid migration and, more importantly, to remove liquid that migrates through the primary liner, thereby reducing the head of liquid on top of the secondary liner, which reduces the rate of liquid migration through the secondary liner, as indicated above. In lined landfills, there is a primary liquid collection layer (called primary leachate collection layer) on top of the primary liner (in the case of a double liner) or on top of the liner (in case of a single liner) to collect leachate and remove it.

26.1.4 DESIGN CONSIDERATIONS

Many of the design issues addressed in Chapter 26 are related to liner systems. Essentially, a liner system must minimize liquid migration, and must perform this function in spite of the *in situ* stresses and environmental conditions to which it is exposed. As indicated in Section 26.1.3, liquid migration is minimized by decreasing the hydraulic head on top of the liner, which requires effective liquid collection. Effective liquid collection requires effective liquid collection layers and effective filters. There are also many instances where liquid collection layers and filters are not used in conjunction with liner systems. This is the case, for example, of the internal drainage system of embankment dams.

Based on the foregoing discussion, four categories of design considerations will be addressed: liquid collection layer design, filter design, liquid migration evaluation, and resistance of liner systems to instability and deformations.

26.2 Design of Liquid Collection Layers

26.2.1 INTRODUCTION TO LIQUID COLLECTION

26.2.1.1 Liquid Collection

The liquid collection layers discussed herein include the liquid collection layers associated with liner systems, as well as liquid collection layers located inside soil masses, such as the liquid collection layers used for the internal drainage of embankment dams, e.g. toe blankets, chimney drains.

Liquid collection plays an important role in the performance of liquid-containing

structures because it is essential to promptly remove liquids from areas where their presence may have a detrimental impact on the performance of the structure. In the case of liner systems, as mentioned in Section 26.1.3, the removal of liquid decreases the liquid head on the liners, thereby decreasing the rate of liquid migration. In the case of liquid collection layers located inside a soil mass, the removal of liquid decreases porewater pressure in the soil mass, thereby increasing the stability of the soil mass; also, the controlled removal of liquids decreases the risk of internal erosion of the soil.

26.2.1.2 Characteristics of Liquid Collection Layers

Liquid collection layers are characterized by their geometry and their hydraulic characteristics. The geometry of a liquid collection layer is characterized by its thickness, its slope and its length (length measured along the slope or, more generally, horizontal projection of the length). The relevant hydraulic characteristic of the material used in the liquid collection layer is its hydraulic conductivity. The relevant hydraulic characteristic of a liquid collection layer is its hydraulic transmissivity. The following relationship exists:

$$\theta_{LCL} = k_{LCL} t_{LCL} \qquad (26.1)$$

where θ_{LCL} = hydraulic transmissivity of the liquid collection layer material, k_{LCL} = hydraulic conductivity (also called coefficient of permeability) of the liquid collection layer material, and t_{LCL} = thickness of the liquid collection layer measured perpendicular to the slope. Equation 26.1 can be used with any set of coherent units. The relevant basis SI units are: θ_{LCL} ($m^2\ s^{-1}$), k_{LCL} ($m\ s^{-1}$), and t_{LCL} (m). Equation 26.1 is used with the subscript 1 for the primary liquid collection layer and the subscript 2 for the secondary liquid collection layer. If the liquid collection layer is a geosynthetic, θ_{LCL} is the hydraulic transmissivity of the geosynthetic.

It should be noted that Eq. 26.1 is based on the assumptions that the flow of liquid in the liquid collection layer is laminar, is parallel to the slope, and is not impeded by capillarity. All three assumptions are generally accepted in current design practice. It should also be noted that Eq. 26.1, as well as all the equations given in Sections 26.2.2 and 26.2.3, is valid for granular as well as geosynthetic liquid collection layers.

26.2.1.3 Materials Used in Liquid Collection Layers

Materials used in liquid collection layers are materials with a high hydraulic conductivity, k_{LCL}. These include granular materials such as gravel and sand, and geosynthetic materials such as geonets and drainage geocomposites. More information on granular materials can be found in Section 25.2 and on geosynthetics in Section 7.4. In the case of geosynthetics, it is easier to characterize the material using the hydraulic transmissivity than the hydraulic conductivity, because the test (see Section 7.4 and 7.7) directly gives the hydraulic transmissivity, and deriving the hydraulic conductivity from the hydraulic transmissivity may not be accurate due to the lack of precision on the measurement of geosynthetic thickness. As pointed out by Williams *et al.* (1984), it is important that testing to measure hydraulic transmissivity be performed under conditions that properly simulate field conditions, in particular the overburden stress, the hydraulic gradient and boundary conditions.

26.2.1.4 Hydraulic Head, Depth and Thickness of Liquid

The rate of liquid migration through a liner is governed by the hydraulic head above the liner. If the liquid does not move (e.g. in the case of a dam or a liquid impoundment), the hydraulic head on top of the liner is equal to the depth of liquid on top of the liner, i.e. $h = D$ in Fig. 26.2a. In the case where the liquid is unconfined and flowing along a

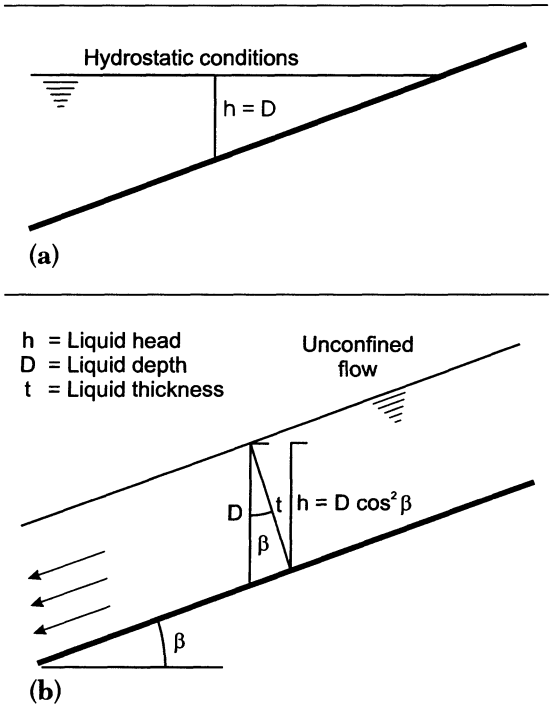


FIGURE 26.2. Head of liquid on top of the liner in the case of a liner on a slope: (a) hydrostatic conditions; and (b) unconfined flow along the slope (after Giroud 1997, © Geosynthetics International, reproduced with permission).

slope, i.e. parallel to a liner resting on a slope, the relationship between the liquid head on top of the liner, h, and the liquid thickness, t, is (Fig. 26.2b):

$$h = t \cos \beta = D \cos^2 \beta \qquad (26.2)$$

where h = hydraulic head on top of the liner; t = thickness of liquid measured perpendicular to the slope; D = depth of liquid, measured vertically; and β = slope angle. The relationship between thickness and depth is:

$$t = D \cos \beta. \qquad (26.3)$$

26.2.1.5 Design of Liquid Collection Layers

The basic principle of the design of liquid collection layers is that the liquid collection layer must be capable of conveying the flow of the collected liquid. This is expressed by the following equation derived from Darcy's equation:

$$Q^* = k_{LCL} t_{LCL} i_{LCL} = \theta_{LCL} i_{LCL} = \theta_{LCL} \sin \beta \qquad (26.4)$$

where Q^* = flow rate per unit width of the liquid collection layer, i_{LCL} = hydraulic gradient in the liquid collection layer (equal to sin β), and β = slope angle of the liquid collection layer. Equation 26.4 can be used with any set of coherent units. The relevant basic SI units are Q^* ($m^2\ s^{-1}$), θ_{LCL} ($m^2\ s^{-1}$), k_{LCL} ($m\ s^{-1}$), t_{LCL} (m) and β (°); i_{LCL} is dimensionless.

For the case of liquid collection layers located inside a soil mass, as for the internal drainage of an embankment dam, the design engineer should evaluate the rate of flow of the collected liquid using geotechnical engineering methods. Methods specific to the liquid collection layers associated with liner systems have been developed and are presented in Sections 26.2.2 and 26.2.3. However, it is important to recognize that the methods presented in Sections 26.2.2 and 26.2.3 are consistent with Eq. 26.4.

26.2.2 DESIGN OF PRIMARY LIQUID COLLECTION LAYERS

26.2.2.1 Analysis of Liquid Flow in a Primary Liquid Collection Layer

At a given time, there is a certain amount of liquid in a primary liquid collection layer. This amount of liquid can be expressed by the depth, thickness or head of liquid on top of the liner (see Section 26.2.1.4). The thickness of liquid is used herein because it can be readily compared to the thickness of the liquid collection layer. The thickness of liquid in the primary liquid collection layer varies along the length of the liquid collection layer. The liquid thickness has a maximum value, $t_{l\max}$, that occurs at a horizontal distance x_m from the top of the liquid collection layer slope (Fig. 26.3). The value of x_m depends on a parameter λ, defined by:

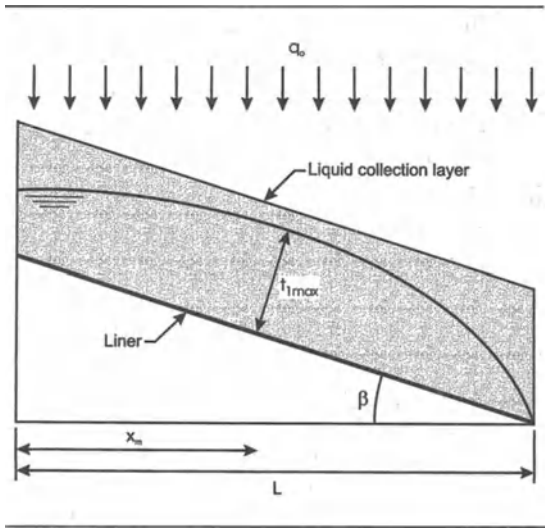


FIGURE 26.3. Liquid flow in a primary liquid collection layer (modified from Giroud & Houlihan 1995).

$$\lambda = \frac{q_o}{k_{LCL1} \tan^2 \beta} \tag{26.5}$$

where q_o = liquid impingement rate, i.e. rate at which liquid impinges the liquid collection layer; k_{LCL1} = hydraulic conductivity of the primary liquid collection layer material; and β = slope angle. Equation 26.5 can be used with any set of coherent units. The relevant basic SI units are: q_o (m s^{-1}) k_{LCL1} (m s^{-1}) and β (°); λ is dimensionless. Herein, q_o is assumed to be uniformly distributed over the entire area of the primary liquid collection layer. Techniques for calculating q_o in landfills are described in Chapter 27.

As shown by Giroud & Houlihan (1995), x_m/L (where L = the horizontal projection of the length of the primary liquid collection layer) is equal to or greater than 0.8, i.e. the maximum of the liquid thickness occurs close to the toe of the slope, if λ is less than 0.15. Such small values of λ are frequent in geosynthetic liner system applications.

Referring to Fig. 26.3, an excellent approximation of the maximum liquid thickness in a primary liquid collection layer under steady-state flow conditions, t_{1max}, is given by the following equation (Giroud & Houlihan 1995):

$$\begin{aligned} t_{1max} &= Lj \frac{(\tan^2 \beta + 4q_o/k_{LCL1})^{1/2} - \tan \beta}{2 \cos \beta} \\ &= Lj \frac{[(1 + 4\lambda)^{1/2} - 1] \tan \beta}{2 \cos \beta} \end{aligned} \tag{26.6}$$

where L = horizontal projection of the length of the primary liquid collection layer, and j = dimensionless coefficient given by:

$$\begin{aligned} j &= 1 - 0.12 \exp\left\{-\left[\log\left(\frac{8q_o}{5k_{LCL1} \tan^2 \beta}\right)^{5/8}\right]^2\right\} \\ &= 1 - 0.12 \exp\left\{-\left[\log\left(\frac{8\lambda}{5}\right)^{5/8}\right]^2\right\}. \end{aligned} \tag{26.7}$$

Values of j are between 0.88 and 1.00. Therefore, the maximum error made by neglecting the dimensionless coefficient j is 12%. As a result, in many practical applications, the following equation, known as Giroud's equation, can be used:

$$\begin{aligned} t_{1max} &= L \frac{(\tan^2 \beta + 4q_o/k_{LCL1})^{1/2} - \tan \beta}{2 \cos \beta} \\ &= L \frac{[(1 + 4\lambda)^{1/2} - 1] \tan \beta}{2 \cos \beta}. \end{aligned} \tag{26.8}$$

For small values of λ (e.g. $\lambda < 0.15$), Eqs 26.6 and 26.8 tend toward:

$$t_{1max} = \frac{q_o L}{k_{LCL1} \sin \beta}. \tag{26.9}$$

Equations 26.6–26.9 can be used with any set of coherent units. The relevant basic SI units are: t_{1max} (m), q_o (m s^{-1}), k_{LCL1} (m s^{-1}), L (m) and β (°); λ is dimensionless.

It is important to note that Eq. 26.9 could have been obtained directly by assuming that the maximum liquid thickness occurs at the toe of the slope (which is a good approximation for $\lambda < 0.15$, as noted above). Then, the flow rate in the liquid collection layer under steady state flow conditions is $q_o L$, i.e. the impingement rate multiplied by the horizontal projection of the length of the liquid collec-

tion layer, and Eq. 26.4, where the maximum liquid thickness is used instead of the thickness of the liquid collection layer, gives the following equation, which is identical to Eq. 26.9:

$$q_o L = k_{LCL} i t_{l\max} = k_{LCL} t_{l\max} \sin \beta. \quad (26.10)$$

26.2.2.2 Design of a Primary Liquid Collection Layer

The design of a primary liquid collection layer consists of checking that the maximum thickness of liquid, $t_{l\max}$, calculated using Eqs. 26.6, 26.7 or 26.8 is less than the thickness of the primary liquid collection layer:

$$t_{l\max} \leq t_{LCL1}. \quad (26.11)$$

If λ is small (e.g. $\lambda < 0.15$), $t_{l\max}$ can be calculated using Eq. 26.9. Hence:

$$\frac{q_o L}{\sin \beta} \leq k_{LCL1} t_{LCL1} = \theta_{LCL1}. \quad (26.12)$$

Therefore, if λ is small (e.g. $\lambda < 0.15$), the design of a primary liquid collection layer consists of checking that $q_o L/\sin \beta$ is less than the hydraulic transmissivity, θ_{LCL1}, of the primary liquid collection layer. For the calculation of t_{LCL1} at the design stage, a factor of safety may be applied to q_o.

It is important to note that Eqs 26.6–26.9 are only valid for steady state flow conditions. Calculations for the case of transient flow conditions are more complex. Practical guidance in the case of transient flow is provided by Giroud & Houlihan (1995).

26.2.2.3 Average Head of Liquid on Top of the Primary Liner for Liquid Migration Evaluation

The rate of liquid migration through the primary liner depends on the head of liquid on top of the primary liner. Since the head of liquid (which is related to the thickness of liquid, as indicated by Eq. 26.2) varies along the slope, it is convenient to use an average liquid head to perform the liquid migration rate calculations. The calculation of the exact value of the average liquid head is complex (Giroud & Houlihan 1995). However, based on numerical values provided by Giroud & Houlihan (1995), it is possible to recommend the following values for the average head of liquid on top of the primary liner:

$$h_{l\text{avg}} = 0.8 t_{l\max} \quad \text{if } \lambda > 0.5 \quad (26.13a)$$

$$h_{l\text{avg}} = 0.7 t_{l\max} \quad \text{if } 0.15 < \lambda \leq 0.5 \quad (26.13b)$$

$$h_{l\text{avg}} = 0.6 t_{l\max} \quad \text{if } 0.01 < \lambda \leq 0.15 \quad (26.13c)$$

$$h_{l\text{avg}} = 0.5 t_{l\max} \quad \text{if } \lambda \leq 0.01. \quad (26.13d)$$

In the last case (i.e. for $\lambda \leq 0.01$), combining Eqs 26.2, 26.9 and 26.13d gives:

$$h_{l\text{avg}} = \frac{q_o L}{2 k_{LCL1} \tan \beta}. \quad (26.14)$$

26.2.3 DESIGN OF SECONDARY LIQUID COLLECTION LAYERS

26.2.3.1 Analysis of Liquid Flow in a Secondary Liquid Collection Layer

Section 26.2.3 addresses the flow of liquid in the secondary liquid collection layer located between the two liners in a double liner system (Fig. 26.4). Since liquid migration through the primary liner of a double liner system occurs essentially through defects, i.e. small holes, of the primary liner geomembrane, and since the number of defects is generally small, the liquid that has migrated through defects of the primary liner generally flows only in portions of the secondary liquid collection layer. These portions are referred to as wetted zones (see Fig. 26.4b). If the defects in the primary liner geomembrane are sufficiently far apart, the wetted zones produced by the various defects do not overlap, and the boundary of the wetted zone related to one defect is approximately a parabola, as shown by Giroud *et al.* (1997a).

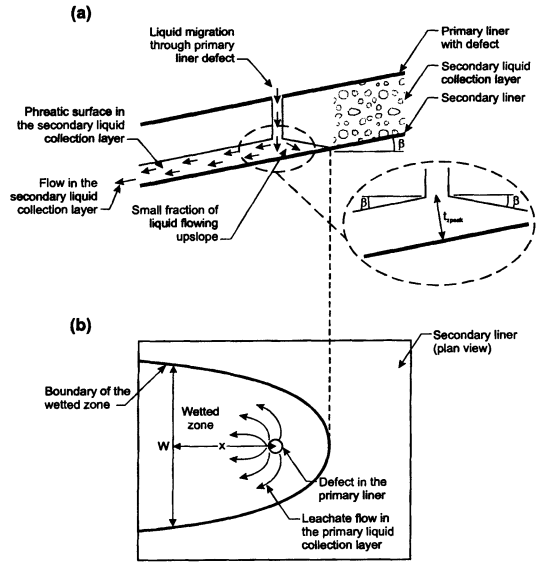


FIGURE 26.4. Liquid flow in the primary liquid collection layer, through a defect in the primary liner, and in the secondary liquid collection layer (leakage detection and collection layer), in the case of a double liner: (a) cross-section; and (b) plan view of the secondary liner (modified from Giroud *et al.* 1997a).

The thickness of liquid in the secondary liquid collection layer has a peak value at the location of each defect in the primary liner. Giroud *et al.* (1997a) showed that the following relationship exists between the rate of liquid migration through a primary liner defect, Q, the hydraulic conductivity of the secondary liquid collection layer, k_{LCL2}, and the thickness of liquid in the secondary liquid collection layer beneath the considered defect, t_{2peak} (Fig. 26.4a):

$$Q = k_{LCL2}\, t_{2peak}^2 \qquad (26.15)$$

where Q = liquid migration rate through the considered defect of the primary liner, k_{LCL2} = hydraulic conductivity of the secondary liquid collection layer material, and t_{2peak} = thickness of liquid in the secondary liquid collection layer at the location of the considered defect of the primary liner. Equation 26.15 can be used with any set of coherent units. The relevant basic SI units are: t_{2peak} (m), Q_{max} (m^3 s^{-1}) and k_{LCL2} (m s^{-1}).

It should be noted that Eq. 26.15 does not depend on the slope of the secondary liquid collection layer. The maximum thickness of liquid in the secondary liquid collection layer, t_{2max}, occurs at the location of the primary liner defect with the largest rate of liquid migration, Q_{max}. It is given by the following equation derived from Eq. 26.15:

$$t_{2max} = \left(\frac{Q_{max}}{k_{LCL2}}\right)^{1/2} \qquad (26.16)$$

where $t_{2\,max}$ = maximum thickness of liquid in the secondary liquid collection layer, Q_{max} = largest rate of liquid migration through a defect of the primary liner, and k_{LCL2} = hydraulic conductivity of the secondary liquid collection layer material. Equation 26.16 can be used with any set of coherent units. The relevant basic SI units are: $t_{2\,max}$ (m), Q_{max} (m^3 s^{-1}) and k_{LCL2} (m s^{-1}).

26.2.3.2 Design of a Secondary Liquid Collection Layer

The design of a secondary liquid collection layer consists of checking that the maximum thickness of liquid calculated as shown above, t_{2max}, is less than the thickness of the secondary liquid collection layer, t_{LCL2}:

$$t_{2max} \leq t_{LCL2}. \qquad (26.17)$$

Combining Eqs 26.16 and 26.17 gives the following condition for the thickness of the secondary liquid collection layer:

$$t_{LCL2} \geq \left(\frac{Q_{max}}{k_{LCL2}}\right)^{1/2}. \qquad (26.18)$$

Equation 26.18 can be used with any set of coherent units. The relevant basic SI units are: t_{LCL2} (m), Q_{max} (m^3 s^{-1}) and k_{LCL2} (m s^{-1}).

It should be noted that Eq. 26.18 is theoretically valid only if the geomembrane defects are sufficiently far apart that the wet zones produced by the different defects do not overlap. From a practical standpoint, however, Eq. 26.18 provides a good approximation of the required secondary liquid collection layer thickness in most typical cases. For the calculation of t_{LCL2} at the design stage, a factor of safety may be applied to Q_{max}. Finally, it should be noted that Eq. 26.18 is only valid for steady state flow conditions.

26.2.3.3 Average Head of Liquid on Top of the Secondary Liner for Liquid Migration Evaluation

To calculate the rate of liquid migration through the secondary liner, i.e. the rate of liquid migration into the ground in the case of a double liner, it is necessary to know the head of liquid on top of the secondary liner. The head of liquid on top of the secondary liner is zero outside the wetted zones, and varies from one point to another inside each wetted zone (see Fig. 26.4). The rigorous calculation of the hydraulic head for each wetted zone and the calculation of the resulting liquid migration rate are very tedious (Giroud *et al.* 1997a). From a practical standpoint, it is preferable to use an approximate approach that consists of calculating an average value of the liquid head over the entire secondary liner, $h_{2\,avg}$, i.e. as if the entire surface area of the secondary liner was uniformly wetted. This was done by Giroud *et al.* (1997a), who assumed that all the defects of the primary liner were identical and considered two scenarios of distribution of the defects in the primary liner. They obtained the following values for the average liquid head on the secondary liner:

$$h_{2avgworst} = \frac{FLQ}{k_{LCL2} \tan \beta} \qquad (26.19)$$

$$h_{2avgrand} = \frac{FLQ}{2k_{LCL2} \tan \beta} \qquad (26.20)$$

where $h_{2avgworst}$ = average head of liquid over the entire secondary liner, in the scenario where all the defects are assumed to be at the top of the primary liner slope ("worst" scenario); $h_{2avgrand}$ = average head of liquid over the entire secondary liner, in the scenario where the defects are assumed to be randomly distributed ("random" scenario); F = frequency of defects, i.e. number of defects per unit area; Q = rate of liquid migration through each one of the defects of the primary liner; and k_{LCL2} = hydraulic conductivity of the secondary liquid collection layer material. Equations 26.19 and 26.20 can be used with any set of coherent units. The relevant basic SI units are: h (m), F (m^{-2}), L (m), Q ($m^3\ s^{-1}$), k ($m\ s^{-1}$) and β (°).

26.3 *Design of Filters*

26.3.1 INTRODUCTION TO FILTRATION

26.3.1.1 Use of Filters in Liquid-Containment Structures

Filters are extensively used in liquid-containment structures. They are typically used between soil and a liquid collection layer, i.e. drainage layer, to protect the liquid collection layer against clogging by soil particles. The use of filters with liquid collection layers associated with liner systems has been discussed in Section 25.2.4.

26.3.1.2 Types of Filters

Two types of filters are used: granular filters (generally sand filters) and geotextile filters. Both types of filters perform the same functions as discussed in Section 26.3.1.3. The characteristics of granular filters are presented in Section 26.3.2.2 and the characteristics of geotextile filters are presented in Section 26.3.2.3.

26.3.1.3 Functions of Filters

The function of a filter in a liner system is to retain the soil while allowing the liquid to

flow as freely as possible. Therefore, the filter must have openings that are large enough to allow free flow of liquid, but small enough to prevent migration of soil particles.

It is important to note that the function of a filter is not to stop particles that are moving, but to prevent particles from moving. If some fine particles are moving toward the filter, and if the filter stops them, these particles will accumulate on or in the filter and will clog it. Situations where fine particles may be moving toward the filter include: (a) internally unstable soils where liquid flow can carry a significant amount of fine particles; and (b) cases where the filter is not placed in close contact with the soil.

It is important to recognize that there are situations, such as the case of internally unstable soils, where a filter is detrimental. Waste is often internally unstable, and filters placed between waste and leachate collection layers may be expected to experience clogging (see Section 26.3.1.5).

26.3.1.4 Importance of Intimate Contact Between Filter and Soil

For soil retention, it is important to have intimate contact between a filter and the adjacent soil (Giroud *et al.* 1977; Giroud 1989, 1996a), and examples of failures due to lack of intimate contact between a geotextile filter and the adjacent soil have been reported (Giroud 1999). Intimate contact between a filter and soil is usually achieved relatively easily with granular filters, but is sometimes difficult to achieve with geotextile filters. If the soil surface is not smooth, it is recommended to use flexible geotextiles that tend to conform to the shape of the soil; also, it is recommended to use rather small aggregate (e.g. aggregate with particles less than 20 mm) on the other side of the geotextile to exert a uniform pressure on the geotextile, thereby forcing the geotextile to conform to the shape of the soil. When a geotextile filter is attached to a geosynthetic drainage layer, the geocomposite thus formed is usually rather rigid and may not be able to conform to the shape of the soil, unless the soil surface is smooth. In such cases, it is necessary to place a layer of sand between the geotextile and the irregular soil surface to ensure intimate contact.

26.3.1.5 Clogging of Filters

Clogging is the decrease of permeability of the filter or the soil in the vicinity of the filter. Clogging results from the accumulation of fine soil particles, biological matter, and/or chemicals in or on the filter, or in the soil in the vicinity of the filter. Clogging by formation or precipitation of chemicals (chemical clogging), by growth of biological matter (biological clogging), or both (biochemical clogging) has been discussed in detail (Giroud 1996a; Rowe 1998a). Also, the development of biological clogging in municipal solid waste landfills is discussed in Sections 25.2.3 and 25.2.4.

26.3.2 RELEVANT CHARACTERISTICS OF SOILS AND FILTERS

26.3.2.1 Characteristics of Soils Relevant to Filter Design

The characteristics of the soil in contact with a filter that are relevant to filter design are the following: the soil hydraulic conductivity, k_s; the particle size distribution curve defined by d_m, the particle size such that m% of the soil particles by mass are smaller than d_m; and the coefficient of uniformity of the particle size distribution curve, C_u, defined by:

$$C_u = \frac{d_{60}}{d_{10}}. \tag{26.21}$$

The linear coefficient of uniformity, C'_u, used in Giroud's retention criterion (see Section 26.3.3.3) is obtained by tracing the tangent to the central portion of the particle size distribution curve of the soil (Fig. 26.5). This tangent intersects the 0% horizontal line for

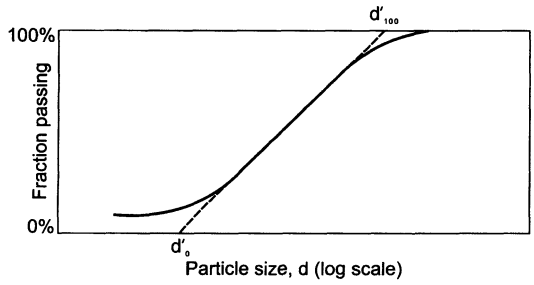


FIGURE 26.5. Determination of the linear coefficient of uniformity.

d'_0 and intersects the 100% horizontal line for d'_{100}. The linear coefficient of uniformity is then given by:

$$C'_u = \left(\frac{d'_{100}}{d'_0}\right)^{0.5}. \tag{26.22}$$

It should be noted that, if the particle size distribution curve of the soil is approximately linear, the coefficient of uniformity and the linear coefficient of uniformity are approximately equal.

26.3.2.2 Characteristics of Granular Filters

A granular filter is characterized by the following properties: average filtration opening size, O_F; porosity, n; particle size distribution curve defined by d_m, the particle size such that $m\%$ of the filter particles by mass are smaller than d_m; and filter hydraulic conductivity, k_{FGRA}. Measurement of the properties of granular materials is discussed in Sections 3.2 and 3.3. Kenney *et al.* (1985) have shown that the following approximate relationship exists:

$$O_F \approx 0.2d_{15}. \tag{26.23}$$

26.3.2.3 Characteristics of Geotextile Filters

A geotextile filter is characterized by the following properties: filtration opening size, O_F, which for practical purposes can be considered approximately equal to the apparent opening size, O_{95}; porosity, n_{FGT} (for nonwoven geotextiles) or relative open area, A_{FGT} (for woven geotextiles); thickness, t_{FGT}; mass per unit area, μ_{FGT}; fiber diameter, d_f; fiber material density, ρ_f; hydraulic conductivity, k_{FGT}; permittivity, ψ_{FGT}. Measurement of geotextile properties is discussed in Section 7.2.

The following basic relationships exist between these properties:

$$k_{FGT} = \psi_{FGT} t_{FGT} \tag{26.24}$$

$$n_{FGT} = 1 - \frac{\mu_{FGT}}{\rho t_{FGT}}. \tag{26.25}$$

In addition to the above rigorous relationships, the following approximate relationship has been developed by Giroud (1996a) for nonwoven geotextiles and is in close agreement with experimental data:

$$\frac{O_F}{d_f} \approx \frac{1}{(1 - n_{FGT})^{1/2}} - 1 + \frac{10 n_{FGT}}{(1 - n_{FGT}) t_{FGT}/d_f}. \tag{26.26}$$

Equation 26.26 makes it possible to evaluate the influence on the filtration opening size of a decrease in thickness and porosity due to compressive stresses. Equations 26.24–26.26 can be used with any set of coherent units. The relevant basic SI units are: O_F (m), t_{FGT} (m), μ_{FGT} (kg m^{-2}), d_f (m), ρ_f (kg m^{-3}), k_{FGT} (m s^{-1}), ψ_{FGT} (s^{-1}); n_{FGT} and A_{FGT} are dimensionless.

26.3.3 DESIGN OF FILTERS

26.3.3.1 Filter Criteria

A filter should satisfy three criteria:

- Permeability criterion: the filter must be permeable enough for free liquid flow.
- Retention criterion: the filter opening size must be small enough to retain soil particles.
- No-clogging criterion: the filter should include a large number of openings so the probability for clogging all of them is small.

These three criteria are discussed below for both granular filters and geotextile filters

26.3.3.2 Permeability Criterion

As shown by Giroud (1996a), a complete permeability criterion includes two requirements for free liquid flow. The first requirement is to prevent excessive pore pressure and can be written as follows (Giroud 1996a), regardless of the type of filter, granular or geotextile:

$$k_F > 10 k_S i_S \tag{26.27}$$

where k_F = filter hydraulic conductivity (k_{FGRA} for a granular filter or k_{FGT} for a geotextile filter), k_S = soil hydraulic conductivity, and i_S = hydraulic gradient in the soil in the vicinity of the filter. Guidance regarding i_S may be found in Table 26.1.

The second requirement is to prevent excessive reduction in flow rate and its expression depends on the type of filter (Giroud 1996a):

$$k_{FGT} > k_S \quad \text{for a geotextile filter} \tag{26.28a}$$

$$k_{FGRA} > 25 k_S \quad \text{for a granular filter} \tag{26.28b}$$

where k_{FGT} = hydraulic conductivity of a geotextile filter, k_{FGRA} = hydraulic conductivity of a granular filter, and k_S = soil hydraulic conductivity.

Based on the classical Hazen's equation and theoretical considerations (Giroud 1996a), the hydraulic conductivity of a granular soil is proportional to the square of the d_{10} or d_{15} of its particle size distribution curve. Therefore, Eq. 26.28b is equivalent to the classical expression of the permeability criterion for granular filters:

$$d_{15F} > 5 d_{15s} \tag{26.29}$$

where $d_{15F} = d_{15}$ of the granular filter; and $d_{15s} = d_{15}$ of the soil (see Sections 26.3.2.1 and 26.3.2.2 for the definition of d_{15}).

Based on the foregoing, the classical permeability criterion for granular filters satisfies the requirement to prevent excessive reduction in flow rate. However, as pointed out above, a complete permeability criterion includes a second requirement (expressed by Eq. 26.27): the requirement to prevent the development of excessive pore pressure. Therefore, it is recommended that, for granular filters, the requirement expressed by Eq. 26.27 be used in addition to the classical criterion expressed by Eq. 26.29.

TABLE 26.1. Typical hydraulic gradients (critical applications may require designing for higher gradients than those given; adapted from Giroud (1988, 1996a) and Luettich *et al.* (1992)

Application	Typical hydraulic gradient
Standard dewatering trench	1.0
Vertical wall drain	1.5
Pavement edge drain	1
Landfill leachate collection/detection removal system	1.5
Landfill leachate collection removal system	1.5
Landfill closure surface water collection removal system	1.5
Dam toe drains	2
Dam clay cores	3 to >10
Inland channel protection	1
Shoreline protection	10
Liquid impoundment with clay liners	>10

TABLE 26.2. Giroud's retention criterion for geotextile filters (adapted from Giroud 1982, 1988, 1994)

Density index of the soil (relative density), I_D		Linear coefficient of uniformity of the soil, C'_u	
		$1 \leq C'_u \leq 3$	$C'_u \geq 3$
Loose soil	$I_D < 35\%$	$O_{95} < (C'_u)^{0.3}\, d_{85}$	$O_{95} < \frac{9}{(C'_u)^{1.7}} d_{85}$
Medium dense soil	$35\% < I_D < 65\%$	$O_{95} < 1.5\,(C'_u)^{0.3}\, d_{85}$	$O_{95} < \frac{13.5}{(C'_u)^{1.7}} d_{85}$
Dense soil	$I_D > 65\%$	$O_{95} < 2\,(C'_u)^{0.3}\, d_{85}$	$O_{95} < \frac{18}{(C'_u)^{1.7}} d_{85}$

26.3.3.3 Retention Criterion

The detailed analysis of the mechanism by which geotextile filters retain soils published by Giroud (1982) led to the geotextile retention criterion presented in Table 26.2. An important characteristic of this criterion is the role played by the particle size distribution curve of the soil characterized by its linear coefficient of uniformity, C'_u, defined in Section 26.3.2.1. Since 1982, a number of studies have led to a variety of retention criteria for geotextile filters; consistent with the approach proposed by Giroud (1982), most of the proposed retention criteria for geotextile filters include as a parameter the coefficient of uniformity of the particle size distribution curve of the soil.

In the case of granular filters, the retention criterion has been expressed as follows ever since the original work on filters by Bertram and Terzaghi in the 1930s:

$$d_{15F} < 5d_{85S} \tag{26.30}$$

where $d_{15F} = d_{15}$ of the granular filter; and $d_{85S} = d_{85}$ of the soil (see Section 26.3.2.1 for the definition of d_{15} and d_{85}).

Combining Eqs 26.23 and 26.30 gives:

$$O_F < d_{85S}. \tag{26.31}$$

In other words, the meaning of Eq. 26.30, i.e. Terzaghi's classical retention criterion for granular filters, is that the filter opening size should be smaller than the d_{85} of the soil.

The rationale used by Giroud (1982) to develop his retention criterion for geotextile filters is not specific to geosynthetics and can be used for any type of filter. Therefore, Giroud's retention criterion for geotextile filters can be used for granular filters, with the value of the filtration opening size of a granular filter given by Eq. 26.23. It is then possible to compare Giroud's retention criterion applied to soils with Terzaghi's classical retention criterion for granular filters. Comparing Eq. 26.31 with Table 26.2 shows that Terzaghi's classical retention criterion for granular filters (represented by Eq. 26.31, which is equivalent to Eq. 26.30) is equivalent to, or more conservative than, Giroud's retention criterion if the coefficient of uniformity of the soil is less than five. In contrast, Terzaghi's classical retention criterion is less conservative than Giroud's retention criterion for soils having a coefficient of uniformity of the soil greater than five. This results from the fact that Terzaghi's retention criterion for granular filters does not take into account the coefficient of uniformity of the soil. As shown by Giroud (1996a), this potential problem can be prevented by using Terzaghi's classical retention criterion for granular filters only on the fraction of the soil particle size distribution curve related to particles smaller than

approximately 5 mm. (This is consistent with the practice often followed by design engineers, which consists of considering only the particles smaller than 4.75 mm when using Terzaghi's filter criteria.)

26.3.3.4 Non-clogging Criterion

To minimize the risk of clogging, the filter should have as many openings as possible. For a given filtration opening size, the number of filter openings is proportional to the porosity of the filter (granular or nonwoven geotextile) or the relative open area (woven geotextile). In the case of granular filters, the porosity is of the order of 0.3; as a result, it is not necessary to include in filter criteria a requirement for the porosity of granular filters. This is why a non-clogging criterion is never mentioned for granular filters. For lack of a better rationale, it has been suggested (Giroud 1985, 1989) that geotextile filters be specified to have a porosity (non-woven geotextiles) or a relative open area (woven geotextiles) greater than 0.3, i.e. the same value as for granular filters. This requirement is easily met by non-woven geotextiles since they typically have a porosity of 0.7–0.9. In contrast, many woven geotextiles do not meet this requirement. Although there are specifications that allow the use of woven geotextile filters with a relative open area as low as 0.04, the authors recommend that woven geotextile filters with a relative open area greater than 0.2 be specified. Woven geotextiles that meet this requirement are available.

26.4 Liquid Migration Through Liners

26.4.1 INTRODUCTION TO LIQUID MIGRATION THROUGH LINERS

26.4.1.1 Types of Liners

All of the liners considered herein are assumed to include a geomembrane. The liners considered are either geomembrane liners or composite liners. In the context of this chapter:

- a composite liner consists of a geomembrane component and a low permeability soil component, i.e. a compacted layer of low permeability soil, or the bentonite layer of a geosynthetic clay liner (GCL); and
- the low permeability soil component of the composite liner is located beneath the geomembrane.

26.4.1.2 The Low Permeability Soil Component of a Composite Liner

When the low permeability soil component of a composite liner is a compacted layer of low permeability soil, this soil generally includes clay and is often referred to as a compacted clay liner (CCL). In the case of a GCL, the low permeability component of the composite liner is a layer of bentonite (which is a variety of clay). There are two types of GCLs: GCLs where the layer of bentonite is encapsulated between two layers of geotextiles, and GCLs where the layer of bentonite is attached to a geomembrane. CCLs are discussed in detail in Sections 25.3.2 and 25.3.3, and GCLs are discussed in detail in Sections 25.3.4, 25.4.2, 25.5.1 and 25.7.2.

The thickness of a CCL is typically between 0.3 and 1.5 m, whereas the thickness of a hydrated GCL depends on the compressive stress applied during hydration and is typically between 5 and 10 mm, i.e. of the order of 100 times less than the thickness of a CCL. The hydraulic conductivity of both CCLs and GCLs depends on the nature of the material, the nature of the liquid, and the applied compressive stress; when the liquid is water or a leachate that does not affect the hydraulic conductivity of clay, including bentonite, the hydraulic conductivity of a CCL is typically between 1×10^{-10} and 1×10^{-9} m s^{-1}, whereas the hydraulic conductivity of a GCL

is typically between 5×10^{-12} and 5×10^{-11} m s^{-1}, i.e. of the order of ten–100 times less than the hydraulic conductivity of a CCL.

26.4.1.3 Geomembranes

Geomembrane material can be permeated by liquids as a result of diffusion and solution. The quantities of liquids that can migrate through geomembrane materials are very small; however, the rate of diffusion of certain organic compounds can be significant, as discussed by Rowe (1998a) and in Sections 25.3, 25.5.3 and 25.5.7. Therefore, permeation of certain chemical compounds (e.g. hydrocarbons and solvents) through geomembranes should be carefully evaluated if these compounds are likely to be present in the contained liquid (even in trace amounts).

Since an intact geomembrane allows negligible permeation of water and other polar liquids, most of the migration of these liquids (e.g. water or any aqueous solution such as leachate from municipal or hazardous solid waste landfills) through a geomembrane liner or a composite liner occurs through geomembrane defects. In this chapter, the only mechanism of liquid migration that is considered is advective flow through geomembrane defects. In other words, in this chapter, geomembranes are treated as impermeable layers with defects.

Studies presented by Giroud & Bonaparte (1989a) have shown that geomembrane liners installed with strict construction quality assurance could be considered having a frequency of one–two defects per 4000 m^2, with a diameter of 2 mm, i.e. a defect area of 3.14×10^{-6} m^2. On the other hand, electric leak detection surveys (Laine 1991) have shown that geomembrane liners installed with strict construction quality assurance have five or more defects per 4000 m^2, with a defect diameter less than 0.5 mm. The number of defects may even be greater after placement of a layer of soil on the installed geomembrane, and is certainly greater in the case of geomembranes installed without strict construction quality assurance. Therefore, it is recommended that design engineers consider different scenarios of defect size and frequency when they calculate the rate of liquid migration through geomembrane liners and composite liners. For the sake of conservatism, a defect area of 1 cm^2 is often considered in design calculations evaluating the rate of liquid migration through primary liners as a first step for the design of secondary liquid collection layers.

26.4.1.4 Liquid Migration Evaluation

The evaluation of liquid migration through liners is an essential aspect of the design of a liquid-containment structure. An early discussion of liquid migration through geomembrane liners was presented by Giroud (1984a). Investigations into liquid migration through composite liners have been performed by Faure (1984), Sherard (1985), Fukuoka (1986), Brown *et al.* (1987), and Jayawickrama *et al.* (1988). From these investigations, Giroud & Bonaparte (1989a, 1989b) developed a systematic semi-empirical methodology for evaluating the rate of liquid migration through composite liners. Most of the equations presented in this chapter were established using this methodology. A detailed theoretical analysis of liquid migration through composite liners has been presented by Rowe (1998a).

The equations presented in this chapter can be used to compare various types of liners from the viewpoint of advective flow. Systematic comparisons presented by Giroud *et al.* (1994b, 1998b) show that the rate of liquid migration through composite liners is typically two to four orders-of-magnitude less than liquid migration through geomembrane liners (with the geomembrane having the same number and size of defects in both cases). Clearly, composite liners should be preferred to geomembrane liners, i.e. geomembranes placed directly on a permeable material. However, in liquid impoundments,

the risk of geomembrane uplift by liquids accumulating between the geomembrane and clay component of a composite liner should be addressed (see Section 26.5.1.5). Comparisons also show that the rate of liquid migration through a composite liner constructed with a given soil having a hydraulic conductivity less than 1×10^{-6} m s^{-1} is approximately three orders-of-magnitude less than through the soil itself. In other words, placing a geomembrane on a soil decreases the rate of liquid migration by a factor of 1000.

The equations presented in this chapter can also be used to compare various types of liner systems from the viewpoint of advective flow. An example of such comparison is presented by Giroud *et al.* (1997d). The same comparison was presented by Lake & Rowe (1999) from the viewpoint of diffusion of organic compounds, and the results of the comparison are different from the results of the comparison based on advective flow. The flows calculated using the equations presented in this chapter can be used as input to contaminant transport models (e.g. Rowe & Booker 1997a), as discussed in Section 25.7.

26.4.2 LIQUID MIGRATION THROUGH COMPOSITE LINERS

26.4.2.1 Ideal Case: Perfect Contact

In the ideal situation where the contact between the geomembrane component and the soil component of a composite liner is perfect, the rate of liquid migration through the composite liner, in the case where the geomembrane defect is circular, is given by the equation (Forchheimer 1930):

$$Q = 4rhk_{UM} \tag{26.32}$$

where Q = rate of liquid migration through the geomembrane defect; r = radius of the geomembrane defect; h = head of liquid on top of the liner; and k_{UM} = hydraulic conductivity of the medium underlying the geomembrane, i.e. the soil component of the composite liner. Equation 26.32 can be used with any set of coherent units. The relevant basic SI units are: Q (m^3 s^{-1}), r (m), h (m) and k_{UM} (m s^{-1}).

26.4.2.2 Description of Liquid Migration Through a Composite Liner

The contact between a geomembrane and the underlying soil is never perfect. There is a small space between the geomembrane and the underlying soil in which some flow can take place. The mechanism of liquid flow through a composite liner is described as follows by Giroud & Bonaparte (1989b): if there is a defect in the geomembrane component of a composite liner, the liquid passes first through the geomembrane defect, then it flows laterally some distance between the geomembrane and the low permeability soil; finally, it infiltrates into and through the low permeability soil layer, which is the second component of the composite liner. Flow in the space between the geomembrane and the low permeability soil is called interface flow, and the area covered by the interface flow is called the wetted area.

26.4.2.3 Quality of Contact Between the Two Components of a Composite Liner

The quality of the contact between the two components of a composite liner, i.e. the geomembrane and the low permeability soil, is one of the key factors governing the rate of flow through the composite liner, because it governs the radius of the wetted area. Good and poor contact conditions have been defined by Bonaparte *et al.* (1989) and Giroud (1997) as:

- good contact conditions correspond to a geomembrane installed, with as few wrinkles as possible, on top of a low permeability soil layer that has been adequately compacted and has a smooth surface; and
- poor contact conditions correspond to a geomembrane that has been installed with a certain number of wrinkles, and/or placed on a low permeability soil that has not been well-compacted and does not appear smooth.

Furthermore, as stated by Giroud (1997):

- for good contact conditions, it is assumed that there is sufficient compressive stress to maintain the geomembrane in contact with the low permeability soil layer; and
- in the case of a GCL, good contact conditions may be assumed because GCLs are usually installed flat, and because the bentonite slurry that may exude from a hydrated GCL contributes to establishing a close contact between the geomembrane and the GCL, provided sufficient compressive stress is applied.

Rowe (1998a) has developed a methodology to evaluate the rate of liquid migration through a defect located in a wrinkle of the geomembrane. He has shown that the rate of liquid migration through a defect located in a wrinkle is significantly greater than the rate of liquid migration through a defect located in an area where the geomembrane is in contact with the underlying low permeability material. This finding confirms the requirement for "good contact" given above. This is especially important given that Soong and Koerner (1998) have shown that geomembrane wrinkles do not significantly flatten once buried by placement of overlying soil layers (i.e. at the location of wrinkles, a gap remains between the geomembrane and the underlying surface). Rowe's equations for calculating leakage through a defect in a wrinkle are given in Section 26.4.2.8.

In liquid migration rate equations, contact quality is represented by a dimensionless contact quality factor, C_q. In the case of a circular defect, a square defect, or a defect with similar dimensions in all directions (sometimes referred to as a quasi-circular defect), the contact quality factor is C_{qo} with:

$$C_{qogood} \leq C_{qo} \leq C_{qopoor} \qquad (26.33)$$

where C_{qogood} = value of C_{qo} in the case of good contact conditions, and C_{qopoor} = value of C_{qo} in the case of poor contact conditions. (The good and poor contact conditions were defined above.) The following values were established semi-empirically (Giroud *et al.* 1989).

$$C_{qogood} = 0.21 \qquad (26.34a)$$

$$C_{qopoor} = 1.15. \qquad (26.34b)$$

In the case of a defect of great length with respect to its width, the contact quality factor is $C_{q\infty}$, with:

$$C_{q\infty good} \leq C_{q\infty} \leq C_{q\infty poor} \qquad (26.35)$$

where $C_{q\infty good}$ = value of $C_{q\infty}$ in the case of good contact conditions, and $C_{q\infty\,poor}$ = value of $C_{q\infty}$ in the case of poor contact conditions. The following values were established semi-empirically (Giroud *et al.* 1992a):

$$C_{q\infty good} = 0.52 \qquad (26.36a)$$

$$C_{q\infty poor} = 1.22. \qquad (26.36b)$$

26.4.2.4 Parameters and Units Used in Equations for Liquid Migration Rate Evaluation

The following notations are used in the equations presented in Sections 26.4.2.5 and 26.4.2.6: Q = rate of liquid migration through a geomembrane defect; Q^* = liquid migration rate per unit length of geomembrane defect in the case where the geomembrane defect has an infinite length; h = hydraulic head on top of the liner; t_{UM} = thickness of the medium underlying the geomembrane, i.e. the low permeability soil component of the composite liner; B = length of a rectangular defect; b = side length of a square defect, width of a rectangular defect, or width of an infinitely long defect; d = diameter of a circular defect; a = defect area; k_{UM} = hydraulic conductivity of the medium underlying the geomembrane, i.e. the low permeability soil component of the composite liner; C_{qo} and $C_{q\infty}$ = contact

quality factors, i.e. dimensionless factors that characterizes the quality of contact between the geomembrane and the underlying low permeability soil. Numerical values of C_{qo} and $C_{q\infty}$ are given in Section 26.4.2.3.

It is important to note that the equations for liquid migration rate presented in Sections 26.4.2.5 and 26.4.2.6 are semi-empirical and can only be used with the following SI units: Q ($m^3\ s^{-1}$), Q^* ($m^2\ s^{-1}$), h (m), t_s (m), B (m), b (m), d (m), a (m^2) and k_{UM} ($m\ s^{-1}$). C_{qo} and $C_{q\infty}$ are dimensionless.

26.4.2.5 General Equations for Liquid Migration Rate

The following equations were developed by Giroud (1997), based on preceding work by Giroud & Bonaparte (1989b) and Giroud *et al.* (1989, 1992a):

- Circular or quasi-circular defect:

$$Q = C_{qo}[1 + 0.1(h/t_{UM})^{0.95}]a^{0.1}h^{0.9}k_{UM}^{0.74} \quad (26.37)$$

hence, for a circular defect:

$$Q = 0.976C_{qo}[1 + 0.1(h/t_{UM})^{0.95}]d^{0.2}h^{0.9}k_{UM}^{0.74}. \quad (26.38)$$

- Square defect:

$$Q = C_{qo}[1 + 0.1(h/t_{UM})^{0.95}]b^{0.2}h^{0.9}k_{UM}^{0.74}. \quad (26.39)$$

- Rectangular defect:

$$Q = C_{qo}[1 + 0.1(h/t_{UM})^{0.95}]b^{0.2}h^{0.9}k_{UM}^{0.74} + C_{q\infty}[1 + 0.2(h/t_{UM})^{0.95}] \times (B - b)b^{0.1}h^{0.45}k_{UM}^{0.87}. \quad (26.40)$$

- Infinitely long defect ($B = \infty$ in Eq. 26.40):

$$Q^* = C_{q\infty}[1 + 0.2(h/t_{UM})^{0.95}]b^{0.1}h^{0.45}k_{UM}^{0.87}. \quad (26.41)$$

Equations 26.37–26.41 must be used with the units defined in Section 26.4.2.4. The parameters in Eqs 26.37–26.41 are defined in Section 26.4.2.4. Values of C_{qo} are given by Eq. 26.34, and values of $C_{q\infty}$ by Eq. 26.36.

26.4.2.6 Equations for Liquid Migration Rate for the Case of Small Hydraulic Heads

In the above equations, the analytical expression of the average hydraulic gradient in the low permeability soil component of the composite liner is given by:

$$i_{avgo} = 1 + 0.1(h/t_{UM})^{0.95}$$

for a defect of finite size (26.42a)

$$i_{avg\infty} = 1 + 0.2(h/t_{UM})^{0.95}$$

for an infinitely long defect. (26.42b)

Equation 26.42a and b shows that the hydraulic gradient is approximately equal to one if the head of liquid above the liner is less than the thickness of the low permeability soil component of the composite liner (a situation that typically exists in landfills where the leachate head above the liner is small, e.g. 0.3 m or less, and the soil component of the composite liner is a CCL with a thickness of 0.3 m or more). Hence, the following equations can be derived from Eqs 26.37–26.41 (but, in reality, were established first, hence the references given hereafter):

- Circular or quasi-circular defect (Giroud *et al.* 1989):

$$Q = C_{qo}a^{0.1}h^{0.9}k_{UM}^{0.74}. \quad (26.43)$$

hence, for a circular defect:

$$Q = 0.976C_{qo}d^{0.2}h^{0.9}k_{UM}^{0.74}. \quad (26.44)$$

- Square defect [1875]

$$Q = C_{qo}b^{0.2}h^{0.9}k_{UM}^{0.74}. \quad (26.45)$$

- Rectangular defect [1875]:

$$Q = C_{qo}b^{0.2}h^{0.9}k_{UM}^{0.74} + C_{q\infty}(B - b)b^{0.1}h^{0.45}k_{UM}^{0.87}. \quad (26.46)$$

- Infinitely long defect (B = ∞ in Eq. 26.46) (Giroud *et al.* 1992):

$$Q^* = C_{q\infty}b^{0.1}h^{0.45}k_{UM}^{0.87}. \quad (26.47)$$

Equations 26.43–26.47 must be used with the units defined in Section 26.4.2.4. The parameters used in Eqs 26.43–26.47 are defined in Section 26.4.2.4. Values of C_{qo} are given by Eq. 26.34 and values of $C_{q\infty}$ by Eq. 26.36.

26.4.2.7 Limitations of the Equations for Liquid Migration Through Composite Liners

The limits of validity of the equations presented in Sections 26.4.2.5 and 26.4.2.6 result from considerations such as: the experimental data supporting the work that led to these equations, restrictions to flow imposed by surface tension and the range of applicability of Bernoulli's equation for free flow through an orifice. These limits can be summarized as folows (Giroud *et al.* 1997c):

- If the defect is circular, the defect diameter should be no less than 0.5 mm and not greater than 25 mm. In the case of defects that are not circular, it is proposed to use these limitations for the defect width.
- The liquid head on top of the geomembrane should be equal to or less than 3 m.
- The hydraulic conductivity of the low permeability soil underlying the geomembrane should be equal to or less than a certain value $k_{UM\,max}$. To ensure a smooth transition between liquid migration rates calculated using Eq. 26.37–26.47 and those calculated using Bernoulli's equation (see Section 26.4.3.1.1), Giroud *et al.* (1997c) propose the following value for $k_{UM\,max}$ in the case where the geomembrane defect is circular:

$$k_{UM\,max} = \left[0.3891 d^{1.8} \Big/ \left\{ C_{qo} \left[1 + 0.1 \left(\frac{h}{t_{UM}} \right)^{0.95} \right] h^{0.4} \right\} \right]^{1/0.74} . \quad (26.48)$$

Equation 26.48 must be used with the units defined in Section 26.4.2.4. Values of $k_{UM\,max}$ calculated using Eq. 26.48 with $C_{qo} = 0.21$ (i.e. values of C_{qo} for good contact conditions, as indicated by Eq. 26.34) and $t_{UM} = 0.6$ m are given in Table 26.3.

26.4.2.8 Leakage Through a Wrinkle

Rowe (1998a) developed the following equation for calculating the flow through a defect in a wrinkle in the geomembrane component of a composite liner:

$$Q = 2L(1 + h/t_{UM})[k_{UM} b + (k_{UM} t_{UM} \theta)^{1/2}] \quad (26.49)$$

where Q = rate of liquid migration through the defect(s) in the wrinkle, L = length of the wrinkle, b = half-width of the wrinkle ($L \gg b$), h = head on top of the liner, t_{UM} = thickness of the low permeability soil component of the composite liner, k_{UM} = hydraulic conductivity of the low permeability soil component of the composite liner, and θ = hydraulic transmissivity of the interface between the geomembrane and soil components of the composite liner away from the wrinkle.

Equation 26.49 is based on the assumption that the rate of liquid migration through the geomembrane defect(s) is sufficient to fill the volume between the geomembrane wrinkle and the top of the low permeability soil component of the composite liner, and that the pressure head at the bottom of the low permeability soil component of the composite liner is zero. More general cases can also be considered, as discussed by Rowe (1998a). Equation 26.49 can be used with any set of coherent units. The relevant basic SI units are: Q ($m^3\ s^{-1}$), L (m), b (m), h (m), t_{UM} (m), k_{UM} ($m\ s^{-1}$), θ ($m^2\ s^{-1}$).

As also indicated by Rowe (1998a), Eq. 26.49 gives an upper limit to the liquid migration rate. A second limit recognizes that the flow may be controlled by: (a) Bernoulli's equation if the hydraulic conductivity of the overlying layer is high enough (see Section 26.4.3.1); and (b) by the capacity of the fluid to drain to the hole. The latter case was examined by Giroud *et al.* (1997b) and can be calculated as discussed in Section 26.4.3.2.

TABLE 26.3. Maximum value, k_{UMmax} (m s^{-1}), of the hydraulic conductivity of the medium underlying the geomembrane for Eqs 26.37–26.47 to be valid with an acceptable approximation in the case where C_{qo} = 0.21 (good contact) and t_{UM} = 0.6 m (adapted from Giroud *et al.* 1997c)

Liquid head on top of the geomembrane, h (m)	Geomembrane defect diameter, d (mm)[a]						
	0.5	1	2	3	5	10	11.284
0.01	2.6×10^{-7}	1.4×10^{-6}	7.5×10^{-6}	2.0×10^{-5}	7.0×10^{-5}	3.8×10^{-4}	5.1×10^{-4}
0.03	1.4×10^{-7}	7.7×10^{-7}	4.1×10^{-6}	1.1×10^{-5}	3.8×10^{-5}	2.1×10^{-4}	2.8×10^{-4}
0.1	7.3×10^{-8}	3.9×10^{-7}	2.1×10^{-6}	5.7×10^{-6}	2.0×10^{-5}	1.1×10^{-4}	1.4×10^{-4}
0.3	3.8×10^{-8}	2.1×10^{-7}	1.1×10^{-6}	3.0×10^{-6}	1.0×10^{-5}	5.6×10^{-5}	7.5×10^{-5}
1	1.8×10^{-8}	9.5×10^{-8}	5.1×10^{-7}	1.4×10^{-6}	4.7×10^{-6}	2.6×10^{-5}	3.4×10^{-5}
3	7.1×10^{-9}	3.8×10^{-8}	2.1×10^{-7}	5.6×10^{-7}	1.9×10^{-6}	1.0×10^{-5}	1.4×10^{-5}

[a] For d = 11.284 mm, a = 1 cm^2.

TABLE 26.4. Minimum value, $k_{UM\,min}$ (m s^{-1}), of the hydraulic conductivity of the medium underlying the geomembrane for Eq. 26.51 (i.e. Bernoulli's equation for free flow through an orifice) to be valid with an acceptable approximation (adapted from Giroud *et al.* 1997c)

Geomembrane defect diameter, d (mm)[a]	0.5	1	2	3	5	10	11.284
$k_{UM\,min}$ (m s^{-1})	2.5×10^{-4}	1.0×10^{-3}	4.0×10^{-3}	9.0×10^{-3}	2.5×10^{-2}	1.0×10^{-1}	1.3×10^{-1}

[a] For d = 11.284 mm, a = 1 cm^2.

For a geomembrane on a CCL, Rowe (1998a) indicated that the hydraulic transmissivity, θ, can be estimated as follows for good contact away from the wrinkle:

$$\log_{10}\theta = 0.07 + 1.036(\log_{10} k_{UM}) + 0.018(\log_{10} k_{UM})^2 \quad (26.50)$$

where Eq. 26.50 is semi-empirical and must be used with units θ ($m^2\ s^{-1}$), k_{UM} ($m\ s^{-1}$). For GCLs, θ may be measured in laboratory tests or estimated from published values, see (Rowe 1998a) for a detailed discussion.

26.4.3 GEOMEMBRANE LINER

26.4.3.1 Geomembrane Overlain and Underlain by Highly Permeable Media

Presentation of the Equation. In the case of a geomembrane liner underlain and overlain by highly permeable media, the rate of liquid migration through a defect in the geomembrane is calculated using the classical Bernoulli's equation for free flow through an orifice, as proposed by Giroud (1984a):

$$Q = 0.6a(2gh)^{1/2} = 0.15\pi d^2(2gh)^{1/2} \quad (26.51)$$

where a = defect area, d = defect diameter in the case of a circular defect, and g = acceleration due to gravity. Equation 26.51 can be used with any set of coherent units. The relevant basic SI units are: a (m^2), d (m), g ($m\ s^{-2}$), h (m).

Limit of Applicability of Bernoulli's Equation. As indicated above, Bernoulli's equation is applicable to geomembranes underlain and overlain by highly permeable media. As shown by Giroud *et al.* (1997c), Bernoulli's equation (Eq. 26.51) provides an acceptable value of the liquid migration rate for values of the hydraulic conductivity of the medium underlying the geomembrane that are greater than $k_{UM\,min}$ given by:

$$k_{UM\,min} = 10^3 d^2 \quad (26.52)$$

with $k_{UM\,min}$ ($m\ s^{-1}$) and d(m). Values of $k_{UM\,min}$ calculated using Eq. 26.52 are given in Table 26.4.

Giroud *et al.* (1997b) have shown that Bernoulli's equation gives the rate of liquid migration through a geomembrane defect with an error of less than 5% if the hydraulic conductivity of the medium overlying the geomembrane, k_{OM}, is greater than:

$$k_{OM\,min} = \frac{30d^2}{h^{3/2}} \quad (26.53)$$

where the following units must be used: d(m), h(m) and $k_{OM\,min}$ ($m\ s^{-1}$).

26.4.3.2 Geomembrane Overlain by a Permeable Medium and Underlain by a Highly Permeable Medium

Presentation of the Equation. When a geomembrane is overlain and underlain by highly permeable media, the rate of liquid migration through a geomembrane defect is given by the classical Bernoulli's equation for free flow through an orifice (Eq. 26.51). Bernoulli's equation sometimes grossly overestimates the rate of liquid migration through a geomembrane defect if the geomembrane is overlain by a medium that is not highly permeable (even though the geomembrane is underlain by a highly permeable medium). In this case, the flow of liquid toward the geomembrane defect is hindered and, as a result, the rate of liquid migration is less than in the ideal case of a geomembrane overlain and underlain by infinitely permeable media. Taking into account the fact that liquid does not flow freely toward the geomembrane defect, Giroud *et al.* (1997b) developed the following equation:

$$h = \left\{ \frac{aq_i}{2k_{OM}\pi} + \frac{Q}{2k_{OM}\pi}\left[\ln\left(\frac{Q}{aq_i}\right) - 1\right] + \frac{1}{4g^2}\left(\frac{Q}{0.6a}\right)^4 \right\}^{1/2} \quad (26.54)$$

where q_i = rate of liquid supply on top of the medium overlying the geomembrane, and k_{OM} = hydraulic conductivity of the medium overlying the geomembrane. Equation 26.54 can be used with any set of coherent units. The

relevant basic SI units are: h (m), a (m^2), q_i (m s^{-1}), k_{OM} (m s^{-1}), Q (m^3 s^{-1}) and g (m s^{-2}).

It should be noted that, if k_{OM} is infinite, Eq. 26.54 becomes identical to Equation 26.51, i.e. Bernoulli's equation for free flow through an orifice.

Use of the Equation. Equation 26.54 cannot be solved for Q. Therefore, an iterative procedure is necessary to calculate Q when h, a, k_{OM} and q_i are known. Alternatively, graphical solutions can be used. An example is shown in Fig. 26.6, and a series of similar graphical solutions is provided by Giroud *et al.* (1997b). Figure 26.6 shows that, in general, Bernoulli's equation overestimates the liquid migration rate. However, Fig. 26.6 also shows that, for values of the hydraulic conductivity of the medium overlying the geomembrane that meet the condition expressed by Eq. 26.53, Bernoulli's equation provides an excellent approximation of the liquid migration rate.

26.4.3.3 Geomembrane Overlain by a Permeable Medium and Underlain by a Semi-permeable Medium

Definition of the Case Considered. The case of a geomembrane overlain by a permeable medium and underlain by a semi-permeable medium is intermediary between the case of a geomembrane overlain and underlain by infinitely permeable media (Section 26.4.3.1) and the case of a composite liner (Section 26.4.2)

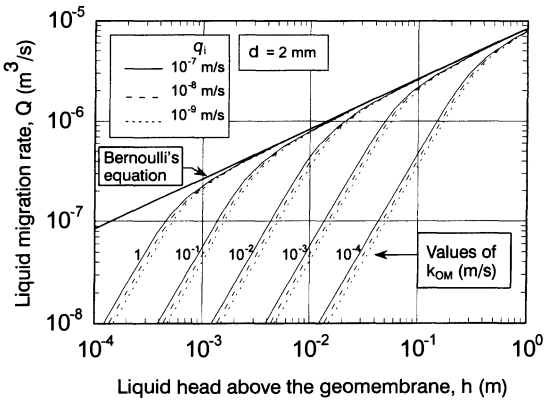


FIGURE 26.6. Graphical solution of Eq. 26.54 for a geomembrane defect having a diameter, d, of 2 mm (after Giroud *et al.* 1997b, © Geosynthetics International, reproduced with permission): q_i = (—) 10^{-7} m s^{-1}, (— — —) 10^{-8} m s^{-1}, (····) 10^{-9} m s^{-1}.

In the context of the liquid migration rate equations discussed herein, a semi-permeable soil is a soil that is not sufficiently permeable to allow the use of Eq. 26.51, i.e. Bernoulli's equation for free flow through an orifice, and too permeable to allow the use of Eqs 26.37–26.47 for composite liners. In other words, the equation presented in this section is valid only for soil hydraulic conductivities of the medium underlying the geomembrane between two limit values, $k_{UM\,max}$ and $k_{UM\,min}$, defined by Eqs 26.48 and 26.52, respectively.

Presentation of the Equation. When a geomembrane is overlain and underlain by infinitely permeable media, the rate of liquid migration through a geomembrane defect is given by Bernoulli's equation for free flow through an orifice (Eq. 26.51 given in Section 26.4.3.1). When a geomembrane is underlain by a low permeability medium, i.e. when the geomembrane and the underlying medium form a composite liner, the rate of liquid migration through a geomembrane defect is given by Giroud's equations (Eqs 26.37–26.47). To evaluate the rate of liquid migration through defects in geomembranes underlain by a semi-permeable medium, i.e. when the hydraulic conductivity, k_{UM}, of the medium underlying the geomembrane is between $k_{UM\,max}$ and $k_{UM\,min}$, Giroud *et al.* (1997c) have developed the following equation:

$$\log Q = 0.3195 + 2\log d + 0.5\log h - 0.74\left(\frac{5 + 2\log d - \log k_{OM}}{m}\right)^m \quad (26.55)$$

where k_{OM} = hydraulic conductivity of the semi-permeable soil, and m = dimensionless exponent given by:

$$m = 4.6380 - 0.4324 \log d + 0.5405 \log h + 1.3514 \log \left[1 + 0.1 \left(\frac{h}{t_{UM}} \right)^{0.95} \right] \quad (26.56)$$

where t_{UM} = the thickness of the semi-permeable soil. Equations 26.55 and 26.56 were used with $C_{qo} = 0.21$, i.e. assuming good contact between the geomembrane and the underlying medium. Equations 26.53 and 26.54 can only be used with the following units: Q ($m^3\ s^{-1}$), d (m), k_{OM} (m s^{-1}), h (m), t_{UM} (m). Also Equation 26.53 is valid only for hydraulic heads equal to or less than 3 m.

Use of the Equation. Figure 26.7 shows a series of curves that represent the rate of liquid migration through a given geomembrane defect (diameter, d = 2 mm) as a function of the hydraulic conductivity of the medium underlying the geomembrane for various liquid heads. Each curve in Fig. 26.7 comprises three portions: the left-hand portion (straight line) represents Eq. 26.38; the right-hand portion (plateau) represents Eq. 26.51; and the central portion (curve) was obtained using Eq. 26.55. Both Eqs 26.38 and 26.51 were used with $C_{qo} = 0.21$ (Eq. 26.34a), i.e. assuming good contact between the geomembrane and the underlying medium. The limit value of the hydraulic conductivity between the left-hand portion and the central portion is k_{UMmax}, given by Eq. 26.48 and Table 26.3. The limit value of the hydraulic conductivity between the central portion and the right-hand portion is k_{UMmin}, given by Eq. 26.52 and Table 26.4. Similar graphs for other values of d are given by Giroud *et al.* (1997c).

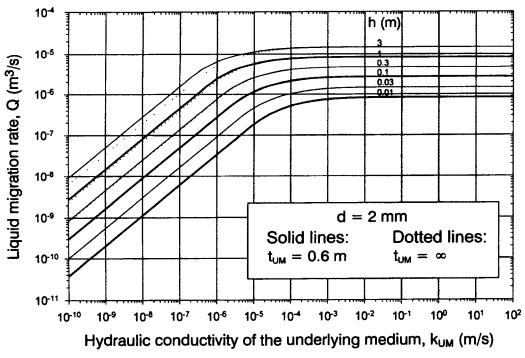


FIGURE 26.7. Rate of liquid migration through a defect having a diameter, d, of 2 mm in a geomembrane underlain by a medium with a hydraulic conductivity, k_{UM}, and overlain by a medium that is significantly more permeable than the underlying medium, for various values of the head of liquid on top of the geomembrane, h (after Giroud *et al.* 1997c, © Geosynthetics International, reproduced with permission): (—) thickness of the medium of hydraulic conductivity, k_{UM}, underlying the geomembrane is t_{UM} = 0.6 m; (····) thickness of the underlying medium is infinite.

26.5 *Stability and Deformations of Linear Systems*

26.5.1 INTRODUCTION

26.5.1.1 Types of Mechanical Actions Applied on Liner Systems

Liner systems are subjected to a variety of mechanical actions that may impact their integrity, such as: (a) instability of soil or waste in contact with the liner system; (b) deformation of soil in contact with the liner system; (c) differential settlement between the soil supporting the liner system and a structure to which the liner system is connected; (d) liner system uplift by fluids; and (e) concentrated stresses applied on the geosynthetic component of a liner system by the materials in contact. These five types of mechanical actions are discussed below.

26.5.1.2 Instability of Soil or Waste in Contact with a Liner System

Instability of soil or waste in contact with a liner system can cause extensive damage to the liner system, in particular to the geosynthetics. Numerous examples of such problems are provided by Rowe (1998a, 1998b) and Giroud (1999). When large masses of soil or waste are involved, general slope stability

analysis methods apply (see Chapter 14). Specific slope stability analysis methods were developed for liner systems on slopes. Details can be found in Giroud & Beech (1989), Koerner & Hwu (1991), Giroud *et al.* (1995a, 1995d), and Koerner & Soong (1998), and in Sections 27.6 (static stability) and 27.7 (seismic stability).

26.5.1.3 Deformation of Soil in Contact with the Liner System

When the medium (e.g. soil, waste) supporting a liner system settles, the liner system may follow the shape of the depressed area or may bridge the depressed area or a portion of it. As a result, the liner system undergoes tensile stresses and strains. This topic is discussed in Section 26.5.2. (Settlement of landfill cover systems is discussed in Section 27.8.4.)

26.5.1.4 Differential Settlement between the Soil Supporting the Liner System and a Structure to which the Liner System is Connected

If differential settlement takes place between the soil supporting the liner system and a structure to which the liner system is connected, the liner system undergoes tensile stresses and strains. This topic is discussed in Section 26.5.3.

26.5.1.5 Uplift of Liner System by Fluids

Liner systems are relatively light and they may be uplifted by pressure applied from underneath by liquids and gas. These situations are addressed by using a drainage system (underdrain) for liquids and/or gas under the liner system. In the case of landfills, a properly designed and operated gas collection system, which is primarily intended to collect gas for energy recovery, prevents the development of high gas pressure in the landfill, thereby minimizing the risk of cover system uplift.

Exposed geomembranes are particularly susceptible to uplift by fluids. The terminology "exposed geomembrane" refers to geomembranes that are not covered with a layer of soil or other material. Exposed geomembranes are used, for example, as liners in many liquid impoundments and as covers in some landfills. The risk of uplifting is high in the case of an exposed geomembrane that is a component of a composite liner for a liquid impoundment. If there is a defect in the geomembrane, which should always be assumed at the design stage, liquid accumulates between the geomembrane and the underlying low permeability soil when the reservoir is full and uplifts the geomembrane in case of drawdown of the reservoir. Therefore, composite liners in liquid impoundments should always be covered with a layer of heavy material, both to minimize the risk of problems due to geomembrane uplift and to protect the geomembrane.

The uplift of exposed geomembrane liners due to suction generated by the wind is an important design consideration. This topic is discussed in Section 26.5.4.

26.5.1.6 Concentrated Stresses Applied on the Geosynthetic Component of a Liner System by the Materials in Contact

Geosynthetics, in particular geomembranes, can be damaged as a result of mechanical actions by materials in contact. For example, the influence of a scratch at the surface of a high density polyethylene geomembrane on its tensile behavior has been quantified in Giroud (1984b, 1994) and Giroud *et al.* (1994a). Even when geomembranes are not damaged by materials in contact, they may be subjected to high concentrated stresses and strains as a result of the size and shape of the materials in contact and the applied stresses. These high concentrated stresses and strains may be detrimental to the long-term performance of the geomembrane.

Geomembranes are generally protected using geotextiles. Based on the foregoing discussion, the geotextile should not only prevent damage to the geomembrane but also minimize the concentrated stresses and strains in-

duced in the geomembrane. These two aspects of geomembrane protection are discussed by Rowe (1998a). The following references are cited by Rowe (1998a) for discussions of geomembrane damage prevention: Giroud *et al.* (1995b); Narejo (1995a, 1995b, 1996); Bishop (1996); Reddy *et al.* (1996); Wilson-Fahmy *et al.* (1996); Narejo *et al.* (1996); Koerner *et al.* (1996); and Badu-Tweneboah *et al.* (1998). The following references are cited by Rowe (1998a) for discussions of concentrated stresses and strains in geomembranes resulting from materials in contact: Brummermann *et al.* (1994); Saathoff & Sehrbrock (1994); Bishop (1996); Seeger & Müler (1996); and Giroud (1996b). Recent publications on the subject include: Badu-Tweneboah *et al.* (1997); Thiel (1997); Reddy *et al.* (1997); Zanzinger & Gartung (1998); and Tognon *et al.* (1999).

26.5.2 GEOSYNTHETIC STRAIN DUE TO SETTLEMENT OF THE SUPPORTING MEDIUM

26.5.2.1 Relationships between Geosynthetic Deflection and Strain

If a geosynthetic is assumed to have a circular shape when it deflects on an infinitely long depression (trough) or a circular depression of the supporting medium (Fig. 26.8), the following relationship exists between the geosynthetic deflection and the average strain in the geosynthetic (Giroud 1981):

$$\varepsilon = 2\Omega \sin^{-1} \frac{1}{2\Omega} - 1 \qquad (26.57a)$$

where:

$$\Omega = (1/4)\{(2y/b) + [b/(2y)]\}$$

for an infinitely long depression (26.57b)

$$\Omega = (1/4)\{(2y/d) + [d/(2y)]\}$$

for a circular depression (26.57c)

where ε = average strain in the geosynthetic, y = geosynthetic deflection, b = width of infinite long depression, d = diameter of circular depression, and Ω = dimensionless factor. It should be noted that Eq. 26.57 is valid only for $y/b < 0.5$, i.e. $\varepsilon < 0.57$ (57%). Numerical values of ε and Ω as a function of y/b or y/d are given in Table 26.5. Equation 26.57b and c can be used with any set of coherent units. The relevant basic SI units are: b (m), d (m) and y (m); Ω is dimensionless.

Giroud (1995) has shown that, for a geosynthetic strain less than 30%, i.e. for a relative deflection (y/b or y/d) less than 0.35, a good approximation of the geosynthetic strain is given by:

$$\varepsilon \approx \frac{8}{3}\left(\frac{y}{b}\right)^2$$ for an infinitely long depression (26.58a)

$$\varepsilon \approx \frac{8}{3}\left(\frac{y}{d}\right)^2$$ for a circular depression. (26.58b)

It should be noted that Eqs 26.57 and 26.58 are valid regardless of the cause of the depression, regardless of the magnitude of the pressure applied on the geosynthetic, and whether the geosynthetic is in contact with the supporting medium (Fig. 26.8a) or bridges the depression (Fig. 26.8b).

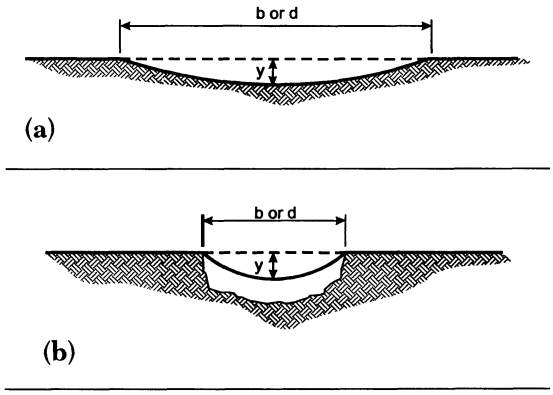


FIGURE 26.8. Geosynthetic deflection: (a) geosynthetic supported by soil; and (b) geosynthetic overlying a void (materials overlying the geomembrane are not shown).

TABLE 26.5. Corresponding values of relative deflection, y/b or y/d, geosynthetic strain, ε, and dimensionless parameter Ω (adapted from Giroud *et al.* 1990)

y/b or y/d	ε (%)	Ω	y/b or y/d	ε (%)	Ω
0.000	0.000	∞	0.242	15.00	0.64
0.010	0.027	12.51	0.250	15.91	0.62
0.020	0.107	6.26	0.260	17.15	0.61
0.030	0.240	4.18	0.270	18.43	0.60
0.040	0.425	3.15	0.280	19.75	0.59
0.050	0.663	2.53	0.282	20.00	0.58
0.060	0.960	2.11	0.290	21.10	0.58
0.061	1.000	2.07	0.300	22.50	0.57
0.070	1.30	1.82	0.310	23.93	0.56
0.080	1.70	1.60	0.317	25.00	0.55
0.087	2.00	1.47	0.320	25.39	0.55
0.090	2.15	1.43	0.330	26.89	0.54
0.100	2.65	1.30	0.340	28.43	0.54
0.107	3.00	1.23	0.350	30.00	0.53
0.110	3.20	1.19	0.360	31.60	0.53
0.120	3.80	1.10	0.370	33.23	0.52
0.123	4.00	1.08	0.380	34.90	0.52
0.130	4.45	1.03	0.381	35.00	0.52
0.138	5.00	0.97	0.390	36.60	0.52
0.140	5.15	0.96	0.400	38.32	0.51
0.150	5.90	0.91	0.410	40.00	0.51
0.151	6.00	0.90	0.420	41.86	0.51
0.160	6.69	0.86	0.430	43.67	0.51
0.164	7.00	0.84	0.437	45.00	0.50
0.170	7.54	0.82	0.440	45.51	0.50
0.175	8.00	0.80	0.450	47.38	0.50
0.180	8.43	0.78	0.460	49.27	0.50
0.186	9.00	0.76	0.464	50.00	0.50
0.190	9.36	0.75	0.470	51.18	0.50
0.197	10.00	0.73	0.480	53.13	0.50
0.200	10.35	0.72	0.490	55.00	0.50
0.210	11.37	0.70	0.500	57.08	0.50
0.216	12.00	0.69	0.562	70.00	0.50
0.220	12.44	0.68	0.631	85.00	0.51
0.230	13.56	0.66	0.696	100.00	0.53
0.240	14.71	0.64	0.819	130.00	0.56

26.5.2.2 Relationships between Geosynthetic Deflection and Tension

Assuming that the geosynthetic has a circular shape when it deflects over a depression, the following relationship exists between the geosynthetic tension, the width of the depression, and the applied pressure, which is assumed to be uniformly distributed on the geosynthetic (Giroud 1981).

$$T = pb\Omega \quad \text{for an infinitely long depression} \tag{26.59a}$$

$$T = pr\Omega \quad \text{for a circular depression} \tag{26.59b}$$

where T = geosynthetic tension, p = pressure normal to the geosynthetic and uniformly distributed over the geosynthetic, b = width of the infinitely long depression, r =

radius of the circular depression, and Ω = dimensionless factor. Equation 26.59a and b can be used with any set of coherent units. The relevant basic SI units are: T (N m^{-1}), b (m), r (m), and p (Pa); Ω is dimensionless.

As pointed out by Giroud (1981), it should be noted that, if the depression over which the geosynthetic deflects is circular, a uniformly distributed pressure does not correspond to a spherical deflection and, conversely, a spherical deflection does not correspond to a uniformly distributed pressure. Therefore, Eq. 26.59b is only approximate. In contrast, if the depression over which the geosynthetic deflects is infinitely long, and if the geosynthetic has uniform characteristics over its entire area, a uniformly distributed pressure does result in a circular shape of the deformed geosynthetic.

26.5.2.3 Evaluation of the Pressure Applied on the Geosynthetic

If the considered geosynthetic is a geomembrane that is not covered with a layer of soil, the pressure applied on the geomembrane is the pressure applied by the liquid. If the geomembrane is overlain by a layer of soil (Fig. 26.9), only a fraction of the overburden load is applied to the geomembrane due to the development of arching in the soil, as the geosynthetic deflects. Several researchers have presented equations that account for arching including: Bonaparte & Berg (1987), Giroud *et al.* (1990), and Poorooshasb (1991). The pressure applied to the geomembrane, as presented by Giroud *et al.* (1990), is given by:

$$p = 2\gamma b[1 - \exp(-0.5H/b)] + q\exp(-0.5H/b)$$
for an infinitely long depression (26.60a)

$$p = 2\gamma r[1 - \exp(-0.5H/b)] + q\exp(-0.5H/b)$$
for a circular depression. (26.60b)

It should be noted that, for $H = 0$, Eq. 26.60a and b gives $p = q$. Combining Eqs 26.59a and 26.60a, and Eqs 26.59b and 26.60b, respectively, gives:

$$T = b\Omega\{2\gamma b[1 - \exp(-0.5H/b)] + q\exp(-0.5H/b)\}$$
for an infinitely long depression (26.61a)

$$T = r\Omega\{2\gamma r[1 - \exp(-0.5H/r)] + q\exp(-0.5H/r)\}$$
for a circular depression. (26.61b)

It should be noted that, for $H = 0$, Eq. 26.61a and b is identical to Eq. 26.59a and b, respectively, since, in this case, $p = q$. Equation 26.60a and b can be used with any set of coherent units. The relevant basic SI units are: b (m), r (m), H (m), p (Pa), q (Pa), T (N m^{-1}) and γ (N, m^{-3}); Ω is dimensionless.

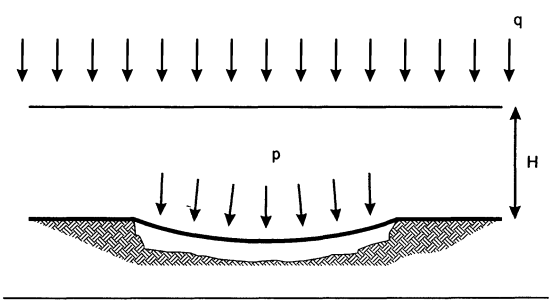


FIGURE 26.9. Geosynthetic deflection under a soil layer.

26.5.2.4 Use of the Equations

Equation 26.61a and b is used to calculate the required geosynthetic tension, T, for a given value of Ω, when all other parameters (b or r, q, H, and γ) are given. The dimensionless parameter Ω depends either on the allowable geosynthetic strain, ε, or the allowable geosynthetic deflection, y (see Eq. 26.57). The allowable geosynthetic strain is the lesser of the maximum design strains for the considered geosynthetic and the strain beyond which the soil layer would be unacceptably deformed or cracked. The allowable geosynthetic deflection is considered when exces-

sive deflection of the soil surface impairs the serviceability of the system. No method is proposed in this chapter to evaluate the deflection of the soil surface; however, in the case of relatively thin soil layers, the soil surface deflection can be assumed to be of the same order as the geosynthetic deflection. In some instances, both the allowable geosynthetic strain and the allowable geosynthetic deflection may need to be considered. Also, if the geosynthetic deforms to the point that it is in contact with the bottom of the depression (Fig. 26.8a), the value of the deflection is given as being the depth of the depression; in this case, the calculated value of the pressure, p, is the difference between the pressure applied on top of the geosynthetic and the reaction of the bottom of the depression beneath the geosynthetic.

Equations 26.57–26.61 can also be used to calculate any of the parameters when the values of all the other parameters are known. For example, values of H, q or Ω can easily be calculated as a function of the other parameters. The calculation of the depression size, i.e. b or r, requires a trial-and-error approach. Detailed examples solved numerically and graphically are presented by Giroud *et al.* (1990).

Engineers using Eqs 26.59–26.61 should use appropriate factors of safety. The factor of safety can be applied to the geosynthetic tension or the applied loads, or both using a partial factor of safety approach.

26.5.3 DIFFERENTIAL SETTLEMENT AT CONNECTION OF LINER SYSTEM TO RIGID STRUCTURES

26.5.3.1 Tension and Strain in the Geomembrane

Geomembranes are generally supported by a compressible medium, such as soil and/or waste, and are sometimes connected to rigid structures, typically made of concrete, metal, or plastic, such as pipes, intake towers, water gate structures, columns, manhole shafts, and gas vents. The compressible medium that supports the geomembrane settles as a result of its own weight and as a result of the loads due to the weight of the materials overlying the geomembrane (e.g. liquid, soil and/or waste). The differential settlement between the compressible medium and the rigid structure induces a tension (force per unit width) and a strain (elongation per unit length) in the geomembrane. In many instances, geomembranes subjected to such differential settlements have undergone excessive tensions and strains, and have failed next to the rigid structure. Giroud (1973, 1977, 1983) has recommended that concrete structures connected to geomembranes be constructed with battered walls (Fig. 26.10) instead of vertical walls to obtain a settlement transition, thereby minimizing the tension and strain in the geomembrane.

This section presents a method to determine the amount of batter of the walls of the rigid structure required to decrease the tension and strain in the geomembrane to an allowable level. The method can also be used to calculate the tension and strain in a geo-

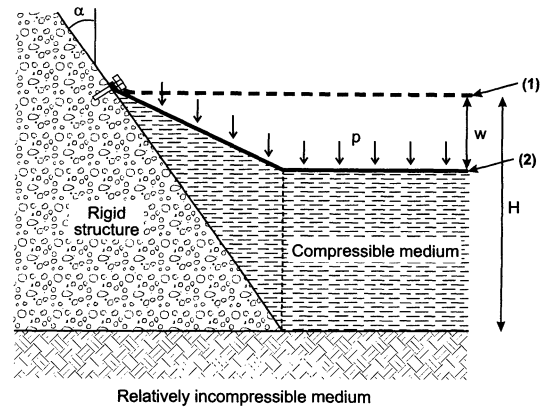


FIGURE 26.10. Geomembrane connected to a battered wall (after Giroud and Soderman 1995, © Geosynthetics International, reproduced with permission): 1 = position of the geomembrane at the time of installation; and 2 = position of the geomembrane after settlement.

membrane for a given wall batter and a given settlement of the medium underlying the geomembrane.

26.5.3.2 Assumptions

The following general assumptions are made:

- The surface of the medium supporting the geomembrane is horizontal and it is uniformly loaded.
- The medium supporting the geomembrane is homogeneous in any horizontal plane, but its properties may vary with depth.
- There is no differential settlement between the structure and the compressible medium at a certain depth, H, below the surface of the compressible medium. This assumption is considered most appropriate if both the structure and the compressible medium rest on a relatively incompressible medium (Fig. 26.10). This assumption is valid with a sufficient approximation if, at the base of the structure, the differential settlement between the structure and the compressible medium is negligible; this situation typically occurs if the compressible medium is a soil whose compression modulus increases as depth increases.
- The geomembrane is mechanically connected to the rigid structure at, or just above, the surface level of the supporting medium at the time of geomembrane installation.
- The problem is two-dimensional, and the geomembrane and the supporting medium are in a plane-strain state.

It should be noted that the last assumption restricts the validity of the equations presented herein to rigid structures of great length perpendicular to the considered cross-section. The equations are not applicable to three-dimensional structures such as circular columns or manholes. Finally, it should be noted that only the settlement of the surface of the compressible medium that occurs after the installation of the geomembrane is considered herein.

26.5.3.3 Presentation of the Method

As shown by Giroud & Soderman (1995) a conservative evaluation of the geomembrane strain at its connection to a wall consists of using the following approximate equation valid for small values of geomembrane strain, e.g. $\varepsilon < 10\%$:

$$\varepsilon_{cons.app} = \tfrac{1}{2}\left(\frac{w/H}{\tan \alpha}\right)^2 \qquad (26.62)$$

where $\varepsilon_{cons.app}$ = conservative and approximate value of the geomembrane strain at its connection to a rigid structure; w settlement of the soil away from the structure; H = thickness of the compressive medium or height of the structure, whichever is less; and α = wall batter, i.e. angle of the wall of the structure with a vertical plane (Fig. 26.10). Equation 26.62 can be used with any set of coherent units. The relevant basic SI units are: w (m), H (m) and α (°); ε is dimensionless.

Similarly, a conservative value of the required wall batter can be obtained from the allowable geomembrane strain, ε_{all}, using the following approximate equation valid for small values of geomembrane strain, e.g. $\varepsilon < 10\%$:

$$\tan \alpha_{cons.app} = \frac{w/H}{(2\varepsilon_{all})^{1/2}}. \qquad (26.63)$$

26.5.3.4 Practical Recommendations

Battering the walls of rigid structures is an effective solution to the problem of differential settlement causing excessive tensions and strains in geomembranes next to their connections with rigid structures. Even though the analysis presented herein is limited to two-dimensional problems, the mechanisms involved are such that wall batter is also expected to be an effective solution for three-dimensional problems. Therefore, it is recommended to use battered walls in structures, of all types and shapes, to which geomembranes are connected.

Causes of excessive settlement next to rigid structures should be avoided. The most common cause is inadequate compaction of the soil in the immediate vicinity of the structure. As heavy equipment cannot effectively compact the soil in the immediate vicinity of structures, small equipment should be used. Structures that deform excessively under lateral loads, such as lateral loads due to earth pressure and compaction-induced stresses, may also cause excessive settlements.

As shown by Giroud & Soderman (1995), the interface friction angles between the geomembrane and the materials in contact can have a significant impact on the magnitude of the tension and strain developed in a geomembrane. In general, the lower the interface friction angle, the lower the tension and strain that develops in the geomembrane. In some instances, it may be possible to reduce the effect of differential settlement by reducing the interface friction angle. Reducing the interface friction angle could be accomplished by selecting a smooth geomembrane rather than a textured geomembrane or by placing a piece of smooth geomembrane, i.e. a "slip sheet", between the geomembrane liner and the underlying medium.

26.5.4 ACTION OF WIND ON GEOMEMBRANES

26.5.4.1 Introduction

When the wind blows over an exposed geomembrane, some portions of the geomembrane are subjected to a suction and can be uplifted. The magnitude of the suction exerted by the wind is discussed in Section 26.5.4.2. Whether a geomembrane is uplifted or not depends on its own weight and the wind velocity (see Section 26.5.4.3). Prevention of geomembrane uplift is discussed in Section 26.5.4.4. If the geomembrane is uplifted, tensile stresses and strains are induced in the geomembrane (see Section 26.5.4.5), and the geomembrane must be anchored at its periphery (see Section 26.5.4.6).

26.5.4.2 Suction Due to Wind

The suction that effectively uplifts the geomembrane, S_e, is given by (Giroud *et al.* 1995d; Zornberg & Giroud 1997):

$$S_e = 0.050\lambda_w V^2 \exp[-(1.252 \times 10^{-4})z] - 9.81\mu_{GM}\cos\beta \quad (26.64a)$$

where S_e = effective suction, λ_w = suction factor, V = wind velocity, z = altitude above sea level, μ_{GM} = mass per unit area of the geomembrane, and β = slope angle. Equation 26.64a can only be used with the following units: S_e (Pa), V (km h^{-1}), z (m), μ_{GM} (kg m^{-2}); λ_w is dimensionless. The right-hand side of Eq. 26.64a comprises two terms: the first term represents the suction applied by the wind on top of the geomembrane, and the second term represents the resistance to uplift resulting from the weight of the geomembrane.

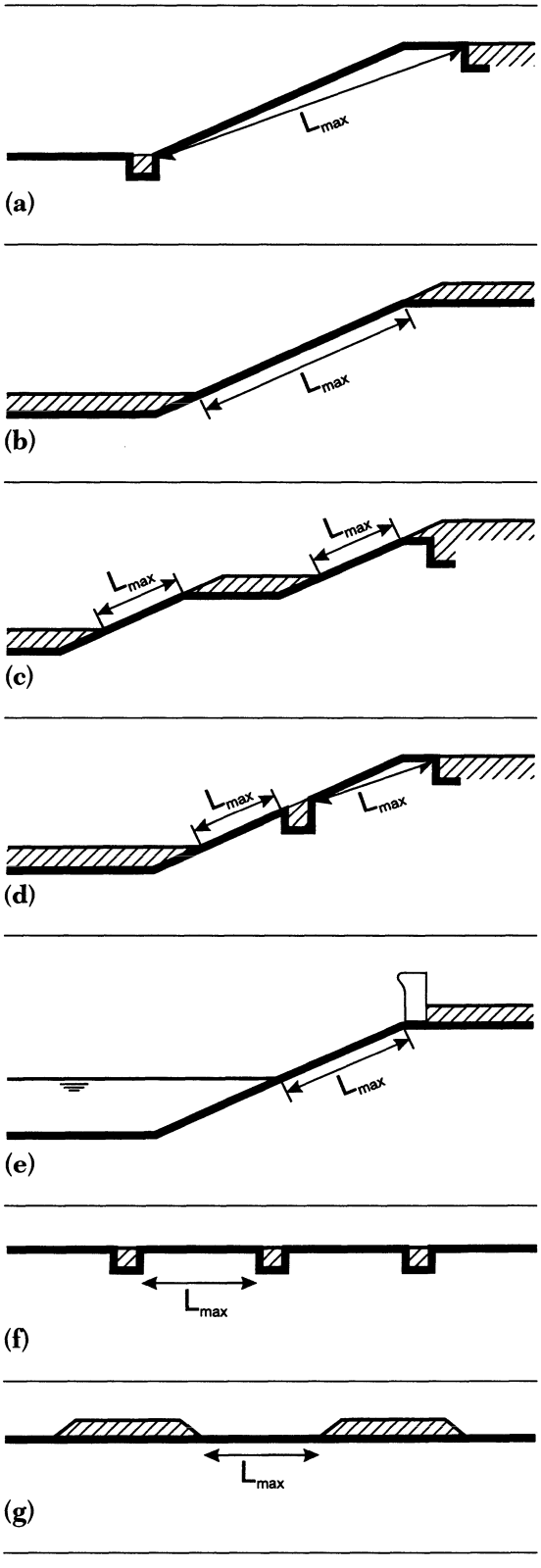
At sea level ($z = 0$), Eq. 26.64a becomes:

$$S_e = 0.050\lambda_w V^2 - 9.81\mu_{GM}\cos\beta \quad (26.64b)$$

with the following units: S_e (Pa), V (km h^{-1}), μ_{GM} (kg m^{-2}).

The suction factor, λ_w, quantifies the fact that the wind suction is not uniformly distributed over the geomembrane. Based on data from wind tunnel tests and the need for extra safety due to gusts of wind, the following values of the suction factor, λ_w, are recommended (Giroud *et al.* 1995c):

- $\lambda_w = 1.00$ if the crest of a slope or the top part of a landfill cover is considered;
- $\lambda_w = 0.70$ if an entire side slope is considered;
- $\lambda_w = 0.85$ for the top third, $\lambda_w = 0.70$ for the middle third, and $\lambda_w = 0.55$ for the bottom third of a slope decomposed in three-thirds by intermediate benches or anchor trenches as shown in Fig. 26.11c and 26.11d; and
- $\lambda_w = 0.40$ in a flat area such as the bottom of a large empty reservoir.



The above values of λ_w can be increased by up to 30% for geomembranes placed on a supporting medium with an unusual geometry likely to increase wind suction. Also, for unusual geometries or large projects for which wind-induced damage of exposed geomembranes may have large financial consequences, wind tunnel tests of reduced-scale models or numerical simulation may be warranted.

26.5.4.3 Resistance to Wind Uplift Due to Geomembrane Self Weight

Based on Eq. 26.64a, it appears that a geomembrane located at altitude z above sea level should not be uplifted by wind if the following condition is met by the geomembrane mass per unit area (Giroud *et al.* 1995c, Zornberg & Giroud 1997):

$$\mu_{GM} \geq \mu_{GM\,req} = \frac{0.0051\lambda_w V^2 \exp[-(1.252 \times 10^{-4})z]}{\cos\beta} \quad (26.65a)$$

with the following units: $\mu_{GM\,req}$ (kg m^{-2}), V(km h^{-1}) and z (m). At sea level, Eq. 26.65 becomes:

$$\mu_{GM} \geq \mu_{GM\,req} = \frac{0.0051\lambda_w V^2}{\cos\beta}. \quad (26.65b)$$

FIGURE 26.11. Typical configurations of a geomembrane exposed to wind: (a) geomembrane anchored in an anchor trench; (b) geomembrane anchored under a pavement or a layer of soil; (c) geomembrane restrained by a soil layer on a bench; (d) geomembrane restrained by an intermediate anchor trench; (e) geomembrane anchored under a structure at the top and restrained by liquid or solids below a certain level; (f) at bottom of reservoir, geomembrane anchored in anchor trenches; (g) at bottom of reservoir, geomembrane anchored by strips of soil or pavement (after Giroud *et al.* 1995c, © Geosynthetics International, reproduced with permission).

TABLE 26.6. Typical density, thickness and mass per unit area for geomembranes, and relationship between mass per unit area and threshold wind velocity (adapted from Giroud *et al.* 1995c)

Type of geomembrane[a]	Geomembrane density, ρ_{GM} (kg m^{-3})	Geomembrane thickness, t_{GM} (mm)	Geomembrane mass per unit area, μ_{GM} (kg m^{-2})	Minimum uplift wind velocity, V_{thresh} (km h^{-1})
PVC	1250[b]	0.5	0.63	11.1
		1.0	1.25	15.7
HDPE	940	1.0	0.94	13.6
		1.5	1.41	16.7
		2.0	1.88	19.2
		2.5	2.35	21.5
CSPE-R	[c]	0.75	0.9	13.3
		0.90	1.15	15.0
		1.15	1.5	17.2
EIA-R	[c]	0.75	1.0	14.0
		1.0	1.3	16.0
Bituminous		3	3.5	26.2
		5	6	34.3

[a] PVC = polyvinyl chloride, HDPE = high density polyethylene, CSPE-R = chlorosulfonated polyethylene-reinforced (commercially known as Hypalon), and EIA-R = ethylene interpolymer alloy-reinforced (commercially known as XR5).
[b] PVC geomembranes have densities typically ranging from 1200 to 1300 kg m^{-3}.
[c] Geomembranes composed of different plies having different densities.

Typical values of geomembrane mass per unit area, density and thickness are given in Table 26.6.

A given geomembrane (defined by its mass per unit area, μ_{GM}) located at altitude z above sea level should not be uplifted if the wind velocity, V, is less than a threshold wind velocity, V_{thresh}, given by the following equation derived from Eq. 26.64a with $S_e = 0$:

$$V_{thresh} = 14.023 \exp[(6.259 \times 10^{-5})z] \times (\mu_{GM} \cos \beta/\lambda_w)^{1/2} \quad (26.66a)$$

with the following units: V_{thresh} (km h^{-1}), z (m) and μ_{GM} (kg m^{-2}). At sea level, Eq. 26.67 becomes:

$$V_{thresh} = 14.023(\mu_{GM} \cos \beta/\lambda_w)^{1/2} \quad (26.66b)$$

The last column of Table 26.6 gives minimum values of the threshold wind velocity, V_{thresh}, for typical geomembranes, calculated using Eq. 26.66b with $\lambda_w = 1$ and $\beta = 0$, i.e. assuming that the geomembrane is located on a horizontal area at sea level, and that the suction factor has a conservative value.

Table 26.6 shows that typical polymeric geomembranes, with masses per unit area ranging between 0.5 and 2 kg m^{-2}, can resist uplift at sea level by winds with velocities ranging between 10 and 20 km h^{-1}; whereas typical bituminous geomembranes, with masses per unit area ranging between 3.5 and 6 kg m^{-2}, can resist uplift at sea level by winds with velocities ranging between 25 and 35 km h^{-1}. It should be noted that the wind velocity values given in Table 26.6 are conservative, i.e. greater wind velocity values would be calculated using a value of λ_w smaller than one and an altitude greater than zero.

26.5.4.4 Prevention of Geomembrane Uplift

Geomembrane uplift by wind can be prevented by covering the geomembrane with a

material that applies a uniform pressure on the geomembrane. The minimum thickness of material required to prevent geomembrane uplift at altitude z above sea level, t_{req}, is given by the following equation derived from Eq. 26.64a with $S_e = 0$ (Giroud *et al.* 1995c; Zornberg & Giroud 1997):

$$t_{req} = \frac{1}{\rho} \times \left\{ -\mu_{GM} + \frac{0.0051 \lambda_w V^2 \exp[-(1.252 \times 10^{-4})z]}{\cos \beta} \right\} \quad (26.67a)$$

where ρ = the density of the material placed on the geomembrane. Equation 26.67a can only be used with the following units: t_{req} (m), μ_{GM} (kg m^{-2}), V (km h^{-1}) and z (m). At sea level, Eq. 26.67a becomes:

$$t_{req} = \frac{1}{\rho} \left(-\mu_{GM} + \frac{0.0051 \lambda_w V^2}{\cos \beta} \right) \quad (26.67b)$$

Using Eq. 26.67b with $\lambda_w = 1$ and $\cos \beta = 1$, it can be shown that approximately 0.2 m of water or 0.1 m of soil are sufficient to prevent geomembrane uplift for wind velocities up to approximately 200 km h^{-1} (assuming that the water or soil is not removed by the wind). It should be noted that 0.2 m of water is equivalent to a mass per unit area of 200 kg m^{-2}. To mobilize the same mass per unit area using sand bags having a mass of 20 kg would require approximately ten bags per square meter, which is impractical. Sand bags having a mass of 20 kg and installed on a 3-m square grid would be equivalent to a uniform thickness of water of 2.2 mm. Using Eq. 67b with $\lambda_w = 1$ and $\cos \beta = 1$, it can be shown that these bags would prevent uplift of a geomembrane with a mass per unit area of 1 kg m^{-2}, i.e. a typical polymeric geomembrane, for wind velocities up to approximately 15 km h^{-1}. These calculations explain why sand bags are effective in preventing geomembrane uplifting only in the case of low velocity winds.

Geomembrane uplift can also be prevented by applying a suction under the geomembrane equal to the effective suction defined by Eq. 26.64. This can be achieved, in the case of the geomembrane cover of a municipal solid waste landfill, by installing and operating a vacuum-based active gas extraction system. These types of systems are common at landfills. The system can be operated to create an effective suction under the geomembrane equal to or larger than that given by Eq. 26.64. In cases where the geomembrane is installed over a landfill without active gas extraction, a suction can be induced under the geomembrane by "suction vents" located at the top of slopes. As indicated by Giroud *et al.* (1995c):

> These vents stabilize the geomembrane by sucking air from beneath the geomembrane when the wind blows, thereby decreasing the air pressure beneath the geomembrane. For the suction vents to work, air located beneath the geomembrane must flow toward the vent when the air vent is exposed to wind-generated suction. If the soil beneath the geomembrane has a low permeability, there is little air beneath the geomembrane. This air will flow toward the vent after the geomembrane has been slightly uplifted. If the soil beneath the geomembrane is permeable there is a significant amount of air entrapped beneath the geomembrane, and while this air is being sucked out by the suction vent, the geomembrane is uplifted. Therefore, in all cases the geomembrane may be uplifted for a short period of time before the suction vents are effective. In cases where the soil beneath the geomembrane has a low permeability, short strips of drainage geocomposites, radiating from the suction vent, have been recommended to help drain the air located beneath the geomembrane. However, the effectiveness of this method has not been evaluated.

Also, according to Giroud *et al.* (1995c):

> To the best of the authors' knowledge, no method is available to design suction vents. [. . .] In a number of projects, suction vents have been

placed every 15 m along the periphery of ponds. The reason for selecting 15 m as the spacing is not known.

Geomembrane uplift can also be prevented by gluing the geomembrane on the supporting medium. This method is effective only if the supporting medium is able to resist tensile forces. This method has been used in the case of a bituminous geomembrane resting on a layer of porous bituminous concrete on the face of an embankment dam (Saintot *et al.* 1993).

More details on methods for preventing geomembrane uplift by wind are provided in Giroud *et al.* (1995c).

26.5.4.5 Analysis of Geomembrane Uplift

If none of the precautions for preventing geomembrane uplift described in Section 26.5.4.4 is taken, an exposed geomembrane can be uplifted. In the analysis that follows, it is assumed that the geomembrane is sealed around its periphery and, as a result, the wind cannot uplift the geomembrane by reaching beneath it. Therefore, the analysis presented in this section is not applicable to a situation that exists during geomembrane installation where a panel is not seamed at its edge, and is not applicable to geomembranes that are torn open.

It is also assumed that the medium under the geomembrane is permeable enough that uplifting of the geomembrane will not be restricted by a decrease in air pressure beneath the geomembrane due to the sudden increase in volume beneath the geomembrane when uplifting begins. In other words, it is assumed that the geomembrane is free to move away from the supporting medium over a certain length. The geomembrane movements are assumed to be restrained at both ends of the geomembrane by anchor trenches, anchor soil layers, or other means. Typical cases are shown in Fig. 26.11, where a length L_{max} is shown. This is the length of exposed geomembrane between two locations where its movements are restrained. The actual length, L, of geomembrane subjected to suction due to wind is equal to, or less than, L_{max}.

The geometry of the uplifted geomembrane can be characterized by four parameters: length of geomembrane subjected to suction due to wind measured along the slope, L; geomembrane strain, ε; geomembrane uplift, u; and angle, θ, between any of the extremities of an uplifted geomembrane and the straight line passing through these two extremities (Fig. 26.12). The following relationships exist between these four parameters (Giroud *et al.* 1995c):

$$\varepsilon = \frac{\theta}{\sin\theta} - 1 \tag{26.68}$$

$$\varepsilon = \frac{1}{2}\left(\frac{2u}{L} + \frac{L}{2u}\right) \times \sin^{-1}\left[2\Big/\left(\frac{2u}{L} + \frac{L}{2u}\right)\right] - 1 \tag{26.69}$$

$$\theta = \sin^{-1}\left[2\Big/\left(\frac{2u}{L} + \frac{L}{2u}\right)\right] = 2\tan^{-1}\left(\frac{2u}{L}\right) \tag{26.70}$$

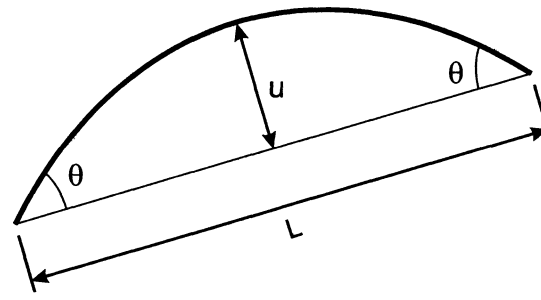


FIGURE 26.12. Geometry of uplifted geomembrane.

$$\frac{u}{L} = \frac{1 - \cos\theta}{2\sin\theta} = \frac{1}{2}\tan\left(\frac{\theta}{2}\right) \quad (26.71)$$

The following relationships exist between effective suction, geomembrane tension and the four parameters defining the geometry of the uplifted geomembrane (Giroud *et al.* 1995c):

$$\varepsilon = \frac{2T}{S_e L}\sin^{-1}\left(\frac{S_e L}{2T}\right) - 1 \quad (26.72)$$

$$\frac{T}{S_e L} = \frac{1}{2\sin\theta} = \frac{1}{4}\left(\frac{2u}{L} + \frac{L}{2u}\right) \quad (26.73)$$

$$\theta = \sin^{-1}\left(\frac{S_e L}{2T}\right) \quad (26.74)$$

$$\frac{u}{L} = \frac{T}{S_e L} - \left[\left(\frac{T}{S_e L}\right)^2 - \frac{1}{4}\right]^{1/2} \quad (26.75)$$

It should be noted that it is not possible to express $T/(S_e L)$ analytically as a function of ε. Therefore, it is useful to tabulate numerical values. Corresponding numerical values of u/L, ε, $T/(S_e L)$ and θ are given in Table 26.7.

Equations 26.68–26.75 and the values given in Table 26.7 make it possible to solve two important problems:

- If S_e and L are known and a geomembrane is characterized by its allowable tension, T_{all}, and allowable strain, ε_{all}, this geomembrane is acceptable regarding wind uplift resistance if its allowable tension is greater than the tension due to geomembrane uplift, which can be calculated using Eq. 26.72 or using the numerical values of ε and $T/(S_e L)$ given in Table 26.7.
- If S_e and L are known and the tension–strain curve of a geomembrane is known, it is possible to calculate the tension and strain in the uplifted geomembrane by trial-and-error using Eq. 26.72 or the numerical values of ε and $T/(S_e L)$ given in Table 26.7.

Having calculated the tension, T, in the geomembrane, it is then possible to calculate the amount of uplift, u, using Eq. 26.75 and the angle θ using Eq. 26.74. Consistency between the calculated values of u/L, ε and θ can then be checked using Eqs 26.68–26.71. It is useful to calculate the angle θ, because it gives the orientation of the geomembrane tension at both extremities of the geomembrane (Fig. 26.12), which is needed to design the anchor trenches or any other anchor systems.

Equations 26.68–26.75 were established based on the assumption that the geomembrane is laying flat, i.e. with no wrinkles, and without contraction when the wind starts blowing. If this assumption is not met, the geomembrane strain, ε, in Eqs 26.68, 26.69 and 26.72 should be replaced by the apparent strain, ε_{app}, defined as the strain that the geomembrane would undergo if it were uplifted off the same amount from an initial position where it lays flat and with no contraction. In other words, the apparent strain is the strain that is calculated from θ using Eq. 26.68 or from u using Eq. 26.69. At the same time, the tension in Eqs 26.72–26.75 is the total tension, i.e. the tension that results from the initial tension, if any, plus the tension due to wind action. As a result, as pointed out by Giroud *et al.* (1995c):

> If a geomembrane has wrinkles when uplifting begins, it is uplifted more, but with a smaller tension, than if the geomembrane has no wrinkles when uplifting begins [and] if a geomembrane is under tension when uplifting begins, it is uplifted less, but with a greater tension, than if the geomembrane is not under tension when uplifting begins.

More details on this topic are provided in Giroud *et al.* (1995c) and Zornberg & Giroud (1997).

TABLE 26.7. Values of the geomembrane normalized tension, $T/(S_eL)$, as a function of the geomembrane strain, ε, the relative uplift, u/L, and the uplift angle, θ (adapted from Giroud *et al.* 1995c)

Relative uplift, u/L (−)	Geomembrane strain, ε (%)	Normalized tension, $T/(S_eL)$ (−)	Uplift angle, θ (°)	Relative uplift, u/L (−)	Geomembrane strain, ε (%)	Normalized tension, $T/(S_eL)$ (−)	Uplift angle, θ (°)
0.000	0.000	∞	0	0.250	15.91	0.63	53.1
0.010	0.027	12.51	2.3	0.260	17.15	0.61	54.9
0.020	0.107	6.26	4.6	0.270	18.43	0.60	56.7
0.030	0.240	4.18	6.9	0.280	19.75	0.59	58.5
0.040	0.426	3.15	9.1	0.2819	20.00	0.58	58.8
0.050	0.665	2.53	11.4	0.2892	21.00	0.58	60.1
0.060	0.957	2.11	13.7	0.290	21.10	0.58	60.2
0.0613	1.000	2.07	14.0	0.2965	22.00	0.57	61.3
0.070	1.30	1.82	15.9	0.300	22.50	0.57	61.9
0.080	1.70	1.60	18.2	0.3035	23.00	0.56	62.5
0.0869	2.00	1.48	19.7	0.310	23.93	0.56	63.6
0.090	2.15	1.43	20.4	0.3105	24.00	0.56	63.7
0.100	2.65	1.30	22.6	0.3174	25.00	0.55	64.8
0.1065	3.00	1.23	24.0	0.320	25.39	0.55	65.2
0.110	3.20	1.19	24.8	0.3241	26.00	0.55	65.9
0.120	3.80	1.10	27.0	0.330	26.89	0.54	66.8
0.1232	4.00	1.08	27.7	0.3307	27.00	0.54	67.0
0.130	4.45	1.03	29.1	0.3373	28.00	0.54	68.0
0.138	5.00	0.97	30.9	0.340	28.43	0.54	68.4
0.140	5.15	0.96	31.3	0.3437	29.00	0.54	69.0
0.150	5.90	0.91	33.4	0.350	30.00	0.53	70.0
0.1513	6.00	0.90	33.7	0.360	31.60	0.53	71.5
0.160	6.69	0.86	35.5	0.370	33.23	0.52	73.0
0.1637	7.00	0.85	36.3	0.380	34.90	0.52	74.5
0.170	7.54	0.82	37.6	0.3806	35.00	0.52	74.6
0.1753	8.00	0.80	38.6	0.390	36.60	0.52	75.9
0.180	8.43	0.78	39.6	0.400	38.32	0.51	77.3
0.1862	9.00	0.76	40.9	0.4096	40.00	0.51	78.6
0.190	9.36	0.75	41.6	0.410	40.08	0.51	78.7
0.1965	10.00	0.73	42.9	0.420	41.86	0.51	80.1
0.200	10.35	0.73	43.6	0.430	43.67	0.51	81.4
0.2064	11.00	0.71	44.9	0.4372	45.00	0.50	82.3
0.210	11.37	0.70	45.6	0.440	45.51	0.50	82.7
0.2159	12.00	0.69	46.7	0.450	47.38	0.50	84.0
0.220	12.44	0.68	47.5	0.460	49.27	0.50	85.2
0.2250	13.00	0.67	48.5	0.4638	50.00	0.50	85.7
0.230	13.56	0.66	49.4	0.470	51.18	0.50	86.5
0.2339	14.00	0.65	50.1	0.480	53.13	0.50	87.7
0.240	14.71	0.64	51.3	0.490	55.09	0.50	88.8
0.2424	15.00	0.64	51.7	0.500	57.08	0.50	90.0

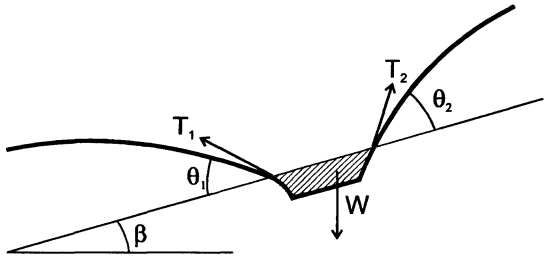


FIGURE 26.13. Geomembrane anchorage to resist uplift by wind.

26.5.4.6 Anchorage of a Geomembrane Subjected to Wind Uplift

The weight of material used to anchor a geomembrane subjected to wind uplift should be greater than the vertical component of the geomembrane tension (Fig. 26.13), hence the following equation (Giroud *et al.* 1999):

$$W = T_1 \sin(\theta_1 - \beta) + T_2 \sin(\theta_2 + \beta) \quad (26.76)$$

where W = weight of material per unit length of anchor trench (kN m^{-1}).

27. COVERS FOR WASTE

R. Bonaparte
E. K. Yanful

27.1 Introduction

Cover systems are used at landfills and other types of waste management units (e.g. waste piles, mine tailings piles, surface impoundments) to contain waste and any waste by-products (e.g. leachate, acid mine drainage, gas), to control moisture and air infiltration into the waste, and to prevent the occurrence of odors, disease vectors, and other nuisances. Cover systems are also used to meet erosion, aesthetic, and other end-use criteria for waste management sites. Cover systems for waste sites may involve only a single soil layer, placed over a mine waste rock pile, for example, or a multicomponent system of soil and geosynthetic layers, placed over a hazardous waste landfill, for example.

This chapter focuses on the hydraulic and geotechnical analysis and design of cover systems and deals with: (a) types of cover systems (Section 27.2); (b) cover system components (Sections 27.3 and 27.4); (c) water balance (Section 27.5); (d) static slope stability (Section 27.6); (e) seismic slope stability (Section 27.7); and (f) settlement (Section 27.8).

27.2 Types of Cover Systems

27.2.1 CLASSIFICATION OF COVER SYSTEMS

At present, cover system designs are based on one or more of three different principles for preventing or minimizing water percolation into waste. Each of these is briefly discussed below.

1. Hydraulic barrier: This type of cover system uses a low permeability physical barrier to impede the downward migration of water into the waste (Fig. 27.1). Hydraulic-barrier materials most commonly include compacted clay layers (CCLs), geosynthetic clay liners (GCLs), geomembranes, and combinations of these materials. These types of barriers are discussed briefly in Section 27.3 (see Chapter 25 for more details). In some countries, e.g. the USA, requirements for cover systems at landfills are developed around the use of hydraulic barriers.

2. Capillary barrier: This type of cover system consists of one or more layers of finer-grained soil overlying one or more layers of coarser-grained soil. Figure 27.2 illustrates the simplest configuration for a capillary barrier: a single clayey soil layer over a sandy soil layer. These systems are discussed in more detail in Section 27.4. At a low degree of soil saturation, i.e. at high matric suction in Fig. 27.2, the hydraulic conductivity of the coarse-grained soil is much less than that of the fine-grained soil. This is the reverse of the condition that occurs when the coarse-grained soil is at a high degree of soil saturation. Capillary barriers either: (i) store water by increased moisture content in the fine-grained soil for subsequent evapotranspiration, or (ii) divert infiltrating water via unsaturated lateral flow

R. K. Rowe (ed.), *Geotechnical and Geoenvironmental Engineering Handbook*
© Kluwer Academic Publishers 2001

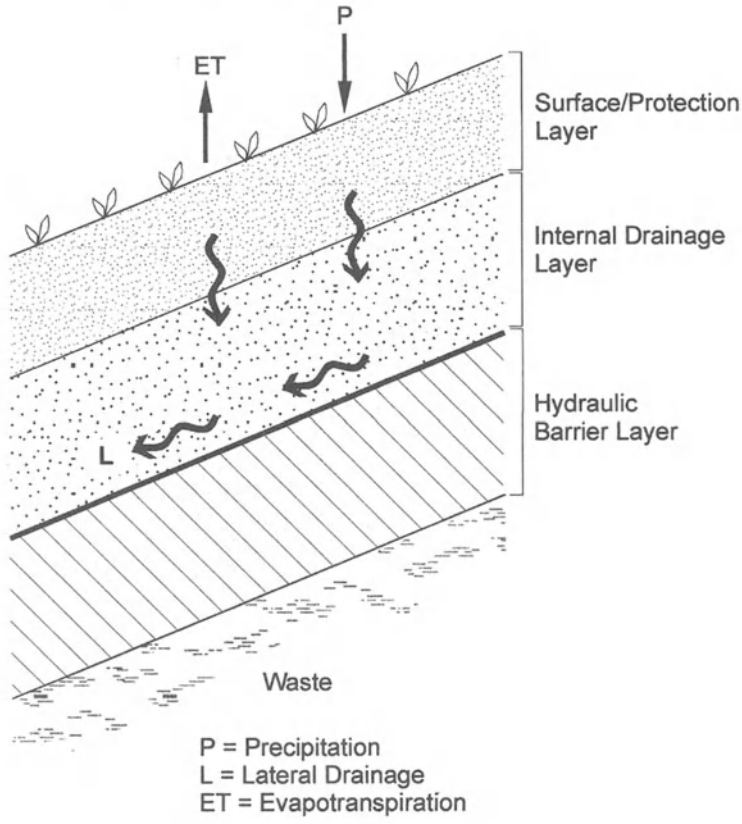


FIGURE 27.1. Hydraulic-barrier cover system.

in the fine-grained soil (above the soil interface). Sometimes a "wicking layer" (with intermediate characteristics to the coarse- and fine-grained layers) is installed between the coarse and fine layers to convey lateral flow. At a high degree of soil saturation in the coarse-grained soil, the capillary effect breaks down and percolation through the system can occur.

3. Evapotranspirative barrier: This type of cover system has also been developed primarily for use at arid and semi-arid sites. Evapotranspirative barriers are covers that consist of a thick layer of relatively fine-grained soil capable of supporting vegetation (Fig. 27.3). Soil thickness can range from about 900 to 1800 mm (Zornberg & Caldwell 1998). Evapotranspirative barriers exploit two characteristics of fine-grained soils: (a) significant soil water storage capacity, i.e. they can store a significant amount of water before gravity drainage; and (b) low hydraulic conductivity, even at high degrees of saturation. Low hydraulic conductivity limits advancement of the soil wetting front during seasonal wet periods (rainfall or snow melt). High water storage capacity allows storage of moisture, which infiltrates until it can later be removed by evapotranspiration. An evapotranspirative barrier must be sufficiently thick that changes in moisture content do not occur near its base, i.e. all changes in soil water storage should occur in the upper portion of the barrier (Fig. 27.3). Otherwise, percolation will occur. The required barrier thickness is a function of the frequency and intensity of precipitation,

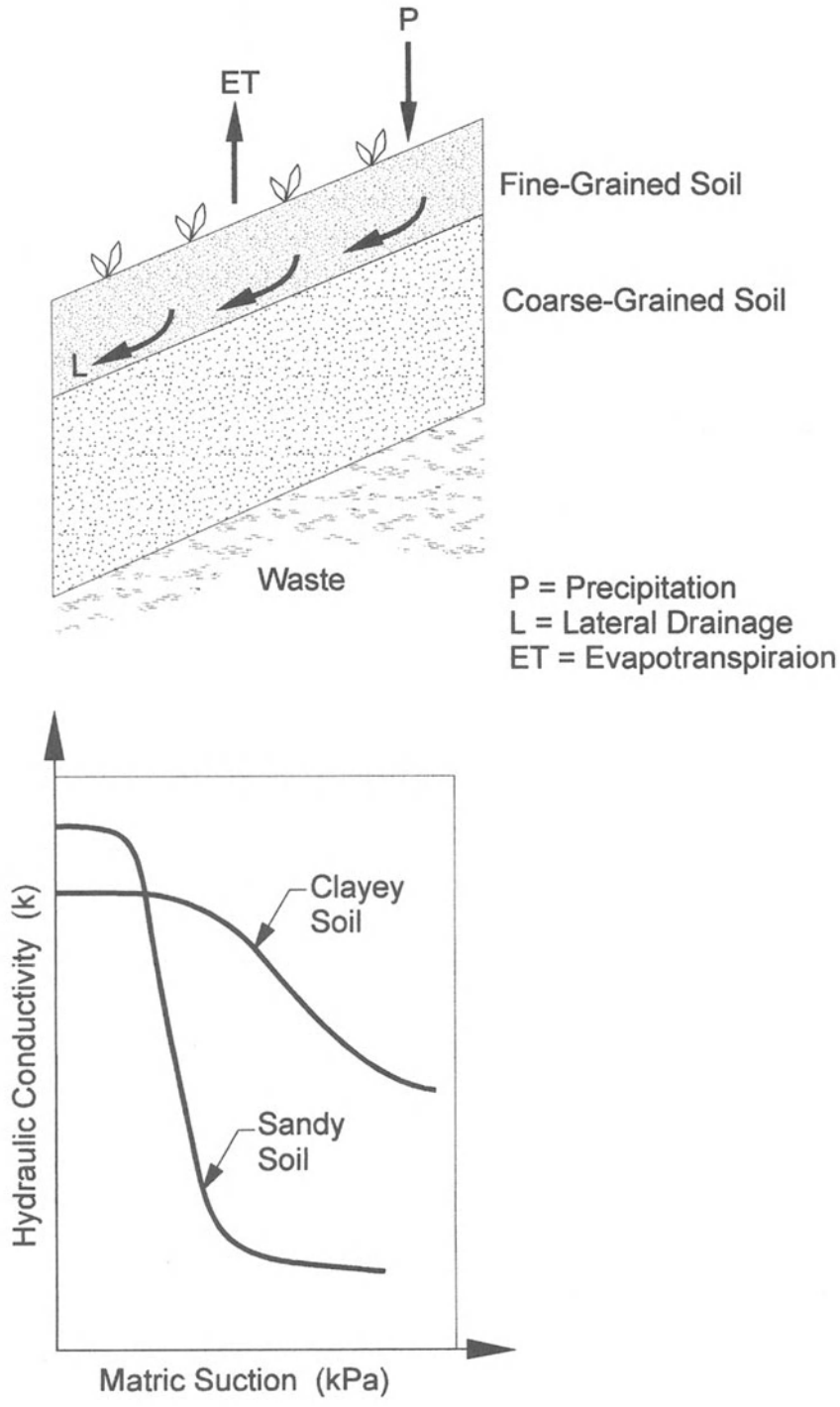


FIGURE 27.2. Capillary-barrier cover system and partially saturated hydraulic conductivity functions.

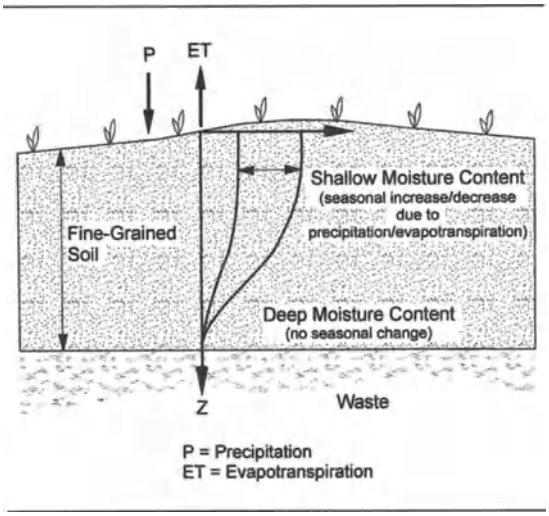


FIGURE 27.3. Evapotranspirative cover system, also called monolayer or monocover (modified from Benson & Khire 1995).

the unsaturated hydraulic properties of the soil, the type and health of cover vegetation, and the rate at which water can be removed by evapotranspiration. Soil types used for construction of evapotranspirative barriers include silty sands, silts and clayey silts.

Different barrier types may be combined in a single cover system. For example, a capillary barrier may be constructed beneath an evapotranspirative barrier.

This chapter focuses primarily on hydraulic-barrier type cover systems, currently the most widely used type of waste cover system, with limited commentary provided on the other two types. It is noted, however, that the use of capillary barriers and evapotranspirative barriers is becoming much more common.

27.2.2 EXAMPLES OF COVER SYSTEMS

Cover systems can be constructed with a wide variety of configurations of soil and geosynthetic layers to satisfy project-specific design criteria. A few examples are presented below. Additional examples can be found in Koerner & Daniel (1997).

Figure 27.4 illustrates two different cover systems for a municipal solid waste (MSW) landfill, one with a CCL hydraulic barrier, the other with a composite hydraulic barrier. For either example, a GCL can be considered as an alternative to the low permeability soil layer. Soil thicknesses will vary based on project-specific conditions. Figure 27.5 presents the cover system cross-section for a low-level radioactive waste disposal facility in the USA with a minimum design life of 200 years. Figure 27.6 shows the cover system used as part of the remediation of an uncontrolled dump site containing hazardous waste. The site is in a marsh. The low bearing capacity of the foundation soil and waste at the site necessitate the use of this lightweight cover system.

Figure 27.7 illustrates the benefits of cover system installation in preventing or minimizing percolation and thereby reducing the potential for waste liquid generation, e.g. leachate, acid mine drainage. This figure shows leachate generation rates after closure for a number of hazardous waste landfill cells (Gross *et al.* 1997). On average, leachate generation rates during the first year after closure were approximately 22% of the rates during the year prior to closure. The average rate for a given year after closure ranged from 1150 l ha^{-1} day^{-1} at one year after closure to less than 1 l ha^{-1} day^{-1} at nine years after closure. Similar data for a MSW landfill cell (in a humid environment precipitation-1000 mm a^{-1}) showed a reduction from 3400 l ha^{-1} day^{-1} during filling to 70 l ha^{-1} day^{-1} at three years after closure (Bonaparte 1995).

27.2.3 GAS GENERATION AND MANAGEMENT

Gas collection and control is necessary at most MSW landfills, at some other types of landfills and surface impoundments, and at some remediation sites. Anaerobic decomposition of organic material is the principal source of gas in solid waste landfills. Some industrial wastes can generate gas by inorganic chemical reactions.

Gas production rates for MSW vary with

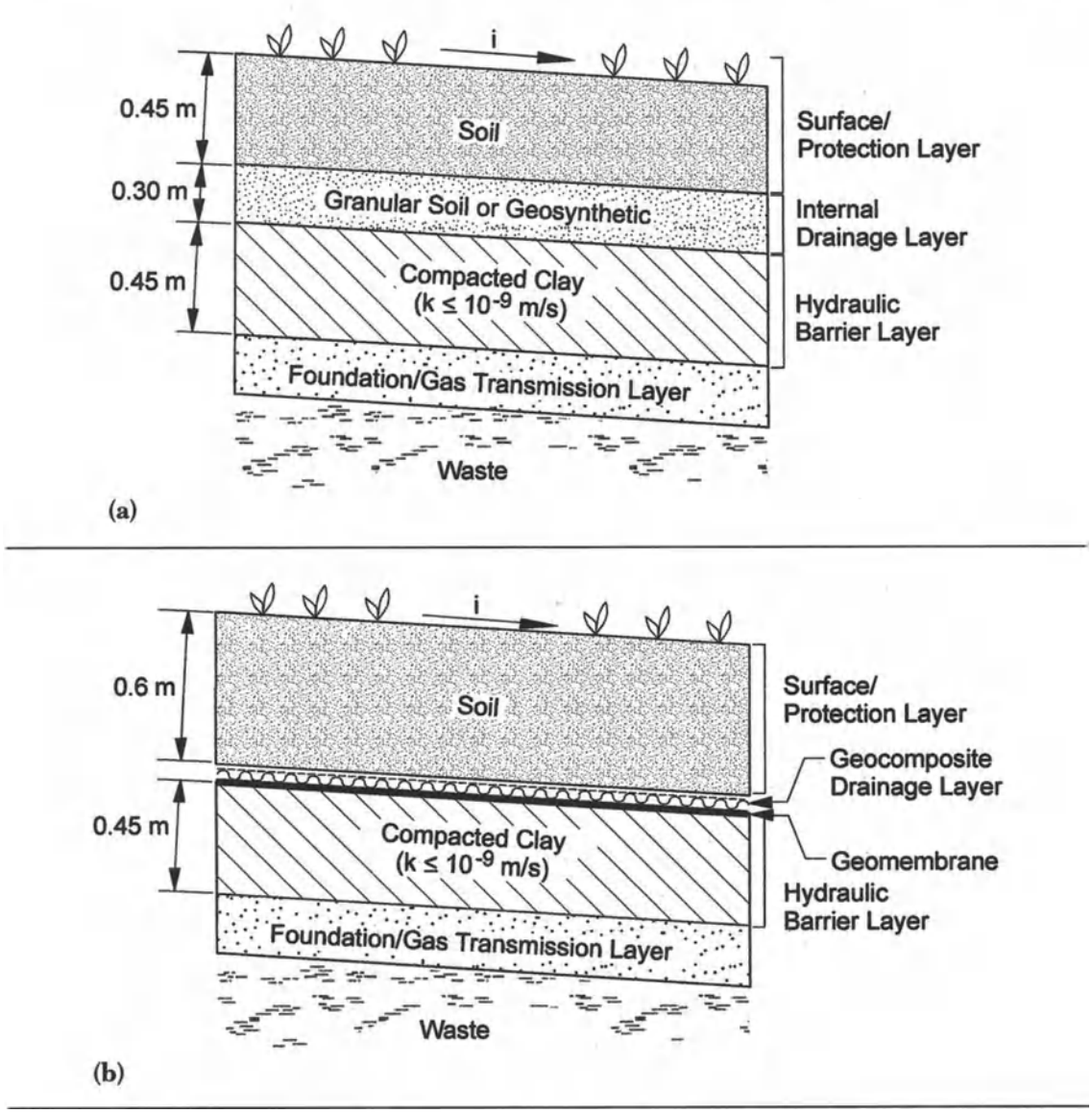


FIGURE 27.4. Example of MSW landfill cover: (a) CCL hydraulic barrier, and (b) composite hydraulic barrier. All thicknesses are typical. Note: i = cover slope (gradient).

the composition and age of waste, waste volume, waste moisture content, and other factors. MSW landfill gas consists mainly of methane and carbon dioxide, with lesser concentrations of nitrogen, oxygen, sulfides, ammonia, and other constituents, and trace concentrations of a variety of volatile organic compounds. Gas generation in a landfill cell can extend over a period of more than 25–50 years, or it can be accelerated through the use of leachate recirculation. Gas generation rates for MSW landfills can be estimated using simplified manual calculations (e.g. Tchobanoglous *et al.* 1993; McBean *et al.* 1995), or computer-based models such as the USEPA landfill air emissions estimation model (USEPA 1996).

Waste-generated gases affect cover sys-

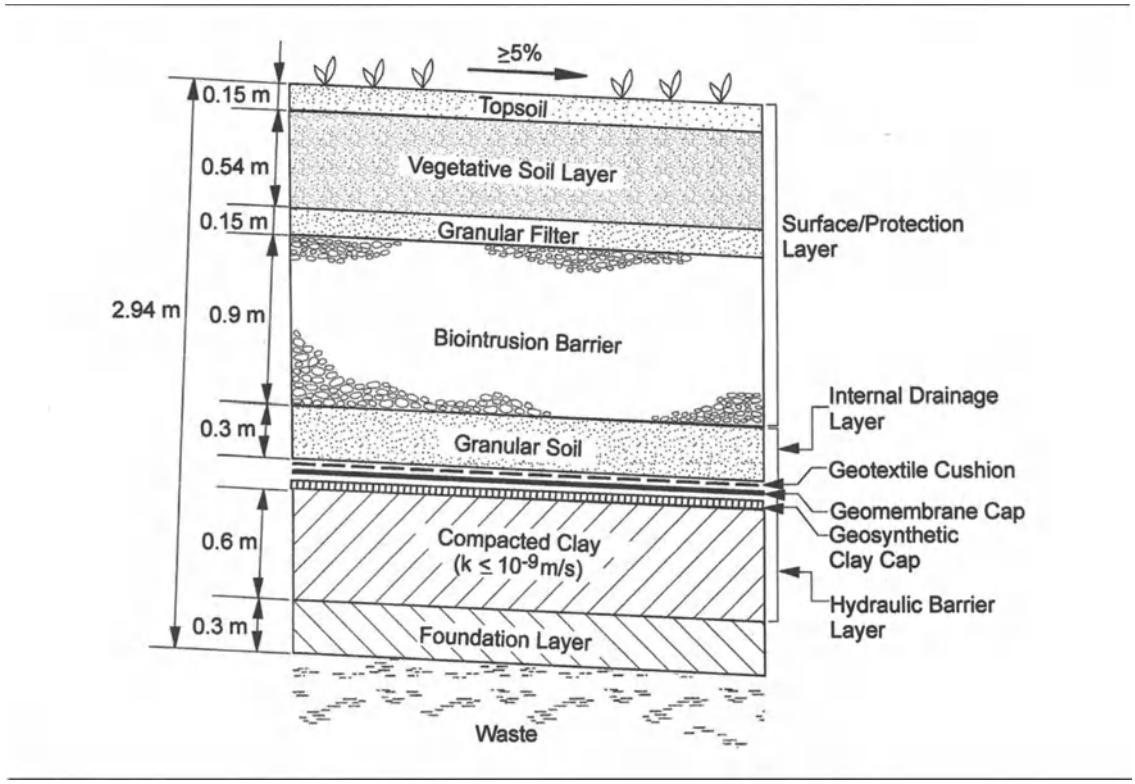


FIGURE 27.5. Example of low-level radioactive waste landfill cover.

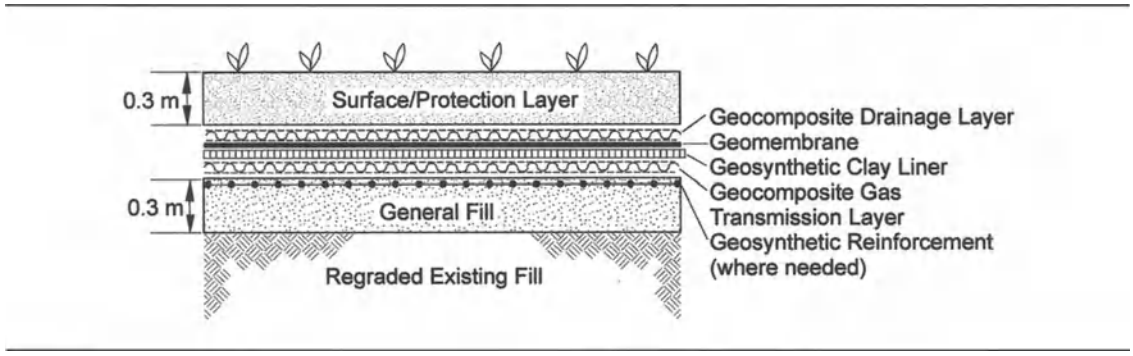


FIGURE 27.6. Example of lightweight site remediation cover over soft waste.

tems in several ways. The presence or absence of gas will influence the selection of the type of hydraulic-barrier layer material. Geomembranes are generally better barriers to gas migration than soils, with the possible exception of intact low permeability soils at or near saturation. Also, it may be necessary to install a gas transmission layer beneath the hydraulic-barrier layer to convey gas to outlets through the cover system. A factor sometimes overlooked in the closure of old landfills and in site remediation is that placement of a cover system will trap any gas being generated by the waste. Gas generation rates at these facilities may be slow enough that gas generation is not even recognized as a design issue. Yet after cover system installation, gas pressure can slowly build up. This process

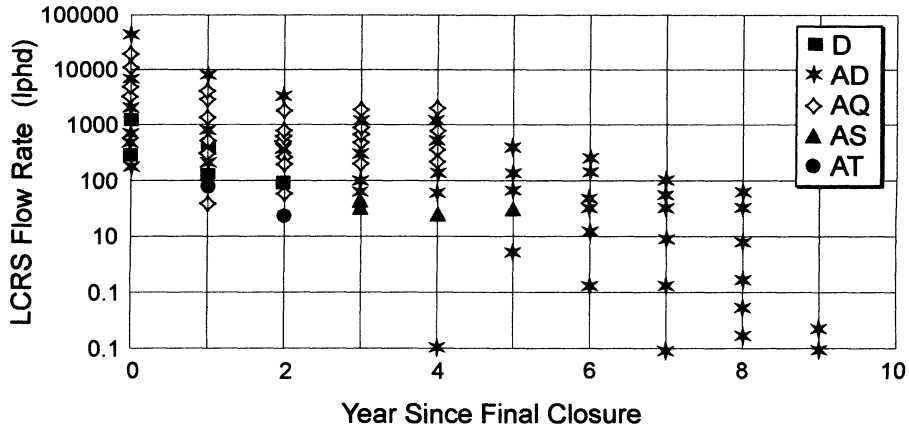


FIGURE 27.7. Leachate generation rates at five hazardous waste landfills in units of liters per hectare per day (lphd = $1\ ha^{-1}\ day^{-1}$). Covers incorporate geomembrane hydraulic barriers (modified from Gross *et al.* 1997). Note: Symbols and letters identify the five landfills in Gross *et al.* (1997).

may eventually lead to one or more of the following: (a) problems with cover system performance, including a reduction in the factor of safety along interfaces in the final cover system below the hydraulic barrier layer; and (b) for unlined or inadequately lined landfills and contaminated source areas, subsurface gas migration. Subsurface gas migration has caused adverse groundwater quality impacts at many landfills.

27.3 Components of Hydraulic-Barrier Cover Systems

27.3.1 TYPICAL COMPONENTS

Components of a typical hydraulic-barrier type cover system are briefly introduced. The usual sequencing of these typical components is illustrated in Fig. 27.8.

27.3.2 SURFACE LAYER

The primary functions of the surface layer are to resist erosion by water and wind, be maintainable, and, depending on the situation, provide a growing medium for vegetation and satisfy project aesthetic, ecological and post-closure land-use criteria.

Materials that may be used for final cover system surface layers include: (a) topsoil, (b) amended topsoil, (c) lightweight soil, (d) riprap, (e) gravel–soil mixtures, (f) asphaltic concrete, and (g) other materials. Of these materials, topsoil is, by far, the one most commonly used. Suitable topsoil will promote growth of vegetation, thereby maximizing the evapotranspirative component of the cover system water balance. Vegetation also decreases stormwater run-off velocities from cover system slopes and reinforces the topsoil; both of these effects reduce the rate of erosion of topsoil in comparison to a topsoil layer without vegetation. In areas where the amount of precipitation is inadequate to support growth of a vegetative layer, riprap, gravel–soil mixtures, asphaltic concrete, or other materials may be used for the surface layer.

27.3.3 PROTECTION LAYER

A protection layer may serve several functions (Daniel & Koerner 1993b): (a) store water that has infiltrated through the surface layer until the water later returns to the atmosphere through evapotranspiration; (b) serve as a barrier to human, burrowing animal, or plant root intrusion; (c) protect underlying lay-

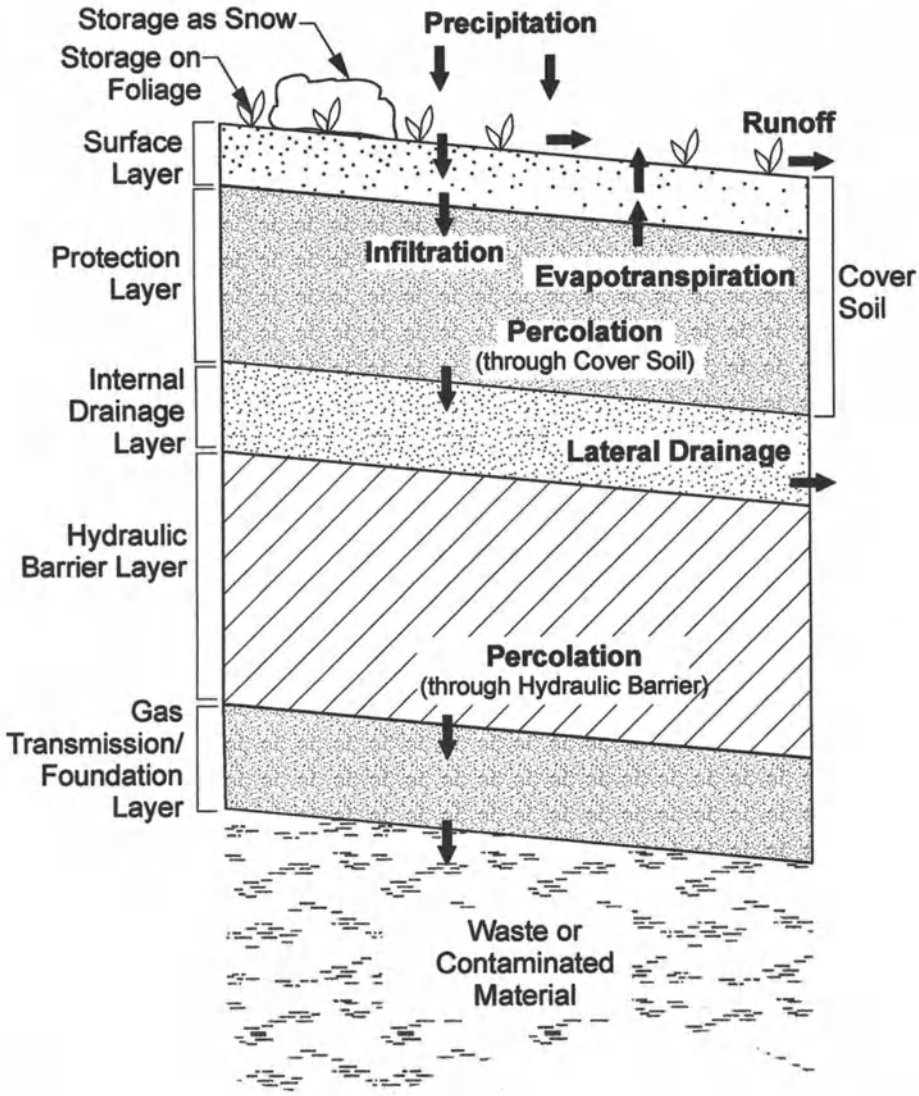


FIGURE 27.8. Identification of typical components of hydraulic-barrier cover system and water movement and storage in cover system.

ers from wet–dry cycles, which could cause cracking of some materials; (d) protect underlying layers from freezing, which could also cause cracking of some materials; and (e) restrict emissions of radon gas for those wastes, such as uranium mill tailings, that emit radon.

On-site or locally available soil is usually suitable for protection layer construction if the primary function of the layer is to serve as a vegetation root zone or for freeze–thaw protection. However, if the primary role of the protection layer is to prevent intrusion by burrowing animals, cobbles, asphaltic concrete or similar materials will typically be required.

27.3.4 INTERNAL DRAINAGE LAYER

In a hydraulic-barrier type cover system, an internal drainage layer may be required

above the hydraulic barrier. The functions of this drainage layer are to: (a) limit the buildup of hydraulic head on the underlying barrier layer, which minimizes percolation of water through the barrier; (b) drain the overlying protection and surface layers, which increases the available water-storage capacity of these layers and helps to minimize erosion of these layers by reducing the time during which the surface and protection layer materials remain saturated with water; and (c) prevent excessive seepage forces in surface, protection, and drainage layer materials, which improves cover system slope stability.

Materials used for drainage layers include sand, gravel, geonets and geocomposite drainage materials (see Chapter 7 for details regarding the different geosynthetics). The material used must have adequate hydraulic conductivity to prevent a buildup of liquid head in the slope and adequate hydraulic transmissivity to laterally convey the design flow rate. If gravel or a geonet is used for the drainage layer, a filter layer will typically need to be placed between the drainage layer and the overlying protection layer. Geotextile filter layers are typically used to achieve this function, although soil filter layers can also be used. If the drainage layer consists of gravel and the underlying barrier layer is a geomembrane, a geotextile cushion layer will typically be needed between the geomembrane and gravel. One of the most important aspects of designing an internal drainage layer is providing for free drainage at the layer discharge point.

27.3.5 HYDRAULIC-BARRIER LAYER

The function of a hydraulic-barrier layer is to minimize percolation of water through the cover system. Properly designed barrier layers can virtually eliminate infiltration into waste. Hydraulic barrier layers also restrict migration of gas or volatile constituents from the waste to the atmosphere. Materials used for barrier layer construction include CCLs, GCLs and geomembranes. These barrier materials may be used alone or in combination.

Historically, CCLs were the most frequently used barrier layer material. Procedures for initial construction of CCL barriers to meet permeability criteria are well-established (see Chapter 25). However, when used alone, CCL barriers in cover systems may not maintain low permeability in the long term. USEPA (1999) describes a number of field case studies where CCL barriers exhibited increasing permeability with time when used alone as waste covers even when overlain by protection and surface layers. This increase is attributed to desiccation cracking, wet–dry and freeze–thaw effects, root penetration, and differential settlement. Field studies by Montgomery & Parsons (1989); Corser & Cranston (1991); Melchior (1997); and the Maine Bureau of Remediation and Waste Management (1997) demonstrate the problem. The USEPA suggests that the best way (USEPA 1999) to maintain low CCL permeability in a cover application is to overlay the CCL with both a geomembrane and an adequate thickness of protection soil.

GCLs are factory fabricated products (see Section 7.6) having attractive features for cover system applications, which include very low saturated hydraulic conductivity (e.g. $k \leq 5 \times 10^{-11}$ m s^{-1}), preservation of low hydraulic conductivity when subjected to differential settlement, and ease of installation. Disadvantages include low hydrated shear strength, potential for increased hydraulic conductivity due to cation exchange reactions under certain conditions, and potential for premature hydration during installation. GCLs are increasingly being used in cover system applications. Additional information on these materials is presented in Chapter 25, Koerner (1998); Daniel & Koerner (1993a); Koerner & Gartung (1995); Koerner & Daniel (1997); and Well (1997). The results of a large-scale test plot program sponsored by the USEPA to evaluate GCL-use in cover

systems are presented in Daniel & Scranton (1996) and Daniel *et al.* (1998).

Geomembranes are factory-manufactured polymeric materials (see Section 7.5) that are widely used as hydraulic barriers in cover systems due to their non-porous structure, flexibility, and ease of installation. Spray-on elastomeric and bituminous membranes are also available, but are rarely used in cover system applications.

27.3.6 GAS TRANSMISSION LAYER

Gas transmission layers may be necessary beneath cover system barrier layers for wastes that generate gas. These layers are designed to have adequate in-plane gas transmissivity to convey gas to passive gas vents, active gas wells, or trenches. Gas transmission layers are typically a necessary complement to systems that utilize passive gas vents. Gas transmission layers may not always be needed for landfills with active gas extraction systems, depending on gas generation rates in the landfill, extraction well spacing, presence or absence of horizontal gas trenches, and other factors. Gas transmission layers may be constructed of granular materials or geosynthetics (geotextiles, geonets or geocomposites). When a granular material is used, a separation layer (typically a geotextile) may be needed to separate the granular material from the overlying barrier layer.

27.3.7 FOUNDATION LAYER

The foundation layer forms the bottom-most component of the cover system. The functions of the foundation layer are to provide grade control for cover system construction, adequate bearing capacity for overlying layers, firm subgrade for compaction of overlying layers, smooth surface for installation of overlying geosynthetics, and, in some applications, buffer zone to reduce the potential effects of waste differential settlements on cover system components. Materials most often used for the foundation layer include on-site or locally available soils. Sometimes, intermediate cover soil already in place is used for all or a portion of the foundation layer. In a few situations, waste material can be used to construct the foundation layer. If constructed of granular material, the foundation layer may also serve as a gas transmission layer.

27.4 Capillary Barrier Cover Systems

As noted in Section 27.2.1, a capillary barrier consists of one or more layers of finer-grained soil overlying one or more layers of coarse-grained soil. At a high matric suction (Fig. 27.2), the hydraulic conductivity of coarse-grained soil is much less than that of fine-grained soil. Under unsaturated flow conditions (high matric suction), moisture movement through the fine-grained soil is greatly impeded when the moisture reaches the interface between the fine- and coarse-grained materials. This fact is used to advantage to design capillary soil barriers. Capillary barriers are finding increasing use in two applications: (a) cover systems for arid sites; and (b) mine waste cover systems.

Capillary barriers are being increasingly used at arid sites where the fine-grained surface layer can be maintained at a low degree of saturation. The critical design condition for these barriers is often winter rain or snow melt. The fine-grained soil layer must be designed to prevent saturation of the layer near the soil interface during these periods. This requires that the fine soil have adequate moisture storage capacity above the soil interface. Also, to be effective, fine-grained soil must not undergo desiccation cracking upon drying. The performance characteristics of these types of cover systems in arid site applications have been discussed by Anderson *et al.* (1993), Benson & Khire (1995), Dwyer (1995, 1998), Fayer *et al.* (1992), Gee *et al.* (1997), and Khire *et al.* (1997).

Capillary barriers are also used in soil covers

for controlling acid production in sulfide mine waste. In this application, the cover system is constructed such that the upper portion of the fine-grained soil layer maintains a high degree of saturation to minimize oxygen intrusion, while the lower portion of the layer remains unsaturated to maintain high matric suction at the soil interface. Under this condition, the coarse layer is not able to transmit a significant amount of moisture downward from the overlying fine-grained layer, and essentially prevents the fine-grained layer from draining. Coarser-grained surface layers are often used with the mine waste covers to increase percolation into, and reduce evapotranspiration from, the fine-grained soil layer. The use of capillary barriers for mine waste covers is discussed by Rasmuson & Eriksson (1987), Nicholson *et al.* (1989), and Yanful & Aubé (1993). Investigations of the performance of capillary barriers in field test plots in Quebec, New Brunswick, and Ontario, Canada, are given in Yanful (1993), Yanful *et al.* (1993a,b), Woyshner & Yanful (1995), and Simms & Yanful (1997).

Figure 27.9 shows a cross-section of the capillary-barrier cover system investigated by Yanful (1993) and Woyshner & Yanful (1995) at the Waite Amulet tailings site in Quebec, Canada. The cover was instrumented with time domain reflectometry (TDR) probes and sensors to measure water content and gaseous oxygen in the various layers. Figure 27.10 shows the volumetric water in the tailings, sand base, and the clay during four years of monitoring from 1990 to 1994. The data indicate that the sand base (the capillary barrier) did not attain a volumetric water content of more than 11% (a degree of saturation of 34%) during the four years. This suggests that during the spring and fall months, at least, there was no significant capillary break and that the overall percolation through the cover system was small. Woyshner & Yanful (1995) measured water percolation in the lysimeters and reported an overall annual percolation that was only 4% of the total precipitation. They also showed that the hydraulic conductivity of the sand

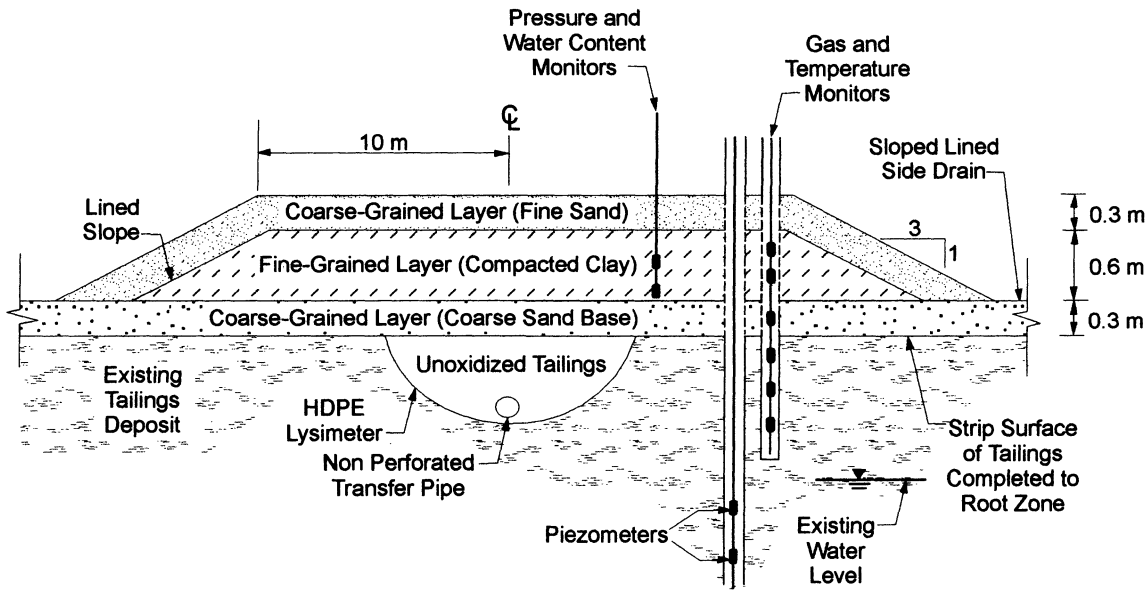


FIGURE 27.9. Capillary-barrier cover system over mine waste at Waite Amulet site, Quebec, Canada (modified from Yanful 1993).

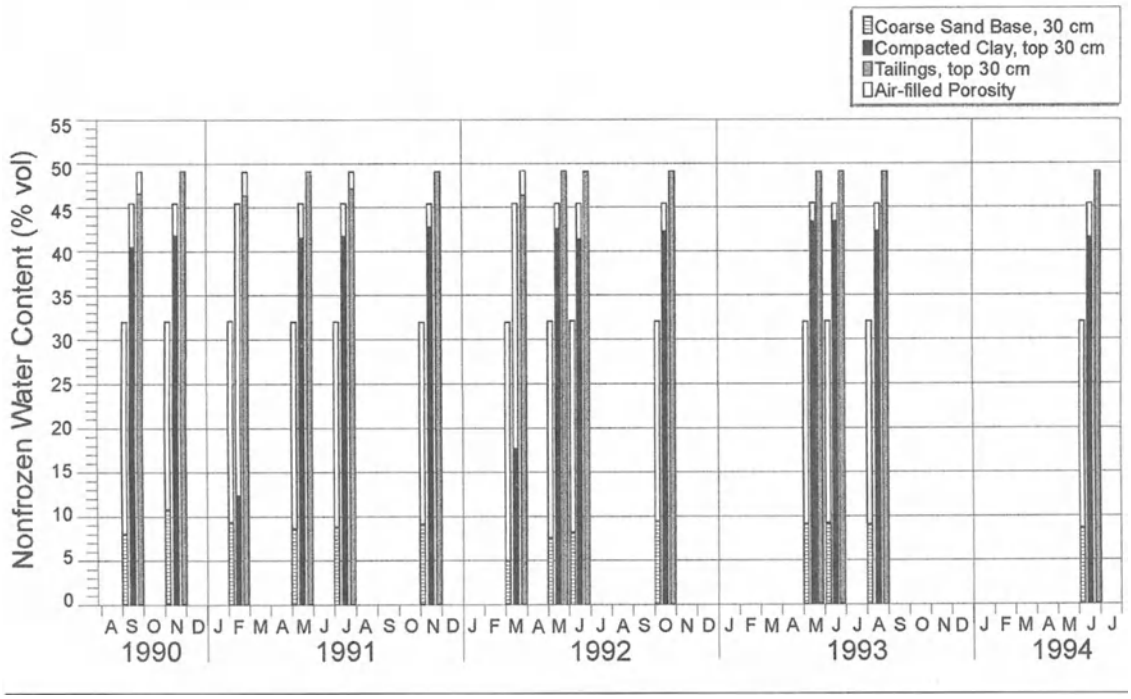


FIGURE 27.10. Water content and air-filled porosity of capillary barrier and mine waste at Waite Amulet site, Quebec, Canada (modified from Woyshner & Yanful 1995).

base capillary barrier would decrease and become lower than that of the clay layer when the suction exceeded 25 kPa.

Figure 27.11 shows oxygen profiles measured in the cover system at different times in 1990 and 1991. The profiles indicate a rapid drop in oxygen concentrations in the clay layer from 12 to about 4%. Yanful (1993) analyzed the data in Fig. 27.11 and calculated an oxygen flux of 0.011 g m^{-2} day^{-1} through the covered tailings. In comparison, the flux through the uncovered tailings was calculated to be 5.83 g m^{-2} day^{-1}, indicating a 99% cover efficiency, based on oxygen diffusion alone.

O'Kane *et al.* (1995) also presented the results of an investigation into the performance of a soil cover consisting of two till layers placed over an acid-producing mine waste rock pile at the Equity Silver mine site in British Columbia, Canada. The function of the cover was to reduce water infiltration and gaseous oxygen ingress into the rock pile. In

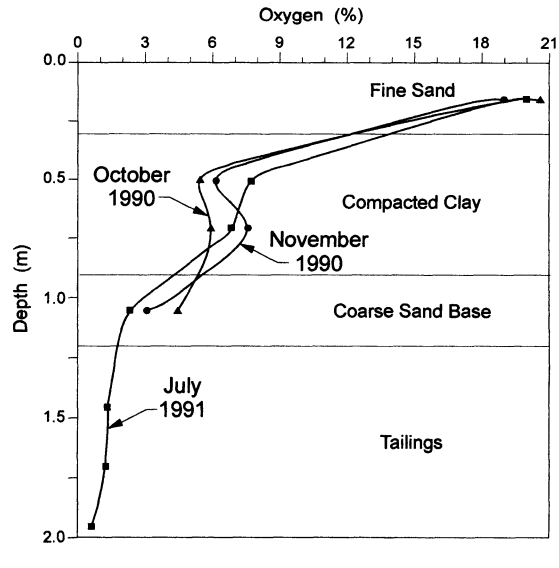


FIGURE 27.11. Field gaseous oxygen profiles in capillary barrier and mine tailings at Waite Amulet site, Quebec, Canada (modified from Yanful 1993).

the design of the cover, the waste rock, being coarse, was relied upon to function as a capillary barrier. The upper 0.3-m thick till layer was loosely placed, while the lower 0.3-m thick till layer was compacted. Suction measurements suggested that the matric suction within the rock pile was similar to the suction at residual saturation. At this suction, the unsaturated hydraulic conductivity of the rock pile would be low and would lead to very little water flow. A water balance evaluation indicated that for these conditions, the overlying compacted till layer would retain a significant portion of its placement water content. The data obtained by O'Kane *et al.* (1995) suggests that the compacted till layer maintained a degree of saturation equal to or higher than the 85% during cyclic wetting and drying.

27.5 *Water Balance*

27.5.1 OVERVIEW

A water balance analysis is used to quantify the percolation of water into and through the cover system. In addition to estimating percolation, water balance analyses of cover systems are used to: (a) develop an understanding of how the various cover system components will function, and identify which water-routing mechanisms are most important; (b) compare the performance of difference cover system designs; and (c) define the performance criteria for various cover system components (e.g. required storage capacity of surface and protection soil layers, required flow capacity of internal drainage layer) so that these components can be designed.

27.5.2 WATER BALANCE CONCEPT

In a water balance analysis, water is routed into and out of a system using a series of calculations that require conservation of water mass. The potential pathways for water movement into and out of a cover system are illustrated in Fig. 27.8. A cover system water balance is expressed in terms of water inflows and outflows and storage changes for a unit area of the system over some arbitrary time interval, e.g. day, as:

$$P = R + ET + \Delta W_{surface} + \Delta W_{foliage} + \Delta W_{soil} + L + PERC \quad (27.1)$$

where P = precipitation (mm day^{-1}), R = run-off (mm day^{-1}), ET = evapotranspiration (mm day^{-1}), $\Delta W_{surface}$ = change in water storage at surface (mm day^{-1}), $\Delta W_{foliage}$ = change in water storage on plant foliage (mm day^{-1}), ΔW_{soil} = change in water storage in cover system soil (mm day^{-1}), L = lateral drainage from internal drainage layer (mm day^{-1}), and $PERC$ = percolation through the cover system (mm day^{-1}). Water is input to the cover system as precipitation in the form of rain or snow, and lost from the cover system by run-off, evapotranspiration, lateral drainage and percolation. Water also is stored on the cover system as ponded water or snow, on plant foliage, and in cover system soils by capillary action. Equation 27.1 is cast above in a time unit of one day; any other time unit could equally well be used.

Infiltration is primarily removed from the cover system by evapotranspiration. Storage of water in soil coupled with removal of water by evapotranspiration are the most important mechanisms for limiting percolation of infiltration. Flow from lateral drainage layers is typically a much smaller component of the water balance than is evapotranspiration. It should be remembered, however, that while the internal drainage layer is typically of secondary importance to the overall cover system water balance, it is of prime importance to cover system slope stability. If even a relatively small amount of potential lateral flow is left undrained in a cover system, hydraulic heads can build up over the hydraulic barrier layer, leading to destabilizing seepage forces on cover system slopes.

Though Eq. 27.1 appears simple, the components of the water balance are dependent

on many factors, difficult to quantify and interrelated. It can be especially difficult to quantify percolation in arid and semi-arid environments, where almost all precipitation is consumed by evapotranspiration. Unlike in wetter climates where actual evapotranspiration may approach the magnitude of potential evapotranspiration, i.e. the process is energy limited, in drier climates actual evapotranspiration is generally much smaller than potential evapotranspiration due to the lack of available water. Evapotranspiration is more difficult to accurately estimate under water-limiting conditions. Because the magnitude of percolation in drier climates is so much smaller than the magnitudes of evapotranspiration and precipitation, relatively small errors in estimated evapotranspiration can result in relatively large errors in estimated percolation. Due to the difficulty in performing accurate analytical water balances, field water balances are often performed using weighing or drainage lysimeters or cover system test plots to better assess the water balances components in drier climates.

Water balance calculations are performed for time intervals that may be shorter than one hour or longer than a year. The time interval to use is dependent on the purpose of the water balance analysis.

27.5.3 WATER BALANCE METHODS

A variety of water balance methods are available to analyze and design cover systems. They range in complexity from relatively simple empirical correlations to sophisticated computer-based finite difference and finite element models. This section describes four of the more widely known and used water balance analysis methods:

- simplified manual method (Koerner & Daniel 1997),
- hydrologic evaluation of landfill performance (HELP) model (Schroeder *et al.* 1994, Schroeder *et al.* 1994),
- leachate estimation and chemistry model (LEACHM) (Hutson & Wagenet 1992), and
- UNSAT-H model (Fayer & Jones 1990).

These are all well-documented, public-domain models that consider the significant water balance processes, e.g. precipitation, run-off, and evapotranspiration, and have been used previously for waste cover water balance analyses. The characteristics of these models are compared in Table 27.1.

27.5.4 SIMPLIFIED MANUAL METHOD

27.5.4.1 Description of Method

Koerner & Daniel (1997) present an updated version of a simplified method for performing manual or computer-spreadsheet water balance calculations first presented in Thornthwaite and Mather (1955, 1957); Fenn *et al.* (1975); and Kmet (1982). In the previous work, only monthly time steps were considered. Koerner & Daniel (1997), however, extended the method to consider a variable time step, e.g. daily, weekly or monthly, to be selected based on the purpose of the analysis.

From the basic concepts of water balance analysis shown in Fig. 27.8 and described by Eq. 27.1, and assuming no water is stored at the surface or intercepted by plants, i.e. $\Delta W_{surface} = \Delta W_{foliage} = 0$, the following relationships are defined for a given time step:

$$P = I + R \tag{27.2}$$

$$I = ET + \Delta W_{soil} + PERC^* \tag{27.3}$$

where I = cover system infiltration (mm day^{-1}); and $PERC^*$ = percolation through cover soil (mm day^{-1}) in Fig. 27.8.

In the simplified formulation (Eq. 27.2), precipitation is partitioned into run-off or infiltration. Run-off is calculated as a fraction of precipitation using a run-off coefficient appropriate for the cover system soil type and slope, i.e. the "rational formula" is used. According to Fenn *et al.* (1975), the rational formula will, in most cases, underestimate run-off.

TABLE 27.1. Comparison of some public-domain water balance models

	Simplified manual method	HELP computer code	LEACHM computer code	UNSAT-H computer code
Calculation scheme	Simplified empirical and mechanistic equations	Quasi two-dimensional water-routing model, with multiple uncoupled subroutines Simplified empirical and mechanistic equations Simplified unsaturated flow model with unit hydraulic gradient	Finite difference model with unsaturated flow model based on Richards partial differential equation User-specified boundary conditions	Finite difference model with unsaturated flow model based on Richards partial differential equation User-specified boundary conditions
Advantages	Easy to perform Few data requirements Any time step Considers lateral drainage	Widely accepted Used to design hydraulic barriers Easy to run simulations Default database of climatic, soils and vegetation data Considers lateral drainage	Mechanistic model Solves unsaturated flow equation Used to design evapotranspirative and capillary barriers May give a better estimate of evapotranspiration in arid climates than the other models	Mechanistic model Solves unsaturated flow equation Flexibility in definition of unsaturated hydraulic conductivity–head–moisture content relationships
Disadvantages	Numerous simplifying assumptions must be made Steady state conditions are assumed All calculations are uncoupled Cannot be used for unsaturated flow	Does not solve unsaturated flow equations Demonstrated overprediction of percolation in many cases Limited to daily climatic data	Only models soil profiles that are no more than 2-m thick Does not consider lateral drainage	High computational demands Unsuitable for parametric evaluation Does not consider lateral drainage
Appropriate use	Instructional tool Design of hydraulic barriers Check of computer simulations Parametric evaluations Calculation of peak lateral drainage from cover system	Design of hydraulic barriers Regulatory compliance demonstrations Parametric evaluations Calculation of peak lateral drainage from cover system	Design of evapotranspirative and capillary barriers (no lateral flow) Parametric evaluations Unsaturated flow analysis	Performance assessment of evapotranspirative and capillary barriers (no lateral flow) Calibration with field data prior to making long-term predictions Unsaturated flow analysis

From Eq. 27.3, water infiltrating the cover soil will evapotranspire, become soil water storage, or percolate downward. In the simplified manual method, evapotranspiration is calculated as a function of the potential evapotranspiration, infiltration, and moisture stored in the soil. Potential evapotranspiration is calculated using an empirical method developed by Thornthwaite & Mather (1955). If more water infiltrates the cover system than can potentially evapotranspire, the excess water is first distributed within the root zone until the soil moisture content is at field capacity. The remaining water is then routed as percolation from the cover soil. If evapotranspiration is greater than infiltration, then stored water is lost from the root zone of the cover system soil until the soil moisture content is at the wilting point.

If water does not flow laterally through an internal drainage layer, percolation through the hydraulic barrier is equal to percolation through the cover soil, i.e. $PERC^* = PERC$. Otherwise:

$$PERC^* = PERC + L. \tag{27.4}$$

In the simplified manual method, Eq. 27.4 is solved iteratively since both *PERC* and *L* are a function of hydraulic head. Assuming steady state conditions, the maximum flow in the internal drainage layer is calculated as:

$$q_m = lL = l(PERC^* - PERC) \tag{27.5}$$

where q_m = maximum flow in internal drainage layer per unit width perpendicular to the direction of flow ($m^2\ s^{-1}$), l = slope length (m), and other terms are as previously defined. The hydraulic transmissivity of the drainage layer must be adequate to accommodate this flow. Using Darcy's equation and the DePuit–Forcheimer assumptions, i.e. line of seepage is assumed to be parallel to the cover system slope and the hydraulic gradient is constant and equal to the sine of the slope angle:

$$T = \frac{l(PERC^* - PERC)}{\sin \beta} FS \tag{27.6}$$

where T = required hydraulic transmissivity of drainage layer ($m^2\ s^{-1}$), β = slope angle (degrees), and FS = factor of safety for flow capacity. Koerner & Daniel (1997) recommend use of a FS value of at least five to ten. The maximum hydraulic head in the drainage is given by:

$$h_m = \frac{q_m}{k \tan \beta} \tag{27.7a}$$

where h_m = maximum hydraulic head (m), k = hydraulic conductivity of drainage medium, and q_m is as defined by Eq. 27.5. The maximum thickness of flow (measured perpendicular to the slope) is obtained from h_m using the equation:

$$t_m = h_m/\cos \beta \tag{27.7b}$$

where t_m = the maximum thickness of flow (m). The design thickness of the internal drainage layer must be larger than t_m in order for pressure head not to build up in the layer.

Percolation through CCL or GCL barrier layers is calculated by Koerner & Daniel (1997) using Darcy's equation (see Chapter 25). Percolation through geomembrane and composite liners is calculated by Koerner & Daniel (1997) using the leakage rate equations developed by Giroud & Bonaparte (1989a,b) (see Chapter 26). Hydraulic head is an input parameter to these equations. It is suggested that h_m evaluated from monthly average water balance calculations be used to calculate leakage rates through hydraulic barriers.

Input data needs for the simplified manual method are minimal. Only precipitation and mean temperature data are required. Koerner & Daniel (1997) provide guidance for selecting all other parameters, e.g. run-off coefficient, root zone depth, and soil water storage capacity. The advantages of the method are its simplicity, ability to use a variable time step, and ability to calculate lateral flows in cover system internal drainage layers. The main disadvantages of the method are the steady state nature of all calculations and the numerous simplifying assumptions. Nonetheless, when

appropriately used, the simplified manual method presents an acceptable approach to the design of hydraulic-barrier type final cover systems. The method is in no way adequate as a simulation or predictive tool, nor is it applicable to the analysis or design of capillary barriers or evapotranspirative barriers.

27.5.4.2 Design of Internal Drainage Layers

Koerner & Daniel (1997) suggest that for sizing the hydraulic requirements of the internal drainage layers, q_m be calculated based on a single storm event. With this approach, the soil above the drainage layer is assumed to be saturated and infiltration into the cover soil is assumed to equal percolation from the cover soil. Accordingly:

$$PERC^* = P - R = P(1 - C) \quad (27.8)$$

where: C = run-off coefficient (dimensionless) obtained from Fenn *et al.* (1975), Table 27.2, or from project-specific information.

Equation 27.5 was developed assuming that:

- the soil is at field capacity before the storm begins,
- there is no evapotranspiration during the storm, and
- the cover soil is sufficiently permeable to accept the calculated infiltration.

TABLE 27.2. Run-off coefficients (adapted from Fenn *et al.* 1975) suggested by Koerner & Daniel (1997) for simplified manual water balance calculations

Description of soil	Slope Description	(%)	Run-off coefficient
Sandy soil	Flat	<2	0.05–0.10
	Average	2–7	0.10–0.15
	Steep	>7	0.15–0.20
Clayey soil	Flat	<7	0.13–0.17
	Average	2–7	0.18–0.22
	Steep	>7	0.25–0.35

Koerner & Daniel (1997) suggest that if the cover soil is not permeable enough to meet this last assumption, $PERC^*$ should be calculated using Eq. 27.9:

$$PERC^* = P(1 - C) \quad \text{when } k_{cs} \geq P(1 - C) \quad (27.9a)$$

$$PERC^* = k_{cs} \quad \text{when } k_{cs} \leq P(1 - C) \quad (27.9b)$$

where k_{cs} = the cover soil saturated hydraulic conductivity in the same units as P. Equation 27.9 can be used to develop a conservative estimate of peak flow into a lateral drainage layer during a single storm event, a capability available in none of the other water balance models considered in this chapter.

27.5.4.3 Refinement to Simplified Manual Method

Equations are available to refine those algorithms in the simplified manual method related to calculating hydraulic head in the internal drainage layer and leakage through a hydraulic-barrier layer containing a geomembrane.

An improved estimate (compared to Eq. 27.7) of maximum hydraulic head in the internal drainage layer can be obtained using the equations from Giroud *et al.* (1992b) and Giroud & Houlihan (1995):

$$h_m = (jl/2)\left[\left(\tan^2\beta + \frac{4PERC^*}{k\cos\beta}\right)^{1/2} - \tan\beta\right] \quad (27.10a)$$

where all terms are as defined previously, and j is given by Eq. 27.10b:

$$j = 1 - 0.12\exp\{-[\log(8\lambda/5)^{5/8}]^2\} \quad (27.10b)$$

where:

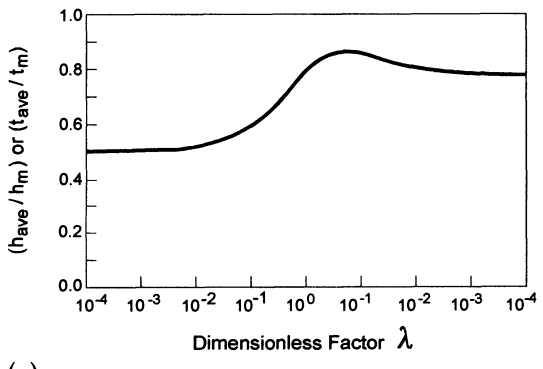
$$\lambda = \frac{PERC^*}{k\tan\beta\sin\beta}. \quad (27.10c)$$

Values of average hydraulic head, h_{ave}, for a given value of h_m can be obtained from Fig. 27.12. For the case of $(PERC^*/k) < 0.25 \tan^2\beta$:

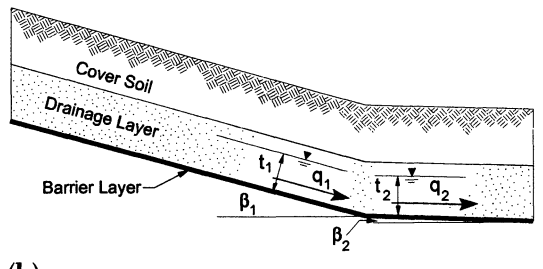
$$h_{ave} = \frac{PERC^* l}{2k \sin \beta \cos \beta}. \qquad (27.11)$$

It is suggested that with the simplified method, h_m be used from single storm event analyses to size the cover system internal drainage layer; h_{ave} can be used to calculate long-term *PERC* values. Similar to the method in Koerner & Daniel (1997), $PERC^*$ to calculate h_m should be derived using hourly water balance calculations for the design storm, and $PERC^*$ to calculate h_{ave} should be derived using monthly water balance calculations.

Improved estimates of leakage rates through geomembrane, geomembrane–GCL, and geomembrane–CCL hydraulic barriers can be obtained using the updated equations developed by Giroud and his coworkers, described in Chapter 26.



(a)



(b)

FIGURE 27.12. Cover system internal drainage layer: (a) values of (h_{ave}/h_m) or (t_{ave}/t_m) modified from Giroud & Houlihan 1995; and (b) flow continuity at slope bench or transition.

27.5.4.4 Design of Slope Transitions

Many cover systems are designed with benches and slopes transitions. Cover system failures have occurred due to hydraulic pressure buildup in the internal drainage layer at the transition. To prevent this condition, flow capacity, q, in the internal drainage layer must not decrease across the transition (Fig. 27.12b).

For many cover systems, the hydraulic gradient on the flatter part of the slope transition will be about one order-of-magnitude lower than the hydraulic gradient on the steeper part. For example, the gradient of a 3H : 1V slope is 0.32, whereas the gradient reduces to 0.03 for a 3% slope inclination typical of a cover system bench. For this condition, to prevent backup of flow and buildup of hydraulic head for an internal drainage layer flowing full, the hydraulic transmissivity of the drainage layer on a cover system bench or slope transition will need to be about one order-of-magnitude larger than that of the drainage layer on the sideslope.

More generally, based on Fig. 27.12b, to prevent hydraulic head buildup:

$$T_2 \geq T_1(\sin \beta_1 / \sin \beta_2) \qquad (27.12)$$

where T = hydraulic transmissivity ($m^2\ s^{-1}$), and β = slope angle (degrees). The subscript "1" refers to the portion of the drainage layer on the steeper upslope side of the transition and the subscript "2" refers to the drainage layer on the flatter downslope side of the transition (Fig. 27.12b). Equation 27.12 can be used directly to analyze geosynthetic

drainage layers for which hydraulic transmissivities are either known or measured in the laboratory. For granular drainage materials where materials are typically specified in terms of a required hydraulic conductivity and thickness, Eq. 27.12 is recast as:

$$k_2 \geq k_1(t_1/t_2)(\sin \beta_1/\sin \beta_2) \quad (27.13)$$

where k = hydraulic conductivity of drainage material (m s^{-1}), and other terms are as defined previously. For Eq. 27.13 to be valid, t_1 and t_2 must be less than the total thickness of the drainage layer.

27.5.5 HELP MODEL

The HELP computer code was developed by the US Army Corps of Engineers Waterways Experimental Station (WES) for the USEPA. At the time of writing, the most recent revision (Version 3.07) can be purchased from NTIS or downloaded from the WES website at http://www.wes.army.mil/el/elmodels. The documentation developed by Schroeder *et al.* (1994a,b) can be downloaded from the USEPA website at http://www.epa.gov/cincl/ or purchased from the US National Technical Information Service, (800) 553-6847. Additional guidance on using the HELP model to evaluate the hydrologic performance of cover systems can be found in USEPA (1991).

The HELP model simulates hydrologic processes for active or closed landfills by performing sequential water balance calculations using a quasi-two-dimensional approach, which considers all flow to be vertical, except at lateral drainage layers, where flow can be vertical or lateral. The simulation is marched forward in time with the water balance processes being considered steady within each time step. The conceptualization of the HELP model is shown in Fig. 27.13. The model can be used to separately evaluate each subsurface profile shown in Fig. 27.13.

The hydrologic processes considered in the model include precipitation, surface water storage, i.e. storage as snow, interception of precipitation by foliage, surface water evaporation, run-off, snow melt, infiltration, plant transpiration, soil water evaporation, soil water storage, vertical flow (saturated and unsaturated) through non-barrier soil layers, vertical percolation (saturated) through soil barrier layers, vertical percolation (saturated) through geomembrane and geomembrane–soil composite barrier layers, and lateral or vertical flow (saturated) through lateral drainage layers.

Run-off in the HELP model is computed using the run-off curve number method of the US Department of Agriculture Soil Conservation Service (USDA-SCS) (USDA-SCS, 1985). Daily run-off is calculated in the model as:

$$R = \frac{(P - 0.2S)^2}{(P + 0.8S)} \quad (27.14)$$

where S = retention parameter (mm day^{-1}), dependent on SCS curve number; and R and P are daily average run-off and precipitation, respectively (mm day^{-1}). The SCS curve number is a function of soil texture, vegetation quality, and cover system slope length and inclination. McBean *et al.* (1995) state that use of daily rainfall averages effectively decreases storm intensity (because the duration of most storms is less than 24 h), resulting in a simulation that overpredicts infiltration and underpredicts run-off.

Evapotranspiration is computed in the HELP model using a two-stage modified Penman energy balance method developed by Ritchie (1972). This method uses the potential evapotranspiration concept as the basis for prediction of surface and soil water evaporation and plant transpiration. The potential evapotranspiration demand is first met by evaporation of water or snow on foliage or on the ground, then soil water evaporation, and finally plant transpiration. Due to the assumptions built into the HELP model,

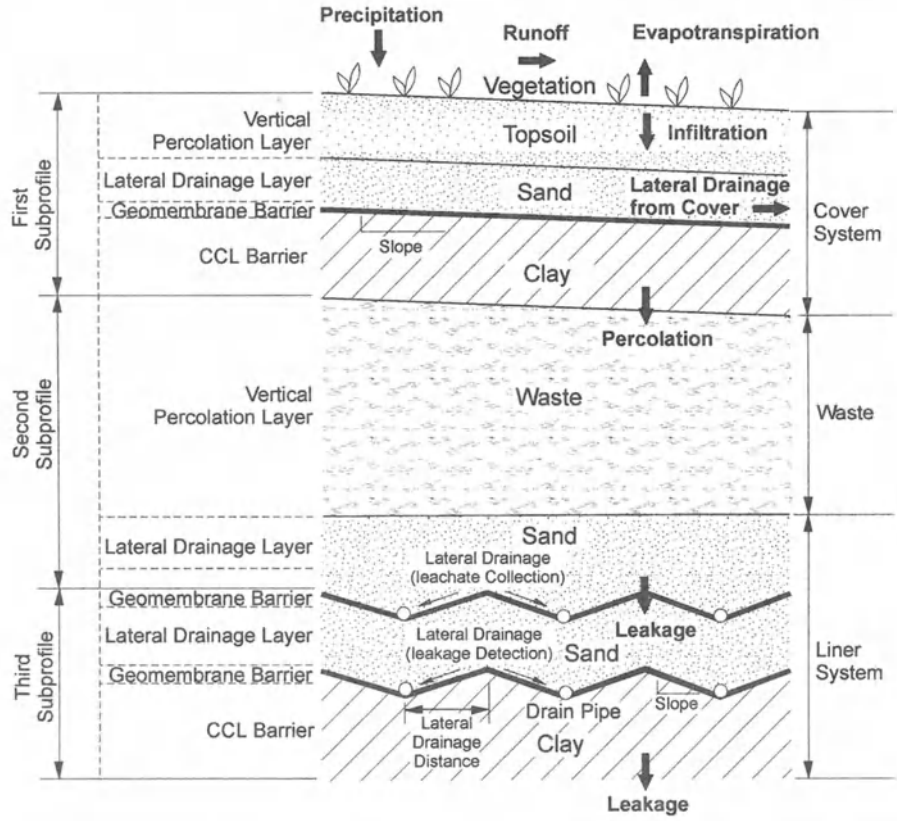


FIGURE 27.13. Conceptualization of HELP water balance model (modified from Schroeder *et al.* 1994a).

evapotranspiration may be underestimated in arid climates. Growth and decay of surface vegetation is modeled using an algorithm taken from the simulator for water resources in rural basins (SWRRB) model (Arnold *et al.* 1989).

Vertical drainage for cover soil, i.e. topsoil and protection, layers for both saturated and unsaturated flow conditions, is computed using Darcy's equation. The HELP model assumes that there is a unit gradient across the vertical percolation layer. The model utilizes an unsaturated hydraulic conductivity and the unit hydraulic gradient to calculate unsaturated flow rates. The unsaturated hydraulic conductivity, k_u (m s^{-1}), is obtained using Campbell's (1974) equation:

$$k_u = k_s[(\theta - \theta_r)/(\theta_s - \theta_r)]^{3+2/\zeta} \quad (27.15)$$

where k_s = saturated hydraulic conductivity of soil layer (m s^{-1}); θ = volumetric moisture content of soil layer (dimensionless); θ_s = volumetric moisture content of soil layer at saturation (dimensionless); θ_r = volumetric moisture content of soil layer at wilting point, typically in the range 0.01–0.10 (dimensionless); and ξ = poresize distribution index (dimensionless), calculated as described in Schroeder *et al.* (1994a,b). As a result of the hybrid formulation given above, the model cannot be used to simulate the physics of water movement through an unsaturated soil layer.

Lateral drainage below a cover soil layer is

modeled by an analytical approximation to the steady state solution of the Boussinesq equation (McEnroe 1993). Vertical percolation through low permeability soil hydraulic barriers is evaluated using Darcy's equation assuming saturated conditions and the calculated average hydraulic gradient across the barrier layer. Vertical percolation through geomembranes and geomembrane–soil composite barriers is evaluated based on the work of Giroud & Bonaparte (1989a,b) and Giroud *et al.* (1992a) (see Chapter 26).

The daily water balance is calculated by a linking process, starting with a surface water balance, then evapotranspiration in the subsurface, and finally subsurface water routing from the surface downward one soil layer at a time. The routing procedure uses a time step that can range from 30 min to 6 h. However, only daily, monthly, annual, and long-term average output data are reported.

Data requirements for Version 3 of the HELP model are summarized in Schroeder *et al.* (1994a,b). The HELP model requires daily and general climatic data, material properties data for the cover system components being modeled, and cover system design data. An important feature of the model is its climatic and material property default data options. Required daily weather data include precipitation, mean temperature, and total global solar radiation.

Due to its method of calculating downward flux and its limiting of upward flux, i.e. no upward flux within or below a barrier layer, the HELP model is not considered a particularly accurate simulation model for cover systems located in arid areas where the subtleties of unsaturated moisture movement can dominate the water balance.

27.5.6 LEACHM MODEL

LEACHM (Hutson & Wagenet 1992) is a one-dimensional finite difference code that was developed to simulate the effects of agricultural management alternatives on the movement of water and chemicals in a shallow soil profile, i.e. to a maximum depth of 2 m. Only the hydrologic component of the model will be discussed further. The code and model documentation may be obtained from the Department of Soil, Crop & Atmospheric Sciences at Cornell University, Ithaca, New York.

LEACHM considers precipitation, run-off, evapotranspiration, soil water storage, and percolation in the water balance. Infiltration of water into the soil profile and vertical drainage are simulated using a finite difference solution to Richards' (Richards 1931) partial differential equation. This equation is obtained by combining the differential form of Darcy's equation for unsteady vertical flow with the one-dimensional differential form of the conservation of mass equation:

$$\frac{\partial \theta}{\partial t} = \frac{\partial}{\partial z}\left[k_u(\theta)\frac{\partial \psi(\theta)}{\partial z} - 1\right] - S(z, t) \qquad (27.16)$$

where Ψ = matric potential head (negative) due to capillary suction forces (N m^{-2}); θ = soil volumetric moisture content (dimensionless); k_u = unsaturated hydraulic conductivity (m s^{-1}); z = vertical co-ordinate, positive downward (m); t = time (s); and $S(z, t)$ = sink term representing uptake by transpiration (s^{-1}).

Unsaturated soil hydraulic conductivity in LEACHM is calculated using the Campbell (1974) relationship. Precipitation in excess of the infiltration capacity of the soil is shed as run-off. Evaporation and transpiration are modeled separately based on the methods of Childs & Hanks (1975). With this method, the potential evaporation and transpiration are first estimated based on the pan evaporation rate, a pan factor, and a crop cover fraction. The actual evaporation is then calculated as the lesser of the potential evaporation and the possible evaporation calculated using Richards' equation and the selected boundary condition. Any remaining poten-

tial evapotranspiration demand is applied to transpiration. However, transpiration is not allowed if the matric potential head of the soil is less than −1500 kPa, the potential corresponding approximately to the soil wilting point.

LEACHM requires that climatic data, soil properties, vegetation data, and initial and boundary conditions be input. Unlike the HELP model, there are no default data; the user must specify each input parameter. Required weather data are precipitation magnitude, rate and start time; minimum and maximum air temperatures; and pan evaporation rate. The precipitation option allows rainfall data for short, intense storms to be input. In the absence of pan evaporation rate data, the rate can be calculated by LEACHM using the Linacre equation (Hutson & Wagenet 1992) with site-specific data, i.e. latitude, elevation, temperature and precipitation. Required soil data are bulk dry density, initial moisture content, saturated hydraulic conductivity, and soil water retention curve. If a soil water retention curve is not available, LEACHM contains a routine to compute fitting parameters for Campbell's soil–water characteristic curve from the particle size distribution, bulk density, and organic matter content of the soil. However, there is considerable uncertainty in the use of the regression equations to compute these parameters.

27.5.7 UNSAT-H

UNSAT-H is a one-dimensional finite-difference water balance model developed at Pacific Northwest Laboratory (Fayer & Jones 1990) to assess the water dynamics of waste disposal facilities at the US Department of Energy Hanford site. The model also simulates soil heat flow and non-isothermal vapor flow. Vapor flow may be an important moisture transport mechanism in near-surface soils in arid climates. UNSAT-H was derived from the UNSAT model of Gupta *et al.* (1978) and has retained many of the same routines. At the time of this writing, Version 2.0 of UNSAT-H is most current. The code can be obtained from the Energy Science and Technology Software Center, Department of Energy, Oak Ridge, Tennessee.

UNSAT-H considers precipitation, run-off, evapotranspiration, soil water storage and percolation in the water balance. Like the LEACHM model, infiltration of water into, and vertical movement of moisture in, the soil profile is governed by a finite difference solution to Richards' partial differential equation. However, the unsaturated soil hydraulic conductivity term in UNSAT-H is calculated using polynomials, Haverkamp functions, Brooks–Corey functions, or van Genuchten functions, rather than the Campbell equation. Precipitation in excess of the infiltration capacity of the soil is shed as run-off. Evaporation and transpiration are considered separately. Evaporation is calculated using one of two approaches:

1. an integrated form of Fick's law of diffusion, which considers the flow of heat to and from the soil surface, the flow of water from the subsurface to the soil surface, and the transfer of water vapor from the soil surface to the atmosphere; or
2. a Penman-type equation, which is a modification of the diffusion equation and is dependent on net radiation and soil heat flux rather than on soil surface temperature.

Transpiration is calculated using a method based on leaf-area index or cheatgrass data and is limited by potential evapotranspiration.

UNSAT-H requires that climatic data, soil properties, vegetation data, and initial and boundary conditions be input. There are no default data; the user must specify each input parameter. The precipitation option allows rainfall data for short, intense storms to be input. Required soil data are fitting parameters for the soil water characteristic functions and the unsaturated hydraulic conductivity functions.

27.5.8 EVALUATION OF MODELS

A number of researchers have performed studies to evaluate the HELP, LEACHM, and/or UNSAT-H models (Thompson & Tyler 1984; Peters *et al.* 1986; Barnes & Rodgers 1988; Peyton & Schroeder 1988; Nyhan 1989; Nichols 1991; Udoh 1991; Fayer *et al.* 1992; Lane *et al.* 1992; Benson *et al.* 1993; Peyton & Schroeder 1993; Martian 1994; Fleenor & King 1995; Khire 1995; Woyshner & Yanful 1995; Khire *et al.* 1997; Webb *et al.* 1997; Zornberg & Caldwell 1998). These studies either simulated field or laboratory water balance data or investigated trends and magnitudes of the different water balance components. The conclusions of these studies are not always in general agreement. For example, some studies found that certain models overpredicted infiltration and/or percolation, whereas other studies concluded just the opposite.

Of all the available studies, the ones reported in Woyshner & Yanful (1995), Khire (1995), and Khire *et al.* (1997) are perhaps most interesting because of the scope and practical applicability of the study to cover system analysis and design.

The study by Woyshner & Yanful (1995), discussed in Section 27.4, used the HELP model to simulate water percolation through a three-layer soil cover test plot at an inactive tailings site near Rouyn-Noranda, Quebec, Canada. The cover system consisted of a compacted varved clay (0.6-m thick) placed between an upper fine sand layer (0.3-m thick), and a lower coarse sand base (0.30-m thick). A thin gravel surface layer was used for erosion protection and the cover was not vegetated. Both field and HELP model results showed that 4% of the total annual precipitation (rainfall and snow melt) percolated through the cover. The HELP model showed good predictive ability for the field conditions reported by Woyshner & Yanful (1995).

The studies by Khire (1995) and Khire *et al.* (1997) involve field water balance evaluations for three cover system test plots at two landfills, one near Atlanta, Georgia ("Live Oak") and the other near East Wenatchee, Washington ("Wenatchee"). The sites were selected to represent humid and semi-arid climates, respectively. The Live Oak test plot has a cover system with a 0.6-m thick CCL barrier overlain by a 0.15-m thick vegetated soil surface layer. In Wenatchee, one test plot has the same cover system as at Live Oak site and the other test plot has a 0.75-m thick sand capillary barrier in lieu of the CCL. Climate, run-off, percolation, and soil moisture data collected between 1992 and 1995 were reported by Khire (1995) and Khire *et al.* (1997); however, data collection was still ongoing as of 1998. Run-off and percolation are collected in tanks and measured, while soil moisture content is measured by time domain reflectrometry.

Khire *et al.* (1997) used their test plot data to assess the predictive capabilities of the HELP and UNSAT-H models and made the following observations from their study:

- Throughout most of the monitoring period, HELP underpredicted run-off for the humid Live Oak site by 740 mm (≈90%) and overpredicted run-off for the semi-arid Wenatchee site with a CCL by 30 mm (≈30%). Cumulative run-off predictions made using UNSAT-H were reasonably accurate for the Live Oak site, i.e. less than 3% error; however, season-to-season differences in run-off amounts were significant. For the Wenatchee site, UNSAT-H underpredicted run-off by 50 mm (≈270%) for the test plot with a CCL, and predicted no run-off for the plot with a capillary barrier. The underpredictions resulted in more water entering the soil in the simulations than in the field. This resulted in higher soil water storage in the simulations than in the field.
- HELP underpredicted evapotranspiration by only 70 mm (≈4%) at the Live Oak site. An accurate prediction of evapotranspiration was not expected, given that more water entered the soil due to the underpre-

diction of run-off. Thus, an overprediction of evapotranspiration was expected unless the potential evapotranspiration demand had already been met. UNSAT-H underpredicted evapotranspiration for the Live Oak site by 300 mm (≈15%). Examination of the water balance equation indicates that underpredicting run-off and predicting evapotranspiration fairly accurately, or vice versa, result in an over-prediction of soil water storage and/or percolation. Both HELP and UNSAT-H overestimated evapotranspiration at the Wenatchee sites by about 20–165 mm (≈20–40%).

- HELP somewhat captured the trends in percolation at the Live Oak site, but overpredicted total percolation by more than 700 mm (≈300%). One reason why percolation was overpredicted was that there was additional water in the soil caused by the underprediction of run-off. Another factor that contributed to the overprediction of percolation by HELP was the assumption that water in the soil flowed vertically downward under a unit hydraulic gradient. Khire (1995) and Khire *et al.* (1997) indicate that under unsaturated conditions the hydraulic gradient in the field rarely equaled "1" and, for most of the time, was oriented vertically upward. UNSAT-H underpredicted percolation for the Live Oak site only slightly, by about 60 mm. Both HELP and UNSAT-H underpredicted percolation for the Wenatchee site with a CCL barrier. However, part of this difference is believed to have been caused by the preferential flow of water and snow melt through cracks and animal burrows during the winter of 1995. Prior to that time, both models had overpredicted percolation. UNSAT-H significantly overpredicted percolation for the Wenatchee site with a capillary barrier. One reason why percolation was overpredicted by over 90 mm (≈2000%) was that there was additional water in the soil caused by the underprediction of run-off.

27.5.9 RECOMMENDATIONS

The specific water balance analysis method and input parameters to use for analysis and design of a cover system should be selected based on the purpose of the analysis and project-specific factors such as climate, type of cover (i.e. hydraulic barrier, capillary barrier or evapotranspirative barrier), and cover system components. Given the inconsistencies in water balance analysis results (e.g. the models sometimes overpredict and sometimes underpredict the various components of the water balance), uncertainties in soil properties and long-term barrier integrity (e.g. CCL hydraulic conductivity may increase over time if the CCL is not adequately protected), and other factors, significant engineering judgment must be applied when performing a water balance analysis for a specific site. The following general recommendations are made regarding the use of water balance methods for the design of cover systems:

- Either the simplified manual method or the HELP model is suitable for analyzing the ability of geomembrane, geomembrane–CCL, or geomembrane–GCL hydraulic barriers to minimize percolation.
- Percolation estimates provided by Gross *et al.* (1997) and summarized in Table 27.3, can be used by design engineers to verify percolation rates calculated on a project-specific basis using either the simplified manual method or the HELP model.
- Either the simplified manual method or the HELP model can be used to design internal drainage layers underlain by hydraulic-barrier layers containing a geomembrane. A discussion of the design storm to use with each method is given at the end of this section.
- Neither the simplified manual method nor HELP is capable of serving as a water balance predictive tool using estimated or default input data. The HELP model has limited capability as a predictive tool when calibrated using site-specific data.
- Any of the water balance analysis methods may be used for evaluating percolation through cover systems with CCL or GCL hydraulic-barrier layers. While methods that incorporate unsaturated flow models are potentially more accurate than methods

TABLE 27.3. Percolation rates through final cover systems with barriers incorporating geomembranes estimated using the HELP model (modified from Gross *et al.* 1997)[a]

Average annual rainfall (mm)	Average percolation rates			
	Geomembrane barrier		Geomembrane–CCL or geomembrane–GCL barrier	
	mm a^{-1}	l ha^{-1} day^{-1}	mm a^{-1}	l ha^{-1} day^{-1}
100–300	0–0.05	0–1	0–0.005	0–0.1
300–600	0.002–03	0.06–9	0.0002–0.03	0.005–0.8
600–800	0.1–1	3–30	0.01–0.1	0.3–3
800–1,000	0.3–2	9–60	0.03–0.2	0.8–5
1,000–1,600	1–5	30–100	0.1–0.5	3–10

[a] Assumptions: (i) fair grass vegetation, (ii) sandy loam and silty clay loam topsoil, (iii) 5 and 20% cover system slopes, (iv) coarse sand and geonet internal drainage layers, and (v) 10-year synthetic weather records.

where saturated conditions are assumed for flow through the hydraulic barrier, the latter methods, i.e. simplified manual method and HELP model, are easier to use. These methods are likely to overpredict actual percolation rates for humid sites.

- For capillary-barrier and evapotranspirative-barrier cover systems, a water balance analysis method that can correctly model unsaturated flow is preferred. Thus, either LEACHM or UNSAT-H is preferable to the HELP model for evaluation of these types of systems.
- For cover systems in any climate that rely on enhanced evapotranspiration to minimize percolation, methods that correctly model unsaturated flow and also allow different vegetation scenarios to be input, such as LEACHM or UNSAT-H, are preferred.
- The literature should be consulted for the best available information on the tendencies of the various water balance models to either underpredict or overpredict the various components of the water balance for both wet and arid climatic conditions. This information should be considered in interpreting the results of project-specific water balance analyses.
- Due to the difficulty in performing accurate analytical water balances, field water balances should be performed, whenever possible, to verify the analytical results. This should especially be the case for alternative cover systems.

An important input parameter in the design of internal drainage layers in hydraulic-barrier type cover systems is rainfall intensity and duration. As previously discussed, the HELP model is limited to using daily rainfall data, and thus does not capture short-term intense peaks in storm events. Koerner & Daniel (1997) have suggested that hourly rainfall data be considered along with the simplified manual method to calculate percolation through the cover soil into the internal drainage layer (*PERC**). They present an example calculation of the sensitivity of *PERC** to the use of monthly, daily, or hourly precipitation data. The example assumes a site near Austin, Texas, with a 100-m long 3H:1V slope and a surface run-off coefficient of 0.4. The results of their analysis were as follows:

- $PERC^* = 0.011$ mm h^{-1}, using the simplified manual method with the average monthly temperature, duration of sunlight and precipitation data from Austin;
- $PERC^* = 1.3$ mm h^{-1}, using the HELP model with default historical daily precipitation data from 1974 to 1977 for San Antonio and all other climatic data generated for Austin; and
- $PERC^* = 50$ mm h^{-1}, using Eq. 27.8 with the probable maximum 6-h precipitation event for the project vicinity, i.e. 500 mm.

Koerner & Daniel (1997) noted that the calculated peak flow rate based on hourly

storm data is more than one order-of-magnitude larger than the calculated peak flow based on daily precipitation values. Because of this, they recommended that hourly precipitation data be considered to conservatively calculate peak flow rates into the drainage layer and to determine if the drainage layer has adequate capacity to transmit the peak flow during extreme storm events.

The authors of this chapter calculated *PERC* * for the same example as above using the HELP model with climatic data generated synthetically for Austin for a 20-year simulation period. For the authors' simulation, *PERC* * = 3.1 mm h^{-1}. This calculated *PERC* * can be compared with the value of 1.3 mm h^{-1} obtained by Koerner & Daniel (1997) using the historical weather data for 1974–1977 for San Antonio. The higher *PERC* * obtained by the authors is primarily due to the fact that the HELP precipitation database for the period 1974–1977 reflects unusually dry weather for certain parts of the USA. More generally, short-duration rainfall records may not contain wet weather cycles or intense storm events, which control design. Also, as noted in Koerner & Daniel (1997), the rate of infiltration into a soil cover will be limited by the hydraulic conductivity of the soil materials. If it is assumed in the above example that the cover soil has a saturated hydraulic conductivity of 1 $\times 10^{-6}$ m s^{-1}, then from Eq. 27.9b, the maximum possible rate of infiltration into the cover for a non-ponded surface condition is 3.6 mm h^{-1}, approximately the rate of percolation calculated with the HELP model and daily rainfall data generated synthetically for Austin, Texas, i.e. 3.1 mm h^{-1}. Thus, for typical cover systems with low to moderately permeable surface and protection layers, it will often be adequate to use the HELP model and a synthetic rainfall record with a sufficiently long simulation period, e.g. 20 years, to calculate lateral drainage and hydraulic head. Alternatively, Eq. 27.9b can be used directly to obtain a conservative value of *PERC* * for design.

27.6 Static Slope Stability

27.6.1 OVERVIEW

Slopes on landfills, waste piles, surface impoundments and other waste containment structures are sometimes quite steep. Slope inclinations can range from flatter than 5H : 1V (11.3°) to steeper than 2.0H : 1V (26.6°). This section addresses issues associated with the static stability of cover system components considering internal or interface downslope sliding of one or more of these components.

The frequency of occurrence of cover system stability failures has been high. More than a dozen case studies of past problems of this nature are described in USEPA (1999). One example of a past problem involved sliding of a protection soil layer over a reinforced GCL in a cover system that did not contain an internal drainage layer. Another example involved a sand drainage layer (itself overlain by a 0.3-m thick topsoil/protection layer) sliding over a textured HDPE geomembrane. In this latter case, the internal drainage layer had inadequate flow capacity and the drainage layer outlets were constricted. With geomembranes, GCLs, CCLs, geotextiles, and geocomposite drainage layers commonly used in a variety of configurations, potential low-shear-strength materials or interfaces must be considered for most designs. Significantly, past failures have involved sliding along each of the geosynthetic interfaces listed in Table 27.4.

27.6.2 LIMIT EQUILIBRIUM ANALYSES

27.6.2.1 Overview

The simplest limit equilibrium (LE) formulation for stability of waste cover systems is to assume infinite slope conditions and neglect the stabilizing influences of passive soil resisting forces at the toe of the slope, any true cohesion/adhesion in cover system materials and interfaces, and tension in the geosynthetic layers. More sophisticated LE formulations can account for these factors. Both the infinite slope and more sophisticated LE for-

TABLE 27.4. Interfaces upon which cover system components have undergone sliding

Cover system component interface sliding
Topsoil/protection layer sliding on:
geotextile cushion layer
geomembrane
GCL
Internal drainage layer sand sliding on:
geomembrane
GCL
Internal drainage layer geosynthetic sliding on:
geomembrane
Geotextile sliding on geomembrane
Geomembrane sliding on:
geotextile
GCL
CCL
GCL sliding on a prepared subgrade

mulations are discussed below. In all of the closed-form, two-dimensional LE solutions, force equilibrium is satisfied in the directions normal and parallel to the slope, but moment equilibrium is ignored.

27.6.2.2 Infinite Slope

For cover system geometries where the cover soil thickness is constant, infinite slope equations provide a simple and conservative basis for design. The degree of conservatism decreases as the ratio of the cover soil thickness to slope increases. In keeping with the approach of Giroud *et al.* (1995b), in this chapter the equations are formulated using buoyant unit weights and seepage forces.

Body seepage forces occur in cover systems when water infiltrating the cover system develops a significant flow component in the downslope as opposed to downward direction. This occurs, for example, when infiltration is blocked by a low permeability hydraulic-barrier layer. If the rate of infiltration is sufficient, hydraulic head will build up above the barrier layer and induce downslope flow. Downslope flow of water has a destabilizing effect on the cover system. The seepage force per unit volume on soil particles in the direction of laminar flow is expressed as:

$$f_w = \gamma_w i \tag{27.17}$$

where f_w = seepage force per unit volume (kN m^{-3}); γ_w = unit weight of water (kN m^{-3}) and i = hydraulic gradient. The concept of a seepage force, F_w (acting parallel to the slope), and buoyant unit weight, W_b (acting vertically), in an infinite soil slope underlain by a hydraulic barrier layer is illustrated in Fig. 27.14. For a 1-m thick cover system at a 3H:1V slope flowing full, the water induces a downslope body seepage force equivalent to a destabilizing shear stress of 3 kPa.

If there is no water flow in an infinite slope, the slope stability factor of safety is given by (Giroud *et al.* 1995b):

$$FS = \frac{\tan \phi_i}{\tan \beta} + \frac{a_i}{\gamma_t t \sin \beta} \tag{27.18}$$

where FS = factor of safety, ϕ_i = angle of internal or interface friction for the critical potential slip surface (degrees), a_i = adhesion (for an interface) or cohesion (for internal strength) for the critical potential slip surface (kN m^{-2}), β = slope angle (degrees), γ_t = average total unit weight of material above the

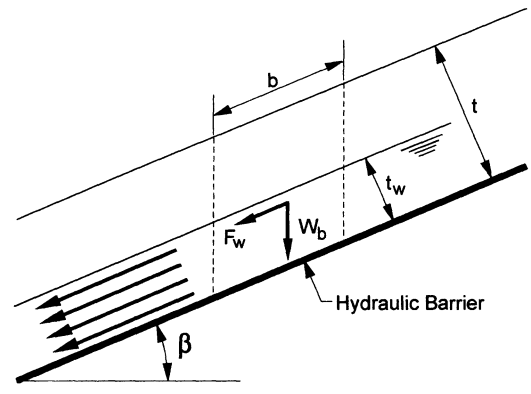


FIGURE 27.14. Seepage force and buoyant unit weight for a soil layer overlying a hydraulic barrier on an infinite slope.

critical potential slip surface (kN m^{-3}), and t = thickness of material above the critical potential slip surface (m). Use of this equation assumes that there is a unique critical potential slip surface in the cover system. For the case of no adhesion or cohesion ($a = 0$), Eq. 27.18 reduces to the classical solution:

$$FS = \tan \phi_i / \tan \beta. \quad (27.19)$$

For full water flow in an internal drainage layer, two conditions need to be considered, stability above the hydraulic-barrier layer, and stability below the hydraulic-barrier layer. Two conditions must be considered because effective stresses above and below a non-porous hydraulic barrier such as geomembrane are different. The infinite slope factor of safety for "full flow" ($t_w = t$ in Fig. 27.14) parallel to the slope along an interface or internal slip surface above the hydraulic-barrier layer is (Giroud *et al.* 1995b):

$$FS_A = \frac{\gamma_b}{\gamma_{sat}} \frac{\tan \phi_a}{\tan \beta} + \frac{a_a}{\gamma_{sat} t \sin \beta} \quad (27.20)$$

where FS_A = factor of safety for critical potential slip surface above the hydraulic-barrier layer (dimensionless), ϕ_a = angle of internal or interface friction for the critical potential slip surface above the hydraulic-barrier layer (degrees), a_a = adhesion (for an interface) or cohesion (for internal strength) for the critical potential slip surface above the hydraulic-barrier layer (kN m^{-2}), γ_b = average buoyant unit weight of material above the critical potential slip surface (kN m^{-3}), γ_{sat} = average saturated unit weight of material above the critical potential slip surface (kN m^{-3}), and all other terms are as previously defined. The buoyant unit weight, γ_b, is equal to the average total unit weight, γ_t, minus the unit weight of water, γ_w.

This factor of safety can be compared with the factor of safety expressed by Eq. 27.18 for the case of no water flow. The comparison shows that for typical soils:

- $FS_{A\ full\ flow}/FS_{no\ flow} \approx 0.5$ if $a_i = 0$; and
- $FS_{full\ flow}/FS_{no\ flow} \approx 0.9$ if $\phi_i = 0$.

Based on these results, for slip surfaces located above the hydraulic-barrier layer, the factor of safety can decrease by a factor of two due to water flow if shearing resistance is generated primarily through friction.

The factor of safety ratios presented above are based on the assumption that the shear strength properties, ϕ_a and a_a, are not influenced by the presence of water. If the presence of water reduces the magnitudes of these parameters, the effects noted in the above comparison would be even more substantial.

The infinite slope factor of safety for "full flow" parallel to the slope along an interface or internal slip surface below a non-porous hydraulic barrier is given by (Giroud *et al.* 1995b):

$$FS_B = \frac{\tan \phi_b}{\tan \beta} + \frac{a_b}{\gamma_{sat} t \sin \beta} \quad (27.21)$$

where FS_B = factor of safety for critical potential slip surface below the hydraulic-barrier layer, ϕ_b and a_b are the interface or internal shear strength parameters for the critical potential slip surface below the hydraulic-barrier layer, and all other terms are as defined previously. It should be noted that the shear strength parameters ϕ_b and a_b, used in Eq. 27.21, will typically be different from the parameters ϕ_a and a_a, used in Eq. 27.20, as the considered interfaces in the two equations are different. This factor of safety is to be compared with the factor of safety expressed by Eq. 27.18 for the case of no water flow. The comparison shows that for typical soils:

- $FS_{B\ full\ flow}/FS_{no\ flow} = 1$ if $a_i = 0$; and
- $FS_{A\ full\ flow}/FS_{no\ flow} \approx 0.9$ if $\phi_i = 0$.

Based on these results, the factor of safety along critical potential slip surfaces below the hydraulic-barrier layer is only affected to a

relatively minor degree by water flow above the hydraulic-barrier layer.

The final infinite slope case to be considered is for "partial-depth" flow ($t_w < t$ in Fig. 27.14) parallel to the slope. The appropriate equations are (Giroud *et al.* 1995b):

$$FS_a = \frac{\gamma_t(t - t_w) + \gamma_b t_w}{\gamma_t(t - t_w) + \gamma_{sat} t_w}\left(\frac{\tan \phi_a}{\tan \beta}\right) + \frac{a_a/\sin \beta}{\gamma_t(t - t_w) + \gamma_{sat} t_w} \quad (27.22)$$

and

$$FS_B = \frac{\tan \phi_b}{\tan \beta} + \frac{a_b/\sin \beta}{\gamma_t(t - t_w) + \gamma_{sat} t_w} \quad (27.23)$$

where t_w = thickness of water flow parallel to the slope (m), as defined in Fig. 27.14, and all other terms are as defined previously.

27.6.2.3 Slope of Finite Length

Equations for the LE evaluation of sloping geosynthetic–soil layered systems (such as a final cover system) for a slope of finite length have been presented by Giroud & Beech (1989); Koerner & Hwu (1991); McKelvey & Deutsch (1991); Bourdeau *et al.* (1993); Druschel & Underwood (1993); Giroud *et al.* (1995a,b); Soong & Koerner (1997); Koerner & Daniel (1997) and Koerner & Soong (1998), among others. The most detailed treatments of the subject have been presented by Koerner and coworkers and Giroud *et al.* (1995a,b). Giroud *et al.* (1995a) have shown that compared with the method they present, the method utilized by Koerner & Hwu (1991) is more rigorous, but somewhat more complicated to use because it requires solution of quadratic equations. The formulation by Giroud *et al.* (1995a,b) involves an approximation that allows expression of the factor of safety as a closed-form algebraic equation where each term in the equation has a distinct physical meaning and is sufficiently accurate for practical purposes.

The two-part wedge considered by Giroud *et al.* (1995a,b) is illustrated in Fig. 27.15. For this condition, the slope stability factor of safety for a slope with constant soil thickness above the critical potential slip surface and for the case of no water flow, i.e. $t_w = 0$ in Fig. 27.15, is given by:

$$FS = \frac{\tan \phi_i}{\tan \beta} + \frac{a_i}{\gamma_t t \sin \beta} + \frac{t}{h}\left[\frac{\sin \phi_s}{2 \sin \beta \cos \beta \cos(\beta + \phi_s)}\right] + \frac{c_s}{\gamma_t h}\left[\frac{\cos \phi_s}{\sin \beta \cos(\beta + \phi_s)}\right] + \frac{T}{\gamma_t h t} \quad (27.24)$$

where ϕ_s = angle of internal friction for the soil material, i.e. protection layer and/or granular internal drainage layer, above the critical potential slip surface (degrees); c_s = cohesion of soil material above the critical potential slip surface (kN m^{-2}); h = height of slope (m), as defined in Fig. 27.15; T = geosynthetic tension above the critical potential slip surface; and all other terms are as defined previously.

The case of partial-depth and full-depth flow of water for a slope of finite height was addressed by Giroud *et al.* (1995b). For the case of a slope of uniform thickness above the critical potential slip surface, the factor of

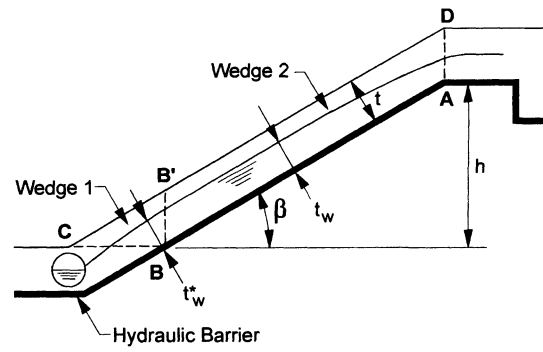


FIGURE 27.15. Definition of two-part wedge and flow thickness for the case of a slope of finite height.

safety above the hydraulic-barrier layer may be calculated using:

$$FS_A = \frac{\gamma_t(t - t_w) + \gamma_b t_w}{\gamma_t(t - t_w) + \gamma_{sat} t_w}\left(\frac{\tan \phi_a}{\tan \beta}\right) + \frac{a_a/\sin \beta}{\gamma_t(t - t_w) + \gamma_{sat} t_w} + \frac{\gamma_t(t - t_w^*) + \gamma_b t_w^*}{\gamma_t(t - t_w) + \gamma_{sat} t_w}\left(\frac{t}{h}\right) \times \left[\frac{\sin \phi_s}{2 \sin \beta \cos(\beta + \phi_s)}\right] + \frac{c_s t/h}{\gamma_t(t - t_w) + \gamma_{sat} t_w} \times \left[\frac{\cos \phi_s}{\sin \beta \cos(\beta + \phi_s)}\right] + \frac{T/h}{\gamma_t(t - t_w) + \gamma_{sat} t_w} \quad (27.25)$$

where t_w^* = thickness of water in Wedge 1 in Fig. 27.15, and all other terms are as defined previously. For potential slip surfaces below a non-porous hydraulic barrier:

$$FS_B = \frac{\tan \phi_b}{\tan \beta} + \frac{a_b/\sin \beta}{\gamma_t(t - t_w) + \gamma_{sat} t_w} + \frac{\gamma_t(t - t_w^*) + \gamma_b t_w^*}{\gamma_t(t - t_w) + \gamma_{sat} t_w}\left(\frac{t}{h}\right) \times \left[\frac{\sin \phi_s}{2 \sin \beta \cos \beta \cos(\beta + \phi_s)}\right] + \frac{c_s t/h}{\gamma_t(t - t_w) + \gamma_{sat} t_w} \times \left[\frac{\cos \phi_s}{\sin \beta \cos(\beta + \phi_s)}\right] + \frac{T/h}{\gamma_t(t - t_w) + \gamma_{sat} t_w} \quad (27.26)$$

When there is full flow of water in Wedge 1 ($t_w = t$) as well as in Wedge 2 ($t_w = t$), Eq. 27.25 gives the following expression for the factor of safety for a critical potential slip surface above the hydraulic-barrier layer:

$$FS_A = \frac{\gamma_b}{\gamma_{sat}}\left(\frac{\tan \phi_a}{\tan \beta}\right) + \frac{a_a}{\gamma_{sat} t \sin \beta} + \frac{\gamma_b}{\gamma_{sat}}\left(\frac{t}{h}\right)\left[\frac{\sin \phi_s}{2 \sin \beta \cos \beta \cos(\beta + \phi_s)}\right] + \frac{c_s}{\gamma_{sat} h}\left[\frac{\cos \phi_s}{\sin \beta \cos(\beta + \phi_s)}\right] + \frac{T}{\gamma_{sat} th} \quad (27.27)$$

and Eq. 27.26 reduces to:

$$FS_B = \frac{\tan \phi_b}{\tan \beta} + \frac{a_b}{\gamma_{sat} t \sin \beta} + \frac{\gamma_b}{\gamma_{sat}}\left(\frac{t}{h}\right)\left[\frac{\sin \phi_s}{2 \sin \beta \cos \beta \cos(\beta + \phi_s)}\right] + \frac{c_s}{\gamma_{sat} h}\left[\frac{\cos \phi_s}{\sin \beta \cos(\beta + \phi_s)}\right] + \frac{T}{\gamma_{sat} th} \quad (27.28)$$

where all terms have been defined previously.

Another case sometimes encountered is that of a tapered cover soil thickness, as illustrated in Fig. 27.16. For this geometry, the

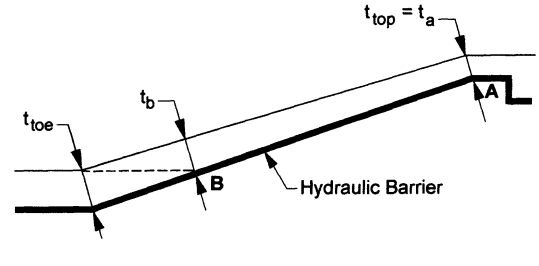


FIGURE 27.16. Definition of slope with a tapered soil layer.

factor of safety for the case of no water pressure is given by the equation:

$$FS = \frac{\tan \phi_i}{\tan \beta} + \frac{t_b}{t_{avg}}\left[\frac{a_i}{\gamma_t t_b \sin \beta} + \frac{t_b}{h}\left[\frac{\sin \phi_s}{\sin(2\beta)\cos(\beta + \phi_s)}\right] + \frac{c_s}{\gamma_t h}\left[\frac{\cos \phi_s}{\sin \beta \cos(\beta + \phi_s)}\right] + \frac{T}{\gamma_t h t_b}\right]. \quad (27.29)$$

where:

$$t_{ave} = (t_a + t_b)/2 \quad (27.30)$$

t_a = thickness of soil layer at point A in Fig. 27.16 (m), and t_b = thickness of soil layer at point B in Fig. 27.16 (m).

Equation 27.29 can also be used to calculate the factor of safety for a tapered slope of height h with a break, as illustrated in Fig. 27.17, by calculating an average soil thickness for the entire slope using the equation:

$$t_{ave} = \frac{t_a}{2}\left(1 + \frac{h_u}{h}\right) + \frac{t_b}{2}\left(1 - \frac{h_u}{h}\right) \quad (27.31)$$

where h_u = height of slope above the break (m), as illustrated in Fig. 27.17.

The equations presented above provide closed-form solutions to a variety of cover system slope stability situations. Some situations are too complex, however, to address using closed-form solutions and are more easily evaluated using commercially available slope stability computer software, e.g. PCSTABL5 (Achilleous 1988), UTEXAS3 (Wright 1991), XSTABL (Sharma 1994), or SLOPE/W (Geo-Slope Int. Ltd.). Available software has the advantage that it can be applied to non-uniform slope, soil cover, and hydraulic head conditions, and can incorporate a pseudo-static seismic coefficient for use in seismic stability evaluations.

The LE method is useful for evaluating cover system stability under most conditions, but is subject to several limitations. With the LE method, material and interface shearing resistances are assumed to be independent of displacement. For geosynthetic materials and interfaces, however, mobilized shearing resistance is not constant but increases with increasing displacement to a peak value. For many materials and interfaces, the shear resistance decreases with increasing displacement, after reaching the peak, ultimately to a "residual" value (Fig. 27.18). This behavior is sometimes referred to as "strain softening." In using the LE method, judgment must be applied to the selection of shear strength values

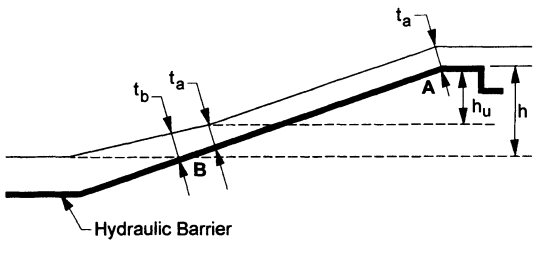


FIGURE 27.17. Definition of slope with a partly tapered soil layer.

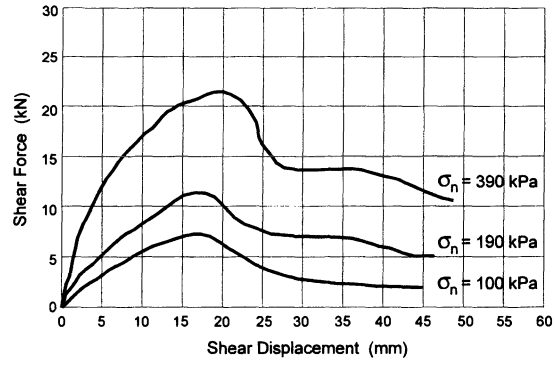


FIGURE 27.18. Result of direct shear test on a GCL illustrating peak and large-displacement shearing resistances.

for strain-softening materials, i.e. peak, residual, or some other value. The LE method is similarly limited with respect to tension forces in cover system geosynthetic components and, therefore, cannot be used to estimate the magnitude and distribution of stresses and deformations in these components.

As a final comment on the LE equations presented in this section, the equations incorporate terms to account for material interface adhesion or internal cohesion, and for geosynthetic tension. Users of these equations should be cautious in selecting adhesion–cohesion and geosynthetic tension values for design. As suggested by Koerner & Daniel (1997), adhesion and cohesion values should be used only when there is clear physical justification. As indicated by the analysis results presented previously, characterization of interface–internal shearing resistance by an adhesion–cohesion term instead of a friction angle will greatly affect the results of slope stability analyses where hydraulic heads are present in the cover system. In general, geosynthetic tension should not be in the equations unless the design includes a geosynthetic reinforcement layer. Other types of geosynthetics, such as geomembranes, geosynthetic drainage layers, etc., are not designed to permanently transmit tensile loads, are potentially subject to significant tensile creep, and typically have a low tensile modulus (which means that the geosynthetic must elongate to generate tension). Even if geosynthetic reinforcement is used, it should only be relied upon for the tensile force, which it can generate at a specified level of deformation. This acceptable level of deformation must be selected considering the overall performance of all system components.

27.6.3 STRESS–DEFORMATION ANALYSES

Stress–deformation analysis methods may be used to account for the stress–strain response of materials and interfaces and, therefore, to predict the distribution of stresses and strains within the cover system components, particularly geosynthetic components. Stress–deformation methods can also account for the effects of construction sequencing. The primary disadvantage of stress–deformation methods is the relatively large effort required to obtain material stress–deformation relationships and perform the calculations compared to the effort required with LE methods.

Several studies have been published on the application of stress–deformation methods to cover systems. For example, Long *et al.* (1993, 1994) describe a finite difference model (GEOSTRES) that considers stress equilibrium and strain compatibility. GEOSTRES uses inelastic, non-linear springs to model the shear resistance–displacement behavior at each interface and to model the axial load–displacement behavior within each component. Wilson-Fahmy and Koerner (1992, 1993) adopted a two-dimensional finite element model to account for stress equilibrium and deformation compatibility in stability analyses of soil–geosynthetic systems on slopes.

27.6.4 SHEAR STRENGTH PARAMETERS

Laboratory testing, using project-specific materials and testing procedures, and conditions representative of the anticipated field application, is typically performed to establish design shear strength parameters for cover system materials and interfaces. The various methods used for laboratory shear strength testing of soils are well-known and are fully described in a number of geotechnical textbooks and laboratory guides (Lambe 1951; Holtz & Kovacs 1981; and Bardet 1997). The most commonly used methods for laboratory shear strength testing of soils are the triaxial compression test and direct shear test.

Currently there are several types of laboratory devices available for the evaluation of shear strength of geosynthetic materials and interfaces. These laboratory devices include:

- large-scale (300 × 300 mm) direct shear box as specified by ASTM Standard D5321,
- conventional (50–100 mm square of circular) direct shear box with testing generally following ASTM D3080,
- torsional shear device (ASTM standard under development),
- tilt table, and
- large-displacement shear box.

Table 27.5 provides a summary of the advantages and disadvantages of the first four devices. Shallenberger & Filz (1996) describe the capabilities and limitations of the large-displacement shear box.

Project-specific shear strength testing programs are designed to simulate the anticipated field conditions by selecting appropriate values for testing procedures and conditions. These include the soil compaction conditions, i.e. water content and density; soil consolidation stress and time; the wetting conditions for the materials and interfaces; the range of applied normal stresses; the direction of shear for geosynthetic interfaces; and the shear displacement rate and magnitude. The potential effects of many of these testing conditions on measured interface shear strength parameters are reported in the literature, e.g. Martin *et al.* 1984; Williams & Houlihan 1987; Seed *et al.* 1988; Giroud *et al.* 1990; Seed & Boulanger 1991; Swan *et al.* 1991; Pasqualini *et al.* 1993; Stark & Poeppel 1994; Bemben & Schulze 1995; Gilbert *et al.* 1995; Nataraj *et al.* 1995; Bonaparte *et al.* 1996; Shallenberger & Filz 1996; Stark & Eid 1996; Stark *et al.* 1996; Dove *et al.* 1997; Eid & Stark 1997; Gilbert *et al.* 1996; Sharma *et al.* 1997; De & Zimme 1998; Sabatini *et al.* 1998; and Snow *et al.* 1998. Particular attention should be given to the following:

- Testing should be performed with materials and boundary conditions representative of the anticipated field conditions.
- Soil materials used in the test should be compacted to representative field conditions. The compaction moisture content for CCLs used in a direct shear testing pro-

TABLE 27.5. Summary of advantages and disadvantages associated with test devices for measuring interface shear strength (adapted from Gilbert *et al.* 1995)

Test device	Advantages	Disadvantages
Large-scale direct shear box	Industry standard Large scale Large displacement Minimal boundary effects	Machine friction Load eccentricity Limited continuous displacement Limited normal stress Expensive
Conventional direct shear box	Experience with soil Inexpensive Large normal stress	Machine friction Load eccentricity Small scale Limited displacement Boundary effects
Torsional shear device	Unlimited continuous displacement	Machine friction Anisotropic shearing Small scale Expensive
Tilt table	Minimal machine effects Minimal boundary effects Inexpensive	Small experience base Limited continuous displacement Limited normal stress No post-peak behavior Large effort to prepare sample

gram should be near the upper limit of acceptable moisture content and near the lower limit of dry unit weight, allowed by the construction specification.

- For geomembrane–CCL interface shear tests, a variety of opinions exist with regard to the application of additional moisture to the interface just prior to assembly of the test specimen. Options include adding no moisture, lightly or moderately "spritzing" water onto the CCL, or submerging the assembled sample. The rationale for any of these techniques is to simulate suspected installation (e.g. rainfall or moisture conditioning) or post-installation (e.g. condensation at the interface or consolidation-induced water movement to the interface) increases in CCL moisture content at the interface. Bowders *et al.* (1997) and Shallenberger & Filz (1996) discuss the contributions of other factors such as thermal gradients and post-compaction thixotrophy on interface stability.
- Hydration (soaking) times for GCL samples should be adequate to achieve minimum strength. Gilbert *et al.* (1996) report hydration times, as determined by cessation of GCL swelling under constant normal stress, for reinforced GCLs of up to 25 days. However, Daniel *et al.* (1993) have shown that full hydration is not always necessary to achieve minimum shear strength. An acceptable approach to hydration is to monitor vertical deformation of the GCL and continue to hydrate until these deformations have ceased under the applied normal stress (see below). When this procedure cannot be performed, a minimum hydration time of 72 h is recommended for GCLs to be tested in a 300-mm direct shear box; however, the user of the data should also be aware that without full hydration the measured strength may be larger than the fully hydrated strength.
- Testing conditions must adequately reflect the field consolidation conditions of the GCL or CCL components. GCLs hydrated as indicated above will be fully consolidated under the normal stress applied during hydration. This normal stress should be equal to that applied by the cover system. Consolidation requirements for CCL components of the cover may be established using ASTM D3080. Specimen consolidation times of 48 h or more may be required for some materials.
- ASTM D5321 recommends that tests be performed at a minimum of three normal stresses, with each test using new test specimens. The three selected normal stresses should bracket the overburden stress applied by the cover system to the material or interface being tested. This is important because many of the materials used in cover systems exhibit a non-linear relationship between interface or internal shear resistance and normal stress. For cover systems, applicable normal stresses will typically be in the range of about 15–50 kPa. Uniformity of normal stress over the entire test specimen must be maintained during consolidation and shearing so as to avoid stress concentrations.
- Shear displacement rates should be selected considering the type of slope stability analysis to be performed and the types of potentially critical materials or interfaces to be tested. For geosynthetic–geosynthetic interfaces (excluding GCLs), the maximum rate allowed by ASTM D5321 of 0.08 mm s^{-1} will generally be acceptable. For long-term stability conditions where the potentially critical material or interface includes a CCL or GCL component, the shear displacement rate should be as slow as reasonably achievable; the default shear displacement rate given in ASTM of 0.08 mm s^{-1} is too fast to achieve drained shearing conditions for CCL and GCL materials. Procedures for estimating shear rates to obtain fully drained conditions for CCL materials are given in ASTM D3080. Procedures and data for determining shear rates to obtain fully drained conditions for GCLs are given in Shan (1993). It is noted, however, that it may not be necessary to achieve fully drained test conditions to obtain test results suitable for long-term analyses. Available data suggest that for design purposes, a shear displacement

rate of not more than 0.0005 mm s^{-1} will produce data appropriate for use in slope stability analyses involving GCL materials and interfaces. In contrast, for the evaluation of seismic stability, shear displacement rates should be as fast as reasonably achievable. For both conditions, testing should be performed using samples fully consolidated under the applied normal stress.

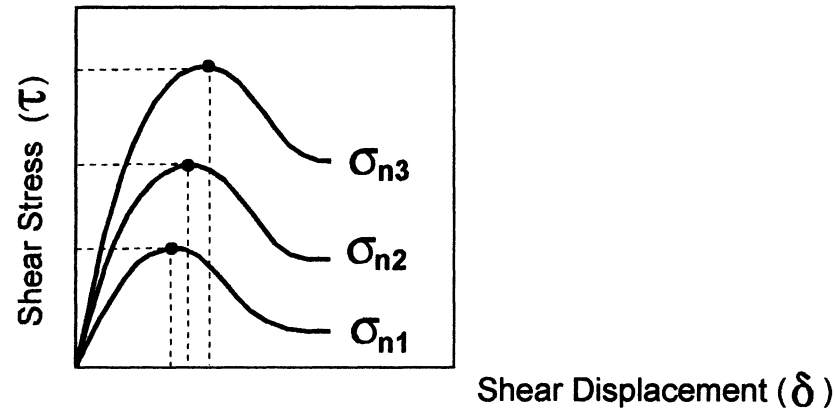
- Tests should be carried out to a shear deformation adequate to evaluate both the peak and large-displacement shear resistance of the interface or material being tested. Many geosynthetic–geosynthetic and soil–geosynthetic interfaces exhibit very significant post-peak reductions in shear strength (Fig. 27.18). ASTM D5321 states that one should "run the test until the applied shear force remains constant with increasing displacement". Torsional ring shear testing (Stark & Poeppel 1994), can be used to evaluate absolute minimum, i.e. residual, shear strengths of soils and geosynthetics for which representative samples can be produced for the small size and torsional shearing mode of this type of test. Alternatively, large-displacement shear box testing (Shallenberger & Filz 1996) can be used to evaluate residual shear strengths for larger-size test specimens in a linear displacement mode. For most practical design applications, true residual strength can be estimated to an acceptable degree of accuracy as 90–95% of the large-displacement direct shear strength obtained from a 300 × 300-mm direct shear test.
- Multicomponent cover systems may have more than one potentially critical slip surface. The shear test program for a project may need to consider several materials or interfaces.
- Some materials exhibit significant manufacturing variability. For example, the degree of texturing on geomembranes and the amount of internal-reinforcing in needle-punched GCLs has been observed to vary significantly from lot to lot. This variability should be considered both in design evaluation of stability and in the selection of project quality control/quality assurance protocols.
- Test results can be interpreted in terms of a secant friction angle that varies as a function of normal stress, or by a tangent friction angle and apparent adhesion (or cohesion for internal strength) applicable to the range of considered normal stresses. Both of these approaches are illustrated in Fig. 27.19. For cover system applications, interface and internal shear strength parameters should be defined in terms of a secant friction angle for cases where hydraulic heads could develop in the cover soil. Since the apparent adhesion/cohesion may not be a true interface or material property, the use of this parameter with high heads could lead to an overprediction of the true slope stability factor of safety.

All of the foregoing factors should be considered in designing a laboratory shear testing program to evaluate interface and material shear strengths and in using the results of the program in slope stability analyses.

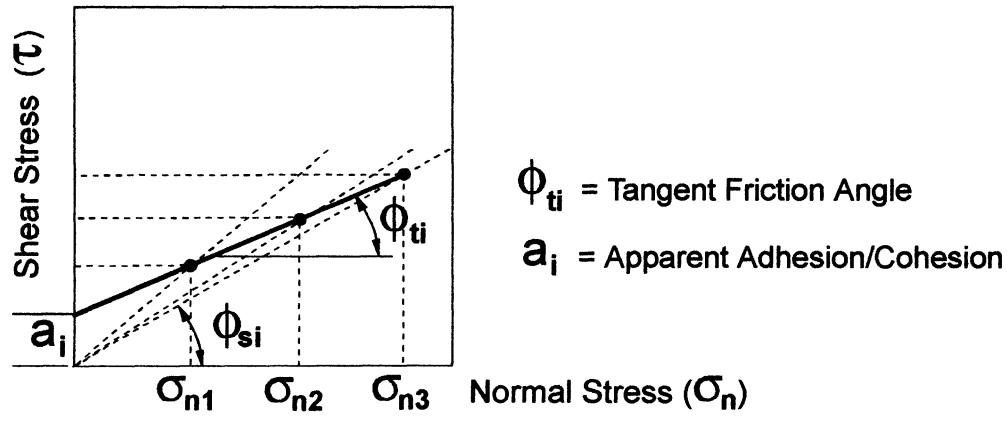
27.6.5 CONSTRUCTION CONSIDERATIONS

The placement of soil over a slope with underlying low shear strength materials or interfaces will induce shear stresses that can reduce slope stability. These shear stresses result from the operation of construction equipment on the slope and, if the soil is pushed down the slope, from the moving soil itself. Construction-induced stresses have been investigated by McKelvey & Deutsch (1991) and Koerner & Daniel (1997). These references present LE equations that can be used to evaluate the effect of construction equipment operation on the stability of the cover system.

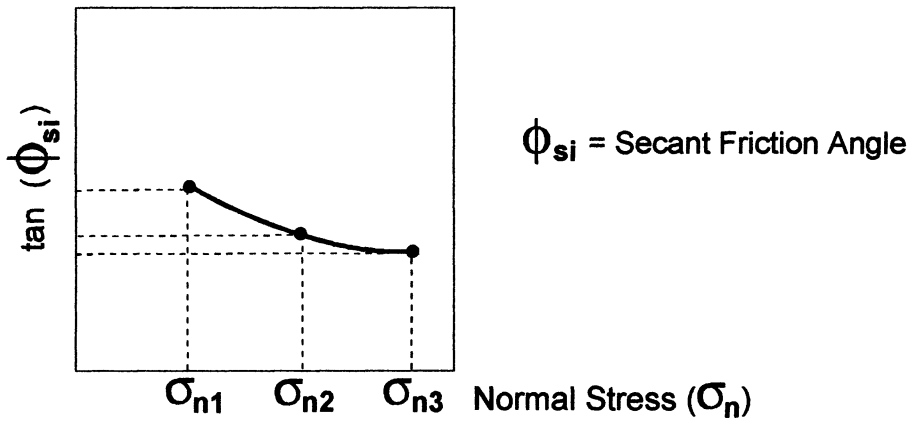
The clear recommendation that comes out of the investigations cited in the previous paragraph is that cover soils should be placed over low shear strength materials and interfaces from the bottom of the slope upward



(a)



(b)



(c)

FIGURE 27.19. Interpretation of interface or internal shear test on cover system components: (a) test results for peak strengths; (b) tangent friction angle, ϕ_{ti}, and apparent adhesion/cohesion, a_i; and (c) secant friction angle, ϕ_{si}. Similar interpretations are applied to large displacement and residual conditions.

and not from the top of the slope downward. The following comments are provided with respect to placement of soil materials in final cover systems:

- by placing cover soils from the bottom of the slope upward, a passive, stabilizing soil wedge is established at the toe of slope prior to placement of soil higher on the slope;
- relatively small, wide-track dozers are recommended for placing the soil cover material; and
- downslope dynamic forces can be limited further by limiting the dozer speed on the slope and by instructing the dozer operator to avoid hard breaking, particularly when backing downslope.

By application of the construction procedures described above, construction-induced impacts to the stability of a cover system slope (designed to conventional slope stability factors of safety described in Section 27.6.6) are minor. For other conditions, (e.g. lower factors of safety than recommended in Section 27.6.6, placement of soil from the top of slope, use of large construction equipment) construction-stage stability should be checked using the procedures described in McKelvey & Deutsch (1991) or Koerner & Daniel (1997).

27.6.6 FACTORS OF SAFETY

LE analysis methods provide a calculated slope stability factor of safety (FS). Minimum acceptable FS values for cover systems depend on project-specific conditions and uncertainties. For example, when cover systems include strain-softening components or interfaces, differing minimum factors of safety are often applied for peak strength analyses and analyses based on large-displacement or residual strength. Other criteria may also influence selection of a minimum acceptable FS, including regulatory requirements, reliability of laboratory test methods, similarity between laboratory testing conditions and field conditions, and completeness of laboratory test data.

A number of technical references discuss the selection of FS for slope stability analyses involving geosynthetic interfaces including Bonaparte *et al.* (1996), Byrne (1994), Koerner & Soong (1998), Liu *et al.* (1997), and Stark & Poeppel (1994). Based on this available information, the following general guidance is provided:

- A minimum acceptable factor of safety (FS_{min}) for static stability analyses of 1.5 will often be adequate for permanent cover system applications where the design is based on peak interface and internal shear strengths. This FS_{min} is applied to normal operating conditions, e.g. no seismic loading, no live loading, and seepage forces, if any, are accounted for assuming a reasonable "average" operating condition.
- A smaller or larger FS_{min} may be considered based on an evaluation of: (a) consequences of cover system failure, and (b) uncertainty associated with each design parameter.
- If the cover system contains geosynthetic materials that exhibit strain-softening internal or interface shear strengths, FS_{min} for large-displacement conditions should also be checked. A FS_{min} of 1.20 is suggested where large-displacement shear strengths are obtained from testing in a direct shear box in accordance with ASTM D5321. For purposes of this evaluation, 50–75 mm of displacement, coupled with the observation that the shear stress–displacement plot is essentially flat at the end of the test is considered to satisfy the large-displacement condition. If true residual shear strengths are obtained using either a torsional-ring or large-displacement shear apparatus, FS_{min} values as low as 1.15 may be considered.
- Cover system designs should be checked for temporary extreme loading conditions. These conditions need to be identified on a case-by-case basis, but generally include

TABLE 27.6. Engineering measures to increase cover system slope stability factor of safety

Use cover system materials that have higher internal or interface shear strengths, as available
Provide for a flatter cover system slope by initially placing waste to a flatter slope (for new facilities) or waste excavation (for existing facilities)
Shorten the slope length through the use of benches or berms
Use perimeter retaining walls or buttresses to achieve a flatter cover system slope angle
Improve cover system internal drainage if hydraulic head buildup is predicted to occur
Utilize geosynthetic reinforcement, but only within the limitations of the approach described in this chapter

extreme storm events, live loads and earthquakes. Design for earthquakes is addressed subsequently. It is recommended that design for temporary extreme loading be based on FS_{min} = 1.25, 1.1 and 1.05 using peak, large-displacement or residual shear strengths, respectively.

If the factor of safety cannot be achieved for a given set of conditions, the engineer can consider a variety of measures to increase slope stability (Table 27.6).

27.7 Seismic Slope Stability

27.7.1 OVERVIEW

Seismic design of engineering structures is discussed in Chapter 21. In this chapter, specific consideration is given to the evaluation of seismic impacts to cover systems for landfills, waste piles, surface impoundments, and other waste containment structures. Impacts may involve either excessive seismic displacement of one or more cover system components or complete instability of the cover system.

27.7.2 SEISMIC HAZARD EVALUATION

The objective of the seismic hazard evaluation is to characterize the design earthquake with respect to the parameters required for engineering analysis (e.g. magnitude, style of faulting, site-to-source distance, peak ground acceleration, and spectral accelerations). The peak horizontal bedrock acceleration at a project site may be estimated using seismic hazard probability maps or site-specific seismic hazard assessments. In the USA, the most widely used such maps are those developed by the US Geological Survey (USGS) depicting peak and spectral horizontal bedrock accelerations having 10, 5, and 2% probability of exceedance in a 50-year period (corresponding to a 90% probability of not being exceeded for 50-, 100- or 250-year periods). These maps are periodically updated to reflect recent developments in the field of seismology. Maps for the USA can be found at the USGS Web site at http://www.geohazards.cr.usgs.gov/eq./. Background information on the development of these maps is provided by Frankel *et al.* (1996). The 90%, 250-year map corresponds to the USEPA prescriptive regulatory criterion for seismic design of MSW landfills.

Seismic hazard maps like those of USGS discussed above usually present the estimated free-field peak horizontal acceleration for a hypothetical bedrock outcrop on level ground at a particular location. If bedrock is not present at or near the ground surface, the peak acceleration may need to be modified to account for local site conditions. The presence of a waste mass will further modify the earthquake ground motions, as discussed subsequently. The primary difficulty associated with using seismic probability maps is that the maps by themselves do not provide information on the magnitude, site-to-source distance, or duration of the earthquake associated with the map acceleration values. For some types of seismic analyses, information on these variables is necessary. Because they

are probabilistically derived, the acceleration values provided on such maps are typically composed of contributions of earthquakes of many different magnitudes from several to many different seismic sources. Each source may be associated with a different site-to-source distance and each magnitude–distance combination with a different duration. The USGS Web site has made information available on the distribution of earthquake magnitudes and site-to-source distances associated with the bedrock accelerations obtained directly from the USGS seismic hazard maps. Using this feature, the peak bedrock acceleration for a given site and recurrence interval is deaggregated by earthquake magnitude and site-to-source distance. Deaggregated spectral accelerations are also provided for spectral periods of 0.2, 0.3, and 1 s. As an example of the information available at the USGS Web site, deaggregated bedrock acceleration and site-to-source data for Evansville, Indiana, are presented in Table 27.7. This table presents the deaggregated analysis results for a probability of exceedence of 2% in 50 years.

In using deaggregated data, such as given in Table 27.7, the engineer should identify the earthquake magnitude and distance combination that encompasses about two-thirds of the seismic hazard. For example, if more than two-thirds of the seismic hazard for a given site is from a small magnitude, near-source earthquake, then seismic analyses should be performed using input variables, e.g. strong motion records appropriate for this type of earthquake event. In some cases, more than one combination of earthquake magnitude and source distance may need to be considered. The values in Table 27.7 for Evansville illustrates such a case: a significant portion (≈40%) of the seismic hazard for Ev-

TABLE 27.7. Deaggregated peak horizontal bedrock accelerations as a percentage of the aggregated peak probabilistic acceleration of 0.328 *g* for Evansville, Indiana, for a 2% probability of exceedence in 50 years (adapted from USGS Web site)

Hypocentral distance (km)	Earthquake magnitude						
	5.0	5.5	6.0	6.5	7.0	7.5	8.0
25	13.888	13.372	9.591	5.787	2.447	1.584	0.000
50	1.507	3.176	4.624	5.054	2.818	2.440	0.000
75	0.093	0.349	0.927	1.737	1.449	1.757	0.000
100	0.011	0.060	0.247	0.670	0.591	0.938	0.000
125	0.002	0.017	0.095	0.348	0.250	0.488	0.000
150	0.000	0.004	0.030	0.143	0.114	0.269	0.000
175	0.000	0.001	0.008	0.050	0.051	0.146	15.718
200	0.000	0.000	0.002	0.019	0.023	0.083	6.904
225	0.000	0.000	0.001	0.007	0.010	0.042	0.000
250	0.000	0.000	0.000	0.003	0.004	0.020	0.000
275	0.000	0.000	0.000	0.001	0.002	0.012	0.000
300	0.000	0.000	0.000	0.000	0.001	0.006	0.000
325	0.000	0.000	0.000	0.000	0.000	0.003	0.000
350	0.000	0.000	0.000	0.000	0.000	0.002	0.000
375	0.000	0.000	0.000	0.000	0.000	0.002	0.000
400	0.000	0.000	0.000	0.000	0.000	0.001	0.000
425	0.000	0.000	0.000	0.000	0.000	0.001	0.000

ansville is derived from earthquakes less than 25 km from the site with magnitudes between 5 and 6 (though the magnitude of some of the local events contributing to the seismic hazard may be as great as 7.5). However, over 20% of the seismic hazard is from a distant earthquake more than 150 km from the site with a magnitude of 8.0. Therefore, for some projects in Evansville, the impact of both local and distant events may warrant consideration.

Due to the reduced uncertainty and greater accuracy, site-specific seismic hazard analyses are preferred to the use of seismic hazard maps for critical structures in regions of high seismic activity. A site-specific seismic hazard analysis involves:

- identification of the seismic sources capable of strong ground motions at the project site,
- evaluation of the seismic potential for each capable source, and
- evaluation of the intensity of the design ground motions at the project site.

Site-specific seismic hazard analyses may be performed using either a deterministic or probabilistic approach. Detailed discussion of this topic is beyond the scope of this chapter. The reader is referred to Reiter (1990), Krinitsky *et al.* (1993), Richardson *et al.* (1995), and Kramer (1996). An example of a site-specific seismic hazard analysis applied to a landfill site (including cover system) in California is given in Kavazanjian *et al.* (1995a).

27.7.3 SEISMIC RESPONSE ANALYSIS

27.7.3.1 Introduction

The seismic hazard assessment as discussed above provides an estimate of peak horizontal accelerations in bedrock for a given site along with information on the causative earthquake event(s). A response analysis is used to estimate the seismically induced motions (e.g. acceleration, velocities, and/or displacements) at the ground surface or in the waste mass cover system. Response analyses are needed because soil layers and waste modify the bedrock motions, sometimes in a manner that can significantly increase damage potential.

27.7.3.2 Material Property Selection

The first step in the seismic response analyses is to characterize the soil and waste material properties needed to perform the analysis. For equivalent linear analyses of vertically propagating shear waves (the most common type of seismic response analysis performed for geotechnical and waste management applications), these properties include total unit weight; dynamic shear modulus, G (kPa); and damping ratio for each material through which the waves propagate. Kramer (1996) provides an extensive review of the available technical literature on the selection of soil and rock properties for response analyses. Guidance on selecting MSW waste properties can be found in Sharma *et al.* (1990), Fassett *et al.* (1994), Richardson *et al.* (1995), Kavazanjian *et al.* (1995b), and Kavazanjian & Matasovic (1995).

Shear modulus and damping ratio curves for the Operating Industries Inc. (OII) site, a large inactive MSW industrial landfill in Monterey Park, California, are presented in Idriss *et al.* (1995), Augello *et al.* (1998) and Matasovic & Kavazanjian (1998). The curves independently developed by these three sets of investigators are shown in Fig. 27.20. These three sets of curves represent the best currently available information for use in estimating strain-dependent shear modulus reduction factors, G/G_{max}, and damping ratios for MSW and other solid waste materials for use in equivalent linear response analyses. The strain-dependent damping ratio is obtained directly from Fig. 27.20. The strain-dependent dynamic shear modulus, G, is obtained by multiplying the shear modulus reduction value from Fig. 27.20 by the small strain shear modulus, G_{max} (kPa), which can be calculated using the equation:

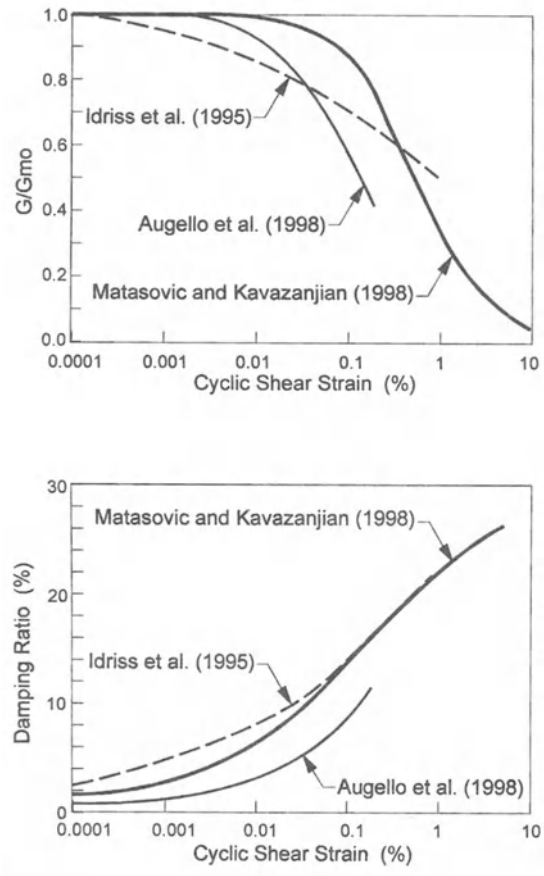


FIGURE 27.20. Estimated OII solid waste landfill shear modulus reduction (G/G_{max}) and damping curves. Data from Idriss *et al.* (1995), Augello *et al.* (1998), and Matasovic & Kavazanjian (1998).

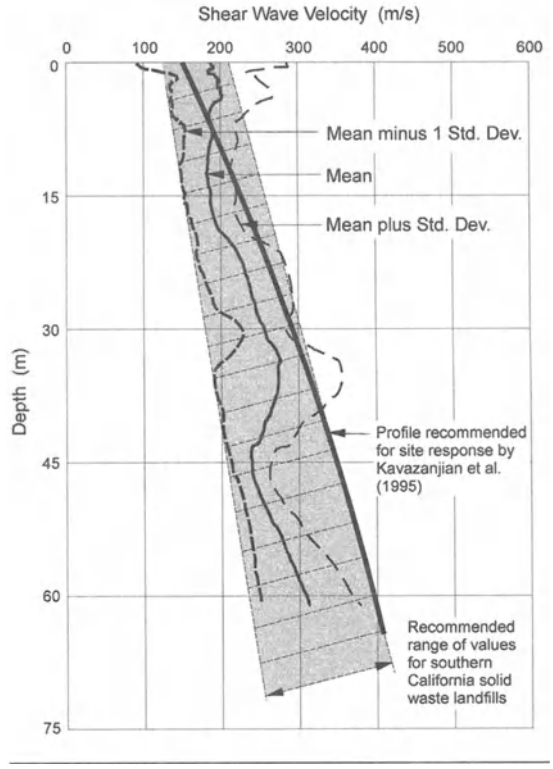


FIGURE 27.21. Shear wave velocities, v_s for southern California solid waste landfills (modified from Kavazanjian *et al.* 1996).

$$G_{max} = \frac{\gamma_t v_s^2}{g} \qquad (27.32)$$

where v_s = shear wave velocity of waste material (m s^{-1}), γ_t = total unit weight of waste (kN m^{-3}) and g = acceleration of gravity (9.8 m s^{-2}). The small-strain shear modulus is ideally obtained from project-specific field testing. For landfills, this type of testing may be conveniently performed with the non-intrusive spectral analysis of surface waves (SASW) technique (Kavazanjian *et al.* 1994, 1996). Intrusive downhole or cross-hole geophysical testing techniques may also be used. In the absence of project-specific testing, the data for southern California landfills from Kavazanjian *et al.* (1996), presented in Fig. 27.21, can be used. It is noted that results obtained from a limited amount of SASW testing of MSW landfills in the eastern USA (unpublished) suggests that shear wave velocities for waste in these facilities may be lower, on average, than shear wave velocities for waste in relatively dry southern California landfills. In the absence of better information, the lower end of the recommended range of shear wave velocities shown in Fig. 27.21 can be used for MSW landfills located in the eastern USA and other temperate to wet climates.

27.7.3.3 Simplified Response Analysis

Simplified approaches to seismic response analyses involve the empirical correlation of peak horizontal waste mass or cover system acceleration, as applicable, to peak bedrock

TABLE 27.8. Earthquake parameters, corresponding peak horizontal bedrock acceleration estimates and peak horizontal accelerations recorded on the top of the Operating Industries Inc. (OII) landfill, California (adapted from Matasovic *et al.* 1998)

Earthquake	Moment magnitude	Style of faulting	Site-to-source distance (km)	Estimated peak-bedrock acceleration (g)	Peak acceleration at top deck (g)
Pasadena, 3 December 1988	5.0	Strike-slip	13	0.075	0.105
Malibu, 19 January 1989	5.0	Thrust	50	0.018	0.009
Joshua Tree, 23 April 1992	6.1	Strike-slip	163	0.006	0.017
Landers, 28 June 1992	7.3	Strike-slip	140	0.032	0.085
Big Bear, 28 June 1992	6.4	Strike-slip	119	0.015	0.049
Mojave Desert, 11 July 1992	5.5	Strike-slip	131	0.004	0.012
Northridge, 17 January 1994	6.7	Thrust	43	0.104	0.230

acceleration. Correlations of this type were first used in geotechnical engineering to relate peak ground accelerations at a site with soil overlying bedrock to peak bedrock accelerations at the same site (e.g. Seed & Idriss 1982; and Idriss 1990). More recently, Bray *et al.* 1995; Kavazanjian & Matasovic 1995; Singh & Sun 1995; Bray & Rathje 1998; and Matasovic *et al.* 1998 have extended this type of relationship to solid waste landfills.

Matasovic *et al.* (1998) compared estimated horizontal bedrock accelerations to recorded peak horizontal accelerations at the OII site. Table 27.8, taken from Matasovic *et al.* (1998), present peak acceleration values (average of two horizontal components) recorded at the crest of the OII landfill versus the estimated peak horizontal bedrock accelerations for the same site. Based on these results, Matasovic *et al.* (1998) concluded that peak horizontal bedrock accelerations from both near-field and far-field earthquakes with peak horizontal bedrock accelerations up to at least 0.15 *g* can be significantly amplified by solid waste landfills. They observed that the curve developed by Harder (1991) for the upper-bound amplification of seismic accelerations in earth dams, shown in Fig. 27.22, provides a conservative upper bound for amplification of peak accelerations for solid waste landfills. They also suggested that the relationship of Idriss (1990) for soft soil sites provides a reasonable representation of average amplification potential of solid waste landfills.

Independent of Matasovic *et al.* (1998), Bray & Rathje (1998) used the non-linear one-dimensional dynamic response analysis D-MOD (Matasovic 1993; Matasovic & Vucetic 1995) to perform parametric analyses of landfill response for a range of waste properties, waste heights, site conditions, and bedrock ground motions. The results of their arametric evaluation for cover systems are given in Fig. 27.22. This figure presents a plot of peak horizontal acceleration at the landfill crest versus peak horizontal bedrock acceler-

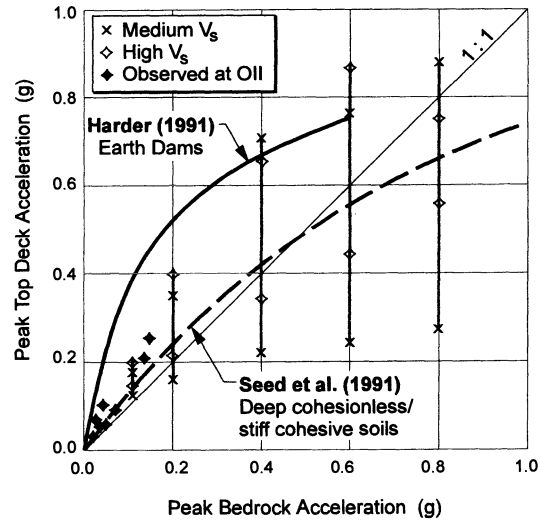


FIGURE 27.22. Results of parametric study comparing calculated peak horizontal acceleration for OII landfill top deck and peak bedrock acceleration (modified from Bray & Rathje 1998). Data from Harder (1991) for earth dams, and Seed *et al.* (1991) for deep cohesionless/stiff cohesive soils. Shear wave velocity v_s: (×) medium, (◇) high, (◆) observed at OII.

ation. They also compared their results to the Harder (1991) and the Seed *et al.* (1991) curves for stiff soil sites. Inspection of Fig. 27.22 shows that the Harder (1991) curve provides a conservative upper bound to the calculated cover system accelerations. Bray & Rathje (1998) note that the large amount of scatter in their parametric analysis results is due in large part to the sensitivity of the results to the input ground motion, i.e. variability among earthquakes. Variability in the assumed foundation conditions and waste profile also influenced the results. These findings are significant and engineers should consider this sensitivity when performing and interpreting the results of seismic response analyses.

Until more data become available, the Harder (1991) curve is recommended as a conservative upper-bound amplification of ground motions for simplified seismic site response of solid waste cover systems. Know-

ing the peak horizontal bedrock acceleration (from a USGS seismic hazard map, other map or site-specific analysis), the Harder (1991) curve can be used to estimate an upper-bound peak horizontal acceleration at the crest of the landfill. Should the Harder (1991) curve result in excessive cover system accelerations, detailed seismic response analyses can be conducted to assess whether a lower value of peak acceleration can be used on a project-specific basis. Site-specific seismic response analyses should also be used for any site where the average shear wave velocity in the upper 30 m of the foundation is less than 120 m s^{-1}, i.e. soft soil sites.

27.7.3.4 Analytical and Numerical Seismic Response Analyses

A one- or two-dimensional seismic site response analysis may be performed where significant cover system accelerations are anticipated or it is necessary to obtain a better estimate of seismically induced motions in the cover system than can be obtained with the simplified approach. These analyses are also recommended for sites with soft soil foundations and for critical facilities or facilities with special features. Such projects include those in regions where very large earthquakes can occur, where waste thicknesses are relatively large, or where cover system material or interface shear strengths are particularly low. The site response analysis is performed considering both the foundation soils and waste mass.

The computer program SHAKE, originally developed by Seed and coworkers (Schnabel *et al.* 1972) and updated by Idriss & Sun (1992), is perhaps the most commonly used computer program for one-dimensional seismic site response analysis. The SHAKE model idealizes the soil (and waste mass) profile as a system of homogeneous, visco-elastic sublayers of infinite horizontal extent. The response of this system is calculated considering vertically propagating shear waves. An equivalent linear analysis accounts for the strain-dependent non-linearity of soil and waste stiffness and damping using an iterative procedure to obtain modulus and damping values that are compatible with the equivalent uniform strain induced in each sublayer. At the outset, a set of properties (shear modulus, damping and total unit weight) is assigned to each sublayer of the soil or waste deposit. The analysis is conducted using these properties and the shear strain induced in each sublayer is calculated. The shear modulus and the damping ratio for each sublayer are then modified based on the applicable relationship between these two properties and shear strain (see Fig. 27.20).

Basic input to SHAKE includes the soil and waste profile, soil and waste properties, and an earthquake acceleration time history. Soil and waste properties include the maximum shear wave velocity, v_s, or maximum (small-strain) shear modulus, G_{max}, and total unit weight, γ_t, for each soil layer plus shear modulus reduction and damping ratio curves for each soil and waste material.

Computer programs are also available for equivalent-linear and truly non-linear two- and three-dimensional seismic site response analyses. A discussion of these more sophisticated models is provided by Kramer (1996). These models are only occasionally used in cover system design practice. Application of these models to the evaluation of cover system earthquake response often may result in lower-intensity seismically induced cover system motions than obtained using the one-dimensional SHAKE analysis. Use of non-linear analysis methods is recommended (Kavazanjian & Matasovic 1995 and Bray & Rathje 1998) when the peak horizontal bedrock acceleration exceeds 0.4 g. Examples of the use of these models include Idriss *et al.* (1995), Augello *et al.* (1998), and Matasovic & Kavazanjian (1998), which use the equivalent-linear two-dimensional finite element program QUAD4M (Hudson *et al.* 1994) to evaluate the seismic response of the OII landfill, and Kavazanjian & Matasovic (1995), Matasovic *et al.* (1998), and Bray & Rathje (1998),

which use the one-dimensional non-linear program D-MOD to evaluate landfill seismic response.

27.7.4. DYNAMIC SHEAR STRENGTH

The dynamic shear strengths of the components and interfaces of a cover system must be estimated to perform seismic slope stability and/or deformation analysis. These estimates are typically based on static or cyclic undrained shear strength tests. Shaking-table laboratory test results and observed earthquake performance of system components are also used to develop information on the performance of these components and interfaces in earthquakes. Information on the cyclic shear strength of soils used in cover systems can be obtained from the geotechnical earthquake engineering literature, e.g. Kramer (1996), Kavazanjian *et al.* (1997). Shear strengths of compacted clays and unsaturated granular soils typically used in cover system construction are not significantly degraded by seismic loading, and cyclic shear strength is assumed to equal static shear strength. Similarly, the limited available data on the cyclic shear strength of interfaces involving geosynthetics (Kavazanjian et al. 1991; Yegian & Lahalf 1992; Augello *et al.* 1995; Yegian *et al.* 1995; and Chaney *et al.* 1997) suggests that cyclic shear strengths can be approximated using the results of static shear strength tests.

27.7.5 SEISMIC STABILITY AND DEFORMATION ANALYSIS

27.7.5.1 Overview

The static LE slope stability analysis methods discussed previously in this document may be adapted for use in the seismic stability evaluation of cover systems. This adaptation can be achieved using a number of different approaches, of which the following three represent the current state of practice:

- the pseudo-static factor of safety method,
- the modified pseudo-static factor of safety method, and
- the permanent seismic deformation method.

27.7.5.2 Pseudo-Static Factor of Safety Method

Due to its simplicity, the pseudo-static factor of safety method remains the most common method of analysis used in practice for seismic design of cover systems. With this approach, the factor of safety for the cover system is calculated using a limit equilibrium analysis that incorporates a specified seismic coefficient, which is applied as a horizontal body force to the potential slide mass. The factor of safety obtained for the calculation is compared to a minimum acceptable factor of safety to determine the adequacy of the design. The seismic coefficient equals the fraction of the weight of the potential failure mass that is applied as a horizontal force to the centroid of the mass in a pseudo-static limit equilibrium stability analysis.

For the case of an infinite slope with no water flow, the pseudo-static factor of safety is given by:

$$FS = \frac{(\cos\beta - k_h \sin\beta)\tan\phi_i}{(\sin\beta + k_h \cos\beta)} + \frac{a_i}{\gamma_t t(\sin\beta + k_h \cos\beta)} \quad (27.33)$$

where k_h = pseudo-static seismic coefficient (dimensionless), and all other terms were defined previously. For the case of a slope of finite length, the pseudo-static factor of safety can be calculated for the case of no water flow using the following approximate solution for sliding on the two-part wedge shown in Fig. 27.15 (Giroud *et al.* 1999):

$$FS = \frac{M}{N}\tan\phi_i + \frac{a_i(1+\tan^2\beta)^{1/2}}{N\gamma_t t} + \left(\frac{t}{2h}\right)\frac{(1+\tan^2\beta)^{/3/2}\tan\phi_s\tan\beta}{1-(N/M)\tan\phi_s}\left(\frac{1+k_h^2}{MN}\right)^2 + \left(\frac{c_s}{\gamma_t h}\right)\frac{\tan\beta(1+\tan^2\beta)}{1-(N/M)\tan\phi_s}\left(\frac{1+k_h^2}{MN^2}\right) + \frac{T\tan\beta}{N\gamma_t h t} \quad (27.34)$$

where M and N are dimensionless parameters given by:

$$M = k_h + \tan \beta \quad (27.35)$$

$$N = 1 - k_h \tan \beta \quad (27.36)$$

and all other terms were defined previously. Note that if $\phi_s = 0$, $c_s = 0$ and $T = 0$, Eq. 27.34 reduces to Eq. 27.33.

The case of a slope of finite length has also been addressed by Koerner & Daniel (1997), which requires the solving of a quadratic equation. For more complicated geometries and slope conditions, design calculations are more easily performed using one of the LE slope stability computer programs described previously. It is common in performing seismic stability analyses of cover systems to assume no water flow in the slope. The rationale for this assumption is that the probability of occurrence of both a design-level earthquake event and a design-level storm event at the same time is extremely low.

The main drawback of the pseudo-static factor of safety approach lies in the difficulty in relating the value of the seismic coefficient to the characteristics of the design earthquake. Use of the peak acceleration at the top of the waste mass as the seismic coefficient, coupled with a pseudo-static factor of safety of 1.0, results in a very conservative design basis. This result would imply no displacement of the cover system during the design earthquake, not even for the milli-seconds during which the peak accelerations are applied. A seismic coefficient smaller than the peak ground acceleration (expressed on a fraction of gravity) is sometimes used, but the magnitude of cover system displacement in this case is unknown.

27.7.5.3 Modified Pseudo-Static Factor of Safety Method

The problem of selecting an appropriate seismic coefficient for the pseudo-static approach can be addressed by implicitly considering the potential for seismically induced deformations. Based on the work of Hynes & Franklin (1984), Richardson *et al.* (1995) suggested that seismically induced displacements in a slope will be less than 0.3 m if the yield acceleration, k_y, defined as the k_h producing a factor of safety of 1.0, is no less than 50% of the peak horizontal acceleration of the slope, i.e. cover system. This result represents an upper-bound value for the seismic deformation calculated by Hynes & Franklin using almost 400 earthquake strong-motion records. The value of k_y required to produce 0.3 m of permanent seismic displacement drops to about 15% of the peak horizontal acceleration if the mean plus one standard deviation curve is considered rather than the upper-bound curve. Other values of k_y can be derived from Fig. 27.23.

Kavazanjian (1998) presented a refined procedure for deriving a displacement-based seismic coefficient value specifically for the design of cover systems for solid waste landfills. Seismic coefficient values for specified levels of permanent seismic displacement are calculated by multiplying a ratio, obtained

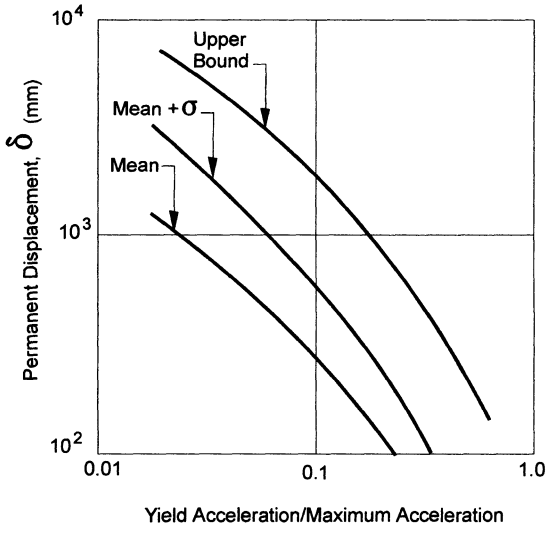


FIGURE 27.23. Hynes & Franklin (1984) permanent seismic displacement chart (modified from Richardson *et al.* 1995).

TABLE 27.9. Ratio of yield acceleration, k_y, to peak acceleration of cover system as a function of calculated permanent seismic displacement (adapted from Hynes & Franklin (1984) curves, shown in Fig. 27.23)

Calculated displacement (mm)	Mean ratio	Mean + σ ratio[a]
100	0.23	0.35
150	0.17	0.27
300	0.08	0.17
500	0.05	0.11
1000	0.03	0.06

[a] σ = standard deviation.

from Table 27.9, by the peak horizontal acceleration of the cover system obtained using the Harder (1991) curve shown in Fig. 27.22. Kavazanjian suggests that for earthquakes of magnitude less than or equal to 6.5 within 10 km of the project site, and for any earthquake of magnitude less than or equal to 5.5, the ratios in the "mean" column of Table 27.9 be used. Kavazanjian further recommends that for earthquakes of magnitude greater than 6.5, and for earthquakes between magnitude 5.5 and 6.5, i.e. more than 10 km from the project site, the ratios in the "mean + σ" column of Table 27.9 be used. Kavazanjian (1998) recommends that seismic coefficients derived using Table 27.9 be used with a factor of safety of 1.0. It is cautioned that the use of peak shear strength parameters with this approach may be unconservative. Shear strength values should be selected considering the displacement value from Table 27.9 associated with the chosen seismic coefficient. Again, this simplified approach is not recommended for soft soil sites.

27.7.5.4 Permanent Seismic Deformation Method

With the permanent seismic deformation method, cumulative permanent seismic deformations are calculated on the basis of that portion of the acceleration–time history of the cover system that exceeds k_y. For the infinite slope case, k_y is calculated using Eq. 27.33 and FS = 1.0. For the case of a finite length slope with uniform soil thickness above the critical potential slip surface, k_y is calculated using Eq. 27.34 and FS = 1.0. For more complex cases, k_y is calculated using a LE slope stability computer program.

The actual calculation of permanent seismic displacement is usually performed using Newmark's "sliding block on a plane" (1965) method of analysis. In a Newmark analysis (1965), acceleration pulses (in the earthquake acceleration–time history) exceeding k_y are double-integrated to calculate the accumulated "permanent" seismic displacement (Fig. 27.24). Theoretically, this calculated permanent displacement is a rigid body displacement that accumulates everywhere along the critical potential slip surface. Typically, only the horizontal component of the

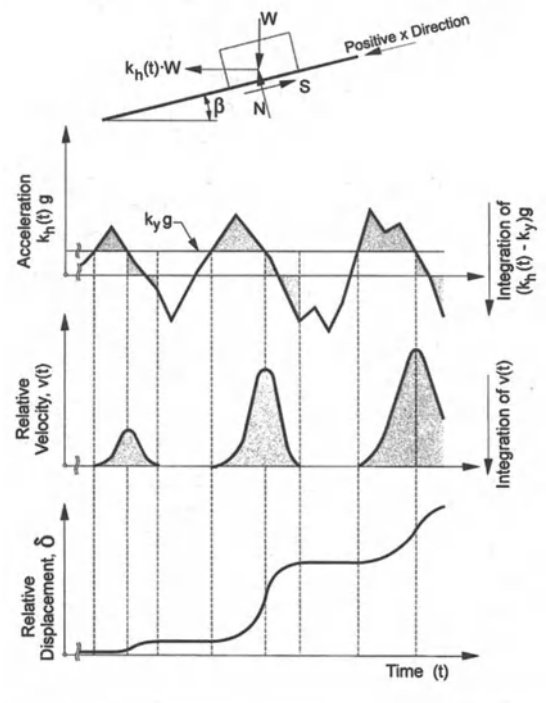


FIGURE 27.24. Basic elements of classical Newmark sliding-block analysis with constant yield acceleration, k_y.

earthquake acceleration–time history is considered in the analysis, and this acceleration is applied parallel to the slip surface. The acceleration–time history of the cover system used in the analysis is obtained from a seismic response analysis. With this approach, the response analysis is "decoupled" from the computation of permanent displacement; i.e. seismic response is calculated assuming no slip displacement between the cover system and landfill, and the cover system displacement is calculated using the results of the seismic response analysis (Bray & Rathje 1998). The decoupled approach is generally conservative (Bray & Rathje 1998) for landfill cover system displacement analyses.

Several PC-based computer programs exist to perform Newmark analyses (Houston *et al.* 1987; Yan *et al.* 1996). These models assume a constant value of k_y. Recognizing that most geosynthetic materials and interfaces exhibit strain-softening shear behavior, a modification to the standard Newmark procedure specifically for cover systems incorporating geosynthetic interfaces was proposed (Matasovic *et al.* 1997). The modified version incorporates a linear k_y degradation model to account for strain-softening materials and interfaces (Fig. 27.25). Matasovic *et al.* (1997) demonstrated the sensitivity of the calculated permanent seismic deformation for a typical geotextile–compacted soil interface and three differing assumptions regarding k_y: (i) constant, based on peak interface shear strength parameters; (ii) constant, based on residual (or large-displacement) interface shear strength parameters; and (iii) degrading, in accordance with Fig. 27.25. Figure 27.26 presents typical calculation results from Matasovic *et al.* (1997) for the post-peak strain-softening exhibited by a compacted soil–geotextile interface. The sensitivity of the calculation results to the k_y assumption is evident.

27.8 *Settlement*

27.8.1 MECHANISMS OF SETTLEMENT

Cover systems may be subject to settlements resulting from a variety of mechanisms. For purposes of evaluating cover system performance, settlements can be considered to have one of three sources (see Fig. 27.27):

1. settlement of foundation soil,
2. settlement due to overall waste mass compressibility, and
3. settlement due to localized mechanisms in the waste.

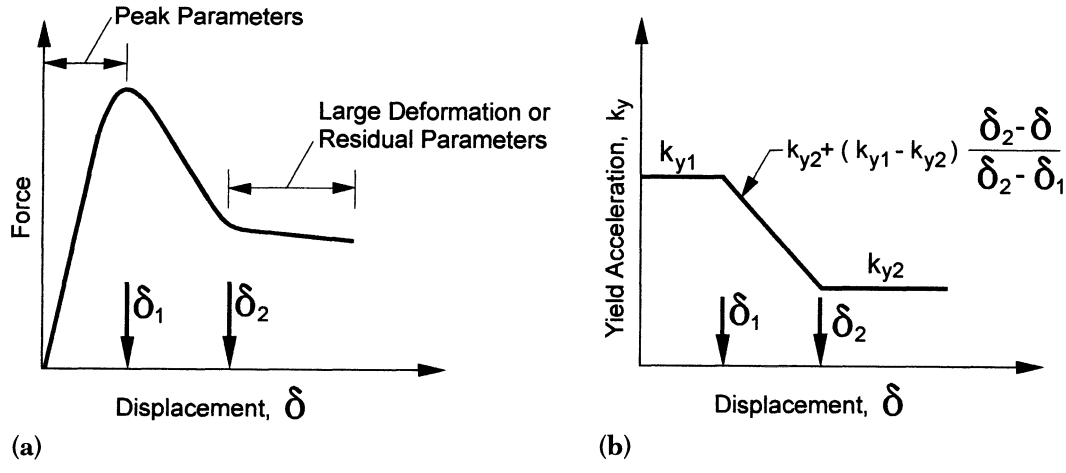


FIGURE 27.25. Yield acceleration degradation model: (a) measured shear force–displacement curve; and (b) yield acceleration degradation (modified from Matasovic *et al.* 1997).

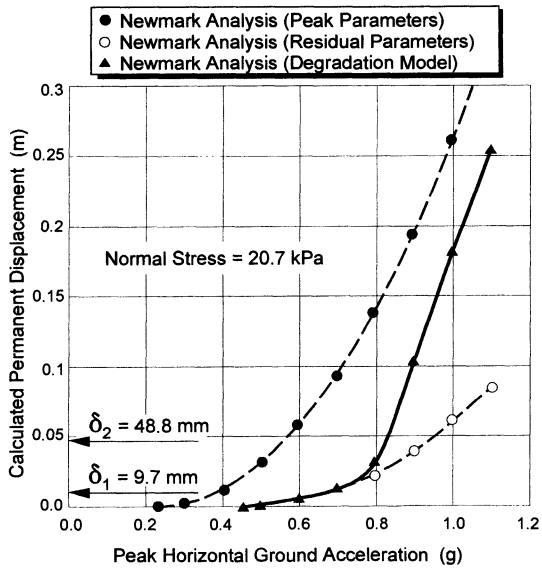


FIGURE 27.26. Results of Newmark seismic deformation analysis for constant and degrading yield acceleration at a normal stress = 20.7 kPa (modified from Matasovic *et al.* 1997): (●) peak parameters; (○) residual parameters; and (▲) degradation model.

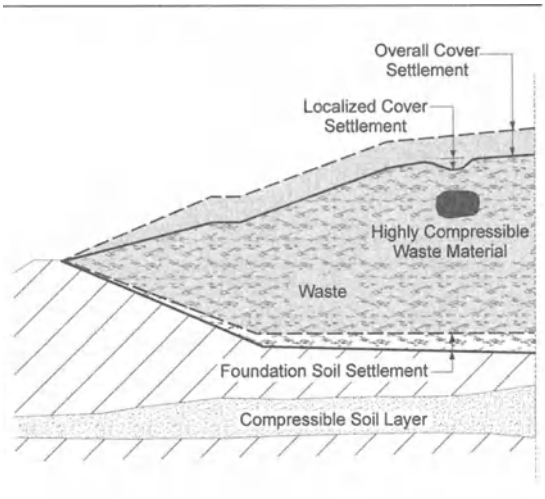


FIGURE 27.27. Sources of cover settlement.

Angular distortion or differential settlement may: (a) induce unacceptable tensile stress and strain in one or more cover system components, which can lead to component tearing or cracking; or (b) cause cover system slopes to change or reverse; which, in turn, can affect the performance of the cover system drainage layer and/or gas collection layer.

27.8.2 SETTLEMENT OF FOUNDATION SOILS

Impacts of foundation settlement on the performance of a cover system are usually not significant. Occasionally, situations arise where foundation settlements are of sufficient magnitude to affect the cover system design. For example, if the waste mass is underlain by a thick layer of soft clay, consolidation settlements can be large. Both primary settlement and long-term secondary settlement should be considered. Calculations are performed using equations from conventional geotechnical engineering practice (see Chapters 2, 3, 9 and 16) and a timeframe at least equal to the active life and post-closure care period of the facility.

27.8.3 OVERALL WASTE COMPRESSION

Overall waste mass compressibility results in area-wide waste mass settlement. The potential for waste settlement is highly dependent on the type of waste. Relative to most other wastes, MSW is very compressible, due to both its initial compressibility when placed and the additional compressibility induced by the biodegradation of the organic component of the MSW. This latter component creates a significant time dependency to waste settlements. Other types of facilities that can undergo large settlements include impoundments containing high-water-content industrial sludges. Materials such as mine waste, ash and slag, construction and demolition waste, and soil waste have relatively lower settlement potential. The following discussion of overall waste settlement primarily focuses on the settlement potential of MSW waste and other highly compressible waste material. The evaluation of ash and soil waste, or other low compressibility inorganic waste, is typically performed using equations for conventional geotechnical engineering practice (see Chapters 2, 3, 9 and 16).

MSW waste compression results from complex factors (Sowers 1973; Edil *et al.* 1990; Sharma & Lewis 1994), including:

- mechanical compression due to self-weight and surface loads;
- ravelling, i.e. movement of fines into larger voids;
- physiochemical changes, including corrosion, oxidation, and combustion; and
- biochemical decomposition under aerobic and anaerobic processes.

The magnitude and rate of MSW settlement are controlled by many factors, among which are the waste fill height, organic content, age, moisture content, degree of compaction, and temperature. Figure 27.28 presents data from Edgers *et al.* (1992), König *et al.* (1996), and Spikula (1996), indicating that MSW land-fills can settle from about 5 to 20% (and even up to 30%) of the initial landfill thickness (measured from the time the landfill first reaches final grade).

A number of methods have been proposed for evaluating the short-term and long-term compression of waste. Three settlement models that have been adopted from geotechnical engineering and applied to waste are: (a) the one-dimensional compression model, (b) the power creep model, and (c) the Gibson & Lo (1961) model. A discussion of the last two models is presented in Edil *et al.* (1990), and they are not discussed further herein. Presently, there is little experience in applying these last two models, and their applicability to the prediction of long-term settlements is questionable (U.S. EPA 1999).

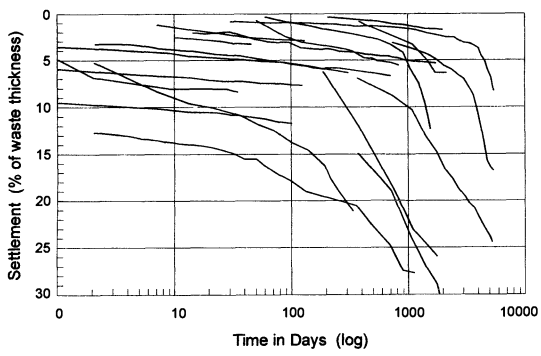


FIGURE 27.28. Total settlement data for MSW landfills, measured from the time the landfill reaches final grade (data from Edgers *et al.* 1992, König *et al.* 1996, and Spikula 1996).

Conventional one-dimensional compression models, e.g. see Sections 2.7.4, 9.4.3, and 16.4.3, have been used to estimate waste settlements. However, it is often assumed that primary self-weight settlement is complete prior to installation of the cover system. Thus, calculated primary settlements are assumed not to directly influence cover system performance.

Cover system performance will be affected, however, by secondary waste settlement. The secondary waste settlement, $s_{\Delta t}$, that occurs between times t_1 and t_2 is calculated with the one-dimensional model using an equation of the form (see also Section 2.7.5):

$$s_{\Delta t} = C_{\alpha\varepsilon} H_1 \log \frac{t_2}{t_1} \qquad (27.37)$$

where $C_{\alpha\varepsilon}$ = modified secondary compression index (dimensionless), H_1 = height of waste at time t_1 (m), t_1 = starting time for the period of secondary compression (s), and $t_2 = t_1$ plus the time duration of secondary compression (s). Use of Eq. 27.37 implies that the magnitude of secondary settlement is independent of the applied stress. A modified form of Eq. 27.37 has been suggested by Bjarngard & Edgers (1990) and Stuglis *et al.* (1995) to account for a variable value of $C_{\alpha\epsilon}$ between "intermediate" and "long-term" secondary compression times. Their equation is formulated herein as:

$$s_{\Delta t} = C_{\alpha\varepsilon 1} H_1 \log \frac{t_2}{t_1} + C_{\alpha\varepsilon 2} H_2 \log \frac{t_3}{t_2} \qquad (27.38)$$

where $C_{\alpha\varepsilon 1}$ = modified secondary compression index during the intermediate secondary compression period (dimensionless), $C_{\alpha\varepsilon 2}$ = modified secondary compression index dur-

ing the long-term secondary compression period (dimensionless), H_1 = height of waste at time t_1 (m), H_2 = height of waste at time t_2 (m), t_1 starting time for the period of secondary compression(s), $t_2 = t_1$ plus the time duration of intermediate secondary compression (s), and $t_3 = t_2$ plus the time duration of long-term secondary compression. Inspection of Fig. 27.28 suggests that for some MSW materials, $C_{\alpha\varepsilon}$ is more or less constant during the period for which data exist, while for other facilities, a variable $C_{\alpha\varepsilon}$ could be used to better fit the data.

The reader should be aware that the choice of a value of $C_{\alpha\varepsilon}$ cannot be made without consideration of the normalization term t_1. For a given $C_{\alpha\varepsilon}$, the calculated value of $s_{\Delta t}$ will be significantly affected by the choice of t_1. Ideally, $C_{\alpha\varepsilon}$ and t_1 should be selected by empirically fitting Eqs 27.37 or 27.38 to field settlement data. In the absence of this type of correlation, it is suggested that t_1 be taken as the time period between when waste reaches final grade and when the cover system is installed over the waste.

Since $C_{\alpha\varepsilon}$ and t_1 are empirically derived and $s_{\Delta t}$ is assumed to be independent of applied effective stress, and since the primary purpose of calculating $s_{\Delta t}$ herein is to assess potential impacts to the performance of the cover system, it is not necessary to subdivide the waste mass into a series of horizontal layers for purposes of calculating $s_{\Delta t}$. With this approach, calculations are performed for increasing time intervals after closure to obtain a relationship between cover system settlement and elapsed time since closure.

Values of $C_{\alpha\varepsilon}$ for MSW reported in the technical literature (Sowers 1973; NAVFAC 1983; Burlingame 1985; Landva & Clark 1990; Fassett *et al.* 1994; Stulgis *et al.* 1995) have generally been in the range of 0.01–0.1. Given the empirical nature of $C_{\alpha\varepsilon}$ and t_1, it is interesting to compare calculated values of $(s_{\Delta t}/H_1)$ obtained using Eq. 27.37 to the range of observed time-dependent post-closure settlements for a number of MSW landfills (Fig. 27.28). For the comparison, the waste mass is considered as a single unit with an average value of t_1 of 100 days (approximately three months). Table 27.10 presents calculated values of $s_{\Delta t}/H_1$ (in percent) for values of $C_{\alpha\varepsilon}$ ranging from 0.01 to 0.1 and post-closure times of 100, 1000 and 10 000 days (to which 100 days are added to obtain t_2 values).

TABLE 27.10. Results of parameter study of calculated post-closure secondary settlements, $S_{\Delta t}$, as a percentage of initial landfill height, H_1

	$(t_2 - t_1)$ (days after closure)		
$C_{\alpha\varepsilon}$	100	1000	10 000
0.01	0.30	1.0	2.0
0.03	0.90	3.1	6.0
0.06	1.8	6.2	12.0
0.10	3.0	10.4	20.0

Based on the calculated values in Table 27.10, $C_{\alpha\varepsilon}$ values less than about 0.03, coupled with t_1 values of 100 days, are too small to model MSW time-dependent settlements. Careful review of the source references used to develop Fig. 27.28 suggests that $C_{\alpha\varepsilon}$ values in the range 0.04–0.08, coupled with t_1 values of about 100 days provide a reasonable modeling of the settlement trends for modern MSW landfills, which are typically filled fairly quickly and compacted using heavy trash compactors. Larger values of $C_{\alpha\varepsilon}$, in the range 0.08–0.12, coupled with t_1 = 100 days, are needed to model the settlement trends in some of the older landfills, where possibly more variable waste was placed under conditions less controlled than for modern landfills. Larger values of $C_{\alpha\varepsilon}$ would also be expected for landfills undergoing leachate recirculation or otherwise managed to increase biological activity and methane production in the waste mass.

If t_1 is assumed to be 30 days rather than 100 days, calculated $s_{\Delta t}/H_1$ values at 10 000

days would be about 25% larger than given in Table 27.10. Thus, if $t_1 = 30$ days is assumed, $C_{\alpha\varepsilon}$ values should be reduced about 25% from the recommended ranges given above. This calculation exercise clearly points out the sensitivity of calculated $s_{\Delta t}/H_1$ values to the magnitude of t_1.

27.8.4 SETTLEMENT DUE TO LOCALIZED MECHANISMS

Localized settlements, in the form of depressions, can develop within the first several years after cover system installation over MSW. These types of localized occurrences appear to be more common in older waste fills where a number of factors may contribute to the problem, including: (a) little initial waste compaction, (b) variable waste characteristics, (c) placement of sludges in the waste fill, and/or (d) poor surface-water control leading to ponding of water on the waste. Localized differential settlement can lead to excessive stress or strain in cover system components (Gilbert & Murphy 1987). Localized differential settlement of waste is generally attributed to one or more of several mechanisms, namely: (a) deterioration and collapse of objects, e.g. drums, in the waste; (b) settlement associated with a highly compressible zone of waste; and (c) migration or raveling of waste particles into underlying voids.

Several analysis methods are available for use in evaluating the potential effects of localized waste settlements on cover system performance. None of the methods have been field calibrated to any significant degree and selection of input parameters to the analyses is based primarily on engineering judgment.

- Murphy & Gilbert (1985) discuss the application of mine subsidence models to the prediction of waste differential settlements.
- Giroud *et al.* (1990) presented an approach based on the uncoupled combined use of the tensioned membrane and soil arching theories for analyzing the stresses and strains in geosynthetics (such as geosynthetic layers within a cover system) that lose foundation support after construction due to development of a foundation void or depression. Poorooshasb (1991) used a somewhat different analytical approach to address a similar problem.
- Jang & Montero (1993) used a boundary element formulation to model deformations around a collapsing void within an existing waste mass.
- Carey *et al.* (1993) performed two-dimensional finite element analyses to evaluate the response of a waste mass containing compressible zones.
- Othman *et al.* (1995) described application of the displacement method of Sagaseta (1987) to evaluate the response of a cover system over a waste mass containing localized compressible zones.

In the situation where differential settlement is likely to occur and the localized depressions cannot be eliminated, the choices are: (a) continuously grading and maintaining the site, (b) installing a thick buffer soil waste prior to cover system construction, or (c) installing a geosynthetic support beneath the cover system. One or more of the analysis methods described above can be used to design soil buffer or geosynthetic (geogrid or high strength geotextile) support systems. The critical design parameters in any such analysis are the locations and dimensions of the anticipated localized depression or void. Since it is generally not possible to predict where such a feature will occur, any buffer soil or reinforcement layer, if used, will typically need to be installed over the entire waste mass.

27.8.5 IMPACTS OF SETTLEMENT ON COVER SYSTEM

In design, settlement profiles accounting for the various settlement mechanisms are developed to evaluate potential impacts to the final

cover system. The evaluation usually considers: (a) post-settlement cover system grades, (b) potential for depressions and ponding in the cover system, and (c) stresses and strains in cover system components. Post-settlement grades should be adequate to shed run-off, prevent ponding, and prevent excessive stress or strain in cover system components, particularly CCL, GCL, and geomembrane hydraulic-barrier layers.

Tensile strains causing cracking in compacted clays have been evaluated by Leonards & Narain 1963; Ajaz & Parry 1975a,b, 1976; Gaind & Char 1983; Chandhari & Char 1985; Jessberger & Stone 1991; and Lozano & Aughenbaugh 1995. Based on these studies, compacted clays tested under unconfined or low confinement conditions exhibit relatively brittle behavior and reach failure at axial extensional strains of 0.02–4%, with most compacted clays exhibiting failure at extensional strains of 0.5% or less. The studies also show that the magnitude of tensile strain causing cracking increases with increasing percentage of fines and water content, and with increasing confining stress.

LaGatta *et al.* (1997) evaluated the impact of differential settlement on the hydraulic conductivity of GCLs overlain by a 600-mm thickness of pea gravel. The results of their evaluation indicate that intact and overlapped samples of needle-punched GCLs can withstand angular distortions of 0.35–0.6, equivalent to tensile strains of up to 5–16%, depending on product, while maintaining a saturated hydraulic conductivity of 1×10^{-9} m s^{-1}, or less. Geotextile-encased, non-reinforced GCL samples (intact and overlapped) were found to be able to maintain a hydraulic conductivity of 1×10^{-9} m s^{-1} up to an angular distortion of 0.1, equivalent to a tensile strain of about 1%. Stitch-bonded geotextile-encased GCL samples (intact) were found to achieve the same hydraulic conductivity criterion up to an angular distortion of 0.35, equivalent to a tensile strain of 5%.

The tensile behavior of geomembranes varies depending on the polymer type, stress-strain characteristics, susceptibility to stress cracking, temperature, and other factors. The present state-of-practice for the design of strain-softening geomembrane barrier layers, e.g. polyethylene geomembranes, is to limit the allowable geomembrane tensile stress (or strain) to the short-term yield value divided by a factor of safety. The allowable tensile stress (or strain) for geomembranes exhibiting strain-hardening behavior is based on the short-term failure (break) value divided by a factor of safety. It should also be remembered that geomembranes are designed to be barrier layers, not tensile inclusions (as is geosynthetic reinforcement, for example). The long-term stress-strain, creep, and brittle fracture behaviors of these materials under stress are not well-understood. To the extent possible, applications should be designed to minimize tensile stresses and elongations in geomembranes.

The authors recommend that when it is necessary to specify allowable geosynthetic tensile stresses and strains, the yield stress and strain of the geomembrane material be determined in a wide-width tension test (for plane deformation) or axisymmetric tension test (for spherical deformation) and that the factor of safety used to calculate the allowable values be at least five. The factor of safety should be applied to the yield values for strain-softening geomembranes and to the failure (break) values for strain-hardening materials. This recommendation should be conservative for virtually all types of commercially available geomembranes used in cover system applications. If a higher value of allowable tensile stress or strain is desired, the engineer must demonstrate that the product to be specified can sustain the allowable values without long-term creep, brittle rupture, or other type of long-term problem. This demonstration must also apply to geomembrane seams.

28. MONITORING OF CONTAMINANTS AND CONSIDERATION OF RISK

E. McBean
K. Schmidtke
W. Dyck
F. Rovers

28.1 Components of a Groundwater Monitoring Program

Groundwater monitoring is a critical component of activities performed at a site where the groundwater may have been adversely impacted by chemicals (i.e. contaminated). The specific purposes of groundwater monitoring will vary depending on the stage of impact identification. The elements of monitoring include:

- initial site characterization using available information;
- refining the site characterization through the installation of boreholes and wells, and sample collection and analysis;
- designing a corrective action; and
- implementing and monitoring a corrective action.

A well-designed sampling and analysis program will:

- provide analytical results of known quality;
- provide a three-dimensional characterization of hydrogeology and chemical presence at the site, including exposure pathways;
- indicate the extent of temporal variability of the chemical concentrations; and
- stay within resource limitations.

The adequacy of a groundwater monitoring program depends upon:

- an adequate characterization of the site hydrogeology,
- the use of appropriate procedures for the collection and analysis of groundwater samples, and
- statistical interpretation of the results.

Inaccurate analytical results cost as much as accurate results initially, but the inaccurate results may later come back to cause more significant problems. The best approach is to perform the program properly from the outset.

This chapter describes the general procedures necessary to ensure that the groundwater monitoring program will achieve the above purposes and some of the statistical procedures frequently used in statistical analyses of monitoring data. Some of the data collection procedures need to be modified based on site-specific factors (e.g. a site with a het-

R. K. Rowe (ed.), *Geotechnical and Geoenvironmental Engineering Handbook*
© Kluwer Academic Publishers 2001

erogeneous subsurface will require more information than a site with a relatively homogeneous subsurface), and the specifics of the regulatory standards applicable to a particular site. Chapters 29 and 30 address the issues of *in situ* containment and treatment of contaminated soil and groundwater, and other aspects of managing contaminated sites.

28.1.1 DETERMINING MONITORING WELL LOCATIONS AND ANALYTICAL PARAMETERS

28.1.1.1 Initial Site Characterization

The initial step in selecting the location of monitoring wells and the analytical parameters requires a review of the existing information in the general vicinity of the site, including: site history, geology, hydrogeology, potential chemical source areas and surface water drainage. This information is used to develop a preliminary conceptual model of the site. The conceptual model should include the following information:

1. Geology underlying the site.
2. Hydrogeology underlying the site (see also Section 24.1):
   - the hydrogeologic units present;
   - vertical and horizontal groundwater flow paths in each hydrogeologic unit, including hydraulic connectivity between waterbearing units;
   - hydraulic conductivity of each unit;
   - horizontal and vertical groundwater gradient and velocity in each unit;
   - structural discontinuities;
   - outside influences, e.g. tidal fluctuations, river stage variations, local pumping influences;
   - local meteorologic conditions, e.g. rainfall, evapotranspiration; and
   - seasonal factors, e.g. snow melt.
3. Chemicals produced, used, stored or disposed at the site.
4. Potential chemical source areas, including properties adjacent to and upgradient of the site.
5. The phase of the chemicals that may be present in the subsurface, i.e. dissolved as aqueous-phase liquid (APL) or as a separate non-aqueous-phase liquid (NAPL), and whether the NAPL is lighter than water (LNAPL) or denser than water (DNAPL).

Examples of sources where information regarding the above can be found include: reports from the US Geologic Survey; historical air photographs; existing water wells or geotechnical borings at, or in the vicinity of, the site; plant operational records if the site was, or is, an operational plant; and local weather stations. If the existing information is insufficient to develop a preliminary site conceptual model, initial activities typically include the installation of a minimum of three boreholes set in a triangular pattern within, and close to, the perimeter of the site. The boreholes are generally installed until a confining layer of significant thickness, which is continuous beneath the site, is encountered. The information obtained regarding the hydrogeology underlying the site is then used to develop the site conceptual model and to assist in selecting monitoring well locations.

Using the conceptual model and assuming chemically impacted groundwater is identified, a corrective action concept (e.g. groundwater pump and treat, soil excavation/treatment/disposal, soil vapor extractions, *in situ* treatment) is then developed.

28.1.1.2 Well Location

During the initial site characterization, a variety of information is obtained and a conceptual model developed. These are then used to identify gaps in the data and to select borehole/monitoring well locations for the subsequent site investigation. These wells must be located so as to further define the geology/hydrogeology and to establish potential groundwater flow and chemical migration pathways underlying the vicinity of the site. Typically, boreholes/monitoring wells are installed in stages. The benefit of this approach

is that information obtained from previous stages can be used to refine the conceptual site model and to assist in selecting the location of wells for subsequent stages to address the identified data gaps. The first stage is generally limited to:

- vertically, the uppermost water-bearing unit down to the first confining layer; and
- horizontally, the areas of concern (AOCs)/potential migration pathways, where no or little data exist.

The reason for limiting the first stage to the first confining layer is that the confining layer may have prevented the migration of chemicals from the site into underlying hydrogeologic units. The decision to investigate units underlying the first confining layer would be based on:

- knowledge that the integrity of the confining layer has been breached by either anthropogenic activities (e.g. installation of a deep building foundation, trenches for subsurface utilities) or that a natural discontinuity exists; or
- monitoring, which shows a potential that the next underlying water-bearing unit may have been adversely impacted.

The evaluation of whether to investigate water-bearing units beneath a confining layer also considers the thickness and potential reactivity of the confining layer in contact with site-specific chemicals. Examples of reactivity include: marl, which is chemically reactive with low pH wastes; and illitic clays, which are reactive with some organic chemicals (e.g. xylene (USEPA 1986a)). Other examples of changes in material properties because of contact with site-related chemicals are described in Abdul *et al.* (1990), Acar *et al.* (1985), Gipson (1985) and Lentz *et al.* (1985).

In situations where multiple hydrogeologic units have been adversely impacted, nested wells, described in Section 28.1.5, are often used. Installation details for overburden and bedrock wells are shown on Figs. 28.1 and 28.2, respectively. Figure 28.3 illustrates alternate capping designs for above-grade and flush-mount casings.

Well locations are typically selected to address AOCs, potential migration pathways, and/or exposure locations to human and environmental receptors. Often, possible migration pathways and the exposure locations are examined using groundwater flow and chemical migration models. Additional details relating to the use of models are presented in numerous sources including API (1988), Bear (1972), Charbeneau *et al.* (1989), USEPA (1985, 1989a), Faust *et al.* (1989), Huyakorn *et al.* (1992), Kaluarchchi & Parker (1989), Kaluarchchi *et al.* (1990), Katyal *et al.* (1991), Mendoza & McAlary (1989), and van der Heijde & Elnawawy (1993).

Once the migration pathways and exposure locations are established, well locations can be selected using either a judgmental, geostatistical (kriging) or random design approach. The judgmental approach uses existing knowledge of the site combined with the objectives of the investigation to select the well locations. For example, if it is known that a chemical leak occurred in an area where there are no wells and the objective is to identify areas with elevated concentrations, a well would likely be placed in the area of the spill. The judgmental approach provides for more efficient use of limited resources by focusing the effort on areas which may pose a risk to human health. The judgmental approach may also support a statistical analysis of the analytical results if the specific well locations within the contaminated area are assigned randomly or in a uniform pattern.

The geostatistical approach (kriging) is an interpolation method using spatial correlation structure to obtain either point or spatially averaged estimates of a parameter, e.g. hydraulic conductivity, from irregularly spaced sparse data sets. Furthermore, it provides an estimate of the accuracy of the interpolated values based on the data configura-

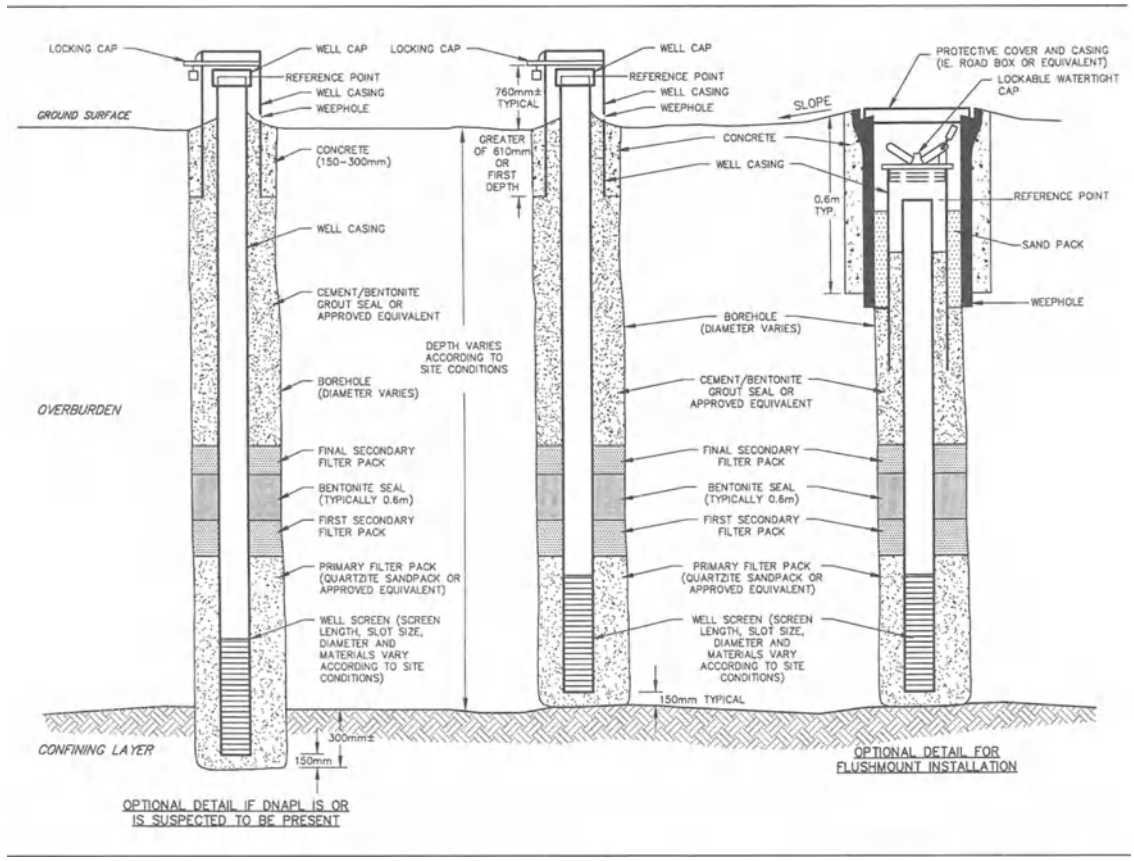


FIGURE 28.1. Typical overburden well installation (center). Left-hand and right-hand figures, respectively show optional detail if DNAPL is, or is suspected, of being present, and flushmount installation.

tion. Areas identified as having a low degree of accuracy are then selected as the next areas from which to obtain information on that parameter. Additional details regarding geostatistical approaches can be found in David (1997), Delhomme (1979), Kafritsas & Bras (1981), and Matheron (1973).

The random approach selects a random pattern of well locations without the use of any previously obtained knowledge.

Systematic grid sampling can be used in both the geostatistical and random design approach. The systematic grid sampling approach uses a defined grid system (e.g. 15 × 15 m) over the site, and can be combined with the random design approach by either randomly selecting which grid block to sample, or by randomly selecting the location within each grid block to sample. If a random design approach is used, the sample design can often be improved by only sampling a given hydrogeologic unit in order to reduce variability. A detailed discussion is provided in Gilbert (1987), Keith (1987, 1990), and USEPA (1989d).

Wells should be located adjacent to permanent features, i.e. fences, buildings, etc., that offer some degree of protection and a reference point for locating the well. Wells located in high traffic areas, road allowance right-of-ways or low lying areas are undesirable and should be avoided if possible. The well locations should be verified prior to placement to confirm clearance from underground or overhead utilities.

An approach to reduce the number of wells otherwise necessary is to combine multiple AOCs into fewer AOCs. The number of AOCs that can be combined will be controlled by

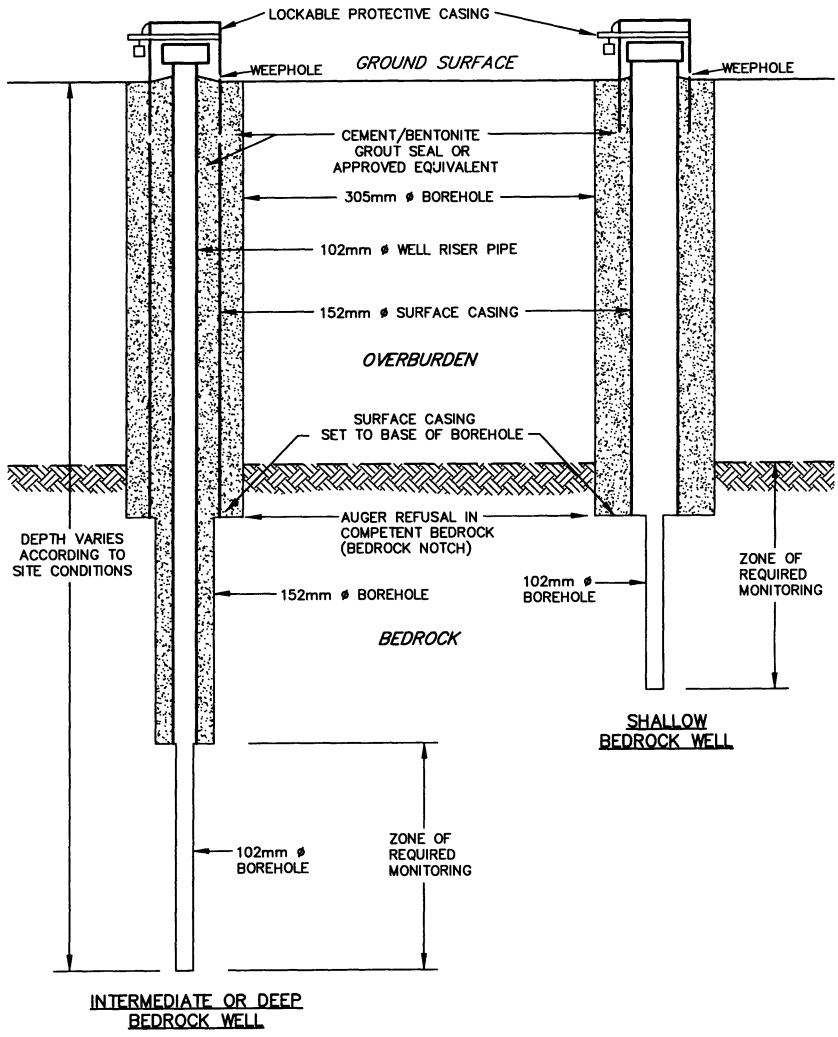


FIGURE 28.2. Typical bedrock well installation: (a) intermediate or deep bedrock well; and (b) shallow bedrock well.

their proximity to each other and the similarity of chemicals which are of potential concern.

The initial number of boreholes/wells for each water-bearing unit underlying an AOC should include one background (upgradient) borehole/well and two boreholes/wells immediately downgradient of the AOC. The background well should be installed upgradient such that it will not be impacted by releases from the AOC. It is expected that information regarding the groundwater flow direction for the site will be available from the initial site characterization activities described in Section 28.1.1.1.

An important consideration in locating monitoring wells within the vertical thickness of a water-bearing unit is the physical–chemical characteristics of the chemicals of concern. Examples of these considerations are LNAPLs and DNAPLs. LNAPLs spread rapidly in the capillary zone just above the groundwater table. DNAPLs, whose migration is governed largely by gravity (i.e. density) and viscosity, generally have a dominant vertical component until con-

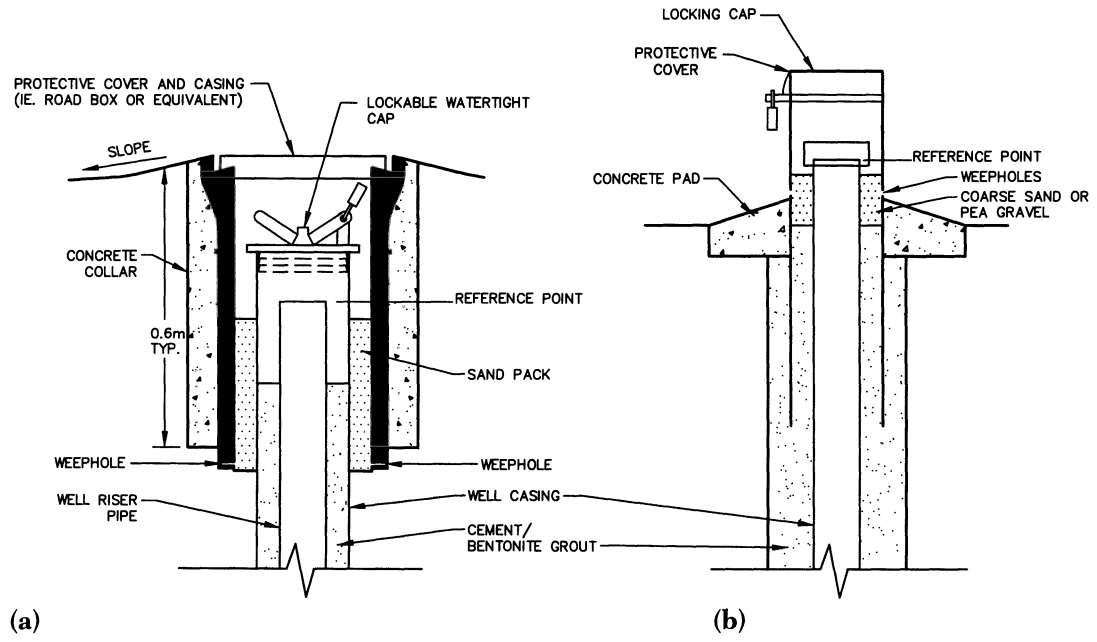


FIGURE 28.3. Protective casing installation: (a) flush mount; and (b) above-grade.

tacting a confining layer. NAPL leaves behind a residual (non-mobile NAPL) as it migrates.

For LNAPLs, the monitoring well-screen should be set so as to straddle the groundwater table. For DNAPLs, the screens should be set at the top of the confining layer and should include a small sump (see Fig. 28.1). The sump will act as a collector for DNAPL. The presence of LNAPL and/or DNAPL may require the installation of more than one well at a sample location (see Section 28.1.5 for nested wells). Additional details regarding NAPL and its effect on well placement can be found in Abdul *et al.* (1989), Blake & Hall (1984), Cohen & Mercer (1993), USEPA (1992d), Gruszczenski (1987), Huling & Weaver (1991), Newell *et al.* (1995), Ostendorf *et al.* (1992), Schwille (1988), and Waterloo Center for Groundwater Research (1989).

For those sites where the background concentrations are close to on-site concentrations, the USEPA (1990) suggests that the number of background samples equals the number of site samples. The reason is to allow the statistical determination of the "true" difference between the background and site concentrations.

The USEPA method uses confidence levels, power and minimum detectable relative difference to calculate the number of samples required for each AOC/exposure pathway. A concern with the USEPA's approach is that for a site where it is difficult to distinguish site-related chemicals from background conditions (i.e. there has been minimal impact at the site and thus there exists a small detectable relative difference), a large number of samples is required when in fact site-related releases may pose no increased health risk and natural attenuation processes can be relied upon to mitigate these low concentrations.

28.1.1.3 Analytical Parameters

Historical information is used to develop a preliminary list of chemicals of potential concern. Factors evaluated to develop this list include:

- uniqueness of the chemical to the site;
- transport properties of the chemical (e.g. is it mobile in the subsurface or is it highly adsorptive);

- chemical stability;

ILM04.0), and Test Methods for Evaluating

described in Borden (1995), Hinchee *et al.* (1995), Klecka *et al.* (1996), and Wiedemeier *et al.* (1995, 1996c).

28.1.1.6 Corrective Action Monitoring

The purpose of corrective action monitoring is to establish whether the corrective action is meeting specified performance criteria. The long-term corrective action monitoring plan should be developed based on site-specific characteristics, the results of chemical migration simulations and the results of exposure pathway/receptor analysis.

1. Chemical concentration performance measures:

- for source control: a decrease in source area concentration to the targeted cleanup level (e.g. maximum concentration limits, MCLs); and no exceedence of MCLs at the downgradient points of compliance.
- for natural attenuation: the rate of concentration decrease between the AOC and exposure location is sufficient to protect the exposure location receptors.

2. Well location: The locations of wells used to monitor corrective action are dependent on the type of corrective action implemented. The locations of these monitoring wells are generally referred to as "points of compliance". Often wells installed for site investigative activities can be used. Examples of the types of corrective action and chemical monitoring wells that are needed are described below.

- Containment: an area of impacted groundwater can be contained physically (e.g. utilize a cap and/or barrier wall), using hydraulics (e.g. extraction wells) or using a combined physical/hydraulic system (e.g. barrier wall with a groundwater collection system within the contained area). Generally, for a hydraulically controlled system, the point of compliance is typically located at a negotiated distance upgradient from the exposure location, but downgradient from the impacted area. The negotiated distance is often calculated using the advective velocity of groundwater flow for a specified number of years (e.g. two-year travel distance). Generally, two or three wells, spread laterally perpendicular to the direction of groundwater flow, are installed at the point of compliance distance for each water-bearing unit to be monitored. In addition to the point of compliance wells, a background well and a well located within the AOC are typically installed.
- Natural attenuation: can be used either as a component of a corrective action (e.g. use pump and treat for source control and let natural attenuation address the portion of the plume downgradient of the zone of capture) or as the sole remedy. The monitoring requirements for natural attenuation are generally more intensive than for other systems because the groundwater monitoring is used to identify chemical migration, intrinsic abiotic and biotic degradation processes, if any, and the need for future action, if any. As an example, evaluation of the feasibility of complete degradation of chlorinated ethylene by anaerobic reductive dechlorination or anaerobic/aerobic degradation would involve careful mapping of the parent compound(s) (PCE, TCE and/or DCE), the degradation products (DCE, vinyl chloride, ethenes/ethanes) and other parameters (Wiedemeier *et al.* 1996c; Carey *et al.* 1997a, 1998).

3. Analytical parameters: The selection of the parameters to be utilized for monitoring the performance of the corrective action is site specific. Typically, the list of parameters is a subgroup of those used to investigate the

site. In addition to the factors described in Section 28.1.1.3, the frequency of detection and magnitude of the concentrations are also considered. It may also be possible to develop a different parameter list for each AOC and/or for each well which monitors a specific AOC.

28.1.2 MONITORING WELL DESIGN AND CONSTRUCTION

28.1.2.1 General

The design and installation of monitoring wells involves the drilling of boreholes into various types of geologic formations. Designing and installing monitoring wells may require several different drilling methods and installation procedures. It is important that the drilling method minimizes disturbance of subsurface materials, not contaminate the subsurface soils and groundwater, and not provide a hydraulic link between different hydrogeologic units. Samples collected from monitoring wells must not be contaminated by drilling fluids or by the drilling procedures. Numerous publications are available describing current monitoring well design and construction procedures. References include Aller *et al.* (1989), ASTM D5092, and Driscoll (1986). Typical design features are illustrated in Figs. 28.1–28.3.

28.1.2.2 Design Considerations

1. Well diameter: The diameter of the well is primarily dictated by the purpose of the installation. In general, wells installed for groundwater monitoring purposes should be at least 5 cm in diameter. This allows small-diameter bladder pumps to be installed for sampling as well as small-diameter bailers and suction tubes.

2. Screen length and placement: The screen length should be consistent with the desired monitored interval and geologic conditions encountered. For delineation of the vertical profile of a groundwater chemical plume, the number of screened intervals and the screen length will be a function of the thickness of the plume and the desired degree of delineation. A fine degree of delineation will require a relatively large number of small screened intervals. Where cost considerations make this impractical or it is desired to identify where the chemical plume is present, larger well-screens on the order of 1.5–3 m can be used. In cases where the water table is being monitored, e.g. for LNAPL, the screen length should accommodate seasonal fluctuations of the water table to allow any floating layer to be drawn into the well when sampling or to utilize nested wells. If DNAPL is, or is suspected to be, present, the borehole should be installed approximately 0.3 m into the top of the confining layer to provide a sump.

3. Well slot size/filter pack material: The slot size of the well-screen must be sized to match the filter pack material. The filter pack material must be sized to match the geologic strata. Additional details regarding the selection of well slot size and gradation of the filter pack material are presented in Driscoll (1986), Hampton & Heuvelhorst (1989), and Hampton *et al.* (1991).

4. Well materials: The materials selected for the well construction must be compatible with the chemicals present in the groundwater and parameter groups selected for chemical analysis to ensure long-term structural integrity and minimal interference with the quality of the groundwater samples. The following well materials are often used:

- stainless steel well-screen and riser pipe,
- stainless steel well-screen and black steel riser pipe, and
- PVC well-screen and riser pipe.

PVC should not be used where solvents are present at significant concentrations. Additional details regarding well material compatibility are presented in McCaulou *et al.* (1995) and references therein.

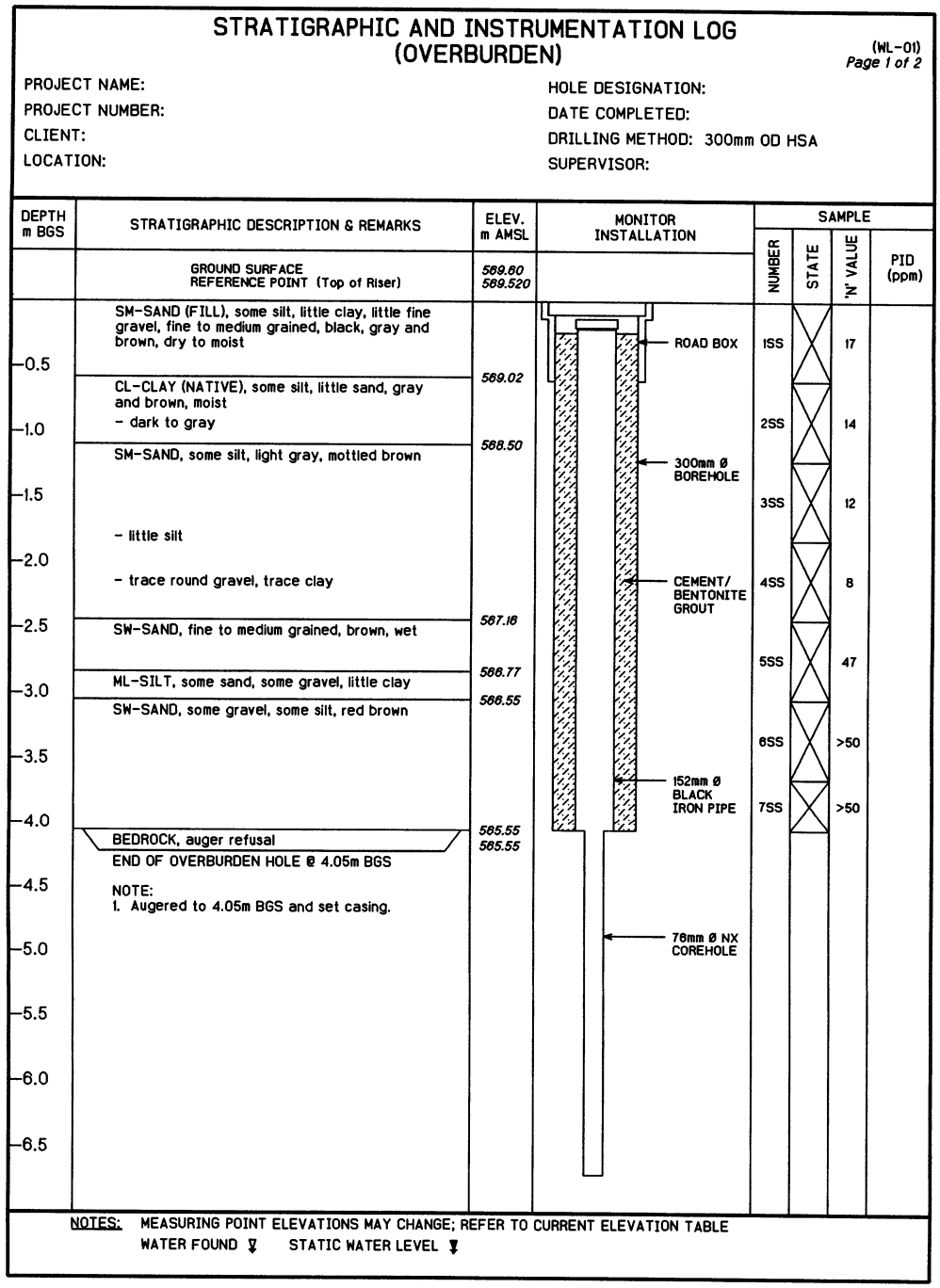


FIGURE 28.4a. Sample stratigraphic and instrumentation logs for overburden well.

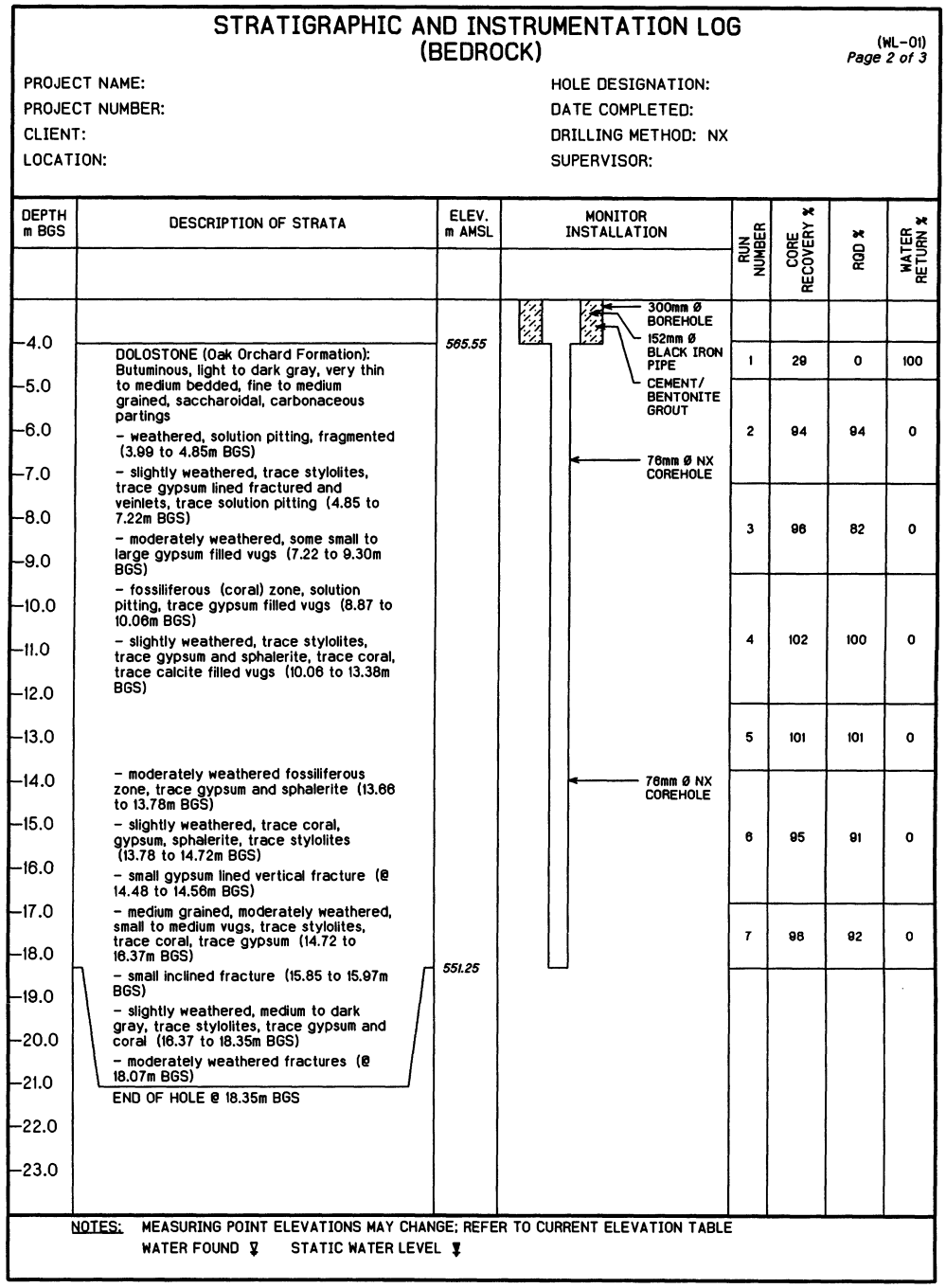


FIGURE 28.4b. Sample stratigraphic and instrumentation log for a bedrock well.

28.1.2.3 Well Installation Documentation

Details of each well installation should be recorded on a stratigraphic and well instrumentation log form. Examples of overburden and bedrock well logs are given in Fig. 28.4a and b, respectively.

28.1.3 GROUNDWATER SAMPLING

28.1.3.1 General

The objective of most groundwater quality monitoring programs is to obtain samples that are representative of existing groundwater conditions, i.e. the physical and chemical properties of the groundwater within a water-bearing unit. The program must include consistent sampling and analysis procedures to ensure that the analytical results are legally and technically defensible.

It is common practice to pre-plan the schedule of sampling activities such that sample collection progresses from "clean" to "dirty" areas in an effort to eliminate the potential for cross-contamination.

One of the most important aspects of groundwater sampling is acquiring samples that are free of suspended silt, sediment or other fine-grained particles. These materials often have a variety of chemical components sorbed to the particle or have the ability to sorb chemicals from the aqueous phase to the particle, which will bias the subsequent analytical results (see Section 24.3.4). The additional field expense to extend purging requirements or modify sampling techniques to achieve sediment free groundwater is minor when considering the implications of gathering data that are unfairly biased.

Additional details regarding groundwater sampling procedures are presented in Barcelona *et al.* (1988), USEPA (1986c, 1987, 1989c, 1991c, and 1992a), Keith (1987, 1990), and Puls and Barcelona (1996).

28.1.3.2 Purging/Sampling Equipment

A variety of purging/sampling devices for groundwater sample collection are available. These include peristaltic pumps, suction pumps, submersible pumps, air-displacement pumps, bladder pumps, inertia pumps and bailers. Table 28.1 presents a guide for selecting the method of best fit.

28.1.3.3 Field Quality Control/Quality Assurance (QC/QA)

The following is a brief discussion defining the common types of field-derived quality control samples, which may be required for a groundwater sampling program to ensure that the investigation results can be used with confidence. It should be noted that a specific project may include all or only some of the following quality control samples.

1. Equipment field blanks: Equipment field blanks are used to determine if cleaning procedures are effective and adequate. The blanks are prepared by collecting distilled deionized water, which has been run through or poured over the cleaned sample collection equipment.
2. Field blanks: A field blank is collected to evaluate the influence of field ambient conditions on the sampling process. Field blank collection is typically performed at a sampling site using distilled deionized water poured directly into the sample container.
3. Field duplicates: Duplicates provide an estimate of total measurement error variance, including variance because of sample collection, preparation, analysis and data processing. During groundwater sample collection, the original and duplicate samples are collected simultaneously by partially filling the original and then the duplicate sample containers, and alternating back and forth until both samples have been fully collected.
4. Trip blanks: Trip blanks are submitted for VOCs only, and are intended to determine if the sample shipping or storage procedures influence the analytical results. Trip blanks are prepared before the sampling event by the laboratory and sent to the site in the shipping container(s) designated for the project. The samples should not be opened.

TABLE 28.1. Purging/sampling equipment usability

Purging/sampling equipment	Acceptable for purging	Acceptable for sample collection						Advantages	Limitations
		VOCs	SVOCs	Pest/ PCBs	Metals	Conventional parameters	Natural attenuation parameters		
Peristaltic pump	Y	N	N	Y	Y	Y	N	Easily transported and used Decontamination not required if well-dedicated tubing is used Minimal maintenance	Limited to a lift of 7.5 m Limited set of parameters that can be sampled
Suction pump	Y	N	N	Y	Y	Y	N	High flow rate minimizes purging time	Limited to a lift of 7.5 m Limited set of parameters that can be sampled
Submersible pump	Y	N	N	Y	Y	Y	N	Can pump water from substantial depth Flow rates vary up to hundreds of l m^{-1} minimizing purging time	More difficult to handle because of weight, rigid piping and electrical requirements Limited set of parameters that can be sampled
Air-displacement pump	Y	N	Y	Y	Y	Y	N	Can pump water from substantial depth Flow rate range from 8 to 12 l m^{-1}	Requires pressurized air source Limited set of parameters that can be sampled
Bladder pump	Y	Y	Y	Y	Y	Y	Y	Can pump water from substantial depth All parameters can be sampled	Small flow rates limit application to low volume wells Labor-intensive decontamination
Inertia pump	Y	Y[a]	Y[a]	Y	Y	Y	N	Decontamination not required if well-dedicated tubing is used	Difficult to collect sediment-free sample
Bailer	Y	Y	Y	Y	Y	Y	N		Not practical for deep wells or for removal of large volumes of water Difficult to collect sediment-free sample

[a] Acceptability is increasing with select state/federal agencies.

COMPANY:	SHIPPED TO (Laboratory Name):	REFERENCE NUMBER:

SAMPLER'S SIGNATURE: _____ PRINTED NAME: _____					No. OF CONTAINERS	PARAMETERS										REMARKS
SEQ. No.	DATE	TIME	SAMPLE No.	SAMPLE TYPE												
TOTAL NUMBER OF CONTAINERS						HEALTH/CHEMICAL HAZARDS										

RELINQUISHED BY:	DATE: TIME:	RECEIVED BY:	DATE: TIME:
① _____		② _____	
RELINQUISHED BY:	DATE: TIME:	RECEIVED BY:	DATE: TIME:
② _____		③ _____	
RELINQUISHED BY:	DATE: TIME:	RECEIVED BY:	DATE: TIME:
③ _____		④ _____	

METHOD OF SHIPMENT:	WAY BILL No.

White —Fully Executed Copy Yellow —Receiving Laboratory Copy Pink —Shipper Copy Goldenrod —Sampler Copy	SAMPLE TEAM: _____ _____	RECEIVED FOR LABORATORY BY: _____ DATE: _____ TIME: _____

FIGURE 28.5. Typical chain-of-custody record.

5. Matrix spike/matrix spike duplicate (MS/MSD): MS/MSD sample volumes are additional sample aliquots provided to the laboratory to evaluate the accuracy and precision of the sample preparation and analysis technique. Typically three times the normal sample aliquot is required to conduct MS/MSD procedures.

28.1.3.4 Documentation

Sample collection and analytical procedures must be accurately documented to substantiate the analysis of the sample, conclusions derived from the results, and the reliability of the results. The documentation includes chain-of-custody (see Fig. 28.5) and field notes. The field notes must document all the events, equipment used and measurements collected during the sampling activities. The field notes must be legible and concise, such that the entire sampling event can be reconstructed later for future reference.

28.1.4 SAMPLING FREQUENCY

The frequency of monitoring the performance of a corrective action is dependent on the groundwater flow and chemical migration rates, the resource value of the groundwater, and the potential exposure pathway to humans and the environment.

Groundwater flow and chemical migration rates are controlled by media characteristics (i.e. f_{oc}, hydraulic conductivity, gradient, porosity, etc., see Chapter 24) and the chemical characteristics (i.e. K_{oc}, solubility, etc., see Section 24.3). Generally, chemical migration

of dissolved substances occurs relatively slowly. An exception to this could be karst or fractured bedrock where the migration occurs in a few discrete highly conductive channels.

The groundwater chemical concentrations generally change slowly or may in fact be stable under pre-corrective action conditions. Thus, the typical monitoring frequency for the first five years of a corrective action is:

- first year: quarterly,
- second and third year: semi-annually,
- fourth and fifth year: annually.

The frequency may need to be modified

ment–bentonite grout. The horizontal spacing between the individual boreholes is a function of the hydrogeologic characteristics of the formation, i.e. the more permeable a formation is, the greater the spacing. Typical spacings in overburden generally range from 3 to 5 m, and in bedrock generally are on the order of 8–10 m. One method to reduce the potential influence of well installation is to place the wells in a line perpendicular to the direction of groundwater flow.

28.2 Statistical Analyses of Monitoring Data

ent). This choice of sampling location is a sensible allocation of resources, but may not meet an assumption of random sampling for a specific statistical model, and therefore another type of statistical analysis should be chosen. Another problematic characteristic of environmental monitoring data is that the data are often censored. That is, the data have a lower limit or, less frequently, an upper limit, beyond which a monitoring result is reported as "not detected" or "off-scale". Statistically, this causes a change in the shape of the data distribution, which may violate assumptions of specific statistical models and require the use of alternate methods. Finally, natural systems tend to be highly complex and variable, and confounding effects such as seasonality, temperature or matrix stratification may need to be extracted to remove noise from the data.

These features stress the difficulty with statistical interpretation of environmental data. There is a need for the analysis procedure to be sensitive to small changes (e.g. early detection of contamination is desirable) and yet a point of diminishing marginal returns also occurs. The result is that the analyst must be inventive in terms of how statistical analyses proceed. For the variety of reasons previously indicated, there is not a single approach to statistical analyses. Instead, what is frequently needed is a series of approaches each of which possess useful attributes that may be appropriate in addressing a particular question.

28.2.1 SOURCES OF VARIABILITY IN MONITORING DATA

The nature of the variability of environmental quality data will greatly influence how the statistical analyses of the data are undertaken. The specifics of statistical analyses will depend upon the way the phenomenon of interest is defined and sampled. In general, the ability of a sample of environmental quality data to characterize the population from which it is drawn is related to such aspects as: (a) the size of the sample, (b) the degree to which it was selected at random, and (c) the degree of independence between the observations comprising the sample.

TABLE 28.2. Features contributing to the variability in groundwater quality measurements

- Sample collection may involve drilling, sampling and laboratory analysis for many water quality constituents. The expense argues for utilization of brief monitoring records, and thus is representative of only some of the potential conditions.
- Sample collection and laboratory analyses have inherent difficulties, resulting in uncertainties in subsequent interpretation of the findings
- Many important groundwater phenomena take years to evolve, making the available timeframe for sampling programs only statistical "windows" of temporally varying processes

Samples of environmental quality are just that, namely subsets of the populations that are of interest. To clarify, a limited number of monitoring samples will never fully describe every condition found in the population, i.e. every possible subset of the environment. The challenge then is to acquire a representative sample that can be used to estimate population parameters with a given probability. Some of the features that contribute to the variability and problems of data analysis in groundwater quality phenomena, are briefly described in Table 28.2. The result is that in many cases, estimates of groundwater quality must be developed from only very brief data records, brief being with respect to both temporal and spatial considerations. Even in cases with substantial quantities of data, there may only be a limited amount that is usable for a specific question.

Although much geotechnical data may be acquired directly, certain measurements may be taken from proxy data. For example, remotely sensed satellite data on vegetation class may be used to estimate the soil types present over a wide area. The validity of these

"data" depends on such features as one's confidence in a particular measurement method, and the reliability of calibration techniques of the instruments, all of which must then be considered when interpreting the data.

In addition to natural variability, the acquisition of monitoring data is also subject to collection and analysis errors. Errors in sampling procedures, inadequate sample storage and preservation techniques, and laboratory analytical errors are examples of errors in environmental data sets. As a demonstration of the multifaceted initiation points for such errors to exist in a data set, further examples of the sources of error in the collection and analysis of groundwater quality data are listed in Table 28.3.

There is always a degree of uncertainty associated with each discrete measurement of environmental quality. In interpreting data, each discrete measurement represents a range of statistically probable values instead of a single value. Uncertainty can be estimated by considering replication and repeatability. Replication is a measure of the variation in results obtained by the same operator in a given laboratory using the same apparatus to make successive determinations on identical test material within a short period of time. Often this is done during quality assurance and quality control testing of a laboratory, to assure that the laboratory results are trustworthy. Replication represents the analytical uncertainty in acquiring monitoring data. Conversely, repeatability is a quantitative expression of the random error associated in the long run with a single operator in a given laboratory obtaining successive results with the same apparatus under constant operating conditions on identical test material. Repeatability is a measure of the natural or sample variability. Note that a systematic error, or bias, in analytical results may be introduced in the field or laboratory due to sampling, handling and/or analysis techniques, and such error may only be detected by making inter-laboratory or inter-technician comparisons using the same samples.

TABLE 28.3. Examples of sources of error in groundwater monitoring data

- Sampling of a non-homogeneous region in which wells and springs intersect more than one water source
- Piezometers and wells that are inadequately flushed out prior to sampling of groundwater so that a sample of the groundwater is not representative of conditions in the soil environment, i.e. cross-contamination
- Sampling stations that are subject to temporal variations of chemical concentrations can exhibit significant sampling error
- An error in the laboratory protocol of the experiment during the laboratory analysis
- Improper preservation techniques. For example, groundwater samples are often particularly susceptible to changes in the pressure of oxygen and carbon dioxide and improper sample storage. Improper preservation techniques can result in an chemical alteration of the sample as it adjusts to new equilibrium conditions, e.g. the pH levels in groundwater samples have been noted as increasing up to 1.0 pH units due to CO_2 escape to the atmosphere during storage
- Volatilization of biodegradation of VOCs may produce low VOC values for many samples depending on factors such as time and space

The fact that sampling errors are inherent in random data does not mean, however, that statistical manipulations and sophistication can in any way overcome faulty data. The quality of any statistical analysis is no better than the quality of the data utilized. Furthermore, statistical considerations cannot be used to replace judgment and careful thought in analyzing data. Statistics must be regarded as a tool or an aid to understanding, but never as a replacement for careful thought.

28.2.2 STATISTICAL SIGNIFICANCE TESTING PROCEDURES

28.2.2.1 Types of Hypotheses

The first consideration that should be made in a statistical evaluation of monitoring data

is to identify the hypothesis that is to be tested. In fact, if at all possible, this should be identified during the design of the monitoring program, before data collection, and used to modify the investigative design as necessary. There are a number of types of hypotheses that are typically encountered in contaminant monitoring programs, which are generally reflective of governing regulation. The first type of hypothesis is that a contaminant concentration is below a standard. For example, if there is a regulatory requirement for groundwater to be of potable quality at a site, then the monitoring data must be evaluated to determine if all contaminants are below the regulated criteria. Another common type of environmental hypothesis is that a given industrial facility or activity does not cause an impact, i.e. a change from background conditions. In this case, monitoring data from potentially impacted areas are compared with those from background or locations known not to be impacted by the potential source. A third type of hypothesis is that a monitoring parameter is increasing/decreasing/not changing at a location over time. For example, an agricultural facility may monitor the salinity of soils over time to determine if the salt balance is being impacted by farm operations. Finally, a fourth type of hypothesis is the "before" and "after" comparison, where it is postulated that a major event has/has not had an environmental impact, such as the completion of a remedial program at a contaminated site.

These alternative types of hypotheses require the use of different statistical techniques. The selection of an appropriate significance test is considered in Section 28.2.2.3 below. The key requirement for the hypothesis to be investigated is that it be *testable*. That is, the investigator must be able to specify an exact outcome, which the data may be compared against. For example, one could test the hypothesis that the mean concentrations of benzene in the groundwater at two locations are equal. This is a testable hypothesis, since the condition of equivalency is an exact outcome (i.e. there is only one way in which the two values can be equal), as compared to the alternative condition that the two means are not equal, which is not exact, since there are an infinite number of ways in which one mean could be greater or less than the other. Another type of testable hypothesis is that the monitoring data fit a specific distribution. For instance, a dispersion model of the transport of a contaminant from a point source release may predict changes in concentrations along a gradient, against which actual monitoring results could be compared to test the significance of the model. The statistical term for the hypothesis to be tested is the *null hypothesis*, which is represented by H_0. If H_0 is shown to be a statistically "unacceptable" hypothesis, then the alternate hypothesis (H_a) may be accepted instead.

28.2.2.2 General Steps of Hypothesis Testing

The general procedure to carry out significant difference testing consists of the following steps:

1. Formulate a suitable (in terms of the problem context) null hypothesis, H_0.
2. Formulate a suitable alternative hypothesis, H_a.
3. Calculate an appropriate test statistic.
4. Define an acceptance/rejection region.
5. Locate the test statistic in the acceptance or rejection region.
6. Reject, or do not reject the null hypothesis.
7. Make a final inference (the proverbial "so what?") to draw a conclusion.

Given the statistical nature of the significance tests, there are two possibilities that can cause differences in observed values. These possibilities are: (a) inherent randomness associated with taking a sample from a population; and (b) an actual effect, i.e. a real differ-

ence, exists. The task of the significance test is then to establish the probabilities of these two possibilities (by defining acceptance and rejection regions) and thereby draw conclusions with a given probability. When a result is obtained which is very unlikely to have arisen by chance, the result is said to be statistically significant. In other words, it is difficult to ascribe the findings to chance, and the difference must, in all common sense, be accepted as a real difference. There is still the possibility that the result happened by chance; and thus, a significance test result is always reported with a probability statement. For example, "the mean benzene concentrations in groundwater upgradient and downgradient of the source area were found to be statistically different at a significance level of 95%." Further discussion of acceptance and rejection regions is presented in Section 28.2.2.4 below.

If a significance test returns a non-significant result, i.e. the null hypothesis is not rejected, it does not follow that there are grounds for supposing this hypothesis to be true, but merely that there are no grounds for supposing it to be false. If a non-significant result occurs, i.e. the null hypothesis is not rejected, then it is appropriate to consider the *power* of the test, which is the probability that the test would have discovered a significant effect if it had been present. Power is discussed in Section 28.2.6 below. As a final note, even if the result proves non-significant, it is equivalent to a verdict of "not proven", and there is still the opportunity to consider further evidence, i.e. more data, which may become available later on.

In response to the significance testing problem, a number of alternative procedures have been proposed. The selection of the best procedure involves careful scrutiny of the characteristics of the problem-at-hand and the assumptions implicit in the particular significance test being considered. This involves not just the choice of significance level, but also the choice of a statistical test, and the requirements of the number of samples. The following section describes the selection of a variety of tests applicable to environmental data.

28.2.2.3 Selection of Appropriate Significance Test

Due to the sheer number of statistical procedures available, a comprehensive treatment is not possible within the scope of this chapter. However, of the many statistical procedures available, certain significance tests stand out due to their wide applicability to environmental data and relatively easily understood mathematical bases. A number of these are presented below, and it is intended that these represent a cross-section of frequently used tests, but also recognizing that data from specific monitoring programs may not require the use of further techniques. A more comprehensive listing of statistical procedures can be found in McBean & Rovers (1998) and Helsel & Hirsch (1992).

Student's t-*test.* The *t*-test is one of the most widely used significance tests. In its various forms, it can be used to compare the observed mean of collected monitoring data against either a single value (e.g. a regulatory criterion), the mean of another data set (e.g. comparing a possible impacted location to a reference location), or the mean of corresponding data from the same sampling locations under different conditions (e.g. before and after a major event). These three forms of this significance test are known, respectively, as the two-sample, one-sample and paired *t*-tests. The *t*-test makes the following assumptions: (a) that the data are independent, i.e. have been randomly sampled; (b) the data are normally distributed; and (c) the variances of the groups of data are equal. The *t*-test is useful in cases where a comparison of a single variable between two groups is to be made. For example, the test could be used

to compare the hydraulic conductivities of soil samples from two locations, or to evaluate if a contaminant's groundwater concentrations in a group of monitoring wells exceeds a given standard. The *t*-test is not useful in cases where more than two groups, more than a single variable, or time series data are to be analyzed. In the first two cases, an ANOVA method is appropriate, while in the third case, a regression or multiple regression approach may be applicable. The *t*-test is introduced in Section 28.2.3.1 below.

Cochran's Approximation to the Behren's Fisher t-test (CABF). In many cases, field data deviate from the assumptions implicit to the application of the *t*-test. This may occur for a variety of reasons such as small sample sizes, large natural variability, non-homogeneity of the sample populations or non-random sampling. The Cochran's approximation to the Behren's Fisher *t*-test (CABF) was developed for cases in which the variances are not equal between the groups to be compared. This occurs relatively frequently in monitoring data, and when the equal variance assumption is shown to be violated, the CABF provides a useful alternative to the standard *t*-test. The CABF is introduced in Section 28.2.3.2 below.

Analysis of Variance (ANOVA). The analysis of variance (ANOVA) is actually a group of statistical procedures that are used to examine differences in mean values across multiple groups and/or multiple variables. The term ANOVA is used when means for one variable are compared across many groups, whereas in the case of multiple variables compared across many groups, the term "multiple ANOVA" (MANOVA) is used. The ANOVA is actually a generalized form of statistical procedures, of which the *t*-test is the special case in which a single variable is compared across only two groups. The ANOVA is useful in evaluating monitoring data across a number of locations. For example, if groundwater from five wells is sampled for a specific contaminant, say benzene, then an ANOVA could be used to test if there are any significant differences in mean benzene concentration between any of the wells. Note that performing a similar comparison by using multiple *t*-tests to compare the wells one pair at a time is laborious and is much less preferred to the ANOVA method, but is possible through the use of special adjustments such as the Bonferroni technique. Application of ANOVA methods is subject to the same assumptions as for the *t*-test; i.e. independence, normality and homogeneity of variance. The use of ANOVA is introduced in Section 28.2.4.1 below.

(Linear) Regression. One of the key goals in monitoring is to establish trends in data over time, distance or some other gradient. For instance, one of the lines of evidence of natural breakdown (biodegradation) of a pollutant in the subsurface is the observation of decreasing concentrations over time. The significance of the pattern of this decrease can be statistically assessed using a regression analysis. The most common form of regression analysis uses a linear model, in which a line is fit through the data points and tested for significance. It is also possible to fit non-linear models using regression models, however, many natural processes fit linear or loglinear patterns, and the regression results for higher-order models may be difficult to interpret. The basic assumptions of regression analysis are: (a) for any given value of the independent variable ("x," or in the example above the time), the observed values of the dependent variable ("y", or the contaminant concentration above) are normally distributed; (b) for a given x, the observed y values are independent of one another; and (c) the sample variances are equal. Furthermore, the regression assumes that the true relationship between the variables is linear (or whatever form of model is being used). A linear regression analysis fits a line through

the observed data, and then actually uses an ANOVA to test whether the line is a significant fit to the observed data. As well, the strength of the relationship between the variables is estimated by calculating a regression coefficient. Regression analysis is introduced in Section 28.2.3.3 below.

It should be noted that regression is often confused with correlation analysis. There are many computational similarities between these two methods, but they have fundamentally different bases. In a regression, the independent variable is known or assumed to cause changes in the dependent variable. In comparison, a correlation analysis simply assesses the degree to which two variables are linearly associated (co-vary), with no assumption of causality. Correlation is also useful in examining monitoring program results; e.g. to investigate the association of the concentrations of different contaminants (i.e. the concentrations of two pesticides in groundwater underlying a farmer's field may be very tightly correlated, but one does not cause the other).

Multiple (Linear) Regression. An extension of the regression model is the formulation of multiple regression models. In these models, a dependent (y) variable is assumed to be a function of a number of independent (x) variables. For example, the pH in soil may be influenced by a number of factors such as soil composition, mineral concentrations, temperature, moisture content and contaminant concentrations. It may be possible in this case to analyze the monitoring data using a multiple regression model and determine if a combination of these variables cause the observed pH. The multiple regression shares the same assumptions as the basic regression model. Regression techniques are particularly useful for predictive purposes, in which the effect on the dependent variable caused by changing an independent variable is estimated. Multiple regression is introduced in Section 28.2.4.2 below.

28.2.2.4 Interpretation of Significance Tests: Acceptance and Rejection Regions

In order to interpret the results of a significance test, acceptance and rejection regions for the test statistic must be defined. Typically, a choice is made based on the degree of certainty desired in identifying significant results. That is, if one desires 95% confidence that a result shown by the statistical test to be significant is in fact truly significant, then this significance level (denoted as "$1 - \alpha$") is used to determine the acceptance and rejection regions of the test statistic. Each statistical test defines the acceptance and rejection regions differently in accordance with the method (e.g. a t-test defines a critical t value, whereas an ANOVA defines a critical F value, etc.); however, they are all usually based on the significance level chosen and the number of samples used.

In conducting statistical inference tests, incorrect conclusions sometimes occur. An acceptance rate is assumed, but what that really means is that an error is made a specified percentage of the time. In reality, because population parameters are being estimated from small samples, the comparison of these means involves the risk of making one of two possible errors, denoted type I or a type II. These describe the balance between two conditions:

1. the risk the procedures will falsely show a significant effect, e.g. that a landfill is causing background values or concentration limits to be exceeded, when in fact the landfill is not causing a problem (false positive); and
2. the risk that the procedures will fail to indicate that background values or concentration limits are being impacted when in fact there is an impact, e.g. the landfill is contaminating the groundwater (false negative).

Table 28.4 illustrates the possibilities when the true environmental condition (truth) is

TABLE 28.4. Outcomes and errors in statistical testing

	Truth	
Decision/inference	H_0	H_a
Accept H_0	No error Probability = $1 - \alpha$	Type II error Probability = β
Accept H_a	Type I error Probability = α	No error Probability = $1 - \beta$ = power

interpreted via a statistical significance test (decision/inference):

- The null hypothesis, H_0, is not rejected and is in fact true, thus no error is made.
- The null hypothesis, H_0, is rejected when it is in fact true (and the alternate hypothesis, H_a, erroneously accepted). This is a Type I error, and its probability is denoted by α. This error is also called a false positive (e.g. a "source" is identified as impacting the groundwater when, in fact, it is not impacting the groundwater; or saying something is present when it is not).
- The null hypothesis, H_0, is rejected and H_a is true and thus no error is made.
- The null hypothesis, H_0, is not rejected and H_a is true. This is a Type II error, denoted by β, and represents the failure to detect an effect, i.e. reject H_0, when there is a significant difference. We accept H_0 when in fact H_a is true. This error is also called a false negative (e.g. a "source" is identified as non-polluting when in fact it is polluting). The result of this type of error, for example, is that a remedial action is not implemented on a contaminating source that is, in fact, degrading the groundwater quality.

The α level represents the probability of making a Type I error. By specifying $\alpha = 0.05$, this indicates that in the long term, the Type I error will be made 5% of the time, i.e. one test in 20 will show an effect when there is none. The probability of a Type II error is represented by β. An important fact is that α and β are not independent, in fact they are related: i.e. if you decrease the possibility of one type of error, you are increasing the possibility of the other. Too often, the desire to make sure that an effect is really happening before flagging an exceedance, i.e. a low α, rate drastically reduces the chances of finding an effect, i.e. β increases. Since the Type II error has environmental consequences, the general approach is to tend to be rather conservative. Further discussion of the power of a statistical test is provided in Section 28.2.6 below.

28.2.3 PROCEDURES FOR SINGLE COMPARISONS

28.2.3.1 Student's *t*-Test

The steps of the *t*-test include:

1. The calculation of the *t*-statistic.
2. Comparison of the calculated value against a critical *t* value (t^*), which is read off a standard table for a given degree of confidence (α) and number of degrees of freedom (df, a function of the sample size).
3. Making a statistical conclusion, i.e. if $t > t^*$, there is a significant difference, if $t < t^*$, there is no evidence of a statistically significant difference in the means.

The student *t*-test can be computed in three forms depending on the type of comparison being made. These are the one-sample, two-sample and the paired *t*-tests.

One-Sample t-*Test.* The one-sample t-test compares a sample mean against a single value, typically either a regulatory standard or population mean. In this case, the t-statistic is calculated using:

$$t = \frac{|\bar{x} - \mu|}{S/(n)^{1/2}} \tag{28.1}$$

where $\bar{x}$ = the sample mean, μ = the population mean (or regulatory standard), S = the standard deviation of the observations, and n = the number of observations. For a one-sample t-test, the number of degrees of freedom is $n - 1$.

Two-Sample t-*Test.* The two-sample t-test compares the mean of one sample against the mean of another sample. The t-statistic for a two-sample comparison is calculated using:

$$t = \frac{|\bar{x}_1 - \bar{x}_2|}{(\mathrm{SE})^{1/2}} \tag{28.2}$$

where $\bar{x}_1$ = the sample mean for the first group, $\bar{x}_2$ = the sample mean for the second group, and SE = the standard error of the difference. If the variances of the two groups are similar, then the standard error is:

$$\mathrm{SE} = \left[\frac{(n_1 - 1)\, S_1^2 + (n_2 - 1)\, S_2^2}{n_1 + n_2 - 2}\right]^{1/2} \tag{28.3}$$

and if the variances are unequal, the standard error is computed as:

$$\mathrm{SE} = \left\{\left[\frac{(n_1 + n_2)}{(n_1 n_2)}\right]\left[\frac{(n_1 - 1)S_1^2 + (n_2 - 1)S_2^2}{n_1 + n_2 - 2}\right]\right\}^{1/2} \tag{28.4}$$

where n_1 and n_2 = the number of observations in the two groups, respectively; and S_1^2 and S_2^2 are the sample variances (squares of the standard deviations). For a two-sample t-test, the number of degrees of freedom is $n_1 + n_2 - 2$.

Paired t-*Test.* The paired t-test uses the same computational sequence as the one-sample t-test, except that the test is performed on the differences between the paired data. For example, if a certain measurement was taken from a group of monitoring wells before and after a major rainstorm, then for each individual well the measurement before the storm would be subtracted from the measurement after the storm, and these differences would be used to carry out the t-test.

Assumption Checking. As noted earlier the assumptions of the t-test are: (a) the data are independent of one another, i.e. have been randomly sampled; (b) the data are normally distributed; and (c) the variances of the groups of data are equal.

The assumption of independence of successive monitoring data requires a well-thought-out sampling design. As much as practical, samples should be acquired in a random order, and under similar conditions. In a geotechnical investigation, this is not always possible; e.g. a soil sample from a borehole must be taken during installation, or it may be impractical to randomly traverse a very large site between successive samples and therefore one area at a time is collected. As well, when prior knowledge is available regarding less- and more-contaminated regions at the site, samples are typically collected in order of increasing chemical concentrations to avoid cross-contamination. However, if the assumption of random sampling was of particular concern, the order of sampling the groundwater monitoring wells on a small- to medium-size site could easily be randomized, and then the assumption of independence could be evaluated by plotting the individual data points in order of collection and visually assessed to see if there is any pattern. If the data are independent, the points will have no discernible pattern and fall in a roughly horizontal band across the graph. If instead the data exhibit an increasing or decreasing

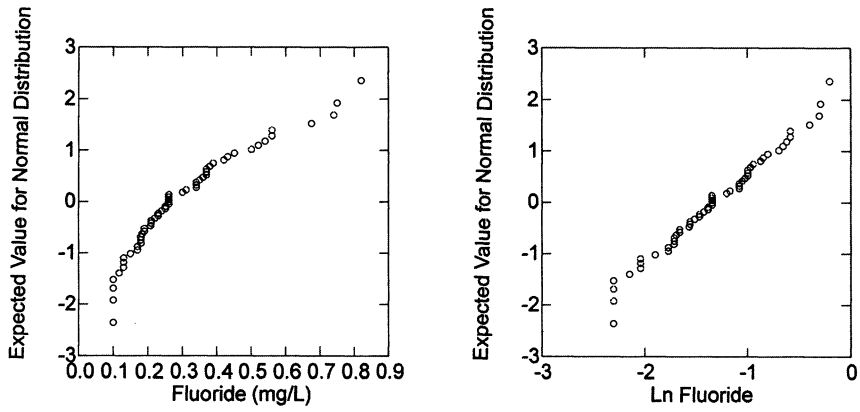


FIGURE 28.6. Cumulative probability plots to assess normality of data.

trend, there is evidence of non-independence.

There are a number of techniques available to assess the assumption of normality for a set of data. The most elegant test of normality is the *cumulative probability plot*, in which the data are plotted using a probability scale for one axis (see Fig. 28.6). Normally distributed data sets are easily identified because they produce a line on such a probability plot. Not only does this plot assess normality, but it can provide useful information that may not be readily apparent from simply looking at the data, such as threshold values, or distinct groups of monitoring results. Another easily performed test of normality is the calculation of the *coefficient of variation* (CV). The CV of a data set is its standard deviation divided by its mean. A CV of greater than one suggests non-normality of the data. A more statistically rigorous alternative is the Shapiro–Wilk test of normality. It is described, along with several other methods, in McBean & Rovers (1998).

The assumption of equal variances, or *homoscedasticity* (from the Greek, "equal scatter"), may be tested by using a number of methods. Like the normality assumption, the simplest test for homoscedasticity is a graphical method: the box plot. A box plot (see Fig. 28.7) is created for each group of data, and the length of the largest box is within about a factor of three of the length of the shortest box, then the variance of the data may be assumed to be equal for the purposes of carrying out a significance test. If not, alternate methods to test for unequal variances should be attempted before concluding that the data are heteroscedastic (unequal variances). These alternates include Levene's F-test, Bartlett's test, Hartley's F_{max} and the log-ANOVA (or Sheffé–Box) test. Detailed descriptions of these tests are given in McBean & Rovers (1998). If a data set is shown to be heteroscedastic, then a data transformation may be needed, using, for example, the log-transformation of the monitoring data.

For further reading about the *t*-test in its various forms, refer to "Student" (1908), Fisher (1925), USEPA (1992c), and McBean & Rovers (1998).

28.2.3.2 Cochran's Approximation to the Behren's Fisher *t*-test

If the variances of the environmental quality data at two locations are not equal, one of the assumptions of the standard *t*-test is violated. In such cases, a useful alternative is the Cochran's approximation to the Behren's Fisher

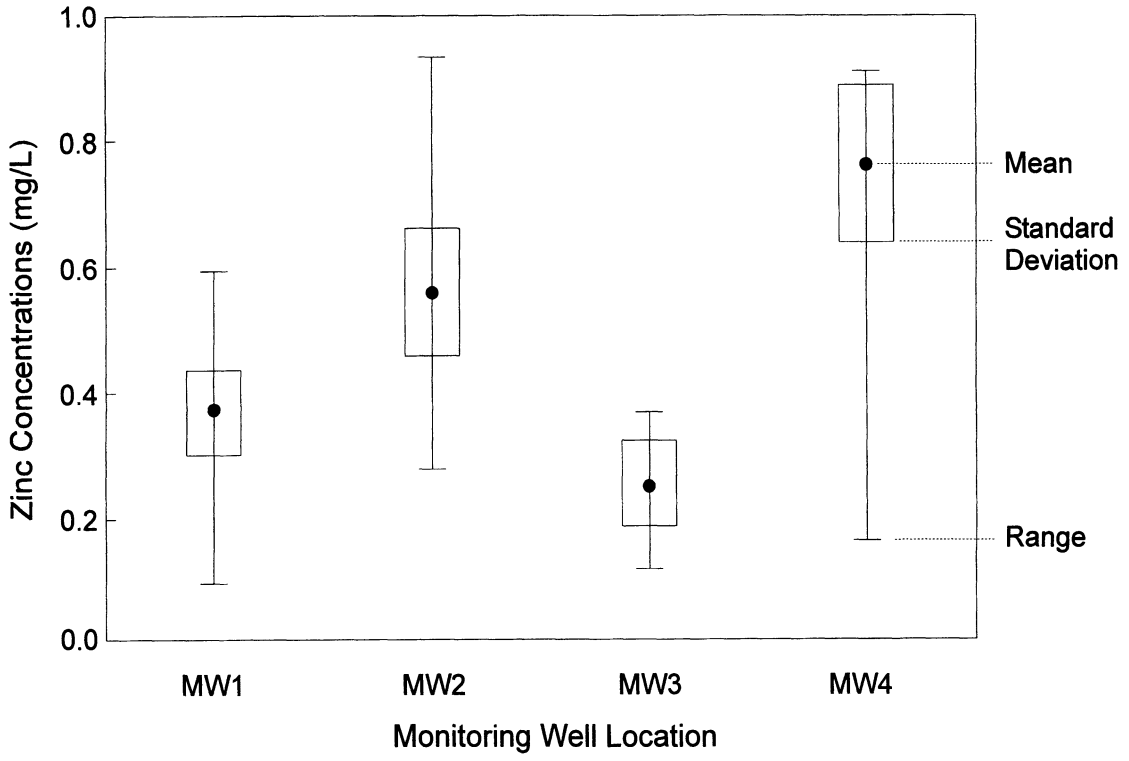


FIGURE 28.7. Example of box plots.

test (CABF). The CABF test functions by relaxing the requirement that the variance of the data at both sampling locations be of the same magnitude by adjusting the degrees of freedom. Cochran's test adjusts the degrees of freedom (df) by weighting the individual t values for each sample. Cochran's test computes the t-statistic from:

$$t = |\bar{x}_1 - \bar{x}_2| \Big/ \left(\frac{S_1^2}{n_1} + \frac{S_2^2}{n_2}\right)^{1/2} \qquad (28.5)$$

The critical t-statistic, t^*, is computed from:

$$t^* = \left[\left(\frac{S_1^2}{n_1}\right)t_1^* + \left(\frac{S_2^2}{n_2}\right)t_2^*\right] \Big/ \left(\frac{S_1^2}{n_1} + \frac{S_2^2}{n_2}\right) \qquad (28.6)$$

where:

$$S_1 = \left[\Sigma \frac{(x_{i1} - \bar{x}_1)^2}{n_1 - 1}\right]^{1/2} \qquad (28.7)$$

and

$$S_2 = \left[\Sigma \frac{(x_{i2} - \bar{x}_2)^2}{n_2 - 1}\right] \qquad (28.8)$$

where the t-values t_1^* and t_2^* are determined from t-tables for df of $n_1 - 1$ and $n_2 - 1$, respectively, at a specified significance level, $1 - \alpha$.

As noted above, CABF allows relaxation of the equality of variances requirement. However, if this assumption is *not* violated, utilization of the approximate test can result in different findings, and the standard t-test should be used instead. This concern was described in detail in McBean *et al.* (1988).

28.2.3.3 Linear Regression

In a regression analysis, a line of best fit is computed, which describes the dependent

variable as a function of the independent variable. The form of the linear regression line is:

$$y = ax + b \tag{28.9}$$

where a = the slope of the line, termed the regression coefficient; and b = the y-intercept of the line (a constant). The equation of the linear regression is usually calculated using the method of least squares, and should be assumed unless specifically stated otherwise. The regression line can be automatically calculated using modern statistical software packages, as well as many spreadsheet programs. If a and b must be manually calculated, the following equations may be used (a mathematical proof for these solutions will not be provided here in the interest of brevity):

$$b = \frac{\Sigma(x_i - \bar{x})\,(y_i - \bar{y})}{\Sigma(x_i - \bar{x})^2} \tag{28.10}$$

$$a = \bar{y} - b\bar{x}. \tag{28.11}$$

Note that these equations apply to the case where there is a single y for each x value, the model to be fit is linear, and the x values are assumed to be known without error (or at least the error in the measurement of x is much lower than the uncertainty in the y measurements). It is possible to fit multiple y values for each x, non-linear, or so-called "random x" models, but techniques for these computations are beyond the scope of this chapter.

The significance of the regression line is tested using an analysis of variance (refer to Section 28.2.4.1) through the calculation of an F statistic.

Interpretation of the linear regression analysis is as follows. First, the significance of the regression model is evaluated using the F-statistic from the ANOVA. If this value is significant with a stated probability of $1 - \alpha$ (typically 95% is used), then the overall regression is said to be a significant fit of the data, i.e. the monitoring data have been shown to exhibit a significant trend. Next, the coefficient of determination, r^2, for the entire model is considered, which yields the proportion of variation in the dependent variable that is explained by the regression, e.g. an r^2 of 0.86 means that the regression explains 86% of the variation in the dependent variable. Following this, a t-test is performed on "b" to test if the regression coefficient of the independent variable is significantly different than zero. If so, this regression coefficient is interpreted as the factor by which the independent variable influences the dependent variable. For example, if a linear regression analysis has yielded a significant fit of depth to groundwater (in mm) over distance (in m), then a value of -10.4 for the regression coefficient means that for every meter of horizontal distance, the water table drops by 10.4 mm.

The assumptions underlying linear regression include those of the t-test, namely: (a) independence, (b) normality, and (c) homoscedasticity. Testing these assumptions should be performed using the methods presented earlier. An additional assumption of linear regression is that the true relationship of the dependent and independent variables is linear. Deviations from linearity will result in a non-significant regression line, and thus this assumption is therefore evaluated as part of the base analysis.

28.2.4 PROCEDURES FOR MULTIPLE COMPARISONS

28.2.4.1 Analysis of Variance (ANOVA)

The various ANOVA procedures are available in modern statistical software packages, as well as some newer spreadsheet programs. It is less common to compute an ANOVA manually; however, the methodology is straightforward as presented below.

The general approach of an ANOVA is to

partition the variation in the data between a number of different terms, and then test these variabilities for significance of the factors (hence the term "analysis of variance"). In order to perform an ANOVA, P mutually exclusive groups of data (e.g. groups of monitoring wells) should have a minimum of three to four samples each, and the total number of samples, n, should exceed the number of groups by at least five (i.e. $n - P \geq 5$).

An ANOVA is performed using the following steps. Note that i denotes the group and j denotes the samples within each group.

1. For each group, the mean value $\bar{x}_i$ is calculated.
2. The grand mean $\bar{x}$ of all data is calculated.
3. For each data point (x_{ij}) in each group, a residual, R_{ij}, is computed as the difference from its group mean, $\bar{x}_i$.
4. Compute the between groups sum of squares:

$$(SS_{between}) = \sum^{P} n_i(\bar{x}_i - \bar{x})^2 \qquad (28.12)$$

(note this value has P − 1 degrees of freedom).

5. Compute the total sum of squares:

$$(SS_{total}) = \sum^{P} \left(\sum^{n_i} x_{ij} - \bar{x} \right)^2 \qquad (28.13)$$

(note this value has n − 1 degrees of freedom).

6. Compute the within groups (residual) sum of squares:

$$(SS_{residual}) = SS_{total} - SS_{between} \qquad (28.14)$$

(note this value has n − P degrees of freedom).

7. Calculate a mean square for the between groups:

$$(MS_{between}) = \frac{SS_{between}}{df}. \qquad (28.15)$$

8. Calculate a mean square for the within groups:

$$(MS_{residual}) = \frac{SS_{residual}}{df}. \qquad (28.16)$$

9. Calculate a test statistic:

$$F = \frac{MS_{between}}{MS_{residual}}. \qquad (28.17)$$

10. Compare the F statistic to a tabulated critical value with P − 1 and n − P degrees of freedom and a given significance level 1 − α.

If the "between sample variation" is significantly greater than the residual (within) variation then the potential exists that the samples were not, in fact, drawn from the same population, but from populations whose average values differed. If this proves to be the situation, in addition to the "within population variation," there exists also a "between population variation." If the calculated F value exceeds the tabulated value, reject the hypothesis of equal well means. Otherwise conclude there is no significant difference between the concentrations at the P wells (groupings). If a significant difference exists, at least one pair of well means is different. To find out which are different, multiple comparisons must be calculated. These comparisons are called *contrasts* in the ANOVA and multiple comparison framework (USEPA, 1989e). These contrasts are usually performed using t-tests with adjusted significance levels to account for error introduced by multiple comparisons. These assure that the total level of significance (1 − α) does not exceed a given limit, e.g. 95%, by adjusting α for the individual comparisons. One such method is the Bonferroni t-statistic, which is outlined in USEPA (1989e) and McBean & Rovers (1998).

28.2.4.2 Multiple Regression

Problems involving more than two variables can be treated in a manner analogous to that for two variables. For example, a dependent variable y may be a function of two dependent variables x_1 and x_2:

$$y = a_1x_1 + a_2x_2 + b_i \qquad (28.18)$$

where a_1, a_2 = the partial correlation coefficients and b = a constant.

The overall multiple correlation coefficient indicates the strength of the relationship between the dependent and independent variables. The partial correlation coefficients indicate the strength of the relationship between a dependent variable and one or more independent variables, with the effects of other independent variables held constant.

Similarly to the two-variable case described in Section 28.2.3.3, a multiple regression model can be fit to monitoring data and a significance test carried out. The assumptions of the multiple regression are the same as for the bivariate case.

28.2.5 NON-PARAMETRIC PROCEDURES

The previous sections have focused on the available procedures for addressing hypothesis testing questions and the identification of trends. However, as noted above, there are significant difficulties with these procedures when a substantial percentage of censored data exist within the data set and/or when there is a failure to adhere to assumptions implicit within the parametric tests. The result is that many existing environmental quality databases are not amenable to analyses by parametric methods. Techniques may not be suitable because of missing data, censored data and changing laboratory techniques or non-normally distributed samples.

A group of tests have been devised in which no assumptions are made about the distribution of the observations. For this reason, the tests are referred to as distribution-free. An array of these alternative tests exists, collectively referred to as "non-parametric" tests. The fundamental characteristic of these procedures is that the ranks of the data are utilized instead of data values (e.g. assigning a rank of "1" to the smallest value, "2" to the second smallest, and so on up to "n" for the largest, nth, observation). A large body of technical literature exists based on analyses of the ranks of the data. The mathematics involved in non-parametric tests are generally very straightforward. The analyses of ranked data are a direct parallel of the more traditional parametric methods as described in previous sections. For data which do not fulfill the necessary assumptions for the parametric analyses, the non-parametric methods are as powerful or, in fact, more powerful than the equivalent parametric tests. The non-parametric methods usually have the additional advantage that they require less burdensome calculations since they are generally not related specifically to the parameters of a given distribution. The major disadvantage of non-parametric methods is that they may be wasteful of information, and usually they have a smaller efficiency than the corresponding parametric methods provided that the assumptions of the standard (parametric) methods can be met. Hamby (1994) discusses many of the features of the non-parametric tests. In large, normally distributed samples, the non-parametric tests have an efficiency of approximately 95% relative to Student's t-test (Hodges & Lehmann 1956) and in small, normally distributed samples, the signed-ranks test (see Section 28.2.5.3) has been shown to have an efficiency slightly higher than this (Klotz 1963). With non-normally distributed data the efficiency of the non-parametric tests relative to the t-test never falls below 86% in large samples and may be greater than 100% for distributions that have long tails (Hodges & Lehmann, 1956).

Non-parametric analyses are performed on the ranks of the data, which has the effect of

equally spacing the datapoints. If two or more observations are tied, each of the observations are assigned the mean of the ranks they would jointly occupy. For example, two observations both having a concentration of 25 mg kg^{-1}, and initially tied for the second and third ranks, will both be assigned a rank of 2.5. Information about relative magnitudes is lost during ranking, but the result is that the assumptions of distributional shape are completely removed. Rank or non-parametric tests are generally tests that do not require any assumptions other than independent samples from continuous populations.

During the last 40 years, the role played by non-parametric tests has undergone considerable change. In the 1950s and 1960s, it was quite common to characterize nonparametric methods as "rough and ready." This attitude has changed now so that practically every introductory statistics text contains a chapter concerning non-parametric, distribution-free or rank methods (Noether, 1981). The non-parametric tests include the Wilcoxon–Mann–Whitney test, the Kruskal–Wallis test, the Wilcoxon signed-ranks test, the Friedman test, Spearman's rank correlation and others. Since the tests are relatively quickly completed, the rank tests are highly useful for the investigator who is doubtful that the data can be regarded as normally distributed.

28.2.5.1 Mann–Whitney (U) Test

The Mann–Whitney (or "U") test is a highly efficient non-parametric test based on rank sums to compare the means of two independent samples. It closely resembles the form of the two-sample *t*-test, but makes no distributional assumptions.

In order to carry out the Mann–Whitney test, the data in each of the two samples are first ordered from lowest to highest values and then the combined data set is ranked. The ranks are then summed for each group. For example, the following measurements from two wells could be ranked as:

Well A	Rank	Well B	Rank
15	2	12	1
20	4	17	3
21	5.5	21	5.5
30	8	25	7
Rank sum	19.5		16.5

The null hypothesis is that the two samples are taken from a common population so that there should be no consistent difference between the two sets of rankings. The Mann–Whitney test is typically carried out using a normal approximation by calculating a Z-statistic from the ranks:

$$Z = \frac{U - \bar{U}}{S_u} = \left[\left(nm + \frac{n(n+1)}{2} - R_1\right) - \frac{nm}{2}\right] \Big/ \left[\frac{nm(n+m+1)}{2}\right] \quad (28.19)$$

where U = the calculated U-statistic, $\bar{U}$ = the mean of the U-distribution, S_u = the standard error, n and m = the respective sample sizes of the groups, and R_1 = the sum of the ranks for the first sample. If both n and m are greater than eight, the distribution of the U-statistic is approximated closely by the standard normal distribution and thus the critical Z-score (Z^*) can be taken from a Z-table for the desired level of confidence. Comparing the calculated Z to the critical Z^*, conclusions can then be made as to whether the null hypothesis of identical population can, or cannot, be rejected. If one sum of the single-sample ranks is sufficiently larger than the other, then the two sample means are considered to be significantly different. For small sample sizes (i.e. n or $m < 8$), the U-statistic is tested directly using a standard reference table of the U-distribution (available in many statistics textbooks).

Use of the Mann–Whitney Test to Test Equality of Variance. If the ranks of the data are assigned in a different way from that outlined above, the U-statistic can be used to test for unequal dispersions or variances. For this type of test, the ranks are assigned "from both ends toward the middle" by assigning Rank 1 to the smallest observation, Ranks 2 and 3 to the largest and second largest observation, Ranks 4 and 5 to the second and third smallest observations and so on. All other aspects of this test for unequal dispersions are identical with those of the Mann–Whitney U test.

28.2.5.2 Spearman's Rank Correlation Coefficient

Spearman's rank correlation coefficient procedure is a very simple ranking technique that can be used to assess inter-laboratory agreement in the order of samples from least to most contaminated. Consider a situation where two laboratories are completing parallel analyses on groundwater quality, and they each analyze the same ten samples for a parameter. To carry out Spearman's rank correlation coefficient test, the samples are ranked from lowest to highest. A difference, d, between the rankings is calculated for each pair of data (e.g., if Laboratory 1 had Sample 5 with a ranking of 3, and Laboratory 2 had Sample 5 ranked as 7, the difference would therefore be $d = 7 - 3 = 4$), and the correlation coefficient is then calculated as:

$$\mathrm{R} = 1 - \frac{6\sum^{n} d_i^2}{n^3 - n} \tag{28.20}$$

where n = the number of samples ranked, and d = the rank difference.

To test the significance of the R value, a t-test is conducted (provided $n > 10$), calculating t as:

$$t = \mathrm{R}\left(\frac{n-2}{1-\mathrm{R}^2}\right)^{1/2} \tag{28.21}$$

with $(n - 2)$ degrees of freedom.

The rank correlation coefficient procedure has been designed so that when the two rankings are identical, R has the value +1: when the rankings are as greatly in disagreement as possible, i.e. one ranking is exactly the reverse of the other, R has the value −1.

28.2.5.3 Sign Test for Paired Observations

This test represents a non-parametric alternative to the paired t-test. The sign test does not depend on the size of numerical values of the differences between paired datapoints, but only on their sign of the differences in their rank order. The assumption of normality is not required in order for this test to be valid. If the difference between the values is expected to equal zero, i.e. a null hypothesis of no difference, we would expect approximately one-half of the differences to be negative and one-half positive. If a small proportion of the differences are either negative or positive relative to the other, we suspect that there might be a real difference and a significance test is carried out.

Applications of the sign test for paired observations are the same as for the paired t-test, and its computation is relatively simple. For example, the fit of a groundwater model could be tested using field data as follows. First, for each location the difference, Z_i, between the observed value, x_i, and the predicted model value, y_i, is calculated as $Z_i = y_i - x_i$. Then, the number of differences greater than zero are counted (denoted by S), as are the number of deviations less than zero (denoted s). Note that differences of zero (i.e. the same ranks in both field and model data are ignored. Finally, the probability that $S < s$ is computed using a binomial expansion, as:

$$\Pr(S < s) = \sum_{k=0}^{S} \frac{m!}{k!(m-k)!}\left(\frac{1}{2}\right)^m \tag{28.22}$$

where m = the number of paired differences Z_i not equal to zero and the counter, k, ranges between zero and S.

With paired observations, the sign test provides a simple test of the null hypothesis that x and y have a common distribution, as opposed to the alternative that x is less than y or x is greater than y.

28.2.5.4 Kruskal–Wallis Test
(or Non-parametric ANOVA)

The Kruskal–Wallis H test is the non-parametric analog of the ANOVA. The method is useful when there are three or more groups present. The Kruskal–Wallis H tests the null hypothesis that k groups of samples come from identical populations against the alternative that the populations have unequal means. The Kruskal–Wallis H test is utilized when the data or the residuals have been found to be significantly different from normal and when a log transformation fails to adequately normalize the data. It does not make any assumptions about the underlying distribution. The H test is conducted in a manner similar to the U test. It requires at least three groups with a minimum sample size of three in each group. As with the U test (see Section 28.2.5.1), all observations are ranked from lowest to highest, and if R_1 is the sum of the ranks occupied by the n_i observations of the ith sample, the test is based on the statistic:

$$H = \frac{12}{n(n+1)}\left(\frac{R_1^2}{n_1} + \frac{R_2^2}{n_2} + \cdots + \frac{R_k^2}{n_k}\right) - 3(n+1) \qquad (28.23)$$

where $n_1, n_2, \ldots, n_k$ are the number of observations in each of the k groups.

When $n_i > 5$ for all i, the distribution of the H statistic is well-approximated by the chi-square distribution with $k - 1$ degrees of freedom if the null hypothesis is true. This forms the basis of the significance test. If the monitoring locations are found to differ, *post hoc* contrasts are needed to determine if and where contamination is present. When small samples are involved ($n_i < 6$), the chi-square approximation can no longer be used as a reliable procedure. In these situations, a table of critical values from the sampling distribution of H must be used. If more than five monitoring locations are involved, the individual comparisons should be performed using $Z_{0.01}$ rather than $Z_{\alpha/(k-1)}$, where $Z_{\alpha/(k-1)}$ is the $[1 - \alpha/(k-1)]$ percentile of the standard normal distribution.

The Kruskal–Wallis test is performed using the following method. First, defining the number of groups by k and the number of observations in each group by n_i, with n being the total number of well observations, let x_{ij} denote the jth observation in the ith group, where j runs from one to the number of observations in the group, n_i and $i = 1, \ldots, k$ groups. The steps of the procedure are then:

1. Rank all the observations from least to greatest within each group. Let R_{ij} denote the rank of the jth observation in the ith group. As a convention, denote the background monitoring location(s) as Group 1. Ties are given the average rank of the tied values, as described in the introduction to this section (28.2.5).
2. Compute the sum of the rank values (R_i) for each group and the average rank (mean R_i) within each group (k groups).
3. Compute the average rank (mean R) of the overall data set.
4. Calculate the Kruskal–Wallis test statistic, H using Equation 28.23.
5. Compare H with appropriate chi-square critical value χ^2, with degrees of freedom equal to $k - 1$, where k = the number of groups.

Equation 28.23 should be modified if there are any tied ranks in the data set. To allow for tied ranks, the calculated value of H is divided by a correction factor to give H*:

$$H^* = H \Big/ \left[1 - \frac{\Sigma(t^3 - t)}{n^3 - n}\right] \qquad (28.24)$$

where t = the number of individual values involved in each set of tied ranks. The summation $\Sigma(t^3 - t)$ must be calculated for each set of tied ranks.

If H^* is greater than χ^2, the null hypothesis H_0 is rejected, indicating that there is a significant difference between at least two of the well groups. If the H statistic is significant, then multiple individual comparisons, i.e. contrasts, must be computed between the groups. This is done by calculating the differences between average ranks of each group, and comparing these to a critical difference C_i, defined as:

$$C_i = Z_{\alpha/(k-1)} \left[\frac{n(n+1)}{12}\right]^{0.5} \left(\frac{1}{n_1} + \frac{1}{n_i}\right)^{0.5} \quad (28.25)$$

where $Z_{\alpha/(k-1)}$ = the upper $\alpha/(k-1)$ percentile from the standard normal distribution, with zero mean and unit variance; and $1 - \alpha$ is the selected level of significance (typically, 95%). If a given difference between two groups exceeds the critical difference, than the two groups are shown to be significantly different.

28.2.6 METHODS FOR CENSORED DATA

As mentioned in the introduction to Section 28.2 above, monitoring records are frequently censored due to the technical limitations of modern analytical techniques. Consequently, a number of procedures for examining data records with varying degrees of censorship have been published. The majority of these procedures assume the data are singly censored, e.g. less than five, as opposed to multiply censored data sets, e.g. the monitoring record consists of concentrations reported as less than five as well as less than 15). Procedures for estimating parameters based on singly censored data sets are examined in Gilbert & Kinnison (1981), Gilliom & Helsel (1986), Gleit (1985), Helsel & Gilliom (1986), Kushner (1976), and Owen & deRouen (1980). Often, a censored data set will exhibit a skewed distribution, which violates the assumptions of the typical significance test methods. The following section therefore presents some alternatives for dealing with censored data in monitoring data.

28.2.6.1 Simple Substitution Methods

If a small proportion of the observations are not detected, one approach is to replace the censored data with a small number, for example, the method detection limit (MDL) divided by two. USEPA recommends the MDL/2 approach if less than 15% of all samples are non-detect, but these simple substitution methods tend to perform poorly in statistical tests when the non-detect percentage is higher (Gilliom & Helsel, 1986). Simple substitution procedures provide a degree of quantification, but may seriously affect subsequent utilization of the parameters in the significance testing. Hashimoto & Trussell (1983) compared several estimators of the mean for censored water quality data. Their examples illustrate the bias caused by three commonly used substitution methods: discarding censored observations, setting all censored observations equal to zero, or assigning the detection limit to all censored observations.

28.2.6.2 Test of Proportions

The test of proportions is a non-parametric procedure, i.e. it does not use the actual monitoring data values directly. Instead, each sample is treated as a one or zero depending on whether the measured concentration is above or below the detection limit. The test of proportions relies on a normal probability approximation to the binomial distribution of zeros and ones and assumes that the sample size is reasonably large. Generally, if the proportion of detected values is denoted by P, and the sample size is n, then the normal approximation is adequate, provided that nP

and $n(1 - P)$ both are greater than or equal to five.

The test of proportions is appropriate for use when the proportion of quantified values (i.e. detects) is small to moderate (e.g. 10–50%) or, if more than 50% of the data are below detection but at least 10% of the observations are quantified. If very few quantified values are reported (<10%), a method based on the Poisson distribution should be used.

A test of proportions might be used, for example, if none of the background well observations are above the MDL, but if all of the compliance well observations are above the detection limit, one would suspect contamination.

28.2.6.3 Plotting Position Procedure

Use of probability paper provides a simple means of estimating the mean and standard deviation in the presence of censored data (McBean & Rovers, 1984). The limitation of this method arises in that sufficient detected data must exist to convince the analyst that the correct type of probability paper is being utilized and that a reasonable line can be fit to the plotted data. This procedure involves fitting the probability distribution to the data above the detection limit and then extrapolating the line to, in turn, estimate the mean and standard deviation. Potential candidate distributions include the normal and log-normal, since the probability plotting papers are readily available and the distributions are generally appropriate to environmental quality data. Additional useful distributions include the binomial, Poisson, Gumbel and log Pearson Type III, among others.

To be successful, a sufficient portion of the data must be in excess of the detection limit to establish that the data are reasonably described by the assumed probability distribution. As well, there must be sufficient quantities of information from which the fitted line can be drawn. For example, with a brief data set, one large value can substantially bias the resulting line (McBean & Rovers, 1984). Mage (1982) describes several techniques for plotting ranked observations on probability paper and drawing lines.

A significant advantage of the probability plotting procedure is that it gives a visual assessment of the data. The analyst can downplay the effect of an individual datapoint if there is a valid rationale for presuming the particular point is a data outlier. The disadvantages of probability plots are that there is no commonly accepted rule for plotting the data and drawing lines by eye, and there is no simple objective way to judge how well the datapoints conform to a straight line (Mage 1982).

28.2.6.4 Cohen's Test

Another procedure for estimating the mean and variance of a censored normal distribution was presented by Cohen (1961). Cohen's test may be applied up to the situation of 50% non-detects. This approach assumes the observed data (detects and non-detects) come from the same normal or log-normal population, but that the non-detect values have been censored at their detection limits. The premise of the technique is based on the censored probability model where we estimate new or adjusted mean and standard deviations. Cohen's method adjusts the sample mean and sample standard deviation to account for data below the detection limit, assuming the data are normally distributed and the detection limit remains the same.

Cohen's method provides maximum likelihood estimates of the mean and variance of a censored normal distribution. Cohen's adjustment may not give valid results if the proportion of non-detects exceeds 50%. McNichols & Davis (1988) found the false positive rate associated with the use of t-tests based on Cohen's method rose substantially

when the fraction of non-detects was greater than 50%. This occurred because the adjusted estimates of the mean and standard deviation are more highly correlated as the percentage of non-detects increases, leading to less reliable statistical tests.

28.2.6.5 Aitchison's Method

When at least 10% of the groundwater samples have a measurable (detected) value of a particular constituent, the mean and variance of the distribution can be approximated using a method developed by Aitchison (1955). Like Cohen's method, the assumption of a particular probability model for the data leads to adjusted estimates of $\bar{x}$ and S. However, Aitchison's adjustment is constructed on the assumption that the non-detect samples are free of contamination, so that all non-detects may be regarded as zero concentrations. To compute Aitchison's adjustment (Aitchison 1955), it is assumed that the detected samples follow an underlying normal distribution. Alternatively, if the detects are found to be log-normally distributed, the entire computation can be carried out using the logarithms of the data instead.

Aitchison's method results in a lower mean than does Cohen's because of the assumption within Aitchison's method that non-detect samples are free of contamination.

28.2.6.6 Maximum Likelihood Estimator and Alternates

The maximum likelihood estimator (MLE) procedure as a way of incorporating the effect of "less thans" in censored data sets is based on assuming an underlying distribution for the entire data set. MLE estimators of distributional parameters (e.g. mean or standard deviation) can then be derived from the uncensored observations. This procedure is useful for data with censored values, but is considerably more complicated than the preceding alternatives and is best accomplished when there are large data sets. For small sample sizes, MLEs are not necessarily minimum variance, unbiased estimates.

An evaluation of MLE performance is presented in Owen & deRouen (1981). They used Monte Carlo techniques to evaluate the performance of MLE methods derived for the log-normal distributions. The technical literature also includes Holland and Fitz-Simmons (1982), which describes a computer program for fitting statistical distributions using the maximum likelihood estimation. Sharma *et al.* (1995a,b) utilize the MLE for parameter estimation in air pathways migration models.

There are several methods for handling regression with censored data. These include the iterative least squares (ILS) method (Schmee & Hahn 1979), the linear unbiased estimate method (Nelson & Hahn 1973), and the MLE method (Dempster *et al.* 1977; Haas & Jacangelo 1993). The ILS method is simpler to implement than the MLE method, and has good statistical convergence properties (Schmee & Hahn 1979). The ILS method was developed for parameter estimation of a linear model with correct censored data, which arose from life-tests.

28.2.6.7 Poisson Model

If more than 50%, but less than 90% of the monitoring records are non-detects, or the assumptions of Cohen's and Aitchison's methods are not met, parametric statistical intervals should generally be abandoned in favor of non-parametric procedures as described in Section 28.2.5. However, there is one final parametric-based procedure, namely the Poisson model, which may be appropriate for application.

Specifically, when 90% or more of the data values are non-detect, the detected samples may be modeled as rare events by using the Poisson distribution. The Poisson model de-

scribes the behavior of a series of independent events over a large number of trials, where the probability of occurrence is low, but remains constant from trial to trial. The Poisson model is similar to the binomial model in that both models represent "counting processes." In the binomial case, non-detects are counted as "misses" or zeros and detects are counted (regardless of contamination level) as "hits" or ones. In the case of the Poisson model, each particle or molecule of contamination (as per the implied assumption implicit in the Poisson distribution model) is counted separately but cumulatively, so that the counts for detected samples with high concentrations are larger than counts for samples with smaller concentrations.

For a detect with concentration of 50 p.p.b., the Poisson count would be 50. Counts for non-detects can be taken as zero or perhaps equal to one-half the detection level (e.g. if the detection level were 10 p.p.b., the Poisson count for a non-detect would be five). Therefore, unlike the binomial model, the Poisson model has the ability to utilize the magnitudes of detected concentrations in statistical tests.

28.2.7 STATISTICAL POWER

The power of a statistical test ($1 - \beta$) is defined as the probability that the test will successfully detect a statistically significant difference. Alternatively, it is the probability of rejecting a null hypothesis when, in fact, it is false and should be rejected. Recall from Section 28.2.2.4 that the two types of statistical errors (I and II) are dependent on one another. If the critical value α is increased in order to reduce the probability of a Type I error, then the probability of a Type II error will increase. Thus, for a specific alternative hypothesis, this will reduce the power of the significance test, which is of concern in monitoring, since failure to detect significant effects can have environmental consequences. A major impact with strict environmental regulations is that they tend to increase power by minimizing the false negative rates (i.e. β, the probability that you conclude that there is contamination when there is) at the expense of increasing the false positive rates (i.e. α, the probability that you conclude that there is contamination when there is none). Simply selecting a test based on its false negative rate is a concern, because a test with a high false positive rate will necessarily have a low false negative rate. In the extreme case in which the false positive rate is 100%, the false negative rate is 0%.

It is therefore desirable to identify a reasonable compromise of β and α values. To come to such a compromise, one can develop power curves. A power curve is a graph of $1 - \beta$ versus the true difference in sample means. Power curves are useful because for a given sample they allow the selection of an optimal test, in the sense that it achieves its intended false positive while simultaneously achieving a reasonable false negative rate. It is noteworthy that the power of a test is a function of the magnitude of the difference considered "significant," i.e. it is much more difficult to have high power for a small difference than for a large difference.

The power of a test may be increased in one or more of the following four ways:

- reducing the variance of the measurements to be tested,
- increasing the size of the difference considered significant,
- increasing the number of samples, and
- using a higher α level.

For example, a test that uses an α of 0.10 will have a higher power (i.e. a lower chance of a Type II error), but also a higher probability of a Type I error, than will a test using the 0.05 level.

As an example of the power calculations, the example of the *t*-test is given for illustra-

tive purposes. For given sample sizes, n_1 and n_2, significance level $(1 - \alpha)$ and effect size (i.e. hypothesized significant difference) between population means, d, the power of the t-test may be estimated (after Zar 1982) by computing:

$$t_{\beta(1)} = \left\{ d \Big/ \left[\frac{2\hat{S}^2}{(2n_1n_2)/(n_1 + n_2)} \right]^{1/2} \right\} - t_\alpha \quad (28.26)$$

where $\hat{S}^2$ = the pooled variance, t_α (one-sided or two-sided depending on the test design) and $t_{\beta(1)}$ (one-sided) = critical values of the t distribution (for $n_1 + n_2 - 2$ degrees of freedom), and n_1 and n_2 = the respective sample sizes.

28.3 *Assessment of Risk Associated with Exceedance of Boundary Criteria*

Risk assessment and risk management may involve use of monitoring (and potentially fate and transport modeling) to estimate the ecological and human health risks associated with a contaminant plume. As discussed in Chapter 22, risk management has become an important part of geoenvironmental engineering. Risk is generally defined as:

$$\text{Risk} = \text{consequence} \times \text{probability of occurrence.} \quad (28.27)$$

In the following, consideration will be given to evaluating the probability of occurrence in the context of information gained from monitoring data. Problem identification and risk management involves exposure assessment (Section 22.5), toxicity assessment (dose-response and hazard identification, Section 22.6), risk characterization (Section 22.7), risk communication (Section 22.8) and, finally, risk management (Section 22.9).

Additional detail regarding some of the subcomponents of the risk assessment process that are of particular relevance to environmental monitoring are presented in the following sections.

28.3.1 MIGRATION PATHWAYS OF ENVIRONMENTAL CONTAMINANTS

Given environmental contamination, a source of potential exposure risk or hazard exists. However, for an environmental risk to occur, two additional components must exist: (a) one or more pathways by which the contaminants may migrate, and (b) a receptor who will be harmed if the exposure is sufficiently large. If any of these three features are zero, there is no risk. Thus, risk assessment is a systematic process for making estimates of all the significant sources and exposure risk pathways that prevail over an entire range of failure modes and/or exposure scenarios (see Chapter 22). When a contaminant is released into the environment, it moves or partitions into the environmental sectors (gaseous, aqueous, solid) according to its physical properties and the properties of the environment. Subsequently, the determination of mobility of the contaminant to create an exposure risk requires development of quantitative estimates of the extent to which these migration pathways are contributing to exposure risk. The availability of environmental monitoring data for the purposes of calibrating the model mobility of the constituents transfer functions greatly improves the confidence in the modeling results.

For some situations, one migration pathway will clearly be the dominant feature. Conversely, for others, a variety of migration pathways may be relevant, which is suggestive of the degree of difficulty sometimes involved in a comprehensive risk assessment. Examples of migration pathways for different media are provided in Table 28.5. The various pathways may include contaminants being transported via one or more media (including air, soils/sediments, surface water and groundwater) to potential receptors (through, for example, inhalation, dermal

TABLE 28.5. Contaminant exposure pathways by medium

Medium	Exposure pathway
Groundwater	Ingestion from drinking
	Inhalation of volatiles
	Dermal absorption from bathing
Surface water	Ingestion from drinking
	Inhalation of volatiles
	Dermal absorption from bathing
	Ingestion during swimming
	Ingestion of contaminated fish
Soil	Ingestion
	Inhalation of particulates
	Inhalation of volatiles
	Ingestion via plant uptake
	Dermal absorption from gardening

contact and ingestion). The existence of various exposure routes to alternative organs within the body (e.g. inhalation suggests that the target organ is likely the lungs, whereas ingestion may result in the target organ being the stomach) indicates that the pathways assessment and exposure risk calculations may require considerable effort.

28.3.2 EXPOSURE ASSESSMENT PROCEDURES

Once a potential migration pathway that could lead to exposure is identified, the magnitude of the potential exposure of a receptor must be evaluated. The exposure assessment aspect of risk assessment includes characterizing the physical and exposure setting (i.e. contaminant distributions leading from sources of environmental contaminants to the points of exposure), identifying significant migration and exposure pathways, and then calculating chemical intakes for all potential receptors. The total exposure of a receptor to a contaminant is the sum of exposures from all migrational pathways.

Mathematical models to quantify the exposure scenarios are important elements of the assessment. Numerous model classification systems exist, including:

- black box models;
- analytical models, and
- numerical models.

The selection of a model to be used is influenced by at least three conditions (McBean *et al.* 1990):

1. the judgment of the investigator in the specific application of the various modeling techniques,
2. the extent of the database, and
3. the physical system being modeled.

Examples of common models used to perform risk calculations by summing over the migrational pathways of exposure levels and probabilities of occurrence are AERIS (1990) and API (1994). A detailed discussion of the pros and cons of some of the available models is found in McTernan & Kaplan (1990) and others.

The risk assessment process reduces a problem into logical pieces. However, important limitations may exist in the models used to solve each of these problems (e.g. characterizing the migration of the constituents from the source to the receptor, the data utilized as inputs to the models, and the scientific understanding of the reference doses). There are always *uncertainties* inherent in a risk assessment, and it is critical that these be quantified to assess the *reliability* of the assessment. Since risk assessment is used to inform a process of managing the risks (see Sections 22.9 and 28.3.3), the degree of certainty associated with the results is a key consideration. In fact, uncertainty can be used to determine the level of effort required for the process; if a risk assessment's results have too much uncertainty, then further field work is performed to collect additional monitoring data, and the risk assessment repeated with better estimates of the input parameters. This process may be iteratively repeated until an acceptable level of uncertainty is achieved. In certain cases, the natural varia-

tion of a parameter may be such that the desired overall uncertainty level may not be achieved (e.g. the hydraulic conductivity of a soil).

28.3.3 DECISIONS ON RISK-BASED CORRECTIVE ACTION

It is noteworthy that, as Lehr (1990) indicates, "risk" is often interpreted as bad — a thing to be avoided — and yet all economic and technological progress requires that human beings take risks. As Wildavsky (1988) indicates, "there can be no safety without risk." Ultimately, the question of risk reduction becomes one of risk management: what levels of environmental exposure risk are acceptable? The resolution to this question is complicated by the many dimensions to the problems that exist. Resolution of such questions for a particular situation involves both risk assessment and risk management:

- Risk assessment: is mainly an objective process that calculates the risk associated with environmental contamination using factual information to define the health effects of exposure of humans and/or the environment to hazardous materials and situations. For example, this involves the quantification of the extent to which a chemical moves from the zone of contaminated groundwater, to create an exposure scenario for a nearby resident via drinking water, and a determination of the deleterious consequences, if any, of that exposure scenario that is the result.
- Risk management: is of necessity a subjective process of weighing policy and remediation alternatives against the calculated risks. This integrates the results of risk assessment, engineering data, and social, economic and political concerns to reach a decision involving the management of the risk.

The breadth of issues involved with reaching risk management decisions is beyond the scope of this chapter. Readers interested in questions of how to manage risks are referred to Chapter 22 and other sources for further reading, e.g. Glickman & Gough (1990) and Asante-Duah (1993). Sufficient attention is paid here only to develop an appreciation of the general magnitudes of various tasks that assist in understanding risks associated with environmental concerns. The risk assessment and management processes are intrinsically based on the statistical procedures presented in Section 28.2, and risk assessment is a logical and important extension of statistical methods to assess monitoring data. The field of environmental risk assessment is enormous and evolving, and it is intended that this section has alerted the reader to its key concepts and generic applications.

28.4 The Case for Innovation: A Unique Visualization Method for Demonstrating Intrinsic Remediation

In recent years, acceptance of monitored natural attenuation as a remedial alternative has gradually increased. It is now becoming recognized that for sites where the immediate risk to environmental or human receptors is minimal, and where the subsurface contaminants present are biodegradable by indigenous micro-organisms, an acceptable and cost-effective solution may be to monitor contaminant concentrations as natural processes carry out the remediation. This alternative may be especially attractive with delicate ecosystems where the disturbance caused by an active remedial alternative (e.g. excavation of soil) may cause more real damage than an existing contaminant plume. As knowledge about biodegration processes increases, the role of natural attenuation in contaminant remediation programs will continue to expand.

Demonstrating the occurrence of natural attenuation at a site is a multicomponent

analysis based on a "weight-of-evidence" approach, which includes such considerations as trend analysis of contaminant concentrations, groundwater dispersion modeling and the evaluation of biodegradation capability (i.e. reduction–oxidation conditions), etc. Up to this point, such evaluation has often been performed through the use of tabulated data and multiple figures mapping the concentration of each parameter at different locations on the site. Recently, a unique visualization software tool (SEQUENCE) was published in the public domain that allows for the simultaneous mapping of multiple monitoring parameters on a single page, which can greatly assist the evaluation of natural attenuation at a site. This tool is presented here as an example of the type of innovation required in the future of contaminant monitoring.

SEQUENCE produces a *radial diagram* map representing the concentrations of a number of chemical parameters simultaneously. The program takes its name from the sequence of reduction–oxidation (REDOX) zones that are observed downgradient of a biodegradable organic contaminant's source area. Biodegradation typically occurs via biological oxidation processes. These processes sequentially consume oxygen, nitrate, manganese, iron, sulphate and carbon dioxide until the contaminant is completely degraded. Thus, changes in concentrations of these parameters may provide evidence that degradation is taking place in the groundwater. These redox parameters can be plotted by SEQUENCE using a modified radial diagram method. An example radial diagram is shown in Fig. 28.8.

On each radial diagram, the site background concentrations are plotted and form the outer line. One or more inner lines are plotted representing the monitoring results at the location. In this way, the conditions at the monitoring location can very quickly be visually compared. On Fig. 28.8, all of the redox parameters show significant changes from background, indicating that this location

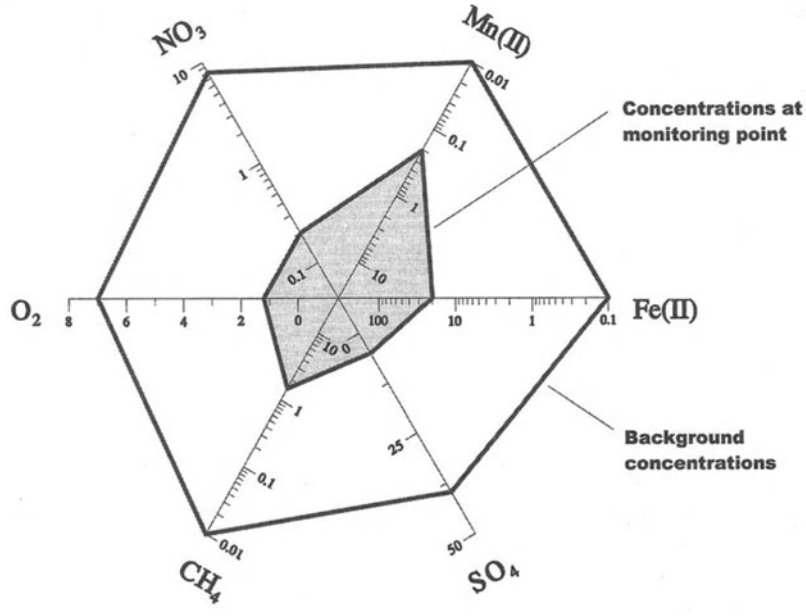


FIGURE 28.8. Example of radial diagram.

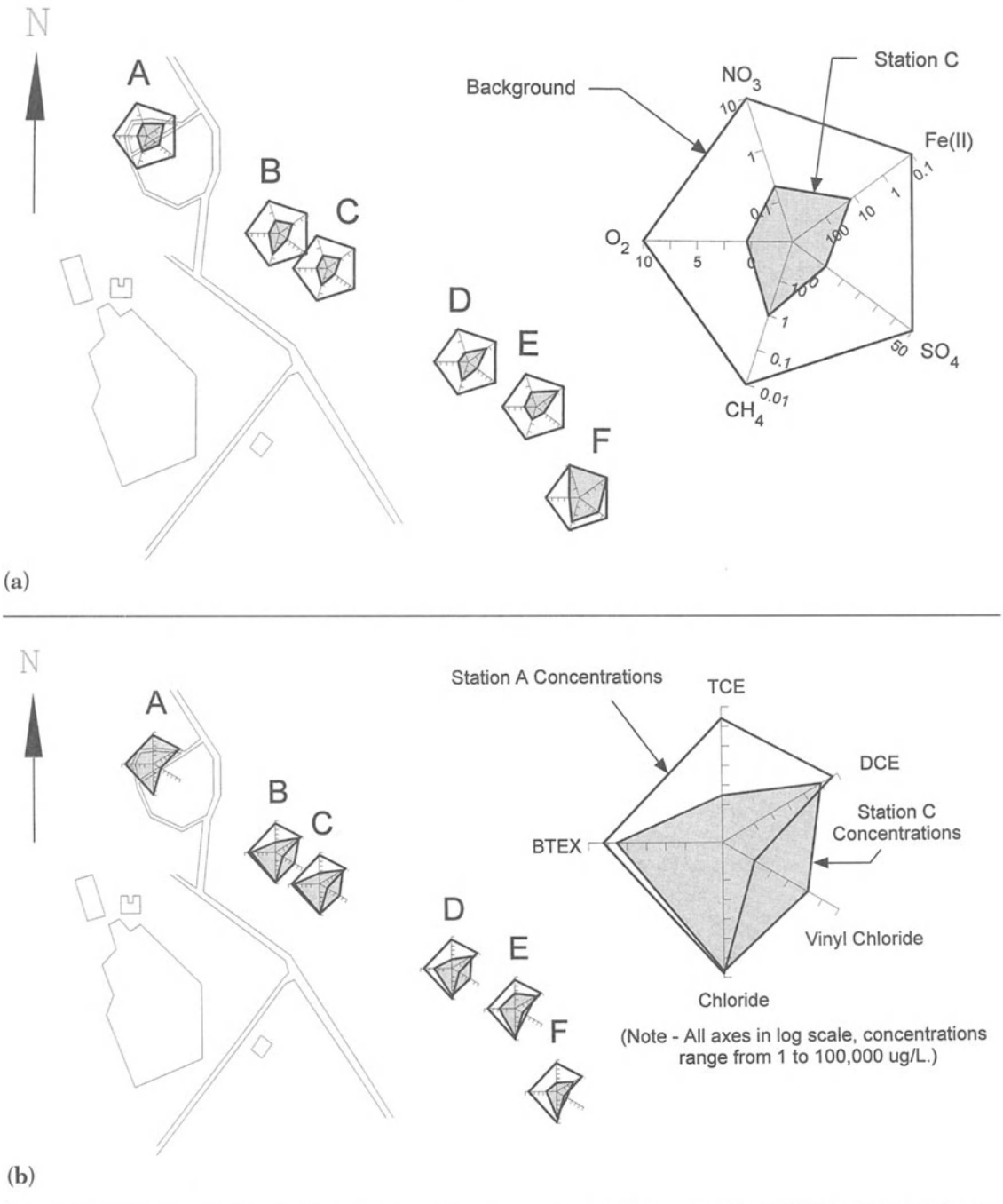


FIGURE 28.9. (a, b) SEQUENCE plots for redox parameters and chemical constituents in groundwater at Plattsburg Air Force Base.

likely is in an advanced stage of biodegradation.

To illustrate the use of this method, consider Fig. 28.9a and b, which presents monitoring data from the Plattsburg Air Force Base (Weidemeir *et al.* 1996). Groundwater flow at the site is in the direction from Station A (upgradient) to Station F (downgradient). Station A is adjacent to a former fire management area that over the years had become contaminated by chlorinated solvents and fuel hydrocarbons in the groundwater. On Fig. 28.9a, notice that at Station A, all of the redox parameters show changes from background concentrations, which is consistent with the occurrence of biodegradation. As the groundwater moves downgradient, the redox parameters gradually return to ambient (although oxygen has not returned to background concentrations by this point) as the contaminant load is decreased by biodegradative removal. This interpretation is supported on Fig. 28.9b, which presents the chemical concentrations at the stations. Clearly, the concentrations of dichloroethene (DCE) and trichloroethene (TCE) decrease with distance. Vinyl chloride (VC), which is an intermediate product in the biodegradation of these substances, first shows an increase in concentrations (as DCE and TCE start breaking down), and then a decrease to non-detected by the last monitoring Station F (as VC is fully biodegraded). Chloride, which is a byproduct of the degradation of chlorinated organics is highest in the region, with the highest contaminant concentrations suggesting active biodegradation occurring at these locations, and also diminishes as the contaminant mass is used up.

SEQUENCE is an example of an innovative approach in the interpretation of monitoring data. It provides a useful visual tool permitting rapid data interpretation and also presents the data in a manner easily explained to the lay public. References treating its theory and application include Carey *et al.* (1996, 1997a,b, 2000), Murphy (1996) and Harris *et al.* (1998).

29. *IN SITU* CONTAINMENT AND TREATMENT OF CONTAMINATED SOIL AND GROUNDWATER

D. J. A. Smyth
R. W. Gillham
D. W. Blowes
J. A. Cherry

29.1 Introduction to Contaminated Sites

29.1.1 CHARACTERISTICS OF CONTAMINATED SITES

Full restoration of contaminated zones in the subsurface, such that unrestricted use of the land or groundwater resources can occur, has proven to be a challenging, costly and often elusive goal. This has been a consequence of the limitations of available remedial technologies, incomplete investigation and definition of the contaminant problem, and the complex and heterogeneous nature of the subsurface. A remedial program for subsurface contamination arising from widespread non-point sources such as the use of agricultural chemicals and fertilizers generally needs to be approached through the implementation of better management practices, such that the introduction of contamination to the subsurface over extensive areas is either reduced or eliminated. For point-source contamination, however, it may be feasible to implement specific programs to reduce or remove contaminants from the subsurface.

Although the release of contaminated water can create plumes of dissolved contaminants in groundwater, it is not uncommon for plumes to emanate from long-term sources, which were introduced to the subsurface through the inappropriate disposal of wastes or inadvertent chemical spills. The nature of impacts from three conceptual models of point-source subsurface contamination is shown in Fig. 29.1. Each model is characterized by a source zone and mobile plumes of dissolved contaminants in groundwater, or possibly vapour-phase contaminants in the vadose zone from sources of volatile organic LNAPL (light, non-aqueous phase liquids) chemicals, such as petroleum hydrocarbons, or DNAPL (dense, non-aqueous phase liquids) chemicals, such as chlorinated solvents, coal tar and creosote. The complexity of these models, and the difficulty associated with remediation, increases as features such as mixed sources of contaminants, heterogeneity of the subsurface, complicated hydrogeological settings associated with fractured clay or rock, or interactions between the contaminants and the subsurface are incorporated. The mass of contaminants associated with the source zone generally far exceeds that associ-

R. K. Rowe (ed.), *Geotechnical and Geoenvironmental Engineering Handbook*
© Kluwer Academic Publishers 2001

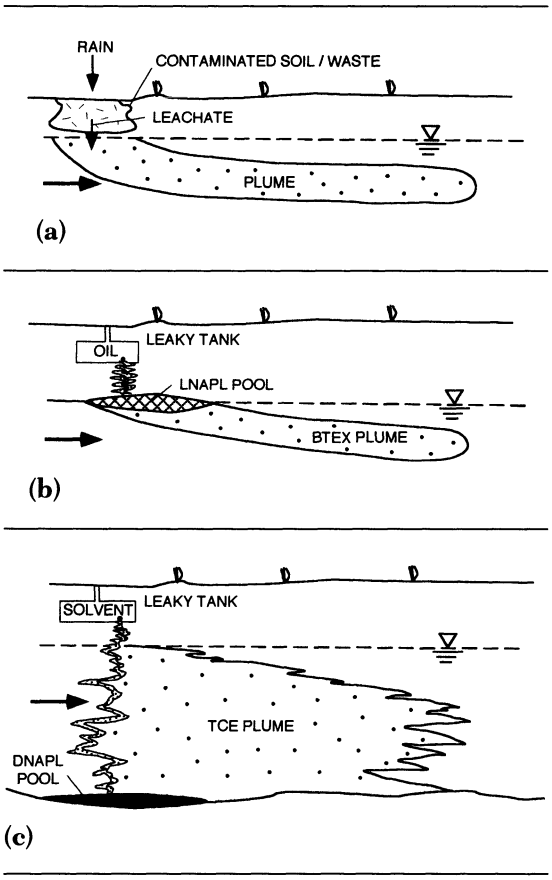


FIGURE 29.1. Conceptual models for three cases of point-source contamination: (a) the non-NAPL case; (b) the LNAPL case; and (c) the DNAPL case (reproduced from Cherry *et al.* 1996 with permission).

ated with plumes (Mackay and Cherry 1989), but mobile contaminants in plumes generally pose more immediate risks to the environment and receptors. Cherry *et al.* (1996) advocate an approach to remediation that clearly recognizes the distinct characteristics of source zones and plumes. It is a rare circumstance for a single remedial technology to be applicable to both source zones and plumes.

This chapter deals with *in situ* containment and treatment of contaminated sites and hence falls within the broader context of geoenvironmental problem identification and risk management. The reader is also referred to Chapter 22 for a discussion of broader issues, Chapter 24 for a discussion of contaminant hydrogeology and migration/attenuation mechanisms, Chapter 25 for a discussion of liner systems and cut-off walls, Chapter 28 for a discussion of monitoring of contaminated sites and Chapter 30 for a discussion of other techniques for dealing with contaminated soil and sites.

29.1.2 OBJECTIVES OF REMEDIATION

The goals of remediation have a significant influence on the development and implementation of remedial plans for contaminated sites. Full restoration of the subsurface is the most stringent goal. It relies on the complete removal or destruction of the contaminants, such that the subsurface is returned to its original condition and groundwater quality could meet health- and ecologically based criteria such as drinking water standards. Generally full restoration is difficult to achieve as it requires complete remediation of subsurface source zones and the mobile plumes of contaminants in both soil vapor and groundwater. Indeed, for many subsurface contamination problems, in particular those involving DNAPL sources, full restoration is generally not technically feasible. Although full restoration was the desired goal of most of the regulatory programs associated with the pioneering efforts in subsurface remediation in the 1980s, such as the Comprehensive Environmental Response, Compensation and Liability Act (CERCLA), better known as Superfund, and the Resource Conservation and Recovery Act (RCRA) in the USA, there has been growing acknowledgment within recent years that partial restoration may be a more practical, affordable and reasonable goal of subsurface remediation. Partial restoration can imply remediation to risk-based criteria, which accommodate some level of contamination in the subsurface, or long-term management or control options to maintain contaminant concentrations at criteria levels in the absence of complete removal or destruction of contamination.

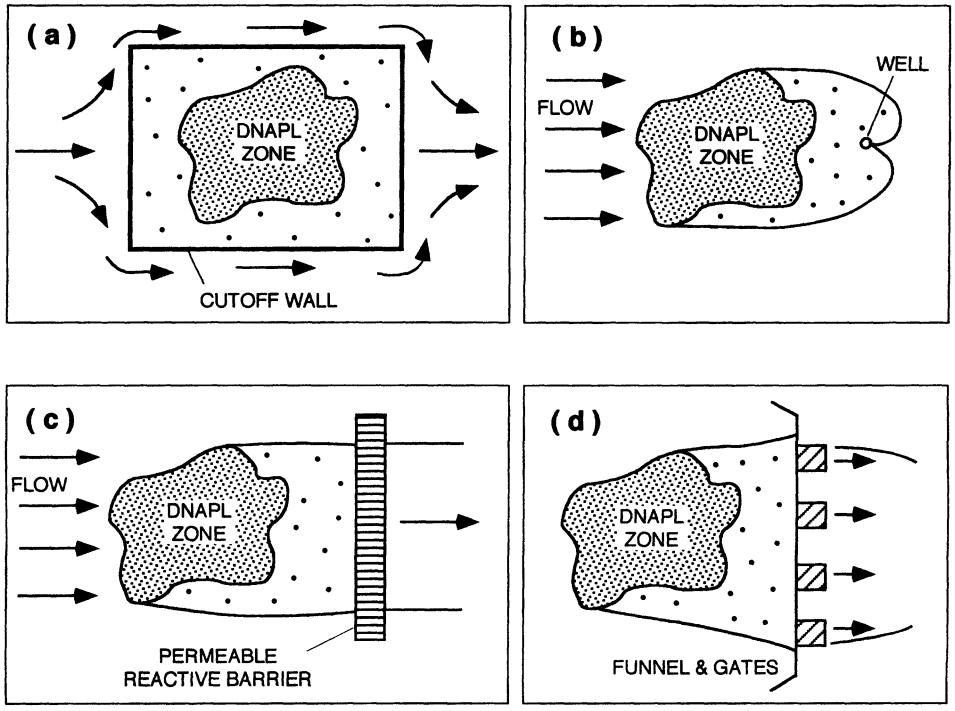


FIGURE 29.2. Engineered remedial actions for subsurface contamination. Actions may include: (a) source-zone isolation, containment or removal; (b) plume control through the use of pump-and-treat systems; (c) passive to semi-passive plume control through the use of permeable reactive walls; or (d) funnel-and-gate systems case (reproduced from Cherry *et al.* 1996 with permission).

A remedial program for contaminated soil and groundwater may involve the implementation of one or a combination of actions to achieve clean-up objectives. At some sites the reliance on natural physical, chemical and biological mechanisms (intrinsic remediation) may reduce contaminant concentrations in the subsurface and achieve clean-up objectives. In other circumstances, as shown in Fig. 29.2, engineered remedial actions, including the following, may also need to be considered:

- Source-zone restoration through the removal or destruction of contaminant mass to eliminate the possibility of further generation of mobile plumes.
- Source-zone isolation or containment through the use of hydraulic or physical barriers in the subsurface.
- Plume control and remediation by active pumping systems or through the use of *in situ* reactive barriers.

29.2 *Intrinsic Remediation*

In some cases, natural attenuation of contamination in the subsurface may be sufficient to achieve remedial goals. Referred to as intrinsic remediation, the approach relies on the development of steady state or shrinking distributions of contaminants within and in the vicinity of a source of contamination.

For intrinsic remediation to be applicable at a site, it is important that concentrations of contaminants within a plume decrease to levels compliant with regulatory or other appropriate criteria before the plume reaches critical receptor or discharge points. In groundwater, the processes of natural attenuation that may cause a contaminant plume to

attain steady state characteristics are dispersion and mass removal by physical, chemical or biological means (see Section 24.3; Cherry 1996; Ward 1996). The reversible sorption/desorption interaction between dissolved-phase contaminants in groundwater and aquifer solids does not cause permanent removal of contaminant mass from plumes, but it may contribute to the apparent development of steady state conditions as a consequence of delaying the advance of plume fronts. Steady state plume conditions in the subsurface may also arise as a consequence of groundwater discharge to surface water. The ability of surface water to assimilate or dilute contaminated discharge will influence the acceptability of this outcome.

The detailed spatial characterization of the contaminant distribution in a plume is necessary to confirm that natural attenuation mechanisms have the potential to achieve the required level of remediation. Cherry (1996) describes the observed presence of high-concentration core zones and lower-concentration fringe areas extending for several hundreds of meters in plumes emanating from actual spills of solvents. The results of inappropriate or sparse monitoring could be used to infer the apparent decrease of contaminant concentrations in the plume with distance from the source, and provide misleading evidence that intrinsic remediation was occurring. It is thus critical that the specific role of the various natural attenuation mechanisms influencing the fate of contaminants can be identified (see Section 24.3; Ward 1996; Wiedemeir *et al.* 1996a).

Aromatic hydrocarbons, including benzene, toluene, ethylbenzene and xylenes (BTEX), typically constitute less than 10% of the composition of gasoline, and even less of heavier petroleum hydrocarbon fuels; however, because of their higher volatility, higher solubility, greater mobility in groundwater, and higher toxicity relative to the predominant alkanes in hydrocarbon fuels, the aromatic hydrocarbons have often been considered as the contaminants of most concern at spill or leak sites. The disappearance of BTEX over relatively modest transport distances in groundwater systems has been documented in Barker *et al.* (1987), Borden (1994), Salanitro (1993), Rifai *et al.* (1995) and elsewhere. These and other studies have shown that the disappearance can be attributed to biodegradation by native microbial organisms in the subsurface, and that the rates of biodegradation are enhanced under aerobic conditions. Biodegradation of BTEX has also been noted to occur under anaerobic conditions, in the presence of terminal electron acceptors other than oxygen, such as nitrate. Under these conditions, however, benzene is more recalcitrant than under aerobic conditions (Barbaro *et al.* 1992; Borden *et al.* 1997a). The persistence of BTEX in plumes at concentrations orders-of-magnitude above drinking water standards more than 200 and 400 m, respectively, from subsurface source zones is documented in Borden *et al.* (1995) and Davis (1997). Thus, the acceptability of intrinsic remediation for petroleum hydrocarbons will depend on the size of the source zone, the aerobic/anaerobic characteristics within the plume, the rate at which oxygen enters the plume from the adjacent groundwater system, and a travel distance to critical receptor points of sufficient length for biodegradation to achieve the necessary decrease in contaminant concentrations. While the prospects are good for the intrinsic remediation of aromatic and aliphatic petroleum hydrocarbons, it has been shown (Squillace *et al.* 1997; Borden *et al.* 1997a) that a gasoline additive, methyl t-butyl ether (MTBE), which has been used extensively in the USA, is resistant to biodegradation in the subsurface, and is a poor candidate for intrinsic remediation.

On the basis of their occurrence in contaminant plumes and drinking water supplies, chlorinated solvents are more recalcitrant than petroleum hydrocarbons (Pankow *et al.* 1996; Mackay & Cherry 1989). McCarty (1996) and Vogel *et al.* (1987) provide the

conceptual framework for the pathways of degradation for the common chlorinated aliphatic compounds such as trichloroethylene (TCE) and tetrachloroethylene (PCE), through intermediate transformation products, which may also be toxic and persistent, such as cis- and trans- 1,2-dichloroethylene (cis-DCE, t-DCE) and vinyl chloride, to innocuous inorganic products such as chloride, carbon dioxide and water. It is, however, very difficult to predict the initiation, extent and rates of degradation (Wiedemeir *et al.* 1996a). In the reductive dechlorination process, the chlorinated solvents act as electron acceptors, and rely on the metabolism of other natural or anthropogenic sources of carbon such as petroleum hydrocarbons as electron donors.

There are many examples of field evidence of the transformation of chlorinated solvents in groundwater, but cases of natural attenuation to levels compliant with regulatory criteria have not been widely documented. Semprini *et al.* (1995), for example, demonstrated the biotransformation and degradation of TCE to the DCE isomers, vinyl chloride and ethene in a sand aquifer in Michigan. The transformation and significant mass loss of TCE as a consequence of the co-metabolic degradation of petroleum hydrocarbons at a site in Plattsburg, New York, is described in Wiedemeir *et al.* (1996b), but the contaminant plume persisted for more than 1.3 km.

The development of steady state and shrinking distributions for various monaromatic and polyaromatic hydrocarbons as a consequence of biodegradation in groundwater downgradient of an experimental coal tar–creosote source is described in King *et al.* (1995). Raven and Beck (1993) also found contaminant plumes of limited areal extent in the vicinity of coal tar and creosote sources at former coal gas sites in Ontario, providing indirect evidence of intrinsic remediation of plumes. Spain (1996) provides a brief review of the potential biodegradability of chloroaromatic compounds including polychlorinated biphenyls (PCBs), nitro-aromatic compounds and pesticides; but the degree to which intrinsic remediation may occur would need to be confirmed on a site-specific basis.

Natural attenuation of inorganic contaminants may also occur as a consequence of transformation or precipitation reactions in the subsurface. Nitrate, which can originate from septic systems, fertilizers or agricultural wastes, may be removed from groundwater by denitrification (Hem 1995), but the availability of labile carbon to support denitrifying bacteria influences the extent to which denitrification may occur in particular groundwater systems (Starr & Gillham 1993). Heavy metals may be among the most toxic contaminants in landfill leachate, but their migration from landfills is generally restricted by mechanisms such as ion exchange, sorption or precipitation of stable solid phases. Yanful *et al.* (1988), for example, documented the precipitation of copper, zinc and lead carbonates, copper hydroxides and a copper organic-phase in the attenuation of metals in leachate at the base of a landfill underlain by carbonate-rich silty clay. The development of different redox environments in plumes from landfills on granular aquifers are identified in Bjerg *et al.* (1995) and Nicholson *et al.* (1983). They suggest that attenuation processes for many contaminants depend on the redox conditions and for some contaminants, such as sulphate, influence the development of the redox conditions in the plume. The reduction of sulphate to sulphide, and the subsequent precipitation of iron and other metal sulphides, is an example of a redox-controlled attenuation mechanism.

29.3 *Source-Zone Restoration*

29.3.1 GOALS AND OBJECTIVES

The goal of source-zone remediation, if full subsurface restoration is to be attained, is to remove or treat contamination to the extent that vapor-phase or aqueous-phase plumes

do not continue to be generated by the source zone. For reactive, soluble or volatile contaminants, the implication of this goal is that nearly complete removal or destruction of the contamination is required. Partial removal of the contaminant mass in the source zone may do little to decrease the characteristics of plumes emanating from the source, and consequently achieve little in the reductions of risks to potential receptors in the vicinity of the contamination (Freeze & McWhorter 1997; Cherry *et al.* 1997; Cherry *et al.* 1996). Thus, a key issue in the performance of a remedial technology is the mass of contamination remaining in the ground, and not necessarily the rates of mass removal or destruction that the technology can attain.

Many of the technologies being proposed for source-zone remediation are emerging technologies, and data pertaining to experience and performance at the field-scale are sparse. There remains significant uncertainty in the potential performance of these emerging technologies, even under the most ideal conditions. This uncertainty is exacerbated in complex or heterogeneous environments, in cases where source-zone contamination is present in both the vadose zone and below the water table, and in cases involving mixtures of contaminants with differing physical or chemical properties. As indicated in Cherry *et al.* (1996), uncertainty in estimates of the mass of contaminants in typical DNAPL source zones casts further uncertainty on quantitative considerations of the performance of a remedial technology and the duration over which it should be applied.

29.3.2 VADOSE-ZONE CONTAMINATION IN THE SOURCE ZONE

For restoration of typical source zones, some effort in the remediation of contaminants in the vadose zone will often be required. The relative importance of contamination is site specific, and is dependent on the type and volume of contaminants, the site geology, and the hydrogeological setting, including the depth to the water table.

29.3.2.1 Excavation

Excavation of a contaminant source for *ex situ* treatment or off-site disposal has been a common approach to shallow soil contamination for the past two decades. For immobile non-NAPL sources of small to modest size, it can be quite successful, but the approach requires approval for treatment and/or disposal of excavated material in a landfill. In some jurisdictions, the use of landfill capacity for the disposal of contaminated soil is discouraged, and the approach may result in the transfer of a contaminant problem from one location to another.

The removal or replacement of faulty underground storage tanks (USTs) or the active spill source is an appropriate first step in responding to NAPL contamination in the subsurface. Excavation of contaminated soil adjacent to tanks has also been broadly applied in attempts to remediate NAPL sites. While there are some prospects for the remediation of NAPL sources entrapped in the vadose zone by excavation, in cases where the NAPL has penetrated through the vadose zone to the water table, the extent of the immiscible-phase contamination in the source zone may not be easily defined, and hence the limits of excavation required for source removal may be difficult to predict or achieve. In many instances, attempts to excavate NAPL source zones may be only partially successful, and some complementary source-zone or plume control remedial action may be necessary. Patrick and Burgess (1992), for sources of petroleum hydrocarbons and solvents, and Feenstra and Cherry (1996), for a source of solvents at a site in Dayton, New Jersey, describe examples of incomplete remediation of NAPL source zones by excavation. At each site, there was a need for complementary

plume control using pump-and-treat systems because remnant contamination source material was left in the subsurface outside and beneath the limits of excavation.

29.3.2.2 Soil Vapor Extraction and Bioventing

Soil vapor extraction (SVE) and bioventing induce the active flow of air through the vadose zone, and have been used to remediate sources of volatile organic contaminants (see Johnson *et al.* 1990; NRC 1994; Fam 1996) and others. Volatile contaminants are transferred to the soil gas from the aqueous, sorbed and immiscible phases of contamination in the soil. The soil gas is drawn under vacuum to the extraction point or points of the SVE system, which induces air flow from the surrounding area through the contaminated zone (see Fig. 29.3). The systems generally incorporate treatment of the effluent vapors, which has important implications to operations, maintenance and costs (Marks *et al.* 1994). The use of SVE to alleviate immediate risks of fires, explosions or the introduction of vapors to buildings from subsurface contamination by volatile organic contaminants has been recognized for more than a decade (Marley & Hoag 1984; O'Connor *et al.* 1984), but SVE is also used extensively for subsurface remediation.

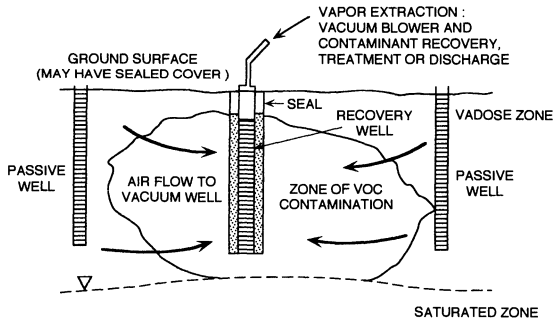


FIGURE 29.3. Elements of a typical soil vapor extraction (SVE)/bioventing system for remediation of VOC contamination in the vadose zone. The key features are the screened well and vacuum pump. Optional features may include passive wells to enhance the flow of air through the zone of contamination, or low permeability ground-surface covers. Upwelling of the water table beneath the vapor extraction wells may inhibit the removal of contaminant mass in these regions.

For recalcitrant chemicals such as chlorinated solvents in the vadose zone, the physical transfer of contaminants to the vapor phase is responsible for active mass removal in the SVE process. When SVE is applied to some contaminants such as petroleum hydrocarbons, biodegradation may result in the *in situ* destruction of some contaminant mass, in addition to the physical removal. This combination is referred to as bioventing. In these cases the introduction of oxygen to enhance biodegradation may be of more importance than mass extraction, so air flow requirements may be moderate in comparison to conventional SVE systems (Marks *et al.* 1994). Performance assessment has generally addressed issues associated with the zone of influence of the SVE system, and the rate and mass removed in effluent gases. Intermittent pumping to identify whether there are contaminant residuals remaining in the source zone is a common and recommended practice. Johnson *et al.* (1990) contrast the simple case of SVE in homogeneously contaminated soils with more complex cases in which contaminant mass may be present in pools of immiscible fluids or trapped within low permeability soil lenses with high moisture content. In these latter cases, air flows adjacent to but not through zones of contamination, and the rate of transfer of contaminant mass to the air stream is diffusion-limited (see Section 25.5). Water-table upwelling may occur in the vicinity of vapor extraction wells, and decreases the effectiveness of SVE operation in deeper parts of the vadose zone.

Flynn *et al.* (1994) experienced initial success in the removal of PCE from a fine to medium sand, but longer-term inefficiencies in the performance of SVE were attributed to heterogeneity within the sand, which con-

tributed to variations in PCE distribution, and non-uniform moisture content and distribution of air flow permeability. Buscheck and Peargin (1991), in a review of more than 140 operating SVE systems, found mass removal rates to decrease exponentially with time until they reached asymptotic removal rates near zero for sites underlain by medium to coarse sediments. At other sites underlain by heterogeneous sediments, the exponential decrease in contaminant removal rates was followed by non-zero asymptotic removal rates. Mass removal following the onset of SVE was attributed to air advection and evaporation, but at later times, diffusion-controlled release of mass from the fine-grained sediments contributed to the long-term presence of contaminants in the soil vapor.

Limitations with respect to mass removal from heterogeneous subsurface environments, and from saturated horizons within and below the capillary fringe, have prompted the application of SVE with complementary remedial actions. Johnson *et al.* (1990) suggest that contaminant mass removal by SVE can be increased if the water table is lowered by pumping, both to counteract the up-welling of the water table induced by lower gas-phase pressures in the immediate vicinity of vacuum extraction wells, and to expose NAPL contamination present within and below the initial capillary fringe.

Air sparging has been used in combination with SVE to remove volatile organic contaminants from water-saturated granular deposits within the capillary fringe and below the water table (Marley *et al.* 1992; Johnson *et al.* 1993). Air sparging consists of the continuous or pulsed injection of air under pressure through wells to depths below the water table. This induces air flow upwards through the contamination towards the vadose zone where capture of the soil gases by SVE is achieved. Contaminant mass may be removed by volatilization to the vapor phase or by enhanced biodegradation (Johnson *et al.* 1993; Hinchee 1993).

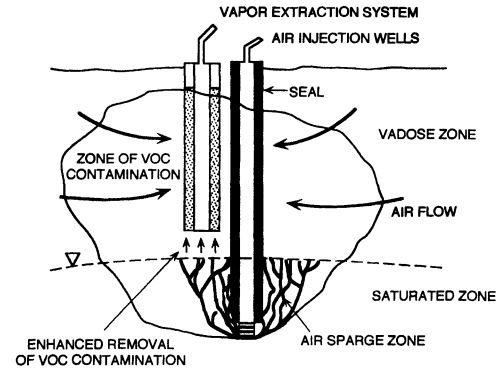


FIGURE 29.4. The elements of a dual soil vapor extraction (SVE)/air sparging system. Air sparging is used to enhance the removal of VOCs within the capillary fringe and beneath the water table. Johnson *et al.* (1993) suggest that the air-sparge zone is characterized by discrete air flow channels.

As shown in Fig. 29.4, it is generally accepted that air flow occurs through discrete channels and not as bubbles distributed in the porous medium (Johnson *et al.* 1993). Although the sparge zone may form a parabolic shape centered on the sparge well in coarse and homogeneous sediments, in heterogeneous soils the air flow channels may occupy a zone of irregular radial dimensions (Marley *et al.* 1992; Ji *et al.* 1993; Lundegard and LaBrecque 1995).

Evidence of decreasing concentrations of chlorinated solvents and petroleum hydrocarbons in groundwater in proximity to air sparge systems is provided in Grubb and Sitar (1994) and Marley *et al.* (1992). Tomlinson *et al.* (1997) provide qualitative evidence for removal of PCE from the subsurface by air sparging, but acknowledge incomplete remediation of a source zone in moderately heterogeneous, fine sands. Within air flow channels, volatilization of contamination to the air phase for transport to the vadose zone occurs rapidly. In areas external to the air channels, which may be large in heterogeneous media, volatilization can only occur after diffusive

transport of contaminants from these inaccessible areas to the air flow channels.

29.3.2.3 Soil Flushing

Another approach to the removal of contaminants from the vadose zone is soil flushing. *In situ* soil flushing is undertaken with the intention of accelerating the movement of contaminants through the vadose zone to the water table, to facilitate their ultimate recovery through a groundwater pumping system (Murdoch *et al.* 1990; Lyman and Nomaw 1990). Water, or another treatment fluid, is introduced to the subsurface above the zone of contamination. The mobilization or destruction of the contaminant occurs as the treatment fluid percolates downward through the zone of contamination. Once it reaches the water table, hydraulic containment and collection of the fluid are generally required. The best prospects for successful application of soil flushing are in granular deposits such as sand or gravel. Furthermore, the treatment fluid should be environmentally acceptable and available at reasonable cost. Issues such as hydraulic containment of the treatment fluid, and its treatment once recovered, may add significantly to the cost of soil flushing.

Soil flushing has not been applied widely at the commercial-scale (Marks *et al.* 1994). The main reasons for this are related to the difficulty of predicting and controlling flow in the vadose zone, and the performance of treatment fluids in mobilizing or destroying the contaminants of concern (Murdoch *et al.* 1990). Soil flushing requires direct contact between the treatment fluid and contaminant. The predictability of fluid movement through the vadose zone is poor because of the inherent heterogeneity of unsaturated soils, and the associated variability of hydraulic conductivity characteristics. As demonstrated by Rudolph *et al.* (1996), the density of measurements required to characterize lateral and vertical fluid flow in the vadose zone would be impractical at most contaminated sites. It would be difficult, for example, to ensure that contamination did not remain in areas between preferential pathways for vertical flow of the treatment fluid. Furthermore, efforts are often complicated by a limited ability to define the spatial distribution of contaminant sources within the vadose zone and the capillary fringe.

The behavior of the treatment fluid may also be dependent on its composition, and the compositions of both the contaminant and the porous material. Though still complex, the behavior of water being used to flush soluble inorganic salts from the vadose zone is more readily predicted than that of reactive solutions for the flushing of organic contaminants. For reactive treatment fluids such as surfactants, mobility can be decreased through interactions between the fluid and porous media (Lyman and Nomaw 1990). Thus, in formations containing fine-grained silt or clay material, or with organic carbon content approaching 1% or more, soil-flushing performance could be reduced. In their review of the technology, Murdoch *et al.* (1990) indicate that field demonstrations of soil flushing have not achieved the efficiencies of remediation projected on the basis of preliminary laboratory work. This reflects the complexities associated with actual site conditions as a consequence of heterogeneous soil conditions, heterogeneous distribution of contaminants, and mixtures of contaminants with different characteristics.

29.3.3 SOURCE-ZONE RESTORATION IN THE GROUNDWATER ZONE

29.3.3.1 Pumping of Immiscible Fluids

The removal of immiscible, mobile NAPL fluids from the subsurface using pumping to induce gradients in the water and immiscible phases is referred to as waterflooding, and has been used for enhanced oil recovery in the petroleum industry for many years (Gerhard *et al.* 1998). In the remediation of petroleum hydrocarbons and other LNAPL fluids,

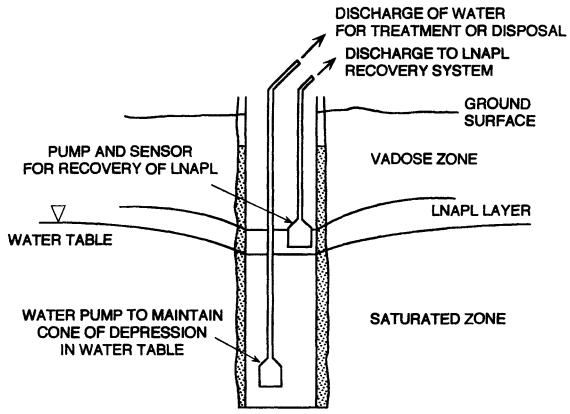


FIGURE 29.5. Typical dual pump system for recovery of LNAPLs such as petroleum hydrocarbons in the subsurface. LNAPL liquid and residual will remain in the subsurface following the removal of the recoverable mobile LNAPL.

the use of free-product recovery pumps in conventional wells or trenches has been adopted for more than 15 years. Dual pumping systems are generally incorporated, one to pump groundwater to create a cone of depression in the water table, and the second to recover the LNAPL as a separate phase (see Fig. 29.5). If removal of mobile LNAPL is successful, residual LNAPL will remain in both the saturated and vadose zones, and may continue to act as a source of dissolved contaminants in groundwater or as a source of contaminant vapors in the vadose zone. In the short term, the concentrations of contaminants in the groundwater and soil plumes may not decrease relative to those present before free-product recovery was undertaken.

Large volumes of DNAPL fluid are not uncommon at coal tar and creosote sites, and free-product recovery by pumping or waterflooding may be feasible (Feenstra *et al.* 1996). At sites with chlorinated solvents, source zones are heterogeneous and direct evidence of DNAPL is rarely encountered in geological cores or monitoring wells. Occasionally, solvent pools have been found in granular aquifers underlain by aquitards, and recovery of thousands of liters of DNAPL fluid has been possible (Cherry *et al.* 1996). While recovery of free-product by waterflooding using wells or horizontal drains reduces the prospects for future remobilization of DNAPL in the source zone, DNAPL residual will remain. Cherry *et al.* (1996) suggest that as much as two-thirds of the contaminant mass might be removed through free-product recovery under the most favorable circumstances. Sale & Applegate (1997) project recovery of as much as 95% of the free-product associated with an extensive pool of creosote-based wood treatment oil at the base of a sand and gravel aquifer. The waterflood system employs a comprehensive network of parallel injection and recovery wells.

29.3.3.2 *In situ* Mass Removal from Source Zones: Chemical Flushing

Although often successful for plume control and remediation, pump-and-treat technology has been ineffective for source-zone restoration, in particular for sources containing NAPL fluids and residual (Mackay & Cherry 1989; NRC 1994; Cherry *et al.* 1996). The failure of pump-and-treat to achieve remediation of contaminant source zones in practical time frames has prompted research and development of alternate source-zone remedial techniques. These techniques either enhance the mass removal efficiencies of flushing by groundwater, or destroy the contaminant mass *in situ* (Cherry *et al.* 1996). Although these technologies have generally originated in other disciplines such as petroleum engineering or water treatment, their applications and objectives in subsurface environments are new. While significant progress has been made, these are currently emerging rather than proven technologies, and their performance in field applications remains to be confirmed.

In recent years there has been a concerted effort to adapt chemical flushing technologies

used to enhance petroleum recovery, to the remediation of subsurface contaminants. The two most common approaches to chemical flushing involve the use of surfactants and co-solvents for enhanced removal of NAPL sources. Although there have been in excess of 20 field demonstrations using surfactants and co-solvents, commercial-scale applications are not yet common (Simpkin *et al.* 1999).

Chemical flushing is achieved by inducing the flow of water containing chemical additives through the contaminant source zone using a system of injection and withdrawal wells (see Fig. 29.6). The water withdrawn from the subsurface requires some form of treatment prior to its recirculation or disposal. Surfactants, or surface active agents, typically act to increase the aqueous solubility of a NAPL, and decrease the NAPL–water interfacial tension, which serves to increase the mobility of the NAPL. Accelerated dissolution, physical mobilization or both can be enhanced by the surfactant selection process (Simkin *et al.* 1999). Alcohols are mutually miscible in both water and NAPL and like surfactants, they can be used to enhance solubility, mobility, or both, of NAPLs in groundwater. At low concentrations, on the order of 5% alcohol or less, solubility enhancement is achieved and remediation would involve flushing of the source zone with many pore volumes of the alcohol–water mixture. At moderate to high concentrations, the alcohol mixes with the NAPL, resulting in a more mobile NAPL with modified physical and chemical characteristics (Simkin *et al.* 1999). Hydraulic containment and recovery of the flushing and modified NAPL fluid is important to avoid inadvertent spread of the contaminated zone.

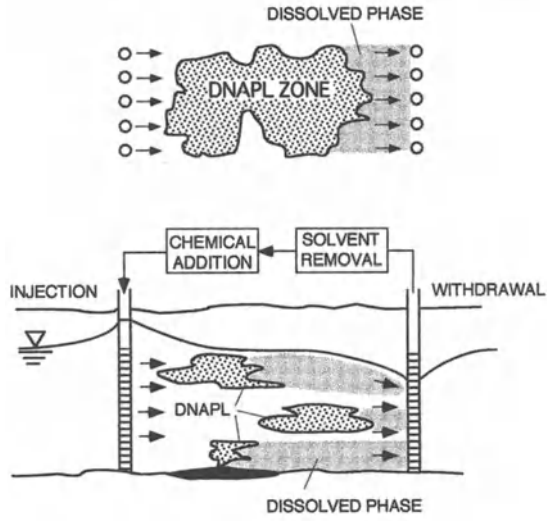


FIGURE 29.6. Chemical flushing for the enhanced removal of NAPL case (reproduced from Cherry *et al.* 1996 with permission). The system includes injection wells for the remedial fluids, and withdrawal wells for the recovery of contaminants and remedial fluids. A forced gradient is maintained between the injection and withdrawal wells.

The performance of chemical flushing technologies is limited by geological heterogeneity and non-uniform NAPL contaminant distribution. A chemical flush generally removes contaminant mass initially from active zones of flushing, such as coarse granular layers or lenses in porous media, or fractures in fractured porous media. Subsequent to this initial mass removal, contaminants move by diffusion from inactive flow zones within low permeability layers or matrix blocks in porous and fractured porous media, respectively, to the active flow pathways, resulting in the slow but continual release of contaminants to the flushing fluid. The use of polymers or foams in the chemical flushing solutions to improve sweep efficiency in heterogeneous settings has been proposed, but research and applications in this area remain in their preliminary stages (Simkin *et al.* 1999). Processes such as sorption and biodegradation of surfactants in the subsurface may detract from performance of chemical flushing methods.

Fountain *et al.* (1996) conducted a highly controlled flush within a containment cell in a fine to medium sand aquifer using an anionic surfactant mixture to enhance dissolution of

a PCE source. Although considerable contaminant mass was removed by flushing more than 20 pore volumes of the surfactant solution through the cell, remnant PCE would quite probably have contributed to the development of dissolved contaminant concentrations in excess of drinking water guidelines in groundwater within the cell in the post-flush period. Costs, and the technical difficulties and uncertainty concerning the degree of success associated with chemical flushing identified by the trials of Fountain *et al.* and others, as documented in Simkin *et al.* (1999), are an impediment to full-scale application of the technology at actual sites.

29.3.3.3 Thermal Flushing Techniques

The petroleum industry has used various thermal flushing techniques to enhance recovery of oil for several decades, but it has only been within the last decade that similar techniques have been applied to subsurface restoration involving organic contaminants (Udell 1997; Sleep 1996). There is a fundamental difference in the objectives of oil-recovery and environmental applications. In subsurface restoration, complete removal of the NAPL source is desired, whereas in the petroleum industry, increased recovery is the objective with minor regard for the amount remaining in the formation. Steam injection is the most common thermal flushing technique, but other approaches such as electrical and radio frequency heating have been explored and may have utility in low permeability media (Udell 1996).

Steam injection is applicable to both LNAPLs and DNAPLs, and is generally operated in combination with water and vapor recovery systems. In steam flushing, steam is injected continuously into the subsurface. Initially the steam condenses, but causes temperatures of soil and fluids to increase. With time a steam front develops, and sweeps away from the injection point. Fluids, including volatile organic contaminants, in the subsurface are volatilized and condense immediately ahead of the steam front. Thus, NAPL that may have been present as immobile residual, may condense as a mobile liquid ahead of the steam front. Ideally this mobile NAPL phase would be recovered through a recovery system, but if capture is incomplete, the contamination could be spread laterally, or to greater depths in the groundwater system if DNAPLs are present. While steam injection enhances potential removal of volatile and semi-volatile NAPL contaminants both below and above the water table, a possible drawback of the technology is the tendency for the steam front to override the contamination as a consequence of the lower density of steam relative to that of water. Other important issues involve the design, operation and maintenance of equipment associated with steam generation and the above-ground handling, treatment or disposal of recovered vapors and fluids (Sleep 1996).

Thermally enhanced subsurface remediation is a recent development, and has no record of commercial application. On the basis of experimental trials, Sleep (1996) reported improved efficiencies for removal of volatile contaminants by steam flushing in sandy soils in comparison to fine-grained and organic-rich soils. Udell (1996) describes two field demonstrations employing thermal enhancements for the removal of solvents and petroleum hydrocarbons from the subsurface. Although the demonstrations achieved considerable mass removal from permeable zones, contaminants remained within, and in proximity to, fine-grained layers. Documentation was not sufficient to determine the degree of cleanup, but clearly full restoration of the sections of the source zones in which the trials were conducted was not achieved.

29.3.3.4 *In situ* Mass Destruction Technologies

In contrast to the use of surfactants or cosolvents for enhanced removal of contaminants from the subsurface, which requires

above-ground treatment or disposal of extracted fluids, *in situ* mass destruction technologies employ injected solutions or materials to promote chemical reactions with the contaminants, without the productoin of toxic degradation products. In addition to active flushing through source zones, it may also be possible to use *in situ* destruction techniques in a semi-passive multiple injection approach (Cherry *et al.* 1996). Experience thus far remains restricted to laboratory and small field-scale trials. The technology faces the same obstacles as chemical flushing with respect to the access of the treatment solution to a heterogeneously distributed source in a heterogeneous geological setting.

Schnarr *et al.* (1998) used potassium permanganate in a series of laboratory and field experiments to degrade NAPL sources containing PCE and TCE. Degradation of the chlorinated alkenes occurs by oxidation, resulting in the formation of carbon dioxide, chloride and manganese dioxide. In two field experiments, conducted within a sheet piling enclosure, in excess of 90% of a homogeneous emplaced source of PCE and 60% of a heterogeneous injected source of PCE and TCE were oxidized *in situ*. While the results suggest promise for the technology, the trial remediation of the heterogeneous source indicates that geological heterogeneity may be difficult to overcome, and implies the need to tailor the design of the injection–extraction system to the configuration of the source. This approach to oxidation is applicable to the chlorinated alkene compounds only, and would not be applicable mixed-solvent sources. Furthermore, the consumption of the oxidant by natural organics in the aquifer in addition to the target compounds, and the precipitation of manganese dioxide in the aquifer may also detract from the performance of the technology.

Other approaches to *in situ* destruction of sources are at an early stage of development. On the basis of laboratory experiments (Lesage *et al.* 1996), a small-scale field trial of biochemical reduction of a solvent source was undertaken. The treatment solutions were expensive, and the highly reducing conditions required for the reaction could not be easily maintained. Barbaro *et al.* (1997) attempted to promote the biodegradation of petroleum hydrocarbon sources through the addition of solutions amended with oxygen and nitrate, but achieved little mass destruction over a period of months. Cherry *et al.* (1996) indicate that biodegradation has also not yet proven to be a one-step remedial action for chlorinated solvent sources. Extending the use of granular iron for treatment of dissolved plumes, as described in Gillham and O'Hannesin (1994), introduction of granular iron into source zones through soil mixing has been proposed for *in situ* destruction of DNAPLs (Gillham *et al.* 1998). Although in the early stages of development, this approach would avoid the need for flushing, and through the mixing process could overcome difficulties presented by geological heterogeneity.

29.4 Source-Zone Isolation and Containment

29.4.1 SOURCE-ZONE ENCLOSURES

In the absence of the technical capability or financial resources to fully restore contaminant source zones, control of contamination emanating from subsurface sources is often an essential component of environmental management of contaminated sites (Freeze and McWhorter 1997). As shown on Fig. 29.2, source-zone containment can be achieved through interim or long-term isolation within an enclosure constructed of low permeability cut-off walls or barriers, long-term hydraulic containment using an active pump-and-treat system, or *in situ* interception and treatment of contaminated groundwater originating from the source by passive

TABLE 29.1. Description and characteristics of common low permeability barrier technologies[a]

Vertical barrier	Materials	Thickness (m)	Hydraulic conductivity (m s^{-1})	Permittivity[b] (s^{-1})	Construction/ installation	Comments
Slurry trench	Soil/bentonite Soil/cement Soil/attapulgite Cement/slag Cement/fly ash	0.5–1.5	1×10^{-9} 1×10^{-8}	$0.7–2 \times 10^{-9}$ $0.7–2 \times 10^{-8}$	Trench excavation and replacement of soil with slurry Backhoe Backhoe/clamshell	Depths of 45 m Removal and disposal of soil may be important issue Difficult in bouldery and bedrock terrain
Soil mixing	Bentonite Cement	1–2	1×10^{-9}	$0.5–1 \times 10^{-9}$	Deep mixing of active soil and grout with augers Overlapping columns	Depths of more than 30 m Minimal removal and disposal of soil Construction possible within confined areas Some native soils may not be suitable
Vibrated beam	Bentonite Cement	0.025–0.1	1×10^{-9}	$1–4 \times 10^{-8}$	Driven H-beam, void filled with grout as beam withdrawn Overlap	Depths of less than 30 m Minimal removal of soil, fluids for disposal Joining of adjacent injections difficult to confirm
Jet grouting	Bentonite Cement Chemical grouts	1–2	1×10^{-8}	$0.5–1 \times 10^{-8}$	Borehole injections of grouts to subsurface Overlapping treated zones or columns	Influence of geological heterogeneity on injection Overlapping of adjacent columns difficult to verify Depth advantages

Geomembranes	PVC (polyvinyl chloride) HDPE (high-density polyethylene) Others	0.001–0.002	1×10^{-14}	$0.5–1 \times 10^{-11}$	Thin polymer sheets or panels Installation in slurry trench or as panels within a steel-driving apparatus, which is subsequently removed Adjacent sheets/panels sealed at joints	Removal and disposal of soil Expense Diffusion of organics through polymer may be concern
Conventional steel sheet piling	Steel sheets Some pre-coated epoxy joints	0.005–0.015	1×10^{-7}	$0.5–2 \times 10^{-5}$	Direct driving using hydraulic-push or vibratory hammers Sheet piles displace soil	Depths of 40 m Strength/confined areas/little waste Difficult in bouldery and bedrock terrain
Sealable-joint steel sheet piling	Steel sheets Grout sealants for joints (bentonite) Cement, modified Cement, chemical polymer	0.75–0.01	$1 \times 10^{-12}–5 \times 10^{-11}$	$1 \times 10^{-14}–1 \times 10^{-8}$	Direct driving using hydraulic-push or vibrating hammers Sheet piles displace soil Flushing and sealing of joints following installation	Depths of 40 m Strength/confined areas/little waste Cavity/seal QA/QC Removable Difficult in bouldery and bedrock terrain

[a] Data from Cherry *et al.* 1996; Mitchell and van Court 1997; Mutch *et al.* 1997; Starr and Cherry 1990.
[b] Permittivity is the ratio of the hydraulic conductivity and the thickness of a barrier.

reactive barriers (Cherry *et al.* 1996). Barrier installations have generally been restricted to depths of less than 50 m, and may have limitations in difficult geological settings such as bouldery terrain or fractured bedrock.

Barriers have been used to provide hydraulic control for civil engineering projects for decades, but their adaptation for the control and isolation of contamination in the subsurface has only occurred within the past two decades (Starr & Cherry 1992; Mutch *et al.* 1997; Cherry *et al.* 1996). The conventional design of enclosures is to achieve low permeability to minimize water flow and the advective transport of contaminants through the barrier wall. Rowe (1996), Mitchell & van Court (1997) and Devlin & Parker (1996), however, indicate that the potential contaminant storage within and movement through barriers as a consequence of diffusion may be important considerations in the design of containment enclosures. The analysis by Devlin & Parker, which invokes controlled pumping within a containment enclosure, suggests that the outward diffusive flux of contaminants can be countered by the inward advective flux of water through barriers such as slurry walls or sealable-joint sheet piling of relatively low hydraulic conductivity. Rowe (1996), however, indicates that, for typical slurry walls, a significant head difference may be required to achieve this objective. For barriers of exceptionally low hydraulic conductivity, such as plastic geomembranes, it is impractical to develop the necessary hydraulic gradients to induce the sufficient inward advective flux of water to overcome the outward diffusive flux of organic contaminants through the plastic polymer.

The hydraulic performance or degree of containment provided by an enclosure can be optimized in situations where the base of the barrier can be keyed into an underlying aquitard or low permeability layer. Where such geological conditions do not exist, or where the depth to an aquitard is too great, the enclosure walls could be terminated within the aquifer. Cherry *et al.* (1996) refer to this situation as a hanging enclosure, and suggest that containment of contaminants can be achieved if the barrier walls extend to a depth below the base of the source zone. To maintain hydraulic containment in a hanging enclosure, higher rates of groundwater pumping from within the enclosure would be necessary than for a keyed enclosure.

The major types of barriers are summarized in Table 29.1 and include: slurry trench, geomembrane in slurry trench, vibrated beam walls, jet grout walls, auger mix walls, conventional steel sheet piling and sealable-joint steel sheet piling. Each type of barrier has its advantages and disadvantages, and the performance of a particular type will be dependent on specific site and project conditions. Permittivity incorporates the ratio of hydraulic conductivity to barrier thickness for comparison of the flux of groundwater through different barriers of typical thickness for a constant drop in head across the barrier (Starr & Cherry 1990).

Physiochemical interactions between barrier materials and contaminants may influence the hydraulic performance of source-zone containment enclosures. Middleton & Cherry (1996) suggest that there is unlikely to be significant increases in hydraulic conductivity of natural and compacted clay barriers as a consequence of exposure to chlorinated solvents or petroleum hydrocarbons. Interaction between clays and water-miscible compounds such as co-solvents and surfactants may cause shrinkage of clay minerals. This could induce increases in hydraulic conductivity, but this would be minimized at depth under adequate confining stresses. Both Middleton & Cherry (1996) and Mitchell & van Court (1997) suggest that the soil–bentonite in barriers, with typically high water content and porosity, may be more susceptible to shrinkage and cracking than compacted natural clays in the presence of

water-miscible and low solubility organic fluids. No examples of barrier failure at field sites were documented. Mitchell & van Court (1997) note that interactions with low pH or high electrolyte groundwaters may increase the hydraulic conductivity of clay barriers, and may also increase degradation of steel sheet-piling barriers. Polymer materials may also be subject to degradative reactions with organic fluids such as aliphatic and aromatic hydrocarbons and chlorinated and petroleum solvents, and their performance in some barrier applications may be questionable (Mitchell & van Court 1997).

29.4.2 COVERS AND BOTTOM BARRIERS

The degree of isolation provided by an enclosure with vertical barriers can be increased, in some circumstances, through the use of emplaced covers. The covers may serve several functions including reduction of infiltration, control of vapor releases, and enhanced isolation of the contaminated subsurface from the biosphere. The use of covers is described in detail in Chapter 27. The cost, required maintenance and longevity of covers relative to the function they serve in improving the isolation of the contaminated material need to be considered in the decision to incorporate covers with enclosures.

In some situations, covers may serve a geochemical control function in the isolation of source zones. For example, the interaction of oxygen with sulphidic-rich mining waste-rock and tailings wastes contributes to the development of acid-mine drainage problems. Incorporation of oxygen-consuming (Reardon & Moddle 1985) or moisture-retaining materials (Nicholson *et al.* 1989) in covers has been suggested as a remedial control for the management of mine waste areas (see also Section 27.4).

Engineered liners serve as floors and bottom barriers in the control and isolation of contaminants at waste management facilities such as landfills (see Section 25.3). Their construction and use for remedial control at existing contaminated sites, however, has not been common. Although technologies for emplacement of bottom barriers have improved in recent years, they are expensive and verification of their emplacement and performance is difficult (Peterson & Landis 1995).

29.5 *In Situ* Plume Control and Remediation

29.5.1 PUMP-AND-TREAT REMEDIATION

Pump-and-treat technology can rarely achieve full restoration of groundwater systems in the vicinity of contaminated sites within reasonable time frames. NRC (1994), in a review of 77 major pump-and-treat systems in the USA, indicated that clean-up goals had been realized at only eight sites, none of which involved complex hydrogeological settings or DNAPL fluids associated with the contaminant source area. Pump-and-treat systems can be used to remove contaminant mass from a plume, causing the plume to shrink toward its source (Mackay & Cherry 1989; NRC 1994; Cherry *et al.* 1996). Thus, it may be possible to control risks to potential receptors arising from dissolved contaminants in plumes. For control of plumes at depths of 30–50 m or more, pump-and-treat may be the most viable and cost-effective technology. The institutional controls, energy consumption and costs of the treatment of the recovered water prior to its discharge or re-injection are long-term liabilities of the technology. In the absence of specific remediation or isolation of source zones, pump-and-treat operations could be required for decades or more in the vicinity of the source.

Figure 29.7 illustrates the conceptual effluent concentrations with time for an array of pumping wells in a pump-and-treat system associated with a plume emanating from a long-term source of contamination below the

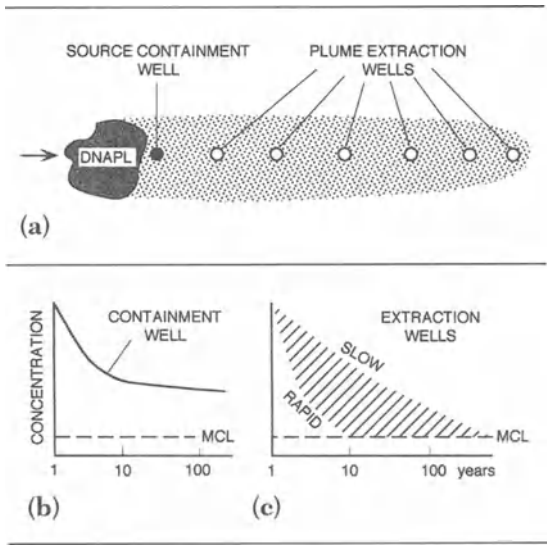


FIGURE 29.7. The conceptual remediation of a source zone and associated plume by pump-and-treat. While remediation of the plume may be achievable over periods of years to decades, the prospects for remediation of the source zone by pump-and-treat are not promising (reproduced from Cherry *et al.* 1996 with permission): (a) plan view; (b) with time at the containment wells; and (c) extraction wells.

water table. For all wells, there is a rapid decline in effluent concentrations immediately following the onset of pumping, followed by a long period of gradually declining concentrations. The quality of the effluent from the source-containment well is influenced by the groundwater quality close to the source, and the effect of dilution by uncontaminated groundwater drawn from surrounding regions as pumping proceeds. The effluent does not, in a practical time frame, attain a quality satisfying environmental guidelines, a direct consequence of continued release of contaminants from the source zone. For the plume extraction wells, contaminant concentrations may decrease to acceptable levels in time frames extending from years to decades or longer. Decreasing contaminant concentrations in effluent from plume extraction wells are a consequence of gradual removal of contaminants from the plume in combination with the introduction of uncontaminated groundwater from adjacent regions of the aquifer systems.

During the period of plume development, the advective transport of most dissolved contaminants is retarded relative to the rate of groundwater flow because of sorptive interactions between the contaminants and aquifer solids. Furthermore, as a consequence of chemical gradients, contaminants invade low permeability lenses, layers or matrix blocks by diffusion adjacent to active flow zones or fractures. With the onset of pumping, the permeable and active zones of groundwater flow within the plume area may be flushed relatively quickly. The gradual release of contaminants by diffusion and desorption, and retardation of their transport to the pumping well, may continue to contaminate groundwater in the active pathways of flow to unacceptable levels for long periods of time. Wood (1996) suggests that the diffusive release of contaminants from the framework and matrix will continue to provide above-background concentrations to groundwater for a period of at least twice the residence time of the contaminants in the aquifer. Even with optimal placement of pumping wells, the gradual release of contaminants by diffusion and desorption causes the volume of groundwater that must be extracted by pumping to far exceed the volume initially occupied by the plume.

Rivett (1993) used a pump-and-treat system to remediate the leading section of a shallow and narrow plume emanating from a source of TCE, PCE and chloroform in a relatively homogeneous sand aquifer at CFB Borden. With peak concentrations ranging from several tens to more than 100 mg l^{-1} in the core, the plume was remediated to concentrations of several micrograms per liter within a period of approximately one year. The amount of groundwater capture was approximately 60 times the original volume of the plume.

The NRC (1994) review of operating systems indicates that pump-and-treat technology has proven to be successful in arresting the advance of contaminant plumes, even in complex hydrogeological settings, including multiple aquifer–aquitard and fractured bedrock environments. Pump-and-treat technology has not, however, been successful in achieving complete restoration of the subsurface. In the absence of specific source-zone remediation or containment, pump-and-treat systems may need to continue to operate for decades or, in some circumstances, centuries to maintain plume control. Furthermore, the energy consumption and costs for long-term operations and maintenance associated with above-ground treatment or disposal of contaminated groundwater, and the potential for wasting uncontaminated groundwater resources, serve to detract from the utility of pump-and-treat systems.

29.5.2 PERMEABLE REACTIVE BARRIERS

29.5.2.1 General Description of Barriers

An alternative which is increasingly being considered for plume control and management at many contaminated sites involves the interception and *in situ* treatment of contaminated groundwater by permeable reactive barriers (Gillham & O'Hannesin 1992; Cherry *et al.* 1996; Cherry 1996; Shoemaker *et al.* 1995; Gillham & Burris 1997; Powell *et al.* 1998).

Permeable reactive barriers have two essential functions. The barrier must facilitate the interception or capture of a contaminant plume at some distance downgradient of the source, and provide treatment or removal of contaminants to acceptable levels. Treatment is achieved within or downgradient of the barrier by one or a combination of physical, chemical or biological processes. The flux of contaminants in groundwater and the efficiency of the proposed treatment technology will influence design parameters such as the thickness and configuration of the permeable barrier system. For example, a minimum residence time for the contaminated groundwater within the treatment media of the barrier is generally required to achieve the appropriate level of treatment. Potential treatment technologies for application in reactive barriers have been identified for a wide range of organic and inorganic contaminants (Shoemaker *et al.* 1995; Gillham & Burris 1997).

In situ treatment zones, created through the injection of chemicals to modify the reactivity of aquifer materials, have been proposed as a method for controlling contaminant migration in groundwater. Brown & Burris (1996), for example, explored the use of cationic surfactants to increase the sorptive retention of chlorinated solvents on aquifer solids. Fruchter *et al.* (1997) have undertaken a trial involving the injection of a sodium dithionite solution to an aquifer at the Hanford site in Washington: to reduce natural iron minerals in the aquifer, and create an anoxic zone where reduction and precipitation of electroactive metals such as chromium will occur. The distribution of solutions and the overall dimensions of the treatment zone are not easily controlled by injection in heterogeneous environments.

The remaining forms of permeable reactive barriers involve the emplacement of treatment materials in the subsurface (see Fig. 29.8). In a permeable wall, the treatment material is emplaced across the entire width and depth of a plume. The wall may consist of material that replaces the native aquifer materials, or it may be a mixture of treatment and native materials. Possible emplacement techniques include open trenching, polymer slurry trenching, overlapping caissons, vertical hydrofracturing, jetting or soil mixing, but most experience to date has been achieved with open-trench methods (Shoemaker *et al.* 1995). The hydraulic conductivity of the wall should be equal to or greater than that of the surrounding aquifer.

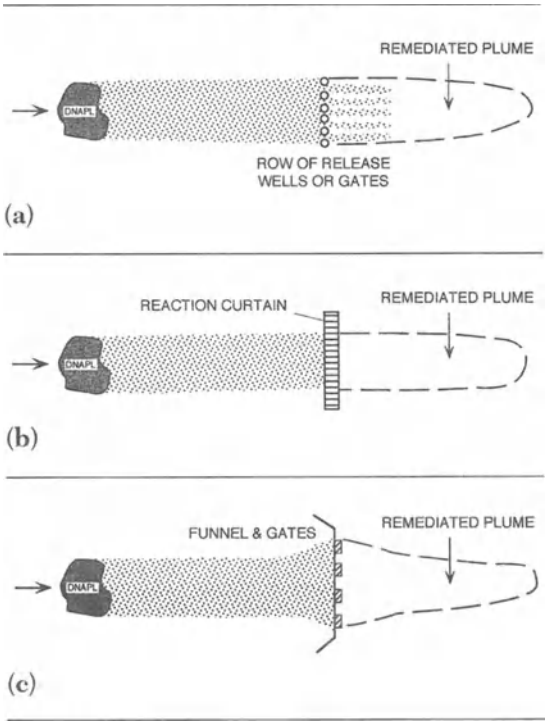


FIGURE 29.8. Possible options for the interception and treatment of contaminant plumes by permeable reactive barriers. Options include: (a) rows of unpumped wells; (b) permeable reactive walls; or (c) funnel-and-gate systems case (reproduced from Cherry *et al.* 1996 with permission).

A second version of the permeable reactive barrier is the funnel-and-gate system (Starr & Cherry 1994). Vertical cut-off walls or barriers of low hydraulic conductivity are installed across a plume to funnel or direct the flow of contaminated groundwater through permeable gates or chambers, in which treatment occurs. The funnels can be installed using any of a number of technologies for the construction of low permeability barriers. The treatment gates can be installed using modifications of the open trenching, polymer slurry trenching or caisson methods applicable to the installation of permeable walls. Gates can be single-chambered, for one-step treatment, or multichambered for situations in which sequential treatment steps may be required to achieve remedial goals (Cherry *et al.* 1996).

A third version of a permeable reactive barrier, which may provide advantages at depth is single or multiple rows of unpumped wells (Wilson & Mackay 1995; Wilson *et al.* 1997). Interception of the plume is achieved through the cumulative effects of convergence of groundwater flow to open wells from the upgradient direction, and subsequent divergent groundwater flow downgradient of the wells. Reactants or nutrients, which induce or enhance degradation reactions, are added to the groundwater in the wells, such that the degradation reactions occur within or downgradient of the wells.

29.5.2.2 Hydraulic Performance of Permeable Barrier Systems

On the basis of numerical simulations for simple hydrogeological systems, Smyth *et al.* (1997) showed that the hydraulic capture for permeable reactive walls, and by inference, passive well systems, appeared to be more favorable than that for funnel-and-gate systems. If the hydraulic conductivity of the treatment material within a permeable reactive wall can be maintained at or in excess of that of the surrounding aquifer, there will be no diversion of groundwater flow around the wall. Thus, the length and depth dimensions of the permeable wall could be established on the basis of width and depth of the plume. The length and depth dimensions for funnel-and-gate systems, however, may need to exceed the width and depth dimensions of the plume (Starr & Cherry 1994; Shikaze *et al.* 1995). Some component of groundwater flow will be diverted around the ends of a funnel-and-gate system, which fully penetrates an aquifer and is keyed into an underlying aquitard, or will be diverted around and beneath a partially penetrating or hanging system in a surficial aquifer (see Fig. 29.9). To ensure the capture of typical plumes, it is likely that funnel-and-gate systems may require several gates across the width of the plume, and need to extend to depths below the base of the

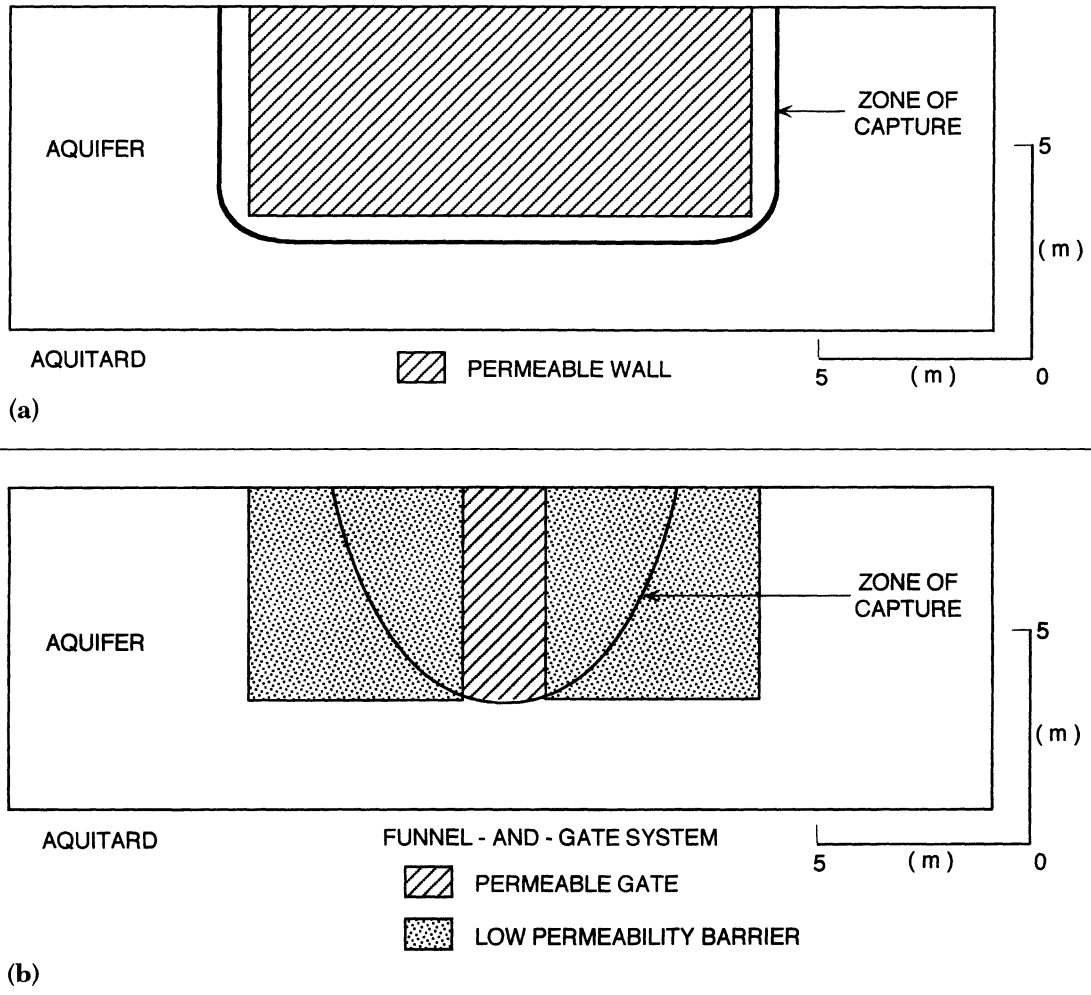


FIGURE 29.9. Sectional views of groundwater flow through permeable reactive barriers. The barrier systems are installed perpendicular to the horizontal groundwater flow direction, and partially penetrate a surficial granular aquifer. For a permeable reactive wall in (a), the zone of capture for groundwater approaching the barrier is slightly greater than the dimensions of the reactive wall if the hydraulic conductivity of the reactive medium exceeds that of the aquifer. In (b), for a funnel-and-gate system with the same reactive medium, the zone of capture is larger than the dimensions of the treatment gate, but some groundwater flow is diverted around the edges and beneath the low permeability funnel walls.

plume at sites where the depth of the plume is not constrained by an underlying aquitard. The flux of groundwater and contaminants through a permeable reactive wall is similar to that through the aquifer. The convergence of flow created by a funnel-and-gate system causes the flux of groundwater and contaminants through the treatment gates to increase by several-fold over that in the aquifer. Thus, to maintain necessary residence times of contaminated groundwater within treatment media, it can be anticipated that the thickness of the treatment zones in the direction of groundwater flow will need to be greater for

funnel-and-gate systems than for permeable walls.

The performance of permeable reactive barriers in demonstrations and commercial applications has largely been inferred from groundwater quality monitoring; i.e. satisfactory water quality downgradient of a reactive barrier reflects satisfactory performance of the barrier. The hydraulic performance of the barrier with respect to the flow rates through the barrier, subtle variations of hydraulic head in the vicinity of the barrier, or zones of capture has proven to be difficult to measure directly.

29.5.2.3 *In situ* Treatment Technologies for Contaminated Groundwater

In situ treatment of contaminated groundwater may be achieved by one or a combination of physical, chemical or biological processes within or downgradient of permeable reactive barriers. The greatest advantage of these systems relative to other plume control technologies arises where treatment proceeds passively, or without the continual need for energy inputs, maintenance or replacement of treatment media, and results in the transformation of contaminants to innocuous and stable degradation products. In many circumstances, completely passive treatment may not be feasible, so semi-passive approaches requiring some maintenance, and operational supervision may be implemented.

Pankow *et al.* (1993) describe the physical treatment of plumes containing VOCs, such as petroleum hydrocarbons and chlorinated solvents, by air sparging in permeable walls or gates. Air is sparged through wells to the base of the treatment wall or gate and, as the resultant bubbles rise toward the water table, the volatile contaminants in the groundwater partition to the vapor phase and their concentrations in the water phase decrease. Collection and treatment of the gas at the water table would normally be required.

A second example of physical treatment of dissolved contamination is a sorptive barrier. This requires the emplacement of a treatment medium in the ground, but designs should incorporate an allowance for periodic replacement. O'Brien & Keyes (1997) implemented groundwater treatment in a modified funnel-and-gate system using activated carbon, which will require replacement at four-year intervals, to remove several organic contaminants including petroleum hydrocarbons, chlorinated solvents and chlorophenols by sorption. Zeolites, which are hydrated aluminosilicates, have also been considered as a sorptive medium. Clinoptilolite has traditionally been used in above-ground operations to remove two radionuclides, cesium and strontium, from water, and has been proposed for *in situ* treatment of contaminated groundwater (Fuhrmann *et al.* 1995).

In contrast to physical treatment options, chemical and biological processes offer the potential to achieve *in situ* treatment through degradation, transformation or precipitation reactions, and avoid the need for above-ground collection or handling of waste materials. Although there are now a range of *in situ* chemical treatment technologies for a variety of inorganic and organic contaminants, an early initiative in the development of permeable reactive barriers was the use of zero-valent iron for the degradation of many of the common chlorinated solvents (Gillham & O'Hannesin 1992, 1994). It is generally agreed that the mechanism for degradation is abiotic reductive dechlorination of the solvent. The reaction appears to be pseudo-first-order with respect to the concentration of the organic, and results in the generation of dissolved chloride, iron and innocuous organic compounds (Orth & Gillham 1996; Matheson & Tratnyek 1994).

Within the past five years, iron-based reactive barriers have been installed at more than 30 sites primarily in the USA, for *in situ* treatment of chlorinated solvents in groundwater. O'Hannesin & Gillham (1998) demon-

strated that the treatment performance of a reactive wall at CFB Borden, containing a 22:78 iron–sand mixture, did not diminish during five years of continuous operation. The wall continued to achieve degradation of 85–90% of TCE and PCE, which were present in the plume at concentrations of as much as 268 and 58 mg l^{-1}, respectively. Although there was evidence of some inorganic mineral precipitation near the upgradient interface of the barrier, coating of reactive surfaces or plugging of pore spaces did not create observable negative impacts on barrier performance. Focht *et al.* (1996) described three commercial examples in which reactive walls or funnel-and-gate systems were installed. Each achieved remediation of contaminated groundwater to regulatory objectives, which generally were based on drinking-water quality guidelines. Projects to date have generally occurred at depths of less than 15 m, but Hubble *et al.* (1997) explored potential barrier installation techniques at depths in excess of 30 m.

Blowes *et al.* (1995) described potential applications of permeable reactive barriers for the removal of metals from groundwaters. Two mechanisms for removal are suggested. In the first, the contaminant is converted to a lower oxidation state, and is removed from solution by precipitation or co-precipitation reactions. In the second, the oxidation state of another constituent associated with the mobile metal of concern is changed by the reactive barrier, resulting in the co-precipitation of the metal.

Blowes *et al.* (1997) installed a permeable wall consisting of granular iron to remove hexavalent chromium (Cr^{VI}) and TCE from a contaminant plume at a coastal site in North Carolina. The barrier, which was installed using a continuous trencher, was 45 m in length and 7.5 m in depth. Cr^{VI} concentrations decrease from in excess of 6 to less than 0.01 mg l^{-1} as a consequence of chemical reduction and the precipitation of low solutibility Cr^{III} oxyhydroxides. TCE concentrations decrease from in excess of 5 to less than 0.005 mg l^{-1} by reductive dechlorination as groundwater flows through the barrier.

In an example of indirect treatment of a contaminant, Benner *et al.* (1997) describe the application of a permeable reactive barrier to remove metals from a plume emanating from sulphidic mine tailings in the Sudbury, Ontario, area. Typical of acid-mine drainage, the contaminant plume contains elevated concentrations of sulphate, iron and other metals. Treatment is achieved by the promotion of sulphate reduction and subsequent co-precipitation of iron and other metal-sulphide mineral phases. The sulphate-reduction process is microbially mediated, and is initiated through the addition to groundwater of carbon for the sulphate-reducing bacteria in the permeable wall. Initial indications are that more than 90% of the soluble iron is removed and alkalinity increases ten-fold as the groundwater passes through the reactive wall. The reactive wall has effectively removed the capacity of groundwater to generate acidity following discharge to receiving surface water. It has been estimated that the wall will function passively for at least 15 years. In another example, microbially mediated sulphate reduction and metal-sulphide precipitation has been investigated as a possible mechanism for removing dissolved uranium from mine-waste waters in New Mexico (Thombre *et al.* 1997).

Robertson & Cherry (1995, 1997) have used various configurations of reactive barriers to promote the removal of nitrate from groundwater, landfill leachate, effluent from septic systems and discharge from agricultural drains. The barrier types have included reactive walls for groundwater plumes, horizontal layers beneath septic beds or reactive chambers. The intent of the remediation is to add carbon to the water to act as an energy source for denitrifying bacteria. In trials to date, 50–80% attenuation of nitrate, at in-

fluent concentrations of as much as 170 mg l^{-1} (NO_3-N), has been achieved, and evidence suggests that the reactive material could function effectively for several decades. Baker *et al.* (1997) demonstrated the use of a mixture of alkaline metal oxides in a reactive barrier to remove more than 85% of the phosphate associated with a septic-system plume at a rural school property. The mechanisms for removal include adsorption and mineral precipitation.

Permeable barriers may also be used to enhance the bioremediation of organic contaminants by native microbial populations in groundwater systems. Conventional approaches to enhanced bioremediation have involved the injection of limiting chemicals or nutrients to the subsurface through wells. The efforts, however, have been frustrated by the difficulty to achieve mixing between the contaminated groundwater and the injected solutions (Gillham & Burris 1997). Permeable barriers provide a mechanism to overcome this limitation. To date, the approach has been to stimulate native microbial activity by modifying geochemical conditions rather than relying on the introduction of isolated or engineered organisms.

Devlin & Barker (1996) developed a semipassive scheme for adding nutrients to a contaminated plume in a permeable wall, and promoting the development of conditions favorable for biodegradation of an organic contaminant downgradient of the wall. In their field trial, anaerobic conditions were created through the addition of an acetate solution to promote the biodegradation of selected chlorinated solvents in groundwater by native microbial populations.

Many petroleum and other hydrocarbons biodegrade readily in groundwater under aerobic conditions. Bowles *et al.* (1995) used air sparging in a funnel-and-gate system to increase dissolved oxygen concentrations to several milligrams per liter to promote the biodegradation of petroleum hydrocarbons in a fractured clay–till environment. This approach was successful because groundwater flow rates, contaminant concentrations and oxygen demands were relatively low. Borden *et al.* (1997b) and Chapman *et al.* (1997) used a proprietary magnesium peroxide powder in barriers consisting of arrays of unpumped wells to release oxygen to plumes containing elevated concentrations of gasoline constituents. While the trials showed promise and partial treatment of the plumes was achieved, BTEX concentrations did not decrease to typical regulatory levels such as drinking-water standards. The limited success of the trials could be attributed to insufficient characterizations of the plumes prior to the trials, an insufficient number of wells within the barrier systems, decreasing oxygen-release rates within several weeks of installation of the peroxide powder, some evidence of biofouling of the wells and oxygen sources and oxygen demands from other organic and inorganic constituents in groundwater. In further work, Wilson *et al.* (1997), for example, explored use of diffusive emitter tubes as an approach to introducing oxygen at elevated concentrations to groundwater in permeable barrier systems.

29.6 *Summary*

Restoration of contaminated soil and groundwater has been a significant environmental issue for only about the last two decades. Progress over this period has been slowed by the poor initial definition of the problem. In particular, the confounding effects of geologic heterogeneity and the occurrence of DNAPLs in the subsurface were not fully appreciated until the late 1980s and early 1990s. With the improved understanding that currently exists, it is reasonable to expect higher rates of development and application of remedial technologies in the future.

At the present time, using developed and emerging technologies, there are few situa-

tions in which the goal of unrestricted use of land and groundwater resources in the vicinity of a contaminated site can be achieved. In some cases this can be a consequence of the limitations of a particular technology, but in virtually all cases, heterogeneity in the hydraulic properties of the geologic materials, in the distribution of contaminants and in the physical characteristics of the contaminants are major contributing factors.

Successful application of existing technologies and the development of new technologies require careful consideration of the effects of heterogeneity, as well as a clear distinction between the characteristics and remedial objectives of source zones and dissolved contaminant plumes.

At many contaminated sites, complete removal or destruction of contaminant mass in the source zone is the most difficult challenge. As an alternative to destruction, there have been successful applications of the use of impermeable barriers to facilitate long-term isolation and containment of source zones. In addition, technologies such as pump-and-treat and, more recently, permeable reactive barriers have been implemented to achieve control and treatment of plumes emanating from sources of a broad range of organic and inorganic contaminants. In the absence of source-zone restoration, source containment and plume remediation, technologies may need to function for prolonged periods. In general more success has been achieved with these technologies for situations where the subsurface source of contaminants occurs within tens of meters of ground surface, and where geological conditions are favorable for the installation of low permeability barriers or permeable reactive barriers. Although improvements in containment and plume control technologies can be anticipated, application to contaminant zones at great depth or in complex geologic settings will continue to be challenging.

Technologies for restoration of source zones, for DNAPL sources in particular, are generally new and not fully developed. With a requirement for complete removal or destruction of contaminant mass, source-zone restoration by flushing technologies will need to overcome limitations arising from heterogeneities in the distribution of contaminant mass and in geological properties. Although there is some promise for *in situ* destruction technologies to overcome these limitations, there have been few full-scale demonstrations to date. Furthermore, the technologies may only be applicable to specific groups of contaminants. Further research, development and demonstration of these technologies are required.

30. MANAGEMENT OF CONTAMINATED SOIL IN ENGINEERING CONSTRUCTION

P. C. Lucia
G. Ford
H. A. Tuchfeld

30.1 Introduction

With the advent of legislation prescribing the handling of contaminated soil and groundwater, the typical scope of a modern site investigation includes consideration of both engineering properties of the soil and groundwater and how to manage any contaminated soil and groundwater in a manner consistent with law, protective of human health and the environment, and in the most cost-effective manner possible. Construction in most urban areas and in some rural areas can lead to the discovery of contaminated soil or groundwater. Linear construction features, such as excavation for pipelines, in an urban area are typically adjacent to numerous sites capable of contaminating soil and groundwater at the construction site, as shown in Fig. 30.1. A business, commercial or industrial building may occupy a site that is the former location of a gas station, dry-cleaning facility, or paint manufacturing or distributing center. The innocent-looking warehouse building in a rural town may be the former site of a pesticide storage or formulating facility. An environmental investigation is required if new construction requires excavation of soil or dewatering where there is reason to believe contamination may exist. The discovery of contaminated soil initiates what can be a complex legal, regulatory and engineering process if the proposed project is to move forward. The engineer must manage the handling of the contaminated soil in a manner that is consistent with good engineering practice, consideration of the legal and regulatory environment of the project, and the cost efficiency and schedule goals of the client.

This chapter discusses the management of contaminated soil leading to a decision on whether the proposed project can move forward or whether the proposed project may not be feasible. Environmental site characterization was examined in Chapter 4. Chapter 22 discussed problem identification and risk management. Chapter 29 has reviewed techniques for *in situ* containment and remediation. The present chapter reviews approaches to contaminated soil management that range from complete removal of the contaminated soil to containment in place. The options available to meet the goals will be discussed, including legal and regulatory considerations, on-site and off-site treatment options, and their limitations and case histories. Guidance regarding this subject is available

R. K. Rowe (ed.), *Geotechnical and Geoenvironmental Engineering Handbook*
© Kluwer Academic Publishers 2001

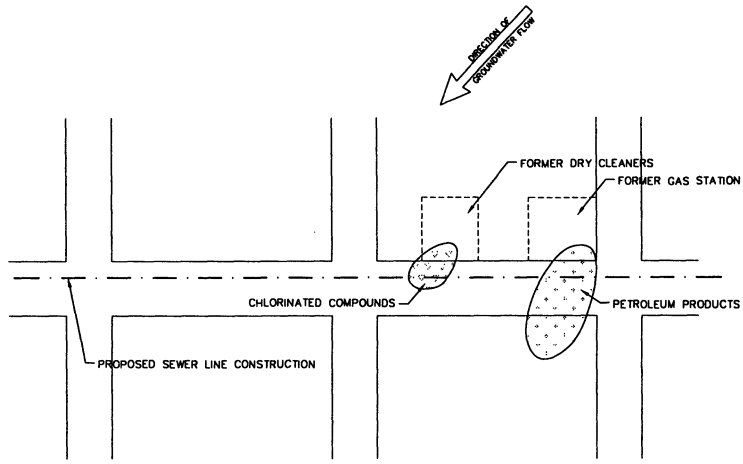


FIGURE 30.1. Example of potential contamination in an urban area.

from a number of USA publications including USEPA (1989f, 1991b, 1992b, 1993a,b, 1994, 1998) and the key governing regulations are given in the US Federal Register (1994).

30.2 Soil Management Goals

When contaminated soil is encountered either during the pre-construction investigation or during construction, a number of important issues arise that include: (a) extent of the soil contamination with respect to the bounds of the proposed project and adjacent properties; (b) legal issues regarding responsibility for the cost of remediation; (c) regulatory issues that must be addressed before initiating remedial actions; and (d) types of options available for managing the contaminated soil and the effects of implementation of such options on the proposed project.

Extending the investigation onto properties not owned by the engineer's client can raise significant legal issues and require site access permission from the adjacent land owner that must be resolved before the engineer can conduct the expanded investigation. The engineer should inform the client that resolution of legal issues beyond the engineer's expertise is needed and then participate with the client in obtaining legal advice from the client's in-house or independent legal counsel. The determination of the source of the contamination can also raise significant issues of legal and financial responsibility and the engineer should work with the client and its counsel to decide if this determination is an objective of the investigation.

If the current owner of the property wishes to recover costs associated with the remediation from prior owners or adjacent property owners, a prescribed investigation and remedial option evaluation methodology and community relations/participation process may be required by law. The engineer should advise the client that determinations and opinions regarding cost recovery, beyond technical matters, are outside of the expertise of the engineer.

An understanding of the regulatory issues and options for managing the contaminated soil are part of developing the soil management goals. The engineer is typically responsible for addressing regulatory issues that may affect remediation and remedial options, often with legal advice regarding interpretation of complex regulatory issues.

One of the most important steps is initially defining the goals of managing the contaminated soil. Many different goals can be considered, including:

- Complete removal: removal of all contaminated soil, possibly including areas beyond those required for the proposed project.
- Non-degradation: partial removal of contaminants or removal of contaminated soil so that the remaining contaminated soil will not contribute to further environmental degradation of present or future groundwater or surface water uses. Non-degradation measures would reduce the potential for significant leaching of contaminants from soil to groundwater.
- Remediation to health-based standards: partial removal of contaminants or contaminated soil so that the remaining contaminated soil does not present a potential existing or future threat to human or ecological health.
- Remediation to the limits of technology-based standards: use of the best available control technology (BACT) to remove as much of the contaminants as technically possible.
- Partial-use restrictions or institutional controls: legal restrictions on areas or resource use, operational measures and/or physical barriers to prevent access to contaminated soils and other media. Examples of use restrictions include deed restrictions to prevent future residential use of a property or to prevent use of groundwater or surface water at a contaminated soil site from being used as a water supply. Operational measures include 24-h security guards to restrict site access and physical barriers including fences, barriers and caps.
- Containment: use of engineered systems (such as caps or subsurface barriers) for minimizing migration of the soil contaminants to locations where human or ecological receptors could be exposed to the contaminants.

A brief summary of the advantages and disadvantages of each of these goals is presented in Table 30.1. Remediating a site to its planned use or eliminating significant health and environmental risks does not always require restoration to original quality. Accordingly, at a growing number of sites, the soil management goals are either containment or remediation to health-based (i.e. human or ecological health) or resource-based (such as protection of underlying groundwater use) standards. A typical approach for achieving such goals is to evaluate the risk associated

TABLE 30.1. Advantages and disadvantages of various potential soil clean-up goals

Goals	Advantages	Disadvantages
Complete restoration	Eliminates risk and liabilities	Difficult to implement
Non-degradation	Reduction of contaminants to a level that prevents further degradation of environment	May be difficult or not practical for many contaminants
Health-based standards	Mitigates risk to human health or environment	Health-based standards are often controversial
Technology-based standard	Allows treatment to the best capabilities of current technology	May not reduce risk sufficiently
Partial-use restrictions	Prevents contact between contaminants and receptors	Ongoing liability and maintenance
Containment	Relatively predictable and reliable; typically less costly than other remediation	Ongoing liability and requires maintenance and monitoring

with exposure to the contaminated soil and to then design a remediation approach that will provide a sufficient level of protection of human health and the environment, i.e. health-based standards; see Chapter 22.

30.3 Soil Management Options

The management of contaminated soils requires consideration of multiple issues that include, along with typical geotechnical concerns:

- Regulatory requirements that may involve a complex series of local, state and federal requirements governing contaminated soil excavation, remediation and disposal.
- Community concerns regarding degree of site clean-up and potential exposure to contaminants (resulting from on-site treatment, off-site hauling and/or containment in place).
- The cost and time schedule required for soil clean-up (including regulatory approval of soil clean-up plan) relative to client expectations and plans.
- Logistical impacts to site preparation, construction, and final land use.

Most construction projects will require the excavation, transportation and disposal of some volume of soil. Excavation of contaminated soil will require a health and safety plan and training for all workers potentially exposed to the contaminants. The level of protection must be consistent with the level of risk to the workers. The more hazardous and the greater the concentration of contaminants in the soil, the greater the level of protection required and, consequently, the greater the cost (and possible duration) of excavating and handling the soil. If the concentration of contaminants in the soil is of a sufficiently high level that the soil needs to be managed as a hazardous waste, then the contractor transporting the soil must be properly licensed to haul hazardous materials. Landfills are permitted to accept hazardous soil consistent with the level of environmental protection incorporated in the design and construction of the facility. All of the above must be considered by the engineer in the excavation, transportation and disposal of contaminated soil from a construction site.

Use of on-site treatment or containment methods is highly dependent on project-specific conditions, including the planned uses of the site and surrounding neighborhood, soil and groundwater conditions, and whether the contaminated soil was discovered long in advance of the project, or during the initial phases of construction. On-site methods tend to be most feasible and successful at sites that are sufficiently large to allow room to implement the methods, and where the treatment option minimizes or eliminates neighborhood exposure issues, particularly at locations where schools, hospitals, houses, childcare centers and the like are relatively distant, or the surrounding areas are commercial or industrial sites.

Processes such as bioremediation (Section 30.5.2.1) and soil vapor extraction (Section 29.3.2.2) require substantial periods of time to reduce the concentrations of contaminants to appropriate levels. These methods may not be feasible in cases where the contamination is discovered after construction has begun or where there is insufficient time to reduce the concentration prior to the beginning of construction. In most cases where contamination is discovered during construction or found to be more extensive than expected, management of the contaminated soil is generally at an appropriate off-site location. Where space is limited for treatment, it is usually necessary to export material from the site quickly, leaving no time for time-consuming on-site treatment or space-consuming containment.

Over the past 15 years, there has been a trend away from simply digging up contaminated soil and hauling it to a landfill. Pres-

ently, soil remediation alternatives are evaluated in the context of risk to human health and the environment (see Chapter 22). In many cases, analysis of both existing and future health risk leads to the conclusion that the contaminated soil presents less risk to the community if it is left relatively undisturbed, or at least not physically hauled from the site. Addressing community concerns regarding contamination left in place is important, and can often be a long and difficult process. Exceptions to this include scenarios in which the contamination has migrated onto adjacent property, where factors such as litigation may control the selection of the remediation alternative, and cases where the contaminants are mobile and may present a threat to groundwater.

In the event that on-site treatment is selected as the preferred alternative for addressing contamination at the construction site, the alternative must also include measures that minimize the risk to the public and local off-site environment during the treatment process. Regulatory and community concerns associated with on-site containment include sufficient demonstration that the mobility of contaminants is adequately reduced such that potential future risk to human health and the environment is considered acceptable.

30.4 *Soil Treatment Technologies*

The applicability of a soil remedial technology is a function of many factors. Evaluation criteria for remedial technologies are presented in Table 30.2. Specific contaminants and their general groupings are presented in Table 30.3. Remedial technologies generally applicable to the contaminant groups are presented in Table 30.4.

The selection of a remediation technology must be made within the constraints of the project's goals and options. The following sections of this chapter describe the most effective and widely used approaches to incorporating soil remediation within a construction project.

30.5 *On-site Treatment Technologies and Containment Options*

The use of on-site treatment technologies at a proposed construction site implies that: (a) the extent and nature of contamination can be treated on site to meet the remediation goals; and (b) the time required to achieve the remediation is allowed within the proposed project schedule. The suitability of any on-site treatment method or containment option is highly dependent on the nature of the

TABLE 30.2. Remedial technology evaluation criteria

Contaminants treated	Technology applicability to all contaminants present
Cost	Capital, operation and maintenance cost
Commercial availability	General availability (beyond pilot scale)
Residuals	Evaluation of whether technology produces solid, liquid or vapor residuals that require additional handling and disposal procedures
Effectiveness	Potential for technology to achieve clean-up goals. How technology addresses reduction in soil contaminant toxicity, mobility and/or mass. Potential to provide long-term effectiveness
Acceptability	Acceptability of technology to the regulators and community
Time	Ability of the technology to achieve the desired results in the time available
Site-specific conditions	Technology effectiveness for the soil conditions at the site

TABLE 30.3. Typical contaminant types

Compound category	Typical contaminants
Halogenated volatile organics	Trichloroethylene (TCE) Perchloroethylene (PCE) 1,1-Dichloroethylene (1,1-DCE) 1,2-Dichloroethylene (1,2-DCE) Methylene chloride Vinyl chloride 1,1-Dichloroethane (1,1-DCA) 1,2-Dichloroethane (1,2-DCA) 1,1,1-Trichloroethane (1,1,1-TCA) Chloroform Carbon tetrachloride
Halogenated semivolatile organics	1,2-Dichlorobenzene 1,3-Dichlorobenzene 1,4-Dichlorobenzene 1,2,4-Trichlorobenzene 2-Chlorophenol 2,4-Dichlorophenol 2,4,5-Trichlorophenol 2,4,6-Trichlorophenol
Non-halogenated volatile organics	Benzene Toluene Xylene Ethylbenzene Acetone Methyl ethyl ketone (MEK) Methyl tertiary butyl ether (MTBE)
Non-halogenated semivolatile organics	Polycyclic aromatic hydrocarbons (PAHs) Acenaphthene Acenaphthylene Anthracene Benzo(a)anthracene Benzo(b)fluoranthane Benzo(k)fluoranthane Benzo(g,h,i)perylene Benzo(a)pyrene Chrysene Fluoranthaene Fluorene Indeno(1,2,3-cd)pyrene Naphthalene Phenanthrene Pyrene Phthalate compounds Bis(2-ethylhexyl)phthalate Di-n-butyl phthalate Others Dibenzofuran Phenol
Fuel hydrocarbons[a] and oxygenates	Fuel hydrocarbons Benzene Toluene Xylene Ethylbenzene Total petroleum hydrocarbons (indicator of petroleum fuel contamination)

TABLE 30.3. (Continued)

Compound category	Typical contaminants
Fuel hydrocarbons[a] and oxygenates	Fuel oxygenates Ethanol Acetone Tert-butanol Methyl tertiary butyl ether (MTBE) Butyl ether (ETBE) Diisopropyl ether (DIPE) Tertiary amyl methyl ether (TAME)
Chlorinated pesticides and PCBs	Polychlorinated biphenyls (PCBs) Aroclor 1016, 1221, 1232, 1242, 1248, 1254, and 1260 Chlorinated organic herbicides 2,4,5-TP (Silvex) 2,4-Dichloroprop Dinoseb Chlorinated organic pesticides Aldrin Chlordane DDT, DDE, DDD Dieldrin Methoxychlor Toxaphene
Inorganics	Arsenic Barium Cadmium Chromium Copper Lead Mercury Nickel Zinc Nitrate Asbestos pH (indicator parameter)

[a] Fuel hydrocarbons are contained in such materials as gasoline, diesel fuel, heating oil, bunker oil and motor oil.

soil and the extent and characteristics of the contamination. An evaluation of the applicability of a treatment method may include a feasibility study, bench-scale testing or even *in situ* pilot scale testing.

30.5.1 REGULATORY CONSIDERATIONS

Commonly encountered soil contaminants during excavation projects (Table 30.3) include petroleum fuel hydrocarbons, metals (including lead), chlorinated volatile organic compounds (including organic solvents), pesticides and herbicides, polycyclic aromatic hydrocarbons (PAHs), polychlorinated biphenyls (PCBs) and asbestos. Different regulatory requirements apply to management of the excavated soil depending on the nature, types and levels of these contaminants, type of site and its history, and regulatory agency (ies) with jurisdiction over the site.

An important first step in assessing the applicable regulatory requirements for the site would be to identify the: (a) locations and history of any present or past underground stor-

TABLE 30.4. Soil treatment technologies generally applicable to compound groups

Compounds	Technology
Halogenated volatile organics	Soil vapor extraction (SVE) Soil flushing Low temperature thermal desorption
Halogenated semivolatile organics	Thermal enhanced SVE Soil washing High temperature thermal desorption Incineration
Non-halogenated volatile organics	Biodegradation Bioventing Soil vapor extraction (SVE) Soil flushing Landfarming Low temperature thermal desorption
Non-halogenated semivolatile organics	Biodegradation Bioventing Thermal enhanced SVE Soil washing Solvent extraction High temperature thermal desorption Incineration
Fuel hydrocarbons	Biodegradation Bioventing Soil vapor extraction (SVE) Landfarming Soil washing Low temperature thermal desorption
Pesticides	Thermally enhanced SVE High temperature thermal desorption Incineration
Inorganics	Solidification Soil washing

age tanks, above-ground storage tanks, waste management units, or disposed waste or spill sites in the subject area; (b) history of past environmental investigations and clean-ups; (c) environmental permitting and regulatory enforcement history; and (d) regulatory agencies that have been involved in the past and those that should be involved in planned excavation of contaminated material and in formulating risk management decisions. This is typically performed through a record search and through discussions with appropriate officials.

The excavation, transport, treatment or containment of contaminated soil typically requires regulatory approval and/or permits. The regulatory process requires definition of the goals of the project and agreement of the regulators on the methodologies and the goals of the project. The client may solicit legal advice to navigate through the complex series of regulations or through problems that

may have a high degree of complexity and/or risk to human health and the environment.

30.5.1.1 Soil Contaminated by Petroleum Fuel Products

Soil at many construction sites is contaminated with petroleum fuel products, such as from existing or past leaking underground gasoline, diesel, and heating or waste oil tanks. When soil is contaminated by petroleum fuel products alone, the regulatory requirements for investigation and management of the contaminated soil are often less stringent than for soil contamination by other potentially hazardous materials, such as chlorinated organic solvents. This is because subsurface contamination by such fuels is believed to typically (depending on the levels of free product and dissolved phase contamination and site setting) pose a lower potential health risk, have limited migration potential in groundwater systems, and have a relatively high biodegradation potential. However, sites where methyl tertiary butyl ether (MTBE) or other anti-knock oxidants associated with gasoline are present may be of greater concern due to the potential higher mobility and toxicity of such compounds.

Sites contaminated only by petroleum fuel products from underground storage tanks typically require a limited site investigation (consisting of installing and sampling soil from several shallow borings in the vicinity of the tank). In the event that soil contaminated by petroleum fuels is identified, such agencies typically require tank removal, removal of free product, remediation of significantly contaminated soil in the immediate vicinity of the site, and possible groundwater contamination assessment. Many state agencies in the USA either directly set minimum clean-up levels and management standards (such as for total petroleum hydrocarbon levels and/or individual petroleum hydrocarbon compounds, petroleum-related metals, and MTBE) or have a tiered health risk-based process for setting clean-up levels and management requirements for petroleum product contaminated soil. Thus, excavated soil from construction sites with petroleum product contamination below such levels (in the absence of MTBE contamination) may be allowed to be used as fill or replaced on site with no or minimal treatment.

30.5.1.2 Soil Contaminated by Hazardous Wastes

The management of soil that is contaminated by constituents other than, or in addition to, petroleum fuels is often subject to more stringent requirements. The highest level of stringency for management of the excavated soils is associated with soil containing hazardous waste or hazardous waste constituents. The federal statute known as the Resource Conservation and Recovery Act (RCRA) regulates the management of hazardous waste from "cradle to the grave", i.e. generation through disposal, in the USA. The US Environmental Protection Agency (USEPA) or a state agency approved by USEPA implements and enforces RCRA. States are required to be at least as stringent as the USEPA in regulating hazardous wastes, and can be more restrictive.

The requirements for identification and management of hazardous wastes under RCRA Subtitle C are contained in 40 "Code of Federal Regulations", 40 CFR 260–268 (USFR 1994). Under RCRA, a contaminated soil may need to be managed as a hazardous waste if it contains a hazardous waste from a specific waste stream or source listed in 40 CFR 261 or is hazardous based on the following characteristics defined in 40 CFR 261: (a) ignitability; (b) corrosivity; (c) reactivity; or (d) toxicity.

Excavated soil which is to be managed as a hazardous waste under RCRA could have the following implications: (a) on-site burial could require RCRA permitting of a double-lined landfill with a leachate collection system, rigorous final cap requirements, groundwater monitoring system, and post-closure maintenance and monitoring; (b) on-site storage of contaminated soil piles could be regulated by RCRA and on-site re-use as fill may be prohibited; (c) off-site disposal would have to be to a licensed Subtitle C (hazardous waste) landfill, incinerator, or other hazardous waste management facility; and (d) either on-site or off-site disposal of the contaminated soil may require pre-treatment prior to land disposal to meet the requirements of 40 CFR 268 (RCRA Land Disposal Restrictions).

On-site burial of soil regulated as hazardous waste would typically be very expensive because of the possible permitting, bottom liner, capping and long-term monitoring requirements. In addition, an on-site disposal facility could require a long lead time for permitting.

If the contaminated soil is to be managed as a hazardous waste, a careful review of the governing regulations, discussions with the site owner/operator and possibly regulators, and a cost-benefit analysis of management options are recommended. Other regulations that should be evaluated for applicability for management of the contaminated soil include the US Comprehensive Environmental Response, Compensation and Liability Act, as amended (CERCLA, or "Superfund"), US Toxic Substances Control Act (TSCA) (which includes the management of PCBs and asbestos), and state and local requirements. In particular, CERCLA applies to certain sites where hazardous substances have been disposed and environmental contamination has resulted. CERCLA requires a remedial investigation and clean-up process, which can be very time consuming and expensive.

30.5.1.3 Soil Contaminated by Non-Hazardous Solid Waste

Solid non-hazardous waste includes materials such as trash, municipal solid waste, used tires and construction demolition debris. Management and disposal of soil that contains these materials is less stringently regulated than soil containing hazardous waste. Off-site disposal of such soil in the USA can be to a RCRA Subtitle D (non-hazardous) landfill, rather than to a RCRA Subtitle C (hazardous waste) landfill. Depending on the characteristics of the contaminated soil and regulatory requirements, on-site disposal of the soil may require a bottom liner and cap, but one less stringently designed than for soil containing hazardous waste.

30.5.2 TREATMENT TECHNOLOGIES

If on-site treatment is to be a viable option, the proposed technology must be cost effective, able to meet the remediation goals within the project schedule, and meet regulatory approval requirements. Treatment technologies that meet these criteria are those that have significant records of success. A great many technologies are available with varying degrees of development. The technologies discussed below are those most widely considered for typical projects.

30.5.2.1 Bioremediation

Soil bioremediation is the process of using naturally occurring or introduced bacteria to decompose toxic organic contaminants into less toxic compounds. This process occurs naturally in many cases (intrinsic or passive bioremediation), or can be induced or accelerated by human interference (extrinsic or engineered bioremediation). Most soils that have not been chemically or thermally sterilized contain naturally occurring bacteria that are capable of breaking down complex organic molecules. Often this process for aero-

bic biodegradation is limited by a lack of sufficient oxygen within the soil.

Aerobic bioremediation consists of inducing conditions that foster the growth and reproduction of carbon-consuming aerobic bacteria within the contaminated zone. By introducing moisture, oxygen and nutrients to the contaminated soil, aerobic bacteria can be induced to thrive and degrade the organic contaminants. This process occurs aerobically, and typically works well on petroleum hydrocarbons and benzene, toluene, ethylbenzene and xylene (BTEX) compounds, and works less well on chlorinated solvents, phenols, PCBs, pesticides, dioxins and other organic compounds (some of which may be more susceptible to anaerobic biodegradation). Water is usually added to the soil during the bioremediation process; therefore, it is most effective for soil that does not contain other highly soluble inorganic contaminants that may affect the environment.

It should be noted that anaerobic bacteria are also capable of metabolizing hydrocarbon compounds, but do so at rates that are typically 10–100 times slower than aerobic bacteria. Thus, anaerobic degradation of hydrocarbon contamination is not often economically feasible.

Bioremediation can be performed *in* or *ex situ*. The primary advantage of *in situ* bioremediation is that it can be performed without excavation of the soil. *In situ* bioremediation's main disadvantage is that it is generally a time-consuming process, and it typically does not result in complete detoxification of contaminants. *Ex situ* bioremediation generally offers the advantage of rapid completion, but usually requires excavation of the contaminated soil and is more practical where contamination occurs at relatively shallow depth.

In situ Bioremediation. *In situ* aerobic bioremediation is most commonly performed on contaminated soil deep in the vadose zone, where the cost to excavate and treat, would be prohibitive. Air and/or moisture is introduced to the contaminated zone by injection through wells. Nutrients may be placed into the contaminated zone through wells, direct injection, or other means. The technique is effective at sites where the soil conditions are favorable for transport of air and fluids, hydraulic conductivities are 10^{-8} m s^{-1} or greater, soil moisture content is in the range 25–85%, and pH values are not extreme.

Aerobic bioremediation in the saturated zone can also be enhanced by increasing the oxygen content in the groundwater through processes such as air sparging or introduction of hydrogen peroxide.

Monitoring of the effectiveness of *in situ* bioremediation is usually accomplished by periodic sampling of the soil to measure contaminant concentrations and bacterial populations. It is typical for the rate of contaminant decomposition to fall off as the process proceeds, such that the decline in concentrations makes an asymptotic approach to detection thresholds. For this reason, *in situ* bioremediation is not the preferred method if the goal is to reduce contaminants to nondetectable levels. The costs of periodic soil sampling may become a significant portion of the total remediation cost.

Ex situ Bioremediation. *Ex situ* bioremediation involves excavating the contaminated soil and treating it above-ground to reduce contaminant concentrations. The treated soil may then be replaced into the ground as compacted fill or disposed off-site, depending upon project requirements. *Ex situ* bioremediation offers the advantage of relatively rapid processing compared to *in situ* bioremediation, ease of monitoring, and it can be used in cases where the site configuration and soil types are not conducive to reasonably efficient *in situ* bioremediation. In particular, where the contamination occurs in highly cohesive clayey soils, it may be impossible to

drive oxygen, moisture and nutrients into the *in situ* pore spaces to induce growth of aerobic bacteria. If the soil is removed from the ground, the soil fabric can be broken up and more surfaces exposed, such that bioremediation becomes feasible. The process works most efficiently in cases where the soil is relatively porous or coarse grained, and when the hydrocarbons are light, short-chain molecules such as fuels or solvents. However, the method can be successfully used on heavier, long-chain hydrocarbons by using longer treatment periods or by adding proprietary enzyme admixtures to facilitate the degrading of heavy hydrocarbons. *Ex situ* bioremediation is typically accomplished by one of two methods:

1. Excavating the contaminated soil and placing it into a bioreactor, where temperature, oxygen, nutrient composition and moisture content are held near optimum for the bacteria, whether native or introduced. This form of bioremediation occurs in a closed, temperature-controlled vessel and the process can be closely monitored and performed regardless of season. This process is usually performed by specialty contractors who use proprietary equipment and procedures.

2. Landfarming of excavated soil. Soil is removed from the ground, placed in shallow lifts or windrows, and water, nutrients (typically nitrogen-rich fertilizer and/or enzymes to assist in breaking down long-chain hydrocarbons) and/or bacteria (if necessary) are applied. The soil is then tilled periodically to introduce air to the pore spaces. This process is continued for a period of days, weeks or months until contaminant concentrations have declined to a target level. In some cases, air, water and nutrients may be supplied to the soil by injection pipes. Landfarming bioremediation is temperature sensitive, and is thus best suited to warm-weather sites, or projects where bioremediation can be carried out over several seasons. Sufficient space is also required for effective landfarming. It should be noted that there are regulatory restrictions and criteria for landfarming of certain wastes in the USA.

The progress of *ex situ* bioremediation is easily monitored by periodic sampling of the soil and testing to determine bacterial density and vigor, and to confirm declining contaminant concentrations. Often, some type of closure sampling and analysis is required to demonstrate that the landfarming operation did not result in contamination of soil beneath the treatment area.

30.5.2.2 Soil Vapor Extraction

As described in greater detail in Section 29.3.2.2, soil vapor extraction is an *in situ* method for removing volatile organic compounds (VOCs) from soil by inducing air flow through the soil using vacuum wells. Contaminant reduction is thought to result from two concurrent processes:

1. The VOCs are volatized and flow through the pore spaces to the wells, where they are carried to the surface for final treatment by combustion, sorption or catalytic decomposition.
2. The increased air flow stimulates the growth of soil bacteria, where present, which consume the VOCs. The basic vapor extraction system is frequently augmented by use of passive soil vents, heating of the soil, surface seals and air sparging (when contaminants are also present in the saturated zone).

Vapor extraction is most applicable when the contamination consists of solvents, gasoline or diesel with a relatively high vapor pressure that is lodged in the vadose zone of a relatively permeable soil. This process may require months to years to substantially reduce contaminant concentrations; therefore, it is most useful in cases where the contaminated soil has been discovered well in advance of

construction or where it can be used in conjunction with the finished project. Under the right circumstances, the method can be effective at removing a large fraction of VOCs from the soil, but cannot remove all contaminants because the rate of removal decreases as the residual concentration of VOCs in the soil decreases. The design of vapor extraction systems must be detailed, site-specific and based on a thorough understanding of the site conditions (see Section 29.3.2.2). Vapor extraction systems can induce local mounding of groundwater, causing migration of dissolved contaminants off-site, and they can draw off-site contaminant vapors inward, unless the system design mitigates these tendencies.

Vapor extraction systems are typically monitored by analyzing the system exhaust for VOCs. When VOC concentrations in the vapor stream decline to low levels, closure sampling of the contaminated soil is usually performed to document that project objectives have been reached.

30.5.2.3 Stabilization

In situ and/or *ex situ* stabilization may be performed to reduce the mobility or exposure hazard of contaminants in soil. *In situ* stabilization can be accomplished by various means, including: (a) conventional or chemical grouting to reduce hydraulic conductivity and/or fix contaminants; and (b) thermal stabilization, ranging from steam or air injection at low temperatures to strip volatiles to high temperature *in situ* vitrification, where soil electrodes are used to melt the soil mass into an inert, glassy mass.

Ex situ stabilization is most commonly done using proprietary processes. A processing plant is placed on site, and the contaminated soil is excavated, stockpiled, processed and then re-used as backfill or disposed off-site. Treatments can be designed to mitigate a range of contaminant characteristics, including: reduction of the solubility of metals; reduction of the mobility and/or toxicity of heavy organics; and removal of petroleum hydrocarbons and/or VOCs. The costs of these *ex situ* processes vary with the type and degree of contamination.

30.5.3 CONTAINMENT OPTIONS

Containment systems (see also Section 29.4) can control (to negligible levels) migration of contaminants to locations where human health or the environment can be impacted. Where contamination is shallow and/or not mobile and migration is not a concern, capping may prevent human or environmental contact and provide acceptable levels of protection. The use of containment can often facilitate the project, but may restrict the project if, for example, excavations were proposed for basements or underground parking. Containment systems may also require long-term monitoring to evaluate their effectiveness and result in additional costs and remaining liability.

30.5.3.1 Capping and Covers

Capping of a contaminated site by the construction of an appropriate cover may be an effective containment option when one or more of the following conditions exists: (a) the contaminants are not mobile in the soil if infiltration of water is mitigated through installation of caps, (b) groundwater is located at a distance from the contaminants such that the reduced infiltration of water due to the cover will mitigate any impacts on groundwater, and (c) the cover provides sufficient protection from contaminant intrusion at the surface and the long-term integrity of the cap can be assured.

The cover must be designed to minimize infiltration, direct surface flows away from the cover surface, and provide long-term durability (see Chapter 27). The decision leading to use of a cover should include an evaluation of the effectiveness of the cap in reducing the mobility of the contaminants, and in reducing

the potential risk to human health and the environment.

The cover can be constructed of a number of low permeability materials designed to minimize infiltration. Often a number of different materials are used in conjunction to provide a combination of low permeability, drainage and durability, as described in detail in Chapter 27.

30.5.3.2 Cut-off Walls

Physical barriers are vertical features in the ground that provide containment of waste. Physical barriers can be formed using a variety of materials. Several of the most commonly used physical barriers are listed in Table 30.5, along with their typical dimensions.

The oldest and most commonly used types of physical barriers are cut-off walls (see Section 25.3.9). Cut-off walls limit migration of contaminated groundwater and leaching of contaminants from contaminated soil by forming a physical impediment to groundwater flow. The effectiveness of the wall is a function of its continuity, its resistance to degradation by contaminants and its resistance to physical degradation. A barrier impedes groundwater flow, and therefore the elevation of groundwater may rise (or "mound") on the upgradient side of the barrier. Other controls may thus be needed to prevent overtopping or flanking of the barrier by contaminated groundwater, such as: (a) groundwater extraction wells or trenches adjacent to the barrier to route mounded groundwater to a discharge point, or (b) permeable segments in the barrier to allow water to pass through controlled locations in the wall.

TABLE 30.5. Types of physical barriers

Barrier type	Width (m)	Maximum depth (m)
Soil–bentonite	0.6–1	25
Cement–bentonite	0.6–1	25
Biopolymer drain	0.6–1	20
Deep mixing	0.75	27
DM structural	0.75	27
Jet grouting	0.5–1	60
Grout curtain	One row	60
Sheet piling	One sheet	45
Geochemical barrier	Varies	Hundreds

Soil–bentonite slurry walls are by far the most common type of physical barrier used in geotechnical and environmental remediation projects. Construction of a slurry wall consists of installing a mixture of soil (or other material) and bentonite clay into a vertical trench to form a very low permeability, vertical barrier to groundwater flow (see Section 25.3.9.1).

The effectiveness of a soil–bentonite slurry wall in preventing migration of contaminants is a function of: (a) the environment of the wall, i.e. the nature of the chemicals in groundwater to which the soil–bentonite mix will be exposed; (b) the percentage of bentonite clay used in the soil–bentonite mix; (c) the type and gradation of soil used, which is typically measured as a percentage of the soil that is finer than the No. 200 USA standard sieve; and (4) the quality of wall construction. The performance of a soil–bentonite slurry wall can be adversely affected by exposure of the wall to VOCs, high levels of aqueous salts (such as those contained in sea water), or non-aqueous phase liquids (NAPLs). Sai and Anderson (1992) reported an increase of two to three orders-of-magnitude in hydraulic conductivity for soil–bentonite slurries that were permeated with the VOCs xylene and methanol. This level of increase may not be typical but illustrates the need to consider clay–permeant compatibility as discussed in Section 25.4.1.

30.5.4 CASE STUDY

In the 1960s, a wastewater treatment plant received soil–sludge waste (waste material) from a refinery. Initially the waste material was described as a non-homogeneous mixture of organic sludge, lead sulfate, dirt, sul-

furic acid (resulting in soil with a low pH), water, tars and wood debris. The waste material was deposited and incorporated into various areas of the facility as fill or to stabilize soil. This occurred more than a decade prior to the passage of major legislation, i.e. RCRA, pertaining to classification and disposal of waste materials.

Subsequent investigations indicated that substances found in soil at the facility included: lead, cadmium and chromium; petroleum hydrocarbons quantified as diesel (TPH-d); BTEX constituents; PAHs; and oil and grease. Groundwater monitoring indicated the presence of only one chemical constituent, benzene, that exceeded a regulatory criterion.

A preliminary risk assessment concluded that the hazardous substances detected did not pose a significant threat to on-site workers and that off-site risk to human health was minimal. However, since the site owner was considering construction of a potential future expansion project on areas of the facility underlain with contaminated soils, the owner proposed taking actions to make the project area suitable for construction of treatment plant facilities.

The subsequent investigations and evaluations addressed the actions to be taken to prevent, minimize or mitigate damage that might otherwise result from a release of hazardous substances at the site at the time hazardous substances actually are moved during construction activities. The specific project goals include:

- excavate soil in the contaminated soil area as required for future treatment plant expansion,
- handle excavated soils in a manner that does not exceed acceptable risk levels to human health and the environment, and
- to the extent possible, provide on-site containment for the contaminated soils.

A baseline risk assessment indicated that the aggregate risk to human health (as hazard index and total theoretical excess cancer risk) fell within the range considered by USEPA to be "safe and protective of the public health" (Federal Register 56(20): 3535, 1991). These conclusions were restricted to occupational exposure only and assumed a future industrial land use. The risk estimates and corresponding exposure calculations would not necessarily hold should a different land use, e.g. unrestricted residential, become important. The facility was a wastewater treatment plant and the future land use was considered unlikely to change.

Four alternatives were identified as feasible and potentially appropriate for the removal action and management of contaminated soil. These alternatives were:

- Alternative 1: no action.
- Alternative 2: consolidate (place excavated contaminated soil in one location on-site)/ treat low pH soil, construct a cover over consolidated soils.
- Alternative 3: consolidate/treat low pH soil, passive bioremediation, construct a cover over consolidated soils.
- Alternative 4: off-site disposal of excavated soil.

Alternative 1 would not meet the primary goal of excavating soil in the contaminated soil area for future treatment-plant expansion. The other three alternatives would all meet this goal. All four alternatives could be implemented within a schedule that compliments the treatment-plant expansion.

The treatment methods for low pH soils proposed for Alternatives 2, 3 and, potentially, 4 were readily available, and have demonstrated performance. The passive bioremediation technology proposed for Alternative 3 was also readily available. However, bioremediation is not very effective on heavy hydrocarbons or PAHs, and is not effective at all on lead. Further, bioremediation has limited success in the type of clayey soils present at the site.

Alternatives 2, 3, and 4 have health and safety requirements related to dust, heavy

equipment and soil contaminants. Risks to workers and the public from dust can be easily mitigated with standard engineering controls, such as keeping soil wet during excavation and consolidation or loading activities. Risks to workers from heavy equipment and soil contaminants can be mitigated by implementing an appropriate health and safety plan, including a hazard analysis, mitigation measures, and appropriate field and medical monitoring in accordance with occupational health and safety requirements.

Alternative 4 posed some additional health and safety risks to the community from the transport of contaminated soil on local streets and highways. However, this risk can be mitigated by using appropriately licensed and experienced haulers.

All alternatives require long-term groundwater monitoring because at least some contaminated soils will remain on site. Alternatives 2 and 3 will also have cover monitoring requirements. However, inspection and maintenance of the cover was anticipated to be easily adapted with minimal impact into the facilities maintenance program. Alternatives 2, 3 and 4 will all require dust and health and safety monitoring during construction. However, this type of monitoring is fairly routine for construction and can be easily implemented.

Alternative 2 was estimated to be the lowest cost alternative. The Alternative 3 cost estimate was higher because of the costs associated with passive bioremediation. Passive bioremediation was not expected to result in a significant benefit over Alternative 2.

Alternatives 1 and 4 were estimated to be the highest cost alternatives. A high estimated cost was associated with the "no action" alternative, due to the anticipated cost of having to locate treatment-plant expansion facilities somewhere other than the proposed expansion area. The high estimated cost of the off-site disposal alternative was associated with transportation and disposal of contaminated materials. Under US law, Alternative 4 would also result in potential long-term liability at the off-site disposal facility.

Alternative 2 (consolidate/treat low pH soil and construct a cover), was the recommended option based on the alternatives evaluation and comparative analysis. Implementation of this alternative would involve the following actions:

- excavate soil in the contaminated soil area,
- segregate and treat low pH soil,
- consolidate excavated material in the on-site disposal area,
- construct a soil cover,
- vegetate the cover,
- perform quality assurance monitoring during construction,
- perform work under an appropriate health and safety plan, and
- perform long-term groundwater monitoring and cover inspection.

The proposed alternative met regulatory requirements, provided a reasonable cost alternative by containing the contaminated soils on site, and provided protection against excessive potential risk to human health and the environment.

30.6 Off-Site Treatment Technologies and Disposal Options

Often, project space and/or schedule constraints dictate that contaminated soil be removed from a site for treatment and final disposal. For instance, in many urban development projects, construction of basements or subsurface parking levels requires that soil be exported from the site to create space underground. In these cases, the decision to perform off-site treatment to reduce contaminants is based on a number of factors, including: (a) cost of treatment versus the cost of disposing of untreated soil, (b) availability of off-site treatment facilities, and (c) regulatory requirements.

Direct hauling and disposal of untreated soil is the simplest alternative for off-site disposal. However, this may also be highest cost choice, owing to the high disposal fees for contaminated waste, and the often great distance (and high transportation costs) to hazardous or regulated waste disposal sites. Treating soil to reduce contaminant concentrations such that it qualifies for non-hazardous or non-regulated disposal will often reduce costs substantially in the following two ways:

- by taking advantage of lower disposal fees, and a generally wider selection of disposal options available for non-hazardous and non-regulated wastes; and
- by reducing transportation costs in most cases, as non-hazardous and non-regulated landfills are more common than hazardous facilities, and may be located closer to the project site.

Information regarding treatment prior to disposal, cost of disposal, and criteria for disposal can be obtained from landfill operators or regulators who permit landfill operations.

30.6.1 REGULATORY CONSIDERATIONS

In the USA, the off-site handling and disposal of contaminated soil are typically governed by three sets of regulations:

- RCRA waste classification and management requirements,
- state and/or local requirements, and
- health and safety requirements to protect both workers handling the soil and the surrounding environment.

Generally, soil classified for management as hazardous waste may only be treated on-site or off-site at a licensed hazardous waste management facility because regulations typically prohibit placing, storing or handling this soil at an interim site. In some cases, it may be cost effective to treat the soil at the project site to reduce the specific contaminants that render it hazardous, then remove the soil to an interim site for additional treatment, followed by final disposal at a permitted non-hazardous waste disposal facility. Frequently, more treatment options are available for soil that is not considered a hazardous waste for management purposes.

Contaminated soil should be hauled to the off-site disposal facility by an experienced and appropriately licensed hazardous waste transporter. In addition, soil that is managed as a hazardous waste must be manifested in accordance with regulatory requirements. Contaminated soil to be disposed at a licensed off-site facility in the USA as a hazardous or non-hazardous waste must not have free liquids. In the event that free liquids are present, the contaminated soil must be stabilized by addition of an appropriate absorbent or solidifying material prior to disposal. There are also regulatory requirements for the manner in which wastes with free liquids are to be transported to disposal sites for stabilization.

30.6.2 DISPOSAL OPTIONS

Disposal options are discussed below for contaminated soil that will be managed as a hazardous waste and for soil that can be managed as non-hazardous waste. Some options, such as incineration or incorporation into asphalt are options for certain oil-contaminated soils, and may, depending upon the constituents and local regulations, be considered regardless of whether the soil needs to be managed as a hazardous waste. Typically, the engineer develops a range of disposal options and facilities from which the client makes a selection based on consideration of long-term liability.

30.6.2.1 Non-Hazardous Waste Landfill

Non-hazardous contaminated soil can be disposed of in a suitable non-hazardous waste landfill. Most jurisdictions have local criteria governing disposal in non-hazardous waste landfills. For example, in California, Class III (non-hazardous waste) landfills frequently ac-

cept soil that contains less than 100 p.p.m. petroleum hydrocarbons (gasoline/BTEX, diesel, or oil and grease), as long as the soil meets all other disposal requirements. The soil is frequently used as daily cover for household waste. Class II landfills are authorized to accept soils containing up to 1000 p.p.m. of various petroleum hydrocarbons, but typically charge substantially higher disposal fees. While disposal fees vary with location, level of business activity, and the landfill's need for daily cover soil, Class II and III disposal fees are generally much lower than hazardous waste disposal fees.

30.6.2.2 Hazardous Waste Landfill

Soil that must be managed as a hazardous waste must be disposed in a licensed off-site hazardous waste disposal facility, e.g. RCRA Subtitle C facility. This option is relatively expensive, and in the USA, could have long-term liabilities. Typically, this option is only considered in those cases where the contaminated soil must be managed as a hazardous waste.

Depending upon the nature and level of the soil contaminants, treatment may be required prior to land disposal within the landfill. The RCRA Land Disposal Restrictions of 40 CFR 268 (USFR 1994) describe the types and level of treatment required for the hazardous waste based on the nature of the contaminants. This treatment could be conducted either on- or off-site. If on-site treatment is considered, it is recommended that the governing regulatory agencies be contacted regarding permitting and other regulatory considerations.

30.6.2.3 Incineration

Incineration at an off-site facility is typically the most expensive option for management of a contaminated soil. It is a potentially viable option when the contaminated soil contains certain levels of chemicals of particularly high toxicity and potential persistence in the environment (such as PCBs or dioxins). The RCRA Land Disposal Restrictions of 40 CFR 268 (1991) lists those types and levels of constituents in hazardous waste that require incineration. One potential advantage of incineration over disposal in a landfill is that the contaminants are destroyed. Thus, the incineration option could have lower long-term liabilities.

Licensed mobile incinerators are available for destruction of particular contaminants. The costs of on-site incineration through use of such mobile incinerators are typically less than at off-site incineration facilities due to the cost savings in transportation. Depending on the nature of the contamination, other types of mobile thermal treatment short of incineration may be viable. Public groups often oppose on-site incineration and the process can often be difficult to permit.

30.6.2.4 Other Off-Site Management Options

In recent years, several other management options have become available for contaminated soil. These include: (a) recycling of contaminated soils for use as road base, and (b) use as fill on construction sites.

These management options can potentially be cost effective, but are very dependent on the waste characteristics. Long-term liability can be high if the waste composition is highly variable, resulting in undetected levels of certain contaminants.

Processes for recycling of contaminated soil for use as road base are usually proprietary. Their use is generally limited to mildly contaminated soil. Re-use of contaminated soil as road base is cost effective only when the project site is not too distant from the recycling facility.

In some cases, contaminated soil may be treated to such an extent that it can be used as fill on construction sites. This alternative is normally restricted to soil that is not highly contaminated, and is also subject to some practical and political restrictions and potential future liability considerations, even when present legal restrictions do not govern. For

example, it is rarely advisable to use formerly contaminated soil, no matter how extensively treated, as backfill at school, hospital or other public facility sites.

30.6.3 TREATMENT TECHNOLOGIES

30.6.3.1 Aeration

Aeration is the process of reducing the concentrations of organic contaminants in soil by evaporation. The technique is effective on high vapor-pressure organic contaminants, such as gasoline, BTEX and light solvents (VOCs). Under favorable conditions, aeration can reduce VOC concentrations to below detection thresholds, such that the soil may be re-used as on-site backfill or as daily cover in a municipal landfill. Aeration is less effective for diesel, and not effective for heavy hydrocarbons. The efficiency of the aeration process depends on the specific hydrocarbon to be aerated, the characteristics of the soil, ambient temperature and humidity, and space available. Aeration is usually an attractive alternative in cases where the weather is warm and relatively dry, enough space is available to allow the placement of soil in thin lifts, and the soil is relatively porous.

The simplest method of aeration is landfarming, where the contaminated soil is spread in thin lifts and tilled periodically to expose more soil to the air. Aeration can also be accomplished, at higher cost, by injection of air into heaps or windrows of soil. Various methods of covering the soil to retain heat and capture escaping VOCs have also been devised, often involving construction of temporary greenhouse-type enclosures.

In many urban areas, the aeration process is regulated by air quality management authorities. These regulations typically limit the amount of contaminated soil that may be exposed to the air each day on the basis of contaminant concentration. In cases where large volumes of soil are highly contaminated, regulations may render open-air aeration impractical. For example, in the San Francisco Bay Area, soil containing more than 5000 p.p.m. (average) VOCs is effectively precluded from open aeration by rules limiting the quantity of soil to be aerated to 0.1 m^3 per day. In such cases aeration may sometimes be accomplished by constructing temporary enclosures with vapor-trapping equipment or by transporting the contaminated soil to an appropriate interim aeration site.

30.6.3.2 Bioremediation/Landfarming

Off-site bioremediation may be performed at virtually any site that meets the basic physical and regulatory requirements. These typically include:

- sufficient space to spread the soil into workable lifts,
- public access capable of being restricted to reduce human exposure to contaminants, and
- adequate run-off and drainage control is possible so that the nearby environment and subsurface soils are not contaminated by run-off or infiltration from the treatment pile.

Although it is theoretically possible to till soils to a depth of about 1.5 m, bioremediation works most efficiently if the soil is spread in lifts 0.5-cm thick or less.

In some cases, it has been convenient and cost effective to construct a temporary treatment area specifically designed for the bioremediation of soil. Such a treatment area may be constructed at the project site, space permitting, at the landfill or other disposal site, or at an interim site. Public agencies such as redevelopment agencies or large commercial entities with very large or multiple sites to clean up have found it cost effective to construct permanent bioremediation treatment areas that can be used for treating soil from multiple sites.

Stockpiled soil is placed in lifts and tilled periodically to introduce air to the pore spaces. This process is continued until contaminant concentrations have declined sufficiently to permit final disposal of the soil.

Treatment progress is monitored by periodic soil sampling. As with on-site bioremediation, usually closure sampling and analysis is required to demonstrate that the landfarming operation did not contaminate soil beneath the treatment area.

30.6.4 CASE STUDY

A large urban building project provides an example of several on- and off-site treatment techniques that were combined to effect a rapid clean-up of an urban site so that a high-rise office building could be constructed. Contaminated fill containing oil, grease, lead and localized pockets of gasoline was discovered on two city blocks in an urban redevelopment area. The proposed buildings included two basement parking levels, requiring all of the contaminated soil to be removed from the site before construction could begin. The combination of oil, grease and lead in the soil rendered it unsuitable for direct disposal at a Class III (non-hazardous) landfill. A pilot study indicated that the soil was amenable to bioremediation to reduce the concentrations of oil and grease.

Various alternatives for direct disposal of the contaminated fill soil were investigated and rejected because of the high cost and the client's unwillingness to become a generator of hazardous waste. *In situ* bioremediation followed by off-site disposal at a non-hazardous landfill was considered and rejected because the *in situ* process could not be completed quickly enough. Landfarming bioremediation on adjacent vacant lots was also rejected because of lack of space and scheduling constraints. Finally, a program of off-site bioremediation for the fill and on-site aeration of soil containing gasoline was adopted. This program met the client's primary objectives, including:

- removing the contaminated soil from the site quickly so that construction of the building could proceed; and
- avoiding the high transportation and disposal costs and potential long-term liability of placing the soil in a hazardous waste facility, the nearest of which was located over 300 km from the project site.

Beginning in early 1990, approximately 25 000 m^3 of contaminated fill were removed from the site and trucked to a Class III landfill in central California. At the landfill, the soil was placed on a specially prepared treatment area constructed of compacted clay, with *in situ* moisture sensors and perimeter drainage channels. Two summer seasons of bioremediation, including weekly tilling of the soil, were required to reduce the oil and grease concentrations from an average of about 500 p.p.m. to less than 100 p.p.m. Bacterial decomposition of the oil and grease essentially stopped during the winter months, owing to excessively high moisture contents and low temperatures. Upon completion of treatment, the soil was used as daily cover in an asbestos disposal unit at the landfill. Closure sampling was performed in the bioremediation area at the landfill to document that the bioremediation process had not resulted in contamination of the treatment area. The total cost to move, treat and dispose of the soil was approximately US\$75 m^{-3}, which compares favorably with estimated Class I disposal costs exceeding US\$150 m^{-3}.

After the fill containing oil and grease had been removed from the urban site, approximately 1500 m^3 of fill and native soil containing gasoline at concentrations up to 4500 p.p.m were excavated, stockpiled, and then spread out and aerated in accordance with local air quality guidelines. When the average gasoline concentrations had declined to non-detectable levels, the soil was placed in a Class III landfill. Finally, closure sampling of the downtown site was performed to document that the contaminated soils had been successfully removed.

REFERENCES

Aas, G., Lacasse, S., Lunne, T. & Hoeg, K. (1986) Use of in-situ tests for foundation design in clay. In *Proceedings of ASCE Geotechnical Engineering Division Specialty Conference, In-Situ '86, on Use of In-Situ Tests in Geotechnical Engineering*, Virginia Tech, Blacksburg, VA. Geotechnical Special Publication No. 6, American Society of Civil Engineer, Reston, VA, pp. 1–30.

AASHTO T-99 (1990a) *The Moisture-Density Relationship of Soils Using a 5.5. lb [2.5 kg] Rammer and a 12 in. [305 mm] Drop*, Standard Specifications for Transportation Materials and Methods of Sampling & Testing, Part II Tests, 15th Ed, American Association of State Highway Transportation Officials, Washington, DC.

AASHTO T-180 (1990b) *The Moisture–Density Relations of Soils Using a 10 lb (4.54 kg) Rammer and a 18 in. (457 mm) Drop*, Standard Specifications for Transportation Materials & Methods of Sampling & Testing, Part II Tests, 15th Ed, American Association of State Highway & Transportation Officials, Washington, DC.

AASHTO (1993) *AASHTO Guide for Design of Pavement Structures*, American Association of State Highway & Transportation Officials, Washington, DC.

AASHTO (1994) *LRFD Bridge Design Specifications, SI Units*, American Association of State of Highway & Transportation Officials, Washington, DC.

AASHTO (1997) *Specification for Highway Bridges*, Interim Report, American Association of State Highway & Transportation Officials, Washington DC.

AASHTO (1998) *DARWin*, American Association of State Highway & Transportation Officials, Washington, DC.

Abdul, A.S., Kia, S.F. & Gibson, T.L. (1989) Limitations of monitoring wells for the detection and quantification of petroleum products in soils and aquifers. *Ground Water Monitoring Review*, **9**(2): 90–99.

Abdul, A.S., Gibson, T.L. & Rai, D.N. (1990) Laboratory study of the flow of some organic solvents and their aqueous solutions through bentonite and kaolin clays. *Ground Water*, **28**(4): 524–533.

Aboshi, H. & Suematsu, N. (1985) The state of the art on sand compaction pile method. In *Soil Improvement Methods, Proceedings of the Third International Geotechnical Seminar*, Nanyang Technological Institute, Singapore.

Abou-matar, H. & Goble, G.G. (1997) SPT dynamic analysis and measurements. *ASCE Journal of Geotechnical & Geoenvironmental Engineering*, Reston, VA, **123**(10): 921–928.

Abrahamson, N.A. & Shedlock, K.M. (1997) Some comparisons between recent ground motion relations. *Seismological Research Letters*, **68**(1): 9–23.

Abrahamson, N.A. & Silva, W.J. (1997) Equations for estimating horizontal response spectra and peak acceleration from western North American earthquakes: a summary of recent work. *Seismological Research Letters*, **68**(1): 94–127.

Abramson, L.W. (1985) Rock wedge stability analysis on a personal computer. In *Proceedings of the 26th US Symposium on Rock Mechanics*, Rapid City, pp. 675–682.

Abramson, L.W. (1997) Ground treatment. Section 3.0 In Schaefer, V.R. (Ed.) *Ground Improvement, Ground Reinforcement, & Ground Treatment: Developments 1987–1997*, Geotechnical Special Publication No. 69, American Society of Civil Engineers, ASCE Press, Reston, VA, pp. 306–371.

Acar, Y.B. & Seals, R.K. (1984) Clay barrier technology for shallow land waste disposal facilities. *Hazardous Waste* **1**: 167–181.

Acar, Y.B., Hamidon, A., Field, S.D. & Scott, L. (1985) The effect of organic fluids on hydraulic conductivity of compacted kaolinite in hydraulic barriers in soil and rock. In Johnson, A.I., Frobel, R.K., Cavalli, N.J. & Petersson, C.B., (Eds) *ASTM STP 874*, American Society for Testing Materials, West Conshohocken, PA, pp. 177–187.

Achilleous, E. (1988) PC STABL5M, User Manual, *Informational Report*, School of Civil Engineering, Purdue University, West Lafayette, 132 p.

ACPA (1992) *Design of Concrete Pavements for City Streets*, American Concrete Pavement Association, Skokie, IL.

Adachi, T., Kimura, M. & Zhang, F. (1994) Analysis of ultimate behaviour of lateral loading of cast-in-place concrete piles by 3-dimensional elasto-plastic FEM. In *Proceedings of the Eighth International Conference on Computer Methods and Advances in Geomechanics*, Morgantown.

Adachi, T., Liu, J., Koike, A. & Zhang, F. (1996) Finite element analysis of Biot's consolidation in slope excavation based on a constitutive model with strain softening. In *Proceedings of the Seventh International Symposium on Landslides*, Trondheim, Vol. 2, pp. 1131–1136.

Adachi, T., Oka, F. & Zhang, F. (1998) An elasto-viscoplastic constitutive model with strain softening. *Soils and Foundations*, **38**(2): 27–35.

Adams, J.I. (1961) Laboratory compression tests on peat. In *Proceedings of the Seventh Muskeg Research Conference*, NRC Technical Memorandum 41, Ottawa, ON, Canada.

Adams, J.I. (1965) The engineering behaviour of a Canadian muskeg. In *Proceedings of the Sixth International Conference on Soil Mechanics & Foundation Engineering*, Montreal, Vol. 1, pp. 3–7.

AERIS Software Inc. (1990) AERIS Model Version 3.0 Technical Manual, Supply & Services Canada, Contract 09SE-DE405-6-6586.

Ahlvin, R. (1991) Origin of developments for structural design of pavements. Technical Report GL9126, US Army Corps of Engineers, Waterways Experiment Station, Vicksburg, MI.

Ahlvin, R.G. (1971). Multiple-wheel heavy gear load pavement tests, Technical Report S-17-17, Vol. 1, U.S. Army Corps Engineers, Waterways Experimental Station, Vicksburg, MS.

Ahmed, S., Lacroix, Y. & Steinbach, J. (1975) Pumping tests in an unconfined aquifer. In *Proceedings of ASCE Geotechnical Engineering Division Specialty Conference on In-Situ Measurement of Soil Properties*, North Carolina State University, Raleigh, NC, June 1–4, 1975, Vol. 1, pp. 1–21.

Ahuja, L.R., Naney, J.W. & Williams, R.D. (1985) Estimating soil–water characteristics from simpler properties and limited data. *Soil Science of America Journal*, **49**: 1100–1105.

Airey, D.W. & Wood, D.M. (1987) An evaluation of direct simple shear tests on clay. *Géotechnique*, **37**(1): 25–35.

AISI (1990) *Modern Sewer Design*, 2nd Edn, American Iron & Steel Institute, Washington, DC.

Aitchison, J. (1955) On the distribution of a positive random variable having a discrete probability mass at the origin. *Journal of American Statistical Association*, **50**: 901–908.

Ajaz, A. & Parry, R.H.G. (1975) Stress–strain behavior of two compacted clays in tension and compression. *Géotechnique*, **25**(3): 495–512.

Ajaz, A. & Parry, R.H.G. (1975) Analysis of bending stresses in soil beams. *Géotechnique*, **25**(3): 586–591.

Ajaz, A. & Parry, R.H.G. (1976) Bending test for compacted clays. *Journal of Geotechnical Engineering Division, ASCE*, Reston, VA, **102**(9): 929–943.

Akagi, T. (1979) Consolidation caused by mandrel-driven sand drains. In *Proceedings of the Sixth Asian Regional Conference on Soil Mechanics & Foundation Engineering*, Singapore, Vol. 1, pp. 125–128.

Aki, K. (1988) Local site effects on strong ground motion, In Van Thun, J.L. (Ed.), *Earthquake Engineering & Soil Dynamic, Recent Advances in Ground-Motion Evaluation*, Geotechnical Special Publication No. 20, American Society of Civil Engineers, Reston, VA, pp. 103–155.

Alberro, J. (1979) Stabilité à long terme des excavations dans la ville de Mexico. *International Symposium of Soil Mechanics*, Oaxaca, Mexico, Vol. 1 pp. 125–143.

Albertsen, M., and an ad hoc Task Force (1986) Beurteilung und Behandlung von Mineralölschadensfallen im Hinblick auf den Grundwasserschutz, Jeil 1, Die wissenschaftlichen Grundlagen zum Verständnis des Verhaltens von Mineralöl im Untergrund. Federal Office of the Environment, LTw S no. 20, 178 p.

Aldrich, H.P. (1956) Frost penetration below highway and airfield pavements. *US Highway Research Board, Bulletin*, **135**: 24–149.

Aller, L., Bennett, T.W., Hackett, G., Petty, R.J., Lehr, J.H., Sedoris, H., Nielsen, D.M. & Denne, J.E. (1989) *Handbook of Practices for the Design and Installation of Ground-Water Monitoring Wells*, EPA/600/4-89/034. National Water Well Association.

Al-Sanad, H. & Aggour, M.S. (1984) Dynamic soil properties from sinusoidal and random vibrations. In *Proceedings of the Eighth World Con-*

ference on Earthquake Engineering, San Francisco, pp. 15–22.

Ambraseys, N.N. (1988) Engineering seismology. *Earthquake Engineering & Structural Dynamics*, **17**: 1–105.

Amos, E.M., Blakeway, D. & Warren, C.D. (1986) Remote sensing techniques in civil engineering surveys. In Hawkins, A.B. (Ed.) *Site Investigation Practice: Assessing BS 5930*, Engineering Geology Special Publication No. 2, Geological Society, London, England, pp. 119–124.

Anagnostou, G. & Kovari, K. (1996) Face stability conditions with earth-pressure-balance shields. *Tunnelling & Underground Space Technology*, **11**(2): 165–173.

Andersland, O.B. & Anderson, D.M. (1978) *Geotechnical Engineering for Cold Regions*, McGraw-Hill, New York.

Andersland, O.B. & Ladanyi, B. (1994) *An Introduction to Frozen Ground Engineering*, Chapman & Hall, New York.

Anderson, D.M. & Morgenstern, N.R. (1973) Physics, chemistry and mechanics of frozen ground. In *Proceedings of The Second International Conference on Permafrost*, Yakutsk, USSR, pp. 257–288.

Anderson, D.M. & Tice, A.R. (1972) Predicting unfrozen water contents in frozen soils from surface area measurements. *Highway Research & Record* **373**: 12–18.

Anderson, J.E., Nowak, R.S., Ratzlaff, T.D. & Markham, O.D. (1993) Managing soil moisture on waste burial sites in arid regions. *Journal of Environmental Quality*, **22**: 2–69.

Anderson, J.N. & Lade, P.V. (1981) The expansion index test. *Geotechnical Testing Journal*, **4**(2): 58–67.

Anderson, L.G. (1968) A modern approach to overburden drilling. *Western Miner*, November.

Anderson, M.P. (1984) Movement of contaminants in groundwater: groundwater transport-advection and dispersion. In National Research Council (U.S.) Geophysics Study Committee (Eds.) *Groundwater Contamination*, NRC Studies in Geophysics. National Academy Press, Washington, DC, pp. 37–45.

Anderson, M.P. & Woessner, W.W. (1992) *Applied Groundwater Modeling Simulation of Flow and Advective Transport*, Academic Press, San Diego, CA.

Andresen, A., Berre, T., Kleven, A. & Lunne, T. (1979) Procedures used to obtain soil parameters for foundation engineering in the North Sea. *Marine Geotechnology*, **3**(3): 1–18.

API (1984) *Recommended Practice for Planning, Designing and Constructing Fixed Offshore Platforms*, 14th Edn. APIRP2A, American Petroleum Institute, Dallas, TX.

API (1988) *Phase Separated Hydrocarbon Contaminant Modeling for Corrective Action*, Publication American Petroleum Institute, 4474, Washington, DC.

API (1993) *Recommended Practice for Planning Designing and Constructing Fixed Offshore Platforms*, American Petroleum Institute, Dallas, TX.

API (1994) *Decision Support System for Exposure and Risk Assessment*, Version 1.0, American Petroleum Institute, Nassau, New York.

Arango, I. (1996) Magnitude scaling factors for soil liquefaction evaluations. *Journal of Geotechnical Engineering, ASCE*, Reston, VA, **122**(11): 929–936.

Arias, A., Sanchez-Sesma, F.J. & Ovando-Shelley, E. (1981) A simplified elastic model for seismic analysis of earth-retaining structures with limited displacements, In *Proceedings of The International Conference on Recent Advances in Geotechnical Earthquake Engineering & Soil Dynamics*, St Louis, MO, Vol. I, 235– 240.

Arman, A. (1978) Current practices in the treatment of soft foundations. In *Soil Improvement, History, Capabilities, and Outlook*, Report by Committee on Placement and Improvement of Soils, Geotechnical Engineering Division, American Society of Civil Engineers, Reston, VA, pp. 30–51.

Armitage, P. & Doll, R. (1961) Stochastic model for carcinogenisis. In Lecam, W. & Heyman, J. (Eds) *Proceedings of the Fourth Berkeley Symposium on Mathematical Statistics & Probability*, Vol. 4, University of California Press, Berkeley, CA.

Arnold, J.G., Williams, J.R., Nicks, A.D. & Sammons, N.B. (1989) *SWRRB, a Simulator for Water Resources in Rural Basins*, Agricultural Research Service, USDA, Texas A&M University Press, College Station, TX.

Arya, L.M. & Paris, J.F. (1981) A physicoempirical model to predict the soil moisture characteristic from particle size distribution and bulk density data. *Soil Science of America Journal*, **45**: 1023–1030.

Arya, S., O'Neil, M. & Pincus, G. (1979) *Design of Structures and Foundations for Vibrating Machines*, Gulf Publishing, Houston, TX.

AS 2870.2 (1990) *Residential Slabs and Footings, Part 2: Guide to Design by Engineering Principles*, Australian Standards, Sydney, Australia.

Asante-Duah, D.K. (1993) *Hazardous Waste Risk Assessment*, Lewis, Boca Raton, FL.

Asaoka, A. (1978) Observational procedure of settlement prediction. *Soils & Foundations*, **18**(4): 87–101.

ASCE (1974) *Subsurface Exploration for Underground Excavation & Heavy Construction. Proceedings of the Geotechnical Engineering Division Specialty Conference*, New England College, Henniker, NH, American Society of Civil Engineers, Reston, VA.

ASCE (1975) *In-Situ Measurement of Soil Properties. Proceedings of ASCE Geotechnical Engineering Division Specialty Conference*, North Carolina State University, Raleigh, NC, June 1–4, American Society of Civil Engineers, Reston, VA.

ASCE (1976) *Subsurface Investigation for Design & Construction of Foundations of Buildings*. ASCE Manuals & Reports on Engineering Practice No. 56, American Society of Civil Engineers, Reston, VA.

ASCE (1978) *Site Characterization & Exploration. Proceedings of the Geotechnical Engineering Division Specialty Conference*, Northwestern University, Evanston, IL, American Society of Civil Engineers, Reston, VA.

ASCE (1986) *Use of In-Situ Tests in Geotechnical Engineering. Proceedings of the ASCE Geotechnical Engineering Division Specialty Conference*, Virginia Tech, Blacksburg, Virginia. Geotechnical Special Publication No. 6, American Society of Civil Engineers, Reston, VA.

ASCE (1995) *Rock Foundations*. Technical Engineering and Design Guides as adapted from the US Army Corps of Engineers, No. 16, American Society of Civil Engineers, Reston, VA.

ASCE (1997) Geotechnical baseline reports for underground construction. In Essex, R.J. (ed.) *Guidelines & Practices*, American Society of Civil Engineers, Reston, VA.

Aspe, J.I. (1988) Polyethylene resins for geomembrane applications. In Koerner, R.M. (ed.) *Geosynthetics Research Institute Conference on the Durability & Aging of Geosynthetics*, Elsevier Applied Science, London, England, pp. 159–176.

ASTM A716 Specification for ductile iron culvert pipe, American Society for Testing and Materials, West Conshohocken, PA.

ASTM A746 Specification for ductile iron gravity sewer pipe, American Society for Testing and Materials, West Conshohocken, PA.

ASTM A796 Standard practice for structural design of corrugated steel pipe, pipe-arches, and arches for storm and sanitary sewers and other buried applications, American Society for Testing and Materials, West Conshohocken, PA.

ASTM A798 Standard practice for installing factory-made corrugated steel pipe for sewers and other applications, American Society for Testing and Materials, West Conshohocken, PA.

ASTM C76 Specification for reinforced concrete culvert, storm drain, and sewer pipe, American Society for Testing and Materials, West Conshohocken, PA.

ASTM C78 *Standard Test Method for Flexural Strength of Concrete (Using Simple Beam With Third-Point Loading)*, American Society for Testing & Materials, West Conshohocken, PA, *http://www.astm.org, Annual Book of ASTM Standards* 4.02.

ASTM C14 Specification for concrete sewer, storm drain, and culvert pipe, American Society for Testing and Materials, West Conshohocken, PA.

ASTM C88 *Standard Test Method for Soundness of Aggregates By Use of Sodium Sulfate or Magnesium Sulfate*, American Society for Testing & Materials, West Conshohocken, PA.

ASTM C131 *Standard Test Method for Resistance to Degradation of Small-Size Coarse Aggregate By Abrasion and Impact in the Los Angeles Machine*. American Society for Testing & Materials, West Conshohocken, PA.

ASTM C123 *Standard Test Method for Lightweight Pieces in Aggregate*. American Society for Testing & Materials, West Conshohocken, PA.

ASTM C301 Test method for vitrified clay pipe, American Society for Testing and Materials, West Conshohocken, PA.

ASTM C655 Standard specification for reinforced concrete D-load culvert, storm drain, and sewer pipe, American Society for Testing and Materials, West Conshohocken, PA.

ASTM D413 *Test Methods for Rubber Property-Adhesion to Flexible Substrate*, West Conshohocken, PA.

ASTM D422-63 *Standard Test Method for Particle-Size Analysis of Soils*, American Society for Testing & Materials, West Conshohocken, PA, *http://www.astm.org, Annual Book of ASTM Standards* 04.08, *Soil & Rock* (I).

ASTM D427-93 *Standard Test Method for Shrinkage Factors of Soils by Mercury Method*, American Society for Testing & Materials, West Conshohocken, PA.

ASTM D638 *Test Method for Tensile Properties of Plastics*, West Conshohocken, PA.

ASTM D698 *Standard Test Methods for Moisture–Density Relations of Soils & Soil Aggregate Mixtures Using 5.5-lb (2.49 kg) Rammer and 12 in (305 mm) Drop* 4.08, American Society for Testing & Materials, West Conshohocken, PA.

ASTM D698-91 *Standard Test Method for Laboratory Compaction Characteristics of Soil Using Standard Effort (12,400 ft-lbf/ft^3* (600 kN.m/m^3)), American Society for Testing & Materials, West Conshohocken, PA.

ASTM D 751 *Test Methods for Coated Fabrics*, West Conshohocken, PA.

ASTM D854-92 *Standard Test Method for Specific Gravity of Soils*, American Society for Testing & Materials, West Conshohocken, PA.

ASTM D882 *Test Methods for Tensile Properties of Thin Plastic Sheeting*, West Conshohocken, PA.

ASTM D1067-92 *Standard Test Methods for Acidity or Alkalinity of Water*, 04.08, American Society for Testing & Materials, West Conshohocken, PA.

ASTM D1194-72 *Standard Test Method for Bearing Capacity of Soil for Static Load and Spread Footings*, 04.08, American Society for Testing & Materials, West Conshohocken, PA.

ASTM D1238 *Standard Test Method for Flow Rates of Thermoplastics by Extrusion Plastometer*, American Society for Testing & Materials, West Conshohocken, PA.

ASTM D1505 *Standard Test Method for Density of Plastics by the Density-Gradient Technique*, American Society for Testing & Materials, West Conshohocken, PA.

ASTM D1556 *Standard Test Method for Density and Unit Weight of Soil in Place by the Sand-Cone Method*, American Society for Testing & Materials, West Conshohocken, PA.

ASTM D1557 *Standard Test Methods for Moisture-Density Relations of Soils and Soil–Aggregate Mixture Using 10-lb (4.54 kg) Rammer and 18 in (457 mm) Drop*, American Society for Testing & Materials, West Conshohocken, PA.

ASTM D1557-91 *Standard Test Method for Laboratory Compaction Characteristics of Soil Using Modified Effort (56,000 ft-lbf/ft^3* (2,700 kN·m/m^3)), American Society for Testing & Materials, West Conshohocken, PA.

ASTM D1883 *Standard Test Method for Bearing Ratio of Laboratory-Compacted Soils*, 4.08, American Society for Testing & Materials, West Conshohocken, PA.

ASTM D2167 *Standard Test Method for Density and Unit Weight of Soil in Place by the Rubber Balloon Method*, American Society for Testing & Materials, West Conshohocken, PA.

ASTM D2216 *Standard Test Method for Laboratory Determination of Water (Moisture) Content of Soil and Rock*, American Society for Testing & Materials, West Conshohocken, PA.

ASTM D2321 Practice for underground installation of thermoplastic pipe for sewers and other gravity-flow applications, American Society for Testing and Materials, West Conshohocken, PA.

ASTM D2412 Standard test method for determination of external loading characteristics of plastic pipe by parallel plastic plate loading, American Society for Testing and Materials, West Conshohocken, PA.

ASTM D2419 *Standard Test Method for Sand Equivalent Value of Soils and Fine Aggregate*, 4.08, American Society for Testing & Materials, West Conshohocken, PA.

ASTM D2434-68 *Standard Test Method for Permeability of Granular Soils (Constant Head)*, American Society for Testing & Materials, West Conshohocken, PA.

ASTM D2487-93 *Standard Test Method for Classification of Soils for Engineering Purposes*, American Society for Testing & Materials, West Conshohocken, PA.

ASTM D2664-86 *Test Method for Triaxial Compressive Strength of Undrained Rock Core Specimens Without Pore Pressure Measurements*, American Society for Testing & Materials, West Conshohocken, PA.

ASTM D2922 *Standard Test Methods for Density of Soil and Soil–Aggregate in Place by Nuclear Methods (Shallow Depth)*, American Society for Testing & Materials, West Conshohocken, PA.

ASTM D2936-84 *Test Method for Direct Tensile Strength of Intact Rock Core Specimens*, American Society for Testing & Materials, West Conshohocken, PA.

ASTM D2938-86 *Test Method for Unconfined Compressive Strength of Intact Rock Core Specimens*, American Society for Testing & Materials, West Conshohocken, PA.

ASTM D2974-87 *Standard Test Methods for Moisture, Ash, and Organic Matter of Peat and Other Organic Soils*, American Society for Testing & Materials, West Conshohocken, PA.

ASTM D3017 *Standard Test Method for Water Content of Soil and Rock in Place by Nuclear Methods (Shallow Depth)*, 04.08, American Society for Testing & Materials, West Conshohocken, PA.

ASTM D3034 Specification for Type PSM poly (vinyl chloride) (PVC) sewer pipe and fittings, American Society for Testing and Materials, West Conshohocken, PA.

ASTM D3080 *Standard Test Method for Direct Shear Test of Soils Under Consolidated Drained Conditions*, 04.08, American Society for Testing & Materials, West Conshohocken, PA.

ASTM D3083 *Specification for Flexible Poly (Vinyl Chloride) Plastic Sheeting for Pond, Canal and Reservoir Lining*, West Conshohocken, PA.

ASTM D3262 Specification for "Fiberglass" (glass-fiber-reinforced thermosetting-resin) sewer pipe, American Society for Testing and Materials, West Conshohocken, PA.

ASTM D3895 *Standard Test Methods for Oxidative-Induction Time of Polyolefins by Differential Scanning Calorimetry*, 04.08, American Society for Testing & Materials, West Conshohocken, PA.

ASTM D4123 *Standard Test Method for Indirect Tension Test for Resilient Modulus of Bituminous Mixtures*, 04.03, American Society for Testing & Materials, West Conshohocken, PA.

ASTM D4253-91 *Standard Test Methods for Maximum Index Density and Unit Weight of Soils Using a Vibratory Table*, American Society for Testing & Materials, West Conshohocken, PA.

ASTM D4254-91 *Standard Test Methods for Minimum Index Density and Unit Weight of Soils and Calculation of Relative Density*, American Society for Testing & Materials, West Conshohocken, PA.

ASTM D4318-95 *Standard Test Method for Liquid Limit, Plastic Limit, and Plasticity Index of Soils*, American Society for Testing & Materials, West Conshohocken, PA.

ASTM D4355 *Standard Test Method for Deterioration of Geotextiles from Exposure to Ultraviolet Light and Water (Xenon-Arc Type Apparatus)*, American Society for Testing & Materials, West Conshohocken, PA.

ASTM D4394 *Test Method for Determining the* in situ *Modulus of Deformation of Rock Mass Using the Rigid Plate Loading Method*, American Society for Testing & Materials. West Conshohocken, PA.

ASTM D4395 *Test Method for Determining the* in situ *Modulus of Deformation of Rock Mass Using the Flexible Plate Loading Method*, American Society for Testing & Materials, West Conshohocken, PA

ASTM D4437 *Practice for Determining the Integrity of Field Seams Used in Joining Flexible Polymeric Sheet Geomembranes*, West Conshohocken, PA.

ASTM D4491 *Standard Test Method for Water Permeability of Geotextiles by Permittivity*, American Society for Testing & Materials, West Conshohocken, PA.

ASTM D4506 *Test Method for Determining the* in situ *Modulus of Deformation of Rock Mass Using a Radical Jacking Test*, American Society for Testing & Materials, West Conshohocken, PA.

ASTM D4595 *Standard Test Method for Tensile Properties of Geotextiles by the Wide-Width Strip Method*, American Society for Testing & Materials, West Conshohocken, PA.

ASTM D4643 *Standard Test Method for Determination of Water (Moisture) Content of Soil by the Microwave Oven Method*, American Society for Testing & Materials, West Conshohocken, PA.

ASTM D4751 *Standard Test Method for Determining Apparent Opening Size of a Geotextile*, American Society for Testing & Materials, West Conshohocken, PA.

ASTM D4791 *Standard Test Method for Flat or Elongated Particles in Coarse Aggregate*, 4.03, American Society for Testing & Materials, West Conshohocken, PA.

ASTM D4829-95 *Standard Test Method for Expansion Index of Soils*, American Society for Testing & Materials, West Conshohocken, PA.

ASTM D4885 *Standard Test Method for Determining Performance Tensile Strength of Geomembranes Using Wide Strip Testing*, American Society for Testing & Materials, West Conshohocken, PA.

ASTM D4971 *Test Method for Determining the* in situ *Modulus of Deformation of Rock Using the Diametrically Loaded 76-mm (3-in) Borehole Jack*, 04.09, American Society for Testing & Materials, West Conshohocken, PA.

ASTM D5084 *Standard Test Method for Mea-*

surement of a Hydraulic Conductivity of Saturated Porous Materials Using a Flexible Wall Permeameter, American Society for Testing & Materials, West Conshohocken, PA.

ASTM D5092 *Standard Practice for Design and Installation of Ground Water Monitoring Wells in Aquifer*, American Society for Testing & Materials, West Conshohocken, PA.

ASTM D5101 *Standard Test Method for Measuring the Soil–Geotextile System Clogging Potential by the Gradient Ratio*, American Society for Testing & Materials, West Conshohocken, PA.

ASTM D5199 *Standard Test Method for Measuring Nominal Thickness of Geotextiles & Geomembranes*, American Society for Testing & Materials, West Conshohocken, PA.

ASTM D5208 *Standard Practice for Operating Fluorescent Ultraviolet (UV) Condensation Apparatus for Exposure of Photo-degradable Plastics*, American Society for Testing & Materials, West Conshohocken, PA.

ASTM D5261 *Standard Test Method for Measuring Mass per Unit Area of Geotextiles*, American Society for Testing & Materials, West Conshohocken, PA.

ASTM D5321 *Standard Test Method for Determining the Coefficient of Soil and Geosynthetic or Geosynthetic and Geosynthetic Friction by the Direct Shear Method*, American Society for Testing & Materials, West Conshohocken, PA.

ASTM D5322 *Standard Practice for Immersion Procedures for Evaluating the Chemical Resistance of Geosynthetics to Liquids*, American Society for Testing & Materials, West Conshohocken, PA.

ASTM D5397 *Standard Test Method for Evaluation of Stress Crack Resistance of Polyolefin Geomembranes using Notched Constant Tension Load Test*, American Society for Testing & Materials, West Conshohocken, PA.

ASTM D5496 *Standard Practice for Field Immersion Testing of Geosynthetics*, American Society for Testing & Materials, West Conshohocken, PA.

ASTM D5617 *Standard Test Methods for Multi-Axial Tension Test for Geosynthetics*, American Society for Testing & Materials, West Conshohocken, PA.

ASTM D5747 *Standard Practice for Tests to Evaluate the Chemical Resistance of Geomembranes to Liquids*, American Society for Testing & Materials, West Conshohocken, PA.

ASTM D5885 *Standard Test Method for Oxidative Induction Time of Polyolefin Geosynthetics by High-Pressure Differential Scanning Calorimetry*, American Society for Testing & Materials, West Conshohocken, PA.

ASTM D5887 *Standard Test Method for Measurement of Index Flux Through Saturated Geosynthetic Clay Liner Specimens Using a Flexible Wall Permeameter*, American Society for Testing & Materials, West Conshohocken, PA.

ASTM D5890 *Standard Test Method for Swell Index of Clay Mineral Component of Geosynthetic Clay Liners*, American Society for Testing & Materials, West Conshohocken, PA.

ASTM D5993 *Standard Test Method for Measuring the Mass Per Unit Area of GCL*, American Society for Testing & Materials, West Conshohocken, PA.

ASTM D5994 *Standard Test Method for Measuring the Core Thickness of Textured Geomembranes*, American Society for Testing & Materials, West Conshohocken, PA.

ASTM E11 *Wire–Cloth Sieves for Testing Purposes*, American Society for Testing & Materials, West Conshohocken, PA, Website: *http://www.astm.org, Annual Book of ASTM Standards* Soil & Rock (I).

ASTM E96 *Standard Test Method for Water Vapor Transmission of Materials*, American Society for Testing & Materials, West Conshohocken, PA.

ASTM E1527-93 *Standard Practice for Environmental Site Assessments: Phase I Environmental Site Assessment Process*, American Society for Testing & Materials, West Conshohocken, PA.

ASTM F679 Specification for Poly(Vinyl Chloride) (PVC) Large-Diameter Plastic Gravity Sewer Pipe and Fittings, American Society for Testing and Materials, West Conshohocken, PA.

ASTM F714 Standard specification for polyethylene (PE) plastic pipe (SDR-PR) based on outside diameter, American Society for Testing and Materials, West Conshohocken, PA.

ASTM F810 Specification for smoothwall polyethylene (PE) pipe for use in drainage and waste disposal aborption fields, American Society for Testing and Materials, West Conshohocken, PA.

ASTM F892 Specification for polyethylene (PE) corrugated pipe with smooth interior and fittings, American Society for Testing and Materials, West Conshohocken, PA.

ASTM F894 Specification for polyethylene (PE) large diameter profiled wall sewer and drain pipe, American Society for Testing and Materials, West Conshohocken, PA.

ASTM F949 Specification for poly(vinyl chloride) (PVC) corrugated sewer pipe with smooth interior and fittings, American Society for Testing and Materials, West Conshohocken, PA.

ASTM (1988) *Vane Shear Strength Testing in Soils: Field and Laboratory Studies*, Special Technical Publication 1014, Richards, A.F. (Ed.), American Society for Testing & Materials, West Conshohocken, PA.

ASTM (1996) Standard Guide for Risk-Based Corrective Action Applied at Petroleum Release Sites. E1739-95 Annual Book of ASTM Standards, Vol. 11.04, American Society for Testing and Materials, West Conshohocken, PA.

ASTM (1997a) *Environmental Sampling*, 2nd Edn, ASTM Standards, Committee D-18 on Soil & Rock, American Society for Testing & Materials, West Conshohocken, PA.

ASTM (1997b) *Environmental Site Characterization*, ASTM Standards, Committees D-18 on Soil & Rock, D-19 on Water, D-34 on Waste Management, E-47 on Biological Effects and Environmental Fate and E-50 on Environmental Assessment, American Society for Testing & Materials, West Conshohocken, PA.

AS 3725 Loads on buried concrete pipes, Standards Australia International Ltd, Sydney.

AS 46060 Loads on buried vitrified clay pipes, Standards Australia International Ltd, Sydney.

AS/NZS 2566.1 Buried flexible pipeline—structural design, Standards Australia International Ltd, Sydney.

Atkinson, J.H. & Bransby, P.L. (1978) *The Mechanics of Soils–An Introduction to Critical State Soil Mechanics*, McGraw-Hill, Maidenhead, England.

Atkinson, J.H. & Mair, R.J. (1981) Soil mechanics aspects of soft ground tunnelling. *Ground Engineering*, **14**(5): 20–28.

Attewell, P.B. & Farmer, I.W. (1976) *Principles of Engineering Geology*, Chapman & Hall, London, England.

Aubery, D. & Chapel, F. (1981) 3-D dynamic analysis of groups of piles and comparisons with experiments. In *Transactions of the Sixth International Conference on Structural Mechanics in Reactor Technology*, Paris.

Augello, A.J., Matasovic, N., Bray, J.D., Kavazanjian, E., Jr., & Seed, R.B. (1995) Evaluation of solid waste landfill performance during the Northridge earthquake, In *Earthquake Design & Performance of Solid Waste Landfills*, Yegian, M.K. and Finn, W.D.L. (Eds.) Geotechnical Special Publication No. 54, American Society of Civil Engineers, Reston, VA, pp. 17–50.

Augello, A.J., Bray, J.D., Abrahamson, N.A., & Seed, R.B. (1998) Dynamic properties of solid waste based on back-analyses of OII landfill. *Journal of Geotechnical Engineering, ASCE*, Reston, VA, **124**(3): 211–222.

August, H. & Tatzky, R. (1984) Permeability of commercially available polymeric liners for hazardous landfill leachate organic constituents. In *Proceedings of International Conference on Geomembranes*, June 20–24, Denver, CO, Vol. I, Industrial Fabrics Association International, Roseville, MN, pp. 163–168.

Avery, S. (1951) Analysis of groundwater lowering adjacent to open water. *Journal of the Soil Mechanics & Foundation Division, ASCE*, Reston, VA, **77**(106): 1–16.

AWWA C905 Standard for PVC water transmission pipe (nominal diameters 14 in. through 36 in.), American Waterworks Association, Denver.

Badu-Tweneboah, K., Giroud, J.P., Carlson, D.S. & Schmertmann, G.R. (1997) Discussion of "Field evaluation of protective covers for landfill geomembrane liners under construction loading" by Reddy *et al.*, *Geosynthetics International*, **4**(5): 543–544.

Badu-Tweneboah, K., Giroud, J.P., Carlson, D.S. & Schmertmann, G.R. (1998) Evaluation of the effectiveness of HDPE geomembrane liner protection. In Rowe, R.K. (Ed.) *Proceedings of the Sixth International Conference on Geosynthetics*, Vol. 1, March 1998, Atlanta, GA, Industrial Fabrics Association International, Roseville, MN, pp. 279–284.

Badv, K. & Rowe, R.K. (1996) Contaminant transport through a soil liner underlain by an unsaturated stone collection layer. *Canadian Geotechnical Journal*, **33**(2): 416–430.

Baez, J.I. (1995) *PhD thesis*, University of Southern California, Los Angeles.

Baguelin, F. & Frank, R. (1979) Theoretical studies of piles using the finite element method. In *Proceedings of the Conference on Numerical Methods in Offshore Piling*, London, Institution of Civil Engineers, Paper No. 11.

Baguelin, F., Jezequel, J.F., LeMee, E. & LeMelhaute, A. (1972) Expansion of cylindrical probes in cohesive soils. *ASCE Journal of Soil*

Mechanics & Foundations Division, Reston, VA, **98**(11): 1129–1142.

Baguelin, F., Jezequel, J.F. & Shields, D.H. (1978) *The Pressuremeter & Foundation Engineering*, Trans Tech Publications, Clausthal, Germany.

Baker, M.J., Blowes, D.W. & Ptacek, C.J. (1997) Phosphorus adsorption and precipitation in a permeable reactive wall: applications for wastewater disposal systems. In *Proceedings of the 1997 International Containment Technology Conference & Exhibition*, February 10–12, St Petersburg, FL, pp. 697–703.

Baker, T.L. & Marienfeld, M.L. (1995) Correlation of outdoor exposure to xenon-arc weatherometer exposure. In *Geosynthetics '95 Conference, Proceedings*, Nashville, TN, IFAI, Roseville, MN, pp. 829–840.

Baker, W.H. (1982) Planning and performance of structural chemical grouting. In Baker, W.H. (Ed.) *Grouting in Geotechnical Engineering*, Proceedings of the Conference, New Orleans, American Society of Civil Engineers, Reston, VA, pp. 515–540.

Baker, W.H., Cording, E.J. & MacPherson, H.H. (1983) Compaction grouting to control ground movements during tunneling. *Underground Space*, **7**: 205–212.

Balaam, B.E., Poulos, H.G. & Brown, P.T. (1977) Settlement analyses of soft clays reinforced with granular piles. In *Proceedings of the Fifth Southeast Asian Conference on Soils Engineering*, Bangkok, pp. 81–92.

Banerjee, P.K. (1978) Analysis of axially and laterally loaded pile groups. In Scott, C.R. (Ed.) *Developments in Soil Mechanics*, Applied Science, London, England, Ch. 9.

Banerjee, P.K. & Davies, T.G. (1977) Analysis of pile groups embedded in Gibson soil. In *Proceedings of the Ninth International Conference on Soil Mechanics & Foundation Engineering*, Vol. 1, pp. 381–386.

Banerjee, S. (1984) Solubility of organic mixtures in water. *Environmental Science Technology*, **18**(8): 587–591.

Bara, J.P. (1978) Collapsible soils and their stabilization. *Soil Improvement, History, Capabilities, & Outlook*, Report by Committee on Placement & Improvement of Soils, Geotechnical Engineering Division, American Society of Civil Engineers, ASCE Press, Reston, VA, pp. 141–152.

Barbaro, J.R., Barker, J.F., Lemon, L.A. & Mayfield, C.I. (1992) Biotransformation of BTEX under anaerobic, denitrifying conditions: field and laboratory observations. *Journal of Contaminant Hydrology*, **11**: 245–272.

Barbaro, J.R., Barker, J.F. & Butler, B.J. (1997) In situ bioremediation of gasoline residuals under mixed electron acceptor conditions. In Situ & *On-Site Bioremediation* **4**(5): 22–26.

Barcelona, M.J., Helfrich, J.A. & Garske, E.E. (1988) Verification of sampling methods and selection of materials for groundwater contamination studies. In Collins, A.G. & Johnson, A.I. (Eds) *Ground-Water Contamination: Field Methods*, ASTM STP 963, American Society for Testing & Materials, West Conshohocken, PA, pp. 221–231.

Bardet, J.P. (1997) *Experimental Soil Mechanics*, Prentice Hall, NJ.

Barkan, D.D. (1962) *Dynamics of Bases & Foundations* (translated from Russian), McGraw-Hill, New York.

Barker, J.F., Patrick, G.C. & Major, D. (1987) Natural attenuation of aromatic hydrocarbons in a shallow sand aquifer. *Ground Water Monitoring Review*, **7**: 64–71.

Barksdale, R.D. (1987) *State of the Art for Design and Construction of Sand Compaction Piles*, Technical Report REMR-GT-4, US Army Corps of Engineers, Washington, DC.

Barksdale, R.D. & Bachus, R.C. (1983) *Design and Construction of Stone Columns*, Vol. I, Report No. FHWA/RD-83/026, Federal Highway Administration, Springfield, VA.

Barnes, D.G., & Dourson, M. (1988) Reference dose (RFD): description and use in health risk assessment. *Regulatory Toxicology and Pharmacology*, **8**: 471–478.

Barnes, F.J. & Rodgers, J.E. (1988) *Evaluation of Hydrologic Models in the Design of Stable Landfill Covers*, EPA Project Summary, EPA/600/S2-88/048, US Environmental Protection Agency, Washington, DC.

Barone, F.S. (1990) *PhD thesis*, University of Western Ontario, London, Ontario.

Barone, F.S., Yanful, E.K., Quigley, R.M. & Rowe, R.K. (1989) Effect of multiple contaminant migration on diffusion and adsorption of some domestic waste contaminants in a natural clayey soil. *Canadian Geotechnical Journal*, **26**: 189–198.

Barone, F.S., Rowe, R.K. & Quigley, R.M. (1992) A laboratory estimation of diffusion and adsorption coefficients for several volatile organics in a natural clayey soil. *Journal of Contaminant Hydrogeology*, **10**: 225–250.

Barone, F.S., Costa, J.M.A. & Ciardullo, L. (1997) Temperatures at the base of a municipal solid waste landfill. In *50th Canadian Geotechnical Conference*, October, Ottawa, Vol. 1 pp. 144–152.

Barron, R.A. (1948) Consolidation of fine-grained soils by drain wells, *Transactions, ASCE*, Reston, VA, **113**: 718–747.

Barton, N. (1973) Review of a new shear strength criterion for rock joints. Engineering Geology, **7**: 287–332.

Barton, N. (1976) The shear strength of rock and rock joints. *International Journal of Rock Mechanics, Mineral Science & Geomechanics Abstracts*, **13**: 1–24.

Barton, N. & Bandis, S.C. (1990) Review of predictive capabilities of JRC-JCS model in engineering practice. In Barton, N. & Stephansson, O. *Proceedings of the International Symposium on Rock Joints*, Leon, Norway, pp. 603–610.

Barton, N. & Choubey, B. (1977) The shear strength of rock joints in theory and practice. *Rock Mechanics*, **10**(1): 1–54.

Barton, N., Lien, R. & Lunde, J. (1974) Engineering classification of rock masses for the design of tunnel support. *Rock Mechanics*, **6**: 189–236.

Bathurst, R.J. & Alfaro, M.C. (1996) Review of seismic design, analysis and performance of geosynthetic reinforced walls, slopes and embankments. Invited keynote paper, *IS-Kyushu '96, Third International Symposium on Earth Reinforcement*, Japan, 12–14 November 1996, Fukuoka, Kyushu, Vol. 2, A.A. Balkema, 887–918.

Bathurst, R.J. & Crowe, E.R. (1992) Recent case histories of flexible geocell retaining walls in North America. In Tatsuoka, F. & Leshchinsky, D. (Eds) *Recent Case Histories of Permanent Geosynthetic-Reinforced Soil Retaining Walls*, 6–7 November 1992, Tokyo, Japan, A.A. Balkema, Rotterdam, pp. 3–20.

Bathurst, R.J. & Simac, M.R. (1994) Geosynthetic reinforced segmental retaining wall structures in North America. Invited keynote paper, *Fifth International Conference on Geotextiles, Geomembranes & Related Products*, Vol. 4, 6–9 September 1994, Singapore, pp. 1275–1298.

Bathurst, R.J., Simac, M.R. & Berg, R.R. (1993) Review of NCMA segmental retaining wall design manual for geosynthetic-reinforced structures. *Transportation Research Record*, **1414**: 16–25.

Baziar, M.H. & Dobry, R. (1995) Residual strength and large-deformation potential of loose silty sands. *ASCE Journal of Geotechnical Engineering Division*, Reston, VA, **121**(12): 896–906.

Bear, J. (1972) *Dynamics of Fluids in Porous Media*, American Elsevier, New York.

Bear, J. (1979) *Hydraulics of Groundwater*, McGraw-Hill, New York.

Bear, J., Tsang, C. & de Marsily, G. (1993) *Flow and Contaminant Transport in Fractured Rock*, Academic Press, San Diego, CA.

Becker, D.E. (1996a) Eighteenth Canadian Geotechnical Colloquium: limit states design for foundations. Part I. An overview of the foundation design process. *Canadian Geotechnical Journal*, **33**(6): 956–983.

Becker, D.E. (1996b) Eighteenth Canadian Geotechnical Symposium: limit states design for foundations. Part II. Development for the National Building Code of Canada. *Canadian Geotechnical Journal*, **33**(6): 984–1007.

Becker, D.E., Crooks, J.H.A. & Been, K. (1988) Interpretation of the field vane test in terms of in-situ and yield stresses. In Richards, A.F. (Ed.) Vane shear strength testing in soils: field and laboratory studies. Special Technical Publication 1014, American Society for Testing & Materials, West Conshohocken, PA, pp. 71–87.

Been, K., Crooks, J.H.A., Becker, D.E. & Jefferies, M.G. (1986) The cone penetration test in sands: Part I. State parameter interpretation. *Géotechnique*, **36**(2): 239–249.

Been, K., Jefferies, M.G., Crooks, J.H.A. & Rothenburg, L. (1987) The cone penetration test in sands: Part II. General inference of state. *Géotechnique*, **37**(3): 285–299.

Bell, A.L. (1993) Jet grouting. In Moseley, M.P. (Ed.), *Ground Improvement*, Blackie Academic & Professional, Blackwood, NJ, pp. 149–174.

Bemben, S.M. & Schulze, D.A. (1995) The influence of testing procedures on clay–geomembrane shear strength measurements. In *Proceedings, Geosynthetics '95 Conference*, Nashville, Industrial Fabrics Association International, Roseville, MN, pp. 1043–1056.

Benner, S.G., Blowes, D.W. & Ptacek, C.J. (1997) A full-scale porous reactive wall for prevention of acid mine drainage. *Ground Water Monitoring & Remediation*, **17**(4): 99–107.

Bennett, R.H. & Hurlbut, M.H. (1986) *Clay Microstructure*, International Human Resources Development Corporation, Boston/Houston/London, 161 p.

Benson, C. & Boutwell, G. (1992) Compaction

control and scale-dependent hydraulic conductivity of clay liners. In *Proceedings 15th Annual Madison Waste Conference*, University of Wisconsin, Madison, pp. 62–83.

Benson, C.H. & Daniel, D.E. (1994) Minimum thickness of compacted soil liners: I. Stochastic models and II. Analysis and case histories. *Journal of Geotechnical Engineering, ASCE*, Reston, VA, **120**(1): 129–172.

Benson, C.H. & Daniel, D.E. (1995) Reply to Discussion by N.F. Fuleihan & A.E.Z. Wissa. *American Society of Geotechnical Engineering*, **121**(6): 506–509.

Benson, C.H. & Khire, M.V. (1995) Earthen covers for arid and semi-arid sites. In *Landfill Closures: Environmental Protection & Land Recovery*, Geotechnical Special Publication No. 53, Dunn, R.J. and Singh, R.P. (Eds.) American Society of Civil Engineers, Reston, VA, pp. 201–217.

Benson, C.H., Khire, M.V. & Bosscher, P.J. (1993) *Final Cover Hydrologic Evaluation, Final Cover—Phase II*, Environmental Geotechnics Report No. 93-4, University of Wisconsin, Madison.

Benson, C.H., Zhai, H. & Wang, X. (1994) Estimating hydraulic conductivity of compacted clay liners. *Journal of Geotechnical Engineering, ASCE*, Reston, VA, **120**(2): 366–387.

Benson, C.H., Daniel, D.E. & Boutwell, G.P. (1999) Field performance of compacted clay liners. *Journal of Geotechnical & Geoenvironmental Engineering, ASCE*, Reston, VA, **125**(5): 390–403.

Beredugo, Y.O. & Novak, M. (1972) Coupled horizontal and rocking vibration of embedded footings. *Canadian Geotechnical Journal*, **9**(4): 477–497.

Berezantzev, V.G., Khristoforov, V. & Golubkov, V. (1961) Load bearing capacity and deformation of piled foundations. In *Proceedings of the Fifth International Conference on Soil Mechanics & Foundation Engineering*, Paris, Vol. 2, pp. 11–15.

Bergado, D.T., Anderson, L.R., Miura, N. & Balasubramaniam, A.S. (1996) *Soft Ground Improvement in Lowland and Other Environments*, ASCE Press, Reston, VA.

Bergen, A.T. & Monismith, C.L. (1973) Characterization of subgrade soils in cold regions for pavement design purposes. *Transportation Research Board Record* **431**: 25–27.

Bermingham, P. & Janes, M. (1989) An innovative approach to load testing of high capacity piles. In *Proceedings of the International Conference on Piling & Deep Foundations*, Vol. 1, pp. 409–413.

BGS (1990) British Geological Society *Proceedings of the Third International Symposium on Pressuremeters*, April 1990, Oxford, Thomas Telford Publishers, London, England.

Bickel, J.O., Kuesel, T.R. & King, E.H. (1996) *Tunnel Engineering Handbook*, 2nd Edn, Chapman & Hall, New York.

Bieniawski, Z.T. (1974) Geomechanics classification of rock masses and its application in tunneling. In *Third International Congress on Rock Mechanics*, Vol. 2A, ISRM, Denver, pp. 27–32.

Bieniawski, Z.T. (1976) Rock mass classifications in rock engineering. In Bieniawski, Z.T. (Ed.) *Proceedings of Symposium on Exploration for Rock Engineering*, Vol. 1, Balkema, Rotterdam, pp. 97–106.

Bieniawski, Z.T. (1978) Determining rock mass deformability: experience from case histories. *International Rock Mechanics, Mineral Science & Geomechanics, Abstracts*, **15**: 237–247.

Bieniawski, Z.T. (1984) *Rock Mechanics Design in Mining and Tunneling*, Balkema, Rotterdam.

Bieniawski, Z.T. (1989) *Engineering Rock Mass Classifications*, New York, Wiley.

Biot, M.A. (1941) General theory of three-dimensional consolidation. *Journal of Applied Physics*, **12**: 155–164.

Biot, M.A. (1955) Theory of elasticity and consolidation for a porous anisotropic solid. *Journal of Applied Physics*, **26**(2): 182–185.

Bishop, A.W. (1955) The use of the slip circle in the stability analysis of slopes. *Géotechnique*, **5**(1): 7–17.

Bishop, A.W. & Bjerrum, L. (1960) The relevance of the triaxial test to the solution of stability problems. In *Proceedings, ASCE Research Conference on Shear Strength of Cohesive Soils*, Boulder, Co, pp. 437–501.

Bishop, A.W. & Blight, G.E. (1963) Some aspects of effective stress in saturated and unsaturated soils. *Geotéchnique*, **2**(3): 177–197.

Bishop, A.W. & Henkel, D.J. (1962) *The Measurement of Soil Properties in the Triaxial Test*, 2nd Edn, Edward Arnold, London, England.

Bishop, D.J. (1996) Discussion of "A Comparison of Puncture Behavior of Smooth and Textured HDPE Geomembranes" and "Three Levels of Geomembrane Puncture Protection" by Narejo, D.B. *Geosynthetics International*, **3**(3): 441–443.

Bjarngard, A. & Edgers, L. (1990) Settlements of municipal solid waste landfills. In *Proceedings, 13th Annual Madison Waste Conference, Madison*, WI.

Bjerg, P.L., Rugge, K., Pedersen, J.K. & Christensen, T.H. (1995) Distribution of redox-sensitive groundwater quality parameters downgradient of a landfill (Grinsted, Denmark). *Environmental Science & Technology*, **29**(5): 1387–1394.

Bjerrum, L. (1963a) Discussion on "Proceedings of the European Conference on Soil Mechanics & Foundation Engineering, Vol. III," *Norwegian Geotechnical Institute Publication*, No. 98, Oslo, Norway, pp. 1–3.

Bjerrum, L. (1963b) Discussion on compressibility of soils. In *Proceedings of the European Conference on Soil Mechanics & Foundation Engineering*, Vol. 2, Wiesbaden, pp. 16–17.

Bjerrum, L. (1972) Embankments on soft ground. In *ASCE Geotechnical Engineering Division Specialty Conference on Performance of Earth & Earth-Supported Structures*, Vol. 2, Purdue University, Lafayette, IN, pp. 1–54.

Bjerrum, L. (1973) Problems of soil mechanics and construction on soft and structurally unstable soils (collapsible, expansive and others). In *Proceedings, Eighth International Conference on Soil Mechanics & Foundation Engineering*, Vol. 3, Moscow, pp. 111–159.

Bjerrum, L. & Andersen, K.H (1972) In-situ measurements of lateral pressures in clay. In *Proceedings, Fifth European Regional Conference on Soil Mechanics & Foundation Engineering*, Vol. 1, Madrid, pp. 11–20.

Bjerrum, L. & Rosenqvist, I.T. (1956) Some experiments with artificially sedimented clays. *Géotechnique*, **6**: 124–136.

Bjerrum, L., Moum, J. & Eide, O. (1967) Application of electro-osmosis on a foundation problem in a Norwegian quick clay. *Géotechnique*, **17**(3): 214–235.

Blake, S.B. & Hall, R.A. (1984) Monitoring petroleum spills with wells: some problems and solutions. In *Proceedings, Fourth National Symposium, On Aquifer Restoration & Ground Water Monitoring*, National Ground Water Association, Dublin, OH, pp. 305–310.

Blaney, G.W., Kausel, E. & Roesset, J.M. (1976) Dynamic stiffness of piles. In *Second International Conference on Numerical Methods in Geomechanics*, Vol. 2, ASCE, Reston, VA, pp. 1001–1012.

Blondeau, F. & Queyroi, D. (1976) Rupture de la tranchée expérimentale de la Bosse-Galin (argile molle). *Bulletin de Liaison des Laboratoires des Ponts et Chaussées*. Numéro spécial III: Stabilité des talus—2: Déblais et remblais, pp. 59–69.

Blondeau, F., Christiansen, M., Guilloux, A. & Schlosser, F. (1984) Talren, méthode de calcul des ouvrages en terre renforcée. In *Proceedings, International Colloquium on* in situ *Reinforcement of Soils & Rocks*, ENPC Press, Paris, pp. 219–224.

Bloomquist D. & Townsend, F.C. (1991) *Development of* in situ *Equipment for Capacity Determinations of Deep Foundations in Florida Limestone*. Report to Florida Department of Transportation, U. Florida, Gainesville, FL.

Blowes, D.W., Ptacek, C.J., Cherry, J.A., Gillham, R.W. & Robertson, W.D. (1995) Passive remediation of groundwater using *in situ* treatment curtains. In Acar, Y.B. & Daniel D.E. (Eds) *Geoenvironment 2000, Characterization, Containment, Remediation & Performance in Environmental Geotechnics*. Geotechnical Special Publication No. 46, Vol. 2, American Society of Civil Engineers, Reston, VA, pp. 1588–1607.

Blowes, D.W., Puls, R.W., Bennett, T.W., Gillham, R.W., Hanton-Fong, C.J. & Ptacek, C.J. (1997) *In-situ* porous reactive wall for treatment of Cr(VI) and trichloroethylene in groundwater. In *Proceedings, 1997 International Containment Technology Conference & Exhibition*, February 10–12, St Petersburg, FL, pp. 851–857.

Boardman, B.T. & Daniel, D.E. (1996) Hydraulic conductivity of desiccated geosynthetic clay liners. *Journal of Geotechnical Engineering, ASCE*, Reston, VA, **122**(3): 204–208.

Bohlke, B.M. (1996) Geotech design reports get a litmus test. *ASCE Civil Engineering*, Reston, VA, **66**(12): 47–49.

Bolt, B.A. (1976) *Nuclear Explosions and Earthquakes: the Parted Veil*, W.H. Freeman, San Francisco, CA.

Bolt, G.H. (1956) Physico-chemical analysis of the compressibility of pure clays. *Géotechnique*, **6**(2): 86–93.

Bolton, M.D. (1986) The strength and dilatancy of sands. *Géotechnique*, **36**(1): 65–78.

Bonaparte, R. (1995) Long-term performance of landfills. Acar, Y.B. & Daniel, D.E. (Eds) *Geoenvironment 2000, Geotechnical Special Publication No. 46*, Vol. 1, American Society of Civil Engineers, Reston, VA, pp. 515–553.

Bonaparte, R. & Berg, R.R. (1987) The use of

geosynthetics to support roadways over sinkhole prone areas. In *Proceedings, Second Multidisciplinary Conference on Sink-holes & Environmental Impact of Karst*, Orlando, FL, pp. 437–445.

Bonaparte, R. & Christopher, B.R. (1987) Design and construction of reinforced embankments over weak foundations. *Transportation & Research Record*, **1153**: 26–39.

Bonaparte, R., Holtz, R.D. & Giroud, J.P. (1987) Soil reinforcement design using geotextiles & geomembranes, In *Geotextile Testing and the Design Engineer*, ASTM, STP 952, American Society for Testing & Materials, West Conshohocken, PA, pp. 69–116.

Bonaparte, R., Giroud, J.P. & Gross, B.A. (1989) Rates of leakage through landfill liners. In *Proceedings, Geosynthetics '89*, Vol. 1, February 1989, San Diego, CA, Industrial Fabrics Association International, Roseville, MN, pp. 18–29.

Bonaparte, R., Othman, M.A., Rad, N.S., Swan, R.H. & Vander Linde, D.L. (1996) Evaluation of various aspects of GCL performance. In *Report of 1995 Workshop on Geosynthetic Clay Liners*, Daniel, D.E. & Scranton, H.B. (Eds) EPA/600/R-96/149, US Environmental Protection Agency National Risk Management Research Laboratory, Cincinnati, Appendix F1–F34.

Bonilla, M.G., Mark, R.K. & Lienkaemper, J.J. (1984) Statistical relations among earthquake magnitude, surface rupture length, and surface fault displacement. *Bulletin of the Seismological Society of America*, **74**: 2379–2411.

Booker, J.R. (1991) Analytic methods in geomechanics, In *Proceedings, Seventh International Conference On Computer Methods & Advances in Geomechanics*, Beer, G., Booker, J.R. & Carter, J.P. (Eds), Vol. 1, pp. 3–14.

Booker, J.R. & Small, J.C. (1983) The analysis of liquid storage tanks on deep elastic foundations. *International Journal for Numerical & Analytical Methods in Geomechanics*, **7**: 187–207.

Boone, S.J. (1995) Ground-movement-related building damage. *Journal of Geotechnical Engineering, ASCE*, Reston, VA, **122**(11): 886–896.

Boore, D.M., Joyner, W.B. & Fumal, T.E. (1993) *Estimation of Response Spectra and Peak Accelerations from Western North American Earthquakes: an Interim Report*, part 2, Open File Report, US Geological Survey, pp. 94–127.

Boore, D.M., Joyner, W.B. & Fumal, T.E. (1997) Equations for estimating horizontal response spectra and peak acceleration from western North American earthquakes: a summary of recent work. *Seismological Research Letters*, **68**(1): 128–153.

Boot, J.C. & Husein, N.M. (1991) Vitrified clay pipes subject to jacking forces. In *Proceedings, Conference on Pipejacking & Microtunnelling '91*, Pipe Jacking Association, London. pp. 6.1–6.9.

Borden, R.C. (1994) Natural bioremediation of hydrocarbon-contaminated ground water. *Handbook of Bioremedation*, CRC Press, Boca Raton, FL, pp. 177–199.

Borden, R.C., Gomez, C.A. & Becker, M.J. (1995) Geochemical indicators of intrinsic bioremediation. *Ground Water*, **33**(2): 180–189.

Borden, R.C., Daniel, R.A., Lebrun, L.E. & Davis, C.W. (1997a) Intrinsic biodegradation of MTBE and BTEX in a gasoline-contaminated aquifer. *Water Resources Research*, **33**(5): 1105–1115.

Borden, R.C., Goin, R.J. & Kao, C.M. (1997b). Control of BTEX migration using a biologically enhanced permeable barrier. *Ground Water Monitoring & Remediation*, **17**(1): 70–80.

Borden, R.H., Holtz, R.D., & Juran, I. (Eds) (1992) *Grouting, Soil Improvement, & Geosynthetics*, Proceedings of the ASCE specialty conference, New Orleans, Geotechnical Special Publication No. 30, American Society of Civil Engineers, ASCE Press, Reston, VA.

Bouchard, R. Leroueil, S. & Marchand, G. (1992) *Aspects géotechniques des étangs pour l'épuration des eaux usées municipales*, Report for Techmat (1992) Inc., Quebec, 111 p.

Bouclin, G. (1990) *MS thesis*, Université Laval, Québec, Canada.

Boudali, M., Leroueil, S. & Murthy, B.R.S. (1994) Viscous behaviour of natural soft clays. In *Proceedings, 13th* International Conference on Soil Mechanics & Foundation Engineering, New Delhi, India, Vol. 1, pp. 411–416.

Bourdeau, P.L., Ludlow, S.J. & Simpson, B.E. (1993) Stability of soil-covered geosynthetic-lined slopes: a parametric study. In *Proceedings, Geosynthetics '93*, Vancouver, BC, Industrial Fabrics Association International, Roseville, MN, Vol. 2, pp. 1511–1521.

Bouyoucos, G.J. (1916) The freezing point method as a new means of measuring the concentration of the soil solution directly in the soil. *Michigan Agricultural College Experimental Station, Technical Bulletin*, **24**: 1–44.

Bowders, J.J., Daniel, D.W., Wellington, J. & Houssidas, V. (1997) Managing desiccation

cracking in compacted clay liners beneath geomembranes. In *Proceedings, Geosynthetics '97* Long Beach, CA, Industrial Fabrics Association International, Roseville, MN, Vol. 1, pp. 527–540.

Bowles, J.E. (1996) *Foundation Analysis & Design*, 5th Ed, McGraw Hill, New York.

Bowles, M., Bentley, L., Barker, J. & Rathgeber, J. (1995) *In-situ* remediation of hydrocarbon contaminated groundwater in low hydraulic conductivity media using trench and gate technology. In *Proceedings (Compact Disk), Fifth Annual Symposium on Groundwater and Soil Remediation (GASReP)*, October 2–6, Toronto, Ontario, Environment Canada.

Bozozuk, M. (1974) Minor principal stress measurements in marine clay with hydraulic fracture tests. In *ASCE Geotechnical Engineering Division Specialty Conference on Subsurface Exploration for Underground Excavation & Heavy Construction*, New England College, Henniker, NH, pp. 333–349.

Brabb, E.E. & Harrod, B.L. (Eds) (1989) *Landslides: Extent and Economic Significance*, In *Proceedings, 28th International Geological Congress: Symposium on Landslides*, Washington, DC.

Brachman, R.W.I. (1999) Mechanical performance of landfill leachate collection pipes *PhD thesis*, University of Western Ontario, London, Canada.

Brady, B.H.G. & Brown, E.T. (1993) *Rock Mechanics for Underground Mining*, 2nd Edn, Chapman & Hall, London, England.

Brady, P.V., Brady, M.V. & Borns, D.J. (1998) *Natural Attenuation—CERCCA, RBCAs and the Future of Environmental Remediation*, Lewis, New York.

Brambati, E., Faccioli, E., Carulli, E., Culchi, F., Onofri, R., Stefanini, R. & Uloigrai, F. (1980) Studio de microzonizzacione sismica dell'are do Tarento (Fruili), (in Italina) Edito da Regione Autonoma Fruili-Venezia, Giulia.

Brandl, H. (1983) Improvement of cohesionless soils, state-of-the-art report. In *Proceedings, Eighth European Conference on Soil Mechanics & Foundation Engineering*, Helsinki, Vol. 3, pp. 1009–1026.

Bray, J.D. & Rathje, E.M. (1998) Earthquake induced displacements of solid waste landfills. *Journal of Geotechnical & Geoenvironmental Engineering, ASCE*, Reston, VA, **124**(3): 242–253.

Bray, J.D., Augello, A.J., Leonards, G.A., Repetto, P.C. & Byrne, R.J. (1995) Seismic stability procedures for solid waste landfills. *Journal of Geotechnical Engineering*, **121**(2): 139–151.

Bright, D.G. (1993) Testing for biological deterioration of geosynthetics in soil reinforcement and stabilization. In Cheng, S.C.J. (Ed.) *Geosynthetic Soil Reinforcement Testing Procedures, ASTM STP 1190*, American Society for Testing & Materials, West Conshohocken, PA, USA, pp. 218–227.

Brindley, G.W. & MacEwan, D. (1953) Structural aspects of mineralogy of clays and related silicates. In *Ceramics, A Symposium*, Green, A.T. & Stewart A.H. (Eds.) British Ceramic Society, London, UK, pp. 15–19.

Britto, A.H. & Gunn, M.J. (1987) *Critical State Soil Mechanics via Finite Elements*, Ellis Horwood, Chichester, UK.

Bromhead, E.N. (1992) *The Stability of Slopes*, Blackie Academic & Professional, Glasgow.

Bromhead, E.N., Cooper, M.R. & Petley, D.J. (1998) The Selborne cutting slope stability experiment (CD-ROM "The Selborne data collection cd").

Broms, B.B. (1964a) Lateral resistance of piles in cohesive soils. *Journal of Soil Mechanics & Foundations, ASCE*, Reston, VA, **90**(2): 27–63.

Broms, B.B. (1964b) Lateral resistance of piles in cohesionless soils. *Journal of Soil Mechanics & Foundations, ASCE*, Reston, VA, **90**(3): 123–156.

Broms, B.B. (1966) Methods of calculating the ultimate bearing capacity of piles—a summary. *Sols Soils*, **18–19**: 21–32.

Broms, B.B. (1979) Problems and solutions to construction in soft clay. In *Proceedings, Sixth Asian Regional Conference on Soil Mechanics & Foundation Engineering*, Singapore, Guest Lecture, Vol. II, pp. 3–38.

Broms, B.B. (1991a) Deep compaction of granular soils. In Fang, H.Y. (Ed.) *Foundation Engineering Handbook*, Van Nostrand Rheinhold, New York, NY, pp. 814–832.

Broms, B.B. (1991b) Stabilization of soil with lime columns. In Fang, H.Y. (Ed.) *Foundation Engineering Handbook*, Van Nostrand Rheinhold, New York, NY, pp. 833–855.

Broms, B.B. (1993) Lime stabilization. In Moseley, M.P. (Ed.) *Ground Improvement*, Blackie Academic & Professional, Blackwood, NJ, pp. 65–99.

Broms, B.B. & Anttikoski, U. (1983) Soil stabilization. *Proceedings, Eighth European Conference on Soil Mechanics & Foundation Engineering*, Helsinki, General Report, Specialty Session 9, Vol. 3, pp. 1298–1301.

Broms, B. & Boman, P. (1978) *Stabilization of Soil with Lime Columns, Design Handbook*, 2nd Edn, Royal Institute of Technology, Stockholm.

Broms, B.B. & Wong, I.H. (1985) Embankment piles. In *Proceedings, Third International Geotechnical Seminar on Soil Improvement Methods*, Singapore.

Brooks, R.H. & Corey, A.T. (1964) *Hydraulic Properties of Porous Materials*, Colorado State University, Hydrology Paper No. 3, p. 27.

Brown, K.W., Thomas, J.C., Lytton, R.L., Jayawickarama, P. & Bahrt, S.C. (1987) *Quantification of Leak Rates Through Holes in Landfill Liners*, report for cooperative agreement CR-810940, EPA Risk Reduction Engineering Research Laboratory, Cincinnati.

Brown, M.J. & Burris, D.R. (1996) Enhanced organic contaminant sorption on soil treated with cationic surfactants. *Ground Water*, **34**(4): 734–744.

Brown, P.T. (1969) Numerical analyses of uniformly loaded circular rafts on elastic layers of finite depth. *Géotechnique*, **19**(2): 301–306.

Brown, P.T. (1975) Strip footing with concentrated loads on deep elastic foundations. *Geotechnical Engineering*, **6**: 1–13.

Brown, S.F. (1996) 36th Rankine Lecture: Soil mechanics in pavement engineering. *Géotechnique*, **46**(3): 383–426.

Brown, S.F. & Pappin, J.W. (1981) Analysis of pavements with granular bases. *Transportation Research Board Record*, **810**: 17–22.

Brown, S.F., Brunton, J.M. & Stock, A.F. (1985) The analytical design of bituminous pavements. *Proceedings, Institution Of Civil Engineers*, London, England. **79**(2): 1–31.

Bruce, D.A. (1992) Recent progress in American pin pile technology. *Grouting, Soil Improvement, & Geosynthetics*, Geotechnical Special Publication No. 30, American Society of Civil Engineers, Reston, VA, pp. 765–777.

Bruce, D.A. (1994a) Pin piles. *Geotechnical News*, **12**(4): 33–36.

Bruce, D.A. (1994b) An overview of grouting developments. *Geotechnical News*, **12**(4): 36–40.

Bruce, D.A. & Jewell, R.A. (1987) Soil nailing: applications and practice. *Ground Engineering*, **20**(1): 21–23.

Brummermann, K., Blümel, W. & Stoewahse, C. (1994) Protection layers for geomembranes: effectiveness and testing procedures. In *Proceedings, Fifth International Conference on Geotextiles, Geomembranes & Related Products*, September 1994, Singapore, Vol. 3, pp. 1003–1006.

Brune, M., Ramke, H.G., Collins, H.J. & Hanert, H. (1994) Incrustation problem in landfill drainage systems. In Christensen, T.H. Cossu, R. & Stegmann, R. (Eds) *Landfilling of Waste: Barriers*, E & FN Spon, London, pp. 569–605.

BS 5400 (1990) *Code of Practice for Steel, Concrete and Composite Bridges*, Part 2, *Highway Loading, British Standards Institution*, London, England.

BS 5930 (1981) *Code of Practice for Site Investigations*. British Standards Institution, London, England.

BS 8006 (1995) *Code of Practice for Strengthened/Reinforced Soils & Other Fills*, British Standards Institution, London, England.

BS 8010 (1987, 1989, 1993) Code of Practice for pipelines. Pipelines on land: design, construction and installation. British Standards Institution, London, England.

Budhu, M. & Davies, T.G. (1987) Nonlinear analysis of laterally loaded piles in cohesionless soils. *Canadian Geotechnical Journal*, **24**: 21–39.

Budhu, M. & Davies, T.G. (1988) Analysis of laterally loaded piles in soft clays. *Journal of Geotechnical Engineering, ASCE*, Reston, VA, **114**(1): 21–39.

Bunce, C.M., Cruden, D.M. & Morgenstern, N.R. (1997) Assessment of the hazard from rock fall on a highway. *Canadian Geotechnical Journal*, **34**(3): 344–356.

Burd, H.J. & Frydman, S. (1997) Bearing capacity of plane-strain footings on layered soils. *Canadian Geotechnical Journal*, **34**: 241–253.

Burdine, N.T. (1953) Relative permeability calculations from pore size distribution data. *Journal of Petroleum Technology*, **5**: 71–78.

Burke, L.M. & Haubert, A.E. (1991) Burying by the bale. *Journal of Civil Engineering, ASCE*, Reston, VA, **61**(8): 58–60.

Burland, J.B. (1973) Shaft friction on piles in clay–a simple fundamental approach. *Ground Engineering*, **6**(3): 30–42.

Burland, J.B. (1990) On the compressibility and shear strength of natural clays. *Géotechnique*, **40**(3): 329–378.

Burland, J.B., Broms, B.B. & de Mello, V.F.B. (1977) Behaviour of foundations and structures, state-of-the-art review. In *IX International Conference on Soil Mechanics & Foundation Engineering*, Tokyo, Vol 3, pp. 495–546.

Burlingame, M.J. (1985) *Construction of a High-*

way on a Sanitary Landfill and Its Long-Term Performance, Transportation Research Record 1031, TRB, Washington, DC: pp. 34–40.

Burns, J.Q. & Richard, R.M. (1964) Attenuation of stresses around buried cylinders. In *Proceedings, Symposium on Soil–Structure Interaction*, Tucson, AZ, American Society for Testing & Materials, West Conshohocken, PA, pp. 379–392.

Burr, J.P., Pender, M.J. & Larkin, T.J. (1997) Dynamic response of laterally excited pile groups. *Journal of Geotechnical & Geoenvironmental Engineering*, **123**1: 1–8.

Buscheck, T.E. & Peargin, T.R. (1991) Summary of nation-wide vapor extraction system performance study. In *Proceedings, Petroleum Hydrocarbons & Organic Chemicals in Ground Water: Prevention, Detection & Restoration*, November 20–22 Houston, TX, National Ground Water Association, pp. 205–220.

Bustamante, M. & Gianeselli, L. (1982) Pile bearing capacity prediction by means of static penetrometer CPT. In *Proceedings*, ESOPT II, Amsterdam, Vol. 2, pp. 492–500.

Butterfield, R. & Banerjee, P.K. (1971) The elastic analysis of compressible piles and pile groups. *Géotechnique*, **21**(1): 43–60.

Butterfield, R. & Douglas, R.A. (1981) *Flexibility Coefficients for the Design of Piles and Pile Groups*. Technical Note 108, CIRIA, London.

Bycroft, G.N. (1956) Forced vibrations of a rigid circular plate on a semi-infinite elastic space and on an elastic stratum. *Philosophical Transactions of the Royal Society*, London, Serial A, **248**: 327–368.

Byrne, P.M., Imrie, A.S. & Morgenstern, N.R. (1994) Results and implications of seismic performance studies for Duncan Dam. *Canadian Geotechnical Journal*, **31**(6): 979–988.

Byrne, P.M., Anderson, D.L. & Jitno, H. (1996) Seismic analysis of large buried culvert structures. *Transportation Research Record*, **1541**: 133–139.

Byrne, R.J. (1994) Design issues with strain-softening interfaces in landfill liners. In *Proceedings, Waste Tech '94 Conference*, National Solid Waste Management Association, Charleston, SC p. 26.

Byrne, R.J., Kendall, J. & Brown, S. (1992) Cause and mechanism of failure of Kettleman Hills Landfill lining material. In *Proceedings of ASCE Conference on Stability & Performance of Slopes & Embankments* II, ASCE Press, Reston, VA, pp. 1–23.

Callanan, J.F. & Kulhawy, F.H. (1985) *Evaluation of Procedures for Predicting Foundation Uplift Movements*. Report, Electric Power Research Institution, No. EPRI EL-4107, Cornell University.

Campanella, R.G. & Weemees, I. (1990) Development and use of an electrical resistivity cone for groundwater contamination studies. *Canadian Geotechnical Journal*, **27**(5): 557–567.

Campanella, R.G. & Robertson, P.K. (1991) Use and interpretation of a research dilatometer. *Canadian Geotechnical Journal*, **28**(1): 113–126.

Campanella, R.G., Davies, M.P., Boyd, T.J. & Everard, J.L. (1994) Geoenvironmental subsurface site characterization using *in-situ* soil testing methods. In *Proceedings, First International Congress on Environmental Geotechnics*, Edmonton, Alberta.

Campbell, G.S. (1974) A simple method for determining unsaturated hydraulic conductivity from moisture retention data. *Soil Science*, **117**(6): 311–314.

Campbell, K.W. (1997) Attenuation relationships for shallow crustal earthquakes based on California strong motion data. *Seismological Research Letters*, **68**(1): 180–189.

CAN/CSA-A5, Portland cement, Canadian Standards Association, Rexdale, Ontario.

CAN/CSA A60 Vitrified clay pipe, Canadian Standards Association, Rexdale, Ontario.

CAN/CSA A257 Concrete culverts, storm drain and sewer pipe, Canadian Standards Association, Rexdale, Ontario.

CAN/CSA B182 Plastic non-pressure pipe, Canadian Standards Association, Rexdale, Ontario.

CAN/CSA C140, Canadian Standards Association, Ottawa. Corrugated steel, Rexdale, Ontario.

Caquot, A. & Kerisel, J. (1966) *Traite de mecanique des sols*, 4th Edn, Gauthier-Villars, Paris.

CARACAS (1998) *Concerted Action on Risk Assessment for Contaminated Sites in the European Union*, European Commission, Brussels, Belgium.

Carey, G.R., Mateyk, M.G., Turchan, G.T., McBean, E.A., Rovers, F.A., Murphy, J.R. & Campbell, J.R. (1996) Application of an innovative visualization method for demonstrating intrinsic remediation at a landfill superfund site. In *Proceedings, API/NGWI Petroleum Hydrocarbons & Organic Chemicals in Groundwater Conference*, Houston, TX.

Carey, G.R., Van Geel, P.J., McBean, E.A. & Rovers, F.A. (1997a) Effect of landfill cap perme-

ability on the natural attenuation of chlorinated solvents below a landfill. In *1997 Canadian Geotechnical Conference Proceedings*, October 20–22, Ottawa, Ontario.

Carey, G.R., Van Geel, P.J., McBean, E.A. & Rovers, F.A. (1997b) An innovative modeling and visualization approach for demonstrating the effectiveness of natural attenuation, presented at the IBC Natural Attenuation '97 Conference, Scottsdale, Arizona, December 8–10.

Carey, G.R., Van Geel, P., Murphy, J., McBean, E., & Rovers, F. (1998) Dimensionality Considerations for a Coupled Biodegradation-Redox Model (BIOREDOX), MODFLOW '98, October 4–8, Denver, Colorado.

Carey, G.R., Van Geel, P.J., Wiedemeier, T.H. & McBean, E.A. (2000) SEQUENCE natural attenuation application for visualizing primary and secondary lines of evidence. *Ground Water Monitoring Review*, in press.

Carey, P.J., Koragappa, N. & Gurda, J.J. (1993) Renewal of old sites, overliner system design, a case study of the Brookhaven Landfill, Long Island, New York. In *Proceedings, Waste Tech '93 Conference*, National Solid Waste Management Association, Marina Del Rey, p. 13

Carrubba, P. (1997) Skin friction of large-diameter piles socketed into rock. *Canadian Geotechnical Journal*, **34**: 230–240.

Carslaw, H.S. & Jaeger, J.C. (1959) *Conduction of Heat in Solids*, 2nd Ed, Oxford University Press, England.

Carter, J.P. & Kulhawy, F.H. (1988) *Analysis and Design of Drilled Shaft Foundations Socketed into Rock*, Report El-5918, Electric Power Research Institute, Palo Alto, CA.

Carter, J.P. & Kulhawy, F.H. (1992) Analysis of laterally loaded shafts in rocks. *Journal of Geotechnical Engineering, ASCE*, Reston, VA, **118**(6):839–855.

Carter, P.G., Pirie, R.M. & Sneddon, M. (1986) Marine site investigations and BS 5930. In Hawkins, A.B. (Ed.) *Site Investigation Practice: Assessing BS 5930*. Geological Society Engineering Geology Special Publication No. 2, Geological Society, London, England, pp. 163–166.

Casagrande, A. (1935) Seepage Through Dams, New England Water Works Association, **2**: 131–172..

Casagrande, L. (1937) Method of hardening soils. U.S. Patent No. 2,099,328.

Casagrande, L. (1952) Electro-osmotic stabilization of soils. *Journal of Boston Society of Civil Engineers*, **39**: 59–83.

Casagrande, L. (1959) *Review of Past and Current Work on Electro-Osmotic Stabilization of Soils*, Harvard Soil Mechanics Series, No. 45, Harvard University Press, Cambridge, MA.

Casagrande, L. (1983) Review of stabilization of soils by means of electro osmosis state of the art. *Geotechnical Section of the BSCE/ASCE*, **69**(2):255–302.

Casagrande, L., Loughney, R.W. & Matich, M.A.J. (1961) Electro-osmotic stabilization of a high slope in loose saturated silt. In *Fifth International Conference of Soil Mechanics & Foundation Engineering*, Paris, Vol. 2, pp. 555–561.

Casagrande, L., Wade, N., Wakely, M. & Loughney, R. (1981) Electro osmosis projects, British Columbia, Canada. In *10th International Conference of Soil Mechanics & Foundation Engineering*, Stockholm, Vol. 2, pp. 607–610.

CCME (1994) *Subsurface Assessment Handbook for Contaminated Sites*, CCME-EPC-NCSRP-48E, Canadian Council of Ministers of the Environment, Winnipeg, Manitoba.

CCME (1996) *A Protocol for the Derivation of Environmental & Human Health Soil Quality Guidelines*. Canadian Council of Ministers of the Environment, Winnipeg, Manitoba.

CDSA (1995) *Dam Safety Guidelines*, Canadian Dam Safety Association, Edmonton, Alberta.

Cedergren, H.R. (1967) *Seepage, Drainage & Flow Nets*, 2nd Edn, Wiley, New York.

Cedergren, H.R. (1989) *Seepage, Drainage, & Flow Nets*, 3rd Edn., Wiley, New York.

Celebi, M. (1987) Topographical and geological amplifications determined from strong motion and aftershock records of the 3 March 1985 Chile earthquake. *Bulletin of the Seismological Society of America*, **77**(4): 1147–1167.

Celebi, M. (1991) Topographical and geological amplification case studies and engineering implications, In *Proceedings, International Workshop on Spatial Variation of Earthquake Ground Motion*, Elsevier Science, B.V. Amsterdam.

CEN (1992) *Geotechnical Design, General Rules*. European Committee for Standardization (CEN), Eurocode 7. Danish Geotechnical Institute, Copenhagen, Denmark.

CEN (1994) *Design Provisions for Earthquake Resistant Structures*, Part 5: *Foundations, Retaining Structure and Geotechnical Aspects*, Eurocode 8, European Committee for Standardization, Central Secretariat, Brussels.

Cernica, J.N. (1995) *Geotechnical Engineering: Soil Mechanics*, Wiley, New York.

CFEM (1992): see CGS (1992).

CGS (1985) *Canadian Foundation Engineering Manual*, 2nd Edn, Canadian Geotechnical Society, Ottawa.

CGS (1992) *Canadian Foundation Engineering Manual*, 3rd Edn, Canadian Geotechnical Society, BiTech Publishers, Richmond, British Columbia.

Challa, P. & Poulos, H.G. (1991) Behaviour of single pile in expansive clay. Geotechnical Engineering, **22**(2): 189–216.

Champ, D.R., Young, J.L., Robertson, D.E. & Abel, K.H. (1984) Chemical speciation of long-lived radionuclides in a shallow groundwater flow system, *Water Pollution Research Journal of Canada*, **19**: 35–54.

Chamberlain, E.J. (1973) A model for predicting the influence of closed-system freeze–thaw on the strength of thawed soil. In *Proceedings, Symposium on Frost Action Roads*, Oslo, pp. 94–97.

Chamberlain, E.J. (1981) *Frost Susceptibility, Review of Index Tests*, Monograph 81–2. US Cold Regions Research and Engineering Laboratory (CRREL).

Chandhari, A.P. & Char, A.N.R. (1985) Flexural behavior of reinforced beams. *Journal of Geotechnical Engineering, ASCE*, Reston, VA, **111**(11): 1328–1333.

Chandler, R.J. (1984) Recent European experience of landslides in over-consolidated clays and soft rocks. In *Proceedings, Fourth International* Symposium on Landslides, Toronto, Vol. 1, pp. 61–81.

Chaney, R.C., Thiel, R., Richardson, G.N. & Cadwallader, M. (1997) Cyclic response of clay–geomembrane interfaces and their impact on the seismic response of lined landfills. In *Proceedings, Geosynthetics '97 Conference*, Long Beach, Industrial Fabrics Association International, Roseville, MN, Vol. 2, pp. 977–987.

Chapelle, F.H. (1993) *Ground-Water Microbiology & Geochemistry*, Wiley, New York.

Chapman, D.N., Falk, C., Rogers, C.D.F. & Stein, D. (1996) Experimental and analytical modelling of pipebursting ground displacements. *Trenchless Technology Research, Tunnelling and Underground Space Technology*, **11**(1): 53–68.

Chapman, S.W., Byerley, B.T., Smyth, D.J.A. & Mackay, D.M. (1997) A pilot test of passive oxygen release for enhancement of *in-situ* bioremediation of BTEX-contaminated groundwater. *Ground Water Monitoring & Remediation*, **17**(2): 93–105.

Chapuis, R.P. (1988) Two case histories of major frost heaving in refrigerated buildings: thermal analyses, repairs and prevention. *Canadian Geotechnical Journal*, **25**(3): 535–540.

Chapuis, R.P. (1990) Sand–bentonite liners: predicting permeability from laboratory tests. *Canadian Geotechnical Journal*, **27**(1): 47–57.

Charbeneau, R.J., Wanakule, N., Chiang, C.Y., Nevin, J.P. & Klein, C.L. (1989) A two-layer model to simulate floating free product recovery: formulation and applications. In *Proceedings, Conference On Petroleum Hydrocarbons and Organic Chemicals in Ground Water: Prevention, Detection, and Restoration*, National Ground Water Association, Dublin, OH, pp. 333–345.

Charles, J.A., Tedd, P., Hughes, A.K. & Lovenbury, H.T. (1996) *Investigating Embankment Dams: A Guide to the Identification and Repair of Defects*, Building Research Establishment Report, Construction Research Communications, Watford, England.

CHBDC (1998) *Buried Structures*, Canadian Highway Bridge Design Code, Section 7, Canadian Standards Association, Rexdale, Ontario.

Chen, L. & Poulos, H.G. (1997) Piles subjected to lateral soil movements. *Journal of Geotechnical & Geoenvironmental Engineering, ASCE*, Reston, VA, **123**(9): 802–811.

Cheney, R.S. (1984) *Permanent Ground Anchors*, Report No. FHWA-DP-68-1, Federal Highway Administration, Springfield, VA.

Cherry, J.A. (1996) Conceptual models for chlorinated solvent plumes and their relevance to intrinsic remediation. In *Symposium on Natural Attenuation of Chlorinated Organics in Groundwater*, September 11–13, Dallas, TX, US Environmental Protection Agency 540/R-96-509, pp. 29–30.

Cherry, J.A., Feenstra, S. & Mackay, D.M. (1996) Concepts for remedation of sites contaminated with DNAPLS. In Pankow, J.F. & Cherry, J.A. (Eds) *Dense Chlorinated Solvents and Other DNAPLs in Groundwater*, Waterloo Press, Rockwood, Ontario, pp. 475–506.

Cherry, J.A., Feenstra, S. & Mackay, D.M. (1997) Developing rational goals for *in situ* remedial technologies. In Ward, C.H., Cherry, J.A. & Scalf, M.R. (Eds) *Subsurface Restoration*. Ann Arbor Press, Chelsea, MI, pp. 75–98.

Childs, E.C. & Collis-George, N. (1950) The per-

meability of porous materials. *Proceedings, Royal Society of London*, **201A**: 392–405.
Childs, S.W. & Hanks, R.J. (1975) Model of soil salinity effects on crop growth. *Soil Science Society of American Journal*, **39**: 617–622.
Choa, V. (1985) Preloading and vertical drains. In *Soil Improvement Methods, Proceedings, Third International Geotechnical Seminar*, Nanyang Technological Institute, Singapore, pp. 87–99.
Chopra, A.K. (1981) *Dynamics of Structures, a Primer*, Earthquake Engineering Research Institute, Oakland, CA.
Choquet, P. & Tanon, D.D.B. (1985) Nomograms for the assessment of toppling failure in rock slopes. In *Proceedings, 26th US Symposium on Rock Mechanics*, South Dakota School of Mines & Technology, Vol. 1, pp. 19–30.
Chow, Y.K. (1986) Analysis of vertically loaded pile groups. *International Journal of Numerical Analytical Methods in Geomechanics*, **10**: 59–72.
Chow, Y.K., Chin, J.T. & Lee, S.L. (1990) Negative skin friction on pile groups. *International Journal of Numerical and Analytical Methods in Geomechanics*, **14**(1): 75–91.
Christian, J.T. & Carrier, W.D. (1978) Janbu, Bjerrum & Kjaernsli's chart reinterpreted. *Canadian Geotechnical Journal*, **15**: 123–128.
Christoulas, S. & Frank, R. (1991) Deformation parameters for pile settlement. In *Proceedings, 10th European Conference on Soil Mechanical and Foundation Engineering*, Florence, Vol. 1, pp. 373–376.
Circeo, L.J. & Mayne, P.W. (1994) *In-situ* thermal stabilization of roads and foundation soils using plasma arc technology. In *Proceedings, Fourth International Conference on Bearing Capacity of Roads and Airfields*. University of Minnesota, Minneapolis.
Clarke, B.G. & Gambin, M.P. (1988) Pressuremeter testing in onshore ground investigations: A report by the ISSMGE Committee TC16. In Robertson, P.K. & Mayne, P.W. (Eds) *Proceedings, First International Conference on Site Characterization, ISC'98*, April 19–22, Atlanta, GA, A.A. Balkema, Rotterdam, pp. 1429–1468.
Clayton, C.R.I. (1990) SPT energy transmission: theory, measurement and significance. *Ground Engineering*, December: 35–43.
Clayton, C.R.I. (1995) *The Standard Penetration Test (SPT): Methods and Use*, Report 143. Construction Industry Research & Information Association (CIRIA), London, England.
Clough, G.W., Smith, E.M. & Sweeney, B.P. (1989) Movement control of excavation support systems by iterative design. *Foundation Engineering: Current Principles and Practices, ASCE* Press, Reston, VA, **2**: 869–882.
Clough, R.W. & Penzien, J. (1993) *Dynamics of Structures*, 2nd Edn, McGraw-Hill, New York.
Clouterre (1991) Recommendations Clouterre 1991. Presses de l'ENPC, Paris (In French). Also Recommendations Clouterre 1991 (Soil nailing recommendations). Published in English by Federal Hyway Administration, Washington, D.C., 301 p.
CMHC (1994) *Phase I ESA Interpretive Guideline*, The Canadian Mortgage and Housing Corporation, Ottawa.
Cohen, A. (1961) Tables for maximum likelihood estimates from singly truncated and singly-censored samples. *Technometrics*, **3**: 535–541.
Cohen, R.M. & Mercer, J.W. (1993) *DNAPL Site Evaluation*, CRC Press, Boca Raton, FL.
Colas, G. & Locat, J. (1993) Glissement et coulée de La Valette dans les Alpes de Haute-Provence: présentation générale et modélisation de la coulée. *Bulletin de Liaison des Laboratoires des Ponts et Chaussées*, **187**: 19–28.
Colas, G., Simon, A., Payani, M. & Pilot, G. (1976). Les glissements de terrain sur l'autoroute A-7 à Rognac, près de l'étang de Berre. *Bulletin de Liaison des Laboratoires des Ponts et Chaussées*, Numéro spécial III, **2**: 70–80.
Cole, D., Bentley, D., Durell, G. & Johnson, T. (1986) *Resilient Modulus of Freeze–Thaw Affected Granular Soils for Pavement Design and Evaluation*, Report 86–4, CRREL.
Collins, B.D. & Znidarcic, D. (1998) Slope stability issues of rainfall induced landslides. In *Proceedings, 11th Danube–European Conference on Soil Mechanics & Geotechnical Engineering (Geotechnical Hazards)*, Poreč, pp. 791–798.
Colwell, R.N. (1983) *Manual of Remote Sensing*, 2nd Edn, American Society of Photogrammetry, New York, NY.
Comer, A.I., Hsuan Y.G. & Konrath, L. (1988) The performance of flexible polypropylene geomembranes in covered and exposed environments. In *Sixth International Geosynthetics Conference*, R.K. Rowe (Ed), Atlanta, GA, IFAI, Roseville, MN.
Cooke, A.J. & Rowe, R.K. (1999) Extension of porosity and surface area models for uniform porous media for studying clogging of landfill collection systems. *Journal of Environmental Engineering, ASCE*, Reston, VA, **125**(2): 126–145.

Coon, R.F. & Merritt, A.H. (1970) *Predicting* in-situ *Modulus of Deformation Using Rock Quality Indexes*, ASTM Special Technical Publication 477, West Conshohocken, PA, pp. 154–173.

Cooper, M.R., Bromhead, E.N., Petley, D.J. & Grant, D.I. (1998) The Selborne cutting stability experiment. *Géotechnique*, **48**(1): 83–101.

Corey, A.T. (1986) *Mechanics of Immiscible Fluids in Porous Media*, Water Resources Publications, Littleton, CO.

Cornell University (1951) Final report on soil solidification research, Ithaca, N.Y.

Cornforth, D.H. (1964) Some experiments on the influence of strain conditions on the strength of sand. *Géotechnique*, **14**: 143–167.

Corser, P. & Cranston, P. (1991) Observation on long-term performance of composite clay liners and covers. In *Proceedings, Geosynthetic Design & Performance*, Vancouver Geotechnical Society, Vancouver, BC.

Costa, J.E. & Baker, V.R. (1981) *Surficial Geology–Building with the Earth*, Wiley, New York.

Coyle, H. & Reese, L.C. (1966) Load transfer for axially loaded piles in clay. *Journal of Soil Mechanics & Foundations Division, ASCE*, Reston, VA, **92**(2): 1–26.

CPCA (1984)*Thickness Design for Concrete Highway and Street Pavements*, Canadian Portland Cement Association, Toronto, Ontario.

Craig, R.F. (1997) *Soil Mechanics*, 6th Edn, E. & F.N. Spon, London, U.K.

Craig, R.N. (1983) *Pipe Jacking: a State-of-the-Art Review*, Technical Note No. 112, Construction Industry Research and Information Association, London.

Croff, A.G., Lomenick, T.F., Lowrie, R.S. & Stow, S.H. (1985) *Evaluation of Five Sedimentary Rocks other than Salt for High Level Waste Repository Siting Purposes*, Oak Ridge National Lab, ORNL/CF-85/2/V2, Oak Ridge, TN.

Croney, D. & Croney, P. (1997) *Design and Performance of Road Pavements*, 3rd Edn, McGraw-Hill, London.

Croney, D., Coleman, J.D. & Black, W.P.M. (1958) Movement and distribution of water in soil in relation to highway design and performance. In *Water and its Conduction in Soils*, Highway Research Board, Special Report, Washington, DC, No. 40, pp. 226–252.

Crooks, J.H.A., Becker, D.E., Jefferies, M.G. & McKenzie, K. (1984) Yield behavior and consolidation. 1: pore pressure response. In *Proceedings, ASCE Symposium on Sedimentation Consolidation Models: Predictions and Validation*, pp. 356–381.

Crouse, C.B. & Cheang, L. (1987) *Dynamic Testing and Analysis of Pile–Group Foundation*, Geotechnical Special Publication No. 11, American Society of Civil Engineers, Reston, VA, pp. 79–98.

Cruden, D.M. & Varnes, D.J. (1996) Landslide types and processes. *Landslides–Investigation and Mitigation*, A.K. Turner & R.L. Schuster (Eds.) Special Report 247, Transportation Research Board, Washington, DC, pp. 36–75.

CSA (1994) *Phase I Environmental Site Assessment*, Canadian Standards Association Report Z768–94, Etobicoke, Ontario.

CSA *Phase II Guideline*, Canadian Standards Association, Toronto, ON.

Dafalias, Y.F. & Herrmann, L.R. (1980) A bounding surface soil plasticity model. In *Proceedings, International Symposium on Soils Under Cyclic and Transient Loading*, Balkema, Rotterdam, pp. 335–345.

Dahlberg, R. (1974) Penetration, pressuremeter, and screw plate tests in a preloaded natural sand deposit. In *Proceedings, European Symposium on Penetration Testing*, 2.2, ESOPT-1, Stockholm, Sweden.

Dakoulas, P. & Gazetas. G. (1986) Seismic shear vibration of embankment dams in semi-cylindrical valleys. *Earthquake Engineering and Structural Dynamics*, **14**: 19–40.

Daniel, D.E. (1998) Landfills for solid and liquid wastes. In *Proceedings, Third International Congress on Environmental Geotechnics*, September, Lisbon, A.A. Balkema, Rotterdam.

Daniel, D.E. & Koerner, R.M. (1993a) *Technical Guidance Document: Quality Assurance and Quality Control for Waste Containment Facilities*, EPA/600/R-93/182, Environmental Protection Agency Risk Reduction Research Laboratory, Cincinnati.

Daniel, D.E. & Koerner, R.M. (1993b) Final cover systems. In Daniel, D.E. (Ed.) *Geotechnical Aspects of Waste Disposal* Chapman & Hall, London, pp. 225–272.

Daniel, D.E. & Koerner, R.M. (1995) *Waste Containment Systems: Guidance for Construction, Quality Assurance, and Quality Control of Liner and Cover Systems*, ASCE Press, Reston, VA.

Daniel, D.E. & Scranton, H.B. (1996) *Report of 1995 Workshop on Geosynthetic Clay Liners*,

EPA/600/R-96/149, US Environmental Protection Agency, National Risk Management Research Laboratory, Cincinnati, OH.

Daniel, D.E. & Shan, H.Y. (1992) *Effects of Partial Wetting of Gundseal on Strength and Hydrocarbon Permeability*, Report submitted to Gundle Lining Systems Inc., Austin, TX.

Daniel, D.E., Anderson, D.C. & Boynton, S.S. (1985) Fixed wall versus flexible wall permeameters. In *Hydraulic Barriers in Soil and Rock*, ASTM STP 874, American Society for Testing & Materials, West Conshohocken, PA, pp. 107–123.

Daniel, D.E., Shan, H.Y. & Anderson, J.D. (1993) Effects of partial wetting on the performance of the bentonite component of a geosynthetic clay liner. In *Proceedings, Geosynthetics '93*, Vancouver, BC, Industrial Fabrics Association International, Roseville, MN, Vol. 3, pp. 1483–1496.

Daniel, D.E., Bowders, J.J. & Gilbert, R.B. (1997) Laboratory hydraulic conductivity testing of GCLs in flexible-wall permeameters. In Well, L.W. (Ed.) *Testing & Acceptance Criteria for Geosynthetic Clay Liners*, ASTM STP 1308 American Society for Testing & Materials, West Conshohocken, PA, USA, pp. 208–228.

Daniel, D.E., Koerner, R.M., Bonaparte, R., Landreth, R.E., Carson, D.A. & Scranton, H.B. (1998) Slope stability of geosynthetic clay liner test plots. *Journal of Geotechnical & Geoenvironmental Engineering, ASCE*, Reston, VA, **124**(7): 628–637.

D'Appolonia, D.J., D'Appolonia, E. & Brissette, R.F. (1970) Settlement of spread footings on sand. *Journal of Soil Mechanics & Foundations Division, ASCE*, Reston, VA, **96**(SM2): 754–762.

Darracott, B.W. & McCann, D.M. (1986) Planning engineering geophysical surveys. In Hawkins, A.B. (Ed.) *Site Investigation Practice: Assessing BS 5930*. Geological Society Engineering Geology Special Publication No. 2, Geological Society, London, England, pp. 85–90.

Darton, N.H. (1909) *Geology and Underground waters of South Dakota*, US Geology Survey, Water Supply Paper 227.

Das, B.M. (1990) *Principles of Foundation Engineering*, PWS Kent, Boston, MA.

Das, B.M. (1995) *Principles of Soil Dynamics*. PWS Kent, Boston, MA.

David, M. (1977) *Geostatistical Ore Reserve Estimation*, Elsevier, New York.

Davidtz, J.C. & Low, P.F. (1970) Relation between crystal lattice configuration and swelling of montmorillonites. *Clays and Clay Minerals*, **18**(6): 325.

Davies, T.G., Sen, R. & Banerjee, P.K. (1985) Dynamic behavior of pile groups in inhomogeneous soil. *Journal of Geotechnical Engineering, ASCE*, Reston, VA, **111**(12): 1365–1379.

Davis, E.H. (1980) Some plasticity solutions relevant to the bearing capacity of rock and fissured clay, J.C. Jaeger Memorial Lecture, In *Proceedings, Third Australia–New Zealand Conference on Geomechanics*, Wellington, New Zealand, Vol. 3, pp. 27–36.

Davis, E.H. & Booker, J.R. (1971) The bearing capacity of strip footings from the point of view of plasticity theory. In *Proceedings, First Australia–New Zealand Conference on Geomechanics*, Institution of Engineers, Melbourne, Australia. Vol. 1, pp. 276–282.

Davis, E.H. & Booker, J.R. (1973) The effect of increasing strength with depth on the bearing capacity of clays. *Géotechnique*, **23**(4): 551–563.

Davis, E.H. & Poulos, H.G. (1968) The use of elastic theory for settlement prediction under three-dimensional conditions. *Géotechnique*, **18**(1): 67–91.

Davis, E.H. & Poulos, H.G. (1972) Rate of settlement under three-dimensional conditions. *Géotechnique*, **22**(1): 95–114.

Davis, G.B. (1997) Intrinsic attenuation of BTEX in groundwater: quantification and monitoring issues (abstract). In *International & On-Site Bioremedation Symposium*, New Orleans, LA, Battelle Press, Columbus, OH, Vol. 4(1), p. 19.

De, A. & Zimme, T.F. (1998) Frictional behavior of landfill liner interfaces with geonets. In *Proceedings*, Rowe, R.E. (Ed.) *Sixth International Conference on Geosynthetics*, Atlanta, GA, Industrial Fabrics Association International, Roseville, MN, Vol. 1, pp. 443–446.

Décourt, L. (1982) Prediction of the bearing capacity of piles based exclusively on N values of the SPT. In *Proceedings, ESOPT II*, Amsterdam, Vol. 1, pp. 29–34.

Décourt, L. (1989) The standard penetration test–State-of-the-art report. In *12th International Conference on Soil Mechanics & Foundation Engineering*, August 13–18, Rio de Janeiro, Brazil.

Décourt, L. (1994) Prediction of settlement of spread footings. In Predicted and Measured Behaviour of Five Spread Footings on Sand, Briaud, J.-L. & Gibbons, R.M. Eds. ASCE Geotechnical Special Publication No. 41,

American Society of Civil Engineers, Reston, VA, pp. 210–213.

Décourt, L. (1995) Prediction of load–settlement relationships for foundations on the basis of the SPT-T. *Ciclo de Conferencias Internationale*, Leonardo Zeevaert, UNAM, Mexico, pp. 85–104.

Décourt, L., Belicanta, A. & Quaresma, Filho, A.R. (1989) Brazilian experience on SPT. In *Proceedings 12th International Conference on Soil Mechanics & Foundation Engineering*, Rio de Janeiro, Supplement, Contributions by Brazilian Society for Soil Mechanics, pp. 49–54.

Deere, D.U. (1964) Technical description of cores for engineering purposes. *Rock Mechanics & Engineering Geology*, **1**: 16–22.

Deere, D.U. & Miller, R.P. (1966) *Engineering Classification and Index Properties for Intact Rock*, Air Force Weapons Laboratory, Report AFWL-TR-65-16, Kirtland Air Force Base, NM.

Deere, D.U., Hendron, A.J., Patton, F.D. & Cording, E.J. (1967) Design of surface and near surface construction in rock. In *Eighth US Symposium on Rock Mechanics*, Minneapolis, pp. 237–303.

Delhomme, J.P. (1979) Spatial variability and uncertainty in groundwater flow parameters: a geostatistical approach, *Water Resources Research*, **15**(2): 269–280.

D'Elia, B., Esu, F., Pellegrino, A. & Pescatore, T.S. (1985) Some effects on natural slope stability induced by the 1980 Italian earthquake. In *Proceedings, 11th International Conference on Soil Mechanics & Foundation Engineering*, San Francisco, CA, Vol. 4, pp. 1943–1949.

D'Elia, B., Picarelli, L., Leroueil, S. & Vaunat, J. (1998) Geotechnical characterisation of slope movements in structurally complex clay soils and stiff jointed clays. *Italian Geotechnical Journal*, **XXXII**(3): 5–32.

de Marsily, G. (1986) *Quantitative Hydrogeology Groundwater Hydrology for Engineers*, Academic Press, Orlando, FL.

Demirtas, R., Karakisa, S., Yatman, A., Baran, B., Zunbul, S., Iravut, Y., Altin, N. & Yilmaz, R. (1996) 1 Ekim 1995 Dinar Depremi Mekanizmasi (in Turkish), *Deprem Arastirma Bulteni* **23**(74): 5–45.

Demond, A.H. & Roberts, P.V. (1987) An examination of relative permeability relations for two-phase flow in porous media. *Water Resources Bulletin*, **23**(4): 617–628.

Dempster, A.P., Laird, N.M. & Rubin, D.B. (1977) Maximum likelihood from incomplete data via the EM algorithm. *Journal of the Royal Statistical Society, Series B. Methodological*, **39**: 1–22.

den Hoedt, G. (1986) Creep and relaxation of geotextile fabrics. *Journal of Geotextiles & Geomembranes*, **4**(2): 83–92.

Deniau, A., Cartier, G., Morbois, A. & Virollet, M. (1981) Un nouveau procédé de drainage: la paroi drainante. *Bulletin de Liaison des Laboratoires des Ponts et Chaussées*, Special XI, **F**: 15–18.

Denver, H. (1982) Modulus of elasticity determined by SPT and CPT. *Proceedings, ESOPT II*, **1**: 35–40.

De Nicola, A. & Randolph, M.F. (1993) Tensile and compressive shaft capacity of piles in sand. *Journal of Geotechnical Engineering, ASCE*, Reston, VA, **119**(12): 1952–1973.

De Ruiter, J. & Beringen, F.L. (1979) Pile foundations for large North Sea structures. *Marine Geotechnics*, **3**(3): 267–314.

Desai, C.S. (1974) Numerical design-analysis for piles in sands. Journal of The Geotechnical Engineering Division, *ASCE*, Reston, VA, **100**(6): 613–635.

Desai, C.S. & Faruque, M.O. (1984) Constitutive model for (geological) materials. *Journal of Engineering Mechanics, ASCE*, Reston, VA, **110**(9): 1391–1408.

Devlin, J.F. & Barker, J.F. (1996) Field investigation of nutrient pulse mixing in an *in situ* biostimulation experiment. *Water Resources Research*, **32**(9): 2869–2877.

Devlin, J.F. & Parker, B.L. (1996) Optimum hydraulic conductivity to limit contaminant flux through cutoff walls. *Ground Water*, **34**(4): 719–726.

DI (1965) *Code of Practice for Foundation Engineering*, Dansk Ingeniorforening, Copenhagen, Denmark, DS415.

Diaz-Rodriquez, J.A., Leroueil, S. & Aleman, J.D. (1992) Yielding of Mexico City clay and other natural clays. *Journal of Geotechnical Engineering Division, ASCE*, Reston, VA, **118**(7): 981–995.

DiMaggio, J.A. (1978) *Stone Columns for Highway Construction*, Demonstration Project No. 46, Report No. FHWA-DP-46-1, Federal Highway Administration, Springfield, VA.

DiMaggio, F.L. & Sandler, I.S. (1971) Material model for granular soils. *Journal of Engineering Mechanics Division, ASCE*, Reston, VA, **97**(3): 935–950.

Dingman, S.L. (1994) *Physical Hydrology*, Macmillan, New York.

DM-7 (1971) *Design Manual for Soil Mechanics*, Foundations and Earth Structures, Department of the Navy, Washington, DC.

Dobry, R. & Gazetas, G. (1985) Dynamic stiffness and damping of foundations by simple methods. In Gazetas, G. & Selig, E.T. (Eds) *Vibration Problems in Geotechnical Engineering*, American Society of Civil Engineers, Reston, VA, USA, pp. 77–107.

Dobry, R. & Gazetas, G. (1988) Simple method for dynamic stiffness and damping of floating pile groups. *Géotechnique*, **38**(4): 557–574.

Dobry, R., Vasquez-Herrera, A., Mohammad, R. & Vucetic, M. (1985) Liquefaction flow failure of silty sand by torsional cyclic tests. *Advances in the Art of Testing Soils under Cyclic Loading Conditions, ASCE Convention*, Detroit, Michigan, ed: V. Khosla, 29–50.

Domenico, P.A. & Schwartz, F.W. (1998) *Physical and Chemical Hydrogeology*, Wiley, New York.

Donald, I.B. (1956) Shear strength measurements in unsaturated non-cohesive soils with negative pore pressures. In *Proceedings, Second Australia–New Zealand Conference on Soil Mechanics & Foundation Engineering*, pp. 200–204.

Donaldson, J.J. (1994) Texturing techniques. In Hsuan, Y.G. & Koerner, R.M. (Eds) *GRI 8 Conference on Geosynthetic Resins, Formulations & Manufacturing*, IFAI, Roseville, MN, pp. 113–122.

Dove, J.E., Frost, J.D., Han, J. & Bachus, R.C. (1997) The influence of geomembrane surface roughness on interface strength. In *Proceedings Geosynthetics '97 Conference*, Long Beach, Industrial Fabrics Association International, Roseville, MN, pp. 863–876.

Dreimanis, A. (1962) Quantitative gasometric determination of calcite and dolomite by using Chittick apparatus. *Journal of Sedimentary Petrology*, **32**(3): 520–529.

Drever, J.I. (1982) *The Geochemistry of Natural Waters*, Prentice-Hall, Englewood Cliffs, NJ.

Driscoll, F.G. (1986) *Groundwater & Wells*, 2nd Edn, Johnson Filtration Systems, St Paul, MN.

Drnevich, V.P. (1976) *Drnevich Resonant Column Apparatus Operating Manual*, Soil Dynamics Instruments, Lexington, KY.

Drucker, D.C., Gibson, R.E. & Henkel, D.J. (1957) Soil mechanics and work-hardening theories of plasticity. *Transactions, ASCE*, Reston, VA, **122**: 338–346.

Drumright, E.E. (1989) *PhD thesis*, Colorado State University, CO.

Druschel, S.J. & Underwood, E.R. (1993) Design of lining and cover system sideslopes. In *Proceedings Geosynthetics '93 Conference*, Vancouver, BC, Industrial Fabrics Association International, Roseville, MN, Vol. 3, pp. 1341–1355.

Dullien, F.A.L. (1979) *Porous Media: Fluid Transport and Pore Structure*, Academic Press, New York.

Duncan, J.M. (1979) Behaviour and design of long-span metal culverts. *Journal of Geotechnical Engineering, ASCE*, Reston, VA, **105**(3): 399–418.

Duncan, J.M. (1992) State-of-the-art: Static stability and deformation analysis. In *Proceedings ASCE Specialty Conference on Stability and Performance of slopes and Embankments – II*, Berkeley, Geotechnical Special Publication No. 31, Vol. 1, pp. 222–266.

Duncan, J.M. (1996) Soil slope stability analysis. In *Landslides—Investigation and Mitigation*, A.K. Turner & R.L. Schuster (Eds.) Special Report 247, Transportation Research Board, Washington, DC, pp. 337–371.

Duncan, J.M. & Buchignani, A.L. (1976) *An Engineering Manual for Slope Stability Studies*, Department of Civil Engineering, University of California, Berkeley.

Duncan, J.M. & Seed, R.B. (1986) Compaction-induced earth pressures under K_o-conditions. *ASCE Journal of Geotechnical Engineering*, Reston, VA, **112**(1): 23–43.

Duncan, J.M. & Wright, S.G. (1980). The accuracy of equilibrium methods of slope stability analysis. *Engineering Geology*, **16**: 5–17.

Duncan, J.M., Williams, G.W., Sehn, A.L. & Seed, R.B. (1991a) Estimation of earth pressures due to compaction. *ASCE Journal of Geotechnical Engineering*, Reston, VA, **117**(12): 1833–1847.

Duncan, J.M., Williams, G.W., Sehn, A.L. & Seed, R.B. (1993b) Discussion. *ASCE Journal of Geotechnical Engineering*, Reston, VA, **119**(7): 1162–1177.

Dunnicliff, J. (1988) *Geotechnical Instrumentation for Monitoring Field Performance*, Wiley, New York.

Dwyer, S.F. (1995) Alternative landfill cover demonstration. In *Landfill Closures: Environmental Protection and Land Recovery*, Geotechnical Special Publication No. 53, Dunn, R.J. and Singh, U.P. (Eds.) American Society of Civil Engineers, Reston, VA, pp. 19–34.

Dwyer, S.F. (1998) Alternative landfill covers pass the test. *Civil Engineering, ASCE*, Reston, VA, **68**(9): 50–52.

Dysli, M. (1990) *Le gel et son action sur les sols et les fondations*, Presses Polytechniques et Universitaires Romandes.

Ebeling, R.M. & Morrison, E.E. (1992) *The Seismic Design of Waterfront Retaining Structures*, Technical Report ITL-92-11, Waterways Experiment Station, Vicksburg, MS.

Eberle, M.A. & von Maubeuge, K. (1997) Measuring the *in-situ* moisture content of geosynthetic clay liners (GCLs) using time domain reflectometry (TDR). In Rowe, R.K. (Ed.) *Proceedings, Sixth International Conference on Geosynthetics*, Atlanta, GA, Industrial Fabrics Association International, Roseville, MN, Vol. 1, pp. 205–210.

Edgers, L., Noble, J.J. & Williams, E. (1992) A Biologic Model for Long-Term Settlement in Landfills, Proc., Conf. on Environmental Technology, Balkan: 177–184.

Edil, T.B. & Dhowian, A.W. (1981) At-rest lateral pressure of peat soils. *Journal of Geotechnical Engineering Division, ASCE*, Reston, VA, **107**(2): 201–217.

Edil, T.B., Ranguette, V.J. & Wuellner, W.W. (1990) Settlement of municipal refuse. In *Geotechnics of Waste Fills – Theory & Practice*, STP 1070, Landua, A. and Knowles E.D. (Eds.) American Society for Testing & Materials, West Conshohocken, PA, pp. 225–239.

Editorial reports on seismic risk. *International Journal on Hydropower and Dams*, **5** (1, 2).

Edlefsen, W.H. & Anderson, A.B.C. (1943) Thermodynamics of soil moisture. *Hilgardia*, **15**(2): 31–298.

Eggestad, A. (1983) Improvement of cohesive soils–state-of-the-art report. In *Proceedings, Eighth European Conference on Soil Mechanics & Foundation Engineering*, Helsinki, Vol. 3, pp. 991–1007.

Ehrig, H.-J. & Scheelhaase, T. (1993) Pollution potential and long term behaviour of sanitary landfills. In *Proceedings, Fourth International Landfill Symposium*, Sardinia, pp. 1203–1255.

Eid, H.T. & Stark, T.D. (1997) Shear behavior of an unreinforced geosynthetic clay liner. *Geosynthetics International*, **4**(6): 645–659.

Eigenbrod, K.D. (1975) Analysis of the pore pressure changes following the excavation of a slope. *Canadian Geotechnical Journal*, **12**(3): 429–440.

Einsele, G. (1992) *Sedimentary Basins*, Springer-Verlag, Berlin.

Einstein, H.H. & Schwartz, C.W. (1979) Simplified analysis for tunnel supports. Journal of *Geotechnical Engineering, ASCE*, Reston, VA, **105**(4): 499–518.

Einstein, H.H., Bischoff, N. & Gofmann, E. (1972) Behavior of invert slabs in swelling shale. In *International Symposium on Underground Openings*, Lucerne, Switzerland, pp. 296–329.

Eith, A.W. & Koerner, R.M. (1992) Field evaluation of geonet flow rate (transmissivity) under increasing load. *Journal of Geotextile & Geomembranes*, **11**(5–6): 153–166.

Eith, A.W., Boschuk, J. & Koerner, R.M. (1991) Prefabricated bentonite clay liners. *Geotextiles & Geomembranes*, **10**: 575–599.

Elias, V. & Christopher, B.R. (1996) *Mechanically Stabilized Earth Walls and Reinforced Soil Slopes; Design and Construction Guidelines*, Report No. FHWA-SA-96-071, US Department of Transportation, Federal Highway Administration, Washington, DC.

Elias, V. & Juran, I. (1991) *Soil Nailing for Stabilization of Highway Slopes and Excavations*, US Department of Transportation, Federal Highway Administration Publication No. FHWA-RD-89-193, Washington, DC.

El-Marsafawi, H., Han, Y.C. & Novak, M. (1992) Dynamic experiments on two pile groups. *Journal of Geotechnical Engineering, ASCE*, Reston, VA, **118**(4): 576–592.

El Naggar, M.H. & Novak, M. (1995a) Nonlinear lateral interaction in pile dynamics. *Journal of Soil Dynamics & Earthquake Engineering*, **14**(2): 141–157.

El Naggar, M.H. & Novak, M. (1995b) Effect of foundation nonlinearity on modal properties of offshore towers. *Journal of Geotechnical Engineering, ASCE*, Reston, VA, **121**(9): 660–668.

El Naggar, M.H. & Novak, M. (1996) Influence of foundation nonlinearity on offshore tower response. *Journal of Geotechnical Engineering, ASCE*, Reston, VA, **122**(9): 717–724.

Eloy-Giorni, C., Pelte, T., Pierson, P. & Margarita, R. (1996) Water diffusion through geomembranes under hydraulic pressure. *Geosynthetics International*, **3**(6): 741–769.

Elsabee, F. & Morray, J.P. (1977) *Dynamic Behavior of Embedded Foundations*, Research Report R77-33, Civil Engineering Department, Massachusetts Institute of Technology, Cambridge, MA.

Emrich, W.J. (1971) Performance study of soil sampler for deep-penetration marine borings.

In *Sampling of Soil & Rock*, ASTM Special Technical Publication 483, American Society for Testing & Materials, West Conshohocken, PA, pp. 30–50.

EN 1401 Plastic piping systems for non-pressure underground drainage and sewerage—unplasticized polyvinyl chloride (PVC-U). European Standard, European Committee for Standardization, Brussels.

EN 12666 Plastics piping systems for non-pressure underground drainage and sewerage-polyethylene (PE), European Standard, European Committee for Standarization, Brussels.

ERES (1998) *Catalogue of Current State Pavement Design Features*, Draft Final Report on NCHRP Project 1-32, ERES Consultants, Champaign, IL, pp. 61821–63915.

Escario, V. & Juca, J. (1989) Strength and deformation of partly saturated soils. *Proceedings, 12th ICSMFE*, Rio de Janeiro, Vol. 3, pp. 43–46.

Esrig, M.I. (1968) Pore pressures, consolidation and electrokinetics. *Journal of Soil Mechanics & Foundation Engineering Division, ASCE*, Reston, VA, **94**(4): 899–921.

Esrig, M.I. & Bachus, R.D. (Eds) (1991) *Deep Foundation Improvements: Design, Construction, and Testing*, Presented at a symposium, Las Vegas, ASTM STP 1089, ASTM, West Conshohocken, PA.

Evans, S.G. (1997) Fatal landslides and landslide risk in Canada. In *Proceedings, International Workshop on Landslide Risk Assessment*, Honolulu, HI; pp. 185–196.

FAA (1987) Federal Aviation Administration Advisory Circular.

FAA (1995a) *LEDFAA User's Manual*, Federal Aviation Administration Advisory Circular ISO/5320-16 Airport Pavement Design for the Boeing 777 Airplane, US Department of Transportation, FAA, Washington, DC.

FAA (1995b) *Airport Pavement Design & Evaluation*, Federal Aviation Administration Advisory Circular ISO/5320-60, US Department of Transportation, FAA, Washington, DC.

Faccioli, E. (1991) Seismic amplification in the presence of geological and topographic irregularities. In *Proceedings, Second International Conference on Recent Advances in Geotechnical Earthquake Engineering & Soil Dynamics*, St Louis, MO, Vol. II, pp. 1779–1797.

Fam, S. (1996) Vapor extraction and bioventing. In Nyer, E.K. (Ed.) In Situ *Treatment Technology*, CRC Lewis, Boca Raton, FL, pp. 101–148.

Fang, H.-Y. (1991) *Foundation Engineering Handbook*, 2nd Edn, Chapman & Hall, New York.

Farmer, I.W. (1968) *Engineering Properties of Rocks*, E. & F.N. Spon Limited, London, England.

Farr, A.M., Houghtalen, R.J. & McWhorter, D.B. (1990) Volume estimation of light nonaqueous phase liquids in porous media. *Groundwater*, **28**: 48–56.

Fassett, J.B., Leonards, G.A. & Repetto, P.C. (1994) Geotechnical properties of municipal solid wastes and their use in landfill design. In *Proceedings, Waste Tech '94 Conference*, National Solid Waste Management Association, Charleston, SC.

Faure, R.M. (1985) Analyse des contraintes dans un talus par la méthode des perturbations. *Revue Française de Géotechnique*, **33**: 49–59.

Faure, R.M., Pham, M., Robinson, J.C. & Jolly, P. (1996) Three dimensional slope stability by the perturbation method. In *Proceedings, Seventh International Symposium on Landslides*, Trondheim, Vol. 2, pp. 1207–1212.

Faure, Y.H. (1984) Design of drain beneath geomembranes: discharge estimation and flow patterns. In *Proceedings, International Conference on Geomembranes*, Denver, CO, Industrial Fabrics Association International, Roseville, MN, Vol. 2, pp. 463–468.

Faust, C.R., Guswa, J.H. & Mercer, J.W. (1989) Simulation of three-dimensional flow of immiscible fluids within and below the unsaturated zone, *Water Resource Research*, **25**(12): 2449–2464.

Faustman, E.M. & Omenn, G.S. (1996) Risk assessment. In Klaassen, C.D. (Ed.) *Casarett & Doull's Toxicology: The Basic Science of Poisons*, 5th Edn, McGraw-Hill, New York, pp. 80–83.

Fay, J.J. & King, R.E. III (1994) Antioxidants for geosynthetic resins and applications, Hsuan, Y.G. & Koerner, R.M. (Eds) *GRI 8 Conference on Geosynthetic Resins, Formulations & Manufacturing*, IFAI, Roseville, MN, pp. 74–91.

Fayer, M. & Jones, T. (1990) *Unsaturated Soil Water and Heat Flow Model, Version 2*, Pacific Northwest Laboratory, Richland, Washington, DC.

Fayer, M.J., Rockhold, M.L. & Campbell, M.D. (1992) Hydrologic modeling of protective barriers: comparison of field data and simulation results. *Soil Science Society of America Journal*, **56**(3): 690–700.

Feenstra, S. & Cherry, J.A. (1996) Diagnosis and assessment of DNAPL sites. In Pankow, J.F. &

J.A. Cherry (Eds) *Dense Chlorinated Solvents and Other DNAPLs in Groundwater*, Waterloo Press, Rockwood, Ontario, pp. 395–474.

Feenstra, S., Cherry, J.A. & Parker, B.L. (1996) Conceptual models for the behavior of DNAPLs in the subsurface. In Pankow, J.F. & J.A. Cherry (Eds) *Dense Chlorinated Solvents and Other DNAPLs in Groundwater*, Waterloo Press, Rockwood, Ontario, pp. 53–88.

Federal Register (1991), **56**(20): 3535.

Fell, R. (1994) Landslide risk assessment and acceptable risk. *Canadian Geotechnical Journal*, **31**(2): 261–272.

Fellenius, B.H. (1989) *Unified Design of Piles and Pile Groups*, Transportation Research Board, Washington, TRB Record 1169, pp. 75–82.

Fellenius, W. (1927) *Erdstatische Berechnungen (Calculation of Stability of Slopes)*, Ernst, Berlin (revised edn 1939).

FEMA (1997) *NEHRP Recommended Provisions for Seismic Regulations for New Buildings, Part 2—Commentary, Federal Emergency Management Agency*, 1994 Edition, Building Seismic Safety Council, Washington, DC.

Fenelli, G.B. & Picarelli, L. (1990) The pore pressure field built up in a rapidly eroded soil mass. *Canadian Geotechnical Journal*, **27**(3): 387–392.

Fenelli, G.B., Silvestri, F. & Picarelli, L. (1992) Deformation process of a hill shaken by the Irpinia earthquake in 1980. In *Proceedings, French–Italian Conference on Slope Stability in Seismic Areas*, Bordighera, pp. 47–62.

Fenn, D.G., Hanley, K.J. & DeGeare, T.V. (1975) *Use of the Water Balance Method for Predicting Leachate Generation from Solid Waste Disposal Sites*, US Environmental Protection Agency, EPA/530/SW-168, Washington, DC.

Fernandez, F. & Quigley, R.M. (1985) Hydraulic conductivity of natural clays permeated with simple liquid hydrocarbons. *Canadian Geotechnical Journal*, **22**: 205–214.

Fernandez, F. & Quigley, R.M. (1988) Viscosity and dielectric constant controls on the hydraulic conductivity of clayey soils permeated with water-soluble organics. *Canadian Geotechnical Journal*, **25**(3): 582–589.

Fernando, N.S.M & Carter, J.P. (1998) Elastic analysis of buried pipes under surface patch loadings. *Journal of Geotechnical & Geoenvironmental Engineering, ASCE*, Reston, VA, **124**(8): 720–728.

Fetzer, C. (1967) Electro-osmotic stabilization of West Branch Dam. *Journal of Soil Mechanics & Foundation Division, ASCE*, Reston, VA, **93**(4): 85–104.

Fetter, C.W. (1994) *Applied Hydrogeology*, Macmillan College Publishing, New York.

FHWA (1987) *Pavement Design, Principles and Practices, FHWA Short Course*, 3rd Revision, Federal Highway Administration & ERES Consultants, Champaign, IL, pp. 61821–63915.

FHWA (1993a) *Recommendations Clouterre 1991* (English translation), *Soil Nailing Recommendations 1991*, Report FHWA-SU-026, Federal Highway Administration, Washington, DC.

FHWA (1993b) *FHWA International Scanning Tour on Soil Nailing*, Federal Highway Administration, US Department of Transportation, Washington, DC.

FHWA (1996) *Mechanically Stabilized Earth Walls and Reinforced Soil Slopes Design and Construction Guidelines*, Federal Highway Administration Demonstration Project 82, Washington, DC.

Finlay, P.J. & Fell, R. (1997) Landslides: risk perception and acceptance. *Canadian Geotechnical Journal*, **34**(2): 169–188.

Finn, W.D.L. (1988) Dynamic analysis in geotechnical engineering. In *Proceedings, Earthquake Engineering & Soil Dynamics II – Recent Advances in Ground Motion Evaluation*, American Society of Civil Engineers, Geotechnical Engineering Division, Park City, UT, pp. 523–591.

Finn, W.D.L. (1990) Analysis of post-liquefaction deformations in soil structures. Invited paper, In *Proceedings, H. Bolton Seed Memorial Symposium*, University of California, Berkeley, Duncan, J.M. (Ed.) Bi-Tech Publishers, Vancouver, Vol. 2, pp. 291–311.

Finn, W.D.L. (1993) Seismic safety evaluation of embankment dams. In *Proceedings, International Workshop on Dam Safety Evaluation*, 26–28 April, Grindewald, Switzerland, Vol. 4, pp. 91–135.

Finn, W.D.L. (1995) Foundation factors for seismic design. In *Proceedings, Seventh Canadian Conference on Earthquake Engineering*, Montreal, pp. 197–204.

Finn, W.D.L. (1999) State of the art of geotechnical earthquake engineering practice. Invited Keynote Lecture, *Seventh International Conference on Soil Dynamics and Earthquake Engineering*, August 10–15, Bergen, Norway.

Finn, W.D.L. & Yogendrakumar, M. (1989) *TARA-3FL: A Program for Analysis of Flow*

Deformations in Soil Structures with Liquefied Zones, Soil Dynamics Group, Department of Civil Engineering, University of British Columbia, Vancouver, BC.

Finn, W.D.L., Yogendrakumar, M., Yoshida, N. & Yoshida, H. (1986) *TARA-3: A Program for Nonlinear Static and Dynamic Effective Stress Analysis*, Soil Dynamics Group, University of BC, Vancouver, BC.

Finn, W.D.L., Ledbetter, R.H., Fleming, R.L. Jr., Templeton, A.E., Forrest, T.W. & Stacy, S.T. (1991) Dam on liquefiable foundation: safety assessment and remediation. In *Proceedings, International Workshop on Remedial Treatment of Potentially Liquefiable Soils*, January, Tsukuba Science City, Japan.

Finn, W.D.L., Wu, G. & Ledbetter, R.H. (1994) Problems in seismic soil–structure interaction. In *Proceedings, Eighth International Conference on Computer Methods and Advances in Geomechanics*, Morgantown, WV, Vol. 1, pp. 139–151.

Finn, W.D.L., Byrne, P.M., Evans, S. & Law, T. (1996) Some geotechnical aspects of the Hyogo-ken-Nanbu (Kobe) earthquake of January 17, 1995. *Canadian Journal of Civil Engineering*, **23**(3): 778–796.

Fisher, R.A. (1925) Applications of Student's distribution. *Metron* **5**: 90–104.

Flaate, K. & Rygg, N. (1964) Sawdust as embankment fill on peat bogs. In *Proceedings, Ninth Muskeg Research Conference*, NRC, ACSSM Technical Memorandum 81, pp. 136–149.

Fleenor, W.E. & King, I.P. (1995) Identifying limitations on use of the HELP model. In *Landfill Closures: Environmental Protection and Land Recovery*, Geotechnical Special Publication No. 53, Dunn, R.J. Sing, U.P. (Eds) American Society of Civil Engineers, Reston, VA, pp. 121–138.

Fleming, I.R., Rowe, R.K. & Cullimore, D.R. (1999) Field observations of clogging in a landfill leachate collection system. *Canadian Geotechnical Journal* **36**(4): 685–707.

Fleming, W.G.K., Weltman, A.J., Randolph, M.F. & Elson, W.K. (1985) *Piling Engineering*, Surrey University Press, Halsted Press, New York.

Fleming, W.G.K., Weltman, A.J., Randolph, M.F. & Elson, W.K. (1992) *Piling Engineering*, 2nd Edn, Halsted Press, New York.

Flynn, D.J., Thomson, N.R. & Farquhar, G.J. (1994) The influence of heterogeneity on the mass removal efficiency on conventional soil vacuum extraction technology: a field study. In *Proceedings, Eighth National Outdoor Action Conference*, May 23–25, Minneapolis, MN, pp. 41–56.

Focht, J.A. & Koch, (1973) Rational analysis of the lateral performance of offshore pile groups. In *Proceedings, Fifth Offshore Technical Conference*, Houston, TX, Vol. 2, pp. 701–708.

Focht, R., Vogan, J. & O'Hannesin, S. (1996) Field application of reactive iron walls for *in-situ* degradation of volatile organic compounds in groundwater. *Remediation*, **6**(3): 81–94.

Folkes, D.J. & Crooks, J.H.A. (1985) Effective stress paths and yielding in soft clays below embankments. *Canadian Geotechnical Journal*, **22**: 357–374.

Forchheimer, P. (1930), *Hydraulik*, 3rd Edn, B.G. Teubner, Leipzig und Berlin.

Foreman, D.E. & Daniel, D.E. (1986) Permeation of compacted clay with organic chemicals. *Journal of Geotechnical Engineering, ASCE*, Reston, VA, **112**: 669–681.

Forsyth, R.A. & Egan, J.P. (1976) *Use of Waste Materials in Embankment Construction*, Transportation Research Record 593, Washington, DC, pp. 3–8.

Fountain, J.C., Starr, R.C., Middleton, T., Beikirch, M., Taylor, C. & Hodge, D. (1996) A controlled field test of surfactant-enhanced aquifer remediation. *Ground Water*, **34**(5): 910–916.

Fox, P.J., Edil, T.B. & Lau, L.T. (1992) C_α/C_c concept applied to compression of peat. *ASCE Journal of Geotechnical Engineering*, Reston, VA, **118**(8): 1256–1263. See also Discussion, **120**(4): 764–770.

Fox, P.J., Roy-Chowdhury, N. & Edil, T.B. (1999) Secondary compression of peat with or without surcharging, Discussion of paper by Mesri *et al.* *ASCE Journal of Geotechnical & Geoenvironmental Engineering*, Reston, VA, **125**(2): 160–162.

Frank, R. & Magnan, J.-P. (1995) Cone penetration testing in France: national report. In *Proceedings, CPT '95*, Linkoping, Swedish Geotechnical Society, Vol. 3, pp. 147–156.

Frank, H.S. & Wen, W.Y. (1957) Structure aspects of ion-solvent interaction in aqueous solutions. A suggested picture of water structure. *Faraday Society Discussions*, **24**: 133–140.

Frankel, F., Mueller, C., Bernhard, T., Perkins, D., Leyendecker, E.V., Dickman, N., Hanson, S. & Hopper, M. (1996) *Interim National Hazard Maps: Documentation*, Draft Report, US Geological Survey, Denver, CO.

Franklin, G. & Chang, F. (1977) *Earthquake Resistance of Earth and Rockfill Dams. 5: Permanent Displacement of Earth Embankments by Newmark Sliding Block Analysis*. Miscellaneous Paper S-71-17, Soils & Pavements Laboratory, US Army Engineer Waterways Experiment Station, Vicksburg, MS.

Fraser, R.A. & Wardle, L.J. (1976) Numerical analysis of rectangular rafts on layered foundations. *Géotechnique*, **26**(4): 613–630.

Freden, S. (1965) Some aspects on the physics of frost heave in mineral soils. *Surface Chemistry*, 79–90.

Fredlund, D.G. (1964) *MSc thesis*, Department of Civil Engineering, University of Alberta, Edmonton.

Fredlund, D.G. (1979) Second Canadian Geotechnical Colloquium: appropriate concepts and technology for unsaturated soils. *Canadian Geotechnical Journal*, **16**(1): 121–139.

Fredlund, D.G. (1992) Background, theory and research related to the use of thermal conductivity matric suction measurements. In *Advances in Measurement of Soil Physical Properties: Bringing Theory into Practice*, San Antonio, Texas, SSSA Special Publication No. 30, Soil Science of America, Eds. G.C. Top, W.D. Reynolds and R.E. Green, Madison, WI, pp. 249–262.

Fredlund, D.G. (1995) Prediction of unsaturated soil functions using the soil–water characteristic curve. In *Proceedings, Bength B. Broms Symposium on Geotechnical Engineering*, December 13–15, Nanyang Technological University, Singapore, River Edge, NJ, World Scientific, pp. 113–133.

Fredlund, D.G. & Krahn, J. (1977) Comparison of slope stability methods of analysis. *Canadian Geotechnical Journal*, **14**(3): 429–439.

Fredlund, D.G. & Morgenstern, N.R. (1977) Stress state variables for unsaturated soils. *Journal of Geotechnical Engineering, ASCE*, Reston, VA, **103**: 447–466.

Fredlund, D.G. & Rahardjo, H. (1993) *Soil Mechanics for Unsaturated Soils*, Wiley, New York.

Fredlund, D.G. & Xing, A. (1994) Equations for the soil–water characteristic curve. *Canadian Geotechnical Journal*, **31**: 521–532.

Fredlund, D.G., Bergan, A.T. & Sauer, E.K. (1975) Deformation characterization of subgrade soils for highways and runways in northern environments. *Canadian Geotechnical Journal*, **12**(2): 213–223.

Fredlund, D.G., Morgenstern, N.R. & Widger, A. (1978) The shear strength of unsaturated soils. *Canadian Geotechnical Journal*, **15**(3): 313–321.

Fredlund, D.G., Xing, A. & Huang, S. (1994) Predicting the permeability function for unsaturated soils using the soil–water characteristic curve. *Canadian Geotechnical Journal*, **31**(4): 533–546.

Fredlund, M.D., Sillers, W.S., Fredlund, D.G. & Wilson, G.W. (1996a) Design of a knowledge-based system for unsaturated soil properties. In *Proceedings, Third Canadian Conference on Computing in Civil Engineering*, August 26–28, Montreal, Quebec, pp. 659–677.

Fredlund, D.G., Xing, A., Fredlund, M.D. & Barbour, S.L. (1996b) The relationship of the unsaturated soil shear strength to the soil–water characteristic curve. *Canadian Geotechnical Journal*, **33**(3): 440–448.

Fredlund, M.D., Fredlund, D.G. & Wilson, G.W. (1997a) Prediction of the soil–water characteristic curve from grain-size distribution and volume–mass properties. In *Proceedings, Third Brazilian Symposium on Unsaturated Soils, NONSAT '97*, April 22–25, Rio de Janeiro, **1**: 13–23.

Fredlund, M.D., Fredlund, D.G. & Wilson, G.W. (1997b) Estimation of unsaturated soil properties using a knowledge-based system. In *Proceedings, Fourth Congress on Computing in Civil Engineering*, June 16–18, American Society of Civil Engineers, Reston, VA, pp. 501–510.

Freeze, R.A. & Cherry, J.A. (1979) *Groundwater*, Prentice-Hall, NJ.

Freeze, R.A. & McWhorter, D.B. (1997) A framework for assessing risk reduction due to DNAPL mass removal from low permeability soils. *Ground Water*, **35**(1): 111–123.

French Standard (1992) *Soil Reinforcement-Backfilled Structures with Inextensible and Flexible Reinforcing Straps or Sheets*, NF, Paris, P 94-220 (English translation).

Fruchter, J.S., Cole, C.R., Williams, M.D., Vermeul, R., Teel, S.S., Amonette, J.E., Szecsody, J.E. & Yabusaki, S.B. (1997) Creation of a subsurface permeable treatment barrier using *in situ* redox manipulation. In *Proceedings, 1997 International Containment Technology Conference & Exhibition*, February 10–12, St Petersburg, FL, pp. 704–710.

Fuhrmann, M., Aloysius, D. & Zhou, I. (1995) Permeable, subsurface sorbent barrier for

^{90}Sr: laboratory studies of natural and synthetic materials. *Waste Management*, **15**(7): 485–493.

Fukuoka, M. (1986) Large Scale Permeability Tests for Geomembrane-Subgrade System. In *Proceedings, Third International Conference on Geotextiles, Geomembranes, & Related Products*, The Hague, The Netherlands, Vol. 3, pp. 917–922.

Fuleihan, N.F. & Wisse, A.E.Z. (1995) Minimum thickness of compacted soil liners: II. Analysis and case histories–Discussion. *Journal of Geotechnical Engineering, ASCE*, Reston, VA, **121**(6): 504–506.

Fung, Y.C. (1977) *A First Course in Continuum Mechanics*, 2nd edn, Prentice-Hall, Englewood Cliffs, NJ.

Gaind, K.J. & Char, A.N.R. (1983) Reinforced soil beams. *Journal of Geotechnical Engineering, ASCE*, Reston, VA, **109**(7): 977–982.

Gallavresi, F. (1992) Grouting improvement of foundation soils (keynote lecture). In *Grouting, Soil Improvement, & Geosynthetics*, Geotechnical Special Publication No. 30, American Society of Civil Engineers, ASCE Press, Reston, VA, pp. 1–38.

Gan, J.K.-M., Fredlund, D.G. & Rahardjo, H. (1988) Determination of the shear strength parameters of an unsaturated soil using the direct shear. *Canadian Geotechnical Journal*, **25**: 500–510.

Gardner, W.R. (1958) Some steady state solutions of the moisture flow equation with application to evaporation from a water table. *Soil Science*, **85**: 228–232.

Gässler, G. & Gudehus, G. (1983) Soil nailing-statistical design. In *Proceedings, VIII ECSMFE*, Helsinki.

Gazetas, G. (1991) Foundation vibrations. Fang, H.Y. (Ed.) In *Foundation Engineering Handbook*, 2nd Edn, Van Nostrand Reinhold, New York.

Gazetas, G. & Dobry, R. (1984) Horizontal response of piles in layered soils. *Journal of Geotechnical Engineering, ASCE*, Reston, VA, **110**(1): 20–40.

Gazetas, G. & Makris, N. (1991) Dynamic pile–soil–pile interaction, part I: Analysis of axial vibration. *Earthquake Engineering & Structural Dynamics*, **20**: 115–132.

Gazetas, G., Fan, K. & Kaynia, A.M. (1993) Dynamic response of pile groups with different configurations. *Journal of Soil Dynamics & Earthquake Engineering*, **12**(4): 239–257.

Gazioglu, S.M. & O'Neill, M.W. (1984) Evaluation of P–Y relationships in cohesive soils. In Meyer, J.R. (Ed.) *Analysis & Design of Pile Foundations*, American Society of Civil Engineers, Reston, VA, pp. 192–213.

Gee, G.W., Anderson, L.W. & Fayer, M.J. (1997) Surface barrier research at the Hanford site. In *Proceedings, International Containment Technology Conference*, February, St Petersburg, FL, pp. 305–311.

Gelhar, L.W., Welty, C. & Rehfeldt, K.R. (1992) A critical review of data on field-scale dispersion in aquifers. *Water Resources Research*, **28**(7): 1955–1974.

Geller, M. (1982) *Compaction Equipment for Asphalt Mixtures*, ASTM STP829, American Society for Testing & Materials, West Conshohocken, PA.

Gemperline, M.C. (1988) Centrifuge modelling of shallow foundations, *Proceedings, ASCE Spring Convention*, ASCE Press, Reston, VA.

Gens, A., Hutchinson, J.N. & Cavounidis, S. (1988) Three-dimensional analysis of slides in cohesive soils. *Géotechnique*, **38**(1): 1–23.

Geological Society (1986) *Site Investigation Practice: Assessing B5 5930*. Geological Society Engineering Geology Special Publication No. 2., Hawkins, A.B. (Ed.) The Geological Society, London, England.

Geo-Slope International Ltd (undated) Slope/W, Calgary, Alberta, Canada (E-mail: *info@geoslope.com*).

Geosynthetics Research Institute GC-1 (1996) *Soil–Filter Core Combined Flow Test*, GSI, Folsom, PA.

Geosynthetics Research Institute GG-1 (1996) *Geogrid Rib Tensile Strength*, GSI, Folsom, PA.

Geosynthetics Research Institute GG-2 (1996) *Geogrid Junction Strength*, GSI, Folsom, PA.

Geosynthetics Research Institute GM-12 (1996) *Asperity Measurement of Textured Geomembranes using a Depth Gage*, GSI, Folsom, PA.

Gerhard, J.I., Kueper, B.H. & Hecox, G. (1998). Waterflooding for the removal of pooled DNAPL. *Ground Water*, **36**(2): 283–292.

Ghaboussi, J. & Momen, H. (1982) Modelling and analysis of cyclic behavior of sands, In Pande, G.N. & Zienkiewicz O.C. (Eds) *Soil Mechanics–Transient & Cyclic Loads*, Wiley, London, England, pp. 313–342.

Ghiassian, H., Hryciw, R.D. & Gray, D.H. (1997) Stabilization of coastal slopes by anchored geosynthetic systems. *Journal of Geotechnical &*

Geoenvironmental Engineering, ASCE, Reston, VA, **123**(8): 736–743.

Ghosh, R.K. (1980) Estimation of soil–moisture characteristics from mechanics properties of soils. *Soil Science Journal*, **130**(2): 60–63.

Gibson, R.E. (1963) An analysis of system flexibility and its effect on time-lag in porewater pressure measurements. *Géotechnique*, **13**(1): 1–11.

Gibson, R.E. & Lo, K.Y. (1961) A theory of soils exhibiting secondary compression. *Acta Polytechnica Scandinavica, C*, **296**(10): 1–15.

Gilbert, P.A. & Murphy, W.L. (1987) *Prediction/Mitigation of Subsidence Damage to Hazardous Waste Landfill Covers*, US Environmental Protection Agency, Hazardous Waste Engineering Research Laboratory, Cincinnati, OH, EPA/600/12/87-025.

Gilbert, R.B., Liu, C.N., Wright, S.G. & Trautwein, S.J. (1995) A double shear test method for measuring interface strength. In *Proceedings, Geosynthetics '95 Conference*, Nashville, Industrial Fabrics Association International, Roseville, MN, Vol. 3, pp. 1017–1029.

Gilbert, R.B., Fernandez, F. & Horsfield, D.W. (1996) Shear strength of reinforced geosynthetic clay liner. *Journal of Geotechnical Engineering, ASCE*, Reston, VA, **122**(4): 259–266.

Gilbert, R.O. (1987) *Statistical Methods for Environmental Pollution Monitoring*, Van Norstrand Reinhold, New York.

Gilbert, R.O. & R.R. Kinneson. (1981) Statistical methods for estimating the mean and variance from radionuclide data sets containing negative, unreported or less-than values. *Health Physics*, **40**: 377–390.

Gillham, R.W. & Burris, D.R. (1997) Recent development in permeable *in situ* treatment walls for remediation of contaminated groundwater. In Ward, C.H., Cherry, J.A. & Scalf, M.R. (Eds) *Subsurface Restoration*, Ann Arbor Press, Chelsea, MI, pp. 343–356.

Gillham, R.W. & O'Hannesin, S.F. (1992) Metal-catalysed abiotic degradation of halogenated organic compounds. In *Proceedings, IAH Conference on Modern Trends in Hydrogeology*, May 10–13, Hamilton, ON, pp. 94–103.

Gillham, R.W. & O'Hannesin, S.F. (1994) Enhanced degradation of halogenated aliphatics by zero-valent iron. *Ground Water*, **32**(6): 958–967.

Gillham, R.W., Major, L., Wadley, S.L.S. & Warren, J. (1998) Advances in the application of zero-valent iron for treatment of groundwater containing VOCs. In *Groundwater Quality: Remediation & Protection Proceedings, GQ'98 Conference*, IAHS Publication No. 250, September 21–25, Tubingen, Germany, pp. 475–481.

Gilliom, R.J. & Helsel, D.R. (1986) Estimation of distributional parameters for censored trace level quality data. 1: Estimation techniques. *Water Resources Research*, **22**: 135–146.

Gipson, A.H., Jr, (1985) Permeability testing on clayey soil and silty sand–bentonite mixture using acid liquor. In *hydraulic barriers in soil and rock*, Johnson, A.I., Frobel, R.K., Cavalli, N.J. & Petersson, C.B. (Eds) ASTM STP 874, American Society for Testing & Materials, West Conshohocken, PA, pp. 140–154.

Girault, D.P. (1987) Analysis of foundations failures in the Mexico earthquakes, 1985: factors involved and lessons learned. In Cassaro, M.A. & Romero, E.M. (Eds.) American Society of Civil Engineers, ASCE Press, Reston, VA, pp. 178–192.

Giroud, J.P. (1973) L'étanchéité des retenues d'eau par feuilles déroulées. *Annales de l'ITBTP*, **312**(TP161): 94–112 (in French).

Giroud, J.P. (1977) Conception de l'étanchéité des ouvrages hydrauliques par géomembranes. In *Proceedings, First International Symposium on Plastic & Rubber Waterproofing in Civil Engineering*, Session 3, Paper 13, June, Liège, Belgium, Vol. 1, pp. 1–17 (in French).

Giroud, J.P. (1981) Designing with geotextiles. *Matériaux et Constructions*, **14**(82): 257–272.

Giroud, J.P. (1982) Filter criteria for geotextiles. In *Proceedings, Second International Conference on Geotextiles*, August, Las Vegas, NV, Vol. 1, pp. 103–108.

Giroud, J.P. (1983) Rapport général sur les bassins revêtus de géomembranes. In *Comptesrendus du colloque sur l'étanchéité superficielle des bassins, barrages et canaux*, February, Paris, France, Vol. II, pp. 75–90d (in French).

Giroud, J.P. (1984a) Impermeability: the myth and a rational approach. In *Proceedings, International Conference on Geomembranes*, June Denver, CO, Vol. 1, pp. 157–162.

Giroud, J.P. (1984b) Analysis of stresses and elongations in geomembranes. In *Proceedings International Conference on Geomembranes*, June, Denver, CO, Industrial Fabrics Association International, Roseville, MN, Vol. 2, pp. 481–486.

Giroud, J.P. (1985) Tomorrow's designs for geotextile applications. In Fluet, J.E. (Ed.) *Geotextile Testing & the Design Engineer*, ASTM STP 952 American Society for Testing & Materials, West Conshohocken, PA, pp. 145–158.

Giroud, J.P. (1988) Review of geotextile filter criteria. In *Proceedings, First Indian Geotextiles Conference*, December, Bombay, India, pp. 1–6.

Giroud, J.P. (1989) Panelist contribution on geotextile filters. In *Proceedings, 12th International Conference on Soil Mechanics & Foundation Engineering*, August Rio de Janeiro, Brazil, Vol. 5, pp. 3105–3106.

Giroud, J.P. (1994) Quantification of geosynthetics behavior (special lecture). In *Proceedings, Fifth International Conference on Geotextiles, Geomembranes & Related Products*, September Singapore, Vol. 4, pp. 1249–1273.

Giroud, J.P. (1995) Determination of geosynthetic strain due to deflection. *Geosynthetics International*, **2**(3): 635–641.

Giroud, J.P. (1996a) Granular filters and geotextile filters. In Lafleur, J. & Rollin, A.L. (Eds) *Proceedings, GeoFilters '96*, May, Montréal, pp. 565–680.

Giroud, J.P. (1996b) Workshop on testing of geosynthetic materials for landfill liners and covers. *IGS News*, **12**(2): 3–4.

Giroud, J.P. (1997) Equations for calculating the rate of liquid migration through composite liners due to geomembrane defects. Special Issue on Liquid Migration Control Using Geosynthetic Liner Systems, *Geosynthetics International* **4**(3–4): 335–348.

Giroud, J.P. (1999) Lessons learned from failures associated with geosynthetics, keynote lecture. In *Proceedings, Geosynthetics '99*, April, Boston, MA, IFAI, Industrial Fabrics Association International, Roseville, MN, Vol. 1, pp. 1–66.

Giroud, J.P. & Beech, J.F. (1989) Stability of soil layers on geosynthetic lining systems. In *Proceedings, Geosynthetics '89*, February San Diego, CA, Industrial Fabrics Association International, Roseville, MN, Vol. 1, pp. 35–46.

Giroud, J.P. & Bonaparte, R. (1989a) Leakage through liners constructed with geomembranes, Part I: geomembrane liners. *Geotextiles & Geomembranes*, **8**(1): 27–67.

Giroud, J.P. & Bonaparte, R. (1989b) Leakage through liners constructed with geomembranes, Part II: composite liners. *Geotextiles & Geomembranes*, **8**(2): 71–111.

Giroud, J.P., Gleason, M.H. & Zornberg, J.G. (1999) Design of geomembrane anchorage against wind action. *Geosynthetics International* **6**(6): 481–507.

Giroud, J.P. & Houlihan, M.F. (1995) Design of leachate collection layers. In *Proceedings, Fifth International Landfill Symposium*, S. Margherita di Pula, Cagliari, Italy, Vol. 2, pp. 613–640.

Giroud, J.P. & Soderman, K.L. (1995) Design of structures connected to geomembranes. *Geosynthetics International*, **2**(2): 379–428.

Giroud, J.P., Gourc, J.P., Bally, P. & Delmas, P. (1977) Comportement d'un textile non tissé dans un barrage en terre (Behaviour of a nonwoven fabric in an earth dam). In *Proceedings, International Conference on the Use of Fabrics in Geotechnics*, April, Paris, France, Vol. 2, pp. 213–218, (in French).

Giroud, J.P. Bonaparte, R., Beech, J.F. & Gross, B.A. (1988) Load carrying capacity of a soil layer supported by a geosynthetic overlying a void. In *Theory and Practice of Earth Reinforcement*, Yamanouchi, T., Miura, N. and Ochiai, H. (Eds.), A.A. Balkema, Rotterdam, pp. 185–190.

Giroud, J.P. Khatami, A. & Badu-Tweneboah, K. (1989) Evaluation of the rate of leakage through composite liners. *Geotextiles & Geomembranes*, **8**(4): 337–340.

Giroud, J.P., Bonaparte, R., Beech, J.F. & Gross, B.A. (1990) Design of soil layer–geosynthetic systems overlying voids. *Geotextiles & Geomembranes*, **9**(1): 11–50.

Giroud, J.P., Badu-Tweneboah, K. & Bonaparte, R. (1992a) Rate of leakage through a composite liner due to geomembrane defects. *Geotextiles & Geomembranes*, **11**(1): 1–28.

Giroud, J.P., Gross, B.A. & Darasse, J. (1992b) *Flow in Leachate Collection Layers–Steady-State Conditions*, GeoSyntec Consultants Internal Report, Boca Raton, FL.

Giroud, J.P., Beech, J.F. & Soderman, K.L. (1994a) Yield of scratched geomembranes, *Geotextiles and Geomembranes*, Vol. 13, No. 4, pp. 231–246.

Giroud, J.P., Badu-Tweneboah, K. & Soderman, K.L. (1994b) Evaluation of landfill liners. In *Proceedings, Fifth International Conference on Geotextiles, Geomembranes & Related Products*, Singapore, Vol. 3, pp. 981–986.

Giroud, J.P., Bachus, R.C. & Bonaparte, R. (1995a) Influence of water flow on the stability of geosynthetic–soil layered systems on slopes. Special Issue on Design of Geomembrane

Applications, *Geosynthetics International*, **2**(6): 1149–1180.

Giroud, J.P., Badu-Tweneboah, K. & Soderman, K.L. (1995b) Theoretical analysis of geomembrane puncture. Special Issue on Design of Geomembrane Applications, *Geosynthetics International*, **2**(6): 1019–1048.

Giroud, J.P., Pelte, T. & Bathurst, R.J. (1995c) Uplift of geomembranes by wind. Special Issue on Design of Geomembrane Applications, *Geosynthetics International*, **2**(6): 897–952 (Erratum, **4**(2): 187–207).

Giroud, J.P., Williams, N.D., Pelte, T. & Beech, J.F. (1995d) Stability of geosynthetic–soil layered systems on slopes. Special Issue on Design of Geomembrane Applications, *Geosynthetics International*, **2**(6): 1115–1148.

Giroud, J.P., Gross, B.A., Bonaparte, R. & McKelvey, J.A. (1997a) Leachate flow in leakage collection layers due to defects in geomembrane liners. Special Issue on Liquid Migration Control Using Geosynthetic Liner Systems, *Geosynthetics International*, **4**(3–4): 215–292.

Giroud, J.P., Khire, M.V. & Soderman, K.L. (1997b) Liquid migration through defects in a geomembrane overlain and underlain by permeable media. Special Issue on Liquid Migration Control Using Geosynthetic Liner Systems, *Geosynthetics International*, **4**(3–4): 293–321.

Giroud, J.P., King, T.D., Sanglerat, T.R., Hadj-Hamou, T. & Khire, M.V. (1997c) Rate of liquid migration through defects in a geomembrane placed on a semi-permeable medium. Special Issue on Liquid Migration Control Using Geosynthetic Liner Systems, *Geosynthetics International*, **4**(3–4): 349–372.

Giroud, J.P., Soderman, K.L. & Badu-Tweneboah, K. (1997d) Optimal configuration of a double liner system including a geomembrane liner and a composite liner. Special Issue on Liquid Migration Control Using Geosynthetic Liner Systems, *Geosynthetics International*, **4**(3–4): 373–389.

Giroud, J.P., Houlihan, M.F., Bachus, R.C. & Qureshi, S. (1998a) Clogging potential of geosynthetic leachate collection layers by fine particles from sand protective layers. In Rowe, R.K. (Ed.) *Proceedings, Sixth International Conference on Geosynthetics*, March, Atlanta, GA, Industrial Fabrics Association International, Roseville, MN, Vol. 1, pp. 185–190.

Giroud, J.P., Soderman, K.L., Khire, M.V. & Badu-Tweneboah, K. (1998b) New developments in landfill liner leakage evaluation. In Rowe, R.K. (Ed.) *Proceedings, Sixth International Conference on Geosynthetics*, March, Atlanta, GA, Industrial Fabrics Association International, Roseville, MN, Vol. 1, pp. 261–268.

Giroud, J.P., Bonaparte, R., Matasovic, N. & Kavazanjian, E., Jr (2000) Approximate solution for pseudo static seismic analysis of landfill cover systems, *Geosynthetics International*, (submitted).

Gleit, A. (1985) Estimation of small normal data sets with detection limits. *Environmental Science & Technology*, **19**: 1201–1206.

Glickman, T.S. & Gough, M. (Eds) (1990) Readings in Risk, *Resources for the Future*, Washington, DC.

Goh, A.T.C., The, C.I. & Wong, K.S. (1997) Analysis of piles subjected to embankment induced lateral soil movements. *Journal of Geotechnical & Geoenvironmental Engineering, ASCE*, Reston, VA, **123**(9): 792–801.

Goldman, L.J., Greenfield, L.I., Damle, A.S., Kingsbury, G.L., Northeim, C.M., and Truesdale, R.S. (1990) *Clay Liners for Waste Management Facilities, Design, Construction & Evaluation*. Noyes Data, NJ.

Goodman, R.E. & Bray, J.W. (1976) Toppling of rock slopes. In *Proceedings, Specialty Conference on Rock Engineering for Foundation & Slopes*, Boulder, CO, American Society of Civil Engineers, ASCE Press, Reston, VA, Vol. 2, pp. 201–234.

Gorelick, S.M., Freeze, R.A., Donohue, D. & Keely, J.F. (1993) *Groundwater Contamination Optimal Capture and Containment*, Lewis, Boca Raton, FL.

Gounaris, V., Anderson, P.R. & Holsen, T.M. (1993) Characteristics and environmental significance of colloids in a landfill leachate. *Environmental Science & Technology*, **27**: 1381–1387.

Graf, E.D. (1992a) Compaction grout. In *Grouting, Soil Improvement, and Geosynthetics*, Geotechnical Special Publication No. 30, American Society of Civil Engineers, ASCE Press, Reston, VA, Vol. 1, pp. 275–287.

Graf, E.D. (1992b) Earthquake support grouting in sands. In *Grouting, Soil Improvement, & Geosynthetics*, Geotechnical Special Publication No. 30, American Society of Civil Engineers, ASCE Press, Reston, VA, Vol. 2, pp. 879–888.

Grant, B.L., McKenna, R.W. & von Maubeuge, K.P. (1997) Investigations of liner leakage rates

and EPA guidelines. In *Environmental Geotechnics*, Bouzza, A., Kodikara, J. and Parker, R. (Eds.) A.A. Balkema, Rotterdam, pp. 315–324.

Grant, R., Christian, J.T. & Vanmarcke, E.H. (1974) Differential settlement of buildings. *Journal of Geotechnical Engineering, ASCE*, Reston, VA, **100**(9): 973–991.

Grassie, N. & Scott, G. (1985) *Polymer Degradation and Stabilization*, Cambridge University Press, England.

Graves, R.W., Pitarka, A. & Somerville, P.G. (1998) Ground motion amplification in the Santa Monica area: effects of shallow basin edge structure. *Bulletin of Seismological Society of America*, **88**(5): 1224–1242.

Gray, D.H. & Leiser, A. (1982) *Biotechnical Slope Protection and Erosion Protection*, Van Nostrand Reinhold, New York, NY.

Gray, D.H. & Sotir, R.B. (1992) Biotechnical stabilization of cut and fill slopes. In *Specialty Conference on Stability & Performance of Slopes and Embankments-II*, Berkeley, Geotechnical Special Publication No. 31, American Society of Civil Engineers, Reston, VA, Vol. 2, pp. 1395–1410.

Gray, D.H. & Sotir, R.B. (1995) *Biotechnical Stabilization of Steepened Slopes*, Transportation Research Record No. 1474, Washington, DC, pp. 23–29.

Gray, D.M. (1970) *Handbook on the Principles of Hydrology*, Canadian National Committee for the International Hydrological Decade, National Research Council of Canada, Ottawa, Canada.

Greenkorn, R.A. (1983) *Flow Phenomena in Porous Media: Fundamentals and Applications in Petroleum, Water and Food Production*, Marcel Dekker, New York.

Greenkorn, R.A. & Kessler, D.P. (1972) *Transfer Operations*, McGraw-Hill, New York.

Gress, J.-C. (1992) Siphon drain: a technic for slope stabilization. In *Proceedings, Sixth International Symposium on Landslides*, Christchurch, Vol. 1, pp. 729–734.

Gress, J.-C. & Faure, R. (1996) Induced streaming electrical potential and water flows through landslides. In *Proceedings, Seventh International Symposium on Landslides*, Trondheim, Vol. 2, pp. 739–742.

GRI GM-10 (1996) *Specification for the Stress Crack Resistance of HDPE Geomembrane Sheet*, GSI, Folsom, PA.

GRI GM-13 (1997) *Specification for HDPE Smooth and Textured Geomembranes*, GSI, Folsom, PA.

Griffin, R.A., Cartwright, K., Shimp, N.F., Steel, J.D., Ruch, R.R., White, W.A., Hughes, G.M. & Gilkeson, R.H. (1976) Attenuation of pollutants in municipal landfill leachate by clay minerals: Part I—column leaching and field verification. Illinois State Geological Survey, Environmental Geology Notes No. 79.

Griffith, A.A. (1921) The phenomena of flow and rupture in solids. *Philosophical Transactions of the Royal Society, London*, **A221**: 163–198.

Griffith, A.A. (1924) Theory of rupture. In *Proceedings, First International Congress Applied Mechanics*, Delft, pp. 55–63.

Gross, B.A., Bonaparte, R. & Othman, M.A. (1997) Inferred performance of surface hydraulic barriers from landfill operational data. In *Proceedings, International Containment Technology Conference*, St Petersburg, FL, pp. 374–380.

Grubb, D.G. & Sitar, N. (1994) *Evaluation of Technologies for* In Situ *Cleanup of DNAPL Contaminated Sites*, EPA/600/R-95/120, US Environmental Protection Agency, Ada, OK, 173 p.

Gruszczenski, T.S. (1987) Determination of a realistic estimate of the actual formation product thickness using monitor wells: a field bailout test. In *Proceedings, Conference On Petroleum-Hydrocarbons and Organic Chemicals in Ground Water: Prevention, Detection, and Restoration*, National Ground Water Association, Dublin, OH, pp. 235–253.

Gschwend, P.M. & Reynolds, M.D. (1987) Monodisperse ferrous phosphate colloids in an anoxic groundwater plume. *Journal of Contaminant Hydrology*, **1**: 309–327.

Gudehus, G. (1972) Lower and upper bounds for stability of earth-retaining structures. In *Proceedings, Fifth European Conference of International Society for Soil Mechanics and Foundation Engineering*, Madrid, **1**: 21–28.

(1990) *Guideline for a Professional Engineer's Duty to Report*, Professional Engineers Ontario, Toronto, ON.

Gullà, G. & Sorbino, G. (1996) Soil suction measurements in a landslide involving weathered gneiss. In *Proceedings, Seventh International Symposium on Landslides*, Trondheim, Vol. 2, pp. 749–754.

Gullick, R.W. (1998) *PhD thesis*, University of Michigan.

Guan, Y. & Fredlund, D.G. (1997) Direct measurement of high soil suction. In *Proceedings,*

Third Brazilian Symposium on Unsaturated Soils, NONSAT '97, April 22–25, Rio de Janeiro, Brazil, **2**: 543–550.

Gumbel, J.E. (1981) Discussion of Pender (1980) *Géotechnique*, **31**(3): 434–436.

Gupta, S.C. & Larson, W.E. (1979) Estimating soil water retention characteristics from particle size distribution, organic matter percent, and bulk density. *Water Resources Research Journal*, **15**(6): 1633–1635.

Gupta, S.K., Tanji, K.K., Nielsen, D.R., Biggar, J.W., Simmon, C.S. & MacIntyre, J.L. (1978) *Field Simulation of Soil-Water Movement with Crop Water Extraction*, Water Science & Engineering Paper No. 4013, Department of Land, Air, & Water Resources, University of California, Davis.

Gutenberg, B. & Richter, C.F. (1944) Frequency of earthquakes in California. *Bulletin of the Seismological Society of America*, **46**: 105–145.

Gysi, H.J., Linder, A. & Leoni, E. (1975) Prestressed diaphragm walls. In *Proceedings, European Conference of International Society for Soil Mechanics and Foundation Engineering*, Vienna, Austria.

Haas, C.N. & Jacangelo, J.G. (1993) Development of regression models with below-detection data. *Journal of Environmental Engineering*, **119**(2): 214–230.

Haas, R., Hudson, W.R. & Zaniewski, J (1994) *Modern Pavement Management*, Krieger, Krieg Malabar, FL.

Hachey, J.E., Plum, R.L., Byrne, J., Killian, A.P. & Jenkens, D.V. (1994) Blast densification of a thick, loose debris flow at Mt St Helens, Washington. *Proceedings, Settlement '94*, Geotechnical Special Publication No. 40, American Society of Civil Engineers, ASCE Press, Reston, VA, Vol. 1, pp. 502–512.

Haimson, B.C. (1978a) The hydrofracturing stress measuring method and recent field results. *International Journal of Rock Mechanics, Mineral Science & Geomechanics, Abstracts*, **15**: 167–178.

Haimson, B.C. (1978b) Underground nuclear power station study. Hydrofracturing stress measurements. Hole UN-1 Darlington G.S. Report No. 78250. Geotechnical Engineering Department, Ontario Hydro.

Haimson, B.C. (1985) SAB-NIAGARA GS NO. 3. Hydrofracturing stress measurements and permeability tests in Holes NF3 and NF4. Report No. 85357. Geotechnical & Hydraulic Engineering Department, Ontario Hydro.

Haimson, B.C. & Fairhurst, C. (1969) *In-situ* stress determination at great depth by means hydraulic fracturing. In *11th US Symposium on Rock Mechanics*, pp. 559–584.

Haimson, B.C. & Lee, C.F. (1980) Hydrofracturing stress determinations at Darlington, Ontario. In *13th Canadian Rock Mechanics Symposium* (The H.R. Rice Memorial Symposium), pp. 42–50.

Haimson, B.C., Tunbridge, L.W., Lee, M.Y. & Cooling, C.M. (1989) Measurement of rock stress using the hydraulic fracturing method in Cornwall, UK – Part II. Data reduction and stress calculation. *International Journal of Rock Mechanics, Mineral Science & Geomechanics, Abstracts*, **26**(5): 361–372.

Hakulinen, M. (1991) Measured full-scale dynamic lateral pile responses in clay and in sand. In *Proceedings, Second International Conference on Recent Advances in Geotechnical Earthquake Engineering & Soil Dynamics*, University of Missouri at Rolla, Rolla, MO, pp. 201–206.

Halse, Y., Koerner, R.M. & Lord, A.E. (1987a) Effect of high levels of alkalinity on geotextiles – Part 1: $Ca(OH)_2$ solution. *Journal of Geotextiles & Geomembranes*, **5**(4): 261–282.

Halse, Y., Koerner, R.M. & Lord, A.E. (1987b) Effect of high levels of alkalinity on geotextiles – Part 2: Na(OH) solution. *Journal of Geotextiles & Geomembranes*, **6**(4): 295–306.

Halton, G., Loughney, R & Winters, E. (1965) Vacuum stabilization of subsoil beneath runway extension at Philadelphia International Airport. In *Sixth International Conference of Soil Mechanics & Foundation Engineering*, Montreal, Vol. 2, pp. 61–65.

Hamby, D.M. (1994) A review of techniques for parameter sensitivity analysis of environmental models. *Environmental Monitoring & Assessment*, **32**: 135–154.

Hampton, D.R. & Heuvelhorst, H.G. (1990) Designing gravel packs to improve separate-phase hydrocarbon recovery: laboratory experiments. In *Proceedings, Conference On Petroleum Hydrocarbons and Organic Chemicals in Ground Water: Prevention, Detection and Restoration*, National Ground Water Association, Dublin, OH, pp. 195–209.

Hampton, D.R., Smith, M.M. & Shank, S.J. (1991) Further laboratory studies of gravel pack design for hydrocarbon recovery wells. In *Proceedings, Conference On Petroleum Hydrocar-*

bons and Organic Chemicals in Ground Water: Prevention, Detection and Restoration, National Ground Water Association, Dublin, OH, pp. 615–629.

Hampton, M.A., Lee, H.J. & Locat, J. (1996) Submarine landslides. *Review in Geophysics*, **34**(1): 33–59.

Handa, S.C. (1984) Foundation performance of very old structures. In *Proceedings, International Conference on Case Histories in Geotechnical Engineering*, Rolla, MO, Vol. I, pp. 201–208.

Handy, R.L., Remens, B., Moldt, S., Lutenegger, A.J. & Trott, G. (1982) *In-situ* stress determination by Iowa stepped blade. *Journal of Geotechnical Engineering, ASCE*, Reston, VA, **108**(11): 1405–1422.

Hanna, T.H. (1982) *Foundations in Tension*, Trans Tech Publications, McGraw-Hill, New York, NY.

Hanna, T.H. (1985) *Field Instrumentation in Geotechnical Engineering*, Trans Tech Publications, Clausthal-Zellerfeld, Germany.

Hanna, A.M. & Meyerhof, G.G. (1980) Design charts for ultimate bearing capacity of foundations on sand overlying soft clay. *Canadian Geotechnical Journal*, **17**: 300–303.

Hanrahan, E.T. (1964) A road failure on peat. *Géotechnique*, **14**(3): 185–202.

Hansbo, S. (1979) Consolidation of clay by band-shaped prefabricated drains. *Ground Engineering*, **12**(5): 16–25.

Hansbo, S. (1981) Consolidation of fine-grained soils by prefabricated drains. In *Proceedings, Tenth International Conference on Soil Mechanics & Foundation Engineering*, Stockholm, Vol. 3, pp. 12–22.

Hansbo, S. (1983) Techno-economic trend on subsoil improvement methods in foundation engineering (special lecture). In *Proceedings Eighth European Conference on Soil Mechanics & Foundation Engineering*, Helsinki, Vol. 3, pp. 1333–1343.

Hansbo, S. (1987) Design aspects of vertical drains and lime column installations. In *Proceedings, Ninth Southeast Asian Geotechnical onference*, Bangkok, Thailand, Vol. 2, pp. 8–12.

Hansbo, S. (1993) Band drains. In Moseley, M.P. (Ed.) Ground Improvement, Blackie Academic & Professional, Blackwood, NJ, pp. 40–64.

Hansen J.B. (1970) *A Revised and Extended Formula for Bearing Capacity*, Danish Geotechnical Institute Bulletin No. 28.

Hanzawa, H. (1989) Evaluation of design parameters for soft clays as related to geological stress history. *Soils & Foundations*, **29**(2): 99–111.

Hanzawa, H., Kishida, T. & Matsuda, E. (1982) Stability analysis with the effective stress method for embankments constructed on an alluvial marine clay. *Soils & Foundations*, **22**(3): 32–46.

Harder, L.F. & Boulanger, R.W. (1997) Application of K_σ and K_α correction factors. In Youd, T.L. & Idriss, I. (Eds) *Proceedings, NCEER Workshop on Evaluation of Liquefaction Resistance of Soils*, December 31, Technical Report, NCEER-7-0022.

Harder, L.F. & Seed, H.B. (1986) *Determination of Penetration Resistance for Coarse-grained Soils Using the Becker Hammer Drill*. Report No. UCB/EERC-86/06, Earthquake Engineering Research Center, University of California, Berkeley.

Harder, L.S., Jr (1991) Performance of earth dams during the Loma Prieta earthquake. In *Proceedings, Second International Conference on Recent Advances in Geotechnical Earthquake Engineering & Soil Dynamics*, St Louis, pp. 11–15.

Hardin, B.O. (1978) The nature of stress–strain behavior of soils. In *Proceedings, Earthquake Engineering & Soil Dynamics*, American Society of Civil Engineers, Reston, VA, Vol. 1, pp. 3–90.

Hardin, B.O. & Drnevich, V.P. (1972) Shear modulus and damping in soils: design equations and curves. *Journal of Soil Mechanics & Foundations Division, ASCE*, Reston, VA, **98**(7): 667–692.

Harris, S.M., Day, S., Roberts, E., Rovers, F.A. & Carey, G.R. (1998) Applications of an innovative method for visualizing natural attenuation. In *Proceedings, First International Conference on Remediation of Chlorinated and Recalcitrant Compounds*, CA, May 18–21 Monterey, Battelle Press, Columbus, OH.

Hartford, D.N. (1997) Dam management in Canada—a Canadian approach to dam safety. In *Proceedings, International Workshop on Risk Based Dam Safety Evaluations*, Trondheim, Norway, Norwegian National Committee of the International Committee on Large Dams.

Hartlén, J. & Wolski, W. (1996) *Embankments on Organic Soils*, Elsevier, Amsterdam.

Hashimoto, L.K. & Trussel R.R. (1983) Evaluating water quality data near the detection limit, In *Proceedings, American Water Works Associ-*

ation Advanced Technology Conference, June 5–9, Las Vegas, NV.

Haslem, R.F. (1986) Pipe jacking forces; from theory to practice. In *Proceedings, Infrastructure, Renovation and Waste Control Centenary Conference*, Manchester, England, North West Association, Institution of Civil Engineers, pp. 173–180.

Hassan, M.H., O'Neill, M.W., Sheikh, S.A. & Ealy, C.D. (1997) Design method for drilled shafts in soft argillaceous rock. *Journal of Geotechnical & Geoenvironmental Engineering*, **123**(3): 272–280.

Hausmann, M.R. (1990) *Engineering Principles of Ground Modification*, McGraw Hill, New York, NY.

Haverkamp, R. & Parlange, J.Y. (1986) Predicting the water-retention curve from particle-size distribution: 1. Sandy soils without organic matter. *Soil Science Journal*, **142**(6): 325–339.

Hayhoe, H.N. & Balchin, D. (1990) Field frost heave measurement and prediction during periods of seasonal frost. *Canadian Geotechnical Journal*, **27**: 393–397.

He, Z., Kennepohl, G., Haas, R. & Cai, Y. (1996) OPAC 2000: a new pavement design system. In *Proceedings Transportation Association of Canada Annual Conference*, Charlottetown, PEI. Proc. CD-ROM Format (no hard copy) ISBN 1-55187-106–8.

Head, K.H. (1986) *Manual of Soil Laboratory Testing*, Volume 3, *Effective Stress Testing*, Pentech Press, London, England.

Health Canada (1993) *Health Risk Determination*. Health Canada, Ottowa, Ontario.

Hearmon, R.F.S. (1961) *An Introduction to Applied Anisotropic Elasticity*, Oxford University Press, England.

HEAST (1997) *Health Effects Assessment Summary Tables FY-1997 Update*, Office of Research & Development, US Environmental Protection Agency, Washington, DC, EPA 540/R-97-036.

Heerten, G., von Maubeuge, K., Simpson, M. & Mills, C. (1993) Manufacturing quality control of geosynthetic clay liners–A manufacturer's perspective. In *Proceedings, Sixth GRI Seminar, MQC/MQA and CQC/CQA of Geosynthetics*, St Paul, MN, IFAI, Roseville, MN, pp. 86–95.

Hefny, A.M. & Lo, K.Y. (1992) The interpretation of horizontal and mixed-mode fractures in hydraulic fracturing tests in rock. *Canadian Geotechnical Journal*, **29**: 902–917.

Hefny, A.M. & Lo, K.Y. (1995) Interpretation of initial stresses from hydraulic fracturing tests at AECL's underground research laboratory, Manitoba. *Canadian Tunnelling Journal*, 123–134.

Hefny, A., Lo, K.Y. & Huang, J.A. (1996) Modeling of long-term time-dependent deformation and stress-dependency of Queenston Shale. *Canadian Tunnelling Journal*, 115–146.

Helenelund, K.B. (1977) *Methods for Reducing Undrained Shear Strength of Soft Clay*, Report No. 2, Swedish Geotechnical Institute, Linköping.

Helsel, D.R. & Gilliom, R.J. (1986) Estimation of distributional parameters for censored trace level water quality data. 2. Verification and applications. *Water Resources Research*, **22**(2): 147–155.

Helsel, D.R. & Hirsch, R.M. (1992) *Statistical Methods in Water Resources* (Studies in Environmental Science 49), Elsevier, Amsterdam.

Hem, J.D. (1995) *Study and Interpretation of the Chemical Characteristics of Natural Water*, United States Geological Survey Water-Supply Paper 2254, 3rd Edn, US Government Printing Office, Washington, DC.

Henkel, D.J. (1956) The effect of overconsolidation on the behaviour of clays during shear. *Géotechnique*, **6**(4): 139–150.

Hewitt, R.D. & Daniel, D.E. (1997) Hydraulic conductivity of geosynthetic clay liners after freeze–thaw. *Journal of Geotechnical & Geoenvironmental Engineering, ASCE*, Reston, VA, **123**(4): 305–313.

Heyman, L. (1965) Measurement of the influence of lateral earth pressure on piles. In *Proceedings, Sixth International Conference on Soil Mechanics & Foundation Engineering*, Montreal, Vol. 2 pp. 257–260.

Herzog, M. (1985) Die Pressenkrafte bei Schildvrieb und Rohrvorpressung im Lockergestein. *Baumaschine & Bautechnik*, **32**: 236–238.

Hilf, J.W. (1991) Compacted fill. In Fang, H. (Ed.) *Foundation Engineering Handbook* 2nd Edn, Van Nostrand Reinhold, New York.

Hill, R. (1983) *The Mathematical Theory of Plasticity*, Oxford Science Publications, Oxford.

Hinchberger, S.D. & Rowe, R.K. (1998) Modelling the rate sensitive characteristics of the Gloucester foundation soil. *Canadian Geotechnical Journal*, **35**(5): 769–789.

Hinchee, R.E. (1993) Bioventing of petroleum hydrocarbons. In *Handbook of Bioremediation*, Robert S. Kerr Environmental Research Laboratory, CRC Press, Boca Raton, FL, pp. 39–60.

Hinchee, R.E., Wilson, J.T. & Downey, D. (1995) *Intrinsic Bioremediation*, Battelle Press, Columbus, OH.

Hirayama, H. (1991) Pile group settlement interaction considering soil nonlinearity. *Computer Methods & Advances in Geomechanic*, Beer, G., Booker, J.R., and Carter, J.P. (Eds.), A.A. Balkema, Rotterdam **1**: 139–144.

Hirt, R.C. & Searle, N.Z. (1964) Wavelength sensitivity or activation spectra of polymers. In *Regional Technical Conference*, Society of Plastics Engineers, Washington, DC, pp. 286–302.

Hittinger, M. (1978) *PhD thesis*, University of California, Berkeley.

Ho, D.Y.F., Fredlund, D.G. & Rahardjo, H. (1992) Volume change indices during loading and unloading of an unsaturated soil. *Canadian Geotechnical Journal*, **29**(2): 195–207.

Hodge, R.A.L. & Freeze, R.A. (1977) Groundwater flow systems and slope stability. *Canadian Geotechnical Journal*, **14**(4): 466–476.

Hodges, J.J., Jr & Lehmann, E.L. (1956) The efficiency of some nonparametric competitors to the *t*-test. *Annals of Mathematical Statistics*, **27**: 324–335.

Hoeg, K. (1968) Stresses against underground structural cylinders. *Journal of Soil Mechanics & Foundation Engineering, ASCE*, Reston, VA, **94**(4): 833–858.

Hoek, E. & Bray, J. (1981) *Rock Slope Engineering*, 3rd Edn, Institute of Mining & Metallurgy, London.

Hoek, E. & Brown, E.T. (1980) Empirical strength criterion for rock masses. *Journal of Geotechnical Engineering Division, ASCE*, Reston, VA, **106**(GT9): 1013–1035.

Hoek, E. & Brown, E.T. (1988) The Hoek–Brown failure criterion–a 1988 update. In Curran, J.C. (Ed.) *Rock Engineering for Underground Excavations, 15th Canadian Rock Mechanics Symposium*, Toronto, pp. 31–38.

Hoek, E., Wood, D. & Shah, S. (1992) A modified Hoek–Brown criterion for jointed rock masses. In Hudson, J.A. (Ed.) *Proceedings, Rock Characterization, Symposium of the International Society of Rock Mechanics, Eurock '92*, British Geological Society, London, pp. 209–214.

Hoek, E., Kaiser, P.K. & Bawden, W.F. (1995) *Support of Underground Excavations in Hard Rock*, Balkema, Rotterdam.

Hoekstra, P. (1969) Water movement and freezing pressures. *Soil Science Society of America, Proceedings*, **33**: 512–518.

Holland, D. & Fitz-Simmons, T. (1982) Fitting statistical distributions to air quality data by the maximum likelihood method. *Atmospheric Environment*, **16**(5): 1971–1076.

Holloway, P.M., Clough, G.W. & Vesic, A.S. (1975) *The Mechanics of Pile–Soil Interaction in* Cohesionless Soils. Soil Mechanic Series No. 39, Duke University School of Engineering, Durham, NC, USA.

Holtz, R.D. (1989) *Treatment of Problem Foundations for Highway Embankments*, NCHRP Synthesis of Highway Practice 147, Transportation Research Board, Washington, DC.

Holtz, R.D. (1990) Design and construction of geosynthetically reinforced embankments on very soft soils. State-of-the-Art Paper, Session 5, Performance of Reinforced Soil Structures. In *Proceedings, International Reinforced Soil Conference*, Glasgow, British Geotechnical Society, pp. 391–402.

Holtz, R.D. (1991) Stress distribution and settlet of shallow foundations. In Fang, H.Y. (Ed.) *Foundation Engineering Handbook*, Van Nostrand Reinhold, New York, NY, pp. 166–222.

Holtz, R.D. & Christopher, B.R. (1987) Characteristics of prefabricated drains for accelerating consolidation. In *Proceedings, Ninth European Conference on Soil Mechanics & Foundation Engineering*, Dublin, Vol. 2, pp. 903–906.

Holtz, R.D. & Holm, G. (1973) Excavation and sampling around some sand drains at Ska-Edeby, Sweden. In *Proceedings, Sixth Scandinavian Geotechnical Meeting*, Trondheim, NGI.

Holtz, R.D. & Holm, G. (1979) Test embankment on an organic silty clay. In *Seventh ECSMFE*, Brighton, Vol. 3, pp. 79–86.

Holtz, R.D. & Kovacs, W.D. (1981) *An Introduction to Geotechnical Engineering*, Prentice Hall, Englewood Cliffs, NJ.

Holtz, R.D. & Schuster, R.L. (1996) Stabilization of soil slopes. *Landslides: Investigation and Mitigation*, Turner, A.K. and Schuster, R.L. (Eds) Transportation Research Board, Washington, DC, Special Report 247, pp. 439–473.

Holtz, R.D. & Wager, O. (1975) Preloading by vacuum-current prospects. *Transportation Research Record*, **548**: 26–29.

Holtz, R.D., Jamiolkowski, M.B., Lancellotta, R. & Pedroni, S. (1991) Prefabricated vertical drains; design and performance. In *CIRIA Ground Engineering Report: Ground Improvement*, Butterworths-Heinemann, London, England.

Holtz, R.D., Christopher, B.R. & Berg, R.B.

(1997) *Geosynthetic Engineering*, BiTech, Vancouver.

Hong Kong Government (1996) *Geoguide 2; Guide to Site Investigation*, Government Publications Centre, Hong Kong Government, Hong Kong.

Hooker, V.E. & Bickel, D.L. (1974) *Overcoring Equipment and Techniques Used in Rock Stress Determinations*, Information Circular 8618, US Bureau of Mines.

Hooper, J.A. (1973) Observations on the behaviour of a piled raft foundation on London clay. *Proceedings, Institute of Civil Engineers*, **55**(2): 855.

Horvath, J.S. (1995) *Geofoam Geosynthetic*, Horvath Engineering, PC, Scarsdale, NY.

Horvath, R.G. (1989) Load–displacement behaviour of socketed piers–Hamilton General Hospital. *Canadian Geotechnical Journal*, **26**: 260–268.

Horvath, R.G., Kenney, T.C. & Kosicki, P. (1983) Method of improving the performance of drilled piers in weak rock. *Canadian Geotechnical Journal*, **20**(4): 758–772.

Houlsby, G.T. (1998) Advanced interpretation of field tests. In Robertson, P.K. & Mayne, P.W. (Eds) *Proceedings First International Conference on Site Characterization – ISC' 98*, April 19–22, Atlanta, GA, Vols. 1 & 2, A.A. Balkema, Rotterdam, pp. 99–112.

Houlsby, G.T. & Jewell, R.A. (1988) Analysis of unreinforced and reinforced embankments on soft clays by plasticity analysis. In *Proceedings, Sixth International Conference on Numerical Methods in Geomechanics*, Innsbruck, Vol. 2, pp. 1443–1448.

Hounslow, A.W. (1995) *Water Quality Data Analysis and Interpretation*, CRC Press, Boca Raton, FL.

Houston, S.L., Houston, W.N. & Padilla, J.M. (1987) Microcomputer-aided evaluation of earthquake-induced permanent slope displacements. *Microcomputers in Civil Engineering*, **2**: 202–222.

Houston, W.N. & Mitchell, J.K. (1969) Property interrelationships in sensitive clays. *Journal of Soil Mechanics & Foundations Division, ASCE*, Reston, VA, **95**(4): 1037–1062.

Howard, A.K. (1977) Modulus of soil reaction values for buried flexible pipe. *Journal of Geotechnical Engineering, ASCE*, Reston, VA, **103**(1): 33–43.

Howard, P.H. (Ed.) (1989–1997) *Handbook of Environmental Fate and Exposure Data for Organic Chemicals*, Lewis, Chelsea, MI.

Howard, P.H. (Ed.) (1991) *Handbook of Environmental Degradation Rates*, Lewis, Chelsea, MI.

Hrudey, S.E. & Pollard S.J.T. (1993) The Challenges of Contaminated Sites; Remediation Approaches in North America, *Environmental Review*, **1**: 55–72.

Hryciw, R.D. (Ed.) (1995) Soil improvement for earthquake hazard mitigation. In *Proceedings, Sessions at the ASCE Convention*, San Diego, Geotechnical Special Publication No. 49, ASCE Press, Reston, VA, p. 141.

Hsuan, Y.G. & Guan, Z. (1997) Evaluation of the oxidation behavior of polyethylene geomembranes using oxidative induction time tests. In Riga, A.T. & Patterson, G.H. (Eds) *Oxidative Behavior of Materials by Thermal Analytical Techniques*, ASTM STP 1326, American Society for Testing & Materials, West Conshohocken, PA, pp. 76–90.

Hsuan, Y.G. & Koerner, R.M. (1995a) The single point–notched constant tension load test: a quality control test for assessing stress crack resistance. *Geosynthetics International*, **2**(5): 831–843.

Hsuan, Y.G. & Koerner, R.M. (1995b) *Long Term Durability of HDPE Geomembranes: Part I–Depletion of Antioxidants*. GRI Report 16, Geosynthetic Research Institute, Philadelphia, PA.

Hsuan, Y.G. & Koerner, R.M. (1998) Antioxidant depletion lifetime in HDPE geomembranes. *Journal of Geotechnical & Geoenvironmental, ASCE*, Reston, VA, **124**(6): 532–541.

Hsuan, Y.G., Koerner, R.M. & Lord, A.E. Jr (1993) A review of the degradation of geosynthetic reinforcing materials and various polymer stabilization methods. In Cheng, S.C.J. (Ed.,) *Geosynthetic Soil Reinforcement Testing Procedures*, ASTM STP 1190, American Society for Testing & Materials, West Conshohocken, PA, pp. 228–243.

Huang, S. (1994) *PhD thesis*, University of Saskatchewan, Saskatoon, Saskatchewan, Canada.

Huang, S., Barbour, S.L. & Fredlund, D.G. (1994) A history of the coefficient of permeability function. In *Sino-Canadian Symposium on Unsaturated/Expansive Soils*, June 7–8, Wuhan, China, pp. 57–80.

Huang, Y.H. (1993) *Pavement Analysis and Design*, Prentice Hall, Englewood Cliffs, NJ.

Hubble, D.W., Gillham, R.W. & Cherry, J.A. (1997) Emplacement of zero-valent metal for remediation of deep contaminant plumes. In

Proceedings, 1997 International Containment Technology Conference & Exhibition, February 10–12, St Petersburg, FL, pp. 872–878.

Hudson, M., Idriss, I.M. & Beikae, M. (1994) *QUAD4M: A Computer Program to Evaluate the Seismic Response of Soil Structures Using Finite Element Procedures and Incorporating a Compliant Base*, University of California, Davis.

Hudson, W.R., Haas, R. & Uddin, W. (1997) *Infrastructure Management*, McGraw-Hill, New York.

Hughes, C.S. (1989) *Compaction of Asphalt Pavement*, National Cooperative Highway Research Program (NCHRP) Synthesis of Highway Practice No. 152, Transportation Research Board, Washington, DC.

Huling, S.G. & Weaver, J.W. (1991) *Ground Water Issue, Dense Nonaqueous Phase Liquids*, EPA/540/4-91/002.

Humphrey, D.N. & Holtz, R.D. (1986) Reinforced embankments–a review of case histories. *Geotextiles & Geomembranes*, **4**(2): 129.

Humphrey, D.N. & Rowe, R.K. (1991) Design of reinforced embankments: recent developments in the state-of-the-art. *Proceedings, ASCE Geotechnical Engineering Congress*, ASCE Special Publication No. 27, American Society of Civil Engineers, ASCE Press, Reston, VA, pp. 1006–1020.

Hungr, O. (1997) Some methods of landslide hazard intensity mapping. In *International Workshop on Landslide Risk Assessment*, Honolulu, HI, pp. 215–226.

Hungr, O., Salgado, F.M. & Byrne, P.M. (1989) Evaluation of a three-dimensional method of slope stability analysis. *Canadian Geotechnical Journal*, **26**(4): 679–686.

Hungr, O., Sobkowicz, J. & Morgan, G.C. (1993) How to economize on natural hazards. *Geotechnical News*, **11**(1): 54–57.

Huntley, D., Hawk, R.N. & Corley, H.P. (1992) Non-aqueous phase hydrocarbon saturations and mobility in a fine-grained, poorly consolidated sandstone. In *Proceedings, 1992 Petroleum Hydrocarbons and Organic Chemicals in Groundwater: Prevention, Detection, and Restoration*, National Groundwater Association, Columbus, OH, pp. 223–237.

Hutchinson, J.N. (1977) Assessment of effectiveness of corrective measures in relation to geological conditions and types of slope movement. *Bulletin of the International Association of Engineering Geologists*, **16**: 131–155.

Hutchinson, J.N. (1987) Mechanisms producing large displacements in landslides on pre-existing shears. *Memoir of the Geological Society of China*, **9**: 175–200.

Hutchinson, J.N. (1988) General report: morphological and geotechnical parameters of landslides in relation to geology and hydrogeology. In *Proceedings, Fifth International Symposium on Landslides*, Lausanne, Vol. 1, pp. 3–35.

Hutson, J.L. & Wagenet, R.J. (1992) *LEACHM Leaching Estimation and Chemistry Model*, Version 3, Department of Soil Crop and Atmospheric Sciences Research Series No. 92–3, New York State College of Agricultural and Life Sciences, Cornell University, Ithaca, NY.

Huyakorn, P.S., Wu, Y.S. & Panday, S. (1992) A comprehensive three-dimensional numerical model for predicting the fate of petroleum hydrocarbons in the subsurface. In *Proceedings, Conference On Petroleum Hydrocarbons and Organic Chemicals in Ground Water: Prevention, Detection, and Restoration*, National Ground Water Association, Dublin, OH, pp. 239–253.

Hvorslev, M.J. (1937) *Über die Festigkeitseigenschaften gestörter bindinger Böden* (København: Danmarks Naturvidenskabelige Samfund) Ingeniørvidenskabelige Skrifter, A45. English translation (1969) *Physical Properties of Remolded Cohesive Soils*, Waterways Experiment Station, Vicksburg, MS, No. 69–5.

Hvorslev, M.J. (1948) *Subsurface Exploration and Sampling of Soils for Civil Engineering Purposes*, US Army Waterways Experiment Station, Vicksburg, MS.

Hvorslev, M.J. (1951) *Time Lag and Permeability in Groundwater Observations*. Bulletin No. 36, US Army, Waterways Experiment Station, Vicksburg, VA.

Hwu, B.-L., Sprague, C.J. & Koerner, R.M. (1990) Geotextile intrusion into geonets. In *Proceedings, Fourth International Conference On Geotextiles, Geomembranes, and Related Products*, G. den Hoedt (Ed). A.A. Balkema, Rotterdam, pp. 351–356.

Hynes, M.E. & Franklin, A.G. (1984) *Rationalizing the Seismic Coefficient Method*, Miscellaneous Paper GL-84-13, US Army Engineer Waterways Experiment Station, Vicksburg, MS.

ICAO (1983) *Aerodrome Design Manual*, Document 9157, *Part 3—Pavements*, International Civil Aviation Organization, Montreal, Canada.

ICBO (1997) *1997 Uniform Building Code, 2, Structural Engineering Design Provisions*, In-

ternational Conference of Building Officials, Whittier, CA.

Idriss, I.M. (1990) Response of soft soil sites ring earthquakes. In *Proceedings, Symposium to Honor Professor H.B. Seed*, Bitech, Vancouver, BC, J.M. Duncan (Ed.) Vol. 2, pp. 273–290.

Idriss, I.M. & Sun, J.I. (1992) *SHAKE91: A Computer Program for Conducting Equivalent Linear Seismic Response Analyses of Horizontally Layered Soil Deposits. User's Manual*, University of California, Davis.

Idriss, I.M., Lysmer, J., Hwang, R. & Seed, H.B. (1973) *QUAD-4: A Computer Program for Evaluating the Seismic Response of Soil Structures by Variable Damping Finite Element Procedures*, Report No. EERC 73-16, University of California at Berkeley.

Idriss, I.M., Fiegel, G., Hudson, M.B., Mundy, P.K. & Herzig, R. (1995) Seismic response of the operating industries landfill. *Earthquake Design and Performance of Solid Waste Landfills*, Geotechnical Special Publication No. 4, Yegian, M.K. and Finn, W.D.L. (Eds.), American Society of Civil Engineers, Reston, VA, pp. 83–118.

Imai, G. & Tang, Y.X. (1992) A constitutive equation of one-dimensional consolidation derived from inter-connected tests. *Soils & Foundations*, **32**(2): 83–96.

Imai, T. & Tonouchi, K. (1982) Correlation of N value with S-wave velocity an shear modulus. In *Proceedings, European Symposium on Penetration Testing, ESOPT-II*, A.A. Balkema, Amsterdam, Vol. 1, pp. 67–72.

Ingles, O.G. (1962) Bonding forces in soils, Part 3: A theory of tensile strength for stabilised and naturally coherent soils. In *Proceedings, First Conference of the Australian Road Research Board*, Vol. 1, pp. 1025–1047.

Inglis, C.E. (1913) Stresses in a plate due to the presence of cracks and sharp corners. *Transactions of the Institution of Naval Architecture*, London, **55**: 219–241.

Ingold, T.S. (1979) The effects of compaction in retaining walls. *Géotechnique*, **29**(3): 265–83.

Institution of Civil Engineers (1996) *Advances in Site Investigation Practice*. Craig, C. (Ed.) Thomas Telford Services, London, England.

International Journal on Hydropower and Dams, Editorial Reports on Seismic Risk, Vol. 5, Issues 1 and 2, Aqua-Media, Sutton, Surrey, UK.

International Standards Organization/DIS 11058 *Determination of Water Permeability Characteristics to the Plane, Without Load, Brussels, Belgium.*

International Standards Organization/DIS 12956 *Determination of the Characteristic Opening Size of Geotextile, Brussels, Belgium.*

International Standards Organization/DIS 12958 *Determination of Water Flow Capacity in their Plane, Brussels, Belgium.*

International Standards Organization/DIS 13431 *Determination of the Tensile Creep and Creep Rupture Behavior, Brussels, Belgium.*

International Standards Organization 10319 *Wide Width Tensile Test, Brussels, Belgium.*

IRIS (1997) *Integrated Risk Information System*, US Environmental Protection Agency. Online search (Internet: http://www.epa.gov/docs/ngispgm3/iris/index.html).

ISC (1998) Geotechnical site characterization. In Robertson, P.K. & Mayne, P.W. *Proceedings, First International Conference on Site Characterization–ISC'98*, April 19–22, Atlanta, Ga, Vols. 1 & 2, A.A. Balkema, Rotterdam.

Ishibashi, I. (1992) Discussion to 'Effects of soil plasticity on cyclic response,' by M. Vucetic & R. Dobry. *Journal of Geotechnical Engineering, ASCE*, Reston, VA, **118**(5): 830–832.

Ishihara, K. (1993) Liquefaction and flow failure during earthquakes, *Géotechnique*, **43**(3): 351–415.

Ishihara, K. (1996) *Soil Behaviour in Earthquake Geotechnics*, Oxford University Press, New York.

Ishihara, K. & Li, S. (1972) Liquefaction of saturated sand in triaxial torsion shear tests. *Soils & Foundations*, **12**(2): 19–39.

ISO 4435 Unplasticized poly(vinyl chloride) (PVC-U) pipes and fittings for buried drainage and sewerage systems; specifications, International Standards Organization, Geneva.

ISO 7186 Ductile iron products for sewage applications, International Standards Organization, Geneva.

ISO 7370 Glass fiber reinforced thermosetting plastics (GRP) pipes and fittings—nominal diameters, specified diameters and standard lengths, International Standards Organization, Geneva.

ISO 8772 High density polyethylene (PE-HD) pipes and fittings for buried drainage and sewerage systems; specifications, International Standards Organization, Geneva.

ISOPT (1988) De Ruiter, J. (Ed.) *Penetration Testing 1988, Proceedings, First International Symposium on Penetration Testing, ISOPT-1*,

March 20–24, Orlando, FL, Vols. 1 & 2, A.A. Balkema, Rotterdam.

ISO/TR 7074 Performance requirements for plastic pipes and fittings for use in underground drainage and sewage, International Standards Organization, Geneva.

ISO/TR 7073 Recommended techniques for the installation of unplasticized poly (vinyl chloride) (PVC-U) buried drains and sewers, International Standards Organization, Geneva.

ISO/TR 10465 Underground installation of flexible glass-reinforced thermosetting resin (GRP) pipes; Part I: Installation procedures, International Standards Organization, Geneva.

ISRM (1978a) Suggested methods for the quantitative description of discontinuities in rock masses. Commission on Standardization of Laboratory and Field Tests. Coordinator: N. Barton. *International Journal of Rock Mechanics, Mineral Science & Geomechanics, Abstracts*, **15**: 319–368.

ISRM (1978b) Suggested methods for determining tensile strength of rock materials. Suggested method for determining indirect tensile strength by the Brazil test. Commission on Standardization of Laboratory and Field Tests. Z.T. Bieniawski and I. Hawkes. *International Journal of Rock Mechanics, Mineral Science & Geomechanics, Abstracts*, **15**: 102–103.

ISRM (1978c) Suggested methods for determining tensile strength of rock materials. Suggested method for determining direct tensile strength. Commission on Standardization of Laboratory and Field Tests. Z.T. Bieniawski and I. Hawkes. *International Journal of Rock Mechanics, Mineral Science & Geomechanics, Abstracts*, **15**: 101–102.

ISRM (1978d) Suggested methods for determining the strength of rock materials in triaxial compression. Commission on Standardization of Laboratory and Field Tests. U.W. Volger and K. Kovari. *International Journal of Rock Mechanics, Mineral Science & Geomechanics, Abstracts*, **15**: 47–51.

ISRM (1979a) Suggested methods for determining *in situ* deformability of rock. Part 1. Suggested method for deformability determination using a plate test (superficial loading). Commission on Standardization of Laboratory and Field Tests. J.H. Coulson (Co-ordinator) *International Journal of Rock Mechanics, Mineral Science & Geomechanics, Abstracts*, **16**: 197–202.

ISRM (1979b) Suggested methods for determining *in situ* deformability of rock. Part 2. Suggested method for field deformability determination using a plate test down a borehole. Commission on Standardization of Laboratory and Field Tests. J.H. Coulson (Co-ordinator) *International Journal of Rock Mechanics, Mineral Science & Geomechanics, Abstracts*, **16**: 202–208.

ISRM (1979c) Suggested methods for determining *in situ* deformability of rock. Part 3. Suggested method for measuring rock mass deformability using a radial jacking test. Commission on Standardization of Laboratory and Field Tests. J.H. Coulson (Co-ordinator) *International Journal of Rock Mechanics, Mineral Science & Geomechanics, Abstracts*, **16**: 208–214.

ISRM (1979d) Suggested methods for determining the uniaxial compressive strength and deformability of rock materials. Commission on Standardization of Laboratory and Field Tests. Co-ordinator: Z.T. Bieniawski. *International Journal of Rock Mechanics, Mineral Science & Geomechanics, Abstracts*, **15**: 135–140.

ISRM (1986) Suggested method for deformability determination using a large flat jack technique. Commission on Testing Methods. J. Loureiro-Pinto (Co-ordinator) *International Journal of Rock Mechanics, Mineral Science & Geomechanics, Abstracts*, **23**: 131–140.

ISRM (1987a) Suggested methods for rock stress determination. Commission on testing Methods. Co-ordinators: K. Kim and J.A. Franklin. *International Journal of Rock Mechanics, Mineral Science & Geomechanics, Abstracts*, **24**(1): 53–73.

ISRM (1987b) Suggested method for deformability determination using a flexible dilatometer. Commission on Testing Methods. B. Ladanyi (Co-ordinator) *International Journal of Rock Mechanics, Mineral Science & Geomechanics, Abstracts*, **24**: 123–134.

ISRM (1989) Suggested methods for laboratory testing of argillaceous swelling rocks. Commission on Standardization of Laboratory and Field Tests. Co-ordinator: H. Einstein. *International Journal of Rock Mechanics, Mineral Science & Geomechanics, Abstracts*, **26**: 415–426.

ISRM (1996) Suggested method for deformability determination using a stiff dilatometer. Commission on Testing Methods. J.L. Yow, Jr. (Co-ordinator) *International Journal of Rock Mechanics, Mineral Science & Geomechanics, Abstracts*, **33**: 733–741.

ISTT (undated) *Trenchless Technology Guidelines*, International Society for Trenchless Technology, London, England.

Itasca (1996) *FLAC* (Version 3.3), *FLAC—Fast Lagrangian Analysis of Continua*, Itasca, Minneapolis, MN.

Ivan, B. (1993) Thermal stability, degradation, and stabilization mechanisms of poly(vinyl chloride). In Clough, R.L., Billingham, N.C. & Gillen, K.T. (Eds) *Polymer Durability*, Advances in Chemistry Series 249, American Chemical Society, New York, NY, USA, pp. 19–32.

Jackson, R.E., Patterson, R.J., Graham, B.W., Bahr, J., Belanger, D., Lockwood, J. and Priddle, M. (1985) *Contaminant Hydrogeology of Toxic Organic Chemicals at a Disposal Site, Gloucester, Ontario*: 1. *Chemical Concepts and Site Assessment*, Environment Canada, *National Hydrological Research Institute*, Paper No. 23, Ottawa.

Jaegar, J.C. & Cook, N.G.W. (1969) Fundamentals of Rock Mechanics, p. 135, Methuen Press.

Jaky, J. (1948) Pressure in silos. In *Proceedings, Second International Conference on Soil Mechanics & Foundations Engineering*, Rotterdam, Holland, Vol. I, pp. 103–107.

Jamiolkowski, M. & Garassino, A. (1977) Soil modulus for laterally loaded piles. In *Proceedings, Special Session No. 10, Ninth International Conferences on Soil Mechanics & Foundation Engineering*, Tokyo, pp. 43–58.

Jamiolkowski, M., Lancellotta, R. & Wolski, W. (1983) Precompression and speeding up consolidation. General Report, Specialty Session 6, *Proceedings, Eighth European Conference on Soil Mechanics & Foundation Engineering*, Helsinki, Vol. 3, pp. 1201–1226. Summary of discussion, pp. 1242–1245.

Jamiolkowski, M., Ladd, C.C., Germaine, J.T. & Lancellotta, R. (1985) New developments in field and laboratory testing of soils. State-of-the-Art Report, *11th International Conference on Soil Mechanics & Foundation Engineering*. San Francisco, CA, Vol. 1, pp. 57–153.

Jamiolkowski, M., Ghionna, V., Lancellotta, R. & Pasqualini, E. (1988) New correlations of penetration tests for design practice. *Proceedings ISOPT-I*, **1**: 263–296.

Jamiolkowski, M., Lancelotta, R. & Lo Presti, D.C.F. (1994) Remarks on the stiffness at small strains of six Italian clays. In Shibuya, S., Mitachi, T. & Miura, S. (Eds) *Proceedings, First International Conference on Pre-Failure Deformation Characteristics of Geomaterials* Sapporo, Japan, Balkema, Rotterdam, Vol. 2, pp. 817–836.

Janbu, N. (1954a) *Stability Analysis of Slopes with Dimensionless Parameters*, Harvard Soil Mechanics Series, Harvard University, Cambridge, MA, No. 46.

Janbu, N. (1954b) Application of composite slip surfaces for stability analysis. In *Proceedings, European Conference on Stability of Earth Slopes*, Stockholm, Vol. 3, pp. 45–49.

Janbu, N. (1963) Soil compressibility as determined by oedometer and triaxial tests. In *Proceedings European Conference on Soil Mechanics & Foundation Engineering*, Wiesbaden, Vol. 1, pp. 19–25.

Janbu, N. (1968) *Slope Stability Computations*, Soil Mechanics & Foundation Engineering Report. Technical University of Norway, Trondheim.

Janbu, N. (1977) Slopes and excavations in normally and slightly overconsolidated clays. In *Proceedings, Ninth International Conference on Soil Mechanics & Foundation Engineering*, Tokyo, Vol. 2, pp. 549–566.

Janbu, N. (1996) Slope stability evaluation in engineering practice. In *Proceedings, Seventh International Symposium on Landslides*, Trondheim, Vol. 1, pp. 17–34.

Janbu, N. & Sennesest, K. (1973) Field compressometer: principles and applications. In *Proceedings, Eighth International Conference on Soil Mechanics & Foundation Engineering*, Moscow, Russia, Vol. 1, pp. 191–198.

Jang, D.J. & Montero, C. (1993) Design of liner systems under vertical expansions: an alternative to geogrids. In *Proceedings, Geosynthetics '93 Conference*, Vancouver, BC, Industrial Fabrics Association International, Roseville, MN, Vol. 3, pp. 1497–1510.

Janssen, H.A. (1895) Versuche uber Getreidedruck in Silozellen. *Zeitschrift des Vereines Deutscher Ingenieure*, **39**(35): 1045–1049.

Japan Highway Public Corporation (1987) *Guide for Design and Construction on Reinforced Slope with Steel Bars*, Japan Highway Public Corporation, Tokyo, Japan.

Jardine, R.J. (1992) Some observations on the kinematic nature of soil stiffness. *Soils & Foundations*, **32**(2): 111–124.

Jardine, R.J. & Hight, D.W. (1987) The behaviour and analysis of embankments on soft clay. In *Embankments on Soft Clays*, Special Publication Bulletin of the Public Works Research Centre, Athens, pp. 159–244.

Jardine, R.J., Potts, D.M., Fourie, A.B. & Burland, J.B. (1986) Studies of the influence of non-linear stress–strain characteristics in soil–structure interaction. *Géotechnique*, **36**(3): 377–396.

Jayawickrama, P., Brown, K.W., Thomas, J.C. & Lytton, R.L. (1988) Leakage rates through flaws in geomembrane liners. *Journal of Environmental Engineering, ASCE*, Reston, VA, **114**(6): 1401–1420.

Jefferies, M.G. (1988) Determination of horizontal geostatic stress in clay with self-bored pressuremeter. *Canadian Geotechnical Journal*, **25**(3): 559–573.

Jefferies, M.G. & Davies, M.P. (1991) Soil classification by the cone penetration test: discussion. *Canadian Geotechnical Journal*, **28**(1): 173–176.

Jefferies, M.G. & Davies, M.P. (1993) Use of CPTU to estimate equivalent SPT N_{60}. *ASTM Geotechnical Testing Journal*, West Conshohocken, PA, **16**(4): 458–468.

Jefferies, M.G., Crooks, J.H.A., Becker, D.E. & Hill, P.R. (1987) Independence of geostatic stress from overconsolidation in some Beaufort Sea clays. *Canadian Geotechnical Journal*, **24**(3): 342–356.

Jessberger, H.L. (Ed.) (1979) *Ground Freezing, Developments in Geotechnical Engineering*, Vol. 26, Elsevier, New York.

Jessberger, H.L. & Stone, K. (1991) Subsidence effects on clay barriers. *Géotechnique*, **41**(2): 185–194.

Jewell, R.A. (1982) A limit equilibrium design method for reinforced embankments on soft foundations. In *Proceedings, Second International Conference on Geotextiles*, Las Vegas, NV, Industrial Fabrics Association International, Roseville, MN, Vol. 2, pp. 671–676.

Jewell, R.A. (1996) *Soil Reinforcement with Geotextiles*, Special Publication No. 123, CIRIA London, England.

Jezequel, F.J. & Mieussens, C. (1975) *In-situ* measurement of coefficients of permeability and consolidation in fine soils. In *Proceedings, ASCE Geotechnical Engineering Division Specialty Conference on* In-Situ *Measurement of Soil Properties*, June 1–4, North Carolina State University, Raleigh, NC, Vol. 1, pp. 208–224.

Ji, W., Dahmani, A., Ahlfeld, D.P., Lin, J.D. & Hill III, E. (1993) Laboratory study of air sparging: air flow visualization. *Ground Water Monitoring & Remediation*, **13**(4): 115–125.

Joffe, Z. & Ranby, B. (1976) Some weathering and UV aging problems of PVC contaminated with Fe-complexes and organic additives: long-term properties of polymers and polymeric materials. In Editors: Ranby, B. & Rabek, J.F. *Journal of Applied Polymer Science: Applied Polymer Symposium 35*, Interscience, New York, NY, USA, pp. 307–320.

Johnson, A.I. (1967) *Specific-Yield-Compilation of Specific Yields for Various Materials*, Water Supply Paper 1662-D, US Geological Survey.

Johnson, K.A. & Sitar, N. (1990) Hydrologic conditions leading to debris-flow initiation. *Canadian Geotechnical Journal*, **27**(6): 789–801.

Johnson, P.C., Stanley, C.C., Kemblowski, M.W., Byers, D.L. & Colthart, J.D. (1990) A practical approach to the design, operation and monitoring of *in-situ* soil venting systems. *Ground Water Monitoring Review*, **10**(2): 159–178.

Johnson, R.L., Johnson, P.C., McWhorter, D.B., Heinchee, R.E. & Goodman, I. (1993) An overview of *in situ* air sparging. *Ground Water Monitoring & Remediation*, **13**(4): 127–135.

Johnson, S.J. (1970a) Precompression for improving foundation soils. *Journal of Soil Mechanics & Foundations Division, ASCE*, Reston, VA, **96**(1): 111–144.

Johnson, S.J. (1970b) Foundation precompression with vertical sand drains. *Journal of Soil Mechanics & Foundations Division, ASCE*, Reston, VA, **96**(1): 145–175.

Johnson, T.C., Cole, D. & Chamberlain, E.J. (1978) *Influence of Freezing and Thawing on the Resilient Properties of a Silt Soil Beneath an Asphalt Concrete Pavement*, Report 78–23, Cold Regions Research and Engineering Laboratory (CRREL).

Johnston, G.H. (1981) *Permafrost. Engineering design and construction*, Associate Committee for Geotechnical Research National Research Council of Canada, Wiley, Toronto.

Jones, C.J.F.P. (1996) *Earth Reinforcement and Soil Structures*, Thomas Telford, London, England.

Jones, C.J.F.P., Fakher, A., Hamir, R. & Nettleton, I.M. (1996) Geosynthetic materials with improved reinforcement capabilities. In Ochiai, M., Yasafuku, N. & Omine, K. (Eds) *Earth Reinforcement*, A.A. Balkema, Rotterdam, Vol. 2, pp. 865–883.

Jorstad, F. (1968) *Snesmelting som arsak til jordskred pa ostlandet ved manedsskiftet april–mai 1966*, Norwegian Geotechnical Institute, Publication No. 75, Oslo, pp. 33–38.

Jorgensen, D.G., Gogel, T. & Signor, D.C. (1982)

Determination of flow in aquifers containing variable-density water. *Groundwater Monitoring Review*, **2**: 29–38.

Joseph, J.B. & Mather, J.D. (1993) Landfill–Does current containment practice represent the best option. In *Proceedings, Fourth International Landfill Symposium*, Cagliari Sardinia, October, pp. 99–107.

Journal of Geotextiles and Geomembranes, Special Issue, **15**(1–3), 1997.

Jumikis, A. (1971) *Foundation Engineering*, Intext Educational, Scranton, PA.

Jung, F. & Phang, W.A. (1974) *Elastic Layer Analysis Related to Performance in Flexible Pavement Design*, Research Report 191, Ministry of Transportation, Ontario, Canada, M#M 1J8.

Juran, I. & Elias, V. (1991) Ground anchors and soil nails in retaining structures. In Fang, H.Y. (Ed.) *Foundation Engineering Handbook*, Van Nostrand Reinhold, New York, NY, pp. 868–905.

Jurgenson, L. (1934) The application of theories of elasticity and plasticity to foundation problems. Boston Society of Civil Engineers, *Contributions to Soil Mechanics* 1925–1940, 184–226.

Kabbaj, M. (1985) *PhD thesis*, Université Laval, Québec.

Kabbaj, M., Tavenas, F. & Leroueil, S. (1988) *In situ* and laboratory stress–strain relationships. *Géotechnique*, **38**(1): 83–100.

Kafritsas, J. & Bras, R.L. (1981) *The Practice of Kriging*, Ralph M. Parsons Laboratory, Report No. 263, Massachusetts Institute of Technology, MA.

Kalteziotis, N., Zervogiannis, F.R., Seve, G. & Berche, J.-C. (1993) Experimental study of landslide stabilization by large diameter piles. In A. Anagnostopoulos, *et al.* (Eds) *Geotechnical Engineering of Hard Soils–Soft Rocks*, Anagnostopoulos, A., Schlosser, F., Kalteziotis, N., and Frank, R. (Eds.) Balkema, Rotterdam, pp. 1115–1124.

Kaluarachchi, J.J. & Parker, J.C. (1989) An efficient finite element model for modeling multiphase flow in porous media. *Water Resources Research*, **25**(1): 43–54.

Kaluarachchi, J.J., Parker, J.C. & Lenhard, R.J. (1990) A numerical model for areal migration of water and light hydrocarbon in unconfined aquifers. *Advanced in Water Resources*, **13**: 29–40.

Kana, D.D., Boyce, L. & Blayney, G.W. (1986) Development of a scale model for the dynamic interaction of a pile in clay. *Journal of Energy Resources Technology, ASME*, Vol. **108**: 254–261.

Karabalis, D.L. & Beskos, D.E. (1985) Dynamic response of 3-D embedded foundations by the boundary element method. In *Second Joint ASCE/ASME Conference*, Albuquerque, p. 34.

Karickhoff, S.W. (1981) Semi-empirical estimation of sorption of hydrophobic pollutants on natural sediments and soils. *Chemosphere*, **10**(8): 833–846.

Karickhoff, S.W. (1984) Organic pollutant sorption in aquatic systems. *Journal of Hydraulic Engineering, ASCE*, Reston, VA, **110**(6): 707–735.

Karickhoff, S.W., Brown, D.S. & Scott, T.A. (1979) Sorption of hydrophobic pollutants on natural sediments. *Water Resources Research*, **13**: 241–248.

Karol, R.H. (1982) Chemical grouts and their properties. In Baker, W.H. (Ed.) *Proceedings, Grouting in Geotechnical Engineering*, New Orleans, American Society of Civil Engineers, ASCE Press, Reston, VA, pp. 359–377.

Karpurapu, R.G. & Bathurst, R.J. (1992) Numerical investigation of controlled yielding of soil retaining wall structures. *Geotextiles & Geomembranes*, **11**(2): 115–131.

Karube, D. (1988) New concept of effective stress in unsaturated soil and its proving test. In *Advanced Triaxial Testing of Soil and Rock*, ASTM STP 977, Eds. R.T. Douglas, R.C. Chaney and M.L. Silver, American Society for Testing & Materials, West Conshohocken, PA, pp. 539–552.

Katchalsky, A. & Curran, P.R. (1967) *Nonequilibrium Thermodynamics in Biophysics*, Harvard University Press, Cambridge, MA.

Katona, M.G. (1978) Analysis of long-span culverts by the finite element method. *Transportation Research Record*, **678**: 59–66.

Katyal, A.K., Kaluarachchi, J.J. & Parker, J.C. (1991) *MOFAT: A Two-Dimensional Finite Element Program for Multiphase Flow and Multicomponent Transport*, Program Documentation and User's Guide, EPA 600/2-91-020.

Kauschinger, J.L., Perry, E.B. & Hankour, R. (1992) Jet grouting: state-of-the-practice, grouting. In *Soil Improvement, & Geosynthetics*, Geotechnical Special Publication No. 30, American Society of Civil Engineers, ASCE Press, Reston, VA, Vol. 1, pp. 169–181.

Kausel, E. & Ushijima, R. (1979) *Vertical and*

Torsional Stiffness of Cylindrical footing, Civil Engineering Department Report R79-6, MIT, Cambridge, MA.

Kausel, E., Roesset, J.M. & Waas, G. (1975) Dynamic analysis of footings on layered media. *Journal of the Engineering Mechanics Division, ASCE*, Reston, VA, **101**(5): 679–693.

Kavazanjian, E., Jr (1998) Current issues in seismic design of geosynthetic cover systems. In R.K. Rowe (Ed.) *Proceedings, Sixth International Conference on Geosynthetics*, Atlanta, GA, Industrial Fabrics Association International, Roseville, MN, Vol. 1, pp. 219–226.

Kavazanjian, E., Jr & Matasovic, N. (1995) Seismic analysis of solid waste landfills. In *Geoenvironment 2000*, Geotechnical Special Publication No. 46, Acar, Y.B. and Daniel, D.E. (Eds.) American Society of Civil Engineers, Reston, VA, Vol. 2, pp. 1066–1080.

Kavazanjian, E., Jr, Hushmand, B. & Martin, G.R. (1991) Frictional base isolation using a layered soil–synthetic liner system. In *Proceedings, Third US Conference on Lifeline Earthquake Engineering*, Los Angeles, Monograph No. 4, pp. 1140–1151.

Kavazanjian, E., Jr, Snow, M.S., Matasovic, N., Poran, C. & Satoh, T. (1994) Non-intrusive Rayleigh wave investigations at solid waste landfills. In *Proceedings, First International Conference on Environmental Geotechnics*, Edmonton, Alberta, pp. 707–712.

Kavazanjian, E., Jr, Bonaparte, R., Johnson, G.W., Martin, G.R. & Matasovic, N. (1995a) Hazard analysis for a large regional landfill. In *Earthquake Design & Performance of Solid Waste Landfill*, Geotechnical Special Publication No. 54, Yegian, M.K. and Finn, W.D.L. (Eds.) American Society of Civil Engineers, Reston, VA, pp. 119–141.

Kavazanjian, E., Jr, Matasovic, N., Bonaparte, R. & Schmertmann, G.R. (1995b) Evaluation of MSW properties for seismic analysis. In *Geoenvironment 2000*, Geotechnical Special Publication No. 46, Acar, Y.B. & Daniel, D.E. (Eds.) American Society of Civil Engineers, Reston, VA, Vol. 2, pp. 1126–1141.

Kavazanjian, E., Jr, Matasovic, N., Stokoe, K.H. & Bray, J.D. (1996) *In situ* shear wave velocity of solid waste from surface wave measurements. In *Proceedings, Second International Conference on Environmental Geotechnics*, Osaka, Japan, Vol. 1, pp. 97–102.

Kavazanjian, E., Jr Matasovic, N., Hadj-Hamou, T. & Sabatini, P.J. (1997) *Geotechnical Earthquake Engineering for Highways, 1. Design Principles*, Geotechnical Engineering Circular No. 3, US Federal Highway Administration, Publication No. FHWA-SA-97-076.

Kawai, T. (1985) *Summary Report on the Development of the Computer Program DIANA–Dynamic Interaction Approach and Non-linear Analysis*, Science University of Tokyo.

Kaynia, A.M. & Kausel, E. (1982) Dynamic behavior of pile groups. In *Second International Conference on Numerical Methods in Offshore Piling*, Austin, TX, pp. 509–532.

Keith, L.H. (1987) *Principles of Environmental Sampling*, American Chemical Society, Washington, DC.

Keith, L.H. (1990) *Environmental Sampling and Analysis*, American Chemical Society, Washington, DC.

Kempton, G., Russell, D., Pierpont, N.D. & Jones, C.J.F.P. (1998) Two- and three-dimensional numerical analysis of the performance of piled embankments. In *Sixth International Conference on Geosynthetics*, Atlanta, GA, R.K. Rowe (Ed.) International Fabrics Association International, Roseville, MN, Vol. 2, pp. 767–772.

Kenney, TC. (1967) The influence of mineralogical composition on the residual strength of natural soils. In *Proceedings, Oslo Geotechnical Conference on the Shear Strength Properties of Natural Soils & Rocks*, Vol. I pp. 123–129.

Kenney, T.C. & Lau, K.C. (1984) Temporal changes of groundwater pressure in a natural slope of nonfissured clay. *Canadian Geotechnical Journal*, **21**(1): 138–146.

Kenney, T.C., Chahal, R, Chiu, E., Ofoegbu, G.I., Omange, G.N. & Ume, C.A. (1985) Controlling constriction sizes of granular filters. *Canadian Geotechnical Journal*, **22**(1): 32–43.

Kersten, M.S. (1949) *Thermal Properties of Soils*, University of Minnesota, Engineering Experiment Station, MN, Bulletin 28.

Kezdi, A. (1975) Lateral earth pressure. In Winterkorn, H.F. & Fang, H-Y. (Eds) *Foundation Engineering Handbook* Van Nostrand Reinhold, New York, pp. 57–220.

Khire, M.V. (1995) *Field Hydrology and Water Balance Modeling of Earthen Final Covers for Waste Containment*, Environmental Geotechnics Report No. 95-5, University of Wisconsin, Madison, WI.

Khire, M.V., Benson, C.H. & Bosscher, P.J. (1997) Water balance modeling of earthen final covers. *Journal of Geotechnical & Geoenviron-*

mental Engineering, ASCE, Reston, VA, **123**(8): 744–754.

Kim, S.K., Hong, W.P. & Kim, Y.M. (1992) Prediction of rainfall-triggered landslides in Korea. In *Proceedings, Sixth International Symposium on Landslides*, Christchurch, Vol. 2, pp. 989–994.

Kimmel, G.E. & Braids, O.C. (1980) Leachate plumes in groundwater from Babylon and Islip landfills, Long Island, New York, Water-Supply Paper 2218, US Geological Survey.

King, K.S., Quigley, R.M., Fernandez, F., Reades, D.W. & Bacopoulos, A. (1993) Hydraulic conductivity and diffusion monitoring of the Keele Valley Landfill liner, Maple, Ontario. *Canadian Geotechnical Journal*, **30**(1): 124–134.

King, M.W.G., Barker, J.F. & Hamilton, K.A. (1995) Natural attenuation of coal tar organics in groundwater. *Intrinsic Bioremedation*, Hinchee, R.E., Wilson, J.T., and Downey, D.C. (Eds.) Battelle Press Inc. Columbus, OH, **3**(1): 171–180.

Kishida, H. & Nakai, S. (1977) Large deflection of single pile inder horizontal load. In *Proceedings, Special Session No. 10, Ninth International Conference on Soil Mechanics & Foundation Engineering*, Tokyo, pp. 87–92.

Kitajima, S. & Uwabe, T. (1979) Analysis on seismic damage in anchored sheet-piling bulkheads. *Report of the Japanese Port & Harbour Research Institute*, **18**(1): 67–130 (in Japanese).

Kjellman, W. (1952) Consolidation of clay soil by means of atmospheric pressure. In *Proceedings, Conference on Soil Stabilization*, Massachusetts Institute of Technology, MA, pp. 258–263.

Klaassen, C.D. & Eaton, D.L. (1991) Principles of toxicology. In Amdur, M.O., Doull, J. & Klaassen, C.D. (Eds) *Casarett & Doull's Toxicology: The Basic Science of Poisons*, 4th Edn, Pergamon Press, New York, pp. 12–49.

Klecka, C.M., Wilson, J.T., Klien, N., West, R., Davis, Weaver, J., Kampbell, D. & Wilson, B. (1996) Intrinsic remediation of chlorinated solvents in groundwater. In *Proceedings, Two Day Conference on Intrinsic Bioremediation*, March 18–19. The Cafe Royal, London.

Klotz, J. (1963) Small sample power and efficiency for the one sample Wilcoxon and normal scores tests. *Annals of Mathematics Statistics*, **34**: 624–632.

Klute, A. & Letey, J. (1958) The dependence of ionic diffusion on the moisture content of nonadsorbing porous media. *Soil Science Society of America Proceedings*, **22**: 213–15.

Kmet, P. (1982) *EPA Water Balance Method–Its Use and Limitations*, Wisconsin Department of Natural Resources, Madison, WI.

Kobayashi, S. & Nishimura, N. (1983) Analysis of dynamic soil–structure interactions by boundary integral equation method. In *Proceedings, Third International Symposium on Numerical Methods in Engineering*, Paris, pp. 353–362.

Kobayashi, K., Yao, S. & Yoshiada, N. (1991) Dynamic compliance of pile group considering nonlinear behaviour around piles. In *Proceedings, Second International Conference on Recent Advances in Geotechnical Earthquake Engineering & Soil Dynamics*, University of Missouri at Rolla, Rolla, MO, pp. 785–792.

Kobori, T., Minai, R. & Suzuki, T. (1971) The dynamical ground compliance of a rectangular foundation on a viscoelastic stratum. *Bulletin Disaster Prevention Research Institute*, **20**: 289–329.

Kobori, T., Minai, R. & Baba, K. (1977) Dynamic behaviour of a laterally loaded pile. In *Ninth International Conference of Soil Mechanics*, Tokyo, pp. 175–180.

Kobori, T., Nakazawa, M., Hijikata, K., Kobayashi, Y., Miura, K., Miyamoto, Y. & Moroi, T. (1991) Study on dynamic characteristics of a pile group foundation. In *Proceedings, Second International Conference on Recent Advances in Geotechnical Earthquake Engineering & Soil Dynamics*, University of Missouri at Rolla, Rolla, MO, pp. 853–860.

Koerner, R.M. (1984) Slope stabilization using anchored geotextiles: anchored spider netting. In *Proceedings, Special Geotechnical Engineering for Roads and Bridges Conference*, PennDot, pp. 1–11.

Koerner, R.M. (1998) *Designing with Geosynthetics*, 4th Edn, Prentice-Hall, Englewood Cliffs, NJ.

Koerner, R.M. & Bove, J. (1983) In-plane hydraulic properties of geotextiles. *Geotechnical Testing Journal*, **6**(4): 190–195.

Koerner, R.M. & Daniel, D.E. (1995) A suggested methodology for assessing the technical equivalency of GCLs to CCLs. In Koerner, R.M., Gartung, E. & Zanzinger H. (Eds) *Geosynthetic Clay Liners*, A.A. Balkema, Rotterdam, pp. 73–100.

Koerner, R.M. & Daniel, D.E. (1997) *Final Covers for Solid Waste Landfills and Abandoned Dumps*, American Society of Civil Engineers, Reston, VA.

Koerner, R.M. & Gartung, E. (1995) *Geosynthetic Clay Liners*, Rotterdam, A.A. Balkema.

Koerner, R.M. & Hwu, B.L. (1991) Stability and tension considerations regarding cover soils on geomembrane-lined slopes. *Geotextiles & Geomembranes*, **10**(4): 335–355.

Koerner, G.R. & Koerner, R.M. (1994) Design of landfill leachate-collection filters. *Journal of Geotechnical Engineering, ASCE*, Reston, VA, **120**(10): 1792–1803.

Koerner, R.M. & Koerner, G.R. (1995) *Leachate Clogging Assessment of Geotextile (and Soil) Landfill Filters*, Report CR-819371, US EPA, Cincinnati, OH.

Koerner, R.M. & Robbins, J.C. (1986) *In situ* stabilization of soil slopes using nailed geosynthetics. In *Proceedings, Third International Conference on Geotextiles*, Vienna, Vol. 2, pp. 395–400.

Koerner, R.M. & Soong, T.Y. (1998) Analysis and design of veneer cover soils, (The Giroud Lecture). In Rowe, R.K. (Ed.) *Proceedings, Sixth International Conference on Geosynthetics*, March, Atlanta, GA, Industrial Fabrics Association International, Roseville, MN, Vol. 1, pp. 1–23.

Koerner, R.M., Koerner, G.R. & Eberlé, M.A. (1996) Out-of-plane tensile behavior of geosynthetic-clay liners. *Gesynthetics International*, **3**(2): 277–296.

Koerner, R.M., Wilson-Fahmy, R.F. & Narejo, D. (1996) Puncture protection of geomembranes Part III: examples. *Geosynthetics International*, **3**(5): 655–675.

Koerner, R.M., Carson, D.A., Daniel, D.E. & Bonaparte, R. (1997) Current status of the Cincinnati GCL test plots. In *Proceedings, GRI-10 Conference on Field Performance of Geosynthetics*, Springfield, PA, pp. 153–182.

Kolbasuk, G.M., Lydick, L.D. & Reed, L.S. (1992) Effects of test procedures on geonet transmissivity results. *Journal of Geotextiles & Geomembranes*, **11**(4–6): 153–166.

König, D., Kockel, R. & Jessberger, H.L. (1996) Zur Beutellung der Standsicherhert und zur Prognose der Setzungen von Mischabfalldeponien. In *Proceedings, 12th Nurnberg Deponieseminar*, 75, Eigenverlag LGA, Nurnberg, pp. 95–117.

Konrad, J.-M. (1987) The influence of heat extraction rate in freezing soils. *Cold Reg. Science & Technology*, **14**: 129–137.

Konrad, J.-M. (1989a) Influence of overconsolidation on the freezing characteristics of a clayey silt. *Canadian Geotechnical Journal*, **26**: 9–21.

Konrad, J.-M. (1989b) Effect of freeze–thaw cycles on the freezing characteristics of a clayey silt at various overconsolidation ratios. *Canadian Geotechnical Journal*, **26**: 217–226.

Konrad, J.-M. (1994) Sixteenth Canadian Geotechnical Colloquium. Frost heave in soils: concepts and engineering. *Canadian Geotechnical Journal*, **2**(31): 223–245.

Konrad, J.-M. (1999) Frost susceptibility related to soil index properties. *Canadian Geotechnical Journal*, **36**(3): 403–417.

Konrad, J.-M. and Duquennoi, C. (1993) A model for water transport and ice lensing in freezing soils. *Water Resources Research*, **29**(9): 3109–3024.

Konrad, J.-M. & Morgenstern, N.R. (1980) A mechanistic theory of ice lens formation in fine-grained soils. *Canadian Geotechnical Journal*, **17**: 473–486.

Konrad, J.-M. & Morgenstern, N.R. (1982a) Prediction of frost heave in the laboratory during transient freezing. *Canadian Geotechnical Journal*, **19**(3), 250–259.

Konrad, J.-M. & Morgenstern, N.R. (1982b) Effects of applied pressure on freezing soils. *Canadian Geotechnical Journal*, **19**(4): 494–505.

Konrad, J.-M. & Morgenstern, N.R. (1983) Frost susceptibility of soils in terms of their segregation potential. In *Proceedings, Fourth International Conference on Permafrost*, Fairbanks, AK, pp. 660–665.

Konrad, J.-M. and Seto, J.T.C. (1994) Frost heave characteristics of undistributed sensitive Champlain sea clay. *Canadian Geotechnical Journal*, **31**: 285–298.

Konrad, J.-M. & Shen, M. (1994) Simulation of retaining wall displacement by frost action using the segregation potential approach. In *Ground Freezing 94*, Fremond, M. (Ed.) Balkema, Rotterdam, pp. 265–270.

Kovacs, W.D. & Leo, E. (1981) Cyclic simple shear of large-scale sand samples: Effects of diameter to height ratio. In *Proceedings, International Conference on Recent Advances in Geotechnical Earthquake Engineering & Soil Dynamics*, St Louis, Vol. 3, pp. 897–907.

Kraft, L.M., Ray, R.P. & Kagawa, T. (1981) Theoretical t–z curves. *Journal of Geotechnical Engineering Division, ASCE*, Reston, VA, **107**(11): 1543–1561.

Krahn, J. & Fredlund, D.G. (1972) On total, matric and osmotic suction. *Journal of Soil Science*, **114**(5): 339–348.

Kramer, S.L. (1996) *Geotechnical Earthquake Engineering*, Prentice Hall, Upper Saddle River, NJ.

Kramer, S.L. & Holtz, R.D. (1991) *Soil Improvement and Foundation Remediation with Emphasis on Seismic Hazards*, Report, University of Washington, Seattle.

Kramer, S.R., McDonald, W.J. & Thomson, J.C. (1992) *An Introduction to Trenchless Technology*, Van Nostrand Reinhold, New York.

Kraus, J.F., Benson, C.H., Erickson, A.E. & Chamberlain, E.J. (1997) Freeze–thaw cycling and hydraulic conductivity of bentonite barriers. *Journal of Geotechnical & Geoenvironmental Engineering, ASCE*, Reston, VA, **123**(3): 229–238.

Krinitzsky, E.L., Gould, J.P. & Edinger, P.H. (1993) *Fundamentals of Earthquake-Resistant Construction*, Wiley, New York.

Kruseman, G.P. & de Ridder, N.A. (1990) *Analysis and Evaluation of Pumping Test Data*, International Institute for Land Reclamation and Improvement, The Netherlands.

Kubo, K. (1965) Experimental study of the behaviour of laterally loaded piles. In *Proceedings, Sixth International Conference on Soil Mechanics & Foundation Engineering*, Montreal, Vol. 2, pp. 275–279.

Kueper, B.H. & Frind, E.O. (1991) Two phase flow in heterogeneous porous media: 2. Model development. *Water Resources Research*, **27**(6): 1059–1070.

Kueper, B.H. & McWorter, D.B. (1991) The behavior of dense, nonaqueous phase liquids in fractured clay and rock. *Groundwater*, **29**(5): 716–728.

Kueper, B.H., Pitts, M., Sale, T.C., Simpkin, T. & Wyatt, K. (1997) Technology practices manual for surfactants and cosolvents. Advanced Applied Technology Demonstration Facility, U.S. Department of Defense.

Kuhlemeyer, R.L. (1979) Static and dynamic laterally loaded floating piles. *Journal of the Geotechnical Engineering Division, ASCE*, Reston, VA, **105**(2): 289–304.

Kulhawy, F.H. (1984) Limiting tip and side resistance: fact or fallacy? In Meyer, J.R. (Ed.) *Analyses & Design of Pile Foundations*, American Society of Civil Engineers, Reston, VA, pp. 80–98.

Kulhawy, F.H. (1991) Drilled shaft foundations. In Fang, H.Y. (Ed.) *Foundation Engineering Handbook*, Van Nostrand, Reinhold, New York, NY, pp. 537–552.

Kulhawy, F.H. & Carter, J.P. (1992) Settlement and bearing capacity of foundations on rock masses. In Bell, F.G. (Ed.) *Engineering in Rock Massess*, Butterworth-Heinemann, Oxford, pp. 231–245.

Kulhawy, F.H. & Carter, J.P. (1992) Socketed foundations in rock masses. In Bell, F.G. (Ed.) *Engineering in Rock Masses, Butterworth-Heinemann*, Oxford, pp. 509–529.

Kulhawy, F.H. & Goodman, R.E. (1987) Foundations in rock. In Bell, F.G. (Ed.) *Ground Engineer's Reference Book*, Butterworths, London, Chapter 55.

Kulhawy, F.H. & Mayne P.W. (1990) *Manual on Estimating Soil Properties for Foundation Design*, Report No. EPRI EL-6800, Cornell University.

Kulhawy, F.H. & Phoon, K. (1993) Drilled shaft side resistance in clay soil to rock. In *Proceedings Conference on Design and Performance of Deep Foundations: Piles and Piers in Soil and Soft Rock*, Geotechnical Special Publication No. 38, American Society of Civil Engineers, Reston, VA, pp. 172–183.

Kunze, R.J., Uehara, G. & Graham, K. (1968) Factors important in the calculation of hydraulic conductivity. *Proceedings, Soil Science of America*, **32**: 760–765.

Kushner, E.J. (1976) On determining the statistical parameters for pollution concentration from a truncated data set. *Atmospheric Environment*, **10**: 975–979.

Kuster, E. (1976) Biological degradation of synthetic polymers. In Ranby, B. & Rabek, J.F. (Eds) *long-term properties of polymers and polymeric materials*, J. of Applied Polymer Science 35, Interscience Publication, New York, NY, USA, pp. 395–404.

Kuwabara, F. & Poulos, H.G. (1989) Downdrag forces in a group of piles. *Journal of the Geotechnical Engineering Division, ASCE*, Reston, VA, **115**(6): 806–818.

Lacasse, S. & Nadim, F. (1994) Reliability issues and future challenges in geotechnical engineering for offshore structures (Plenum Paper). In *Seventh International Conference on the Behaviour of Offshore Structures, BOSS'94*, Massachusetts Institute of Technology, MA, Cambridge, pp. 9–38.

Ladanyi, B. (1977) Friction and end bearing tests on bedrock for high capacity socket design: Discussion. *Canadian Geotechnical Journal*, **14**: 153–155.

Ladanyi, B. & Archambault, G. (1970) Simulation

of shear behavior of a jointed rock mass. In *Proceedings, 11th Symposium on Rock Mechanics*, American Institute of Mechanical Engineers, New York, pp. 105–125.

Ladanyi, B. & Roy, A. (1971) Some aspects of bearing capacity of rock mass. In *Proceedings, Seventh Canadian Symposium on Rock Mechanics*, Edmonton, pp. 161–190.

Ladanyi, B., Dufour, R., Larocque, G.S., Samson, L. & Scott, J.S. (1974) *Report of the Subcommittee on Foundations and Near-Surface Structures to the Canadian Advisory Committee on Rock Mechanics.*

Ladd, C.C. (1969) The prediction of *in situ* stress strain behaviour of soft saturated clay during undrained shear. *Proc. Bolkesjo Symp.*, Norway, Norwegian Geotechnical Institute, Oslo, pp. 14–20.

Ladd, C.C. (1991) Stability evaluation during staged construct. *Journal of Geotechnical Engineering, ASCE*, Reston, VA, **117**(4): 540–615.

Ladd, C.C. & Foott, R. (1974) New design procedure for stability of soft clays. *Journal of Geotechnical Engineering Division, ASCE*, Reston, VA, **100**(7): 763–786.

Ladd, C.C., Foott, R., Ishihara, K., Schlosser, F. & Poulos, H.G. (1977) Stress–deformation and strength characteristics, state-of-the-art report. In *Proceedings, Ninth International Conference on Soil Mechanics and Foundation Engineering*, Tokyo, Vol. 2, pp. 421–494.

Lade, P.V. (1977) Elasto-plastic stress–strain theory for cohesionless soil with curved yield surfaces. *International Journal of Solids & Structures*, **13**: 1019–1035.

Lade, P.V. & Kim, M.K. (1995) Single hardening constitutive model for soil, rock and concrete. *International Journal of Solids & Structures*, **32**(14): 1963–1978.

Lade, P.V. & Yamamuro, J.A. (1993) Stability of granular materials in postpeak softening regime. *Journal of Engineering Mechanics, ASCE*, Reston, VA, **119**(1): 128–144.

Laflamme, J.F. & Leroueil, S. (1999) *Analyse des pressions interstitielles mesurées aux sites d'excavation de Saint-Hilaire et de Rivière-Vachon, Québec.* Report GCT-99-10, Prepared for Ministère des Transports du Quèbec, Université Laval, Québec.

Lafleur, J. & Lefebvre, G. (1980) Groundwater regime associated with slope stability in Champlain clay deposits. *Canadian Geotechnical Journal*, **17**(1): 44–53.

Lafleur, J., Silvestri, V., Asselin, R. & Soulié, M. (1988) Behaviour of a test excavation in soft Champlain Sea clay. *Canadian Geotechnical Journal*, **25**(4): 705–715.

LaGatta, M.D., Boardman, B.T., Cooley, B.H. & Daniel, D.E. (1997) Geosynthetic clay liners subjected to differential settlement. *Journal of Geotechnical & Geoenvironmental Engineering, ASCE*, Reston, VA, **123**(5): 402–410.

Laine, D.L. (1991) Analysis of pinhole seam leaks located in geomembrane liners using the electrical leak location method: case histories. In *Proceedings, Geosynthetics '91*, Atlanta, GA, Industrial Fabrics Association International, Roseville, MN, Vol. 1, pp. 239–253.

Lake, C.B. & Rowe, R.K. (1999) The role of contaminant transport in two different geomembrane/geosynthetic clay liner composite liner designs. *Proceedings, Geosynthetics '99*, April, Boston, MA, Industrial Fabrics Association International, Roseville, MN, Vol. 1, pp. 661–670.

Lake, C.B. & Rowe, R.K. (2000a) *Swelling Characteristic of Needlepunched, Thermally Treated GCLs*, Geotextiles and Geomembranes **18**(2): 77–102.

Lake, C.B. & Rowe, R.K. (2000b) *Diffusion of Sodium and Chloride Through Geosynthetic Clay Liners*, Geotextiles and Geomembranes, **18**(2): 103–132.

Lam, T.S.K., Yau, J.H.W. & Permchitt, J. (1991) Side resistance of a rock-socketed caisson. *Hong Kong Engineer*, **19**(2): 17–28.

Lambe, T.W. (1951) *Soil Testing for Engineers*, Wiley, New York.

Lambe, T.W. (1958a) The structure of compacted clay. *Journal of the Soil Mechanics & Foundation Division, ASCE*, Reston, VA, **84**(2): 1654/1–34.

Lambe, T.W. (1958b) The engineering behaviour of compacted clay. *Journal of Soil Mechanics & Foundation Division, ASCE*, Reston, VA, **84**(2): 1655/1–35.

Lambe, T.W. (1964) Methods of estimating settlement. *Journal of the Soil Mechanics & Foundation Division, ASCE*, Reston, VA, **90**(5): 43–67.

Lambe, T.W. (1967) Stress path method. *Journal of the Soil Mechanics & Foundation Division, ASCE*, Reston, VA, **93**(6): 309–331.

Lambe, T.W. & Whitman, R.V. (1979) *Soil mechanics, SI Version*, Wiley, New York.

Landva, A.O. (1980) Vane testing in peat. *Canadian Geotechnical Journal*, **17**(1): 1–19.

Landva, A.O. & Clark, J.I. (1990) Geotechnics of waste fill. In *Geotechnics of Waste Fills–Theory & Practice*, STP 1070, Landua, A. and Knowles, E.D. (Eds.) American Society for Testing & Materials, West Conshohocken, PA, pp. 86–106.

Landva, A.O. & La Rochelle, P. (1983) Compressibility and shear characteristics of Radforth peats. In *Testing of Peats & Organic Soils*, STP 820, P.M. Jarrett (Ed.) ASTM American Society for Testing & Materials, West Conshohocken, PA, pp. 157–191.

Landva, A.O. & Pheeney, P.E. (1980) Peat fabric and structure. *Canadian Geotechnical Journal*, **17**(3): 416–435.

Landva, A.O., Korpijaakko, E.O. & Pheeney, P.E. (1983) Geotechnical classification of peats and organic soils. In *STP 820*, P.M. Jarrett (Ed.) American Society for Testing & Materials, West Conshohocken, PA, pp. 37–51.

Lane, D.T., Benson, C.H. & Bosscher, P.J. (1992) *Hydrologic Observations and Modeling Assessments of Landfill Covers*, Environmental Geotechnics Report No. 92-10, University of Wisconsin, Madison, WI.

Larsson, R. (1980) Undrained shear strength in stability calculations of embankments and foundations on soft clays. *Canadian Geotechnical Journal*, **17**(4): 591–602.

Larsson, R. (1986) *Consolidation of Soft Soils*, Swedish Geotechnical Institute Report No. 29, Linköping, Sweden.

Lav, M.A., Carter, J.P. & Booker, J.R. (1995) The effect of fissures on the bearing capacity of clay. In *Proceedings, 14th Australasian Conference on the Mechanics of Structures & Materials*, Hobart, pp. 38–43.

Law, K.T. (1985) Use of field vane tests under earth structures. *11th International Conference on Soil Mechanics & Foundation Engineering*, San Francisco, Vol. 2, pp. 893–898.

Law, K.T. & Bozozuk, M. (1979) A method of estimating excess pore pressures beneath em bankments on sensitive clays. *Canadian Geotechnical Journal*, **16**(4): 691–702.

Lawson, C.R. (1986) Geosynthetics in soil reinforcement. In *Proceedings, Symposium on Geotoxtiles in Civil Engineering*, Institution of Engineers Australia, Newcastle, pp. 1–35.

Lea, N.D. & Brawner, C.O. (1963) *Highway Design and Construction Over Peat Deposits in the Lower Mainland of British Columbia*, Highway Research Board Research Record, No. 7, Washington, DC, pp. 1–33.

Leach, G. & Reed, K. (1989) Observations and assessment of the disturbance caused by displacement methods of trenchless construction. In *Proceedings, Fourth International Conference on Trenchless Construction for Utilities, NO-DIG '89* April, London, International Society for Trenchless Technology, London, England, pp. 67–78.

Leblanc, D.R. & Celia, M.A. (1991) *Density-induced downward movement of solutes during a natural-gradient tracer test, Cape Cod, Massachusetts*, Resources Investigation Report 91-4034, US Geological Survey Water, pp. 10–14.

Lebuis, J., Robert, J.M. & Rissmann, P. (1983) Regional mapping of landslides hazard in Québec. In *Symposium on Slopes in Soft Clays*, Linköping, SGI Report No. 17, pp. 205–262.

Lechner, P. (1994) Design criteria for leachate drainage and collection systems. In *Landfilling of Waste: Barriers*. T.H. Christensen, R. Cossu & R. Stegmann (Eds.), E & FN Spon, London, UK, pp. 519–530.

Ledbetter, R.H. & Finn, W.D.L. (1993) *Development and evaluation of remediation strategies by deformation analyses*. In *Proceedings, Special Technical Publication, Geotechnical Practice in Dam Rehabilitation*, April 15–28, American Society of Civil Engineers, Reston, VA.

Lee, C.Y., Poulos, H.G. & Hull, T.H. (1991) Effect of seafloor instability on offshore pile foundations. Canadian Geotechnical Journal, **28**(5): 729, 737.

Lee, I.K. (1993) Analysis and performance of raft and pile-raft systems (keynote lecture). In *Third International Conference on Case Histories in Geotechnical Engineering*, St. Louis.

Lee, K.L. & Singh, A. (1971) Relative density and relative compaction. *Journal of the Soil Mechanics & Foundations Division, ASCE*, Reston, VA, **97**(7): 1049–1052.

Lee, K.L. & Seed, H.B. (1967) Drained strength characteristics of sands. *Journal of the Soil Mechanics & Foundations Division, ASCE*, Reston, VA, **93**(6): 117–141.

Lee, K.L., Jones, C.J.F.P. Sullivan, W.R. & Trolinger, W. (1995) Failure and deformation of four reinforced earth walls in Eastern Tennessee, USA. *Géotechnique*, **45**(4): 749–752.

Lee, M. & Finn, W.D.L. (1978) *DESRA-2: Dynamic Effective Stress Response Analysis of Soil Deposits with Energy Transmitting Boundary Including Assessment of Liquefaction Potential*, Report No. 38, Soil Mechanics Services, University of British Columbia, Vancouver, BC.

Lee, M.K., Lum, K.Y. & Hartford, D.N.D. (1998) Calculation of the seismic risk of an earth dam susceptible to liquefaction. In Dakoulas, P. & Yegian, M. (Eds.), Earthquake Engineering and Soil Dynamics III. Geotechnical Special Publication No. 75. American Society of Civil Engineers, Reston, VA, pp. 1451–1460.

Lee, S.L., Chow, Y.K., Karunaratne, G.P. & Wong, K.Y. (1988) Rational wave equation model for pile driving analysis. *Journal of Geotechnical Engineering, ASCE*, Reston, VA, **114**(3): 306–325.

Leeman, E.R. (1968) The determination of the complete state of stress in rock in a single borehole-laboratory and underground measurements. *International Journal of Rock Mechanics & Mineral Science*, **5**: 31–56.

Lefebvre, G. (1981) Fourth Canadian Geotechnical Colloquium: Strength and slope stability in Canadian soft clay deposits. *Canadian Geotechnical Journal*, **18**(3): 420–442.

Lefebvre, G., Langlois, P., Lupien, C. & Lavallée, J.-G. (1984) Laboratory testing and *in situ* behaviour of peat as embankment foundation. *Canadian Geotechnical Journal*, **21**(2): 322–337.

Lefebvre, G., Paré, J.J. & Dascal, O. (1987) Undrained shear strength in the surficial weathered crust. *Canadian Geotechnical Journal*, **24**(1): 23–34.

Leflaivre, E, Khay, M. & Blivet, J.C. (1983) Un nouveau material: le Texsol. *Bulletin de Liason du Laboratoire des Ponts et Chaussees*, **125**: 105–114.

Legget, R.F. (1962) *Geology in Engineering*, McGraw-Hill, 2nd Edn, New York.

Legget, R.F. & Hatheway, A.W. (1988) *Geology & Engineering*, McGraw-Hill, New York.

Lehr, J.H. (1990) Toxicological risk assessment distortions: Part III a different look at environmentalism. *Ground Water*, **28**(3): 330–340.

Lenhard, R.J. & Parker, J.C. (1990) Estimation of free hydrocarbon volume from fluid levels in monitoring wells. *Groundwater*, **28**, 57–67.

Lenhard, R.J., Johnson, T.G. & Parker, J.C. (1993) Experimental observations of non-aqueous-phase liquid subsurface movement. *Journal of Contaminant Hydrology*, **12**: 79–101.

Lentz, R.W., Horst, W.D. & Uppot, J.O. (1985) The permeability of clay to acidic and caustic permeants. In Johnson, A.I., Frobel, R.K., Cavalli, N.J. & Pettersson, C.B. (Eds) *Hydraulic Barriers in Soil and Rock*, STP 874, American Society for Testing & Materials, West Conshohocken, PA, pp. 127–139.

Leonards, G.A. (1962) *Foundation Engineering*, McGraw Hill, New York.

Leonards, G.A. (1972) Settlement of pile foundations in granular soil. *Proceedings, Conference Perf. Earth & Earth-Supp. Structures, ASCE*, Reston, VA, **2**: 1169–1184.

Leonards, G.A. (1979) Stability of slopes in soft clays (special lecture). *Sixth Panamerican Conference on Soil Mechanics & Foundation Engineering*, Lima.

Leonards, G.A. & Narain, J. (1963) Flexibility of clay and cracking of earth dams. *Journal of the Soil Mechanics & Foundations Division, ASCE*, Reston, VA, **89**(2): 47–98.

Leonards, G.A., Cutter, W.A. & Holtz, R.D. (1980) Dynamic compaction of granular soils. *Journal of Geotechnical Engineering, ASCE*, Reston, VA, **106**(1): 35–44.

Leong, E.C. & H. Rahardjo (1997a) A review on soil–water characteristic curve equations. *Journal of Geotechnical Engineering, ASCE*, Reston, VA, **123**(12): 1106–1117.

Leong, E.C. & H. Rahardjo (1997b) Permeability functions for unsaturated soils. *Journal of Geotechnical Engineering*, ASCE, Reston, VA, **123**(12): 1118–1126.

Leroueil, S. (1988) Recent developments in consolidation of natural clays: 10th Canadian Geotechnical Colloquium. *Canadian Geotechnical Journal*, **25**(1): 85–107.

Leroueil, S. (1996) Compressibility of clays: fundamental and practical aspects. *Journal of Geotechnical Engineering*, ASCE, Reston, VA, **122**(7): 534–543.

Leroueil, S. (1997) Critical state soil mechanics and the behaviour of real soils. In Almeida, M. (Ed.) *Proceedings, International Symposium on Recent Developments in Soil & Pavement Mechanics*, Rio de Janeiro, Brazil, pp. 41–80. A.A. Balkema, Brookfield, Vermont.

Leroueil, S. (2000) 39th Rankine Lecture: Cuts and natural slopes: movement and failure mechanisms. *Géotechnique* (in press).

Leroueil, S. & Jamiolkowski, M. (1991) Exploration of soft soil and determination of design parameters, (General Report, Session 1). *GeoCoast '91*, Yokohama, Vol. 2, pp. 969–998.

Leroueil, S. & Locat, J. (1998) Slope movements: geotechnical characterization, risk assessment and mitigation. In *Proceedings, 11th Danube–European Conference on Soil Mechanics & Geotechnical Engineering*, Poreč, Croatia, pp. 95–106.

Leroueil, S. & Marques, M.E.S. (1996) Impor-

tance of strain rate and temperature effects in geotechnical engineering. *ASCE Convention*, Geotechnical Special Publication No. 61 Washington, DC, pp. 1–60.

Leroueil, S. & Tavenas, F. (1986) Discussion on 'Effective stress paths and yielding in soft clays below embankments' by D.J. Folkes & J.H.A. Crooks. *Canadian Geotechnical Journal*, **23**(3): 410–413.

Leroueil, S. & Vaughan, P.R. (1990) The general and congruent effects of structure in natural soils and weak rocks. *Géotechnique*, **40**(3): 467–488.

Leroueil, S., Tavenas, F., Trak, B., La Rochelle, P. & Roy, M. (1978a) Construction pore pressures in clay foundations under embankments, Part I: the Saint-Alban test fills. *Canadian Geotechnical Journal*, **15**(1): 54–65.

Leroueil, S., Tavenas, F., Mieussens, C. & Peignaud, M. (1978b) Construction pore pressures in clay foundations under embankments, Part II: generalized behaviour. *Canadian Geotechnical Journal*, **15**(1): 66–82.

Leroueil, S., Tavenas, F. & Le Bihan, J.-P. (1983) Propriétés caractéristiques des argiles de l'est du Canada. *Canadian Geotechnical Journal*, **20**(4): 681–705.

Leroueil, S., Kabbaj, M., Tavenas, F. & Bouchard, R. (1985a) Stress–strain–strain rate relation for the compressibility of sensitive natural clays. *Géotechnique*, **35**(2): 159–180.

Leroueil, S., Magnan, J.-P. & Tavenas, F. (1985b) *Remblais sur argiles molles*. Lavoisier-Technique et Documentation, France. English version *Embankment on Soft Clays*, Ellis Horwood, Chichester, UK.

Leroueil, S., La Rochelle, P., Tavenas, F. & Roy, M. (1990) Remarks on the stability of temporary cuts. *Canadian Geotechnical Journal*, **27**(5): 687–692.

Leroueil, S., Tardif, J., Roy, M., LaRochelle, P. & Konrad, J.-M. (1991) Effects of frost on the mechanical behaviour of Champlain Sea clays. *Canadian Geotechnical Journal* **28**: 690–697.

Leroueil, S., Le Bihan, J.P. & Bouchard, R. (1992a) Remarks on the design of clay liners in lagoons as hydraulic barriers. *Canadian Geotechnical Journal*, **29**: 512–515.

Leroueil, S., Le Bihan, J.P. & Bouchard, R. (1992b) Discussion of water content–density criteria for compacted soil liners by D. Daniel, & C. Benson. *Journal of Geotechnical Engineering, ASCE*, Reston, VA, **118**(2): 963–965.

Leroueil, S., Demers, D., La Rochelle, P., Martel, G. & Virely, D. (1995) Practical applications of the piezocone in Champlain sea clays. In *Proceedings, International Symposium on Cone Penetration Testing*, CPT-95, Linköping, pp. 515–522.

Leroueil, S., Perret, D. & Locat, J. (1996a) Strain rate and structuring effects on the compressibility of a young clay. Session on Measuring and Modeling Time Dependent Soil Behavior, *ASCE Convention*, Geological Special Publication No. 61, Washington, DC, pp. 137–150.

Leroueil, S., Vaunat, J., Picarelli, L., Locat, J., Faure, R.M. & Lee, H. (1996b) A geotechnical characterization of slope movements. In *Proceedings, Seventh International Symposium on Landslides*, Trondheim, Vol. 1, pp. 53–74.

Lesage, S., Brown, S. & Millar, K. (1996) Vitamin B12-catalyzed dechlorination of perchloroethylene present as residual DNAPL. *Ground Water Monitoring & Remediation*, **16**(4): 76–85.

Leshchinsky, D., Ling, H.I. & Hanks, G.A. (1995) Unified design approach to geosynthetic reinforced slopes and segmental walls. *Geosynthetics International*, **2**(5): 845–881.

Leussink, H. & Wenz, K.P. (1969) Storage yard foundations on soft cohesive soils. In *Proceedings, Seventh International Conference on Soil Mechanics & Foundation Engineering*, Mexico City, Vol. 2, pp. 149–155.

Levy, J.F. (1970) Sonic pulse method of testing cast-*in-situ* concrete piles. *Ground* Engineering, **3**(3): 17–19.

Li, A.L. & Rowe, R.K. (1999) Reinforced embankments and the effect of consolidation on soft cohesive soil deposits. In *Geosynthetics '99*, Boston. Industrial Fabrics Association International, Roseville, MN, pp. 477–490.

Li, J., Cameron, D.A. & Mills, K.G. (1996) Numerical modelling of covers and slabs subject to seasonal surface suction changes. In *Seventh Australia–New Zealand Conference on Geomechanics*, 1–5 July, Adelaide, M.B. Jaksa, W.S. Kaggwa & D.A. Cameron (Eds.), pp. 424–429.

Liao, S.S.C. & Whitman, R.V. (1986) Overburden correction factors for SPT in sand. *Journal of Geotechnical Engineering*, ASCE, Reston, VA, **112**(3): 373–377.

Liao, S.S.C., Veneziano, D. & Whitman, R.V. (1988) Regression models for evaluating liquefaction probability. *Journal of Geotechnical Engineering, ASCE*, Reston, VA, **114**(4): 389–411.

Liao, S.T. & Roesset, J.M. (1997) Identification of defects in piles through dynamic testing. *In-*

ternational Journal of Numerical Analytical Methods in Geomechanics, **21**(4): 277–291.

Little, A.D. Inc. (1985) *Resistance of Flexible Membrane Liners to Chemicals and Wastes*, US EPA Report PB86–119955, Cincinnati, OH.

Littlejohn, G.S. (1993) Chemical grouting. In Moseley, M.P. (Ed.) *Ground Improvement*, Blackie Academic & Professional, Blackwood, NJ, pp. 100–130.

Liu, C.N., Gilbert, R.B., Thiel, R.S. & Wright, S.G. (1997) What is an appropriate factor of safety for landfill cover slopes. In *Proceedings, Geosynthetics '97 Conference*, Long Beach, Industrial Fabrics Association International, Roseville, MN, Vol. 1, pp. 481–496.

Lo, K.Y. (1962) Shear strength properties of a sample of volcanic material of the Valley of Mexico. *Géotechnique*, **22**(4): 303–318.

Lo, K.Y. (1970) The operational strength of fissured clays. *Géotechnique*, **20**: 57–74.

Lo, K.Y. (1978) Regional distribution of *in-situ* horizontal stresses in rocks of Southern Ontario. *Canadian Geotechnical Journal*, **15**(3): 371–381.

Lo, K.Y. (1986) Recent advances in design and evaluation of performance of underground structures in rocks. *Tunnelling & Underground Space Technology*, **4**(2): 171–183.

Lo, K.Y. & Cooke, B.H. (1989) Foundation design for the Skydome Stadium, Toronto. *Canadian Geotechnical Journal*, **26**: 22–33.

Lo, K.Y. & Grass, J.D. (1994) Recent experience with safety assessment of concrete dams on rock foundations. In *Proceedings, Canadian Dam Safety Conference*, October, Winnipeg, pp. 231–250.

Lo, K.Y. & Hefny, A.M. (1993) The evaluation of *in-situ* stresses by hydraulic fracturing tests in anisotropic rocks with mixed-mode fractures. *Canadian Tunnelling Journal*: 59–73.

Lo, K.Y. & Hefny, A.M. (1996) Design of tunnels in rock with long-term time-dependent and nonlinearly stress-dependent deformation. *Canadian Tunnelling Journal*: 179–214.

Lo, K.Y. & Hefny, A.M. (1998) Statistical analysis of the strength of the contact between concrete dams and rock foundations. In *First Annual Conference System Stewardship for Dams & Reservoirs*, September 27–October 1, The Canadian Dam Association, Halifax, NS, pp. 18–33.

Lo, K.Y. & Hori, M. (1979) Deformation and strength properties of some rocks in Southern Ontario. *Canadian Geotechnical Journal*, **16**: 108–120.

Lo, K.Y. & Lee, F. (1974) An evaluation of the stability of natural slopes in plastic Champlain clays. *Canadian Geotechnical Journal*, **11**(1): 165–181.

Lo, K.Y. & Lee, Y.N. (1990) Time dependent deformation behavior of Queenston Shale. *Canadian Geotechnical Journal*, **27**: 461–471.

Lo, K.Y. & Lukajic, B. (1984) Predicted and measured stresses and displacements around the Darlington intake tunnel. *Canadian Geotechnical Journal*, **21**: 147–165.

Lo, K.Y. & Morin, J.P. (1972) Strength anisotropy and time effects of two sensitive clays *Canadian Geotechnical Journal*, **9**(3): 261–277.

Lo, K.Y. & Stermac, A.G. (1965) Failure of an embankment founded on varved clay. *Canadian Geotechnical Journal*, **2**(3): 234–253.

Lo, K.Y. & Yuen, C.M.K. (1981) Design of tunnel lining in rock for long term effects. *Canadian Geotechnical Journal*, **18**: 24–39.

Lo, K.Y., Wai, R.S.C., Palmer, J.H.L. & Quigley, R.M. (1978) Time-dependent deformation of shaly rocks in Southern Ontario. *Canadian Geotechnical Journal*, **15**: 537–547.

Lo, K.Y., Devata, M. & Yuen, C.M.K. (1979a) Performance of a shallow tunnel in a shaly rock with high horizontal stresses. London, ON. Canada. *Tunnelling*, 1–12.

Lo, K.Y., Lukajic, B., Yuen, C.M.K. & Hori, M. (1979b) *In situ* stress measurement in rock overhang at the Ontario Power Generating Station, Niagara Falls. In *Fourth International Congress on Rock Mechanics*, Montreux, Switzerland, Vol. 2, pp. 343–351.

Lo, K.Y., Lukajic, B. & Ogawa, T. (1984) Predicting settlement due to tunneling in clays. *Proceedings, Tunnelling in Soil & Rock, ASCE*, Reston, VA, May 14–18, Atlanta, GA, pp. 128–155.

Lo, K.Y., Cooke, B.H. & Dunbar, D.D. (1987a) Design of buried structures in squeezing rock in Toronto, Canada. *Canadian Geotechnical Journal*, **24**: 232–241.

Lo, K.Y., Yung, T.C.B. & Lukajic, B. (1987b) A field method for the determination of rock mass modulus. *Canadian Geotechnical Journal*, **24**: 406–413.

Lo, K.Y., Lukajic, B., Wang, S., Ogawa, T. & Tsui, K.K. (1990) Evaluation of strength parameters of concrete–rock interface for dam safety assessment. In *Proceedings, Canadian Dam Safety Conference*, September, Toronto, pp. 71–94.

Lo, K.Y., Ogawa, T., Lukajic, B., Smith, G.F. &

Tang, J.H.K. (1991a) The evaluation of stability of existing concrete dams on rock foundations and remedial measures. In *Proceedings, 17th International Congress, International Commission on Large Dams*, Vienna, Austria, pp. 963–990.

Lo, K.Y., Ogawa, T., Lukajic, B. & Dupak, D. (1991b) Measurements of strength parameters of concrete–rock contact at the dam–foundation interface. *Geotechnical Testing Journal, ASTM*, West Conshohocken, PA, **14**(4): 383–394.

Lo, K.Y., Inculet, I.I. & Ho, K.S. (1991c) Field test of electroosmotic strengthening of soft sensitive clay. *Canadian Geotechnical Journal*, **28**(1): 74–83.

Lo, K.Y., Ho, M.S.F., Hefny, A.M. & Adeghe, L. (1997) Measurements of laboratory rates of concrete expansion in Saunders Dam. *The Canadian Geotechnical Conference*, October 20–22, Golden Jubilee, Ottawa, Ontario, pp. 582–592.

Lo, M.C. (1992) *PhD thesis*, University of Texas.

Locat, J. & Leroueil, S. (1997) Landslides risk assessment in sensitive clays: pre-failure, failure, and post-failure issues. *IUGS Workshop on Landslide Risk Assessment*, Honolulu, pp. 261–270.

Loi, J., Fredlund, D.G., Gan, J.K-M. & Widger, R.A. (1992) Monitoring soil suction in an indoor test track facility. *Transportation Research Record*, **1362**: 101–110.

Long, J.H., Daly, J.J. & Gilbert, R.B. (1993) *Structural Integrity of Geosynthetic Lining and Cover Systems for Solid Waste Landfills*, Department of Civil Engineering, University of Illinois, Project No. OSWR 06-005.

Long, J.H., Gilbert, R.B. & Daly, J.J. (1994) Geosynthetic loads in landfill slopes: displacement compatibility. *Journal of Geotechnical Engineering, ASCE*, Reston, VA, **120**(11): 2009–2025.

Lopes, R.F., DuBois, D., Barone, F.S., Matchett, D. & Quigley, R.M. (1992) An evaluation of compacted Question Shale as clay liner material for a landfill. In *Proceedings, 45th Canadian Geotechnical Conferences*, October, Toronto, pp. 71-1–71-10.

Loudon, P.A. (1967) *PhD thesis*, University of Cambridge, England.

Loughney R.W. (1954) Electricity Stiffens Clay Fivefold for Electric Power Plant Excavation. Construction Methods & Equipment **36**(8): 70–82.

Louis, C. (1969) *PhD thesis*, University of Karlsruhe, Germany. Translated by the Rock Mechanics Department, Imperial College, Report 10, London, England.

Lovell, C. (1957) Temperature effects on phase composition and strength of partially frozen soil. *Hwy. Research Board Bulletin* **168**: 74–95.

Low, P.F. (1987) Structural component of the swelling pressure of clay. *Langmuir*, **3**: 18–25.

Low, P.F. (1992) Interparticle forces in clay suspensions: flocculation, viscous flow and swelling. In Güven, N. & Pollastro, R.M. (Eds) *CMS Workshop Lectures, 4: Clay Water Interface and its Rheological Implications*, Clay Minerals Society, pp. 157–190.

Lowe, J. & Zaccheo, P.F. (1991) Subsurface exploration and sampling. In Fang, H.Y. (Ed.) *Foundation Engineering Handbook*, 2nd Edn. Van Nostrand Reinhold, New York, pp. 1–71.

Lozano, N. & Aughenbaugh, N.R. (1995) Flexibility of fine-grained soils. In *Geoenvironment 2000*, Geotechnical Special Publication No. 46, Acar, Y.B. and Daniel, D.C. (Eds.) American Society of Civil Engineers, Reston, VA, Vol. 1, pp. 844–858.

Luco, J.E. & Hadjian, A.H. (1974) Two-dimensional approximations to the three-dimensional soil–structure interaction problem. *Nuclear Engineering & Design*, **31**(2): 195–203.

Luco, J.E. & Westmann, R.A. (1971) Dynamic response of circular footings. *Journal of Engineering Mechanics Division, ASCE*, Reston, VA, **97**(6): 1381–1395.

Luettich, S.M. & Williams, N.D. (1989) Design of vertical drains using the hydraulic conductivity ratio analysis. In *Proceedings Geosynthetics '89*, IFAI, Roseville, MN, pp. 95–103.

Luettich, S.M., Giroud, J.P. & Bachus, R.C. (1992) Geotextile filter design guide. *Geotextiles & Geomembranes*, **11**(4–6): 355–370.

Lukas, R.G. (1986) *Dynamic Compaction for Highway Construction Volume I: Design and Construction Guidelines*, Report, No. FHWA/RD-86/133, Federal Highway Administration, Springfield, VA.

Lukas, R.G. (1995) *Dynamic Compaction*, Geotechnical Engineering Circular No. 1, Report FHWA-SA-95-037, Federal Highway Administration, Springfield, VA.

Lukas, R.G. (1997) Delayed soil improvement after dynamic compaction. In *Ground Improvement, Ground Reinforcement, and*

Ground Treatment: Developments 1987–1997, V.R. Schaefer (Ed.) *ASCE* Press, Reston, VA.

Lundegard, P.D. & Labrecque, D. (1995) Air sparging in a sandy aquifer (Florence, Oregon): Actual and apparent radius of influence. *Journal of Contaminant Hydrology*, **19**(1): 1–28.

Lunne, T., Eide, O. & de Ruiter, J. (1976) Correlations between cone resistance and vane shear strength in some Scandinavian soft to medium stiff clays. *Canadian Geotechnical Journal*, **13**(4): 430–441.

Lunne, T., Lacasse, S. & Rad, N.S. (1990) SPT, CPT, pressuremeter testing and recent developments on *in-situ* testing of soils. Part 1: all tests except SPT (state-of-the-art report). In *12th International Conference on Soil Mechanics & Foundation Engineering*, August 13–18, Rio de Janeiro, Brazil.

Lunne, T., Powell, J.J.M. & Robertson, P.K. (1996) Use of piezocone tests in non-textbook soils. In Craig, C. (Ed.) *Proceedings, International Conference on Advances in Site Investigation Practice*, March 30–31, London, Thomas Telford, London, England, pp. 438–451.

Lunne, T., Robertson, P.K. & Powell, J.J.M. (1997) *Cone Penetration Testing*, Blackie, London, England.

Lupien, C., Lefebvre, G., Rosenberg, P., Pare, J.J. & Lavallée, J.G. (1983) The use of fabrics for improving the placement of till on peat foundation. *62nd Annual Meeting of The Transportation Research Board*, January 17–21. Washington, DC.

Lupini, J.F., Skinner, A.E. & Vaughan, P.-R. (1981) The drained residual strength of cohesive soils. *Géotechnique*, **31**(2): 181–213.

Luster, J. (1986) Physical loss of stabilizers from polymers. In Scott, G. (Ed.) *Developments in Polymer Stabilization – 2*, Applied Science, London, pp. 185–240.

Lutenegger, A.J., DeGroot, D.J., Mirza, C. & Bozozuk, M. (1995) *Recommended Guidelines for Sealing Geotechnical Exploratory Holes*, Transportation Research Board, National Research Council, National Cooperative Highway Research Program, NCHRP Report 378.

Lyman, W.J. & Nomaw, D.C. (1990) *Assessing UST Corrective Action Technologies: Site Assessment and Selection of Unsaturated Zone Treatment Technologies*, Report EPA/600/2-90/011, US Environmental Protection Agency, Cincinnati, OH, 107 p.

Lyman, W.J., Reehl, W.F. & Rosenblatt, D.H. (1982) *Handbook of Chemical Property Estimation Methods: Environmental Behavior of Organic Compounds*, McGraw-Hill, New York.

Lysmer, J. & Kuhlemeyer, R.L. (1969) Finite dynamic model for infinite media. *Journal of Engineering Mechanics Division, ASCE*, Reston, VA, **95**(4): 859–877.

Lysmer, J., Udaka, T., Tsai, C.F. & Seed, H.B. (1975) *FLUSH–A computer program for approximate 3-D analysis of soil structure interaction problems*, Report No. EERC 75–30, Earthquake Engineering Research Centre, University of California, Berkeley.

MacFarlane, I.C. (Ed.) (1969) *Muskeg Engineering Handbook*, University of Toronto Press, Toronto, ON.

MacFarlane, I.C. & Rutka, A. (1959) Evaluation of road performance over muskeg in Ontario. In *Proceedings, 14th Convention of the Canadian Good Roads Association*, Vancouver, BC, pp. 396–405.

Mackay, D.M. & Vogel T.M. (1985) Groundwater contamination by organic chemicals: uncertainties in assessing impact, Hitchon, B. & Trudell, M. (Eds), *Second Canadian/American Conference on Hydrogeology*. National Water Well Association, Dublin, OH, pp. 50–59.

Mackay, D.M., Freyberg, D.L. & Roberts, P.V. (1986) A natural gradient experiment on solute transport in a sand aquifer. 1. Approach and overview of plume movement. *Water Resources Research*, **22**(13): 2017–2029.

Mackay, D., Shiu, W.Y. & Ma, K.C. (1992–1997) *Illustrated Handbook of Physical–Chemical Properties of Environmental Fate for Organic Chemicals*, Lewis, Boca Raton, FL.

Mackay, D.M. & Cherry, J.A. (1989) Groundwater contamination: limits of pump-and-treat remediation. *Environmental Science & Technology*, **23**(6): 630–636.

MacKay, P. (1997) *MESc thesis*, University of Western Ontario, London, Canada.

Madsen, F.T. & Mitchell, J.K. (1988) Chemical effects on clay fabric and hydraulic conductivity. In Baccini, P. (Ed.) *The Landfill, Reactor and Final Storage*. Lecture Notes in Earth Sciences 20, Berlin, Springer, pp. 201–251.

Mage, D.T. (1982) An objective graphical method for testing normal distributional assumptions using probability plots. *The American Statistician*, **36**(2): 116–120.

Magnan, J.P. (1987) Prediction and behavior of embankments – Settlements and improvements (State-of-the-art report). *International*

Symposium on Geotechnical Engineering of Soft Soils, Mexico City, Vol. 2, pp. 87–123.

Magnan, J.P. (1992) Le rôle du fluage dans les calculs de consolidation et de tassement des sols compressibles. *Bulletin de Liaison des Laboratoires des Ponts et Chaussées*, **180**: 19–24.

Magnan, J.-P. & Deroy, J.-M. (1980) Analyse graphique des tassements observés sous les ouvrages. *Bulletin de Liaison des Laboratoires des Ponts et Chaussées*, **109**: 45–52.

Maidment, D.R. (1993) *Handbook of Hydrology*, McGraw-Hill, New York.

Maine Bureau of Remediation & Waste Management (1997) *An Assessment of Landfill Cover System Barrier Layers Hydraulic Performance*, Augusta, ME.

Mair, R.J. (1987) Discussion on tunnel face pressures in soft clay. In *Proceedings, Eighth Asian Regional Conference on Soil Mechanics & Foundation Engineering*, Kyoto, Japan, Vol. 2, p. 290.

Mair, R.J. & Wood, D.M. (1987) *Pressuremeter Testing Methods and Interpretation*, Construction Industry Research and Information Association (CIRIA), Ground Engineering Report: *In-Situ* Testing. Butterworths, London, England.

Mair, R.J., Taylor, R.N. & Bracegirdle, A. (1993) Subsurface settlement profiles above tunnels in clays. *Géotechnique*, **43**(2): 315–320.

Major, A. (1962) *Dynamics in Civil Engineering*, Akademical Kiado, Budapest, Vols. I–IV.

Makris, N. & Gazetas, G. (1992) Dynamic pile–soil–pile interaction. Part II: Lateral and seismic response. *Earthquake Engineering & Structural Dynamics*, **21**: 145–162.

Mandel, J. & Salençon, J. (1972) Force portante d'un sol sur une assise rigide (étude théorique). *Géotechnique*, **22**(1): 79–93.

Mansur, C.I. & Kaufman, R.I. (1962) Dewatering. In Leonards, G.A. (Ed.) *Foundation Engineering*, McGraw-Hill, New York, pp. 241–350.

Marchetti, S. (1980) *In situ* tests by flat dilatometer. *Journal of Geotechnical Engineering, ASCE*, Reston, VA, **106**(3): 299–321.

Marchetti, S. & Crapps, D.K. (1981) *Flat Dilatometer Manual*, Gainesville, FL.

Marcuson, W.F., Hynes, M.E. & Franklin, A.G. (1992) Seismic stability and permanent deformation analyses: the last twenty five years. In Seed, R.B. & Boulanger, R.W. (Eds) *Proceedings, ASCE Specialty Conference on Stability and Performance of Slopes and Embankments – II*, Geotechnical Special Publication No. 31, American Society of Civil Engineers, Reston, VA, Vol. I, pp. 552–592.

Marks, P.J., Wujcik, W.J. & Loncar, A.F. (1994) *Remediation Technologies Screening Matrix and Reference Guide*, 2nd Edn, NTIS PB95-104782, *Department of Defense Environmental Technology Transfer Committee*, Washington, DC, 461 p.

Marle, C.M. (1981) *Multiphase Flow in Porous Media*, Gulf Publishing, Houston, TX.

Marley, M.C. & Hoag, G.E. (1984) Induced soil venting for recovery/restoration of gasoline hydrocarbons in the vadose zone. In *Proceedings, Petroleum Hydrocarbons & Organic Chemicals in Ground Water*, November 5–7, Houston, TX, National Ground Water Association, pp. 473–503.

Marley, M.C., Hazebrouck, D.J. & Walsh, M.T. (1992) The application of *in situ* air sparging as an innovative soils and ground water remediation technology. *Ground Water Monitoring Review*, **12**(2): 137–145.

Marshall, T.J. (1958) A relation between permeability and size distribution of pores. *Journal of Soil Science*, **9**: 1–8.

Marsland, A. (1986) The choice of test methods in site investigation. In Hawkins, A.B. (Ed.) *Site Investigation Practice: Assessing BS 5930*. Engineering Geology Special Publication No. 2, Geological Society, London, England, pp. 289–297.

Marston, A. & Anderson, A.O. (1913) The theory of loads on pipes in ditches and tests on cement and clay drain, tile and sewer pipe. Bulletin 31, Engineering Experimental Station, Iowa State College.

Martian, P. (1994) *Calibration of HELP Version 2.0 and Performance Assessment of Three Infiltration Barrier Designs for Hanford Site Remediation*, Draft A, DOE/RL-93-33, Idaho National Engineering Laboratory, Idaho Falls.

Martin, G.R. & Dobry, R. (1994) Earthquake site response and seismic code provisions. *NCEER Bulletin*, **8**(4): 1–6, Buffalo, NY.

Martin, G.R., Finn, W.D.L. and Seed, H.B. (1975) Fundamentals of liquefaction under cyclic loading. *Journal of the Geotechnical Engineering Division, ASCE*, Reston, VA, **101**(GT5): 423–438.

Martin, J.P., Koerner, R.M. & Whitty, J.E. (1984) Experimental friction evaluation of slippage between geomembranes, geotextiles, & soils. In *Proceedings, International Conference on*

Geomembranes, Denver, CO, Industrial Fabrics Association International, Roseville, MN, pp. 191–196.

Massarsch, K.R. (1975) New method for measurement of lateral earth pressure in cohesive soils. *Canadian Geotechnical Journal*, **12**(1): 142–146.

Massarsch, K.R. (1986) Lateral earth pressure at rest in clay. In *Proceedings, Fourth International Geotechnical Seminar*, Singapore, pp. 203–209.

Massarsch, K.R., Holtz, R.D., Holm, B.G. & Fredriksson, A. (1975) Measurement of horizontal *in-situ* stresses. In *Proceedings, ASCE Geotechnical Engineering Division Specialty Conference on* In-Situ *Measurement of Soil Properties*, June 1–4, North Carolina State University, Raleigh, NC, Vol. 1, pp. 266–286.

Masuda, K., Saseki, F., Urao, K. Veno, K. & Miyamoto, Y. (1986) Simulation analysis of forced vibration test of actual pile foundation by thin layer method. In *Proceedings, Annual Meeting of Architectural Institute of Japan*, Architectural Institute of Japan.

Matar, M. & Salençon, J. (1977) Capacité portante d'une semelle filante sur sol purement cohérent d'épaisseur limitée et de cohésion variable avec la profondeur. *Annales de l'Institut Technique du Bâtiment et des Traveaux Publics, Sols et Fondations*, **352**: 95–107.

Matasovic, N. (1993) *PhD dissertation*, Department of Civil Engineering, University of California, Los Angeles, NV.

Matasovic, N. & Kavazanjian, E., Jr (1998) Cyclic characterization of OII landfill waste. *Journal of Geotechnical & Geoenvironmental Engineering, ASCE*, Reston, VA, **124**(3): 186–196.

Matasovic, N. & Vucetic, M. (1995) Seismic response of soil deposits composed of fully saturated clay and sand layers. In *Proceedings, First International Conference on Earthquake Geotechnical Engineering*, Tokyo, Japan, Vol. 1, pp. 611–616.

Matasovic, N., Kavazanjian, E., Jr & Yan, L. (1997) Newmark deformation analysis with degrading yield acceleration. In *Proceedings, Geosynthetics '97 Conference*, Long Beach, Industrial Fabrics Association International, Roseville, MN, Vol. 2, pp. 989–1000.

Matasovic, N., Kavazanjian, E., Jr. & Anderson, R.L. (1998) Performance of solid waste landfills in earthquakes. *Earthquake Spectra*, **14**(2): 319–334.

Matheron, G. (1973) The intrinsic random functions and their applications. *Advances Appl. Prob.*, **5**: 439–468.

Matheson, L.J. & Tratnyek, P.G. (1994) Processes affecting remediation of contaminated groundwater by dehalogenation with iron. *Environmental Science & Technology*, **28**(11): 2045–2053.

Mathis, H. & Munson, W.E. (1987) *Retaining Wall Failure at Northern Ditch*, Report, Geotechnical Branch, Kentucky Department of Highways, Frankfort.

Matlock, H. (1970) Correlations for design of laterally loaded piles in soft clay. Proceedings, Second *Offshore Technology Conference*, Houston, TX, Vol. 1, pp. 577–594.

Matlock, H. & Foo, S.C. (1980) Axial analysis of piles using a hysteretic and degrading soil model. *Proceedings, Conference on Numerical Methods in Offshore Engineering*, Institution of Civil Engineers, London, pp. 165–185.

Matlock, H., Foo, H.C. & Bryant, L.M. (1978) Simulation of lateral pile behaviour under earthquake motion. *Proceedings, ASCE Speciality Conference on Earthquake Engineering & Soil Dynamics*, Pasadena, CA, Vol. 2, pp. 1065–1084.

Matsui, T. (1993) Case studies on cast-in-place bored piles and some considerations for design. *Proceedings BAP II*, Ghent, Balkema, Rotterdam, pp. 77–102.

Matsuo, H. & Ohara, S. (1960) Dynamic porewater pressure acting on quay walls during earthquakes. *Proceedings, Third World Conference on Earthquake Engineering*, New Zealand, Vol. 1, pp. 130–140.

Matsuzawa, H., Ishibashi, I. & Kawamura, M. (1985) Dynamic soil and water pressures of submerged soils. *Journal of Geotechnical Engineering*, ASCE, Reston, VA, **111**(10): 1161–1176.

Maugeri, M. & Motta, E. (1991) Stresses on piles used to stabilize landslides. In D. Bell, (Ed.) *Landslides*, Balkema, Rotterdam, pp. 785–790.

Mayhew, H.C. & Harding, H.M. (1986) *The Design of Concrete Roads*, TRRL RR87, Transport & Road Research Laboratory, Crowthorne, England.

Mayne, P.W. & Kulhawy, F.H. (1982) K_0–OCR relationships in soil. *Journal of Geotechnical Engineering Division, ASCE*, Reston, VA, **108**(6): 851–872.

Mayne, P.W. & Rix, G.J. (1993) G_{max}–q_c relationships for clays. *Geotechnical Testing Journal, ASTM*, West Conshohocken, PA, **16**(1): 54–60.

Mayne, P.W., Robertson, P.K. & Lunne, T. (1998) Clay stress history evaluated from seismic piezocone tests. In Robertson, P.K. & Mayne, P.W. (Eds) *Proceedings, First International Conference on Site Characterization–ISC'98*, April 19–22, Atlanta, GA, Vols. 1 & 2, Balkema, Rotterdam, pp. 1113–1118.

McBean, E.A. & Rovers, F.A. (1984) Alternatives for handling detection limit data in impact assessments. *Ground Water Monitoring Review*, Spring **4**: 42–44.

McBean, E.A. & Rovers, F.A. (1998) *Statistical Procedures for Analysis of Environmental Monitoring Data and Risk Assessment*. Prentice Hall, NJ.

McBean, E., Kompter, M. & Rovers F. (1988) A critical examination of approximations implicit in Cochran's procedure. *Ground Water Monitoring Review*, Winter, **8**: 83–87.

McBean, E., Rovers, F. & Schmidtke, K. (1990) Risk assessments using relatively simple mathematical models. In McTernan, W.F. & Kaplan, E. (Eds.) *Risk Assessment for Groundwater Pollution Control*, American Society of Civil Engineers, Reston, VA.

McBean, E.A., Mosher, F.R. & Rovers, F.A. (1993) Reliability-based design for leachate collection systems. In Christensen, T.H., Cossu, R. & Stegmann, R. (Eds), *Proceedings, Fourth International Landfill Symposium*, S. Margherita di Pula, Sardinia, pp. 433–441.

McBean, E.A., Rovers, F.A. & Farquhar, G.J. (1995) *Solid Waste Landfill Engineering & Design*, Prentice Hall, Englewood Cliffs, NJ.

McCaulou, D.R., Jewett, D.G. & Huling, S.G. (1995) *Ground Water Issue, Non-Aqueous Phase Liquids Compatibility with Materials Used in Well Construction, Sampling and Remediation*, EPA/540/5-95/503. Office of Solid Waste and Emergency Response, Washington, DC.

McCarthy, J.F. & Zachara, J.M. (1989) Subsurface transport of contaminants. *Environmental Science & Technology*, **23**(5): 496–502.

McCarty, P.L., Reinhard, M. & Rittmann, B.E. (1981) Trace organics in groundwater. Environmental Science & Technology, **15**(1): 40–51.

McCarty, P.L. (1996) Biotic and abiotic transformation of chlorinated solvents in groundwater. In *Symposium on Natural Attenuation of Chlorinated Organics in Groundwater*, September 11–13, Dallas, TX, 540/R-96-509, US Environmental Protection Agency, pp. 5–9.

McClelland, B. (1972) Techniques used in soil sampling at sea. *Offshore*, **32**(3): 51–57.

McDonald, L.A. (1997) Status of risk assessment of dams in Australia. In *Proceedings, International Workshop on Risk Based Dam Safety Evaluations*, Trondheim, Norway, Norwegian National Committee of the International Committee on Large Dams.

McEnroe, B.M. (1993) Maximum saturated depth over landfill liner. *Journal of Environmental Engineering*, **119**(2): 262–270.

McGrath, T.J. (1998) "Pipe-soil interactions during backfill placement" *PhD thesis*, The University of Massachusetts, Amherst.

McGrath, T.J. & Kurdziel, J.B. (1991) SPIDA method for reinforced concrete pipe design. *Journal of Transportation Engineering, ASCE*, Reston, VA, **117**(4): 371–381.

McKay, L.D. & Trudell, M.R. (1989) The sorption of trichloroethylene in clayey till. *Symposium of Groundwater Contamination*, June 14–15, Saskatoon, Saskatchewan, Paper E-40.

McKelvey, J.A. & Deutsch, W.L . (1991) The effect of equipment loading and tapered soil layers on geosynthetic lined landfill slopes. In *Proceedings, 14th Annual Madison Waste Conference*, University of Wisconsin, Madison, pp. 395–411.

McNichols, R.J. & Davis, C.B. (1988) Statistical issues and problems in ground water detection monitoring at hazardous waste facilities, *Ground Water Monitoring Review*, Fall, **8**: 135–150.

McTernan, W.F. & Kaplan, E. (Eds) (1990) *Risk Assessment for Groundwater Pollution Control*, American Society of Civil Engineers, Reston, VA.

McTrans, *McTrans ELSYM5*, University of Florida, Transportation Research Center, Gainesville, FL (*http://www-mcrans.ce.ufl.edu/*).

McVay, M.C., Townsend, F.C. & Williams, R.C. (1992) Design of socketed drilled shafts in limestone. *Journal of Geotechnical Engineering, ASCE*, Reston, VA, **118**(10): 1626–1637.

Meek, J.W. & Veletsos, A.S. (1974) Simple models for foundations in lateral and rocking motions. *Proceedings, Fifth World Conference on Earthquake Engineering*, Rome, Vol. 2, pp. 2610–2613.

Meek, J.W. & Wolf, J.P. (1992a) Cone models for homogeneous soil. *Journal of Geotechnical Engineering, ASCE*, Reston, VA, **118**(4): 667–685.

Meek, J.W. & Wolf, J.P. (1992b) Cone models for soil layer on rigid rock. *Journal of Geotechnical Engineering, ASCE*, Reston, VA, **118**(4): 686–703.

Meek, J.W. & Wolf, J.P. (1994) Cone models for an embedded foundation. *Journal of Geotechnical Engineering, ASCE*, Reston, VA, **120**(1): 60–80.

Mejia, L.H. & Seed, H.B. (1983) Comparison of 2-D and 3-D dynamic analysis of earth dams. *Journal Geotechnical Engineering, ASCE*, Reston, VA, **109**(11): 1383–1398.

Melchior, S. (1997) *In-situ* studies on the performance of landfill caps. In *Proceedings, International Containment Technology Conference*, February, St Petersburg, FL, pp. 365–373.

Mellor, M. & Hawkes, I. (1971) Measurement of tensile strength by diametral compression of disks and annuli. *Engineering Geology*, **5**: 173–225.

MELT (1993) *Regles techniques de conception et de calcul des fondations des ouvrages de genie civil*. CCTG, Fascicule No. 62, Titre V, Min. de L'Equipement du Lodgement et des Transport, Paris.

MEND (1993) *Soilcover User's Manual for an Evaporative Flux Model*, University of Saskatchewan, Saskatoon, Canada.

Mendoza, C.A. & McAlary, T.A. (1989) Modeling of groundwater contamination caused by organic solvent vapors. *Ground Water*, **28**(2): 199–206.

Mercer, F.B., Andrawes, K.Z., McGown, A. & Hytiris, N. (1984) A new method of soil stabilisation. In *Polymer Grid Reinforcement*, Thomas Telford, London, pp. 224–249.

Mercer, J.W. & Cohen, R.M. (1990) A review of immiscible fluids in the subsurface: properties, models, characterization, and remediation, *Journal of Contaminant Hydrology*, **6**: 107–163.

Mesri, G. (1975) Discussion on 'New design procedure for stability of soft clays'. *Journal of Geotechnical Engineering Division, ASCE*, Reston, VA, **101**(4): 409–412.

Mesri, G. (1987) The fourth law of soil mechanics: the law of compressibility. *International Symposium on Geotechnical Engineering of Soft Soils*, Mexico City, Vol. 2, pp. 179–187.

Mesri, G. & Choi, Y.K. (1985) Settlement analysis of embankments on soft clays. *Journal of Geotechnical Engineering Division, ASCE*, Reston, VA, **111**(4): 441–464.

Mesri, G. & Feng, T.-W. (1991) Surcharging to reduce secondary settlements. In *Proceedings, Geo-Coast '91*, Yokohama, pp. 359–364.

Mesri, G. & Godlewski, R.M. (1977) Time and stress compressibility interrelationship. *Journal of Geotechnical Engineering Division, ASCE*, Reston, VA, **103**(5): 417–430.

Mesri, G., Lo, D.O.D. & Feng, T.W. (1994) Settlement of embankments on soft clays. In *Proceedings, Conference on Vertical & Horizontal Deformations of Foundations & Embankments: Settlement '94*, Geotechnical Special Publication No. 40, American Society of Civil Engineers, Reston, VA, Vol. 1, pp. 8–56.

Mesri, G., Shahien, M. & Feng, T.W. (1995) Compressibility parameters during primary consolidation. *International Symposium on Compression & Consolidation of Clayey Soils IS-Hiroshima '95*, Hiroshima, Vol. 2, pp. 1021–1037.

Mesri, G., Stark, T.D., Ajlouni, M.A. & Chen, C.S. (1997) Secondary compression of peat with or without surcharging. *J of Geotechnical Geoenvironmental Engineering, ASCE*, Reston, VA, **123**(5): 411–421.

Mesri, G., Stark, T.D., Ajlouni, M.A. & Chen, C.S. (1999) Closure to discussion of Secondary compression of peat with or without surcharging. *J of Geotechnical Geoenvironmental Engineering, ASCE*, Reston, VA, **125**(2): 164–165.

Meyerhof, G.G. (1953) The bearing capacity of foundations under eccentric and inclined loads. In *Proceedings, Third International Conference on Soil Mechanics & Foundation Engineering*, Zürich, Vol. 1, pp. 440–445.

Meyerhof, G.G. (1956) Penetration tests and bearing capacity of cohesionless soils. *Journal of Soil Mechanics & Foundations Division, ASCE*, Reston, VA, **82**(1): 1–19.

Meyerhof, G.G. (1963) Some recent research on the bearing capacity of foundations. *Canadian Geotechnical Journal*, **1**(1): 16–26.

Meyerhof, G.G. (1974) Ultimate bearing capacity of footings on a sand layer overlying clay. *Canadian Geotechnical Journal*, **11**: 223–229

Meyerhof, G.G. (1976) Bearing capacity and settlement of pile foundations. *Journal of Geotechnical Engineering Division, ASCE*, Reston, VA, **102**(3): 195–228.

Meyerhof, G.G. (1995) Behaviour of pile foundations under special loading consitions. 1994 R.M. Hardy keynote address. *Canadian Geotechnical Journal*, **32**(2): 204–222.

Meyerhof, G.G. & Adams, J.I. (1968) The ultimate uplift capacity of foundations. *Canadian Geotechnical Journal*, **5**(4): 225–244.

Meyerhof, G.G. & Sastry, V.V.R.N. (1978) Bearing capacity of piles in layered soils: Part I & Part II. Canadian Geotechnical Journal, **15**(2): 171–189.

Michalowski, R.L. (1998) Limit analysis in stability calculations of reinforced soil structures. *Geotextiles & Geomembranes*, **16**(6): 311–331.

Michalowski, R.L. & Shi, L. (1995) Bearing capacity of footings over two-layer foundation soils. *Journal Geotechnical Engineering Division, ASCE*, Reston, VA, **121**(5): 421–428.

Middendorp, P., Bermingham, P. & Kuiper, B. (1992) Statnamic load testing of foundation piles. In *Proceedings, Fourth International Conference on Application. of Stress Wave Theory to Piles*, The Hague, Balkema, Rotterdam, pp. 581–588.

Middleton, T. & Cherry, J.A. (1996) The effects of chlorinated solvents on the permeability of clays. In Pankow, J.F. & Cherry J.A. (Eds) *Dense Chlorinated Solvents and Other DNAPLs in Groundwater*, Waterloo Educational Services Inc, Rockwood, Ontario, pp. 313–336.

Mikkelsen, P.E. (1996) Field instrumentation. In Turner, A.K. and Schuster, R.L. (Eds) *Landslides: Investigation and Mitigation*, Special Report 247, Transportation Research Board, Washington, DC, 278–316.

Miller, C.T., Poirier-McNeill, M.M. & Mayer, A.S. (1990) Dissolution of trapped nonaqueous phase liquids: mass transfer characteristics. *Water Resources Research*, **26**(11): 2783–2796.

Miller, R.D. (1972) Freezing and heaving of saturated and unsaturated soils. *Highway Research Record*, **393**: 1–11.

Milligan, G.W.E. & Ripley, K.J. (1989) Packing materials in jacked pipe joints. *Proceedings, Fourth International Conference on Trenchless Construction for Utilities, NO-DIG '89*, April, London, International Society for Trenchless Technology, London, UK, pp. 39–48.

Milligan, V. (1975) Field measurement of permeability in soil and rock. In *Proceedings, ASCE Geotechnical Engineering Division Specialty Conference on* In-Situ *Measurement of Soil Properties*, June 1–4, North Carolina State University, Raleigh, NC Vol. 2, pp. 3–36.

Ministères des Transports (1979) *Direction générale des transports interieurs-les ouvrages en Terre Armée–recommendations et règles de l'art*, Paris.

Mitchell, J.K. (1978) *In-situ* techniques for site characterization. In *Proceedings, ASCE Geotechnical Engineering Division Specialty Conference on Site Characterization and Exploration*, Northwestern University, Evanston, IL, pp. 107–129.

Mitchell, J.K. (1981) Soil improvement — State-of-the-art report. In *Proceedings, Tenth International Conference on Soil Mechanics & Foundation Engineering*, Stockholm, Vol. 4, pp. 506–565.

Mitchell, J.K. (1986a) Practical problems form surprising soil behavior, 20th Terzaghi lecture. *Journal of Geotechnical Engineering, ASCE*, Reston, VA, **112**(3): 259–289.

Mitchell, J.K. (1986b) Ground improvement evaluation by *in-situ* tests. In *Proceedings, In Situ '86*, Blacksburg, VA, Geotechnical Special Publication No. 6, American Society of Civil Engineers, ASCE Press, Reston, VA, pp. 221–236.

Mitchell, J.K. (1988) New developments in penetration tests and equipment, In De Ruiter, J. (Ed.) *Proceedings, First International Symposium on Penetration Testing, ISOPT-1*, March 20–24, Orlando, FL, A.A. Balkema, Rotterdam, Vol. 1, pp. 245–261.

Mitchell, J.K. (1991) Conduction phenomena: from theory to geotechnical practice. *Géotechnique*, **41**(3): 299–340.

Mitchell, J.K. (1993) *Fundamentals of Soil Behavior*, 2nd Edn, Wiley, New York.

Mitchell, J.K. & Christopher, B.R. (1990) North American practice in reinforced soil systems. In *Design and Performance of Earth Retaining Structures*, Lambe, P.C. and Hansen, L.A. (Eds.) American Society of Civil Engineers, Reston, VA, pp. 322–346.

Mitchell, J.K. & Gardner, W.S. (1975) *In-situ* measurement of volume change characteristics. In *Proceedings, ASCE Geotechnical Engineering Division Specialty Conference on* In-Situ *Measurement of Soil Properties*, June 1–4, North Carolina State University, Raleigh, NC, Vol. 2, pp. 279–345.

Mitchell, J.K. & Solymar, Z.V. (1984) Time-dependent strength gain in freshly deposited or densified sand. *Journal of Geotechnical Engineering, ASCE*, Reston, VA, **110**(11): 1559–1576.

Mitchell, J.K. & van Court, W.A.N. (1997) Barrier design and installation: walls and covers. In Ward, C.H., Cherry, J.A. & Scalf, M.R. (Eds.) *Subsurface Restoration*, Ann Arbor Press, Chelsea, MI, pp. 175–197.

Mitchell, J.K. & Villet, W.C.B. (1987) *Reinforcement of Earth Slopes and Embankments*, Na-

tional Cooperative Highway Research Program Report 290, Transportation Research Board, National Research Council, Washington, DC.

Mitchell, J.K., Hooper, D.R. & Campanella, R.G. (1965) Permeability of compacted clay. *Journal of the Soil Mechanics & Foundation Division, ASCE*, Reston, VA, **91**(4): 41–65.

Mitchell, J.K., Baxter, C.D.P. & Munson, T.C. (1995) Performance of improved ground during earthquakes. In *Soil Improvement for Earthquake Hazard Mitigation*, Geotechnical Special Publication No. 49, R.D. Hryciw (Ed.) American Society of Civil Engineers, Reston, VA, pp. 1–36.

Mitchell, R.J. & Eden, W.J. (1972) Measured movements of clay slopes in the Ottawa area. *Canadian Journal of Earth Sciences*, **9**: 1001–1013.

Mizuno, H. & Iiba, M. (1992) Dynamic effects of backfill and piles on foundation impedance. In *Proceedings, 10th World Conference on Earthquake Engineering*, Madrid, Spain, Vol. 3, pp. 1823–1828.

MoEE (1993) *Interim Guidelines for the Assessment and Management of Petroleum Contaminated Sites in Ontario*, Ministry of Environment & Energy, Toronto, Ontario.

MoEE (1994) *Proposed Guideline for the Clean-up of Contaminated Sites in Ontario*, Ministry of Environment & Energy, Toronto, Ontario.

MoEE (1996a) The challenge of contaminated sites: remediation approaches in North America. In *Guidance on Sampling & Analytical Methods for Use at Contaminated Sites in Ontario*, Ontario Ministry of Environment & Energy, Standards Development Branch, Toronto, Ontario.

MoEE (1996b) *Guidance on Sampling and Analytical Methods for Use at Contaminated Sites in Ontario*, Ontario Ministry of Environment and Energy Standards Development Branch, Toronto, ON.

MoE (1997) *Guideline for Use at Contaminated Sites in Ontario*. Revised February 1997, Ontario Ministry of Environment, and supporting documents, Toronto, Ontario.

MoE (1998) *Landfill Standards: A Guideline on the Regulatory and Approval Requirements for New or Expanding Landfilling Sites*, and Ontario Regulation 232/98, *Ontario Gazette*, pp. 131–22, 983–996.

Molenaar, A.A.A. (1983) *PhD dissertation*, Delft University of Technology, Delft, Holland.

Mononobe, N. & Matsuo, H. (1929) On the determination of earth pressures during earthquakes. *Proceedings, World Engineering Congress*, 9 p.

Montgomery, J.H. & Welkom, L.M. (1990) *Groundwater Chemicals Desk Reference*, Lewis, Chelsea, MI.

Montgomery, R.J. & Parsons, L.J. (1989) The Omega Hills final cover test plot study: three-year data summary. *Annual Meeting of the National Solid Waste Management Association*, Washington, DC.

Moore, C.A. (1983) *Landfill and Surface Impoundment Performance Evaluation*, SW-869, US EPA, Cincinnati, OH.

Moore, I.D. (1987) The elastic stability of shallow buried tubes. *Géotechnique*, **37**(2): 151–161.

Moore, I.D. (1988) Static response of deeply buried elliptical tubes. *Journal of Geotechnical Engineering, ASCE*, Reston, VA, **114**(6): 672–687.

Moore, I.D. (1989) Elastic buckling of buried flexible tubes – a review of theory and experiment. *Journal of Geotechnical Engineering*, ASCE, Reston, VA, **115**(3): 340–358.

Moore, I.D. (1990) Three dimensional response of elastic tubes. *Solids & Structures*, **26**(4): 391–400.

Moore, I.D. (1994) *Profiled HDPE Pipe Response Under Parallel Plate Loading*, Special Technical Publication 1222, Buried Plastic Pipe Technology, American Society for Testing & Materials, West Conshohocken, PA, **2**: 25–40.

Moore, I.D. & Brachman, R.W.I. (1994) Three dimensional analysis of flexible circular cylinders. *Journal of Geotechnical Engineering, ASCE*, Reston, VA, **120**(10): 1829–1844.

Moore, I.D. & Laidlaw, T.C. (1997) Corrugation buckling in HDPE pipes – measurements and analysis. Paper No. 97-0565, *TRB Annual Meeting*, Washington, DC.

Moore, I.D., Haggag, A. & Selig, E.T. (1994) Buckling strength of flexible cylinders with nonuniform elastic support. *Solids & Structures*, **31**(22): 3041–3058.

Morel, F. (1983) *Principles of Aquatic Chemistry*, Wiley, New York.

Moretrench American Corporation (1967) *Dewatering Systems Applicable to Different Soils*, Moretrench American Corporation, Rockaway, NJ.

Morgan, G.C. (1997) A regulatory perspective on slope hazards and associated risks to life. In *Proceedings, International Workshop on Landslide Risk Assessment*, Honolulu, HI, pp. 285–295.

Morgan, T.A. & Panek, L.A. (1963) *A method for determining stress in rock*. Report of Investigations No. 6312, Bureau of Mines, United States Department of the Interior, Denver, Colorado.

Morgenstern, N.R. (1992) Keynote Paper. The role of analysis in the evaluation of slope stability. In *Proceedings, Sixth International Symposium on Landslides*, Christchurch, Vol. 3, pp. 1615–1629.

Morgenstern, N.R. (1995) Managing risk in geotechnical engineering. In *Proceedings, Tenth Panamerican Conference on Soil Mechanics & Foundation Engineering*, Guadalajara, Vol. 4.

Morgenstern, N.R. & Nixon, J.F. (1971) One dimensional consolidation of thawing soils. *Canadian Geotechnical Journal*, **8**(4): 558–565.

Morgenstern, N.R. & Price, V.E. (1965) The analysis of the stability of general slip surfaces. *Géotechnique*, **15**(1): 79–93.

Morgenstern, N.R. & Sego, D.C. (1981) Performance of temporary tie-backs under winter conditions. *Canadian Geotechnical Journal*, **18**: 566–572.

Morin, P., Leroueil, S. & Samson, L. (1983) Preconsolidation pressure of Champlain clays, Part I—*in situ* determination. *Canadian Geotechnical Journal*, **20**(4): 782–802.

Morin, W.J. & Todor, P.C. (1977) *Laterites and Lateritic Soils and the Problem Soils of the Tropics*, US Agency for International Development, A10/csd 3682.

Moriwaki, Y., Beikae, M. & Idriss, I.M. (1988) Nonlinear seismic analysis of the upper San Fernando Dam under the 1971 San Fernando Earthquake. In *Proceedings, Ninth World Conference on Earthquake Engineering*, Tokyo & Kyoto, Japan, Vol. III, pp. 237–241.

Morrison, R.T. & Boyd, R.N. (1992) *Organic Chemistry*, 6th Edn, Prentice Hall, Englewood Cliffs, NJ, USA.

Moseley, M.P. (Ed.) (1993) *Ground Improvement*, Blackie Academic & Professional, Blackwood, NJ.

Moseley, M.P. & Priebe, H.J. (1993) Vibro techniques. In Moseley, M.P. (Ed.) *Ground Improvement*, Blackie Academic & Professional, Blackwood, NJ, pp. 1–19.

Mroz, Z., Norris, V.A. & Zienkiewicz, O.C. (1981) An anisotropic, critical state model for soils subject to cyclic loading. *Géotechnique*, **31**(4): 451–469.

MTO (1990) *Pavement Design & Rehabilitation Manual*, Publication No. 500-90-01, Ministry of Transportation of Ontario, Downsview, Ontario, Canada.

Mualem, Y. (1976a) A new model for predicting the hydraulic conductivity of unsaturated porous media. *Water Resources Research*, **12**: 513–522.

Mualem, Y. (1976b) Hysteretical models for prediction of the hydraulic conductivity of unsaturated porous media. *Water Resources Research*, **12**: 1248–1254.

Mualem, Y. (1986) Hydraulic conductivity of unsaturated soils: prediction and formulas. In Klute, A. (Ed.) Methods of Soil Analysis, No. 9, Part 1, American Society of Agronomy, Madison, WI, pp. 799–823.

Munfakh, G.A. (1997a) Ground improvement engineering–the state of the US practice: Part 1. methods. *Ground Improvement*, **1**(4): 193–214.

Munfakh, G.A. (1997b) Ground improvement engineering–the state of the US practice: Part 2. applications. *Ground Improvement*, **1**(4): 215–222.

Munfakh, G.A., Abramson, L.W., Barksdale, R.D. & Juran, I. (1987) *In-situ* ground reinforcement. In *Soil Improvement–A Ten Year Update*. Geotechnical Special Publication No. 12, American Society of Civil Engineers, Reston, VA, pp. 1–67.

Murchison, J.M. & O'Neill, M.W. (1984) Evaluation of *P–Y* relationships in cohesionless soils. In Meyer, J.R. (Ed.) *Analysis & Design of Pile Foundations*, American Society of Civil Engineers, Reston, VA, pp. 174–191.

Murdoch, L., Patterson, B. Lasonsky, G. & Harrar, W. (1990) *Technologies of Delivery or Recovery for the Remediation of Hazardous Waste Sites*, Report EPA/600/2-89/066 US Environmental Protection Agency, Cincinnati, OH, 96 p.

Murphy, J.R. (1996) *Understanding and Evaluating Natural Attenuation, Application at Metamora Landfill Site*, Poster Presentation at NGWA/API Petroleum Hydrocarbons & Organic Chemicals in Groundwater Conference, November 13–15, Houston, TX.

Murphy, W.L. & Gilbert, P.A. (1985) *Settlement and Cover Subsidence of Hazardous Waste Landfill*, EPA/600/2-85/035, US Environmental Protection Agency Hazardous Waste Engineering Research Laboratory, Cincinnati.

Murray, R.T. & Irwin, M.J. (1981) *A preliminary Study of TRRL Anchored Earth*, TRRL Supplementary Report 674, Transport & Road Research Laboratory, Crowthorne, UK.

Musser, S.C. (1996) Utah DOT's testing program to determine the soil–structure interaction of pile groups under lateral loads. In *Proceedings, Fourth Caltrans Seismic Research Workshop*, California Department of Transportation, Sacramento.

Mutch, R.D., Ash, R.E. & Caputi, J.R. (1997) New technologies for subsurface barrier wall construction. In *Barrier Technologies for Environmental Management* (Summary of a Workshop), National Academy Press, Washington, DC, D-23-34.

Myles, B. (1993) Practical Aspects of Soil Nailing, Amerad Jord, Svenska Geotechniska Foreningen, Uppsala, September.

Mylleville, B.L.J. & Rowe, R.K. (1988) Some considerations in the design of geosynthetic reinforced embankments on clayey foundations. In *Proceedings, Third Canadian Symposium on Geosynthetics*, October, 29–33, Kitchener, Ontario.

Mylleville, B.L.J. & Rowe, R.K. (1991) On the design of reinforced embankments on soft brittle clays. In *Proceedings, Geosynthetics 91*, February, Atlanta, GA, Industrial Fabrics Association International, Roseville, MN, Vol. 1, pp. 395–408.

Mylonakis, G., Nikolaou, A. & Gazetas, G. (1997) Soil–pile–bridge seismic interaction: kinematic and inertial effects. Part I soft soil. *Journal of Earthquake Engineering & Structural Dynamics*, **26**(3): 337–359.

Myrand, D., Gillham, R.W., Cherry, J.A. & Johnson, R.L. (1987). *Diffusion of Volatile Organic Compounds in Natural Clay Deposits*, University of Waterloo, Waterloo, Ontario, Canada.

Naeim, F. & Lew, M. (1995) On the use of design spectrum compatible motions. *Earthquake spectra*, **III**(1): 111–128.

Nagase, A. (1967) The $\phi = 0$ analysis of stability and unconfined compression strength. *Soils & Foundations*, **11**(4): 35–45.

Narejo, D.B. (1995a) A comparison of puncture behavior of smooth and textured HDPE geomembranes. *Geosynthetics International*, **2**(4): 699–705.

Narejo, D.B. (1995b) Three levels of geomembrane puncture protection. *Geosynthetics International*, **2**(4): 765–769.

Narejo, D.B. (1996) Closure of discussion of 'A comparison of puncture behavior of smooth and textured HDPE geomembranes' and 'Three levels of geomembrane puncture protection.' *Geosynthetics International*, **3**(3): 443–444.

Narejo, D., Koerner, R.M. & Wilson-Fahmy, R.F. (1996) Puncture protection of geomembranes. Part II: experimental. *Geosynthetics International*, **3**(5): 629–653.

Narin Van Court, W.A. & Mitchell, J.K. (1995) New insights into explosive compaction of loose, saturated cohesionless soils. In *Soil Improvement for Earthquake Hazard Mitigation*, Geotechnical Special Publication No. 49, American Society of Civil Engineers, R.D. Hryciw (Ed.), Reston, VA, pp. 51–65.

Nataraj, M.S., Magauti, R.S. & McManis, K.L. (1995). Interface frictional characteristics of Geosynthetics. In *Proceedings, Geosynthetics '95 Conference*, Nashville, TN, Industrial Fabrics Association International, Roseville, MN, Vol. 3, pp. 1057–1069.

Nauroy, J.F., Bruey, F., Le Tirant, P. & Kervadec, J.-P. (1986) Design and installation of piles in calcareous formations. In *Proceedings, Third International Conference on Numerical Methods in Offshore Piling*, Nantes, pp. 461–480.

NavFac (1982) *Soil Mechanics. Design Manual 7.1*. Department of the Navy Naval Facilities Engineering Command, Alexandria, VA, US Government Printing Office, Washington, DC.

NavFac (1983) *Soil Dynamics, Deep Stabilization, & Special Geotechnical Construction, Design Manual 7.3*, US Navy Facilities Command, Alexandria, VA, pp. 77–78.

Nayak, N.V. & Christensen, R.W. (1971). Swelling characteristics of compacted, expansive soils. *Clays & Clay Minerals*, **19**(4): 251–261.

Naylor, D.J. & Hooper, J.A. (1974) An effective stress finite element analysis to predict the short and long term behaviour of a piled raft foundation on London clay. In *Proceedings, Conference On Settlement of Structures*, Cambridge, pp. 394–402.

NCEER (1997) Proceedings of the NCEER workshop on evolution of liquefaction resistance of soils. T.L. Voud & I. Idriss (Eds.), Technical Report, NCEER-7-0022.

Neely, W.B. (1985) Hydrolysis. In Neely, W.B. & Blau, G.E. (Eds) *Environmental Exposure from Chemicals*, Vol. 1, CRC Press, Boca Raton, FL, pp. 157–173.

Nelson, J.D. & Miller, D.J. (1992) *Expansive Soils. Problems and Practice in Foundation and Pavement Engineering*, Wiley Interscience, New York.

Nelson, W. & Hahn, G.J. (1973) Linear estimation of a regression relationship from censored

data–Part II: best linear unbiased estimation and theory. *Technometrics*, **15**(1): 133–150.

Nersesova, Z. & Tsytovich, N.A. (1963) Unfrozen water in frozen soils. In *Proceedings, First International Conference on Permafrost*, Purdue University, Lafayette, IN, pp. 230–234.

Newell, C., Acree, S.D. Ross, R.R. & Hulling, S.G. (1995) *Ground Water Issue: Light Nonaqueous Phase Liquids*, EPA/540/S-95/500. Office of Solid Waste and Emergency Response, Washington, DC.

Newmark, N. (1965) Effects of earthquakes on Dams and Embankments, Geotechnique, 15(2): 139–160.

Newmark, N.M. (1965) Effects of earthquakes on dams and embankments. *Géotechnique*, **15**(2): 139–160.

New South Wales (1996) *Design of Reinforced Soil Walls*, RTA QA Specification R57, New South Wales Road and Traffic Authority, Surry Hills, NSW, Australia.

Nichols, W.E. (1991) *Comparative Simulations of a Two-Layer Landfill Barrier Using the HELP Version 2.0 & UNSAT-H Version 2.0 Computer Codes*, PNL-7583, Pacific Northwest Laboratory, Richland, Washington, DC.

Nicholson, R.V., Cherry, J.A. & Reardon, E.J. (1983) Migration of contaminants at a landfill: a case study, 6. Hydrogochemistry. *Journal of Hydrology* **63**(1/2): 131–176.

Nicholson, R.V., Gillham, R.W., Cherry, J.A. & Reardon, E.J. (1989) Reduction of acid generation in mine tailings through the use of moisture-retaining cover layers as oxygen barriers. *Canadian Geotechnical Journal*, **26**(1): 1–8.

Nielsen, D.M. (1991) *Practical Handbook of Ground-Water Monitoring*, Lewis, Chelsea, MI.

Nixon, J.F. (1991) Discrete ice lense theory for frost heave in soils. *Canadian Geotechnical Journal*, **28**(6): 843–859.

Noether, G.E. (1981) Comment. *The American Statistician*, **35**(3): 129.

Nogami, T. (1980) Dynamic stiffness and damping of pile groups in inhomogeneous soil. In *Proceedings Session on Dynamic Response of Pile Foundations: Analytical Aspects, ASCE National Convention*, October, FL, pp. 31–52.

Nogami, T. & Novak, M. (1976) Soil–pile interaction in vertical vibration. *International Journal of Earthquake Engineering & Structural Dynamics*, **4**(3): 277–293.

Noorany, I. (1972) Underwater soil sampling and testing–a state-of-the-art review. In *Underwater Soil Sampling, Testing & Construction Control*, Special Publication 501, American Society for Testing & Materials, West Conshohocken, PA, pp. 3–41.

Nordal, R.S. & Refsdal, G. (1989) Frost protection in design and construction. *VTT Symposium '95, Frost in Geotechnical Engineering*, Saariselka, Finland, Vol. 1, pp. 127–164.

Nordlund, R.L. (1963) Bearing capacity of piles in cohesionless soils. *Journal of Soil Mechanics & Foundational Division, ASCE*, Reston, VA, **89**(3): 1–35.

Norris, P. & Milligan, G.W.E. (1992) Frictional resistance of jacked concrete pipes at full scale. *Proceedings International Conference on Trenchless Technology, NO-DIG 92*, Paris, Balkema, Rotterdam, pp. 121–128.

Norrish, N.I. & Wyllie, D.C. (1996) Rock slope stability analysis. *Landslides – Investigation & Mitigation*, A.K. Turner & R.L. Schuster (Eds.) Special Report 247, Transportation Research Board, Washington, DC, pp. 391–425.

Norton, D. & Knapp, R. (1977) Transport phenomena in hydrothermal systems: Nature of porosity. *American Journal of Science*, **27**: 913–936.

Novak, M. (1974) Dynamic stiffness and damping of piles. *Canadian Geotechnical Journal*, **11**: 574–598.

Novak, M. (1979) Soil–pile interaction under dynamic loads. In *Proceedings, International Symposium on Numerical Methods in Off-Shore Pilling*, London, England, pp. 41–50.

Novak, M. & Aboul-Ella, F. (1978) Impedance functions of piles in layered media. *Journal of the Engineering Mechanics Division, ASCE*, Reston, VA, **104**(3): 643–661.

Novak, M. & Beredugo, Y.O. (1972) Vertical vibration of embedded footings. *Journal of Soil Mechanics & Foundations Division, ASCE*, Reston, VA, **98**(SM12): 1291–1310.

Novak, M. & El-Sharnouby, B. (1983) Stiffness and damping constants of single piles. *Journal of Geotechnical Engineering Division, ASCE*, Reston, VA, **109**(7): 961–974.

Novak, M. & El-Sharnouby, B. (1984) Evaluation of dynamic experiments on pile group. *Journal of Geotechnical Engineering, ASCE*, Reston, VA, **110**(6): 738–756.

Novak, M. & Grigg, R.F. (1976) Dynamic experiments with small pile foundations. *Canadian Geotechnical Journal*, **13**(4): 372–385.

Novak, M. & Kim, T.C. (1981) Resonant column technique for dynamic testing of cohesive soils. *Canadian Geotechnical Journal*, **18**(3): 448–455.

Novak, M. & Mitwally, H. (1987) Random response of offshore towers with pile–soil–pile interaction. In *Proceeding, Sixth International Symposium on Offshore Mechanics & Arctic Engineering*, Houston, TX, Vol. 1, pp. 329–336.

Novak, M. & Nogami, T. (1977) Soil-pile interaction in horizontal vibration. *International Journal of Earthquake Engineering & Structure Dynamics*, **5**(3): 263–282.

Novak, M. & Sachs, K. (1973) Torsional and coupled vibrations of embedded footings. *International Journal of Earthquake Engineering & Structure Dynamics*, **2**(1): 11–33.

Novak, M. & Sheta, M. (1980) Approximate approach to contact problems of piles. In *Proceedings, Geotechnical Engineering Division, ASCE National Convention, Dynamic Response of Pile Foundations: Analytical Aspects*, October, FL, pp. 53–79.

Novak, M., Nogami, T. & Aboul-Ella, F. (1978) Dynamic soil reactions for plane stain case. *Journal of the Engineering Mechanics Division, ASCE*, Reston, VA, **104**(4): 953–959.

Novak, M., El Naggar, M.H., Sheta, M., El-Hifnawy, L., El-Marsafawi, H. & Ramadan, O. (1999) *DYNA5 a Computer Program for Calculation of Foundation Response to Dynamic Loads*, Geotechnical Research Centre, The University of Western Ontario, London, Ontario.

NRC (1994) National Research Council *Alternatives for Ground Water Cleanup*, National Academy Press, Washington, DC.

NRC (1985) National Research Council, *Liquefaction of Soils During Earthquakes*, National Academy Press, Washington, DC.

NRC (1996) National Research Council, *Rock Fractures & Fluid Flow: Contemporary Understanding & Applications*, National Academy Press, Washington, DC.

NRCC (1995a) *National Building Code of Canada*, National Research Council of Canada, Ottawa.

NRCC (1995b) *User's Guide – NBC 1995, Structural Commentaries (Part 4)*, National Research Council of Canada, Ottawa.

Nunn, M.E. & Merrill, D.B. (1997) *Review of Flexible and Composite Design Methods*, TRL Paper PA/3298/97, Transport Research Laboratory, Crowthorne, Berkshire, UK.

Nyhan, J.W. (1989) *Hydrologic Modeling to Predict Performance of Shallow Land Burial Cover Designs at the Los Alamos National Laboratory*, LA-11533-MS, Los Alamos National Laboratory, Los Alamos, NM.

Oda, M. (1972) Initial fabrics and their relations to mechanical properties of granular materials. *Soils & Foundations*, **12**(1): 17–37.

O'Brien, K. & Keyes, G. (1997) Implementation of a funnel-and-gate remediation system. *Proceedings, International Containment Technology Conference* (US Department of Energy/ Dupont Company/US Environmental Protection Agency), February 9–12, St Petersburg, FL, pp. 895–901.

O'Connor, M.J., Agar, J.G. & King, R.D. (1984) Practical experience in the management of hydrocarbon vapours in the subsurface. In *Proceedings, Petroleum Hydrocarbons & Organic Chemicals in Ground Water*, November 5–7, Houston, TX, National Ground Water Association, pp. 519–533.

O'Donnell, S.A., Rumar, R.R. & Mitchell, J.K. (1995) *Assessment of Barrier Containment Technologies. A Comprehensive Treatment for Environmental Remedial Applications*, Report PB96-180583.

O'Hannesin, S.F. & Gillham, R.W. (1998) Long-term performance of an *in situ* iron wall for remediation of VOCs. *Ground Water*, **36**(1): 164–170.

Ohsaki, Y. & Iwasaki, R. (1973) On dynamic shear moduli and Poisson's ratio of soil deposits. *Soils & Foundations*, **13**(4): 61–73.

Oliveira, R. & Graca, J.C. (1987) *In situ* testing of rocks. In Bell, F.G. (Ed.) *Ground Engineer's Reference Book*, Butterworths, London, England, Chapter 26.

Okabe, S. (1926) General theory of earth pressures. *Journal Japan Society of Civil Engineering*, Tokyo, **12**(1).

Okamoto, S. (1973) *Introduction to Earthquake Engineering*, University of Tokyo Press, Tokyo, Japan.

O'Kane, M., Wilson, G.W., Barbour, S.L. & Swanson, D.A. (1995) Aspects on the performance of the till cover system at Equity Silver Mines Ltd. *Proceedings, Sudbury 95 – Mining & the Environment*, May 28–June 1, Sudbury, Ontario, Canada, Vol. 2, pp. 565–573.

Olson, R.E. (1974) Shearing strength of kaolinite, illite, & montmorillonite. *Journal of Geotechnical Engineering Division, ASCE*, Reston, VA, **100**(11): 1215–1229.

O'Neil, D.A., Baldi, G. & Della Torre, A. (1996) The multi-functional Envirocone® test system. In Craig C. (Ed.) *Proceedings, International Conference on Advances in Site Investigation*

Practice, March 30–31, London, Thomas Telford, London, England, pp. 421–437.

O'Neill, M.W. (1983) Group action in offshore piles. In *Proceedings, ASCE Conference of Geotechnical Practice in* Offshore Engineering, Austin, TX, pp. 25–64.

O'Neill, M.W. & Ha, H.B. (1982) Comparative modelling of vertical pile groups. In *Proceedings, Second International Conference on Numerical Methods in Offshore Piling*, Austin, TX, pp. 399–418.

O'Neill, M.W., Ghazzaly, O.I. & Ha, H.B. (1977) Analysis of three-dimensional pile groups with nonlinear soil response and pile–soil–pile interaction. In *Proceedings, Ninth OTC*, Houston, TX, Paper OTC 2838, pp. 245–256.

Onodera, T.F. (1963) Dynamic investigation of foundation rocks *in situ*. In *Proceedings Fifth US Rock Mechanics Symposium*, University of Minnesota, pp. 517–533.

Ontario MBS (1993) *Contaminant Recognition and Management*, Environmental Advisory Services Unit, Realty Group, Toronto, ON.

OPSD (1994) *Ontario Provincial Standards for Roads and Municipal Services*, Vol. 3, *Drawings for Roads, Barriers, Drainage, Sanitary Sewers, Watermains and Structures*, OPSD 509 and 510 Series, Ontario Provincial Standards, St Catharines, Ontario.

O'Reilly, M.P. & New, B.M. (1982) Settlements above tunnels in the United Kingdom – their magnitude and prediction. In *Proceedings, Tunnelling 82 Symposium*, Institute of Mining and Metallurgy, London, England, pp. 173–181.

O'Reilly, M.P. & Rogers, C.D.F. (1987) Pipe jacking forces. In *Proceedings, International Conference on Foundations & Tunnels*, Edinburgh, Engineering Technics Press, Edinburgh, Scotland, pp. 201–208.

O'Rourke, T.D. (1987) Lateral stability of compressible walls. *Géotechnique*, **37**(2): 145–149.

O'Rourke, T.D. & Jones, C.J.F.P. (1990) Overview of earth retention systems 1970–1990. In *Design & Performance of Earth Retaining Structures*, Lambe, P.C. and Hansen, L.A. (Eds.) American Society of Civil Engineers, Reston, VA, pp. 22–51.

Orth, W.S. & Gillham, R.W. (1996) Dechlorination of trichloroethene in aqueous solution using Fe^{o}. *Environmental Science & Technology*, **30**: 66–71.

Ortigao, J.A.R. (1980) *DSc, thesis*, Federal University of Rio de Janeiro.

Ostendorf, D.W., Moyer, E.E., Richards, R.J., Hinlein, E.S., Xie, Y. & Rajan, R.V. (1992) *LNAPL Distribution and Hydrocarbon Vapor Transport in the Capillary Fringe*, EPA/600/R-92/247.

Osterberg, J.O. (1957) Influence values for vertical stresses in a semi-infinite mass due to an embankment loading. In *Proceedings, Fourth International Conference on Soil Mechanics and Foundation Engineering*, London, Vol. 1, pp. 393–394.

Osterberg, J.O. (1978) Failures in exploration programs. In *Proceedings, ASCE Geotechnical Engineering Division Specialty Conference on Site Characterization & Exploration*, Northwestern University, Evanston, IL, pp. 3–9.

Osterberg, J. (1989) New device for load testing driven and drilled shafts separates friction and end bearing. In *Proceedings, International Conference on Piling & Deep Foundations*, London, pp. 421–427.

Osterberg, J.O. & Gill, S.A. (1973) Load transfer mechanism for piers socketed in hard soils or rock. In *Proceedings, Ninth Canadian Rock Mechanics Symposium*, Montreal, PQ, pp. 235–262.

Othman, M.A. & Benson, C.H. (1993) Effect of freeze–thaw on the hydraulic conductivity and morphology of compacted clay. *Canadian Geotechnical Journal*, **30**(2): 236–246.

Othman, M.A., Bonaparte, R., Gross, B.A. & Schmertmann, G.R. (1995) Design of MSW landfill final cover systems. In *Landfill Closures: Environmental Protection & Land Recovery*, Geotechnical Special Publication No. 53, Dunn, R.J. and Singh U.P. (Eds.) American Society of Civil Engineers, Reston, VA, pp. 218–257.

Ottaviani, M. (1975) Three-dimensional finite element analysis of vertically loaded pile groups. *Géotechnique*, **25**(2): 159–174.

Owen, W.J. & DeRouen, T.A. (1980) Estimation of the mean for lognormal data containing zeroes and left-censored values, with application to the measurement of worker exposure to air contaminants. *Biometrics*, **36**: 707–719.

Palmeira, E.M., Pereira, J.H.F. & da Silva, A.R.L. (1998) Backanalyses of geosynthetic reinforced embankments on soft soils. *Geotextiles & Geomembranes*, **16**(5): 273–292.

Palmer, J.H.L. & Lo, K.Y. (1976) *In-situ* measurements in some near-surface rock formations—Thorold, Ontario. *Canadian Geotechnical Journal*, **13**(1): 1–7.

Pande, G.N. & Pietruszczak, S. (1982) Reflecting surface model for soils. In *Proceedings, International Symposium on Numerical Models in Geomechanics*, Balkema, Rotterdam, The Netherlands, pp. 50–64.

Pankow, J.F., Johnson, R.L. & Cherry, J.A. (1993) Air sparging in gate wells in cutoff walls and trenches for control of plumes of volatile organic compounds (VOCs). *Ground Water*, **31**(4): 654–663.

Pankow, J.F., Feenstra, S., Cherry, J.A. & Ryan, C. (1996) Dense chlorinated solvents in groundwater: background and history of the problem. In Pankow, J.F. & Cherry, J.A. (Eds) *Dense Chlorinated Solvents & Other DNAPLs in Groundwater*, Waterloo Press, Rockwood, Ontario, pp. 1–52.

Paolucci, R. & Pecker, A. (1997) Seismic bearing capacity of shallow strip foundations on dry soils. *Soils & Foundations*, **37**(3): 95–105.

Papagiannakis, A.T. & Schwartz, C.W. (Eds) (1998) *Application of Geotechnical Principles in Pavement Engineering*, Geotechnical Special Publication No. 85, American Society of Civil Engineers, Reston, VA.

Park, J.K., Sakti, J.P. & Hooper J.A. (1995) Effectiveness of geomembranes as barriers of organic compounds. In *Proceedings, Geosynthetics 95*, February, Industrial Fabrics Association International, Roseville, MN, IFAI, Vol. 3, pp. 879–892.

Parry, R.H.G. (1968) Field and laboratory behaviour of a lightly overconsolidated clay. *Géotechnique*, **18**(2): 151–171.

Parry, R.H.G. (1977) Estimating bearing capacity in sand from SPT values. *Journal of Geotechnical Engineering Division, ASCE*, Reston, VA, **103**(9): 1014–1019.

Pasqualini, E., Roccato, M. and Sani, D. (1993) Shear resistance of the interfaces of composite liners. In *Proceedings, Sardinia '93 Fourth International Landfill Symposium*, Cagliari, Italy, Vo. 2, pp. 1457–1471.

Paterson, W.D.O. (1987) *Road Deterioration and Maintenance Effects: Models for Planning & Management*, Johns Hopkins University Press, Baltimore, Maryland, MD.

Patrick, G.C. & Burgess, A.S. (1992) Field studies of non-aqueous phase liquids at two sites in California's Santa Clara Valley. In Weyer, K.U. (Ed.) *Subsurface Contamination by Immiscible Fluids*, Balkema, Rotterdam, pp. 489–501.

Patton, F.D. (1966) Multiple mode of shear failure in rock. In *Proceedings, First Congress of the International Society for Rock Mechanics*, Lisbon, Vol. 1, pp. 509–513.

Paulin, M.J., Phillips, R., Clark, J.I., Trigg, A. & Konuk, I. (1998) A full scale investigation into pipeline/soil interaction. *51st Canadian Geotechnical Conference*, Edmonton, AB, Vol. 1, pp. 241–248.

PCA (1984) *Thickness Design for Concrete Highway and Street Pavements*, Portland Cement Association, Skokie, IL.

PCA (1992) *Design of Concrete Pavements for City Streets*, Information Series 184, Portland Cement Association, Skokie, IL.

Peck, R.B. (1969a) Advantages and limitations of the observational method in applied soil mechanics. Ninth Rankine Lecture. *Géotechnique*, **19**(2): 171–187.

Peck, R.B. (1969b) Deep excavations and tunnelling in soft ground. In *Proceedings, Seventh International Conference, International Society for Soil Mechanics and Foundation Engineering*, Mexico.

Peck, R.B. (1973) Influence of non-technical factors on the quality of embankment dams. In *Embankment-Dam Engineering, Casagrande Volume*, R.C. Hirschfield & S.S. Poulos (Eds.), Wiley, New York, pp. 201–208.

Peck, R.B. (1976) Rock foundations for structures. In *Proceedings, Rock Engineering for foundations & Slopes*, August 15–18, University of Colorado, Boulder, CO, Vol. 2, pp. 1–21.

Peck, R.B., Hanson, W.E. & Thornburn, T.H. (1974) *Foundation Engineering*, 2nd Edn, Wiley, New York,

Pecker, A. (1996) Seismic bearing capacity of shallow foundations. In *Proceedings, 11th World Conference Earthquake Engineering*, Paper No. 2076, Acapulco, Mexico.

Pells, P.J.N. & Turner, R.M. (1979) Elastic solutions for the design and analysis of rock-socketed piles. *Canadian Geotechnical Journal*, **16**: 481–487.

Pender, M.J. (1996) *Aseismic Foundation Design Analysis*, University of Auckland, New Zealand.

Penner, E. (1974) Uplift forces on foundations in frost heaving soils. *Canadian Geotechnical Journal*, **11**(3): 323–338.

Penner, E. & Goodrich, L.E. (1980) Location of segregated ice in frost susceptible soil. In *Proceedings, Second International Symposium on Ground Freezing*, Trondheim, Norway, pp. 626–639.

Penrose, W.R., Polzer, W.L., Essington, E.H.,

Nelson, D.M. & Orlandini, K.A. (1990) Mobility of plutonium and americium through a shallow aquifer in a semiarid region. *Environmental Science & Technology*, **24**: 228–234.

Penzien, J., Scheffey, C.F. & Parmelee, R.A. (1964) Seismic analysis of bridges on long piles. *Journal of the Engineering Mechanics Division, ASCE*, Reston, VA, **90**(3): 223–254.

Pereira, A.T. (1977) *Procedures for Development of CBR Design Curves*, Instruction Report 5-77-1, US Army Corps of Engineers, Vicksburg, MS.

Pessaran, A. (1995) *Hydraulic Characterization of Sand*, M. Eng. Report, University of Saskatchewan, Saskatoon, Canada.

Peters, N., Warner, R.S., Coates, A.L., Logsdon, D.S. & Grube, W.E. (1986) Applicability of the HELP Model in Multilayer Cover Design: A Field Verification and Modeling Assessment. In *Land Disposal of Hazardous Waste–Proceedings, 1986 Research Symposium*, US Environmental Protection Agency, Cincinnati.

Peterson, M.E. & Landis, R.C. (1995) Artificially emplaced floors and bottom barriers. In Rumer, R.R. & Mitchell, J.K. (Eds) *Assessment of Barrier Containment Technologies: A Comprehensive Treatment for Environmental Remediation Applications*, US Department of Energy/US Environmental Protection Agency/Dupont Company, pp. 185–209.

Petrov, R.J. & Rowe, R.K. (1997) Geosynthetic clay liner compatibility by hydraulic conductivity testing: Factors impacting performance. *Canadian Geotechnical Journal*, **34**(6): 863–885.

Petrov, R.J., Rowe, R.K. & Quigley, R.M. (1997a) Comparison of laboratory measured GCL hydraulic conductivity based on three permeameter types. *Geotechnical Testing Journal*, **20**(1): 49–62.

Petrov, R.J., Rowe, R.K. & Quigley, R.M. (1997b) Selected factors influencing GCL hydraulic conductivity. *Journal of Geotechnical & Geoenvironmental Engineering, ASCE*, Reston, VA, **123**(8): 683–695.

Peyton, R.L. & Schroeder, P.R. (1988) Field verification of HELP model for landfills. *Journal of Environmental Engineering, ASCE*, Reston, VA, **114**(2): 247–269.

Peyton, R.L. & Schroeder, P.R. (1993) Water balance for landfills. In Daniel, D.E. (Ed.) *Geotechnical Practice for Waste Disposal*, Chapman & Hall, London, pp. 214–243.

PFRA (1951) *South Saskatchewan River Project: Report on Geological Test Drift-Dam Site 10*, Prairie Farm Rehabilitation Administration, Department of Regional Economic Expansion, Canada.

Pickens, J.F., Grisak, G.E., Avis, J.D., Belanger, D.W. & Thury, M. (1987) Analysis and interpretation of borehole hydraulic tests in deep boreholes: principles, model development and applications. *Water Resources Research*, **23**: 1341–1376.

Pillai, V.S. & Byrne, P.M. (1994) Effect of overburden pressure on liquefaction resistance of sand. *Canadian Geotechnical Journal*, **31**(1): 53–60.

Pilot, G. (1972) Study of five embankments on soft soils. In *Proceeding, ASCE Specialty Conference on Performance of Earth & Earth-Supported Structures*, Purdue University, Lafayette, IN, Vol. 1, 81–99.

Pilot, G. & Moreau, M. (1973) *La stabilité des remblais sur sols mous*, Abaques de calcul, Eyrolles, Paris.

Pilot, G., Trak, B. & La Rochelle, P. (1982) Effective stress analysis of the stability of embankments on soft soils. *Canadian Geotechnical Journal*, **19**(4): 433–450.

PJA (1995) *Guide to Best Practice for the Installation of Pipe Jacks and Microtunnels*, Pipe Jacking Association, London, England.

Piwoni, M.D., & Keeley, J.W. (1990) *Ground Water Issue: Basic Concepts of Contaminant Sorption at Hazardous Waste Sites*, EPA/540/4-90/053. Office of Solid Waste and Emergency Response, Washington, DC.

Pohlman, K.F., Icopini, G.A., McArthur, R.D. & Rosal, C.G. (1994) *Evaluation of sampling and field-filtration methods for the analysis of trace metals in ground water*, EPA/600/R-94/119.

Polo, J.M. & Clemente, J. (1988) Pile group settlement using independent shaft and point loads. *Journal of Geotechnical Engineering, ASCE*, Reston, VA, **114**(4): 469–487.

Polshin, D.E. & Tokar, R.A. (1957) Maximum allowable non-uniform settlement of structures. In *Proceedings, Fourth International Conference on Soil Mechanics & Foundation Engineering*, Vol. 1, pp. 402–405.

Poorooshasb, H.B. (1991) Load settlement response of a compacted fill layer supported by a geosynthetic overlying a void. *Geotextiles & Geomembranes*, **10**(3): 179–201.

Poorooshasb, H.B. & Pietruszczak, S. (1985) On yielding and flow of sand; a generalized two-surface model. *Computers & Geotechnics*, **1**(1): 33–58.

Porter, L.K., Kemper, W.D., Jackson, R.D. & Stewart, B.A. (1960) Chloride diffusion in soils as influenced by moisture content. *Soil Science Society of America Proceedings*, **24**: 460–463.

Potts, D.M., Kovacevic, N. & Vaughan, P.R. (1997) Delayed collapse of cut slopes in stiff clay. *Géotechnique*, **47**(5): 953–982.

Poulos, H.G. (1968) Analysis of the settlement of pile groups. *Géotechnique*, **18**: 449–471.

Poulos, H.G. (1971a) Behaviour of laterally loaded piles: I-single piles. *Journal of Soil Mechanics & Foundation Division, ASCE*, Reston, VA, **97**(5): 711–731.

Poulos, H.G. (1971b) Behaviour of laterally loaded piles: II-pile groups. *Journal of Soil Mechanics & Foundation Division, ASCE*, Reston, VA, **97**(5): 733–751.

Poulos, H.G. (1972) Difficulties in prediction of horizontal deformations of foundations. Journal of Soil Mechanics & Foundation Division, *ASCE*, Reston, VA, **98**(8): 843–848.

Poulos, H.G. (1973) Load–deflection prediction for laterally loaded piles. *Australian Geomechanics Journal*, **3**(1): 1–8.

Poulos, H.G. (1977) Estimation of pile group settlement. *Ground Engineering*, March: **10**: 40–50.

Poulos, H.G. (1979a) Settlement of single piles in non-homogeneous soil. *Journal of Geotechnical Engineering Division, ASCE*, Reston, VA, **105**(5): 627–641.

Poulos, H.G. (1979b) Group factors for pile deflection estimation. *Journal of Geotechnical Engineering Division, ASCE*, Reston, VA, **105**(5): 627–641.

Poulos, H.G. (1982a) Developments in the analysis of static and cyclic lateral response of piles. In *Proceedings, Fourth International Conference on Numerical Methods in Geomechanics*, Edmonton, Vol. 3, pp. 1117–1135.

Poulos, H.G. (1982b) Single pile response to cyclic lateral load. *Journal of Geotechnical Engineering, ASCE*, Reston, VA, **108**(3): 355–375.

Poulos, H.G. (1985) Ultimate lateral pile capacity in two-layer soil. *Geotechnical Engineering*, **16**(1): 25–37.

Poulos, H.G. (1987) Piles and piling. In Bell, F.G. (Ed.) *Ground Engineer's Reference Book*, Butterworths, London, England.

Poulos, H.G. (1988a) Cyclic stability diagram for axially loaded piles. *Journal of Geotechnical Engineering, ASCE*, Reston, VA, **114**(8): 877–895.

Poulos, H.G. (1988b) *Marine geotechnics*, Unwin Hyman, London.

Poulos, H.G. (1989) Pile behaviour-theory and application. *Géotechnique*, **39**(3): 365–415.

Poulos, H.G. (1993) Settlement of bored pile groups. In *Proceedings BAP II*, Ghent, Balkema, Rotterdam, W.F. van Impe (Ed.) pp. 103–117.

Poulos, H.G. (1994a) Settlement prediction for driven piles and pile groups. In *Vertical & Horizontal Deformations of Foundations & Embankments*, Geotechnical Special Publication No. 40, American Society of Civil Engineers, Reston, VA, Vol. 2, pp. 1629–1649.

Poulos, H.G. (1994b) Analysis and design of piles through embankments. In *Proceedings International Conference on Design & Construction of Deep Foundations*, Orlando, FL, Vol. 3, pp. 1403–1421.

Poulos, H.G. (1996) A comparison of methods for the design of piles through embankments. In *Proceedings 12th SE Asian Geotechnical Conference*, Kuala Lumpur, Vol. 2, pp. 157–167.

Poulos, H.G. (1997a) Failure of a building supported on piles. In *Proceedings International Conference On Foundation Failures*, Singapore, Institute of Engineers Singapore, pp. 53–66.

Poulos, H.G. (1997b) Piles subjected to negative friction: a procedure for design. *Geotechnical Engineering*, **28**(1): 23–44.

Poulos, H.G. & Chen L. (1996) Pile response due to unsupported excavation-induced lateral soil movements. Canadian Geotechnical Journal, **33**: 670–677.

Poulos, H.G. & Chen, L. (1997) Pile response due to excavation-induced lateral soil movement. *Journal of Geotechnical & Geoenvironmental Engineering, ASCE*, Reston, VA, **123**(2): 94–99.

Poulos, H.G. & Davis, E.H. (1974) *Elastic Solutions for Soils and Rocks*, Wiley, New York. Reprinted 1991 by University of Sydney.

Poulos, H.G. & Davis, E.H. (1980) *Pile Foundation Analysis and Design*, Wiley, New York.

Poulos, H.G. & Hewitt, C.M. (1986) Axial interaction between dissimilar piles in a group. In *Proceedings, Third International Conference on Numerical Methods in Offshore Piling*, Nantes, pp. 253–270.

Poulos, H.G. & Hull, T.S. (1989) The role of analytical geomechanics in foundation engineering. *Foundation Engineering: Current Principles and Practices, ASCE*, Reston, VA, **2**: 1578–1606.

Poulos, H.G. & Mattes, N. (1969) The behaviour

of axially loaded end bearing piles. *Géotechnique*, **19**(2): 185–300.

Poulos, H.G. & Randolph, M.F. (1983) A study of two methods for pile group analysis. *J. Geotechnical Engineering Division, ASCE*, Reston, VA, **109**(3): pp. 355–372.

Powell, J.J.M. & Shields, H.S. (1995) Field studies of the full displacement pressuremeter in clays. In *Proceedings, Fourth International Symposium on Pressuremeters (ISP4)*, May, Sherbrooke, Quebec, Canada, pp. 239–248.

Powell, J.J.M. & Uglow, I.M. (1985) A comparison of Menard, self-boring and push-in pressuremeter tests in a stiff clay till. IN *Proceedings Conference Offshore Site Investigation, Advances in Underwater Technology & Offshore Engineering*, London, UK, Vol. 3, pp. 201–217.

Powell, J.J.M. & Uglow, I.M. (1988) The interpretation of the Marchetti dilatometer test in UK clays. In *Proceedings, Conference on Penetration Testing in the UK*, July, Birmingham, Thomas Telford, London, UK, pp. 269–273.

Powell, R.M., Puls, R.W., Blowes, D.W., Vogan, J.L., Gillham, R.W., Powell, P.D., Schultz, D., Sivavec, T. and Landis, R. (1998) *Permeable Reactive Barrier Technologies for Contaminant Remediation*, US Environmental Protection Agency, US Office of Research & Development, US Office of Solid Waste & Emergency Response, EPA/600/R-98/125. Washington, DC, 94 p.

Powell, W.D., Potter, J.F., Mayhew, H.C. & Nunn, M.E. (1984) *The Structural Design of Bituminous Roads*, Department of Transport, TRRL Report LR1132, Crowthorne, Berkshire, UK.

Powers, J.P. (1991) Dewatering and groundwater control. In Fang, H.Y. (Ed.) *Foundation Engineering Handbook*, 2nd Edn, Van Nostrand Reinhold, New York, NY, pp. 236–248.

Powers, J.P. (1992) *Construction Dewatering–New Methods and Applications*, 2nd Edn, Wiley, New York, NY.

Powrie, W. (1997) *Soil mechanics–Concepts and Applications*, E. & F.N. Spon, London, UK.

Prakash, S. & Puri, V.K. (1988) *Foundations for Machines: Analysis and Design*, Wiley, New York.

Prandtl, L.C. (1920) Uber die harte plastischen korper. *Nachr. K. Ges. Wiss. Gott., Math.-Phys.* **K1**: 74–85.

Pressley, J.S. & Poulos, H.G. (1986) Finite element analysis of mechanisms of pile group behaviour. *International Journal of Numerical Analysis Methods in Geomechanics*, **10**: 213–221.

Preston, J.N. (1996) *Analytical Pavement Design*, SPDM-PC, Highways & Transportation-Shell, Delft.

Prevost, J.-H. (1978) Plasticity theory for soil stress–strain behavior. *Journal of Engineering Mechanics Division, ASCE*, Reston, VA, **104**(5): 1177–1194.

Prevost, J.H. (1981) *DYNAFLOW: A Nonlinear Transient Finite Element Analysis Program*, Princeton University, Princeton, NJ.

Prevost, J.H. & Scanlan, R.H. (1983) Dynamic soil–structure interaction: centrifugal modelling. *Journal of Soil Dynamics & Earthquake Engineering*, **2**(4): 212–221.

Pritchard, M.A. & Savigny, K.W. (1990) Numerical modeling of toppling. *Canadian Geotechnical Journal*, **27**(6): 823–834.

Puls, R.W. & Barcelona, M.J. (1989) Filtration of groundwater samples for metals analyses. *Hazardous Waste & Hazardous Materials*, **6**(4): 385–393.

Puls, R.W. & Barcelona, M.J. (1996) *Ground Water Issue: Low-Flow (Minimal Drawdown) Ground Water Sampling Procedures*, EPA/540/5-95/504. Office of Solid Waste and Emergency Response, Washington, DC.

Puls, R.W. & Paul, C.J. (1995) Low-flow purging and sampling of groundwater monitoring wells with dedicated systems. *Groundwater Monitoring & Remediation*, **XV**(1): 116–123.

Puls, R.W. & Powell, R.M. (1992) Transport of inorganic colloids through natural aquifer material: Implications for contaminant transport. Environmental Science & Technology, **26**(3): 614–621.

Puls, R.W., Clark, D.A., Bledsoe, B., Powell, R.M. & Paul, C.J. (1992) Metals in groundwater: Sampling artifacts and reproducibility. *Hazardous Waste & Hazardous Materials*, **9**(2): 149–162.

PWRI (1992) *Design and Construction Manual for Reinforced Soil Structures Using Geotextiles*, Internal Report No. 3117, Public Works Research Institute, Ministry of Construction, Tsukuba, Japan (in Japanese).

Pyke, R., Seed, H.B. & Chan, C.K. (1975) Settlement of sands under multi-directional loading. *Journal of Geotechnical Engineering Division, ASCE*, Reston, VA, **101**(4): 379–398.

Qian, J.H., Zhao, W.B., Cheung, W.B. Cheung, Y.K. & Lee, P.K.K. (1992) The theory and prac-

tice of vacuum preloading. *Computers & Geotechnics*, **13**: 103–118.

Quigley, R.M., Yanful, E.K. & Fernandez, F. (1987) Ion transfer by diffusion through clay barriers. *Geotechnical Practice for Waste Disposal, ASCE Press*, Reston, VA, 137–158.

Raabe, A.W. & Esters, K. (1993) Soilfracturing techniques for terminating settlements and restoring levels of buildings and structures, In Moseley, M.P. (Ed.) *Ground Improvement*, Blackie Academic & Professional, Blackwood, NJ, pp. 175–192.

Radhakrishnan, R. & Leung, C.F. (1989) Load transfer behavior of rock-socketed piles. *Journal of Geotechnical Engineering*, **115**(6): 755–768.

Randolph, M.F. (1981) Response of flexible piles to lateral loading. *Géotechnique*, **31**(2): 247–259.

Randolph, M.F. (1983) Design considerations for offshore piles. In *ASCE Special Conference on Geotechnical Practice in Offshore Engineering*, Austin, TX, pp. 422–439.

Randolph, M.F. (1992) *Settlement of Pile Groups*, Lecture No. 4, Modern Methods of Pile Design, University of Sydney, Sydney, Aust.

Randolph, M.F. (1994a) *RATZ. Load transfer analysis of axially loaded piles, Users Manual*, University of Western Australia.

Randolph, M.F. (1994b) Design methods for pile groups and piled rafts. In *Proceedings, 13th International Conference Soil Mechanics & Foundations Engineering*, **5**: 61–82.

Randolph, M.F. & Simons, H. (1986) An improved soil model for one-dimensional pile driving analysis. In *Proceedings, Third International Conference on Numerical Methods in Offshore Piling*, Nantes, pp. 3–17.

Randolph, M.F. & Wroth, C.P. (1978) Analysis of deformation of vertically loaded piles. *Journal of Geotechnical Engineering Division, ASCE*, Reston, VA, **104**(12): 1465–1488.

Randolph, M.F. & Wroth, C.P. (1979) An analysis of the vertical deformation of pile groups. *Géotechnique*, **29**(4): 423–439.

Ranganatham, B.V. & Satyanarayana, B. (1965) A rational method of predicting swelling potential for compacted expansive clays. In *Proceedings, Sixth International Conference on Soil Mechanics & Foundation Engineering*, Montreal, Canada, Vol. 1, pp. 92–96.

Rao, P.S.C., Lee, L.S. & Wood, A.L. (1991) *Solubility, Sorption, and Transport of Hydrophobic Organic Chemicals in Complex Mixtures*, Environmental Research Brief, EPA/600/M-91/009. Robert S. Kerr, Environmental Research Laboratories, Ada, OK.

Rapoport, N.Ya., Livanova, N.M. & Miller, V.B. (1977) On the influence of internal stress on the kinetics of oxidation of oriented polypropylene. *Vysokomol. Soyed.* **A18**(9): 2045–2049. (Translated in *Poly. Sci. USSR*, **18**: 2336–2341).

Rasmuson, A. & Eriksson, J.C. (1986) *Capillary Barriers in Covers for Mine Tailings*, National Swedish Environmental Protection Board, Report 3307.

Raulin, P., Rouques, G. & Toubol, A. (1972) *Calcul de la stabilité des pentes en rupture non circulaire*, Research Report No. 36, Laboratoire Central des Ponts et Chaussées, Paris.

Rausch, E. (1950) *Maschinen Fundamente*, VDI-Verlag, Dusseldorf, pp. 107–232.

Rausche, F., Goble, G.G. & Likins, G. (1985) Dynamic determination of pile capacity. *Journal of Geotechnical Engineering, ASCE*, Reston, VA, **111**(3): 367–387.

Raven, K.G. & Beck, P. (1993) Coal tar and creosote contamination in Ontario. In Wayer, K.U. (Ed.) *Subsurface Contamination by Immiscible Fluids*, Balkema, Rotterdam, pp. 401–440.

Raymond, G.P. (1969) Construction method and stability of embankments on muskeg. *Canadian Geotechnical Journal*, **6**: 81–96.

Raymond, G.P. & Giroud, J.P. (1993) *Geosynthetics Case Histories*, ISSMFE Technical Committee TC9 Publication, Bitech, Richmond, BC, Canada.

Reardon, E.J. & Moddle, P.M. (1985) Gas diffusion co-efficient measurements on uranium mill tailings: implications to cover layer design. *Uranium* **2**: 111–131.

Reddy, K.R., Bandi, S.R., Rohr, J.J., Finy, M. & Siebken, J. (1996) Field evaluation of protective covers for landfill geomembrane liners under construction loading. *Geosynthetics International*, **3**(6): 679–700.

Reddy, K.R., Bandi, S.R., Rohr, J.J., Finy, M. & Siebken, J. (1997) Closure of discussions of 'Field evaluation of protective covers for landfill geomembrane liners under construction loading' by Reddy *et al. Geosynthetics, International*, **4**(5): 543–546.

Reese, L.C., O'Neill, M.W. & Smith, R.E. (1970) Generalized analysis of pile foundations. Journal of *Soil Mechanics & Foundational Division, ASCE*, Reston, VA, **96**(1): 235.

Reese, L.C., Cox, W.R. & Koop, F.D. (1974) Analysis of laterally loaded piles in sand. In *Pro-*

ceedings, Sixth Offshore Technology Conference, Houston, TX, paper OTC 2080, pp. 473–483.

Reid, W.M. & Buchanan, N.W. (1984) Bridge approach support piling. In *Proceedings, Conference on Piling & Ground Treatment*, Thomas Telford, London, England, pp. 267–274.

Reissner, E. (1936) Stationare, axialsymmetrische durch eine schuttelnde masseerregte schwigungen eines homogenen elastischen halbraumes. (in German) *Ingenieur-Archiv*, **7**(6): 381–396.

Reiter, L. (1990) *Earthquake Hazard Analysis: Issues and Insights*, Columbia University Press, New York.

Richards, B.G. (1965) Measurement of the free energy of soil moisture by the psychometric technique using thermisters. In *Moisture Equilibria & Moisture Changes in Soils Beneath Covered Areas*, A Symposium in Print, Australia, Butterworths, pp. 35–46.

Richards, L.A. (1931) Capillary conduction of liquids in porous mediums. *Physics*, **1**: 318–333.

Richards, R. & Elms, D. (1979) Seismic behaviour of gravity retaining walls. *Journal of the Geotechnical Engineering Division, ASCE*, Reston, VA, **105**(4): 449–464.

Richardson, G.N., Kavazanjian, E., Jr. & Matasovic, N. (1995) RCRA Subtitle D (258) *Seismic Design Guidance for Municipal Solid Waste Landfill Facilities*, Report No. EPA/600/R-95/051,US Environmental Protection Agency, Office of Research & Development, Washington, DC.

Richardson, H.W. (1953) Electric curtain stabilizes wet ground for deep excavation. *Construction Methods & Equipment*, **35**(4):52–58.

Richart, F.E. (1975) Foundation vibrations. In Fang, H.Y. (Ed.) *Foundation Engineering Handbook*, Van Nostrand Reinhold, New York, pp. 673–699.

Richart, F.E., Hall, J.R. & Woods, R.D. (1970) *Vibrations of Soils and Foundations*, Pentice-Hall, Englewood Cliffs, NJ.

Richter, C.F. (1958) *Elementary Seismology*, W.H. Freeman, San Francisco, CA.

Rickards, I. (1994) APSDS: a structural design system for airport and industrial pavements. In *Proceedings, Ninth Australian Asphalt Pavement Association Conference*, Surfers Paradise, Queensland, Australia.

Ridley, A.M. (1993) *PhD thesis*, Imperial College, London, UK.

Ridley, A.M. & Burland, J.B. (1993) A new instrument for the measurement of soil moisture suction. *Géotechnique*, **43**: 321–324.

Rieke, R., Vinson, T.S., Mageau, D.W. (1983) The role of specific surface area and related index properties in the frost heave susceptibility of soils. In *Proceedings, Fourth International Conference on Permafrost*, Fairbanks, Alaska, pp. 1066–1071.

Rifai, H.S., Borden, R.C., Wilson, J.T. & Ward, C.H. (1995) Intrinsic bioattenuation for subsurface restoration. In Hinchee, R.E., Wilson, J.R. & Downey, D.C. (Eds) *Intrinsic Remediation, Third International* In Situ & *On-Site Bioreclamation Symposium*, Battelle Press, Columbus, OH, Vol. 3(1), pp. 1–30.

Risk Engineering Inc. (1997) *EZ-FRISK Computer Program 4.0*, Boulder, CO.

Ripley, C.F. & Leonoff, C.E. (1961) Embankment settlement behaviour on deep peat. In *Proceedings, Seventh Muskeg Research Conference*, Technical Memorandum No. 71, National Research Council of Canada, Ottawa, ON, pp. 185–204.

Ritchie, J.T. (1972) Model for predicting evaporation from a row crop with incomplete cover. *Water Resources Research*, **8**(5): 1204–1213.

Rittmann, B.E., Fleming, I. & Rowe, R.K. (1996) Leachate chemistry: its implications for clogging. In *North American Water & Environment Congress '96*, June, Anaheim, CA, Paper 4 (CD Rom).

Rivard, P.J. & Lu, Y. (1978) Shear strength of soft fissured clays. *Canadian Geotechnical Journal*, **15**(3): 382–390.

Rivett, M.O. (1993) A field evaluation of pump-and-treat remediation. In *Joint CSCE–ASCE National Conference on Environmental Engineering*, July 12–14, Montreal, pp. 1171–1178.

Rixner, J.J., Kraemer, S.R. & Smith, A.D. (1986a) *Prefabricated Vertical Drains, 1: Engineering Guidelines*, Report No. FHWA-RD-86/168. Federal Highway Administration, Springfield, VA.

Rixner, J.J., Kraemer, S.R. & Smith, A.D. (1986b) *Prefabricated Vertical Drains, 2: Summary of Research Effort*, Report No. FHWA-RD-86/169. Federal Highway Administration, Springfield, VA.

Robert, Y. (1997) A few comments on pile design. *Canadian Geotechnical Journal*, **34**: 560–567.

Roberts, F.L., Kandhal, P.S., Brown, E.R., Lee, D-Y, and Kennedy, T.W. (1996) *Hot Mix As-*

phalt Materials, Mixture Design & Construction, National Asphalt Pavement Association, Lanham, MD.

Robertson, P.K. (1986) *In-situ* testing and its application to foundation engineering. *Canadian Geotechnical Journal*, **23**(4): 573–594.

Robertson, P.K. (1990) Soil classification using the cone penetration test. *Canadian Geotechnical Journal*, **27**(1): 151–158.

Robertson, P.K. & Campanella, R.G. (1983) Interpretation of cone penetration tests. Part I: Sand; Part II: Clay. *Canadian Geotechnical Journal*, **20**(4): 718–733.

Robertson, P.K. & Campanella, R.G. (1985) Liquefaction potential of sands using the cone penetration test. *Journal of the Geotechnical Division, ASCE*, Reston, VA, **111**(3): 298–307.

Robertson, P.K., Sully, J.P., Woeller, D.J., Lunne, T. & Gillespie, D.G. (1992) Estimating coefficient of consolidation from piezocone tests. *Canadian Geotechnical Journal*, **29**(4): 551–557.

Robertson, P.K., Lunne, T. & Powell, J.J.M. (1996) Application of penetration tests for geo-environmental purposes. In Craig, C. (Ed.) *Proceedings, International Conference on Advances in Site Investigation Practice*, March 30–31, London, Thomas Telford, London, pp. 407–420.

Robertson, P.K., Lunne, T. & Powell, J.J.M. (1998) Geo-environmental applications of penetration testing. In Robertson, P.K. & Mayne, P.W. (Eds) *Proceedings, First International Conference on Site Characterization–ISC'98*, April 19–22, Atlanta GA, Vols. 1 & 2, A.A. Balkema, Rotterdam, pp. 35–48.

Robertson, W.D. & Cherry, J.A. (1995) *In situ* denitrification of septic system nitrate using reactive porous media barriers: field trials. *Ground Water*, **33**(1): 99–111.

Robertson, W.D. & Cherry, J.A. (1997) Long term performance of the Waterloo denitrification barrier. In *Proceedings, International-Containment Technology Conference*, (US Department of Energy/Dupont Company/US Environmental Protection Agency), February 9–12, St Petersburg, FL pp. 691–696.

Robinsky, E.I. & Bespflug, K.E. (1973) Design of insulated foundations. *Journal of Geotechnical Engineering, ASCE*, Reston, VA, **99**(9): 649–667.

Robinson, H.D. & Gronow, J.R. (1993). A review of landfill leachate composition in the UK. In *Proceedings, Fourth International Landfill Symposium*, Sardinia, pp. 821–832.

Robinson, R.A. & Stokes, R.H. (1970) *Electrolyte Solutions*, Butterworths, London, UK.

Rocha, M. & Silverio, A. (1969) A new method for the complete determination of the state of stress in rock masses. *Géotechnique*, **19**: 116–132.

Rogers, C.D.F. & Chapman, D.N. (1995a) Ground movements caused by trenchless pipe installation techniques. In *Transportation Research Record* 1514, Transportation Research Board, Washington, DC pp. 37–48.

Rogers, C.D.F. & Chapman, D.N. (1995b) An experimental study of pipebursting in sand. *Geotechnical Engineering, Proceedings Institution of Civil Engineers*, **113**(1): 38–50.

Rogers, C.D.F. & Chapman, D.N. (1995c) Ground displacements caused by pipebursting. In *Proceedings of Trenchless Asia 95*, February, Singapore, International Society for Trenchless Technology, London, UK.

Rogers, C.D.F. & Chapman, D.N. (1998) Analytical modelling of ground movements associated with trenchless pipelaying operations. *Geotechnical Engineering, Institution of Civil Engineers*, **131**: 210–222.

Rollins, K.M. (1994) *In-Situ* deep soil improvement. In *Proceedings, Sessions at the ASCE National Convention*, Atlanta, GA, Geotechnical Special Publication No. 45, American Society of Civil Engineers, ASCE Press, Reston, VA.

Rollins, K.M. & Kim, J.H. (1994) US experience with dynamic compaction of collapsible soils. In *In-Situ Deep Soil Improvement*, Geotechnical Special Publication No. 45, American Society of Civil Engineers, ASCE Press, Reston, VA, pp. 26–43.

Roscoe, K.H. & Burland, J.B. (1968) On the generalized stress–strain behaviour of 'wet' clay. In Heymann, J. & Leckie, F.A. (Eds) *Engineering Plasticity*, Cambridge University Press, Cambridge, England, pp. 535–609.

Roscoe, K.H., Schofield, A.N. & Wroth, C.P. (1958) On the yielding of soils. *Géotechnique*, **8**(1): 22–52.

Rosenberg, P. & Journeaux, N.L. (1976) Friction and end bearing tests on bedrock for high capacity socket design. *Canadian Geotechnical Journal*, **13**: 114–124.

Roth, W.H. (1985) *Evaluation of Earthquake Induced Deformations of Pleasant Valley Dam*, Report for the City of Los Angeles, Dames & Moore, Los Angeles.

Rouhani, S., Srivastava, R.M., Desbarats, A.J.,

Cromer, M.V. & Johnson, A.I. (1996) *Geostatistics for Environmental & Geotechnical Applications*, Special Technical Publication 1283, American Society for Testing & Materials, West Conshohocken, PA.

Rowe, P.W. (1952) Anchored sheet pile walls. *Proceedings, Institution of Civil Engineers*, London, England, 1(1): 27–70.

Rowe, P.W. (1957) Sheet pile walls in clay. *Proceedings, Institution of Civil Engineers*, London, England, **7**: 629–654.

Rowe, R.K. (1982) The analysis of an embankment constructed on a geotextile. In *Proceedings, Second International Conference on Geotextiles*, Las Vegas, NA, Industrial Fabrics Association International, Roseville, MN, Vol. 2, pp. 677–682.

Rowe, R.K. (1984) *Recommendations for the Use of Geotextile Reinforcement in the Design of Low Embankments on Very Soft/Weak Soils*, Research Report GEOT-1-84, Faculty of Engineering Science, The University of Western Ontario.

Rowe, R.K. (1988) Contaminant migration through groundwater: The role of modeling in the design of barriers. *Canadian Geotechnical Journal*, **25**(4): 778–798.

Rowe, R.K. (1992) Some challenging applications of geotextiles in filtration and drainage. In *Geotextiles in Filtration & Drainage*, Corbet, S. and King, J. (Eds.) Thomas Telford, London, England, pp. 1–12.

Rowe, R.K. (1994) *Leachate Characterization*, Report to Interim Waste Authority, October 1994. see also Rowe, R.K. (1995) Leachate characterization for MSW landfills. In *Proceedings Fifth International Landfill Symposium*, Sardinia, Italy, Vol. 2, pp. 327–344.

Rowe, R.K. (1995) Considerations in the design of hydraulic control layers. In *Proceedings, Fifth International Landfill Symposium*, Cagliari, Sardinia, Italy, October. Vol. 1, pp. 103–114.

Rowe, R.K. (1996) The role of diffusion and modelling and its impact on groundwater quality. In Areal, M. (Ed.) *Advances in Groundwater Pollution Control & Remediation*, Kluwer Academic Publishers, Netherlands, pp. 371–403.

Rowe, R.K. (1997a) Reinforced embankment behaviour: lessons from a number of case histories. In Almeida, M. (Ed.) *Proceedings, Symposium on Recent Developments in Soil & Pavement Mechanics*, June, Rio de Janeiro, A.A. Balkema, Rotterdam, pp. 147–160.

Rowe, R.K. (1997b) The design of landfill barrier systems: should there be a choice? *Ground Engineering*, **August**: 36–39.

Rowe, R.K. (1998a) Geosynthetics and the minimization of contaminant migration through barrier systems beneath solid waste. In *Proceedings, Sixth International Conference on Geosynthetics*, March, Atlanta, GA, pp. 27–102.

Rowe, R.K. (1998b) From the past to the future of landfill engineering through case histories. In *Proceedings, Fourth International Conference on Case Histories in Geotechnical Engineering*, St Louis, pp. 145–166.

Rowe, R.K. & Armitage, H.H. (1984) *Design of Piles Socketed into Weak Rock*, Research Report GEOT-11-84, University of Western Ontario, London, Ontario.

Rowe, R.K. & Armitage, H.H. (1987) Theoretical solutions for axial deformation of drilled shafts in rock. *Canadian Geotechnical Journal*, **24**: 114–125.

Rowe, R.K. & Armitage, H.H. (1987a) A design method for drilled piers in soft rock. *Canadian Geotechnical Journal*, **24**: 126–142.

Rowe, R.K. & Armitage, H.H. (1987b) A new design method for drilled piers in soft rock: implications relating to three published case histories. In *Proceedings, International Congress on Rock Mechanics*, Montreal, Canada, Vol. 2, pp. 497–502.

Rowe, R.K. & Badv, K. (1996a) Chloride migration through clayey silt underlain by fine sand or silt. *Journal of Geotechnical Engineering, ASCE*, Reston, VA, **122**(1): 60–68.

Rowe, R.K. & Badv, K. (1996b) Advective-diffusive contaminant migration in unsaturated sand and gravel. *Journal of Geotechnical Engineering, ASCE*, Reston, VA, **122**(12): 965–975.

Rowe, R.K. & Barone, F.S. (1991) *Diffusion Tests for Chloride and Dichloromethane in Halton Till*, Report of the Geotechnical Research Centre, University of Western Ontario, London, Ontario, Canada.

Rowe, R.K. & Booker, J.R. (1981a) The behaviour of footings on a non-homogeneous soil mass with a crust. Part I: strip footings. *Canadian Geotechnical Journal*, **18**(2): 250–264.

Rowe, R.K. & Booker, J.R. (1981b) The behaviour of footings on a non-homogeneous soil mass with a crust. Part II: circular footings. *Canadian Geotechnical Journal*, **18**(2): 265–279.

Rowe, R.K. & Booker, J.R. (1989) Analysis of contaminant transport through fractured rock at an Ontario landfill. In *Proceedings, Third Interna-*

tional Symposium on Numerical Methods in Geomechanics, Niagara Falls, pp. 383–390.

Rowe, R.K. & Booker, J.R. (1997a) *POLLUTE v.6.3—ID Pollutant Migration Through a Non-homogeneous soil*, © 1983, 1990, 1994, 1997, GAEA Environmental Engineering, Whitby, ON, Canada.

Rowe, R.K. & Booker, J.R. (1997b) Recent advances in modelling contaminant impact due to clogging (keynote paper). In *Ninth International Conference of the Association for Computer Methods & Advances in Geomechanics*, November, Wuhan, China, Vol. 1, pp. 43–56.

Rowe, R.K. & Davis, E.H. (1982a) The behaviour of anchor plates in clay. *Géotechnique*, **32**(1): 9–23.

Rowe, R.K. & Davis, E.H. (1982b) The behaviour of anchor plates in sand. *Géotechnique*, **32**(1): 25–41.

Rowe, R.K. & Fleming, I.R. (1998) Estimating the time for clogging of leachate collection systems. In *Proceedings, Third International Congress on Environmental Geotechnics*, September, Lisbon, vol. 1, pp. 23–28.

Rowe, R.K. & Lake, C.B. (1999) Geosynthetic clay liner research and design applications. In *Proceedings, Seventh International Landfill Symposium*, October, S. Margherita di Pula, Cagliari, Sardinia, Vol 3, pp. 181–188.

Rowe, R.K. & Li, A.L. (1999) Reinforced embankments over soft foundations under undrained and partially drained conditions. *Geotextiles & Geomembranes*, **17**(3): 129–146.

Rowe, R.K. & Mylleville, B.L.J. (1989) Consideration of strain in the design of reinforced embankments. In *Proceedings, Geosynthetics '89*, San Diego, Industrial Fabrics Association International, Roseville, MN, pp. 124–135.

Rowe, R.K. & Mylleville, B.L.J. (1990) Implications of adopting an allowable geosynthetic strain in estimating stability. In *Fourth International Conference on Geotextiles, Geomembranes & Related Products*, The Hague, Vol. 1, pp. 131–136.

Rowe, R.K. & Mylleville, B.L.J. (1993) The stability of embankments reinforced with steel. *Canadian Geotechnical Journal*, **30**(5): 768–780.

Rowe, R.K. & Mylleville, B.L.J. (1996) A geogrid reinforced embankment on peat over organic silt: a case history. *Canadian Geotechnical Journal*, **33**(1): 106–122.

Rowe, R.K. & Seychuk, J.L. (1995) Alleged nonperformance of a geotextile filter. In *Proceedings, Proc Pan-American Conference on Soil Mechanics & Foundation Engineering*, October, Guadalajara, Mexico, Vol. 3, pp. 1654–1667.

Rowe, R.K. & Soderman, K.L. (1984) Comparison of predicted and observed behaviour of two test embankments. *Geotextiles & Geomembranes*, **1**(1): 143.

Rowe, R.K. & Soderman, K.L. (1985a) An approximate method for estimating the stability of geotextile reinforced embankments. *Canadian Geotechnical Journal*, **22**(3): 392–398.

Rowe, R.K. & Soderman, K.L. (1985b) Geotextile reinforcement of embankments on peat. *Geotextiles & Geomembranes*, **2**(4): 277–297.

Rowe, R.K. & Soderman, K.L. (1986) Reinforced embankments on very poor foundations. *Geotextiles & Geomembranes*, **4**(1): 65–81.

Rowe, R.K. & Soderman, K.L. (1987) Stabilization of very soft soils using high strength geosynthetics: the role of finite element analyses. *Geotextiles & Geomembranes*, **6**(1): 53.

Rowe, R.K. & Weaver, T.R. (1997) Contaminant transport in groundwater. In *Proceedings, First Australian–New Zealand Conference on Environmental Geotechnics*, Bouzza, A., Kodikara, J. and Parker, R. (Eds.) November, Melbourne, pp. 97–114.

Rowe, R.K., MacLean, M.D. & Barsvary, A.K. (1984a) The observed behaviour of a geotextile reinforced embankment constructed on peat. *Canadian Geotechnical Journal*, **21**(2): 289–304.

Rowe, R.K., MacLean, M.D. & Soderman, K.L. (1984b) Analyses of a geotextile reinforced embankment constructed on peat. *Canadian Geotechnical Journal*, **21**(3): 563–576.

Rowe, R.K., Caers, C.J. & Barone, F. (1988) Laboratory determination of diffusion and distribution coefficients of contaminants using undisturbed clayey soil. *Canadian Geotechnical Journal*, **25**(1): 108–118.

Rowe, R.K., Caers, C.J. & Chan, C. (1993) Evaluation of a compacted till liner test pad constructed over a granular subliner contingency layer. *Canadian Geotechnical Journal*, **30**(4): 667–689.

Rowe, R.K., Hrapovic, L. & Kosaric, N. (1995a) Diffusion of chloride and dichloro-methane through an HDPE geomembrane. *Geosynthetics International*, **2**(3): 507–536.

Rowe, R.K., Quigley, R.M. & Booker, J.R. (1995b) *Clayey Barrier Systems for Waste Disposal and Facilities*, E. & F.N. Spon. London, U.K.

Rowe, R.K., Fleming, I., Cullimore, R., Kosaric, N. & Quigley, R.M. (1995c) *A Research Study of Clogging and Encrustation in Leachate Collection Systems in Municipal Solid Waste Landfills*, Report to Interim Waste Authority Ltd, Geotechnical Research Centre, University of Western Ontario.

Rowe, R.K., Gnanendran, C.T., Landva, A.O. & Valsangkar, A.J. (1995d) Construction and performance of a full-scale geotextile reinforced test embankment, Sackville, New Brunswick. *Canadian Geotechnical Journal*, **32**: 512–534; and (1996) *Canadian Geotechnical Journal*, Erratum. **33**: 208.

Rowe, R.K., Caers, C.J. & Chan, C. (1996a) The design and operation of a state-of-the-art landfill facility. In *Fourth Canadian Society for Civil Engineering Environmental Engineering Specialty Conference*, May 4, Edmonton, pp. 179–190.

Rowe, R.K., Hrapovic, L. & Armstrong, M.D. (1996b) Diffusion of organic pollutants through HDPE geomembrane and composite liners and its influence on groundwater quality. In *Proceedings, First European Geosynthetics Conference*, October, Maastricht, pp. 737–742.

Rowe, R.K., Petrov, R.J. & Lake, C. (1997a) Compatibility testing and diffusion through GCLs. In *Proceedings, Sixth International Landfill Symposium*, October, S. Margherita di Pula, Cagliari, Italy, Vol. 3, pp. 301–310.

Rowe, R.K., Cooke, A.J., Rittmann, B.E. & Fleming, I.R. (1997b) Some considerations in numerical modelling of leachate collection system clogging, (lead lecture). In *Sixth International Symposium on Numerical Methods in Geomechanics*, July, Montreal, pp. 277–282.

Rowe, R.K., Fleming, I.R., Armstrong, M.D., Millward, S.C., VanGulck, J. & Cullimore, R.D. (1997c) Clogging of leachate collection systems: some preliminary experimental findings. In *Proceedings, 50th Canadian Geotechnical Conference*, October, Ottawa, Vol. 1, pp. 153–160.

Rowe, R.K., Fleming, I.R., Armstrong, M.D., Cooke, A.J., Cullimore, R.D., Rittmann, B.E., Bennett, P. & Longstaffe, F.J. (1997d) Recent advances in understanding the clogging of leachate collection systems. In *Proceedings, Sixth International Landfill Symposium*, October, S. Margherita di Pula, Cagliari, Italy, Vol. 3, pp. 383–392.

Rowe, R.K., Lake, C.B. & Petrov, R.J. (1998a) *Test Apparatus and Procedures for Assessing Inorganic Diffusion Coefficients for Geosynthetic Clay Liners*, Geotechnical Research Centre Report, University of Western Ontario.

Rowe, R.K., Caers, C.J., Reynolds, G. & Chan, C. (1998b) *Design of the Halton Landfill*, GEOT-4-98, Faculty of Engineering Science, University of Western Ontario.

Rowe, R.K., Caers, C.J., Reynolds, G. & Chan, C. (2000) Design and construction of the barrier system for the Halton Landfill, *Canadian Geotechnical Journal*, **37**(3): 662–675.

Rowe, R.K., Armstrong, M.D. & Cullimore, D.R. (2000a) *Mass Loading and the Rate of Clogging due to Municipal Solid Waste Leachate*, *Canadian Geotechnical Journal* **37**(2): 355–370.

Rowe, R.K., Armstrong, M.D. & Cullimore, D.R. (2000b) *Particle Size and Clogging of Granular Media Permeated with Leachate. Journal of Geotechnical & Geoenvironmental Engineering, ASCE,* Reston, VA (In press).

Rubright, R. & Welsh, J. (1993) Compaction grouting. In Moseley, M.P. (Ed.) *Ground Improvement*, Blackie Academic & Professional, Blackwood, NJ, pp. 131–148.

Rudolph, D.L., Kachanoski, G.R., Celia, M.A., Leblanc, D.R. & Stevens, J.H. (1996) Infiltration and solute transport experiments in unsaturated sand and gravel, Cape Cod, Massachusetts. Experimental design and overview of results. *Water Resources Research*, **32**(2): 519–532.

Ruhl, J.L. & Daniel, D.E. (1997) Geosynthetic clay liners permeated with chemical solutions and leachates. *Journal of Geotechnical & Geoenvironmental Engineering, ASCE*, Reston, VA, **123**(4): 369–380.

Rumer, R.R. & Mitchell, J.K. (1995) Assessment of barrier containment technologies—a comprehensive treatment for environmental applications. National Technical Information Services, Springfield, VA.

Russam, K. (1958) An investigation into the soil moisture conditions under roads in Trinidad, B.W.I. *Geotéchnique*, **8**: 55–71.

Saada, A. & Bianchini, G.S. (Eds) (1987) *Proceedings, International Workshop on Constitutive Equations for Granular Non-Cohesive Soils*, July 22–24, Case Western Reserve University, Cleveland, Ohio, A.A. Balkema.

Saathoff, F. & Sehrbrock, U. (1994) Indicators for selection of protection layers for geomembranes. In *Proceedings, Fifth International*

Conference on Geotextiles, Geomembranes & Related Products, September, Singapore, Vol. 3, pp. 1019–1022.

Sabatini, P.J., Schmertmann, G.R. & Swan, R.H. (1998) Issues in clay/textured geomembrane interface testing. In Rowe, R.K. (Ed.) *Proceedings, Sixth International Conference on Geomembranes*, Atlanta, GA, Industrial Fabrics Association International, Roseville, MN, Vol. 1, pp. 423–426.

Sadigh, K., Chang, C.-Y., Egan, J.A., Makdisi, F. & Youngs, R.R. (1997) SEA96—A new predictive relation for earthquake ground motions in extensional tectonic Regimes. *Seismological Research Letters*, **68**(1): 190–198.

Sagaseta, C. (1987) Analysis of undrained soil deformation due to ground loss. *Géotechnique* **37**(3): 301–320.

Sai, J.O. & Anderson, D.C. (1991) Barrier wall materials for containment of dense nonaqueous phase liquid (DNAPL). *Hazardous Waste & Hazardous Materials*, **9**(4): 317–330.

Saintot, J., Isambert, F., Simon, B. & Potié, G. (1993) Barrage de Borfloc'h Belle-Ile-en-Mer—Borfloc'h Dam Belle-Ile-en-Mer. In *Proceedings, Rencontres* 93, CFGG, Joué-les-Tours, France, Vol. 2, pp. 315–324 (in French & English).

Salanitro, J.P. (1993) The role of bioattenuation in the management of aromatic hydrocarbon plumes in aquifers. *Ground Water Monitoring & Remediation*, **13**(4): 150–161.

Sale, T.C. & Applegate, D. (1997) Mobile NAPL recovery: conceptual, field and mathematical considerations. *Ground Water*, **35**(3): 418–426.

Sällfors, G., Larsson, R. & Ottosson, E. (1996) New Swedish national rules for slope stability analysis. In *Proceedings, Seventh International Symposium on Landslides*, Trondheim, Vol. 1, pp. 377–380.

Salman, A., Elias, V. Juan, I. Lu, S. & Pearce, E. (1997) Durability of geosynthetics based on accelerated laboratory testing. In *Geosynthetics '97*, Long Breach, CA, IFAI, Roseville, MN, pp. 217–234.

Salman, A., Elias, V. & DiMillio, A. (1998) The effect of oxygen pressure, temperature and manufacturing processes on laboratory degradation of polypropylene geosynthetics. In *Proceedings, Sixth International Conference on Geosynthetics*, R.K. Rowe (Ed), Atlanta, GA, IFAI, Roseville, MN, pp. 683–690.

Sara, M.N. (1991) Ground-water monitoring system design. In Nielsen, D.M. (Ed.) *Practical Handbook of Ground-Water Monitoring* Lewis, Chelsea, MI, pp. 17–68.

Sarma, S.K. (1973) Stability analysis of embankments and slopes. *Géotechnique*, **23**(3): 423–433.

Saul, W.E. (1968) Static and dynamic analysis of pile foundations, *Journal of Structural Division, ASCE*, Reston, VA, **94**(ST5): 1077–1100.

Schaefer, V.R. (Ed.) (1997) *Ground Improvement, Ground Reinforcement, and Ground Treatment: Developments 1987–1997*, Geotechnical Special Publication No. 69, American Society of Civil Engineers, Reston, VA.

Schincariol, R.A., Schwartz, F.W. & Mendoza, C.A. (1994) On the generation of instabilities in variable density flow. *Water Resources Research*, **30**(4): 913–927.

Schincariol, R.A., Schwartz, F.W. & Mendoza, C.A. (1997) Instabilities in variable density flows: Stability and sensitivity analyses for homogeneous and heterogeneous media. *Water Resources Research*, **33**(1): 31–41.

Schlosser, F. (1982). Behaviour and design of soil nailing. In *Proceedings, Symposium on Recent Developments in Ground Improvement Techniques*, Bangkok, pp. 299–413.

Schmee, J. & Hahn, G.J. (1979) A simple method for regression analysis with censored data. *Technometrics*, **21**: 417–432.

Schmertmann, J.H. (1970) Static cone to compute static settlement over sand. *Journal of Soil Mechanics & Foundations Division, ASCE*, Reston, VA, **96**(3): 1011–1043.

Schmertmann, J.H. (1975) Measurement of *in-situ* shear strength. In *Proceedings, ASCE Geotechnical Engineering Division Specialty Conference on* In-Situ *Measurement of Soil Properties*, June 1–4, North Carolina State University, Raleigh, NC, Vol. II, pp. 57–138.

Schmertmann, J. (1978) *Guidelines for Cone Penetration test–in Performance and Design*, US Department of Transportation, Federal Highways Administration, Washington, DC.

Schmertmann, J.H. (1986) Suggested method for performing the flat dilatometer test. ASTM Subcommittee D.18.02. *ASTM Geotechnical Testing Journal*, **9**(2): 99–102.

Schmertmann, J.H. (1991) The mechanical aging of soils. 25th Terzaghi lecture. *Journal of Geotechnical Engineering, ASCE*, Reston, VA, **117**(9): 1288–1330.

Schmertmann, J.H., Hartman, J.P. & Brown, P.R.

(1978) Improved strain factor diagrams. *Journal of Geotechnical Engineering Division, ASCE*, Reston, VA, **104**(8): 1131–1135.

Schmertmann, J.H., Baker, W., Gupta, R. & Kessler, K. (1986) CPT/DMT QC of ground modification at a power plant. In *Use of* In Situ *Tests in Geotechnical Engineering*, Geotechnical Special Publication No. 6, American Society of Civil Engineers, ASCE Press, Reston, VA, pp. 985–1001.

Schmidt, B. (1966) Discussion of Earth pressures at rest related to stress history. *Canadian Geotechnical Journal*, **3**(4): 239–242.

Schmidt, H.M., Pas F.W.T., Risseeuw, P. & Voskamp W. (1994) The hydrolytic stability of PET yarns under medium alkaline conditions. In *Proceedings, Fifth International Conference*, September, Singapore, pp. 1153–1158.

Schnabel, H. (1982) *Tiebacks in Foundation Engineering and Construction*, McGraw-Hill, New York, NY.

Schnabel, P., Lysmer, J. & Seed, H.B. (1972) *SHAKE: A Computer Program for Earthquake Response Analysis of Horizontally Layered Sites*, Report No. EERC 72-12, Earthquake Engineering Research Center, University of California, Berkeley, CA.

Schnarr, M.J., Truax, C.T., Farquhar, G.J., Hood, E.D., Gonullu, T. & Stickney, B, (1998) Experiments using potassium permanganate to remediate trichloroethylene and perchloroethylene DNAPLs. *Journal of Contaminant Hydrology*, **29**: 205–224.

Schofield, A.N. & Wroth, C.P. (1968) *Critical State Soil Mechanics*, McGraw-Hill, London.

Schroeder, P.R., Lloyd, C.M. & Zappi, P.A. (1994) *The Hydrologic Evaluation of Landfill Performance (HELP) Model: User's Guide for Version* 3, EPA/600/R-94/168a, US Environmental Protection Agency, Risk Reduction Engineering Laboratory, Cinncinnati, OH.

Schroeder, P.R., Dozier, T.S., Zappi, P.A., McEnroe, B.M., Sjostrom, J.W. & Peyton, R.L. (1994) *The Hydrologic Evaluation of Landfill Performance (HELP) Model: Engineering Documentation for Version* 3, EPA/600/R-94/168b, US Environmental Protection Agency Risk Reduction Engineering Laboratory, Cincinnati, OH.

Schuster, R.L. (1995) Keynote paper: Recent advances in slope stabilization. In *Proceedings, Sixth International Symposium on Landslides*, Christchurch, Vol. 3, pp. 1715–1725.

Schuster, R.L. (1996) Socioeconomic significance of landslides. *Landslides – Investigation and Mitigation*, Special Report 247, A.K. Turner & R.L. Schuster (Eds.) Transportation Research Board, Washington, DC, pp. 12–35.

Schwartz, D.P. & Coppersmith, K.J. (1984) Fault behaviour and characteristic earthquakes from the Wasatch and San Andreas faults. *Journal of Geophysical Research*, **89**: 5681–5698.

Schwarzenbach, R.P. & Giger, W. (1985) Behavior and fate of halogenated hydrocarbons in groundwater. In Ward, C.H. Giger, W. & McCarty, P.L. (Eds) *Groundwater Quality*, Wiley-Interscience, New York, pp. 446–471.

Schwarzenbach, R.P. & Westall, J. (1981) Transport of nonpolar organic compounds from surface water to groundwater–laboratory studies. *Environmental Science & Technology*, **15**: 1300–1367.

Schwille, F. (1988) *Dense Chlorinated Solvents in Porous and Fractured Media: Model Experiments*, translated by J.F. Pankow, Lewis, Chelsea, MI.

Scott, R.F., Liu, H.P. & Ting, J. (1977) Dynamic pile tests by centrifuge modelling. In *Proceedings, Sixth World Conference on Earthquake Engineering*, New Delhi, India, Vol. 4, pp. 199–203.

Scott, R.F., Ting, J. & Lee, J (1982) Comparison of centrifuge and full-scale dynamic pile tests. In *Proceedings, International Conference on Soil Dynamics & Earthquake Engineering*, Southampton, Vol. 1, pp. 299–309.

SCW (1981) *Stability of Slopes Constructed with Polyester Reinforcing Fabric*, Study Centre for Road Construction, Arnhem, The Netherlands.

SEBJ (1983) *Experts Committee on Soft Clays from the NBR Complex. Final report*, Société d'Énergie de la Baie James Montréal, Québec, Canada.

Seed, H.B. (1979a) Soil liquefaction and cyclic mobility evaluation for level ground during earthquakes. *Journal of the Geotechnical Engineering Division, ASCE*, Reston, VA, **105**(2): 201–255.

Seed, H.B. (1979b) Considerations in the earthquake-resistant design of earth and rockfill dams. *Géotechnique*, **29**(3): 215–263.

Seed, H.B. (1987) Design problems in soil liquefaction. *Journal of Geotechnical Engineering, ASCE*, Reston, VA, **113**(7): 827–845.

Seed, H.B. & Idriss, I.M. (1970) *Soil Moduli and Damping Factors for Dynamic Response Analyses*, Report EERC 70-10, College of Engineering, University of California, Berkeley, CA.

Seed, H.B. & Idriss, I.M. (1971) Simplified proce-

dures for evaluating soil liquefaction potential. *Journal of Soil Mechanics & Foundations Division, ASCE*, Reston, VA, **97**(9): 1249–1273.

Seed, H.B. & Idriss, I.M. (1982) *Ground Motions and Soil Liquefaction During Earthquakes*, Monograph No. 5, Earthquake Engineering Research Institute, Berkeley.

Seed, H.B. & Lee, K.L. (1967) Undrained strength characteristics of cohesionless soils. *Journal of Soil Mechanics & Foundations Division, ASCE*, Reston, VA, **93**(6): 333–360.

Seed, R.B. & Raines, J.R. (1988) *Failure of Flexible Long-span Culverts under Exceptional Live Load*, Transportation Research Record No. 1191, pp. 22–20.

Seed, H.B. & Wilson, S.D. (1966) The Turnagain Heights Landslides, Anchorage, Alaska. In *Proceedings, ASCE Specialty Conference on Stability & Performance of Slopes & Embankments*, Reston, VA, pp. 357–385.

Seed, H.B., Mitchell, J.K. & Chan, C.K. (1960) The strength of compacted cohesive soils. In *ASCE Research Conference on the Strength of Cohesive Soils*, Boulder, CO, pp. 877–964.

Seed, H.B., Mitchell, J.K. & Chan, C.K. (1962a) Swell and swell pressure characteristics of compacted clays. *Highway Research Board Bulletin* **313**: 12–39.

Seed, H.B., Woodward Jr, R.J. & Lundgren, R. (1962b) Prediction of swelling potential for compacted clays. *Journal of Soil Mechanics & Foundations Division, ASCE*, Reston, VA, **88**(3): 53–97.

Seed, H.B., Lee, K.L., Idriss, I.M. & Makdisi, F.F. (1975) The slides in the San Fernando Dams during the earthquake of February 9, 1971. *Journal of Earthquake Engineering Division, ASCE*, Reston, VA, **101**(7): 651–688.

Seed, H.B., Tokimatsu, K., Harder, L.F. & Chung, R.M. (1985) The influence of SPT procedures in soil liquefaction resistance evaluations. *Journal of Geotechnical Engineering, ASCE*, Reston, VA, **111**(12): 1425–1445.

Seed, H.B., Seed, R.B., Harder, L.F. Jr & Jong, H.-L. (1989) *Re-evaluation of the Lower San Fernando Dam, Report 2, Examination of the Post-earthquake Slide of February 9, 1971*, Department of the Army, US Army Corps of Engineers, Washington, DC.

Seed, H.B., Tokimatsu, K., Harder, L.F. & Chung, R.M. (1985) Influence of SPT procedures in soil liquefaction resistance evaluations. *Journal of Geotechnical Engineering, ASCE*, Reston, VA, **111**(12): 1425–1445.

Seed, R.B. & Boulanger, R.W. (1991) Smooth HDPE–clay linear interface shear strengths: compaction effects. *Journal of Geotechnical Engineering, ASCE*, Reston, VA, **117**(4): 686–693.

Seed, R.B. & Harder, L.F. Jr. (1990) SPT-based analysis of cyclic pore pressure generation and undrained residual strength. In *Proceedings, H. Bolton Seed Memorial Symposium*, May, Bi-Tech, pp. 351–376.

Seed, R.B., Mitchell, J.K. & Seed, H.B. (1988) *Slope Stability Failure Investigation: Landfill Unit B-19, Phase I-A, Kettleman Hills, California*, Report No. UCB/GT/88-01, University of California at Berkeley, Berkeley.

Seed, R.B., Dickenson, S. & Mok, C.M. (1991) Seismic response analyses of soft and deep cohesive sites: a brief summary of recent lessons. In *Proceedings, First Annual CALTRANS Seismic Research Seminar*, CALTRANS, Sacramento.

Seeger, S. & Müller, W. (1996) Requirements and testing of protective layer systems for geomembranes. *Geotextiles & Geomembranes*, **14**: 365–376.

Sego, D.C., Robertson, P.K., Sasitharan, S., Kilpatrick, B.L. & Pillai, V.S. (1994) Ground freezing and sampling of foundation soils at Duncan Dam. *Canadian Geotechnical Journal*, **31**(6): 939–950.

Selig, E.T. (1990) Soil properties for plastic pipe installations. In Buczala, G.S. & Cassidy, M.J. (Eds) *Buried Plastic Pipe Technology*, Special Technical Publication 1093, American Society for Testing & Materials, West Conshohocken, PA, pp. 141–158.

Selvadurai, A.P.S. (1979) *Elastic Analysis of Soil–Foundation Interaction*, Elsevier, New York.

Selvadurai, A.P.S. (1985) Numerical simulation of soil–pipeline interaction in a ground subsidence zone. In Jeyapalan, J.K. (Ed.) *International Conference On Advances in Underground Pipeline Engineering*, Madison, WI, pp. 311–319.

Semple, R.M. & Rigden, W.J. (1984) Shaft capacity of driven piles in clay. *Analysis & Design of Pile Foundations, ASCE* Press, Reston, VA, pp. 59–79.

Semprini, L., Kitandis, P.K., Kampbell, D.H. & Wilson, J.T. (1995) Anaerobic transformation of chlorinated aliphatic hydrocarbons in a sand aquifer based on spatial chemical distributions. *Water Resources Research*, **31**(4): 1051–1062.

Serrano, A. & Olalla, C. (1994) Ultimate bearing

capacity of rock masses. *International Journal of Rock Mechanics Mineral Science & Geomechanics Abstracts*, **31**(2): 93–106.

Serrano, A. & Olalla, C. (1996) Ultimate bearing capacity of rock masses. *International Journal of Rock Mechanical Mineral Science & Geomechanics Abstracts*, **33**(4): 327–345.

Sève, G. (1998) *PhD thesis*, École Nationale des Ponts et Chaussées, Paris.

Sève, G. & Durville, J.-L. (1995) Surveillance des glissements de terrain. In *Proceedings, 11th European Conference on Soil Mechanics & Foundation Engineering*, Copenhagen, Vol. 4, pp. 115–120.

Sève, G. & Leca, E. (1995) Stabilization of landslide using large diameter piles. In *Proceedings, 11th European Conference on Soil Mechanics & Foundation Engineering*, Copenhagen, Vol. 6, pp. 179–184.

Sève, G. & Pouget, P. (1998) *Guide technique sur la stabilisation des glissements de terrain*. Techniques et Méthodes des Laboratories des Ponts et Chausseées, Paris.

Shackelford, C.D. & Daniel, D.E. (1991a) Diffusion in saturated soil. I: Background. *Journal of Geotechnical Engineering, ASCE*, Reston, VA, **117**(3): 467–506.

Shackelford, C.D. & Daniel, D.E. (1991b) Diffusion in saturated soil. II: Results for compacted clay. *Journal of Geotechnical Engineering, ASCE*, Reston, VA, **117**(3): 485–506.

Shahin, M.Y. & Crovetti, J.A. (1987) Determining the effects of utility cut patching on the service life prediction of asphalt concrete pavements. In *Proceedings, Second North American Conference on Managing Pavements*, Toronto, Canada, Vol. 1, pp. 225–236.

Shallenberger, W.C. & Filz, G.M. (1996) Interface strength determination using a large displacement shear box. In *Proceedings, Second International Conference on Environmental Geotechnics*, Osaka, Japan, Vol. 1, pp. 147–152.

Shan, H.-Y. (1993) *PhD dissertation*, University of Texas, Austin, TX.

Shan, H.-Y. & Daniel, D.E. (1991) Results of laboratory tests on a geotextile/bentonite linear material. In *Proceedings, Geosynthetics '91*, Industrial Fabrics Association International, Roseville, MN, Vol. 2, pp. 517–535.

Shang, J.Q. (1998) Electroosmotic enhanced preloading consolidation via vertical drains. *Canadian Geotechnical Journal*, **35**(4): 491–499.

Shang, J.Q., Lo, K.Y. & Huang, K.M. (1996) On influencing factors in electro-osmotic consolidation. *Journal of Geotechnical Engineering*, South East Asia Geotechnical Society, **27**(2): 23–26.

Shang, J.Q., Tang, M. & Z. Miao, (1998) Vacuum preloading consolidation of reclaimed land: a case study. *Canadian Geotechnical Journal*, **35**(5): 740–749.

Sharma, S. (1994) *XSTABL, Reference Manual, Version* 5, Interactive Software Designs, Inc., Moscow, ID.

Sharma, H.D. & Lewis, S.P. (1994) *Waste Containment Systems, Waste Stabilization, & Landfills, Design & Evaluation*, Wiley, New York.

Sharma, H.D., Dukes, M.T. & Olsen, D.M. (1990) Field measurements of dynamic moduli and Poisson's ratios of refuse and underlying soils at a landfill site. In *Geotechnics of Waste Landfills – Theory & Practice*, STP 1070, Landva, A. & Knowles, E.D. (Eds.) American Society for Testing & Materials, West Conshohocken, PA, pp. 57–70.

Sharma, H.D., Hullings, D.E. & Greguras, F.D. (1997) Interface strength tests and application to landfill design. In *Proceedings, Geosynthetics '87 Conference*, Long Beach, CA, Vol. 2, pp. 913–926.

Sharma, M., Thomson, N.R. & McBean, E.A. (1995) Linear regression analyses with censored data: estimation of PAH washout ratios and dry deposition velocities to a snow surface. *Canadian Journal of Civil Engineering*: **22**(4): 819–833.

Sharma, M., McBean, E.A. & Thomson, N.R. (1995) Maximum likelihood method for parameter estimation with below-detection data. *Journal of the Environmental Engineering Division, ASCE*, Reston, VA, **11**: 776–784.

Sherard, J.L. (1985) The upstream zone in concrete–face rockfill dams. In Cooke, J.B. & Sherard, J.L. (Eds) *Proceedings, Symposium on Concrete Face Rockfill Dams–Design, Construction, and Performance*, American Society of Civil Engineers, Reston, VA, pp. 618–641.

Sherif, M., Ishibashi, I. & Lee, C. (1982) Earth pressure against rigid retaining Walls. *Journal of the Geotechnical Engineering Division, ASCE*, Reston, VA, **108**(5): 679–695.

Sheta, M. & Novak, M. (1982) Vertical vibration of pile groups. *Journal of Geotechnical Engineering Division, ASCE*, Reston, VA, **108**(4): 570–590.

Shi, X. & Richards, Jr. R. (1995) Seismic bearing capacity with variable shear transfer. In

Kramer, S. & Siddharthan, R. (Eds) *Earthquake Induced Movements and Seismic Remediation of Existing Foundations and Abutments*, Geotechnical Special Publication No. 55, American Society of Civil Engineers, Reston, VA, pp. 17–32.

Shikaze, S., Austrins, C.D., Smyth, D.J.A., Cherry, J.A., Barker, J. & Sudicky, E. (1995) The hydraulics of a funnel-and-gate system. A three-dimensional numerical analysis. *Solutions '95: Proceedings, IAH International Congress*, June, Edmonton, AB.

Shields, D., Chandler, N. & Garnier, J. (1990) Bearing capacity of foundations in slopes. *Journal of Geotechnical Division, ASCE*, Reston, VA, **116**(3): 528–537.

Shoemaker, S.H., Greiner, J.F. & Gillham, R.W. (1995) Permeable reactive barriers. In Rumer, R.R. & Mitchell, J.K. (Eds), *Assessment of Barrier Containment Technologies: A Comprehensive Treatment for Environmental Remediation Applications*. US Department of Energy/US Environmental Protection Agency/Dupont Company, pp. 301–353.

Shoukry, S.N. (Ed.) (1998) Finite element for pavement analysis and design. *Proc., First National Symposium on 3D Finite Element Modeling for Pavement Analysis and Design*, November, West Virginia University, Morgantown, WV-ISBN 093 7058-49-1, pp. 1–305.

SHRP (1994) *The Superpave Mix Design Manual for New Construction and Overlays*, Report A-407, Strategic Highway Research Program, Washington, DC.

Siddle, H.J., Jones, D.B. & Warren, C.D. (1986) The use of tracer techniques to assess groundwater flows in site investigations. In Hawkins, A.B. (Ed.) *Site Investigation Practice: Assessing BS 5930*. Geological Society Engineering Geology Special Publication No. 2, London, England, pp. 375–384.

Sieh, K.E. & Jahns, R.H. (1984) Holocene activity of the San Andreas Fault at Wallace Creek, California. *Bulletin Geological Society of America*, **90**: 883–896.

Silva, W.J. (1988) *Soil Response to Earthquake Ground Motion*, EERI Report NP-5747, Electric Power Research Institute, Palo Alto, CA.

Silva, W.J. & Lee, K. (1987) *WES RASCAL Code for Synthesizing Earthquake Ground Motions*, Department of the Army, US Army Corps of Engineers, Washington, DC.

Simac, M.R., Bathurst, R.J., Berg, R.R. & Lothspeich, S.E. (1993) *National Concrete Masonry Association Segmental Retaining Wall Design Manual*, National Concrete Masonry Association, Herndon, VA.

Simac, M.R., Bathurst, R.J. & Fennessey, T.W. (1997a) Case study of a hybrid gabion basket geosynthetic reinforced soil wall. *Ground Improvement*, **1**(1): 9–17.

Simac, M.R., Bathurst, R.J. & Fennessey, T.W. (1997b) Design of gabion–geosynthetic retaining walls on the Tellico Plains to Robbinsville Highway. In *Geosynthetics'97*, Industrial Fabrics Association International, Roseville, MN, March, Vol. 1, pp. 11–13.

Simms, P.H. & Yanful, E.K. (1997) Monitoring, analysis, and performance of an engineered soil cover near London, Ontario. In *Proceedings, 50th Canadian Geotechnical Conference*, Ottawa, Vol. 1, pp. 42–49.

Simkin, T.J., Sale, T.C., Kueper, B.H., Pitts, M.J., and Wyatt, K. (1999). *Surfactants and Cosolvents for NAPL Remediation: A Technology Practices Manual.* (Eds.) Lowe, D.F., Oubre, C.L., and Ward, C.H. Lewis Publishers, Boca Raton, Floida, 448 p.

Sims, R.C. (1990) Soil remediation techniques at uncontrolled hazardous waste sites: a critical review. *Journal of the Air & Waste Management Association*, **40**(5): 704–732.

Singh, S. & Sun, J.I. (1995) Seismic evaluation of municipal solid waste landfills. In *Geoenvironment 2000*, Acar, Y.B. and Daniel, D.E. (Eds.) Geotechnical Special Publication No. 46, American Society of Civil Engineers, Reston, VA, Vol. 2, pp. 1081–1096.

Sinha, J. & Poulos, H.G. (1996) Behaviour of stiffened raft foundations. In *Seventh Aust–NZ Conference on Geomechanics*, 1–5 July, Adelaide. M.B. Jaksa, W.S. Kaggwa & D.A. Cameron (Eds.), pp. 704–709.

Site Investigation Steering Group, ICE (1993) *Site Investigation in Construction. Part 1: Without Site Investigation Ground is a Hazard; Part 2: Planning, Procurement & Quality Management; Part 3: Specification for Ground Investigation; & Part 4: Guidelines for the Safe Investigation by Drilling of Landfills & Contaminated Land*, Thomas Telford, London, England.

Skempton, A.W. (1957) Discussion. *Proceedings, Institution of Civil Engineers*, **7**: 305–307.

Skempton, A.W. (1964) Long-term stability of clay slopes. *Géotechnique*, **14**(2): 77–101.

Skempton, A.W. (1977) Slope stability of cuttings in brown London clay. *Proceedings, Ninth In-*

ternational Conference on Soil Mechanics & Foundation Engineering, Tokyo, Vol. 3, pp. 261–270.

Skempton, A.W. (1985) Residual strength of clays in landslides, folded strata and the laboratory. *Géotechnique*, **35**(1): 3–18.

Skempton, A.W. (1986) Standard penetration test procedures and the effects in sands of overburden pressure, relative density, particle size, aging and overconsolidation. *Géotechnique*, **36**(3): 425–447.

Skempton, A.W. & MacDonald, D.H. (1956) The allowable settlement of buildings. *Proceedings, Institution of Civil Engineers*, **5**: 727–768.

Sleep, B. (1996) Steam injection for *in-situ* remediation of DNAPLs in low permeability media. In In Situ *Remediation of DNAPL Compounds in Low Permeability Media:Fate/Transport, In Situ Control Technologies & Risk*, ORNL/TM-13305, Oak Ridge National Laboratory, Oak Ridges, TN, **13**: 1–13.

Slemmons, D.B., Bodin, P. & Zhang, X. (1989) Determination of earthquake size from surface faulting events. In *Proceedings, International Seminar on Seismic Zonation*, Guangshou, China.

Sloan, S.W. & Randolph, M.F. (1982) Numerical prediction of collapse loads using finite element methods. *International Journal for Numerical & Analytical Methods in Geomechanics*, **6**: 47–76.

Sloan, S.W. & Yu, H.S. (1996) Rigorous plasticity solutions for the bearing capacity factor N_γ. In *Proceedings, Seventh Aust–NZ. Conference on Geomechanics*, 1–5 July, Adelaide, M.B. Jaksa, W.S. Kaggwa & D.A. Cameron (Eds.), pp. 544–550.

Slocombe, B.C. (1993) Dynamic Compaction. In Moseley, M.P. (Ed.) *Ground Improvement*, Blackie Academic & Professional, Blackwood, NJ, pp. 20–39.

Small, J.C. & Booker, J.R. (1986) Finite layer analysis of layered elastic materials using a flexibility approach, Part 2. circular and rectangular loadings. *International Journal for Numerical Methods in Engineering*, **23**: 959–978.

Small, J.C. & Booker, J.R. (1996) *User's manuals for FLEA (Finite Layer Elastic Analysis) and FLAC (Finite Layer Analysis of Consolidation)*, Centre for Geotechnical Research, The University of Sydney.

Smith, D.W. (Ed.) (1986) *Cold climate utilities manual*, Canadian Society for Civil Engineering, Montreal, Quebec.

Smith, E.A.L. (1960) Pile driving analysis by the wave equation. *Journal of Soil Mechanics & Foundations Division, ASCE*, Reston, VA, **86**(4): 35–61.

Smith, L.A., Means, J.L. Chen, A., Alleman, B., Chapman, C.C., Tixier, J.S., Brauning, S.E., Gavaskar, A. & Royer, M.D. *Remedial Options for Metals-Contaminated Sites*, Battelle Memorial Institute, Columbus, OH.

Smyth, D.J.A., Shikaze, S.G. & Cherry, J.A. (1997) Hydraulic performance of permeable barriers for *in situ* treatment of contaminated groundwater. *Land Contamination & Reclamation*, **5**(3): 131–137.

Snow, M., Mansour, R., Swan, R.H., Jr & Kavazanjian, E., Jr (1998) Variability of interface shear strengths. In Rowe, R.K. (Ed.) *Proceedings, Sixth International Conference on Geomembranes*, Atlanta, GA, Industrial Fabrics Association International, Roseville, MN, Vol. 1, pp. 439–442.

Soderman, L. & Milligan, V. (1961) Capacity of friction piles in varved clay increased by electro osmosis. In *Fifth International Conference of Soil Mechanics & Foundation Engineering*, Paris, Vol. 2, pp. 143–147.

Sokolovskii, V.V. (1960) *Statics of Soil Media*, Butterworth, London, England.

Sokolovskii, V.V. (1965) *Statics of Granular Media*, Pergamon Press, London, England.

Solymar, Z.V. (1984) Compaction of alluvial sands by deep blasting. *Canadian Geotechnical Journal*, **21**(2): 305–321.

Solymar, Z.V. & Mitchell, J.K. (1986) Blasting densifies sand. *Civil Engineering, ASCE*, Reston, VA, **56**(3): 46–48.

Solymar, Z.V. & Reed, D.J. (1986) A comparison of foundation compaction techniques. *Canadian Geotechnical Journal*, **23**(3): 271–280.

Solymar, Z.V., Iloabachie, B.C., Gupta, R.C. & Williams, L.R. (1984) Earth foundation treatment at Jebba Dam site. *Journal of Geotechnical Engineering, ASCE*, Reston, VA, **110**(10): 1415–1430.

Somerville, P.G. (1998) Emerging art: earthquake ground motion. In Dakoulas, P., Yegian, M. & Holtz, R.D. (Eds.) *Proceedings, Geotechnical Earthquake Engineering in Soil Dynamics III*, Geotechnical Special Publication No. 75, American Society of Civil Engineers, Reston, VA, Vol. 1, pp. 1–38.

Somerville, P.G. & Graves, R.W. (1996) Strong ground motions of the Kobe, Japan earthquake

of January 17, 1995, and development of forward rupture directivity applicable in California. In *Proceedings, Western Regional Technical* Seminar of Earthquake *Engineering for Dams*, April 11–12, Sacramento, CA, Association of State Dam Safety Officials.

Soong, T.Y. & Koerner, R.M. (1997) *The Design of Drainage Systems Over Geosynthetically Lined Slopes*, GRI Report No. 19, Geosynthetic Research Institute, Drexel University, Philadelphia, PA.

Soong, T.Y. & Koerner, R.M. (1998) Laboratory study of high density polyethylene geomembrane waves. In Rowe, R.K. (Ed.) *Proceedings, Sixth International Conference on Geosynthetics*, March, Atlanta, GA, Vol. 1, Industrial Fabrics Association International, Roseville, MN, pp. 301–306.

Sowers, G.F. (1973) Settlement of waste disposal fills. In *Proceedings, Eighth International Conference on Soil Mechanics & Foundation Engineering*, Moscow, pp. 207–210.

Sowers, G.F. (1979) *Introductory Soil Mechanics and Foundations: Geotechnical Engineering*, 4th Edn, MacMillan, New York.

Sowers, G.B. & Sowers, G.F. (1970) *Introductory Soil Mechanics and Foundations*, 3rd Edn, MacMillan, New York.

Spain, J. (1996) Future vision: compounds with potential for natural attenuation. In *Symposium on Natural Attenuation of Chlorinated Organics in Groundwater*, September 11–13, Dallas, Tx, 540/R-96-509, US Environmental Protection Agency pp. 128–132.

Spangler, M.J. (1956) Stresses in pressure pipelines and protective casting pipes. *Journal of Structural Engineering, ASCE*, Reston, VA, **82**: 1–33.

Spangler, M.J. & Handy, R.L. (1973) *Soil Engineering*, Intext Educational, New York.

Spencer, E. (1967) A method of analysis of the stability of embankments assuming parallel inter-slice forces. *Géotechnique*, **17**(1): 11–26.

Spikula, D. (1996) Subsidence performance of landfills: a seven-year review. In *Proceedings, GRI-10 Conference on Field Performance of Geosynthetics & Geosynthetic Related Systems*, Geosynthetic Research Institute, Philadelphia, PA, pp. 237–244.

Sposito, G. (1984) *The Surface Chemistry of Soils*, Oxford University Press, New York.

Sprague, C.J. (1990) Leachate compatibility of polyester needlepunched nonwoven geotextiles. In Koerner, R.M. (Ed.) *Geosynthetic Testing for Waste Containment Applications, ASTM STP 1081*, American Society for Testing & Materials, West Conshohocken, PA, USA, pp. 212–224.

Sprute, R.H. & Kelsh, R.H. (1980) Dewatering fine-particle suspensions with direct current. In *Proceedings, International Symposium of Fine Particle Process*, Las Vegas, NV, Vol. 2, pp. 1828–1844.

Squillace, P.J., Pankow, J.F., Korte, N.E. & Zogorski, J.S. (1997) Review of the environmental behavior and fate of methyl tert-bretyl ethel. *Environmental Toxicology & Chemistry*, **16**(9): 1836–1844.

SSA (1997) Special issue. *Seismological Research Letters*, **68**(1): 1–255.

Stagg, K.G. (1968) *In situ* tests on the rock mass. In Stagg, K.G. & Zienkiewicz, O.C. (Eds), *Rock Mechanics in Engineering Practice*, Wiley, Chichester, pp. 125–156.

Stain, R.T. & Williams, H.T. (1991) Interpretation of sonic coring results–a research project. In *Proceedings, Fourth International Conference on Piling & Deep Foundations*, Stresa, Balkema, Rotterdam.

Stark, T.D. & Eid, H.T. (1993) Modified Bromhead ring shear apparatus. *Geotechnical Testing Journal, ASTM*, West Conshohocken, PA, **16**(1): 100–107.

Stark, T.D. & Eid, H.T. (1996) Shear behavior of reinforced geosynthetic clay liners. *Geosynthetics International*, **3**(6): 771–786.

Stark, T.D. & Olson (1995) Liquefaction Resistance Using CPT and Field Case Histories. ASCE Journal of Geotechnical Engineering, Reston, VA, **121**(12): 856–869.

Stark, T.D. & Poeppel, A.R. (1994) Landfill liner interface strengths from torsional-ring-shear tests. *Journal of Geotechnical Engineering, ASCE*, Reston, VA, **120**,(3): 597–615.

Stark, T.D., Williamson, T.A. & Eid, H.T. (1996) HDPE geomembrane–geotextile interface shear strength. *Journal of Geotechnical Engineering, ASCE*, Reston, VA, **122**(3): 197–203.

St-Arnaud, G., Morel, R. & Lavallée, J.-G. (1992) *Comportement de la fondation argileuse traitée avec des drains synthétiques sous le remblai d'essai Olga-C*, Internal Report, Hydro-Québec, Service géologie et structures, Montréal, Canada.

Starr, R.C. & Cherry, J.A. (1990) *In situ* barriers for groundwater pollution control. In *Conference on Prevention & Treatment of Soil & Groundwater Contamination in the Petroleum*

Refining & Distribution Industry, October 16–17, Montreal, PQ.

Starr, R.C., & Cherry, J.A. (1992) Applications of low permeability cutoff walls for groundwater pollution control. In *Proceedings, 45th* Canadian Geotechnical Conference, October 26–28, Toronto, ON.

Starr, R.C. & Gillham, R.W. (1993) Denitrification and organic carbon availability in two aquifers. *Ground Water*, **31**(6): 934–947.

Starr, R.C. & Cherry, J.A. (1994) Passive *in situ* remediation of contaminated groundwater: the funnel and gate system. *Ground Water*, **32**(3): 465–476.

Stas, C.V. & Kulhawy F.H. (1984) *Critical Evaluation of Design Methods for Foundations Under Axial Uplift and Compression Loading*, EPRI Report EL-3771, Cornell University.

Stefan, J. (1891) Uber die Theorie des Eisbildung, insbesondere uber die Eisbildung im Polameere. Ann. Phys. u. Chem., Neue Folge, **42**(2): 269–286.

Stein, D., Möllers, K. & Bielecki, R., (1989) Microtunnelling, Ernst & Sohn, Berlin.

Stephens, D.B. (1996) *Vadose Zone Hydrology*, CRC Lewis, Boca Raton, FL.

Stermac, A.G., Lo, K.Y., & Barsvary, A. (1967) The performance of an embankment founded on a deep deposit of carved clay. *Canadian Geotechnical Journal*, **4**(1):45–61.

Stewart, D.P., Jewell, R.J. & Randolph, M.F. (1994) Design of piled bridge abutments on soft clay for loading from lateral soil movements. *Geotechnique*, **14**(2): 277–296.

Stocker, M.F., Korber, G.W., Gassler, G. & Gudehus, G. (1979) Soil nailing. In *C.R. Coll. Int. Reinforcement des Sols*, Paris, pp. 105–118.

Stollenwerk, K.G. (1991) *Simulation of Molybdate Sorption with Diffuse Layer Surface-Complexation Model*, Water Resources Investigations Report 91–4034, US Geological Survey, pp. 47–52.

Stroud, M.A. (1974) The Standard Penetration Test in insensitive clays and soft rocks. Proceedings European Symposium on Penetration Testing, Stockholm **2**: 367–375.

Stulgis, R.P., Soydemir, C. & Telgener, R.J. (1995) Predicting landfill settlement. In *Geoenvironment 2000*, Geotechnical Special Publication No. 46, Acar, Y.B. and Daniel D.E. (Eds.) American Society of Civil Engineers, Reston, VA, Vol. 2, pp. 980–993.

STUDENT (W. Gossen) (1908) The probable error of a mean. *Biometrika*, **54**: 1–25.

Stumm, W. & Morgan, J.J. (1996) *Aquatic Chemistry: Chemical Equilibria and Rates in Natural Waters*, 3rd Edn, Wiley, New York.

Sui, T.L., Na, W.J. & Li, D.Z. (1988) Distribution of horizontal frost heaving forces on test retaining wall. In *Proceedings, Fourth Chinese Conference on Glaciology & Geocryology* pp. 108–113. (in Chinese).

Sullivan, W.R., Reese, L.C. & Fenske, C.W. (1979) Unified method for analysis of laterally loaded piles in clay. In *Conference on Numerical Methods in Offshore Piling*, Institution of Civil Engineers, London, pp. 135–146.

Suzuki, Y., Taye, Y., Tokimatsu, K. & Kubota, Y. (1995). Correlation between CPT Data and Dynamic Properties of In-Situ Frozen Samples. Proceedings of the Third International Conference on Recent Advances in Geotechnical Earthquake Engineering and Soil Dynamics, St. Louis, Missouri, April 2–7, 1995. Prakash, Shamsher (Ed.). University of Missouri Rolla, 1995, Vol. 1, pp. 249–252.

Swan, R.H., Bonaparte, R., Bachus, R.C., Rivette, C.A. & Spikula, D.R. (1991) Effect of soil compaction conditions on geomembrane–soil interface strength. *Geotextiles & Geomembranes*, **10**(5): 523–529.

Swane, I.C. & Poulos, H.G. (1984) Shakedown analysis of laterally loaded pile tested in stiff clay. In *Proceedings, Fourth Aust–NZ Conference* on Geomechanics, Perth, Vol. 1, pp. 165–169.

Swedish Geotechnical Society (1995) *CPT'95: Proceedings, International Symposium on Cone Penetration Testing*, October 4–5, Linkoping, Sweden, Vols 1–3, Swedish Geotechnical Institute.

Swedish Road Board (1974) *Bankpälming, särtryck ur verksamhetshan doken, (Embankment Piles)*, Report TV121, Au 110:1 kap 4.2.8.06 och del ii kap 4.3.1 Sweden (in Swedish).

Sy, A. (1996) Pile Dynamics and impact *in-situ* penetration tests. *Canadian Geotechnical Journal*, **34**(6): 952–973.

Sy, A. & Campanella, R.G. (1991a) Wave equation modelling of the SPT. In *Proceedings, ASCE Geotechnical Engineering Congress 1991*, Boulder, CO, Geotechnical Special Publication No. 27, Vol. 1, pp. 225–240.

Sy, A. & Campanella, R.G. (1991b) An alternative method of measuring SPT energy. *Proceedings, Second International Conference on Recent Advances in Geotechnical Engineering & Soil Dynamics*, St Louis, MO, Vol 1, pp. 499–505.

Sy, A & Campanella, R.G. (1992a) Dynamic performance of the Becker hammer and penetration test. In *Proceedings, 45th Canadian Geotechnical Conference*, Toronto, Ontario, Paper 24.

Sy, A. & Campanella, R.G. (1992b) Dynamic measurements of the Becker penetration test with implications for pile driving analysis. In *Proceedings, Fourth International Conference on the Application of Stress-Wave Theory to Piles*. The Hague, The Netherlands, A.A. Balkema Publishers, Rotterdam, pp. 471–478.

Sy, A. & Campanella, R.G. (1994) Becker and standard penetration tests (BPT–SPT) correlations with consideration of casing friction. *Canadian Geotechnical Journal*, **31**: 343–356.

TAC (1997) *Pavement Design and Management Guide*, Transportation Association of Canada, Ottawa, Ontario.

TAI (1983) *Asphalt Overlays for Highways and Streets*, Manual Series No. 17, The Asphalt Institute, Lexington, KY.

TAI (1987a) *Soil Manual*, Asphalt Institute Manual Series No. 10, The Asphalt Institute, Lexington, KY.

TAI (1987b) *Asphalt Pavements for Air Carrier Airports*, Manual Series No. 11, The Asphalt Institute, Lexington, KY.

TAI (1988) *The Asphalt Handbook*, Manual Series No. 4, The Asphalt Institute, Lexington, KY.

TAI (1991a) *Thickness Design – Asphalt Pavements for Highways and Streets*, Manual Series No. 1, The Asphalt Institute, Lexington, KY.

TAI (1991b) *Computer Program CP-4 Thickness Design of Highways and Overlays (HWY)*, The Asphalt Institute, Lexington, KY.

Tajimi, H (1969) Dynamic analysis of a structure embedded in an elastic stratum. In *Proceedings Fourth World Conference on Earthquake Engineering*, Chile, Vol. III, 53–69.

Takahashi, T. (1991) *Debris flow*, Balkema, Rotterdam.

Tarbuck, E.J. & Lutgens, F.K. (1996) *Earth–An Introduction to Physical Geology*, 5th Edn, Prentice Hall, Upper Saddle River, NJ.

TA Siedlungsabfall (1993) Technische anleitung zur verwertung, behandlung und sonstigen entsorgung von Siedlungsabfallen, bundesanzeiger.

Task Force No. 27 (1991) *Guidelines for the Design of Mechanically Stabilized Earth Walls*, AASHTO–AGC–ARTBA Joint Committee, Washington, DC.

Tatsuoka, F. & Kohata, Y. (1994) Stiffness of hard soils and soft rock in engineering applications. In Shibuya, S., Mitachi, T. & Miura S. (Eds) *Proceedings, First International Conference on Pre-Failure Deformation Characteristics of Geomaterials*, Sapporo, Japan, Balkema, Rotterdam, Vol. 2, pp. 947–1063.

Tavenas, F. & Leroueil, S. (1977) Effects of stresses and time on yielding of clays. In *Proceedings, Ninth International Conference on Soil Mechanics & Foundation Engineering*, Tokyo, Vol. 1, pp. 319–326.

Tavenas, F. & Leroueil, S. (1980) The behaviour of embankments on clay foundations. *Canadian Geotechnical Journal*, **17**(2): 236–260.

Tavenas, F. & Leroueil, S. (1981) Creep and failure of slopes in clays. *Canadian Geotechnical Journal*, **18**(1): 106–120.

Tavenas, F. & Leroueil, S. (1987) State-of-the-art on laboratory and *in-situ* stress–strain–time behavior of soft clays. In *Proceedings, International Symposium on Geotechnical Engineering of Soft Soils*, Mexico City, pp. 1–46.

Tavenas, F., Blanchette, G., Leroueil, S., Roy, M. & LaRochelle, P. (1975) Difficulties in the *in-situ* determination of K_0 in soft sensitive clays. In *Proceedings, ASCE Geotechnical Engineering Division Specialty Conference on*, In-Situ *Measurement of Soil Properties*, June 1–4, North Carolina State University, Raleigh, NC, Vol. 1 pp. 450–476.

Tavenas, F., Blanchet, R., Garneau, R. & Leroueil, S. (1978) The stability of stage-constructed embankments on soft clays. *Canadian Geotechnical Journal*, **15**(2): 283–305.

Tavenas, F., Mieussens, C. & Bourges, F. (1979) Lateral displacements in clay foundations under embankments. *Canadian Geotechnical Journal*, **16**(3): 532–550.

Tavenas, F., Trak, B. & Leroueil, S. (1980) Remarks on the validity of stability analyses. *Canadian Geotechnical Journal*, **17**(1): 61–73.

Tavenas, F., Flon, P., Leroueil, S. & Lebuis, J. (1983a) Remolding energy and risk of slide retrogression in sensitive clays. *Symposium on Slope Stability*, Linköping, Sweden, SGI Report No. 17, pp. 423–454.

Tavenas, F., Jean, P., Leblond, P. & Leroueil, S. (1983b) The permeability of natural clays, Part II: permeability characteristics. *Canadian Geotechnical Journal*, **20**(4): 645–660.

Tawfig, K.S., Aggour, M.S. & Al-Sanad, H. (1988) Dynamic properties of cohesive soils from impulse testing. In *Proceedings, Ninth World*

Conference on Earthquake Engineering, Tokyo, Vol. 3, pp. 11–16.

Taylor, D.W. (1948) *Fundamentals of Soil Behavior*, Wiley, New York.

Taylor, M.B. & Erikson, J.S. (1996) Accelerated site characterization. *ASTM Standardization News*, **June**: 34–39.

Tchepak, S. (1997) Private communication.

Tchobanoglous, G., Theisen, H. & Vigil, S. (1993) *Integrated Solid Waste Management*, McGraw-Hill, New York.

Tedd, P., Powell, J.J.M., Charles, J.A. & Uglow, I.M. (1990) *In-situ* measurement of earth pressure using push-in-spade-shaped pressure cells–10 years experience. In *Proceedings, Conference on Geotechnical Instrumentation in Practice*, April 1989, Nottingham, Thomas Telford, London, pp. 701–715.

Terzaghi, K. (1923) Die Berechnung der Durchlassigkeitziffer des Tones aus dem Verlauf der hydrodynamischen Spannungserscheinungen. Original paper published in 1923 and reprinted in *From Theory to Practice in Soil Mechanics*, Wiley, New York, pp. 133–146.

Terzaghi, K. (1925) *Erdbaumechanik auf bodenphysikalischer*, Grundlag, Franz Deuticke, Vienna.

Terzaghi, K. (1943) *Theoretical Soil Mechanics*, Wiley, New York.

Terzaghi, K. & Peck, R.B. (1967) *Soil Mechanics in Engineering Practice*, 2nd Edn, Wiley, New York.

Terzaghi, K., Peck, R.B. & Mesri, G. (1996) *Soil Mechanics in Engineering Practice*, 3rd Edn, Wiley, New York.

Thevanayagam, S. & Nesarajah, S. (Eds) (1996) *International Workshop on Technology Transfer for Vacuum-Induced Consolidation: Engineering and Practice*, Report of a workshop sponsored by the National Science Foundation, Port of Los Angeles, and ISSMFE TC-17, Los Angeles, CA.

Thevanayagam, S., Kavananjian, E., Jacob, A. & Juran, I. (1994) Prospects of vacuum-assisted consolidation for ground improvement of coastal and offshore fills. In Rollins, K.M. (Ed.) In Situ *Deep Soil Improvement*, Special Publication 45, American Society of Civil Engineers, ASCE Press, Reston, VA, pp. 90–105.

Thibodeaux, L.J. (1996) *Environmental Chemodynamics: Movement of Chemicals in Air, Water & Soil*, 2nd Edn, Wiley, New York.

Thiel, R.S. (1997) Discussion of 'Field evaluation of protective covers for landfill geomembrane liners under construction loading' by Reddy *et al. Geosynthetics International*, **4**(5): 543.

Thomas, R.W. & Ancelet, C.R. (1993) The effect of temperature, pressure and oven aging on the high pressure oxidative induction time of different types of stabilizers. In *Geosynthetics '93*, Nashville, TN, IFAI, Roseville, MN, pp. 915–924.

Thombre, M.S., Thomson, B.M. & Barton, L.L. (1997) Use of a permeable biological reaction barrier for groundwater remediation at Uranium Mill Tailings Remedial Action (UMTRA) site. In *Proceedings, International Containment Technology Conference*, February 9–21, St. Petersburg, FL, US Department of Energy/ Dupont Company/US Environmental Protection Agency, pp. 744–750.

Thompson, F.L. & Tyler, S.W. (1984) *Comparison of Two Groundwater Flow Models–UNSATID & HELP*, EPRI CS-3695, Electric Power Research Institute, Palo Alto, CA.

Thompson, R.W. (1997) Evaluation protocol for repair for residences damaged by expansive soils. In Houston, S.L. & Fredlund, D.G. (Eds) *Unsaturated Soil Engineering Practice*, Geotechnical Special Publication No. 68, American Society of Civil Engineers, Reston, VA, pp. 255–276.

Thomson, J. (1993) *Pipejacking and Microtunnelling*, Blackie Academic Publishers, Glasgow.

Thornthwaite, C.W. & Mather, J.R. (1955) The water balance. *Publications in Climatology*, **8**(1): 104.

Thornthwaite, C.W. & Mather, J.R. (1957) Instructions and tables for computing potential evapotranspiration and the water balance. *Publications in Climatology*, **10**(3): 185–311.

Ting, J.M. & Scott, R.F. (1984) Static and dynamic lateral pile group action. In *Proceedings, Eighth World Conference on Earthquake Engineering*, San Francisco, Vol. III, pp. 641–648.

Tognon, A.R., Rowe, R.K. & Moore, I.D. (1999) *Large Scale Testing of Geomembrane Protection Layers*, GEOT-16-99, Faculty of Engineering Science, University of Western Ontario, London, Canada.

Tokimatsu, K. & Seed, H.B. (1987) Evaluation of settlements in sands due to earthquake shaking. *Journal of Geotechnical Engineering, ASCE*, Reston, VA, **113**(8):861–879.

Tomlinson, D.W., Thomson, N.R. & Johnson, R.L. (1997) Performance assessment of *in situ* air sparging for the removal of tetrachloroethylene from a mildly heterogeneous sand aquifer.

In *Proceedings, 1997 Petroleum Hydrocarbons & Organic Chemicals in Ground Water: Prevention, Detection & Remediation*, November 12–14, Houston, TX, API/AGWA.

Tomlinson, M.J. (1957) The adhesion of piles driven into clay soils. In *Proceedings, Fourth International Conference on Soil Mechanics & Foundation Engineering*, London, England, Vol. 2, pp. 66–71.

Tomlinson, M.J. (1977) *Pile Design and Construction*, Viewpoint London, England.

Tomlinson, M.J. (1986) *Foundation Design and Construction*, 5th Edn., Longman, Harlow, England.

Tomlinson, M.J. (1995) *Foundation Design and Construction*, 6th Edn., Longman, Harlow, England.

Tòth, P.S. (1993) *In situ* soil mixing. In Moseley, M.P. (Ed.) *Ground Improvement*, Blackie Academic & Professional, Blackwood, NJ, pp. 193–204.

Trak, B., La Rochelle, P., Tavenas, F., Leroueil, S. & Roy, M. (1980) A new approach to the stability analysis of embankments on sensitive clays. *Canadian Geotechnical Journal*, **17**(4): 526–544.

Trast, J. & Benson, C.H. (1995) Estimating field hydraulic conductivity at various effective stresses. *Journal of Geotechnical Engineering, ASCE*, Reston, VA, **121**(10): 736–740.

Trautmann, C.H. & O'Rourke, T.D. (1985) Lateral force–displacement response of buried pipe. *Journal of Geotechnical Engineering, ASCE*, Reston, VA, **111**(9): 1077–1092.

Trautmann, C.H., O'Rourke, T.D. & Kulhawy, F.H. (1985) Uplift force–displacement response of buried pipe. *Journal of Geotechnical Engineering, ASCE*, Reston, VA, **111**(9): 1061–1076.

TRB (1986) *Shared Experience in Geotechnical Engineering: Wick Drains*, Transportation Research Circular No. 309, Transportation Research Board, Washington, DC.

TRB (1998) Transportation Research Board, *Catalog of Current State Pavement Design Features*, NCHRP Project 1–32 Report, Transportation Research Board, Washington, DC, (CD-ROM only).

Trochanis, A.M., Bielak J. & Christiano, P. (1988) *A Three-Dimensional Nonlinear Study of Piles Leading to the Development of a Simplified Model*, Technical Report, Grant No. ECE-86/1060, Carnegie Mellon University, Pittsburg, PA, USA.

Trochanis, A.M., Bielak, J. & Christiano, P. (1991) Three-dimensional nonlinear study of piles. *Journal of Geotechnical Engineering, ASCE*, Reston, VA, **117**(3): 429–447.

Trow, W.A. & Lo, K.Y. (1989) Horizontal displacements induced by rock excavation: Scotia Plaza, Toronto. *Canadian Geotechnical Journal*, **26**: 114–121.

Turner, A.K. & Schuster, R.L. (1996) *Landslides: Investigation and Mitigation*, Special Report 247, Transportation Research Board, Washington, DC.

Turner, M.J. (1997) *Integrity Testing in Piling Practice*, Report 144, Construction Industry Research and Information Association (CIRIA), London, England.

Tuzuki, M., Inada, O. & Yamagishi, M. (1992) Field testing and analysis of dynamic loaded pile group. In *Proceedings, 10th World Conference on Earthquake Engineering*, Madrid, Spain, Vol. 3, pp. 1787–1790.

Udell, K.S. (1996) Thermal treatment of low permeability soils using electrical resistance heating. In In situ *Remediation of DNAPL Compounds in Low Permeability Media: Fate/Transport*, In Situ *Control Technologies & Risk Reduction*, Siegrist, R.L. & Walden, T.L., (Eds.) ORNL/TM-13305, Oak Ridge National Laboratory, Oak Ridges, TN, pp. **15**: 1–18.

Udell, K.S. (1997) Thermally enhanced removal of liquid hydrocarbons contaminants from soils & groundwater. In. Ward, C.H., Cherry, J.A. & Scalf, M.R. (Eds.) *Subsurface Restoration*, Ann Arbor Press, Chelsea, MI pp. 251–270.

Udoh, F.D. (1991) *Minimization of Infiltration into Mining Stockpiles Using Low Permeability Covers*, Dissertation Proposal, Department of Materials Science & Engineering, University of Wisconsin, Madison, WI.

Ullidtz, P. (1987) *Pavement Analysis*, Elsevier, Amsterdam.

Ullidtz, P. (1998) *Modelling Flexible Pavement Response and Performance*, Polyteknisk Forlag, Anker Engelunds Vej 1, DK-2800, Lyngby, Denmark.

Ulrich, C.M. & Kuhlemeyer, R.L. (1973) Coupled rocking and lateral vibrations of embedded footings. *Canadian Geotechnical Journal*, **10**(2): 145–160.

United States Office of the Federal Register (1994) *Code of Federal Regulations, 40, Protection of the Environment*, National Archives and Records Administration, pp. 260–268.

Urciuoli, G. (1990) *Contributo alla caratterizzazione geotecnica delle frane dell'Appennino*, Report of the Istituto di Tecnica delle Fondazioni e Costruzioni in Terra, Universita di Napoli Federico II.

US Army (1966) *Arctic and Subarctic Construction: Calculation Methods for Determination of Depths of Freeze and Thaw in Soils*, Technical Manual TM5-852-6/AFM 88-19.

US Army (1983) *Dewatering and Groundwater Control*, Army Joint Departments of the Army, the Air Force & Navy, Technical Manual TM-5-818-5/AFM88-5, Chapter 6/NAVFAC P-418, Washington, DC.

USDA-SCS (1985) *National Engineering Handbook, Section 4, Hydrology*, US Government Printing Office, Washington, DC.

USEPA (1984) 40 CFR Part 136 *Guidelines Establishing Test Procedures for the Analysis of Pollutants Under the Clean Water Act*, October 26, and all subsequent revisions (Federal Register). United States Government Printing Office, Pittsburg, PA.

USEPA (1985) *Modelling Remedial Actions at Uncontrolled Hazardous Waste Sites*, EPA/540/2-85/001.

USEPA (1986a) *RCRA Ground-Water Monitoring Technical Enforcement Guidance Document*, OSWER-9950.1.

USEPA (1986b) *Superfund Health Evaluation Manual*, EPA/540-1-86.

USEPA (1986c) *Test Methods for Evaluating Solid Waste, Physical/Chemical Methods*, 3rd Edn, November (with all subsequent revisions).

USEPA (1987) *A Compendium of Superfund Field Operations Methods*, EPA/540/P-87/001.

USEPA (1989a) *Seminar Publication: Transport and Fate of Contaminants in Subsurface*, EPA/625/4-89/019.

USEPA (1989b) *Integrated Risk Information System (IRIS) Database*, Office of Research & Development.

USEPA (1989c) *RCRA Facility Guidance*, Vols I–IV, EPA/530/SW-89/031.

USEPA (1989d) *Methods for Evaluating Attainment of Cleanup Standards*, Vol. 1, *Soils and Solids Media*, EPA/230/2-89/042.

USEPA (1989e) *Statistical Analysis of Groundwater Monitoring Data at RCRA Facilities*, Interim Final Guidance, Office, of Solid Waste, EPA/530/SW-89/026.

USEPA (1989f) *Risk Assessment Guidance for Superfund*, Vol. 1, *Human Health Evaluation Manual*, Part A, Environmental Protection Agency, Washington, DC.

USEPA (1990) *Guidance for Data Usability in Risk Assessment–Interim Final*, EPA/540/G-90/008.

USEPA (1991a) *Design and Construction of RCRA/CERCLA Final Covers*, EPA/625/4-91/025, US. Environmental Protection Agency, Office of Research & Development, Washington, DC.

USEPA (1991b). *Site Characterization for Subsurface Remediation*, Seminar Publication, EPA/625/4-91/026, Office of Emergency & Remedial Response, Washington, DC.

USEPA (1991c) *Compendium of ERT Groundwater Sampling Procedures*, EPA/540-91.007.

USEPA (1992a) *RCRA Ground-Water Monitoring: Draft Technical Guidance*, EPA/530-R-93-001, Office of Solid Waste, US Environmental Protection Agency, Washington, DC.

USEPA (1992b) *Bioremediation of Hazardous Wastes*, EPA/600/R-92/126, Office of Research & Development, Washington, DC.

USEPA (1992c) *Statistical Analysis of Ground-Water Monitoring Data at RCRA Facilities: Addendum to Interim Final Guidance*, Office of Solid Waste, Washington, DC. Draft.

USEPA (1992d) *Dense Non-Aqueous Phase Liquids–A Workshop Summary*, April 16–18, 1991, Dallas, TX, EPA/600/R-92/030, US Environmental Protection Agency, Washington, DC.

USEPA (1993a) *Solidification/Stabilization and its Application to Waste Materials*, Technical Resource Document, EPA/530-R-93/012, office of Research & Development, Washington, DC.

USEPA (1993b) *Remediation Technologies Screening Matrix and Reference Guide. Solid Waste & Emergency Response* (OS-110W), EPA-542-B-93-005.

USEPA (1994) *Evaluation of Technologies for* In situ *Cleanup of DNAPL Contaminated Sites*, EPA/600/R-94/120, Office of Research & Development, Washington, DC.

USEPA (1996) *Enabling Document for the New Source Performance Standards and Emissions Guidelines for Municipal Solid Waste Landfills*, EPA-453/R-96-004, US Environmental Protection Agency, Atmospheric Pollution Prevention Division, Washington, DC.

USEPA (1997) *Framework for Environmental Health Risk Management*, Presidential/Congressional Commission on Risk Assessment & Risk Management, Final Report, Vol. 1.

USEPA (1998) *Evaluation of Subsurface Engi-*

neered Barriers at Waste Sites, EPA 542-R-98-005, Office of Solid Waste & Emergency Response (5102G).

USEPA (2000) Technical Guidance for RCRA/CERCLA Final Covers, US Environmental Protection Agency Superfund Office, Washington, DC (in preparation).

USEPA *ILM04.0 USEPA Contract Laboratory Program (CLP) Statement of Work (SOW) for Inorganic Analysis.*

USEPA, *OLM03.2. USEPA Contract Laboratory Program (CLP) Statement of Work (SOW) for Organic Analysis.*

US Navy (1983) *Soil Dynamics, Deep Stabilization, and Special Geotechnical Construction*, Design Manual 7.3, Naval Facilities Engineering Command, Alexandria, VA.

Uthayakumar, M. & Vaid, Y.P. (1998) Static liquefaction of sand under multiaxial loading. *Canadian Geotechnical Journal*, **35**(2): 273–283.

Vaid, Y.P. & Chern, J.C. (1985) Cyclic and monotonic undrained response of saturated sands. *Advances in the Art of Testing Soils Under Cyclic Conditions*, American Society of Civil Engineers, Reston, VA, 120–147.

Vaid, Y.P. & Negussey, D. (1988) *Preparation of Reconstituted Sand Specimens*, Advanced Triaxial Testing of Soils & Rock, ASTM STP 977, American Society for Testing & Materials, West Conshohocken, PA, pp. 405–417.

Vaid, Y.P. & Sivathayalan, S. (1996) Static and cyclic liquefaction potential of Fraser Delta sand in simple shear and triaxial tests. *Canadian Geotechnical Journal*, **33**(2): 281–289.

Vaid, Y.P. & Thomas, J. (1994) Post liquefaction behaviour of sand. In *Proceedings, 13th International Conference on Soil Mechanics & Foundation Engineering*, New Delhi, India.

Vaid, Y.P., Sivathayalan, S. & Stedman, D. (1999) Influence of specimen reconstituting method on the undrained response of sand. *ASTM Geotechnical Testing Journal*, West Conshohocken, PA, **22**(3): 187–195.

Vaid, Y.P., Stedman, D. & Sivathayalan, S. (2000) K_o and K_α factors in cyclic liquefaction. Canadian Geotechnical Journal, submitted.

van Bavel, C.H.M. (1952) Gaseous diffusion and porosity in porous media. *Soil Sciences*, **73**: 91–104.

Van der Molen, W.H. & Van Ommen, H.C. (1988) Transport of solutes in soils and aquifers. *Journal of Hydrology*, **100**: 433–451.

Vanapalli, S.K. (1994) *PhD thesis*, University of Saskatchewan, Saskatoon, Canada.

Vanapalli, S., Fredlund, D.G., Pufahl, D.E. & Clifton, A.W. (1996) Model for the prediction of shear strength with respect to soil suction. *Canadian Geotechnical Journal*, **33**(3): 379–392.

van der Heijde, P.K.M. & Elnawawy, O.A. (1993) *Compilation of Ground-water Models*, EPA/600/2-93/118. Robert S. Kerr, Environmental Research Laboratories, Ada, OK.

Vandevivere, P. & Baveye, P. (1992) Effect of bacterial extracellular polymers on the saturated hydraulic conductivity of sand columns. *Applied & Environmental Microbiology*, **58**: 1690–1698.

van Genuchten, M.Th. (1980) A closed-form equation of predicting the hydraulic conductivity of unsaturated soils. *Soil Science of America Journal*, **44**: 892–898.

Van Impe, W.F. (1989) *Soil Improvement Techniques and their Evolution*, Rotterdam, Balkema, Netherlands.

Van Impe, W.F. (1991) Deformations of deep foundations. In *Proceedings, 10th European Conference on Soil Mechanics & Foundation Engineering*, Florence, Vol. 3, pp. 1031–1062.

Van Olphen, H. (1977) *An Introduction to Clay Colloid Chemistry*, 2nd Edn., Wiley Interscience, New York, 318 p.

Van Weele, A.F. (1957) A method of separating the bearing capacity of a test pile into skin friction and point resistance. In *Proceedings, Fourth International Conference on Soil Mechanics & Foundation Engineering*, London, Vol. 2, pp. 76.

Varnes, D.J. (1978) Slope movement types and processes. In *Landslides: Analysis & Control*, R.L. Schuster & R. Krizek (Eds.) Special Report 176, Transportation Research Board, Washington, DC, pp. 11–33.

Varnes, D.J. & the IAGE Commission on Landslides & Other Mass Movements on Slopes (1984) *Landslide Hazard Zonation–A Review of the Principles and Practice*, UNESCO, Paris.

Veletsos, A.S. & Nair, V.V.D. (1974) Torsional vibration of viscoelastic foundation. *Journal of the Geotechnical Division, ASCE*, Reston, VA, **100**(3): 225–246.

Veletsos, A.S. & Verbic, B. (1973) Vibration of viscoelastic foundations. *Earthquake Engineering & Structural Dynamics*, **2**: 87–102.

Veletsos, A.S. & Wei, Y.T. (1971) Lateral and rocking vibrations of footings. *Journal of Soil Mechanics & Foundations Division, ASCE*, Reston, VA, **97**(9): 1227–1248.

Veletsos, A.S. & Younan, A.H. (1994) Dynamic

soil pressures on rigid vertical walls. *Earthquake Engineering and Structural Dynamics*, **23**: 275–301.

Veletsos, A.S., Parikh, V.H. & Younan, A.H. (1995) Dynamic response of a pair of walls retaining a visco-elastic solid. *Earthquake Engineering and Structural Dynamics*, **24**: 1567–1589.

Vesic, A.S. (1969) *Experiments with Instrumented Pile Groups in Sand*, American Society for Testing & Materials, West Conshohocken, PA, STP 444 pp. 177–222.

Vesic, A.S. (1973) Analysis of ultimate loads of shallow foundations. *Journal of Soil Mechanics & Foundations Division, ASCE*, Reston, VA, **99** (SM1): 45–73.

Vesic, A.S. (1975) Bearing capacity of shallow foundations. In Winterkorn, H.F. & Fang, H.-Y. (Eds) *Foundation Engineering Handbook*, Van Nostrand Reinhold, New York.

Viggiani, C. (1981) Ultimate lateral load on piles used to stabilize landslides. In *Proceedings, 10th International Conference on Soil Mechanics & Foundation Engineering*, Stockholm, Vol. 3, pp. 555–560.

Vink, P. (1986) Loss of UV stabilizers from polyolefins during photo-oxidation. In Scott, G. (Ed.) *Developments in Polymer Stabilization–3*, Applied Science, London, England, pp. 117–138.

Vogel, T.M., Criddle, C.S. & McCarty, P.L. (1987) Transformation of halogenated aliphatic compounds. *Environmental Science & Technology*, **21**: 722–736.

Vrymoed, J. (1975) *Dynamic Analysis of Oroville Dam*, Office Report, Department of Water Resources, State of California.

Vucetic, M. & Dobry, R. (1991) Effect of soil plasticity on cyclic response. *Journal of Geotechnical Engineering, ASCE*, Reston, VA, **117**(1): 89–107.

Waas, G. & Hartmann, H.G. (1981) Pile foundations subjected to dynamic horizontal loads. In *European Simulation Meeting Modelling & Simulation of Large Scale Structural Systems*, Capri, Italy.

Wager, O. & Holtz, R.D. (1976) Reinforcing embankments by short sheet piling and tie rods. In *Proceedings International Symposium on New Horizons in Construction Materials*, Lehigh University, Vol. I, pp. 177–185.

Wagner, A.A. (1957) The use of the Unified Soil Classification System by the Bureau of Reclamation. In *Proceedings, Fourth International Conference on Soil Mechanics & Foundation Engineering*, London, England, Vol. I, pp. 125–134.

Walsh, J.B. (1965) The effect of cracks on the compressibility of rock. *Journal of Geophysical Research*, **70**: 381–389.

Walton, W.C. (1962) *Selected Analytical Methods for Well and Aquifer Evaluation*, State of Illinois, Bulletin No. 49, Urbana, IL.

Ward, C.H. (1996) Introductory talk: Where are we now? Moving to a risk-based approach. In *Symposium on Natural Attenuation of Chlorinated Organics in Groundwater*, September 11–13, Dallas, TX, 540/R-96-509, US Environmental Protection Agency, pp. 1–3.

Ward, W.H., Coates, D.J. & Tedd, P. (1976) Performance of Tunnel Support Systems in the Four Fathom Mudstone Tunnelling, '76 Institution Mining & Metallurgy, London, pp. 329–340.

Wardle, L.J. (1996) *CIRLY User's Manual, Version 3.0*, MINCAD Systems, Richmond, Australia.

Wardle, L.J. & Rodway, B. (1995) Development and application of an improved airport pavement design method. In *1995 Transportation Congress*, San Diego, American Society of Civil Engineers, ASCE Press, Reston VA.

Wardle, L.J. & Rodway, B. (1998a) Layered elastic pavement design–recent developments. In *Proceedings, Transport 98*, ARRB Transport Research, Vermont South, Victoria, Australia.

Wardle, L.J. & Rodway, B. (1998b) Recent developments in flexible aircraft pavement design using the layered elastic method. In *Proceedings, Third International Conference on Road & Airfield Pavement Technology*, Beijing, Vol. 2, Huajie International. pp. 882–890.

Warner, J. (1982) Compaction grouting—the first thirty years. In Baker, W.H. (Ed.) *Proceedings, Grouting in Geotechnical Engineering*, New Orleans, American Society of Civil Engineers, ASCE Press, Reston, VA, pp. 694–707.

Warner, J., Schmidt, N., Reed, J., Shepardson, D., Lamb, R. & Wong, W. (1992) Recent advances in compaction grouting technology. In Borden, R.H. Holtz, R.D. & Juran, I. (Ed.) *Grouting, Soil Improvement & Geosynthetics, Proceedings*, New Orleans, Geotechnical Special Publication No. 30, American Society of Civil Engineers, ASCE Press, Reston, VA, pp. 252–264.

Waterloo Centre For Ground Water Research (1989) Short Course, University of Waterloo,

Dense Immiscible Phase Liquid Contaminants in Porous and Fractured Media, Kitchener, Ontario, Canada.

Watts, K.S. & Charles, J.A. (1988) *In-situ* measurement of vertical and horizontal stress from a vertical borehole. *Géotechnique*, **38**(4): 619–626.

Wayne, M.H. & Koerner, R.M. (1993) Correlation between long term flow testing and current geotextile filtration design practice. In *Proceedings, Geosynthetics '93*, IFAI, Roseville, MN, pp. 501–517.

Weatherby, D.E. (1982) *Tiebacks*, Report No. FHW A/RD-81/047, Federal Highway Administration, Springfield, VA.

Weaver, K. (1991) *Dam Foundation Grouting*, American Society of Civil Engineers, ASCE Press, Reston, VA.

Webb, M.C., McGrath, T.J., Zoladz, G.V. & Selig, E.T. (1995) *Field Test Data from Pipe Installation Study*, Geotechnical Report No. NSF95-438I, Department of Civil & Environmental Engineering, University of Massachusetts, Amherst, MA.

Webb, M.C., Sussmann, J. & Selig, E.T. (1999) *Large Span Culvert Field Test Results*, NCHRP Project 12–45, Department of Civil & Environmental Engineering, University of Massachusetts, Amherst, MA.

Webb, S.W., McCord, J.T. & Dwyer, S.F. (1997) Prediction of tilted capillary barrier performance. In *Proceedings, International Containment Technology Conference*, February, St Petersburg, FL, pp. 296–302.

Weber, Jr, W.G. (1969) Performance of embankments constructed over peat. In *Proceedings, Journal of the Soil Mechanics & Foundations Division, ASCE*, Reston, VA, **95**(1): 53–76.

Well, L.W. (1997) *Testing and Acceptance Criteria for Geosynthetic Clay Liners*, ASTM STP 1308, American Society for Testing Materials, West Conshohocken, PA.

Welsh, J.P. (1986) *In situ* testing for ground modification techniques. In *Proceedings*, In Situ *'86*, Blacksburg, VA, Geotechnical Special Publication No. 6, American Society of Civil Engineers, ASCE Press, Reston, VA, pp. 322–335.

Welsh, J.P. (Ed.) (1987) *Soil Improvement—A Ten Year Update*, Geotechnical Special Publication No. 12, American Society of Civil Engineers, ASCE Press, Reston, VA.

Welsh, J.P., Anderson, R.D., Barksdale, R.P., Satyapriya, C.K., Tumay, M.T. & Wahls, H.E. (1987) Densification. In Welsh, J.P. (Ed.) *Soil Improvement–A Ten Year Update*, Geotechnical Special Publication No. 12, American Society of Civil Engineers, Reston, VA, pp. 67–97.

West, G. (1986) Desk studies, air photograph interpretation and reconnaissance for site investigation. In Hawkins, A.B. (Ed.) *Site Investigation Practice: Assessing BS 5930*, Engineering Geology Special Publication No. 2, Geological Society, London, England, pp. 9–16.

Westergaard, H. (1931) Water pressure on dams during earthquakes. *Transactions of ASCE*, Reston, VA, No. 98 Paper No. 1835: 418–433.

Wheeler, S.J. (1991) Alternative framework for unsaturated soil behavior. *Géotechnique*, **41**(2): 257–261.

Wheeler, S.J. & Sivakumar, V. (1992) Critical state concepts for unsaturated soil. *Proceedings, Seventh International Conference on Expansive Soils*, August 3–5, Dallas, TX, Vol. 1, pp. 167–172.

White, H.L. & Layer, J.P. (1960) The corrugated metal culvert as a compression ring. *Highway Research Board Proceedings*, **39**: 389–397.

White, N.F., Duke, H.R., Sundae, D.K. & Corey, A.T. (1970) Physics of desaturation in porous materials. *Irrigation & Drainage Division, ASCE*, Reston, VA, **96**: 165–191.

Whitman, J. & Christian, J. (1990) Seismic response of retaining structures. In *Symposium Seismic Design for World Port 2020*, Port of Los Angeles, Los Angeles, CA.

Whitman, R.V. (1984) Evaluating calculated risk in geotechnical engineering (17th Terzaghi Lecture). *Journal of Geotechnical Engineering*, **110**(2): 145–188.

Whitman, R. & Liao, S. (1985) *Seismic Design of Retaining Walls*, Miscellaneous Paper GL-85-1, US Army Engineer Waterways Experiment Station, Vicksburg, MS.

Whitman, R.V. & Richart, F.E. Jr (1967) Design procedures for dynamically loaded foundations. *Journal of the Soil Mechanics & Foundations Division, ASCE*, Reston, VA, **93**(6): 169–193.

Whittaker, M., Pollard, S.J.T. & Fallick, A.E. (1995) Characterisation of refractory wastes at heavy oil-contaminated sites: a review of conventional and novel analytical methods. *Environmental Technology*, **16**: 1009–1033.

Whittaker, M., Sprenger, J.G.S. & DuBois, D.D. (1998) Assessing the key components of credible risk assessment at contaminated sites. *Environmental Science & Engineering*, **10**(6): 102–103.

Whittle, R.W. (1996) Recent developments in the cone pressuremeter. In Craig, C. (Ed.) *Proceedings, International Conference on Advances in Site Investigation Practice*, March 30–31, 1995, Thomas Telford, London, England, pp. 533–546.

Whittlestone, A.P. & Ljunggren, C. (1996) A new technique for *in-situ* stress measurement by overcoring. In Craig C. (Ed.) *Proceedings, International Conference Advances in Site Investigation Practice*, March 30–31, 1995, London, Thomas Telford, London, England, pp. 499–509.

Wieczorek, G.F., Lips, E.W. & Ellen, S.D. (1989) Debris flows and hyperconcentrated floods along the Wasatch front, Utah, 1983 & 1984. *Bulletin of the International Association of Engineering Geologists*, **26**(2): 191–208.

Wiedemeier, T.H., Wilson, J.T. Kampbell, D.H., Miller, R.N. & Hansen, J.E. (1995) *Technical Principals of Implementing Intrinsic Remediation with Long-Term Monitoring for Natural Attenuation of Fuel Contamination Dissolved in Groundwater*, US Air Force Center for Environmental Excellence, Technology Transfer Division, Brooks Air Force Base, San Antonio, TX.

Wiedemeir, T.H., Swanson, M.A., Moutoux, D.E., Wilson, J.T., Kampbell, D.H., Hansen, J.E. & Haas, P. (1996a) Overview of technical protocol for natural attenuation of chlorinated aliphatic hydrocarbons in ground water under development for the US Air Force Center of Excellence. In *Symposium on Natural Attenuation of Chlorinated Organics in Groundwater*, September 11–13, Dallas, TX, 540/R-96-509, US Environmental Protection Agency pp. 35–59.

Wiedemeir, T.H., Wilson, J.T. & Kampbell, D.H. (1996b) Natural attenuation of chlorinated aliphatic hydrocarbons at Plattsburgh Air Force Base, New York. In *Symposium on Natural Attenuation of Chlorinated Organics in Groundwater*, September 11–13, Dallas, TX, 540/R-96-509, US Environmental Protection Agency, pp. 65–68.

Wiedemeier, T.H., Swanson, M.A., Moutoux, D.E., Gordon, E.K., Wilson, J.T., Wilson, B.H., Kampbell, D.H., Hansen, J.E., Haas, P. & Chapelle, F.H. (1996) *Technical Protocol for Evaluating Natural Attenuation of Chlorinated Solvents in Groundwater*, Draft Revision 1, Air Force Center for Environmental Excellence, Technology Transfer Division, Brooks Air Force Base, San Antonio, TX.

Wildavsky, A. (1988) *Searching for Safety*, Transaction Publishers, New Brunswick, NJ.

Wilkinson, W.B. (1967) A note on the constant head test to measure soil permeability *in-situ*. *Géotechnique*, **17**(2): 68–71.

Wilkinson, W.B. (1968) Constant head *in-situ* permeability tests in clay strata. *Géotechnique*, **18**(2): 177–194.

Williams, A.F. & Pells, P.J.N. (1981) Side resistance rock sockets in sandstone, mudstone and shale. *Canadian Geotechnical Journal*, **18**(4): 502–513.

Williams, J.G. (1984) *Fracture Mechanics of Polymers*, Ellis Horwood, Ltd, Chichester, England.

Williams, N.D. & Abouzakhm, M.A. (1989) Evaluation of geotextile–soil filtration characteristics using the hydraulic conductivity ratio analysis. *Journal of Geotextiles & Geomembranes*, **8**(1): 1–26.

Williams, N.D. & Houlihan, M.F. (1987) Evaluation of interface friction properties between geosynthetics and soils. In *Proceedings, Geosynthetics '87 Conference*, New Orleans, Industrial Fabrics Association International, Roseville, MN, Vol. 2, pp. 616–627.

Williams, N., Giroud, J.P. & Bonaparte, R. (1984) Properties of plastic nets for liquid and gas drainage associated with geomembranes. In *Proceedings, International Conference on Geomembranes*, June Denver, CO, Vol. 2, pp. 399–404.

Wilson, G.W. (1990) *PhD thesis*, University of Saskatchewan, Saskatoon, Canada.

Wilson, G.W., Fredlund, D.G. & Barbour, S.L. (1994) Coupled soil–atmosphere modeling for evaporation. *Canadian Geotechnical Journal*, **31**(2): 151–161.

Wilson, G.W., Barbour, S.L. & Fredlund D.G. (1997) The effect of soil suction on evaporative fluxes from soil surfaces. *Canadian Geotechnical Journal*, **33**(4): 145–155.

Wilson, J.L. & Conrad, S.H. (1984) Is physical displacement of residual hydrocarbons a realistic possibility in aquifer restoration? In *Proceedings, NWWA/API Conference on Petroleum Hydrocarbons & Organic Chemicals in Groundwater–Prevention, Detection, & Restoration*, National Water Well Association, Dublin, OH, pp. 274–298.

Wilson, R.D. & Mackay, D.M. (1995) A method for passive release of solutes from an unpumped well. *Ground Water*, **33**(6): 936–945.

Wilson, R.D., Mackay, D.M. & Cherry, J.A.

(1997) Arrays of unpumped wells for plume migration control by semi-passive *in situ* remediation. *Ground Water Monitoring & Remediation*, **17**(3): 185–193.

Wilson-Fahmy, R.F. & Koerner, R.M. (1992) *Stability Analysis of Multi-Lined Slopes in Landfill Applications*, GRI Report No. 8, Geosynthetic Research Institute, Drexel University.

Wilson-Fahmy, R.F. & Koerner, R.M. (1993) Finite element analysis of stability of cover soil on geomembrane-lined slopes. In *Proceedings, Geosynthetics '93 Conference*, February Vancouver, BC, Industrial Fabrics Association International, Roseville, MN, Vol. 3, pp. 1425–1438.

Wilson-Fahmy, R.G., Koerner, R.M. & Fleck, J.A. (1993) Unconfined and confined wide width testing of geosynthetics. In Cheng, S.J. (Ed.) *ASTM STP 1190*, American Society for Testing & Materials, West Conshohocken, PA, pp. 44–63.

Wilson-Fahmy, R.F., Narejo, D. & Koerner, R.M. (1996) Puncture protection of geomembranes. Part I: theory. *Geosynthetics International*, **3**(5): 605–628.

Winterkorn, H.F. & Pamukcu, S. (1991) Soil stabilization and grouting. In Fang, H.Y. (Ed.) *Foundation Engineering Handbook*, Van Nostrand Reinhold, New York, NY, pp. 317–378.

Wolf, J.P. (1995) *Foundation Vibration Analysis Using Simple Physical Models*, Prentice-Hall, Englewood Cliffs, NJ.

Wolf, J.P. & Darbre, G.R. (1984) Dynamic-stiffness matrix of soil by the boundary-element method: embedded foundations. *Earthquake Engineering & Structural Dynamics*, **12**: 401–416.

Wolf, J.P. & Darbre, G.R. (1986) Nonlinear soil–structure interaction analysis based on the boundary-element method in time domain with application to embedded foundation. *Earthquake Engineering & Structural Dynamics*, **14**: 83–101.

Wolf, J.P. & von Arx, G.A. (1978) Impedance functions of a group of vertical piles. In *Proceedings, ASCE Specialty Conference on Earthquake Engineering & Soil Dynamics*, Pasadena, CA, Vol. II, pp. 1024–1041.

Wolf, J.P., von Arx, G.A., de Barros, F.C.P. & Kakubo, M. (1981) Seismic analysis of the pile foundation of the reactor building on the NPP Angra 2. *Nuclear Engineering & Design*, **65**(3): 329–341.

Wolf, J.P., Meek, J.W. & Song, Ch. (1992) Cone models for a pile foundation. In Prakash, S. (Ed.) *Piles Under Dynamic Loads*, Geotechnical Special Publication No. 34, American Society of Civil Engineers, Reston, VA, pp. 94–113.

Wong, L.C. & Haug, M.D. (1991) Cyclical closed-system freeze–thaw permeability testing of soil liner & cover materials. *Canadian Geotechnical Journal*, **28**(6): 784–793.

Wood, D.M. (1990) *Soil Behaviour and Critical State Soil Mechanics*, Cambridge University Press, Cambridge, England.

Wood, D.M., Jendele, L., Chan, A.H.C. & Cooper, M.R. (1995) Slope failure by pore pressure recharge: numerical analysis. In *Proceedings, 11th European Conference on Soil Mechanics & Foundation Engineering*, Copenhagen, Vol. 6, pp. 1–8.

Wood, J. (1973) *Earthquake-induced Soil Pressures on Structures*, Report No. EERL 73-05, California Institute of Technology, Pasadena, CA.

Wood, W.W. (1996) Diffusion: the source of confusion. *Ground Water*, **34**(2): 193.

Woods, R.I. & Jewell, R.A. (1990) A computer design method for reinforced soil structures. *Geotextiles & Geomembranes*, **9**(3): 233–259.

Woodward, R., Gardner, W.S. & Greer, D.M. (1972) *Drilled Pier Foundations*, McGraw Hill, New York.

Worotnicki, G. & Walton, R.J. (1976) Triaxial 'hollow inclusion' gauges for the determination of rock stress *in situ*. *Proceedings, ISRM Symposium on Investigation of Stress in Rock & Advances in Shear Measurement*, Sydney supplement, pp. 1–8.

Woyshner, M.R. & Yanful, E.K. (1995) Modelling and field measurements of water percolation through an experimental soil cover on mine tailings. *Canadian Geotechnical Journal*, **32**(4): 601–609.

Wright, S.G. (1991) *UTEXAS3—A Computer Program for Slope Stability Calculations*, Department of Civil Engineering, University of Texas, Austin, TX.

Wroth, C.P. (1984) The interpretation of *in-situ* soil tests, 24th Rankine Lecture. *Géotechnique*, **34**: 449–489.

Wroth, C.P. (1988) Penetration testing – a more rigorous approach to interpretation. In De-Ruiter, J. (Ed.) *Proceedings First International Symposium on Penetration Testing*, ISOPT-1, Orlando, FL, Vol. 1, A.A. Balkema, Rotterdam, pp. 303–311.

Wroth, C.P. & Wood, D.M. (1978) The correla-

tion of index properties with some basic engineering properties of soils. *Canadian Geotechnical Journal*, **15**(2): 137–145.

Wu, G. & Finn, W.D.L. (1996) Seismic pressure against rigid walls. In *Analysis and Design of Retaining Structures Against Earthquakes*, Geotechnical Special Publication No. 60, American Society of Civil Engineers, Reston, VA, pp. 1–19.

Wu, G. & Finn, W.D.L. (1999) Seismic lateral pressures for the design of rigid walls. *Canadian Geotechnical Journal*, **36**(3): 509–522.

Wu, T.H. (1976) *Soil Mechanics*, Allyn & Bacon, Boston, MA.

Wyllie, D.C. (1992) *Foundations on Rock*, Chapman & Hall, London, England.

Wyllie, D.C. & Norrish, N.I. (1996a) Rock strength properties and their measurement. In *Landslides—Investigation and Mitigation*, Special Report 247, Turner, A.K. & Schuster, R.L. (Eds.) Transportation Research Board, Washington, DC, pp. 372–390.

Wyllie, D.C. & Norrish, N.I. (1996b) Stabilization of rock slopes. In *Landslides – Investigation & Mitigation*, Special Report 247, Turner, Transportation Research Board, Washington, DC, Turner, A.K. & Schuster, R.L. (Eds.) pp. 473–504.

Wyss, M. (1979) Estimating Maximum Expectable Magnitude of Earthquakes from Fault Dimensions, *Geology* 7: 336–340.

Yan, L., Matasovic, N. & Kavazanjian, E., Jr. (1996) *YSLIPPM_A Computer Program for Simulation of Dynamic Behaviour of a Rigid Block on an Inclined Plane and Calculation of Permanent Displacements of the Block, User's Manual*, GeoSyntec Consultants, Huntington Beach, CA.

Yanful, E.K. (1993) Oxygen diffusion through soil covers on sulphidic mill tailings. *Journal of Geotechnical Engineering, ASCE*, Reston, VA, **119**(8): 1207–1228.

Yanful, E.K. & Aubé, B. (1993) Modelling moisture-retaining soil covers. In *Proceedings, Joint Canadian Society of Civil Engineers—American Society of Civil Engineers National Conference on Environmental Engineering*, Montreal, Canada, pp. 273–280.

Yanful, E.K., Nesbitt, H.W. & Quigley, R.M. (1988) Heavy metal migration at a landfill site, Sarnia, Ontario, Canada – I. Thermodynamic assessment and chemical interpretations. *Applied Geochemistry*, **3**: 522–533.

Yanful, E.K., Bell, A.V. & Woyshner, M.R. (1993a) Design of a composite soil cover for an experimental waste rock pile near Newcastle, New Brunswick, Canada. *Canadian Geotechnical Journal*, **30**(4): 578–587.

Yanful, E.K., Riley, M.D., Woyshner, M.R. & Duncan, J. (1993b) Construction and monitoring of a composite soil cover on an experimental waste rock pile near Newcastle, New Brunswick, Canada. *Canadian Geotechnical Journal*, **30**(4): 588–599.

Yang, D.S. (1994) The applications of soil mix walls in the United States. *Geotechnical News*, **12**(4): 44–47.

Yang, D.S. & Takeshima, S. (1994) Soil mix walls in difficult ground. In In-Situ *Deep Soil Improvement*, Geotechnical Special Publication No. 45. K.M. Rollins (Ed.) American Society of Civil Engineers, ASCE Press, Reston, VA, 106–120.

Yang, D.S., Yagihashi, J.N. & Yoshizawa, S.S. (1998) Swing method for deep mixing. In *Soil Improvement for Big Digs*, Geotechnical Special Publication No. 81, A. Maher & D.S. Yang (Eds.) American Society of Civil Engineers, pp. 111–121, ASCE Press, Reston, VA.

Yasuda, S., Ishihara, K., Harada, K. & Shinkawa, N. (1996) Effectiveness of the ground improvement on the susceptibility of liquefaction observed during the 1995 Hyogoken Nanbu (Kobe) earthquake. In *Proceedings, 11th World Conference on Earthquake Engineering*, Mexico.

Yaws, C.L. (1995) *Handbook of Transport Property Data*, Gulf Publishing Company, Houston, TX.

Yegian, M.K. & Lahalf, A.M. (1992) Dynamic interface shear strength properties of geomembranes & geotextiles. *Journal of Geotechnical Engineering, ASCE*, Reston, VA, **118**(5): 760–779.

Yegian, M.K., Yee, Z.Y. & Harb, J.N. (1995) Seismic response of geosynthetic–soil systems. In *Geoenvironment 2000*, Geotechnical Special Publication No. 46, Acar, Y.B. and Daniel, D.E. (Eds.) American Society of Civil Engineers, Reston, VA, Vol. 2, pp. 1113–1125.

Yeung, A.T.-C. & Mitchell, J.K. (1992) Coupled fluid, chemical, and electrical flows in soil. *Géotechnique*, **43**(4).

Yim, G. & Godin, M. (1993) Long-term heat aging stabilization study of polyethylene and its relationship with oxidative induction time (OIT). In *Geosynthetics '93*, Nashville, TN, IFAI, Roseville, MN, pp. 803–816.

Yong, R.N. (1985) Interaction of clay and industrial waste: a summary review. In Hitchon B. & Trudell, M. (Eds) *Second Canadian/American Conference on Hydrogeology*, National Water Well Association, Westerville, OH, pp. 13–25.

Yood, T.L. & Idris, I. (Eds) (1997) *Proceedings, NCEER Workshop on Evaluation of Liquefaction Resistance of Soils*, Technical Report, NCEER-7-0022.

Yoshida, R., Fredlund, D.G. & Hamilton, J.J. (1983) The prediction of heave of a slab-on-grade floor on Regina clay. *Geotechnical Journal*, **20**(1): 69–81.

Yoshimi, Y., Hatanaka, M. & Oh-oka, H. (1978) Undisturbed sampling of saturated sands by freezing. *Soils & Foundations*, **18**(3): 59–71.

Yoshimine, M., Ishihara, K. & Vargas, W. (1998) Effect of principal stress direction and intermediate principal stress on undrained shear behaviour of sand, *Soils & Foundations*, **38**(3): 179–188.

Youd, T.L. (1973) Factors controlling maximum and minimum densities of sands. In *Evaluation of Relative Density and Its Role in Geotechnical Projects Involving Cohesionless Soils*, ASTM STP 523, American Society for Testing & Materials, West Conshohocken, PA, (Eds.) E.T. Selig and R.S. Ladd, pp. 98–112.

Youd, T.L. & Noble, S.K. (1998) Magnitude scaling factors. In Youd, T.L. (Ed.) *Draft Report, NCEER Workshop on Evaluation of Liquefaction Resistance*, Brigham Young University, Provo, UT.

Young, O.C. & Trott, J.J. (1984) *Buried Rigid Pipes: Structural Design of Pipelines*, Elsevier, London, England.

Youngs, R.R., Chiou, S.-J., Silva, W.J. & Humphrey, J.R. (1997) Strong motion attenuation relationships for subduction zone earthquakes. *Seismological Research Letters*, **68**(1): 58–73.

Yu, P. & Richart, F.E., Jr (1984) Stress ratio effects on shear modulus of dry sands. *Journal of Geotechnical Engineering, ASCE*, Reston, VA, **110**(3): 331–345.

Zanzinger, H. & Gartung, E. (1998) Efficiency of puncture protection layers. In Rowe, R.K. (Ed.) *Proceedings, Sixth International Conference on Geosynthetics*, Vol. 1, March, Atlanta, GA, Industrial Fabrics Association International, Roseville, MN, pp. 301–306.

Zar, J.H. (1982) Power and statistical significance impact evaluation. *Ground Water Monitoring Review*, Summer **2**: 33–35.

Zhang, B.Q. & Small, J.C. (1994) Finite layer analysis of soil-raft-structure interaction. In *Proceedings, XIII International Conference on Soil Mechanics & Foundation Engineering*, January 5–10, New Delhi, India, Vol. 2, pp. 587–590.

Zhang, C. & Moore, I.D. (1998) *Finite Element Analysis of Thermoplastic Pipes*, Transportation Research Record No. 1624, pp. 225–230.

Zhang, H., Schwartz, F.W., Wood, W.W., Garabedian, S.P. & LeBlanc, D.R. (1998) Simulation of variable-density flow and transport of reactive and nonreactive solutes during a tracer test at Cape Cod, Massachusetts. *Water Resources Research*, **34**(1): 67–82.

Zienkiewicz, O.C. (1979) *The Finite Element Method*, 3rd Edn, McGraw-Hill, London, England.

Zornberg, J.G. & Caldwell, J.A. (1998) Design of monocovers for landfills in arid locations. In *Third International Conference on Environmental Geotechnics*, ISSMFE, September, Lisbon, (in press).

Zornberg, J.G. & Giroud, J.P. (1997) Uplift of geomembranes by wind—Extension of equations. *Geosynthetics International*, **4**(2): 187–207, Erratum 6(6): 521–522.

INDEX

Page numbers in *italics* indicate figures. Page numbers followed by "t" indicate tables.

A

AASHTO, 379–380, 388
Acetic acid
 diffusion coefficient, 783
 partitioning coefficient, range, 784
Acetone
 diffusion coefficient, 778, 783
 Henry's law constant, 732
 partitioning coefficient, range, 784
ACGIH. *See* American Conference of Governmental Industrial Hygienists
Acid-base reactions, hydrogeology, *730*, 730–731
Acids
 chemical resistance guidelines, 775
 as contaminants, 671
Adjacent structures
 excavations, rock, effect on, 310
 influence on, with trenchless technology, 588
Admixtures, soil stabilization by, 430
Adsorbed water, properties of, 696–697
Advantages, limitations of, 90t
Advection, hydrogeology, 721
Aeration, contamination, 965
Agency for Toxic Substances and Disease Registry, 683
Air
 thermal, soil, 449
 thermal properties, 597
Air-displacement pump, for groundwater sampling, 891
Air Force Total Petroleum Hydrocarbon Criteria Working Group, 683
Airfield pavement, 382–386
 comparative thicknesses, 383–386
 failure, 386
 thickness design, *384*, 384–386, *385*
 types, 383–386
Aitchison's method, censored data analysis, 911–912
Alcohols, chemical resistance guidelines, 775
Aliphatic hydrocarbons, chemical resistance guidelines, 775
Alkalinity, in groundwater analysis, 198
Allophane
 clay, 694
 physicochemistry, 694
Alluvial deposits, soil, 9
Alluvium, shield tip resistance pressure, 576
Aluminum
 as pipe material, 543
 thermal properties, 597
American Conference of Governmental Industrial Hygienists, 683
Ammonia, diffusion coefficient, 783
Amphibole, 148
Analysis of variance, 898, 904–905
Andesite, geological classification, 149
Angular roundness, 45
Anhydrite
 density, 47
 porosity, 713
Aniline, diffusion coefficient, 778, 783
ANOVA, non-parametric, 909–910
Aquifers, hydrogeology, 711–712
Aquitards, 711–712, 751–752
Arching
 buried pipe, *553*, 553–554
 reinforcement over voids, 536
Arenaceous rock, classification, 149
Argillaceous rock, classification, 149
Aromatic hydrocarbons, chemical resistance guidelines, 775
Arsenic, as contaminant, 671
Artificial ground freezing, *448*, 448–449, 449t
Asphalt, 366
Asphalt concrete, 371–372
 thickness, 378
Asphalt Institute method, flexible road pavement technology, 380–382, *381*, *382*
Asphalt layers, 365–366
ATSDR. *See* Agency for Toxic Substances and Disease Registry
Attapulgite
 Atterberg limit, 48
 clay, 694
 density, 47
 physicochemistry, 694
Attenuation of solutes, 729–737
Atterberg limits, 46–48, 47t
 liquid limit, 46–47
Auger boring, 570, 573
Augite, 148
 density, 47
 geological classification, 149
Auto industry, contaminants, 671

B

Backfill selection, buried pipe, 560–561
Bailer, for groundwater sampling, 891
Bark, as fill material, 433
Barrier geocomposites, 188
Barrier systems, 739–824
 collection systems, geotextile "filters" for leachate, *745*, 745–747, 746t
 contaminant impact assessment, 787–788
 diffusion through barriers, 775–785
  clays, intact, compacted, diffusion through, 777–778, 778t
  dissolved-phase diffusion, through porous media, 776–781
 double composite liners, 769
 drainage layers, hydraulic capacity of, *741*, 741–742, 742t
 geomembrane
  diffusion through, 782–785, 783t, 784t
  liners, 768
 geosynthetic clay liners, 761–765
 hydraulic containment, 765–768, *766*, *767*
 leachate collection

drainage material, service life of, 748–751, *749*
pipes, 751
systems
biologically induced clogging, *743*, 743–745, *744*
granular drainage material in, 747–748
liquid migration through, 801–809
liner compatibility with leachate, 770–775
clay-permeant interaction, *771*, 771–772
GCL-permeant interaction, 772–774, 773t, *774*
geomembrane-permeant interaction, 774–775, 775t
liner stability, 788, 810–816
liner systems, 751–770, 789–790
equivalence of, 787–788
liner temperature, 785–786, *786*, 786t
low permeability liners, 751–770
compacted clay liners, 752–761
geological barriers, 751–752
particulate clogging, in drainage layers, 742–743
porous media, gaseous-phase diffusion through, *781*, 781–782
single composite liners, *768*, 768–769
soil-bentonite liners, 761
transmissive layers, 739–751, 790–796
vertical cut-off walls, 769–770
geomembranes, 770
sheet pile walls, 770
slurry trench walls, 769–770
Basalt, geological classification, 149
Base heave, tall building on rock foundation, 310
Bases, as contaminants, 671
Basic soil mechanics, 7–42
BCE. *See* British Columbia Ministry of Environment, Lands and Parks
Beam, vibrated, low permeability barrier, 934
Bearing capacity
shallow foundation, 224–240, *225*
non-uniform soils, 232–240
clay layer, *238*, 239, *239*, 239–240, *240*
fissured clays, *235*, 235–237, *236*
footings on slopes, *237*, 237–238
layered soils, 238–240
strength increasing with depth, *234*, 234–235
finite depth, 235, *235*
infinitely deep, 234–235
uniform soils, 225–232, *226*
base tilt, 230
drained case, *227*, 227–228
finite depth, soil layers, 232, 232t
footing shape, effect of, 228
general formulae, 229–232, 230t, *231*
foundation depth, 230
foundation shapes, 230
inclined loading, 230
net bearing capacity, 228–229
surface slope, 230
Terzaghi's factors, 228
undrained case, 227
unsaturated soil, 140
Becker penetration test, 91
advantages, limitations of, 89
applicability, 88
Behren, Fisher t-test, Cochran's approximation to, 898, 902–903
Bentonite
cement, physical barrier, 960
soil, physical barrier, 960
Benzene
diffusion coefficient, 778, 783
Henry's law constant, 732
partitioning coefficient, range, 784
Berms, 488
Bicarbonate alkalinity, in groundwater analysis, 198
Biopolymer drain, physical barrier, 960
Bioremediation, contamination, 956–958, 965–966
Biotechnical stabilization, slopes, 459
Biotite, 148
density, 47
thermal properties, 597
bis- (2 ethylhexyl)phthalate, Henry's law constant, 732
Bituminous concrete, thermal properties, 597
Bladder pump, for groundwater sampling, 891
Blast densification, 431, 454
Bored shafts, advantages, disadvantages of, 263
Boreholes, sealing of, in site characterization, 86–87
Bottom barriers, source-zone isolation, 937
Boulder, ASTM sieve number, 44
Boundary conditions
evapotranspiration, unsaturated soil, 124–125, *125*
unsaturated soil, 122–125, *123*
evaporation, 124–125, *125*
flux boundary condition, prediction of, 124–125, *125*
BPT. *See* Becker penetration test
Braced excavations, *519*, 519–520, *520*, *521*
Brazilian test, 157–159
Breccia, 149
Bridging, with slope movement, 423
British Columbia Ministry of Environment, Lands and Parks, 683
Brittle material, failure criteria, 164–166
Griffith criterion, *164*, 164–165
Hoek-Brown failure criterion, 165t, 165–166, *166*
BS 8006 method, reinforcement over voids, 537
Buckling, buried pipe, 559–560
Building, tall, on rock foundation, 305–318
adjacent structures, effect of excavations, 310
allowable bearing pressure, 305–309, 307t, *308*, *309*
base heave, 310
bearing capacity, 305, 306t
design considerations, 305–310
differential settlement, 309
Bulk storage depots, contaminants, 671
Buried pipe, 541–568
arching, *553*, 553–554
backfill selection, 560–561
buckling, 559–560
concrete storm sewer, 561–564, 562t
construction loading, 548
deflection, 556–559
design standards, 544t, 545
drainage pipe, polyethylene, 565t, 566t, 566–567, 567t
expirical limits, 556
flexible pipe, classification for, 554t, 554–555, 555t
fluid loading, 548
limiting values, 555–556
loads, 545–550, *546*
non-circular pipes, 556
pipe stiffness, 550–551
pipe types, 541–542, 543t
soil-pipe interaction, 551–553
soil properties and, 550–551, 551t
steel culvert, large diameter, corrugated, 564t, 564–566
stress, strain, 559
surface live loads, 548
thrust, 555–556
trench installation, 546–548, *547*, 547t

trench loading, *vs.* embankment loading, 563–564
wall properties and, 550
Buried structures. *See also* Buried pipe
cold and, 612
influence on, with trenchless technology, 588
2-butanone, Henry's law constant, 732
Butyric acid, diffusion coefficient, 783
Byphenyls, polychlorinated, contaminants, 671

C

CABF. *See* Cochran's approximation to Behren's Fisher t-test
Cadmium, as contaminant, 671
Caisson. *See* Drilled shafts
Calcareous rock, classification, 149
Calcite, 148
density, 47
Calcium hardness, in groundwater analysis, 198
California Environmental Protection Agency, 683
Canadian Centre of Occupational Health and Safety, 683
Canadian Council of Ministers of Environment, 683
Cantilever walls, gravity and, *516,* 516–517
Capillary barrier cover systems, 834–837, *835, 836*
Capillary rise, in sediments, 712t
Capping, with contamination, 959–960; *see also* Covers
Carbon dioxide, diffusion coefficient, 783
Carbon tetrachloride, partitioning coefficient, range, 784
Carbonaceous rock, classification, 149
Carbonate alkalinity, in groundwater analysis, 198
Cast-in-situ piles, base driven, advantages, disadvantages of, 263
Cast iron, as pipe material, 543
CCME. *See* Canadian Council of Ministers of Environment
CCOHS. *See* Canadian Centre of Occupational Health and Safety
Cellular concrete, as fill material, 433
Cement, bentonite, physical barrier, 960
Cemented soil, shield tip resistance pressure, 576
Censored data, analysis of, 910–913
Aitchison's method, 911–912
Cohen's test, 911
maximum likelihood estimator, 912
plotting position procedure, 911
Poisson model, 912–913
simple substitution methods, 910
test of proportions, 910–911
Chalk, porosity, 713
Channel protection, inland, 799
Chemical admixtures, stabilization, soil improvement, 444
Chemical flushing, 930–932, *931*
Chemical resistance guidelines, geomembranes, 775t
Chemical stabilization, for soil improvement, 443–452
Chloride
diffusion coefficient, 778
in groundwater analysis, 198
partitioning coefficient, range, 784
Chlorinated pesticides, containment, 953
Chlorinated solvents
chemical resistance guidelines, 775
contaminants, 671
Chlorine, diffusion coefficient, 783
Chlorite
clay, 694
density, 47
physicochemistry, 694
Chlorobenzene
Henry's law constant, 732
partitioning coefficient, range, 784
Chloroform
diffusion coefficient, 778, 783
Henry's law constant, 732
partitioning coefficient, range, 784
Chloroethane, Henry's law constant, 732
Chromium, as contaminant, 671
Circular rafts, 253–255, *255*
Clam shells, as fill material, 433
Clay, 149
ASTM sieve number, 44
behavior after end of construction, 466
drainage, hydraulic conductivity, 54
drained behavior of, 33–34, *34*
effective strength parameters, *61,* 61–62, *62*
expanded, as fill material, 433
geosynthetic, liners, 761–765
intact, compacted, diffusion through, 777–778, 778t
marine, drainage, hydraulic conductivity, 54
mineral characteristics, 694–695, 695t
mixed-layer, 694
as pipe material, 543
pipe-soil interface coefficient, 578
shield tip resistance pressure, 576
soft, reinforced embankments on, 488–494
thermal properties, 597
Clay fabric, 10
Clay foundations
under embankments, 463–468
reinforced embankments on, *468,* 468–470, *470*
Clay liner
functions, 174
geosynthetic, defined, 173
geosynthetic, *186,* 186–187
endurance properties, 187
hydraulic properties, 186
physical properties, 186
liquid impoundment, 799
Clay minerals
Atterberg limits, 48t
physicochemistry, 692–694, *693*
Clay-water-electrolyte system, physicochemistry, 697–701
double layer
interactions, *699,* 699–700
repulsion, 700–701
ion distributions, *698,* 698–699
Clean-up goals, soil, 949t
Clogging, 743–750, 797
Cluster sampling, 669
Coal, 149
Coarse-grained particle, ASTM sieve number, 44
Cobble, ASTM sieve number, 44
Cochran's approximation to Behren's Fisher t-test, 898, 902–903
Cohen's test, censored data analysis, 911
Coherent gravity method, retaining, reinforcement, *528,* 528–530
Cold climate (region), 593–614
buried structures, 612
design considerations, 610–611
earth retaining structures, 611
excavations, 611
foundations, 611
frost susceptibility, 609–610
soils, 609–610
highways, 612–613
frost heave, *612,* 612–613
pavement design, 613–614
thaw-weakening, 613
ice formation, freezing soils, 600–609
frost depth, prediction of, 606–608
frost heave prediction, *608,* 608–609
ice lens, *601,* 601–602
segregation potential, 602–603

field conditions, 603–606
SP_{field}
empirical correlations, 606, *606*
field observations, *605*, 605–606
laboratory freezing tests, *604*, 604–605, *605*
thaw weakening, 609
unfrozen water content, 600, *600*
water migration, *601*, 601–602
shallow foundation, 257–258
thermal boundary conditions, 596–600
freezing indices, *598*, 598–600, *599*, 599t
thermal properties, 593–600
soils, 595–596
heat capacity, 595–596
heat flow, through, 593–595
latent heat, 596, *596*
thermal conductivity, 595, *595*
thermal resistance, 596, 597t
Collection systems, geotextile "filters" in leachate, *745*, 745–747, 746t
Colloids, 738
Combined footings, 224
Communication, of contaminant risk, 686–687
external, 686
internal, 686–687
Compaction
liner, 752–761
pavement, 364–366
relative, soil, 46
soil, 364–365
Compaction grouting
for soil improvement, 452–453
for soil stabilization, 431
Compaction piles
for soil improvement, 456
for soil stabilization, 431
Complete restoration, as soil clean-up goal, 949
Complexation reactions, hydrogeology, 737, *737*
Composite pavement, 361
Compressibility, soil, 19–28, 55–58, 56t
elasticity, 19–20
expansion, 21–22, *22*
modulus variation, *20*, 20–21
preconsolidation pressure, 56, *56*
Compressible pipe, stiffness, 554
Compressive creep, geosynthetics, 181, 182t
Conceptual pathway model, *678*, 679
Concrete
flexural strength, 387
reinforced, as pipe material, 543
thermal properties, 597
Concrete dam, on rock foundation, 318–335
Barrett chute dam, 329–334
bonded, unbonded contacts, strength envelopes of, 322–325, *323*, 324t, 325t
bonded contact, 322
data from records, extraction of, 326, *326*
deign provisions, *329*, 329–330
field investigation, 321–322, 322t, 330
high uplift pressures, 330–334, *331*
stability, 331t, 334
analysis methods, 326–329, *328*
strength parameters, design analysis, 330
unbonded contact, 322
weakly bonded contact, 322
Concrete pipes, pipe-soil interface coefficient, 578
Concrete storm sewer, 561–564, 562t
Conductivity
groundwater, 198
soil, 708–710
flows, effects of, 710
thermal, soil, 449
Consolidation, soil, 55–58, 434–443
coefficient of, *57*, 57–58, 450
dewatering, 434
groundwater control, 434
one-dimensional, 23–26, *24*, *25*
preloading, surcharge, 434–436, *435*
vacuum, preloading by, *436*, 436–437, *437*
vertical drains, consolidation with, 437–441, *438*, 438t
Containment
with contamination, 959–960
capping, 959–960
cut-off walls, 769–770, 960, 960t
geocomposites, 188
as soil clean-up goal, 949
Contaminants
hydrogeology, 711–738
acid-base reactions, *730*, 730–731
advection, 721
complexation reactions, 737, *737*
cosolvation, 737–738
Darcy flux, 715
diffusion, 721–723, 722t
dispersion, 723–724, *724*
dissolved solutes, attenuation of, 729–737
hydraulic characteristics of sources, 720
hydrogeologic controls, 716–719, *718*
hydrogeological environments, 711–716
aquifers, 711–712
hydraulic head, 714–716, *715*
porosity, 712–714, 713t
saturated zone, 711, 712t
hydrolysis, 736–737
Karst system, 717–719
loading history, 720
mass transport processes, 721–724
multiphase flow, 724–729, *725*, *726*, *727*, *729*
oxidation-reduction reactions, 736
physical, chemical properties of, 719
point sources, 720
solution, 731–733, 732t
sorption, 733–736, 734t
sources of, 719–720
transport, 721–738
identification, 670–674
analytical parameters, 673–674
contaminant partitioning, 672, *673*
contaminant weathering, 672–673
hazards associated with, 670–671, 671t
inorganic contamination, 670–671
organic contamination, 671
requirements, 670
by industry, 671t
monitoring, 879–920
boundary criteria, exceedance of, risk assessment, 914–916
groundwater monitoring program
components of, 879–893
documentation, 892, *892*
groundwater sampling, 890–892
monitoring well
locations, 880–886
nests, 893
sampling frequency, 892–893
statistical analyses
analysis of variance, 898
Behren, Fisher t-test, Cochran's approximation to, 898
censored data, 910–913
Aitchison's method, 911–912
Cohen's test, 911
maximum likelihood estimator, 912
plotting position procedure, 911
Poisson model, 912–913
simple substitution methods, 910
test of proportions, 910–911
linear regression, 898–899

monitoring data, 893–914
multiple comparisons, 904–906
analysis of variance, 904–905
multiple regression, 906
multiple regression, 899
non-parametric procedures, 906–910
Kruskal-Wallis test, 909–910
Mann-Whitney (U) test, 907–908
Spearman's rank correlation coefficient, 908
significance tests, interpretation of, 899–900, 900t
single comparisons, procedures for, 900–904
Behren, Fisher t-test, Cochran's approximation to, 902–903
linear regression, 903–904
student's t-test, 900–902
statistical power, 913
student's t-test, 897–898
visualization method, 916–919, *917*, *918*
physical, chemical properties of, 719
sources of, 719–720
transport, 721–738
types, 952–953t
Contamination
containment, 959–960
capping, 959–960
covers, 959–960
cut-off walls, 769–770, 960, 960t
hazardous wastes, soil contaminated by, 955–956
non-hazardous solid waste, soil contaminated by, 956
off-site treatment technologies, 962–966
disposal, 963–965
hazardous waste landfill, 964
incineration, 964
non-hazardous waste landfill, 963–964
regulatory issues, 963
treatment, 965–966
aeration, 965
bioremediation, 965–966
petroleum fuel products, soil contaminated by, 955
regulatory issues, 953–956
remediation
intrinsic, 923–925
objectives of, 922–923, *923*
sites, characteristics of, 921–922, *922*
in situ containment, treatment, 921–946
in situ plume control, 937–944
permeable reactive barriers, 939–944
hydraulic performance of, 940–942, *941*
pump-and-treat remediation, 937–939, *938*
soil
characterization of, 104–105
goals, 948–950, 949t
groundwater, *in situ* containment, treatment, 921–946
management of, 947–966
options, 950–951
treatment technologies, 951, 951t, 952–953t, 954t
source-zone
isolation, 933–937
bottom barriers, 937
covers, 937
enclosures, 933–937, 934–935t
restoration, 925–933
goals, 925–926
in groundwater zone, 929–933
chemical flushing, 930–932, *931*
immiscible fluids, pumping of, 929–930, *930*
in situ mass destruction technologies, 932–933
thermal flushing techniques, 932
Vadose-zone contamination in source zone, 926–929
excavation, 926–927
soil flushing, 929
soil vapor extraction, 927, 927–928, *928*
treatment technologies, 956–959
bioremediation, 956–958
ex situ bioremediation, 957–958
in situ bioremediation, 957
soil vapor extraction, 958–959
stabilization, 959
Continuous flight auger piles, advantages, disadvantages of, 263
Continuous seismic reflection profilters, method, procedure, 84
Copper
as contaminant, 671
in groundwater analysis, 198
thermal properties, 449, 597
Corrugated steel, as pipe material, 543
Cosolvation, hydrogeology, 737–738
Coulomb
failure criterion, soil mechanics, *34*
wedge methods, *513*, 513–515
Coupled flows, 709–710, 710t
Covers
for containment, 937, 959–960
waste, 825–878
CPT. *See* Static cone penetration test
CPTS. *See* Seismic cone-penetration test
CPTU. *See* Piezo-cone-penetration test
Creep. *See also* Compressive creep
reduction, 195
soil, 26–28, *27*, 58, 58t
p-cresol
diffusion coefficient, 783
Henry's law constant, 732
Critical pressure. *See* Hydraulic fracturing
Cross-anisotropic rocks, deformation parameters, 155–157
Crosshole seismic test, applicabilty, 88
Crude petroleum solvents, chemical resistance guidelines, 775
Crystalline rock, fractured, porosity, 713
Culvert, steel, large diameter, corrugated, 564t, 564–566
Curtain, grout, 960
Cut-off walls
with contamination, 960, 960t
freezing, 214
grouting, 214
vertical, 769–770
Cyanide, contaminants, 671
Cyclic loading
pile foundations, 271–273, *272*
single piles, 290–292
Cyclohexane, partitioning coefficient, range, 784

D

Dam, concrete, on rock foundation, 318–335
Barrett chute dam, 329–334
bonded contact, 322
strength envelopes of, 322–325, *323*, 324t, 325t
data from records, extraction of, 326, *326*
deign provisions, *329*, 329–330
field investigation, 321–322, 322t, 330
high uplift pressures, 330–334, *331*
stability analysis, 326–329, *328*, 331t, 334
strength parameters, design analysis, 330
unbonded contact, 322
weakly bonded contact, 322
Dam clay cores, 799
Dam toe drains, 799
Damping
determination of, soil mechanics, 40–41
shear modulus, soils, *66*, 67

Darcy flux, 714–715
Darcy's law, 13, 199, 714
Darcy velocity: *see* Darcy flux
DCPT. *See* Dynamic cone-penetration test
De novo synthesis of toxicity information, 683
Deep foundations, 344–350
 pile groups, impedance functions of, 347–348
 pile-soil-pile interaction, 346–347
 piles
  batter, 348
  experimental studies on response of, 349–350
   centrifugal modeling, 350
   full-scale field tests, 349
   small prototype field tests, 349–350
   small-scale laboratory tests, 350
  impedance functions of, *344,* 344–346, *345, 346*
  non-linear response of, 348, *348*
  seismic response of, 349
Deep soil mixing
 for soil improvement, 445
 for soil stabilization, 430
Deflection, buried pipe, 556–559
Deformation
 parameters, cross-anisotropic rocks, 155–157
 properties, rock, 154–159, *155*
 soil, 706–708
Degreasers, contaminants, 671
Degree of saturation, defined, 12
Densification, for physical stabilization, 452–457
Density
 defined, 12
 dry, defined, 12
 relative, soil, 46
 of solids
  defined, 12
  relative, defined, 12
 of water, defined, 12
Density index, 12, 45–46
Depth recorders, method, procedure, 84
Design, site characterization, *74,* 74–80
Dewatering
 area, 206–207
 site characterization, 197–220
 for slope stabilization, 457
 soil, 430
 specialty contractor, responsibility of, 220
 specifications, 218–220
 specified complete groundwater control system, 219
 specified end result, 219
 specified minimum groundwater control system, 219
 system, 208–214
 cut-off walls
  freezing, 214
  grouting, 214
  design of, 214–218
  electro-osmosis, 213, *213, 214*
  filter packs, *216,* 216–217, *217,* 217t
  fittings, 217–218
  installation, 218
  open pumping, 214
  operation, 218
  permanent, 218
  piping, 217–218
  pump units, 217
  recharge, 214
  removal of, 218
  soil stabilization systems, 208–213
  vacuum applied to soil, 208–213, *213*
  well-screens, 215–216
 trench, 799
Diaphragm walls, 520–523, *522*
Dichlorobenzene
 diffusion coefficient, 783
 Henry's law constant, 732
Dichloroethane, 784
 diffusion coefficient, 783
 Henry's law constant, 732
 partitioning coefficient, range, 784
Dichloromethane
 diffusion coefficient, 778, 783
 Henry's law constant, 732
 partitioning coefficient, range, 784
Diffusion
 hydrogeology, 721–723, 722t
 through barriers, 775–785
  clays, intact, compacted, diffusion through, 777–778, 778t
  dissolved-phase diffusion, through porous media, 776–781
  gaseous phase, 781–782
  geomembranes, 782–785
  GCL's, 778–780
  temperature, effect of, 786
  unsaturated soil, 780–781
Diffusion coefficient, 783t
 effective, 722, 722t, 723t
 fine-grained soils, 709, 778t, 779t
 geomembranes, 784t, 785t
 GCLS, 778–780
 porous media, 721–722
 unsaturated soil, 782
Dilatometer test, 94
 advantages, limitations of, 90
 applicability, 88
 rock mass modulus, 312
Diorite, geological classification, 149
1,4 dioxane, diffusion coefficient, 778
Directional drilling, 573–574
Discrete frequency occurrence, earthquake, 618–619
Dispersion, hydrogeology, 723–724, *724*
Disposal, contamination, 963–965
Dissolved solids
 attenuation of, 729–737
 in groundwater analysis, 198
Disturbed soils, 58
DMT. *See* Dilatometer test
DNAPL, 719, 724–729, 769, 880–884, 921–945
Dolerite, geological classification, 149
Dolomite, 148
 density, 47
 porosity, 713
Dolomitic limestone, 149
Double composite liners, 769
Double sampling, 669
DP. *See* Dynamic probing
Drainage, *205,* 205–206
 pavement, *363,* 363–364
 site characterization, 197–220
Drainage layers, hydraulic capacity of, *741,* 741–742, 742t, 790–796
Drains
 biopolymer, physical barrier, 960
 dam toe, 799
 pavement edge, 799
 pipe, polyethylene, 565t, 566t, 566–567, 567t
 subhorizontal, 425
 trench, 425
 vertical
  prefabricated, 441–443
  wall, 799
 wall, vertical, 799
Drilled shafts, advantages, disadvantages of, 263
Drilling
 directional, 573–574
 guided, 582–583
Drop in potential, method, procedure, 83
Dry density, defined, 12
Dry unit weight, soil mass, defined, 12
Ductile iron, as pipe material, 543
Dutch cone. *See* Static cone penetration test
Dynamic compaction
 for soil improvement, 453–454
 for soil stabilization, 431

Dynamic cone-penetration test, 91
advantages, limitations of, 89
applicability, 88
Dynamic loads, types of, 337–338
Dynamic probing, advantages, limitations of, 89
Dynamic properties, soil, 40–42, 64–67
modulus, determination of, 40–41
seismic stability, 41–42
shear modulus, damping, 64–67, 65t, *66*

E

E-logs, method, procedure, 83
Earth pressure theory, 508–516
compaction stresses, 513, *513*
Coulomb wedge methods, *513,* 513–515
Rankine earth pressure theory, 508–513, *510, 511, 512*
Earth retaining structures, 501–538
cold temperatures, 611
retaining wall, selection of, 504–506
types of, 501–504, 502t, *503*
Earthquakes, 615–660
covers, 850–871
discrete frequency occurrence, 618–619
embankment dams, 652–654
foundations, seismic design of, 640–642
ground motions, 622–627
basic elements, 622, *622*
confirmation dynamic analyses, 625
crustal earthquakes, 625–627, 626t
effects of soil conditions on, 627–632, *628*
response spectra, 622–623, *623*
simple design spectra, 623–624, *624*
site-specific response spectra, 624–625
subduction zone earthquakes, 627
uniform hazard spectra, 625
liquefaction, 642–649
Becker penetration test, 647
seismic settlement, *647,* 647t, 647–648, *648*
shear-wave velocity, 646, *646*
magnitude, 617–618, 619
from fault break, fault area, 620
maximum, estimation of, *619,* 619–620
Newmark's deformation analysis, *652*
occurrence, 615–616, *616*
post-liquefaction deformations, 649–652
probability of occurrence, 620
residual strength, 649–652
retaining structures, seismic design of, 633–640, *634*
seismic risk in, 654–659
seismic soil-structure interaction, 632–633
seismology, 615–620
source zones, 619
statistics, 618, *618*
wave propagation, 620–622
buried pipes, strains in, *621,* 621–622
elements of, 620
ground, strains in, 620–621
wave type, 616–617, *617*
Echo-sounding. *See* Depth recorders
Effective vertical stress
ground, 18–19
in ground, state of, 18–19
Elastic properties, soils, 55–56
Elasto-plasticity, soil, 36–40
Cam clay model, 37–39, *38*
critical state soil mechanics, 36–37, *37*
Electric field intensity, electro-osmotic consolidation, soil, 450
Electrical conductivity
electro-osmotic consolidation, soil, 450
fine-grained soils, 709
Electrical conductors, contaminants, 671
Electrical resistivity, method, procedure, 83
Electrical stabilization, for soil improvement, 443–452
Electro-kinetic stabilization, for soil improvement, *449,* 449–452, 450t
Electro-osmosis
dewatering system, 213, *213, 214*
soil stabilization, 431
Electro-osmotic conductivity, fine-grained soils, 709
Electro-osmotic permeability, electro-osmotic consolidation, soil, 450
Electro-osmotic stabilization, for soil improvement, *449,* 449–452, 450t
Electrokinetic stabilization, soil, 431
Embankments, 541–568
berms, 488
clay, behavior after end of construction, 466
clay foundations
under embankments, 463–468
reinforced embankments on, *468,* 468–470, *470*
consolidation, 481–483
primary consolidation, 481–483, *482*
structuring effects, 483, *483*
viscous effects, 483, *483*
dams, earthquake, 652–654
lateral displacements, *480,* 480–481
over peat, 463–500
over soft soil, 463–500
peat, 463–500
peat, reinforced embankments on, 495–497
peat deposits under embankments, 470–473
during, after construction, 472–473
peat characteristics, 470–471, *471*
pore pressures, 471–472, *472*
piles
in, near, 299
reinforcement, 537
pore pressures, 467–468
reduction, 195
reinforcement of, 456–457
settlements, 473–480
construction settlement, 474–475
of embankments on peat, 478–480
long-term settlement, 475–477, *476*
reinforcement, effect of, 477–478
stress distribution under, *473,* 473–474
several stages, construction in, 486
CPT tip resistance approach, 487
field vane test approach, 487
SHANSEP approach, 487
vertical effective stress approach, 487
soft clay, reinforced embankments on, 488–494
stability, 484–487
estimation of, 486, *486*
mobilized shear strength, evaluation of, 484–486, *485*
one stage construction, 484–486
weathered crust, strength of, 486, *486*
stage construction, 467, *467*
Empty cavity pipe, stiffness, 554
Enclosures, source-zone isolation, 933–937, 934–935t
Endurance properties
geosynthetics, 177–179, *178,* 179t
geotextiles, 175
Engineering, geoenvironmental
barrier systems, 739–788. *See also* Barrier systems
contaminants
hydrogeology, 711–738
monitoring of, 879–920
risk, 879–920. *See also* Contaminants

in situ containment, treatment, 921–946
contaminated soil, groundwater, *in situ* containment, treatment, 921–946
liquid-containing structures, geosynthetics, 789–824. *See also* Liquid-containing structures
physicochemistry of soils for, 691–710
problem identification, 663–690
risk management, 663–690
waste, covers for, 825–878. *See also* Waste
Environmental sampling strategies, 669t
Erosion control, reduction, 195
Ethylbenzene
diffusion coefficient, 783
Henry's law constant, 732
partitioning coefficient, range, 784
Evaluation criteria, remedial technology, 951t
Evaporation, unsaturated soil, 124–125, *125*
Evapotranspiration, unsaturated soil, 124–125, *125*, 837–845
Excavation
cold temperature, 611
piles near, 299
techniques, 570–582
Existing information, in site characterization, review of, 80
Expansive soils, pile foundations, 296, *296*
Exposure to contaminants, assessment of, 679–681
Externally imposed ground movements, pile response to, 293–299
Extrusion, geosynthetics, 181

F

Fabric, soil, 9–11
Fabric-property interrelationships, physicochemistry, *704*, 704–705
Face stability, trenchless technology and, 574–576, *575*, 576t
Failure criteria, brittle material, 164–166
Griffith criterion, *164*, 164–165
Hoek-Brown failure criterion, 165t, 165–166, *166*
Failure movement, slopes, *406*, 406–407, *407*
Feldspar, 148
density, 47
thermal properties, 597
Ferruginous rock, classification, 149
Field tests, applicability of, summary, 88t
Field vane test, 92
advantages, limitations of, 89
applicability, 88
Fill materials, lightweight, 433t
Fill soils, imported, contaminants, 671
Filter packs, dewatering system, *216*, 216–217, *217*, 217t
Filters, 796–797
characteristics of, 797–798
clogging of, 745, 797
design of, 796–801
functions of, 796
soil, contact between, 797
Fine-grained particles, 44
Flat jack test, rock mass modulus, field tests, 311
Flexible pavement, 361
AASHTO design method, 379–380
Asphalt Institute method, 380–382, *381*, *382*
overlay, design methods, 391–392, *392*
structural design, 377–382
Flexible pipe
classification for, 554t, 554–555, 555t
stiffness, 554
Flexural strength, concrete, 387
Flow parameters, fine-grained soils, 709t
Fluoride, in groundwater analysis, 198
Flux boundary condition, unsaturated soil, 124–125, *125*
Fly ash, as fill material, 433
Footings
combined, 224
pad, 223–224
trip, 223, *223*
Foundations
cold temperatures, 611
dynamics of, 337–360
deep foundations, 344–350
pile batter, 348
pile foundations, seismic response of, 349
pile groups, impedance functions of, 347–348
pile-soil-pile interaction, 346–347
piles
experimental studies on response of, 349–350
centrifugal modeling, 350
full-scale field tests, 349
small prototype field tests, 349–350
small-scale laboratory tests, 350
impedance functions of, *344*, 344–346, *345*, *346*
non-linear response of, 348, *348*
design objectives, 337
dynamic loads, types of, 337–338
hammer foundations, 355–360
design criteria, *355*, 355–356, 356t
one mass foundation, response of, 356–357, *357*
two mass foundation, response of, 357–359, *358*
types of, 355
machine foundations, 350–355
rigid foundations
coupled response of, *351*, 351–353
one degree-of-freedom, 350–351
six degrees-of-freedom, *353*, 353–355
shallow foundations, 338–344
embedment effects, 341–343, *342*, 342t, 343t
impedance functions of, *338*, 338–341, *339*, 339t, *340*, 341t
layer on halfspace, impedance functions of, 343–344
types of foundations, 338
earthquake, seismic design of, 640–642
pile, 261–304. *See also* Pile foundation
reinforcement of, 456–457
on rock, 305–306. *See also* Rock, foundation on
shallow, 223–260. *See also* Shallow foundation
Fractured crystalline rock, porosity, 713
Free swell test, rock, 160–162, 161t, *162*
Freezing
artificial, ground, *448*, 448–449, 449t
cut-off walls, 214
Freezing indices, *598*, 598–600, *599*, 599t
Freezing soils, ice formation, 600–609
frost depth, prediction of, 606–608
frost heave prediction, *608*, 608–609
ice lens, *601*, 601–602
segregation potential, 602–603
field conditions, 603–606
SP_{field}
empirical correlations, 606, *606*
field observations, *605*, 605–606
laboratory freezing tests, *604*, 604–605, *605*
thaw weakening, 609
unfrozen water content, 600, *600*
water migration, *601*, 601–602
Friction angle, shear strength, discontinuities, rock, 166–168, *167*

Frost heave, highways, *612,* 612–613
Frost susceptibility, soils, 609–610
Fuel dispensing, contaminants, 671
Fuel hydrocarbons
 containment, 952, 953
 soil treatment technology, 954
Fuel products, soil contaminated by, 955
FVT. *See* Field vane test

G

Gabbro, geological classification, 149
Gas generation, waste cover, management, 828–831
GCL. *see* Geosynthetic clay liners
Geochemical barrier, physical barrier, 960
Geocomposites
 containment, 188
 defined, 170
 drainage, 188
 filtration, 188
 functions, 174
 geosynthetics, 187–188
  barrier geocomposites, 188
  containment geocomposites, 188
  drainage geocomposites, 188
  filtration geocomposites, 188
  reinforcement geocomposites, 188
  separation geocomposites, 187–188
 reinforcement, 188
 separation, 187–188
Geoenvironmental engineering, 661–966
 barrier systems, 739–788. *See also* Barrier systems
 contaminants
  hydrogeology, 711–738
  monitoring of, 879–920
  risk, 879–920. *See also* Contaminants
  in situ containment, treatment, 921–946
 contaminated soil, groundwater, *in situ* containment, treatment, 921–946
 liquid-containing structures
  geosynthetics, 789–824. *See also* Liquid-containing structures
  geosynthetics in, 789–824
 overview, 3
 physicochemistry of soils for, 691–710
 problem identification, 663–690
 risk management, 663–690
 waste, covers for, 825–878. *See also* Waste
Geoenvironmental problem identification, 663–690
 contaminant identification, 670–674
  analytical parameters, 673–674
  contaminant partitioning, 672, *673*
  contaminant weathering, 672–673
  contaminants, hazards associated with, 670–671, 671t
  inorganic contamination, 670–671
  organic contamination, 671
  requirements, 670
 exposure assessment, 679–681
 problem formulation, 674–679
  conceptual pathway model, *678,* 679
  contaminants, 675
  pathways, 675–678, *676–677*
  receptors, 675, *675*
 regulatory issues, 665–667
 risk-based site management, 664, *664, 665,* 666t
 risk characterization, 684
 risk communication, 686–687
  external, 686
  internal, 686–687
 risk management, 687–690
  options, selection of, 687–688, *688*
  success, monitoring of, 689
 sampling strategies, 669t, 669–670
 site assessment, 667–670
  procedural components, 667–669
 toxicity assessment, 681–684
Geogrids
 defined, 173
 functions, 174
 geosynthetics, 179–180
  endurance, 180
  mechanical, 180
  physical, 180
Geologic cycle, soil, 8–9
Geologic formation, classification, soil, 7–11
Geomembranes, 182–185, 770, 802
 chemical resistance guidelines, 775t
 defined, 173
 diffusion through, 782–785, 783t, 784t
 endurance properties, 184–185
 functions, 174
 liners, 768, 801–809
 low permeability barrier, 935
 mechanical properties, 183t, 183–184, *184, 185*
  peel test on seams, 183
  shear test on seams, 183
  tensile test on sheet, 183
 wind action on, 817–824
Geonets
 compressive creep, 181, 182t
 defined, 173
 endurance, 181–182
 extrusion, 181
 functions, 174
 hydraulic, 181
 intrusion, 181
 mechanical, 181
 physical, 181
 properties, 180–182
Geophysical methods
 land, 83t
 offshore, 84t
Geosynthetics, 173–196
 allowable strength, 192–193, 193t
 in concrete, 366–368, *368*
 endurance properties, 177–179, *178,* 179t, 773–774
 functions, 174, 174t
 geocomposite properties, 187–188
  barrier geocomposites, 188
  containment geocomposites, 188
  drainage geocomposites, 188
  filtration geocomposites, 188
  reinforcement geocomposites, 188
  separation geocomposites, 187–188
 geogrid properties, 179–180
  endurance properties, 180
  mechanical properties, 180
  physical properties, 180
 geomembrane properties, 182–185
  endurance properties, 184–185
  mechanical properties, 183t, 183–184, *184, 185*
   peel test on seams, 183
   shear test on seams, 183
   tensile test on sheet, 183
  physical properties, 182–183
 geonet properties, 180–182
  compressive creep, 181, 182t
  endurance properties, 181–182
  extrusion, 181
  hydraulic properties, 181
  intrusion, 181
  mechanical, 181
  physical, 181
 geotextile properties, 174–179
 hydraulic properties, 176–177, 177t
  percent open area, 176
  permeability, 177
  porosity, 176
 limit states approach, 193, 194t, 522–527
 liner systems, 762–765, 768–769, 789–790, *790*
 liquid flow applications, 193–194, 195t
 mechanical properties, 174–176, 175t, *176, 177*
 physical properties, 174, 175t

polymers
degradation mechanisms, 188–192
biological degradation, 191
hydrolytic degradation, 191–192
oxidation degradation, 188–190
accelerated test, 190
polyolefins, *189*, 189–190
ultraviolet degradation, 190–191
oxidation degradation, lifetime prediction, 190
reinforcement, for soil stabilization, 431
site characterization, 173–196
tensile behavior, wide-width test specimens, 176
test methods, 174–179
Geosynthetic clay liners, 186, 186–187, 762–765, 773–774
defined, 173
endurance properties, 187
hydraulic properties, 186, 762–764, 773–774
physical properties, 186
diffusion through, 778–780
equivalence with CCL, 787–788
Geotechnical engineering, overview, 3
Geotextiles
defined, 173
filters, 745–747, 798
functions, 174
properties, 175t
Gibbsite, density, 47
Glacial till, drainage, hydraulic conductivity, 54
Glass, thermal properties, 597
Glass-reinforced plastic, as pipe material, 543
Gneiss
classification, 150
thermal properties, 597
Grain-size distribution, soil, 43–45, 44t, *45*
Granite
geological classification, 149
porosity, 713
thermal properties, 449, 597
Granular, filters, 798
Granular bases, pavement, 372, 373t
Granular densities, soils, 47t
Granular soil
densities for, 47t
fabric of, 10
maximum, minimum densities for, 47t
Gravel
capillary rise in, 712
drainage, hydraulic conductivity, 54, 739–745, 747–750
fine, ASTM sieve number, 44
medium, ASTM sieve number, 44
pipe-soil interface coefficient, 578
shield tip resistance pressure, 576
Gravelly sands, thermal properties, 597
Gravity, method, procedure, 83
Griffith criterion, brittle material, *164*, 164–165
Gritstone, 149
Ground anchors
for slope stabilization, 457
for soil stabilization, 431
Ground displacement, techniques involving, 582–588
Ground freezing, artificial, *448*, 448–449, 449t
Ground motions, 586–588, *587*
calculation of, 579–580, *580*
earthquake, 622–627
basic elements, 622, *622*
confirmation dynamic analyses, 625
crustal earthquakes, 625–627, 626t
effects of soil conditions on, 627–632, *628*
response spectra, 622–623, *623*
simple design spectra, 623–624, *624*
site-specific response spectra, 624–625
subduction zone earthquakes, 627
uniform hazard spectra, 625
externally imposed, pile response to, 293–299
sources of, 293–294, *294*
Groundwater
characterization
piezometric pressures, 101–102
sampling, 101–102
conditions, assessment of, 207–208, *208*, 208t
contaminated, *in situ* containment, treatment, 921–946
control, slope stabilization, 457
monitoring program
components of, 879–893
documentation, 892, *892*
groundwater sampling, 890–892
monitoring well locations, 880–886
monitoring well nests, 893
sampling frequency, 892–893
table, porewater pressure, 18
Group, soil, assigning, 50
Group effects, pile foundations, 271, 272t
Grout curtain, physical barrier, 960
Grouting
compaction, 431, 452–453
cut-off walls, 214
jet, 431, 447, 934, 960
low permeability barrier, 934
physical barrier, 960
permeation, 430, 445–447, *446*
GRP. *See* Glass-reinforced plastic
Guided drilling, 570, 582–583
Gypsum, density, 47

H

Halloysite
clay, 693
density, 47
physicochemistry, 693
Halogenated semivolatile organics
containment, 952
soil treatment technology, 954
Halogenated volatile organics
containment, 952
soil treatment technology, 954
Hammer foundations, 355–360
design criteria, *355*, 355–356, 356t
one mass foundation, response of, 356–357, *357*
two mass foundation, response of, 357–359, *358*
types of, 355
Hardness, in groundwater analysis, 198
Hazard, slope movement, 421–422
Hazardous wastes. *See also* Contamination
landfill, 964
soil contaminated by, 955–956
Health-based standards, as soil cleanup goal, 949
Health Effects Assessment Summary Tables, 683
HEAST. *See* Health effects assessment summary tables
Heat capacity, soils, 595–596
Heat flow, through soils, 593–595
Heave, expansive soil, volume change, *145*, 145–146
Heavy metals
chemical resistance guidelines, 775
as contaminants, 671
HELP model
water balance, waste cover, 843–845, *844*
Hematite, 148
density, 47
Heptane, partitioning coefficient, range, 784
n-hexane, partitioning coefficient, range, 784
High resolution reflection, method, procedure, 83
Highways, cold temperatures, 612–613

frost heave, *612,* 612–613
pavement design, 613–614
thaw-weakening, 613
Hoek-Brown failure criterion, brittle material, 165t, 165–166, *166*
Home heating, contaminants, 671
Horizontal directional drilling, 570
Horizontal stress, 168–172. *See also* Lateral earth pressure
in ground, state of, 19
hydraulic fracturing, *171,* 171–172, *172*
United States Bureau of Mines, 168–171, *169,* 169t, *170*
Hornblende, 148
density, 47
geological classification, 149
Hornfels, classification, 150
Hvorslev surface, *32*
Hydraulic barrier cover systems
components of, 831–834
foundation layer, 834
gas transmission layer, 834
hydraulic-barrier layer, 752–765, 833–834
internal drainage layer, 833
protection layer, 831–833
surface layer, 831
Hydraulic conductivity, 13, 51–54, 54t, 199, 212–213
electro-osmotic consolidation, soil, 450
fine-grained soils, 709
function, unsaturated soil, *126,* 126–128, *127,* 130–133, *131*
laboratory hydraulic conductivity tests, 51–54, 759–760
test, applicability, 88
values, correlations, 54, 54t
von Post classification, 52t
Hydraulic containment, 765–768, *766, 767*
Hydraulic fracturing. *See also* Piezometer probe
horizontal stresses, *171,* 171–172, *172*
test, advantages, limitations of, 90
Hydraulic head, 714–716, *715*
Hydraulic properties
geosynthetics, 176–177, 177t
percent open area, 176, 746
permeability, 177
porosity, 176
geotextiles, 175
Hydraulic pumping test, applicability, 88
Hydraulic trap. *See* Hydraulic containment
Hydrocarbons
chemical resistance guidelines, 775
fuel
containment, 952
soil treatment technology, 954
petroleum, contaminants, 671
Hydrogen, diffusion coefficient, 783
Hydrogeologic controls, 716–719, *718*
Hydrogeological environments
aquifer recharge, 714–716, *715*
aquifier discharge, 714–716, *715*
aquitards, 711–712
flux, 714–716, *715*
hydraulic conductivity, 712–714, 713t
specific yield, 712–714, 713t
storativity, 712–714, 713t
transmissivity, 712–714, 713t
unsaturated zone, 711, 712t
velocity, 714–716, *715*
Hydrogeology, 197–198, *198,* 198t
contaminant, 711–738
acid-base reactions, *730,* 730–731
advection, 721–724
colloidal transport, 737–738
complexation reactions, 737, *737*
cosolvation, 737–738
Darcy flux, 715
Darcy velocity; *see* Darcy flux
diffusion, 721–724, 722t
dispersion, 723–724, *724*
solutes, 721–724
dissolved solutes, attenuation of, 729–737
fractured system, 717–719
hydraulic characteristics of sources, 720
hydrogeologic controls, 716–719, *718*
hydrogeological environments, 711–716
aquifers, 711–712
hydraulic head, 714–716, *715*
porosity, 712–714, 713t
saturated zone, 711, 712t
hydrolysis, 736–737
Karst system, 717–719
lithology, 716–719, *718*
loading history, 720
mass transport processes, 721–724
multiphase flow, 724–729, *725, 726, 727, 729*
non-point sources, 720
oxidation-reduction reactions, 736
physical, chemical properties of, 719
point sources, 720
precipitation reactions, 731–733, 732t
solution, 731–733, 732t
sorption, 733–736, 734t
sources of, 719–720
stratigraphy, 716–719, *718*
transport, 721–738
volatilization, 731–733, 732t
Hydrology, 197–205
basic flow equations, 198–200, *199, 200, 201, 202*
graphical approach, 200–205, *203, 204*
Hydrolysis, 736–737
Hydrolytic degradation, polymers, 191–192
Hydromechanical compaction, 456
Hydroxide alkalinity, in groundwater analysis, 198

I

Ice, 449
formation, freezing soils, 600–609
frost depth, prediction of, 606–608
frost heave prediction, *608,* 608–609
ice lens, *601,* 601–602
segregation potential, 602–603
field conditions, 603–606
SP_{field}
empirical correlations, 606, *606*
field observations, *605,* 605–606
laboratory freezing tests, *604,* 604–605, *605*
thaw weakening, 609
unfrozen water content, 600, *600*
water migration, *601,* 601–602
physicochemistry, 695–696
thermal properties, 449, 597
Igneous rock
formation, 8
geological classification of, 149t
Illite
Atterberg limit, 48
clay, 694
compatibility, 771–772
density, 47
physicochemistry, or hydrous mica, 694
Immiscible fluids, groundwater zone, pumping of, 929–930, *930*
Imported fill soils, contaminants, 671
In situ testing
advantages, limitations, 89t
applicability of, summary, 88t
characterization, 87t, 87–95, 88t, 89–90t
data, 268–271
Incineration, contamination, 964
Index tests, soils, 43–51
Atterberg limits, 46–48, 47t
activity, 48

clay minerals, 48t
liquid limit, 46–47
plasticity index, 47t, 47–48
shrinkage limit, 48
density index, 45–46
expansion index, 48–49
grain-size distribution, 43–45, 44t, *45*
granular soil, maximum, minimum densities for, 47t
liquidity index, 48
minerals, relative density of, 47t
organic material, content of, 49–51
particle shape, 45, *45*, 45t
particle sizes, 44t
plasticity chart, *49*
relative compaction, 46
relative density, 46
roundness criteria, 45t
sensitivity, 49
void ratios, maximum, minimum, 45, *46*, 47t
Indirect tension test. *See* Brazilian test
Industrial landfill, contaminants, 671
Inertia pump, for groundwater sampling, 891
Infrastructure, buried, influence on, with trenchless technology, 588
Inland channel protection, 799
Inorganics
containment, 953
soil treatment technology, 954
Insulation, thermal properties, 597
Integrity testing, pile foundations, *303*, 303–304, *304*
Intrusion
geosynthetics, 181
for soil improvement, 445–447, *446*
Inundation, for soil improvement, 456
Ion exchange, soils, 701–702
microfabric, 703
particle associations, fabric scale, 703, *703*
soil fabric, *702*, 702–705
Iron
cast, as pipe material, 543
as contaminant, 671
ductile, as pipe material, 543
in groundwater analysis, 198
Iron oxide, 148
Ironstone, 149

J

Jacking
pipe, 570–573
shafts, 581
Jet grouting
low permeability barrier, 934
physical barrier, 960
for soil improvement, 447
for soil stabilization, 431
Joint configurations, concrete, 389, *389*
Joint steel sheet piling, sealable, low permeability barrier, 935
Joints, rock, shear strength, discontinuities, 168, 168t
Judgment sampling, 669

K

K_α, 645
Kaolinite, 148
Atterberg limit, 48
clay, 693
density, 47
physicochemistry, 693
Karst system, in hydrogeology, 717–719
KM, 644
KO, 19, 54–55
KOC, 732
KOW, 732

L

Laboratory hydraulic conductivity tests, soils, 51–54
Lacustrine deposits, 9
Landfarming, with contamination, 965–966
Landfill
closure surface water collection removal system, 799
contaminants, 671
hazardous, 964
leachate
collection, removal system, 739–750, 799
reduction, 195
non-hazardous, 963–964
temperature, 785–786
see also Barrier systems and covers
Latent heat, soils, 596, *596*
Lateral earth pressure, unsaturated soil, 140–141, *141*
Lateral ground movements, piles subjected to, 296–299, *297*, *298*
Lateral loading, pile foundations, 283–292
lateral deflection, single piles, 285–287
linear elastic solutions, 285t, 285–287, 286t
non-linear solutions, 287, *288*, *289*
p-y analysis, 285
single piles
cyclic loading, 290–292
group effects, 287–288, *290*
parameters, 288–290, 290t, 291t
ultimate lateral capacity, 283–284
pile groups, 284
single piles, 283–284, 284t
Layered soil, shallow foundation, 246, *247*
Leachate
collection, 790–796
biologically induced clogging, *743*, 743–745, *744*
drainage material, service life of, 748–751, *749*
granular drainage material in, 747–748
pipes, 751
liner compatibility with, 770–775
LEACHM model, water balance, waste cover, 845–846
Lead, as contaminant, 671
Leakage. *See* Liquid migration
Life-cycle period, rigid pavement, 387–388
Lightweight fill
materials, 433t
for soil improvement, 432–433, 433t
Lime-cement columns, 444–445
for soil stabilization, 430
Limestone, 149
porosity, 713
thermal properties, 597
Limit state design, shallow foundation, 258–259
Linear regression, 898–899
Liners
clay, 186–187
geosynthetic, 761–765
properties, 186–187
compatibility with leachate, 770–775
clay-permeant interaction, *771*, 771–772
GCL-permeant interaction, 772–774, 773t, *774*
geomembrane-permeant interaction, 774–775, 775t
double composite, 769
geomembrane, 768
geosynthetic clay, 761–765
liquid migration through, 801–810
low permeability, 751–770
single composite, *768*, 768–769
soil-bentonite, 761
stability, 788
systems, equivalence of, 787–788
temperature, 785–786, *786*, 786t
Liquefaction, earthquake, 642–649
Becker penetration test, 647

seismic settlement, *647*, 647t, 647–648, *648*
shear-wave velocity, 646, *646*
Liquid collection. *See* Leachate
Liquid-containing structures, 789–824
dam clay cores, 799
dam toe drains, 799
deformations, 810–824
dewatering trench, 799
filters, 796–797
characteristics of, 797–798
clogging of, 797
design of, 796–801
functions of, 796
geotextile, 798
granular, 798
in liquid-containment structures, 796
soil, contact between, 797
types of, 796
geosynthetic liner systems, 789–790, *790*
geosynthetic strain, 812–815
inland channel protection, 799
landfill
closure surface water collection removal system, 799
leachate collection, removal system, 799
liquid collection, 790–791
layers
characteristics of, 791
design of, 790–796
materials used in, 791
primary, design of, 792–794
secondary, design of, 794–796
liquid impoundment, clay liners, 799
liquid migration, through liners, 801–810
pavement edge drain, 799
permeability, criterion, 799t, 799–800
shoreline protection, 799
vertical wall drain, 799
wind, action on geomembranes, 817–824
Liquid flow applications, geosynthetics, 193–194, 195t
Liquid migration, through liners, 801–810
LNAPL, 719, 728–729, 880–884, 921–945
Loam, pipe-soil interface coefficient, 578
Low permeability barrier technologies, 934t
Low permeability liners, 751–770
compacted clay liners, 752–761
geological barriers, 751–752
Lubrication, trenchless technology, 580–581

M

Machine foundations, 350–355
rigid foundations
coupled response of, *351*, 351–353
one degree-of-freedom, 350–351
six degrees-of-freedom, *353*, 353–355
Magnesium hardness, in groundwater analysis, 198
Magnetite, density, 47
Manganese
as contaminant, 671
in groundwater analysis, 198
Mann-Whitney (U) test, 907–908
Mapping, site characterization, 81
Marble, classification, 150
Marine clay, drainage, hydraulic conductivity, 54
Marine deposits, 9
Mass movements, 397–428
processes, hydrogeology, 721–724
slopes, 397–428
Massachusetts Department of Environmental Protection, 683
Mat foundation, 224
Matric suction, unsaturated soil, 121–122, *122*
Maximum likelihood estimator, censored data analysis of, 912
MDEP. *See* Massachusetts Department of Environmental Protection
Mechanical properties, geotextiles, 175
Medium sand, drainage, hydraulic conductivity, 54
Mercury, as contaminant, 671
Metal plating operations, contaminants, 671
Metals, heavy, chemical resistance guidelines, 775
Metamorphic rock
classification, 150t
formation, 8
Methyl ethyl ketone
diffusion coefficient, 783
partitioning coefficient, range, 784
Mica, 148
geological classification, 149
hydrous, clay, 694
physicochemistry, 694
Micro-piles, for soil stabilization, 431
Microgranite, geological classification, 149
Micropiles, for slope stabilization, 458–459
Microtunneling, 570–573
Mills, pulp, contaminants, 671
Mine tailings, contaminants, 671
Minerals
density of, 47t
non-clay, in soils, 692
relative density of, 47t
rock-forming, 147, 148t
soil forming, 7–8, 8t
thermal properties, 597
Minimum groundwater control system, 219
Mining, contaminants, 671
Mohr-Coulomb failure criterion, *34*
Mohr-Coulomb failure envelope, unsaturated soils, *134*
Mohr's circle, 13–16, *14*, *15*, *16*
Moling, 570, 582–583
Monitoring of contaminants, 879–920
Montmorillonite
Atterberg limit, 48
density, 47
Mudstone, 149
diffusion, chloride, 723
thermal properties, 597
Multigrain fabrics, soils, 703–704
Multiple comparisons, 904–906
analysis of variance, 904–905
multiple regression, 906
Multiple regression, 899, 906
Multistage sampling, 669
Municipal landfill, contaminants, 671
Muscovite, 148
density, 47

N

Na-Ca-feldspars, density, 47
Nails, soil. *See under* Soil
Naphthalene, Henry's law constant, 732
NAPL, 719, 724–729, 880–884, 921–945
National Institute for Occupational Safety and Health, 683
National Institute of Health, National Toxicology Program, 683
National Toxicology Program, 683
Negative friction, pile foundations, 294–296, *295*
Newmark's deformation analysis, earthquake, *652*
NIH. *See* National Institute of Health
NIOSH. *See* National Institute for Occupational Safety and Health
Nitrate, in groundwater analysis, 198
Nitrogen, diffusion coefficient, 783

Non-aqueous phase liquids (NAPLs), 719–720
Non-chlorinated solvents, contaminants, 671
Non-circular pipes, 556
Non-degradation, as soil clean-up goal, 949
Non-halogenated semivolatile organics
 containment, 952
 soil treatment technology, 954
Non-halogenated volatile organics
 containment, 952
 soil treatment technology, 954
Non-hazardous waste
 landfill, 963–964
 soil contaminated by, 956
Non-parametric procedures, Kruskal-Wallis test, 909–910
NTP. *See* National Toxicology Program

O

Obsidian, geological classification, 149
Occupational Safety and Health Association, 683
n-octane, partitioning coefficient, range, 784
Off-site treatment technologies, contamination, 962–966
 aeration, 965
 bioremediation, 965–966
 disposal, 963–965
  hazardous waste landfill, 964
  incineration, 964
  non-hazardous waste landfill, 963–964
 regulatory issues, 963
Olivine, 148
 density, 47
OMOE. *See* Ontario Ministry of Environment
OMOL. *See* Ontario Ministry of Labour
Ontario Ministry of Environment, 683
Ontario Ministry of Labour, 683
Open pumping, dewatering system, 214
Organic matter, in soils, 695
Orthoclase, 148
 geological classification, 149
 mica, geological classification, 149
OSHA. *See* Occupational Safety and Health Association
Osmotic suction, unsaturated soil, 121–122, *122*
Ottawa sand, void ratio, 47
Oxidation degradation, polymers, 188–190
Oxidation-reduction reactions, hydrogeology, 736
Oxygen, diffusion coefficient, 783
Oxygenates
 chemical resistance guidelines, 775
 containment, 952

P

Pad footings, 223–224
PAHs. *See* Polynuclear aromatic hydrocarbons
Painting operations, contaminants, 671
Partial-use restrictions, as soil clean-up goal, 949
Particle shape, 45, *45*, 45t
Particle sizes, 44t
Partitioning coefficient, ranges, 784t
Pavement, 361–396
 AASHTO thickness design procedure AASHTO 1993, 388
 airfield pavement, 382–386
  comparative thicknesses, 383–386
  failure, 386
  thickness design, *384*, 384–386, *385*
  types, 383–386
 asphalt concrete, 371–372
 cold temperatures, 613–614
 compaction, 364–366
  asphalt, 366
   compaction equipment, 366
  asphalt layers, 365–366
  basic principles, 364
  construction equipment for, 365
  soils, 364–365, *365*
 composite pavement, 361
 design, 361–396
  economic evaluation of, 393
  inputs, 371–375
 drainage, *363*, 363–364
 engineering properties, 362–363
environment effects, 368–369
environmental considerations, 361–369
flexible, 361
 overlay, design methods, 391–392, *392*
 road
  AASHTO design method, 379–380
  Asphalt Institute method, 380–382, *381*, *382*
  structural design, 377–382
 geosynthetics in, 366–368, *368*
 geotechnical considerations, 361–369
 granular bases, subbases, 372, 373t
 joint
  configurations, 389, *389*
  in design, 389
 material, properties, 371–375
 overlays, 391–392
 Portland Cement Association, thickness design procedure, 388–389
 Portland cement concrete, 372
 reinforcement steel, 372–373
 reliability, 392–393
 rigid, 361
  thickness, 387–388
   flexural strength, concrete, 387
   life-cycle period, 387–388
   subbase support, 387
   subgrade, 387
  types of, 386–387
 roads, rigid pavements for, structural design, 386–391
 soils investigation, 362–363
 structural design methods, 370–371
 thickness, 378t
  design methods, 388
 traffic loads, 374–375, 375t
Pavement edge drain, 799
PCBs. *See* Polychlorinated byphenyls
PCE. *See* Tetrachloroethane
Peat
 characteristics, 470–471, *471*
 classification of, 51t
 compressed bales of, as fill material, 433
 deposits under embankments, 470–473
  during, after construction, 472–473
  pore pressures, 471–472, *472*
 dried, pulverized, as fill material, 433
 embankments over, 463–500
 fine-fibrous, 50
 reinforced embankments on, 495–497
 thermal properties, 597
Pentachloro-phenol, Henry's law constant, 732
Peridotite, geological classification, 149
Peristaltic pump, for groundwater sampling, 891
Permeability
 function, unsaturated soil, *129*, 129–130, *130*
 geosynthetics, 177
 intrinsic, 712–713
 see also Hydraulic conductivity

Permeation grouting, 445–447, *446*
 for soil stabilization, 430
Pesticides
 contaminants, 671
 soil treatment technology, 954
Petroleum
 fuel products, soil contaminated by, 955
 hydrocarbons, contaminants, 671
 solvents, crude, chemical resistance guidelines, 775
Phenol
 contaminants, 671
 Henry's law constant, 732
Phosphate, in groundwater analysis, 198
Phosphatic rock, classification, 149
Phyllite, classification, 150
Physical barriers, types, 960t
Physicochemistry, soils, 691–710
 allophane, 694
 attapulgite, 694
 chlorite, 694
 clay
  mineral characteristics, 694–695, 695t
  mineral structures, 692–694, *693*
 clay-water-electrolyte system, 697–701
  double layer
   interactions, *699*, 699–700
   repulsion, 700–701
  ion distributions, *698*, 698–699
 fabric-property interrelationships, *704*, 704–705
 halloysite, 693
 illite, 694
 ion exchange, 701–702
 microfabric, 703
 particle associations, fabric scale, 703, *703*
 soil fabric, *702*, 702–705
 kaolinite, 693
 macrofabric, 703
 mineral compositions, 691
 minifabric, 703
 mixed-layer clays, 694
 multigrain fabrics, 703–704
 non-clay minerals, in soils, 692
 organic matter, in soils, 695
 silicate minerals, 691–692, *692*
 single-grain fabrics, 703
 smectite minerals, 693
 soil mineralogy, 691–695
 soil properties, 705–710
  conductivity properties, 708–710
   coupled flows, 709–710, 710t
   direct flows, 708–709, *709*, 709t
   flows, effects of, 710
  deformation, 706–708
  strength, 706–707, *707*
  stress-strain behavior, 707, *708*
  stress-strain-time behavior, 707–708
  volume change properties, 705–706
 soil water, 695–697
  adsorbed water, properties of, 696–697
  dissolved ions, 696, *696*
  ice, 695–696
  water adsorption, by soils, 696, *697*
 vermiculite, 694
PIEZ, 97
Piezo-cone penetration test, 92, 93
 advantages, limitations of, 89
 applicability, 88
Piezometer probe, applicability, 88
Piezometric pressures, groundwater characterization, 101–102
Pile foundations, 261–304. *See also* Piles; Piling
 cyclic loading, 271–273, *272*
 design, 261–262
 embankments, piles in, near, 299
 excavation, piles near, 299
 expansive soils, 296, *296*
 externally imposed ground movements, pile response to, 293–299
 ground movement, sources of, 293–294, *294*
 group effects, 271, 272t
 integrity testing, *303*, 303–304, *304*
 lateral ground movements, piles subjected to, 296–299, *297*, *298*
 lateral loading, 283–292
  lateral deflection, single piles, 285–287
   linear elastic solutions, 285t, 285–287, 286t
   non-linear solutions, 287, *288*, *289*
   p-y analysis, 285
  single piles
   cyclic loading, 290–292
   group effects, 287–288, *290*
   parameters, 288–290, 290t, 291t
  ultimate lateral capacity, 283–284
   pile groups, 284
   single piles, 283–284, 284t
 load capacity, 263–273
  dynamic calculation methods, 263–264
  gravel, 268
  layered soils, 267–268, *269*
  non-cohesive soils, 266–267, *267*, 267t, 268t
  sand, 268
   calcareous, 268
   dense, 268
   loose, 268
  saturated clay soils, 264–265, *265*, 265–266
  silt, 268
  soil type, 268
  static calculation methods, 264–268
 load testing, 299–304
  dynamic pile testing, 300–301
  load distribution, 302–303
  results, 02–303
  soil stiffness, 303
  static load testing, 300
  statnamic testing, 301–302, *302*
  ultimate load, 302
 negative friction, 294–296, *295*
 pile groups, analysis of, 292–293
  elastic-based computer methods, 293, 293t
 settlement prediction, 273–283
  analysis methods, 273–278
  design charts, *274*, 274–275, *275*, *276*
  group settlement, 275–280, 278–280, *279*
  non-linear analysis, 275, *277*
 in situ test data, 268–271
 slopes, unstable, piles in, 299
 standard penetration test, 268–271, 270t
 static cone penetration test, 268, 270t
 types of piles, 262–263, 263t
 uplift capacity, 271
Piles
 cast-in-situ, base driven, advantages, disadvantages of, 263
 compaction, soil stabilization, 431
 continuous flight auger, advantages, disadvantages of, 263
 embankment, reinforcement, 537
 in embankments, 299
 groups, analysis of, 292–293
  elastic-based computer methods, 293, 293t
 socketed, into rock, *313*, 313–318
 types, advantages, disadvantages of, 263t
Piling
 joint steel sheet, sealable, low permeability barrier, 935
 sheet
  physical barrier, 960
  steel, conventional, low permeability barrier, 935

Pin piles, for stabilization, 431, 458–459
Pipe
 buried, 541–568
  arching, *553*, 553–554
  backfill selection, 560–561
  buckling, 559–560
  concrete storm sewer, 561–564, 562t
  construction loading, 548
  culverts, 556
  deflection, 556–559
  design standards, 544t, 545
  drainage pipe, polyethylene, 565t, 566t, 566–567, 567t
  expirical limits, 556
  flexible pipe, classification for, 554t, 553–555, 555t
  fluid loading, 548
  installation, 560–561
  limiting values, 555–556
  loads, 545–550, *546*
  moment, 555–556
  non-circular pipes, 556
  rigid pipe, classification for, 554t, 553–555, 555t
  soil-pipe interaction, 551–553
  soil properties, 550–551, 551t
  steel culvert, large diameter, corrugated, 564t, 564–566
  stiffness, 550–551
  stress, strain, 559
  surface live loads, 548
  thrust, 555–556
  trench
   installation, 546–548, *547*, 547t
   loading *vs.* embankment loading, 563–564
  types, 541–542, 543t
  wall properties and, 550
 bursting, 570, 583–584
 collection, leachate, 751
 design standards, 544t
 dewatering system, 217–218
 jacking, 570–573
 materials, 543
 ramming, 570, 584
 stiffness, categories, 543t, 554t
Pipe-soil interface coefficient, 578, 578t
Pipelines. *See also* Pipe
 friction, *576*, 576–579, *577*, *578*, 578t
 trenchless technology, *576*, 576–579, *577*, *578*, 578t
 void stability, 585–586
 rehabilitation techniques, 588–591
Plagioclase, 148
 geological classification, 149
Plastic
 chips, recycled, thermal properties, 597
 glass-reinforced, as pipe material, 543
 waste blocks, compressed, as fill material, 433
Plate-bearing test, applicability, 88
Plate-load test, 94
 advantages, limitations of, 90
 rock mass modulus, field tests, 311
 site characterization
PLT. *See* Plate-load test
Plume control, *in situ*, 937–944
 permeable reactive barriers, 939–944
  hydraulic performance of, 940–942, *941*
 pump-and-treat remediation, 937–939, *938*
PMT. *See* Pressuremeter test
Point sources, hydrogeology, 720
Poisson model, censored data analysis, 912–913
Poisson's ratio, 55, 55t
 approximate values of, 55t
Polychlorinated byphenyls, 671, 719, 953
Polyethylene drainage pipe, 565t, 566t, 566–567, 567t
Polymers
 degradation mechanisms, 188–192
  biological degradation, 191
  hydrolytic degradation, 191–192
  oxidation degradation, 188–190
   accelerated test, 190
   polyolefins, *189*, 189–190
  ultraviolet degradation, 190–191
 oxidation degradation, lifetime prediction, 190
Polynuclear aromatic hydrocarbons, contaminants, 671
Polyolefins, *189*, 189–190
Polypropylene, extruded, as fill material, 433
Polystyrene
 expanded, as fill material, 433
 thermal properties, 597
Polyvinylchloride
 pipe, 544
 thermal properties, 597
Pore pressures, embankments, 467–468
Porewater pressure, groundwater table, 18
Porosity
 defined, 12, 712
 effective, 712
 fine-grained soils, 709
 geosynthetics, 176
 hydrogeology, 712–714, 713t
 rock, 713t
 total, 712
Porous media, gaseous-phase diffusion through, *781*, 781–782
Portland Cement Association, thickness design procedure, 388–389
Portland cement concrete, 372
Position procedure, plotting, censored data analysis, 911
Post-failure movement, slopes, 407–408
Post-liquefaction deformations, earthquakes, 649–652
Potassium, diffusion coefficient, 778
Power consumption, hourly, electro-osmotic consolidation, soil, 450
Power stations
 contaminants, 671
 thermal, contaminants, 671
Pre-failure movement, slopes, *405*, 405–406
Precast concrete, advantages, disadvantages of, 263
Preconsolidation pressure, soils, 56, *56*
Prefabricated vertical drains, 441–443
Preloading, soil, 430, 431, 452
Pressure cells test, applicability, 88
Pressure plate apparatus, soil-water characteristic curves, *116*
Pressure tunnel test, rock mass modulus, field tests, 311
Pressuremeter test, 93
 advantages, limitations of, 90
 applicability, 88
Prestraining, for soil stabilization, 431
Probability sampling, 669
Propanoic acid, partitioning coefficient, range, 784
Property assessment, site characterization, 107–146
Propionic acid, diffusion coefficient, 783
Protection of structures, with slope movement, 423
Pulp mills, contaminants, 671
Pump units, dewatering system, 217
Pumps, for groundwater sampling, 891
PVC. *See* Polyvinylchloride

Pyrophyllite, density, 47
Pyroxene, 148

Q

Quartz, 148
 density, 47
 geological classification, 149
 thermal properties, 597
Quartzite, 149
 classification, 150
 thermal properties, 597

R

Radial jacking test, rock mass modulus, field tests, 311
Raft foundation, 224, 252–257
 circular rafts, 253–255, *255*
 of general shape, 256
 rectangular rafts, 255–256, *256*, *257*
 strip rafts, 253, *253*, *254*
Ramming, pipe, 584
Random sampling, 669
Rankine earth pressure theory, 508–513, *510*, *511*, *512*
Reactivation movement, slopes, *408*, 408–409
Reactive soils, shallow foundation, 257
 rafts on, 257
 Recharge, dewatering system, 214
 Recompression, soil, 57, *57*
 Rectangular rafts, 255–256, *256*, *257*
 Recycled plastic chips, thermal properties, 597
 Reduction factors, range of, 195t
 Regulatory issues, toxicity exposure, 665–667
 Reinforced concrete
  advantages, disadvantages of, 263
 as pipe material, 543
Reinforced embankments, 456–457, 537
Reinforced slopes, 501–538, *506*
Reinforced soil walls, 523–531
Reinforcement over voids, 535–537
Reinforcement steel, pavement, 372–373
Relative compaction, soil, 46
Relative density
 soil, 46
 solids, defined, 12
Relocation, with slope movement, 423
Remediation. *See also* Contaminants
 intrinsic, 923–925
 objectives of, 922–923, *923*
 technology, evaluation criteria, 951t
Remolded soils, 58
Remote sensing, in site characterization, 80–81
Removal, unstable materials, with slope movement, 423
Residues from wood industry, as fill material, 433
Restoration, complete, as soil clean-up goal, 949
Retaining structures. *See also* Walls
 cantilever walls, gravity and, *516*, 516–517
 conventional, 516–522
 cut-offs, 520–523, *522*
 diaphragm walls, 520–523, *522*
 earth, types of, 501–504, 502t, *503*
 earthquake, seismic design of, 633–640, *634*
 selection of, 504–506
 sheet pile walls, 517–518, *518*
 soil walls, reinforced, 523–531
Rhyolite, geological classification, 149
Rice hull ash, as fill material, 433
Rigid pavement, 361
 thickness, 387–388
  flexural strength, concrete, 387
  life-cycle period, 387–388
  subbase support, 387
  subgrade, 387
 types of, 386–387
Rigid pipe, stiffness, 554
Risk assessment. *See also* Contaminants
 consultants, 683
 slope movement, 420–423
Risk management, 663–690, *664*, *665*, 666t
 contaminant identification, 670–674
  analytical parameters, 673–674
  hazards associated with, 670–671, 671t
  inorganic contamination, 670–671
  organic contamination, 671
  partitioning, 672, *673*
  requirements, 670
  weathering, 672–673
 exposure assessment, 679–681
 options, selection of, 687–688, *688*
 problem formulation, 674–679
  conceptual pathway model, *678*, 679
  contaminants, 675
  pathways, 675–678, *676–677*
  receptors, 675, *675*
 regulatory issues, 665–667
 risk-based site management, 664, *664*, *665*, 666t
 risk characterization, 684
 risk communication, 686–687
  external, 686
  internal, 686–687
 sampling strategies, 669t, 669–670
 site assessment, 667–670
  procedural components, 667–669
 success, monitoring of, 689
 toxicity assessment, 681–684
Risk monitoring, contaminants, 879–920
Roads
 pavement, flexible, AASHTO design method, 379–380
 rigid pavements for, structural design, 386–391
Rock
 foundation on, 305–306
 buildings, tall, foundations for, 305–318
 concrete dams on, 318–335
  Barrett chute dam, 329–334
  bonded contact, 322
  data from records, extraction of, 326, *326*
  deign provisions, *329*, 329–330
  field investigation, 321–322, 322t, 330
  high uplift pressures, 330–334, *331*
  stability analysis, methods, 326–329, *328*
  strength parameters, design analysis, 330
  unbonded contact, 322
  strength envelopes of, 322–325, *323*, 324t, 325t
  weakly bonded contact, 322
 rock mass modulus, field tests, 310–313, 311–312t, *313*
  dilatometer test, 312
  dynamic tests, 312
  large flat jack test, 311
  plate load test, 311
  pressure tunnel test, 311
  radial jacking test, 311
  stress relief test, 312
  tunnel relaxation test, 312
 socketed piles into rock, *313*, 313–318
  average side shear, 314–316, 315t, *316*
  design, 316–318, *317*, *318*, *319*
  end bearing resistance, 314
  shaft resistance, 314
 tall buildings, 305–318
  adjacent structures, effect of excavations, 310

allowable bearing pressure, 305–309, 307t, *308, 309*
base heave, 310
bearing capacity, 305, 306t
design considerations, 305–310
differential settlement, 309
free swell test, 160–162, 161t, *162*
igneous
formation, 8
geological classification of, 149t
metamorphic
classification, 150t
formation, 8
sedimentary
classification, 149t
formation, 8
thermal properties, 597
types, 7–8, 8t
Rock-forming minerals, 147, 148t
Rock joints, shear strength, discontinuities, 168, 168t
Rock mass modulus, field tests, 310–313, 311–312t, *313*
Rock mechanics, 147–172, *157,* 158t
classifications, 147–154, 148t
deformation, 154–159, *155*
parameters, cross-anisotropic rocks, 155–157
failure criteria, brittle material, 164–166
Griffith criterion, *164,* 164–165
Hoek-Brown failure criterion, 165t, 165–166, *166*
horizontal stresses, 168–172
calculations, 169t, 170, *170*
hydraulic fracturing, *171,* 171–172, *172*
United States Bureau of Mines, 168–171, *169,* 169t, *170*
rock classifications, 147–154
engineering classification, 150t, 150–154, *151, 152, 153,* 153t, *154*
rock-forming minerals, 147
shear strength
discontinuities, 166
description, 166
friction angle, 166–168, *167*
rock joints, results of tests on, 168, 168t
measurement, 166
site characterization, 147–172
strength, 154–159, *155*
stress-train relationships, cross-anisotropic rocks, 155–157
tensile strength tests, 157–159
Brazilian test, 157–159
direct tension test, 159
time-dependent deformation, 159–164, *160,* 161t
free swell test, 160–162, 161t, *162*
semi-confined swell test, 162–164, *163*
triaxial compression test, 159
triaxial extension test, 159
types of rocks, 147–154, 148t
uniaxial compression test, 155, *155, 156,* 157
Root piles, for stabilization, 431, 458–459
Roundness
class, described, 45
criteria, 45t
Rudaceous rock, classification, 149

S

Saline rock, classification, 149
Salt
chemical resistance guidelines, 775
porosity, 713
Sampling, haphazard, 669
Sampling methods, site characterization, 84–87, 85t
Sand
capillary rise in, 712
coarse
ASTM sieve number, 44
drainage, hydraulic conductivity, 54
drained behavior of, 28–31, *29, 30*
fine, 47
ASTM sieve number, 44
drainage, hydraulic conductivity, 54
footings on, settlement of, 247–250
medium
ASTM sieve number, 44
drainage, hydraulic conductivity, 54
micaceous, void ratio, 47
pipe-soil interface coefficient, 578
shield tip resistance pressure, 576
silty
drainage, hydraulic conductivity, 54
void ratio, 47
undrained behavior of, *30,* 31
Sand layer, non-uniform soils, shallow foundation, *238,* 239, *239*
Sandstone, 149
diffusion, chloride, 723
porosity, 713
thermal properties, 597
Saturated unit weight, defined, 12
Saturation, degree of, defined, 12
Sawdust
as fill material, 433
thermal properties, 597
SBP. *See* Self-boring pressuremeter
Schist, classification, 150
Screw piles, advantages, disadvantages of, 263
Screw-plate test
applicability, 88
site characterization, 94
Sealing of boreholes, in site characterization, 86–87
Search sampling, 669
Sedimentary rock
classification, 149t
formation, 8
Sediments, capillary rise, 712t
Seepage. *See also* Groundwater
site characterization, 197–220
through saturated soil, 11–13
through unsaturated soil, 125–134
hydraulic conductivity function, *126,* 126–128, *127,* 130–133, *131*
Mohr-Coulomb failure envelope, unsaturated soils, *134*
permeability function, *129,* 129–130, *130*
study state, formulation of, 134
unsteady state seepage analysis, 134
water storage function, 128, *128,* 130–133, *131,* 133
Seismic cone-penetration test, 97, 98
advantages, limitations of, 89
Seismic refraction, method, procedure, 83
Seismic risk, earthquake, 654–659
Seismic soil-structure interaction, earthquake, 632–633
Seismic stability, waste cover, 862–872
deformation analysis, 869–872
dynamic shear strength, 869
seismic hazard evaluation, 862–864, 863t
seismic response analysis, 864–869
Seismology, earthquake, 615–620
Self-boring pressuremeter, advantages, limitations of, 90
Semi-confined swell test, rock, 162–164, *163*
Semi-rigid pipe, stiffness, 554
Semivolatile organics
halogenated
containment, 952
soil treatment technology, 954
non-halogenated
containment, 952
soil treatment technology, 954
Sensing, remote, in site characterization, 80–81

Serpentine, density, 47
Settlement, 240–246
 computation, 240–242
 limits of, 240, 241t
 prediction, pile foundations, 273–283
  analysis methods, 273–274, 275–278
  design charts, *274*, 274–275, *275*, *276*
  group settlements, 278–280, *279*
  non-linear analysis, 275, *277*
  pile group settlement, 275–280
 rate of, *244*, 244–246, *245*
 theory of elasticity, 242–244
  one-dimensional conditions, 242
  three-dimensional problems, 242–244, *243*, *244*
Sewage, contaminants, 671
Sewer, concrete, 561–564, 562t
Shaft, jacking, 581
Shale, 149
 diffusion, chloride, 723
 porosity, 713
 thermal, soil, 449
Shallow foundation, 223–260, 338–344
 bearing capacity, 224–240, *225*
  non-uniform soils, 232–240
   clay layer, *238*, 239, *239*, 239–240, *240*
   fissured clays, *235*, 235–237, *236*
   footings on slopes, *237*, 237–238
   layered soils, 238–240
   sand layer, *238*, 239, *239*
   strength increasing with depth, *234*, 234–235
    finite depth, 235, *235*
    infinitely deep, 234–235
    strip loading on, 234–235
  uniform soils, 225–232, *226*
   base tilt, 230
   drained case, *227*, 227–228
   finite depth, soil layers, 232, 232t
   footing shape, effect of, 228
   general formulae, 229–232, 230t, *231*
    foundation depth, 230
    foundation shapes, 230
    inclined loading, 230
   net bearing capacity, 228–229
   surface slope, 230
   Terzaghi's factors, 228
   undrained case, 227
 cold climates, 257–258
 combined footings, 224
 embedment effects, 341–343, *342*, 342t, 343t
 impedance functions of, *338*, 338–341, *339*, 339t, *340*, 341t
 inspection, 224
 layer on halfspace, impedance functions of, 343–344
 limit state design, 258–259
 mat foundation, 224
 numerical approaches, 246–252
  bearing criteria, settlement, 250–252, *251*
  layered soil, 246, *247*
  non-linear materials, 246
  sand, footings on, settlement of, 247–250
  soil parameter estimation, 252
  standard penetration test, 247–249, *248*
  static cone penetrometer, 249, *250*
 pad footings, 223–224
 raft foundation, 224, 252–257
  circular rafts, 253–255, *255*
  of general shape, 256
  rectangular rafts, 255–256, *256*, *257*
  strip rafts, 253, *253*, *254*
 reactive soils, 257
  rafts on, 257
 settlement, 240–246
  computation, 240–242
  limits of, 240, 241t
  rate of, *244*, 244–246, *245*
  theory of elasticity, 242–244
   one-dimensional conditions, 242
   three-dimensional problems, 242–244, *243*, *244*
 trip footings, 223, *223*
 types, 223–224
Shape, particle, 45, *45*, 45t
Shear modulus, damping, soils, 64–67, 65t, *66*
Shear strength, 34–36
 discontinuities
  rock, 166
   description, 166
   friction angle, 166–168, *167*
  rock joints, results of tests on, 168, 168t
 measurement, 166
 soils, 59–64
  effective strength parameters, *60*, 60–62
   clays, *61*, 61–62, *62*
  soil behavior, laboratory determination of, 59–60
  undrained shear strength, 62–64
   normally consolidated clays, 62–63, *63*
   overconsolidated clays, 63–64, *64*
 strength characterization, *34*, 34–35, *35*, 35–36
 undrained, soils, 62–64
 unsaturated soil, *134*, 134–141, *135*
  bearing capacity problems, 140
  lateral earth pressure problems, 140–141, *141*
  slope stability problems, 141, *142*
  soil suction, *135*, 135–136, *136*, 136–137
  soil-water characteristic curve, 137–140
Sheet pile
 physical barrier, 960
 walls, 517–518, *518*, 770
Shield tip resistance pressures, 576t
Shoreline protection, 799
Shrinkage, soil, *58*, 58–59, 59t
Side scan sonar, method, procedure, 84
Siderite, density, 47
Significance tests, interpretation of, 899–900, 900t
Silica, in groundwater analysis, 198
Silicate minerals, physicochemistry, 691–692, *692*
Siliceous rock, classification, 149
Silt
 ASTM sieve number, 44
 coarse
  ASTM sieve number, 44
  capillary rise in, 712
 fine
  ASTM sieve number, 44
  capillary rise in, 712
 loess, drainage, hydraulic conductivity, 54
 medium, ASTM sieve number, 44
 shield tip resistance pressure, 576
 thermal properties, 597
 uniform, inorganic, void ratio, 47
Silver, as contaminant, 671
Simple substitution methods, censored data analysis, 910
Single comparisons, procedures for, 900–904
 Behren, Fisher t-test, Cochran's approximation to, 902–903
 linear regression, 903–904
 student's t-test, 900–902
Single-grain fabrics, physicochemistry, 703
Site characterization, 69–106
 codes of practice, 75
 contaminated land, 104–105
 contracts, 80
 cost, 79
 design, *74*, 74–80
 dewatering, 197–220
 drainage, 197–220
 engineering characteristics
  in situ tests, 96–98, 98t, 99t

statistical methods, 96–98
environmental site characterization, 103–106
field equipment, 78
field instrumentation, 100–101
flowchart, *72*, 72–73
geosynthetics, 173–196
groundwater characterization, 101–103
piezometric pressures, 102–103
sampling, 101–102
in situ hydraulic conductivity tests, 103
water levels, 102–103
guidelines, 75
integrated approach, 70–73, *71*
investigation
aerial photographs, 80–81
backfiling, 86–87
background, 80
Becker penetration test, 91–92
borehole drilling, 84–87, 85t
components, methods, 80–95
continuous seismic reflection profilers, method, procedure, 84
depth recorders, method, procedure, 84
dilatometer test, 93–94
dynamic cone-penetration test, 91
dynamic probing, 91
existing information, review of, 80
field reconnaissance, 81
field testing, 87t, 87–95, 88t, 89–90t
field vane test, 92
geophysical surveys, 81–84, 83t, 84t
horizontal stress, *in situ*, 94–95
mapping, 81
Piezo-cone penetration test, 92–93
plate-load test, 94
pressuremeter test, 93
remote sensing, 80–81
sampling methods, 84–87, 85t
screw-plate test, 94
sealing of boreholes, 86–87
side scan sonar, method, procedure, 84
in situ testing, 87t, 87–95, 88t, 89–90t
standard penetration test, 89–91
landfills, 104–105
need for, 69–70
objectives of, 70
observational approach, monitoring, 97–101
offshore investigations, 79–80
planning, *74*, 74–80
process, 70–73, *71*
property assessment, 107–146
quality management, site investigation, 75
reporting, 73
rock mechanics, 147–172
scope of investigation, 75–78, *77*
seepage, 197–220
soils, engineering properties of, 43–68
test methods, 78
unsaturated soil, 107–146
Slate, classification, 150
Slopes, 397–428
anchor systems, 427, *427*
counterforts, 425
drainage systems, 424–426, *426*
drawdown, rapid, 402
dynamic loading, 402
earth retaining systems, 424
earthworks, 424, *424*
failure movement, *406*, 406–407, *407*
flow nets, 402–403, *403*
galleries, 425
groundwater conditions, 399–404
clays, excavations in, *401*, 401–402
triggering factors, water, 402, *402*
water flow conditions, 399–401
mass movements, 397–428
mitigation, movement, 423–427
bridging, 423
protection of structures, 423
relocation, 423
unstable materials, removal of, 423
movement, *404*, 404–409
elements at risk, 421
hazard, 421–422
risk assessment, 420–423
tolerable risk, *422*, 422t, 422–423
total risk, 420–421
types of, 399, *400*
post-failure movement, 407–408
pre-failure movement, *405*, 405–406
rainfall, intense, 402
reactivation movement, *408*, 408–409
reduction, 195
reinforced, 501–538, 531–535
rock slopes, 404, *404*
in situ reinforcement, 426–427
snowmelt, 402
stability
analysis, 409–420
drawdown, rapid, 412
global method, perturbation method, 414–415, *415*
infinite slope, *411*, 411–412
open fissures, 412
planar failure, 415–416, *417*
seismic forces, 412
slices, methods of, *412*, 412–414, *413*, *414*
submerged slopes, 412
toppling failure, 418–420, *419*
wedge failure, 416–418, *418*
unsaturated soil, 141, *142*
waste cover, 850–862
construction, 859–861
limit equilibrium analyses, 851–856
safety, 861–862, 862t
shear strength parameters, 857t, 857–859, 860t
stress-deformation analyses, 856
stabilization, 457–459
trench, drains, 425
tunnels, drainage, 425
unstable, piles in, 299
vegetation, 427
warning systems, with movement, 427–428, 428t
wells, drainage, 425
Slurry trench
low permeability barrier, 934
walls, 769–770
Smectite minerals, 693
clay, 693
Smelting operations, contaminants, 671
Snow, thermal properties, 597
Socketed piles into rock, *313*, 313–318
average side shear, 314–316, 315t, *316*
design, 316–318, *317*, *318*, *319*
end bearing resistance, 314
shaft resistance, 314
Sodium, diffusion coefficient, 778
Soft soil, embankments over, 463–500
Soil
classification, 50t, 51, 51t, 52t, 53t
chart, 50t
clean-up goals, 949t
clogging, blinding, reduction, 195
contaminated
management of, 947–966
in situ containment, treatment, 921–946
engineering properties, 43–68
amorphous-granular peat, 50
attapulgite, density, 47
augite, density, 47
biotite, 47
calcite, 47
chlorite, 47
coarse-fibrous peat, 50
coarse-grained soils, 50

compressibility, 55–58, 56t
preconsolidation pressure, 56, *56*
consolidation, 55–58
coefficient of, *57*, 57–58
creep, 58, 58t
disturbed soils, 58
dolomite, 47
dynamic properties, 64–67
shear modulus, damping, 64–67, 65t, *66*
elastic properties, 55–56
fine-fibrous peat, 50
fine-grained soils, 50
gibbsite, 47
gypsum, 47
halloysite, density, 47
hematite, density, 47
highly organic soils, 50
hornblende, 47
hydraulic conductivity, 51–54
laboratory hydraulic conductivity tests, 51–54
soils, 54t
values, correlations, 54, 54t
von Post classification, 52t
illite, 47
index tests, 43–51
Atterberg limits, 46–48, 47t
activity, 48
clay minerals, 48t
liquid limit, 46–47
plastic limit, 47
plasticity index, 47t, 47–48
shrinkage limit, 48
density index, 45–46
expansion index, 48–49
grain-size distribution, 43–45, 44t, *45*
granular soil, maximum, minimum densities for, 47t
liquidity index, 48
minerals, relative density of, 47t
organic material, content of, 49–51
particle shape, 45, *45*, 45t
particle sizes, 44t
plasticity chart, *49*
relative compaction, 46
relative density, 46
roundness criteria, 45t
sensitivity, 49
void ratios, maximum, minimum, 45, *46*, 47t
K-feldspars, 47
kaolinite, 47
magnetite, 47
montmorillonite, density, 47
muscovite, density, 47
Na-Ca-feldspars, 47
names, group, assigning, 50
olivine, 47
peat structure, classification of, 51t
Poisson's ratio, 55, 55t
approximate values of, 55t
pyrophyllite, 47
quartz, 47
remolded soils, 58
at rest stress state, 54–55
normally consolidated soils, 54
overconsolidated soils, 54–55
serpentine, 47
shear strength, 59–64
effective strength parameters, *60*, 60–62
clays, *61*, 61–62, *62*
soil behavior, laboratory determination of, 59–60
undrained shear strength, 62–64
normally consolidated clays, 62–63, *63*
overconsolidated clays, 63–64, *64*
shrinkage, *58*, 58–59, 59t
siderite, density, 47
soil classification, 50t, 51, 51t, 52t, 53t
chart, 50t
swelling, *58*, 58–59, 59t
recompression, 57, *57*
symbols, group, soil, assigning, 50
talc, density, 47
virgin compression, 56t, 56–57, *57*
Young's modulus, 55, 55t
engineering properties of, 43–68
fill, imported, contaminants, 671
filter, contact between, 797
fine-grained, 50
frost susceptibility, 609–610
granular, densities for, 47t
improvement, 429–461
blast densification, 454
chemical admixtures, stabilization by, 444
chemical stabilization, 443–452
compaction grouting, 452–453
compaction piles, 456
consolidation, 434–443
dewatering, 434
groundwater control, 434
preloading, surcharge, 434–436, *435*
vacuum, preloading by, *436*, 436–437, *437*
vertical drains, consolidation with, 437–441, *438*, 438t
deep soil mixing, 445
dynamic compaction, 453–454
electrical stabilization, 443–452
electro-kinetic stabilization, *449*, 449–452, 450t
electro-osmotic stabilization, *449*, 449–452, 450t
embankments, reinforcement of, 456–457
evaluation of, 459–462
foundations, reinforcement of, 456–457
ground freezing, artificial, *448*, 448–449, 449t
hydromechanical compaction, 456
intrusion, 445–447, *446*
inundation, 456
jet grouting, 447
lightweight fill, 432–433, 433t
lime-cement columns, 444–445
methods, 430–431t
permeation grouting, 445–447, *446*
physical stabilization, densification, 452–457
preloading, 452
removal, 433–434
replacement, 433–434
slope stabilization, 457–459
biotechnical stabilization, 459
dewatering, 457
ground anchors, 457
groundwater control, 457
micropiles, 458–459
pin piles, 458–459
root piles, 458–459
soil nailing, 457–458, *458*
tiebacks, 457
thermal stabilization, 443–452
thermal treatment, 447–448
verification, 459–462
vertical drains, prefabricated, 441–443
vibro-compaction, 454–456
vibro-replacement, 454–456
mass, dry unit weight, defined, 12
mechanics, 7–42
alluvial deposits, 9
compressibility, 19–28
elasticity, 19–20
expansion, 21–22, *22*
modulus variation, *20*, 20–21
consolidation, one-dimensional, 23–26, *24*, *25*
Coulomb's failure criterion, *34*
creep, 26–28, *27*
damping, determination of, 40–41
dynamic soil behavior, 40–42
modulus, determination of, 40–41
seismic stability, 41–42

elasto-plasticity, 36–40
Cam clay model, 37–39, *38*
critical state soil mechanics, 36–37, *37*
forming minerals, 7–8, 8t
geologic formation, classification, soil, 7–11
Hvorslev surface, *32*
igneous rock, formation, 8
lacustrine deposits, 9
marine deposits, 9
metamorphic rock, formation, 8
minerals, soil forming, 7–8, 8t
Mohr-Coulomb failure criterion, *34*
Mohr's circle, 13–15, *14, 15,* 15–16, *16*
p-q diagram, 17
rock groups, 8t
rock types, 7–8, 8t
s-t diagram, 16, *16*
sedimentary rock, formation, 8
seepage, through saturated soil, 11–13
basic head equations, 11–13
shear strength, 34–36
effective strength characterization, *34,* 34–35, *35*
total strength characterization, 35–36
mixing, low permeability barrier, 934
nailing, 431, 457–458, *458,* 530–531, 531t
organic, 50
parameter estimation, shallow foundation, 252
phases
relationships, *11*
relationships among, *11*
physicochemistry, 691–710
soil water, 695–697
pipe, interface friction coefficients, 578t
properties, 705–710
defined, 12
relationships, 11, *11,* 12t
reinforcement, 506–507
soft, embankments over, 463–500
stabilization
dewatering system, 208–213
geosynthetic reinforcement for, 431
systems, 208–213
strain, 15–16, *16*
strength behavior, *28,* 28–34
stress, 13–15, *14, 15,* 17–19
effective stress principle, 17
effective vertical stress, 18–19
groundwater table, porewater pressure, 18
horizontal stress, 19
paths, 16–17
representations, 16–17
total vertical stress, 17–18
stress-strain, *28,* 28–34
clay
drained behavior of, 33–34, *34*
normally consolidated, undrained behavior of, 31, *31*
overconsolidated, undrained behavior of, 31–33, *32, 33*
sand
drained behavior of, 28–31, *29, 30*
undrained behavior of, *30,* 31
suction, unsaturated soil, *135,* 135–136, *136,* 136–137
thermal properties, 449, 449t, 595–597
treatment technologies, 954t
types, 7–11
clay fabric, 10
Darcy's law, 13
geologic cycle, 8–9
granular soils, fabric of, 10
hydraulic conductivity, 13
soil fabric, 9–11
soil forming processes, 8–9
undrained shear strength, 62–64
unsaturated, 107–146
site characterization, 107–146
walls, reinforced, 523–531
water, physicochemistry, 696, *697*
water characteristic curve, 110
estimation of, *118,* 118–120, *120*
laboratory measurement, *116,* 116–118, *117,* 118t
mathematical form for, 115t, 115–116
pressure plate apparatus, *116*
residual conditions, 113–115, *114*
stages, 111
unsaturated soil, 110, 137–140
Weald clay, drained triaxial compression test data for, *34*
Soil-bentonite liners, 761
Soil-forming minerals, 7–8, 8t
Soil-pipe interaction, 551–553
Soil-vapor extraction, 927–928, 958–959
Solids
density of
defined, 12
relative, defined, 12
unit weight, defined, 12
Sorption, hydrogeology, 733–736, 734t
Source-zone isolation, 933–937
covers, 937
enclosures, 933–937, 934–935t
Source-zone restoration, 925–933
goals, 925–926
Source zones, earthquake, 619
Spearman's rank correlation coefficient, 908
Specific storage, 714
Specified complete groundwater control system, 219
Specified minimum groundwater control system, 219
SPT. *See* Standard penetration test
Stabilization of contaminants, 959
Standard penetration test, 97, 98
advantages, limitations of, 89
applicability, 88
pile foundations, 268–271, 270t
shallow foundation, 247–249, *248*
Static cone penetration test, pile foundations, 268, 270t
Static cone penetrometer, shallow foundation, 249, *250*
Statistical analyses
analysis of variance, 898
Behren, Fisher t-test, Cochran's approximation to, 898
censored data, 910–913
Aitchison's method, 911–912
Cohen's test, 911
maximum likelihood estimator, 912
plotting position procedure, 911
Poisson model, 912–913
simple substitution methods, 910
test of proportions, 910–911
linear regression, 898–899
monitoring data, 893–914
multiple comparisons, 904–906
analysis of variance, 904–905
multiple regression, 906
multiple regression, 899
non-parametric procedures, 906–910
Kruskal-Wallis test, 909–910
Mann-Whitney (U) test, 907–908
Spearman's rank correlation coefficient, 908
significance tests, interpretation of, 899–900, 900t
single comparisons, procedures for, 900–904
Behren, Fisher t-test, Cochran's approximation to, 902–903
linear regression, 903–904
student's t-test, 900–902
statistical power, 913
student's t-test, 897–898
Steel
corrugated, as pipe material, 543
culvert, large diameter, corrugated, 564t, 564–566
pipe, pipe-soil interface coefficient, 578

reinforcement, pavement, 372–373
sheet piling, conventional, low permeability barrier, 935
thermal properties, 597
Stepped-blade, 90
Stiffness, pipe, 550–551, 554t
performance limits, 543t
Storativity, 713
Storm sewer, concrete, 561–564, 562t
Strain, soil and, 15–16, *16*
Stratified random sampling, 669
Straw fibers, thermal properties, 597
Strength, 706–708. *See also* Shear strength
rock, 154–159, *155*
soil, *28*, 28–34, 706–707, *707*
Stress
ground, 13–15, *14*, *15*
state of, 17–19
effective stress principle, 17
effective vertical stress, 18–19
groundwater table, porewater pressure, 18
total vertical stress, 17–18
paths, 16–17
relief test, rock mass modulus, field tests, 312
representations, 16–17
state, soil, at rest, 54–55
normally consolidated soils, 54
overconsolidated soils, 54–55
state variables, unsaturated soil, 120–122
matric suction, 121–122, *122*
osmotic suction, 121–122, *122*
total suction, 121–122, *122*
Stress-strain, *28*, 28–34
clay
drained behavior of, 33–34, *34*
normally consolidated, undrained behavior of, 31, *31*
overconsolidated, undrained behavior of, 31–33, *32*, *33*
sand
drained behavior of, 28–31, *29*, *30*
undrained behavior of, *30*, 31
soil, 707, *708*
Stress-strain-time behavior, soil, 707–708
Strip footings, 223, *223*
Strip rafts, 253, *253*, *254*
Student's t-test, 897–898
Subangular roundness, 45
Subbase support, rigid pavement, 387
Submerged unit weight, defined, 12
Submersible pump, for groundwater sampling, 891
Substitution methods, censored data analysis, 910
Suction pump, for groundwater sampling, 891
Sulfate, in groundwater analysis, 198
Surcharging, soil, 430
Swelling, soil, 57, *57*, *58*, 58–59, 59t
Syenite, geological classification, 149
Symbols, soil, assigning, 50
Systematic sampling, 669

T

Tailings ponds, contaminants, 671
Talc, density, 47
Tall buildings on rock foundation, 305–318
adjacent structures, effect of excavations, 310
allowable bearing pressure, 305–309, 307t, *308*, *309*
base heave, 310
bearing capacity, 305, 306t
design considerations, 305–310
differential settlement, 309
TCE. *See* Trichloroethene
Technology-based standard, as soil clean-up goal, 949
Temperature, in groundwater analysis, 198
Tensile strength tests, rock, 157–159
Brazilian test, 157–159
direct tension test, 159
Tension membrane theory, reinforcement over voids, 536
TERA. *See* Toxicology Excellence for Risk Assessment
Test methods, in site characterization, 78
Test of proportions, censored data analysis, 910–911
Testing laboratories, toxicology, 683
Tetrachloroethane
Henry's law constant, 732
partitioning coefficient, range, 784
Thaw-weakening, highways, 613
Thermal boundary conditions, 596–600
freezing indices, *598*, 598–600, *599*, 599t
thawing indices at ground surface, *598*, 598–600, *599*, 599t
Thermal conductivity
fine-grained soils, 709
soils, 595, *595*
Thermal flushing techniques, 932
Thermal power stations, contaminants, 671
Thermal properties, 597t
soil, 449t, 595–596
heat capacity, 595–596
latent heat, 596, *596*
thermal conductivity, 595, *595*
thermal resistance, 596, 597t
Thermal slope stabilization, 443–452
Thermal treatment, for soil improvement, 447–448
Thermoplastics, as pipe material, 543
Thickness, pavement, 388
Thrust, buried pipe, 555–556
Tiebacks, 457, 524–528
for soil stabilization, 431
Time-dependent deformation, rock, 159–164, *160*, 161t
free swell test, 160–162, 161t, *162*
semi-confined swell test, 162–164, *163*
Tire chips, thermal properties, 597
Tires, used, as fill material, 433
Toe drains, dam, 799
Tolerable risk, slope movement, *422*, 422t, 422–423
Toluene
diffusion coefficient, 778, 783
Henry's law constant, 732
partitioning coefficient, range, 784
Total risk, slope movement, 420–421
Total suction, unsaturated soil, 121–122, *122*
Total unit weight, defined, 12
Toxic heavy metals, as contaminants, 671
Toxicity assessment, 681–684
Toxicology, testing laboratories, 683
Toxicology for Risk Assessment, 683
TPHCWG. *See* U.S. Air Force Total Petroleum Hydrocarbon Criteria Working Group
Trachyte, geological classification, 149
Traffic loads, pavement, 374–375, 375t
Trans-1,2 dichlorethene, Henry's law constant, 732
Transmissive layers, 739–751
Transmissivity, 713
Transport, contaminant, 721–738
Trench
dewatering, 799
installation, buried pipe, 546–548, *547*, 547t
loading, *vs.* embankment loading, 563–564
Trench drains, 425
Trench walls, slurry, 769–770
Trenchless technology, 569–592
adjacent structures, influence on, 588
auger boring, 573
buried infrastructure, influence on, 588

directional drilling, 573–574
excavation, techniques, 570–582
face stability, 574–576, *575*, 576t
geotechnical engineering, 574–582
ground displacement, techniques involving, 582–588
ground movements, 586–588, *587*
calculation of, 579–580, *580*
guided drilling, 582–583
jacking shafts, 581
lubrication, 580–581
methods, 570t
microtunneling, 570–573
moling, 582–583
pipe
bursting, 583–584
jacking, 570–573
ramming, 584
pipeline
friction, *576*, 576–579, *577*, *578*, 578t
void stability, 585–586
rehabilitation techniques, 588–591
tunnel stability, *576*, 576–579, *577*, *578*, 578t
void
creation, 584–585
stability, pipeline friction, 585–586
Triaxial compression test, rock, 159
Triaxial extension test, rock, 159
Trichloroethene
diffusion coefficient, 778
Henry's law constant, 732
partitioning coefficient, range, 784
Tunnel, stability of, *576*, 576–579, *577*, *578*, 578t
Tunnel relaxation test, rock mass modulus, field tests, 312
Turbidity, in groundwater analysis, 198

U

Ultraviolet degradation, polymers, 190–191
Underdrains, reduction, 195
Uniaxial compression test, rock, 155, *155*, *156*, 157
Unit weight
defined, 12
dry, soil mass, defined, 12
saturated, defined, 12
solids, defined, 12
submerged, defined, 12
total, defined, 12
water, defined, 12
UNSAT-H, water balance, waste cover, 846–847
Unsaturated soil
boundary conditions, 122–125, *123*
evaporation, 124–125, *125*
evapotranspiration, 124–125, *125*
flux boundary condition, prediction of, 124–125, *125*
overview, 109–110, *110*
property assessment, 107–146
seepage through, 125–134
hydraulic conductivity function, *126*, 126–128, *127*, 130–133, *131*
Mohr-Coulomb failure envelope, unsaturated soils, *134*
permeability function, *129*, 129–130, *130*
study state, formulation of, 134
unsteady state seepage analysis, 134
water storage function, 128, *128*, 130–133, *131*
shear strength, *134*, 134–141, *135*
bearing capacity problems, 140
lateral earth pressure problems, 140–141, *141*
slope stability problems, 141, *142*
soil suction, *135*, 135–136, *136*, 136–137
soil-water characteristic curve, 137–140
in site characterization, 107–146
soil-water characteristic curves, 110
estimation of, *118*, 118–120, *120*
laboratory measurement, *116*, 116–118, *117*, 118t
mathematical form for, 115t, 115–116
pressure plate apparatus, *116*
residual conditions, 113–115, *114*
stages, 111
stress state variables, 120–122
matric suction, 121–122, *122*
osmotic suction, 121–122, *122*
total suction, 121–122, *122*
volume change, 141–146, *143*, *144*
heave, expansive soil, *145*, 145–146
measurement, 144–145
volume change moduli, *144*, 145
Unsteady state seepage analysis, unsaturated soil, 134
Uphole, downhole, and cross-hole, method, procedure, 83
Uplift capacity, pile foundations, 271
U.S. Air Force Total Petroleum Hydrocarbon Criteria Working Group, 683
U.S. Bureau of Mines, horizontal stresses tests, 168–171, *169*, 169t, *170*
USBM. *See* U.S. Bureau of Mines

V

Vacuum, to soil, dewatering system, 208–213, *213*
Vadose-zone contamination in source zone, 926–929
excavation, 926–927
soil flushing, 929
soil vapor extraction, *927*, 927–928, *928*
Velocity
Darcy, *see* Darcy flux
Groundwater, 13, 716
Verification, soil improvement, 459–462
Vermiculite
clay, 694
physicochemistry, 694
Vertical cut-off walls, 769–770
geomembranes, 770
sheet pile walls, 770
slurry trench walls, 769–770
Vertical drains, 430
prefabricated, 441–443
wall, 799
Vertical stress, effective
ground, 18–19
in ground, state of, 18–19
Vibrated beam, low permeability barrier, 934
Vibration, method, procedure, 83
Vibrocompaction, 431, 454–456
Vibroreplacement, 431, 454–456
Vinyl chloride, Henry's law constant, 732
Virgin compression, soil, 56t, 56–57, *57*
Visualization method, 916–919, *917*, *918*
Vitrified clay pipe, 544
Void creation, trenchless technology, 584–585
Void ratio
defined, 12
maximum, minimum, 45, *46*, 47t
Void stability, pipeline friction, 585–586
Voids, reinforcement over, 535–537
arching, 536
BS 8006 method, 537
combined arching, tension membrane theory, 536
tension membrane theory, 536

Volatile organics
halogenated
containment, 952
soil treatment technology, 954
non-halogenated
containment, 952
soil treatment technology, 954
Volume change, soil
properties, 705–706
unsaturated, 141–146, *143, 144*
heave, expansive soil, *145,* 145–146
measurement, 144–145
moduli, *144,* 145
volume change moduli, *144,* 145
Volumetric water content, defined, 12
Von Post classification, soils, 52t

W

Wall drain, vertical, 799
Walls
cantilever, gravity and, *516,* 516–517
cut-off, with contamination, 960, 960t
diaphragm, 520–523, *522*
reduction, 195
retaining, selection of, 504–506
sheet pile, 517–518, *518*
soil, reinforced, 523–531
Warning systems, slope movement, 427–428, 428t
Waste covers, 825–878
capillary barrier cover systems, 834–837, *835, 836*
classification, 825–828, *826, 827, 828*
examples of, 828, *829, 830, 831*
gas generation, management, 828–831
hydraulic barrier cover systems
components of, 831–834
foundation layer, 834
gas transmission layer, 834
hydraulic-barrier layer, 833–834
internal drainage layer, 833
protection layer, 831–833
surface layer, 831
seismic stability, 862–872
deformation analysis, 869–872
dynamic shear strength, 869
seismic hazard evaluation, 862–864, 863t
seismic response analysis, 864–869
settlement, 872–877
due to localized mechanisms, 876
foundation soils, 873
impact of, on cover system, 876–877
mechanisms of, 872–873, *873*
waste compression, 873–876, *874,* 875t
static slope stability, 850–862
construction, 859–861
limit equilibrium analyses, 851–856
safety, 861–862, 862t
shear strength parameters, 857t, 857–859, 860t
stress-deformation analyses, 856
water balance, 837–850
evaluation of models, 847–848
HELP model, 843–845, *844*
LEACHM model, 845–846
simplified manual method, 838–843
UNSAT-H, 846–847
Waste landfill
hazardous, 964
non-hazardous, 963–964
Water
density of, defined, 12
diffusion coefficient, 783
partitioning coefficient, range, 784
thermal properties, 449, 597
unit weight, defined, 12
Water adsorption, by soils, 696, *697*
Water balance, waste cover, 837–850
evaluation of models, 847–848
HELP computer code, 839
HELP model, 843–845, *844*
LEACHM computer code, 839
LEACHM model, 845–846
simplified manual method, 838–843
UNSAT-H, 846–847
UNSAT-H computer code, 839
Water content
defined, 12
volumetric, defined, 12
Water storage function, unsaturated soil, 128, *128,* 130–133, *131*
Water supplies, contaminants to, 671
Wave propagation, earthquake, 620–622
buried pipes, strains in, *621,* 621–622
elements of, 620
ground, strains in, 620–621
Wave type, earthquake, 616–617, *617*
Weald clay, drained triaxial compression test data for, *34*
Weathered crust, strength of, 486, *486*
Well, monitoring, locations, 880–886
Well-screens, dewatering system, 215–216
WHO. *See* World Health Organization
Wind, action on geomembranes, 817–824
Wood bark, thermal properties, 597
Wood chips, thermal properties, 597
Wood industry, residues from, as fill material, 433
Wood treatment, contaminants from, 671
World Health Organization, 683

X

Xylene
diffusion coefficient, 783
partitioning coefficient, range, 784

Y

Young's modulus, 55, 55t

Z

Zinc
as contaminant, 671
diffusion coefficient, 778

CONVERSION FACTORS US TO SI UNITS

	Multiply	by	to obtain
Length	ft	3.048×10^{-1}	m
	mile	1.609	km
Area	ft^{-2}	9.290×10^{-2}	m^2
	acre	4.047×10^{3}	m^2
	mi^2	2.590	km^2
Volume	ft^3	2.832×10^{-2}	m^3
	U.S. gal	3.785×10^{-3}	m^3
	U.K. gal	4.546×10^{-3}	m^3
	ft^3	2.832×10	ℓ
	U.S. gal	3.785	ℓ
	U.K. gal	4.546	ℓ
Velocity	ft s^{-1}	3.048×10^{-1}	m s^{-1} (m/s)
Acceleration	ft s^{-2} (ft/s^2)	3.048×10^{-1}	m s^{-2} (m/s^2)
Mass	lb_m	4.536×10^{-1}	kg
	ton	1.016×10^{3}	kg
Force and Weight	lb_f	4.448	N
Pressure and Stress	psf	4.788×10	Pa or N m^{-2} (N/m^2)
	psi	6.895×10^{3}	Pa or N m^{-2} (N/m^2)
	atm	1.013×10^{5}	Pa or N m^{-2} (N/m^2)
	atm	1.013	bar
Work and Energy	ft-lb_f	1.356	J
	calorie	4.187	J
Mass Density	lb_m ft^{-3} (lb_m/ft^3)	1.602×10	kg m^{-3} (kg/m^3)
Weight Density	lb_f ft^{-3} (lb_f/ft^3)	1.571×10^{2}	N m^{-3} (N/m^3)
Discharge	ft^3 s^{-1} (ft^3/s)	2.832×10^{-2}	m^3 s^{-1} (m^3/s)
	ft^3 s^{-1} (ft^3/s)	2.832×10	ℓ s^{-1} (ℓ/s)
	U.S. gal min^{-1} (gal/min)	6.309×10^{-5}	m^3 s^{-1} (m^3/s)
	U.S. gal min^{-1} (gal/min)	6.309×10^{-2}	ℓ s^{-1} (ℓ/s)
	U.S. gal min^{-1} (gal/min)	7.576×10^{-5}	m^3 m^3 s^{-1} (m^3/s)
	U.S. gal min^{-1} (gal/min)	7.576×10^{-2}	ℓ s^{-1} (ℓ/s)
Hydraulic	ft s^{-1} (ft/s)	3.048×10^{-1}	m s^{-1} (m/s)
Conductivity	U.S. gal day^{-1} ft^{-2} (gal/day/ft^2)	4.720×10^{-7}	m s^{-1} (m/s)
Transmissivity	ft^2 s^{-1} (ft^2/s)	9.290×10^{-2}	m^2 s^{-1} (m^2/s)
	U.S. gal day^{-1} ft^{-1} (gal/day/ft)	1.438×10^{-7}	m^2 s^{-1} (m^2/s)